Digitized by the Internet Archive
in 2026

https://archive.org/details/symposium-international-on-combustion_1957

SIXTH SYMPOSIUM

(INTERNATIONAL)

ON

COMBUSTION

At Yale University
New Haven, Connecticut
August 19–24, 1956

Published for
THE COMBUSTION INSTITUTE

REINHOLD PUBLISHING CORPORATION
New York
CHAPMAN & HALL, Ltd., LONDON

Copyright 1957 by

The Combustion Institute
1st reprinting 1971

All rights reserved

Brief quotations from this book for purposes of scientific discussion will be permitted.

Library of Congress Catalog Card Numbers: 57-13313

Printed in the United States of America

PREFACE

The Sixth Symposium (International) on Combustion, the first of the combustion symposia to be conducted under the auspices of The Combustion Institute, was held at Yale University, New Haven, Connecticut, August 19 through 24, 1956.

Combustion in its broadest concept provided the theme of the technical meetings. The very arduous task of review of the papers and arrangement of the program was ably discharged by the Papers Subcommittee. There were thirty-seven papers on the structure and propagation of laminar flames, six on the structure and propagation of turbulent flames, eight on high speed reactions, eight on flame stabilization in fast streams, nine dealing with instability in combustion chambers, eight on the combustion of solid fuels, eleven on the combustion of explosives and solid propellants, nine on the evaporation and combustion of droplets and sprays, nine covering experimental and analytical techniques, and twenty on applications of combustion.

Resumés of three interesting panel discussions are given in this publication.

The assistance of members of the Explosives Technology Division of the U. S. Bureau of Mines in reading proof of this volume was very much appreciated.

Of the 698 participants at the symposium, 31 were from Great Britain, 19 from Canada, five from France, three each from Belgium, Japan, Sweden, and the Union of Soviet Socialist Republics, and one each from Germany, Holland, Norway, and Spain. Of the United States registrants, 99 were Federal employes, 124 were from educational institutions, and 369 represented industry.

The Department of the Air Force generously provided transportation for a number of the overseas delegates.

It is desired to acknowledge the partial support of this symposium by the United States Department of the Air Force through the Office of Scientific Research of the Air Research and Development Command, by the United States Department of the Army through the Office of Ordnance Research, and by the United States Department of the Navy through the Office of Naval Research.

The Finance Subcommittee enlisted the cooperation and financial support of the following organizations, to whom grateful acknowledgment is made:

Aerojet-General Corporation
Aircooled Motors, Inc.
Air Reduction Company
American Gas Association
American Gas and Electric Service Corporation
Atlantic Research Corporation
Bechtel Corporation
Bell Aircraft Corporation
Bethlehem Steel Company
Boeing Airplane Company
Godfrey L. Cabot, Inc.
California Research Corporation
Canadian Industries, Ltd.
Caterpillar Tractor Company
Cities Service Research and Development Company
Combustion Engineering, Inc.
Combustion and Explosives Research, Inc.
Continental Aviation & Engineering Corp.
Continental Oil Company
Cummins Engine Company, Inc.
Douglas Aircraft Company, Inc.
E. I. du Pont de Nemours & Company
Esso Research and Engineering Company
Ethyl Corporation
Experiment Incorporated
Fairchild Engine Division
The Fluor Corporation, Ltd.
Ford Motor Company
The Garrett Corporation
General Dynamics Corporation
General Electric Company
    Aircraft Gas Turbine Division
    Research Laboratory
General Motors Corporation
    Allison Engine Division
    G. M. Research Laboratories
Gulf Research & Development Company
Hauck Manufacturing Company
International Harvester Company
The M. W. Kellogg Company
Koppers Company, Inc.
Linde Air Products Company
The Arthur D. Little Foundation
The Lummus Company
Lycoming Divison, AVCO

Marquardt Aircraft Company
Mine Safety Appliances Company
Minneapolis-Honeywell Regulator Company
National Airoil Burner Company, Inc.
National Northern
Olin-Mathieson Chemical Corporation
Owens-Corning Fiberglas Corporation
Phillips Petroleum Company
Pittsburgh Consolidation Coal Company
Pittsburgh Plate Glass Company
Pratt & Whitney Aircraft Division
The Pure Oil Company
Reaction Motors, Inc.
Richfield Oil Corporation
Shell Development Company
Sinclair Refining Company
Socony Mobil Oil Company, Inc.
Southwest Research Institute
Standard Oil Company (Indiana)
Standard Oil Company (Ohio)
Sun Oil Company
The Texas Company
Thompson Products, Inc.
Union Oil Company of California
United States Steel Corporation
Universal Oil Products Company
Westinghouse Electric Corporation
Worthington Corporation
Wright Aeronautical Division

The sincere gratitude of all who attended the symposium is extended to President A. Whitney Griswold, of Yale University, for making available the facilities of the University. Special thanks are due also to the Yale Subcommittees on Arrangements who provided admirably for the comfort and pleasure of the participants.

Members of the Institute were deeply grieved by the untimely death on August 8 of Professor Walter J. Wohlenberg, who was admired and respected as a friend, a colleague, and an outstanding scientist. Professor Wohlenberg had participated energetically in the work of the Yale Subcommittees and his selfless efforts contributed greatly to the success of the symposium.

THE COMBUSTION INSTITUTE

A non-profit professional society, incorporated in 1954, to promote the science and application of combustion and to disseminate knowledge in this field.

Officers

President . . . . . Bernard Lewis
Vice President . . . . . Hoyt C. Hottel
Treasurer . . . . . Stewart Way
Assistant Treasurer . . . . . Bernard M. Sturgis
Secretary . . . . . Glenn C. Williams

Executive Office

Union Trust Building, Pittsburgh 19, Pennsylvania
Mrs. Helen G. Barnes, Executive Secretary

Board of Directors

Mr. J. L. Cooley	California Research Corporation
Professor Newman A. Hall	Yale University
Dr. Amos G. Horney	Office of Scientific Research
Professor H. C. Hottel	Massachusetts Institute of Technology
Dr. Bernard Lewis	Combustion and Explosives Research, Inc.
Mr. J. B. Macauley	Ethyl Corporation
Mr. A. J. Nerad	General Electric Company
Dr. Walter T. Olson	NACA Lewis Flight Propulsion Laboratory
Dr. Robert N. Pease	Princeton University
Dr. Edward H. Seymour	Reaction Motors, Inc.
Dr. B. M. Sturgis	E. I. du Pont de Nemours & Company, Inc.
Dr. W. J. Sweeney	Esso Research and Engineering Company
Dr. Stewart Way	Westinghouse Research Laboratories
Professor Glenn C. Williams	Massachusetts Institute of Technology
Dr. Lloyd L. Withrow	General Motors Research Laboratories

The Combustion Institute Committee

United States

Professor Glenn C. Williams, Chairman	Massachusetts Institute of Technology
Dr. David Altman	Aeronutronic Systems, Inc.
Mr. J. L. Cooley	California Research Corporation
Dr. George Glockler	Office of Ordnance Research
Dr. J. P. Longwell	Esso Research and Engineering Company
Dr. Walter T. Olson	NACA Lewis Flight Propulsion Laboratory

Great Britain

Sir Alfred C. Egerton, *Chairman*	Imperial College of Science and Technology, London
Dr. J. S. Clarke, *Secretary*	Joseph Lucas Limited, Birmingham
Dr. J. W. Linnett	Queen's College, Oxford
Dr. Peter Lloyd	National Gas Turbine Establishment, Farnborough
Professor O. A. Saunders	Imperial College of Science and Technology, London

Australia	
Mr. W. B. Kennedy	Aeronautical Research Laboratories, Melbourne
Belgium	
Dr. Louis Deffet	Centre de Recherches pour l'Industrie des Produits Explosifs, Brussels
France	
Professor Paul Laffitte	Faculté des Sciences de l'Université de Paris
Germany	
Professor Wilhelm Jost	Chemisches Institut der Universität, Göttingen
India	
Dr. M. S. Thacker	Council of Scientific and Industrial Research, New Delhi
Italy	
Professor Cesare Codegone	Politechnico di Torino
Japan	
Professor Sakae Yagi	University of Tokyo
Netherlands	
Professor J. J. Broeze	Electrotechnische Industrie voorheen Willem Smit & Company, Slikkerveer
Spain	
Dr. Gregorio Millán	Instituto Nacional di Tecnica Aeronáutica, Madrid
Sweden	
Professor Ernst H. W. Weibull	Bockamöllan, Brösarps Station
Switzerland	
Professor K. Clusius	Physikalisch-Chemisches Institute der Universität, Zürich
Turkey	
Professor Hikmet Binark	Teknik Üniversitesi, Istanbul

1956 SYMPOSIUM SUBCOMMITTEES

Papers Subcommittee

Dr. Walter T. Olson, *Chairman*	NACA Lewis Flight Propulsion Laboratory
Dr. David Altman	Aeronutronic Systems, Inc.
Dr. W. H. Avery	The Johns Hopkins University
Dr. Lyman G. Bonner	Allegany Ballistics Laboratory
Dr. Mathew M. Braidech	National Board of Fire Underwriters
Mr. Edmund D. Brown	United Aircraft Corporation
Dr. David S. Burgess	U. S. Bureau of Mines
Dr. Hartwell F. Calcote	AeroChem Research Laboratories, Inc.
Dr. J. S. Clarke	Joseph Lucas Limited, England
Professor L. G. Crocco	Princeton University
Mr. Jean Fabri	Office National d'Études et de Recherches Aéronautiques, France
Dr. Ernest F. Fiock	Phillips Petroleum Company
Dr. R. D. Geckler	Aerojet-General Corporation
Dr. Melvin Gerstein	NACA Lewis Flight Propulsion Laboratory
Professor Wilhelm Jost	University of Göttingen, Germany
Mr. Béla Karlovitz	Combustion and Explosives Research, Inc.
Professor G. B. Kistiakowsky	Harvard University
Professor Paul Laffitte	University of Paris, France
Dr. J. W. Linnett	Oxford University, England
Dr. J. P. Longwell	Esso Research and Engineering Company
Dr. Frank E. Marble	California Institute of Technology
Dr. George H. Markstein	Cornell Aeronautical Laboratory
Dr. Gregorio Millán	Instituto Nacional di Tecnica Aeronáutica, Spain
Dr. George E. Moore	General Electric Company
Dr. B. P. Mullins	National Gas Turbine Establishment, England
Mr. P. S. Myers	University of Wisconsin
Dr. S. S. Penner	California Institute of Technology
Dr. Ernst H. W. Schmidt	Lehrstuhl fur Technische Thermodynamik, Munich, Germany
Professor F. Schultz-Grunow	Technische Hochschule, Aachen, Germany
Dr. Arch C. Scurlock	Atlantic Research Corporation
Dr. Ellis B. Rifkin	Ethyl Corporation
Professor Kurt Wohl	University of Delaware
Dr. Cornelis Zwikker	National Luchtvaart Laboratorium, Amsterdam, Holland

Finance Subcommittee

Mr. Walter E. Lobo, *Chairman*	The M. W. Kellogg Company
Mr. Richard C. Alden	Phillips Petroleum Company
Dr. J. Bennett Hill	Sun Oil Company
Mr. W. G. Lovell	Ethyl Corporation
Mr. A. L. Lyman	California Research Corporation
Dr. Jerry McAfee	Gulf Research & Development Company

Yale Subcommittee on Arrangements

General

Professor W. J. Wohlenberg, *Chairman*
Professor B. F. Dodge
Dr. Loomis Havemeyer
Mr. R. A. Holden (Secretary of the University)
Professor T. T. Holme
Professor F. W. Keator
Dr. J. G. Kirkwood
Professor L. C. Lichty
Mr. R. A. Toti
Professor C. A. Walker
Dean Dana Young

Entertainment

Professor T. T. Holme, *Chairman*
Professor H. A. Lepper
Professor W. E. Milligan
Mr. R. A. Toti

Ladies

Mrs. C. T. G. Looney, *Chairman*
Mrs. B. F. Dodge
Mrs. T. T. Holme
Mrs. H. A. Lepper, Jr.
Mrs. F. T. McNamara
Mrs. W. J. Wohlenberg
Mrs. Dana Young

Registration and Program

Professor F. W. Keator, *Executive Chairman*
Professor D. R. Olson, *Deputy Chairman*
Professor R. H. Bretton
Mr. J. E. Gibson
Dr. Loomis Havemeyer
Professor C. T. G. Looney
Professor R. R. Shank
Professor F. J. Zimmermann

CONTENTS

Introduction to the Sixth Symposium (International) on Combustion, Yale University, New Haven, Connecticut, August 19–24, 1956, by Walter T. Olson xxiii

STRUCTURE AND PROPAGATION OF LAMINAR FLAMES

*1. The Present Status of the Theory of Laminar Flame Propagation. *Theodore Von Kármán* .. 1
2. Ends and Means in Flame Theory. *D. B. Spalding* 12
3. Limits of Inflammability. *J. W. Linnett and C. J. S. M. Simpson* 20
4. The Effect of Fuel Type and Pressure on Flame Quenching. *A. E. Potter, Jr. and A. L. Berlad* 27
5. A Principle of Mixing Similarity and Its Application to Inhomogeneous Combustion. *William G. Browne and Hugh N. Powell* 37
6. Chain Branching and Flame Propagation. *A. Van Tiggelen and J. Deckers* 61
7. Correlations of Burning Velocity, Quenching Distances, and Minimum Ignition Energies for Hydrocarbon-Oxygen-Nitrogen Systems. *Richard S. Brokaw and Melvin Gerstein* 66
8. The Influence of Pressure on Flame Speed. *Mitchell Gilbert* 74
9. The Effect of Pressure on the Laminar Burning Velocity of Methane-Oxygen-Nitrogen Mixtures. *Donald Smith and John T. Agnew* 83
10. Influence of Physical and Chemical Factors on Burning Velocity. *E. S. Golovina and G. G. Fyodorov* 88
*11. The Structure of Laminar Flames. *Robert M. Fristrom* 96
12. Flame Attachment Zone of Laminar, Premixed Methane-Air Flames. *Arthur L. Thomas and Richard H. Wilhelm* 111
13. Mass Spectrometer Studies of Fuel Concentration in the Dark Space of Laminar Bunsen Flames. *John F. Byrne* 120
14. Flame Propagation in Cylindrical Tubes Near the Quenching Limit. *J. M. Singer and G. von Elbe* 127
15. Cool Flames of Pentane-Oxygen Mixtures. *Michel Lucquin and Paul Laffitte* 130
16. The Dependence of Flame Temperature on Mass Burning Velocity. *W. E. Kaskan* 134
17. Spectroscopic Study of Some Alcohol Flames: Flame Temperatures and Their Influence on the Intensity Changes in Various Bands. *N. R. Tawde and B. B. Laud* 143
18. Burning Velocities of Mixtures of Nitrous Oxide, Carbon Monoxide, Nitrogen and Water. *C. J. S. M. Simpson and J. W. Linnett* 149
19. Ignition Limits and Products of the Multistage Flames of Propane-Nitrogen Dioxide Mixtures. *Albert L. Myerson, Francis R. Taylor and Barbara G. Faunce* 154
20. Burning Structure and Stability of *n*-Butane-Nitrogen Dioxide Flames in Air. *E. Miller and H. J. Setzer* 164
21. Spectroscopic Investigation of *n*-Butane-NO_2 Flames. *W. W. Wharton, T. D. Violett and E. Miller* 173
22. The Methyl Nitrite Decomposition Flame. *E. A. Arden and J. Powling* 177
23. Reduction of Nitric Oxide in Flames and the Decomposition Flame of Methyl Nitrite. *Peter Gray and M. W. T. Pratt* 183
24. Multiple Reaction Zones in Low Pressure Flames with Ethyl and Methyl Nitrate, Methyl Nitrite and Nitromethane. *A. R. Hall and H. G. Wolfhard* 190
25. Flame Properties and the Kinetics of Chain-Branching Reactions. *J. Calvin Giddings and J. O. Hirschfelder* 199
26. Theoretical Study of the Hydrogen-Bromine Flame. *Edwin S. Campbell* 213
27. The Chemical Steady State in HBr Flames. *Mitchell Gilbert and David Altman* 222
28. Stability of the Ozone Flame Propagation. *J. B. Rosen* 236
29. Carbon Formation in Quenched Flat Flames at 1600°K. *C. P. Fenimore, G. W. Jones and G. E. Moore* 242

30. Carbon Formation from Acetylene. *F. C. Stehling, J. D. Frazee and Robbin C. Anderson*... 247
31. The Propagation and Stability of the Decomposition Flame of Hydrazine. *Peter Gray, J. C Lee and (in part) H. A. Leach and D. C. Taylor*..... 255
32. The Ozone to Oxygen Flame. *A. G. Streng and A. V. Grosse*..... 264
33. A Study of Hydrogen Diffusion Flames. *Edgar R. Stephens, William E. Scott, Joseph A. Golden and Barbara Faunce*..... 273
34. On the Burning Velocity of Moist Carbon Monoxide-Oxygen-Nitrogen Mixtures. *Karl Scheller*..... 280
35. Some Recent Experimental Results on the Flammability Regions of Various Gases and Combustible Vapors at Low Pressures. *Ralph Delbourgo and Paul Laffitte*..... 288
36. The Effect of Preheating on Flame Radiation and Flame Shape. *H. Guénebaut and A. G. Gaydon*..... 292
37. Effect of Initial Mixture Temperature on the Burning Velocity of Benzene-Air, *n*-Heptane-Air, and Isooctane-Air Mixtures. *Sheldon Heimel and Robert C. Weast*..... 296

STRUCTURE AND PROPAGATION OF TURBULENT FLAMES

38. Turbulent Burning Velocities of Natural Gas-Air Flames with Pipe-Flow Turbulence. *J. Kenneth Richmond, Joseph M. Singer, E. B. Cook, James R. Oxendine, Joseph Grumer and David S. Burgess*..... 303
39. Turbulent Diffusion Flames. *Masanaga Kunugi and Hiroshi Jinno*..... 311
40. Combustion of a Turbulent Jet in Burners with Preliminary Mixing. *V. N. Ievlev*..... 317
41. Growth Rates of Turbulent Free Flames. *William R. Mickelsen and Norman E. Ernstein*.. 325
42. On the Structure of Turbulent Flames. *K. Wohl and Collaborators*..... 333
43. Combustion in Turbulent Gas Streams. *H. Iida*..... 341

HIGH SPEED REACTIONS

*44. Heat Conductivity in Polyatomic, Electronically Excited, or Chemically Reacting Mixtures. III. *Joseph O. Hirschfelder*..... 351
45. Spectra of the Detonation of Oxygen with H_2, CO and Hydrocarbons. *H. Gg. Wagner*.... 366
46. On the Specification of Transient Nonequilibrium Systems. *Kurt E. Shuler*..... 371
47. Calculation of Detonation Characteristics. *Tsutomu Hikita and Taro Kihara*..... 375
48. Study of Shock Waves from High Explosives. *Tsutomo Hikita, Tetsuro Asaba and Kuniaki Yoneda*..... 379
49. A Shock-Tube Study of Flame Front-Pressure Wave Interaction. *G. H. Markstein*..... 387
50. Combustion Studies in a Stirred Reactor. *H. C. Hottel, G. C. Williams and M. L. Baker*... 398
51. A Discussion of the Relations Existing Between Limiting Energy Release Rates and Blow-out for Hydrocarbon Fuels. *Walter J. Wohlenberg*..... 411

FLAME STABILIZATION IN FAST STREAMS

52. Ignition in the Laminar Wake of a Flat Plate. *S. I. Cheng and A. A. Kovitz*..... 418
53. Boundary Layer Effects on Stability Characteristics of Bluff-Body Flameholders. *G. C. Williams, P. T. Woo and C. W. Shipman*..... 427
54. Some Effects of Fuel Reactivity and Heat Loss on Flame Stabilization. *Malcolm A. Weiss, James C. Rohrer and John P. Longwell*..... 439
55. The Influence of the Initial Temperature of a Combustible Mixture and of the Ambient Pressure on the Stabilization Limits. *L. N. Khitrin and S. A. Goldenberg*..... 448
56. Flame Stabilization in Volatile Fuel Sprays. *H. C. Hottel, C. P. Marion and W. P. Jensen*.. 451
57. Flame Stabilization in Gases Flowing Cyclonically: Flow Characteristics, Temperatures, and Gas Analyses. *Lyle F. Albright and Lloyd G. Alexander*..... 464
58. Flame Stabilization by Means of Annular Fluid Jets. *D. G. Shepherd*..... 472
59. A Contribution to the Study of Flame Stability in Ducts. *B. C. Dutta, D. G. Martin and N. P. W. Moore*..... 481

INSTABILITY IN COMBUSTION CHAMBERS

60. Influence of the Injector Pressure Drop on Low Frequency Instability in Liquid Propellant Rockets. *M. Barrère and J. J. Bernard* 487
61. Some Stability Tests on an Axially Symmetric Combustor. *A. A. Putnam and W. R. Dennis*. 493
62. An Analysis of Unstable Combustion of Premixed Gases. *H. J. Merk* 500
63. The Growth of Disturbances in a Flame-Generated Shear Region. *Perry L. Blackshear, Jr.*.. 512

IGNITION

64. Spark Ignition of Flowing Gases Using Long-Duration Discharges. *Clyde C. Swett, Jr.*.... 523
65. Ignition and Combustion in a Laminar Boundary Layer Over a Hot Surface. *Tau-Yi Toong*. 532
66. The Flammability Characteristics of the System H_2-NO-N_2O-Air. *F. E. Scott, R. W. Van Dolah and M. G. Zabetakis* 540
67. Thermal Theory of Ignition of Gas Mixtures: Limiting Conditions. *L. N. Khitrin and S. A. Goldenberg* 545
68. Ignition of Flowing Gases by Heated Wires. *Seiichiro Kumagai and Itsuro Kimura*..... 554

COMBUSTION OF SOLID FUELS

*69. Report on Progress in Combustion of Solid Fuels. *A. A. Orning* 559
70. Fundamental Principles of Carbon Combustion and Factors Intensifying the Burning of Solid Fuels. *L. N. Khitrin* 565
71. Solving Problems of Heterogeneous Combustion by the Method of Averaging Equations. *O. A. Tsukhanova* 573
72. The Combustion of Solid Fuels in Fixed Beds. *Mutsuo Koizumi* 577
73. Studies on Combustion and Gasification of Pulverized Coal in a Model Cyclone Generator. *Sakae Yagi and Daizo Kunii* 584
74. Flame Propagation in Pulverized Coal-Air Mixtures. *Hisao Hattori* 590
75. Studies of Pulverized Coal Flames. *B. Ghosh, D. Basu and N. K. Roy* 595
76. Radiative Transfer in Dust Flames. *H. M. Cassel, I. Liebman and W. K. Mock*..... 602

COMBUSTION OF EXPLOSIVES AND SOLID PROPELLANTS

77. Ignition of Explosives. *C. H. Johansson, A. Persson and H. L. Selberg*..... 606
78. The Combustion and Explosion of Crystals. *F. P. Bowden, B. L. Evans and A. D. Yoffe*... 609
79. Deflagration of Ammonium Perchlorate. *Raymond Friedman, R. G. Nugent, K. E. Rumbel and A. C. Scurlock* 612
80. Transition-State Theory of the Linear Rate of Decomposition of Ammonium Perchlorate. *Robert D. Schultz and Albert O. Dekker* 618
81. Some Developments in the Theory of Thermal Explosions. *G. B. Cook*..... 626
82. Effect of the Charge Diameter on the Velocity of Detonation Waves in Gas Mixtures. *N. Manson and H. Guénoche* 631
83. Detonation in Media of Variable Density. *L. I. Sedov*..... 635
84. The Effect of Slight Confinement on the Detonation Waves in Solid Explosives. *L. Deffet and J. Boucart* 642
85. Post-Detonation Pressure and Thermal Studies of Solid High Explosives in a Closed Chamber. *William S. Filler* 648
86. The Detonability of Certain Rocket Propellants. *John R. Scholl, H. W. Byington and R. L. Potter* 657
87. A Mathematical Method to Predict the Effects of Erosive Burning in Solid-Propellant Rockets. *J. M. Lenoir and G. Robillard*..... 663

EVAPORATION AND COMBUSTION OF DROPLETS AND SPRAYS

*88. Combustion of Fuel Sprays. *Seiichiro Kumagai*..... 668
89. Application of the Onsager Theory to the Transfer Phenomenon in Evaporation and Combustion Processes. *A. V. Luikov*..... 675

90. Atomization, Acceleration, and Vaporization of Liquid Fuels. *Robert D. Ingebo* 684
91. Liquid Fuel Atomization. *R. P. Fraser* 687
92. Flame Propagation Through Air-Fuel Foams. *A. Thomas* 701
93. Dynamic Factors Affecting the Combustion of Liquid Spheres. *George A. Agoston, Henry Wise and Willis A. Rosser* 708
94. Combustion Rates of Freely Falling Fuel Drops in a Hot Atmosphere. *J. A. Bolt and M. A. Saad* 717
95. Combustion of Fuel Droplets in a Falling Chamber. *Seiichiro Kumagai and Hiroshi Isoda* .. 726
96. On the Combustion of a Liquid Fuel Spray. *C. C. Miesse* 732

EXPERIMENTAL AND ANALYTICAL TECHNIQUES IN COMBUSTION

*97. Pyrometry of High Velocity Gases. *I. Warshawsky* 739
98. Photopyrometric Determination of the Temperature of a Burning, Moving Particle. *V. A. Popov* 751
99. Thermoelectric Probes for Measuring High Temperatures in Gas Streams: Their Application to the Study of Flames Stabilized by Obstacles. *G. Matton and C. Fouré* 757
100. A Self-Calibrating High Speed Photographic Pyrometer. *J. Tyroler* 763
101. Application of Optical Methods to Combustion Research. *F. J. Weinberg* 765
102. Ionization Studies of Flames Stabilized in Rapid Flow. *G. Matton* 770
103. A Detector for Combustible Hydrocarbons in Air. *Harold M. Brewster* 774
104. A Micrographic Device for the Study of Rapidly Moving Mists and Its Application to Research on Carburization in Internal Combustion Engines. *Willy Diamant* 776
105. An Apparatus for Studying the Burning of Dust Clouds. *Lloyd E. Line, Jr., Wendall J. Clark and James C. Rahman* 779

APPLICATIONS OF COMBUSTION

106. The Suppression of Methane/Air Ignitions by Fine Powders. *J. E. Dolan* 787
107. Fire Extinguishment by Means of Dry Powder. *C. S. McCamy, H. Shoub and T. G. Lee* ... 795
108. The Effect of Certain Halogenated Methanes on Pre-mixed and Diffusion Flames. *F. H. Garner, R. Long, A. J. Graham and A. Badakhshan* 802
109. Effects of Halogenated Extinguishing Agents on Flame Quenching and a Chemical Interpretation of Their Action. *Frank E. Belles and Cleveland O'Neal, Jr.* 806
110. The Rocket Motor as a Chemical Reactor (Illustrated by Nitrogen Fixation). *I. J. Weisenberg and P. F. Winternitz* 813
111. Chemical Reactions in Adiabatic Compression. *V. N. Kondratiev, A. M. Markevitch, Yu. N. Ryabinin and I. I. Tamm* 821
112. The Effect of Pipe Diameter on the Thermal Decomposition of Acetylenes. *Herbert H. Nelson* 823
113. The Production of Hydrogen Peroxide Via Combustion: Conditions for the Synthesis and Isolation in High Yield from the Combustion of Aliphatic Alcohols. *C. F. Cullis and E. J. Newitt* 827
114. Techniques for the Study of Air Flow and Fuel Droplet Distribution in Combustion Systems. *B. V. Poulston and E. F. Winter* 833
115. Experimental Investigation of Rapid Combustion of Low Grade Gaseous Fuel. *Teikichi Ōtsuka and Hisao Hattori* 843
116. Similitude Study of Idealized Combustors. *E. C. Woodward* 849
117. Some Applications of Combustion Theory to Gas Turbine Development. *V. W. Greenhough and A. H. Lefebvre* 858
118. Correlation of Turbine-Engine Combustion Efficiency with Theoretical Equations. *J. Howard Childs and Charles C. Graves* 869
119. A Detonation Wave Theory of Gasoline Engine Knock. *J. C. Firey* 878
120. Flame Quenching at the Walls of an Internal Combustion Engine. *W. A. Daniel* 886
121. Comparison of Emission Spectra of Low Temperature Combustion Reactions Produced in an Engine and in a Flat-Flame Burner. *J. T. Agnew, W. G. Agnew and K. Wark, Jr.* 894

122. Studies of the Spontaneous Ignition Tendencies of Sulfur-Containing Organic Compounds with White Fuming Nitric Acid by the Drop-Test Method. *Murray P. Strier and Louis R. Rapp* 902
123. The Behavior of the System Triethylamine—White Fuming Nitric Acid under Conditions of Rapid Mixing. *Rose L. Schalla and Edward A. Fletcher* 911
124. Some Fluid Dynamic Aspects of Laminar Diffusion Flames. *H. N. Powell and W. G. Browne* 918
125. Physical Methods for Improving Combustion. *Yukichi Asakawa* 923

PANEL DISCUSSIONS

1. Future Problems in Combustion Research. Panel Members: Walter T. Olson, *Chairman*, Louis Deffet, Carl Hugo Johansson, Tsutomu Hikita, V. N. Kondratiev H. Gg. Wagner, Guenther von Elbe, J. S. Clarke 930
2. High Speed Reactions. Panel Members: Arthur Kantrowitz, *Chairman*, James A. Fay, David Garvin, J. O. Hirschfelder, Paul Kydd, A. A. Westenberg 937
3. Flame Stabilization in Fast Streams. Panel Members: E. D. Brown, *Chairman*, M. Barrère, Béla Karlovitz, J. P. Longwell, G. C. Williams, E. E. Zukoski 941

*Invited Papers

LIST OF AUTHORS

Albright, Lyle F., School of Chemical Engineering, Purdue University, Lafayette, Indiana... 464
Alexander, Lloyd G., Oak Ridge National Laboratory, Oak Ridge, Tennessee..... 464
Agnew, John T., School of Mechanical Engineering, Purdue University, Lafayette, Indiana. 83, 894
Agnew, William G., Fuels and Lubricants Department, General Motors Corporation, Box 188, North End Station, Detroit 2, Michigan..... 894
Agoston, George A., Chemical Physics Department, Stanford Research Institute, Menlo Park, California..... 708
Altman, David, Aeronutronic Systems, Inc., 1234 Air Way, Glendale, California..... 222
Anderson, Robbin C., Department of Chemistry, University of Texas, Austin 12, Texas..... 247
Arden, E. A., Ministry of Supply E.R.D.E., Powdermill Lane, Waltham Abbey, Essex, England 177
Asaba, Tetsuro, Faculty of Engineering, University of Tokyo, Bunkyo-Ku, Tokyo, Japan.... 379
Asakawa, Yukichi, Nihon University, Technical College, Surugadai, Tokyo, Japan..... 923
Badakhshan, A., Department of Chemical Engineering, The University, Edgbaston, Birmingham, England..... 802
Baker, M. L., Shell Chemical Corporation, Houston, Texas..... 398
Barrère, M., O.N.E.R.A., 25, Avenue de la Division-Leclerc, Chatillon-sous- Bagneux, France 487, 941
Basu, D., Fuel Research Institute, Jealgora (Bihar), India..... 595
Belles, Frank E., Lewis Flight Propulsion Laboratory, National Advisory Committee for Aeronautics, Cleveland 11, Ohio..... 806
Berlad, A. L., Consolidated Vultee Aircraft Corporation, San Diego, California..... 27
Bernard, J. J., O.N.E.R.A., 25, Avenue de la Division-Leclerc, Chatillon-sous-Bagneux, France. 487
Blackshear, Perry L., Jr., National Advisory Committee for Aeronautics, Lewis Flight Propulsion Laboratory, Cleveland 11, Ohio..... 512
Bolt, Jay A., Department of Mechanical and Industrial Engineering, University of Michigan, Ann Arbor, Michigan..... 717
Boucart, J., Centre de Recherches, Tir National, Place des Carabiniers, Bruxelles, Belgium... 642
Bowden, F. Philip, Department of Physical Chemistry, University of Cambridge, Free School Lane, Cambridge, England..... 609
Brewster, Harold M. (U. S. Naval Air Turbine Test Station). Present Address: Products Research Division. Esso Research and Engineering Co., P. O. Box 51, Linden, New Jersey.. 774
Brokaw, Richard S., National Advisory Committee for Aeronautics, Lewis Flight Propulsion Laboratory, Cleveland 11, Ohio..... 66
Brown, Edmund D., Pratt & Whitney Aircraft, East Hartford 8, Connecticut..... 941
Browne, William G., General Electric Company, Aircraft Gas Turbine Division, Evendale, Ohio..... 37, 918
Burgess, David S., U. S. Bureau of Mines, 4800 Forbes Street, Pittsburgh 13, Pennsylvania... 303
Byington, H. W., Rocket Combustion Research, Bell Aircraft Corporation, P. O. Box 1, Buffalo 5, New York..... 657
Byrne, John F., Battelle Memorial Institute, 505 King Avenue, Comlubus 1, Ohio..... 120
Campbell, Edwin S., Department of Chemistry, New York University, New York 53, New York..... 213
Cassel, Hans M., U. S. Bureau of Mines, 4800 Forbes Street, Pittsburgh 13, Pennsylvania.... 602
Cheng, Sin-I, Department of Aeronautical Engineering, Princeton University, Princeton, New Jersey..... 418
Childs, J. Howard, National Advisory Committee for Aeronautics, Lewis Flight Propulsion Laboratory, Cleveland 11, Ohio..... 869
Clarke, J. S., Joseph Lucas Ltd., Birmingham 19, England..... 930
Clark, Wendall J., Experiment Incorporated, Richmond, Virginia..... 779

Cook, E. B., U. S. Bureau of Mines, 4800 Forbes Street, Pittsburgh 13, Pennsylvania 303
Cook, G. B., Ministry of Supply, Armament Research and Development Establishment, Fort Halstead, Sevenoakes, Kent, England 626
Cullis, C. F., Chemistry Department, Imperial College of Science and Technology, South Kensington, London S. W. 7, England 827
Daniel, Wayne A., Fuels and Lubricants Department, General Motors Corporation, Box 188, North End Station, Detroit 2, Michigan 886
Deckers, Jacques, 85 Avenue Van Ryswyck, Anvers, Belgium 61
Deffet, L., Centre de Recherches, Tir National, Place des Carabiniers, Bruxelles, Belgium. 642, 930
Dekker, Albert O., Aerojet-General Corporation, Azusa, California 618
Delbourgo, Ralph, Faculté des Sciences de Paris, Laboratoire de Chimie Générale, Université de Paris, Paris V^0, France 288
Dennis, W. R., Battelle Memorial Institute, Columbus 1, Ohio 493
Diamant, Willy, 3 Avenue de la Marne, Champigny, Seine, France 776
Dolan, J. E., Research Department, Nobel Division, Imperial Chemical Industries Limited, Stevenston, Ayrshire, Scotland 787
Dutta, B. C., D. Napier & Son, Ltd., Acton Vale, London W. 3, England 481
Ernstein, Norman E., National Advisory Committee for Aeronautics, Lewis Flight Propulsion Laboratory, Cleveland 11, Ohio 325
Evans, B. L., Department of Physical Chemistry, University of Cambridge, Free School Lane, Cambridge, England 609
Faunce, Barbara, The Franklin Institute, Laboratories for Research and Development, Philadelphia 3, Pennsylvania 154, 273
Fay, James A., Massachusetts Institute of Technology, Cambridge 39, Massachusetts 937
Fenimore, Charles P., Research Laboratory, General Electric Company, P. O. Box 1088, Schenectady, New York 242
Filler, William S., U. S. Naval Ordnance Laboratory, White Oak, Silver Spring, Maryland ... 648
Firey, J. C., Department of Mechanical Engineering, University of Washington, Seattle 5, Washington 878
Fletcher, Edward A., National Advisory Committee for Aeronautics, Lewis Flight Propulsion Laboratory, Cleveland 11, Ohio 911
Fouré, C., O.N.E.R.A., 25 Avenue de la Division-Leclerc, Chatillon-sous-Bagneux, France 757
Fraser, R. P., Tir-Na-N'og, Kingston Hill, Surrey, England 687
Frazee, J. D., Department of Chemistry, University of Texas, Austin 12, Texas 247
Friedman, Raymond, Atlantic Research Corporation, Alexandria, Virginia 612
Fristrom, Robert M., Applied Physics Laboratory, The Johns Hopkins University, 8621 Georgia Avenue, Silver Spring, Maryland 96
Fyodorov, G. G., Institute of Energetics, USSR Academy of Sciences, Moscow, USSR 88
Garner, F. H., University of Birmingham, Edgbaston, Birmingham 15, England 802
Garvin, David, Princeton University, Princeton, New Jersey 937
Gaydon, A. G., Imperial College of Science and Technology, London, S. W. 7, England 292
Gerstein, Melvin, National Advisory Committee for Aeronautics, Lewis Flight Propulsion Laboratory, Cleveland 11, Ohio 66
Ghosh, B., Jadavpur University, Calcutta, India 595
Giddings, J. Calvin, The University of Wisconsin, Naval Research Laboratory, P. O. Box 2127, Madison, Wisconsin 199
Gilbert, Mitchell, Jet Propulsion Laboratory, California Institute of Technology, 4800 Oak Grove Drive, Pasadena 3, California 74, 222
Golden, Joseph A., Special Defense Projects Department, General Electric Company, Philadelphia, Pennsylvania 273
Goldenberg, S. A., Institute of Energetics, USSR Academy of Sciences, Moscow, USSR. 448, 545
Golovina, E. S., Institute of Energetics, USSR Academy of Sciences, Moscow, USSR 88
Graham, A. J., Department of Chemical Engineering, The University, Edgbaston, Birmingham, England 802

GRAVES, Charles C., National Advisory Committee for Aeronautics, Lewis Flight Propulsion Laboratory, Cleveland 11, Ohio 869
GRAY, PETER, School of Chemistry, The University, Leeds 2, Yorkshire, England 183, 255
GREENHOUGH, V. W., Combustion Department, Rolls-Royce Limited, Derby, England 858
GROSSE, A. V., Research Institute, Temple University, Philadelphia 44, Pennsylvania 264
GRUMER, JOSEPH, U. S. Bureau of Mines, 4800 Forbes Street, Pittsburgh 13, Pennsylvania 303
GUÉNEBAUT, H., Faculté des Sciences, Université de Dijon, France 292
GUÉNOCHE, HENRI, Institut Français du Petrole, 1, Place Aristide Briand, Bellevue, S.-&-O., France 631
HALL, A. R., R. A. E., Rocket Propulsion Department, Ministry of Supply, Westcott near Aylesbury, Bucks, England 190
HATTORI, HISAO, Resources Research Institute, Agency of Industrial Science and Technology, Kawaguchi-Saitama, Japan 590, 843
HEIMEL, SHELDON, National Advisory Committee for Aeronautics, Lewis Flight Propulsion Laboratory, Cleveland 11, Ohio 296
HIKITA, TSUTOMU, The Faculty of Engineering, The University of Tokyo, Bunkyo-Ku, Tokyo, Japan 375, 379, 930
HIRSCHFELDER, J. O., Naval Research Laboratory, University of Wisconsin, P. O. Box 2127, Madison 6, Wisconsin 199, 351, 937
HOTTEL, HOYT C., Fuel Engineering, Massachusetts Institute of Technology, Cambridge 39, Massachusetts 398, 451
IEVLEV, V. N., Institute of Energetics, USSR Academy of Sciences, Moscow, USSR 317
IIDA, HEIHACHIRO, Transportation Technical Research Institute, 700 Shinkawa, Mitaka, Tokyo, Japan 341
INGEBO, ROBERT D., National Advisory Committee for Aeronautics, Lewis Flight Propulsion Laboratory, Cleveland 11, Ohio 684
ISODA, HIROSHI, Department of Aeronautics, University of Tokyo, Bunkyo-Ku, Tokyo, Japan .. 726
JENSEN, WILLIAM PAUL, Massachusetts Institute of Technology, Cambridge 39, Massachusetts. 451
JINNO, HIROSHI, Department of Industrial Chemistry, Kyoto University, Kyoto, Japan 311
JOHANSSON, CARL HUGO, Nitroglycerin AB, Vinterviken, Stockholm, Sweden 606, 930
JONES, G. W., Research Laboratory, General Electric Company, P. O. Box 1088, Schenectady, New York 242
KANTROWITZ, ARTHUR, AVCO Research Laboratory, Everett 49, Massachusetts 937
KARLOVITZ, BÉLA, Combustion and Explosives Research, Inc., 200 Alcoa Building, Pittsburgh 19, Pennsylvania 941
KASKAN, WALTER E., Research Laboratory, General Electric Company, P. O. Box 1088, Schenectady, New York 134
KHITRIN, L. N., USSR Academy of Sciences, Moscow, USSR 448, 545, 565
KIHARA, TARO, Faculty of Science, University of Tokyo, Bunkyo-Ku, Tokyo, Japan 375
KIMURA, ITSURO, Department of Aeronautics, University of Tokyo, Bunkyo-Ku, Tokyo, Japan. 554
KOIZUMI, MUTSUO, Shigengijutsu-Shikenjo, Resources Research Institute, Agency of Industrial Science and Technology, Kawaguchi-Saitama, Japan 577
KONDRATIEV, V. N., USSR Academy of Sciences, 14, B. Kaluzhskaja, Moscow, USSR 930
KOVITZ, ARTHUR A., Department of Aeronautical Engineering, Princeton University, Princeton, New Jersey 418
KUMAGAI, SEIICHIRO, Department of Aeronautics, University of Tokyo, Bunkyo-Ku, Tokyo, Japan 554, 668, 726
KUNII, DAIZO, Department of Chemical Engineering, University of Tokyo, Tokyo, Japan 584
KUNUGI, MASANAGA, Faculty of Engineering, Kyoto University, Kyoto, Japan 311
KYDD, PAUL, Harvard University, Cambridge 38, Massachusetts 937
LAFFITTE, PAUL, Laboratoire de Chimie Générale, L'Université de Paris, 1, rue Victor-Cousin, Paris V^{0}, France 130, 288
LAUD, B. B., Department of Physics, University of Poona, Poona, India 143
LEACH, H. A. The University, Leeds 2, England 255

Lee, J. C., Department of Chemical Engineering, University of Cambridge, Tennis Court Road, Cambridge, England 255
Lee, T. G., National Bureau of Standards, Washington 25, D. C. 795
Lefebvre, A. H., Combustion Department, Rolls-Royce Limited, Derby, England 858
Lenoir, J. M., Jet Propulsion Laboratory, California Institute of Technology, 4800 Oak Grove Drive, Pasadena 3, California 663
Liebman, I., U. S. Bureau of Mines, 4800 Forbes Street, Pittsburgh 13, Pennsylvania 602
Line, Lloyd E., Jr., Experiment Incorporated, Richmond 2, Virginia 779
Linnett, J. W., Queen's College, Oxford, England 20, 149
Long, R., Department of Chemical Engineering, The University, Edgbaston, Birmingham, England 802
Longwell, J. P., Esso Research and Engineering Company, P. O. Box 121, Linden, New Jersey 439, 941
Lucquin, Michel, Laboratoire de Chimie Générale, L'Université de Paris, 1, rue Victor-Cousin, Paris V^{0}, France 130
Luikov, A. V., Institute of Energetics, USSR Academy of Sciences, Moscow, USSR 675
McCamy, C. S., National Bureau of Standards, Washington 25, D. C. 795
Manson, N., Faculté des Sciences, Poitiers, Vienne, France 631
Marion, Charles Parker, The Texas Company, Montebello, California 451
Markevitch, A. M., USSR Academy of Sciences, Moscow, USSR 821
Markstein, George H., Combustion Section, Cornell Aeronautical Laboratory, Inc., 4455 Genesee Street, Buffalo 21, New York 387
Martin, D. G., City & Guilds College, Imperial College, Exhibition Road, London, S. W. 7, England 81
Matton, G., O.N.E.R.A., 25, Avenue de la Division-Leclerc, Chatillon-sous-Bagneux, France 757, 770
Merk, H. J., Koninklijke/Shell-Laboratorium, Delft van de N. V. DeBataafsche Petroleum Maatschappij, The Hague, Holland 500
Mickelsen, William R., Fuels and Combustion Division, National Advisory Committee for Aeronautics, Lewis Flight Propulsion Laboratory, Cleveland 11, Ohio 325
Miesse, C. C., Armour Research Foundation of the Illinois Institute of Technology, 10 West 35th Street, Chicago 16, Illinois 732
Miller, Eugene, Ordnance Missile Research Laboratories, Redstone Arsenal, Huntsville, Alabama 164, 173
Mock, W. K., U. S. Bureau of Mines, 4800 Forbes Street, Pittsburgh 13, Pennsylvania 602
Moore, George E., Research Laboratory, General Electric Company, The Knolls, Schenectady, New York 242
Moore, N. P. W., City & Guilds College, Imperial College, London, S. W. 7, England 481
Myerson, Albert L., The Special Defense Projects Dept., General Electric Co., Philadelphia 4, Pennsylvania 154
Nelson, Herbert H., Plastics Division, Monsanto Chemical Company, Texas City, Texas 823
Newitt, E. J., Chemistry Department, Imperial College of Science and Technology, South Kensington, London, S. W. 7, England 827
Nugent, R. G., Atlantic Research Corporation, Alexandria, Virginia 612
Olson, Walter T., NACA Lewis Flight Propulsion Laboratory, Cleveland 11, Ohio ..... xxiii, 930
Ōtsuka, Teikichi, Resources Research Institute, Agency of Industrial Science and Technology, Kawaguchi-Saitama, Japan 843
Oxendine, J. R., Aerial Reconnaissance Laboratory, Wright-Patterson Air Force Base, Ohio 303
O'Neal, Cleveland, Jr., National Advisory Committee for Aeronautics, Lewis Flight Propulsion Laboratory, Cleveland, 11, Ohio 806
Orning, A. A., Combustion Section, U. S. Bureau of Mines, Pittsburgh 13, Pennsylvania 559
Persson, Algot, Nitroglycerin A. B. Vinterviken, Stockholm S V, Sweden 606
Popov, V. A., Institute of Energetics, USSR Academy of Sciences, Moscow, USSR 751

Potter, A. E., Jr., National Advisory Committee for Aeronautics, Lewis Flight Propulsion Laboratory, Cleveland 11, Ohio 27
Potter, R. L., Rocket Combustion Research, Bell Aircraft Corporation, P. O. Box 1, Buffalo 5, New York 657
Poulston, B. V. "Shell" Research Limited, Thornton Research Centre, P. O. Box 1, Chester, England 833
Powell, Hugh N., General Electric Company, Aircraft Gas Turbine Division, Building 300, Evendale, Ohio 37, 918
Powling, J., Ministry of Supply—E.R.D.E., Powdermill Lane, Waltham Abbey, Essex, England 177
Pratt, M. W. T., School of Chemistry, The University, Leeds 2, England 183
Putnam, Abbott A., Battelle Memorial Institute, 505 King Avenue, Columbus 1, Ohio 493
Rahman, James C., Experiment Incorporated, Richmond 2, Virginia 779
Rapp, Louis R., Hughes Tool Co., Culver City, California 902
Richmond, J. Kenneth, U. S. Bureau of Mines, 4800 Forbes Street, Pittsburgh 13, Pennsylvania 303
Robillard, G., Jet Propulsion Laboratory, California Institute of Technology, 4800 Oak Grove Drive, Pasadena 3, California 663
Rohrer, James C., Esso Research & Engineering Company, P. O. Box 121, Linden, New Jersey 439
Rosen, J. B., Shell Development Company, Emeryville, California 236
Rosser, Willis A., Stanford Research Institute, SRI Building 404C, 5th Street, Stanford Village, Menlo Park, California 708
Roy, N. K., College of Engineering & Technology, Jadavpur University, Calcutta, India 595
Rumbel, K. E., Atlantic Research Corporation, Alexandria, Virginia 612
Ryabinin, Yu. N., USSR Academy of Sciences, Moscow, USSR 821
Saad, M. A., Department of Mechanical Engineering, Lehigh University, Bethlehem, Pennsylvania 717
Schalla, Rose L., National Advisory Committee for Aeronautics, Lewis Flight Propulsion Laboratory, Cleveland 11, Ohio 911
Scheller, Karl, Aeronautical Research Laboratory, Wright Air Development Center, Wright-Patterson Air Force Base, Ohio 280
Scholl, John R., Rocket Department, Bell Aircraft Corporation, P. O. Box 1, Buffalo 5, New York 657
Schultz, Robert D., Aerojet-General Corporation, Azusa, California 618
Scott, Frank E., U. S. Bureau of Mines, 4800 Forbes Street, Pittsburgh 13, Pennsylvania 540
Scott, William E., The Franklin Institute, Laboratories for Research and Development, Philadelphia 3, Pennsylvania 273
Scurlock, Arch C., Atlantic Research Corporation, 901 South Columbus Avenue, Alexandria, Virginia 612
Sedov, L. I., USSR Academy of Sciences, Zone U, 84, Moscow B-234, USSR 635
Selberg, Henrik L., Nitroglycerin Aktiebolaget, Vinterviken, Stockholm S V, Sweden 606
Setzer, Herbert J., Research Laboratories, Ordnance Missile Laboratories, Redstone Arsenal, Huntsville, Alabama 164
Shepherd, D. G., College of Engineering, Cornell University, Ithaca, New York 472
Shipman, C. W., Department of Chemical Engineering, Massachusetts Institute of Technology, Cambridge 39, Massachusetts 427
Shoub, H., National Bureau of Standards, Washington 25, D. C. 795
Shuler, Kurt E., National Bureau of Standards, Washington 25, D. C. 371
Simpson, C. J. S. M., Queen's College, Oxford, England 20, 149
Singer, Joseph M., U. S. Bureau of Mines, 4800 Forbes Street, Pittsburgh 13, Pennsylvania 127, 303
Smith, Donald, Department of Chemical Engineering, Purdue University, Lafayette, Indiana. 83
Spalding, D. B., Mechanical Engineering Department, Imperial College of Science & Technology, London, S. W. 7, England 12
Stehling, F. C., Department of Chemistry, University of Texas, Austin 12, Texas 247

Stephens, Edgar R., The Franklin Institute Laboratories for Research and Development, Philadelphia 3, Pennsylvania ... 273
Streng, Alex G., Research Institute, Temple University, 4150 Henry Avenue, Philadelphia 44, Pennsylvania ... 264
Strier, Murray P., Research Laboratories, Air Reduction Co., Inc., Murray Hill, New Jersey. 902
Swett, Clyde C., Jr., National Advisory Committee for Aeronautics, Lewis Flight Propulsion Laboratory, Cleveland 11, Ohio ... 523
Tamm, I. I., USSR Academy of Sciences, Moscow, USSR ... 821
Taylor, D. C., The University, Leeds 2, England ... 255
Taylor, Francis R., The Franklin Institute Research Laboratories, Philadelphia 3, Pennsylvania ... 154
Tawde, N. R., Department of Physics, Karnatak University, Dharwar, India ... 143
Thomas, Arthur L., E. I. du Pont de Nemours & Company, Parlin, New Jersey ... 111
Thomas, A., Thornton Research Centre, "Shell" Research Ltd., P. O. Box 1, Chester, England. 701
Toong, T. Y., Department of Mechanical Engineering, Sloan Laboratories, Massachusetts Institute of Technology, Cambridge 39, Massachusetts ... 532
Tsukhanova, O. A., Institute of Energetics, USSR Academy of Sciences, Moscow, USSR ... 573
Tyroler, J. F., Pyrotechnics Section, Samuel Feltman Ammunition Laboratories, Picatinny Arsenal, Dover, New Jersey ... 763
van Dolah, Robert W., U. S. Bureau of Mines, 4800 Forbes Street, Pittsburgh 13, Pennsylvania ... 540
Van Tiggelen, A., Université de Louvain, 98, rue de Namur, Louvain, Belgium ... 61
Violett, T. D., Research Laboratories, Ordnance Missile Laboratories, Redstone Arsenal, Huntsville, Alabama ... 173
von Elbe, Guenther, Combustion and Explosives Research, Inc., 200 Alcoa Building, Pittsburgh 19, Pennsylvania ... 127, 930
von Kármán, Theodore, 1501 South Marengo Avenue, Pasadena, California ... 1
Wagner, H. Gg., Physikalisch-chemisches Institut der Universität Göttingen, Bürgerstr. 50, Göttingen, Germany ... 366, 930
Wark, K., Jr., Mechanical Engineering Department, Purdue University, West Lafayette, Indiana ... 894
Warshawsky, I., National Advisory Committee for Aeronautics, Lewis Flight Propulsion Laboratory, Cleveland 11, Ohio ... 739
Weast, Robert C., National Advisory Committee for Aeronautics, Lewis Flight Propulsion Laboratory, Cleveland 11, Ohio ... 296
Weinberg, F. J., Department of Chemical Engineering, Imperial College of Science & Technology, South Kensington, London, S. W. 7, England ... 765
Weisenberg, I. J., Reaction Motors, Incorporated, Denville, New Jersey ... 813
Weiss, Malcolm A., Esso Research & Engineering Company, P. O. Box 121, Linden, New Jersey ... 439
Westenberg, A. A., Applied Physics Laboratory, The Johns Hopkins University, Silver Spring Maryland ... 937
Wharton, W. W., Research Laboratories, Ordnance Missile Laboratories, Redstone Arsenal, Huntsville, Alabama ... 173
Wilhelm, Richard H., Department of Chemical Engineering, Princeton University, Princeton, New Jersey ... 111
Williams, Glenn C., Department of Chemical Engineering, Massachusetts Institute of Technology, Cambridge 39, Massachusetts ... 398, 427, 941
Winter, E. F., The Shell Petroleum Company, Thornton Research Centre, P. O. Box 1, Chester, England ... 833
Winternitz, P. F., College of Chemical Engineering, New York University, New York 53, New York ... 813
Wise, Henry, Stanford Research Institute, SRI Bldg. 404C, 5th Street, Stanford Village, Menlo Park, California ... 708

Wohl, Kurt, Department of Chemical Engineering, University of Delaware, Newark, Delaware. 333
Wohlenberg, Walter J., Mason Laboratory, Yale University, 400 Temple Street, New Haven 10, Connecticut (Deceased) 411
Wolfhard, Hans G., U. S. Bureau of Mines, 4800 Forbes Street, Pittsburgh 13, Pennsylvania.. 190
Woo, P. T., California Research Corporation, Richmond, California 427
Woodward, E. C., Research Laboratories, Westinghouse Electric Corporation, East Pittsburgh, Pennsylvania 849
Yagi, Sakae, Department of Chemical Engineering, University of Tokyo, Tokyo, Japan 584
Yoffe, A. D., Department of Physical Chemistry, University of Cambridge, Free School Lane, Cambridge, England 609
Yoneda, Kuniaki, Faculty of Engineering, University of Tokyo, Bunkyo-Ku, Tokyo, Japan... 379
Zabetakis, Michael G., U. S. Bureau of Mines, 4800 Forbes Street, Pittsburgh 13, Pennsylvania 540
Zukoski, E. E., Jet Propulsion Laboratory, California Institute of Technology, Pasadena 3, California 941

INTRODUCTION

By WALTER T. OLSON*

The Sixth International Symposium on Combustion shows no diminution in the high output of research on combustion and combustion-related topics that has characterized this field during the last dozen years. Laboratories in government, industry, and universities throughout the world have continued to produce data and knowledge in the broad area of combustion at a high rate. Much of this productivity is due to the financial sponsorship of a government usually desirous of furthering some particular application of combustion. This productivity of the combustion scientists is reflected both by the appearance of a number of other, often more specialized, combustion conferences and by more papers than ever being proposed for the Sixth Symposium; the 125 papers published in this volume represent a selection from 196 papers originally proposed.

The continuing purpose of this series of international symposia is to compile important research papers, to summarize and coordinate work in the combustion field, and to provide that free forum of scrutiny and debate that is so essential to good science. Because of the tremendous growth of the field, a quite comprehensive or broad agenda was programmed for the Sixth Symposium. This broad treatment of combustion is in contrast to the Fifth Symposium (1954) which emphasized the physical aspects of combustion, particularly wave phenomena and turbulence, and to the Fourth Symposium (1952) which emphasized the chemical aspects of combustion, particularly reaction kinetics. The particular agenda topics of the Sixth Symposium are included either because considerable new data or new theories and concepts are available, or because the topic is currently of great interest.

Ignition and flame phenomena in homogeneous combustible mixtures occupy the attention of many of the scientists in the combustion field. More papers were submitted in this general area than in any other area of research.

Efforts continue to simplify or to solve the equations for laminar flame propagation. Predictions of most flame phenomena from fundamental reaction steps appear to be nearly hopelessly complex; the reaction kinetics are just too involved. In a typical approach, however, the flame is treated as a one-dimensional flow problem; equations of conservation of mass and energy are written, and pressure is assumed invariant across the flame. In general, the further simplifying assumption is made that reactions of intermediates are very rapid compared to the over-all reaction, the so-called steady-state assumption. In addition to new contributions on this problem, an invited paper by Dr. Theodore von Kármán summarizes the present status of the theory of laminar flame propagation.

Collateral attacks on the chemical and physical details governing flame phenomena include probing flames for profiles of gas velocity, temperature, composition, and gas properties. An invited paper by Mr. R. M. Fristrom discusses the present understanding of the structure of the laminar flame front. Also, it is possible to measure the effects of parameters, such as pressure, surface-to-volume ratio, temperature, and diluents on flame phenomena, and to deduce the underlying mechanisms that may have produced the observed effects. Spectra of flames are also available.

Another approach to simplification of the laminar flame problem treats flames for which the reaction steps are simple and known, for example, hydrogen bromine flames, or hydrazine decomposition.

Investigations of the structural details of turbulent flames have continued, but no certainty exists about their structure. Accordingly, no general theory for predicting turbulent flame phenomena yet exists. A valuable new technique is the heavily stirred reactor in which extreme turbulence produces maximum heat-release rates from fuel-air mixtures; also the pressure and concentration dependence of heat-release rate is measured.

Ignition phenomena, like laminar flame phenomena, have been treated with relations between the flow or transport of energy and the ensuing combustion reactions; an Arrhenius rate equation for a second order reaction is assumed to be operative for the over-all combustion reaction. This

* Chief, Propulsion Chemistry Division, NACA Lewis Flight Propulsion Laboratory.

point of view is applied to a variety of situations: Minimum spark energy, ignition from hot surfaces, and limiting conditions.

Because of the relation to explosives and rocket propellants, ignition and flame phenomena of systems of fuel with oxides of nitrogen have been receiving detailed attention, as have nitro, nitrite, and nitrate compounds. This research is, therefore, discussed in the symposium.

A topic related to flame propagation in homogeneous combustible mixtures that is currently attracting great attention is fast, high temperature reactions. The topic is pertinent in an increasing number of situations: External flow and heat transfer with hypersonic flight, high temperature jet engines and rockets, high temperature chemical processes, and upper atmosphere studies, for examples, as well as the familiar ones of explosions, detonations, and flames. The fundamental problems of interest are to determine the equilibrium states of species and energy at high temperatures, to determine the actual concentrations and energy distributions obtained, and to determine the rates at which species and energy states appear and disappear. New experimental techniques and methods are required and are being used. Theoretical work, too, is advancing in this important area, aided in part by machine computing methods that permit integration of equations expressing rates of transport, exchange of energy, and transport and reaction of species. As an example of the kinds of problem encountered in this general area, the invited paper by Dr. J. O. Hirschfelder deals with heat conductivity in polyatomic electronically-excited or chemically reacting gases. A round-table session discusses the many new or refined experimental methods, such as sampling and analysis, mass spectrography, and shock tube and spectra for analysis of flames and detonation; and flash photolysis, atomic flames, and molecular beams for studies of the simpler parts of reactions.

Combustion problems of condensed states are of great technical importance. The burning rate of a single liquid fuel droplet has been shown to be proportional to its diameter for many conditions. Recent work predicts trajectories of droplets from drag data for evaporating or burning drops. Atomization to produce a statistical distribution of drops or a spray and the subsequent combustion of sprays have also been under study. The invited paper by Dr. Seiichiro Kumagai reviews the status of the knowledge of combustion of fuel sprays.

Papers were invited on the combustion of solid fuels because of the tremendous technologic importance of combustion of coal in the world's economy. The results of research on the combustion of coal in pulverized form appear in this symposium. Here the mechanism parallels in most physical principles that of liquid sprays; one big exception is that a much higher fraction of the heat is transferred by radiation in dust flames than in burning liquids.

A big problem in the formulation and preparation of explosives is to interpret and predict their sensitivity to ignition, combustion, and explosion for the different ways of formulating and fabricating them. A part of this problem is the desire to predict the effect of manufacturing techniques on the subsequent rate of explosion. The idea that the compression of air inclusions promotes ignition of explosives under impact has led to detailed researches on the effects of the form, shape, and size of solid particles of explosives on their sensitivity to ignition, combustion, and explosion. A highly interesting area of work is that having to do with research on the effects of imperfections and cracks on the rates of combustion and explosion.

One important application of combustion is in high heat release devices for flight propulsion. Stabilization of flames in fast streams has, accordingly, been a topic of intensive research for the past several years. A round-table discussion is devoted to the mechanism by which flame is anchored to a bluff body in a combustible stream; different rate determining steps are hypothesized for the ignition of unburned gases by burned gases in the stabilizer wake. Experiments on some variants of flame stabilization are described. Several organizations have intensively studied the relations between individual processes and combustion limits and efficiency for gas turbine combustors; information reveals that often chemical reaction rates provided the slow, or limiting step to the over-all combustion process. The importance of the fuel preparation step and of air flow patterns, however, is also stressed. A number of papers, including an invited paper by Mr. I. Warshawsky on temperature measurements, describe experimental techniques for studying combustion in high velocity streams.

Another important application area that has seen progress is in reciprocating engines, where the problem of the relation between unburned fuel and smog is taking the place of primary importance formerly occupied by engine knock.

Researches on ignition and combustion of rocket fuels by nitric acid, on fire extinguishing by powders and by halogenated agents, and on syntheses of chemicals by combustion processes are areas of great topical interest and are areas in which data have been released in the last two years, both from military classification and from proprietary interests.

In summary, new data are appearing at a continuing or increasingly high rate. Many of these data are analyzed empirically or semi-empirically with the aid of simple concepts. As a result the engineer concerned with applications has been provided with practical guide lines, and the scientist concerned with fundamental mechanisms has been given additional clues and puzzle pieces to resolve.

The practitioner has certainly profited in recent years. A number of fields of combustion applications are vastly better equipped with data and concepts than they were just a decade ago. Just since the Fifth Symposium, scientific and engineering understanding of several aspects of high-speed combustion, for example, flameholding, high heat release burning, and droplet combustion, have reached a modestly satisfactory level. The theoretician has reached a more mature and sophisticated understanding of the many processes involved in combustion. No revolutionary new discovery or concept or large generalization has appeared recently, however. Currently emphasized research on the kinetics and energetics of simpler molecules and reactions can be expected to be more amenable to important generalizations than research on hydrocarbon-air flames has been.

The range of applications of combustion and of the scientific disciplines used in combustion research is most impressive. There is no doubt that technology and science in this field will advance in the same increasing fashion as have other areas of technology and science in the modern world.

Structure and Propagation of Laminar Flames

1

THE PRESENT STATUS OF THE THEORY OF LAMINAR FLAME PROPAGATION

By THEODORE VON KÁRMÁN
(WITH COOPERATION OF GREGORIO MILLÁN AND S. S. PENNER)

1. Formulation of the Problem

There seems to be general agreement between the scientific workers engaged in the theory of laminar flame propagation that the theory shall be based on the application of the equations of conservation of mass, momentum and energy to a one-dimensional flow of a mixture which is unburned at the "cold boundary" and approaches an equilibrium state at the "hot boundary." It is assumed that the flow can be considered as that of a continuous gas, that chemical kinetics furnishes the necessary expressions for the quantities entering into the conservation equations due to chemical changes, and finally that the transfer phenomena are determined by full knowledge of the heat transfer coefficient and the laws of diffusion.

We have to satisfy the equations for the conservation of matter and energy. The law of conservation of momentum is taken care of by the assumption that pressure variations can be neglected.

The conservation of total mass requires for a one-dimensional flow that

$$\rho v = m \tag{1}$$

where m is the constant mass flow per unit cross-sectional area.

The continuity equation for the species, j, requires that

$$m \frac{d\epsilon_j}{dx} = w_j \tag{2}$$

where w_j is the mass rate of production per unit volume of the species, j.

The rate of production can be expressed in terms of the specific reaction rates, k_r, of the individual reactions in which the species j participates, and in terms of the stoichiometric coefficients ν'_{jr} and ν''_{jr} for the forward and backward reactions, respectively, in the following way:

$$w_j = M_j \sum_r (\nu''_{jr} - \nu'_{jr}) k_r \left(\frac{p}{RT}\right)^{n_r} \prod_{i=1}^{s} (X_i)^{\nu'_r} \tag{3}$$

where the exponent $n_r = \sum_{i=1}^{s} \nu'_{ir}$. The preceding formula follows from the law of mass action.

For the specific rate of reaction, we write the semitheoretical equation:

$$k_r = B_r \left(\frac{T}{T_f}\right)^{\alpha_r} \exp\left(-\frac{A_r}{RT}\right) \tag{4}$$

The quantity A_r is called the activation energy, the factor $B_r \left(\frac{T}{T_f}\right)^{\alpha_r}$ the frequency factor.

The diffusion equations express the relation between the fractional mass flow rate ϵ_j and the weight ratio Y_j of the species j in the form

$$\epsilon_j = Y_j \left(1 + \frac{V_j}{v}\right) \tag{5}$$

Following Curtiss and Hirschfelder,[1] we use the expression for the diffusion stream in terms of the binary diffusion coefficients, D_{jk}, *viz.*,

$$\frac{dX_j}{dx} = \frac{m}{c_t} \sum_k \frac{1}{D_{jk}} \left(X_j \frac{\epsilon_k}{M_k} - X_k \frac{\epsilon_j}{M_j}\right) \tag{6}$$

Finally, the equation for the conservation of energy reads:

$$\frac{\lambda}{m_h \bar{C}_p} \frac{dT}{dx} = T - T_f + \sum_i (\epsilon_i - \epsilon_{if}) \frac{h_i^0}{\bar{C}_p} \tag{7}$$

where ϵ_{if} is the final value of the mass flow ratio ϵ_j.

It is seen that the last equation enables us to eliminate the space coordinate, x, and for a reaction scheme involving s species, one has to deter-

mine $2(s-1)$ dependent variables ϵ_j and x_j as functions of the independent variable, T. The remaining variables, ϵ_s and X_s, are determined by the conditions that the algebraic sum of the ϵ_j and X_j must be equal to unity.

However, we have to satisfy $2(s-1)$ boundary conditions for the ϵ_j and X_j at $T = T_0$ and $T = T_f$. The values of the ϵ_j and X_j for $T = T_0$ are given by the initial state of the unburned gas and the values for $T = T_f$ by the chemical equilibrium between the products. Therefore, it is seen that the boundary conditions cannot be satisfied for arbitrary values of the parameter m, and the problem of laminar flame propagation culminates in the determination of an eigenvalue of the mass flow, m, for which all boundary conditions can be satisfied.

The system of differential equations can be written, after introduction of a dimensionless variable $\theta = \frac{T}{T_f}$ and the corresponding notations $\theta_0 = \frac{T_0}{T_f}$ and $\theta_a = \frac{A_r}{RT_f}$, in the following form:

$$\frac{d\epsilon_j}{d\theta} = \frac{\lambda}{m^2\overline{C}_p} \frac{w_j}{(\theta - 1) + \sum (\epsilon_j - \epsilon_{jf}) \left(\frac{h_j^0}{\overline{C}_p T_f}\right)} \tag{8a}$$

$$\frac{dX_j}{d\theta} = \frac{\lambda}{\overline{C}_p} \left(\frac{RT}{p}\right) \frac{\sum_k \frac{1}{D_{jk}} \left(X_j \frac{\epsilon_k}{M_k} - X_k \frac{\epsilon_j}{M_j}\right)}{(\theta - 1) + \sum_i (\epsilon_j - \epsilon_{jf}) \left(\frac{h_j^0}{\overline{C}_p T_f}\right)} \tag{8b}$$

2. Methods of Solution. The Problem of the Cold Boundary

One easily recognizes by computing a simple example that the problem stated in the foregoing paragraph, strictly speaking, has no solution. It appears necessary to assume that the chemical changes do not start at the initial temperature, T_0, but at a higher temperature, T_i, which is called the ignition temperature. Computing a simple example, such as the case of a one-step unimolecular reaction, Millán and I found[2] that the value of the mass flow, m, becomes infinite if the ignition temperature coincides with the initial temperature, and becomes zero if the ignition temperature is equal to the final temperature, T_f. However, the eigenvalue considered as a function of T_i remains practically constant over a large interval of T_i, at least in the case that the activation energy is large in comparison with the quantity, RT_f.

We concluded that in most cases it must be possible to determine a value of the velocity of the propagation of the laminar flame, which is practically independent of the ignition process.

Hirschfelder, Curtiss and Campbell[3] proposed to eliminate the difficulty arising from the boundary condition at the cold boundary by means of the assumption of a flameholder which is represented mathematically by a heat sink of small intensity. This means that the temperature as a function of the coordinate x starts at $x = 0$ with a small but finite value of the gradient dT/dx. The intensity of the heat sink is given by $(-\lambda(dt/dx))_{x=0}$. Then it can be shown—as was first pointed out by Emmons[4] for the case of the simple thermal theory—that the eigenvalue which satisfies the condition at the hot end and the new condition at the cold boundary is insensitive to the assumed intensity of the heat sink. To be sure, when the heat loss at the flame holder converges to zero, the computed flame velocity increases to infinity.

The result obtained by Millán and myself holds for both the pure thermal theory of flame propagation and the complete theory which takes into account the diffusion. For this second case, Hirschfelder, Curtiss and Campbell,[3, 5] propose that, in addition to the heat sink, the existence of a filter be assumed which prevents the diffusion of the burned gas products into the unburned gas upstream of the heat sink. This assumption, however, has the disadvantage that the composition of the gas at $x = 0$ is a priori unknown and, therefore, it is difficult to start the integration of the system of differential equations at the cold boundary. The procedure applied by Hirschfelder and his school until 1954 consisted of calculating by numeric integration a sequence of temperature *vs.* mass ratio curves which satisfy the boundary conditions at the hot boundary. These curves correspond to a sequence of chosen values of the flame velocity or the mass flow. Then one tries to interpolate a curve which satisfies approximately the conditions at the cold boundary and obtains by this interpolation the eigenvalue sought for. It appears that by replacing the method of point by point integration of the differential equations by an integral method, the difficulty created by the boundary conditions at the cold boundary disappears at least for reactions with not too small activation energies. The method is applicable both to the thermal

and the complete theory, i.e., the theory taking into account both heat conduction and diffusion.

In our joint publications (with Millán and Penner[2, 6, 7]) in the years 1952–1953, we tried to develop such a method, which is relatively simple and sufficiently accurate for the computation of the flame velocity. Since 1954, after the British mathematician Klein joined the Wisconsin group, this group also uses, in addition to the numerical point by point integration procedure, an integral equation method, which by iteration furnishes the solution of the flame equations and the value of the flame velocity.[8] The first step of this method is very similar to the procedure proposed previously by our group.

Fundamentally, our procedure is similar to the methods proposed by Zeldovich, Frank-Kamenetski, and Semenow,[9] and by Boyr and Corner.[10] We believe, however, that our method is somewhat more systematic and leads to fair accuracy already for the first step of the calculation.

Before I try to describe our method and compare it with the methods of the authors quoted, I want to note that a group of other authors published so-called pure diffusional theories of laminar flame propagation. The common fundamental idea of these latter theories is the concept that the presence of "active centers" in the reaction zone determines the flame velocity. Tanford and Pease[11] analyzed various mechanisms producing atom and radical concentrations, such as equilibrium production in the burned gas and diffusion from the hot boundary. They arrived at the conclusion that in most cases the diffusion of atoms or radicals from the burned gases into the reaction zone is the governing mechanism. Van Tiggelen[12] calculates for chain reactions the probability of chain branching and chain breaking for active centers which move from the burned gas into the reaction zone. He obtains from the analysis of such a mechanism a simple expression for the progression of the flame into the unburned gas. The theory of Gaydon and Wolfhard[13] is also based on the picture that the diffusion of atoms or radicals from the burned gas into the unburned gas determines the propagation velocity of the flame.

I will not say that the formulae developed by these authors are not useful for comparative studies of certain reactions; for example, for a quick determination of the dependence of the flame velocity on the initial concentrations of the reaction partners. Nevertheless, I believe that the good accordance with experiments is sometimes more a matter of good luck in the choice of the numerical parameters than a proof for the correct description of the phenomena. In my belief, all these diffusional theories tend toward oversimplification of the problem of laminar flame propagation.

3. The Proposed Integral Method for Computation of the Flame Velocity

The method proposed and actually used in our calculations can be described in the following way:

The main assumption is that the behavior of the functions ϵ_j and X_j near the hot boundary, $\theta = 1$, has an overwhelming influence on the value of the flame velocity. Therefore, for the first approximation, approximate expressions for these functions are used which correspond to their behavior near $\theta = 1$.

Concerning the diffusion process, it is known from the pioneering work of Lewis and von Elbe[14] and Semenow[15] that, in the special case of two species for which the Lewis number $\left(\text{ratio between the binary diffusion coefficient, } D, \text{ and the thermal diffusivity, } \frac{\lambda}{C_p \rho}\right)$ is equal to one, the weight ratio of each component is a linear function of the temperature.[7] This corresponds to the rule—correct for this special case—that the sum of the thermal and chemical enthalpies of the gas mixture remains constant through the flame zone. Correspondingly, in the general case, we assume that Y_j and X_j behave as linear functions near $\theta = 1$.

The behavior of ϵ_j near $\theta = 1$ is evaluated from the Equation (8a) and depends largely on the order of the reactions considered.

The first approximation for the burning velocity is obtained by integration of the Equation (8b) between the limits $\theta = \theta_0$ and $\theta = 1$ and substituting for the functions ϵ_j and X_j the approximate expressions established as indicated above.

Jointly with Millán[16] we have compared, for a simple case, the results obtained by our method with those obtained from the so-called Semenow formula and by the method of Boys and Corner. The comparison was made for an idealized reaction of first order. We consider only two components in the mixture, reactants and products. We assume for the sake of simplicity that both the molecular weight and the specific heat of the mixture are constant; furthermore, that the

thermal conductivity is independent of the composition and varies proportionally with the temperature of the mixture. Finally, we assume that the diffusion coefficient between the two components is equal to the thermal diffusivity of the mixture.

Because of the last assumption, the mass ratio of the products, Y, can be assumed to be a linear function of the temperature in the form

$$Y = \frac{\theta - \theta_0}{1 - \theta_0} \tag{9}$$

The differential equation for the fractional mass flow ratio, ϵ, of the products can be written in the form

$$\frac{d\epsilon}{d\theta} = \frac{\lambda}{m^2 \bar{C}_p} \frac{w}{(\theta - 1) + (1 - \theta_0)(1 - \epsilon)} \tag{10}$$

For the rate of production of the products, we write

$$w = k \frac{1 - Y}{\theta} \exp\left(-\frac{\theta_a}{\theta}\right) \tag{11}$$

where k is a constant. The factor $(1 - Y)/\theta$ corresponds to the assumption that the reaction is of the first order.

Thus, after substituting for Y the expression $(\theta - \theta_0)/(1 - \theta_0)$ and writing $\lambda = \lambda_f \theta$, we obtain from Equation (10)

$$\frac{d\epsilon}{d\theta} = \Lambda \frac{(1 - \theta) \exp\left(-\theta_a \frac{1 - \theta}{\theta}\right)}{(\theta - 1) + (1 - \theta_0)(1 - \epsilon)} \tag{12}$$

where the parameter Λ is defined by

$$\Lambda = \frac{\lambda_f k \exp(-\theta_0)}{m^2 \bar{C}_p (1 - \theta_0)} \tag{13}$$

The factor $e^{-\theta_a}$ is included for convenience in the definition of Λ; otherwise Λ would be a very large number.

The problem of the burning velocity is reduced to the determination of the value for the parameter Λ which allows that the boundary conditions $\epsilon = 0$ for $\theta = \theta_0$ and $\epsilon = 1$ for $\theta = 1$ be satisfied.

The consideration that the behavior of ϵ near $\theta \equiv 1$ has an overwhelming influence on the correct value of Λ allows us to obtain a simple approximate formula which I would consider a zero-order approximation. We neglect in the denominator the quantity $(\theta - 1)$ in comparison with $(1 - \theta_0)(1 - \epsilon)$. This corresponds to neglecting in the energy balance the change of the heat content of the mixture in comparison with the heat transfer by conduction and the heat production by chemical reaction.

Then we readily obtain the equation

$$(1 - \epsilon)\, d\epsilon = \Lambda \frac{d\theta}{1 - \theta_0} (1 - \theta) \exp\left(-\theta_a \frac{1 - \theta}{\theta}\right) \tag{14}$$

in which the variables appear separated. Integrating this equation between the limits $\theta = \theta_0$ and $\theta = 1$, we obtain the zero-order approximation for the quantity $1/\sqrt{\Lambda}$ which is proportional to the burning velocity, S_b, i.e.,

$$\frac{1}{\sqrt{\Lambda}} = \sqrt{\frac{2I}{1 - \theta_0}} \tag{15}$$

where I denotes the integral

$$I = \int_{\theta_0}^{1} (1 - \theta) \exp\left(-\theta_a \frac{1 - \theta}{\theta}\right) d\theta \tag{16}$$

which can be easily evaluated.

If we want a better, say a first-order approximation, we approximate the quantity $(\theta - 1)$ which we neglected above, by an expression valid near $\theta = 1$. Setting

$$1 - \theta = \alpha(1 - \epsilon) \tag{17}$$

we evidently obtain from Equation (12) the relation

$$\frac{1}{\alpha} = \Lambda \frac{1}{-1 + \frac{1}{\alpha}(1 - \theta_0)} \tag{18}$$

Using this value for α, we find after integration

$$\frac{1}{\sqrt{\Lambda}} = \sqrt{\frac{2I}{1 - \theta_0 - \sqrt{2I}}} \tag{19}$$

In most cases this first-order approximation is satisfactory. A further improvement of the approximation can be obtained by computing the correction term $(\theta - 1)$ from numerical integration of Equation (12).

Comparing now our result first with the well-known Semenow formula, it is interesting to find that Semenow, Zeldovich and Frank-Kamenetski obtained an approximation for the value of S_b which corresponds exactly to our zero-order approximation. However, they proceeded to evaluate the integral I by means of a semiconvergent expansion in powers of $1/\theta_a$. In our notation

this leads to the expression

$$\frac{1}{\sqrt{\Lambda}} = \frac{1}{\theta_a}\sqrt{\frac{2}{1-\theta_0}} \qquad (20)$$

This formula, as will be clarified in the discussion of Figure 1, is greatly inferior to our first-order approximation.

The procedure of Boys and Corner has the following common feature with our method: they use the linear relation between $(1 - \epsilon)$ and $(1 - \theta)$ which is expressed by Equation (17). But they substitute the expression for $(1 - \epsilon)$ in the denominator of Equation (12). I believe this procedure is fundamentally wrong because one retains in the denominator the small quantity $(1 - \theta)$ and approximates the relatively large quantity $(1 - \epsilon)$ in terms of $(1 - \theta)$. The consequence is a large error in the first-order approximation and a slow convergence of the iteration process which is, in general, quite laborious.

In Figure 1 we represent the error in the evaluation of S_b for the three methods in the special case $\theta_0 = 0.125$. The ratio between the approximate values of $1/\sqrt{\Lambda}$ and the exact value obtained by careful numerical integration is plotted as a function of θ_a. It is seen that our zero-order approximation is better than the result obtained from the Zeldovich-Semenow formula and from the first-order approximation of Boys and Corner. The figure also includes the results of our first-order approximation corresponding to Equation (19) as well as the results derived from the Boys-Corner procedure by a further iteration. It is seen that both of our approximations involve a smaller error than the values obtained from the rather laborious iteration of Boys and Corner.

Similar comparative calculations have been made for the case of a second-order reaction and for values of the Lewis-Semenow number different from unity. These calculations led to the same general conclusions as were discussed above.

In the case of chain reactions (reactions in which atoms or free radicals play a role), the assumption that the mass or mole ratios can be approximated by linear functions of $(1 - \theta)$ is restricted to the main reactants and reaction products, i.e., to the stable species. The concentrations of the radicals are approximated by functions whose forms are determined by the chain-initiating, chain-branching and chain-breaking reactions. The procedure followed for chain reactions will be clear from the examples treated in the following Section 4. Particularly, I want to show the application of the steady-state assumption to the computation of the flame velocity in the case of simple chain reactions.

4. Application of the Steady-State Assumption

The application of the steady-state assumption to the problem of the computation of the flame velocity in the case of chain reactions was proposed in 1953 by the present writer and Penner

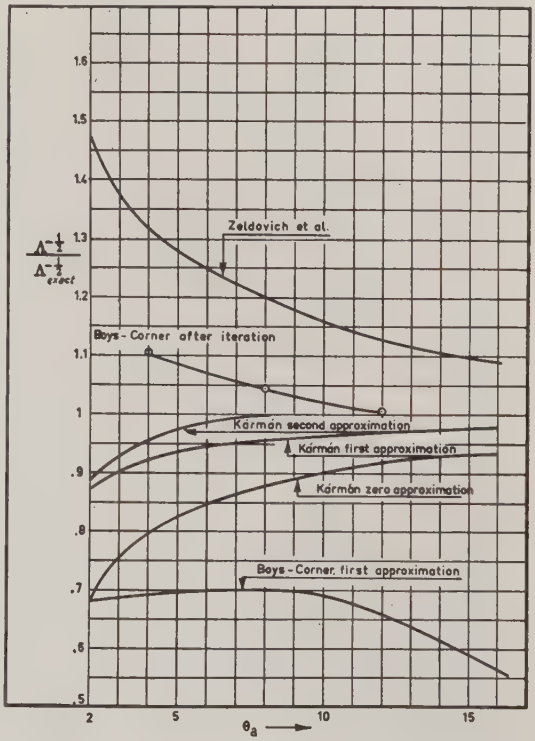

FIG. 1. Comparison between various semi-analytical methods for computation of the flame velocity.

in connection with the theory of the ozone decomposition flame.[7]

The principle involved in the steady-state approximation is the following: one assumes that the production and removal of every species of radicals compensate each other in every cross-sectional element of the flow. If we apply these conditions to all species of radicals, we obtain definite expressions for the radical concentrations as functions of the temperature and the mole fractions of the main reactants. Therefore, the system of reactions is reduced to a scheme in which only the main reactants enter. Then the computation of the flame velocity can be pursued

by means of any of the methods mentioned and explained in the foregoing Section 3.

It is noted that the assumption of the steady-state condition for the concentrations of radicals is based on a physical picture diametrically opposite to that underlying the so-called diffusional theories. The diffusion of the radicals from the burned gas into the flame zone—the most important process from the viewpoint of the diffusion theories—is neglected in our theory. The distribution of the radicals throughout the

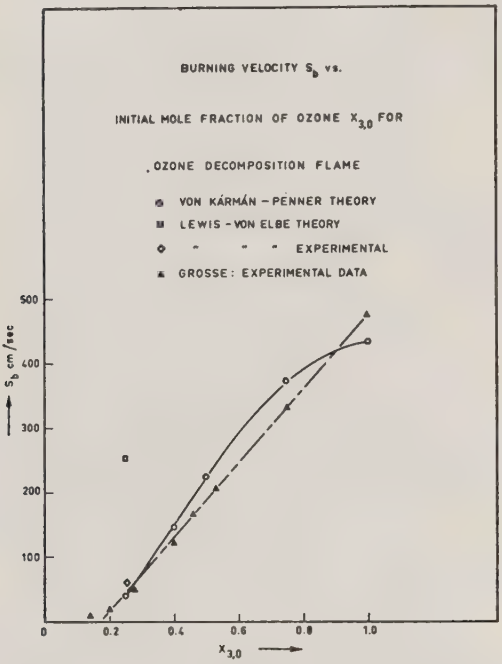

FIG. 2. The ozone dissociation; comparison between compiled and measured values of the burning velocity.

flame zone is computed from the balance between their production and disappearance by chemical reactions.

I want to present the results of calculation for three typical chain reactions for which the chemical kinetics data are sufficiently well known and experimental data are available so that a judgment on the validity and value of the steady-state assumption can be formed.

A. OZONE DECOMPOSITION

The scheme of reactions involved in the ozone decomposition flame is assumed to be the following:

$$O_3 + G \rightarrow O + O_2 + G \tag{1}$$

$$O + O_2 + G \rightarrow O_3 + G \tag{2}$$

$$O + O_3 \rightarrow 2O_2 \tag{3}$$

$$2O_2 \rightarrow O + O_3 \tag{4}$$

$$O_2 + G \rightarrow 2O + G \tag{5}$$

$$2O + G \rightarrow O_2 + G \tag{6}$$

Here G represents any of the three species O, O_2, or O_3.

The examination of available chemical kinetics data (Ref. 17) shows that the reactions (4) and (5) have extremely high activation energies in comparison with the other reactions; for reactions (2) and (6) the frequency factor is of a very small order of magnitude. One concludes that the rate governing reactions are reactions (1) and (3).

The condition that the production of O atoms according to the reaction (1) is balanced by their removal by means of reaction (3) leads to the following formula for the mole fraction X_1 of the oxygen atoms

$$X_1 = 1.48 \exp(-7.30/\theta) \tag{21}$$

The problem of the ozone decomposition flame has now been reduced to the solution of the following two equations:

$$\frac{d\epsilon_3}{d\theta} = -\Lambda \frac{\left(\frac{X_3}{\theta}\right) \exp\left(-\frac{9.719}{\theta}\right)}{\theta - 1 + \left(\frac{h_3^0}{\bar{C}_p T_f}\right)\epsilon_3} \tag{22a}$$

$$\frac{dX_3}{d\theta} = \frac{\lambda_f}{\bar{C}_p}\left(\frac{RT_f}{p}\right)\frac{1}{D_{23}} \frac{\frac{9}{10}X_3 - \frac{3}{5}\epsilon_3 - \frac{3}{10}X_3\epsilon_3}{\theta - 1 + \left(\frac{h_3^0}{\bar{C}_p T_f}\right)\epsilon_3} \tag{22b}$$

where

$$\Lambda = 2\lambda_f M_3 \left(\frac{p}{RT_f}\right)^2 B_1/m^2\bar{C}_p$$

[B_1 denotes the frequency factor for reaction (1)]. The laminar flame velocity S_b is obtained, as usual, from the relation

$$S_b = \frac{m}{\rho_0} \tag{23}$$

In Figure 2 we have plotted the following data: (1) The computed values of S_b according to the steady-state approximation for the following values of the initial ratio X_{30} (mole fraction of ozone): 0.25, 0.40, 0.50, 0.75 and 1.00. (2) The experimentally measured values of S_b. The

value for $X_3 = 0.25$ is taken from the publication of Lewis and von Elbe.[18] All other values were obtained by Grosse.[19]

It is seen that the general trends of the experimental and the computed values are in fair accordance; the maximum deviation is of the order of 15 to 20 per cent. The value of S_b for $X_{30} = 0.25$ was computed by Hirschfelder and his group by numerical integration of the system of equations without using the steady-state assumption.[17] Near the final adiabatic flame temperature, temperature intervals as small as one-tenth of a degree had to be used in the numerical integration. Nevertheless, the deviation between his and our results for the value of $X_{30} = 0.25$ is no more than 10 per cent.

However, if one assumes—as Lewis and von Elbe did[18]—that the atom concentration X_1 is determined by the equilibrium condition between O_3, O, and O_2, i.e., by the balance between the reactions (1) and (2), then one obtains a value for S_b which is more than five times larger than the measured value for $X_{30} = 0.25$. We have also calculated the burning velocity according to the assumption used by Lewis and von Elbe for other values of the initial concentration, namely, for $X_{30} = 0.50$, 0.75 and 1.00. We have found that, using the hypothesis of Lewis and von Elbe,[18] the computed value agrees for $X_{30} = 0.65$; for $X_{30} = 1.00$ the computed value becomes 40 per cent smaller than the measured value. As a matter of fact, the computed values are relatively insensitive to the initial concentration of O_3 and to the flame temperature, whereas the measured values, for the same range of initial concentrations, change in a ratio of about 1:10. In this connection, it is worthwhile to mention that the early measurements of S_b by Lewis and von Elbe are in good accord with the more extensive study of Grosse.[19]

B. HYDRAZINE DECOMPOSITION FLAME

In the matter of the hydrazine decomposition, a small accident occurred in the past both to the Wisconsin group[20] and to our group.[7] We all considered the first order reaction

$$N_2H_4 \rightarrow 2NH_2$$

as the rate-governing step. We all used a numerical value for the heat conduction coefficient which was given in a paper of Murray and Hall[21] as ten times larger than the actual value because of a common misprint. We obtained perfect agreement between the numerical integration of the Wisconsin group and our semianalytical method but too high numerical values for the burning velocity compared with the measurements.

Spalding[22] took up the problem again in 1955 and introduced a chain reaction scheme proposed by Adams,[23] as follows:

$$A \rightarrow 2B, \text{ radical production}$$

$$B + A \rightarrow B + 2C, \text{ chain propagation}$$

$$B + B + G \rightarrow 2\,C + G, \text{ chain breaking}$$

In this scheme no difference is made between the radicals NH_2, H or other radicals which may be present. A denotes hydrazine and C end products. Spalding used for the computation of the radical concentration and for the burning velocity a numerical integration method which starts from an arbitrary temperature profile through the flame zone and tries to follow the transient process which converges to the stationary state. He uses the assumption that the sum of the thermal and chemical enthalpies remains constant throughout the flame zone so that the mass fraction of the hydrazine is a linear function of the temperature.

Using the same assumption and the same chemical data, Millán and Sanz[24] recalculated Spalding's result using our way of computation, then they computed the burning velocity using the steady-state assumption. The first calculation is more laborious because, if one uses the steady-state condition, the mass fraction of the radicals is explicitly given as a function of the mass fraction of the hydrazine and the temperature; thus, one has to deal only with one differential equation for the fractional mass flow ratio of the hydrazine. If the steady-state assumption is not used, one has a system of simultaneous differential equations for the fractional mass flow ratio of the hydrazine and both the mass fraction and the fractional mass flow ratios of the radicals.

Figure 3 shows the result of these calculations including comparison with the available experimental values. The burning velocity is plotted as a function of the flame temperature. Spalding gave two theoretical values of the burning velocity corresponding to one hot and one cool flame. These values were in good agrement with the observations. The recalculation according to our semianalytical method agreed with Spalding's results. The figure shows in addition three other theoretical values for intermediate temperatures. The general trend of the calculated burning velocities is in fair agreement with the experimen-

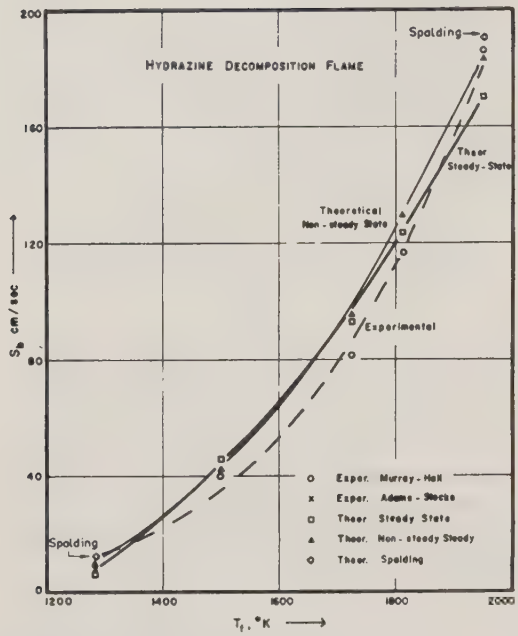

FIG. 3. Hydrazine decomposition flame; comparison between compiled and measured values of the burning velocity.

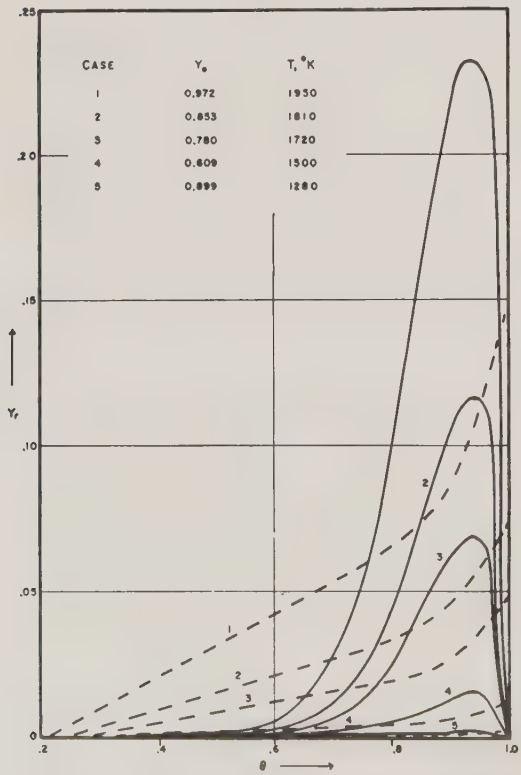

FIG. 4. Radical concentration vs temperature; computed with and without the use of the steady-state assumption for the case of hydrazine decomposition.

tal curve. Finally, the burning velocity has been computed for the same cases using the steady-state assumption. These values are also shown in Figure 3.

It is rather remarkable how little the theoretical values based on the steady-state assumption differ from the values calculated without the use of this assumption.

In order to find out the reason for this rather surprising state of affairs, Millán and Sanz compared the radical concentrations computed with and without the steady-state assumption. The

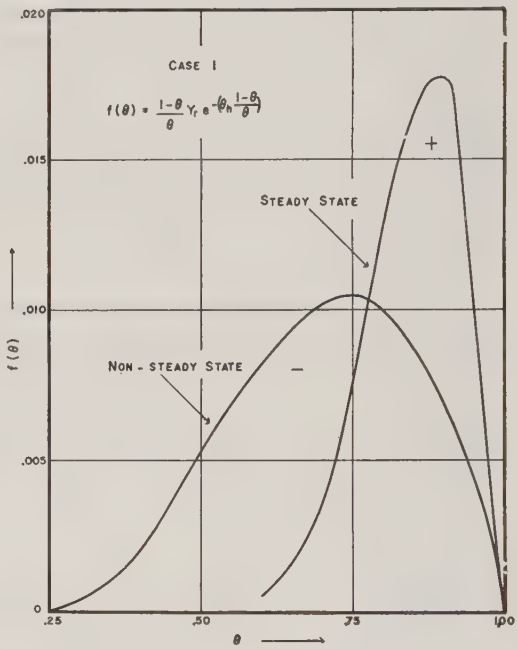

FIG. 5. The integrand used in the computation of the burning velocity in the case of the hydrazine dissociation with and without use of the steady-state assumption.

results of this investigation are shown in Figures 4 and 5. It appears from Figure 4 that the steady-state assumption (full lines) has the effect of exaggerating the radical concentration near the hot boundary. This was also found by Spalding, although the effect is much smaller than indicated in his paper. Spalding concluded that because of this effect the steady-state assumption overestimates the burning velocity. This conclusion seems to be false because, for example, in the case of the hot flame, as shown in Figure 3, the theoretical value calculated with the use of the steady-state assumption is considerably lower than Spalding's value. The explanation of this apparent contradiction is given in Figure 5

In Section 3 of this paper we have shown that the first-order approximation to the burning velocity is obtained in terms of a definite integral, I, over a given function of the nondimensional temperature, θ. Figure 5 shows the corresponding function which enters as the integrand in the analogous computation in the case of the hydrazine flame. One sees that the steady-state assumption overestimates the integrand near the hot boundary because it overestimates the radical concentration. However, this effect is compensated by the fact that the same assumption underestimates the radical concentration and the magnitude of the integrand in the lower temperature range since it neglects the diffusion of the radicals. This is clearly shown also in Figure 4.

The conclusion is that, at least in the case of the hydrazine flame, the steady-state assumption leads to a fair estimate of the magnitude of the burning velocity and its dependence on the flame-temperature but does not necessarily give a correct picture of the actual radical concentration.

C. THE HYDROGEN BROMINE FLAME

The reaction between hydrogen and bromine, forming hydrogen bromide, is of great interest because it is a rare example of a chain reaction whose reaction mechanism and rate constants are well defined and have been determined experimentally.[25] As a matter of fact, this reaction played an important part in the history of the knowledge of chain reactions.[26]

The reaction scheme is the following:

(1) $Br_2 + G \rightarrow 2\,Br + G$ radical production

(2) $Br + H_2 \rightarrow HBr + H$ chain propagation

(3) $H + Br_2 \rightarrow HBr + Br$ chain propagation

(4) $HBr + H \rightarrow H_2 + Br$ chain propagation

(5) $2Br + G \rightarrow Br_2 + G$ chain breaking

where G denotes any of the chemical species present.

The steady-state assumption requires that the number of H atoms produced by reaction (2) be equal to the sum of the number of H atoms removed by the reactions (3) and (4). Furthermore, the total number of Br atoms produced by reactions (1), (3) and (4) has to be equal to the number removed by reactions (2) and (5). These conditions lead to the following equation for the production of HBr molecules in unit time:

$$\frac{d(\mathrm{HBr})}{dt} = (\mathrm{const})\,\frac{(H_2)\,(Br_2)^{3/2}}{(Br_2) + (\mathrm{const})\,(HBr)} \qquad (24)$$

It is seen that this Equation (24) contains only the main or stable reactants, H_2 and Br_2, and the product, HBr. The proportionality factors are a known function of the temperature.

The present author, jointly with Penner,[27] applied this equation to the computation of the burning velocity with the additional assumption that the mass fraction of the radicals, H and Br, are small in comparison with the mass fractions of the stable reaction partners; in other words, that in the expressions for the conservation of the numbers of Br and H atoms through the flame zone, i.e., $2(Br_2) + (HBr) + (Br) = 2(Br_2)_0$ and $2(H_2) + (H) + (HBr) = 2(H_2)_0$ the quantities (Br) and (H) can be neglected. As a matter of fact, the H concentration is always small; however, as was first pointed out by

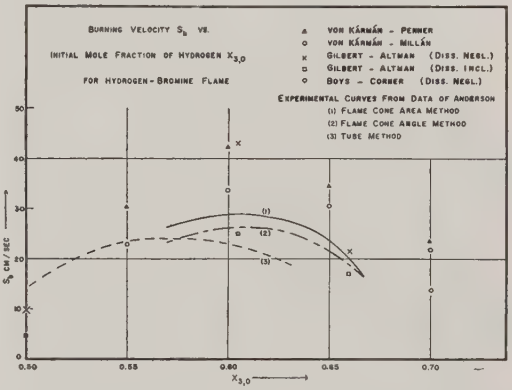

FIG. 6. The hydrogen bromine flame; computed and measured values of the burning velocity for hydrogen-rich mixtures.

Gilbert and Altman[28] the concentration of Br is not negligible. This is especially true for the hydrogen-rich mixtures.

Figure 6 represents the experimental curves for the burning velocity, S_b, plotted as a function of the initial mole ratio of H_2 in the interval between the stoichiometric mole ratio $X_{2,0} = X_{3,0} = 0.5$ and the mole ratio $X_{3,0} = 0.67$.

The observations were made by Anderson.[29] Curves (1) and (2) were obtained by observations of the flame cone, measuring the flame cone area and the cone angle respectively. Curve (3) was obtained from observations of flame propagation in a tube.

The first calculations of the author and Penner, as shown in the same figure, led to values of the flame speed which are definitely too high. Then Millán introduced a correction, which takes into

account the presence of Br atoms due to the dissociation of Br_2.

Instead of the relation $2(Br_2) + (HBr) = 2(Br_2)_0$ the complete equation $2(Br_2) + (Br) + (HBr) = 2(Br_2)_0$ is used and the quantity Br is determined from the steady-state condition $d(Br)/dt = 0$. According to this condition (Br) is proportional to $\sqrt{(Br_2)}$. Therefore, for hydrogen-rich mixtures, $(Br_2) \rightarrow 0$ at the hot boundary and the Br concentration becomes even larger than the Br_2 concentration and reduces the latter very considerably. The reduction of (Br_2) means —according to Equation (24)—a reduction of the over-all reaction rate and of the burning velocity.

As I mentioned before, Gilbert and Altman pointed out previously the importance of this correction for dissociation.[28] However, they carried out the computation of the correction only for the pure thermal theory. Then they computed the burning velocity including the effect of diffusion but neglecting the influence of the presence of (Br) atoms due to dissociation. In order to include the effect of dissociation they simply applied the same percentage reduction which they had obtained from the thermal theory. This assumption is rather arbitrary and overestimates the influence of dissociation which is, in general, less for a reaction with diffusion than for a pure thermal process. In addition, Gilbert and Altman followed the procedure of Boys and Corner and the apparent coincidence between the computed and measured values is essentially due to the fact that the first approximation of Boys and Corner furnishes too low values for the burning velocity, as we have shown in Figure 1. For example, Millán calculated for $X_{3,0} = 0.7$ the burning velocity using first our method without and with dissociation and then the Boys-Corner approximation without dissociation. These results are also shown in Figure 6. It is seen that the value computed by the Boys-Corner approximation, without taking into account dissociation, lies even below our value corrected for dissociation.

If we apply the same equations to the case of bromine-rich mixtures, we obtain values for the burning velocity which decrease rather rapidly with the increasing initial bromine concentration but are finite for arbitrary bromine-hydrogen ratios. The experimental evidence shows that it is not possible to obtain a stable flame if the bromine-hydrogen ratio is larger than the stoichiometric ratio. It is possible that this apparent instability is a consequence of the environment, for example, of heat removal from the flame. In fact it can be shown—as suggested by Spalding[30]—that, if the external cooling of the mixture is taken into account, below and above certain well-defined initial mixture ratios there is no real eigenvalue at all.

Summary

Summarizing our considerations concerning the present status of the theory of laminar flame propagation, I wish to state:

(1) That it appears in cases in which the reaction-scheme and the corresponding chemical kinetics are well-defined, a semianalytical method, as presented in this paper, makes a relatively easy determination of the flame velocity possible. There is no necessity for radical simplifying assumptions such as are introduced, for example, in the pure diffusion theories.

(2) There is no necessity to take recourse to laborious numerical integration of the differential equations, although the use of digital computers may facilitate such methods.

(3) It appears that in the cases dealt with until now, the steady-state assumption facilitates a rather quick determination of the flame velocity of a chain reaction, even in those cases where it does not furnish an exact picture for the distribution of the radicals through the flame zone.

(4) It is believed that in order to make further progress in the theory, the most urgent need is a better knowledge of the reaction schemes and the chemical kinetics of the important chain reactions. Especially more exact data are necessary concerning the presence and distribution of the radicals involved.

A paper by K. A. Wilde [J. Chem. Phys. *22*, 1788 (1954)] has recently come to our attention. The procedure used by this author for the integration of the simple one-step flame reaction is the same as that used in our first approximation except that ϵ is assumed to vary as $([\theta = \theta_0)/(1 - \theta_0)]^{n+1}$. Here the exponent n is determined by equating the limiting slope of $[(\theta - \theta_0)/(1 - \theta_0)]^n$ to the limiting slope of $\{\exp[-\theta_a(1 - \theta)/\theta]\}$. This procedure leads to the relation

$$\frac{1}{\sqrt{\Lambda}} = \sqrt{\frac{2I}{1 - \theta_0}\left[1 + \frac{2}{\theta_a(1 - \theta_0)}\right]} \qquad \text{(A-1)}$$

which is similar to our Equation (19). For sufficiently large values of θ_a, i.e., small values of I, Equations (A-1) and (19) become evidently equivalent. We have evaluated $1/\sqrt{\Lambda}$ according to Equation (A-1) and find the results to be less accurate than our second approximation for

$\theta_a \geqslant 5$ but to be better at smaller values of θ_a. Equation (A-1) gives results which are superior to those determined from Equation (19) for $\theta_a < 8$ but are roughly comparable [with $\sqrt{\Lambda}$ about as much too small according to Equation (A-1) as it is too large according to Equation (19)] for larger values of θ_a.

Nomenclature

ϵ_j fractional mass flow rate of the species j
Y_j weight fraction of the species j
X_j mole fraction of the species j
$\bar{C}_p$ average specific heat
h_j^0 standard specific formation enthalpy of the species j
C_t total concentration, i.e., number of moles of mixture in unit volume
T_0 initial temperature of mixture
T_f final temperature of mixture
M_j molecular weight of the species j
λ heat conduction coefficient of the mixture
ρ density of the mixture
v mean mass velocity of the mixture
V_j diffusion velocity of the species j

REFERENCES

1. Curtiss, C. F., and Hirschfelder, J. O.: J. Chem. Phys., *17*, 550, (1949).
2. von Kármán, T., and Millán, G.: *Anniversary Volume on Applied Mechanics*, pp. 55–69. Haarlem, N. V. de Technische Uitgeverig H. Stam, 1953.
3. Hirschfelder, J. O., Curtiss, C. F., and Campbell, D. E.: *Fourth Symposium (International) on Combustion*, pp. 190–210. Baltimore, The Williams & Wilkins Co., 1953.
4. Emmons, H. W.: Harvard University Report, 1950.
5. Round Table Discussion: *Fourth Symposium (International) on Combustion*, pp. 919–922. Baltimore, The Williams & Wilkins Co., 1953.
6. von Kármán, T., and Penner, S. S.: *Scientific Papers Presented to Max Born*, pp. 49–58. Edinburgh, Oliver and Boyd, 1953.
7. von Kármán, T., and Penner, S. S.: *Selected Combustion Problems*, I pp. 1-41. London, Butterworths Scientific Publications, 1954.
8. Klein, G.: University of Wisconsin Naval Research Lab. Report, September 1954, February 1955, and April 1955.
9. Zeldovich, Y. B., Frank-Kamenetski, D. A., and Semenow, N. N.: J. Exptl. Theoret. Phys., *10*, 1427 (1940); English translation in NACA Tech. Memo. No. 1084.
10. Boys, S. F., and Corner, J.: Proc. Roy. Soc., *197A*, 90 (1949); Corner, J.: Proc. Roy. Soc., *198A*, 388 (1949).
11. Tanford, C., and Pease, R. N.: J. Chem. Phys., *15*, 431, 433 (1947).
12. Van Tiggelen, A.: Mem. Acad. Roy. Belg. (Sciences), *27*, 1 (1952).
13. Gaydon, A. G., and Wolfhard, H. G.: *Flames, Their Structure, Radiation and Temperature*. London, Chapman and Hall, 1953.
14. Lewis, B., and von Elbe, G.: *Combustion, Flames and Explosions of Gases, p. 351* et. seq. New York, Academic Press, Inc., 1951.
15. Semenow, N. N.: Adv. Phys. Sci. (Moscow), *24*, 433 (1940); English translation in NACA Tech. Memo 1026.
16. von Kármán, T., and Millán, G.: Comparison of three analytical methods for computing laminar flame propagation (1950). Unpublished.
17. Hirschfelder, J. O., Curtiss, C. F., and Campbell, D. E., J. Phys. Chem., *57*, 403 (1953).
18. Lewis, B., and von Elbe, G.: J. Chem. Phys., *2*, 283, 537 (1934).
19. von Grosse, A.: *Sixth Symposium (International) on Combustion*, New York, Reinhold Publ. Corp., 1957.
20. Hirschfelder, J. O., Curtiss, C. F., Bird, R. B., and Spatz, E. L.: *The Molecular Theory of Gases and Liquids*. New York, John Wiley and Sons, Inc., 1954.
21. Murray, R. C., and Hall, A. R.: Trans. Faraday Soc., *47*, 743 (1951).
22. Spalding, D. B.: The Theory of Flame Phenomena with a Chain Reaction. Phil. Trans., Jan. 1956.
23. Adams, G. K., and Stocks, G. W.: *Fourth Symposium (International) on Combustion*, pp. 239–248. Baltimore, The Williams & Wilkins Co., 1953.
24. Millán, G., and Sanz, J.: Report, June 1956, on contract No. AF61(514)—734C, ARDC European Office.
25. Campbell, E. S., and Hirschfelder, J. O.: University of Wisconsin Naval Research Lab., Report CF-2108, Nov. 1953.
26. Bodenstein, M., and Lind, S. C.: Z. Physik. Chem., *57*, 116 (1906); Bodenstein, M., and Jung, G.: Z. Physik. Chem., *121*, 127 (1906).
27. von kármán, T., Penner, S. S., and Millán, G.: Technical Report No. 16, Contract DA-04-495-Ord-446, California Institute of Technology, Pasadena, 1956.
28. Gilbert, M., and Altman, D.: *Sixth Symposium (International) on Combustion*, New York, Reinhold Publ. Corp., 1957.
29. Anderson, R. C.: *Combustion Researches and Reviews, 1956*. London, Butterworths Scientific Publications, 1956.
30. Spalding, D. B.: Personal note.

2

ENDS AND MEANS IN FLAME THEORY

By D. B. SPALDING

1. Purposes of this Paper

Although the research chemist and the design engineer both need to predict flame phenomena theoretically, there is at present little general understanding of what can and cannot be achieved by flame theory. This paper gives a brief review of current achievements for the benefit of nonspecialists (sections 2 and 3).

The whole field of theoretical flame problems which interest chemists and engineers is very large. Review shows, however, that almost all the work has been done in one corner of this field: the one-dimensional laminar flame. One result has been that the theoretical methods developed there are useful only for this flame; continued neglect of two- and three-dimensional problems is therefore encouraged. In section 4 of this paper some methods are suggested which, while being applicable to the one-dimensional flame, can also be extended to flames of more practical importance. Some of these methods are being developed in the author's laboratory. It is hoped that this section will interest the specialist in flame theory.

2. The Aims of Flame Theory

(2.1) THE NATURE OF FLAME THEORY

Three bodies of knowledge form the basis of the theory of flames: (a) Reaction kinetics: the relation of the volumetric rates of chemical change to the local gas composition and temperature in a differential volume. (b) Transport phenomena: the relations of the fluxes across the boundaries of the differential volume, of work, heat and matter, to the gradients of velocity, temperature and composition normal to those boundaries. (c) The conservation laws of matter, momentum and energy, together with the thermodynamic properties of materials. These laws relate the fluxes to the volumetric rates of change.

Flame theory has the task of combining (a) (b) and (c) so as to predict what sort of flame will ensue when given reactants are caused to flow into a given combustion chamber under given conditions; the general statements about the infinitesimal volumes have to be added up to see what they demand in the behavior of the particular whole.

(2.2) PURPOSES OF FLAME THEORY

Flame theory has two main purposes. The first is practical. Combustion chamber testing is expensive. A theory which reliably predicts the result of an experiment, without the need to conduct the experiment, speeds and cheapens development. In this branch of flame theory, the reaction kinetic and transport data are regarded as known; the interest is in the effect of changing the geometry and flow conditions. Usually the assumed reaction kinetics have to be simplified.

Flame theory is also used with a fundamental aim in view. Measurements on simple flames are often easier than direct measurement of reaction kinetic data. A reliable theory enables the latter to be deduced from the former. In this branch of flame theory, the geometry and flow conditions are usually as simple as possible; the interest is in the effect of changes in the assumed reaction kinetics, and full justice has to be done to complex kinetic schemes.

Theoretically considered, the differences between the practical and fundamental branches of the subject lie only in the varying number of dependent and independent variables, and in the nature of the boundary conditions. Similarities exceed differences.

3. Present Achievements of Flame Theory

The object of this section is to state what types of flame have been dealt with so far, to classify the theories of the various investigators, and to point out differences and similarities.

(3.1) THE ONE-DIMENSIONAL LAMINAR PRE-MIXED ADIABATIC FLAME

The inner cone of the Bunsen burner has claimed the greatest attention among investigators. The problem is this: given data about the reaction kinetics and transport properties of the mixture, what will be the distribution of temperature and gas composition along a line normal to the flame, and what must be the velocity of flow along this line? Since these questions can also be answered experimentally, comparison of theory and experiment is a check on the data.

In the simplest case the reaction is single-step

and the resultant diffusivity equals thermal diffusivity, for then it suffices to consider the temperature variation—composition being linked to temperature in a known way. A single differential equation must be solved. If the diffusivities are not equal, both temperature and composition must be watched; then two simultaneous equations must be solved. Increasing complexity of the reaction increases the number of equations by one for each new reactant that is involved. Each of these differential equations has the same independent variable, viz. distance.

The subject of applied mathematics is highly developed and provides many techniques which may be applied to these equations. The apparent differences between "theories" of flame propagation, which so bewilder the onlooker, are usually only differences of notation or of procedure; each investigator chooses the mathematical tool which is best suited to his own situation. These differences of method have often obscured the fact that the differences between the solutions obtained in given cases are very slight.

Differences in the solutions exist because every mathematical method is to some extent approximate. In some methods approximation is inherent, for example where it is desired to present the result as an algebraic formula. Such are the methods of Zeldovich and Frank-Kamenetsky,[1] Boys and Corner,[2] Adams,[3] and von Kármán and Penner.[4] In other methods, where the result is to be presented as a set of numbers valid for particular cases, the degree of approximation can be reduced to zero merely by taking more trouble in computation. Such are the methods of Hirschfelder, Curtiss, and Campbell,[5] who integrate the equations numerically; of Hirschfelder's associates (Klein[6] and Schatzki[7]), who use respectively solutions by successive quadrature and by relaxation; and of Spalding,[8] who obtains the steady flame speed as an asymptotic solution of the unsteady state equations.

All of these methods have been applied with success to problems where there are only two dependent variables, usually the case of a single-step reaction with unequal diffusivities. All of them become difficult to use when there are more dependent variables, as in chain reactions of the hydrogen-bromine type, to take a popular example. Solutions to these complex flame problems have been delayed by the search for the best mathematical procedures, but the certainty of success is not in question.

In addition to the above-mentioned researches, "theories" of the one-dimensional flame exist which do not start from consideration of the fundamentals mentioned in section 2.1, but attempt to take a short cut by assuming, in the light of intuition, that a single property or process is dominant in flame propagation. Such, for example, are the "diffusion theory" of Tanford and Pease,[9] the "excess enthalpy hypothesis" of Lewis and von Elbe,[10] and the "H-radical momentum theory" of Manson.[11] In the view of the author it is now time to put aside these "short-cut" theories. Although the insight which some of them have afforded in the past has been valuable, they now confuse rather than simplify. The effort that is still wasted in discussing the relative merits of "thermal" or "diffusional" theories could be more usefully employed.

(3.2) MULTI-DIMENSIONAL STEADY LAMINAR PREMIXED FLAMES

Very few problems of this type have been studied. Von Kármán and Millán[12] have considered effects near the wall when a flame propagates through gas at rest in a tube. Marble and Adamson[13] have studied the mixing and reaction of adjacent semi-infinite streams of equal velocity and ultimate composition but different temperature. The transient method mentioned in 3.1 has been applied to the mixing of finite jets of equal velocity.[8] No other work of this type is known to the author.[a]

(3.3) TURBULENT FLAMES

There are no turbulent flame theories in the sense of this paper.[b] Tentative extension of laminar results to turbulent conditions is usually made by postulating augmented transport properties. This is made necessary by present ignorance of the proper differential description of turbulence even without combustion; the relations between time-mean reaction rates and time-mean concentrations also await investigation.

Most practical flames are turbulent. Satis-

[a] Karlovitz, Knapschaefer, and Wells[14] discussed flames in the presence of velocity gradients in a "short-cut" theory, assuming the laminar flame speed to be a constant of the mixture, irrespective of the local flow.

[b] "Short-cut" theories by Karlovitz, Denniston, and Wells[15] and Scurlock and Grover[16] exist. They assume that turbulent flames are composed of laminar ones. Many doubt whether this is a helpful assumption, e.g., Summerfield, Reiter, Kebely, and Mascolo.[17]

factory ways of writing the differential equations governing turbulence must be discovered if theory alone is to predict flame phenomena. Section 4.32 of this paper indicates how a combination of theory and model experiment makes prediction possible already.

(3.4) IDEALIZATIONS OF FLAMES IN STEADY-FLOW ENGINES

An idealized flow system which has features in common with some engine flames is the homogeneous reaction zone of Avery and Hart,[33] in which variations in both space and time are assumed absent. Longwell, Frost, and Weiss[34] have shown how, for a single dependent variable, the gas condition can be calculated as a function of the steady-flow rate. Cases of two dependent variables have also been considered in connection with chain reactions[8b] and radiation heat transfer.[35] In each case it is found that the flame must be extinguished when the flow rate exceeds a critical value. The homogeneous reaction zone represents a simple limiting case, and future work must account for the spatial inhomogeneities arising in real combustion systems due to the finite transport rates. Spalding[8a] deals with one such case: the cylindrical vortex with uniform diffusivity. This exhibits extinction phenomena also, as must all steady-flow systems whether homogeneous or not.

(3.5) NON-PRE-MIXED FLAMES

Particularly simple (aerodynamic) considerations govern flame position when fuel and oxidant flow in separately. Pioneer investigations in this field by Nusselt[18] and Burke and Schumann[19] have been followed by Hottel,[20] Fay,[21] Spalding,[22] and many others. The rate of fuel consumption is calculable without knowledge of the reaction kinetics. But few workers[23, 24] have studied the extinction of this flame type, when chemical reaction becomes controlling, yet this phenomenon sets the limit to aircraft engine performance at high altitude.

(3.6) COMMENTS

The research chemist has more reason to be pleased with the present achievements of flame theory than has the engineer, because the Bunsen burner is his chosen laboratory tool. Even so, serious use of theory in making reaction kinetic deductions from flame measurements has scarcely begun, partly because the right theoretical problems have not been solved, but still more because the available solutions are cast in forms which chemists find obscure.

The engineer on the other hand will look in vain for adequate theories of flame propagation in boundary layers, of the effect of velocity ratio on propagation from pilot flames, on ignition in static and moving gases, etc., to name only laminar flame phenomena of interest to him. Nor will current work on one-dimensional flames throw much light on these multi-dimensional ones; entirely different techniques appear suitable for the latter, as will be seen.

The final section of this paper is intended to interest the specialist in the multi-dimensional problems by suggesting theoretical and other methods which are not restricted to the one-dimensional flame.

4. "Source-and-Sink" Methods

The mathematical theory of heat conduction with heat sources but without convection is highly developed. It is built on the Poisson equation which involves second derivatives of temperature with respect to distance, and a source term. Analytical solutions often involve the integration of Green's function for the prescribed boundary conditions (e.g., Carslaw and Jaeger[25]). Numerical solution by relaxation methods is an established technique.[26, 27] Analogues of various kinds have been widely used.[28] If there is only one independent variable, numerical integration is particularly easy (e.g., Hartree[29]). These techniques will here be given the generic name "source-and-sink methods," since they all involve the source concept explicitly or implicitly.

If flame problems can be expressed in terms of Poisson-like equations the above techniques become available. This is the aim of the methods to be described below. Because of the complicated nature of the source (reaction rate) terms, analytical methods are often out of the question; nevertheless, the Green's function approach may be used in iterative numerical methods, and forms the basis of the analogues. Transformations are indicated which in simple cases eliminate the convection term from the flame equations, so making them of the Poisson form.

Discussion of these methods begins with the one-dimensional flame because of its familiarity.

(4.1) NUMERICAL PROCEDURES

(4.1.1) *One-dimensional flames*

For simplicity, a flame with one dependent variable (temperature) will be considered. In

terms of a dimensionless space co-ordinate y, the equation of conservation is

$$\frac{d^2\tau}{dy^2} - \frac{d\tau}{dy} = -\lambda\phi(\tau) \qquad (1)$$

Terms on the left-hand side represent molecular transport and convection respectively; ϕ is a function of τ and represents volumetric reaction rate; λ is related to burning velocity, and represents the eigenvalue to be determined.

Most workers[14] have followed Zeldovich and Frank-Kamenetsky in transforming the equation to new variables $p\left(\equiv \frac{d\tau}{dy}\right)$ and τ, giving

$$p\frac{dp}{d\tau} - p = -\lambda\phi(\tau) \qquad (2)$$

It is this transformation which, in the past, has turned flame theory away from the main stream of heat and mass transfer theory. It is advantageous for approximate methods but, since the equation is now first order, is not amenable to the "source-and-sink" techniques. It does not appear capable of extension to multidimensional flames.

The methods to be described do not make this transformation but operate either directly on Equation (1) or on transformations of it which are still of second order.

(4.1.2) *"Catalyst-plug" boundary conditions*

An often-discussed difficulty of flame theory arises because the analytical expression for reaction rate has a finite, though very small, value in the gas stream before it approaches the flame. This difficulty is avoided by some authors by assuming the reaction rate terms to be exactly, instead of nearly, zero below a certain temperature. Hirschfelder, Curtiss, and Campbell[5] have instead introduced a fictitious "cold plug" at the upstream boundary and suppose that the flame must always lose a small but finite amount of heat to this plug.

A less widely known difficulty of flame theory arises at the hot boundary where, in the real flame, temperature and concentration gradients become zero. Since the reaction rate is also zero there, Equation (2) shows that

$$\left(\frac{dp}{d\tau}\right)_{\tau=1} = 1 - \lambda\frac{0}{0} = \text{indeterminate} \qquad (3)$$

Special devices must therefore be used before the integration from the hot boundary can begin, e.g., expansion in series.

The author circumvents the difficulty, which arises whatever the form of the equations, by introducing a fictitious "catalyst-plug" at the hot boundary which always supplies a small but finite amount of heat to the flame. It may be thought of as an adiabatic porous catalyst into which the gas flows and which brings about thermodynamic equilibrium at its upstream surface. Solutions for the value of λ are then obtainable for any finite temperature gradient at the plug surface. The required value for zero temperature gradient cannot be obtained directly; it must be determined by extrapolation.

(4.1.3) *Discussion of Equation (1) in terms of sources and sinks*

Solution of Equation (1) involves obtaining the temperature distribution through the flame. If the R.H.S. of Equation (1) were everywhere very small (except at the catalyst plug surface,

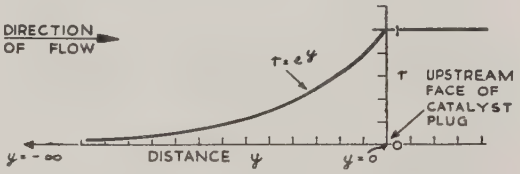

FIG. 1. Temperature distribution in one-dimensional gas stream if λ is very small (negligible reaction except at plug face).

of course), this distribution would simply be an exponential decay curve upstream of the plug and a horizontal line downstream of the plug (Fig. 1). This distribution is the effect of a unit plane source of heat normal to the stream direction, situated at the plug surface. If the source were situated farther upstream, the distribution curve would merely be shifted correspondingly. Now the R.H.S. of Equation (1) is linear, so that, if two sources are present, the temperature at any point is the sum of the temperatures which would prevail there due to each source individually. In particular the temperature distribution due to a unit source at $y = \eta$ and a unit sink at the hot plug ($y = 0$) is shown in Figure 2. Curves such as this are easily calculated for any value of η. Suppose their ordinate is $G(y,\eta)$.

Now the R.H.S. of Equation (1) states how the heat sources are distributed albeit with respect to temperature. The foregoing discussion shows that the temperature distribution which solves the equation is the sum of the effects of all the sources in the flame region, these effects being determinable from the curves such as Figure 2

and from the function ϕ. In mathematical form this is stated by re-writing Equation (1), together with its boundary conditions, as an integral equation:

$$-\infty < y \leqslant 0, \quad \tau(y) = e^{y} + \lambda \int_{-\infty}^{0} G(y,\eta), \quad \phi(\tau)\, d\eta$$

where

$$\begin{aligned} G(y,\eta) &= 1 - e^{y}, & \operatorname{Ln} \eta \leqslant y \leqslant 0 \\ G(y,\eta) &= e^{y-\eta} - e^{y}, & \operatorname{Ln} y \leqslant \eta \leqslant 0 \end{aligned} \tag{4}$$

$G(y,\eta)$, the integrating kernel of Equation (3), is the Green's function of the problem.

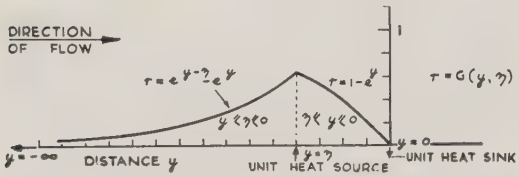

FIG. 2. Temperature distribution $G(y, \eta)$ in gas stream caused by unit heat source at $y = \eta$ and unit heat sink at $y = 0$ (plug surface). $\eta = -1$ in this case.

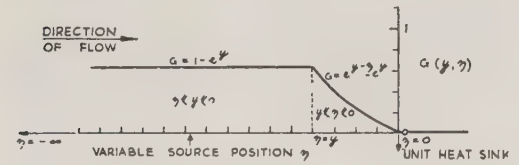

FIG. 3. Influence function (Green's function) $G(y, \eta)$ showing temperature rise incurred at y when a unit source is placed at η and a unit sink at the catalyst plug ($\eta = 0$). $y = -1$ in this case.

The idea of a Green's function can perhaps be made acceptable to engineers by pointing out the similarity of Figure 2, for example, to a bending moment diagram representing the effects at all points (y) of a beam when a force is placed at a given point (η). Alternatively $G(y,\eta)$ may be plotted as in Figure 3. This curve represents the effects at one point (y) for various positions (η) of the source; its engineering analogy is the "influence line" of structural theory. It is notable that if the source is upstream of y its effect at y is independent of source position.

(4.1.4.) *Methods of solution*

Since $\phi(\tau)$ in Equation (4) can be given definite values only when τ is known as a function of y, iterative methods of solving Equation (4) suggest themselves. A τ distribution is assumed as a first approximation, the corresponding ϕ is calculated, and Equation (4) is used to give a new approximation for τ. If this is done point by point, the space having first been divided up into finite intervals, the procedure is essentially one of relaxation; if, for speed, sources are adjusted simultaneously at all points, the procedure is essentially one of successive quadrature performed by means of tables of $G(y,\eta)$.

This procedure, or variants of it, can be applied to the general case where there are several dependent variables. The arithmetic, though simple, is heavy; automatic devices soon become necessary. Apart from digital computers, analogue devices such as those mentioned later may be used; indeed analogues represent the most suitable means of carrying out solutions of this nature.

(4.1.5) *Flames in more than one dimension*

As far as the one-dimensional flame is concerned, the above method is just one among many. It is presented here because it can be extended, in either its numerical or analogue form, to multi-dimensional flames—that is, to partial differential equations. The only essential change lies in the extended nature of the Green's function which must represent the influence of a heat source at point A on the temperature at point B, wherever these points are situated. If an analogue is used it is not necessary to evaluate these influences explicitly; they are "built-in" to the apparatus.

(4.1.6) *Transformations of the conservation equations*

Numerical integration, relaxation techniques, and analogues all deal with second-order differential equations most happily when the first derivative is absent. A number of transformations make this possible provided that, although heat and matter flow may be multi-dimensional, the general stream velocity is uniform. They will be indicated for the one-dimensional flame only.

The dependent variable in Equation (1) can be transformed by putting

$$\tau = te^{y/2} \tag{5}$$

Then Equation (1) becomes

$$\frac{d^2t}{dy^2} = \frac{1}{4}\, t - \lambda e^{-y/2}\phi(\tau) \tag{6}$$

Thus the first derivative has been eliminated at the cost of introducing a new source term and

making the original source term depend upon position. It is still amenable to the various source-and-sink techniques, and is particularly suitable for expression in finite difference form and solution by relaxation. Computation is unnecessary at points so far upstream that chemical reaction has become negligible, for the exponential nature of the solution is known there; that y goes to infinity is not a serious disadvantage. This transformation has been used to solve analytically the heat conduction problems with moving heat sources encountered, for example, in welding.[30]

As an alternative, the independent variable may be transformed by putting

$$\xi = e^{y} \tag{7}$$

Then Equation (1) becomes

$$\frac{d^2\tau}{d\xi^2} = -\lambda \frac{\phi(\tau)}{\xi^2} \tag{8}$$

This has the advantage that the independent variable only varies between 0 and 1 in the whole flame region. It is usually preferable to Equation (6) for one-dimensional problems.

A different but related transformation which is of relevance to the electric analogue follows from multiplying Equation (1) by e^{-y} giving

$$\frac{d}{dy}\left(e^{-y}\frac{d\tau}{dy}\right) = e^{-y}\phi(\tau) \tag{9}$$

In finite difference form this is easily simulated electrically, and y of course varies from 0 to $-\infty$.

Each of these transformations has its own special features. Which to use depends on the details of the problem and the solution technique which is to be used. Source-and-sink methods are applicable in each case. None of these transformations works when the flow velocity is not uniform.

(4.1.7) *Other applications of source-and-sink methods*

The method of solving transient problems mentioned in section 3.1 involves the use of sources and sinks; it makes use of the linearity of all terms of the equation, except that for reaction rate, when distance and time are the independent variables.

The distribution of chemical reaction in steady diffusion flames (section 3.4) can be studied by obvious modification of the techniques mentioned above. In this case the source and sink magnitudes depend on position in a new way, only having finite values in a restricted region. The boundary conditions are such as to make numerical integration very difficult; relaxation or successive quadrature are possible, however, as is the use of an analogue.

(4.1.8) *Closing note*

The above formulations have not yet been tried with any very complicated flames. They are mentioned here to indicate that there are many more ways of solving flame problems theoretically than the current literature of the subject would suggest.

(4.2.) ANALOGUE METHODS FOR PROBLEMS WITH PRESCRIBED FLOW

When the flow is not uniform, as for example in laminar boundary layer problems, the calculation of the Green's functions is a formidable task. This is avoided if a device is constructed which obeys the same differential equation as does the flame, i.e., if an analogue is used. An electric analogue for example must be so constructed that a unit current source at point A produces a voltage increase at point B which is proportional to the temperature rise at the corresponding point b in the flame when a unit heat source is present at the corresponding point a. Since they automatically satisfy the differential equation and the boundary conditions, analogues may be regarded as having "built-in" Green's functions. Usually the simulation must be of a finite-difference nature, at least as far as the source terms are concerned.

Electrical and other analogues for heat transfer and diffusion problems are well known[28] and will not be described. Here some modifications needed for solving flame problems will be mentioned. It is assumed that the flow pattern and the transport properties are known beforehand.

(4.2.1) *Fully electrical analogues*

Electrical resistance networks with controllable current inputs at the mesh-points obey Poisson's equation in finite difference form. Transformations of the flame equations into the Poisson form have been described above.

The analogue for Equation (6), for example, is a line of equal resistance in series representing the left-hand side; a set of equal resistances connecting each junction of the line to ground, representing the $\frac{1}{4}t$ term; and a controlled current input at each junction to represent the reaction rate term. One end of the resistor line is held at

a fixed voltage above ground; this corresponds to the hot plug. The other end, theoretically at infinity, is at ground voltage. The current sources are adjusted successively until they accord with the local voltages for an arbitrary value of λ. The current taken from the terminating battery is a measure of the temperature gradient at the hot plug. For problems with many dependent variables, many such networks are required, interconnected at least through the input currents. With several independent variables, several networks are cross-connected electrically.

Equation (7) can be simulated more easily: the line of resistance is finite in length, and the leaks to ground are absent. Equation (9), on the other hand, requires an infinite line of series resistances, but these decrease in value the greater the distance from the hot plug; leakage resistors are absent. This technique and others are described by Johnson and Alley.[31]

Problems with nonuniform velocity cannot be described by Poisson-type equations by any transformation known to the author; the convection terms cannot be eliminated. If network analogues are to be used for these problems, they must incorporate resistances which have different values according to which end they are seen from. Suitable devices are described by Soroka;[28] they involve electronic equipment.

(4.2.2) *Electro-thermal analogues*

When simulation of convection terms is unavoidable, a thermal resistance network may be used in place of the electrical one. Mesh-points are connected by metal tubes; thermal conduction occurs along thin walls while fluid flows through them with a distribution of velocities which simulates that appropriate to the flame. Electrical resistances wound around the tubes provide concentrated heat sources, and thermocouples measure the local temperature. The external control relates the rate of heat input to the temperature, which represents the dependent variable of the flame problem.

This technique has not so far been used. Although somewhat clumsy, it offers an inexpensive means of investigating flame phenomena in boundary layers where the velocity distribution, although complex, can be calculated without knowledge of the flame pattern.

(4.3) ANALOGUES FOR FLAMES IN COMPLEX AERODYNAMIC FIELDS

In engineering equipment, flow is usually turbulent and multi-dimensional, and moreover involves regions of mixing and recirculating flow which aerodynamics can at present neither predict nor describe in detail sufficient as a basis for flame theory. This difficulty must be surmounted if flame theory is to serve practical ends. Two ways of doing so are here described. The first is simple in concept but difficult in practice; it has not been used. The second involves an analogue which avoids these difficulties; it has been in operation since mid-1954.

(4.3.1) *Experiment on models, combined with calculation*

An early step in one of the theoretical methods (section 4.1) is the calculation of the Green's function relating temperature increment at one point to heat source increment at another. This is impossible for complex turbulent flow fields. However, these influence coefficients could be determined experimentally, by making a dynamically similar model of the flow system (combustion chamber) and, for example, measuring the concentration of a tracer at position A when a thin stream of tracer is supplied at B; this would be done at a sufficient number of point-pairs to characterize the flow.

The next step, iterative solution of the conservation equations in integral form, then follows. Though straightforward, it demands much computation even in relatively simple cases. Thus both the initial experimental step and the following computational step are time-consuming.

(4.3.2) *Electro-thermal analogue*

The experimental step in the above method is eliminated and the computational step shortened by use of an electro-thermal analogue. A model of the combustion chamber is constructed through which air flows simulating the reactive gas. Distributed through the model are thermocouples measuring the air temperature and electric resistance wires providing heat. External controls relate local heat input to local air temperature in a way similar to the prescribed reaction rate function. The flow in the model automatically ensures that temperature increments resulting from a heat source increment are distributed through the flow space in the correct manner.

The analogue constructed at the Cambridge University Engineering Laboratory and now operating at Imperial College[32] solves two-dimensional turbulent flow problems with a single dependent variable. The reaction-rate function used is rectangular in shape for simplicity. Control of heaters is automatic. Each solution takes

about one minute. The heater-thermocouple elements are permanently in position; changes in combustion chamber shape are made by interposing metal baffles.

The main limitations of this type of analogue are inability to simulate the density changes consequent on reaction, and inability to account for the effects of two-phase flow (spray combustion). Separate introduction of fuel (assumed gaseous) and air is simulated by a preliminary temperature-distribution experiment with a heat source simulating fuel injection; the local reaction rate is adjusted to accord with the local fuel/air ratio. Heat losses and complex reaction schemes may in principle be simulated by simultaneous use of several analogues with cross-coupled source terms. Further development will be directed to these points, to use of three dimensions and the better simulation of reaction-rate-temperature functions.

5. Conclusions

The theoretical flame problems dealt with by the design engineer and research chemist have much in common, differing only in the relative number of dependent and independent variables.

Methods are becoming available for solving most of these problems. The analogue methods which are most suitable for complex flow patterns are similar in spirit to numerical methods which may be used for solving the more familiar problems of the one-dimensional laminar flame.

6. Acknowledgment

The electro-thermal analogue described in section 4.3.2 has been developed as part of an extra-departmental research sponsored by the Mechanical Engineering Research Laboratory of the Department of Scientific Research.

REFERENCES

1. Zeldovich, Y. B., and Frank-Kamenetsky, D. A.: J. Phys. Chem. Moscow, *12*, 100, (1938).
2. Boys, S. F., and Corner, J.: Proc. Roy. Soc., *A197*, 90, (1949); Corner, J.: Proc. Roy. Soc., *A198*, 388 (1949).
3. Adams, E. N.: See Henkel, M. J., Spaulding, W. P., and Hirschfelder, J. O.: *Third Symposium on Combustion*, p. 21. Baltimore, The Williams & Wilkins Co., 1949.
4. von Kármán, T., and Penner, S.: *Selected Combustion Problems*, p. 5. London, Butterworth's 1954.
5. Hirschfelder, J. O., Curtiss, C. F., and Campbell, D. E.: *Fourth Symposium (International) on Combustion*, p. 190. Baltimore, The Williams & Wilkins Co., 1953.
6. Klein, G.: University of Wisconsin SQUID—1 (1955).
7. Schatzki, T. K.: University of Wisconsin CM 853 (1955).
8. Spalding, D. B.: (a) Aircraft Engineering, *25*, 264 (1953); (b) Phil. Trans. Roy. Soc., *A249*, 1 (1956).
9. Tanford, C., and Pease, R. N.: J. Chem. Phys., *15*, 433 (1947).
10. Lewis, B., and von Elbe, G.: *Combustion, Flames and Explosions*. New York, Academic Press, 1951.
11. Manson, N.: Rev. Inst. Fr. Pétrole, *4*, 338 (1949).
12. von Kármán, T., and Millan, G.: *Fourth Symposium (International) on Combustion*, p. 173. Baltimore, The Williams & Wilkins Co., 1953.
13. Marble, F. E., and Adamson, T. C.: *Selected Combustion Problems*, p. 111. London, Butterworth's, 1954.
14. Karlovitz, B., Knapschaefer, D. H., and Wells, F. E.: *Fourth Symposium (International) on Combustion*, p. 613. Baltimore, The Williams & Wilkins Co., 1953.
15. Karlovitz, B., Denniston, D. W., and Wells, F. E.: J. chem. Phys., *19*, 541 (1951).
16. Scurlock, A. C., and Grover, J. H.: *Selected Combustion Problems*, p. 215. London, Butterworth's, 1954.
17. Summerfield, M., Reiter, S. H., Kebely, K., and Mascolo, R. W.: Jet Propulsion, *25*, 377 (1955).
18. Nusselt, W.: Z.V.D.I., *60*, 102 (1916).
19. Burke, S., and Schumann, T.: Ind. Eng. Chem., *20*, 998 (1928).
20. Hottel, H. C.: *Fourth Symposium (International) on Combustion*, p. 97. Baltimore, The Williams & Wilkins Co., 1953.
21. Fay, J. A.: J. Aero. Sci., *21*, 681 (1954).
22. Spalding, D. B.: Proc. I. Mech. E., *168*, 545 (1954).
23. Zeldovich, Y. B.: J. Tech. Phys. Moscow, *19*, 1199 (1949); trans. as NACA Tech. Memo 1296 (1951).
24. Spalding, D. B.: Fuel, *33*, 253 (1954).
25. Carslaw, H. S., and Jaeger, J. C.: *Conduction of Heat in Solids*. New York, Oxford Univ. Press, 1947.
26. Emmons, H. W.: Trans. A.S.M.E., *65*, 607 (1943).
27. Dusinberre, G. M.: *Numerical Analysis of Heat Flow*. New York, McGraw-Hill, 1949.
28. Soroka, W. W.: *Analog Methods in Computation and Simulation*. New York, McGraw-Hill, 1954.
29. Hartree, D. R.: *Numerical Analysis*, New York, Oxford Univ. Press, 1952.

30. Rosenthal, D.: Trans. A.S.M.E., *68*, 849 (1946).
31. Johnson, W. C., and Alley, R. E.: Rep. 3. ONR. Contract N6 105, Task Order VI June 1948.
32. Spalding, D. B.: Proc. I. Mech, E., to be published.
33. Avery, W. H., and Hart, R. W.: Ind. Eng. Chem. *45* 1634 (1953).
34. Longwell, J. P., Frost, E. E., and Weiss, M. A.: Ind. Eng. Chem., 1628 (1953).
35. Spalding, D. B., and Tall, B. S.: Aero Quarterly, *5*, 195 (1954).

3

LIMITS OF INFLAMMABILITY

By J. W. LINNETT AND C. J. S. M. SIMPSON

Introduction

Many experimental determinations have been made of limits of inflammability, but less has been done on the theory of the problem, and, at the present time, there is no agreed explanation of why composition limits are observed. Recent work has been concerned mainly with suggesting features that might account for the existence of a finite limit of composition; there has been little attempt to see whether the known facts support the suggestions.

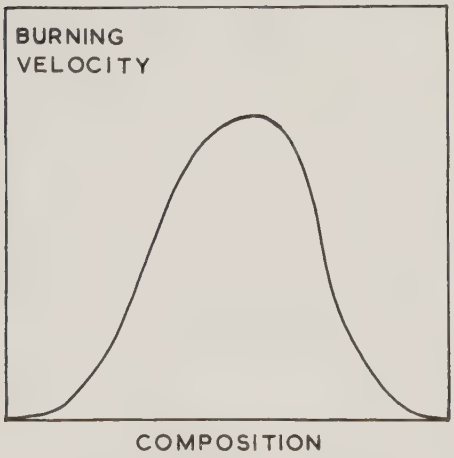

Fig. 1. Probable theoretical variation of burning velocity with composition (diagrammatic).

Why is there this difficulty regarding the existence of limits? The recent steady-state treatments of flame propagation are thorough.[1] However, they include no factor that would account for the existence of limits. Theoretically steady-state solutions (see also Layzer[2]) can exist over the whole composition range, so that present theories of this type would probably predict a burning velocity curve of the form shown in Figure 1. (Figure 1 is not to scale.) Theory will predict that the burning velocity will be close to zero for a range of compositions near each end of the curve (*i.e.*, the "tails" will be much closer to the composition axis than is drawn).

Because of this situation it has been necessary to try to account for limits by additional suggestions. One of these has been to consider the effect of perturbations on the steady-state condition.[3] It has been shown that for some mixtures a perturbation would die away while for others it would grow and the flame would fail to return to its steady-state condition.

Before examining these ideas it is important to consider the question: Does experimental evidence indicate whether an infinite horizontal plane flame moving through a quiescent homogeneous mixture would or would not show a composition limit of inflammability? The answer is not certain for no such flames have been studied. The nearest approach is provided by the circular flat flame burner of Powling,[4] Egerton and Thabet[5] and Badami and Egerton.[6] But this is only about 3 in. across so that convection between the hot products from the flame and the surrounding gases may be important. If the answer to the above question were "Yes, such flames would show a limit," a second may need to be asked, namely: Are the limits usually determined close to or far from the limits that might exist for such infinite undisturbed plane flames?

Examination of Some Limits

Here it is only practicable in attempting to answer the above questions to consider the results for one or two gas mixtures. Table 1 lists some results for methane + air mixtures at room temperature and atmospheric pressure. Those for the lower limit spread over a relatively wide range of 1 per cent (from 5 to 6) even if data for 2½-cm tubes are excluded. The upper limit spreads over 2 per cent. The limit is considerably dependent on conditions. Table 2 shows results for ethylene + air mixtures in which all major components have approximately the same molecular weights. For the lower limit the results range from 2.7 to 3.4 and for the upper limit from 15 to 34 per cent (excluding 2½-cm tube results). For the lower limit of ethane + air mixtures Badami and Egerton give 2.53, Jones 3.00 and White for 5- and 7½-cm tubes, figures ranging from 3.12 to 3.32 per cent. For the lower limit of butane + air mixtures Badami and Egerton give 1.40, Egerton and Powling, 1.93, and Jones, 1.86 per cent.

The results for any limit spread over a considerable range. That the range is considerable may be stressed by remarking that the calculated flame temperatures for the lower limit mixtures of butane + air flames observed by Egerton and Powling and by Badami and Egerton are 1445 and 1114°C respectively. The difference between the calculated flame temperatures for Jones and Badami and Egerton's limit mixtures for propane + air and for ethane + air are about 130 and 200°C respectively. Considering the great effect of temperature on rate of reaction, these differences seem surprisingly large.

Table 1. Methane + Air Limits

Results from Bone and Townend,[7] Jost,[8] Lewis and von Elbe,[9] Badami, and Egerton[6] and Egerton and Powling[10]

Tube Diam.	Direction of Propagation	Limits		Workers
		Lower	Upper	
cm				
7.5	Up	5.35	14.85	White
7.5	Horiz.	5.40	13.95	White
7.5	Down	5.95	13.35	White
5.0	Up	5.40	14.25	White
5.0	Horiz.	5.65	13.95	White
5.0	Down	6.12	13.25	White
2.5	Up	5.80	13.2	White
2.5	Horiz.	6.20	12.9	White
2.5	Down	6.30	12.8	White
2	Down	6.0	13.1	Mason and Wheeler
16 (sphere)	Up	5.6	14.8	Wheeler
8	Down	6.0	13.0	Terres and Plentz
5	Up	5.0	15.0	Jones
5	Up	5.26	14.3	Egerton and Powling
5	Up	5.2	14.0	Coward and Hartwell
6	Stat (D)	5.31	—	Badami and Egerton

Table 2. Ethylene + Air Limits

Results from Bone and Townend,[7] Lewis and von Elbe[9] and Badami and Egerton[6]

Tube Diam.	Direction of Propagation	Limits		Workers
		Lower	Upper	
cm				
7.5	Up	3.02	34.0	White
7.5	Horiz.	3.20	23.7	White
7.5	Down	3.33	15.5	White
5.0	Up	3.13	33.3	White
5.0	Horiz.	3.25	22.4	White
5.0	Down	3.42	15.3	White
2.5	Up	3.15	27.6	White
2.5	Horiz.	3.30	14.0	White
2.5	Down	3.45	13.7	White
5	Up	2.75	28.6	Jones
6	Stat (D)	2.72	—	Badami and Egerton

The experimental results presented above do not encourage the conclusion that any determined limits are *necessarily* near to an *"absolute"* limit of inflammability. It has been argued that experiments in tubes of increasing diameter indicate that a *true* limit is being approached. For example, for methane + air lower limits for upward propagation White gives 5.8, 5.4 and 5.35 per cent in tubes of diameter 2½, 5 and 7½ cm respectively. But results for varying tube size do not always show the same convergent pattern as the above (*e.g.*, Table 2 and also Laffitte and Elston[11] quoted by Lewis and von Elbe[12]). Moreover Badami and Egerton[6] have found that flames can be supported on the flat flame burner in mixtures which are much leaner than the lean limits found by White in tubes of diameter 5 and 7½ cm (for which wall effects have been said to be negligible) and by Jones in tubes of similar dimensions.

The considerable dependence of the limits on conditions suggests that the observed limits are decided by factors which are dependent on the experimental arrangement, such as perhaps the flow or convection pattern (and/or heat loss). In examining the experimental results there appears to be little evidence for concluding that the limits observed at the present time are in any sense absolute or even approach ones that are absolute. If this interpretation is correct, it is possible that explanations of limits of the type of Rosen,[13] and of the type of Van Tiggelen[14] and of Weinberg[15] are not appropriate to the limits recorded in the literature, for all these treatments relate to the detail of the internal structure of the flame front and such properties would hardly be expected to lead to the limits being so dependent on conditions. For example Van Tiggelen[14] and Weinberg[15] suggest that, in mixtures which lie outside the limits of inflammability, the heat of reaction cannot bring the mixture to a temperature at which the chain process becomes effectively branching. The limit is therefore the mixture for which, in the flame front, chain branching processes can just outweigh chain breaking processes. It is not easy to see how changes in this balance could account for differences of several hundred degrees in the limit flame temperatures for tube and flat flame burner experiments. Egerton and his co-workers have demonstrated impressively that it is possible to maintain flames in much leaner mixtures than had previously been thought possible. But there seems no reason to believe that no device exists capable of extending the range further. In fact, the extent of the dependence of limits on conditions suggests that it may well be possible to construct such a device. If this is so then we must look for explanations of the limits that are observed in terms of relations between the maintenance of the flame front and the surroundings and circumstances of that flame.

Rosen[13] has examined the behavior of a perturbation in the temperature distribution in the flame front. He concludes that, for some mixtures, the temperature distribution will return to the steady-state distribution while, for others, the perturbation will grow without limit. This suggests that there may be *real* limits of inflammability for infinite plane flames.

One factor that is clearly important in some cases in affecting limits of inflammability is the diffusion of one of the combustible components through the mixtures. This is probably very important in hydrogen + air lower limit mixtures. The same may also be true for the rich limits of organic vapor + air flames for which the limit is also very dependent on the direction of propagation. This phenomenon has been reviewed most instructively by Markstein[16] who discusses, *inter alia*, the instability of flames near the inflammability limits.

Flames in Tubes

A flame front separates hot burnt gas of low density from cold unburnt gas of higher density. There must therefore be convection effects in most flames. The consequences of convection on the shape of a flame traveling along a horizontal tube has been discussed by Hoare and Linnett.[17] They observed that the flame either traveled as a hemisphere along the tube or as a "tipped" flame with the leading part at the top of the tube. The flow of burnt gas away from the flame and along the tube tends to confer a hemispherical shape on the flame. Convection tends to modify this, but appears to be effective in doing so only if the flame is moving sufficiently slowly. The effect of convection was shown to be greater the wider the tube.

When a flame travels up a tube from an open to a closed end the flow will tend to make the flame axially symmetric and roughly hemispheric. Convection will tend to draw the centre of the flame up the tube so elongating it, increasing the flame area, and hence also the speed of movement. The effect will be greater the greater the tube diameter. But, if the flame is traveling down the tube, convection will tend to flatten it, reduce its

area and hence its speed of movement. So a greater fraction of the heat produced will be lost to the wall during downward than upward movement. This will tend to make limits wider for upward than for downward propagation. It is interesting that the percentage separation of limits for upward and downard propagation changes little with tube diameter (*cf.* White[7]). This is difficult to understand solely in terms of the effect of diameter on heat loss, but convection will tend to have greater effect in wider tubes and therefore cause a greater difference between the flame speeds for upward and downward propagation. This will tend to cause a greater difference in heat loss and would therefore oppose the simple effect of tube diameter.

Another interesting feature of White's results is that the limit for horizontal propagation is closer to the limit for downward propagation for narrow tubes (2½ cm) but seems usually to move towards the limit for upward propagation in wider tubes (7½ cm). Take, for example, his results for carbon monoxide + air lower limits. For upward, horizontal and downward propagation in a 2½-cm tube these are 13.2, 15.9 and 16.3; in a 5-cm tube 13.1, 14.1 and 15.7, and in a 7½-cm tube 12.8, 13.6 and 15.3 per cent. It would be interesting to know whether this is a general phenomenon; it is commonly found in White's results. A possible explanation may be that, in the narrow tube, where effects of convection are smaller, the flame in the horizontal tube is not greatly distorted from a hemisphere. Therefore, because it is probably easier to elongate the hemisphere in upward propagation than to flatten it in downward, the shape for horizontal propagation may be more like that for downward than for upward propagation. In the larger horizontal tube however the shape of the flame will be more affected by convection, and will probably have a leading front at the top of the tube with a long trailing front spreading back towards the bottom of the tube. Convection may convert the upward traveling flame to something similar; namely elongate the flame with a leading front in the middle and long trailing edges towards the walls. The flame traveling downward will however remain compact even in the wide tube for convection tends to flatten it. So convection may cause the upward and horizontally moving limit flames to become more alike as the tube diameter is increased.

Flat Flames

Convectional effects may also affect the flames on the flat flame burner. The hot gases above the flame are surrounded by cooler gases. Consequently they tend to accelerate upwards and to raise the flame from the burner. A gauze is placed above the flame, its presence being necessary, in part, it may be presumed, to modify this convectional flow. However it may be that, as the mixture is made leaner, the burning velocity smaller, and the gas flow smaller, a point is reached where the flow momentum is reduced so much that convectional effects can again operate and the flame ceases to be able to maintain itself on the burner. That such an explanation of the limit is possible is suggested by the fact that all limit flames have similar burning velocities and therefore flow momentum (see later).

An alternative reason for the limits observed on the flat flame burner may be sought in the nature of the flow pattern. Egerton and Thabet[5] (*cf.* also Wohl, Kapp and Gazley[18]) have shown that the gas flow becomes slightly divergent above the burner port. The flame settles at such a height that the flow and burning velocity balance. The divergence of the flow may decrease as the flow rate (*i.e.*, the burning velocity) decreases so that it becomes more difficult to maintain a flame at the burner. On this basis also the limit would be expected to be decided by a limiting burning velocity.

Burning Velocities at Limits

Jost,[19] when discussing limits, says that the smaller the burning velocity, the more will disturbances by conduction etc. make themselves felt and the more will limits depend on external factors. This is probably why (he goes on) it is generally not possible to observe burning velocities below a certain limit, frequently in the neighbourhood of 10 to 20 cm per sec.[19] This impression, not limited to Jost, that the reduction of the velocity below a certain value leads to a failure to propagate suggests that features like conduction and convection are more important than features like the details of the mechanism of the chemical reaction.

It might be argued that the limits observed in tubes are fixed by features such as the above and therefore tend to show a limiting burning velocity but that the leaner limits of Badami and Egerton do not show this behavior. This does not seem to be borne out by the results recorded in Tables 4

and 10 of the paper by Badami and Egerton. In the first of these it can be seen that, for mixtures of air with saturated hydrocarbons (methane to butane), ethylene and cyanogen, the burning velocities at the limits vary from 3.38 to 3.82 (a range of about 13 per cent of the lower figure). Since the variation for the four saturated hydrocarbons is not regular, there is a possibility that the recorded limiting burning velocities for any given hydrocarbon is not precise. For three carbon monoxide + air mixtures with varying water content the limit burning velocities are 3.12, 4.20 and 3.52 cm per sec. They are in the same range though with a greater spread (the variation does not occur regularly with water content). In their second table (Table 10) Badami and Egerton omit the carbon monoxide + air mixtures. They list the flame temperatures and it is found that the temperature rise varies from 1076 to 1574°C (a range of 46 per cent on the lower figure; the percentage range for the flame temperatures in °K is 36 per cent.) The excess enthalpy at the limit, calculated by the procedure of Burgoyne and Weinberg,[20] for the five hydrocarbons varies from 0.238 to 0.323 (a range of 35 per cent). So, for the hydrocarbon (saturated and unsaturated) and cyanogen, the factor which varies least is the limit burning velocity. Therefore the evidence favors slightly the conclusion that this is the factor fixing the limit in these experiments rather than any of the others tested.

From the graphs of Badami and Egerton[6] it will be seen that the burning velocity varies rapidly with composition near the limit. So, if the stability of the flame is affected by the speed at which it is moving, the percentage composition of the limit will appear precisely determined even though the limiting speed is not an exact quantity. A behavior somewhat analogous to this was noted by Hoare and Linnett[17] for the transition between upright and "tipped" flames in horizontal tubes.

Bechert[21] has attempted a treatment of limits by supposing that flames with velocities lower than 1 cm/sec cannot propagate. This is an undesirably arbitrary assumption but it may be that, for a given experimental arrangement, a situation like this exists, the limiting velocity depending primarily on the experimental arrangement and only secondarily on the particular mixture.

Effect of Pressure on Limits

If the pressure in a container is reduced below atmospheric pressure the effect of the walls on the flame is likely to increase (*e.g.*, rates of diffusion increase). To avoid consequences of this effect it is probably more valuable to examine the effect of increasing the pressure. The results[7, 8] for this on the limits are rather uncertain when the effects are small but the larger effects are definite. As regards the latter, the range of inflammability for carbon monoxide + air mixtures is decreased at both limits by raising the pressure (1 atmos 14.2 to 71 per cent; 10 atmos 17.8 to 62.8; 30 atmos 20.6 to 56.8). For hydrogen and hydrocarbon + air mixtures the range at the upper limit is increased (*e.g.*, for hydrogen at 1, 30 and 75 atmos 68.4, 71.9 and 74.2 per cent respectively). For these mixtures the range at the lower limit is little affected although, in the case of methane and ethane and perhaps hydrogen, there seems to be some evidence that it is decreased (*e.g.*, methane, 1 and 6 atmos, 6.0 and 6.4 per cent; ethane, 1 and 6 atmos, 3.13 and 3.22 per cent).

The ordinary effect of pressure on rate of reaction might lead one to expect that the range of inflammability would be increased as the pressure is raised. The behavior of carbon monoxide + air mixtures is the reverse of this.

In homogeneous systems explosion limits are observed. These are of two types: thermal and chain-branching. For thermal explosion limits the temperature of the limit decreases as the pressure is raised; for chain branching explosions, at the second limit, the temperature of the limit increases as the pressure is raised. The behavior of carbon monoxide + air inflammability limits is therefore analogous to the second chain branching explosion limit while the behavior of hydrogen and of hydrocarbon + air upper limits is analogous to that of thermal explosion limits (or of the third chain branching explosion limit of hydrogen + oxygen mixtures). The result for carbon monoxide + air mixtures therefore suggests that chain branching processes and their competition with breaking reactions may be important in these flames. The effect of pressure on the upper limits of hydrogen and hydrocarbon + air flames is, however, consistent with a purely thermal behavior.

If the value of the burning velocity is important in deciding the limit, another way or regarding the effect of pressure is to consider the effect of pressure on the burning velocity. It has been concluded that this is given by

$$V_b \alpha P^{\frac{1}{2}(n-2)} \qquad (1)$$

where n is the order of the reaction.[22] Therefore

the velocity, V_b, increases with the pressure, P, if n is greater than 2, but decreases with pressure if n is less than 2. The effect of pressure on the convection effect in a flame is uncertain but, from the above results and Equation (1), one would conclude that the rate controlling reactions occurring in carbon monoxide + air flames are of a lower order than those occurring in hydrogen or hydrocarbon + air flames at the upper limits.

It is not possible to be certain of the interpretation of the effect of pressure on the limits, but it is interesting that pressure exerts all types of effects on the range of inflammability for different systems. This would repay further study perhaps in conjunction with measurements of the effect of pressure on burning velocity for mixtures near the limits.

Other Factors Affecting Limits

An increase of temperature always increases the range of inflammability. Moreover it has been shown that the magnitude of the effect is such that the limit temperature remains approximately constant. This is understandable if reaction rate governs the burning velocity, and either of these is important at the limit because reaction rates are much more dependent on temperature than on composition (*cf.* Dixon-Lewis[23]).

Egerton and Powling[10] showed that, in many cases, the effect of additives on the lean limit could be deduced solely from their thermal properties. They, and Burgoyne and Williams-Leir,[24] did observe, however, that organic halides had inhibiting effects presumably because of an ability to remove radicals. Dixon-Lewis and Linnett,[25] working at the hydrogen + air upper limit, showed that organic substances had an inhibiting effect, raising the limit flame temperature, and suggested that, at the relatively low limit flame temperatures the organic molecules were chain breaking because of their ability to remove atoms by processes such as $RH + H = R + H_2$, replacing them by less reactive organic radicals. This proposal is consistent with the conclusions of Baldwin, Corney and Simmons.[26] These substances therefore appear to affect the limit by virtue of an ability to affect the rate.

The effect of inert gases on limits has been discussed by Egerton and Powling[10] and Mellish and Linnett.[27] It is interesting, in relation to what has been said earlier (*cf.* Markstein[16]) that the effect of different inert gases on the hydrogen + nitrous oxide upper limit appears to be paralleled by their effect on the diffusion coefficient of the mixture rather than on the thermal conductivity.

Clusius and Gutschmidt[28] have made most interesting observations on hydrogen and deuterium lower limits. These and the views of Goldman[29] have been discussed by Markstein.[16]

Conclusion

Lewis and von Elbe[30] have suggested that limits of inflammability are caused by there being a transition from a composition range in which the flame front is stable to a disturbance to one in which the disturbance, once started, grows and destroys the flame front. This type of approach is also adopted by Rosen. Both considered disturbances which were intimately connected with the fine structure of the flame front. However, it is equally possible to consider a similar approach in relation to a distortion of the shape or form of the flame front such as might be occasioned by the flow characteristics of the experimental arrangement or by a convectional disturbance. There exists, therefore, the possibility that the limit appears at that composition at which the flame becomes unstable to a change in the curvature or extent or form of the flame front.

When employing burners, the determined limit may be that at which it becomes impossible to maintain the flame in its position at the burner port. There seems to be some evidence that this may be the factor deciding the limits in the burner. But if this is accepted it is important to remember that the ranges of inflammability obtained by Badami and Egerton are wider than in any tube. This achievement of Egerton and his co-workers is of great and far-reaching importance for it has shown that the limits obtained in tubes (even the widest ones) are not fundamental.

Summary

It appears to us that there is no convincing experimental evidence for the existence of fundamental limits of inflammability although theory suggests that there probably are such limits. It also appears that there is no experimental evidence proving that any limits that have been observed in gaseous systems are fundamental and, in fact, the great dependence on conditions favors the opinion that there is a considerable difference between the observed limits and any possible fundamental limit.

REFERENCES

1. Hirschfelder, J. O., Curtiss, C. F., Henkel, M. J., Spalding, W. P., and Hummel, H.: *Third Symposium on Combustion, Flame and Explosion Phenomena*, pp. 121, 127, 135. Baltimore, The Williams & Wilkins Co., 1949.
2. Layzer, D.: J. Chem. Physics, *22*, 222, 229 (1954).
3. Lewis, B., and von Elbe, G.: *Combustion, Flames and Explosions*, p. 369. New York, Academic Press, 1951.
4. Powling, J.: Fuel, *28*, 25 (1949).
5. Egerton, A. C., and Thabet, S. K.: Proc. Roy. Soc., *A211*, 445 (1952).
6. Badami, G. N., and Egerton, A. C.: Proc. Roy. Soc., *A228*, 297 (1955).
7. Bone, W. A., and Townend, D. T. A.: *Flame and Combustion in Gases*, pp. 92–102. London, Longmans Green, 1927.
8. Jost, W.: *Explosion and Combustion Processes in Gases*, pp. 124–133. New York, McGraw-Hill Book Co., 1946.
9. Lewis, B., and von Elbe, G.: *Combustion, Flames and Explosions*, p. 749. New York, Academic Press, 1951.
10. Egerton, A. C., and Powling, J.: Proc. Roy. Soc., *A193*, 172, 190 (1948).
11. Laffitte, P., and Elston, J.: Rev. inst. franc. petrole, *4*, 502 (1949).
12. Lewis, B., and von Elbe, G.: *Combustion, Flames and Explosions*, p. 335. New York, Academic Press, 1951.
13. Rosen, J. B.: J. Chem. Phys., *22*, 733, 743 (1954).
14. Van Tiggelen, A.: Bull. Soc. Chim. Belges, *55*, 202, (1947).
15. Weinberg, F. J.: Proc. Roy. Soc., *A230*, 331 (1955).
16. Markstein, G. H.: *Fourth Symposium (International) on Combustion*, p. 44. Baltimore, The Williams & Wilkins Co., 1953.
17. Hoare, M. F., and Linnett, J. W.: Trans. Faraday Soc., *49*, 1038 (1953).
18. Wohl, K., Kapp, N. M., and Gazley, C.: *Third Symposium on Combustion, Flame and Explosion Phenomena*, p. 3. Baltimore, The Williams & Wilkins Co., 1949.
19. Jost, W.: *Explosion and Combustion Processes in Gases*, p. 124. New York, McGraw-Hill Book Co., 1946.
20. Burgoyne, J. H., and Weinberg, F. J.: Fuel, *33*, 436 (1954).
21. Bechert, K.: Z. Elektrochem. *54*, 239 (1950); Ann. Physik (Leipzig), (6) *4*, 191 (1949); *5*, 349 (1950).
22. Boys, S. F., and Corner, J.: Proc. Roy. Soc., *A197*, 90 (1949); Friedman, R.: J. Am. Rocket Soc., *23*, 349 (1953).
23. Dixon-Lewis, G.: AGARD Combustion Colloquium, Liege, 1955.
24. Burgoyne, J. H., and Williams-Leir, G.: Proc. Roy. Soc., *A193*, 525 (1948).
25. Dixon-Lewis, G., and Linnett, J. W.: Proc. Roy. Soc., *A210*, 48 (1951).
26. Baldwin, R. R., Corney, N. S., and Simmons, R. F.: *Fifth Symposium (International) on Combustion*, p. 502. New York, Reinhold Publishing Corp., 1955.
27. Mellish, C. E., and Linnett, J. W.: *Fourth Symposium (International) on Combustion*, p. 407. Baltimore, The Williams & Wilkins Co., 1953.
28. Clusius, K., and Gutschmidt, H.: Naturwiss, *22*, 693 (1934); Böhm, G., and Clusius, K.: Z. Naturforsch., *3a*, 386 (1948); *5a*, 514 (1950).
29. Goldmann, F.: Z. physik. Chem., *B5*, 307 (1929).
30. Lewis, B., and von Elbe, G.: AGARD Combustion Colloquium, Liege, 1955.

Discussion by G. Dixon-Lewis*

The authors have suggested that, among other things, convection effects may be important in determining limits of flame propagation in some circumstances. In this comment some work carried out by Dr. G. L. Isles and myself on flat flame limits will be briefly described. We have used a flat flame burner with the chimney top covered by a perforated plate which could be heated electrically. The flame speed *vs.* composition curves have been measured near the lower limit for methane-air mixtures using different temperature levels in the system (the burner matrix is heated by radiation from the top plate, and reaches a steady-state temperature). It was found that even with the top plate heated to about 900°C, so that an unignited stream of combustible mixture just inside the limit was ignited at the plate, a limiting burning velocity of about 2.4 cm/sec was obtained, the mixture containing 3.67 per cent methane and the matrix preheat temperature being 279°C. On weakening the mixture, the flame tried to flow through the plate. If a smaller total gas flow were used the flame became smaller in area, but still gave the same limit and the same limit burning velocity even though just inside the limit the top plate was hot enough to ignite the mixture. The reason for this seems to be that at the low flow rates used, convection is important in determining the linear gas velocity entering the flame. To investigate this further some streak photographs of powder particles entrained in the flame gases were taken, both with the burner operating with the top plate heated to the high temperature, and

* The University of Leeds, England.

with operation under normal conditions without external heat supply. Photographs were taken and compared with and without the flame ignited. The influence of convection is clearly shown. It seems to us, therefore, that this type of downward propagating flame presents a case more of a limiting burning velocity determined largely by convectional gas velocities, and that the limit composition is that composition which can give the limit burning velocity.

4

THE EFFECT OF FUEL TYPE AND PRESSURE ON FLAME QUENCHING

By A. E. POTTER, JR., AND A. L. BERLAD

Introduction

Previous flame-quenching research at this laboratory has explored such topics as the effect of oxygen concentration, inert diluents, and tube geometry on flame quenching.[1, 2, 3] The present work is an extension of these studies, and is concerned with the effect of fuel type on quenching. Most of the measurements were made using liquid hydrocarbons, because of the general lack of such data and the industrial importance of liquid fuels. Eight hydrocarbons and hydrogen were chosen for study; the effect of fuel concentration and pressure on the quenching distance were determined. Some of the hydrocarbons (propane, isooctance, and benzene) have been studied by Friedman.[4] The discussion is divided in two parts: The first is concerned with the effect of fuel type and concentration on the quenching distance, and the second deals with the pressure exponent of the quenching distance.

Experimental

APPARATUS

A schematic diagram of the apparatus is shown in Figure 1. The adjustable slot burner, and the means for maintaining any desired pressure around it, have been previously described.[1] As before, air and gaseous fuels were metered by critical flow orifices. Liquid fuels were injected by a metering pump into the air stream, and were vaporized in a long coil of steam-heated copper tubing. The metering pump was a commercially available model, and consisted of two pistons mechanically coupled so as to produce a nearly continuous flow. Small flow fluctuations were removed by pumping through a 20-ft length of gum-rubber tubing. Water was pumped through the metering pump and the rubber tubing. The water displaced mercury which in turn displaced the fuel into the vaporizor. Because of the problems associated with pumping fuels at low pressure (dissolved gases and boiling), it was necessary to hold the pressure constant and near atmospheric at the point of fuel injection. This was done by placing a pressure-relief valve in the line downstream from the fuel-vaporizing section. The rubber diaphragm of the pressure-relief valve was replaced by a teflon diaphragm.

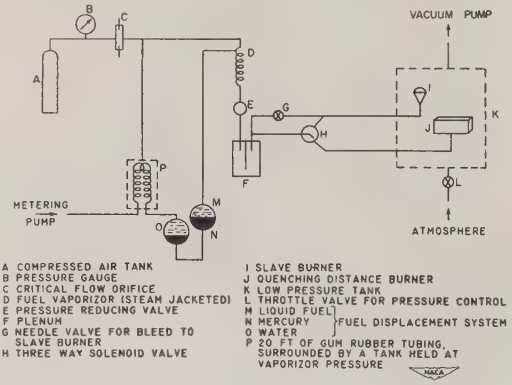
VACUUM PUMP
ATMOSPHERE
METERING PUMP
A COMPRESSED AIR TANK
B PRESSURE GAUGE
C CRITICAL FLOW ORIFICE
D FUEL VAPORIZOR (STEAM JACKETED)
E PRESSURE REDUCING VALVE
F PLENUM
G NEEDLE VALVE FOR BLEED TO SLAVE BURNER
H THREE WAY SOLENOID VALVE
I SLAVE BURNER
J QUENCHING DISTANCE BURNER
K LOW PRESSURE TANK
L THROTTLE VALVE FOR PRESSURE CONTROL
M LIQUID FUEL
N MERCURY
O WATER
FUEL DISPLACEMENT SYSTEM
P 20 FT OF GUM RUBBER TUBING, SURROUNDED BY A TANK HELD AT VAPORIZOR PRESSURE
NACA

FIG. 1. Quenching distance apparatus for liquid fuels.

The flow of fuel-air mixture to the slot burner could be interrupted by a three-way solenoid valve, which diverted the flow to a slave burner, located next to the slot burner inside the pressure tank. A pilot flame was kept constantly burning on the slave burner to provide instant ignition when flow was switched to the slave burner. The slave burner was not used for experiments with hydrogen-air flames; the flow was interrupted by a simple shutoff valve.

For hydrocarbons, the fuel-air mixture was heated to 105±5°C by resistance heaters; the

slot burner was held at 105±2°C by circulating steam through its walls. Quenching measurements on the hydrogen flames were made at 40°C.

PROCEDURE

First, a flame was established atop the slot burner. Then, flow to the burner was interrupted by switching the flow to the slave burner. The flame would then either flash back or be quenched. The experiment was repeated at various pressures to determine the pressure above which the flame flashed back, and below which it was quenched. This pressure is called the limiting pressure. The limiting pressure was determined as a function of fuel concentration at three different slot widths. For hydrocarbons, the slot widths were 0.305, 0.508, and 0.762 cm, and the slot length was 12.7 cm. For hydrogen, the slot widths were 0.132, 0.213, and 0.323 cm, and the slot length was 5 cm.

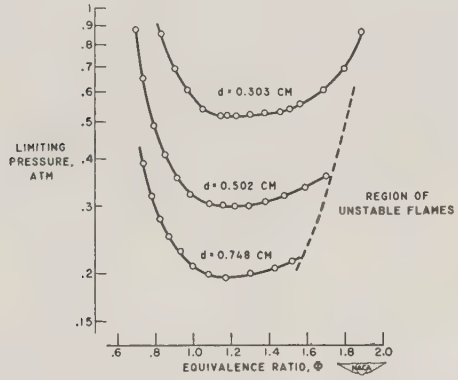

FIG. 2. Limiting pressure as a function of equivalence ratio for n-decane-air flames.

MATERIALS

The materials used and their purity are given in the following list. Purity for liquids was determined either by melting curve determinations or by refractive index. For gases, the manufacturers' stated purity is given.

Compound	*Mole Per Cent*
Propane	99+
Benzene	99.9
Isooctane	99.1
n-Decane	99+
1-Decene	99+
n-Hexane	99.2
1-Hexene	99+
n-Butyl benzene	99+
Hydrogen	98+

The air used was taken from high-pressure cylinders, and consequently was quite dry.

Results and Discussion

Three factors were varied in these experiments: quenching distance, pressure, and equivalence ratio. Discussion of the results is easier if only two variables are considered at a time. The variation of quenching distance at constant pressure with equivalence ratio will be discussed first; the variation of the pressure exponent of quenching distance will be discussed second.

In order to compare the quenching data on a common basis, the experimental rectangular slot widths were reduced to their equivalent plane parallel plate-quenching distances by application of the tube-geometry equation given by Berland and Potter.[3] All quenching distances given in this paper have been so corrected. The largest correction was 1.8 per cent.

Limiting pressure was determined as a function of equivalence ratio at constant quenching distance. An example of the experimental results is given in Figure 2, where data for n-decane-air flames are plotted. Points interpolated from the experimental curves for all the flames studies are given in Table I. In order to put the data into a more convenient form, the experimental curves were cross-plotted to find quenching distance as a function of pressure at constant equivalence ratio. At constant equivalence ratio, quenching distance d as a function of pressure p can be represented by an equation of the form $(d/d^0) = (p/p^0)^n$. The points cross-plotted from the experimental data were fitted to this equation to find the constants d^0 (quenching distance at one atmosphere) and n (pressure exponent of quenching distance) at each equivalence ratio. The calculated values of d^0 and n for all the compounds studied are listed in Table 2. For comparison, Friedman[4, 5] reports the following quenching distances at 1 atmos and temperatures corresponding to this research: propane, 0.185 cm, benzene, 0.173 cm, isooctane, 0.215, and hydrogen, 0.0530 cm. Friedman's[5] hydrogen-air data was corrected to 1 atmos, assuming an average barometric pressure of 740 mm Hg at Madison. All the data were corrected to plane parallel plates.

QUENCHING DISTANCE AT CONSTANT PRESSURE

The hydrocarbons studied can be divided into three groups: saturated, unsaturated, and aromatic.

TABLE 1. LIMITING PRESSURE AS A FUNCTION OF EQUIVALENCE RATIO AT CONSTANT QUENCHING DISTANCE

Fuel	ϕ	p_i, atmos at d = 0.748 cm	p_i, atmos at d = 0.502 cm	p_i, atmos at d = 0.303 cm
Propane	0.70	0.378	0.622	—
	0.80	0.266	0.423	0.789
	1.00	0.202	0.322	0.565
	1.15	0.194	0.312	0.537
	1.30	0.214	0.339	0.582
	1.50	0.288	0.468	0.795
	1.60	0.344	0.566	0.964
	1.70	0.419	0.718	—
	1.80	0.551	0.912	—
Benzene	0.70	0.341	0.582	—
	0.80	0.255	0.396	0.712
	1.00	0.190	0.297	0.525
	1.15	0.184	0.284	0.496
	1.30	0.191	0.300	0.518
	1.50	0.219	0.353	0.608
	1.70	0.286	0.451	0.769
	1.80	0.343	0.535	0.882
Hexene-1	0.70	0.374	0.635	—
	0.80	0.260	0.433	0.815
	1.00	0.193	0.306	0.515
	1.15	0.188	0.289	0.492
	1.30	0.200	0.300	0.508
	1.50	0.235	0.344	0.579
	1.70	0.289	0.422	0.777
n-Hexane	0.70	0.411	0.695	—
	0.80	0.282	0.464	0.886
	1.00	0.204	0.321	0.564
	1.15	0.194	0.304	0.528
	1.30	0.207	0.320	0.548
	1.50	0.239	0.374	0.606
	1.60	0.269	0.414	0.659
	1.70	0.314	0.474	0.754
	1.80	0.373	0.565	1.015*
Isooctane	0.80	0.474	0.728	—
	1.00	0.257	0.377	0.746
	1.15	0.222	0.350	0.610
	1.30	0.218	0.338	0.573
	1.50	0.236	0.362	0.593
	1.70	0.270	0.395	0.714
	1.80	0.292	0.436	0.872
n-Butyl benzene	0.70	0.461	0.856	—
	0.80	0.307	0.541	1.016*
	1.00	0.216	0.343	0.624
	1.15	0.204	0.320	0.562
	1.30	0.208	0.328	0.553
	1.50	0.223	0.350	0.576
	1.70	0.249	0.390	0.609
	1.80	0.266	0.416	0.633
Decene-1	0.70	0.478	0.745	—
	0.80	0.312	0.509	0.973
	1.00	0.212	0.314	0.559
	1.15	0.191	0.291	0.506
	1.30	0.194	0.297	0.500
	1.50	0.207	0.318	0.525
	1.70	0.227	0.368	0.586
	1.80	—	0.404*	0.632
n-Decane	0.70	0.468	0.819	—
	0.80	0.297	0.464	0.966
	1.00	0.210	0.319	0.575
	1.15	0.194	0.302	0.521
	1.30	0.197	0.303	0.521
	1.50	0.213	0.324	0.537
	1.60	0.225	0.340	0.565
	1.70	0.237*	0.359	0.610
	1.80	—	0.382*	0.691
		d = 0.316 cm	d = 0.210 cm	d = 0.131 cm
Hydrogen	0.50	0.291	0.422	0.672
	0.60	0.255	0.355	0.551
	0.70	0.231	0.321	0.497
	0.80	0.214	0.301	0.462
	0.90	0.203	0.288	0.439
	1.00	0.196	0.281	0.425
	1.20	0.193	0.279	0.425
	1.40	0.201	0.289	0.443
	1.60	0.213	0.307	0.472
	1.80	0.229	0.332	0.509
	2.00	0.246	0.359	0.549

* Extrapolated point.

Values of d^0 (quenching distance at 1 atmos) for four saturated hydrocarbons are plotted against equivalence ratio in Figure 3a. It is seen that for lean mixtures the quenching distance increases as the carbon chain is lengthened, going from propane to *n*-hexane to *n*-decane. Branching of the carbon chain evidently has a powerful effect, as shown by the upward displacement of the quenching distance of isooctane. It is interesting to note that the burning velocities vary in exactly the opposite manner, being smallest for isooctane and largest for propane. As the mixture is made richer, the quenching distance curves converge and eventually cross one another. Finally, in mixtures richer than $\phi = 1.5$, it is found that the quenching distances have arranged themselves inversely with molecular weight: propane has the largest quenching distance, *n*-decane the smallest.

In Figure 3b, two unsaturated straight-chain

TABLE 2. QUENCHING DISTANCE AS A FUNCTION OF PRESSURE AT CONSTANT EQUIVALENCE RATIO; CONSTANTS* IN THE EQUATION $\frac{d}{d^0} = \left(\frac{p}{p^\circ}\right)^n$

Fuel	ϕ	d°	n
		cm	
Propane	0.7	0.343	−0.80
	0.8	0.248	−0.83
	1.0	0.184	−0.88
	1.15	0.170	−0.89
	1.3	0.187	−0.90
	1.5	0.250	−0.89
	1.6	0.297	−0.88
	1.7	0.393	−0.74
	1.8	0.467	−0.79
Benzene	0.7	0.335	−0.75
	0.8	0.224	−0.88
	1.0	0.171	−0.88
	1.15	0.160	−0.91
	1.3	0.167	−0.91
	1.5	0.196	−0.89
	1.7	0.240	−0.91
	1.8	0.271	−0.96
Hexene-1	0.7	0.356	−0.75
	0.8	0.258	−0.79
	1.0	0.166	−0.92
	1.15	0.156	−0.94
	1.3	0.157	−0.97
	1.5	0.174	−1.00
	1.7	0.238	−0.91
n-Hexane	0.7	0.381	−0.76
	0.8	0.275	−0.79
	1.0	0.182	−0.89
	1.15	0.170	−0.91
	1.3	0.173	−0.93
	1.5	0.188	−0.97
	1.6	0.201	−1.01
	1.7	0.228	−1.03
	1.8	0.310	−0.88
Isooctane	0.8	0.374	−0.93
	1.0	0.233	−0.84
	1.15	0.195	−0.89
	1.3	0.181	−0.94
	1.5	0.183	−0.98
	1.7	0.220	−0.92
	1.8	0.267	−0.82
n-Butyl benzene	0.70	0.454	−0.65
	0.80	0.309	−0.76
	1.00	0.203	−0.85
	1.15	0.182	−0.89
	1.30	0.176	−0.92
	1.50	0.181	−0.95
	1.70	0.187	−1.01
	1.80	0.193	−1.04
Decene-1	0.70	0.386	−0.90
	0.80	0.289	−0.79
	1.00	0.175	−0.93
	1.15	0.160	−0.93
	1.30	0.157	−0.95
	1.50	0.163	−0.97
	1.70	0.186	−0.95
n-Decane	0.70	0.422	−0.71
	0.80	0.291	−0.76
	1.00	0.183	−0.89
	1.15	0.167	−0.92
	1.30	0.165	−0.93
	1.50	0.166	−0.99
	1.60	0.174	−0.98
	1.70	0.189	−0.96
Hydrogen	0.50	0.0858	−1.051
	0.60	0.0658	−1.139
	0.70	0.0583	−1.145
	0.80	0.0539	−1.142
	0.90	0.0511	−1.141
	1.00	0.0495	−1.138
	1.20	0.0505	−1.116
	1.40	0.0528	−1.114
	1.60	0.0570	−1.106
	1.80	0.0622	−1.102
	2.00	0.0680	−1.097

* p^0 is taken as 1 atmos; then d^0 is the quenching distance at 1 atmos.

hydrocarbons, hexene-1 and decene-1, are compared. As before, the relative order is altered in going from lean to rich mixtures, so that the heaviest hydrocarbon has the smallest quenching distance in rich mixtures.

In Figure 3c, two aromatic compounds, benzene and *n*-butyl benzene, are compared. Again, the striking effect of molecular weight is demonstrated by the reversal of order in going from lean to rich mixtures.

Since rich quenching distances appear to be controlled by different processes than lean and stoichiometric quenching distances, it seems reasonable to discuss them separately.

STOICHIOMETRIC QUENCHING DISTANCE

As several investigators have noticed,[4, 5, 6, 7] stoichiometric quenching distance is closely related to the burning velocity. An equation relating the two can be obtained by combining a thermal quenching equation[8] and the Semenov burning velocity equation. The result is

$$Ud = \frac{RT_0}{p}\sqrt{\frac{2\lambda_q\lambda_F FGW_F}{C_{p,q}C_{p,F}W_q}} \qquad (1)$$

A list of symbols is given at the conclusion of this paper. The ratio of thermodiffusivity to mass diffusivity, and the ratio of moles product to moles reactant, which appear in the Semenov equation, have not been included, since these factors are not considered in the thermal quenching equation.

It is interesting to note that several of the terms in Equation (1) can be combined into one having the character of a thermodiffusivity. This "thermodiffusivity" is given the symbol α^*, which is defined in the symbol list. Thus, the product of burning velocity and quenching distance is a function primarily of three things. One is a "thermodiffusivity." Another is F, the fraction of the total heat produced by the flame that the flame must retain in order to exist. The third is activation energy of the flame reaction, since the activation energy together with F determines the value of W_F/W_q. Of course, the geometry of the tube is also important and is accounted for by G, the geometrical factor.[3]

The assumption that F is constant has been found satisfactory for hydrocarbon-air flames.[2] The "thermodiffusivity" and activation energy do not change very much among the hydrocarbon-air flames studies in this research.[9] Consequently, one would expect the product Ud to be nearly constant for these flames; *i.e.*, quenching distance should vary approximately inversely as the burning velocity. This is indeed the case, as is shown in Table 3, where values of Ud for the flames of this research are given.

The assumption F equals a constant is satisfactory for many flames.[10] This can be seen in Figure 4, where the correlation of some Ud values taken from the experimental literature with values calculated from equation (1) is shown. A value of 0.78 for F was assumed for all flames. Flames of hydrocarbon-oxygen-inert gas mixtures are well correlated; data for different initial temperatures, hydrocarbons, oxygen concentrations and inert gases (N_2, A and He) are included. Data for N_2O-hydrocarbon, hydrogen-air and the H_2-Br_2 flames are also correlated fairly well. Data for NO-hydrocarbon and the ethylene oxide decomposition flames are not correlated. Because the assumption F is constant seems satisfactory for most flames, the product Ud is directly proportional to α^*, and increases with the size of the activation energy relative to the flame temperature.

For calculation of Figure 4, Semenov's formulation of W was used for both the free and quenched flame. When necessary, activation energies were calculated from lean limit flame

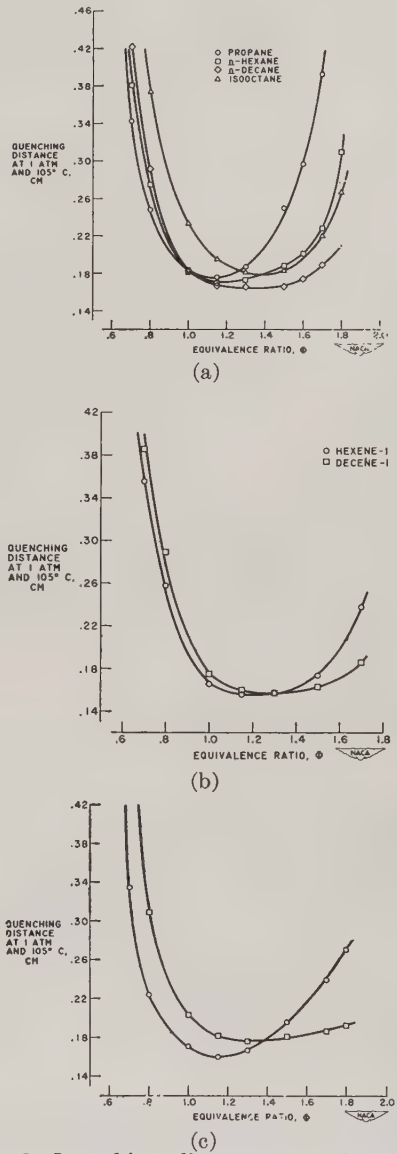

FIG. 3. Quenching distance as a function of equivalence ratio. (a) Saturated hydrocarbons; (b) unsaturated hydrocarbons; (c) aromatic hydrocarbons.

temperatures.[9] Otherwise, low temperature activation energies were used. Burning velocities were taken from references 9, 12, 13, 14, 15, 16, and 17, quenching distances from references 1, 2, 6, 7, 11, 18, and 19, and lean flammability limits from references 9, 20, and 21. Thermal conductivities were calculated using the methods

of references 22 and 23. Further details of the calculation may be found in reference 10.

The quotient of burning velocity and quenching distance can be obtained in a way similar to the way in which the product is obtained. When this is done, it is found that terms involving heat transport tend to cancel, but the average reaction velocities in free and quenched flame multiply one another. Consequently, the quotient is a measure of the average reaction velocity in the flame.

Table 3. Quenching Distance and Burning Velocity* at 105°C, 1 Atmos and $\phi = 1.0$ for Some Hydrocarbon-Air Flames

Fuel	d	U	dU
	cm	*cm/sec*	*cm²/sec*
Hexene-1	0.166	65.6	10.9
Benzene	0.171	63.4	10.8
Decene-1	0.175	59.3	10.4
n-Hexane	0.182	59.1	10.8
n-Decane	0.183	55.5	10.2
Propane	0.184	60.1	11.1
n-Butyl benzene	0.203	53.2	10.8
Isooctane	0.233	43.4	10.1

* Calculated from data of Dugger,[12] Simon,[13] and Wagner and Dugger;[14] all sets of data used contained a value for propane, so that all data were normalized to propane = 40 cm/sec at 25°C.

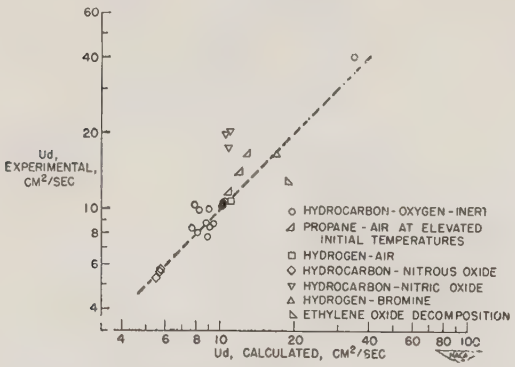

Fig. 4. Correlation of the product of burning velocity and quenching distance.

Rich Quenching Distance

Quenching distance for rich hydrocarbon flames is fairly reproducible, and is thus of value in characterizing rich flames. Quite different results are obtained depending upon whether propagation is upward or downward. In general, the plots of limiting pressure as a function of equivalence ratio are lobed for upward propagation, as though two or more paraboloids were superimposed.[24] The lobes do not appear for downward propagation; apparently only the first of the paraboloids is obtained. The experimental results reported in this paper are for downward propagation.

Under some conditions, particularly at low pressures, rich flames were obtained which did not give reproducible results. These flames were quenched if the flow was interrupted, but would flash back through the flow if disturbed with a spark or gust of air. The flame appeared to be open at the top, and separated into a number of small cells as it flashed back. Such flames were obtained for *n*-decane, decene-1, *n*-butyl benzene, and hexene-1. The general region in which these flames were observed is shown in Figure 2, where data for *n*-decane is plotted.

For rich hydrocarbon-air flames, quenching distance is primarily a function of the molecular weight of the hydrocarbon. Chemical factors, such as determine the lean quenching distance, do not seem to be of great importance. The dependence of rich quenching distance on molecular weight is shown in Figure 5. It is found that the quenching distance varies as the -0.3 power of molecular weight at $\phi = 1.5$ and as the -0.5 power at $\phi = 1.7$. The dependence of quenching distance on molecular weight is probably the result of preferential diffusion in the cellular flames encountered. Spalding[25] has pointed out that the fuel, oxygen, and heat flows must be considered separately in three-dimensional flames, such as cellular flames. The result is that the fuel:oxygen ratio at various stations within the flame may be quite different from the ratio anticipated from the composition of the unburned gas. Because of this, the over-all reaction rate in the flame may be quite different from what was expected. Since the quenching distance decreases as molecular weight increases, the reaction rate seems to have been speeded up by preferential diffusion. (The quenching distance is inversely proportional to the square root of the reaction rate.)

It is interesting to note that Markstein[26] has observed cell size in cellular flames to vary as the inverse one-third power of the molecular weight at $\phi = 1.4$. Quenching distance varies with molecular weight in the identical fashion at this equivalence ratio. This indicates a definite relation between cell size and quenching distance. Friedman[27] has suggested that such a relation should exist.

PRESSURE DEPENDENCE OF THE QUENCHING DISTANCE

The exponents which describe the pressure dependence of the quenching distance are given in Table 2. The pressure exponent n is negative, so that the quenching distance increases with decreasing pressure. The absolute value of n increases from lean to stoichiometric, reaches a maximum somewhat rich of stoichiometric, and usually decreases again as the mixture becomes very rich. These general features of the pressure exponent are quite well known. Somewhat less familiar is the close relation of the pressure exponent to the order of the global reaction. The pressure exponent of the quenching distance is the sum of two terms: one is one-half the order of the reaction and the other is a function of the pressure dependence of the flame temperature. In order to see the relative importance of these two terms, we shall formulate them in detail. This can be done from consideration of a thermal quenching equation[8]

$$d^2 = \frac{FG\lambda_q N X_f}{C_{p,q} W_q} \tag{2}$$

The following assumptions were made:

(1) The reaction velocity W_q varies as p^m. All other terms in the equation are independent of pressure.

(2) The reaction velocity W_q varies as $\exp(-E/RT_q)$.

(3) The temperature dependence of all other terms in the quenching equation can be approximated by simple powers of temperature. Then, all these temperature dependences can be lumped into one term which varies as T_q^r. Equation (2) can now be rewritten as follows

$$d^2 = KT_q^r p^{-m} e^{(E/RT_q)} \tag{3}$$

All the pressure- and temperature-independent parts of Equation (2) have been combined into the constant K. By taking the natural logarithm of both sides and differentiating with respect to $\ln p$, we obtain

$$\frac{D \ln d}{D \ln p} = \frac{1}{2}\left(r - \frac{E}{RT_q}\right)\frac{D \ln T_q}{D \ln p} - \frac{m}{2} \tag{4}$$

By definition,

$$n = \frac{D \ln d}{D \ln p} \tag{5}$$

Combining Equations (4) and (5),

$$n = \frac{1}{2}\left(r - \frac{E}{RT_q}\right)\frac{D \ln T_q}{D \ln p} - \frac{m}{2} \tag{6}$$

The value of r is difficult to establish, owing to uncertainties in the temperature dependences to be used for various terms. Fortunately, the final result is only slightly affected by the value chosen for r. We shall assume that r is 1.5. Since F is about 0.7 for most flames, $T_q \approx 0.7\ T_F$. With these assumptions, Equation (6) becomes

$$2n = \left(1.5 - \frac{1.43E}{RT_F}\right)\frac{D \ln T_F}{D \ln p} - m \tag{7}$$

For flames in which dissociation is negligible, the pressure dependence of flame temperature is negligible. For such flames, the order of the global reaction m is simply the negative of twice the pressure exponent n. Dissociation is quite extensive in most hydrocarbon flames, and the effect

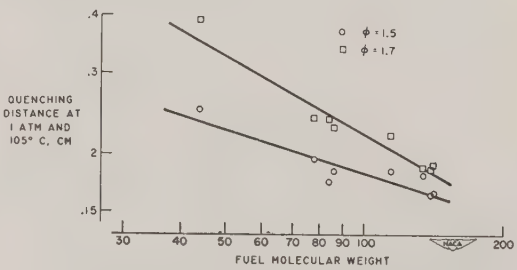

FIG. 5. Quenching distance in rich mixtures as a function of fuel molecular weight.

of the pressure dependence of flame temperature on the observed pressure exponent must be taken into account. Since the order of the global reaction is often of interest, the observed pressure exponents were used with Equation (7) to compute values of m. For these calculations, the pressure dependence of flame temperature must be known. Data concerning this are given by Berlad,[1] Potter and Berlad,[2] Simon and her associates,[6] and Edse,[28] for various hydrocarbon-oxygen-inert and hydrogen-oxygen flames. A plot of $(D \ln T_F)/(D \ln p)$ from these sources against T_F for lean flames gave a smooth curve on which most of the data fell. Values of $(D \ln T_F)/(D \ln p)$ for correction of the observed pressure exponents were taken from this curve. Flame temperatures for the hydrocarbon-air flames were calculated from the graphs of Vichnievsky and his associates.[29] The activation energy for all the hydrocarbon-air flames was assumed to be 38 kcal/mole and for the hydrogen-air flames was taken as 23 kcal/mole.

Table 4. Order of the Global Reaction for Various Flames

Flame System	ϕ	T_F at 1 atmos	m
		°K	
Propane-air	0.7	1927	1.56
	0.8	2080	1.57
	1.0	2291	1.60
Propane-argon "air"	0.593	2099	1.68
	0.738	2381	1.68
	0.864	2481	1.65
	1.000	2557	1.71
Propane-helium "air"	0.738	2381	1.50
	0.864	2481	1.53
	1.000	2557	1.63
Hydrogen-air	0.5	1633	2.08
	1.0	2318	2.17
	2.0	1998	2.16
Benzene-air	0.7	2021	1.44
	0.8	2174	1.64
	1.0	2363	1.61
Hexene-1-air	0.7	1976	1.45
	0.8	2127	1.58
	1.0	2320	1.68
n-Hexane-air	0.7	1940	1.48
	0.8	2088	1.49
	1.0	2297	1.62
Isooctane-air	1.0	2293	1.52
n-Butyl benzene-air	0.7	1978	1.25
	0.8	2134	1.42
	1.0	2336	1.53
Decene-1-air	0.8	2112	1.48
	1.0	2312	1.70
n-Decane-air	0.7	1962	1.37
	0.8	2103	1.41
	1.0	2300	1.62

Table 5. Comparison of Pressure Exponents for Burning Velocity and Quenching Distance

Flame System	ϕ	n	s	s(calc.)
Propane-air.....	1.0	−0.88	−0.05	−0.12
Propane-air.....	0.8	−0.83	−0.20	−0.17
Hydrogen-air....	1.0	−1.14	+0.09	+0.14
Hydrogen-air....	2.0	−1.10	+0.10	+0.10

The pressure dependence of flame temperature contributes about 10 per cent to n at $\phi = 1.0$ and 3 per cent at $\phi = 0.7$. The calculated values of m are given in Table 4. It was thought that the change in pressure exponent with equivalence ratio might be wholly accounted for by the pressure dependence of flame temperature term. This does not seem to be the case, as the order itself is seen to increase with fuel concentration. This may indicate that the flame reaction has two or more competing paths whose relative importance changes with flame temperature. Alternatively, the fuel concentration may affect the reaction path. Experiments which show the effect of flame temperature on reaction order at constant fuel and oxygen concentration are necessary to settle this point.

It is interesting that the order is changed by substitution of helium for argon. This may suggest that third-order reactions with the inert acting as "third body" are important in the flame. Rabinowitch[30] has found that the velocity of atom recombination reactions is approximately halved when helium is substituted for argon.

The pressure exponent of burning velocity is also affected by the pressure dependence of flame temperature. The Semenov burning-velocity equation can be used to obtain the pressure exponent of burning velocity s in the following form:

$$s = \frac{m - 2}{2} + \frac{1}{2}\left(r' + \frac{E}{RT_F}\right)\frac{D \ln T_F}{D \ln p} \tag{8}$$

Equations (6) and (8) can be combined to relate the pressure exponents of burning velocity and quenching distance. We obtain

$$s = -(1 + n) + \frac{1}{2}\left(r - \frac{E}{RT_q}\right)\frac{D \ln T_q}{D \ln p} + \frac{1}{2}\left(r' + \frac{E}{RT_F}\right)\frac{D \ln T_F}{D \ln p} \tag{9}$$

If r and r' are assumed to be about 1.5 and $T_q \approx 0.7\ T_F$, the terms involving the pressure dependence of flame temperature almost cancel one another, and can be neglected. Then we can write

$$s = -(1 + n) \tag{10}$$

Some pressure exponents for burning velocity and quenching distance are compared in Table 5. The burning velocity exponents were taken from Manton and Milliken.[31] The values of s calculated

by Equation (10) compare moderately well with the experimental values.

Manton and Milliken[31] have noticed that the pressure exponent of burning velocity is a function of burning velocity. Because of the close relation of burning velocity to quenching distance, it was thought that a similar relation should be found for quenching distance. This is indeed the case, as is shown in Figure 6. Here, the pressure exponent n is plotted against the quenching distance at 1 atmos. Quenching data for flames of propane with argon and helium "airs"[2] are included. There is considerable scatter of the data, but a definite correlation can be observed. The data can be represented by a single straight line with the apparent exception of the helium "air" flames. No quenching data for $\phi > 1.0$ are included in the plot.

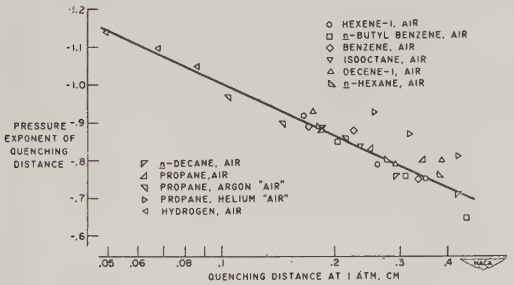

FIG. 6. Pressure exponent as a function of quenching distance.

It is felt that the correlation observed between the pressure exponent and the quenching distance is the result of their dependence on a third independent variable. A good share of the variation of pressure exponent with equivalence ratio can be explained if one takes into account the pressure dependence of flame temperature, itself a function of flame temperature. Thus a good share of the variation of pressure exponent is explicable as the result of variation of the flame temperature. In addition, if the global reaction is a complex chain reaction, it is quite reasonable to expect the order to change with temperature. Thus, the third independent variable may be flame temperature. Helpful experiments to determine whether or not flame temperature alone is the independent variable include determination of pressure exponents for systems other than hydrocarbon-oxygen-inert, and for systems in which flame temperature is changed at constant fuel and oxygen concentration.

Conclusions

The following conclusions can be drawn from the experimental results:

(1) For stoichiometric hydrocarbon-air flames, the quenching distance varies inversely with the burning velocity.

(2) For rich hydrocarbon-air flames, the quenching distance is a function of fuel molecular weight. The dependence of quenching distance on molecular weight is similar to the dependence of cell size in cellular flames on molecular weight.

(3) The observed pressure exponent is composed of two terms. One is one-half the order of the reaction, the other is a function of the pressure dependence of flame temperature. A good share of the change in pressure exponent with equivalence ratio is caused by the term involving the pressure dependence of flame temperature.

(4) The pressure exponents for burning velocity and quenching distance are simply related.

Nomenclature

C_v heat capacity, cal/(deg) (mole)
$\overline{C_p}$ average heat capacity, cal/(deg) (mole)
d quenching distance, cm
F fraction of the heat produced by the flame which the flame must retain in order to exist
G geometrical factor which relates the quenching properties of various tube geometries
K a constant
m order of the global flame reaction
N Avogadro's number
n pressure exponent of the quenching distance
p pressure, atmos
R gas constant
r temperature exponent, quenching distance equation
r' temperature exponent, burning velocity equation
s pressure exponent of the burning velocity
T temperature, °K
U burning velocity, cm/sec
W average flame reaction rate; average rate of disappearance of fuel, molecules/(cm)^3(sec)
X_f fuel mole fraction
α^* "thermodiffusivity," $\dfrac{RT_0}{p}\sqrt{\dfrac{\lambda_q\lambda_F}{C_{p,q}C_{p,}}}$
λ thermal conductivity, cal/(cm) (deg) (sec)
ϕ equivalence ratio

SUBSCRIPTS:

$_F$ flame
$_0$ initial
$_q$ quenched flame

REFERENCES

1. Berlad, A. L.: J. Phys. Chem., *58*, 1023 (1954).
2. Potter, A. E., Jr., and Berlad, A. L.: J. Phys. Chem., *60*, 97 (1956).
3. Berlad, A. L., and Potter, A. E., Jr.: *Fifth Symposium (International) on Combustion*, p. 728. New York, Reinhold Publ. Corp., 1955.
4. Friedman, R., and Johnston, W. C.: J. Chem. Phys., *20*, 919 (1952).
5. Friedman, R.: *Third Symposium on Combustion, Flame and Explosion Phenomena*. p. 110. Baltimore, The Williams & Wilkins Co., 1949.
6. Simon, D. M., Belles, F. E., and Spakowski, A. E.: *Fourth Symposium (International) on Combustion*, p. 126. Baltimore, The Williams & Wilkins Co., 1953.
7. Parker, W. G., and Wolfhard, H. G.: *Fourth Symposium (International) on Combustion*, p. 420. Baltimore, The Williams & Wilkins Co., 1953.
8. Potter, A. E., Jr., and Berlad, A. L.: *A Thermal Equation for Flame Quenching*, NACA Report 1264, 1956.
9. Fenn, J. B., and Calcote, H. F.: *Fourth Symposium (International) on Combustion*, p. 231. Baltimore, The Williams & Wilkins Co., 1953.
10. Potter, A. E., Jr., and Berlad, A. L.: *A Relation Between Burning Velocity and Quenching Distance*. NACA TN 3882, November, 1956.
11. Friedman, R., and Burke, E.: *Fifth Symposium (International) on Combustion*, p. 596. New York, Reinhold Publ. Corp., 1955.
12. Dugger, G. L.: *Effect of Initial Mixture Temperature on Flame Speeds of Methane-Air, Propane-Air and, Ethylene-Air Flames*. NACA TN 2374, May 1951.
13. Simon, D. M.: J. Am. Chem. Soc., *73*, 422 (1951).
14. Wagner, P., and Dugger, G. L.: J. Am. Chem. Soc., *77*, 227 (1955).
15. Ladenburg, R. V., Lewis, B., Pease, R. N., and Taylor, H. S.: *Physical Measurements in Gas Dynamics and Combustion*, Section K by E. F. Fiock, p. 409, Princeton, N. J., Princeton Univ. Press, 1954.
16. Wagner, P.: *Burning Velocities of Various Premixed Turbulent Propane Flames on Open Burners*. NACA TN 3575, Oct. 1955.
17. Botha, L. P., and Spalding, D. B.: Proc. Roy. Soc. (London), *225A*, 71 (1954).
18. Friedman, R., and Johnston, W. C.: J. Appl. Phys., *21*, 791 (1950).
19. Harris, M. E., Grumer, J., von Elbe, G., and Lewis, B.: *Third Symposium on Combustion Flame and Explosion Phenomena*, p. 80. Baltimore, The Williams & Wilkins Co., 1949.
20. Egerton, A. C., and Thabet, S. K.: Proc. Roy. Soc., *A211*, 445 (1952).
21. Coward, H. F., and Jones, G. W.: U. S. Bur. Mines, Bull. No. 503, 1952.
22. Hirschfelder, J. O., Curtiss, C. F., and Bird, R. B.: *Molecular Theory of Gases and Liquids*, Chap. 8. New York, John Wiley Sons, Inc., 1954.
23. Lindsay, A. L., and Bromley, L. H.: Ind. Eng. Chem., *42*, 1508 (1950).
24. DiPiazza, J. T., Gerstein, M., and Weast, R. C.: Ind. Eng. Chem., *43*, 2721 (1951).
25. Spalding, D. B.: *Some Fundamentals of Combustion*, p. 177. New York, Academic Press, 1955.
26. Markstein, F. H.: *Fourth Symposium (International) on Combustion*, p. 44. Baltimore, The Williams & Wilkins Co., 1953.
27. Friedman, R.: *J. Aeronaut Sci., 18*, 499 (1951).
28. Edse, R.: *Studies on Burner Flames of Hydrogen-Oxygen Mixtures at High Pressures*. WADC Tech. Rep. 52–59 April 1952.
29. Vichnievsky, R., Sale, R., and Marcadet, J.: Jet Prop., *25*, 105 (1955).
30. Rabinowitch, E.: Trans. Faraday Soc., *31*, 283 (1937).
31. Manton, J., and Milliken, B. B.: *Study of Pressure Dependence of Burning Velocity by the Spherical Vessel Method*. Proj. Squid Tech. Rep. BUM-12-P, July, 1955.

5

A PRINCIPLE OF MIXING SIMILARITY AND ITS APPLICATION TO INHOMOGENEOUS COMBUSTION

By WILLIAM G. BROWNE AND HUGH N. POWELL

Introduction

An adequate and consistent physicochemical picture of laminar diffusion flames is essential to a general theory of inhomogeneous combustion. In particular, by exploiting the uncomplicated fluid dynamic nature of these flames, we may hope to formulate general physicochemical principles which are also applicable to the structurally much more complicated turbulent flames of applied interest.

For an analytical approach to inhomogeneous combustion, it is interesting to note that the paper by Burke and Schumann[1] in 1928 is still the classic reference. Indeed, conceptually speaking, it has dominated most of the subsequent analytical work on the gross structure of diffusion flames. On the other hand our phenomenologic knowledge and qualitative understanding in this field have increased greatly since 1928. The spectroscopic investigations of Wolfhard and Parker[2] on the detail structure of the laminar diffusion burning zone are particularly significant in this respect.

THE BURKE AND SCHUMANN AND JOST FORMULATIONS

Let us review certain characteristics of the series of analytic-experimental investigations which began with Burke and Schumann. Their paper has retained its stature largely because of a twofold contribution: (1) By introducing the concept of an effectively infinite reaction rate into their analytical model, they were able to eliminate reaction-rate considerations and thereby define a "flame surface" entirely in terms of the well-known Fick's law equation for unsteady-state diffusion. (2) The appearance of the typical laboratory laminar diffusion flame is in immediate accord with both their flame surface approximation and the over-all geometries which their theory predicts.

Jost[3] and others have questioned the meaningfulness of Burke and Schumann's rigorous mathematical development because of their highly simplified physical picture. As an alternative, Jost proposed a much simpler formulation which altogether ignores chemical reactions and their rates. He shows that many of the essential features of the Burke and Schumann analysis can be deduced from the Einstein "random walk" equation, $\overline{x^2} = 2Dt$. Mathematically, this is not surprising since the dimensionless group, $(x/2\sqrt{Dt})$, appears in some form as the argument of most Fick's law solutions. Wohl, Gazley, and Kapp[4] extended Jost's basic approach and used it on experimental studies of laminar fuel jets. Simultaneously and independently, Hottel and Hawthorne,[5] following the conceptual lead of Burke and Schumann, also studied laminar fuel jets. More recently, Barr[6] applied a modified Burke and Schumann analysis to studies of enclosed laminar diffusion flames with unequal fuel and air-stream velocities. In a separate paper (in the present volume) the present authors[7] conclude, that, if due allowance is made for fluid dynamic effects, there is no clear experimental evidence for questioning the physicochemical validity of the Burke and Schumann formulation insofar as the gross structure is defined by "thin" burning zones.

The important distinction is that, on the one hand, the Burke and Schumann formulation rests on the introduction of a specific constraint, *i.e.*, that of an effectively infinite chemical reaction rate. On the other hand, the largely intuitive Jost formulation involves no chemical considerations, no physically observable "burning surface," and yet (after Jost, and Wohl and his associates) it lends itself to experimental correlations with about equal facility. This situation generates the definite impression that more than a mathematical accident is involved in the formulation of the two approaches, *i.e.*, there is some underlying physical explanation which is not yet clear.

THE WOLFHARD AND PARKER CONCEPT AND ITS CONSEQUENCES

The detail structure of flame zones has been investigated spectroscopically by Wolfhard and Parker,[2] who have shown that *local states of chemical equilibrium may exist in a flame zone of a distinctly finite thickness.* They advance a well-founded thermodynamic argument that such a situation must result when diffusion is completely

rate-controlling. *It therefore appears that the infinitely thin Burke and Schumann "flame surface" cannot be regarded as a legitimate extrapolation to the case of an infinite reaction rate*—a conclusion which tends to undermine the physicochemical significance of their approach despite its success in dealing with the gross structure of laminar diffusion flames.

Two theoretical papers have appeared which modify and extend the original Burke and Schumann type of analytical model to allow for finite reaction rates. Zeldovitch[8] treated the case of a single, isolated diffusion burning zone; Powell[9] treated the case of many parallel, laminar, diffusion flame burning zones in which the diffusive mixing rate may be independently varied by appropriate changes in the burner. The final expression in the latter paper was shown to be in accord with the essential gross structure characteristics of both completely premixed, *i.e.*, reaction-controlled, and completely diffusion-controlled flames. Zeldovitch obtained somewhat equivalent results for the single flame case. However, despite this degree of success, unless a common ground is found for describing both the gross and the detail structure of diffusion flames in the limiting case of an infinite reaction rate, the physicochemical significance of these latter two papers is uncertain because of their basically Burke and Schumann parentage.

In the foregoing discussion we have confined our attention to those works which have a direct bearing on the analytical description of laminar diffusion flame structure. Wohl and Shipman[10] have written an interpretative review of the more general literature on inhomogeneous combustion, and Barr[11] has compiled an extensive annotated bibliography of the literature.

The specific objectives of the present paper are to justify theoretically and experimentally an approach to inhomogeneous combustion which provides a common physical basis for both the Burke and Schumann formulation and the Jost formulation: one which reconciles them with the spectroscopically observed detail structure of the flame zone, which accounts for laminar flame zone thickness behavior, and which is independent of the geometry and flow state of the flame gases. In reality, our approach is not entirely new; several previous investigators—Burke and Schumann, Wolfhard and Parker, and Spalding—have already used various elements of it, as will be noted.

Theoretical Basis for "Mixing Similarity"

BASIC THEORETICAL ASSUMPTIONS

Let it be assumed that ordinary molecular diffusion is the dominating molecular transport mechanism in a diffusion flame, *i.e.*, in comparison, thermal diffusion will be considered as having a negligible influence.

Let it also be assumed that the diffusion of any chemical species can be treated in terms of a common diffusion coefficient, D. Let this assumption be restated in another way: Regardless of what mean value of D is associated with the chemical composition, temperature and pressure at a particular point in the field, the diffusion of any of the species at that point can be treated in terms of this D, no restrictions being placed on how D varies with state variables.

These are the only two physicochemical assumptions which will be introduced into the theoretical development, and it ultimately appears that the physical realism of our whole viewpoint hinges on the degree to which these key assumptions are justified by experiment.

ALLOWANCE FOR DIFFUSIVE MASS FLOW

Although the majority of the literature on diffusion phenomena employs the g-mol concentration per unit volume of a species, c_i, as the concentration or driving force variable, these formulations are not usually applicable to combustion work because of the presence of temperature gradients. Such isothermally valid expressions may be re-expressed in terms of the mol fraction gradient by substituting $(\partial c_i/\partial x) = c(\partial \alpha_i/\partial x)$ (For the sake of simplicity we will deal with one-dimensional diffusion only, the multidimensional processes being identical in form except for the use of vector notation.) This leads directly to the expression,

$$j_i' = -Dc \frac{\partial \alpha_i}{\partial x} \tag{1}$$

which is in a form suitable for nonisothermal applications.[a] An alternate form is in terms of the

[a] One of the authors (H. N. P.) has investigated this point by carrying out a simplified "hard elastic sphere" kinetic theory analysis for diffusion in a nonisothermal system. It was found that when the "velocity persistence effect" is allowed for, as in the case of heat conduction, the relation takes on the necessary form of Equation (1).

partial pressure gradient, $j_i' = -(D/RT)(\partial p_i/\partial x)$. The Equation (1) formulation of diffusive flows has been frequently used in combustion work.

In Equation (1) j_i is the diffusive current in g-mols of i/cm² × sec through a surface which is normal to the direction of flow along the x axis. A condition in the derivation of this expression is that such a surface move with the gas as a whole so that the total flow rate of all molecules which cross it from both directions is zero, as is in accord with the obvious conditions, $\sum_i \alpha_i = 1$ and $\sum_i (\partial\alpha_i/\partial x) = 0$, from which:

$$\sum_i j_i' = 0 = -Dc\sum_i (\partial\alpha_i/\partial x) \qquad (2)$$

The surface so defined then has the average convective velocity (if any) of all the molecules in its vicinity.

The *mass flow* of i through this surface is obtained by multiplying j_i' by m_i, the molecular weight of the i molecules.

$$j_i' m_i = -Dcm_i\left(\frac{\partial\alpha_i}{\partial x}\right) \qquad (3)$$

It is now apparent that in the general case when all the m_i's are not equal, $\sum_i j_i m_i \neq 0$ and *there is a net mass flow across this surface of zero net molecular flow.* Let this mass flow be formulated as $\rho\Delta u_m$ g/cm² × sec in which ρ g/cm³ is the mass density of the gas at the surface and Δu_m cm/sec is the velocity of the mass flow relative to the surface.

$$\rho\Delta u_m = \sum_i j_i' m_i = -Dc\sum_i m_i\left(\frac{\partial\alpha_i}{\partial x}\right) \qquad (4)$$

Therefore, for any point on the x axis we can define a reference surface which has a velocity such that either (a) the net molecular flow across it is zero or (b) the net mass flow across it is zero. The velocity of the surface by the second definition, relative to that of the first, is Δu_m, and that by the first relative to the second is $-\Delta u_m$.

In order to illustrate this picture with a simple system, consider the molecular flows at the interface of two gases, "a" and "b," at the instant when a separating partition has "vanished." The v's are the rms molecular speeds relative to the stagnant system. We introduce the condition, $m_a > m_b$. It is seen that, for zero molecular flow, the surface will have a velocity in the direction of the lighter "b" gas moving into the heavier "a" gas; for zero mass flow it will have the opposite velocity of the heavier "a" gas moving into the lighter "b" gas. Furthermore it is apparent that, since no external force has been applied to the system, there will be no mass motion of the system as a whole, but that, within the system, *local mass flows, purely diffusive in origin, will persist so long as there are mean molecular weight gradients.* We note also that since the two definitions arise entirely from applications of different criteria, neither is more "correct" than the other in a fundamental sense, and finally that neither gives a surface with a zero or constant velocity with respect to a laboratory coordinate system.

TABLE 1

Initial Conditions	Equations	× Flow Components
$T_a = T_b$, $p_a = p_b$ from which $c_a = c_b$, and $\frac{1}{2}m_a v_a^2 = \frac{1}{2}m_b v_b^2$ with $m_a > m_b$	$\frac{v_a}{v_b} = \sqrt{\frac{m_b}{m_a}} < 1$	$\lvert c_a v_a \rvert_x < \lvert c_b v_b \rvert_x$ (molecular flow)
	$\frac{m_a v_a}{m_b v_b} = \sqrt{\frac{m_a}{m_b}} > 1$	$\lvert c_a m_a v_a \rvert_x > \lvert c_b m_b v_b \rvert_x$ (mass flow)

However, from an application standpoint, the zero mass flow surface may have certain advantages. The total convective g-mol flow through the surface of zero mass flow is $-c\Delta u_m$, which is rendered explicit by Equation (4) and the relation $\rho = cm$.

$$-c\Delta u_m = -\frac{\rho}{m}\Delta u_m = -\frac{1}{m}\sum_i j_i' m_i = \frac{Dc}{m}\sum_i m_i\left(\frac{\partial\alpha_i}{\partial x}\right) \qquad (5)$$

The convective g-mol flow of i through this surface is

$$\Delta j_i = -\alpha_i c\Delta u_m \qquad (6)$$

Then, in accord with the definition, $m = \sum_i$

$m_i\alpha_i$, from which

$$\frac{\partial m}{\partial x} = \sum_i m_i \left(\frac{\partial \alpha_i}{\partial x}\right),$$

we obtain from Equations (5) and (6):

$$\Delta j_i = \alpha_i \frac{Dc}{m}\left(\frac{\partial m}{\partial x}\right) \tag{7}$$

The total diffusive plus convective g-mol flow of i through the surface of zero mass flow is then,

$$j_i = j_i' + \Delta j_i = -Dc\left(\frac{\partial \alpha_i}{\partial x}\right) + \frac{Dc\alpha_i}{m}\left(\frac{\partial m}{\partial x}\right) \tag{8}$$

which can be put into the forms,

$$\begin{aligned} j_i &= -Dcm\left[\frac{1}{m}\left(\frac{\partial \alpha_i}{\partial x}\right) - \frac{\alpha_i}{m^2}\left(\frac{\partial m}{\partial x}\right)\right] \\ &= -D\rho \frac{\partial(\alpha_i/m)}{\partial x} \end{aligned} \tag{9}$$

or, finally

$$j_i = -D\rho\left(\frac{\partial n_i}{\partial x}\right) \tag{10}$$

in which $\alpha_i/m = n_i$ g-mols of i/g of mixture.

Comparisons of Equations (10) and (1) bring out the changes shown in Table 2. From Equation (9) it is seen that, in general, when $(\partial m/\partial x) \neq 0$, $j_i \neq j_i'$.

For application to combustion-diffusion problems, the Equation (10) formulation has the following advantages:

(1) Molecular diffusion is placed on the same basis as heat conduction and momentum transfer, *i.e.*, all three are defined as purely conductive flows across reference planes of zero convective mass flow, independently of mean molecular weight gradients. Indeed, the $D\rho$ of Equation (10) is dimensionally identical with the viscosity, μ, the two usually being conveniently related by means of the Schmidt number, $(\mu/D\rho)$.

(2) Inasmuch as the concentration variable, n_i g-mols of i/g of mixture, is referred to a unit mass of gas, it has a direct, one-to-one correspondence with the amount of i species present, independently of the mean molecular weight—*and changes in mean molecular weight*—of the gross mixture at that point. The definition of n_i is therefore independent of the molecularity of the various reactions which may be occurring, as is also consistent with the conservation of mass in chemical reactions.

For these reasons we will adopt the Equation (10) rather than the Equation (1) formulation. While the Equation (10) formulation is not new to the literature, the present authors are not aware of any previous development which clearly distinguishes its properties from the Equation (1) type of formulation and which establishes its significance for multicomponent systems.

TABLE 2

	Current	Coefficient	Concentration Variable
Equation (1), reference plane of zero mol flow	$j_i' \dfrac{\text{g-mols i}}{\text{cm}^2 \times \text{sec}}$	$(Dc) \dfrac{\text{g-mols}}{\text{cm} \times \text{sec}}$	$\alpha_i \dfrac{\text{g-mol of i}}{\text{g-mol of mixture}}$
Equation (10), reference plane of zero mass flow	$j_i \dfrac{\text{g-mols i}}{\text{cm}^2 \times \text{sec}}$	$(D\rho) \dfrac{\text{g}}{\text{cm} \times \text{sec}}$	$n_i \dfrac{\text{g-mols of i}}{\text{g of mixture}}$

THE "MIXING SIMILARITY" PRINCIPLE

The general rate balance for unsteady-state diffusion and reaction in a gas in terms of n_i is

$$\left(\frac{dn_i}{dt}\right)_{\text{total}} = \left(\frac{dn_i}{dt}\right)_{\text{diffusion}} + \left(\frac{dn_i}{dt}\right)_{\text{reaction}} \tag{11}$$

or, more explicitly,

$$\left(\frac{dn_i}{dt}\right)_{\text{total}} = \frac{1}{\rho}\nabla\cdot(D\rho\nabla n_i) + \left(\frac{dn_i}{dt}\right)_{\text{reaction}} \tag{12}$$

in which the first term on the right accounts for diffusion (in generalized coordinates) and the second term for reaction.

Now let Equation (12) be multiplied through by $\nu_{E,i}$ which is defined as:

$$\nu_{E,i} = \frac{\text{g-atoms of element E}}{\text{g-mol of species i}}$$

(For example, if E = C (carbon) and i = C_2H_2, then $\nu_{E,i} = 2$; and if E = C and i = H_2O, then $\nu_{E,i} = 0$, etc.) Then sum the resulting expression over all i.

$$\left[\frac{d\left(\sum_i \nu_{E,i} n_i\right)}{dt}\right] = \frac{1}{\rho}\,\nabla\cdot\left(D\nabla \sum_i \nu_{E,i} n_i\right) + \left[\frac{d\left(\sum_i \nu_{E,i} n_i\right)}{dt}\right]_{\text{reaction}} \tag{13}$$

The group $\sum_i \nu_{E,i} n_i$ will be recognized as the total number of g-atoms of the element E per g of mixture which may be designated N_E.

$$\sum_i \nu_{E,i} n_i = N_E \frac{\text{g-atoms of E}}{\text{g of mixture}} \tag{14}$$

Now we come to the crux of the whole development. *Since chemical reactions neither create nor destroy atoms, and since mass is conserved in chemical reactions* (noting that the N_E is on a per unit mass basis), then

$$\left[\frac{d\left(\sum_i \nu_{E,i} n_i\right)}{dt}\right]_{\text{reaction}} = \left[\frac{dN_E}{dt}\right]_{\text{reaction}} = 0 \tag{15}$$

and Equation (13) becomes (in cartesian coordinates)

$$\frac{dN_E}{dt} = \frac{1}{\rho}\left[\frac{\partial}{\partial x}\left(D\rho\frac{\partial N_E}{\partial x}\right) + \frac{\partial}{\partial y}\left(D\rho\frac{\partial N_E}{\partial y}\right) + \frac{\partial}{\partial z}\left(D\rho\frac{\partial N_E}{\partial z}\right)\right] \tag{16}$$

for any element E, *independently of chemical composition or reaction rate.*

Also, since the quantity $A_E N_E$ is merely the weight fraction of the element E, Equation (16) is subject to the normalization conditions,

$$\sum A_E N_E = 1 \tag{17}$$

and

$$\sum_E A_E N_E^j = 0 \tag{18}$$

in which N_E^j is any arbitrary jth derivative of N_E.

Spalding,[12] in a treatment of burning from a liquid surface, was apparently the first investigator to explicitly introduce "atomic conservation," Equation (15), into a general transport equation.

An immediate consequence of the Equation (16) generalization may be illustrated by considering a hydrocarbon-air system. In the initial pure fuel the concentrations of the H and C atoms, N_H° and N_C° respectively, are fixed by the chemical composition of the fuel and therefore have exactly similar initial distributions; and since we may designate E = H or E = C in Equation (16) without in any way altering the relationships, it follows then that *the elements* H *and* C *have exactly similar distributions everywhere, independently of time and all chemical considerations,*

$$\frac{N_H}{N_H^\circ} = \frac{N_C}{N_C^\circ} \tag{19}$$

and similarly for the O *and* N *distributions.*

$$\frac{N_O}{N_O^\circ} = \frac{N_N}{N_N^\circ} \tag{20}$$

The full implications of this principle, together with comments on its implicit use by other investigators, will be discussed in the section, "Application of Results."

EXPERIMENTAL APPROACH AND OBJECTIVES

The first objective is to ascertain the degree of agreement between experiment and the mixing similarity theory, as formulated by Equations (19) and (20). The approach consists of obtaining chemical analyses of gas samples which have been drawn from local zones across a number of flat, laminar, hydrocarbon-air diffusion flames. The average values of the differences, $N_H/N_H^\circ - N_C/N_C^\circ$ and $N_N/N_N^\circ - N_O/N_O^\circ$, will be taken as the criteria of agreement between theory and experiment. This test is to be only on the *similarity* of the distributions as distinct from the form of the distributions.

The second objective is to analyze the experimental N_E distributions in terms of an analytically derived equation, and thereby calculate the effective diffusion coefficients which give the best fit to the data. Inasmuch as mixing similarity is implicit in this second treatment, it provides an additional test of the principle. However, a number of additional constraints and simplifying assumptions must be introduced in order to obtain a manageable, closed-form mathematical expression. Therefore, it is assumed that we have a physical system for which the following conditions are justified.

(a) A steady-state, two-dimensional (x and y) combustion and flow regime exists; from which

$$\frac{dN_E}{dt} = u_y\left(\frac{\partial N_E}{\partial y}\right) + u_x\left(\frac{\partial N_E}{\partial x}\right)$$

(b) Diffusive mixing is effectively confined to the x dimension; *i.e.*, we need consider only the x

component term in the right-hand member of Equation (16).

(c) If this x component term is expanded and the temperature dependencies $D \sim T^{1.75}$ and $\rho \sim T^{-1}$ are introduced,

$$\frac{1}{\rho}\frac{\partial}{\partial x}\left(D\rho\frac{\partial N_E}{\partial x}\right) = D_o\left(\frac{T}{T_o}\right)^{1.75}\left[\frac{\partial^2 N_E}{\partial x^2} + 0.75\frac{\partial \ln T}{\partial x}\left(\frac{\partial N_E}{\partial x}\right)\right] \tag{21}$$

then, in the right-hand member of the above expression, the second term in the brackets may be considered negligible in comparison to the first.

(d) The flow velocity, u, makes a constant average angle, θ, with the y axis; the x- and y-axis components of u are therefore related by: $u_x/u_y = \tan\theta$.

(e) In the high-temperature region u_y varies with T so that the group,

$$\frac{D_o}{u_y}\left(\frac{T}{T_0}\right)^{1.75} = k\left(\frac{D}{u}\right)_0$$

may be regarded as independent of T. k is a correction factor which accounts for "hydrodynamic effects" and variations of initial stream temperature.

(f) For all $y < 0$ the streams are separated by a negligibly thin partition; both streams are infinite in extent to either side of $x = 0$. The boundary conditions are therefore:

$$\text{for } y < 0, \quad N_E = \begin{cases} N_E^\circ, \text{ for all } x > 0 \\ 0, \text{ for all } x < 0 \end{cases}$$
$$\text{for } y > 0, \quad N_E = \begin{cases} N_E^\circ, \text{ for } x = \infty \\ 0, \text{ for } x = -\infty \end{cases} \tag{22}$$

and inversely for the x relations of an atomic species initially on the $-x$ side of the partition.

With these constraints and simplifications, Equation (16) becomes

$$\frac{\partial N_E}{\partial y} = k\left(\frac{D}{u}\right)_0\left(\frac{\partial^2 N_E}{\partial x^2}\right) - \tan\theta\frac{\partial N_E}{\partial x} \tag{23}$$

which upon integration and introduction of the Equations (22) boundary conditions, yields

$$\frac{N_E}{N_E^\circ} = \frac{1}{2}\left[1 \pm \operatorname{erf}\left(\frac{x - x_0}{\lambda}\right)\right] \tag{24}$$

the sign depending on which stream originally contained E, and in which

$$\lambda = 2\sqrt{k\left(\frac{D}{u}\right)_0 y} \tag{25}$$

$$x_0 = y\tan\theta \tag{26}$$

It is seen that, in consequence of the necessary conditions of Equations (17) and (18) on Equation (24), the x_0's and λ's for all E elements in a given flame must be equal.

The criteria of agreement between theory and experiment includes consideration of three independent variables. The first two, p and u_0, are seen to enter directly into the λ of Equation (24) (noting that $D \sim p^{-1}$). Thirdly, since the diffusion equation is derived on a basis which allows for diffusive mass flows, a butane-air flame was also investigated to check the theory on a system with widely varying molecular weights.

The degree to which our flames justify the conditions and assumptions (a) through (f) is best considered in the light of the experimental results.

Experimental Equipment and Procedure

GAS-HANDLING SYSTEM

Compressed-cylinder air and liquefied hydrocarbon gases (95 per cent ethane and 99 per cent butane) were used in all experiments. It was important that we be able to measure and control our flow variables accurately and reproducibly, since the positioning of the steep concentration region is sensitive to the stream velocities. Upstream pressure regulation for each stream was provided by Nullmatic pressure regulators. A watch-jewel critical flow orifice system (after Anderson and Friedman[13]) metered the air stream. Sets of capillary flow tubes, each consisting of about 12 ft of $\frac{1}{8}$-in. copper tubing formed into a $\frac{3}{4}$-in. diameter coil, were utilized for metering the fuel gases. With this arrangement viscous flow was maintained up to Reynolds numbers of 7000 to 8000, and the whole assembly was immersed in a constant-temperature bath. Calibrations were made with wet test meters which had been checked against a water-displacement apparatus. The maximum uncertainty of the volumetric flow measurements was within ± 1 per cent for the air and $\pm\frac{1}{2}$ per cent for the fuel. The burning chamber pressure was regulated by a cartesian manostat which was located in the combustion products exhaust line and which, in turn, discharged into a vacuum pumping system.

THE BURNER

Figure 1 illustrates the general design of the burner. A series of 5-100-mesh/in. stainless-steel screens established flat velocity profiles prior to combustion. A sheet-metal chimney was fitted to the burner proper to prevent an influx of outside air or gas which otherwise circulated down into the burner from the top, causing instability. The burner assembly was contained in an outer chamber (not shown in Fig. 1) within which the burning pressure level was maintained.

SAMPLING SYSTEM AND EXPERIMENTAL PROCEDURE

Figure 2 illustrates the probe and associated apparatus. A volumetric sampling rate of 1 to 2 cm^3/sec (referred to the burner pressure but at room temperature) was established in order to achieve a reasonable time for collecting a sample. This sampling rate yields an effective resolution distance $\Delta x = 0.37$ cm in the burner in the worst instance. The resulting error in atomic concentration is quite small. (See "Evaluation of Effective Diffusion Coefficients.")

A permanently mounted camera viewed the burner and probe by means of a schlieren system. As each sample was collected, a photograph permanently recorded the position of the probe relative to the burner. The uncertainty in the location was less than ± 0.025 cm.

The sampling lines were wrapped with electric heating tape to prevent water condensation from the sample; the sample then passed through a dew-point indicator where the water concentration was ascertained from the dew point, the gauge pressure in the indicator, and the barometric pressure; subsequently the sample was dried with $CaSO_4$ and compressed by a Toeppler pump to atmospheric pressure; the sample was then collected by mercury displacement in a 350-cc bulb. The sampling apparatus was purged by displacing 15 to 20 times the system's total volume before taking a sample.

SAMPLING ANALYSIS AND DATA REDUCTION

The dry gas samples were analyzed by the F. C. Broeman Co., Chemists, Cincinnati, Ohio. With a few modifications, standard gas-analysis procedures were adhered to; randomly chosen control samples were analyzed by the authors. The samples were analyzed for the following constituents: CO_2, Illuminants (considered as C_2H_4 for ethane, and C_4H_8 for butane flames), O_2, H_2, CO, CH_4, C_2H_6 (or C_4H_{10}), and N_2.

After factoring in the water content of the original sample the chemical composition of the "wet" samples was calculated in terms of the g-mol fractions, α_i. Then, after noting that in Equation (12), $n_i = \alpha_i/m$ and that $m = \sum_i m_i\alpha_i$, N_E was calculated by:

$$N_E = \frac{1}{m} \sum_i \nu_{E,i}\alpha_i \tag{27}$$

This quantity was then normalized to N_E/N_E° in which N_E° is the value of N_E in the pure air or fuel.

Air	C_2H_6	C_4H_{10}
$N_O^\circ = \frac{2(0.2095)}{28.97} = 0.01446$	$N_H^{\circ\prime} = \frac{6}{30.07} = 0.19753$	$N_H^\circ = \frac{10}{58.12} = 0.17205$
$N_N^\circ = \frac{2(0.7905)}{28.97} = 0.05457$	$N_C^\circ = \frac{2}{30.07} = 0.06651$	$N_C^\circ = \frac{4}{58.12} = 0.06882$

The values 28.97, 30.07 and 58.12, are the molecular weights of air, ethane and butane, respectively. Tables 1A and 2A in the appendix show a complete set of analyses for a typical flame, (F).

EXPERIMENTAL LIMITATIONS

Figure 3 shows how the nine flames which we studied are related to the independent variables, p and u_o, and also the various practical limits to these variables. Figures 4 through 12 show the experimental N_E/N_E° distributions for these flames plotted against the burner's x coordinate. In all the flames the data showed that the gases are pure air or fuel at the extremes; the scale of the graphs does not permit the inclusion of all these points.

The deposition of solid carbon in the probe intake hole did not permit a complete data traverse in the higher pressure flames which manifested a luminous carbon zone. Indeed, it was difficult even to approach this zone because a "front" of carbon deposit was observed to move slowly out along the probe surface (as much as 1 to 1.5 mm) from the main deposit which formed where the probe traversed the luminous zone. Presumably, this was connected with the effective radius of the sampling

volume in the burner, there being no evidence of solid-phase carbon in the gas which was co-planar with these carbon deposit "extensions." Therefore, inasmuch as the position of the data points which bracket the carbon zone depended on the amount of "extended" carbon deposit which had formed on the probe, the regions without data points in Figures 4, 5, 6 and 7, are not particularly indicative of the location of the carbon zone. Attempts to locate its position by other means were not successful; it did not register observable schlieren and the necessary depth of field was too great for accurate conventional photography. Visual methods were not sufficiently reproducible.

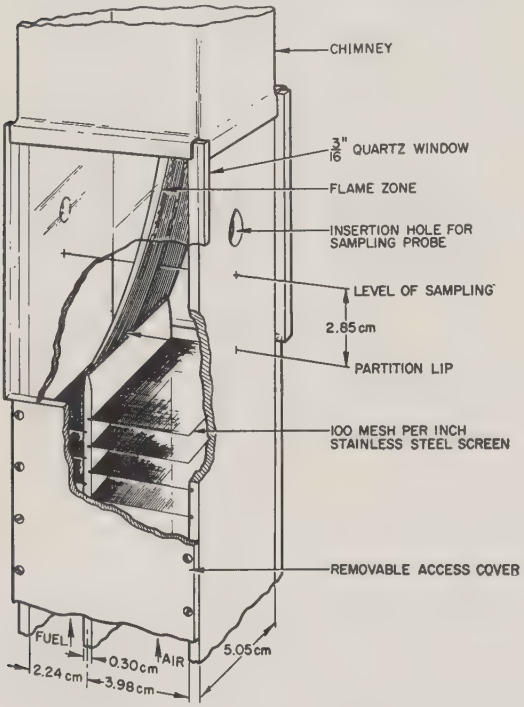

FIG. 1. Burner construction.

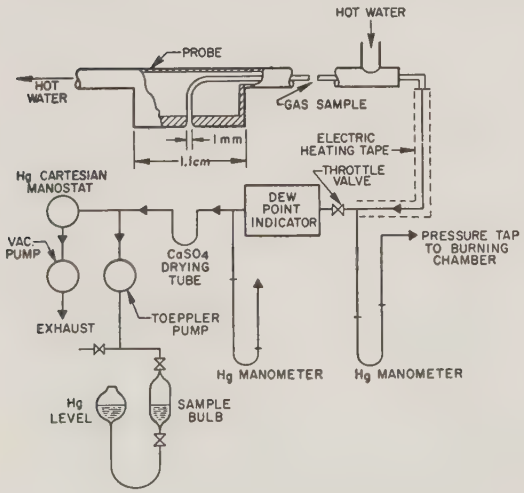

FIG. 2. Flow diagram of gas sampling apparatus.

The curves which are shown in Figures 4 through 12 are not the best representation of each individual flame's data, but are derived from a consistent analytic representation of all the flames. The indicated theoretical stoichiometric compositions in each figure is located with respect to this analytic curve.

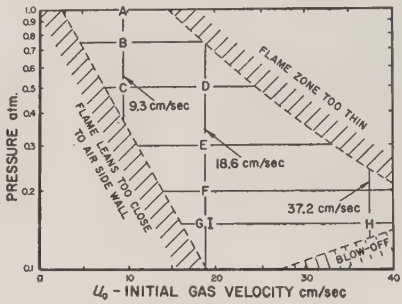

FIG. 3. Map of pressure-velocity operating limits. All flames are ethane-air except for I which is butane-air.

Analysis and Discussion of Data

EXPERIMENTAL JUSTIFICATION FOR "MIXING SIMILARITY"

The theoretical Equations (19) and (20) predict $(N_H/N_H^\circ) - (N_C/N_C^\circ) = \delta_{H\text{-}C} = 0$ and $(N_N/N_N^\circ - N_O/N_O^\circ) = \delta_{N\text{-}O} = 0$. Our object now is to show the degree to which the data fulfill these equations by evaluating an average experimental $\delta_{H\text{-}C}$ and $\delta_{N\text{-}O}$ as defined below. The sense of the formula is indicated by the integral representation at the right, φ being an average N_E/N_E° for the appropriate pair of elements.

$$\bar{\delta} = \frac{\sum (A_k^{k+1}\delta)\,(\Delta_k^{k+1}\varphi)}{\sum (A_k^{k+1}\varphi)\,(\Delta_k^{k+1}\varphi)} \rightleftharpoons \frac{\int \delta d\varphi}{\int \varphi d\varphi} \qquad (28)$$

The subscript $(_k)$ identifies data from the plane at burner position x_k. The symbols A_k^{k+1} and Δ_k^{k+1} indicate "average" and "difference" respectively for the data at x_k and x_{k+1}, as is consistent with the following definitions (for H-C differences):

$$(A^{k+1}\delta) = \tfrac{1}{2}[(N_H/N_H^\circ)_{k+1} - (N_C/N_C)_{k+1} + (N_H/N_H)_k - (N_C/N_C)_k] \qquad (29)$$

$$(\Delta_k^{k+1}\varphi) = \tfrac{1}{2}[(N_H/N_H^\circ)_{k+1} + (N_C/N_C^\circ)_{k+1} - (N_H/N_H^\circ)_k - (N_C/N_C^\circ)_k] \quad (30)$$

$$(A_k^{k+1}\varphi) = \tfrac{1}{4}[(N_H/N_H^\circ)_{k+1} + (N_C/N_C^\circ)_{k+1} + (N_H/N_H^\circ)_k + (N_C/N_C^\circ)_k] \quad (31)$$

and similarly for the N-O differences.

There were three reasons for choosing this method of averaging. First, each difference, $(A_k^{k+1}\delta)$, is weighted according to the increment, $(\Delta_k^{k+1}\varphi)$; therefore an irregular x axis spacing or "clustering" of the data does not arbitrarily weight $\bar{\delta}$, as small increments are associated with a close spacing, and vice versa. Secondly, since $0 < (A_k^{k+1}\varphi) < 1$, the summations tend toward stationary values as near limiting values of $(A_k^{k+1}\varphi)$ are included, *i.e.*, it is not possible to arbitrarily "improve" the over-all results by including many points in the pure air or fuel streams where the H-C and N-O differences are necessarily small. Thirdly, no theoretical relationships are implicit in Equations (28), (29), (30) and (31). As only the experimental (N_E/N_E°) values are involved, the magnitude of the $\bar{\delta}$'s is a measure only of the similarity of the mixing, independently of the spatial distributions of the N_E's which result from mixing. This method gives the greatest weight to the differences in the region of the steepest N_E/N_E° gradient.

Of course the $\bar{\delta}$ values are still influenced by the number and accuracy of the data involved. Also, since the averaging equations do not allow for higher than first-order differences, there is a certain characteristic error of the averaging technique itself. A measure of this latter error is the value of the denominator in Equation (28), relative to its ideal value 0.5 when the limits on φ are 0 and 1.

Table 3 lists the values of $\bar{\delta}_{H\text{-}C}$ and $\bar{\delta}_{N\text{-}O}$ as calculated from the data which is plotted in Figures 4 through 12. Averages are shown over three ranges: the fuel and air sides (with respect to the x_0 plane), and an over-all average. In all cases the values of the denominator in Equation (28) was within 0.48 and 0.51 for the over-all average, indicating that the intrinsic error of the averaging procedure is quite small.

Since N_E is simply the number of g-atoms of E per g of mixture, it is independent of all chemical and mean molecular weight changes which may occur either while drawing the sample or subsequently; its determination is subject only to the procedural errors and uncertainties of chemically analyzing a sample.

Table 3: Observed Departures from Exact Similarity

Numerical $\bar{\delta}$'s are in per cent

Flame	A	B	C	D	E	F	G	H	I	Av.
p (atmos)	1.0	0.75	0.50	0.50	0.30	0.20	0.15	0.15	0.15	
u_0 (cm/sec)	9.3	9.3	9.3	18.6	18.6	18.6	18.6	37.2	18.6	
$\bar{\delta}_{H\text{-}C}$										
fuel side	+1.3	+0.1	+1.2	−1.0	+0.9	+0.6	+0.8	+0.4	−0.3	+0.3
air side	+5.5	+0.6	+1.8	+2.2	+2.7	−0.2	−1.8	−4.1	−5.4	+0.1
over-all	+2.4	+0.2	+1.4	0.0	+1.4	−0.1	−0.1	−0.7	−1.2	+0.3
$\bar{\delta}_{N\text{-}O}$										
fuel side	−5.1	−3.8	−2.8	+4.0	+19.5	+17.8	+14.5	+11.2	+8.8	+7.1
air side	+7.8	+2.0	+1.7	−1.0	+7.2	+2.7	+6.0	+3.4	+1.5	+3.5
over-all	+4.5	+0.4	+0.8	+0.1	+9.9	+5.4	+7.3	+5.5	+4.0	+4.2

It is immediately apparent from Figures 4 through 12 that most of the scatter in the data probably originates with the chemical analyses of the samples. The way in which chemical-analysis errors influence the final results is shown for the air-side by Table 4, which deals with a hypothetical analysis of a 100-ml "wet" sample of an ideal stoichiometric (C_2H_6-air products) mixture. The volumetric analysis errors which we deem reasonable are indicated under each constituent. In the case of H_2O, the dewpoint temperature and pressure uncertainties are shown. Although such an ideal mixture contains no H_2, CO or O_2, the analyst does not know this and, in trying to analyze for them, may introduce errors. It is assumed that preliminary tests have

shown the absence of hydrocarbon constituents. Each column shows the effect of the individual constituent error on the four calculated results, all other errors taken as zero.

Table 4 shows that, since N_2 is present in the mixture we take 20 ml and mix it with 80 ml of O_2 in order to insure adequate excess O_2 for the combustion step. This mixture now contains 4 ml of N_2. Now, assuming that the accumulative errors of the combustion step and the subsequent

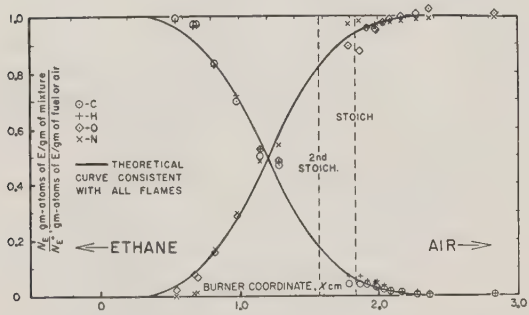

FIG. 4. Flame A. Ethane-air, p = 1.0 atmos, u_0 = 9.3 cm/sec.

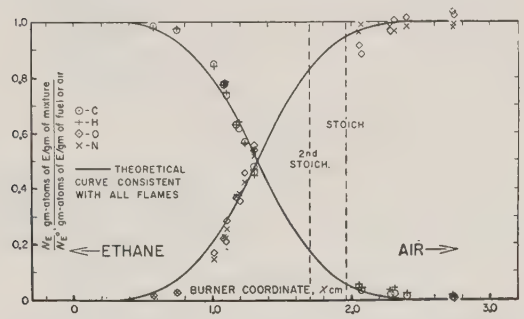

FIG. 5. Flame B. Ethane-air, p = 0.75 atmos, u_0 = 9.3 cm/sec.

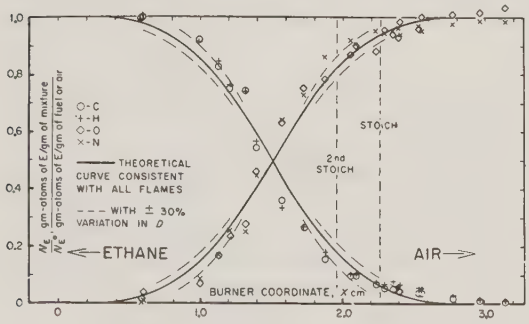

FIG. 6. Flame C. Ethane-air, p = 0.50 atmos, u_0 = 9.3 cm/sec.

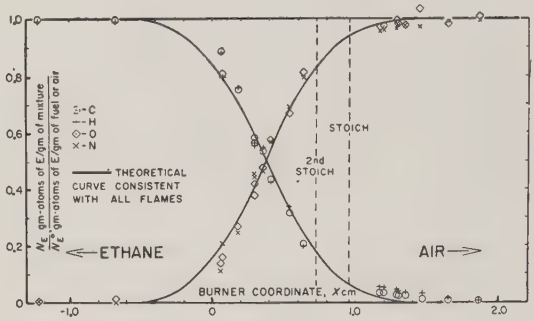

FIG. 7. Flame D. Ethane-air, p = 0.50 atmos, u_0 = 18.6 cm/sec.

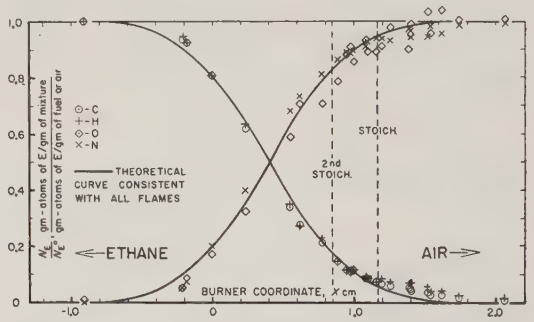

FIG. 8. Flame E. Ethane-air, p = 0.30 atmos, u_0 = 18.6 cm/sec.

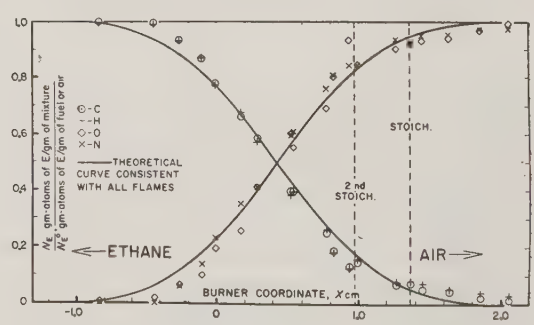

FIG. 9. Flame F. Ethane-air, p = 0.20 atmos, u_0 = 18.6 cm/sec.

greatest amount, the N_N/N_N° determination is subject to the least error and that the N_C/N_C° is subject to the greatest error from the CO analysis.

On the fuel side the picture is considerably more complex, and a table of analysis errors would be unduly complicated. By way of illustration, however, consider a simple mixture of 20 per cent N_2 and 80 per cent C_2H_6. In order to analyze this CO_2 and excess O_2 absorptions is 1 ml, the error in N_N/N_N° which follows from the 4 ml of N_2 residue is 25 per cent, N_N/N_N° being in the range of 0.25. Therefore, we are strongly inclined to believe that the appreciable fuel-side $\delta_{N\text{-}O}$ differences in Table 3 are largely due to analysis error. Otherwise, we have to make the improbable postulate that O-containing compounds, largely CO and

H_2O in this region, diffuse much more slowly than N_2. Another possible source of error, for both air and fuel sides, is that small amounts of formic acid and formaldehyde were removed in the $CaSO_4$-drying tubes; the characteristic odor of these substances was detected on several occasions when the spent $CaSO_4$ was being replaced.

The per cent uncertainties in the chemical analyses, as illustrated by Table 4 for the air side and by the foregoing discussion for the fuel side, are observed to be commensurate with or greater than the observed per cent departures from exact similarity in Table 3. Therefore, noting that the chemical-analysis error which is associated with each constituent is sure to have a systematic component, *we conclude that the deviations from exact similarity in the actual flame gases are, at the most commensurate with and probably less than, those shown in Table 3.*

Our final views on mixing similarity are summarized at the end of the paper.

EVALUATION OF THE EFFECTIVE DIFFUSION COEFFICIENTS

Equation (24) was fitted by the minimum chi-square criterion (virtually equivalent to a least-square fit) to the N_E/N_E° vs x data of each element for the nine flames. At the suggestion of Mr. G. P. Williams (General Electric Co.), this was effected by an application of the "normit" technique[14] for analyzing biologic data in terms of an error-function curve. In normit coordinates the error function becomes a straight line and curve fitting is very easily accomplished. The transformation is not well suited to handling limiting values of N_E/N_E° as it tends to $\pm\infty$; consequently only data in the range, $0.01 < N_E/N_E^\circ < 0.99$, was used in evaluating the λ's. Care was taken to modify the "weighting functions" to allow for the experimentally independent nature of our data points, in contrast to the accumulative nature of the data in the usual biologic problem. All calculations were carried out on an IBM Model 607 electronic computor. It has been pointed out that, in consequence of mixing similarity, a formal requirement Equations (17) and (18) is that the same x_0's and λ's obtain for all elements in a given flame. The variations between experimental x_0's and λ's therefore provide an additional criterion for mixing similarity, as well as of the applicability of Equation (24). The average λ's for the (H + C) and (N + O) data were obtained by treating the H and C data as indistinguishable, and similarly for the N and O. Comparisons between them provide a measure of the over-all consistency of the Equation (24) correlation. See Table 3A (appendix).

The effective diffusion coefficients for each

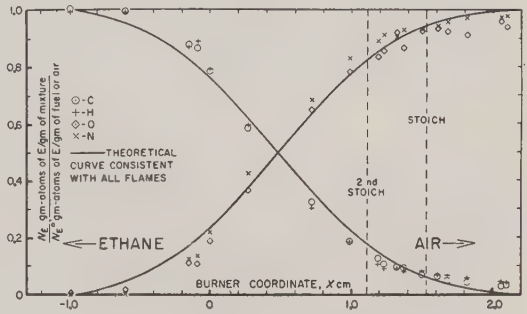

FIG. 10. Flame G. Ethane-air, $p = 0.15$ atmos, $u_0 = 18.6$ cm/sec.

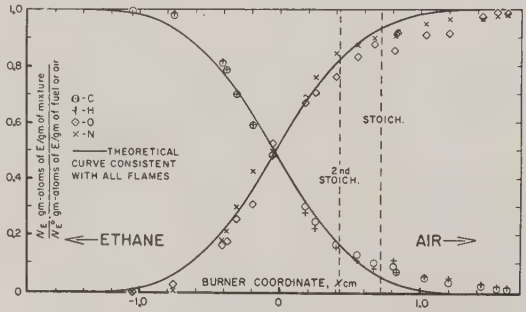

FIG. 11. Flame H. Ethane-air, $p = 0.15$ atmos, $u_0 = 37.2$ cm/sec.

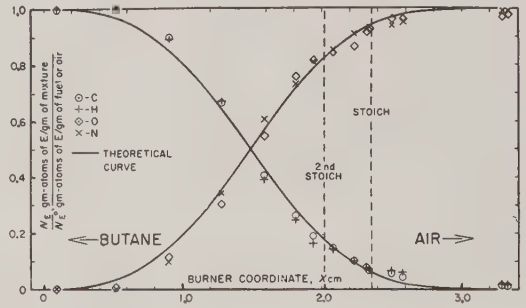

FIG. 12. Flame I. Butane-air, $p = 0.15$ atmos, $u_0 = 18.6$ cm/sec.

element were calculated from the λ's of Table 3A in the appendix by means of a rearranged Equation (25), all values being referred to 1 atmos by introducing the theoretical pressure dependence.

$$D_1 = \tfrac{1}{4}(u_0/ky)(p/p_1)\lambda^2 \qquad (32)$$

Flow balances show that due to the lateral displacement of the mixing mid-plane from $x = 0$

to $x = x_0$, the average velocity of this region increases. k then is the correction factor which relates the x- and y-averaged mixing-region velocity to the initial u_0. Because of the increased viscosity in the high-temperature region to the air side of x_0, we have given the air-side velocity ratio a weight of 0.75 rather than 0.50.[b]

$$1/k = \frac{1}{2}\left[1 + \left(0.75\,\frac{3.94}{3.94 - x_0} + 0.25\,\frac{2.24}{2.24 + x_0}\right)\right] \tag{33}$$

3.94 cm and 2.24 cm are the air-side and fuel-side duct widths (Fig. 1).

Inasmuch as λ is more directly experimental than D_1, the final average D_1 was computed from the average of the $\sqrt{D_1}$'s for each element excluding flame H.

Figure 14 summarizes graphically the results shown in Table 3A in the appendix. A measure of the effectiveness of the *over-all correlation* is provided by comparisons of the experimental λ's and the "theoretical" λ's which were obtained by back-calculation from the final average D_1, using the tabular u_0, p and k values. A graphical comparison is provided by the plots of Equation (24) in Figures 4 through 12, which use the theoretical λ's and average X_o's.

TABLE 4. EFFECT OF CHEMICAL ANALYSIS ERRORS ON CALCULATED N_E/N_E° RATIOS FOR AN IDEAL STOICHIOMETRIC MIXTURE (C_2H_6-AIR PRODUCTS)

The + volumetric error is arbitrary; the per cent errors are in parentheses; those greater than 2.0 are in italics.

Constituent	H_2O	CO_2	N_2	CO	H_2	O_2
mol fr. α_i	0.1648	0.1098	0.7254	0	0	0
Vol. error	+1°F at 30°F or $\frac{1 \text{ mm}}{25 \text{ mm}}$ Hg	$\frac{+0.5 \text{ ml}}{100 \text{ ml}}$	$\frac{+1.0 \text{ ml}}{100 \text{ ml}}$	$\frac{+1.0 \text{ ml}}{100 \text{ ml}}$	$\frac{+1.0 \text{ ml}}{100 \text{ ml}}$	$\frac{+1.0 \text{ ml}}{100 \text{ ml}}$
$\frac{N_C}{N_C^\circ} = 0.0585$	−0.0004 (−0.8)	+0.0026 (*+4.5*)	−0.0021 (*−3.6*)	+0.0053 (*+9.1*)	−0.0006 (−1.0)	−0.0006 (−1.0)
$\frac{N_H}{N_H^\circ} = 0.0585$	+0.0023 (*+4.0*)	−0.0004 (−0.6)	−0.0021 (*−3.6*)	−0.0006 (−1.0)	+0.0036 (*+6.1*)	−0.0006 (−1.0)
$\frac{N_O}{N_O^\circ} = 0.9415$	+0.0118 (+1.3)	+0.0220 (*+3.4*)	−0.0342 (*−3.6*)	+0.0186 (*+2.0*)	−0.0094 (−1.0)	+0.0430 (*+4.6*)
$\frac{N_N}{N_N^\circ} = 0.9415$	−0.0075 (−0.8)	−0.0052 (−0.6)	+0.0130 (+1.4)	−0.0094 (−1.0)	−0.0094 (−1.0)	−0.0094 (−1.0)

In the case of flame A, k also includes a temperature correction on the group $(D/u) \sim (400°K/300°K)^{0.75} = 1.242$ to account for the increased initial stream temperature, as measured. The burner for flame A was not enclosed in the outer chamber and the approach duct became quite warm, presumably by radiation from the large luminous excess fuel flame at the top. No such heating of the approach duct was noted for the other flames, their gases not contacting room air because of the outer chamber. The initial gas temperature was taken to be ~300°K.

[b] In another paper[7] we gave an equal weight at $y = y_1 = u_0^2/2g$, but in the presens case, $y \geqslant 16\ (u_0^2/2g)$ and it is reasonable to expect much greater viscosity effects.

The analytical validity of Equation (24) and the resulting evaluations of D depends on several approximations and assumptions which have been pointed out previously.

First, there is the possibility that inadequate spatial resolution of the sampling might introduce an excessive error into the measured N_E/N_E° distributions with x. We can investigate this possibility by evaluating the equation,

$$\Delta(N_E/N_E^\circ) = \frac{\int_{x-\frac{1}{2}\Delta x}^{x+\frac{1}{2}\Delta x} (N_E/N_E^\circ)\,dx}{\Delta x} - (N_E/N_E^\circ) \tag{34}$$

in which (N_E/N_E°) is the "exact" value at x by

Equation (24); the integral term is the average value of the sample from a region Δx cm wide; $\Delta(N_E/N_E^\circ)$ is the resulting error. By integrating, then uniformly expanding all the resulting functions of $(x \pm \frac{1}{2}\Delta x)/\lambda$ in a Taylor series (including all third-derivative terms), Equation (34) reduces to:

$$\Delta(N_E/N_E^\circ) = \pm \frac{(\Delta x/\lambda)^2}{12\sqrt{\pi}} \left(\frac{x - x_o}{\lambda}\right) e^{-(x-x_o/\lambda)^2} \quad (35)$$

Then, noting that

$$(x - x_0)/\lambda \exp\left[-\left(\frac{x - x_0}{\lambda}\right)^2\right]$$

is a maximum at $(x - x_0)/\lambda = \pm 1/\sqrt{2}$, we obtain:

$$\Delta(N_E/N_E^\circ)_{max.} = \pm 0.020 \left(\frac{\Delta x}{\lambda}\right)^2 \quad (36)$$

Then, introducing the maximum experimental $\Delta x \simeq 0.37$ cm for flame C, and with $\lambda \simeq 0.68$ cm (from Table 3A), we obtain a $\Delta(N_E/N_E^\circ)_{max} \simeq 0.006$ which is much smaller than the largest chemical-analysis error as typified by Table 4. This analysis shows that our spatial resolution was quite adequate for determining atom distributions, but is inadequate for extracting much information on the detailed chemical distributions.

The generally close correlation in form between the experimental N_E/N_E° distributions and the Equation (24) curves substantiates the reasonableness of assumptions (a) through (f) which were listed at the end of the theoretical development. Assumption (b), which states in effect that the y-axis diffusion components are negligible in comparison to the x-axis component, is of special interest since it is subject to some degree of independent experimental control. If Equation (24) is in fact valid, then it must satisfy the inequality,

$$\left|\frac{\partial^2 N_E}{\partial x^2}\right| \gg \left|\frac{\partial^2 N_E}{\partial y^2}\right|$$

at all conditions of experimental interest. By performing the indicated differentiations of Equation (24) (noting Equation (25) and neglecting variations of x_0 with y), the above inequality reduces to:

$$1 \gg \left|\frac{1}{4}\left(\frac{\lambda}{y}\right)^2 \left[\frac{3}{2} - \left(\frac{x - x_0}{\lambda}\right)^2\right]\right|$$

Therefore, except when $(x - x_0)$ is too large to be of interest, for the worst condition when $x = x_0$ and $\lambda \simeq 0.94$ for flame G, we obtain

$$1 \gg \frac{1}{4}\left(\frac{0.94}{2.85}\right)^2 \frac{3}{2} = 0.044.$$

In fact, the lower left shaded line in Figure 3, in addition to the reason given in the figure, also roughly defines the region below which y-axis diffusion is commensurate with the x-axis component.

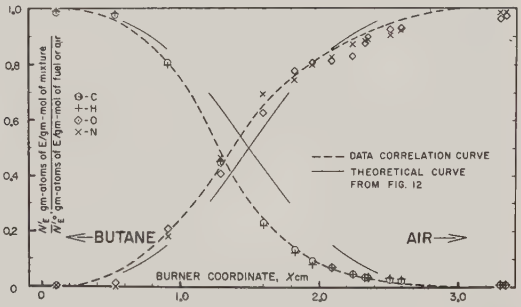

FIG. 13. Flame I. Butane-air, $p = 0.15$ atmos, $u_0 = 18.6$ cm/sec. (With same data as Fig. 12 plotted on a "per g-mol" rather than "per gram" of mixture basis.)

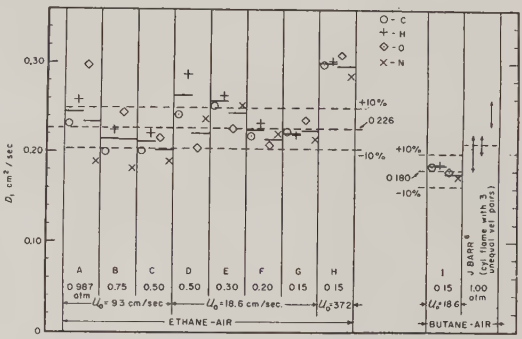

FIG. 14. Diffusion coefficients (corrected to 1.0 atmos and at ~300°K) for flames A-I, together with other values of interest.

Concerning the effects of a local variation in D, *it is important to note that the partial differential Equation* (16) *is only a constraint relation between the time and space derivatives of* N_E; *the value of a local* N_E *and its derivatives at any instant still depends on the space-time integrals of all the preceding changes throughout the field.* Therefore, the effect of a local variation in D on both the local N_E value and on the over-all distribution is much smaller than would appear to be indicated by a purely local application of the differential Equation (16) alone. The significance of the mean D of Equations (24) and (25) is analogous to that of a mean heat capacity which is defined over a large

temperature range, and which therefore has a much weaker dependence on the final T than the true, point-function heat capacity for that final T.

Therefore, since the region of high temperature is considerably displaced from the center of the mixing region at x_0, and furthermore since it occupies a comparatively narrow portion of the total mixing zone, we would not expect the uncertainties in (D/u) which are connected with this region to have a strong influence on the over-all N_E/N_E° distributions, as is observed to be the case. Only in the flame-zone region are systematic departures from Equation (24) noted, and they are not large at that.

In general it appears that chemical-analysis errors are responsible for most of the scatter in

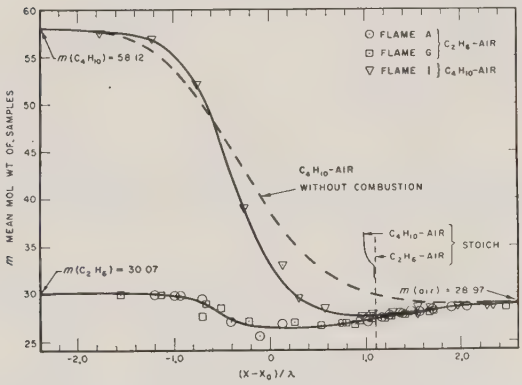

FIG. 15. Sample m's through the mixing and reaction zone. At the extreme left the experimental points fall above the theoretical "without combustion" curve because the λ does not permit an exact fit of the very rich points (see Fig. 12).

the D_1's of Figure 14. Unfortunately, the functional dependence of D_1 on the N_E/N_E° values is an extremely strong one and, in spite of a good over-all correlation in form, moderate chemical-analysis uncertainties are greatly amplified in the computation of an effective D_1. The nature of this relationship is illustrated inversely in Figure 6, the dashed lines showing the comparatively small effects of rather large ($\pm 30\%$) deviations in D_1.

The markedly high mean D_1 for flame H is obviously connected with the unsymmetrical N_E/N_E° distributions which are apparent in Figure 11. This lack of symmetry, contrasting with all the other flames, possibly stems from an interaction between the sampling probe and the high gas velocity (u_0 = 37.2 cm/sec) for this flame. The D_1 for flame H was not included in the average D_1 for the ethane-air flames.

Nevertheless, the general agreement among the D_1's for seven of the eight ethane-air flames—even with wide variations in velocity and pressure—lead us to regard the resulting mean $D_1 = 0.23$ cm²/sec for all ethane-air flames (Table 3A) as a physically significant quantity which is constant and known within ± 10 per cent (including all flame-average D_1's and 17 out of 28 of the D_1's for the individual elements).

It is perhaps surprising that the mean D_1 for the butane-air flame (I) is only $\sim$ 18 per cent less than that for the ethane flames. A clue to the probable reason appears in Figure 15. Any discrepancy between the mean molecular weight of the samples and that of the actual flame gases is very probably such as to make the sample m's larger. Therefore, taking the Figure 15 data as representative of the flame m's, the butane-air sample molecular weights are seen to become coincident with the two sets of ethane-air data well to the rich side of the stoichiometric when all are on a common "reduced distance" basis. Comparisons with the "no-combustion" butane-air curve indicate that the heavy butane molecules decompose to lighter species, and that in a major portion of the mixing and reaction region the gas composition is about the same as for ethane fuel. We may infer then that the same is approximately true for any hydrocarbon fuel, and that consequently D_1 *is very weakly dependent on the fuel's molecular weight, even for those heavy enough to be initially liquid.*

Our quantitative result for butane-air combustion is in surprisingly good agreement with that of Barr[6] pertaining to "calor gas" (butane-propane mixture) flames with air as shown in Figure 14. Barr obtained these results with a completely different geometry (cylindrically symmetric) and with different and varying fuel and air-stream velocities. Burke and Schumann's effective D_1 for methane-air flames, 0.44 cm²/sec, appears somewhat high. (The foregoing figure includes a -13 per cent hydrodynamic correction taken from Table 1 of a separate paper.[7]

Final results: $\begin{cases} \text{ethane-air flames, } D_1 \text{ cm}^2/\text{sec} = 0.23 \pm 10\% \\ \text{butane-air flames, } D_1 \text{ cm}^2/\text{sec} = 0.18 \pm 10\% \end{cases}$ $\left.\begin{matrix} \\ \\ \end{matrix}\right\}$ at 1 atmos and $\sim$300°K.

EXPERIMENTAL JUSTIFICATION FOR THE "PER UNIT MASS" DIFFUSION FORMULATION

Figure 12 shows the butane-air data on the same basis as all the other flames, *i.e.*, employing N_E g-atoms of E/g of mixture, as is consistent with Equation (10). In contrast, Figure 13 shows

the same experimental data analyzed in terms of N'_E g-atoms of E/g-mol of mixture, as is consistent with Equation (1).

The much closer correspondence between the Figure 12 representation and the analytic error function curve is in accord with the theoretically predicted advantage of the Equation (10) formulation in the presence of molecular weight gradients. Noting that $N'_E = mN_E$, the reason for the observed change in shape of the curves is obvious from Figure 15. With the ethane-air data the difference between the N_E/N°_E and N_E/N'°_E methods of correlation, though less than for the butane-air, is still quite pronounced. Indeed, it is doubtful that any quantitatively significant D's could have been determined from our experimental approach if the Figure 13 correlation had been generally used.

Application of Results

PREVIOUS APPLICATIONS OF MIXING SIMILARITY

Burke and Schumann,[1] in 1928, were apparently the first to make an implicit use of this principle. They determined an effective diffusion coefficient for a CO-air flame by correlating experimental data with theoretical curves which were derived by considering "the interdiffusion of the two gases to take place as though no flame were present" (followed by a reaction to completion). The strikingly good over-all correlation which they show in their Figure 8, constitutes strong support for the validity of mixing similarity in CO-air flames.

More recently, Wolfhard and Parker[2] spectroscopically determined the distribution of the temperature and the concentrations of OH and O_2 molecules through a portion of a NH_3-O_2 diffusion flame. They then showed that these distributions were mutually consistent with local states of chemical equilibrium. Although no explicit statement is made as to how they defined the complete O, H, N system, it is virtually certain that they used a fixed ratio, $N_H/N_N = 3$, so that equilibrium data on NH_3-O_2 systems could be employed, allowing the N_O/N_H ratio to vary across the flame as they indicate. Therefore, in principle, the consistency of their results as so interpreted constitutes a verification of the correctness of the $N_H/N_N = 3$ ratio and consequently of mixing similarity; or, inversely, mixing similarity is a condition for the success of the interpretation procedure which they applied to their results. Quantitatively, this argument is not strongly conclusive since the equilibrium, $2H_2O + O_2 \rightleftharpoons 4OH$, is not strongly pressure sensitive. In other words, if the partial pressure of N_2 deviated somewhat from that indicated by similarity, the resulting effect on the partial pressure of OH might be commensurate with the uncertainty of measurement.

Although Spalding[12] introduced a condition which is similar to our mixing similarity in his analytical treatment of burning from a liquid surface, his final experimental results are not sufficiently dependent on this single factor to be easily interpretable in terms of mixing similarity.

A BASIS FOR THE DETAILED STRUCTURE OF LAMINAR DIFFUSION FLAME ZONES

Let us accept the principle of mixing similarity as a working hypothesis and investigate some of its consequences.

First, a suitable composition variable must be defined. The equivalence ratio, r, is awkward because of its unsymmetrical representation of the lean and rich composition ranges. Consequently, we will adopt a function, M, defined by

$$M = \frac{r}{1+r} = \frac{2N_C + \frac{1}{2}N_H}{2N_C + \frac{1}{2}N_H + N_O} = \frac{N_f}{N_f + N_{ox}} \tag{37}$$

in which

$N_f = 2N_C + \frac{1}{2}N_H$ = oxygen equivalent of fuel, g-atoms/g of mixture

$N_{ox} = N_O$ = g-atoms of oxygen/g of mixture

In general, $0 < M < \frac{1}{2}$ for lean, and $\frac{1}{2} < M < 1$ for rich mixtures. At the stoichiometric, $N_f = N_{ox}$ and $M = \frac{1}{2}$. In a pure hydrocarbon fuel, $M_f = 1$; but if the fuel is, say, CH_3OH, then

$$M_f = \frac{2(1) + \frac{1}{2}(4)}{2(1) + \frac{1}{2}(4) + 1} = 0.80.$$

Similarly, if the oxidant is H- and C-free (say, air of O_2), $M_{ox} = 0$, but if it is vitiated air, then $M_{ox} > 0$.

For the case of pure hydrocarbon combustion, Equation (37) can be put into a very convenient form by normalizing each variable by its value, N°_f or N°_{ox}, in the pure hydrocarbon and oxidant (H- and C-free) streams, respectively. Then, from the stoichiometric equation

$$C_{\nu(C)}H_{\nu(H)} + (2\nu_C + \tfrac{1}{2}\nu_H)(O) \rightarrow \nu_C(CO_2) + \tfrac{1}{2}\nu_H(H_2O)$$

we observe that since $N^\circ_{ox} = \nu_O/m_{ox}$ and $N^\circ_f =$

$(2\nu_C + \frac{1}{2}\nu_H)/m_f$, it follows that;

$$\frac{N^\circ_{ox}}{N^\circ_f}\left[\frac{\nu_O/m_{ox}}{(2\nu_C + \frac{1}{2}\nu_H)/m_f}\right] = \frac{m_f}{m_{ox}} F_s = f_s = \frac{12.01 + 1.008(\nu_H/\nu_C)}{[16.00 + A_{In}(\nu_{In}/\nu_O)][2 + \frac{1}{2}(\nu_H/\nu_C)]} \tag{38}$$

in which ν_O is the g-atoms of O per g-mol of the oxidant (C- and H-free) which has a mean molecular weight, $m_{ox} = (16.00\ \nu_O + A_{In}\nu_{In})$. ν_{In} is the g-atoms of nonparticipating (or inert) elements per g-mol of mixture, and A_{In} is their average atomic weight. F_s is the g-mol ratio and f_s *is the weight ratio of fuel to oxidant* (C- *and* H-*free*) *for a stoichiometric mixture.* The formulation at the far right conveniently expresses f_s as a function *only* of the system's H-to-C ratio

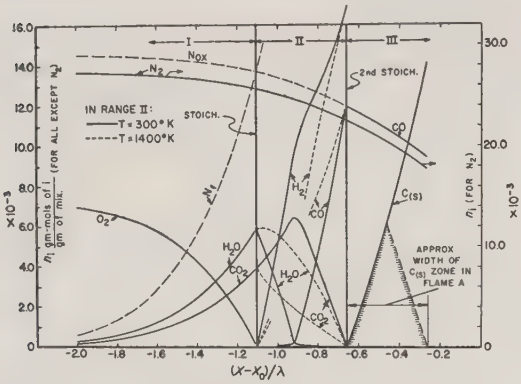

FIG. 16. Idealized equilibrium composition distribution through an ethane-air flame zone (on a room temperature basis, except as noted).

(ν_H/ν_C), and inert-to-O ratio (ν_{In}/ν_O), and the respective atomic weights. Equation (37) now becomes:

$$M = \frac{\left(\frac{N_f}{N^\circ_f}\right)}{\left(\frac{N_f}{N^\circ_f}\right) + f_s\left(\frac{N_{ox}}{N^\circ_{ox}}\right)} \tag{39}$$

	In Pure Hydrocarbon Fuel	In H- and C-Free Oxidant	In Oxidant Containing H and C in Same Ratio as in Fuel
N_f/N°_f	1	0	>0
N_{ox}/N°_{ox}	0	1	<1
M	1	0	$M_{ox} > 0$

The last column takes into account either a homogeneous premixing with some fuel or vitiation with combustion products; the N_f and N_{ox} in this oxidant must be evaluated accordingly, N°_{ox} still being defined on the H- and C-free (or original oxidant) basis. In any of the above cases, f_s remains fixed as defined by Equation (38).

Now it is apparent that by invoking mixing similarity, N_f/N°_f and N_{ox}/N°_{ox} can be expressed in terms of the Fick's law solution, which is appropriate to the geometry of interest. In the case of a flat, laminar, hydrocarbon-oxidant (C- and H-free) flame, considering Equation (24) to be applicable, there results:

$$N_f/N^\circ_f = \tfrac{1}{2}\left[1 + \operatorname{erf}\left(\frac{x - x_0}{\lambda}\right)\right] \quad \text{and} \quad N_{ox}/N^\circ_{ox} = \tfrac{1}{2}\left[1 - \operatorname{erf}\left(\frac{x - x_0}{\lambda}\right)\right] \tag{40}$$

The signs on the error functions locate the oxidant to the left side of x_0 and the fuel to the right, an orientation which is opposite to that of our experimental data, but which is later convenient.

At $x - x_0 = -\infty$, $N_f/N^\circ_f = 0$ and $N_{ox}/N^\circ_{ox} = 1$; at $x - x_0 = +\infty$, $N_f/N^\circ_f = 1$ and $N_{ox}/N^\circ_{ox} = 0$. After substituting Equation (40) into Equation (39) and simplifying, there results

$$M = \frac{1 + \operatorname{erf}\left(\frac{x - x_0}{\lambda}\right)}{(1 + f_s) + (1 - f_s)\operatorname{erf}\left(\frac{x - x_0}{\lambda}\right)} \tag{41}$$

or by rearrangement,

$$\frac{x - x_0}{\lambda} = -\operatorname{erf}^{-1}\left[\frac{1 - M(1 + f_s)}{1 - M(1 - f_s)}\right] \tag{42}$$

Now inasmuch as the atomic distributions are everywhere determined, we can derive a great deal of information on the chemical distributions in the flame even in the absence of information on the temperature distribution, *i.e.*, by considering the reactions in each local zone to be complete at room temperature. We thereby obtain a simplified, *i.e.*, no-dissociation, description of the chemical distribution toward which chemical reactions strive to bring the system—a distribution which may actually be approached if the kinetic circumstances are favorable, as Wolfhard and Parker have shown in the case of a NH_3-O_2 flame.

Three separate and distinct composition ranges are needed to describe all mixture proportions. These are labeled with Roman numerals in Figure 16.

$M = \frac{1}{2}$ identifies the stoichiometric composi-

tion, corresponding to a maximum in CO_2 and H_2O and the disappearance of O_2 in region I, and the appearance of CO and H_2 in region II. $M = M'_s$ identifies the "second stoichiometric" composition which is associated with the lower oxidation state of carbon, *i.e.*, in accord with the equation:

$$C_{\nu(C)}H_{\nu(H)} + \nu_C(O) \rightarrow \nu_C(CO) + \tfrac{1}{2}\nu_H(H_2)$$

For this condition, $N_O = N_C$, and since the O requirements are reduced by the factor $\nu_C/(2\nu_C + \frac{1}{2}\nu_H)$ relative to the stoichiometric, we obtain f'_s, second stoichiometric fuel/air weight ratio.

$$f'_s = [2 + \tfrac{1}{2}(\nu_H/\nu_C)]f_s \tag{43}$$

From Equation (37),

$$M'_s = \frac{2N_C + \frac{1}{2}N_H}{3N_C + \frac{1}{2}N_H} = \frac{2 + \frac{1}{2}(\nu_H/\nu_C)}{3 + \frac{1}{2}(\nu_H/\nu_C)} = \frac{f'_s/f_s}{1 + f'_s/f_s} \tag{44}$$

in which (ν_H/ν_C) is the H-to-C atom ratio of the fuel. $M = M'_s$ identifies the maximum of CO and the disappearance of CO_2 and H_2O in range II and the appearance of $C_{(s)}$ in range III. Thermodynamically speaking, solid carbon exists even to the pure fuel, $M = 1$, composition. The absence of solid carbon in pure hydrocarbons, *e.g.*, C_2H_6, merely reflects the fact that, these substances are reasonably stable at ordinary T's and p's, although they are not in chemical equilibrium. The greater tendency of unsaturated hydrocarbons toward solid carbon formation in diffusion flames is consistent with their markedly greater excess free energy. CH_4 is the most stable pure hydrocarbon.

The reduced distance coordinates of the two stoichiometric compositions are conveniently given by substituting $M = \frac{1}{2}$ and Equation (44), respectively, into Equation (42).

$$\frac{x_s - x_0}{\lambda} = \text{erf}^{-1}\left[\frac{1 - f_s}{1 + f_s}\right] \tag{45}$$

(for the stoichiometric at $M = \frac{1}{2}$)

$$\frac{x'_s - x_0}{\lambda} = \text{erf}^{-1}\left[\frac{1 - f'_s}{1 + f'_s}\right] \tag{46}$$

(for the "second stoichiometric" at $M = M'_s$)

The chemical compositions in Figure 16 were computed from the concentrations of the elements at each value of M, and then were plotted against $(x - x_0)/\lambda$ with the aid of Equation (42). In range II the water-gas equilibrium, $CO_2 + H_2 \rightleftarrows CO + H_2O$, at 298°K was used to calculate the solid-line curves. At flame temperatures, a marked rightward shift of the equilibrium alters the distributions; the dotted-line curves pertain to a representative temperature of 1400°K. An investigation of the thermodynamic criteria on the presence of solid carbon has shown that both the amount and the exact M'_s composition are virtually independent of T and p, at least in the range $M'_s < M < 0.85$. Therefore the $n_{C(s)}$ curve of Figure 16 is closely representative of the *maximum* amounts of solid carbon which can be formed within a diffusion flame burning zone, and the $M = M'_s$ composition effectively defines the thermodynamic boundary of the solid carbon zone for all T and p.

It is now possible to draw a number of deductions from Figure 16, bearing in mind that we are dealing with a simplified and limiting case distribution.

(a) Since the relations between the room temperature n_i's and M are independent of the geometry, *the ordinate values of the n_i's for any particular M are equally valid for any surface characterized by that M, regardless of its geometry.* The spatial distribution of these n_i's, being determined by the spatial distribution of M, varies from case to case. In the particular case of a flat flame as represented in Figure 16, every value of $(x - x_0)/\lambda$ identifies a parabolic-shaped constant M surface having the equation (in the x, y plane),

$$(x - x_0)^2 = [\text{erf}^{-1}(M, f_s)]^2 k(D/u)_0 y \tag{47}$$

in which $[\text{erf}^{-1}(M, f_s)]$ is given explicitly by the right-hand member of Equation (41). Figure 16 therefore conveniently embodies all portions of an entire flat flame.

(b) If we limit our analysis to the principal constituents that are dealt with in Figure 16 it is seen that, in order for localized chemical equilibrium to be achieved, all reactions must be instantaneous and confined to the $M = \frac{1}{2}$ and $M = M'_s$ surfaces. Therefore, except for the fact that we have two such reaction surfaces for hydrocarbon flames, *the picture is virtually identical with Burke and Schumann's.*

(c) Reactions in a volume space—rather than in surfaces as above—are consistent with localized chemical equilibrium, but actually occur only as a result of dissociation phenomena which were excluded from consideration in paragraph (b) above. In fact, if local equilibrium prevails in

a flame zone and the gases are reversibly cooled to room temperature while holding the M distribution fixed, the resulting chemical distribution is that shown by Figure 16. Therefore, we conclude that *there is no basic conflict between the concept of Burke and Schumann, as portrayed in Figure* 16, *and that of Wolfhard and Parker. The consideration of dissociation phenomena in a volume space is equivalent to adding another degree of refinement and descriptiveness to a more elementary, but still basically sound, conceptual picture.* This conclusion reestablishes not only the conceptual validity of the Burke and Schumann formulation in the limiting case of infinite reaction rates, but also the finite reaction-rate treatments of Zeldovitch[8] and Powell.[9] All these treatments, however, are still

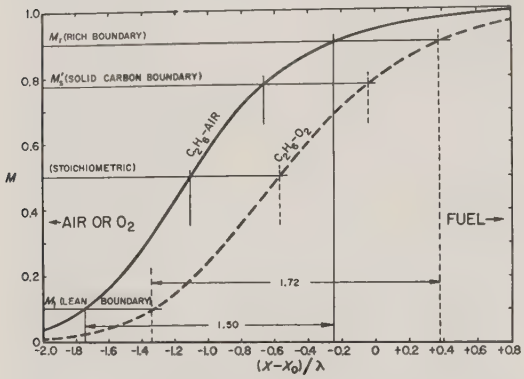

FIG. 17. Composition parameter, M, vs reduced distance for ethane-air and ethane-O_2 flames [equation (41) with the stoichiometric fuel/air weight ratios, $f_s = 0.0621$ and $f_s = 0.2685$, respectively].

subject to an additional complication (for hydrocarbon flames) as discussed in the following paragraph.

(d) Even on the basis of the simplified representation of an infinite reaction-rate flame zone as portrayed by Figure 16, the flame zone would still appear to have a finite thickness because the two reaction planes are necessarily separated by a finite distance; a NH_3-O_2 flame, on the other hand, has only a single "reaction surface." To the eye, the flame zone is usually characterized by the radiation of luminescent solid carbon and the chemiluminescent radiation of various electronically excited species which are produced in the reaction. The latter species tend to diffuse away from their zones of origin and, depending on their mean lifetimes in a given local environment, give a false visual impression of the regions of chemical activity. *We therefore conclude that there is no direct connection between the thickness of a visible flame zone and the velocity of the reactions within it.*

A "thickness" is nevertheless a quantity of interest. Therefore, let the lean and rich "boundaries" of the flame be defined by the particular values, $M_l = 0.10$ and $M_r = 0.90$, respectively, as are shown on the Figure 17 plot of Equation (41). Since $(x_l - x_r)/\lambda = -1.50$ is fixed, we obtain an exact relation, $(x_l - x_r) \sim 1/\sqrt{p}$, at constant u_o and y—in agreement with approximate observations on the visible thickness. Furthermore, on the same basis Figure 17 shows that a C_2H_6-O_2 flame is thicker than a C_2H_6-air flame under the same conditions—in agreement with experimental observations which are difficult to explain on a reaction-rate basis.

(e) The carbon zone at $y = 2.85$ cm in flame A (at 1 atmos) was observed to be approximately 2.0 to 2.5 mm thick. Therefore, relative to the air-side boundary of the carbon zone at $(x_s' - x_0)/\lambda = -0.660$, with $\lambda \simeq 0.6$ cm we obtain an observed reduced thickness $\Delta(x - x_0)/\lambda \simeq 0.4$, as shown in Figure 16. Now, assuming the maximum carbon concentration to be in the center of the carbon zone and, in addition, assuming that this amount corresponds to the thermodynamic, *i.e.*, maximum possible, concentration as given by the $n_{C(s)}$ curve, we find that a maximum of only ~22 per cent of the total carbon present in this zone can be in the form of solid phase carbon. Therefore, even if the effective diffusivity of the carbon particles were zero in the local carbon zone of this most luminous of all the flames which we studied, the mean diffusivity of carbon, as an element, decreases by only a corresponding 22 per cent. More realistically, we note that it is the group $(D\nu)_{C,C(s)}$ which contributes to the diffusion of carbon as an element. And because $\nu_{C,C(s)}$ is necessarily large for particles, there is a compensation effect for small values of $D_{C,C(s)}$. Undoubtedly, such considerations, together with the weak effects of local variations in D on the over-all distribution of an element, account in part for the high degree of similarity which we found for the H and C distributions.

LIMITATIONS ON VALIDITY OF MIXING SIMILARITY

Despite the fact that the presence of a solid carbon phase did not markedly disturb the similarity of the H and C distributions under our experimental conditions, and despite the semi-

theoretical deductions which support these observations, *it is nevertheless obvious that mixing similarity does not hold when free soot escapes from a flame.* It would appear from the foregoing considerations that residence time at a particular T and p, and the agglomeration rate of the particles, have a bearing on the formation and escape of free soot. Fortunately, there are wide ranges of conditions of scientific and applied interest for which free soot formation does not occur, and for which mixing similarity may be considered applicable to the degree which has been experimentally demonstrated.

It might also be expected that marked deviations from similarity occur at the other extreme when a majority of the element H is carried by the rapidly diffusing H_2. In this connection, the remarkably close verification of chemical equilibrium which Wolfhard and Parker observed in a NH_3-O_2 flame supports the thesis that similarity may be applicable in such systems even with the large amounts of H_2 which their equilibrium composition curves show for rich mixtures. In a $(H_2 + N_2)$-air flame, however, Wolfhard[15] reports flame temperatures which are several hundred degrees higher than the maximum theoretical adiabatic flame temperatures of an equivalent pre-mixed system; this he attributes to the greater diffusivity of H_2—indicating a departure from similarity.

Unfortunately, there seems to be no simple and reliable way of theoretically predicting how great the departures from similarity will be in any given system. We note, however, that complexity of chemical composition in a flame tends to enhance similarity as it reduces the opportunity for a single molecular species to dominate the transport of a particular element. Finally, we also point out that exact similarity almost always prevails initially and that it must also prevail in the final homogeneous system; therefore, any trend away from similarity must undergo a reversal at some stage in order to approach the necessary final state.

MIXING SIMILARITY AS A BASIS FOR THE GROSS STRUCTURE OF LAMINAR DIFFUSION FLAMES

As a result of similarity in the distribution of the respective fuel and oxidant elements, the mixing in any inhomogeneous fuel-oxidant system becomes, on the atomic level, a problem in binary mixing only. Let the structure of this field be defined by the pattern of constant M surfaces. Equation (37) severally defines M in terms of the equivalence ratio, r, the element concentrations, N_E, and the binary variables N_f and N_{ox}, *all the definitions being independent of chemical, i.e., molecular level considerations.* Each so-defined constant M surface also identifies, on either a "no-reaction" or a "complete-reaction-at-room-temperature" basis, a coincident surface of constant chemical composition. While the reaction velocity in any local volume is determined by the usual kinetic variables, reactant concentrations, chain carriers, collision rates, etc., these variables must be consistent with and subject to the independent process of atomic diffusion, as conveniently described in terms of the binary variables, N_f and N_{ox}, and the constant M surfaces. *Chemical reactions influence the geometry of the constant M surfaces only in a rather indirect way, namely, via the macroscopic effects of heat release on fluid dynamic factors, e.g., turbulence, and the dependence of D on the state variables, temperature and composition.* In laminar diffusion flames these latter influences modify, but do not basically change, the structure of the field in relation to that of the isothermal, no-combustion case.

Inasmuch as the particular $M = \frac{1}{2}$ surface is coincident with Burke and Schumann's "flame surface," if the latter formulation is divorced from the logic of its derivation it may be regarded, in effect, as a particular application of mixing similarity for predicting the geometry of the stoichiometric surface. The only formal differences are that mixing similarity deals with more physically significant variables and is on a basis which is consistent with heat and momentum transfer. However, from the standpoint of the underlying logic, an important difference is that the structure of the flame, as defined by the geometry of the constant M surfaces, is independent of reaction rates, except indirectly as noted above. The fast reaction-rate limitation which is implicit in the Burke and Schumann approach arises only as a consequence of their analytical model which was based upon considerations of *molecular* instead of *atomic* distributions. While conceptually sound, and appropriate to an elementary treatment of fast reactions, this limitation is irrelevant and unnecessary for structural considerations. Indeed, atoms may be regarded as exhibiting a "random walk" behavior which is statistically independent of the nature of the molecules in which they are combined. This explains why Jost's application of the Einstein diffusion equation is in basic agree-

ment with experiment in spite of its neglect of chemical considerations. Mixing similarity therefore provides a common physical basis for both the Burke and Schumann formulation and the Jost formulation.

Mixing similarity, in addition to retaining the considerable experimental support which the Burke and Schumann formulation has received since 1928, provides a more general basis for analytical descriptions of diffusion flame structure. By replacing the single Burke and Schumann "flame surface" with a family of constant M surfaces that are distributed in depth, it is possible to define the structure of the more diffuse flames which are encountered at low pressures or when burning with O_2. The same approach which we have illustrated for the flat flame case obviously can be applied to other geometries with only appropriate changes in the mathematical procedures.

Because of its importance in laboratory investigations, the cylindrical geometry deserves special comment. For a steady-state system with a basically one-dimensional (vertical) flow field, and neglecting the derivatives of D, the cylindrical coordinate form of Equation (16) is:

$$\frac{\partial N_E}{\partial y} = \frac{D}{u}\left[\frac{\partial^2 N_E}{\partial r^2} + \frac{1}{r}\frac{\partial N_E}{\partial r} + \frac{\partial^2 N_E}{\partial y^2}\right] \quad (48)$$

If the boundary conditions and the mass flows of the fuel and oxidant streams are held constant, *i.e.*, (D/u) is constant, then only a fixed N_E distribution for each E is possible by Equation (48). Consequently, not only the "flame height" but the entire geometry of the flame as determined by the constant M surfaces is independent of pressure (except when pressure-dependent fluid dynamic effects, or free soot formation, disrupt the picture). This generalization is strongly supported by the work of Barr.[6] On the other hand, if u is held constant while the pressure is varied, then the axial height of the constant M surfaces vary directly with the pressure *so long as the y-axis diffusion is negligible in comparison to the radial component*—in accord with Burke and Schumann's solution for the $M = \frac{1}{2}$ surface for this condition. However, as the pressure is decreased, the decreasing slopes of the constant M surfaces give an increasing weight to the $\partial^2 N_E/\partial y^2$ term in Equation (48); the flame zone thereby becomes not only thickened because of the increase in D, but flattened because of y-axis diffusion.

We venture the foregoing as an explanation for the marked changes in geometry with pressure which Gaydon and Wolfhard[16] show in Figure 6.2 (Ch. VI) of their book. Although they do not state whether the sketches pertain to constant u or constant ρu conditions, it is nevertheless apparent that in the two lower pressure flames the y-axis gradients are commensurate with the radial gradients. We therefore feel that these flame geometries probably can be explained entirely from diffusional considerations by invoking the mixing similarity principle.

Summary[c]

We have endeavored to demonstrate theoretically and experimentally that, in the inhomogeneous combustion of hydrocarbon-air systems, a high degree of similarity prevails in the distribution of the initial fuel (H and C) and oxidant (O and N) elements, respectively—subject to the limitation that free soot does not escape from the flame. The same data were used to establish the effective mean diffusion coefficient of the elements in ethane-air flames, (D_1 cm²/sec = 0.23 ± 10 per cent) and butane-air flames (D_1 cm²/sec = 0.18 ± 10 per cent). There is good reason to believe that this same range of values holds for the inhomogeneous combustion (with air) of any hydrocarbon, regardless of its molecular weight.

The data were treated in terms of analytical expressions which, theoretically, are valid in the presence of gradients and variations in the mean molecular weight of the gases. The butane-air flame analysis strongly supports this theoretical prediction.

On the basis of mixing similarity, a picture was developed which is in accord with a wide variety of observations on both the gross and detailed structure of laminar diffusion flames, and which provides a common physical basis for the work of Burke and Schumann, of Jost, and of Wolfhard and Parker.

Mixing similarity clearly delineates the domains of diffusional, chemical kinetic, thermo-

[c] Supplementary information (Tables similar to 1A and 2A, appendix, for all flames) has been deposited as Document Number 4981 with the ADI Auxiliary Publications Project, Photoduplication Service, Library of Congress, Washington 25, D. C. A copy may be secured by citing the Document number and by remitting $2.50 for photoprints or $1.75 for 35-mm microfilm. Advance payment is required. Make checks or money orders payable to: Chief, Photoduplication Service, Library of Congress.

dynamic and fluid dynamic phenomena. Although, for reasons of mathematical simplicity and illustrative clarity, we have dealt entirely with laminar diffusion flames, the general physicochemical principles are applicable to any flow regime.

Acknowledgments

The authors wish to gratefully acknowledge the considerable skill and unfailing ingenuity which Mr. Maynard Cook has brought to bear on the experimental phase of our work. We also wish to thank Mrs. Shirley Feltman for her invaluable aid in carrying out the many laborious calculations which were involved in preparing this paper.

We would also like to note that the interest and attention to detail with which the firm of F. C. Broeman Co., Chemists, handled our sample analyses was an important factor in establishing the feasibility of our over-all experimental approach.

APPENDIX

Table 1A. Sample Analyses for Flame F (in Mol Per Cent)

Sample No.	CO_2	Ill*	O_2	H_2	CO	C_2H_6	CH_4	N_2	H_2O
49	3.9	0.0	10.1	0.2	0.1	0.1	0.2	74.2	11.2
50	7.4	0.1	1.7	0.0	0.8	0.3	0.5	71.1	18.1
51	7.8	0.5	0.0	2.3	3.2	0.0	0.6	69.0	16.6
52	7.5	3.4	0.0	1.9	4.8	0.0	4.9	61.2	16.3
53	5.9	5.1	0.0	0.6	1.2	8.4	10.1	55.0	13.7
54	4.7	5.2	0.0	2.8	4.3	24.5	4.0	44.4	10.1
55	4.5	5.5	0.0	1.3	2.8	21.7	10.0	44.5	9.7
56	7.7	0.4	0.0	1.6	3.4	0.2	1.3	68.1	17.3
57	6.6	0.0	4.3	0.2	0.4	0.8	0.0	72.1	15.6
58	6.2	4.9	0.0	1.5	3.9	3.3	7.2	58.5	14.5
60	0.1	0.0	19.9	0.0	0.0	0.5	0.0	79.0	0.5
61	2.6	0.0	14.0	0.1	0.0	0.3	0.0	75.4	7.6
62	0.0	2.6	0.0	0.1	0.0	97.2	0.0	0.0	0.1
63	0.0	2.4	0.0	0.2	0.1	97.1	0.0	0.0	0.2
64	0.2	3.6	0.0	0.3	0.1	93.3	2.0	0.0	0.3
65	0.4	2.8	0.0	0.8	0.7	85.8	3.1	5.1	1.3
66	1.4	3.6	0.0	1.6	1.0	66.5	4.0	18.2	3.7
67	3.3	4.6	0.0	1.2	3.4	44.4	4.5	31.7	6.9
186	6.6	3.8	0.0	4.2	3.5	2.3	3.9	60.3	15.4
187	2.3	3.7	0.0	1.0	0.3	50.2	10.5	26.6	5.4
188	0.9	2.7	0.0	0.2	0.0	77.8	4.9	11.1	2.4

* Illuminants taken as C_2H_4.

TABLE 2A. N_E/N_E° AND BURNER POSITIONS FOR FLAME F

Sample No.	x_{cm}	N_C/N_C°	N_H/N_H°	N_O/N_O°	N_N/N_N°	m
49	1.86	0.024	0.043	0.972	0.975	27.84
50	1.45	0.053	0.074	0.933	0.950	27.39
51	1.27	0.070	0.078	0.905	0.938	26.92
52	0.94	0.136	0.132	0.937	0.844	26.50
53	0.78	0.252	0.265	0.696	0.762	26.39
54	0.53	0.402	0.388	0.606	0.600	27.05
55	0.54	0.403	0.402	0.555	0.610	26.67
56	1.37	0.076	0.084	0.922	0.925	26.94
57	1.64	0.047	0.054	0.941	0.954	27.64
58	0.83	0.192	0.183	0.805	0.812	26.36
60	2.83	0.006	0.007	0.968	1.004	28.77
61	2.06	0.017	0.031	0.995	0.978	28.20
62	−1.32	1.001	0.993	0.002	0.000	29.98
63	−0.83	1.000	0.992	0.007	0.000	29.94
64	−0.44	0.997	0.988	0.020	0.000	29.56
65	−0.26	0.936	0.933	0.066	0.063	29.13
66	0.00	0.781	0.775	0.197	0.235	28.34
67	0.30	0.588	0.573	0.416	0.415	27.91
186	1.00	0.151	0.162	0.849	0.849	26.01
187	0.18	0.664	0.679	0.259	0.356	27.35
188	−0.10	0.868	0.871	0.100	0.140	28.88

TABLE 3A. EXPERIMENTAL x_o'S, λ'S AND D'S

$D_1 = D$ corrected to 1 atmos and 300°K, see Equations (32) and (33). All theoretical curves in Figures 4 through 12 are from the average x_o's and "theoretical" λ's listed below.

Flame	A	B	C	D	E	F	G	H	I
u_0 (cm/sec)	9.3	9.3	9.3	18.6	18.6	18.6	18.6	37.2	18.6
p (atmos)	0.987	0.75	0.50	0.50	0.30	0.20	0.15	0.15	0.15
x_0 cm									
C	1.20	1.31	1.50	0.38	0.40	0.42	0.47	−0.03	1.49
H	1.22	1.32	1.51	0.38	0.41	0.42	0.47	−0.04	1.48
O	1.23	1.32	1.51	0.39	0.46	0.46	0.54	0.01	1.52
N	1.20	1.32	1.50	0.38	0.38	0.40	0.44	−0.05	1.49
Av.	+1.21	+1.32	+1.51	+0.38	+0.41	+0.43	+0.48	−0.03	1.49
λ cm									
C	0.564	0.532	0.650	0.538	0.707	0.807	0.938	0.779	0.796
H	0.592	0.566	0.674	0.585	0.724	0.831	0.931	0.786	0.805
O	0.639	0.590	0.669	0.500	0.671	0.788	0.966	0.794	0.788
N	0.509	0.510	0.626	0.553	0.723	0.812	0.922	0.763	0.775
C + H	0.580	0.553	0.662	0.561	0.715	0.819	0.935	0.782	0.800
O + N	0.566	0.552	0.643	0.514	0.697	0.799	0.943	0.778	0.782
Theor.	0.557	0.568	0.684	0.520	0.670	0.821	0.946	0.679	0.790
k (dimensionless)	1.107	0.875	0.846	0.979	0.976	0.975	0.971	1.001	0.849
D_1 (cm²/sec)									
C	0.213	0.198	0.203	0.241	0.251	0.218	0.222	0.297	0.183
H	0.258	0.224	0.219	0.285	0.262	0.231	0.219	0.302	0.187
O	0.297	0.244	0.215	0.204	0.225	0.207	0.235	0.308	0.179
N	0.189	0.182	0.189	0.237	0.262	0.220	0.214	0.284	0.173
C + H	0.245	0.214	0.211	0.262	0.256	0.224	0.220	0.299	0.184
O + N	0.233	0.213	0.201	0.220	0.243	0.214	0.224	0.296	0.176
Av.				0.226					0.180

Nomenclature

Symbol	*Units*	*Meaning*
A_E	grams/g-atom	atomic weight of element E
c, c_i	g-mols/cm³	g-mol concentration per unit volume; all species, or species i, respectively.
D, D_o, D_1	cm²/sec	diffusion coefficient; general, at initial conditions, or at 1 atmos and 300°K, respectively
E	—	chemical element, C, H, etc.
f_s, f_s'	dimensionless	fuel/oxidant weight ratio; at the stoichiometric, and "second stoichiometric," respectively, see Equations (38) and (43)
i	—	chemical species, H_2O, CO etc.
j_i, j_i'	g-mols/(cm² × sec)	diffusive current of species i across a plane of zero net mass, or mol flow, respectively
k	dimensionless	"hydrodynamic" and initial temperature correction factor, see Equation (33)
M, M_s, M_s'	dimensionless	mixture proportion variable; $M_s = \frac{1}{2}$, at the stoichiometric; M_s' at the "second stoichiometric." See Equations (37), (39) and (44)

Nomenclature (*continued*)

m, m_i	grams/g-mol	molecular weight of mixture, or of i species, respectively
N_E , N_E°	g-atoms/gram	atom concentration of E per g of mixture; general, or per g of initial fuel or oxidant, respectively
N_f , N_{ox} N_f° , N_{ox}°	g-atoms/gram	equivalent oxygen atom concentrations; of fuel, or oxidant, atoms in a mixture. Superscript (°) denotes pure hydrocarbon or oxidant.
n_i	g-mols/gram	mol concentration of i per g of mixture
p	atmos	absolute pressure
r	dimensionless	equivalence ratio
r	cm	radius
T	°K	temperature
t	sec	time
u, u_0	cm/sec	gas velocity; general, and initial, respectively
x, x_0	cm	horizontal distance; general, and horizontal displacement of mixing mid-plane, respectively
y, z	cm	distance, vertical, and depth dimensions
α_i	dimensionless	mol fraction of i
δ, $\bar{\delta}$	dimensionless	difference, and average difference, respectively of N_E/N_E° for two E elements
$\nu_{E,i}$	dimensionless	g-atoms of E per g-mol of i
ρ	grams/cm^3	density
θ	degrees	mean angular displacement of mixing mid-plane
λ	cm	diffusive mixing constant for flat flame, see Equation (25)

REFERENCES

1. Burke, S. P., and Schumann, T. E. W.: Ind. Eng. Chem., *20*, 998 (1928).
2. Wolfhard, H. G., and Parker, W. G.: Proc. Phys. Soc. A, *65*, 2 (1952).
3. Jost, W.: *Explosion and Combustion Processes in Gases*, p. 212. New York, McGraw-Hill, 1946.
4. Wohl, K., Gazley, C., and Kapp, N.: *Third Symposium on Combustion, Flame and Explosion Phenomena*, p. 288. Baltimore, The Williams & Wilkins Co., 1949.
5. Hottel, H. C., and Hawthorne, W. R.: *Third Symposium on Combustion, Flame and Explosion Phenomena*, p. 254. Baltimore, The Williams & Wilkins Co., 1949.
6. Barr, J.: Fuel, *XXVIII-9*, 200 (1949).
7. Powell, H. N., and Browne, W. G.: *Sixth Symposium (International) on Combustion*, p. 918. New York, Reinhold Publ. Corp., 1957.
8. Zeldovitch, Y. B.: NACA TM1296 (1951).
9. Powell, H. N.: *Fifth Symposium (International) on Combustion*, p. 290. New York, Reinhold Publ. Corp., 1955.
10. Wohl, K., and Shipman, C. W.: *Combustion Processes*, Section I. Princeton, N. J., Princeton Univ. Press, 1956.
11. Barr, J.: AGARD Memorandum AG11/M7 (1954).
12. Spalding, D. B.: *Fourth Symposium (International) on Combustion*, p. 847. Baltimore, The Williams & Wilkins Co., 1953.
13. Anderson, J. W., and Friedman, R.: Rev. Sci. Instr. *20*, 61 (1949).
14. Berkson, J.: J. Am. Stat. Assoc., *50*, No. 270, 529 (1955).
15. Wolfhard, H. G.: *Selected Combustion Problems*, p. 519. London, Butterworth, 1954.
16. Gaydon, A. G., and Wolfhard, H. G.: *Flames; Their Structure, Radiation and Temperature*, Ch. 6. London, Chapman & Hall, 1953.

6

CHAIN BRANCHING AND FLAME PROPAGATION

By A. VAN TIGGELEN AND J. DECKERS

1. Introduction

The primary purpose of this paper is to establish certain basic principles governing the reaction kinetics in stationary premixed flames. It is not our intention to make a comparative study of the theories which have been elaborated on a more rigorous mathematical base and which lead to complex equations that are applicable only to a few unusually simple cases. It is precisely the complexity of the usual cases which led us to a completely different point of view. Instead of using continuity equations whose solution is very intricate, but which are strictly valid at every location in the flame, we have considered the individual molecule, radical or free atom in the flame reaction zone. Accordingly, it was necessary to describe for each species some kind of "mean molecule" whose behavior is the "most probable." It is then sufficient if our deductions are not in conflict with the general laws of thermodynamics; the good agreement with experimental data in all possible cases and the practical utility of the derived relations are the best justification of our point of view.

2. Flames and the Theory of Collisions

The approach outlined above requires the interpretation of flame reaction kinetics on the basis of the collision theory. As the flame front corresponds to a continuous transition zone from the state of unburned gases to that of burned products, the characteristic parameters of the temperature of the flammable mixture (density, composition, refractive index, etc.) vary from the initial to the final values. The difficulties lie precisely in deriving equations which represent the variation of all these parameters across the flame front. To avoid these difficulties it is useful to introduce certain mean values that make it possible to treat the flame front as a homogeneous region of constant temperature, T. We have already proposed[1] the following relation for T:

$$T = T_0 + 0.74\ (T_f - T_0)$$

where T_0 and T_f are, respectively, the initial and the final flame temperatures. If V_0 and x_0 are, respectively, the burning velocity and the flame front thickness, the mean time spent by each molecule in the flame is given by:

$$t = \frac{x_0}{V} = \frac{x_0 T_0}{V_0 T}\ .$$

The ratio T_0/T is introduced because V_0 refers to the cold unburned gases, whereas the temperature reaches the mean value T in the flame front.

During the time, t, each molecule undergoes Z_t collisions given by the simple relation:

$$Z_t = \frac{ct}{\lambda} = \frac{x_0 T_0 c}{V_0 T \lambda}$$

where c and λ are the molecular mean velocity and the mean free path. We can replace c by its value $(2\sqrt{2RT}/\sqrt{\pi M})$ and λ by $(\lambda_0 T P_0/P T_0)$ where P is the actual pressure and P_0 the standard atmospheric pressure (760 mm Hg). For the most common gases, λ_0 (mean free path at standard conditions) is equal to 10^{-5} and M (mean molecular weight) is equal to approximately 30. Accordingly, Z_t becomes

$$Z_t = 2.1\ \frac{x_0}{V_0}\ \frac{P}{P_0 T^{3/2}}\ 10^{13}$$

Values for Z_t and t are given in Table 1 for a few stoichiometric fuel/oxygen flames diluted with nitrogen at atmospheric pressure; it has been shown[2] that x_0 is equal to the distance, s, between the luminous zone and the region revealed by the schlieren method, divided by 4.7.

3. Necessity of Chain Reactions

During its short stay in the flame front each molecule, which according to the stoichiometry of the global flame reaction must be changed into the burned compound, must take part in at least one effective collision in order to evolve into the final product. Two different ways can be considered: (1) a primary reaction analogous to that which occurs in slow combustion; (2) an effective collision with a chain carrier represented by the symbol R without any further specification.

Let us consider the first possibility and let us even suppose that a collision with any molecule is effective provided there is a sufficient activation energy. Now, this necessary activation en-

ergy must be at least equal to the value E_s which has been determined in studies on slow combustion. For example: > 100 kcal for H_2/O_2 ;[7] ~ 85 kcal for CH_4/O_2 ;[8, 9] 50 kcal for NH_3/O_2 ;[10] 35 kcal for C_2H_2/O_2 ;[11] 40 kcal for C_2H_4/O_2 ;[12] ~ 50 kcal for hydrocarbons and C_6H_6/O_2 ;[13] 47 kcal for NH_3/N_2O.[14] The number of effective collisions, granting steric factors equal to unity, is given by

$$Z_{t(\text{eff.})} = Z_t e^{-E_s/RT}$$

In all the cases in Table 1, $Z_{t\,(\text{eff.})}$ is much smaller than one. This proves the impossibility of a pure thermal explosion.

The second possibility, i.e., attack of a molecule by a chain carrier, corresponds to an elementary process with a much smaller activation energy. It would, for example, be the case of a fuel molecule RH colliding with an OH radical: $RH + OH \rightarrow R + H_2O$. All exchange reactions of that type have an activation energy of about 5 to 10 kcal as a mean value for a chain propagation step. The number of effective collisions now becomes

$$Z_{t\cdot\text{eff.}} = f \cdot Z_t e^{-\sim 8.000/RT} \frac{[R]}{p}$$

where f is a steric factor, probably near to unity. The radical concentration $([R]/p)$ needs to be large enough to make this last expression at least equal to one. This shows the possibility of a chain explosion if a sufficient mean radical concentration is maintained in the flame front.

TABLE 1

Stoichiometric Fuel/Oxidant	N_2	$x_s = \frac{s}{4.7}$ 10^3 cm	V_0	Tf°K	T	t 10^6 sec	Zt 10^{-4}
	per cent		*cm/sec*				
H_2/O_2 (3)	50	—	290	2370	1830	—	—
H_2/O_2 (3)	65	—	164	2100	1630	—	—
CH_4/O_2 (3)	65	6.0	66	2370	1830	14.6	2.47
CH_4/O_2	73	11.5	34	2110	1638	60.5	1.08
C_2H_6/O_2 (4)	59	3.0 (5)	140	2560	1971	3.2	0.52
C_2H_6/O_2	75	7.2 (5)	57	2197	1702	21.7	3.82
C_2H_4/O_2 (2)	60	2.5	180	2563	1973	2.1	0.34
C_2H_4/O_2	76	6.3	55	2112	1639	20.5	3.67
C_2H_2/O_2 (2)	71	2.5	165	2446	1886	2.4	0.39
C_2H_2/O_2	81	5.7	63	2040	1586	16.7	3.04
C_3H_8/O_2 (3)	64	4.0	102	2520	1941	5.9	0.97
C_3H_8/O_2	80	11.7	31	2070	1608	68.8	12.44
C_6H_6/O_2 (4)	69	3.9 (5)	107	2423	1869	5.7	0.96
C_6H_6/O_2	79	10.0 (5)	36	2046	1590	51.2	9.31
CO/O_2 (2)	0	6.6	63	2740	2104	14.6	2.31
($H_2 < 0.2\%$)	39	10.8	34	2334	1803	51.6	8.82
CO/O_2 (4)	0	6.0	76	2740	2104	11.0	1.74
1% H_2	39	9.5	40	2334	1803	38.6	6.59
CO/O_2 (2)	0	3.4	139	2740	2104	3.4	0.54
5% H_2	39	6.0	71	2334	1803	13.7	2.35
NH_3/O_2 (4)	0	4.3 (5)	127	2692	2068	4.8	0.77
NH_3/O_2	35	10.1 (5)	48	2416	1864	33.1	5.56
H_2/N_2O (6)	35	3.5	155	2521	1942	3.4	0.56
H_2N_2O	55	9.0	48	2008	1562	35.2	6.45
C_2H_2/N_2O (6)	20	2.6	156	2848	2184	2.2	0.35
C_2H_2/N_2O	50	5.5	71	2455	1893	12.0	2.00
CO/N_2O (6)	0	10.9	34	2650	2037	46.1	7.41
H_2 % < 0.2	40	24.6	16	2268	1755	256.8	44.45
NH_3/N_2O (6)	0	4.7	89	2619	2014	7.7	1.24
NH_3/N_2O	25	8.8	46	2450	1889	29.7	4.95

4. General Mechanism of a Chain Reaction

Let us now consider a typical chain reaction according to a very general scheme. Let us consider a flammable mixture of gas A (oxidant) and

gas B (fuel) that burns according to the stoichiometric equation

$$A + B \rightarrow C + D$$

This reaction follows a very general mechanism that will be illustrated in the special case of CH_4/O_2 :

In general	Example
Primary step (i): not specified → X (radical) or Y (radical)	$CH_4 \rightarrow CH_2 + H_2$ followed by $CH_2 + O_2 \rightarrow CHO + OH$
Propagation steps:	
p: B + Y → X + C	$CH_4 + OH \rightarrow CH_3 + H_2O$
p': A + X → Y + D	$CH_3 + O_2 \rightarrow CH_2O + OH$
Chain termination: (f) not specified	
Chain branching (r) A + X → 2Y + E	$CH_3 + O_2 \rightarrow CH + 2OH$

E_i , E_p , E_p' and E_r are the corresponding activation energies. Bracketed symbols ([A] [B] . . . . .) will be used for partial pressures, [R] represents the sum [X] + [Y], and will be used when the nature of radical is not specified. If τ is the mean duration of one link in the propagating chain (this means the time after which an X radical is reobtained after having been changed into a Y radical by the successive reactions p and p'), we may write that $\tau = \tau_x + \tau_y$, where τ_x and τ_y are the mean lifetimes of radicals X and Y.

Evidently we have

$$\tau_x/\tau_y = [B]e^{-E_p/RT}/[A]e^{-E_{p'}/RT} \qquad (1)$$

We have assumed that all steric factors and collision diameters are equal; eventually a correction could be brought to this last equation. The probability of a radical R really being a radical X is given by τ_x/τ. The probability υ for a radical R to undergo in any collision a branching reaction is now equal to

$$\upsilon = \frac{\tau_x[A]e^{-E_r/RT}}{\tau p} = \frac{[A]e^{-E_r/RT}[B]e^{-E_p/RT}}{p([B]e^{-E_p/RT} + [A]\ e^{-E_{p'}/RT})} \qquad (2)$$

where p is the total pressure. Eventually this last equation could be multiplied by a steric factor. The corresponding probability of a chain termination will be represented by β. Because of the alternation of reactions p and p' we can introduce the concept of a mean molecular weight (M) of the chain carriers in the following way

$$M = (M_x\tau_x + M_y\tau_y)/\tau \qquad (3)$$

Evidently if $\tau_y \gg \tau_x$ (which means that reaction p' is much faster than reaction p, and this would be the case if $E_p \gg E_p'$) M is approximately equal to M_y .

5. Importance of Chain Branching

It was shown above that the reaction of a molecule in the flame front occurs with the highest probability when colliding with a chain carrier, but that a sufficient concentration of chain carriers must be maintained. This is made possible by the countercurrent diffusion of active radicals and many authors have taken this diffusion into account. Two facts, however, have been neglected to date: (1) The continuous alternation of the radicals (from X to Y, etc.) because of the reactions which they undergo during diffusion. (2) The losses of radicals by chain termination reactions and back diffusion. To compensate for the losses, chain branching becomes necessary. It occurs while the chain carriers diffuse ahead of the flame front toward the unburned gases.

The equation of Smoluchowsky gives the total number of collisions Z_t when a particle diffuses over a given linear distance, d:

$$Z_t = \frac{3\pi\ d^2}{4\lambda^2} \qquad (4)$$

In order to compensate all losses each chain carrier has to diffuse over a distance, d, such that branching occurs once. Therefore

$$Z_t(\upsilon - \beta) = 1 = \frac{3\pi\ d^2(\upsilon - \beta)}{4\lambda^2} \qquad (5)$$

This is the simplest relation for the quiescence of premixed flames.

6. Burning Velocity Equation

When a particle diffuses over a distance, d, the time elapsed is given by

$$d^2 = 2Dt$$

The diffusion coefficient being equal to $D = \lambda c/3$, we have $d^2 = 2\lambda ct/3$. Corresponding to a displacement, d, we may derive a mean diffusion velocity for each particle; it varies inversely with the displacement:

$$\frac{d}{t} = \frac{2\lambda c}{3\ d} \qquad (6)$$

If we introduce the value of d as given by Equation (5) into (6) we obtain:

$$\frac{d}{t} = c\sqrt{\frac{\pi}{3}(v - \beta)}$$

The mean projection of this velocity on the normal to the flame front gives the diffusion velocity of chain carriers perpendicular to the flame front. For the steady state the burning velocity, V, is then equal to the last equation multiplied by $2/\pi$, the mean value of the cosine:

$$V = \frac{d2}{t\pi} = \frac{2c}{\sqrt{3\pi}}\sqrt{(v - \beta)}$$

V represents, of course, the burning velocity in gases at a mean temperature, T.

In practice V_0 is measured for the cold gases.

TABLE 2

Fuel	Oxidant O_2	Oxidant N_2O
	kcal	*kcal*
H_2	18	28.5
CO(0.2% H_2)	22	28.5
CO(1% H_2)	18	?
C_2H_2	31	40
CH_4	40	?
C_2H_6	39	?
C_3H_8	39	?
C_2H_4	36	?
C_6H_6	40	?

Because of mass conservation

$$V_0 = VT_0/T = \frac{2cT_0}{T\sqrt{3\pi}}\sqrt{(v - \beta)} \qquad (7)$$

the mean velocity of radicals, c, can be replaced by its value from gas kinetics: $c = \sqrt{8RT/\pi M}$ (M = mean molecular weight of chain carriers).

It follows that

$$V_0 = \frac{4T_0}{\pi}\sqrt{\frac{2R(v - \beta)}{3MT}} \qquad (8)$$

This relation is the basic expression of burning velocity. It explains flammability limits when $v = \beta$; it was proposed for the first time in connection with methane/air flames[15] and generalized in a later publication where it was applied to hydrogen/oxygen flames.[1] Subsequently many different laminar flames have been successfully tested on the basis of this theory.[2] In particular the importance of the activation energy of the branching reaction can be shown.[4, 6, 16, 17]

Combining Equations (8), (1), (2), and (3), a more detailed relation for flame velocity can be written in the following successive equations (β can be neglected for mixture composition which is far enough from flammability limits):

$$V_0 = \frac{4T_0}{\pi}\sqrt{\frac{2R}{3T}}\sqrt{\frac{\tau_x[\mathrm{A}]e^{-E_r/RT}}{p(M_x\tau_x + M_y\tau_y)}}$$

$$V_0 = \frac{4T_0}{\pi}\sqrt{\frac{2R}{3T}}\sqrt{\frac{[\mathrm{A}][\mathrm{B}]e^{-(E_r+E_p)/RT}}{p(M_x[\mathrm{B}]e^{-E_p/RT} + M_y[\mathrm{A}]e^{-E_p/RT})}} \qquad (9)$$

This relation shows that the apparent over-all activation energy, E, of the branching reaction lies between $(E_r + E_p - E_{p'})$ and E_r ; so that $(E_r + E_p - E_{p'}) > E > E_r$. It shows also that the order of the over-all branching reaction with respect to A and B varies between 0 and 1, but that the sum of the orders is equal to unity. Therefore we now may write

$$V_0 = \frac{4T_0}{\pi}\sqrt{\frac{2R}{3MT}}\sqrt{\frac{[\mathrm{A}]^a[\mathrm{B}]^b e^{-E/RT}}{p^{(a+b)}}} \qquad (10)$$

where $(a + b) = 1$ which, in the most common case, is the total over-all order minus unity of the branching reaction. Furthermore, it should be borne in mind that the branching reaction must be of the first order with respect to the radical concentration; the total over-all order is thus equal to $a + b + 1 = 2$.

In some cases, however, the apparent order of the branching reaction may become larger than $(a + b + 1) = 2$; this occurs for example by hydrogen/oxygen flames[4, 6] and by hydrogen containing carbon monoxide flames[17] where we observed that $(a + b + 1) = 3$. The explanation of this must be found in the necessity of two successive collisions in the branching process, for example, $H + O_2 \rightarrow OH + O$ followed by $O + H_2 \rightarrow OH + H$.

Over-all activation energies for the branching reaction have been measured for different flames.[4, 6, 16, 17] They are given in Table 2.

7. Flame Front Thickness and Related Values

Equation (5) in Section 5 gives us the distance, d, through which the chain carriers must diffuse ahead of the flame in order to undergo the branching reaction once. This happens in the reaction zone and we may assume, therefore, that $2\ d/\pi$

is equal to the flame front thickness x_0 :

$$x_0 = \frac{4\lambda}{\pi\sqrt{3\pi}\sqrt{(v-\beta)}} \tag{11}$$

Combining with Equation (8) we obtain

$$V_0 x_0 = \frac{16\lambda T_0}{3\pi^2\sqrt{\pi}}\sqrt{\frac{2R}{MT}}$$

Now at atmospheric pressure and for ordinary gases

$$\lambda = \lambda_0{}^T/T_0 = 10^{-5T}/T_0$$

Replacing in the last equation:

$$V_0 x_0 = \frac{16\sqrt{2R}\cdot 10^{-5}}{3\pi^2\sqrt{\pi}}\sqrt{\frac{T}{M}} = 3.9\sqrt{\frac{T}{M}}\cdot 10^{-2}$$

This may be written:

$$V_0/\sqrt{T} = \frac{3.9\cdot 10^{-2}}{\sqrt{M}}\frac{1}{x_0} \tag{12}$$

If M may be considered constant, this equation represents a straight line giving $V_0/\sqrt{T}$ in function of $1/x_0$. Very different flammable mixtures have been shown[2, 6] to obey remarkably the relation in Equation (12); the slope of a plot of $V_0/\sqrt{T}$ *vs.* $1/x_0$ has exactly the expected value. This seems to be an indication as to the identity of chain carriers in all cases considered here. The most durable radical responsible for chain propagation is probably OH,[4, 6] except near the hydrogen-free, carbon monoxide flame.[2] From the concept of flame front thickness it is easy to derive all related concepts, such as quenching distances and minimum ignition energy. This last quantity, H, could be defined as the energy needed to heat the mean temperature, T, a spherical volume of gas of radius (bx_0), where b is a constant proportionality factor.

Accordingly:

$$H = \frac{4\pi}{3}(bx_0)^3(T - T_0)\rho C_p = \frac{4\pi b^3}{3}x_0^3(T - T_0)\rho C_p$$

where ρ = density and C_p = specific heat at constant pressure. From the relation in Equation (12) between V_0 and x_0 , and from $\rho = \rho_0 T_0/T$, we have

$$H = \left(\frac{3.9\cdot 10^{-2}4\pi b^3 C_p T_0 \rho_0}{3\sqrt{M}}\right)\cdot\frac{x_0^2}{V_0}\cdot\left(\frac{T - T_0}{\sqrt{T}}\right) \tag{13}$$

This equation shows the experimental relation between H and the ratio x_0^2/V_0 assuming that the flame front thickness, x_0 , is proportional to the quenching distance, d. The relation in Equation (13) is equivalent, therefore, to the equation proposed by Lewis and von Elbe.[18] All constants between brackets are known (M = 17 for the usual fuels) except b which might be taken as the proportionality factor between the flame front thickness and the quenching distance.

Acknowledgments

The authors express their thanks to the Fonds National de la Recherche Scientifique and to the European Office of the Air Research and Development Command (USAF) for financial support from its European Office (Contract AF-61 (514) 814). J. Deckers is indebted, also, to the I.R.S.I.A. for a post-graduate fellowship.

REFERENCES

1. van Tiggelen, A.: Mem. Acad. Roy. Sc. Belg. (Cl. Sc.), *47*, 1 (1952).
2. van Wonterghem, J., and van Tiggelen, A.: Bull. Soc. Chim. Belg., *63*, 235 (1954).
3. Morgan, G. H., and Kane, W. R.: *Fourth Symposium (International) on Combustion*, p. 313. Baltimore, The Williams & Wilkins Co., 1953.
4. van Wonterghem, J., and van Tiggelen, A.: Bull. Soc. Chim. Belg., *64*, 99 (1955).
5. van Wonterghem, J.: Unpublished data from Ph.D. Thesis, Louvain, 1955.
6. van Wonterghem, J., and van Tiggelen, A.: Bull. Soc. Chim. Belg., *64*, 780 (1955).
7. Wilbourn, A. H., and Hinshelwood, C. N.: Proc. Roy. Soc., *A185*, 353 (1946).
8. Vanpée, A.: Ann. Mines Belg., *47*, 1053 (1948).
9. Wynen, J., and van Tiggelen, A.: Bull. Soc. Belg., *57*, 446 (1948).
10. Verwimp, J., and van Tiggelen, A.: Bull. Soc. Chim. Belg., *62*, 205 (1953).
11. Jost, W.: *Explosion and Combustion Processes in Gases*, p. 403. New York, McGraw-Hill Book Co., 1946.
12. Thompson, H. W., and Hinshelwood, C. N.: Proc. Roy. Soc., *A125*, 277 (1929).
13. Jost, W.: *Explosion and Combustion Processes in Gases*, p. 468. New York, McGraw-Hill Book Co., 1946.
14. Volders, A., and van Tiggelen, A.: Bull. Soc. Chim. Belg., *64*, 736 (1955).
15. van Tiggelen, A.: Bull. Soc. Chim. Belg., *55*, 202 (1946).
16. van Wonterghem, J., and van Tiggelen, A.: *Fifth Symposium (International) on Combustion*, p. 637. New York, Reinhold Publ. Corp., 1955.
17. Slootmaekers, J., and van Tiggelen, A.: Bull. Soc. Chim. Belg., *65*, in press.

18. Lewis, B., and von Elbe, G.: *Combustion, Flames and Explosions of Gases*, p. 413. New York, Academic Press, 1951.

Author's Reply

(*In reply to a remark by Dr. T. von Kármán*) We wish to point out that our theory does not have any common point with the theory of Tanford and Pease. In particular, no radical concentration appears in the final formula we have proposed for the burning velocity. In fact, the chain carrier concentration at any point of the flame front is assumed to be entirely dependent on the branched chain reaction kinetics and is not, in any way, connected with the equilibrium concentration in the burned gases.

7

CORRELATIONS OF BURNING VELOCITY, QUENCHING DISTANCES, AND MINIMUM IGNITION ENERGIES FOR HYDROCARBON-OXYGEN-NITROGEN SYSTEMS

By RICHARD S. BROKAW and MELVIN GERSTEIN

Introduction

Over the past several years, extensive measurements have been made of the fundamental combustion properties of hydrocarbons in air and, to a lesser extent, in oxygen or in atmospheres of varying oxygen-nitrogen ratio. Such data have often been interpreted in terms of specific theories of flame propagation, quenching, or ignition, with the primary purpose of testing these theories.

The aim of the correlations presented in this paper is somewhat different. We wish to predict the values of these properties under conditions where measurement may be difficult or impossible—for example, at the high temperatures and low pressures which are encountered in turbojet afterburners.

For this purpose, it is desirable that the correlation chosen should reproduce the available experimental data as closely as possible. Insofar as simple theoretical relationships accomplish this, well and good. Where theory fails, it is abandoned in favor of a more accurate empiricism without further apology.

The correlations are derived from data on propane, inasmuch as combustion properties of propane have been determined over a very broad range of conditions. They may be applied to practical fuels without serious error, since burning velocities, quenching distances and ignition energies for saturated hydrocarbons are similar.

These correlations are used to calculate the effect of initial temperature on fundamental combustion properties. Initial temperature may be raised either by preheating or by preburning. Both cases are considered.

Development of Correlations for Fundamental Combustion Properties

Correlations of burning velocity, quenching distance, and minimum ignition energy for propane flames were obtained in the following fashion. First, an expression for burning velocity was developed using the Semenov-Zeldovich-Frank-Kamenetsky equation as a starting point, but altering the expression empirically to give a better fit to the experimental data. The experimental data were fitted using an activation energy and a multiplicative factor as disposable constants. Data on the effect of initial temperature[1, 2] and oxygen concentration[3] on burning velocities of propane flames were used to establish the correlation for burning velocity.

The correlation of quenching distance was obtained from the relationship used for burning velocity, assuming that burning velocity and quenching distance are related by the expression

$$u_f d \propto \frac{\lambda}{C_p} \frac{T_0}{P} \tag{1}$$

where u_f is the burning velocity, d the quenching distance, λ the thermal conductivity, C_p the molar heat capacity, T_0 the initial temperature, and P the pressure. This relationship, suggested by Spalding,[4] is also implicit in the equation for the burning velocity-quenching distance product

proposed by Potter and Berlad.[5] In this fashion an expression relating quenching distance to initial concentrations, pressure, and initial and flame temperatures was obtained. Quenching data on the effect of oxygen concentration[6] and initial temperature[7] were fitted, using the activation energy from the burning velocity, with a multiplicative factor as a disposable constant.

Finally, the correlation of minimum ignition energies was developed in a form consistent with the burning velocity and quenching distance correlations using the equation of Lewis and von Elbe[8]

$$H \propto \frac{\lambda d^2}{u_f} (T_f - T_0) \qquad (2)$$

where H is the minimum ignition energy and T_f is the flame temperature. Data on the effect of oxygen concentration on ignition energy[9] for propane-oxygen-nitrogen mixtures were used to obtain the correlation.

The development of these expressions will be set forth in greater detail in the remainder of this section.

BURNING VELOCITY

The Semenov-Zeldovich-Frank-Kamenetsky equation for burning velocity may be cast in the form

$$u_f = \frac{RT_0}{P} \sqrt{\frac{2\lambda_f}{X_f \overline{C}_p} \frac{\int_0^{T_f} \omega \, dT}{T_f - T_0}} \qquad (3)$$

where X_f is the mole fraction of combustible in the unburned gas, λ_f is the thermal conductivity at flame temperature, $\overline{C}_p$ a mean molar heat capacity, and ω is the chemical reaction rate. This expression assumes thermal and mass diffusivities equal and neglects the change in number of moles of gas across the flame.

Data on the effect of pressure on quenching distance and burning velocity suggest for hydrocarbon-air flames an over-all reaction order of somewhat less than two. Further, the blowout of a homogeneous reactor correlates assuming a reaction of order 1.8.[10] We have likewise assumed an over-all order of 1.8. It was convenient to arbitrarily choose this total order as one with respect to fuel concentration and 0.8 with respect to oxygen, since the correlations were then independent of fuel concentration.

Following Semenov, and using the conventional Arrhenius expression for reaction rate we obtained

$$\int_0^{T_f} \omega \, dT \simeq C_f' C_{O_2}'^{0.8} AZ \frac{RT_f^2}{E} e^{-ER/T_f} \qquad (4)$$

where C_f' and C_{O_2}' are effective concentrations of fuel and oxygen, A is a steric factor, Z a collision number, and E an activation energy. For flames with first-order kinetics or *stoichiometric* second-order kinetics the effective concentrations are given by

$$C' = C \frac{T_0}{T_f} \left(\frac{\frac{RT_f^2}{E}}{T_f - T_0} \right) \qquad (5)$$

where the C is the initial concentration. However, it was found that data on the effect of oxygen concentration and initial temperature on flame velocity could be correlated by a single activation energy only if the term $(T_f - T_0)$ was replaced by T_f in the concentration expression. Then for stoichiometric mixtures, we have

$$C' \simeq C \frac{R}{E} T_0 \propto \frac{XP}{E}$$

For nonstoichiometric mixtures, somewhat more complex concentration terms are called for in the Semenov equation (see, *e.g.*, Dugger and Simon[11]). These account for the fact that when flame temperature is held constant flame speeds (and accordingly, reaction rates) are higher in off-stoichiometric mixtures. This has been experimentally demonstrated by Botha and Spalding.[12] However, the Semenov relationship greatly overcompensates for this effect; indeed double maxima in the flame-speed curves are predicted.[11] The reason for this may perhaps be that, even if the over-all reaction rate may be expressed by a simple order, the reaction is proceeding to an equilibrium rather than to completion. The rate expressions for reactions approaching equilibrium differ considerably from equations for reactions going to completion.[13] In any event, data for air were well correlated using for the concentration terms

$$\left.\begin{aligned} C' &\propto \frac{XP}{E\varphi}, \qquad \varphi \leq 1 \\ &\propto \frac{\varphi XP}{E}, \qquad \varphi \geq 1 \end{aligned}\right\} \qquad (6)$$

where φ is the equivalence ratio.

Combining Equations (3), (4) and (6) yields

$$u_f \propto \begin{cases} \dfrac{T_0}{E^{1.4}P^{0.1}}\left(Z\dfrac{\lambda_f}{\bar{C}_p}\right)^{\frac{1}{2}} \\ \dfrac{T_f}{(T_f - T_0)^{\frac{1}{2}}}\dfrac{X_{O_2}^{0.4}}{\varphi^{0.9}}\, e^{-E/2RT_f}, & \varphi \geq 1 \\ \propto \dfrac{T_0}{E^{1.4}P^{0.1}}\left(Z\dfrac{\lambda_f}{\bar{C}_p}\right)^{\frac{1}{2}} \\ \dfrac{T_f}{(T_f - T_0)^{\frac{1}{2}}}\varphi^{0.9}X_{O_2}^{0.4}\, e^{-E/2RT_f}, & \varphi \geq 1 \end{cases} \tag{7}$$

In essence, then, this is a Semenov equation, with concentration terms extensively and empirically altered to better fit the experimental data.

Assuming that the quantity $(Z(\lambda_f/\bar{C}_p))$ is proportional to the flame temperature, a plot of $\log U$, where

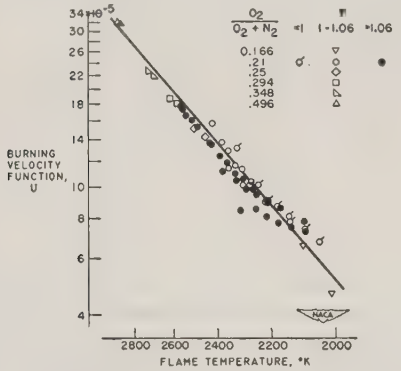

FIG. 1. Burning velocity correlation (C_3H_8-O_2-N_2 mixtures).

$$U \equiv u_f \frac{P^{0.1}(T_f - T_0)^{\frac{1}{2}}}{T_0 T_f^{3/2}}\frac{\varphi^{0.9}}{X_{O_2}^{0.4}}, \qquad \varphi \leq 1$$

$$\equiv u_f \frac{P^{0.1}(T_f - T_0)^{\frac{1}{2}}}{T_0 T_f^{3/2}\varphi^{0.9}X_{O_2}^{0.4}}, \qquad \varphi \geq 1$$

versus $1/T_f$ should be linear.

Such a plot is shown in Figure 1. The experimental data are those of Dugger[1] (T_0 = 200–616°K, φ = 0.8–1.36), and Dugger, Weast, and Heimel[2] on the effect of initial temperature on propane-air burning velocities (T_0 = 616–894°K, φ = 1.15), and the data of Dugger and Graab[3] on the effect of oxygen concentration on propane burning velocities (T_0 = 311, 422°K, φ = 1.0–1.06, $O_2/(O_2 + N_2)$ = 0.166 − 0.496). Eighty-five per cent of the data points lie within ±10 per cent of the line shown in the figure. The resulting equation for burning velocity is

$$\begin{aligned} \log u_f = {} & \log T_0 + \tfrac{3}{2}\log T_f \\ & + 0.4\log X_{O_2} - 0.1\log P \\ & - \tfrac{1}{2}\log(T_f - T_0) - 1.6994 \\ & - \frac{5180}{T_f}\begin{cases} -0.9\log\varphi, & \varphi \leq 1 \\ +0.9\log\varphi, & \varphi \geq 1 \end{cases} \end{aligned} \tag{8}$$

where the flame velocities are obtained in cm/sec, temperatures are in degrees Kelvin and oxygen concentration is expressed as mole fraction. The data are correlated by an activation energy of 47.3 kcal/mole ($E = 5180 \times 2.303 \times 2 \times R$).

Some rough calculations suggested that Equation (7) is also applicable to mixtures where the thermal conductivity and heat capacity have been altered by dilution with argon or helium in place of nitrogen. In this event the thermal conductivity-heat capacity ratio in Equation (7) must be adjusted accordingly. For example, the ratio of the burning velocities of methane in helium and argon "airs" is 1.87 for stoichiometric mixtures;[14] the ratio of the square root of the thermal conductivities of these mixtures at flame temperature is 1.96 (calculated using the methods of Hirschfelder, Curtiss, and Bird,[15] and Lindsay and Bromley.[16])

QUENCHING DISTANCE

The form of the quenching distance equation is obtained immediately by combining Equations (1) and (7):

$$d \propto \begin{cases} \dfrac{E^{1.4}}{P^{0.9}}\left(\dfrac{\lambda_f}{\bar{C}_p Z}\right)^{\frac{1}{2}}\dfrac{(T_f - T_0)^{\frac{1}{2}}}{T_f} \\ \qquad \cdot \dfrac{\varphi^{0.9}}{X_{O_2}^{0.4}}\, e^{E/2RT_f}, & \varphi \leq 1 \\ \propto \dfrac{E^{1.4}}{P^{0.9}}\left(\dfrac{\lambda_f}{\bar{C}_p Z}\right)^{\frac{1}{2}}\dfrac{(T_f - T_0)^{\frac{1}{2}}}{T_f} \\ \qquad \cdot \dfrac{e^{E/2RT_f}}{X_{O_2}^{0.4}\varphi^{0.9}}, & \varphi \geq 1 \end{cases} \tag{9}$$

Assuming the quantity $(\lambda_f/\bar{C}_p Z)$ to be independent of flame temperature, a plot of $\log D$, where

$$D \equiv dP^{0.9}\frac{T_f}{(T_f - T_0)^{\frac{1}{2}}}\frac{X_{O_2}^{0.4}}{\varphi^{0.9}}, \qquad \varphi \leq 1$$

$$\equiv dP^{0.9}\frac{T_f}{(T_f - T_0)^{\frac{1}{2}}}X_{O_2}^{0.4}\varphi^{0.9}, \qquad \varphi \geq 1$$

versus $1/T_f$ should be linear.

Experimental quenching distances (essentially plane parallel plates) for propane-oxygen-nitrogen mixtures are plotted in this fashion in Figure 2. Data are those of Berlad[6] (T_0 = 300°K, $O_2/(O_2 + N_2)$ = 0.17–0.70) and Friedman and Johnston[7] (T_0 = 300–557°K, $O_2/(O_2 + N_2)$ = 0.21). Data in the equivalence ratio range of 0.5–1.5 are included. Although the values for air (circles) fall reasonably close to the line, rich and lean points for higher oxygen concentrations are less well represented. This suggests that the empirical concentration equation (Eq. (6)) is not as suitable at high oxygen concentrations for very rich and lean equivalence ratios. The line of Figure 2 has been drawn giving added weight to points closest to the stoichiometric composition and atmospheric pressure. The slope has been chosen to be the same as that of the flame-velocity correlation (Fig. 1). Data of Figure 2 cover a much broader range of equivalence ratio than those of Figure 1. Furthermore, pressures vary from 0.11 to 1 atmos. When restricted to data similar to that of Figure 1, the correlation of Figure 2 is almost as good. The expression for quenching distance is

$$\left.\begin{aligned} \log d = & -0.9 \log P - \log T_f \\ & + \tfrac{1}{2} \log (T_f - T_0) \\ & - 0.4 \log X_{O_2} - 1.5701 \\ & + \frac{5180}{T_f} + \begin{cases} 0.9 \log \varphi, & \varphi \leq 1 \\ -0.9 \log \varphi, & \varphi \geq 1 \end{cases} \end{aligned}\right\} \quad (10)$$

where quenching distances are in centimeters, temperatures in degrees Kelvin, and oxygen concentration as mole fraction.

Some mention should perhaps be made concerning the pressure dependence of the quenching distance. In mixtures with high flame temperatures, the flame temperature itself is markedly pressure dependent. Thus, although pressure appears in Equations (9) and (10) explicitly to the inverse 0.9 power, a somewhat higher inverse power will be obtained for the pressure dependence of the quenching distance. Actually, the data for stoichiometric air flames will be reproduced somewhat more closely if low pressure values are computed without considering the change of flame temperature with pressure (simply use $d \propto P^{-0.9}$).

The fact that quenching distances and burning velocities are well correlated by the same activation energy indicates that Equation (1) applies rather well to the propane-oxygen-nitrogen system. The form is

$$u_f d = 5.38 \times 10^{-4} \frac{T_0}{P} T_f^{\frac{1}{2}}$$

where the quenching distance is for plane parallel plates.

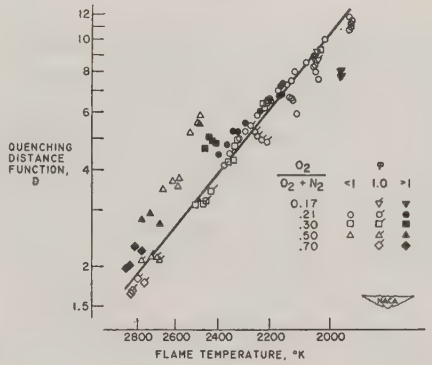

FIG. 2. Quenching distance correlation (C_3H_8-O_2-N_2 mixtures).

MINIMUM IGNITION ENERGY

Combining Equations (2), (7), and (9) we obtain:

$$\begin{aligned} H &\propto \frac{E^{4.2}}{T_0 P^{1.7}} \left(\overline{C}_p^{\frac{1}{2}} \frac{\lambda_f^{3/2}}{Z^{3/2}} \right) \frac{(T_f - T_0)^{5/2}}{T_f^3} \\ &\quad \cdot \left(\frac{\varphi^{2.7}}{X_{O_2}^{1.2}} \right) e^{3E/2RT_f}, \qquad \varphi \leq 1 \\ &\propto \frac{E^{4.2}}{T_0 P^{1.7}} \left(\overline{C}_p^{\frac{1}{2}} \frac{\lambda_f^{3/2}}{Z^{3/2}} \right) \frac{(T_f - T_0)^{5/2}}{T_f^3} \\ &\quad \cdot \frac{e^{3E/2RT_f}}{\varphi^{2.7} X^{1.2}}, \qquad \varphi \geq 1 \end{aligned} \quad (11)$$

If it is assumed that the quantity $(\overline{C}_p^{1/2} \lambda_f^{3/2} / Z^{3/2})$ is independent of temperature, then a plot of the quantity $\log h$, where

$$\begin{aligned} h &\equiv H T_0 P^{1.7} \frac{T_f^3}{(T_f - T_0)^{5/2}} \frac{X_{O_2}^{1.2}}{\varphi^{2.7}}, \qquad \varphi \leq 1 \\ &\equiv H T_0 P^{1.7} \frac{T_f^3}{(T_f - T_0)^{5/2}} X_{O_2}^{1.2} \varphi^{2.7}, \qquad \varphi \geq 1 \end{aligned}$$

against reciprocal flame temperature should be linear.

However, for various hydrocarbons in air, it has been observed that the minima in the ignition energy curves shift toward richer than stoichiometric equivalence ratios as the molecular weight of the fuel increases.[9] Lewis and von Elbe[8] sug-

gest that this is a result of diffusion processes. Spalding[4] further proposes that the equivalence ratio of the minimum, φ' is displaced from stoichiometric, and is given by

$$\varphi' = \left(\frac{D_{O_2}}{D_f}\right)^{\frac{1}{2}} \tag{12}$$

where D_{O_2} and D_f are diffusion coefficients of oxygen and fuel respectively. This relationship seems to work rather well for hydrocarbons in air. Thus, for propane-air flames the minimum occurs at $\varphi' = 1.28$; Equation (12) predicts $\varphi' = 1.33$. This is not an adequate picture, however, since for propane-oxygen flames the minimum occurs very close to the stoichiometric fuel-air ratio. Furthermore, the data of King and Calcote[17] on

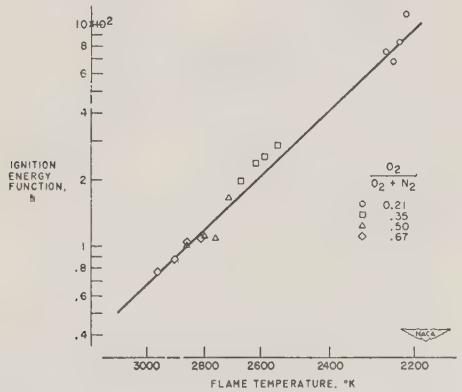

FIG. 3. Minimum ignition energy correlation (C_3H_8-O_2-N_2 mixtures).

pentane-air ignition energies indicate that the position of the minimum shifts toward stoichiometric as the initial temperature is raised.

In view of these uncertainties, we have applied Equation (11) to the minima in the ignition energy-concentration curves for C_3H_8-O_2-N_2 mixtures ($O_2/(O_2 + N_2) = 0.21$–0.67, $P = 0.2$–1.0 atmos).[9] These were correlated using *stoichiometric* concentrations and flame temperatures. The plot of log$h$ versus reciprocal flame temperature is shown in Figure 3. The equation for minimum ignition energy is

$$\left.\begin{aligned} \log H = &-1.7 \log P - \log T_0 \\ &- 1.2 \log X_{O_2} - 3 \log T_f \\ &+ \frac{5}{2}\log(T_f - T_0) + \frac{9402}{T_f} \\ &- 1.306 \begin{cases} + 2.7 \log\varphi, & \varphi \leq 1 \\ - 2.7 \log\varphi, & \varphi \geq 1 \end{cases} \end{aligned}\right\} \tag{13}$$

Bear in mind that although equivalence ratio has been included for completeness, it has not been tested. This equation should give ignition energy-equivalence ratio curves of the proper shape. However, the experimental curve will be displaced from the calculated curve, with the experimental minimum falling at an equivalence ratio intermediate between the φ of the calculation and $(D_{O_2}/D_f)^{\frac{1}{2}}$ times the φ of the calculation.

The activation energy of the correlation is 28.6 kcal/mole, significantly lower than the value common to both the burning velocity and quenching distance correlations. Nevertheless, effects of pressure, oxygen concentration and (as we shall presently see) initial temperature are well described. This suggests that Equation (2) is qualitatively correct; its failure as a quantitative expression may arise from the fact that it applies steady-state properties (flame velocity, flame temperatures, etc.) to a situation where these properties are not valid.

In summary, these correlations suggest that the adiabatic flame temperature is a decisive factor in determining burning velocities, quenching distances and ignition energies. Although the experimental data generally encompass a rather narrow range of initial temperatures, flame temperatures vary from about 2000° to 3000°K. It is believed, therefore, that these correlations may be used with some confidence for initial conditions of temperature, pressure and oxygen concentration where data are not available. The effects of fuel concentration are less well predicted. For burning velocities and quenching distances results will be best for mixtures close to the stoichiometric fuel-oxidant ratio.

Some Applications: Estimation of the Effect of Initial Temperatures on Burning Velocity, Quenching Distance, and Minimum Ignition Energy

As examples of the manner in which the correlations of the previous section may be applied, the effects of initial temperature on burning velocity, quenching distance and minimum ignition energy have been calculated. Two cases have been considered. First, the initial temperature is raised by preheating. This would correspond, for example, to increased stagnation temperatures associated with high Mach number flight. In the second case, initial temperature is raised by preburning air at 300°K. This corresponds to the increased inlet temperatures of afterburners.

These two methods of raising the initial temperature differ in two important respects: With preheating, flame temperatures are also raised; with preburning, flame temperature is unchanged. Also, with preheating, oxygen concentration remains constant; with preburning it decreases.

In calculating the preburning cases the possible chemical effects of carbon dioxide and water which arise from the primary combustion have been neglected. In the most extreme case calculated carbon dioxide and water comprise slightly more than 10 per cent of the total mixture; nitrogen is still the major diluent (about 75 per cent). Neglecting the carbon dioxide and water should cause the calculation of the preburning cases to be very slightly optimistic.

Preheating cases were calculated up to 1000°K, corresponding to a flight Mach number of 4.25 in the troposphere.[18] Preburning cases were considered up to 1200°K (1700°F). This temperature is very considerably higher than present day afterburner inlet (turbine outlet) temperatures.

Although these calculations were made for the propane-air system, combustion properties of saturated hydrocarbons are generally similar, so that the results should represent the behavior of practical hydrocarbon fuels rather well.

Burning velocities, quenching distances and ignition energies are individually discussed below.

BURNING VELOCITY

Burning velocities for stoichiometric mixtures, calculated from Equation (8) are shown in Figure 4. Experimental data on the effect of preheating[1, 2] are also included. Note that when initial temperature is raised 600° (from 300° to 900°K) the burning velocity with preheating is twice the burning velocity with preburning.

In either case, flame velocity increases with initial temperature. However, it would be fallacious to assume that preburning makes combustion faster. The mass, or number of moles, of fuel-air mixture which are consumed by a unit flame surface area in unit time changes very little with preburning. This effect is illustrated in Figure 5, where $u_f(300/T_0)$ is plotted against initial temperature; the temperature ratio accounts for the changing density. Combustion is faster with preheating, but not with preburning.

QUENCHING DISTANCE

Quenching distances for stoichiometric mixtures, together with experimental preheating values[7] are shown in Figure 6. Preheating markedly decreases the quenching distance. The slight decrease in quenching distance with preburning is due to the fact that heat losses from the flame are reduced ($T_f - T_0$ is smaller) as the initial temperature rises.

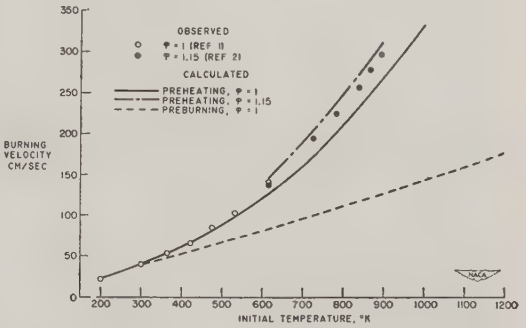

FIG. 4. Effect of initial temperature on burning velocity (1 atmos).

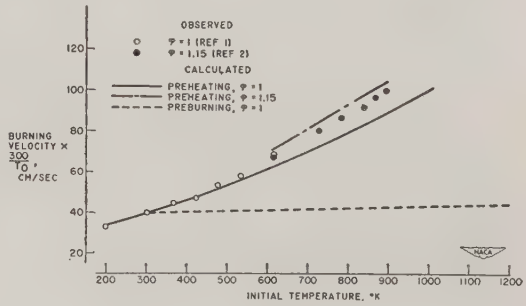

FIG. 5. Effect of initial temperature on relative mass burning rate (1 atmos).

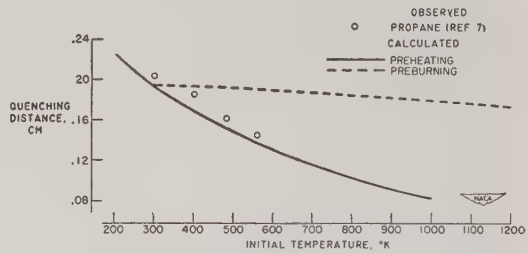

FIG. 6. Effect of initial temperature on quenching distance (1 atmos).

MINIMUM IGNITION ENERGY

Results are shown in Figure 7. Since ignition energies vary by almost two orders of magnitude, a semilog plot was used. These were calculated using Equation (13) with stoichiometric flame temperatures and concentrations. The values correspond, however, to the minima of the ignition energy curves, and would be observed at

somewhat richer equivalence ratios. The experimental minima observed by King and Calcote for preheated pentane air mixtures are also included. Their value at 300°K is more than twofold greater than values for other hydrocarbons (CH_4, C_2H_6, C_3H_8, C_4H_{10}, C_6H_{14}, C_7H_{16}) observed by Blanc, Guest, von Elbe, and Lewis.[9] Nonetheless, the relative effect of initial temperature is well predicted. At 1000°K the preburning ignition energy is 3½ times the preheating ignition energy.

In conclusion, these calculations show that combustion becomes easier (burning velocity rises, quenching distance and minimum ignition energy fall) as the initial temperature is raised by

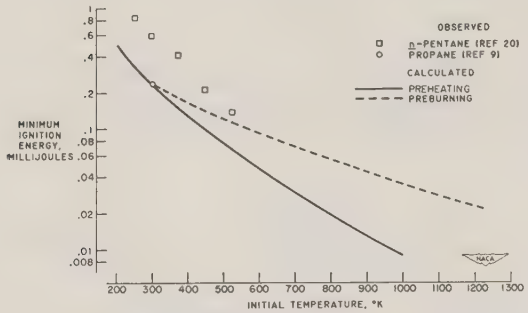

FIG. 7. Effect of initial temperature on minimum ignition energy (1 atmos).

preheating. With preburning effects are much less marked; the mass burning rate and the quenching distance are only slightly changed.

Concluding Remarks

Equations for burning velocity, quenching distance and minimum ignition energy have been developed empirically, using existing experimental data. The equations were shown to fit a wide variation of these flame properties with initial temperature, oxygen concentration and equivalence ratio; thus they may be used with a fair degree of confidence to predict values under conditions where experimental data is either lacking or difficult to obtain. One such application to conditions of preheating with and without vitiation was demonstrated.

REFERENCES

1. DUGGER, G. L.: NACA Report 1061, (1952).
2. DUGGER, G. L., WEAST, R. C., AND HEIMEL, S.: *Fifth Symposium (International) on Combustion*, p. 589. New York, Reinhold Publ. Corp., 1955.
3. DUGGER, G. L., AND GRAAB, D. D.: *Fourth Symposium (International) on Combustion*, p. 302. Baltimore, The Williams & Wilkins Co., 1953.
4. SPALDING, D. B.: *Some Fundamentals of Combustion*, p. 171. New York, Academic Press, 1955.
5. POTTER, A. E., JR., AND BERLAD, A. L.: NACA Technical Note 3398 (1955).
6. BERLAD, A. L.: NACA Research Memorandum E53K30 (1954).
7. FRIEDMAN, R., AND JOHNSTON, W. C.: J. Appl. Phys., *21*, 791 (1950).
8. LEWIS, B., AND VON ELBE, G.: *Combustion, Flames and Explosions of Gases*, p. 413. New York, Academic Press, 1951.
9. BLANC, M. V., GUEST, P. G., VON ELBE, G., AND LEWIS, B.: *Third Symposium on Combustion Flame, and Explosion Phenomena*, p. 363. Baltimore, The Williams & Wilkins Co., 1949.
10. LONGWELL, J. P., AND WEISS, M. A.: Ind. Eng. Chem., *47*, 1634 (1955).
11. DUGGER, G. L., AND SIMON, D. M.: *Fourth Symposium (International) on Combustion*, p. 336. Baltimore, The Williams & Wilkins Co., 1953.
12. BOTHA, J. P., AND SPALDING, D. B.: Proc. Roy. Soc., *225A*, 71 (1954).
13. GLASSTONE, S.: *Textbook of Physical Chemistry*, 2nd edition, pp. 1069–1073, New York, Van Nostrand, 1946.
14. CLINGMAN, W. H., JR.: Princeton Univ. Ph.D. Thesis, Table XV (Sept. 1954).
15. HIRSCHFELDER, J. O., CURTISS, C. F., AND BIRD, R. B.: *Molecular Theory of Gases and Liquids*, p. 534. New York, John Wiley & Sons, Inc., 1954.
16. LINDSAY, A. L., AND BROMLEY, L. A.: Ind. Eng. Chem., *42*, 1508 (1950).
17. KING, I. R., AND CALCOTE, H. F.: J. Chem. Phys., *23*, 2444 (1955).
18. Ames Research Staff, NACA Report 1135 (1953).

DISCUSSION BY R. S. BROKAW

The correlations of burning velocity and quenching distance presented above all include pressure dependences for the various flame properties. Let us examine these pressure dependences in greater detail. Four flame propagation properties will be considered, namely: Burning velocity, u_f, which measures the normal velocity of flame propagation; quenching distance, d, which indicates whether or not a flame will propagate; minimum ignition energy, h, which specifies the energy required to start a flame propagating; and the critical velocity gradient for flashback, g, which defines the conditions under which the flame will propagate upstream from a burner port.

According to simple thermal theories of flame propagation the pressure dependences of burning velocity,* quenching distance,* minimum ignition energy,* and critical flashback velocity gradient† are as follows:

$$u_f \propto p^{(m/2)-1},\ d \propto p^{-m/2},\ h \propto p^{1-3m/2},\ \text{and}\ g \propto p^{m-1}.$$

The quantity, m, describes the pressure dependence of the flame reaction rate ($\omega \propto p^m$). Accordingly, we can construct the following functions of the flame propagation properties which are proportional to the flame reaction rates.

$$f(u_f) = u_f^2 p^2 \propto \omega \propto p^m$$

$$f(d) = d^{-2} \propto \omega \propto p^m$$

$$f(h) = (p/h)^{2/3} \propto \omega \propto p^m$$

$$f(g) = pg \propto \omega \propto p^m$$

Plots of the logarithms of these functions versus the logarithm of the pressure should yield straight lines of slope m. Such plots are shown in Figure 1 (5 per cent C_3H_8-air) and Figure 2 (stoichiometric H_2-air). Sources of the experimental data are indicated on the figures. In each figure a single slope has been chosen to represent the four types of plots. These slopes ($m = 1.88$ for 5 per cent C_3H_8, $m = 2.17$ for stoichiometric H_2) fit the burning velocity, quenching distance, and flashback data very well; somewhat different slopes would have been selected to best fit the ignition energies alone.

As has already been indicated, the exponent, m, is concerned with the pressure dependence of the flame reaction rate. Experimentally, m is found to vary with fuel and oxygen concentrations. A tentative explanation of this is as follows: In simple thermal theories (such as the burning velocity theory of Semenov, Zeldovich, and Frank-Kamenetski) the flame reaction rates are related to the flame temperature.

$$\omega \propto p^m \propto p^n e^{-E/RT_f}$$

(actually, the flame temperature also appears preexponentially, but the principal influence is in the exponent. A more detailed treatment of this type is presented by Potter and Berlad‡. Accordingly,

$$m = \frac{d \ln \omega}{d \ln p} = n + \frac{E}{R}\left(\frac{1}{T_f}\frac{d \ln T_f}{d \ln p}\right)$$

It is seen that m is the sum of two terms; n, the global reaction order and a second term which corrects for the variation of flame temperature with pressure. A plot of m versus $(1/T_f)(d \ln T_f/d \ln p)$ should yield a straight line of intercept n and slope E/R. Such a plot for stoichiometric C_3H_8-O_2-N_2

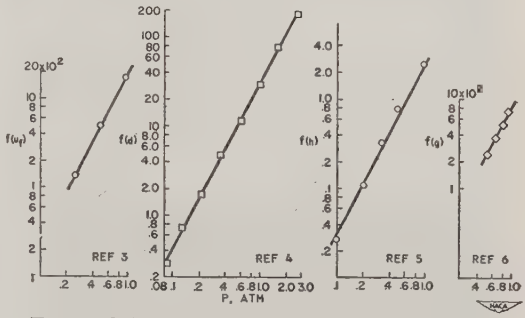

FIG. 1. Effect of pressure on U_f, d, h, and g functions for 5 per cent propane in air. Slope, 1.88.

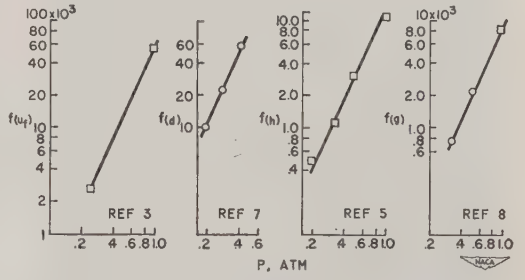

FIG. 2. Effect of pressure on U_f, d, h, and g functions for stoichiometric H_2-air. Slope, 2.17.

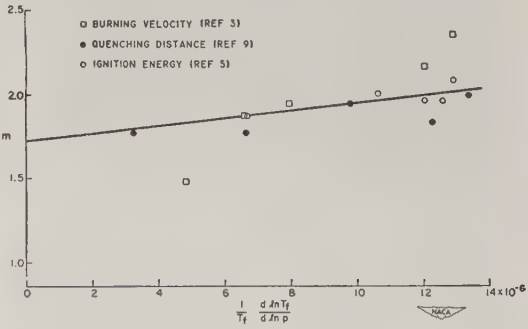

FIG. 3. Variation of m with flame temperature pressure dependence. Stoichiometric propane flames.

flames is shown in Figure 3. Although the data scatter considerably, the line fits the quenching distance and ignition energy data rather well. Burning velocities for very slow and very fast flames fit less well. The line has been drawn to correspond to an activation energy of 45 kcal/mole, a reasonable value for hydrocarbon combustion. Admittedly a steeper slope might have been chosen. It is noteworthy that the apparent reac-

* D. B. Spalding: *Some Fundamentals of Combustion*, p. 190. New York, Academic Press, Inc., 1955.

† A. L. Berlad and A. E. Potter: J. Phys. Chem., to be published.

‡ A. E. Potter and A. L. Berlad: *Sixth Symposium (International) on Combustion*, p. 27. New York, Reinhold Publ. Corp., 1957.

tion order (about 1.7) is close to the value used to correlate blowout data for combustion in the homogeneous reactor (1.8).*

However, this type of reasoning probably only partially explains the variation of m with fuel and oxygen concentrations. It would indeed be fortuitous if the complex of reactions occurring in a hydrocarbon flame could under all conditions be described by a single global reaction order.

In conclusion, it appears that the interrelationships among pressure dependences of the various flame propagation properties are rather well described by simple thermal considerations. Thus experimental determinations of a single flame property may suffice to describe the behavior of the other properties. The quenching distance is most easily measured with good precision. In fact, in precise low pressure measurements of the other properties quenching effects must be considered and minimized.†

* J. P. Longwell and M. A. Weiss: Ind. Eng. Chem., *47*, 1634 (1955).

† Additional references:

J. Manton and B. B. Milliken: Proceedings of the Gas Dynamics Symposium on Aerothermochemistry, Aug. 22–24, 1955, p. 151. Northwestern University, Evanston, 1956.

R. Friedman and W. C. Johnston: J. Appl. Phys., *21*, 791 (1950).

B. Lewis and G. Von Elbe: *Combustion, Flames and Explosions of Gases*. New York, Academic Press, Inc., 1951.

J. E. Garside and B. Jackson: *Fourth Symposium (International) on Combustion*, p. 545. Baltimore, The Williams & Wilkins Co., 1953.

B. D. Fine: NACA TN 3833.

A. L. Berlad: J. Phys. Chem., *58*, 1023 (1954).

8

THE INFLUENCE OF PRESSURE ON FLAME SPEED[a]

By MITCHELL GILBERT

1. Introduction

The modern theory of flame propagation indicates that the pressure is an important parameter arising primarily in the effective over-all order of the chemical reactions. Variation of the flame speed with P^n, where $0 \geq n \geq -\frac{1}{2}$, suggests second- to first-order kinetics, and $0 \leq n \leq \frac{1}{2}$ suggests second- to third-order kinetics. Second-order processes would be expected to occur most frequently, and flame speed independent of pressure should result. However, a complicating factor is the relative behavior of diffusive and thermal transport processes. If the ratio of these effects (expressed as the Prandtl number divided by the Schmidt number) is truly independent of temperature and local chemical composition, then theory predicts flame speed invariant with pressure for second-order kinetics. Variations of the ratio probably occur, and it may be expected that the correlation mentioned above will not be precise. It may be noted that flame temperatures and equilibrium compositions depend sufficiently on pressure to cause variations in the Schmidt and Prandtl numbers.

In the present paper, experimental data on the effects of pressure are presented, in the range of pressure below one atmos, for eight fuels. No startling effects are noted and the data are valuable primarily for adding to the completeness of the literature. However, in the course of the experiments an opportunity arose to examine the influence of the method of measuring flame speed. It was found that, in some previously observed results at subatmospheric pressures, deviations from a linear logarithmic law, $\ln U = a + n \ln P$, occurred. These results were commonly ascribed, by various investigators including the present author as well, to quenching influences of the burner port or wall. Recent experiments at this Laboratory, however, indicated that these quenching influences were minor. Thus, by using a schlieren-type method for determining flame area, it is shown that the luminous-cone boundary is not proper for determining flame speed, although at elevated pressures no significant error

[a] This paper presents the results of one phase of research carried out at the Jet Propulsion Laboratory, California Institute of Technology under Contract No. DA-04-495-Ord 18, sponsored by the Department of the Army, Ordnance Corps.

is introduced through its use. The new method of measuring flame speed involves deflections of wire-grid shadows to determine the flame boundary. In addition a measure of flame thickness is provided.

2. Experimental Technique

Flame speeds were measured in a vacuum system described in detail elsewhere.[1] Bunsen-type flames were established on long cylindrical ducts. Some of the ducts were provided with short nozzle inserts in order to increase the range of duct diameter for the experiments. This was necessary because the variation of the stability limits of low-pressure flames requires increase in burner size as the pressure is lowered.[1, 2] The control of pressure and flow are such as to produce flames of remarkable stability. In addition, low-pressure flames are relatively free of influence due to the nature and behavior of the external atmosphere.

Most of the flame speeds reported here were measured by determining the area of the inner boundary of the luminous cone. A single convex lens, with a 9-in. focal length and 5-in. diameter, projected the flame image onto a transparent plastic screen, and the inner boundary was visually traced. Magnification was 1:1. Flow volume divided by area gives a flame speed averaged over the surface.

Some lack of agreement in pressure dependence of flame speed has been noted among various investigators. Consequently, some flame-speed measurements were repeated using a schlieren technique, since this method, for experimental and theoretical reasons, has found wide acceptance. Experiments evaluating flame-speed measurement techniques indicate that the schlieren cone, from the point of view of providing a boundary most consistent with the definition of flame speed, is satisfactory because the temperature rise is quite small up to this boundary. Furthermore, geometric assumptions appear to be satisfied because the stream lines remain parallel up to the schlieren boundary. Broeze,[3] Linnett,[4] and Gerstein[5] summarize the physical considerations involved and make strong arguments for the validity of the schlieren boundary.

An interesting variation of the ordinary schlieren method was used. Instead of a knife-edge stop in a double-mirror Z-system, one can interpose a grid of parallel wires. The grid is conveniently placed between the image plane of the flame and the image of the light source. Burgoyne and Weinberg[6, 7] in a simpler version of this technique, used parallel open slits to study a flat flame. These authors and Wright[8] discuss the formation of the slit image and wire shadow on the image plane. It is clear that deflections in the shadow or slit are produced by index-of-refraction gradients normal to the light path. The magnitude of the deflection is essentially the counterpart of the intensity variation produced on the image plane by the combination of a refracting source and a schlieren knife-edge. Figure

FIG. 1. Wire-shadow patterns produced by a propane-air flame (mole ratio 0.044, pressure 249 mm Hg abs).

1 shows the wire shadow pattern deflected by a flame. The associated diffraction pattern is also visible. A grid composed of 0.010-in. wires about $\frac{1}{8}$ in. apart was used to produce the patterns of Figure 1.

The peak deflections are of interest. It can be shown that the peak intensity of the ordinary schlieren image and the peak deflections of the wire shadows represent the maximum of the function

$$(1/\mu)(d\mu/dx)\sin\theta$$

or

$$(-1/T^2)(dT/dx)$$

for the beam at right angles to the gradient. Thus the schlieren boundary, or the boundary defined by the locus of peak deviations in Figure 1, is seen theoretically to represent a flame boundary of lower temperature than the inner luminous cone, and lies farther upstream than the luminous boundary. Indeed, it lies far enough upstream toward the unburned gas to provide a good determination of the flame speed, and supporting evidence is presented in this paper. Right and left photographs such as Figure 1 were taken for some of the flames, and comparison was made between flame speeds determined by the inner and Weinberg in that deflections can be magnified enormously by bringing the wire grid closer to the image plane of the schlieren light source. At low pressures the gradients are diminished and deflections become quite small, but by changing the grid position respectable deflections can again be obtained. The wire shadows concurrently separate, and a closer grid construction must be employed if the flame image is to be defined by a sufficient number of peaks.

The conical-cylindrical geometry of the flame introduces some optical distortion, primarily in the colder region of the flame where the light beam

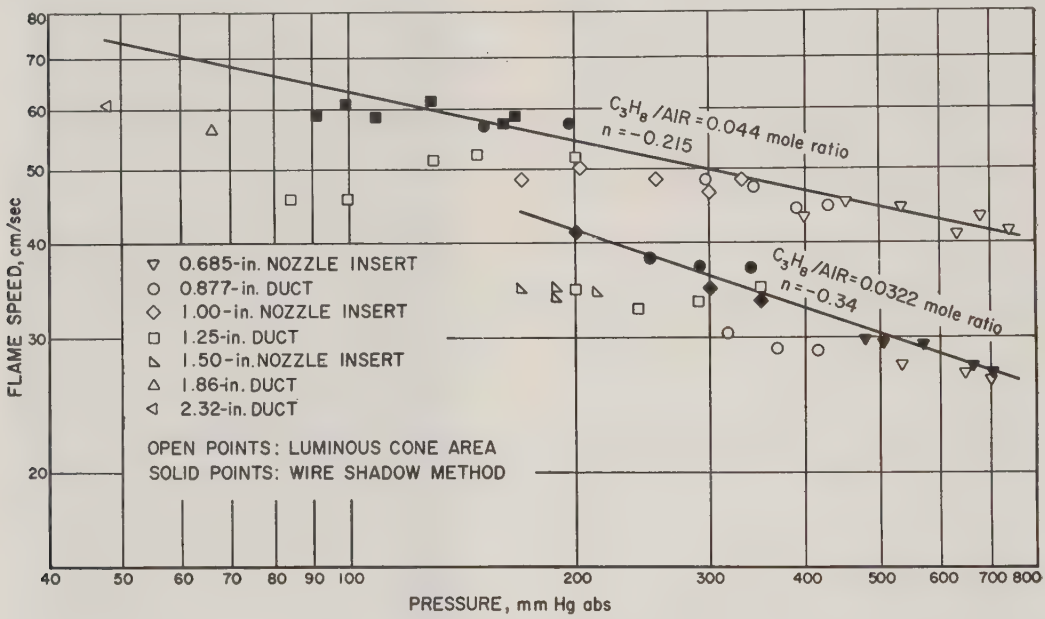

FIG. 2. Flame speed vs pressure for two propane-air mixtures.

luminous-cone area and by the area defined from the locus of peak deflections of the wire shadows.

Brief discussion may be made of some additional factors involved in using the shadow deflection method. First, the peak deviations are determined at the central bright line of the wire shadow. Second, although the trace of a single wire is, in principle, capable of giving the refractive index or temperature distribution in the reaction zone of the flame, as pointed out by Burgoyne and Weinberg,[6, 7] the quantitative accuracy is not as yet very great. For purposes of measuring flame speed, however, the maximum deflection point (determined by a tangent to the peak, parallel to the undeviated shadow) is quite definitive. The present optical system has a significant advantage over that used by Burgoyne must pass through the reaction zone twice at a small angle to the gradient, and then through a long path length of cooler gas. It can be shown that in the region of maximum deflection the perturbing effects of the flame geometry are small, due to variation of path length and variation of gradient along the path (a slight upstream shift is caused). Good over-all temperature distributions can probably be obtained only for plane flames. Further consideration of the properties of the wire-shadow technique and its physical applications will be deferred to a later publication.

3. Results and Discussion

The figures show flame speeds for a large number of systems. Most of the data give flame speeds

obtained from the area of the inner luminous boundary. The flame speeds for the faster-burning flames appear to be independent of pressure below one atmosphere, while the slower-burning flames show a behavior characterized by $U \propto P^n$. Such a power law is valid if the data can be represented by straight lines in the log plots, despite an obvious falling off toward low pressures (Figs. 2 to 8).

The use of the straight line in Figures 2, 3 and 4 stems from the observation that as the duct size s increased the straight-line behavior of the data is extended. It would appear that for extremely large ducts a linear asymptote should be valid. An attempt to explain the deviation of the data from a power law was made by Cullen.[9] Assuming that a quenching effect exists, arising from the burner port or wall, Cullen derived an expression which seemed to indicate that for Peclet numbers below 200, based on the observed flame speed, burner exit diameter, and operating pressure, the data would fall away from the linear asymptote. The correlation was quite convincing; the present author had reached the same conclusion on the basis of early experimental data at this Laboratory, but the present research shows that the correlation is invalid.

When recently the wire-shadow technique (see the solid points in Figures 2, 3 and 4) was used with some low-pressure flames previously studied by the luminous-cone method, it was noted that the data do not exhibit the deviation from the power law. At extremely low pressures there is some indication, as would be expected, that a falling off of flame speed occurs part of which may be attributable to the quenching implied in Cullen's analysis based on the effects of burner rim.

The linear logarithmic behavior of the wire-shadow data suggests a more natural explanation for the falling off of the luminous-cone-boundary

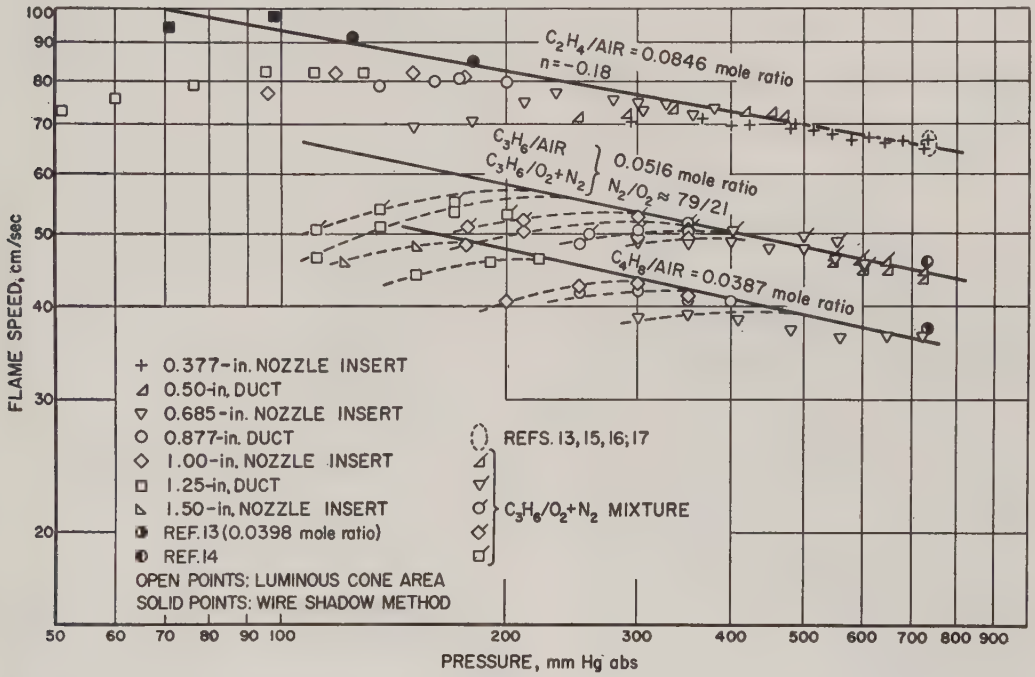

FIG. 3. Flame speed vs pressure for ethylene-air, propylene-air, and isobutylene-air.

data. This explanation is based on the increase in separation between the inner luminous boundary and the schlieren or wire-shadow boundary, as the pressure is reduced. Assume, in Figure 9, that the solid cone represents the wire shadow, or true boundary, and that the dotted cone represents the inner luminous boundary. If the separation of these boundaries is δ (experimentally δ should be of the order of reaction-zone thickness), then mean free path considerations dictate that $\delta \propto 1/P$, or $\delta = \delta_0 P_0/P$, where δ_0, P_0 represent flame thickness and pressure at 1 atmos. The ratio of flame areas, the luminous-cone area to wire-shadow cone area, is then, for $\delta \ll r$.

$$\frac{A_{1c}}{A_{ws}} \approx 1 + \frac{2\delta}{r} = 1 + \frac{2\delta_0 P_0}{rP} \qquad (1)$$

If it is assumed that the power law holds, then

$$U[P] = U_0(P/P_0)^n = (Q/A_{ws})(P/P_0)^n \qquad (2)$$

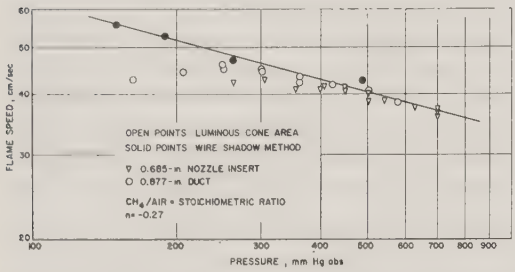

FIG. 4. Flame speed vs pressure for methane-air stoichiometric mixture.

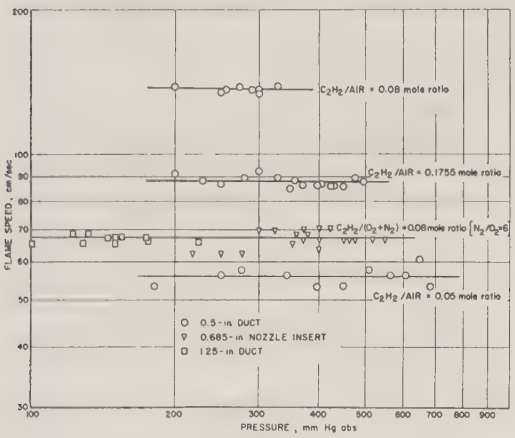

FIG. 5. Flame speed vs pressure for acetylene-air and acetylene-oxygen-nitrogen mixtures.

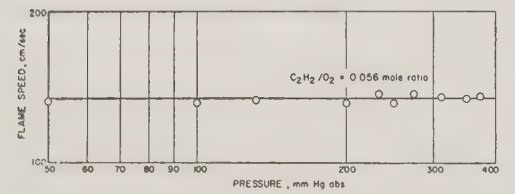

FIG. 6. Flame speed vs pressure for an acetylene-oxygen mixture, 0.5-in. duct.

Thus the use of the flame area A_{1c} instead of the correct one, A_{ws}, would result in an apparent flame speed

$$U'[P] = (Q/A_{1c})(P/P_0)^n \qquad (3)$$

and using Equations (1) and (2)

$$U' = \frac{U_0(P/P_0)^n}{1 + (2\delta_0 P_0/rP)} \qquad (4)$$

The denominator of the right-hand side of Equation (4) determines the deviation of the flame speed from a power law. In fact, the deviation at any pressure is

$$\Delta U = U - U' \approx (2U_0\delta_0/r)(P/P_0)^{n-1} \qquad (5)$$

and upon examination it is seen that the observed deviation from the power law can, through the use of Equation (5), give a measure of δ_0 :

$$\delta_0 = (r\Delta U/2U_0)(P/P_0)^{1-n} \qquad (6)$$

For example, for the methane-air flame n =

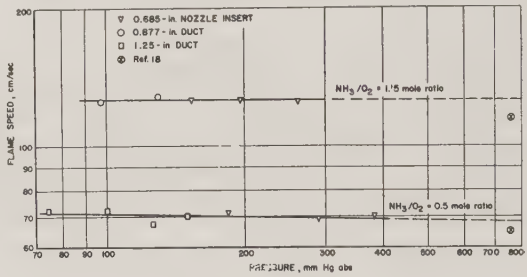

FIG. 7. Flame speed vs pressure for ammonia-oxygen mixtures.

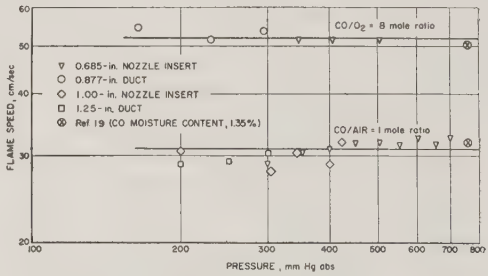

FIG. 8. Flame speed vs pressure for carbon monoxide-oxygen and carbon monoxide-air mixtures.

-0.27, U_0 = 36 cm/sec, and at 162 mm Hg abs the luminous-cone-area flame speed deviates from the linear asymptote by about 12 cm/sec in an 0.877-in.-diameter duct (Fig. 4). The calculated value of δ_0 is 0.026 cm. Morgan and Kane[10] measured the distance from the schlieren boundary to what is effectively the middle of the luminous cone. Thus their measurement should be two to four times δ_0. Morgan's and Kane's value of 0.048 cm is therefore comparable with this author's calculated value.

From the foregoing analysis, the reason for the accidental correlation found by Cullen[9] becomes clear. The correlation with Peclet number, $\rho D U c_p/\lambda$, can be reduced to purely a function of Reynolds number by noting that the Prandtl

number is practically constant with pressure and varies only slightly for similar hydrocarbon fuel-air mixtures. Now, if one recognizes the fact that δ_0 in Equation (4) is an inverse function of flame speed, then it follows that the quantity $\delta_0 P_0/rP$ can also be replaced by a function of the Reynolds number. Thus, the observations of Cullen[9] are explained without recourse to quenching as their origin.

Figures 10 through 17 summarize flame speed for some faster-burning systems. Propane-oxygen and acetylene-oxygen systems could, because of the high flame speeds, be burned down to pressures of a few millimeters of mercury. Part of the effects noticed at very low pressures may be attributed to true quenching. For example, in

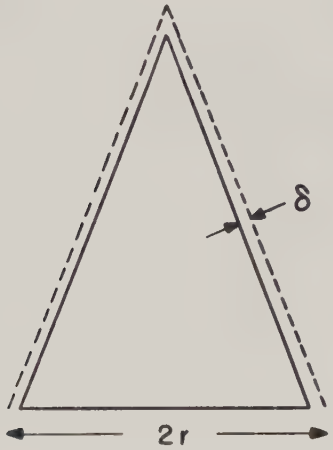

FIG. 9. Diagram of a conical flame.

Figures 13 and 16, flat flames are observed to yield lower flame speeds than conical flames, at a given pressure and burner diameter. It is not unreasonable to assume that this is partly due to the greater value of the ratio of wetted perimeter to flame area for the flat flame as compared with the conical flame. That the effect seems accentuated in the smaller (1.25-in.) duct is consistent with the expected increase in wetted-perimeter/flame-area ratio as duct size is decreased.

Nevertheless, for a given duct even the very-low-pressure data are influenced by the deviation introduced through use of the luminous-cone boundary. Referring to Figures 15d and 17, one can estimate the reaction-zone thickness δ_0 for the propane-oxygen system. At 10 mm Hg abs, the deviation in flame speed from a linear behavior (in this case $n \sim 0$) is about 75 cm/sec; $U_0 = 325$ cm/sec at a mole ratio of 0.11. The calculated value of δ_0 is 0.003 cm, which compares with 0.0094 cm observed by Morgan and Kane at a mole ratio of 0.20 (a mixture having the same flame speed as the 0.11 mixture). As predicted, their value is about three times δ_0.

Some consideration can be given to the question of the flame speed vs pressure behavior of the very-fast-burning systems. Lewis[11] has indicated that in these systems $U \propto P^n$ where $n \geq 0$. The flame speed should then fall appreciably as the pressure is reduced. For example, one can roughly estimate that acetylene-oxygen flame speed should decrease by a factor of 1.5 between 760 and 100 mm Hg. A good check is not available since the present data are for very lean mixtures

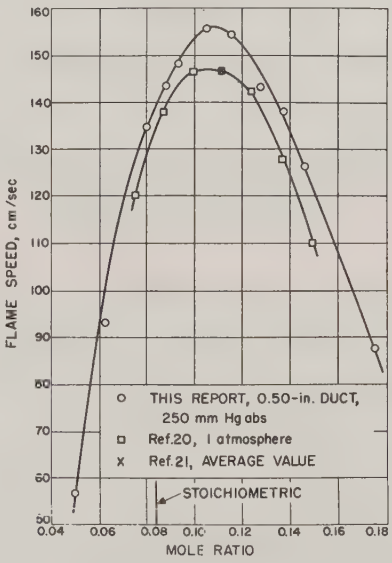

FIG. 10. Effect of mole ratio on flame speed of acetylene-air mixtures.

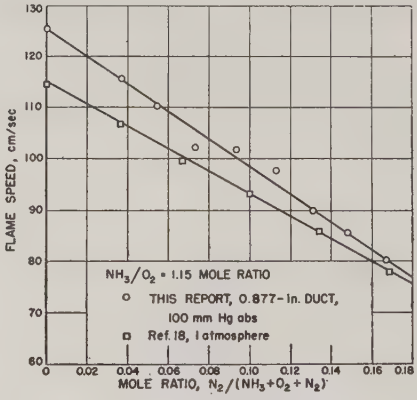

FIG. 11. Effect of nitrogen addition on flame speed of an ammonia-oxygen mixture.

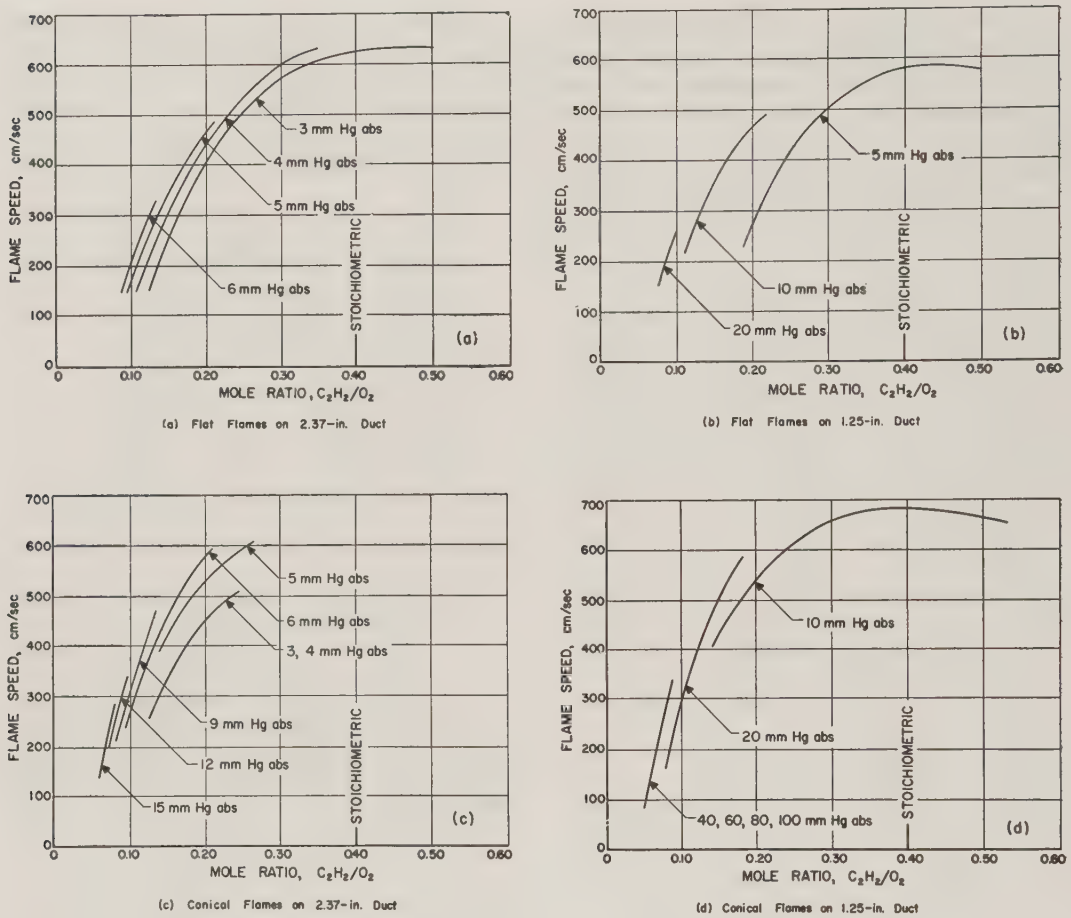

FIG. 12. Variation of flame speed with mole ratio for acetylene-oxygen at low pressures (curves represent experimental data with mean scatter 0–2 per cent).

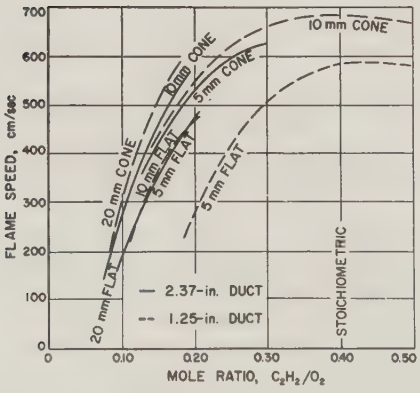

FIG. 13. Comparison of acetylene-oxygen flame speeds at low pressures (5–20 mm Hg abs) showing effects of flame shape and duct size.

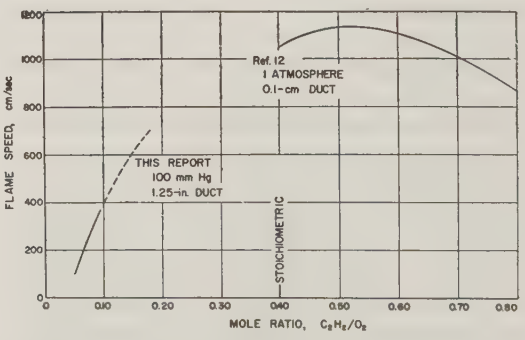

FIG. 14. Acetylene-oxygen flame speeds, limiting values of present research extrapolated using Fig. 12.

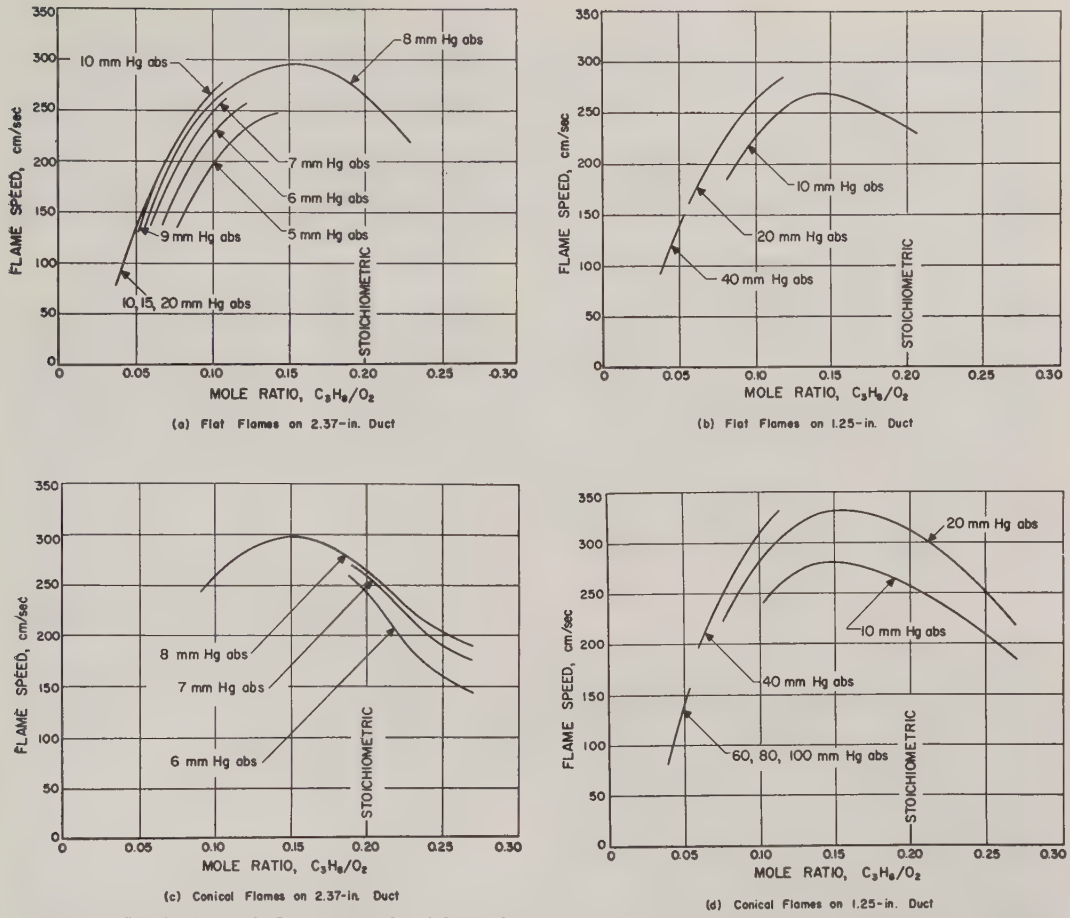
FLAME SPEED, cm/sec
MOLE RATIO, C_3H_8/O_2
10 mm Hg abs
8 mm Hg abs
7 mm Hg abs
6 mm Hg abs
9 mm Hg abs
5 mm Hg abs
10, 15, 20 mm Hg abs
STOICHIOMETRIC
(a) Flat Flames on 2.37-in. Duct
10 mm Hg abs
20 mm Hg abs
40 mm Hg abs
(b) Flat Flames on 1.25-in. Duct
8 mm Hg abs
7 mm Hg abs
6 mm Hg abs
(c) Conical Flames on 2.37-in. Duct
20 mm Hg abs
10 mm Hg abs
40 mm Hg abs
60, 80, 100 mm Hg abs
(d) Conical Flames on 1.25-in. Duct

FIG. 15. Variation of flame speed with mole ratio for propane-oxygen at low pressures (curves represent experimental data with mean scatter less than 1 per cent).

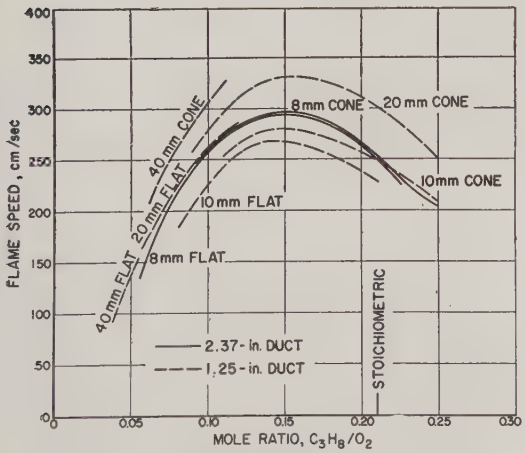

FIG. 16. Comparison of propane-oxygen flame speeds at low pressures (8–40 mm Hg abs) showing effects of flame shape and duct size.

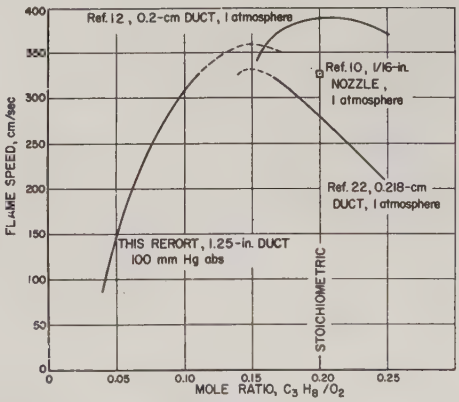
FLAME SPEED, cm/sec
MOLE RATIO, C_3H_8/O_2
Ref. 12, 0.2-cm DUCT, 1 atmosphere
Ref. 10, 1/16-in. NOZZLE, 1 atmosphere
Ref. 22, 0.218-cm DUCT, 1 atmosphere
THIS REPORT, 1.25-in. DUCT 100 mm Hg abs
STOICHIOMETRIC

FIG. 17. Propane-oxygen flame speeds, limiting values (low pressure) of present research compared with 1-atmos data.

and could not be readily extended to stoichiometric mixtures, and the only comparable data (12) occur at 1 atmos for richer mixtures. However, Figure 14 presents the available fragments of data and shows that it is not at all evident that Bartholomé's data would lie above the low-pressure data if the experimental range of mixtures were extended.

In Figure 17 a comparison of high- and low-pressure data for propane-oxygen again do not suggest any decrease of flame speed as pressure is reduced. Here the data are extensive enough to be more forceful.

With regard to the slope of the flame speed vs pressure data in some of the figures, it may be noted that where the line is drawn through the data obtained only for luminous-cone areas without the confirmation of wire-shadow measurements, the slope is probably underestimated.

4. Conclusions

Experimental data on the variation of flame speed with pressure in the subatmospheric range indicate that slow-burning flames have varying pressure dependence; in general, flame speed increases as pressure decreases. Fast flames are independent of pressure. The present data on very fast flames, propane and acetylene with oxygen, on comparison with the literature did not indicate any direct pressure dependence sufficient to cause an appreciable *decrease* of flame speed as pressure is lowered.

Flame boundaries obtained with a wire-shadow technique comparable to a schlieren method indicate that flame speed obeys a power law $U \propto P^n$. The data tend to affirm the schlieren boundary as the correct one for flame-speed measurement. In the cases studied (methane, propane, ethylene), deviations from this power law, observed when the luminous inner boundary is used for flame-speed determination, are shown to be caused by the separation of the schlieren and luminous boundaries as the pressure is lowered. Quenching processes do not appear to be responsible, and in fact probably enter only at considerably lower pressures than those at which deviations from the power law are first observed with the luminous boundary. The range of n observed was $0 \geq n \geq -\frac{1}{3}$.

Simple theory indicates that the deviation of flame speed from the power law provides a measure of the flame thickness. Values so obtained are comparable with other researches.

When kinetics for a particular flame are available, laminar flame theory predicts the pressure dependence of the flame speed. The extent of departure of experiment from such theory can, if the flame kinetics have a reasonably firm basis, provide information on the actual variation of transport processes with pressure and other contingent parameters.

Acknowledgments

The author gratefully acknowledges the help of George A. Eriksen, Lieutenant, USN; William McK. Pardee, Lieutenant Commander, USN; and John M. Charles, Lieutenant, USN, who obtained a major portion of the data with great care and fidelity. The valuable discussions with Dr. Hamilton Wright are also acknowledged.

Nomenclature

A_{lc} = area of inner luminous-cone boundary
A_{ws} = area of boundary defined by peak deflections of wire shadows
n = exponent of pressure in flame-speed equation
P = pressure
P_0 = atmospheric pressure
Q = total volume flow through flame
r = radius of flame base or burner duct
T = temperature
U = flame speed
U' = flame speed observed using inner luminous-cone boundary
U_0 = flame speed at atmospheric pressure
x = distance normal to flame front
δ = flame thickness (distance between schlieren and luminous boundaries)
δ_0 = flame thickness at atmospheric pressure
$\Delta U = U - U'$
η = gas viscosity
μ = index of refraction of flame gases
ρ = gas density
θ = angle between light beam and index-of-refraction gradient

REFERENCES

1. Gilbert, M.: California Institute of Technology, Jet Propulsion Laboratory, Pasadena, Report No. 4-54 (1949).
2. Wolfhard, H. G.: Z. tech. Phys., *24*, 206 (1943).
3. Broeze, J. J.: *Third Symposium (International) on Combustion*, pp. 146–155. Baltimore, The Williams & Wilkins Co., 1949.
4. Linnett, J. W.: *Fourth Symposium (International) on Combustion*, pp. 20–35. Baltimore, The Williams & Wilkins Co., 1953.

5. Gerstein, M.: Ref. 4, pp. 35–43.
6. Burgoyne, J. H., and Weinberg, F.: Ref. 4, pp. 294–302.
7. Burgoyne, J. H., and Weinberg, F.: Proc. Roy. Soc. *224A*, 286 (1954).
8. Wright, F. H.: California Institute of Technology, Pasadena, Ph.D. Thesis, 1948.
9. Cullen, R. E.: Trans. Am. Soc. Mech. Engrs., *75*, 43 (1953).
10. Morgan, G. H., and Kane, W. R.: Ref. 4, pp. 313–320.
11. Lewis, B.: *Selected Combustion Problems, AGARD*, 176 ff. London, Butterworth, 1954.
12. Bartholomé, E.: Z. Elektrochem., *53*, 191 (1949).
13. Gerstein, M., Levine, O., and Wong, E. L.: J. Am. Chem. Soc., *73*, 418 (1951).
14. Gray, K. L., Linnett, J. W., and Mellish, C. E.: Trans. Faraday Soc., *48*, 1155 (1952).
15. Pickering, H. S., and Linnett, J. W.: Trans. Faraday Soc., *47*, 1101 (1951).
16. Conan, H. R., and Linnett, J. W.: Trans. Faraday Soc., *47*, 981 (1951).
17. Dugger, G. L., and Simon, D. M.: NACA RM E52J13 (1953).
18. Ausloos, P., and Van Tiggelen, A.: Bull. soc. chim. Belges, *60*, 433 (1951).
19. Jahn, G.: *Der Zündvorgang in Gasgemischen*. Berlin, Oldenbourg, 1934.
20. Smith, F. A.: Chem. Revs., *21*, 389 (1937).
21. Wheatley, P. J., and Linnett, J. W.: Trans. Faraday Soc., *48*, 338 (1952).
22. Damköhler, G.: Z. Elektrochem., *46*, 601 (1940).

9

THE EFFECT OF PRESSURE ON THE LAMINAR BURNING VELOCITY OF METHANE-OXYGEN-NITROGEN MIXTURES

By DONALD SMITH and JOHN T. AGNEW

Introduction

The laminar burning velocity, commonly symbolized by S_u, is recognized as one of the most basic parameters in the science of combustion. Considerable effort is being made to develop adequate theories by means of which this parameter can be calculated for a given fuel-oxidant mixture. The adequacy of these theories is invariably tested by comparison with experimental results. More experimental data is needed, particularly relative to the effect of pressure on the laminar burning velocity of hydrocarbon fuels. Very little experimental data exists in the pressure range above one atmosphere. The data reported here covers a pressure range up to 20 atmos. The pressure coefficient of burning velocity has been determined in a 10-in. spherical bomb for three mixtures; $CH_4 + 2O_2$, $CH_4 + 2O_2 + 2.25N_2$, and $CH_4 + 2O_2 + 7.56N_2$ (methane-air), all mixtures being initially at room temperature.

Description of Experimental Methods

These studies have been carried out by means of the constant-volume bomb method. This method was chosen primarily for two reasons First, propagation of the flame front is every where perpendicular to the unburned gas, a strict requirement for accurate measurements of the laminar burning velocity. Secondly, the bomb method is well adapted for studies in the high pressure range. It is realized that the bomb method has some disadvantages, chief among which is the question of full energy release in the thin reaction zone. This must be assumed in order to make the calculation of the adiabatic explosion pressure, P_e, and ultimately the value of S_u.

The use of the constant-volume bomb technique has been discussed in detail by Lewis and von Elbe,[1] by Manton, von Elbe, and Lewis,[2] and by Manton and Millikan.[3] The basic relationships employed for the determination of S_u are as follows:

$$P_e = \left(\frac{M_b T_e}{M_i T_i}\right) \tag{1}$$

$$n = \frac{P - P_i}{P_e - P_i} \tag{2}$$

$$\left(\frac{r_b}{a}\right)^3 = 1 - \left(\frac{P_i}{P}\right)^{1/k_u} \left(\frac{P_e - P}{P_e - P_i}\right) \tag{3}$$

$$S_u = \frac{dr_b/dt}{1 + \frac{1}{k_u}\left(\frac{P_e}{P} - 1\right)} \qquad (4)$$

In these equations:

n = fraction of total charge burned
r_b = flame radius
P_i = initial pressure
P = actual instantaneous pressure at any time t
dr_b/dt = slope of curves shown in Figures 3, 4, and 5
k_u = ratio of specific heats for the unburned charge
T_e = Thermodynamic equilibrium flame temperature for adiabatic constant volume combustion
P_e = Thermodynamic equilibrium pressure corresponding to T_e
M_b = moles of burned gas
M_i = moles of unburned gas
T_i = initial temperature

Equation 2, which states that the fraction of charge burned is proportional to the pressure rise is only true for adiabatic conditions and for small values of n, of the order of one per cent. This is the order of n during the first few centimeters of flame travel in the constant-volume bomb. P_e is evaluated on the assumption of complete combustion, allowing for dissociation of CO_2 and H_2O to O_2, CO, H_2 and OH. P_e is always greater than the actual maximum pressure observed due to lack of adiabatic conditions during the late stages of the combustion process.

The investigators mentioned above have shown that the method gives quite reliable and accurate results by taking both pressure data and photographic flame travel data simultaneously. Manton and Millikan[3] have presented very interesting results concerning the pressure coefficient of burning velocity for a wide range of hydrocarbon-oxygen-inert gas mixtures at atmospheric pressure and below.

In the constant-volume bomb technique, the use of pressure-time data for the determination of S_u is somewhat difficult since a very sensitive pressure gauge is required to record the small pressure rise associated with the first few centimeters of flame travel (during which travel the determination of burning velocity is made). At the same time, this sensitive pressure gauge must be protected against the ultimate high pressure which develops upon completion of combustion of the entire charge. For example, with an initial pressure of one atmosphere, the pressure rise at the time S_u is determined might be of the order of 0.005 atmos., whereas the total pressure rise would be of the order of 6 atmos.

A different method for determining the flame position as a function of time was used in this work, utilizing ionization gaps located at strategic positions. Four positions of the ionization gaps were utilized and were spaced at approximately equal intervals along a radius of the spherical cavity. The outermost gap was approximately four-tenths of the way from the central ignition gap to the vessel wall. As the flame front passed the ionization gaps, a corresponding deflection was observed on an oscilloscope screen and recorded with a drum camera. Figure 1 is a diagrammatic sketch of the experimental apparatus including the electrical circuit used to produce the sequence of events on an oscilloscope screen. Figure 2 is a typical oscilloscope trace and Figures 3, 4, and 5 are typical experimental results for the three mixtures studied, the data in these figures being for an initial pressure of one atmos. For the stoichiometric methane-air mixture sphericity of propagation was confirmed by locating an ionization gap at a constant distance from the ignition gap along a number of radii. The spark ignition gap was 0.010 in. for pressures up to 10 atmos, and 0.003 in. at 20 atmos. The ionization gaps were 0.020 in. placed perpendicular to the direction of propagation. Both the spark gap and ionization gaps were between pointed steel

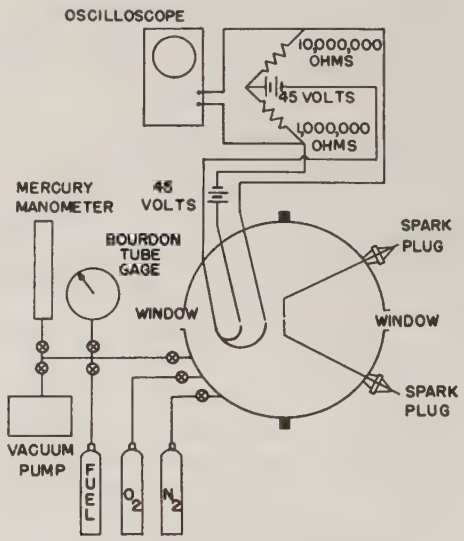

FIG. 1. Diagram of apparatus.

electrodes 0.0625 in. in diameter. The ignition spark was a pure capacitance spark generated by 0.00625 μf at 4560 v, or an energy of 65 mj. The spark gap was energized by closing a snap switch, so that the 65 mj of energy were actually dissipated across two gaps, the external switch and the internal gap. The minimum ignition energy for a stoichiometric methane-air mixture, with bare steel electrodes forming a 0.010 in. gap is of the order of 8 mj.[1]

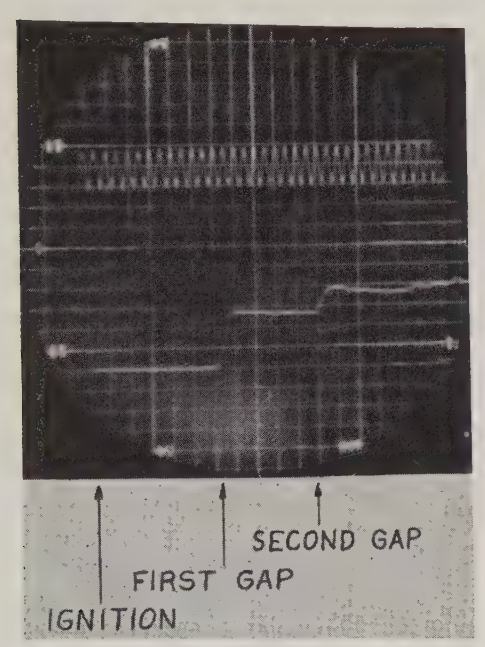

FIG. 2. Typical oscilloscope trace.

Effect of Pressure on the Laminar Burning Velocity

Figure 6 shows the results of our work and of several other investigators as to the effect of pressure on S_u for a stoichiometric methane-air mixture. The Wolfhard data may not be accurately represented since it was transferred from a slide projected by Dr. Wolfhard at a recent lecture at Purdue University. However, his values, obtained by a burner method were, in general, somewhat lower than ours. The Egerton and Lefebvre data[4] were obtained by a tube method. Manton and Millikan[3] have suggested that the variation of burning velocity with pressure for most hydrocarbon-oxygen-inert gas mixtures may be represented by the relation;

$$\frac{(S_u)_a}{(S_u)_b} = \left(\frac{P_a}{P_b}\right)^n \qquad (5)$$

and that the value for n for a stoichiometric methane-air mixture is about -0.09. This value of n is based upon measurements at two pressures, 1.0 and 0.1 atmos. The data shown in

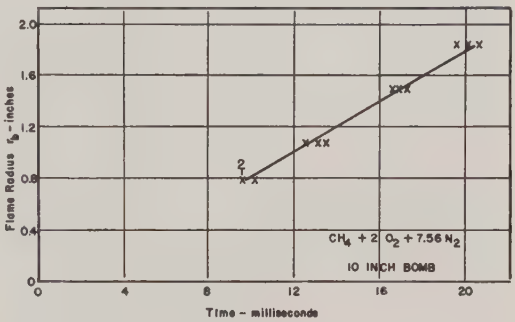

FIG. 3. Experimental flame travel data for methane-air mixture.

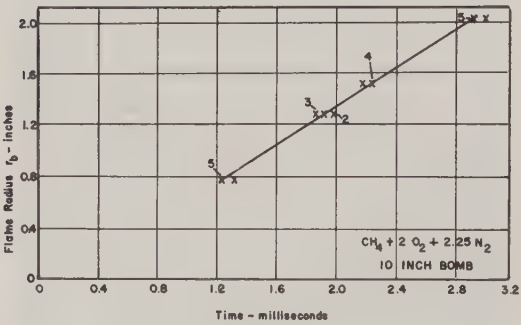

FIG. 4. Experimental flame travel data for $CH_4 + 2O_2 + 2.25N_2$ mixture.

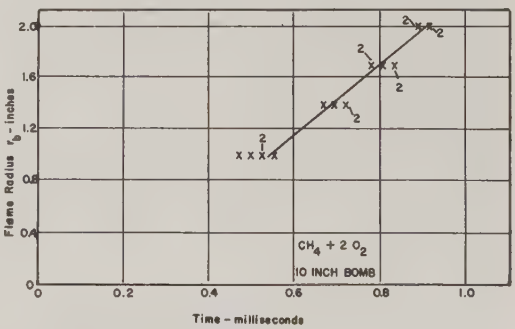

FIG. 5. Experimental flame travel data for methane-oxygen mixture.

Figure 6 for these investigators is an extension of this equation, with the -0.09 exponent, to a pressure of 20 atmos. Our data would indicate that the pressure dependency is not representable by the simple relationship shown in Equation 5. As shown in Figure 6, our data is accurately represented by the relationship;

$$\frac{S_u}{S_{u_1}} = e^{0.3(1-P^{0.54})} \tag{6}$$

where S_u is the laminar burning velocity at pressure, P, and S_{u_1} is the laminar burning velocity at a pressure of one atmos.

This equation gives a value of 44.4 cm/sec for S_u at 0.1 atmos., which checks quite closely the experimental value of Manton and Millikan.

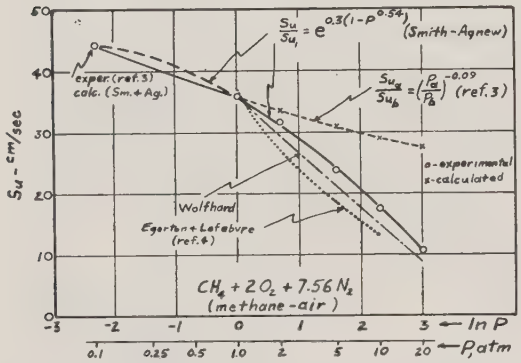

FIG. 6. Burning velocity as a function of pressure for stoichiometric methane-air mixture.

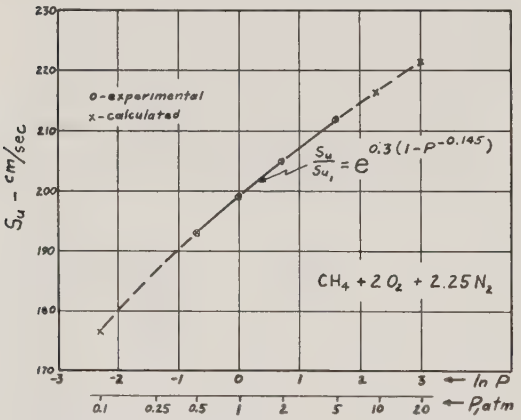

FIG. 7. Burning velocity as a function of pressure for 42.8 per cent nitrogen mixture.

Figure 7 shows the results obtained for the $CH_4 + 2O_2 + 2.25N_2$ mixture. It will be noticed immediately that the values of S_u are much higher than for the methane-air mixture, and furthermore that the pressure coefficient is now positive rather than negative. An equation which accurately fits the curve shown in Figure 7 is;

$$\frac{S_u}{S_{u_1}} = e^{0.3(1-P^{-0.145})} \tag{7}$$

Both equations 6 and 7 have the same general form;

$$\frac{S_u}{S_{u_1}} = e^{b(1-P^x)} \tag{8}$$

where b and x are experimentally determined constants. The rather striking result was that the constant b was within one per cent of 0.3 for both the methane-air and the $CH_4 + 2O_2 + 2.25N_2$ mixtures.

The third mixture studied was a stoichiometric methane-oxygen mixture. There is considerable

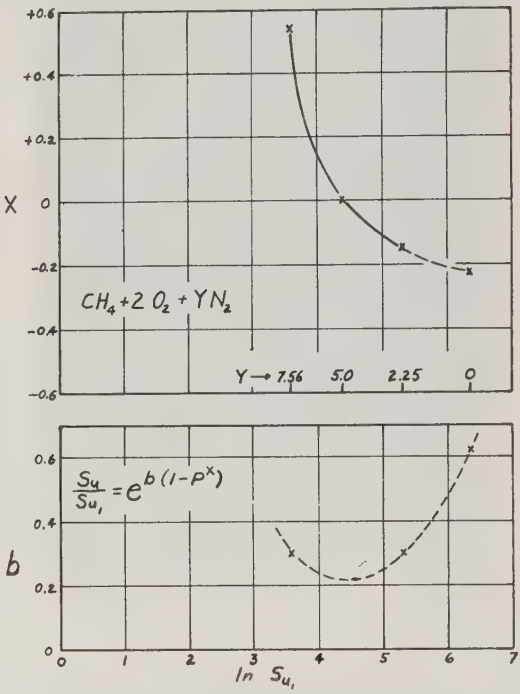

FIG. 8. Relationship between burning velocity the experimental parameters b and x, and the nitrogen content of the mixture.

discrepancy in the literature both as to the actual value of S_u for this mixture at one atmos pressure and as to the pressure coefficient of the burning velocity. Wolfhard (5) has indicated that his results with the burner method show little, if any, pressure dependency of S_u for this mixture. We have measured S_u for the $CH_4 + 2O_2$ mixture at only two pressures, 0.1 and 1.0 atmos. The values obtained were 386 and 564 cm/sec respectively, indicating a positive pressure dependency for this mixture. In order to compare the magnitude of this pressure dependency with that obtained with the other two mixtures investigated, the method shown in Figure 8 was used.

The upper curve in this figure is a plot of the pressure exponent, x, in equation 8 as a function of ln S_{u_1} (the atmospheric pressure value). The values of x of $+0.54$ and -0.145 are for the methane-air and $CH_4 + 2O_2 + 2.25N_2$ mixtures. The data of Manton and Millikan indicate that a $CH_4 + 2O_2 + 5N_2$ mixture should have zero pressure dependency and a burning velocity of approximately 80 cm/sec. This point has been included on the curve and the curve then extrapolated to ln S_{u_1} equal to 6.34 (S_{u_1} equal to 564 cm/sec) which was obtained experimentally. This extrapolation resulted in a value for x of -0.21. Using this value of x and the experimental S_u values at 0.1 and 1.0 atmos of 386 and 564 cm/sec, an equation of the same form as equation 8 was derived for the methane-oxygen mixture as

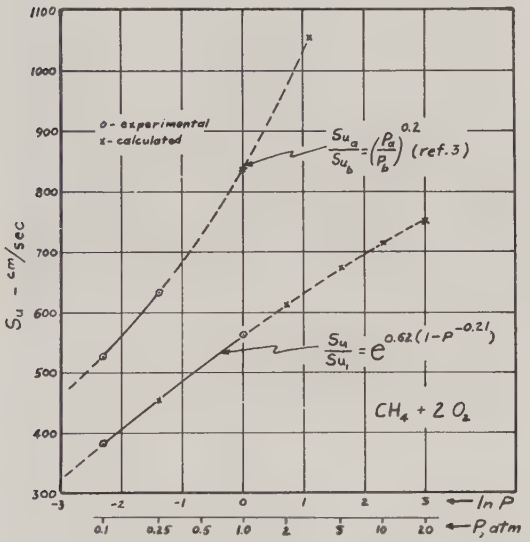

FIG. 9. Burning velocity as a function of pressure for stoichiometric methane-oxygen mixture.

$$\frac{S_u}{S_{u_1}} = e^{0.62(1-P^{-0.21})} \qquad (9)$$

This equation has been plotted in Figure 9 along with the Manton and Millikan equation for this mixture, the dotted portion of each curve indicating an extension of the experimental data according to the appropriate equation. It is for this mixture that the greatest deviation exists (in the low pressure experimental range) between the data of Manton and Millikan and our data. Singer and Heimel (see Lewis and von Elbe,[1] p. 467) using the burner cone frustrum method obtained a value of approximately 450 cm/sec for S_u of a stoichiometric methane-oxygen mixture at a pressure of one atmosphere.

The lower curve in Figure 8 is a plot of the b value in Equation 8 as a function of ln S_{u_1} for the three mixtures investigated, the value for the methane-oxygen mixture being subject to the methods described above. It is, of course, almost impossible to draw any conclusions from such sparse data, but it is interesting to note that a minimum in the b curve is indicated in the region where Manton and Millikan have observed zero pressure dependence. These results also indicate a definite positive pressure dependence of S_u for the methane-oxygen mixture.

Summary and Conclusions

The laminar burning velocity of a stoichiometric methane-air mixture (71.6 per cent nitrogen) decreases markedly as the pressure is increased from one to twenty atmos. This pressure relationship is not representable by a single value of n in the relationship given in Equation 5. The burning velocity for the $CH_4 + 2O_2 + 2.25 N_2$ mixture (42.8 per cent nitrogen) increases as the pressure increases from 0.5 to 5.0 atmos. Experimental data show also that a stoichiometric methane-oxygen mixture has a positive pressure dependence. Equations 6, 7, and 9 accurately represent the pressure dependence of laminar burning velocity for these three mixtures, respectively, all of these equations being of the general form given in Equation 8. It should be noted that the form of Equation 8 is such that a negative value of x indicates a positive pressure dependence and vice versa.

The positive pressure dependence indicates a high order or reaction which is rather disturbing. However, it is to be noted also, that the possible objection that excitation lag might cause false results in the bomb method applies just as well to the methane-air mixture as to the methane-oxygen mixture. Fair agreement among the various investigators exists for the methane-air mixture up to a pressure of 20 atmos, but considerable discrepancy remains regarding the actual values of and the pressure dependency of S_u for the methane-oxygen mixture. This lack of agreement will undoubtedly be resolved by more research by the various investigators.

REFERENCES

1. LEWIS, B., AND VON ELBE, G.: *Combustion, Flames and Explosions*. New York, Academic Press, Inc., 1951.
2. MANTON, J., VON ELBE, G., AND LEWIS, B.:

Fourth Symposium (International) on Combustion. Baltimore, The Williams & Wilkins Co., 1953.
3. Manton, J., and Millikan, B. B.: *Gas Dynamics Symposium on Aerothermochemistry.* Evanston, Illinois, August 1955. See also Lewis, B. (discussion): *Selected Combustion Problems, AGARD,* p. 177. London, Butterworths Scientific Publications, 1954.
4. Egerton, A., and Lefebvre, A.: Proc. Roy. Soc., *A222,* 206 (1954).
5. Private communication.

10

INFLUENCE OF PHYSICAL AND CHEMICAL FACTORS ON BURNING VELOCITY

By E. S. Golovina and G. G. Fyodorov

Introduction

The principal objective of this study was to determine the effect of the chemical characteristics of a combustible mixture on the fundamental burning velocity. Changes in the rate of the chemical process were effected by varying the oxygen content in mixtures containing benzene, hexane or a hexene-hexane fraction (40 per cent hexene and 60 per cent hexane). The oxygen content was changed by replacing nitrogen with oxygen, going from 16.4 per cent O_2 to a pure oxygen atmosphere. The experimental method consisted of varying the content of the fuel by replacing nitrogen in fuel—O_2-N_2 mixtures with a fixed oxygen content. In this way, a system of U_n (normal burning velocity) curves was obtained over the maximum possible range of fuel concentrations, each curve corresponding to a constant oxygen concentration.

Experimental Procedure

The burning velocity measurements were made with a Bunsen-type burner. Because of the high burning velocities in oxygen-containing mixtures and the necessity of maintaining a laminar regime of flow, it was necessary to use narrow burners and decrease the burner diameter from $d = 3$ mm to $d = 2$ mm and then to $d = 1.45$ mm as the oxygen content was increased. Check tests showed that at sufficiently high burning velocities, of the order of those of oxygen flames, changing the burner diameter did not change the normal velocity values appreciably.

With such small burners, the most difficult experimental problem was to obtain a low, stable feed rate for the fuel and to measure it. This problem was solved successfully by using narrow capillary tubes through which the fuel was fed to a vaporizer, from which its vapors were removed by a nitrogen or oxygen stream. Changes in the feed rate of the combustible were effected by varying the location of the capillary tube with respect to the liquid level in the feed reservoir, or by using a capillary tube of a different diameter. The capillary tube made it possible to obtain a stable feed of the combustible with an accuracy of 0.01 cc/min. The burning velocity was determined from photographs of the flame cone on the burner by measuring the angle 2α at the apex of the cone and calculating U from the relationship

$$U = \overline{W} \sin\alpha$$

in which $\overline{W}$ is the mean flow velocity at the burner port. The spectral line-reversal method also was used to measure the temperature at the cone apex for the mixture giving the maximum burning velocity and for the stoichiometric mixture.

The composition and temperature of the combustion products were determined by thermodynamic calculations for a wide range of hexane concentrations and for O_2 concentrations varying within the limits mentioned above.

Results

Figure 1 shows the burning velocity in benzene-oxygen mixtures as a function of the fuel content of the mixture expressed in per cent. With the exception of the extreme upper curve, representing $C_6H_6 + O_2$ mixtures in which the content of each of the components is a variable, the oxygen content for each curve is constant. Similar curves for hexane mixtures are given in Figure 2. The

figures show a large increase in the burning velocity range due to an increase in the upper limit. The lower limit may, without serious error, be considered constant over the entire range of oxygen concentrations. When the oxygen content of the mixture is increased the relative positions of the maximum velocity and of the stoichiometric mixtures are shifted (the maximum velocity and stoichiometric mixtures are indicated by dashes); for mixtures with a large oxygen concentration, the velocity maximum is shifted with respect to the stoichiometric mixture towards the region of lean mixtures.

It is preferable to express the burning velocity as a function of the ratio of the contents of the fuel and the oxidizing agent. The most convenient method of expressing the ratio is in moles of fuel to moles of oxidizing agent. In Figures 3 and 4 the mean experimental data of Figures 1 and 2 are plotted using such a system of coordinates. The resulting curves exhibit several interesting features. First, the maximum values of the burning velocity for mixtures containing up to 50 per cent oxygen occur at a constant value of the ratio

$$K_m = \frac{C_6 \cdot H_6}{O_2} = A$$

For benzene $K_m = 0.165$; for hexane (for mixtures with an O_2 concentration of up to 60 per cent) $K_m = 0.118$. Similar treatment of the data of Jahn[1] and Dennues[2] for methane indicates that the relationship covers that gas as well, K_m being equal to 0.565 if the oxygen concentration does not exceed 50 per cent. The expression is also true for CO and H_2. It is not possible however, to determine the actual numerical value from the data of Jahn inasmuch as they were not obtained at constant values of the O_2 content in the mixtures, but in "atmospheres" ($O_2 + N_2$ or $O_2 + CO_2$). For fuels, such as CO and H_2, with a wide burning velocity range, numerical values of K_m calculated from such experimental data would be in error.

A constant ratio of the per cent combustible to the per cent oxygen at maximum velocity appears to be a general rule for various fuels. This ratio evidently corresponds to optimum conditions for the chemical reaction in the flame front.

Practical recommendations can be made from the results obtained: the concentration of the combustible at the maximum burning velocity in a mixture with air can be used for determining the concentration at maximum velocity for mixtures with other oxygen concentrations up

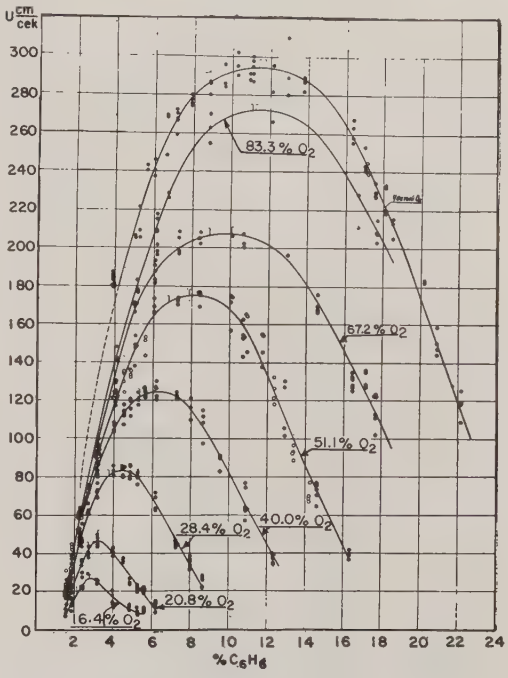

FIG. 1.

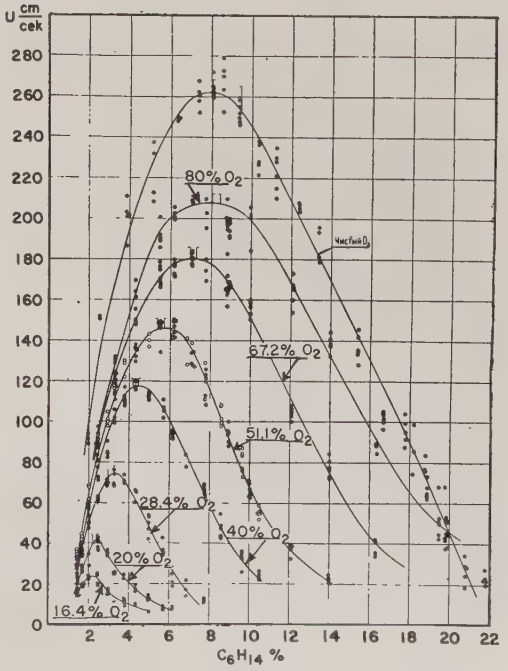

FIG. 2.

to 60 per cent, and with a decrease in accuracy of about 10 per cent for even higher oxygen

concentrations. Thus, if for an air mixture

$$K_m = \frac{\text{Fuel content}}{20.8} = A$$

then, for any oxygen concentration,

$$\text{Per cent fuel} = A \cdot \text{per cent } O_2$$

For mixtures containing more than 50 to 60 per cent oxygen, the burning velocity maximum gradually shifts toward the lean mixture region; for mixtures with an oxygen concentration above 80 per cent, the maximum is found at ratios leaner than the stoichiometric. An attempt to explain this is made below.

Let us now consider the question of limits. It is difficult to determine values at the limits accurately, especially at the upper limit, by the experimental method used in this study. However, in spite of some scattering it will be seen that on the right all the curves approach some constant limiting value of K. Consequently, the upper concentration limit for flame propagation is not given by some constant value of the fuel content of the mixture, but by a constant ratio of the fuel content to the oxygen content. Thus, K for benzene is approximately 0.3; for hexane, it is approximately 0.27. The upper limit of the fuel content for various oxygen contents can easily be computed from these values. Similar results were also obtained for mixtures with a hexene-hexane fraction.

For some of the benzene and hexane mixtures, in addition to the burning velocity, the flame temperature was measured over the entire range of O_2 concentrations. The temperature at the apex of the cone, measured by the spectral line-reversal method, was recorded. A tungsten-ribbon-filament temperature lamp with a tem-

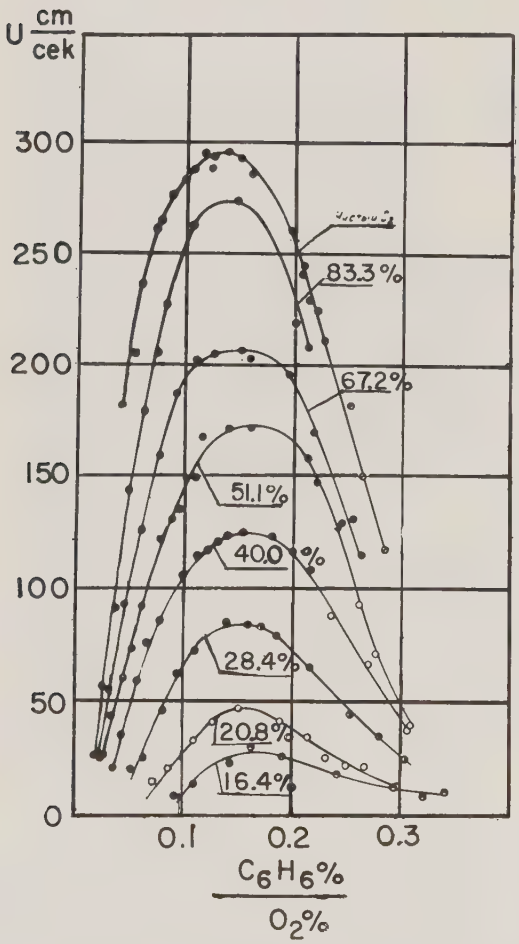

Fig. 3.

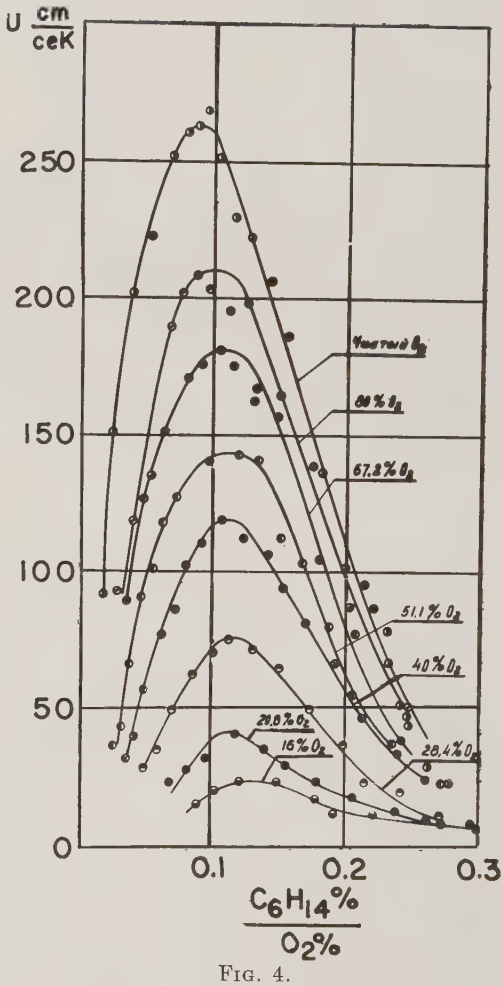

Fig. 4.

perature range of from 1500° to 2400°C was used as a standard source; for higher temperatures an electric arc with a neutral absorbing screen was used. For hexane, the temperature and composition of the combustion products was determined by thermodynamic calculations over the complete range of fuel and oxygen concentrations. Results of the calculations can be given only in part here. The measured and the calculated temperature values for hexane mixtures are given in Figure 5. The experimental data for benzene mixtures are given in Table 1.

As will be seen from Figure 5, in the region of lean mixtures changes in the oxygen content do not affect the flame temperature. It is significant at the flame of an 80 per cent oxygen mixture

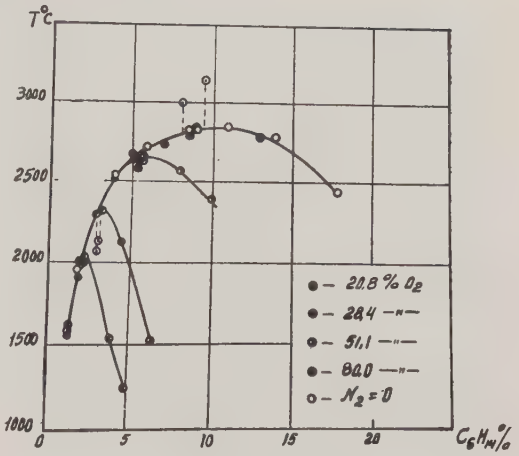

Fig. 5.

Table 1

O_2	C_6H_6	T	U	O_2	C_6H_6	T	U
per cent	*per cent*	°C	*cm/sec*	*per cent*	*per cent*	°C	*cm/sec*
16.4	2.20 stoich	1830	20.0	51.5	6.75 stoich	2710	171
	2.85 max	1960	26.0		7.9 max	2840	175
20.8	2.75 stoich	1940	40	67.2	8.92 stoich	2950	211
	3.20 max	1990	45		10.1 max	3040	212
28.4	3.8 stoich	2240	80.5	83.3	11.10 stoich	3190	270
	4.4 max	2310	82.0		11.25 max	3190	270
40.0	5.35 stoich	2630	122	88.2	11.8 stoich	3270	287
	6.20 max	2700	126	88.6	11.4 max	3190	287

has the same temperature as a pure oxygen flame. At oxygen contents below 67 per cent, for each concentration curve, the location along the curve of maximum temperature and the location of maximum burning velocity coincide. At oxygen contents above 67 per cent, the burning velocity maximum shifts with respect to the temperature maximum in the direction of the lean mixtures. The fact that the measured temperatures are considerably higher than calculated ones for a pure oxygen flame is surprising and has not yet been explained. The difference amounts to almost 300°C.

Following the example of Gaydon and Wolfhard[3] and Linnett,[4] it is interesting to correlate the temperature values for the flame front and the composition of the combustion products, especially the concentrations of the atoms and radicals O, OH and H, with the burning velocity. Although the temperature and composition values were calculated for the entire range of fuel and oxygen concentrations, in this paper space permits consideration only of the mixture corresponding to the maximum burning velocity. The data for this case are represented in Figure 6, where the dots represent experimental data and the solid line is the calculated temperature curve.

Initially, for mixtures with an O_2 content of less than 70 per cent, the burning velocity curve closely follows the pattern of the temperature curve. At O_2 content values above 70 per cent, the temperature remains virtually constant, but the flame velocity once again begins to rise rapidly. Evidently, there is a change in the chemical reaction at this point due to the high temperatures developed in the flame front. It should be noted that when N_2 is replaced by O_2 in the range 80 per cent to zero, the physical properties of the mixture, including λ and C_p, which are of special interest, do not undergo any significant changes that could have any appreciable influence on the value of the burning velocity.

The rate of chemical transformations in the reaction zone is a function of the temperature, the effective concentration of the fuel and

oxidizing agent, and the concentration of the active radicals; it is clearly the main factor controlling flame propagation. For mixtures containing over 70 per cent oxygen, which corresponds to a temperature above 2700°C, the increase in the rate of chemical transformation is evidently the result of an increase in the part played in the combustion zone by the active atoms and radicals which form in increasing quantities due to the growth of chains and the dissociation of combustion products. As a result, the temperature level remains virtually unchanged and this, in turn, can have its specific effects on the mechanism of flame propagation.

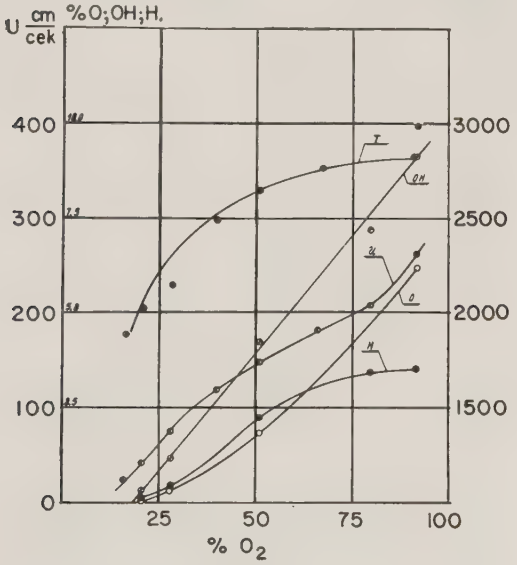

FIG. 6.

The changes in the relationships governing flame propagation at O_2 contents above 60 per cent have already been mentioned: the fact that the maximum burning velocity and the temperature maximum do not coincide; the shift of the velocity maximum towards the lean mixtures region; the end of the linear character of the curve for the flame propagation velocity *vs* the oxygen content of the mixture, etc. These changes undoubtedly are the result of the changes in the chemical reaction, which is ultimately a function of the temperature of the process. For the hydrocarbons under consideration, the most important part is probably played by the OH radical, whereas the H atom content is the factor in the pattern of the increase in the burning velocity, as can be seen in Figure 10. In the region of rich combustible mixtures, in spite of the considerable increase of the H content in the products, the increase in U is slow and follows the course of the increase in temperature and the OH and O content.

The above results do not support the conclusions of those authors[5] who propose the pure diffusion theory of flame propagation and assign the decisive role to diffusion into the fresh mixture of active particles, especially to the diffusion of H atoms.

Discussion

The laws governing the burning velocity lead to: (1) A general empirical equation for calculating the approximate burning velocity with a minimum amount of data; (2) Information regarding the kinetic characteristics of the process in the flame front.

The burning velocity curves can be described by a parabolic equation of the type

$$(x - x^m)^2 = -2p(U - U^m)$$

where x^m and U^m are the coordinates of the vertex of the parabola; p is the parameter, x is the concentration of fuel in the mixture. The equation may be rewritten as follows

$$U = U^m - \frac{(x - x^m)^2}{2p}$$

The parameter, p, may be expressed in terms of the values of x and U for the lower limit, $*x_0$ and U^0. Then,

$$U = U^m - \left(\frac{x - x^m}{x_0 - x^m}\right)^2 (U^m - U^0) \qquad (1)$$

Let us now determine how the quantities entering into the equation depend on the oxygen concentration.

There are considerable experimental data[6, 7] to show that both in air and in oxygen mixtures the lower limit of the burning velocity and the burning velocity at the limit are approximately constant in value, which is in agreement with theoretical considerations. On the basis of our data, the values of the normal burning velocity, U^0, and of the concentration at the lower limit, x_0, can also be considered to be approximately independent of the oxygen concentration. As was noted above, the concentration of the fuel in mixtures of maximum burning velocity can be determined from the simple relationship:

$$x^m = K_m \cdot O_2\%$$

in which K_m is constant for each fuel. For such mixtures the relationship between U^m and the O_2 content (for both mixtures investigated at oxygen contents of up to 50 per cent) is found to be linear, and the analytical expression is

$$U^m = B(O_2 - O_2^0) \qquad (2)$$

where B is a constant depending on the fuel (for benzene, $B = 4.3$, for hexane, $B = 4.0$, for methane, $B = 6.72$ and for CO, $B = 11$) and O_2^0 is the lower limit oxygen concentration for the given fuel. Our data yield $O_2^0 = 10$ per cent for benzene and $O_2^0 = 10.2$ per cent for hexane. Egerton and Thabet[8] give O_2^0 values for a number of hydrocarbons that are fairly close to our results, e.g., 11.5 per cent for methane, 11.0 per cent for propane and 11.5 per cent for butane. Equation (2) can be used to transform Equation (1) as follows

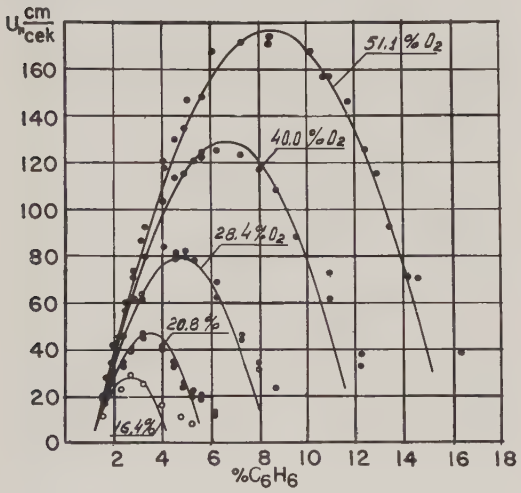

FIG. 7.

$$U = U^0 \left(\frac{x^m - x}{x_0 - x^m}\right)^2 + \left[1 - \left(\frac{x^m - x}{x_0 - x^m}\right)^2\right] B(O_2 - O_2^0) \qquad (3)$$

Figures 7 and 8 show the accuracy with which Equations (1) and (3) fit the experimental data for benzene and methane (Equation (1)). The dots represent experimental data; the curves are calculated. Although Equations (1) and (3) were obtained by purely empirical methods, they are very convenient for estimating the burning velocities of mixtures with various oxygen concentrations.

The second problem which can be considered on the basis of the experimental data obtained in this study is that of the basic kinetic characteristics of combustion in the flame front.

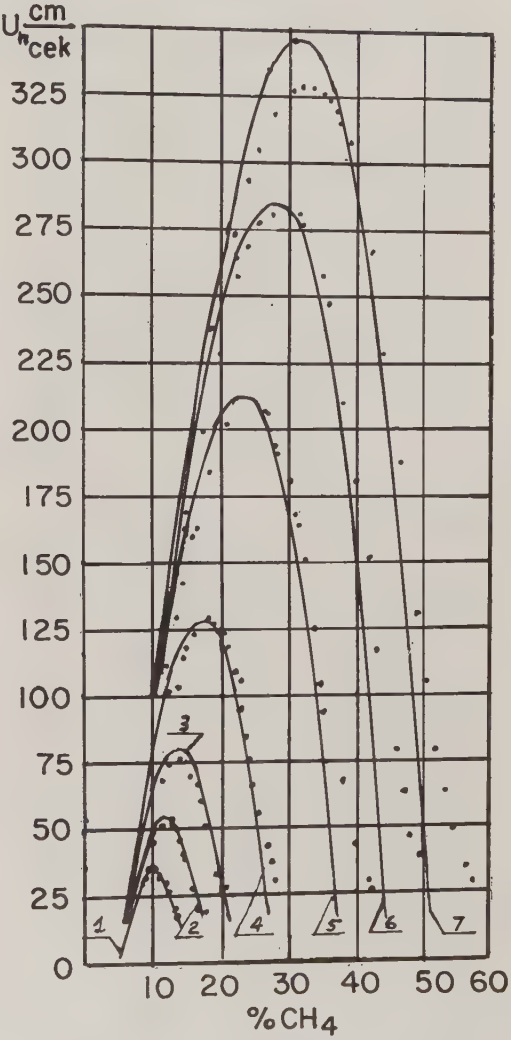

1—79%N_2 + 21%O_2
2—75%N_2 + 25%O_2
3—70%N_2 + 30%O_2
4—60%N_2 + 40%O_2
5—40%N_2 + 60%O_2
6—20%N_2 + 80%O_2
7—1.5%N_2 + 98.5%O_2

FIG. 8.

To date, no hard and fast point of view has been developed on the relation between the burning velocity and the characteristics of the chemical process in the combustion zone. Numerous theoretical equations have been proposed but the most rigorous statement and solution of the problem is that of Zeldovich and Semenov.[9]

In its most general form the relationship is expressed by the equation:

$$U = \sqrt{A \frac{dm}{dt}} \qquad (4)$$

where A is a quantity depending on the physical

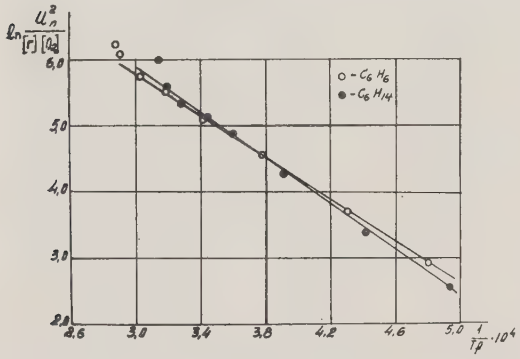

Fig. 9.

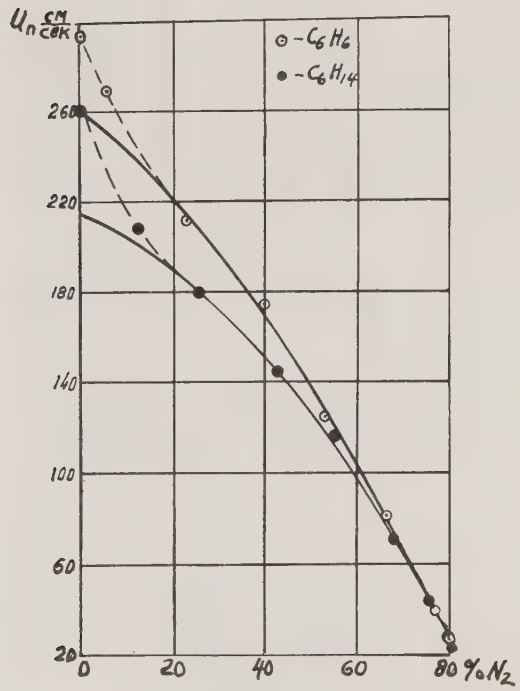

Fig. 10.

properties of the combustible mixture in the flame zone (λ, C_p, ζ, etc.) and dm/dt is the rate of the chemical reaction in the combustion zone. Assuming that the over-all reaction is of the second order, its rate, expressed in terms of the classical Arrhenius equation, can be written as follows:

$$\frac{dm}{dt} = K_0 \cdot e^{-E/RT} [O_2][F]$$

$[O_2]$ and $[F]$ are averages of the active concentration of the oxidizing agent and the combustible component in the combustion zone. Let us assume that the reaction takes place principally at T_f, the maximum temperature in the flame front and that A is independent of the temperature. We obtain the following expression, which can be used for analyzing the process

$$U = \sqrt{A \cdot K_0 \cdot e^{-E/RT} [O_2][F]} \qquad (5)$$

Let us first consider the mixture of maximum burning velocity. The value of T_f for such a mixture is determined experimentally. The mean effective concentration of the fuel in the reaction zone according to Semenov is given by the expression

$$[F]_{\text{eff}} = \frac{\zeta_0 \cdot \bar{C}_p \cdot T_0 \cdot R \cdot T_f}{\theta' \cdot E}$$

which may be written more simply as

$$[F]_{\text{eff}} = C_1 \cdot \bar{C}_p \cdot T_f$$

inasmuch as all the quantities except $\bar{C}_p$ and T_f are constant in value for a given combustible mixture. For the mixtures under discussion, which correspond to the maximum burning velocities, experiments show that:

$$\frac{E}{O_2} = K_m$$

Assuming that this expression is also valid for the flame zone:

$$[F][O_2] = C(\bar{C}_p \cdot T_f)^2$$

and (6)

$$U = \sqrt{B \cdot e^{-E/RT_f} (\bar{C}_p \cdot T_f)^2}$$

The activation energy of the combustibles used may be determined from experimental values for U_m and T_f. If $\ln U^2/[O_2][E]$ is plotted as a function of $1/T_f$ our data lie very closely along a straight line. This shows that the Arrhenius equation is valid for the chemical reaction over a wide range of oxygen concentrations. Only at the very highest oxygen concentrations, at $O_2 >$ 70 per cent, do the plotted points deviate from a straight line, which also points towards a change in the laws governing the process. The straight

lines of Figure 9 correspond to benzene and hexane mixtures. The values of the energy of activation determined from the slopes of the straight lines are 31,600 kcal/mole for benzene and 34,000 kcal for hexane. The values for benzene are somewhat larger than those obtained by Fenn and Calcote.[10] This may be a result of the numerous assumptions made both by us and by these authors. Introducing the value obtained for B, we obtain the following expressions for the maximum burning velocity for benzene mixtures:

$$U = \sqrt{3.94e^{-31600/RT_f} \cdot \bar{C}_p^2 \cdot T_f^2} \qquad (7)$$

and for hexane mixtures

$$U = \sqrt{5.99e^{-34000/RT_f} \cdot \bar{C}_p^2 \cdot T_f^2} \qquad (8)$$

These equations are satisfied by the experimental data quite accurately. The solid line curves of Figure 10 were calculated using Equations (7) and (8). Thus, the initial assumption that in combustible mixtures of maximum burning velocity, the over-all chemical process is governed by relationships for second-order reactions, was generally confirmed. It is natural now to attempt to apply Equations (7) and (8) not only to data for maximum velocity gas mixtures but to data for other mixtures as well. We may assume that in the rich mixture region, for any O_2 = constant curve, only that part of the mixture will be effective which conforms to the mixture of maximum velocity. Increasing the excess of the fuel (in place of N_2) only alters the composition of the diluent and leads to some changes in the physical properties of the mixture. The most important change is in the value of the specific heat. This affects the temperature developed in the flame front, which in turn decreases the rate of the chemical reaction. The increase in the number of effective molecular collisions due to the increased fuel content would not be very large in this case, because the excess of the fuel over the value for the maximum velocity mixture is only a few per cent. This means that the influence of the concentration factor $[O_2][F]$ will be relatively small compared to the influence of the temperature relationship factor, and that in Equation (5) the change in $[O_2][F]$ will be negligible as compared with that in $e^{-E/RT}$. An estimate showed that for O_2 = constant curves, the influence of T_f on U in the rich mixtures region is two orders higher than the increase in the number of collisions. The picture is similar for the branch of the velocity curve corresponding to lean mixtures. Therefore, assuming the factor $[F][O_2]$ to be constant and equal to the maximum velocity value, $[F^m][O_2]$ over the entire O_2 = constant curve, let us apply Equations (7) and (8) to the experimental data, using the value of T_f obtained by thermodynamic calculations. Experimental results and calculated results (solid curves) are given for benzene mixtures containing 20.8 per cent and 28.4 per cent O_2 (Fig. 11) and for hexane mixtures (Fig. 12). The coincidence is quite good in both cases.

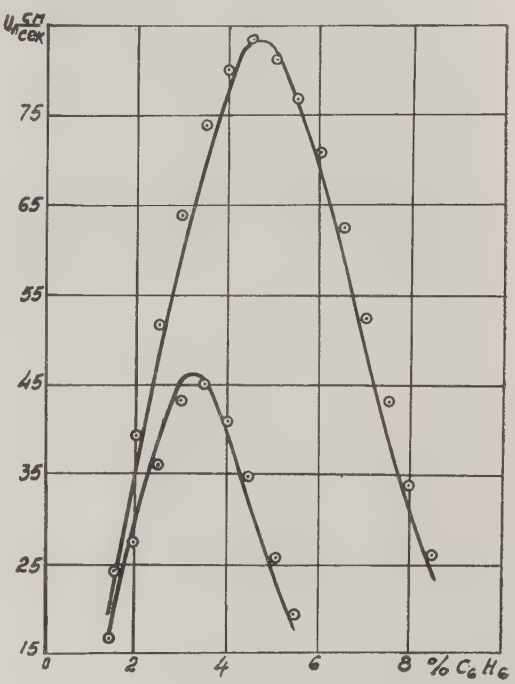

FIG. 11.

At higher concentrations of oxygen the discrepancy is larger. This is further confirmation of the concept that in mixtures with a constant oxygen content, when the fuel content—and, consequently, the nitrogen content—is varied, the changes which take place in the flame velocity are principally due to changes in the rate of the chemical reaction resulting from changes in the temperature of the flame front.

The idea has often been advanced that in lean mixtures the excess oxygen represents an inert addition and does not have any effect on the course of the reaction. For lean mixtures (not for those approaching the lower limit), for a fixed concentration of the fuel, there is a notice-

able increase in the burning velocity when higher concentrations of oxygen are used in the mixtures (see Fig. 1). At the same time, as was noted for Figure 5, the temperature in the flame front does not change when the oxygen concentration alone is increased and the content of the combustible component remains constant. Obviously, for these mixtures the increase in U is not due to the temperature factor, nor is there any change in the physical properties of the mixture. Thus, for a pure nitrogen diluent $\lambda_{N_2} = 5.95 \times 10^{-5}$ cal/cm sec °C, and for pure oxygen $\lambda_{O_2} = 5.99 \times 10^{-5}$ cal/cm sec °C. The specific heat values of oxygen and nitrogen also are close. Therefore the increase of U with an increase in the oxygen content of a mixture should be attributed only to an increase in the rate of collisions of the oxygen and combustible molecules, that is, to an increase in the rate of the chemical reaction.

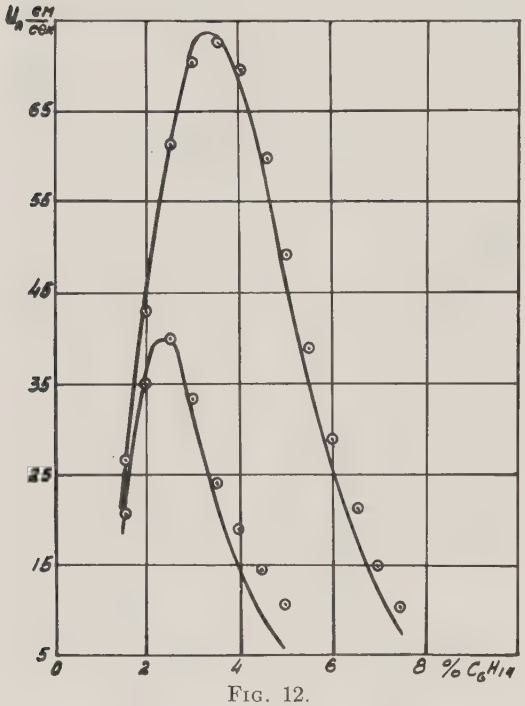

FIG. 12.

Acknowledgments

This investigation was carried out under the direction of L. N. Khitrin, Corresponding Member of the USSR Academy of Sciences, to whom the authors express their deep thanks. A. V. Sorokina, Technical Laboratory Assistant, also took part in the investigation.

REFERENCES

1. JAHN, G.: *Der Zündvorgang in Gasgemischen* (Dissertation). Karlsruhe, 1934.
2. DENUES, A. R. T., AND HUFF, W. J.: J. Am. Chem. Soc., *62*, 3045 (1940).
3. GAYDON, A., AND WOLFHARD, H.: *Flames.* London, Chapman and Hall, 1953.
4. LINNETT, J. W., AND WHEATLEY, P. J.: Trans. Faraday Soc., *45*, 33 (1949).
5. TANFORD AND PEASE: J. Chem. Phys., *15*, 433, 861 (1947).
6. Jost, W.: *Explosions und Verbrennungsvorgänge in Gasen.* Berlin, Springer, 1939.
7. BARCKY, G. A.: *Investigation of the Combustion of Carbon Monoxide* (Dissertation). Moscow, 1945.
8. EGERTON, A. C., AND THABET, S. K.: Proc. Roy. Soc., *A211*, 445 1952.
9. SEMENOV, N. N.: Uspekhi Fisicheskikh Nauk, (Progress of Physical Science), *24*, 433 (1940). (Translated as N.A.C.A. Tech. Memo. No. 1026 (1942)).
10. FENN, J., AND CALCOTE, H.: *Fourth Symposium (International) on Combustion*, pp. 231–239. Baltimore, The Williams & Wilkins Co., 1953. *See also* Voprosi Raketnoi Tekniki, 1955.

11

THE STRUCTURE OF LAMINAR FLAMES

By ROBERT M. FRISTROM

1. Introduction

The study of laminar-flame structure provides an insight into the nature of the combustion processes in flames. These processes are complex because of the interaction of chemical reaction, convection, thermal conduction, and diffusion. Formal equations can be written for flame systems[1] relating conservation of energy, mass, and atomic species with the differential equations of diffusion, conduction, and species production. In ideal cases, these equations can be solved, and

they provide the basis for the interpretation of experimental studies. Confirmatory experimental work is required, however, and in complex flames the experimental approach has proven to be less difficult.

Flame structure is generally used to describe two properties of flames, the macroscopic structure or flame-front geometry and the microscopic structure as described by detailed temperature and composition profiles. Microscopic flame structure is the primary subject of this survey, but flame geometry will be discussed particularly with relation to the detailed microscopic structure.

The systems under discussion are premixed, laminar flames. A number of other interesting combustion systems such as cool flames, polyhedral flames, and diffusion flames will be discussed only briefly. Laminar flames can be completely described by a set of unidimensional profiles or graphs[2] that relate the state of the gas with distance through the flame front. The coordinate usually chosen is the distance normal to the flame front and measured from the center of the luminous zone (Fig. 1). These profiles depend only upon the initial state (temperature, composition, and pressure) of the unburned gas.

Satisfactory interpretation of such data would clarify many vexing problems concerning combustion mechanism and would provide chemists with a wealth of new kinetic information on reactions that are too fast to be studied by ordinary techniques.

2. Flame Geometry

Visual observation of simple conical hydrocarbon-air flames indicates that there are at least three distinct regions of measurable thickness (Fig. 1)—preluminous, luminous, and postluminous. The thin luminous zone is the most conspicuous feature of this flame. Gouy suggested in 1881[3] that the shape of such conical flames could be explained by assuming that the flame propagates normal to itself at a constant velocity that exactly matches the component of incoming gas velocity normal to the luminous surface. The concept of burning velocity has been a fruitful one and has underlain much of combustion research in the past 50 years. This simple picture has been criticized[4, 5, 6] but recent detailed measurement of flow patterns through flame fronts of a number of hydrocarbon flames[2] has shown that in many and probably most cases the concept of a constant burning velocity is capable of quantitatively explaining flame front geometry (Fig. 2). This concept can be generalized to include all of the isothermal surfaces from the point of initial temperature rise to the outer edge of the luminous region. Complications arise primarily because of the aerody-

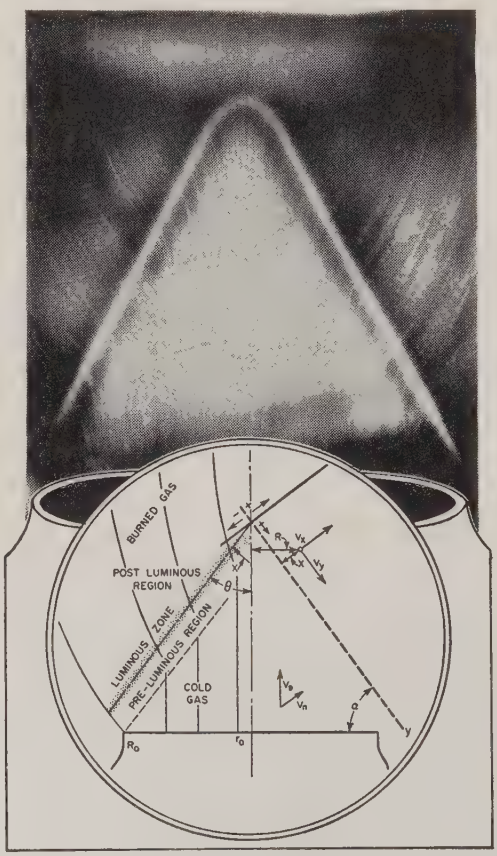

FIG. 1. Macroscopic flame structure—flame geometry. Pictured is a propane-air flame saturated with MgO dust. Illumination is at right angles with a high-intensity photoflash bulb. This picture clearly shows the preluminous reaction region ahead of the luminous zone; the faint luminous mantel which marks the post-luminous reaction region is obscured by the particle images. The positions of the various reaction regions in the flame and the coordinates used in the analysis of the flame geometry are shown in the insert. X and Y are flame front coordinates; R's are burner coordinates; V's are velocities; and Greek letters are angles.

namic effect which a flame has on uniform velocity profiles provided by nozzles. Hydrocarbon flames possess a further complication since the reaction is not complete at the outer edge of the luminous zone, and heat release from the oxidation of CO and H_2, formed in the flame front, continues over an extended region of space (post luminous region, see Fig. 1). This latter complication is by no means a unique

phenomenon though it is absent in simple flame systems.

In spite of aerodynamic and chemical complications, the luminous zone geometry is primarily an aerodynamic problem in which the flame can be treated as a mathematical discontinuity. The approach and following flow is laminar, inviscid, and steady, and the state of the gas is known in both regions. Momentum, mass, and energy are conserved across the discontinuity. Even this simplified three-dimensional flow problem has not been solved, but

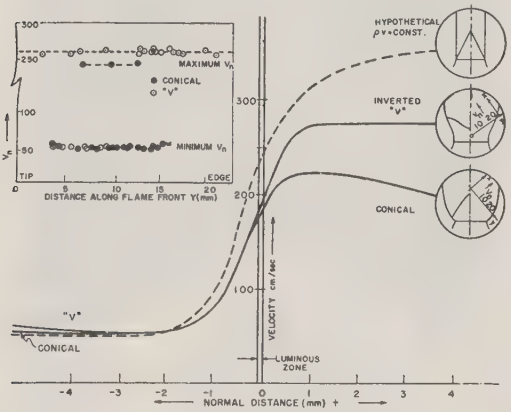

FIG. 2. Normal velocity profiles. The normal velocity profiles for two geometries of the stoichiometric, quarter-atmosphere propane-air flame are compared with the theoretical velocity curve for a flame with no lateral expansion (i.e. where $\rho V =$ const). The insert shows a cross plot of the data against position along the flame front. The data indicate that the normal velocity profile is a function only of the normal distance through the flame front and that burning velocity (the minimum velocity) does not depend upon flame geometry or the initial gas velocity. The unidimensionality of temperature and composition profiles has also been checked experimentally for this system (Refs. 2, 45).

several theoretical studies[7, 8] of two-dimensional systems have been made. These studies show good correlation with experimental flame shapes, and in particular the assumption of constant burning velocity has been shown to be consistent with the existence of a rounded flame tip. Experimental studies of the flow through three-dimensional flame tips indicate that this is the case if one considers the burning velocity to be the velocity normal to the luminous reaction region measured at some consistent point, for example, the inner edge of the luminous zone. Normal velocity in this reaction region appears to be insensitive to flow variations in either the approach or following flow, and has a constant value everywhere along the flame front.

This simple picture is inadequate to describe polyhedral flames and turbulent flames.

3. Microscopic Structure of Flame Fronts

CHARACTERIZATION OF FLAME FRONTS

In order to describe completely laminar flame fronts a model and a suitable set of profiles must be provided. The model chosen by most workers is a simple unidimensional one in which flame-front properties are described by a single set of profiles giving the state of the gas as a function of some distance parameter. With minor modifications this simple model can be adapted to describe accurately three-dimensional Bunsen flames.[2]

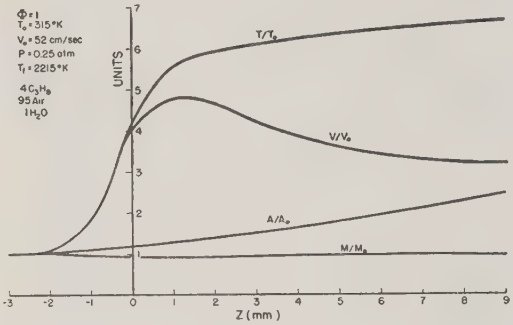

FIG. 3. Characteristic aerodynamic and temperature profiles. Relative velocity, area expansion ratios, average molecular weight, and temperature profiles are given for the stoichiometric quarter-atmosphere propane-air flame. These profiles were obtained by particle track studies combined with composition data from microprobe sampling studies (Refs. 2, 44, and 48).

The aerodynamic and thermodynamic parameters in the flame front depend only upon a single coordinate, the distance normal to the flame front (Fig. 1). It is a good approximation, therefore, to speak of a single reaction course which describes a flame and which depends only on the initial temperature, pressure, and composition. In spite of the excellence of the unidimensional approximation, account must be taken of expansion of the stream tubes passing through the flame front (Figs. 2 and 3), in the case of a stoichiometric propane-air flame at 0.25 atmos; this effect amounts to about 20 per cent. Such expansion does not preclude a unidimensional description, however, and the problem is analogous to the aerodynamic problem of one-dimensional flow in a pipe of expanding cross section. The primary effect is to require the introduction of area expansion into the conservation equa-

tions.[9] The qualitative effect of neglecting this expansion is a distortion of the distance scale.

Variables

In order to describe a flame to which this model applies a set of profiles is required which gives the properties as a function of some single variable. In experimental work, the variable usually chosen is the distance normal to the luminous zone, whereas in theoretical work it is more convenient to choose temperature as the independent variable. A set of profiles convenient for experimental work would be temperature, velocity, and composition as a function of distance. A set suitable for theoretical work is temperature gradient, velocity, and composition as a function of temperature. These sets can be transformed into one another.[9]

same form, and the characteristic thicknesses would be expected to vary inversely with burning velocity and pressure. This qualitative behavior is observed in experimental studies of flame front thickness (Table 1).

FLAME FRONT THICKNESS

A first approximation to the structure of flame fronts can be made by characterizing them with thickness. A number of such measurements of characteristic thickness of flame fronts have been made[9, 10, 11, 12, 13, 14] by measuring thickness of the luminous region or the distance between the schlieren image and the luminous zone. The schlieren image has been shown to be located close to the region of the initial temperature rise.[11] Another method is to measure the pressure profile of the flame.[10] Some caution is necessary in interpreting such data since the flame thickness may not be a direct measure of the reaction region.[2] However, these measurements furnish a useful characterization of flame fronts.

Table 1. Characteristic Propane-Air Flame Front Thicknesses

ϕ	P atmos	V_0 cm/sec	d(Thermal)	$d(H_2)$	$d(CO_2)$	Ref.
			cm	*cm*	*cm*	
1	0.25	50	0.27 calc	0.8 calc	0.17 calc	45
			0.25 exp	0.5 exp	0.25 exp	
1	1.0	50	0.065 calc	0.2 calc	0.04 calc	17
			0.067 exp	—	—	
0.6	0.059	20	2.7 calc	12.5 calc	—	29
			2.2 exp	—	—	
0.6	1.00	8	0.4 calc	1.2 calc	0.25 calc	28
			0.22 exp	—	—	

SOURCE OF FLAME STRUCTURE

Since flames possess spatial structure susceptible to measurement, it is instructive to consider what processes are responsible for this structure. Four processes should contribute to the thermal and compositional structure of the flame front: these are (a) spatially extended reactions, (b) thermal conduction, (c) diffusion, and (d) thermal diffusion. The first process is of particular interest to chemists, but it can only be studied by an analysis that includes the other processes. Thermal diffusion can be shown to be negligible compared with the other processes.[1] Table 1 gives values for the thickness of ideal flames calculated by assuming that only a single process, diffusion, or thermal conduction is important in determining flame front thickness. These values are compared with experimentally determined flame front thicknesses; it is significant that the major part of the observed structure of hydrocarbon flame fronts could be due to these two processes. Both diffusion and thermal conduction obey a differential equation of the

EXPERIMENTAL DETERMINATION OF FLAME FRONT STRUCTURE

The experimental study of the structure of laminar flame fronts involves the determination of the set of characteristic profiles. They can be divided into three general but interrelated types—aerodynamic, thermal, and compositional. A number of techniques that have been devised for making these measurements will be discussed.

In order to study flame fronts quantitatively it is necessary to determine the state of the gas at each point in the flame front. A complete description can be given by three sets of profiles that give the pointwise aerodynamic, temperature, and compositional properties of the gas. It must also be assumed that the postulates of

nonequilibrium thermodynamics are applicable (see Hirschfelder, Curtiss and Bird,[1] p. 18 ff). The other properties of the flame front can then be calculated if the parameters of thermal conductivity and diffusion are available either from experiments on other systems or from calculations.

Although the information desired can be neatly classified under the above three categories, the experimental results often provide only indirect measurement of the quantities of interest, and auxiliary information is required for their interpretation. This situation is not unusual, but it does mean that fairly complete sets of profiles are necessary to provide unambiguous interpretations. For example, the aerodynamic measurements yield directly a density profile that can be interpreted in terms of temperature if the average molecular weight profile (*i.e.*, composition profiles) is known or in terms of an average molecular profile if the temperature is known.

Aerodynamic measurements

The aerodynamic measurements of gas velocity and stream tube cross sectional area would be unnecessary if the Bunsen flames were truly one dimensional. Because of lateral expansion of the gas, the product of density, velocity, and stream tube cross section is constant rather than the product of density and velocity as is assumed in simple one-dimensional flame models. Thus, although the properties of the flame depend only upon one distance coordinate, two aerodynamic profiles must be measured, the normal velocity and the stream tube cross section.[a] This problem can be compared with that of one-dimensional flow in a pipe of expanding cross section.[2]

Particle track measurements. The most versatile technique for studying aerodynamic profiles is the particle track method in which microscopic dust particles are introduced in the gas stream, and their paths are recorded photographically by using high-intensity illumination systems. If a repetitive source of illumination is used, velocity profiles can be measured directly from the resulting picture; if, on the other hand, prolonged illumination is used, streamlines are obtained which can be used to determine the area expansion profiles of the flame front. With certain assumptions streamlines have been used to estimate the velocity profile. This method has been used by several investigators[2, 14, 15, 16, 17, 18] who have shown that reliable measurements can be made using the repetitive illumination technique.

Pressure profile measurements. Another method used to study the aerodynamic structure of flames is the measurement of the pressure profile through the flame front. Pressure drop can be related to the normal velocity by considering momentum conservation in the flame front. These measurements are difficult to make because of the small pressure differences (approximately 0.05 in. of water total pressure), and a quantitative interpretation of these data has not been made.[10]

Temperature measurements

Temperature profile measurements were among the first to be made.[19] They can be interpreted with the aid of estimated composition profiles and the assumption that ρv = constant, but such an analysis is subject to error because of the expansion of stream tubes, and possible errors in the assumed composition profile.[2, 18] In the case of flame fronts there has been some debate as to whether it is meaningful to speak of a single temperature profile since reaction rates may be comparable with the molecular relaxation times. In this event it would be necessary to specify several temperatures, translational, rotational, vibrational, and/or electronic or in an extreme case to specify a set of population distributions for all molecular energy levels of each species. The question of a single temperature profile arose because of the lack of equilibrium in the emission spectra of certain radicals which occur in flames such as OH, CH, C_2. These species show spectral vibrational and rotational temperatures in excess of the calculated adiabatic flame temperatures. The problem has been discussed in some detail,[20] and appears to have been resolved by recent studies of OH fluorescence[21] which showed that the OH radical emission was quenched by every collision so that the distribution is characteristic of a reaction rather than thermal equilibrium. In flames a translational temperature that describes the collisional rate of the species involved at every point can be defined in terms of a thermodynamic or gas scale. The question of equilibrium with respect to the excitation of the internal degrees of freedom of the reacting molecule requires a more thorough study since highly excited reaction species could be formed both by chain branching or by diffusion from the adjacent high-temperature region. It should be pointed out, however, that just because some highly excited

[a] Two rather than three profiles are sufficient because flame properties do not change along two of the coordinates.

species are formed out of equilibrium and are conspicuous because of their visual emission, it does not follow that the major part of the reaction could not be explained in terms of thermal equilibrium excitation. These species in the luminous region account for only a few tenths of a per cent of the molecules at their point of emission and only a fraction of a per cent of the total energy involved in the flame. There is no direct evidence that they are an integral part of the oxidations scheme in hydrocarbon flames.

These questions of equilibrium must be deferred to more detailed studies which will someday be made of flame front processes. Detailed arguments have been given by several authors.[17, 18, 20]

Particle track measurements. Particle track measurements of the flow pattern through the flame front yields a density profile that can be interpreted as a temperature profile. In essence, the method uses the flame gases as a gas thermometer. Since gas thermometry is one of the methods of establishing the thermodynamic temperature scale, the method is a rather basic one. In spite of the reliability of gas thermometry, however, several difficulties exist; namely, the necessity of knowing the average molecular weight profile and the laboriousness of the data reduction. These techniques have been described in the previous section. Measurements can be made which have a reproducibility of 2 per cent and a resolution better than 0.05 mm. The early studies using this method[16, 17] used streak pictures of the streamlines which required the assumption of a function for describing the velocity profile parallel to the flame front for interpretation. Unfortunately, the simple velocity pattern assumed in these measurements gave results that must be corrected in the light of the detailed measurements that have been made. In particular, temperatures above adiabatic flame temperature probably do not occur in flame fronts. The temperature maxima reported in these studies[17, 18] can be attributed to (a) the failure of the parallel component of velocity to follow the assumed pattern, (b) the failure of the average molecular weight to follow a simple monotonic pattern, and (c) the incorrect assignment of the position of attainment of final adiabatic flame temperature.

The improved particle track techniques using repetitive illumination[2, 18] for making direct measurements of both components of velocity have resolved these problems, and reliable measurements can now be made using these methods.

Optical methods. Several optical methods have been used to measure temperature profiles. Within certain limits the density of the gas can be derived from these measurements and related to the temperature with an assumed molecular weight profile and equation of state as is done in the particle track method. This method is less direct than the particle track technique and involves several experimental and interpretational difficulties. However, profiles of excellent precision have been obtained, and optical methods possess the unique advantage of not disturbing the flame.

Several techniques have been suggested and used for these measurements; they will be grouped according to whether they measure the optical density or one of its derivatives.

The use of interferometry to measure gas density in flames was proposed a number of years ago.[22]

Using light of several different wave lengths makes possible the measurement of both temperature and composition. Aside from the general intricacy of interferometric measurements, several major difficulties are involved:

(1) In order to obtain the desired sensitivity the pattern must be interpreted to a fraction of a fringe.

(2) Because of the fact that refractive index depends both upon composition and temperature, it is especially necessary to know the composition profile. In particular, such species as H_2 and free radicals may have a pronounced effect on the measurements.

(3) Interpretation of the pattern involves using either an extended flat flame or a conical flame with circular symmetry. In the case of the flat flame, the end effects become very important since the fringe deflection is integrated along the total light path and, in the second case, the symmetry must be as perfect as the resolution desired and it must be assumed that in the region of interpretation the isothermal and isocompositional surfaces do lie accurately parallel to one another or, in other words, that flame front properties are independent of lateral position along the flame front. In addition there are mathematical complexities in reduction of data on conical flames since it involves the solution of a nonlinear differential equation.

None of these difficulties are insuperable, but the technique has not been used for detailed profile studies.

A second optical method is the schlieren tech-

nique in which the deflection of a narrow light beam is measured; this deflection is proportional to $(1/\rho)d\rho/dx$, or in special cases approximately $(1/T)dT/dx$. This method has the unique advantage of measuring directly an important flame variable, the temperature derivative, as well as the usual optical advantage of not disturbing the flame front. Its disadvantages include those mentioned in connection with interference measurements as well as the additional problem of having to integrate in order to obtain temperature. The end effects are particularly pronounced because of the $1/T$ factor which very heavily weights the derivatives in the cooler end region. The alternative method of interpreting the deflections in a conical flame does not appear to have been used. The accuracy of the method is limited by the necessity of using small deflections in obtaining the necessary resolution. Diffraction effects connected with the slit edges also impair the resolution.

In spite of these difficulties several temperature profiles have been measured using these techniques.[23, 24, 25, 26] Detailed discussions of the problems involved have been given by the individual authors. These profiles appear to be reproducible and to give reasonable results. The general problem of quantitative interpretation of schlieren patterns has been discussed.[27] Two sources of errors would appear to merit closer attention. These are the neglect of the effect of composition variation and the problem of establishing accurately flat flames.

The shadowgraph method has been used for determining flame geometries, but it does not appear to have been developed into a quantitative method. It does not seem to offer significant advantages over the schlieren techniques.

Thermocouple techniques. One of the most obvious methods of making temperature surveys is that of putting a thermocouple into the flame. Unfortunately there are several major limitations to this method:

(1) The thermocouple must not affect the flame; *i.e.*, it must be very small and must be made of noncatalytic material.

(2) Accurate corrections for radiation losses must be known. This is an involved problem which is only partially solved.

(3) The thermocouple material must be able to withstand the temperatures. (This, in general, limits the method to flames where the maximum flame temperature is below 2000°K.)

(4) It must be ascertained whether the thermocouple is in thermal equilibrium with the gas.

This method was one of the first to be applied to flame structure studies,[19] and has been highly developed in recent years,[28, 29] The use of small oxide-coated platinum rhodium thermocouples reduces the necessary corrections to a few degrees and appears to give reliable profiles. This method does not require composition data for its interpretation, but very sophisticated arguments are required to show that the thermocouple does not disturb the flame and is in equilibrium with the flame. These problems have been discussed in detail by workers in the field.[19, 28, 29]

Resistance thermometer measurements. Resistance thermometer measurements are related to thermocouple measurements. Accuracy is limited by the corrections necessary and the problems of catalysis and general disturbance of the flame. The necessary corrections in these measurements are high. Reproducible measurements have been made with good spatial resolution.

A discussion of the general theory and practice of these measurements can be found in standard texts, and the application to flame measurements is given.[30]

Spectroscopic measurements. A very attractive method of making flame temperature measurements is the spectroscopic (or photometric) method. The theory of the measurement is straightforward.[20] The population of energy levels of the emitter is assumed to be in equilibrium, and since emission is proportional to the population of the excited state, the relative intensity of emission at two different known wave lengths can be directly related to the temperature. If one is dealing with a continuum or near continuum, a simple two-color measurement is sufficient. More precise measurements can be made, however, by using individual vibrational-rotational lines or vibration bands. The former measurements require spectroscopes of rather high resolution (about a tenth of a wave number in the case of rotational transitions), and such instrumentation is not often available in the laboratory for this type of measurement. The visible and ultraviolet emission of the various radical species, OH, CH, C_2,[20, 31] as well as the infrared emission of stable species such as CO, CO_2, H_2O, HBr, and HCl, has been successfully used for these measurements. In a number of flame studies a foreign species that emits in a

convenient region of the spectrum has been introduced to make the measurements. Among the species that have been used are the alkali metals,[15] iron,[20] and HCl.[32] None of these additives can be used at low temperatures. An additive that would be useful in this region is iodine, which has been used for engine studies,[33] but not in laminar flame studies.

This method has the advantage of having no upper limit to the temperatures that can be measured. If the components of the flame can be used for this study, there is no disturbance of the flame itself. (In cases where an additive is necessary, minute amounts will often suffice.) There are three major limitations to the method: (a) The spatial resolution is poor and the interference of edge gases which are cooler is quite pronounced. (b) Present studies have been limited to high-temperature regions of the flame. (c) There is some question as to whether the emitters are in thermal equilibrium with their surroundings.[20]

The use of an absorption technique might solve the resolution problem, but this makes the question of the effects of self absorption doubly important. These methods have been very successful in studying the high temperature regions of hydrocarbon flames where resolution is not of extreme importance.[15, 34, 35, 36] Resolution of the order of 0.5 mm can be obtained by this technique.

Other methods. X-ray[37] and α particles[38] have been used to make temperature measurements in flames since their absorption is a direct function of the density of the gas. The problem of interpretation of the flame density in terms of temperature are similar to those of the particle track method. These techniques do not appear to have been used in making profile measurements in flames, but the x-ray absorption has been used recently[39] to measure density profiles in detonation waves.

The velocity of sound in a gas is a function of temperature (also molecular weight and ratio of specific heats), and has been used to measure flame temperatures[40] but not to make high resolution profiles. The technique used thus far (schlieren photographs of sound waves) lacks spatial resolving power, and detailed composition profiles would be necessary to make the analysis.

In principle, any method of temperature measurement can be used for these studies provided that (a) the measurements can be made at sufficiently high temperature, (b) accurate corrections for radiation, etc., are available, and (c) the measuring apparatus can be scaled down to give adequate resolution.

Composition measurements

Composition measurements are of primary importance in understanding the chemical processes that occur in flames. A qualitative interpretation of these data provides clues to the course of the reaction, and kinetic constants can be obtained from quantitative interpretation of the data. Two experimental techniques have been used—direct spectroscopic analysis and sample withdrawal using a fine quartz probe. Both methods have advantages, but the second method has been more generally successful.

Spectroscopic methods. The most direct method of making composition measurements is to choose a suitable wave length or band of light that is absorbed and determine the amount of light absorbed in a known path length in the flame. A number of problems are involved in making such measurements: (a) It is difficult to produce and maintain a narrow light beam in the presence of strong density gradients. (b) Flames are not optically dense in the visible region so that work must be done either in the infrared or ultraviolet regions. (c) For proper interpretation of the results, single lines should be used (so that Beer's law is obeyed), and the temperature should be known so that its effect on the population of the energy levels can be determined. (d) Suitably flat flames are difficult to produce and may be inhomogeneous in the region close to the grid or sintered disc used to stabilize them. (e) End effects tend to confuse the measurement.

For these reasons very few composition profiles have been made using these techniques.[31, 41, 42]

If a species is in thermal equilibrium and the temperature is known, the intensity of emission can be used to measure concentration. The optical problems are even more severe here than in the case of absorption spectroscopy, and only very low resolution has been possible. Such measurements have been made only in the high-temperature region of the flame. A number of studies have been made of the emission of such radical species as CH, OH, and C_2 in the after-burning region.[32, 33, 34, 35, 36] The interpretation of such data is difficult since it is not easy to establish what reactions are connected with the emission and

what relationship exists between the emission and the concentration of the species.

Probe sampling techniques.—Taking a sample from a reacting mixture, rapidly quenching it, and then analyzing it is one of the classic methods used in studying kinetics. The application of this technique to flame studies gives rise to a number of problems: (a) Since distance rather than time

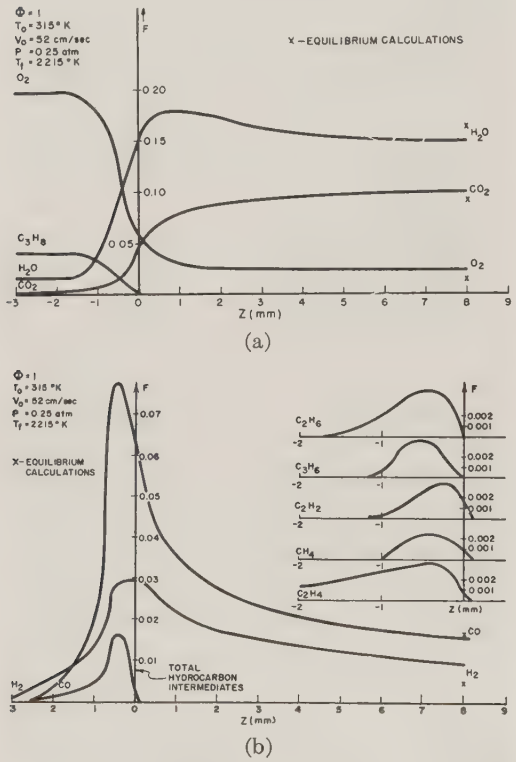

FIG. 4. Characteristic composition profiles. Composition profiles are given for the various stable species found in the quarter-atmosphere stoichiometric propane-air flame front. Figure 4a gives profiles for the reactants and major products. Figure 4b gives the profiles of the various intermediate species. These data were obtained using a microprobe technique with mass spectrographic analysis (Refs. 44 and 45).

is the important variable, resolution is a problem. (b) Since a probe must be introduced, the questions as to what affect this has on the flame must be answered. (c) The problem of interpretation of the sample becomes important.[43]

This technique is limited to flame temperatures below the softening point of the probe material and can only be used for species which are stable to sampling. The limitations and justification of the techniques have been discussed in some detail[43, 44, 45, 46, 47] with the conclusion that the results are reasonable and self consistent. A number of questions concerning the probe effect on the flame have not been completely answered; however, work is continuing and these problems should eventually be clarified. It would appear reasonable to accept these data (Fig. 4) until better information becomes available.

Once the sample is taken it can be analyzed by any suitable technique. Because of the limitations of sample size[b] only two analytical techniques have been used for these studies although several others would appear to offer some promise. The most versatile method has been mass spectrometry which is ideally suited to the analysis of small complex gas samples. If a simple freezeout separation technique is used, a sample of partially burned hydrocarbon can be analyzed quantitatively for 15 different molecular species.[44, 45]

Even more complex mixtures can be handled.[48] Although mass spectrometry is by far the most useful and versatile technique available, it has limitations.

The second method that has been used in these studies is a simple freezeout technique in which the sample is fractionated using one or more low-temperature baths which quantitatively freeze out components.

This method has obvious limitations, but has been used to analyze for CO and CO_2 in the afterburning region of propane-air flames.[47] It could be extended to include other components and systems, but it is too slow for the complex analyses involved in hydrocarbon flames.

A promising method which has not been used yet is gas chromatography. This method would appear to be ideal for the analysis of complex mixtures of hydrocarbon-air or oxygenated compounds; for example, optical isomers can be analyzed by this technique.

Infrared analysis offers some special advantages, but the ordinary commercial instruments require rather large samples (50 cc-atmos). This method has been used in the study of cool flames.[41]

Free radical and atom concentration profiles. The determination of free radical and atomic composition profiles deserves special mention. These

[b] The average sample size, 300 μl (0.3 cc-atmos) is determined by the requirement that the removal shall not disturb the flame. The sample could be increased in size by taking it over a longer period of time, although this time is limited by stability of the flame front.

profiles are important but are difficult to measure. Ordinary sampling techniques are not effective because of the reactivity of the radicals. Three techniques have been devised for the detection of radicals in flames—thermocouple, spectroscopic, and mass spectroscopic (Fig. 5). The interpretation of the thermocouple data is complicated, but the problems can be resolved.[49] The spectroscopic method is difficult because of the low optical density of flames and the complication of edge effects. Mass spectroscopic studies are complicated by multitudinous interferences by stable molecular species. Several successful studies of this type have been made. However, the determination of absolute concentration has not been possible with these methods, and the spatial resolution is poor in the case of the spectroscopic work and very difficult to interpret in the case of the mass spectroscopic studies. In spite of these limitations such measurements are of great importance in flame studies, and it is hoped that eventually techniques will be improved or devised so that quantitative concentration profiles of free radicals and atoms will be available for study.

4. Interpretation of Laminar-Flame Structure

Ideally, the interpretation of the experimental data obtained from the study of the structure of laminar flame fronts yields two types of information: (a) determination of the relative importance of the various processes that occur in flame fronts, *i.e.*, diffusion, heat conduction, and reaction, and (b) determination of the reaction schemes involved in flame reactions and a quantitative evaluation of the reaction rates and their associated constants. The former type is of vital importance in understanding the mechanism of flame process and is of the most immediate importance. The latter, however, opens a wide new field of fast reactions for kinetic study and may ultimately be of greater value.

MECHANISM OF COMBUSTION: FLAME EQUATIONS

If the usual assumptions of nonequilibrium thermodynamics are made,[1] thermodynamic functions can be defined at each point in the flame, and a set of equations relating conservation of mass, atomic species, and energy, together with the differential equation of diffusion, heat induction, and species production, can be written formally defining the flame process. These equations form a set of nonlinear differential equations that are solvable in ideal cases.[1, 48] The solution of the flame equations is an eigen-value problem in which the mass rate of flow or burning velocity plays the part of the eigen value. If the flame kinetics, diffusion constants, and thermal conductivities are known, the flame properties can be calculated from these equations. Most flames are too difficult to treat by this technique. However, a number of ideal flames have been solved, and work is underway on the H_2-Br_2 flame using high-speed computing machine techniques.[50] These techniques are too difficult to apply to complex flames such as hydrocarbons, but the flame equations provide a solid basis for the interpretation of experimental studies of such flames. This combination of theoretical and experimental work should finally provide the solution to the many vexing problems of combustion and allow the detailed study of the kinetics of flame reactions.

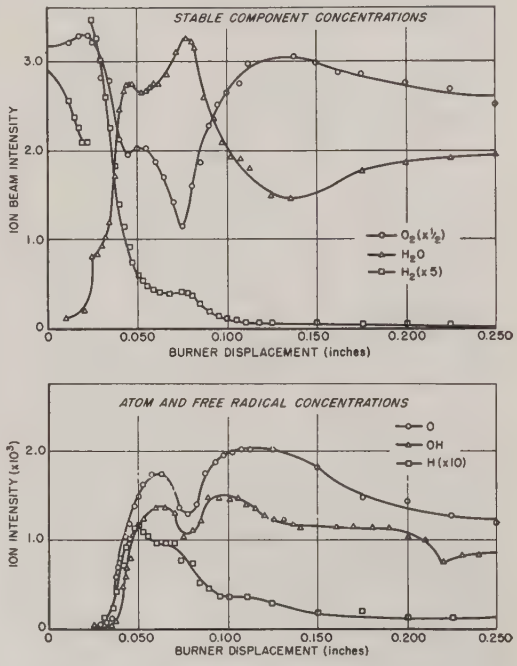

FIG. 5. Free radical and atomic species in a hydrogen-oxygen diffusion flame. Mass spectrometer ion current for various radical species in the hydrogen-oxygen diffusion flame is plotted against distance above the burner. Results were obtained using a molecular beam sampling mass spectrometer (Ref. 43).

INTERPRETATION OF EXPERIMENTAL RESULTS OF FLAME-PROFILE STUDIES

Because of the strong interaction between reaction, thermal conduction, and diffusion that oc-

curs in flames, it is necessary to have a relatively complete set of profiles and a suitable formulation of the flame equations. This discussion will assume that there is available an aerodynamic profile, a temperature profile, and a complete composition profile (excluding reactive species such as free radicals and atoms), and that the diffusion coefficients and thermal conductivities are available. As has been indicated such information can be obtained using presently available techniques, and the discussion will be illustrated

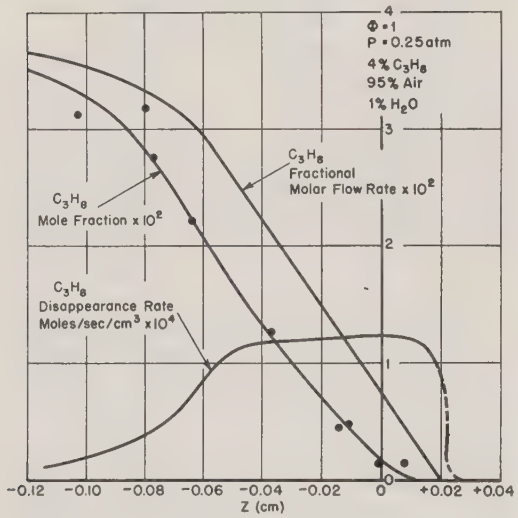

FIG. 6. Composition, fractional molar rate of flow, and disappearance rate of propane. The difference between the stationary concentration at a point and the flux past that point is illustrated by the two profiles for propane in the stoichiometric propane-air flame front (quarter atmosphere). Concentration (mole fraction) and fractional molar rate of flow are plotted against normal distance through the flame front. (Ref. 46.) The propane disappearance calculated from this preliminary curve is given in units of moles per sec per cm^3. Accuracy of this curve is determined by the second derivative of the experimental data and calculations of diffusion coefficients.

with a propane-air flame which has been recently studied.[45, 46] Less extensive profiles can be analyzed by making suitable assumptions,[26, 29] but some caution must be used in interpreting the results. The methods used will obviously depend upon the information available and what information is desired. The problem is too involved for discussion in this paper.

Modified flame equations for interpreting experimental data

As has been indicated, the experimental data are obtained as a series of profiles relating the various measured properties with distance through the flame front. In most formulations of the flame equations temperature has been chosen as the dependent variable. A transformed set of equations is therefore required. One such set has been formulated.[9] These equations express conservation of mass, of atomic species, and of energy; conservation of momentum is not included because of the low velocity of flames.

The equations are used to treat the experimental data by both numerical and graphical methods.

Composition and fractional mass rates of flow. As has been previously mentioned, there are two composition variables that are of interest: the ordinary concentration, *i.e.*, the number of molecules per cc, and the fractional mass rate of flow, which is the fraction of the total flow at a particular point due to a given species. Because of the effects of diffusion, these two variables will, in general, be different (Fig. 6). Experimentally, composition profiles are usually available (Fig. 4), and the fractional mass rates of flow can be derived. It is necessary to know diffusion coefficients for this computation. Since most flames are multicomponent systems, the multicomponent diffusion coefficients should be used. Fortunately, in the case of hydrocarbon air systems, where N_2 is the major component, binary diffusion coefficients can be used. The required diffusion coefficients are not all available, and almost no experimental data are available above 100°C. It is therefore necessary to have a method of extrapolating the data to the high temperatures required in flame studies (2000°K). In principle, kinetic theory provides a method for calculating diffusion coefficients. The problem has been discussed at some length,[1] and equations and tables for making the computations for most common molecules are given by Hirschfelder, Curtiss and Bird.[1] These equations should be tested over an extended temperature range and more data should be provided for polar molecules and species such as free radicals that may have abnormal transport properties.[51]

Enthalpy flux. In a flame, three processes must be considered in the calculation of enthalpy flux. They are convection, thermal conduction, and diffusion. In general, none of these effects are negligible. If thermal conduction is the most important effect, then there will be an enthalpy maximum in the flame front, whereas if diffusion is the most important effect, there will be a minimum in the enthalpy curve. Only one case has

been treated thus far in which diffusion has not been neglected;[46] here an enthalpy minimum was found. The sign of the specific enthalpy in the flame front does not appear to be of fundamental importance in flame propagation since it depends upon the relative magnitudes of the diffusional and thermal conduction energy fluxes.

Species production rates. One of the most important results that can be derived from these measurements is the rates of appearance and disappearance of the various molecular species (Fig. 6). These rates are directly related to the kinetics in the flame front and can be used to determine the heat release rate.

Heat release rate. An interesting property of flame fronts that can be deduced from these measurements is the heat release rate. It can be calculated in two ways using either temperature or compositional curves. Figure 7 gives the results of such calculations in a typical case.

Flame kinetics. One of the most important facets of this work is the possibility of interpreting the data in terms of the kinetics of the flame reactions. The discussion which follows is an outline of some of the possibilities of the method. Quantitative application obviously must be made carefully since several sources of error cannot be accurately evaluated at present. These problems should eventually be resolved, and these techniques are expected to provide an important method for the study of reaction kinetics.

In the flame used to illustrate this review a number of interesting observations can be made. It appears logical to consider the flame in two regions—the fast reaction region which extends from the beginning of reaction to the outer edge of the luminous zone and the afterburning region beyond the reaction zone (Figs. 1 and 2). The first region is normally associated with flame propagation; here the gradients are steep and a unidimensional description applies. The reactions are essentially those of cracking of the hydrocarbon and oxidation to form primarily CO and H_2O with some H_2 and CO_2. It is significant that no oxygenated compounds, such as alcohols, aldehydes, etc., are formed in this region. In particular this indicates that the dominant oxidation processes in flames are different than those in low-temperature oxidations and cool flames where formaldehyde is an important intermediate and many oxygen containing compounds are found. This pattern is in all of the hydrocarbon flames that have been studied, stoichoimetric and fuel rich ($\phi = 1.25$) propane-air flames as well as the methane diffusion flame.[45, 46, 48, 52, 53] The primary process in the secondary region is the oxidation of CO to form CO_2. In this secondary reaction region transport processes are relatively unimportant, and it can probably be treated as a homogenous reaction which occurs in the environment provided by the initial combustion.

These data allow one to calculate rate constants for the production and disappearance of species. Wherever radical concentrations can be estimated, measured, or eliminated from the reaction schemes by the steady state approximation, it is possible to make kinetic studies of the reactions involved in much the usual manner. If the steady state approximation is not obeyed, then radical concentrations must be determined by measurement or some auxiliary assumption if detailed kinetics and constants are desired. Any specific reaction scheme can be, of course, directly compared with the data providing an excellent criterion for evaluating theories.

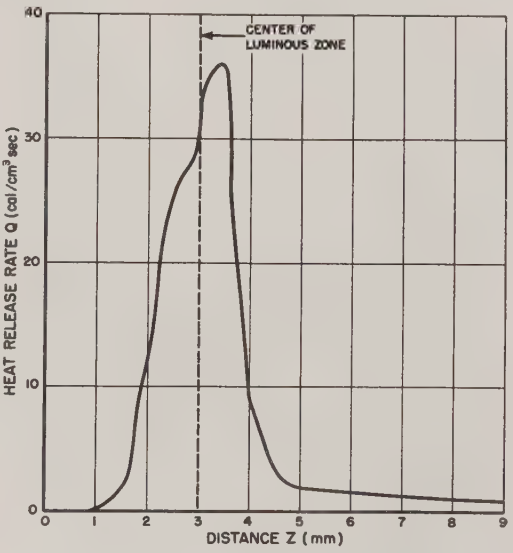

FIG. 7. Heat release rate. The rate of heat release in a propane-air flame front (stoichiometric, quarter-atmosphere) is given as a function of position. This curve is calculated from the temperature profile using estimated thermal conductivities (Ref. 46).

5. Literature Survey

Since this is a relatively new field, much of the literature is in the form of reports that have not been formally published. An effort was made to make as complete a survey as possible; the presently available literature is summarized in

TABLE 2. FLAME-PROFILE DATA

System	Press	Temp.	V_0	Data Avail.	Technique	Ref.
(a) Laminar Flames						
	atmos	*°K*	*cm/sec*			
H_2 + 0.5 Air	0.392	1500	(164)	*T*	*O*	23
CH_4 + 9.32 Air	1.00	2200	36	*T*	*O*	24
C_2H_2 + 6.33 O_2	0.00565	2900	(270)	*T*	*Th*	19
C_2H_2 + 8.37 Air	0.015		(149)	*T*	*Th*	54
C_2H_2 + 10.3 Air	0.0158		(138)	*T*	*Th*	54
C_2H_2 + 14.3 Air	0.0195		(118)	*T*	*Th*	54
C_2H_4 + 45 Air (434°K)	1.00	1160	3.97	*T, A*	*O*	26
C_3H_8 + 45.9 Air (329°K)	0.0594	1050	21	*T, C, A*	*Th, Pr*	28, 47
C_3H_8 + 24 Air (315°K)	0.25	2215	52	*T, C, A*	*P, Pr*	2, 44, 45, 46
C_3H_8 + 19.1 Air (315°K)	0.275	2200	50	*T, C, A*	*P, Pr*	18, 52
C_3H_8 + 17.6 Air	0.54	1990		*T*	*Ps*	17
C_3H_8 + 21.3 Air	0.76	2250		*T*	*Ps*	17
C_3H_8 + 21.7 Air	1.00	2300		*T*	*Ps*	17
C_3H_8 + 22.9 Air	1.00	2310		*T*	*Ps*	17
C_3H_8 + 24.8 Air	1.00	2300		*T*	*Ps*	17
C_3H_8 + 25.6 Air	1.00	2200		*T*	*Ps*	17
C_2H_4O (Ethylene Oxide)	0.9	1211	3.8	*T*	*Th*	55
"Natural Gas" + 8.1 Air	1.00	1740		*M*	*Na*	15
"Natural Gas" + 10.5 Air	1.00	1865		*M*	*Na*	15
"Natural Gas" + 12.3 Air	1.00	1755		*M*	*Na*	15
"Natural Gas" + 13.2 O_2	1.00	1800		*M*	*Na*	15

(b) Diffusion Flames

System	Data Avail.	Technique	Ref.
H_2-O_2	*C*	*MS*	43
CH_4-O_2	*C, T*	*MS, Th, Sp*	43, 57
CH_4-Air	*T, C*	*Th, Pr, MS*	56, 48
C_2H_4-O_2	*T, C*	*Sp*	57
Candle	*T, C*	*Th, MS*	20 (p. 134), 53
NH_3-O_2	*T, C*	*Sp*	57

V_0 Burning velocity. Values in parentheses were not given by the original authors and represent estimates.

T_f Calculated adiabatic flame temperature. Values given in parentheses were not given by the original authors and represent estimates.

T Temperature profile

C Composition profile

A Analysis of profile

M Temperature map of post-luminous region

O Optical techniques

Sp Spectroscopic techniques

Th Thermocouple techniques

P Particle track techniques using direct velocity measurements

Ps Particle track technique using streak photographs. (These data were indirect measurements and need correction in light of new particle track measurements.)

Na Sodium line reversal method

Table 2. A surprising number of systems have been studied. No complete analysis is available at present.

Work is progressing in the study of several related systems: (a) cool flames, (b) diffusion flames, and (c) detonations and decomposition flames. The techniques used in these studies are similar to those that have been described in con-

nection with the laminar flame studies. Because of space limitations, they will not be discussed.

GENERAL EXPERIMENTAL TECHNIQUES

A number of special techniques have been developed which are useful in these studies, such as gas handling techniques, designs of burners and housings for special measurements, and auxiliary equipment (pressure measuring devices, optical equipment, etc.). Many of these techniques are only incompletely described in flame-profile literature. A listing of papers giving such experimental techniques has been compiled and is given in Table 3. This listing provides a supplement to the references on specific studies.

6. Summary

A number of techniques have been developed recently which have made it possible to make reproducible and apparently meaningful measurements of the important properties of the flame front. The results take the form of a series of profiles of the properties as a function of distance through the flame front. The properties that have been measured include temperature, gas velocity and time, and composition. Such profiles determine the state of the gas at each point in the flame front, and the transport properties can be calculated.

Interpreting these data with the flame equations gives a quantitative measure of the importance of the various processes that occur in flame fronts. With some limitations the data are both qualitative and quantitative.

The model on which these considerations are based has been critically discussed, and the various techniques and measurements have been reviewed and discussed with regard to their limitations and possible extension. These studies are believed to be opening up a new field in the study of very fast reactions.

Table 3. Special Techniques

Techniques	Ref.
Burner systems	59
Flat flame burners	60
Constant velocity nozzles	61, 62
Critical flow orifice gas metering	63
High intensity repetitive illumination	64

Acknowledgment

The author would like to acknowledge the many instructive conversations which he has had with contributors to this field. It is a pleasure to work in a field where information is generously shared. In particular he owes a debt to his associates at the Applied Physics Laboratory whose interest and help have often been of great value. Particular thanks are due to Dr. W. H. Avery, who introduced this author to the combustion field; to Dr. A. A. Westenberg, and to Mr. R. Prescott, who have been close associates in this work.

REFERENCES

1. Hirschfelder, J. O., Curtiss, C. F., and Bird, R. B.: *Molecular Theory of Gases and Liquids*. New York, John Wiley and Sons, 1954.
2. Fristrom, R. M.: J. Chem. Phys., *24*, 888–894 (1956).
3. Gouy, G.: Ann. Chim. Phys. (5) *18*, 27 (1879).
4. Gerstein, M.: *Fourth Symposium (International) on Combustion*, pp. 35–42. The Williams and Wilkins Co., Baltimore, 1953.
5. Garner, F. H., Long, R., and Thorley, B.: *Fourth Symposium (International) on Combustion*, pp. 386–91, Baltimore, The Williams and Wilkins Co., 1953.
6. Uberoi, M.: J. Chem. Phys., *22*, 1784 (1954).
7. Ball, G.: *Study of a Two-Dimensional Flame*. Combustion Lab. Report No. 19, Harvard University, 1951.
8. Gross A. and Esch R.: Jet Prop., *24*, 96–101 (1954).
9. Westenberg, A.: *The Analysis of Experimental Data on Laminar Flame Structure*. APL/JHU/CM-870, 1956.
10. Quinn, J.: *Measurement of Laminar Flame Front Thickness at Atmospheric Pressure as a Function of Composition*. Combustion Aerodynamic Lab. Report No. 5, Harvard University, 1953.
11. Weinberg, F.: Fuel *35*, 161–65 (1956).
12. Wolfhard, H., Z. tech. Phys., *24*, 206 (1943).
13. Van Wonterghem, J., and Van Tiggelen, A.: Bull. Soc. Chim. Belges, *63*, 235–60 (1954).
14. Smith, S.: Chem. Rev. *21*, 389 (1937).
15. von Elbe, G., and Lewis, B.: J. Chem. Phys., *11*, 75 (1943).
16. Anderson, J. W., and Fein, R. S.: J. Chem. phys., *17*, 1268 (1949).
17. Fristrom, R. M., Prescott, R., Neumann, R., and Avery, W. H.: *Fourth Symposium (International) on Combustion*, Baltimore, p. 268. The Williams and Wilkins Co., 1953.
18. Fristrom, R. M., Avery, W. H., Prescott,

R., AND MATTUCK, A.: J. Chem. Phys., *22*, 106–109 (1954).

19. KLAUKENS, H, AND WOLFHARD, H. G.: Proc. Roy. Soc., *A193*, 512 (1948).
20. GAYDON, A. G., AND WOLFHARD, H. G.: Flames, Chap. IX and XI. London, Chapman and Hall, 1953.
21. BROIDA, H. P., AND CARRINGTON, T.: J. Chem. Phys., *23*, 2202 (1955).
22. OLSEN, H. L.: *Third Symposium on Combustion*, Flame and Explosion Phenomena, pp. 663–67. Baltimore, The Williams & Wilkins Co., 1949.
23. DIXON-LEWIS, G.: *Fourth Symposium (International) on Combustion*, pp. 263–267. Baltimore, The Williams & Wilkins Co., 1953.
24. DIXON-LEWIS, G., AND WILSON, M.: Trans. Faraday Soc., *47*, 1106 (1951).
25. BURGOYNE, J. H., AND WEINBERG, F.: *Fourth Symposium (International) on Combustion*, pp. 294–302, Baltimore, The Williams & Wilkins Co., 1953.
26. BURGOYNE, J. H., AND WEINBERG, F.: Proc. Roy. Soc., *A224*, 286–308 (1954).
27. SCHARDEIN, H.: *Verhandl. deut. Ing. Forschungsheft, B5*, 367, 1934.
28. FRIEDMAN, R.: *Fourth Symposium (International) on Combustion*, p. 259. Baltimore, The Williams & Wilkins Co., 1953.
29. FRIEDMAN, R., AND BURKE, E.: J. Chem. Phys., *22*, 824 (1954).
30. GILBERT, M., AND LOBDELL, J. H.: *Fourth Symposium (International) on Combustion*, pp. 285–294. Baltimore, The Williams & Wilkins Co., 1953.
31. GAYDON, A. G., AND WOLFHARD, H. G.: Proc. Roy. Soc., *A194*, 169 (1948).
32. SILVERMAN, S.: *Third Symposium on Combustion*, Flame and Explosion Phenomena, pp. 498–500. Baltimore, The Williams & Wilkins Co., 1949.
33. BECK, N. J., CHEN, S. K., UYEHARA, O. A., WINANS, J. G., AND MYERS, P. S.: *Fifth Symposium (International) on Combustion*, pp. 412–23. New York, Reinhold Publishing Corp., 1955.
34. WOHL, K., AND WELTY, F.: *Fifth Symposium (International) on Combustion*, pp. 746–53. New York, Reinhold Publishing Corp., 1955.
35. AUSLOOS, P., AND VAN TIGGELEN, A.: *Fourth Symposium (International) on Combustion*, pp. 252–259. Baltimore, The Williams & Wilkins Co., 1953.
36. BARRERE, S.: Recherche Areonaut (Paris) No. 46, 15–24 (1955), CA 6132i *50*, (1956).
37. WELTMANN, R. AND KUHNS, P.: NACA Tech. Note No. 2580, (1951).
38. SHIROKDAR, A.: Phil. Mag., *15*, 426 (1933).
39. KISTIAKOWSKY, G. B., AND KYDD, P.: J. Chem. Phys., *23*, 271 (1955).
40. MARLOW, D. NISENWANGER, C. AND CADY, W.: J. Appl. Phys., *20*, 771 (1949).
41. DONOVAN, R., AND AGNEW, W.: J. Chem. Phys., *23*, 1592–96 (1955).
42. GAYDON, A. G., AND WOLFHARD, H. G.: Proc. Roy. Soc., *A194*, 169 (1948).
43. FONER, S., AND HUDSON, R.: J. Chem. Phys., *21*, 1374–82 (1953).
44. PRESCOTT, R., HUDSON, FONER, AND AVERY, W. H.: J. Chem. Phys., *22*, 145–146 (1954).
45. FRISTROM, R. M., PRESCOTT, R., AND GRUNFELDER, C.: APL/JHU CM 858 (1955).
46. FRISTROM, R. M., AND WESTENBERG, A: APL/JHU CM *875*, 1955.
47. FRIEDMAN, R., AND CYPHERS,: J. Chem. Phys., *23*, 1875 (1955).
48. SMITH, S., AND GORDON, A.: J. Phys. Chem., *60*, 759–63 (1956).
49. LEAH, A. S., AND CARPENTER, N.: *Fourth Symposium (International) on Combustion*, p. 274. Baltimore, The Williams & Wilkins Co., 1953.
50. Campbell, E.: Univ. of Wisc. Naval Res. Lab. Reports; APL/JHU CF 2108, 2109, CM-819, 849 (1950–1956).
51. HIRSCHFELDER, J. O., AND ELIASON, M.: *Univ. of Wisc. Naval Research Lab. Tech. Report WIS-AF-1*, (1956).
52. SMITH, S., AND GORDON, A.: J. Chem. Phys., *22*, 1150 (1954).
53. RAEZER, S., AND FRISTROM, R. M.: Private communication.
54. GAYDON, A. G., AND WOLFHARD, H. G.: Proc. Roy. Soc., *A196*, 105–113 (1949).
55. FRIEDMAN, R., AND BURKE, E.: Sci. Paper No. 1813, Westinghouse Research Lab., East Pittsburg, Pa. (1954).
56. HOTTEL, H. C., AND HAWTHORNE, W. R.: *Third Symposium on Combustion*, Flame and Explosion Phenomena, pp. 254–65. Baltimore, The Williams & Wilkins Co., 1949.
57. WOLFHARD, H. G., AND PARKER, W. G.: Proc. Phys. Soc., *A65*, 2 (1952).
58. KLEIN, G.: Univ. of Wis. Naval Res. Lab. Reports: Squid 1, Squid 3 (1955).
59. FRISTROM, R. M., AND RAEZER, S.: APL/JH UCF 2553 (1956).
60. BOTHA, J., AND SPALDING, D. B.: Proc. Roy. Soc., *A225*, 71 (1954).
61. MACHE, H., AND HEBRA, A.: *Wiener Akademie Sitzungberichte Ableitung IIa 150* band 157 (1941).
62. ANDERSEN, J. W.: Rev. Sci. Inst., *19*, 822 (1948).
63. ANDERSEN, J. W., AND FRIEDMAN, R.: Rev. Sci. Inst., *20*, 61 (1949).
64. FRISTROM, R. M.: Photo. Eng., *4*, 74 (1953).

12

FLAME ATTACHMENT ZONE OF LAMINAR, PREMIXED METHANE-AIR FLAMES[a]

By ARTHUR L. THOMAS[b] AND RICHARD H. WILHELM

Introduction

Present work is concerned with the attachment of flames to surfaces. Laminar flames were chosen for initial study; featured is the effect of the compositional control of the flame attachment zone on flame properties.

It is well known that a flame seated or stabilized on the end of a tube through which a premixed combustible mixture of hydrocarbon and air is passing in laminar flow can station itself on the rim of the tube between two limiting values of the gas flow, for any given composition of the premixed combustible gas. As the flow rate is decreased, a critical flow is reached at which the flame no longer sits on the rim of the burner but travels down through the tube or flashes back.[4] If the gas flow rate is increased, a critical maximum flow is reached above which the flame will rise from or blow off[4] the rim of the burner and eventually become extinguished as it separates itself with increasing distance from the burner.

The concept of critical boundary velocity gradient as a rational means of correlating flame flashback and blowoff stability limits for burners of different diameters has been explained well in several places.[3, 4, 7, 8] With decreasing tube size, a diameter is reached for a given fuel-oxidant mixture below which flashback does not occur. This critical diameter is the quenching distance.[4] However, as the premixed combustible gas flow is reduced, although the flame will not flash back, it will rise from the burner, as in blowoff, and can be extinguished. Below this critical flow rate a flame will not stabilize on the rim of the tube. This limit of stability is the extinction limit.[4]

This paper makes experimental inquiry into:

(1) The effect of the introduction of small amounts of gases into the zone of flame attachment on flame stability. Also a comparison of the behavior of such locally introduced gases compared to the results of experiments when the entire flame is surrounded by an atmosphere of the gas in question.

(2) The effect of geometrical factors on flame stability: spacing of the injection slots from a central rectangular orifice and angle of the lip of the burner.

To elucidate these points, blowoff, flashback and extinction limits were determined, and burning velocity measurements were made on a rectangular burner. Injection slots for auxiliary gas introduction on the burner were spaced 3 mm from the rectangular orifice edge. Additional experiments were performed on a rectangular burner with 1 mm slot spacing and on a cylindrical burner with a circular orifice surrounding it for auxiliary gas introduction. These additional experiments, which are consistent with those reported here, are presented elsewhere.[6]

Experimental

Two burner arrangements were used: rectangular burner with injection slots for auxiliary gas introduction and a jacketed rectangular burner for environmental gas control.

Pertinent details of the burner are given in Figure 1. Chambers between the gas inlets to the injection slots and the injection slots were packed with steel wool to aid gas distribution. The burner was water cooled. One side of the burner could be moved in and out by releasing the end plate and bottom plate screws to provide different, adjustable orifice widths. Four orifice widths were used: 0.159, 0.238, 0.320 and 0.397 cm.

The jacket for the burner was constructed of sheet metal and plexiglas. Jacket dimensions were width: 14.0 cm, length: 25.3 cm, and height: 60 cm. Three sides of the jacket were metal, the fourth, plexiglas. Each side was constructed of two parallel sheets, spaced 1.2 cm apart. Holes appropriately fashioned into the sides of the jacket permitted fitting the burner with its heat exchange inlet and outlet tubes, premixed gas and injection gas tubes, and thermocouple into the jacket.

The gas entering the jacket as atmosphere had six inlets in the form of ¼ in. o.d. holes at the bottom through which copper tubes were sold-

[a] This research was supported by the United States Air Force under Contract No. AF 33(038)-23976 monitored by the Office of Scientific Research.

[b] Present address: E. I. du Pont de Nemours & Co., Inc., Photo Products Department, Parlin, New Jersey.

ered. These tubes were covered with a bed of glass wool.

Because of the large cross-sectional area of the jacket it was necessary to minimize convection currents from becoming established within the jacket due to interaction of air in the room and the hot gases rising from the jacket. To accomplish this, a copper screen was placed over the top and an asbestos board was mounted 1½ inches above the screen. Cooling water also was circulated in the channel surrounding the jacket to minimize thermal convection.

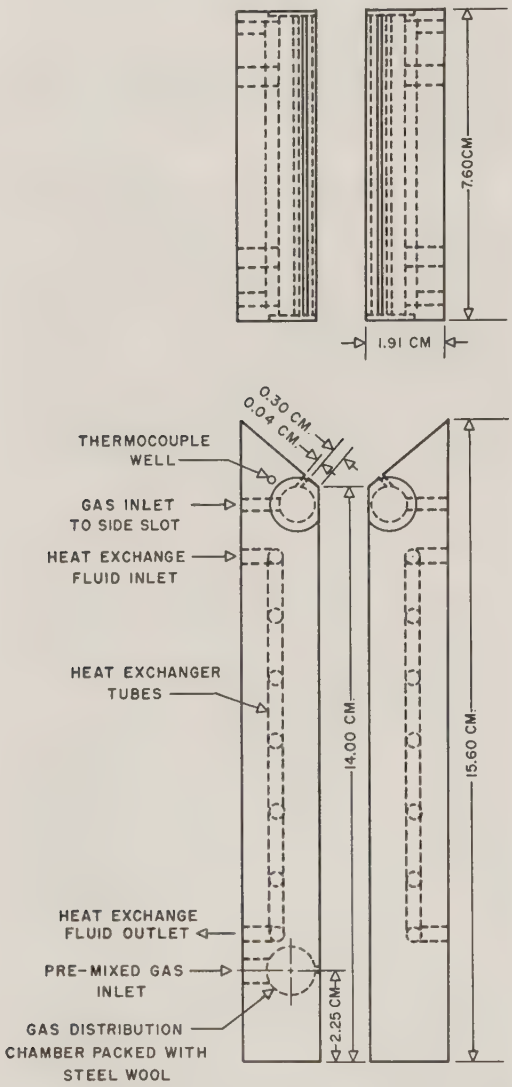

FIG. 1. Top and end views of essential features of rectangular burner without end and bottom plates.

Premixed combustion gases as well as auxiliary gases for attachment zone control were metered with calibrated rotameters.

Methane in the premixed methane-air stream was technical grade 96.0 per cent Matheson, the major impurities being ethane, propane, nitrogen and oxygen. Auxiliary methane for the injection slots was c.p. grade. Gases other than air used for introduction in the side slot or into surrounding atmospheres were better than 99.5 per cent pure.

The burner length was sufficiently long for laminar Poiseuille flow to be established and the critical Reynolds number was not exceeded. Flame stability data were obtained in laminar flow except for certain methane and hydrogen injection data, given in Figures 10, 11 and 12.

Temperature of the burner was measured by means of an iron-constantan thermocouple which was movable throughout the length of a thermocouple well. Temperature readings were obtained from a Leeds and Northrup Portable Precision Potentiometer.

The temperature level in the burner was maintained within 2°C by circulation of coolant through heat exchange tubes.

In determining stability limits, the procedure was to obtain a stable flame, then increase or decrease the air or methane flow rate in the premixed gas until the flame either blew off, flashed back or was extinguished upon an incremental change in flow.

Results

RANGE OF VARIABLES

Burner:

Geometry: rectangular
Sizes: rectangular orifice width 0.159 to 0.397 cm
Premixed combustible gas: methane-air
Auxiliary gases introduced at flame attachment zone: air, oxygen, helium, nitrogen, carbon dioxide, hydrogen, methane
Atmospheres surrounding burner: air, oxygen, helium, nitrogen, carbon dioxide
Temperature of premixed gas and atmosphere: room temperature
Temperature of burner surface: 20 to 55°C

Experimental results are presented graphically. Blowoff stability results in the presence and absence of auxiliary gases issuing from the side slots are presented in Figures 3, 4, 5, 6, 7, 8, 9, 10, 11 and 12. The auxiliary gas flow ratio, in per cent,

designates the following relationship: (auxiliary gas flow/main stream methane flow) $\times 100$.

Blowoff stability results for the burner when immersed in an atmosphere within a jacket are given in Figures 13, 14, 15 and 16.

Special experiments were performed in conjunction with jacketed burner experiments which established that over a fourfold range (0.85 to 3.94 cm/sec) of flow rate of the environmental gas, blowoff limits on the burner were not affected. The jacket gas flow rate for the data here reported was in the middle of this range (1.3 cm/sec).

Burning velocity measurements were made by means of the total area method and are presented in Figure 17. The object here was to determine whether the addition of auxiliary combustible in the local attachment zone affects the average adiabatic flame velocity as the limiting blowoff condition is approached.

In the graphical presentation of results gas composition is expressed as equivalence ratio and blowoff velocity as critical boundary velocity gradient. Equivalence ratio is defined as: (moles fuel)/(moles fuel + moles air) divided by the same ratio at stoichiometric.

The critical boundary velocity gradient of Lewis and von Elbe[3, 4] is here defined for a rectangular orifice as $\frac{g = -6\, u_{Av}}{d}$, where u_{Av} is the area average velocity and d is the rectangular orifice width. Subscripted values of this variable, g_B and g_F, denote critical gradients at blowoff and flashback, respectively.

Discussion

As frame of reference a laminar flame model of the flame attachment region is considered. The model is consistent with recent views.

Three main parts of the laminar flame are recognized: The tip, the main adiabatic part, B, and the attachment zone, C. See Figure 2.

A complement of conservation balances are operative in the x direction as has been much discussed in the literature on combustion. Because the flame temperature also decreases within the combustion wave, from B to C, as a result of the presence of a heat and radical sink and because of gas dilution at C, the flame velocity decreases continuously in the y direction toward C. In this direction (Fig. 2), there is a net flux of heat toward C. There is simultaneoulsy presumed to be a propagation of energy in both directions of the y coordinate, through free radical concentration gradients, with a net flux toward C.

A small zone of the flame, at C, is considered to serve as a continuous ignition source of the main flame, B, by energy propagation in the y direction from C. There is a feedback loop because the zone of ignition itself is maintained by heat flow from the main flame, along y, in addition to x component contributions. When the feedback loop can not be maintained, the flame becomes extinguished. The ignition region is anchored in a hydrodynamically protected region, close to the

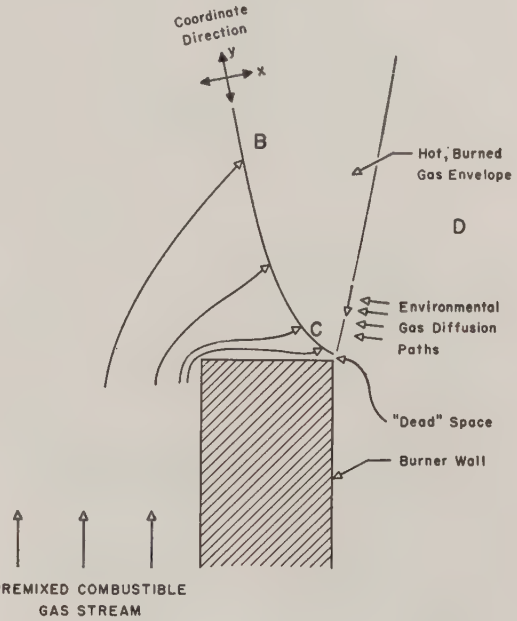

FIG. 2. Schematic diagram of premixed flame stabilized at rim of burner.

burner rim, and this position is within a normal boundary layer distance.

The mechanism of blowoff with increasing bulk combustible gas velocity may be visualized as follows: blowoff occurs when the feedback loop between the main flame and the ignition zone is broken. This action is assumed to take place when the zone has been so cooled and diluted by diffusive introduction of surrounding gases that the dilute limit of flammability is reached and continuous ignition near the surface may no longer take place. A condition of instability ensues; the ignition zone is extinguished and the rest of the flame follows. Contrariwise, conditions of high stability have been achieved, as has been shown experimentally in the work here described, when the ignition zone remains lighted long after the

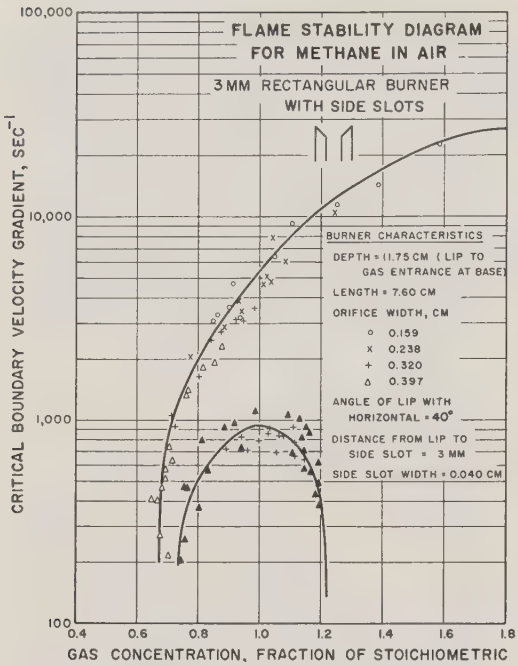

FIG. 3. Stability diagram for premixed methane-air flames at 1 atmos pressure.

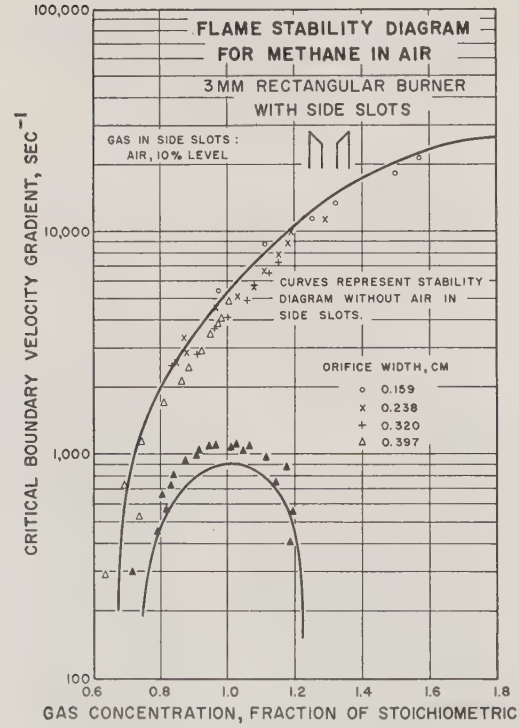

FIG. 4. Stability diagram for premixed methane-air flames at 1 atmos pressure with air injection.

top of the flame has disappeared at high gas flows, and when the bulk gas composition approaches the lower limit of flammability. In effect the introduction of auxiliary combustible gas at the ignition zone C has made this zone more stable than the adiabatic region, B.

Fresh combustible or oxidant *mass* is introduced into the attachment complex by diffusional processes. In the well-known case of a pilot light placed near the attachment zone, the alternate, *heat*, is furnished to the ignition zone. In the present arrangement for influencing the local mass concentration of combustible, the amount of auxiliary gas may be so small that by itself it can not support a flame. A pilot light by contrast commonly is supplied with premixed combustible and oxidizer gases and it maintains itself. In the present arrangement, the auxiliary, such as methane or oxygen, must first mix with other gases in the attachment zone before it can take part in the local combustion process.

EXPERIMENTAL BOUNDARY VELOCITY GRADIENTS

Stability diagrams in this work show that the concept of critical boundary velocity gradient correlates well the results of the rectangular burner system in atmospheres of air, oxygen and inert gases. These results are consistent with data for butane-air flames stabilized in air.[5] The values of g_B and g_F at any given premixed gas composition for flames stabilized in a given atmosphere are greater for rectangular burner systems than for cylindrical burner systems.

An explanation for the difference in g between rectangular and cylindrical geometries is found by consideration of the quenching distance. The minimum quenching distances for methane-air flames are[4] 0.32 cm for a tubular orifice and 0.25 cm for a rectangular orifice. This difference is accounted for by the ratio of burner rim perimeter to cross-sectional area which for a tube is twice that for a rectangular channel. The reason for the difference between g_B for tubular and rectangular burners would be the same as for g_F except that the significance of quenching or penetration distance at blowoff involves not only thermal quenching but quenching by material diffusion as well.

FLASHBACK AND EXTINCTION

Figures 3 to 16 indicate that for rectangular burner systems flashback is independent of atmosphere or auxiliary injection gas at the 10 per cent and 20 per cent levels. Flashback data points

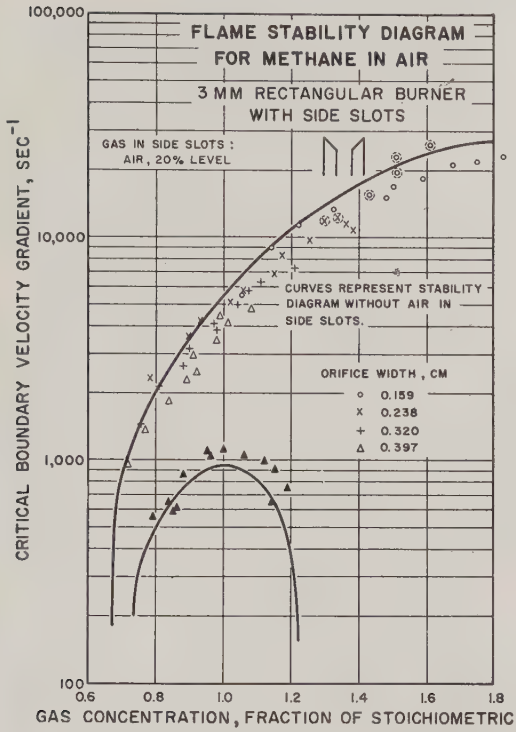

FIG. 5. Stability diagram for premixed methane-air flames at 1 atmos pressure with air injection.

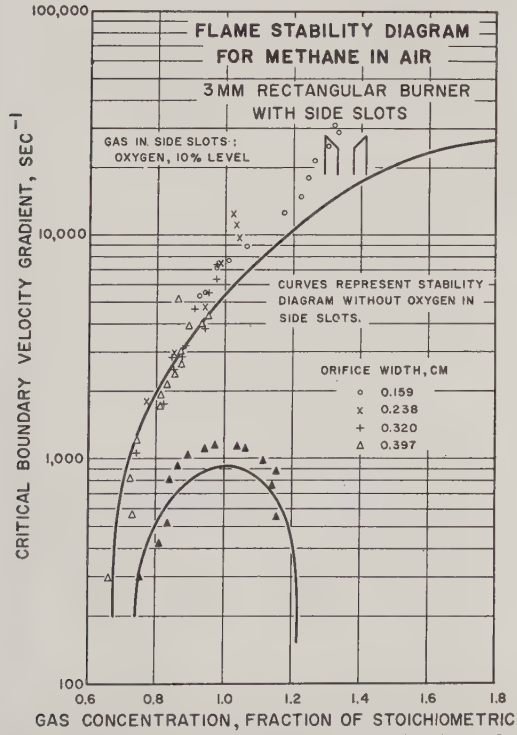

FIG. 6. Stability diagram for premixed methane-air flames at 1 atmos pressure with oxygen injection.

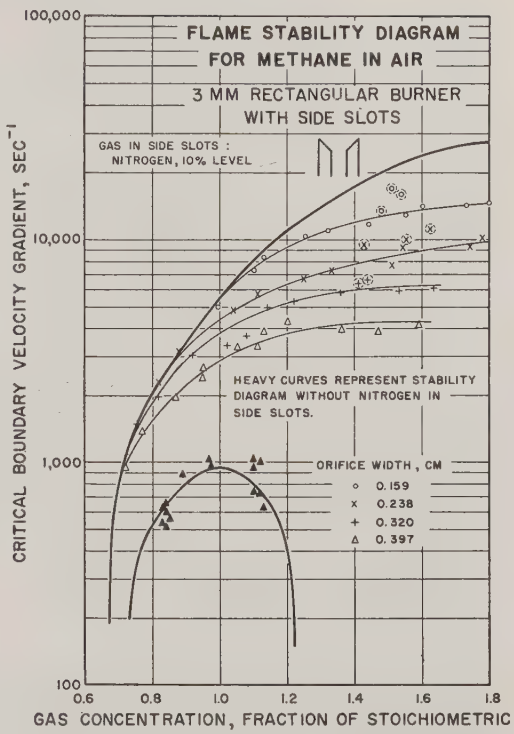

FIG. 7. Stability diagram for premixed methane-air flames at 1 atmos pressure with nitrogen injection.

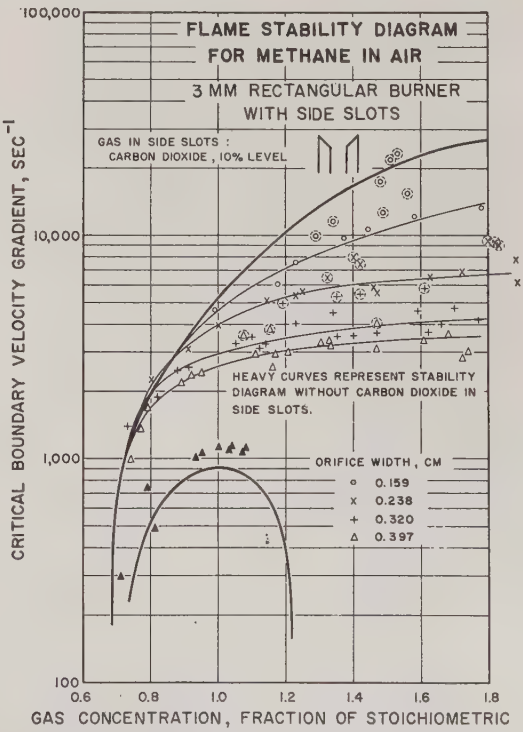

FIG. 8. Stability diagram for premixed methane-air flames at 1 atmos pressure with carbon dioxide injection.

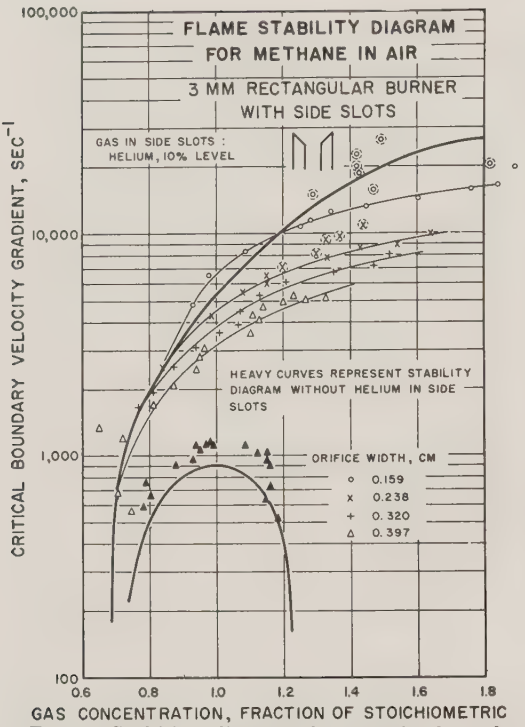

FIG. 9. Stability diagram for premixed methane-air flames at 1 atmos pressure with helium injection.

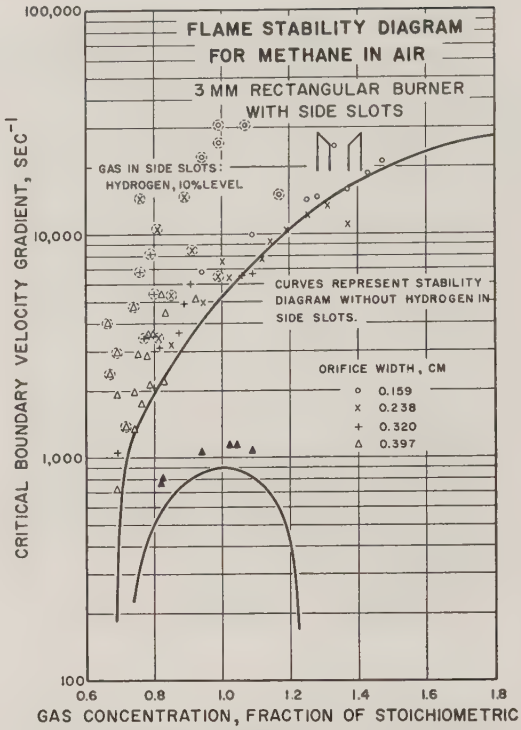

FIG. 11. Stability diagram for premixed methane-air flames at 1 atmos pressure with hydrogen injection.

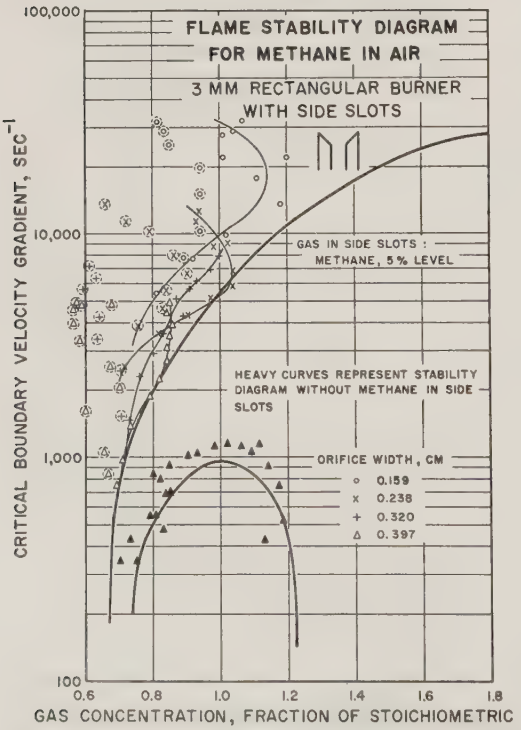

FIG. 10. Stability diagram for premixed methane-air flames at 1 atmos pressure with methane injection.

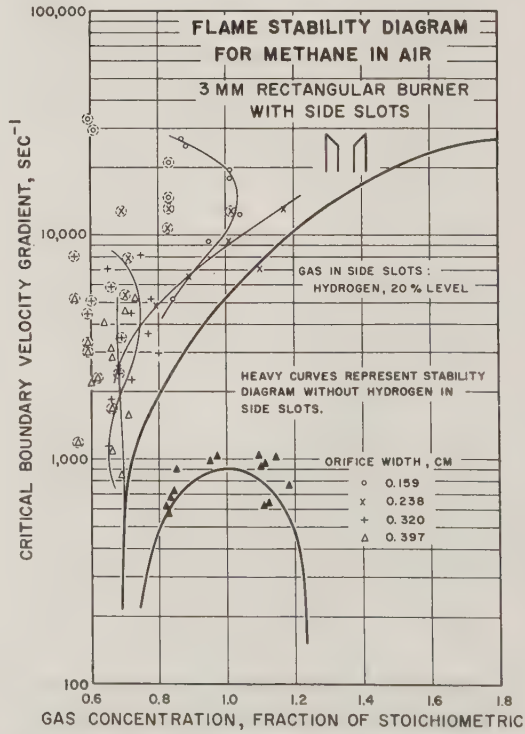

FIG. 12. Stability diagram for premixed methane-air flames at 1 atmos pressure with hydrogen injection.

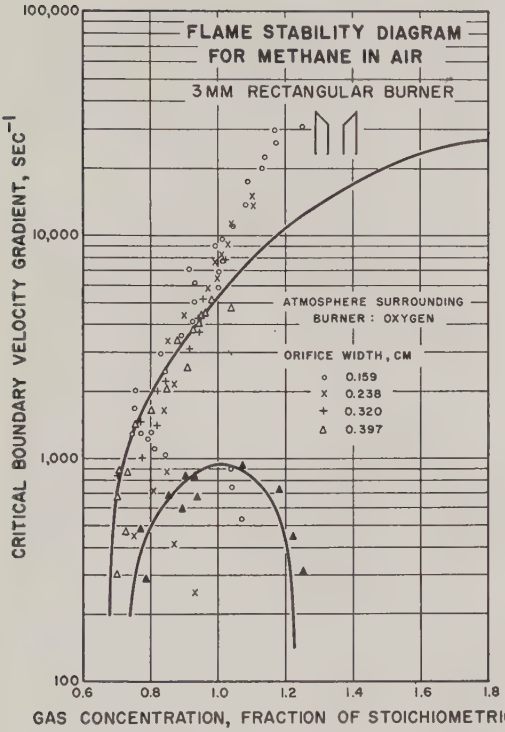

FIG. 13. Stability diagram for premixed methane-air flames at 1 atmos pressure in an oxygen atmosphere.

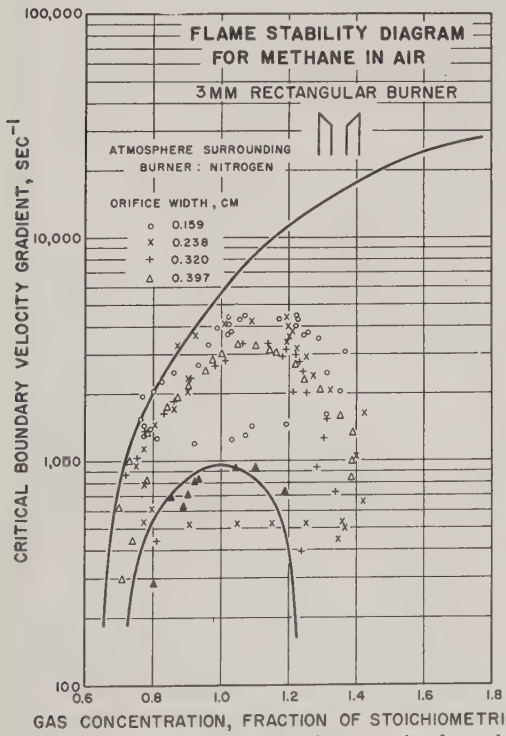

FIG. 14. Stability diagram for premixed methane-air flames at 1 atmos pressure in a nitrogen atmosphere.

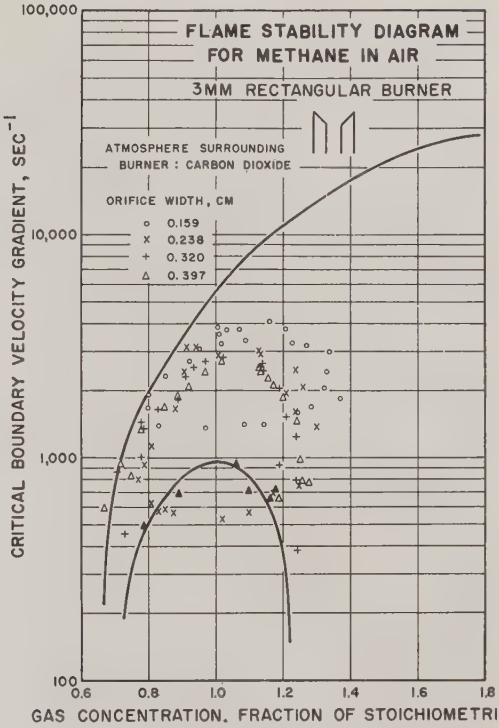

FIG. 15. Stability diagram for premixed methane-air flames at 1 atmos pressure in a carbon dioxide atmosphere.

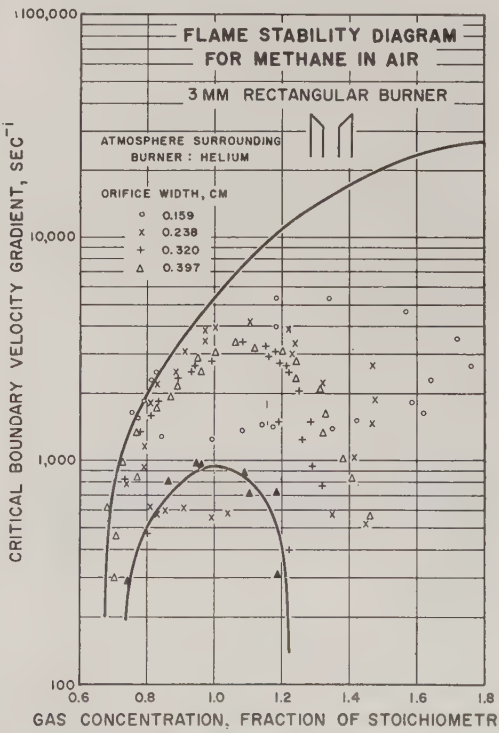

FIG. 16. Stability diagram for premixed methane-air flames at 1 atmos pressure in a helium atmosphere.

are in each case clustered about a lower, clearly identifiable curve.

The extinction data do not correlate on a unique critical boundary velocity curve. The data were obtained at orifice widths of 0.159 and 0.238 cm. These widths are less than the quenching distance; the point of equality of gas and burning velocities is closer to the center of the orifice so that the critical boundary gradient principle does not apply. The flame is extinguished at a higher gas velocity at the 0.159 cm width than at the 0.238 cm width; quenching by the walls of the burner is more effective at 0.159 cm than at 0.238 cm wall spacing.

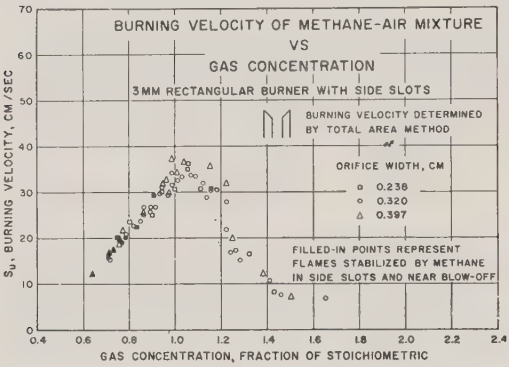
BURNING VELOCITY OF METHANE-AIR MIXTURE
VS
GAS CONCENTRATION
3MM RECTANGULAR BURNER WITH SIDE SLOTS
BURNING VELOCITY DETERMINED BY TOTAL AREA METHOD
ORIFICE WIDTH, CM
0.238
0.320
0.397
FILLED-IN POINTS REPRESENT FLAMES STABILIZED BY METHANE IN SIDE SLOTS AND NEAR BLOW-OFF
S_u, BURNING VELOCITY, CM/SEC
GAS CONCENTRATION, FRACTION OF STOICHIOMETRIC

FIG. 17. Effect on average burning velocity of methane injection at base of premixed methane-air flames at 1 atmos.

BLOWOFF

In the figures presenting the results for blowoff there are two kinds of points, *i.e.*, points enclosed or not enclosed in dotted circles. In Figures 10, 11 and 12 in which auxiliary hydrogen or methane is added, the unenclosed points represent initial rupture at some point in the flame sheet and the enclosed points represent conditions at which the last vestige of flame disappears. In the sequence of events the flame first ruptures far from the burner and it disappears finally in the close vicinity of the burner surface.

Air injection at the 10 per cent and 20 per cent levels yielded substantially the same blowoff curves. See Figures 4 and 5. These results indicate that the influence of auxiliary gases on blowoff, at least at less than the 20 per cent level, was not hydrodynamic.

When the auxiliary gases were inerts, CO_2, He and N_2, unenclosed and enclosed points in Figures 7, 8 and 9 continued to signify initial and final blowoff conditions respectively. However, in these instances the final flame tended to be at a distance from the attachment surface, a condition which usually is designated as "lift".

It is noted that, in contrast to the "standard" curves, boundary velocity gradient curves when auxiliary inerts are added are separate and distinct for different orifice sizes. Let "l" refer to large orifice width and "s" refer to small orifice width. Then, although for a given value of F, $g_l < g_s$, it is true experimentally that $V_l > V_s$ (V = total bulk orifice flow) so that (inert flow)$_l$ > (inert flow)$_s$. Therefore, at a given F at blowoff, the flame attachment zone is blanketed with more inert gas in the large orifice than in the small orifice; in terms of g, the larger the orifice width, the more the blowoff curve is depressed. As F decreases, the separate g curves approach one another because of the decreasing amount of auxiliary inert gas. The extent of the lowering of the critical boundary velocity gradients was in the order He < N_2 < CO_2.

The fact that auxiliary helium depressed blowoff less than nitrogen may be due to the higher diffusivity of helium; the issuing helium is rapidly dissipated in the surrounding atmosphere.

With auxiliary inerts, at the two smallest orifice widths and at $F > 1$, one side of the laminar flame would tend to rise up or blow off before the other side, and upon ceasing to rise, yielded a turbulent diffusion flame above the orifice with the laminar flame still stabilized on one side of the burner; then the laminar flame would blow off completely leaving a turbulent diffusion flame stabilized in space above the burner, then this flame would blow out. Data in Figures 7, 8 and 9 indicate that this sequence of events occurred with small changes in g.

Figure 6 shows that the presence of oxygen in the flame attachment zone in the F range studied correlates well in terms of g. Effects of diffusion as a mechanism for the existence of flames directly over the injection slots were observed when oxygen issued as auxiliary at low pre-mixed methane-air flow rates at $F > 1$. The stabilized flame was accompanied by a periodic "buzzing" noise the frequency of which increased with increasing air flow through the main orifice, with the amplitude going to zero at about stoichiometric, at $F = 1$. The flame sheet oscillated over an injection slot; a small blue diffusion flame about 1 mm high directly over the slot would alternately be ignited and extinguished. When this diffusion flame formed, the base of the main flame stabilized above the burner would move

further away from the orifice. Above $F \cong 1.8$, the two flames formed a continuous front with no oscillations.

The hydrogen data in Figures 11 and 12 show that the presence of the 20 per cent level of hydrogen increased blowoff stability more than the 10 per cent level. The flame attachment zone, in other words, responds to changes in concentration of the locally introduced gas.

Not only does auxiliary hydrogen supply gas for combustion with the ambient air at the flame base but it also provides a system with a potentially higher burning velocity at the flame attachment zone than if the same quantity of methane were supplied at the zone because of the normally higher burning velocity of hydrogen-air flames. However, methane at the 5 per cent level appeared to affect blowoff stability more than hydrogen at the 10 per cent level possibly because the hydrogen diffused away rapidly from the combustion zone or because the hydrogen concentration was too low. At a 10 per cent methane-air mixture, the burning velocity is about 38 cm/sec whereas the burning velocity of a 10 per cent hydrogen-air mixture appears to extrapolate to close to zero.[4]

In inert atmospheres the order of increasing blowoff stability is $CO_2 < N_2 \cong He$ with the maximum stability in all cases at $F \cong 1.1$. See Figures 14, 15 and 16. At the two orifice widths at greater than the quenching distance the blowoff data correlate well in terms of critical boundary velocity gradient, in agreement with results elsewhere[8] with butane-air flame cylindrical tube systems in an atmosphere of carbon dioxide.

At $F < 1$ the blowoff limits are almost independent of the surrounding atmosphere. At $F < 1$ the main orifice gas stream contains an excess of oxidant so that air or oxygen diffusing into the attachment zone behaves as inert atmosphere. See Figures 13, 14, 15 and 16.

Figures 14, 15 and 16 also show stability loops formed by blowoff and extinction curves.

Blowoff curves in inert atmospheres seem to indicate that, *per se*, carbon dioxide is an excellent flame quenching material. For given composition of combustible, oxygen and inert mixture this would be expected, on the basis of relative burning velocities, which, at stoichiometric, are $He:N_2:CO_2 \approx 12:3.4:1$,[1,4] where $[\text{inert}/(\text{inert} + 0_2)] = 0.79$.

The burner was fitted with a horizontal lip and stability curves determined. The end plates extended 4 cm above the surface of the burner to prevent endwise diffusion of air into the flame. The results were the same as with the burner with lips at 40° with the horizontal.

Burning velocity measurements of flames near blowoff for flames stabilized in different atmospheres or with auxiliary gas present at the flame base indicate that the average bulk burning velocity is unaffected by atmosphere or auxiliary gas. Auxiliary gas, if added to the premixed combustible stream, would shift F and S_{Av}. The shift for auxiliary air, oxygen or nitrogen is negligible. For the methane case, S_{Av} would change by about 10 per cent. The actual increase of severalfold in g_B indicates that the addition of methane at the flame attachment zone resulted in a local influence. Hydrogen would increase S_{Av} up to twice the actual value.

REFERENCES

1. Clingman, W. H., Brokaw, R. S., and Pease, R. N.: *Fourth Symposium (International) on Combustion*, p. 310. Baltimore, The Williams & Wilkins Co., 1953.
2. Cullen, R. E.: Project MX-833, Contract No. AF. W33-038-ac-21100, VMM-81, University of Michigan, 1950.
3. Lewis, B., and von Elbe, G.: J. Chem. Phys., *11*, 75 (1943).
4. Lewis, B., and von Elbe, G.: *Combustion, Flames and Explosions*. New York, Academic Press, 1951.
5. MacCallum, N. R. L.: Fuel, *35*, 169 (1956).
6. Thomas, A. L.: Ph.D. Dissertation, Princeton University, 1956.
7. von Elbe, G., and Mentser, M.: J. Chem. Phys., *13*, 89 (1945).
8. Wohl, K., Kapp, N. M., and Gazley, C.: *Third Symposium on Combustion, Flame and Explosion Phenomena*, p. 3. Baltimore, The Williams & Wilkins Co., 1949.

13

MASS SPECTROMETER STUDIES OF FUEL CONCENTRATION IN THE DARK SPACE OF LAMINAR BUNSEN FLAMES

By JOHN F. BYRNE

The experimental investigation to be described was undertaken to obtain information on the concentration of the gases in the dark space between the flame and the end of the burner tube of a Bunsen burner. The measurements of the concentration of gases involved the use of a fine probe with which samples of the gases, in the region of the dark space between the flame and the burner, were withdrawn for analysis with a mass spectrometer.

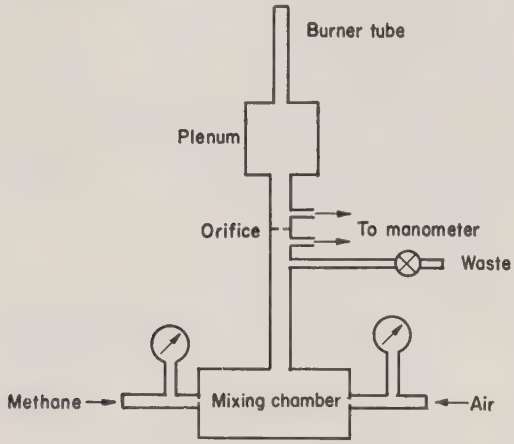

FIG. 1. Burner and flow-control system.

The first part of this paper deals with the experimental arrangements and the method of test. The second part gives a description of the profiles of concentration of gases found in the dark space for the condition near flame blowoff.

Part I. Apparatus and Method of Test

THE BURNER

Figure 1 is a schematic drawing of the burner and flow-control system. The length of the burner tube always exceeded 50 diameters of the tube to insure laminar flow at the burner port formed by the square edge of the cut end of the cylindrical tube.

The fuel used was bottled methane, with a stated purity of 96 per cent. Methane was selected because it has a molecular weight of 16; thus, there are no ion masses in the mass spectrum from methane that can be confused with either nitrogen (28) or oxygen(32). Although the parent ion mass (16) was indistinguishable either from doubly ionized oxygen $O_{(32)}{}^{++}$ or from $O_{(16)}{}^{+}$, the methyl ion fragment $CH^{3}{}_{(15)}$ is present in practically the same intensity as the parent ion, and is free of interference. Thus, mass 15 was used to follow the concentration of methane.

The field of interest in these experiments consisted of the region between the lip of the burner and the base of a flame that one sees in a flame photograph. The maximum separation of the base of the flame from the lip of the burner was approximately 0.030 in. The horizontal distance over which this separation occurred was also about 0.030 in. Within this small area, it was possible to obtain gas samples from the vicinity of the tip of the probe representative of spherical regions calculated from gas flow to be approximately 0.0015 in. in diameter. This was accomplished by sampling through a small Vycor capillary which could be moved to sample the entire region of interest between the flame and the port of the burner. A typical capillary was measured and was found to have an internal diameter of 0.0012 in. and an external diameter of 0.0025 in.

Figure 2 shows the relative position of the probe, the flame and the burner in a typical experiment. The probe was set at the desired vertical distance above the lip of the burner. The horizontal position of the probe was measured from the inside edge of the port of the burner. The desired position of the probe always was approached from the same direction to avoid backlash in the micrometer screw.

A mechanical pump was operated continuously to withdraw the sample through the probe. The pressure in the pump line depended on the dimensions of the particular probe in use. This, in itself, caused no difficulty. However, during an experiment, the tip of the probe could traverse regions that varied widely in temperature, depending on the position of the probe relative to the flame. Since the rate of gas flow through the probe is dependent on viscosity, the flow varied by as much as a factor of 2. This change in flow caused the pressure in the pump line to vary, and the variation had to be taken into account.

A tracer method was used to obtain a flow factor for compensating the variations in flow through the probe. Nitrogen was used as the tracer gas; in effect, the ratio of N_2 to CH_4 was measured. Since changes in flow owing to temperature change are the same for both gases, the ratio can be used to follow changes in concentration, provided the tracer gas is always present in unvarying concentration. Because of interdiffusion of the air and the primary mixture in the region under the base of the flame, the concentration of N_2 is not exactly invariant in the region. Nevertheless, the measurements were based on the concentration of nitrogen at the center of the jet. By this means, the uncertainty in the concentration of methane was least in regions where the concentration was highest.

Table 1 gives typical values of flow factors within the probe, for different positions of the probe in the gases of the dark space. The factors were obtained by taking the ratio of the nitrogen peak in the mass spectrometer for the position at which the flow factor was desired to the peak at the center of the jet. For example, at the position 0.0, the flow factor was found from the ratio 1130/2440 to be 0.46; hence, the flow through the probe at this point was only 46 per cent of the flow through the probe at the center of the jet.

To illustrate the use of the flow factors in computing the concentration of methane, suppose the concentration of methane in the primary mixture was 10 per cent by volume. Further, suppose that the height of the methane peak in the mass spectrometer was 200 units for the probe in the center of the jet, and that the height of the peak dropped to 70 units at the 0.0 position. Using, for this example, the flow factors in Table 1, the calculation of the percentage concentration of methane at 0.0 position would run as follows:

$$10 \times \frac{70}{200} \times \frac{1}{0.46} = 6.2$$

In practice, the flow factor was measured for each position of the probe, for every sample of gas that was analyzed.

INVESTIGATION OF THE POSSIBLE EFFECT OF CARBON MONOXIDE ON THE MEASURED FLOW FACTORS

The possibility was considered that CO might be present, under the base of a flame, and thus cause error in the measurement of the concentration of nitrogen, since the mass spectrometer could not distinguish between the parent peaks of N_2 and CO. To answer the question, the concentration of argon under the flame was compared to the concentration of nitrogen plus carbon monoxide. Since there are no products of a methane-air flame which interfere in the mass spectrum with argon 40, the ratio of the intensity

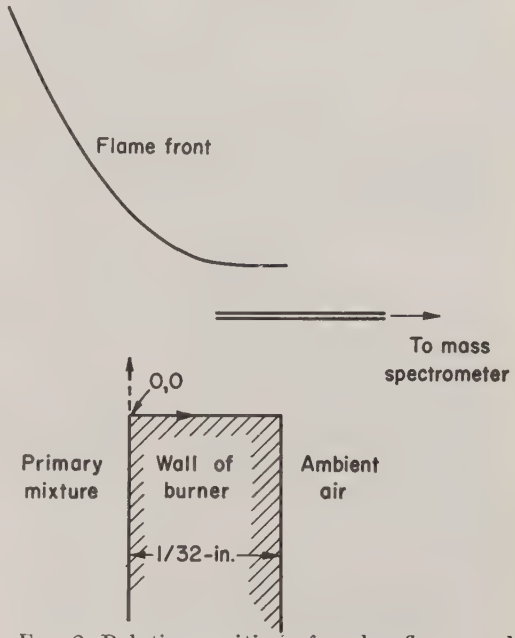

FIG. 2. Relative position of probe, flame, and one edge of burner for one setting of probe.

TABLE 1. FLOW FACTORS AS DETERMINED BY NITROGEN-TRACER METHOD

¼-in. tube; 9.45 per cent CH_4 in air; flow = 0.083 cfm. Probe at 0.015 in. above burner.

Position of probe relative to inner edge of burner, thousandths of an inch	−125	−50	−20	−10	0.0	+10	+20	+30	+40
Nitrogen peak, in mass spectrometer, arbitrary units	2440	1810	1295	1185	1130	1180	1200	1360	1530
Relative gas flow through the probe	1	0.74	0.53	0.48	0.46	0.48	0.49	0.56	0.63

of the ion current at mass 40 to the current at mass 28 would be constant only if CO was not present or, if present, was constant in concentration in the region in which the measurements were made.

Table 2 shows the results of a traverse of the probe at a height of 0.015 in. above the lip of a ¼-in. burner tube. The primary mixture was 11.7 per cent methane in air.

The ratio $A/[N_2 + CO(?)]$ varied somewhat erratically; however, the variation is probably not greater than the error involved in these measurements. It was concluded that CO does not occur in appreciable quantities in the dark space of the methane-air flames, and that nitrogen is satisfactory for use as a tracer for measuring relative volume rates of flow through the probe.

Table 2. Measurements Showing the Absence of Appreciable Carbon Monoxide in Gases under Methane Flame

Position of probe relative to inner edge of burner, thousandths of an inch	−125	−50	−20	−10	0.0	+10	+20	+30	+40
Argon peak, arbitrary units	181	124	102	89	86	83	93	102	119
Nitrogen + CO peak, arbitrary units	2440	1810	1205	1185	1130	1180	1200	1360	1530
Ratio, $A/[N_2 + CO(?)]$	0.074	0.069	0.078	0.075	0.076	0.070	0.077	0.075	0.078

Part II. Distribution of Gases in the Dark Space for a Methane-Air Bunsen Flame Near Blowoff

It was a matter of some interest to determine the concentration pattern of the fuel component in the dark space between the flame and the burner. In the first place, such information was unavailable, and in the second place, some insight might be gained about the flow pattern in this small, but important, region in which the particle tracer method has not yielded much information. Particular attention was given to flames near the point of blowoff with the aim of finding whether there was something unique in the concentration pattern of the fuel component at blowoff.

A methane-air flame was established on a cylindrical tube of 3/16-in. ID having a 1/32-in. wall. The concentration of methane in the primary mixture was 11.7 per cent by volume, and the average velocity of the mixture was 8 fps, which was as near to the velocity at blowoff as could be maintained for the necessary period of time required for the experiments. Having established the above conditions, the concentration of methane was determined point-by-point as described in Part I.

Table 3 gives a complete set of data for a typical survey. A typical calculation to obtain the concentration of methane at a point proceeded as follows. Taking the point $h = 0$, $d = 0$, as an example, the CH_3 peak was found to be 432 units from which 40 units residual reading were subtracted. The ratio of the N_2 peak at 0.0 to that at −0.085 (center of jet) was 45.2/48 = 0.94, since the nitrogen residual was negligible. This ratio indicated that, at 0.0, the gas flow rate through the probe was 94 per cent of the flow rate for the probe in the center of the jet.

Figure 3 is a plot of the concentrations of methane shown in Table 3. The decrease in concentration of methane, with increase in the height of the probe above the burner, shows that some small amount of methane is present even beyond the rim of the burner tube. A rapid and linear decrease in the concentration of methane occurs over an interval of about 0.030 in., but the last 1 per cent of methane disappears gradually.

Figure 4, obtained from Figure 3 by cross-plotting, shows the lines of constant concentration of methane above the burner and below the flame front. The lines of concentration of methane in the space between the lip of the burner and the base of the flame in Figure 4 can be visualized as arising from a combination of mass flow from the jet and interdiffusion of the ambient gases with the gases of the jet. In the main, the effect of diffusion appears to predominate over the effect of mass flow.

The extension of the flame front into a region of extremely low fuel concentration is of interest, as shown in Figure 4. For a flame to exist in this region, where the mixture is far leaner than the lean limit, a supply of heat or of free radicals must exist.

TABLE 3. DATA OBTAINED IN SURVEY OF THE DARK SPACE BETWEEN THE BURNER AND THE BASE OF A METHANE-AIR FLAME, 11.7 PER CENT CH_4 IN AIR

h^* = 0.001										
d†	−85	−30	−20	−10	0.0	+10	+20	+30	+40	+50
CH_3, observed‡	531	513	506	495	432	270	169	92	65.7	52.5
CH_3 −40° (residual)	491	473	466	455	392	230	129	52	25.7	12.5
N_2, observed‡	48.0	46.5	46.5	45.7	45.2	47.0	49.0	50.2	52.0	53.8
Flow factor, N_2/N_2 (−0.085)	1.00	0.97	0.97	0.95	0.94	0.98	1.02	1.04	1.08	1.12
CH_4, per cent	11.7	11.6	11.5	11.4	9.9	5.6	3.0	1.2	0.56	0.27
h = 0.010										
CH_3, observed	546	446	446	433	346	242	147	84.0	55.0	45.5
CH_3 −40° (residual)	504	406	406	393	306	202	107	44	15	5.5
N_2, observed	49.2	41.2	41.5	41.6	41.7	42.5	44.0	45.5	48.0	49.5
Flow factor, N_2/N_2 (−0.085)	1	0.84	0.84	0.85	0.85	0.87	0.90	0.93	0.98	1.01
CH_4, per cent	11.7	11.2	11.2	10.7	8.4	5.4	2.8	1.1	0.35	0.13
h = 0.020										
CH_3, observed	550	400	398	376	303	204	116	63	48	46
CH_3 −40° (residual)	510	360	358	336	263	164	76	23	8	6
N_2, observed	48.5	37	37	36	37	39	40.5	43.5	45.7	48.5
Flow factor, N_2/N_2 (−0.085)	1.00	0.76	0.76	0.74	0.76	0.80	0.83	0.90	0.94	1.00
CH_4, per cent	11.7	10.9	10.8	10.4	8.2	4.7	2.1	0.57	0.10	0
h = 0.030										
CH_3, observed	594	381	376	342	265	159	62	44	44	40
CH_3 −40° (residual)	540	341	336	302	225	119	22	4	4	0
N_2, observed	49.0	34.5	34.5	34.0	35.0	36.5	39.0	40.5	41.0	45.0
Flow factor, N_2/N_2 (−0.085)	1.00	0.70	0.70	0.69	0.71	0.74	0.80	0.83	0.84	0.92
CH_4, per cent	11.7	10.5	10.3	9.5	6.8	3.5	0.60	0.10	0.10	0

* h = height of probe above lip of burner.

† d = horizontal position of probe relative to inner wall of burner, thousandths of an inch.

‡ Observed output of amplifier, arbitrary units.

Figure 5 shows lines of constant concentration of methane above the edge of a burner tube when a flame is not present. In this instance, the con-

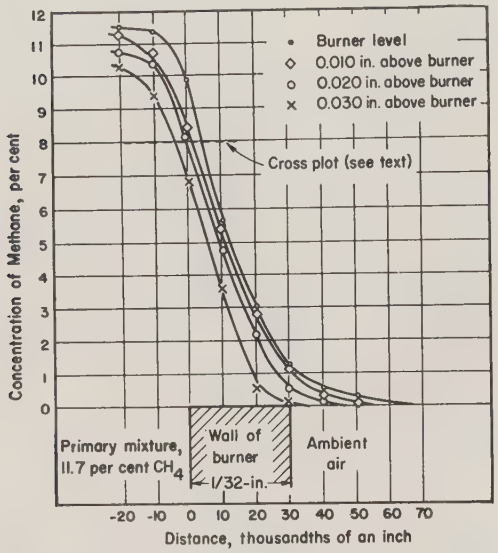

FIG. 3. Concentration of methane in dark space between flame and burner.

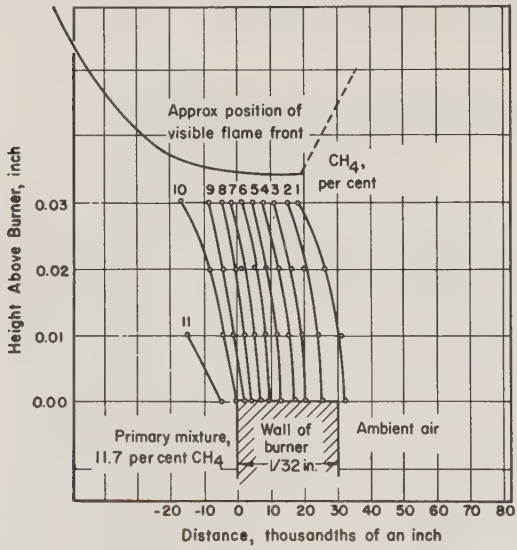

FIG. 4. Lines of constant concentration of methane under base of methane-air flame.

centration of methane in the primary mixture was 11.4 per cent, slightly less than that used for the flame study that resulted in the data for Figure 4, although the velocity of the primary mixture was 8 fps in both instances. Comparison of the two figures shows that the concentration profiles have a noticeable curvature when a flame is present.

EFFECT OF MIXTURE VELOCITY ON CONCENTRATION OF METHANE IN DARK SPACE

The effect of the velocity of the primary mixture on the pattern of concentration of fuel in the dark space was investigated, using a $\frac{3}{16}$-in. ID burner through which a primary mixture of 10.9 per cent methane in air was passed. The concentration pattern was determined for two velocities of the primary mixture. Inasmuch as experience had shown that the profiles of constant concentration were smooth lines, measurements were confined to two levels: one near the level of the

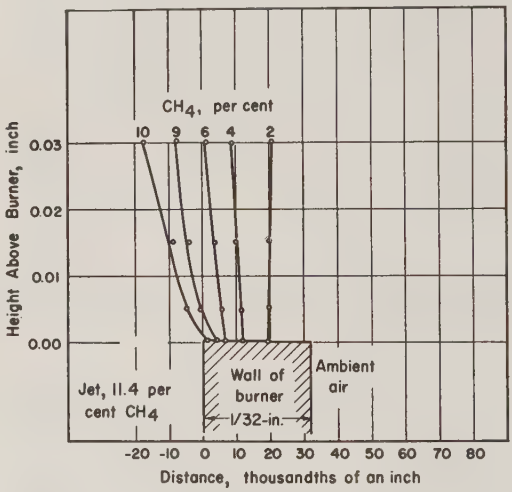

FIG. 5. Concentration profile of a free jet with no flame.

burner, and the other at a height of 0.025 in. above the burner.

Figure 6 shows plots of the methane concentrations obtained; an increase in velocity is accompanied by an increase in the concentration of methane at a given point. The decrease in concentration, as the probe is moved away from the axis of the burner, is similar to that shown in Figure 3.

Figure 7, which was obtained by cross plotting from Figure 6, shows typical shifts, with velocity, in lines of constant concentration of methane. The solid lines, connecting points of equal concentration for a velocity of 4.9 fps of the primary mixture, become displaced to the corresponding dashed lines when the velocity is increased to 6.6 fps. The changes are understandable in terms of the time available for the loss of methane or

the addition of air by diffusion. However, the general effect of an increase in the velocity of the jet is to increase the concentration of methane at any point in the dark space. The specific effect of an increase in velocity will be to increase the burning velocity of the mixture at a given point, provided one selects the point where, initially, the concentration of the fuel component is on the lean side of the stoichiometric mixture.

The effect, then, of an increase in the velocity of the primary mixture is, on the one hand, to increase burning velocity by increasing the concentration of the fuel component in the dark

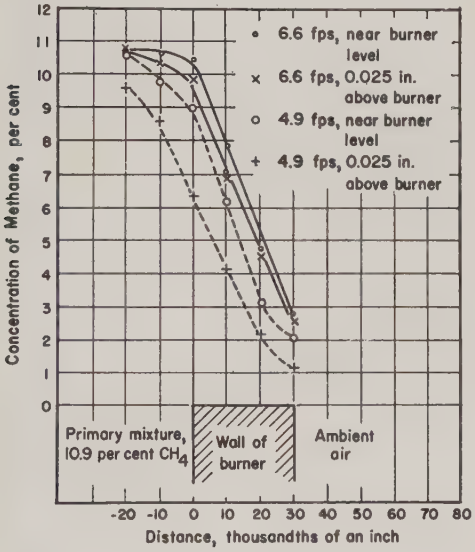
Concentration of Methane, per cent
Distance, thousandths of an inch
• 6.6 fps, near burner level
× 6.6 fps, 0.025 in. above burner
○ 4.9 fps, near burner level
+ 4.9 fps, 0.025 in. above burner
Primary mixture, 10.9 per cent CH4
Wall of burner
Ambient air

FIG. 6. Concentration of methane in dark space for two velocities and for two levels above burner.

space. On the other hand, an increase in velocity increases the upward component of gas velocity in the dark space—through the process of diffusion of momentum from the jet. It would be difficult to predict the net effect on flame stability of these two competing processes. Another factor, which may be of possibly great importance to flame stability, ought to be considered in relation to the problem of the stability of a flame. This factor is the presence of combustion products, particularly CO_2, in the dark space of a laminar methane flame.

CONCENTRATION OF CARBON DIOXIDE IN THE DARK SPACE AT BLOWOFF

Figure 8 shows the concentration of CO_2 in the gases of the dark space of flame of 10.7 per cent CH_4 in air. The flame was near the point of blowoff, since the mixture velocity was 7.7 fps; consequently, the results are pertinent to the discussion of the problem of flame stability. A

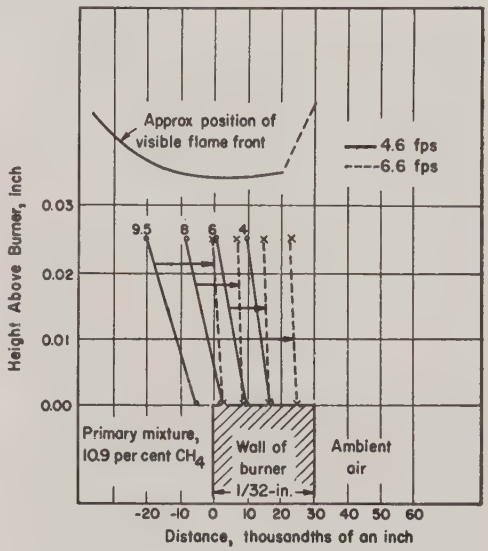

FIG. 7. Effect of increase in velocity of primary mixture on profiles of constant concentration of methane.

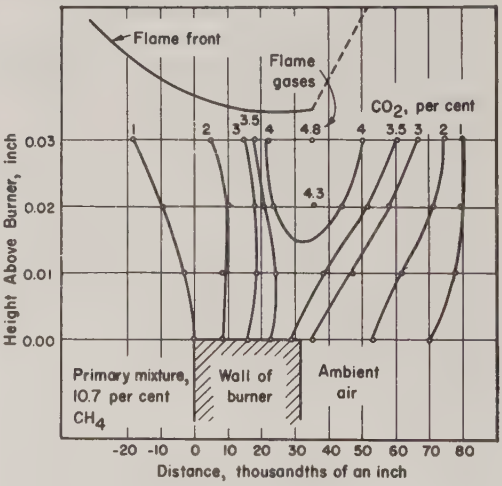

FIG. 8. Concentration profile of CO_2 in dark space of laminar methane-air flame.

striking feature of Figure 8 is that it shows CO_2 to be present not only in the dark space near the flame but also in the dark space near the lip of the burner.

Comparison of Figure 8 with Figure 4 shows that the region in which CO_2 increases in concentration corresponds generally to the region in which the concentration of methane decreases.

Nevertheless, the CO_2 in the dark space does not appear to be the result of the combustion of CH_4 in the dark space.

The principal reason for considering that combustion does not occur in the dark space itself is that CO_2 was found in equal concentration near both the relatively cool burner and the hot flame. It would be expected that combustion in the dark space would occur with much more vigor in the immediate vicinity of the visible flame front. If such combustion should occur, the concentration of CO_2 would be much higher in the dark space near to the flame than it would be in the dark space near to the burner.

Combustion in the dark space does not have to occur to account for the presence of CO_2 in that region. It is possible that the CO_2 comes from the flame gases by recirculation, as indicated by the arrow near the tip of the flame in Figure 8.

The importance to the flame stability problem of an influx of CO_2 near the anchored edge of a methane-air flame may lie in the effect of the CO_2 as a diluent to the combustible mixture in the region of the anchored edge of the flame. Furthermore, the quantity of CO_2 in the region near the edge of the flame should increase with an increase in the velocity of the primary mixture. This increase would be brought about through the process in which the main jet entrains more and more of the ambient gases as the velocity of the jet is increased more and more.

Another important diluent that affects the stability of laminar Bunsen flames is the air that enters from below the burner into the region near the anchored edge of the flame. In contrast to CO_2, which probably can reduce the burning velocity of the combustible mixture at the edge of the flame, air that enters this region may have less effect on the flame than the CO_2, since the air contains oxygen which may assist the combustion process.

To sum up, with the use of a mass spectrometer, it has been possible to measure the concentration of the CH_4 and of CO_2 in the dark space between the lip of a Bunsen burner and the base of methane-air flames. Mass flow of the primary mixture into the dark space appears to be highly modified by inward diffusion of ambient gases, including air and CO_2.

Conclusions

In regard to conclusions that can be reached about the problem of flame stability, it can be said that the results of this investigation show: (1) that an increase in velocity of the primary jet increases the concentration of the fuel component at a given point in the dark space, and, thus, opposes the tendency of the increase in velocity to produce a condition of blowoff. Coincident with an increase in velocity of the primary mixture, one can predict an increase in the concentration of CO_2 by recirculation of burned gases into the flame-holding region. This CO_2, as a diluent, may reduce flame stability by reducing the burning velocity of the combustible mixture in the region critical to the stability of the flame.

The results of this study indicate some of the complexity of the problem of flame stability. With few exceptions, all of the complexities are subsumed by the correlation parameter, velocity-gradient at the wall of the burner tube. This parameter has been found by Lewis, von Elbe and co-workers[1] to correlate the data on blow-off of flames of one primary mixture, regardless of the diameter of the burner tube. In the light of the present study, it would appear that the success of the velocity-gradient parameter in the correlations rests on the ability of the parameter to specify uniquely the conditions of flow in the dark space.

Acknowledgments

The work described in this paper was conducted under the sponsorship of the Aeronautical Research Laboratory, Wright Air Development Center. The assistance of Leonard H. Mauk in obtaining many of the data is gratefully acknowledged.

REFERENCE

1. Lewis, B., and von Elbe, G.: *Combustion, Flames, and Explosions of Gases*, pp. 241, 282, New York, Academic Press, 1951.

14

FLAME PROPAGATION IN CYLINDRICAL TUBES NEAR THE QUENCHING LIMIT[a]

By J. M. SINGER AND G. VON ELBE[b]

Introduction

Flame propagation through various methane-air mixtures contained in tubes of near quenching distance has been studied by the Bureau of Mines. The tubes were mounted vertically; the lower end was closed, and the flame was propagated downward from the open to the closed end. Lewis and von Elbe[1] have assumed that the change of cross section of the stream tubes passing through the moving combustion wave is very small in channels near the quenching distance, so that the flow lines are maintained substantially parallel to the channel wall. A large temperature gradient in the burned gas from wall to center prevents isothermal Poiseuille flow and the corresponding spreading of flow lines in the unburned gas. According to this model, the more or less hemispherical curvature of the flame surface is the result of a decrease of burning velocity over the tube cross section. This decrease is due to heat flow to the wall. The burning velocity becomes zero near the wall and increases toward the axis of the tube. The linear flame speed is identical with the axial burning velocity. According to Lewis and von Elbe's theory of the structure of combustion waves near solid surfaces,[2] the axial burning velocity and hence the linear flame speed at quenching is approximately equal to the standard burning velocity.

To test this theory, linear flame speeds at near quenching limits were determined experimentally. Also, the corresponding dead space distance between flame and inside wall was measured and compared with the value predicted from theory. In addition, dead space distances were compared with the interconal distances between schlieren and luminous outlines of burner flames.

Apparatus and Experiments

Methane-air mixtures of various compositions were spark-ignited at the open end of vertical tubes 30 cm long. Mixtures of varying composition were prepared in gas reservoirs by the partial-pressure method. The thoroughly mixed gas mixture was introduced to a spark igniter chamber and flame tube that had been previously evacuated. The flame channels were precision-bore Pyrex-glass tubes equipped at both ends with tapered-joint connections for interchangeability. To dampen vibratory motion of the flame, a glass-wool plug was placed at the top of the igniter chamber. In operation, the igniter cover was carefully slid off and the gas mixture spark-ignited. Igniter volume and diameter were large, to avoid spurious spark effects in the flame tube. The flame front moved down the wide igniter tube into the narrow flame channel, where the speed was measured at various positions by means of two photocells placed 5 cm apart. In most instances the flame front was a meniscus of approximately hemispherical shape. Flame radiation was received by each photocell and transmitted by means of an amplifier to a Dumont 208 cathode-ray oscillograph coupled to a low-frequency linear time-base generator, Dumont type 215. Both a 60-cycle calibration sine wave and an impulse-interrupted linear single-sweep trace are shown in Figure 1. The circuit diagram and firing synchronization unit are indicated in Figure 2. Flame oscillations were occasionally noted. After flame oscillation, a horizontal linear pattern of water condensate could be observed on the inside wall, probably due to rapid compression and expansion. To investigate the effect of constricting the flow of burned gas, brass diaphragms containing holes of various diameters were placed at the open end of the flame igniter along with the glass-wool plug. An opening of approximately 10 per cent of the flame-tube diameter gave most stable and reproducible flame propagation, the flame speed increasing slightly (4 to 6 cm/sec) with increasing constriction. When flame speeds were measured in the present experiments, no restriction was at the open end other than the glass-wool plug.

Dead space distances could be determined from photographs by means of a 24× enlarging comparator, the approximate error being 0.5 per cent.

[a] This research is a part of the work being carried out at the Bureau of Mines on project NA onr 25-47, NR 098 117, supported by the Office of Naval Research.

[b] Present address: Combustion and Explosives Research, Inc., Pittsburgh, Pa.

For comparison, in a separate experiment, schlieren-luminous interconal distances were obtained for various methane-air flames stabilized on cylindrical burner tubes in free space.

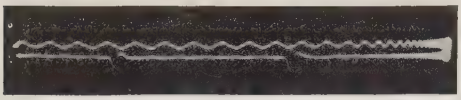

FIG. 1. Typical oscillograph picture showing experimental and calibration lines.

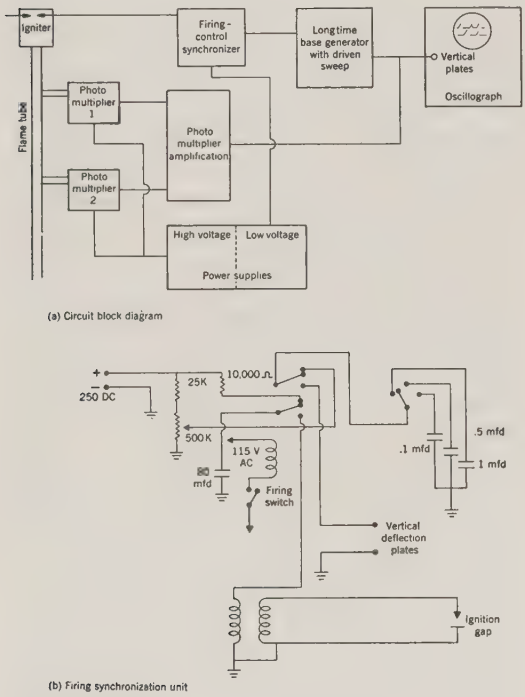

FIG. 2. Electronic circuits for determination of flame velocities.

Data and Discussion

LINEAR FLAME-SPEED MEASUREMENT

The problem of obtaining uniform flame movement in large tubes not near the quenching distance has been pointed out recently by Wheatley[3] and Hoare and Linnett.[4] The hydrodynamics of flames propagating in large tubes has been treated by Jost,[5] Ball,[6] and Lewis and von Elbe.[7]

Few investigators have studied flame propagation in very narrow channels. At near quenching limits, uniform flame movement in downward propagation is usually attained within a few centimeters after the ignition. Occasionally, steady state may not be reached after the flame enters the flame tube, resulting in extinction before the entire flame tube is traversed. In the initial movement, nonsymmetrical tilting of flame front increases the instability and leads to lower linear flame speeds and apparent burning velocities.

Figure 3 shows the downward flame speed within tubes of various diameters for several methane-air mixtures. The figure includes flames that traversed only a partial length of the flame tube before extinction. In Table 1 are linear flame speeds for some methane-air mixtures very close to the quenching limit (within ½ to 1 mm.). Also listed for comparison are the standard burning velocities obtained by Manton and Milliken.[8] In part "b" of the table, the flame speeds are seen to be less than the standard burning velocity when the flame does not traverse more that ¼ of the flame tube before extinction. Observed agreement between the linear flame speeds and standard burning velocity confirms the prediction by Lewis and von Elbe[1] that stream tubes are not expanded when passing through the flame front in tubes of near quenching diameter. Similarly, Payman and Wheeler[9] have obtained flame speeds in horizontal tubes approaching the quenching limit that approximately equal the standard burning velocity for methane-air mixtures.

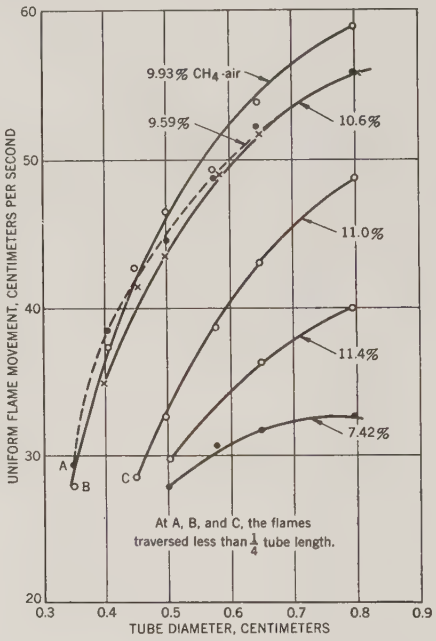

FIG. 3. Linear flame speeds, cm/sec, for methane-air mixtures at 1 atmos, 25° C.

DEAD-SPACE DATA

The dead-space distances between flame and

wall for various methane-air mixtures and tube diameters are shown in Figure 4. It is seen that these distances increase sharply for lean and rich mixtures. Because of the laborious calculation involved, comparison of the measured dead space with the value from theory is limited to the 10 per cent methane-air mixture. For this mixture the dead-space distance is calculated to be 0.45 mm.,[c] in satisfactory agreement with the experimental value, which is 0.432 mm. Similarly, satisfactory agreement has been previously reported for theoretical and experimental quenching distances.[12]

Table 1. Linear Flame Speeds for Methane-Air Mixtures in Tubes That Are Close to the Quenching Limit

Tube Diameter	Composition	Linear Flame Speed	S_u*
cm	%	*cm/sec*	*cm/sec*
(a) Entire flame tube traversed by flame			
0.399	9.94	37.3	36
0.399	9.59	38.3	37.8
0.399	10.6	35.0	35.0
0.498	11.4	29.4	29
0.498	7.42	28.0	25
0.498	11.0	32.1	32.5
0.498	10.6	36.6	35.5
0.498	10.7	35.0	35.4
(b) Extinction of flame during travel			
0.352	9.59	29.4	36.9
0.352	9.93	28.0	36.8
0.456	11.0	29.0	32.5

* Manton, J., and Milliken, B. B.[8]

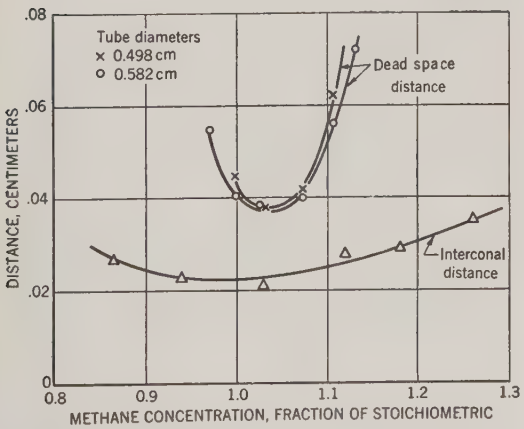

Fig. 4. Comparison of dead space distance and interconal luminous-schlieren distance.

There is also shown in Figure 4 the distance between the schlieren and luminous outlines in flames on cylindrical burner tubes. It is seen that these interconal distances are much smaller than the dead-space distances; that is, the temperature gradient from the luminous zone into the unburned gas is considerably steeper than the temperature gradient from the luminous zone to the wall. This difference is evidently due to the decrease of burning velocity in the vicinity of a heat sink, such as a tube wall, which considerably flattens the temperature gradient. The interconal distance seems to be less sensitive to change of mixture composition than the dead-space distance, reflecting the fact that, as the burning velocity is decreased by enriching or leaning the mixture, the heat loss from a flame to a sink becomes relatively larger. However, quantitative interpretation of these effects does not seem feasible.

Conclusions

(1) The measured data of linear flame speeds confirms the prediction by Lewis and von Elbe[1] that the linear flame speed approximately equals the standard burning velocity in channels of near quenching dimensions.

(2) The difference between the dead-space distances and interconal luminous-schlieren distances conforms to qualitative theoretical expectations. Computation of the theoretical dead-space distance for a specific mixture of methane-air (10 per cent methane-air) shows satisfactory agreement with the experimental value.

Acknowledgments

The authors wish to thank the members of the Branch of Physical Sciences of the Bureau of Mines, U. S. Department of the Interior, for their cooperation—especially J. Grumer for many helpful discussions. The electronic circuits and firing synchronization units were constructed by Frank C. Gibson.

REFERENCES

1. Lewis, B., and von Elbe, G.: *Combustion Flames and Explosions of Gases*, p. 326. New York, Academic Press, 1951.
2. Lewis, B., and von Elbe, G.: *Combustion, Flames and Explosions of Gases*, pp. 379–388. New York. Academic Press, 1951.

[c] In dimensionless units, ν is approximately 7.5.[10] Division of ν by $a = 164$ cm^{-1} yields 0.45 mm.[11]

3. Wheatley, P. J.: Fuel, *29*, 80 (1950).
4. Hoare, M. F., and Linnett, J. W.: Trans. Faraday Soc., *49*, 1038 (1953).
5. Jost, W.: *Explosion and Combustion Processes in Gases*, p. 80. New York, McGraw-Hill, 1946.
6. Ball, G.: A Study of a Two-Dimensional Flame, Combustion Project Report, Harvard Univ., July 1951.
7. Lewis, B., and von Elbe, G.: *Combustion, Flames and Explosions of Gases*, p. 317. New York, Academic Press, 1951.
8. Manton, J., and Milliken, B. B.: *Proceedings, Gas Dynamics Symposium on Aerothermochemistry*, p. 151. Evanston, Ind., Northwestern Univ. Press, 1956.
9. Payman, W., and Wheeler, R. V.: J. Chem. Soc., 1251 (1923); 1835 (1932).
10. Lewis, B., and von Elbe, G.: *Combustion, Flames, and Explosions of Gases*, fig. 171, p. 386. New York, Academic Press, 1951.
11. Lewis, B., and von Elbe, G.: *Combustion, Flames, and Explosions of Gases*, table 13, p. 418. New York, Academic Press, 1951.
12. Lewis, B., and von Elbe, G.: *Combustion, Flames, and Explosions of Gases*, table 15, p. 426. New York, Academic Press, 1951

15

COOL FLAMES OF PENTANE-OXYGEN MIXTURES

By MICHEL LUCQUIN and PAUL LAFFITTE

Introduction

Explosion limits of cool and second-stage flames offer numerous special characteristics that are more or less directly related to the chemical oxidation mechanism, and have led the authors to make a detailed study of the morphologic aspect of these phenomena, including the influence of added chemical agents. The present paper gives a number of the experimental results obtained.

Complete explosion low temperature diagrams of hydrocarbon oxygen mixtures which include the three parameters of pressure, temperature and concentration, had not been determined previously. Pentane was chosen for this investigation, first, because it has been little studied, and second, because it is easy to investigate experimentally as it is situated between the relatively small propane and butane molecules that have rather long time lags and the heavier molecules which burn too rapidly.

Experimental

We used the statical constant volume method known as the "pyrometer" method. Observations were made either visually or by differential manometer recordings. The reaction vessel was a Pyrex cylinder, 10 cm long and with a 22 mm i.d. To improve temperature control, the vessel was surrounded by a Duralumin jacket. Taking into account information given in the literature, we were able to obtain reproducible results.

Phillipps' Research Grade 99.9 per cent pentane was used. The oxygen was commercial grade and the same cylinder was used throughout. It was purified over copper oxide and soda lime and dried over phosphorus pentoxide. It was 99 per cent pure as tested by pyrogallol.

Determination of the Pressure-Temperature-Concentration Diagram

A number of isochors were determined and used to derive isobars and isotherms.

Isochors (pressure-temperature diagram)

Isochors were determined for mixtures containing 80, 66.66, 50, 33.33, 20, 11.11, 4 and 2 per cent pentane. A certain number of isochors only are reproduced here.

33.33 per cent mixture[1]

Figure 1 shows two-stage ignition limits which are particularly easy to determine in this case. There are several maximums and minimums, and their possible relation to the chemical mechanism will be shown later. Curves 1, 2, 3, 4, and 5 represent the number of cool flames obtained inside each region. The first cool flame limit presents a higher temperature lobe, as reported earlier by Malherbe and Walsh.[2] Contrary to the previous hypothesis of Laffitte and Freling,[3] there seem to be no relation between the

multiple flame regions and these two lobes. The pressure recordings show that at high temperature the waves produced by the occurrence of multiple flames progressively disappear with the superposed slow reaction (Fig. 6c). In this case it becomes impossible to determine a limit that has any physical meaning, as it depends solely on the sensitivity of the gauge.

Four and two per cent mixtures

Figure 2 shows the 4 per cent diagram where a small cool flame region (Curve 2) still exists, and the 2 per cent where it has completely disappeared. The high temperature lobe grows as the pentane concentration decreases. This appears even more clearly when all the diagrams obtained are examined successively.

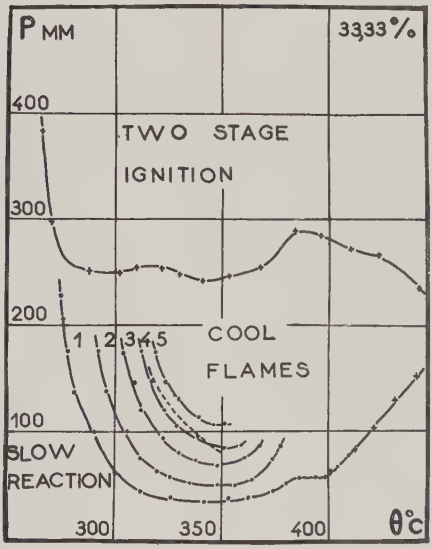

FIG. 1. Explosion limits for 33.33 per cent pentane-oxygen mixture.

Other mixtures

The number of cool flames obtained depends on the concentration of the mixture as will be seen upon examining the isotherms. The second lobe cannot be detected for mixtures richer than 50 per cent.

ISOTHERMS (PRESSURE-CONCENTRATION DIAGRAM)

Only the 350°C[4] isotherm is shown (Fig. 3). This temperature corresponds approximately to the minimum of the isochors. It is therefore for this isotherm that the regions are widest.

Cool flames

The curves for each region reach a minimum value for approximately the same mixture (33 per cent). This is also the case for other temperatures. It is for this mixture that the number of cool flames is maximum. It is always equal to five whatever the vessel dimensions, and provided the temperature is strictly homogeneous, this number cannot be increased. This is to be related to the number of multiple cool flames found for other hydrocarbons: 5 for butane (Bardwell[5]); 5 for propane (Newitt and Thornes[6]); 4 (at least) for ethane (Knox and Norrish[7]). The first cool flame region is particularly wide. A cool flame can be detected for concentrations extending from 2 to 96 per cent. Induced pyrolysis—if it occurs at this temperature—could well be a slow cool-flame reaction, as the presence of a very

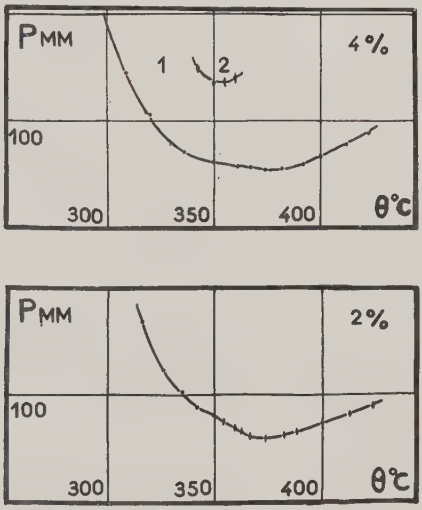

FIG. 2. Explosion limits for 2 and 4 per cent pentane-oxygen mixtures.

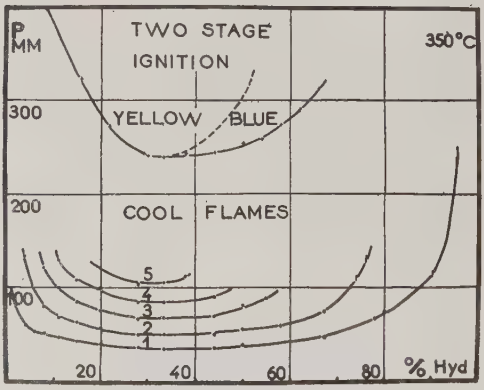

FIG. 3. Explosion limits at 350°C.

small amount of one of the constituents in the other is enough to produce a cool flame. We feel that this view is correct, at least in the case of acetaldehyde, and results obtained by Niclause[8] on induced pyrolysis should be interpreted in this way.

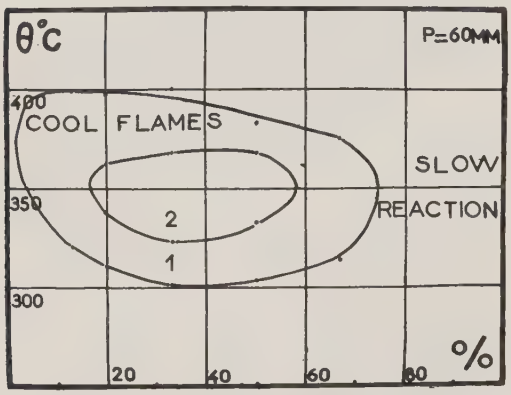

FIG. 4. Explosion limits at 60 mm Hg.

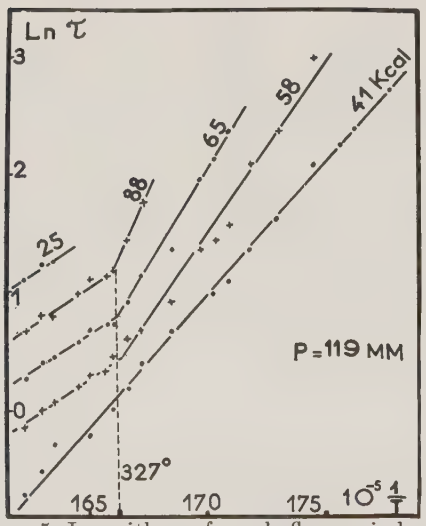

FIG. 5. Logarithm of cool flames induction period against reciprocal of absolute temperature at 119 mm Hg pressure.

Two-stage ignition

The two-stage ignition limit has been determined. At high concentrations of hydrocarbon, the second-stage flame is blue and similar to the cool flame which precedes it. As the oxygen content increases, its intensity increases. At the same time, the center becomes yellow and this color extends progressively to the whole flame which often becomes violent enough to break the apparatus. The minimum of this region coincides with the cool flame minimum, which shows that the normal flame forms from the products of the cool flame. Points located at the left of the minimum were obtained by increasing the pressure, rather than by decreasing it in the usual manner. Although this may not be a recommended technique, it proved the only possible one after violent explosions shattered the inlet stopcock and tubes repeatedly. The two regions located at each end of the diagram are now well determined and can be studied without hazard. In particular, the stoichiometric mixture can be studied down to a pressure of 350 mm of mercury.

ISOBARS (TEMPERATURE-CONCENTRATION DIAGRAM)

Figure 4 shows an isobar obtained at a pressure of 60 mm of mercury. As the pressure is low, the cool flame regions are closed. At low concentrations the widening of the first limit shows the importance assumed by the second lobe under these conditions.

Shape of the Flame Curves

The first flame is always different from the others. There are several reasons for this: Its limit curve is the only one that has two lobes. The curve obtained shows a marked peak, whereas consecutive flames appear simply as waves that disappear progressively in the slow reaction when the temperature increases (Fig. 6c). The first flame is much less influenced and is the only one observed in small reaction vessels. A carbon black deposit suppresses multicool flames.

Relative importance of multicool flames and their time lags

As we have seen, the flames become less important as the temperature increases. However, multicool flames react much more to this influence than does the first one. Figure 6c shows a typical curve. When five, four, or even three, cool flames are present, one can see how the importance of the consecutive flames decreases from the last to the second as this is translated by the height of each wave on the recording. However, the last flame, the nearest to its limit, is more important than the ones before. After the first flame, it is always the last which is the most marked. The time lags between these consecutive flames increase in the same manner from the second to the last one, but they do not vary regularly with the temperature as is the case for the

first one. This is clearly apparent in Figure 5 where the logarithm of the time lag is plotted against the reciprocal of the absolute temperature. For a given pressure, there is one temperature for which the slope of the curve changes suddenly. Referring these results to the pressure-temperature diagram in Figure 1, we obtained the line represented by dashes. On the high temperature side, the time lags vary little. They are, however, still at a finite interval, one from the other, when the multicool flames disappear in the slow reaction which is superposed. Figure 5 gives the temperature coefficient for each flame.

Discussion

Without involving a great number of hypotheses, our observations have led us to a number of conclusions which may well have some bearing on the flame and oxidation mechanisms.

Normally, the second-stage flame is closely linked to the first cool flame and probably to the slow reaction which is superposed. The cool flame is followed by a pseudo-induction period (Fig. 6a). This must be due to some sort of compensation because for a given pressure, the second-stage flame immediately follows the cool flame (Fig. 6b). There is no case of a limit which is not preceded by a slow reaction. The influence of added chemical agents, either homogeneous or heterogeneous, should give us information on the nature and behavior of this limit and therefore on the second-stage flame through the studying of their influence on these maxima, and minima, and also on the induction periods.

Whenever normal ignition cannot take place, periodicity occurs. To understand our results on the importance of cool flames, one must postulate an action of the initial reaction products on the multicool flames. This action is modified by their decay with time and thus gives a particular aspect to each flame. If, as Bardwell and Hinshelwood[9] think, the flame is mainly a peroxidic phenomenon it is also necessary to consider the perturbing influence of certain products on the nature, rate of formation, and the critical concentration of these peroxides. For several reasons, the aldehydes produced at the beginning of the reaction and especially by the first cool flame might be held responsible for this interaction. It is known that the addition of higher aldehydes always decreases the induction periods of cool flames.[10] In our case, their concentration also tends to diminish with time as the induction period between the second and the last increases. The second-stage ignition limit and its slow reaction are both very sensitive to the addition of aldehydes. As aldehydes are found in combustion products they must play an important role. Accordingly, we think that aldehydes connected with the slow reaction must have a perturbing effect on the relatively independent cool flame mechanism. This interpretation agrees with the views of Frank-Kamenetzki[11] on the periodical influence of peroxides and aldehydes, and of Walsh[12] on the condensation of peroxides and aldehydes favoring explosion.

At high temperature, in particular as far as the induction periods are concerned (Fig. 5), the mechanism of this interaction may be modified.

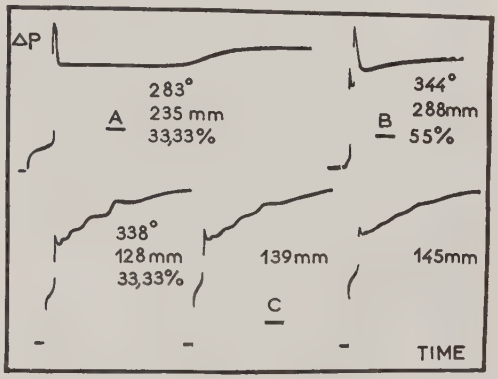

FIG. 6. Recording for various flames of pressure variation with time: (A) Cool flame in single flame region; (B) two-stage ignition; (C) multicool flames in five flame regions.

This perturbation then may be related to the existence of the second lobe in the first cool flame region and to the maximum of the two-stage ignition at 390°C.

REFERENCES

1. LUCQUIN, M., AND LAFFITTE, P.: Compt. Rendu., *240*, 1095 (1955).
2. MALHERBE, F. E., AND WALSH, A. D.: Trans. Faraday Soc., *46*, 835 (1950).
3. LAFFITTE, P., AND FRELING, E.: Inst. Internat. de Congrès Solvay, 8° Conseil de Chimie, Bruxelles, 1950, p. 119.
4. LUCQUIN, M., BEN-AIM, R., AND LAFFITTE, P.: Compt. Rendu., *241*, 949 (1955).
5. BARDWELL, J.: *Fifth Symposium (International) on Combustion*, p. 529. New York, Reinhold Publ. Corp., 1955.
6. NEWITT, D. M., AND THORNES, L. S.: J. Chem. Soc., 1656 (1937).

7. Knox, J. H., and Norrish, R. G.: Trans. Faraday Soc., *50*, 928 (1954).
8. Niclause, M.: Thèse Nancy, p. 18, fig. 3, 1953.
9. Bardwell, J., and Hinshelwood, C.: Proc. Roy. Soc., *A205*, 375 (1951).
10. Neumann, M., and Feklikof, G.: Zhur. Fiz. Khim., *28*, 1439 (1954).
11. Frank-Kamenetzki, D. A.: Zhur. Fiz. Khim., *14*, 30 (1940).
12. Walsh, A. D.: Trans. Faraday Soc., *43*, 297 (1947).

16

THE DEPENDENCE OF FLAME TEMPERATURE ON MASS BURNING VELOCITY

By W. E. KASKAN

Introduction

The cooled porous metal burner is a powerful new tool for the study of premixed laminar flames.[1, 2] Whereas the flame temperature of an unquenched or adiabatic flame is a unique function of the state of the unburned gas, the final temperature of a flame burning on a cooled porous metal burner can, within limits, be fixed independent of the properties of the unburned gas.

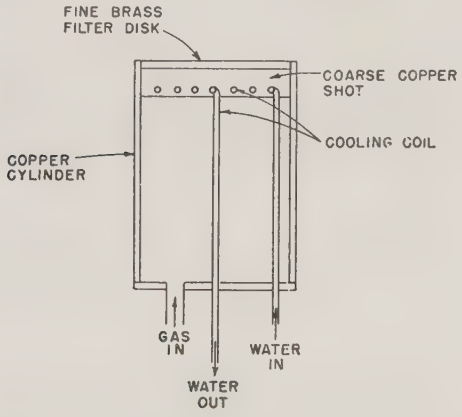

Fig. 1. Diagram of cooled porous metal burner.

For a given fuel-oxidant system, for example, it is possible to produce flames over a wide range of final temperature all with the same initial composition. To a much more limited extent it is possible to effect this by precooling. However as has been pointed out by Botha and Spalding,[1] it is possible to cool a flame on a porous burner to a temperature lower than that which would result from the adiabatic combustion starting from the absolute zero. Flames on porous burners offer other advantages for study. They are very stable, their position in space being fixed by the position of the burner surface. They can also be made quite flat, independent of the size of the burner.

The work reported here began as a study of quenching. Specifically, it was desired to investigate by means of porous burners the effect of cooling on burning velocity with the hope that it might be possible to extrapolate the data to zero burning velocity to obtain an absolute measure of quenching. This did not turn out to be possible. However, in the course of the work a simple and hitherto unreported relationship between mass burning velocity and flame temperature was observed. This paper presents the data on this relationship for various mixtures of a number of fuels with air, as well as some data on H_2-"air" flames in which the N_2 in air has been replaced with He, CO_2, and A.

Apparatus

Water-cooled porous metal burners 1.5 to 3 in. in diameter were used. The burners were constructed as is indicated in Figure 1. The filter disk, coarse shot, cooling coil, and copper cylinder were sintered together in a single operation. The filter disk, a commercially available item made from approximately 0.001-in. diameter shot, served to control the flow, whereas the coarse portion, made of 0.020-in. diameter shot, served to provide good thermal contact between the cooling coil and the filter disk.

The velocity of gas issuing from these burners was found not to be uniform over the surface. This was determined in several ways: by probing with a thermistor anemometer in the absence of a flame; by probing with a thermocouple in the presence of a flame; and by visual observation

of a flame near blowoff. Therefore, each of the burners was mapped by taking thermocouple readings at a number of regularly spaced points over the burner surface. At a given point, the maximum flame temperature was an approximately linear function of flow velocity, for small changes in flow velocity, so that an arithmetic average thermocouple reading was correlated with the average flow velocity. In making such a map, it was found that for the lean flames which were used in the process the observed maximum temperature would start to drop rather sharply a few millimeters from the edge of the burner. This was attributed to the interdiffusion of cold air, and these readings were discarded in computing the average. This is equivalent to assuming that the average flow in the outer annulus of the burner was the same as that for the central core, an assumption that really cannot be justified except by noting that the velocities arrived at in this way from one burner to the next agreed with each other to within 5 per cent. From these maps, a point on each burner was chosen which was surrounded by a relatively large region of constant velocity. The local velocity in terms of the average velocity was evaluated for this point from the mapping data, and all subsequent measurements were made over this point.

The temperatures were measured with quartz-coated Pt-Pt 10 per cent Rh thermocouples made from 0.0005-in. diameter wire.[3, 4] Each of the fine wires was 1 to 1.5 cm long and was flame-welded to support leads of the same material 0.010 in. in diameter. The assembly was Y-shaped, with the heavy wires forming the Y and in turn being supported by a length of two-holed ceramic tubing, and with the fine wires strung across the top of the Y. The heavy wires were bent so as to put the fine wires in tension; thus the fine wires could be held taut and parallel to the burner surface.

The junction itself was made by carefully manipulating the fine wires, previously welded to the support leads, under a microscope so that they butted together, and then discharging a small condenser through them. When properly done, this sometimes resulted in a junction which was very nearly a butt-weld, and usually in a weld which was less than twice the wire diameter. These junctions represented such a small perturbation of the otherwise nearly cylindrical character of the fine wires that the thermocouples were considered as cylinders for the purposes of calculating radiation corrections.

Catalytic heating of Pt-Pt 10 per cent Rh thermocouples upstream of the temperature maximum in a lean C_3H_8 air flame has been reported,[3] as has been catalytic heating of Pt 10 per cent Rh wires at and downstream of this point in CO and hydrocarbon flames.[5] However, in a C_2H_2-O_2 flame[6] catalytic effects were not reported at the position of the temperature maximum. Coatings of a ceramic[3] or of fused quartz[5] have been reported to reduce or eliminate this effect.

Because of the general desirability of fused quartz as a coating material, its use in the present case was investigated. It was found possible to coat the thermocouples with a quite uniform glassy film of fused quartz by immersing the thermocouple in the hot gases from a flame in which a small amount of hexamethyldisiloxane had been burned. The flame was held on a porous metal burner and was adjusted so that the thermocouple temperature was about 1800°K at the start of the coating process. At temperatures higher than 1800°K there was tendency for the silica to agglomerate into little beads along the wire, as if the silica were fluid enough to flow and did not wet the metal well. At too low a temperature the coating was powdery.

It has been reported[5] that emissivities of quartz-coated Pt 10 per cent Rh resistance wires have been calculated using the method and data of Pirani.[7] It is not clear how this was done, since the data of Pirani are for very much thicker sections of fused quartz at temperatures much lower than those encountered here. Consequently, it was desired to make some direct estimates of emissivity by comparing the temperature of a thermocouple before and after coating under identical flame conditions. To do this, however, the test flame had to be one in which there was no observable catalytic heating.

A comparison was made of the temperatures of coated and uncoated thermocouples in the neighborhood and downstream of the maximum temperature. In some flames the effects observed were similar to those previously reported by Leah and Carpenter, and are what would be expected if the flame gases were not in equilibrium downstream of the maximum temperature. The bare wires attain a higher temperature than the coated wires because of their lower emissivity and because of the catalytic heating which occurs on their surface. As the flame gases pass downstream they approach equilibrium and the difference in wire temperatures decreases. Once equilibrium has been attained, this difference

becomes constant, and both temperatures decrease slowly because of the cooling of the gas by radiation.

As a further check on this picture, theoretical temperature gradients were calculated, assuming that the temperature drops only because of loss of energy by radiation. Data on the emissivity of H_2O and CO_2 of Hottel[8] were used assuming no self-absorption.[9] It was found that, in those flames in which the temperature gradient measured by both coated and uncoated couples agreed to within about 10 per cent, the theoretical gradient also agreed to within 10 to 20 per cent of the experimental. On the other hand, when the two experimental gradients did not agree, the theoretical gradient was found also not to agree, and to be higher than that measured by the coated couple. This is consistent with the assumption that the equality of the two gradients indicates the absence of appreciable catalytic heating of the uncoated thermocouple.

Lean H_2-air flames, free of catalytic heating according to the criterion above, were employed to estimate ϵ, the coated thermocouple emissivity. For the purpose of estimating heat transfer to the wire, the following correlation of Reynolds number (Re) and Nusselt number (Nu) for cylinders was used.[10]

$$\mathrm{Nu} = 0.8\ (\mathrm{Re})^{0.25} \tag{1}$$

The constants in Equation (1) were obtained by extrapolating as a straight line the curve given by McAdams[10] to the low Re values encountered in this work. Since

$$\mathrm{Nu} = \frac{hD}{\lambda} \tag{2}$$

where h = heat transfer coefficient, D = wire diameter, and λ = thermal conductivity of gas at wire temperature, T_w, and

$$\mathrm{Re} = \frac{D\rho v}{\eta} \tag{3}$$

where (ρv) = mass flow, η = viscosity at wire temperature, and the over-all heat balance equation for a unit length of cylinder is

$$h\Delta T_{\mathrm{rad}} = \epsilon\sigma T^4 \tag{4}$$

where σ is the Stefan-Boltzmann constant, and ΔT_{rad} is the radiation correction, then, from Equations (1) through (4),

$$\Delta T_{\mathrm{rad}} = \frac{1.25\ \epsilon\sigma T_w^4 D^{0.75}}{\lambda}\left(\frac{\eta}{\rho v}\right)^{0.25} \tag{5}$$

In applying this equation, the values of η and λ for air[11] were taken, due to the difficulty of estimating transport properties of multicomponent mixtures. ϵ for the bare wires (assumed to be the same for this purpose) was taken as 0.16, and D before and after coating was estimated with a microscope. The gas temperature was first determined by calculating the radiation correction for the uncoated wire, and then the emissivity of the coated wire calculated from the gas temperature and the measured ΔT_{rad}. Since only low-velocity, low-temperature H_2-air flames were found to be sufficiently noncatalytic for this purpose, these experiments were carried out in the temperature range of 1300° to 1550°K only. Values of $\epsilon = 0.22 \pm 0.02$ were obtained. At higher temperatures, for example at the coating temperature of about 1800°K, similar calculations (ignoring the existence of catalytic heating) gave values of $\epsilon = 0.3$. Since this value is undoubtedly too high, a constant value of 0.22 for ϵ, independent of temperature, was assumed.

Gases and Metering

Except for C_2H_2 and CO, all gases were used without purification. Acetone was removed from C_2H_2 by passing through an activated charcoal trap. $Fe(CO)_5$ was removed from CO by a dry-ice cold trap followed by an activated charcoal trap. The CO contained about 1 per cent of H_2, as determined by mass-spectrometric analysis. It was necessary that removal of $Fe(CO)_5$ be quite complete, since otherwise iron oxide would deposit on the thermocouple and drastically change the radiation correction. Thermocouples used in CO flames were always checked after use to insure that this had not happened.

All metering was done with critical flow orifices which were calibrated by liquid displacement techniques.

Procedure

The burners were mounted so that flow was upward, and a screen was placed about 2 cm above the burner so as to impede the upward flow of the hot gases (see below). The two-holed ceramic tube which supported the thermocouple was mounted on a micromanipulator which allowed thermocouple movement in all directions. In order to minimize conduction errors, the heavy lead wires were bent to pull the fine wires straight, and the fine wires were placed parallel to the burner surface. With each flame

the thermocouple was moved up and down perpendicular to the burner surface to locate the maximum temperature. All readings were taken over the point on the burner previously chosen by the mapping procedure. Cooling was generally accomplished by a flow of about 20 cc/sec of water at about 50°C. Data for some mixtures were obtained with only one burner, and for others two or more were used.

The factors limiting the range in which data could be obtained were, on the high velocity side, the breakdown of the silica coating, and on the low velocity side, flame instability. At thermocouple temperatures higher than 1800° to 1900°K, there was a tendency for the silica coating to agglomerate into droplets, thus exposing the bare wire and allowing catalytic heating of the thermocouple. At the low velocity end, as the velocity of any lean or stoichiometric mixture was lowered the edges of the flame would eventually begin to flicker. At first this would not affect the stability of the reading of a thermocouple located near the center of the burner, but a further decrease in velocity would result in thermocouple instability. It was found that a screen placed above the burner would reduce this tendency. Even with the screen, continued reduction of the flow eventually resulted in instability which was observed in the center of the burner. Since it was felt that the beginning at least of this instability was due to the effect of the dense cold surrounding air displacing the less dense hot gases, a phenomenon extraneous to the experiment, all of the work was done with such a screen. It was shown that the presence of a screen had no effect on the observed temperatures of stable flames. The use of a screen offered an additional advantage in that with it the flow of hot gases was more nearly one-dimensional than without it. This was deduced from the fact that visual observation of a shadow of the flame showed that the boundary between hot and cold gas was more nearly vertical just above the burner with the screen than otherwise.

Radiation corrections were calculated with Equation (5). The transport properties employed were those for air[11] or for the inert gas[12] which was substituted for the N_2 in the air in some of the experiments. Except for the data taken with He "air," radiation corrections ranged from about 40°C at the lowest velocities to about 100°C at the highest. For the He "air" experiments they ranged from 7° to 12°C.

Results

Measurements of maximum flame temperature as a function of flow velocity were made on several compositions each for flames with air of CH_4, C_2H_2, C_2H_4, C_2H_6, C_3H_8, H_2, CO (containing about 1 per cent H_2) and CO + H_2. In addition, data were obtained for H_2 with three other kinds of "air" in which the N_2 was replaced with He, A, or CO_2. The data are shown plotted in Figures 2 to 10 in the form of logarithm of the burning velocity against the

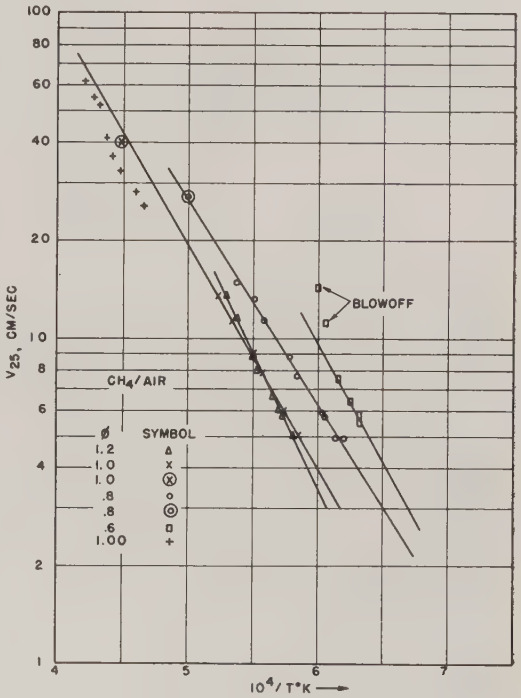

FIG. 2. Burning velocities of methane-air mixtures. Points marked: △, ×, ○, and □, this work; ⊗ Ref. 20; ◎, Ref. 21;, + Ref. 13.

reciprocal of the maximum flame temperature. The units of the burning velocity, V_{25}, are cm/sec of unburned gas measured at 25°C and 1 atmos. The V_{25} are thus proportional to mass velocities, but the proportionality constant is different for each mixture. Composition is expressed by ϕ, which is the ratio of the actual fuel/air ratio to that of the stoichiometric mixture. The temperatures are the thermocouple temperatures plus radiation correction.

As can be seen from the figures, with the exception of rich C_2H_2- and H_2-air, all of the plots are within experimental error straight lines. Thus the burning velocity of any mixture, with those

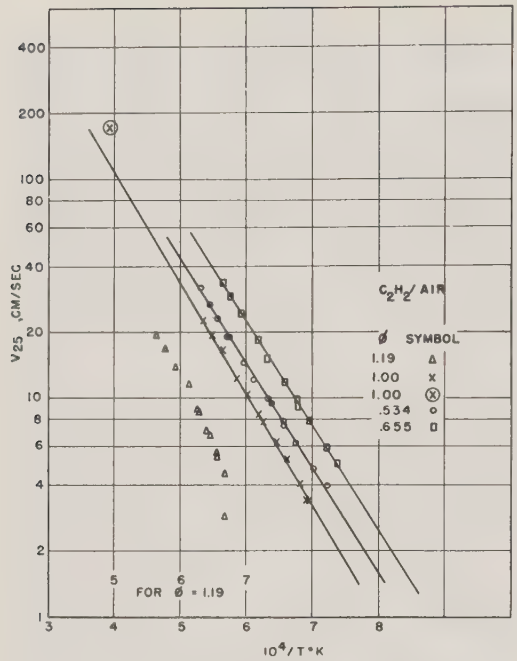

FIG. 3. Burning velocities of acetylene-air mixtures. Points marked: △, x, o, and □, this work; ⊗, Ref. 22. Abscissae for $\phi = 1.19$ points displaced as indicated.

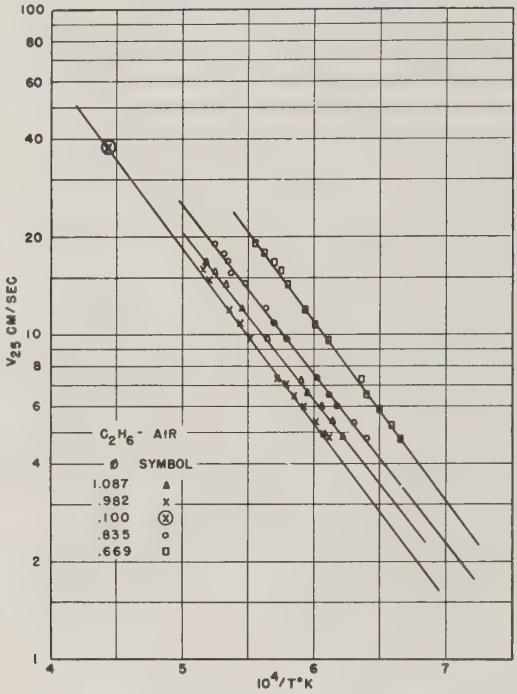

FIG. 5. Burning velocities of ethane-air mixtures. Points marked: △, x, o, and □, this work; ⊗, Ref. 24.

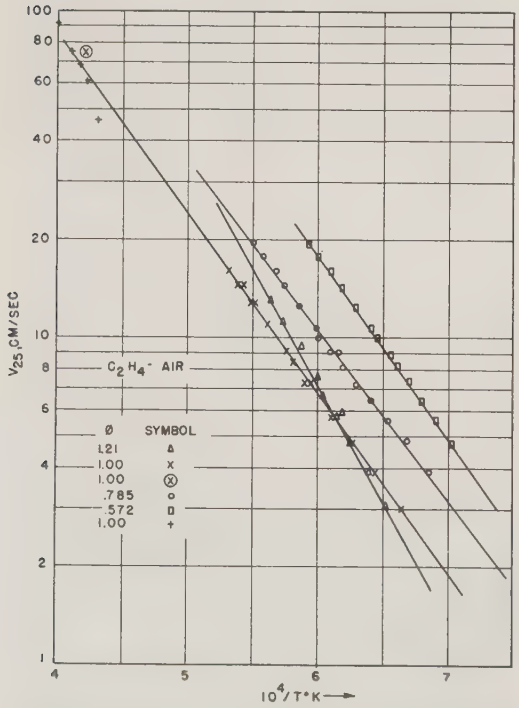

FIG. 4. Burning velocities of ethylene-air flames. Points marked: △, x, o, and □, this work; ⊗, Ref. 23; +, Ref. 13.

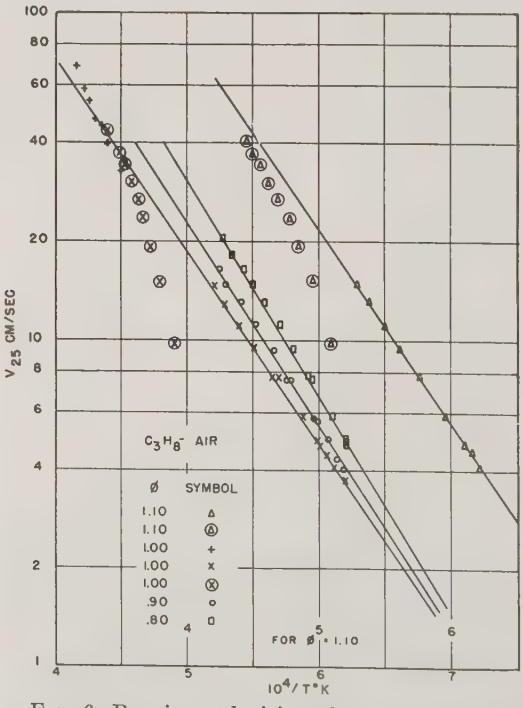

FIG. 6. Burning velocities of propane-air mixtures. Points marked: △, x, o, □, this work; Ⓐ and ⊗, Ref. 1; +, Ref. 13. Abscissae of $\phi = 1.10$ points displaced as indicated.

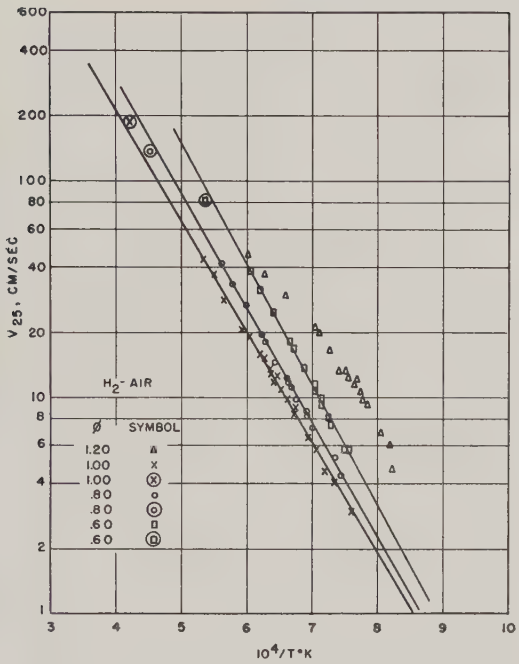

FIG. 7. Burning velocities of hydrogen-air flames. Points marked: △, x, o, and △, this work; ⊗, ◎, and ⊙, Ref. 25.

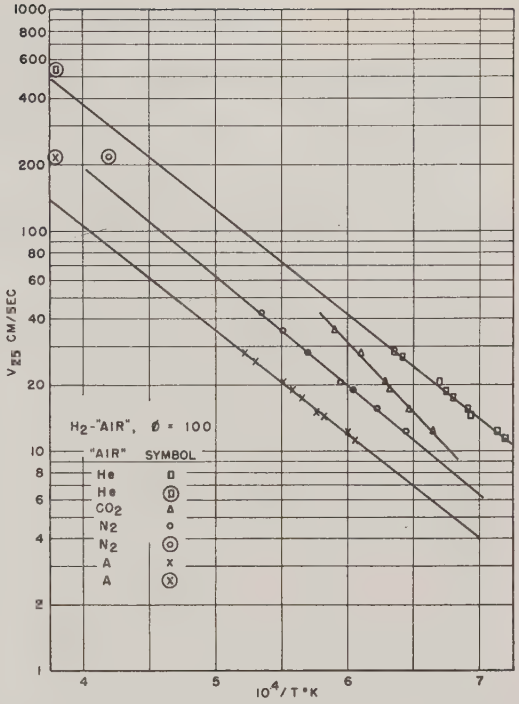

FIG. 9. Burning velocities of hydrogen-"air" mixtures at $\phi = 1.00$. "Airs" made by replacing nitrogen in air with an equal amount of diluent indicated. Points marked: △, x, o, and □, this work; ⊙, ◎, and ⊗, Ref. 22.

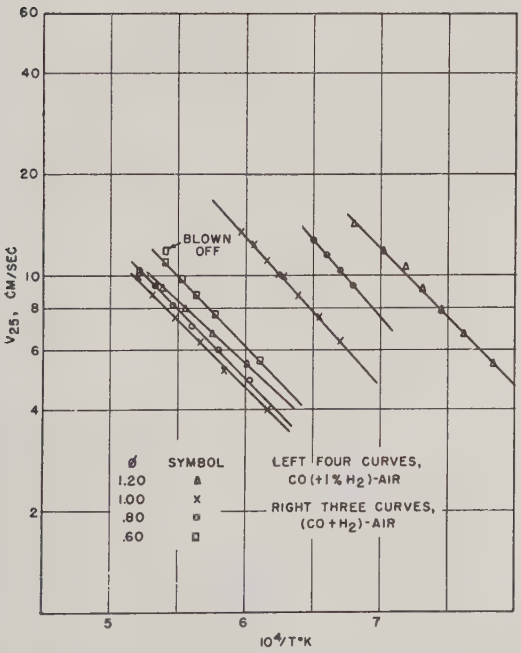

FIG. 8. Burning velocities of carbon monoxide-air mixtures, and of mixtures with air of an equimolar mixture of carbon monoxide and hydrogen. The carbon monoxide contained 1 per cent of hydrogen.

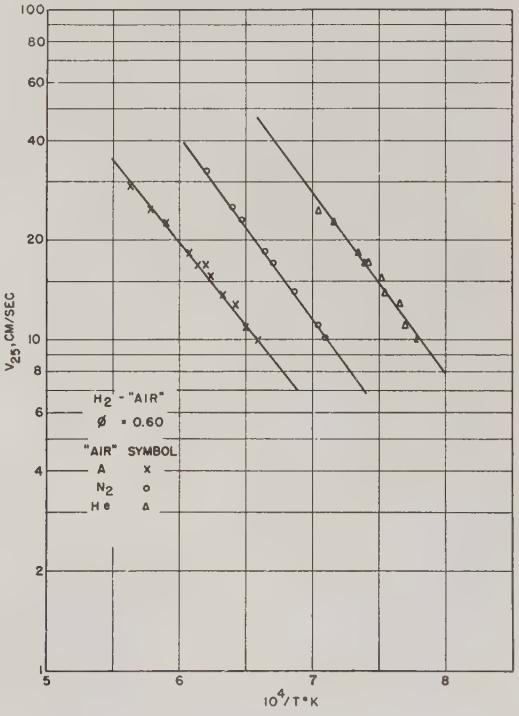

FIG. 10. Burning velocities of hydrogen-"air" mixtures at $\phi = 0.60$. "Airs" made by replacing nitrogen in air with an equal amount of diluent indicated.

two exceptions, can be expressed by an equation of the form

$$V_{25}^2 = ke^{-E/RT} \tag{6}$$

where k is a constant characteristic of the mixture, T is the maximum flame temperature and

TABLE 1

Fuel	Oxidizer	ϕ	E (kcal/mol)
CH_4	air	1.20	73
		1.00	65
		0.80	56
		0.60	60
C_2H_2	air	1.00	47
		0.83	43
		0.65	44
C_2H_4	air	1.21	65
		1.00	50
		0.78	48
		0.57	52
C_2H_6	air	1.08	47
		0.98	50
		0.83	49
		0.67	49
C_3H_8	air	1.10	54
		1.00	53
		0.90	54
		0.80	58
H_2	air	1.00	47
		0.80	49
		0.60	50
H_2	A "air"	1.00	44
		0.60	47
H_2	He "air"	1.00	44
		0.60	48
H_2	CO_2 "air"	1.00	59
$CO(+1\%\ H_2)$	air	1.20	34
		1.00	37
		0.80	38
		0.60	38
$(CO + H_2)$	air	1.20	36
		1.00	40
		0.80	44

E is an "activation energy." The use of the second power of velocity of course is not required by the data but conforms with common usage and facilitates comparison with other work. The E's reported here are, of course, not activation energies in the strict sense of the word, since they do not refer to reaction rates per unit volume. The term will be used by analogy, since the E's can be used to describe in an analogous way the temperature dependence of the over-all rate of consumption of fresh gas. Table 1 lists the activation energies as calculated from equations of the form of Equation (6).

Discussion

No attempt at a comprehensive comparison with other published work has been made. A few experimental adiabatic burning velocity points have been plotted in the figures and for these the temperatures are the calculated adiabatic flame temperatures. More detailed comparisons have been made with the work of Dugger[13] and of Botha and Spalding.[1] In the former, data are presented on the dependence of normal burning velocity on temperature for CH_4-, C_2H_4-, and C_3H_8-air flames. The points for the stoichiometric mixtures have been plotted on Figures 2, 4, and 6. The velocities of Dugger[13] have been converted to V_{25}, and the temperatures are the calculated adiabatic flame temperatures.[14] The agreement with the line extrapolated from our data is only fair with respect to both magnitudes and temperature dependence. This is perhaps not surprising, in view of the rather long extrapolation necessary and the difficulties inherent in measuring burning velocities.

A direct comparison with the work of Botha and Spalding should be possible, since our mixture compositions were chosen to be identical with some of theirs, and the methods differ only in that the temperatures reported here were directly measured, whereas those of Botha and Spalding were calculated from the mass flow, heat transferred to the burner, and adiabatic flame temperatures. The results of Botha and Spalding for two mixtures are shown in Figure 6; their results for the other two mixtures in Figure 6 look very similar, and were omitted to avoid confusion. The agreement is poor at lower velocities, but reasonably good at higher velocities with the lines extrapolated from our data. Some, if not all, of this difference can be attributed to the fact that combustion is not in general complete at the position of maximum temperature[15, 16] so that Botha's and Spalding's calculated temperatures are too high.

The major sources of error in this work are probably in the determination of the local velocity, the emissivity, and in the use of the transport properties of air or pure diluent. The first of these is difficult to assess, since it requires a knowledge of the flow near the burner edge. The fact that the mapping procedure gave results agreeing to within 5 per cent for burners of dif-

ferent diameters suggests that the error in the velocity is no larger than 5 per cent. The low temperature emissivity, judging from its reproducibility, is in error by no more than 10 per cent, corresponding to an error of 5°C in flame temperature. This is about the uncertainty in a given flame temperature, as judged by its day-to-day reproducibility. The emissivity at the higher temperatures is in more doubt. If the value $\epsilon = 0.3$, obtained under the coating conditions at 1800°K, were correct the corresponding errors in temperatures in this region would be 30 to 40°C.

It is difficult to assess the effect of the use of thermal conductivities of air or diluent gas. This was done for the sake of simplicity and because it was not the intention in this work to obtain accurate burning velocities. As an indication of the over-all accuracy of the measurements, however, it may be noted that the measured temperature of the two "blowoff" points on Figure 2 are 1653 and 1667°K. The calculated adiabatic flame temperature for this mixture, which is one which would be expected to reach equilibrium very rapidly,[15] is 1675°K, assuming an initial temperature of 50°C. This agreement is quite good, and suggests that no large errors have been made in evaluating the radiation correction.

In general, then, the lack of close agreement between the extrapolations of our data and published adiabatic burning velocities is not so serious as it first appears. This follows from the inherent difficulty in measuring burning velocities and from the fact that deviations from equilibrium are to be expected. It seems quite possible that relations of the form of Equation (6) are of general validity for the correlation of burning velocity with temperature. Their use in prediction is limited by the fact that actual, and not theoretical, flame temperatures are required. However, in those cases where equilibrium is reached rather rapidly, they should be immediately applicable.

Of greater consequence is the question of the chemical kinetic significance of the results reported here. That they are characteristic of the burning process itself is shown by the data in Figures 9 and 10. With the exception of CO_2, the slopes are independent of the nature of the diluent. The anomalous behavior of CO_2-containing flames may be related to the fact that these flames had a well-defined blue luminous zone. The source of this luminosity is not known as yet, but its absence with the other diluents suggests a specific effect which might disqualify CO_2 as an inert gas.

That such good straight-line correlations were obtained is somewhat surprising, since maximum temperatures were plotted, and all reactions must take place at temperatures lower than these. If kinetic significance is to be ascribed to these activation energies it seems that one must conclude that the rate controlling part of the chemical reaction takes place at a temperature which is approximately a constant fraction of the final temperature. This would appear to be a remarkable coincidence unless this constant fraction were always approximately 1, that is, unless the rate-controlling reactions are those that occur near the maximum temperature. This is similar to the assumption made in some thermal theories of flame propagation.[17]

Two recent publications report compositions of gases sampled from various points within C_3H_8-air flames.[18, 19] Both of these papers show that in the high-temperature regions of the flame the remaining unoxidized material is mainly CO. Recent work in this laboratory, based on sampling downstream of the maximum temperature, suggest that this can be generalized to include most lean and stoichiometric hydrocarbon flames.[15] These observations, together with the observed similarity of temperature dependence of burning velocity of various hydrocarbon flames reported here, and the implication that the high-temperature reactions are rate-controlling, all suggest that the high-temperature oxidation of CO may be the rate-controlling process in lean and stoichiometric hydrocarbon flames.

In this connection, it is of interest to compare the data for corresponding mixtures of the various fuels with air. This has been done in Figure 11, in which the curves for the mixture ϕ equal or nearly equal to 0.8 have been plotted. The most striking feature in this figure is the effect of H_2 on the over-all rate of CO oxidation in flames. Whereas the curves for corresponding CO and H_2 flames are widely different, the curve for the $(CO + H_2)$ flame lies very close to that for H_2 alone. That is, at a given temperature, replacement of half of the H_2 by CO changes the burning velocity by very little. The initial presence of molecular H_2 catalyzed the CO oxidation, in accord with the well-known effect of H_2 on adiabatic CO flames.

Among the hydrocarbons, as one goes from the saturates, which form a group, through C_2H_4 to C_2H_2, the $(H_2 + CO)$ curve is approached both

in magnitude and temperature dependence. This is also the order of decreasing low temperature stability for these hydrocarbons. This suggests that mixtures of H_2 and CO may in a sense represent limiting cases for hydrocarbon combustion, and that the rate of burning perhaps depends on how nearly or how quickly the products of the initial breakup of hydrocarbon in the flame correspond to those present in flames of mixtures of H_2 and CO.

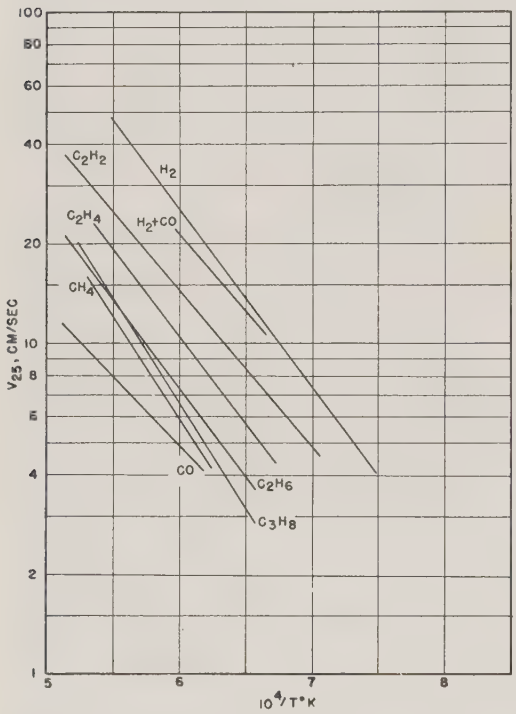

FIG. 11. Burning velocities of various fuels with air, all at ϕ equal or nearly equal to 0.80.

Summary

The temperature dependence of burning velocity has been investigated by means of cooled porous metal burners and fine quartz-coated Pt-Pt 10 per cent Rh thermocouples. It has been shown that, for nearly all of the mixtures studied, the logarithm of the mass burning velocity is a linear function of the reciprocal of the measured flame temperature in the range from 1300° to 1900°K. A comparison with adiabatic burning velocities suggests that this correlation may be valid at higher temperatures. It is suggested that the results imply that the high-temperature flame reactions are rate-limiting in the flames studied.

Acknowledgments

The author wishes to express his gratitude to M. D. Tupper, who developed the method for "butt-welding" the thermocouples, and to H. W. Barber, who made a major portion of the measurements.

REFERENCES

1. Botha, J. P., and Spalding, D. B.: Proc. Roy. Soc., *A225*, 71 (1954).
2. Wohl, K.: *Fourth Symposium (International) on Combustion*, p. 68. Baltimore, The Williams & Wilkins Co., 1953.
3. Friedman, R.: *Fourth Symposium (International) on Combustion*, p. 259. Baltimore, The Williams & Wilkins Co., 1953.
4. Friedman, R., and Burke, E.: J. Chem. Phys., *22*, 824 (1954).
5. Leah, A. S., and Carpenter, N.: *Fourth Symposium (International) on Combustion*, p. 274. Baltimore, The Williams & Wilkins Co., 1953.
6. Gilbert, M., and Lobdell, J. H.: *Fourth Symposium (International) on Combustion*, p. 285. Baltimore, The Williams & Wilkins Co., 1953.
7. Pirani, M.: J. Sci. Instr., *16*, 377 (1939).
8. McAdams, W. H.: *Heat Transmission*, Ed. 3, pp. 83, 85. New York, McGraw-Hill, 1954.
9. *Ibid.*, p. 87.
10. *Ibid.*, p. 259.
11. *The NBS-NACA Tables of Properties of Gases*, National Bureau of Standards, Washington (1950).
12. Hirschfelder, J. O., Curtiss, C. F., and Bird, R. B.: *Molecular Theory of Gases and Liquids*, pp. 528, 534, 1110. New York, John Wiley & Sons, 1954.
13. Dugger, G. L.: NACA Report 1061, 1952.
14. In part from Smith, R. W., Edwards, H. E., and Brinkley, S. R.: Bur. Mines Rep. Invest., 4938 (1953).
15. Fenimore, C. P.: To be published.
16. Wohl, K., and Welty, F.: *Fifth Symposium (International) on Combustion*, p. 746. New York, Reinhold Publ. Corp., 1955.
17. See, for example, Semenov, N. N.: NACA TM 1026 (1942).
18. Prescott, R., Hudson, R. L., Foner, S. N., and Avery, W. H.: J. Chem. Phys., *22*, 145 (1954).
19. Friedman, R., and Cyphers, J. A.: J. Chem. Phys., *23*, 1875 (1955).
20. Lewis, B., and von Elbe, G.: *Combustion, Flames and Explosions*, p. 467. New York, Academic Press, 1951.
21. Clingman, W. H., Brokaw, R. S., and Pease,

R. N.: *Fourth Symposium (International) on Combustion*, p. 310. Baltimore, The Williams & Wilkins Co., 1953.

22. Morgan, G. H., and Kane, W. R.: *Fourth Symposium (International) on Combustion*, p. 313. Baltimore, The Williams & Wilkins Co., 1953.

23. Dugger, G. L., and Graab, D. D.: NACA RM E52J24 (1953).

24. Gerstein, M., Levine, O., and Wong, E. L.: J. Am. Chem. Soc., *73*, 418 (1951).

25. Data of Jahn, G.: Reproduced in *Combustion, Flames and Explosions*, p. 460. New York, Academic Press, 1951.

17

SPECTROSCOPIC STUDY OF SOME ALCOHOL FLAMES: FLAME TEMPERATURES AND THEIR INFLUENCE ON THE INTENSITY CHANGES IN VARIOUS BANDS

By N. R. TAWDE and B. B. LAUD

Introduction

The inner cone of a flame seems to have received very little systematic attention from workers in the field of combustion spectroscopy. It is in the inner cone that a molecule of combustible vapor or gas first meets the oxygen molecule and hence the spectral and thermal changes which take place there are of the utmost importance.

In the present investigation, it is proposed: (1) to study simultaneously the general growth and decay of several spectral radicals in the flame as a function of their relative intensities; (2) to measure the temperatures of the inner and outer flame cones; (3) to see if there is any correlation between them.

For this study, we have chosen flames of alcohol vapor, as they give spectra similar to hydrocarbons, which play an essential part in chemical industry. It is believed that an investigation of this type carried out on elementary fuels such as simple alcohols, may yield a good deal of factual information that will greatly contribute to the understanding of the different processes involved in the combustion of complex fuels.

Initially methyl alcohol was used but following a sudden shortage of this material in the course of investigation, we substituted the next alcohol in the series, ethyl alcohol (strength: 99.68 per cent; density: 0.0793 g/cc), which was available in adequate supply. It was found that the various molecular band systems, C_2(Swan λ5165), CH(λ4315), HCO(λ3377) and OH(λ3064), could readily be followed in its flame radiations.

Experimental

The flames were produced by premixing alcohol vapor with air in various proportions. To study such a flame, it must be possible to stabilize it for any given length of time. With gaseous fuels, this is achieved without much difficulty by maintaining a uniform flow of gases to the burner. With liquid fuels, however, the rate of evaporation is a factor of primary importance and must be taken into account in designing the system. To this end, the system described below was evolved after a number of trials and improvements.

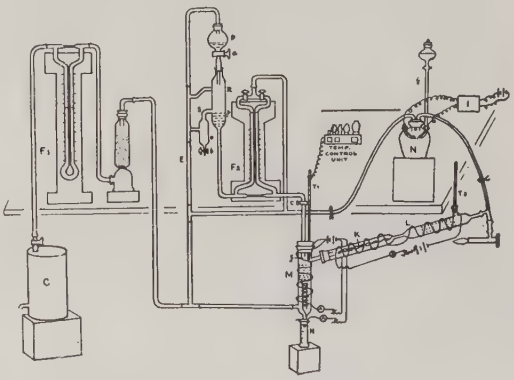

Fig. 1. Alcohol flow system.

A. Technique of Alcohol-Flow-System and Flames

A diagram of the system is shown in Figure 1. A blower is used to pump air under small pressure into a small pressure chamber, *C*; this pre-

vents surging of air-supply. The air then passes through a calibrated flow meter, F_1, to the vaporizing chamber, M. Alcohol, contained in the separating funnel, P, is allowed to fall drop by drop into the reservoir, R, from which it passes through the flow meter, F_2, and falls into the vaporizing chamber, M.

The vaporizing chamber is a cylindrical tube about 43 cm high and 2.5 cm in diameter. A long thin electrical heating element is placed in the tube, directly in the path of the incoming air. The tube is kept heated internally and externally by electric heating elements, so as to vaporize uniformly and completely the liquid alcohol that falls into it.

The alcohol vapor and air pass to the mixing chamber, K, where mixing is perfected and then through the flame-trap, L, to the burner. The mixing chamber and the flame-trap are also heated electrically from outside to prevent any cooling of the mixture while it passes through them. That there was no fall of temperature during the passage was indicated by the thermometer, T_2, introduced at the end of the flame-trap. The mixture was kept throughout at 79.5°C, before being fed to the burner.

The next step was to make the system work efficiently with a minimum of attention. This was achieved by means of a specially designed electronic temperature control unit, which operated automatically and kept the temperature constant to within ±0.2°C.

To obtain the desired air-fuel ratios, the alcohol flow was kept constant and the air flow varied. In all, twelve flames produced in this way were examined. They corresponded to the following air/fuel ratios: 5.2, 5.7, 6.0, 6.4, 6.7, 7.0, 7.5, 8.1, 8.5, 8.8, 9.4 and 9.8, which lie on either side of the stoichiometric mixture (air/fuel ratio = 9.0).

An ordinary Meker burner with open end, 1.7 cm in diameter, and a 40 mesh screen was used. As the air was premixed, the usual air passage at the foot of the burner was closed. To vary the air-fuel ratio gradually, it was found convenient to remove the nipple at the base of the burner.

With the alcohol flow system perfected in this way, flames of graded air-fuel compositions were obtained. These were subjected to: (1) temperature measurements by line-reversal method; (2) quantitative spectral intensity measurements of the various radicals appearing in the flame.

B. FLAME TEMPERATURES

Flame temperatures were measured by the sodium line-reversal method. The validity of the method has been discussed in detail by Lewis and von Elbe,[1] Loomis and Perrott,[2] and others. The optical system used was similar to that described by Jones, Lewis, Friauf and Perrott.[3] The precision of the temperature measurements was of the order of ±10°C.

Coloring of the flames was achieved by introduction of sodium by the sparking method. The chief advantage of this method is that it leaves an adequate concentration of the salt in the inner cone, while introducing a minimum amount of water vapor in the flame.

C. MEASUREMENT OF INTENSITIES

Photographic techniques and procedures were used to follow accurately the changes in intensity of the various band systems associated with variation in the air/fuel ratio. Owing to the extensive spectral region over which the molecular radicals C_2, CH, OH and HCO were spread, the usual rigorous process of heterochromatic photometry could not be used, but the nearest approach to the method, *viz.*, the proportionality of intensity to the optical density was used. Necessary precautions for eliminating or minimizing as far as possible the defects inherent in the process were observed.

The spectra were photographed on a small Hilger quartz instrument. A recording Moll (type A) microphotometer was used for the microphotometry of the final plates.

Observations and Results

Observations were begun with the flame requiring the least air to change its initial luminous appearance to a just nonluminous one. Under these conditions, the dull green tinge of the inner cone passes through bright green, blue and bluish-violet to violet at the blowoff stage, with gradual increase of the air added to the initial, constant pressure of the alcohol vapor. These color changes are accompanied by great alterations in the intensities of the four band systems occurring in the reaction zone.

A. Temperatures

Line-reversal temperatures of both the inner and outer cones, observed for the twelve flames of graded air/fuel ratios, are shown graphically in Figure 2.

B. Intensity changes in the spectra of different molecular radicals

An idea of the relative intensity variations in the four band systems associated with the change

in the air-fuel ratio can be had from the picture of the spectra obtained at various air-fuel ratios shown in Figure 3.

A quantitative study of this variation was made by measuring the relative intensities of the representative bands, *viz.*, C_2(Swan λ5165), CH(λ4315), OH(λ3064) and HCO(λ3377). These variations were followed consistently, throughout the whole range of mixtures, starting with some arbitrary intensity value for the initial mixture composition. These intensity variations are recorded graphically in Figure 4.

It may be noted that the HCO system is a close chain of many overlapping bands, for which the background intensities were difficult to extropolate correctly. However, with due care, a general pattern of relative rise and fall of the group was obtained. The figures for intensities in this case are not expected to be as precise as for other radicals.

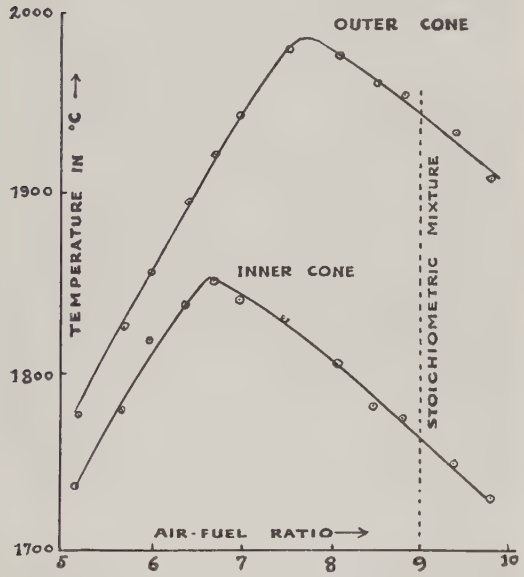

FIG. 2. Variation of translational temperatures with air-fuel ratio.

Discussion and Conclusions

A. FLAME TEMPERATURES

The results of translational temperatures represented in Figure 2 bring out the following broad features:

(1) There is a virtually smooth variation of temperature with the oxygen content of the combustible mixture, both in the inner and in the outer cone.

(2) The temperature has a definite maximum for flame of a particular air-fuel composition.

(3) The position of maximum temperature is different for the inner and outer cones. Both lie on the rich side of the stoichiometric mixture, but the inner cone maximum is relatively further

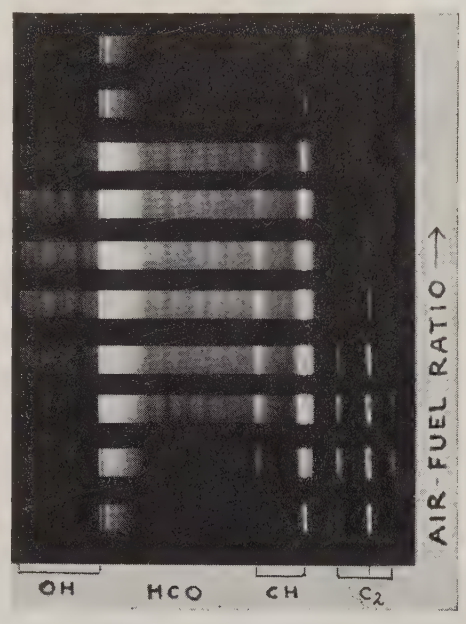

FIG. 3. Intensity changes with air-fuel ratio.

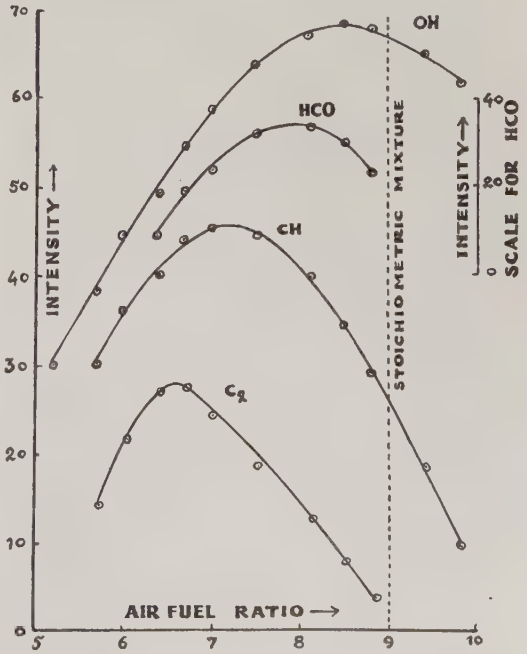

FIG. 4. Variation of intensities of C_2, CH, OH, and HCO with air-fuel ratio.

away from it than the outer one. The maximum temperatures, determined graphically, are given in Table 1.

TABLE 1

Flame Cones	Air/Fuel Ratio	Temp.	Temp. at the Stoichiometric Mixtures (Air/Fuel Ratio = 9)
		°C	
Inner	6.6	1850	1765
Outer	7.7	1985	1943

It is also evident from Figure 2 that the course of the temperatures runs almost parallel in both cones. Further, although the intake of energy resulting in higher temperature in both cases is steep, its dissipation is more gradual with the increasing oxygen proportion in the mixtures.

It is relatively easier to formulate the course of the combustion processes in the outer cone than in the inner cone. In the outer cone there is no free alcohol burning, and the difficult question as to what happens when alcohol molecules meet oxygen molecules does not arise.

The location of the maximum temperatures in the outer cone on the richer side of stoichiometric can be accounted for on the basis of dissociation of the products of combustion taking place in the flame. Jones, Lewis, Friauf and Perrott[3] observed similar shifts for a number of hydrocarbon flames. To explain them, they calculated theoretical flame temperatures allowing for dissociation. The theoretical maxims were found to agree fairly well with the observed ones.

In the inner cone, however, there is a relatively larger departure of the position of maximum from the stoichiometric mixture which needs examination. The shift cannot be explained in terms of the dissociation of the combustion products, especially because of the lower temperature of the inner cone. That the chemical reaction progresses with the increasing content of oxygen appears clear from the fact that the intensity of the OH band increases very steadily until the maximum is reached in the close approach to the stoichiometric mixture; which further shows that the reaction is more active at the correct mixture. Hence it is not impossible that the energy release is maximum for the stoichiometric mixture. The flame temperature, however, does not seem to follow the same course as that of energy release. The disharmony between the energy release and the consequent temperature attained must be attributed to some influence causing progressive removal of a part of available energy of the chemical reaction.

Such an influence is likely to be due to (1) a grid which may bring about increasing heat losses, and (2) energy loss to C_2 molecule to dissociate as evidenced in the simultaneous rapid fall of the Swan band intensities. As to the first influence, *viz.*, grid losses, nothing definite can be said unless we obtain some estimate of their variation.

Gaydon and Wolfhard[4] point out that although the line-reversal method is probably a satisfactory method at atmospheric pressure for the main body of the flame, the emission of the sodium lines is often abnormally intense in the inner cone, because the atoms are excited by collision with active species formed in the combustion processes, so that the effective temperature of the sodium atoms exceeds that for thermal equilibrium.

However, the temperatures in the inner cone observed by us in the present investigation were not high. They vary from 1735°C at one extreme, to 1728°C at the other extreme, by passing through the maximum of 1850°C for a mixture in between. Here we find it difficult to reconcile our results with the observations of Gaydon and Wolfhard.[4] As regards the sensitivity of our observations, we are confident that they represent the true state of affairs.

B. INTENSITY VARIATIONS

It is interesting to see whether the temperature variations presented above have any bearing on the corresponding intensity variations of the representative spectral radicals in the flames examined. Accordingly, the observed intensities were plotted for C_2(λ5165), CH(λ4315), HCO(λ3377) and OH(λ3064) bands, together with the temperatures of the flame cones (Fig. 5).

It will be seen that the C_2 band (λ5165) increases in intensity as the air-supply is increased, reaching its maximum for the ratio of 6.6. Further increase in the air-supply brings about a rapid fall in intensity, with some bands disappearing at the violet stage.

The CH band (λ4315) similarly gains in intensity with increasing air-supply, but continues to do so even after the C_2 has reached its maximum at the ratio 6.6 and has begun to weaken. While C_2 is still weakening, CH is gradually enriched until it reaches its peak intensity at the

ratio of 7.2. After this the fall in intensity is very gradual in contrast to the behavior of C_2 which suffers extreme changes both on the increase and on the decrease sides. The CH band at λ3872 was noted to behave similarly.

The variation of OH is entirely different. The gain in its intensity with the progressive increase of the air-supply is much slower; also the band reaches its maximum (ratio, 8.6) near the stoichiometic mixture (ratio, 9.0) after which there is a slight decrease.

The intensities of HCO bands (subject to the limitations indicated above) show that the general trend of rise and fall is similar to the bands of CH and OH, and that the maximum is somewhere between those of CH and OH about the ratio 7.9.

Thus it will be seen that all the radicals C_2, CH, HCO and OH undergo maxima of intensities over the range of mixtures examined, but the course of attaining the maximum and its position on the scale of air-fuel ratio differ to an appreciable extent from radical to radical.

To understand the true nature of the variation of intensity of the bands it is necessary to probe into the changes over the complete range, beginning with the stage when the flame is just nonluminous to the blowoff stage; otherwise wrong conclusions are likely. For instance, the statement by Smith[5] that the minimum air-supply favored the emission of C_2 band system, while the excess of air caused its almost complete disappearance, is not in itself complete and requires supplementing. It will be observed that Smith's interpretation is true if attention is confined to the range from the blue-green stage to the blowoff stage. The minimum air-supply needed to make the flame nonluminous gives the first dull-green stage and the intensity of Swan bands is very low showing that the intensity of the Swan bands falls with a minimum air-supply as well as with an excess supply.

Similarly, Bell's[6] observation that the intensities of OH, CH and C_2, bands in the methane flame diminished as the percentage of methane was increased is partly true. This variation will be observed if the mixture composition is changed from the blue-green stage to the dull-green stage. If, however, changes are noticed from the blowoff stage to the blue-green stage, the increase in the hydrocarbon content will show an increase in the intensity of the bands instead of a diminution.

Thus while the above observations are true statements of fact, they represent only a partial aspect of one whole range of phenomena. It is essential, therefore, to investigate the changes over the complete range of the mixture compositions.

C. INFLUENCE OF TEMPERATURE ON INTENSITY AND ACTIVATION MECHANISM

Figure 5 reveals that the maximum of intensity curve of C_2 band coincides with maximum temperature of the inner cone. Intensity maxima of the other molecular radicals do not show any such

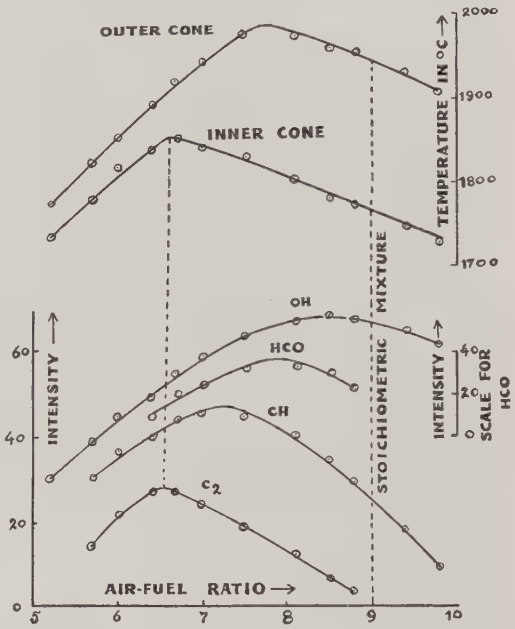

FIG. 5. Variation of temperatures and intensities with air-fuel ratio.

coincidence with the temperature of the inner or outer cone. There thus appears to be a close dependence of temperature on the production of C_2. To examine this point closely, a graph of intensity against temperature was prepared (Fig. 6). It shows that the intensity is directly proportional to the temperature from the origin to the maximum. This suggests that the production of C_2 may be a consequence of thermal effects. After the maximum, the character of the relation changes and the curve shows a somewhat exponential variation. The following reaction has been proposed to explain the formation of the C_2 molecule:

$$CH + CH \rightarrow C_2 + H_2 + 26 \text{ kcal}$$

As Gaydon[7] has pointed out, although this reaction is highly exothermic it does not provide enough energy for the electronic activation of the C_2 molecule.

We have observed that with a relatively low air-supply that is, at about the dull-green stage, the C_2 and OH bands are stronger than CH bands. Therefore, it is difficult to believe that CH is responsible for the formation of C_2. The data on the intensity temperature variation suggest that it is the thermal effects rather than the chemical effects that play an important role in the formation of C_2.

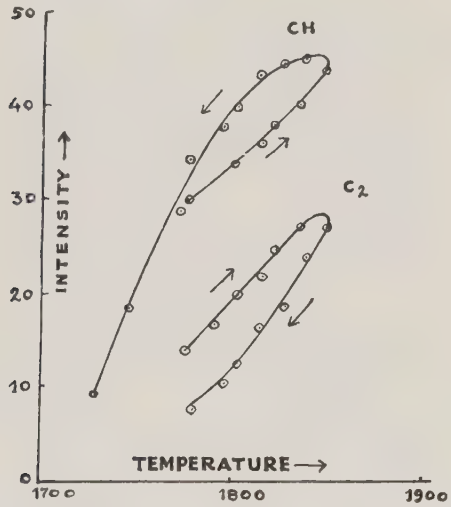

FIG. 6. Variation of intensities of C_2 and CH with flame temperature.

The variation of intensity of CH with temperature is different from that of C_2, and difficult to interpret. We cannot attribute the formation of CH to purely thermal causes. On the contrary, the fact that CH is relatively very weak in comparison to C_2 and OH in the early dull-green stages of the flame tends to indicate that the reaction $C_2 + OH \rightarrow CH + CO$ is most probably operative for the formation of CH, as suggested by Bonhoeffer and Haber,[8] and Pannetier and Gaydon.[9]

In sharp contrast to the variation of C_2 and CH, is the behavior of OH and HCO. Intensity of OH does not seem to bear any relationship to the temperature. This observation is in agreement with the generally accepted view that OH in the inner cone results from chemiluminescence. The variation of HCO is similar to that of OH. It is found to be independent of temperature.

Herman and Hornbeck[10] have made an interesting suggestion with respect to these bands. In their opinion, no such molecular radicals really exist. According to them, the apparent groups of bands in the region 3000 to 4000 Å, attributed to HCO molecule, are structures resulting from the overlapping of the band systems: (1) Deslanders d'Azambuja system of C_2, $^1\pi_g - {}^1\pi_u$; (2) the Schumann-Runge system of O_2, $^3\Sigma_u - {}^3\Sigma_g$; (3) OH(λ3428 Å); (4) CH(λ3628 Å). This hypothesis is based on the fact that the authors observed these bands in the spectra of ethylene and methane burning with oxygen at the stoichiometric mixture. Now, it has been observed here that the HCO bands undergo systematic variation, i.e., the intensities rise or fall with the air-fuel ratio. If Herman and Hornbeck's suggestion is accepted and their hypothesis holds, then the component bands of complex total phenomena, described as HCO by them, must run a parallel course of intensity variation. While the particular bands of C_2, CH, OH and O_2 referred to above were not examined by us for intensity variation, we feel that three of them would, in all probability, follow the intensities of C_2(Swan), CH(λ4315, λ3872), and OH(λ3064). But these do not run a concurrent course, as seen from our observations, and hence would not give a regular systematic variation of HCO on the basis of Herman and Hornbeck's suggestion. As the experimental intensity variation of HCO is not what one would expect from Herman and Hornbeck's line of argument, one cannot easily accept their point of view about HCO.

It should be mentioned, however, that in a later paper, Herman, Hornbeck and Laidler[11] state that although in their opinion there is no unequivocal spectroscopic evidence that these bands are emitted by HCO, they tend to favor this identification as the kinetic mechanism suggested by them makes it seem likely that the HCO radical is produced exothermally. They have suggested a detailed mechanism for the production and activation of HCO in acetylene flames.

Two attempts have been made to obtain direct evidence for attributing hydrocarbon flame bands to HCO. Murphy and Schoen[12] attempted to determine the emitter by utilizing isotope effects through deuterium substitution. A definite shift observed by them provides conclusive evidence that one or more hydrogen atoms are involved in the structure of the emitter.

A similar attempt to use the isotope effect was

made by Vaidya.[13] From the small change in the vibrational frequency of the A band system, he concludes that though it is present in the emitter, the vibration which gives rise to the hydrocarbon flame bands is such that H does not participate in it directly. As regards the likely nature of the other vibration concerned, he concludes from the experiments of Dyne and Style,[14] who obtained the A bands by fluorescent excitation of formaldehyde, that the vibrator must be $C = 0$. Thus, according to them, the emitter has to be HCO. Calculation of the mass factor from the isotope effect leads to the same conclusion.

The observations of Murphy and Schoen,[12] and of Vaidya,[13] in conjunction with our own observations, give reasonable support to the view that the hydrocarbon flame bands are due to the HCO radical.

Acknowledgment

This work forms part of the research program carried out under a scheme approved by the Fuel Research Committee and supported by the Council of Scientific and Industrial Research, India. It was done at the Spectroscopy Laboratories of the Institute of Science, Bombay, when the authors were working there. One of the authors (Laud) is indebted to the Council for the Award of Research Assistantship on the scheme. The authors wish to thank Dr. W. M. Vaidya of the N. P. L., New Delhi, for much helpful advice and consultation.

REFERENCES

1. Lewis, B., and von Elbe, G.: *Combustion, Flames and Explosions of Gases*. New York, Academic Press, 1951.
2. Loomis, A. G. and Perrott, G. St. J.: Ind. Eng. Chem., *20*, 1004 (1928).
3. Jones, G. W. Lewis, B., Friauf, J. B. and Perrott G. St. J.: J. Am. Chem. Soc., *53*, 869 (1931).
4. Gaydon, A. G., and Wolfhard, H. G.: Proc. Roy. Soc., *A194*, 169 (1948).
5. Smith, E. C. W.: Proc. Roy. Soc., *A174*, 110 (1940).
6. Bell, J.: Proc. Roy. Soc., *A158*, 429 (1937).
7. Gaydon, A. G.: *Spectroscopy and Combustion Theory*, Chapman & Hall, London, 1948.
8. Bonhoeffer, K. F. and Haber, F.: Zeit. Physik. Chem., *A137*, 263 (1928).
9. Pannetier, G. and Gaydon, A. G.: C. R. Acad. Sci., Paris, *225*, 1300 (1947).
10. Herman, R. C. and Hornbeck, G. A.: J. Chem. Phys., *17*, 1344 (1949).
11. Herman, R. C. Hornbeck, G. A. and Laidler, K. J.: Science, *112*, 497 (1950).
12. Murphy, G. M. and Schoen, L.: J. Chem. Phys., *19*, 380 (1951).
13. Vaidya, W. M.: Proc. Phys. Soc., *A64*, 428 (1951).
14. Dyne, P. G. and Style, W. G.: Discuss. Faraday. Soc., *2*, 159 (1947).

18

BURNING VELOCITIES OF MIXTURES OF NITROUS OXIDE, CARBON MONOXIDE, NITROGEN AND WATER

By C. J. S. M. SIMPSON and J. W. LINNETT

Introduction

Measurements have been made at Oxford by H. S. Pickering[1] of the kinetics of the oxidation of carbon monoxide by nitrous oxide at about 600°C and of the effect of added water on this. The object of the experiments described here was to see how far the burning velocities of carbon monoxide + nitrous oxide flames changed with composition in a manner to be expected from the low temperature kinetics, investigated under homogeneous conditions.

The two observations of Pickering that it was proposed to investigate were: (a) For small amounts of water the rate of oxidation in a given carbon monoxide + nitrous oxide mixture increased as the pressure of water vapor was increased; but, with larger amounts, the rate approached a limiting value and became independent of the pressure of water vapor. (b) For given pressures of nitrous oxide and water the rate of oxidation of carbon monoxide decreased as the carbon monoxide pressure was increased, provid-

ing that the pressure of water vapor was such that the rate was independent of the pressure of water vapor.

In order to see whether the above kinetic behavior is apparent in carbon monoxide + nitrous oxide flames, the effect of varying composition on the burning velocity was studied for the following: (1) Mixtures in which the relative amounts of carbon monoxide, nitrous oxide and nitrogen were kept constant, the pressure of water vapor added to this constant mixture being varied. (2) Mixtures of carbon monoxide, nitrous oxide, nitrogen and water vapor in which the percentages of nitrous oxide and water vapor were kept constant, but in which the relative amounts of carbon monoxide and nitrogen were varied. In all cases the carbon monoxide was in excess of the nitrous oxide, so that the flame temperature did not vary.

In order to obtain the requisite variation of water content in series (1), it was necessary to carry out the experiments above room temperature; in fact, 50°C was used.

Van Wonterghem and Van Tiggelen[2] have recently made some measurements of the burning velocities of carbon monoxide + nitrous oxide + nitrogen mixtures. All these mixtures were free from water although the carbon monoxide contained a small but unknown amount of hydrogen. Their results cannot therefore be used to investigate variations of either type (1) or type (2), for behavior (b) was observed by Pickering when a considerable amount of water was present. It is unfortunately impossible also to check any results of the above authors against ours because the initial temperature was different, and all our mixtures were much weaker in nitrous oxide than those studied by them.

Experimental Method

The burning velocities were determined by the burner method, schlieren photography being used.[3] The radius of the vertical burner tube was 0.536 cm and it was 120 cm long. It was water-jacketed, the water flowing through an electrically heated tube before passing into the bottom of the jacket, which was lagged. The temperature of the water was measured immediately after leaving the top. The temperature of the gas at the top of the flame tube was found to be 0.8°C greater than the temperature of the water, measured as above.

To produce the schlieren picture, light from a 500-watt Osira mercury vapor lamp was focused onto a vertical slit. Light from this slit was made parallel with an f2.9 lens of 8 in. focal length. It then passed through the flame and was brought to a focus by an f2.5 lens of 7 in. focal length. At the focus was placed a vertical wire. The light deflected by the flame past the wire fell on a photographic plate fitted with a shutter and placed so that the schlieren picture of the flame was in focus. The magnification was measured by photographing an object of known dimensions placed above the burner port. In order to obtain good photographs, the amount of light from the flame reaching the photographic plate was reduced by placing a screen with a small hole in it in the same plane as the schlieren wire.

PREPARATION OF GASES

Carbon monoxide from a cylinder was used. To remove any hydrogen this probably contained the gas was mixed with chlorine, both gases being bubbled through concentrated sulfuric acid to register the flow and to remove any iron carbonyl. The mixture was passed through a silica tube at about 1000°C and then through two towers containing pumice wetted with caustic soda solution to remove chlorine, hydrogen chloride and phosgene although formation of the last compound was most unlikely. From these the gas passed through beds of calcium chloride and sofnalite followed by a trap cooled in liquid air. From this it flowed to the flow-meter, at which the pressure drop across a capillary was measured.

The equilibrium constant for the reaction

$$H_2 + Cl_2 = 2HCl$$

is about 10^{-17} at 1000°C (i.e., strongly favoring hydrogen chloride formation), and the data of Pease[4] suggest that the reaction rate at this temperature will be such that effective equilibrium will be attained during the half second the gases spend in the furnace. Therefore, virtually all the hydrogen will be converted to hydrogen chloride and removed from the carbon monoxide.

Nitrous oxide from a cylinder for dental use was employed. It was passed through alkaline hydrosulfite solution to remove oxygen, then dried with calcium chloride. This was followed by a trap cooled in solid carbon dioxide in cellosolve.

Nitrogen from a cylinder was passed through alkaline hydrosulfite solution, a bed of calcium chloride granules and a trap cooled in liquid air. The flow rates of all these gases were obtained by measuring the pressure drop across a capillary.

The three gases were brought together and the

mixture passed over the surface of water in four horizontal tubes half filled with water and immersed in a thermostat. That the gas was saturated was shown by the fact that the first tube lost a lot of water, the second much less, and in the third and fourth there was no visible loss of water. The thermostat could be controlled over a wide temperature range to vary the water content. From the saturators to the burner the tubes were electrically heated to prevent condensation. At the bottom of the burner tube there was a sintered metal disk which acted as a flame trap.

In calculating the total gas flow rate from the burner port, allowance was made for the temperature rise and for the addition of water vapor.

Table 1. Measured Burning Velocities at Various Positions on the Cone for a "Dry" Mixture Containing 50 per cent CO, 25 per cent N_2O and 25 per cent N_2

Room temperature, 18°C; gas temperature at top of burner tube, 50.8°C; tube radius, 0.536 cm; total flow rate from flow-meters, 75 cc/sec; Mean burning velocity = 40 cm/sec

Radius Relative to Tube Radius Where Cone Angle Measured	Angle Between Cone Edge and Vertical	Linear Flow Rate Relative to That at Center	Burning Velocity
			cm/sec
0.890	41	0.207	25
0.752	29	0.434	38½
0.656	22	0.570	40
0.600	19½	0.640	40
0.546	18½	0.698	41
0.506	17	0.744	40½
0.465	15½	0.783	39½
0.422	15½	0.822	40½
0.385	15	0.852	40½
0.352	14½	0.876	40½
0.313	13½	0.902	39
0.276	14	0.924	41½
0.245	14	0.940	42
0.210	14	0.956	43
0.173	13½	0.970	42
0.138	14½	0.981	45½

CALCULATION OF BURNING VELOCITY

The schlieren photograph of a flame was projected in an enlarger of measured magnification onto graph paper and the cone diameter at a series of measured heights determined to half a millimeter. From these, the angles between the edge of the cone and the vertical (α) at various radii could be calculated and, assuming parabolic flow across the burner tube, the burning velocity (V_b) could be calculated using the formula

$$V_b = V_f \cdot \sin \alpha$$

where V_f is the linear gas velocity at the particular radius. The results for one mixture are tabulated in Table 1, and for two other mixtures shown graphically in Figures 1 and 2. For all these mixtures it will be seen that there is a region of the flame cone over which the burning velocity is constant. Near the tip the burning

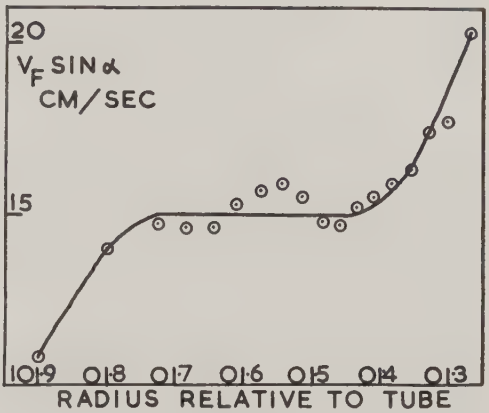

Fig. 1. Measured burning velocities at various cone radii for a flame containing, in the dry gas mixture, 60 per cent of CO, 15 per cent of N_2O and 25 per cent of N_2 to which water had been added to a pressure of 33.7 mm. Gas temperature, 50°C.

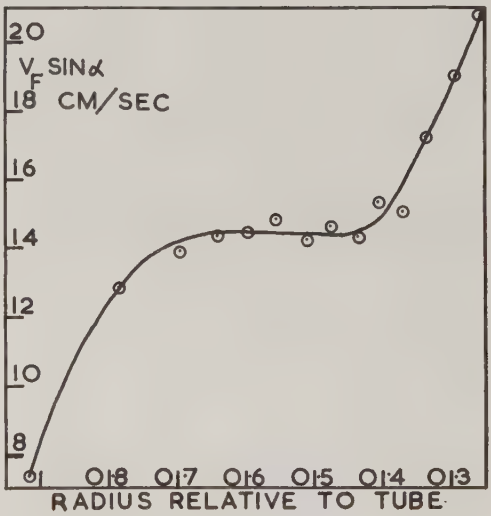

Fig. 2. Measured burning velocities at various cone radii for a flame containing, in the dry gas mixture, 30 per cent of CO, 15 per cent of N_2O and 55 per cent of N_2 to which water had been added to a pressure of 13.4 mm. Gas temperature, 50°C.

velocity is higher than the value over the constant region, and near the base lower. For all the flames studied, there was a region of constant burning velocity where the effects of tip and burner wall were apparently negligible. The mean value for this constant region was taken to be the burning velocity of the mixture under investigation.

Table 2. Burning Velocities (V_b) of Some Mixtures Containing in the Dry Gas 60 per cent CO, 15 per cent N_2O and 25 per cent N_2 to Which had been Added Varying Vapor pressures of Water Vapor

Pressure, atmospheric; gas temperature, 50°C

Experiment Number	Water Pressure	Burning Velocity
	mm	*cm/sec*
1	0	13¾
10	4.6	16½
11	6.7	17¾
6	9.6	18
7	9.6	18½
5	13.0	18¼
4	17.8	17¾
9	22.3	16¾
2	25.2	15¾
8	28.2	15
3	33.7	15

Table 3. Burning Velocities (V_b) of Some Mixtures Containing in the Dry Gas 15 per cent N_2O, x per cent CO and $(85 - x)$ per cent N_2 to Which 13.4 mm Water Vapor had been Added

Pressure, atmospheric; gas temperature, 50°C; calculated flame temperatures, in °K, are also listed

Experiment Number	Per Cent of CO	Per Cent of N_2	V_b	Calculated Flame Temperature
			cm/sec	*°K*
3	30	55	14¼	—
5	40	45	15½	1822
1	60	25	18	1818
4	75	10	16¾	—
2	85	0	16¼	1819

Experimental Results

In Table 2 are listed the measured burning velocities of a number of mixtures containing 60 per cent carbon monoxide, 15 per cent nitrous oxide and 25 per cent nitrogen in the dry gas, to which had been added varying pressures of water vapor. In Table 3 are listed the measured burning velocities of mixtures containing 15 per cent nitrous oxide, x per cent carbon monoxide and $(85 - x)$ per cent nitrogen in the dry gas, x varying from 30 to 85, to which had been added 13.4 mm of water vapor. This percentage of water was chosen as it was the percentage for which the variation of burning velocity with water content is small (*cf.* Table 2 and Figure 3). This corresponded, therefore, most satisfactorily with the conditions chosen by Pickering for the study of the kinetics of the wet reaction. The results in Tables 2 and 3 are shown graphically in Figures 3 and 4.

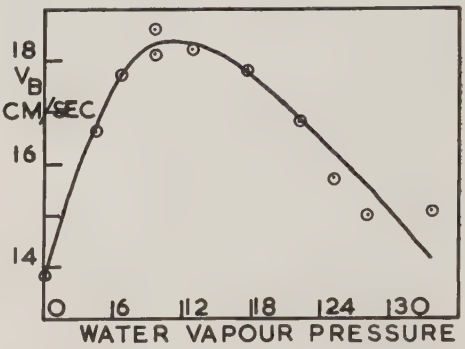

Fig. 3. Dependence of burning velocity (V_b) on the pressure of added water vapor for mixtures containing, in the dry gas, 60 per cent of CO, 15 per cent of N_2O and 25 per cent of N_2. Gas temperature, 50°C.

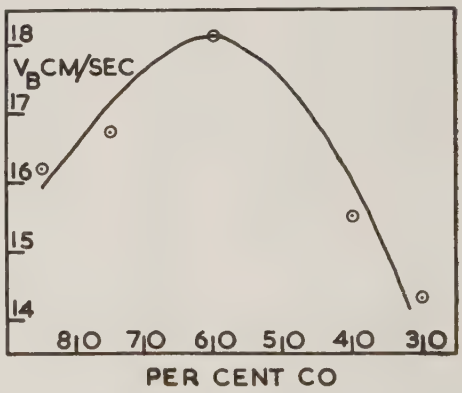

Fig. 4. Dependence of burning velocity (V_b) on the percentage of CO for mixtures containing, in the dry gas, 15 per cent of N_2O, the remaining 85 per cent being CO and N_2, to which 13.4 mm. of water vapor had been added. Gas temperature, 50°C.

From Figure 3 it will be seen that, as the

amount of water is increased, the burning velocity first increases and then decreases. The actual water content of the so-called "dry" mixture is not known but the method used in the production of the gases suggests that it will be low. Figure 4 shows that as carbon monoxide is replaced by nitrogen, the burning velocity first increases and then decreases. The equilibrium flame temperatures of three of the above mixtures were calculated. The results which are listed in the last column of Table 3, show that the calculated flame temperature does not change as carbon monoxide is replaced by nitrogen over the range studied.

Discussion

The fact that, for all cones, there was a region for which ($V_f \cdot \sin \alpha$) was constant implies that a genuine burning velocity is being determined. We feel that it is better to use the present procedure than to consider a truncated portion of the cone, dividing its area into the volume flowing through it per second. With that method there is no guarantee that the portion being considered is a region over which the burning velocity is constant. The method used here also has the advantage that the value given for the burning velocity is the mean of a number of values of $V_f \cdot \sin \alpha$.

The schlieren photographs obtained using the mixtures listed in Tables 3 and 4 were not as sharp as those obtained using a coal gas + air flame. This suggests that the flame front is thicker for the flames studied here, and it is possible therefore that these mixtures might be well suited for temperature distribution studies. Mixtures containing somewhat more nitrous oxide than 15 per cent, which were therefore faster burning, gave sharper schlieren photographs suggesting that the flame front was then less thick.

The results listed in Table 2 and graphed in Figure 3 are easily understood on the basis of the kinetic observations at 600°C. The first additions of water increase the burning velocity. Further additions of water do not increase the rate of reaction at constant temperature (*cf.* kinetic results) so that, in the flame, the consequences of the cooling effect of water (i.e., lowering of the flame temperature) become important and the burning velocity falls as more water is added. The initial rise and subsequent fall of the curve in Figure 3 are therefore to be expected.

The results in Figure 4 are much less easy to understand. The rise in burning velocity as the carbon monoxide percentage is reduced from 85 to 60 is what would be expected on the basis of the low temperature kinetics. But one would not expect the decrease observed as the carbon monoxide percentage is reduced from 60 to 30. This cannot be accounted for by a reduction in the theoretical flame temperature (*cf.* Table 3) although, of course, it may be that equilibrium is not established and theoretical flame temperatures do not therefore apply. This may be especially important for flames containing carbon monoxide (*cf.* Leah and Carpenter[5]). An alternative explanation is that the kinetics of the oxidation in the neighborhood of the flame temperature are not the same as at the lower temperature. However, one must not overlook the fact that the surprising kinetic result that an increase in reaction rate occurs when the partial pressure of carbon monoxide is reduced is paralleled by the flame result that an increase in the burning velocity occurs when the percentage of carbon monoxide is reduced from 85 to 60. It seems probable therefore that the system would repay further study.

Summary

The effects of composition on the burning velocities of the carbon monoxide + nitrous oxide flames studied are to a considerable extent what would be expected from the results of the low temperature kinetics, although not entirely so.

REFERENCES

1. Pickering, H. S.: Thesis, Oxford University, 1952.
2. Van Wontergehm, J., and Van Tiggelen, A.: Bull. Soc. Chim. Belges, *64*, 780 (1955).
3. Conan, H. R., and Linnett, J. W.: Trans. Faraday Soc., *47*, 981 (1951); Gray, K. L., Linnett, J. W., and Mellish, C. E.: Trans. Faraday Soc., *48*, 1155 (1952).
4. Pease, R. N.: J. Am. Chem. Soc., *56*, 2388 (1934).
5. Leah, A. S., and Carpenter, N.: *Fourth Symposium (International) on Combustion*, p. 274. Baltimore, The Williams & Wilkins Co., 1953.

19

IGNITION LIMITS AND PRODUCTS OF THE MULTISTAGE FLAMES OF PROPANE-NITROGEN DIOXIDE MIXTURES[a]

By ALBERT L. MYERSON, FRANCIS R. TAYLOR AND BARBARA G. FAUNCE

Introduction

Two-stage ignition, consisting of a cool flame followed by a hot flame, has been studied extensively in the case of hydrocarbon-oxygen mixtures.[1] Such ignition also has been described by Maizus and Emanuel[2] for propane-oxygen mixtures containing nitrogen dioxide added as a catalyst. For hydrocarbon-nitrogen dioxide mixtures, multistage ignition had not been observed prior to the present work, although Yoffe[3] had reported two modes of inflammation with hydrocarbons from ethane to pentane. One mode was the emission of blue luminescence, and the other was violent explosion.

This paper presents the results of our observations of the inflammation of mixtures of propane and nitrogen dioxide. Cool and multistage flames are described in terms of their radiation intensity-time traces and their occurrence as a function of pressure, composition and temperature. The products of each of the flames in a representative series have been analyzed quantitatively. The results are discussed in terms of possible reaction mechanisms. Important evidence is deduced for the formation of an addition complex of fuel molecule with nitrogen dioxide in the initiation step, as opposed to the theory of hydrogen abstraction. Conclusions are reached concerning the initiation and propagation of the second stage flame.

Experimental

MATERIALS

Nitrogen dioxide and instrument grade propane were obtained from the Matheson Company. The propane gas had a minimum purity of 99.9 per cent and was used as such. Nitrogen dioxide had a minimum purity of 99 per cent and contained traces of water and lower oxides of nitrogen. Purification of the nitrogen dioxide was achieved by passing the gas through phosphorous pentoxide into a glass transfer system. Here, the nitrogen dioxide was collected in a liquid nitrogen trap, warmed to 0°C and exposed to an atmosphere of oxygen overnight to convert the lower oxides to nitrogen dioxide. The liquid was redistilled, cooled, and the oxygen removed by pumping.

APPARATUS AND PROCEDURE FOR IGNITION STUDIES

An all-Pyrex vacuum system was used for transferring and mixing the gases at the desired temperatures and pressures. All stopcocks and ground glass joints were lubricated with Kel-F or similar fluorocarbon grease. The pressure of the nitrogen dioxide was measured by means of a senstive Pyrex spiral used as a nullpoint differential gauge in conjunction with an accurate mercury manometer. The movement of the spiral resulting from a change in pressure was determined by the deflection of a light beam reflected from a small mirror mounted on the axis of the coil. The movement of the reflected beam was followed on a horizontal glass scale. With this scale, a pressure change of 1 mm of mercury caused a 0.2 mm deflection of the projected light beam when the coil mirror was 1 m from the scale.

Mixtures were prepared by first introducing propane at a calculated pressure into a 100-cc Pyrex vessel. Nitrogen dioxide at a higher pressure was then admitted to an adjoining 500-cc flask. The stopcock connecting these two flasks was then opened, resulting in the desired mixture of reactants at a pressure predetermined through calibration. Finally, the stopcock connecting the 100-cc flask to the 58-cc reaction vessel evacuated to less than 1 μ was opened quickly giving the required final pressure. Corrections[4] were made for the equilibrium between nitrogen tetroxide and nitrogen dioxide. It was assumed that conversion of nitrogen tetroxide to nitrogen dioxide was complete and instantaneous upon admission of the mixture to the reaction vessel at 400°C or 503°C.

The reaction vessel was a spherical, quartz flask with a volume of 58 cc and was connected

[a] This research was performed under Contract AF33(616)-2456 with the Chemistry Research Branch of Wright Air Development Center. Some of the work on ignition limits and radiation-time traces of the flames, was presented orally at the Delaware Valley Regional Meeting and the Dallas National Meeting of the American Chemical Society in 1956.

to the mixture reservoir by 2-mm bore quartz capillary tubing. The reaction flask was maintained at a constant temperature of 400°C or 503°C in an L and L Dyna-trol furnace with an electronic circuit containing the bridge provided proportional control to a small wattage intermittent heater, and a constant heavy duty heater maintained the temperature at an appropriate minimum level. The temperature was measured to ± 0.1°C with a calibrated platinum *vs* platinum—13 per cent rhodium thermocouple.

The flames in the reaction flask were observed visually through a tube projecting through the furnace wall. The intensity-time trace of the flames was observed on an oscilloscope. A large ceramic tube containing a quartz optical system was used to direct the radiation emitted by the flame to a 1P28 photomultiplier detector. The signal resulting from the flame was impressed on the Y-deflection plates of the oscilloscope which was set for driven sweep. The trace was photographed with a Polaroid camera. Examples of the traces are shown in Figures 1a, 1b, and 2.

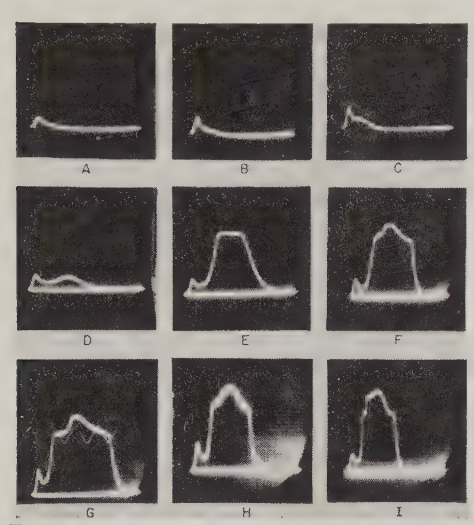

FIG. 1a. Oscilloscope traces of radiation from thermally ignited mixtures of propane and nitrogen dioxide. Initial temperature, 400°C; pressure, 314 mm Hg. These traces, together with those of Fig. 1b, show the effect upon the flame development of gradually increasing the proportion of nitrogen dioxide from 66.8 per cent for A, to 72.5 per cent for N of Fig. 1b. The duration of the sweep is approximately 70 milliseconds. In these and succeeding traces, the sweep proceeds from left to right.

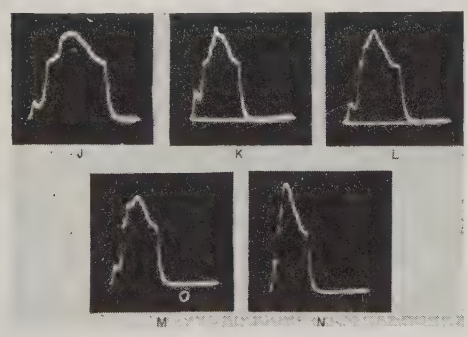

FIG. 1b. Oscilloscope traces of radiation from thermally ignited mixtures of propane and nitrogen dioxide. These traces represent a continuation of the series of Fig. 1a 400°C and 314 mm Hg.

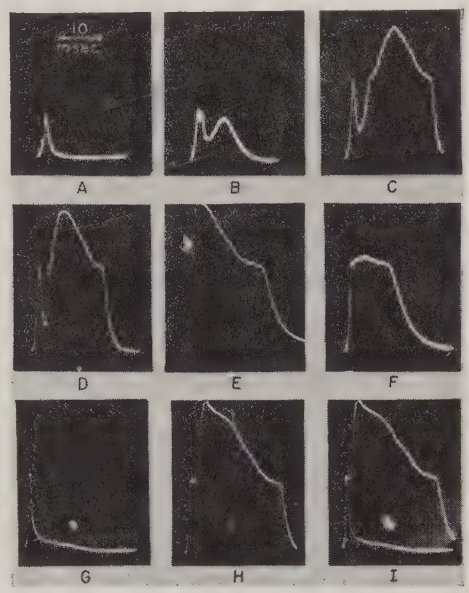

FIG. 2. Oscilloscope traces of radiation from thermally ignited mixtures of propane and nitrogen dioxide. A through F represent a series at 503°C and a pressure of 104 mm Hg. The proportion of nitrogen dioxide increases from 71.2 per cent in A, to 75.2 per cent in D; E = 84 per cent and F = 96.2 per cent. Traces G and H at 72 per cent and 75 per cent of nitrogen dioxide respectively, are superimposed in I. Both G and H were ignited at 503°C and 208 mm Hg.

internal volume greater than one cubic foot. A squirrel-cage fan was installed inside the furnace, and connected to an electronically controlled motor by means of a special shaft and bearing. The temperature was controlled by means of a platinum resistance wire which functioned as one arm of a Wheatstone bridge. A specially designed

It is our intention to interpret the unusual contours of the flame traces at some later date. However, it should be mentioned that the ratio of the peak intensity of the second stage flame to that of the first is much greater than indicated

on the traces. This is because of the selective radiation (probably blue) of the first stage and the inability of the photomultiplier to detect the blackbody radiation of the second stage beyond 7000Å.

METHOD OF ANALYSIS

Because of the high volatility of the products at the temperatures employed it was possible to make a complete infrared analysis for each flame with a single gaseous sample. Analyses were carried out with a Perkin-Elmer Model 12 Recording Infrared Spectrometer which was equipped with a new Model 81 A AC amplifier. An all-Pyrex 10-cm absorption cell with sodium chloride windows was used. The cell was connected, by means of a ball-joint, to a line separated by a stopcock from the capillary lead to the reaction vessel. The stopcock was opened as soon as possible after ignition (e.g., one-half min) allowing approximately 80 per cent of the product gases to escape into the evacuated Perkin-Elmer absorption cell.

Corrections were made for water and carbon dioxide in the atmosphere and cell-face by running a blank under identical spectrometric conditions. The latter consists of a coating of sodium nitrate formed on the surface of the salt windows by the reaction of sodium chloride and nitrogen dioxide in the presence of water. The other product is nitrosyl chloride. The absorption caused by the cell-face is responsible for the only serious scatter of data observed, namely the case of methane. The methane band used for analysis adjoins the broad cell-face absorption band.

Quantitative determinations of the products were made by comparison of their absorption spectra with those of references consisting of known pressures of the pure gas in the same cell, under identical spectrometric conditions. The reference pressures were selected to cover the actual pressures of the product being analyzed, so that deviations from the simplified absorption laws did not affect the results. All product samples and all references were pressurized to 1 atmos with nitrogen. The analyses are expressed as moles of product formed per mole of propane consumed or reacted.

All of the gases used as references were obtained from the Matheson Company except HCN which was prepared from sodium cyanide and sulfuric acid.

Results

THE IGNITION LIMITS AND FLAMES OF PROPANE-NITROGEN DIOXIDE MIXTURES

Visual observation of thermally ignited mixtures of propane and nitrogen dioxide at 400°C and 503°C shows that orange-red, blue-white or white flames of varying intensity are produced, their exact nature depending upon the pressure and composition. By means of the apparatus described, oscilloscope traces of the intensity of the total radiation have resolved these flames into two general types: (a) single stage, relatively weak, cool flames of which traces A of Figure 1 and A of Figure 2 are examples, and (b) multistage flames consisting of one flame of type (a) quickly followed by a hot or intense flame of which traces F of Figure 1a and C of Figure 2 are examples.

The occurrence of these and similar flames as a function of temperature, pressure and composition are shown in Figures 3 and 4. The limits have been determined at 400°C and 503°C, and cover a range of total pressures varying from 0 to 360 mm of mercury. The composition of the mixtures examined varies from 55 per cent to 95 per cent nitrogen dioxide.

The flame transitions which determine the boundary between single cool flames and multistage flames are illustrated by traces A through E of Figure 1a (400°C) and traces A through C of Figure 2 (503°C).

Trace A of Figure 1a is that of a typical cool flame at 400°C. Mathematically it is interesting to note that the trace, with its concave exponential rise and fall, is an almost perfect example of a reaction rate-time plot of a nondegenerate chain branching process in which the rate tends to infinity[5]. In trace B of Figure 1a, at 67.6 per cent nitrogen dioxide the embryo hot flame appears. Very slight increments in the per cent of nitrogen dioxide, at this stage, result in large increases in the intensity of the developing hot flame. These changes are seen in traces C, D and E of Figure 1a with a true hot flame stage first attained in trace E at 68.8 per cent nitrogen dioxide.

As the per cent of nitrogen dioxide is increased further, the induction time τ, between the first and second flames, decreases. This is true at 503°C as well as 400°C. Here τ is defined as the time lapse between the peak of the cool flame and a point of equal radiation intensity on the rise of the hot flame.

Figure 5 shows the interesting relationships which exist among the peak intensities of cool and hot flames of an isobaric series. The peak intensities are plotted as a function of per cent nitrogen dioxide for a series of flames at 503°C. A similar plot with data at 400°C would differ in one important respect. At 400°C the peak intensity of the hot flame continues to increase with increasing per cent of nitrogen dioxide until the entire flame process ceases completely at approximately 98 per cent nitrogen dioxide.

From this series of flame studies it is apparent that the short duration, low intensity flame must reach a critical intensity before the hot flames can develop. An interesting example of this is provided by the traces G, H and I of Figure 2. These are traces of the radiation from mixtures containing 72 (G) and 75 (H) per cent nitrogen dioxide. With the former per cent (G), a cool flame of critical intensity is produced since the hot flame is in its embryo stage. With the latter per cent (H), a full scale hot flame is produced. Trace I consists of G superimposed on H. The resulting trace I shows that the cool flame process is a part of the multistage flame and that at 503°C, once the cool flame reaches its critical intensity, further increase in the per cent of nitrogen dioxide does not cause an increase in cool flame intensity.

The limit (Figure 3) separating single cool flames from a zone of nonluminous reaction is an interesting one. The lack of dependence on composition is unusual for a system of two reactants, whether the initiation process is thermal or chain branching. However, such a limit can be explained by postulating that it is the chemiluminescence limit of a single intermediate compound, the existence of which is suggested by the nature of all of these flames. It would be assumed that the ignition occurs through chain branching with destruction of active centers at the wall, so that the total pressure would be the final controlling independent variable.

The effect of temperature on the second pressure-composition limit, as shown on Figure 4, is quite pronounced, in contrast to the negligible effect of temperature on the first limit. Such an effect could be explained on the basis of increased thermal decomposition of an inhibiting intermediate with increased temperature. Another factor that may contribute to this effect is the increased rate and extent of decomposition of nitrogen dioxide at 503°C compared to the rate and extent at 400°C.

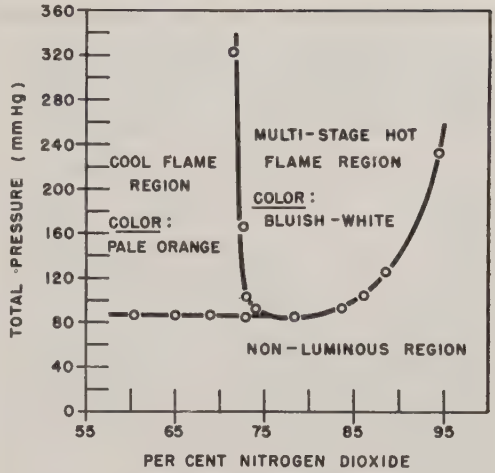

FIG. 3. Pressure-composition ignition limits for propane-nitrogen dioxide mixtures in a 58-cc spherical, quartz flask at 400°C.

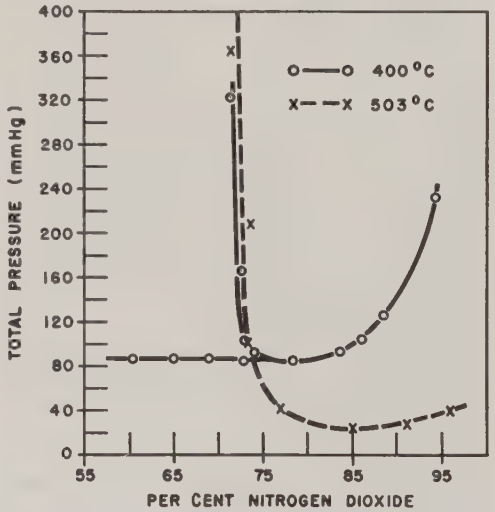

FIG. 4. Pressure-composition ignition limits for propane-nitrogen dioxide mixtures in a 58-cc spherical, quartz flask at 400°C and 503°C.

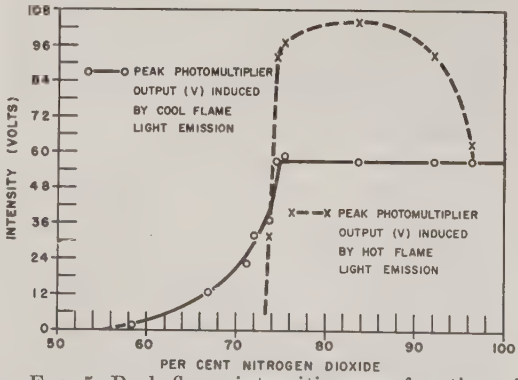

FIG. 5. Peak flame intensities as a function of the per cent of nitrogen dioxide. Temperature, 503°C; pressure, 104 mm Hg.

PRODUCTS OF THE COOL AND MULTISTAGE FLAMES

Analyses have been made of the products of the flames represented by oscilloscope traces A through N of Figure 1a and b. These flames comprise an isobaric series in which the total pressure of each reacting mixture is approximately 314 mm of mercury. The temperature of each experiment is 400°C while the per cent of nitrogen dioxide varies from 42.3 to 72.5. We have found that the order in which the flame traces have been arranged is not always that of increasing per cent of nitrogen dioxide. This is due, of course, to the difficulty of reproducing precisely, a flame of a mixture corresponding to boundary conditions. In such a region, the nature of the flames varies radically with changes of a few tenths of a per cent of nitrogen dioxide. In addition to inaccuracies in pressure measurements, wall conditions may change sufficiently on occasion, to shift the boundary by a significant amount. Outside the boundary region, reproducibility of a given flame is surprisingly precise. Consequently the multistage flames have been arranged in decreasing order of the induction time, τ, between the first and second flame stages, as previously defined. This order receives corroboration in that it is essentially the same as the order of increasing intensity of the second or hot flame stage. Most important, this sequence correlates quite reasonably with the changes in the concentration of the various products. The order of the cool flames observed at relatively widely separated per cents of nitrogen dioxide, is the same by per cent or by intensity.

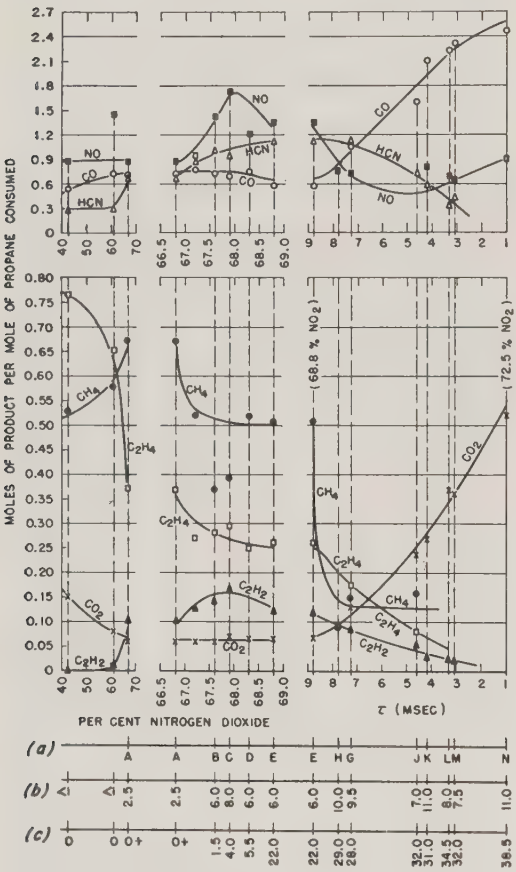

FIG. 6. Effect of the per cent of nitrogen dioxide on the moles of products formed per mole of propane consumed. In the region between 68.8 and 72.5 per cent nitrogen dioxide, the induction time (τ) between the two stages is used as the independent variable (τ is a decreasing function of the per cent of nitrogen dioxide). A through N of line (a) refer to the traces of Figs. 1a and 1b. The values given on lines (b) and (c) are the peak intensities, in arbitrary units, of the cool flames and hot flames respectively, as indicated by the photomultiplier output.

The relation between the concentrations of the various products formed and the type of flame which produces the products can best be seen through the graphical representation of Figure 6. The most desirable and logical independent variable for such a graph is the per cent of nitrogen dioxide. However, it has been necessary to separate the x-axis into three sections, each with a different range in composition. The first section, up to 66.8 per cent nitrogen dioxide, employs the actual per cent of nitrogen dioxide. However, the second section represents the critical region between 66.8 and 68.8 per cent nitrogen dioxide. Per cent assignment is impracticable here, as previously mentioned, due to the difficulty in precisely correlating composition and flame-type in this small range. These flames have therefore been arranged in order of increasing hot flame intensity. The two per cent interval was divided into equal parts and the resulting per cents assigned to the flames in question. Since the per cent increments are so small, and since the order is the important factor, no significant error is introduced by this method of plotting. In the third section from 68.8 to 72.5 per cent nitrogen dioxide, the product concentrations, quite logically, have been plotted as a function of the induction time, τ.

As an aid in the interpretation of the graph, an additional assignment of the x-coordinate has been made at the bottom of the graph. This provides values, in arbitrary units, for the relative intensities of the first and second flame stages,

so that one can readily correlate the products with the type of flame which produces them.

It is apparent from Figure 6 that the products assume varying importance depending on the type of flame which produces them. The significance of these data will be discussed in the following section.

Recently a thorough study has been made of the radiation emission of C_3H_8-NO_2 two-stage flames. It was found that the flatness and irregularities of the intensity-time patterns of the hot-flame stage of these processes result from saturation in the light detecting equipment. The factors influencing the degree of saturation are multiplier phototube characteristics, value of dynode resistance and magnitude and regulation of the detector input voltage. In order to minimize these factors a unit was built consisting of an RCA 1P28 multiplier phototube using 10 K dynode resistors and powered by a well-regulated, low impedance power supply. The voltage is applied through a special feed-back circuit which continuously varies the voltage across the dynodes from 850 volts at the low light level of the cool flame stage to 250 volts at the high light level of the hot flame stage. Resulting intensity-time traces reveal the hot flame radiation to have a shape similar to that of the cool flame but an intensity approximately fifty to a hundred times greater. This work will be presented in a later publication.

Discussion

Consideration of the products of the cool flame yields information important to the understanding of the general mechanism of reactions of nitrogen dioxide, as well as to elucidation of the specific reactions herein under consideration.

THE INITIATING COOL FLAME REACTION

For many years it has been suggested that the rate-controlling step for reactions involving the attack of nitrogen dioxide, or the oxygen molecule, on hydrocarbons and their derivatives is hydrogen abstraction. In the case of nitrogen dioxide and a hydrocarbon

$$RH + NO_2 \rightarrow R\cdot + HNO_2 \qquad (1)$$

A number of examples of the postulation of this step are cited in a letter by Walsh[6] for the cases of formaldehyde, acetaldehyde and glyoxal. Furthermore, this step is suggested by Hass, Dorsky and Hodge,[7] for the case of pure hydrocarbons in which the hydrogen atom is a secondary one. The formation of secondary nitroparaffins found by Yoffe[3] to result from the slow reaction of nitrogen dioxide and normal pentane was considered to be additional evidence for the validity of this reaction.

However, Walsh, in the letter cited, has presented significant evidence for the premise that the formation of a complex between nitrogen dioxide and the fuel molecule is the rate-controlling step in such reactions. The reasoning involves a correlation between the reaction rates of nitrogen dioxide with a number of fuels, and the first ionization potential (i.e., that of the most loosely bound electron) of the fuel. Thus the oxidation of the fuel would begin with the step

$$RH + NO_2 \rightarrow RH\cdot NO_2 \qquad (2)$$

No final conclusions were reached as to whether the second step involves decomposition of the product, or reaction of the complex with another molecule of nitrogen dioxide.

In the present case, analysis has shown that the cool flame is accompanied by considerable reaction. In the case of trace A of Figure 1a, about 20 per cent of the propane was decomposed. In the succeeding discussion no inference has been made as to the fraction of the reacting molecules which is involved with the production of chemiluminescence. In view of the relatively minute pressures of alkyl nitrites needed for chemiluminescence,[8] it is likely that the fraction is very small. But the increasing extent of decomposition with the increase in cool flame intensity is certain from the present work. The criticality of the intensity of the cool flame and consequently the criticality of the temperature of the flame, or of the concentration of the products, in triggering the second stage flame has also been shown.

If the attack on the propane molecule during the cool flame is initiated and propagated through hydrogen abstraction by either nitrogen dioxide or other radicals there is not much question that the isopropyl radical would be formed:

$$CH_3CH_2CH_3 + NO_2 \rightarrow CH_3CHCH_3 + HNO_2 \qquad (3)$$

The secondary hydrogen atom is the more labile or weakly bound. Also, as previously mentioned,[3] the secondary nitroparaffins were the more important nitroparaffins produced by the slow reaction between nitrogen dioxide and pentane at

220°C to 300°C. The reaction of the propyl radical with nitrogen dioxide follows readily to produce 2-nitropropane and/or isopropyl nitrite:

$$CH_3\dot{C}HCH_3 + NO_2 \rightarrow CH_3CH(NO_2)CH_3 \quad (4a)$$

or

$$CH_3\dot{C}HCH_3 + NO_2 \rightarrow CH_3CH(ONO)CH_3 \quad (4b)$$

Since addition of nitrogen dioxide to an ethyl radical is slightly more exothermic when the product is a nitrite, it has been suggested[6] that the activation energy may be lower for the nitrite. Should this be the case the difference would probably be small, and one would expect that in the present case, reaction would proceed through Reaction (4a) as well as Reaction (4b).

Now the products of the thermal decompositions of 2-nitropropane and isopropyl nitrite have been studied recently by a number of groups: 2-nitropropane by K. A. Wilde[9] and Gray, Yoffe and Roselaar,[10] and isopropyl nitrite by Levy[11] and Colburn.[12] The nitroparaffins are much more stable than the alkyl nitrites. The only decomposition rate available for isopropyl nitrite is one obtained from Levy's work[11] at 181°C. From this and the activation energy of the RO—NO bond,[8] an approximate lower limit for the rate can be calculated. This indicates that almost complete decomposition would take place in a matter of milliseconds at 400°C.

In contrast, the half-life of 2-nitropropane, as calculated from Wilde's work, is approximately one-half minute. Although some fraction of a minute is entailed in transferring the products from the hot reaction flask in the present experiments, one would expect to find detectable amounts of the nitroparaffin in the products if the reaction proceeded by the abstraction of secondary hydrogens and subsequent formation of 2-nitropropane during the cool flame period. It is possible, of course, that the decomposition of the nitroparaffin may be accelerated by the presence of excess nitrogen dioxide. On the basis of a rate measured by Harnsberger,[13] the reaction of nitrogen dioxide with nitromethane is not significantly different from the rate of nitromethane's thermal decomposition. At high pressures, Mueller[14] noted little effect of nitrogen dioxide on the thermal decomposition of nitromethane. The effect of nitrogen dioxide may be very different, of course, for the case of other nitroparaffins.

The major products[9] of the thermal decomposition of 2-nitropropane (and 1-nitropropane) are propylene, nitric oxide and water. Minor products are hydrogen cyanide, nitrogen dioxide, aldehydes and carbon dioxide. Although the present analyses have revealed hydrogen cyanide (as a major product) and nitric oxide, no propylene has been found. Instead ethylene is the major product. If a secondary hydrogen is removed from propane, there does not seem to be any mechanism of high probability for returning it. This return is essential if ethylene is to be formed from the propyl radical at a succeeding stage.

The same objection holds if Reaction (4b) is postulated even though the alkyl nitrites, unlike the nitroparaffins, do exhibit chemiluminescent or cool flame decomposition. According to Levy[11] and Colburn[12] the principal products of the thermal decomposition of isopropyl nitrite at 200°C are acetone, hydrogen cyanide and nitric oxide. Again, the formation of ethylene from acetone is even more improbable than it is from the isopropyl nitrite itself. It appears, then, that the explanation for the presence of ethylene as the major hydrocarbon product involves the formation of a complex. The facts require that the carbon-carbon bond of propane break without the loss of a secondary hydrogen. If a complex is formed as previously indicated by Reaction (2) then

$$CH_3CH_2CH_3 + NO_2 \rightarrow CH_3CH_2(NO_2)CH_3 \quad (5a)$$

or

$$CH_3CH_2CH_3 + NO_2 \rightarrow CH_3CH_2(ONO)CH_3 \quad (5b)$$

The second step may proceed either by further reaction with another molecule of nitrogen dioxide, which would probably require only a small activation energy

$$CH_3CH_2(NO_2)CH_3 + NO_2 \rightarrow \text{products} \quad (6a)$$

$$CH_3CH_2(ONO)CH_3 + NO_2 \rightarrow \text{products} \quad (6b)$$

and/or by decomposition of the complex, which would involve larger activation energies

$$CH_3CH_2(NO_2)CH_3 \rightarrow CH_3CH_2NO_2 + CH_3\cdot \quad (7a)$$

$$CH_3CH_2(ONO)CH_3 \rightarrow CH_3CH_2ONO + CH_3\cdot \quad (7b)$$

All of these reactions leave open the possibility of breaking a carbon-carbon bond without the removal of a secondary hydrogen atom. The thermal decomposition of nitroethane[10] at 430°C to 485°C produces ethylene, nitric oxide, methane and carbon monoxide as major products. all in

approximately equivalent amounts, along with formaldehyde, water and hydrogen cyanide. The relatively slow decomposition of the nitroparaffins was discussed previously. It is possible that the presence of nitrogen dioxide and of a branching mechanism may result in the rapid reaction observed. It is also possible that the decomposition may proceed through the nitrite mode as in Reaction (6b) or Reaction (7b), which may produce the products observed at the rate observed.

The mechanisms by which products such as hydrogen cyanide, methane, ethylene, nitric oxide and carbon monoxide are produced from nitrites and nitroparaffins have been discussed fully in many of the papers previously referred to[8, 9, 10, 11, 12] and in others. No further discussion of this point will be made here.

SECOND STAGE REACTIONS

It has been shown that the production of nitric oxide by the cool flame becomes much larger when the embryo second stage makes its first detectable appearances. A close comparison of the peak intensities for cool flames with the corresponding nitric oxide production, reveals excellent correlation between the increases in both. It is not until a relatively intense hot flame is produced that the nitric oxide concentration drops significantly. Therefore, oxidation by nitric oxide is apparently not responsible for the creation of the second stage flame. However, when the latter becomes sufficiently intense and the gas temperature therefore sufficiently high, nitric oxide begins its role as oxidant, and corresponding increases in flame intensity can be noted. Corroborating this point, we find that the significant drop in nitric oxide production corresponds precisely to the equally significant decrease in methane production. Patry and Engel[15] studied the reaction between nitric oxide and methane at temperatures up to 1100°C. They found that 70 per cent of the nitric oxide was converted in 3 seconds at this temperature, to form hydrogen cyanide, water and hydrogen:

$$CH_4 + NO \rightarrow HCN + H_2O + \tfrac{1}{2} H_2 \qquad (8)$$

It will be noted that the production of hydrogen cyanide continues to increase with increasing hot flame intensity, or at least does not suffer a decrease, even after the aforementioned sudden drop in methane takes place. With further hot flame development a gradual decrease in concentration takes place. This relative persistence of the hydrogen cyanide is quite likely, then, to be related to the nitric oxide-methane reaction. It would probably disappear at an earlier stage without this replenishment. Its complete disappearance occurs rather abruptly as the induction time τ approaches zero. This would seem to imply that it does not appear as a product at this stage, because its normal production during the first stage flame is prevented by the early onset of the second stage process.

SECOND STAGE INITIATION

The only major product formed by the cool flames which is capable of explosive reaction with nitrogen dioxide under conditions of the cool flame, is ethylene.[16] It will be noted that its production, which is relatively quite high after a pure cool flame, drops abruptly with the first vestiges of the embryo second stage flame. It should be borne in mind that the actual intensities of the second stage flames are far greater, relative to those of the first stage flames, than appear from the traces. This was indicated earlier in this article. Ethylene production decreases rapidly thereafter, with increasing intensity of the hot flames. It is the only fuel molecule whose concentration decreases as the smaller second stage flames first begin to appear. Futhermore, this decrease parallels the increase in nitric oxide production for the first embryo two-stage flames observed. Also, quite significantly, there is a ten-fold increase in acetylene production, at the identical and previously noted stage at which the ethylene production falls. This quite logically could follow from the formation of dinitroethylene and nitroethyl nitrite both produced[16] by the reaction of nitrogen dioxide and ethylene; for example;

$$C_2H_4 (NO_2)_2 \rightarrow C_2H_2 + 2HNO_2 \qquad (9)$$

This involves one additional step identical to the first step in the formation of ethylene from nitroethane. The mechanism of the formation of the latter is discussed by Wilde,[9] Gray, Yoffe and Roselaar,[10] and others.

There is still another easily noted discontinuity at this same stage. This is the sudden rise in the production of hydrogen cyanide. This would follow from the reaction of methyl radicals with the increased concentration of nitric oxide. Evidence for this type of reaction is discussed by Levy[11] and others.

Summary

The ignition of mixtures of propane and nitrogen dioxide proceeds through a one- or two-stage

process. The intensity of a relatively cool first stage flame increases with increasing per cent of nitrogen dioxide until a critical intensity is reached. Very small increments in the per cent of nitrogen dioxide then result in the rapid growth of an intense second stage, or hot, flame. Further increases in nitrogen dioxide concentration result eventually in eliminating both flames. There is also a sharply defined limit of pressure, independent of composition over a considerable range, below which no luminosity is exhibited.

The cool flame appears to be due to a branched chain process. The principal products are nitric oxide, ethylene, carbon monoxide, methane and hydrogen cyanide. The presence of ethylene, rather than propylene, is significant. Also important is the manner in which the product distribution of these species varies with increase in the intensities of the first and second stages of the flames. It has been concluded, from these facts, that the initial reaction between propane and nitrogen dioxide probably occurs through the formation of a complex rather than through hydrogen abstraction.

Also, it has been deduced from the changes in product distribution that the second stage flame is initiated by the reaction between ethylene, produced by the first flame, and nitrogen dioxide. When this flame becomes sufficiently hot other reactions begin to take place, including the oxidation of methane by nitric oxide.

REFERENCES

1. Lewis, B., and von Elbe, G.: *Combustion, Flames and Explosions of Gases*, Ch. 4. New York, Academic Press, 1951.
2. Maizus, Z. K., and Emanuel, N. M.: Proc. Acad. Sci. USSR, *95*, 1009 (1954).
3. Yoffe, A. D.: Research, *6*, 11s (1953).
4. Myerson, A. L., Taylor, F. R., and Faunce, B. G.: Franklin Institute Laboratories, Interim Technical Report No. I-2452-1 to Wright Air Development Center, Contract No. AF 33(616)-2456, December 31, 1955.
5. Semenoff, N.: *Chemical Kinetics and Chain Reactions*, Section 14. Oxford, Clarendon Press, 1935.
6. Walsh, A. D.: Fuel, *33*, 243 (1954).
7. Hass, H. B., Dorsky, J., and Hodge, E. B.: Ind. Eng. Chem., *33*, 1138 (1941).
8. Gray, P.: Proc. Roy. Soc., *A 221*, 462 (1954).
9. Wilde, K. A.: Ind. Eng. Chem., *48*, 769 (1956).
10. Gray, P., Yoffe, A. D., and Roselaar, L.: Trans. Faraday Soc., *51*, 1489 (1955).
11. Levy, J.: NAVORD Report 3833, U. S. Naval Ordnance Laboratory, White Oak, Md., November 1954.
12. Colburn, C. B.: Redstone Arsenal Research Division, Rohm and Haas Company, private communication to J. Levy.[11]
13. Harnsberger, H. F.: Dissertation, University of California, 1951.
14. Mueller, K. H.: J. Am. Chem. Soc., *77*, 3459 (1955).
15. Patry, M., and Engel, G.: Compt. rend., *231*, 1302 (1950).
16. Cottrell, T. L., and Graham, T. E.: J. Chem. Soc., 556 (1953).

Discussion by A. D. Yoffe*

Myerson, Taylor and Faunce have presented a most interesting and valuable paper on the ignition of propane-nitrogen dioxide mixtures. It may be of interest to outline some results which have been obtained using a similar system. The spontaneous ignition limits of *n*-pentane-NO_2 mixtures have been measured in the temperature range 300° to 525°C, and this has been mentioned in a brief note.†

When *n*-C_5H_{12}-NO_2 mixtures are admitted to a hot cylindrical quartz vessel (length 26 cm, diam 2.8 cm) it is found that reaction is already rapid at 252°C. Thus for a mixture containing 7.3 cm C_5H_{12} and 14.5 cm NO_2 the time for half of the NO_2 to disappear is 3 min. The variation of the initial rate of reaction (expressed as the disappearance of NO_2 in cm/sec) as a function of temperature for two different values of the total pressure is given in Figure 1. An indication of the change in the initial rate of reaction with increasing pressure of NO_2 for a constant value of pC_5H_{12} at 252°C is shown in Figure 2. More results are needed in order to obtain quantitative relations between the rate of reaction and the pressure of the reactants.

Above 300°C flames may be seen above a certain critical pressure,† and two regions of inflammation exist; in the first region a faint luminescence is observed and in the second region at a higher critical pressure there is an explosion accompanied by a white flash. There is an induction period of several seconds before the inflammation. The explosion limit at 422°C has been plotted in Figure 3, curve a, and the limit at 511°C is given by curve 1. At these higher temperatures multiple flames can be seen, depending on the total pressure inside the vessel. Thus in the region above curve 1, only a single flame is observed after an induction period of about 1 to 1½ sec. The color of the flame at the limit is dependent on the partial pressure of the NO_2 and may be white, orange or blue; the intensity of the flame at the limit is low. In the region above curve 2, two flames may be seen. The first is a white flash (and frequently accom-

* University of Cambridge.

† A. D. Yoffe: Research, *6*, 75 (1953).

panied by an audible click) which occurs shortly after admitting the mixture. The second flame appears shortly after the first and is usually of lower intensity than the first. In the region above the dotted line 3, there are three successive flashes. The ignition limit of n-C_5H_{12}-O_2 mixtures at 511°C has also been determined and is plotted in Figure 4 for comparison. The flame obtained with these mixtures appears after a much longer induction period, i.e., 9½ to 13 sec.

Iso-pentane-nitrogen dioxide mixtures behave in a manner similar to n-pentane. For example when the mole fraction of NO_2 is 0.86 the first limit at 511°C is about 4.0 cm and the limit for two flames is about 16 cm. Ethane also gives multiple flames with NO_2 at 511°C, and in this system the flame is frequently ignited locally and may be seen to travel along the length of the vessel. The ignition limit of a methane-nitrogen dioxide mixture at 511°C is much higher than for the higher hydrocarbons. When the mole fraction of the NO_2 is 0.62 the limit is at about 11.5 cm, and there is a time lag of about 1 to 1½ sec before the flash. The critical pressure limit rises steeply as the mole fraction of the NO_2 is raised above 0.75. Only single flames have been observed. No attempt was made to determine whether methane gives multiple flames, as it was not convenient to use very high pressures in the apparatus.

Gas analysis of the products of ignition at 511°C have also been made. A typical result for a mixture of n-C_5H_{12}-NO_2 at the first limit when the mole fraction of the NO_2 is 0.86 is; NO, 46 per cent; CO_2, 9 per cent; H_2, 10 per cent; CO, 17 per cent; N_2, 16 per cent; other gases, 2 per cent; water was not determined, formaldehyde was also formed but not estimated.

There is strong evidence* that the low temperature reactions (<300°C) proceed by a free radical mechanism, the initial step being hydrogen abstraction by NO_2. The inflammation of hydrocarbon-nitrogen dioxide mixtures is a complex process and a simple interpretation of the results can not be given on the results so far obtained. Some of the possible steps have been discussed.† At temperatures in the region of 400° to 500°C it does not seem profitable to consider the formation of a stable complex* between a saturated hydrocarbon and NO_2 as suggested by Myerson, Taylor and Faunce. The dissociation of nitrogen dioxide into nitric oxide and oxygen must be taken into account at these temperatures, and it may explain in part the incidence of the multiple flames.

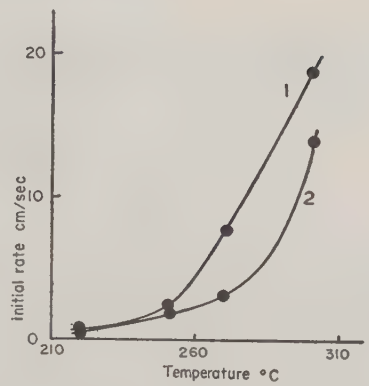

FIG. 1. Variation of initial reaction rate (expressed as disappearance of NO_2 in cm/sec) with temperature. Curve 1: pC_5H_{12} 4.7 cm, pNO_2 19.1 cm; Curve 2: pC_5H_{12} 3.6 cm, pNO_2 14.6 cm.

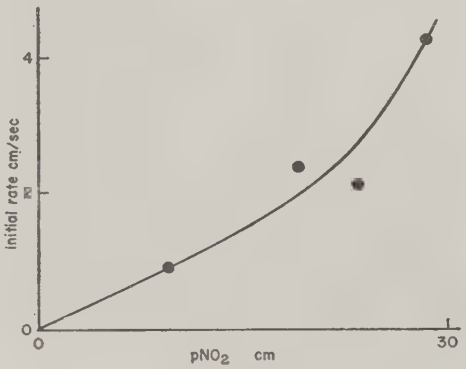

FIG. 2. Variation of initial reaction rate with pressure of NO_2. Temperature 252°C; pressure of C_5H_{12} 4.7 cm Hg.

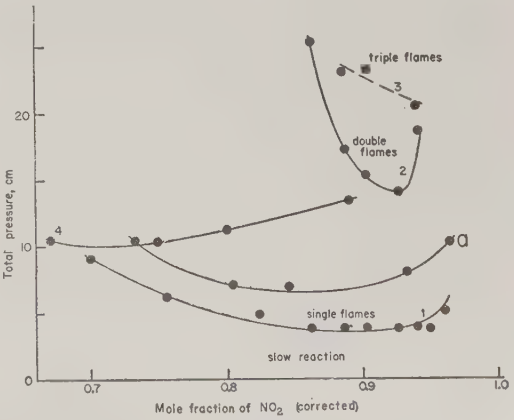

FIG. 3. Regions of inflammation of n-C_5H_2-NO_2 mixtures. Curve a: 422°C; curves 1, 2, 3: 511°C; curve 4 is the ignition limit of an n-C_5H_{12}-O_2 mixture and is included for comparison.

* P. Gray and A. D. Yoffe: Chem. Rev., *55*, 1069 (1955); Quart. Rev. Chem. Soc. *9*, 362 (1955).

20

BURNING STRUCTURE AND STABILITY OF *n*-BUTANE-NITROGEN DIOXIDE FLAMES IN AIR[a]

By E. MILLER AND H. J. SETZER

Introduction

Parker and Wolfhard[1] point out that information on the properties of flames supported by oxidants other than air or oxygen is meager, doubtlessly because of the wider technical application of air and oxygen flames. Because of an interest in chemical propellants for rocket propulsion, we have made a laboratory study of premixed *n*-butane-NO_2 flames burning in air.

The experimental program reported here comprises spark shadowgraphs and direct photographs of these flames under various conditions, laminar flame velocities, blowoff measurements for four tubes, 0.396 cm, 0.706 cm, 0.847 cm and 1.026 cm i.d. and flashback measurements for the latter three tubes. With the largest tube, the effect of tube wall temperature on flashback stability was studied in the range 65° to 260°C. Similar studies were conducted for blowoff stability, with the 0.706 cm tube, between 83° and 180°C. A simplified analysis of the effect of tube wall temperature is presented which correlates the flashback and blowoff data satisfactorily.

Apparatus and Procedure

The *n*-butane (CP, 99 per cent purity) and the nitrogen dioxide (98 per cent purity) were obtained from commercial sources and used without further purification. The gases were metered separately in rotameters calibrated in place with a wet test meter. A fluorinated hydrocarbon oil was used as the working fluid in the wet-test meter for the nitrogen dioxide, and water for the butane. Particularly in the case of the nitrogen dioxide gases, it was necessary to heat and to insulate the flow system and burner tube in order to prevent condensation in the lines. Gas temperatures were maintained at about 35° ± 5°C throughout the tests.

The butane and nitrogen dioxide were mixed in a tee leading into the burner tube. The burner tubes were approximately 100 diameters long, allowing sufficient length for mixing and establishment of a fully developed velocity profile. The last 10 cm of each burner tube was cooled by an open water-jacket; the tube tip temperature was maintained at a desired magnitude by adjusting the level of the water below the tip. The wall temperature was measured with an iron-constantan thermocouple peened into the tube 1 mm from the tip. The temperature at the tube tip was estimated.

The procedure in determining the critical flashback or blowoff condition was to adjust the mixture ratio and total gas flow so that a stable flame was obtained. Then, either the fuel or oxidizer flow was increased or decreased until flashback or blowoff occurred. The water level in the cooling jacket was adjusted, as required, in order to maintain the tube wall temperature to within ±9°C. In the experiments with constant tube wall temperature, the tube wall was maintained at 83°C.

The volume of the gases used in the calculation is based on the temperature of the cool gas in the burner tube. The equilibrium composition of $N_2O_4 \rightleftharpoons 2NO_2$ was calculated using the data of Verhoeck and Daniels.[2] The butane concentration is reported on a weight basis to avoid confusion in presentation of the results.

A double mirror arrangement was used for the shadow photography. The flame was set in the path of parallel light between the mirrors. f/4 mirrors of 4 ft focal length were used. The flash source was an argon filled, high intensity lamp available commercially. The flash was synchronized with the camera shutter set at 1/100 sec. The flash duration itself was of the order of a μsec.

Theory

The critical boundary velocity gradients for flashback, g_F, and blowoff, g_B, were computed from the equations developed originally by Lewis and von Elbe[3] for laminar flow in the burner tube:

$$g_F = \frac{8\bar{u}}{D} \sim \frac{S_u}{X_F} \qquad (1)$$

[a] This research was supported by the Office of Ordnance Research and the Research and Development Division, Office of the Chief of Ordnance. Contribution Number 27, Research Laboratories, Ordnance Missile Laboratories, Redstone Arsenal.

$$g_B = \frac{8\bar{u}}{D} \sim \frac{S_u}{X_B} \tag{1a}$$

The critical boundary velocity gradients for blowoff in the turbulent region were calculated from

$$g_B = \frac{0.023\bar{u}^{1.8}\nu^{0.8}}{D^{0.2}} \tag{1b}$$

u is the average stream velocity of flashback or blowoff, D is the tube diameter, ν the kinematic viscosity, S_u the flame velocity and X_F and X_B the penetration distance for flashback and blowoff respectively.

Equations (1), (1a) and (1b) reasonably apply to an isothermal case in which the tube wall and the unburned gas are at the same temperature. Experimentally, it was found difficult to keep the burner tube tip at the same temperature as the unburned gas. A marked dependence was observed between flashback or blowoff stability and tube wall temperature. See Figures 1 and 3.

Qualitatively, an increase in tube wall temperature should cause two effects; the quenching effect of the wall on the flame should change and the velocity gradient at the wall should decrease because of an increase in the viscosity of the gas near the wall. For hydrocarbon-nitrogen dioxide flames, in which a relatively cool inner cone is surrounded by a hot outer cone, little effect on the flame velocity or the final flame temperature would be expected.

From Wohl,[4] there can be written

$$T_i - T_w = \left(\frac{dT}{dx}\right)_w \frac{\alpha}{S}\left[e^{(S/\alpha)X_1} - 1\right] \tag{2}$$

where T_i and T_w are the ignition and wall temperatures respectively; $(dT/dx)_w$ is the temperature gradient at the wall; α is the thermal diffusivity of the gases, S the flame velocity and X_1 the distance of the cold wall from the point of ignition.

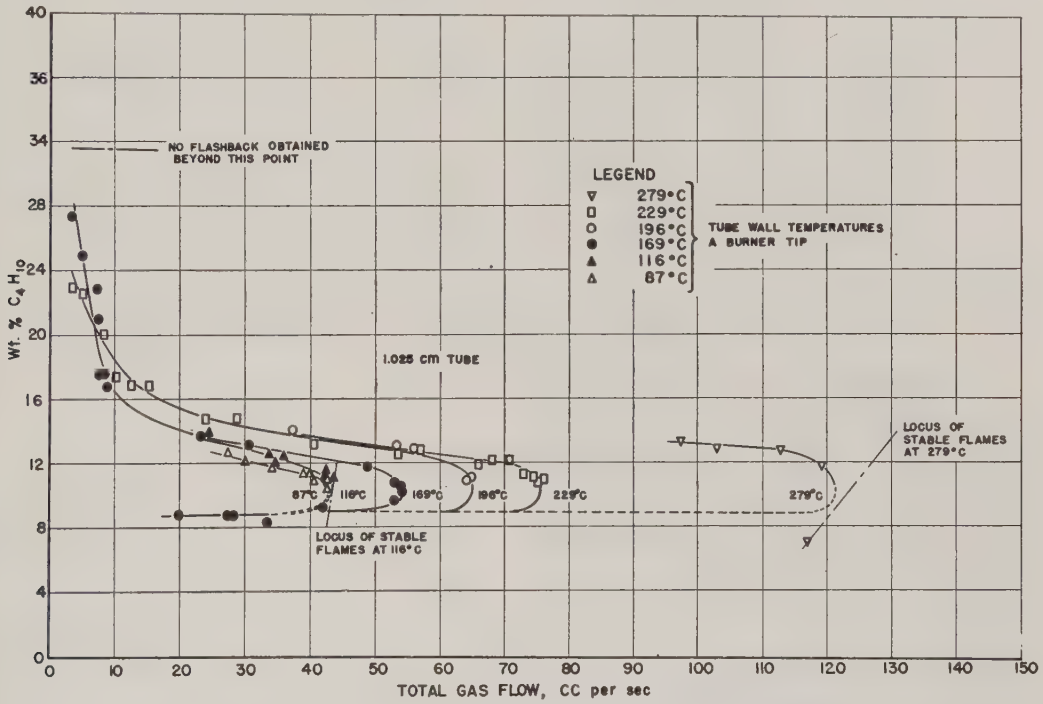

FIG. 1. Flashback limits as a function of tube wall temperature.

For the flame velocities encountered in this system, it is sufficient to approximate $\exp(SX_1/\alpha)$ by $(1 + SX_1/\alpha)$; therefore, Equation (2) becomes

$$T_i - T_w \cong \left(\frac{dT}{dx}\right)_w X_1 \tag{2a}$$

Since

$$\left(\frac{dT}{dx}\right)_w = \frac{S}{\alpha}(T_f^a - T_f) \tag{3}$$

Where T_f^a and T_f are the adiabatic and actual

flame temperatures respectively, there can be written by combining Equations (2a) and (3)

$$X_1 \cong \frac{\alpha}{S}\frac{T_i - T_w}{T_f^a - T_f} \quad \text{where} \quad T_w \neq T_i \,. \tag{4}$$

Further, the velocity gradient at the wall is inversely proportional to the viscosity of the gas at the wall. Therefore, the velocity gradient at the wall decreases as $\overline{T}^{0.6}$, if X_1 is small compared

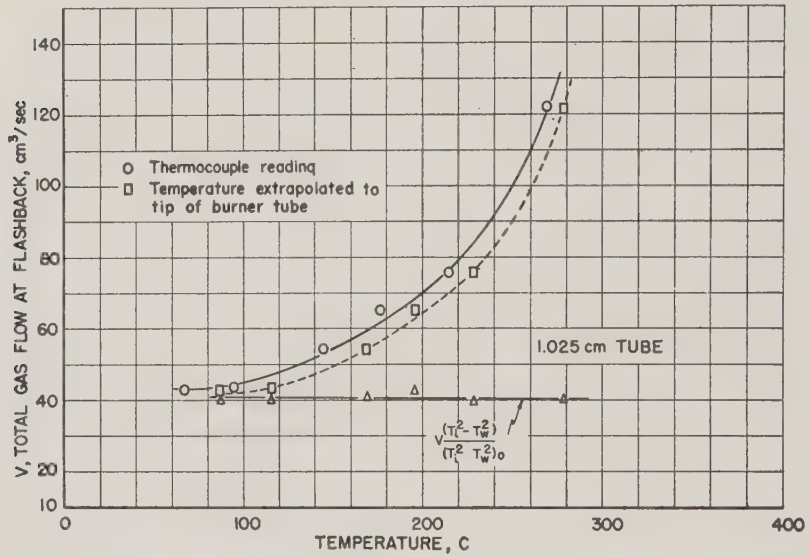

FIG. 2. Maximum total gas flow at flashback as a function of tube wall temperature.

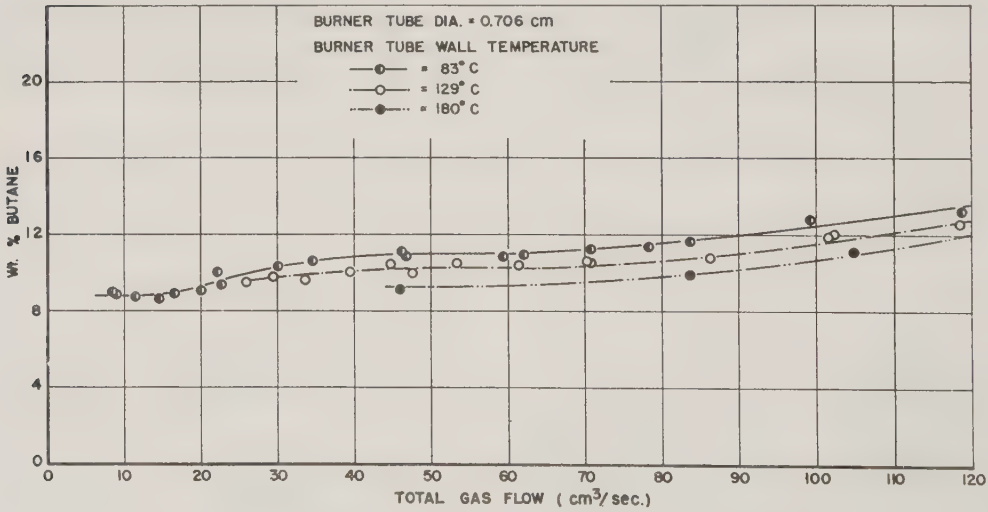

FIG. 3. Blowoff limits as a function of tube wall temperature.

If the average temperature, $\overline{T}$, of the gases between X_1 and the wall is taken as $(T_i + T_w)/2$ and α assumed proportional to $\overline{T}^{1.6}$,

$$X_1 \propto (T_i + T_w)^{1.6}(T_i - T_w) \tag{4a}$$

with S and $(T_f^a - T_f)$ assumed constant. Equation (4a) predicts a maximum penetration distance at $T_w \sim 0.25\, T_i$.

with the diameter of the tube. The velocity gradient at the wall calculated from the parabolic velocity profile of isothermal, laminar flow is too large by a factor proportional to $\overline{T}^{0.6}$.

Finally, there is obtained, if X_B or X_F is proportional to X_1,

$$\bar{u} \propto \frac{\bar{T}^{0.6}}{\bar{T}^{1.6}(T_i - T_w)} = \frac{1}{T_i^2 - T_w^2} \tag{5}$$

or $\bar{u}(T_i^2 - T_w^2)$ is independent of tube wall temperature.

Results and Discussion

A. FLASHBACK AND BLOWOFF CHARACTERISTICS

1. Effect of tube wall temperature

Figure 1 shows a correlation of the weight per cent butane in the mixture at flashback for the 1.026 cm tube as a function of critical total gas flow with tube wall temperature as a parameter. In Figure 2 there is plotted the maximum total gas flow for flashback in this tube, i.e., at 10.3 per cent butane, versus the tube tip temperature. The strong effect of tube wall temperature on flashback stability is quite evident in these figures. The effect is greatest at the higher temperatures. Below 115°C there is almost no effect of tube wall temperature on flashback.

The behavior is consistent with the analysis given in the theory. As the tube wall temperature is increased, a higher gas velocity is required to prevent flashback. In Figure 2 there is plotted also the quantity,

$$V \frac{(T_i^2 - T_w^2)}{(T_i^2 - T_w^2)_o}$$

versus the tube wall temperature, where V is the total gas flow at flashback or blowoff. The subscript, o, signifies an arbitrary reference wall temperature which is used to reduce the data to the same basis. At 10.3 per cent butane, a $T_i = 623$°K (350°C) satisfactorily correlates the results. At 12 per cent butane, a $T_i = 613$°K (340°C) correlated the data. No attempt was made to correlate all the data, since the slope of the flashback curves makes the absolute value of gas flow at flashback somewhat indefinite.

Blowoff data at different tube tip temperatures are shown in Figure 3. In this case also, an increase in tip temperature caused a higher gas flow requirement in order to blow off the flame. At 11 per cent butane, a $T_i = 588$°K (315°C) correlated the blowoff data.

The magnitude of T_i obtained is low compared with the value normally observed for hydrocarbon-air flames. However, an appreciable reaction of hydrogen with nitrogen dioxide occurs at temperatures as low as 300°C, probably initiated by the direct addition of nitrogen dioxide to the hydrogen.[5] If an analogous reaction takes place between the butane and nitrogen dioxide, then an ignition temperature of about 350°C is reasonable. In addition, the flame temperature of the inner cone of the flame can be as low as 700°C;[1] therefore, again, a 350°C ignition temperature is reasonable. Much significance should not be placed on the variation in T_i observed, considering the simplifying assumptions made in the analysis. Until further evidence is obtained for the ignition temperatures of butane-nitrogen dioxide, however, it is best to consider T_i as a fictitious temperature used to correlate the data.

2. Constant tube wall temperature

Figures 4 and 5 summarize the flashback and blowoff limits found, for the tubes studied, at a constant tube wall temperature of 83°C. The curves resemble the data reported for butane-air flames[6] but are displaced toward the richer side of stoichiometry, i.e., an equivalence ratio of 1.3 for nitrogen dioxide flames as compared with 1.1 for air flames.

Stoichiometry for flashback and blowoff of the butane-nitrogen dioxide flames is considered here as being combustion to CO_2, H_2O and NO (8.84 per cent butane). It seems reasonable to consider the reaction of the inner cone to control the stability of the flames. On the other hand, as shown in Figure 11 described further below, the burning velocity variation of the inner cone shows a maximum at about 15 per cent butane, or close to a stoichiometry based on CO_2, H_2O and N_2 (16.2 per cent butane). It is not likely, however, considering the behavior of hydrocarbon and air flames, that the maximum g_F occurs at lean mixtures.

X_F values were calculated from the experimental values obtained for g_F and S_u. The variation of X_F with per cent butane is shown in Figure 6. X_F is greatest for lean and rich mixtures. The composition at the minimum X_F corresponds approximately with the composition for maximum g_F. This agrees with the variation of penetration distance reported for butane-air flames.[6] Also, the calculated penetration distances are the same magnitude as those observed in air flames.

B. BURNING STRUCTURE

1. Laminar flames

A series of direct and spark shadow photographs were taken of laminar flames in the range shown in Figure 7. The flow conditions ranged from lean mixtures near blowoff to very rich mixtures.

The hydrocarbon-nitrogen dioxide flame is described, in general[1] as consisting of two main

reaction cones. The inner cone, emitting a continuous yellow color, qualitatively consists of the decomposition of NO_2 and a hydrocarbon-oxygen flame diluted with NO; the outer cone, which is violet in color, is the hotter one in which the richer, the outer cone becomes brighter and the inner cone dimmer. Figure 8b is a direct photograph of a typical rich, double cone flame at 19 per cent butane. At very rich mixtures, the two cones separate, as shown in Figure 8c.

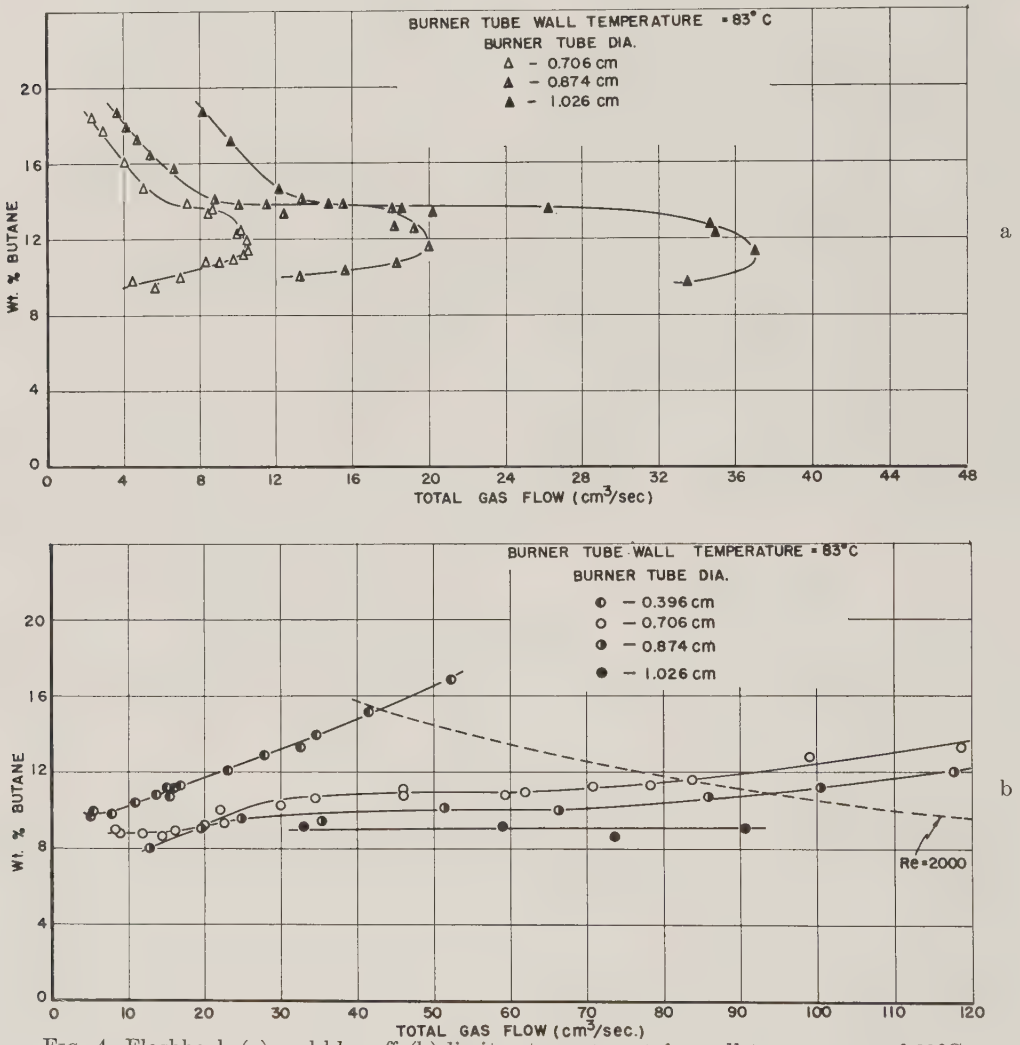

FIG. 4. Flashback (a) and blowoff (b) limits at constant tube wall temperature of 83°C.

partly oxidized fuel burns with NO diluted with combustion products from the first cone

A lean flame with a single cone can be stabilized in air, however. Figure 8a is a direct photograph of such a lean flame near blowoff in which only the inner cone is present. The outer cone does not exist at this mixture. As the mixture is made richer in butane, a rough, bluish-white reaction zone appears above the inner cone, and at 16.5 per cent butane it becomes defined and readily visible. As the mixture is made still

The spark shadowgraphs of these flames are shown in Figures 8d, 8e, and 8f. Outside of the main reaction cone there is a faint truncated cone visible. Surprisingly, the shadowgraph of the lean single cone flame (Fig. 8d) closely resembles the shadowgraph of a rich double cone flame (Fig. 8e). By superimposing the shadowgraphs of rich and lean flames on the direct photographs and correcting for differences in magnification, it is found that the direct image and the shadowgraph of the inner cone coincide closely. The faint

truncated cone of the shadowgraph apparently does not necessarily coincide with the second visible cone. It is believed that this faint second cone is associated with the reaction of NO and the partially oxidized fuel remaining after passage through the first cone.

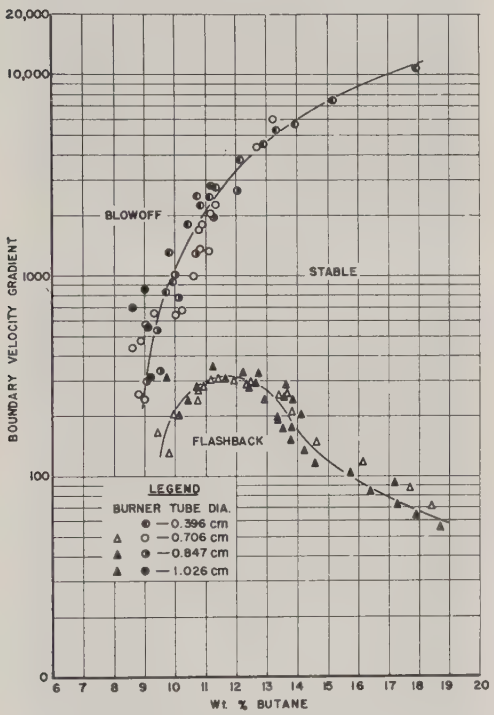

FIG. 5. Flashback and blowoff critical boundary velocity gradients at constant tube wall temperature of 83°C.

2. Turbulent flames

Figures 9a and 9b are spark shadowgraphs of butane-nitrogen dioxide flames in the near turbulent flame region. The conditions of flow and mixture ratio are shown in Figure 7.

Here again, in these shadowgraphs, only a single reaction cone shadow is visible. However, it is rather irregular in appearance, suggesting that the burning takes place on the surface of eddy balls. In addition, instead of an outer cone as noted for the laminar flames, the reaction of NO and partly oxidized fuel takes place in an irregular structure with an appearance of "strings" or possibly cells. As was the case for the laminar flames, the direct photographs did not show this zone.

In Figure 10, a shadowgraph is shown of a rich lifted flame at a total gas flow of about 325 cc/sec. The turbulent structure of the cool jet is evident and it continues with an increase in scale into the flame region. This flame has much the appearance of a lifted butane-air flame.

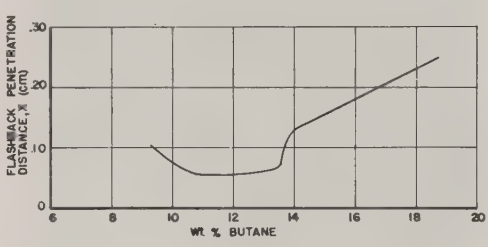

FIG. 6. Variation of flashback penetration distance with per cent butane in mixture.

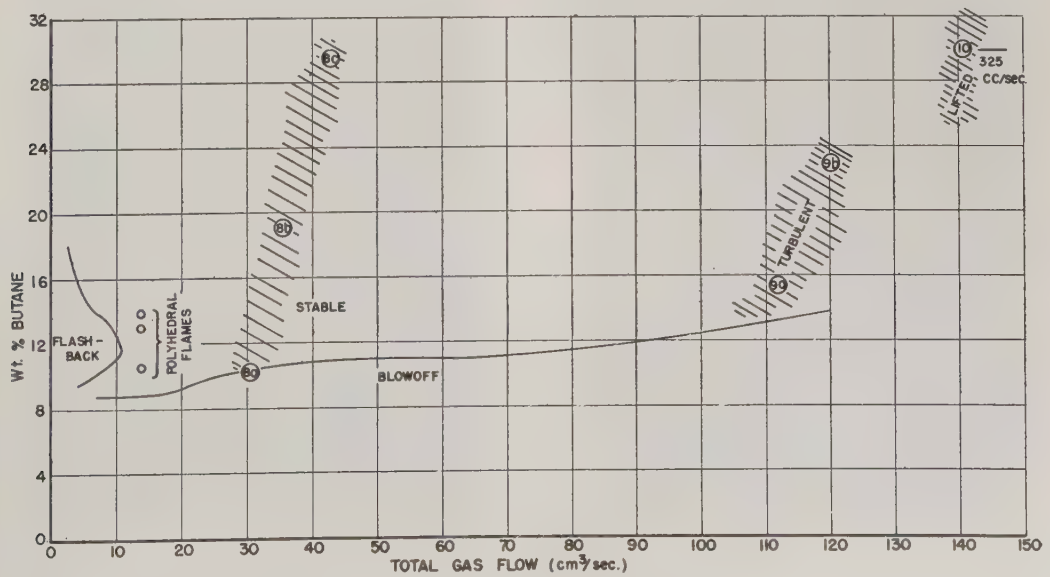

FIG. 7. Per cent butane in mixture and total gas flow conditions for duct and shadow photographs.

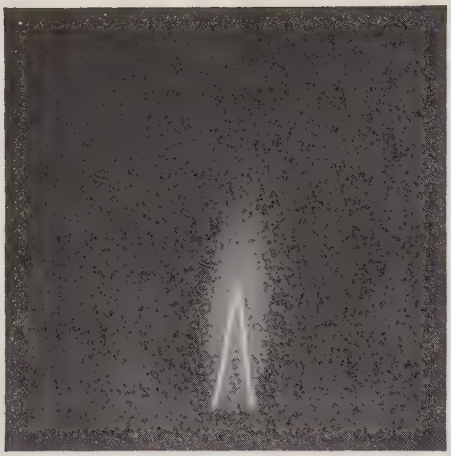

a

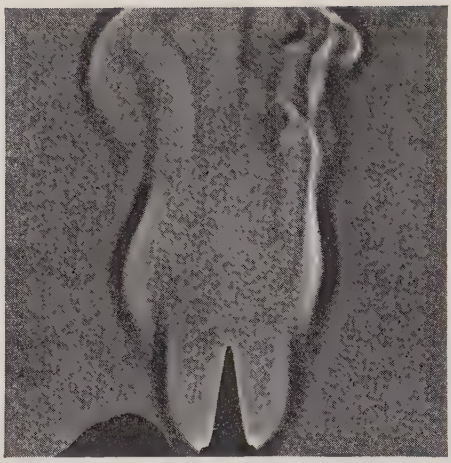

d

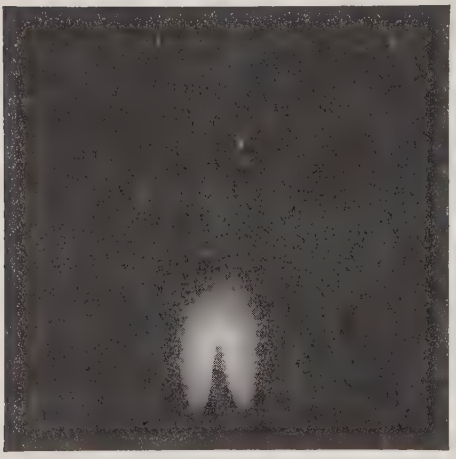

b

e

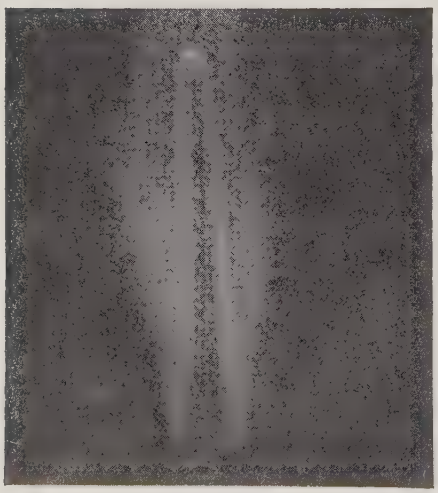

c

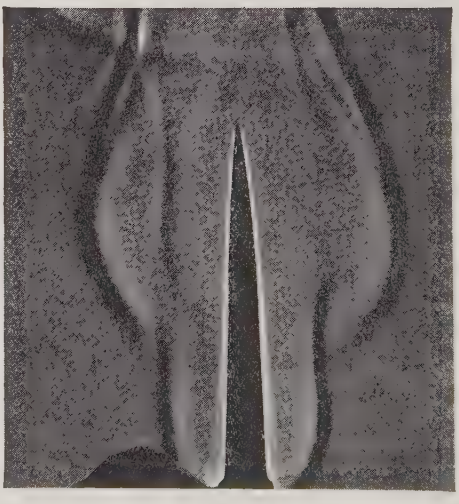

f

FIG. 8. Direct and shadow photographs of lean and rich laminar flames.

3. Polyhedral flames

Polyhedral flames of 3, 4 and 6 sides were observed on the 0.706-cm tube near flashback at stoichiometric and moderately rich mixtures (based on the inner cone reaction). The number of sides of the polyhedral increased with increasing butane in the mixture. The polyhedral flame involves the inner cone only, as far as can be seen visually. The outer "cone" at these conditions exists as an indefinite, bluish-white reaction zone above the inner cone. The formation of the polyhedral occurred only near flashback in the region shown in Figure 7. At lower total gas flow ratios and 11 per cent butane, tilted flames were observed. At higher gas flows, the flame appearance was "normal." At richer mixtures and lower gas flow, near the flashback condition, dish-shaped and flat flames were observed. Tentatively, it may be concluded that polyhedral flames will occur for this flame system, only for moderately rich mixtures near flashback.

C. LAMINAR FLAME VELOCITIES

In Figure, 11, the average laminar flame velocities as a function of per cent butane in the mixture is given. The flame velocities were calculated from the total area of the cone, from both direct and shadow photographs, and the total gas flow. The inner visible edge of the inner cone was used from the direct photographs, and the outer visible shadow edge from the shadowgraphs.

a b

FIG. 9. Shadowgraphs of near stoichiometric and rich turbulent flames.

The shadowgraphs data yielded somewhat lower burning velocities than those obtained from the direct photographs. The maximum flame velocity calculated from the direct photographs is 19.8 cm/sec at 16 per cent butane and from the shadowgraphs, 18.3 cm/sec at 14.6 per cent butane. Based on a stoichiometry of CO_2, H_2O and NO, the maxima occur at 1.81 and 1.65 of stoichiometry respectively. Based on a stoichiometry of CO_2, H_2O and N_2, the maxima occur at 0.99 and 0.90 respectively. Although it is reasonable to base the stoichiometry of the inner cone on a reaction that does not involve NO, this would

suggest that the maximum flame velocity occurs at an extremely rich mixture. Therefore, it must be concluded that conduction and radiation from the outer cone to the inner cone have a strong influence and that the maximum flame velocity occurs close to the overall stoichiometry of the flame.

Parker and Wolfhard[1] report a flame velocity for ethane and nitrogen dioxide at over-all stoichiometry as 20 cm/sec. Their calculations were based on all the N_2O_4 being present as NO_2. Changing their basis of calculation to that used here yields a value of about 16 cm/sec.

Anomalously, the per cent butane at which the maxima of the flashback critical velocity and the laminar burning velocity curves are found differ considerably. Comparison of Figures 5 and 11 shows that the peak in the burning velocity curve falls at a much richer mixture than that of the flashback curves. In butane-air flames the per cent butane at which the two peaks occur is almost the same. As mentioned above, the calculated penetration distance for the butane-nitrogen dioxide flames do exhibit a minimum at a mixture coinciding approximately with the percentage butane for maximum g_F.

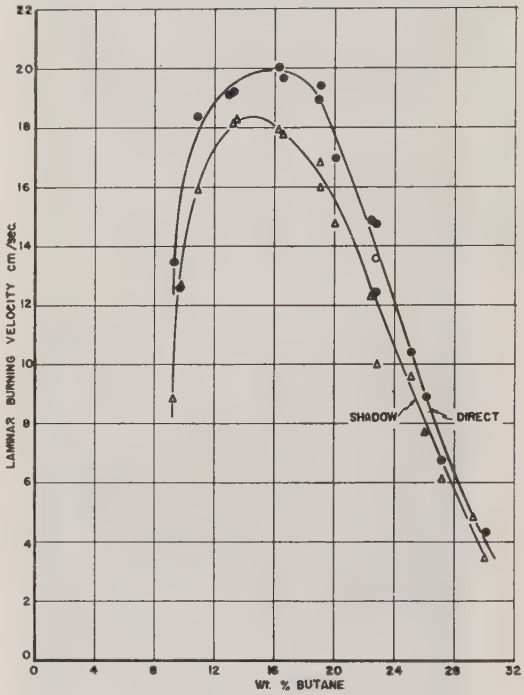

FIG. 11. Laminar flame velocities as a function of per cent butane in mixture.

FIG. 10. Shadowgraph of rich lifted flame.

Acknowledgment

The authors wish to express appreciation to C. W. Manry and Harwell Gregg for their assistance in conducting these experiments.

REFERENCES

1. PARKER, W. G., AND WOLFHARD, H. G.: *Fourth Symposium (International) on Combustion*, p. 420. Baltimore, The Williams & Wilkins Co., 1953.
2. VERHOECK, F. H., AND DANIELS, F.: J. Am. Chem. Soc., *53*, 1250 (1931).
3. LEWIS, B., AND VON ELBE, G.: *Combustion, Flames and Explosions of Gases*, p. 279. New York, Academic Press, 1951.
4. WOHL, K.: *Fourth Symposium (International) on Combustion*, p. 68. Baltimore, The Williams & Wilkins Co., 1953.
5. ROSSER, W. A., AND WISE, H.: Jet Propulsion Laboratory Progress Report No. 20-282 (1955).
6. WOHL, K., KAPP, N. M., AND GAZLEY, C.: *Third Symposium on Combustion, Flame and Explosion Phenomena*, p. 3. Baltimore, The Williams & Wilkins Co., 1949.

21

SPECTROSCOPIC INVESTIGATION OF *n*-BUTANE-NO_2 FLAMES[a]

By W. W. WHARTON, T. D. VIOLETT AND E. MILLER

Introduction

The project from which this paper is taken was initiated to study the combustion processes which may occur in flames supported by oxidants other than air. The results of a spectroscopic study of *n*-butane-NO_2 flames burning in air are reported here.

A modified Egerton burner[1] has been developed which produces a flat flame. The flame thus produced has been traversed optically, from the premixed gases, through the various stages of combustion to the combustion products. This procedure has afforded a knowledge of the rise and decay of various species in the flame as evidenced by their emission spectra.

Apparatus and Procedure

A schematic drawing of the burner used to produce a flat flame is shown in Figure 1. It consists of a cylindrical tube with six laminarizing screens and spacers, a grid and a water-cooled jacket. Thin sheets of corrugated stainless steel are bundled together snugly to form the grid. The openings in the grid are approximately 0.01 in. square and the total open area is about thirty per cent of the total surface.

Under suitable conditions the butane-NO_2 flame produces two discrete reaction zones. With the burner used, two zones occur for mixture ratios on the fuel rich side of stoichiometry based on the end products of CO_2, H_2O and N_2. As stoichiometry is approached, the zone farther from the burner base blows off leaving a pale yellow single cone. A general description of the appearance of flames of these gases is given by Wolfhard and Parker[2] and Miller and Setzer.[3]

In order to traverse the flame optically, an auxiliary optical system and a micrometer traversing mechanism were designed and constructed. A schematic of the optical system is shown in Figure 2. The spherical mirror, M-1, is mounted so that light from the burner or from an auxiliary source may be focused onto the monochromator slit, S-2. The two positions of the spherical mirror are fixed by dowel pin stops. Slit S-1 is an aperture controlling slit. Its width may be set from 0 to 2.5 cm with an accuracy better than 0.01 mm. The setting of this slit together with the entrance slit of the monochromator controls the average cross section of the flame viewed by the spectrometer. For this work the aperture slit width was 2 mm and the entrance slit 0.02 mm. The average cross section

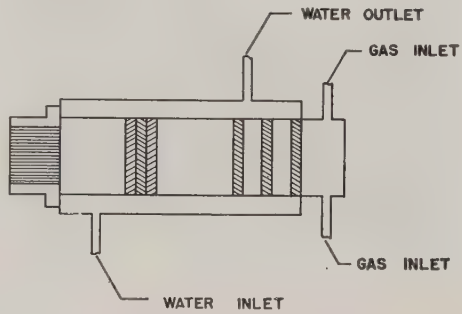

FIG. 1. Schematic of flat flame burner.

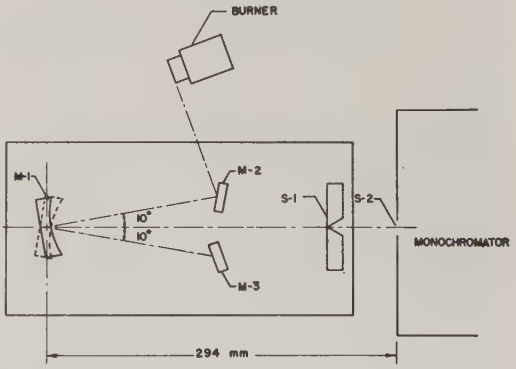

FIG. 2. Schematic of optical system.

of the flame viewed with these settings was about 0.137 mm.

The working part of the traversing mechanism consists of a 3-in. stainless steel bolt which drives the burner mount. This bolt has machined $\frac{1}{32}$-in. threads and is turned by a knob having 100 equally spaced divisions around its circumference. This makes possible the accurate positioning of the burner to $\frac{1}{3200}$ of an inch. Figure 3 shows a picture of the assembled traversing mechanism, burner and optical system attached to the spectrometer.

[a] This research was supported by the Office of Ordnance Research and the Research and Development Division, Office of the Chief of Ordnance. Contribution Number 28, Research Laboratories, Ordnance Missile Laboratories, Redstone Arsenal.

The flow system consists of flow-meters, surge vessels, constant temperature bath, mixing chamber and heat exchangers. Figure 4 shows a schematic of the flow system. Schilling design flow-meters having removable orifices were used. A $\frac{1}{20}$-cu ft wet-test meter was used to calibrate the flow-meters. The wet-test meter was calibrated against a standard liter. Fluorinated hydrocarbon oil, saturated with the appropriate gas, was used as the manometer fluids and as the working fluid

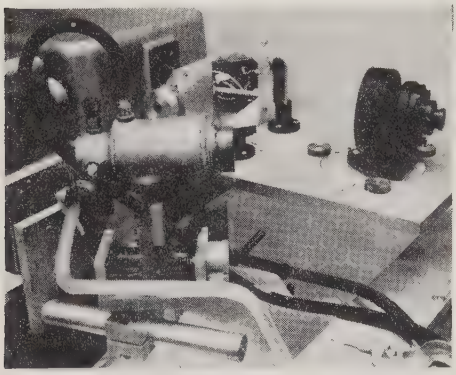

FIG. 3. Close-up of burner, traversing mechanism and optical system.

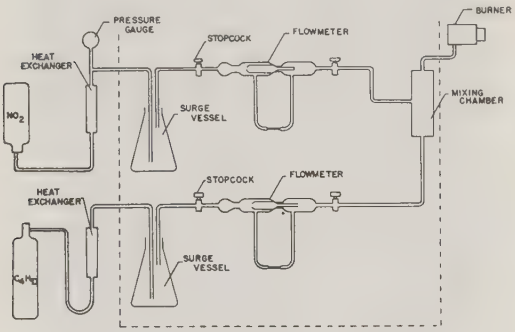

FIG. 4. Schematic of flow system.

in the wet-test meter. The equilibrium decomposition of $N_2O_4 \rightleftharpoons 2\ NO_2$ was calculated from the data of Verhoeck and Daniels.[4] CP grade butane and commercial grade (98 per cent) NO_2 were used without further purification.

A 3-liter Erlenmeyer flask in the butane and NO_2 lines is used to damp oscillations. These have proved effective enough that traverses of the flame front in $\frac{1}{320}$-in. steps have been reproducible.

The flow-meters, surge vessels and mixing chamber are submerged in a large constant temperature bath. The bath is maintained at a constant temperature of 40°C to prevent condensation of the NO_2 and to enable accurate metering and flow stability of the gases. The butane and NO_2 were vaporized in suitable heat exchangers. Figure 5 shows the constant temperature bath and most of the associated equipment.

The spherical mirror, M-1, (Fig. 2) is placed exactly 2 focal lengths from the entrance slit of the monochromator. The burner is mounted so that a light placed behind the entrance slit is focused at the center of the grid. This positions the burner so that magnification is unity.

The "base" of the burner was determined by

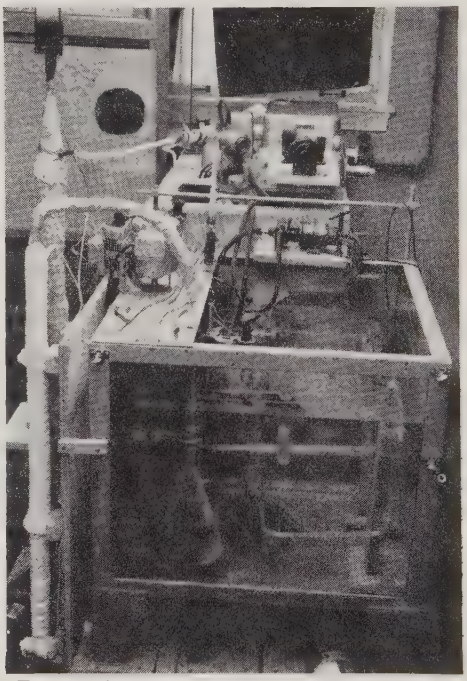

FIG. 5. Complete flame study apparatus.

moving the burner past the slit until the background radiation was 0 at all wavelengths. Although this position closely approximates the grid surface it is not necessarily the true base. All measurements of distances into the flame reported in this paper were measured relative to the "base" determined in the above manner. Distances into the flame are measured quite accurately by the precision micrometer screw of the traversing mechanism.

The gas flow is essentially parallel to the burner axis over the region studied. Therefore, the burner is mounted horizontally and rotated in the horizontal plane until the sharpest possible image appears on the slit. Moving the burner in any one degree of freedom upsets the positioning of other

degrees of freedom. Some time is required by trial and error methods to initially position the burner. No attempt was made to remove atmospheric CO_2 and H_2O from the optical path. This would have little effect on the ultraviolet and visible region studied.

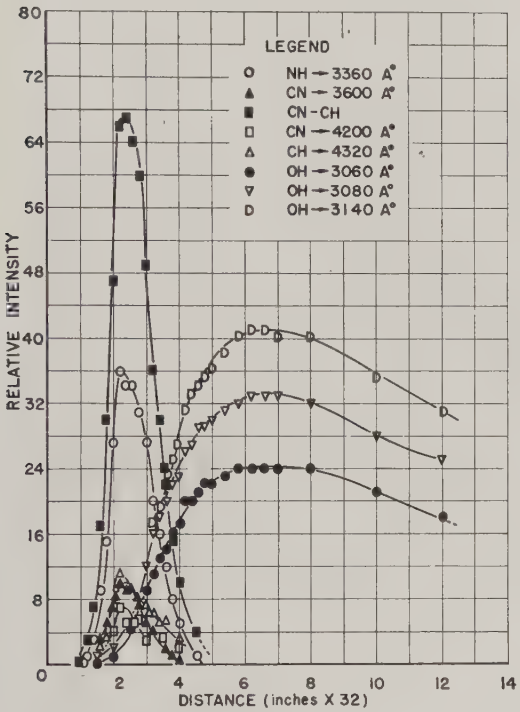

FIG. 6. Relative intensity as a function of distance from burner base (22.2 per cent butane by weight).

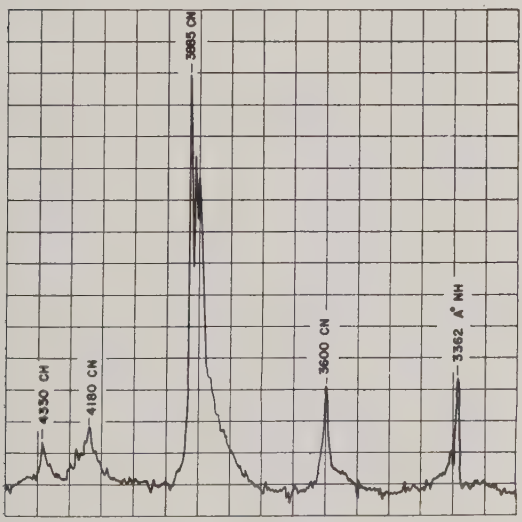

FIG. 7. Emission spectra of butane-NO_2 flame position 1.

Results and Discussion

The flame front has been traversed in steps as small as $\frac{1}{320}$ of an inch. Such traversals present a very detailed picture of the rise and decay of radiation from various species. This is presented graphically in Figure 6 for the composition 22.2 weight per cent butane. Radiation from CN, CH and NH reaches maximum intensity in the burning zones close to the base. OH radiation, which is weak in this region, builds up to a maxima farther out in the flame where the CN, CH and NH radicals have disappeared. The largest peak in Figure 6 is radiation emitted by the 3900 Å CH band overlapping the CN band at 3890 Å.

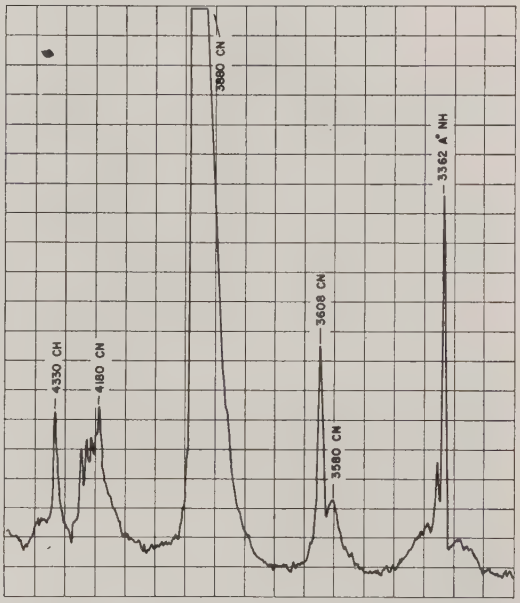

FIG. 8. Emission spectra of butane-NO_2 flame position 2.

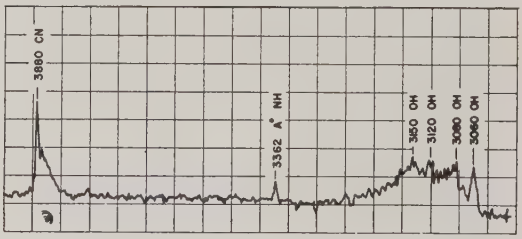

FIG. 9. Emission spectra of butane-NO_2 flame position 3.

Figures 7, 8, 9 and 10 show the effect of the position of the flame on the recorded spectra. Figures 7, 8 and 9 show the same spectral range at consecutive $\frac{1}{32}$-in. intervals. Figure 10 shows

the manner in which the OH band builds up as a function of distance into the flame ($\frac{1}{32}$-in. intervals).

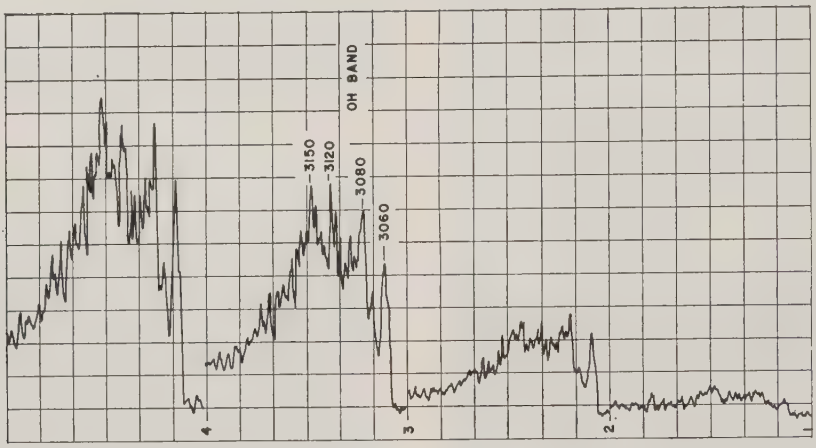

FIG. 10. OH band at consecutive $\frac{1}{32}$ in. steps.

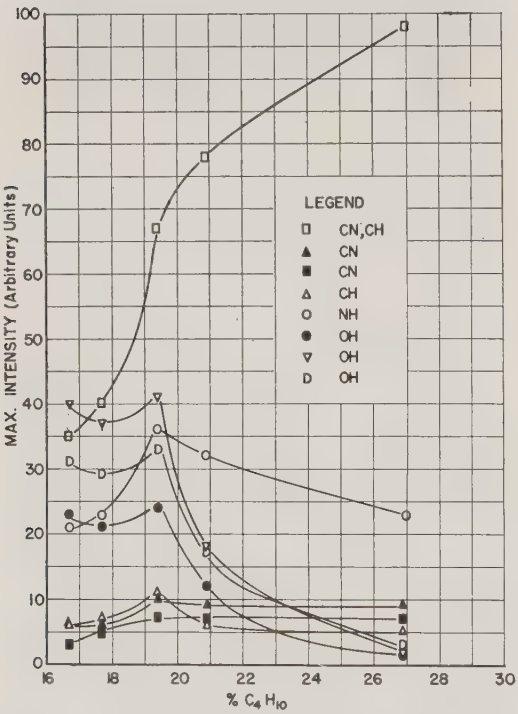

FIG. 11. Maximum intensity as a function of per cent butane.

The percentage composition of the flame has a profound effect on the intensity of the radiation. Figure 11 shows graphically the maximum intensity of the various emitters as a function of weight per cent butane. At about 19 per cent butane CN radiation tends to build up to a constant value. CH, OH and NH radiation have a maximum intensity at this composition. The odd shape of the OH and NH curves to the left of the maximum is probably due to a flow effect. The total flow was not constant but gradually decreased as the percent of butane was increased (38 to 23.6 cc/sec). Since the maximum intensity is dependent to some extent on the total flow, the data could be corrected to constant total flow by dividing the maximum intensity by some power of the total flow. Since the points to the left of the graph would be reduced in value most, this would not change the over-all picture but should have the effect of removing the discontinuity in the curve with a maximum somewhere around 19 per cent butane. The CN, CH curve increases continuously over the entire range studied. The bulge results from the CH having a maximum at this point.

Wolfhard and Parker[2] report that OH radiation maximizes past the primary reaction zones in various hydrocarbon-NO_2 and in some hydrocarbon-NO flames. Slight C_2 radiation has been observed. Similar results have been observed in this work except no C_2 radiation has been detected. Wohl and Welty,[5] on the other hand, have studied butane-air flames and find that OH radiation in these flames is a maximum within the primary reaction zone. Further they find strong C_2 radiation. It is suggested, therefore, that within the outer primary reaction zone for butane-NO_2, the following exothermic reaction takes place:

$$C_2 + OH \rightarrow CO + CH$$

This reaction evidently removes both C_2 and OH.

From the gray halo in the mantle of the flames, it may be concluded that NO is decomposing outside of the primary reaction zones. This is confirmed by some of the spark shadowgraphs taken of butane-NO_2 flames.[3] The flame temperature, therefore, should be at a maximum outside of the main reaction zones due to the energy release from the NO. The intense OH radiation appearing in this region could then be accounted for by additional formation of OH from either the reaction of oxygen, from the NO decomposition, with hydrocarbon fragments or from the dissociation of water. Very probably both occur to some extent.

Additional evidence that OH is formed by reaction of oxygen from the NO decomposition with various fuel fragments formed initially may be seen in Figure 6. All of the radicals except OH reach their maximum intensity at the same point in the primary reaction region. Only weak OH radiation is observed here. The OH radical appears in appreciable intensity just passed the maximum for the other emitters and reaches its maximum at approximately the point where the other emission is negligible.

Since OH is observed in the reaction zone of butane-air flames, it would appear that its radiative life time is short relative to the time required for the OH to traverse the flame front. Wolfhard and Parker[2] give evidence that radiation in hydrocarbon-NO_2 flames is thermal in nature. These observations indicate that the OH radical is formed at or near the point in the flame where the radiation is detected.

REFERENCES

1. Egerton, A. C., and Sen, D.: *Fourth Symposium (International) on Combustion*, p. 321. Baltimore, The Williams & Wilkins Co., 1953.
2. Wolfhard, H. G., and Parker, W. G.: *Fifth Symposium (International) on Combustion*, p. 718. New York, Reinhold Publ. Corp., 1955.
3. Miller, E., and Setzer, H.: *Sixth Symposium (International) on Combustion*, p. 164. New York, Reinhold Publ. Corp., 1957.
4. Verhoeck, F. H., and Daniels, F.: J. Am. Chem. Soc., 1250 (1934).
5. Wohl, K., and Welty, F.: *Fifth Symposium (International) on Combustion*, p. 746. New York, Reinhold Publ. Corp., 1955.

22

THE METHYL NITRITE DECOMPOSITION FLAME

By E. A. ARDEN and J. POWLING

Introduction

The combustion process of aliphatic nitric esters, including cordites, may be divided into two broad phases. In the first, decomposition of the ester takes place very rapidly but the reactions do not proceed to chemical equilibrium since most of the nitrogen content of the system remains as nitric oxide. After a time delay, the length of which depends on the pressure, reduction of the NO in the reaction products appears to take place in a second flame zone in which thermodynamic equilibrium is reached. Up to quite high combustion pressures (e.g., >1500 psi) this second phase of reaction is too remote from the burning surface of the ester to influence its rate of consumption and the latter is usually controlled almost entirely by the reactions in the first phase. For example at atmospheric pressure the secondary flame, involving final reduction of NO, is absent altogether yet stable flames of decomposing nitric esters (of sufficient energy) can still be obtained. In the case of ethyl nitrate[1] it has been shown by analyses of first-stage products that the greater part of the nitrogen content remains as NO and in the cooler flames of the propyl nitrates[2] products of the first-stage of reaction include major quantities of nitrites and nitro compounds in addition to NO. An important observation from these flames was that although the greater part of the NO remained unreduced at the end of the atmospheric pressure reaction, a limited amount was reduced to N_2 in every case and this reaction proceeded far more rapidly in the flame front than in the hotter and apparently equally reducing atmosphere of the products behind the flame front.

The low pressure, relatively low temperature reactions of NO are of prime importance in the combustion of nitric ester propellants: reduction of NO by organic molecules or hydrogen is usually a highly exothermic process, and the extent of such reactions occurring in the first, rate-controlling stage will be a major influence on the rate of burning.

It was recently discovered[3] that methyl nitrite will sustain a self decomposition flame at relatively low pressure (atmospheric) and the maximum temperature of this flame is too low for the thermal decomposition of nitric oxide. The energy released in the flame must, nevertheless, depend

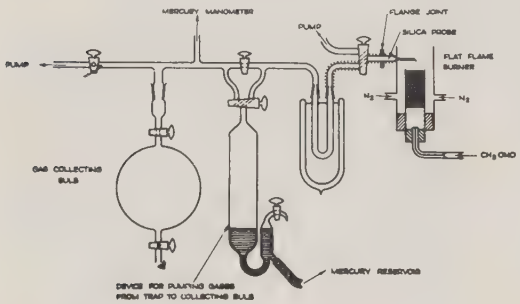

FIG. 1. Burner and sampling apparatus.

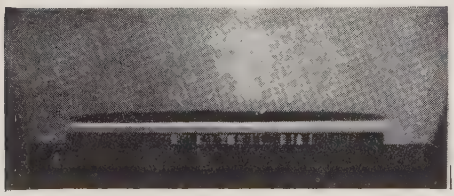

FIG. 2. Shadowgraph of the flame.

entirely on oxidation of organic fragments by NO. Certain unknown species are capable of reduction of NO with relative ease in this flame whereas in somewhat similar nitric ester flames, e.g., methyl nitrate,[4] the reaction is very limited. Therefore, in addition to being of considerable interest itself, the methyl nitrite flame provides a very valuable system for the study of the low pressure, low temperature, flame reactions of NO which are important in nitric ester propellant combustion. The simplicity of the reactant is of particular advantage in the study of the reactions taking place in complex combustion processes.

A fairly detailed analysis of the changes of temperature and of reaction products and intermediates has been made in the pure methyl nitrite decomposition flame.

Experimental

PREPARATION AND STORAGE OF METHYL NITRITE

Methyl nitrite is a gas at room temperature, condensing at −18°C to a yellow liquid. It was prepared from methanol, $NaNO_2$, and dilute H_2SO_4 by the method of Gray and Style,[5] and stored in a 2-liter metal cylinder at room temperature in a separate compartment away from the operator.

APPARATUS

The methyl nitrite flame was stabilized very easily at atmospheric pressure in a flat flame burner[6] 3.8 cm in diameter. A diagram of the burner and the sampling system is shown in Figure 1. The flame was almost invisible and was detected using a shadow technique; Figure 2 shows a shadowgraph of the flame. Measurements of chemical composition and temperature of the flame were made at intervals through the flame.

Samples of the burning gas were withdrawn slowly (~300 cc in 5–10 min) from the flame by means of a fine silica probe and frozen rapidly in a liquid nitrogen trap.

IDENTIFICATION AND ANALYSIS OF THE PRODUCTS OF COMBUSTION

The products were identified by their infrared spectra, and complete quantitative analyses of the samples collected were carried out. A gaseous fraction was analyzed by chemical and infrared methods. A vapor and a liquid fraction were estimated by infrared measurements alone, the infrared cell being maintained at 120°C, if necessary. Water could not be analyzed satisfactorily in the vapor phase by the infrared method but it could be estimated directly by the Fischer titration method, since none of the other substances present in the liquid were found to interfere with the reaction.

FLAME TEMPERATURE MEASUREMENTS

Measurements of flame temperature were made with a platinum/platinum–10 per cent rhodium thermocouple, covered with a thin coating of Pyrex glass and stretched horizontally through the flame. The over-all thickness of the thermocouples was not greater than 0.3 mm. The inflection in the temperature distribution curve (Fig. 4, at 1 mm) is thought to be real since there is supporting evidence from shadow photographs

of the flame (Fig. 2) which reveal a second shadow above the first. Smooth curves are obtained on each individual determination of the temperature distribution but the actual values of the maximum temperature showed some variation (Fig. 4) presumably because of changes in heat lost from the burner due to variation of external conditions.

FLAME PROPAGATION TESTS

The ability of certain gas mixtures, containing CH_3ONO, NO, etc., to propagate flame was tested in a vertical glass cylinder about 5 cm i.d. and 25 cm long. A hot wire igniting coil was located towards the lower end of the tube and the latter was closed at the bottom by a wide pressure release valve, set to operate at 1 atmos (abs). The whole tube and the evacuating, filling and sampling leads were electrically heated to permit the testing of less volatile fuels (e.g., formaldehyde). A diagram of the apparatus is shown in Figure 3.

BURNING VELOCITY

The burning velocity of the methyl nitrite flame relative to the vapor at 200°C, the steady degree of preheat in burner used, was found to be 7.5 cm/sec.

Results and Discussion

The course of events taking place in the flame, as far as it is revealed by the changes in chemical composition of its (more stable) ingredients and in its temperature, is shown in Figure 4; the temperature distribution is given in the upper part of the graph and the quantitative combustion product distribution on the same distance scale below. The number of moles of the nitrite required to give the amounts of products shown in Figure 4 is estimated from the mean of a carbon and a nitrogen balance, both of which seem fairly reliable.

The main events in the flame may be briefly summarized as follows: the methyl nitrite vapor, heated to about 160 to 200°C by radiation via the burner matrix, enters the flame zone and decomposition appears to be complete before the inflection in the temperature curve, i.e., below 700°C. The over-all reaction in this first stage is almost quantitatively according to Reaction (1) which is approximately thermoneutral. (The thermochemical data used is mostly that given by Gray[3]).

$$CH_3ONO \rightarrow \tfrac{1}{2}\ CH_3OH + \tfrac{1}{2}\ CH_2O + NO - 1\ \text{kcal} \qquad (1)$$

Exothermic reaction then proceeds between the

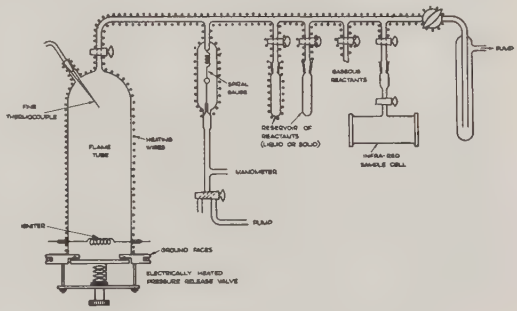

FIG. 3. Diagram of apparatus.

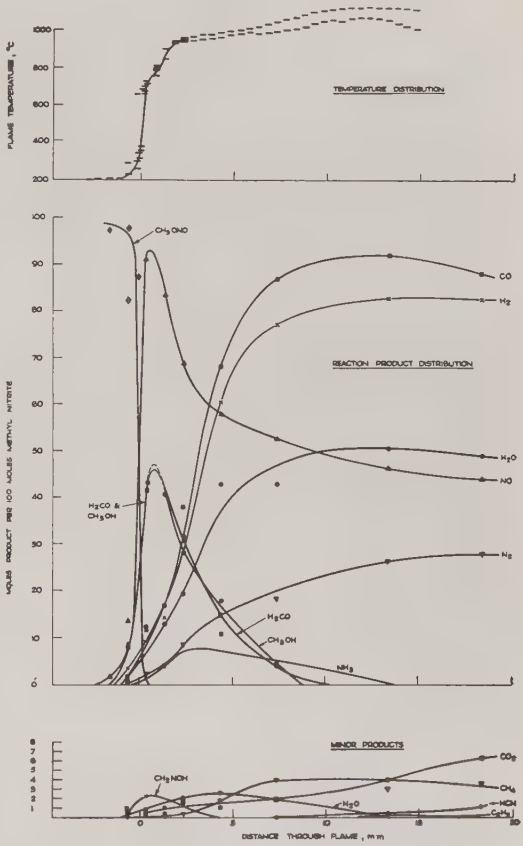

FIG. 4. Temperature and product distribution in methyl nitrite flame.

NO and the other products of Reaction (1) or their degradation products, to give water and nitrogen. This reaction does not continue after the degradation of the methanol and the formaldehyde to CO and H_2, which is complete about 9

mm from the flame front, and approximately ½ of the NO remains unreduced in the final gases at about 1100°C. The reactions consuming the nitrous ester could be:

$$CH_3ONO \rightarrow CH_3O\cdot + NO - \sim 38 \text{ kcal} \quad (2)$$

$$CH_3O\cdot + CH_3ONO \rightarrow CH_3OH + CH_2O + NO - \sim 37 \text{ kcal} \quad (3)$$

Reaction (2) is considered to be the initial step in the thermal decomposition of methyl nitrite[7], but the subsequent steps in the reactions of the products of Reaction (2) are still uncertain. Steacie and Shaw[7] have suggested Reactions (4) and (5) below to account for the main products.

$$CH_3O\cdot \rightarrow CH_2O + H\cdot - \sim 25 \text{ kcal} \quad (4)$$

$$H\cdot + CH_3O\cdot \rightarrow CH_3OH + \sim 100 \text{ kcal} \quad (5)$$

Reaction (5) would seem unlikely as a major reaction in flames. Rice and Rodowskas,[9] for ethyl nitrite, suggest another nonchain radical process in which the nitrous ester itself is attacked by radicals. The analogous sequence of reactions for methyl nitrite would be (2), (3) and (4) and in addition the Reaction (6).

$$H\cdot + CH_3ONO \rightarrow H_2 + CH_2O + NO + 41 \text{ kcal} \quad (6)$$

In this work there is evidence that Reaction (6) does not take place to any appreciable extent since the amount of hydrogen found when all the nitrite has disappeared is quite small and this small amount is in any case probably formed from the decomposition of H_2CO and CH_3OH (Fig. 4). Although Reaction (3) would seem the most feasible step to follow Reaction (2) it, has been assumed by Gray and Style[5] to be unimportant in the photodecomposition of methyl nitrite and the analogous reaction in the ethyl nitrite decomposition (Reaction (7)) has been discounted by Levy.[10]

$$CH_3CH_2O\cdot + CH_3CH_2ONO \rightarrow CH_3CH_2OH + [CH_3CHONO] \quad (7)$$

The presence of major quantities of N_2O was reported in the work of Gray and Style[5] and of Levy,[10] and to explain this, Reaction (2) and (3) alone were, of course, inadequate. Gray and Style suggested that hydrogen atoms were produced in Reaction (4) and some combined with NO to give HNO. The HNO produced N_2O according to

$$2HNO \rightarrow N_2O + H_2O + \sim 88 \text{ kcal} \quad (8)$$

A similar source of N_2O was suggested by Levy who considered NOH to be the result of reaction between ethoxy radicals and NO:

$$CH_3H_2O\cdot + NO \rightarrow NOH + CH_3CHO \quad (9)$$

The NOH degenerated to N_2O and H_2O and perhaps also to NO, N_2 and H_2O. In the flame decomposition reported here, N_2O is observed to be only a very minor product, especially at the end of the first stage, namely when all the nitrite has decomposed almost quantitatively to CH_3OH, CH_2O and NO. To account for the final products of the first stage of the flame decomposition, reactions similar to (8) and (9) are therefore not necessary but it is possible that N_2O is an intermediate in the formation of N_2 in the *later* stages of the flame. Further evidence is required to decide whether Reaction (3) alone follows (2) to give the first stage products. A more complex route, starting with Reaction (4) may take place at the higher temperatures in the flame front. Useful information on this matter is provided by the effects observed when NO is added to the flame; this is discussed later.

The NO formed in the flame front is reduced in what will be termed here the second stage of the flame; that is, the phase of reaction which takes place in the products of the initial decomposition (beyond 0.5 mm, Fig. 4). The only reactants in major quantities at the beginning of the second stage are, as already stated, NO, CH_3OH and H_2CO which make up 42 per cent, 19 per cent and 20 per cent by volume respectively, of the gases. The exothermic reactions which maintain flame propagation in methyl nitrite must take place in these ingredients and it is observed that reduction of NO ceases when all the CH_3OH and the H_2CO has disappeared. This observation immediately presents an interesting problem because in the isopropyl nitrate flame,[2] these three ingredients are present in roughly the same proportions, yet extensive reduction of NO does not take place. The differences between the two systems are that, firstly, in the isopropyl nitrate flame numerous other ingredients are present as well and that, secondly, the maximum temperature is only about 450°C so that the CH_3OH and H_2CO are not decomposing very rapidly. The two more obvious suggestions for absence of reaction of NO are either that the active species, which is produced in the CH_3OH/H_2CO system and attacks NO, is more readily consumed by the other ingredients of the isopropyl nitrate flame or that it is not produced sufficiently rapidly at temperatures up to 450°C.

It would be reasonable to suggest that hydrogen atoms, produced in the high temperature decomposition of CH_3OH or H_2CO, might be responsible for the reduction of NO. The reaction between H· and NO has been considered by various authors without positive conclusion. For instance, Hinshelwood[11, 12] concluded that hydrogen atoms do not take part in the thermal reaction between NO and H_2 at 1000°K, whereas Taylor and Tanford[13] suggest that they are responsible for the reduction of NO according to the following reactions:

$$H\cdot + NO \rightarrow HNO \quad (10)$$

$$2HNO \rightarrow N_2O + H_2O \quad (8)$$

$$N_2O + H\cdot \rightarrow N_2 + \cdot OH + 62 \text{ kcal} \quad (11)$$

$$H\cdot + HNO \rightarrow H_2 + NO\cdot + \sim 55 \text{ kcal} \quad (12)$$

Adams, Parker, and Wolfhard[14] do not favor Reactions such as (10) and (8) as steps in the high temperature flame of NO and H_2. There is good evidence, however, that NO reacts readily with hydrogen atoms, at least at low temperature, to give HNO,[15] and the reaction with hydrocarbon free radicals is well known if little understood.

In the explosion of methyl nitrite vapor in the glass cylinder at a constant pressure of 1 atmos, it was found that the addition of NO to the nitrite increased the vigor of the explosion. This seems a rather remarkable fact when it is remembered that about 50 per cent of the NO produced by the pure nitrite remains unchanged in the final flame gases. Also, the dilution limit of inflammability of CH_3ONO in NO is very much lower than that of CH_3ONO in N_2. All mixtures of more than 17.6 per cent (vol.) CH_3ONO in NO are, in fact, capable of propagating flame at atmospheric pressure whereas the dilution limit of CH_3ONO in N_2 is 42.8 per cent. Dilution of CH_3ONO with four times its volume of NO does not result in complete oxidation of the flame reaction products. Preliminary infrared analyses of the products of such a mixture show that (1) most of the NO remains unchanged; (2) less CO and CO_2 are formed from the nitrite than in the absence of added NO; (3) CO remains a major ingredient of the final flame gases in spite of excess oxidant; (4) the amount of N_2O is increased considerably; and (5) there appears to be little, if any, methanol formed. The inhibition of the formation of CH_3OH when NO is added to the nitrite is particularly significant and has been verified by stabilizing flame of NO/CH_3ONO in the flat flame burner and extracting samples of the product at known distances from the flame front as for the pure nitrite. Table 1 compares the amounts of products (per 100 mol CH_3ONO) from a flame in pure CH_3ONO with those from a flame in 62 per cent NO/38 per cent CH_3ONO. The samples were extracted from both flames at 0.3 mm and 2.3 mm. It is seen that considerably more NO has been reduced to N_2 in the NO-diluted system and H_2O is the main over-all oxidation product of the reaction. The amount of H_2CO is little changed in contrast to the CH_3OH which is much reduced. Such changes might well be the result of a reaction such as Reaction (13) taking place in excess of NO, followed by the degeneration of HNO formed. The flame is not the usual lower limit flame in which the deficient fuel is oxidized completely as is the case when CH_3ONO is diluted with N_2O or air. In these latter cases, lower limit figures of ~5.1 per cent and ~3.6 per cent are obtained and oxidation is complete.

Table 1. Moles of Reaction Product Derived from Mixture Containing 100 Moles CH_3ONO

(Samples taken at distances of 0.3 and 2.3 mm)

Product	100% CH_3ONO		38% CH_3ONO 62% NO	
	0.3	2.3	0.3	2.3
CH_3ONO	0	0	42.9	13.5
NO	91.3	68.8	171	170
CH_3OH	41.6	28.3	9.2	3.5
H_2CO	43.2	38.0	25.2	32.2
H_2	9.0	30.5	19.8	47.1
CO	11.8	31.6	18.8	41.5
CO_2	0.4	1.7	1.0	1.7
H_2O	12.4	19.5	23.8	46.0
N_2	2.2	8.6	17.4	41.5
N_2O	0.8	2.1	4.9	5.2
CH_2:NOH	2.2	1.3	1.0	0.7
CH_4	0.1	0.4	0	0.7
NH_3	1.6	7.6	4.0	8.6
HCOOH	—	—	1.9	5.5

Under conditions in which CH_3ONO will ignite and propagate flame freely, it has been found impossible to ignite a gas mixture of 2 mol NO, 1 mol H_2CO and 1 mol CH_3OH. This is rather remarkable because CH_3ONO breaks down, thermoneutrally, to these products in the first stage of the flame. Gray[16] has observed pre-ignition glows, which he associates with presence of alkoxy radicals, in the thermal decomposition of CH_3ONO but was unable to see them in the above mixture

of NO, H_2CO and CH_3OH at 300–420°C, nor was reaction detected in the latter.

An inference from these experiments with nitric oxide-diluted CH_3ONO is that NO reacts with the early intermediates of the CH_3ONO breakdown which, in the absence of large amounts of NO would react rapidly with CH_3ONO. The most likely possibilities for such intermediates would seem to be $CH_3O\cdot$ from Reaction (2), or $H\cdot$ from Reaction (2) plus (4), especially since addition of NO to the early stages of the flame inhibits the formation of CH_3OH. Reaction with $CH_3O\cdot$ could proceed according to Reaction (13) for example:

$$CH_3O\cdot + NO \rightarrow HNO + H_2CO + \sim 24 \text{ kcal} \quad (13)$$

It is less likely that $CH_3O\cdot$ is generated beyond about 0.5 mm (Fig. 4) yet in the pure methyl nitrite flame practically all the NO is reduced after this distance. It is not unreasonable to suppose, however, that hydrogen atoms are generated during the decomposition of the nitrite and also during the decomposition of H_2CO and CH_3OH and that if the NO concentration is sufficiently high the latter will be reduced by these atoms according to Reaction (10), before they are removed by reaction with other molecules. In the photolysis of methyl nitrite, Gray and Style have suggested that the CH_3O, produced in the first step of the degradation, breaks down further to give H_2CO and $H\cdot$ (Reaction (14)). Reaction (3) was apparently not adequate to describe the appearance of the CH_3OH and they suggested that it was formed in a reaction of $H\cdot$ with CH_3ONO (Reaction (15))

$$CH_3O\cdot \rightarrow CH_2O + H\cdot - 25 \text{ kcal} \quad (14)$$

$$H\cdot + CH_3ONO \rightarrow CH_3OH + NO + 62 \text{ kcal} \quad (15)$$

If Reaction (14) also occurs in the relatively high temperature flame decomposition of the nitrite, then the NO-reducing reactions could be essentially the same in both stages of the flame. J. H. Gray (reported by P. Gray[16]) has suggested that the formation of major quantities of N_2O and N_2 in the photolysis of methyl nitrite rather than NO as in thermal decomposition is due to the reduction of NO by hydrogen atoms, the latter being formed from $CH_3O\cdot$ in the early stages of decomposition by the excess energy of the irradiating light or, in later stages, by the photolysis of H_2CO. The high temperature of the CH_3ONO decomposition in the flame might also cause further decomposition of $CH_3O\cdot$ to CH_2O and $H\cdot$ but, although it is agreed that hydrogen atoms are produced in the photolysis of H_2CO and probably in the photolysis of CH_3OH, it is uncertain whether they would be involved in the high temperature thermal decomposition (see Steacie[17]). If they are produced from $CH_3O\cdot$ in the flame then they must be consumed, in the pure CH_3ONO flame, only by reactions giving CH_3OH such as (15) because of the almost quantitative yields of products according to the over-all Reaction (1). The analytical data show that only the hydrogen of the aldehyde and the alcohol is oxidized (to H_2O) by NO. The yield of CO from the CH_3OH and H_2CO decompositions is almost quantitative, only minor quantities of CO_2 being detected. It is interesting to note from Figure 4 that the rates of decomposition of both H_2CO and CH_3OH are the same in the flame over the temperature range ~750 to ~1000°C. This suggests that the two decompositions are linked by a common radical process; such a link could be a hydrogen atom. However, there is much evidence that NO reacts with many free radicals, and there are no more than indications from the experimental data here that hydrogen atoms are responsible for the reduction in the methyl nitrite flame.

Acknowledgment

The authors are grateful to Mr. J. Scrivener for assistance in part of the work.

REFERENCES

1. Needham, D. P., and Powling, J.: Proc. Roy. Soc., *A232*, 337 (1955).
2. Powling, J.: XIV International Congress of Pure and Applied Chemistry, Zurich, 1955.
3. Gray, P., Hall, A. R., and Wolfhard, H. G.: Proc. Roy. Soc., *A232*, 389 (1955).
4. Adams, G. K., and Scrivener, J.: Unpublished M.O.S. Report.
5. Gray, J. A., and Style, D. W. G.: Trans. Faraday Soc., *48*, 1137 (1952).
6. Powling, J., Fuel, *28* (*2*), 25 (1949).
7. Steacie, E. W. R., and Shaw, G. T.: Proc. Roy. Soc., *A146*, 388 (1934).
8. Steacie, E. W. R., and Calder, J.: Chem. Phys., *4*, 96 (1936).
9. Rice, F. O., and Rodowskas, E. L.: J. Am. Chem. Soc., *57*, 350 (1935).
10. Levy, J. B.: J. Am. Chem. Soc., *75*, 1801 (1953).
11. Hinshelwood, C. N., and Green, T. E.: J. Chem. Soc., 730 (1926).
12. Hinshelwood, C. N., and Mitchell, J. W.: J. Chem. Soc., 378 (1936).
13. Taylor, J. A., and Tanford, C.: J. Chem. Phys., *12*, 47 (1944).
14. Adams, G. K., Parker, W. G., and Wolf-

HARD, H. G.: Discuss. Faraday Soc., *14*, 97 (1953).
15. HARTECK, P.: Ber. deut. chem. Ges., *1366*, 423 (1933).
16. GRAY, P.: Proc. Roy. Soc., *A221*, 462 (1954).
17. STEACIE, E. W. R.: *Atomic and Free Radical Reactions*, Ed. 2, pp. 205, 215, 616. New York, Reinhold Publ. Corp., 1954.

23

REDUCTION OF NITRIC OXIDE IN FLAMES AND THE DECOMPOSITION FLAME OF METHYL NITRITE

By PETER GRAY AND M. W. T. PRATT

Introduction

The observation that, in general, nitric oxide is not readily reduced to nitrogen in a flame poses one of the serious present-day problems of combustion. Modern propellants are frequently based on oxygen compounds of nitrogen (e.g., mono-fuels such as nitroalkanes or nitrate esters, and bi-fuels such as kerosene-nitric acid mixtures). Propellants such as these are much more efficient if reduction of their nitrogen content takes place beyond nitric oxide. This usually requires elevated temperatures and pressures. In a flame such an effect is cumulative: the less the nitric oxide which reacts, the cooler is the flame; the cooler the flame, the less nitric oxide reacts.

A remarkable flame which depends for its existence on the reduction of nitric oxide is the decomposition flame of methyl nitrite, CH_3ONO, discovered by Gray, Hall and Wolfhard[1] in 1955. This flame is important not only for the extensive reactions of nitric oxide which occur in it, but also for its value in testing current theories of flame propagation.

The principal properties of the flame have been examined, and analysis made of the products of decomposition. The diffusion flames of methyl and ethyl nitrites with oxygen have also been examined.

Experimental and Results

PREPARATION OF METHYL AND ETHYL NITRITES

Ethyl nitrite was prepared as a pale yellow liquid (bp. 17°C) by adding aqueous sulfuric acid to a mixture of an excess of ethanol and a saturated solution of sodium nitrite. It was washed with caustic soda and water, and dried over anhydrous calcium chloride.

Methyl nitrite was made by the method of Gray and Style as described by Gray, Hall and Wolfhard.[1]

THE DECOMPOSITION FLAME OF METHYL NITRITE

When a stream of methyl nitrite vapor issuing from the mouth of an upright cylindrical glass tube a few cm in diameter is ignited, it burns in the air as a lambent diffusion flame, grayish-yellow in color. At the inner surface of the diffusion flame an orange-red zone forms as a cone at the mouth of the tube. If the flow rate of methyl nitrite vapor is reduced, this faint orange-red inner flame detaches itself from the outer diffusion flame and slowly descends the tube as a flat disk surmounted by a feeble conical afterglow of the same color, easily visible in a darkened room.[1] No oxygen is necessary for its propagation, and after it has entered the tube it is not affected if the diffusion flame at the mouth is extinguished. It is the decomposition flame of pure methyl nitrite, shown diagrammatically in Figure 1. Downstream of the decomposition flame a white, polymeric deposit smelling strongly of formaldehyde forms on the walls of the tube. Where this becomes strongly heated it decomposes and chars to a brown resinous material.

PROPERTIES OF THE DECOMPOSITION FLAME OF METHYL NITRITE

1. Quenching diameter

The decomposition flame of methyl nitrite will still burn steadily in a Pyrex tube having an internal diameter of only 0.7 cm. The flame can just be seen in a darkened room as a luminous red dot in the center of the tube. On extinction of the upper diffusion flame, the decomposition

flame continues to burn, often rising slowly up the tube. (This rising is probably because the burning velocity of the flame decreases when the tube walls are no longer warmed by the diffusion flame.) When the decomposition flame has risen

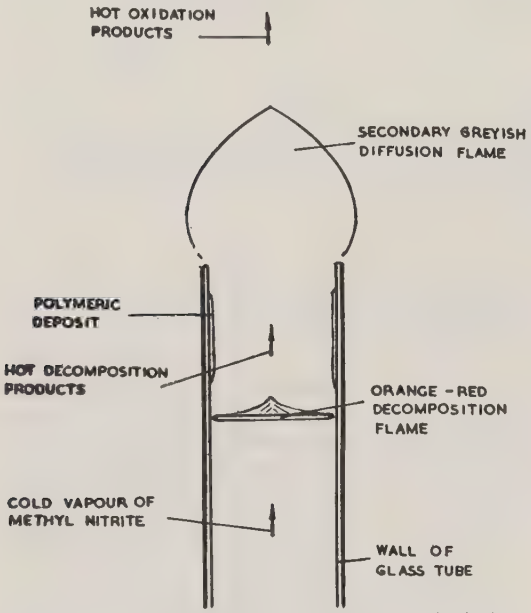

FIG. 1. Combustion of gaseous methyl nitrite. Primary decomposition flame of pure methyl nitrite burning in complete absence of air, followed by secondary diffusion flame in air.

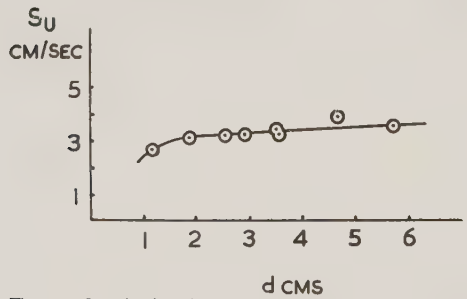

FIG. 2. Variation in the burning velocity (S_u cm sec^{-1}) with the tube diameter (d. cm) for the methyl nitrite decomposition flame burning inside a cylindrical tube. Temperature of the unburned gas 18°C.

to within a few mm of the top of the tube, the diffusion flame re-ignites. In still smaller tubes, of 0.65 and 0.53 cm diameter, although the decomposition flame is no longer visible, the re-ignition of the diffusion flame several seconds after it has been extinguished indicates that an extremely feeble decomposition flame is still propagated even in these narrow tubes.

2. Effect of tube diameter upon burning velocity

The burning velocity relative to the unburned gas, S_u, has been measured in a series of upright cylindrical Pyrex glass tubes of various diameters.

In tubes of diameter between 2 and 4 cm the decomposition flame appears to be perfectly flat and apparently equal in area to the cross-section of the tube and its burning velocity is calculated on that assumption. Thus, if A is the internal area (cm^2) of the burning tube and Q the volume flow rate of unburned vapor in ml sec^{-1} necessary to maintain a stationary flame, then $Q = S_u A$ or $S_u = Q/A$. The flame shrinks away from the walls in tubes narrower than 1.5 cm diameter. A capillary flow meter, calibrated against a soap film meter, was used to give a quickly read measurement of volume rate of flow.

It is impracticable to maintain an absolutely constant rate of flow of methyl nitrite vapor through the burning tube for a long period of time, so in each tube the rate of rise or fall of the flame inside the tube was compared every few seconds with the flow rate. By interpolation the rate of flow necessary to maintain an exactly stationary flame is found.

As shown in Figure 2, S_u varies only very slowly with the tube diameter, d, over a large fraction of the tube diameter range studied.

3. Influence of initial temperature of vapor on flame speed

To determine the dependence of linear flame speed, S_u, upon the temperature, t°C, of the unburned gas, the methyl nitrite vapor was preheated by passage through an electrically heated burning tube of internal diameter 2.56 cm. Temperatures of the unburned gas were measured by a chromel-alumel thermocouple inside the burning tube and a few cm below the decomposition flame. The burning velocity was determined as before. The graph of S_u against t°C is shown in Figure 3. Values of S_u are corrected for expansion of the vapor during preheating, and refer to the rate of flame propagation relative to the unburned preheated gas.

When the temperature of the preheated unburned gas is much above 120°C the flame flickers considerably, accurate measurements consequently becoming very difficult to make. At temperatures above 175°C, but not below, the decomposition flame will burn steadily down the whole length of the burning tube when the supply of methyl nitrite is suddenly cut off. At 240°C and

higher temperatures no decomposition flame can be obtained.

The fact that temperatures above 175°C are necessary for the flame to burn steadily down the tube when the vapor flow is stopped suggests that heating of the walls either by the decomposition flame or by the diffusion flame is important in determining the quenching distances reported in Section 1.

4. *Value of the final flame temperature*

Uncoated chromel-alumel thermocouples (of different sizes) were used to give an estimate of the temperature of the decomposition flame. It was found to be 1100°C. This crude value which may be subject to errors due to radiation losses and surface catalysis is close to that of 1080°C calculated (*vide infra*) from product analyses neglecting any heat losses.

CHEMICAL ANALYSIS OF THE PRODUCTS OF THE DECOMPOSITION FLAME

Qualitative analysis showed the following compounds to be present among the products of the decomposition flame: carbon monoxide, hydrogen, water, methanol, nitric and nitrous oxides, nitrogen, formaldehyde and its polymer, formaldoxime and hexamethylene tetramine ($C_6H_{12}N_4$). No significant amounts of other products have been found. Table 1, column 1 lists the amounts of these products found experimentally per hundred moles of methyl nitrite burned, together with the resulting element balance. To obtain a stoichiometrically balanced equation for the over-all reaction the mole numbers listed in column 2 have been adopted. Very little adjustment to the experimental values is necessary for this.

A flow system was used to simplify the analytical problems by providing large amounts of products. The flame was usually burned for about an hour. After drying and metering, the methyl nitrite was burned at the mouth of a jacketed glass tube. A duct, heated in order to prevent condensation near the flame itself, led the products from the flame into a train of five traps, in which products of different volatility could be separated by fractional condensation. The first two traps were maintained at 0°C; the last three traps at liquid oxygen or solid carbon dioxide temperatures. The uncondensed gaseous residue was metered before discharge.

For analysis, products were divided into the following groups: solid residues and the fraction condensing in the traps at 0° to −78°C; those uncondensed at −78°C; and those uncondensed at −170°C.

The methyl nitrite container plus contents were weighed before ignition and after extinction of the flame.

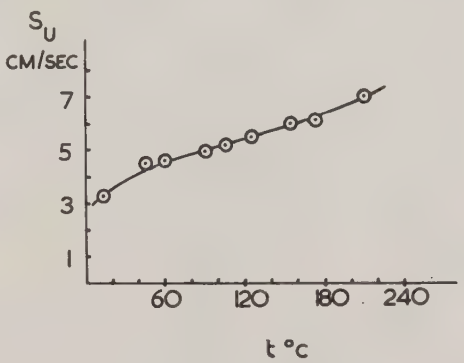

FIG. 3. Variation in the burning velocity (S_u cm sec^{-1}) with the temperature (t°C) of the preheated unburned gas for the methyl nitrite decomposition flame burning in a tube 2.56 cm in diameter. S_u is measured relative to the hot unburned gas.

TABLE 1. PRODUCTS OF THE DECOMPOSITION FLAME OF METHYL NITRITE TOGETHER WITH ELEMENT BALANCES FOUND EXPERIMENTALLY, AND ADJUSTED PRODUCT YIELDS TO GIVE A STOICHIOMETRIC BALANCE

Units are moles per 100 moles of methyl nitrite burned

Product	Moles Found Experimentally	Adjusted Yield to Give Stoichiometric Balance
CO	84	77
H_2	59	64
H_2O	51	51
NO	35	34
N_2O	26	24
CH_3OH	11	11
N_2	5	5
CH_2NOH	2	2
$C_6H_{12}N_4$	1.5	1.5
CH_2O	1	1
Element Balance		
C	107	100
H	289	300
O	210	200
N	105	100

1. *Products uncondensed at liquid air temperatures* (CO, H_2, N_2)

Of the products listed above, CO, H_2 and N_2 do not condense in traps cooled with liquid air. To determine each of these in terms of moles per

mole CH_3ONO burned, two measurements are necessary: (1) determination of total number of moles of this gaseous mixture formed per mole CH_3ONO burned; (2) determination of percentage composition of the mixture.

The first determination is made very simply by measuring flow rates before and after condensation: number of moles $CO + H_2 + N_2$ formed/number of moles CH_3ONO burned = volume flow rate of non condensables/volume flow rate of $CH_3ONO = 1.50$. The percentage composition was found in a conventional gas analysis apparatus.

2. Products condensed at liquid air temperatures but volatile at −78°C (N_2O, NO)

After passing through three traps kept at approximately −78°C by solid carbon dioxide, there were 2.12 moles/mole uncondensed products. Samples of this colorless gas were analyzed for CO_2 and NO by measuring in a gas burette the absorption in caustic soda and ferrous sulfate solution respectively. The amount of CO_2 present was negligible.

The only other product condensed by liquid oxygen but not by solid carbon dioxide was N_2O, and its yield was derived in two ways: (1) from the difference in the uncondensed product ratio in the two cases and (2) by an independent infrared absorption of the gaseous products not condensed at −78°C.

3. Products condensed at −78°C (CH_2O *and* $(CH_2O)_n$; CH_3OH; H_2O; $C_6H_{12}N_4$; CH_2NOH).

The greater part of these condensable products (16 g per mole, 61 g, of methyl nitrite burned) was always trapped as a colorless liquid in the first two traps although these were cooled only by ice. The products were separated by vacuum distillation into a liquid and a white solid residue.

The *liquid* consisted of *water* and *methanol* which were easily separated by fractional distillation and weighed (first fraction, methanol, bp. 64.7°C/760 mm, R.I. 1.33/15°C; second fraction, water, bp. 100°C/760 mm, R.I. 1.33/15°C).

The *solid residue* in the traps combined with the white solid condensed in the duct represented only 5 per cent by weight of the total products. It was examined chemically and by infrared spectroscopy and consisted largely of *hexamethylene-tetramine*, $C_6H_{12}N_4$, together with *paraformaldehyde*, $(CH_2O)_n$, and *formaldoxine*, CH_2NOH. Quantitative element analysis of the solid gave (w/w per cent) carbon 44.0, hydrogen 7.55, nitrogen 34.4, oxygen (by difference) 14.0. Simple mole ratios of the above products satisfying this analysis and used in the stoichiometric equation in Table 1 are hexamethylene tetramine 1.5 (64 w/w per cent): CH_2NOH 2 (27 per cent): CH_2O 1 (9 per cent). These correspond to the weight percentages carbon 43.6, hydrogen 7.9, nitrogen 33.9, oxygen 14.6, in good agreement with experimental figures above.

EXOTHERMICITY ($-\Delta H$) OF THE OVER-ALL FLAME REACTION

The reactions occurring in the flame may be represented by the stoichiometric equation:

$$\begin{aligned} CH_3ONO \rightarrow\ & 0.77\ CO + 0.64\ H_2 + 0.42\ H_2O\ (g) \\ & + 0.34\ NO + 0.24\ N_2O + 0.05\ N_2 \\ & + 0.11\ CH_3OH\ (g) + 0.10\ CH_2O\ (g) \\ & + 0.06\ NH_3 + 0.02\ CH_2NOH \qquad (1) \end{aligned}$$

In Equation (1) gaseous formaldehyde and gaseous ammonia replace the solid hexamethylene tetramine actually isolated by the analytical techniques used, since it is probable that the hexamethylene tetramine is not formed until well after the main reaction zone and contributes nothing to the heat of the flame:

$$6CH_2O + 4NH_3 \rightarrow C_6H_{12}N_4 + 6H_2O$$

Recent thermochemical data[2, 3] have been used to derive the enthalpy increase corresponding to Equation (1). It is $\Delta H = -26.4$ kcal mole^{-1}. Even if hexamethylene tetramine formation is allowed for, ΔH is altered by less than 2.5 kcal mole^{-1}.

SPECTROSCOPIC EXAMINATION OF THE DECOMPOSITION FLAME OF METHYL NITRITE

The decomposition flame of methyl nitrite burning inside a glass tube is too feeble for convenient spectrographic study. To permit a larger flat flame to be maintained a sintered disk burner was used. On this, large flat flames identical in appearance with the methyl nitrite decomposition flame could be burned provided a small amount (0.1 mole/mole CH_3ONO) of oxygen was added. Spectrographic analysis of such a flame using the methods described by Gray, Hall and Wolfhard[1] revealed two important features: (1) pyrolysis was extensive before the luminous zone was

reached, (2) the nitric oxide was formed before the luminous zone, and only partially consumed during it.

THE DECOMPOSITION FLAME OF ETHYL NITRITE

Ethyl nitrite was burned in a vertical glass tube as before. On reducing the flow, the diffusion flame became saddle-shaped but no flame could be seen to descend the tube. However, when the experiment was repeated in a darkened room a definite white smoke-like ring was seen to descend into the tube, only to disappear after a few seconds.

In his work on the ethyl nitrate decomposition flame Wolfhard[4] reported that the first reaction zone of the flame was invisible in daylight, but just visible in the dark, when it was seen to have a gray color. Its passage was sometimes observed just as a cloud of smoke moving up the combustion tube, the smoke-ring being formed by condensation of formaldehyde behind the flame front.

The similarity of the phenomenon described by Wolfhard to that observed during the burning of ethyl nitrite suggests that ethyl nitrite may also possess a decomposition flame. The "smoke-ring" in this case would soon vanish, condensation of formaldehyde against the tube walls ceasing when the walls become heated.

THE DIFFUSION FLAME OF METHYL NITRITE

The diffusion flame of methyl nitrite was examined in a burner invented by Parker and Wolfhard in which the fuel and oxygen passed up two adjacent rectangular tubes, surrounded by a shield through which a current of an inert gas was maintained. Figure 4 shows the nature of the flame obtained. On the oxygen-rich side is a bright yellow zone *L* and on the nitrite side an orange-red zone *N*. In the middle is the main reaction zone *M* which is blue in color.

Spectra of the flame in emission and absorption were obtained from a horizontal section across the flame 4 mm above the burner top. The absorption spectrum of methyl nitrite was detectable outside the zone *N*. The absorption spectrum of nitric oxide was found between the methyl nitrite region and the onset of zone *N*. Nitric oxide decreased in concentration, and its disappearance coincided with the onset of emission of CN and NH from the red zone *N*. From the hot main reaction zone continuous radiation was emitted and OH bands were seen. Towards the oxygen side the Schumann-Runge bands of oxygen were visible. The yellow zone *L* emitted only continuous radiation. No carbon was formed.

The flame may be represented diagrammatically by the scheme:

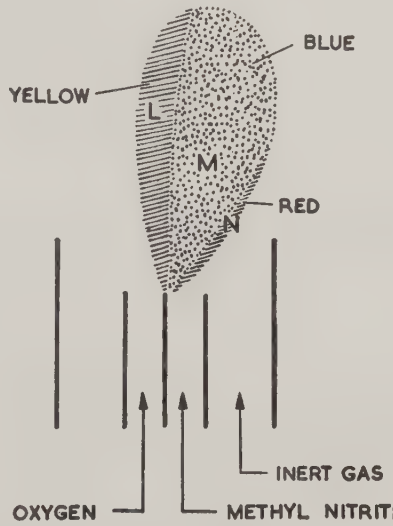

FIG. 4. Methyl nitrite diffusion flame with oxygen.

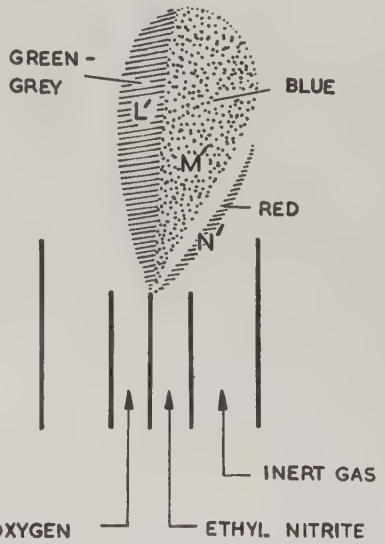

FIG. 5. Ethyl nitrite diffusion flame with oxygen.

	L	M	N	
Oxygen supply	Yellow continuum	Blue OH and continuum	Orange-red CN and NH	Methyl nitrite supply

THE DIFFUSION FLAME OF ETHYL NITRITE

The diffusion flame of ethyl nitrite was examined on the same burner, its appearance being as shown in Figure 5. On the oxygen side is a gray-green zone L' which merges into the hot middle zone M', blue in color. Between M' and the orange-red zone N' situated on the ethyl nitrite side is a definite dark space.

Diagrammatically the flame is:

	L′	M′		N′	
Oxygen supply	Green-gray	Blue	Dark space	Orange-red	Ethyl nitrite supply

Discussion

THE DECOMPOSITION FLAME OF METHYL NITRITE

The decomposition flame of methyl nitrite has a number of interesting properties. Its low burning velocity ($S_u \sim 3.2$ cm sec^{-1}) makes it one of the slowest flames known. Now in many systems a low burning velocity, S_u, is accompanied by a large quenching diameter, d_Q : often the product, $S_u d_Q$, is approximately constant, having a characteristic value for each particular flame system. Thus for oxygen-hydrocarbon-inert gas systems at 1 atmos, $S_u d_Q \sim 12$ cm^2 sec^{-1}; for hydrocarbon-nitric oxide flames $S_u d_Q \sim 30$ cm^2 sec^{-1}. However, although the methyl nitrite decomposition flame might be expected to belong to this latter class, for it the product $S_u d_Q \sim 3$ cm^2 sec^{-1} and the quenching diameter is less than 1 cm. It is possible, therefore, that the reactions occurring to support the flame are new in combustion experience; the small quenching diameter requires reactions occurring readily at relatively low temperatures.

The chemical analyses show very clearly the extent to which reaction has occurred, and although the details of reaction mechanism cannot yet be resolved a number of general statements may be made.

The initial step in thermal decomposition of the alkyl nitrites has been shown to be fission of the O—N bond, the weakest in the molecule, yielding nitric oxide and an alkoxy radical:

$$CH_3ONO \rightarrow CH_3O + NO$$

$$E \sim 37 \text{ kcal mole}^{-1} \quad (2)$$

According to Steacie and Shaw[6] thermal decomposition at 200°C ends with the formation of methanol, formaldehyde and nitric oxide, a reaction which is approximately thermoneutral:

$$CH_3ONO \rightarrow 0.5\ CH_3OH + 0.5\ CH_2O + NO$$

$$\Delta H \sim \text{zero} \quad (3)$$

In the flame, with a final temperature between 1000 and 1500°C, reaction is much more extensive than Equation (3). The most striking features are the reduction of a large part of the nitric oxide to nitrous oxide, nitrogen and even ammonia and the ultimate survival of very little formaldehyde.

Formaldehyde, if formed in the early stages of reaction, probably undergoes pyrolysis in the subsequent higher temperatures. The small amount which escapes may have passed through the cool rim of the flame close to the tube wall. It is thought that the hexamethylene tetramine formed originates in a similar way, *viz.*, that some of the formaldehyde which escapes pyrolysis is attacked by ammonia from the flame reactions. The traces of carbon dioxide present may arise in part from the water gas reaction between CO and H_2O; the ratio $(P_{CO_2}P_{H_2}/P_{CO}P_{H_2O})$ is very much less than corresponds to thermal equilibrium at the temperature of the flame.

However, despite the extent which decomposition has reached, the survival of a considerable proportion of methanol (accounting for about 10% of the carbon balance) does suggest that the initiation reaction in Equation (2) is still of importance, since it is difficult to devise an alternative precursor to methanol. If the suggestion in Equation (1) is true, that the processes in the red zone, N, of the nitrite-oxygen diffusion flame are substantially the same as in the nitrite decomposition flame then the spectroscopic evidence is that reaction with organic fragments (other than CO and H_2) is contributing to the removal of NO, leaving three plausible species as the active agent: methanol, formaldehyde or the methoxy radical. So far our attempts to ignite methanol-formaldehyde-nitric oxide mixtures have not been successful[7] and we favor an interpretation in terms of direct NO—CH_3O reaction. This, together with the question of water formation represent the chief remaining problems of this system.

The reaction corresponding to Equation (1) implies an adiabatic flame temperature of 1080°C.

The effect of initial temperature observed in the experiments with preheated methyl nitrite is remarkable. No decomposition flame occurred when the vapor was preheated to 240°C or above.

When the vapor is preheated, some decomposition occurs well before the flame is reached to yield products which are at least unable to take part in the self-sustaining reactions of the flame, or even able to impede them. The half life of methyl nitrite at 240°C is[6] 170 sec; its residence time in the heated tube is about 7 sec, i.e., enough for only 2 to 3 per cent decomposition. However, this is apparently able to extinguish the flame.

At lower temperatures the linear rate of burning relative to the preheated gas increases with increasing temperature. The increase (Fig. 3) is approximately proportional to the absolute temperature, so that the mass rate of burning is virtually unaltered.

A self-decomposition flame, such as that of methyl nitrite, is a very convenient system in which to test theories of flame propagation. No substances are involved other than the decomposing material itself, so that the system is more simple chemically than one in which mixtures are burned.

The thermal theory of flame propagation, developed by Zeldovich, Frank-Kamenetskii and Semenov[8] leads, for a first-order reaction, to the relation:

$$S_u^2 = (2\lambda^*\rho b/\rho_u^2 L)(1/[T_b - T_u]) \\ (RT_b^2/E)^2 \cdot A e^{-E/RT_b} \qquad (4)$$

In the case of the methyl nitrite decomposition flame represented by Equation (1), L, the heat of combustion, is taken as 432 cal per g; T_b and T_u, the temperatures of the burned and unburned gases as 1350° and 290°K respectively. Values of ρ_b and ρ_u, the densities of the burned and unburned gases, and λ^*, the mean thermal conductivity (cal cm^{-1} sec^{-1} $°C^{-1}$) of the burned gases were calculated.

If A and E, the frequency factor and activation energy of the flame reaction, have the values given by Steacie and Shaw[6] for the thermal decomposition, *viz.*, $A = 1.84 \times 10^{13}$ sec^{-1} and $E =$ 36,400 cal, then Equation (4) leads to $S_u = 120$ cm sec^{-1}.

The difference between this figure and the experimental value $S_u \sim 3.2$ cm sec^{-1}, together with the differences found by chemical analysis between the products of the flame and slow decomposition suggest that the initial step, Equation (2) does not control the rate of the decomposition flame.

THE DIFFUSION FLAMES

The diffusion flames of methyl and ethyl nitrites with oxygen have complex structures, each consisting of several sharply differentiated and clearly defined reaction zones.

The main reaction zone, M, blue in color, is situated in the middle of the flame. Most of the heat releasing reactions occur in this zone and it is intensely hot, its high temperature being shown by the strong OH band emission which it gives out. On the fuel side, an important point which the spectrographic evidence has brought out is that nearly all the methyl nitrite undergoes pyrolysis to nitric oxide and organic fragments before the first luminous reaction zone N is reached. From this zone emission due to NH and CN is obtained.

The work of Wolfhard, Parker, and Gaydon[5] has proved that generally emission of CN and NH bands is characteristic of the oxidation of nitrogen oxides by organic fragments (i.e., species other than H_2 or CO).

The first luminous reaction zone, N, of the diffusion flame, orange-red in color, has a strikingly similar appearance to the decomposition flame of pure methyl nitrite, burning either alone inside a tube or mixed with a little oxygen, on the sintered disk burner. It is probable that the reactions taking place in this first zone of the diffusion flame are closely related to those occurring in the decomposition flame.

The diffusion flame of ethyl nitrite shows the same general features as that of methyl nitrite. The same complex structure of well-differentiated reaction zones is observed. An interesting point of difference is that for this flame a dark space separates the initial and the main reaction zones.

Acknowledgments

We thank Dr. A. R. Hall of the Royal Aircraft Establishment, Westcott, and Dr. H. G. Wolfhard of the U. S. Bureau of Mines, Pittsburgh, for their comments and for their help with spectroscopic experiments, and Dr. J. C. Lee of Cambridge for valuable discussions. We also thank the D. S. I. R. for a grant to M. W. T. Pratt.

REFERENCES

1. Gray, P., Hall, A. R., and Wolfhard, H. G.: Proc. Roy. Soc. (London), *A232*, 389 (1955).
2. *Selected Values of Chemical Thermodynamic Properties*. National Bureau of Standards

Circular 500, U. S. Dept. of Commerce, Washington, D. C., 1952.
3. Baldrey, J. A., Lotzgesell, J. A., and Style, D. W. G.: Private communication.
4. Wolfhard, H. G.: Fuel, *34*, 60 (1955).
5. Wolfhard, H. G., and Parker, W. G.: *Fifth Symposium (International) on Combustion*, p. 718. New York, Reinhold Publ. Corp., 1955; Parker, W. G., and Wolfhard, H. G.: *Fourth Symposium (International) on Combustion*, p. 420. Baltimore, The Williams & Wilkins Co., 1953; Gaydon, A. G., and Wolfhard, H. G.: *Flames: Their Structure, Radiation and Temperature*. London, Chapman and Hall, Ltd., 1953.
6. Steacie, E. W. R., and Shaw, G. T.: Proc. Roy. Soc. (London), *A146*, 388 (1934).
7. Gray, P.: Proc. Roy. Soc. (London), *A221*, 462 (1954).
8. Zeldovich, Y. B., and Frank-Kamenetskii, D. A.: Acta Physicochim. U.R.S.S., *9*, 341 (1938). Semenov, N. N.: Prog. Phys. Sci. U.S.S.R., *24*, 433 (1940). Translated as N.A.C.A. Technical memo. 1026.

24

MULTIPLE REACTION ZONES IN LOW PRESSURE FLAMES WITH ETHYL AND METHYL NITRATE, METHYL NITRITE AND NITROMETHANE

By A. R. HALL and H. G. WOLFHARD

Introduction

Methyl nitrate and ethyl nitrate will burn at low pressure without the addition of an oxidizer. Whereas the decomposition flame of ethyl nitrate has only one faintly luminous reaction zone,[1] methyl nitrate has two distinctly separated zones of different color, the first zone emitting formaldehyde bands and the second continuous light in the visible.[2] On adding oxygen to these decomposition flames a multitude of phenomena occur which are described in this paper. Methyl nitrite and nitromethane, although not able to form a decomposition flame at low pressure, burn readily with oxygen and at low pressures form up to three separate reaction zones. The spectrum and condition for formation of each of these zones are recorded in this paper and the data are used to derive some tentative reaction schemes for the nitrobodies under consideration.

Experimental

The methyl nitrate, methyl nitrite and nitric oxide used were prepared as previously described[2] and monomeric formaldehyde vapor was produced by heating commercial paraformaldehyde and keeping the delivery tube and burner at 120°C. All the other chemicals used were the commercially available materials.

To distinguish the emission spectra of the separate regions of the multiple-zone flames from each other and from that of the burned gas, and also to reveal any distinctions within each of these or of other flame regions studied, the flames were stabilized, where possible, as flat reaction zones and examined end-on. Flat flames were obtained at low pressures either on open-mouthed cylindrical tubes, on tubes with a "port" consisting of a porous disk (2.8 cm diam) of sintered stainless steel which was jacketed with water at 50°C, or in a Pyrex cone (4 cm diam at large end and 50 cm long).

An advantage of stabilizing the flame in a cone where the gases are introduced at the apex is that the flame automatically adopts the position where its burning velocity just counterbalances the local linear rate of flow. When the cone is mounted vertically, apex downwards, it is possible to maintain the flames as flat disks by adjusting the pressure and the flow rate. The burning velocity of such flames can be readily computed when the flow rate and the cone dimensions are known. Such determinations were made earlier with pure ethyl nitrate[1] and these have now been extended to ethyl nitrate/air mixtures.

In order to raise the adiabatic flame temperature of one or two of the mixtures studied these were exploded in a closed vessel, for a flame propagated under constant volume conditions has a temperature several hundred degrees higher than the flame in the same mixture burning at constant pressure. The explosion vessel consisted of a Pyrex tube, 2½ cm diam by 20 cm

long, with plane quartz windows at the ends, through which light from the flames was focused on the spectrograph. Platinum electrodes were mounted in a side tube to keep the light of the spark away from the spectrograph slit. An average of ten explosions sufficed to produce acceptable spectra with a Raman instrument.

Properties of Ethyl Nitrate-Air Flames

Premixed flames of gaseous ethyl nitrate and air possess one, two or three distinct luminous regions depending on the mixture strength and experimental conditions.

Pure ethyl nitrate will propagate a self-decomposition flame[1] consisting of a single region of very pale gray, as depicted in Figure 1a. A mixture of ethyl nitrate/air in the ratio of about 2:3, if ignited with a spark, may propagate the above type of flame in conjunction with a second orange region a short distance away on the downstream side, as shown in Figure 1b. With mixtures of about stoichiometric proportions a third, violet region appears after, and in contact with, the orange region, which is now much thinner, as illustrated in Figure 1c; the velocity of this flame is much greater than either of the other two. The burning velocities of the three types of flames, when stabilized as flat disks in a Pyrex cone, are shown in Figure 2; two different types of flames with different burning velocities may exist even at the same pressure for one mixture strength of ethyl nitrate and air. For example, if air is added to an already existing pure decomposition flame burning at a pressure below 150 mm Hg in the conical vessel, no second orange reaction zone will form, and the flame extinguishes before the mixture strength becomes stoichiometric. Both zones will form, however, when the proper gaseous mixture is ignited by a spark. Thus the second zone seems to be an independent flame which need separate ignition. Above 150 mm Hg this property disappears and the second zone forms by itself on adding air to the pure decomposition flame. The third zone forms spontaneously from the 2-zone flame, on increasing the air, and the burning velocity is appreciably increased. The flame stabilizes itself lower down in the conical burner. Decreasing the air content of a mixture supporting a 3-reaction zone flame will usually extinguish the flame, no doubt because the disappearance of the third zone causes too sudden a reduction in burning velocity.

Using the symbols I, II and III to denote the flames with 1, 2 and 3 zones respectively, then the ability to convert one type of flame into another in the conical burner by altering the mixture ratio and pressure can be represented thus:

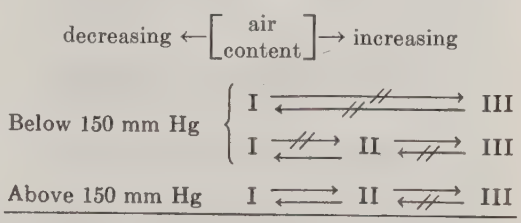

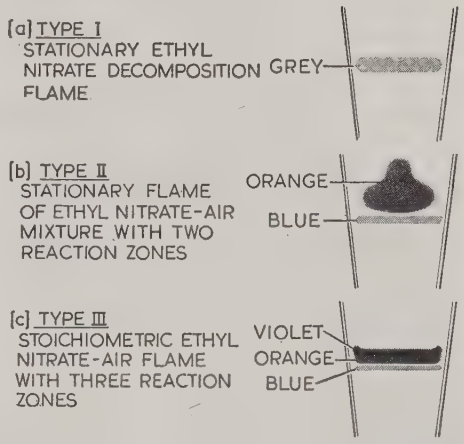

FIG. 1. Structure of flat flames with ethyl nitrate stabilized in a Pyrex cone at low pressure.

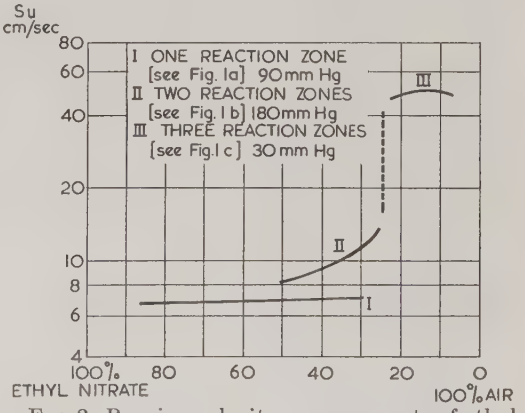

FIG. 2. Burning velocity measurements of ethyl nitrate/air mixtures.

Spectra of Flames with Ethyl Nitrate and Methyl Nitrite, etc.

The self-decomposition flame of ethyl nitrate alone is too weak to produce a spectrum. However, addition of small amounts of oxygen or nitrogen dioxide appreciably increase the flame luminosity without changing the structure of the reaction zone except to produce a more decidedly blue color. The spectrum of the decomposition

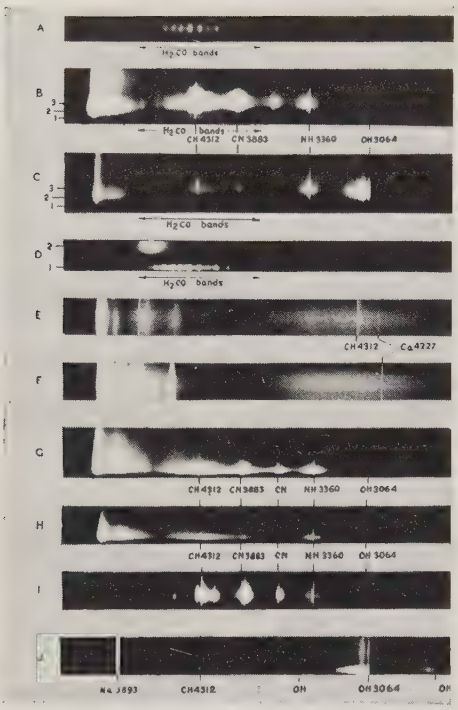

KEY TO FIG. 3: The records in Figs. 3 and 4 are emission spectra of flat, pre-mixed flames seen end-on, unless otherwise stated. The lower edge of each spectrum corresponds to the leading surface of the particular flame. Where more than one zone has been recorded with the multiple zone flames the zones are marked 1, 2, 3 at the L.H. edge; in a number of such cases only the 3rd zone, characterized by bands of CN, NH, etc., was recorded. The gas mixtures were stoichiometric, or near-stoichiometric, except in the case of 3A. The annotations denote wavelength in Angstrom units.

The spectra in Fig. 3 were obtained with a Hilger Raman spectrograph, aperture F/4, with a quartz set except for E and F for which a glass set was used. In B, G, H and I the OH bands are partially absorbed by Pyrex glass.

A. Ethyl nitrate/small amount O_2 . First zone only. Pyrex cone. Pressure, 1.3 cm Hg. Plate, HP3. Slit 0.15 mm. Exposure, 4½ min.

B. Ethyl nitrate/O_2 . 3 zones. Pyrex cone. Pressure, 1.3 cm Hg. Plate, HP3. Slit, 0.15 mm. Exposure, 4½ min.

C. Methyl nitrite/O_2 . 3 zones. 4 cm dia. tube. Pressure, 1.2 cm Hg. Plate, HP3. Slit, 0.03 mm. Exposure, 5 min.

D. Ethyl nitrate/NO_2 . 2 zones. Pyrex cone. Pressure, 3.0 cm Hg. Plate, Zenith. Slit, 0.25 mm. Exposure 15 min.

E. Ethyl nitrate/O_2 . Explosion flame. Initial pressure, 8 cm Hg. Plate, HP3. Slit, 0.05 mm. 10 explosions.

F. Methyl nitrate/O_2 . Explosion flame. Initial pressure, 8 cm Hg. Plate, HP3. Slit, 0.05 mm. 8 explosions.

G. Nitromethane/air. 2 zones. Sintered disc, 2.8 cm dia. Pressure, 8 cm Hg. Plate, HP3. Slit, 0.1 mm. Exposure, 1 min.

H. Methyl nitrite/air. 3 zones. Sintered disc, 2.8 cm dia. Pressure, 15 cm Hg. Plate, HP3. Slit, 0.1 mm. Exposure, 5 min.

flame into which small amounts of oxygen were introduced is shown in Figure 3A. It consists solely of the formaldehyde bands, as emitted by "cool" flames.

Increasing amounts of oxygen produce a second and third zone as in air flames. By maintaining a flat, relatively steady 3-zone flame of ethyl nitrate with oxygen on a burner at low pressure it has been possible to distinguish the spectra of each of the zones, as shown with small dispersion in Figure 3B; the actual separation of the first and second zones is better than can be judged from the spectrum because of inevitable, small flame movements during its recording; the second and third zones, however, do actually overlap slightly. It can be seen that the second zone emits only a continuum in the red and yellow and that the bands of C_2 , CH, CN, NH, OH and NO come from the third zone; the spectrum of the latter is shown with higher dispersion in Figure 4A.

The 3-zone oxygen flames with methyl nitrite and ethyl nitrate are quite alike in appearance except that the third, violet zone is much less intense with the methyl nitrite. A spectrum of an approximately stoichiometric methyl nitrite/oxygen flame is shown in Figures 3C and 4B for comparison with the ethyl nitrate/oxygen flame spectrum of Figures 3B and 4A. The strengths of the heads of the OH bands are roughly comparable, (Figs. 4A and 4B), and it can be seen that the C_2 , CH and CN bands are much weaker in the methyl nitrite spectrum (Fig. 4B) and that the rotational temperature of the OH band is much greater with the ethyl nitrate flame (Fig. 4A). Both the spectra show that the intensity of the OH bands is much greater in the reaction zone than in the burned gases and also that the plane of maximum intensity of the emission of OH bands is slightly lower, i.e., the emission comes earlier in the flame zone, than that of the CH, CN and NO γ-bands and to a lesser degree of the NH bands.

The weakness of the CN and NH bands with the methyl nitrite/oxygen flame points to only a restricted reaction between organic compounds or residues and an oxide of nitrogen in the third zone and indeed analysis of the products of a flame with a methyl nitrite/oxygen mixture, to which enough oxygen had been added to maintain

I. Ethyl nitrate/air. 3 zones. Sintered disc, 2.8 cm dia. Pressure, 7 cm Hg. Plate, Zenith. Slit, 0.05 mm. Exposure, 1½ min.

J. Formaldehyde/O_2 . 1½ cm dia. tube. Pressure, 2 cm Hg. Plate, HP3. Slit, 0.1 mm. Exposure, 3 min.

fully the third zone, gave a composition corresponding to the following overall reaction:

$$10CH_3ONO + 9O_2 \rightarrow$$
$$N_2 + 8NO + H_2 + 4CO + 6CO_2 + 14H_2O$$

The N_2 content of the products shows that little oxide of nitrogen can have reacted and that an appreciable amount of NO remains unburned in spite of the excess fuel.

is shown in Figure 3D; only the formaldehyde bands of the first zone and the continuum of the second zone are present. No banded spectrum is emitted in, or beyond, this second zone except for some mixtures with which extremely weak bands of CH, CN and NH can be recorded; but no mixture produces a flame with a visible third zone. The second, yellow zone is quite bright; indeed, addition of even small amounts of NO_2

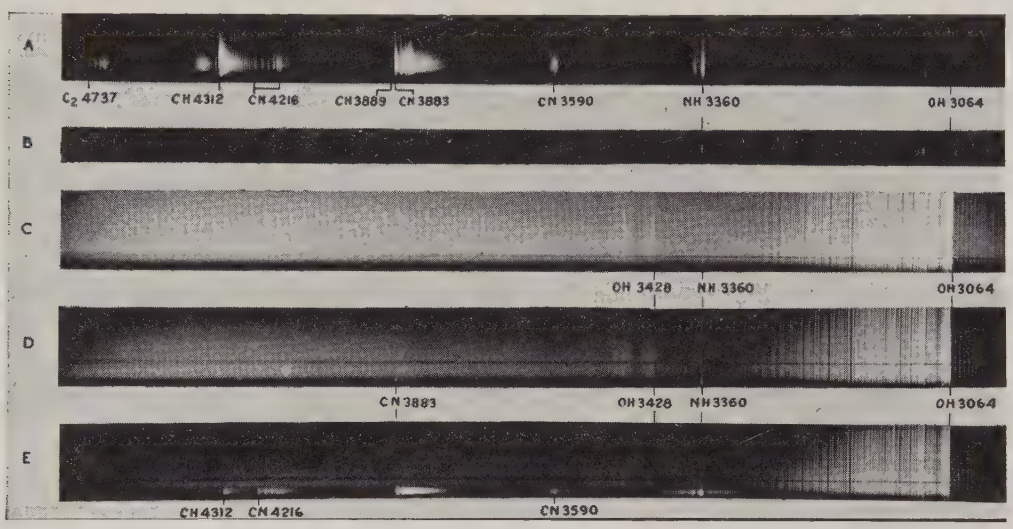

KEY TO FIG. 4: See Key to Fig. 3. The spectra in Fig. 4 were obtained with a Hilger medium spec trograph (quartz set).

A. Ethyl nitrate/O_2 . 3 zones. 2 cm dia. tube. Pressure, 2.3 cm Hg. Plate, Zenith. Slit, 0.03 mm. Exposure, 5 min.
B. Methyl nitrite/O_2 . 3 zones. 2 cm dia. tube. Pressure, 2.2 cm Hg. Plate, Zenith. Slit, 0.03 mm. Exposure, 5 min.
C. Formaldehyde/NO. 2 cm dia. tube. Pressure, atmospheric. Plate, HP3. Slit, 0.03 mm. Exposure, 40 sec.
D. Methyl alcohol/NO. 1½ cm dia. tube. Pressure, atmospheric. Plate, HP3. Slit, 0.03 mm. Exposure, 3 min.
E. Methane/NO. 1 cm dia. tube. Pressure, atmospheric. Plate, HP3. Slit, 0.03 mm. Exposure ½ min.

Analysis of the combustion products of the equivalent flame with ethyl nitrate gave a composition corresponding approximately to the following over-all reaction:

$$32C_2H_5ONO_2 + 33O_2 \rightarrow 36CO + 28CO_2$$
$$+ 18H_2 + 8NO + 12N_2 + 62H_2O$$

It is clear that most of the NO initially produced has reacted.

The spectra of methyl nitrite and ethyl nitrate/air flames are very similar to the corresponding oxygen flames. Details can be seen from Figures 3H and 3I, respectively, as well as from Table 1.

The spectrum of a flame with ethyl nitrate/NO_2 to the air or oxygen flames of ethyl nitrate or methyl nitrite with 2 or 3 zones makes the second yellow zone much more intense.

Spectra of Explosion Flames with Methyl Nitrate, etc.

When stabilized on a burner at low pressures neither the self-decomposition flame of methyl nitrate, nor any flame in mixtures with oxygen, possesses the third luminous zone, and no bands of C_2, CH, CN, NH, OH or NO are emitted. The absence of this zone, in contrast to the 3-zone flame with methyl nitrite/oxygen, has been attributed to the lower flame temperature.[2]

To induce combustion between the unburned

fuel residues and nitric oxide, which clearly escape from the first two regions of the methyl nitrate flames, methyl nitrate vapor alone and also in a bright bluish flame was propagated. The intensity of the blue flame quite obscured any yellow radiation. This effectively 2-staged reac-

Table 1. Spectral Emission of Multi-Zone Flames with Nitrobodies at Low Pressure

Fuel/Oxidizer System*	1st Zone (Blue) (Formaldehyde Bands)	2nd Zone (Orange) (Continuous Emission)	3rd Zone (Violet) (Band Emission)
Methyl nitrate (CH_3ONO_2)	Very strong (No change on addition of O_2)	Very strong	Absent
Methyl nitrate (explosion flame in closed vessel)	(Masked by 3rd zone)		Only OH and continuum
Methyl nitrite/O_2 (CH_3ONO)	Medium	Weak	Weak bands of C_2, CH, CN, NH, and NO. OH stronger in reaction zone than in burned gas but appears to have normal rotational temperature. OH slightly below CH and CN.
Nitromethane/O_2 (CH_3NO_2)	Absent	Strong	Very strong bands of C_2, CH, CN, NH, NO and OH. OH stronger in reaction zone than in burned gas and with high rotational temperature.
Ethyl nitrate ($C_2H_5ONO_2$)	Very weak	Absent	Absent
Ethyl nitrate + small amount O_2	Strong	Strong depending on amount of O_2	Absent
Ethyl nitrate/O_2	Strong	Strong	Very strong bands of C_2, CH, CN, NH, NO and OH. OH stronger in reaction zone than in burned gas and with high rotational temperature. OH slightly below CH and CN.
Ethyl nitrate/air	As with oxygen flame, but weaker; all three zones clearly visible		
Nitromethane/air	Absent	Strong	Strong bands of C_2, CH, CN, NH and OH.
Methyl nitrite/air	Weak	Medium	No 3rd zone distinguishable but weak bands of CN, NH and OH are present within the 2nd zone. OH has apparently normal rotational temperature.

* Mixtures with air or oxygen were near-stoichiometric, unless otherwise stated.

stoichiometric proportions with oxygen was exploded by a spark in the closed vessel. With initial pressures below 5 cm Hg only feebly luminous flames of a dull yellow color, undoubtedly corresponding to the stationary flames with 2 zones, were observed, but at a pressure of 8 cm Hg tion with methyl nitrate (the blue flame following the yellow flame after a few msec) was first suspected by Zeldovich and Shaulov[3] and later detected by a schlieren method by Adams and Scrivener.[4]

The spectrum of the blue flame was obtained

with a stoichiometric mixture of methyl nitrate/oxygen at an initial pressure of 8 cm Hg using a Hilger Raman spectrograph; Figure 3F shows a spectrum taken with the glass set. Spectra taken with the quartz set reveal only OH bands, besides the continuous radiation which is also visible in Figure 3F. The presence of strong OH bands is confirmatory evidence of the onset of a third step in the reaction. No bands due to CH, CN or NH are obtained under any conditions. Calcium was apparently present as an impurity as seen by some calcium oxide bands in the red end of the spectrum (Fig. 3F).

It has to be remembered, however, that the spectra of explosion flames do not distinguish between radiation from the reaction zone and that from the burned gases (chiefly OH and continua). Any band emission from the reaction zone therefore tends to be masked by the continua from the burned gases and in any case it must appear weaker relative to the OH bands than in the spectra with a flat, stationary burner flame. So it is still possible that CH, CN and NH bands are emitted from the third zone of the methyl nitrate/oxygen flame but they must be extremely weak if they are present at all, for these bands are reasonably strong with similar explosion flames with ethyl nitrate/oxygen mixtures (Fig. 3E). The pure methyl nitrate decomposition flame exhibits the same spectrum as the methyl nitrate/oxygen flame. The CN and NH bands of methyl nitrite/oxygen explosion flames are also too weak to show up in the spectrum.

Flames with Nitromethane: Comparison with Methyl Nitrite

As nitromethane (CH_3NO_2) and methyl nitrite (CH_3ONO) are isomeric, with almost identical heats of formation, it is instructive to compare their combustion characteristics.

Methyl nitrite supports a self-decomposition flame at atmospheric pressure. An attempt was therefore made to get such a flame with nitromethane at 1 atmos, but without any success, although burners up to 20 cm diam were used in order to minimize heat losses from the flame. Even small additions of air or oxygen did not induce flame propagation. It is known that nitromethane decomposes in a self-sustained manner at pressures of 20 atmos, at least in the presence of a catalyst.[5] Methyl nitrite is also influenced by pressure in this respect,[2] so the difference between the two compounds may be one of degree rather than of kind; nevertheless, it is probably significant.

Nitromethane certainly burns easily with near-stoichiometric amounts of air or oxygen at low pressures and two luminous, adjacent regions, the first yellow and the second violet may be distinguished as depicted in Figure 5. These zones correspond in the general nature of their light emission to the second and third zones of the methyl nitrite/oxygen flame; the first zone of the latter, characterized by the formaldehyde bands, is never observed with the nitromethane flames. The final, violet zone of the nitromethane flames emits CH, CN and NH bands at least as strongly as the violet zone of the ethyl nitrate/oxygen flame, in contrast to the weak emission of the methyl nitrite/oxygen flame. The rotational temperature of the OH also seems to be as high as in the ethyl nitrate/oxygen flame. The intensity of the OH bands is much greater in the reaction zone than in the burned gases.

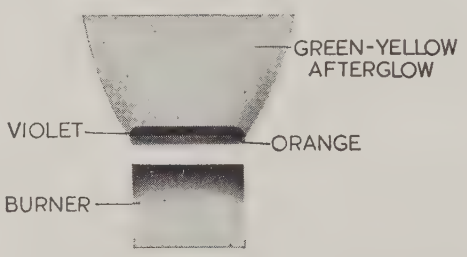

FIG. 5. Structure of flat burner flame with nitromethane/oxygen at low pressures.

The spectrum of the air flame with nitromethane (Fig. 3G) more closely resembles that with ethyl nitrate (Fig. 3I) than that with methyl nitrite (Fig. 3H) in that its CH and CN bands are strong and its OH band displays a high rotational temperature.

The main details of all the above flames and their spectra are summarized in Table 1.

The self-decomposition flame with methyl nitrite at 1 atmos was previously described as too feebly luminous for direct spectroscopy.[2] However, by obtaining a more stable flame and by using a Hilger Raman spectrograph (quartz set) with a wide slit, it has proved possible to record a weak spectrum with an exposure of twenty minutes. This spectrum consists solely of a continuum in the red and yellow: no formaldehyde bands are present.

The Spectra of Flames of Formaldehyde and Methyl Alcohol with O_2, NO and NO_2

To provide further essential data for the fuller interpretation of the spectra given by the separate reaction zones of the nitrobodies under investigation the spectra of formldehyde and methyl alcohol with oxides of nitrogen were recently obtained,[6] as these compounds are known to occur as intermediates.[7]

At 1 atmos the flames of formaldehyde with NO have large quenching diameters. Formaldehyde cannot therefore conveniently be burned with nitric oxide at low pressures. In both these respects formaldehyde resembles H_2 and CO rather than hydrocarbons (other than methane). The spectrum of the flame at atmospheric pressure, shown in Figure 4C, is identical with that of a flame of H_2/NO, i.e., it consists solely of OH bands and the Schumann Runge bands of O_2, together with extremely weak NH bands which are probably due to N_2O as an impurity in the NO; no excess OH radiation is present in the reaction zone.

A formaldehyde/NO_2 flame at atmospheric pressure was found to emit only a yellow continuum similar to that from the second luminous zones mentioned above; however, very weak OH bands do show up with long exposures with a Hilger Raman instrument. It is clear that only partial combustion takes place, as is the case with H_2/NO_2 and CO/NO_2 flames.

In the spectra of flames of methyl alcohol with O_2 and with NO at 1 atmos, the C_2 and CH bands are stronger with the oxygen flame. With the flames with NO the CN and NH bands are quite prominent, as shown in Figure 4D, although they are not nearly so strong as they are in flames of methane/NO, as shown in Figure 4E. Methyl alcohol is clearly appreciably more "organic" in character than formaldehyde.

Discussion and Conclusions

A number of flames supported by oxides of nitrogen at atmospheric pressure consist of two zones distinguishable by color and spectra and sometimes separated by a nonluminous gap. Such effects are given by hydrocarbons burning with nitrogen dioxide and by hydrogen burning with a mixture of oxygen and nitric oxide.[9] It has been shown that the first zones result from reaction between fuel and NO_2, and fuel and O_2, respectively, and that the second zones are due to reaction between fuel and NO, as the latter reactions need a higher temperature and proceed more slowly than the former. It has also been shown that nitric oxide reacts in one of two ways depending on the chemical nature of the fuel: with hydrocarbons, and especially with ammonia, reaction occurs at moderate temperature by radical mechanisms but in the absence of suitable radicals, as in flames with hydrogen or carbon monoxide, the nitric oxide will only support combustion where the final flame temperature is sufficiently high to allow it to release its oxygen rapidly enough by thermal decomposition.[10]

Although it is not yet possible to describe in detail the chemical reactions in these separate luminous zones enough experimental material is now available to discuss their general nature.

GENERAL NATURE OF THE SEPARATE REACTION ZONES

1. First zone

The first, blue reaction zone, characterized by the emission of formaldehyde bands, occurs in low-pressure flames of oxygen with ethyl nitrate, methyl nitrate and methyl nitrite but not with nitromethane or mixtures of hydrocarbons and any oxide of nitrogen. The only other hot flame which emits these bands is the one with methyl alcohol/oxygen,[8] notably at low pressure where H_2CO bands occur fairly early in the flame, i.e., in the relatively lower temperature region. The bands are also emitted from "cool" and "blue" flames (*e.g.*, Topps and Townend[11]). All this strongly suggests that the presence of alkoxy groups (RCH_2O) is required for this band emission, for a variety of compounds are formed in "cool" flames which would allow alkoxy radicals to be formed. Indeed, there are other similarities between "cool" flames and these first zones which emit formaldehyde bands, such as their low temperatures.

As work with "cool" flames has shown, the emission of formaldehyde bands is most probably only incidental to the main chemical reaction (*e.g.*, Topps and Townend[11]), but it may still be directly connected with reactions occurring early on in the flame which are important for reactions giving rise to self-decomposition flames. Thus, although nitromethane is isomeric with methyl nitrite it has no apparent tendency to form a self-decomposition flame at atmospheric pressure. Now in the self-decomposition flame of methyl nitrite at 1 atmos a small proportion of nitric oxide must be reduced as otherwise the reaction

can only be thermoneutral.[2] The alkoxy radical may play a vital part in this reduction.

2. Second zone

As far as the spectrographic characteristics are concerned this zone is present in all the multiple-zone flames mentioned above (although its intensity varies from flame to flame) and with premixed flames of NO_2 with hydrocarbons, CO and H_2.[12] Absorption spectroscopy with premixed hydrocarbon/NO_2 flames has also shown that the NO_2 has at least largely disappeared before this region of the flame, that NO escapes through this region[12] and that the temperatures with very fuel rich mixtures may be as low as 780°C;[9] when a further zone is allowed to form it has the characteristics of the third zone in the flames with the nitrobodies.

Not only are zones of this particular radiation apparently confined to flames involving NO_2 but the same emission is produced when NO_2 is brought into contact with hot oxygen in the absence of an oxidation reaction with fuels, as is seen when NO_2 is mixed with the oxygen supporting a diffusion flame with hydrogen, for the yellow zone appears on the oxidant side of the normal reaction zone;[12] the same effect is obtained with carbon monoxide. The great strengthening of the yellow zone on addition of NO_2 to the flames with ethyl nitrate, etc., has already been noted.

It is thus difficult to avoid the conclusion that the radiation arises from reactions which involve nitrogen dioxide molecules, at least initially. The heat release reactions which enable this yellow zone to propagate must be oxidation reactions mainly involving either NO_2 or O_2 or both, but not NO.

3. Third zone

A third zone can be produced with all the nitrobodies studied in the present work. Bands of C_2, CH, CN, NH, OH and NO are emitted (except with methyl nitrate) and this shows that organic fuels are reacting with either NO or N_2O or both; the strength of the CN bands is an indication of the extent of these reactions and this fact, together with the analysis of the burned gases given above, show that such reactions are important with the ethyl nitrate and nitromethane flames but hardly occur with methyl nitrite. However, some of the spectra reveal high rotational temperatures in the OH bands and these are not produced by NO flames; furthermore, it is known that when organic fuels burn with NO there is no excess intensity of OH in the reaction zone compared with the burned gases immediately after this zone,[12] as is observed, for example, with the third zone of the ethyl nitrate/O_2 flame.

Consideration of the behavior of flames with all the relevant simpler fuels with O_2, NO or N_2O in these two respects enables more specific conclusions to be drawn about the reactions in the third zone of each of the nitrobodies concerned. This data on the OH radiation is summarized in Table 2. The case of ethylene is typical of other hydrocarbons. Some of the differences are of degree rather than of kind but they are sufficiently marked for the present purpose. It can be seen that whereas hydrocarbons exhibit both types of "abnormal" OH radiation when burned with O_2, and neither when burned with NO, CO and H_2 never give either. Formaldehyde and methyl alcohol occupy an intermediate position in that in the flames with O_2 the OH is stronger in the reaction zone than in the burned gas but the rotational temperatures are normal (Fig. 3J).

Table 2. Excess Intensities and High Rotational Temperatures of OH Bands in the Spectra of some Flames with O_2, NO and N_2O

Fuel/Oxidizer System	OH Stronger in Reaction Zone than in Burned Gases	High Rotational Temperature of OH in Reaction Zone	Ref.
H_2/O_2	No	No	8
H_2/NO	No	No	12
H_2/N_2O	Yes	Moderately high	8
CO/O_2	No	No	8
C_2H_4/O_2	Yes	Yes	8
C_2H_4/NO	No	No	12
$HCHO/O_2$	Yes	No	8
HCHO/NO	No	No	
$HCHO/N_2O$	Yes	Unknown (presumably no)	8
CH_3OH/O_2	Yes	Very moderately	8
CH_3OH/N_2O	Yes	No	8
CH_3OH/NO	No	No	

It is clear that excess OH radiation in the third zone of the flames with the nitrobodies is due to reaction between organic compounds or formaldehyde with O_2 or N_2O (and/or H_2 with N_2O) (Table 2); in the absence of high rotational temperatures in the OH band any excess OH

radiation must be ascribed to reaction between formaldehyde or methyl alcohol and O_2.

MORE SPECIFIC NATURE OF THE REACTIONS IN THE SEPARATE NITROBODIES

At least a simplified picture can now be produced, on the basis of the foregoing evidence, of the main reactions responsible for the zones in the various low pressure flames with nitrobodies. This is outlined below. (The equations have not been balanced.)

A. Methyl nitrate self-decomposition flame

1st zone The ester breaks down to small molecules early in the reaction, possibly according to $CH_3ONO_2 \rightarrow CH_3O + NO_2 \rightarrow CO + H_2$ (and/or H_2CO) + $NO + O_2 + NO_2$

2nd zone $H_2 + CO + O_2 + NO_2 \rightarrow CO + CO_2 + H_2 + H_2O + NO$

3rd zone H_2, CO, and/or H_2CO react readily with NO only at temperatures higher than those obtainable in methyl nitrate flames burning at constant (low) pressure, hence the absence of the third zone with burner flames; at low initial pressures the necessary temperatures are only obtainable in explosion flames. Addition of oxygen does not materially alter the reactions.

B. Methyl nitrite flame with stoichiometric amount of oxygen

1st zone Most of the ester breaks down to small fuel fragments, formaldehyde and NO but larger organic molecules, presumably mainly methyl alcohol, are also formed and possibly some N_2O.

2nd zone No important reactions occur.

3rd zone $HCHO + O_2 \rightarrow CO + CO_2 + H_2 + H_2O$. The organic fuels burn with available O_2 and any N_2O and then with some of the NO giving rise to some CN and NH bands. The reactions with O_2 effectively precede those with N_2O and NO.

C. Nitromethane flame with stoichiometric amount of oxygen

1st zone Absent.

2nd zone $CH_3NO_2 \rightarrow CH_3 + NO_2$. Further oxidation with O_2 and NO_2

3rd zone Organic molecules, presumably built up from initial fragments such as CH_3 and CH_2, etc., react readily with O_2 and then a little later in the flame with NO.

D. Ethyl nitrate flame with stoichiometric amount of oxygen

1st zone The ester breaks down into NO_2 and formaldehyde, acetaldehyde and other organic molecules of a similar size.

2nd zone Partial combustion of the fuel molecules with NO_2.

3rd zone The oxygen is first consumed by the organic (and other) fuels and the latter then react with NO.

Acknowledgments

The authors wish to express their thanks to Mr. G. Hayward for assistance in obtaining the burning velocities and to Dr. G. A. Heath for the analysis of the combustion products with methyl nitrite and ethyl nitrate.

REFERENCES

1. Wolfhard, H. G.: Fuel, *34*, 60 (1955).
2. Gray, P., Hall, A. R., and Wolfhard, H. G.: Proc. Roy. Soc., *A232*, 389 (1955).
3. Zeldovich, Y. B., and Shaulov, Y. K.: J. Phys. Chem., U.S.S.R., *20*, 1359 (1946).
4. Adams, G. K., and Scrivener, J.: *Fifth Symposium (International) on Combustion*, p. 656. New York, Reinhold Publ. Corp., 1955.
5. Zwicky, F., and Ross, C. C., S. A. E. J., *57*, 22 (1949).
6. Hall, A. R., McCoubrey, J. C., and Wolfhard, H. G.: In press.
7. Needham, D. P., and Powling, J.: Proc. Roy. Soc., *A232*, 337 (1955).
8. Gaydon, A. G., and Wolfhard, H. G.: *Third Symposium on Combustion, Flame and Explosion Phenomena*, p. 504. Baltimore, The Williams & Wilkins Co., 1949.
9. Parker, W. G., and Wolfhard, H. G.: *Fourth Symposium (International) on Combustion*, p. 420. Baltimore, The Williams & Wilkins Co., 1953.
10. Adams, G. K., Parker, W. G., and Wolfhard, H. G.: Discuss. Faraday Soc., *14*, 97 (1953).
11. Topps, J. E. C., and Townend, D. T. A.: Trans. Faraday Soc., *42*, 345 (1946).
12. Wolfhard, H. G., and Parker, W. G.: *Fifth Symposium (International) on Combustion*, p. 718. New York, Reinhold Publ. Corp., 1955.

Discussion by Joseph B. Levy*

The work on the flames of nitrite esters fits in very well with the studies on the kinetics and

* Atlantic Research Corporation, Alexandria, Virginia.

mechanism of the thermal decomposition of these compounds.*† As a result of those studies, the following mechanism has been proposed and strong evidence presented for it. It is written for ethyl nitrite since that ester was the one investigated, but it is, it seems, equally applicable to methyl nitrite as well.

$$C_2H_5ONO \underset{k_{-1}}{\overset{k_1}{\rightleftharpoons}} C_2H_5O\cdot + NO \qquad (1)$$

$$C_2H_5O\cdot + NO \xrightarrow{k_2} NOH + CH_3CHO \qquad (2)$$

$$2NOH \rightarrow N_2O + H_2O \qquad (3)$$

$$C_2H_5O\cdot + NOH \rightarrow C_2H_5OH + NO \qquad (4)$$

If this is treated kinetically making the usual steady state assumptions and making the plausible assumption that $k_{-1} \gg k_2$ the rate expression found is

$$\frac{-d \ln (C_2H_5ONO)}{dt} = \frac{k_1 k_2}{k_{-1} + k_2}$$

The nondependence of the rate on the nitric oxide pressure, which was firmly established in these studies, arises because nitric oxide reacts with the ethoxyl radical to push the reaction back in step (1) and to carry the reaction forward in step (2). In nitrite esters having no hydrogen on the alpha carbon, the addition of nitric oxide depresses the rate in proportion to the amount added. This has been shown experimentally for *t*-butyl nitrite.

This mechanism can explain why, for example, the mixture of *t*-butyl nitrite and nitric oxide made up by Dr. Powling to approximate the composition of methyl nitrite, did not burn. It would appear that reaction (2) is a key reaction for the burning process. In the flame, the fate of the NOH species may very well be different from that indicated in the equations above for the slow decomposition. Thus, at the higher temperatures found in the flame the reaction $NOH \rightarrow NO + H$ may become important.

It may also be pointed out that there is strong evidence‡ that reactions of the type

$$CH_3O\cdot + CH_3ONO \rightarrow CH_3OH + H_2O + NO$$

are not important in the thermal decomposition reaction. The course taken there is better explained by steps (2) to (4) written above. There is no apparent reason why the same should not be true in the nitrite decomposition flames.

With respect to the NOH species, it is difficult to write a step for the formation of nitrous oxide in a gas phase reaction. As a consequence, whenever nitrous oxide is found as a product, its formation is usually explained by the step

$$2\ NOH \rightarrow N_2O + H_2O$$

This explanation probably has its source in the well-known fact that when salts of hyponitrous acid are acidified, even at low temperatures, nitrous oxide is immediately evolved.

$$Ag_2N_2O_2 + 2\ H^+ \rightarrow [H_2N_2O_2] + 2\ Ag^+$$

$$[H_2N_2O_2] \rightarrow N_2O + H_2O$$

* J. B. Levy: J. Am. Chem. Soc., *78*, 1780 (1956).

† J. B. Levy: Ind. Eng. Chem., *48*, 762 (1956).

‡ J. B. Levy: J. Am. Chem. Soc., *75*, 1801 (1953).

25

FLAME PROPERTIES AND THE KINETICS OF CHAIN-BRANCHING REACTIONS[a]

By J. CALVIN GIDDINGS AND J. O. HIRSCHFELDER

Introduction

The great majority of flames of practical interest involves a complicated set of reactions leading to the degradation of chemical energy.

[a] This work was carried out at the University of Wisconsin Naval Research Laboratory under Contract N6-ori-105 with the Office of Naval Research.

The outstanding feature of many reaction schemes is the presence of one or more chain-branching reactions, *i.e.*, reactions in which one active particle enters as reactant, and two are produced as product. The properties of static reacting systems involving such reactions have received extensive theoretical and experimental investigations,[1] and have been shown to possess

unique characteristics. In some cases explosion limits are well defined; in many cases the concentration of active particles greatly exceeds the pseudo-equilibrium concentration with respect to the reactants. This generally leads to a much larger reaction rate than that expected from more familiar mechanisms.

The features of a flame supported in part by a chain-branching reaction have often been the subject of speculation. There have been neither theoretical nor experimental techniques available to assess the properties of these flames. There are, however, a large number of flames governed by nonbranching reactions that have been examined theoretically by the methods of Hirschfelder and Curtiss.[2, 3] These investigations have provided sufficient information to answer many outstanding questions relating to flame propagation. The role played by diffusion, heat conduction, and chemical kinetics, along with the usefulness of various approximations, have been studied. It is our aim to extend these methods to chain-branching flames.

In the present paper, calculations have been made of the flame velocity and chemical profiles for the prototype chain-branching system with a second-order chain-breaking step (which we shall refer to as SOB).

$$2B \xrightarrow{k_1} A \qquad \text{(chain-breaking)}$$

$$B + A \xrightarrow{k_2} 2B + C \qquad \text{(chain-branching)}$$

The values of the assumed diffusion coefficients were varied greatly without appreciably affecting either the flame velocity or the chemical profiles. This result can be explained on the basis of the very short lifetime of the free radical B (of the order of 10^{-6} sec) which makes it virtually impossible for B to migrate an appreciable distance before being destroyed. The qualitative results of the SOB flame are very similar to those of the nonbranching ABC and the AB^2C flames in which the reverse reactions (including chain starting) were considered.

We conclude that whenever the free radicals in the hot part of a flame have sufficiently short mean lives, the flame velocity and chemical and temperature profiles can be approximated by replacing the detailed chemical kinetics by a pseudo-one-step chemical reaction in which the concentrations of the free radicals are taken to be pseudo-stationary state values. Direct calculation show that such modifications change the flame velocity of the SOB by only 6 per cent; the flame velocity of ABC by 0.5 per cent; and the flame velocity of AB^2C by 13 per cent.

In the following discussion, we will compare the features of the SOB scheme with actual kinetic mechanisms, particularly as found in hydrogen combustion. At this stage of development, it would be impossible to study any of the known chain-branching flames with all of the recognized reaction steps included. Simple systems such as hydrogen and oxygen or methane and oxygen are so complicated kinetically that even reaction under static conditions can not be accurately described. Thus, for a flame study, we must necessarily find simple reaction schemes that will support a hypothetical flame with all of the important features of a real flame. These schemes will be devised from the following general considerations.

Aside from molecular mechanisms, which we will assume unimportant, there are four classes of radical (active-particle) reactions which are found in kinetic studies. These are chain-initiating, chain-propagating, chain-branching, and chain-breaking reactions. Some of the important steps of hydrogen combustion illustrate the nature of these reactions.

$$\begin{aligned}
H_2 &\rightarrow 2H && \text{(chain-initiating)}\\
H + O_2 &\rightarrow OH + O && \text{(chain-branching)}\\
OH + H_2 &\rightarrow H_2O + H && \text{(chain-propagating)}\\
O + H_2 &\rightarrow OH + H && \text{(chain-branching)}\\
H + O_2 &\rightarrow H_2O && \text{(chain-breaking)}\\
H + O_2 &\rightarrow HO_2 && \text{(chain-breaking)}
\end{aligned} \qquad (1)$$

The HO_2 of the last reaction is assumed to be an inactive particle—for this reason the reaction is labeled chain-breaking. A more complete description of these and similar reactions can be found in Jost.[1] In order to find simple yet meaningful reaction schemes for the above hydrogen combustion, the following considerations are needed. When, and only when, the over-all reaction is proceeding rapidly, chain-initiating reactions can be neglected. This is a result of the ease with which radicals are produced through branching reactions. As will be shown later, the chain-initiating step can be neglected with a second-order breaking scheme, but must be included if the chain is first-order breaking.

Chain-propagating steps can be omitted. These merely effect the change from one radical to

another. Our treatment must be simple to the extent that only one radical is allowed. Since we will consider only one radical, just one chain-branching step is needed.

There are two chain-breaking steps written in the above reaction sequence. One is first order, and the other is second order in the radical concentration. It can be shown that a fundamentally different chain reaction results depending upon which is the terminal step. A chain with a first-order breaking step is usually of the Semenoff type (see Jost). We will outline simple reaction schemes for both chain reactions, but at this time present numerical calculations only for flame supported by a chain reaction not of the Semenoff type.

If we attempted to find a reaction scheme for a Semenoff chain while neglecting initiating and propagating steps, we would get something like

$$\begin{aligned} \mathrm{B} &\xrightarrow{k_2} \mathrm{C} && \text{(chain-breaking)} \\ \mathrm{B} + \mathrm{A} &\xrightarrow{k_3} 2\mathrm{B} + \mathrm{C} && \text{(chain-branching)} \end{aligned} \tag{2}$$

where A, B, and C are reactant, active particle, and product, respectively. The steady-state condition is,

$$\frac{d\,[\mathrm{B}]}{dt} = 0 = k_3[\mathrm{A}][\mathrm{B}] - k_2[\mathrm{B}] \tag{3}$$

and can be satisfied, in general, only for [B] = 0. This condition, of course, means that the reaction is not proceeding at all, hence a chain-initiating step must be included in this sequence. Thus we arrive at a three-component reaction scheme which very simply describes a Semenoff chain (first-order chain-breaking flame, which we shall refer to as FOB).

$$\begin{aligned} \mathrm{A} &\xrightarrow{k_1} 2\mathrm{B} \\ \mathrm{B} &\xrightarrow{k_2} \mathrm{C} && \text{(FOB)} \\ \mathrm{B} + \mathrm{A} &\xrightarrow{k_3} 2\mathrm{B} + \mathrm{C} \end{aligned} \tag{4}$$

The steady-state condition yields a value for [B],

$$[\mathrm{B}] = \frac{2k_1[\mathrm{A}]}{k_2 - k_3[\mathrm{A}]}, \tag{5}$$

which goes to infinity for certain finite values of k_2, k_3, and [A]. This is the point that describes the very rapid reaction typical of an explosion limit. Flames supported by such reaction sequences very naturally fall into two categories. The explosion limit may, or may not, be reached at some point in the flame front. Calculations on this Semenoff chain flame are now in progress and will be discussed at a later time.

We can now proceed to the branching chain that is terminated by a second-order radical reaction. It is found that the initiating step can be successfully omitted in this case. The simple SOB reaction scheme that fulfills all necessary requirements is,

$$\begin{aligned} 2\mathrm{B} &\xrightarrow{k_1} \mathrm{A} && \text{(chain- breaking)} \\ \mathrm{B} + \mathrm{A} &\xrightarrow{k_2} 2\mathrm{B} + \mathrm{C} && \text{(chain- branching)} \end{aligned} \tag{6}$$

The steady-state condition is seen to be,

$$\begin{aligned} \frac{d\,[\mathrm{B}]}{dt} &= 0 = k_2[\mathrm{B}][\mathrm{A}] - 2k_1[\mathrm{B}]^2 \\ [\mathrm{B}] &= \frac{k_2[\mathrm{A}]}{2k_1} \end{aligned} \tag{7}$$

and the rate of formation of product molecules is,

$$\frac{d\,[\mathrm{C}]}{dt} = k_2[\mathrm{B}][\mathrm{A}] = \frac{k_2^2[\mathrm{A}]^2}{2k_1} = -\frac{2d[\mathrm{A}]}{dt} \tag{8}$$

Hence the over-all reaction, to the steady-state approximation, proceeds with the second order.

The reaction scheme described by Equation (6) is not patterned after a particular reacting system—the requirements of its derivation were that it be simple, and that it be a second-order branching chain. However, Equation (6) may resemble a real, but different, reaction sequence in many ways. If we choose the following reactions involved in hydrogen combustion from Equation (1),

$$\begin{aligned} \mathrm{OH} + \mathrm{H_2} &\xrightarrow{k_4} \mathrm{H_2O} + \mathrm{H} \\ \mathrm{H} + \mathrm{O_2} &\xrightarrow{k_5} \mathrm{OH} + \mathrm{O} \\ \mathrm{O} + \mathrm{H_2} &\xrightarrow{k_6} \mathrm{OH} + \mathrm{H} \\ \mathrm{H} + \mathrm{OH} &\xrightarrow{k_7} \mathrm{H_2O} \end{aligned} \tag{9}$$

we notice many features not included in (6). There are three radicals and two chain-branching steps. There is one chain-propagating step, where in Equation (6) there is none. Also the chain-breaking step yields a product molecule, whereas in Equation (6) a reactant molecule is produced.

We may apply the steady-state condition to Equation (9) by setting the time derivatives of [H], [OH], and [O] equal to zero. The resulting

steady-state rate of formation of product is,

$$\frac{d\,[H_2O]}{dt} = \frac{2k_4k_5[H_2][O_2]}{k_7} \tag{10}$$

Since Equation (10) is similar to Equation (8), the SOB reaction mechanism (6) is kinetically similar to the reaction scheme (9). Both expressions are second order in reactant concentration. The chain-branching rate constant, k_2, is equivalent to twice the geometric mean of a branching rate constant and a propagating rate constant, k_4 and k_5, all of which describe bimolecular reactions. Both chain-breaking rate constants, k_1 and k_7, appear in the denominator to the first power.

Despite the similarity of Equations (10) and (8), it may be argued that a flame supported by the respective reaction sequences is quite different. The last reaction of Equation (9), for instance, actually proceeds with third-body restrictions. But with little added difficulty, k_1 can be made to include these restrictions. It might also be argued that the similarity in steady-state approximations is meaningless—that this condition does not hold in the flame front. Our calculations, however, show that the steady-state condition is quite valid for a large range of parameters.

The Flame Equations

The general equations for one-dimensional flame propagation are outlined by Hirschfelder and his associates.[2] Kinetic energy and viscosity are neglected in the usual manner. Throughout the paper we will assume a constant specific heat per gram, equal for all components. Also, the perfect gas law is assumed.

Several methods have been developed which allow for a solution to the flame equations. The series expansion method,[4] the relaxation method,[5] and the integral equation method[6] have all been used with success. We have used the integral equation method, developed by Klein, throughout the paper. The results have been found very satisfactory. The symbols in the nomenclature list at the end of this paper arise in its application.

The condition of constant specific heat gives b the value, $b = b_i$ for all i, and, with this, L becomes $L = \sum h_i G_i^\infty + b\,(\tau^\infty - \tau)$.

For a treatment of the flame problem by successive approximations to an integral equation, under general conditions, the original report by Klein[6] should be read. We will treat the equations with the special techniques that apply to the problem at hand. The flame equations for an arbitrary reaction scheme, and with constant and equal specific heat, are

$$g\frac{dg_i}{d\tau} = qbsR_i \tag{11}$$

$$g\frac{dx_i}{d\tau} = \sum \frac{1}{\delta_{ij}}\,(x_i g_j - x_j g_i) \tag{12}$$

$$bg = G - L \tag{13}$$

These equations, along with the conditions,

$$x_A + x_B + x_C = 1 \tag{14}$$

$$g_A + (g_B + g_C)/2 = 1 \tag{15}$$

specify all flame properties. Instead of using the various R_i, the rate of production of species i, it is convenient to reduce everything to R_1 and R_2, the respective rates of the two reactions in Equation (6). Thus $R_A = R_1 - R_2$, $R_B = R_2 - 2R_1$, and $R_C = R_2$. With the use of Equation (14) and Equation (15) it is possible to eliminate one equation from Equation (11) and one from Equation (12). The equations to be solved are

$$g\frac{dg_A}{d\tau} = qbs(R_1 - R_2) \tag{16}$$

$$g\frac{dg_B}{d\tau} = qbs(R_2 - 2R_1) \tag{17}$$

$$g\frac{dx_A}{d\tau} = \frac{1}{\delta_{AB}}\,(x_A g_B - x_B g_A) + \frac{1}{\delta_{AC}}\,(x_A g_C - x_C g_A) \tag{18}$$

$$g\frac{dx_B}{d\tau} = \frac{1}{\delta_{AB}}\,(x_B g_A - x_A g_B) + \frac{1}{\delta_{BC}}\,(x_B g_C - x_C g_B) \tag{19}$$

$$bg = g_A + g_B - L \tag{20}$$

There are more unknowns than equations in the above, but x_C, g_C, and g_B can be eliminated through Equations (14), (15), and (20). We now add Equations (16) and (17) together and get

$$g\frac{d}{d\tau}\,(g_A + g_B) = -qbsR_1 \tag{21}$$

Again using Equation (20), and considering that $dL/d\tau = -b$, we arrive at Klein's principal flame equation

$$g\left(1 - \frac{dg}{d\tau}\right) = qsR_1 \tag{22}$$

Rearranging the terms in Equations (17), (18), and (19), the following equations result

$$s(R_2 - 2R_1) = \frac{g}{bq}\frac{dg_B}{d\tau} \tag{23}$$

$$\frac{dx_A}{d\tau} + x_A\left(\frac{bg + L - 2\delta_{AC}^{-1} - g_B\delta_{AB}^{-1}}{g}\right) \tag{24}$$

$$= \frac{x_B(\delta_{AC}^{-1} - \delta_{AB}^{-1})(bg + L - g_B) + \delta_{AC}^{-1}(g_B - bg - L)}{g}$$

$$g_B = \frac{g\dfrac{dx_B}{d\tau} - x_B[2\delta_{BC}^{-1} + (\delta_{AB}^{-1} - 2\delta_{BC}^{-1})(bg + L)]}{(\delta_{BC}^{-1} - \delta_{AB}^{-1})(x_A + x_B) + \delta_{BC}^{-1}(x_B - 1)} \tag{25}$$

It is the last four equations, with the appropriate diffusion parameters, that must be simultaneously solved. Klein suggests a number of approaches to the problem. We have separated the equations into two parts. With an assumed x_B, equation (22) yields g and the eigenvalue q. With this g and q, Equations (23), (24), and (25) are solved to obtain consistent values of x_B, x_A, and g_B. The solution of Equations (23), (24), and (25) is straightforward. Equation (23) is quadratic in x_B, Equation (24) is a linear differential equation in x_A, and Equation (25) is a simple algebraic equation in g_B. The convergence to a simultaneous solution was found to be rapid, involving perhaps three cycles for better than one per cent accuracy.

The solution of the Abel equation (Equation (22)) is not so easily obtained. It is this equation for which Klein suggests successive approximations to an integral equation.[6] Thus, after a single integration, Equation (22) becomes,

$$\frac{1}{2}g^2 = q\int_{\tau}^{\tau^\infty} sR_1\,d\tau - \int_{\tau}^{\tau^\infty} g\,d\tau \tag{26}$$

After a higher approximation to the g is obtained from this equation, a new eigenvalue is obtained

$$q = \int_{\tau^0}^{\tau^\infty} g\,d\tau \Big/ \int_{\tau^0}^{\tau^\infty} sR_1\,d\tau \tag{27}$$

This equation results from the boundary conditions, *i.e.*, $g(\tau^0) = g(\tau^\infty) = 0$. Thus with any reasonable g_0 and q_0 for input, g and q can be obtained to any desired degree of accuracy. The convergence of Equation (26) is rapid except near the hot boundary. Thus more points were added to the numerical procedure for large τ. The cycle, Equations (26) and (27), needed repetition of the order of ten times to make the hot boundary values satisfactory. For this reason, the numerical solutions of g and q were obtained with the use of the IBM 650 Magnetic Drum Calculator at the University of Wisconsin Numerical Analysis laboratory.

In selecting the parameters that apply to Equation (6) we have drawn heavily on the $H_2 + O_2$ reaction. Since the sequence, Equation (9), is very incomplete, especially regarding chain-breaking steps, we do not expect more than a very general description of hydrogen combustion. Nevertheless, it is a convenient place to begin.

The first step in the imitation of the $H_2 + O_2$ flame is the requirement that Equation (10) resemble Equation (8) at all temperatures. Thus we make the activation energy for k_1 equal to zero. Geib[7] has estimated that the activation energy for k_4 and k_5 are 7 kcals and 14 kcals, respectively. The activation energy of k_2 must equal the mean of these two values such that k_4k_5 has the same temperature dependence as k_2^2. We will use the approximate value of 10 kcals, then, for this activation energy. It might be added that the frequency factor of both reactions, that is, the ν in $k = \nu\exp(-E/RT)$, has been set equal to 10^{13} cm^3 mole^{-1}sec^{-1} at T = 3000°K ($\nu^\infty = 10^{13}$). The temperature dependence of ν will be discussed shortly. A number of other parameters agree to a greater or lesser extent with the hydrogen problem. These are,

P = one atmosphere

T^∞ = 3000°K

T^0 = 300°K

m_A = 20

λ^∞ = 10^{-3} cal cm^{-1} sec^{-1} deg^{-1}

b = 3.7037

h_B = 2

and, as a result,

$m_B = m_C = 10$

$\tau^0 = 0.03$

$\tau^\infty = 0.3$

Concerning the Equation (22), it is convenient for qsR_1 to have temperature dependent terms only as they appear in X_B. The term s is given the value $(\tau/\tau^\infty)^{\frac{1}{2}}$, in accordance with simple kinetic theory. The eigenvalue, q, is constant.

TABLE 1. FLAME RESULTS

τ	$g = \frac{d\tau}{d\zeta}$	x_A	g_B	x_B	x_B^*
Case I ($\delta_{AC} = \delta_{AB} = \delta_{BC} = 1$) $v_f = 55.1$ cm/sec					
.30	0	0	0	0	0
.29	.00335	.02187	.00441	.00199	.00193
.28	.01003	.04398	.00868	.00376	.00365
.27	.01818	.06667	.01241	.00531	.00517
.26	.02766	.09183	.01580	.00676	.00663
.25	.03802	.11891	.01808	.00805	.00795
.24	.04865	.14746	.01937	.00911	.00907
.23	.05909	.17769	.01959	.00995	.00997
.22	.06896	.20951	.01871	.01055	.01065
.21	.07790	.24285	.01684	.01089	.01107
.20	.08559	.27769	.01420	.01097	.01123
.19	.09177	.31398	.01100	.01080	.01112
.18	.09624	.35168	.00753	.01040	.01075
.17	.09886	.39072	.00410	.00976	.01014
.16	.09955	.43104	.00096	.00894	.00929
.15	.09831	.47252	−.00164	.00796	.00826
.14	.09522	.51504	−.00323	.00687	.00709
.13	.09042	.55849	−.00439	.00572	.00583
.12	.08414	.60268	−.00469	.00457	.00456
.11	.07664	.64743	−.00436	.00350	.00334
.10	.06820	.69254	−.00344	.00255	.00226
.09	.05911	.73814	−.00235	.00175	.00138
.08	.04959	.78412	−.00147	.00113	.00073
.07	.03983	.83130	−.00082	.00068	.00031
.06	.02994	.88121	−.00036	.00039	.00010
.05	.01999	.94086	−.00011	.00020	.00002
.04	.01001	.97661	−.00002	.00008	0
.03	0	1.00000	0	0	0
Case II ($\delta_{AC} = 1$, $\delta_{AB} = \delta_{BC} = 2$) $v_f = 54.8$ cm/sec					
.30	0	0	0	0	0
.29	.00329	.02131	.00494	.00197	.00188
.28	.00996	.04340	.01035	.00374	.00360
.27	.01816	.06582	.01503	.00528	.00511
.26	.02758	.09053	.01923	.00670	.00654
.25	.03778	.11716	.02205	.00794	.00783
.24	.04817	.14533	.02334	.00897	.00894
23	.05833	.17528	.02305	.00977	.00984
.22	.06788	.20692	.02116	.01033	.01052
.21	.07649	.24019	.01784	.01064	.01095
.20	.08386	.27504	.01340	.01071	.01112
.19	.08974	.31150	.00836	.01054	.01103
.19	.09398	.34944	.00316	.01015	.01068
.17	.09647	.38886	−.00213	.00957	.01009
.16	.09711	.42957	−.00684	.00878	.00926
.15	.09590	.47149	−.00979	.00786	.00824
.14	.09295	.51453	−.01147	.00688	.00708
.13	.08844	.55842	−.01280	.00585	.00583

TABLE 1.—*Continued*

τ	$g = \frac{d\tau}{d\zeta}$	x_A	g_B	x_B	x_B^*
Case II ($\delta_{AC} = 1$, $\delta_{AB} = \delta_{BC} = 2$) $v_f = 54.8$ cm/sec—*Continued*					
.12	.08249	.60301	−.01271	.00475	.00456
.11	.07531	.64802	−.01053	.00372	.00335
.10	.06720	.69349	−.00805	.00285	.00227
.09	.05842	.73924	−.00616	.00210	.00138
.08	.04915	.78540	−.00421	.00144	.00073
.07	.03956	.83252	−.00236	.00095	.00032
.06	.02978	.88229	−.00117	.00060	.00010
.05	.01990	.94185	−.00051	.00035	.00002
.04	.00996	.97729	−.00018	.00017	0
.03	0	1.00000	0	0	0

τ	$g = \frac{d\tau}{d\zeta}$	x_A	g_B	x_B	x_B^*	$g = \frac{d\tau}{d\zeta}$	x_A
Case III ($\delta_{AC} = \delta_{AB} = \delta_{BC} = 0$) $v_f = 91.8$ cm/sec						Modified ($\delta_{AC} = 1$) $v_f = 58.3$ cm/sec	
.30	0	0	0	0	0	0	0
.29	.00399	.02421	.00462	.00237	.00214	.00468	.02379
.28	.00870	.05148	.00856	.00450	.00427	.01122	.04864
.27	.01420	.08194	.01218	.00659	.00636	.01926	.07319
.26	.02087	.11705	.01558	.00870	.00846	.02870	.09995
.25	.02880	.15791	.01866	.01080	.01056	.03906	.12850
.24	.03790	.20533	.02132	.01285	.01262	.04975	.15830
.23	.04779	.25967	.02344	.01476	.01457	.06029	.18962
.22	.05816	.32134	.02491	.01646	.01633	.07031	.22231
.21	.06858	.39034	.02566	.01784	.01779	.07943	.25629
.20	.07856	.46610	.02564	.01879	.01884	.08732	.29147
.19	.08757	.54714	.02483	.01921	.01938	.09370	.32783
.18	.09503	.63095	.02329	.01900	.01929	.09834	.36528
.17	.10039	.71361	.02110	.01808	.01851	.10106	.40380
.16	.10322	.79064	.01841	.01648	.01705	.10179	.44333
.15	.10326	.85736	.01538	.01429	.01499	.10051	.48376
.14	.10055	.91058	.01223	.01168	.01253	.09728	.52502
.13	.09534	.94914	.00912	.00890	.00991	.09226	.56712
.12	.08811	.97420	.00623	.00610	.00737	.08568	.60977
.11	.07939	.98864	.00354	.00349	.00511	.07784	.65313
.10	.06982	.99551	.00163	.00162	.00325	.06906	.69697
.09	.05994	.99773	.00093	.00093	.00187	.05966	.74132
.08	.04998	.99892	.00046	.00046	.00093	.04990	.78644
.07	.04000	.99961	.00019	.00019	.00038	.03998	.83280
.06	.03	.99988	.00006	.00006	.00011	.03	.88211
.05	.02	.99998	.00001	.00001	.00002	.02	.94139
.04	.01	1.00000	0	0	0	.01	.97683
.03	0	1.00000	0	0	0	0	1

We have for the rate of reaction 1, $R_1 = \nu x_B^2 n^2$. Since n is inversely proportional to temperature, ν must increase with the 3/2 power of temperature to fulfill the condition. Thus $\nu = \nu^\infty(\tau/\tau^\infty)^{3/2}$

The calculations were carried out for three examples in which the diffusion constants were varied:

Case I $\delta_{AC} = \delta_{AB} = \delta_{BC} = 1$
Case II $\delta_{AC} = 1$ $\delta_{AB} = \delta_{BC} = 2$
Case III $\delta_{AC} = \delta_{AB} = \delta_{BC} = 0$

The results are presented in Table 1. Here v_f is the flame velocity and x_B^* is the steady state mole fraction of B as given by Equation (7). The profiles for x_B, x_B^*, g_B, and g are shown in Figure 1.

In the limit that k_2 becomes small compared to k_1, it is expected that the flame velocity and the temperature and chemical profiles should approach those for a modified problem. In the modified SOB, for the purposes of the chemical kinetics, the concentration of B is maintained at its steady state value as given by Equation (7) but for the purposes of the diffusion and

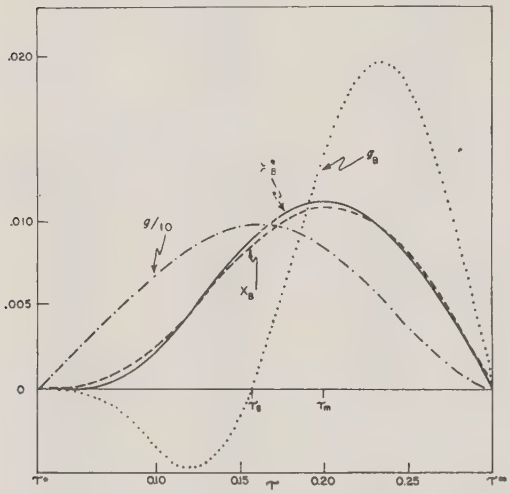

FIG. 1. Case I ($\delta_{AC} = \delta_{AD} = \delta_{BC} = 1$), values of g, g_B, x_B and the steady state value, x_B^*.

temperature gradient equations the existence of B is ignored. Thus the modified SOB corresponds to a flame with a single chemical step, A + A → A + 2C, and the chemical kinetics as given by Equation (8). The calculational results for a modified SOB with $\delta_{AC} = 1$ and all other constants the same as in the previous examples are given in Table 1. The calculated flame velocity, $v_f = 58.3$ cm/sec, is surprisingly close to the flame velocities, 55.1 and 54.8 cm/sec, found for examples I and II. Thus the modified SOB is indeed a good approximation for the particular choice of parameters considered.

The flame velocity in Case III where diffusion is considered negligible is approximately 1.7 times that of Case I. This result is reminiscent of the simple A → B flame where the flame velocity for $\delta = 0$ is 1.8 times that for $\delta = 1$.

Discussion

In Figure 1, one sees many features usually appearing in chain-reacting flames. First of all, the mole fraction or concentration of the free radicals is almost equal to its steady-state value. We shall presently discuss the conditions under which this occurs. The value for the free radical concentration generally passes through a maximum at some temperature, τ_m, (in this case $\tau_m = 0.20$). At temperatures higher than τ_m the free radicals diffuse in the direction of the flow velocity towards the hot boundary, and at lower temperatures they diffuse against the flow velocity. Then at a temperature τ_g (in this case $\tau_g = 0.16$) slightly lower than τ_m the diffusion velocity becomes exactly equal in magnitude to the flow velocity but opposite in direction. At τ_g the value of g_B becomes zero. For temperatures lower than τ_g, the free radicals on the average move towards the flame holder and g_B is negative; whereas for higher temperatures the net flow of free radicals is towards the hot boundary and g_B is positive. The purely diffusional theories of flame propagation such as that of Tanford and Pease[8] assume that for *all* temperatures the net flow of the free radicals is towards the flame holder. Since most of the chemical reactions take place between the temperatures τ^∞ and τ_g, it follows that such diffusional theories are qualitatively wrong. The following detailed calculations give the same sort of results as we obtain with the SOB and lead to the same conclusions: (1) the calculations of Klein,[6] Schatzki,[5] and Hirschfelder and E. Campbell[9] on the ABC flame; (2) the calculations of Hirschfelder, Curtiss, and D. Campbell[10] on the ozone flame; (3) the preliminary calculations of Klein[6] and Schatzki[5] on the AB^2C flame[5, 6]; and (4) the preliminary and as yet unpublished results on the HBr flame.

Since radicals are constantly diffusing away from the reaction zone, the question naturally arises as to the ability of this zone to keep a normal supply of radicals despite the continuous depletion effect. By a normal supply, we mean that which exists under stationary conditions, the steady-state value. For a flame supported by the Semenoff kinetics, the question of course, is meaningless at all points near and above the explosion limit. In our case, consideration of the departure from steady-state concentrations is very instructive, hence we shall briefly discuss

some of the processes contributing to this departure.

The concentration of radicals in a particular zone in the flame front is influenced by the concentration in other zones in a number of ways. The diffusion process tends to bring its value to the mean value of the preceding and following zones. Diffusion considerations aside, the radical concentration is influenced by the flow process itself. Since the gas mixture is flowing forward through our stationary coordinate system, each zone in the combustion wave inherits—and modifies—the properties of a preceding zone. These properties are changed by such chemical processes as will bring the reaction mixture toward the steady-state values appropriate to the new conditions.

The reaction rate of the radical is an important factor in the consideration of flames. For each radical that can be ascribed a steady-state concentration, a relaxation time, t_B, exists. (All physical and chemical processes in a combustion zone are directed towards restoring an equilibrium condition, and for each a relaxation time exists. Of these processes, we speak here only of the radical relaxation time.) This is, essentially, the time it takes for the radical concentration to proceed most of the way to pseudo-equilibrium (steady-state). Almost all radical reactions are fast reactions proceeding with little or no activation energy. For this reason, the psueudo-equilibration in radical concentration is a rapid process with a short relaxation time.

As an example, we can calculate the relaxation time for our chain-branching kinetic system described by Equation (6). With ϵ defined by $x_B = x_B^*(1 + \epsilon)$, we get $dx_B/dt = x_B^* d\epsilon/dt$, since x_B^* can be considered as slowly varying. This can be equated to a like term derived from Equation (7) after substituting $nx_B = (B)$, *i.e.*,

$$\frac{d\epsilon}{dt} = -\frac{nk_2^2x_A^2}{2k_1x_B^*}\epsilon = -k_2nx_A\epsilon \tag{28}$$

The relaxation time is most conveniently defined as the ratio of the extent of departure from the pseudo-equilibrium condition to the rate of annihilation of that departure,

$$t_B = \frac{\epsilon}{-d\epsilon/dt} = (k_2nx_A)^{-1} \tag{29}$$

(t_B is also the time which sees a decrease in ϵ by $1/e$, as shown by integration of Equation (28)). For the numerical example of a flame just considered, $t_B \sim 10^{-6}$ in the reaction zone.

One can also define a time, t_A, characteristic of the rate of the over-all reaction. If [A] is the concentration of a reactant and $-d[A]/dt$ is the net rate of destruction of A when all of the free radicals are maintained at their steady-state concentrations, then

$$t_A = \frac{[A]}{-\frac{d[A]}{dt}} \tag{30}$$

For the SOB flame it follows from Equation (8) that

$$t_A = \frac{4k_1}{k_2^2(A)} \tag{31}$$

It would seem that the ratio t_B/t_A should provide a criterion for the validity of the pseudo-stationary state concentrations of the free radicals.[b] If t_B/t_A in the hot part of the flame is very small compared to unity, the pseudo-steady state and the corresponding modification of the flame calculations (as in the modified SOB example) should be a good approximation. In the cold part of the flame, the pseudo-steady state approximation is usually very poor but there are so few free radicals in the cold part of the flame that this does not appreciably affect the chemical kinetics or the flame velocity. If t_B/t_A is of the order of unity in the hot part of the flame, then the pseudo-stationary state approximation is not applicable. In the case of the HBr flame it is found that the pseudo-steady state approximation can be used for the H atoms but not for the Br atoms. In the AB^2C flame, Klein and Schatzki found that the pseudo-stationary state approximation is not satisfactory for the particular set of constants which they assumed. Thus, we cannot conclude that the pseudo-steady state approximation is generally applicable. But it is very useful in those cases where it does apply.

For the SOB flame, it follows from Equations (29) and (31) that

$$t_B/t_A = k_2/4k_1 = \tfrac{1}{4}\exp(-E/RT) = \tfrac{1}{4}\exp(-0.503/\tau) \tag{32}$$

The over-all chemical reactions proceed at their

[b] Y. Zeldovich and N. Semenov[11] state that a necessary condition for the steady-state approximation is the short lifetime of the active centers in comparison to the duration of the reaction. However, they did not further develop this notion.

maximum rate when τ is in the vicinity of τ_m. At this temperature $t_B/t_A = 1/50$.

The qualitative nature of the departure from quasi-equilibrium can be explained on the basis of very simple considerations. Let us simplify the multi-component diffusion equations by assuming that the free radical B diffuses through the mixture of other components (regarded as a single specie) with a diffusion coefficient, D_B. Then combining the equation of continuity with

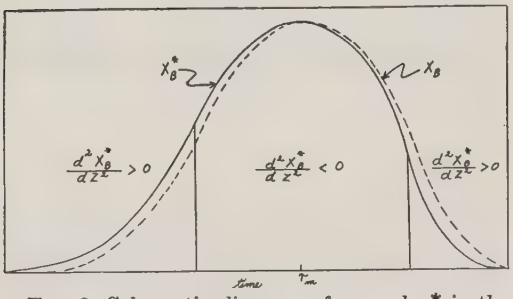

FIG. 2. Schematic diagram of x_B and x_B^* in the flame zone.

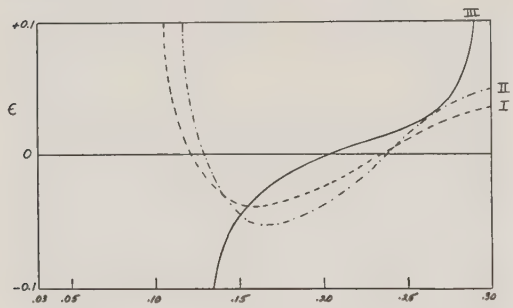

FIG. 3. Illustrating the variation of ϵ with the nature of the flame.

the equation for diffusion,[2]

$$M \frac{dX_B}{dz} = m_B R_B + \frac{d}{dz}\left(nD_B \frac{dX_B}{dz}\right) \qquad (33)$$

And since the value of nD_B does not change rapidly we can ignore its variation. Also X_B is almost equal to X_B^*. Thus

$$R_B = \frac{M}{m_B}\frac{dX_B^*}{dZ} - nD_B \frac{d^2X_B^*}{dZ^2} \qquad (34)$$

For the SOB flame

$$R_B - \epsilon(2k_1 n^2 x_B^{*2}) \qquad (35)$$

Let us consider two cases.

(1) When the coefficients of diffusion for the free radicals are zero, the radicals move through the flame with the flow velocity. For the SOB flame,

$$\epsilon_0 = -\frac{M}{m_B}\frac{dX_B^*}{dz} \Big/ (2k_1 n^2 X_B^{*2}) \qquad (36)$$

Since x_B^* reaches a maximum at τ_m, dx_B^*/dz is positive for temperatures less than τ_m and negative for higher temperatures. Correspondingly, ϵ is negative for low temperatures, zero for τ_m, and positive for higher temperatures. This is shown in Figure 3 and Table 2 for Case III. This behavior of ϵ may be traced to a time-lag in the concentration of the free radicals. If at each point, pseudo-steady state equilibrium were attained, the mole fraction of free radicals would follow the solid curve in Figure 2. Because of the finite relaxation times there must be a time lag first in the formation of the free radicals and then in their decrease. The result is that the mole fractions of free radicals, x_B, actually follows the dotted line in Figure 2 which is similar to the solid curve but shifted towards the right.

(2) When the diffusion coefficients of the free radicals are not zero, the value of ϵ is determined by a diffusional effect as well as the time-lag. From Equations (34), (35), and (36) it follows that

$$\epsilon = \epsilon_0 + \frac{nD_B}{m_B}\frac{d^2X_B^*}{dz^2} \Big/ (2k_1 n^2 X_B^{*2}) \qquad (37)$$

Thus the effect of diffusion in the SOB flame is to increase ϵ when $d^2x_B^*/dz^2$ is positive and decrease it when $d^2x_B^*/dz^2$ is negative. In Figure 2 it appears that in both the very low and very high temperature ranges this second derivative is positive. In Figure 3 and in Table 2 we see that in accord with our qualitative arguments, for Cases I and II ϵ is positive for small temperatures and high temperatures but negative for the intermediate range. In the low temperature zone, diffusion is far more important than the free radical lag due to chemical kinetics.

In those cases where t_B/t_A is small so that the pseudo-steady state approximation can be expected to apply, a higher approximation, giving the corrections, can be obtained in the following manner. First a modified flame problem is solved in which for the purposes of the chemical kinetics x_B is assumed to be equal to x_B^*, but for the purposes of the diffusion and temperature gradient equations, the existence of B is ignored. From this approximation the profiles of x_A and g are obtained as well as a first estimate of q. Next an

approximate expression for g_B is obtained using x_B^* in the diffusion equation, (25). Then the derivative of this g_B is used in conjunction with the rate Equation (23) to obtain an expression for ϵ. In Figure 4 a comparison is made between ϵ calculated exactly with ϵ calculated in this approximate fashion. It is seen that the two functions do not differ appreciably.

The calculations of Klein[6] on the ABC flame provides an excellent example of the deviations from the pseudo-steady state. In the ABC flame, A is the reactant, B is the free radical, and C is the product. The reaction scheme is

$$\begin{aligned} A + X &\underset{k_9}{\overset{k_8}{\rightleftharpoons}} B + X \\ A + B &\underset{\omega k_8}{\overset{\omega k_9}{\rightleftharpoons}} B + C \end{aligned} \tag{38}$$

Here X stands for a molecule of A, B, or C. The specific heats at constant pressure of A, B, and C are all equal and equal to $5R$ (where R is the gas constant). The energies of formation of C, A, and B are 0, 29800 cal/mole, and 59600 cal/mole respectively. The value of T^∞ is 3270°K and T^0 is 300°K. The reaction rates are

$$\frac{d[B]}{dt} = nk_8[A] - nk_9[B] \tag{39}$$

$$\frac{d[A]}{dt} = -\omega(k_9[A][B] - k_8[B][C]) - (nk_8[A] - nk_9[B]) \tag{40}$$

where

$$k_9 = 10^{13}\ \text{cm}^3\text{mole}^{-1}\text{sec}^{-1}$$

And

$$k_8 = k_9 \exp(-15000/T)$$

Let the reduced temperature be $\tau = T/15000$ and the reduced diffusion coefficient be $\delta_{AB} = \delta_{AC} = \delta_{BC} = 1$. The constant ω is a very interesting parameter since it affects t_A but not t_B. From Equation (39) it is easy to show that $t_B = (nk^9)^{-1}$. And from Equation (40) if we neglect the small effect of the back reaction, it follows that $t_A = (\omega n k_9 x_B^*)^{-1}$. Thus

$$t_B/t_A = \omega x_B^* \tag{41}$$

Since x_B^* reaches a maximum value of 0.00076, t_B/t_A is small if ω is 1, 10, or 100. But t_B/t_A becomes unity when ω gets around 1000. Thus the pseudo-steady state should apply for small values of ω but the deviations should become progressively larger as ω gets larger.

TABLE 2. THE VALUES OF ϵ FOR CASES I, II, AND III

T	τ	Case I	Case II	Case III
3000	0.30			
2900	0.29	.0336	.0462	.1093
2800	0.28	.0305	.0396	.0540
2700	0.27	.0259	.0337	.0361
2600	0.26	.0195	.0245	.0286
2500	0.25	.0119	.0139	.0228
2400	0.24	.0049	.0035	.0176
2300	0.23	−.0023	−.0073	.0126
2200	0.22	−.0094	−.0180	.0077
2100	0.21	−.0162	−.0280	.0027
2000	0.20	−.0228	−.0370	−.0028
1900	0.19	−.0285	−.0448	−.0085
1800	0.18	−.0333	−.0499	−.0152
1700	0.17	−.0367	−.0515	−.0231
1600	0.16	−.0383	−.0518	−.0330
1500	0.15	−.0368	−.0471	−.0467
1400	0.14	−.0309	−.0285	−.0674
1300	0.13	−.0189	.0028	−.1020
1200	0.12	.0035	.0418	−.1715
1100	0.11	.0458	.1114	−.3167
1000	0.10	.1243	.2589	−.5008
900	0.09	.2669	.5170	−.5004
800	0.08	.5448	.9725	−.5002
700	0.07	1.1760	2.0035	−.5001
600	0.06	2.8880	4.9837	−.5000
500	0.05	8.9850	16.3950	−.5000
400	0.04	45.9950	99.3110	−.5000
300	0.03	0	0	0

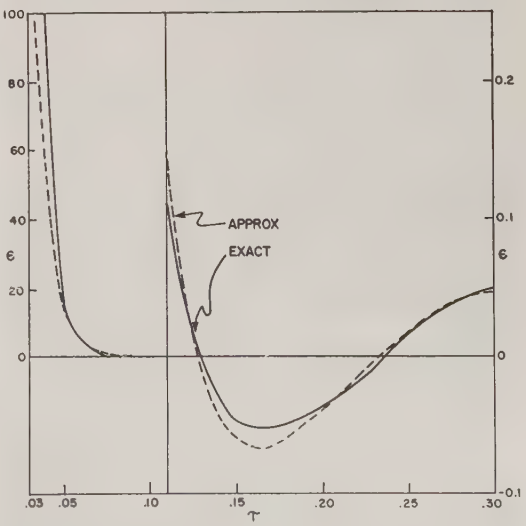

FIG. 4. Comparison of exact and approximate methods for Case II.

Klein[6] studied the behavior of this flame as a function of ω. For small values of ω where the pseudo-steady state applies, the flame velocity is given by

$$v_f = a(\omega)^{\frac{1}{2}} \tag{42}$$

where a is a constant depending on the value assumed for the molecular weight, the coefficient of heat conductivity, etc. For larger values of ω,

$$v_f = a[\omega + 7.023 \times 10^{-7}\omega^2 - 1.69 \times 10^{-9}\omega^3 + 4 \times 10^{-12}\omega^4]^{\frac{1}{2}} \tag{43}$$

It appears that this series converges rapidly if ω is less than 100 or 200 and for such cases the flame velocity is near to its steady-state value. However, as ω approaches 1000 the series expansion for the flame velocity does not converge rapidly and the steady-state approximation is no longer useful.

In a similar manner, Klein expressed x_B as a power series. Letting $x_B = x_B^*(1 + \epsilon)$,

$$\epsilon = b\omega + c\omega^2 + d\omega^3 \tag{44}$$

where b, c, and d are functions of the temperatures given in Table 3. The corresponding values of ϵ are given in Table 4 for $\omega = 1$, 10, 100, and 1000. Here again it is clear that the pseudo-steady state is a good approximation if ω is less than 100 or 200 but becomes poor if ω approaches 1000. The general behavior of ϵ as a function of temperature is very similar to that which we found for the SOB flame.

Table 3. The Coefficient Terms in the ω Expansion (From Klein[6])

T	τ(Klein)	$b \times 10^2$	$c \times 10^4$	$d \times 10^6$
3270	0.218	0	0	0
3210	0.214	.0151	.0008	.0000
3150	0.210	.0219	.0009	−.0003
3000	0.20	.0092	−.0072	−.0014
2850	0.19	−.0301	−.0117	.0099
2700	0.18	.0759	.0087	.0198
2500	0.17	−.1090	.0532	−.0281
2400	0.16	−.1128	.0717	−.0837
2250	0.15	−.0749	.0465	−.0590
2100	0.14	.0113	−.0419	.0482
1950	0.13	.1472	−.1650	.1970
1800	0.12	.3288	−.2525	.2116
1650	0.11	.5495	−.2235	−.0037
1500	0.10	.8044	−.0122	−.3541
1350	0.09	1.0899	.4332	−.6079
1200	0.08	1.4162	1.2080	−.4752
1050	0.07	1.7970	2.5945	.5806
900	0.06	2.2438	5.3990	5.0153
600	0.04	3.8000	220.0000	1000.
300	0.02	∞	∞	∞

Flame Velocity

The prediction of a flames velocity, and the elucidation of factors effecting it, has long been a major goal in the theory of flame propagation. The flame velocity is of no more inherent interest than many other properties, but if a correlation with experimental data is desired, it alone can be accurately compared. It has so far been found impossible to accurately measure temperature, concentrations, etc., in a hydrodynamic system containing the tremendous gradients typical of a flame. The situation is further complicated, as pointed out by Gaydon and Wolfhard,[12] by the fact that in most real flames, the problem is three-dimensional. Thus, with an abundance of published data, the flame velocity becomes the connecting link between theory and experiment.

Ever since a thermal (heat conduction) theory of flame propagation was proposed by Mallard and Le Chatelier[13] in 1883, refinements have been made in the calculations of flame velocity. A problem about which much has been written, and curiously, a problem that still evokes much controversy,[14] is the comparative role played by heat conduction and material diffusion in the propagation of a flame. Originally the argument concerned simple flames, of the A → B type, but these flames are now well understood. However, a change in the chemical reactions and components supporting a flame could conceivably change the entire relationship between conduction, diffusion, and flame velocity. Hence the results of the A → B flame have little bearing upon the complicated chain-branching flames that presently occupy the center of attention. The calculations we present concerning flame velocity, of course, may not lead to general conclusions. However, our results are tremendously different from those of the radical-diffusion school. It can be seriously doubted if a change in kinetics would change our results by the difference of the two theories. Thus it is felt that radical-diffusion theories must be regarded with suspicion until more evidence in their support is found.

A contention of the radical-diffusion school is that radicals must diffuse from either the reaction

or the burned region into the pre-reaction zone. In this zone they are essential for causing reaction to proceed or in initiating chains. Thus the flame velocity, by one theory,[8] is assumed to increase with the square root of the radical diffusion coefficients. This theory assumes that radicals originate in the burned region, but for a chain branching reaction this is unlikely. Hence our previous examples, Case I and Case II, can be very usefully applied. The diffusion coefficients of the radical, B, in Case II, are just double concentration in the cold zone irrespective of origin. The initiation of chains is no problem if the relaxation time is short; when the temperature becomes high enough for reaction to proceed, the radicals will be there, diffusion or not. If the relaxation time is long, chain initiating radicals obtained by diffusion might be useful, but these radicals would very likely contribute more to the flame velocity had they not diffused away from the reaction zone at all. This is in accord with the Eyring theory[16] that the influence of added

TABLE 4. ϵ AS A FUNCTION OF ω FOR THE ABC FLAME

T	τ(Klein)	$\omega = 1$	$\omega = 10$	$\omega = 100$	$\omega = 1000$
3270	0.218	0	0	0	0
3210	0.214	.0002	.0015	.0159	.2680
3150	0.210	.0002	.0022	.0225	.0453
3000	0.20	.0001	.0009	.0006	−2.0650
2850	0.19	−.0003	−.0031	−.0319	8.4480
2700	0.18	−.0008	−.0075	−.0475	19.8620
2550	0.17	−.0011	−.0104	−.0868	−24.1450
2400	0.16	−.0011	−.0106	−.1248	−77.6870
2250	0.15	−.0007	−.0071	−.0874	−55.1470
2100	0.14	.0001	.0008	.0177	44.1510
1950	0.13	.0015	.0133	.1792	181.9800
1800	0.12	.0033	.0306	.2878	189.5900
1650	0.11	.0055	.0527	.3223	−20.5970
1500	0.10	.0080	.0799	.4372	−347.2700
1350	0.09	.0109	.1127	.9152	−553.7200
1200	0.08	.0143	.1532	2.1490	−340.2300
1050	0.07	.0182	.2062	4.9721	858.0400
900	0.06	.0230	.2834	12.6580	5577.6000
600	0.04	.0610	3.5800	1223.8000	1022000.
300	0.02	∞	∞	∞	∞

those in Case I. Hence an increase in flame velocity by $\sqrt{2}$ is expected but a small decrease is found.

Case I ($\delta_{AC} = \delta_{AB} = \delta_{BC} = 1$) — $v_f = 55.1$ cm/sec

Case II ($\delta_{AC} = 1\delta_{AB} = \delta_{BC} = 2$) — $v_f = 54.8$ cm/sec

One of the diffusion arguments advanced was that chain reactions must be initiated in the cold zone by radicals originating in the reaction zone. This argument was supported by the observation that chain-initiating substances do not effect the flame velocity.[15] Hence it was assumed that the cold-zone radical concentration was independent of the cold-zone kinetics—an apparently valid conclusion, but, in our estimation not an important one. Our results indicate that the flame velocity is relatively independent of the radical reaction is important only if it occurs where the reaction rate already has a maximum value.

Acknowledgment

The authors owe a great deal of thanks to the computation staff at the University of Wisconsin Naval Research Laboratory. Mrs. Phyllis Reese took a great deal of responsibility for the over-all computational procedures as did Mrs. Marianne Schanzenbach for the machine calculations. Without their help, this work would have been next to impossible. The results reported here were made possible through the support of Project SQUID, Princeton University.

Nomenclature

$\hat{C}_i$ specific heat per gram of i
x_i mole fraction of component i

G_i fractional mass flow of i
M ρv
ρ density (g/cm³)
p pressure
v mean mass velocity
z coordinate normal to flame
n total moles per unit volume
R gas constant per mole
T temperature, Kelvin scale
m_i molecular weight of i
$\hat{H}_i$ enthalpy per unit mass of i
R_i production rate (moles/cm³) of i
D_{ij} binary diffusion coefficient
λ heat conductivity (cal $cm^{-1}sec^{-1}deg^{-1}$)

$g = \dfrac{d\tau}{d\zeta}$ reduced temperature gradient

$\tau = \dfrac{RT}{m\hat{H}}$ reduced temperature

$\zeta = \dfrac{MbRZ}{m\lambda}$ reduced distance

EIGENVALUE:

$$q = \frac{\lambda^{\infty} m^2}{Rb^2M^2}$$

$$m = \sum m_i x_i^0$$

$$\hat{H} = \sum (\hat{H}_i^{\infty} - \hat{H}_c^{\infty}) G_i^0$$

$$b = \sum b_i G_i^0$$

$$b_i = m\hat{C}_i/R$$

$$g_i = mG_i/m_i$$

$$s = \lambda/\lambda^{\infty}$$

$$\delta_{ij} = D_{ij}NRb/\lambda$$

$$G = \sum h_i G_i$$

$$h_i = (\hat{H}_i^{\infty} - \hat{H}_c^{\infty})/\hat{H}$$

$$L = \sum h_i G_i^{\infty} + (\tau^{\infty} - \tau)(\sum b_i G_i^0)$$

SUPERSCRIPTS:

0 value at cold boundary
∞ value at hot boundary

SUBSCRIPT:

e product molecule of our chain-branching flame

REFERENCES

1. Jost, W.: *Explosion and Combustion Processes in Gases.* New York, McGraw-Hill, 1946.
2. Hirschfelder, J. O., Curtiss, C. F., and Bird, R. B.: *Molecular Theory of Gases and Liquids,* Chap. 11. New York, John Wiley & Sons, 1954.
3. Hirschfelder, J. O., Curtiss, C. F., and Campbell, Dorothy E.: *Fourth Symposium (International) on Combustion.* Baltimore, The Williams & Wilkins Co., 1953.
4. Hirschfelder, J. O., and Campbell, E. S.: Univ. of Wisconsin Naval Res. Lab., Rep. CM-784, May (1953).
5. Schatzki, T. F.: Univ. of Wisconsin Naval Res. Lab., Rep. CM-853, Sept. (1955).
6. Klein, G.: Univ. of Wisconsin Naval Res. Lab., Rep. SQUID-1, Feb. (1955), SQUID-2, Feb. (1955).
7. Geib, ——: In Jost, W.: *Explosion and Combustion Processes in Gases,* pp. 317–320. New York, McGraw-Hill, 1946.
8. Tanford, C., and Pease, R. N.: J. Chem. Phys., *15*, 861 (1947).
9. Campbell, E. S.: University of Wisconsin Naval Research Laboratory Report CM-847, July (1955).
10. Hirschfelder, J. O., Curtiss, C. F., and Campbell, Dorothy E.: J. Phys. Chem. *57*, 403 (1953).
11. Zeldovich, Y., and Semenov, N.: J. Exptl. and Theoret. Phys. (USSR), *10*, 1116 (1940); English translation in N. A. C. A. Tech. Memo. 1084.
12. Gaydon, A. G., and Wolfhard, H. G.: *Flames: Their Structure, Radiation and Temperature,* p. 81, London, Chapman and Hall, Ltd., 1953.
13. Mallard and Le Chatelier: Ann. Mines, *4*, 274 (1883).
14. Evans, Marjorie W.: Princeton University, Project SQUID, Technical Report No. 27, (1951), page 6 et. seq.
15. Gaydon, A. G., and Wolfhard, H. G.: *Flames: Their Structure, Radiation and Temperature,* p. 87. London, Chapman and Hall, Ltd., 1953.
16. Eyring, H., Giddings, J. C., and Tensmeyer, L. G.: J. Chem. Phys., *24*, 857 (1956).

26

THEORETICAL STUDY OF THE HYDROGEN-BROMINE FLAME

By EDWIN S. CAMPBELL

I. Introduction

The study of the hydrodynamic equations for a one-dimensional steady-state hydrogen-bromine flame has been undertaken as part of a theoretical attack upon the controversy over the relative importance of processes such as diffusion and thermal conduction. Several factors lend interest to the study of simplified versions of our previous treatment of the hydrogen-bromine flame.[1, 2] From a conceptual point of view, alteration of the equations in a limited and theoretically intelligible way forms a necessary step in our attempt to discover what is and what is not important to the steady-state flame; from a numerical point of view, it seemed possible that the integration of a simpler model might yield a clue to the source of the difficulty we had met in our first attempt to integrate the more complete equation system.[2]

The particular simplification discussed in this paper had two main bases. First, since question had been raised concerning the validity of the steady-state approximation for Br atoms at the high temperatures found in flames,[3] it appeared to be of theoretical interest to determine the exact effect of such an assumption.[a] Second, it seemed possible that the lack of equilibrium between Br and Br_2 predicted by our earlier studies[2] might well be responsible mathematically for the difficulty we encountered in our integration. This lead to the investigation of models whose most important difference from our complete version lay in the assumption of a steady state[a] with respect to Br atoms. The exact distinction between the two versions of the flame is defined in the following section.

II. Specific Statement of the Approximations of the Simplified Model

A. SUMMARY OF THE EQUATIONS FOR A STEADY-STATE FLAME

The following discussion will be given in terms of the notation employed in previous reports. These reports should be consulted for explanation of the notation,[1] for reference to the general development and approximations of the flame equations,[b] application to hydrogen-bromine[1] and numerical values assumed for parameters.[c] In order to provide a convenient reference, the definitions of symbols have been omitted from the text and summarized under Nomenclature.

The hydrodynamic equations for the one-dimensional steady state can be written as follows: (a) an equation of continuity for the component γ in terms of the fractional mass rate of flow, G_γ,

$$\frac{dG_\gamma(z)}{dz} = \frac{m_\gamma}{M} R_\gamma \tag{1}$$

(b) a diffusion equation for each component α,

$$\frac{dx_\alpha(z)}{dz} = \frac{M}{n} \sum_\gamma D_{\alpha\gamma}^{-1} \left\{ \frac{x_\alpha G_\gamma}{m_\gamma} - \frac{x_\gamma G_\alpha}{m_\alpha} \right\} \tag{2}$$

(c) an equation of energy balance,

$$\frac{dT(z)}{dz} = \frac{M}{\lambda} \sum_\beta \frac{1}{m_\beta} \left\{ H_\beta G_\beta - \lim_{z \to \infty} H_\beta G_\beta \right\} \tag{3}$$

(d) The perfect gas equation as an equation of state. For flames which have burning velocities on the order of a few hundred cm-sec^{-1} or less, the pressure variation is in general believed to be negligible. Consequently the equation of motion is ignored and the relation between density and temperature is obtained from the perfect gas equation.[d]

It is convenient to adopt as a general notation for any of the Equations (1), (2) and (3):

$$\frac{du_i(z)}{dz} = F_{u_i} \tag{4}$$

B. SIMPLIFICATION OF THE MORE COMPLETE MODEL

The more complete model of our earlier studies of hydrogen-bromine assumed that the flame

[a] The steady-state is discussed under Assumptions (I–III) of Section II of this paper.

[b] See Campbell, Hughes and Buehler[1], p. 3 ff.

[c] See: Campbell, Hughes and Buehler[1], Appendix B; Campbell and Hirschfelder[9]; Campbell[4], Appendix B. 2; Campbell[7], Appendix B. 2.

[d] In one case a pressure change of $\sim$ 0.003 per cent was estimated for a flame speed of 30 cm^{-1} and p = 1 atmos.[8]

could be described by five homogeneous gas reactions:

$$\begin{aligned}
&(1)\ X + Br_2 \rightleftarrows 2\,Br + X' \\
&(2)\ X + H_2 \rightleftarrows 2\,H + X' \\
&(3)\ H_2 + Br \rightleftarrows HBr + H \\
&(4)\ H + Br_2 \rightleftarrows HBr + Br \\
&(5)\ H + Br + X \rightleftarrows HBr + X'
\end{aligned} \tag{5}$$

X: any of the constituents of the gas mixture.

This more complete model will be designated hereafter by [*c*]. The simplifying assumptions which reduce [*c*] are:

Assumption I. R_5 is negligible

Since calculations in the hot temperature region indicated that reaction (5) contributes at most about a per cent to the rate of production of any chemical species apart from H, it was ignored.[e] This implied that R_{Br}, the net rate of production of Br atoms, would be given by the equation

$$\begin{aligned}
R_{Br} &= R_1 - R_3 + R_4 - R_5 \\
&\simeq R_1 - R_3 + R_4
\end{aligned} \tag{6}$$

Assumption II. R_2 is negligible, $R_H = 0$

Calculations based on studies in the hot temperature region[2] also showed that R_3 and R_4 were on the order of 100 times larger than the net rate of production of H atoms,

$$R_H = R_2 + R_3 - R_4 - R_5, \tag{7}$$

which in turn dominated R_2 and R_5 except in the small t interval surrounding the point where R_H passes through zero. The steady-state approximation for H therefore reduces to

$$R_H \simeq R_3 - R_4 \simeq 0 \tag{8}$$

This simplifies Equation (6) for the rate of production of bromine atom to

$$R_{Br} \simeq R_1. \tag{9}$$

This approximation for R_{Br} is reasonable since in general R_1 appears to be on the order of 100 times as large as $R_3 - R_4$.

Assumption III. $R_{Br} \simeq R_1 = 0$

The previous study of [*c*][2] indicated that the steady-state approximation for Br is very poor for the parameters currently assigned to the specific rate constants for Reaction (1). Nevertheless, as one step toward discovering what factors affect a free-radical flame significantly, it was desirable to determine how sensitive the mole-fractions and fractional mass rates of flow were to this approximation. It was also of interest to see whether this approximation would succeed in removing the difficulty found in the numerical integration of [*c*], and if so, what number would have to be assigned to the eigenvalue, M, the mass rate of flow,[f] in order to satisfy the cold boundary conditions.

Assumption IV. Alternative approximations for the Free-radical G_γ and for diffusion

Model [I. a] for Diffusion. The F_{x_α} for the major components were approximated as follows:

$$\begin{aligned}
F_{x_\alpha} = \frac{M}{n} \sum_{\nu\epsilon\{Br,H,Br_2,H_2,HBr\}} &\{x_\alpha G_\nu/m_\nu \\
- x_\nu G_\alpha/m_\alpha\}/D_{\alpha\nu} &\simeq \frac{M}{n} \sum_{\nu\epsilon\{Br_2,H_2,HBr\}} \\
&\{x_\alpha G_\nu/m_\nu - x_\nu G_\alpha/m_\alpha\}/D_{\alpha\nu}
\end{aligned} \tag{10}$$

At about 50°C below the hot boundary temperature the errors introduced in model [*c*] by the omission of the free-radical x_ν, G_ν in the diffusion equations for Br_2 and H_2 were respectively, 7.7 per cent and 3.3 per cent.[g]

Two assumptions were introduced in order to keep the hot boundary values for the G_γ and the F_{x_α} in the models [*c*] and [*I. a*] identical: (1) The linear relations which are exact for the G_γ in [*c*][h] were used:

$$\frac{G_{HBr}}{m_{HBr}} = \frac{G_{H_2}(t_o)}{m_H} - \frac{2G_{Br_2}}{m_{Br_2}} - \frac{G_{Br}}{m_{Br}} \tag{11.a}$$

$$\frac{G_{H_2}}{m_{H_2}} = \frac{G_{Br_2}}{m_{Br_2}} + \frac{G_{Br}}{m_{Br_2}} - \frac{G_H}{m_{H_2}} \tag{11.b}$$

(2) The free radical G_γ in Equation (11) was given the constant values correct for [*c*] at the hot boundary:

$$G_{Br}(t) = G_{Br}(t_o), \qquad G_H(t) = G_H(t_o). \tag{12}$$

[e] See Assumption II which states in what sense R_5 is unimportant even for R_H.

[f] For a discussion of M as an eigenvalue, see Campbell, Hughes and Buehler[1], p. 8–9.

[g] These figures are taken from integrations using $M = 2.1 \times 10^{-2}$.

[h] These equations are obtained from the Equations IG. 3 f.g. of Campbell, Hughes and Buehler[1], p. 10, for the 50 mole-per cent hydrogen-bromine fuel.

Model [I. b] for diffusion. The general F_{x_α} of Equation (2) was used for both models [*I. b*] and [*c*]. In the exact linear relations given by Equation (11) the free-radical G_γ was assumed to be linear functions of t which had the correct values at the hot and cold boundaries, t_o and t_c respectively:

$$G_{Br}(t) = G_{Br}(t_o)\ [1 - t/t_c] \qquad (13.a)$$

$$G_H(t) = G_H(t_o)\ [1 - t/t_c] \qquad (13.b)$$

Since neither G_{Br} nor G_H even closely approximates a linear function, the sole virtue of Equations (13.a,b) is that they do preserve the boundary conditions. The effect of these approximations is discussed in Section IV.B.

In the preceding group of approximations, the simplification of the kinetics is more serious than that of diffusion. The worst assumption is that the net rate of production of Br is zero. The only difference between the kinetic model used for both [*I. a*] and [*I. b*] and the one conventionally used to describe hydrogen-bromine kinetics in static systems at temperatures less than 650°K is that the conventional model ignores the reverse of Reaction (4), R_4^r. Now the currently used boundary conditions require that

$$\lim_{t\to+\infty} F_{G_{Br_2}} = \lim_{t\to+\infty} -(m_{Br}R_4)/M = 0. \qquad (14)$$

Therefore, when the reverse of Reaction (4) is ignored, the limiting value of either x_{Br_2} or x_H must be set equal to zero. R_4^r was left in the reaction schema for two reasons: (1) It seemed desirable to maintain the hot boundary mole-fractions of [*c*]; (2) As shown by the ratios of R_4^r/R_4^f of Table 1, R_4^r makes an appreciable contribution in the neighborhood of the hot boundary.

III. Integration of the Flame Equations for Models [*I. a*] and [*I. b*]

A. EQUATIONS AND BOUNDARY CONDITIONS USED

The foregoing assumptions which simplify model [*c*] to models [*I. a*] or [*I. b*] reduce the number of linearly independent G_γ (t) to one and give three algebraic relations between the mole-fractions. G_{Br_2}, x_{Br_2}, and x_{H_2} were selected as the variables to be obtained by integrating differential equations. The equations used for the calculation[i] and the parameter values[j] have been tabulated in other reports.

[i] See Appendices B. 1 of Campbell[4, 7].

[j] See Appendices B. 2 of Campbell[4, 7].

The hot boundary values are the same for each of the three models studied.[k] For [*c*] and [*I. b*] the cold boundary values were

$$\frac{G_{Br_2}(t_c)}{m_{Br_2}} = \frac{G_{H_2}(t_c)}{m_{H_2}}, \qquad (15)$$

$$G_{Br}(t_c) = G_H(t_c) = G_{HBr}(t_c) = 0;$$

for [*I. a*], the cold boundary values were

$$\frac{G_{Br_2}(t_c)}{m_{Br_2}} = \frac{G_{H_2}(t_c)}{m_{H_2}} - \frac{G_{Br}(t_o)}{m_{Br_2}} + \frac{G_H(t_o)}{m_{H_2}} \qquad (16)$$

$$G_{HBr}(t_c) = 0,\ G_{Br}(t_c) = G_{Br}(t_o),$$

$$G_H(t_c) = G_H(t_o)$$

In the search for the eigenvalue, M, which would give solution curves satisfying the cold boundary conditions[l] the equations of [*I. a*] and of [*I. b*] were each integrated for two different choices of M.

TABLE 1. CONTRIBUTION OF R_4^r TO R_4 IN MODEL [I. b]

$T°$	R_4^r/R_4^f
1738	1.0
1732	0.562
1712	0.191
1648	0.0437
1565	0.0147

Legend: $R_4^f = f_4^f x_{Br_2} x_H$, $R_4^r = f_4^r x_{Br} x_{HBr}$.
The calculations are for $M = 0.082$ g-cm^{-2}-sec^{-1}.

B. METHOD OF SOLUTION FOR THE NEIGHBORHOOD OF THE HOT BOUNDARY, t_o.

The numerical integration was initiated by constructing the successive coefficients,

$$(u_j; t_o)_n = (d^n u_j/dt^n)_{t_o}/n! \qquad (17)$$

in power series expansions of approximately the twentieth order about the point $t_o = 0$.[l]

[k] See Campbell, Hughes and Buehler[1], p. 6, 7 for a discussion of the hot boundary conditions. A slight numerical inconsistency in the parameters assigned to the specific rates leads to a difference in the sixth digit between the value for x_H in [*C*] and that in [I.a] and [I.b].

[l] The techniques used have been reported by Campbell, Hughes and Buehler[1] and are being submitted for publication.

These coefficients[m] were used to calculate (a) the values[n] for the variables $\{G_{Br_2}, x_{Br}, x_H, x_{Br_2}, x_{H_2}, x_{HBr}\}$ in [*I. a*] and [*I. b*]; (b) the values for the derivatives[n] $\{(d\,G_{Br_2}/dt), (d\,x_{Br_2}/dt), (d\,x_{H_2}/dt)\}$ in [*I. b*] at points t off the hot boundary.

The series calculations were checked for self-consistency by computing first derivatives at points off the hot boundary using two distinct numerical procedures: Process I: (a) Compute the function values

$$(u; t_q)_0 = u(t_q) = \sum_{n \geq 0} (u; t_0)_n t_q^n \qquad (18)$$

(b) Compute the first derivatives at t_q using the function values computed in step (a) and the formulae

$$(u; t_q)_1 = (du/dt)_{t_q} = [F_u/F_t]_{t_q} \qquad (19)$$

Process II: Compute the first derivatives at t_q from the derived series

$$(u; t_q)_1 = \sum_{n \geq 1} n(u; t_0)_n t_q^{n-1} \qquad (20)$$

For $-t \leqslant 0.0032$ the values for $u = x_{Br_2}$ or x_{H_2} agreed to within a few digits in the eighth figure. For $u = G_{Br_2}$, there was an increasing discrepancy with decreasing t even though the contribution of the last term to the series sum was completely negligible. Although this indicates that the higher coefficients may be subject to some error, this discrepancy is only in the seventh digit at the point $t = -0.0032$ where the next integration step was begun.

C. METHOD USED TO EXTEND THE SOLUTION TOWARD THE COLD BOUNDARY

Beyond the range of convergence of the series expansion about $t_o = 0$, the solutions were continued for both models [*I. a*] and [*I. b*] using a six-point implicit backward difference formula. The non-linear relations given by the implicit formula were solved by the Newton-Raphson technique.[o]

Sharp changes in the vicinity of the cold boundary required the use of a much smaller interval. For this reason the Runge-Kutta procedure was adopted as an explicit method which would allow the adjustment of the interval size at any time.[p]

Both the results of the backward difference and the Runge-Kutta Integrations were checked for consistency with Weddle's Rule.

The interval size for the backward difference integration was chosen so that the results usually satisfied the rule within a discrepancy of a few units in the seventh or eighth digit. The exceptions were: (a) the discrepancies for G_{Br_2} after G_{Br_2} had risen to within a per cent or so of its final value; (b) in the case of Model [*I. b*] for $M = 0.075$, the discrepancies for G_{Br_2} which were allowed to appear in the sixth digit for a range of t. For the Runge-Kutta integration, agreement was maintained to at least the first four digits.

The numerical results which have been tabulated in other reports[o, p] are summarized in the graphs on the following page.

IV. Discussion of Results

A. COMPARISON OF [*I. b*] WITH ANOTHER SIMPLIFIED MODEL

First, let us compare the numerical integration of [*I. b*] with results obtained by Klein[5] in his studies of solving flame equations by means of successive approximations to an integral equation. He introduced the following simplification of the hydrogen-bromine flame:

Assumptions which are the same for model [*I. b*] and for Klein's model: (1) R_2, R_5 are negligible, $R_H = 0$, $R_1 = 0$.

Assumptions which Klein's model makes which [*I. b*] does not: (2) The reverse reactions of (3) and (4) are negligible.

The combination of Assumptions (1) and (2) implies:

$$R_{HBr} = 2\,f_3^f \{f_1^f/f_1^r\}^{\frac{1}{2}} x_{H_2} x_{Br_2}^{\frac{1}{2}} \qquad (21.a)$$

(3) Since (21.a) would cause the chemical reaction to go to completion, this equation is modified to give

$$R_{HBr} = 2f_3^f \{f_1^f/f_1^r\}^{\frac{1}{2}} \{x_{H_2} x_{Br_2}^{\frac{1}{2}} - x_{H_2}(t_o)[x_{Br_2}(t_o)]^{\frac{1}{2}}\} \qquad (21.b)$$

(4) Klein chose to demand consistency at the

[m] The coefficients have been tabulated in Appendices C, Campbell[4, 7].

[n] The values have been tabulated in Appendices D, Campbell[4, 7].

[o] The general form of the equations used has been summarized in Appendix E, Campbell[4]. Some specific formulae are given in Appendix E, Campbell[7]. The numerical results have been tabulated in Appendices F, Campbell[4, 7].

[p] The equations used have been tabulated in Appendices G and the results in Appendices H of Campbell[4, 7].

Graphs of the Flame Variables for a Fuel Consisting of an Equimolar Hydrogen-Bromine Mixture

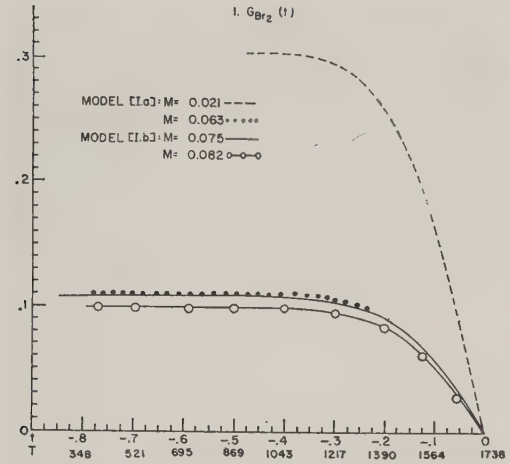

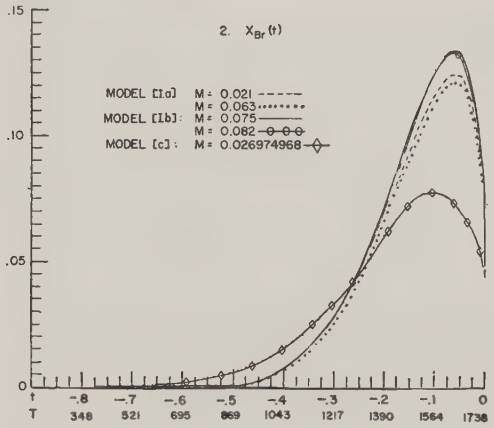

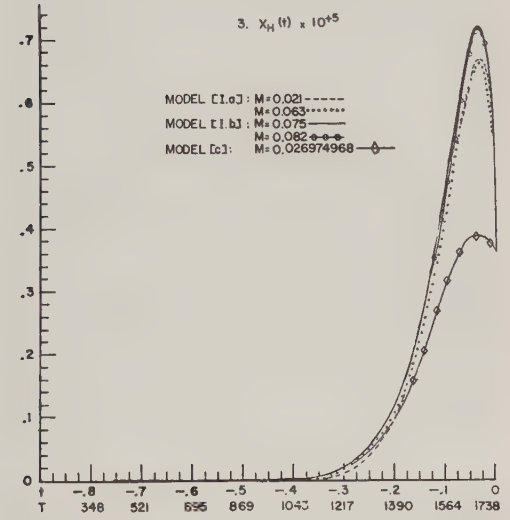

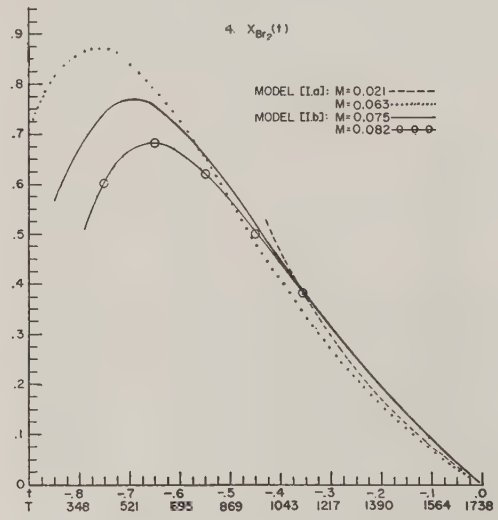

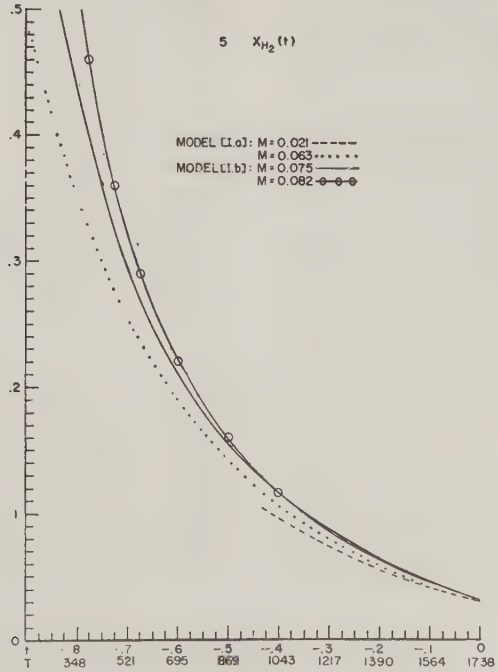

cold boundary. Since the original version of [*c*] supposed that

$$G_{\mathrm{Br_2}}(t_c)/m_{\mathrm{Br_2}} = G_{\mathrm{H_2}}(t_c)/m_{\mathrm{H_2}} \tag{22}$$

and since for Klein's model

$$R_{\mathrm{Br_2}} = R_{\mathrm{H_2}} \tag{23}$$

it follows that

$$\frac{G_{\mathrm{Br_2}}(t)}{m_{\mathrm{Br_2}}} \equiv \frac{G_{\mathrm{H_2}}(t)}{m_{\mathrm{H_2}}} \tag{24}$$

Equation (24) together with the hot boundary conditions on $F_{x_{\mathrm{Br_2}}}$ and $F_{x_{\mathrm{H_2}}}$ implies that

$$x_{\mathrm{H_2}}(t_o) = x_{\mathrm{Br_2}}(t_o). \tag{25}$$

TABLE 2. $\{(u_j)_{\mathrm{G.\,K.}} - (u_j)_{[I.b]}\}/(u_j)_{[I.b]}$

t	$u_j = x_{\mathrm{Br_2}}$	$u_j = x_{\mathrm{H_2}}$	$u_j = G_{\mathrm{Br_2}}$
0	22.0	1.7	23.0
−0.02585	3.2	1.7	1.4
−0.06332	1.3	1.3	0.50
−0.1008	0.76	1.2	0.28
−0.1383	0.56	1.1	0.15
−0.1757	0.38	0.89	0.090
−0.2507	0.24	0.76	0.036
−0.3256	0.17	0.62	−0.0051
−0.4005	0.12	0.47	−0.0030
−0.4755	0.065	0.36	−0.0070
−0.5504	0.031	0.28	−0.0070
−0.6253	−0.022	0.20	−0.0070
−0.7003	−0.069	0.15	−0.0070
−0.7752	−0.074	0.068	−0.0070

Legend: $(u_j)_{\mathrm{G.\,K.}}$: The value of the variable u_j computed by G. Klein.

$(u_j)_{[I.b]}$: The value of the variable u_j computed by model [*I.b*] with $M = 0.082$.

(5) All free-radical terms in $F_{x_{\mathrm{Br_2}}}$ and $F_{x_{\mathrm{H_2}}}$ are neglected and some arithmetic parameters are slightly modified for the sake of computational simplicity.

By far the most serious approximation made by Klein but not by Model [*I. b*] was to neglect the reverse of reaction (3) and then to insert the arbitrary term into (21. b).

Table 2 shows that the curves for the two models are qualitatively but not quantitatively similar. Naturally the two curves for $G_{\mathrm{Br_2}}$ become more alike as $G_{\mathrm{Br_2}}$ approaches its plateau value. For $x_{\mathrm{Br_2}}$ the curves are roughly similar for $t < ca.\ -0.4$. The discrepancies for each of the three variables at $t = -0.78$ are not due to Klein's approximations but are due primarily to the slight error in the M used in integrating the equations for [*I. b*]. In his attempt to fit the cold boundary conditions Klein used $M = 0.143$ g−cm^{-2}−sec^{-1} compared with 0.082 for [*I. b*] and an experimental value for hydrogen bromine of *ca.* 0.021. Since $M[G_{\mathrm{Br_2}}(t_c) - G_{\mathrm{Br_2}}(t_o)]$ is approximately constant, the value $M = 0.0828$ should allow [*I. b*] to satisfy the cold boundary condition $G_{\mathrm{Br_2}}(t_c) = 0.9887$. The value $M = 0.0820$ gave $G_{\mathrm{Br_2}}(t_c) = 0.997$.

B. EFFECT OF THE ALTERNATIVE APPROXIMATIONS OF [*I. a*] AND [*I. b*] FOR G_{Br} AND G_{H} IN THE DIFFUSION EQUATIONS

The graphs shown above of $x_{\mathrm{Br_2}}$ (T) and $x_{\mathrm{H_2}}$ (T) for [*I. a*] differ significantly from those for [*I. b*]. This difference is to be attributed primarily to two causes: (1) the omission of the explicit free-radical terms from (10) for [*I. a*] and their inclusion for [*I. b*]; (2) the failure of (12) for the G_{Br} of [*I. a*] to satisfy the cold boundary conditions. The terms in G_{H} do not make as important a numerical contribution as do those for G_{Br}.

The striking effect at t_c of the failure of [*I. a*] to satisfy the cold boundary conditions on the G_γ may be interpreted heuristically in the following way. By definition the cold boundary temperature t_c is defined by the condition

$$[F_t]_{t_c} \simeq 0 \tag{26}$$

i.e., at least two among those terms whose sum gives F_t are larger than F_t itself.[q] As is physically reasonable, it has been found in previous flame studies that there appears to be a range of t values within which t_c may be chosen which will make relatively little difference to the solution of the flame equations. This is true as long as $F_t \simeq 0$ in the sense defined above, but has not yet approached "too close" to zero.

The first effect of the failure of the G_γ (t) to approach the correct limiting value as $t \to t_c$ is just to pick out another value t_q at which $F_t \to 0$. If $t_q > t_c$, then the equations in t have a singularity at t_q; if $t_q < t_c$, then it is necessary to integrate the flame equations for values of t below those attained in the physical flame in order to determine the character of the x_β (t) in the neighborhood of the cold boundary, t_c. That is, it is expected that the curves will be

[q] See Campbell, Hughes and Buehler [1], p. 7, for a brief discussion of this point.

stretched and misshapen but that their qualitative character will be preserved.

The second effect of the failure of the $G_\gamma(t)$ to approach the correct limiting value as $t \to t_c$ depends on both the F_{x_α} and F_t. The two statements that $[F_t]_{t_c} \simeq 0$ and that t_c can be chosen over a range of values clearly implies that the F_{x_α} are approaching zero also. Otherwise, the $dx_\alpha/dt = F_{x_\alpha}/F_t$ would be becoming large and the exact choice of t_c would critically affect the solution. Now the F_{x_α} are of the form

$$F_{x_\alpha} = \frac{M}{n} \sum_\nu \{x_\alpha G_\nu/m_\nu - x_\nu G_\alpha/m_\alpha\}/D_{\alpha\nu} \qquad (27)$$

Since the $D_{\alpha\nu}$ are linearly independent in general, therefore,

$$\frac{x_\nu m_\nu}{x_\alpha m_\alpha} \to \frac{G_\nu}{G_\alpha} \qquad (28)$$

$$\frac{\sum_\nu x_\nu m_\nu}{x_\alpha m_\alpha} \to \frac{\sum_\nu G_\nu}{G_\alpha} = \frac{1}{G_\alpha}. \qquad (29)$$

Thus according to Equation (29), the x_α all approach the limiting values consistent with negligible diffusion.[r] However, since $[I.\ a]$ makes an appreciable error in the linear relations among the G_γ at the cold boundary, it must make an error in the limiting values for the x_ν.

C. SOME CONSEQUENCES OF THE BASIC PHYSICAL AND MATHEMATICAL FLAME MODEL

One of the major goals of this study is to determine the effect of the approximations which reduce model $[c]$ to $[I.\ a]$ or $[I.\ b]$. The comparison of these models requires a brief discussion of the mathematical and physical implications of the boundary conditions which have been applied.

Since there is in general no experimental data about the mole-fractions, mass rates of flow, and temperature at any given point in the high temperature region in a flame, it has been necessary to limit consideration to those flames which can be approximately described by an asymptotic approach to equilibrium:[s]

$$\lim_{z\to+\infty} du_i(z)/dz = \lim_{z\to+\infty} F_{ui} = 0 \qquad (30)$$

For present purposes, the only relevant feature of the cold boundary conditions is the requirement that the G_γ reach pre-assigned values at a temperature t_c.[s] In general, if these conditions on the G_γ are the only ones to be satisfied, one would expect that the conditions at the hot boundary should be just sufficient to define a solution with a number of arbitrary constants equal to the number of linearly independent G_γ. In a numerical integration from the hot boundary these parameters will represent eigenvalues.

Since there are reasons for integrating from the hot to the cold boundary, the first mathematical problem is to determine how to initiate the solution to a set of non-linear equations with asymptotic boundary conditions. One technique is to transform the independent variable from distance to one of the flame variables such as T and to begin the solution at

$$T_\infty = \lim_{z\to+\infty} T(z) \qquad (31)$$

Unfortunately, Equation (30) implies that the differential equations

$$du_i(T)/dT = F_{ui}/F_T \qquad (32)$$

are not defined at T_∞. In order to define the problem in a mathematically convenient fashion an added restriction has been imposed to determine whether a set of functions $\{u_j(T)\}$ will be an acceptable solution: the set $\{u_j(T)\}$ will be admissible as a solution only if each $u_j(T)$ possesses at least a one-sided derivative with respect to T at T_∞ of some pre-assigned order N. The effect of this restriction can be shown to depend upon the roots of a characteristic equation and a certain set of N-1 matrices in the following way:

(a) For each choice of the single eigenvalue, M, there are P distinct sets of possible first derivatives where P is the number of distinct roots of this characteristic equation.[t] However, there are heuristic physical reasons for selecting a particular one of these sets.[u]

(b) Provided each of the N-1 matrices is non-singular,[v] then each of the P sets of first derivatives determines its own unique set of

---

[r] Recall that in general

$$G_\alpha = (m_\alpha v_\alpha x_\alpha)/\sum_\nu m_\nu x_\nu v_\nu ,$$

and Equation (29) holds provided $v_\nu = v_\alpha$ for all ν.

[s] See Campbell, Hughes and Buehler[1]: p. 6, 7 discuss the conditions at the hot boundary; p. 4, 5 those at the cold boundary.

[t] See Equation (IIA. 13), p. 16, of Campbell, Hughes and Buehler[1].

[u] This is the set of coefficient matrices for the linear equation systems of Equation (IIB. 15), p. 23 of Campbell, Hughes and Buehler[1].

[v] See p. E.8–11 of Appendix E of Campbell, Hughes and Buehler[1].

derivatives of order two through N. Thus each of the P sets of derivatives corresponds to a different solution to the system of the flame equations which (1) satisfies the hot boundary conditions and (2) belongs to the restricted class depending upon exactly one eigenvalue.

The obvious question is, can such a restricted class contain a solution to the flame equations which also satisfies the cold boundary conditions when there is more than one linearly independent G_γ ? Mathematically the answer would seem to be no. However, there is the possibility that although a solution in this restricted class might not satisfy the cold boundary conditions exactly, it might satisfy the conditions sufficiently well for the purposes of physical approximation and might be a sufficiently good approximation for all T to the solution of the exact mathematical problem. Indeed, preliminary results indicate that when the set of linearly independent G_γ consists of G_γ for only one component in addition to free-radicals which follow a steady-state approximation within about a per cent over the region of the flame through which significant chemical reaction occurs, then a solution can be found in this single eigenvalue class which will satisfy the cold boundary conditions rather well.

As a part of the first stage of this study mathematical methods have been developed for treating this type of single eigenvalue problem. The method yields the solution to a full equation system such as [*c*], and thus determines the extent to which the system deviates from the steady-state approximation which is assumed in [*I. b*].[6]

The preceding method does not apply to free-radicals which do not follow roughly a steady-state relation. Unfortunately, in this case preliminary studies of model [*c*] indicate that a solution in the restricted class will not approximate the true solution and that a more general solution which depends on more than one eigenvalue is required. Numerical procedures for determining these more general solutions are currently being studied.

D. COMPARISON OF THE INTEGRATION OF MODELS [*I. a*] AND [*I. b*] WITH PRELIMINARY RESULTS ON [*c*]

1. Eigenvalue problem for [*c*]

All studies of [*c*] which will be discussed in this paper were based on attempts to seek a solution in the restricted class which has the mass-rate of flow, M, as its single eigenvalue. The three linearly independent G_γ for the hydrogen-bromine flame can be taken as G_{H_2}, G_{Br}, and G_H. Although H appears to obey the steady-state approximation to within a per cent over the region of the flame where significant chemical reaction occurs, Br does not. Consequently, as pointed out in the preceding section, by adjusting M, both G_{Br} and G_H can be made to approach their pre-assigned values

$$G_{Br}(t_c) = G_H(t_c) = 0 \tag{33.a}$$

but G_{H_2} cannot,

$$\lim_{t \to t_c} G_{H_2}(t) \nrightarrow G_{H_2}(t_c) \tag{33.b}$$

Thus the failure of Br atom to follow the steady-state implies that even an approximation to the solution of the flame equations must depend upon at least two eigenvalues.

2. Sensitivity of [*c*] *to M*

The divergence of Br from the steady-state produces an extraordinary sensitivity to the mass rate of flow, M. In general, free-radical G_γ (T) first climb to a positive maximum, then pass through a negative minimum and approach zero asymptotically from the negative side of the axis. If M is too large, then G_{Br} will fail to pass through a maximum, or, if it passes through a maximum, will fail to pass through a sufficiently deep minimum. In either case it diverges toward positive infinity. If M is too small, then G_{Br} will pass through a maximum, decrease too rapidly, and will either fail to pass through a negative minimum, or, if it passes through a minimum, it subsequently attains a negative maximum. In either case it diverges toward negative infinity. The equations for x_{Br} and G_{Br} are so cross-linked that sensible solutions for x_{Br} and G_{Br} within two or three hundred degrees above the cold boundary temperature seem to depend upon the seventh and eighth digits of M! Of course, such dependence lies within the uncertainty introduced by rounding error of the calculations.

3. Comparison of numerical results for [*I. a*] *and* [*I. b*] *with those for* [*c*]

Although [*c*] is essentially a two eigenvalue problem, it is interesting to compare the free-radical mole-fractions for models [*I. a*] and [*I. b*], which are rigorously single eigenvalue problems, with the single eigenvalue solution for

[c] which causes G_{Br} and G_H but not G_{H_2} to attain the correct cold boundary values. The graphs show that the incorrect application of the steady-state approximation to Br causes both x_{Br} and x_H to pass through much too sharp a maximum. Since G_{Br_2} and G_{H_2} both approach too large limiting values at the cold boundary, therefore x_{Br_2} and x_{H_2} do also. This agrees with the heuristic discussion of Section IV. B.

V. Summary

The ultimate goal of understanding the role of reaction kinetics, thermal conductivity, and diffusion in a free-radical flame will depend upon developing methods of solution for a multi-eigenvalue problem.

Present progress can be summarized as follows. Two extreme types of free-radical behavior have been found in the hydrogen-bromine flame. H[w] approximately follows a steady-state and Br does not. These two types of free-radical behavior must necessarily be treated by different mathematical methods.

The failure of the steady-state for Br makes the hydrogen-bromine flame extraordinarily sensitive to the reaction kinetics of Br and to the mass rate of flow. The mole-fractions and fractional mass rates of flow have been calculated and graphed as functions of temperature for a simplified kinetic model which incorrectly assumes a steady-state with respect to Br. For this model with a fuel consisting of an equimolar hydrogen-bromine mixture, $M = 0.082$ g-cm^{-2} $-$sec^{-1} caused G_{Br_2} to approach a limiting value of 0.997 at the cold boundary. The M which would cause G_{Br_2} to approach the theoretical value of 0.989, was estimated as 0.0828. This compares with an approximate experimental value of 0.021.[x]

Numerical procedures for integrating a system of simultaneous first order ordinary differential equations of the mathematical type which describes a certain type of free-radical flame have been developed. This type of flame has one linearly independent G_γ in addition to G_γ which approximately follow a steady-state.

[w] i.e., in general the difference between the rate of production of H and the rate of consumption of H is less than one one-hundredth the rate of production of H.

[x] This estimate is based on the observation that $\{[G_{Br}(t_c) - G_{Br}(t_0)]M\} \sim$ constant. For the experimental value see Campbell, Hughes and Bueheler[1], footnote 5 of p. 4 and p. 9.

Acknowledgment

This work is built upon the theoretical development of flame theory by Professors J. O. Hirschfelder and C. F. Curtiss and has benefited from critical discussions with Drs. G. Klein and T. Schatzki.

I would like to express my appreciation to Professor Hirschfelder for advice, encouragement, and support, which those who have been fortunate in working with him have enjoyed. Thanks is also due to the computing and secretarial staff for their work which made this study possible.

Nomenclature

$D_{\alpha\gamma}$	Binary diffusion coefficient of species α and γ in cm^2- sec^{-1}.
F_{u_i}	The function of the variables of the set $\{u_j\}$ such that $du_i(z)/dz = F_{u_i}[\{u_j(z)\}]$
G_γ	$m_\gamma n_\gamma v_\gamma / \left(\sum_\beta m_\beta n_\beta v_\beta\right)$, the fractional contribution of component γ to the mass rate of flow, M.
H_β	The enthalpy of component β in cal-mole^{-1}. The reference state is taken as the elementary substance at 0°K.
$[I.a]$, $[I.b]$	Designations for two different simplified kinetic models; *cf.* Section II.B.
M	$\sum_\beta m_\beta n_\beta v_\beta$, the mass rate of flow in g-cm^{-2}-sec^{-1}.
R_β	The rate of production of component β in mole-cm^{-3}-sec^{-1}.
R_i^f, R_i^r	The rate of the forward (reverse) half of the i-th reaction of Equation (5); the units are mole-cm^{-3}-sec^{-1}.
R_i	$R_i^f - R_i^r$, the net rate of the i-th reaction of Equation (5); the units are mole-cm^{-3}-sec^{-1}
T	The temperature in degrees absolute.
T_∞	$\lim_{z \to +\infty} T(z)$
$[c]$	A symbol for the more complete model for the hydrogen-bromine flame. cf. Section II. B.
f_i^f, f_i^r	Specific rate constants for the forward (reverse) half of the i-th reaction of equation (5) when the concentrations are expressed in mole-fractions.
m_γ	The molecular weight of component γ in g-mole^{-1}.
n_β	The concentration of component β in mole-cm^{-3}.
n	$\sum_\beta n_\beta$, the total gas concentration in mole-cm^{-3}.

t	$(T - T_\infty)/T_\infty$, a reduced temperature.
t_c	The value of t at the cold boundary.
t_o	The value of t at the hot boundary.
u_j	Any variable.
$(u_j ; t_o)_n$	$(du_j^n/dt^n)/n!$
v_β	The average velocity of molecules of component β in the units of cm-sec^{-1} with respect to a fixed axis system.
x_β	The mole-fraction of component β.
z	A distance coordinate in the units of cm.
λ	The coefficient of thermal conductivity in the units of cal-deg^{-1}-cm^{-1}-sec^{-1}.

REFERENCES

1. Campbell, E. S., Hughes, D. R., and Buehler, R. J.: CF-2109, University of Wisconsin Naval Research Laboratory, October, 1953.
2. Campbell, E. S., Schatzki, T. F.: CM-819, University of Wisconsin Naval Research Laboratory, September, 1954.
3. Benson, S. W.: J. Chem. Phys., *20*, 1605–1612 (1952).
4. Campbell, E. S.: CM-849, University of Wisconsin Naval Research Laboratory, July, 1955.
5. Klein, G.: University of Wisconsin Naval Research Laboratory, Squid 3, April 1955.
6. Campbell, E. S.: CM-846, University of Wisconsin Naval Research Laboratory, July, 1955.
7. Campbell, E. S.: University of Wisconsin Naval Research Laboratory, CM-882, August, 1956.
8. Hirschfelder, J. O., and Curtiss, C. F.: J. Chem. Phys., *17*, 1076–1081 (1949), Appendix B.

27

THE CHEMICAL STEADY STATE IN HBr FLAMES[a]

By MITCHELL GILBERT and DAVID ALTMAN

1. Introduction

The chemical-steady-state hypothesis as a feature of the propagation of HBr flames has been studied. This hypothesis, which assumes that, in many static systems reacting isothermally, the reactions involving intermediate chemical species are much more rapid than the over-all chemical reaction has recently been employed[1, 2, 3, 4] in the high-temperature regions of flames.

On the other hand, the validity of steady-state chemical kinetics at high temperatures has been questioned.[5] Among other factors the possible adverse effect of diffusion processes on the steady-state has been mentioned.

Interest in extending flame propagation concepts to the HBr flame stems from the following facts concerning this system: (1) The kinetics in static systems has been well investigated, and there is general agreement with regard to the rate constants. (2) The reaction involves a chain mechanism, and such behavior is typical of most flames that have been studied. Hence it is hoped that simplifications evolved from this study may be applicable to other more complicated systems. (3) The applicability of the low-temperature steady-state mechanism measured statically has been challenged at high temperatures,[5] and it would be interesting to inquire whether or not this uncertainty also exists in a flame system. (4) The molecular diffusivities of the flame species (H_2, Br_2, HBr, H, Br) are widely different and offer a good opportunity for testing the validity of simplifications to the diffusion treatment. Specifically, approximations based on the assignment of unity to the Lewis number (ratio of Schmidt to Prandtl number) would not a priori be considered valid.

The full consideration of the chemical steady state in this paper establishes the validity of the approximation for HBr flames on the basis (1) that the local chemical time of establishing steady-state concentrations is small compared with the flow time of the gases and (2) that the high-temperature reaction rate approaches the steady-state value in the flame.

2. The Problem of Steady State

Deviations from steady-state behavior in flames can occur because of either or both of the following reasons:

[a] This paper presents the results of one phase of research carried out at the Jet Propulsion Laboratory, California Institute of Technology under Contract No. DA-04-495-Ord 18, sponsored by the Department of the Army, Ordnance Corps.

(1) In a static isothermal system at high temperature the reaction rate may be so fast that the individual rates of the chain steps cannot maintain approximately constant concentration of chain carriers. As shown by Benson,[5] this lack in rate can be estimated from the time to reach steady state.

(2) Assuming steady state for the isothermal system, the reaction rate in a flame may deviate from local steady state because the rates of the individual chain steps cannot keep up with the rate of change of temperature in a gas element. One may refer to this deficiency as the dynamical lag.

It is of interest, therefore, to examine the behavior of the HBr system with respect to these two conditions in an average environment of a typical flame.

A. KINETICS

The kinetics and specific-rate constants suggested in homogeneous, static, gaseous systems are as follows:[6, 7, 8]

(1) $Br_2 + X \rightarrow 2Br + X$

$$k_1 = 1.44(10^{18})T^{-1}e^{-46053/RT}\text{cm}^3/\text{mol sec}$$

(2) $Br + H_2 \rightarrow HBr + H$

$$k_2 = 3.46(10^{10})T\ e^{-16640/RT}\text{cm}^3/\text{mol sec}$$

(3) $H + Br_2 \rightarrow HBr + Br$

$$k_3 = 6.43(10^{12})T^{\frac{1}{2}}e^{-1109/RT}\text{cm}^3/\text{mol sec}$$

(4) $HBr + H \rightarrow H_2 + Br$

$$k_4 = 7.65(10^{11})T^{\frac{1}{2}}e^{-1109/RT}\text{cm}^2/\text{mol sec}$$

(5) $2Br + X \rightarrow Br_2 + X$

$$k_5 = 10^{16}\text{cm}^6/\text{mol}^2\text{sec}$$

The values of rate constants are those of Campbell and Hirschfelder[23] and differ slightly from those used by Cooley and Anderson.[9] Campbell and Hirschfelder's values are preferred because they represent the Br_2-Br equilibrium more closely in the high-temperature region than do those of Cooley and Anderson.

From the above kinetics it follows that the rates of changes of the various species are, in general, for constant volume systems

$$\frac{d[Br_2]}{dt} = k_5[Br]^2[X] - k_1[Br_2][X] - k_3[H][Br_2] \tag{1}$$

$$\frac{d[HBr]}{dt} = k_2[Br][H_2] + k_3[H][Br_2] - k_4[H][HBr] \tag{2}$$

$$\frac{d[H]}{dt} = k_2[Br][H_2] - k_3[H][Br_2] - k_4[H][HBr] \tag{3}$$

$$\frac{d[Br]}{dt} = 2k_1[Br_2][X] - 2k_5[Br]^2[X] - k_2[Br][H_2] + k_3[H][Br_2] + k_4[H][HBr] \tag{4}$$

B. THE STATIC ISOTHERMAL SYSTEM

A sufficient condition for the steady-state hypothesis is that the concentrations of radical in the chain remain negligibly small compared with those of the major species. Under this circumstance Equations (3) and (4) are set equal to zero, and the rate of formation of HBr, Equation (2), becomes the steady-state form

$$\frac{d[HBr]}{dt} = \frac{2k_2(k_1/k_5)^{\frac{1}{2}}[H_2][Br_2]^{\frac{1}{2}}}{1 + (k_4/k_3)([HBr]/[Br_2])} = \frac{8.3(10^{11})T^{3/4}e^{-39667/RT}[H_2][Br_2]^{\frac{1}{2}}}{1 + (0.119[HBr]/[Br_2])} \tag{5}$$

However, the sufficient condition for the steady state is not necessary for the approximate use of the hypothesis since moderate mole fractions of an intermediate may not cause appreciable deviations from steady state. In HBr systems the H atom can certainly be expected to satisfy the condition up to quite elevated temperatures (mole fraction $\sim 10^{-4}$), but the Br atom does not satisfy the condition of low-mole fraction. When only the H-atom concentration is at steady state, the net reaction rate is modified as follows:

$$\frac{d[HBr]}{dt} = \frac{2k_2[H_2][Br]}{1 + (k_4/k_3)[HBr]/[Br_2]} \tag{5'}$$

where [Br] represents the actual nonsteady-state concentration. Insertion of the steady-state (equilibrium) value for [Br] into Equation (5′) leads directly to Equation (5).

Applying the condition of negligible time variance implied in the steady state only to H atom, Equation (3) is set equal to zero, and the behavior of Equation (4) is then investigated for its deviation from steady state (zero). Equations (1) to (4) then condense to

$$\frac{d[\mathrm{Br}]}{dt} = 2k_1[\mathrm{Br_2}][X] - 2k_5[\mathrm{Br}]^2[X] \tag{6}$$

$$\frac{d[\mathrm{Br_2}]}{dt} = -\frac{1}{2}\frac{d[\mathrm{Br}]}{dt} - \frac{k_2[\mathrm{Br}][\mathrm{H_2}]}{1 + (k_4[\mathrm{HBr}]/k_3[\mathrm{Br_2}])} \tag{7}$$

These two simultaneous, first-order, nonlinear equations were integrated on the Jet Propulsion Laboratory electronic differential analyzer for isothermal behavior, with two sets of initial conditions, in a constant-volume system.

Case II

$$t = 0; \quad [\mathrm{Br}] = 0$$
$$[\mathrm{H_2}] = [\mathrm{Br_2}]$$
$$[\mathrm{HBr}] = 0$$

Case II corresponds to a mixture of H_2 and Br_2 mixed cold and instantaneously heated to the reaction temperature. The heat of reaction is removed as in Case I. Case II obviously represents the system where Br atom builds up in the initial period as reaction proceeds.

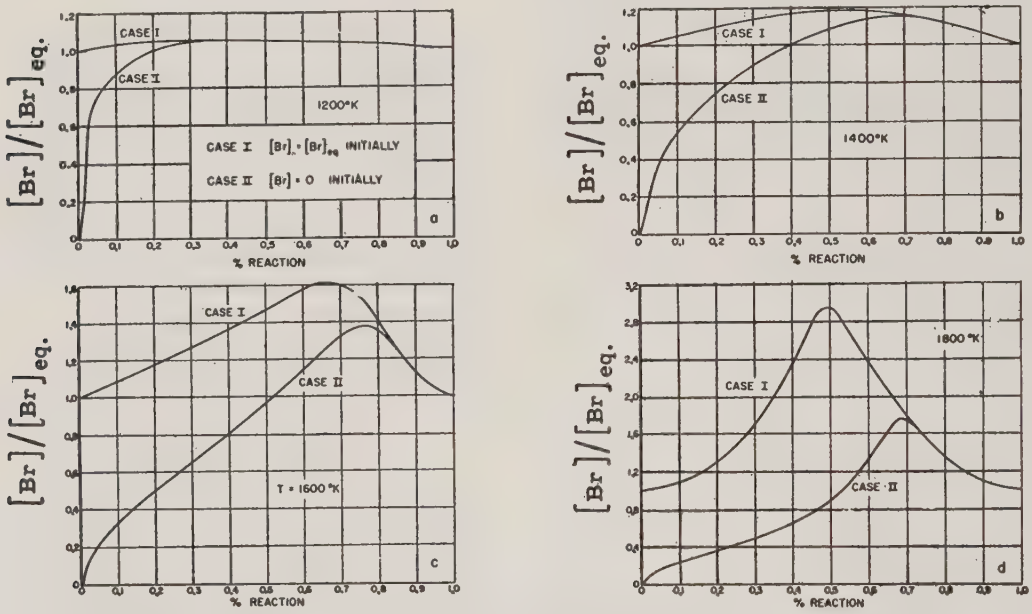

FIG. 1. Kinetics of static isothermal systems. Ratio of actual to steady-state vs per cent reaction in the stoichiometric mixture.

Case I

$$t = 0; \quad [\mathrm{Br}]^2/[\mathrm{Br_2}] = k_1/k_5$$
$$[\mathrm{H_2}] = [\mathrm{Br_2}] + \tfrac{1}{2}[\mathrm{Br}]$$
$$[\mathrm{HBr}] = 0$$

Case I thus corresponds to a stoichiometric reacting mixture of H_2 and Br_2 which is formed by heating the reactants separately to the reaction temperature and at equilibrium instantaneously mixing the reactants. The heat of reaction is removed to keep the ensuing reaction isothermal. Case I thus corresponds to a system starting at the steady state since the bromine atom is initially in equilibrium with the molecule and $d[\mathrm{Br}]/dt = 0$.

The solutions give [Br], $[Br_2]$, and [HBr] as a function of time for the temperature chosen, i.e., 1000, 1200, 1400, 1600, and 1800°K. Figure 1 is a plot of $[\mathrm{Br}]/\sqrt{k_1[\mathrm{Br_2}]/k_5}$ as ordinate *vs.* the per cent reaction as abscissa. The ordinate is a measure of the ratio of actual reaction rate to steady-state reaction rate since $\sqrt{k_1[\mathrm{Br_2}]/k_5}$ is equilibrium [Br](*Cf.* Eqs. 5 and 5′).

It is interesting to note that for Case I, the systems immediately exceed the steady-state behavior and do not return until final equilibrium is reached. However, up to 1200°K the isothermal reaction exceeds steady state only negligibly. The average values of reaction rate are 2, 7, 18, and 47 per cent in excess of steady state

for temperatures 1200, 1400, 1600, and 1800°K respectively.

For Case II the system behavior is also startling in that the reaction rate starting from its initial zero value exceeds the steady state, with a final behavior identical with that of Case I. Although as the temperature of the isothermal reaction exceeds 1200°K, a larger and larger fraction of the reaction is completed prior to reaching the steady-state rate, nevertheless the average rates fall short of steady state by only about 2, 7, 15, and 20 per cent for 1200, 1400, 1600, and 1800°K, respectively. From the results of Cases I and II, it is seen that deviations from steady state are not appreciable in static systems with reaction distributed in the range of 1000 to 1700°K, and concentrated around 1400°K, as occurs in a typical flame. It is probable that Case I refers more closely to the condition in a flame.

C. DYNAMICAL LAG

Assuming that steady-state behavior in the isothermal systems holds, the dynamical lag can be estimated from a treatment of the following problem: Consider the system at steady state at temperature T_1 and impose an instantaneous temperature jump to T_2. The time to reach an arbitrary fraction of steady-state-level characteristic of T_2 may be compared with the time of passage of an element of gas from a region at T_1 to one at T_2. This time ratio may be considered as an indication of the dynamical lag.

Considering Equation (6) in terms of this problem, following Benson[5] one assigns values of k_1, k_5, $[X]$, and $[Br_2]$ characteristic of T_2 and integrates the equation with respect to [Br]. The result is

$$t = -\frac{1}{\gamma} \ln \phi + \frac{1}{\gamma} \ln \left(\frac{[Br]_{T_2} + [Br]}{[Br]_{T_2} + [Br]_{T_1}} \right) \quad (8)$$

where

$$\gamma = (4[X] \sqrt{k_1 k_5 [Br_2]})_{T_2} \quad (9)$$

$$\phi = \frac{[Br]_{T_2} - [Br]}{[Br]_{T_2} - [Br]_{T_1}}; \quad (10)$$

$$\phi_{t=0} = 1, \qquad \phi_{t\to\infty} \to 0$$

and the T subscript refers to the temperature at which the species is at the steady-state value. For small intervals of temperature $T_2 - T_1$, the second term in Equation (8) may be neglected and the following approximate relation obtained:

$$\phi \cong e^{-\gamma t} \quad (11)$$

where $1/\gamma$ is a characteristic time constant for ϕ to fall to $1/e$, ϕ being the fractional deviation from steady state.

In Table 1 the values of the time constants $1/\gamma$ are calculated as a function of T for the HBr flame in the mixture containing 39 per cent Br_2 initially (the fastest burning mixture). The required concentrations of Br_2 are obtained from calculations in Section 3 and the total concentration $[X] = P/R_1T$. The rate constants k_1 and k_5 are calculated from expressions given in Section 2-A. It will be seen that, except close to the hot and cold boundaries where practically no reaction occurs, the characteristic times are of the order of 10^{-5} second. Upon comparison with the over-all dynamical time in this flame (0.00022 sec), the ratio of chemical time to dynamical time is seen to be of the order of 0.05. This fact alone indicates that gross adjustment to steady state is probable.

Table 1. The Dynamical Time Constant $1/\gamma$ as a Function of Temperature in a Mixture Containing 39 Per Cent Bromine Initially

T	$1/\gamma$
°K	sec × 10^5
1000	4.79
1100	2.01
1200	0.985
1300	0.571
1350	0.510
1400	0.520
1500	0.939
1550	4.71

D. THE STATIC "FLAMELIKE" SYSTEM

Having established the fact that the deviations from steady state in the static-isothermal and dynamical systems taken separately are not serious, it is now desirable to investigate more precisely the lag in a system containing both effects simultaneously. The simplest such system is one in which the reactants, after mixing, are permitted to react and heat at a rate corresponding to that of a flame. The system is imagined to be in contact with a bath capable of removing or supplying heat to maintain the rate of heating at any desired level. Thus the static system becomes

"flamelike" in all respects except diffusive transport. For simplicity constant heating rates are assumed ($dT/dt = r$). The same sets of initial conditions are applied as in the isothermal cases, with the initial temperature merely specified at any value below which negligible reaction would have occurred in the corresponding flame system. This prescription is consistent with the fact that in flowing flame gases, heating takes place over a

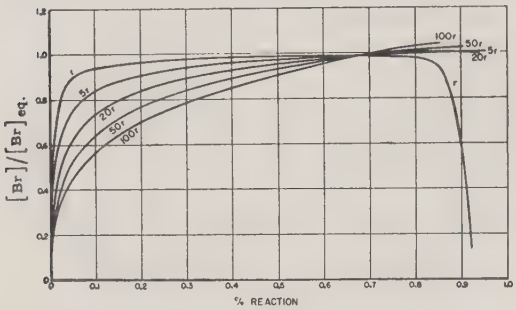

FIG. 2. Kinetics of static nonisothermal systems. Ratio of actual to steady-state rate vs per cent reaction in the stoichiometric mixture. $r = 2.65 \times 10^5$ °K/sec.

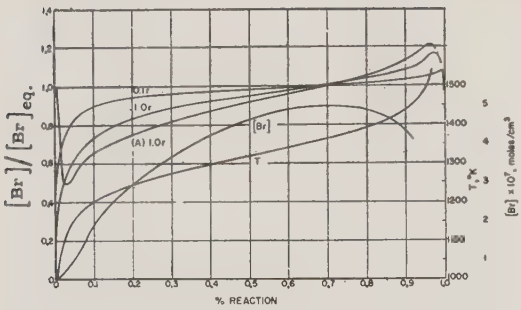

FIG. 3. Kinetics of static nonisothermal system. Ratio of actual to steady-state rate vs per cent reaction in a mixture of 61 per cent hydrogen and 39 per cent bromine. Curve (A): Variation of [Br] and T with progress of reaction for $r = 2.65 \times 10^6$ °K/sec.

considerable temperature range by heat conduction, without occurrence of appreciable reaction.

Dividing Equations (6) and (7) by dT/dt, there are obtained

$$\frac{d[\mathrm{Br}]}{dT} = \frac{1}{r}\{2k_1(T)[\mathrm{Br_2}][X] - 2k_5[\mathrm{Br}]^2[X]\} \qquad (12)$$

$$\frac{d[\mathrm{Br_2}]}{dT} = -\frac{1}{2}\frac{d[\mathrm{Br}]}{dT} - \frac{k_2(T)[\mathrm{Br}][\mathrm{H_2}]}{r(1 + 0.119[\mathrm{HBr}]/[\mathrm{Br_2}])} \qquad (12a)$$

Because of the wide variations of k_1 and k_2 with temperature, the equations are more accurately integrated on the JPL electronic digital computer. Solutions were obtained at various values of r for two mixtures of reactants, stoichiometric and 39 per cent bromine. Integrations were run to temperatures near the flame temperatures. The *a priori* values of r chosen were at 2.65×10^5°K/sec for the stoichiometric mixture and 2.65×10^6°K/sec for the 39 per cent bromine system. These average values were based on experimental flame speeds[9] and temperature distributions of the actual flames calculated from flame theory. Figures 2 and 3 are plots of the results using the same coordinates as Figure 1.

It is observed that the "flamelike" systems do not deviate greatly from the steady state for the heating rates approximating the average heating rate of the actual flame. Figure 2 shows that the nonisothermal stoichiometric system is on the average within 95 per cent of the steady state, and Figure 3 indicates that the 39 per cent bromine system (fastest burning mixture) has an average reaction rate within 87 per cent of the chemical-steady-state rate. It may be concluded, therefore, that one may employ the steady-state reaction rate in HBr flames (*cf.* Eq. 5), incurring errors of the order of only 10 per cent in reaction rate or 5 per cent in flame-speed calculations.

The treatments of the nonisothermal static systems bear strong resemblance to the results of later flame calculations despite the fact that the imposed heating rate cannot duplicate exactly the complicated heating rate over the entire flame, and as a consequence the integrations cannot match the final boundary conditions of a flame. An interesting similarity is noted from Figure 3 in that the rate exceeds the steady-state value at around 70 per cent reaction, then rises to a maximum, and drops near the last stage of reaction. Figure 3 shows this point to correspond with the temperature of maximum-Br-atom concentration. Just such behavior is also expected in the actual flame on the basis of the dynamical lag. Deviations from steady state can be readily visualized, which are of interest in explaining the detailed instantaneous behavior of the reaction in a flame, but are not considered sufficiently great, as an integrated average, to cause appreciable error in flame calculations.

3. The Flame Equations Neglecting Diffusion

A. DERIVATION

The problem of one-dimensional flame propagation has been subjected to fairly complete formulations in the past ten years.[3, 10, 11, 12, 13, 14]

The flame equations are treated briefly here. The basic relations and mathematical development are given elsewhere.[15, 16] The nomenclature follows that used by Boys and Corner.[10] The conservation of mass and energy, the constant pressure and steady condition of the flow, and the enthalpy relations

$$H = \Sigma \epsilon_i \Delta H_{fi} + c(T - T_o) \tag{13}$$

$$H - H_m = Q(\epsilon_{2m} - \epsilon_2) - Q_d(\epsilon_4 - \epsilon_{4m}) - c(T_m - T) \tag{14}$$

provide the basis for the flame equations. It should be noted that a general form of the enthalpy relation is used to facilitate incorporation of the effect of dissociation as expressed by Q_d, which represents the heat of dissociation of bromine molecules to bromine atoms.

Since it has been shown in Section 2 that the steady-state formation rate, Equation (5), is justifiable in the flame, there is obtained the rate of change of the mass fraction of HBr.

$$\frac{d\epsilon_2}{dt} = \frac{8.3(10^{11}) W_2 T^{3/4} e^{-39667/RT} \rho^{\frac{1}{2}} \epsilon_1 \epsilon_3^{\frac{1}{2}}}{W_1 W_3^{\frac{1}{2}}(1 + 0.238\epsilon_2/\epsilon_3)} \tag{15}$$

A convenient form of the flame equation can be developed by introducing a dimensionless formulation, expressing all the mass fractions of species ϵ_i in terms of the single species HBr (ϵ_2), determining the bromine dissociation corrections to be included in the concentration and enthalpy terms and finally condensing the proper equations.

A dimensionless mass fraction of species, i, and a dimensionless temperature are defined, respectively,

$$\epsilon_i^* = \frac{\epsilon_{im} - \epsilon_i}{\epsilon_{im} - \epsilon_{io}} \tag{16}$$

and

$$\eta = \frac{T_m - T}{T_m - T_o} = \frac{c(T_m - T)}{Q\epsilon_{2m} + Q_d\epsilon_{4m}} \tag{17}$$

Thus $1 - \eta$ and $1 - \epsilon_i^*$ indicate the fractional approach of temperature and composition to final flame values.

To carry out the conversion of ϵ_i to ϵ_2^*, it is first noted that the chemical equation representing the reaction for the stoichiometry of both hydrogen- and bromine-rich systems may be given as

$$aH_2 + bBr_2 \rightarrow 2HBr + (a - 1)H_2 + (b - 1)Br_2 \tag{18}$$

where $a = 1$ for $b \geqslant 1$, and $b = 1$ for $a \geqslant 1$. But for the small effects of bromine dissociation it is noted that the average molecular weight remains constant during reaction. With this approximation the average molecular weight $\overline{W} \approx (aW_1 + bW_3)/(a + b)$.

It can readily be shown from the stoichiometry that the concentrations of species in moles per gram of mixture at any point in the flame are

$$\frac{\epsilon_1}{W_1} = \frac{a - 1 + \epsilon_2^*}{\overline{W}(a + b)} \tag{19}$$

$$\frac{\epsilon_2}{W_2} = \frac{2(1 - \epsilon_2^*)}{\overline{W}(a + b)} \tag{20}$$

$$\frac{\epsilon_3}{W_3} = \frac{b - 1 + \epsilon_2^*}{\overline{W}(a + b)} - \frac{\epsilon_4}{2W_4} = \frac{b - 1 + \epsilon_2^* - \Delta^*}{\overline{W}(a + b)} \tag{21}$$

where ϵ_4/W_4 are the moles of bromine atoms per gram of mixture, produced by dissociation of Br_2, and Δ^* is the quantity $\epsilon_4\overline{W}(a + b)/2W_4$. The latter quantity is determined from the definition of the equilibrium constant, K_p, for the $1/2Br_2 \rightleftarrows Br$ equilibrium, which was assumed to hold in the HBr reaction scheme under steady state. A good approximation obtained when $\Delta^* \ll a + b$ is

$$\Delta^* = \frac{K_p^2(a + b)}{8P}\left[\left(1 + \frac{16P[b - 1 + \epsilon_2^*]}{K_p^2[a + b]}\right)^{\frac{1}{2}} - 1\right] \tag{22}$$

Since K_p is a function only of T, Equation (22) may be plotted as a function of T for unit pressure and various values of a and ϵ_2^*. Figure 4 is such a plot for the case of $a = 1.562$ (39 per cent Br_2).

With thermodynamic data for the heat of reaction Q and for the heat of dissociation of bromine molecules to bromine atoms Equations (16) and (17) (noting that $\overline{W}\epsilon_{2m}(a + b) \approx 2W_2$) can be incorporated into Equation (14) to yield

$$H - H_m \approx (Q\epsilon_{2m} + Q_d\epsilon_{4m}) \cdot \left[\frac{\epsilon_2^* - [1 - 1.87\Delta_m^*]\eta + 1.87(\Delta^* - \Delta_m^*)}{1 - 1.87\Delta_m^*}\right] \tag{23}$$

Now combining Equations (15), (16), (17),

(19), (20), (21) and (23) with the basic conservation and flow conditions there is obtained the complete flame equation, without diffusion

$$\frac{d\epsilon_2^*}{d\eta} = \frac{A(a-1+\epsilon_2^*)(b-1+\epsilon_2^*-\Delta^*)^{3/2} \cdot (1-1.87\Delta_m^*)e^{-(E/RT_m)(\beta\eta/1-\beta\eta)}}{(b-0.762+0.762\epsilon_2^*-\Delta^*)\{\epsilon_2^* - [1-1.87\Delta_m^*]\eta + 1.87(\Delta^*-\Delta_m^*)\}(1-\beta\eta)^{3/4}} \quad (24)$$

where to very close approximation, using average

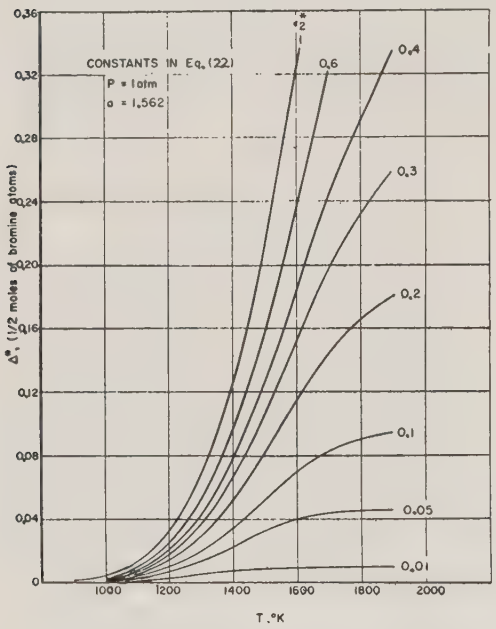

FIG. 4. Equilibrium, ½ Br ⇌ Br, as a function of temperature and mass fraction of HBr.

values for λ and c

$$A = \frac{4.15(10^{11})\bar{\lambda}\overline{W}P^{3/2}e^{-E/RT_m}}{M^2\bar{c}R_1^{3/2}T_m^{3/4}(a+b)^{\frac{1}{2}}} \quad (25)$$

From the definitions it is now observed that ϵ_2^* and η vary from zero at the hot boundary ($T = T_m$) to unity at the cold boundary ($T = T_0$).

B. DETERMINATION OF THE FLAME SPEED NEGLECTING DIFFUSION

Equation (24) can be numerically integrated and M obtained as the eigenvalue which permits the integration, started at the cold boundary, to satisfy the hot-boundary condition $\eta \to 0$, $\epsilon_2^* \to 0$. Charts such as Figure 4 are used during the integration to provide proper values of Δ^*, Δ_m^* being fixed by the equilibrium hot-boundary value ϵ_{4m}. For values of b less than and not exceeding 1.1, the value of $\Delta_m^* \ll 1$ and can be neglected in comparison with Δ^* throughout the calculation. Thus when $a \gg 1$ ($b = 1$), Equation (24) can be rewritten in a very good form to read

$$\frac{d\epsilon_2^*}{d\eta} = \frac{A(a-1+\epsilon_2^*) \cdot (\epsilon_2^*-\Delta^*)^{3/2}e^{-(E/RT_m)(\beta\eta/1-\beta\eta)}}{(0.238+0.762\epsilon_2^*-\Delta^*) \cdot (\epsilon_2^*-\eta+1.87\Delta^*)(1-\beta\eta)^{3/4}} \quad (24')$$

In column 6 of Table 2 is given the results of numerical integrations of Equation (24′) for several initial mixtures of H_2 and Br_2. For comparison the results of solution of Equation (24′) neglecting bromine dissociation (Δ^*, $\Delta_m^* = 0$) are included (*cf.* column 5 of Table 2) to show the large effect of neglecting Br_2 dissociation. The Br_2 dissociation becomes appreciable at higher temperatures; in fact the Br-atom concentration not only peaks but exceeds the bromine-molecule concentration in a region of flame where part of the reaction is occurring. Thus the chemical rate is reduced considerably (cf. Section 3-C) when dissociation occurs. Since M^2 varies directly with the rate of reaction, Equation (24′) gives a much lower value for M when dissociation is included.

In column 5 of Table 2 results are given obtained by analytical solution of Equation (24′) with $\Delta^* = 0$. Also included are values obtained analytically by Mileson[1] which for inclusion in this table are corrected for any differences between the values of $\bar{\lambda}$, $\bar{c}$, T_m, and specific rate constants used in his calculations and those used in the present calculations. Because of a difference in the methods of analytical solution, Table 2 also includes numerical integrations of Equation (24′) for $\Delta^* = 0$. It is seen that the present treatment gives similar agreement with numerical methods of solution. It is recognized of course that all the analytical solutions give flame speeds that are unrealistic due to the neglect of dissociation as well as the neglect of diffusion, as can be seen by reference to the corresponding experimental data in column 9 of Table 2.

Figure 5 is a plot of the result of numerical integrations, ϵ_2^* versus η. Figure 6 shows the partial pressure of Br_2 molecule (atmos) as a function of temperature and the Br-atom distribution, which of course corresponds to the steady state. Figure 7 shows the spatial distributions of Br and H (also the steady-state distribution). Figure 7 also shows the spatial dis-

tribution of temperature, and Figure 8 gives the temperature-time relationship corresponding to Figure 7. In the calculations for Figures 7 and 8 an experimental value of the flame speed was used in order that realistic numbers could be obtained for use in Section 2.

c. Discussion of the "thermal" flame calculations

The calculations for the "thermal" HBr flame have been made primarily to investigate the approach of H- and Br-atom concentrations to the values given by the principle of chemical stationarity. The flame equations developed neglected diffusion, and therefore it is not surprising that measured and calculated flame speeds do not agree. However, the principle of chemical stationarity coupled with consideration of diffusion and dissociation leads to far better agreement between calculated and measured values.

A basic discrepancy between these calculations and those of Mileson[1] lies in the consideration of the effects of bromine dissociation on flame

Table 2. HBr Flame Speeds

1 Br_2	2 a	3 T_0	4 T_m	Diffusion Neglected: 5 Bromine dissociation neglected	Diffusion Neglected: 6 Bromine dissociation included	Diffusion Included: 7 Bromine dissociation neglected	Diffusion Included: 8 Bromine dissociation included	9 Experimental values*
per cent		°K	°K	*cm/sec*	*cm/sec*	*cm/sec*	*cm/sec*	*cm/sec*
33	2	323	1427	71,† 67,‡ 75§	52†	21.6¶	(17)‖	10 to 23
33	2	483	1560	—	—	68.5¶	—	72
39	1.562	323	1570	107,† 95,‡ 95§	62†	43¶	(25)‖	20 to 32
50	1	323	1700	77,‡ 67,‡ 61§	37†	10¶	(4.8)‖	0 to 12

* Cf. Refs. (9) (20) (21) 22)
† Numerical integration
‡ Analytic solution
§ Analytic solution based on Reference 1
¶ Analytic solution (Cf. Equations 56 and 60)
‖ Estimates based on ratio of column 5 to column 6 (Cf. Section 7)

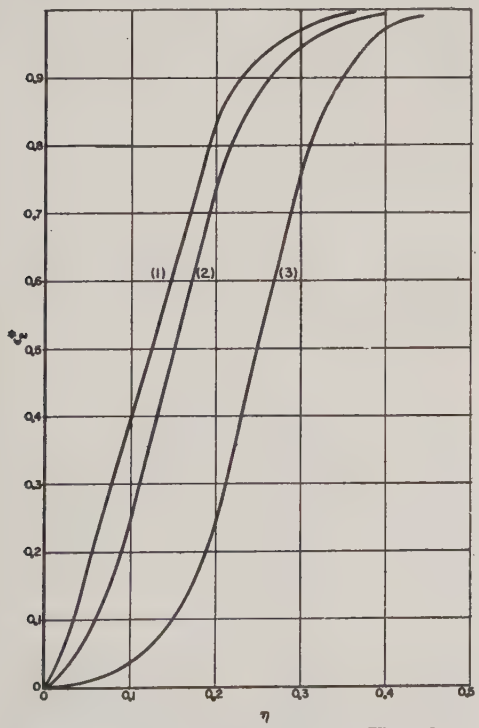

Fig. 5. Numerical integrations of HBr thermal flame equation, including dissociation of bromine. (1) 33 per cent bromine mixture, $M = 0.107$ ($U_0 = 52$ cm/sec); (2) 39 per cent bromine mixture, $M = 0.146$ (62 cm/sec); (3) stoichiometric (50%) bromine mixture, $M = 0.11$ (37 cm/sec)

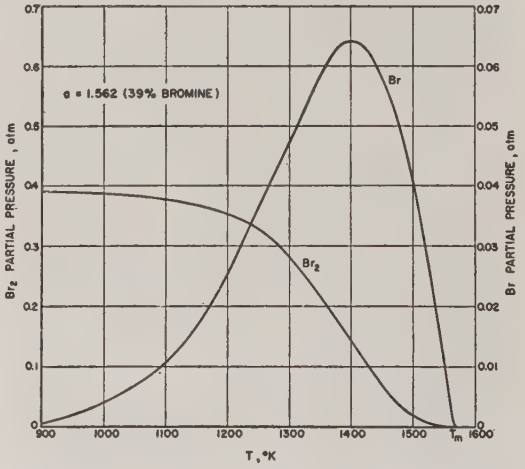

Fig. 6. Partial pressure of bromine-molecule and bromine-atom as a function of temperature in the thermal flame.

speed, which the latter considers negligible. In Table 2, however, the results of numerical integration of Equation (24′) shows the effect of bromine dissociation to be a major one. The physical

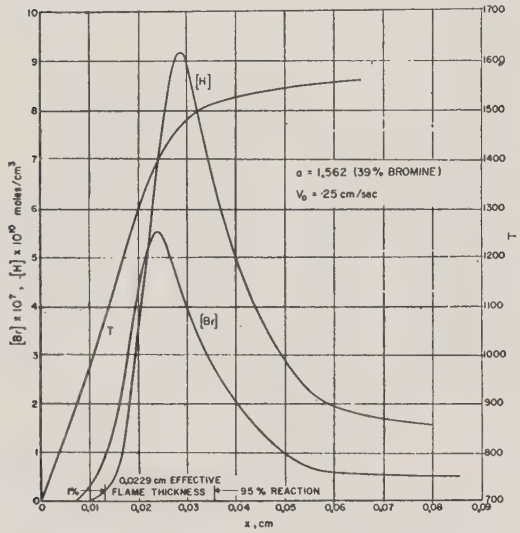

FIG. 7. Bromine- and hydrogen-atom concentrations and temperature as a function of distance in the thermal flame.

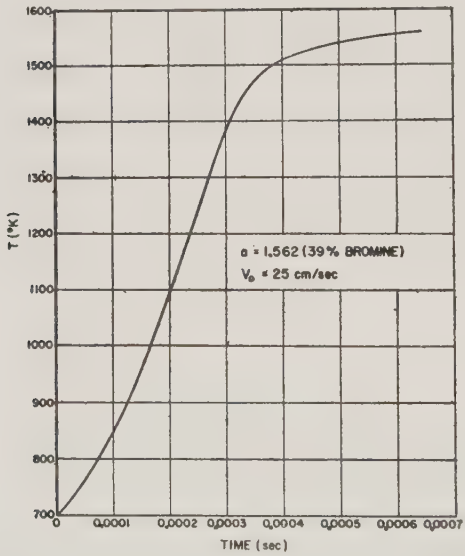

FIG. 8. Temperature—time behavior for HBr thermal flame.

basis is readily understood. The dissociation of bromine in an extensive region near the hot boundary leads to the situation where bromine-atom concentration equals and then far exceeds the bromine-molecule concentration. This condition holds for a very wide range of reactant mixtures, and most particularly near stoichiometric. As a consequence the reaction rate term in Equation (24′) will be appreciably decreased by the large decrease in the bromine-molecule concentration.

4. Derivation of the Flame Equations with Diffusion

For a two-component system Boys and Corner[10] have given the energy and mass-balance equations as

$$-\frac{d}{dx}\left(\lambda\frac{dT}{dx}\right)+Mc\frac{dT}{dx}-\rho\mathcal{R}Q=0 \qquad (26)$$

$$-\frac{d}{dx}\left(\rho\mathcal{D}\frac{d\epsilon}{dx}\right)+M\frac{d\epsilon}{dx}-\rho\mathcal{R}=0 \qquad (27)$$

As the subsequent formulation will show, a great simplification in treatment can be effected if the form of Equation (27) is also employed for a multicomponent system with a suitably defined diffusion coefficient $\mathcal{D}_i$.

In the H_2-Br_2 system, two net reaction rates must be considered for the four dominant species H_2, HBr, Br_2 and Br. One involves the net formation of HBr ($\mathcal{R}_2 = dG_2/dT$) and the other involves the net formation of Br ($\mathcal{R}_4 = dG_4/dt$). Thus, the energy equation must be modified to read:

$$-\frac{d}{dx}\left(\lambda\frac{dT}{dx}\right)+Mc\frac{dT}{dx}-\rho(Q\mathcal{R}_2+Q_d\mathcal{R}_4)=0 \qquad (26')$$

The four mass-balance equations can be written in terms of $\mathcal{R}_2$ and $\mathcal{R}_4$ noting that $\mathcal{R}_1 = -1/2\mathcal{R}_2$, $\mathcal{R}_3 = -1/2(\mathcal{R}_2 + \mathcal{R}_4)$.

$$-\frac{d}{dx}\left(\rho\mathcal{D}_i\frac{d\epsilon_i}{dx}\right)+M\frac{d\epsilon_i}{dx}+\rho\mathcal{R}_i=0 \qquad (27')$$

It is clear that an appreciable complication is caused by the incorporation of the dissociation rate $\mathcal{R}_4$ since there appears to be no simple way of combining Equation (26′) and Equations (27′). In order that the equations may be handled analytically, it will be desirable therefore to neglect $\mathcal{R}_4$, which as was shown earlier is important only in the latter stages of reaction. Then from a comparison obtained with and without dissociation in the "thermal" model, approximate corrections may be applied to the final results. The formulations given in Equation (27′) assume that each component diffuses as in a binary system with the remaining species con-

sidered as some sort of average molecule. Such a representation of the multicomponent system is assumed here, and in Section 5, $\mathfrak{D}_i$ is given in terms of the true binary coefficients $\mathfrak{D}_{ij}$.

Define the mass fraction of the gas flow contributed by the ith species,

$$G_i = \epsilon_i - (\rho \mathfrak{D}_i / M)(d\epsilon_i/dx) \tag{28}$$

Since $\Sigma G_i = \Sigma \epsilon_i = 1$

$$\Sigma \mathfrak{D}_i \frac{d\epsilon_i}{dx} = 0 \tag{29}$$

The rate of production of HBr in mol/cm³/sec is given by the steady-state rate expression

$$\frac{d[\mathrm{HBr}]}{dt} = \frac{\rho}{W_2}\frac{dG_2}{dt} = \frac{2k_2(k_1/k_5)^{\frac{1}{2}} e^{-E/RT} \epsilon_1 \epsilon_3^{1/2} \rho^{3/2} T^{3/4}}{W_1 W_3^{1/2}(1 + k_4 W_3 \epsilon_2 / k_3 W_2 \epsilon_3)} \tag{30}$$

where $2k_2(k_1/k_5)^{\frac{1}{2}} = 8.3(10^{11})$ cm$^{3/2}$ mol$^{\frac{1}{2}}$ sec and $k_4/k_3 = 0.119$.

From Equations (26′), (27′) and (28) there is obtained on integration neglecting $\mathfrak{R}_4$

$$\frac{dT}{dx} = \frac{M}{\lambda}[Q(G_{2m} - G_2) - c(T_m - T)] \tag{31}$$

which holds for the boundary conditions: $T = T_m$, $G_2 = G_{2m}$, $dT/dx = 0$ at the hot boundary, and $T = T_o$, $G_2 = 0$, $dT/dx = 0$ at the cold boundary.

From the foregoing equations the flame equations can be obtained,

$$\frac{d\epsilon_i}{dT} = \frac{\lambda(\epsilon_i - G_i)}{\rho \mathfrak{D}_i [Q(G_{2m} - G_2) - c(T_m - T)]} \tag{32}$$

$$\frac{dG_2}{dT} = \frac{8.3(10^{11})\lambda \overline{W}^{3/2} W_2 P^{3/2} e^{-E/RT} \epsilon_1 \epsilon_3^{1/2}}{M^2 W_1 W_3^{1/2} R_1^{3/2} T^{3/4}[Q(G_{2m} - G_2) - c(T_m - T)][1 + 0.119(W_3\epsilon_2/W_2\epsilon_3)]} \tag{33}$$

Define the dimensionless quantities

$$G_i^* = \frac{G_{im} - G_i}{G_{im} - G_{io}} \tag{34}$$

$$\alpha_i = \frac{\lambda}{\rho \mathfrak{D}_i c} \tag{35}$$

It can be shown from a mass and atom balance for the flame that the general dimensionless criterion

$$G_1^* \approx G_2^* \approx G_3^* \equiv G^* \tag{36}$$

holds, which permits significant simplification leading to a solution of the flame problem with diffusion. In the presence of diffusion the relations employed for the mass fractions are

$$\epsilon_1 = \frac{W_1}{\overline{W}(a + b)}(a - 1 + \epsilon_1^*) \tag{37}$$

$$\epsilon_2 = \frac{2W_2}{\overline{W}(a + b)}(1 - \epsilon_2^*) \tag{38}$$

$$\epsilon_3 = \frac{W_3}{\overline{W}(a + b)}(b - 1 + \epsilon_3^*) \tag{39}$$

Equations (32) and (33), with the foregoing, become

$$\frac{d\epsilon_i^*}{d\eta} = \frac{a_i(G^* - \epsilon_i^*)}{G^* - \eta} \tag{40}$$

and

$$\frac{dG^*}{d\eta} \frac{A(a - 1 + \epsilon_1^*)(b - 1 + \epsilon_3^*)^{3/2} \cdot e^{-(E/RT_m)(\beta\eta/1-\beta\eta)}}{(G^* - \eta)[(b - 1 + \epsilon_3^*) + 0.238(1 - \epsilon_2^*)](1 - \beta\eta)^{3/4}} \tag{41}$$

where a and b are the number of moles of H_2 and Br_2 in the reactants initially. All the stoichiometry is included by letting $b = 1$ for $a \geqslant 1$, and $a = 1$ for $b \geqslant 1$. The parameter, A, is defined as follows:

$$A = \frac{8.3(10^{11})\bar{\lambda} P^{3/2} W_2 e^{-E/RT_m}}{M^2 \bar{c} G_{2m} R_1^{3/2} T_m^{3/4}(a + b)^{3/2}} \tag{42}$$

The solution to the flame problem is contained in Equations (40) and (41) and is to be obtained by Boys and Corner's method of using the solution of the "hot-boundary" equations as the first approximation. The latter is resubstituted into Equation (41), and the quadrature solution of the resulting equation leads to a particular value of M as the second approximation.

Evaluation of the α_i term is the remaining preparatory step before attempting the solution to the flame problem with diffusion. This is described by Gilbert and Altman.[16]

5. The Effective-Mass-Diffusion Coefficients

Curtiss and Hirschfelder[17] give as the rigorous form of the mass flow due to diffusion in a multicomponent mixture

$$n_i W_i V_i = \left(\frac{W_i n^2}{\rho}\right) \sum_{k \neq i} W_k D_{ik} \frac{dy_k}{dx} \tag{43}$$

where continuity requires that $\sum n_i W_i V_i = 0$. Equation (43) is readily shown to reduce rigorously for a binary mixture ($D_{ik} = \mathfrak{D}_{ik}$) to the form

$$n_i W_i V_i = -\left(\frac{W_i \rho}{\overline{W}}\right) \frac{1 - \epsilon_i}{\sum_{j \neq i} y_j / \mathfrak{D}_{ij}} \frac{dy_i}{dx} \tag{44}$$

Equation (44) also holds very well for the ith species in a multicomponent mixture when $y \ll 1$, and is still found to be a good approximation where the y_i terms are not small. In physical terms, the validity of this approximation implies that a ternary system (and probably multicomponent) can be considered as a binary system if the suitable average property for the mixture can be chosen.

A formal identification now can be made between Equation (44) and the diffusive flux $\rho \mathfrak{D}_i (d\epsilon_i/dx)$ appearing in Equation (27′) where, obviously, the diffusion coefficient must also be interpreted to be effectively a binary coefficient.

For the HBr flame where $\overline{W}$ varies much less than ϵ_i in the region of reaction it can be shown then that

$$\mathfrak{D}_i = \frac{1 - \epsilon_i}{y_j / \mathfrak{D}_{ij} + y_k / \mathfrak{D}_{ik}} \tag{45}$$

The $\mathfrak{D}_i$ terms are clearly functions of composition, as well as of T and P through the dependence of $\mathfrak{D}_{ij}$.

6. The Diffusion of Minor Species

Prior to presenting the solution to the flame problem it is worthwhile to estimate a further deviation from the steady state, introduced by the diffusion of the minor species. The Br- and H-atom concentrations can be expected to depart from the steady-state distribution in a manner determined by the relative magnitudes of the terms in the mass-balance Equation (27) for these species.

Writing Equation (27′) in terms of concentration of species $i([i] = \rho \epsilon_i / W_i)$, and employing a suitably chosen constant value for $\mathfrak{D}_i$ in order to simplify the estimates, there is obtained for H and Br

$$-\mathfrak{D}_{\mathrm{H}} \frac{d^2[\mathrm{H}]}{dx^2} + U \frac{d[\mathrm{H}]}{dx} - \overline{\mathfrak{R}}_{\mathrm{H}} = 0 \tag{46}$$

$$-\mathfrak{D}_{\mathrm{Br}} \frac{d^2[\mathrm{Br}]}{dx^2} + U \frac{d[\mathrm{Br}]}{dx} - \overline{\mathfrak{R}}_{\mathrm{Br}} = 0 \tag{47}$$

where $\overline{\mathfrak{R}}_{\mathrm{H}}$ and $\overline{\mathfrak{R}}_{\mathrm{Br}}$ are net rates of formation of H and Br atoms in units of mol/cm³ sec. When the true steady-state distributions hold $\overline{\mathfrak{R}}_{\mathrm{H}}$ and $\overline{\mathfrak{R}}_{\mathrm{Br}}$ are zero, as determined by the expressions

$$\overline{\mathfrak{R}}_{\mathrm{H}} = k_2[\mathrm{H_2}][\mathrm{Br}] - k_3[\mathrm{Br_2}][\mathrm{H}] - k_4[\mathrm{HBr}][\mathrm{H}] \tag{3}$$

$$\overline{\mathfrak{R}}_{\mathrm{Br}} = k_1[\mathrm{Br_2}][X] - k_5[\mathrm{Br}]^2[X] - \overline{\mathfrak{R}}_{\mathrm{H}} \tag{4}$$

Setting Equations (3) and (4) equal to zero leads to expressions for the values of the local steady-state concentrations of H and Br. However, in the general case, the perturbed concentrations of H and Br can be obtained from Equations (3), (4), (46) and (47) in the first approximation as

$$[\mathrm{H}] = \frac{k_2[\mathrm{H_2}][\mathrm{Br}] + \delta_{\mathrm{H}}}{k_3[\mathrm{Br_2}] + k_4[\mathrm{HBr}]} \tag{48}$$

$$[\mathrm{Br}] = \left(\frac{k_1[\mathrm{Br_2}][X] + \delta_{\mathrm{Br}}}{k_5[X]}\right)^{\frac{1}{2}} \tag{49}$$

where

$$\delta_{\mathrm{H}} = \mathfrak{D}_{\mathrm{H}} \frac{d^2[\mathrm{H}]}{dx^2} - U \frac{d[\mathrm{H}]}{dx} \tag{50}$$

$$\delta_{\mathrm{Br}} = \mathfrak{D}_{\mathrm{Br}} \frac{d^2[\mathrm{Br}]}{dx^2} - U \frac{d[\mathrm{Br}]}{dx} \tag{51}$$

The ratios $\delta_{\mathrm{H}}/k_2[\mathrm{H_2}][\mathrm{Br}]$ and $\delta_{\mathrm{Br}}/k_1[\mathrm{Br_2}][X]$ are therefore measures of the perturbation of the chemical steady state by transport of the minor species. An estimate of magnitude is made by considering the distributions [H] and [Br] versus x obtained for steady state, without diffusion, for the flame mixture with 39 per cent bromine. The first and second derivatives are calculated; $\mathfrak{D}_i$ is estimated, and $U(x)$ is given by $U_0 T(x)/T_0$. Values of $\mathfrak{D}_{\mathrm{H}}$20 cm²/sec and $\mathfrak{D}_{\mathrm{Br}}$ 0.5 cm²/sec were chosen. The [$\mathrm{Br_2}$] and [$\mathrm{H_2}$] distributions (including the effect of their respective diffusion) are estimated, and the preceding rates are calculated.

As may be expected, the exceedingly low concentration of H atoms leads to negligible correction to the steady-state value of [H], due to transport. For Br atoms, however, their concentration is not negligible and the corrections are given in Table 3 (designating the steady-state

value as $[Br]_{ss}$):

TABLE 3

T°K	$[Br]/[Br]_{ss}$
1135	0.78
1300	0.80
1400	0.93
1470	1.11
1512	1.20

Since as it turns out the over-all flame reaction rate ($\sim 2k_2[H_2][Br]$) peaks around 1400°K and falls to ½ values at approximately 1250 and 1470°K, it is clear that the effective average value of $[Br]/[Br]_{ss}$ will be about 0.9. Thus, roughly, the transport of Br atoms perturbs the steady state by about 10 per cent, and this would result in a 5 per cent error in flame speed, over the steady state.

Although this conclusion applied to the 39 per cent Br_2 mixture, it is not expected that the result will be appreciably different for other mixture ratios. At lower Br_2 concentrations, the lower Br atom concentration will reduce the diffusive flux, and at higher Br_2 concentrations the lower flame speeds will increase the flame thickness, thereby reducing the concentration gradient.

As noted in Section 2, a 5-per cent error in the same direction was incurred by failure to kinetically follow the steady state owing to dynamical-lag considerations. In short, the steady-state treatment of the HBr flame in this paper can be expected to incur an over-all error of 10 per cent, exclusive of uncertainties in other pertinent parameters.

7. Solution of the Flame Equations

Near the hot boundary, as $T \to T_m$; ϵ_i^* , G^*, and $\eta \to 0$, Equation (41) becomes in the case of $a \geqslant 1$ $(b = 1)$.

$$\frac{dG^*}{d\eta} = \frac{A'\epsilon_3^{*3/2}}{G^* - \eta} \tag{52}$$

where

$$A' = \frac{A(a-1)}{0.238} \tag{53}$$

The hot-boundary form of Equation (40) is determined from the considerations that the exponential factor in the chemical rate usually causes G^* to vary much more rapidly than ϵ_i or η near the hot boundary. Therefore near the hot boundary it is found that

$$\frac{d\epsilon_i^*}{d\eta} \approx \alpha_i ; \quad \text{and} \quad \epsilon_i^* \approx \alpha_i \eta \tag{54}$$

That such behavior occurs has been shown in the theoretical treatments[11, 18] of the general effect of diffusion on the variation of ϵ and G with η and is the basis of von Kármán's analytical treatment of the HBr "thermal" flame equations.[1] The approximation $G^* \gg \eta$ occupies the same role in the flame with diffusion as does the approximation $\epsilon^* \gg \eta$ in the flame without diffusion, near the hot boundary.

Using Equation (54) with $i = 3$ in Equation (52), there is obtained upon integration, for the solution in the vicinity of the hot boundary,

$$G^* \approx [0.8A'\alpha_3^{3/2}\eta^{5/2}]^{\frac{1}{2}} \tag{55}$$

As the second approximation Equation (55) is combined with Equation (41) for $a \geqslant 1$, $b = 1$ to give, separating variables

$$\int_0^1 dG^* = 1 = \int_0^1 \frac{\begin{array}{r} 0.238A'\alpha_3^{3/2}\eta^{1/2} \\ \cdot(a - 1 + \alpha_1\eta) \\ \cdot e^{-(E/RTm)(\beta\eta/1-\beta\eta)} \end{array}}{\begin{array}{l} (a-1)(1-\beta\eta)^{3/4} \\ \cdot(\alpha_3\eta + 0.238[1 - \alpha_2\eta]) \\ \cdot([0.8A'\alpha_3^{3/2}]^{\frac{1}{2}}\eta^{1/4} - 1) \end{array}} d\eta \tag{56}$$

The irregular behavior of the integrand in Equation (56) near $\eta = 0$ does not affect the final calculation. A finite limiting behavior actually occurs near the hot boundary as has been shown in the literature, and the attachment of the correct limiting slope near $\eta = 0$ does not change the value of the integral appreciably (*cf.* Mileson[1] and Appendix of Gilbert and Altman[15]).

Equation (56) is the final flame equation with the variables separated and can be evaluated by numerical or other methods. The value of A' which satisfies this equation then determines M^2 through Equations (53) and (42).

A further simplification of Equation (56) may be noted from the fact that $A' \gg 1$ for the flames of interest. Equation (56) becomes

$$\int_0^1 \frac{\begin{array}{r} 0.266\alpha_3^{3/4}A'^{1/2}\eta^{1/4}(a - 1 + \alpha_1\eta) \\ \cdot e^{-(E/RTm)(\beta\eta/1-\beta\eta)} \end{array}}{\begin{array}{l} (a-1)(1-\beta\eta)^{3/4} \\ \cdot(\alpha_3\eta + 0.238[1 - \alpha_2\eta]) \end{array}} d\eta = 1 \tag{57}$$

Flame Speed Calculation at $a = 2$

In this case, the following constants are characteristic of the mixture: $\alpha_1 = 0.32$, $\alpha_2 = \alpha_3 = 2.5$

(cf. Appendix of Gilbert and Altman[16]), $T_m = 1427°K$, $T_0 = 323°K$, $\bar{c} = 0.137$ cal/gm°K, $G_{2m} = 0.9877$, $\bar{\lambda} = 0.00025$ cal/cm sec°K, $\beta = 0.775$, $E = 39{,}667$ cal, $A' = 0.485/M^2$. Equation (57) becomes:

$$\int_0^1 \frac{(1 + 0.32\eta)\eta^{1/4} e^{-10.8\eta/(1-.775\eta)}}{(1 + 8\eta)(1 - 0.775\eta)^{3/4}}\, d\eta = 0.64M$$

A graphical integration of this equation gives a value of 21.6 cm/sec for the flame speed.

Flame Speed Calculation at Stoichiometric ($a = 1$)

The flame equation for the stoichiometric case, $a = 1$, $b = 1$, is obtained from Equation (41) and leads to the hot-boundary form

$$\frac{dG^*}{d\eta} = \frac{A\epsilon_1^* \epsilon_3^{*3/2}}{0.238(G^* - \eta)} \tag{58}$$

Equation (40) also applies and again leads to the hot-boundary form, Equation (54). Using the approximation $G^* \gg \eta$, Equations (54) and (58) are combined to give

$$G^* \approx (2.4\alpha_1\alpha_3^{3/2} A\eta^{7/2})^{\frac{1}{2}} \tag{59}$$

The second approximation, combining Equations (59) and (41), for $a, b = 1$ is

$$\int_0^1 dG^* = 1 = \int_0^1 \frac{\begin{matrix} A\alpha_1\alpha_3^{3/2}\eta^{3/2} \\ \cdot e^{-(E/RTm)(\beta\eta/1-\beta\eta)} \end{matrix}}{\begin{matrix} (1 - \beta\eta)^{3/4} \\ \cdot (\alpha_3\eta + 0.238[1 - \alpha_2\eta]) \\ \cdot ([2.4\alpha_1\alpha_3^{3/2}A]^{\frac{1}{2}}\eta^{3/4} - 1) \end{matrix}} d\eta \tag{60}$$

In this case $a = b = 1$, $\alpha_1 = 0.2$, $\alpha_2 = \alpha_3 = 1$, $T_m = 1700°K$, $T_0 = 323°K$, $\bar{c} = 0.1$ cal/gm°K, $G_{2m} = 0.947$, $\bar{\lambda} = 0.000137$ cal/cm sec°K, $\beta = 0.8$, $E = 39{,}667$ cal, $A = 1.337/M^2$. Graphical integration gives a value of ~10 cm/sec for the flame speed.

Before comparing the calculated and experimental values of the flame speed it is necessary to evaluate the correction required for failure to include bromine dissociation in the flame equation. The inclusion of this correction complicates the flame equation greatly. However, by numerical integration it was shown (Section 3) that in the case without diffusion the calculated flame speed is reduced by almost a factor of two. A similar factor can, qualitatively, be expected to apply to Equation (30) and thus to Equations (33), (56) and (60), in the case with diffusion. The reason for this is that the major way in which the inclusion of bromine dissociation affects the equation is to alter the term ϵ_3 by the amount of bromine present as atoms, and the enthalpy term $H\text{-}H_m$. It may be noted that in any case flame speed varies as $[\mathcal{R}_2(\epsilon_1, \epsilon_2, \epsilon_3)/(H\text{-}H_m)]^{\frac{1}{2}}$. Thus dissociation lowers the speed because the appearance of Br atom, which reduces ϵ_3, lowers $\mathcal{R}_2$ and raises $H\text{-}H_m$, as is clear from Equations (14) and (15). Since the above expression commonly governs the behavior of flame speed for both the diffusive and nondiffusive treatments, and since Br atom concentration is determined mainly by the $Br_2 = 2Br$ equilibrium, a correction of similar magnitude may be expected to account for dissociation in the flame with diffusion. A further consideration shows that the lowering observed in the "thermal" flame should be an upper limit. This is so because ϵ_3, though not far different in flames with or without diffusion, is certainly smaller in the former and leads to smaller equilibrium Br-atom concentrations.

The foregoing analysis suggests that the correction factors obtained through numerical integration in Section 3, for the effect of bromine dissociation, can be applied to the flame equations solved in the present paper. Table 2 summarizes the flame speeds calculated for HBr systems with column 8 derived from column 7 by application of the correction factors obtained in Section 3. A comparison of column 8 with column 9, the experimental values of flame speeds, indicates that the final calculated values represent excellent mean values of the observed flame speeds considering the inherent uncertainties in some of the basic physical constants.

8. Discussion

The over-all agreement between the calculated and experimental values of flame speeds for the HBr flame including diffusion indicates the basic correctness of the physical assumptions. The chemical steady state holds approximately, and the values for the thermal conduction and diffusion parameters are probably of about the right magnitude.

There is general satisfaction with the correctness of complete formulations of flame equations as given by Hirschfelder and co-workers.[2, 19] Nevertheless, the solution of these equations for all but the simpler systems is rather involved and leaves something to be desired with regard to the extraction of physical understanding concerning the behavior of flame propagation with complex reaction. Drastic approximation of the physical details of flames has sometimes led to

partial understanding of flame propagation as a result of a few cases of good agreement between experimental and calculated values of the flame speed (through the liberal use of empirical correlation constants). But a more prevalent result has been the establishment of confidence in physical models that are seriously incomplete or erroneous in basic details.

One example has been the development of diffusion theories based solely on H atoms or other atoms as the controlling factor in propagation velocity of some flames. The empirical success of these theories has rested on magnitudes of atom concentrations of the order of the hot-boundary equilibrium value. Yet it appears to be probable from the present paper that flames which depend on the fast reactions of atomic species in a chain mechanism will maintain atom concentrations in the critical zones of reaction that are an order of magnitude or greater than the final equilibrium values.

Attempts that have been made to relate the burning velocity of the HBr flame to the diffusion of minor species can now be seen to be incorrect. There are first the obvious magnitude errors due to the existence of steady-state maxima within the flame instead of concentration profiles governed by diffusion from the adiabatic-flame-temperature region. Equally important is the fact that only the diffusion of the major species has any significant bearing on the HBr flame. Thus physical reasoning indicates that once the kinetics are fixed by steady-state considerations for the minor species there can be no H or Br diffusion mechanism controlling flame speed simply because diffusion has no great influence on the minor species distribution in the reaction zone.

Some comment can also be made regarding the so-called constant-enthalpy treatment of the flame equation, which is based on the condition that all $\alpha_i = 1$. Such treatment of the flame equations would be physically invalid because of the large deviations of α_1 from 1, as seen in this paper. Using Equation (60) for the stoichiometric flame, as an example, setting all $\alpha_i = 1$ would result in a calculated flame speed of ~22 cm/sec. This value compares with 10 cm/sec for the calculation with $\alpha_1 = 0.2$ for hydrogen.

Nomenclature

A, A'	hot boundary constants.
a	initial moles $H_2 (b = 1)$.
b	initial moles $Br_2 (a = 1)$.
c	mean specific heat at constant pressure
$\mathfrak{D}_i$	effective diffusion coefficient for species i in mixture.
$\mathfrak{D}_{ij}$	true binary diffusion coefficient for species i and j.
D_{ij}	multicomponent diffusion coefficient.
E	activation energy.
G_i	mass fraction of species i in mass rate of flow.
G_{im} , G_{io}	mass fraction of i in rate of flow, at boundaries.
G_i^*	dimensionless mass fraction of i in rate of flow.
H	specific enthalpy of mixture.
$-\Delta H_{fi}$	molar heat of formation of species i.
$[i]$, n_i	concentration of species i (mol/cm³).
k	specific chemical rate constant.
K_p	equilibrium constant for $\frac{1}{2}\ Br_2 \rightleftarrows Br$.
M	total mass rate of flow per unit area.
n, $[X]$	total concentration (mol/cm³).
P	pressure.
Q	heat of reaction per gram of HBr formed.
Q_d	heat of dissociation reaction per gram of Br atoms (negative).
$\mathfrak{R}_i$	grams of species i produced per g of mixture/sec.
$\overline{\mathfrak{R}}_i$	moles of species i produced per cm³ per sec.
R	gas constant, energy units.
R_1	gas constant, mechanical units.
T	temperature.
T_m	adiabatic flame temperature.
T_0	initial temperature.
t	time.
U	gas speed (cm/sec).
U_0	flame speed (cm/sec).
V_i	diffusion velocity for species i.
W_i	molecular weight of species i.
$\bar{W}$	average molecular weight of mixture.
x	distance.
y_i	mole fraction of species i in mixture.
α_i	ratio of Schmidt to Prandtl number for species i.
β	$(T_m - T_0)/T_m$.
ϵ_i	mass fraction of species i, gram/gram mixture.
ϵ_{im} , ϵ_{io}	mass fraction of i at hot and cold boundaries, respectively.
ϵ_i^*	dimensionless mass fraction of species i.
$\epsilon_1, \epsilon_2, \epsilon_3, \epsilon_4$,	mass fractions of H_2 , HBr, Br_2 and Br, respectively.
γ	time constant, sec^{-1}, for attainment of steady state.
$2\Delta^*$	moles of Br atoms in $(a + b)$ moles of mixture, (cf. Equation 22).
Δ_m^*	hot boundary value of Δ^*.
λ_i	thermal conductivity of species i.

λ thermal conductivity of mixture.
η dimensionless temperature.
ρ density of gas mixture.
ϕ fractional deviation from steady-state concentration of bromine atoms (cf. Equation 10).

SUBSCRIPTS

m, o = hot and cold boundary values, respectively. 1, 2, 3, 4 = species identity, H_2, HBr, Br_2, Br, respectively.

REFERENCES

1. Mileson, D. F.: Report No. 6, California Institute of Technology, July, 1954.
2. Giddings, J. C., and Hirschfelder, J. O.: SQUID-5, Series 8, University of Wisconsin, May 3, 1956.
3. Von Kármán, T., and Penner, S. S.: *Fundamental Approach to Laminar Flame Propagation, Selected Combustion Problems.* London, Butterworth Scientific Publications, 1954.
4. Gilbert, M., and Altman, D.: Progress Report No. 20–278, Jet Propulsion Laboratory, June 6, 1955.
5. Benson, S. W.: J. Chem. Phys., *20*, 1605 (1952).
6. Christiansen, J. A.: Det Ang Danshe Videnskabeknes Selskab Mathematiskfysiske Meddelelser, *1*, 3 (1919).
7. Herzfeld, K. F.: Ann. Physik, *56*, 635 (1919).
8. Polanyi, M.: Z. Elektrochemie, *26*, (Nos. 3 and 4), 1920.
9. Cooley, S. D., and Anderson, R. C.: Ind. Eng. Chem., *44*, 1402 (1952).
10. Boys, S. F., and Corner, J.: Proc. Roy. Soc., *A197*, 90 (1949).
11. Corner, J.: Proc. Roy. Soc., *A198*, 388 (1949).
12. Hirschfelder, J. O., and Curtiss, C. F.: *Third Symposium on Combustion, Flame and Explosion Phenomena*, pp. 121–140. Baltimore, The Williams & Wilkins Co., 1949.
13. Hirschfelder, J. O., Curtiss, C. F., and Bird, R. B.: *Molecular Theory of Gases and Liquids.* New York, John Wiley & Sons, 1954.
14. Lewis, B., and von Elbe, G.: *J. Chem. Phys.*, *2*, 537 (1934).
15. Gilbert, M., and Altman, D.: Progress Report No. 20-276, Jet Propulsion Laboratory, June 6, 1955.
16. Gilbert, M., and Altman, D.: Progress Report No. 20-277, Jet Propulsion Laboratory, June 6, 1955.
17. Curtiss, C. F., and Hirschfelder, J. O.: J. Chem. Phys., *17*, 550 (1949).
18. Hirschfelder, J. O., Curtiss, C. F., and Campbell, D. E.: *Fourth Symposium (International) on Combustion*, pp. 190–211. Baltimore, The Williams & Wilkins Co., 1953.
19. Campbell, E. S., Hughes, D. R., and Buehler, R. J.: CF 2109, University of Wisconsin, October 19, 1953.
20. Cooley, S. D., Lasater, J. A., and Anderson, R. C.: J. Am. Chem. Soc., *74*, 739 (1952).
21. Cooley, S. D., and Anderson, R. C.: J. Am. Chem. Soc., *77*, 235 (1955).
22. Hellwig, K., and Anderson, R. C.: J. Am. Chem. Soc., *77*, 232 (1955).
23. Campbell, E. S., and Hirschfelder, J. O.: CF 2108, University of Wisconsin, Nov. 17, 1953.

28

STABILITY OF THE OZONE FLAME PROPAGATION[a]

By J. B. ROSEN

Introduction

The physical significance of the steady-state solution to the equations of laminar flame propagation is closely related to whether or not the solutions considered are stable. The stability of a steady-state solution is determined by the behavior of the solution to the complete time-dependent equations starting with an initial condition which is a perturbed steady-state solution. If the perturbed time-dependent solution approaches the original steady-state solution, the solution considered is stable; if not, it is unstable.

[a] This research was supported by the United States Air Force under Contract No. AF 33(038)-23976 monitored by the Office of Scientific Research, while the author was at the Forrestal Research Center, Princeton University, Princeton, New Jersey.

An unstable solution cannot represent a physically realizable steady flame propagation since the temperature and concentration profiles given by such a steady-state solution would not be obtained from a developing ignition source. Furthermore, if it were possible to impose such a steady-state profile, it would alter with time as a result of the growth of small random fluctuations (e.g., in the reaction rate).

A general theory of laminar flame stability has previously been given.[1] In this paper the theory is applied to investigate the stability of the steady-state ozone flame propagation. The steady-state equations used to describe the process as well as the chemical kinetic and transport coefficients are those given and solved by Hirschfelder, Curtiss, and Campbell.[2] Some simplifications in the steady-state solution given by von Kármán and Penner[3] are also used.

Ozone Flame System

The ozone flame reaction is a three-component system, the components being O_3, O_2, and O atom. The time-dependent system of equations representing the constant pressure ozone flame consists of the energy blance equation, the conservation of mass equation, and the continuity equations for two of the three components. As a matter of convenience, the continuity equations for the two components O_3 and O are used. The continuity equations are written in terms of the weight fractions, Y, of O_3 and Y_1 of O. The concentration of O_2 is then immediately given by $Y_2 = 1 - Y_1 - Y$. The complete unsteady-state equations for such a multicomponent system have previously been given,[4] including a diffusion equation for each component. In the present case the concentration of O atom, Y_1, relative to unity is sufficiently small so that we may take $Y_2 = 1 - Y$ as far as the conservation and diffusion equations are concerned and treat the O atom as a trace component. This permits the two diffusion equations to be treated as binary diffusion equations, which results in a considerable simplification. In particular, the diffusion and continuity equations for each component can be combined, resulting in a single continuity equation for each of the components O_3 and O. The combined continuity equation is a second order equation including a diffusion term and the rate of production of the component considered.

The energy equation relates the rate of increase of the temperature to the local increase in energy due to thermal conduction and the net heat release due to chemical reaction. The gas density, ρ, can be eliminated from the equations by the use of the equation of state in the form $\rho T = \text{const.}$, since we assume a constant pressure flame. The resulting energy equation, two continuity equations, and conservation of mass equation for the simplified two-component system can then be given as the following four dimensionless equations.

$$\Phi^{-1}\Phi_\theta + \Omega\Phi_z - \Phi_{zz} + \frac{1}{\beta}(cP + c_1P_1) = 0 \quad (1)$$

$$\Phi^{-1}Y_\theta - \delta Y_{zz} + \Omega Y_z - \beta^{-1}P = 0 \quad (2)$$

$$\Phi^{-1}(Y_1)_\theta - \delta(Y_1)_{zz} + \Omega(Y_1)_z - \beta^{-1}P_1 = 0 \quad (3)$$

$$(\Phi^{-1})_\theta + \Omega_z = 0 \quad (4)$$

In these equations, $\Phi = T/T_o$ is the reduced temperature, where T is the gas temperature and T_o its value in the unburned gas, Ω is the ratio of the mass flow to its steady-state constant value, and δ is the reduced diffusion constant. P and P_1 are rates of production of O_3 and O, respectively, due to chemical reaction and are explicit nonlinear functions of Φ, Y, and Y_1. β is a constant, the value of which is an eigenvalue of the steady-state equations and determines the steady-state flame velocity. c is the reduced value of the difference between the specific enthalpy of O_3 and O_2 at $T = T_o$. c_1 similarly represents the enthalpy difference in O and O_2. The independent variables θ and z are the reduced time and distance variables, respectively. All quantities are defined in the Table of Nomenclature, and the values of the dimensionless parameters used are given in the Appendix. The flow of combustible gas through the flame zone is assumed to be from $z = -\infty$ toward $z = \infty$, with $z = 0$ located at the temperature profile inflection point. The composition and temperature of the mixture at $z = -\infty$ are those of the unburned (cold) gas while at $z = \infty$ the equilibrium values at the adiabatic flame temperature are obtained. The Equations (1) through (4) together with appropriate boundary and initial conditions determine the four quantities, Φ, Y, Y_1, and Ω.

The rate functions, P and P_1, are determined by the chemical kinetics of the flame reaction. The kinetic equations describing the rates of production of O atom and O_2 from O_3 are taken to be

$$O_3 + G \underset{r_1'}{\overset{r_1}{\rightleftharpoons}} O + O_2 + G \qquad (5)$$

$$O + O_3 \xrightarrow{r_3} 2O_2 \qquad (6)$$

where G represents any other particle. The validity of approximating the complete reaction scheme by these two relations has been discussed.[3] Except as the combustion reactions go to completion and the ratio of O to O_3 becomes greater than unity, the reverse reaction (r_1') of Equation (5) may be neglected. Since the reaction zone where the heat release is greatest is the important part of the flame from the point of view of stability, only the forward reactions with rates r_1 and r_3 are considered. These rates have been given,[2] and in terms of the dimensionless variables used here are given by

$$r_1 = (Y/2\Phi) \exp(-\sigma/\Phi) \qquad (7)$$

$$r_3 = (k_1 Y Y_1/2\Phi) \exp(-\sigma_1/\Phi) \qquad (8)$$

The fuel O_3 is decreased by both Equations (5) and (6) so that

$$P = -r_1 - r_3 , \qquad (9)$$

while O atoms are produced by Equation (5) and lost by Equation (6) giving

$$P_1 = 1/3(r_1 - r_3) \qquad (10)$$

The steady-state solution of Equations (1) through (4) is obtained by setting the time derivative term in each equation identically equal to zero. This gives immediately Ω = const. = 1 from Equation (4). For the steady state, the approximation $P_1 = 0$, $r_1 = r_3$ is good except as $z \to \infty$. This gives Y_1 as a function of Φ only by the relation

$$k_1 Y_1 = \exp\left(\frac{\sigma_1 - \sigma}{\Phi}\right) \qquad (11)$$

The steady-state value of P is then given by using Equation (11) in Equation (8) for r_3 which gives

$$P = -(Y/\Phi) \exp(-\sigma/\Phi) \qquad (9a)$$

A departure from the simple Equations (11) and (9a) will occur for time-dependent solutions depending on the rate of change of Φ with time.

The resulting steady-state Equations (1), (2) and (3) given here are equivalent to those given and solved for the eigenvalue, β, in Hirschfelder, Curtiss and Campbell[2] and von Kármán and Penner.[3] The steady-state values of Φ, Y, and Y_1 as functions of z which are needed in the present stability analysis, were obtained by numerical integration of the steady-state equations. The eigenvalue, β, and therefore the steady-state flame velocity, was determined as part of the numerical integration procedure for each of the five cases considered.

Linearized Stability Equations

The method of determining the stability of the steady-state solution for a particular set of parameter values consists of linearizing the time-dependent equations with respect to the steady-state solution and solving this linearized system for a temperature perturbation equivalent to a point source heat release. The linearized system is obtained by letting

$$\begin{aligned} \Phi &= [\Phi] + \tau \\ Y &= [Y] + y \\ Y_1 &= [Y_1] + \frac{\mu}{3\gamma} \\ \Omega &= 1 + m \end{aligned} \qquad (12)$$

where the brackets $[\square]$, denote the steady-state value and γ is a scale factor. These expressions are substituted in Equations (1) through (4) and terms of second order in the perturbations τ, m, y and μ are neglected. The steady-state terms drop out leaving the following system of four linear partial differential equations in the four pertubations.

$$-\tau_{zz} + \tau_z + a_3\tau + a_4\tau_\theta + a_5 m + a_6 y + a_7\mu = 0 \qquad (13a)$$

$$y_\theta + a_8(y_z - \delta y_{zz}) + a_9 y + a_{10}\tau + a_{11} m + a_{12}\mu = 0 \qquad (13b)$$

$$\mu_\theta + a_8(\mu_z - \delta\mu_{zz}) + \gamma a_{12}\mu + \gamma a_{13}\tau = 0 \qquad (13c)$$

$$\tau_\theta + a_{14} m_z = 0 \qquad (13d)$$

The coefficients, a_i, are determined by the steady-state solution and are constant in time. They are, however, functions of the space variable, z, some of them being rather strong functions. The values of the coefficients are given in the Appendix in terms of the steady-state values of Φ, Y, and Y_1 and the partial derivatives of P and P_1 evaluated at the steady state.

In order to test the stability of a particular steady-state solution, the Equations (13) are integrated numerically with the corresponding

coefficients and appropriate initial and boundary conditions. The initial condition chosen as a stability test function is the Gaussian distribution function for the temperature perturbation

$$\tau = \theta^{-b^2 z^2} \tag{14}$$

This corresponds to the temperature disturbance shortly after the release of an instantaneous heat source. The initial values chosen for y and μ are $y = 0$ and $\mu = \mu^*$, where μ^* is the steady-state value of μ obtained by linearizing Equation (11), and is given by

$$\mu^* = -\frac{a_{13}}{a_{12}}\tau \tag{15}$$

The subsequent value of τ as given by Equations (13) is then computed for a sufficient number of time steps to decide definitely whether it is increasing continually with time or decaying to zero. It is found that the ultimate growth or decay of the perturbation as determined numerically does not depend on the initial condition chosen, although the number of time steps required to make a decision will depend on the function chosen. The initial values in Equations (14) and (15) are the most satisfactory for minimizing the computation required.

In order to carry out the numerical integration, it is necessary to replace the infinite space interval $(-\infty < z < \infty)$ by a finite interval. This is done by limiting consideration to the z interval over which the coefficients $a_i(z)$ have an appreciable variation $(-L \leqslant z \leqslant L)$. Physically, this corresponds to the flame zone over which measurable changes in temperature and concentrations occur. The boundary conditions imposed at $z = \pm L$ are that $\tau_z = y_z = \mu_z = m_z = 0$. The value of the constant, b, in the initial condition in Equation (14) is taken as $b = 4/L$.

The numerical integration is carried out by replacing Equations (13) by an equivalent difference equation system where the space range $-L \leqslant z \leqslant L$ is divided into 40 intervals of length $\ell = L/20$. The size of the time step, h, that can be taken is limited by $h \leqslant \ell^2/4\Phi_f$, in order that the stability criterion be satisfied for the numerical procedure used for this type of parabolic equation. Between 200 and 300 of such time steps are usually required to determine the stability of a particular steady-state solution. A high-speed digital calculator was used in carrying out these numerical integrations.

Results and Discussion

The stability of the steady-state solution has been investigated by the method described for five different cases of ozone flame propagation. The cases chosen were all for $T_o = 300°C$ and at 0.821 atmospheric pressure, so that the data of Hirschfelder, Curtiss and Campbell[2] could be used. The values of the dimensionless parameters used in computing the steady-state solutions and the coefficients $a_i(z)$ are listed in the Appendix. These values for the dimensionless parameters were obtained from the physical and kinetic constants for the ozone flame given in Hirschfelder, Curtiss and Campbell.[2] Three initial concentrations of O_3 were considered, $Y_o = \frac{1}{3}$, $Y_o = \frac{1}{2}$, and $Y_o = 1.0$, and the stability of the corresponding steady-state solution was determined for no diffusion ($\delta = 0$) and for an average value of the diffusion coefficient ($\delta = 1.0$).

Table 1. Stability of Ozone Flame
$T_0 = 300°C$, $p = 0.821$ atmos.

Y_o	δ	Ta_{diab}	U	Stable
		°C	*cm/sec*	
$\frac{1}{3}$	1	1250	42	No
$\frac{1}{3}$	0	1250	88	No
$\frac{1}{2}$	1	1725	169	Yes
1.0	1	3153	986	Yes
1.0	0	3153	1560	Yes

The essential results of these calculations may be stated as follows: (1) The steady state ozone flame propagation is stable for high initial O_3 concentration, $Y_o = 1$ and $Y_o = \frac{1}{2}$; but becomes unstable for the more dilute case of $Y_o = \frac{1}{3}$. (2) The inclusion of the O atom diffusion term ($\delta = 1$) has a stabilizing effect as compared with no diffusion ($\delta = 0$). The $Y_o = \frac{1}{3}$ case, however, is unstable even with diffusion.

These stability results are shown in Table 1. The values of Y_o and δ for the five cases calculated are shown, the last column indicating whether or not the case has a stable steady-state solution. In addition, the calculated adiabatic flame temperature is given as well as the flame velocity computed from the steady-state flame equations for the five cases considered. These velocities correspond to those of Hirschfelder, Curtiss and Campbell[2] and von Kármán and Penner[3] for those cases which have been calculated in the references.

The way in which the initial τ perturbation

behaves is shown in Table 2. The computed values are listed of τ, y, and μ at the space point $z = 0$, as given by Equations (13) and the initial condition in Equation (14). Also listed are the values of $\mu^*(\tau)$ and $y^*(\tau)$ which μ and y would have if the relation between these quantities and τ were the same as in the steady state. $\mu^*(\tau)$ has

Table 2. Results of Numerical Solution

θ	τ	y	y^*	μ	μ^*
$Y_o = \frac{1}{3}$, $\delta = 1.0$, unstable					
0	1.000	0	−0.381	0.537	0.537
2	1.454	−0.092	−0.553	0.752	0.781
4	1.827	−0.190	−0.696	0.949	0.981
6	2.177	−0.284	−0.830	1.13	1.17
8	2.506	−0.373	−0.955	1.30	1.35
10	2.813	−0.458	−1.07	1.46	1.51
$Y_o = 1$, $\delta = 1$, stable					
0	1.000	0	−0.204	0.102	0.102
2	1.129	−0.046	−0.228	0.086	0.115
4	1.150	−0.084	−0.235	0.087	0.117
6	1.140	−0.111	−0.232	0.088	0.116
$\tau_{max} = 1.15$ occurs at $\theta = 4.16$					
$Y_o = 1$, $\delta = 0$, stable					
0	1.000	0	−0.204	0.102	0.102
2	1.176	−0.051	−0.240	0.102	0.120
4	1.236	−0.096	−0.252	0.106	0.126
6	1.245	−0.127	−0.254	0.109	0.127
7.9	1.223	−0.144	−0.250	0.108	0.125
$\tau_{max} = 1.246$ occurs at $\theta = 5.44$					

previously been given by Equation (15). The value of y^* is given in an analogous fashion as

$$y^* = \left[\frac{dY}{d\Phi}\right]_{ss} \tau \qquad (16)$$

Table 2 for the case $Y_o = \frac{1}{3}$, $\delta = 1$, shows an unstable case in which the initial τ perturbation grows continually with time.

The case $Y_o = 1$, $\delta = 1$, in Table 2 is stable. Here the value of τ at $z = 0$ first increases, goes through a maximum, and then continually decreases. The maximum value of τ and the time at which it is reached are given as good indications of relative stability in observing the effect of diffusion. The last case listed in Table 2 is identical with the previous case except that $\delta = 0$. It is seen that a higher maximum is reached for no diffusion, i.e., it is less stable. The value of μ relative to μ^* is seen to be smaller as a result of diffusion. Similarly, for the unstable case $Y_o = \frac{1}{3}$, the value of τ is always greater for $\delta = 0$ than for $\delta = 1$ at the corresponding time θ.

An understanding of the relative importance of the terms in Equations (13) on stability can be obtained by considering only Equation (13a) as a relation for τ_θ. If the general time dependence of τ is given by $\tau \sim e^{-\lambda\theta}$, then $\lambda > 0$ is stable and $\lambda < 0$ is unstable. It can be shown[5] that if in Equation (13a) we have

$$m = 0, \quad y = y^*(\tau), \quad \text{and} \quad \mu = \mu^*(\tau)$$

then τ will be just stable, i.e., $\lambda = 0$.

We can consider Equation (13a) as an equation involving only τ and its derivatives and represent the terms m, y and μ as proportional to τ, where the factor of proportionality will depend on z. A function $S(z)$ can then be defined by

$$S(z)\tau = a_5 m + a_6(y^* - y) + a_7(\mu^* - \mu) \qquad (17)$$

Equation (13a) can then be written as

$$-\tau_{zz} + \tau_z + A_3\tau + a_4\tau_\theta = S(z)\tau \qquad (18)$$

where $A_3(z)$ is a new coefficient which depends on z only. For $S = 0$, the temperature perturbation τ is just stable. If for all z, $S(z) \geq O$, τ is unstable, while if $S(z) \leq 0$, τ is stable. Thus, the effect of the perturbations m, y and μ on stability can be seen by their effect on the sign of $S(z)$ as given by Equation (17). The coefficients a_5, a_6, and a_7 are such that $a_5 \geq 0$, $a_6 \leq 0$, $a_7 \leq 0$. Then, in general, it can be seen that in order to have a stabilizing effect we must have $y^* - y > 0$ for the O_3 perturbation, $\mu^* - \mu > 0$ for the O atom perturbation and $m > 0$ for the mass flow perturbation. Reference to Table 2 shows that y never becomes sufficiently negative to be a stabilizing influence while the O atom term μ is always stabilizing. The mass flow term, m, is always positive and therefore has a stabilizing effect. Since O atom diffusion tends to lower the peak value of μ at $z = 0$, this is a stable effect. Thus, stability or instability appears to depend on the combined result of all these effects rather than on any specific term.

The relationship of the type of instability shown here to flammability limits and detonation limits will be determined by comparison of the results given here, and additional similar results, with experimental data on limits for the ozone flame as soon as such data are available.

Appendix

COEFFICIENTS OF LINEARIZED EQUATIONS

$$a_3 = \left(\frac{\bar{\sigma}}{\Phi} - 1\right)\frac{cP}{\beta\Phi}$$

$$a_4 = \Phi^{-1}$$

$$a_5 = \Phi_z$$

$$a_6 = -c\beta^{-1}S$$

$$a_7 = -\left(c + \frac{c_1}{3}\right)Y\beta^{-1}S_1$$

$$a_8 = \Phi$$

$$a_9 = \Phi\beta^{-1}S$$

$$a_{10} = -\left(\frac{\sigma + \sigma_1}{2\Phi} - 1\right)\beta^{-1}P$$

$$a_{11} = \Phi Y_z$$

$$a_{12} = \Phi Y\beta^{-1}S_1$$

$$a_{13} = \left(\frac{\sigma - \sigma_1}{2\Phi}\right)\beta^{-1}P$$

$$a_{14} = -\Phi^2$$

$$\bar{\sigma} = \frac{1}{2}\left[\left(1 - \frac{c_1}{3c}\right)\sigma + \left(1 + \frac{c_1}{3c}\right)\sigma_1\right]$$

$$P = -YS$$

$$S = \Phi^{-1}\exp(-\sigma/\Phi)$$

$$S_1 = \Phi^{-1}\exp\left(\frac{\sigma_1 - \sigma}{\Phi_f} - \frac{\sigma_1}{\Phi}\right)$$

PARAMETER VALUES USED

$c = 9.51$
$c_1 = 48.47$
$k = 1.207 \times 10^{10}$
$k_1 = 0.4796$
$\sigma = 40.50$
$\sigma_1 = 10.07$

Nomenclature

$c = (h_3 - h_2)/c_pT_o$
$c_1 = (h_1 - h_2)/c_pT_o$
c_p = specific heat
D = binary diffusion coefficient
E = activation energy for r_3
E_1 = activation energy for r_1
h_i = specific enthalpy of $i^{\text{-th}}$ component ($i = 1, 2, 3$)
k = frequency factor
k_1 = frequency factor ratio
M = mass flow
m = mass flow perturbation
P = rate of production of O_3
P_1 = rate of production of O
T = temperature
t = time
U = flame velocity
x = distance
Y = weight fraction O_3 (fuel)
y = weight fraction O_3 perturbation
Y_1 = weight fraction O atom
$z = Ux/\alpha$ = reduced distance
α = thermal diffusivity
$\beta = U^2/k\alpha$
$\gamma = \frac{k_1}{6}\exp\left(\frac{\sigma - \sigma_1}{\Phi_f}\right)$ = scale factor for O perturbation
$\delta = D/\alpha$ = reduced diffusion coefficient
$\theta = U^2t/\alpha$ = reduced time
μ = weight fraction O perturbation
ρ = density
$\sigma = E/RT_o$ = reduced activation energy
$\sigma_1 = E_1/RT_o$ = reduced activation energy
τ = temperature perturbation
$\Phi = T/T_o$ = reduced temperature
$\Omega = M/M_o$ = reduced mass flow

SUBSCRIPTS

o = value in unburned gas
f = value in burned gas

REFERENCES

1. Rosen, J. B.: J. Chem. Phys., *22*, 733, 743 (1954).
2. Hirschfelder, J. O., Curtiss, C. F., and Campbell, D. E.: J. Phys. Chem., *57*, 403 (1953).
3. von Kármán, T., and Penner, S. S.: *Selected Combustion Problems*, pp. 5–41. Butterworths Scientific Publications, London, 1954.
4. Rosen, J. B.: J. Chem. Phys., *22*, 742 (1954).
5. Wehner, J. F., and Rosen, J. B.: To be published in Combustion and Flame.

29

CARBON FORMATION IN QUENCHED FLAT FLAMES AT 1600°K

By C. P. FENIMORE, G. W. JONES AND G. E. MOORE

Introduction

Carbon formation in flames has been discussed a good deal recently.[1-4] Porter believes that, in most cases at least, acetylene is a common intermediate and that this adds to a growing carbon particle with simultaneous loss of hydrogen. The experimental support for this view is not derived from flame studies, however.

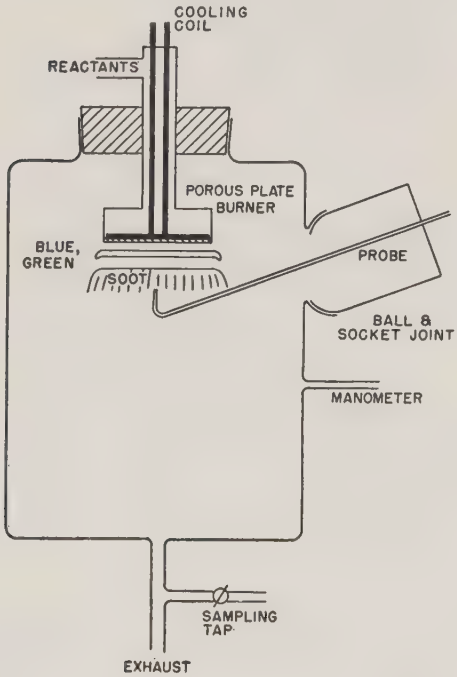

FIG. 1. Schematic experimental arrangement.

Premixed flat flames possess a blue or green reaction zone, a nonluminous dead space downstream of thickness comparable to the blue layer, and if the pressure and mixture strength are right, a yellow zone of luminous carbon particles beyond the dead space. Since carbon first appears well out in the burned gas, the acetylene theory implies that its growth should be independent of fuel or mixture strength except as these variables give different yields of acetylene to deposit carbon and different yields of oxidizing agents to oppose it.

We have attempted to test whether carbon growth correlates with the composition of the burned gas from flat premixed flames and if so, to determine whether acetylene is the chief carbon producer.

Experimental Details

We use porous metal burners in closed vessels to permit burning at various pressures, and limit burning rate and temperature by limiting the flow of reactants. The flames, cooled from the upstream side, cannot strike back. The burners are $\frac{3}{32}$-in. thick sintered bronze plates soldered into brass holders and cooled by water coils of $\frac{1}{8}$-in. copper tubing pushed against the upstream side. They produce the flat flames described in the Introduction. The burner is shown schematically in Figure 1.

A fraction of one per cent of the burned gas is withdrawn through a critical flow quartz probe in the flame, or a few per cent through a sampling tap downstream of the flame. Probe samples taken in a plane 2 cm from the face of a 3.3-cm diam. burner at various radial distances from the center give the same O:C:H: ratios as those fed. Therefore, our flames do not exhibit preferential radial diffusion. Since the probe frequently plugs with carbon, most samples are taken through the downstream tap. Samples from the two sources give the same analysis when the probe is placed within the carbon zone and the reactant flow is about 25 cc/sec (S.T.P.).

The gas sample is passed through liquid nitrogen traps, compressed to one atmosphere, measured, and analyzed for CO, H_2, CH_4, O_2 and N_2. The traps are warmed to -80°C and CO_2, C_2 and C_3 hydrocarbons swept out in a stream of helium. These products are measured and analyzed. Water is swept out after further warming and absorbed. The helium stream is then cooled again to condense any heavy product, benzene for example, and this is measured and burned in a stream of nitrogen over hot copper oxide. Benzene has been characterized by its mass spectrometer pattern also. When the pressure is high enough to condense water, this is inferred by assuming enough to force agreement of the C:H and C:O ratios with those taken. The products determined account for 100 $\pm$ 4 per cent of the atoms fed.

Temperature of the carbon zone is measured by the two-color method using interference filters of passing bands 548 and 657 mμ, and adopting Hottel and Broughton's variation of absorption coefficient with wavelength. This amounts to assuming that our carbon scatters light the same as does the carbon in diffusion flames with which these authors worked. The assumption may be tolerable: electron microscope photographs of soot from our premixed propane and butane flames strongly resemble photographs of carbon from diffusion flames. Soot caught on grids in the carbon zone forms spiral curlicues, and samples brushed from the cold walls are mostly spheres of some 300A° diam.

With 25 cc/sec flow on a 3.3-cm diam burner, the hottest region of the carbon zone is 1610 ± 20°K at 20 cm P, and 1560 ± 20°K at 60 cm regardless of fuel or mixture strength. Increasing mass flow per unit area fourfold increases temperature 50 ± 20°K. The measurements are difficult because absorption strength is low and temperature falls rapidly as one moves downstream in the carbon zone. Over this very limited temperature range, no marked dependence of carbon growth on temperature is noted, and we consider our results virtually an isothermal study at about 1600°K.

Soot is determined by mounting the burner in a Vycor vessel with a long leg packed with Vycor wool at its downstream end. Soot deposits on the walls and on the wool, at least the last 6 in. of the wool remaining clean. The vessel is evacuated an hour or more after the flame is shut off, the deposited soot burned in oxygen, and the dried carbon dioxide absorbed.

Reactants, mostly Matheson C. P. gases used without purification, are metered through critical flow orifices and well mixed. The flow measurements are believed to be accurate to about 1 per cent. Liquid fuels are vaporized into the oxygen stream. The tubing and cooling water to the burner are heated to prevent condensation, when necessary. In one case, naphthalene, the cooling water was replaced with warm air.

Onset of Soot Formation

The yellow carbon luminescence of a rich flat premixed flame fades abruptly as pressure is sufficiently lowered but mass flow and mixture strength held constant. The yellow clearly appears or disappears over a 1 cm pressure range. The pressure at which carbon just appears is designated P_c.

P_c is unchanged whether the flame burns downwards against a rising gas stream or upwards, or if it is surrounded by an annular sheath of nitrogen or of leaner flame in a double burner. P_c is higher the leaner the mixture or the greater the mass flow per unit area of burner. Figure 2 shows some values of P_c for various fuels and O/C ratios, and for two different flows per unit area. If the flow through the smaller burner is decreased to give the same flow per unit area as was used for the larger burner, the small burner

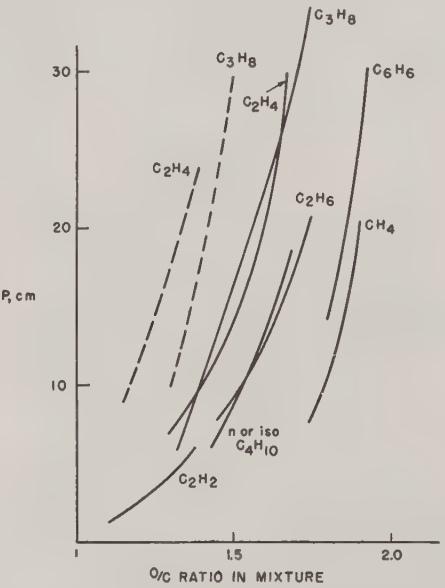

FIG. 2. Pressure at which soot is just formed in hydrocarbon, oxygen flames. Solid curves obtained with 3.3 cm diam. burner, dashed curves with 1.6 cm burner. Flow was 25 cc/sec for both burners (STP).

values of P_c fall and coincide with those for the larger burner.*

The onset of carbon is influenced by added

* With reference to Fig. 2, the question was asked at the meeting, does the onset of soot still depend on pressure if flames are burnt with constant linear flow of reactants? Or does the division between clear and sooty flames then occur at a fixed mixture strength, independent of pressure? For ethylene and propane flames, most of the dependence of P_c on mixture strength disappears at constant linear flow. Thus from Fig. 2, to lower P_c by a factor of four one must decrease the O/C ratio by about 25% at constant mass flow, but by only 6 to 10% at constant linear flow. However, our criterion for the onset of soot holds in either case: Fig. 4 contains sets of points for which linear flow was constant and mass flow varied fourfold.

gases. To keep P_c unchanged in a propane oxygen flame after diluting by various gases (diluent/O_2 = 0.5), the O_2/C_3H_8 ratio in the reactants must be increased 13 per cent if hydrogen is added, decreased 6 to 8 per cent if nitrogen, argon, helium, carbon monoxide, or dioxide is added, and decreased 15 per cent if water is added. Other trials of this nature show that added carbon oxides are effectively inert under our conditions, but added hydrogen and water are not.

At a fixed mass flow, burned gas composition changes only slowly with pressure. This contrasts with the marked effect of pressure on the formation of carbon.

The burned gas contains almost no oxygen,

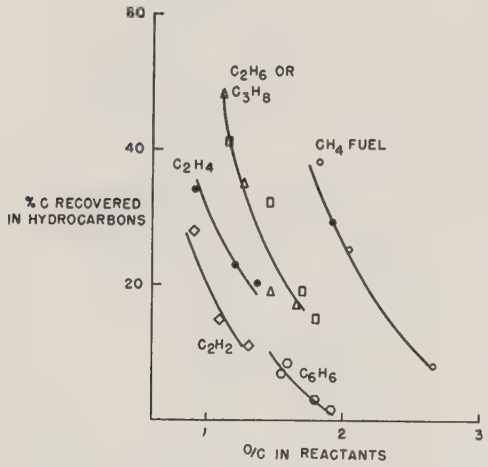

FIG. 3. Hydrocarbons in burnt gas from flames on 3.3 cm diam. burner. Flow = 25 cc/sec (STP) $P = P_c$ approx.

but large and nonequilibrium quantities of hydrocarbons. Acetylene and methane are formed in largest amount, ethylene in considerably less. Flames of methane, propane, ethylene, and acetylene give burned gases in which the ratio of methane to acetylene is about 5, 1, 0.3, and 0 respectively. Benzene is very small unless benzene itself is the fuel. For nonbenzene flames, the ratio of benzene to acetylene is 0.006 $\pm$ 0.002. The fraction of carbon fed which is recovered as hydrocarbons is plotted in Figure 3 for several fuels.

It may be worth noting that the recovery of acetylene in the burned gas from flames of most other fuels is greater than from flames of acetylene itself at a constant O/C ratio. Consequently, the observation that under some conditions, generally not of constant temperature, premixed flames of ethane form soot more readily than do flames of acetylene is not really evidence against the acetylene theory of carbon formation as is sometimes held.[3]

P_c is lower the greater the yield of hydrocarbons. At high mass flow per unit area, high P_c is associated with a small recovery of hydrocarbons. When mass flow is decreased so that P_c falls, the recovery of hydrocarbons increases.

If we try to correlate the pressures of the most important constituents, water, hydrogen, and hydrocarbons, then considering first only the analyses in which acetylene is the principal hydrocarbon, we find that

$$2P_{C_2H_2} = 0.6\ P_{H_2O}/P_{H_2}^{\frac{1}{2}} \text{ at } P_c$$

When methane occurs as a major constituent, we find that if we suppose it too makes a contribution to soot formation, less than that of acetylene but more than $\frac{1}{3}$ as great, our data for all flames except benzene correlate rather well with a similar expression. In benzene flames, P_c occurs at much lower partial pressures of hydrocarbons. If we fit our data with the obvious extension

$$P_{CH_4} + 2P_{C_2H_2} + \alpha P_{C_6H_6} = 0.6 P_{H_2O}/P_{H_2}^{\frac{1}{2}} \text{ at } P_c$$

our results require α near 100 (Fig. 4). We estimate our error in determining the pressure of hydrocarbons at about 15 per cent and most values in Figure 3 fall this close to the line over a tenfold change in P_c and the various partial pressures.

This correlation suggests that soot grows by deposition of carbon from simple hydrocarbons and that the growth is opposed by oxidation by hydroxyl, proportional to $P_{H_2O}/P_{H_2}^{\frac{1}{2}}$. Or perhaps that growth is by some reaction product of hydrocarbon with hydrogen atoms, and oxidation is by water. If oxidation is by hydroxyl radicals, one can rationalize the existence of a dead space between the blue-green reaction zone and the zone of carbon formation. It is reasonable to postulate that a large (perhaps nonequilibrium) concentration of hydroxyl exists in the reaction zone, and that this must decay somewhat before soot growth can occur.

It is surprising that methane when weighted for its smaller carbon content is about as effective as acetylene. Possibly the conversion, methane $\rightarrow$ acetylene in the burnt gas is faster than acetylene $\rightarrow$ soot, and even the methane found gives

soot only via acetylene, for we never find a burned gas free of acetylene. Benzene cannot give soot *via* acetylene, however, because it is 17 times as effective as acetylene, even when allowance is made for its greater carbon content. This conclusion agrees with Smith's and Gordon's recent finding that carbon may be formed from benzene in diffusion flames as well as from acetylene.[6]

Examination of Soot

The interpretation that soot growth depends on

$$(P_{CH_4} + 2P_{C_2H_2}) - 0.6\frac{P_{H_2O}}{P_{H_2}^{\frac{1}{2}}} = F$$

implies that particle size should increase with increasing value of the expression. This is difficult to prove or disprove. Soot from our flames always appears about the same size in the electron microscope, but the objects visible are aggregates of crystallites.

Samples collected on quartz slips placed near the flames reveal suggestive differences when examined by electron diffraction (Table 1).

From *iso*butane flames, soot crystallinity and yield increase with F and therefore the carbon crystallites may indeed grow with increasing F. Ethane soot resembles the butane soot formed at nearly equal F, not the butane soot formed in similar yield at much lower F. Therefore at equal F, the two soots are probably composed of crystallites of the same size, and the different yields are due to different numbers of crystallites.

Some soots were collected from propane flames with O/C = 1.39, and stored several days in a vacuum at room temperature before analysis. Their composition was 94.2 per cent C, 3.2 per cent H, independent of the soot yield (1.5 to 12 per cent of C present in the burned gas as methane or acetylene) or of the value of F (varied from 0.4 to 4.0).

Since we suppose that soot grows by virtue of a change in the relative frequency of deposition and oxidation reactions, we thought it possible that soot might change in composition with changing F. But no change is apparent.

Soot Yield from Smoke Flames

Figure 5 is a plot of soot yield against

$$R = (P_{CH_4} + 2P_{C_2H_2})P^{\frac{1}{2}}H_2/P_{H_2O}$$

Yield is based on carbon in the burned gas as methane or acetylene. If based on total carbon in the fuel, the yield is generally less than 2 per cent. Most fuels were burned at two mixture strengths, two flow rates, and several different pressures to obtain the data for Figure 5.

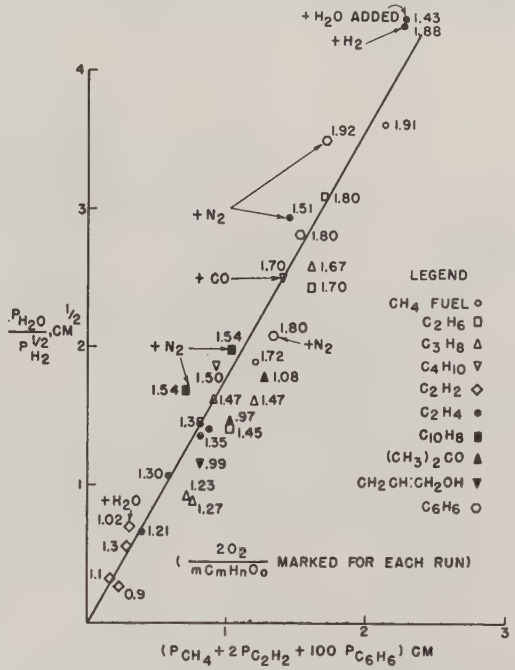

FIG. 4. Partial pressures in burnt gas when formation of carbon is just zero. O/C ratio indicated for each run.

TABLE 1. DIFFRACTION PATTERNS OF SOOT*

Fuel	P	F†	Soot Yield‡	Pattern
	cm			
iso-C_4H_{10}	26	0.9	1	Amorphous, 2 broad rings
iso-C_4H_{10}	60	3.3	8	Much more crystalline, 4 strongest rings of graphite §
C_2H_6	60	2.9	1.4	

* All flames burnt with O/C ratio = 1.56.

† $F = (P_{CH_4} + 2\,P_{C^2H_2}) - 0.6\,P_{H_2O}/P_{H_2}^{\frac{1}{2}}$.

‡ Yield as per cent of C in $CH_4 + C_2H_2$ in burned gas.

§ Rings observed: 1.20. 1.74, 1.96, 3.37.

For all fuels, soot yield approaches zero at R = 0.6. This confirms visual observation. But at greater R, the yield depends on fuel burned and increases in the order CH_4, C_2H_6, C_2H_4, C_3H_8, *n*-C_4H_{10} C_2H_2, *iso*-C_4H_{10}, *neo*-C_5H_{12}.

At constant R, soot yield depends roughly

linearly on fuel composition for mixtures of ethane and *iso*butane. Mixing two moles of hydrogen with *iso*butane decreases soot yield about fourfold, although carbon first forms at $R = 0.6$ still. Added carbon monoxide or nitrogen leaves yield unchanged as a function of R.

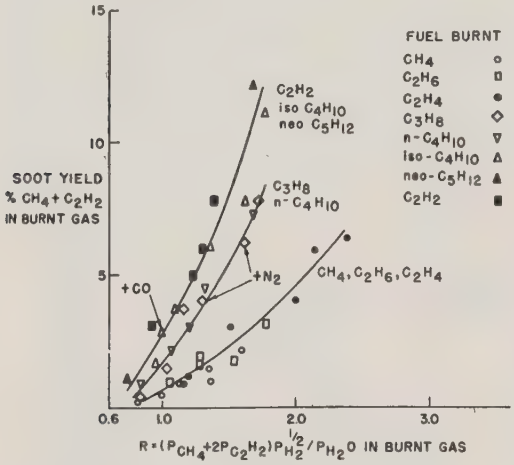

FIG. 5. Soot yield of smoky flames on a 3.3 cm diam. burner.

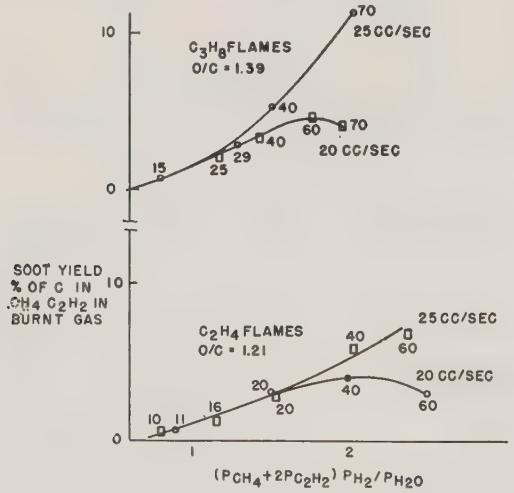

FIG. 6. Soot yield from flames showing decrease in yield at high pressures and low flow rates. Pressures, cm, indicaded for each point.

Sulfur trioxide is reported to promote carbon formation[7] and we find that its addition, about 0.2 mole per cent of *iso*butane, increases soot by 40 per cent but does not change R. The effect cannot be systematically studied because most of this additive does not pass the porous burner. In the instance cited, 0.8 per cent sulfur trioxide was added but only ¼ of this emerged in the flame. Subsequent runs without the additive gave high soot yields unless the burner was well cleaned.

Iron carbonyl or ferrocene at concentrations of one iron to 10^3–10^4 carbon atoms, affect neither soot yield nor R from propane flames.

In the preceding sections, we have suggested that the growth of individual soot particles depends only on the burned gas and is usually proportional to

$$P_{CH_4} + 2P_{C_2H_2} - 0.6P_{H_2O}/P_{H_2}^{\frac{1}{2}}$$

Since the quantity of soot is equal to the number of nuclei x net growth, the rough correlation of Figure 5 can be forced into agreement with the suggested growth expression by making appropriate assumptions about the number of nuclei. However, different soot yields from different fuels at constant R would then indicate that nucleation is not determined by gross composition and pressure of the burned gas only.

We have found some more direct evidence that nucleation is affected by occurrences early in the flame, in the blue-green luminous zone or even further upstream. At low enough flows of reactants or high enough pressures, the blue-green zone is largely quenched by the burner face, and then the yield of soot decreases considerably below that shown in Figure 5 (see Fig. 6). The temperature of the carbon zone is unchanged, ±20°K, whether the green zone is partially quenched or not. When the green reaction zone stands off from the burner appreciably, as it did in the flames plotted in Figure 5, soot yield at constant R is independent of further decrease in pressure or increase in flow rate.

A decrease in soot yield with quenching of the green zone is reminiscent of Gaydon and Fairbairn's[4] suggestion that C_2 can nucleate soot growth. Our observation, however, does not discriminate between C_2 and any other readily quenched species present in the zone of vigorous oxidation.

REFERENCES

1. GAYDON, A. G., AND WOLFHARD, H. G.: *Flames*. Chapman and Hall, London, 1953.
2. PORTER, G.: *Fourth Symposium (International) on Combustion*. The Williams and Wilkins Co., Baltimore, 1953.
3. STREET, J. C., AND THOMAS, A.: Fuel, *34*, 4 (1955).

4. *Fifth Symposium (International) on Combustion.* Reinhold Publ. Corp., New York, 1955.
5. Hottel, H. C., and Broughton, F. P.: Ind. Eng. Chem., Anal. Ed., *4*, 166 (1932).
6. Smith, S. R., and Gordon, A. S.: J. Phys. Chem., *60*, 759 (1956).
7. Gaydon, A. G., and Whittingham, G.: Proc. Roy. Soc., *189*, 314 (1947).

30

CARBON FORMATION FROM ACETYLENE

By F. C. STEHLING, J. D. FRAZEE, and ROBBIN C. ANDERSON

Introduction

The problem of carbon formation in combustion systems has been of continuing interest because it involves processes by which large aggregates of atoms or molecules must be built up under conditions such that the normal expectation is for degradation or fragmentation of molecules to occur. It is of particular interest in connection with acetylene reactions, which have potential significance in connection with general mechanisms of carbon formation.[1, 2] In the decomposition, or self-combustion, flames of acetylene, carbon formation occurs as part of the flame propagation reactions.

In earlier reports[3, 4, 5] it was noted that three types of carbon were found in the products of flame propagation in acetylene in straight tubes. One was a "vitreous" carbon, similar to that observed by Wolfhard and Parker[6] in oxygen-acetylene diffusion flames. This could be formed also by reaction of hot acetylene on a porcelain surface. It is formed by a surface reaction and is not, therefore, considered in the present discussion.

Two types of gas carbon were also formed. The first was found in the region of the hot-wire igniter. It was gray and graphitic in appearance and rather dry. The second type was a very black carbon found farther down the flame tubes. It was rather greasy. Extraction and distillation tests showed that colored, liquid, polymeric materials could be extracted from both, the black carbon showing more extractable material than the gray. Electron microscope observations showed both to be aggregates of small particles in the "reticulated chain" structure. These small particles were in the range of 800 to 2000 Å in diameter, with those of the gray type being consistently somewhat smaller than the black. The carbon reacts further if exposed to hot acetylene.[7]

The present report summarizes further information on the gas carbon obtained from studies of the actual conditions of particle formation in the thermal reaction of acetylene, for comparison with the results observed in flame propagation. X-ray measurements have also been used to get certain additional information about the particles.

Materials, Apparatus, and Procedures

In general, the materials used in the various tests were of the best grade commercially available. The 2,4,6-octatriyne was from a sample kindly supplied by Dr. John Happel of the Department of Chemical Engineering, New York University. The acetylene was passed through sodium bisulfite to remove acetone and then dried over calcium chloride and calcium sulfate.

Carbon "Gel"

This was a distinctive material formed from the liquid polymeric materials collected in the bottom of a reactor tube used for flow experiments on acetylene reactions. When a flame in a gas mixture of 1 per cent oxygen in acetylene passed along the surface of this liquid deposit, the material reacted suddenly, forming a voluminous product which was a spongy, or gel-like, aggregate of carbon particles. (If the residue was preheated to 450°C in helium for a time, it was more difficult to get reaction, and the carbon eventually formed was glazed or "vitreous" rather than spongy.)

A carbon gel similar to that above was also

formed when crystals of octatriyne were merely heated to about 130°C in an inert atmosphere.

X-RAY STUDIES

The x-ray pictures were taken with a flat-film camera using a Machlett tube. The carbon black samples were mounted in a specially designed holder by a technique developed by Dr. S. H. Simonsen.[8] The following conditions were adopted, after testing, as giving the best pictures:

Wt. of sample: 10 mg	Exposure time: 30 min
Collimating pinholes	Radiation
Back: 0.025 in.	Cu target
Front: 0.040 in.	Ni filter
Film-to-specimen dist.: 4.636 cm	
Tube current: 15 ma	Tube voltage: 35 kv

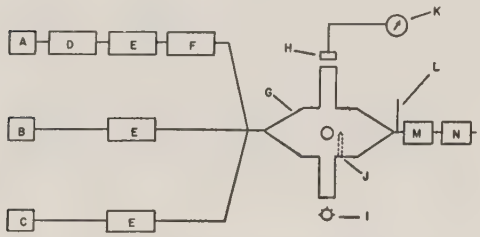

FIG. 1. Diagram of apparatus.

A Acetylene source	H Photocell
B Helium source	I Light source
C Additive source	J Thermocouple
D Purification tower	K Microammeter
E Flowmeter	L Manometer
F Filter	M Cold trap
G Vycor reactor	N Filter

The line widths of the diffuse diffraction maxima were determined by scanning with a recording microphotometer and measuring the breadth of the lines on the tracings at half-height.

STUDIES OF PARTICLE FORMATION

A schematic diagram of the apparatus used in these experiments is shown in Figure 1. The overall design permitted the flow of a constant concentration of acetylene diluted with helium through a reactor at a constant temperature, pressure, and flow rate. Any one of these factors could be varied independently and its effect determined. Provisions were included so that gaseous, liquid, or solid additives could be introduced. The presence and relative amounts of particles of carbon or condensed polymer were determined by the light transmission through the reaction chamber.

The reaction vessel is essentially a cylinder of Vycor, about 20 cm long and 6 cm i.d. and tapered at both ends. Projecting from the chamber were three side-arm extensions with plane quartz windows sealed to the ends, through which the light transmission was measured.

The reactor was heated by means of a resistance-wire coil wrapped around the chamber. Temperatures up to 900°C could be obtained. A chromal-alumel thermocouple was inserted into a thin-walled well placed near the center of the reactor to determine the temperature of the reacting gas mixture.

A preheater was used to vary on occasion the temperature of the incoming reagents. It also served as a mixing chamber for gases. A very fine filter (a Type AA filter membrane manufactured by the Millipore Filter Corporation) was inserted ahead of the preheater to remove dust particles, etc., from the incoming gases.

A Sylvania photoflood lamp was used as light source. The detector of the transmitted light was a Weston Photronic cell, with the photocurrent indicated by a microammeter.

In all the experiments the total flow rate of gas was held constant, and the volume concentration of the acetylene and other constituent obtained from the flow rate of each constituent divided by the total (acetylene, diluent, and additive) flow rate. The separate flow rates for each gas were measured before mixing by orifice-type flow meters calibrated for the particular gas involved. These flow rates were reproducible within about one or two per cent over a range from 5 to 1000 cm/min.

The vapors of liquid additives such as benzene and toluene were introduced by bubbling the helium diluent through the liquid. The percentage of additive was varied by altering the fraction of the helium passing through the saturator.

The addition of 2,4,6-octatriyne, which is normally solid, was accomplished by putting a few mg of the additive in a porcelain boat in the gas stream. The percentage of octatriyne was increased by raising the temperature of the additive and the carrier gas with heating lamps. The vapor pressure of the solid is not known, but it is probably close to that of a compound of nearly the same molecular weight, octatriene-5,7-yne-3, which has a vapor pressure of 20 mm. at 40°C.[9]

SAMPLING OF PARTICLES FORMED

Since the turbidity data obtained from the light-transmission measurements would make no

distinction between different types of particles, liquid or solid, samples of the product in the gas stream were collected on another Millipore filter in a cold-trap placed just after the reactor. Other samples were collected on a small removable Pyrex plate placed on the end of a glass rod which was inserted into the reactor from the downstream end. The plate was thus projected into the center of the reaction region where carbon and polymer deposited upon it. The deposits were examined visually and microscopically and analyzed for carbon and hydrogen content.

Results

X-RAY DATA

The x-ray patterns were, as might be expected, similar to those for acetylene blacks. There was no indication of true graphite crystals, but diffuse patterns like that of graphite show up distinctly. Some typical results are shown in Table 1.

The increased line-width for the black carbon as contrasted to gray indicates smaller crystallites. The larger particle size shown by electron-microscope pictures seems therefore to result from a coating of polymeric hydrocarbons. This would be consistent with the results on extraction with benzene.[4] These variations and the results with ethylene oxide, which accelerates the flames very markedly,[10] indicate that more rapid reaction gives larger crystallites of actual carbon, but that in slower reaction these may become coated fairly readily.

It may be noted also that the particles in the carbon gel formed by decomposition of liquid polymeric product seem very similar to those formed in the flames.

PARTICLE FORMATION

The method used here for observing particle formation from acetylene, i.e., by measuring the turbidity of the gas stream, does not distinguish between effects of a large number of small particles or a smaller number of large particles. The interpretations are, therefore, based upon *comparative* data for similar conditions rather than upon the absolute values of intensities.

A constant flow rate was used for these comparative measurements. Preliminary tests, starting with a freshly cleaned or a "dirty" reactor, indicated that the observed effects were not controlled by surface reactions. Variations in the purification trains and the filters showed also that the particle formation was not being determined by dust particles, vapor, etc., brought in by the reacting gases.

By diluting the acetylene with helium, it is possible to vary over a wide range the conditions for appearance of particles. The general appearance of the gas system, the samples collected on filters, and the microscopic observations of particles collected on a plate showed that the first effect observable—at about 20 per cent acetylene at 600°C—is formation of a mist of light yellow liquid. Increasing the temperature to 700°C and then 800°C will give first droplets of darker and darker liquid and then black solid particles. Analysis of the particles at 700°C showed 93.7 per cent carbon and 5.8 per cent hydrogen, approximately $(C_8H_6)_x$. Analysis of particles at 800°C gave 95.6 per cent carbon and 4.2 per cent hydrogen, or $(C_8H_4)_x$. In general, the 600°C range gives liquid product, the 800°C solid (800°C is comparable with average temperatures which occur in the decomposition flames[3]).

Table 1. Line-Widths of Carbon Black Samples

Sample	Width Half-height (cm)
Spectroscopic graphite	0.52
From C_2H_2 flame at 1500 mm	
Gray carbon	3.3
Black carbon	4.6
From flame in C_2H_2 at 1500 mm + 0.53 per cent C_2H_4O	
Gray carbon	3.2
Black carbon	4.7
From flame in C_2H_2 at 1500 mm + 8.32 per cent C_2H_4O	
Gray carbon	3.3
Black carbon	3.3
Carbon gel from liquid polymer	4.2

Similar variations in the particles occur if the percentage acetylene is increased, or if an accelerator such as oxygen is added. At higher temperatures, the relative effect of the oxygen was less; and at 800°C the effect of oxygen in decreasing carbon formation shows up with more than 1 to 2 per cent oxygen, becoming more pronounced with higher percentages of acetylene.

Data typical of the effects of additives are shown in Figure 2, which includes curves for results with added oxygen and different acetylene concentrations. Figure 3 shows results for nitric oxide, which inhibits particle formation, ethylene

oxide, which is an accelerator like oxygen, and benzene, which has no appreciable effect. Ethylene oxide was even more effective as accelerator at 600°C, but had very little effect at 800°C.

Propylene tended to inhibit reaction at 600°C

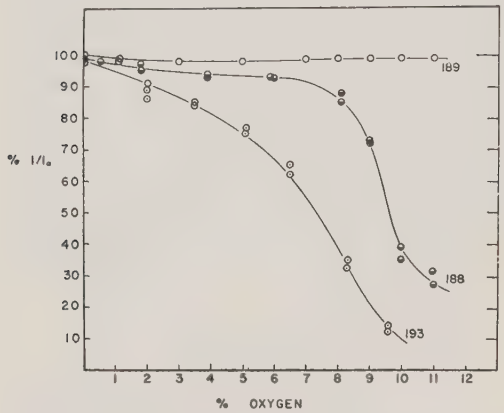

FIG. 2. Effect of oxygen additive at 600°C.

Run 189: 8.8% C_2H_2, 600°C, 1000 cc/min. Run 188: 14.9% C_2H_2, 600°C, 1000 cc/min. Run 193: 19.9% C_2H_2, 600°C, 1000 cc/min.

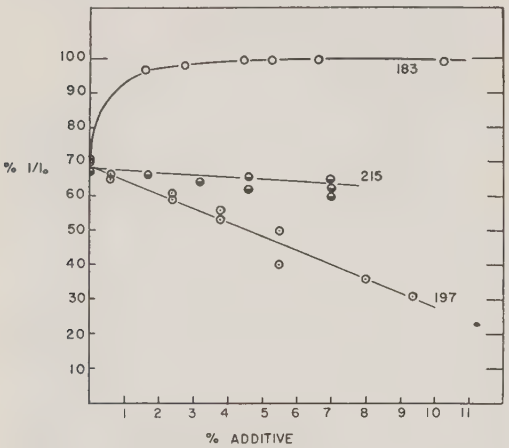

FIG. 3. Effect of promoter, inhibitor, and ineffective additive.

Run 183: 5.0% C_2H_2, nitric oxide additive, 700°C, 1000 cc/min. Run 215: 14.7% C_2H_2, benzene additive, 700°C, 1000 cc/min. Run 197: 15.0% C_2H_2, ethylene oxide additive, 700°C, 1000 cc/min.

and 700°C for low concentrations of acetylene, but at higher concentrations and temperatures it actually accelerated reaction (Fig. 4). Similarly, propane was a diluent at 600°C but tended to accelerate reaction at 700°C or 800°C.

Comparative data on certain hydrocarbons which are of interest as possible intermediates in the reaction system are shown in Table 2. The $\Delta(I/I_0)$ tabulated is:

I/I_0 (for C_2H_2 alone) $-$ I/I_0 (with additive)

The values given are averages of two or more runs in each case.

As a further check on the effects of the additives samples of the products from the toluene tests were analyzed for carbon and hydrogen. At 700°C, with 20 per cent acetylene and 4.4 per cent toluene, the products were 93.7 per cent carbon and 5.6 per cent hydrogen, virtually the same as for the pure acetylene. At 800°C the particles were 96.0 per cent carbon and 4.0 per cent hydrogen, again essentially the same as for the acetylene alone.

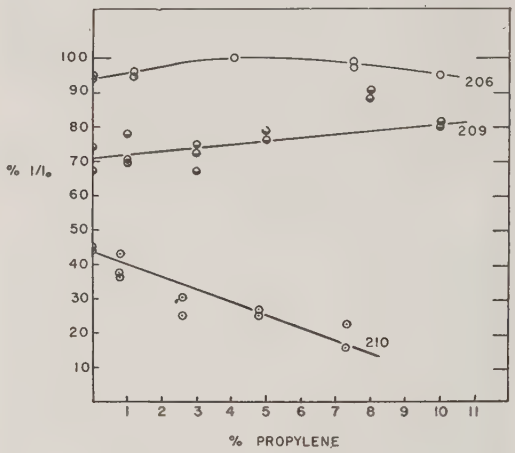

FIG. 4. Effect of propylene additive at various temperatures.

Run 206: 20.0% C_2H_2, 600°C, 1000 cc/min. Run 209: 15.0% C_2H_2, 700°C, 1000 cc/min. Run 210: 9.0% C_2H_2, 800°C, 1000 cc/min.

Discussion

Once reaction is started, the problem of carbon formation is that of building up a platelet system of condensed rings similar to a plane of a crystal of graphite. No single simple picture can be given for a carbon particle and there is no reason to expect a single reaction mechanism to be applicable, but a common structure is observable made up of graphitic planes which vary in orientation and orderliness. They differ from graphite itself in the spacing between planes and in the extent of orientation of planes with respect to one another. This degree of orientation is affected by the amount of residual hydrogen present and by cross-links between the planes, particularly where traces of oxygen may be involved.

In chemical structure, the gas carbons may be considered as highly complex and condensed hydrocarbons (*cf.* Hofmann,[11]), hydrogen being present to some extent in almost all samples. The reactivity of fresh carbon surfaces or particles in many instances indicates also that they are unsaturated or even free radical in character.[11, 12] This is borne out by recent results on paramagnetic resonance of chars.[13] The work of Rosalind Franklin and others[14, 15, 16] shows that at temperatures of 1000°C and above, dehydrogenation and fusion reactions may result in growth by polynuclear condensation of whole layers or groups of layers, but at lower temperatures growth is probably by addition or reaction of smaller molecules. It is the latter type, which represents the earliest stage of carbon formation, which is of particular interest here.

The x-ray data obtained here are consistent with the above picture of carbon formation and indicate also that liquid polymeric products tend to form with the carbon at lower temperatures.

For acetylenic carbons, Hofmann and Wilm[17] found the smallest crystallite size to be 13 Å by 21 Å, Clark, Eckert and Burton[18] found planes of 10–60 Å, Grisdale,[12] diameters of less than 50 Å, and Parker and Wolfhard[5] primary particles of 13 Å by 21 Å. The basic problem in carbon formation therefore involves mechanisms whereby a platelet of fused-ring structures containing about 100 carbon atoms may be built up. With acetylene as starting material, extensive combination obviously must occur.

One possibility is that of a simple molecular combination, such as

$$3C_2H_2 \longrightarrow C_6H_6 \qquad \Delta H = -138 \text{ kcal} \qquad (1)$$

Sufficient energy would be released either for dissociation or ring opening, and this is probably an important source of energy and thus of active particles in the early stages of reaction.

Once formed, however, benzene cannot react very readily to form condensed-ring structures. In pyrolysis, diphenyl is formed readily, but not naphthalene or anthracene. Aromatic hydrocarbons are well-known as products of the pyrolysis of acetylene at relatively low temperatures, but the spectra of the decomposition flames[19] and of diffusion flames[5] show no evidence of their presence and Porter did not detect them in flash photolysis.[1] The tests with benzene as additive

TABLE 2

Temp. of Reaction	Per Cent Additive	Per Cent C_2H_2	$\Delta(I/I_0)$
		Benzene	
°C.			
600	2	9	0.00
	3.4	9	0.00
600	2	20	0.02
	3.6	20	0.03
700	2.1	9	0.00
	5.4	9	0.05
	10.5	9	0.09
800	1.7	5	0.00
	3.2	5	0.01
		Toluene	
600	1.2	9.1	0.02
	3.6	9.1	0.02
700	1.2	9.1	0.00
	3.6	9.1	0.08
800	1.2	0	(0.1 ref. to I_0)
	4.2	0	(0.06 ref. to I_0)
	1.2	5	0.16
	4.2	5	0.35
800	4.2	14.1	0.34
		Naphthalene	
600	2.5	21	0.00
700	2.5	13	0.02
		21	0.00
800	2.5	0	(0.01 ref. to I_0)
		5	0.04
		9	0.11
		13	0.16
		Anthracene	
700	2	9	0.18
		13	0.20
		20	0.13
730	2	0	(0.02 ref. to I_0)
		13	0.13
800	2	5	0.33
	4	5	0.59
	2	13	0.14
	4	13	0.24
		Octatriyne	
700	(90°)*	14	0.06
	(100°)*		0.17

* Indicates temperature to which solid is heated.

in carbon formation and in the reaction with solid carbon[4] indicate it acts essentially as a diluent.

Furthermore, it has already been noted that the occurrence of decomposition flames and the related effects of increased concentration of acetylene, increased temperature, and additives such as oxygen and ethylene oxide clearly indicate a free-radical mechanism of reaction.[5, 10] The parallel results shown above for carbon formation indicate the same type mechanism is involved there. The inhibition by nitric oxide and the variations in effects of propylene and propane at different temperatures are also best explainable by such a mechanism.

One possibility of a simple free-radical process might be of the type

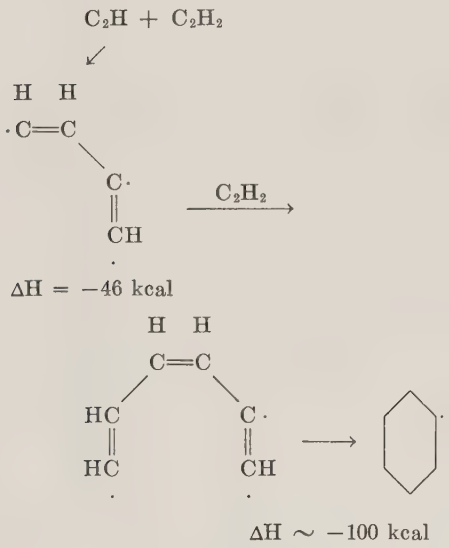

(2)

(Thermodynamic data are not directly available for all the compounds and radicals used in these and other equations, but where necessary reasonable estimates can be made from group contributions.[5]) This may release sufficient energy so that reactions such as

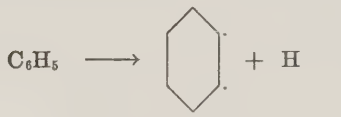

(3)

and

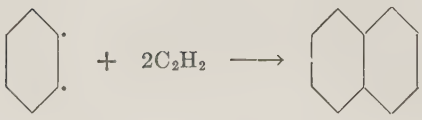

(4)

might follow. This is, however, subject to some of the same objections as the molecular mechanisms, in particular because of the lack of reactivity of benzene in the experimental systems.

The effectiveness of toluene, naphthalene and anthracene as additives show that ring structures are important in this system, but Reactions (1) and (2) do not seem to be a good source for these.

There is an alternative to Reaction (2) which is feasible under reaction conditions, although it would not be expected to show up in ordinary stable products. This involves simply a different orientation during reaction:

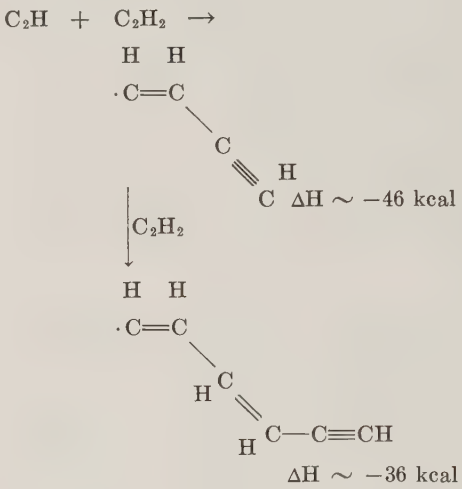

(5)

This may be followed by a reaction:

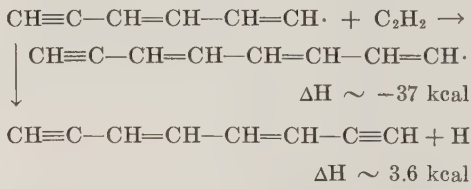

(6)

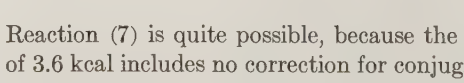

(7)

Reaction (7) is quite possible, because the value of 3.6 kcal includes no correction for conjugation. Available data on structures of acetylene, butadiene, etc., indicate Reactions (5) and (6) are as probable as Reaction (2).

Under reaction conditions such as are involved here, with high temperatures and relatively high free radical concentrations, dehydrogenation steps must be expected to be mixed in with the combinations (*cf.* Porter,[1]). Recent data on hydrocarbon decomposition (*cf.* Hinshelwood *et al.*[20]) indicate this may involve occasional elimination of molecular H_2, but free-radical stripping seems more likely. Compare, for instance, the

following:

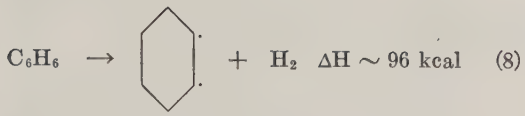

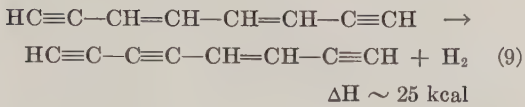

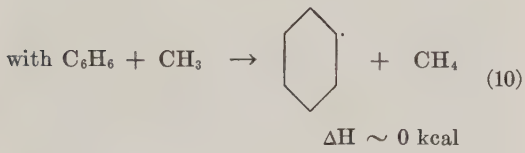

In Reaction (10), O_2, H and other active groups may also be involved, as in Reaction (1).

If concentration and temperature conditions are such that hydrogen stripping occurs fairly readily, reactions such as (5), (6) and (7) may lead to structures such as the octatriyne and the molecules or free radicals may combine:

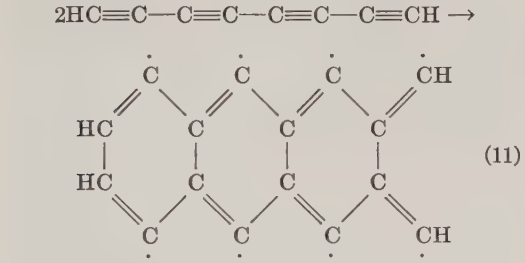

Four- or six-carbon groups might also be involved in such reactions. It is evident that a group of these might react in a sort of thermal explosion to start a platelet of condensed-ring structure such as that found for the gas carbons. This would be analogous to the chemical complex type of nucleation which Turkevich, Stevenson, and Hillier[21] have suggested for gold sols and which has in recent years also been applied to certain precipitation reactions such as that of iron hydroxide. The collection and partial orientation of molecules which might occur in formation of a liquid droplet or a solid crystallite would favor such reactions. However, with such highly unsaturated molecules, it would be very difficult to distinguish between a cluster of molecules and a microdroplet or crystal.

The results obtained with the octatriyne in forming the carbon gel indicate that such reactions are feasible and can occur much more rapidly than can condensation of aromatics to larger polycyclic structures. Reactions of the latter type are well-known, as, for example, in the recent results of Kinney and Delbel[16] and Nunn, Walker, and Kinney,[22] but the nature of the carbon and the various fragment molecules formed indicate that fragmentation is an initial stage for gas-phase reactions.

The carbon gel formation from the liquid reaction product of acetylene, and the effect of octatriyne on the acetylene reaction indicate that such reactions are of importance in carbon formation from acetylene. The effects of such straight-chain unsaturated compounds on the reaction systems must be taken into account as well as that of aromatics.

The possibilities of polymerization reactions such as Reaction (1) and free radical reactions involving aromatic structures as in Reactions (2), (3) and (4) or straight-chain unsaturates as in Reactions (5), (6) and (11) could give rise to a wide variety of reaction products and conditions, a variety which is consistent with that observed for the acetylene system. In general, low temperatures, and the presence of diluents would favor simple polymerization to give liquid hydrocarbons. High temperatures and concentrations, the presence of free-radical sources, etc., should favor free-radical formation and hydrogen-stripping reactions, which would lead to carbon formation.

Acknowledgments

The authors wish to express their thanks to Dr. S. H. Simonsen who made the x-ray pictures and to Mr. William Robertson and Mr. Gene Morrow for assistance with some of the experiments. We wish also to acknowledge the support of this work in part by a grant from the Petroleum Research Fund of the American Chemical Society and in part by the Office of Scientific Research of the U. S. Air Research and Development Command, Baltimore, Maryland.

REFERENCES

1. Porter, G.: *Fourth Symposium (International) on Combustion*, p. 248. The Williams & Wilkins Co., Baltimore, 1953.
2. Cole, D., and Minkoff, G. J.: Fuel *35*, 135 (1956).
3. Prout, W. E., and Anderson, R. C.: Fuel *33*, 125 (1954).
4. Frazee, J. D., and Anderson, R. C.: Paper presented at Am. Chem. Soc. Meeting, Chicago, Ill., Sept., 1953. (*Cf.* Tech. Rept.

No. 8, Contract AF 18(600)-430, Univ. of Texas, Aug., 1953).

5. Westbrook, E. A., Hellwig, K., and Anderson, R. C.: *Fifth Symposium (International) on Combustion*, p. 631. Reinhold Publ. Corp., New York, 1955.
6. Parker, W. G., and Wolfhard, H. G.: J. Chem. Soc. *1950*, 2038.
7. Tesner, P. A., and Echeistova, A. I.: Doklady Akad. Nauk SSSR, *87*, 1029 (1952); Chem. Abs., *47*, 6210f (1953).
8. Simonsen, S. H., and Anderson, R. C.: Tech. Note 22, No. OSR-TN-55-222, Contract AF 18(600)-430, Univ. of Texas, July, 1955.
9. Egloff, G.: *Physical Constants of Hydrocarbons*, p. 395. Reinhold Publ. Corp., New York, 1939.
10. Munson, M. S. B., Westbrook, E. A., and Anderson, R. C.: Paper presented at Am. Chem. Soc. Meeting, Minneapolis, Minn., Sept., 1955. (*Cf.* Tech. Note 17, No. OSR-TN-55-17, Contract AF 18(600)-430, Univ. of Texas, Jan., 1955).
11. Hofmann, U.: Naturwissenschaften, *32*, 260 (1944).
12. Grisdale, R. O.: J. Appl. Phys., *24*, 1082 (1953).
13. Ingram, D. J. E.: Discuss. Far. Soc., *19*, 179 (1955); Ingram, D. J. E., and Tapley, J. G.: Chem. & Ind., *1955*, 568.
14. Franklin, R.: Proc. Roy. Soc., *A209*, 196 (1951).
15. Schaefer, W. D., Smith, W. T., and Polley, M. H.: Ind. Eng. Chem., *45*, 1721 (1953).
16. Kinney, C. R., and Delbel, E.: Ind. Eng. Chem., *46*, 548 (1954).
17. Hofmann, U., and Wilm, D.: Z. Elektrochem., *42*, 504 (1936).
18. Clark, G. L., Eckert, A. C., and Burton, R. L.: Ind. Eng. Chem., *41*, 201 (1949).
19. Robertson, W. W., Humphreys, N., and Anderson, R. C.: J. Chem. Phys., *21*, 2093 (1953).
20. Hinshelwood, et al.: Proc. Roy. Soc. (London), *A231*, 145 (1955); *A225*, 64 (1954); *A214*, 471 (1952).
21. Turkevich, J., Stevenson, P. C., and Hillier, J.: Discuss. Far. Soc., *11*. 55 (1951).
22. Nunn, R. C., Walker, P. L., Jr., and Kinney, C. R.: Paper presented at Am. Chem. Soc. Meeting, Dallas, Texas, April, 1956.

Discussion by Bernard Greifer*

A clue to the structure of hydrocarbons synthesized during soot formation may be obtained by mounting a flat, polished NaCl or KBr plate in the flame so as to collect a thin uniform deposit. The plate may then be easily handled so as to obtain infrared, ultraviolet, and even x-ray spectra. It might be interesting to investigate the effect of varying the sampling height of the NaCl plate above the burner.† It is possible that the solvent extraction itself caused the observed polymerization of the hydrocarbons in the soot.

Author's Reply

The suggestion is an interesting one, but will involve some fairly marked experimental difficulties. We have been making somewhat similar tests on samples collected by various means and find the spectra are very complex, as might be expected; also the hydrocarbons foul a sodium chloride plate quite badly, requiring regrinding for cleaning.

The extraction tests mentioned above were made at room temperature, so there is very little likelihood of any polymerization in this. Care does, of course, have to be used in interpretation of results because of polymerization which can occur in the stages when samples are in process of cooling down.

* U. S. Bureau of Mines, Pittsburgh, Pennsylvania.

† A. A. Orning and B. Greifer: Fuel, *35*, 381 (1956).

31

THE PROPAGATION AND STABILITY OF THE DECOMPOSITION FLAME OF HYDRAZINE

By PETER GRAY, J. C. LEE AND (IN PART) H. A. LEACH AND D. C. TAYLOR

Introduction

Pre-eminent among problems facing the theory of laminar flame propagation is the prediction of the properties of flames from the kinetics of the chemical reactions occurring in them. Such predictions require, *inter alia*, knowledge of the kinetic order and activation energy of the over-all decomposition reaction under the conditions of the flame. This in turn requires extrapolation of experimental data on reaction kinetics, usually far beyond the range in which their validity is sure.

An alternative approach uses measurements made on the laminar flame to derive the form of kinetic equations governing reactions in the flame, and then compares this with the kinetic behavior observed at lower temperatures. This approach is adopted here.

The rigorous solution of the flame equations for even an elementary, single-step, reaction requires lengthy calculations and for this reason their excessive chemical complexity hinders the use of this information in testing flame theories, although in the past most information has been derived from studies of hydrocarbon flames. Flames which are chemically much less complicated may be expected to supply suitable data more readily.

The most simple flames known are those supported by the exothermic breakdown of a single compound and among these the hydrazine decomposition flame stands out. Hydrazine decomposition produces only nitrogen, hydrogen and ammonia. Thus, chemical analysis is easy and stoichiometry and thermochemistry are clear cut. The kinetics of the initial step in homogeneous decomposition (N—N bond fission) are known[1] as a function of temperature. The spontaneous[2, 3] and spark[4] ignitions have been observed. The gaseous decomposition flame has been stabilized on burners[5, 6] at atmospheric pressure. The decomposition flame has been burned above the surface of the liquid.[7, 8] Furthermore, some theoretical work has also been done on this system[9, 10] in an attempt to predict the flame velocity from the kinetics of the initial step in homogeneous decomposition.

Two fundamental properties of the hydrazine flame are (1) the dependence of flame speed on pressure from which the over-all kinetic order of reaction may be found, and (2) the dependence of flame speed on temperature from which the over-all activation energy may be found. The primary purpose of this work is to supply this information experimentally, to examine its theoretical implications, and to see how they may be interpreted.

Two experimental methods have been used. In the first, flame speeds of gaseous hydrazine have been measured by the closed vessel method. This permits the accurate control of initial pressure and temperature and avoids the hazards of the considerable flow of heated hydrazine necessary for a normal burner technique. The pressure range which can be studied in a glass vessel extends from very low values up to about 10 cm Hg.

In the second method the pressure range between 10 cm Hg and atmospheric has been examined by burning liquid hydrazine in narrow tubes.[6, 7] This provided the secondary purpose of this work—to examine the validity of this simple technique. In tubes, the flame is not adiabatic but subject to strong quenching influences as a result of lateral heat losses. This difficulty has been pointed out by Gray and Kay[8] but not previously overcome. An attempt has now been made to allow for these varying heat losses.

Experimental

MATERIALS

Concentrated hydrazine, containing approximately 98 per cent N_2H_4 by weight, was dehydrated by refluxing for 2 to 3 hr over fused caustic soda at 120 to 150 mm Hg in an atmosphere of nitrogen, followed by distillation under similar conditions. Analysis by the iodate method[11] gave 99.9 to 100.2 per cent N_2H_4. The samples were stored in the absence of air. All other gases were taken from cylinders, the noncondensable ones being passed through a liquid oxygen trap to remove water vapor.

APPARATUS AND PROCEDURE USED IN CLOSED VESSEL EXPERIMENTS

The combustion vessel was a squat glass cylinder 20 cm diam and 20 cm depth which could be evacuated to 10^{-4} mm Hg by a two-stage pump. The electrodes of 1 mm diam tungsten wire with rounded tips projected horizontally from side arms leaving a spark gap of 4.6 mm at the center of the vessel. To prevent condensation of the hydrazine the vessel was enclosed in an air thermostat maintained at 62°C.

The movement of the flame was followed by the schlieren optical technique. The field of view was restricted to a narrow section of the flame along its vertical diameter. The progress of the flame in this direction was recorded as a V-shaped trace on a film moving horizontally in a drum camera. The speed of the drum was found by timing the revolution of a spindle driven through a reduction gear. A spark from the secondary of an ignition coil was used to ignite the gas and the spark energy was never grossly in excess of the minimum required.

The flame traces showed that in most cases, after a short initial period of acceleration, the movement of the flame was uniform until it reached a diameter of 9 to 10 cm. On the enlarged traces tangents were drawn at a point corresponding to a flame diameter of 6 cm, i.e., where the radius of the flame sphere, $r_b = 0.3R$, where R is the radius of the vessel. There was no significant difference between the slopes of the upper and lower traces. The estimated error in the flame speed is about 2 per cent.

At the lowest pressures and with mixtures containing helium or hydrogen of high thermal conductivity, the initial acceleration extended over a greater distance and the length of the straight portion of the trace was correspondingly reduced. In these cases, the measured value of the flame speed may be a few per cent too low.

INTERPRETATION OF FLAME TRACES

Lewis and von Elbe[12] have given a detailed account of the processes which occur when gas is ignited at the center of a closed vessel. As the flame travels to the walls, the pressure rises and both the burned and unburned gases are compressed. As a result, the movement of the flame depends on both the burning rate and the gas flow. However, during the initial phase of the combustion, the increase in pressure is small and the linear speed of the flame, S_l, is very close to the speed relative to the burned gas, S_b. Even when the radius of the flame sphere, r_b, is $0.3R$ (where R is the radius of the vessel) the pressure has risen by only 3 per cent and S is $0.98\ S_b$. The speed of the flame measured at this point is therefore essentially the speed relative to the burned gas at the initial pressure.

RESULTS OF CLOSED VESSEL MEASUREMENTS

Products of the decomposition flame

The products from the decomposition flame of liquid hydrazine were unaffected by changes in pressure and corresponded closely to the equation

$$N_2H_4 = NH_3 + \tfrac{1}{2}N_2 + \tfrac{1}{2}H_2$$

Murray and Hall[5] and Hall[13] found that the same products were formed by the flame of gaseous hydrazine on a burner at atmospheric and at low pressures. In each of these circumstances, the flame burns under constant pressure. Similarly in a closed vessel, the pressure is virtually constant during the initial stage of the combustion and in the region where flame speeds were measured it is most probable that the same mode of decomposition occurs.

The *final* products after complete combustion of hydrazine in the closed vessel are not of course the same as the products formed in the initial stages. The major part of the hydrazine burns close to the walls after being adiabatically compressed, at the same time compressing the hot gases produced in the earlier phase of the decomposition. Under these conditions much higher temperatures are reached compared with the constant pressure flame and secondary decomposition of ammonia is likely to take place. Unless the hydrazine is strongly diluted with an inert gas to reduce the temperature, the final products may be expected to contain less ammonia. In agreement with this, analysis of the final products showed that they were the same as the products of the constant pressure flame only for a mixture of 1 mole N_2H_4 diluted with 1.5 moles N_2. With smaller proportions of added nitrogen, less ammonia was found, the products from pure hydrazine being given by

$$N_2H_4 = 0.72NH_3 + 0.64N_2 + 0.93H_2$$

Influence of pressure on flame speed

A four-fold change in pressure from 2 to 8 cm Hg produced little variation in the flame speed of

pure hydrazine (Fig. 1). The small decrease in speed at low pressures is probably due to the method of measurement. The thermal theory of flame propagation predicts[14] that the flame speed will vary with pressure according to $S_b \propto P^{(n-2)/2}$, where n is the kinetic order of the chemical reaction controlling the flame. The pressure independence shown by hydrazine indicates that $(n - 2)/2 = 0$, i.e., the reaction is second order.

The calculated final flame temperature is 1904°K and thus the flame speed at 5 cm Hg, $S_b = 1330$ cm/sec, is equivalent to a speed relative to the unburned gas, $S_u = 117$ cm/sec. At atmospheric pressure and a higher initial temperature (150°C), Murray and Hall[5] found $S_u = 200$ cm/sec.

FLAME SPEEDS IN MIXTURES WITH DILUENTS

The addition of the diluents helium, argon, nitrogen, hydrogen and ammonia decreased the speed of the hydrazine decomposition flame. The speed was measured for different partial pressures of each added diluent at a fixed hydrazine pressure of 5.02 cm Hg (Table 1, Fig. 2). The range

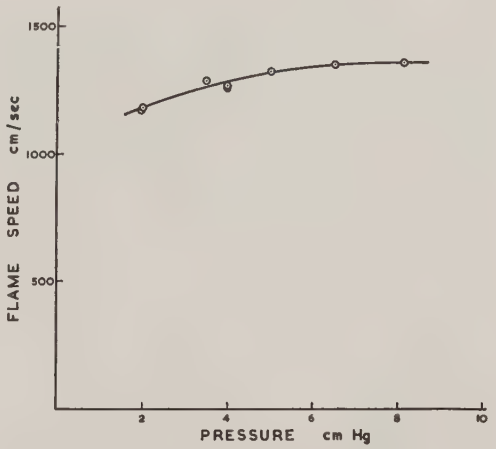

FIG. 1. Effect of pressure on the flame speed of pure hydrazine.

TABLE 1. FLAME SPEEDS IN MIXTURES OF HYDRAZINE WITH DILUENTS

Hydrazine pressure 5.02 cm Hg. Initial temperature 62°C

Diluent	Pressure of Diluent cm Hg	Flame speed S_b cm/sec	Flame Temperature T_b°K	Reciprocal Flame Temperature $\frac{1}{T_b} \times 10^3$	Thermal Conductivity $\lambda \times 10^6$ cal/cm, sec°C	$\text{Log}_{10}\left\{\frac{S_b^2(T_b - T_u)^2}{\lambda T_b^6}\right\} + 6$
—	—	1330	1904	0.5252	759	2.078
					650*	2.145*
He	0.99	1070	1846	0.5417	781	1.924
	1.88	852	1797	0.5565	795	1.763
	2.02	814	1790	0.5587	797	1.728
A	1.01	1050	1845	0.5420	686	1.966
	2.02	770	1790	0.5587	625	1.785
	3.02	644	1738	0.5754	573	1.714
	4.00	478	1690	0.5917	531	1.540
	5.02	400	1645	0.6079	493	1.449
	6.02	314	1602	0.6242	461	1.308
	7.00	234	1563	0.6398	432	1.118
	7.99	174	1526	0.6553	407	0.922
					337*	1.004*
N_2	1.24	823	1792	0.5580	668	1.813
	2.50	547	1694	0.5903	594	1.595
	5.02	233	1534	0.6519	489	1.089
H_2	0.84	1020	1831	0.5461	796	1.893
	2.64	636	1696	0.5896	844	1.572
NH_3	0.74	869	1790	0.5587	712	1.834

* λ calculated by the method of Lindsay and Bromley.[16]

of measurements for hydrogen and helium was limited by the difficulty of igniting these mixtures.

Effect of heat capacity

The inert diluent lowers the flame temperature and Figure 2 illustrates that nitrogen and hydrogen of higher heat capacity than argon and helium were more effective in decreasing the flame speed. Flame temperatures for the adiabatic combustion of the mixtures at constant pressure and an initial temperature of 62°C were calcu-

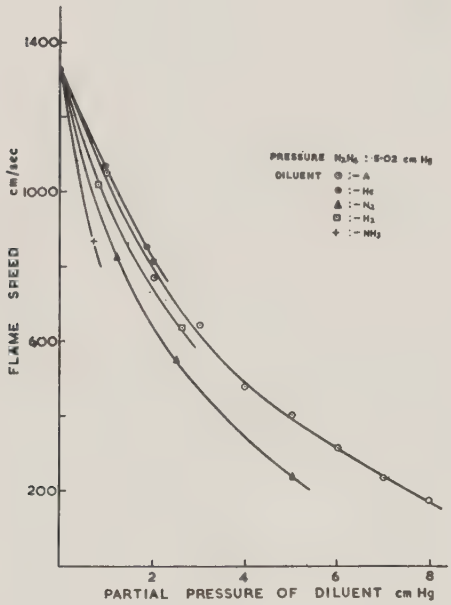

FIG. 2. Flame speeds in mixtures of hydrazine with diluents.

lated on the basis of the equation

$$N_2H_4(g) = NH_3 + \tfrac{1}{2}N_2 + \tfrac{1}{2}H_2$$

$$\Delta H^\circ = -33.74 \text{ kcal/mole}$$

The enthalpy of ammonia was taken from Justi's tables and the enthalpies of the other gases from tables of the National Bureau of Standards. The flame temperatures are listed in Table 1 and the parallel between temperature and flame speed shows clearly that the dominant effect of the addition of the inert diluent is the lowering of the flame temperature.

Effect of thermal conductivity

The inert gas also changes the thermal conductivity. Comparison of helium with argon and hydrogen with nitrogen (Fig. 2) shows that the flame speed was higher in mixtures of high thermal conductivity. (On theoretical grounds, it is the thermal conductivity of the *products* at the final temperature which is most important in determining the flame speed.) This value of the thermal conductivity was calculated for each mixture as shown in Table 1.

In deriving the thermal conductivity the viscosities of the pure gases at temperatures between 1500 and 1900°K were calculated by the method described by Hirschfelder, Curtis and Bird.[15] The values of the collision integrals were taken from the tables based on the Lennard-Jones function for the intermolecular potential. The thermal conductivity of each gas was then found from the viscosity using the Eucken assumption. Two procedures were used to calculate the thermal conductivity of the mixture. The first used a simple molar average. However, as this is known to give too much weight to the components with high thermal conductivities the more realistic but lengthier method of Lindsay and Bromley[16] was also used as a check.

APPARATUS AND PROCEDURE USED IN TUBE EXPERIMENTS

A narrow glass tube was completely filled with liquid hydrazine which was then ignited with a small flame. As the hydrazine was consumed the decomposition flame followed the liquid surface as it receded down the tube leaving at the mouth a diffusion flame of the products burning in air.

To study the effect of pressure on the flame, the tube was enclosed in a large vessel evacuated by a pump.

The burning rate of the decomposition flame was measured by timing the movement of the liquid surface between marks on the tube, keeping the pressure constant. Several determinations of the burning rate were made and the mean value taken. This rate is proportional to the mass rate of flow of hydrazine per unit area. To convert this experimentally measured burning rate into the flame speed relative to the burned gas for use in Equations such as (1) and (2) we use the relation:

$$S_M = S_b\rho_b$$

Thus in interpreting these results it must be borne in mind that a flame for which S_b is independent of pressure will show S_M proportional

to the pressure, since ρ_b is itself proportional to the pressure.

RESULTS OF TUBE EXPERIMENTS

Analysis of products

For analysis of the flame products, the tube containing the burning hydrazine was connected to a sampling tube fitted with taps at each end. The product gases were allowed to stream through the tube and sweep out the air before the taps were closed. Samples were collected under two different pressures and analyzed (Table 2). Pure hydrazine was used to avoid condensation of water. If any water is present, ammonia analyses give low values.

Effect of varying lateral heat losses

As the flame burns down the tube, heat is transferred to the walls and lost at the outer surface to the surroundings. When the tube is surrounded by air its outside is heated above 100°C. The lateral heat loss was varied by immersing the tube in a water-bath held at different temperatures. In one experiment at atmospheric pressure, when the temperature of the bath was 90°C, the flame travelled more slowly than in air, but would not propagate at 80°C.

Measurement of extinction pressures

As the pressure was reduced, the thickness of the decomposition flame increased, the gap between the flame and the walls of the tube became slightly larger, and finally the flame was extinguished. Near the extinction pressure, the flame was rather unstable and a slight bubbling of the liquid or a mechanical shock put out the flame.

The (lower) pressure limit for the propagation of the decomposition flame was measured in four different tubes covering a range of diameters. In a smaller tube extinction of the flame occurred at a higher pressure. The flame also became less stable when the hydrazine was diluted with water, the extinction pressure in a particular tube being increased.

This variation of the extinction pressure with tube diameter and hydrazine concentration is very similar to the quenching effects found with burner flames of premixed gases, where the quenching diameter is roughly inversely proportional to the pressure. To illustrate that the same relation holds for the extinction of the hydrazine flame, the experimental results are presented in Figure 3 as the reciprocal of the extinction pressure plotted against the tube diameter. Each point represents the mean value of several individual determinations.

The effect of hydrazine concentration on the extinction of the decomposition flame at high pressures was determined by Adams and Stocks.[7]

Table 2. Products of Decomposition Flame of Liquid Hydrazine

Pressure	Moles Product/Mole N_2H_4			Element Balance of Analysis H/N
	NH_3	H_2	N_2	
cm Hg				
30–35	1.016	0.477	0.492	1.980
76	1.020	0.470	0.490	1.997

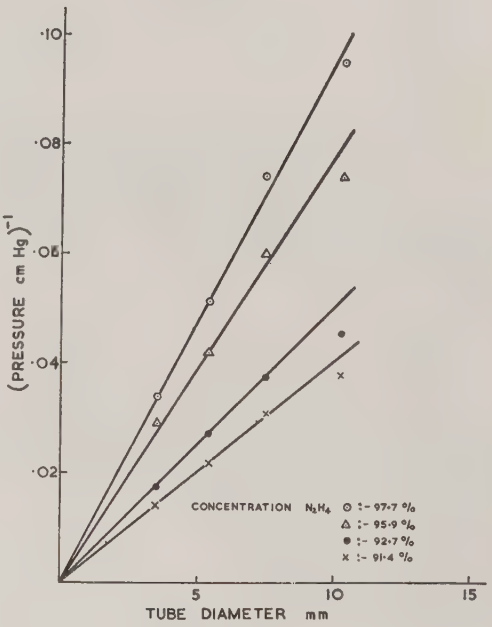

Fig. 3. Extinction pressures for the decomposition flame of liquid hydrazine.

The new measurements on the low pressure extinction, combined with the previous results, define the whole region of pressure and composition for the stable propagation of the flame in a tube of 5-mm diam (Fig. 4).

Measurement of Burning Rates

For a given tube, the burning rate increased with pressure while at constant pressure the rate was smaller in tubes of larger diameter (Fig. 5).

Diluting the hydrazine with water reduced the burning rate. Burning rates over the whole region of pressure and composition where propagation

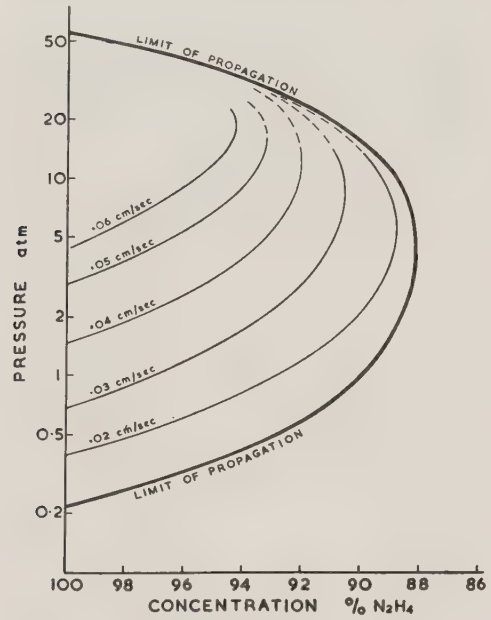

FIG. 4. Limits of stability and burning rates of the decomposition flame of liquid hydrazine in a tube of 5 mm diameter. Results above 1 atmos from Ref. 4.

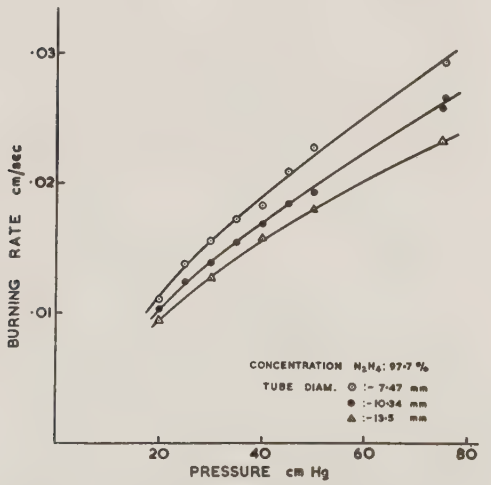

FIG. 5. Burning rates of liquid hydrazine containing 97.7 per cent N_2H_4 by weight.

can occur are illustrated in Figure 4. In Figure 4 the three dimensional surface corresponding to the variation of the burning velocity with pressure and concentration is represented as a series of contour lines of equal burning rates lying inside the boundaries of stable propagation on the pressure concentration chart.

Correction of Burning Rates for Effect of Quenching

The theory of flame propagation deals with the simple case of a plane adiabatic flame. In tubes the flame is not adiabatic and to apply the theory comparison of burning rates at different pressures should be made under comparable quenching conditions. As pointed out by Wolfhard,[17] this can be done by working with a different tube for each pressure so that the tube diameter is always a constant multiple of the quenching diameter.

For 97.7 per cent hydrazine, the quenching diameter at four different pressures was taken from Figure 3. Then at each of these pressures the burning rate in a tube of five times the appropriate quenching diameter was found by interpolating between the curves shown in Figure 5. When the burning rate so derived is plotted against pressure (Fig. 6) the result is a straight line through the origin.

The mass rate of burning, corrected for the influence of quenching effects, is thus proportional to the pressure. This corresponds to a flame speed relative to the burned gases, i.e., S_b, independent of the pressure.

Discussion

1. THE DECOMPOSITION FLAME OF GASEOUS HYDRAZINE

The products formed during the initial stage of the explosion in the closed vessel correspond to the equation

$$N_2H_4 = NH_3 + \tfrac{1}{2}N_2 + \tfrac{1}{2}H_2$$

$$\Delta H^\circ = -33.74 \text{ kcal/mole}$$

although the final products are influenced by the high temperatures reached in the later stages and contain a smaller proportion of ammonia.

The speed of the flame of pure hydrazine, measured with respect to the initial products in the closed vessel, was virtually independent of the pressure between 2 and 8 cm Hg, indicating that the over-all reaction in the flame is second order and not first as has previously been accepted.

The addition of inert diluents decreased the flame speed. Comparison of different diluents showed that this decrease was mainly due to the lowering of the flame temperature, and that

the thermal conductivity influenced the speed to a smaller extent. This behavior is in agreement with the Semenov[14] theory of flame propagation which, for a second order reaction leads to the relation:

$$S_b^2 = \frac{2\lambda}{P_u L} \cdot Ba_u \cdot \frac{1}{(T_b - T_u)^2} \cdot \left(\frac{RT_b^2}{E}\right)^3 \cdot e^{-ER/T_b} \quad (1)$$

The partial pressure of hydrazine was the same for each mixture so that a_u and the product $L\rho_u$

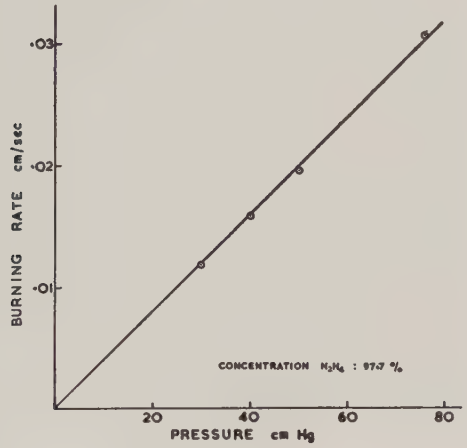

FIG. 6. Burning rate of liquid hydrazine corrected for the influence of quenching.

were constant. Thus rearranging Equation (1)

$$\mathrm{Log}_{10} \frac{S_b^2(T_b - T_u)^2}{\lambda T_b^6} = \frac{E}{2.3R} \cdot \frac{1}{T_b} + \text{const} \quad (2)$$

The expression on the left hand side of Equation (2) has been evaluated (Table 1) and plotted against $1/T_b$ in Figure 7. The points all lie fairly close to a single straight line as required by the theory, although a slight deviation occurs at the low temperature end. Thermal conductivities of the mixtures were calculated as molar averages. However, the relative positions of points at the ends of the line are not significantly changed when thermal conductivities are calculated by the method of Lindsay and Bromley and it is unlikely that more refined calculation of the conductivities of other mixtures would change the shape or slope of the graph appreciably. The slope of a line fitted to the more numerous argon points corresponds to an activation energy E = 36 kcal/mole.

Both this activation energy, 36 kcal, and the value derived from burner flames,[5,7] 30 to 45 kcal., are considerably less than the activation energy required[1] for the reaction

$$N_2H_4 \rightarrow 2NH_2 \qquad E = 60 \text{ kcal mole}^{-1}$$

Moreover, using this reaction in the accurate numerical calculation[9,10] of the burning velocity gives a value of only 30 cm/sec compared with 200 cm/sec experimentally.[6] This shows that the initial fission of N_2H_4 to $2NH_2$ cannot be the sole

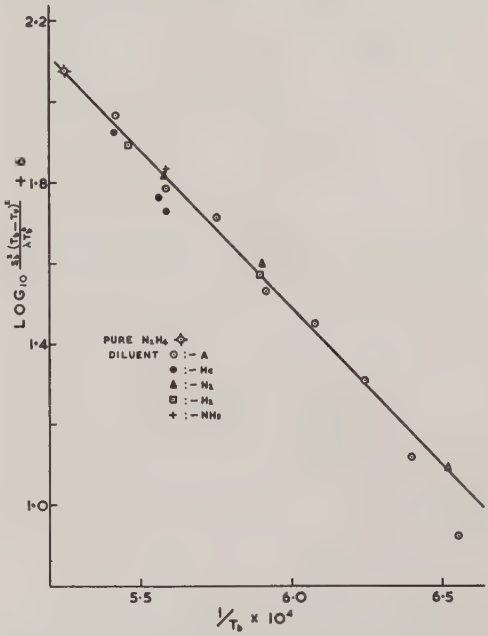

FIG. 7. Application of the Semenov theory to flame speeds in mixtures with diluents.

rate determining step. A chain reaction is probably involved.

The mechanism of this reaction has been discussed by Adams and Stocks,[7] who proposed the scheme

$$N_2H_4 \rightarrow 2NH_2 \qquad \text{initiation}$$

$$\left.\begin{aligned} NH_2 + N_2H_4 &\rightarrow NH_3 + N_2H_3 \\ N_2H_3 &\rightarrow N_2 + H_2 + H \\ H + N_2H_4 &\rightarrow NH_3 + NH_2 \end{aligned}\right\} \text{ propagation}$$

followed by termination steps of second order with respect to the chain carriers. The roles of NH_2 and H as chain carriers in this reaction sequence are very similar. If X represents any chain carrier, the mechanism in its most general

form becomes:

$$N_2H_4 \rightarrow 2X$$
$$\text{Rate} = k_1(N_2H_4)$$
$$X + N_2H_4 \rightarrow X + \text{Products}$$
$$\text{Rate} = k_2(X)(N_2H_4)$$
$$X + X \rightarrow \text{Products}$$
$$\text{Rate} = k_3(X)^2.$$

Applying the stationary state principle, the rate of decomposition of hydrazine by the propagation step is $k_2(2k_1/k_3)^{\frac{1}{2}}(N_2H_4)^{\frac{3}{2}}$. This can be second order in relation to the total pressure only if k_1 is proportional to the pressure and k_2 independent of pressure. These are conditions most likely to hold at low pressures, where the rate of the initiation step might be determined by the rate of activation of the hydrazine and termination by three body collisions would be infrequent. Termination would then occur by reactions such as:

$$H + N_2H_3 \rightarrow N_2 + 2H_2$$
$$NH_2 + N_2H_3 \rightarrow NH_3 + N_2 + H_2$$
$$2NH_2 \rightarrow N_2 + 2H_2$$

because a third body would be required for the reactions

$$H + H \rightarrow H_2 \qquad H + NH_2 \rightarrow NH_3$$

This chain mechanism for the reaction is thus consistent with the observed second order behavior of the hydrazine flame at low pressures.

2. THE DECOMPOSITION FLAME OF LIQUID HYDRAZINE

The study of decomposition flames of liquids burning in narrow tubes is easy and convenient. The liquid appears to act only as a reservoir to supply fresh vapor to the flame burning the gas phase above the meniscus. Work can be carried out with quite small amounts of liquid—a useful consideration when explosive liquids are being investigated. However, the conditions differ from those used in the definitions of burning velocity and they certainly do not satisfy the requirements of theoretical models of flames from which heat losses are absent. Instead, heat is lost to the walls of the tube and at low pressures the flame is extinguished. The extinction pressure was found to be inversely proportional to the tube diameter, suggesting that the flame is quenched in a manner similar to the quenching of gas flames on burners.[17] The flame is also extinguished at high pressures[7] so propagation can occur only within a limited range of pressure. Dilution of the hydrazine with water both decreases the upper pressure limit and increases the lower pressure limit until a concentration is reached where the two limits coalesce. The complete region of stability in a 5 mm diameter tube is shown in Figure 4.

In passing from the lower to the upper pressure boundary of this region (Fig. 4) the mass rate of burning increases with increasing pressure, although the speed of the gas flowing through the flame decreases. In the low pressure part of the region, the burning rate is certainly influenced by heat losses which tend to quench the flame, for the burning rate was decreased when the tube was surrounded by water. To compensate for quenching effects, the diameter of the tube in which the burning rate is measured should be increased as the pressure is reduced so that burning rates are measured in tubes which are always a constant multiple of the quenching diameter. When rates determined in this way are compared it is found that the mass rate of burning is proportional to the pressure and the flame speed relative to the burned gas, S_b, independent of pressure. If the Semenov theory[14] is applicable to the data corrected in this way this means a second-order rate-controlling step in agreement with the closed vessel results. If the burning rates are not corrected for quenching the mass rate of burning does not depend on the pressure in any simple way and formulae of the type $S_M \propto P^\alpha$ cannot be satisfied by a constant value for α. Thus by taking quenching into account it is possible to correct some of the deficiencies of the tube method. However, other factors which vary with tube diameter also influence the rate. Thus, in spite of increased heat losses expected, the mass rate of burning is actually higher in tubes of smaller diameter (Fig. 5). The flame front is possibly more curved[7] in the smaller tubes and its greater area causes an increase in the mass rate of burning. Longitudinal conduction of heat in the walls of the tube may also be important. Until the burning rate can be corrected for these effects, it is clear that the simple method of burning liquids in tubes cannot yield such reliable quantitative information about the speed of the adiabatic flame as other methods.

Acknowledgments

We are grateful to Dr. G. K. Adams of the E. R. D. E., Waltham Abbey, and to Dr. A. R. Hall of R. A. E., Westcott, for helpful discussions.

We also thank the Royal Society of London for a Research Grant for equipment and Professor T. R. C. Fox for the facilities which enabled this work to be carried out.

Nomenclature

S_b , S_u	linear flame speeds relative to the burned and unburned gas, cm/sec
S_M	mass rate of burning per unit area of flame surface, g/sec cm^2
T_b , T_u	temperatures of the burned and unburned gas, °K
ρ_b , ρ_u	density of the burned and unburned gas mixture, g/cm^3
a_u	concentration of reactant in unburned gas, moles/cm^3
L	heat ($-\Delta$H) of combustion of the gas mixture, cal/g
λ	thermal conductivity of burned gas, cal/cm sec °C
R	gas constant, cal/mole °K
E	energy of activation, kcal/mole
n	order of reaction.
B	pre-exponential rate constant such that: reaction velocity (moles/cm^3 sec) = $a^n B \exp(-E/\mathbf{R}T)$.

REFERENCES

1. Szwarc, M.: Proc. Roy. Soc., *A198*, 267 (1949).
2. Gray, P., and Lee, J. C.: Trans. Faraday Soc., *50*, 719 (1954); Research, *7*, S2 (1954).
3. Gray, P., and Lee, J. C.: *Fifth Symposium (International) on Combustion*, p. 692. New York, Reinhold Publ. Corp., 1955.
4. Bamford, C. H.: Trans. Faraday Soc., *35*, 1239 (1939).
5. Murray, R. C., and Hall, A. R.: Trans. Faraday Soc., *47*, 743 (1951).
6. Pannetier, G., and Guedeney, F.: Compt. rend., *238*, 898 (1954).
7. Adams, G. K., and Stocks, G. W.: *Fourth Symposium (International) on Combustion*, p. 239. Baltimore, The Williams & Wilkins Co., 1953.
8. Gray, P., and Kay, J. C.: Research, *8*, S3 (1955).
9. Hirschfelder, J. O., Curtiss, C. F., and Campbell, D. E.: J. Phys. Chem., *57*, 403 (1953). See also Hirschfelder, Curtis and Bird,[15] p. 764.
10. von Karman, T., and Penner, S. S.: *Selected Combustion Problems*, p. 5. London, Butterworths Scientific Publications, 1954.
11. Penneman, R. A., and Audrieth, L. F.: Ind. Eng. Chem. (Anal.), *20*, 1058 (1948).
12. Lewis, B., and von Elbe, G.: *Combustion, Flames and Explosions*, p. 448. New York, Academic Press, 1951.
13. Hall, A. R.: Private communication, 1956.
14. Semenov, N. N.: Prog. Phys. Sci. (U.S.S.R.), *24*, 433 (1940); (translated as NACA Tech. Memo No. 1026).
15. Hirschfelder, J. O., Curtis, C. F., and Bird, R. B.: *Molecular Theory of Gases and Liquids*, Chap. 8. New York, John Wiley & Sons, 1954.
16. Lindsay, A. L., and Bromley, L. A.: Ind. Eng. Chem., *42*, 1508 (1950).
17. Wolfhard, H. G.: Z. tech. Phys., *24*, 206 (1949).

Discussion by A. R. Hall

For the same reasons as Dr. Gray, Dr. Wolfhard and I determined the pressure dependence of the burning velocity of flames supported by hydrazine vapor (97 per cent) at 120°C. Murray and Hall* had obtained the velocity at atmospheric pressure by the burner method, measuring the total cone area, so we extended this technique to obtain velocities at 3, 7 and 15 cm Hg; care was taken to ensure that inevitable heat losses from the flames did not vitiate the comparative measurements of the burning velocities. The velocities were found to be relatively constant at around 185 cm/sec even over the wide pressure range from 1 atmos to 1/25 atmos. Some interesting spectrographic observations were also recorded with both the self-decomposition and oxygenated flames of hydrazine, etc. A full report of this work is in press elsewhere.

Author's Reply

The experiments reported by Dr. Hall and his collaborators afford excellent confirmation of our findings. They use a different experimental technique. Not only do they find, as we do, that the burning velocity, S_U , is independent of pressure but the numerical values they report, 200 and 185 cm sec^{-1} referring to initial temperatures of 150° and 120°C, respectively, in 97 per cent N_2H_4 are also in good agreement with our value of 120 cm sec^{-1} at an initial temperature of 60°C in 100 per cent hydrazine.

* R. C. Murray and A. R. Hall: Trans. Faraday Soc., *47*, 743 (1951).

32

THE OZONE TO OXYGEN FLAME[a]

By A. G. STRENG AND A. V. GROSSE

Introduction

In the last few years our laboratories have been devoting a lot of effort to the production of high temperatures by chemical means. The two prerequisites for producing high temperatures are (a) a reaction with a high heat release, and (b) thermal stability of the reaction products.

Among the most thermally stable molecules known are carbon monoxide and nitrogen. By combusting cyanogen to these products temperatures of 4800°K have been produced at 1 atmos[1]

TABLE 1

	At 1 Atmos	At 3.00 Atmos	At 30 Atmos
$(CN)_2 + O_2 \rightarrow 2\ CO + N_2$	4850°K	4960	—5090
$(CN)_2 + \frac{2}{3}O_3 \rightarrow 2\ CO + N_2$	5170°K	5310	5530

TABLE 2

	Atmos 1.0	.10	40.82 (= 600 Psia)
$(C_4N_2)_g + 2\ O_2 \rightarrow 4\ CO + N_2$			
$\Delta H_{298}^{\circ} = -254.6$	5261°	5573°	5748°
$(C_4N_2)_g + \frac{4}{3}O_3 \rightarrow 4\ CO + N_2$			
$\Delta H_{298}^{\circ} = -299.9$	5516°	5936°	6100°

and by combusting them under pressure 5050°K have been attained.[2] Recently, by combusting a new type of compounds, namely, the carbon subnitrides, specifically, (C_4N_2), again to carbon monoxide and nitrogen, a temperature of 5260°K at 1 atmos was reached.[3] This is due to the fact that the endothermic heat of formation of C_4N_2 (ΔH_f° at 298°K = +149.81 kcal/mole) is substantially greater than that of cyanogen (ΔH_{298}° = +73.84 kcal/mole). It was obvious that by combining these endothermic fuels with an endothermic oxidizer, still higher temperatures might be reached. An obvious substitute for oxygen is *ozone*, since it has the advantage of giving the same products of combustion. The heat of "combustion" of ozone, in line with the stoichiometric equation

$$O_3 \rightarrow 1.5\ O_2 + 33.92\ \text{kcal/mole}$$

is H_f° at 291°K = −33.92 kcal/mole (see p. 265). Thus a substitution of O_2 by O_3 would raise appreciably the temperatures of the above flames. As a comparison of the temperatures obtainable with ozone and oxygen in the cyanogen combustion, the figures given in Table 1 are of interest.

Whereas the above calculations are only approximate, accurate calculations[3] were carried out in the case of C_4N_2, and are given in Table 2.

Similar increases might be expected in a large number of other flames. Furthermore, the substitution of oxygen by ozone in all oxygen containing flames studied so far gives an excellent opportunity to obtain a large number of new experimental data of the various combustion parameters and thus provide existing theories with fresh material.

In order to investigate the combustion of other substances with ozone, it is important to explore first the ozone flame alone.

The direct combustion of ozone (or ozone-oxygen mixtures) to oxygen would be the simplest flame of all since it involves only the transformation of one allotropic form of an element into another. Only atomic oxygen is possible as an intermediate in such a flame, outside of the "fuel," O_3, and the "product of combustion," O_2.

In recent years a number of studies have been devoted to ozone, particularly to its method of preparation, handling and storage and explosive decomposition. The Armour Research Foundation has been prominent in this field, and the literature is fully reviewed by Thorp.[4]

The stability of ozone and the rates of decomposition or explosion have been investigated at the Armour Research Foundation, and their results are summarized in Figure 1, which is reproduced here for ready reference. This figure shows the relationship between the decomposition velocity of ozone in cm/sec *vs* the ozone concentration. At the Armour Research Foundation four types of decomposition have been observed and designated as follows:[5] (a) "Normal

[a] This research was supported by the United States Air Force through the Air Force Office of Scientific Research of the Air Research & Development Command under Contract No. AF 18(600)-1475.

decomposition," in the range of 0 to 20 wt per cent ozone; (b) "Self-sustaining decomposition," in the range of 20 to 48 wt per cent ozone; (c) "Deflagration," in the range of 48 to 54 wt per cent O_3, and (d) "Detonation," in the range of 54 to 100 wt per cent O_3.

The detonation velocity is assumed to be constant from 54 per cent on, and equals approximately 2150 m/sec.[6]

Point "C'" of Figure 1 at 48 wt per cent O_3, has been determined from experimental data in the Armour Research Foundation Laboratories[6] to be approximately 240 m/sec. The whole interpretation given in Thorp's book implies that no steady flame could be produced in concentrated ozone and that detonation would invariably result with ozone mixtures above 54 per cent. It is likely that the same tacit assumption that explosions or detonations would result prevented earlier workers from producing a steady ozone flame and studying its properties.

Lewis and von Elbe[7, 8] have studied the flame propagation of an explosion in a spherical vessel. From the experimentally observed rate of pressure increase with time they have been able to calculate the flame velocity. Such a flame, however, is not stable in time but has a constantly increasing velocity. It does not prove that a steady flame would actually burn from a standard tip.

The temperatures of the ozone-oxygen flames are discussed in detail on page 266. The 100 per cent ozone flame has a calculated temperature of 2677°K. In view of this substantial temperature one would expect that concentrated ozone-oxygen mixtures would burn to oxygen in a regular manner from a burner tip, assuming that conditions can be found to avoid explosion or detonation. Such conditions have been found and we will describe in this paper how ozone can be burned to oxygen, from a simple burner tip, in the whole range from 17 per cent to 100 per cent ozone.

As inorganic chemists our interest was primarily to learn how to burn pure ozone and to use it to combust a whole gamut of fuels. In addition, however, the pure ozone flame has a particular theoretical interest to physical chemists. It is, as stressed previously, the simplest flame since the only possible intermediates are oxygen atoms.

Lewis and von Elbe[9, 10] were the first to attempt to develop a modern combustion wave theory and they used the ozone flame as a model.

During the last few years Hirschfelder, Curtis and Campbell,[11, 12] on the one hand, and von Kármán and Penner[13] on the other, have developed mathematical methods for finding exact solutions for the flame velocity and have applied them to the ozone flame. Recently, Sandri[14] has

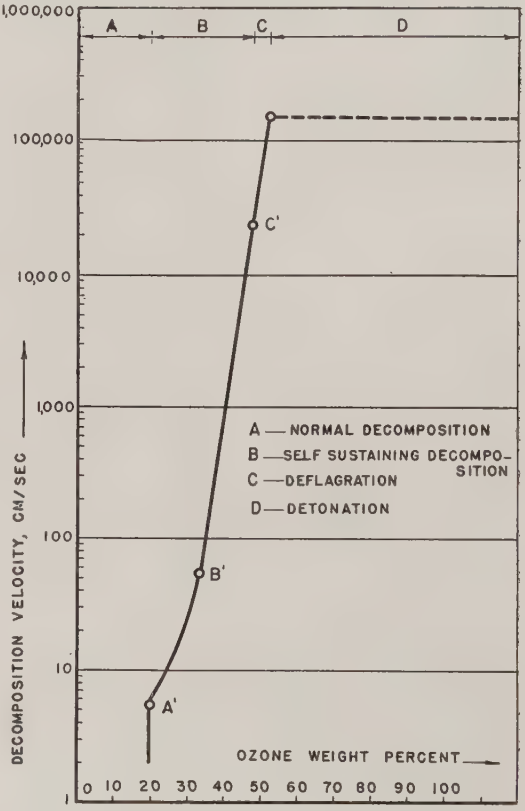

FIG. 1. Decomposition velocities of gaseous ozone-oxygen mixtures.

simplified the theory. The theories are valuable, not because they may give accurate calculated burning velocities, but primarily because they give a much deeper insight into the mechanism and the sequence of events which take place in the flame front. Knowing the experimental flame velocities one can interpret them in the light of theory and get an insight into the actual conditions that prevail in the flame front.

A comparison of our experimental burning velocities with the above theoretical calculations is made on page 272.

The Temperature of Ozone → Oxygen Flames

The flame temperatures can be calculated readily since the enthalpy data and dissociation constants of oxygen are known with great accuracy.

TABLE 3

Mole %O_3	Mole %O_2	Flame Temperature at 1.0 Atmos and 298°K Initial Gas Temperature
100.00	0.00	2677°K.
66.67	33.33	2277
40.00	60.00	1687
18.18	81.82	1027
0.00	100.00	298

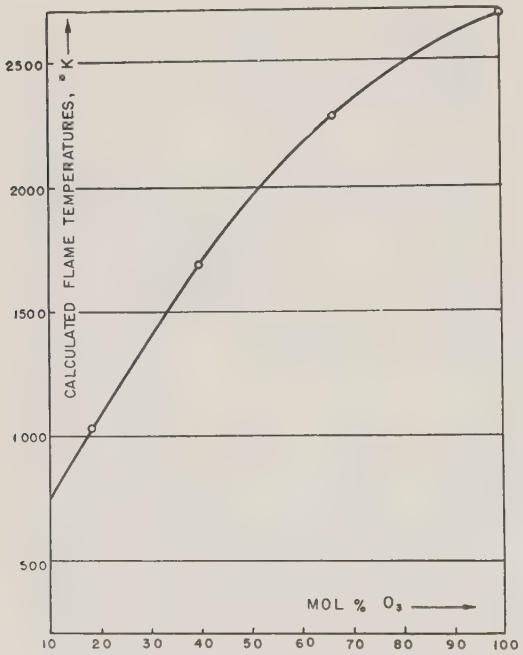

FIG. 2. $O_3 \rightarrow O_2$ flame temperature (1.0 atmos pressure, 298° K initial temperature).

The heat of "combustion" of ozone, i.e., the ΔH of the reaction

$$O_3 \rightarrow 1.5\ O_2$$

has been determined by Günther, Wassmuth and Schryver[15] by exploding ozone in a calorimetric bomb, at constant volume and 18°C to

$$-34{,}220 \pm 180 \text{ cal/mole}$$

Correcting for the expansion of oxygen to constant pressure

ΔH at 1 atmos pressure and 291°K

$$= -33{,}923 \pm 180 \text{ cal/mole } O_3$$

This value checks, within the small experimental error, with an earlier determination of Kailan and St. John.[16] The above value has been used by Kassel, Lewis and von Elbe and many others. In our calculations we used Kelley's[17] enthalpy tables for O_2 (Kelley's tables are in good agreement with the recent NACA tables), and Lewis and von Elbe[18] values for the dissociation constants and energy of oxygen. The dissociation of oxygen in the flame is small and even in the 100 per cent ozone flame, at equilibrium, only 2.5 mol per cent of O_2 is dissociated into oxygen atoms.

The calculated flame temperatures, as a function of composition, are shown in Table 3. They are shown in graph form in Figure 2. Thus the flame temperature of pure ozone is appreciable; it is higher than the methane-air (2148°K) or carbon monoxide-air (2370°K) flames. In view of this fact it was felt that if detonability could be avoided a continuous visible flame should be obtainable.

Experimental

PREPARATION OF OXYGEN-OZONE MIXTURES AND PURE OZONE

The simplest methods for the preparation of ozone are based, since Schoenbein's discovery in 1840, on the silent electrical discharge. The literature is thoroughly reviewed in Thorp's book on Ozone Technology.[4]

We have been using a standard commercial ozonator, the Welsbach Corporation having loaned us their Model T-23.

DETAILS OF PREPARATION AND PURIFICATION

A sketch of our apparatus is shown in Figure 3. As a starting material we used the purest oxygen which was available, the so-called "breathing oxygen." In line with the teaching of the Thorp patent (U. S. 2,700,648, January 25, 1955), we have given special attention to the elimination of all organic impurities in the ozone produced. This was done, as described in the above patent, by passing a stream of oxygen before the ozonator, through a stainless steel tube (No. 1) containing copper oxide heated to 700°C. In this tube traces of organic compounds (of the order of a few parts per million), are oxidized to CO_2 and H_2O, which was then absorbed in a tube (No.

2) filled with calcium sulfate, ascarite and anhydrone.

The ozonator produces ozone in a concentration of 3 to 6 vol per cent. The ozone-containing

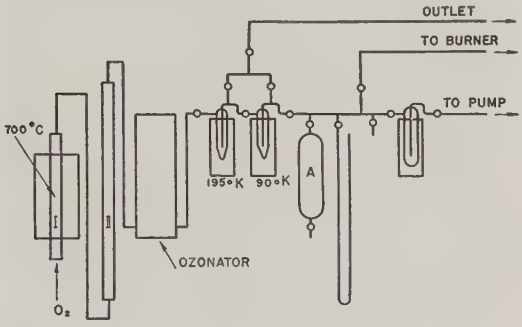

FIG. 3. O_3-preparation apparatus.

stream is first passed through a dry-ice trap and the O_3 is completely condensed with comparatively small amounts of oxygen in a liquid oxygen trap. The boiling points of ozone and oxygen ($-111.9°C \pm 0.3$ and $-183.0°C$) are sufficiently far apart that separation of the two can be readily achieved by standard vacuum techniques.

The vapor pressure and boiling point of pure ozone have been accurately determined, the most recent data being by Jenkins and Birdsall.[19] The last authors also give details regarding the elimination of the last traces of oxygen from ozone.

The 100 per cent pure ozone was then carefully vaporized into a vacuum system of known volume (Tube A), the pressure recorded, and then the ozone either used as such or mixed with known volumes of oxygen to prepare any desired mixture.

As is well known, traces of organic matter will initiate the decomposition or explosion of ozone. For this reason no organic lubricants can be used for stopcocks. We have found that the fluorocarbon lubricants, which were originally developed at Columbia University for the separation process of the uranium isotopes by the diffusion method, are stable against ozone.[20] It was originally determined that they are stable against elementary fluorine and also against oxygen at temperatures in the range of 200–300°C under pressure. In view of the electronegativity of fluorine it could be expected they would not be attacked by ozone, which later proved to be the case. We have also found that the Kel-F lubricants, produced by the Kellogg Company, which are polymers of monochlorotrifluoroethylene, are also resistant to ozone. Both of these fluorine lubricants permit the use of an ordinary vacuum system with regular glass stopcocks.

TABLE 4. DECOMPOSITION OF O_3 ON STORAGE

O_3 Mole %	T°K	P mm Hg	Time Days	Volume, cm^3 (0°C, 760 mm)		Amount of O_3 Decomposed	Rate of Decomposition, per cent/Day
				Initial	Final		
40	296–99	740	7	240	242	4.2% in 7 days	0.6
50	273	766	3	137	138	2.9% in 3 days	0.9
50	296–97	600	5	134	135.5	4.5% in 5 days	0.9
100	195	754	8	90	90	No noticeable decomposition	0.0
100	296	757	1	657	660	0.9% in 1 day	≃0.9

Stability of Ozone Mixtures

The stability of our ozone mixtures and pure 100 per cent ozone is illustrated in Table 4. It should be understood that these tests were not made to find optimum stability conditions for the storage of ozone, but only to show to what extent decomposition may occur in our experiments.

The data in the tables show that 100 per cent ozone can be kept at $-78°C$ (dry ice temperature) for long periods of time without noticeable decomposition (less than 0.10 per cent). At room temperature (23°C), the decomposition of ozone is noticeable over a period of days. However, since we used our ozone mixtures within an hour after preparation, we can be sure that the concentration has remained constant (within less than 0.10 per cent).

Stability of Ozone in the Presence of Water and the Solubility of O_3

Ozone decomposes more readily in the presence of water. It has been demonstrated at the Armour

Research Foundation that very dilute aqueous solutions of perchloric acid decreased the rate of decomposition. Since we were using water in our burner tip experiments (see page 269) special stability tests were made.

TABLE 5. SOLUBILITY OF 100 PER CENT O_3 IN WATER

°C	Bunsen Coefficient α (= liter O_3 @ N.T.P./liter H_2O)	g O_3/l H_2O
0	0.53	1.13
10	0.41	0.88
20	0.32	0.69
30	0.26	0.56
40	0.21	0.45
50	0.17	0.37
60	0.14	0.31

TABLE 6. THE BURNING CHARACTERISTICS OF THE GASEOUS OZONE + OXYGEN MIXTURES IN HORIZONTAL GLASS TUBES AT +23°C AND 1.0 ATMOS PRESSURE

(Length = 1.0 m, diam = 0.95 cm)

Mole % O_3 in Mixture	Number of Experiments Performed	Burning Characteristics
5.0	1	No inflammation
10.0	1	No inflammation
15.0	2	No inflammation
16.0	2	No inflammation
17.0	2	Slow uniform burning
20.0	2	Slow uniform burning
25.0	1	Slow uniform burning
30.0	2	Uniform burning with slight noise
40.0	1	Noisy burning, faster than above
50.0	1	Fast noisy burning
55.0	1	Fast noisy burning
63.0	1	Fast noisy burning
70.0	1	Very fast burning with explosive knock. Tube broke
85.0	1	Very fast burning with explosive knock. Tube broke
100.0	1	Very fast burning with explosive knock. Tube broke

Eighty-one cm^3 of 30 mol per cent O_3, 70 mole per cent O_2 were allowed to stand with 5.0 cc of 0.01 molar perchloric acid first for a period of 20 hr at 0°C; no change in volume was observed. After an additional period of 24 hr at 24°C there was still no noticeable decomposition of ozone.

Thus it can be concluded that in our burning experiments, which were completed in less than an hour after ozone was stored over water, no significant decomposition could possibly take place.

For ready reference the solubility of 100 per cent ozone in water as determined by Briner and Perrottet[21] is given in Table 5.

The solutions of ozone in water follow Henry's law, i.e., are proportional to the partial pressure of ozone.

Since explosions or detonations may occur, water is, from the safety standpoint, by far the best liquid medium to contain ozone under ordinary laboratory conditions.

Experimental Determination of the Burning Velocity

Two methods were used to determine the burning velocity: (a) the open tube method; and (b) the burning tip method.

The advantages of the open tube method are simplicity and safety. They were carried out first because they gave a good general, although not very accurate, picture of the behavior of various ozone-oxygen mixtures and of pure ozone. Mixtures above 30 per cent ozone burned too rapidly for an accurate velocity determination. The open tube method was inferior to the burner method for higher O_3 concentrations. This was due to two reasons. Our time measuring system was very primitive and became less accurate for the faster burning mixtures; secondly, it involved assumptions in regard to the geometrical shape of the flame front.

THE OPEN TUBE METHOD

Pyrex glass tubes, of about 1 m in length and varying in diam from 1.2 to 0.2 cm, sealed at one end and provided with a glass ground joint and a stopcock at the other, were filled with the desired oxygen-ozone mixture. The mixtures were burned in tubes in a horizontal position in a dark room and the propagation of the flame front observed visually and clocked with a precision stop-watch as it passed through two marks at a known distance between them.

They were ignited by means of a hot platinum wire. The tubes were filled with the desired mixture at slightly above atmospheric pressure. When the glass joint was taken out a hot platinum wire was quickly inserted for a distance of an inch or two into the tube; in nearly all cases it ignited the ozone. The observations recorded for various mixtures are given in Table 6.

Thus mixtures containing less than 17 mole per cent O_3 do not ignite. The ozone flame has a blue color with a typical pink cast. The flame is not bright and does not compare in luminosity with any hydrocarbon flames. Whereas the above refers to dry mixtures it was found that water vapor suppresses the color, so that in the range of 17 to 30 per cent O_3 the flame is not visible.

The above experiments showed that ozone mixtures can be burned at concentrations even above 50 per cent.

In order to test the influence of varying tube diameters, the following series of tests were run, see Table 7.

As a perusal of the data will show, the observed burning velocity for tube diameters changing from 1.2 cm down to 0.4 cm are constant within experimental error. The observed burning velocities, V_{obs}, were converted into normal burning velocities, V_n, by assuming, in most cases, a hemispheric flame front. Obviously, the exact front could have been determined by instantaneous photographic techniques, but in view of the lack of time and equipment this was deemed unnecessary.

The relationship

$$\Pi r^2 V_{obs} = \frac{4\Pi r^2}{2} V_n, \qquad \text{or} \qquad V_n = \tfrac{1}{2} V_{obs}$$

holds, where r is radius of the tube.

These data, for the range 17 to 25 per cent O_3, are included in the final results or Table 8.

BURNER TIP EXPERIMENTS

The burner tip experiments were carried out in standard apparatus, using Pyrex glass or aluminum tips with an inner diameter of 3 to 0.65 mm.

The apparatus used by us is shown in Figure 4. It consisted essentially of a water gas holder containing the desired oxygen-ozone mixture. A constant flow of ozone was provided by adding water to this gas holder at a constant rate. The gas mixture was ignited by means of a hot platinum wire after a steady gas rate had been attained. The flames could be readily observed by the standard schlieren method at all concentrations above 30 mole per cent. Direct measurements and photographs were taken of the flame. Above 50 per cent ozone the flame could be readily observed with the naked eye. The 100 per cent ozone burns with a blue flame with a pink cast. The flame is characterized by a very high concentration of oxygen atoms. A strip of paper inserted into the flame ignites immediately. Schlieren pictures of a 53 mole per cent and 100 per cent ozone flame are shown in Figures 5 and 6, respectively.

The results of our measurements are given in Table 8, and a plot of the points obtained is shown on Figure 7. Essentially the burning velocity of ozone is a straight-line function of the ozone concentrations in the whole range from the ignition point of 17 mole per cent ozone to 100 per cent ozone. The points below 30 per cent ozone should be considered preliminary and will be determined with greater accuracy in future.

Table 7. Burning Velocities of O_3 to O_2 Mixtures in Tubes of Varying Diameters

Mole % O_3 in Mixture	Observed Burning Velocities, cm/sec at 23°C and 1.0 Atmos				
	i.d. = 1.2 cm	i.d. = 1.0 cm	i.d. = 0.8 cm	i.d. = 0.6 cm	i.d. = 0.4 cm
17.0	21.5	19.2	—	—	—
20.0	36.4	33.3	—	—	—
25.0	—	58.3	62.1	64.2	62.0
30.0	—	70.0	82.0	81.5	81.1
				83.7	81.5

Table 8. Experimental Burning Velocities of Ozone-Oxygen Mixtures (at 1.0 Atmos and 300°K)

Mole % O_3 (±0.2%) in $O_3 + O_2$ Mixture	Burning Velocities
	cm/sec
17.0	9.2
20.0	18.2
28.0	52.2
40.0	125
46.0	166
53.0	210
75.0	331
100.0	475

Our measurements were all carried out in the laminar flow region and the Reynolds number of our flows was below 2000.

The burning velocity can be expressed, in a first approximation, in the form of a linear equation, namely,

$$v = 5.63 \cdot x - 88.8$$

where x is the ozone concentration in mole per cent in the range of 17 to 100 per cent and v is

the burning velocity in cm/sec. The burning velocity of pure ozone, equalling 475 cm/sec at 300°K and 1.0 atmos is comparatively low. There is no difficulty in burning pure ozone for substantial periods of time, without explosion or detonation, as long as the gas rate is constant.

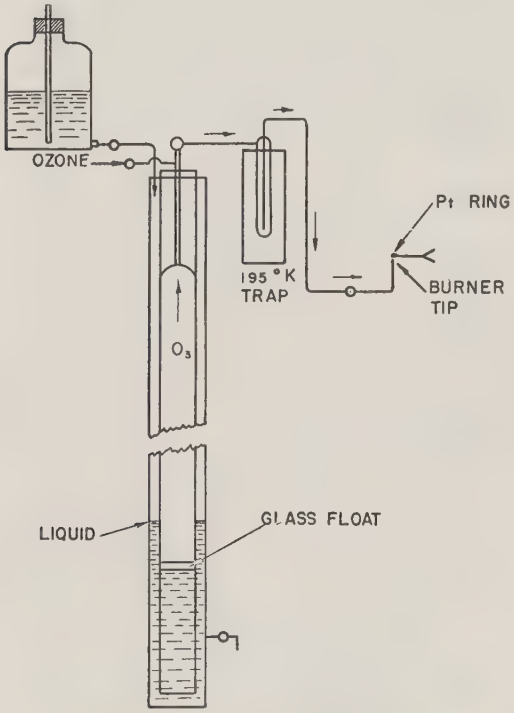

FIG. 4. O_3-burning apparatus.

FIG. 5. Schlieren photograph of 53 mol per cent O_3 + 47 mol per cent O_2 flame. (Rate = 7.7 cc/sec through 1.3 mm i. d. tip.)

PRESSURE OF THE PURE OZONE FLAME

It is of interest to note that the flame pressure of 100 per cent ozone calculated from the following simple relationship:[22]

$$p_u - p_b = \xi_u V^2(\xi_u/\xi_b - 1)$$

(where p and ξ are pressure and gas density, respectively, while the subscripts, b and u, refer to the burned and unburned gas), is 4.1 mm Hg.

FIG. 6. Schlieren photograph of 100 per cent ozone flame. (Rate = 8.23 cc/sec through 0.66 mm tip.)

This is equal to the pressures of the fastest flame described in the literature (for example, oxyacetylene = 4.1 mm and oxyhydrogen = 2.2 mm Hg, both close to the stoichiometric point). The recently described premixed H_2-F_2 flame has a flame pressure up to $\simeq$100 mm.[23]

RELATIONSHIP BETWEEN BURNING AND DETONATION VELOCITIES

Now that the normal burning velocities of ozone combustion or decomposition have been experimentally determined, over the whole range, we can take a fresh look at the relationships expressed in Figure 1. The burning velocities are the lower limit for the propagation of a steady flame front in ozone. The hydrodynamic theory of detonation establishes the upper limit or the

velocity of a detonation wave.[24, 25] This theory has been proven experimentally in a large number of cases, so that it can be applied without hesitation also to our system.

We have calculated detonation velocities using an approximate method described by Taylor[26] but adequate for our comparative purposes.

The results are given in Table 9 (initial conditions: 300°K 1.0 atmos).

The relationship between combustion and detonation velocities for the gaseous O_3-O_2 system is shown in Figure 8. Thus instead of the single

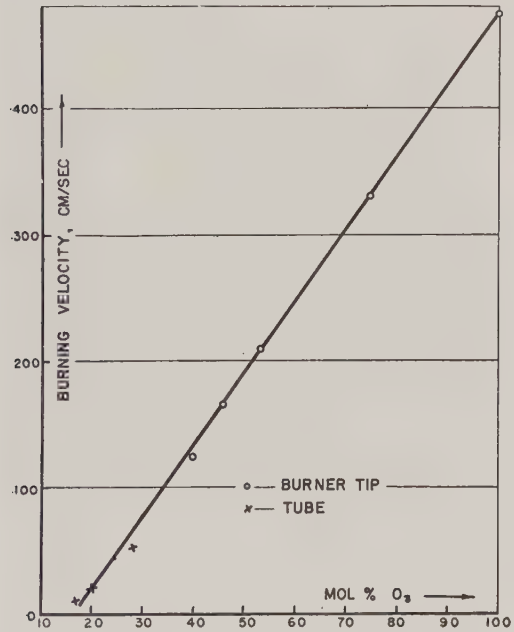

FIG. 7. Burning velocity vs mol per cent O_3.

path of decomposition shown in Figure 1, we have an infinite number of paths from a steady combustion to a steady detonation wave. A steady combustion front can be accelerated to a full detonation depending on the amount of ozone present, the geometrical dimensions of the system (particularly the length and diameter of a tube), the strength of the initiating shock or impulse and the presence of catalytic agents, sensitizers, initiators or impurities (in addition to change of initial pressure or temperature). Thus the whole region between the two curves of Figure 8 is one of unstable decomposition velocities. The time which is necessary for a combustion wave to accelerate to a detonation wave will depend also on the factors just enumerated. For example, a 30 per cent O_3-O_2 mixture will burn steadily at the rate indicated; however, if properly initiated within a suitable geometry and if adequate amounts of the mixture are present it *may* detonate with a steady velocity of ≃1200 m/sec. Similarly, pure ozone will burn with a velocity of

TABLE 9. DETONATION VELOCITIES OF GASEOUS O_3-O_2 MIXTURES

Mole % O_3 in O_3-O_2 Gaseous Mxture	Energy Release in Cal/G Mixture	Detonation Velocity in M/Sec
12.5	125	808
25	236	1110
50	425	1492
100	709	1950

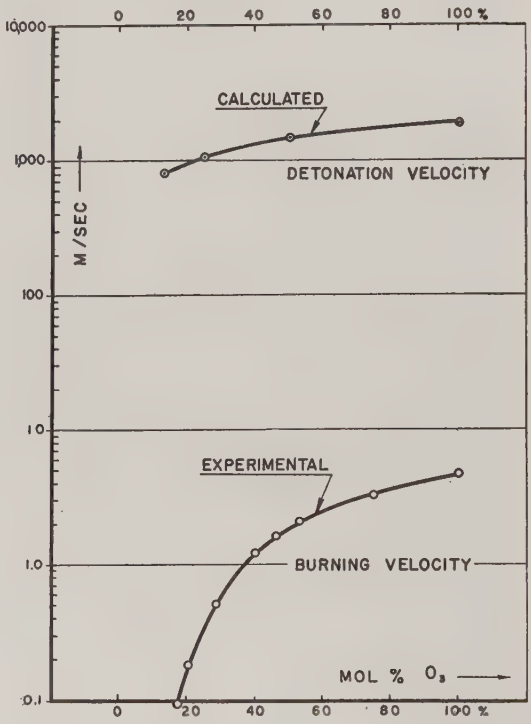

FIG. 8. Combustion and detonation velocities of gaseous O_3-O_2 mixtures at 1 atmos and 298° K.

475 cm/sec, but can be accelerated to the detonation velocity of 1950 m/sec. Obviously, in view of the much larger energy content of pure ozone (see Table 9) a much smaller impulse will be required to initiate its detonation.

Therefore, the "detonation" velocities given in Figure 1 do not characterize the particular ozone-oxygen mixtures but rather the conglomerate of random factors used in experimentation.

Comparison of Experimental with Theoretical Burning Velocities

Doctor von Kármán and his associates have kindly calculated the theoretical burning velocities of ozone flames for the whole range including 100 per cent ozone. They compared their values with ours and Dr. von Kármán has shown at this symposium[27] that they are in close agreement.

OZONE FLAMES WITH COMBUSTIBLE GASES

The way is now open to substitute ozone for ozygen in various flames.

Some preliminary experiments were carried out. A 27.5 O_3 to 72.5 mole per cent O_2 mixture was burned in a diffusion flame, with an excess of hydrogen, carbon monoxide and cyanogen. The ozone was fed to an inner quartz tube of 2.0 mm i.d., surrounded by an outer Vycor tube with an i.d. = 4.0 mm.

Steady flames were observed in all three cases with only one well-defined inner cone. In general appearance and color the flame did *not* differ from the corresponding oxygen flames.

Acknowledgments

Acknowledgment is due to the Office of Ordnance Research, Contract DA-36-034-ORD-1489, for their support of the preliminary stage of this work.

We are also grateful to the Welsbach Corporation for the loan of their Model T-23 Ozonator, and to Messrs. C. S. Stokes and A. D. Kirshenbaum for their assistance in some of the experiments.

REFERENCES

1. Conway, J. B., Wilson, R. H., Jr., and Grosse, A. V.: J. Am. Chem. Soc., *75*, 499 (1953).
2. Conway, J. B., Smith, W. F. R., Liddell, W. J., and Grosse, A. V.: J. Am. Chem. Soc., *77*, 2026 (1955).
3. Kirshenbaum, A. D., and Grosse, A. V.: J. Am. Chem. Soc., *78*, 2020 (1956); Grosse, A. V., and Kirshenbaum, A. D.: Technical Note No. 1, Report Control No. AFOSR-TN-56-13, Contract No. AF 18(600)-1475, Project No. 7-7968, dated December 15, 1955, U. S. Air Force, Office of Scientific Research & Development Command, Building Temporary T, Wing 4, 14th St., and Constitution Ave., Washington, D. C.
4. Thorp, C. E.: *Bibliography of Ozone Technology*, Vol. I, 1954; Vol. II, 1955. Chicago. Armour Research Foundation of Illinois Institute of Technology.
5. Thorp, C. E., *Bibliography of Ozone Technology*, Vol. II, p. 33. Chicago, Armour Research Foundation of Illinois Institute of Technology, 1955.
6. Thorp, C. E., *Bibliography of Ozone Technology*, Vol. II, p. 40. Chicago, Armour Research Foundation of Illinois Institute of Technology, 1955.
7. Lewis, B., and von Elbe, G.: J. Chem. Phys., *2*, 283 (1934).
8. Lewis, B., and von Elbe, G.: *Combustion, Flames and Explosions*, pp. 457–458. New York, Academic Press, 1951.
9. Lewis, B., and von Elbe, G.: J. Chem. Phys., *2*, 537 (1934).
10. Lewis, B., and von Elbe, G.: *Combustion, Flames and Explosions*, p. 344. New York, Academic Press, 1951.
11. Hirschfelder, J. O., Curtiss, C. F., and Campbell, D. E.: J. Phys. Chem., *57*, 403 (1953).
12. Hirschfelder, J. O., Curtiss, C. F., and Campbell, D. E.: *Fourth Symposium (International) on Combustion*, p. 197. Baltimore, The Williams & Wilkins Co., 1953.
13. von Kármán, T., and Penner, S. S.: Selected Combustion Problems, AGARD. Combustion Colloquium, Cambridge University, England, pp. 5–41 (1953); Chem. Abstracts, *48*, 10409^e (1954).
14. Sandri, R.: Canad. J. Chem., *34*, 313, 324, 331 (1956).
15. Günther, P., Wassmuth, E., and Schryver, L. A.: Z. physik. Chem., *A158*, 297–304 (1932).
16. Kailan and St. John: Z. anorg. u. allgem. Chem., *68*, 243 (1910).
17. Kelley, K. K.: U. S. Bureau of Mines, Bull. No. 476, p. 130, 1949.
18. Lewis, B., and von Elbe, G.: *Combustion, Flames and Explosions*, p. 742. New York, Academic Press, 1951.
19. Jenkins, A. C., and Birdsall, C. M.: J. Chem. Phys., *20*, 1158–1161 (1952).
20. Grosse, A. V.: S. A. M. Labs. Columbia University, Report A-211, July, 1942; Cady, G. H., et al.: Ind. Eng. Chem., *39*, (1947); see also National Nuclear Energy Series, Division VII, Vol. I, Chap. 30 (L. Spiegler), pp. 485–539, 1951.
21. Briner, E., and Perrottet, E.: Helv. Chim. Acta, *22*, 397–404 (1949).
22. Lewis, B., and von Elbe, G.: *Combustion,*

Flames and Explosions, p. 240. New York, Academic Press, 1951.
23. Grosse, A. V., and Kirshenbaum, A. D.: J. Am. Chem. Soc., *77*, 5012 (1955).
24. Lewis, B., and von Elbe, G.: *Combustion, Flames and Explosions*, pp. 590–611. New York, Academic Press, 1951.
25. Taylor, J.: *Detonation in Condensed Explosives*, pp. 54–110. Oxford, England, Clarendon Press, 1952.
26. Taylor, J.: *Detonation in Condensed Explosives*, p. 82. Oxford, England, Clarenden Press, 1952.
27. von Karman, T.: *Sixth Symposium (International) on Combustion*, p. 1. New York, Reinhold Publ. Corp., 1957.

33

A STUDY OF HYDROGEN DIFFUSION FLAMES[a]

By EDGAR R. STEPHENS, WILLIAM E. SCOTT, JOSEPH A. GOLDEN, and BARBARA FAUNCE

Introduction

There are a number of combustion systems in which inorganic additives can play a pronounced role. The antiknock activity of lead tetraethyl, the use of sodium carbonate to control fire damp ignition from mine explosives, the use of potassium compounds to suppress afterburning from aircraft engines and muzzle flash from guns, and the recently-announced use of dicyclopentadienyl iron to control soot formation in oil burners are all examples of this use of inorganic compounds to modify or control combustion processes. In most of these cases little information is available on the mechanism by which the inorganic additive operates. The small amounts of additive necessary to produce marked changes in the over-all performance of the combustion system make it probable that these effects are not to be explained on a gross thermal basis. It seems much more likely that the inorganic additive enters into the combustion mechanism itself by some specific reactions involving the chain carriers by which the combustion reactions are propagated. All these combustion systems are quite complex so that attempts to study the mechanism by using the system itself are severely limited.

We have been using a simpler combustion system to study the role of inorganic substances in flame reactions. This is the diffusion flame of hydrogen burning in air. Our work is based on the discoveries of Smith,[1] Arthur,[2] and Arthur and Townend.[3] The first of these authors studied the radiation from solid substances under flame impact. He found that samples of calcium oxide when activated with small quantities of other substances (e.g., compounds of bismuth, antimony, etc.) will luminesce when in contact with a diffusion flame of hydrogen in air. Smith demonstrated first that this luminescent radiation is not thermal in origin. He showed that it was excited by the impact of free hydrogen atoms on the surface of the luminescent substance. This was a very useful discovery since it made available a technique for the detection of hydrogen atoms in flames.

Experiments by Arthur[2] disclosed some interesting properties of the diffusion flame itself. Arthur found that the luminescence could be quenched by the addition to the flame of quite small quantities of a wide variety of substances. Methane, ethane, sulfur dioxide, toluene, benzene and a number of other compounds were found to be effective quenchers for the luminescence. A more striking observation was that the ubiquitous D-lines of sodium were quenched by these same additives in a manner parallel to the quenching of the luminescence. Quenching of the luminescence was attributed to the removal of the hydrogen atoms from the flame. Since the sodium radiation was also quenched it was concluded that the hydrogen atoms were in some way necessary for the production or the excitation of atomic sodium in the flame.

[a]This research was supported by the Ammunition Branch, Research and Development Division, Office of the Chief of Ordnance, U. S. Army Contract DA-36-034-ORD-738RD.

Our first experiments were directed toward determination of which of these two possibilities was in fact correct. These experiments, which involved measurements of the sodium atom concentration in the flame by absorption spectroscopy, were reported some time ago.[4] It was found that unexcited sodium was *not* present in the quenched flame. From this we concluded that the *formation* of atomic sodium in such a flame

Table 1. Absorption by Atomic Potassium in a Hydrogen Diffusion Flame

Conc of SO_2 Added to H_2	Per Cent Absorption	
vol. per cent	4044 Å	4047 Å
0	45.9	27.2
0.12	22.7	12.7
0.21	15.3	6.3
0.36	11.8	6.6
0.62	0	0

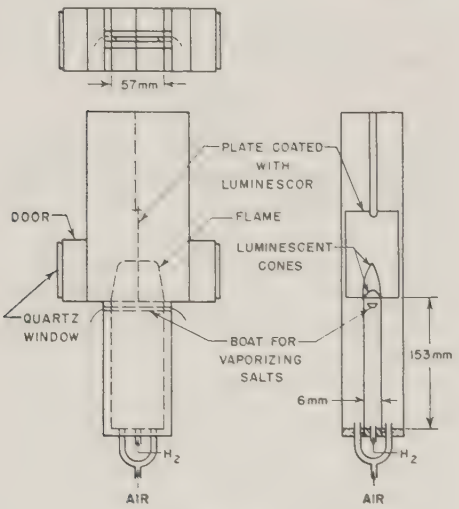

Fig. 1. Diffusion burner.

was dependent on the presence of hydrogen atoms in the flame. This indicated that hydrogen atoms were necessary for the production rather than the excitation of atomic sodium in the flame. The reaction proposed by Arthur and Townend was thus verified:

$$H + NaX \rightarrow Na + HX \qquad (1)$$

This reaction was considered to be of importance since it involves the removal of a chain-carrying hydrogen atom from the flame zone. If the sodium atom is incapable of continuing the reaction chain, then this reaction, if it is rapid, could have a very pronounced influence on the behavior of flames themselves. This and similar reactions may be involved in some of the combustion systems mentioned previously.

The present paper is concerned with further experiments with diffusion flames of hydrogen that were carried out to learn more about reactions of this type.

Potassium Compounds in the Diffusion Flame

Our first experiments on diffusion flames involved examination of the sodium D-line in absorption in a hydrogen diffusion flame as a function of amount of a quenching gas added. As stated above, this experiment indicated that the concentration of atomic sodium in the flame decreases as a quenching gas (in this case sulfur dioxide) is added. This experiment has been repeated using potassium chloride as the inorganic additive. Higher dispersion was obtained by using a Bausch and Lomb Littrow spectrograph. The remainder of the optical system and the burner were the same as those used previously. The photographic plates were measured with a recording densitometer and the fractional absorption at the wavelengths of the potassium doublet was computed. The data are given in Table 1.

It is clear that the absorption by atomic potassium and therefore its concentration in the flame decrease as sulfur dioxide is added. Thus this alkali metal behaves in the same way as sodium. Presumably it also is produced in the diffusion flame by a reaction involving atomic hydrogen:

$$H + KX \rightarrow HX + K \qquad (2)$$

Several other quenching gases were also studied briefly. Methane, ethylene and carbon dioxide will also quench the D-lines of atomic sodium. Absorption measurements were not made with these quenchers.

Quenching of Luminescence by Salts

If, as is argued above, the alkali metal salts are capable of reacting with hydrogen atoms in a flame then it should be possible to quench the luminescence from a substance such as CaO(Bi) by adding a sufficient concentration of an alkali metal salt to reduce the hydrogen atom concentration. To test this postulate a new diffusion burner was constructed. This burner is shown in

Figure 1. Hydrogen is fed into the bottom of a rectangular channel which is flanked on each side by a similar channel carrying air for combustion. A boat for vaporizing salts into the flame was constructed from ceramic tubing. A small coil of resistance wire inside the tube serves as a heating element. This system permits much higher salt concentrations to be attained and also allows control over the salt concentration. A flat piece of metal coated with a luminescent substance (CaO activated with one per cent bismuth) is inserted vertically into this flame. The luminescence appears where the flame front intersects the flat surface. With this probe in place, a salt, e.g., sodium chloride, can be vaporized into the flame. Figure 2 shows photographs of this experiment. The emission of sodium becomes bright at the higher concentrations of sodium so that the quenching of luminescence is not so apparent in the photographs. Visually the disappearance of the blue luminescence can easily be distinguished. Potassium chloride, thallous chloride, and metallic lead were all effective in quenching luminescence. Heating the vaporizer boat with no salt in it failed to quench luminescence, showing that quenching was not due to the heat added to the flame by the boat itself. These observations show that the reaction between salt and hydrogen atoms is rapid enough to remove a significant portion of the hydrogen atoms.

The Inner Cone

The photographs (Figure 2) of the luminescence caused by the flame show clearly the shape of the main flame front. This shape agrees at least qualitatively with that predicted by Burke and Schumann.[5] However, close examination of the luminescent probe disclosed the presence of a small inner cone just above the rim of the burner. This apparently indicated the presence of a combustion zone in a region which should have contained pure hydrogen. However, analysis of the hydrogen stream indicated the presence of about ¼ per cent oxygen. When this was removed from the hydrogen supply with a "deoxo" purifier, the inner cone disappeared. Thus the inner cone is apparently an extremely rich hydrogen-oxygen premixed flame. It apparently depends for its stability on the presence of the main flame front. It is stabilized by either the conduction of heat or the diffusion of chain-carrying atoms or radicals back from the main flame front. The role of the main flame zone in stabilizing the inner cone was more clearly demonstrated by some experiments in which the concentration of oxygen in the air stream was

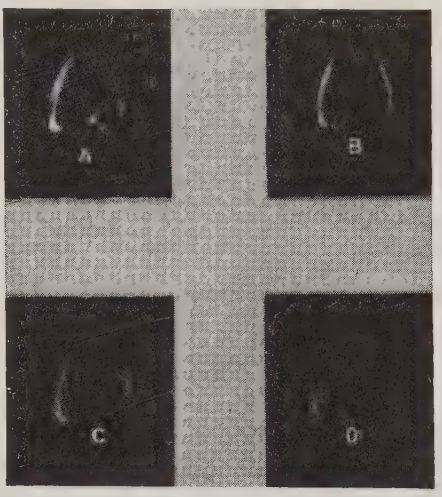

FIG. 2. Quenching of luminescence by sodium chloride. Flame conditions 1.14 l/min. H_2 ; 4.23 l/min. air. (A) 0 watts; (B) 94.6 watts; (C) 108 watts; (D) 129 watts. Wattage indicated is to salt vaporizer.

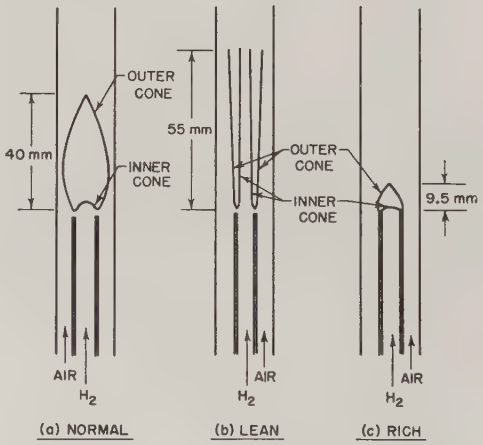

FIG. 3. Shape of the diffusion flame with enriched and with diluted air. (a) 20 per cent O_2 in air. 1.62 l/min. H_2 ; 3.85 l/min air. (b) 8 per cent O_2 in air. 1.62 l/min H_2 ; 3.55 l/min N_2 ; 0.30 l/min O_2 . (c) 38 per cent O_2 in air. 1.62 l/min H_2 ; 2.40 l/min N_2 ; 1.45 l/min O_2 .

changed. For these experiments the flow rates of hydrogen and air were maintained constant but the composition of the air was changed. A schematic diagram of the results is shown in Figure 3. As the air was diluted with nitrogen both cones became larger and opened up at the top. When the air was enriched with oxygen

both cones decreased in size until the inner cone became almost parallel with the burner rim. The changes in shape which the main flame front

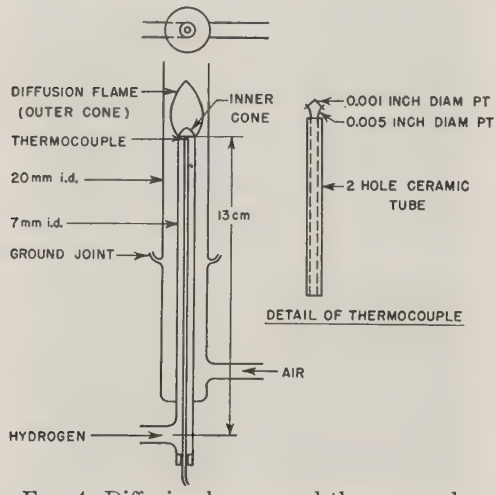

FIG. 4. Diffusion burner and thermocouple assembly.

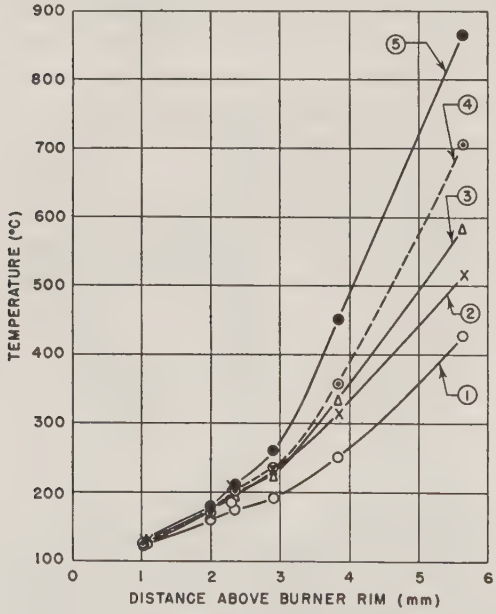

FIG. 5. Axial temperature of diffusion flame with oxygen added to the hydrogen flow (ceramic coated Pt-Pt, Rh thermocouple). (1) No O_2 added; (2) unpurified H_2 ; (3) 0.61 per cent O_2 ; (4) 1.2 per cent O_2 ; (5) 1.8 per cent O_2 .

undergoes as the oxygen concentration is decreased are in accord with the Burke and Schumann theory of diffusion flames. The dependence of the inner cone on the main flame zone is clearly shown by the way its shape and position follow that of the outer cone.

This stabilization of the inner cone by the outer cone is of particular interest from the point of view of the theories of flame propagation. The comparatively large separation between the inner cone and the outer cone which supports it permits experiments to determine whether a heat conduction mechanism or a radical diffusion mechanism is important. In an attempt to distinguish between these two mechanisms temperature measurements were made along the burner axis through the inner cone.

For those experiments the concentric tube burner shown in Figure 4 was used. Thermocouples were brought into the flame from below with a piece of two-hole ceramic tubing. The thermocouple junctions were prepared from 0.001-in. diam platinum and platinum-rhodium wires which were in turn welded to larger diameter support wires of the same metals. Two cathetometers were used to position the thermocouple both vertically and horizontally. The hydrogen was purified by passage through a "deoxo" purifier followed by a drying tube. It was then metered into the center tube of the burner. Air was likewise metered into the outer section of the burner. A third flow-meter was used to add small amounts of oxygen to the hydrogen stream.

Since the platinum thermocouple wires were expected to be catalytically active and thus not register the true gas temperature they were coated with a special ceramic developed by the National Bureau of Standards and previously used as an inactive thermocouple coating by Friedman.[6] This ceramic (designated A-418) was applied from a water suspension and fired at 1000°C.

In measurements such as these it must be assumed that the thermocouple junction is at the same temperature as the gas with which it is in contact. This will not be true if its rate of heat loss by radiation and conduction down the leads is large compared to the rate of heat transfer from gas to thermocouple. The present measurements are less susceptible to these errors than many flame temperature measurements with thermocouples because the temperatures involved are fairly low. A calculation of the temperature error due to heat loss by radiation showed that this error is indeed small. That lead conductions are also small was demonstrated by comparing the temperatures measured by two thermocouples of different diameter (both were coated with the ceramic described above). Fairly good agreement was obtained. Probably the most important

error arose from uncertainty in positioning of the thermocouple junction.

Data obtained with a ceramic-coated platinum, platinum-rhodium thermocouple are plotted in Figure 5. At 1 mm above the burner rim addition of oxygen to the hydrogen stream causes no increase in temperature. Above this point addition of oxygen causes an increase in temperature. The increase in temperature is more clearly shown in Figure 6 where it is plotted against distance. At each position the temperature increase caused by the addition of various amounts of oxygen is measured without moving the thermocouple. Errors caused by uncertainty in the thermocouple position are thus minimized. This set of data indicates that release of heat by the added oxygen begins at a relatively low temperature. The position of the inner cone under these conditions was estimated using a rod coated with luminescor. These measurements are summarized in Table 2. From these data it can be estimated that the reaction begins at a temperature of about 150 to 160°C. This seems a very low temperature for a thermal ignition mechanism.

One unexplained feature of these data is the magnitude of the temperature increases. It was expected that the maximum temperature increase caused by oxygen addition would correspond to the adiabatic flame temperature of the mixture. For these very rich mixtures, the calculated flame temperatures are quite low. They are indicated in Figure 6. This discrepancy may be caused by catalytic activity of the surface.

Similar data were taken with uncoated platinum, platinum-rhodium thermocouples. The catalytic activity of these metal surfaces introduces complications in the interpretation of the data. These metals not only catalyze the recombination of hydrogen atoms but may also catalyze the oxidation itself. The data are shown in Figure 7. Temperatures recorded are consistently higher than those measured by the coated thermocouple. The increase in temperature arising from surface catalysis was obtained by difference between the curves of Figures 5 and 7. The differences are shown in Figure 8. These plots all show a pronounced maximum in the region of the inner cone. This may be correlated tentatively with the presence of excess hydrogen atoms in this region.

The Excitation of Luminescence

The entire interpretation of these diffusion flame experiments rests on the use of the luminescent substance as a detector for the presence of hydrogen atoms. Smith's experiments, which were reported in detail only recently,[1] indicated that the recombination of hydrogen atoms on the surface was responsible for the excitation of luminescence. Work by Neunhoffer,[7] however, suggested that charged particles were responsible for the excitation of luminescence.

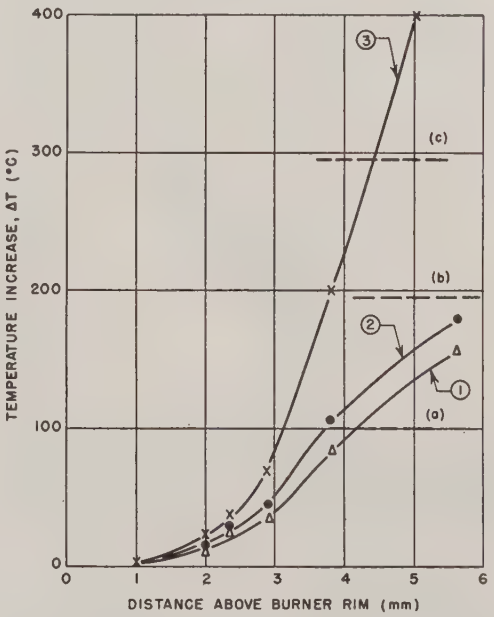

FIG. 6. Temperature increase caused by addition of oxygen to the hydrogen flow (ceramic coated Pt-Pt, Rh thermocouple). (1) 0.61 per cent O_2 ; (2) 1.2 per cent O_2 ; (3) 1.8 per cent O_2 . (a), (b), and (c) are the calculated adiabatic flame temperatures for 0.61, 1.2 and 1.8 per cent O_2 respectively.

TABLE 2. POSITION OF INNER CONE

O_2 Conc (volume per cent)	0.25	0.61	1.2	1.8
Height above burner rim (mm)	1.64	1.64	1.88	1.88
Thickness (mm)	2.20	2.73	2.80	3.45

The chief differences between the experiments reported by these two investigators were: (1) The chemical nature of the luminescent substance. Neunhoffer used zinc beryllium silicate, and Smith used calcium oxide activated with bismuth. (2) Smith heated his sample and Neunhoffer did not.

In order to clarify this situation, a discharge tube for producing hydrogen atoms was constructed as shown schematically in Figure 9.

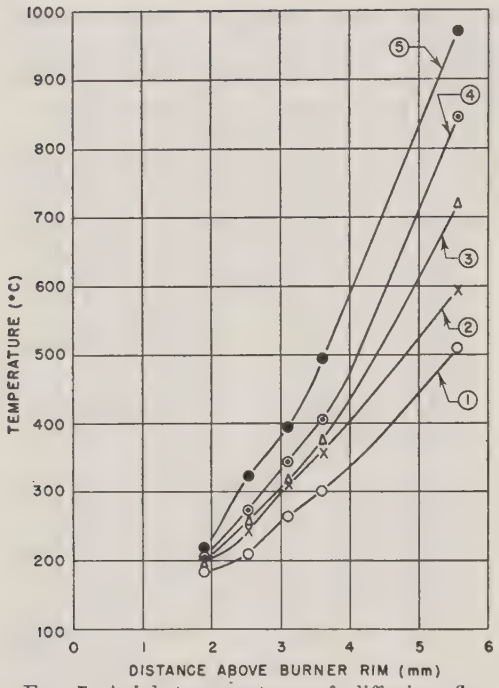

FIG. 7. Axial temperature of diffusion flame with oxygen added to the hydrogen flow (uncoated Pt-Pt, Rh thermocouple). (1) No O_2 added; (2) unpurified H_2 ; (3) 0.61 per cent O_2 ; (4) 1.2 per cent O_2 ; (5) 1.8 per cent O_2 .

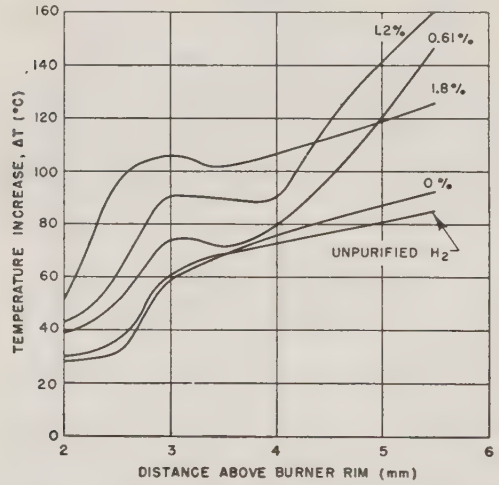

FIG. 8. Temperature increase caused by addition of oxygen to the hydrogen flow (uncoated Pt-Pt, Rh thermocouple).

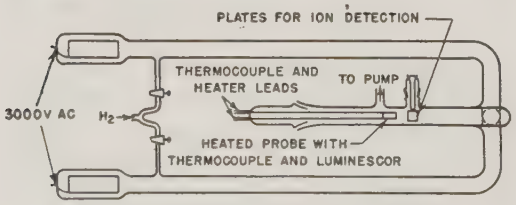

FIG. 9. Hydrogen discharge tube.

This apparatus is similar to that used by Neunhoffer and Smith. A discharge is maintained between cylindrical aluminum electrodes sealed into the ends of a "U" shaped Pyrex tube (32 mm i.d.). Power for the discharge is supplied by a 3,000 v, 1 kva transformer with a 10-h choke in series with each electrode to act as a ballast. Dry hydrogen is metered into both arms of the tube. From the closed end of the "U" the gas passes into a side arm containing the test assembly and is exhausted by a high capacity pump. Since the hydrogen atoms generated in the discharge have a comparatively long lifetime, they are carried with the gas into the side arm. A small heated probe placed in the side arm is coated with luminescent substances to be tested. A pair of parallel plates was positioned upstream from the test sample. Their original purpose was to remove ions from the gas stream by applying a dc potential to these plates. This did not prove practical so the plates were eventually used as a detector for ions. The walls of the tube were coated with metaphosphoric acid to reduce the rate of atom recombination.

In order to determine whether ions or uncharged atoms were responsible for the luminescence it was necessary to provide a method for removing ions and not the atoms for the gas stream. This was accomplished by bringing a 7,500-oersted magnet up to the side arm upstream from the plates. When this was done it was observed that the current between the two plates decreased nearly to zero. This was taken to indicate effective removal of ions from the gas stream. The data obtained for various luminescors are summarized in Table 3.

It is clear that removal of ions had no effect on the luminescence. At room temperature zinc beryllium silicate gives a pale red-orange luminescence while the bismuth-activated calcium oxide gives a blue luminescence. With increased surface temperature, the silicate coating assumes a bright yellow color while the blue color of the calcium oxide bismuth becomes more intense; at no time are they visibly affected by the presence or absence of ions. By adjusting the discharge tube system to an unstable condition whereby the coatings are exposed to an excess of ions, the silicate coating becomes bright yellow while the color of the CaO(Bi) remains unaffected. Under these conditions the silicate can be returned to its former red-orange color by bringing a magnetic field close to the discharge tube upstream from the sample. Thus Neunhoffer's results can be

reconciled with those of Smith. Zinc beryllium silicate will luminesce in the presence of either atoms alone or ions plus atoms at room temperature. Neunhoffer's discharge probably produced an excess of ions which gave rise to a bright yellow luminescence. When these were removed the pale red-orange luminescence caused by atoms was probably hardly visible so that he concluded that free atoms do not excite luminescence.

Table 3. Luminescence Caused by Atoms and by Ions

Tube Conditions: H_2 flow = 13.5 cc/min; Pressure = 0.43 mm Hg; Discharge: 145 ma at ~ 2200 v

Temperature of Probe	Current Through Ion Collection Plates*	Luminescence		
		$ZnBeSiO_4$	CaO(Bi)	
°C	μ a	color	color	
28	1.15	Pale red-orange	Pale blue	
	0 †	Pale red-orange	Pale blue	
157	1.25	Pale red-orange	Pale blue	
	0 †	Pale red-orange	Pale blue	
361	1.8	Pale red-orange	Bright blue	
	0 †	Pale red-orange	Bright blue	
415	1.8	Pale yellow	Bright blue	
	0 †	Pale yellow	Bright blue	
421	1.5	Bright yellow	Bright blue	
	0 †	Bright yellow	Bright blue	
529	3.0	Yellow	Blue	
	0.3 †	Yellow	Blue	
		$CaSO_4MnSO_4$	CaO(Bi)	$CaOMnSO_4H_2O$
		color	color	color
30	0.9	Pale orange	No lum.	Pale green
	0 †	Pale orange	No lum.	Pale green
52	—	Pale orange	Pale blue	Pale green
363	0.9	Pale orange	Pale blue	Pale green
	0.15†	Pale orange	Pale blue	Pale green
533	1.1	Pale orange	Pale blue	Pale green
	0.05†	Pale orange	Pale blue	Pale green
423	0.15	Yellow	Pale blue	Pale blue
	0 †	Yellow	Pale blue	Pale blue
127	0.15	Bright yellow	Pale blue	Bright green
	0	Bright yellow	Pale blue	Bright green
45	0.7	Yellow	Pale blue	Green
	0 †	Yellow	Pale blue	Green

* A potential of 50 v dc was applied to these ion collector plates.

† A 7,500-oersted magnet was held near the tube upstream from the ion collector plates and the probe.

Summary

(1) Both atomic sodium and atomic potassium are produced in a hydrogen diffusion flame by a reaction involving atomic hydrogen.

(2) This reaction is sufficiently rapid to reduce significantly the concentration of hydrogen atoms in the flame.

(3) An inner cone is observed when a small amount of oxygen is present in the hydrogen that is burned as a diffusion flame. This is regarded as a premixed flame stabilized by the presence of the main diffusion flame.

(4) Measurements of the temperature along the axis of the diffusion flame yield data which favor an atom diffusion mechanism rather than a heat conduction mechanism for the stabilization of the inner cone.

(5) Hydrogen atoms generated in a discharge tube will excite both a preparation of calcium oxide activated with bismuth and zinc beryllium silicate to luminescence. This luminescence is

brighter at higher temperature. Zinc beryllium silicate will also luminesce when subjected to ions.

(6) The luminescence of these materials is a valid test for hydrogen atoms in diffusion flames.

REFERENCES

1. Smith, E. C. W.: Second Arthur Duckham Fellowship Report, Copyright Publication No. 237/100 of the Institution of Gas Engineers, 1 Grosvenor Place, London, S.W.1.
2. Arthur, J. R.: Nature, *165*, 557 (1950).
3. Arthur, J. R., and Townend, D. T. A.: Symposium on Energy Transfer in Hot Gases, U. S. Department of Commerce, National Bureau of Standards Circular 523.
4. Linder, L., Scott, W. E., and Stephens, E. R.: J. Chem. Phys., *21*, 161 (1953).
5. Burke, S. P., and Schumann, T. E. W.: Ind. Eng. Chem., *20*, 998 (1928).
6. Friedman, R.: *Fourth Symposium (International) on Combustion*, p. 259. Baltimore, The Williams & Wilkins Co., 1953.
7. Neunhoffer, O.: Z. Physik. Chem., *197*, 179 (1951).

34

ON THE BURNING VELOCITY OF MOIST CARBON MONOXIDE-OXYGEN-NITROGEN MIXTURES

By KARL SCHELLER

Introduction

Tanford and Pease[1] have derived an expression for the burning velocity based upon the concept that the flame speed of a combustible mixture is controlled primarily by the rate at which active particles (chiefly hydrogen atoms) diffuse into and react with the unburned fuel. They have applied their equation to the experimental results of Jahn[2] on moist carbon monoxide-oxygen-nitrogen mixtures reporting an excellent correlation of the data in confirmation of their theory

In an earlier, elegant paper on the mechanism of CO combustion, Zeldovitch and Semenov[3] were able to explain most of the qualitative and many of the quantitative details of the CO flames. They emphasized the role of chemical kinetics in the combustion process and gave an expression for the flame velocity in terms of the reaction rate and the thermal properties of the combustible mixtures. A method was developed for accounting for the dilution of the unburned mixtures by back diffusion of products from the burned gases, but no consideration was given to the diffusion of active species from the hot flame boundary. Indeed their calculations of the free radical concentrations in the reaction zone indicated that they were an order of magnitude greater than the equilibrium concentrations at the adiabatic flame temperature (2000°C).

This work was undertaken to explore the discrepancy between the two theories and attempt to explain their agreement with the experimental data on CO flame velocities. It will be shown that Jahn's data and the calculations of Tanford and Pease support a point of view diametrically opposed to theirs, which ignores the effects of diffusion and correlates the burning velocities in terms of the kinetic mechanisms at the flame front. The approach here is different from that of Hoare and Linnett[4] who have shown that Jahn's measurements are consistent with the relation of Mallard and Le Chatelier[5] for the burning velocity, if one assumes that the effect of moisture is to reduce the ignition temperature of carbon monoxide mixtures.

I. Application of Semenov Theory to Jahn's Data

Semenov, Zeldovitch and Frank-Kamenetski[6] have developed a theory of flame propagation based upon the assumption that the bulk of the chemical reaction in the flame occurs in a zone very near to the adiabatic flame temperature. They have given especial attention to the chain character of the combustion reaction and postulated a kinetic scheme for the oxidation of CO in the presence of moisture involving the following

steps:[3]

I. $H + O_2 \rightarrow OH + O$

II. $CO + OH \rightarrow CO_2 + H$

III. $CO + O \rightarrow CO_2$

IV. $O + H_2 \rightleftharpoons OH + H$ (equilibrium)

V. $H_2 + OH \rightleftharpoons H_2O + H$ (equilibrium)

Analysis of this sequence of reactions indicates that the rate of CO oxidation in the flame, W, will be given to good approximation by

$$W = Ze^{(25000/RT_f)}[CO]_{eff}[H_2O]_0 \qquad (1)$$

in which Z is the kinetic frequency of collision for a bimolecular reation, T_f is the adiabatic flame temperature, $[H_2O]_0$ is the initial concentration of water in the combustible mixtures and $[CO]_{eff}$ is the effective concentration of carbon monoxide in the reaction zone (i.e., the initial concentration of CO corrected for dilution by back diffusion of the products computed in accordance with their theory). The kinetic equation leads to the following relationship for the flame velocity

$$U_0 = \left\{\frac{2\lambda Z}{\rho_0}\cdot\frac{Q'}{L\rho_0}\cdot\frac{1}{L}\cdot\frac{RT_f^2}{E}\left(\frac{T_0}{T_f}\right)^2 [H_2O]_0[CO]_{eff}e^{-(25000/RT_f)}\right\}^{\frac{1}{2}} \qquad (2)$$

where the symbols have the following meaning: λ = thermal conductivity, assumed independent of mixture composition and proportional to $T_f^{\frac{3}{2}}$; Q' = heat of combustion per mole of CO in the mixture; ρ_0 = density of unburned mixture at initial temperature; L = heat of combustion per unit weight of the initial mixture including diluents; E = activation energy, 25,000 kcal/g-mol; T_f = adiabatic flame temperature; T_0 = initial temperature of the mixture. Introducing appropriate values for the thermodynamic and kinetic parameters, they obtain the expression

$$U_0 = \text{const} \cdot [T_f e^{-(25000/RT_f)}[H_2O]_0[CO]_{eff}/[CO_2]_f^2]^{\frac{1}{2}} \qquad (3)$$

the concentration $[CO_2]_f$ representing the stoichiometric quantity of CO_2 formed in the combustion reaction. Equation (3) has been confirmed quite nicely, in a qualitative manner, by the work of Barsky and Zeldovitch.[7] They measured the variation of burning velocity with initial water content for mixtures of carbon monoxide, oxygen and nitrogen of specified composition and found it to be proportional to $[H_2O]_0^{\frac{1}{2}}$. They varied the CO and O_2 concentrations at constant flame temperature (in separate experiments) and showed the burning velocity to be proportional to the effective CO concentration and virtually independent of the oxygen content in the reaction zone.

The data of Jahn, for the mixtures analyzed by Tanford and Pease, were reduced in accordance with Equation (3) and are plotted in Figure 1.

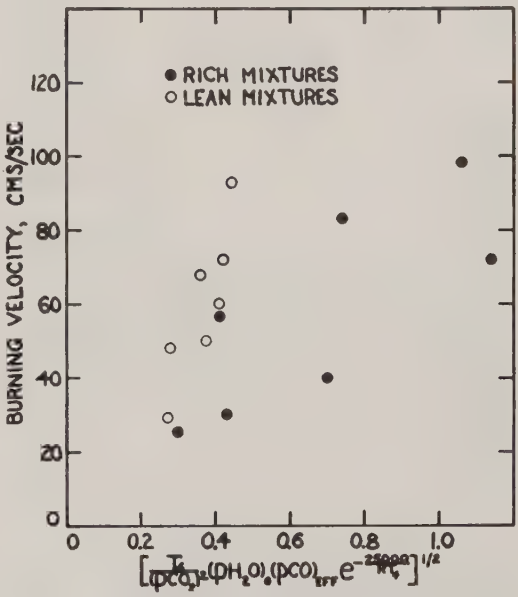

FIG. 1. Reduction of Jahn's carbon monoxide-data in accordance with the Semenov-Zeldovitch Frank-Kamenetsky theory.

The correlation is quite disappointing, in view of the excellent qualitative predictions of the theory, and cannot be reconciled with the linear relationship expected from the equation. Rich and lean mixtures have been distinguished by separate symbols, since they seem to follow different trends. One explanation for the wide scatter in the correlation suggests itself upon study of the graph. It appears that the carbon monoxide content in the reaction zone of lean and near stoichiometric rich mixtures may have been greatly underestimated by the method used in accounting for the back diffusion of the products. We shall bear this in mind in formulating a simplified model of the combustion wave.

II. Application of a Simplified Version of the Semenov Theory to Jahn's Data

In view of the success of the Semonov-Zeldovitch-Frank-Kamenetski theory in predicting many of the features of moist carbon monoxide flames and the plausible scheme it postulates for the kinetics of the combustion reaction, one is reluctant to abandon the basic features of the model on which it is based.

Let us simplify the model by neglecting the back diffusion of combustion product entirely and assume that the combustion reaction takes place in a narrow zone close to the adiabatic flame temperature in a mixture identical in

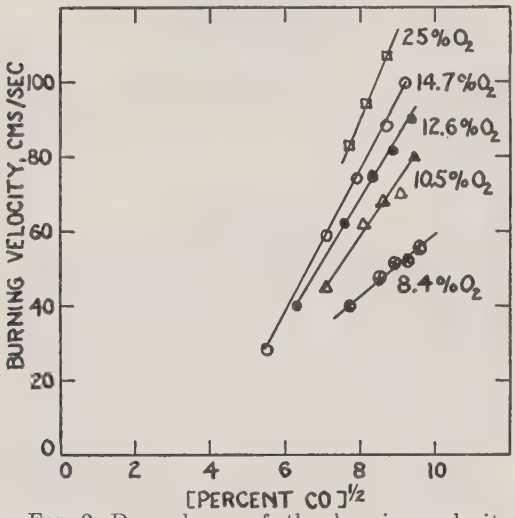

FIG. 2. Dependence of the burning velocity upon the initial carbon monoxide content in CO mixtures at a constant flame temperature.

composition (mole fractions) with the unburned gas. We adopt the kinetic scheme of Zeldovitch and Semenov with some modifications. In place of Reaction III, we introduce (for reasons that will be discussed later) a bimolecular reaction between carbon monoxide and water vapor, viz.:

$$\text{III}'.\ CO + H_2O \rightarrow CO_2 + H_2$$

In addition we remove the equilibrium requirement from Reaction V, preferring to believe that at the temperatures we are concerned with the thermal dissociation of water determines the equilibrium water content. The latter assumption very considerably simplifies the calculation of the composition of the reacting mixtures.

Upon the foregoing basis, the rate of oxidation of carbon monoxide is given by

$$W = k_{II}[CO][OH] + k_{III'}.[CO][H_2O]_{eq} \quad (4)$$

$[H_2O]_{eq}$ denoting the equilibrium water concentration at the adiabatic flame temperature. It is understood that in terms of our model the concentration of carbon monoxide is determined by pCO, the mole fraction of CO in the fresh gas, and the molar density at the adiabatic flame temperature. This assumption demands some justification. It implies that the flame speed of moist carbon monoxide mixtures should be related in a linear manner to the square root of the initial CO content at a fixed percentage of moisture and a constant adiabatic flame temperature. That this is indeed so is shown by Figure 2, in which Jahn's data has been crossplotted to demonstrate the effect of increasing mole fraction of carbon monoxide in rich CO flames at a fixed percentage of oxygen. The substitution of carbon monoxide for nitrogen in rich mixtures has practically no effect on the adiabatic flame temperature. It should be mentioned that we have been anticipated in this form of presentation of the burning velocity data by Behrens,[8] who is, however, willing to accept such a plot as indicative of the kinetics of the flame reaction, without the theoretical considerations of the Semenov theory.

Values must now be obtained for the specific reaction rates k_{II} and $k_{III'}$, in order to use Equation (4) for the correlation of the burning velocities. It will be assumed first that k_{II} and $k_{III'}$ do not differ greatly from one another. This assumption is certainly open to question, for Reaction III′ might be expected to be much slower than Reaction II. However, in our ignorance of the actual relative reaction rates, we shall arbitrarily take them as equal. The specific reaction rate, k, is written in the form, $k = AZe^{-(E/RT_f)}$ where A is Arrhenius preexponential factor. The expression for the rate of oxidation of CO then becomes

$$W = AZ\left(\frac{T_0}{T_f}\right)^2 \rho_0^2 p\text{CO}(p\text{OH} + p\text{H}_2\text{O}_{eq})e^{-(E/RT_f)} \quad (5)$$

and the burning velocity is

$$U_0 = \left[2\lambda ZA\left(\frac{T_0}{T_f}\right)^2 \cdot \frac{Q'}{L^2} \cdot \frac{RT_f^2}{E} \cdot p\text{CO}(p\text{OH} + p\text{H}_2\text{O}_{eq})e^{-(E/RT_f)}\right]^{\frac{1}{2}} \quad (6)$$

We can reduce Equation (6) by noting that L,

the heat of combustion per unit weight of the mixture may be written as

$$L = \bar{C}_p(T_f - T_0) = \bar{C}_p T_f(1 - T_0/T_f) \cong \bar{C}_p T_f$$

in which $\overline{C}p$ is an average specific heat for all the combustible mixtures. Furthermore, from the kinetic theory of ideal gases we may say that λZ is proportional to T_f, the adiabatic flame temperature. According to the theory of absolute reaction rates, the Arrhenius constant A has a temperature dependence represented by T^x, where x is determined from the partition functions for the reaction species. For the reaction between two diatomic molecules, x has a value of -1 or $-3/2$, depending upon the nature of the activated complex formed. For the reaction between a diatomic molecule and a polyatomic molecule $x = -3/2$. Thus to the accuracy of our approximate treatment

$$\lambda Z A \approx \text{const}$$

Introducing these considerations into Equation (6), we find that:

$$U_0 = \text{constant} \cdot \left[\left(\frac{T_0}{T_f} \right)^2 \cdot p\text{CO}(p\text{OH} + p\text{H}_2\text{O})_{eq} e^{-(E R/T_f)} \right]^{\frac{1}{2}} \quad (7)$$

Equation (7) satisfies the same qualitative criteria as the Semenov-Zeldovitch-Frank Kamenetski relationship. It requires that the burning velocity be independent of the initial oxygen content at constant combustion temperature. A crossplot of Jahn's data for lean mixtures at fixed carbon monoxide percentage, shown in Figure 3, is in reasonable accord with this requirement. This observation allows one to determine an appropriate value for the activation energy, E, in the burning velocity expression. For a fixed carbon monoxide content and a constant percentage of moisture, a change in the oxygen concentration is equivalent to changing the temperature at which the oxidation of carbon monoxide is worked out in the flame. If this assumption has some validity, a graph of $U_0(T_f/T_0)$ against the reciprocal of the absolute flame temperature in semilogarithmic coordinates should yield a straight line of slope $E/2R$ for each of the mixtures of specified composition. This has been done in Figure 4 for the range of CO percentages of interest. The resulting plots are quite linear and sensibly parallel in slope.

The point that deviates markedly from the 40 per cent CO line was calculated for a very lean (60 per cent O_2) mixture, where the slight influence of O_2 on the oxidation kinetics makes itself noticeable. The activation energy corresponding to the slope of the family of lines is approxi-

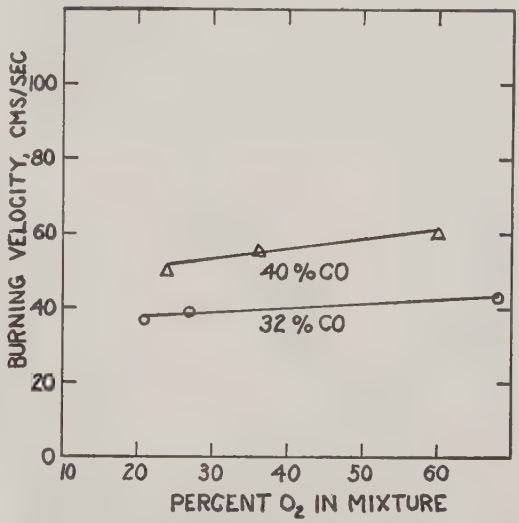

FIG. 3. Relationship between burning velocity and initial oxygen content in CO mixtures at a constant flame temperature.

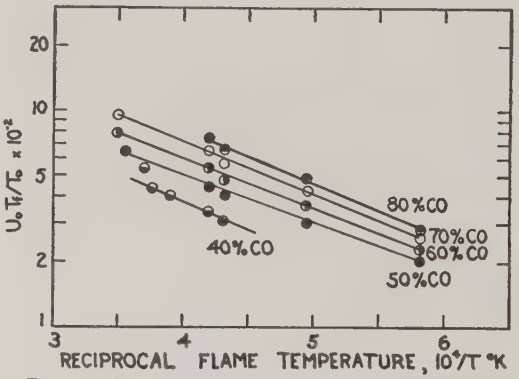

FIG. 4. Plot of the burning velocity against the reciprocal of the flame temperature (°K) for mixtures with a constant carbon monoxide and moisture content.

mately 22,000 kcal/g-mol. This value is not, of course, an accurate measure of the chemical activation energy for the reaction we have postulated. It includes the effects of the change in thermal conductivity with temperature (only approximately compensated for in Equation (7)) as well as the change in CO concentration in the reaction zone due to diffusion. The activation energy determined in the present work is quite

independent of mixture composition, in contrast to the findings of Barsky and Zeldovitch who report values of the activation energy ranging from 19.4 to 73 kcal/g-mol as a function of composition. A discussion of this discrepancy is outside the scope of the present writing, particularly in view of the probability that none of the values quoted here reliably represent the chemical activation energy for the reactions occurring in the flame.

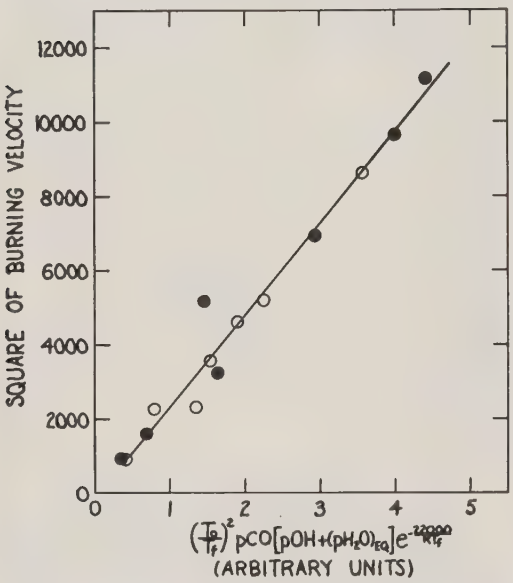

FIG. 5. Reduction of Jahn's carbon monoxide data in accordance with the proposed theory.

TABLE 1. ADIABATIC FLAME TEMPERATURE AND EQUILIBRIUM CONCENTRATIONS FOR JAHN'S CO MIXTURES

pCO	Concentrations, Atmos × 10^4			Flame Temp	U_0 OBS.
	I. Rich Mixtures				
per cent	pH	pOH	pH$_2$O eq.	(°K)	Cm/sec
35	0.1	—	100	1730	25.5
40	2.5	3.4	47	2320	30
40	3.8	4.9	103	2320	40
45	16.0	58.0	111	2710	57
80	29	39	38	2860	72
60	38	90	114	2850	83
70	52	102	133	2900	98
80	59	78	153	2860	106
	II. Lean Mixtures				
26.5	0.7	20.6	80	2320	29.5
40	5.6	56	34	2720	48
40	11.6	56	112	2660	50
40	9.2	88	89	2720	60
60	24	86	40	2930	68
50	24	91	108	2810	72
60	29	134	102	2930	93

The preceeding analysis predicts that the square of the burning velocity of moist carbon monoxide mixtures will be a linear function of

$$\left(\frac{T_0}{T_f}\right)^2 [p\mathrm{CO}(p\mathrm{OH} + p\mathrm{H_2O_{eq}})e^{-(22000/RT_f)}]$$

This conclusion is tested in Figure 5. The correlation exhibited here is fully as satisfactory as that of Tanford and Pease and is based upon their calculations of the adiabatic flame temperatures and equilibrium concentrations of hydrogen and hydroxyl radicals in the burned gases. Their reported values were used to calculate the equilibrium water concentrations, with the aid of the equilibrium constants tabulated by Lewis and von Elbe.[5] Pertinent data for the plot are collected in Table 1. The rich and lean mixtures have been separately identified in this graph to delineate any possible differences in the fit of the correlation between the two types of mixtures. Apparently there are none, a fact which offers some satisfaction, since one would intuitively expect the same reaction mechanism to be operative in both lean and rich mixtures. By way of contrast, it may be mentioned that the analysis of Barsky and Zeldovitch[7] shows the rate of oxidation of carbon monoxide to be first order with respect to water concentration in rich mixtures and of fractional order ($\frac{1}{2}$) in lean mixtures.

If the carbon monoxide concentration in Equation (7) is corrected for the effect of diffusion by the method of Zeldovitch and Frank-Kamenetski, a significant change is effected in the burning velocity correlation (Fig. 6). Separate lines are obtained for rich and lean mixtures and neither seem to fit the data quite as well as the original relationship, which embraced all mixtures. This result offers supporting evidence for our view that the effect of diffusion in diluting the concentration of combustible is overestimated by the Semenov-Zeldovitch-Frank-Kamenetski theory of flame propagation.

III. Critical Comparison Between the Tanford-Pease and Proposed Theory

The fact that both the Tanford-Pease and the present ideas are supported by the same data,

indicates that the assumptions made in both cases are overwhelming the essential differences in the roles assigned to the active particles. A more critical comparison of the two views is needed to elucidate the effect of active particles on the combustion mechanisms of carbon monoxide. This may be obtained by analyzing the effect of varying water content on the burning velocity of a carbon monoxide oxygen mixture of fixed composition. If the water content is not excessive (<2 per cent) the variation in adiabatic flame temperature will be negligible. Under these circumstances, the physical, thermal and chemical (i.e., specific reaction rate either local or average) properties may be regarded as invariant for all mixtures. Thus the only parameter to be considered is the concentration of active particles in the burned gas. The measurements of McDonald[9] on 80 per cent CO-20 per cent O_2 lend themselves readily to this purpose.

Both the Tanford-Pease and the present theory predict a linear relationship between the square of the burning velocity, U_0^2 and a radical concentration function equal to $(p\mathrm{H}/B_{\mathrm{H}} + 0.15\ p\mathrm{H})$ for the Tanford-Pease theory and represented by $(p\mathrm{OH} + p\mathrm{H_2O_{eq}})$ in our views. Tests of this prediction for each of the theories are compared in Figure 7, based upon the equilibrium concentrations listed in Table 2. Radical concentrations were calculated from the equilibrium constants tabulated by Lewis and von Elbe for the flame temperatures and hydrogen atom concentrations reported by McDonald. The factor, B_{H} (1.39), correcting for the hydrogen atom loss due to chemical processes was taken from the data of Tanford and Pease. It is evident, upon inspection of Figure 7, that the Tanford-Pease theory gives a much poorer correlation of McDonald's burning velocity data than do the present ideas. In addition to a marked departure from linearity, the Tanford-Pease correlation implies that the flame speed of the dry mixture may be very close to zero. On the other hand, the correlation developed by us indicates that the burning velocity of the dry mixture is 35 cm/sec, a value in surprisingly close agreement with the experimental value of 34 to 35.2 cm/sec. It thus appears, that when the two theories are compared under conditions that require the least number of questionable assumptions regarding the physical, chemical, and thermal properties of the combustible mixture, our correlation is improved appreciably while the Tanford-Pease correlation deteriorates. Hence, there are grounds for reasonable doubt of the supposition that the diffusion of hydrogen atoms is the controlling factor in the combustion of moist carbon monoxide mixtures.

In postulating our kinetic scheme for the oxidation of CO in the presence of moisture, we selected the water gas reaction in preference to the reaction between carbon monoxide and oxygen atoms as a second mechanism for the production of CO_2 and assumed that the equilibrium concentration of water is determined by the reaction

VI. $\mathrm{H_2O} \rightleftharpoons \mathrm{H} + \mathrm{OH}$

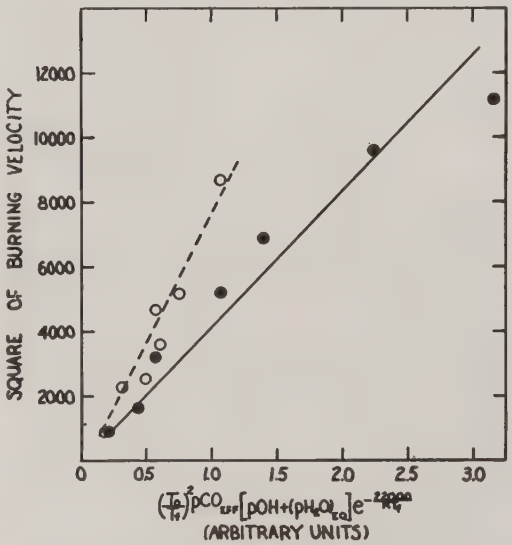

FIG. 6. Reduction of Jahn's data in accordance with the proposed theory. CO concentration in the reaction zone corrected for diffusion.

We deferred the discussion of the basis for our choice to a later time. This matter will now be considered with reference to the data for 80 per cent CO-20 per cent O_2 mixtures.

The average flame temperature of these mixtures is 2850°K, with a maximum deviation from this value of less than 1 per cent. The equilibrium constant for Reaction V at this temperature is readily obtained from the tabulation of Lewis and von Elbe and is equal to

$$K_5 = \frac{(p\mathrm{H_2})(p\mathrm{OH})}{(p\mathrm{H_2O})(p\mathrm{H})} = 0.3$$

The equilibrium concentrations calculated upon the assumption that Reaction VI is satisfied when substituted into the expression for K_5 give values

ranging from 0.2 to 0.32. It appears that within the limits of the accuracy of the calculation both equilibria are satisfied under these flame conditions and will yield approximately the same values for the radical concentrations.

The kinetic scheme of Zeldovitch and Semenov, under their postulate of a steady state with respect to the radical concentrations in the reaction zone, leads to the result that the rate of

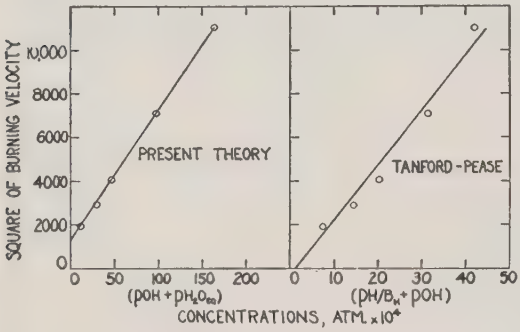

FIG. 7. Comparison of correlations obtained with Tanford-Pease and proposed theory on 80 per cent CO-20 per cent O_2 mixtures containing added water.

TABLE 2. ADIABATIC FLAME TEMPERATURES AND EQUILIBRIUM CONCENTRATIONS IN 80 PER CENT CO-20 PER CENT O_2 MIXTURES

H_2O added	Flame Temp	Concentrations, Atmos × 10^4		
		pH	pOH	pH$_2$O$_{eq}$
per cent	°K			
0.12	2870	8.5	8.0	2.65
0.31	2865	16.5	18.8	10.8
0.50	2861	22.5	26.6	20.7
1.03	2850	34.0	44.6	52.1
1.78	2837	45.0	64.0	100.0

oxidation of carbon monoxide is given rigorously by

$$W = 2k_{II}[CO][O] = 2k_I[O_2]_{eff}[H]$$

For the conditions we are considering (constant O_2 composition, essentially constant flame temperature), this implies that the burning velocity should be directly proportional to the square root of the hydrogen atom concentration in the reaction zone and therefore, as we have already indicated, to the square root of the equilibrium hydrogen atom concentration. This prediction is not borne out by McDonald's measurements and calculations which show the flame speed to be proportional to the 1.26 power of the hydrogen atom concentration in the burned gases. It seems that the kinetic scheme we have advanced is better supported by the experimental data than is the Semenov-Zeldovitch reaction mechanism. This result is quite surprising; it would be expected *a priori* that the reaction between CO and oxygen would be much more plausible under flame conditions than the presumably slow bimolecular reaction between carbon monoxide and water vapor. Certainly further evidence is needed before the place of the latter reaction in the combustion mechanism of carbon monoxide can be accepted as established.

McDonald's experiments with heavy water indicate that it has less effect than an equal quantity of ordinary water on the burning velocity of his carbon monoxide mixtures. Furthermore, the difference in effect increased with increasing concentration of water. The ratio of the flame velocity with H_2O to the flame velocity with D_2O varied from 1.13 to 1.24 for the lowest to the highest water concentrations reported in his tabulated experimental values. This behavior may be explained upon the basis of the present theory.

A correlation of the burning velocity data against the radical concentration function for heavy water additions exhibits the same type of behavior as that found for mixtures of carbon monoxide containing ordinary water. Both relationships are expressible in the form:

$$U_0^2 = KR + U_A^2 \tag{8}$$

where U_A is the burning velocity of the dry mixture, K is product of the thermal and physical parameters of the mixture multiplied by the specific reaction rate (see Equation (6)) and R is the concentration function $p\mathrm{CO}(p\mathrm{OH} + p\mathrm{H_2O_{eq}})$ or $p\mathrm{CO}(p\mathrm{OD} + p\mathrm{D_2O_{eq}})$. For small water additions (< 2 per cent) the radical concentrations are not significantly affected by the substitution of deuterium for hydrogen in a given quantity of water. Upon comparing the correlations for ordinary and heavy water, it is found that the slope, K, of the line for heavy water is less than that for ordinary water. Since the physical and thermal properties of these mixtures are practically identical, the difference in K must arise from a difference in the reaction rate constants. It is instructive, therefore, to compare

the reactivity of the OH radical with the OD radical.

An expression for isotope substitution on the rate of reaction has been derived by Biegeleisen.[10] In cases where the rate is determined by rupture of the chemical bond, A-B, between two atoms, his theoretical treatment predicts that the ratio of the reaction rate constants will be given in its simplest and most approximate form by

$$\frac{k}{k^*} = \left[\frac{M_B^*}{M_B}\left(\frac{M_A + M_B}{M_A + M_B^*}\right)\right]^{\frac{1}{2}}$$

In which M_A is the mass of atom, A, and M_B^* are the masses of atom, B, and its isotope respectively. For the case of OH and OD

$$\frac{k_{OH}}{k_{OD}} = \left[2 \cdot \frac{17}{18}\right]^{\frac{1}{2}} = 1.37$$

A more refined calculation,[11] taking into consideration the partition functions of the reactants and of the activated complex, gives a value of 1.33 for the ratio of the reaction rates. Presumably the reactivities of ordinary and heavy water would be in about the same ratio. The square root relationship between reaction rate and burning velocity requires that the flame speeds of H_2O to D_2O-bearing mixtures be in the ratio of 1.17 to 1, a value in good agreement with observation. If the contribution of the burning velocities of the dry mixtures is included in our considerations, we have from Equation (8)

$$\frac{U_{H_2O}}{U_{D_2O}} = \left[\frac{k_{OH}R + U_A^2}{k_{OD}R + U_A^2}\right]^{\frac{1}{2}}$$

a relationship which states that the ratio of the burning velocities of the two types of mixtures should increase with increasing water content and approach a constant value at higher values of the flame speed. This is in satisfactory qualitative accord with experiment.

If we accept McDonald's relationship between the burning velocity of these mixtures and the hydrogen atom concentration, $U_0 \alpha (p\mathrm{H})^{1.26}$ and assume that the flame speeds are affected only by the relative diffusion rates of hydrogen atoms as compared to deuterium atoms, the ratio U_{H_2O}/U_{D_2O} would be expected to be equal to $(D_H/D_D)^{1.26} = (1.4)^{1.26} = 1.52$, a prediction in rather poor agreement with the measurements.

Thus it appears that our present views, which emphasize the chemical kinetic aspects of the flame, explain the effect of substitution of deuterium for hydrogen in moist carbon monoxide mixtures better than does the premise that the burning velocity is controlled primarily by the diffusion of hydrogen atoms from the burned gases.

Summary

(1) It has been shown that the Tanford-Pease analysis of Jahn's burning velocity data on moist carbon monoxide mixtures does not necessarily support their views regarding the mechanism of flame propagation.

(2) A model of the combustion wave has been postulated which ignores the effects of diffusion and correlates the burning velocities in terms of the kinetic mechanisms at the flame front. This has been found to give a satisfactory fit with the experimental results of Jahn.

(3) A critical comparison of the two flame theories has been made on mixtures consisting of 80 per cent CO and 20 per cent O_2 with varying amounts of water. Under these circumstances, free from most of the doubtful assumptions made regarding the thermal, physical and chemical properties of Jahn's mixtures, the present views have been found to correlate the experimental data in a more satisfactory manner than the Tanford-Pease theory.

(4) The effect of heavy water on the burning velocity of moist carbon monoxide mixtures has been explained in terms of the difference in reactivity between the OH and OD radical. The agreement of the predicted variation in burning velocity with experiment is satisfactory.

(5) It is believed that these results indicate that the diffusion of hydrogen atoms from the burned gases may not be the controlling factor in the combustion of moist carbon monoxide mixtures.

REFERENCES

1. Tanford, C., and Pease, R. N.: J. Chem. Phys., *10*, 861 (1947).
2. Jahn, G.: Der Zündvergang in Gasgemisch. Berlin, Oldenbourg, 1934.
3. Zeldovitch, Y. B., and Semenov, N. N.: Zhur. Exp. Teor. Fiz., *12*, 1427 (1940).
4. Hoare, M. F., and Linnett, J. W.: J. Chem. Phys., *16*, 747 (1948).
5. Lewis, B., and von Elbe, G.: *Combustion*,

Flames and Explosions of Gases, p. 342. New York, Academic Press, 1951.
6. Semenov, N. N.: Progress Phys. Sci. (U.S.S.R.), *24*, 439–486 (1940); NACA Tech. Memo No. 1026.
7. Barsky, G. A., and Zeldovitch, Y. B.: Zhur. Fiz. Khim., *25*, 523 (1951).
8. Behrens, H.: Z. physik. Chem., *195*, 225 (1950).
9. McDonald, G. E.: NACA Research Memo. No. E53108, 1954.
10. Biegelson, J.: J. Chem. Phys., *17*, 425 (1949).
11. Rutner, E., Scheller, K., and McLain, W.: To be published.

35

SOME RECENT EXPERIMENTAL RESULTS ON THE FLAMMABILITY REGIONS OF VARIOUS GASES AND COMBUSTIBLE VAPORS AT LOW PRESSURES

By RALPH DELBOURGO and PAUL LAFFITTE

The present paper summarizes a number of current investigations on the flammability regions of various mixtures, determined by electric spark at reduced pressure and carried out by Monique Charton (spectrography), Jean Combourieu (flame propagation), Gisèle Dalmai (influence of geometrical factors), Raoul Graziotti (propagability ranges of diethyl ether), and Nicole P. Prot (analytical determinations).

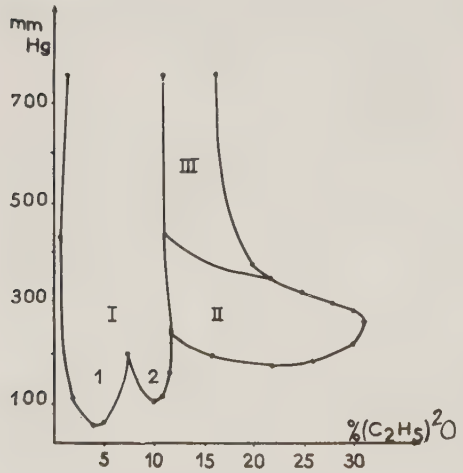

Fig. 1. Flammability regions of ethyl ether-air mixtures. Electric spark—normal temperature.

Introduction

The authors have shown previously[1] that when mixtures of air and hydrocarbons heavier than ethane are ignited by a train of condensed sparks at reduced pressure, they present a flammability region divided into two lobes in which the types of flames are different (*"first region"* flames for low hydrocarbon concentrations, and *"second region"* flames for rich mixtures). As reported previously,[2] these rich lobes must not be mistaken for cool-flame regions of similar shape, such as that observed for diethyl ether at low pressures.

Evidence of this effect is provided by Graziotti[3] who studied the flammability regions of diethyl ether-air mixtures. The experimental arrangement used by Graziotti is the same as that which the authors used to determine the two-lobe regions of propane-air and butane-air mixtures. In particular, the tube length and diameter, and the ignition source were those described previously. Graziotti showed that when a combustible vapor can support a cool flame at reduced pressure and under the given experimental conditions, its flammability region has not two but three distinct lobes. This has proved to be the case with diethyl ether-air mixtures. Figure 1 shows the complete region for these mixtures. It can be seen that the cool flame region as determined by known cool flame criteria, lies along the second region for still higher combustible concentrations. All types of flames already described are present. The region is divided into three parts, part I being the normal two-lobe region, part II the cool-flame region, and part III the second-stage flame region. Additional evidence that rich lobes are not to be identified with cool-flame regions is provided by a spectrographic study of flames of the two lobes, using various concentrations of butane in air over the whole region. Figure 2 shows the emission spectra obtained with flames

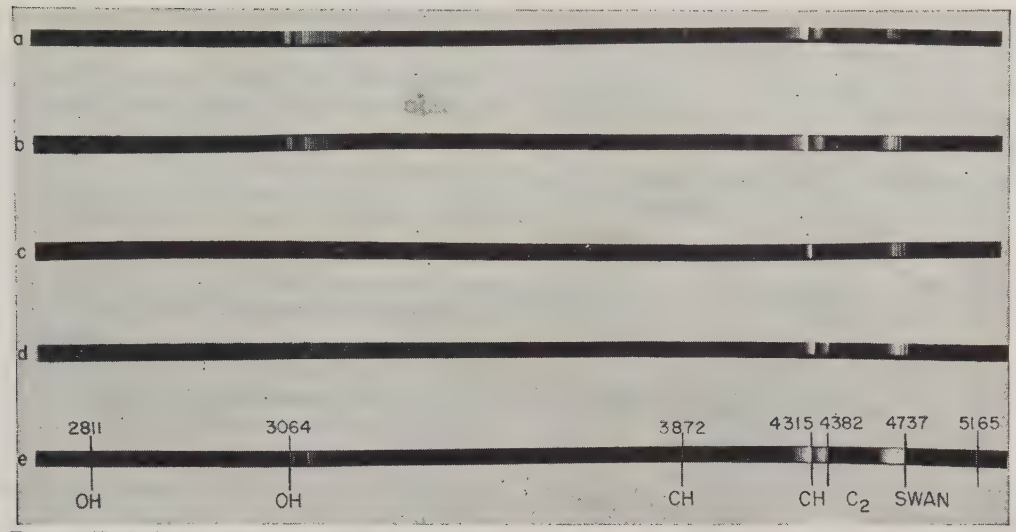

FIG. 2. Emission spectra of butane-air flames 250 mm pressure a = 3.3% C_4H_{10}; b = 4.3%; c = 5.25%; d = 6.1%; e = 8.0%.

of given composition in each of the two regions. *Qualitatively the emission spectra are those of normal flames* (C_2, CH and OH bands) and at no hydrocarbon concentration does the well-known formaldehyde fluorescence spectrum, characteristic of cool flames, appear.

Experimental

To study quantitatively both the condensable products of these flames and their spectrographic emission, an apparatus was constructed with a flow-type conical arrangement that stabilized any type of flame (Fig. 3). In principle, the apparatus consists of a conical Pyrex flame tube with a water jacket. The tube is 80 cm long and its diameter decreases steadily from 4 cm at one end to 2 cm at the other. Three traps (T_0, T_1, T_2), normally immersed in liquid nitrogen, make it possible to sample the condensable products along the tube, moving away from the flame. A fourth trap (T_3) is still farther away from the flame outside the water jacket. Two tungsten electrodes are used to produce high-tension sparks across the gap. Once ignited, the flame travels through the tube and is quenched at some point along it, usually at the place shown in the figure, by regulating the pumping velocity and the mixture feed with the valves shown.

The metering and mixing system includes precision flowmeters, mercury manometers, filtering and desiccating (P_2O_5) tubes. Each gas has an independent 10-liter vessel to damp out pressure variations. The two constituents of the mixture flow into a third 10-liter vessel through a T-joint and the mixture is fed from there to the flame tube through a needle valve. The pressure is recorded by a mercury manometer placed at the tube inlet. The high pumping velocity necessary is provided by a 150-l/min oil vacuum pump. With this setup flames can be stabilized and kept constant for several hours. As a rule, a two-hour run was sufficient to obtain enough condensable products for analysis. In some cases longer times were necessary for a correct spectrum to be obtained. To study the flame spectra, the tube was placed on the spectrograph bench. A standard type Adam Hilger apparatus was used for these determinations.

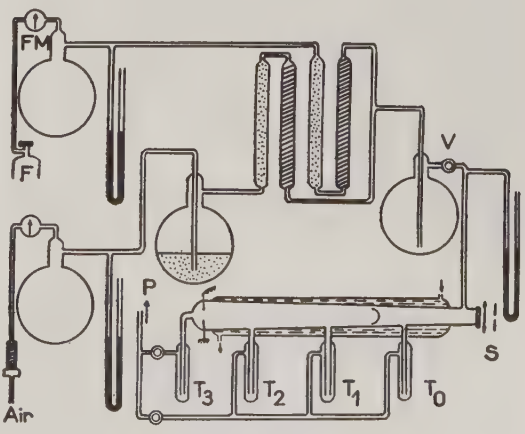

FIG. 3. Flow type apparatus for flame stabilization at reduced pressure.

Data Obtained

The condensable material was analyzed by Mrs. Nicole P. Prot, mainly by polarography, using an electrolytic cell with saturated calomel reference electrode. The basic solution was 0. IN lithium chloride. Samples were purged with pure nitrogen for a period of 15 minutes; tylose is

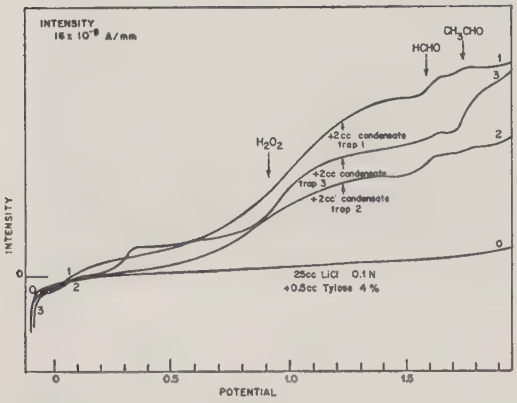

FIG. 4. Polarogram of condensable products.

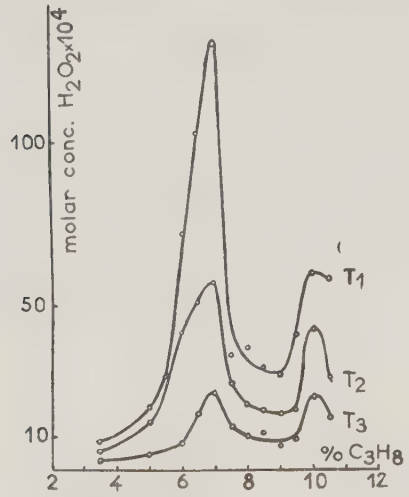

FIG. 5. Hydrogen peroxide concentration against combustible mixture.

used as maximum suppressor. The polarographic half-wave potential of hydrogen peroxide is well known (−0.9 volts). A typical polarogram obtained is shown in Figure 4 where waves of hydrogen peroxide, together with waves of formaldehyde and acetaldehyde, are clearly visible. This technique was applied to flames of various propane mixtures across the whole flammability region for a pressure of 250 mm Hg. The condensable products were allowed to come to room temperature before analysis. The standard procedure was adopted throughout in these determinations and, for many reasons, the results should be considered as purely relative, but nevertheless comparable. Figure 5 shows the variation of hydrogen peroxide concentrations in products of flames of propane-air mixtures with 3.5 per cent to 10.5 per cent propane. (H_2O_2 expressed as molarity of H_2O_2 solutions). As was to be expected, hydrogen peroxide formation is maximum in trap 1, i.e., nearest the flame; it decreases rapidly as we move away from the flame (traps 2 and 3). The amount of H_2O_2 obtained increases with the hydrocarbon content of the mixture, reaching a maximum at 7 per cent (stoichiometric mixture $\simeq$ 4 per cent). It then decreases almost to the minimum value, after which it rises again

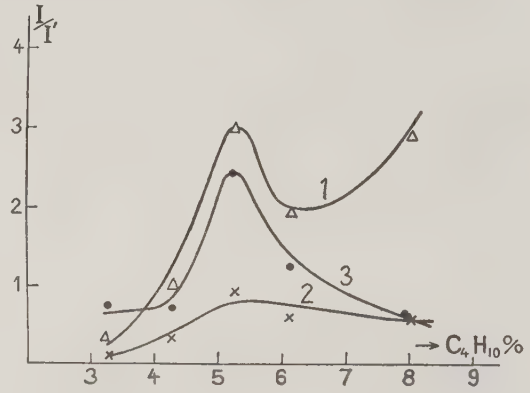

FIG. 6. Free radical intensity ratio against combustible mixture.

to another maximum at 10 per cent. Peroxides other than H_2O_2 have not been detected; they may be present but masked by the importance of the hydrogen peroxide wave.

Parallel to this work, the spectrographic emission of butane-air flames at the same reduced pressure was studied by Charton,[5] who showed that the mixtures for which the flames change their color and shape can be characterized spectrographically. Figure 6 shows variations of the the following intensity ratios:

$$(1)\ \frac{I_{C_2}(0.0)}{I_{CH}(3900)} \quad (2)\ \frac{I_{C_2}(1.0)}{I_{CH}(4300)} \quad (3)\ \frac{I_{CH}(4300)}{I_{CH}(3900)}$$

against the butane concentration. The maximum of these curves is situated between 5 and 6 per cent.

Concomitant to these quantitative studies on stabilized flames, Dalmai[6] and Combourieu[7] de-

termined the influence of certain physical factors on propagation and therefore on the shape of the limiting curves. The apparatus used is of the conventional type already described by the authors. Figure 7 shows that geometric parameters, such as diameter variations, are likely to have a great influence on the shape of these curves. Increasing the tube diameter tends to lower the critical pressure obtained, especially for mixtures with partial propagation and flame quenching, i.e., mixtures giving rise to the characteristic two-lobe shape.

Suppressing certain vibrations can make propagation complete, whereas closed tube conditions make it partial and therefore alter the shape of the flammability region. However, Mallard and Le Chatelier recordings throughout the reduced pressure region show that propagation varies little with pressure and greatly with concentration. Propagation is vibratory throughout the entire region and is not limited to those mixtures that lead to flame quenching. The conclusion that two-lobe regions are due exclusively to physical factors[8] seems to contribute only to one aspect of a complex question. Figure 8 shows schematically drawn recordings of typical flame propagations.

Conclusion

The determination of flammability limits having some practical application has always led investigators to adopt a certain number of criteria as, for instance, the minimum tube length and diameter, a known ignition source and total propagation. Once determined, these experimental conditions are kept constant except when it is desired to study a single phenomenon as a function of any one of these parameters. Obviously the limits obtained and the shape of the range determined are a function of these parameters. In particular, it has been established that in closed tubes the criterion of total propagation, for a constant tube length, diameter and ignition source may lead to flammability regions with complex features.

In some cases, certain geometric factors, such as tube diameter, and changes of the propagation regime produced by opening one end of the tube, can alter the shape of these regions without explaining the phenomena occurring inside them. Making the propagation complete in a region of flame quenching and partial propagation does not suggest any explanation for this quenching. It merely shows that specific factors can have a definite action on a flame propagating along a tube.

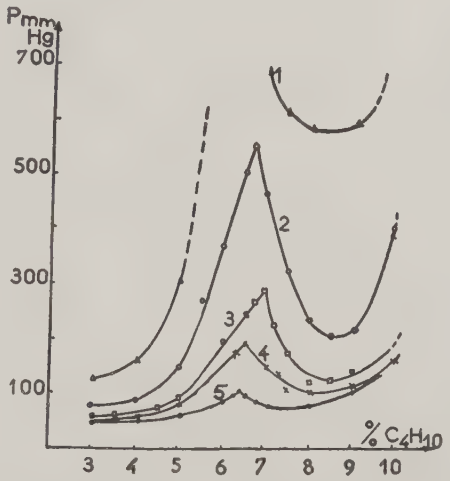

FIG. 7. Influence of diameter on low-pressure flammability region of butane-air mixtures. 1 = 17 mm; 2 = 22.5 mm; 3 = 32.5 mm; 4 = 40 mm; 5 = 55 mm.

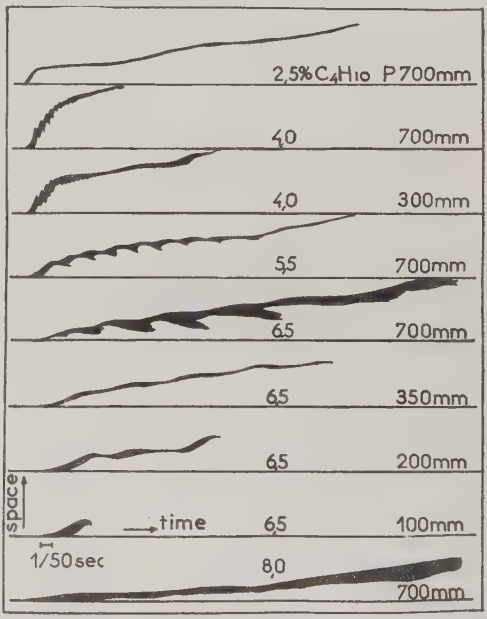

FIG. 8. Propagation regime of various mixtures at various pressures.

Investigation of any mixture, first as regards its reaction products, especially hydrogen peroxide formation, and second as regards the free radicals emitted, has shown definitely that mixtures for which flame quenching occurs (propane or butane) lead to particular values of the proper-

ties considered (whether it is H_2O_2 formed, or a free radical intensity ratio). Although there may not be any obvious link between these properties, and the flammability region as determined by a static closed-tube method, a parallel can be drawn between this special behavior and the fact that the same mixtures do not give total propagation under a given set of conditions.

Bearing in mind the influence of walls and surfaces on the limits and on the regions studied, together with this same influence on H_2O_2 formation or radical deactivation, the authors are planning a study of the influence of treated surfaces on the character of the flammability regions and on H_2O_2 formation.

In this way a number of chemical factors may be shown to have an influence on flame propagation, leading to total propagation for a mixture which might otherwise have shown flame quenching. This will again alter the shape of the region proving once more how complex the whole problem is and that there is no unequivocal answer.

In the present state of their work, the authors feel that further experimental data is needed before conclusions can be drawn.

REFERENCES

1. Laffitte, P., and Delbourgo, R.: *Fourth Symposium (International) on Combustion*, p. 114. Baltimore, The Williams & Wilkins Co., 1953.
2. Delbourgo, R., and Laffitte, P.: Compt. rend., *233*, 1612 (1951).
3. Graziotti, R., and Laffitte, P.: Compt. rend., *239*, 1640 (1954).
4. Prot, N., Delbourgo, R., and Laffitte, P.: Compt. rend., *241*, 1306 (1955).
5. Charton, M., and Laffitte, P.: Compt. rend., *242*, 640 (1956).
6. Dalmai, G., Delbourgo, R., and Laffitte, P.: Compt. rend., *240*, 192 (1955).
7. Combourieu, J.: Personal communication. Results to be published.
8. Guénoche, H., Fréling, E., and Dugleux, P.: Rev. Inst. Fr. du Pétrole, *10*, 1209 (1955)

36

THE EFFECT OF PREHEATING ON FLAME RADIATION AND FLAME SHAPE

By H. GUÉNEBAUT and A. G. GAYDON

Introduction

It was discovered by von Helmholtz[1] in 1890 that preheating the gases of a Bunsen-type flame caused a decrease in total flame radiation, although such preheating must increase the final equilibrium flame temperature and might be expected to produce an increase in thermal radiation from the flame. This result was apparently confirmed by Haslam, Lovell and Hunneman;[2] from their graph, it appears that preheating the air supply to 1100°F reduces the radiation, per unit flame area, to about 60 per cent of the value before preheating. These results have been quoted (e.g., by Garner and Johnson[3] and by Gaydon[4]) as evidence that the infrared radiation from flames may be partly of chemical rather than thermal origin. It is known[4] that a large part of the visible and near ultraviolet radiation from Bunsen-type flames comes from the reaction zone, or inner cone, and is emitted by radicals like CH and C_2, which are certainly not in chemical equilibrium and probably not in thermal equilibrium either. However, in stationary flames, it appears that the infrared radiation comes from the interconal gases and outer sheath of burned gases rather than from the inner cone[5] and is emitted by the stable combustion products, CO_2 and H_2O, with a small contribution from CO and OH which are present to some extent in the equilibrium gas mixture.

There does not appear to be any recent work on the effect of preheating on the infrared radiation from premixed flames, although similar effects have been reported by Guyomard[6] in diffusion flames. The older work by Haslam, Lovell and Hunneman[2] was carried out under ill-defined flame conditions; they used a long horizontal pipe with openings along it to give a continuous length of flame; it is not clear whether the flow was laminar or turbulent. They also speak of the possibility of prereactions occurring in the pipe. This paper, therefore, reports new

measurements on a better defined flame with laminar flow. The effect of the preheating on the flame shape and general flow pattern has been noted. Experiments have been carried out mainly with methane/air flames, as methane has a relatively high ignition temperature and no "cool flame" region, so that slow combustion in the preheating region is less likely.

Experimental

The air and methane were metered with rotameter flow-meters and mixed in a simple metal mixing chamber. The mixture then passed up a long (60 cm) quartz tube of 1 cm i.d. This long tube gave ample time for the preheating and enabled a laminar flow pattern to be properly established so that a steady symmetrical flame was maintained on the top of the tube. This quartz tube was heated by a winding of nichrome wire, and was lagged with asbestos and enclosed in a water-cooled brass tube which suppressed any radiation from the heated tube.

The temperature to which the gases were preheated was measured with a small platinum-rhodium thermocouple. This was inserted into the gas stream just inside the top of the burner mouth. No corrections were made for radiation losses; these would be largely compensated by radiation from the burner walls. Measurements of preheat temperature were made in a stream of air, with the methane supply cut off, to prevent catalytic heating of the couple. Temperatures up to 750°C could be attained. Below 600°, there did not appear to be any reaction in the preheat tube, but above this temperature the unignited gases smelled very slightly of formaldehyde.

The radiation measurements were made with a Hilger Schwartz thermopile and sensitive galvanometer. For measurements of total radiation, the thermopile was placed at a considerable distance from the flame so that the whole flame came within the angle "seen" by the thermopile. A rough inverse square law check was made to see that there was no error due to light failing to reach the sensitive surface of the thermopile. A black screen behind the flame served to reduce scattered light or radiation reflected from the flame. Differences in temperature of the water-cooled tube and of surroundings gave a small deflection of the galvanometer without the flame. This was always measured before igniting the flame, with a small piece of black card covering the hot unignited gas stream, or with the gas flow momentarily stopped.

Most measurements were taken with the thermopile exposed to all wavelengths. For some measurements, a quartz window was interposed. This was transparent to about 4 μ and served to transmit the main 2.8 μ band of H_2O and CO_2 but to reduce the intensity of the strong 4.4 μ band of CO_2.

For study of variation with height above the burner mouth, an asbestos slot was interposed between the flame and thermopile, close to the former. This slot was made of a double thickness of asbestos and the horizontal rectangular slot was 0.8 by 3.2 cm. For these measurements, the distance between the thermopile and the flame was reduced to 23 cm, and the slot was 4 cm from the flame. In making measurements, the thermopile and slot were fixed so that the light traveled horizontally and the flame was progressively racked down.

The flame shape has also been studied by schlieren photography, using a conventional lens and knife-edge system, with single-spark photography. Owing to the length of the flame, it was necessary to study the flame of unheated gases in two sections, and of heated gases in three sections.

Results

For constant initial flow rates of methane and air, measured at room temperature, the total flame radiation was measured without preheating and with various preheat temperatures up to 750°C. This was done for several flow rates and mixture strengths. All the results showed that for this experimental set-up the total radiation did not change significantly for preheat temperatures up to about 500°C and that, above this temperature, there was a small increase in total flame radiation. In a few cases there was a slight minimum in radiation at a preheat to about 400°C.

Substantially similar results were obtained at various total flow rates within the range within which stable flames could be maintained. The results of a few observations with the quartz window absorbing the far infrared were also similar.

Measurements of radiation at various flame heights showed that without preheating the flame radiation rose fairly rapidly with height above the burner mouth, to reach a maximum

near the tip of the inner cone, then falling steadily and fairly quickly to a very low value at the top of the flame. With preheating, the increased burning velocity caused the inner cone to be much shorter. The radiation rose with height, as before, but not to such a high value, so that its maximum value, now slightly above the tip of the inner cone, was only about $\frac{2}{3}$ of the previous maximum value without preheating. However, the subsequent fall in radiation with height was less rapid and, towards the top of the

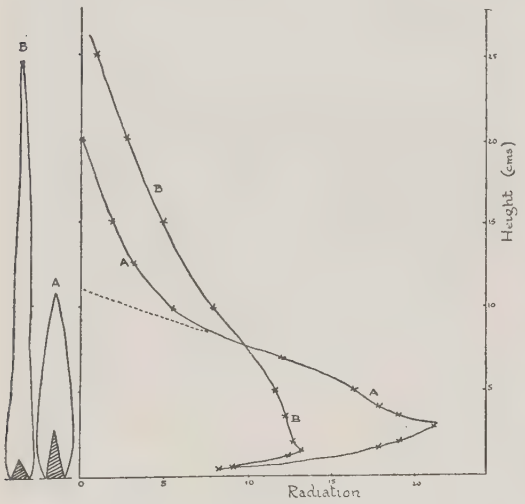

FIG. 1. Graphs of radiation, in arbitrary units (galvanometer deflection), against height above burner mouth for a slightly rich methane/air flame. Methane flow 13.3 cc/sec, air flow 113 cc/sec. Curve A without preheating, curve B with mixture preheated to 550°C. On the left of the graphs are shown the forms of the flame, as deduced by measurement of height of inner cone, with and without preheating.

now longer flame, the radiation exceeded that from the flame without preheating. Measurements of the total areas under the curves showed that these were almost equal, corresponding to equal total flame radiation. A typical set of measurements for a slightly rich methane/air flame is plotted in Figure 1.

Simultaneous observations of the flame showed that, as well as the shortening of the inner cone and lengthening of the outer cone, the flame became thinner. A representation of the flame shape, with and without preheating, is shown on the left of the curves in Figure 1.

The change in flame shape is well shown by the schlieren photographs, as illustrated in Figure 2. The flame with preheating has a shorter inner cone, is thinner and much longer, and the

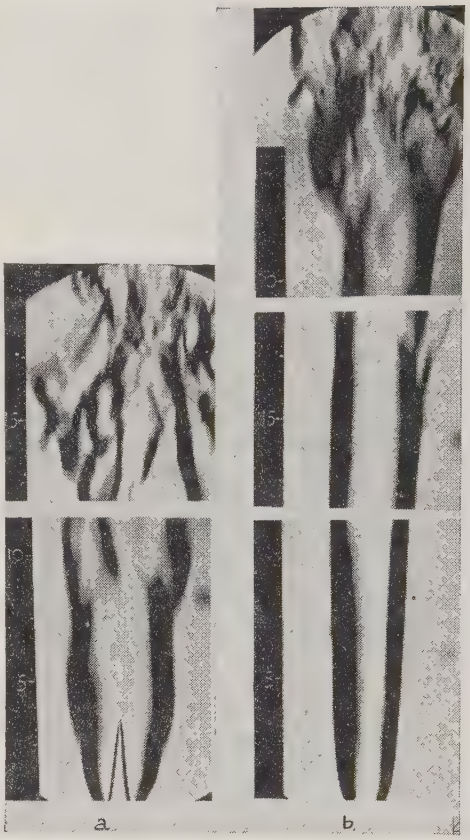

FIG. 2. Instantaneous schlieren photographs of methane/air flames (methane flow 13 cc/sec, air 160 cc/sec). (a) Without preheating (2 sections); (b) with preheating (3 sections). The black scale on the left shows the height, in cm, above the burner.

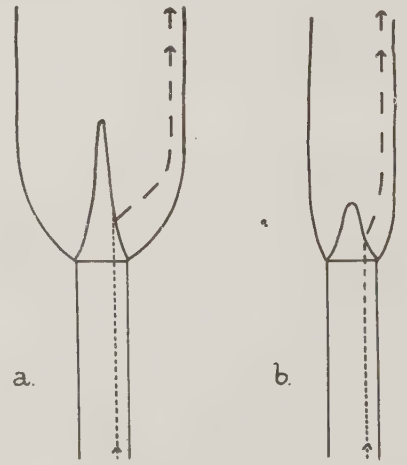

FIG. 3. Flow line without and with preheating.

height to turbulence is much greater. This increased height to turbulence means that the hot gases travel as a coherent stream for a greater distance. As soon as turbulence sets in, the more

rapid mixing with cool air will quench the flame radiation.

Discussion

The main change in radiation can be explained by the accompanying change in flame shape, the reduced cross-sectional area near the tip of the inner cone giving lower radiation here, and the greater length accounting for the greater amount at the top of the flame.

The change in flame shape can be accounted for by two effects: (1) The preheating causes an expansion and increase in velocity as the gases pass up the tube, so that they leave the burner mouth at about 2½ times their former velocity, so giving a faster jet of gas and a tendency to a longer flame. (2) The increased burning velocity with preheating alters the angle of the inner cone. The unheated gas gives a long inner cone and, as the gases pass through the flame front, they expand from around 300°K to the final flame temperature and receive an outward acceleration due to this expansion to six or seven times the previous volume. With preheating, the expansion across the flame front has a greater upward and a smaller outward component, because of the changed cone angle. Also, since the gases have been preheated, to perhaps 800°K, the expansion across the flame front is only by a factor of perhaps 2½ instead of 6 or 7. Thus, the outward flow of gas, which leads to a wide flame, is reduced, while the greater upward velocity gives a longer flame. These effects are illustrated in Figure 3.

It will be noticed that the curves in Figure 1 both show a small but sharp peak in radiation near the tip of the inner cone. The visible and near ultraviolet emission from C_2, CH and OH is, of course, much greater in the inner cone region than elsewhere and may account for this small peak in total radiation. Alternatively, there may really be a slightly greater amount of infrared radiation from the region in or near the flame front. It is, however, quite clear that these results show that the changes in radiation observed by von Helmholtz[1] and by Haslam, Lovell and Hunneman[2] are due mainly to changes in flame shape and do not indicate that there is any major chemical or disequilibrium contribution to the infrared emission.

Certain other observations have also suggested that flame radiation was not entirely thermal in origin. Thus, the well-known influence of moisture, or added hydrogen, in decreasing the infrared radiation from carbon monoxide flames is accompanied by a change in flame speed and thus presumably also of flame shape and dimensions. Changes in flame radiation can only be used in discussion of fundamental processes if full allowance for alterations in flame shape and temperature distribution, also of secondary effects like self-absorption of the radiation, can be made. The effect of preheating on flame radiation does not show that the infrared radiation is other than thermal.

The interpretation of Guyomard's results for diffusion flames[6] may differ from that for premixed flames. He made a careful study of flames under both laminar and turbulent flow conditions. In diffusion flames there are gradients of both temperature and composition across the flame front. It is likely that preheating will vary the relative positions of these, and probable that, with preheating, the pyrolysis to form solid carbon may occur in a region of similar temperature but lower oxygen concentration. The carbon particles will then not be heated so rapidly by oxidation, and so may be at lower temperature and radiate less.

REFERENCES

1. von Helmholtz, R.: *Die Licht und Warmstrahlung verbrennende Gase.* Berlin, 1890.
2. Haslam, R. T., Lovell, W. C., and Hunneman, R. D.: Ind. Eng. Chem., *17*, 272 (1925).
3. Garner, W. E., and Johnson, C. H.: Phil. Mag., *3*, 97 (1927).
4. Gaydon, A. G.: *Spectroscopy and Combustion Theory.* London, Chapman and Hall, 1948.
5. Hartley, H.: Inst. Gas Eng. Trans., p. 466 (1932–3).
6. Guyomard, F.: Compt. rend.: *233*, 237 (1951).

37

EFFECT OF INITIAL MIXTURE TEMPERATURE ON THE BURNING VELOCITY OF BENZENE-AIR, *n*-HEPTANE-AIR, AND ISOOCTANE-AIR MIXTURES

By SHELDON HEIMEL AND ROBERT C. WEAST

Introduction

Theories of flame propagation introduce temperature-dependent properties of the combustible mixture such as thermal conductivity and reaction rate. Consideration of the effect of initial temperature on such properties for a given combustible should make it possible to determine how well theoretical and experimental burning velocities agree as this parameter is varied.

Dugger[1] has shown that, for the gaseous fuels, propane, ethylene, and methane, maximum burning velocities predicted by both a thermal and a diffusion theory agreed with experiment to within 20 per cent in the temperature range of about 200° to 615°K. The same order of agreement was obtained by Dugger and Graab[2] for 2,2,4-trimethylpentane (hereinafter called *iso*octane) in oxygen-nitrogen mixtures at 311° and 422°K, with oxygen-nitrogen mole ratio ranging approximately from 0.205 to 1.000. The present investigation reports burning velocities for the liquid fuels, benzene, *n*-heptane, and *iso*octane, as a function of composition at initial temperatures ranging from 300° to 700°K. A comparison was made between the experimental data for each fuel and the relative effects of temperature on burning velocities predicted by the thermal and diffusion theories. Activation energies fitted to the initial temperature data were used rather than values from slow oxidation used previously.[1]

Experimental Procedure

The liquid fuel was vaporized in a turbulent air stream and the mixture passed through a heated burner tube. The fuel-air mixture was burned in an open flame, which was photographed using schlieren optics.

TABLE 1. FUEL PROPERTIES

Fuel	Molecular Weight	Density, g/cm³ at 20°C	Boiling Point,	Stoichiometric F/A,	Minimum purity	Source
			°F	vol %	mole %	
C_6H_6	78.1	0.879	176.2	2.791	98.9	Barrett
n-C_7H_{16}	100.2	.684	209.2	1.903	99.6	Phillips
i-C_8H_{18}	114.2	.692	210.6	1.674	99.5	Phillips

FUELS AND AIR

Some data relative to the fuels are listed in Table 1. Fuel-air ratio by volume was calculated on the basis of air consisting of 3.76 volumes N_2 to 1.00 volume O_2.

For this investigation, laboratory service air containing approximately 0.3 volume per cent water was used.

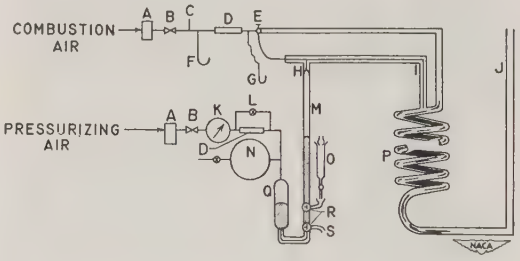

FIG. 1. Experimental apparatus.

A Air filter
B Nullmatic pressure regulator
C Thermocouple
D Critical-flow orifice
E Combustion-air valve
F Upstream manometer
G Downstream manometer
H Glass capillary tee
I Vertical extension of capillary
J Burner tube
K Gauge, 0–100 lb/sq in.
L By-pass valve
M Precision-bore tube
N Plenum chamber
O Fuel storage bulb
P Helical vaporizing coil
Q Mercury reservoir
R Three-way stopcock
S Drain

METERING SYSTEM

The liquid-fuel feed system was of the Calcote type.[3] Liquid fuel was driven up through a precision-bore tube *M* (Fig. 1) by air pressure from the plenum chamber, *N*. The rate of pressure rise in the plenum was held constant by a critical flow orifice, *D*.[4] Thus, the liquid fuel from the tube, *M*, was forced into the side arm of a glass capillary tee, *H*.

The metered combustion air was divided by the valve, *E*, so that part flowed into the capillary (*H* and *I*) and the remainder went directly into the helical copper coil, *P*. The first part broke

up the stream of liquid fuel into droplets. The second part vaporized the droplets in the coil and formed the vapor-air mixture.[5] The resulting vapor-air mixture then flowed into the heated burner, *J* (see below).

The fuel feed tube was a 80-cm length of precision-bore glass tubing, with an inside diameter of 6.602 mm. The tube was calibrated with each fuel by timing the rise of the mercury-fuel interface at various pressures upstream of a given orifice at a known upstream temperature. Fuel vapor flow at downstream temperature and pressure was calculated from the straight-line relation between upstream pressure and linear feed rate.

BURNER TUBE AND TEMPERATURE CONTROL

The heated burner tube detailed in Figure 2 received the mixture from the vaporizing coil after the mixture passed through a connecting length of tubing which contained a flashback arrester, *F*. The burner was a stainless steel tube of 0.998 cm i.d. The upright portion of the tube above the the thermocouple, *C*, was about 100 diam. long, insuring laminar flow. The burner tube was wrapped with four individually controlled lengths of asbestos-covered heating wire, *G*, to permit regulation of the tube-wall temperature.

Temperatures were measured at the following positions: A: gas temperature at the port by an aspirating thermocouple[6] positioned as shown between runs; B: lip temperature; C: gas temperature about half-way up the vertical tube; D: wall temperature; E: gas temperature.

In addition, a bare wire thermocouple was used to monitor gas temperatures between the port and thermocouple, *C*, between runs. All thermocouples were iron-constantan, except *C* which was chromel-alumel to withstand the thermal effect of flashback. Gas temperatures from A to C were maintained within 15°F of one another.

Burning velocity was determined from schlieren photographs of the flame by a total area method.[2] Measurements were based on the outside edge of the image.

Results and Discussion

BURNING VELOCITIES

In Figure 3, burning velocity for each fuel is plotted against two composition variables: (1) equivalence ratio, Φ, and (2) mass air-fuel ratio, *A/F*. The over-all range of initial mixture temperatures was 298° to 707°K. The mass flow did not vary greatly. Thus, only very few critical-flow orifices were required. As a result, the stream-flow Reynolds number was limited between 380 and 1300.

It is believed that no preflame reaction occurred during the short periods (<1 sec) necessary to preheat benzene-air, *n*-heptane-air and *iso*octane-air to their respective maximum temperatures of 700°, 579°, and 707°K. This conclusion is supported by the fact that only the usual amount of data scatter was actually observed up to and including the higher temperatures used. This can be interpreted on the basis of the large scatter and eventual decrease in burning velocity obtained with propane-air flames when preflame reaction did occur.[7] Since the preflame reactions

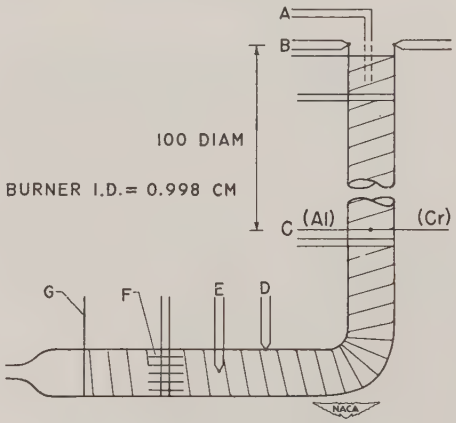

FIG. 2. Burner assembly.

Thermocouples (A–E)
A Aspirating
B Lip
C Bare Chromel-Alumel
D Wall
E Gas
F Flashback arrester
G Heating wire (4 sections)

which affect the burning velocity are very sensitive to temperature variations, it seems reasonable to relate the absence of large data scatter for the liquid fuels with the absence of preflame reaction.

Norrish and Taylor[8] have carried out complete analyses of the products of oxidation of benzene in a flow system at atmospheric pressure. They observed no evidence of low-temperature oxidation in the temperature range 473° to 873°K, which is well above the range of the present investigation.

The curves for benzene-air (Fig. 3a) show a maximum burning velocity at an average Φ = 1.046. The corresponding Φ's for *n*-heptane-air and *iso*octane-air are 1.060 and 1.033, respectively (Figs. 3b and c). The burning velocity

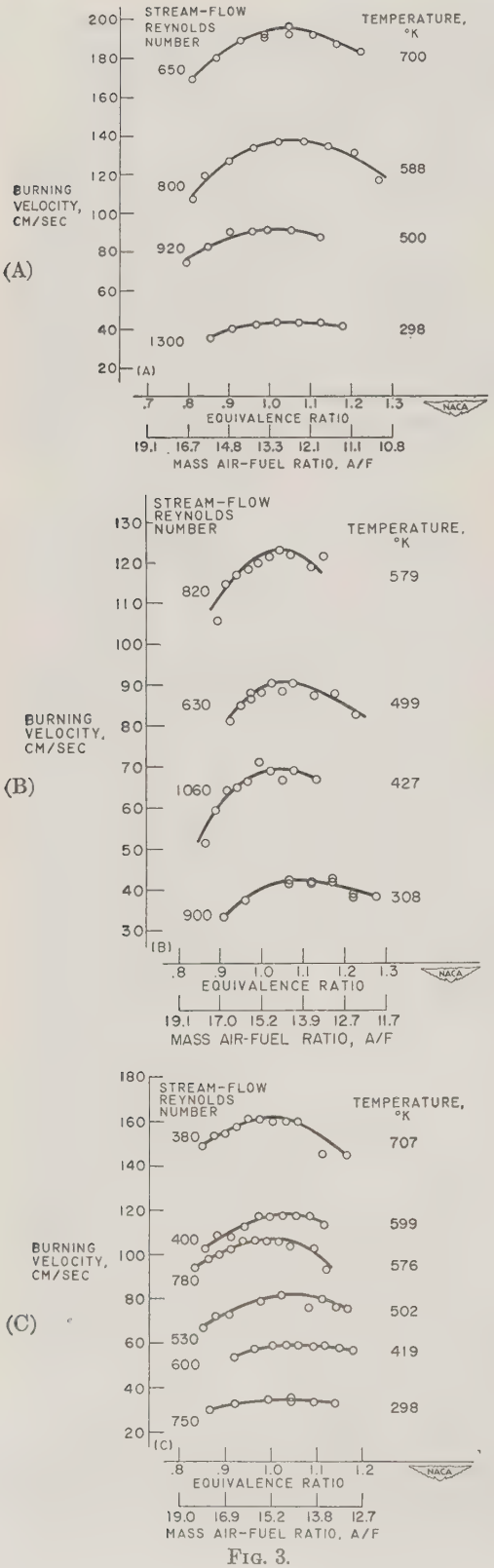

FIG. 3.

maxima from Figure 3, as well as maxima from replicate runs, are plotted against initial mixture temperature in Figure 4 to illustrate the reproducibility of the maxima.

An empirical equation of the form

$$u = b + cT_0^n \tag{3}$$

was fitted to the data by plotting $\log_{10}(u - b)$ against $\log_{10} T_0$. For each fuel, b, c, and n are constants. The constant, b, was determined by trial and error. Least-square treatment of c and n

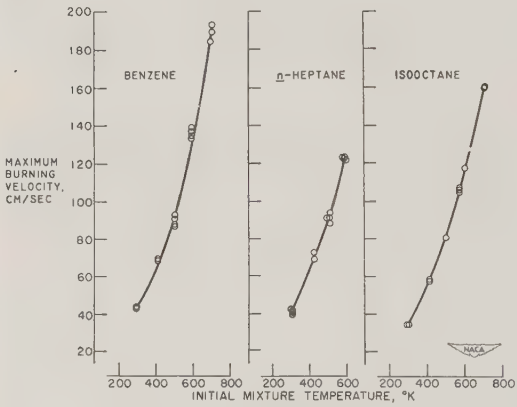

FIG. 4. Effect of initial temperature on maximum burning velocity.

gave the following equations: for benzene at $T_0 =$ 298° to 700°K,

$$u = 30.0 + 7.910 \times 10^{-7} T_0^{2.92} \tag{4}$$

for n-heptane at $T_0 = 308°$ to 579°K,

$$u = 19.8 + 2.493 \times 10^{-5} T_0^{2.39} \tag{5}$$

and for *iso*octane at $T_0 = 298°$ to 707°K,

$$u = 12.1 + 8.362 \times 10^{-5} T_0^{2.19} \tag{6}$$

Equation (6) may be compared with the analogous equation from Dugger and Graab:[2]

$$u = 0.01193 T_0^{1.40} \tag{7}$$

For example, at $T_0 = 700$°K, Equation (6) gives 154.4 cm/sec, Equation (7) gives 114.7 cm/sec, and the experimental burning velocity is 158.4 cm/sec. Consequently, Equation (6) is applicable over a much wider temperature range than Equation (7).

The least-square burning velocity maxima are given in Table 2. The data of Table 2 may be

FIG. 3. Burning velocity as function of equivalence ratio and mass air-fuel ratio at various initial mixture temperatures.
(A) Benzene-air flames; (B) n-Heptane-air flames; (C) *Iso*octane-air flames.

used to show the variation of burning velocity with equilibrium flame temperature. (See below for calculation of flame temperature.) In contrast with initial temperature, a small increase in flame temperature is accompanied by a large increase in burning velocity.

This is reasonable since the per cent of fuel by volume does not exceed three per cent at maximum burning velocity.

Since the mixtures being considered are substantially stoichiometric, the following form of Semenov's bimolecular equation[9] was used:

Table 2. Predicted Relative Burning Velocities of Benzene, *n*-Heptane, and Isooctane

Fuel	Equivalence Ratio*	Activation Energy, kcal/mole		Initial Temperature, °K	Flame Temperature, °K†	Equilibrium Radical Pressure (1 atmos total pressure), atmos. × 10^5‡				Maximum Burning Velocity, cm/sec			
										Predicted, relative to 298°K		Experimental	Experimental least-squares
		Semenov bimolecular	Tanford-Pease			P_H	P_{OH}	P_O	$\Sigma P_i D_{i,r}$	Semenov bimolecular	Tanford-Pease		
Benzene	1.046	43	23.5	298	2355	68.2	284	57.2	784	43.6	43.6	43.6	43.6
	(2.92			418	2403	99.6	358	86.5	1065	74.5	76.1	68.7	66.6
	vol.			500	2438	112.6	411	107.8	1250	102.0	103.1	91.0	91.8
	per			588	2471	137.8	470	136.3	1503	137.4	138.5	137.5	129.2
	cent)			700	2517	177.7	563	185.7	1904	194.0	194.0	194.0	195.1
n-Heptane	1.060	34	11.6	298	2287	65.8	239	25.4	692	40.4	40.4	40.4§	41.9
	(2.02			308	2292	66.2	247	27.1	705	42.5	42.3	43.0	43.0
	vol.			427	2346	97.8	335	55.2	1026	71.4	73.0	69.4	72.5
	per			499	2380	115.6	389	58.4	1198	93.9	94.0	90.8	96.6
	cent)			579	2415	143.3	460	78.4	1470	123.2	123.2	123.2	129.5
*Iso*octane	1.033	39	16.4	298	2281	55.1	260	31.1	649	35.0	35.0	35.0	35.0
	(1.73			419	2337	79.0	333	49.0	900	59.3	59.5	59.6	61.2
	vol.			502	2375	98.2	396	65.0	1110	82.0	81.8	81.8	84.8
	per			576	2408	121.0	462	84.0	1340	106.7	106.1	107.0	110.0
	cent)			599	2418	130.0	485	89.9	1420	115.0	114.8	118.2	118.7
				707	2464	173.0	607	126.0	1860	161.2	161.2	161.2	164.9

* Fraction of stoichiometric fuel-air ratio at which maximum burning velocity occurred.
† Theoretical adiabatic flame temperature computed by method of Huff, Gordon and Morrell.[13]
‡ Computed by method of Huff, Gordon and Morrell.[13]
§ Obtained from Figure 4 by extrapolation.

Estimation of Activation Energy from Effect of Initial Temperature on Maximum Burning Velocity

To estimate the over-all or global activation energy of the flame reaction, the thermal bimolecular equation of Semenov[9] and the active-particle diffusion equation of Tanford[10] and Tanford and Pease[11] have been reduced to functions of temperature. In the final forms of the Semenov and Tanford-Pease equations, the temperature-independent properties of the mixture have been eliminated, and the temperature-dependent properties have been made proportional to powers of T corresponding to the same properties for air.[1]

$$u^2 = \frac{2\lambda_f K a_0 c_{p,f}^2}{\rho_0 \bar{c}_p^3}\left(\frac{T_0}{T_f}\right)^2\left(\frac{\lambda}{c_p \rho D}\right)_f^2\left(\frac{n_1}{n_2}\right)^2 \cdot\left(\frac{RT_f^2}{E}\right)^3 \frac{\exp\,(-E/RT_f)}{(T_f - T_0)^3} \tag{8}$$

Dugger[1] has shown that this equation can be closely approximated by

$$u^2 \propto T_0^2 T_f^5 \frac{\exp\,(-E/RT_f)}{(T_f - T_0)^3} \tag{9}$$

The reduced form of the Tanford-Pease equation[1] was modified to include the variation of k_i with temperature.[2] $D_H : D_O : D_{OH} = 6.5 : 1 : 1$ from Linnett and Hoare.[12]

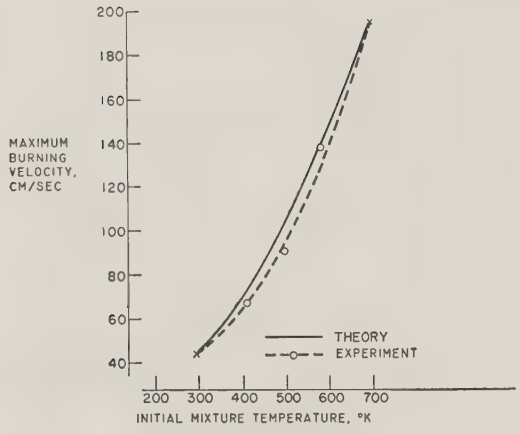

(A)

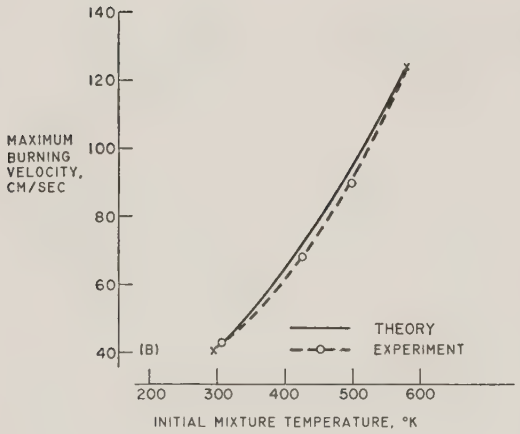

(B)

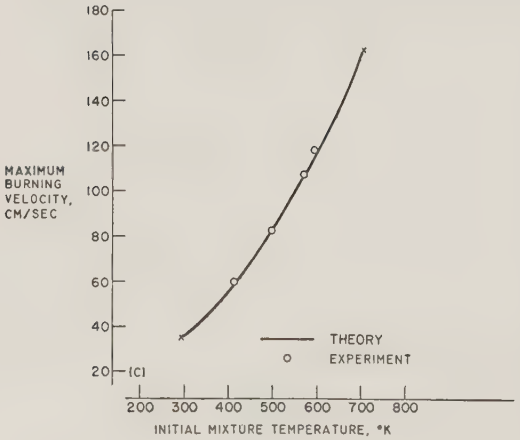

(C)

FIG. 5. Effect of initial mixture temperature on maximum burning velocity. Comparison of predicted curves (based on 298°K) with experiment. (A) Benzene; (B) *n*-Heptane; (C) *Iso*octane.

Each reduced equation was solved for that activation energy which would equate the predicted and experimental burning velocities at the extreme values of initial temperature. This procedure minimized the influence of small changes in burning velocity on the calculated activation energy. At the maximum burning velocity, flame temperature and active-particle concentrations were calculated by a matrix method[13] with heats of formation published by the Bureau of Standards.[14] The largest uncertainty in the calculation of the relative active particle concentrations is the two per cent uncertainty in the original choice of the concentration of hydrocarbon in air for maximum burning velocity.[15] For example, a 1.8 per cent decrease in heptane concentration from 2.26 per cent produces a 3.8 per cent increase in relative particle concentration.

Table 2 shows that the activation energies calculated from the Tanford-Pease equation are about half of those calculated from the Semenov equation.

COMPARISON OF EXPERIMENTAL DATA WITH RELATIVE VALUES PREDICTED BY THEORETICAL EQUATIONS

In order to validate the activation energies, predicted burning velocities, normalized with respect to the experimental burning velocities at the extreme initial temperatures, were calculated from the two theoretical equations using the calculated values of E.

Figure 5 illustrates comparisons of the relative effect of initial mixture temperature on maximum burning velocities as predicted by the reduced equations for benzene, *n*-heptane, and *iso*octane. The values used in plotting both the experimental dashed curve and the predicted points are presented in Table 2. The extremities of each expermental curve are marked X to indicate that the method of calculation forces the predicted burning velocities to coincide with the experimental data at these initial temperatures.

Figure 5 and Table 2 show that the burning velocities predicted by both the thermal theory equation and the diffusion theory equation did not deviate by more than 5.1 per cent from those obtained experimentally, for benzene, *n*-heptane, and *iso*octane in the temperature ranges studied. In the entire range of temperatures, the values predicted by the two theories are essentially the same.

The goodness of fit of the theoretical burning

velocities, in order of increasing goodness, is benzene; *n*-heptane; *iso*octane. The predicted burning velocities for benzene and *n*-heptane are higher than the experimental values whereas the predicted burning velocities for *iso*octane are slightly lower than the experimental values.

Concluding Remarks

Dugger[1] obtained linear correlations between maximum burning velocity and either ($6.5\ P_H + P_{OH} + P_O$) or P_H alone for gaseous mixtures of constant composition but varying initial temperature. In the current investigation such correlations were found only for *iso*octane. *Iso*octane also showed linear correlations between maximum burning velocity and P_O as well as P_{OH}.

Longwell and Weiss[16] were able to correlate blow-off limits in a stirred reactor burning *iso*octane in air. A good correlation was obtained with an E of 40 kcal/mole and a bimolecular mechanism, using the same rate constant for both the lean and rich data. (A somewhat better fit of the rich blow-off limits was obtained with an E of 42 kcal/mole and a 1.8 reaction order.) The E of 40 kcal/mole compares well with the E of 39 kcal/mole obtained in the Semenov theory correlation.

Except for the aforementioned agreement in activation energy, the assumptions made in reducing both the Semenov and Tanford-Pease equations, and the absence of independently measured flame temperatures, radical concentrations and activation energies make it impossible to decide the relative merits of the two theories.

Summary of Results

An investigation of the effect of initial mixture temperature on the laminar burning velocities of benzene-air, *n*-heptane-air, and *iso*octane-air mixtures gave the following results:

(1) Empirical equations for maximum burning velocity u (cm/sec; based on the outer edge of the schlieren image of the flame cone) for use in the temperature ranges indicated were: for benzene, at an initial mixture temperature T_0 of 298° to 700°K,

$$u = 30.0 + 7.910 \times 10^{-7} T_0^{2.92}$$

for *n*-heptane, for $T_0 = 308°$ to 579°K,

$$u = 19.8 + 2.493 \times 10^{-5} T_0^{2.39}$$

and for *iso*octane for $T_0 = 298°$ to 707°K,

$$u = 12.1 + 8.362 \times 10^{-5} T_0^{2.19}$$

(2) Relative burning velocities predicted by both the thermal bimolecular equation presented by Semenov and the diffusional equation of Tanford and Pease did not deviate by more than 5.1 per cent from the experimental burning velocities for the temperatures and fuels studied. *Iso*octane gave the best, and benzene the poorest agreement. The values predicted by the two theories were essentially the same.

(3) When maximum burning velocity was plotted against effective concentration of active species, a straight-line correlation was found for *iso*octane. Benzene and *n*-heptane gave linear correlations only over a limited range of burning velocities and effective radical concentrations.

Nomenclature

A/F	mass air-fuel ratio
a	number of molecules of combustible per unit volume
b, c	constants in empirical equation for a given fuel
c_p	specific heat at constant pressure, cal/(g)(°K)
$\bar{c}_p$	mean specific heat at constant pressure, T_0 to T_f, cal/(g)(°K)
d	diameter of burner tube, cm
D	diffusion coefficient, cm²/sec
$D_{i,r}$	relative diffusion coefficient of i^{th} radical with respect to other radicals, cm²/sec
E	activation energy, kcal/g-mole
exp	base of Napierian logarithmic system raised to power in parentheses following exp
i.d.	inner diameter of burner tube, cm
K	frequency factor from specific rate equation, cm³/(two molecules)(sec)
k_i	specific rate constant for reaction between i^{th} radical and combustible material, cm³/(two molecules)(sec)
n	constant exponent in empirical equation for given fuel
n_1/n_2	moles of reactants per mole of products from stoichiometric equation
P_i	equilibrium mole fraction or partial pressure of i^{th} species at the flame front
$P_iD_{i,r}$	effective relative mole fraction or partial pressure of i^{th} species at the flame front
R	universal gas constant, kcal/(g-mole)(°K)
Re	stream-flow Reynolds number, $d\bar{u}\rho/\mu$, dimensionless
T	absolute temperature, °K
T_f	adiabatic flame temperature, °K
u	maximum burning velocity, varying Φ at constant T_0, cm/sec
$\bar{u}$	average stream velocity, $4V/\pi d^2$, cm/sec

V volumetric stream velocity, cm^3/sec
λ thermal conductivity, cal/cm(sec)(°K)
μ absolute viscosity of mixture, poise, g/(cm)(sec)
ρ density of mixture, g/cm^3
Φ equivalence ratio, fraction of stoichiometric fuel-oxygen ratio

SUBSCRIPTS

0 property of reactants at initial conditions
f property of products at flame temperature

REFERENCES

1. Dugger, G. L.: NACA Report 1061, 1952.
2. Dugger, G. L., and Graab, D. D.: *Fourth Symposium (International) on Combustion*, pp. 302–310. Baltimore, The Williams & Wilkins Co., 1953.
3. Calcote, H. F.: Anal. Chem., *22*, 1058–1060 (1950).
4. Anderson, J. W., and Friedman, R.: Rev. Sci. Instruments, *20*, 61–66 (1949).
5. Clark, T. P.: Ind. Eng. Chem., *45*, 2786 (1953).
6. Whitesel, H. A.: In *Temperature. Its Measurement and Control in Science and Industry*, p. 851. New York, Reinhold Publ. Corp., 1941.
7. Dugger, G. L., Weast, R. C., and Heimel, S.: *Fifth Symposium (International) on Combustion*, p. 593. New York, Reinhold Publ. Corp., 1955.
8. Norrish, R. G. W., and Taylor, G. W.: Proc. Roy. Soc., *A234*, 160–177 (1956).
9. Semenov, N. N.: NACA TM 1026, 1942.
10. Tanford, C., and Pease, R. N.: J. Chem. Phys., *15*, 861–865 (1947).
11. Tanford, C.: *Third Symposium on Combustion, Flame and Explosion Phenomena*, pp. 140–146. Baltimore, The Williams & Wilkins Co., 1949.
12. Linnett, J. W., and Hoare, M. F.: *Third Symposium on Combustion, Flame and Explosion Phenomena*, pp. 195–203. Baltimore, The Williams & Wilkins Co., 1949.
13. Huff, V. N., Gordon, S., and Morrell, V. E.: NACA Report 1037, 1951.
14. Rossini, F. D., *et al.*: Circular C461, Nat. Bureau Standards, 1947.
15. Simon, D. M.: J. Am. Chem. Soc., *73*, 422–425 (1951).
16. Longwell, J. P., and Weiss, M. A.: Ind. Eng. Chem., *47*, 1634 (1955).

Structure and Propagation of Turbulent Flames

38

TURBULENT BURNING VELOCITIES OF NATURAL GAS-AIR FLAMES WITH PIPE-FLOW TURBULENCE[a]

By J. KENNETH RICHMOND, JOSEPH M. SINGER, E. B. COOK, JAMES R. OXENDINE,[b] JOSEPH GRUMER AND DAVID S. BURGESS

Introduction

The evaluation of existing theories of turbulent burning requires precise techniques for measuring local turbulent burning velocities throughout the flame brush. With such techniques, proposed equations describing turbulent combustion can be tested, and the existence and nature of flame-generated turbulence can be examined. Considerable data already are available for the burning velocity averaged over the whole flame, and a good deal is known about turbulence in the approach flow; but information is needed on the trends of burning velocity and the degree of turbulence within the flame brush. The present paper proposes some solutions to these latter problems.

Measurements and Related Calculations

Four sets of experiments were performed on a 1¼-in. i.d., 9-ft-long burner tube at Re = 10,000, 25,000, 50,000 and 100,000, respectively. In each instance a flame of a stoichiometric mixture of Pittsburgh natural gas-air was stabilized on top of the tube by an annular flame of hydrogen-air. A concentric flow of secondary air was provided; the mean flow matched that of the burner, except at Re = 100,000, where it was half-matched. The experimental setup was identical with that used by Karlovitz, Denniston and Wells.[1] Fully developed pipe-flow turbulence was assumed. The burning velocity was defined, by analogy with that of a laminar Bunsen flame, in terms of the mean flame position and the direction of the approach flow.

PHOTOMETER

Turbulent combustion does not occur in a narrow zone but is spread out over a region known as the flame "brush," the boundaries of which are not sharply defined. For purposes of burning-velocity calculations, the position of the flame is defined by its mean position within the brush, taken as the locus of maximum luminosity at about 4315Å. To make rapid measurements of relative flame luminosity across the turbulent brush, an instrument called the "flame-radiation photometer" was developed, which consists of a focusing lens and a 1P21 photomultiplier tube that views the flame image through an aperture 0.013 in. in diam. The photomultiplier tube is supplied with an appropriate battery power supply, signal attenuator, and a galvanometer with a sensitivity of 0.0001 μa/mm. The flame image is scanned horizontally and vertically. The circuit is relatively stable, its time constant of 13 sec being much larger than that of the turbulent fluctuations in the flame. Therefore all measurements are time-average. Within the range of light levels involved, the current output of the photomultiplier tube is proportional to the light intensity. To evaluate accurately the luminosity from the flame, the light from one emitter species was considered. For this purpose, the light from the flame was passed through a narrow band-pass filter with the pass-band centered at 4315Å and a half-width of about 70Å. This corresponds to an intense spectral band due to the CH radical in the flame.

[a]This research was supported by the U. S. Air Force through the Air Force Office of Scientific Research of the Air Research and Development Command.

[b] Present address: Aerial Reconnaissance Laboratory, Wright-Patterson Air Force Base, Ohio.

The photometer was calibrated spatially by viewing an illuminated calibration screen inserted firmly in the burner tube in place of the flame. This screen consisted of a lucite strip on which a grid had been ruled accurately. In this way distances from the center-line of flow and from the burner rim could be accurately determined.

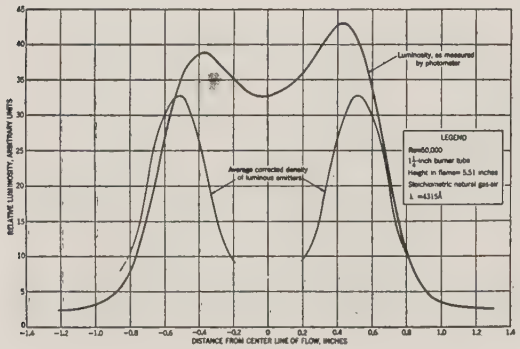
RELATIVE LUMINOSITY, ARBITRARY UNITS
DISTANCE FROM CENTER LINE OF FLOW, INCHES
Luminosity, as measured by photometer
Average corrected density of luminous emitters
LEGEND

FIG. 1. Apparent distribution of luminous emitters, with corresponding distribution corrected for cylindrical curvature.

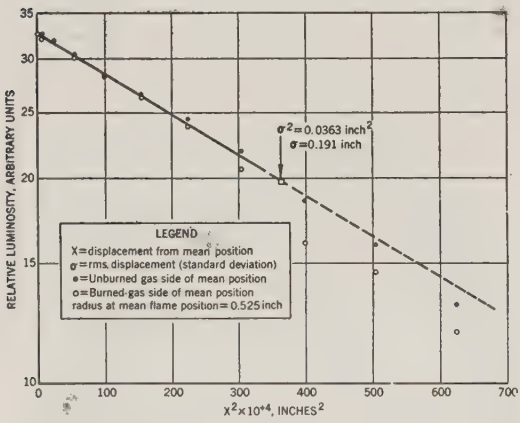

FIG. 2. Corrected density of luminous emitters as a function of displacement from mean position. Same conditions as in Fig. 1.

The apparent mean position of the flame, which is the locus of maximum luminosity as observed by the photometer, compared favorably with results obtained by densitometric analysis of long-exposure flame photographs.

As the burner tube is cylindrical, the apparent distribution of luminosity across the flame, observed at a distance, does not correspond to the actual radial distribution, because light is emitted not only from the front and back of the flame but also from the sides. Corrections for flame curvature were applied to the experimental turbulent flames, following the procedure described by Hübner and Klaükens[2] and Clark.[3] As the corrections must be applied stepwise, a large number of simultaneous equations were needed to obtain good resolution, the radial interval chosen being 0.025 in. A large, triangular matrix was set up and solved. For the very thick flames calculations were performed on a UNIVAC 60 computer. The result of these calculations is the corrected radial distribution of luminosity across the flame brush. Figure 1 shows the raw data as given by the photometer in a typical case, plus the corrected curve, averaged for both sides of the flame.

The corrected flame-luminosity distribution yields (a) the position of maximum luminosity, taken as the flame position for burning-velocity computations; and (b) a measure of flame-brush thickness, to be correlated with considerations of turbulent diffusion within the flame brush. Figure 2 shows the same corrected luminosity distribution plotted as the logarithm of relative luminosity versus the square of the displacement from the mean position. The normal probability function, $y = ke^{-x^2}$, represents the data very well, with points on both sides of the mean position fitting the distribution for about 85 per cent of the area under the curve. The standard deviation of this curve, or the rms displacement from the mean position, is a useful measure of the thickness of the flame brush.

PITOT TUBE

The magnitude and direction of approach flow gas through the mean position is determined by Pitot- and static-tube traversals of the approach flow gas. Results were checked against flow-meter readings by integrating the velocities over the burner mouth. Because of the pilot flame, relatively large values of static pressure were found, especially with small burner-gas flows. In the presence of main flame, pilot flame, and surrounding air flow, the pattern of divergence did not vary systematically with variation in Reynolds number.

As the burning velocity is defined in terms of the unburned gas, velocities in the unburned gas were extrapolated through the flame brush to the mean flame position, as is done with laminar flames. An example of such extrapolation is shown in Figure 3, where the approach flow velocity at a given height is plotted as a function of the radius squared. At the burner mouth the

experimental velocity profile fits the Nikuradse distribution very well, but higher in the flame the distribution rapidly flattens out, due primarily to drag of the surrounding air flow. In some instances, the data are better represented by an exponential distribution or by a quadratic parabola. The infinite series corresponding to these three functions are identical for the first two terms, and subsequent terms are significant only for large values of radius. Choice of a function does not affect appreciably the final values of burning velocity. For each of the four flames studied the extrapolated velocity of approach flow along the mean flame locus was substantially constant; i.e., the flame assumed a position close to a constant velocity contour.

The radial distribution of velocities in the unburned gas and extrapolated into the flame, at each level above the burner mouth, were integrated analytically over the cross-sectional area to give radial distributions of mass flow. The direction of approach flow in the flame was found by plotting the lines of constant included mass flow. Figure 4 shows a chart of selected lines of constant included mass flow and the mean flame position.

ELECTRONIC PROBE

Another parameter of interest in turbulent combustion, especially in developing theories of burning velocity, is the intensity of turbulence in the approach flow and in the flame itself. Unless otherwise indicated, the term "turbulence" (or "turbulent intensity") as used here refers to the rms value of the fluctuation velocity in cm/sec. The radial component of approach flow turbulence, v', and the axial component, u', are based on experiments carried out at Langley Field[4] with hot-wire anemometers on a burner-tube arrangment of similar design to that at the Bureau of Mines.

The electronic probe[5] has been used to measure turbulence in the flame itself.[6] It is assumed that the ionization peak associated with a flame front may serve as a tracer for turbulent fluctuations of the gas with which the flame is associated. This assumption does not depend necessarily on any particular flame brush structure, but the process may be illustrated by the wrinkled combustion-wave model, each wrinkle being considered to originate at the burner rim, with all radial displacements from the flame's mean position being taken as zero. The wrinkle is carried downstream at a nearly constant velocity, U_F; at any height in the flame its age or diffusion time, t, is defined as H/U_F. Meanwhile the displacement from mean flame position of any

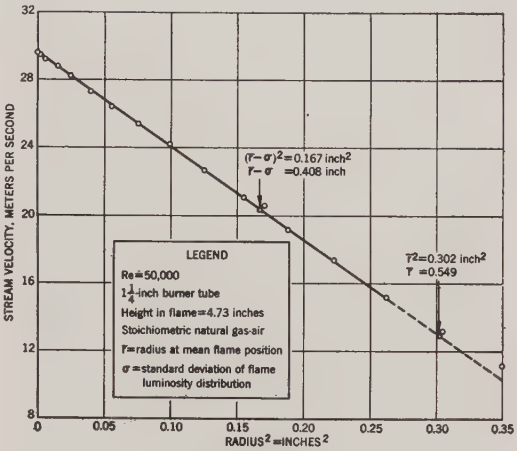

FIG. 3. Burner flow velocity distribution extrapolated to mean flame position.

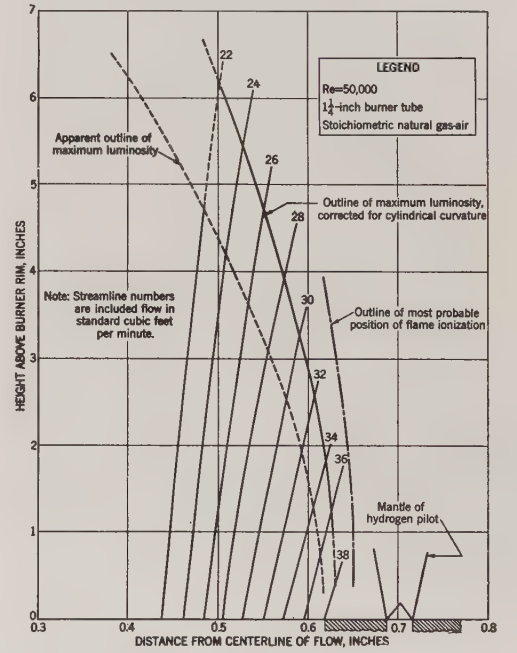

FIG. 4. Flame contours, corrected and uncorrected for cylindrical curvature, with lines of constant included mass flow.

point on the wrinkle is determined by the radial fluctuation velocity, v, of the approach gas with which this particular element of flame is associated. For short downstream distances, the rms displacement of all points on all wrinkles, σ, is equal to $v't$ or $v'H/U_F$.

The bare probe wire is mounted at a given height in the flame brush, where it meets a succession of flame wrinkles. Probe data determine the relative frequencies with which the wire encounters displacements of various magnitudes. A plot of probe-meter readings versus horizontal displacement of the probe-wire tip fits that of the probability integral.[5] An example is shown at the left of Figure 5, with the corresponding probability curve obtained by differentiation. The standard deviation of this probability curve is known to be the rms displacement of all ionization peaks from their mean position at this particular height; it is taken as equal to the rms displacement of all points on the wrinkled flame front from the front's mean position. Thus the rms level of turbulence at the flame front is associated with rms rate at which the flame brush thickens with (downstream) diffusion time.

The right side of Figure 5 is a plot of σ vs. height in the flame, evaluated both by the electronic probe and by the photometer. Also shown are corresponding values of σ of the approach flow turbulence, as calculated from the hot-wire anemometer measurements of v' in cold gas flow, $\sigma = v'H/U_F$. Conversely, the ratio of σ/H of the probe may be used to compute v' in the flame itself by multiplying by U_F,

$$v' = \sigma/t = (\sigma/H)U_F$$

For flames of $Re = 50{,}000$ and 100,000, the values of v' in the flame computed in this manner agree very well with the values of approach flow turbulence. Furthermore, as the plot of σ vs. H is linear, v' is constant with height in each flame, within the region studied. This result does not admit the possibility of appreciable flame-generated turbulence. At present, it appears that the rate of flame-brush thickening, as indicated by the photometer, is determined also by factors other than the turbulent intensity in the flame brush.

Burning-Velocity Computations

Two general methods for computing total turbulent burning velocity are the angle method and the area method. Both depend on a knowledge of magnitude and direction of flow velocities.

Derived by analogy from similar techniques with laminar Bunsen flames, the angle method was first used for turbulent flames by Karlovitz, Denniston and Wells.[1] With this method, the burning velocity can be computed point-by-point in the flame. The total turbulent burning velocity is $S_T = U_F \sin \alpha$, where α is the angle formed by the approach flow of unburned gas with the tangent to the mean flame position at the same point. Figure 6 shows the details of such a pointwise computation of burning velocity. For convenience, the angle, α, is divided into two parts to show both the rate of change of the slope of flame position and that of flow divergence as the observer moves downstream. In all cases, the angle of divergence is of the same order of magnitude as that of the flame and should not be neglected. As the values of U_F are fairly constant in each flame, the change of burning velocity depends essentially on the change of α with height. The angles may be measured graphically or computed analytically from the empirical functions describing flow divergence and mean flame position.

With the area or frustum method the burning velocity is determined directly from a divergence chart (Fig. 3) and equals the included flow in a flow tube passing through the mean flame position divided by the lateral surface area, considered to be a frustum. The total area method gives results that might be misleading, even though on the average it may agree with the angle method, over a limited region. The apparent average burning velocity of the upper portion of a flame (above the inner apex of the inner cone) through which about $\frac{1}{2}$ to $\frac{2}{3}$ of the flow passes, is usually about twice that of the frustums chosen for measurement. Above the apex of the inner cone there is no assurance that the burning velocity is measured relative to the initial cold gas. At the base of the flame, for about 1 in. above the burner rim, the apparent burning velocity is quite low, since there is a considerable surface of flame with very little main flow passing through (as shown by Pitot tube). Burning velocity measurements in this region are meaningless because the mean flame position is not determined exclusively by the main flow.

Discussion of Results

Figures 7a, 7b, 7c and 7d compare burning velocity data obtained by the various experimental methods and with the theoretical equation, $S_T = S_L + v'$, at $Re = 10{,}000$, 25,000, 50,000 and 100,000. For the latter two flows, the angle and frustum methods give consistent results; and the burning velocity is constant with

height, a fact that is consistent with constant flame turbulence. At the lower flows the agreement between methods is poor, due in part to large divergence of flow, small magnitude of Pitot tube pressures, proportionately larger static pressures, heating of Pitot tube by radiation from flame, etc. Moreover, with the smaller flows, the burning velocity increases slightly with height, although the somewhat tentative probe measurements possible under these conditions do not show any change in turbulence with height.

The results of all the burning velocity calculations are compared in Figure 8, where the effect of v' (or, to be more precise, of s') on S_t is normalized by plotting the ratio S_t/s' versus radius of mean flame position ($S_t = S_T - S_L$). These two general trends indicate that the results may be divided into 2 parts for purposes of discussion, i.e., first, the data for Re = 50,000 and 100,000; second, the data for Re = 10,000 and 25,000.

For Re = 50,000 and 100,000 the burning velocity is virtually constant with height and radius in the flame over the region where reliable measurements could be made. Contrary to the present experimental data, Scurlock and Grover[7] predicted an increase in burning velocity with height, as a result of eddy diffusion and laminar burning only. Karlovitz, Denniston and Wells[1] predicted an increase due to flame-generated turbulence. The relationship, $S_T = S_L + v'$, suggested by Damköhler and by Karlovitz (in the absence of flame-generated turbulence) correlates these results very well.

There is considerable disagreement between S_t and v' for Re = 10,000 and 25,000. In both instances the measured burning velocity is considerably higher than would have been predicted from consideration of approach flow turbulence alone. Correspondingly the apparent rate of flame brush thickening as measured with the photometer is greatly augmented although constant with height, and the electronic probe indicates an apparent increase in turbulence intensity in the flame over that of the approach flow, but also constant with height. Any concept of flame-generated turbulence that might be introduced at this point must take into account this linearity of σ vs. H.

Assuming that the actual rate of turbulent diffusion within the flame remains unchanged, the following tentative explanations are proposed for the above results, again using the wrinkled wave concept as illustration. Figure 9 represents horizontal sections of hypothetical continuous flame fronts; in Figure 9a the mean flame position has negligible curvature; A–A represents the mean position the flame would have taken if S_L were zero; as the average fluctuation is zero, the turbulent fluctuations do not in themselves

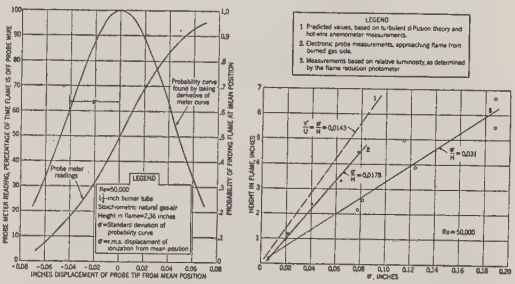
LEGEND
Probability curve found by taking derivative of σ meter curve
Probe meter readings
Re=50,000
Height in flame=2.36 inches
INCHES DISPLACEMENT OF PROBE TIP FROM MEAN POSITION
PROBABILITY OF FINDING FLAME AT MEAN POSITION
HEIGHT IN FLAME, INCHES
Re=50,000

FIG. 5. Turbulence intensity measurements with the electronic probe.

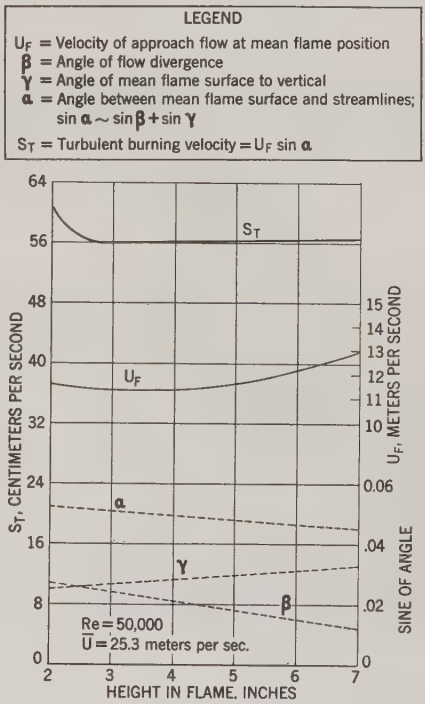
LEGEND
U_F = Velocity of approach flow at mean flame position
β = Angle of flow divergence
γ = Angle of mean flame surface to vertical
α = Angle between mean flame surface and streamlines; sin α ~ sin β + sin γ
S_T = Turbulent burning velocity = U_F sin α
S_T
U_F
α
γ
β
Re = 50,000
U = 25.3 meters per sec.
S_T, CENTIMETERS PER SECOND
U_F, METERS PER SECOND
SINE OF ANGLE
HEIGHT IN FLAME, INCHES

FIG. 6. Summary of turbulent burning velocity calculations by the angle method.

contribute to advancement of the front. $S_L \cdot t$ represents the front advancement to be expected from laminar burning normal to the mean flame front, and $S_t \cdot t$ represents the advancement resulting from the combustion of pockets of unburned gas.[c] In line with the equation developed by

[c] The fluctuations on A–A are considerably smoothed in the actual flame front.

Karlovitz, S_t very nearly equals v'. Although the drawing is hypothetical, the relative magnitudes of S_L, v' and of turbulent scale are made consistent with values in the 50,000 *Re* flame that was studied here. As before, $t = H/U_F$. The same process is shown in Figure 9b but with the mean flame position bent to form the arc of a circle. Here the net flame advancement $S_t \cdot t_V$ $v' \cdot t$ due to merging flame indentations. In both instances the effect of laminar burning is to smooth out the wrinkles caused by turbulence; however the effect is greater on the unburned side of the curved flame.

Although the foregoing curvature effect could account for the upward trend of burning velocities at small radii of curvature (see Fig. 8), it

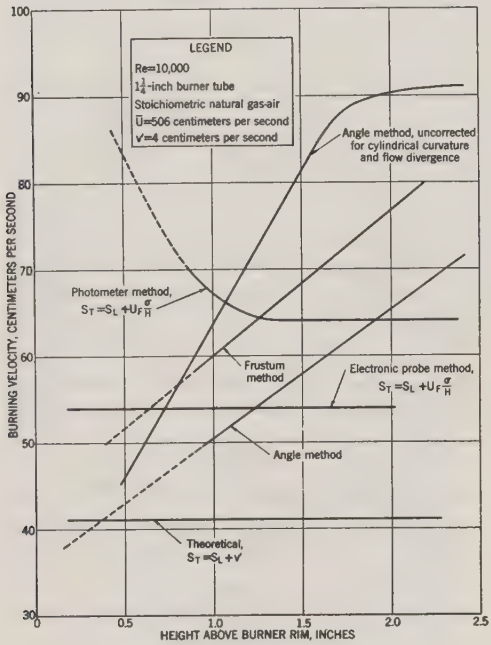
LEGEND
Re=10,000
1¼-inch burner tube
Stoichiometric natural gas-air
Ū=506 centimeters per second
v'=4 centimeters per second
Angle method, uncorrected for cylindrical curvature and flow divergence
Photometer method, $S_T = S_L + U_F \frac{\sigma}{H}$
Frustum method
Electronic probe method, $S_T = S_L + U_F \frac{\sigma}{H}$
Angle method
Theoretical, $S_T = S_L + v'$
BURNING VELOCITY, CENTIMETERS PER SECOND
HEIGHT ABOVE BURNER RIM, INCHES

(A)

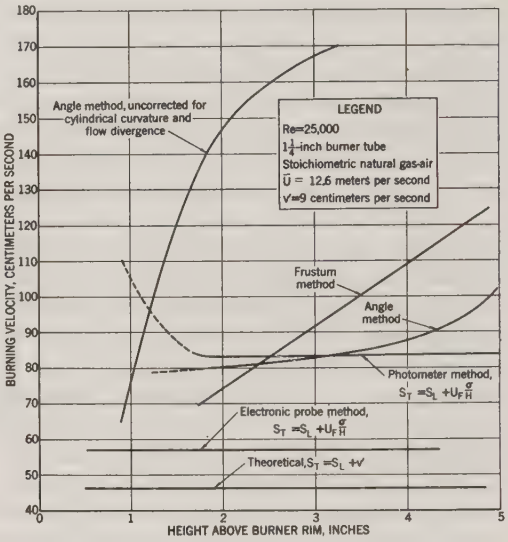
Angle method, uncorrected for cylindrical curvature and flow divergence
LEGEND
Re=25,000
1¼-inch burner tube
Stoichiometric natural gas-air
Ū = 12.6 meters per second
v'=9 centimeters per second
Frustum method
Angle method
Photometer method, $S_T = S_L + U_F \frac{\sigma}{H}$
Electronic probe method, $S_T = S_L + U_F \frac{\sigma}{H}$
Theoretical, $S_T = S_L + v'$
BURNING VELOCITY, CENTIMETERS PER SECOND
HEIGHT ABOVE BURNER RIM, INCHES

(B)

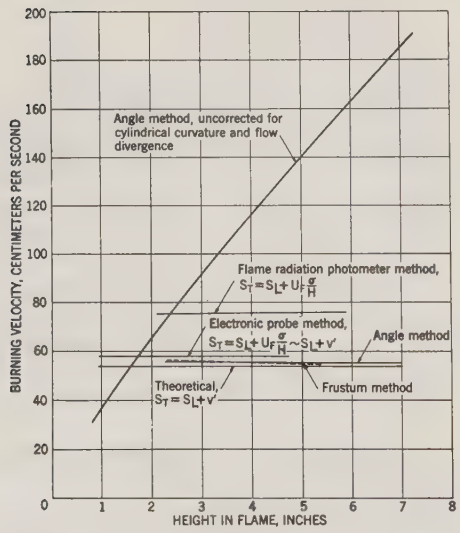
Angle method, uncorrected for cylindrical curvature and flow divergence
Flame radiation photometer method, $S_T = S_L + U_F \frac{\sigma}{H}$
Electronic probe method, $S_T = S_L + U_F \frac{\sigma}{H} \sim S_L + v'$
Angle method
Theoretical, $S_T = S_L + v'$
Frustum method
BURNING VELOCITY, CENTIMETERS PER SECOND
HEIGHT IN FLAME, INCHES
Stoichiometric natural gas-air flame Burner tube I. D. = 1¼ inches
Re = 50,000 v' = 17 centimeters per second Ū = 25.3 meters per sec.

(C)

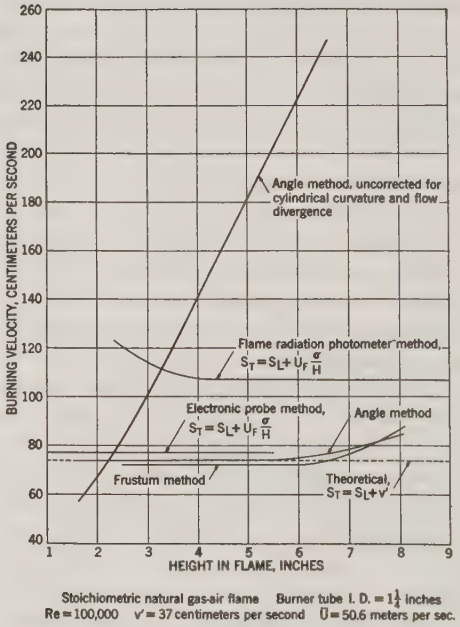
Angle method, uncorrected for cylindrical curvature and flow divergence
Flame radiation photometer method, $S_T = S_L + U_F \frac{\sigma}{H}$
Electronic probe method, $S_T = S_L + U_F \frac{\sigma}{H}$
Angle method
Frustum method
Theoretical, $S_T = S_L + v'$
BURNING VELOCITY, CENTIMETERS PER SECOND
HEIGHT IN FLAME, INCHES
Stoichiometric natural gas-air flame Burner tube I. D. = 1¼ inches
Re = 100,000 v' = 37 centimeters per second Ū = 50.6 meters per sec.

(D)

FIG. 7. Summary of turbulent burning velocity data.

does not account for the fact that the burning velocity for Re = 25,000 is greater than for Re = 50,000, at the same radius of curvature. Reexamination of Figure 9 shows that the amount of smoothing depends on (a) the relative values of $S_L \cdot t$ and of turbulent scale;[d] and (b) the relative values of v' and S_L. When v' is large, as in Figure 9, the resulting flame front bears a resemblance to the fluctuations on A–A, and the electronic probe may be expected to give values of rms displacement that are reasonably close to $v' \cdot t$ or $S_t \cdot t$. However when $v' \ll S_L$, the resulting flame front bears little resemblance to the turbulent fluctuations and its advancement is much greater than $v' \cdot t$; the smaller indentations are almost completely erased and the mean flame position is affected mainly by a few large fluctuations—an effect that is exaggerated by flame-front curvature. It is as though the random distribution of fluctuating velocities has been acted upon by a high-pass velocity filter. Both the electronic probe and the photometer tend to support this conclusion, but it is still not clear where one should expect to find luminosity and ionization peaks in a burned-out indentation of the flame front.

Comparison with Data of Other Investigators

Our burning velocities at 10,000 and 25,000 Re may be compared with the empirical equation of Bollinger and Williams,[8] $S_T = S_L d^{2 \cdot 6} \cdot 0.18\ Re^{0 \cdot 24}$ derived from measurements based on the total area method. However, the 50,000 and 100,000 Re flames fall far outside the range of experimental conditions for which the Bollinger and Williams equation was derived (Table 1). The agreement at low Reynolds number may be somewhat fortuitous, as there are canceling errors in the total area method at high and at low heights in the flame, as pointed out above. At high Reynolds numbers the contribution of low burning velocity near the burner rim becomes relatively less significant.

The present results would agree well with the experiments of Karlovitz, Denniston and Wells[1] had these investigators applied the same corrections for stream divergence and for flame curvature that are discussed here.

Wohl and Shore[9] measured burning velocities by the total area method, neglecting flame-curvature corrections and using a 1-in. burner tube with a stoichiometric mixture of methane-air for Re = 8850 and an approach flow velocity of 540 cm/sec (this corresponds roughly to the present measurement at Re = 10,000). The ratio v'/U for a bare tube was assumed to be 0.053. Wohl reported a value of about 72 cm/sec as compared with the present value of about 60 cm/sec.

The theory developed by Scurlock and Grover[7] can be applied to the experimental conditions described here. The comparison in this instance

[d] Crudely represented by the average base of the triangles representing fluctuations. Scale may be considered to be constant in these experiments, since only one burner diameter was used.

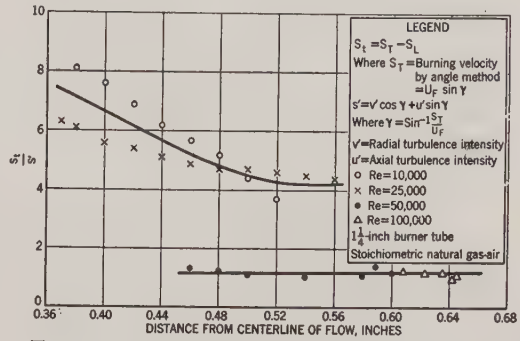
LEGEND
$S_t = S_T - S_L$
Where S_T = Burning velocity by angle method = $U_F \sin \gamma$
$s' = v' \cos \gamma + u' \sin \gamma$
Where $\gamma = \sin^{-1} \frac{S_T}{U_F}$
v' = Radial turbulence intensity
u' = Axial turbulence intensity
o Re=10,000
× Re=25,000
• Re=50,000
△ Re=100,000
1½-inch burner tube
Stoichiometric natural gas-air
s'/v
DISTANCE FROM CENTERLINE OF FLOW, INCHES

Fig. 8. Effect of mean flame curvature and turbulence intensity on turbulent burning velocity.

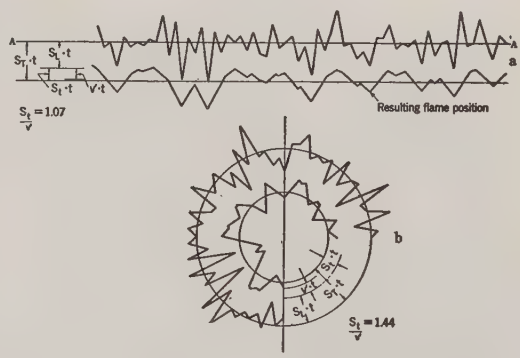

Fig. 9. Diagrams to show effect of mean flame curvature on total burning velocity.

Table 1

Re	S_T, cm/sec	
	Bollinger and Williams, empirical equation	Present work, central portion of flame
10,000	64	60
25,000	80	88
50,000	(91)	55
100,000	(111)	72

is based on their consideration of effects due to eddy diffusion and flame propagation only, omitting flame-generated turbulence (Table 2). Scurlock's theory predicts an increase in burning velocity with height, even in the absence of flame-generated turbulence.

The electronic probe data indicating the lack of flame-generated turbulence agrees with the findings of Westenberg,[10] who measured the turbulence intensity in a stream by the method of helium diffusion, with and without flame.

Conclusions

The burning velocities in the range of Re = 50,000 to 100,000 on a 1¼-in. burner tube with pipe flow turbulence can be predicted quite well by the equation $S_T = S_L + v'$ over a range of flame surface, excluding the base and top. This conclusion is supported by the electronic probe,

TABLE 2

v'/S_L	Height in Flame	Re	S_T, cm/sec	
			Scurlock	Present work
	in.			
0.5	1	50,000	37	56
.5	6	50,000	59	55
1.0	1	100,000	37	72
1.0	7	100,000	83	77

which indicates a constant degree of turbulence in the flame equal to the approach flow turbulence. Burning velocities considerably higher than those predicted by this equation are found to prevail in the region of Re = 10,000 to 25,000. This is confirmed both by the photometer and electronic probe, which also indicate that the apparent rate of flame spreading and of flame-level ionization do not increase with height over the central flame-brush region. A tentative explanation has been given based on purely geometric considerations. In addition, the results of the present work are inconsistent with existing concepts of flame-generated turbulence.

REFERENCES

1. Karlovitz, B., Denniston, D. W., Jr., and Wells, F. E.: J. Chem. Phys., *19*, 541 (1951).
2. Hübner, H. J., and Klaükens, H.: Ann. Physik, *5*, 39 (1941), S. 33–50.
3. Clark, T. P.: NACA Tech. Note 2246, 1951.
4. Little, B. H., Jr., and Wilbur, S. W.: NACA Tech. Note 2361, 1951.
5. Karlovitz, B., Denniston, D. W., Jr., Knapschaefer, D. H., and Wells, F. E.: *Fourth Symposium (International) on Combustion*, p. 613. Baltimore, The Williams & Wilkins Co., 1953.
6. Denniston, D. W., Jr., Oxendine, J. R., Knapschaefer, D. H., Karlovitz, B., and Burgess, D. S.: J. Appl. Phys., in press.
7. Scurlock, A. C., and Grover, J. H.: *Fourth Symposium (International) on Combustion*, p. 645. Baltimore, The Williams & Wilkins Co., 1953.
8. Bollinger, L. M., and Williams, D. T.: NACA Report 932, 1949.
9. Wohl, K., and Shore, L.: Ind. Eng. Chem., *47*, 828 (1955).
10. Westenberg, A. A.: J. Chem. Phys., *22*, 814 (1954).

Discussion by Burton D. Fine

The extrapolation of the results of Bollinger and Williams to high stream velocities may be questionable on two grounds: First, the actual measurements for their largest burner (1⅛ in. diam) covered a small range of Reynolds numbers (6,000 to 11,000) so that even if actual measurements over that range were fairly precise an extrapolation of results for a burner 1¼ in. diam to a Reynolds number of 100,000 could be significantly in error. Second, the mean flame areas were not measured directly by Bollinger and Williams but, rather, were computed from an empirical relation involving the area, flame height and burner diameter. This relation would not necessarily hold in an extrapolated region.

TABLE 1

Reynolds Number	U_T Richmond, *et al.*	U_T Fine and Wagner
	cm/sec	*cm/sec*
10,000	60	69
15,000	—	80
20,000	—	80
25,000	86	69
35,000	—	69
45,000	—	79
50,000	55	76
55,000	—	84
60,000	—	83
70,000	—	86
100,000	72	—

As part of a study of turbulent bunsen flames done at the NACA,* turbulent burning velocities were measured for stoichiometric propane-air

* B. Fine and P. Wagner: NACA TN 3277, 1956.

flames in a 1¼ in. burner over a range of stream velocities corresponding to Reynolds numbers between 10,000 and 70,000. The mean flame surface was measured from photographs and no correction was made for flame-front curvature. The results shown in Table 1 indicate that trends shown from Bollinger and Williams' data are, in fact, not followed at higher stream velocities. Between Reynolds numbers of 15,000 and 70,000 the "total area" turbulent burning velocity is constant and equal to about 80 cm/sec. This is in good agreement with results reported by the angle method.

It was observed, however, that for smaller burners in the range ¼in. to ⅝ in. the "total area" turbulent burning velocity did increase with stream velocity and trends reported by Bollinger and Williams were approximately followed.

Author's Reply

The NACA data are interesting in that they show (in agreement with our data) a trend of relatively large values of burning velocity at low Reynolds numbers and a distinct minimum at intermediate Reynolds numbers. Although the numerical agreement may be somewhat fortuitous, as pointed out in the text, the trend is significant, indicating a transition of some kind in the mode of flame propagation.

39

TURBULENT DIFFUSION FLAMES

By MASANAGA KUNUGI and HIROSHI JINNO

Introduction

Turbulent flames may be divided into two broad categories, namely turbulent diffusion flames and turbulent flames propagating in homogeneous mixtures of fuel and oxidant. Much less attention has been paid to the former than to the latter in fundamental research, though the former is the very type now used in industrial furnaces.

Research by Hawthorne, Weddell and Hottel,[1] by Wohl, Gazley and Kapp,[2] by Yagi and Saji,[3] and by Hottel[4] with turbulent jet flames in open air, and also with liquid jets of alkali discharging into a reservoir containing acid, have enhanced our basic knowledge of turbulent diffusion flames. Their results indicate that mixing of fuel and air by eddy diffusion is the principal factor controlling the rate of burning.

From the practical point of view, studies of turbulent diffusion flames cannot be considered complete until the characteristic features of the turbulent diffusion flames in an enclosed space, namely, the influences of the restriction of air, the presence of constraining walls, and the entrainment of the recirculated gases, are understood.

The present paper reports the results of investigations on flat turbulent diffusion flames formed by separate gas and air jets issuing from narrow rectangular ports into a confined space, and discusses the characteristics of such flames, using cold models.

Experimental Procedure and Results

The experiments were carried out in a combustion chamber having a rectangular cross section 2 by 7 cm and 30 cm high, as shown in Figure 1. City gas and air were introduced upward from the center bottom at various velocities, using a demountable rectangular burner with two adjoining ports.

Provisions were made to determine the composition, temperature and velocity of the flame along the lines passing vertically through the center line of the broader wall of the chamber at five different levels. For gas-sampling and measuring the temperature and pressure, several holes were made in the walls. They were 5 mm in diam, and were spaced 1 or 5 cm apart. These holes, except the one used for the measurement, were closed with asbestos plates. The narrower wall was equipped with plate glass windows at intervals of 5 cm for observing the flame. The channel of the rectangular burner was 20 mm long and 1 to 3 mm wide. The thickness of the partition wall between the ports was 2 mm. City gas and air were introduced at room temperature under nearly atmospheric pressure. The average

composition of the gas used was CO_2 2.9, C_nH_m 2.1, O_2 1.0, CO 14.2, H_2 27.6, CH_4 15.4, N_2 36.8 per cent.

The chemical analysis of gas in the flame was made by physical methods using the thermal conductivity of carbon dioxide and hydrogen and thermomagnetic property of oxygen.

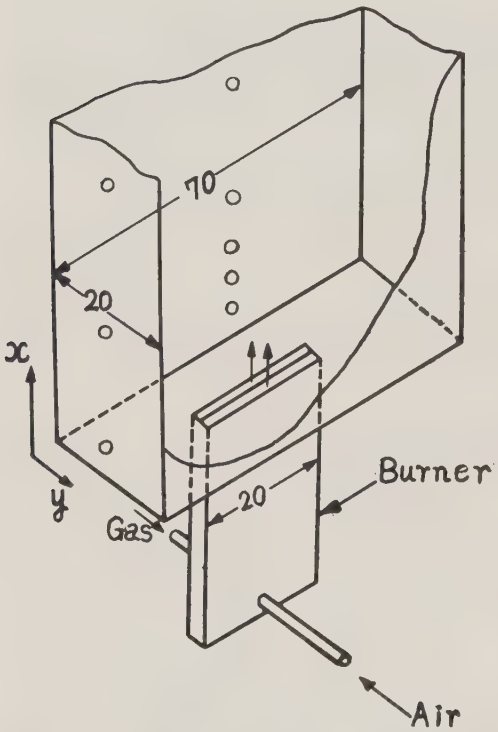

FIG. 1. Schematic diagram of apparatus. Scale in mm.

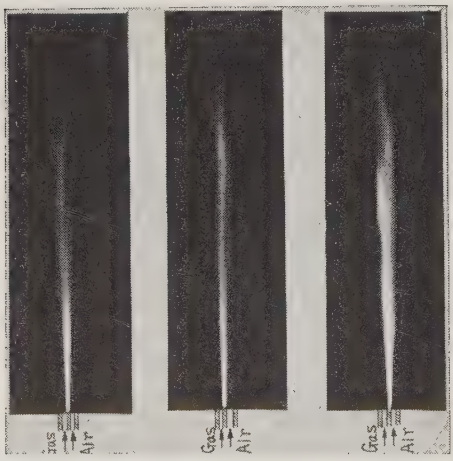

FIG. 2. Direct photograph of flat diffusion flames in a confined space. (a) V_g = 4 l/min, V_a = 12 l/min, u_g = 1.7 m/sec, u_a = 5.1 m/sec; (b) V_g = 4 l/min, V_a = 12 l/min, $u_g = u_a$ = 3.3 m/sec; (c) V_g = 4 l/min, V_a = 13.2 l/min, u_g = 1.7 m/sec, u_a = 5.5 m/sec.

Sampling was carried out through a thin quartz tube of 1 mm inner diameter at such a rate that the intake velocity at the mouth piece was of the same order as the average velocity of the gas stream there. The composition of the gas might have suffered some change at the time of sampling through the cooling from the combustion temperature to that at which the sample was stored for analysis. This variation, however, may be negligible, because the coexisting fuel and oxidant are observed in the sample.

The temperature at different points in the flame was measured by a bare, thin platinum-platinum rhodium thermocouple of 60 μ in diameter. Taking into consideration the radiation and the possible catalytic action at the metal surface, the measurements thus made could be designated as apparent temperatures.

A small quartz Pitot tube was arranged so as to permit the determination of impact pressure. The pressure was measured by a Chattock-type manometer with a cathetometer. In cold experiments the velocities at different points in the stream were measured by a hot-wire anemometer 60 μ in diam and 3 mm long.

For various values of the gas port velocity u_g, the air port velocity u_a, the amount of gas V_g, and the amount of air V_a (ranging from u_g = 1.6 $\sim$ 7.6 m/sec, u_a = 3.2 $\sim$ 7.6 m/sec, V_g = 4.0 $\sim$ 11.7 l/min, V_a = 7.0 $\sim$ 22.5 l/min), the composition, the apparent temperature at the burning zone, and the impact and static pressures were measured at five different levels, i.e., x = 1, 2, 5, 10, 15 cm from the bottom of the combustion chamber.

Direct photographs up to 20 cm from the burner are reproduced in Figure 2, where a refers to the case when gas and air are introduced at different port velocities, namely, u_g = 1.7 m/sec for gas, and u_a = 5.1 m/sec for air, and b refers to the case at the same velocity of $u_a = u_g$ = 3.3 m/sec from ports having different areas in order to retain the same excess air rate. Figure 2c represents the flame burning with a larger excess air. In order to photograph the narrower walls of the combustion chamber, they were equipped with plate glass windows of 2 by 20 cm.

The visible portion of a flame shown in the photographic records has a width of 3 to 5 mm near the ports. It is mainly a luminous blue

towards the air side, and a yellowish red towards the fuel side.

In these photographs the exposures were as long as $\frac{1}{25}$ sec, which obviously is too long for photographing the real state of turbulence. The photographs indicate, however, some sign of flickering, especially at the upper part of the flames, while near the burner they incline toward the air port side.

Two typical concentration profiles of CO_2, H_2 and O_2 are presented in Figure 3a and b

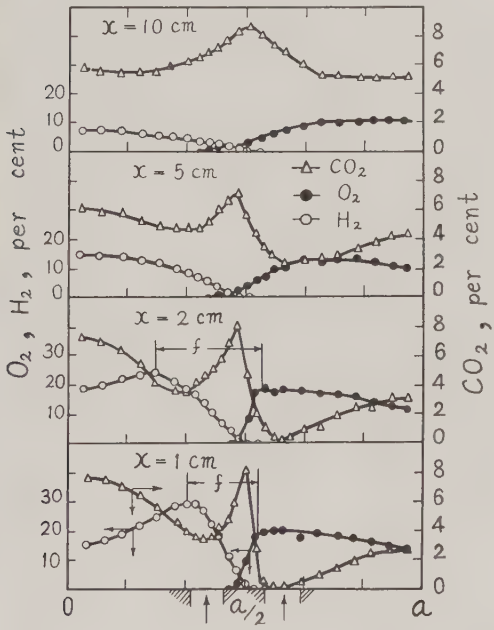

FIG. 3a. Concentration profiles of the city gas flame. Port velocity $u_g = 1.7$ m/sec, $u_a = 5.1$ m/sec, $V_g = 4$ l/min, $V_a = 12$ l/min. a is the width of combustion chamber ($a = 20$ mm).

under the same experimental conditions as in Figure 2a and b. The vertical axis on the right indicates the percentage of H_2 and O_2 ; that on the left indicates the CO_2 concentration.

To ascertain how the actual flame pattern may be represented with the mixing process in a cold jet, some comparative studies were carried out on hot and cold jets under the same conditions. The results are shown in Figure 3c.

Inspection of the curves in Figure 3a and b shows that the concentration of the combustion products reaches a maximum around the points where there is no oxygen, and then decreases on either side. Both fuel and air are diluted more and more by the combustion products from the combustion zone and from the surrounding atmosphere. The curves at the levels $x = 1$, and $x = 2$ cm show that there is a fairly strong recirculation of the combustion products around the main stream.

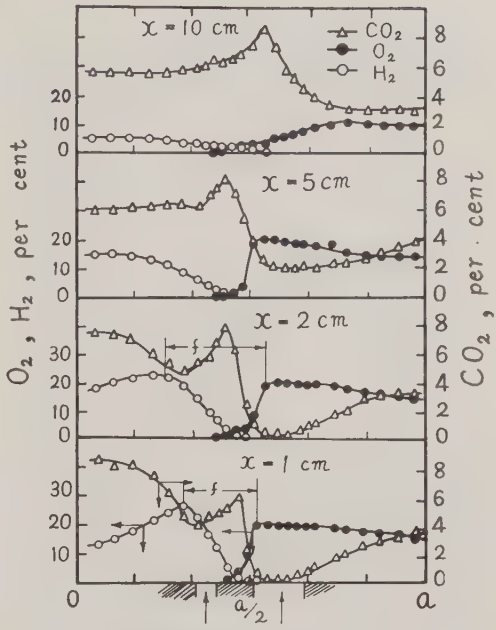

FIG. 3b. Concentration profiles of the city gas flame burning in limited air. Port velocity = $u_g = u_a = 3.3$ m/sec, amount of gas $V_g = 4.0$ l/min, amount of air $V_a = 12$ l/min.

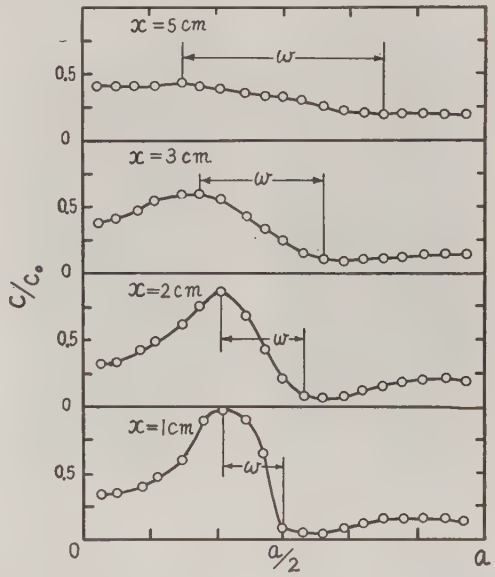

FIG. 3c. Concentration profiles in cold jets. Port velocity of gas $u_g = 1.7$ m/sec; port velocity of air $u_a = 5.1$ m/sec; c/c_0 = ratio of hydrogen in fluid at any point and in initial fluid.

The range f indicated in the figure (see Fig. 3a and b), representing concentration patterns in the flame, corresponds on the one hand to the

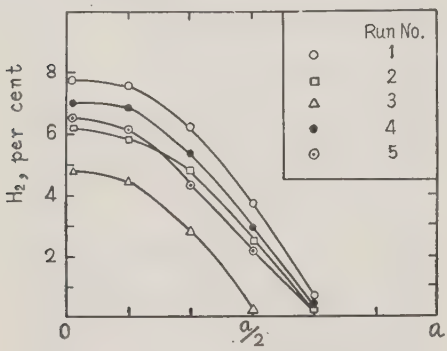

FIG. 4. Hydrogen concentration patterns of flames at the level x = 15 cm. a is the width of combustion chamber.

Run No.	V_g(l/min)	V_a(l/min)	u_g(m/sec)	u_a(m/sec)
1	5.4	8.2	2.2	3.6
2	5.4	10.8	2.2	4.5
3	5.4	13.2	2.2	5.6
4	5.4	10.8	3.6	5.4
5	5.4	10.8	4.5	4.5

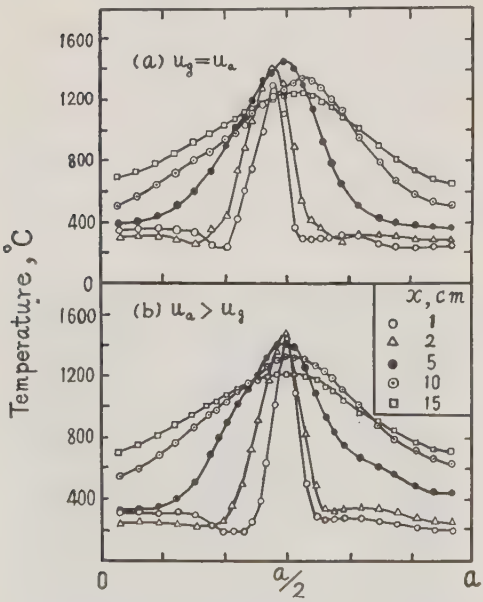

FIG. 5. Temperature distributions in the city gas flames. (a) V_g = 4 l/min, V_a = 12 l/min, u_g = 3.3 m/sec, u_a = 3.3 m/sec; (b) V_g = 4 l/min, V_a = 12 l/min, u_g = 1.7 m/sec, u_a = 5.1 m/sec. a is the width of combustion chamber.

mixing zone, w (see Fig. 3c) of the cold jet, and on the other to the width measured from the point where concentration gradient dc/dy of hydrogen becomes zero to the point where that of oxygen becomes zero. It should be noted that the width, f, is larger than the width of the corresponding visible zone, and that the growth of f with increasing x has a trend similar to that of the mixing zone in the cold state with increasing x.

The curves in Figure 3a appear very similar to those in Figure 3b. However, close inspection shows that the maximum of the CO_2 curve in Figure 3a lies somewhat nearer to the air side than in Figure 3b, and that the maximum of CO_2 curve is situated on the oxidant side of the reaction zone where the maximum temperature is attained. Observation of the flame shows that turbulence begins in the upper regions of the flame at some distance from the port. It was found that the sample which gives the time average value of the gas composition contains both unburned gas and oxygen as will be seen from the curves of Figure 3a and b.

The curves in Figure 3c indicate clearly that the width of the mixing zone increases with the axial distance from the burner. Although actual combustion does not take place in this experiment, the point where $c/c_0 \cong 0.3$ should correspond to the flame tip, because at this point the gas mixture contains the theoretical amount of air required for complete combustion. Thus it is suggested that the course of the combustion in diffusion flames can be predicted from the mixing process of the two streams in cold models.

The hydrogen concentration patterns of flames with various excess air ratios and relative port velocities at the level x = 15 cm are shown in Figure 4. These curves make it clear that the effect of the excess air ratio on the burning rate in the flame is preponderant (see runs 1, 2 and 3), whereas the relative port velocities of gas and air are of secondary importance as the air/gas ratio is constant (see runs 2, 4 and 5).

Typical temperature distributions in the flame are shown in Figure 5a and b. The figures indicate that near the burner port the flame temperature increases somewhat with increasing difference between the gas and air velocities, whereas in the upper part of the flame the relative velocity at the burner seems to have virtually no influence on the temperature distribution.

Representative velocity profiles are shown in Figure 6, together with those of the cold air model. They show the similarity of the velocity profiles of the hot and cold jets. Moreover it is interesting to note that the velocity of the hot jet is not much larger than that of the cold jet.

To visualize the flow patterns, the authors carried out some experiments with water models using plastic spheres (grading: 100 to 150 mesh, density: 1.0) coated with aluminum powder as tracer. Water was supplied downward into a chamber of 2 by 7 by 30 cm from ports of the same size as those used in the hot experiments. A carbon arc was used as the light source. Through a slit and a high-speed rotating disc, a vertical sheet of light 1 mm thick was projected into the chamber. The tracks of the particles in the illuminated area of the water jets were photographed with a lens of large aperture. In Figure 7 the tracks described by the tracer particles in the chamber are reproduced. When the water flows very slowly (Fig. 7a), the flow is laminar. When there is a difference between the velocities of the two jets, i.e., $u_g = 22$ cm/sec, $u_a = 57$ cm/sec, the jet with the lower velocity is drawn into the other (Fig. 7b). These figures show that turbulence begins to occur in jets even if the Reynolds numbers at the ports are as low as 800 and 1600, respectively.

Having measured the composition, temperature, and velocity of the gases in the combustion zone of a burning flame it becomes possible to calculate the combustion ratio taking into account the lateral distribution of the flow velocity. The average value α of the ratio of the concentration of unburned hydrogen at any cross section normal to the x-axis to the mass flow rate of hydrogen V_H at the burner port may be expressed as

$$\alpha = \frac{1}{\bar{V}_H} \int_0^a cu \frac{T_0}{T} dy \qquad (1)$$

where c is the concentration of hydrogen, u the flow velocity, α the width of the combustion chamber, and T and T_0 the flame temperature and the initial temperature.

Figure 8 gives the relations between average factor burned $(1 - \alpha)$ and flame travel x under different conditions. The experimental conditions in runs 1 and 2 are the same as in Figure 3a and b. In run 3 the gas was burned with less excess air and the burned gas in the combustion chamber was equal in amount to that of the above cases. The figures show that the difference in the combustion ratio, due to the different factors named above, becomes less marked especially near the flame tip ($x = 15$ cm).

Conclusion

The present series of experiments were carried out under conditions such that the gas flow in the burner was distinctly laminar with a Reynolds number of about 1000, although the jet issuing into the combustion chamber was confirmed to be in considerable turbulence.

Comparison between the results of the cold and

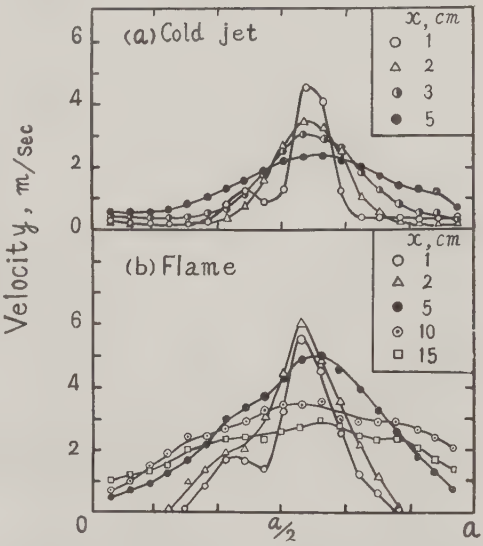

FIG. 6. Velocity profiles of flame and cold jet. $V_g = 4$ l/min, $V_a = 12$ l/min, $u_g = 1.7$ m/sec, $u_a = 5.1$ m/sec.

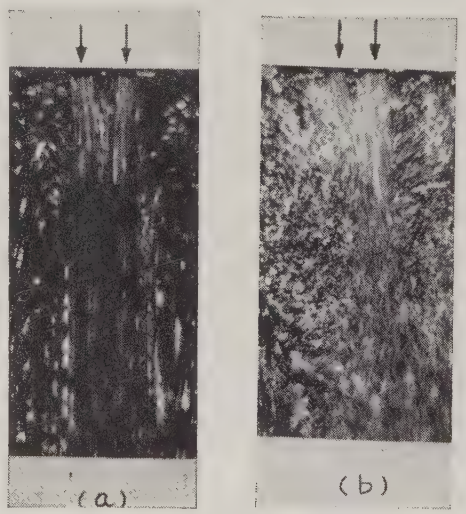

FIG. 7. Flow patterns of two liquid jets in an enclosed space. Time between interruptions: (a) 0.17 s, (b) 0.12 s. Port velocities: (a) $u_g = u_a = 11$ cm/sec, (b) $u_g = 22$ cm/sec, $u_a = 57$ cm/sec. Reynolds number: (a) $Re = 400$, (b) $Re = 800$ and 1600 in the ports.

the hot experiments suggests that the degree of turbulence in both cases does not differ greatly, because no major difference in the flow velocity or the width of jet expanse can be detected. In other words, there is a type of flame in which the flame-generated turbulence exerts at best only a minor influence.

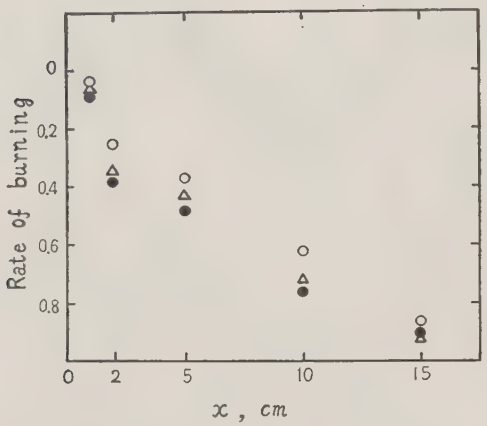

FIG. 8. Variation of axial combustion ratio in the flames.

Run No.	Symbols	V_g(l/min)	V_a(l/min)	u_a/u_g
1	○	4	12	1
2	●	4	12	3
3	△	5.3	10.8	2

Obviously an important and necessary condition for the burning of a diffusion flame is the contact of fuel and air. Hence, the rate of mixing of gas and air would have a pronounced effect on the burning rate as may be seen from the results of the present experiments. However, for combustion in an enclosed space the amount of air supply is limited, and there are complex recirculations that vary according to the dimension of the combustion chamber. Both may be regarded as being influential on the burning velocity.

Although it is not possible now for the authors to evaluate exactly the influence of recirculations on the burning rate, the fact that the flame length becomes shorter with the increasing excess air rate leads us to surmise that the dilution of gas and air by the combustion products would tend to suppress the burning rate.

Combustion in diffusion flames is simply the mixing process of fuel, air and combustion products, each having different chemical compositions. In other words, it is the mixing process of a nonhomogeneous system that cannot be exactly reproduced by the result of the model experiments with an air jet in open air.

Based on the measurement of the distribution of gases and on temperature data, it seems very probable that a flame envelope is the locus of the points at which $dc/dy = 0$, where dc/dy is the concentration gradient normal to the jet axis. Therefore, the flame envelope will be wider than the blue luminous zone of the flame that appears in the photographic record. Moreover, it has been observed that this luminous zone occurs near the air port, especially near the port opening. The position of this zone seems to have been influenced by the width of the air port as well as by the port velocity.

REFERENCES

1. HOTTEL, H. C., AND HAWTHORNE, W. R.: *Third Symposium on Combustion, Flame and Explosion Phenomena*, p. 266. Baltimore, The Williams & Wilkins Co., 1949.
2. WOHL, K., GAZLEY, C., AND KAPP, N.: *Third Symposium on Combustion, Flame and Explosion Phenomena*, p. 288. Baltimore, The Williams & Wilkins Co., 1949.
3. YAGI, S., AND SAJI, K.: *Fourth Symposium (International) on Combustion*, p. 771. Baltimore, The Williams & Wilkins Co., 1953.
4. HOTTEL, H. C.: *Fourth Symposium (International) on Combustion*, p. 97. Baltimore, The Williams & Wilkins Co., 1953.

40

COMBUSTION OF A TURBULENT JET IN BURNERS WITH PRELIMINARY MIXING

By V. N. IEVLEV

Experience obtained in utilizing combustible gases as fuels shows that, of the various kinds of existing gas burners, the tunnel-type burners with premixing offer definite advantages. Theoretically, this type of burner should have maximum performance indices, inasmuch as the mixture undergoing combustion is formed beforehand.

In spite of the wide use of tunnel-type burners in industry, for instance in the USSR, the actual mechanism of the combustion process which takes place in them is not as clear as it should be. This constitutes a very serious obstacle in designing rational types of these burners, and especially of large unit-capacity burners.

The few existing studies of the combustion process in tunnel-type burners generally are linked to some one, physical or chemical, aspect of the process, and the conclusions derived for this particular aspect have been applied to the process as a whole. Individual facts observed during these studies have, of course, helped to uncover certain features of the combustion process in tunnels, but at the same time they have led to a large number of different, often contradictory, points of view on the mechanism of combustion. This question is discussed in considerable detail in the special Soviet literature.[1, 2, 3]

The present investigation, designed as a first step in a systematic study of the process of combustion in tunnel burners, deals with the general problems of ignition and combustion in turbulent jets, and covers all the various aspects of the process, including physical and chemical factors.

The immediate objectives of the investigation were: (1) To determine the mechanism of the process of combustion in a tunnel and to discover how it differs from an ordinary jet process; also, to determine the effect of the tunnel on the combustion process; and (2) To study the individual stages of the combustion process and the laws which govern them and to discover methods of influencing both the individual stages and the process as a whole.

The fuel used in the investigation was a mixture of air and Moscow city gas with a heat of combustion of about 7,700 kg/cal/m^3. The concentration of CO_2 and pressures were measured both at points over the cross section and at points along the axis of flow. On the basis of data on CO_2 distribution, plots were made of fields and curves for the relative degree of combustion $(\kappa)^a$ characterizing the process of combustion of the initial fuel mixture as it moves away from the burner. A characterization of the combustion process based on the change in the ratio CO_2: CO_2^{max} differs somewhat from a characterization based on full incomplete combustion inasmuch as the city gas contains hydrogen. However, in our tests the possible error due to this remained within the limits of accuracy of the other measurements.

On the basis of the experimental data, fields and curves were also plotted showing variations in pressure and velocities. The velocities were calculated from measurements of pressure and temperature at fixed points of the combustion zone.

On the basis of the large volume of observations and the theoretical analysis given by Khitrin,[4] it is natural to assume that combustion in a tunnel is a volume process of combustion of a chemically homogeneous gas mixture, differing only in that it takes place in the specific conditions created by the tunnel. Accordingly, in this investigation, those aspects of combustion in a tunnel were studied which are usually typical for the combustion of a free jet of combustible mixture: (1) The conditions under which ignition takes place and its character; (2) The specific features of the formation of a continuous front; and (3) the course of combustion of the gas-air mixture.

A large number of papers have been devoted to problems of combustion of free turbulent jets of premixed gases.[5-10]

In the course of our investigation, we first obtained the characteristics for combustion in free turbulent jets. We then compared both

[a] By the relative degree of combustion based on CO_2 (κ) we mean the percentage ratio of the actual concentration (CO_2) at the point considered to the maximum concentration (CO_2^{max}) which would result by complete combustion of an air-gas mixture of the composition used.

types of combustion and determined the characteristics of the individual stages. In conclusion some attention was devoted to intensifying the combustion process in tunnel-type burners.

The tests were made using burners with premixing. The burner tube was 30 mm in diam and

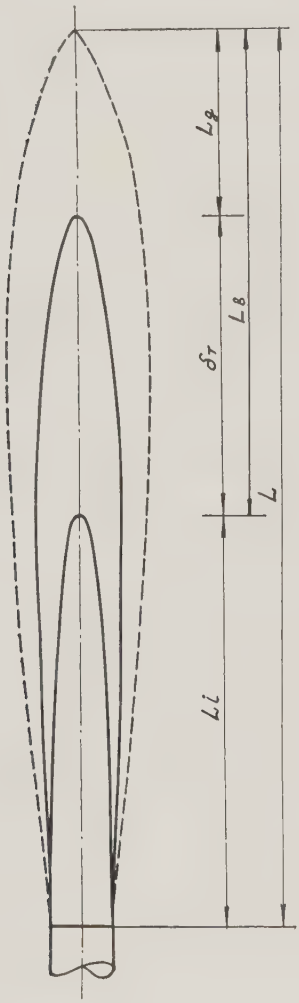

FIG. 1. Sketch of free burning jet.

200 mm long. When the process of combustion of an unenclosed jet was being studied, the burner was equipped with a gas-oxygen ignition ring; when the process of combustion in a tunnel was under investigation, the burner was placed at the end of an 80 mm diam tunnel. Some stages of the study were tested on industrial burners with a tube diameter of 66 or 90 mm and mounted at the end of a 260 mm diam tunnel.

The tests were made with a gas-air mixture feed velocity of from 10 to 30 m/sec, and with values of the surplus air coefficient, α, ranging from 0.86 to 1.37.

Visual examination of a free burning jet shows separate zones which together make up the total length of the jet (Fig. 1). These zones are: (1) The zone extending from the burner tube to the point where the axial stream ignites (L_i), i.e., the nucleus along which the flame spreads from the periphery to the center and covers the entire cross section of the jet; (2) The zone of bright luminescence (δ_T) between the surface of the nucleus and the outer cone which determines the turbulent front of the flame; and (3) The zone of faint luminescence L_g in which combustion is completed.

From the field of the κ value which, as was pointed out above, describes the process of combustion of the initial gas mixture, we can determine the specific features of each individual zone and of the over-all combustion process.

Figure 2a represents the field of the κ values (iso-concentration lines); it shows that there is an internal part of the burning jet—a nucleus—the borders of which are given by the zero value of the κ line, where there is neither combustion nor mixing. Farther, there is a region where the κ values show a sharp rise, which is typical of intense combustion. The initial 80 to 90 per cent of the rise occurs very rapidly, the remaining increase to 100 per cent takes place slowly. The process is especially slow for the combustion of the last 3 to 5 per cent.

Figure 2b shows not only the κ-value field but also the location of the zone of constant values of the surplus air coefficient, α; i.e., the zone in which no influence is exerted by the surrounding atmosphere. That zone is about 2d (tube diam) in length and covers the entire nucleus of the burning jet and a large part of the zone of combustion.

If the representation of the κ-values field and the picture of the free burning jet (Fig. 2c) are examined simultaneously it can be seen that the nucleus approximately coincides with the zone of zero κ values. Some shift of the borders of the nucleus from the line of zero κ values is evidently explained by the fact that luminescence of the front becomes visible only in regions where the value of κ has reached about 5 per cent. The border of the external cone, i.e., the flame front, is given by a κ curve equal to about 90 per cent. The remaining 10 per cent undergoes combustion

outside the visible front. Inasmuch as the aim of the investigation was to determine the nature of the process of combustion in the tunnel of a burner, a comparison is made in Figure 3 of the κ field for a free burning jet and for the process the fact that in a tunnel the jet cannot expand freely, nor can fresh air from the surrounding atmosphere penetrate to the jet axis to increase the concentration of the oxidizing agent in the tunnel.

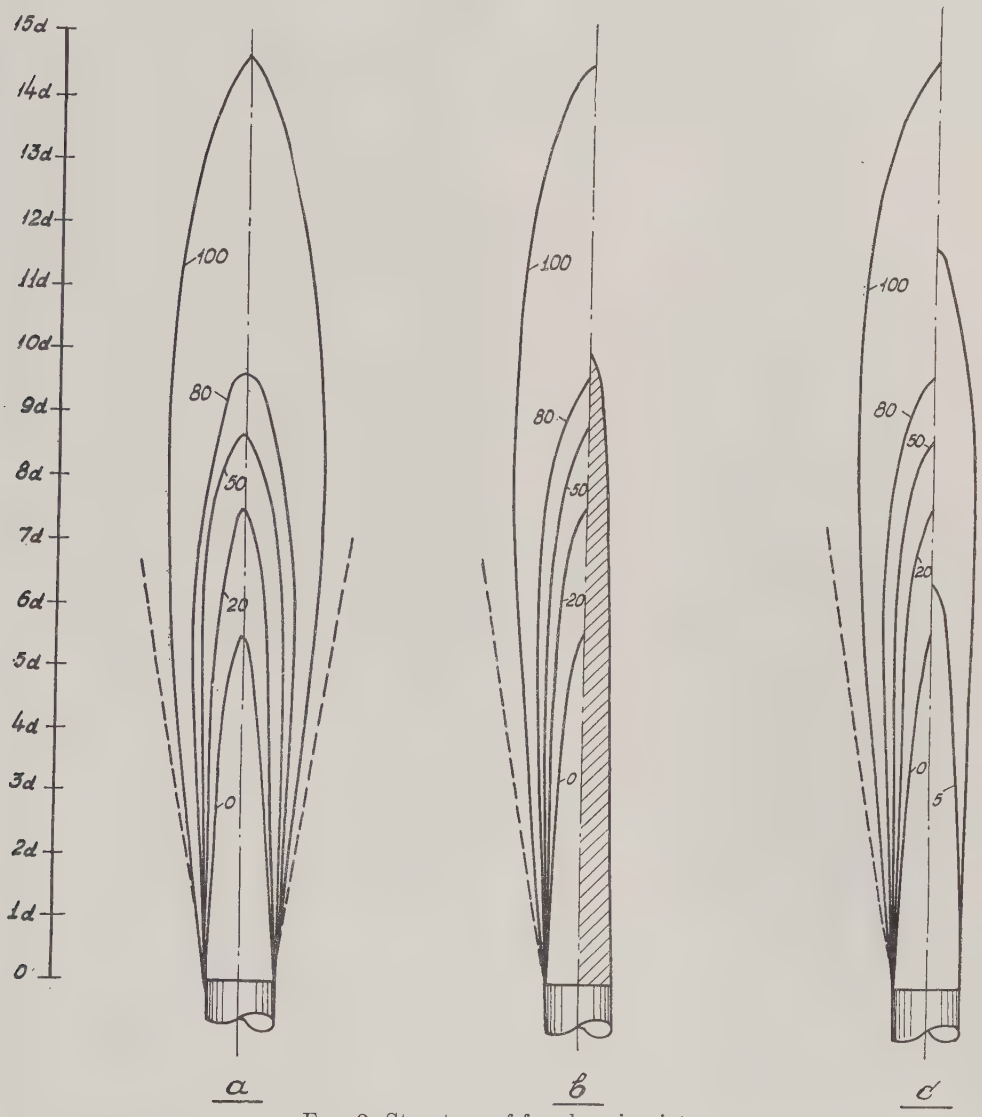

FIG. 2. Structure of free burning jet.

in a tunnel. This comparison indicates that the structure of the κ field is similar in both cases (especially in the zone of κ values up to 80 per cent) not only with respect to the general pattern but also to the absolute values in the various zones. Some differences in the width of the "flame" and in the length required for complete combustion (κ = 100 per cent) are explained by

Judging from the distribution of the κ lines, it may be stated with confidence that the three typical zones described above (Fig. 1) also exist in tunnels.

From Figure 3 it follows that the combustion front in a tunnel begins in the immediate vicinity of the burner tube, at its circumference, and resembles an elongated nucleus that is very like a

cone in shape. Thus, from a study of the pattern of the κ values in a free-burning jet and in a tunnel, the conclusion can be drawn that combustion in a tunnel is essentially analogous to that of a free-burning jet.

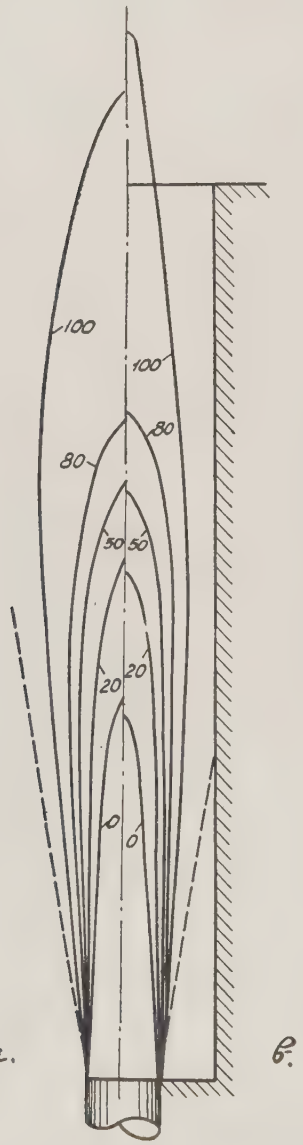

FIG. 3. κ-field in burning jet (a) and in duct (b).

It should be noted that between the tunnel wall and the region described by the lines κ = 100 per cent (Fig. 3), there exists a zone of products of complete combustion which excludes the possibility of any direct influence of the incandescent tunnel wall on the chemical process of combustion in the jet.

The pressure field (Fig. 4) shows that at the head of the tunnel there exists a zone of negative pressure values in which there is a reverse motion, or circulation, of the combustion products from the periphery of the burning jet to its root in a region located about 4d (tube diameters) from the tube.

The continuous supply to the jet root of high temperature combustion products that are prevented from cooling by the incandescent refractory wall of the tunnel provides stable ignition of the jet of fresh combustible mixture from the circumference. As a result, tunnel burners with properly selected dimensions do not require the use of special ignition devices during operation, and the fuel mixture is ignited automatically by circulation to the jet root of high temperature combustion products. In contrast to this, stable burning of a free jet at values of $\alpha > 1$ and at high feed velocities of the combustible mixture is possible only if artificial ignition is provided, for instance, by means of an ignition ring.

The spreading angle of a burning jet in a refractory tunnel is close to that of a free jet whether hot or cold (*ca.* 22°).

The spreading angle value determines the length of the zone of negative pressures. An increase in the spreading angle leads to a decrease in the length of the zone. Higher feed velocities of the gas-air mixture result in smaller spreading angles and increase the length of the negative pressure zone. Changing the ratio of the diameter of the tunnel and the tube (D:d) also changes the spreading angle which increases when the ratio, D:d, increases. The experiments carried out in this study suggest that tunnels with different diameters but with equal values of the ratio, D:d, are aerodynamic analogues for the combustion of a given mixture.

As is self-evident and as can be seen in Figure 3, the combustion process occupies the greatest length along the jet axis, so that when combustion is completed along the axis we may assume that it is completed over the entire cross section of the flow. On this basis, further study of the combustion process, of its individual stages and the laws governing them, were carried out along the flow axis.

In the case of a free burning jet (Fig. 5a), the variations of κ along the flow axis, or the so-called "combustion curve," begin essentially in the region at the end of the nucleus where a sharp rise in the combustion curve occurs, followed by an inflection and a smooth approach to κ = 100

per cent. It was found that this is the universal shape for this curve and that, as can be seen below, it is fitted by a definite expression.

Similarly there is a typical shape for the curve of relative flow velocities, W, in a free burning jet. Initially, in the nucleus of the jet, the values of the velocity in the flame front decrease. They then increase abruptly[b] due to a sharp rise in the temperature as a result of combustion, and to conditions in the flame front which, to some extent, hamper expansion of the combustion products. Once most of the combustible mixture is ignited, curve W gradually decreases to zero.

The combustion process along the flow axis for a refractory tunnel is described by a curve (Fig. 5b) of a similar nature. The curve shows that, in so far as this characteristic is concerned, the combustion process along the tunnel axis develops in the same fashion as in a free burning jet and that the incandescent tunnel walls have no influence on the dimensions of the burning jet. To support this conclusion, a series of tests were made in a water-cooled steel tunnel, thus excluding the possibility of any effects of incandescent surfaces on the combustion process. The ignition process of the combustible mixture was simulated by an "igniting ring." For this case also (Fig. 5c), the "combustion curves" and the change of flow-velocity curves were similar in nature to those obtained earlier.

The experiments in a free burning jet and in tunnels—both with refractory and with water-cooled walls—show that when a combustible mixture burns under identical conditions, and when there is stable ignition, the general patterns of the combustion process along the flow axis are virtually identical and the "combustion curves" coincide quite closely (Fig. 6). This makes it possible to apply the relationships observed along the axis for free burning jets to the case of combustion in a tunnel.

Up to this point, consideration of the combustion process was limited to constant conditions of feeding the combustible mixture and to constant feed composition. The influence of such individual factors on the combustion process was determined experimentally.

The value of the air surplus coefficient, α, which mainly affects the kinetic characteristic of the mixture, has a marked influence on the character of the "combustion curves." For values of α from 1.0 to 1.2, the curves are closer to the origin of the coordinate system (Fig. 7a) and rise more sharply than for $\alpha < 1.0$ and $\alpha > 1.2$.

Increasing the feed velocity of the combustible mixture—an aerodynamic factor—in all cases increases the length of the nucleus (Fig. 7b) and the over-all length of the burning jet, i.e., to a corresponding shift away from the origin of the coordinate system of the "combustion curves" and change of velocity curves. An increase in the tube diameter from 30 mm to 90 mm causes a decrease in the relative length (L/d) of the burning jet (Fig. 7c).

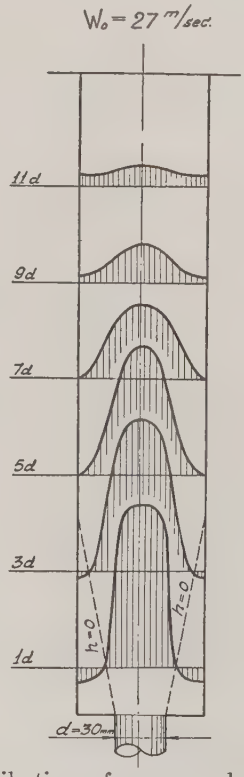

FIG. 4. Distribution of pressure head in duct.

As was pointed out above, the length of the burning jet (Fig. 1) is the sum of the length of the nucleus, the width of the flame front and the length of the zone of completed combustion. The experimental data given here show that both combustion stages, combustion in the front and completed combustion, are covered by a common "combustion curve" which describes the process from the beginning of ignition of the jet to the

[b] It should be noted that the quantitative evaluation of the abrupt increase is conditional to a certain degree inasmuch as the velocity was not measured directly but was calculated from pressure and temperature measurements.

formation of the final products. It is therefore more expedient to divide the length of the burning jet into two parts differing in physical character: (1) Part L_i, corresponding to the nucleus of the burning jet, along which the process of initial ignition over the entire cross section of the jet is completed and which depends on the laws governing the spread of the flame from the circumference to the center of the jet; $L_i/d = f(W, d, \alpha)$ is determined experimentally; (2) Part L_b, whose length is determined by the "combustion curve," which follows the law:

$$\kappa = 1 - e^{-K(L_b/cl)^3},$$

where K is a constant which depends on the values of W, d and U_n (the normal burning velocity)

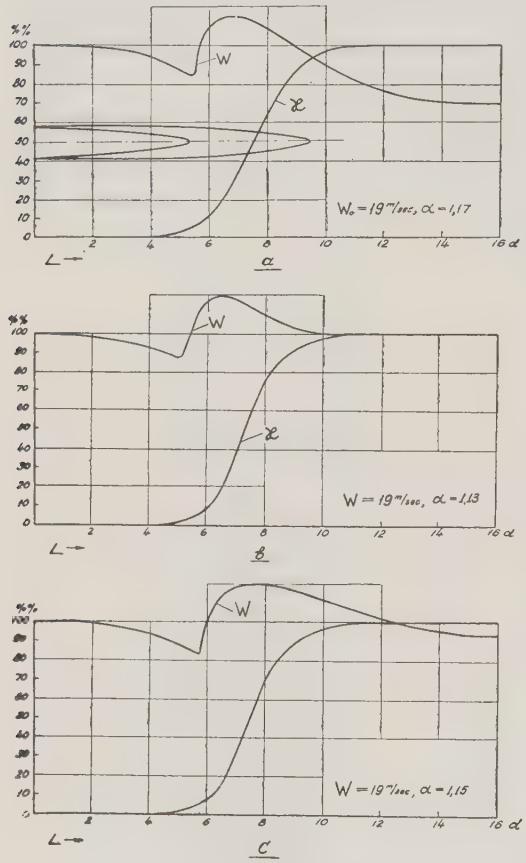

FIG. 5. Curves of combustion efficiency (κ) and velocity stream (W). (a) free burning jet; (b) high refractory duct; (c) cooled duct.

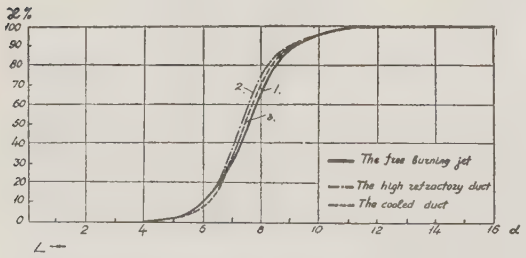

FIG. 6. Comparison of the curves of combustion efficiency in free burning jet (1), in high refractory duct (2), and in cooled duct (3).

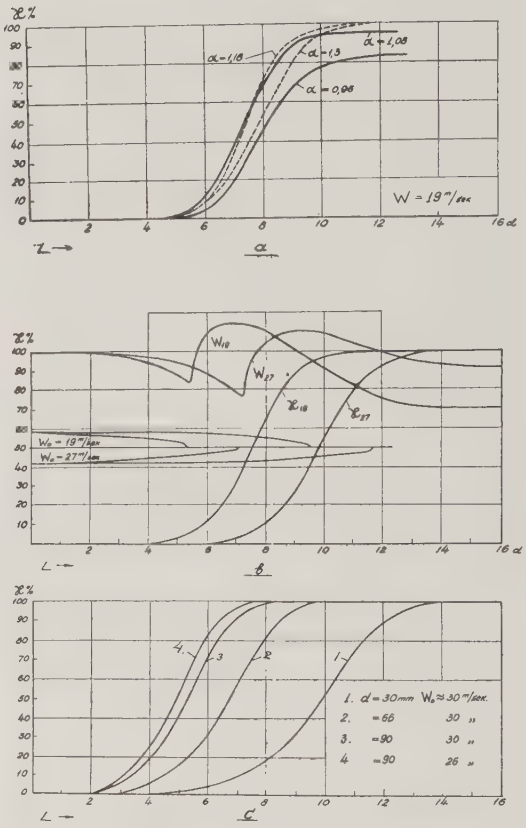

FIG. 7. Influence of α (a), W (b) and d (c) on process of combustion.

and is determined experimentally; L_b is the distance from the zero point of the "combustion curve"; d is the diameter of the burner tube.

When the value of the constant, K, has been determined, for a given value of the degree of combustion, 99 per cent for example, an expression for L_b can be obtained from the "combustion curve" equation:

$$\frac{L_b}{d} = \frac{1.66}{\sqrt[3]{K}}$$

Experimental data indicate that the K is virtu-

ally independent of the test conditions (values of W and d).

"Combustion curves" calculated from the above equation correspond satisfactorily to experimental data of various authors.

The efficiency of combustion in a tunnel depends on the rate of heat liberation. Decreasing the length of the burning jet increases the rate of heat liberation in the tunnel.

The over-all length of the burning jet is made up of two parts:

$$L = L_i + L_b$$

The quantity L_i is largely connected with the aerodynamic organization of the process and with the tube dimensions. Consequently the simplest way to change the quantity L is to change L_i.

The length of L_i can be decreased by: (1) decreasing the dimensions of the burner tube, as, for instance, in multichannel burners; (2) providing supplementary ignition sources, for example, along the jet axis.

The first measure is not altogether expedient inasmuch as combustion becomes less stable when the diameter is decreased, especially at forced regimes of operation. On the other hand the introduction into the tunnel of attachments placed along the axis of flow near the tube and representing poorly streamlined bodies, for example, cone-shaped ones, brings about major changes in the aerodynamic pattern of the jet in the vicinity of the tube (Fig. 8). The jet becomes more turbulent and the ignition perimeter is increased; as a result, ignition of the gas-air mixture takes place not only at the jet root, from the periphery, but also at the edges of the cone-shaped attachments inside the jet. All this leads to more effective ignition, and, consequently, to a decrease in the length, L_i.

Experiments carried out with burners with tube diameters of 30, 66 and 90 mm, respectively, at a feed velocity of the combustible mixture of about 30 m/sec, showed that introduction of a cone-shaped attachment into the tunnel decreases the length of the burning jet more than twofold and causes a corresponding increase in the rate of heat liberation ($Q:V$) in the "active volume"[c] of the tunnel (from 14 million to 43 million kcal/m³hr for the introduction of a smooth cone-shaped attachment and to 100 million kcal/m³hr for the introduction of a cone-shaped attachment with blades—a so-called vortex generator).

The increase of the rate of heat liberation in the tunnel by introduction of cone-shaped attachments leads to an increase in the hydraulic resistance of the system. However, it is possible to find a position of the cone for which the resistance of the system will be at a minimum and the rate of heat liberation will be at a maximum (Table 1). The best results were obtained when cones with a diameter about two thirds the diameter of the tube were introduced into the tunnel at a distance from the tube approximately equal to the attachment diameter.

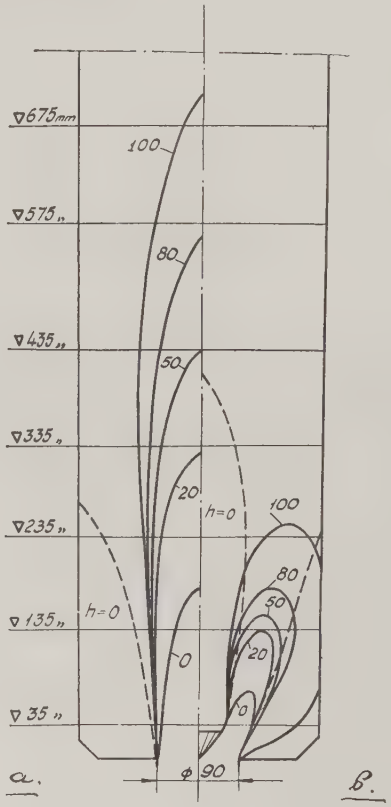

FIG. 8. κ-fields in high refractory duct. (a) Empty duct, (b) duct with conic insert.

[c] That part of the tunnel volume in which the combustion process is completed.

Summary

As a result of this study, a clear picture has been obtained of the nature of the combustion process in tunnel-type burners. It coincides with

that of combustion in a free turbulent jet. All the laws governing combustion in a free jet can be applied, therefore, to combustion in a tunnel. The tunnel does not exert any significant influence on the burning process itself, but acts as an efficient and convenient flame stabilizer, which provides stable ignition of the combustible mixture entering the tunnel.

The study has led to a subdivision of the burning jet into two zones. The laws governing the processes in these zones may be applied to developing methods of calculation for pre-mixed gas burners.

Table 1

D	d	D/d	Type of Cone-shaped Attachment	W_0	W_T	h_0 (mm water)	h (mm water)	$h:h_0$	Q_0	Q	Q/Q_0	Q_0/V	Q/V	$Q/V:Q_0/V_0$
mm	*mm*		*diam mm l, mm*	*m/sec*	*m/sec*			*per cent*	*thousands kcal/hr*	*thousands kcal/hr*	*per cent*	*millions kcal/m³/hr*	*millions kcal/m³/hr*	*per cent*
120	30	4	Empty tunnel	35	2.1	100	—	100	60	—	100	14.2	—	100
120	30	4	15 8	35	2.2	100	115	115	60	60	100	14.2	30.0	210
120	30	4	20 8	35	2.2	100	175	175	60	60	100	14.2	30.0	210
120	30	4	20 20	35	2.2	100	140	140	60	60	100	14.2	30.0	210
120	30	4	Vortex generator	35	2.2	100	120	120	60	60	100	14.2	100.0	700
260	66	4	Empty tunnel	33	2.1	75	—	100	285	—	100	9.9	—	100
260	66	4	60 30	33	2.2	75	152	200	285	268	94	9.9	17.3	175
260	66	4	60 60	35	2.4	78	125	160	303	325	107	10.4	21.0	202
260	66	4	45 60	35	2.4	78	108	138	303	315	104	10.4	25.4	244
80	30	2.7	Empty tunnel	30	4.2	90	—	110	56	—	100	25.0	—	100
80	30	2.7	Vortex generator	27	3.8	85	115	135	50	45	90	22.3	100	450
260	90	2.9	Empty tunnel	30	3.6	33	—	100	436	—	100	15.5	—	100
260	90	2.9	60 30	27	3.4	28	59	210	392	430	100	14.0	38.5	275
260	90	2.9	60 60	27	3.4	28	45	160	395	445	113	14.0	42.5	302
260	90	2.9	45 20	27	3.4	28	63	225	392	424	108	14.0	33.0	235
260	90	2.9	45 60	26	3.3	27	40	148	390	470	120	13.9	33.0	235

Finally, the study indicates practical measures, connected mainly with the design of the burner, which lead to a reduction in the length of the burning jet and to a corresponding increase in the efficiency of combustion in a tunnel.

Acknowledgment

The author expresses deep thanks to Corresponding Member of the USSR Academy of Sciences, L. N. Khitrin, under whose direction this study was carried out, for his active aid in its fulfillment.

Nomenclature

D	tunnel diameter, mm
d	tube diameter, mm
diam	attachment (cone) diameter, mm
l	distance from tube to attachment, mm
W_0	feed velocity of the gas-air mixture in m/sec at standard conditions
W_T	mean velocity of flow in the tunnel, m/sec at standard conditions
h_0	hydraulic resistance of empty tunnel, mm of water column
h	hydraulic resistance of tunnel containing attachment, mm of water column
$h:h_0$	relative increase in resistance of the device (based on the empty tunnel) in per cent
Q_0	rate of heat liberation in empty tunnel, thousands of kcal/hr
Q	rate of heat liberation in tunnel containing attachment, thousands of kcal/hr
Q/Q_0	relative increase in rate of heat liberation in tunnel as a result of introducing attachment (based on the empty tunnel) in per cent
Q_0/V_0	rate of heat liberation in "active" volume of empty tunnel, millions of kcal/m³/hr
Q/V	rate of heat liberation in "active" volume of tunnel containing an attachment, millions of kcal/m³/hr
$Q/V:Q_0/V_0$	relative increase in the rate of heat liberation in "active" volume of tunnel as a result of introducing an

attachment (based on the empty tunnel) in per cent.

REFERENCES

1. Arceyev, A. V.: *Combustion of Industrial Gases*. 1952.
2. Ravitch, M. B.: *Surface Flameless Combustion*. Moscow-Leningrad, 1949.
3. Groshev, M. B.: *Torchless Burning of Gas*. 1950.
4. Khitrin, L. N.: Bull. Acad. Sci. USSR, No. 3, 1953.
5. Shelkin, K. I.: J. Tech. Phys., *9–10*, 1943.
6. Damköhler, G.: National Advisory Committee for Aeronautics, TM 1112, 1947.
7. Karlovitz, B., et al.: *Fourth Symposium (International) on Combustion*, p. 613. Baltimore, The Williams & Wilkins Co., 1949.
8. Leason, D. B.: Fuel, No. 10, 1951.
9. Karlovitz, B.: *Fourth Symposium (International) on Combustion*, p. 60. Baltimore, The Williams & Wilkins Co., 1949.
10. Summerfield, M., et al.: Jet Propulsion, *25*, 377–84, 1955.

41

GROWTH RATES OF TURBULENT FREE FLAMES

By WILLIAM R. MICKELSEN and NORMAN E. ERNSTEIN

Introduction

Extensive investigations have been made of the propagation rate of turbulent flames in Bunsen burners[1, 2, 3, 4] and turbulent flames seated on bluff bodies in premixed fuel-air streams.[5, 6, 7] In these investigations, the propagation rate has been given in terms of a turbulent flame speed S_T defined as:

$$S_T = U\left(\frac{A_a}{\overline{A}}\right) \tag{1}$$

where U is the approach stream velocity, A_a is the cross-sectional area of an approach stream tube and $\overline{A}$ is the smoothed time average area of the flame surface bordered by the stream tube. These definitions are clarified in Figure 1. Turbulent flame speeds measured in this way are generally subject to a number of difficulties. These difficulties include: (a) large fluctuations in instantaneous flame front position, which introduce uncertainty in the evaluation of the mean area, $\overline{A}$, (b) the existence of "piloting zones," which may affect the burning rate of the flame, (c) large velocity differences between the burned and unburned gas streams, which may introduce turbulence in addition to that in the approach stream, and (d) curvature of unburned gas streamlines, which introduces uncertainty in the evaluation of the approach stream tube area, A_a.

To avoid the difficulties present in conventional turbulent flame speed experiments, a study was made of the growth of free flames carried along in a flowing, turbulent, homogeneous mixture of gaseous propane and air.[8] The free flame growth was characterized by an effective turbulent flame

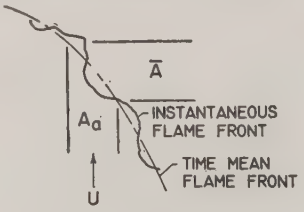

Fig. 1. Stabilized flame.

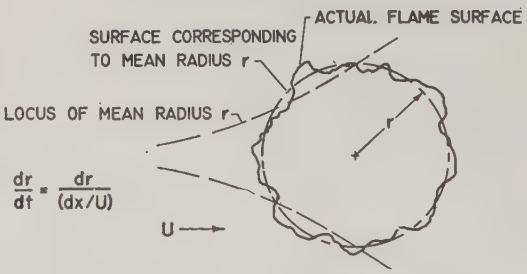

Fig. 2. Free flame.

speed, S_T, derived from a mass flow balance across an infinitesimally thin flame front.[9]

$$S_T = \left(\frac{\rho_F}{\rho_a}\right)\left(\frac{dr}{dt}\right) \tag{2}$$

where (ρ_F/ρ_a) is the density ratio of burned to

unburned gas, respectively, and (dr/dt) is the time rate of change of the free flame globule radius. This definition is clarified in Figure 2.

Previous experimental data have shown that the flame speeds of stabilized flames are increased in the presence of turbulence. Recent theoretical treatments attributed this increase to flame front wrinkling by the large turbulent eddies, and to increased heat and mass transfer due to the turbulent eddies smaller than the flame front thickness. The flame front wrinkling and diffusion processes can be characterized by the principles of turbulent diffusion set forth by Taylor[10] in terms of the

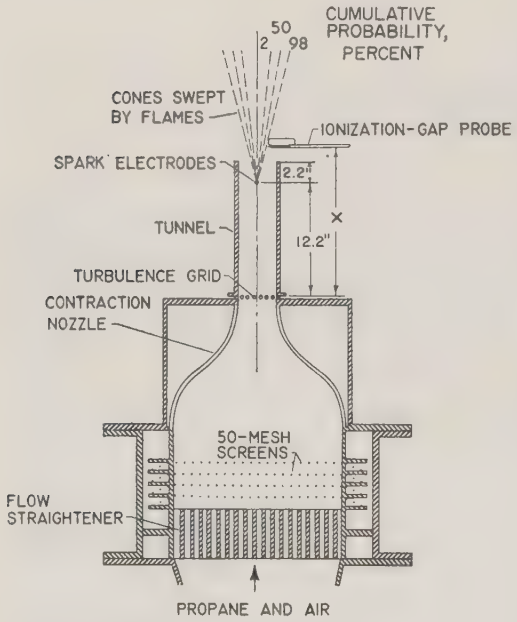

FIG. 3. Combustion tunnel.

turbulent diffusion coefficient, D, and the fluid particle displacement, X:

$$D = \frac{1}{2}\frac{\overline{dX^2}}{dt} = \overline{u^2}\int_0^t \mathcal{R}\, dt \qquad (3)$$

where $\mathcal{R}$ is the mean value of the correlation between velocities of discrete fluid particles over the time interval, t. Since both u and $\mathcal{R}$ have probability distributions, then D and X are expected to be statistical variables also. Following these concepts, the turbulent flame speed should also be a statistical variable with a distribution about a mean value. In contrast to most previous experiments, the present investigation considers turbulent flame propagation from the standpoint of statistical measurement and analysis.

Apparatus and Procedure

The following turbulent propane-air mixture was generated by blowing the premixed gas through a 4- by 4-in. square low-turbulence wind tunnel of conventional design (Fig. 3). The turbulence was introduced by placing one of three wire grids across the gas stream at the tunnel throat. The velocity fluctuations, u, in the stream flow direction, x, were defined by the intensity $\sqrt{\overline{u^2}}$ and the correlation coefficient $f = \overline{u_0 u_\xi}/\overline{u^2}$, u_0 and u_ξ are separated in space by the distance, ξ, and the bars indicate time averages. The turbulence was complicated by the presence of a 136 db sound field (originating in the exhaust system) so that hot-wire anemometer measurements of $\sqrt{\overline{u^2}}$ and f included the sound velocity fluctuations through the relation:[11]

$$\overline{u^2} = \overline{u_s^2} + \overline{u_t^2} \qquad (4)$$

The sound velocity fluctuations $\sqrt{\overline{u_s^2}}$ had a constant value of 0.96 ft/sec throughout the investigation, and the turbulence velocity fluctuations $\sqrt{\overline{u_t^2}}$ were varied by changing the grid size and the stream velocity. The correlation coefficient, f, was varied by changing the grid size, and was assumed to be independent of stream velocity. Correlation coefficients measured downstream from the three grids are shown in Figure 4.

The free flames were ignited by single sparks produced across electrodes protruding from the tunnel walls to the tunnel axis. The spark power supply was of the capacitive type and could be adjusted for sparking rates up to five per second. The growth of the free flames was observed by photographic, ionization-gap, or photo-multiplier tube instrumentation.

The photographic data were obtained with a 16-mm, high-speed, motion-picture camera in a schlieren optical system. The photographic observations were made in a glass walled, enclosed version of the apparatus shown in Figure 3. The photographic data were analyzed by projecting the 16-mm motion picture film record of each flame-globule expansion onto a film viewer. A typical photographic record is shown in Figure 5a. The outline of each globule was traced to permit measuring its area and calculating a mean radius. The mean radius was plotted against time for each flame globule of the sequence, as shown in Figure 5b. The slope of a straight line faired through such a series of experimental points is dr/dt. The effective turbulent flame speed was

then calculated by multiplying dr/dt by the expansion factor ρ_F/ρ_a as shown in Equation (2).

From sets of 30 or more flame speeds obtained in this manner for identical fuel-air-flow conditions, the cumulative probability of occurrence of flames having these flames speeds was calculated.[12] To illustrate the statistical nature of these data, the turbulent flame speeds of a typical set of data are plotted against cumulative probability of occurrence in Figure 5c. Each data point represents the effective flame speeds of a single free flame.

Having established the statistical character of the effective turbulent flame speed, instrumentation was devised for the convenient measurement of free flames in quantities large enough to form true statistical samples. An ionization-gap probe technique was used whereby thousands of free flames could be measured conveniently at fixed stream conditions. The physical orientation of the ionization-gap probe is shown in Figure 3. The ionization-gap probe, together with an electro-mechanical counter, indicated the number of flames N_P reaching a given radius or larger. A photo-multiplier tube with another counter indicated the total number of flames, N_t, so that the cumulative probability of occurrence, $(N_t - N_P)/N_t$, of free-flame radii could be measured for a wide range of effective turbulent flame speeds. Typical data are shown in Figure 6 for two distances down-stream from the spark electrodes. Each data point on this figure represents at least 1,000 free flames. For a given cumulative probability, the effective turbulent flame speed was determined from Equation (2) with the Δr measured between the faired curves shown in Figure 6.

For additional verification of the statistical variation of effective flame speed, a photo-multiplier unit was substituted for the ionization-gap probe for a portion of the experimental program. Light from the spark and the free flame passed through a narrow slit parallel and coincident with the duct axis before entering the photomultiplier tube. The voltage signal from the tube was assumed proportional to the free flame size, so that relative values of effective turbulent flame speed could be measured from oscillograms.

Verification of the Experimental Method

With the aid of the three techniques of observation listed above, a number of assumptions inherent in the equation defining effective free flame speed (Eq. (2)) were verified. The assumptions

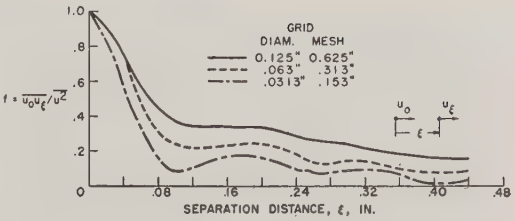

FIG. 4. Correlation coefficient f for each of three grids (curves faired from original data). Mean stream velocity 68.5 fps.

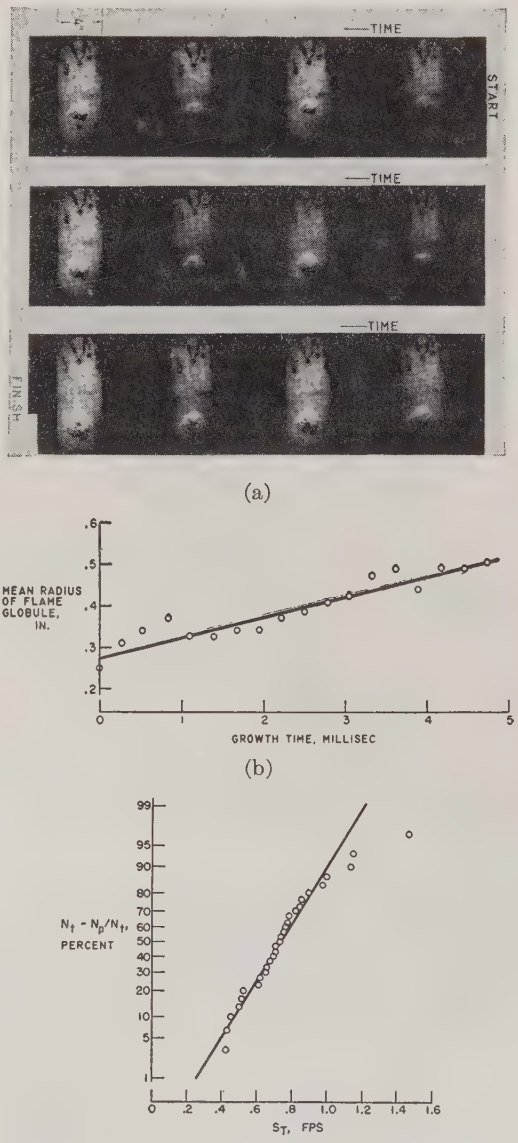

FIG. 5. Typical turbulent flame-speed data from enclosed tunnel. (a) Typical photographic records, film speed, approximately 3600 frames per second; (b) flame-globule expansion history; (c) cumulative probability of turbulent flame speed.

and their verification are discussed in the following paragraphs.

Photographic data of the flame globule growth in the enclosed tunnel were analyzed to determine whether the globules had preferential growth directions. This analysis was made by measuring globule diameters at four angles of rotation from the tunnel axis. Although each globule had different growth rates along the four diameters, no consistent relation between growth rate and direction was found. This observation supports the use of a mean radius in the photographic method of flame-speed measurement, the use of a single radial direction in the ionization-gap method, and the use of a single diameter in the photomultiplier method of flame-growth observation.

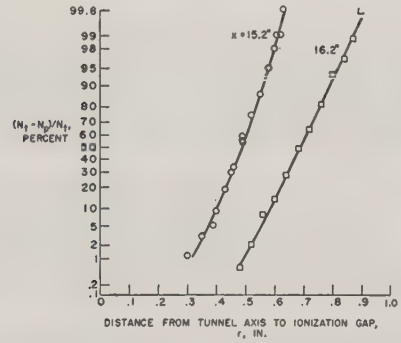

FIG. 6. Typical probability distribution of free-flame size. Stream velocity, 70 fps; grid, 0.125 in. wire diameter by 0.625 in. mesh.

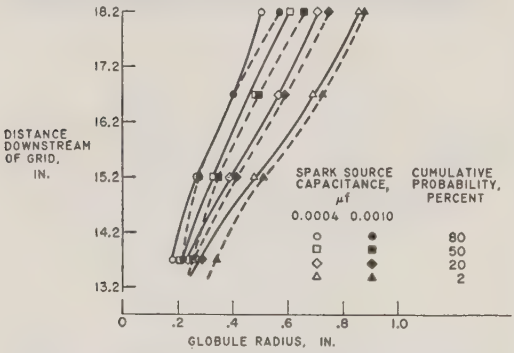

FIG. 7. Effect of spark energy on flame-globule growth.

In order to determine whether the fluctuations in flame-globule-growth rates, illustrated by Figure 3b, were due to pressure fluctuations in the enclosed tunnel, the data were inspected for possible phase relations between the fluctuations in growth rate along four diametral directions. Since no frequency-phase relation was found from these data, it was concluded that pressure fluctuations were not responsible for the fluctuations in globule-growth rate. Additional measurements with a wall-mounted pressure pickup indicated the absence of significant pressure pulsations in the enclosed tunnel.

The effect of buoyancy of the hot flame globule on its axial velocity was determined by measuring the distance from the spark electrodes to the globule center on each flame of photographic sequences such as shown in Figure 5a. The axial velocities calculated from such measurements agreed closely in all cases with the measured stream velocity, which indicated that the buoyancy effect was negligible.

As shown by Equation (2), the rate of thermal expansion of the flame globule is from 7 to 8 times as great as the effective turbulent flame speed. In order to determine whether the unburned-gas motion caused by this thermal expansion was purely radial (from the globule center), simultaneous oscillograph records were made in the free-jet installation with the ionization-gap probe and a shielded hot-wire anemometer probe. The ionization-gap trace indicated the flame-globule passage, and the anemometer trace was proportional to the instantaneous stream velocity. Inspection of 60 such records indicated no axial change in mean stream velocity and therefore no circumferential flow of unburned gases about the sphere.

In order to determine the effect of spark energy on the flame-globule growth, two series of runs were made in the free-jet installation under identical stream and fuel conditions but with spark source energies differing by a factor of 2.5. As shown in Figure 7, cumulative probabilities of flame-globule sizes were measured at a series of axial positions with the ionization-gap instrumentation for two spark source capacitors of 0.0004 and 0.0010 μf. The data of Figure 7 show an increase in initial flame-globule size, but no change in turbulent flame speed between the axial positions $x = 15.2$ and 16.2 in.

Additional information on the relation between the spark characteristics and the flame-globule growth was obtained with the photo-multiplier instrumentation. With this instrumentation, oscillographs were obtained in the free-jet installation showing spark light intensity and flame light intensity as a function of time for 151 consecutive flame globules at constant mean stream and fuel conditions. Typical oscillographs ob-

tained by this method are shown in Figure 8. Special tests indicated that the portion of the trace due to the spark light intensity was proportional to spark current. Statistical analysis showed that the magnitudes of the peak spark light intensity approximated a normal probability distribution. The flame speed of the globule was taken as proportional to the slope of the portion of the oscillograph trace due to flame light intensity. The group of 151 consecutive runs are shown in Figure 9, in which peak spark light intensity is plotted against flame speed for each particular flame globule. The statistical correlation coefficient for these data was determined with Pearson's product moment formula and was found to have an absolute value of | 0.17 | for a possible range of zero to | 1.0 |. The low value of the statistical correlation coefficient is interpreted to indicate that variations in spark current had no effect on turbulent flame speed.

The cumulative probability of occurrence of slopes measured from the series of 151 photomultiplier oscillographs is shown in Figure 10. The statistical distribution of flame speeds measured by this method is interpreted as additional proof of the randomness of the phenomena.

The ionization-gap method assumes that all flame globules have a common origin point. In order to determine the error introduced by this assumption, "origin points" were measured from the series of 151 photo-multiplier traces by extrapolating the slope of the flame light intensity trace to the time axis, as shown in Figure 8. The origin points showed a statistical variation in position, and the theoretical error introduced into flame speeds determined by the ionization-gap method was calculated to be ±2.5 per cent or less, within one standard deviation of origin position. The error in flame speed due to shift in origin point is small compared with the variations in flame speed actually measured by the photographic, the ionization-gap, and the photomultiplier tube methods.

Results and Discussion

Effective turbulent flame speeds were measured in the enclosed-tunnel and free-jet installations over a range of propane-air and turbulence conditions as shown in Table 1. The longitudinal turbulence scales L_f for the enclosed tunnel were determined from turbulence spectrum measurements, and the lateral turbulence scales L_g were calculated through the isotropic turbulence relation $L_g = 0.5\, L_f$. The values of L_g for the free jet were obtained by fitting the exponential curve $e^{-\xi/L_g}$ to graphs of the lateral correlation coefficient, g, where g was determined from the longitudinal correlation coefficient, f, through the isotropic turbulence relation $g = f + 0.5\, \xi(df/d\xi)$.

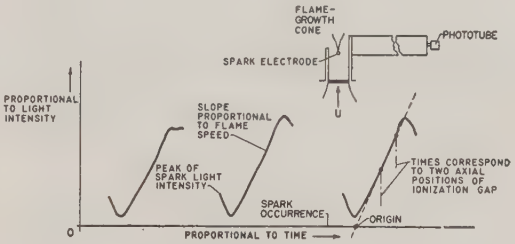

FIG. 8. Typical oscillographs depicting spark occurrence and flame growth.

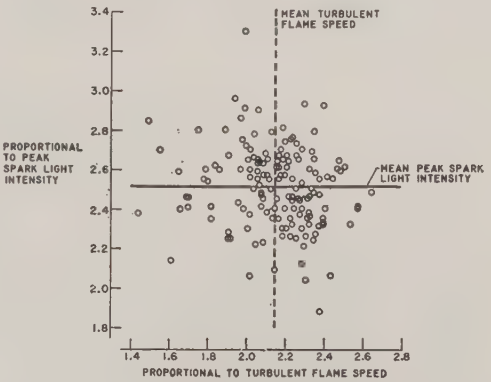

FIG. 9. Correlation between spark light intensity and turbulent flame speed.

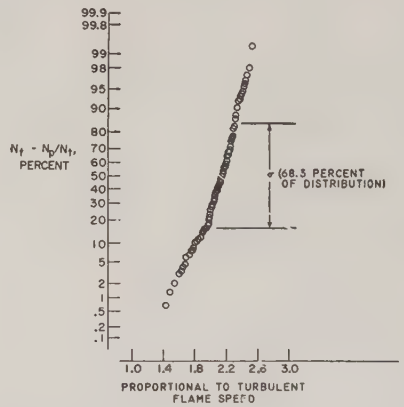

FIG. 10. Statistical variation of turbulent flame speed as determined from photomultiplier oscillograms.

To find the effect of the velocity fluctuation, $\sqrt{\overline{u^2}}$, on the probability distribution, effective speeds of the turbulent free flame were measured

over a range of stream velocities at a constant propane-air weight ratio of 0.07 with a single turbulence grid. These data are plotted in Figure 11 against cumulative probability of occurrence with the velocity fluctuation $\sqrt{\overline{u^2}}$ as a parameter. The statistical variation of effective flame speed is quite apparent, and the probability distribution curves show greater effective flame speeds for the higher velocity fluctuations. From Figure 11, it is seen that the probability density of effective flame speeds is roughly Gaussian (a straight line on probability coordinates) in the range shown, and that the standard deviation is greater for the large velocity fluctuations. These observations are consistent with the discussion in the Introduction, since turbulent velocities generally have been observed to have a Gaussian probability density.[13]

To find the effect of fuel-air weight ratio on the probability distribution of free flame growth rate, a series of data were taken at constant stream and turbulence conditions. These data are shown in Figure 12 where cumulative probability of occurrence is plotted against effective turbulent flame speed. The laminar flame speed measured by the Bunsen burner method[14] is marked on each distribution curve, and shows that the maximum flame speeds for the turbulent free flame and the laminar Bunsen flame occur at the same fuel-air weight ratio. The probability distribution curve for the 0.063 (stoichiometric) and 0.070 fuel-air weight ratios are roughly Gaussian. As the fuel-air weight ratio departs farther from the stoichiometric, the distribution curves depart from the Gaussian form, and have larger standard deviations. The data in Figure 12 show an increasing proportion of sublaminar flame

TABLE 1

Grid Size		Stream Velocity, U	Longitudinal Velocity Fluctuation Intensity, $\sqrt{\overline{u^2}}$	Lateral Turbulence Scale, L_g	Propane-Air Weight Ratio	Distance Downstream of Grid, x
Diam	Mesh					
			Free Jet			
in.	*in.*	*ft/sec*	*ft/sec*	*in.*		*in.*
0.125	0.625	35 to 105	1.18 to 2.60	0.0645	0.07	15.2 to 16.2
0.125	0.625	70	1.69	0.0645	0.056 to 0.09	15.2 to 16.2
0.063	0.313	70	1.34	0.0587	0.058 to 0.084	15.2 to 16.2
0.0313	0.156	70	1.17	0.0437	0.053 to 0.084	15.2 to 16.2
			Enclosed Tunnel			
0.125	0.625	35 to 140	0.81 to 3.51	0.08 to 0.13	0.045 (approx.)	6.3 to 15.3

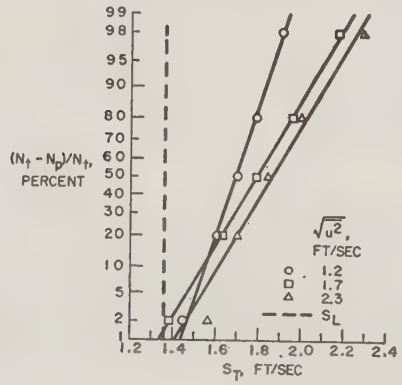

FIG. 11. Turbulent flame speed as a function of cumulative probability of occurrence with longitudinal velocity fluctuation intensity as a parameter. Grid, 0.125 in. diameter by 0.625 in. mesh; propane-air weight ratio, 0.07.

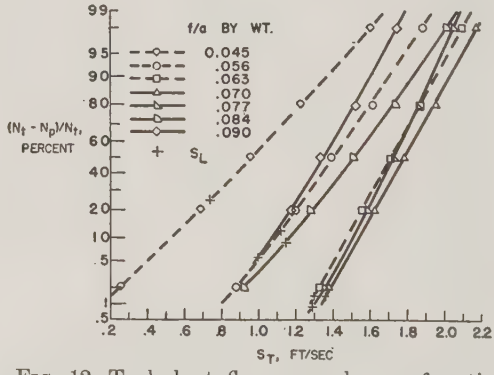

FIG. 12. Turbulent flame speed as a function of cumulative probability of occurrence with fuel-air weight ratio as a parameter. Grid, 0.125 in. diameter by 0.625 in. mesh; stream velocity, 70 fps; turbulence intensity, 1.7 fps.

speeds as the fuel-air ratio departs farther from stoichiometric. Botha and Spalding[15] found that for a given decrease in flame temperature, the laminar flame speed suffers progressively greater decreases from the adiabatic value as the fuel-air ratio departs farther from stoichiometric. From these observations, it is reasonable to conclude that the turbulence had a cooling effect on some of the free flames.

The effect of the turbulence correlation coefficient on the turbulent propagation of the free flame was investigated by the use of the three turbulence generating grids. As shown by Figure 4, increases in the grid dimensions resulted in larger values of the scale, L_f, defined by the equation

$$L_f = \int_0^\infty f \, d\xi \tag{5}$$

The effect of the correlation coefficient, f, on the ratio of turbulent to laminar flame speed, S_T/S_L, is shown in Figure 13 where the data are plotted against fuel-air weight ratio for each grid size with cumulative probability as a parameter. As the correlation coefficient becomes smaller, an increase is noted in the proportion of free flames having speeds less than the laminar. This may be due to a greater diffusive action of the turbulence as the turbulence scale becomes smaller, thereby causing decreases in the flame temperature and therefore the laminar flame speed.

The turbulent flame speed theory proposed by Tucker[16] is compared with the free flame speed data in Figures 13 and 14. The Tucker theory is based on a wave analysis of the interaction of low intensity turbulence with an infinitesimally thin flame front, and results in the equation:

$$\frac{S_T}{S_L} = 1 + f\left(\frac{T_F}{T_a}\right)\frac{\overline{u^2}}{S_L^2} \tag{6}$$

where $f(T_F/T_a)$ is a function of the flame and unburned gas temperatures. The theory neglects second order and higher values of the ratio $\overline{u^2}/S_L^2$, but conforms well to the free flame data over ranges where this assumption becomes uncertain.

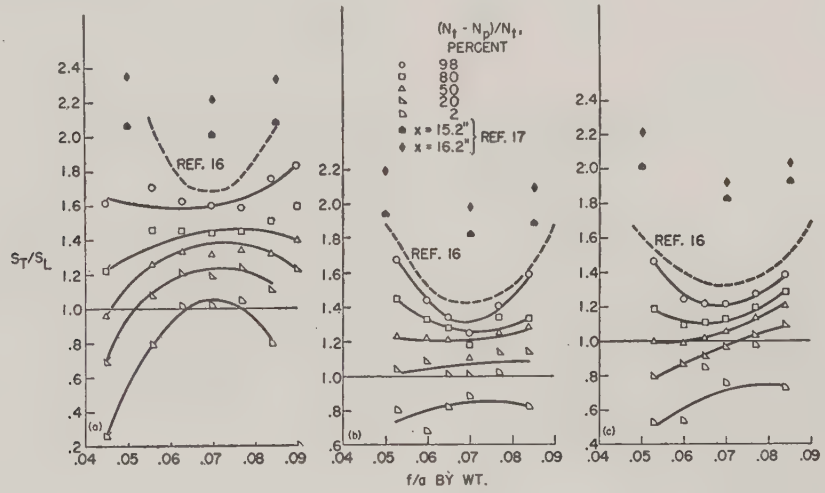

FIG. 13. Comparison of turbulent flame speed data with theories from references 15 and 16. (Open symbols denote free-jet data; tailed symbols, enclosed tunnel data.) (a) Grid, 0.125 in. diameter by 0.625 in. mesh; (b) grid, 0.063 in. diameter by 0.313 in. mesh; (c) grid, 0.0313 in. diameter by 0.156 in. mesh.

The turbulent flame theory proposed by Scurlock and Grover[17] is compared with the free flame data in Figures 13 and 14. The theory assumes that the turbulent flame has an increased propagation rate by virtue of cone shaped wrinkles; where the ratio of cone height to base diameter is proportional to $(\overline{X_{tot}^2}/L_g^2)^{\frac{1}{2}}$. The analysis results in the equation

$$\frac{S_T}{S_L} = \left[1 + 4\left(\frac{\overline{X_{tot}^2}}{L_g^2}\right)\right]^{\frac{1}{2}} \tag{7}$$

where the mean square displacement $\overline{X_{tot}^2}$ is in-

creased by turbulence and flame generated turbulence, but reduced by the wrinkled smoothing effect of the local laminar flame speed, S_L. In the present investigation, the flame generated turbulence was assumed negligible (as predicted by the Tucker theory[16]), so that $\overline{X_{tot}^2}$ was calculated from the relation

$$\sqrt{\overline{X_{tot}^2}} = \int_0^{\Delta t} \left\{ \frac{1}{2\sqrt{\overline{X_T^2}}} \frac{d\overline{X_T^2}}{dt} - \frac{S_L}{4} \left[\left(1 + 4 \frac{\overline{X_T^2}}{L_g^2} \right)^{\frac{1}{2}} - 1 \right] \right\} dt \tag{8}$$

The contribution $\overline{X_T^2}$ due to "turbulent wrinkling" was determined from

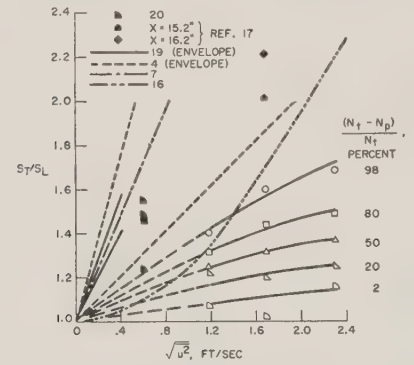

FIG. 14. Comparison of turbulent flame speed data with those of other investigations.

$$\overline{X_T^2} = \overline{2u^2} \int_0^{\Delta t} \int_0^{\Delta t} \mathcal{R}\, g_t\, dt\, dt \tag{9}$$

The Lagrangian correlation coefficient, $\mathcal{R}$, was found from the correlation coefficient, f, through the independent variable transformation, $\xi = 0.6\sqrt{\overline{u_t^2}}$.[18] The correlation coefficient, g_t, was found from the lateral correlation coefficient, g, through the transformation, $\xi = S_L t$. The theory predicts that the turbulent flame speed approaches an asymptotic value after a time greater than the characteristic time of the turbulence $L_g/\sqrt{\overline{u^2}}$. Because the growth times encountered in the present experiment were less than the characteristic time of the turbulence, the ratio, S_T/S_L, was calculated for the two growth times corresponding to the two ionization gap stations. From inspection of Figures 13 and 14 it is evident that the Scurlock-Grover theory falls well above the data.

Turbulent flame speeds measured by other methods are compared with the free-flame data in Figure 14. The Bunsen burner,[7] the nozzle burner,[4] and the flame tube[19] data all fall above the free flame speeds of the present experiment and another similar experiment.[20] Better agreement between the data could be obtained if the free flame data were plotted against the turbulence intensity, $\sqrt{\overline{u_t^2}}$, instead of the velocity fluctuation, $\sqrt{\overline{u^2}}$, thereby eliminating the velocity contributions due to sound. This procedure is questionable, since little is known about the effect of sound on flame propagation.

Conclusions

From the results of the investigation, the following conclusions are drawn.

(1) The propagation rate of a free turbulent flame is a statistical variable having a probability of occurrence band bounded by a zero propagation rate and possibly an upper bound well above the laminar flame speed.

(2) The propagation rate of a free turbulent flame is substantially less than those previously measured for stabilized flames.

(3) The statistical spread of turbulent free-flame propagation rates is markedly wider in both the lean and rich fuel-air-ratio regions.

(4) Values calculated from the Tucker theory for turbulent free-flame propagation apparently form an upper limit for the statistical spread of free-flame propagation rates in the regions where the velocity fluctuations are small.

REFERENCES

1. HOTTEL, WILLIAMS, AND LEVINE: *Fourth Symposium (International) on Combustion*, p. 636. Baltimore, The Williams & Wilkins Co., 1953.
2. KARLOVITZ, B., DENNISTON, D. W., JR., AND WELLS, F. E.: J. Chem. Phys. *19*, 541 (1951).
3. BOLLINGER, L. M., AND WILLIAMS, D. T.: NACA Rep. 932 (1949).
4. WRIGHT, F. H.: California Institute of Technology Jet Propulsion Laboratory Progress Report 3-21 (1950).
5. SCURLOCK, A. C.: Massachusetts Institute of Technology Meteor Report 19 (1948).
6. WILLIAMS, HOTTEL, AND SCURLOCK: *Third Symposium on Combustion, Flame and Explosion Phenomena*, p. 21. Baltimore, The Williams & Wilkins Co., 1949.
7. WOHL, SHORE, VON ROSENBERG, AND WEIL: *Fourth Symposium (International) on Combustion*, p. 620. Baltimore, The Williams & Wilkins Co., 1953.
8. MICKELSEN, W. R., AND ERNSTEIN, N. E.: NACA TN 3456 (1955).

9. Stevens, F. W.: NACA TR 176 (1923).
10. Taylor, G. I.: Proc. London Math. Soc., *20*, 196 (1922).
11. Mickelsen, W. R., and Laurence, J. C., NACA RM E53F19 (1953).
12. Mickelsen, W. R.: M. S. Thesis, Case Institute of Technology, 1953.
13. Batchelor, G. K.: Australian J. Sci. Research, 2, 437 (1949).
14. Dugger, G. L.: NACA TR 1061 (1952). Also J. Am. Chem. Soc., *72*, 5271 (1950).
15. Botha, J. P., and Spalding, D. B.: Proc. Royal Soc. (London), *A225*, 71 (1954).
16. Tucker, M.: NACA TN 3407 (1955).
17. Scurlock, A. C., and Grover, J. H.: *Fourth Symposium (International) on Combustion*, p. 645. Baltimore, The Williams & Wilkins Co., 1953.
18. Mickelsen, W. R.: NACA TN 3570 (1955).
19. Leason, D. B.: Fuel, *30*, 233 (1951).
20. Bolz, R. E., and Burlage, H.: Jet Propulsion, *25*, 265 (1955).

42

ON THE STRUCTURE OF TURBULENT FLAMES[a]

By K. WOHL, and Collaborators[b]

There exists at present a considerable uncertainty about the structure of "turbulent" flames. A weak disturbance will make a flame front wrinkled. Larger disturbances will cause progressive disintegration which will take the form first of ruptures, then of isolated flame front elements (balls of fire, flamelets) and possibly of a quasi-homogeneous distribution of the reaction zone in depth. The latter form of burning is approached at extreme degrees of mixing at which the rate of burning approaches a maximum value; its realization in turbulent flames with smaller burning rates is controversial (Summerfield, Reiter, Kebely and Mascolo,[1] and Kovasznay[2]). As long as burning occurs in laminar flame front elements, either connected or isolated, the instantaneous loci of flame luminosity practically coincide with those of a "sudden" transition from unburned to burned. The average maximum luminosity of the flame brush will then be observed where combustion, defined as oxygen consumption, is half completed. For the case of a "homogeneously" distributed reaction zone Summerfield predicted that in analogy to the laminar flame front maximum luminosity would be observed where combustion were about 85 per cent complete.

We have made a comparative study of the progress of the chemical combustion process in a number of turbulent flames and the local luminosity of these flames as obtained by a densitometric evaluation of direct photographs.

1. Enclosed Flames at Atmospheric Pressure

By H. E. von ROSENBERG, R. C. SCHILLY, and C. W. SHIPMAN

Various homogeneous propane-air mixtures were burned in a horizontal duct of 2 in. inner height, 1.5 in. inner width and 10 inches length. The 2 in. vertical walls consisted of quartz plates. The flames were held by a plate of ¼ in. thickness which extended between the center lines of the quartz walls. Due to an arrangement similar to that described by Scurlock[3] the initial velocity profile was flat and the cold stream turbulence was below 0.4 per cent as was ascertained with the help of a hot-wire anemometer.[4] The velocity was 60 ft/sec.

The stoichiometric flame was sampled with a water-cooled probe. Care was taken to sample with a velocity equal to the local velocity of the flame gases at the position of the probe tip. In order to find the local gas velocity the impact pressure and static pressure at the point of analysis were measured, and preliminary values of temperature and density were obtained from analysis of samples drawn with a tentative sam-

[a] This work was sponsored by Project SQUID which is supported by the Office of Naval Research under contract N6-ori-105, T.O. III, NR-098-038. Reproduction in full or in part is permitted for any use of the United States Government.

[b] See the single chapters of this article.

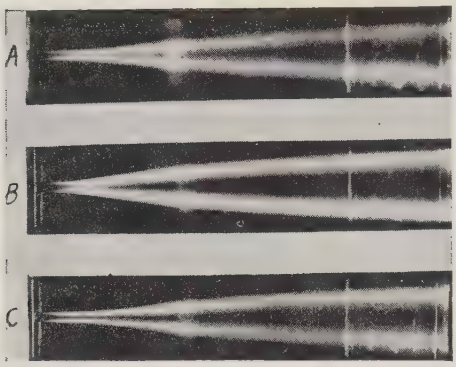

FIG. 1. Direct photographs of propane-air flames burning at 1 atmos in a rectangular duct. Turbulence below 0.4 per cent. A, lean flame, 3.38 per cent propane; B, stoichiometric flame, 4.03 per cent propane; C, rich flame, 6.54 per cent propane.

FIG. 2. Instantaneous schlieren photographs of flames of Fig. 1.

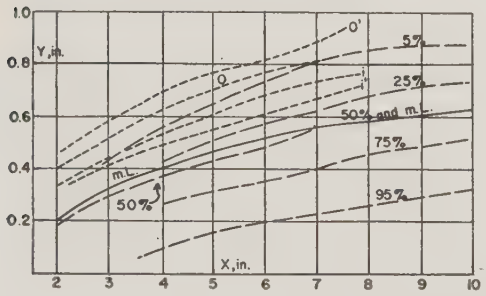

FIG. 3. Contours of chemical composition, luminosity and schlieren image of stoichiometric flame of Fig. 1 and Fig. 2B.

X = distance from flame holder in flow direction
Y = distance from central plane of duct perpendicular to flow direction.

m.L. ——— line of maximum luminosity
— — — lines of indicated per cent of oxygen consumption
- - - - - - schlieren image contours
i, inner contour (Schilly)
i', inner contour (von Rosenberg)
o, outer contour (Schilly)
o', outer contour (von Rosenberg)

pling velocity. Pitot pressure and density yielded a first gas velocity value. Shipman and von Rosenberg repeated the sampling with this velocity and recalculated the density and gas velocity. The correct sampling velocity could thus be found by trial and error. The details of this method will be discussed by authors mentioned at another place.

In addition, direct pictures of lean, stoichiometric and rich propane-air flames were taken at the same conditions (Fig. 1) and evaluated densitometrically with respect to the lines of maximum flame luminosity. Also instantaneous schlieren pictures of the same flames were obtained (Fig. 2). The "flame front region" was determined from the schlieren pictures by connecting the highest points of the larger bulges by a smooth line and also the lowest points of the more outspoken valleys. The "flame front" was then supposed to be between these outer and inner contours.

Figure 3 assembles a large number of curves characteristic of the upper half of the stoichiometric flame burning in the horizontal duct. The line of maximum luminosity (solid) is seen to coincide very well with the line of 50 per cent oxygen consumption (long dashes) in the downstream section of the flame and to be slightly premature in the upstream section. The lines of 5, 25, 75, and 95 per cent oxygen consumption are also inserted. Two inner (i) and outer (o) contours of the schlieren picture are added (short dashes). The curves indicated by i and o pertain to flames produced by Schilly, those indicated by i' and o' to flames produced by von Rosenberg. For unknown reasons, the latter show stronger waves of a somewhat regular nature. But the average positions of the two schlieren "flame fronts" coincide very well. It is noticed that combustion has progressed at the place of the average "flame front" position in the upstream region of the flame by less than 5 per cent, in the downstream region by somewhat more than 5 per cent. The line of maximum luminosity is far inside the inner contour even of von Rosenberg's flame (curve i'). For lean and rich propane-air flames no reliable chemical analytical data are available at present, but the relationship of the schlieren picture contours to the line of maximum luminosity (Figs. 4 and 5) is the same that was found for the stoichiometric flame.

Thus there seems to occur generally only little combustion in the schlieren front, i.e., at the places of maximum gradient of density. Most of the gas breaks through this front unburned or

quite incompletely burned. The idea that burning in the schlieren front proceeds to the CO-stage would not account for the observations at all. The form in which combustion continues behind the schlieren front is open to question. The result that the line of maximum luminosity coincides so closely with that of 50 per cent oxygen combustion suggests combustion of pockets or streaks of combustible material by way of flame front elements which are similar to laminar flame fronts. Burning in a quasi-homogeneously distributed burning zone would, according to Summerfield, Reiter, Kebely and Mascolo,[1] lead to belated luminosity as mentioned.

One point may be added: The quenching of the combustion reaction through cooling in the sampling probe is independent of sampling velocity.[5] In the reported experiments it can probably be considered to be instantaneous. If, however, a reaction would have occurred in the probe the true oxygen consumption would have been less than the one measured, i.e., the maximum luminosity curve in Figure 3 would become premature and the schlieren contours still more premature

2. General Considerations

A. DISSOLUTION OF FLAME FRONT

The conclusion just drawn seems plausible since the criterion which Kovasznay[2] has given for the dissolution of a flame front

$$\frac{\text{Typical velocity gradient in approaching cold flow}}{\text{Typical velocity gradient in laminar flame}} = \alpha > 1$$

does not seem to be fulfilled for the flames under consideration. Kovasznay writes for the above ratio

$$\alpha = \frac{u'\Delta_o}{\lambda S_o}$$

(u' = root mean square turbulent velocity fluctuation, λ = microscale of turbulence in the flow, S_o = laminar burning velocity, Δ_o = thickness of laminar flame front.) It is suggested to modify the term for the typical velocity gradient in the laminary flame and to write

$$\alpha = \frac{u'\Delta_o T_o}{\lambda S_o (T_f - T_o)} > 1 \qquad (1)$$

(T_o = cold flow temperature, T_f = maximum flame temperature). There follows that low pressure (large Δ_o) and excess of one of the combustion partners (small S_o, large Δ_o, small T_f) favor the dissolution of the flame front. For the stoichiometric propane-air flame considered we have[6] $\Delta_o = 0.0124$ cm, $T_o = 293°K$, $S_o = 39$ cm/sec, $T_f = 2207°K$, mean cold flow velocity $U_o = 1830$ cm/sec, i.e., $\alpha = 0.089\ (u'/U_o)/\lambda$. Even with a λ-value as small as 0.2 cm and a (u'/U_o)-value as high as 0.05, α would only reach the value 0.022. For the lean and rich flame α is larger but remains far below the value 1.

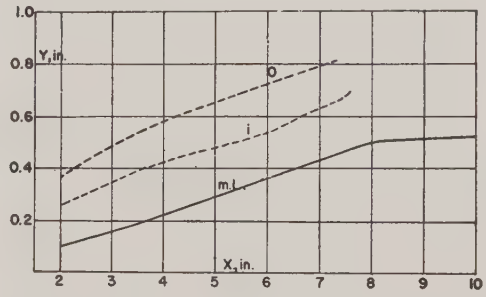

FIG. 4. Contours of luminosity and schlieren image of lean flame of Fig. 1 and Fig. 2A. Symbols: see Fig. 3.

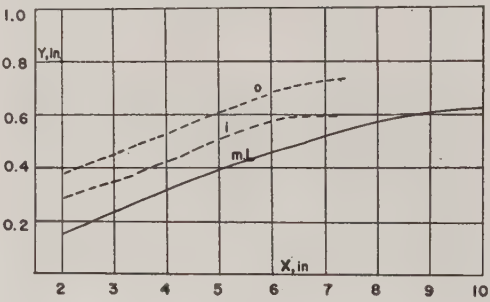

FIG. 5. Contours of luminosity and schlieren image of rich flame of Fig. 1 and Fig. 2C. Symbols: see Fig. 3.

It seems that Kovasznay's criterion $\alpha > 1$ leads to a dissolution of the flame front only if an additional criterion is fulfilled which is $\lambda/\Delta_o > 1$. Usually, if $\lambda/\Delta_o > 1$ holds the condition $\ell_1/\Delta_o > 1$ (ℓ_1 = Lagrangian scale) will also be fulfilled. In the distributed reaction zone, the mean time for combustion τ_t is determined by the mean chemical reaction time

$$t^* = \frac{\Delta_o T_o}{S_o \bar{T}} \qquad (2)$$

($\bar{T}$ = average flame front temperature) and the mean lifetime of an eddy or mixing time

$$\tau = \frac{\ell_1}{u'} \qquad (3)$$

The ratio of these two periods

$$\beta = \frac{t^*}{\tau} = \frac{u'\Delta_o T_o}{\ell_1 S_o \bar{T}} \tag{4}$$

bears a strong resemblance to Kovasznay's term, α (Eq. (1)). For the mean combustion time we write

$$\tau_t = t^* + \tau \quad \text{or} \quad \frac{\tau_t}{t^*} = 1 + \frac{1}{\beta} \tag{5}$$

It is seen that the factor, β, is decisive for the question of how close the reaction rate in a distributed turbulent flame comes to the chemical reaction rate in a laminar flame front.

If $\lambda/\Delta_o < 1$ a smooth flame front will exist which is somewhat thickened by turbulence. Normally $\ell_1/\Delta_o < 1$ will then hold as well. Damköhler[7] and Shelkin[8] treated this case by operating with a turbulent diffusivity

$$\epsilon = u'\ell_1 \tag{6}$$

i.e., by assuming tacitly that $\tau < t^*$ or $\beta > 1$. They found

$$\frac{S}{S_o} = \frac{\Delta}{\Delta_o} = \sqrt{\frac{\nu + \epsilon}{\nu}} = \sqrt{1 + \frac{u'\ell_1 T_o}{\Delta_o S_o \bar{T}}} \tag{7}$$

(S = burning velocity of a flame front element, Δ = thickness of a flame front element, ν = kinematic viscosity). The last term in the above sequence implies $\nu = \Delta_o S_o \bar{T}/T_o$ (see, e.g.,[6] Eqs. (1) and (2)). Equation (7) is not likely to lead to large effects.

If $\ell_1/\Delta_o < 1$ and $\beta < 1$, the eddy diffusivity becomes

$$\epsilon = (u')^2 t^* \tag{8}$$

from which there follows with the help of Eq. 2 and 7

$$\frac{S}{S_o} = \frac{\Delta}{\Delta_o} = \sqrt{1 + \left(\frac{u'T_o}{S_o \bar{T}}\right)^2} \tag{9}$$

If $\ell_1/\Delta_o > 1$ and $\alpha < 1$ a distorted (wrinkled) flame front exists. The corresponding average turbulent burning velocity S_t has been expressed by Shelkin[8] for the case of $u'/S_o < 1$ by the historically important equation

$$\frac{S_t}{S} = \sqrt{1 + \left(\frac{2u'}{S_o}\right)^2} \tag{10}$$

which resembles Equation (9). (For $u'/S_o > 1$ there would follow by Shelkin's method $S_t/S = \sqrt{1 + 8u'/S_o}$.) At these conditions the part of the spectrum of scale below Δ_o increases S_o and leads, according to the method used by Wohl,[6] for $\beta < 1$ (i.e., for the case of Equation (8)) to Equation (9), and for $\beta > 1$ (i.e., for the case of Equation (6)) to the equation

$$\frac{S}{S_o} = \sqrt{1 + \frac{u'\Delta_o}{\ell_1 S_o}} \tag{11}$$

which contains essentially the term β (see Wohl[6]). But frequently, if $\beta > 1$, there will be $\alpha > 1$, so that no flame front would exist at all.

B. SAMPLING

Hirschfelder (see, e.g., Hirschfelder, Curtiss and Bird[9]) drew attention to the difference between the mass fraction, x_j, of a species at any place in a steady state-flame reaction zone and the fractional mass flow, x_j^s, of this species, i.e., the fraction which passes through a plane perpendicular to the direction of flow. The relationship between these two quantities in one-dimensional flow is

$$x_j^s = x_j \left(\frac{U_m + U_j^{(D)}}{U_m}\right)$$

(U_m = mass average velocity, $U_j^{(D)}$ = diffusion velocity of species j). The distinction plays an important part in the theory of von Karman and Penner[10] and has been considered in the evaluation of experimental data for the laminar flame front by Fristrom, Prescott and Grunfelder.[11] It should apply in some way also to the reaction zone of turbulent flames. The continuity equations lead to the result that the chemical reaction rate r_j (the production of mass of species j per cc and sec) is given by $r_j = m\dfrac{dx_j^s}{dz}$ (m = constant mass velocity, z = length in direction of flow). Integration of this equation yields the degree of conversion (e.g., oxygen consumption). In order to find the latter it is therefore desirable to measure x_j^s.

It appears to us that this quantity, x_j^s, is obtained directly by sampling if the velocity of sampling equals the local gas velocity as was the case in the experiments on stoichiometric propane-air flames reported above. If the sampling velocity is increased the effect of diffusion is minimized so that the fraction sampled comes closer to mass fraction, x_j. A decrease of sampling velocity should yield a result more different from x_j than x_j^s. In propane-air flames the diffusion velocity of the reactant oxygen is positive and that of the product CO_2 is negative so that

$x^s_{O_2} > x_{O_2}$ and $x^s_{CO_2} < x_{CO_2}$. One therefore should find in a reacting gas mixture with increasing sampling velocity an increasing oxygen consumption. This is the same effect of sampling rate which occurs if a gas is inhomogeneous, consisting of a mixture of hot light eddies of combustion products and heavy eddies of reactants.[12, 13, 14]

3. Open Flames at Atmospheric Pressure

By R. M. ZIELINSKI

The relationship between luminosity and progress of combustion has also been tested with open butane-air flames burning from a cooled tube of 1-in. i.d. in a chamber of 10 in. by 10 in. cross-section through which a slow stream of nitrogen was flowing. The flame was held at the rim by a stoichiometric butane-oxygen flame burning from an annulus. The main stream velocity was 49 ft/sec. The flow rate of the pilot mixture was 1 per cent of that of the main flow. The approach turbulence was varied by placing screens in the tube as was described by Wohl and Shore.[15]

Sampling was carried out with a water-cooled probe. The sampling velocity was probably about equal to the maximum local velocity in the flame (pitot pressure measurements carried out by Mr. J. L. Waldron and temperature estimates yielded a maximum local velocity of 2900 cm/sec which agrees with the average velocity estimated from the time of collecting the gas sample). Flame photographs were evaluated with a densitometer, and the true luminosity per cc in the plane through the burner axis was ascertained from the observed luminosity by a stepwise procedure.

The results are shown in Table 1. On the average the points of maximum luminosity in the flame axis lie 5.3 mm below the points of 50 per cent oxygen consumption and the points of maximum luminosity in two flame cross-sections at lower heights lie on the average closer to the axis by 0.6 mm than the points of 50 per cent oxygen consumption.

These differences are small and since they do not vary with conditions in a recognizable regular fashion the result is interpreted as an essential coincidence of maximum luminosity and 50 per cent oxygen consumption. Sampling with too high a velocity and incomplete quenching of the reaction in the probe would make the true oxygen consumption to be smaller than found so that luminosity would be premature. These results, therefore, favor again the model of flame front burning over that of a continuously distributed reaction.

Table 1. Open Butane-Air Flames

Points of maximum luminosity (subscript ml) and of 50 per cent consumption of reactable oxygen (subscript 50). Burner tube diameter 1 in. Cold stream velocity 49 ft/sec

		Per Cent Butane				
		3.13 (stoich.)		3.91		4.69
		Per Cent Turbulence				
		5	9	<1	5	5
Height above burner in flame axis	h_{50}, cm	25.6	14.2	21.0	15.7	14.9
	h_{ml}, cm	24.8	14.55	19.1	15.5	14.8
	$h_{50}-h_{ml}$	+0.8	−0.35	+1.9	+0.2	+0.1
Distance from flame axis at $\frac{1}{3}\ h_{ml}$	r_{50}, cm	1.27	1.36	1.30	1.20	1.42
	r_{ml}, cm	1.23	1.36	1.23	1.23	1.25
	$r_{50}-r_{ml}$	+0.04	0	+0.07	−0.03	+0.17
Distance from flame axis at $\frac{2}{3}\ h_{ml}$	r_{50}, cm	0.96	1.29	1.10	1.12	1.12
	r_{ml}, cm	0.94	1.08	1.04	1.11	1.09
	$r_{50}-r_{ml}$	+0.02	+0.20	+0.06	+0.01	+0.03

The sign + signifies premature luminosity, the sign − signifies belated luminosity.

4. Enclosed Flame at 0.2 Atmospheres

By D. H. ARCHER and W. M. JACOBI

A similar investigation as described in Sections 1 and 3 has been made for butane-air flames burning at 0.2 atmos in a vertical water-cooled tube

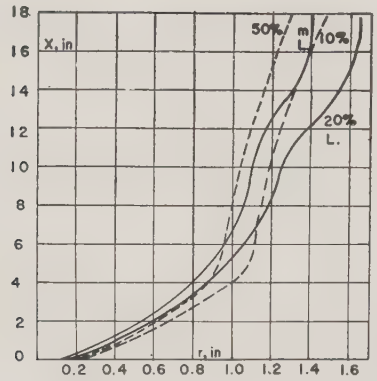

FIG. 6. Contours of chemical composition and luminosity of stoichiometric butane-air flame (3.18 per cent), burning at 0.2 atmos in a tube. Intensity of turbulence 0.6 per cent, average cold flow velocity 32 ft/sec.

X = distance from pilot in direction of flow
r = distance from tube axis
m.L. ——— line of maximum luminosity
20%L. ——— line of 20 per cent of maximum luminosity
— — — line of indicated per cent of oxygen consumption

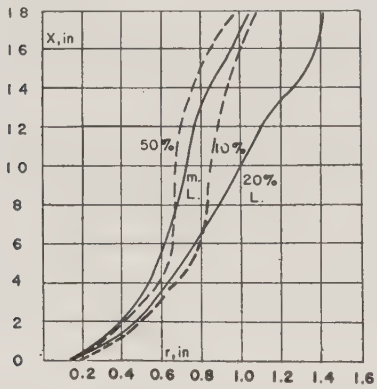

FIG. 7. Flame similar to that of Fig. 6. Intensity of turbulence 0.6 per cent, velocity 68 ft/sec.

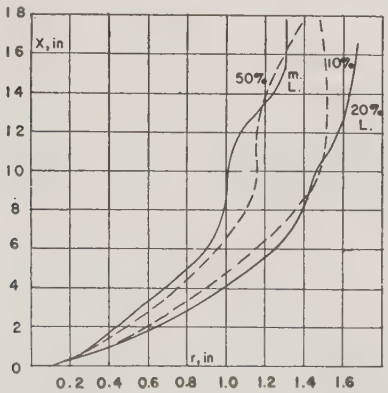

FIG. 8. Flame similar to that of Fig. 6. Intensity of turbulence 7 per cent, velocity 32 ft/sec.

of 3 in. diam from a central stoichiometric H_2-O_2 pilot flame. Experiments showed that the flame composition outside the pilot was not affected by variation of the pilot flame. The turbulence level of the approach stream was varied with the help of screens. Gas samples have been collected by means of a water-cooled probe. The same probe was used for measuring the pitot pressure, which enabled the determination of local velocities as described in Section 1. The measurements have been carried out for 4 conditions at several distances behind the pilot (Figs. 6, 7, 8 and 9 and Table 2), and for many other conditions at 17.8 in. behind the pilot (Table 3). Direct photographs have been taken and densitometrically evaluated for all conditions at numer-

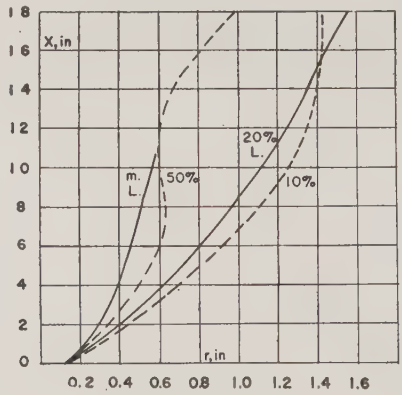

FIG. 9. Flame similar to that of Fig. 6. Intensity of turbulence 7 per cent, velocity 68 ft/sec.

ous distances behind the pilot. The distortions caused by the water mantle around the burner tube have been taken into consideration, and the true luminosity per cc in the plane through the tube axis has been determined by a stepwise procedure.

A variation of the mean sampling velocity from about 13 per cent lower than stream velocity to about 39 per cent higher had an insignificant effect on the analytical result. Concerning the question of quenching of the combustion reaction in the probe, it was estimated that it would take 2.10^{-5} sec to cool the combustion products to 760°C. This period compares favorably with the mean reaction time in the laminar flame which, at 0.2 atmos, is about 4.10^{-4} sec (see Eq. (2), $\Delta_o = 0.062$ cm, $S_o = 40$ cm/sec, $\bar{T}/T_o = 4$).

These experimental data are being used here to make a comparison between the points of maximum luminosity and 50 per cent consumption of reactable oxygen in a horizontal cross-section,

and between the outer points of 20 per cent of maximum luminosity and those of 10 per cent-oxygen consumption in a horizontal cross-section. in Table 3 in such a manner that it is indicated by the signs + or − whether a certain luminosity occurs further away from the axis than the pre-

Table 2. Stoichiometric Butane-Air Flames at 0.2 Atmos in a Circular Duct

Cross-sections at various distances from the pilot. The signs + and − pertain to the difference between the distance of a point of a certain luminoisty from the axis and the distance of a point of certain consumption of reactable oxygen from the axis in the same cross-section. *The sign + signifies premature luminosity, the sign − signifies belated luminosity.* Two signs signify a large difference; a sign in parentheses signifies a small difference.

	Velocity ft/sec	0.6 Per Cent Turbulence		7.0 Per Cent Turbulence	
		X^*	Sign	X^*	Sign
		in.		*in.*	
Points of maximum luminosity and 50 per cent O_2-consumption	31	0–6.0	−	0–13	—
		6–17.8	+	13–17.8	0
	68	0–7.4	−	0–12	−
				12	0
		7.4–17.8	(+)	12–17.8	−
Points of 20 per cent of maximum luminosity and 10 per cent O_2-consumption	31	0–7.0	−	2–10	+
				10	0
		7.0–17.8	+	10–17.8	+
		0–7.0	(−)	0–15	−
	68	7.0–17.8	++	15–17.8	(+)

* X = distance downstream of pilot flame.

Table 3. Butane-Air Flames Burning from a Pilot Flame at 0.2 Atmos in a Circular Duct

Cross-section at 17.8 inches distance from the pilot. The meaning of the signs is explained in Table 2

	Velocity	Per Cent Butane in Butane-Air Mixture								
		3.13 Per Cent (Stoich.)			~2.5 Per Cent			~4 Per Cent		
		Per Cent Turbulence			Per Cent Turbulence			Per Cent Turbulence		
		0.6	4.8	7.0	0.6	4.8	7.0	0.6	4.8	7.0
	ft/sec									
Points of maximum luminosity and 50 per cent O_2-consumption	31	+		0	+		−	+		−
	68	(+)		−			− −			− −
	115	(+)	−	(−)	+	−	+	(+)		−
Points of 20 per cent of maximum luminosity and 10 per cent O_2-consumption	31	+	+	+	+		(+)	+	+	+
	68	++	(+)	(+)	+		−	+	+	+
	115	+	+	0	+	(+)	−	(+)	+	(−)

Figures 6, 7, 8 and 9 show the detailed results found for a stoichiometric flame at average cold stream velocities of 32 ft/sec and 68 ft/sec and turbulence levels of 0.6 per cent and 7 per cent. The other data, all pertaining to a cross-section 17.8 in. downstream of the pilot, are summarized sumed corresponding oxygen consumption, i.e., prematurely, or whether it occurs belatedly. Especially small differences are indicated by a parenthesis, especially large ones by a doubling of the sign. The same method has been used in Table 2 to sum up the relationships between

luminosity and oxygen consumption at various distances from the pilot as they can be read from Figures 6, 7, 8 and 9.

The conclusions for the case of low approach turbulence which can be drawn from Figures 6 and 7 and the left half of Table 2 are that on the whole the loci of maximum luminosity are close to those of 50 per cent oxygen consumption: near the flame holder the luminosity occurs belatedly, far away from it prematurely. It is in agreement with these findings that, according to Table 3, the maximum luminosity at low approach turbulence and *large* distances from the Pitot tube is invariably premature. With increasing approach turbulence the maximum luminosity shifts, according to all evidence, especially that in Table 3, to points of higher oxygen consumption. This tendency is strongest with lean and rich flames for which the luminosity at higher turbulence lies (with one exception) at values of oxygen consumption larger than 50 per cent. This indicates that at these conditions combustion occurs to some degree in a "homogeneously" distributed reaction zone (Summerfield, Reiter, Kebely and Mascolo[1]), in agreement with the conclusion drawn from Kovasznay's Equation (1) in Section 2, that "low pressure and excess of one of the combustion partners favor the dissolution of the flame front."

For the luminosity equal to 20 per cent of its maximum value there is a general tendency to occur prematurely compared with the consumption of 10 per cent of the reactable oxygen. This is possibly due to the fact that the first stages of combustion, concerned with the formation of CO rather than with its further oxidation, are connected with a stronger luminosity. Close to the flame holder, though, the "20 per cent luminosity" occurs again mostly belatedly although not quite as much as the maximum luminosity (Table 2).

At the highest velocity of 115 ft/sec an increase of turbulence causes the 20 per cent luminosity points to shift to higher oxygen consumption, least for the stoichiometric and most for the lean flame. This is assumed to be the result of a dissolution of the flame front at conditions of highest absolute intensity of turbulence, in agreement with the conclusions drawn in the preceeding paragraph.

REFERENCES

1. Summerfield, M., Reiter, S. H., Kebely, V., and Mascolo, R. W.: Jet Propulsion, *25*, 377 (1955).
2. Kovasznay, L. S. G.: Jet Propulsion *26*, 485 (1956)
3. Scurlock, A. C.: Meteor Report No. 19, Massachusetts Institute of Technology, May 1948.
4. Wohl, K., Shore, L., von Rosenberg, H. E., and Weil, C. W.: *Fourth Symposium (International) on Combustion*, p. 620. Baltimore, The Williams & Wilkins Co., 1953.
5. Archer, D. H.: Doctor Thesis, University of Delaware, Sept. 1953.
6. Wohl, K.: *Fourth Symposium (International) on Combustion*, p. 68. Baltimore, The Williams & Wilkins Co., 1953
7. Damköhler, G.: Z. Elektrochem., *46*, 601 (1940).
8. Shelkin, K. I.: NACA Tech. Memo No. 1110 (1947).
9. Hirschfelder, J., Curtiss, C., and Bird, R.: *Molecular Theory of Gases and Liquids*, p. 778. New York, John Wiley and Sons, 1954.
10. von Kármán, T., and Penner, S. S.: *Selected Combustion Problems (Agard)*, p. 5. London, Butterworths Scientific Publications, 1954.
11. Fristrom, R. M., Prescott, R., and Grunfelder, C.: Johns Hopkins University, Appl. Phys. Labor., Rep. CM-858, December 1955.
12. Muhlbauer, H. G.: M. S. Thesis, University of Delaware, June 1950.
13. Schmidt, H. M.: M. S. Thesis, University of Delaware, June 1950.
14. von Rosenberg, H. E.: Doctor Thesis, University of Delaware, June 1955.
15. Wohl, K., and Shore, L.: Ind. Eng. Chem., *47*, 828 (1955).

43

COMBUSTION IN TURBULENT GAS STREAMS

By H. IIDA

A. Influence of the Flame Front on the Flow

1. INTRODUCTION

The study of the flow resulting from the release of chemical energy in the form of heat is one of the most important problems for combustion in gas turbines and jet engines. In most cases the phenomena are very complicated, involving mixing of fuel and air with recirculating flow, and chemical reaction. Because of this interference between aerodynamics and chemical kinetics, the problem has been treated only for two cases: (1) the combustion zone is regarded as a continuous heat source, (2) it is considered as a flame front of infinitesimal thickness in a homogeneous mixture.

The former case has been treated by Hicks[1] and by the author.[2] The present paper is concerned with the second case, in which the flame velocity is assumed to be small compared to the approach velocity. We can then simplify the fundamental equation of flow with a flame front, and by introducing the Crocco transformation used in boundary layer theory, the equation can be linearized yielding a new integral equation of the second kind. The solution of this integral equation agrees with the results of Scurlock,[3] and Fabri,[5] and is in good agreement with our experiments in turbulent gas streams. However, when the turbulent intensity is increased, the difference between theory and experiment in the neighborhood of flame boundary grows owing to the thickness of flame front.

2. GENERAL EQUATIONS

The equations for two-dimensional steady flow with a flame front, neglecting viscosity and heat conduction, are the following:

Momentum equations

$$\rho = \left(u \frac{\partial u}{\partial x} + v \frac{\partial u}{\partial y} \right) = - \frac{\partial p}{\partial x} \tag{1a}$$

$$\rho = \left(u \frac{\partial v}{\partial x} + v \frac{\partial v}{\partial y} \right) = - \frac{\partial p}{\partial y} \tag{1b}$$

Continuity equation

$$\frac{\partial (\rho u)}{\partial x} + \frac{\partial (\rho v)}{\partial y} = 0 \tag{2}$$

Energy equation and equation of state

$$Q = i + \tfrac{1}{2} q^2 = \lambda Q_0 \tag{3}$$

$$p = R \rho T \tag{4}$$

In these equations p, ρ, T denote respectively the pressure, density, and absolute temperature of the gas mixture, Q is the total enthalpy per unit mass of the mixture, R is the gas constant, λ is the ratio of the total enthalpies of the burned and unburned gas; u and v are the components of the flow velocity along the x and y axes (Fig. 1).

The boundary conditions are the following:

$$\begin{aligned} &\text{(i)} && x = -\infty,\ u = V,\ v = 0 \\ &\text{(ii)} && y = 0,\ y = \pm b,\ v = 0 \end{aligned} \tag{5}$$

where V is the uniform velocity at an infinite distance upstream.

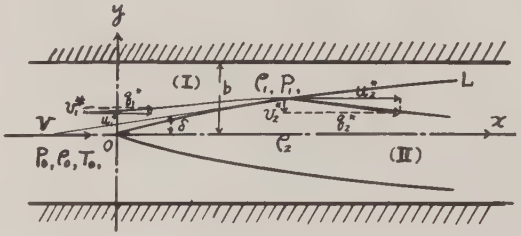

FIG. 1. (I) Unburned mixture; (II) burned gas; L, flame front.

The velocity gradient across the flame front is obtained by the usual equations for flow discontinuity:

$$u_2^* = u_1^* + S_b (\mu - 1) \sin S \tag{6a}$$

$$v_2^* = v_1^* - S_b (\mu - 1) \cos S \tag{6b}$$

where S_b = the normal combustion velocity; $_1^*$ denotes velocities upstream of the flame front; $_2^*$ denotes velocities downstream of the flame front; $\mu = P_1^*/\rho_2^*$. The flow of the burned gases is rotational and necessitates the use of a stream function ψ. If ω denotes the vorticity of the burned gas flow, the following relation between ω, ψ, and S (entropy of the burned gas) can be obtained:

$$\frac{\rho_0}{\rho} \omega = T \frac{dS}{d\psi} - \frac{dQ}{d\psi} \tag{7}$$

when λ = constant,

$$\frac{\rho_0}{\rho}\left(\frac{\partial v}{\partial x} - \frac{\partial u}{\partial y}\right) = T\frac{dS}{d\psi} \tag{8}$$

3. LINEARIZATION

As in all rotational flow problems, determination of the flame front position and the velocity distribution is very complicated. However, the normal propagation velocity of the flame is actually quite small compared to the flow velocity, i.e., $S_b \ll V$. If we regard V as 0 (1) and S_b as 0 (ϵ), u, x can be shown as 0 (1) and v, y as 0 (ϵ). In the same manner, one may write

$$\frac{\partial u}{\partial y} = 0\left(\frac{1}{\epsilon}\right), \qquad \frac{\partial u}{\partial x}, \qquad \frac{\partial u}{\partial y} = 0(1), \qquad \frac{\partial v}{\partial x} = 0(\epsilon)$$

If the term of 0 (ϵ) and higher order may be neglected in regard to that of 0 (1) order, the following approximate equations of flow result from the system of Equations (1a), (1b), (2), (3), (4) and (8).

$$\rho\left(u\frac{\partial u}{\partial x} + v\frac{\partial u}{\partial y}\right) = -\frac{\partial p}{\partial x}, \qquad 0 = -\frac{\partial p}{\partial y} \tag{9}$$

$$\frac{\partial(\rho u)}{\partial x} + \frac{\partial(\rho v)}{\partial y} = 0 \tag{10}$$

$$C_pT + \tfrac{1}{2}u^2 = \lambda Q_0 \tag{11}$$

$$p = R\rho T = p(x) \tag{12}$$

$$-\frac{\rho_0}{\rho}\frac{\partial u}{\partial y} = T\frac{dS}{d\psi} \tag{13}$$

where C_p is the specific heat at constant pressure. The boundary conditions are:

$$\begin{aligned} &\text{(i)} && x = 0,\ u = V,\ v = 0 \\ &\text{(ii)} && y = 0, \pm b,\ \mathrm{v} = 0 \\ &\text{(iii)} && u_2^* = u_1^*,\ v_2^* = v_1^* - (\mu - 1)\,S_b \end{aligned} \tag{14}$$

where

$$S_b = u_1^*\frac{dy^*}{dx} - v_1^*.$$

For simplicity, we introduce a nondimensional variable:

$$x/b \equiv x,\ y/b \equiv y,\ u/V \equiv u,\ v/V \equiv v,\ \rho/\rho_0 \equiv \rho$$

$$T/T_0 \equiv t,\ S/C_p \equiv s,\ p/p_0 \equiv p,\ \psi/V_b \equiv \psi,$$

$$S_b/V \equiv S_b$$

In the unburned region (I) Figure 1

$$S = \text{const}, \qquad \frac{\partial u}{\partial y} = 0, \qquad u = u_1(x) \tag{15}$$

from Equation (9)

$$\rho_1 u u' = -\frac{dp}{dx} \tag{16}$$

where

$$\rho_1 = \left\{1 - \frac{k-1}{2}M^2(u^2 - 1)\right\}^{1/k-1};$$

M = Mach number at uniform flow; k = ratio of specific heats. Integrating Equations (10) and (16) for the conditions $y = 1$, $v_1 = 0$, $\psi_1 = 1$, we obtain the following results:

$$v_1 = \frac{1 - y}{\rho_1}\frac{d(\rho_1 u_1)}{dx} \tag{17}$$

$$\psi = 1 - (1 - y)\rho_1 u_1 \tag{18}$$

In the burned region (II), Figure 1, using Crocco transformation, as follows,

$$\xi = x,\ u = u(x_1 y) \tag{19}$$

Therefore,

$$\frac{\partial}{\partial x} = \frac{\partial}{\partial \xi} - \frac{y\xi}{yu}\frac{\partial}{\partial u}, \qquad \frac{\partial}{\partial y} = \frac{1}{yu}\frac{\partial}{\partial u} \tag{20}$$

and Equations (9) and (10) can be expressed as

$$\rho v = \rho u y\xi - \frac{dp}{d\xi}yu \tag{21}$$

$$\rho u = \frac{\partial \psi}{\partial y} = \frac{1}{yu}\frac{\partial \psi}{\partial u} \tag{22}$$

$$\rho v = -\frac{\partial \psi}{\partial x} = -\frac{\partial \psi}{\partial \xi} + \frac{y\xi}{yu}\frac{\partial \psi}{\partial u} \tag{23}$$

From Equations (21), (22) and (16), we obtain the fundamental equation

$$\frac{\partial^2 \psi}{\partial u_1^2} + \frac{\rho_1}{\rho}\frac{\partial \psi}{\partial u_1^2} = 0 \tag{24}$$

where

$$\rho = \frac{1 - \dfrac{k-1}{2}M^2(u_1^2 - 1)}{\lambda - \dfrac{k-1}{2}M^2(u^2 - \lambda)}$$

This partial differential equation of first order

can be solved easily by the characteristic equation,

$$\frac{\lambda\, du_1^2}{1 - \frac{k-1}{2} M^2(u_1^2 - 1)} = \frac{\lambda\, du^2}{\lambda - \frac{k-1}{2} M^2(u^2 - \lambda)} \tag{25}$$

so that the solution of Equation (24) takes the simple form

$$\psi = \psi(\zeta) \tag{26}$$

where

$$\zeta = \frac{2\lambda}{(k-1)M^2} \log e \frac{\lambda - \frac{k-1}{2} M^2(u^2 - \lambda)}{1 - \frac{k-1}{2} M^2(u_1^2 - 1)} + \text{const}$$

The entropy of flow may be derived from Equation (13), as follows:

$$\frac{ds}{dt} = -\frac{k-1}{\rho t} M^2 \frac{\partial u}{\partial y}, \tag{27}$$

where

$$t = \lambda - \frac{k-1}{2} M^2(u^2 - \lambda)$$

The integrated form of this equation, satisfying the boundary conditions $x = 0, u = u_1 = 1$, $S = s_0$, is given by

$$s - s_0 \log e \frac{\lambda - \frac{k-1}{2} M^2(u^2 - \lambda)}{\left\{\lambda + \frac{k-1}{2} M^2(\lambda - 1)\right\} \cdot \left\{1 - \frac{k-1}{2} M^2(u_1^2 - 1)\right\}} \tag{28}$$

On the axis of the duct, $\psi = 0, S = s_0, u = um$, one obtains the following result, which corresponds to the extended formula in compressible flow involving a flame front, derived by Tsien.[4]

$$u_m = \sqrt{1 + \left\{\lambda + \frac{k-1}{2} M^2(\lambda - 1)\right\}(u_1^2 - 1)} \tag{29}$$

From Equation (26), the relation between ζ and s can be obtained, putting $u = um$, $\zeta = 0$;

$$\zeta = \frac{2\lambda}{(k-1)M^2}(s - s_0) \tag{30}$$

4. INTEGRAL EQUATIONS

Let us consider an incompressible case and simplify the above equations. Putting $M = 0$, $\rho_1 = 1$, $\rho = 1/\lambda$, in the unburned region (I),

$$v_1 = (1 - y)u_1', \quad \psi_1 = 1 - (1 - y)u \tag{31}$$

in the burned region (II),

$$\psi = \psi(\zeta), \qquad \zeta = \lambda(u_1^2 - 1) - (u^2 - 1) \tag{32}$$

$$\frac{\partial y}{\partial u} = -2\lambda\psi'(\zeta) \tag{33a}$$

or

$$\frac{\partial y}{\partial \zeta} = \frac{\lambda}{\sqrt{\lambda(u_1^2 - 1) - (\zeta - 1)}} \psi'(\zeta) \tag{33b}$$

Integrating this equation at boundary conditions:

$$\zeta = 0, y = 0, u = u_m = \sqrt{1 + \lambda(u_1^2 - 1)}$$

we obtain the equation

$$y = \lambda \int_0^s \frac{\psi'(\zeta)}{\sqrt{u_m^2 - \zeta}}\, d\zeta = \frac{\lambda\psi(\zeta)}{\sqrt{u_m^2 - \zeta}} - \frac{\lambda}{2} \int_0^s \frac{\psi(\zeta)}{(u_m^2 - \zeta)^{3/2}}\, d\zeta \tag{34}$$

For the flame front condition,

$$u = u_1, \zeta = \zeta_1 = (\lambda - 1)(u_1^2 - 1), \quad \psi(\zeta_1) = 1 - (1 - y^*)u_1 \tag{35}$$

where y^* is the value of y at any point of the flame front, we can write

$$\psi(\zeta_1) = \frac{\sqrt{\zeta_1 + \lambda - 1} - \sqrt{\lambda - 1}}{(\lambda - 1)^{3/2}} + \frac{\lambda}{2} \int_0^{s_1} \frac{\sqrt{\zeta_1 + \lambda - 1}}{\{\lambda\zeta_1 - (\lambda - 1)(\zeta - 1)\}^{3/2}} \psi(\zeta)\, d\zeta \tag{36}$$

an integral equation of the second kind, where $\psi(\zeta_1)$ characteristic of the burned fraction of the total mass flow is the function of the entropy term, ζ_1. This equation can be solved by successive integration, and the calculated results are shown in Figure 2. An example of the velocity distribution over a cross section of the flame front shows the same results as obtained by

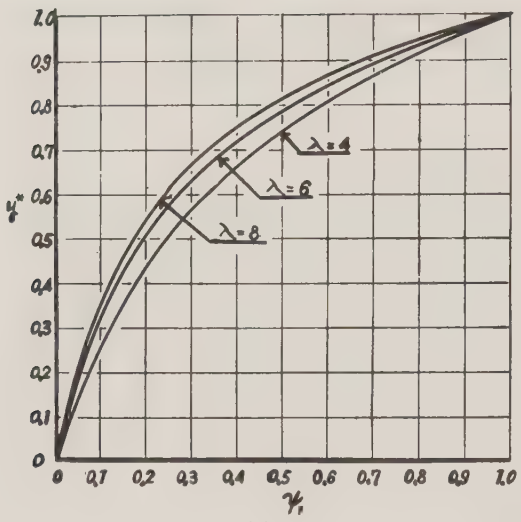

(a)

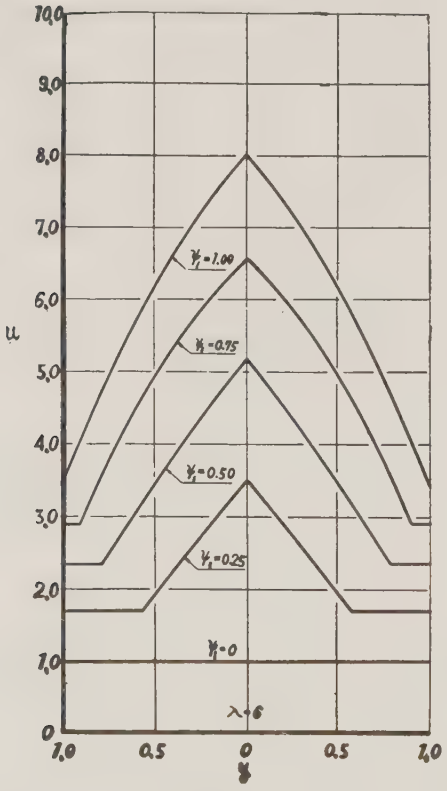

(b)

FIG. 2.

Scurlock (3) and Fabri, Siestrunck and Fouré: (Fig. 2).

From Equations (14) and (18), we obtain the burning velocity, S_b, in the form

$$S_b = \frac{d\psi_1}{d\alpha}.$$

$$(S_b)_0 = \frac{1}{\lambda}\left(\frac{dy^*}{dx}\right)_{x=0} \tag{37}$$

$$\overline{S_b} = \frac{1}{x_1}\int_0^{x_1} S_b\, dx = \frac{\psi_1}{x_1}$$

With this, we can estimate the burning velocity at any point of the flame front and its mean value for combustion in a turbulent gas stream.

5. COMPARISON BETWEEN THEORETICAL PREDICTIONS AND EXPERIMENTAL DATA

The experimental apparatus employed (Figs. 3 and 4) was such that a homogenous mixture of air and gaseous fuel at atmospheric pressure and a temperature of 300°K could be introduced into a combustion chamber of constant rectangular cross section (18 cm by 5 cm). Two opposite walls of fused quartz made it possible to observe the

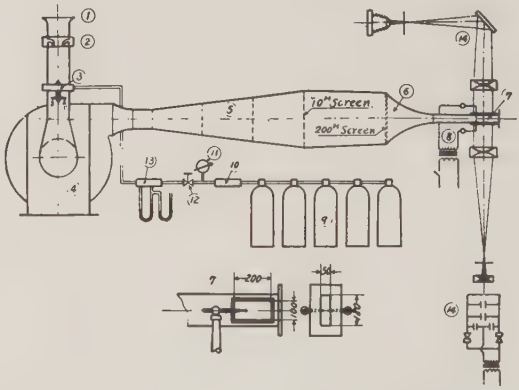

FIG. 3. (1) Air inlet; (2) air flow meter; (3) fuel gas injector; (4) 15-hp blower; (5) diffuser; (6) 32:1 nozzle; (7) combustion chamber; (8) ignition spark gap or flame holder; (9) propane gas bomb; (10) collecting chamber; (11) pressure gauge; (12) regulator valve; (13) gas flow meter; (14) apparatus for flash schlieren photography.

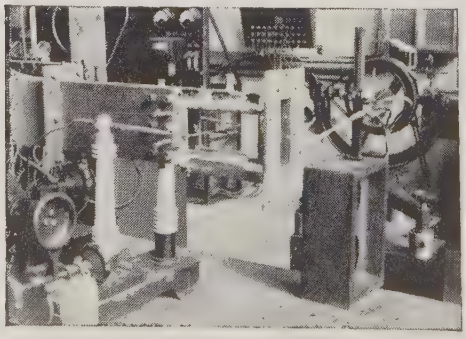

FIG. 4.

flame continuously and to obtain instantaneous schlieren photographs. Measurements showed that the velocity profile was flat and that the turbulence intensity was 0.5 to 2.0 per cent. The fuel used for all the work was propane gas (molecular weight, 44.6). The flameholder was a single cylinder of 1 mm diameter, oriented with its axis normal to the flow and placed 51.5 cm from the chamber outlet for all the experiments. The maximum combustion chamber entrance velocity was 20 m/sec, and λ could be changed from 4.0 to 7.0 by means of varying air-fuel ratio, in which the flame temperature was measured by Pt to Pt. Rh. thermocouple, calibrated by the line-reversal method.

A comparison of theoretical predictions with experimental data is shown in Figure 5, for the relation between u_1 and u_m, and u_1 and y^*, and in Figure 6a and Figure 6b, where the turbulence of the approach flow was 0.54 and 1.65 per cent. The theoretical curves were in good agreement with experiments, but when the turbulence intensity was increased the discrepancy between theory and experiment in the neighborhood of the flame front grew increasingly. This fact seems to be caused by additional turbulence generated by the flame, through a steep gradient of the velocity component parallel to the flame surface in enclosed duct.

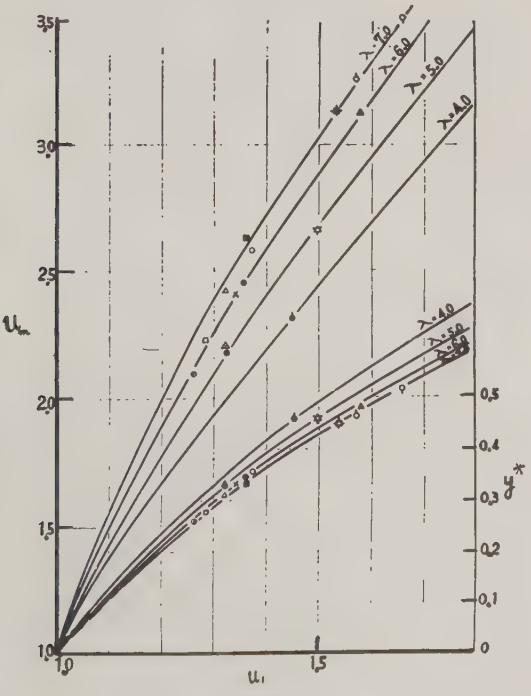

FIG. 5.

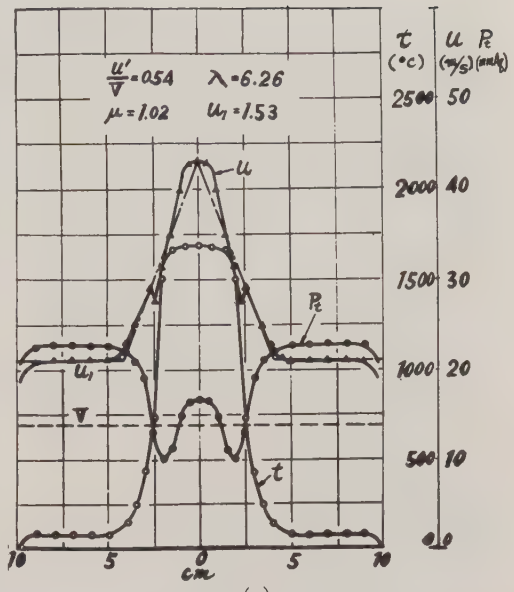

(a)

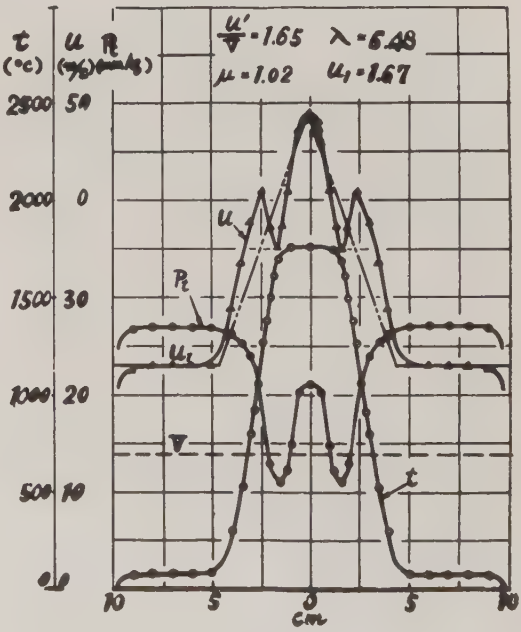

(b)

FIG. 6.

6. CONCLUSIONS

An approximate solution of the rotational flow problems involving a flame front in a two-dimensional parallel duct is proposed, assuming a small flame velocity compared to the approach velocity. Its predictions are in good agreement with experiments in a low turbulent gas stream when a small diameter flameholder is used, but as the turbu-

lence intensity is increased about 2 per cent, the discrepancy near the flame front grows remarkably. This seems to be closely connected with the increase of flame velocity due to flame-generated turbulence in the flow. From this theory, some new formulas for calculating the burning velocity from the geometric shape of the flame front are obtained.

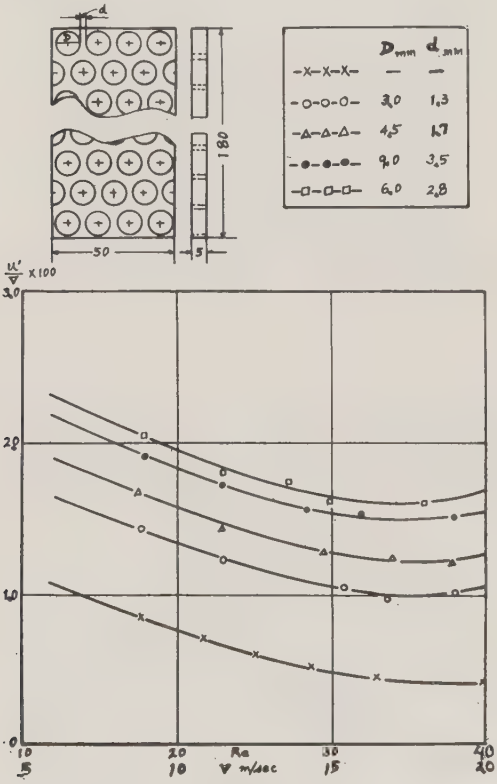

FIG. 7.

B. Some Effects of Turbulence on Combustion

1. INTRODUCTION

The effect of turbulence on combustion has been treated theoretically by Damköhler,[6] Schelkin,[7] Karlovitz, Denniston and Wells,[8] Williams, Hottel and Scurlock,[9] and Tucker,[10] while the additional effect of turbulence created by the turbulent flame was established experimentally by Karlovitz, Denniston and Wells.[8] However, a quantitative agreement between theory and experiment cannot be expected with data obtained for open Bunsen burner flames and flames enclosed in ducts, owing to boundary effects or the existence of a wake behind the flameholder.

In this paper, burning velocities are measured by both direct and flash schlieren photography in a turbulent gas stream, using propane-air mixtures ignited by intermittent spark gap and a small cylindrical flameholder. The comparison between theory and experiment was verified for the effect of different structures of the flame front.

2. APPARATUS AND PROCEDURE

As in (A), the experimental apparatus (Figs. 3 and 4) was constructed so that the mixture flows through a section consisting of a diffuser with an angle of 14.5°, four 10-mesh and two 200-mesh screens and a 32:1 contraction ratio nozzle. The mixture enters the combustion chamber with a turbulence intensity of 0.5 to 2.0 per cent and a flat velocity profile, which can be changed by four different turbulence generators placed at the entrance of duct (Fig. 7). The turbulence intensity was measured by the thermal diffusion method using platinum wire with a 30-μ diam.

Characteristics of the fuel-gases used are:

C_2H_6	5.9 per cent
C_3H_8	75 per cent
C_4H_{10}	15.5 per cent
C_5H_{12}	3.6 per cent

Stoichiometric mixture ratio: 15.5

The premixed gas was ignited by intermittent spark gap (1 mm) using a neon transformer (50 cycle, 100 primary voltage, and 15,000 secondary voltage) and a cylindrical flameholder of 1 mm diameter. The combustion chamber entrance velocity could be varied up to 20 m/sec and air-fuel ratio from 12 to 27.

3. RESULTS AND DISCUSSION

The burning velocity, S_b was calculated from flame shapes by use of Equation (37) as follows:

a. Burning velocity at ignition point $(S_b)_{x=0}$

As the velocity gradient near the ignition point is very small and the effect of additional turbulence created by the flame front can be neglected, one may consider that the increments of flame velocity are due solely to the approach stream turbulence.

Figures 8a and 8b show some experimental results, the former corresponding to the case of spark ignition and the latter representing the case of cylindrical flameholder, calculated on the basis of laminar flame speed, S. The curves (a)

and (b) are the theoretical predictions given by Karlovitz and Schelkin, respectively, in which μ and u' express the equivalence ratio and the turbulence intensity, respectively.

The increment of flame velocity with varying air-fuel ratio approaches curve (a) for a stoichiometric mixture and curve (b) for lean or rich mixtures (Figs. 8a and 8b). The difference between the case of spark ignition and the case of a cylindrical flameholder for lean and rich mixtures seems to be due to different flame structure, the former having a cellular structure and the latter a nearly planar flame front as shown later in schlieren flash photographs (Figs. 12 to 15). Comparison of this difference is shown clearly in Figures 9a and 9b, based on the air-fuel ratio.

The effect of flame front curvature on burning velocity, as Markstein[11] has pointed out in his studies on instability phenomena in combustion waves, must be considered in problems of turbulent flame propagation and structure.

b. Mean flame velocity, $\overline{S_b}$

Figures 10a and 10b show the results of measurements of mean burning velocities from the

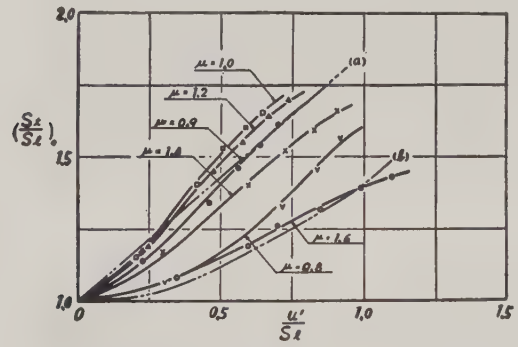

(a)

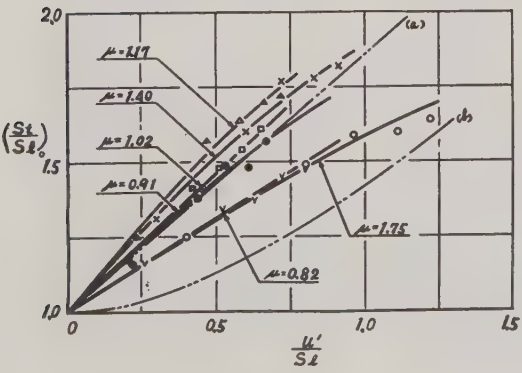

(b)

FIG. 8.

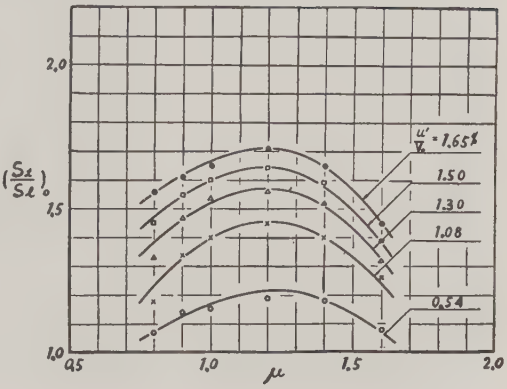

(a)

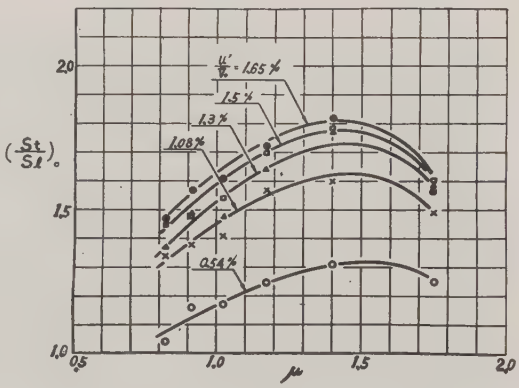

(b)

FIG. 9.

ignition point to the end of the quartz window, (a distance of 13.5 cm). In this case, the discrepancy between two kinds of ignition method for lean or rich mixture ratios becomes marked, and near the stoichiometric composition the experimental value of flame velocity is much higher than the theoretical predictions. This is attributed to additional turbulence generated by the flame front where a strong vorticity of flow occurs, producing a steep velocity gradient as mentioned in (A), in the burned gas. This velocity gradient grows steep as the flame angle increases, so that the difference between theoretical and experimental values of $\overline{S_b}$ is remarkable near the stoichiometric composition, where the flame angle is largest and is influenced by approach turbulences. For an enclosed flame, the approach turbulence has considerable effect on flame-generated turbulence indirect, i.e., the turbulent flame propagation velocity.

c. Burning velocity along flame front (S_b)

The burning velocity along flame front was calculated by Equation (37) for a turbulence intensity of 0.54 and 1.65 per cent, respectively (Fig. 11). The turbulent flame velocity corresponding to an upper limit of flame-generated turbulence presented by Karlovitz, Denniston and Wells[8], is shown in Figure 11 with dotted line for spark ignition and cylindrical flameholder. This maximum value of flame velocity seems to indicate its suitability for low approach turbulence intensity, but it cannot be applied for strong approach turbulent flow in an enclosed duct.

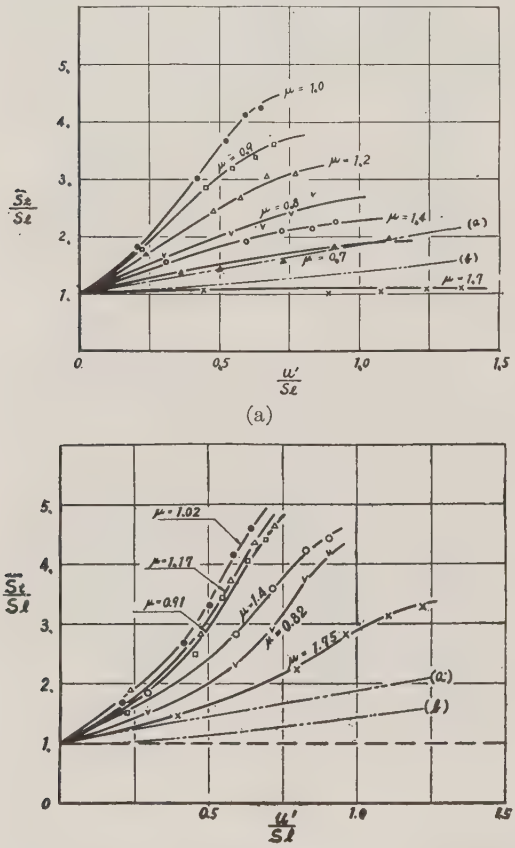

Fig. 10.

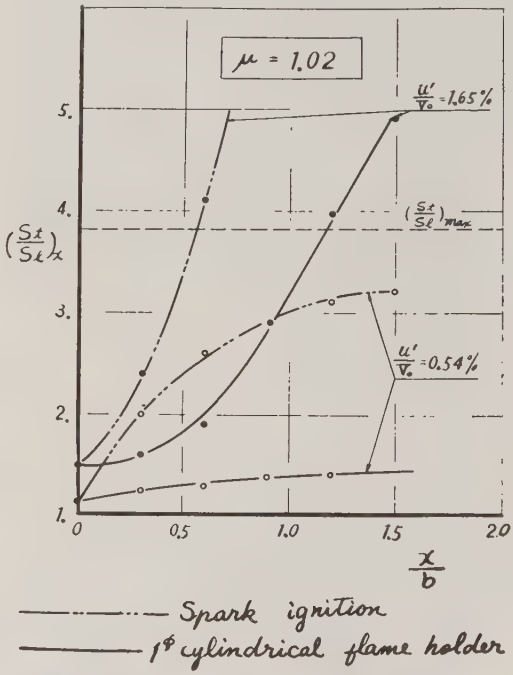

Fig. 11.

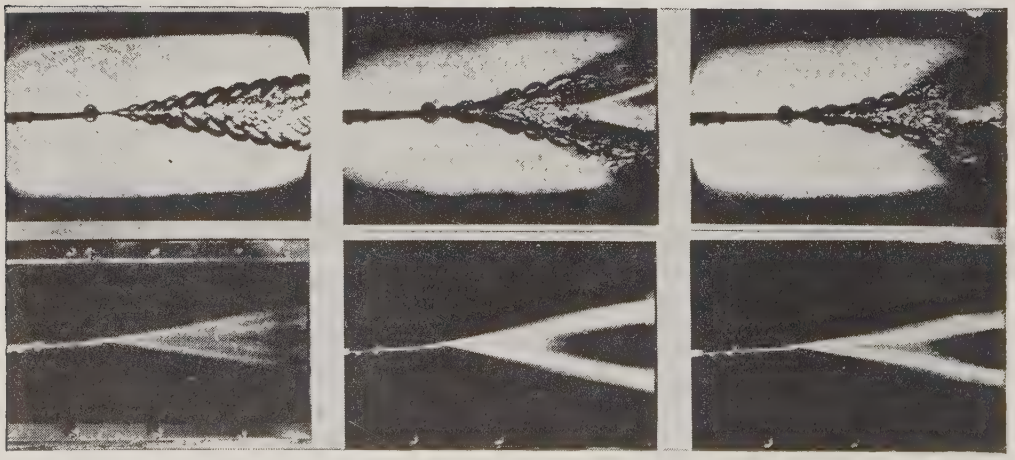

Fig. 12a. $\mu = 1.40 \quad \frac{\mu'}{v} \times 100 = 0.54$

Fig. 12b. $\mu = 1.03 \quad \frac{\mu'}{v} \times 100 = 0.54$

Fig. 12c. $\mu = 0.83 \quad \frac{\mu'}{v} \times 100 = 0.54$

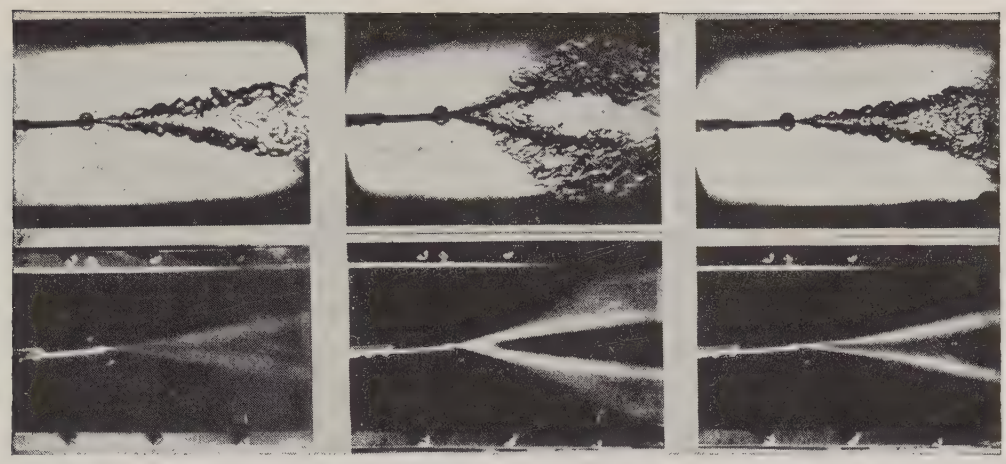

FIG. 13a. FIG. 13b. FIG. 13c.

$\mu = 1.40 \quad \frac{\mu'}{v} \times 100 = 1.65$ $\mu = 1.03 \quad \frac{\mu'}{v} \times 100 = 1.65$ $\mu = 0.83 \quad \frac{\mu'}{v} \times 100 = 1.65$

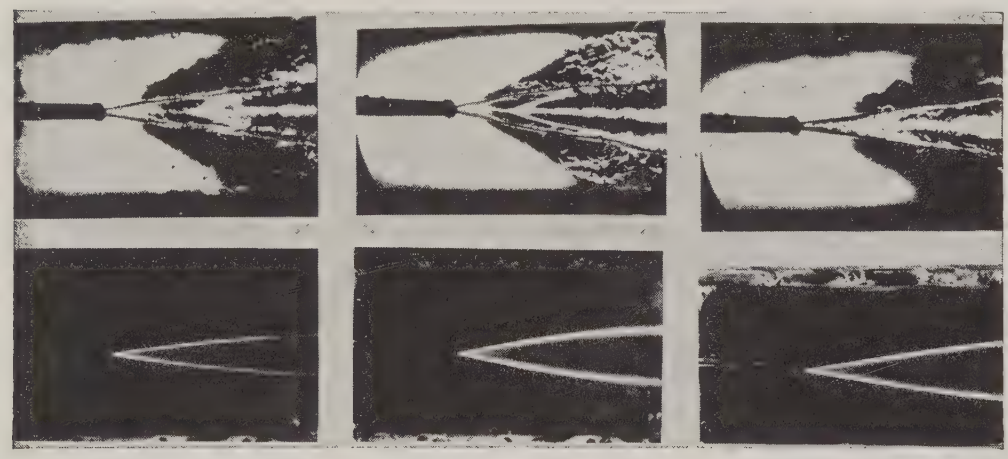

FIG. 14a. FIG. 14b. FIG. 14c.

$\mu = 1.40 \quad \frac{\mu'}{v} \times 100 = 0.54$ $\mu = 1.03 \quad \frac{\mu'}{v} \times 100 = 0.54$ $\mu = 0.83 \quad \frac{\mu'}{v} \times 100 = 0.54$

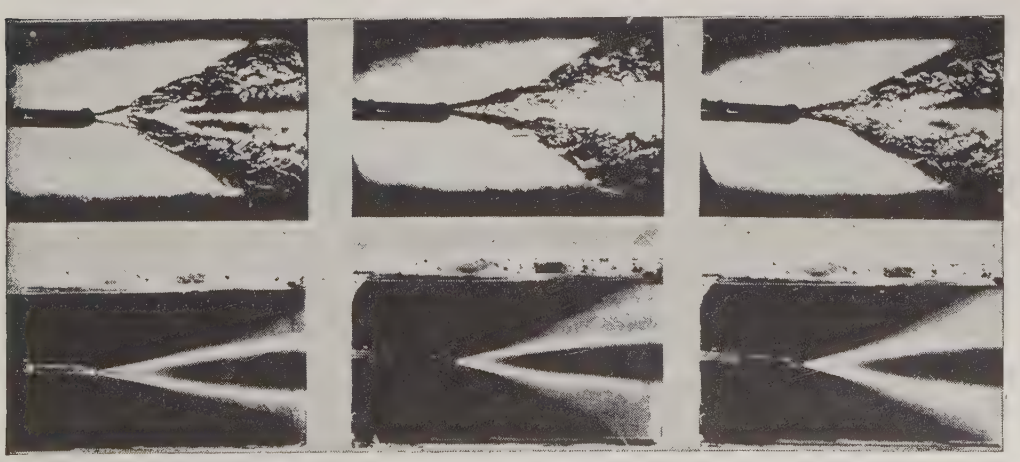

FIG. 15a. FIG. 15b. FIG. 15c.

$\mu = 1.40 \quad \frac{\mu'}{v} \times 100 = 1.65$ $\mu = 1.03 \quad \frac{\mu'}{v} \times 100 = 1.60$ $\mu = 0.83 \quad \frac{\mu'}{v} \times 100 = 1.65$

d. Schlieren photographs

Both direct and flash schlieren photography were used to study flame phenomena and the structure of the flame front. Typical direct and flash photographs (ca. 10 μsec duration) are shown in Figures 12 to 15. The approach flow velocity is 14 m/sec, the approach turbulence intensities are 0.54 and 1.65 per cent and the equivalent ratios are 0.83, 1.02 and 1.40, respectively. Figures 12 and 13 were taken for spark ignition and Figures 14 and 15 for cylindrical flameholder; the approach turbulence intensity in Figures 12 and 14 was 0.54 per cent and in Figures 13 and 15, 1.65 per cent; inlet compositions are noted on each photograph.

The significant factors in these photographs were found to be: (1) By spark ignition in low-turbulence gas mixtures, we obtain regular cellular flames, which are gradually destroyed by flame-generated turbulence or by increased approach turbulence. The frequency of spark ignition by an alternating current is about twenty times the actual frequency of the neon transformer (60 cycle/sec). (2) For a cylindrical flameholder, the flame front shows an almost plane discontinuity, which is also destroyed by additional turbulence caused by the approach turbulence.

Unfortunately the fact that the temperature gradient on the fused quartz walls interfered with a clear schlieren image downstream of the ignition point made it impossible to determine the maximum value of the burning velocity in these experiments.

4. CONCLUSIONS

The above investigation on turbulent flames in a closed duct can be summarized as follows:

(1) The increase in the burning velocity due to turbulence of the approach flow is comparatively small for spark-gap and small flameholder ignition. It is in good agreement with the theory of Karlovitz for stoichiometric mixtures and approaches Schelkin's formula for rich and lean mixtures.

(2) The additional effect due to flame-generated turbulence along the flame front increases with the approach turbulence intensity and is considerably greater for spark ignition than for a rod stabilizer. This difference between the two types of ignition is due to the complex cellular structure of the flame front, which may be one of the most important problems in relation to the creation of additional turbulence.

Acknowledgments

The author wishes to express his gratitude to Mr. K. Nakata of the Transportation Technical Research Institute for advice in the course of this investigation, and to Messrs. Y. Uematsu and H. Fukuda for assistance in the experimental work.

REFERENCES

1. Hicks, B. L.: *Third Symposium on Combustion, Flame and Explosion Phenomena*, p. 212. Baltimore, The Williams & Wilkins Co., 1949.
2. Iida, H.: Trans. Soc. Mech. Eng. (Japan), *17*, No. 58 (1951).
3. Scurlock, A. C.: Meteor Report No. 19 Fuel Research Laboratory, Massachusetts Institute of Technology, July, 1948.
4. Tsien, H. S.: J. Appl. Mech., *73*, 188 (1951).
5. Fabri, J., Siestrunck, R., and Fouré, C.: *Fourth Symposium (International) on Combustion*, p. 448. Baltimore, The Williams & Wilkins Co., 1953.
6. Damköhler, G.: NACA Tech. Memo No. 1112 (1947).
7. Schelkin, K. I.: NACA Tech Memo No. 1110 (1947).
8. Karlovitz, B., Denniston, D. W., and Wells, F. E.: J. Chem. Phys., *19*, 541 (1951).
9. Williams, G. C., Hottel, H. C., and Scurlock, A. C.: *Third Symposium on Combustion, Flame and Explosion Phenomena*, p. 21. Baltimore, The Williams & Wilkins Co., 1949.
10. Tucker, M.: NACA Tech. Memo No. 3407 (1955).
11. Markstein, G. H.: J. Aero. Sci., (1951).

HIGH SPEED REACTIONS

44

HEAT CONDUCTIVITY IN POLYATOMIC, ELECTRONICALLY EXCITED, OR CHEMICALLY REACTING MIXTURES. III[a]

By JOSEPH O. HIRSCHFELDER

The heat conductivity of gases at high temperatures plays an important role in determining the temperature profile of a flame, the structure of a shock, and the heat transfer to the surface of a supersonic vehicle. The present paper is the third in a series which attempts to survey some of the problems in the estimation of heat conductivity.[1,2] Since heat conductivity is a very complex phenomenon there are many different types of problems to be considered.

First, one must distinguish between the determination of the heat flux alone and the determination of the detailed temperature and chemical profiles. If one is only interested in the heat flux, the problem is comparatively simple. The heat flux is determined largely by the chemical composition and temperature at the hot and the cold surfaces of the cell and is almost independent of the chemical reactions which take place in between. In sharp contrast, the chemical and temperature profiles are sensitive to reaction rates, the coefficients of diffusion, and the relaxation times. Because of the present effort to interpret and predict the detailed structure of flames, strong shocks, and detonations we seek to make this detailed analysis.

Then, there is the question of whether the heat flux is proportional to the temperature gradient, or whether the conduction is "non-Fourier." We find that the presence of metastable electronic or molecular species in the gas mixture leads to heat fluxes which depend sensitively on the boundary conditions and cannot be expressed in terms of an effective coefficient of thermal conductivity. This behavior is quite analogous to non-Newtonian viscous flow where the momentum flux is not proportional to the velocity gradient. The "non-Fourier" behavior might be expected for extremely hot air which contains "active" nitrogen, "active" oxygen and many other metastable species. The large temperature gradients in strong shocks would also lead to "non-Fourier" heat conductivity.

The coefficient of heat conductivity is increased as a result of chemical reactions. We find that the coefficient of heat conductivity is almost proportional to the specific heat of the chemically reacting gas mixture. At very low temperatures and very high temperatures the specific heat is an average of the specific heats of the components. However, at intermediate temperatures there is an additional term which is due to the change in chemical composition with temperature. The magnitude of this chemical contribution to the specific heat depends on the entropy change. For a dissociative reaction where entropy strongly favors the dissociated products, the coefficient of heat conductivity can be 10 to 15 times its normal value. However, for unimolecular or bimolecular reactions with little change in entropy the increase in heat conductivity may only amount to 15% or 20%.

The coefficient of thermal conductivity for a polyatomic gas is usually taken to be the product of the coefficient of thermal conductivity (assuming the gas to be monatomic) times the Eucken factor, $(4/15)(C_v/R) + (3/5)$. We derive an improved Eucken factor, $0.354\ (C_v/R) + 0.469$. In the derivation, each quantum state of the pure substance is regarded as a separate chemical species. Three assumptions are required (two explicit and one implicit):

[a] This work was carried out at the University of Wisconsin Naval Research Laboratory under Contract NOrd 15884 with the Naval Bureau of Ordnance.

(1) It is assumed that equilibrium is maintained at each point between the chemical composition and the local temperature. For gases containing metastable quantum states this condition is not fulfilled. The effect of the metastable states is to lower the heat conductivity if the temperature is lower than the transition temperature at which the reaction is proceeding the fastest, and to increase the heat conductivity if the temperature is much higher than the transition temperature. The presence of metastable constituents also complicates the problem of satisfying the boundary conditions. This results in a dependence of the apparent coefficient of thermal conductivity on the cell size as well as on the temperature difference between the boundary surfaces.

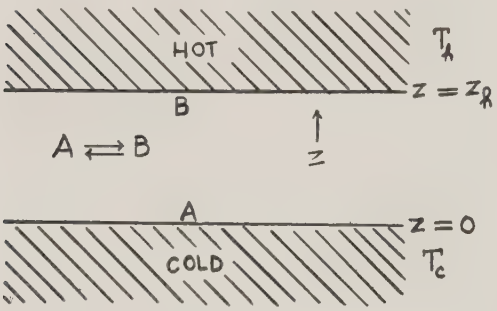

FIG. 1. Assumed heat conductivity cell.

(2) The coefficient of diffusion is assumed to be the same for all molecules. This assumption is probably good except for electronically excited atoms or molecules which have collision diameters much larger than for ordinary molecules. Excited molecules contribute comparatively little to the heat conductivity since their coefficients of diffusion (which vary inversely as the square of the collision diameter) are very small.

(3) In using the macroscopic flux equations, the assumption is implied that the non-adiabatic collisions do not appreciably distort the molecular distribution functions. This assumption should be excellent for both the electronic and the vibrational degrees of freedom since only once collision out of hundreds or thousands involves changes in the electronic or vibrational quantum numbers. However, at very low temperatures (air at minus 100°C or polar gases at room temperature) the Eucken factor does not seem to be applicable to the rotational degrees of freedom. Changes occur in the rotational quantum numbers in almost every collision. Curtiss and Muckenfuss[3] have shown that these rotational transitions lead to rather large distortions of the molecular distribution functions of rigid spheroids and the same sort of anomalously small coefficient of thermal conductivity which is found at low temperature. However, at higher temperatures the experimental data indicates that this distortional effect becomes unimportant and the Eucken correction is applicable to the rotational as well as to the vibrational and electronic degrees of freedom.

The heat conductivity of a polyatomic gas mixture is considered in much the same manner as of a pure polyatomic gas. This leads to a generalization of the Eucken treatment which involves the coefficients of self and ordinary diffusion for all of the components, in addition to the Eucken type factors for the pure components and the coefficient of thermal conductivity for the "monatomic" mixture. The resulting formula gives excellent agreement with the experimental data.

Engineers are always surprised to find that whereas the Prandtl numbers vary by only a few per cent from one pure gas to another, the Prandtl number for a mixture may be as small as one-half of the value for the pure components or else the Prandtl number for the mixture may be considerably larger than the value for the pure components. This behavior should be expected since it might occur even if the coefficient of viscosity, the coefficient of thermal conductivity, and the specific heat per mole of mixture each varied linearly with the composition. Actually, the reciprocal of the coefficient of thermal conductivity usually varies almost linearly with the composition. The coefficient of viscosity varies in an anomalous manner with composition and often possesses either a maximum or a minimum. Thus we conclude that it is far better to deal directly with the coefficient of thermal conductivity than to use Prandtl numbers for mixtures.

In the present paper, we shall confine our attention to the steady state conditions which result when a chemically reacting gas mixture is placed in a cell between two parallel plates. The plate at the bottom is maintained at the cold temperature, T_c, and the plate at the top is held at the hot temperature, T_h. As shown in Figure 1, z is the distance from the cold plate and z_h is the thickness of the cell. The chemical and temperature profiles as well as the heat flux, q, depend upon the homogeneous and heterogeneous reaction rates as well as on the physical and thermal properties. As Prigogine and Buess[4] have pointed out, the chemical profile corresponds to a chemi-

cally controlled thermal diffusion. Indeed, if the cell were rotated so that the hot and cold plates were parallel we could obtain the same sort of chemical separations as occur in a Clusius column.

Waelbroeck, Lafleur and Prigogine[5] have considered the problem of heat transfer in a chemically reacting mixture from the standpoint of the thermodynamics of irreversible processes. This leads to identically the same approximation as we obtain from assuming that the chemical composition is in equilibrium with the local temperature. Prigogine considers the dissociative equilibrium $A \rightleftarrows 2B$ in connection with the heat conductivity of N_2O_4 and of compressed argon. He also considers the possibility of using this chemically controlled thermal diffusion to separate mixtures in the liquid phase. However, he finds that the effect is very small in the liquid phase.

In all our equations, we neglect the terms which involve the coefficients of thermal diffusion. Prigogine considers these thermal diffusion terms very carefully and concludes that they are orders of magnitude too small to have an appreciable effect on the thermal conductivity.

I. The General Equation

The general equations for the one-dimensional steady state heat transfer are readily obtained from *Molecular Theory of Gases and Liquids*[6] and have been discussed in detail in Part I of this series.[1] After the steady state has been established, the mass average velocity is everywhere zero, but due to the chemical reactions, the diffusion velocities of the individual chemical species are functions of z, the distance from the cold plate. Besides the temperature, T, the dependent variables are the mole fraction, x_i, and the number flux, g_i, of the i-th chemical component. If n is the number of moles of the gas mixture per cm³ and V_i is the diffusion velocity of molecules of the i-th kind, then the net number of moles of i moving from smaller towards larger z through a cm² of area (perpendicular to the z axis) in one second is

$$g_i = nx_iV_i \tag{1}$$

Since the diffusion velocities are defined relative to the mass average velocity, it follows that if M_i is the molecular weight of the i-th species,

$$\sum_i M_ig_i = 0 \tag{2}$$

The values of g_i at the hot and at the cold boundaries are determined by the rates of the heterogeneous chemical reactions taking place on these surfaces. Thus if S_{ic} is the net number of moles of "i" formed per cm² of the cold surface per second, the value of g_i at the cold boundary is $(g_i)_c = S_{ic}$; and if S_{ih} is the net number of moles of "i" formed per cm² of the hot surface per second, the value of g_i at the hot surface is $(g_i)_h = -S_{ih}$. In general the S_{ic} and the S_{ih} are functions of the chemical compositions at the two surfaces, $(x_j)_c$ and $(x_j)_h$; the two temperatures, T_c and T_h; and the nature of the surfaces. If the surfaces are chemically inert and have no catalytic activity,

$$S_{ic} = S_{ih} = 0 \quad \text{and} \quad (g_i)_c = (g_i)_h = 0$$

The variation of the g_i with z can be expressed in terms of the homogeneous chemical reaction rates. If R_i is the net number of moles of "i" formed per cm³ per sec, then the equations of continuity give

$$dg_i/dz = R_i \tag{3}$$

Here the R_i are functions of the chemical composition, x_j, and the local temperature, T.

In terms of the usual binary diffusion coefficients, $\mathfrak{D}_{ij}$, the equations of multicomponent diffusion are

$$dx_i/dz = \sum_j (x_ig_j - x_jg_i)/n\mathfrak{D}_{ij} \tag{4}$$

However, the equations, Equation (4), of multicomponent diffusion can be solved for a particular g_i. In this case the equations are expressed in terms of the multicomponent diffusion coefficients, D_{ij}, and the density $\rho = n\sum_i M_ix_i$. Thus,

$$g_i = -(n^2/\rho) \sum_j D_{ij}M_j\, dx_j/dz \tag{5}$$

The multicomponent diffusion coefficients can be obtained from the molecular weights, the mole fractions, and the ordinary binary diffusion coefficients by evaluating a set of determinants.[7] Unlike the binary diffusion coefficients, the multicomponent diffusion coefficients vary a great deal with the chemical composition of the mixture. In Equations (4) and (5), we have omitted the thermal diffusion terms as well as the diffusion due to pressure gradients and external forces, since they are usually of second order importance as compared to ordinary density gradient diffusion which we are considering.

The energy flux, q, is independent of z for the

steady state. Again neglecting thermal diffusion, it is made up of two terms. The first term is the coefficient of heat conductivity, λ, times the temperature gradient. Here λ is the λ(mix) of Equation (76) or (77) taking into account the physical mixture of the chemical components but not the chemical reactions which take place between them. The second term is the energy transported by the diffusion of the molecules, which is the sum of the number fluxes times the corresponding enthalpies per mole, H_i. Thus, the energy flux is

$$q = -\lambda\, dT/dz + \sum_i g_i H_i \tag{6}$$

The energy flux, q, is a constant independent of z. If the temperatures of the two boundary surfaces are specified, then q is determined mathematically as an "eigenvalue;" that is, we adjust the value of q until we can satisfy the boundary conditions: at $z = 0$, $T = T_c$ and $(g_i)_c = S_{ic}$ and at $z = z_h$, $T = T_h$ and $(g_i)_h = -S_{ih}$. There are no boundary conditions for the mole fractions.

The nature of the solutions to the heat transfer equations has been thoroughly discussed in Part I.[1] If the reaction rates are fast either in the forward or else in the reverse direction so that there are no metastable molecules in the system, then one can obtain an excellent approximation to the heat flux by assuming that the chemical composition is maintained in equilibrium with the local temperature. Indeed, this is the approximation that is obtained from the thermodynamics of irreversible processes. However, from a mathematical standpoint, the local equilibrium relations for x_i and g_i are unsatisfactory since they satisfy neither the original differential equations nor do they satisfy the boundary conditions. We use the subscript "e" to designate the functions calculated on the assumption of local equilibrium. The x_{ie} are functions of the temperature and pressure as determined by solving the set of simultaneous algebraic equations,

$$R_i(x_{1e}, x_{2e}, \cdots, T, P) = 0 \quad i = 1, 2, \cdots \tag{7}$$

The g_{ie} are products of the temperature gradient times functions of the temperature and pressure,

$$g_{ie} = -(dT/dz)(n^2/\rho) \sum_j D_{ij} M_j (dx_{je}/dT) \tag{8}$$

The heat flux can then be expressed in terms of an effective coefficient of thermal conductivity, λ',

$$q = -\lambda' dT/dz \tag{9}$$

where

$$\lambda' = \lambda + (n^2/\rho) \sum_j D_{ij} M_j (dx_{je}/dT) \tag{10}$$

The local equilibrium functions are the first approximation to a true particular solution to the differential equations for heat transfer. We call this particular solution the *principal* solution and designate it by the subscript "p." The x_{ip} and the g_{ip} are functions not only of the temperature and pressure, but also of the derivatives: dT/dz, d^2T/dz^2, d^3T/dz^3, $\cdots$. The principal solution, like the equilibrium solution, does not satisfy the boundary conditions. There is an asymptotically converging iterative procedure for approximating the principal solution. Let us designate the order of the approximation by the subscripts 1, 2, $\cdots$. The x_{i1} are determined by solving the set of simultaneous algebraic equations.

$$R_i(x_{11}, x_{21}, \cdots, T, P) = d(g_{ie})/dz \qquad i = 1, 2, \cdots \tag{11}$$

The g_{i1} are then formed from the x_{i1} by the relations,

$$g_{i1} = -(n^2/\rho) \sum_j D_{ij} M_j (dx_{j1}/dz) \tag{12}$$

The x_{i2} are then formed by replacing dg_{ie}/dz by dg_{i1}/dz in Equation (11); the g_{i2} are obtained by replacing x_{j1} by x_{j2} in Equation (12). Thus the approximation procedure may be carried out to any desired order. In a typical unimolecular reaction, the difference between x_{i1} and x_{ie} is of the order of 10^{-12}; in a typical dissociation reaction it might be of the order of 10^{-8}. The differences between the g_{i1} and the g_{ie} are usually correspondingly small. Thus the local equilibrium and the principal solutions are usually sensibly equivalent. We shall consider the deviations from the local equilibrium solution presently in the special case of a unimolecular reaction.

The complete solution to the heat transfer equations is the principal solution plus the sum of the integration constants times transients. The integration constants are then adjusted so as to satisfy the boundary conditions. The transients vary as $\exp(dz)$ and as $\exp(-dz)$ where d is the boundary layer thickness. We find that d^2 is approximately equal to the product of the coefficient of diffusion and the relaxation time for the chemical reaction, τ. Here τ is meant to be the reciprocal of the sum of the reaction rates in the forward and in the reverse directions. If d is very

small compared to z_h, the width of the cell, these transient terms can be added to or subtracted from the principal solution so as to satisfy the boundary conditions without sensibly affecting the heat flux. In a typical unimolecular reaction, d is of the order of 10^{-6} cm; in a typical dissociation reaction it is of the order of 10^{-4} cm.

In order to understand the basic phenomena without getting bogged down in mathematical complexity let us consider two highly idealized examples, one corresponding to a unimolecular reaction and the other to a dissociation reaction.

II. Example: Unimolecular Reaction, A $\rightleftarrows$ B

First, let us consider the unimolecular reaction, A $\rightleftarrows$ B. Here the rate of the forward reaction is $nk_f x_a$ and the rate of the reverse reaction is $nk_r x_b$. The functions k_f and k_r are called the rate constants (although they may be functions of the temperature). The mole fraction $x_a = 1 - x_b$ and it is convenient to express all of our relations in terms of x_b. Let us define a temperature θ such that $\theta = (H_b - H_a)/R$ where H_a and H_b are the molal enthalpies of a and of b and R is the usual gas constant. The basic equations for heat transfer are then

$$dg_b/dz = nk_f(1 - x_b) - nk_r x_b = n(k_f + k_r)(x_{be} - x_b) \tag{13}$$

$$g_b = -n\mathfrak{D}_{ab}\, dx_b/dz \tag{14}$$

$$q = -\lambda dT/dz - R\theta n\mathfrak{D}_{ab}\, dx_b/dz \tag{15}$$

In order to simplify our example as much as possible, let us assume that λ, θ, $n\mathfrak{D}_{ab}$, and $\mathfrak{D}_{ab}/k_r$ are all constants. In addition it is convenient to introduce the dimensionless constant, or Lewis number,

$$\delta = n\mathfrak{D}_{ab}C_{pf}/\lambda$$

Here C_{pf} is the specific heat at constant pressure per mole of either A or B under conditions such that no chemical reaction takes place. According to our best estimates of experimental data for many substances, the value of δ is very nearly unity. To complete the specification of the rate constants, we write the expression for the equilibrium composition,

$$x_{be}/(1 - x_{be}) = k_f/k_r = \exp[(S/R) - (\theta/T)] \tag{16}$$

Here S is the entropy change in the reaction, $S = S_b - S_a$. We can now examine the characteristics of heat transfer through a gaseous mixture containing A and B.

1. THE HEAT FLUX

Since λ and $R\theta n\mathfrak{D}_{ab}$ are assumed to be constants, Equation (15) integrates exactly to give

$$-qz/\lambda = (T - T_c) + \delta\theta(C_{pf}/R)^{-1}(x_b - x_{bc}) \tag{17}$$

or integrating all the way across the cell to $z = z_h$,

$$-qz_h/\lambda = (T_h - T_c) + \delta\theta(C_{pf}/R)^{-1}(x_{bh} - x_{bc}) \tag{18}$$

Thus the heat flux is determined by the temperature and chemical composition at the two boundaries. The chemical composition at the two boundaries, however, is determined both by the homogeneous and by the heterogeneous reaction rates. The maximum heat flux is obtained when the homogeneous and/or heterogeneous reaction rates are sufficiently fast to establish chemical equilibrium at both the hot and the cold surfaces, i.e.,

$$x_{bh} - x_{bc} = (x_{be})_{T_h} - (x_{be})_{T_c} \tag{19}$$

2. SURFACE CHEMICAL REACTIONS

According to the Hertz-Knudsen[8] equation, the number of molecules hitting a square centimeter of surface in one second is

$$r = nkT(2\pi mkT)^{-\frac{1}{2}} = 444P(MT)^{-\frac{1}{2}} \text{ moles/cm}^2 - \text{sec} \tag{20}$$

Here M is the molecular weight of the substance and P is the pressure in atmospheres. We can define the catalytic efficiency of the surface, $\epsilon(T)$, such that if a molecule of B hits the surface, the probability of it being converted to A is ϵx_{ae}; and if a molecule of A hits the surface, the probability of it being coverted to B is ϵx_{be}. The catalytic efficiency, ϵ, represents the fraction of molecules hitting the surface which come off with a composition in thermal equilibrium with the surface. Thus ϵ is analogous to the accommodation coefficient. For a metallic surface, a good catalytic efficiency would be of the order of 10^{-2} to 10^{-3}. A ceramic surface might have an efficiency of around 10^{-6}. The precise determination of $\epsilon(T)$ for a particular example requires a great deal of difficult experimentation and theory.[7] If we know the rate of the surface chemical reactions in one direction, then by the principle of microscopic reversibility and a knowledge of the equilibrium constant we know the rate in the reverse direction. Thus for the A $\rightleftarrows$ B reaction it is reasonable to suppose that S_{bc} and S_{bh} have the functional form,

$$S_b = 444P(MT)^{-\frac{1}{2}}\epsilon(x_{be} - x_b) \text{ moles/cm}^2 - \text{sec} \quad (21)$$

It will be remembered that the boundary conditions are that $g_{bc} = S_{bc}$ and $g_{bh} = -S_{bh}$. If the catalytic efficiency is zero then $g_{bc} = g_{bh} = 0$. For most cases, however, it is more reasonable to suppose that the catalytic efficiency is sufficiently large to maintain chemical equilibrium at the surfaces of the cell.

It is interesting to consider a hypothetical example where the reaction rates for the homogeneous reactions are all zero so that the only chemical reactions occur on the surface.

Example: reactions on surface, no homogeneous reactions

If there are no homogeneous reactions, $R_b = 0$ and g_b = constant. Then from Equation (14) it follows that x_b must vary linearly with z,

$$x_b = x_{bc} - g_b(n\mathfrak{D}_{ab})^{-1}z \quad (22)$$

and since $x_b = x_{bh}$ when $z = z_h$,

$$g_b = (n\mathfrak{D}_{ab}/z_h)(x_{bc} - x_{bh}) \quad (23)$$

In order to simplify the expressions let us suppose that

$\epsilon_c T_c^{-\frac{1}{2}} = \epsilon_h T_h^{-\frac{1}{2}}$ and let

$$\beta = 444P(MT_c)^{-\frac{1}{2}}(n\mathfrak{D}_{ab})^{-1}\epsilon_c z_h$$

Then since $g_b = S_{bc} = -S_{bh}$ it follows that

$$x_{bc} - x_{bh} = \beta[(x_{be})_c - x_{bc})] = -\beta[(x_{be})_h - x_{bh}] \quad (24)$$

Solving for x_{bc} and x_{bh},

$$\begin{aligned} x_{bc} &= [(1 + \beta)(x_{be})_c + (x_{be})_h]/(2 + \beta) \\ x_{bh} &= [(x_{be})_c + (1 + \beta)(x_{be})_h]/(2 + \beta) \end{aligned} \quad (25)$$

From which it follows that

$$g_b = (n\mathfrak{D}_{ab}/z_h)[\beta/(2 + \beta)][(x_{be})_c - (x_{be})_h] \quad (26)$$

And the heat flux, Equation (18), is for this case

$$\begin{aligned} -qz_h/\lambda = (T_h - T_c) + \theta(C_{pf}/R)^{-1} \\ \times (\beta/(2 + \beta))((x_{be})_h - (x_{be})_c) \end{aligned} \quad (27)$$

Thus, the greater is β or the catalytic activity ϵ, the greater is the heat flux. The maximum heat flux occurs in the limit that β is infinite in which case $x_b = x_{be}$ on the two surfaces. From Equation (17) it follows that since x_b varies linearly with z, the temperature must also vary linearly with z.

In examples where both homogeneous and heterogeneous reactions occur, the treatment of the boundary conditions remains very much the same as for the simple case we have just considered, with the exceptions that g_b is no longer constant and x_b is no longer a linear function of z.

3. THE LOCAL EQUILIBRIUM SOLUTION

The local equilibrium solution is very simple for the unimolecular reaction example. From Equation (16),

$$x_{be} = [1 + \exp(-(S/R) + (\theta/T))]^{-1} \quad (28)$$

From Equation (14),

$$\begin{aligned} g_{be} &= -n\mathfrak{D}_{ab}(dT/dz)(dx_{be}/dT) \\ &= n\mathfrak{D}_{ab}(dT/dz)x_{be}(1 - x_{be})\theta/T^2 \end{aligned} \quad (29)$$

And from Equations (9), (10) and (15), $q = -\lambda'(dT/dz)$ where

$$\begin{aligned} \lambda' &= \lambda + n\mathfrak{D}_{ab}Rx_{be}(1 - x_{be})(\theta/T)^2 \\ &= \lambda[1 + \delta(R/C_{pf})x_{be}(1 - x_{be})(\theta/T)^2] \end{aligned} \quad (30)$$

It is perhaps more significant to express the effective coefficient of thermal conductivity in terms of the specific heats. Since the enthalpy per mole of mixture of A and B is

$$H = x_aH_a + x_bH_b = H_a + x_bR\theta \quad (31)$$

it follows that C_{pe} (the specific heat at constant pressure assuming that the chemical composition is maintained in equilibrium with the temperature) is given by

$$C_{pe} - C_{pf} = R\theta dx_{be}/dT = Rx_{be}(1 - x_{be})(\theta/T)^2 \quad (32)$$

Thus the effective coefficient of thermal conductivity is given by

$$\lambda'/\lambda = 1 + \delta((C_{pe}/C_{pf}) - 1) \quad (33)$$

Or letting $\delta = 1$, which is reasonably close to the values found from experimental data for a number of cases,

$$\lambda'/\lambda = C_{pe}/C_{pf} \quad (33')$$

Figure 2 shows the temperature as a function of $(-qz/\lambda)$ which is obtained for the special case of $S/R = 0$, $\delta = 1$, $\theta = 1000°\text{K}$, $C_{pf}/R = 5/2$, $T_c = 200°\text{K}$, $T_h = 2000°\text{K}$. On this same graph there are two straight lines. One straight line corresponds to the temperature versus $(-qz/\lambda)$ if there were no chemical reaction, the other straight line corresponds to the case where we assumed that chemical equilibrium is attained on the two surfaces by catalytic reactions but no reactions occur in the gas phase. One is indeed impressed with the smallness of the effect of chemical reac-

tions in this example. The values of λ'/λ versus T are given in Figure 3. The maximum value of $\lambda'/\lambda = C_{pe}/C_{pf}$ is approximately 1.18 and occurs at a temperature around 400°K. The reason for this small chemical effect is that we have assumed that S/R is zero.

The magnitude of the maximum value of $\lambda'/\lambda = C_{pe}/C_{pf}$ depends upon the value of S/R. Let us define the transition temperature, T_t, as the temperature at which C_{pe}/C_{pf} is largest. Using Equations (28) and (32) it is easy to show that θ/T_t is related to S/R by the transcendental equation,

$$\exp(S/R) = [(\theta/T_t) - 2] \times [(\theta/T_t) + 2]^{-1} \exp(\theta/T_t) \quad (34)$$

And $(C_{pe} - C_{pf})_{\max}/R$ is simply related to θ/T_t,

$$(C_{pe} - C_{pf})_{\max}/R = (\theta/2T_t)^2 - 1 \quad (35)$$

At the transition temperature, the equilibrium composition is

$$(x_{be})_{T_t} = (\tfrac{1}{2}) - (T_t/\theta) \quad (36)$$

The values of S/R and $(C_{pe} - C_{pf})_{\max}/R$ are given in Table 1 for different values of θ/T_t. First of all one sees that, regardless of entropy, the transition temperature can never be greater than $\theta/2$. Then it appears that the larger is S/R, the greater is the maximum value of the specific heat. For large values of S/R, entropy strongly favors the high energy product B and therefore lowers the transition temperature. If C_{pf}/R is taken to be 5/2 as in the above example, then

$$(\lambda'/\lambda)_{\max} = 0.4\,(C_{pe} - C_{pf})_{\max}/R + 1 \quad (37)$$

The values of $(\lambda'/\lambda)_{\max}$ for various values of θ/T_t are given in Table 1. For unimolecular reactions, large values of S/R are unusual and therefore the effect of chemical reactions on the coefficient of thermal conductivity is not usually large. This is in contrast to dissociation reactions where there is generally a large entropy change favoring the dissociation products. We shall consider this case presently.

4. THE PRINCIPAL SOLUTION

It is easy to examine the deviations of x_b from the local equilibrium solution, x_{be}. Equations (13) and (14) can be rearranged into the form,

$$x_b = x_{be} + (1 - x_{be})(\mathfrak{D}_{ab}/k_r)d^2x_b/dz^2 \quad (38)$$

And both sides of Equation (15) can be differentiated to give

$$d^2x_b/dz^2 = -(\delta\theta)^{-1}(C_{pf}/R)d^2T/dz^2 \quad (39)$$

Substituting Equation (39) into Equation (38),

$$x_b = x_{be} - (\mathfrak{D}_{ab}/k_r)(\delta\theta)^{-1} \times (C_{pf}/R)(1 - x_{be})(d^2T/dz^2) \quad (40)$$

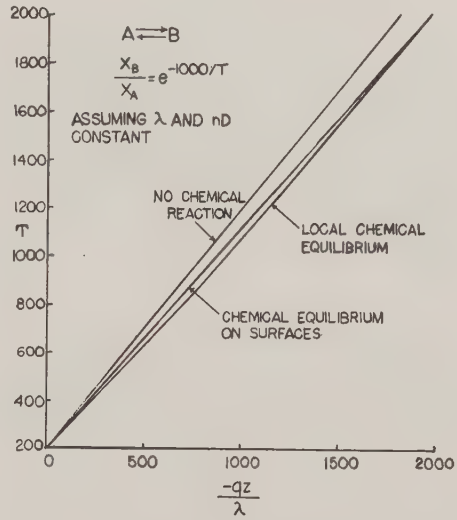

FIG. 2. Variation of temperature with distance for a hypothetical unimolecular reaction taking place in a thermoconduction cell.

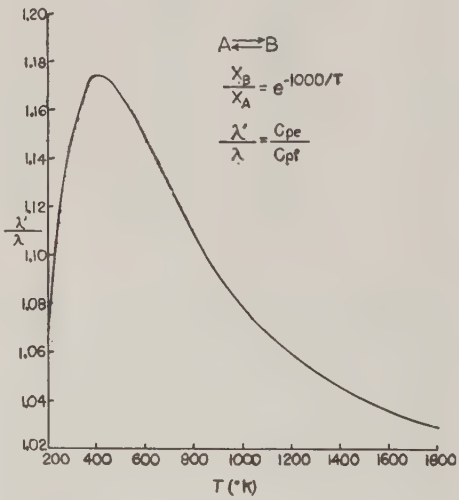

FIG. 3. Effect of chemical reaction on coefficient of heat conductivity for a hypothetical unimolecular reaction.

At temperatures somewhat below the transition temperature, d^2T/dz^2 is negative so that x_b is somewhat greater than x_{be}; whereas for temperatures somewhat larger than the transition temperature, d^2T/dz^2 is positive so that x_b is somewhat less than x_{be}. In order to establish

orders of magnitude, let us consider a typical unimolecular reaction with $k_r = 10^{12}$ sec^{-1}, $\mathfrak{D}_{ab} = 1$ cm^2/sec, $\delta = 1$, and $(C_{pf}/R) = 5/2$. Then for this example

$$x_b = x_{be} - 2.5 \times 10^{-12}(1 - x_{be})(d^2(T/\theta)/dz^2) \quad (41)$$

In a cell where the temperature change might take place in one centimeter, the difference between x_b and x_{be} would be of the order of 10^{-12}. For such a reaction, in order for the difference between x_b and x_{be} to be appreciable, one would have to consider a strong shock in which the temperature change takes place in a few hundred Ångstrom. Under such drastic conditions neither our treatment nor the usual kinetic theory of gases

Table 1

The Maximum Value of the Specific Heat Attained in a Unimolecular Reaction at a Transition Temperature, T_t, as a Function of the Entropy Change in the Reaction, S. Here θR is the Enthalpy Change in the Reaction

θ/T_t	(S/R)	$\frac{(C_{pe}-C_{pf})_{\max}}{R}$	$\left(\frac{\lambda'}{\lambda}\right)_{\max}$
2	$-\infty$	0	1
2.25	−0.5832	0.2656	1.106
2.4	+0.0021	0.4400	1.176
2.5	0.3028	0.5625	1.225
2.75	0.9042	0.8906	1.356
3	1.3906	1.2500	1.500
3.5	2.2007	2.0625	1.825
4	2.9014	3.0000	2.200
5	4.1527	5.2500	3.100
7.5	6.9535	13.0625	6.225
10	9.5945	24.0000	10.600

is valid. However, if B is a metastable substance so that k_r is of the order of 10^2 to 10^4, then the difference between x_b and x_{be} might be large under a wide variety of practical circumstances.

Let us define the function d which we shall later identify with the boundary layer thickness,

$$d^2 = \mathfrak{D}_{ab}/(k_f + k_r) = (\mathfrak{D}_{ab}/k_r)(1 - x_{be}) \quad (42)$$

Also we shall continue to define the effective coefficient of thermal conductivity, λ', by the equation $q = -\lambda' dT/dz$ so that

$$\lambda' = \lambda + R\theta n\mathfrak{D}_{ab}(dx_b/dz)/(dT/dz) \quad (43)$$

This leads to the relation

$$\lambda'/\lambda = 1 + \delta((C_{pe}/C_{pf}) - 1) + d^2[x_{be}\theta T^{-2}d^2T/dz^2 - (d^3T/dz^3)/(dT/dz)] \quad (44)$$

An analysis shows that the correction term, except for metastable components, is usually very small. For temperatures somewhat lower than T_t, the correction term is negative; whereas for temperatures somewhat greater than T_t, the correction term is positive.

Equations (41) and (44) comprise the principal solution to the flame equations. For cases where the coefficients of diffusion, thermal conductivity, etc., are not constant and where the chemical kinetics is more complex, it is not generally possible to obtain the principal solution without making approximations. In those cases one must resort to the iterative procedure discussed previously.

5. The Transients and the Fitting of the Boundary Conditions

The nature of the transients and the fitting of the boundary conditions has been discussed at some length in Part I.[1] Equation (38) can be written in the form,

$$d^2(d^2x_b/dz^2) = x_b - x_{be} \quad (45)$$

If the boundary layer is truly thin, then in the small boundary layer region we can assume that d and x_{be} are constant so that

$$x_b = x_{be} + c_1 \exp(z/d) + c_2 \exp(-z/d) \quad (46)$$

Also

$$g_b = g_{be} - (n\mathfrak{D}_{ab}/d) \times (c_1 \exp(z/d) - c_2 \exp(-z/d)) \quad (47)$$

Since d is very small, i.e., of the order of 10^{-6} cm for a typical unimolecular reaction, an extremely small value for either c_1 or c_2 will suffice to adjust the value of g_b at the boundary to satisfy the required boundary conditions. At the cold boundary c_1 is set equal to 0 whereas at the hot boundary it is c_2 which is set equal to 0. We have seen from Equation (18) it is the values of x_{bc} and x_{bh} which determine the heat flux. At the cold boundary $x_{bc} = x_{be} + c_2$. Thus if d is truly small, then c_2 will be small and little error is made in assuming that x_{bc} is given by the local equilibrium solution. A similar argument holds for the hot boundary.

III. Example Dissociative Reaction, $A \rightleftarrows 2B$

Inasmuch as in Part I[1] we have given a detailed discussion of the oxygen dissociation, $O_2 \rightleftarrows 2O$, and Prigogine and his co-workers have discussed the N_2O_4 dissociation quite thoroughly,

we need not go into much detail here. The point of most interest in the case of the dissociative reaction is that λ'/λ can be as large as 10 or 15 in contrast to the unimolecular case where λ'/λ is usually only slightly larger than unity. We shall explain this effect in terms of the large entropy change in favor of the dissociation products.

If we let $\delta = \hat{C}_{pf}\rho\,\mathfrak{D}_{ab}/\lambda$, then to the local equilibrium approximation,

$$\lambda'/\lambda = 1 + \delta(2 - x_{be})[(\hat{C}_{pe}/\hat{C}_{pf}) - 1] \quad (48)$$

The values of δ are surely of the order of unity but may vary by as much as a factor of two with composition (depending on the critical volumes and critical temperatures of the A and B molecules). The values of $\hat{C}_{pf}$ and $\hat{C}_{pe}$ are readily determined. Here $\hat{C}_{pf}$ is the specific heat of one gram of the mixture at constant pressure if the chemical composition is frozen, whereas $\hat{C}_{pe}$ is the same specific heat except that the chemical composition is maintained in equilibrium with the temperature. The enthalpy per gram of mixture, $\hat{H}$, is equal to the enthalpy per cm^3, $n(x_aH_a + x_bH_b)$, divided by the number of grams per cm^3, $n(x_aM_a + x_bM_b)$. Thus

$$\hat{H} = \hat{H}_b - \theta R M_b^{-1}(2 - x_b)^{-1} \quad (49)$$

Here $\theta = 2H_b - H_a$ where H_a and H_b are the enthalpies per mole of the A and B respectively. If we let $S = 2S_b - S_a$, then the equilibrium constant for the reaction is

$$x_{be}^2/(1 - x_{be}) = P^{-1}\exp[(S/R) - (\theta/T)] \quad (50)$$

Differentiating Equation (49) and making use of Equation (50),

$$\begin{aligned} M_b(\hat{C}_{pe} - \hat{C}_{pf})/R &= \theta(2 - x_{be})^{-2}dx_{be}/dT \\ &= x_{be}(1 - x_{be})(2 - x_{be})^{-3}(\theta/T)^2 \end{aligned} \quad (51)$$

The maximum value of $\hat{C}_{pe} - \hat{C}_{pf}$ occurs at the transition temperature, T_t. It is easy to show that

$$\begin{aligned} \exp[(S/R) - \ln P] &= 2[(\theta/T_t) - 4] \\ &\times [(\theta/T_t) + 2]^{-1}\exp(\theta/T_t) \end{aligned} \quad (52)$$

At the transition temperature, x_{be} is designated by x_{bt}. It is given by the relation,

$$\begin{aligned} x_{bt} = [(\theta/T_t) + 2]^{-1}\,[&-((\theta/T_t) - 4) \\ &+ (3(\theta/T_t)((\theta/T_t) - 4))^{\frac{1}{2}}] \end{aligned} \quad (53)$$

The maximum value of $M_b(\hat{C}_{pe} - \hat{C}_{pf})/R$ is then found by substituting T_t and x_{bt} into Equation (51). The results are shown in Table 2. In order to estimate λ'/λ let us assume that $\delta = 1$ and that $M_b\hat{C}_{pf} = 5R/2$. Then the maximum value of (λ'/λ) is given by

$$\begin{aligned} (\lambda'/\lambda)_{\max} &= 1 + 0.4\,(1 - 2x_{bt}) \\ &\times (\hat{C}_{pe} - \hat{C}_{pf})_{\max}M_b/R \end{aligned} \quad (54)$$

For the dissociative reaction, the largest value of T_t is $\theta/4$, and as in the case of the unimolecular reaction, the greater is S/R the larger is the maximum value of the specific heat and the heat conductivity. In the dissociative case the normal value of S/R is around 15 so that the normal expectancy is for a large value of λ'/λ in the vicinity of T_t.

TABLE 2

THE MAXIMUM VALUE OF THE SPECIFIC HEAT ATTAINED IN A DISSOCIATIVE REACTION AT A TRANSITION TEMPERATURE, T_t, AS A FUNCTION OF THE ENTROPY CHANGE, S. HERE θR IS THE ENTHALPY CHANGE IN THE REACTION

θ/T_t	$(S/R) - \ln P$	x_{bt}	$M_b(\hat{C}_{pe} - \hat{C}_{pf})_{\max}/R$	$(\lambda'/\lambda)_{\max}$
4.0	$-\infty$	0.0000	0.0000	1.000
4.5	2.63	0.3228	0.938	1.629
5.0	3.75	0.4104	1.506	1.958
7.5	7.19	0.5657	4.684	3.687
10.0	10.00	0.6180	8.944	5.944
15.0	15.26	0.6617	21.013	12.249
20.0	20.37	0.6811	37.869	20.978

IV. Heat Conductivity of a Pure Polyatomic Gas

The problems involved in the estimation of the coefficient of thermal conductivity of a polyatomic gas can be divided into three classes: (1) The derivation of the Eucken type correction factor and the choice of the best constants to use in it. (2) The corrections to the coefficient of thermal conductivity resulting from the distortion of the molecular distribution functions due to the nonadiabatic collisions. (3) The estimation of the coefficient of heat conductivity for electronically excited molecules.

1. THE EUCKEN-TYPE CORRECTION FACTOR[2]

The Eucken-type factor for the heat conductivity of a polyatomic gas follows easily from Equation (10). Let λ be the coefficient of thermal conductivity of the polyatomic gas and let λ

(mon) be the coefficient of thermal conductivity which one would estimate if the molecules possessed no internal degrees of freedom. Then if we consider each of the quantum states of the molecules as a separate chemical species,

$$\lambda = \lambda(\text{mon}) + \sum_{i,j} H_i n D_{ij} dx_i/dT \qquad (55)$$

Here the D_{ij} are the multicomponent diffusion coefficients. If the different quantum states have different coefficients of diffusion, Equation (55) is as far as one goes in writing a convenient expression for the coefficient of thermal conductivity. This is the case for electronically excited molecules. However, for normal molecules the assumption is usually made that the coefficients of diffusion are the same regardless of the quantum state. For these normal molecules we can derive a somewhat simpler expression. Going back to Equation (4), setting each of the binary coefficients $\mathfrak{D}_{ij}$ equal to the self diffusion coefficient, $\mathfrak{D}$, and making use of the fact that since the molecular weights are the same for all species, $\sum_j g_j = 0$ and $\sum_j x_j = 1$, it follows that

$$g_i = -(n\mathfrak{D})dx_i/dz \qquad (56)$$

Then from Equation (6),

$$\lambda = \lambda\ (\text{mon}) + (n\mathfrak{D}) \sum_i H_i\, dx_i/dT \qquad (57)$$

But the enthalpy per mole of gas is $H = \sum_i x_i H_i$ so that the specific heat at constant pressure is

$$C_p = \sum_i x_i\, dH_i/dT + \sum_i H_i dx_i/dT \qquad (58)$$

The first term is the specific heat that the gas would have if the molecules had no internal degrees of freedom, that is $5R/2$. Thus the summation in Equation (57) is just equal to $C_p - 5R/2$ and

$$\lambda = \lambda(\text{mon}) + (n\mathfrak{D})(C_p - 5R/2) \qquad (59)$$

It is convenient to introduce a dimensionless parameter

$$\delta_f = (5R/2)(n\mathfrak{D})/\lambda\ (\text{mon}) \qquad (60)$$

Then

$$\lambda/\lambda(\text{mon}) = (1 - \delta_f) + (\tfrac{2}{5})\delta_f(C_p/R) \qquad (61)$$

The right hand side of Equation (61) is exactly the Eucken factor if one assumes that $\delta_f = \tfrac{2}{3}$. However Eucken arrived at this value on the basis of the most simplified kinetic theory arguments. In Part II,[2] we have computed δ_f on the assumption that the molecules interact according to various potential energy laws for spherical molecules. For either the Lennard-Jones (6–12) or the Buckingham (6-exp) potentials, $\delta_f = 0.885$ to within a couple of per cent. This theoretical value varies only slightly with temperature and with the assumed potential law. Using $\delta_f = 0.885$, we obtain the Eucken-type correction factor,

$$\begin{aligned}\lambda/\lambda(\text{mon}) &= 0.115 + 0.354C_p/R \\ &= 0.469 + 0.354C_v/R\end{aligned} \qquad (62)$$

The value of δ_f can be determined from a knowledge of the experimental Prandtl numbers, $\text{Pr} = \eta C_p/M\lambda$. This requires that we assume that the viscosity for a polyatomic gas is not affected by the internal degrees of freedom of the molecule. If this is the case, then

$$\eta = (\tfrac{4}{15})M\lambda(\text{mon})/R \qquad (63)$$

Thus

$$\begin{aligned}(1/\text{Pr}) &= (\tfrac{15}{4})(R/C_p)[\lambda/\lambda(\text{mon})] \\ &= (R/C_p)[(\tfrac{15}{4}) + (\tfrac{3}{2})\delta_f(C_p - (\tfrac{5}{2})R)/R]\end{aligned} \qquad (64)$$

The factor $(3/2)\delta_f$ has frequently been called f_{int}, or the rate of transport of the energy of the internal degrees of freedom. Vines and Bennett[9] have made a thorough study of f_{int} for a large variety of molecules. They find that the best value for nonpolar molecules is $f_{\text{int}} = 1.27$ or $\delta_f = 0.85$. This is in excellent agreement with our theoretical value, $\delta_f = 0.885$.

2. CORRECTIONS DUE TO FREQUENT NONADIABATIC COLLISIONS

In using the macroscopic transport equations to consider the heat flux in a chemically reacting gas mixture, we have made the implicit assumption that the nonadiabatic collisions themselves did not distort the molecular distribution functions and thereby produce anomalous transport coefficients. This difficulty is not apt to arise in the case of either vibrational or electronic degrees of freedom since vibrational or electronic transitions usually occur so seldom (one transition in more than a thousand collisions). However, rotational transitions occur in almost every collision. Our concern is therefore centered on the validity of our treatment with respect to the rotational degrees of freedom.

Uhlenbeck, Wang and de Boer[10, 11] have developed a rigorous formal theory of the transport properties in a polyatomic gas. They consider each quantum state of the molecule to be a separate chemical species. For each species there is a separate Boltzman equation. In addition to the usual adiabatic collision terms on the right hand side, there are terms which involve the differential scattering cross-sections, $I_{ij}^{kl}(\theta, \phi)$. These cross-sections give the probability that a molecule in quantum state "i" and possessing a specified velocity will collide with a molecule in state "j" having a specified velocity and that, after the collision, the two molecules will have changed their quantum states to k and l respectively. Their trajectories will be deflected through specified angles and the molecules will possess specified new velocities. Uhlenbeck, Wang and de Boer have formally solved the transport equations and have expressed the coefficient of thermal conductivity in terms of the differential scattering cross-sections. They have showed that in the limit that the nonadiabatic collisions are infrequent as compared to the adiabatic collisions, the local chemical equilibrium treatment leading to the Eucken type formula for the heat conductivity is valid. However, when the nonadiabatic collisions occur frequently the molecular distribution functions become distorted and this distortion affects the coefficient of thermal conductivity. Unfortunately the differential scattering cross-sections have not yet been calculated for any practical cases so that it is difficult to estimate the importance of this distortional effect from the Uhlenbeck, Wang and de Boer treatment.

A gas made up of perfectly rough spheres is one of the two examples of rotational-translation interaction for which the theory has been completely worked out. Table 3 gives the results of Pidduck's[12] calculations. Here I is the moment of inertia, m the mass and σ the diameter of the spherical molecules. If all of the mass were concentrated at the center, $4I/m\sigma^2$ would be 0; if the mass were uniformly distributed throughout the sphere, $4I/m\sigma^2$ would equal 0.4; if all of the mass were concentrated in its outermost spherical shell of radius $\sigma/2$, $4I/m\sigma^2$ would equal $\frac{2}{3}$. In Table 3, the λ_s (mon), η_s, and $\mathfrak{D}_s$ are the usual coefficients of thermal conductivity, viscosity and self-diffusion for (smooth) rigid monatomic molecules without internal degrees of freedom, Pr is the Prandtl number, $\mathrm{Pr} = \eta C_p/M\lambda$, and S the Schmidt number, $\mathrm{S} = \eta/\rho\mathfrak{D}$. For (smooth) rigid monatomic molecules, $\mathrm{Pr} = \frac{2}{3}$ and $\mathrm{S} = \frac{5}{6}$. At first sight it seems surprising that the Prandtl number for a rough sphere with all of its mass concentrated at the center should be different from the (smooth) rigid monatomic spheres; however, this is due to the interchange of rotational energy even in this limiting case. We can calculate λ/λ_s (mon) and the Prandtl number to be expected for the rough spheres on the basis of the Eucken-type factor for the coefficient of thermal conductivity, using Equations (61) and (64). If we take $\delta_f = 0.800$, which is correct for smooth rigid monatomic molecules, λ/λ_s (mon) = 1.480 and Pr = 0.721. Thus in the limit that the mass of the rough sphere is concentrated at its center, the Eucken-type factor

Table 3

The Transport Properties for Rough Spheres

$4I/m\sigma^2$	λ/λ_s(mon)	η/η_s	$\mathfrak{D}/\mathfrak{D}_s$	Pr	S
0.0	1.480	1.000	1.000	0.721	0.833
0.1	1.482	0.995	0.917	0.716	0.904
0.2	1.501	1.005	0.857	0.714	0.977
0.3	1.519	1.024	0.813	0.719	1.050
0.4	1.533	1.050	0.778	0.731	1.125
0.5	1.543	1.080	0.750	0.747	1.200
0.6	1.550	1.113	0.727	0.766	1.275

is exactly correct. The Eucken-type procedure leads to Prandtl numbers which agree with the exact calculations to within one percent until $4I/m\sigma^2 = 0.4$. If we had used $\delta_f = 0.85$, we would have obtained for the rough sphere, λ/λ_s(mon) = 1.510 and Pr = 0.706; or if $\delta_f = 0.885$, λ/λ_s (mon) = 1.531 and Pr = 0.697. Both of these estimates of the Prandtl number would have been in good agreement with the actual values. Thus we conclude that, at least in the case of the rough spheres, the errors introduced by the use of the macroscopic transport equations are small.

The only other example of rotational-translational interaction for which the transport properties have been calculated is the case of rigid spheroids. Table 4 gives the Prandtl numbers which result from the preliminary calculations of Curtiss and Muckenfuss.[3] The Prandtl numbers which we would estimate on the basis of the Eucken-type factor are the same as for the case of the rough spheres, Pr = 0.721, 0.706, or 0.697

depending on whether $\delta_f = 0.800, 0.850$, or 0.885. It is seen that the deviations from the Eucken-type result become large both as the molecule

Table 4

Prandtl Numbers for Rigid Spheroids

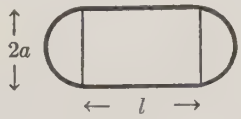

I/ma^2	$l/2a = 0.4$	$l/2a = 0.8$	$l/2a = 1.0$
0.25	0.716	0.854	0.960
0.50	0.716	0.751	0.804
0.75	0.716	0.725	0.753

Table 5

Prandtl Numbers at Low Temperatures[14]

	−200°C	−150°C	−100°C	−50°C	0°C
CO	0.80	0.78	0.77	0.75	0.74
N_2	0.76	0.77	0.75	0.74	0.72
NO	—	0.83	0.80	0.77	0.75
O_2	0.77	0.76	0.75	0.73	0.71
N_2O	—	—	0.78	0.77	0.76
CO_2	—	—	—	0.79	0.78
CH_4	0.80	0.77	0.75	0.74	0.74
Air	0.77	0.77	0.75	0.73	0.72

Table 6

Prandtl Numbers for Polar Gases[9] at 80°C

Substance	Prandtl Number	Dipole Moment *debyes*
Acetaldehyde	0.90	2.7
Water	1.07	1.83
Acetonitrile	0.94	—
Ammonia	0.86	1.47
Methyl alcohol	0.89	1.66
Acetone	0.85	2.74
Methyl chloride	0.80	1.89
Ethyl chloride	0.79	2.02
Chloroform	0.79	1.05

becomes more asymmetrical and as the moment of inertia, I, becomes small.

From the two examples of rotational-translational interaction, one sees that the deviations from the Eucken-type expected behavior manifest themselves by unusually large values of the Prandtl number. It is therefore interesting to examine the experimental data and see under what conditions large Prandtl numbers are found. Table 5 gives the results of some of the low temperature measurements of Keyes.[14] These large low temperature Prandtl numbers must be explained on the basis of the distortion of the distribution function as the result of translational-rotational interactions. A similar explanation must be given for the very large Prandtl numbers of polar substances,[9] as shown in Table 6. Inasmuch as two polar molecules interact at separations of the order of four or five kinetic theory collision diameters to exchange quanta of rotational energy, it is not surprising that they should behave in this manner.

V. Heat Conductivity of an Electronically Excited Gas

The heat conductivity of an electronically excited gas or a gas made up of electronically degenerate free atoms or molecules is very difficult to estimate. First of all, there are usually a large number of potential energy curves for the various sorts of intermolecular collisions. For example, if two oxygen atoms in their ground states collide, the collision can follow, with a priori statistical probability, any one of 81 different potential energy curves. Up to the present time, these potential energy curves have not been determined either for the interaction of the two atoms or for any other example of corresponding complexity. Then there is the question as to whether we could do a good job of estimating the transport properties if we were presented with the set of potential energy curves. At the present time, we have not even succeeded in determining the transport properties for hypothetical polar molecules which satisfy the simple Stockmayer potential. Thus we must seek rather crude approximations which are intended to give orders of magnitude or semi-quantitative estimates of the heat conductivity. Two methods for making rough approximations are suggested by the work of Hirschfelder and Eliason.[15] The first requires no knowledge of the potential energy curves, the second provides an estimate of the transport properties once the potential energy curves are known.

1. Estimation of Collision Diameter for an Atom in Either a Ground or Excited State

On a strictly empirical basis Hirschfelder and Eliason[15] found that the collision diameter of an

atom is equal to twice the mean radius, $\bar{r}$, of an electron in its outermost orbital plus 1.8 Ångstrom:

$$\sigma = 2\bar{r} + 1.8 \text{ Ångstrom} \quad (65)$$

Here σ is intended to mean the distance of closest approach of two molecules colliding with zero relative velocity. The $\bar{r}$ is readily computed on the basis of Slater screening constants,

$$\bar{r} = (\tfrac{1}{2})n^*(2n^* + 1)(Z - S)a_o \quad (66)$$

Here Z is the atomic number; n^* is the effective principal quantum number of the outermost shell; S is the Slater screening constant for this shell; and a_o is the radius of the Bohr orbit. Table 7 compares the calculated with the experimental values of σ for the noble gases and provides estimates of σ for other cases where no experimental data is available. The giant size of the excited states is quite surprising. For example, the first excited state of argon has a collision diameter of 9.80 A as compared to the ground state of argon for which $\sigma = 3.45$ A. This accounts for the large pressure broadening of excited molecules.

It is interesting to note that $\bar{r}$ is very nearly equal to the covalent binding radius. Thus if R is the equilibrium separation in a diatomic molecule, R_{ab} is very nearly equal to $\bar{r}_a + \bar{r}_b$ as seen in Table 8. Also in Table 8 is given a comparison between the experimental collision diameters and the values calculated on the basis of the empirical formula,

$$\sigma(\text{diatomic}) = (\tfrac{4}{5})(\bar{r}_a + \bar{r}_b) + 1.8 \text{ Ångstrom} \quad (67)$$

2. ESTIMATION OF THE TRANSPORT COEFFICIENTS AND SECOND VIRIAL COEFFICIENT FROM POTENTIAL ENERGY CURVES[15]

Most of the potential energy curves usually encountered in collisions between chemically active or electronically excited atoms or molecules are either of the purely repulsive type or else have a very deep minimum in the potential energy. For both of these types Hirschfelder and Eliason[15] found that it is easy to make a rather good approximation to the transport properties and second virial coefficient in the following manner. Let us define the quantities: σ (heat), σ (visc), σ (diff), σ (virial) as the effective collision diameters which, when substituted into the kinetic theory expressions for the interaction of rigid sphere molecules, give the correct values for the coefficients of thermal conductivity, viscosity, diffusion, and the second virial coefficient respectively. The problem is to determine these effective collision diameters in terms of simple properties of the given potential energy function, $E(r)$. The following equation has been found to work quite well,

$$E(\sigma) = \theta kT \quad (68)$$

TABLE 7

CALCULATED AND EXPERIMENTAL VALUES OF ATOMIC COLLISION DIAMETERS[15]

Atom	Electron Configuration	σ (calc) $2\bar{r}$ (A) + 1.8 (A)	σ (exp) (A)
	A. Ground States		
H	1s	3.38	
He	$(1s)^2$	2.73	2.58
C	$(1s)^2(2s)^2(2p)^2$	3.42	
N	$(1s)^2(2s)^2(2p)^3$	2.88	
O	$(1s)^2(2s)^2(2p)^4$	2.96	
Ne	$(1s)^2(2s)^2(2p)^6$	2.70	2.79
Cl	$(1s)^2(2s)^2(2p)^6(3s)^2(3p)^5$	3.62	
A	$(1s)^2(2s)^2(2p)^6(3s)^2(3p)^6$	3.45	3.42
Br	$\ldots (4s)^2(4p)^5$	3.96	
Kr	$\ldots (4s)^2(4p)^6$	3.56	3.61
Xe	$\ldots (5s)^2(5p)^6$	4.11	4.06
	B. Excited States		
H	(2s) or (2p)	7.10	
H	(3s) or (3p) or (3d)	12.86	
He	(1s)(2s) or (1s)(2p)	6.40	
Ne	$\ldots (2s)^2(2p)^5(3s)^1$	7.20	
N	$\ldots (2s)^2(2p)^2(3s)^1$	8.74	
O	$\ldots (2s)^2(2p)^3(3s)^1$	8.14	
A	$\ldots (3s)^2(3p)^5(4s)^1$	9.80	
Kr	$\ldots (4s)^2(4p)^5(5s)^1$	11.08	
Xe	$\ldots (5s)^2(5p)^5(6s)^1$	11.96	

TABLE 8

COLLISION DIAMETERS FOR DIATOMIC MOLECULES

	$\bar{r}_a + \bar{r}_b$ (A)	R_{ab} (exp) (A)	σ (calc) (A)	σ (exp) (A)
H_2	1.58	0.75	3.9	2.9
N_2	1.08	1.09	3.2	3.7
O_2	1.16	1.20	3.4	3.5
Cl_2	1.82	1.98	4.2	4.2
Br_2	2.16	2.28	4.7	4.3
CO	1.39	1.13	3.3	3.5
NO	1.12	1.15	3.7	3.7

Here the θ is a number independent of temperature and characteristic of the type of potential energy curve and the characteristic property under consideration. The set of values for θ are given in Table 9. For inverse power potentials, the θ are rigorously independent of temperature. For the Buckingham or the Lennard-Jones potentials, the values of θ vary only slightly with temperature, as long as the minimum in the potential energy curve is larger than $1.5\,kT$.

TABLE 9

VALUES OF θ REQUIRED TO CALCULATE VARIOUS PROPERTIES[15] WHICH RESULT FROM A GIVEN INTERMOLECULAR POTENTIAL

	θ (heat) = θ (visc)	θ (diff)	θ (virial)
Steep repulsive potential (varying as r^{-12})	0.83	1.85	0.44
Moderately long range repulsive potential (varying as r^{-6})	0.91	1.70	0.32
Long range repulsive potential (varying as r^{-4})	0.96	1.59	0.18
Deep minimum attractive potential	−0.58	−0.60	—

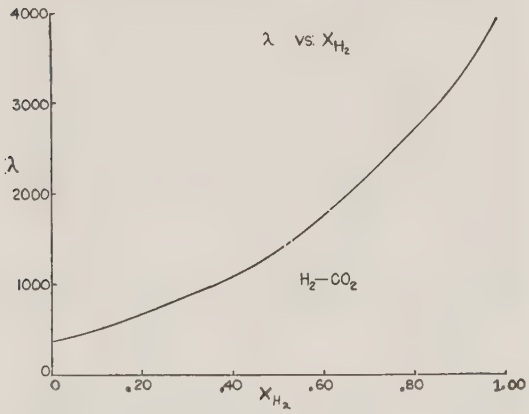

FIG. 4. Coefficient of thermal conductivity in units of 10^{-7} cal cm^{-1} sec^{-1} deg^{-1} vs composition for an H_2-CO_2 gas mixture.[13]

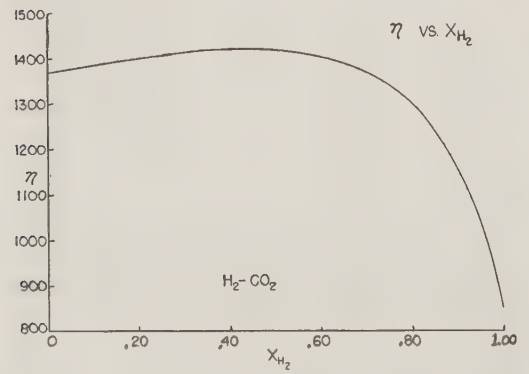

FIG. 5. Coefficient of viscosity in units of 10^{-7} g cm^{-1} sec^{-1} vs composition for an H_2-CO_2 gas mixture.[13]

VI. Heat Conductivity in a Polyatomic Gas Mixture

Figures 4, 5 and 6 show the variation of the coefficient of thermal conductivity, the coefficient of viscosity, and the Prandtl number for a H_2-CO_2 mixture at 0°C and 1 atmos. This is typical of the behavior of polyatomic gas mixtures. The coefficient of thermal conductivity varies smoothly with composition and in fact the reciprocal of the thermal conductivity varies almost linearly with the mole fraction. The coefficient of viscosity, however, varies in an anomalous fashion with composition. For the H_2-CO_2 mixture it has a maximum value, but for other mixtures it has a minimum. The Prandtl number possesses a minimum value of approximately one half of the Prandtl numbers for either of the pure components. The large difference between the molecular weights of the two components leads to the minimum. For other mixtures, the Prandtl number has a maximum value. The Prandtl numbers for a number of different mixtures at 0°C and 1 atmos are given in Table 10. It is therefore clear that although there is very little variation in the Prandtl numbers for pure substances, the Prandtl numbers for mixtures show a large variation.

Actually we can derive a Eucken-type relation to express the coefficient of thermal conductivity of a polyatomic gas mixture λ(mix) in terms of the coefficient of thermal conductivity which the mixture would possess if the molecules had no internal degrees of freedom, λ(mon-mix). Let us consider a mixture of molecules A and B. We shall consider each quantum state of each molecule to be a separate species, and suppose that the coefficients of diffusion are independent of the quantum state. Then the variation of the mole fraction of the "i"th state of molecule A is given by Equation (4) and can be written in the form,

$$dx_{ai}/dz = \sum_j (x_{ai}g_{aj} - x_{aj}g_{ai})/n\mathfrak{D}_{aa} + \sum_j (x_{ai}g_{bj} - x_{bj}g_{ai})/n\mathfrak{D}_{ab} \tag{69}$$

And a similar relation holds for the dx_{bi}/dz. If there is no chemical reaction between molecules

of A and molecules of B, then when a steady state is reached

$$g_a = \sum_j g_{aj} = 0 \quad \text{and} \quad g_b = \sum_j g_{bj} = 0 \tag{70}$$

Also we have the identities

$$x_a = \sum_j x_{aj} \quad \text{and} \quad x_b = \sum_j x_{bj} \tag{71}$$

Thus Equation (69) and the similar relation for dx_{bi}/dz become

$$\begin{aligned} dx_{ai}/dz &= -g_{ai}(x_a/n\mathfrak{D}_{aa} + x_b/n\mathfrak{D}_{ab}) \\ dx_{bi}/dz &= -g_{bi}(x_b/n\mathfrak{D}_{bb} + x_a/n\mathfrak{D}_{ab}) \end{aligned} \tag{72}$$

Thus Equation (69) gives

$$\lambda(\text{mix}) = \lambda(\text{mon-mix}) - \left[\sum_i g_{ai}H_{ai} + \sum_i g_{bi}H_{bi}\right]/(dT/dz)$$

$$\begin{aligned} \lambda(\text{mix}) = \lambda(\text{mon-mix}) &+ [x_a/n\mathfrak{D}_{aa} + x_b/n\mathfrak{D}_{ab}]^{-1} \sum_i H_{ai}\, dx_{ai}/dT \\ &+ [x_b/n\mathfrak{D}_{bb} + x_a/n\mathfrak{D}_{ab}]^{-1} \sum_i H_{bi}\, dx_{bi}/dT \end{aligned} \tag{73}$$

But in the approximation of local chemical equilibrium,

$$\begin{aligned} \sum_i H_{ai}\, dx_{ai}/dT &= x_a(C_{pa} - 5R/2) \\ \sum_i H_{bi}\, dx_{bi}/dT &= x_b(C_{pb} - 5R/2) \end{aligned} \tag{74}$$

And so the coefficient of thermal conductivity becomes

$$\begin{aligned} \lambda(\text{mix}) = \lambda(\text{mon-mix}) &+ x_a(C_{pa} - 5R/2) \\ &\times [x_a/n\mathfrak{D}_{aa} + x_b/n\mathfrak{D}_{ab}]^{-1} \\ &+ x_b(C_{pb} - 5R/2)[x_b/n\mathfrak{D}_{bb} + x_a/n\mathfrak{D}_{ab}]^{-1} \end{aligned} \tag{75}$$

Or making use of the Eucken-type expressions for the thermal conductivity of a pure polyatomic gas, we obtain

$$\begin{aligned} \lambda(\text{mix}) = \lambda(\text{mon-mix}) &+ x_a[x_a + x_b(\mathfrak{D}_{aa}/\mathfrak{D}_{ab})]^{-1}[\lambda_a - \lambda_a(\text{mon})] \\ &+ x_b[x_b + x_a(\mathfrak{D}_{bb}/\mathfrak{D}_{ab})]^{-1}[\lambda_b - \lambda_b(\text{mon})] \end{aligned} \tag{76}$$

Thus Equation (76) gives the Eucken-type correction for the coefficient of the thermal conductivity of a polyatomic gas mixture. It is altogether reasonable that the coefficients of both self-diffusion and ordinary diffusion should enter into this relation. Table 11 shows the excellent agreement which is obtained between experiment and theory for the case of a H_2-CO_2 mixture at 0°C and 1 atmos. The agreement which is obtained is slightly better than is obtained using

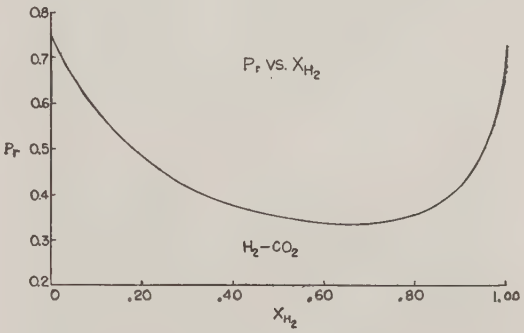

FIG. 6. Prandtl number vs composition for a H_2-CO_2 gas mixture.[13]

TABLE 10

THE PRANDTL NUMBER FOR GAS MIXTURES.[16] THE x_1 IS THE MOLE FRACTION OF THE LIGHTER COMPONENT

	$x_1 = 0$	$x_1 = .25$	$x_1 = .50$	$x_1 = .75$	$x_1 = 1.00$
H_2-O_2	0.716	0.509	0.413	0.418	0.720
H_2-A	0.683	0.434	0.362	0.368	0.717
N_2-A	0.677	1.038	1.145	1.168	0.730
H_e-A	0.670	0.496	0.437	0.466	0.705
H_2-CO_2	0.751	0.448	0.354	0.345	0.717
H_2-CO	0.802	0.550	0.463	0.443	0.716
H_2-N_2	0.764	0.560	0.478	0.473	0.716
H_2-N_2O	0.772	0.471	0.365	0.344	0.717

TABLE 11

COMPARISON OF THEORY AND EXPERIMENT FOR THE COEFFICIENT OF THERMAL CONDUCTIVITY OF AN H_2-CO_2 GAS MIXTURE AT 0°C AND 1 ATMOS.

xH_2	λ(mix) in 10^{-7} cal cm^{-1} sec^{-1} deg^{-1} Experiment[16]	Calculation
0.000	360	360
0.100	510	505
0.142	570	572
0.250	770	763
0.355	1000	982
0.500	1350	1350
0.750	2270	2291
0.901	3150	3195
1.000	4040	4040

the empirical formula which corresponds to multiplying the λ(mon-mix) by the linearly averaged Eucken-type correction for the two pure components. Equation (76) can be generalized to a

multicomponent mixture in which case,

$$\lambda(\text{mix}) = \lambda(\text{mon-mix}) + \sum_i (x_i/\mathfrak{D}_{ii})(\lambda_i - \lambda_i(\text{mon})) \Big(\sum_j x_j/\mathfrak{D}_{ij}\Big)^{-1} \quad (77)$$

Acknowledgments

The author wishes to extend his heartiest thanks to J. W. Linnett for his help, his encouragement, and his many suggestions during the preparation of this manuscript. Thanks are also due to Jan de Boer and to C. F. Curtiss for many interesting discussions; to Miss Beatrice Belda and Miss Florence Daul for typing the manuscript in record time; and to my wife for proofreading and correcting my errors.

REFERENCES

1. Hirschfelder, J. O.: WIS-ONR-18, University of Wisconsin Naval Research Laboratory (Feb. 1956). J. Chem. Phys., *26*, 274 (1957).
2. Hirschfelder, J. O.: WIS-ONR-22, University of Wisconsin Naval Research Laboratory (April 1956). J. Chem. Phys., *26*, 282 (1957).
3. Curtiss, C. F., and Muckenfuss, C.: WIS-NSF-6, University of Wisconsin Naval Research Laboratory (Nov. 1955). J. Chem. Phys., *26*, 1619 (1957). Here $Pr = \frac{80}{111}\frac{(\eta/\eta_s)}{(\lambda/\lambda_s)}$.
4. Prigogine, I., and Buess, R.: Acad. Roy. Belg., *38* (Series 5), 711, 851 (1952).
5. Waelbroeck, F., Lafleur, S., and Prigogine, I.: Physica, *21*, 667 (1955).
6. Hirschfelder, J. O., Curtiss, C. F., and Bird, R. B.: *Molecular Theory of Gases and Liquids*, p. 746. New York, John Wiley & Sons, 1954.
7. Ref. 6, p. 541.
8. Glasstone, S., Laidler, K., and Eyring H.: *Rate Processes*, p. 351. New York, McGraw-Hill Book Co., 1941.
9. Vines, R. G., and Bennett, L. A.: J. Chem. Phys., *22*, 360 (1954).
10. Uhlenbeck, G. E., Wang, C. S., and de Boer. To be published. We wish to thank the authors for the use of their manuscript prior to publication.
11. Ref. 6, p. 501.
12. Pidduck, F. B.: Proc. Roy. Soc., *A101* (1922).
13. Ref. 6, p. 507.
14. Keyes, F. G.: SQUID Tech. Rept., 37, Massachusetts Institute of Technology (April 1952).
15. Hirschfelder, J. O., and Eliason, M. A.: WIS-AF-1, University of Wisconsin Naval Research Laboratory (May 1956). Monograph of New York Acad. Sci., *Unstable Chemical Species: Free Radicals, Ions, and Excited Molecules* (1957).
16. Ref. 6, p. 577.

45

SPECTRA OF THE DETONATION OF OXYGEN WITH H_2, CO AND HYDROCARBONS

By H. Gg. WAGNER

Introduction

The theory of the hydrodynamics of detonation developed by Chapman and Jouget makes it possible to calculate the velocity of a stationary detonation if the thermodynamic data are given for all the reactants.[8,9] Generally, the calculated values for the detonation velocities of gases agree well with the experimental values. In these calculations it is not necessary to consider the particular mechanism of the reaction. However, certain effects that accompany detonation, raise the problem of the mechanism of the reaction, e.g., the limits of detonation and the behavior of detonation near these limits, the dependence of the detonation velocity on the tube diameter, etc.

The present paper describes experiments on the establishment of equilibrium in detonations especially with respect to the rotational and vibrational degrees of freedom. For this purpose, the emission spectra of different detonations were

examined, and temperatures of rotation and vibration were calculated where possible. In all these experiments, the initial gas mixtures were at room temperature and atmospheric pressure. The spectra were studied in three different apparatuses. Two spectographs were used, a Hilger E_3 with quartz optics and a Steinheil two-prism quartz instrument.

Experimental Procedure

FIRST APPARATUS

In a nonreflecting brass tube, 1.5 cm in diameter, the detonation traveled toward the slit of the spectroscope; the end of the tube was kept open (Fig. 1). The length l_1 was between 1 and 1.5 meters. The length l_2 was so chosen that the detonation showed good stability upon entering the portion l_1 of the tube. At the closed end, there was a spark gap for ignition.

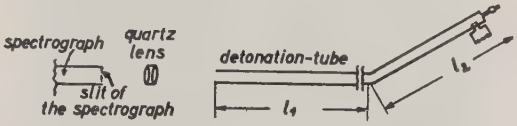

FIG. 1. Apparatus for observing spectra from detonations traveling toward the slit.

SECOND APPARATUS

A nonreflecting brass tube of square cross section was equipped with a removable quartz window in one wall. Through this window, the inside of the tube could be projected on the slit of the spectograph, using a quartz objective (Fig. 2).

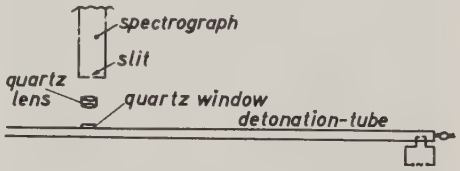

FIG. 2. Apparatus for observing spectra from detonations traveling perpendicular to the slit.

THIRD APPARATUS

In the first two apparatuses, a photographic plate was used as a receiver. Here a mobile slit was placed in the focal plane of the spectograph, and a multiplier, with the anode directly connected over a cathode-follower to a cathode-ray oscilloscope, was used as the indicator. Photographs were taken with the cathode-ray tube. The time of rise in this apparatus was 2.0×10^{-7} sec. The gas mixtures were prepared from commercial products and exact compositions were made using capillary flowmeters.

In the following paragraphs the spectra of H_2 and oxygen, CO and oxygen, and different hydrocarbon-O_2 detonations are dealt with. Only the discussion of the results is attempted without stressing details.

THE OH SPECTRUM IN THE H_2-O_2 DETONATION

Comparison of the spectra of burner flames with spectra detonations shows that detonation spectra are less resolved than the burner flames (Fig. 3). If one compares the intensity distribution in the spectra of detonations and flames[45], the 0—0 transition of the OH[7] bands being taken as constant for purpose of comparison, then transitions with higher quantum numbers are stronger in detonations than in flames. The intensity does not decrease from 1—0 to 3—2 as in a flame but it seems to increase from 1—0 to 3—2. The 3—3 transition seems to be much more excited in a detonation than in a flame.

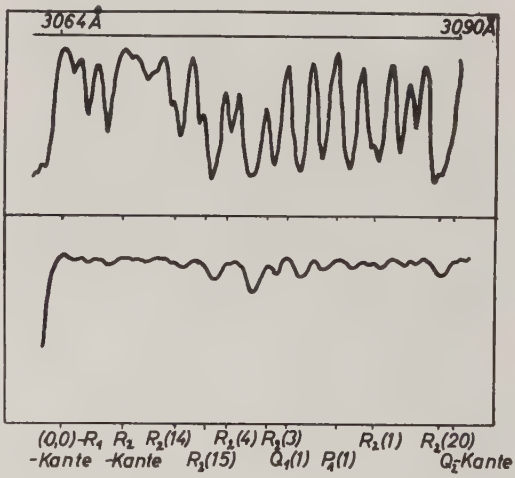

FIG. 3. Photometer curve for a $2H_2 + O_2$ flame and a $2H_2 + O_2$ detonation near the 0—0 transition of the OH bands.

By calculating the intensity distribution for the temperatures 3000°K and 4000°K, it is observed that the relative intensity of the higher vibrational transitions, compared to the intensity of 0—0, is only slightly stronger at 4000°K. In the different rotational branches, too, the relative intensity of the lines with higher rotational quantum numbers increases somewhat when temperature rises from 3000°K to 4000°K.

Comparison of the intensity distribution ob-

served in detonations with the intensity distribution for 4000°K calculated on the basis of observed flame spectra at 3000°K shows considerable deviation for the higher quantum states.

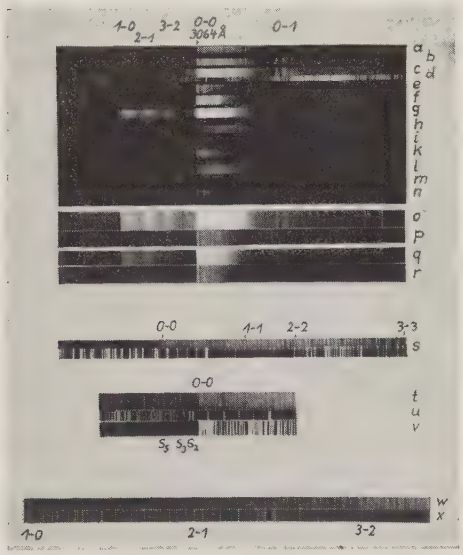

FIG. 4. Spectra of hydrogen-oxygen detonations. a,b,c, detonations in a stoichiometric mixture seen from the front with Hilger E 3 (100, 150 and 200 detonations); d,u, iron arc; e,f,g, $2H_2 + O_2$ flames; h, detonation of $H_2 + O_2$; i,k, $H_2 + O_2$ flame; l, detonation of $3H_2 + O_2$; m,n, $3H_2 + O_2$ flame; o,p, detonations of stoichiometric mixtures seen from the side with Hilger E 3; q,r, $2H_2 + O_2$ flames; s, detonation of $2H_2 + O_2$ seen from the front side with higher dispersion (Steinheil); t, region near the 0—0 head of the same spectrum as in s; v, region of the flame spectrum as in t; w, region between the 1—0 and the 3—2 transition of a spectrum as in s; x, region between the 1—0 and the 3—2 transition.

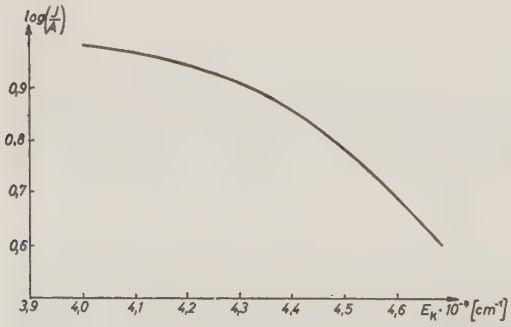

FIG. 5. Plot of ln I/A against E for the P_2 lines of the 0—0 transition of the OH bands.

Another difference between flame and detonation spectra is the marked pressure broadening of the lines in the detonation spectra (Fig. 4t, v). As a result, the number of lines for investigation is considerably reduced.

Evaluating the rotational temperature using the lines of parameter $K = 25$ from the P_2 branch of the 0—0 transition (ln I/A plotted as function E), one does not obtain a linear relation, from the slope of which the rotational temperature could be determined, but only a curve (Fig. 5).

For higher quantum numbers, the slope of the line gives a rotational temperature of 6000°K; for the lower quantum numbers, the rotational temperature rises to 20,000°K and more. The evaluation of the S lines of the 0—0 transition and of lines of 1—0 transition, gives similar results as to rotational temperature. Examination of the 3—3 transition, however, shows rotational temperatures not far from the calculated adiabatic temperatures. From the lines P_1, 6, 8, 3, 10, 12, etc., of the 3—3 transition, the rotational temperature is found to be approximately $T_r \approx$ 4000°K.

Investigation of the exposures obtained from the side points to the same conclusion, except that the deviations between adiabatic and rotational temperatures decrease.

Difficulties in the examination of the spectra arise not only from the pressure broadening of lines, but also from the weak continuum extending over the whole spectrum. The intensity of this continuum could be determined only at few points. Thus, the spectral analysis may involve a somewhat large relative error, which reduces the accuracy of the temperature data, in some cases as much as 10 per cent.

Effects of the Length of the Luminous Zone on Temperature

If a detonation traveling in a tube is observed from the side, the intensity distribution appears as a function of time (Fig. 6). After an extremely short rise, the intensity slowly decreases. The gradual temperature drop in the hot gases behind the detonation front may be observed from the relative intensities of two appropriate curves plotted as a function of time, e.g., lines from the 3—3 transition. The pressure drop can be measured directly. For known values of p and T, the decrease of the OH concentration may be evaluated.

If the lateral exposure leads to a rotational temperature T_g, the temperature T_m building up in the Chapman-Jouget plane or immediately behind it, may be calculated from the relation $T_m = T_g/(1 - BT_g)$. The coefficient B depends essentially on the tube diameter. In the experiments referred to here B was smaller in every case

than 10^{-5}. This means that the error associated with this parameter in the determination of the temperature is relatively small.

Another important factor in the determination of the temperature is the self-absorption.[2-5, 10, 11, 12] In the standard procedure for determining temperatures from spectra, it is supposed[1] that the light arriving at the photographic plate has the same intensity distribution as that emitted by the molecules, i.e., that between the originating point of the radiation and the receiver no absorption modifying the relative intensity takes place.

In a H_2O detonation, two factors give us reason to expect that self-absorption will play an important part, independent of the method of observation used: (1) The concentration of OH is very high. (2) The length of the radiating zone is large. For exposure from the side it is relatively simple to determine the influence of the self-absorption. If T_s is the temperature determined from the relative intensity of two lines lying closely together, the temperature T corrected for self-absorption[2] may be obtained from

$$T = \frac{T_s}{1 + \frac{RT_s}{\Delta E} \ln F}; \qquad \Delta E = E_1 - E_2$$

$$F = \frac{\alpha_2}{\alpha_1} \left(\frac{1 - \exp(-\alpha_1 x)}{1 - \exp(-\alpha_2 x)} \right)$$

The coefficient of absorption α for the maxima of the lines may be evaluated.

If self-absorption is taken into consideration, it will be seen that the evaluated lines of the transitions 0—0, 1—0, and 3—3 of the OH bands in H_2-O_2 detonation show no deviation of the rotational temperatures from the adiabatic temperature calculated by Berets, Green and Kistiakowsky[14] within the limits of precision that can be reached with the different apparatus. Lines with lower rotational quantum numbers could not be evaluated. It may be assumed that they would give the same results.

If the intensities for different vibrational states are compared without taking account of self-absorption, some important deviations from equilibrium distribution are observed. Taking the self-absorption into consideration, the deviation from the equilibrium distribution is only small. An insignificant overpopulation of the higher states may not be excluded with certainty.

Mixtures of CO_2 with Oxygen

Mixtures of CO-O_2 are of special interest for investigations on detonations; the reaction rate of the mixture may be changed by small additions of H_2 or H_2O over a large domain without significantly altering any of the thermodynamic properties of the mixture which, according to the theory of Chapman and Jouget, are of importance.

The light emission of the CO-O_2 detonation in the visible region is very intense up to the limits of detonation if the addition of H_2 or H_2O is not too great.

Figure 7t shows the spectrum of a $2CO + O_2$ flame with 3.5 per cent H_2 in the CO. The OH and the CO-flame bands are clearly visible.

FIG. 6. Light emission as a function of time: a $2H_2 + O_2$ detonation seen from the side (P_2 line in the 0—0 transition of OH).

Spectra of CO detonations obtained from the front with the Hilger E 3 spectograph also are presented (Fig. 7u, v, w). The detonation of this mixture shows a spectrum that is very similar to the spectra of the flame. Whereas the structure of the CO-flame bands[6, 10] may be observed in the flame, they are completely absent in the detonation. The intensity of the OH bands decreases noticeably in comparison with the intensity of the CO flame bands. In a mixture of $CO + O_2$, the CO-bands are less intense and the OH bands appear stronger.

Figure 7q, r, s shows the spectrum of $2CO + O_2$, with 3 per cent H_2 in the CO detonation seen from the side, and exposures of only the hot gases behind the detonation zone. These were obtained by closing the tube with a diaphragm. The tube was charged with the mixture up to the diaphragm. In the region of the tube before the diaphragm was a window that transmitted ultra-

violet light. This part of the tube was charged with N_2. The window was 1 to 4 cm from the diaphragm. It was opened before starting the detonation. It may be noticed that the intensity of the OH bands decreases less rapidly than that

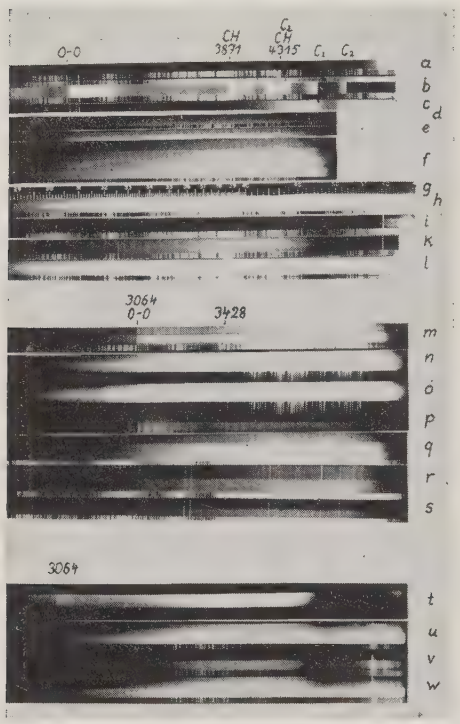

FIG. 7. Spectra of CO and hydrocarbons with oxygen, observed with Hilger E 3 detonations all seen from the front side except q,r,s. a, flame $3C_2H_4 + O_2$; b, flame $C_2H_4 + 3O_2$; c, flame $C_2H_4 + O_2$; d, detonation $C_2H_4 + 9O_2$; e, detonation $C_2H_4 + 8O_2$; f, detonation $C_2H_4 + 3O_2$; g, approximate wavelength scale; h, detonation $C_2H_4 + 3O_2$; i, detonation $C_2H_4 + O_2$; k, detonation $C_2H_2 + 9O_2$; l, detonation $C_2H_2 + 4O_2$; m, detonation $CH_4 + 3O_2$; n, detonation $CH_4 + 3O_2$; o, detonation $CH_4 + 1.5O_2$; p, detonation $CH_4 + 4.5O_2$; q, detonation of $2CO + O_2$ observed from the side; r,s, hot gases 1 and 4 cm behind the detonation front observed from the side ($2CO + O_2$); t, flame $2CO + O_2$ with 3% H_2 in the CO; u, detonation $2CO + O_2$ with 3% H_2 in the CO; v, detonation $CO + O_2$ with 3% H_2 in the CO; w, detonation $2CO + O_2$ with 5% in the CO.

of the CO flame bands. The analysis of the OH bands with respect to rotational temperatures is particularly uncertain because of the superimposed CO-flame bands.

Spectra of Some Hydrocarbon-Oxygen Detonations

Figure 7a, b, c gives the spectrum of a stoichiometric C_2H_4 flame (Hilger E 3). The OH bands of the transitions 1—0 to 0—1, the C_2 bands and the CH bands[6, 13] appear clearly together with a weak continuum in the violet region.

In the detonation spectra of mixtures whose compositions vary from $C_2H_4 + O_2$ to $C_2H_4 + 9O_2$, a continuum appears near the stoichiometric that extends from the ultraviolet to the red region. The OH bands are faint. If mixtures with a higher C_2H_2 concentration are used, the continuum disappears partially. Where there are impurities there is a weak continuum that increases in intensity from the yellow to the red region. The same continuum appears in $C_2H_4 + O_2$ flames, and its intensity decreases toward the shorter wavelengths with increasing content of C_2H_4 in the flame. It may be concluded that this continuum is due to particles of soot. Incandescent soot particles may also be responsible for the continuum in the detonation although no soot particles are obtained by refrigeration of the hot gases. The soot continuum disappears completely if a mixture with a high O_2 content is substituted for one with a high content of C_2H_4. On the other hand, a weak continuum appears superimposed on the OH and Schumann-Runge bands. There is evidence of the CH bands at 4315 Å also. In the stoichiometric mixture this continuum, which is weak in mixtures with high O_2 content, appears essentially stronger and extends to longer wavelengths. It is very similar to the continuum of the CO detonation.

Spectra similar to those of C_2H_4-oxygen detonations are obtained from CH_4-O_2 detonations. In the region of excess oxygen, the continuum is weak, increases toward the stoichiometric region, and decreases again for mixtures with a high CH_4 content. In detonations with CH_4, the OH bands appear with higher intensity than in C_2H_4.

For $C_2H_2 + 9O_2$ the spectrum is very similar to that of CH_4 and C_2H_4 mixtures with a high oxygen content. The continuum appears much stronger for $C_2H_2 + 4O_2$ than for $C_2H_2 + 9O_2$.

Experiments made to date do not establish definitely whether the continuum that appears in hydrocarbons and reaches a maximum in intensity between 4000 and 4500 Å in mixtures with a high oxygen content has the same origin as the continuum appearing in a CO combustion. The position of the maximum intensity might indicate it. The intensity of the violet continuum of stoichiometric mixtures of C_2H_4, CH_4, CO with oxygen and of $C_2H_2 + 9O_2$ increases appreciably towards the region of longer wave-

length if one starts from mixtures with high oxygen content.

Whether and to what extent the soot continuum plays a part here cannot be discussed until the investigations in the region of higher wavelengths are finished.

Acknowledgments

Grateful appreciation is extended to the Deutsche Forschungsgemeinschaft for financial support, to Drs. G. Spener and Th. Just for their assistance, and especially to Professor Wilhelm Jost for his kind interest and valuable discussions throughout this investigation.

REFERENCES

1. Herzberg, G.: *Spectra of Diatomic Molecules*. D. Van Nostrand Company, New York, 1950.
2. Cowan, R. D., and Dieke, G. H.: Rev. Mod. Phys., *20*, 418, (1948).
3. Shuler, K. E.: J. Chem. Phys., *21*, 624 (1953).
4. Broida, H. P., and Shuler, K. E.: J. Chem. Phys., *20*, 168 (1952).
5. Laidler, K. J., and Shuler, K. E.: Chem. Rev., *48*, 153 (1951).
6. Gaydon, A. G.: *Spectroscopy and Combustion Theory*. London, Chapman and Hall, 1948.
7. Dieke, G. H., and Crosswhite, H. N.: *The Ultraviolet Bands of OH*. Baltimore, The Johns Hopkins University Press, 1948.
8. Jost, W.: *Explosion and Combustion Processes in Gases*. Berlin, New York, McGraw-Hill Book Co., 1946.
9. Lewis, B., and von Elbe, G.: *Combustion Flames and Explosions of Gases*. New York, Academic Press, 1951.
10. *Energy Transfer in Hot Gases*. National Bureau of Standards Circular 523.
11. Penner, S. S.: J. Chem. Phys., *19*, 272 (1951).
12. Penner, S. S., and Weber, D.: J. Chem. Phys., *19*, 1351 (1951).
13. Pearse, R. W. B., and Gaydon, A. G.: *The Identification of Molecular Spectra*. New York, John Wiley & Sons, 1950.
14. Berets, D., Green, E., and Kistiakowsky, G. B.: J. Am. Chem. Soc., *72*, 1080, 1086 (1950).
15. Spener, G., Wagner, H. Gg.: Z. phys. Chem. N. F. 2, 312–319 (1954).

46

ON THE SPECIFICATION OF TRANSIENT NONEQUILIBRIUM SYSTEMS[a]

By KURT E. SHULER

Introduction

One of the important problems in the field of high-temperature chemical kinetics concerns the exchange and the distribution of the energy liberated in highly exothermic combustion systems. As has been pointed out by the author in a previous communication,[1] the energy liberated in such reactions often appears to go preferentially into specific degrees of freedom of the reaction products, so that the reaction system will contain rotationally, vibrationally or electronically excited species in excess of their equilibrium concentration. An example of this is furnished by the reaction

$$H + O_3 \rightarrow OH(^2\Pi, v = 9) + O_2 \qquad (1)$$

studied by McKinley, Garvin, and Boudart,[2] where the OH is formed preferentially in the ninth vibrational level of the electronic ground state. It would appear that the heat of reaction ($\Delta H = -82.5$ kcal) goes almost exclusively into the vibrational excitation of the OH radicals rather than into the equilibrium-equipartitional excitation of all the (quantum-mechanically accessible) degrees of freedom of OH and O_2. Another example is given by the reactions

$$O + NO_2 \rightarrow NO + O_2(^3\Sigma_g^-, v = 8) \qquad (2)$$

$$O + ClO_2 \rightarrow ClO + O_2(^3\Sigma_g^-, v = 8) \qquad (3)$$

recently studied by Lipscomb, Norrish, and Thrush,[3] where it appears that a considerable fraction of the heat of these reactions goes preferentially into the vibrational excitation of the O_2 molecules in the ground electronic state.

The occurrence of these reactions raises the question, among others, as to the specification of

[a] This work was supported by the U. S. Atomic Energy Commission.

such nonequilibrium systems. Temperature, for instance, is a distribution parameter which is defined strictly only for equilibrium-canonical distributions and therefore is not applicable to systems which depart from the equilibrium Boltzmann distribution to any considerable extent.[4] The simple relation between the energy E in each degree of freedom and the temperature T

$$E = \tfrac{1}{2}kT \tag{4}$$

is true only for equilibrium-equipartition systems and can therefore not be applied to the specification of nonequilibrium systems of the type discussed here. In general, a nonequilibrium system can no longer be specified by a single "statistical" parameter—such as the temperature —but requires instead the explicit introduction of all the relevant "molecular" quantities such as, for instance, radiative and collisional transition probabilities, impact parameters, or scattering cross sections which determine the transient properties of the system.[1] In a formal way a nonequilibrium system could be specified by some function S of the transient distribution function $f(t)$ such that

$$S = S[f(t)] \text{ and } f(t) = f(\text{molecular parameters}, t) \tag{5}$$

In order to carry out such a program it is necessary to have some detailed information about the (time-dependent) distribution function $f(t)$ for various nonequilibrium systems.

The author, in collaboration with R. J. Rubin and E. W. Montroll, has recently initiated a study on the relaxation of vibrational nonequilibrium distributions[5, 6] which is to furnish the information required for the evaluation of Equation (5) above. Since the mathematical aspects of these studies are discussed in detail by Rubin and Shuler[5] and Montroll and Shuler,[6] we shall limit ourselves here to the presentation of some of the more important results, without derivations or proofs, and utilize the space instead for a more detailed discussion of some of the physical implications.

The Relaxation of a System of Harmonic Oscillators

As one of our models (Gedanken-Experiment) for the study of vibrational nonequilibrium distributions, we have chosen a system of harmonic oscillators contained in a large excess of inert gas which acts as a *constant temperature* heat bath. The oscillators are excited to a vibrational nonequilibrium distribution by irradiation with a short-duration, high-intensity beam of light, or by exothermic chemical reactions of the type discussed above. After the light source has been turned off, or after the cessation of the reaction, the system will readjust to its final equilibrium state. If the concentration of the oscillators is sufficiently small, and the energy absorbed by the oscillators during the excitation is not too large, the heat bath can be considered to remain, to within a good approximation, at its equilibrium temperature T throughout the relaxation process. In this model, the concentration of the excited oscillators is also made sufficiently small so that the relaxation process is of first order with respect to the concentration of the oscillators. The relaxation of the oscillators to their final equilibrium distribution is assumed to proceed both by inelastic collisions between the oscillators and the heat-bath molecules and by radiative transitions.

If one uses the Landau-Teller transition probabilities[7] for the collisional and transitions of the oscillators and the Einstein transition probabilities for the radiative transition, it can be shown[5, 6] that the collisional and radiative relaxation process is govered by the set of differential difference equations

$$\frac{dx_n(t)}{dt} = \kappa\{ne^{-\theta}x_{n-1} - [n + (n+1)e^{-\theta}]x_n + (n+1)x_{n+1}\} \tag{6}$$

$$n = 0, 1, \cdots, \infty$$

where κ is a simple and known function of the collisional and radiative transition probabilities whose exact form depends upon the energy transfer mechanism of the relaxation process. In these equations, $x_n(t)$ is the fraction of oscillators in the vibrational energy level n at time t; $\theta = h\nu/kT$, with ν equal to the vibrational frequency of the harmonic oscillator and T equal to the final equilibrium temperature of the system. The introduction of the generating function

$$G(z, t) = \sum_{n=0}^{\infty} z^n x_n(t) \tag{7}$$

which is defined so that the coefficient of z^n is the fraction of molecules, $x_n(t)$, in level n at time t, and the introduction of the dimensionless time

$$\tau = \kappa t(1 - e^{-\theta}) \tag{8}$$

leads to the general and exact solution of Equation (6)

$$G(z, t) = \frac{(1 - e^{\theta})}{(z - e^{\theta}) - (z - 1)e^{-\tau}} \cdot G_0\left[\frac{(z - 1)e^{-\tau}e^{\theta} - (z - e^{\theta})}{(z - 1)e^{-\tau} - (z - e^{\theta})}\right] \tag{9}$$

where the x_n (t)'s are again the coefficients of z^n and where G_0 is determined by the initial distribution x_n (0) at time $t = 0$. As $t \longrightarrow \infty$ (and hence as $\tau \longrightarrow \infty$), one finds, since G_0 $(1) = 1$, that

$$x_n(\infty) = (1 - e^{-\theta})e^{-n\theta} \tag{10}$$

which is the Boltzmann distribution for a set of harmonic oscillators with $\theta = h\nu/kT$. This approach to the final equilibrium distribution as $t \longrightarrow \infty$ is a property of the system which is independent of the form of the initial vibrational nonequilibrium distribution x_n (0).

The initial distribution of the vibrationally excited OH radicals in reaction (1) corresponds mathematically to a δ function where all the molecules are formed initially in one vibrational level n_0, *i.e.*

$$x_n(0) = \delta(n - n_0) \tag{11}$$

The time-dependent distribution x_n (t) which corresponds to this initial distribution is found to be[6]

$$x_n(t) = \frac{(1 - e^{\theta})e^{n_0\theta}}{(e^{-\tau} - e^{\theta})}\left(\frac{e^{-\tau} - 1}{e^{-\tau} - e^{\theta}}\right)^{n_0+n} \cdot F(-n, -n_0, 1; u^2) \tag{12}$$

where

$$u = \frac{\sinh \tfrac{1}{2}\theta}{\sinh \tfrac{1}{2}\tau} \tag{12a}$$

and where F is the hypergeometric function. Even though Equation (12) appears to be quite complicated, it can readily be used to determine, for instance, the total energy $E(t)$ of the system of oscillators at any time t

$$E(t) = h\nu \sum_{n=0}^{\infty} n x_n(t) \tag{13}$$

It can furthermore be used to determine various related quantities, such as the fraction $x_n^*(t)$ of oscillators with energy greater than some critical energy $E^* = n^*h\nu$, *i.e.*

$$x_n^*(t) = \sum_{n=n^*}^{\infty} x_n(t) \tag{14}$$

These, and related quantities, can serve as the "specification parameters" S defined in Equation (5), since the distribution function $f(t) = x_n(t)$ is known explicitly as a function of time and of the molecular parameters which in the model studied here are the collisional and radiative transition probabilities appearing in the "rate constant" κ of Equation (6).

A particularly interesting case arises when the initial vibrational distribution of the oscillators is a Boltzmann distribution with a temperature $T_0 \neq T$. The intial distribution of the oscillators is then given by

$$x_n(0) = (1 - e^{-\theta_0})e^{-n\theta_0} \tag{15}$$

with $\theta_0 = h\nu/kT_0$. Substitution of Equation (15) into Equation (9) leads to

$$x_n(t) = (1 - e^{-\Theta})e^{-n\Theta} \tag{16}$$

for the time-dependent nonequilibrium distribution x_n (t) where

$$\Theta = \log\left\{\frac{e^{-\tau}(1 - e^{\theta-\theta_0}) - e^{\theta}(1 - e^{-\theta_0})}{e^{-\tau}(1 - e^{\theta-\theta_0}) - (1 - e^{-\theta_0})}\right\} \tag{16a}$$

It will be noted that the time-dependent distribution (16) remains a Boltzmann distribution at all times t, with $\Theta = h\nu/k\mathfrak{I}$, and $\mathfrak{I}$ (t) equal to the "temperature" of the distribution. For this particular nonequilibrium case it is thus possible to define a "temperature" $\mathfrak{I}$ (t) which can serve to specify the nonequilibrium system at all times t. As can readily be verified from Equation (16a), $\mathfrak{I}$ $(0) = T_0$ and $\mathfrak{I}$ $(\infty) = T$. The behavior of the temperature $\mathfrak{I}$ as a function of the dimensionless time τ is shown in Figure 1 for various values of θ_0 and θ.

The Relaxation of the Internal Energy

As pointed out previously,[1] the internal energy can be used to specify the time-dependent behavior of a nonequilibrium system if it is known explicitly as a function of time and of the molecular parameters of the system. Bethe and Teller[8] have shown that it is possible to obtain such an explicit relation for the internal energy for the harmonic oscillator relaxation model.[b] If Equa-

[b] This has also been demonstrated by Montroll and Shuler,[6] who derived a general expression for the relaxation of the moments of the distribution. The internal energy of the distribution corresponds to the first moment (see Eq. (13)).

tion (6) is multiplied on both sides by $nh\nu$ and then summed over all n, one obtains, using Equation (13) for $E(t)$,

$$\frac{dE(t)}{dt} = \kappa(1 - e^{-\theta})\left[\frac{h\nu}{e^{\theta} - 1} - E(t)\right] \qquad (17)$$

The internal energy of a system of harmonic oscillators in their equilibrium Boltzmann distribu-

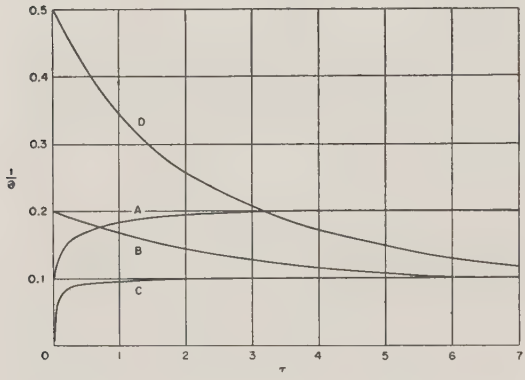

FIG. 1. The "temperacure" $1/\Theta = \mathfrak{Z}\left(\frac{k}{h\nu}\right)$ as a function of the time $\mathfrak{Z}$ for the relaxation of an initial Boltzmann distribution with $T_0 \neq T$.

Curve A:	$\theta_0 = 10$	$\theta = 5$	$T_0 = \frac{1}{2}T$
Curve B:	$\theta_0 = 5$	$\theta = 10$	$T_0 = 2T$
Curve C:	$\theta_0 = 20$	$\theta = 10$	$T_0 = \frac{1}{2}T$
Curve D:	$\theta_0 = 2$	$\theta = 10$	$T_0 = 5T$

tion (as $t \rightarrow \infty$) is given by

$$E(\infty) = \frac{h\nu}{e^{\theta} - 1} \qquad (17a)$$

Substitution of Equation (17a) into Equation (17) leads to the differential equation

$$\frac{dE(t)}{dt} = \kappa(1 - e^{-\theta})[E(\infty) - E(t)] \qquad (17b)$$

for the relaxation of the energy. Its solution is

$$\frac{E(t) - E(\infty)}{E(0) - E(\infty)} = e^{-\kappa(1-e^{-\theta})t} = e^{-\tau} \qquad (17c)$$

where $E(0)$ is the internal energy of the initial distribution at time $t = 0$. Equation (17c) is remarkable in its simplicity. It states that the internal energy $E(t)$ at any time t can readily be determined from a knowledge of the internal energy of the initial and final distributions and the value of the molecular parameter κ. For sufficiently simple cases this parameter can be obtained from quantum mechanical calculations.[9] Another interesting aspect of Equation (17c) is the fact that $E(t)$ is independent of the form of the initial distribution of the oscillators, but depends only upon the energy of the initial distribution. This means that a knowledge of the amount of energy liberated in the system, or added to the system, suffices for the determination of the energy at any time t; it is not necessary that the initial *distribution* of the energy be known for this calculation. The internal energy $E(t)$ thus forms a very convenient parameter for the specification of transient nonequilibrium distributions.

It should be borne in mind that the results obtained above have been derived for the specific model of a system of harmonic oscillators contained in a large constant-temperature heat bath. Whether analogously simple relations hold for other systems remains to be seen. Work on this problem is now in progress.

REFERENCES

1. SHULER, K. E.: *Fifth Symposium on Combustion*, pp. 56–74. New York, Reinhold Publ. Corp., 1955.
2. MCKINLEY, J. D., GARVIN, D., AND BOUDART, M. J.: J. Chem. Phys., *23*, 784 (1955).
3. LIPSCOMB, F. J., NORRISH, R. G. W., AND THRUSH, B. A.: Proc. Roy. Soc. (London), *233A*, 455 (1956).
4. See *e.g.* the discussion by HERZFELD, K. F. in *Temperature, Its Measurement and Control in in Science and Industry*, Vol. II, pp. 233–251. Reinhold Publ. Corp., New York, 1955.
5. RUBIN, R. J., AND SHULER, K. E.: J. Chem. Phys., *25*, 59 (1956).
6. MONTROLL, E. W., AND SHULER, K. E.: J. Chem. Phys., *26*, 454–464 (1957).
7. LANDAU, L., AND TELLER, E.: Physik. Z. Sowjetunion, *10*, 34 (1936).
8. BETHE, H. A., AND TELLER, E.: Deviations from Thermal Equilibrium in Shock Waves, Ballistic Research Labs., Report X-117, 1941.
9. See *e.g.* SCHWARTZ, R. N., AND HERZFELD, K. F.: J. Chem. Phys., *22*, 767 (1954).

47

CALCULATION OF DETONATION CHARACTERISTICS

By TSUTOMU HIKITA AND TARO KIHARA

I. Introduction

Detonation characteristics of condensed explosives have been calculated by different authors on the basis of the hydro-thermodynamic theory of detonation developed by Hugoniot, Chapman and Jouguet.[1] In making such calculations the proper evaluation of an equation of state for the detonation gases is of utmost importance, but unfortunately exact information as to the state of the molecules during detonation is not yet available. Most authors (Schmidt,[2] Cook,[3] Jones and Miller,[4] Brinkley and Wilson,[5] Cottrell and Paterson[6] and Kihara and Hikita[9]) have assigned values to the parameters in an assumed equation of state, using observed detonation velocities. This treatment, however, is a conventional one and the correctness of the values of the parameters must be reconsidered from the purely theoretical point of view.

Various procedures have been proposed for the absolute calculation of detonation characteristics. Jones[7] used an equation of state which was introduced on the assumption that the detonation gases behave like a solid, but it is probable that this equation of state does not apply to high temperature detonation gases. Paterson[8] in his absolute calculation used a virial expansion type of equation of state which offers some resemblance to our equation of state, but differs from it with respect to the form of intermolecular potential employed since he regards the gases as rigid molecules.

Our treatment is based on the following idea. In a gas, simple molecules, such as H_2, N_2, CO, CH_4, etc., are nearly spherically symmetric and intermolecular potentials can be approximated by the so-called Lennard-Jones potential,

$$U(r) = \lambda r^{-n} - \mu r^{-6} \qquad (1.1)$$

where r is the intermolecular distance; λ and n are molecular constants. At high temperatures the attractive part of the potential is negligible and the model, Equation (1.1), reduces to

$$U(r) = \lambda r^{-n} \qquad (1.2)$$

$\lambda^{3/n}$ being proportional to the molecular volume. In the following, Equation (1.2) is used throughout. The values of $\lambda^{3/n}$ in $Å^3(eV)$ determined from compressibility data by use of Equation (1.1) are, for $n = 12$, as follows:

> 8 for H_2, 18 for O_2, 21.5 for N_2 and CO, 27 for CH_4, 30 for CO_2 and probably 17 for H_2O

For a gas mixture, where the molecules do not differ greatly in size, the equation of state can be approximated by the equation of state of a pure gas with the averaged constant given by

$$\lambda^{3/n} = \Sigma\, \lambda_i^{3/n} x_i \; ; \qquad \Sigma\, x_i = 1 \qquad (1.3)$$

where λ_i is the molecular constant of i-th species whose molar fraction is x_i.

In a previous paper[9] the present authors developed a theory of detonation using the intermolecular potential, Equation (1.2). The values of $\lambda^{3/n}$ determined from observed detonation velocities, however, were noticeably (about 30 per cent) smaller than the values determined from compressibility data. The cause of this discrepancy was not clear.

Essentially the hydro-thermodynamic theory of detonation applies to ideal detonations with infinitely fast rates of chemical reactions. We must distinguish between real detonations and these ideal ones. The aim of the present paper is to calculate propagation velocities of the ideal detonations by use of the "real" potential constant derived from compressibility data, and to compare results of the calculation with observed detonation velocities. If our theory is exact, the difference between these two will indicate the deviation of the real reaction rate from ideal infinity.

II. Caloric and Thermal Equation of State of Gases at High Temperatures[9]

For the potential, Equation (1.2), the internal energy E per unit mass is simply given by

$$E = N\left[\frac{3}{2}kT + \frac{3}{n}(Pv - kT)\right] + N\epsilon_i \qquad (2.1)$$

(v = volume per molecule, N = number of gas molecules per unit mass, P = pressure, T = temperature, k = Boltzmann's constant). Here ϵ_i denotes the energy due to internal degrees of

freedom (rotational and vibrational) of a molecule. In the temperature range $1500 \leq T \leq 5500°K$, ϵ_i is given to sufficient accuracy by

$$2\epsilon_i/kT = \varphi - \theta/T \tag{2.2}$$

where

$$\begin{aligned}\varphi - \theta/T &= 3.4 - 2000/T \text{ for } H_2\\ &= 3.9 - 2300/T \text{ for } N_2\\ &= 3.9 - 2100/T \text{ for CO}\\ &= 8.0 - 6300/T \text{ for } H_2O\\ &= 9.8 - 5500/T \text{ for } CO_2\\ &= 19.6 - 16900/T \text{ for } CH_4\end{aligned}$$

For gas mixtures, we need to take only average values. Thus in the case of $2N_2 + 4H_2O + 3CO_2 + 2CO$, which corresponds to the gas mixture produced by a PETN-detonation, we obtain

$$\varphi - \theta/T = 7.0 - 4600/T$$

For the potential, Equation (1.2), the equation of state of a gas is of the form

$$\frac{kT}{Pv} = f(x), \qquad x \equiv \left(\frac{\lambda}{Pv}\right)^{3/n} \frac{1}{v} \tag{2.3}$$

The function $f(x)$ can be evaluated both for very small and very large densities. An approximation obtained by interpolation is

$$f(x) = \frac{1 - \alpha x}{1 + ax + bx^2 + cx^3}, \tag{2.4}$$

the constant for $n = 12$ being $a = 0.998$, $b = 1.411$, $c = -1.773$, $\alpha = 1.569$.

Introducing Equation (2.3) into Equation (2.1) we have

$$E = NPv\left[\frac{3}{n} + F(x)\right] - q \tag{2.5}$$

where

$$q = \frac{k}{2} N\theta \tag{2.6}$$

$$F(x) = \frac{1}{2}\left(3 - \frac{6}{n} + \varphi\right) f(x) \tag{2.7}$$

In the following we choose $n = 12$ and use the values of $\lambda^{3/n}$ given in Section I together with Equation (1.3). (Calculated detonation velocities do not greatly depend on the adopted index n.)

III. Ideal Detonations on the Assumption of Homogeneity

The caloric and thermal equations of state, Equations (2.5) and (2.3), are capable of application to the hydro-thermodynamic theory of one-dimensional propagation of detonation.

Let V_0 be the initial volume and Q the heat released by the reaction per gram of explosives, and let P_0 be the initial pressure. Then the final pressure P and the specific volume V after completion of the reaction must satisfy the Rankine-Hugoniot relation

$$\tfrac{1}{2}(P + P_0)(V_0 - V) = E - Q \tag{3.1}$$

where E denotes the increase of internal energy per gram of the reaction product. When E is known as a function of V and P, the relation can be represented by a curve in V-P plane called the Rankine-Hugoniot curve. V and P are determined by Equation (3.1) and a supplementary condition

$$\frac{dP}{dV} = -\frac{P - P_0}{V_0 - V} \tag{3.2}$$

known as the Chapman-Jouguet hypothesis.

Using V and P determined in this way, the detonation velocity, D, and the particle velocity, W, can be calculated from

$$\frac{V_0 - V}{V_0} = \frac{(P - P_0)V_0}{D^2} = \frac{W}{D} \tag{3.3}$$

It is to be noted that Equations (3.1) and (3.3) are derived from the conservation law of mass, momentum and energy. In the following, we neglect P_0 by comparison with P.

Introducing Equation (2.5) into Equation (3.1) and using $V = Nv$ and $n = 12$, we have

$$\tfrac{1}{2}PV_0 = NPv[\tfrac{3}{4} + F(x)] - (Q + q) \tag{3.4}$$

while the Chapman-Jouguet condition, Equation (3.2), takes the form

$$\begin{aligned}\frac{1}{2}V_0 = Nv\left[\frac{1}{2} + \frac{1}{4}F(x) - \frac{1}{4}xF'(x)\right]\\ - (V_0 - Nv)\frac{\delta}{\delta v}\left[v\left\{\frac{3}{4} + F(x)\right\}\right]\end{aligned}$$

which can be converted to

$$\tfrac{1}{2}V_0[F(x) + \tfrac{5}{4}G(x)] = Nv[F(x) + \tfrac{3}{4}G(x)] \tag{3.5}$$

where

$$G(x) = 1 - xF'(x)$$

Using $f(x)$ given by Equation (2.4), we know Nv/V_0, $NPv/(Q + q)$ and $NkT/(Q + q)$ as functions of x. The corresponding initial density, $1/V_0$, of the explosive is given by the relationship

$$\frac{N}{V_0}\left(\frac{N\lambda}{Q+q}\right)^{\frac{1}{2}} = \frac{Nv}{V_0}\left(\frac{NPv}{Q+q}\right)^{\frac{1}{2}} x$$

The propagation velocity can be calculated by use of Equation (3.3).

In this section we assume that the product of a chemical reaction is a homogeneous phase composed of simple gas molecules. In particular, we assume the following decomposition equations. (The water-gas equilibrium plays a small role and can be ignored.)

For PETN, (*a*) $C(CH_2ONO_2)_4 = 2N_2 + 4H_2O + 3CO_2 + 2CO$; $-\Delta H = 1400$ cal/gram: for tetryl, (*a*) $2C_6H_2(NO_2)_3NCH_3NO_2 = 5N_2 + 3H_2O + 13CO + CH_4$; $-\Delta H = 1050$ cal/gram: for TNT, (*a*) $2C_6H_2CH_3(NO_2)_3 = 3N_2 + 12CO + 2CH_4 + H_2$; $-\Delta H = 785$ cal/gram: for nitroguanidine, (*a*) $HN{:}C(NH_2)NHNO_2 = 2N_2 + H_2O + CO + H_2$; $-\Delta H = 625$ cal/gram: for ammonium nitrate, (*a*) $2NH_4NO_3 = 2N_2 + 4H_2O + O_2$; $-\Delta H = 380$ cal/gram.

The results of the calculations for propagation velocities are shown by curves *a* in Figures 1 to 5. The observed velocities at high densities are noticeably smaller than the calculated ideal velocities; ammonium nitrate shows great discrepancy even at low densities.

IV. Ideal Detonations on the Assumption of Thermal Equilibrium

An investigation was made to determine how the calculated velocities vary with the decomposition equation chosen. For this purpose, the composition of the detonation products was assumed to be in thermal equilibrium. Exact calculations of equilibrium composition using theoretical values of detonation characteristics can be performed by means of the ordinary thermodynamic relations[10] together with the equations of state for gases and solids. In this paper, however, we describe only the results for the following assumed compositions because the exact calculation offers only a slight shift from these.

For tetryl, (*b*) $2C_7H_5N_5O_8 = 5N_2 + 5H_2O + 11CO + 3C$; $-\Delta H = 1040$ cal/gram: for TNT, (b_1) $2C_7H_5N_3O_6 = 3N_2 + 5H_2O + 7CO + 7C$;

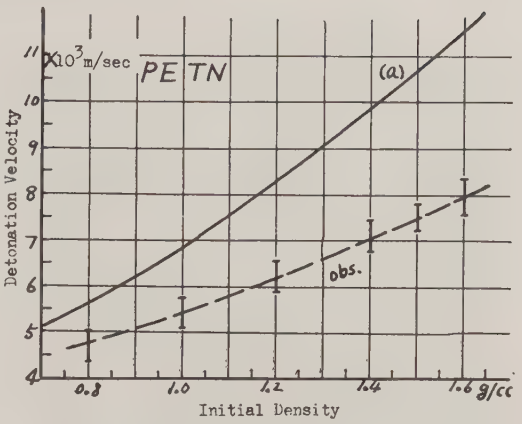

FIG. 1. Ideal and observed detonation velocity of PETN.
(a) PETN = $2N_2 + 4H_2O + 3CO_2 + 2CO$

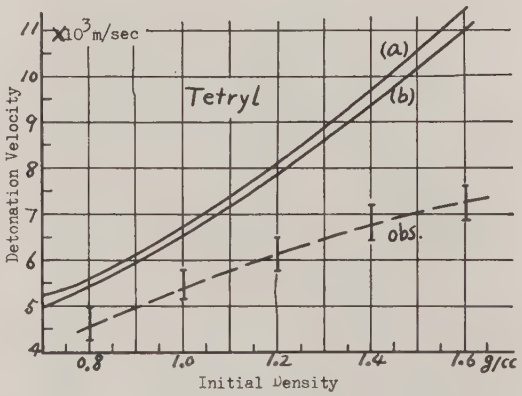

FIG. 2. Ideal and observed detonation velocities of tetryl.
(a) 2(tetryl) = $5N_2 + 3H_2O + 13CO + CH_4$
(b) 2(tetryl) = $5N_2 + 5H_2O + 11CO + 3C$

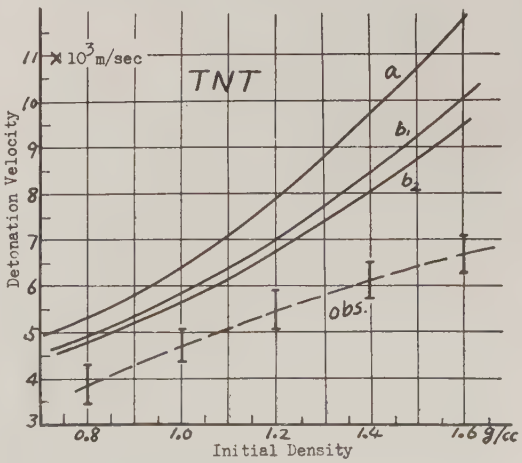

FIG. 3. Ideal and observed detonation velocity of TNT.
(a) 2(TNT) = $3N_2 + 12CO + 2CH_4 + H_2$
(b_1) 2(TNT) = $3N_2 + 5H_2O + 7CO + 7C$
(b_2) 2(TNT) = $3N_2 + 5H_2O + CO + 3CO_2 + 10C$

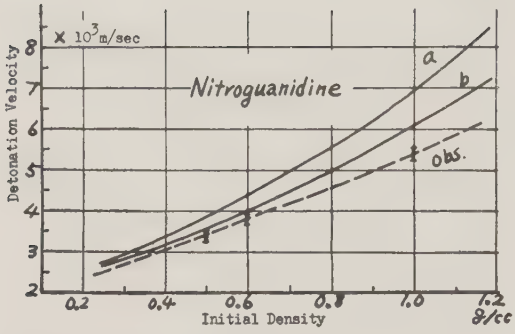

FIG. 4. Ideal and observed detonation velocity of nitroguanidine.
(a) nitroguanidine = $2N_2 + H_2O + CO + H_2$
(b) nitroguanidine = $2N_2 + 2H_2O + C$

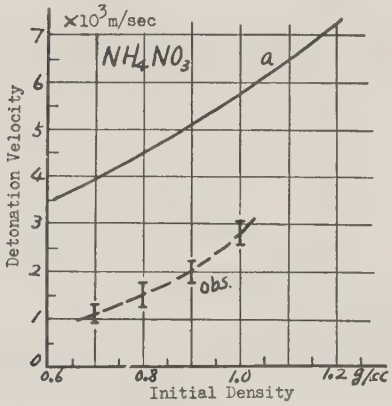

FIG. 5. Ideal and observed detonation velocity of ammonium nitrate.
(a) $2NH_4NO_3 = 2N_2 + 4H_2O + O_2$

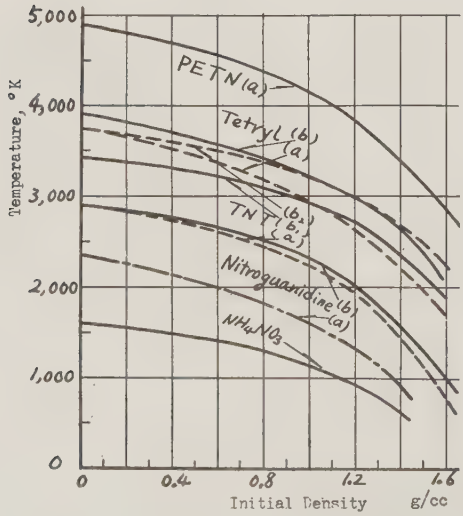

FIG. 6. Ideal detonation temperatures.

$-\Delta H = 1000$ cal/gram, (b_2) $2C_7H_5N_3O_6 = 3N_2 + 5H_2O + CO + 3CO_2 + 10C$; $-\Delta H = 1270$ cal/gram: for nitroguanidine, (b) $CH_4N_4O_2 = 2N_2 + 2H_2O + C$; $-\Delta H = 920$ cal/gram. Here free carbon is assumed to form β-graphite.

For graphite at high pressures, the volume per carbon atom can be approximated by

$$v_c = v_c(P) = v^*(1 + 4\kappa P)^{-\frac{1}{4}} \qquad (4.1)$$

where $v^* = 9.1$ Å^3, $\kappa = 3.0\ 10^{-6}$ bar^{-1}. The volume V per gram after completion of the reaction is, in this case, $Nv + N^*v_c$, where N and N^* denote the number of gas molecules and of solid carbon atoms, respectively. Let us further approximate the internal energy per atom by

$$\frac{kT}{2}\left(6 - \frac{\theta^*}{T}\right) - \int_{v^*}^{v_c(P)} P dv_c(P) \qquad (4.2)$$

where $\theta^* = 3000$°K.

Using the thermal and caloric equations of state for carbon, together with those for gases, we can calculate detonation characteristics for this case. The equations corresponding to Equations (3.4) and (3.5) are, respectively,

$$\frac{1}{2}P(V_0 - N^*v_c) + N^*\int_{v^*}^{v_c(P)} P dv_c = NPv\left[\frac{3}{4} + F(x)\right] - (Q + q)$$

and

$$\frac{1}{2}\left[V_0 + N^*P^2\frac{d}{dP}\left(\frac{v_c}{P}\right)\right]\left[F(x) + \frac{5}{4}G(x)\right] = Nv\left[F(x) + \frac{3}{4}G(x)\right]$$

where, in the present case,

$$q = k(N\theta + N^*\theta^*)/2,$$

$$F(x) = \frac{1}{2}\left(3 - \frac{1}{2} + \varphi + \frac{6N^*}{N}\right)f(x).$$

The results of calculation for propagation velocity are shown by curves b in Figures 1 to 5. The observed velocities at high densities are again noticeably smaller than the calculated ideal velocities. This fact may indicate that the assumption of an infinitely fast rate of reaction does not accurately apply to detonations of condensed explosives.

V. Other Characteristics

Calculated values of temperature, T, and pressure, P, are shown in Figures 6 and 7 although these values cannot be considered accurate for

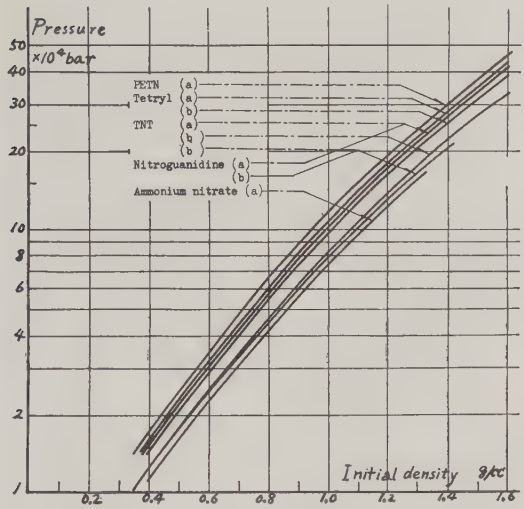

FIG. 7. Ideal detonation pressures.

high density explosives. Curves *a* are for the assumption of homogeneity and *b* for that of thermal equilibrium.

VI. Conclusion

In conclusion the absolute calculation of detonation characteristics on the basis of molecular constants derived from the compressibility data gives higher detonation velocities than the real ones, especially for high density explosives.

To find the true cause of this discrepancy, further theoretical and experimental investigations are needed. At the present time we are inclined to think that the problem may exceed the scope of the hydro-thermodynamic theory of detonation, and that it must be supplemented by some chemico-kinetical considerations. The fact that the sensitivity of explosives usually drops as the initial density increases may support this view.

REFERENCES

1. JOUGUET, E.: *Mechanique des Explosifs*. Paris, Doin et Fils, 1917.
2. SCHMIDT, A.: Z. ges. Schiess-u. Sprengstoff., *30*, 364 (1935); *31*, 220, 243 (1936).
3. COOK, M. A.: J. Chem. Phys., *15*, 518 (1947); *16*, 1081 (1948).
4. JONES, H., AND MILLER, A. R.: Proc. Roy. Soc., London, *A194*, 480 (1948).
5. BRINKLEY, S. R., AND WILSON, E. B.: OSRD Rept. No. 1231 (PB-18859) (1954).
6. COTTRELL, T. L., AND PATERSON, S.: Proc. Roy. Soc., London, *A213*, 214, 1952.
7. JONES, H.: *Third Symposium on Combustion, Flames and Explosion Phenomena*, p. 590. Baltimore, The Williams & Wilkins Co., 1949.
8. PATERSON, S.: Research, *1*, 221 (1948).
9. KIHARA, T., AND HIKITA, T.: *Fourth Symposium (International) on Combustion*, p. 458. Baltimore, The Williams & Wilkins Co., 1953.
10. ROSSINI, F. D.: *Thermodynamics and Physics of Matter*, p. 307. Princeton, Princeton University Press, 1955.

48

STUDY OF SHOCK WAVES FROM HIGH EXPLOSIVES

By TSUTOMU HIKITA, TETSURO ASABA AND KUNIAKI YONEDA

The study of luminous phenomena that accompany the detonation of condensed explosives is of interest in connection with both detonation and shock mechanisms. In recent years, photographic studies by Muraour[1] have shown that the luminosity associated with detonation is emitted mainly by the shock wave produced in the ambient gas. In particular, a shock wave confined in a tube is less attenuated and generally highly luminous over a rather long distance, whereas the light due to detonation gases is comparatively weak except in the case of a secondary combustion or recompression during the expansion of the detonation gases.

The present paper describes investigations of the luminous phenomena produced by detonation of an explosive charged in a glass or other transparent tube. This includes: (1) measurement and calculation of the initial propagation velocities of explosive-produced shock waves in various gases; (2) study of the dark zone that exists directly above the charge surface and which is to be associated with the shock formation length and with the detonation wave structure; (3) spectroscopic study of temperature measurement for explosive-produced shock waves.

Shock Wave Velocity, Its Measurement and Calculation

Figure 1 illustrates the experimental arrangement used to measure shock wave velocities. A glass tube, 13 mm in inner diameter and 1 m long,

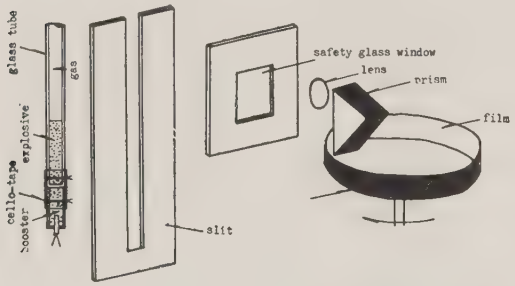

FIG. 1. Experimental arrangement.

in the lower part of which 15 g of pentaerythritol-tetranitrate (PETN) is charged at the density of ~1.0 g/cc (after evacuation, the tube space is filled with a gas) has been used as a high-explosive shock tube.

The reaction is initiated by 4 g of PETN (density ~0.8 g/cc) used as a booster charge which, in turn, is detonated by an electric blasting cap. A high-speed rotating-drum camera is used for measuring time-distance relation of the luminous phenomena traveling down the shock tube. The camera consists essentially of a drum that has a slot on its inner periphery of 54.3 cm to hold a 35-mm film; the drum is directly connected to a universal motor giving a maximum film speed of 160 m per second. The rotating speed of the drum is fixed through the measurement of the frequency of the alternating current induced in a pick-up by a magnet mounted on the shaft of the motor. The camera set is operated under a reduced pressure of about 20 mm Hg. In this experiment the tube axis is directed perpendicularly to the motion of the film.

PETN-produced shock waves are generally highly luminous except in a light gas like hydrogen or in a polyatomic gas like butane. Even in such gases the time when the shock wave arrives at the top end of the tube is clearly indicated by a bright luminosity, due to the collision with the solid wall; knowing this, we can estimate the mean shock velocities.

As a preliminary test, the interference effects of glass cracks and of "boundary disturbances" (recently found by Shreffler and Christian[2]) on the shock traces have been investigated. In this experiment the internal reflection from glass cracks whose propagation velocity may exceed 5300 m/sec[3] was found to give no interference (Fig. 7). While the boundary disturbances were certainly observed for argon or chlorine shocks, at least in the initial period of shock formation the masking action of the boundary disturbances was considered negligible.

Thus the shock velocities can be obtained from the slopes measured along the image-fronts in the streak photographs. Reproducibility of the measurement is satisfactory, the deviations from mean values being within 5 per cent.

Sample photographs are shown in Figure 2, and the observed velocities are summarized in Table 1, together with the approximate values of the attenuation constant K in the following equation[4]

$$\frac{1}{D} = \frac{1}{D_0} + Kx$$

where D is the observed shock velocity at a distance x from the charge surface and D_0 the value of D for $x = 2 \sim 4$ cm, the values for $x = 0$ being uncertain.

CALCULATION OF SHOCK WAVE PARAMETERS

The initial velocity and other characteristics of an explosive-produced shock wave have been calculated theoretically by means of the so-called "matching technique,"[5] where it is assumed that across the boundary between the explosive and the air the pressure as well as the material velocities remain constant in both the shock wave emitted into air and the rarefaction wave reflected back in detonation gases. Moreover, it is assumed that the lateral and forward-moving rarefactions which inevitably follow the real detonation wave can be neglected. We assume implicitly that the shock formation occurs instantaneously, and the detonation wave can be represented by Chapman-Jouguet variables, the existence of a reaction zone being ignored.

In order to find the pressure P and the material velocity U in an explosive-produced shock wave, we must know two possible relations between P and U in both shock and rarefaction waves: a common value of P or U to both waves is what we want.

P-U relation in shock waves in air or any other gas has been derived from the Rankine-Hugoniot shock equations on the assumption that the gas is perfect, and that only the translational and rotational freedoms of the gas molecules are excited during shock formation; naturally some ionization or dissociation occurs, but in so far as the P-U relation is concerned the error due to this last assumption may not be serious—although temperature values must be corrected. The P-U relation in the rarefaction wave has been obtained by the numerical integration of the Riemann function

$$\sigma = \int_{V_2}^{V} \sqrt{-\left(\frac{\partial P}{\partial V}\right)_S}\, dV$$

as the material velocity is

$$U = W - \sigma$$

where W is the material velocity in the detonation wave.

In calculating the above equations, the Kihara-Hikita equation of state for high temperature gases was applied with satisfactory results.[6, 7] Calculated P-U relations in rarefaction waves in detonation products of PETN of densities 0.8, 1.0, 1.2 and 1.6 g/cc are shown in Figure 3, together with the calculated results of P-U relations in shock waves in hydrogen, methane, butane, chlorine, and argon gas at 1 atmos, and in air at various pressures.

Table 1 summarizes the calculated values of characteristics of shock waves produced in various gases from PETN of density 1.0 g/cc.

It will be seen (Table 1) that in less resistant hydrogen gas the shock wave travels at a high velocity and with little attenuation, the situation being similar to that in air at a reduced pressure of 50 mm Hg. In argon gas, a strong shock with high temperature and pressure is formed but is followed by rapid attenuation.

In spite of the many simplifications involved in the calculation, the agreement of the initial shock velocities with the observed values is good if we consider that the observed data are for shock waves at a distance of 2∼4 cm from the charge surface—those for a distance of 0∼2 cm being higher but rather uncertain.

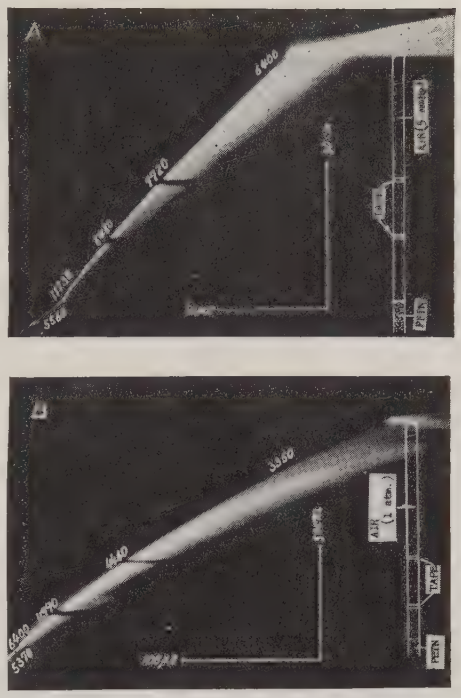

FIG. 2. Examples of streak photographs of the luminous phenomena produced in the explosive shock tubes (glass).
(A) PETN (Δ = 1.0 g/cc) — Air (5 mm Hg)
(B) PETN (Δ = 0.9 g/cc) — Air (1 atmos.)

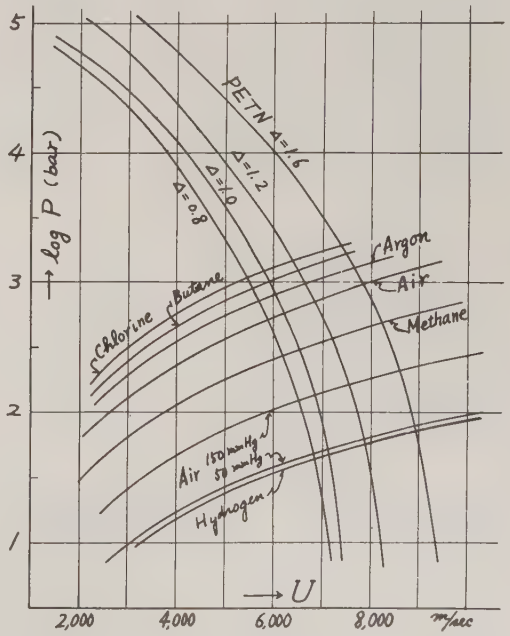

FIG. 3. Pressure-material velocity relations in rarefaction waves in PETN-gas and in shock waves in various gases.

If shock formation were instantaneous, as assumed in the above calculation, a microshock wave similar to that in Figure 2 might form even in the air space among particles of granular explosives. Paterson[8] recently calculated the temperature of a shock front that precedes the detonation zone in a granular explosive, and obtained an enormous shock front temperature, far higher than those we have calculated for PETN-produced shock waves.

A high air pocket temperature (hot spot) probably is an important factor for initiating the detonation reaction (Bowden-Yoffe[9]). However, in the narrow intergranular space, the hot spot may not grow enough to become an intense shock at a super-high temperature, because the hot spot loses its energy, in turn, for exciting the explosive particles. Knowledge concerning the shock formation length may be of help on this point.

Table 1. Characteristics of the Shock Wave Produced in a Gas by the Detonation of PETN (Density = 1.0 g/cc), whose Chapman-Jouguet Characteristics are: Detonation Velocity = 5550 m/sec, Pressure = 8×10^4 bar, Temperature = 4160°K, Material Velocity = 1400 m/sec, Density ($1/V_2$) = 1.37 g/cc, and Observed Detonation Velocity = 5500 ± 100 m/sec

Gas in Shock Tube	Characteristics					
	Calculated				Observed	
	Pressure P (bar)	Temperature (transl. + rotat.) T (°K)	Material velocity U (m/sec)	Initial shock velocity D_0 (m/sec)	Initial shock velocity* D_0 (m/sec)	Attenuation constant† $K \times 10^5$ (sec/m²)
Hydrogen (1 atmos)	55	3100	7400	9100	8300	6.7
Argon (1 atmos)	850	63200	6170	8220	7550	35.0
Air (1 atmos)	590	29000	6370	7660	6900	22.0
Methane (1 atmos)	320	14900	6670	7810	7100	22.5
iso-Butane (1 atmos)	1000	42000	6000	7000	6300	47.5
Chlorine (1 atmos)	1200	56600	5920	6700	6200	38.0
Air (150 mm Hg)	150	35800	7070	8510	8500	—
Air (50 mm Hg)	52	38300	7430	8900	9500	7.5
Air (1 mm Hg)	—	—	—	—	12400	5.5
Air (100 atmos)	17300	8600	3660	4200	—	—

* Values at the distance of 2 ~ 4 cm from charge surface.
† values in $1/D = 1/D_0 + Kx$, $x = 0 \sim 1$ meter.

Study of Dark Zone

The discontinuous nature of the luminous phenomena that occur across the boundary between the surface of an explosive and a surrounding gas atmosphere has been observed in many photographic records of detonations,[10] but no proper explanation for the phenomenon has been given.

Between the intense luminosity due to the shock wave in air and the weak luminosity due to the detonation wave in an explosive, a less luminous zone exists; in the following we shall call it the dark zone.

Many fully-exposed still-photographs of the luminous phenomena produced in high-explosive shock tubes have been taken through a red filter (6000 to 6500 Å), which makes it easy to distinguish clearly the relative intensity of the light from each part of the tube. Glass mainly was used for the tube because it has the strength needed to extinguish the external-shock luminosity. Although cracks in glass often propagate with a speed comparable to that of air shocks in a tube, its real fracture is always delayed behind the passage of shocks, and a pattern of cracks is recorded on the still-photographs without disturbing the dark zone measurement. Sample photographs showing the dark zone are given in Figure 4.

Approximate values of dark zone widths measured from photographic records for shock tube systems consisting of glass tube, argon gas, and various sorts of explosives are summarized in Table 2.

The dark zone widths seem to depend upon the property of the shock-forming gas as well as the manner of detonation of shock-producing ex-

plosive; e.g., it seems that the dark zone is shortest with gases of high density and low specific heat, and with explosives of high detonation velocity and rapid completion of detonation reaction without solid particles entrained. The role of solid particles is to be emphasized; the dark zone widths for carbon-producing explosives (TNT, tetryl, picric acid, nitroguanidine) or for explosives mixed with an inert matter (PETN + common salt or graphite) are rather longer than those for explosives that yield only gaseous products (PETN or nitroglycerine). The solid particle, whether reaction product or inert diluent or detonating particle, may retard shock formation by penetrating and disturbing the wave front which is on its way to shock formation.

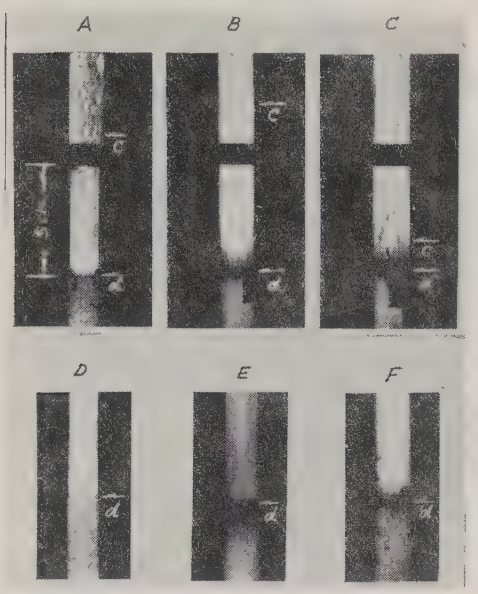

FIG. 4. Examples of still-photographs showing the dark zone phenomena for argon shocks in glass tube.
(A) PETN 70 + graphite 30 (Δ = 0.98)
(B) nitroguanidine (Δ = 0.72)
(C) nitroguanidine (Δ = 0.55)
(D) PETN (Δ = 0.85)
(E) picric acid (Δ = 0.85)
(F) TNT (Δ = 0.95)

From the above results, we take the dark zone as a measure of the shock formation length and draw a schematic diagram of time-distance relation of the wave phenomena in a high-explosive shock tube as shown in Figure 5.

The dotted lines which form a delta zone (Fig. 5) represent the reaction paths of explosive particles that are thrown into the outer atmosphere after the arrival of the detonation front to the charge surface; the full lines are for reaction paths in the detonation wave itself. The expanding delta zone will give rise to a compression wave in the outer atmosphere but not an instantaneous rise to a shock wave of high intensity owing to

TABLE 2. DARK ZONE WIDTHS MEASURED FROM STILL-PHOTOGRAPHIC RECORDS FOR SHOCK TUBE CONSISTING OF GLASS TUBE (13-mm BORE), ARGON (OR HYDROGEN) GAS AND VARIOUS EXPLOSIVES.

Explosive	Density	Dark Zone Width
	g/cc	*mm*
PETN	0.85	<0.5 (~4 mm in H_2)
PETN + NaCl		
7:3	0.98	~1 (~10 mm in H_2)
5:5	1.10	3 ~ 6 (~13 mm in H_2)
PETN + graphite		
7:3	0.98	2 ~ 3
5:5	0.95	7 ~ 9
Nitroglycerine	1.6	<0.5
TNT	0.95	3 ~ 6
TNT + NaCl		
95:5	0.98	4 ~ 8
90:10	1.0	6 ~ 10
85:15	1.1	10 ~ 20
80:20	1.15	15 ~ 30
Nitroguanidine	0.72	6 ~ 10
Tetryl	0.85	2 ~ 6
Picric acid	0.85	2 ~ 5

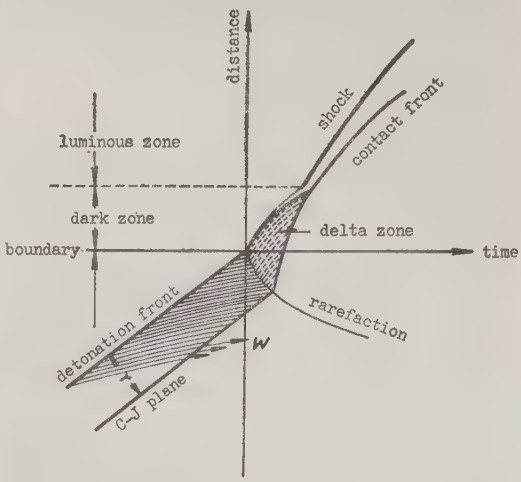

FIG. 5. Schematic diagram for shock formation.

its rapid attenuation and, in addition, probably to the disturbing effect of flying explosive particles; for the compression wave to grow into a substantial form of shock wave, it will need some distance—that is to say, a shock formation length or a dark zone—which may be terminated near the point of completion of the reaction. For high explosives yielding only gaseous products, this distance of dark zone is very short (less than 0.5 mm); in the case of solid-producing explosives the solid particles outrunning the delta zone and weakening the growing shock prolong the distance of dark zone greatly.

Thus the real process of shock formation may be too complicated to formulate strictly but, at least for explosives with a short shock formation length, like PETN, we can apply the ordinary method of calculation approximately—as we have done in the preceding section.

Streak photographs taken through the red filter for similar samples show the same dark zone phenomena as in Figure 6. (They show that the main luminosity, probably due to shock waves, lasts only for 4~6 μsec.)

As in the case of shock formation in the outer atmosphere, a dark zone phenomenon has been found in the contact transmission of a detonation wave from one explosive to another less sensitive one. Thus, in Figure 6, a dark zone exists in the initial period of the TNT or nitroguanidine detonation which is transmitted from PETN, whereas the PETN detonation transmitted from TNT or nitroguanidine shows no appreciable dark zone.

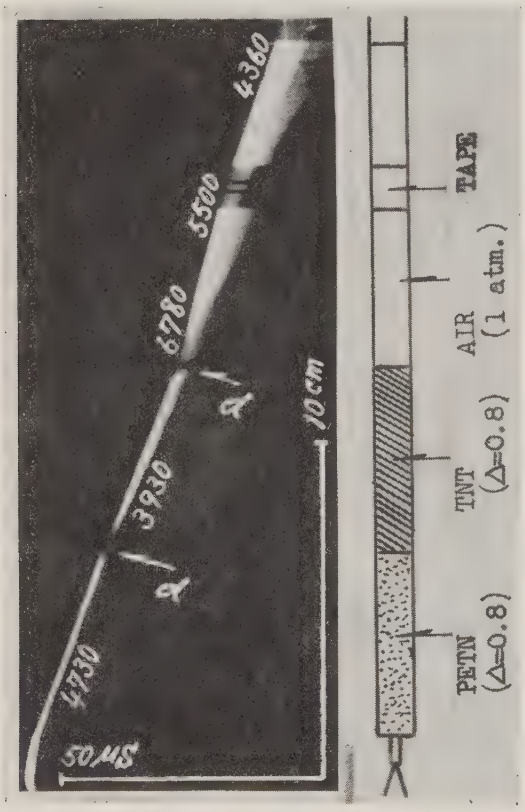

Fig. 6. Streak photograph of detonation transmission from PETN to TNT.

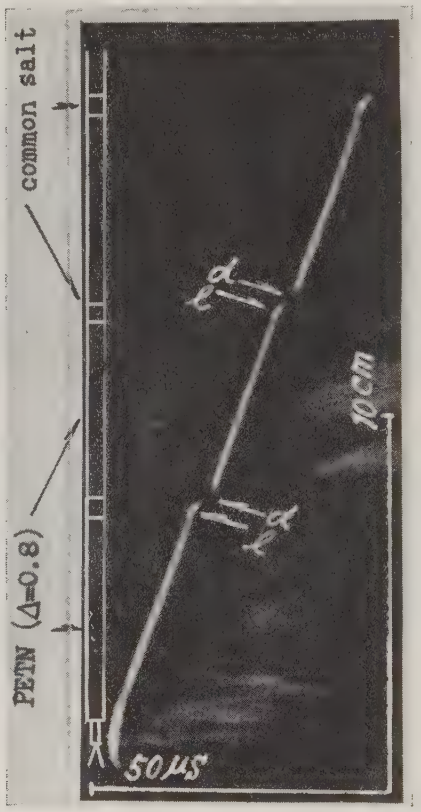

Fig. 7. Streak photograph of a zebra charge in glass tube (celluloid tube gives a similar image).

Furthermore, similar dark zones can be seen in the detonation of a "zebra" charge, where granular common salt of 5-mm width is placed in alternate layers with PETN.

Figure 7 shows that the salt zone temporarily interrupts the progress of the detonation wave and delays the initiation of the adjacent PETN layer for 3.4 μsec, and that the first part of the salt zone emits a bright light due to the collision with the detonation wave,[11] but thereafter a dark

zone follows. The same phenomena are clearly observed in a still-photograph of the same zebra charge. The situation is similar when naphthalene, graphite or a sheet of paper is used in place of common salt in the charge, although the luminous part is shorter than that for common salt.

From the above observations we conclude that: (1) The dark zone appearing just above the charge surface is a measure of shock formation length, which is determined by the nature of both surrounding atmosphere and detonation wave; in particular, solid particles entrained play an important role. (2) The pure shock front preceding the detonation wave in a granular explosive

FIG. 8. Spectrum of PETN-produced air shock, Method (b). (a) Shows the method of having copper particles suspended in air.

emits a light of moderate intensity by producing microshocks in the air space between granules, the energy of the micro-shocks being used to initiate an endothermal decomposition of the explosive. (The formation of microshocks may depend upon factors similar to those mentioned by Muraour.[1] (3) When a detonation wave collides against an inert or less reactive solid it is temporarily dammed up and raised to a higher temperature but, owing to the event, the steady form of the detonation wave being destroyed, a decayed shock front precedes the detonation zone and a dark zone forms which persists until the detonation wave recovers its steady form in the next explosive layers.

Spectroscopic Measurement of Shock Wave Temperature

Some spectroscopic measurements of detonation or shock temperatures have been performed by Muraour,[12] Alentzev,[13] Fox[14] and others. They obtained the color temperatures, assuming blackbody radiation for the luminosities from the detonation. Recently, Kantrovitz *et al.*[15] measured the temperatures of argon shocks by means of Unsöld's or Baranger's theory.

However, these methods cannot be applied to the temperature measurement of an air shock from a PETN detonation, because its spectrum contains numerous metallic lines due to impurites and CN bands superimposed on the background of weak continuum, the oxygen or nitrogen lines being obscure.

Therefore, in this experiment, we adopted the two-line method developed by Ornstein and his group[16] and, for reference, the method of Spier and Smit-Miessen[17] who used the unresolved CN bands.

For a Boltzmann radiator, the next formula applies and gives the relative intensities of two atomic or ionic lines with different initial levels

$$\frac{I'}{I} = \frac{A'g'\nu' \exp(-E'/kT)}{Ag\nu \exp(-E/kT)}$$

where A is the transition probability, g is the statistical weight of the excited level with energy E which gives rise to the line with frequency ν, T is the absolute temperature of the radiator and k is the Boltzmann constant.

If the excited atoms in the air shock are in thermal equilibrium, the temperature of the air shock can be obtained by comparing the intensities of two metallic lines, but the spectrum of the air shock from PETN has no lines suitable for that purpose. Accordingly, we have tried to insert intentionally the copper lines of 5106, 5153 and

5220 (+5218) Å, because they are not disturbed by lines or bands of other elements in the shocks and, in addition, they exist in a narrow wave length range (this is desirable from the standpoint of both film sensitivity for different wave lengths and deviations from the reciprocity law). Copper lines have been introduced (a) by mixing a small quantity (1 per cent) of fine copper powder with PETN or (b) by suspending the copper particles in air through the electric spark between copper electrodes in which a small quantity of granular copper chloride is held, as shown in Figure 8(a).

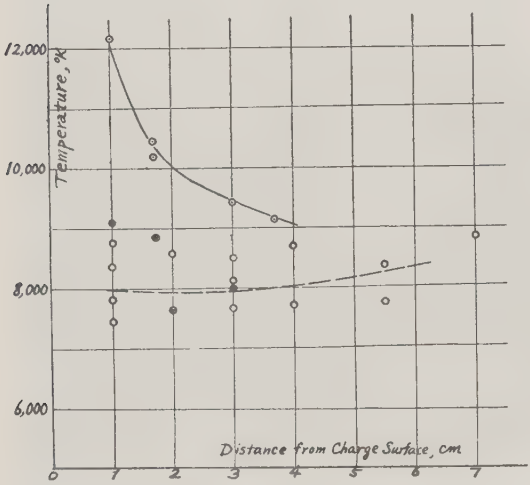

FIG. 9. Observed values of air shock temperatures. ⊙ from the two lines of copper suspended in air by spark; ○ from the two lines of copper mixed in explosive; ● from unresolved CN-bands.

The experimental arrangement is similar to the previous one (Fig. 1). A Hilger-type quartz spectrograph with Kodak tri-X film replaces the rotating-drum camera. A glass tube of 18-mm bore and PETN of 0.8 ~ 0.9 g/cc density are used. Together with the shock spectrum, the standardized tungsten lamp is spectrographed through a rotating sector which enables us to express the spectrum densities by corresponding intensities; the "intensity-area" of a line, i.e., area of the intensity-wave length diagram, is found by subtracting the part of the background continuum. Furthermore, we corrected the self-absorption effect by comparing the intensities of two lines which have the same excitation level (copper lines of 5153 and 5220 Å) by use of the equation expressing the weakening by self-absorption

$$\frac{I(resultant)}{I(Planck)} = 1 - \exp\left[-\frac{I(initial)}{I(Planck)}\right]$$

where $I(resultant)$ is the intensity actually observed $I(initial)$ the intensity before self-absorption, and $I(Planck)$ the intensity in radiation equilibrium. Transition probabilities of copper were found from the data of van Lingen.[18]

Figure 8(a) is an example of the spectrum of PETN-produced air shock. Figure 9 summarizes the values of air shock temperatures obtained by applying the two-line method for the spectra which were obtained according to methods (a) and (b) mentioned above. The values determined through the analysis of unresolved CN bands of (0–0) and (1–1) also were received.

In method (a), where copper was mixed with PETN, the temperature values were found to be relatively low (of the same order as the temperature values of CN radicals) and to remain almost constant along the shock path; in method (b), where copper was suspended in air, the highest temperature was obtained near the origin of the shock formation (in the dark zone, lines and bands are very weak) and the temperature values decreased along the shock path.

It is to be noted that the temperature value obtained here is either an effective excitational temperature of copper atoms entrained in the shock wave and in the detonation gases, or an effective vibrational temperature of CN radicals produced in the shock or detonation gases and not the temperature of the air itself which forms the shock wave.

The problem is whether or not the copper atoms are in thermal equilibrium in the shock wave; in this respect method (b) seems preferable to others, although its accuracy is not so clear.

Acknowledgment

The authors are indebted to Mr. S. Kitaoka for his assistance in the experimental work.

REFERENCES

1. MURAOUR, H.: Memor. Artil. Fr., *23*, 867 (1949).
2. SHREFFLER, R. G., AND CHRISTIAN, R. H.: J. Appl. Phys., *25*, 324 (1954).
3. TAYLOR, J.: *Detonation in Condensed Explosives*, p. 31. New York, Oxford Univ. Press, 1952.
4. SAVITT, J., AND STRESAU, R. H. F.: J. Appl. Phys., *25*, 89 (1954).
5. KISTIAKOWSKY, G. B., AND WILSON, E. B., JR.: OSRD Rept. 114 (1941).

6. Kihara, T., and Hikita, T.: *Fourth Symposium on Combustion*, p. 458. Baltimore, The Williams & Wilkins Co., 1953.
7. Hikita, T., and Yoneda, K.: Proc. Japan. Fifth Natl. Cong. for Appl. Mechanics, 367, (1955).
8. Paterson, S.: *Fifth Symposium on Combustion*, p. 672. New York, Reinhold Publ. Corp., 1955.
9. Bowden, F., and Yoffe, A. D.: *The Initiation and Growth of Explosions in Liquid and Solid*. New York, Cambridge Univ. Press, 1952.
10. Parisot, A.: Memor. Artil. Fr., *18*, 499 (1939).
11. Paterson, S.: Nature, *167*, 479 (1941).
12. Muraour, H.: Chim. et Ind., *47*, 3 (1942).
13. Alentzev, M., et al.: Exptl. Theoret. Phys. U.S.S.R., *16*, 990 (1946).
14. Fox, J. C.: PB Rept. 36957 (1945).
15. Kantrovitz, A., et al.: J. Appl. Phys., *26*, 83 (1955).
16. Ornstein, L. S., and Brinkman, H.: Physica, *1*, 797 (1934).
17. Spier, J. L., and Smit-Miessen, M. M.: Physica, *9*, 193, 922 (1942).
18. van Lingen: Physica, *1*, 797 (1934).

49

A SHOCK-TUBE STUDY OF FLAME FRONT-PRESSURE WAVE INTERACTION[a]

By G. H. MARKSTEIN

Introduction

Many applications of combustion in a gaseous medium, and particularly those in jet and rocket propulsion, require burning rates far in excess of those corresponding to laminar flame propagation. It is generally recognized that these rates are achieved by the interaction of the flame with more or less random flow disturbances that are often somewhat loosely called "turbulence." Apparently because of this terminology, recent studies have concentrated on interactions of pipe flow or grid-generated turbulence with open or enclosed flames while, in comparison, the study of interactions with other kinds of flow disturbance has been neglected.

Linearized perturbation analysis[1] has shown that in a flow devoid of rapid changes of average variables any random disturbance can be decomposed into three modes that are in first-order approximation independent of each other: namely, a vorticity mode (eddy turbulence), a pressure mode (random sound), and entropy spottiness. Whenever the average flow variables are subject to rapid changes, however, such as occur during passage through grids, shock waves, flame fronts, or changes of cross section of a duct, the three modes become strongly coupled in first order.

Thus, in a turbulent flame all three disturbance modes must be present. This may be of minor importance with open flames, since the pressure mode will be dissipated by sound radiating from the flame, and the entropy mode will appear only in the burned gases in the form of temperature and density fluctuations. In the case of flames enclosed in a duct, however, the pressure disturbances may become as significant as eddy turbulence, for the energy contained in pressure waves will in general become trapped in the various resonance modes of the duct. The combustion process in ducts is therefore generally accompanied by intense sound waves that may include random noise as well as resonance oscillations. Undoubtedly these pressure waves must affect the flame in various ways, but the nature of these interactions is at present ill understood.

The large majority of previous studies of pressure wave-flame front interactions was concerned with spontaneous generation of sound and vibrations by flames. A complete bibliography and adequate discussion of the numerous investigations in this field would be beyond the scope of this paper. Among their results, the following are of particular significance in relation to the present work:

(1) The rate of flame propagation in tubes during "vibratory movement" exceeds that during

[a] This research was conducted under the auspices of Project SQUID, jointly sponsored by the Office of Naval Research, Department of the Navy, Office of Scientific Research, Department of the Air Force, and Office of Ordnance Research, Department of the Army.

"uniform movement" appreciably. This was observed in the earliest work on the phenomenon[2] and confirmed in many subsequent studies.

(2) Both the amplitudes of the vibrations and the associated flame-propagation rates can be varied within wide ranges by terminating the open end of the flame tube with diaphragms of various diameters.[3]

(3) During vibratory movement of moderate or large amplitude, flames undergo recurrent changes of structure.[5, 6, 7, 8]

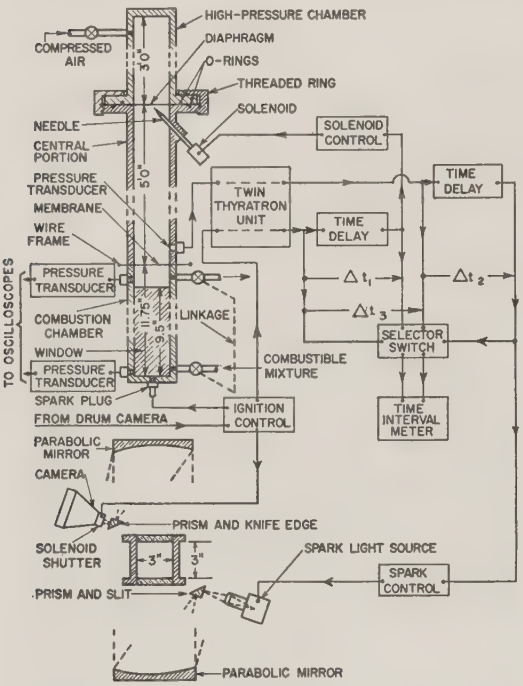

FIG. 1. Schematic diagram of apparatus.

Although the studies of spontaneous flame vibrations yielded these important results, the mechanism of the phenomena has remained somewhat obscure, and little quantitative information has been derived from them. One reason may be that, with any spontaneous phenomenon that is due to some feedback mechanism, it is difficult if not impossible to distinguish between causes and effects; another reason may lie in the complicated nature of the pressure and flow transients during large-amplitude vibratory movement.

It appears therefore desirable to study the effects of externally generated pressure disturbances of simple wave shape on flames propagating in tubes. Surprisingly, only one previous investigation of this type,[9] in which sound waves were used as disturbance, appears to have been undertaken, with rather inconclusive results. In the present work the problem is attacked somewhat differently, by subjecting a flame to shock-wave disturbances. A brief account of preliminary work by this method has been published elsewhere.[10] The design of the present apparatus does not permit the study of the interaction of a single shock wave with the flame, but rather that of a head-on collision between flame and shock wave followed by interaction with the wave transmitted by the flame and reflected at the bottom of the combustion chamber. Although this complicates the observed phenomena, it has the advantage of allowing the investigation of two different interactions in a single experiment. The technique appears adaptable for studying many other types of interactions with only minor modifications of apparatus.

Experimental

The apparatus is shown schematically in Figure 1. The shock tube consisted of a high-pressure chamber, a central portion, and a combustion chamber of the indicated lengths and of 3- by 3-in. internal cross section. It was mounted vertically, with the combustion chamber at the bottom, in order to avoid asymmetric flame shapes due to gravity effects.

Preceding each run, a diaphragm was inserted between the high-pressure chamber and the central portion, and clamped between the indicated O-rings by means of the threaded ring. The choice of diaphragm material depended on diaphragm pressure: up to about 7 psi one layer of cellophane was found to be suitable; from 7 to 15 psi two layers of cellophane were used; from 15 to 25 psi photographic film stock was best suited.

The combustion chamber was separated from the central portion by a thin collodion membrane held between two cork-rubber gaskets. The membranes were prepared by pouring a few drops of a commercially available collodion solution ("Testor's Microfilm") on water and, after evaporation of the solvent, lifting the film off with a wire frame. On the basis of interference colors the thickness of the membranes was estimated to be in the range of 300 to 600 mμ. Although they were heavier than those employed in studies of refraction of shock waves at gaseous interfaces,[11] their effect on the shock wave was considered negligible on the basis of results obtained by Jahn.[11] Note that in the present work the mem-

brane breaks shortly after ignition and prior to passage of the shock wave, whereas in the interface study it is broken by the shock wave.

The combustion chamber was filled with combustile mixture by flushing it for at least 10 min. The flow entering and leaving through the valves indicated in Figure 1 had to be kept small in order to prevent the chamber pressure from rising more than a few inches of water above ambient pressure and causing rupture of the membrane. In the present work *n*-butane-air mixtures, mostly in stoichiometric proportion, were used. They were prepared by metering air and fuel separately with rotameters. In order to obtain accurate rotameter readings, the total flow had to be much larger than the portion used for flushing the combustion chamber. The excess was burned off on an auxiliary burner; the appearance of this flame provided a rough check on mixture composition. The small fraction of the flow used for filling the combustion chamber was metered by a third rotameter. Before closing the valves, the mixture escaping through the upper valve was tested by burning it on a small nozzle. The blowoff flow of this flame furnished a rather sensitive test of attainment of uniform and correct mixture composition in the chamber. The valves were then closed in succession by the indicated linkage, which was designed so that the outflow valve closed somewhat later than the inflow valve. Thus, the chamber pressure dropped to ambient pressure during this operation. Finally, compressed air was admitted to the high-pressure chamber. The pressure was preset with a regulator valve and measured with a precision gauge with an error of less than ± 0.05 psi.

The cycle of operation of the device was initiated by igniting the combustible mixture with a spark plug located in the center of the bottom of the combustion chamber. In preliminary work, it had been found that in spite of the use of stoichiometric mixtures the initial flame surface was not free of some irregularities. Most of these could be eliminated by removing the grounded side electrode of the spark plug. A conventional 6-v battery ignition circuit was used. The instant of ignition was determined by a synchronous motor-driven multicam timer (Industrial Timer Corporation Type MC) that was started by the "Event" switch of the recording drum-camera. The timing accuracy of the 2-sec cycle timer used was about ± 2 msec, sufficient to insure synchronization of the streak and oscillograph records.

In preliminary work,[9] the time interval between ignition and rupture of the shock-tube diaphragm could not be varied at will, and was found to scatter also at least by ± 2 msec. There were three independent sources for this scatter: variations (1) in the operation of a relay that served as ignition and shock-tube solenoid control, (2) in the operation of the solenoid, and (3) in the bulging of the diaphragm. It appeared impossible to eliminate this last cause of timing scatter entirely. Its influence was reduced appreciably, however, by increasing the acceleration of the diaphragm-piercing needle. This was achieved by energizing the solenoid, originally designed for 115-v ac operation, through the discharge of a 300-μF capacitor charged to 450 v. The instant at which this occurred was determined as follows: a voltage pulse from the ignition coil triggered one circuit in the twin thyratron unit (Fig. 1), the output pulse of this thyratron was fed into an electronic time-delay generator (Rutherford Model A-2) which, after a preset interval Δt_1, triggered a type 3022 thyratron that in turn discharged the capacitor through the solenoid. The time interval Δt_1 was set at 15.0 msec for the majority of the runs discussed in the present paper.

A pressure transducer located 2.5 in. above the top of the combustion chamber served the dual purpose of measuring the time interval Δt_3 between ignition and arrival of the shock wave at this transducer, and of timing the spark-light source. An electrokinetic transducer[12] was used for this purpose; although its frequency response was inadequate for pressure recording in shock-tube work, its simplicity and large output made it ideally suited for triggering applications. The pulse from this transducer fired the other circuit of the twin thyratron unit. The output of this thyratron triggered the spark light-source after a time interval Δt_2 provided by another electronic time-delay generator (Dumont Type 326).

By means of a selector switch, the proper starting and stopping pulses could be fed into an electronic time-interval meter (Berkeley Model 5510) for measuring any one of the intervals Δt_1, Δt_2 or Δt_3. The first two were preset before the runs, while the last one was measured during the experiments. The interval Δt_3 was found to exceed Δt_1 by about 8 msec, of which about 5 msec corresponded to the time the shock wave traveled

from the diaphragm to the transducer, the rest to the interval between energizing the solenoid and breaking the diaphragm. For constant setting of Δt_1 and of diaphragm pressure, Δt_3 scattered by about ± 0.1 msec. Since Δ_1 varied by only about ± 15 μsec, the scatter of Δt_3 was primarily due to variations of diaphragm bulging that affected the instant of its perforation by the needle. As the undisturbed flame traveled only about 0.1 in. in the interval of 0.2 msec, this unavoidable scatter was considered tolerable.

The interaction phenomenon was studied by means of spark schlieren photography, schlieren streak records, and by recording of pressure and of flame-radiation transients. The conventional Z-type schlieren system indicated in the plan

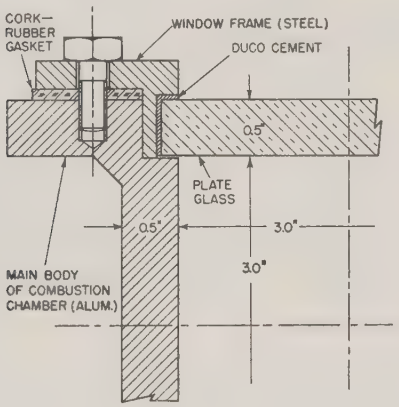

FIG. 2. Design of combustion chamber windows.

view at the bottom of Figure 1 consisted of two 12-in. diameter 5-ft focal-length parabolic mirrors and the usual prisms, slit and knife edge. Horizontal orientation of spark, slit and knife edge was used. The spark was triggered by an auxiliary "teaser" electrode connected to an induction coil that was energized by a thyratron-controlled condenser discharge. The delay between firing of the thyratron and of the spark was measured by means of a photoelectric cell with the time-interval meter. With correct polarity of the induction coil, this delay was found to be 7 ± 1 μsec. In order to avoid fogging of the films by flame radiation, the camera shutter had to be operated at a short exposure synchronized with the spark. A shutter setting of $\frac{1}{100}$ sec was found to be satisfactory. Synchronization was achieved by means of a shutter solenoid operated by the multicam timer in the ignition control unit.

The schlieren photographs were taken through plate-glass windows that allowed a full view of the interior of the combustion chamber from the bottom to a height of 9.5 in. Details of the window design are shown in Figure 2. The glass plates were sealed into steel window frames by means of Duco cement. The frames were designed so that a small gap remained between the glass and the body of the combustion chamber and thus no strain was exerted on the glass. The plates were not entirely free from striations that are faintly visible on the schlieren photographs shown below.

The streak records were taken on 70-mm film with a drum camera (Southern Instruments, Ltd. Model M-1020) that was modified by replacing its original lens with one of 9-in. focal length and by incorporating the solenoid-operated shutter. When a film speed of 50 ft/sec was used, a shutter setting of $\frac{1}{25}$ sec with proper synchronization of camera and shutter gave nonoverlapping records that included the instant of ignition, the interaction, and several returns of the shock wave owing to reflections at the ends of the tube. A 100-w zirconium arc light source was used with the schlieren system described above. The combustion-chamber window that faced the camera was blocked except for a central vertical slot of $\frac{1}{16}$-in. width. A time base was provided by means of a flash tube (Sylvania type R1130B) operated at 10,000 pulses/sec.

Pressure transients were recorded by means of two condenser-type transducers (Rutishauser pickup Model HR-3 and electronic indicator Type ST-12) located 0.5 in. above the bottom and 2.0 in. below the top of the combustion chamber, respectively. Flame radiation in a direction normal to the shock-tube axis was collected by one of the schlieren mirrors and was recorded with a type 931A photo-multiplier placed at the mirror focus. The combustion-chamber window facing the other mirror was blocked with white cardboard in these runs. The previously mentioned drum camera, with its original lens of 3-in. focal length, and two dual-beam oscilloscopes (Dumont Model 322A) were used for recording the transients. The scopes were arranged at right angles to each other and the four traces were displayed simultaneously by means of an optical beam splitter. The fourth channel provided a 0.1-msec time base. No special provision was necessary for recording the instant of ignition, since the photo-multiplier

trace recorded a strong deflection at this instant, owing to pickup of a voltage pulse by this high-impedance device. A film speed of 50 ft/sec was used.

Results and Discussion

SPARK SCHLIEREN PHOTOGRAPHS

The early stages of the interaction between a stoichiometric butane-air flame and a shock wave of pressure ratio 1.3 are shown in Figure 3. The photograph to the left shows the flame a few μsec before the start of interaction. The origin of the time scale used in this and the following figures was arbitrarily selected as the instant of this first photograph. The times referred to in the following photographs were obtained from their respective Δt_2 settings by subtracting that for the first photograph: 0.6 msec. The time elapsed between ignition and the origin of the time scale was thus $\Delta t_3 + 0.6$ msec, or 23.6 ± 0.1 msec for this series of runs.

The major portion of the flame surface shown in the first photograph is devoid of any irregularities. As mentioned before, this was achieved by removing the side electrode of the spark plug. The origin of the remaining distortions near the bottom of the combustion chamber is obscure but, since their shape recurred in many of these photographs, they were presumably caused by minor irregularities of the bottom of the combustion chamber. The shock wave, and weak secondary waves originating at the junction of the combustion chamber and the central portion of the shock tube, are visible above the flame.

The second photograph shows the incident shock wave intersecting the flame, and the rarefaction wave reflected by the flame. The transmitted shock wave is only very faintly visible on the original photograph and therefore has been traced by a dashed line. A phenomenon related to irregular refraction of shock waves at interfaces[13] takes place at the outer portion of the flame that is steeply inclined with respect to the shock wave. Owing to the high speed of sound in the burned gas, the transmitted shock wave coming from the central portion of the flame has here propagated ahead of the intersection between incident shock and flame and created a retransmitted wave in the unburned gas that is well visible in the photograph.

The third photograph shows a somewhat later stage. The incident shock in the unburned gas surrounding the flame and the reflected rarefaction wave are still visible, but the transmitted shock is not discernible in this photograph or any others that were taken during this stage of the interaction. The complicated pattern of waves

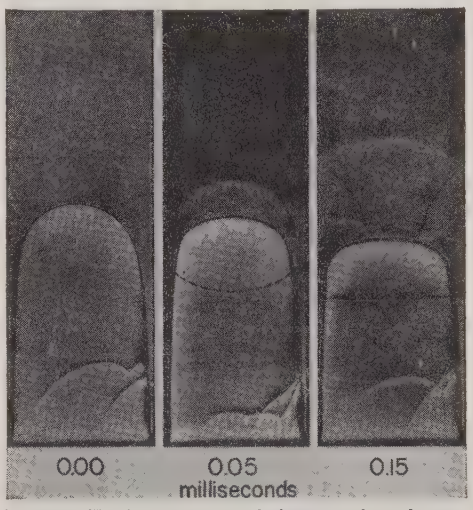

FIG. 3. Early stages of interaction between stoichiometric butane-air flame and shock wave of pressure ratio 1.3 (diaphragm pressure 10 psig). Ignition 23.6 msec. before origin of time scale.

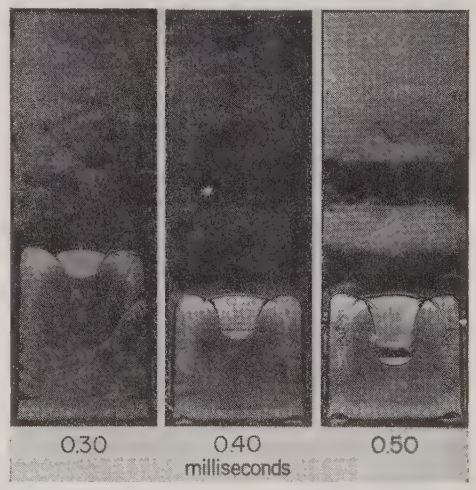

FIG. 4. Beginning of flame inversion under conditions of Fig. 3.

visible above the flame results from multiple reflections of the rarefaction wave at the walls and at the flame front.

Up to this point the interaction has proceeded as one would expect on the basis of theoretical considerations:[14] essentially, the flame has acted like a contact surface separating unburned and

burned gases. Figure 4 shows the beginning of a new stage of the interaction phenomenon that starts in the photograph to the left with the formation of a smooth indentation in the center of the flame. At the same time a dark band, indicating an upward-propagating compression wave, appears just above the flame. The streak records discussed below showed that this wave is identical with the shock wave transmitted by the flame and reflected at the bottom of the combustion chamber. Its appearance as a broad band is presumably due to distortion of its shape owing to the two interactions with the curved flame surface.

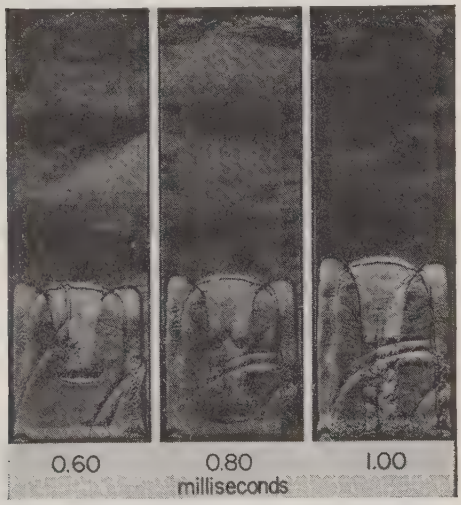

FIG. 5. Further development of inverted flame under conditions of Fig. 3.

The coincidence of flame indentation and passage of the reflected wave was found to be accidental and merely due to the particular choice of the time interval Δt_1. The streak records (see below) showed that for a longer interval (*e.g.*, $\Delta t_1 = 20$ msec), the indentation started before arrival of the reflected wave.

The next two photographs and those of Figure 5 show that the indentation continues to move downward and gradually develops into a "spike" of unburned gas that penetrates into the burned gas and finally impinges at the bottom of the combustion chamber. The surprising persistence of rapid downward motion of the spike, despite the upward acceleration of the gases by the reflected shock wave, seems to be understandable only on the basis of Taylor instability.[15, 16, 17] This acceleration is indeed in the right direction for causing instability of the flame front. However, in view of the impulsive acceleration of very short duration associated with passage of a shock wave, the concept of Taylor instability may have to be modified considerably. Constant acceleration acting on a slightly wavy contact surface (or flame front) creates positive or negative restoring forces, depending on whether it acts in the stabilizing or unstabilizing direction. If, however, the acceleration acts only during a very short time interval, these forces will be of equally short duration and will thus create flow velocities that later on persist with little change. One may thus conclude that in this case the interface distortions will grow approximately linearly with time after the interaction, regardless of the direction of passage of the shock wave. The final deformations will be in the opposite or in the same direction as the initial ones, depending on whether the acceleration was "stabilizing" or "unstabilizing" in the Taylor sense.

The conclusions of this conjecture seem to be well borne out by the results of the present study. The incident shock wave accelerates the flame in the "stabilizing" direction and causes indeed an indentation in the center of the flame front, thereby reversing its original shape. The transmitted wave, after reflection at the bottom of the chamber, traverses the flame at a time when this indentation has just started to form. Since this wave accelerates the flame in the "unstabilizing" direction, it enhances the indentation, causing its transformation into a spike.

Several additional features of interest can be seen in Figures 4 and 5. The tip of the spike is seen to detach from the stem and to broaden into a cap. Figure 5 shows that the edge of this cap begins to shed a fine-grained trail. The surface of the stem, which initially remains smooth, begins to fold about 0.8 msec after the start of interaction; in the last photograph of Figure 5 it looks like the typical schlieren image of a turbulent flame. The flattening of the tip and the disintegration of the surface of the spike have been discussed in connection with Taylor instability.[17] The formation of the spike and the roughening of its surface must be accompanied by an increase of flame surface area and thus of instantaneous volumetric rate of burning. This should cause emission of compression waves by the flame,[14] and indeed the photographs show a second dark band emerging from the flame at 0.5 msec. At 0.8 msec, the first shock wave, visible below the top of the photograph, has straightened, the second wave is

seen below, and several weak additional compression waves can be seen closer to the flame.

The irregular disturbance visible near the top of the photographs of Figure 5 is the contact surface between air and combustible mixture that also contains fragments of the membrane that initially separated these gases. This interface at first moves upward after ignition, but later is pushed down by the incident shock wave and the reflected rarefaction wave, comes into the field of view, and finally moves up again under the influence of the upward-propagating compression waves.

The final stages of the interaction are shown in Figure 6. The inversion of the flame into a deeply drawn-out funnel is seen to persist, accompanied by further development of turbulent flame structure. Very fine-grained structure appears to develop near the bottom of the combustion chamber, presumably owing to the impact of the spike at the bottom, which seems to set up a circulation outward along the bottom, upward along the walls and down again in the center. The structure of the flame gradually becomes coarser, and the last photograph shows that the leading edge of the flame has become essentially laminar, consisting of four lobes that move up along the walls of the chamber. The changes of flame structure that occur during this final stage of the phenomenon are rather gradual, and for this reason no further emission of pressure waves by the flame can be detected on the photographs.

The interaction of a stoichiometric butane-air flame with a stronger shock wave of pressure ratio 1.6 is shown in Figures 7, 8, and 9. The first photograph differs little from the analogous one in Figure 3, except that the transmitted wave is better visible for this stronger shock. The following three photographs show that the formation of the spike occurs more rapidly for the stronger shock wave. A very fine-grained structure appears early in the process, and throughout the later stages the flame appears more highly turbulent than for the weaker shock wave. The compression waves emitted by the flame are seen to steepen more rapidly into shock waves; the last photograph of Figure 8, for instance, shows two fully developed shock waves near the top, followed by another steep compression wave and several weaker waves.

The last photograph of Figure 9, taken 5.4 msec after the beginning of interaction, shows, in addition to the strong density gradients of the turbulent flame funnel, some weaker gradients in the burned gas. In earlier work, using high-speed motion pictures,[10] it was observed that these

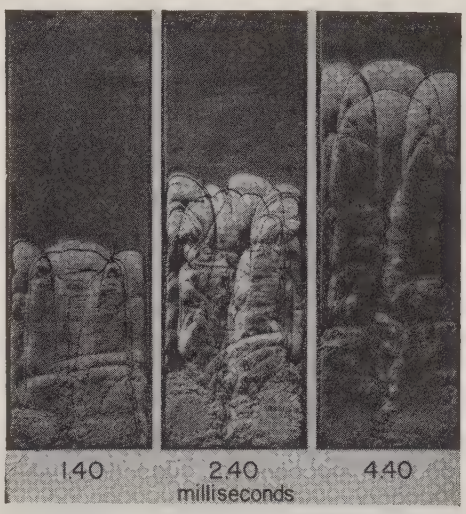

FIG. 6. Final stages of interaction under conditions of Fig. 3.

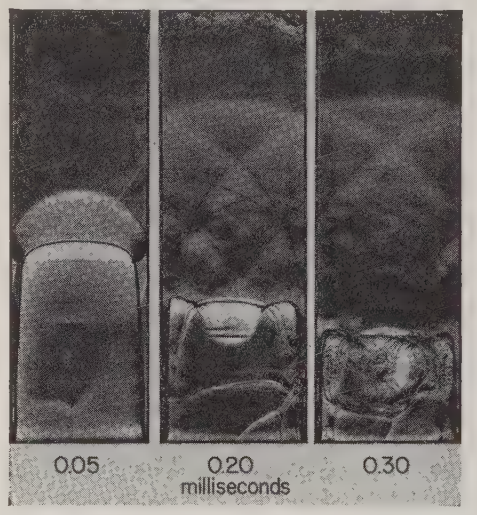

FIG. 7. Initial stages of interaction between stoichiometric butane-air flame and shock wave of pressure ratio 1.6 (diaphragm pressure 25 psig). Ignition 24.0 msec before origin of time scale.

gradients persist for an appreciable time after burning has ceased. Thus they are of the nature of entropy spottiness left behind by the turbulent flame.

A series of photographs was also taken of the interaction of a rich butane-air flame, of equivalence ratio 1.38, and a shock wave of pressure

ratio 1.3. Despite the cellular structure of the undisturbed flame, the interaction was found to proceed very similarly to that of the stoichiometric flame. The later stages, in particular, starting with development of the spike, were indistinguishable from those in the stoichiometric case. These photographs are therefore not reproduced here.

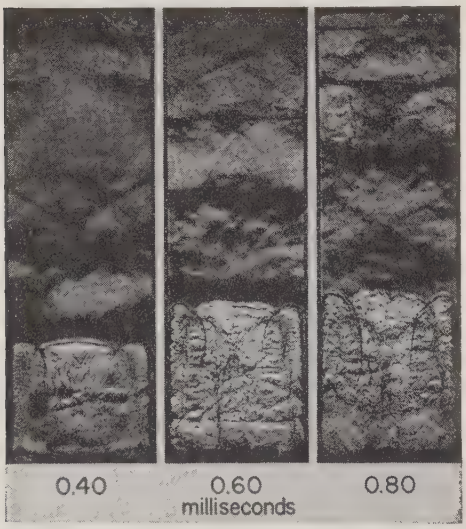

FIG. 8. Development of inverted flame under conditions of Fig. 7.

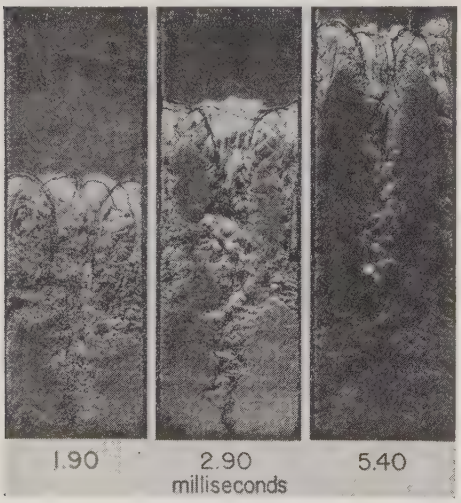

FIG. 9. Final stages of interaction under conditions of Fig. 7.

The results obtained by spark photographs agree with observations on spontaneous vibratory flame movement. The inversion of flame shape, or periodic formation of spikes of unburned gas penetrating into the burned gas, has been described by various authors.[6, 18, 19] The increase of average flame-propagation rate during vibratory movement is understandable on the basis of the periodic formation of turbulent flame funnels, and the emission of secondary compression waves by the flame provides the driving mechanism. Note also that the vibration-induced cell structure[5] which occurs during vibratory movement of small amplitude may be regarded as a periodic inversion of flame cells, and its analysis[20] as a generalization of Taylor instability.

STREAK RECORDS

While the interaction phenomenon can be understood only on the basis of its three-dimensional nature revealed by the spark photographs, a quantitative analysis useful for application of the wave-diagram method[21] to combustion phenomena in nonsteady compressible flow must necessarily replace the problem by an equivalent one-dimensional description. Therefore, the derivation of equivalent one-dimensional boundary conditions for pressure-wave reflection and transmission at a flame front will be a primary aim of future work using the techniques described in the present paper. In addition to the pressure and radiation records discussed below, experimentally derived wave diagrams will be required for this purpose. Simplified and approximate wave diagrams can be constructed from the spark photographs. As an example, the diagram for interaction of a stoichiometric butane-air flame with a shock wave of pressure ratio 1.3 is shown in Figure 10; the appearance of the photographs at several stages is sketched in the lower part of the figure.

More complete and accurate wave diagrams that can be evaluated in terms of wave and particle velocities were obtained by means of streak records; three of these are shown in Figure 11. The main features of these records can be readily identified by comparison with Figure 10. The incident shock wave, the reflected rarefaction wave, the flame front and its gradual transformation into a turbulent burning zone, and the compression waves emerging from the flame during and after interaction are clearly discernible. The transmitted shock wave and its reflection from the bottom of the combustion chamber were again only rather faintly visible on the original records, and were therefore traced as dashed

lines. For interaction with $\Delta t_1 = 20.0$ msec, as mentioned earlier, the flame indentation can be seen to occur before the return of the transmitted shock wave to the flame front.

A feature that was not included in Figure 10 is the contact region between unburned mixture and air, that shows up as a broad band in the upper parts of the top and bottom records of Figure 11. The slope of this band yields the particle velocity in the contact region. Particle paths are also visible more faintly in the unburned gas following the interaction, presumably owing to slight density spottiness caused by the intersecting waves. Weak waves propagating in either direction can also be seen in this region, so that all three characteristics are visible there. Some of the faint lines, however, are due to oblique secondary waves; since their slopes do not correspond to true wave speeds, they must be avoided in the evaluation of the records.

The very prominent streaks in the turbulent flame zone indicate the movement of burning gas particles. Near the bottom of the combustion chamber two diagonally intersecting systems of streaks are visible, confirming the formation of a circulation after impingement of the spike at the bottom.

Evaluation of the records showed, in general, good agreement with theoretically expected wave speeds and particle velocities. The measured speeds of the incident and the transmitted shock waves were used for computing the ratio T_b/T_u of the absolute temperatures of burned and unburned gases in the following manner. The shock-pressure ratio and thus the Mach number of the incident wave was known and was further checked by the measured particle velocity behind the shock. A trial pressure ratio of the transmitted shock wave was calculated from the relation for transmission of a weak wave,[14] using an assumed value for T_b/T_u . From the known wave speed in the burned gas and this pressure ratio, a value of T_b/T_u was obtained and was used for improving the calculation of the pressure ratio. This iteration converged very rapidly; the final values of T_b/T_u obtained from several records were all in the range between 7.0 and 7.5—the latter corresponding closely to adiabatic flame temperature of a stoichiometric butane-air mixture.

For as yet undetermined reasons, the particle velocity behind the reflected rarefaction wave, as well as the pressure change across this wave, as measured on the oscillographic records (see below) corresponded to appreciably lower temperature ratios. Early emission by the flame of compression waves that weakened the rarefaction wave may have been the cause of this discrepancy.

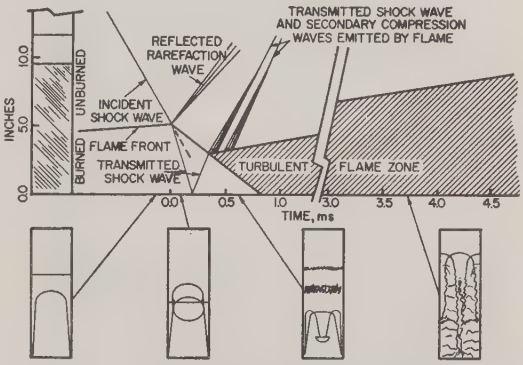

FIG. 10. Simplified wave diagram of interaction between stoichiometric butane-air flame and shock wave of pressure ratio 1.3.

FIG. 11. Streak records of interaction between stoichiometric butane-air flames and shock waves. *Top:* shock pressure ratio 1.3, $\Delta t_1 = 1.50$ msec; *center:* shock pressure ratio 1.3, $\Delta t_1 = 20.0$ msec; *bottom:* shock pressure ratio 1.6, $\Delta t_1 = 15.0$ msec.

It seemed of particular interest to compare the measured velocity of downward motion of the tip of the spike with the computed particle velocity in the burned gas behind the transmitted shock wave. For an incident shock wave of pressure ratio 1.3, the spike velocity was found to be about 570 ft/sec, while the particle velocity

should be only about 320 ft/sec. Similarly, for a shock-pressure ratio of 1.6, the spike velocity was 980 ft/sec compared with a theoretical particle velocity of 640 ft/sec. These results show clearly that the interaction generated a circulation, downward in the center and upward near the walls, that was superposed on the flow calculated on the basis of one-dimensional theory, and further confirm the mechanism of modified Taylor instability discussed earlier.

PRESSURE AND RADIATION TRANSIENTS

A portion of a drum-camera record of flame radiation and pressure transients during interaction of a stoichiometric butane-air flame with a shock wave of pressure ratio 1.3 is shown in Figure 12. The upper pressure trace, taken with the transducer placed 2.0 inches below the top

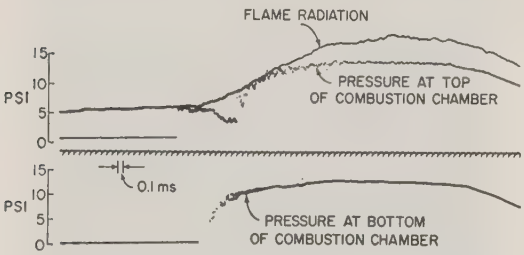

FIG. 12. Oscillograph record of pressure and flame radiation transients during interaction between stoichiometric butane-air flame and shock wave of pressure ratio 1.3.

of the combustion chamber, shows the arrival of the incident shock wave, which occurred 23.2 msec after ignition, followed by an interval of constant pressure of 0.7 msec in duration. This is followed by the rarefaction wave reflected by the flame, the transmitted wave and, finally, the secondary compression waves emitted by the flame. The times of arrival of these waves agree well with those derived from the spark photographs and streak records, as can be verified by drawing a horizontal line at the location of the transducer through the wave diagrams (Figs. 10 and 11). The lower trace, corresponding to the pressure 0.5 in. above the bottom of the combustion chamber, shows the arrival of the transmitted shock wave followed by a succession of compression waves.

The information that may be of greatest interest is the excess pressure rise owing to the combustion process. Both traces show a slight rise preceding interaction. The maxima of both traces exceed the diaphragm pressure of 10 psi by about 3 psi. Detailed evaluation and interpretation of pressure records taken under various conditions, for the purpose of obtaining equivalent one-dimensional boundary conditions at the flame front, will be carried out as a separate investigation by Dr. G. Rudinger of this Laboratory.

It appeared desirable to obtain some measure of instantaneous volumetric burning rate, independently from the information that may be derivable from pressure records and experimental wave diagrams. For this purpose, flame-radiation records were taken simultaneously with the pressure records. It is realized that radiation may depend on other variables besides burning rate. At least one influence, that of changes of flame structure owing to turbulence, appears to be negligible.[22] The effect of pressure on flame radiation apparently has not been studied adequately in the pressure range of interest in the present work.

The radiation transient shown in the top trace of Figure 11 shows an initial rise preceding interaction, followed by a steeper approximately linear rise that finally tapers off to a maximum. The steeper rise starts 23.5 msec after ignition, *i.e.*, at the beginning of interaction, and the maximum occurs about 3.7 msec later. Neither the passage of the incident shock wave nor that of the transmitted wave reflected from the bottom seems to cause any sudden changes of flame radiation, and one may thus conclude that direct effects of pressure on radiation were not significant.

Thus, the radiation transient would seem to yield at least an approximate measure of instantaneous volumetric burning rate. Insofar as this interpretation may be correct, the result agrees with that of the spark photographs, which showed the gradual formation of a turbulent flame funnel after the shock waves had traversed the flame. The maximum of radiation occurred before the flame began to move upward beyond the edge of the window, and may thus indicate the beginning of decay of flame turbulence. The last photograph in Figure 6, taken at a time beyond the maximum, indeed shows reappearance of laminar structure in a portion of the flame.

A series of records of interactions between stoichiometric butane-air flames and shock waves of various pressure ratios was taken. There was some doubt whether the time interval between ignition and arrival of the shock wave at the flame may have an appreciable effect on the

course of interaction. An auxiliary series was therefore first taken, for which the pressure ratio, 1.3, was held constant while the time interval Δt_1 was varied from 13.0 to 17.0 msec. No significant changes of the radiation records could be detected over this range. In the series with varying pressure ratio, Δt_1 was adjusted in such a way that the interval Δt_3 remained constant at 23.0 $\pm$0.1 msec.

The results of these runs are shown in Figure 13. A comparison run taken with flame alone is also included. The rate of rise of the radiation after the start of interaction, as well as the maximum radiation is seen to increase with increasing shock pressure ratio, while the time required for reaching the maximum decreases. Unfortunately, the maxima for flame alone and for shock-pressure ratio 1.15 occured so late that the flame may have moved partly beyond the edge of the window, and their significance is therefore doubtful. An attempt was made to overcome this difficulty by collecting the radiation by means of a boresight prism inserted into the shock tube in the vicinity of the diaphragm, but this method gave unsatisfactory results and was abandoned. The ratio of the maximum radiation to the radiation emitted by the flame in the comparison run without shock-wave interaction at the same instant after ignition may be regarded as a measure of the effect of the shock wave on burning rate. Figure 14 shows a plot of this ratio as a function of shock-pressure ratio.

Summary and Conclusion

The interaction of initially laminar stoichiometric butane-air flames with shock waves of several pressure ratios has been investigated. Schlieren spark photographs and streak records showed that reflection and transmission of the incident shock wave coming from the side of the unburned gas initially took place according to theoretical expectation. Later on, however, interaction of the flame with the incident wave and with the wave transmitted by the flame and reflected at the bottom of the combustion chamber led to formation of a spike of unburned gas that penetrated rapidly into the burned gas. The resulting inverted flame assumed a turbulent structure that persisted for several msec after the wave interaction. The mechanism responsible for flame inversion has been tentatively identified with a modified version of Taylor instability.

Transients of pressure near the bottom and the top of the combustion chamber, and of flame radiation, were recorded. Detailed evaluation of

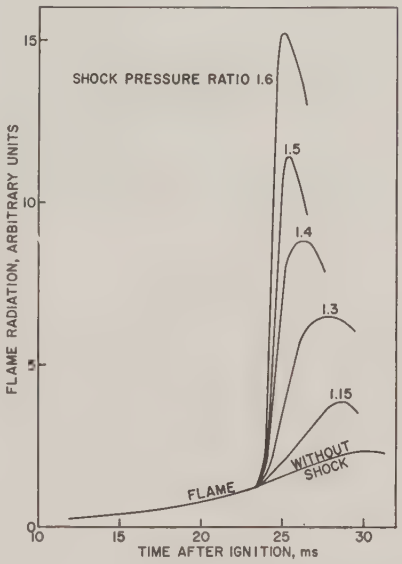

FIG. 13. Flame radiation transients during interaction of stoichiometric butane-air flames with shock waves of various pressure ratios.

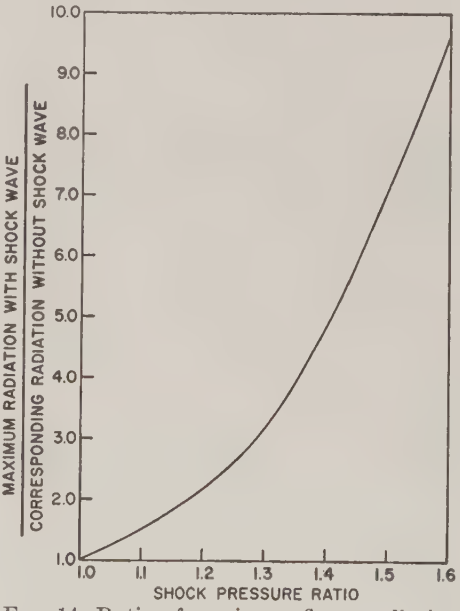

FIG. 14. Ratio of maximum flame radiation to radiation emitted by flame without shock wave interaction at the same instant after ignition.

these records in terms of equivalent one-dimensional boundary conditions at the flame front has not yet been carried out. The radiation transients showed gradual increases during and after wave

interaction leading to maxima that depended on shock-pressure ratio. The absence of abrupt changes of radiation during passage of the shock waves through the flame led to the conclusion that the radiation may be regarded at least as a rough measure of instantaneous burning rate. For the strongest shock wave of pressure ratio 1.6 that was used, the radiation maximum was 9.6 times larger than the radiation emitted by the flame without wave interaction at the same instant after ignition.

Acknowledgments

The author is greatly indebted to Dr. G. Rudinger for many valuable suggestions and discussions, and to Messrs. L. M. Somers and R. Phibbs for assistance in the design and construction of apparatus and in the performance of the experiments. In earlier work, Mr. D. Schwartz provided valuable assistance.

REFERENCES

1. Kovasznay, L. S. G.: J. Aeronaut. Sci., *20*, 657 (1953).
2. Mallard, E., and Le Chatelier, H.: Ann. Mines, *8* (4), 274 (1883).
3. Guénoche, H., and Laffitte, P.: Compt. rend., *222*, 1394 (1946); Guénoche, H., Manson, N., and Monnot, G.: Compt. rend., *226*, 69, 163 (1948); Guénoche, H.: Rev. Inst. français du Pétrole, *4*, 15, 48 (1949).
4. *Fourth Symposium (International) on Combustion*, Baltimore, The Williams & Wilkins Co., 1953.
5. Markstein, G. H.: J. Aeronaut. Sci., *18*, 199 (1951); Ref. 4, p. 44.
6. Schmidt, E., Steinicke, H., and Neubert, V.: Ref. 4, p. 658.
7. Kaskan, W. E.: Ref. 4, p. 575.
8. Guénoche, H., and Jouy, M.: Ref. 4, p. 403; Compt. rend., *236*, 2295 (1953).
9. Ehret, L., Neubert, U., and Hahnemann, H.: Z. angew. Phys., *4*, 126 (1952).
10. Markstein, G. H., and Schwartz, D.: Jet Propulsion, *25*, 174 (1955).
11. Jahn, R. G.: Princeton University Technical Report II-16 (June 1954).
12. Hardway, E. V.: Instruments *26*, 1186 (1953).
13. Jahn, R. G., Princeton University Technical Report II-19 (April 1955).
14. Chu, B.-T.: Ref. 4, p. 603.
15. Taylor, Sir G.: Proc. Roy. Soc. (London), *A201*, 192 (1950); Lewis, D. J.: Proc. Roy. Soc. (London), *A202*, 81 (1950).
16. Allred, J. C., and Blount, G. H.: Los Alamos Report LA-1600 (Nov. 1953).
17. Birkhoff, G.: Los Almos Report LA-1862 (Dec. 1954).
18. Ellis, O. C. de C.: Fuel, *7*, 452 (1928).
19. Jost, W.: *Explosion and Combustion Processes in Gases*, p. 144. New York, McGraw-Hill, 1946.
20. Markstein, G. H., and Squire, W.: J. Acoust. Soc. Am., *27*, 416 (1955).
21. Rudinger, G.: *Wave Diagrams for Nonsteady Flow in Ducts*. New York, Van Nostrand, 1955.
22. Clark, T. P., and Bittker, D. A.: NACA RM E54F29 (Aug. 1954).

50

COMBUSTION STUDIES IN A STIRRED REACTOR

By H. C. HOTTEL, G. C. WILLIAMS and M. L. BAKER[a]

The study of intense mixing as applied to combustion has a two-fold significance: (a) all high-output combustion systems give evidence of dependence on the principle of quickening the reaction of the components of the feed by mixing them with hot products, and (b) the combustion rates attained in some of these systems are so high as to indicate that they can be and in some cases are chemically limited. The studies reported here were made to compare—under conditions of as intense mixing of premixed entering fuel and air with their products of combustion as appeared feasible to attain—the combustion rates of two fuels differing in chemical structure but identical in molecular weight and *atomic* composition and, after adiabatic combustion to equilibrium, iden-

[a] Present address, Shell Chemical Corp., Houston, Texas.

tical in all properties. Secondary objectives were the examination of the effects of varying the feed-hole size to vary the mixing, and the determination of reaction order.

The principle of evaluating chemical rate-controlling processes in combustion by feeding a well-stirred system to the quench-point was first applied by Longwell and Weiss,[1] who employed a spherical reactor to which a homogeneous fuel-air mixture was admitted through a central feed source and from which reaction products left through outlet holes on the external surface of the combustion chamber. The method appeared to have great potentialities for establishing the significance of any chemical limitations on combustion, and the present authors have employed a quite similar device. The principle on which the method is dependent will be reviewed briefly.

If the combustion is controlled by chemical kinetics, the rate of combustion of fuel yN_F (where N_F is the molal fuel feed rate and y is the fraction consumed by combustion) may be tentatively described by the following equation:

$$yN_F = ke^{-E/RT}Vc_F^{\alpha}c_O^{\beta} \qquad (1)$$

where V is the reactor volume and c_F and c_O are the concentrations of fuel and oxygen, respectively.

The assumptions that the reaction is of order α in fuel and β in oxygen and involves no intermediates and that the effect of temperature can be allowed for by the conventional Arrhenius expression may appear naive; they should be considered at this point heuristic assumptions, justified if they correlate the data. Accordingly, the constants, E and k, should not be given the significance "activation" energy and "collision factor" which they have in describing a single chemical act; but they would have fundamental significance if one reaction in the combustion process were much slower than all the rest. In general, these terms refer to a gross chemical change which may take place in a great number of steps.

If the perfect gas laws are used in order to replace c_F and c_O by f_F (P/RT) and f_O (P/RT) where f represents mole fraction, Equation (1) becomes

$$yN_F = ke^{-E/RT}Vf_F^{\alpha}f_O^{\beta}(P/RT)^{\alpha+\beta} \qquad (2)$$

If it is assumed for simplicity that the temperature attained and the gas composition are unique functions of y, the fraction reacted, then y, f_F and f_O may be calculated from an energy balance as a function of temperature and fuel-air ratio, ϕ; and Equation (2) becomes, after substituting n (the reaction order) for $(\alpha + \beta)$

$$N_F/kP^nV = d(E, T, \phi, \beta, n - \alpha) \qquad (3)$$

Typical plots of temperature versus the group, N_F/kP^nV for a fixed value of ϕ, for $\alpha = 1$ and $n = 2$ and for two assumed values of activation energy, E, are presented in Figure 1. For reactions with low values of activation energy the

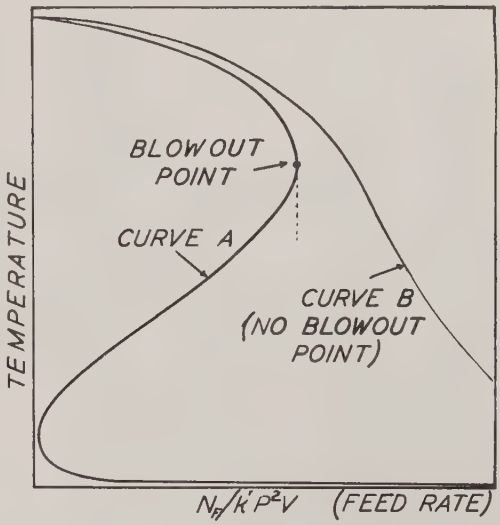

FIG. 1. Characteristic curves of temperature vs generalized rate for well-stirred reactors. Effect of activation energy: low (curve B) vs high (curve A).

operating characteristics of a completely stirred reactor would conform to Curve B. For highly exothermic reactions of high activation energy, i.e., for combustion processes, the reactor follows Curve A, with its stable branch (heavy line), its unstable branch or ignition condition (lighter line), and its bottom branch, numerically indistinguishable from the x-axis unless preheat is high, and following from the form of rate equation used, predicting a finite reaction rate at *any* temperature above zero. The fact that blowout occurs at point x allows inferences concerning reaction rates and reaction kinetics to be made from experiments on blowout in stirred reactors, since N_F/VP^n at blowout becomes a unique function of air-fuel ratio of a form dependent on the postulated mechanism.

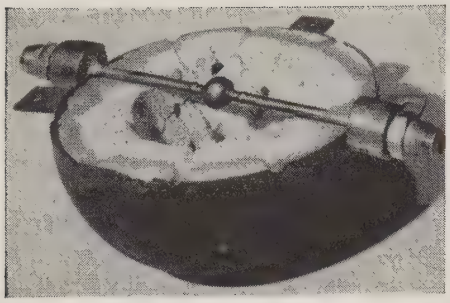

FIG. 2. Combustion chamber and inner feed sphere (partially assembled).

TABLE 1

"Fuel" A	"Fuel" B
57.7% propane	57.7% acetone
31.0% carbon dioxide	26.8% water
11.3% oxygen	15.5% ethylene

Common Properties

Molecular weight	42.7
Empirical formula	$C_{2.04}H_{4.62}O_{0.85}$
Enthalpy of combustion (per mole of fuel at 300°K)	508,000 Btu
Stoichiometric air requirement, moles/mole of fuel	13.20
Moles products per mole reactants (stoichiometric)	1.046
Adiabatic flame temperature of stoichiometric mixture at 300°K	2270°K

TABLE 2. RANGE OF VARIABLES STUDIES

Fuel flow rate	4×10^{-5}–11×10^{-5} lb moles/sec (.017–.050 g moles/sec)
Air flow rate	55×10^{-5}–225×10^{-5} lb moles/sec (0.25–1.02 g moles/sec)
Reactor pressure	0.09–0.81 atmos
Residence time	2–5 msec
Generalized fuel fraction	0.32–0.50 (lean)
	0.61–0.68 (rich)
Equivalence ratio	0.47–1.0; 1.56–2.12
Feed temperature	580–740°R (320–410°K)
Reactor volume	0.021–0.023 ft.^{3} (0.59–0.65 l)
Size of feed holes	0.030 in. and 0.055 in.

TABLE 3. PURITY OF THE FUELS

Carbon dioxide	99.5
Oxygen	99.5–99.7
Acetone	99.
Ethylene	96.1
2.8 per cent ethane	
0.7 per cent methane	
0.4 per cent carbon dioxide	
Propane	92–96

Experimental

The spherical combustion chamber used was much like that of Longwell and Weiss.[1] Figure 2 shows a partly assembled unit. The inside diameter was 4 inches; the insulating lining of the stainless steel shell was 3000°F-kaolin insulating brick 1.75 in. thick. Sixty nearly uniformly spaced ¼-in. holes in the insulation served as gas exit ports. The feed source was a stainless steel sphere ¾-in. in diameter provided with 80 feed ports spaced similarly to exit ports and supported in the center of the combustion chamber by two stainless steel feed arms entering opposed on a diameter. The cool incoming gases kept the feed source and its supporting arms from melting.

The properties, both unique and common, of the two fuel mixtures studied are presented in Table 1. The range of variables studied is shown in Table 2. A complete description of the apparatus is given by Baker.[2]

Unfortunately, the magnitude of the fuel consumption dictated use of components of commercial purity, given in Table 3. Still more unfortunately, the manifolding of propane cylinders caused loss of knowledge of exact composition of the two batches used; and, as the results will indicate, reactor performance was significantly affected, possibly by the variation in propylene content, 0 to 1.5 per cent, the butane, 1.5 to 5.7, or the ethane, 0.8 to 2.1. Reference to fuel A_1 or A_2 indicates the propane batch used.

Experiments consisted of measurements of blowout flow rates and analyses of gas samples withdrawn from the reaction zone. The first 6 columns of Table 4 present the blowout data, including air rate, N_A, fuel rate, N_F, chamber pressure, P, feed temperature, T, and generalized fuel fraction, F (the ratio, fuel/(fuel + fuel equivalent to the air used); varying from 0 (air) to 0.5 (stoichiometric) to 1.0 (fuel), and equal to (equivalence ratio)/(equivalence ratio + 1)). Because the blowout flow rate is rather sensitive to feed temperature and the latter was not controlled, a correction of the data to a common fuel temperature is desirable before correlation. Since the feed temperature never varied more than 110°F from the mean temperature of 630R, the temperature correction factor formulated by Longwell and Weiss,[1] although not strictly applicable to the present data, was considered adequate, and was used. It appears as column 7 of Table 4.

The blowout data of Table 4 are grouped ac-

TABLE 4. SUMMARY OF DATA AND CALCULATIONS

Run No.	Air Rate, $N_A \times 10^5$ lb moles/sec	Fuel Rate, $N_F \times 10^5$ lb moles/sec	Pressure, atmos abs	Inlet Temp, °R	Gen. Fuel Fract., F	Correction Factor* to 630°R	$\frac{N_A}{VP^{1.3}}$ Corrected to 630	$\frac{N_A}{VP^{1.8}}$ Corrected to 630
Fuel A (Batch-1 Propane); $V = 0.0226$ ft³; 0.030 in. holes								
9	117.	4.69	0.227	595	0.346	1.15	0.411	0.863
10	119.	4.26	0.278	620	0.321	1.05	0.277	0.526
11	104.	4.88	0.167	630	0.383	1.00	0.381	0.93
12	144.	5.32	0.330	604	0.328	1.12	0.303	0.53
13†	95.9	5.36	0.140	599	0.424	1.08	0.596	1.58
14	101.	5.40	0.144	610	0.414	1.06	0.594	1.56
38	111.	4.56	0.216	582	0.352	1.20	0.429	0.919
39	102.	4.69	0.0170	593	0.377	1.13	0.517	1.25
40	105.	4.51	0.0191	617	0.361	1.05	0.418	0.953
41	108.	5.46	0.160	606	0.40	1.08	0.559	1.41
42‡	112.	6.31	0.146	630	0.427	1.0	0.604	1.60
43	109.	6.31	0.139	630	0.432	1.0	0.627	1.69
44	104.	3.99	0.269	606	0.341	1.10	0.278	0.539
48	56.8	7.99	0.368	642	0.65	0.972	0.0894	0.148
49	55.8	7.78	0.376	625	0.648	1.02	0.0896	0.146
50	63.6	8.33	0.257	612	0.633	1.06	0.175	0.344
51	63.1	9.70	0.592	608	0.67	1.09	0.0601	0.0782
52	61.1	9.81	0.697	606	0.68	1.10	0.044	0.0569
53	55.1	7.69	0.33	605	0.648	1.10	0.113	0.197
53a	55.6	7.67	0.336	652	0.649	0.927	0.0937	0.162
55a	66.5	7.33	0.175	664	0.593	0.91	0.26	0.615
56	59.6	9.64	0.81	636	0.68	0.971	0.0336	0.0374
Fuel A (Batch-1 Propane); $V = 0.0226$ ft³; 0.055-in. holes								
16	109.	6.20	0.178	543	0.428	1.24	0.565	1.38
17	121.	6.76	0.193	548	0.424	1.23	0.555	1.27
18	136.	5.60	0.367	549	0.353	1.36	0.300	0.497
19	122.	5.67	0.252	544	0.38	1.33	0.433	0.866
21	161.	5.88	0.598	588	0.325	1.20	0.167	0.216
22	195.	7.77	0.604	577	0.345	1.24	0.205	0.264
23	163.	5.83	0.785	581	0.321	1.25	0.124	0.139
24	136.	4.89	0.612	585	0.322	1.23	0.140	0.179
25	173.	7.84	0.321	556	0.375	1.28	0.431	0.761
26	132.	7.92	0.174	561	0.441	1.16	0.664	1.60
27	226.	10.9	0.345	570	0.388	1.20	0.479	0.818
28	199.	10.7	0.256	625	0.416	1.02	0.529	1.03
29	172.	7.66	0.335	579	0.371	1.19	0.375	0.647
30	97.3	4.63	0.203	650	0.386	0.935	0.319	0.705
31	88.6	5.38	0.129	677	0.445	0.902	0.505	1.38
32	129.0	5.33	0.313	684	0.353	0.813	0.209	0.374
34	143.	7.64	0.185	643	0.413	0.975	0.551	1.29
57	60.7	7.90	0.301	600	0.632	1.11	0.143	0.262
58	61.0	9.02	0.492	631	0.661	0.99	0.0673	0.0963
59	67.8	6.87	0.174	566	0.573	1.19	0.347	0.84
60	88.5	11.4	0.262	649	0.629	0.945	0.211	0.412
61	88.3	11.4	0.322	632	0.629	0.99	0.170	0.267
62	82.0	11.4	0.418	643	0.646	0.953	0.107	0.166
63	82.8	11.4	0.524	590	0.645	1.16	0.0993	0.138
64	77.6	11.4	0.670	600	0.659	1.02	0.0592	0.724

TABLE 4—*Continued*

Run No.	Air Rate, $N_A \times 10^5$ lb moles/sec	Fuel Rate, $N_F \times 10^6$, lb moles/sec	Pressure, atmos abs	Inlet Temp, °R	Gen. Fuel Fract., F	Correction Factor* to 630°R	$\frac{N_A}{VP^{1.3}}$ Corrected to 630	$\frac{N_A}{VP^{1.8}}$ Corrected to 630
Fuel A (Batch-2 Propane); V = 0.0208 ft³; 0.030-in. holes (best data)								
65	106.	4.59	0.220	607	0.363	1.09	0.400	0.855
65a	105.	4.57	0.220	600	0.355	1.11	0.403	0.861
66	107.	4.58	0.22	612	0.361	1.06	0.359	0.843
67	124.	4.92	0.293	625	0.343	1.02	0.302	0.558
68	100.	4.87	0.166	660	0.392	0.918	0.457	1.13
70	117.	4.87	0.241	677	0.355	0.833	0.299	0.61
71	119.	4.21	0.399	664	0.319	0.852	0.161	0.254
73	119.	4.44	0.331	627	0.33	1.02	0.244	0.424
75	92.0	4.42	0.155	675	0.388	0.863	0.434	1.09
76	98.6	3.52	0.340	647	0.32	0.927	0.179	0.307
77	88.8	3.52	0.221	637	0.344	0.971	0.294	0.624
78	92.4	3.38	0.293	622	0.326	1.04	0.227	0.419
79	121.	4.41	0.393	607	0.325	1.11	0.216	0.346
80	100.	5.41	0.167	626	0.417	1.01	0.501	1.23
81	107.	5.94	0.167	636	0.423	0.98	0.52	1.28
82	93.3	4.23	0.198	598	0.374	1.11	0.405	0.923
83	110.	5.21	0.202	630	0.385	1.0	0.423	0.927
84	106.	5.87	0.168	637	0.422	0.98	0.505	1.22
84a	105.	6.01	0.165	637	0.43	0.98	0.516	1.27
85	103.	5.37	0.165	648	0.408	0.962	0.494	1.22
86‡	74.1	3.39	0.162	632	0.377	0.995	0.378	0.933
87	55.4	3.51	0.0913	677	0.456	0.889	0.538	1.78
88	80.5	4.35	0.131	665	0.417	0.918	0.501	1.39
90	62.4	2.67	0.109	704	0.493	0.88	0.463	1.43
91	80.4	2.88	0.119	692	0.45	0.87	0.532	1.52
92	71.4	2.94	0.105	707	0.483	0.87	0.563	1.71
Fuel B; V = 0.0226 ft³; 0.055-in. holes								
101	126.	6.65	0.299	612	0.411	1.04	0.28	0.511
102	141.	6.71	0.533	620	0.387	1.04	0.146	0.205
103	128.	6.10	0.358	610	0.386	1.06	0.228	0.38
104	128.	6.12	0.358	610	0.387	1.06	0.227	0.38
105	154.	6.74	0.635	625	0.367	1.02	0.126	0.158
106	134.	7.85	0.230	612	0.433	1.05	0.422	0.88
107	125.	7.85	0.187	610	0.454	1.05	0.484	1.12
Fuel B; V = 0.0226 ft³; 0.030-in. holes								
108	87.5	4.92	0.148	727	0.425	0.788	0.368	0.954
109	102.	4.90	0.226	685	0.388	0.848	0.266	0.563
110	117.	4.90	0.319	701	0.356	0.757	0.173	0.307
111	116.	4.47	0.497	711	0.338	0.715	0.091	0.129
112	112.	4.46	0.399	735	0.345	0.658	0.108	0.170
113	112.	4.46	0.399	735	0.345	0.658	0.108	0.170

* Using correction of Longwell and Weiss[1] for feed temperature.

† Premature blowout; questionable.

‡ Bad point.

General: Run numbers omitted were incomplete or plainly faulty; reasons given in original notebooks. Numbering starts at 101 with Fuel B. Runs 65–92 (best data) follow Run 113 chronologically.

cording to fuel used, size of holes in central feed sphere, and whether on the lean or fuel-rich side of stoichiometric. Fuels A and B were compared only on the lean side of stoichiometric, no data being obtained for rich mixtures of fuel B because of extreme difficulties from feed-sphere burnout. Because the original batch of propane cylinders was depleted before sufficient data were taken, the last and best runs on fuel A, runs 65 to 92, using the small-feed-hole reactor, were made with a new batch.

Blowout Data

The preliminary analysis has indicated that the quantity N_F/VP^n (or N_A/VP^n) at blowout should be a unique function of air-fuel ratio or of the generalized fuel fraction, F. Accordingly, the first step in data analysis is the determination of reaction order n. The only data considered good enough for this, in view of the modest range of pressure variation studied, are the lean data on fuel A_2 with the 0.030-in. feed holes. A preliminary plot of data on N_A *vs.* F was made, with pressures indicated on the points. Rough isopiestic lines were faired through the data. Then six different F's were chosen such that each was near a number of data points, and each point was projected, parallel to the estimated isopiestics, to the F-value nearest it. Figure 3 shows the resulting data, N_F *vs.* P, on logarithmic coordinates; and Figure 4 (triangles) shows the slopes of the curves of Figure 3.

Although the pressure range of the data in Figure 3 at any fixed composition, F, is inadequate for an accurate determination of the slope or pressure exponent n, the triangles of Figure 4 indicate that the slopes at different F's are fairly consistent in predicting a value of n of 1.3. Since this is possibly in conflict with the value of 1.8 recommended by Longwell and Weiss,[1] their data were reexamined. All their lean-mixture data on reactors of identical feed design (reactors 3a, 3b, 3c, 3e; 31 points) appear in Figure 5 as N_A/V at blowout *vs.* F, with chamber pressure appearing beside each datum point. Correction of each point to that value of F near which other data appear allows the plotting, analogously to Figure 3, of N_A/V *vs.* P, for the different F's (Fig. 6). The lines so obtained are impressively straight; their slopes, representing n, appear as the circle points of Figure 4 for comparison with the present results. For a generalized fuel fraction, F, from 0.37 to 0.50 (an equivalence ratio of 0.58 to 1.0) an average value for n of 1.7 to

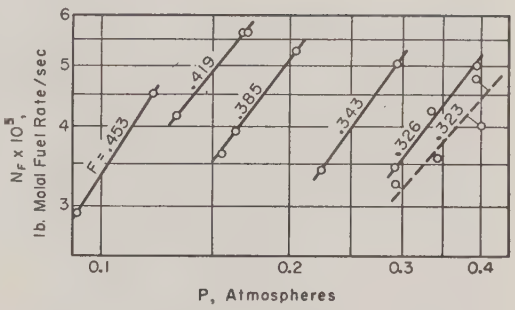

FIG. 3. Effect of pressure on feed rate at blowout, for constant values of F (generalized fuel fraction). Fuel A_2, feed holes 0.030 in.

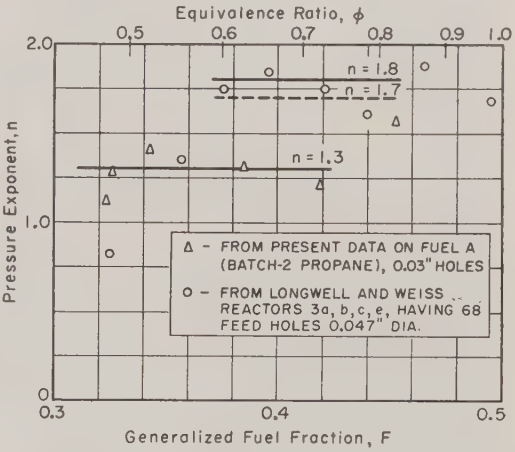
Equivalence Ratio, ϕ
Pressure Exponent, n
Generalized Fuel Fraction, F
n = 1.8
n = 1.7
n = 1.3
Δ - FROM PRESENT DATA ON FUEL A (BATCH-2 PROPANE), 0.03" HOLES
o - FROM LONGWELL AND WEISS REACTORS 3a, b, c, e, HAVING 68 FEED HOLES 0.047" DIA.

FIG. 4. Pressure exponent, n, in dependence on generalized fuel fraction, F.

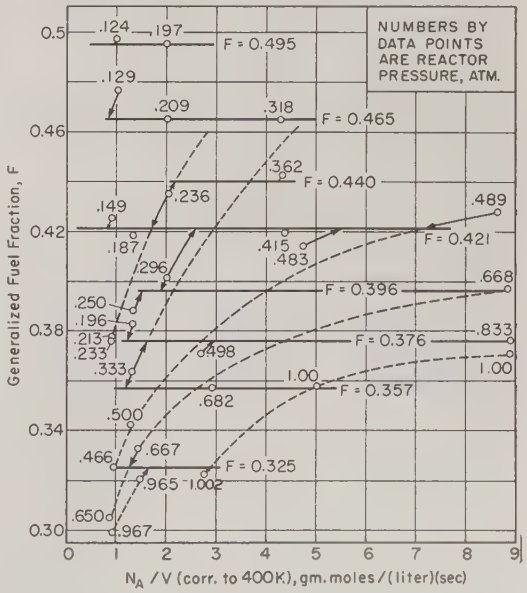
NUMBERS BY DATA POINTS ARE REACTOR PRESSURE, ATM.
F = 0.495
F = 0.465
F = 0.440
F = 0.421
F = 0.396
F = 0.376
F = 0.357
F = 0.325
Generalized Fuel Fraction, F
N_A / V (corr. to 400K), gm. moles / (liter)(sec)

FIG. 5. Blowout data of Longwell and Weiss[1] on iso-octane. (Dotted lines represent estimated isopiestics for use in data interpolation).

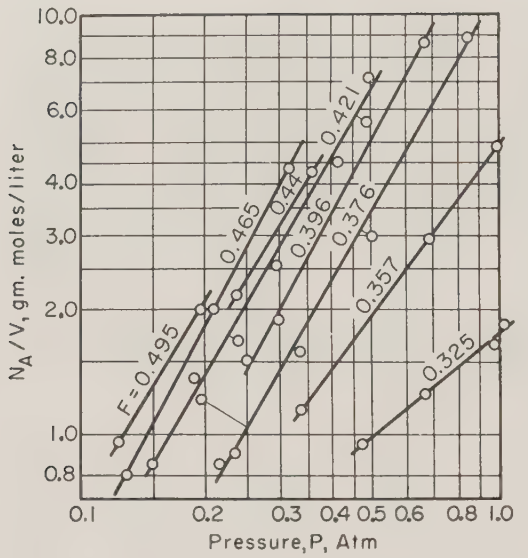

FIG. 6. Effect of pressure on feed rate at blowout. Data of Longwell and Weiss[1] for eight values of generalized fuel fraction, F.

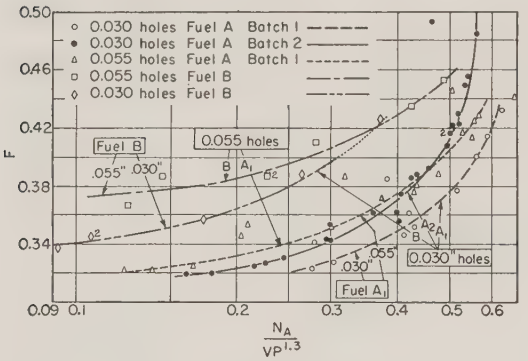

FIG. 7. Relation between generalized fuel fraction, F, and blowout parameter, N_A/VP^n, assuming a value for n of 1.3.

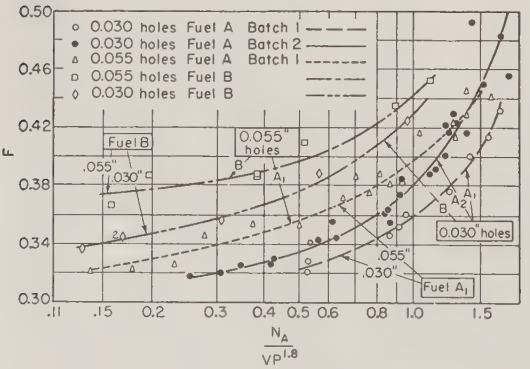

FIG. 8. Relation between generalized fuel fraction, F, and blowout parameter, N_A/VP^n, assuming a value for n of 1.8.

1.8 appears to be well established. There is a suggestion from the data, however, that n may decrease for leaner mixtures, and that part of the difference between the n of 1.3 from the present data and the value recommended by Longwell and Weiss is due to the difference in the range of F's covered. The possible significance of the difference will be discussed later.

Based on the value of n of 1.3 established from the present data on Fuel A only, the quantity, $N_A/VP^{1.3}$, was plotted *vs.* F, for all the data on each of the fuels and on each of the feed-hole sizes (Fig. 7). For comparison the same data are plotted in Figure 8 using Longwell and Weiss' value of n of 1.8. The data will be used to discuss the effects on the reaction of fuel type, feed-hole size and pressure.

An object of the experiments was to find whether, with fuels so chosen as to perform identically if chemical reaction is not controlling, there is any difference between fuels. Fuel B was found to react more slowly than A for each of the two feed-hole systems used (top line *vs.* short-dashed line, 0.055-in. feed holes; second line *vs.* bottom dashed line (A_1) or *vs.* solid line (A_2), 0.030-in. feed holes). The blowout feed rate for fuel A was 2 to 3.5 times as great as for B, the difference being greatest for lean mixtures.

The effect of feed-hole size appears in results both on fuel B and on fuel A_1. Figure 7 indicates that for each of these the effect of decreasing hole size is to raise the blowout feed rate; and comparison on the basis of $n = 1.8$ instead of 1.3 accentuates the effect (Figure 8). The effect is less pronounced the closer the approach of mixture ratio to stoichiometric. The data support the conclusion that, in general, the higher mass velocity of feed associated with the higher pressure drop necessary to maintain a given flow through smaller holes causes combustion to be maintained up to higher values of feed rate. The most plausible explanation is that mixing has thereby been improved and that consequently mixing has not been completely eliminated as a factor in the stirred reactor. That this may cause the pressure exponent, "n," to be modified may be shown by the following dimensional analysis: Consider two dimensionally similar combustion systems fed with the same mixture at the same temperature, and operated at such pressures and feed rates that similarity is maintained in the two patterns of combustion progress. In the two

systems the double ratio

(feed rate) : (diffusion rate) :

(chemical reaction rate)

will be the same at blowout. This ratio is expressible as

$$N:(A\mathfrak{D}\ dc/dr):kVc^n$$

where N is the molal feed rate, A and V are diffusion area and reaction volume, respectively, $\mathfrak{D}$ is the diffusivity and dc/dr is the concentration gradient. Setting in the proportionality of L^2 and L^3 to A and V, and of c/L to dc/dr, and substituting fP/RT for c, one has

$$N:L\frac{\mathfrak{D}P}{RT}f:kL^3\left(\frac{P}{RT}\right)^n f^n$$

Blowout in dimensionally similar systems is then characterized by a relation between the dimensionless ratios formable from the above, or

$$f\left(\frac{N_{BO}RT}{L\mathfrak{D}Pf},\qquad \frac{N_{BO}}{kL^3}\left(\frac{RT}{fP}\right)^n = 0\right) \tag{4}$$

For the simpler case where diffusional resistance is negligible the first of these groups disappears as a factor and the second becomes a constant; or, considering only the effect of pressure,

$$\frac{N_{BO}}{L^3} \equiv \frac{N_{BO}}{V} \propto P^n \tag{5}$$

This is the presumed case of present interest. If, however, it is the chemical resistance which is negligible, the first term in Equation (4) is constant at blowout, or

$$\frac{N_{BO}}{L^3} \equiv \frac{N_{BO}}{V} \propto \mathfrak{D}P \tag{6}$$

Three sub-cases are of interest, molecular diffusion, eddy diffusion caused by subsonic jets, and eddy diffusion in choked-jet systems. In the first, $\mathfrak{D}P$ is constant and N_{BO}/V is independent of P. In the second case $\mathfrak{D}$ is replaced by eddy diffusivity $\mathcal{E}$, proportional to the product of a characteristic velocity and dimension or to U_0L, and since U_0 for a constant molal rate N is proportional to P^{-1}, $\mathcal{E}$ is likewise; and again N_{BO}/V is independent of P. For choked-jet systems Rousso and Kochendorfer's[3] study indicates a proportionality of mixing or diffusion rate to the cube-root of the free-space pressure, or an effective diffusivity proportional to $P^{-\frac{1}{3}}$, making N_{BO}/V proportional to $P^{\frac{1}{3}}$. From all this it appears that, under conditions of combustion controlled in part by chemical and in part by diffusional resistance, any pressure exponent from n to 0 is not unreasonable.

The maximum value of the flow rate parameter $N_A/VP^{1.3}$ for fuel A is, according to Figure 7, about 0.65 lb moles air/sec ft^3 atmos$^{1.3}$; and the maximum occurs near the stoichiometric

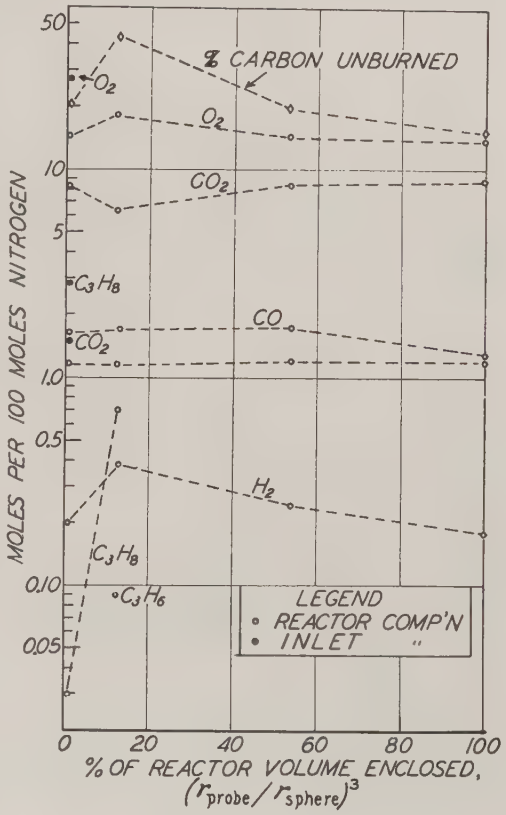

FIG. 9. Dependence of gas composition on location in sphere (fuel A; feed-holes 0.030 in.; $F = 0.339$; $N_F = 4.46 \times 10^{-5}$ lb moles/sec).

composition. On the basis of measured efflux gas composition it is estimated that about 90 per cent of the fuel is oxidized to carbon dioxide and water at blowout. This corresponds to a heat release rate of 80 million Btu/hr ft^3 atmos$^{1.3}$. If however the pressure exponent of 1.8 is accepted, Figure 8 indicates that the above numbers are replaced by 1.8 lb moles air/sec ft^3 atmos$^{1.8}$ and 220 $\times$ 10^6 Bru/hr ft^3 atmos$^{1.8}$. The change emphasizes the considerable effect of choice of n on the estimated performance at higher pressures than those covered in the experiments.

Sampling Data

Data on gas sampling from the reactor appear in Figures 9 and 10, and in Table 5. The figures present comparisons of traverses of the chamber when fed with fuel A at the same fuel feed rate and at about the same generalized fuel fraction, but with the two different sizes of inner-sphere feed holes, 0.030 in. and 0.055 in. Gas composition and carbon-unburnedness are plotted *vs.* probe position expressed as fraction of the reactor volume lying inside the radius at which the probe is located. Carbon-unburnedness is defined as the atoms of incompletely oxidized carbon per atom of oxidizable carbon fed, i.e., exclusive of the carbon fed in Mixture A as carbon dioxide.

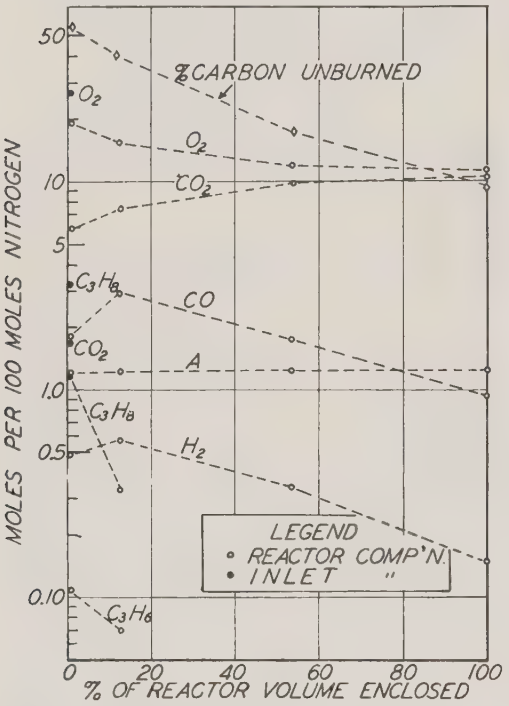

FIG. 10. Dependence of gas composition on location (fuel A; feed-holes 0.055 in.; $F = 0.371$; $N_F = 4.48 \times 10^{-5}$ lb moles/sec).

Consider first the small feed-hole data (Fig. 9). The apparently anomalous distribution probably was a consequence of traversing as indicated in Figure 11. The distance between feed holes was about 0.15 in. and the exact position of the probe tip could not be determined with this accuracy. Consequently the probe could easily have passed through a jet emerging from the feed source and into a recirculation zone adjacent to the feed source between holes. The data indicate the outer half of the reactor to be fairly uniform in composition, and substantially the same as in the recirculation zone between jets at their base. Figure 10, showing data on the large-hole feed source, indicates a steeper composition gradient in the sphere, center to outer wall; and it confirms the conclusion from the blowout data that mixing is less adequate when the larger feed holes are used.

Unfortunately, the efficiencies of combustion for the two sizes of hole cannot be directly compared because the sampling traverse made with the small-hole apparatus was carried out beyond the blowout conditions for that with the large holes. It was deemed best to carry out these sampling traverses as close to blowout as possible lest the reactor appear more homogeneous during the traverse than it typically was. For traverses carried out far from blowout, where the residence times are long and reaction rates slow due to depletion of the reactants, it is likely that the mixing process would be rapid enough to yield a much more nearly homogeneous reaction zone.

The efflux gases from the reactor, fed successively with each of the two fuel mixtures, are compared in Table 5, which presents analyses of samples taken under essentially the same conditions of flow rate and generalized fuel fraction and within 10 per cent of the same pressure. The samples were stored under pressure and analyzed with a mass spectrometer. The carbon-nitrogen ratio in these samples, somewhat lower than that metered, was corrected to the metered value by assuming the discrepancy was caused by an inleak of air in the sampling lines. The analyses were then checked for consistency by calculating the water formation by an oxygen balance and by a hydrogen balance.

The gas analyses of Table 5 support the conclusions of Longwell and Weiss[1] that the efflux gases from stirred reactors operating on lean mixtures contain no unreacted fuel, that the only partially burned fuels present in measurable quantities are carbon monoxide and hydrogen, and that the fraction of fuel-carbon appearing as CO is much greater than the fraction of fuel-hydrogen appearing as H_2.

The calculated gas temperature appearing in Table 5 was obtained by assuming adiabatic reaction to the composition found by analysis. The next line of the table represents the degree of incompleteness of the reaction on a temperature-rise basis; and below that is the incomplete-

ness based on consumable oxygen. The two criteria are in good agreement in indicating that for both pairs of runs the incompleteness of reaction is greater for mixture B. Comparison of gas compositions indicates that the difference is due to unburned carbon monoxide.

It is to be recalled that in fuel A a significant fraction of the carbon enters in the burned state as CO_2, whereas in fuel B a part of the hydrogen enters burned. It follows that if the carbon burns via carbon monoxide and the latter burns more slowly than hydrogen, fuel B would be expected to burn more slowly than A. This is supported by the gas analyses as well as by the blowout

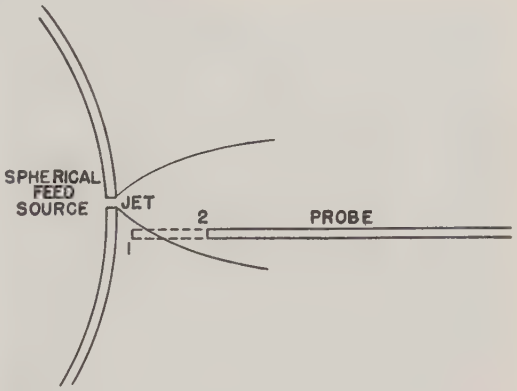

FIG. 11. Possible probe sampling positions.

TABLE 5. EFFECT OF FUEL TYPE (A VS B) ON COMPOSITION OF REACTOR EFFLUX GASES

Sample identification	M	P	N	Q
Fuel mixture	A	B	A	B
Total feed rate $\times 10^5$ (lb mole/sec)	107.7	106.0	100.0	98.9
Generalized fuel fraction	0.364	0.364	0.384	0.381
Reactor pressure, atmos	0.334	0.308	0.334	0.307
Analysis (moles/100 moles N_2)				
Oxygen	11.74	12.85	10.72	11.76
Carbon dioxide	8.95	8.16	10.31	9.24
Carbon monoxide	2.36	2.86	1.97	2.96
Hydrogen	0.30	0.25	0.30	0.17
Water (from hydrogen balance)	12.46	12.54	13.40	13.59
Gas temperature (°R)				
Exit	2846	2809	3062	2931
Inlet	638	634	643	623
Unaccomplished fractional temp. rise $\frac{T_{ad.fl.}-T}{T_{ad.fl.}-T_{inlet}}$	0.084	0.098	0.062	0.095
Unreacted O_2 usable, expressed as per cent of originally usable O_2*	8.3	10.3	6.5	9.5
Per cent C appearing as CO	21	26.6	15.9	24.4

* Calculated on the assumption that any oxygen in the fuel, except O_2 as such, entered already used.

results previously presented. Further evidence of the tendency of CO to be consumed more slowly than H_2 comes from evaluation of the water-gas equilibrium criterion $(CO)(H_2O)/(CO_2)(H_2)$ for eight reactor gas samples, five from mixture A and three from B. The criterion as evaluated from gas analyses was higher than the equilibrium constant corresponding to the reactor temperature, by a factor of 3 to 5 for fuel A and more than 7 for fuel B.

Comparison of Several Reaction Schemes

A numerical analysis of the behavior of a completely stirred adiabatic reactor was made in order to delineate the effects of activation energy, inlet temperature and reaction scheme or superficial mechanism. The following four reaction schemes were considered.

Case I.

The incoming fuel and air react to form carbon dioxide and water only. All unreacted propane leaves the reactor as such. This assumption is quite unrealistic but is included to cover the general case of a reaction in which the formation of intermediates is unimportant.

Case II.

The fuel and air react instantaneously to form carbon monoxide and water, followed by the combustion of carbon monoxide at a finite rate. Necessarily following from this assumed mecha-

nism is the instantaneous release of a large fraction of the enthalpy of combustion (approximately half) as the fuel-air mixture is fed to the reactor. This introduces an important difference between Case II and Longwell and Weiss' equation 4a and 4b[1] which are based on the assumption that, although the production of CO is instantaneous, no correspondingly instantaneous energy conversion occurs. Case II is, of course, inapplicable for rich mixtures in which there is not enough oxygen to convert all of the hydrogen

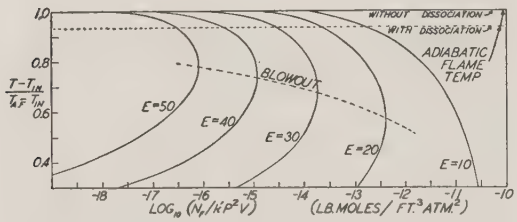

FIG. 12. Effect of activation energy on reactor operation (stoichiometric mixture; inlet temperature 300°K).

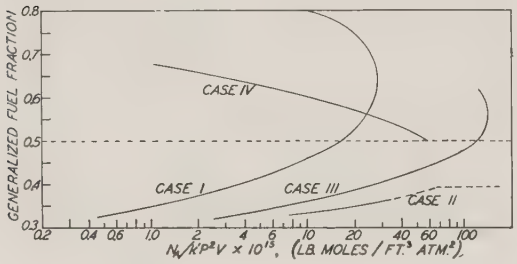

FIG. 13. Relation between generalized fuel fraction, F, and blowout parameter $N_A/k'P^2V$. Comparison of four reaction schemes. (E = 40 kcal/g mol; T_{in} = 300°K).

to water and all of the carbon to carbon monoxide.

Case III.

The fuel and air react instantaneously to form hydrogen and carbon monoxide and these in turn are oxidized at relative rates such that water-gas equilibrium is maintained.

Case IV.

This is applicable only to rich mixtures. It is assumed that propane and air react, in the ratio in which they appear in the feed, at a finite rate to form carbon monoxide and hydrogen, that these latter react also at finite rates to form carbon dioxide and water, and that water-gas equilibrium is maintained.

Plots of the type appearing in Figure 1 were prepared, for a number of fuel-air ratios for each of the above cases. The effect of activation energy on these rates for a stoichiometric mixture following reaction scheme I is shown in Figure 12. Since no account was taken of dissociation, the maximum hypothetical temperature corresponds to complete reaction to carbon dioxide and water and is therefore higher than the equilibrium adiabatic flame temperature. However, interest is chiefly in the characteristics of blowout (dotted line), a condition where the temperature is enough lower to make errors due to ignoring dissociation unimportant. A comparison of the four cases for an activation energy of 40 kcal/g mole and a reaction first order in fuel and first order in oxygen is presented in Figure 13. For the assumptions of Case II, mixtures richer than a certain fuel-air ratio generate enough heat from the hypothesized instantaneous reaction to water and carbon monoxide to make blowout impossible. For Cases I and III the calculated maximum blowout flow rate occurs for mixtures richer than stoichiometric, rather than at stoichiometric as might be predicted without full cognizance of the large dilution effect of the nitrogen in the air. Because of this dilution the decrease in reaction rate due to temperature reduction by fuel enrichment beyond stoichiometric is more than compensated by the increase in rate due to increased fuel concentration. The fuel-air ratio corresponding to the maximum blowout flow-rate parameter for fixed values of activation energy, feed enthalpy, and overall reaction order will obviously increase with increased reaction order in fuel and with increased dilution of oxidant with inerts.

The shapes of the curves shown in Figure 13 can be compared with the experimental data. Since the abscissa is plotted on a logarithmic scale, its multiplication by a constant simply shifts the curves horizontally without distorting their shapes. If the over-all reaction order n is known, the experimental data can be plotted on an overlay on Figure 13, with abscissa N_A/VP^n. Horizontal shift then permits match to the best curve and simultaneous determination of k', the "collision" factor. Unfortunately, however, at fuel-air ratios leaner or richer than stoichiometric the shape of the calculated curve is not a very sensitive function of the values assumed for reaction order with respect to air and fuel and for activation energy. For example, for lean mixtures increasing activation energy may largely

be compensated by increasing reaction order with respect to fuel; the shape of the curve for Case I on the lean side would remain nearly unchanged if reaction order were changed from first order in air and first order in fuel to half order in air and one and one-half order in fuel and the activation energy were increased from 40 to 50 kcal. Near stoichiometric mixtures, however, the difference in the two assumptions becomes somewhat more apparent.

Assuming the reaction to be first order in air and first order in fuel, and comparing the experimental data with the calculations for Case III on the lean side, one finds an "activation energy" of 30 kcal/g mole (based on the oxidation of carbon monoxide) with a "collision factor" of 16×10^{13} cm³/sec gmole. For the rich side the "activation energy" is 50 kcal/gmole (based on the oxidation of propane, Case IV) with a "collision factor" of 9.1×10^{17} cm³/sec gmole.

None of the reaction schemes presented here can properly be said to fit the data well.

Further Comparison with Earlier Data

Figure 14 presents a comparison of the present data on mixture A with those of Longwell and Weiss on iso-octane. The data of both studies are plotted to the abscissa used by Longwell and Weiss, based on a pressure exponent of 1.8; and both are corrected to the same feed temperature of 400°K. The "air" flow rates for the present data are adjusted to include the carbon dioxide and oxygen of mixture A; so for purposes of comparison of the data from the two studies mixture A can be considered to be propane burning in gas containing about 21 per cent oxygen. With this adjustment residence times for iso-octane and for mixture A are within one or two per cent of each other for a given value of N_A/V. Inspection of Figure 14 shows that the blowout flow rate of the present study exceeds by a factor of about 3 that of Longwell and Weiss for quite lean and quite rich mixtures, and is about eight-tenths their value near stoichiometric. The present data were not corrected for heat loss; those of Longwell and Weiss were. Since runs at the lowest pressure—and therefore those with the highest ratio of heat loss rate to heat generation rate—were made near stoichiometric, correction of the present data for heat loss would increase the blowoff feed rate near stoichiometric a small amount to give rates in closer agreement with the earlier experiments.

The less pronounced peaking of the present blowoff data near stoichiometric corresponds to a lower energy of activation than that applicable to the earlier data.

The cause of the different shapes of the two blowout curves of Figure 14 is difficult to establish. Possibly the explanation lies in the difference between isooctane and propane diluted with carbon dioxide, although both fuels appear to be limited in burning rate by the reactions of carbon monoxide. The difference in mixing intensity employed in the two sets of experiments may account for the difference, but this point is con-

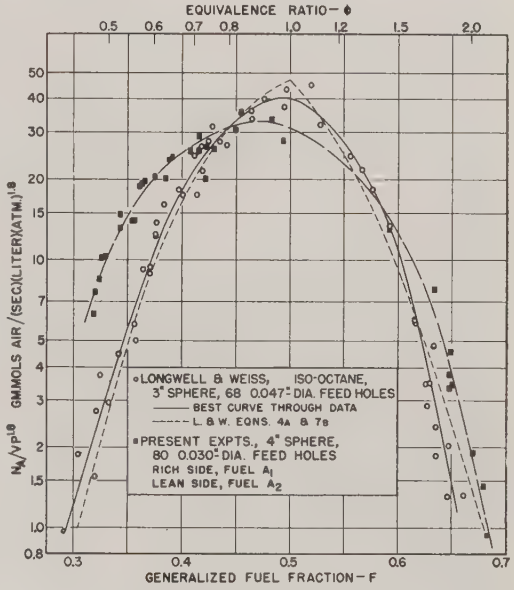

FIG. 14. Comparison of present data on fuel A with those of Longwell and Weiss[1] (Present data corrected to a feed temperature of 400°K for comparison.)

fused. The results presented in Figure 7 indicated that smaller holes produce better mixing; and smaller holes were used here than in the earlier work. But if there is a mixing limitation on the burning rate, its effect should be more apparent near stoichiometric composition than near the rich or lean limits where a lesser mixing rate should be adequate to keep pace with the chemical rate. Better mixing should by this argument cause greater rather than less peaking of curves such as those of Figure 14. It is apparent that the mixing role in well-stirred reactors has not been adequately established.

The effect of heat losses on stirred-reactor performance has not been considered here. At a given value of generalized fuel fraction, heat losses

cause greater reduction in blowout flow rate with decreasing flow rates (long residence times) and corresponding decreasing pressures. Consequently, the rate of change of blowout flow rate with pressure is greater for a nonadiabatic reactor than for an adiabatic reactor, and values of n uncorrected for the effects of heat losses are high. DeZubay and Woodward[4] have calculated the effect of reactor wall temperature on the blowout flow rates for well-stirred reactors. Measurements of temperature gradients through the insulating walls of the reactor used in the present study, and similar measurements made by Weiss[5] lead to the conclusion that the estimated coefficient for convective heat transfer from the gas to the reactor wall used by DeZubay and Woodward was probably an order of magnitude less than that occurring in the experiments reported here and those of Longwell and Weiss. A rather elaborate numerical calculation was made of heat losses for one condition of operation, with allowance for the effect that heat transfer from gas along the exit-hole walls has in minimizing the outward losses from the interior surface of the reactor walls.[2] The model used was oversimplified and the result is consequently not of high accuracy, but it offers some guidance as to how to modify the results of simple calculations based on the assumption of radial heat flow through the shell. On the basis of this study it was concluded that the experimentally determined pressure exponent n should be reduced by about 0.1 to allow for wall losses.

The value of the pressure exponent, n, is of considerable practical importance if blowoff curves from stirred reactors operating at low pressure are to be used as guides to the performance of full-scale equipment operating at higher pressure. Longwell and Weiss' data provide a better basis for establishing the pressure exponent, n, than the present data. Arguments have been presented here, however, which indicate a possible variation of n with air-fuel ratio for two reasons: (1) If mixing has not been eliminated as a factor, n may be expected to vary downwards from its true value for a chemically-controlled system, and the relative importance of mixing and chemistry may be expected to vary with air-fuel ratio. (2) No reaction scheme yet proposed has produced a good enough fit to the data to justify assuming n constant; in fact, a normal consequence of fitting an empirical reaction scheme would be the introduction of an n which varies with composition. A pressure exponent varying from 1.7 at stoichiometric to 1.0 at $F = 0.32$ (equivalence ratio 0.47) would not be in significant disagreement with either of the sets of n-values appearing in Figure 4.

Conclusions

The well-stirred reactor differentiates fuels which are identical in density, atomic composition and thermal properties, but which are different chemically.

The energy of activation required to fit the data is consistent with that expected from chemically controlled reactions.

Changing the hole size of the feed system changes the performance in the direction expected from the assumption that mixing resistance has not been completely eliminated.

The pressure exponent on the reaction lies between 1 and 1.7, has an average value of 1.3 for the experiments reported here, and probably varies with fuel-air ratio.

The conclusions of Longwell and Weiss, that the gas throughout most of the volume of a stirred reactor fed with lean hydrocarbon-air mixtures contains carbon monoxide and hydrogen but negligible unreacted fuel, are confirmed.

The well-stirred reactor yields results which depend primarily on chemical resistance to combustion, and it consequently has great utility for the study of gross chemical kinetics under conditions approaching practise; but the assumption that the system is perfectly stirred is not in accord with all the data.

Nomenclature

$c_F(c_O)$	concentration of fuel (oxygen) in reactor
$\mathfrak{D}$	molecular diffusivity
$\mathcal{E}$	eddy diffusivity
E	"activation energy" (kcal/g. mole)
F	generalized fuel fraction, (fuel/(fuel + fuel-equivalent of air)
$f_F(f_O)$	mole fraction fuel (oxygen)
k'	"collision factor"
L	characteristic length
n	pressure exponent (over-all order of reaction if chemical kinetics is controlling
$N_A(N_F)$	molal flow rate of air (fuel), (lb moles/sec) (sometimes subscript BO is added to indicate blowout conditions)
P	absolute pressure
R	gas constant
T	Reactor temperature, deg. abs.
$T_{\text{ad. fl.}}$	adiabatic flame temperature, deg. abs.
T_{inlet}	inlet feed temperature, deg. abs.
U_0	characteristic velocity

V reactor volume
y fraction fuel reacted
α order of reaction with respect to fuel
β order of reaction with respect to oxygen
ϕ fuel-air ratio
ψ function of

REFERENCES

1. Longwell, J. P., and Weiss, M. A.: Ind. Eng. Chem., *47*, 1634–1637 (1955).
2. Baker, M. L.: Sc. D. Thesis in Chemical Engineering, Massachusetts Institute of Technology, May 1956.
3. Rousso, M. D., and Kochendorfer, F. D.: NACA RM351F18, 1951.
4. DeZubay, E. A., and Woodward, E. C.: *Fifth Symposium (International) on Combustion*, pp. 329–335. New York, Reinhold Publ. Corp., 1955.
5. Weiss, M. A.: Personal communication, 1955.

51

A DISCUSSION OF THE RELATIONS EXISTING BETWEEN LIMITING ENERGY RELEASE RATES AND BLOWOUT FOR HYDROCARBON FUELS

By WALTER J. WOHLENBERG

1. Introduction

The blowout under consideration is that designated by Longwell and Weiss[2] as "reaction-rate-induced blowout." It is defined by them as a blowout because the chemical reaction *itself* is not fast enough to maintain combustion with a further increase in input rate to the reaction chamber even when the molecular distribution is uniform. Henceforth this condition will usually be referred to merely as blowout.

The reaction under consideration is second order and occurs at constant pressure, with the input rate to the furnace cavity steady and with a molecularly uniform distribution between the fuel and air entering the cavity. Beginning at entrance and continuing to the exit, combustion progress is one-dimensional in terms of the fraction of fuel burned. The molecular distribution at any point beyond entrance in the path of combustion progress is uniform with respect to the constituents which are present in the vicinity of that point as a result of the combustion progress which occurred along the path preceding that point.

In so far as the rate of reaction may be influenced by the molecular distribution, the above pattern of it is that which provides for the maximum rate of combustion progress from any given fraction fuel burned to any larger fraction of it burned, and so also for the maximum rate of progress from fraction burned zero at entrance to any subsequent fraction burned greater than zero. Turbulence can not, in the above sense, be the means of further finite improvement in the preceding pattern of molecular distribution, once it has been attained. This conclusion appears unavoidable, at least to the author.

Values of the potential time mean energy release rates per unit volume of a flame, which contains the preceding optimum pattern of molecular distribution may be computed by means of Equations (7e) through (10) in an earlier paper.[1] Such a value times the volume of the flame is thus the steady-state value of the potential release rate for the whole flame. In the integration which leads to the above equations, it is assumed, in addition to the conditions outlined in the second paragraph, that:

(a) The rise from entrance to flame temperature is instantaneous, and the flame temperature level, T, is constant in the direction of the flame axis.

(b) The level T of the flame temperature is that resulting at the flame end for zero *heat loss* from the flame itself, including, however, the effects of dissociation at high temperatures, and;

(c) An effective reaction rate of the molecular collision mechanism within the flame as determined by values assigned to the energy of activation.

A value of the potential time mean release rate, which has been computed based on the assumption that all of the conditions outlined in preceding paragraphs are fulfilled, for any given case,

represents the maximum possible magnitude of it for that case, provided the correct value of energy of activation has been included. When first dealing with this problem, the author had no reliable information on the latter, and so included two sets of results: one, Figure 3 of an earlier paper based on

$$E = 50{,}000 \text{ cal/g-mol} = 90{,}000 \text{ Btu/lb-mol}$$

and the other, Figure 4 of the same paper based on[1]

$$E = 33{,}000 \text{ cal/g-mol} = 59{,}600 \text{ Btu/lb-mol}$$

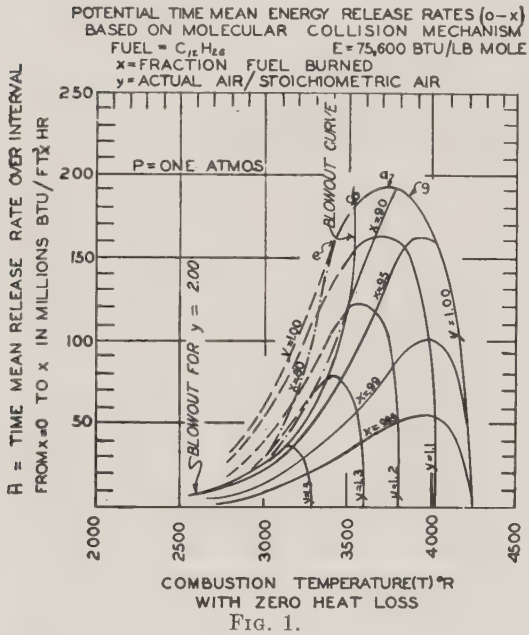

FIG. 1.

2. Results of Longwell and Weiss

This wide spread in values of E leaves us in the dark relative to the real magnitudes of potential time mean release rates. Recently, the above authors have published[2] their evaluation

$$E = 42{,}000 \text{ cal/g-mol} = 75{,}600 \text{ Btu/lb-mol}$$

for isooctane and heptane. This is based on those experimentally determined values of the input rates, to their reaction chamber, at which blowout occurred.

Note now that the conditions realized in the Longwell and Weiss experiments must have been very close to those which had been assumed by the author, as previously outlined, with the exception that in Longwell and Weiss, high turbulence was superimposed at entrance, the latter primarily as a means toward realization of the instantaneous temperature rise from entrance to flame temperature levels. Those authors state it should also aid toward realization of uniformity of the flame temperature level throughout the reaction chamber itself. The reader is reminded that both of these conditions were assumed to exist by this author,[1] but turbulence was *not* mentioned as a means of accomplishing them.

Although the fundamental pattern of conditions which control the rate of reaction must, as just explained, be very nearly the same in the author's earlier paper[1] and in Longwell and Weiss,[2] there is a difference in fuels, the results in the author's being based on dodecane and those in Longwell and Weiss, as before noted, on isooctane and heptane. It was found that the latter two were interchangeable as to results and it can be shown that, with reference to their apparent potentiality for rate of releasing energy, all three fuels are nearly alike, dodecane being slightly on the low side if the same value of energy of activation applies to all three fuels. This, of course, it should, when the matter is viewed in the light of the preceding discussion.

Accordingly, the pattern of results on energy release rate included in the author's paper[1] for dodecane has been corrected so as to be based on the value of E from Longwell and Weiss[2] and thus leads to Figure 1. Although developed for the special fuel dodecane, the curves shown should, in view of the preceding discussion, also be closely representative of those which would have emerged for isooctane. This, as will become evident later on, is especially true with reference to the set of conditions of most concern to us, *i.e.*, those associated with blowout. This is fortunate, because the development of such a set of results starting from scratch with a different fuel would involve much labor and time that is unnecessary in the correction of available data for a given fuel so as to fit a changed value of E.

The curves in Figure 1 other than that for blowout are plotted so as to pass through (x, y, T) values included in Table 1. Ordinate values of release rates $\bar{H}$ are time mean values over the interval from time θ = zero to time θ associated with fraction burned x, the latter being, of course, the value of x associated with the point in the $(\bar{H}, T)$ field under consideration. The reader is reminded that relations shown in Figure 1 are for a steady state of firing into a furnace cavity maintained at a steady pressure and with zero

heat loss from the flame. It is noted that under these conditions, the location of a point in the above field is fixed when the values of any pair of the group (x, y, T) are known. Hence for a given $y = c$, a value assigned to x fixes the values of both T and $\bar{H}$.

Consider a case in which a furnace cavity is just of the length necessary to accommodate reaction progress to $x = 0.99$ with $y = 1.00$. Reference to Figure 1 discloses the time mean release rate for a flame with this endpoint condition to be approximately 39.6×10^6 Btu/ft^3 $\times$ hr and temperature $T \approx 4230$°R. Now suppose the input rate to the preceding furnace cavity to be increased while holding y constant. This decreases the time interval θ necessary to traverse the cavity with a resultant decrease in the fraction burned at exit, *i.e.*, at the flame end. Whatever this decreased value of x, it must, in view of the preceding discussion, be located at some point on $y = 1.00$ and in the direction of decreasing x along it. If the input rate is increased to its maximum value, *i.e.*, that of blowout, the flame endpoint will land at (b) in Figure 1 after having passed through the energy peak at (a). If the input rate is now decreased, the endpoint travels in the reverse direction back over the curve of $y = 1.00$, since it can be shown that to travel from (b) downwardly on the left-hand branch of $y = 1.00$ violates the second law of thermodynamics. This applies to any curve $y = c$, and so it is seen that the whole range of operating conditions, as defined above, is contained in the area to the *right of the blowout* curve in Figure 1.

3. Input Rates at Blowout vs Those at Peak Values of Potential Time Mean Energy Release Rates

Attention is called to the position in Figure 1 of the peaks on the $y = c$ curves relative to those where the blowout line cuts through them. The latter are to the left of the former. Hence the release rates at the peaks of the y curves are greater than they are at the blowout, location of the latter being, as before noted, at the point on the y curve, where the rate of input is a maximum.

With reference to the pattern of results disclosed in Figure 1, a relatively simple procedure suffices for the determination of this location. It falls on a given y curve at that point where the ratio, which may be succinctly represented as:

$$[\bar{H}/x]_{y=c} = I \qquad (1)$$

attains its maximum value. In this,

$$\bar{H} \equiv 3600 \cdot \left(\frac{d\bar{H}}{d\theta} \right)_{0}^{x} \qquad (2)$$

= time mean release rate (Btu/ft^3 $\times$ hr) over interval $(0 - x)$, for the conditions associated with the point on $y = c$ curve where fraction burned is x. Notation on right-hand side of Equation (2) is that employed in Equation (1).

In further explanation, it is noted that for any given point in the field of Figure 1, the value I of the above ratio is proportional to the fuel rate required to attain the release rate $\bar{H}$, because the

Table 1. Energy Release Conditions for E = 42,000 cal/g-mol = 75,600 Btu/lb-mol

	y	T°R	θ (sec)	Release Rate Btu/ft^3 $\times$ hr
			$\times 10^{-3}$	$\times 10^6$
$x = 0.999$	1.00	4288	1.00	3.04
	1.10	4010	0.730	53.30
	1.20	3800	0.726	51.20
	1.30	3590	0.860	38.0
	1.50	3260	1.83	20.0
	2.00	2630	21.4	1.53
$x = 0.99$	1.00	4220	0.500	39.6
	1.10	4000	0.403	101.0
	1.20	3780	0.430	85.5
	1.30	3550	0.560	57.0
	1.50	3250	1.110	28.4
	2.00	2630	13.70	2.46
$x = 0.95$	1.00	4030	0.200	159.6
	1.10	3820	0.173	156.0
	1.20	3640	0.330	115.0
	1.30	3420	0.400	76.2
	1.50	3140	1.058	35.3
	2.00	2560	12.04	2.81
$x = 0.90$	1.00	3760	0.250	192.0
	1.10	3640	0.238	163.0
	1.20	3480	0.306	119.2
	1.30	3300	0.500	71.8
	1.50	3020	1.20	29.5
	2.00	2470	15.10	2.33
$x = 0.80$	1.00	3430	0.250	160.5
	1.10	3290	0.332	122.0
	1.20	3140	0.542	68.4
	1.30	3000	1.00	30.0
	1.50	2780	2.02	16.3
	2.00	2310	26.4	1.24

energy released per pound of fuel is proportional to burned fraction x. For a given y the ratio is thus proportional also to the *total input rate* (*fuel plus air*) required to attain the release rate ($\bar{H}$). Thus it becomes clear that the maximum value of Equation (1) must fall on $y = c$ at exactly the condition of "reaction-rate-induced" blowout as defined by Longwell and Weiss.

It is of special importance to note that variations of $\bar{H}$ and x along any given y curve are *not* proportional to each other as the peak is approached from the right. They are not even in the same sense, $\bar{H}$ increasing and x decreasing. The two curves $(I)_{y=c}$ vs x and $(\bar{H})_{y=c}$ vs x

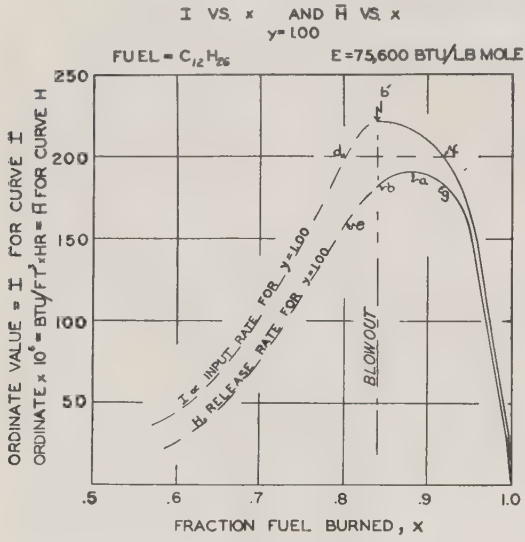

Fig. 2.

can *not* therefore peak at the same value of x, or, as shown in Figure 1, at the same value of T.

This is more clearly illustrated in Figure 2 where the two curves I vs x and $\bar{H}$ vs x each for $y = 1.00$ are shown on the same chart. In further explanation it is noted that in the vicinity of (a) the value of $(\bar{H})_{y=c}$ remains nearly constant while x continues to decrease in passing over the peak from right to left. Hence the ratio $[\bar{H}/x]_{y=c} \equiv (I)_{y=c}$ is still increasing in this passage over energy peak (a). Beyond this $(\bar{H})_{y=c}$ itself decreases at an accelerated rate and so the peak value of the ratio $(I)_{y=c}$ is soon attained.

Thus it is apparent that relative positions of energy release and blowout peaks can, for the range of mixture conditions included in Figures 1 and 2, be no others than those shown. It follows that within this range of conditions the stability of combustion at the peak of energy release is greater than it is at blowout, or, it is finite there, rather than infinitesimal, the latter being its value at blowout.

For the stoichiometric mixture the release rate at the energy peak is about 5 per cent greater than at blowout. This difference decreases with increasing (air/fuel). At $y = 1.5$, it appears to be so small as to be almost negligible and so might be very difficult to check in experiment. Nevertheless, there is a finite difference in the stability of combustion at the two points, *i.e.*, it is finite at the energy peak and infinitesimal at blowout. The chief effect of the left shift of the blowout peak with reference to the energy peak is thus to increase the stability of combustion at the energy peak as compared to that which would exist there if the two peaks coincided.

The preceding argument should apply for the mixture range from the stoichiometric through the lean side even when energy is lost as heat from the flame. This in itself does not alter the fact that $(\bar{H})_{y=c}$ remains nearly constant over an interval of (x) centered on the peak while x is still decreasing at an accelerated rate. It is, of course, assumed that neither the heat loss nor the leanness of the mixture nor their combined effects are so large as to reduce the flame temperature to such an extent as to interfere appreciably with combustion progress. This would probably occur, for a molecularly uniform distribution, when the value of y is considerably in excess of 2. It would certainly be the case with $y = 3$.

With reference to rich mixtures, so little is known of the details of the reaction progress that it is not clear just how (x) might vary with $(\bar{H})_{y=c}$ near the peak. It is conceivable that it might remain nearly constant or even increase. When the latter is true it is impossible to exceed the release rate associated with the conditions where $(I)_{y=c}$ is a maximum, *i.e.*, those associated with blowout.

4. Comparison with Results from Longwell and Weiss

In order to test the validity of the preceding conclusions, reference is again to blowout data as determined by Longwell and Weiss.[2] This is contained in the table below their Figure 20, where, as defined

$$\phi \equiv 1/y \qquad \text{and} \qquad \epsilon = x$$

The range of conditions for this comparison are those represented in Figure 1, *i.e.*, a pressure of

one atmos and a mixture range from the stoichiometric through the lean side, including $y = 2.0$. Plotting the data from the above-mentioned table, and also those from the author's earlier paper[1] in the planes y vs x and y vs T leads to the results shown in Table 2.

Considering the nature of the problem, it appears to the author that the agreement between the two sets of values of x at blowout for given values of y is exceedingly good. The higher temperature values obtained by Longwell and Weiss[2] as compared to those of the author[1] are largely accounted for by differences in entering temperatures, *i.e.*, 720°R for Longwell and Weiss as compared to 492°R for the author. Furthermore, such differences, as will be explained directly, can have only a secondary effect on those characteristics of the pattern disclosed in Figure 1, which determines the relation between the values of x and y at blowout.

In reviewing the reasons for this, attention is called to the fact that for a reaction of the second order, or for one approximating this order, the proportional influence of the product of concentrations of fuel and oxygen over the path of combustion progress is so overpowering on the form taken by the function

$$\left[\begin{array}{l}\text{Maximum rate of in-}\\ \text{put, } i.e.,\text{ blowout}\end{array}\right]_{y=c} = \phi(x, y)_{y=c} \qquad (3a)$$

in the pattern

$$\bar{H} = \phi\ (x, y, T) \qquad (3b)$$

shown by Figure 1, that everything else is secondary to it. As evidence of this is the agreement just shown between results for the author[1] and Longwell and Weiss[2] in Table 2, the former being based on a second order reaction with entering temperature of 492°R, and the latter on a 1.8 order reaction with entering temperature of 720°R, the value of 1.8 for the order of the reaction in the latter case being a result of the experimental investigation by Longwell and Weiss.[2]

5. Comparison of Energy Release Rate Values Contained in Wohlenberg[1] with Those Contained in Longwell and Weiss[2]

On the basis of the conditions associated with *blowout for* the stoichiometric mixture $y = 1.00$, Longwell and Weiss[2] arrive at the value

$$3.0 \times 10^8 \text{ Btu/ft}^3 \times \text{hr}$$

The condition which corresponds to this for the author[1] is located at point (b) in Figures 1 and 2, *i.e.*, at the point where the blowout curve meets the curve $y = 1.00$. Inspection shows the ordinate value at this point to be

$$182.0 \times 10^6 = 1.82 \times 10^8 \text{ Btu/ft}^3 \times \text{hr}$$

The latter value is associated with $T = 3530$°R and the preceding value with $T = 3660$°R. Correcting the former by a multiplier 1.06 for the fuel dodecane to isooctane and by a multiplier of 1.385 for temperatures 3530° to 3660°, the author's result in energy release rate at blowout for $y = 1.00$ is

$$2.67 \times 10^8 \text{ Btu/ft}^3 \times \text{hr}$$

which is within about 11 per cent of the Longwell and Weiss result for the same condition.

TABLE 2

P = one atmos

E = 42,000 cal/g-mol = 75,600 Btu/lb-mol

y	x at blowout from Wohlenberg[1]	x at blowout from Longwell and Weiss[2]	Temp. at blowout from Wohlenberg[1]	Temp. at blowout from Longwell and Weiss[2]
1.00	0.84	0.83	3520°R	3670°R
1.10	0.88	0.87−	3530	3610
1.20	0.90	0.88+	3480	3530
1.30	0.91+	0.90−	3370	3400
1.50	0.93+	0.91+	3050	3150
2.00	0.95	0.93	2560	2680

Considering the nature of the problem, this is probably much closer than should be expected. It may well be the result of a number of errors which accidentally cancel each other. In one respect, however, the result does not appear to meet expectations. It is on the low side, whereas it should have been on the high side because the author's assumed conditions are, as before noted, those which should yield the maximum value of release rate possible to any given case. This, of course, is the same goal which Longwell and Weiss have attempted to reach in their experimental reaction chamber. The actual performance must, however, necessarily fall short of the author's[1] result, if his theory and theirs, including their experimental procedure are correct in all respects. That, of course, is not true, on either side. Neither does it appear possible, in view of earlier discussion on the subject, that it could be accounted for by the turbulence superimposed in the experiments of Longwell and Weiss,[2] nor can

it be accounted for on the basis of the intermediate products of the reaction. Observation relative to the effect of the latter in Longwell and Weiss[2] indicates that, if anything, their presence slows down the reaction rate. This effect is, however, largely included when the value assigned to the energy of activation is that which resulted from an experiment in which the controls were designed to yield the very reaction conditions which are under investigation. The value of it so found has been employed by both the author[1] and Longwell and Weiss.[2]

Thus the explanation must, it appears, lie at least partly in the values of other constants employed in the two cases. In Longwell and Weiss[2] these are the result of correlation between experiment and a dimensional equation which relates the input rate to the coordinates of the process. In the author's paper[1] they are based directly on the molecular constants of the kinetic theory of gases, the equation itself emerging from an application of that theory to the process under consideration. It, too, is of course dimensionally consistent. One of the constants employed in this equation depends on the value employed for the mean free path length of the fuel molecule when present in the furnace gases. This depends in turn on the diameter of the fuel molecule itself. Both stages of this determination necessitate assumptions in order to arrive at results. The same general comments are no doubt applicable to some of the other constants contained in the work of both the author[1] and Longwell and Weiss.[2] In the light of this it seems quite clear that there is nothing in the relation between the magnitudes of the preceding values of energy release rate for the author and Longwell and Weiss which has any real significance as to which of the two should be the greater. This leaves it as it was; the result from the author's work[1] would be larger than that from Longwell and Weiss,[2] if theory were complete and experiment perfect.

6. Influence of Pressure and Temperature

In the preceding comparisons, results were based on a furnace pressure of one atmos. A question arises then as to the influence of a change in this pressure. In the attempt to answer this it is noted that the (P, T) function contained in the equation from the author[1] is equal to $(P/T)^{1/5}$ times that contained in the equation from Longwell and Weiss.[2] On this basis the results for energy release rate from the author[1] would exceed those from Longwell and Weiss[2] by about 60 per cent if the pressure were increased to ten atmos from one atmos.

A decrease of pressure to 0.1 atmos just about maintains the proportions but reverses the statement. The effect of this on the pattern which shows the relation between y and x at blowout would of course be small because the pressure effect enters merely as a variable stretching or shrinking factor on the ordinate scale in Figure 1. It has, as before noted, only a secondary effect on the form taken by function (3a). Thus it is seen that such agreement as exists between the two sets of values for a pressure of one atmos is not unduly strained by changes of pressure within the above range.

In such respects, temperature has even less influence than pressure because the fifth root of it lies between 4.7 and 5.3 for the whole range of temperature values within which combustion is stable. Hence the maximum difference between values of release rate because of the preceding difference in the temperature function included in Wohlenberg[1] and Longwell and Weiss[2] must be much less than is indicated by the ratio $5.3/4.7 = 1.13$, or it is considerably less than 13 per cent. Again it is noted that this influence appears as a variable stretching or shrinking factor on the ordinate scale in Figure 1, which has only a secondary effect on the relation between x and y at blowout. In this case the secondary effect of the variable, *i.e.*, of temperature, on the form taken by function (3a) is very small indeed.

7. Summary

For the range of mixture conditions from the stoichiometric through a limited range on the lean side including twice the stoichiometric air supply, the pattern of results yielded by the author's equation for potential time mean release rates is in exceedingly good agreement with results based on experiment as reported by Longwell and Weiss.[2]

Insertion of appropriate data from this pattern in the proportionality factor on input, $[\overline{H}/x]_{y=c}$, leads to results of x for the maximum input rate, *i.e.*, that at which "reaction-rate-induced" blowout occurs, which also are in close agreement with the Longwell and Weiss results for it. In addition to the above, these results show definitely, for the range of mixture conditions covered in the preceding discussion, that these blowout points fall beyond the peak of energy release in

the direction of decreasing fraction fuel burned and thus land in positions where the energy release rate is less than it is at the energy peaks. This difference is greatest for the stoichiometric mixture, being about 5 per cent for that case. It becomes negligible, in a practical sense, when the air supply is increased to more than 1.2 times the stoichiometric. Thus it appears that the chief effect of the left shift of the blowout peak is to provide for a finite stability of the combustion process at the energy peak.

In continuing this summary it seems appropriate to review briefly the basic conditions which are associated with Wohlenberg[1] as compared to those which are associated with Longwell and Weiss.[2] Both formulations involve the energy of activation in the usual way, the value assigned to it being that of its experimental determination in Longwell and Weiss.[2] This, in part at least, takes into account the effect of intermediate reaction products on the result for both cases. The reaction in Wohlenberg[1] is assumed to be of the second order whereas that of Longwell and Weiss[2] is found on the basis of experimental results to approximate the 1.8 order. This difference in order of reaction may be in part a result of intermediate reaction products. Values of other constants in Longwell and Weiss[2] are from experiment, whereas those in Wohlenberg[1] are based on the molecular constants of the kinetic theory of gases. Finally, when all of this is viewed against the background of the close agreement in results between Wohlenberg[1] and Longwell and Weiss,[2] it appears that, if the intermediate stages of the reaction are influential in the results, then, a considerable part, perhaps the larger part, of it is included in both formulations when the appropriate value is assigned to the energy of activation.

REFERENCES

1. Wohlenberg, W. J.: *Fourth Symposium (International) on Combustion*, Equations (7e) through (10), p. 800. The Williams & Wilkins Co., Baltimore, 1953.
2. Longwell, J. P., and Weiss, M. A.: Heat Release Rates in Hydrocarbon Combustion. Joint Conference on Combustion, M.I.T., June 1955. Published by The Institution of Mechanical Engineers, 1 Birdcage Walk, Westminster, London, S.W.1.
3. Jeans, J.: *The Dynamical Theory of Gases*, 4th ed. New York, Dover Publications, 1954.

Flame Stabilization in Fast Streams

52

IGNITION IN THE LAMINAR WAKE OF A FLAT PLATE[a]

By S. I. CHENG AND A. A. KOVITZ

1. Introduction

The development of high output combustors brings into focus the problem of flame stabilization within a duct through which the combustible mixture is flowing at high velocity. Since the mixture velocity is usually much greater than the burning velocity some device is necessary for the successful anchoring of the combustion region within the desired volume. This problem is solved by providing for a relatively stagnant region in which a pilot flame can exist and which acts as a continuous source of ignition for the high velocity gases. In the case of ram-jet combustion chambers a solution is sought by placing bluff bodies in the stream which provide a region of low velocity in their wake where a pilot flame may exist.

This paper will be concerned with the type of interaction occurring between hot, combustion products and cool, combustible mixtures. It is this interaction, between the hot gases in the immediate wake of a bluff body and the main flow of cool, combustible gas, which is generally recognized as being a major factor in flame stabilization.

The concept of flame initiation at the boundary between a hot stream consisting of combustion products and a cool, combustible stream has been idealized by Marble and Adamson[1]. They considered two flows, one a cool, combustible mixture, and the other its hot combustion products. These streams begin to mix at a certain point and through the processes of mass diffusion, viscous mixing, thermal conduction and chemical reaction a laminar flame finally develops at a certain distance downstream of the initial contact point. The model is two-dimensional and all significant variations of temperature, concentration, and velocity take place in a very thin layer between the two streams. Because of these assumptions the Prandtl boundary layer approximations are employed to reduce the mathematical complexity without introducing undue errors.

An important length is introduced with the following definition: it is the distance downstream from the initial contact point at which a local maximum in the temperature profile first appears, *i.e.*, at this distance the heat release due to chemical reaction is just sufficient to compensate for conduction loss. Marble and Adamson determined this length for the case when the initial velocities of the two streams were uniform and equal. They also showed that if the initial velocities were uniform but unequal this "ignition length" was linearly dependent on the initial velocity of the hot stream. In both cases this length depended exponentially on the hot stream temperatures.

The restriction of uniform initial velocity profiles is an important one, as will be subsequently shown. In the following analysis this assumption will be dropped and Blasius profiles will be used for the initial velocity distribution at the end of a flat plate of finite length. Conservation laws will be written under the boundary layer approximation following Marble and Adamson. As a result the pressure is uniform throughout the field. Assuming viscosity proportional to absolute temperature the Howarth transformation is used to separate the momentum and continuity equations from the energy and species equations. With this separation Goldstein's solution for incompressible flow in the wake of a flat plate can be directly incorporated into the energy and species equations.

Two, second order, simultaneous, partial dif-

[a] This research is part of the work under OOR DA-36, ORD-2183, sponsored by the Office of Ordnance Research, U. S. Army.

ferential equations for temperature and concentration of combustible present themselves for solution, each containing a first order Arrhenius factor giving the effect of chemical reaction. These equations are solved using a method similar to that used by Goldstein in obtaining his wake flow results.

By matching solutions for large and small values of the independent variable, it is shown that only one numerical computation need be made to cover a wide range of initial conditions.

The essential difference between Marble and Adamson's analysis and the present one is, of course, the initial condition on the velocity profile. The uniform velocity assumption, coupled with step function initial conditions on the temperature and concentration fields results in the use of error functions to express the zeroth order solution. However, when step function initial conditions on temperature and concentration are embedded in an initially non-uniform velocity field the zeroth order solution cannot be expressed in terms of an error function. This substantially complicates the solution of higher order terms.

In any physical system involving mixing of two streams the velocity field must be non-uniform. Since convection plays a significant role in the mixing processes one can expect non-uniformities in velocity to be important. Roughly speaking the interaction, in the case of an initially non-uniform velocity field, should be expected to proceed in similar fashion to that in a uniform flow, the major difference being a contraction of the overall process toward the point of initiation. This expectation is inferred from the nature of the flow field in the wake of a flat plate in which case the flow is stagnant at the trailing edge and remains slow moving for some distance downstream.

The foreshortening toward the origin is substantiated in the following analysis. Furthermore, the temperature profiles have the same general shape as in the uniform flow case. Marble and Adamson show that the initial bulge in the temperature profile occurs at the outer edge of the velocity boundary layer in the case of initially unequal but uniform velocity profiles. For symmetric non-uniform profiles this is no longer true, as will be shown. The first local temperature maximum is, in fact, found deep within the boundary layer and much closer to the trailing edge, its exact location depending upon the flat plate length. The non-uniform initial condition brings into the problem the upstream geometry. The flat plate is a simple geometry but, nevertheless, will bring out essential dimensionless parameters and how the geometry enters into the determination of the bulge. Such dimensionless parameters will help in extrapolation of numerical results when necessary.

2. Analytical Formulation

The general hydrodynamic equations with heat addition in a multispecied fluid have been given by Hirschfelder, Curtiss and Bird[2] and reviewed by Adamson[3]. Adamson also reduced these general equations to their boundary layer form. In what follows, the symbols used will, in the main, be those used by Marble and Adamson[1].

For a two-component system with first order chemical kinetics the governing equations, under the boundary layer approximation, are

$$\frac{\partial}{\partial x_0}(\rho u_0) + \frac{\partial}{\partial y_0}(\rho v_0) = 0$$

$$\rho u_0 \frac{\partial u_0}{\partial x_0} + \rho v_0 \frac{\partial u_0}{\partial y_0} = \frac{\partial}{\partial y_0}\left(\mu \frac{\partial u_0}{\partial y_0}\right)$$

$$\rho u_0 \frac{\partial T}{\partial x_0} + \rho v_0 \frac{\partial T}{\partial y_0} = \frac{\partial}{\partial y_0}\left[\frac{\mu}{\mathrm{Pr}} \frac{\partial T}{\partial y_0}\right] + \frac{\Delta H_{12}}{C_p \tau} \rho K e^{-(A/RT)} \tag{1}$$

$$\rho u_0 \frac{\partial K}{\partial x_0} + \rho v_0 \frac{\partial K}{\partial y_0} = \frac{\partial}{\partial y_0}\left[\frac{\mu}{\mathrm{Sc}} \frac{\partial K}{\partial y_0}\right] - \frac{1}{\tau} \rho K e^{-(A/RT)}$$

$$P = \rho \mathcal{R} T / \bar{M}$$

The first equation is the overall mass continuity balance. The second is the momentum equation. Pressure is uniform throughout the flow field since in the boundary layer approximation $\partial P/\partial y_0$ can be neglected and for flow along a flat plate $\partial P/\partial x_0$ vanishes. Combustion introduces no difficulties in this assumption, for even in the case of a fully developed flame the change in pressure across the flame front is neglected. The third expresses energy conservation with the last term giving the heat release due to chemical reaction. It is assumed that viscous dissipation is small compared to the other terms in the heat balance. The fourth equation states that the concentration of combustible changes due to diffusion and consumption by chemical reaction.

The last equation assumes that the medium acts as a single perfect gas.

Note that these five equations are all hopelessly interdependent. However, if it is assumed that $\rho\mu$ = constant throughout the field then the Howarth[4] transformation may be used to uncouple the continuity and momentum equations from the remaining three equations.

$$\frac{\partial u_1}{\partial x_1} + \frac{\partial v_1}{\partial y_1} = 0$$

$$u_1 \frac{\partial u_1}{\partial x_1} + v_1 \frac{\partial u_1}{\partial y_1} = \nu \frac{\partial^2 u_1}{\partial y_1^2}$$

$$u_1 \frac{\partial T}{\partial x_1} + v_1 \frac{\partial T}{\partial y_1} = \nu/\mathrm{Pr} \frac{\partial^2 T}{\partial y_1^2} + \frac{\Delta H_{12}}{C_p T} K e^{-(A/RT)} \tag{2}$$

$$u_1 \frac{\partial K}{\partial x_1} + v_1 \frac{\partial K}{\partial y_1} = \nu/\mathrm{Sc} \frac{\partial^2 K}{\partial y_1^2} - \frac{1}{\tau} K e^{-(A/RT)}$$

where the transformation

$$y_1 = \int_0^{y_0} \rho/\rho_I \, dy_0 , \qquad x_1 = x_0 \tag{3}$$

has been used. Note that the Howarth transformation only contracts the lateral dimension y_0. The longitudinal dimension is not affected. If one is only interested in quantities in the longitudinal dimension, the inverse transformation need not be carried out. The equation of state remains as a means of getting back to the x_0, y_0 variables after the temperature field has been determined from Equation (2).

The system of Equations (2) is in terms of an incompressible formulation which has left the first two equations independent of the last two equations. They can be solved and their solution used to determine T and K.

Through the use of the nondimensional variables u, v, x, y, ϑ (defined in the list of symbols) the equations may finally be put into a form more convenient for solution. The coordinates and initial conditions are shown in Figure 1.

$$\left.\begin{aligned} u_x + v_y &= 0 \\ uu_x + vu_y &= u_{yy} \end{aligned}\right\} \tag{4}$$

$$\left.\begin{aligned} u\vartheta_x + v\vartheta_y &= \frac{1}{\mathrm{Pr}} \vartheta_{yy} + BKe^{-\vartheta_a/\vartheta} \\ uK_x + vK_y &= \frac{1}{\mathrm{Sc}} K_{yy} - CKe^{-\vartheta_a/\vartheta} \end{aligned}\right\} \tag{5}$$

The boundary conditions on ϑ and K will be taken to be the same as those used by Marble and Adamson[1]. Furthermore, in order to make a direct comparison with their results the numerical example will use the same physical constants, namely the constants appropriate to azomethane.

3. Goldstein's Solution for the Wake

Goldstein[5] solved Equation (4) for the wake of a flat plate, the solution being approximately valid in the neighborhood of the end of the plate, excluding the trailing edge. He determined the velocity field separately in the region of small y and large y and forced the two solutions to join smoothly at some intermediate value of y. His solution may be summarized as follows:

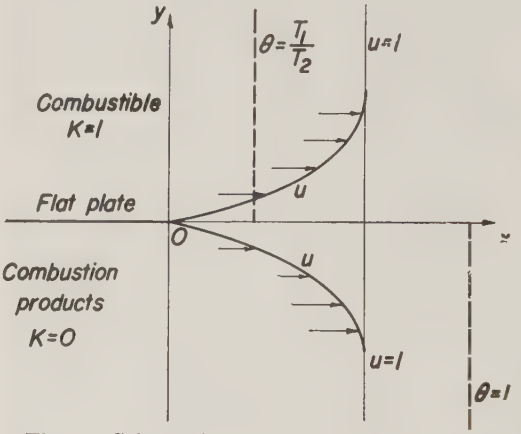

Fig. 1. Schematic of initial conditions and coordinate system.

For small y:

$$u = \frac{1}{3} \sum_{l=0}^{\infty} b_{3l+1} \xi^{3l+1}$$

$$v = \frac{1}{3} \sum_{k=0}^{\infty} c_{3k-1} \xi^{3k-1} \tag{6}$$

where

$$b_{3l+1} = f'_{3l}(\eta), \qquad c_{3k-1} = \eta f'_{3k}(\eta) - (3k+2) f_{3k}(\eta)$$

For large y:

$$u = \psi'_0(y) + \xi \psi'_1(y) + \xi^2 \frac{\psi'_2(y)}{2!} + \cdots$$

$$v = -\frac{1}{3} \xi^{-2} \psi_1(y) - \frac{2}{3} \xi^{-1} \frac{\psi_2(y)}{2!} - \frac{3}{3} \frac{\psi_3(y)}{3!} - \cdots$$

where

$$\psi_0' = u_0(y), \qquad \psi_1' = Au_0', \qquad \psi_2'/2! = \frac{A^2}{2!}u_0'', \ \cdots$$

$u_0(y)$ = Blasius profile

A, B, etc. are known constants. The functions f_0, f_3, f_6 have been tabulated by Goldstein and recalculated for smaller mesh size as part of this work.

4. Solution of Temperature and Concentration Fields

The solutions of Equation (5) will follow along the lines Goldstein[5] used in calculating the velocity field. Goldstein's solution is valid only for $y \gtrless 0$, a circumstance arising from the fact that the Blasius initial condition holds only for $y \gtrless 0$, the velocity field being symmetric with respect to y. Therefore, the temperature and concentration fields being unsymmetric will have to be solved in the two half-planes separately and joined smoothly along the x-axis.

Series solutions, in the region of small y, are assumed of the form

$$\vartheta(\xi, \eta) = \sum_{r=0}^{\infty} \xi^r \vartheta_r(\eta), \qquad K(\xi, \eta) = \sum_{r=0}^{\infty} \xi^r K_r(\eta) \quad (8)$$

in both upper and lower half-planes. The boundary conditions will be satisfied if

$$\lim_{\bar{\eta}\to\infty} \bar{\vartheta}_0 = 1, \qquad \lim_{\eta\to\infty} \vartheta_0 = T_{\mathrm{I}}/T_{\mathrm{II}} = \Lambda$$

$$\lim_{\bar{\eta}\to\infty} \bar{\vartheta}_r/\bar{\eta}^r = \lim_{\eta\to\infty} \vartheta_r/\eta^r = \lim_{\bar{\eta}\to\infty} \bar{K}_r/\bar{\eta}^r = \lim_{\eta\to\infty} K_r/\eta^r = 0 \quad (9)$$

$$\lim_{\bar{\eta}\to\infty} \bar{K}_0 = 0, \qquad \lim_{\eta\to\infty} K_0 = 1$$

Substituting Equations (6) and (8) into Equation (5) and setting coefficients of like powers of ξ equal to zero results in a series of equations for ϑ_r and K_r.

$$\left.\begin{aligned} \vartheta_r'' + \lambda_2 f_0 \vartheta_r' - \lambda_r f_0' \vartheta_r &= \mathrm{Pr} I_r \\ K_r'' + \lambda_2 f_0 K_r' - \underline{\lambda}_r f_0' K_r &= \mathrm{Sc} H_r \end{aligned}\right\} \quad (10)$$

where

$$\lambda_r = r\,\mathrm{Pr}, \qquad \underline{\lambda}_r = r\mathrm{Sc}$$

and

$$I_0 = I_1 = H_0 = H_1 = 0$$

$$I_2 = -9BK_0 e^{-\vartheta_a/\vartheta_0}, \ \cdots$$

$$H_2 = 9CK_0 e^{-\vartheta_a/\vartheta_0}, \ \cdots$$

Since all boundary conditions are applied at $\eta \to \infty$ the asymptotic form of Equation (10) must be known. Using Goldstein's result

$$f_0 \sim \tfrac{1}{2}\alpha_1(\eta + \delta_0)^2, \qquad f_0' \sim \alpha_1(\eta + \delta_0)$$

it can be shown that the homogeneous part of Equation (10) has the form

$$\vartheta_r'' + a(\eta + \delta_0)^2 \vartheta_r' - ra(\eta + \delta_0)\vartheta_r = 0$$

where

$$a = \alpha_1 \qquad \mathrm{Pr} = 5.977\ \mathrm{Pr} \quad (11)$$

Particular solutions must be constructed from the consecutively obtained asymptotic solutions. As it can be shown, Equation (11) is reducible to Whittaker's Equation[6], the asymptotic form of the solutions being known.

The solutions for small and large η can be matched at some intermediate value of η in both half-planes to determine the slope and value of $\vartheta_r(\eta)$ at $\eta = 0$. This gives approximate values from which to begin the numerical integration necessary for the determination of ϑ_r throughout the range of the variable, η.

The final problem in the solution of the temperature-concentration field involves using the velocity distribution valid only for large y. Strictly speaking, this solution of ϑ and K for large y must be obtained and then forced to match the solution for small y at some intermediate value. Fortunately, the phenomena of physical interest occur within the region of validity of the solution for small y. Therefore, the other solution will not be considered here.

Details of the mathematical development, including the above mentioned matching of solutions for large and small y, will be published separately at a later date, as well as by Kovitz[7].

5. Calculation of First Few Terms of Solution

The equation for ϑ_0 is given by

$$\vartheta_0'' + 2\mathrm{Pr}\vartheta_0' = 0 \quad (12)$$

The asymptotic form of its solution is

$$\vartheta_0 \sim A_0\eta^{-2}e^{-(a/3)\eta^3}\{1 + \sum_1 a_n^{(0)}\eta^{-3n}\} + \Lambda,$$
$$\bar{\vartheta}_0 \sim \bar{A}_0\bar{\eta}^{-2}e^{-(a/3)\bar{\eta}^3}\{1 + \sum_1 a_n^{(0)}\bar{\eta}^{-3n}\} + 1 \tag{13}$$

From the matching of the solution for small η with the solution for large η it can be shown that

$$\vartheta_0(\eta, \mathrm{Pr}, \Lambda) = \tfrac{1}{2}(1 + \Lambda) + \frac{1 - \Lambda}{1 - \Lambda^*} \tag{14}$$
$$[\vartheta_0(\eta, \mathrm{Pr}, \Lambda^*) - \tfrac{1}{2}(1 + \Lambda^*)]$$

Thus, one numerical calculation of ϑ_0 for a particular $\Lambda = \Lambda^*$ and Pr will suffice to obtain ϑ_0 for all $\Lambda = T_{\mathrm{I}}/T_{\mathrm{II}}$.

The numerical result, for azomethane, is given in Figure 2, for the same physical parameters catalogued in the Appendix.

The equation for K_0 is

$$K_0'' + 2\mathrm{Sc}f_0K_0' = 0 \tag{15}$$

and its asymptotic solution is

$$K_0 \sim E_0\eta^{-2}e^{-(b/3)\eta^3}\{1 + \sum_1 b_n^{(0)}\eta^{-3n}\} + 1,$$
$$\bar{K}_0 \sim \bar{E}_0\bar{\eta}^{-2}e^{-(b/3)\bar{\eta}^3}\{1 + \sum_1 b_n^{(0)}\bar{\eta}^{-3n}\} \tag{16}$$

where $b = \alpha_1\mathrm{Sc}$.

It is important to determine accurately the behavior of K_0 in the asymptotic region in the lower, hot stream where it must vanish exponentially. The reason is physically clear if one notices the fact that the temperature bulge must first occur near the highest temperature where the concentration is very low. It is necessary to match the asymptotic form to the machine calculated result at a point where $\bar{E}_0$ as given by the asymptotic form is stationary and use the asymptotic form from the matching point $\bar{\eta}_m$ toward higher values of $\bar{\eta}$ (corresponding to smaller $\bar{K}_0$). The machine calculation involves at least an error of the order of 10^{-6} which leads to the calculated values of $\bar{K}_0$ in those regions fluctuating at this order of magnitude instead of asymptoting to zero exponentially. Such deviation is not tolerable in the hot stream because it enters into the calculation of ϑ_2 as a factor of the inhomogeneous part I_2 with a multiplying constant of the order of 10^{13}, and yet must asymptote to zero exponentially! The computation of ϑ_2 would therefore not be possible without the proper matching. I_2 is a measure of chemical reaction and as such must vanish deep down in the lower stream. K_0 is shown in Figure 2 and the asymptotic matching in Figure 3.

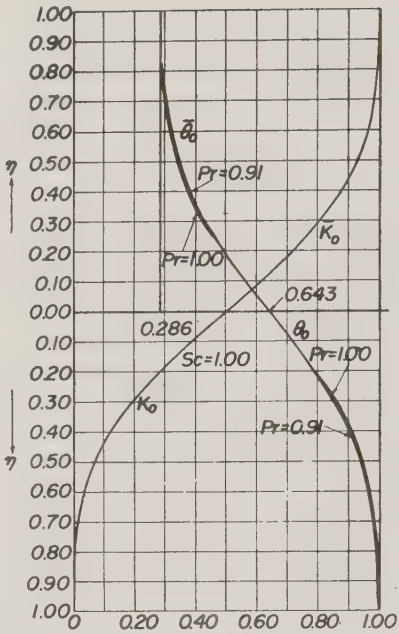

Fig. 2. Plot of $\theta_0(\eta)$ and $K_0(\eta)$. Upper and lower half-plane notation reversed.

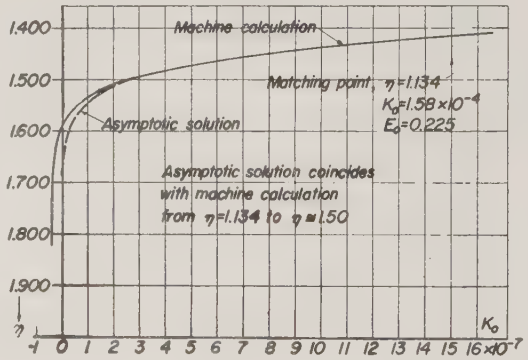

Fig. 3. Matching of $\bar{K}_0(\bar{\eta})$ from machine calculation with asymptotic form of $\bar{K}_0(\bar{\eta})$. All quantities are in lower half-phase.

The equation for ϑ_1 is

$$\vartheta_1'' + \mathrm{Pr}\, f_0\vartheta_1' - \mathrm{Pr}\, f_0'\vartheta_1 = 0 \tag{17}$$

The asymptotic form of its solution is

$$\vartheta_1 \sim A_1\eta^{-2}e^{-(a/3)\eta^3}\{1 + \sum_1 a_n^{(1)}\eta^{-3n}\},$$
$$\bar{\vartheta}_1 \sim \bar{A}_1\bar{\eta}^{-3}e^{-(a/3)\bar{\eta}^3}\{1 + \sum_1 a_n^{(1)}\bar{\eta}^{-3n}\} \tag{18}$$

If the matching procedure is used to determine the six remaining free constants in the solution of ϑ_1 it may be shown that all constants must

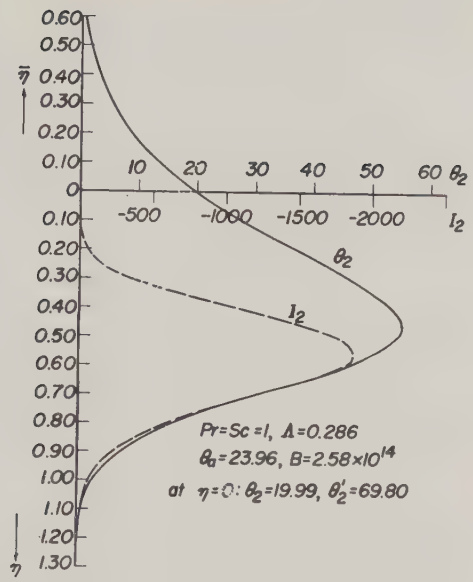

Fig. 4. Plot of $\theta_2(\eta)$ and $I_2(\eta)$. η and $\bar{\eta}$ are reversed.

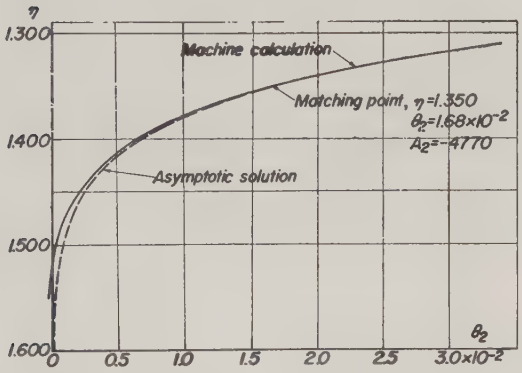

Fig. 5. Matching of $\theta_2(\bar{\eta})$ from machine calculation with asymptotic form of $\bar{\theta}_2(\bar{\eta})$. All quantities are in lower half-plane.

vanish. Therefore

$$\vartheta_1 = \bar{\vartheta}_1 \equiv 0 \tag{19}$$

The equation for ϑ_2 is

$$\vartheta_2'' + 2\,\mathrm{Pr}\, f_0 \vartheta_2' - 2\,\mathrm{Pr}\, f_0' \vartheta_2 = -9B\,\mathrm{Pr}\, K_0 e^{-\vartheta_a/\vartheta_0} \tag{20}$$

For large η,

$$-9B\ \mathrm{Pr}\ K_0 e^{-\vartheta_a/\vartheta_0} \approx -9B\ \mathrm{Pr}\ e^{-\vartheta_a/\Lambda} \approx 0$$

For large $\bar{\eta}$,

$$-9B\ \mathrm{Pr}\ \bar{K}_0 e^{-\vartheta_a/\bar{\vartheta}_0} \approx$$

$$-9B\ \mathrm{Pr}\ \bar{E}_0 \bar{\eta}^{-2} e^{-(b/3)\bar{\eta}^3}(1 + b_1^{(0)}\bar{\eta}^{-3} + \cdots) e^{-\vartheta_a}$$

Then the asymptotic form of its solution is

$$\theta_2 \sim \eta^{-4} e^{-(a/3)\eta^3} \left\{1 + \sum_1 a_n^{(2)} \eta^{-3n}\right\}$$

$$\bar{\vartheta}_2 \sim \bar{A}_2 \bar{\eta}^{-4} e^{-(a/3)\bar{\eta}^3} \left\{1 + \sum_1 a_n^{(2)} \bar{\eta}^{-3n}\right\}$$

$$+ \frac{9B\ \mathrm{Pr}\ \bar{E}_0}{a} e^{-\vartheta_a} e^{-(b/3)\bar{\eta}^3} \left\{\bar{\eta}^{-3} - \frac{b_1^{(0)}}{2}\bar{\eta}^{-6} + \cdots\right\} \tag{21}$$

It is seen that the particular solution of $\bar{\vartheta}_2$ becomes the dominating term as $\bar{\eta} \to \infty$ but, nevertheless, $\bar{\vartheta}_2(\bar{\eta} = \infty) = 0$ as required.

Since B appears linearly in the particular solutions both for large and small η it can be shown from the matching of the two solutions that

$$\vartheta_2(\eta, \mathrm{Pr}, \mathrm{Sc}, \Lambda, \vartheta_a, B) = \frac{B}{B^*}\vartheta_2(\eta, \mathrm{Pr}, \mathrm{Sc}, \Lambda, \vartheta_a, B^*) \tag{22}$$

Thus, the dependence of ϑ_2 on the important parameter, B, has been extracted.

The numerical result for ϑ_2 and its matching using Equation (21) are shown in Figures 4 and 5.

ϑ_3 turned out to be much smaller than ϑ_2 and $\xi^4\vartheta_4$ can be neglected compared to $\xi^2\vartheta_2$, at least to the value of ξ where the first bulge appeared.

The solution to the temperature field, considering only the first two nonvanishing terms can then be written, for the lower half-plane, as

$$\bar{\vartheta}(\xi, \bar{\eta}, \mathrm{Pr}, \mathrm{Sc}, \vartheta_a, \Lambda, B, C) = \tfrac{1}{2}(1 + \Lambda) + \frac{1 - \Lambda}{1 - \Lambda^*}\left[\bar{\vartheta}_0(\bar{\eta}, \mathrm{Pr}, \Lambda^*) - \tfrac{1}{2}(1 + \Lambda^*)\right] + \xi^2 \frac{B}{B^*}\bar{\vartheta}_2(\bar{\eta}, \mathrm{Pr}, \mathrm{Sc}, \vartheta_a, \Lambda, B^*) \tag{23}$$

When $\bar{\eta}$ is large a further simplification is possible. Then, $\bar{\vartheta}_0 \approxeq 1$, independent of Λ. It can be shown therefore that

$$\bar{\vartheta}_2(\bar{\eta}, \mathrm{Pr}, \mathrm{Sc}, \Lambda, \vartheta_a, B) \cong \frac{B}{B^*} e^{-\vartheta_a + \vartheta_a^*} \cdot \vartheta_2(\bar{\eta}, \mathrm{Pr}, \mathrm{Sc}, \vartheta_a^*, B^*) \tag{24}$$

For large $\bar{\eta}$ the dependence of $\bar{\vartheta}_2$ on ϑ_a has been extracted and there is independence of $\bar{\vartheta}_2$ on Λ. The reasonableness of this result is apparent from Equation (20) which shows ϑ_0 appearing only in the inhomogeneous term. With ϑ_0 replaced by unity a solution must be obtained which is independent of Λ. Physically, this implies that the rate of heat release due to chemical reaction deep in the lower stream is quite inde-

pendent of the initial temperature of the cool stream.

These results will be extremely important in the following section.

6. Location of the First Local Maximum in the Temperature Profile and Discussion

As combustible material diffuses into the region of high temperature it is converted into combustion products with associated heat release. The rate of conversion is strongly dependent on the temperature, through the Arrhenius factor. The distance downstream at which the first local maximum forms is an important measure of the future rate of development of the temperature profile to its ultimate laminar flame configuration, in which the local maximum has become an almost discontinuous jump at the flame front. Marble and Adamson[1] discuss this point at length, noting that this initial "bulge" marks the result of sufficient accumulation of heat due to chemical reaction to overcome the local loss of heat to the upper stream by conduction. Subsequent to this initial "bulge" the chemical rate rapidly increases as ξ increases because concentration of combustible increases with ξ. The process takes on the character of a temperature wave propagating upward into the cooler, combustible mixture. Figure 6 shows the results of calculation for azomethane.

This length, ξ_i, can be determined by formulating the two conditions that must hold at the initial bulge. Before formation of the bulge $\bar{\vartheta}_{\bar{\eta}} > 0$ and $\bar{\vartheta}_{\bar{\eta}\bar{\eta}} < 0$ for all finite $\bar{\eta}$. The bulge is defined by $\bar{\vartheta}_{\bar{\eta}} = 0$ and just after its formation an inflection point must occur after which $\bar{\vartheta}_{\bar{\eta}\bar{\eta}} > 0$. Therefore, the first bulge is given by

$$\begin{aligned} \bar{\vartheta}_{\bar{\eta}} &= \bar{\vartheta}_0'(\bar{\eta}_i) + \xi_i^2 \bar{\vartheta}_2'(\bar{\eta}_i) + \cdots = 0 \\ \bar{\vartheta}_{\bar{\eta}\bar{\eta}} &= \bar{\vartheta}_0''(\bar{\eta}_i) + \xi_i^2 \bar{\vartheta}_2''(\bar{\eta}_i) + \cdots = 0 \end{aligned} \tag{25}$$

Considering only the first two terms these conditions are equivalent to Marble and Adamson's statement that the initial maximum occurs where

$$\left.\frac{d\xi}{d\bar{\eta}}\right|_{\bar{\eta}=\bar{\eta}_i} = \frac{d}{d\bar{\eta}} \sqrt{-\frac{\bar{\vartheta}_0'}{\bar{\vartheta}_2'}}\Bigg|_{\bar{\eta}=\bar{\eta}_i} = 0$$

From Equation (25) the initial local maximum occurs at

$$\xi_i = \sqrt{-\frac{\bar{\vartheta}_0'}{\bar{\vartheta}_2'}}\Bigg|_{\bar{\eta}=\bar{\eta}_i} \tag{26}$$

Using Equations (14) and (24) this gives

$$\xi_i^2 = \frac{1-\Lambda}{1-\Lambda^*} \frac{B^*}{B} e^{\vartheta_a - \vartheta_a^* \xi_i^{*2}} \tag{27}$$

For azomethane, using the physical constants given in the Appendix, one can calculate $\bar{\eta}_i = 2.40$, $\xi_i^* = 0.0484$, $x_{1_i} = 0.00452$ cm. Then,

$$\xi_i^2 \cong 3.22 \frac{1-\Lambda}{B} e^{\vartheta_a} \tag{28}$$

From this, substituting for B and Λ,

$$x_{1_i} \cong 2.9\, u_{\mathrm{I}} \left(\frac{u_{\mathrm{I}}}{l}\right)^{\frac{1}{2}} \left[(T_{\mathrm{II}} - T_{\mathrm{I}}) \frac{\tau c_p}{\Delta H_{12}} e^{\vartheta_a} \right]^{3/2} \tag{29}$$

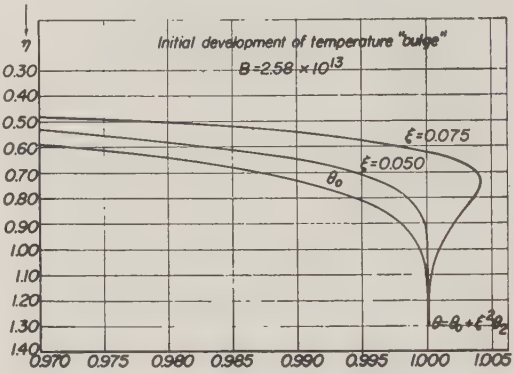

Fig. 6. Development of temperature profiles due to chemical reaction near bulge. Lower half-plane.

The large value, $\bar{\eta}_i = 2.40$, justifies a posteriori the approximations used in obtaining Equation (24).

Adamson,[3] for Pr = 0.91, Sc = 1.00 gets $\tilde{x}_{1_i} = 0.071$ cm. Adamson's calculations indicate that extrapolation to Pr = Sc = 1 gives $\tilde{x}_{1_i} \cong 0.068$ cm. Therefore, for this particular example the ratio of ignition lengths in uniform and non-uniform flow is

$$\tilde{x}_{1_i}/x_{1_i} \cong 15$$

The result evidently shows that the distance to the first local temperature maximum is greatly reduced in the case of non-uniform initial velocity profiles when $l = 10$ cm. Even when $l = 1$ cm (corresponding to $\xi_i \cong 0.15$), $x_{1_i} \cong 0.0143$ cm, a length still considerably smaller than Adamson's $\tilde{x}_{1_i} \cong 0.068$ cm.

The first bulge forms at $\bar{\eta}_i = 2.40$, $\xi_i = 0.0484$. This is equivalent to

$$\bar{y}_i = 3\xi_i \bar{\eta}_i = 0.348$$

At $\bar{y}_i = 0.348$, $x_{1_i}/l \leqslant 0.0005$, Goldstein shows that $u \cong 0.25$, which is deep within the retarded layer. This is contrary to Adamson's[3] result for uniform but unequal initial velocity profiles in which he shows the first bulge to appear at the edge of the velocity layer.

Another observation to be made concerns the shape of the temperature profiles in uniform and non-uniform flow. As seen from Figure 7 they are virtually of the same form but displaced along the x_1-axis. The major difference between them is the rapidity with which they asymptote to $\vartheta = 1$. The results for non-uniform profiles show a slightly faster rise to the free stream temperature which may in this case be attributed to the inflow of mass from the hot, free stream.

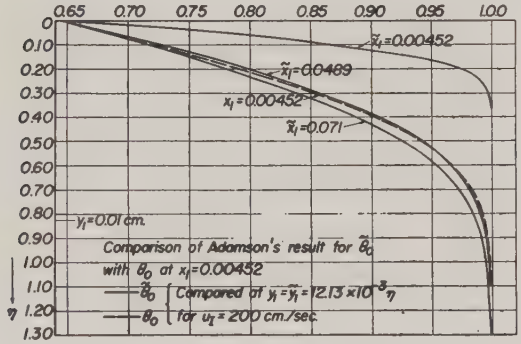

Fig. 7. Comparison of temperature profiles in uniform and nonuniform flow. Lower half-plane.

Adamson[3] has shown that

$$x_{1_i} \propto u_I e^{\vartheta_a} \tag{30}$$

From Equation (29)

$$x_{1_i} \propto (u_I e^{\vartheta_a})^{3/2} \tag{31}$$

keeping all other parameters constant. Thus, for a given l, x_{1_i} is more sensitive to free stream velocity and ϑ_a (*i.e.*, initial temperature of the hot stream) than in the uniform flow case. This is physically reasonable since as free stream temperature is reduced, the first local maximum would form further downstream in regions of higher velocity which, in turn, tends to further increase x_{1_i}.

In the over-all picture of the bulge formation one may look upon the solution with velocity boundary layers as quite similar to the pure mixing case except that the effective free stream velocity is smaller. This results in a contraction toward the origin, $x_1 = 0$, of the temperature, concentration field, at least for values of x_1, less than the ignition length. Furthermore, the depth y_i at which the initial bulge forms is also reduced because of the forementioned inflow of mass from the free stream.

The constants which completely characterize the problem, both as regards boundary conditions and combustible, are ϑ_a, B, C, and Λ. Their effects on x_{1_i}, within the two term approximation to ϑ, are summarized in Equation (29). It is seen that x_{1_i} is more sensitive to changes in u_I than in l. This is physically reasonable since the slope of the Blasius profile at the trailing edge of a flat plate of length l is given by

$$\left.\frac{\partial u_1}{\partial y_1}\right|_{x1=y1=0} \propto u_I^{3/2}/l^{1/2}$$

The larger this slope, the larger the average velocity in the wake, and so, the farther downstream the initial bulge. This slope has the same dependence on u_I and l as x_{1_i}.

If it is assumed that the combustible be diluted by some inert gas, the change in A is negligible compared to changes in ΔH_{12}. Then the dominating importance of chemistry, through the influence of ΔH_{12} compared to geometry is shown, for increasing l (tending to decrease x_{1_i}) and decreasing ΔH_{12} (tending to increase x_{1_i}) results in a net increase in x_{1_i} if both are changed proportionately.

7. Conclusions

The effect of preformed velocity boundary layers on the interaction of a cool, combustible stream with its hot, combustion products can be summarized as follows:

(1) The distance to the first local maximum in the temperature distribution is greatly reduced by velocity boundary layers.

(2) The first bulge is formed deep in the retarded velocity layer in contrast to the result with uniform, but unequal initial velocities.

(3) The shape of the temperature profiles is similar in uniform and nonuniform flow, at least in the immediate vicinity of the trailing edge.

(4) In comparison to uniform flow there is a contraction of the temperature, concentration field toward the initial contact point between the two streams and their dividing streamline.

(5) As shown by Equation (29) the distance to the first local temperature maximum is proportional to the $\frac{3}{2}$ power of the free stream ve-

locity and to the $-\frac{1}{2}$ power of the flat plate length. Furthermore, equal relative changes in combustible properties and geometry (through changes in flat plate length) show the ignition length to be more sensitive to the former.

Summary

The interaction of a cool, combustible mixture with its hot combustion products is studied from the point of view of determining where the first local maximum in the temperature profile occurs with respect to the initial contact point between the two streams. This work represents a modification of Marble and Adamson's study of a similar interaction in which the effect of preformed velocity boundary layers in the two flows was not considered.

Marble and Adamson determined this "ignition length" for a system with first order chemical kinetics assuming the velocities of the two streams were uniform before mixing. They found that this length depended linearly on the velocity of the hot stream and exponentially on the hot stream temperature.

The inclusion of non-uniform velocity boundary layers considerably changes the results. There is a foreshortening of the temperature and concentration fields both toward the origin and the x_1-axis. The distance to the first bulge, for the same combustible, is proportional to the slope of the velocity profiles at the initial contact point between the two streams. Furthermore, the "ignition length" becomes more sensitive to velocity and temperature changes than in the uniform flow.

Nondimensional scaling factors are discussed which show the dominance of free stream velocity and chemistry compared to geometry in determining the "ignition length."

Appendix: Numerical Calculations

The physical constants appropriate to azomethane, taken from Adamson[3] are as follows:

$$\tau = 10^{-14}\ \text{sec}, \qquad \Delta H_{12}/C_p T_{II} = 1.29,$$

$$A = 50\ \text{kcal/mol},$$

$$R = 1.987\ \text{cal/mol °K}, \quad \text{Pr} = 0.91, \quad \text{Sc} = 1.00$$

Adamson also chose

$$T_I = 300°\text{K}, \quad T_{II} = 1050°\text{K},$$

$$u_I = u_{II} = 200\ \text{cm/sec}$$

The numerical example worked out here was calculated using, in addition $l = 10$ cm. Furthermore, Pr = 1.00 was used for simplicity, since the result is not very sensitive to Pr, as seen from Figure 2. Then one gets

$$\vartheta_a = 23.96, \qquad B = 2.58 \times 10^{13}, \qquad C = 2.00 \times 10^{13}$$

Figure 2 shows the results for ϑ_0 and K_0. The difference between the curves of ϑ_0 for Pr = 1.00 and Pr = 0.91 is quite small. With Pr = 1.00 slightly higher temperatures prevail in the lower stream. This explains the slightly smaller value of $\tilde{x}_{1_i}$ obtained from Adamson's[3] result when it is extrapolated to Pr = 1.00.

The asymptotic matching of $\bar{K}_0$ with $\bar{K}_0$ as given by Equation (16) is shown in Figure 3.

ϑ_2 and I_2 are shown in Figure 4. The rate of chemical reaction, as measured by I_2, is clearly seen to peak sharply in the lower stream at $\bar{\eta} = 0.45$. Figure 5 exhibits the asymptotic matching of $\bar{\vartheta}_2$ with $\bar{\vartheta}_2$ given by Equation (21).

In Figure 6 the net effect of chemical reaction on the temperature profile is shown for two values of ξ. The lowest value, $\xi = 0.050$ is, essentially, at the first bulge.

Nomenclature

A	activation energy, cal/mole/°K
$a_n^{(r)}$, $b_n^{(r)}$	dimensionless coefficients appearing in asymptotic solutions
B	dimensionless constant, $4l\Delta H_{12}/u_{I\tau}C_pT_{II}$
C	dimensionless constant, $4l/u_{I\tau}$
c_p	specific heat at constant pressure, cal/gm/°K
$\bar{E}_0$	dimensionless constant in asymptotic solution for $\bar{K}_0$
ΔH_{12}	heat release due to chemical reaction per unit mass of combustible
K	dimensionless local relative mass concentration of combustible
l	length of flat plate, cm
$\bar{M}$	average molecular weight of mixture
P	static pressure
Pr	Prandtl number, $c_p\mu/\lambda$
$\mathfrak{R}$	universal gas constant, cal/mole/°K
R	Reynolds number, $4lu_I/\nu$
Sc	Schmidt number, $\mu/\rho D$, where D = binary diffusion coefficient
T	local stream temperature, °K
T_I, T_{II}	initial temperature of cool and hot stream respectively
u_0, v_0	local axial and transverse velocity in compressible flow, cm/sec
u_1, v_1	local axial and transverse velocity in corresponding incompressible flow, cm/sec

u_I free stream velocity

u, v dimensionless axial and transverse velocity: u_1/u_I , $R^{\frac{1}{2}}v_1/u_I$

$u_0(y)$ dimensionless Blasius velocity profile at $x = 0$

x_0 , y_0 axial and transverse distance coordinates in compressible flow, cm, origin at trailing edge of flat plate

x_1 , y_1 axial and transverse distance coordinates in corresponding incompressible flow, cm

x, y dimensionless axial and transverse distance coordinates: $x_1/4l$, $R^{\frac{1}{2}}y_1/4l$

x_i , y_i dimensionless axial and transverse coordinates of first local temperature maximum

$\tilde{x}_{1i}$ coordinate of first local temperature maximum from Adamson's solution, cm

δ_0 dimensionless constant = 0.3408

η dimensionless variable, $y/3\xi$

$\bar{\eta}_m$ approximate boundary of diffusion layer in lower half-plane

$\tilde{\eta}$ dimensionless transverse coordinate used by Adamson, $y_1\sqrt{u_I/\nu x_1}$

ϑ dimensionless local stream temperature, T/T_{II}

$\tilde{\vartheta}_0$ dimensionless zeroth order temperature solution from Adamson

ϑ_a dimensionless activation energy, A/RT_{II}

λ coefficient of thermal conductivity, cal/gm/sec/°K

Λ temperature ratio, T_I/T_{II}

μ dynamic viscosity, gm/cm/sec

ν kinematic viscosity, μ/ρ, cm²/sec

ξ dimensionless variable, $x^{\frac{1}{3}}$

ξ_i , η_i dimensionless coordinates of first local maximum in temperature

ρ density of mixture, gm/cm³

ρ_I density of combustible before mixing

τ characteristic time of chemical reaction, sec

$\bar{(\ )}$ quantities in lower half-plane

$\tilde{(\ )}$ quantities in the case of uniform profiles

REFERENCES

1. Marble, F. E., and Adamson, T. C., Jr.: Jet Propulsion, *24*, 85 (1954).
2. Hirschfelder, J. O., Curtiss, C. F., Bird, R. B., and Spatz, E. L.: *Kinetic Theory of Gases*, Chap. 7, pp. 88–97. University of Wisconsin, CF 1500-A, February, 1952.
3. Adamson, T. C., Jr.: Ph.D. Thesis, California Institute of Technology, Pasadena, California (1954).
4. Howarth, P. L.: Proc. Roy. Soc. London, *A194*, 16 (1948).
5. Goldstein, S.: Proc. Cambridge Phil. Soc., *26*, 1 (1930).
6. Whittaker, E. T., and Watson, G. N.: *Modern Analysis*, Ed. 4, pp. 337–343. Cambridge University Press, 1952.
7. Kovitz, A. A.: Ph.D. Thesis, Dept. of Aeronautical Engineering, Princeton University, Princeton, N. J. (1956).

53

BOUNDARY LAYER EFFECTS ON STABILITY CHARACTERISTICS OF BLUFF-BODY FLAMEHOLDERS

By G. C. WILLIAMS, P. T. WOO[a] and C. W. SHIPMAN

Introduction

In the design of the ram-jet combustion chamber or turbo-jet afterburner one of the primary problems is that of stabilizing the flame. This is because the high heat release rate per unit volume (synonymous with high feed rates of fuel and oxidant) and small cross-section required by such burners result in inlet velocities many times the normal burning velocity of the fuel-oxidant systems used. It is usual to employ bluff (unstreamlined) bodies as stabilizers, often in the form of a network of V-shaped gutters. Relatively little quantitative information is available for prediction of the performance of such stabilizers, although some empirical rules have been developed. Certainly no quantitative picture of the mechanisms of stabilization and blowout has been given, although some qualitative conclusions are rather firmly established.

Studies of the stability limits of flames on bluff bodies in homogeneous streams of gaseous

[a] Present address, California Research Corporation.

fuel and air (all fuel oxidant systems discussed herein are of this type) by Scurlock,[13, 17] Longwell, Chenevy, Clark and Frost[5], Baddour and Carr,[1] De Zubay,[2] and many others indicate generally that the range of fuel-air ratios and velocities allowable for stable operation for geometrically similar flameholders at a given condition of approach stream turbulence, temperature, and combustion chamber geometry may be shown by plotting the group $U_{BO}/d^n P^m$ versus ϕ, the equivalence ratio.

Experimental efforts to establish the nature of the flow pattern about bluff bodies on which a stable flame is maintained have not defined the flow patterns completely. Longwell[6] and Nicholson and Field[8] have shown the existence of a recirculation zone in the immediate wake of the stabilizer, and it has been assumed that this recirculation zone takes the form of a pair of eddies as in isothermal flow.[3] Nicholson concluded from photographs of particles in the immediate wake that the eddy-pair is unstable. Zukoski, in unpublished work,[17] reports a Karman vortex trail downstream of a residual (stable but nonpropagating) flame, but this is unconfirmed in other work.[14] Schlieren cinematography of flames in the process of blowing out has shown eddy shedding clearly.[8, 14] No schlieren photograph of a stable flame, no matter how turbulent, has revealed either a density pattern or a motion of the flame fronts attributable to eddy shedding. It can be argued that the high temperatures and acceleration due to the reaction cause the vorticity of the free vortex layers to be dissipated rapidly and that the velocity gradients causing vorticity are decreased when a stable flame is maintained, consequently reducing the tendency to eddy shedding.

Studies of the effects of variation in fuel type, stabilizer dimension, and approach stream turbulence on the limits of stable operation by Scurlock,[13] and observations of flame color near the stabilizer led Baddour and Carr[1] and Williams[16] to postulate that molecular diffusion between the main stream of combustible mixture and the recirculating gases in the wake could cause the mixture burning in the immediate wake of the flameholder to be significantly different from the feed mixture, provided the fuel and oxidant have sufficiently different molecular diffusion coefficients and provided the flow at the edge of the immediate wake is laminar. These postulations by Baddour and Carr were confirmed, first by the data of Williams and Shipman[14, 18] who showed that the atomic composition of the gases on the downstream side of the stabilizers was significantly different from that of the feed, and later by Zukoski.[19, 20] In the former work only propane-air mixtures were used, and it was found that the gases in the immediate wake (recirculating gases) were completely burned and that their atomic composition was different from that of the feed, tending, however, toward that of the approach stream with increasing approach stream velocity, stabilizer size, and noise generated by the flame. This behavior parallels the transition to turbulence in the free vortex layers found in studies of isothermal flow about bluff objects[3] and was indicated qualitatively by schlieren photographs of the flames. The latter work showed in addition that the effect of other fuels, hydrogen and methane, followed the predictions of Baddour and Carr. In addition, Zukoski measured the conditions of transition to turbulence of the flame surrounding the recirculation zone, finding the transition to be a function of the Reynolds number *and* the characterizing dimension of geometrically similar stabilizers.

As a result of the studies described above it seems reasonably well established that the mechanism by which flame is stabilized on bluff objects at high velocities is different from that so well established for flames burning above tubes in that initiation of the reaction in the unburned feed does not take place by self propagation of the flame into the fresh gas, but rather by exchange of energy and mass between a stream of hot combustion products recirculated in the eddy region and the unburned gas separating from the stabilizer. Several authors seem to agree on this point.[13, 18, 20] It has been argued, however, that separation of the boundary layer from a bluff object supplies a region of relatively low velocity at a point sufficiently far from any quenching surface that the initiation of flame does take place by self propagation of the flame. Under such circumstances the effect of molecular diffusion could still be of some importance.

The mechanism of blowout is not so clearly defined, and at least three different mechanisms have been proposed in the literature[6, 8, 18] with several others being proposed less formally.

Experimental

As a means of examining further the mechanism of flame initiation, it was decided to eliminate the argument dependent on low velocity unburned

gas by removing the boundary layer from a bluff body used as a stabilizer, and to measure the effects on limits of stable operation and composition of the immediate wake.

In terms of the mechanism of flame initiation in the fresh gas by exchange of matter and energy between the burned recirculating gases and the unburned gases surrounding them, removal of the boundary layer would have three major effects. First, the unburned gas would initially contact the recirculating gas at relative velocities

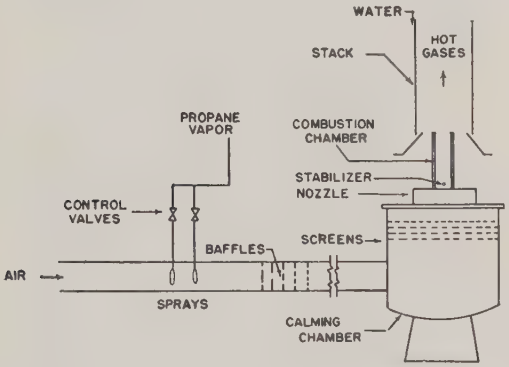

Fig. 1. Schematic diagram of apparatus.

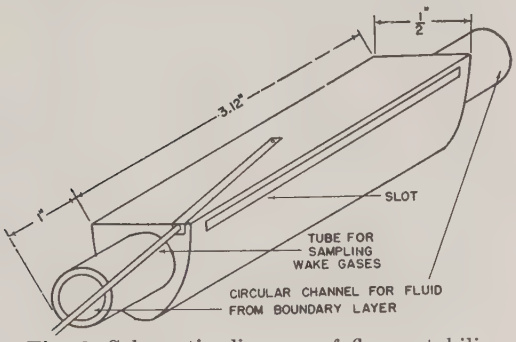

Fig. 2. Schematic diagram of flame stabilizer.

comparable to that of the approach stream. Second, the thickness of the free vortex layer established between the recirculating fluid and its surroundings would be decreased, presumably delaying transition to turbulence, *i.e.*, the zone of contact would be laminar over a greater fraction of its length. Third, since the stabilizer itself is allowed to assume an equilibrium temperature, the boundary layer is probably preheated somewhat as a consequence. Removal of the boundary layer would also remove this preheated gas, and the unburned gases making contact with the burned gas would be cooler as a result.

Two other related effects of boundary layer removal are of interest. The increased velocity of the unburned gas means that the zone of diffusion between the burned and unburned gas will be thinner and molecular diffusion more rapid as a consequence. In some cases removal of the boundary layer would place fluid having a greater momentum near the boundary, and this might shift the point of separation of the boundary layer farther downstream. If the body has a flat trailing edge, however, this delay would not be of any moment.

APPARATUS

Figure 1 is a schematic diagram of the apparatus used. The combustion chamber was 3.17 in. square in cross-section and 10 in. long, the flameholders being located 2 in. from the entrance and midway between two of the walls. One wall of the chamber was of Vycor glass. A premixed stream of propane and air was fed to the combustion chamber through a calming section and a nozzle of 30:1 contraction ratio, insuring an homogeneous feed stream of low turbulence and flat velocity profile. All data were taken with the feed at about 70°F and the exhaust of the chamber at atmospheric pressure.

The flame stabilizers were semi-cylindroids extending the full width of the chamber. The flat side, corresponding to the minor axis, faced directly downstream. The elliptical cross-section was selected because it allowed the formation of a suitable boundary layer on the upstream side and provided a definite point of flow separation at its downstream edge. The ratio of the major to the minor axis of the ellipses was arbitrarily set at two, and stabilizers with minor axes of ½ and ¼ in. were used. Slots milled along the trailing edges of each stabilizer communicated with a cylindrical channel inside the stabilizer and allowed withdrawal of the boundary layer. The locations and widths of the slots were as follows:

Stabilizer (Minor axis)	Slot Width	Distance from Trailing edge
in.	*in.*	*in.*
½	0.016	0.048
¼	0.010	0.025

The rate of fluid withdrawal was measured by means of an orifice. Figure 2 is a drawing of the ½-in. stabilizer.

Gas samples were withdrawn from the immediate wake through a stainless steel tube im-

bedded in the downstream face of the ½-in. stabilizer and through a water-cooled probe of 1/16 in. outside diameter, held flush with the downstream side of the ¼-in. stabilizer. The rate of sampling was measured by means of a capillary flow meter. The sampling rate was arbitrarily selected as one per cent of the volume flow rate specified by the product of the volume of a cube having the characteristic dimension of the stabilizer and the frequency of eddy shedding obtained from data on isothermal flow. The gas samples were analyzed by the Orsat technique, unburned hydrocarbons being determined by slow combustion with oxygen over a hot platinum filament.

The stability limits of the stabilizers, both with and without boundary layer removal, were established at each velocity by maintaining constant air flow and varying the fuel flow rate until blowout occurred. For those data with boundary layer removal, the mass rate of withdrawal was kept constant for a given air flow rate.

Effect of Boundary Layer Removal on Blowout

The effects of boundary layer removal on the blowout using the ½-in. stabilizer are shown in Figure 3 for lean mixtures and in Figure 4 for rich mixtures. In these figures the equivalence ratio at blowout, ϕ, is plotted against the suction parameter, λ, for constant entrance velocity. The suction parameter is defined as

$$\lambda \equiv W_s/(U_0 d)^{\frac{1}{2}} \qquad (1)$$

This definition is a consequence of boundary layer theory which states that the displacement thickness of the boundary layer is proportional to the square root of the Reynolds number. So defined, the suction parameter is a measure of the ratio of the flow through the slots to the boundary layer flow.

The pertinent features of Figure 3 (lean limit blowout) are that the removal of the boundary layer causes a shift to higher equivalence ratios (richer mixtures), that the shift decreases with increasing velocity, and that the equivalence ratio approaches an asymptotic value with increasing values of the suction parameter. Study of Figure 4 (rich limit blowout) shows that boundary layer removal has a mild effect of shifting the equivalence ratio at blowout to richer mixtures at low velocity, that this effect increases with velocity to a maximum, falling off again at higher velocity, and that at the highest velocity studied the effect of boundary layer removal is a shift to less rich mixtures. As in Figure 3, the equivalence ratio at blowout approaches an asymptote with increasing rate of flow through the slots.

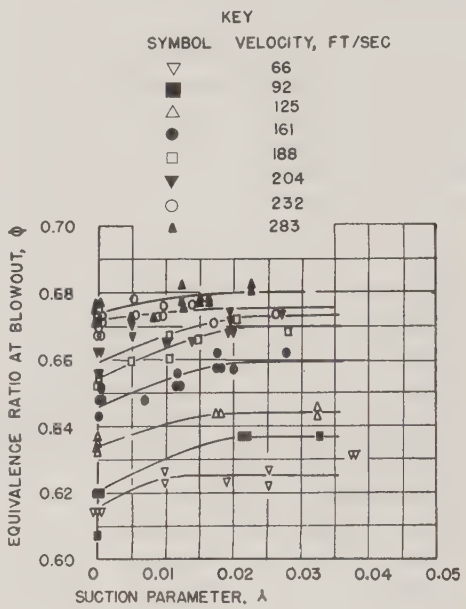

Fig. 3. Effect of boundary layer on lean limit, ½-inch stabilizer.

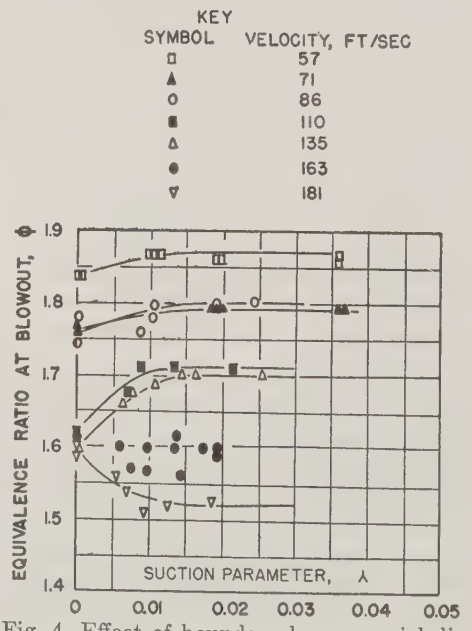

Fig. 4. Effect of boundary layer on rich limit, ½-inch stabilizer.

The value of λ at which the curves of Figures 3 and 4 reach the asymptote is defined as λ^*.

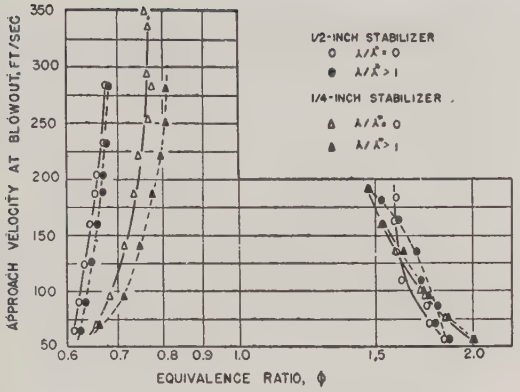

Fig. 5. Stability limits.

This value is believed to indicate the suction rate at which all of the boundary layer is removed. A further increase in suction rate, within limits, should have no effect.

Data obtained using the ¼-in. stabilizer were different from those obtained with the ½-in. flameholder in some respects. The effect of boundary layer removal on the lean limit was, generally speaking, a shift to richer mixtures as with the larger stabilizer, but the amount of the shift increased with increasing velocity, a trend opposite to that found for the larger flameholder. The effect of boundary layer removal on the rich limits of the ¼-in. stabilizer was generally a shift to richer mixtures, the amount of the shift (in terms of equivalence ratio) being small in any case and passing from a negligible value at low velocities through a maximum to a negligible value at high velocities. The shift of the rich limit to leaner mixtures noted for the data obtained from the ½-in. stabilizer was not found with the smaller unit at the highest velocity studied (192 ft/sec).

It was found that during operation the flat side of the ¼-in. flameholder warped so that the width of the slots was not uniform. Hence the rate of removal of fluid through the slots was not uniform over the length of the stabilizer. While this undoubtedly influenced the shape of the curves of equivalence ratio at blowout versus the suction parameter, the trends given above are believed to be valid, since the curves of the equivalence ratio at blowout became asymptotic with increasing values of the suction parameter as did those for the larger stabilizer.

Figure 5 shows the stability limit data plotted on the usual co-ordinates of approach velocity at blowout versus equivalence ratio. It is interesting to note that at low velocities the ¼-in. stabilizer has wider rich limits than the ½-in. stabilizer. This has been noted often in other work and is probably due to a change in mechanism of blowout.

Effect of Boundary Layer Removal on Gas Composition in the Immediate Wake

As indicated in the Introduction molecular diffusion across the incipient flame zone in the region corresponding to the free vortex layers would be expected to cause a difference between atomic compositions of the wake and of the feed mixture. As a measure of the effect, the parameter

$$\alpha \equiv (\Sigma C/N_2)_w/(\Sigma C/N_2)_0 \qquad (2)$$

(where the subscript w refers to the wake and the subscript $_0$ refers to the feed mixture) has been used.[18, 19] (This is Zukoski and Marble's Λ.[20])

Data obtained from the present experiments are shown in Figures 6 and 7 for the ¼-in. and ½-in. stabilizers respectively, with feed composition and λ/λ^* as parameters. Figures 8 and 9 show the velocities and equivalence ratios at which the samples were taken. For reference,

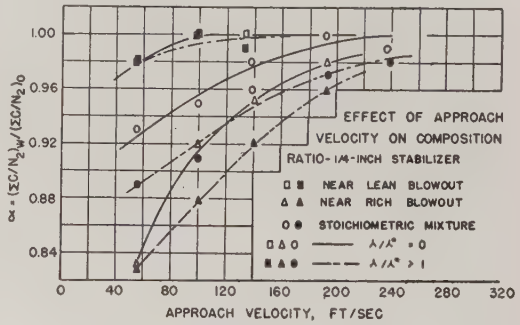
EFFECT OF APPROACH VELOCITY ON COMPOSITION RATIO- 1/4-INCH STABILIZER
NEAR LEAN BLOWOUT
NEAR RICH BLOWOUT
STOICHIOMETRIC MIXTURE
APPROACH VELOCITY, FT/SEC

Fig. 6. Effect of approach velocity on composition ratio, ¼-inch stabilizer.

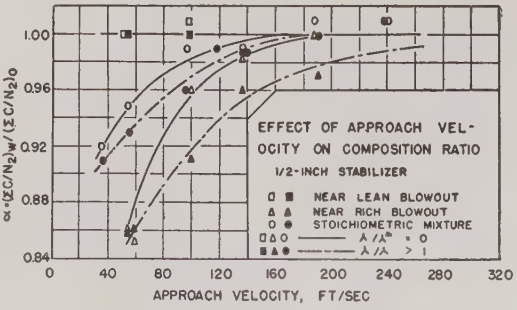

Fig. 7. Effect of approach velocity on composition ratio, ½-inch stabilizer.

the stability limits of the systems are indicated, and in Figure 9 the effect of the cooled sampling probe on the stability limits of the ¼-in. stabilizer is also shown.

It is immediately obvious that α approaches unity as velocity is increased, and that removal of the boundary layer decreases the value of α. The strong influence of feed composition on α will be discussed later.

Physically, α is a measure of the relative concentrations of carbon-containing compounds in the wake and in the feed. Since the carbon-containing products of combustion (CO_2, CO) have higher molecular diffusion coefficients than does the fuel, steady state requires a lower concentration of carbon atoms in the wake than in the feed mixture. For purposes of analysis of the effects of molecular diffusion on the stability, however, a parameter showing the relative rates of diffusion of fuel and oxidant would be more desirable. For this purpose a parameter called "excess oxygen" (ξ) has been defined equal to the moles of oxygen per mole of nitrogen in excess of that required for complete combustion

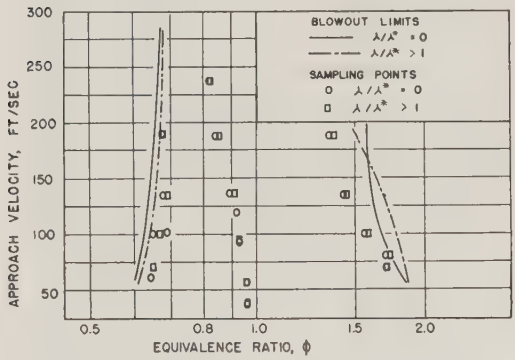

Fig. 8 Approach stream conditions for sampling (½-inch stabilizer).

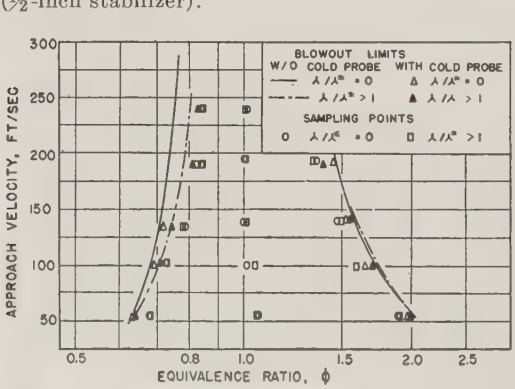

Fig. 9. Approach stream conditions for sampling (¼-inch stabilizer).

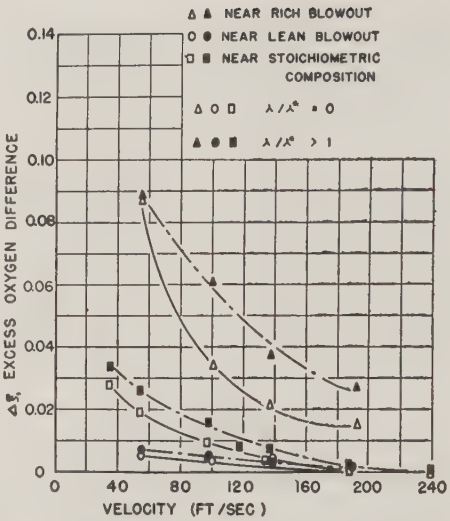

Fig. 10. Effect of velocity and composition on excess oxygen difference, ½-inch stabilizer.

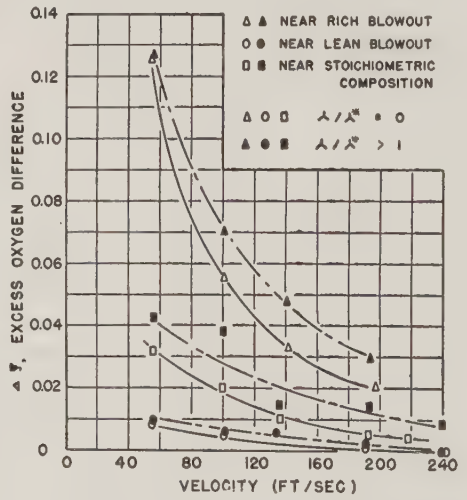

Fig. 11. Effect of velocity and composition on excess oxygen difference, ¼-inch stabilizer.

of the mixture of CO_2 and H_2O. (For rich mixtures ξ will be negative.) The difference in atomic compositions of the wake and feed stream will then be represented by

$$\Delta\xi = \xi_w - \xi_0 \qquad (3)$$

A positive value of $\Delta\xi$ indicates the wake composition to be "leaner" than that of the feed. (This cannot be converted to a change in equivalence ratio because the carbon-hydrogen ratio of the wake gases can be significantly different from that of the fuel). The data of Figures 6 and 7 are plotted on this basis in Figures 10 and 11. The additional information to be obtained from

these plots is that the effect of molecular diffusion is to cause the wake composition to be "leaner" than the feed composition in accordance with the hypothesis of Baddour and Carr.[1]

None of the gas samples contained unburned fuel, even for those conditions near blowout. However, it should be pointed out that due to the steep slope of the stability limit curves, a data point "near blowout" as measured by equivalence ratio was actually quite far removed from blowout velocity (Figs. 8 and 9). This is in part due to the difficulty of control of fuel-air ratio

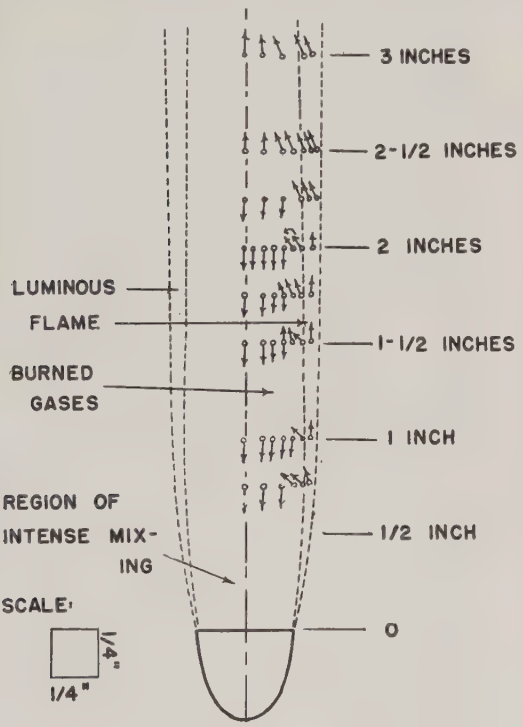

Fig. 12. Results of probing.

and in part due to the unstable character of the system itself, preventing stable operation closer to the blowout points for periods long enough to obtain a gas sample. Further, even the attempts to take samples at stoichiometric composition left something to be desired (Fig. 8).

Experiments on Determination of the Flow Pattern in the Wake Near the Stabilizer

Some indications of the flow patterns in the wake near the stabilizer were obtained by inserting at various locations in the wake region a ceramic rod of 0.038 in. diameter coated with sodium chloride. The mean direction of the flow was indicated by the characteristic yellow glow of the sodium particles. These studies were conducted using the ½-in. stabilizer at an approach velocity of 118 ft/sec and an equivalence ratio of 0.67. The results are shown in Figure 12. For a distance of about ½ in. downstream of the stabilizer, insertion of the rod at any point between the flame fronts immediately colored the entire region, and it was concluded that this is a region of rapid mixing. A hydrodynamic explanation for this has not been found, and more study is indicated. For a distance of about five stabilizer widths downstream, an upstream motion was found at the center of the wake, while a downstream motion was found at the edges of the flame zone. This figure of five stabilizer widths for the length of the recirculation zone does not agree with the value of about two obtained by other experimenters[5, 8] and found also for isothermal flow.[3] It is, however, comparable to the length of residual flames.[14]

As a result of these studies the hypothetical model of Figure 12 was drawn. In this model it is assumed, in accordance with the results of the probing, that any gases entering the region about one stabilizer diameter downstream of the flameholder are immediately mixed and distributed throughout the entire region. Material enters this region by molecular diffusion, eddy diffusion, and recirculation. Material leaves this region by molecular diffusion, eddy diffusion, and a bulk flow assumed to be about equal to that entering by recirculation. The material leaving the wake by bulk flow passes along a boundary over which there is sufficient eddy diffusion to bring its atomic composition to that of the feed stream, and it may be assumed that it is this material which is recirculated.

Semi-Theoretical Analysis of Transfer of Mass Into and Out of the Immediate Wake

Exact solutions of the problem of diffusion between the recirculation zone and the main stream are not available. Even an approximate attempt is hindered by lack of knowledge of the flow pattern in the wake of a bluff object on which a flame is stabilized. Rough attempts to predict the effect of molecular diffusion have been made,[14] and Marble and Adamson[7] have treated the problem of interaction between parallel streams of burned and unburned gas with no initial velocity gradient. In no case has an attempt been made to include the effect of eddy diffusion.

By using the model of Figure 13 and making

several simplifying assumptions, steady-state material balances can be written on the immediate wake for each atomic species. It should be emphasized that the model of Figure 13 is based on the results obtained in the present experiments only, and other more conventional models, based on isothermal flow patterns, will yield similar equations. Indeed, other models could be developed based on the present experiments. The simplifying assumptions are:

(1) Thermal diffusion can be neglected.

(2) Composition gradients are linear.

(3) The compositions on the two sides of the vortex layers can be represented by suitable averages.

(4) The thicknesses of the laminar and turbulent diffusion zones may each be represented by a suitable average.

(5) The mole fraction of nitrogen at all points is large, permitting the driving forces for diffusion to be represented by the gradient of the ratio of the moles of diffusing component to that of nitrogen.

(6) The gas entering the immediate wake by recirculation has the same composition as the feed stream, and the bulk flow out of the immediate wake has the same composition as the immediate wake. (The moles of nitrogen entering or leaving the immediate wake per unit time by bulk flow are designated by B.)

(7) The mole fraction of propane in the immediate wake, and the mole fractions of carbon monoxide, hydrogen, water, and carbon dioxide in the main stream are negligiby small.

With these broad assumptions steady-state material balances can be written on the eddy zone for carbon, oxygen, and hydrogen, *viz.*:

Carbon balance:

$$(Y_{w,CO_2} + Y_{w,CO}) - 3Y_{0,C_3} = \frac{2x_L L}{\delta_L B'} (D_{CO_2}\Delta Y_{CO_2} + D_{CO}\Delta Y_{CO} + 3D_{C_3}\Delta Y_{C_3}) \quad (4)$$

Hydrogen balance:

$$(Y_{w,H_2} + Y_{w,H_2O}) - 4Y_{0,C_3} = \frac{2x_L L}{\delta_L B'} (4D_{C_3}\Delta Y_{C_3} + D_{H_2}\Delta Y_{H_2O} + D_{H_2}\Delta Y_{H_2}) \quad (5)$$

Oxygen balance:

$$(Y_{w,O_2} + \tfrac{1}{2}Y_{w,CO} + Y_{w,CO_2} + \tfrac{1}{2}Y_{w,H_2O}) - Y_{0,O_2} = \frac{2x_L L}{\delta_L B'} (D_{O_2}\Delta Y_{O_2} + \tfrac{1}{2}D_{CO}\Delta Y_{CO} + D_{CO_2}\Delta Y_{CO_2} + \tfrac{1}{2}D_{H_2O}\Delta Y_{H_2O}) \quad (6)$$

In these equations

$$B' = B + 2\frac{Ex_t L}{\delta_t} \quad (7)$$

and

$$\Delta Y = Y_0 - Y_w \quad (8)$$

Nomenclature may be found in the table at the end of this paper.

Equation (4) may be put in a form to give α directly by division of both sides by $3Y_{0,C_3}$ and rearranging, *viz.*:

$$\frac{Y_{w,CO_2} + Y_{w,CO}}{3Y_{0,C_3}} = \alpha = \frac{2x_L L}{\delta_L B'} \cdot \frac{(D_{CO_2}\Delta Y_{CO_2} + D_{CO}\Delta Y_{CO} + 3D_{C_3}\Delta Y_{C_3})}{3Y_{0,C_3}} + 1 \quad (9)$$

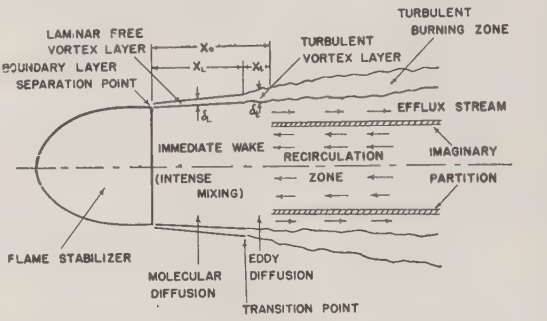

Fig. 13. Hypothetical model of flames held on bluff bodies.

Thus it can be seen that α is a function, not only of the character of the vortex layer as indicated by the group $x_L/\delta_L B'$, but also a function of the feed composition. This is clearly indicated by Figures 6 and 7.

Equations can be written in the same manner as Equations (4), (5) and (6) to give the excess oxygen difference between the wake and feed mixtures.

$$\Delta\xi = \xi_w - \xi_0 = (Y_{w,O_2} - \tfrac{1}{2}Y_{w,CO} - \tfrac{1}{2}Y_{w,H_2}) - (Y_{0,O_2} - 5Y_{0,C_3}) = \frac{2x_L L}{\delta_L B'} \cdot (D_{O_2}\Delta Y_{O_2} - \tfrac{1}{2}D_{CO}\Delta Y_{CO} - \tfrac{1}{2}D_{H_2}\Delta Y_{H_2} - 5D_{C_3}\Delta Y_{C_3}) \quad (10)$$

Again it is obvious that $\Delta\xi$ is a function of the flow pattern and the composition of the feed. Presumably it would be possible to normalize the curves of Figures 6, 7, 10, and 11 by dividing α and $\Delta\xi$ by the terms in parenthesis on the right

hand sides of Equations (9) and (10) respectively, but the approximations of the equations hardly justify such a procedure. Furthermore, the quantity B is unknown but is probably a function of the temperature of the products of combustion.

From Equations (9) and (10) it can be seen that α and $\Delta\xi$ will be functions of the flow pattern as the group $x_L/\delta_L B'$ is varied. While the

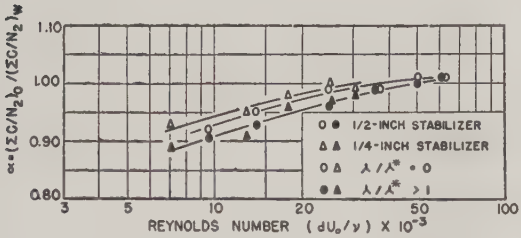

Fig. 14. Effect of Reynolds number on composition ratio (stoichiometric mixtures).

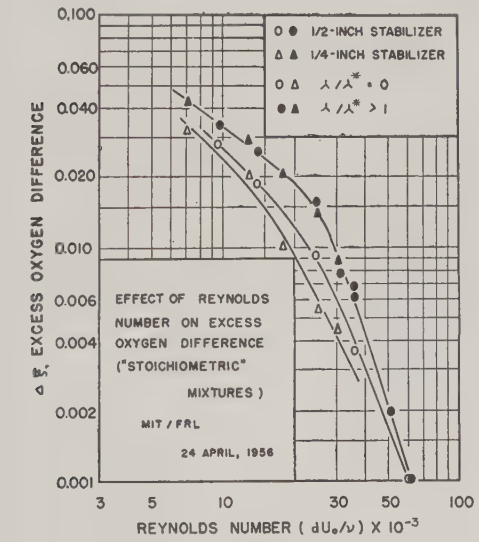

Fig. 15. Effect of Reynolds number on excess oxygen difference ("stoichiometric" mixtures).

flow pattern has been well defined for isothermal flow, the effects of boundary layer removal and/or combustion are not known. It is reasonable to expect that x_L/δ_L will decrease and that B' will increase with Reynolds number. Further, since the volume of recirculating gases depends on the size of the eddy region, the mass of these gases (B) will be a function of the temperature. Removal of the boundary layer would be expected to increase x_L/δ_L as indicated in the Experimental section.

With the aid of Equations (9) and (10) an explanation of Figures 6, 7, 10 and 11 will be given. For any one curve it would be expected that $\Delta\xi$ would decrease and α would approach unity with increasing velocity because of the decrease in the group $x_L/\delta_L B'$, bearing in mind that there is an additional effect of variation in composition, particularly for the curves near rich and lean blowout. That is, as the velocity increases, the length over which the free vortex layer remains laminar decreases due to the increased rate of shear. There will be some velocity at which the laminar portion of the free vortex layers is so small that the composition of the wake and of the free stream are nearly the same. The data of Figures 6, 7, 10 and 11 behave well in this respect.

The effect of boundary layer removal on the group $x_L/\delta_L B'$, would probably be an increase, but this simple statement needs further clarification. At very low velocities, where nearly the entire length of the vortex layers is laminar, removal of the boundary layer would not be expected to influence x_L greatly. As indicated in the Experimental section of this paper, boundary layer removal might decrease δ_L. Thus, one would conclude that α and $\Delta\xi$ might not be as greatly altered by removing the boundary layer at low velocities as at intermediate velocities. This expectation is realized in the curves of α and $\Delta\xi$ versus velocity for mixtures near rich blowout for both stabilizers (Figs. 6, 7, 10 and 11). The situation is not clear for the other compositions. For a better comparison, α and $\Delta\xi$ have been plotted against Reynolds number based on stabilizer minor axis for nearly constant composition in Figures 14 and 15 respectively. (It is noted that there is no justification in terms of the experimental data for the use of the Reynolds number because the viscosity was not varied. Furthermore, it has not been shown that the Reynolds number should be a correlating parameter.) In Figure 15, where the over-all pattern of results may be seen, the predicted smaller effect of boundary layer removal at low Reynolds number is borne out to some degree. Figure 14 does not show the effect. In general it must be concluded that removal of the boundary layer increases the rate of molecular diffusion even at low Reynolds numbers, because the thickness of the diffusion zone is decreased.

At high velocities, where nearly the entire length of the vortex layers would be expected to be turbulent, boundary layer removal might delay transition to turbulence, but at sufficiently high velocities the delay would be negligible.

Furthermore, as the velocity is increased the eddy diffusivity and recirculation rate would be expected to increase, increasing the value of B'. Thus, at high Reynolds numbers (velocities) the effect of boundary layer removal on α and $\Delta\xi$ would be small. These expectations are amply fulfilled by the data.

One other feature of the curves remains to be explained. This feature is particularly obvious in Figure 15 where it can be seen that (a) the effect of boundary layer removal on $\Delta\xi$ is greater for the $\frac{1}{4}$-in. stabilizer than for the $\frac{1}{2}$-in. stabilizer at constant Reynolds number, and (b) that the use of the Reynolds number as a parameter correlates the data from both stabilizers with the boundary layer removed.

One obvious explanation for the failure of a correlation of $\Delta\xi$ with Reynolds number for the case of the unaltered boundary layer is the variation in feed composition, *i.e.*, the effect is not real. However, Williams and Shipman[18] concluded from schlieren photographs of flames stabilized on circular cylinders that the Reynolds number did not characterize the flame structure and found that the pressure distribution on the surface of the flameholders was a function of stabilizer diameter at constant Reynolds number. Zukoski,[19] using water-cooled cylinders as flameholders, found that the Reynolds number at which the vortex layers became completely turbulent increased with the stabilizer diameter. Another possible explanation for the phenomenon is that when the boundary layer is removed, the gases in the wake are contacted by cold, unburned gases, giving rise to similar boundary conditions for the vortex layers of both sizes of stabilizer, with respect to both temperature and velocity gradient. For the case of the unaltered boundary layer it is possible that the temperature of the fluid separating from the flameholder would depend on the size of the flameholder. Thus, in the former case the Reynolds number might well be a correlating parameter, while in the latter case it would not. It might be assumed that this argument is negated by Zukoski's measurements with cooled flameholders, but unless it is established that the cooling gives rise to similar boundary conditions, the question must remain open.

Figure 15 may also be used to compare the data of Zukoski[19] and of Williams and Shipman[18] with the present work. Zukoski found from schlieren photographs that the Reynolds number for complete transition to turbulence in the free vortex layers was between 1×10^4 and 4×10^4, depending on the stabilizer diameter and shape. From measurements of gas composition in the wake Zukoski found the critical Reynolds number to be 4×10^3. The data of Williams and Shipman allow calculation of a critical Reynolds number of about 2.5×10^4. The present data (Fig. 15) indicate a critical Reynolds number of about 5 to 7 $\times 10^4$. Sampling rates for the work of Williams and Shipman and for the present experiments were much lower than those used by Zukoski. Undoubtedly such factors as noise generated by the flame and variations in flameholder geometry also influence the critical Reynolds number. There does seem to be a qualitative agreement, however, realizing the limitation that the Reynolds number is not a general correlating parameter.

The effect of boundary layer removal on the range of equivalence ratios and velocities over which stable operation can be maintained can be dependent on two effects. First, the modification of the composition of the immediate wake could make the flame more stable for a given feed if the shift of composition were toward the stoichiometric mixture, *et contra*. Second, removal of the boundary layer means that the unburned gases contacting the burned gases in the immediate wake will, in general, be cooler (because they have not been in contact with the hot flameholder) which should have an adverse effect on the stability.

For example, for lean mixtures, the gases contacting the burned gases in the wake will be cooler when the boundary layer is removed, and, due to diffusion, the mixture burning in the vortex layers would be fuel lean compared with the feed when propane or a higher hydrocarbon is the fuel. One would expect, then, that removal of the boundary layer would curtail the lean limit of stable operation. Further, one would expect the effect of boundary layer removal to follow the alteration in composition in some measure. That is, at low Reynolds numbers (small stabilizer and low velocity) the alteration of composition is not great, and the change in the blowout limit is due primarily to the decrease in temperature of the unburned gas. As the velocity and/or stabilizer dimension is increased (increase of Reynolds number) the alteration of composition becomes appreciable, and this effect is added to that of the cooler unburned gas. Finally, for high velocities and large stabilizer sizes, the alteration in composition is again small, the stability limit

being affected primarily by the cold fresh gas. These general expectations are amply borne out by the data, the results from the ¼-in. stabilizer showing an increased change of the stability limits with increasing velocity and the results from the ½-in. stabilizer showing a decreased alteration with increasing velocity, limits in all cases being curtailed.

For rich mixtures the effect of diffusion would be to extend the rich limit, *i.e.*, the mixture burning in the vortex layers would be leaner in fuel than the feed. However, the cooler unburned gases would curtail the rich limit. Thus, there are two opposing effects. At high velocities, where the change of composition due to removal of the boundary layer is small, the limit would be curtailed by the "cold gas" effect, while at lower velocities the effect of diffusion could be more important. The data of Figure 4 bear out such predictions, the rich limit being extended at low velocities due to the diffusion and curtailed at high velocities due to the cooler unburned gas.

Conclusions

The role of the boundary layer in the stabilization of flame by bluff objects seems to be twofold. First, it determines the aerodynamic character of the zone of contact between the burned gas in the immediate wake of the stabilizer and the unburned gas of the feed stream. Second, by its contact with the stabilizer, its presence means that the unburned gases coming into the zone of initial combustion have been preheated. That the boundary layer moves relatively slowly seems to be of little moment except as it influences the character of the zone of contact (laminar or turbulent) between burned and unburned gas. The dual role of the boundary layer is shown in the effect of boundary layer removal on the stability limits. There is a consistent shift of blowout composition to broader limits commensurate with the shift in atomic composition of the immediate wake toward the stoichiometric, and conversely; and there is a curtailment of the limits of stability where the effect of lack of preheating overshadows the shift of composition.

These effects of boundary layer removal seem to substantiate the conclusion that ignition of the fresh feed takes place by contact of and mass and energy transfer between the burned gases of the immediate wake and the unburned gases in the free vortex layers. It also emphasizes the fact that a region of slowly moving unburned gas is not required for stability in these circumstances (at least in the initial stages).

From the practical point of view the results of the present experiments, as well as earlier ones, seem to indicate that while for burners operating at atmospheric pressure the influence of molecular diffusion is probably negligible, at high altitudes, where the pressure may be as low as 0.2 atmos. and the feed temperature may be as high as 600°F, the Reynolds number may well be reduced below the critical values of 1 to 5×10^4, and molecular diffusion would then be of importance.

Acknowledgments

The able assistance of A. C. Tobey in all experiments is gratefully acknowledged.

The research reported here was done in connection with Contract N6-ori-105, Task Order III for Project Squid, a cooperative research project in jet propulsion under the sponsorship of the Office of Naval Research, Department of the Navy, the Office of Ordnance Research, Department of the Army, and the Office of Scientific Research, Department of the Air Force. The authors acknowledge with thanks the sponsorship of the study and the permission to publish this paper.

Nomenclature and Abbreviations

B	moles of nitrogen per unit of time entering wake by recirculation
B'	defined by Equation (8)
d	characteristic dimension of bluff object, *i.e.*, diameter of a cylinder, minor axis of an ellipse
D	molecular diffusivity, moles/time × distance
E	eddy diffusivity, moles/time × distance. This is the product of the eddy diffusivity normally used and the mol density.
L	length of stabilizer
m	empirical exponent
n	empirical exponent
P	pressure
S_L	normal burning velocity for laminar flow
U	velocity at combustion chamber entrance, ft/sec
W_s	mass rate of flow through slots in flameholder (lb/min)

x_t turbulent length of free vortex layers

x_L laminar length of free vortex layers

Y_{O_2}, Y_{C_3}, Y_{H_2}, Y_{H_2O} mole ratio of subscript component to nitrogen

ΔY difference between the values of Y in the free stream and the wake

GREEK

α ratio of total carbon per mole of nitrogen in the wake to that of the free stream

δ_L thickness of laminar diffusion zone

δ_t thickness of turbulent diffusion zone

ξ excess oxygen. Moles of oxygen per mole of nitrogen in excess of that required to burn the mixture completely

λ suction parameter. Defined by Equation (1)

ν kinematic viscosity

ϕ equivalence ratio (ratio of fuel supplied to that stoichiometrically required)

SUBSCRIPTS

0 free stream

w wake

L laminar

t turbulent

C_3 propane (other chemical species denoted by their chemical symbols)

BO blowout condition

REFERENCES

1. Baddour, R. F., and Carr, L. D.: S. M. Thesis, Department of Chemical Engineering, Massachusetts Institute of Technology (1949).
2. DeZubay, E. A.: Aero. Digest, *61*, 54–56 and 102–104 (1950).
3. Goldstein, S. (ed.): *Modern Developments in Fluid Dynamics*. Oxford at the Clarendon Press, 1938.
4. Kovasnay, L. S. G.: Proc. Roy. Soc. (London), *A198*, 174–190 (1949).
5. Longwell, J. P., Chenevy, J. E., Clark, W. W., and Frost, E. E.: *Third Symposium on Combustion, Flame, and Explosion Phenomena*, p. 40. Baltimore, The Williams & Wilkins Co., 1949.
6. Longwell, J. P., et al.: Ind. Eng. Chem., *45*, 1629 (1953).
7. Marble, F. E., and Adamson, T. C.: Ignition and Combustion in a Laminar Mixing Zone, in *Selected Combustion Problems (AGARD)*. London, Butterworths, 1954.
8. Nicholson, H. M., and Field, J. P.: *Third Symposium on Combustion, Flame, and Explosion Phenomena*, p. 44. Baltimore, The Williams & Wilkins Co., 1949.
9. Roshko, A.: On the Development of Turbulent Wakes from Vortex Streets. NACA TN 2913, March, 1953.
10. Roshko, A.: J. Aeronaut. Sci. *22*, 124 (1955).
11. Schiller, L., and Linke, W.: Pressure and Frictional Resistance of a Cylinder at Reynolds Numbers 5000 to 40,000. NACA TM 715, July (1933).
12. Schram, C.: S. B. Thesis, Department of Chemical Engineering, Massachusetts Institute of Technology (1951).
13. Scurlock, A. C.: Flame Stabilization and Propagation in High Velocity Gas Streams. Meteor Report 19, Fuels Research Laboratory, Massachusetts Institute of Technology (1948).
14. Shipman, C. W.: Sc.D. Thesis, Dept. of Chemical Engineering, Massachusetts Institute of Technology (1952).
15. Spalding, D. B.: *Gas Turbine Series*, Vol. 2, p. 192. New York, Academic Press, 1955.
16. Williams, G. C.: J. Aeronaut. Sci., *16*, 12, 714 (1949).
17. Williams, G. C., Hottel, H. C., and Scurlock, A. C.: *Third Symposium on Combustion, Flame, and Explosion Phenomena*, p. 21. Baltimore, The Williams & Wilkins Co., 1949.
18. Williams, G. C., and Shipman, C. W.: *Fourth Symposium (International) on Combustion*. p. 733. Baltimore, The Williams & Wilkins Co., 1953.
19. Zukoski, E. E.: Ph.D. Thesis, California Institute of Technology (1954).
20. Zukoski, E. E., and Marble, I. E.: The Role of Wake Transition in the Process of Flame Stabilization on Bluff Bodies, in *AGARD, Combustion Research and Reviews*. London, Butterworths, 1955.

54

SOME EFFECTS OF FUEL REACTIVITY AND HEAT LOSS ON FLAME STABILIZATION

By MALCOLM A. WEISS, JAMES C. ROHRER AND JOHN P. LONGWELL

In published studies of flame stabilization in turbulent air streams, emphasis has usually been placed on varying pressure, velocity, and stabilizer geometry for both baffles, e.g., Weir, Rogers and Cullen[1] and DeZubay,[2] and cans, e.g., Weiss and Longwell[3] and Probert.[4] Despite the work already done, there is still no clear understanding of the details of the stabilization mechanism. A number of theories have been published, e.g., Mullins,[5] Spalding,[6] and Longwell, Frost and Weiss,[7] which describe performance in terms of a physical model and some combustion characteristic of the fuel. These theories usually account reasonably well for the known effects of pressure, velocity, and stabilizer size. Although different measures of fuel chemical reactivity are assumed in each, few results of systematic changes in fuel reactivity have been published against which to test these measures. Furthermore, the effect of heat losses from the stabilization zone would be expected to be different for each theory. Therefore, in this study, interest was centered on effects due to the chemical nature of the fuel, and to heat transfer from the walls of a typical can. For the tests, large stabilizers were used, both cans and baffles. In this way, wall effects were minimized and the stabilizers were close in size to stabilizers suitable for practical applications. The fuel-air mixing variable was eliminated by testing with completely homogeneous mixtures of fuel and air approaching at about 400°K.

Effects of Fuel Type

In order to determine the influence of chemical variables on flame stability, a series of tests was conducted in which lean blowout equivalence ratios were measured with eight fuels of widely varying reactivity, ranging from hydrogen to isopropyl chloride. The stabilizers tested included a 1-in. V-gutter, a 2-in. cone baffle, a 3-in. and a 6-in. diameter cylindrical single-stage can, and two 2 by 10-in. rectangular single-stage cans. Each stabilizer was mounted near the end of a 10-in. pipe exhausting to the atmosphere; details of mounting and stabilizer geometry are shown in Figure 1. The pipe itself consisted of a straight section about 20 diameters long, preceded by two perforated velocity distribution plates (the second of which choked). Upstream of these plates, fuel was injected and mixed with the air at a constant humidity of 0.025 lb water/lb air. The flow approaching the stabilizer was homogeneous and probably was close to equilibrium turbulent pipe flow. A measured velocity profile did correspond to the profile for fully developed pipe flow. The test procedure was to ignite the stabilizer with a spark at a relatively rich mixture of air and fuel and then gradually to decrease the fuel rate until the flame blew out. This sequence was immediately repeated one or two more times to check the blowout point, usually with excellent reproducibility. Once the point had been established for one fuel, the entire procedure would be repeated for another fuel, and then for a third or fourth fuel, if necessary. The fuels burned were of commercial purity, used as received. They included isopropyl chloride, isooctane, heptane, benzene, tetralin, propylene oxide, carbon disulfide, and hydrogen. Testing of hydrogen was made practicable by the commercial availability of tank trailers, each containing 30,000 to 50,000 SCF.

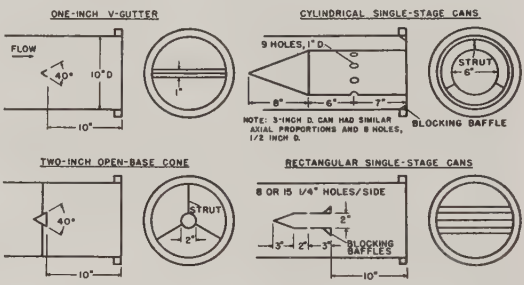

Fig. 1. Mounting of flame stabilizers near end of a ten-inch pipe.

In the test series described above, nothing was changed but the nature of the fuel and the fuel rate; that is, air rate, temperature, pressure, and geometry were held fixed. The observed results then consisted of the lean blowout equivalence ratio varying with the chemical nature of the fuel, all other conditions constant.

A recurring problem in almost all large scale combustion measurements is the lack of repro-

ducibility of data from one day to another under presumably identical conditions. Because some accuracy was desired in these studies, a reference fuel technique was used to minimize the effects of poor reproducibility. That is, every fuel tested was compared on the same day to a reference fuel, chosen here to be isooctane. The technique becomes clearer on examining the results of Figure 2. Figure 2 shows, for a 1-in. V-gutter stabilizer, the relation between lean blowout equivalence ratio and duct air flow for all the fuels tested on the several dates on which tests were conducted.

For example, consider the data of July 18, 1955, in Figure 2, the circular points. On this date propylene oxide, benzene, and isooctane were tested. Interpolating between the data points, the air rate corresponding to isooctane blowout at an equivalence ratio of 0.600 is 7.6 lb/sec. (The reference equivalence ratio for isooctane was chosen, arbitrarily, as 0.600.) At this same air rate, interpolating between the data points for propylene oxide and benzene, the propylene oxide equivalence ratio is 0.480 and the benzene equivalence ratio is 0.535. On November 9, 1955, isooctane was compared to carbon disulfide in the same apparatus. This time, the isooctane blowout point at an equivalence ratio of 0.600 was 6.4 lb/sec and at this air rate on the same date, carbon disulfide blew out at an equivalence ratio of 0.327. Similarly, on other dates and in other stabilizers, the blowouts for various fuels were determined by direct comparison on the same dates with the reference isooctane blowouts. In this way, day-to-day variations in the specific air mass flows at blowout had minimum effect on the results. Variations during a single day were usually negligible; this was checked by determining the reference fuel blowout both before and after all other runs.

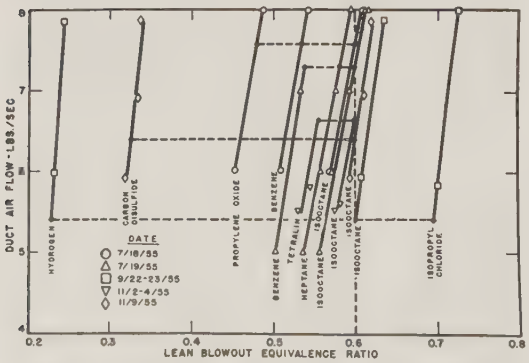

Fig. 2. Blowout data from a one-inch V-gutter.

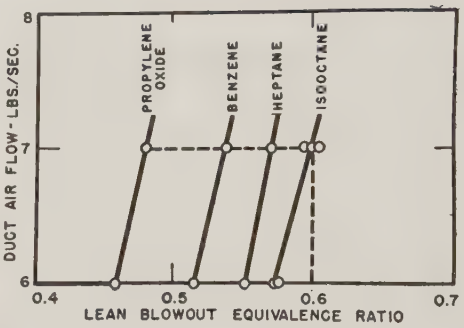

Fig. 3. Blowout data from a two-inch cone baffle.

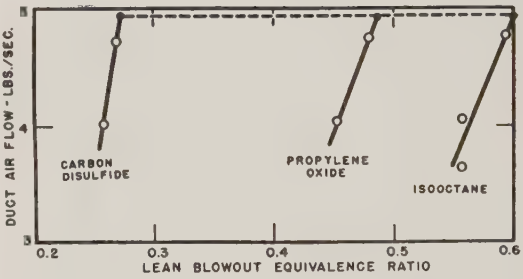

Fig. 4. Blowout data from a three-inch diameter single-stage can.

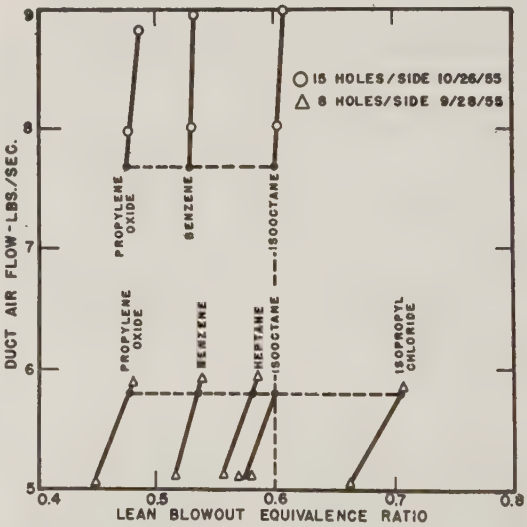

Fig. 5. Blowout data from two-inch thick single-stage rectangular cans.

All the data points taken are shown in Figures 2, 3, 4, and 5. The summarized results, based on the reference value of 0.600 for isooctane, are given in Table 1. (Table 1 also lists several results for a 6-in. cylindrical can which was operated at a single air rate.) For each fuel, a mean blowout equivalence ratio (again, relative to the 0.600 isooctane reference) was computed along

with its standard deviation (expressed as a per cent of the mean value). All of the stabilizers showed the same relative effect of fuel reactivity; this is demonstrated by the low standard deviations in Table 1. (One notable exception is carbon disulfide; there is no obvious explanation for the lack of agreement with this fuel.) In fact, the results among stabilizers are reproducible within the precision of experimental measurement. Of interest is the fact that the average duct mass flow for blowout of the 1-in. V-gutter at the reference conditions is 7 lb/sec, equal to the duct mass flow for blowout of the 2-in. cone baffle at these conditions. This result confirms the conclusion by Longwell, Chenevey, Clark and Frost[8] that the mean hydraulic radius of a baffle is its significant dimension in turbulent flame stabilization.

fuel, as measured in his apparatus, is regarded as significant in the stabilization process. In Mullins' model, there is a mixing zone at the edge of a baffle recirculation zone. In this mixing zone, an approaching mass $(1 - x)$ of unburned gases at temperature, T_1, mixes rapidly with a recirculating mass x of completely burned gases at the flame temperature, T_5. The adiabatic mixing of these two masses results in temperature, T_3. Incipient blowout occurs when the time of recirculation of the mixture at T_3 is just equal to the ignition delay, τ, of that mixture at T_3. If, as in the experiments here, geometry, inlet temperature, and velocity are held constant, Mullins' theory results in the following criterion for blowout:

$$\tau\sqrt{T_3} = C \qquad (1)$$

Table 1. Summarized Lean Blowout Equivalence Ratios

Fuel	One-In. V-Gutter	Two-In. Cone Baffle	Rectangular Cans		Cylindrical Cans		Mean	Standard Deviation	Calculated Flame Temperature
			8 Holes	15 Holes	3-In.	6-In.			
								% of mean	*°K*
Isopropyl chloride	0.697	—	0.705	—	—	—	0.701	0.8	1886
Isooctane	0.600	0.600	0.600	0.600	0.600	0.494	0.600	—	1789
Heptane	0.583	0.572	0.580	—	—	0.482	0.578	1.0	1749
Tetralin	0.554	—	—	—	—	—	0.554	—	1725
Benzene	0.535, 0.538	0.537	0.535	0.529	—	0.451	0.535	0.7	1722
Propylene oxide	0.480	0.480	0.477	0.475	0.484	0.404	0.479	0.7	1634
Carbon disulfide	0.327	—	—	—	0.272	—	0.300	13	1101
Hydrogen	0.229	—	—	—	—	—	0.229	—	1095

Note: Mean and standard deviation calculated excluding 6-in. cylindrical can data. Flame temperatures computed for mean equivalence ratio with mixture entering at 400°K.

It is instructive to compare the dependence of blowout equivalence ratio on chemical fuel type with what one would predict from various blowout theories. First, it is clear that any purely aerothermodynamic theory that neglects chemical factors cannot account for the results. The last column of Table 1 lists computed flame temperatures at the mean blowout equivalence ratios. These flame temperatures range from about 1100 to 1900°K for the various fuels tested. Because blowout flame temperature varies so greatly as a result of changing only the chemical fuel type, temperature *per se* cannot control the blowout process. Some chemical property of the fuel must be introduced into any general blowout theory. Several chemical properties have already been proposed as important influences and these proposals may be examined individually.

In a theory by Mullins,[5] ignition delay of a

where C is a constant. If the variation of specific heat with temperature is neglected for convenience, T_3 is related to the inlet temperature, T_1, the final temperature, T_5, and the recirculating fraction, x, by

$$T_3 = (1 - x)T_1 + xT_5 \qquad (2)$$

For the reference fuel, isooctane, values of x were assumed and the corresponding values of T_3 were computed. The τ corresponding to each T_3 was obtained from Mullins' original data[9] and, using Equation (1), various values of C were computed, each value appropriate to the original x chosen. After C is established by the reference fuel, it is used for other fuels. Thus, choosing an x and its C, T_5 was altered to satisfy Equations (1) and (2) for any particular fuel. But since T_5 depends only on the equivalence ratio of a particular fuel, the equivalence ratio is established.

In this way, the equivalence ratio at blowout can be predicted for any fuel operated in the same apparatus under constant conditions.

These computations were performed for the fuels tested here. The x chosen was 0.57, found by trial to give the best average agreement between predicted and observed equivalence ratios. Equivalence ratios so calculated are shown in Table 2. The agreement with observed values is reference fuel. The x values are shown in Table 2 and are seen to vary from less than 20 per cent to more than 90 per cent, an unreasonable range for fixed geometry and operating conditions. These results lead one to the conclusion that ignition delay, at least when operating in the model proposed by Mullins, is not always controlling blowout under the conditions of these experiments.

Table 2. Results Predicted by Various Blowout Theories

Fuel	Observed Mean Φ	Ignition Delay			Laminar Flame Velocity		Spherical Reactor	
		Predicted Φ, $x = 0.57$	Error	Values of x to match mean Φ	Predicted Φ, constant S_u	Error	Predicted Φ, constant load	Error
			per cent			*per cent*		*per cent*
Isopropyl chloride	0.701	—	—	—	0.67	−6	0.700	0
Isooctane	0.600	0.600	—	—	0.600	—	0.600	—
Heptane	0.578	0.562	−3	0.538	0.59	+2	0.585	+1
Tetralin	0.554	0.579	+5	0.662	0.57	+3	0.545	−2
Benzene	0.535	0.548	+2	0.610	0.55	+3	0.545	+2
Propylene oxide	0.479	0.449	−6	0.479	0.53	+11	0.478	0
Carbon disulfide	0.300	0.478	+59	<0.2	0.45	+50	—	—
Hydrogen	0.229	0.303	+32	>0.9	0.4	+75	0.24	+5

Note: Φ = Equivalence ratio.

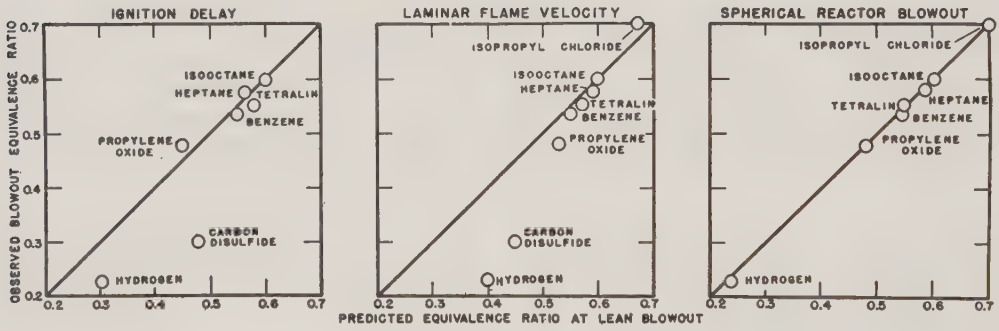

Fig. 6. Comparison of observed stabilizer blowouts with predictions of three blowout theories.

rather poor for fuels with reactivity much different from isooctane. Figure 6 illustrates this better. (The ignition delay times used were those of Mullins' original data;[9] ignition delay data for hydrogen were measured at a pressure of 0.9 rather than at 1.0 atmos abs. No data on ignition delays of isopropyl chloride were available.)

An alternate method of matching the data would be to use the value of T_5 corresponding to the observed equivalence ratio and to satisfy Equations (1) and (2) by use of the proper x. Such a calculation results in a different recirculation fraction, x, for each fuel when paired with the

In a theory of flame stabilization set forth by Spalding,[6] the following relation was proposed as the criterion for flame extinction

$$V \sim dpS_u^2 \tag{3}$$

where V is the blowout velocity, d the baffle dimension, p the pressure, and S_u the laminar flame velocity. Scurlock [10] has also suggested that blowout velocity is a direct function of laminar flame velocity; in addition to flame velocity, flame temperature was also said to explicitly affect blowout velocity, although the exact dependence on flame temperature was not made

clear. If flame velocity alone is the measure of chemical reactivity meaningful in baffle stabilization, then two fuels should blow out (in the same apparatus under identical operating conditions) at equivalence ratios such that their laminar flame velocities are equal. Table 2 lists, for the fuels tested here, equivalence ratios calculated by matching the test fuel laminar flame velocity to the reference fuel laminar flame velocity. These calculated equivlaence ratios are quite approximate; few data have been published on laminar flame velocities of these fuels at an inlet temperature of 400°K and at equivalence ratios as lean as those of the stabilizer blowout tests. Therefore, the values tabulated are (usually long) extrapolations from scattered information published in several sources. This extrapolation error is considered to be larger than errors due to measurement of flame velocities in different pieces of apparatus by different investigators.

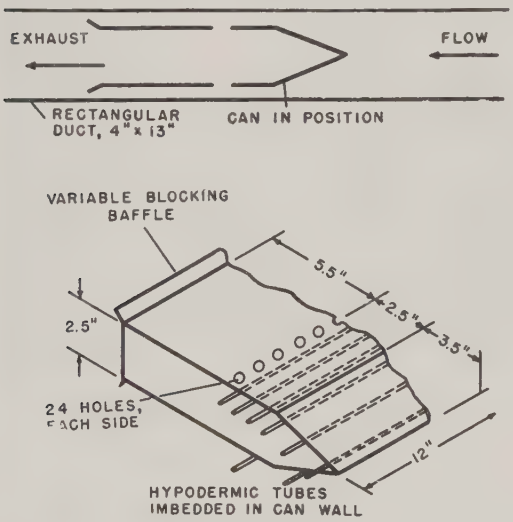

Fig. 7. Apparatus for heat transfer study.

The errors in laminar flame velocity theory prediction of the observed data are reasonable if the fuel reactivity does not vary greatly from that of isooctane. However, the errors increase rapidly from propylene oxide, to carbon disulfide, to hydrogen. There is a distinct trend in the results which is more obvious in the center section of Figure 6 where the data are plotted. Although there is a correlation (i.e., all the points are close to a single smooth curve), there is no direct correspondence (which would occur if all the points fell on the 45° line) and, therefore, laminar flame velocity is not suitable as the sole measure of reactivity in a stabilization theory.

Other combustion properties have been suggested as important in the flame stabilization process—minimum ignition energy, lean flammability limit, and quenching distance, for example. However, no specific stabilization mechanisms involving these properties have been described, and available data are limited as to fuel type, equivalence ratio, and inlet temperature.

One final mechanism was proposed[7] in which stabilization was assumed to be controlled by the rate of homogeneous reaction between fuel and oxygen in the stabilizer recirculation zone. Overall rates of reaction of all the fuels tested here (except carbon disulfide) were measured in the spherical reactor described by Longwell and Weiss.[11] For each fuel, the equivalence ratio at which the sphere loading factor—sphere air flow (g/sec) divided by sphere volume (liters) and pressure$^{1.8}$ (atmos $^{1.8}$)—was 8.92 was determined. At 400°K, 8.92 was the loading factor at which isooctane blew out[11] at an equivalence ratio of 0.600. The results are shown in the final columns of Table 2. Only for hydrogen is the difference between observed and predicted equivalence ratio as much as 5 per cent. In particular, the right part of Figure 6 shows the direct correspondence between spherical reactor blowouts and practical stabilizer blowouts. The precision with which the blowouts are matched is about equal to the precision of the experimental determination of blowout in the spherical reactor or practical stabilizer separately. (The relative ranking of fuels in the 6-in. cylindrical can, with an isooctane blowout equivalence ratio of 0.494, is also accurately predicted by spherical reactor blowouts.)

Measurements by Westenberg[12] in the immediate wake of flame holding baffles show that the wake is not completely mixed and thus is not entirely homogeneous in composition and temperature. A similar conclusion was reached by Weiss and Longwell[3] in their study of cylindrical can recirculation zones. Therefore, if recirculation zones are not perfectly mixed, and yet the dependence of stability on fuel type is the same as in a very vigorously mixed system, then a well-mixed local region in the recirculation zone could control stability. In the wake of a baffle, for example, such a zone might occur near the baffle edge where recirculating hot gases mix with the passing cold stream.

Recirculation Zone Heat Losses

Different stabilization mechanisms predict different effects of heat loss from the primary

stabilizing region. Therefore, it was hoped that some understanding of the flame stabilization mechanism in a can recirculation zone could be gotten by a study of heat transfer from that zone. Because no data were available, equipment was constructed to measure the heat transfer from a typical can recirculation zone operated under typical conditions. This equipment is illustrated in Figure 7; details of the can and mounting of the can in a two-dimensional (4 by 12 in.) duct are shown. Narrow slots were milled in the recirculation zone walls. In these slots, lengths of hypodermic tubing were laid and the slots then brazed over, renewing the flush surfaces. Thermocouples were inserted into the hypodermic tubing to measure metal temperatures.

With this equipment, a total of eight runs were made varying static pressure (the can exhaust led to a steam ejector), mass flow, equivalence ratio and hole size. The run conditions are shown in Table 3. As in previous testing, the approach fuel-air stream was completely homogeneous (the fuel was solvent naphtha) and entered at about 380°K.

For each run condition, equilibrium wall temperature profiles were measured by the embedded thermocouples. These profiles could be used to measure heat losses from the recirculation zone by a simulation technique (because neither inner nor outer heat transfer coefficient was known with any confidence). This was done by placing ten cylindrical electrical heaters, partially insulated from each other and most with independently variable power input, inside the recirculation zone—defining the recirculation zone as the entire can volume upstream of the entry holes. The can was then replaced in the air stream, as before, but with no burning occurring. Input to the heaters was varied until the wall temperature profiles reasonably matched the wall temperature profiles observed under each of the sets of burning conditions. Because the outside coefficients and temperature differentials were the same in both cases, the measured electrical power input was then equal to the total heat losses while burning. One example of the matching of the normal profile by the use of these heaters is shown in Figure 8.

Table 3. Results of Can Heat Transfer Studies

Approach velocity, ft/sec	70	105	140	70	70	70	52	140
Maximum velocity outside recirculation zone, ft/sec	180	270	360	180	180	180	135	360
Air mass flow into can holes, lb/sec	.040	.071	0.119	.099	0.107	.083	0.119	0.211
Can hole diameters, in	0.266	0.266	0.266	0.266	0.266	0.375	0.375	0.375
Upstream pressure, atmos abs	⅓	⅓	⅓	⅔	⅓	⅓	⅔	⅓
Equivalence ratio	0.58	0.62	0.70	0.56	0.71	0.63	0.56	0.66
Calculated flame temperature, °F	2,560	2,650	2,820	2,510	2,840	2,670	2,510	2,730
Average can wall temperature, °F	760	780	760	740	880	760	700	710
Total electrical power input to match profile, Btu/hr	8,000	9,100	11,400	10,600	11,200	8,000	8,100	9,900
Estimated radiant heat loss, Btu/hr	2,100	2,800	2,700	2,400	4,100	2,600	2,300	2,300
Estimated convection heat loss, Btu/hr	5,900	6,300	8,700	8,200	7,100	5,400	5,800	7,600
Estimated inside convection coefficient, Btu/hr/ft²/°F	4.0	4.4	5.0	5.4	5.2	3.8	4.0	4.5
Estimated outside convection coefficient, Btu/hr/ft²/°F	9.8	10.1	14.5	14.2	9.7	9.0	10.9	13.9

Total electrical heat loads required to match each profile are listed in Table 3. Outside heat losses are the sum of radiation and convection losses. The radiation losses (to the outer duct walls at an average temperature of about 380°K) were estimated using an emissivity of 0.6 to 0.8 for the can wall. (The can wall was painted with a high-temperature green paint and these emissivities were recommended by the paint manufacturer in the temperature range used.) From the balance—the convection losses—the average outside convection coefficients listed in Table 3 were calculated, based on average wall temperatures. Inside the can, assuming gas temperatures to be equal to theoretical flame temperatures, the estimated inside convection coefficients of

Table 3 resulted. However, inside gas temperatures were probably significantly lower than theoretical, because of heat losses and possibly also of combustion inefficiency. Therefore, the

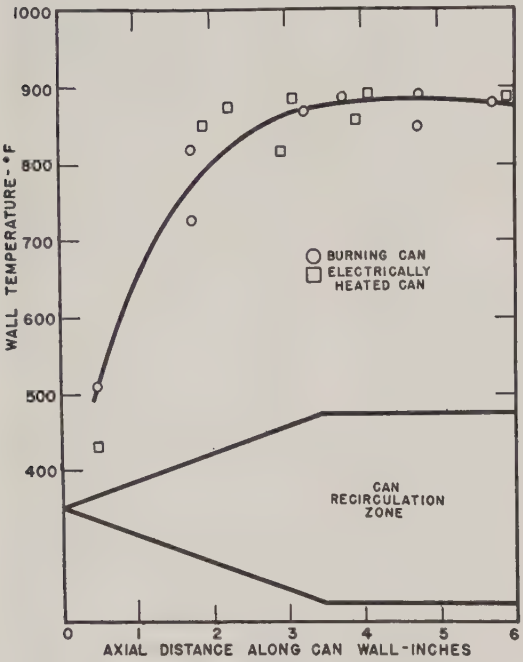

Fig. 8. Typical match of can wall temperature profiles.

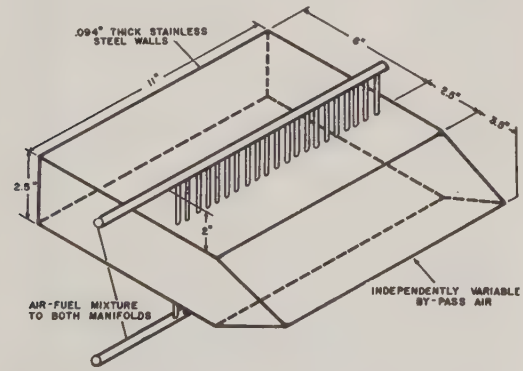

Fig. 9. Details of uninsulated can for heat loss effect study.

calculated coefficients are only approximate averages. Note that the outer convection coefficient is about two to three times as great as the inner coefficient.

For the restricted ranges of variables studied, the outside convection coefficient increased about linearly from 9.0 to 14.2 (Btu/hr ft²°F) as maximum mass velocity outside the can increased from 3.5 to 7.0 (lb/sec ft²). No simple correlation for the inside coefficient was found.

Over-all heat losses measured in this study were estimated to range from 6 to 30 per cent of the heat liberated in the recirculation zone. (These estimates assume that 25 per cent of the flow through the can holes entered the recirculation zone and burned completely.) A heat loss that great could be expected to seriously affect stability. If, for example, the recirculation zone were perfectly mixed, these heat losses would reduce heat release rates to 60 per cent to 5 per cent, respectively, of the rates in an adiabatic zone. Therefore, a definitive test was planned to determine the effect of heat losses on stability.

First, the can illustrated in Figure 9 was constructed. The can was mounted—similar to the mounting of Figure 7—in a rectangular duct 14 in. deep by 10¾ in. high. A homogeneous mixture of air and naphtha was fed to the manifolds and then down through the individual feed tubes to the can. The object here was to make the mass and direction of the jets entering the can independent of all other geometric and operating variables. An independently variable flow of air in the duct simulated the external cooling effect of normal immersion of the can in its air stream. Table 4 lists the conditions of operation of this can and the observed lean blowout equivalence ratios.

Next, a can was constructed that was geometrically almost identical to the can of Figure 9 but which had minimum heat losses. The "can" itself consisted of a void hollowed out of a surrounding mass of insulating fire-brick. Manifolds provided for fuel-air entry, as before, and the hollow space conformed in size and shape to the steel can. The construction is shown in Figure 10. This can, it was believed, would show the ultimate gain possible with this geometry as a result of insulation. Details of performance of the fire-brick can are also listed in Table 4.

A comparison of the stability of insulated and uninsulated cans is shown in Figure 11. Here, a loading factor shown by Weiss and Longwell[3] to be useful for correlating can stability data is plotted against blowout equivalence ratio. (The loading factor, $A/VP^{1.8}$, was corrected to a uniform inlet temperature of 380°K by correction factors of Longwell and Weiss.[11] Actual inlet temperatures varied between 370 and 400°K. The value of A used was the total manifold air flow although it is understood that only a part of this flow ever enters the recirculation zone.) The results show that the insulated can blows out at approximately twice as great a loading factor

Table 4. Stability Limits of Rectangular Cans

Can	A, Manifold Air Flow	P, Static Pressure	Equivalence Ratio at Lean Blowout	$A/VP^{1.8}$	Notes
	lb/sec	*atmos abs*			
Uninsulated can of Figure 9	0.035	1/3	0.62	4.2	By-pass air at 300°F
	0.055	1/3	0.66	6.7	past can with max-
	0.076	1/3	0.70	8.9	imum velocity of
	0.076	2/3	0.58	2.5	200 ft/sec
Uninsulated can of Figure 9	0.034	1/3	0.64	3.9	No by-pass air
	0.056	1/3	0.67	6.7	
	0.079	1/3	0.68	9.0	
	0.078	2/3	0.55	2.5	
Fire-brick can of Figure 10	0.041	1/4	0.60	8.7	
	0.043	1/3	0.53	4.7	
	0.057	1/3	0.59	5.8	
	0.069	1/3	0.59	7.0	
	0.090	1/3	0.63	8.6	
	0.089	2/3	0.50	2.5	

Note: V = can volume (ft^3), 0.062 for steel can and 0.068 for brick can.

for a given equivalence ratio as the uninsulated can. By-pass air has relatively little effect on stability of the uninsulated can.

Of most significance was the relatively small improvement resulting from the drastic insulation provided. It was estimated that recirculation zone heat losses from the uninsulated can with by-pass air averaged about 20 per cent of heat liberation rate. From the fire-brick can, heat losses averaged about 6 per cent. Were the recirculation zone homogeneous, this reduction in heat loss would result in more than a four-fold improvement in heat release ratio (i.e., allowable loading at blowout). Therefore, one concludes that gases near the can walls have largely left the zone of primary stabilization and are not returned to it to any great extent. If this were not so, temperature of the primary stabilization zone would depend more on heat lost from gases near the wall and, regardless of the stabilization mechanism assumed, the can would be more heat-loss sensitive than observed. Further evidence that the can recirculation zone is not completely mixed arises when comparing the

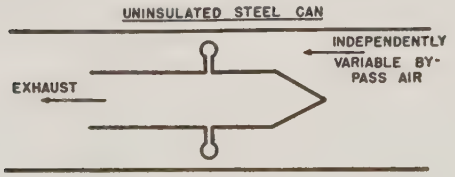

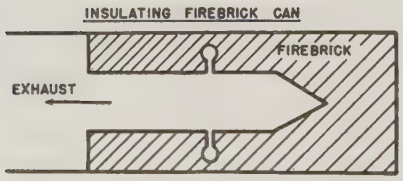

Fig. 10. Uninsulated and insulated cans mounted in two-dimensional duct.

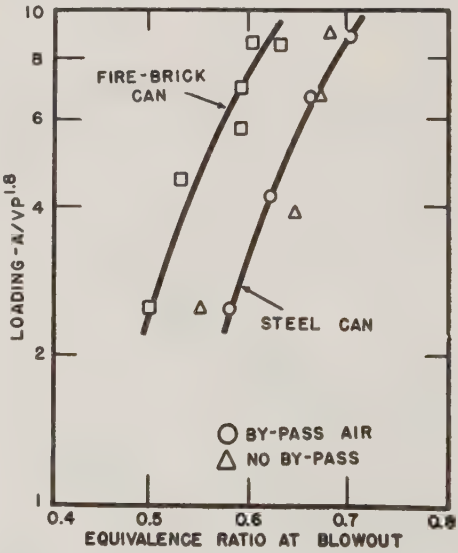

Fig. 11. Comparison of insulated and uninsulated can stability.

loading factors at blowout with those from the spherical reactor.[11] This comparison shows that, for the equivalence ratios tested, even the firebrick can blows out at heat release rates only 20 to 25 per cent as large as those observed in the spherical reactor. (The calculation again assumes 25 per cent of the mass flow entering the can to burn in the recirculation zone.)

Some flow tracing experiments were made in the recirculation zone of a can similar to that of Figure 7 while burning under conditions like those of the fifth column of Table 3. Argon was injected into the recirculation zone with variation in both the design and location of the injector. A small probe was used to remove gas samples from other parts of the recirculation zone and the argon concentration measured with a mass spectrometer. The results showed qualitatively a fair degree of mixing in the recirculation zone but by no means enough to validly assume homogeneity throughout. About half of the mass in the entering jets was directed upstream after impingement. (This result tended to be confirmed by visual observation of the jets which showed them to impinge at an angle close to 180°.) However, only about a quarter of the total flow penetrated a significant distance into the recirculation zone; the remainder was turned quickly and swept downstream by the hot recirculating gases.

Conclusions

The similar behavior of fuels in both cans and baffles at lean blowout suggests a common basic stabilization mechanism. Such a mechanism must take chemical reactivity of the fuel into account. Of the "basic" measurements of chemical reactivity, homogeneous reaction rates as measured in the spherical reactor best predict the observed data. However, the recirculation zone of neither a baffle nor a can is completely homogeneous. This has been demonstrated by earlier flow tracing studies and by the work here. Further confirmation occurs in the results of heat loss measurements which show a smaller gain to result from reducing heat losses than would be obtained in a completely homogeneous system.

All of the results obtained are consistent with a stabilization mechanism in which homogeneous reaction controls the flame nucleus; but this reaction occurs in some local region of the recirculation zone. Because the drastic can insulation used had a relatively small effect on recirculation zone stability, one would expect little aid to stabilization from practical insulation. The volume occupied by insulation could be better used to enlarge the combustion space in the recirculation zone. These conclusions apply to large stabilizers in fully turbulent homogeneous flow at low pressures.

Acknowledgment

This work was performed for the Bureau of Ordnance, Department of the Navy, in cooperation with the Applied Physics Laboratory, The Johns Hopkins University.

REFERENCES

1. Weir, A., Rogers, D. E., and Cullen, R. E.: Willow Run Research Center, University of Michigan Report UMM-74, September 1950.
2. DeZubay, E. A.: Aero Dig., *61*, 54 (1950).
3. Weiss, M. A., and Longwell, J. P.: Jet Propulsion, *26*, 749 (1956).
4. Probert, R. P.: Application of Research to Gas-Turbine Combustion Problems. ASME-IME Joint Conference on Combustion, Section 5, Gas Turbines, June 1955, p. 70.
5. Mullins, B. P.: In *Combustion Researches and Reviews, 1955*, p. 87. London, Butterworth, 1955.
6. Spalding, D. B.: *Some Fundamentals of Combustion*, p. 185. New York, Academic Press, 1955.
7. Longwell, J. P., Frost, E. E., and Weiss, M. A.: Ind. Eng. Chem., *45*, 1629 (1953).
8. Longwell, J. P., Chenevey, J. E., Clark, W. W., and Frost, E. E.: *"Third Symposium on Combustion, Flame and Explosion Phenomena*, p. 40. Baltimore, The Williams & Wilkins Co., 1949.
9. Mullins, B. P.: Fuel, *32*, 343, 363, 467, 481 (1953).
10. Scurlock, A. C.: M.I.T. Fuel Research Laboratory Meteor Report No. 19, July 1948.
11. Longwell, J. P., and Weiss, M. A.: Ind. Eng. Chem., *47*, 1634 (1955).
12. Westenberg, A. A., Berl, W. G., and Rice, J. L.: Applied Physics Laboratory, The Johns Hopkins University, Report CM-844, June 1955.

55

THE INFLUENCE OF THE INITIAL TEMPERATURE OF A COMBUSTIBLE MIXTURE AND OF THE AMBIENT PRESSURE ON THE STABILIZATION LIMITS

By L. N. KHITRIN AND S. A. GOLDENBERG

In a previous paper[1] the authors showed that the condition for stabilizing a flame by a bluff body can be obtained from the analysis of the critical conditions for the ignition of a flowing combustible mixture,[2] expressed as

$$Re_{cr} = A \cdot S^{(1/\beta)} \tag{1}$$

where $Re_{cr} = W_0 d/\nu$; W_0 is the critical velocity of the flow near the stabilizer fringe at blowoff; d is a typical dimension of the stabilizer; ν is the coefficient of the kinematic viscosity of the mixture; $S = ud/a$; u is the normal velocity of the flame; $a = \lambda/C_p\rho$ is the coefficient of the thermal conductivity of the mixtures; β indicates the degree of reaction which depends on the configuration of the stabilizer and the law of heat transfer; A is a coefficient. In other words, Equation (1) can be written as

$$\frac{W_0 d}{\nu} = A \left(\frac{ud}{a}\right)^{(1/\beta)} \tag{2}$$

It is of interest to ascertain the influence of the initial temperature of the mixture and of the ambient pressure on the stabilization limits. This is also of importance from the practical viewpoint, as many high heat release furnaces operate under conditions differing from "normal."

If the purely thermal mechanism of igniting gas mixtures in the flow governs the process of stabilizing the flame, it is evident that the relation between the parameters which form part of the stabilization criterion and the initial temperature of the mixture, T, and the pressure, P, must be established in order to evaluate the effect of T and P.

Assuming by way of approximation, and in accordance with the kinetic theory of gases, that $a \approx \nu \approx D$, we can write that

$$a = a_0 \frac{(T/T_0)^n}{(P/P_0)} \tag{3}$$

The normal velocity of the flame as a function of T and P can be expressed in a general way as follows

$$u = u_0 \frac{(T/T_0)^m}{(P/P_0)^k} \tag{4}$$

where the subscript 0 designates normal conditions (e.g., $P_0 = 760$ mm or $P = 1$ atmos and $T_0 = 293$°K).

If Equations (3) and (4) are substituted in Equation (2), we obtain the following general expression

$$Re_{cr} = A \cdot S_0^{1/\beta} \frac{(T/T_0)^{n+(1/\beta)(m-n)}}{(P/P_0)^{1+(1/\beta)(k-1)}} \tag{5}$$

For a special case,[1] a number of published results on the stabilization of the flame by bluff bodies give $\beta = 0.5$. Hence, Equation (5) can be replaced by a simpler expression

$$Re^0_{cr} = A \cdot S_0^2 \left(\frac{T}{T_0}\right)^{2m-n} \left(\frac{P}{P_0}\right)^{1-2k} \tag{6}$$

The temperature dependence $a = \lambda/C_p\rho$ as well as of D can be expressed in the first approximation as

$$a = a_0 \left(\frac{T}{T_0}\right)^{1.75}$$

For the dependence of u on T and P, the reader is referred to published experimental results[3, 4] that show the influence of the initial temperature of CH_4-air, C_2H_4-air and C_3H_8-air mixtures on the normal flame velocity over a wide range of temperatures (−124° to 342°C).

Figure 1 presents the dependence of maximum values of u on the initial temperature of the mixture. An analysis of these data, made by us, was used successfully to establish with sufficient accuracy the value of the index of degree, M, in Equation (4). In Figure 2, index u_0' and T_0' designate the initial values of these magnitudes. Figure 2 shows that for all the above combustible mixtures $M \approx 1.7$.

The influence of pressure on the normal flame velocity can be determined both from theoretical considerations and from published experimental data. The various theories of the normal flame velocity, which are chiefly based on the thermal mechanism of flame propagation,[5, 6, 7, 8] can be reduced to the following general relation

$$u \propto \sqrt{\frac{\lambda}{C_p\rho} F(C, T)} \tag{7}$$

where $F(C, T)$ is a function of the rate of the chemical reaction. If C is expressed in relative concentrations, then we know that $dm/dt \propto P^{\nu-1}$, where ν is the order of reaction and $\lambda/C_p\rho \propto 1/P$. Hence $u \propto P^{(\nu/2)-1}$, where P is the pressure.

For a reaction of the second order, u does not depend on P, i.e., $u \propto P^0$, and for a reaction of the first order $u \propto P^{-\frac{1}{2}}$. Experimental data for a number of hydrocarbon-air mixtures show that the order of the reaction is fractional[9] ($u \propto P^{-\frac{1}{4}}$). On the other hand, for a number of oxygen mixtures it approximates the second order of $u \propto P^0$. Consequently, the index of degree K in Equation (4) can range from zero to 0.25.

Taking this result into account, Equation (6) gives us

$$Re_{cr}^0 = A \cdot S_0^2 \left(\frac{T}{T_0}\right)^{1.65} \left(\frac{P}{P_0}\right) \tag{8}$$

(for a reaction of the second order, when $K = 0$), or:

$$Re_{cr}^0 = A \cdot S_0^2 \left(\frac{T}{T_0}\right)^{1.65} \left(\frac{P}{P_0}\right)^{0.5} \tag{8'}$$

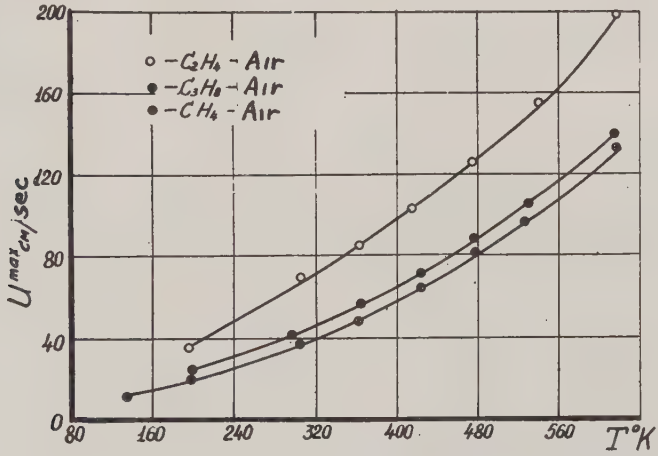

Fig. 1. Effect of initial temperature of combustible mixtures on the burning velocity (Dugg and Heimel[4]).

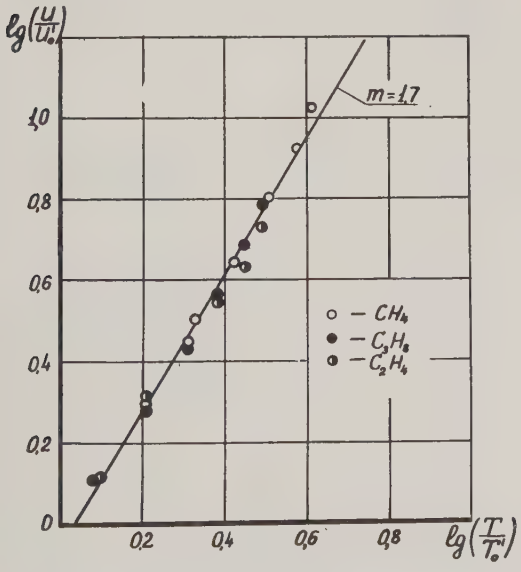

Fig. 2. Correlation of data on effect of initial temperature of combustible mixtures on the burning velocity.

(for a reaction of the order $\nu = 1.5$, when $K = 0.25$).

In 1955, experiments aimed at investigating the influence of the initial temperature of a methane-air mixture on the process of flame stabilization were conducted by L. A. Volodina at the Laboratory of Intensification of Furnace Processes of the Institute of Energetics USSR Academy of Sciences. The experiments were performed at atmospheric pressure on a conical stabilizer ($d = 7$ mm) and the initial temperature of the mixture ranged from 20° to 400°C.

In the case of the normal flame velocity of the CH_4-air mixture its dependence on the temperature has been established near stoichiometric (see Fig. 1). This makes the analysis of experimental results obtained by Volodina on the stabilization of the flame, likewise near stoichiometric, of definite interest. Figure 3 presents the results of the analysis of the primary experimental data of Volodina. The flow velocities at which blowoff of the flame occurs are plotted on the

ordinate axis, and the temperatures of the mixture on the abscissa axis. (W_0 being the critical flow velocity at $T_0 = 293°$).

As seen from Figure 3, the experimental results near stoichiometric are rather well defined by Equation (6) with the value of the degree index at T/T_0 being equal to 1.62, which agrees with Equation (8).

To check the relation between the stabilization criterion and pressure established by us, we used the available experimental data. For this purpose we expressed equation (8) as follows:

$$\frac{W_0 d}{\nu_0} = A \left(\frac{u_0 d}{a_0}\right)^2 \left(\frac{T}{T_0}\right)^{1.65} \left(\frac{P}{P_0}\right)$$

or

$$\frac{W_0}{P \cdot d \cdot T^{1.65}} = B u_0^2 \qquad (9)$$

The right hand part of Equation (9) appears to depend on the concentration or on fuel air ratio, F/A, of the mixture. Hence it can be expressed as

$$\frac{F}{A} = \varphi \left(\frac{W_0}{P \cdot d \cdot T^{1.65}}\right) \qquad (10)$$

In a number of papers,[10, 11, 12] Equation (10) is termed the stability parameter. These papers cite the results of experiments carried out by E. A. DeZubay concerning the influence of pressure on the limit of stability during the combustion of a propane-air mixture. The flame stabilizer was a flat, round disk (with the range of change in variables $W_0 = 12 \div 167$ m/sec; $P = 0.2 \div 1$ kg/cm^2 and $d = 6 \div 25$ mm). These experimental results concerning stabilization are quite adequately defined by the following stability parameter:

$$\frac{F}{A} = \varphi \left(\frac{W_0}{P^{0.95} \cdot d^{0.85} \cdot T^{1.7}}\right) \qquad (11)$$

Thus the stability parameter in Equation (11) established experimentally on the basis of tests dealing with flame stabilization in a flowing mixture, when the pressure and initial temperature of the mixture change, agrees fairly well with Equation (10) derived on the basis of theoretical considerations. There is some deviation in the case of the degree index at d, which appears to be connected with the peculiarity of the stabilizer configuration.[13] At the same time, as has been established by DeZubay, Equation (11), the experimental results for a hydrogen-air mixture with a changing pressure but where $T = T_0$ are defined by the following stability parameter:

$$\frac{F}{A} = \varphi_1 \left(\frac{W_0}{P^{0.61} \cdot d^{0.74}}\right) \qquad (12)$$

As regards pressure dependence, Equation (12) is in better agreement with Equation (8′). This shows that the index of degree may change with the pressure ranging from 0.5 to 1.0 depending on the order of the reaction. Hence, the theoretical analysis of the dependence of the stabilization criterion on the ambient pressure and initial temperature of the mixture is confirmed by experimental results.

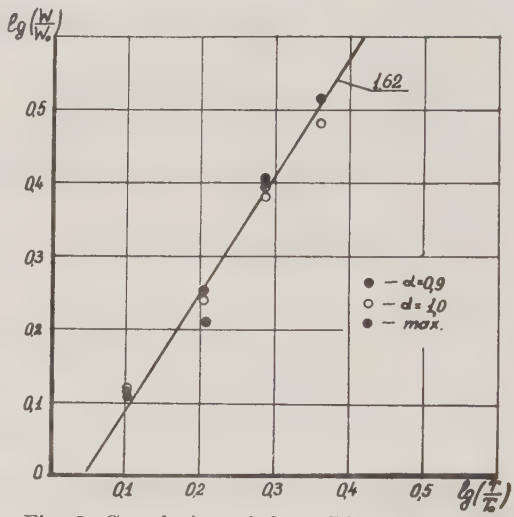

Fig. 3. Correlation of data. Blowoff velocities vs initial temperature of combustible mixture (CH_4-air). α = coefficient of excess air $\left(\frac{\text{air}}{\text{air (stoich)}}\right)$.

It is worth noting that the stability parameter in Equation (10), as noted elsewhere,[11, 12] also can be applied effectively to more complex systems such as large-scale combustion chambers of ramjet engines and thrust chambers.

REFERENCES

1. Khitrin, L. N., and Goldenberg, S. A.: Reports of the USSR Academy of Sciences, vol. *103*, no. 5, 1955.
2. Khitrin, L. N., and Goldenberg, S. A.: Reports of the USSR Academy of Sciences, vol. 103, no. 2, no. 3, 1955.
3. Gaydon, A. G., and Wolfhard, H. G.:

Flames, Their Structure, Radiation and Temperature. New York, Macmillan Co., 1954.
4. Dugger, G. L., and Heimel, S.: NACA Tech. Note, No. 2624, 1952.
5. Zeldovich, Y. B., and Frank-Kamenetzki, A. D.: J. Phys. Chem., *12*, 100 (1938).
6. Semionov, N. N., Uspekhi fizicheskikh nauk, *24*, installment 4, (1940).
7. Boys, S. F., and Corner, J.: Proc. Roy. Soc., *A197*, 90 (1949).
8. Corner, J.: Proc. Roy. Soc., *A198*, 388 (1949).
9. Egerton, A. C., and Sen, D.: *Fourth Symposium (International) on Combustion.* Baltimore, The Williams & Wilkins Co., 1953.
10. Longwell, J. P.: *Fourth Symposium (International) on Combustion.* Baltimore, The Williams & Wilkins Co., 1953.
11. Friedman, J., Bennet, W. J., and Zwick, E. B.: *Fourth Symposium (International) on Combustion*, Baltimore, The Williams & Wilkins Co., 1953.
12. Bjerklie, J.: J. Propulsion, *25*, 227–234 (1955).
13. Spalding, D., and Tall, B.: Aero. Quart., *5*, 195–217 (1954). (See translation in Voprosy raketnoi tekhniki, No. 4, 1955.)

56

FLAME STABILIZATION IN VOLATILE FUEL SPRAYS

By H. C. HOTTEL, C. P. MARION and W. P. JENSEN

Introduction

Stabilization of flames in high-velocity streams of air containing fuel vapor and fuel droplets can be accomplished by use of a bluff-object flameholder which produces in the space immediately downstream of it an eddy zone of low velocity where a pilot flame can be established and from which ignition of combustible in the main stream can be accomplished. No general theory of flame stabilization behind bluff objects is yet available, although the mechanism of stabilization in high velocity streams of homogeneous fuel-air mixtures is fairly well understood.[1, 2, 3, 4] The study of flame stabilization in high-velocity fuel sprays is much less advanced because of its greater complexity. Moreover, less effort has been devoted to study of this problem with burners of geometry simple enough to yield the sort of fundamental information which has been obtained in studies of flame-stabilization with homogeneous air-fuel mixtures. The present paper reports a study of the flame-holding properties of a cylindrical rod in fuel sprays, with special emphasis on the influence of fuel volatility.

Several distinct processes must precede and influence the combustion of liquid fuel sprays. The first of these, atomization of the fuel, determines the initial drop size and size distribution and is itself influenced by fuel properties, nozzle characteristics, atomization technique and pressure. The subsequent processes of vaporizing the droplets and of mixing vapor and liquid droplets with the air are strongly influenced by fuel volatility and by the temperature, velocity and turbulence of the air stream.

Flame stabilization itself is governed in part by the following factors which have been studied in the work here reported: (a) fuel type and volatility, (b) fuel/air ratio, (c) velocity of the air stream, (d) initial drop size and (e) fractional vaporization of the fuel. Other factors which influence flame stabilization but which were not varied or specifically controlled are the size, shape, and temperature of the flameholder; drop size distribution; combustion chamber geometry; and the pressure, temperature, and turbulence of the approach stream.

Air atomization of liquids in orifices and nozzles has been studied by Nukiyama and Tanasawa[5] and by Lewis, *et al.*,[6] who showed that the surface-volume mean diameter of the spray drops is a function of liquid properties and of atomizing velocity, i.e., the relative velocity between gas and liquid; drop size decreases with increased atomizing velocity. Fledderman and Hanson[7] have applied the Froessling equation[8] for droplet vaporization to sprays of drops in turbulent air streams. Mixing and distribution of liquids in high velocity air streams has been investigated by Longwell and Weiss[9] who have been able to predict distribution occurring downstream of point sources and nonpoint sources of liquid.

The collection of liquid droplets on a circular cylinder, from a spray cloud moving at high velocity transversely to the cylinder, has been studied both experimentally and analytically by Langmuir and Blodgett.[10] They defined a collection efficiency function, E_c, as the fraction which impinged on the collector, of the total mass of liquid drops approaching through the projected area of the collector. The collection efficiency in an air stream of given state properties was found to be a direct function of drop diameter, liquid density, and stream velocity, and an inverse function of cylinder diameter.

Stabilization of flames in a spray of diesel fuel was studied by Hottel, May, Williams, and Maddocks.[11] Hottel and May proposed a flame stabilization mechanism based, as with gaseous mixtures, on maintenance of a pilot flame in the primary eddy zone. The theory was found to be consistent with data on the individual effects of drop size, flow velocity, rod diameter, and independently-controlled rod temperature, and with the use of flame-holding rods having external fins or internal ceramic insulation. May[12] also examined the effect of fuel volatility by using mixtures of propane and diesel fuel to simulate fuels of various vapor pressures. Marked increase of the maximum stable burning velocity and extension of the fuel-rich stability limits were achieved by the addition of propane.

The principal objectives of the present investigation were (a) to measure flame stability limits in evenly distributed sprays for a series of volatile fuels in air, and (b) to study the effect of fuel volatility on the mechanism of flame stabilization.

Development of Flame Stabilization Criteria

ANALYSIS OF STABILIZATION MECHANISM

Some insight into the complex processes involved in flame stabilization can be gained from an analysis of phenomena in the region of the pilot flame. Such an analysis has been made[13] on the basis of the qualitative theory of Hottel, May, Williams and Maddocks[11] which showed the interdependence between eddy temperature and the ratio of fuel to air in the eddy. To make the analysis possible it was assumed that approach-stream temperature and pressure, drop-size distribution, turbulence, and distribution of fuel drops and vapor were not variables. Equations developed in the analysis and presented below are based on unit length of a cylindrical flameholder mounted transversely to the flow. Results of the analysis cannot be made quantitative for lack of detailed knowledge of the processes at the flameholder, but with certain assumptions the final form of the expressions can be used to describe qualitatively the effects of independent variables on flame stability.

When a stream of spray droplets impinges on a flameholder the maintenance of a pilot flame in its wake is believed to depend on the following processes:

(1) Production in the eddy zone of a combustible mixture of composition f_{vE} (weight ratio of vaporized fuel to air). Further,

$$f_{vE} = fF_v + \Delta \tag{1}$$

in which f is the fuel/air ratio in the feed, F_v is its fractional vaporization in the approach stream, and Δ is the increment in vapor-air ratio due to vaporization of collected fuel from the flameholder.

(2) Combustion of this mixture to produce a temperature, T_E, defined as the average effective temperature of the recirculating eddy gases.

(3) Transfer of heat from the flame and burned products at T_E to the flameholder and collected fuel at a rate sufficient to supply energy for (a) vaporizing fuel to provide the increment Δ, and (b) heating all the collected fuel to a temperature, T_L, at which the remainder is sloughed off by the shearing force of the passing stream.

(4) Diffusion of the vapor from the collected liquid, at elevated temperature, T_L, to the pilot flame.

It is assumed that in the eddy zone the only fuel to burn is vapor. Eddy temperature, T_E, is related to the mixture composition, $fF_v + \Delta$, by the thermodynamic relation for adiabatic flame temperature.

$$T_E = \psi(fF_v + \Delta) \tag{2}$$

This function, ψ, has been computed conventionally[14] for the experimental fuels in question. A typical resultant curve is shown in Figure 1, marked Equation (2).

Expressions for processes 1, 3, and 4 above have been derived and combined to yield a second relation between T_E and Δ:

$$T_E = T_s\left(\frac{C_4VR\Delta}{A_{RL}N_{Re}^{0.6}T_f^{1.5}}\right)^{\frac{1}{a}} + \left(\frac{C_1VR\Delta + [C_2N_{Re}^{0.6} + C_3Vf(1 - F_v)E_c] \times \left[T_s\left(\frac{C_4VR\Delta}{A_{RL}N_{Re}^{0.6}T_f^{1.5}}\right)^{\frac{1}{a}} - T\right]}{\pi(A_{\quad E} + A_{RL})C_HK_{fE}N_{Re}^{0.6}}\right) \tag{3}$$

This expresses the relation between the vaporization, Δ, and the eddy-zone temperature, T_E, necessary to produce the vaporization. The first term represents the collected-fuel temperature, T_L. The second term, representing the difference between T_E and T_L, includes a term (containing C_1) for the latent heat of vaporization of collected fuel, a term (containing C_2) for heat lost to the passing stream, and a term (containing C_3) for sensible heat required to raise collected fuel from the approach-stream temperature T to T_L. Other factors in Equation (3) are identified in the table of nomenclature at the conclusion of this paper.

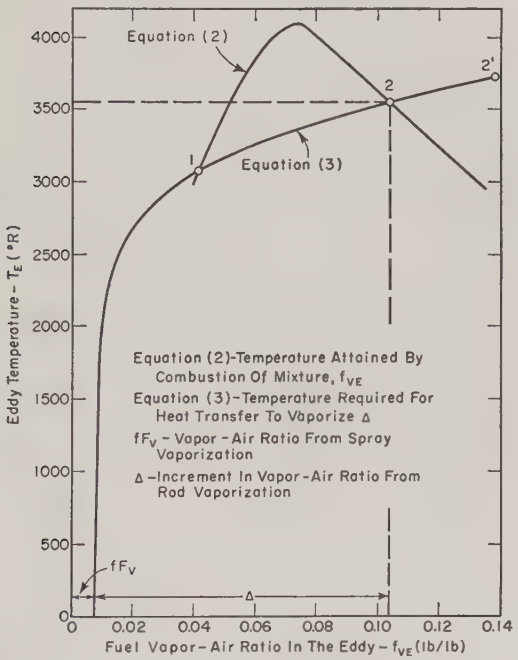

Fig. 1. Flame stability criteria.

The terms A_{RL} and A_{RE} in Equation (3) refer to wetted and dry areas, respectively, on the flameholder, areas effective for receiving heat from the eddy zone; they are sketched in Figure 4.

The function represented by Equation (3) has been plotted in Figure 1 with an assumed value for R, the ratio of air entering the eddy zone to air which approaches through the projected area of the flameholder, and with calculated values for the constants, C_1, C_2, C_3, C_4, and C_H, which depend only upon fuel properties. Approximately known empirical constants were used in the equations for diffusion and heat transfer; methods of calculation have been presented elsewhere.[13]

FLAME STABILITY CRITERIA

The condition for existence of a stable flame is that the curves (Fig. 1) representing Equations (2) and (3) must intersect. At intersections 1 and 2, heat supplied to the flameholder would vaporize just enough fuel to produce mixture ratios f_{vE_1} and f_{vE_2}, which on burning would yield temperatures T_{E_1} and T_{E_2}. Consideration of a slight perturbation of T_E or f_{vE} shows that only point 2 would be stable while point 1 would be metastable.

A further restriction on the construction of Figure 1 is that the ends of curve 2 are limits fixed by the approach-stream velocity, analogous to rich and lean limits in homogeneous fuel-air mixtures. Thus the requirements for flame stability in a gaseous mixture are added to those peculiar to fuel sprays, in which at least a portion of the fuel vapor must be supplied to the pilot flame by vaporization of collected fuel. An additional limitation is that the extension of curve 3 has a finite limit at 2′, corresponding to the fuel-droplet collection rate.

Throughout this paper the identification of stability limits as rich or lean refers to the fuel/air ratio of the approach stream, f, whereas the nature of the stability limit is controlled by the ratio, f_{vE}, of vaporized-fuel to air in the eddy, which may be either a direct or an inverse function of f. Considering first fuels of slight volatility, the limits resulting from changes in fuel rate at a fairly low velocity are shown in Figure 2a. Stable intersections of curves 2 and 3 occur at points 1, 2, and 3 which represent fuel/air ratios progressively decreased in the eddy zone and progressively increased in the free stream. Translation of the stable point toward a smaller value of f_{vE} is caused by increasing the approach-stream fuel/air ratio and consequently the fuel-collection rate at the stabilizer. The difference between f_{vE} at 2 and f at 2′ corresponds to unevaporated fuel sloughed from the stabilizer. Intersection 3 represents the eddy composition and temperature corresponding to a maximum fuel/air ratio in the feed stream. This is the "slough-limited blowout," a rich limit due to excessive sloughing of heated fuel, as described by Hottel, May, Williams, and Maddocks.[11]

For the limiting condition at which point 1′ approaches point 1, sloughing ceases, all collected fuel is evaporated, and the following expression should hold

$$\Delta = f_{vE} - fF_v = \frac{f(1 - F_v)E_C}{R} \qquad (4)$$

With a further reduction in approach-stream fuel/air ratio and consequently in collection rate, there would be an excess of heat beyond that required to vaporize all the collected fuel. Since there is no way for this excess energy to be absorbed without further increase in the rod temperature, no new equilibrium could be established. The rod rapidly would become dry and vapor bound in the fashion observed experimentally by May and Maddocks. This lean-limit condition will be called "vapor-bound blowout."

In volatile-fuel sprays stability limits must depend also on the fractional spray vaporization in the approach stream, F_v. If, as in the above example, little fuel is vaporized in the approaching spray, increasing the fuel rate affects the collection rate principally and leads to a rich limit as illustrated at 3 in Figure 2a. If the fuel is considerably more volatile than corresponds to the example of Figure 2a, fractional vaporization in the approach stream becomes of major significance. This case is represented by Figure 2b. Increments of fuel flow here affect the vapor concentration fF_v in the approach stream much more than the collection rate; thus from a fuel-lean limit near 1, T_E falls toward a rich limit at 3, analogous to that for homogeneous mixtures and hereafter to be called "rich-wet blowout."

Experimental Procedure

APPARATUS

Flame-stability measurements with the various fuels were made with the apparatus shown in Figure 3, which consisted of four main parts: Approach Section, Atomizing Section, Preparation or Mixing Section, and Combustion Chamber or Test Section.

The Approach Section included a diffuser, calming chamber, and nozzle, each having a square cross section. A fuel manifold consisting of three straight copper tubes extending in parallel across the calming chamber delivered fuel to the Atomizing Section through hypodermic tubes (three tubes from each copper tube) which projected through the approach nozzle. The downstream end of the plaster approach nozzle was a $3\frac{1}{8}$-in. steel passage which contained pressure taps on its inside surfaces and thin transverse struts designed to center the downstream ends of the fuel tubes at the entrance to the Atomizing Section.

To distribute fuel spray evenly across the test section, air atomization was accomplished in a nest of nine identical venturi passages with an L/D ratio of 6. The preparation length for mixing and vaporization was made variable in order to provide independent control over the elapsed time between atomization and combustion of the spray. These preparation sections were lengths of square steel tubing, $3\frac{1}{8}$-in. inside. At the downstream end of each was a trough for collection of

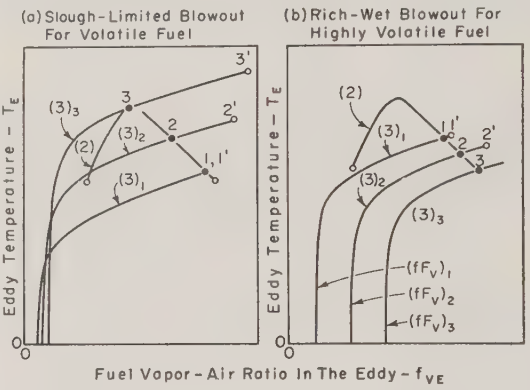

Fig. 2. Blowout limits for volatile fuels.

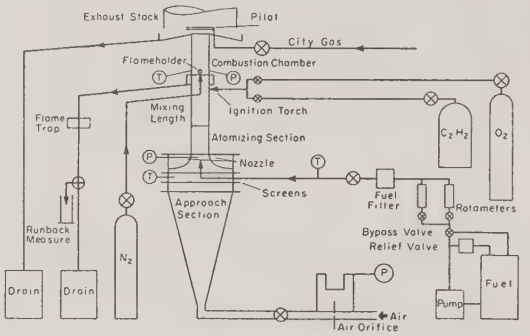

Fig. 3. Apparatus for study of flame stabilization in fuel sprays.

that liquid fuel which had deposited on the walls of the Mixing Section.

To permit independent control of atomizing velocity, preparation time, and mixture velocity in the combustion chamber, seven different atomizing nests and five mixing tubes were used. Throat areas, A_A, of the venturis and lengths, L_M, of the tubes provided velocity and time combinations in geometric progression, with a ratio of 5/4.

The combustion chamber or Test Section was a 10-in. length of the same $3\frac{1}{8}$-in. square tubing with a front face of vycor glass. The flameholder was a stainless steel rod, $2\frac{3}{4}$ in. long by $\frac{1}{8}$ in. in

diam supported horizontally between the window and the back wall by smaller tubes silver-soldered to the two ends. Through holes in these tubes, nitrogen was blown to prevent liquid fuel running onto the stabilizer from the wall surfaces of the chamber. For traversing the combustion chamber, the large glass window was replaced by a small window and a steel plate which supported the sampling probe or Pitot tube.

Oil-free air was supplied at ambient temperature and 100 psig to the approach system through control valves and a metering orifice from a carbon ring compressor at rates up to 0.5 lb/sec.

Table 1. Fuel Distillation Data

Fuel	I.B.P.	10%	20%	30%	50%	80%	90%	Final
Diesel, Fuel D...	350	436	457		505		594	653
Fuel C.....	406	423		432	442	463	476	497
Fuel B.....	324	330			338		367	387
Naphtha, Fuel A.	250	256			261		272	290

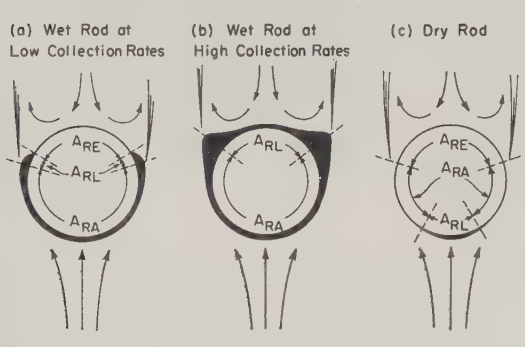
(a) Wet Rod at Low Collection Rates
(b) Wet Rod at High Collection Rates
(c) Dry Rod
ARE
ARL
ARA
ARA - Fractional Surface Area for Heat Transfer to the Air
ARE - Fractional Surface Area (Dry) Exposed to the Eddy
ARL - Fractional Surface Area for Heat Transfer to Liquid

Fig. 4. Flameholder surface conditions.

Ignition was accomplished with an acetylene torch inserted through a hole near the downstream end of the mixing section. The exhaust system consisted of a water-cooled stack and water-collection tray.

The fuels were petroleum fractions in the volatility range between diesel fuel and gasoline, with distillation data as shown in Table 1. Fuel A was a narrow-cut varnish makers' and painters' naphtha containing 25% naphthenes and about 73% paraffins. Fuel B was a Stoddard solvent conforming to NBS specification CS340 and containing nearly equal amounts of aromatics, naphthenes, and paraffins. Fuel C was a narrow-cut so-called "deodorized kerosene", containing mainly paraffins.

ROCEDURE

Rich and lean limits of stable combustion were determined at the desired values of combustion chamber velocity by first setting the air rate for one of the control values of atomizing velocity, 400, 500 or 625 fps; then, after admission and ignition of fuel, the fuel rate was altered stepwise until the flame failed. This process was repeated with sufficiently small changes in fuel rate to establish the equilibrium value of fuel/air ratio at blowout. When stable combustion at the higher design values of atomizing velocity could not be obtained with diesel fuel or fuel C, ignition was accomplished at a lower velocity and a fixed fuel rate. Gradual increase of air velocity at this fuel rate was used to approach blowout, and the technique was repeated at other fuel rates to define a curve of velocity maxima.

The fuel/air ratio of the inlet spray was determined from the difference between the rates of fuel feed and collection at the walls. During stable combustion wall-collection rates were measured near rich and lean limits and extrapolated to the blowout conditions.

Experimental Results

COLD FLOW IN THE COMBUSTION CHAMBER

Pitot-tube and sampling-probe traverses were made to determine the patterns of local velocity, fuel/air ratio, and fractional spray vaporization. The local flow velocity was found to be uniform to within ½ in. of the walls. With naphtha, the profile of local fuel/air ratio was flat across the entire test section. With diesel fuel, the mixture was richer near the center of the chamber than at the walls. Estimates of the fractional vaporization of naphtha were made by analyzing samples of the fuel-air mixture withdrawn at various fractions of the main stream velocity. These tests showed that fractional spray vaporization increased from the center of the chamber toward the walls, which were always covered by a film of liquid fuel. At the walls the measured fractional vaporization closely approached equilibrium values calculated by the method of Brown.[15]

VISUAL OBSERVATIONS OF FLAMEHOLDER CONDITIONS

Four conditions of the flameholder surface were observed, and the first three are sketched in Figure 4. The four conditions are: (1a) Wet rod, with all the surface upstream of the flame fronts covered by a continuous film of liquid fuel, as

shown in Figure 4a. (1b) Wet rod, with a film of liquid fuel covering the entire rod, including the downstream portion between the flame fronts (Fig. 4b). (2a) Semi-dry rod, with only a narrow region extending slightly downstream from the upstream stagnation line wetted by fuel, which is vaporized at the collection rate. This is also called the "dry-rod" condition, and in Figure 4c the area and thickness of liquid film for dry-rod collection is probably exaggerated. (2b) Completely dry rod, without effectual collection, apparently vapor-bound and always attended by flame blowout.

In sprays of fuel B, fuel C and diesel fuel, combustion was sustained only with a wet flameholder; rich limits were always reached with the rod wet. Lean-limit blowout occurred at low velocities just as the flameholder became dry, but at higher velocities in the wet-rod state. One exception to this generalization was found with fuel B and fuel C in a very narrow range near the lean limit. In a light beam, drops of these fuels could be seen to spatter on the upstream side of the rod and disappear. No continuous film formation (as in Figure 4c) took place, but apparently drops were able to maintain a stable flame by collecting and evaporating from the nearly dry surface. Although this droplet behavior could not be directly observed with naphtha, perhaps because of the smaller drop size or greater evaporation rate, the stability-limit data show that naphtha could also collect on and evaporate from a "dry rod."

In the case of naphtha, stable flames were found over wide ranges with the rod either wet or semi-dry. To illustrate flameholder behavior with this fuel, Figure 5 shows the experimental stability limits for an atomizing velocity of 400 fps and a preparation time of 0.0244 sec. (On the line KCH along which the rod became dry as fuel/air ratio was decreased, only one point, H, was actually measured). Lean limits were always reached with the rod completely dry, rich limits with the rod either wet or dry. Stable combustion in either of these states could be initiated at such points as A, J, or N in Figure 5. Following ignition, adjustment of fuel/air ratio or velocity caused transitions from the one state to the other and/or blowout, as indicated by the cross-hatched portions of the figure.

Two visual observations confirmed the occurrence of the vapor-binding phenomenon. One was the failure of fuel drops to collect on the stabilizer when it was heated by a torch to accomplish dry-rod ignition of naphtha. The other was persistence of the dry-rod condition at lean limits for a definite period of time after blowout, until the stabilizer became cool enough to resume fuel collection. Two fine blue lines marked the origins of the flame fronts very close to the edges of the collected fuel film on the flameholder (Fig. 4a). As the rod became dry, these lines became discontinuous and then disappeared; with naphtha this change was accompanied by a characteristic color change of the pilot flame from greenish-blue to purplish-blue.

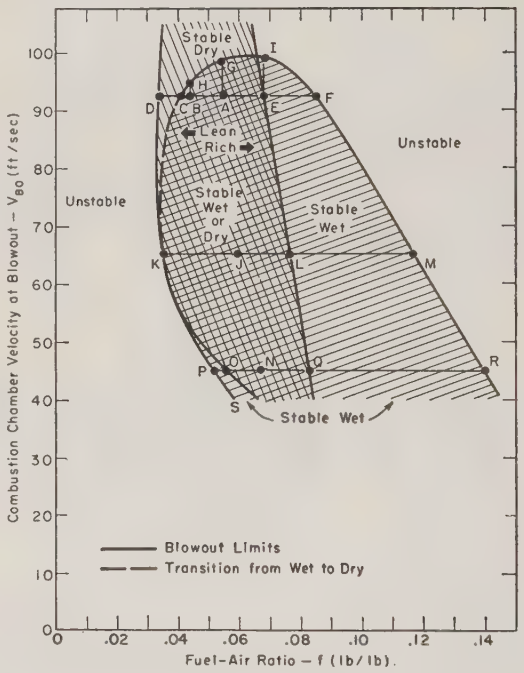

Fig. 5. Flameholder conditions with naphtha, fuel A.

FLAME STABILITY DATA

The principal experimental results represent the relations at blowout among five variables, initial mean drop size, d_{o1}, preparation time, θ, total fuel/air ratio, corrected for collection at the walls, f, velocity, V, and fuel type. Values of d_{o1} were calculated from the equations of Nukiyama and Tanasawa[5] for orifice atomization and are regarded only as showing the correct relative magnitude for venturi-atomized droplets. Figures 6, 7, 8, and 9 inclusive show experimental stability-limit curves for the four fuels, naphtha, fuel B, fuel C, and diesel fuel, at particular drop sizes and preparation times. Each curve is a plot of air velocity at the inlet of the combustion

chamber *vs.* fuel/air ratio, and would be continuous but for the limitation on air velocity

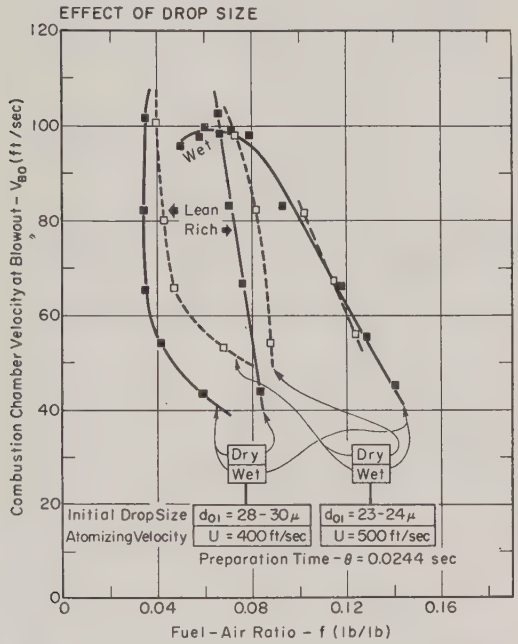

Fig. 6. Flame stability limits for naphtha, fuel A.

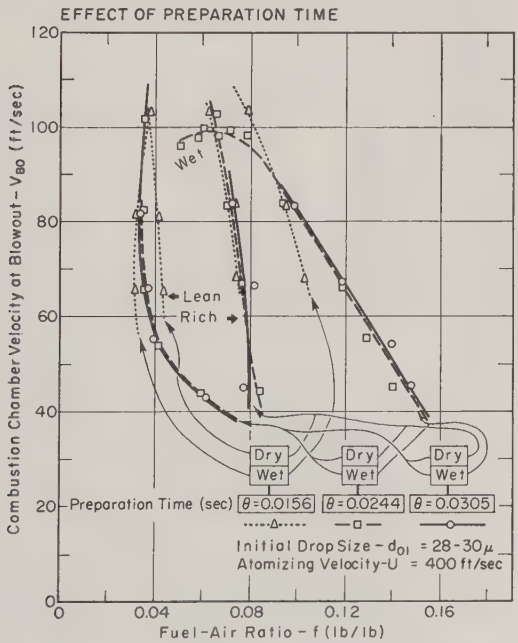

Fig. 7. Flame stability limits for naphtha, fuel A.

imposed by the compressor output which restricts the curves to separate branches for rich and lean limits. The indicated preparation times were computed from the geometry of the atomizing and mixing sections and from the air velocities at the test chamber corresponding to the control atomizing velocities. The two values of drop size indicated on each curve are averages for all points on the lean and rich branches, respectively. Drop sizes were somewhat larger for the rich-limit flames than for the lean, mainly because of the effect of fuel/air ratio. In the laboratory the control variable was atomizing velocity, and it did not seem practicable to adjust for the small effect of fuel rate on drop size during operation of the apparatus.

In Figures 6 and 7, which show the effect of drop size and preparation time upon stability limits for naphtha, the condition of the flameholder during approach to the limit has been distinguished as wet or dry, corresponding to the conditions shown in Figure 4. Many of the lean limit curves are identical for approaching from either condition.

Figures 8 and 9 show the effect of fuel type at two different drop sizes. The dry and wet notation for the naphtha curves appear as before, while for the other fuels the few vapor-bound blowouts at low velocity lie below the line marked "wet rod/dry rod." Included in Figure 8 is Williams, Hottel, and Scurlock's correlation[1] of their data for gaseous propane.

Discussion of Results

THEORY OF DRY-ROD STABILIZATION

Equation (3) above was derived for a stabilizer with wetted upstream surfaces which collected all impinging drops. The discussion needs to be extended to cover the phenomenon of stabilization on a nearly dry flameholder, a situation which differs markedly from the phenomena studied by May and used as the basis for analysis of wet-rod stabilization. The new analysis can be started with an equation written for the stage of transition from a wet- to a dry-rod condition, as follows:

$$f_{vE} = fF_v + \frac{f(1 - F_v)E_c}{R} \tag{4}$$

From the previous work on drop collection,[10] it may be expected that under dry-rod conditions the collection efficiency function can be approximated in the following form

$$E_c = K_c' \frac{V^\alpha d_o^\beta}{D^\gamma T_E^\epsilon} \tag{5}$$

in which K_c', α, β, γ, and ϵ are empirical constants

for reasonable ranges of approach-stream velocity, V, drop size d_o and flameholder diameter, D. The factor, T_E^{ϵ}, has been introduced to account for the vapor-binding phenomenon. As eddy temperature, T_E, rises, rod temperature also rises; when the difference between the temperature of the upstream surface of the rod and that of the approach stream becomes large, the surface becomes vapor-bound and drops cannot collect.

Equation (5) is substituted into Equation (4) to give

$$f_{vE} = fF_v + \frac{K_c f(1 - F_v) V^{\alpha} d_o^{\beta}}{RD^{\gamma} T_E^{\epsilon}} \qquad (6)$$

with a new constant, K_c. For a particular fuel, flameholder, and set of values of the stream properties, Equation (6) may be simplified to

$$f_{vE} = fF_v + \frac{K_D}{T} \qquad (7)$$

from which its form has been sketched in Figure 10. This is a plot of f_{vE} *vs.* T_E to show the suggested mechanism for dry-rod stabilization. The curve of Equation (3) has been included to emphasize the difference between wet-rod and dry-rod conditions.

At very high values of eddy-zone (and rod) temperature, droplet collection cannot occur, so the vertical line, $f_{vE} = fF_v$, is an asymptote for curve 6 as well as curve 3. As eddy and rod temperatures fall along curve 6, collection increases until point D for stable, equilibrium combustion is reached. In this dry-rod case the lean-branch intersection D is stable, rather than D″. At D, if a small increment in eddy temperature reduces the collection rate and hence f_{vE}, the leaner mixture leads to a lower value of eddy temperature, in the restoring direction. At D″, however, the increased rod-surface temperature and reduced collection rate caused by an increment in eddy temperature would cause the latter to increase further.

The effects of independent variables on stability limits with the semi-dry flameholder are illustrated by curves 6 in Figure 10b. Point 1 corresponds to the minimum and point 3 to the maximum stable fuel rate. A slight increase in over-all fuel/air ratio over that of point 3 raises curve 6 to a position $(6)_4$ which can no longer intersect any value of eddy temperature specified by Equation (2). T_{E_3} corresponds to the eddy composition at 4″ on the new $(6)_4$ curve, a mixture ratio which would cause the eddy temperature to fall, allowing further collection, overenrichment, and a "dry-rich blowout" such as

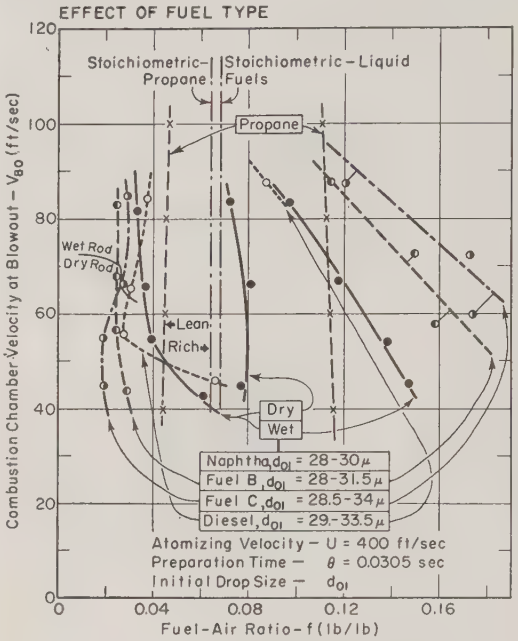

Fig. 8. Flame stability limits.

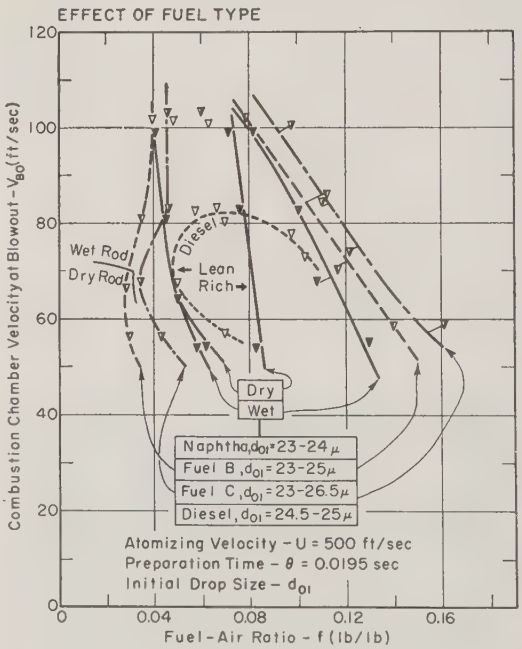

Fig. 9. Flame stability limits.

represented by line ELQ in Figure 5. This dry-rich blowout may be reached by increasing fuel/air ratio or drop size, either of which would raise curve 6 by increasing the collection rate. Con-

verse reasoning applies to the "dry-lean" blowout, which is the lean limit at point 1 in Figure 10b.

With other variables constant, an increment in velocity narrows the limits for stable eddy-zone fuel/air ratios and thus shortens the curve of Equation (2) in Figure 10b at both ends. Equation (5) shows, however, that increased velocity should augment the collection rate (because of increased drop momentum). If the exponent, α, for the velocity, V, in Equation (6) is greater than unity and thus permits dominance over the factor, R (a direct function of V) in the denominator, the net effect of a velocity increase would be to raise the position of curve 6 and the equilibrium eddy-

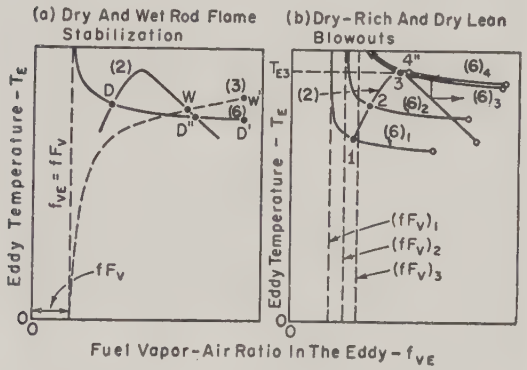

Fig. 10. Dry-rod flame stabilization.

TABLE 2. FLAME STABILITY LIMITS

Type of Blowout	*Approach Condition*	*Illustration*
Dry-lean	Dry rod	Fig. 10b, point 1
Dry-rich	Dry rod	Fig. 10b, point 3
Vapor-bound	Wet rod	Fig. 2a, point 1
Slough-limited	Wet rod	Fig. 2a, point 3
Rich-wet	Wet rod	Fig. 2b, point 3

zone temperature. Depending on the fuel rate, the limit finally reached as velocity is increased could be either a dry-lean or a dry-rich blowout. At the optimum fuel rate, the maximum stable burning velocity, V_{max} would be reached at point 3, but with curve 2 reduced to a single point at the maximum eddy-zone temperature.

INTERPRETATION OF EXPERIMENTAL RESULTS

To facilitate discussion of the experimental data (Figures 5 to 9) in the light of Equations (2), (3) and (6), a compilation of blowout-types is presented in Table 2.

Dry-rod stability limits of naphtha

As shown by Figure 5, lean limits are leaner with the wet than with the dry-rod condition, at low velocity where collection efficiency is poor. The final cause of blowout in either case is vapor-binding with the rod overheated. The collection efficiency of the wetted rod is greater because its entire upstream surface is cool enough for drops to collect. Therefore, if approach to the lean limit is made with the rod essentially dry, it becomes vapor bound at a higher fuel rate than if the approach is made with a wetted rod.

Collection efficiency is markedly improved by increased velocity. Therefore, when vapor binding begins at high velocity, the eddy-zone temperature may first increase to a maximum and then decrease, following curve (2) Figure 10a from W, at which vapor-binding would begin when W′ becomes coincident with it, to D, at which a new dry-rod equilibrium may be established. Further reduction of the fuel-air ratio would lead to dry-lean blowout, such as that at D in Figure 5.

At very high velocities, near the wet-rod maximum in Figure 5, an increase of the air rate with the flameholder wet caused a blowout rather than a transition to the dry-rod condition. It is believed that this failure of the system to make the transition was due to its greater sensitivity, at very high velocity, to changes in temperature and collection rate. After vapor-binding begins, the transition requires a rapid increase of rod temperature and decrease in collection rate. At high velocity, where the range of stable fuel/air ratios is narrow and the turbulence is great, it is probable that fluctuations of temperature or composition in the eddy zone cause a blowout before dry-rod steady-state conditions can be established.

The effect of initial drop size at constant preparation time is shown in Figure 6. The marked extension of lean limits with increased drop size is due to increased collection efficiency. The negative slope of the lean stability limits at low velocity is explained by the fact that the collection-efficiency function increases with velocity most rapidly at low velocity. The fact that dry-rich limits are made leaner by increased drop size also reflects the attendant increased collection efficiency.

The effect of preparation time is illustrated by Figure 7, which shows that between the two larger values of preparation time there was no significant difference in stability limits with the flameholder either wetted or dry; but that interesting effects were observed when the time for prevaporization of fuel was reduced to 0.0156 sec, half of the largest value. The shorter preparation time decreased the fractional spray vaporization, F_v, but increased the size of the drops arriving at the

flameholder. In this case the vapor-bound lean limit was made leaner because the improved collection efficiency due to larger drop size allowed leaner over-all fuel/air ratios to be reached before vapor binding occurred. On the other hand, the dry-rod lean limit was made richer by decreased preparation time. This result is taken to mean that spray vaporization in the approach stream is more important for effective dry-rod than wet-rod stabilization.

Vapor-bound lean limits

Almost all of the lean stability limits at low velocity were vapor-bound blowouts, indicated below the line marked "wet rod/dry rod" in Figures 8 and 9, which compare data for the four fuels. Additional data[13] also show extension of these limits to leaner fuel/air ratios with increases in drop size and velocity, due to improved collection rate. Within the precision of the data, variations in preparation time showed no discernible effect on the vapor-bound lean limit.

The progressive extension of vapor-bound blowouts to leaner limits as fuel volatility was decreased (from naphtha to fuel B to fuel C in Figure 8 and from naphtha to fuel B in Figure 9) is predicted by Equation (4). This shows that with identical velocity, fuel/air ratio, and initial drop size the flame of a more volatile fuel should reach the vapor-binding condition sooner because of greater spray vaporization (a lower value of $(1\text{-}F_v)$) and poorer collection efficiency (due to reduced drop size at the flameholder). The relationship breaks down, however, for the deisel fuel data, possibly because of unknown or uncontrolled factors, perhaps peculiar to the apparatus.

Maximum stable burning velocity

When velocity is increased the range of stable fuel/air ratios in the eddy-zone is diminished, as with flames of homogeneous fuel-air mixtures. The maximum velocity, with the other independent variables fixed, is attained when this range on the curve of Equation (2) is reduced to a single point at the maximum attainable eddy-zone temperature. Through that point a unique curve of Equation (3) or (6), corresponding to the optimum fuel/air ratio, must pass. In discussions earlier in this paper, eddy-zone temperature has been treated as a unique function of eddy-zone composition, equal to the adiabatic flame temperature. This was a simplification used where conclusions regarding flame stability could be drawn simply from consideration of the movement of curve (3) or (6) relative to curve (2). Actually, at a given velocity, fuel/air ratio, and drop size the curves of eddy temperature versus eddy fuel/air ratio (Eq. 2) for wet-rod stabilization would be higher with more volatile fuels. These curves would be still higher for dry-rod stabilization and highest for gaseous fuels with an artificially heated flameholder. This relationship results from the progressively reduced abstraction of energy from the eddy region to heat the flameholder and the collected fuel. Since the maximum available eddy-zone temperature is higher with a more volatile fuel, a higher velocity can be reached before the stable range of vapor-air ratios in the eddy zone becomes reduced to a point. This reasoning is borne out by the work of Russi, Cornet and Cornog[16] with gaseous fuels. The experimental data on velocity maxima from the investigation reported here are consistent with the above reasoning. As shown in Figures 6 and 7 for naphtha, a maximum velocity was found for wet-rod stabilization; but at the same preparation time and identical drop size, no peak was reached with the flameholder dry. Further support for the theory is given by Figure 9, in which only the least volatile fuel, diesel, shows a maximum velocity. Similar data[13] for smaller drop sizes consistently showed higher maximum stable velocities with increased fuel volatility and with transition to the dry-rod condition.

Wet-rod lean limits

At velocities above the line marked "wet-rod/dry-rod" in Figures 8 and 9, the lean limits for fuel B, fuel C and diesel fuel occurred with the flameholder wetted, as in Figure 4a. At velocities below that line, as explained above, reduction of fuel flow progressively enriched the eddy-zone mixture, (by fuel vaporization from the rod at a greater rate because of reduced heat loss to sloughing fuel), until the vapor-binding condition was reached and fuel collection stopped. With the greater collection rate which occurs at high velocity the flameholder can still be wetted at blowout; and liquid fuel is still sloughing from it when the lean stability limit is reached. This limit corresponds to an eddy-zone fuel/air ratio that has become too rich to lie within the narrowed range of stable eddy-zone compositions at high velocity.

Wet-rod rich limits

Before examination of the data it would be advisable to reconsider two assumptions explicit

in the derivation of Equation (3). These were (a) that all of the collected fuel is heated to the temperature, T_L, before being vaporized or sloughed off, and (b) that the composition of collected fuel remains unchanged from its original composition. Near the lean limit, when the collected fuel forms only a thin layer, the first assumption is probably justified. With the high collection rates (Figure 4b) that occur near rich limits, it is likely that a considerable fraction of sloughed fuel is not heated to the high temperature of the fuel surface at or between the flame fronts, the area from which most of the vaporized

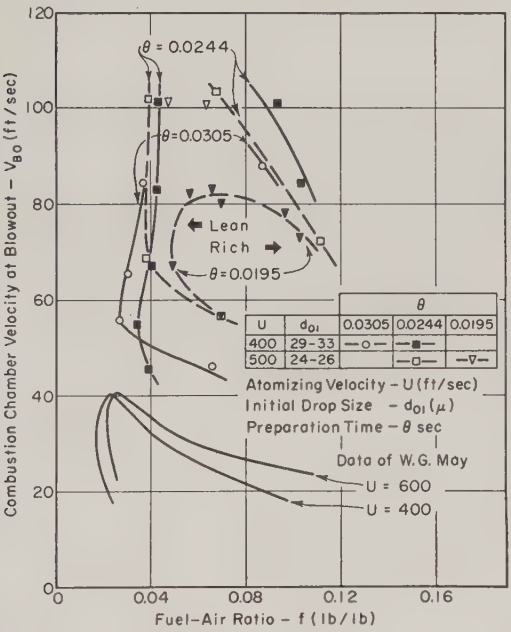

Fig. 11. Flame stability limits for diesel.

fuel would be expected to enter the eddy zone. Under these conditions only the most volatile portions of the fuel would be vaporized and the composition of the collected layer would vary with collection rate. Thus an increase in collection rate could cause an increase in the rate of feed of fuel vapor (mainly the more volatile fractions) to the eddy zone, without requiring any considerable change in the rate of heat removal from the flameholder. With a relatively nonvolatile fuel, on the other hand, the increased collection rate could lead only to a slough-limited blowout.

For every case in which the effect of drop size was measurable, increased drop sizes caused the rich limits to become leaner, a result attributable to increased collection rate and excessive enrichment of the pilot zone by rod-vaporized fuel. It follows, also, that the most volatile fuel should have the leanest rich limits. Figures 8 and 9 show this to be the case for naphtha, fuel B, and fuel C. The exceptional behavior of diesel fuel indicates that diesel flames were subject to slough-limited blowouts (i.e., excessive abstraction of heat by sloughed fuel); this result is consistent with those of Hottel, May, Williams and Maddocks.[11]

For naphtha alone, Figure 7 shows essentially identical rich limits at the two larger values of preparation time and a leaner rich limit at low velocity when the preparation time was much shorter. This effect at low velocity is compatible with the rich-wet blowout mechanism, in this case caused by increased collection of volatile components. Longer preparation time produces increased spray vaporization. This enriches the approach stream but at the same time tends to strip the most volatile components from the fuel drops which are subsequently collected by the rod. With the moderately volatile fuels studied here, rod vaporization is believed to be the principal source of fuel vapor for the eddy region; so the net enrichment of the eddy would be reduced by increased preparation time.

This attainment of rich stability limits with a rich-wet blowout caused by increasing the collection rate implies a shift in behavior of the flameholder system which can be explained with the aid of Figures 2a and 2b. From a lean limit such as at point 1, Figure 2a, increasing fuel flow would cause movement of the system toward intermediate points like 2, which represents a slightly increased vapor concentration in the approach stream and a considerably reduced rate of vaporization of fuel from the rod. There would also be a considerable increase in heat removal from the rod by sloughed fuel. At some point in the process, depending upon fuel volatility and composition of the collected liquid, there appears to be a shift, with increased collection rate, toward increased rod vaporization. This reversal might be expected to occur when the downstream surface of the rod becomes flooded, as in Figure 4b, and subsequent action of the system would be identified with Figure 2b. The increase of hot collected-fuel surface exposed to the eddy would increase the supply of fuel vapor to the eddy region and cause a rich-wet blowout, as at point 3 in Figure 2b. For the least volatile of fuels used, diesel, this shift in flameholder action apparently does not occur, since the data indicate that rich limits for flames

in diesel sprays were always slough-limited blowouts.

Comparison of present and earlier data on diesel fuel flames

The stable combustion range of diesel fuel in the apparatus used for this investigation was markedly different from that measured by May, as shown in Figure 11. There the data for diesel flames on an unheated flameholder of 0.132-in. diam are replotted from Figure 7 of the earlier paper.[11] The differences can best be explained by considering differences in the apparatus. May's burner was of 3 by 3-in. cross section (like the present one), but was preceded by a large convergent nozzle between it and the atomizing section. From 60 to 85 per cent of the injected fuel returned as runback to a tray at the atomizing section, so that only 15 to 40 per cent remained in the spray reaching the combustion chamber. It is reasonable to assume that the nozzle had a classifying effect, allowing only the smallest droplets to enter the combustion chamber. Decreased drop size has been shown here to reduce the maximum stable velocity.

The average residence time in the large mixing section and nozzle of May's apparatus must have been about 8 times as long as in the present apparatus at comparable velocities in the combustion chamber; so in May's apparatus equilibrium vaporization must have been much more nearly approached. While only a small fraction of the diesel spray would have been vaporized even at equilibrium, it is reasonable to suppose that the more volatile components would have been stripped out and that the spray collected by the flameholder must have been less volatile. This effect would explain both a lowering of the maximum velocity, compared with results in the present work, and the shift of stability to leaner over all fuel/air ratios, as observed.

May's rich and lean limits were satisfactorily explained by the mechanisms of slough-limited and vapor-bound blowouts, respectively. These mechanisms also explain diesel stability limits at low velocities with the apparatus used in the present work; at high velocities with diesel fuel the wet-rod lean limit is believed to be caused by increased collection and over-enrichment of the eddy zone by vaporization of rod-collected fuel. The pronounced extension of rich limits and increase of maximum velocity by addition of propane in May's work[11] is consistent with the present experimental results for increased fuel volatility and fractional spray vaporization and with the prediction of higher velocity maxima for more volatile fuels.

Conclusions

(1) Flame stabilization in a high-velocity spray of volatile fuel droplets depends upon maintaining a pilot flame in the wake of a flameholder.

(2) The fuel-vapor/air ratio supplied to the pilot-zone flame results from vaporization of both fuel droplets in the approach stream and liquid fuel collected on the flameholder.

(3) In the eddy region the fuel-vapor/air ratio (a) must lie within rich and lean limits determined by approach-stream velocity, as with homogeneous fuel/air mixtures, and (b) must have a composition which satisfies the conditions for steady-state mass and heat exchange between eddy zone and rod. These conditions come from the following relationships: (*1*) Eddy-zone composition determines the combustion temperature of the pilot flame. (*2*) This temperature determines the heat-transfer rate to the flameholder and collected fuel. (*3*) Heat transfer fixes the rate of vaporizing collected fuel which, to satisfy the condition for stability, must be that value which maintains the above eddy composition.

(4) Depending on the ratio of prevaporized fuel to rod-vaporized fuel, stable flames can be maintained with the stabilizer wetted by a continuous film of collected fuel or almost completely dry. (a) In the wet-rod state, some of the fuel collecting on the wetted surfaces is vaporized; the remainder is sloughed off by the passing stream. The heat transfer from the eddy zone to wetted stabilizers causes fuel to vaporize at a rate sufficient to maintain the fuel-vapor/air ratio in the eddy zone slightly fuel-rich. (b) In the "dry-rod" state only a narrow strip of flameholder surface, extending slightly downstream from the upstream stagnation line of the rod, is wetted with fuel, all of which is vaporized at the collection rate. For dry-rod stabilization, the heat transfer rate to the stabilizer maintains it at a high temperature which permits only enough droplet collection to provide an eddy composition near stoichiometric or slightly lean.

(5) The proposed mechanisms of flame stabilization are consistent with curves of blowout velocity versus approach-stream fuel/air ratio, measured for four different fuels on a $\frac{1}{8}$-in. rod flameholder and with independent control of initial mean drop size and elapsed time from atomization to combustion. (a) Higher peak

blowout velocities were attained with larger drop sizes, with longer preparation times, and with more volatile fuels. With volatile naphtha the maximum velocity at a given fuel/air ratio was higher for dry-rod than for wet-rod stabilization. Maximum velocity was reached with the eddy-zone temperature at a maximum (near the stoichiometric eddy mixture). (b) At low velocity, fuel-lean limits were reached when heat transferred to the rod exceeded requirements and the rod became too hot (vapor bound) to collect fuel. At a given combustion-chamber velocity the lean limits were made leaner by reduced fuel volatility, by reduced preparation time, and by increased drop size. (c) At high velocity, lean limits with the less volatile fuels were caused by excessive enrichment of the pilot eddy. These blowouts were characterized by wet flameholders because of the greater collection rate at higher velocity and were extended to leaner mixtures by increased fuel volatility. In the case of naphtha, high-velocity lean limits were reached at complete vapor binding after transition to the dry-rod condition and were extended to leaner mixtures by increasing drop size and preparation time. (d) Rich limits with a dry (but not vapor-bound) stabilizer were caused by overenrichment of the eddy zone. These limits were made richer by decreased drop size and were reached at much lower fuel rates than when the rod was wet. (e) Rich limits with a wetted stabilizer were extended by decreased drop size, increased preparation time, and decreased fuel volatility. These blowouts resulted from increased collection rate rather than from increased vapor in the approach stream. With diesel fuel, the increased collection rate caused the eddy to become too lean as less fuel was vaporized, because of heat loss to the slightly volatile collected liquid blown off the stabilizer. With the more volatile fuels, blowouts apparently were caused by increasing concentration of volatile constituents in the rod-collected fuel, which made the eddy zone become too rich to maintain the pilot flame.

Data

Complete tables of data and experimental procedure are given by Marion[13].

Acknowledgment

Grateful acknowledgment of financial support in the early stages of this work is made to Project Meteor, administered by the Bureau of Ordnance, Department of the Navy, under Contract Nord 9661; in the later stage to Project SQUID, which is jointly supported by the Office of Naval Research, the Office of Ordnance Research (Army), and the Office of Scientific Research (Air Force) under Contract N6-ori-105, Task Order III, NR-098-038. One of the authors (C. P. Marion) wishes also to acknowledge the financial support by the Standard Oil Company, Indiana, and the William S. Knudsen Fellowship which sponsored him during part of the period of this work.

Nomenclature

A_R fractional surface area of rod stabilizer per unit length
A_{RA} effective for heat transfer from rod to air
A_{RE} effective for heat transfer from eddy to rod
A_{RL} effective liquid surface for vaporization and heat acceptance
a constant to express variation of vapor pressure with temperature
C_1 constant
D flameholder diameter
d_o surface-volume mean drop diameter
d_{o1} initial value of d_o
E_c collection efficiency
F_v weight fraction of spray vaporized
f over-all fuel/air ratio by weight
f_{vE} vapor fuel/air ratio in pilot eddy
K_i constant
k_{fE} thermal conductivity of gas film between eddy and flameholder
N_{Re} Reynold's number
R ratio of air burned in the eddy zone to air which would flow through the upstream projected area of the flameholder
T temperature, degrees F absolute, of fuel/air mixture in approach stream
T_E average effective temperature of eddy gases for heat transfer to flameholder system
T_f gas-film temperature
T_L liquid-surface temperature
T_s arbitrary standard temperature
U atomizing velocity—relative velocity between air and liquid ($U = V_A - V_F$)
V gas velocity entering combustion chamber
V_A velocity of air at atomization
V_{BO} flame blowout velocity
V_F velocity of fuel at atomization
V_{max} maximum stable burning velocity
Δ vapor fuel/air ratio in the eddy from rod vaporization only
θ preparation time
ψ functional relationship between adiabatic flame temperature and fuel/air ratio

SUBSCRIPTS

A air
c collection or collected

E eddy
F fuel
f film
L liquid
R rod
v vapor or vaporized

REFERENCES

1. Williams, G. C., Hottel, H. C., and Scurlock, A. C.: *Third Symposium on Combustion, Flame and Explosion Phenomena*, p. 21. Baltimore, The Williams & Wilkins Co., 1949.
2. Caldwell, F. R., Ruegg, F. W., Olsen, L. O., and Broida, H. P.: Sixty-third through Seventy-first Reports of Progress on the Combustion Chamber Research Program, National Bur. Stds. Reports, U. S. Dept. of Commerce, Washington, D. C., July 1949.
3. Longwell, J. P., Frost, E. E., and Weiss, M. A.: Ind. Eng. Chem., *45*, 667 (1953).
4. Zukowski, E. E., and Marble, F. E.: *Combustion Researches and Reviews*, p. 167, London, Butterworths Scientific Publications, 1955.
5. Nukiyama, S., and Tanasawa, Y.: Trans. Soc. Mech. Eng. (Japan), *4*, 14, 15, 86, 93 (1938); *5*, 18, 63, 68 (1939); *6*, 22, 23 (1940).
6. Lewis, H. C., Edwards, D. G., Goglia, M. J., Rice, R. I., and Smith, L. W.: Div. 10, NDRC, OSRD; OSRD No. 6345, Oct. 10, 1945.
7. Fledderman, R. G., and Hanson, A. R.: University of Michigan Engr. Res. Inst., Rept. No. CMM667, June 20, 1951.
8. Froessling, N.: Gerlands Beitr. Geophys., *52*, 170 (1938).
9. Longwell, J. P., and Weiss, M. A.: Ind. Eng. Chem., *45*, 667 (1953).
10. Langmuir, I., and Blodgett, K. B.: Report No. 5418, Dayton, Ohio, U. S. Air Force, Air Materiel Command, Wright-Patterson Air Force Base, February 19, 1946.
11. Hottel, H. C., May, W. G., Williams, G. C., and Maddocks, F. E.: *Fourth Symposium (International) on Combustion*, p. 715. Baltimore, The Williams & Wilkins Co., 1953.
12. May, W. G.: Sc.D. Thesis, Dept. Chem. Eng., Massachusetts Institute of Technology, 1949.
13. Marion, C. P.: Sc.D. Thesis, Dept. Chem. Eng., Massachusetts Institute of Technology, 1952.
14. Hottel, H. C., Williams, G. C., and Satterfield, C. N.: *Thermodynamic Charts for Combustion Processes*. New York, John Wiley and Sons, Inc., 1949.
15. Brown, G. G.: University of Michigan Engr. Res. Bulletin No. 14, May 1930.
16. Russi, M. J., Cornet, I., and Cornog, R.: *Fourth Symposium (International) on Combustion*, p. 743, Baltimore, The Williams & Wilkins Co., 1953.

57

FLAME STABLIZATION IN GASES FLOWING CYCLONICALLY: FLOW CHARACTERISTICS, TEMPERATURES, AND GAS ANALYSES

By LYLE F. ALBRIGHT[a] and LLOYD G. ALEXANDER[b]

Cyclonic flow principles have been used extensively in the combustion of coal and oil, but only to a limited extent in the combustion of gaseous fuels. The term "cyclonic flow" as used here designates spiral motion of a fluid around its flow axis.

Three investigations[2, 4, 5] have been made of the flow patterns of air flowing cyclonically in cylindrical ducts. Qualitatively, the results are similar. In the annular region next to the wall of the duct, a forward cyclonic flow occurred, *i.e.*, the axial component of the flow was toward the duct outlet. The static pressures near the axis of the duct were lower than at the duct wall, and a weak reverse cyclonic flow occurred here.

Preliminary results for cyclonic burners with gases have been reported by several investigators.[3, 11, 12, 14] In some cases the burners were designated "vortex burners." The air, at least, was always introduced so that it possessed a tangential velocity component and so flowed cyclonically. Garner and Cheetham[3] measured

[a] Present address: Purdue University, Lafayette, Indiana.

[b] Present address: Oak Ridge National Laboratory, Oak Ridge, Tennessee.

the impact pressures in the cyclonic combustion chamber. The pressures at the axis were found to be lower than those elsewhere. Pistor[12] reports some gas analyses for the flame of a cyclonic free jet. Stone and Wade[14] indicate that gaseous fuels can be used in cyclonic burners designed for coal or oil. Kurz[6, 7, 8, 9] states that cyclonic burners can be used to determine the compatibility of various gaseous fuels.

Hottel and Person[4] also studied cyclonic flames in ducts. The flow patterns in the flames were found to be similar qualitatively to those in air only. The combustion efficiencies of the flames studied were dependent primarily on the fuel-air ratio and the length of the duct. Efficiencies varied from 20 to 99 per cent, and heat release rates in the flames were as high as 1,700,000 Btu/hr/cu ft. Calculations made with their data indicate that the highest flow rates were equivalent to a superficial velocity of 13 fps. Superficial velocity is defined as the velocity the gas would have if passed through the duct linearly, unburned, and at room conditions.

Albright and Alexander[1] have reported that cyclonic flames can be stabilized in emergent cyclonic free jets up to 100 fps. and in ducts up to 700 fps. Combustion was sometimes incomplete, and pressure drops through the apparatus were high. Cyclonic equipment could probably be designed, however, which would reduce pressure losses considerably. Recently Plaster[13] has analyzed the gases resulting from several cyclonic flames. He used a small cyclonic apparatus[1] and collected gas samples at various locations in and near the flame through a water-cooled sampling tube. Combustion in ducts was complete only when the flame front extended to the wall of the duct. Otherwise the gas flowing near the wall escaped combustion.

In the investigation reported here, flow characteristics, temperatures, and chemical compositions of flames stabilized in ducts by cyclonic motion were studied.

Apparatus Used

Natural gas and air were metered, by means of sharp-edged orifices, to the cyclonic nozzle (see Fig. 1). The natural gas contained approximately 90 per cent methane, 5 per cent ethane, and the remainder air. The natural gas and air were mixed and introduced through the annulus of the cyclonic nozzle. The mixture then flowed through the vanes into the swirl chamber of the nozzle. If desired, the natural gas could be introduced separately through the ⅛-in. pipe penetrating along the axis of the nozzle.

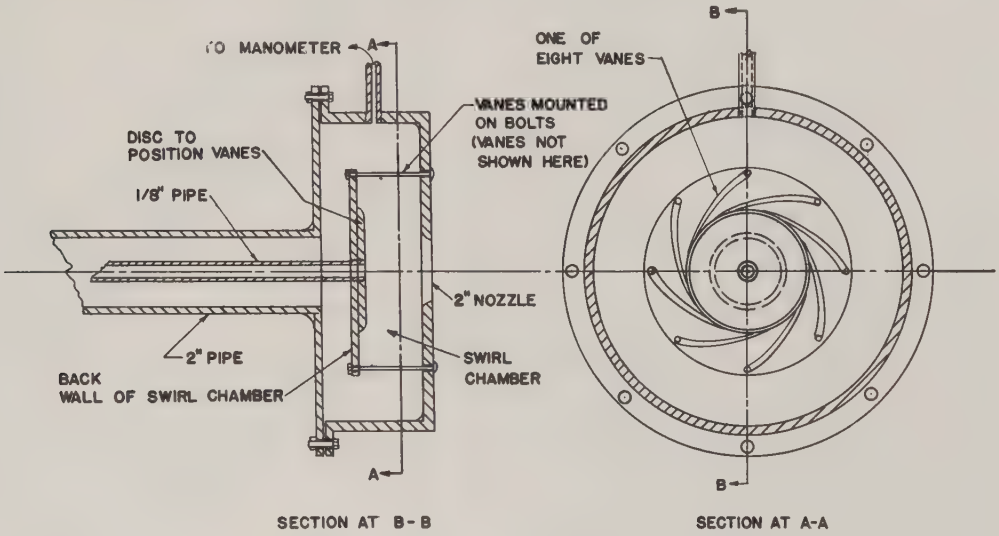

Fig. 1. Cyclonic combustion nozzle.

A glass or metal duct with a 2-in. i.d. was attached to the face plate of the cyclonic apparatus at the 2-in. nozzle. The lengths of the ducts varied from 6 to 36 in. The duct used when flow measurements were made was 19¼ in. long; two ⅛-in. holes, 180 deg apart, were drilled at distances of 1¼, 4, 8¼, 16, and 19 in. from the duct inlet. These holes were provided for the water-cooled impact tube shown in Figure 2. The tube was mounted on the duct in two sliding and

turning joints, so that it could be rotated through 360 deg. A collar with set screw was used to position the impact tube vertically. A pointer attached to the collar was used to read the horizontal angle on a 360-deg protractor.

Impact-tube pressures were recorded for various flow conditions at intervals of 10 deg over a range of at least 50 to 60 deg on each side of the angle for maximum pressure. Plots made of the

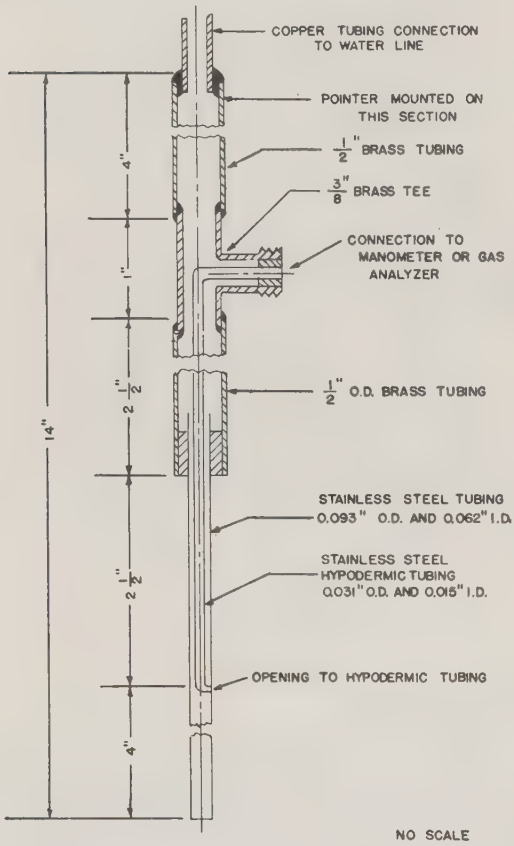

Fig. 2. Water-cooled impact tube and gas analyzer.

pressure versus the angle were always symmetrical within experimental accuracy. The maximum pressure was considered the total pressure, and the corresponding angle as the flow angle. The pressure indicated at 51 deg from the maximum pressure was taken as the static pressure. This orientation had been determined by calibration of the impact tube in linear free jet streams.

The impact tube was also used to collect samples of gas from the flame. Samples were analyzed with a Standard Burrell Gas Analysis Apparatus. Temperature measurements in the flames were made with an unprotected chromel-alumel thermocouple, which withstood temperatures up to 2600°F but failed at higher temperatures.

Flow Patterns of Air in a Duct

The vanes of the cyclonic nozzle were positioned on the circumference of a 5-in. disc. At superficial velocities of 12.9, 56, and 65 fps, pressure drops through the cyclonic nozzle were 0.15, 2.5, and 3.8 in. of Hg, respectively. Meas-

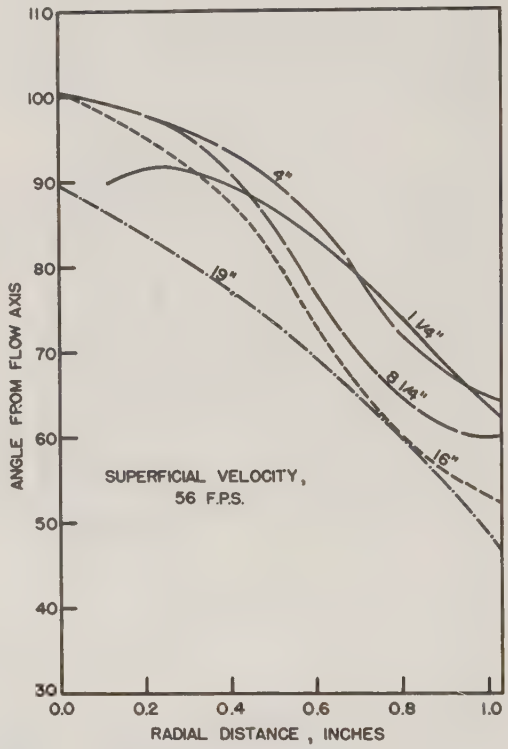

Fig. 3. Flow angles of air flowing cyclonically in 19¼ in. duct.

urements were taken across the diameter at distances of 1¼, 4, 8¼, 16, and 19 in. from the duct inlet.

The flow angles and the impact and static pressures at 56 fps are shown in Figures 3 and 4. The flow angles were generally reproducible within about 2 deg as determined by frequent checks at a given setting and by the good agreement of the data with typical curves (Fig. 3). At the axis, however, the accuracy of the measurements was much less since the total and static pressure were nearly equal in many cases. Errors as high as 10 to 20 deg may have occurred here. Impact and static pressure measurements were in

general reproducible within at least 0.5 in. of water.

A flow angle of zero corresponds to a forward flow parallel to the flow axis. Flow angles of up to 90 deg represent forward cyclonic flow. Angles of above 90 deg indicate reverse cyclonic flow. A strong forward cyclonic flow was found to occur at all radii greater than about 0.5 in. At the duct outlet, the forward cyclone extended over the entire cross-sectional area of the tube.

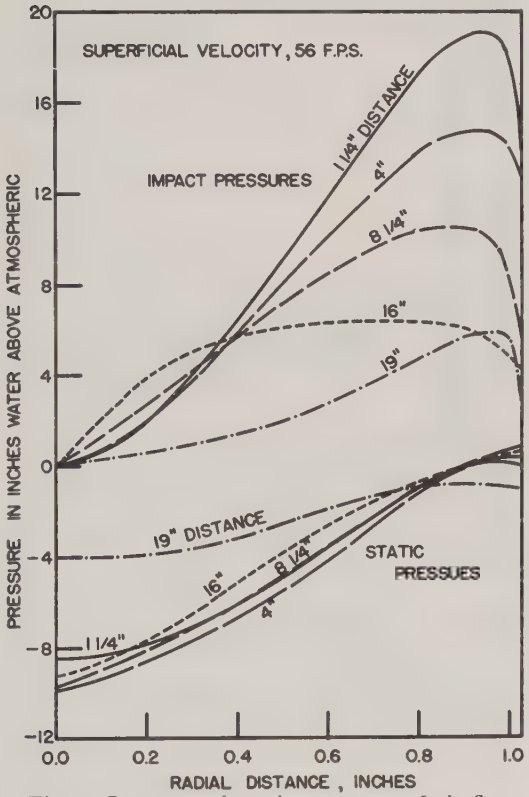

Fig. 4. Impact and static pressures of air flowing cyclonically in 19¼ in. duct.

At distances of from 4 to 16 in., a reverse cyclone was present at radial distances of less than about 0.5 in. At 1¼ in. from the inlet, a weak forward cyclonic flow was found near the duct axis, and the reverse cyclone was present in the annular region from about 0.15 to 0.40 in. of radial distance. The flow angles for a given distance from the inlet were found to be essentially identical for all three superficial velocities. The impact pressure was essentially proportional to the superficial velocity squared. It was generally zero at the axis, increased to a maximum at radial distances of from about 0.7 to 0.95 in., and then decreased as the wall of the duct was approached. At radii greater than 0.4 in., the impact pressure decreased with increased distance along the duct. In some cases, this trend was reversed at radial distances of less than 0.4 in. The static pressure for all flows was approximately atmospheric near the duct wall. At the axis, the static pressure was always below atmospheric and generally increased as the duct outlet was approached. These pressure differentials along the axis were undoubtedly the cause of the reverse flow. As a rule, the flow became more linear at increased distances in the duct. The air-flow measurements were compared to those reported by other investigators,[2, 4, 5] with good agreement.

Since a reverse flow of gases occurred only at shorter horizontal distances in the duct, there was some radial movement in the gases as the net flow of gases is constant along the length of the duct. The amount of radial flow was, however, probably small and relatively insignificant.

The impact tube used was subject to error due to distortion of the flow pattern by the tube itself. Further, the small rotation of the hole in the wall of the impact tube as the angle of the tube was changed may have caused error—especially near the flow axis where, for symmetrical flow, the tangential velocity components must be zero. In some cases the flow angles near the axis were apparently greater than zero, implying cyclonic motion. Yet a small impact pressure was sometimes measured. It is thought that the impact pressure was actually zero, and that the error was caused mainly by the rotation of the hole in the tube wall.

The superficial velocity of the air flowing in the duct was calculated by graphic integration. Velocities calculated in this manner were found to agree within about 5 per cent of each other and with the values calculated from the meter readings. Values of angular momentum were calculated by graphic integration. When the logarithm of angular momentum was plotted *vs* the horizontal distance, the points for each air flow fall on a straight line, as shown in Figure 5. The slopes of these lines are equal. The angular momentum flow values for a given horizontal distance can be plotted *vs* the velocity squared. A straight line passing through the origin was found to correlate the values at all distances according to the equation:

$$M = 0.000613\, v^2 e - 0.0419\, L \qquad (1)$$

where M = angular momentum in lb mass,

ft^2/sec^2; v = superficial velocity, fps.; and L = distance in duct, in. This equation is probably applicable only to the system studied here. Angular momentum is also presumably a function of the gas density; the length, diameter, and roughness of the duct; and the intensity of cyclonic flow.

Cyclonic Flames in Ducts

Cyclonic flames were stabilized in several ducts up to 36 in. in length when the vanes of the nozzle were positioned by discs 3.0 to 4.5 in. in diameter. When the air and natural gas were mixed prior to entry into the cyclonic nozzle, the flames tended to flash back and burn between and before the vanes. Flashbacks caused the apparatus to heat rapidly, and might have damaged it if the flames had not been extinguished. When air alone was introduced through the vanes, and the gas entered through the $\frac{1}{8}$-in. axial pipe, flashback was prevented.

In the case of premixed air and natural gas, flashbacks were eliminated by positioning the vanes with a 5-in. disc and thereby increasing the gas velocity between the vanes. The flames obtained were similar to those obtained by Albright and Alexander,[1] who used a smaller cyclonic apparatus that probably produced a more intense cyclonic flow field. At air-to-natural gas mole ratios greater than approximately 7:1, flames were stabilized in the ducts in the form of hollow cylinders which extended to the back wall of the swirl chamber, and protruded from the exit of the duct. The color of the flames generally was most intense at air-to-gas ratios of about 9:1. At higher ratios, the flames became less intense and smaller in both diameter and length. At ratios of from about 12:1 to 15:1, the flames blew out. Just before blowout, the flames became very indistinct, and the exhaust gases from them were relatively cool.

Pertinent information about five flames studied extensively in a duct $19\frac{1}{4}$ in. long is given in Table 1. The exhaust gases from Flame 1 were relatively cool, and the heat release seemed to be low. Neither Flame 1 nor Flame 2 touched or appreciably heated the duct wall. The gases from Flame 2 were hotter than those from Flame 1, but not as hot as those from Flame 3. The exhaust gases from Flames 3, 4, and 5 were hot. Flames 3 and 4 touched the duct wall at the duct outlet. Flame 5 touched the wall several inches from the end and heated the tip of the duct to incandescence.

When a duct 12 in. long was attached to the cyclonic nozzle, the flames obtained were similar to those obtained with the $19\frac{1}{4}$-in. duct. At air-to-gas mole ratios of from about 8:1 to 9:1, and at superficial velocities up to about 35 fps. the flames touched the duct wall at the outlet. Combustion in these flames appeared to be complete.

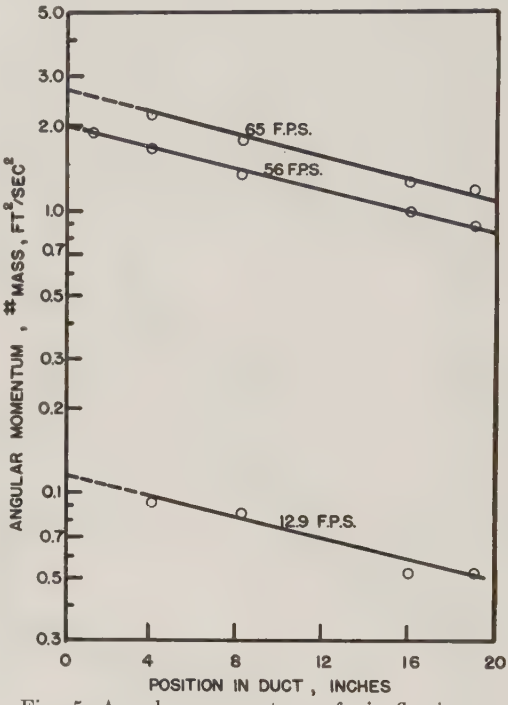

Fig. 5. Angular momentum of air flowing cyclonically in $19\frac{1}{4}$ in. duct.

Table 1. Flow Conditions of Flame Studied in Duct $19\frac{1}{4}$ In. Long

Flame Designation	Natural Gas Flow	Air Flow	Air-to-Gas Mole Ratio	Superficial Velocity in Duct	Pressure Drop Through Burner
	cfm	*cfm*		*fps*	*in. Hg*
1	4.9	72	14.7	56	2.5
2	5.7	70	12.3	55	2.4
3	6.4	69	10.8	55	2.4
4	9.0	87	9.7	69	3.9
5	1.4	16.5	11.8	12.9	0.15

Flow Measurements in Ducted Flames

Measurements were made to determine the characteristics of the flow in the five flames. The data are somewhat less accurate than those for air, since relatively small changes in the air or

natural gas flows had rather pronounced effects upon the measurements. The experimental data for each flame, however, yielded smooth curves,

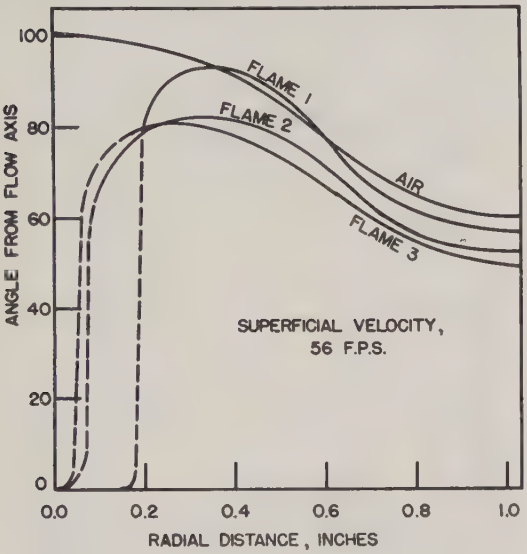

Fig. 6. Flow angles in air and flames at 8¼ in. distance in 19¼ in. duct.

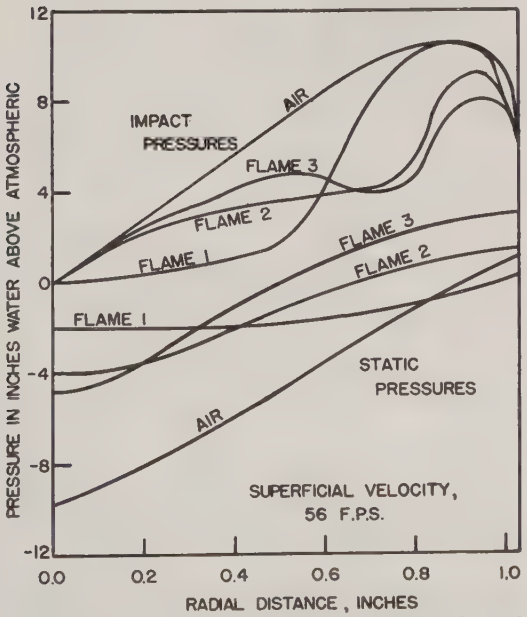

Fig. 7. Impact and static pressures in air and flames at 8¼ in. distance in 19¼ in. duct.

and the flow characteristics of the flames were found to be quite different in several respects from those of air. A comparison is shown in Figures 6 and 7, which compare air and Flames 1 to 3—all of which had superficial velocities of about 56 fps. Figure 6, which presents the flow angles at 8¼ in. from the inlet, indicates that in general the flow angles decreased in the following order: air, Flame 1, Flame 2, and Flame 3. Only Flame 1 and air exhibited any reverse flow at this distance. At the flow axis, all three flames had forward linear flow.

Figure 7 compares the impact and static pressures of air and Flames 1 to 3 at 8¼ in. The maximum impact pressures decreased in the following order: air, Flame 1, Flame 2, and Flame 3. The impact pressure of Flame 3 passed through two maxima at radial positions of about 0.55 and 0.95 in. The other impact-pressure curves passed through only one maximum at about 0.90 in. In general, the static pressures increased in the following order: air, Flame 1, Flame 2, and Flame 3. At the flow axis, the air exhibited a considerably lower pressure than did any of the three flames.

The differences in the flow patterns as shown by Figures 6 and 7 were probably caused primarily by heat release in the gases. Angular momentum was, however, unaffected by combustion. The slight decrease of angular momentum—in the following order: air, Flame 1, Flame 2, and Flame 3—is attributed to changes in the mass of material flowing. Although the entering gas volumes were essentially constant, the air-to-natural gas ratios varied, and the density of the natural gas was somewhat less than that of air.

The flow angles and impact pressures of all flames decreased in general with increased distance in the duct. An exception to this rule occurred in some cases at radial positions near the flow axis, where the impact pressures increased with distance. Both Flames 2 and 3 exhibited reverse flow only at the 1¼-in. distance. The reverse flows in these flames were not pronounced, since the maximum angles recorded were only 92 deg. Reverse flow occurred between radii of 0.45 to 0.65 in. At the flow axis, the flow angles for these two flames indicated a forward flow. Flame 1, however, had reverse linear flow along the axis at distances of 1¼ and 4 in. from the inlet. At other distances, it was found to have forward linear flow.

The impact pressures of Flame 3 showed two maxima at sections 1¼, 4, 8¼, and 16 in. from the inlet, but not at 19 in. Flame 2 also showed two maxima at several distances. Flame 1, however, exhibited only one maximum. The static pressures at the flow axis for Flame 3 were nearly equal at all distances. Near the wall of the duct

the static pressures, in general, decreased with distance.

Temperature Measurements in Flames

Temperatures were measured in Flames 1 to 3. Typical results are shown in Figure 8, which represents Flame 3 at the section of 1¼ in. The temperature data were reproducible within about 50°F. Near the duct wall the temperature was only slightly above room temperature, but it rose sharply a short distance from the wall, and passed through a maximum at radii lying between 0.40 and 0.60 in. The positions of the maxima occurred nearest the axis for Flame 1 and farthest for Flame 3. The temperatures at the axis were in general about 100 to 200°F lower than the maxima. Temperature measurements of Flame 3 were highest, ranging up to 2610°F, and those of Flame 1 were lowest, ranging up to 1900°F.

The temperature measurements were of course subject to errors due to conduction, radiation, and surface reactions. No attempt was made to correct for these. The conduction errors appear to have been relatively small, since the thermocouple readings at both the top and bottom sides of the duct were nearly equal. It is hoped that the values reported give at least a qualitative picture of the temperatures. Table 2 indicates the location of the 1400°F isotherm. The radial distances are probably accurate to within 0.03 in. This isotherm was arbitrarily taken as coinciding with the flame front.

Gas Analyses in Flames

Gas samples were collected using the water-cooled tube at 1¼, 8¼, and 19 in. distances for Flames 1 to 3. The data in general were reproducible within about 0.3 to 0.4 per cent for a particular component. Typical results are shown in Figure 9, which represents Flame 3 at 1¼ in. from the inlet. The gases flowing in the annular region between the flame and the duct wall were completely unburned. This analysis compared closely with one calculated with flow measurements of the orifices. Samples taken inside the flame had the same analysis independent of the distance from the inlet and, in general, indicated almost complete combustion. The transition region from no combustion to almost complete combustion was about 0.20 in. in thickness. The outer edge of this region probably represented the flame front. Flame-front location determined in this manner always agreed within 0.02 in. with those shown in Table 2. Analyses at the duct outlet indicate that the flame front had reached the duct wall for Flame 3, but not for Flames 1 and 2.

The analyses across the flame were similar at all sections along the duct. It is, therefore, not surprising that the temperature distributions for a given flame were similar at all distances also. Since the analyses indicate that combustion was essentially complete near the axis, there was no heat release in this region due to combustion. The gases here tended to cool because of radiation to the cool walls. This effect was counter-balanced in part by heat transfer from the surround-

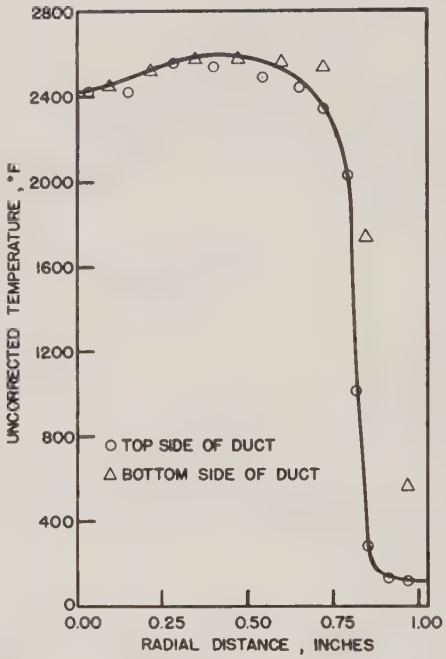

Fig. 8. Temperature distribution of flame 3 at 1¼ in. distance in 19¼ in. duct.

Table 2. Flame Front of Flames in Duct 19¼ In. Long

Horizontal Distance	Radial Distance, Flame 1	Radial Distance, Flame 2	Radial Distance, Flame 3
in.	*in.*	*in.*	*in.*
1¼	0.60	0.77	0.81
4	0.62	0.77	0.78
8¼	0.61	0.76	0.78
16	0.58	0.83	0.94
19	0.58	0.85	1.03

Radius of duct, 1.03 in. Flame front considered to be point where thermocouple read 1400°.

ing flame. This is one possible explanation for the existence of the lower temperatures noted at the axis. Another explanation might be that the tube was acting as a Ranque tube, in which temperatures near the axis are lower than those at the wall.[2]

The differences in the maximum temperatures measured for Flames 1, 2, and 3 are explained primarily by the degree of excess air in the combustible gas mixtures. The analyses of this investigation were by no means complete, since no determinations were made of unstable free radicals or partially oxidized hydrocarbons such as aldehydes whose odors were sometimes noted. The analyses are, however, probably sufficiently complete and accurate to indicate the extent of combustion.

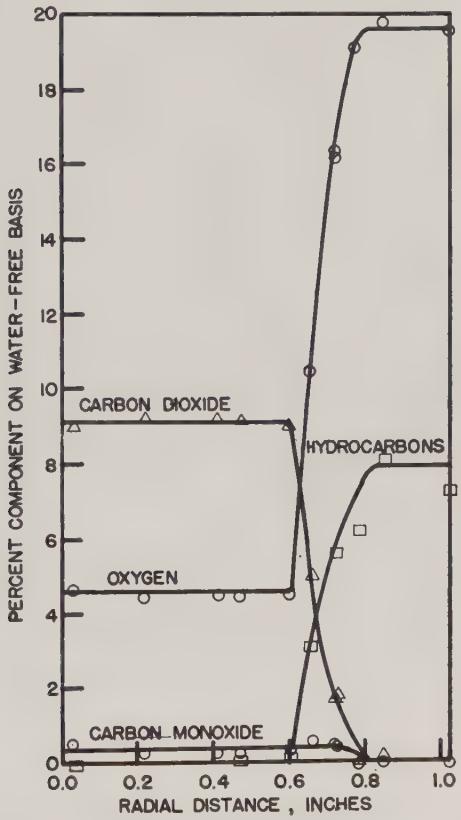

Fig. 9. Gas analysis in flame 3 at 1¼ in. distance in 19¼ in. duct.

Discussion of Cyclonic Flames

Flame stabilization in ducts was postulated earlier[1, 4, 11, 12] as being caused by a reverse flow along the axis. The fact that such a flow was observed lends support to this hypothesis. The results of this investigation indicate that the reverse flow may have extended back in the cyclonic nozzle itself. The flame was probably initiated in the cyclonic nozzle at the outer diameter of the reverse-flow pattern. The existence of the hollow cylindrical flame observed inside the nozzle is compatible with this theory. The flame initiated in the nozzle presumably traveled through the combustible gas mixture in both axial and radial directions. The degree of combustion obtained in a given duct depended, then, largely on the radius of the flame front at the duct outlet.[13] Variations of the radial positions were probably affected by differences in the flame velocities in the combustible mixtures. These velocities were, of course, dependent on the gas compositions, flame temperatures, and shearing rates. The flame location also depended on the time the gases spent in the duct. Increased residence time can be obtained by decreasing the superficial velocity for a given duct, or by increasing the duct length for a given superficial velocity. Increasing the residence time allows the flame to approach the wall. A comparison of Flames 2 and 5 shows this clearly. More complete combustion would presumably have been obtained for Flame 2 if the duct length had been increased.

The rate of heat release was calculated for several flames in which combustion was thought to be complete from the flow rate and heats of combustion of the natural gas.[10] The volume charged to the flame includes the volume of the duct plus approximate volumes of the flame extending from the ends. The heat releases for Flames 3 and 4 were about 8,000,000 and 10,000,000 Btu/hr/cu ft respectively. A similar value was found for a flame in a duct 12 in. long. Pressure drops for these flames of 1.5 to 3.9 in. of Hg are comparable to losses in typical burners.

Calculations were made for some of Plaster's cyclonic flames.[13] Heat-release rates were as high as 26,000,000 Btu/hr/cu ft, but pressure drops in the burner ranged from about 5 to 26 in. of Hg. Both his burner and the one used here probably could be modified so that pressure drops would be decreased without changing the degree of cyclonic flow. On the basis of the preliminary evidence the duct length to a particular nozzle can be varied rather widely without affecting the maximum rate of heat release obtainable. The differences of the rates of heat release for the two cyclonic nozzles were probably caused by at least two factors: the degree or intensity of cyclonic

flow and the duct diameter. The intensity of cyclonic flow may be of particular interest, since it is no doubt related to pressure drop in the apparatus.

The heat release rates of 8,000,000 to 26,000,000 Btu/hr/cu ft are high compared to the results of Hottel and Person,[4] who reported a value of 1,700,000 for one of their flames, which they compared to a typical value of 4,000,000 for aircraft gas-turbine combustors. Their flames, however, had low superficial velocities, and they indicated that their equipment was capable of higher rates of heat release.

Summary

The aerodynamic and thermal structures of flames stabilized by cyclonic flow in 2-in. i.d. ducts 6 to 36 in. long were investigated. The flames had the form of hollow cylinders extending the length of the duct. The flames were approximately 0.2 in. thick. Unburned gas flowed with high axial and rotational velocity in the annular region surrounding the flame. The interior region of the hollow flame was filled with completely burned gases. Here the axial velocity was low, and in some cases was directed upstream. Heat release rates of the 2-in. burner ranged as high as 10,000,000 Btu/hr/cu ft. Flame temperatures up to 2600°F (uncorrected) were observed, but the duct wall was not heated significantly except when the flame touched it.

Acknowledgment

The National Advisory Committee for Aeronautics, who supported this research, are thanked for their permission to publish the results. Messrs. P. L. Pickard, Walter Morrison, D. I. Davis, M. S. Fales, and W. J. Sadler helped collect data.

REFERENCES

1. Albright, L. F., and Alexander, L. G.: Jet Propulsion *26*, 867–73 (1956).
2. Eckert, E. R. G., and Hartnett, J. P.: *Proceedings of the Fourth Midwestern Conference on Fluid Mechanics* pp. 69–92, Purdue University, Lafayette, Indiana (1955).
3. Garner, F. H., and Cheetham, H. A.: J. Inst. Petroleum, *37*, 554 (1951).
4. Hottel, H. C., and Person, R. A.: *Fourth Symposium (International) on Combustion*, Baltimore, The Williams & Wilkins Co., 1953.
5. Iinoya, K.: Nagoya Univ. *5* (No. 2), 131 (1953).
6. Kurz, P. F.: Ind. Eng. Chem., *45*, 2072 (1953).
7. Kurz, P. F.: Ind. Eng. Chem., *46*, 746 (1954).
8. Kurz, P. F.: Rev. Sci. Instr., *25*, 418 (1954).
9. Kurz, P. R.: Ind. Eng. Chem., *46*, 1311 (1954).
10. Lewis, B., and von Elbe, G.: *Combustion, Flames, and Explosions*. New York, Academic Press, 1951.
11. Moore, N. P. W., and Martin, D. G.: Fuel, *32*, 393 (1953).
12. Pistor, R.: Chem. Ing. Tech., *26*, 207 (1954).
13. Plaster, W. E.: M. Chem. Engr. Thesis, Univ. of Oklahoma (1955).
14. Stone, V. L., and Wade, I. L.: Mech. Eng., *74*, 359 (1952).

58

FLAME STABILIZATION BY MEANS OF ANNULAR FLUID JETS

By D. G. SHEPHERD

Flame stabilization data were obtained for propane-air mixtures in an annular duct, the stabilization being obtained by the injection of pure air or of a stoichiometric propane-air mixture perpendicularly outwards into the main stream from the inner tube of the annulus. Tests were also made using annular metal discs similary located, for the purposes of comparison. Injection velocities up to 300 fps were used, the annular injection gap width varying from 0.010 to 0.030 in. The duct was $2\frac{3}{8}$ in. i.d., with the inner injection tube $\frac{1}{2}$ in. in diameter. Blowout velocities up to 160 fps were obtained, with stable regions having a mixture-strength range somewhat greater than that of conventional solid baffles. Somewhat higher velocities were obtainable with injection of a stoichiometric mixture than with pure air, but not markedly so. Extrapolation of results to higher injection velocities indicated the possibility of a successful stabiliz-

ing system for the high-velocity gas streams which are met with in propulsion power plants; as, for example, in the exhaust pipes of turbo-jets.

Introduction

Flame stabilization by means of metal baffles has been studied fairly extensively, both for practical application and for an understanding of flame behavior. Solid baffle systems, however, are subject to the disadvantage that they have to provide for adequate stabilization at extreme conditions, leading to undesirable drag effects or pressure loss under normal conditions. A baffle system which can be regulated according to the nature of the duty required, or which gives no obstruction to the fluid stream when not required, obviously has some advantages. Such a system can be provided if the baffles are fluid rather than solid, and an initial investigation into the possibilities of injecting fluid perpendicularly to the main stream was the subject of the research reported here. An annular duct was chosen to provide symmetry and to minimize undesirable three-dimensional effects, with the fluid acting as the stabilizing medium being injected from the inner tube to minimize the quantity of higher-velocity fluid required.

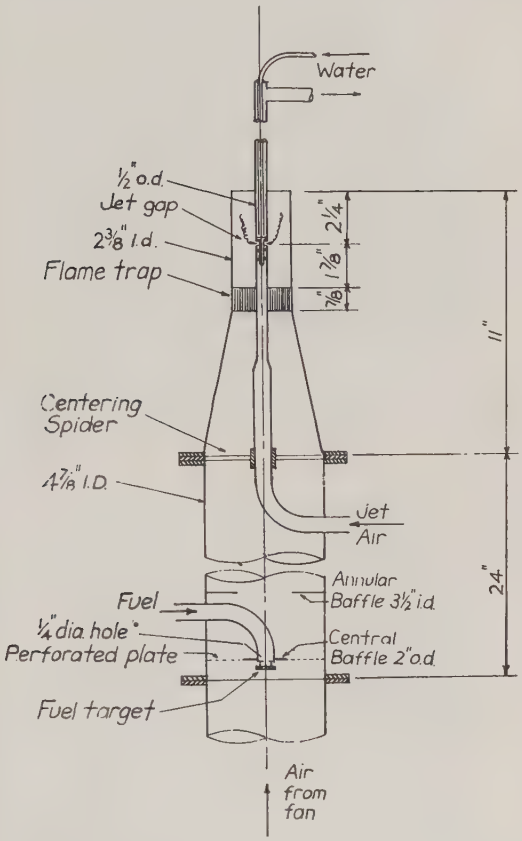

Fig. 1. Diagrammatic representation of apparatus.

Apparatus and Procedure

The essential features of the duct are shown in Figure 1, with an enlarged view of the injection region shown in Figure 2. The air supply was at approximately atmospheric conditions. The fuel used was propane of 99 per cent purity or better, the fuel being mixed with the air as shown in Figure 1. Fuel and air were metered separately.

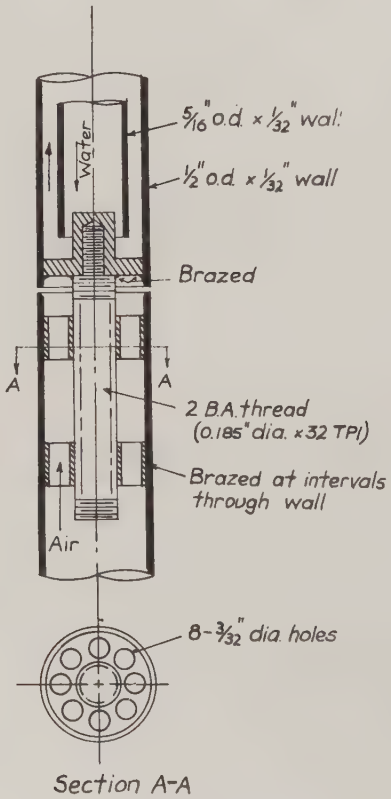

Fig. 2. Detail of injection region.

Figure 2 shows details of the injection system, the screw-thread arrangement for varying the width of the injection gap, and the water-cooled tube downstream of the gap. The walls of the tube forming the annular injection orifice were rounded-off on the inside, but the exact contour was not precise.

A flame trap of the Amal type was inserted

immediately following the nozzle of the 2⅜-in. tube. This flame trap consisted of a ⅞-in. wide strip, alternately plain and 0.025-in. corrugated, wound spirally around the inner tube to fill the annulus.

The annular metal baffles were made of steel 0.023 in. thick, centered on the 2-B.A. thread, and clamped firmly by screwing down the top half of the central tube.

Initially the central injection tube was made of stainless steel and uncooled; but it was found that, when at red heat or over, the extinction limit was uncertain, as the stabilization region would move slowly along the tube dependent on its local temperature.[1] The change to a water-cooled brass tube produced a definite extinction point which was reproducible. The flow rate of the water was such as to produce no appreciable rise of temperature, and therefore the temperature of the inner tube can be considered to be about 50 to 60°F.

The stabilization region was small and, as the duct length where combustion occurred was small, the outer pipe remained relatively cool—except for the tests with the largest slot width, in which the flame nearly filled the duct at the exit. No measurements were taken of the outer pipe temperature.

The injection velocities used are referred to as "100 fps," "125 fps," "200 fps," and "300 fps." However, it was not possible to keep these figures exact, and the range of values over all the tests were respectively 98 to 102, 124 to 126, 204 to 210, 256 to 264, and 313 to 321 fps, with the averages being 100, 125, 207, 260, and 317 fps. Because of these variations, and since the velocities are computed from continuity with an orifice discharge coefficient of unity (as the value of this was uncertain in view of the varying shape of the injector gap), these velocities must be considered as nominal. They will, henceforth, be referred to in the round-figure numbers, but the mean values given above have been used in computations. Velocities of 100, 200 and 300 fps were the standard values, with the intermediate values used in only one or two instances.

Three gap widths were used, nominally 0.010, 0.020, and 0.030 in. as set from the angle of advance on the screw thread; on measurement with the thickness gauge, they were 0.0095, 0.019, and 0.0285 in. Smaller gaps were tried, but the play in the screw thread led to lack of parallelism and the results were discarded. Larger gaps were impossible, due to limitations of fuel and air supplied; this likewise prohibited data for the largest gap (0.0285 in.) at the highest velocity (300 fps).

Results

Space forbids giving plots to include all the experimental points, but some representative figures are shown. Figure 3 shows a plot to demonstrate the degree of consistency obtained with a large number of experimental points. Figure 4, for the 0.0095-in. gap at 250 fps jet mixture, illustrates a plot with the smallest number (10) of separate points. The majority of the plots contained about 16 separate points. In the case of the larger gaps at the higher jet velocities, it was impossible to plot the region of peak velocity owing to limitations of air and fuel supply; Figure 5 shows the extreme case of this. Later figures show the extrapolated regions in broken lines and Figure 5 then shows the actual data of the extreme case for which extrapolation was necessary. The curves for the solid baffles are

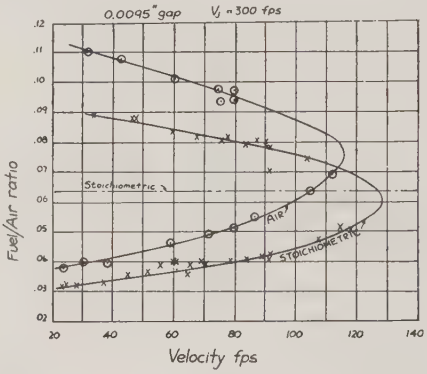

Fig. 3. Stability diagram for 0.0095 in. gap at 300 fps.

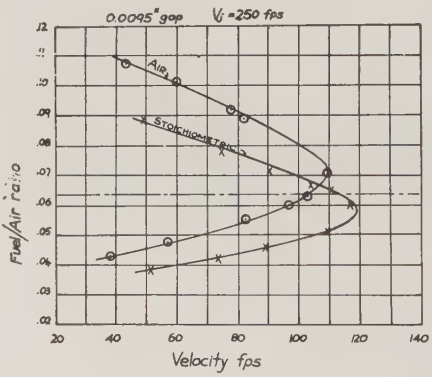

Fig. 4. Stability diagram for 0.0095 in. gap at 250 fps.

shown in Figure 6, with all the experimental points included, as these form a homogeneous group without confusing overlapping of curves.

Comparative results are shown in Figures 7 to 11, inclusive, with the separate points omitted but with the extrapolated regions shown in broken line. Figures 7 to 9 show the results for the three different gap widths, respectively, for the different jet velocities used. The curves for

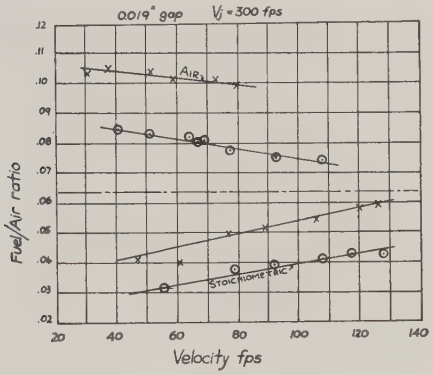

Fig. 5. Stability diagram for 0.019 in. gap at 300 fps.

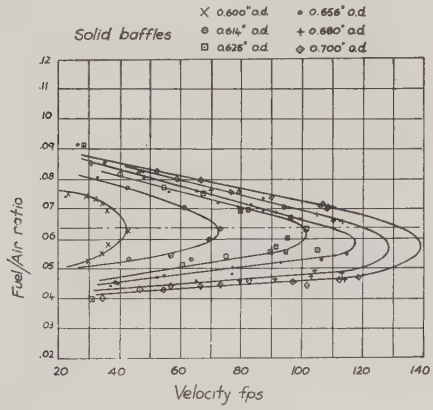

Fig. 6. Stability diagram for solid annular baffles.

injection of pure air are shown in heavy lines, and those for the stoichiometric mixture in thin lines. Figures 10 and 11 are cross-plots showing, respectively, all the results for injection of pure air together and the results for injection of stoichiometric mixture together. In these two figures, the extrapolated regions are not shown separately in broken lines, as this representation has been taken over to differentiate between the jet velocities.

Figures 7 to 9 show consistent results in that increase of jet velocity V_j increases the blowout velocity V_{bo} and Figures 10 and 11 show that, for a given jet velocity, V_{bo} increases with gap width. For air injection, the peak blowout velocities occur at mixtures richer than stoichiometric as would be expected. From Figure 10, an average fuel:air ratio at peak velocity has the value of about 0.078 (corresponding to an equivalence ratio of 1.23) compared with the stoichiometric value of 0.0636. From Figure 11, showing the

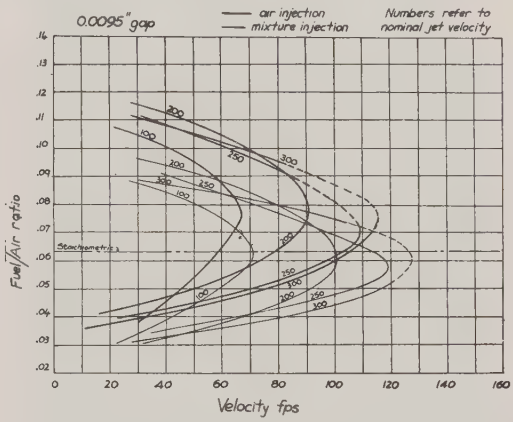

Fig. 7. Comparison of stability diagrams for 0.0095 in. gap.

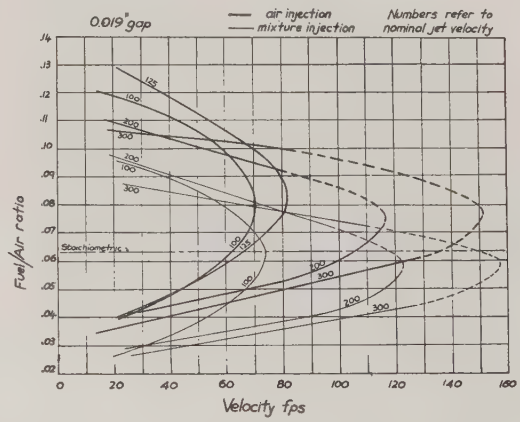

Fig. 8. Comparison of stability diagrams for 0.019 in. gap.

results for the injection of stoichiometric mixture, it is seen that the peak velocities do not all correspond exactly with the stoichiometric mixture of the main flow, with a slight tendency towards leaner mixtures for the larger gap widths. It is more usual to find peak velocities occurring on the rich side when not at the stoichiometric, which has been explained on the basis of the effect of the relative diffusivities of the fuel and air at lower Reynolds numbers. In this instance, the data show a tendency to the lean side with increase of Reynolds number. This may be due to

a nonhomogeneous main-stream mixture (fuel rich towards the center of the duct) but, as the effect is relatively small and is most pronounced in the cases requiring the greatest extrapolation, no emphasis is placed on this observation.

The results for mixture injection show that a higher blowout velocity is obtained than for air injection, and that the range of stable burning is

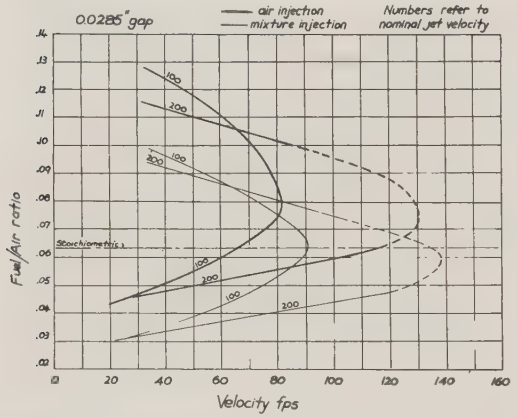

Fig. 9. Comparison of stability diagrams for 0.0285 in. gap.

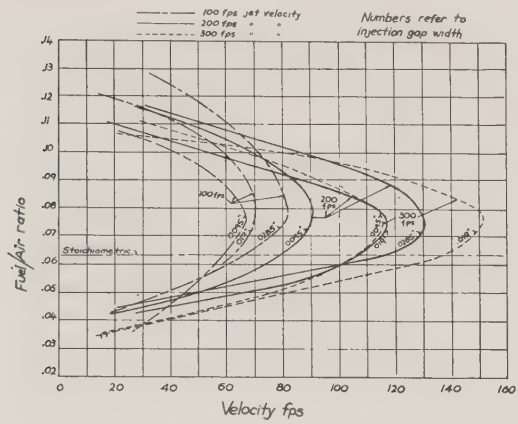

Fig. 10. Comparison of stability diagrams for all gaps, air injection.

likewise greater. Both these effects are to be expected, as air injection inherently involves a weaker stabilization zone. However, the effects are not large (about 5 to 8 per cent for blowout velocity), so one can conclude that mixing of the main stream and the jet stream is very rapid and must occur before the critical combustion zone is reached.

It may be mentioned at this point that this series of tests permitted data to be taken only with an injection stream of stoichiometric composition, although some qualitative tests were run at other mixture strengths. The effect of injecting pure propane was tried, but stabilization was very poor and no data were taken.

The stability data for solid annular baffles, as shown in Figure 6, show a similar trend towards a leaner mixture strength at peak velocity with increase of baffle size, which corresponds to increased jet velocity. Peak values of V_{bo} increase with increase of baffle size. These results were

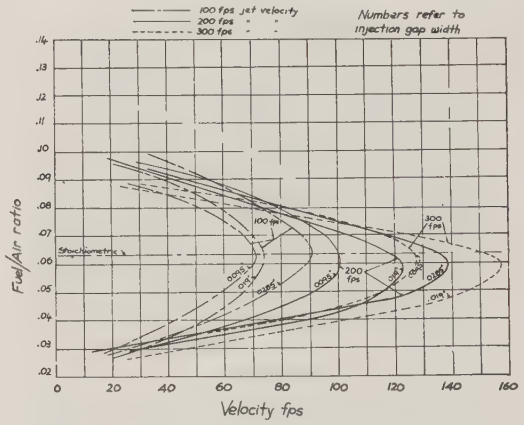

Fig. 11. Comparison of stability diagrams for all gaps, mixture injection.

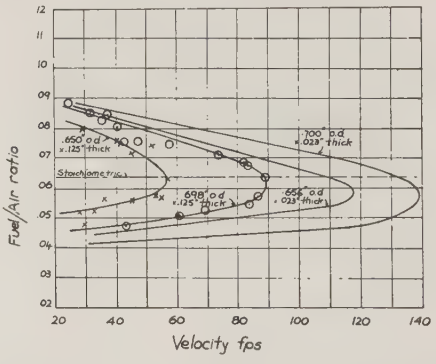

Fig. 12. Stability diagrams for solid baffles showing effect of baffle thickness.

obtained only after due consideration had been given to the thickness of the baffle. Initially, flat washers of different sizes were used as baffles, but it was found that inconsistent results were obtained: increase of baffle diameter did not always increase the stability limits as might be expected. Figure 12 shows some results, consisting of two curves reproduced from Figure 6, the 0.656-in. and 0.700-in. diameter sheet-metal baffles of 0.023-in. thickness, and two plots of results of 0.650-in. and 0.698-in. diameter baffles of 0.125-in. thickness. It is seen that these thick baffles materially reduced the stability limits.

The inside diameter was 0.5 in., so that the thick baffles were closer to cylinders than to discs, as the ratio of thickness (in the flow direction) to height (perpendicular to flow direction) was greater than unity. It was found that a thickness of 0.070 in. gave the same result as one of 0.023 in., although the maximum thickness:height ratio for the baffles to act as thin discs was not

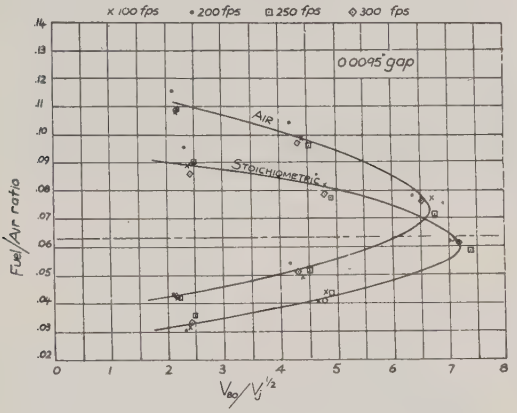

Fig. 13. Correlation of stability limits for 0.0095 in. gap.

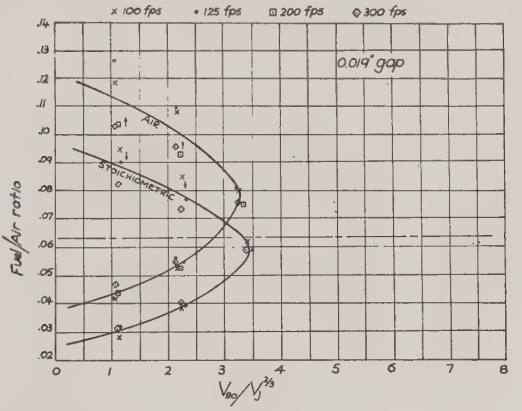

Fig. 14. Correlation of stability limits for 0.019 in. gap.

investigated. One test was run with a disc of 0.125-in. thickness radiussed on the upstream side to give a parallel section of 0.023-in. thickness, and this gave a similar stability curve to the sheet-metal disc of 0.023-in. thickness.

Correlation of Results

A general correlation of results can be made taking into account the parameters of jet velocity, jet mixture-strength, and width of jet gap. It results in a plot with points within the general limits of scatter of much published stability data, but a less-generalized presentation seems more advisable until data on a wider range of variables are available.

The correlation of the jet-velocity parameter is shown in Figures 13, 14 and 15 for the 0.0095-, 0.019-, and 0.0285-in. gaps, respectively. The separate points shown were calculated from the curves of Figures 10 to 12, using the peak velocity and values of $\frac{1}{3}$ and $\frac{2}{3}$ of the peak velocity. Exponents of variables in the correlating parameters are all expressed as simple fractions, although closer correlation can be obtained by using decimal exponents, but at this stage of the investigation it seems unwise to give the appearance of greater precision.

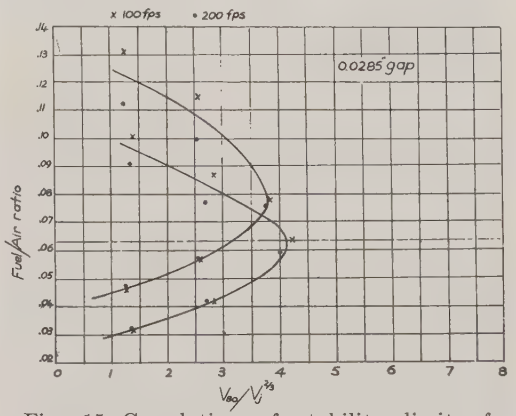

Fig. 15. Correlation of stability limits for 0.0285 in. gap.

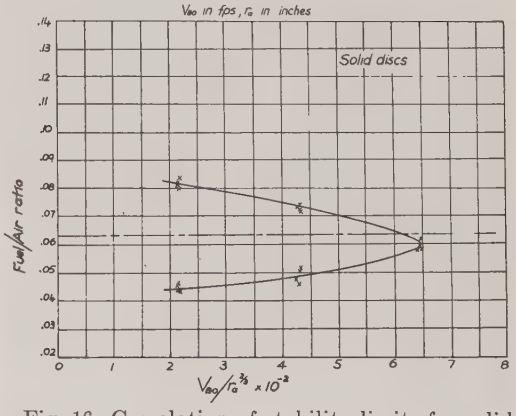

Fig. 16. Correlation of stability limits for solid baffles.

Figure 13, for the smallest injection gap, shows that, for the four values of jet velocity used, $V_{bo}/V_j^{\frac{1}{2}}$ is a correlating parameter. Figures 14 and 15, for the two larger gaps, show that $V_{bo}/V_j^{\frac{2}{3}}$ is a correlating parameter. The peak values and

lean mixture-strength values give very good correlation, while the rich side yields more scatter. which is common. While the narrowest gap can be correlated within present general limits of scatter of stability data with $V_j^{\frac{3}{4}}$, the plot using $V_j^{\frac{1}{2}}$ is so clearly defined, both for air and stoichiometric-mixture injection, that a different mechanism is indicated. The range of fuel:air ratio for stable burning at a given velocity is rather wider than that for most solid baffles with propane as fuel, being over 2:1 at 50 per cent of the blowout velocity.

Correlation of the solid annular baffle data is shown in Figure 16 with $V_{bo}/r_a^{\frac{3}{4}}$ as parameter, r_a being the annulus height perpendicular to flow. The four baffles of largest size correlate very well, particularly for the peak velocity, but the two baffles of smallest size have not been included as they give much lower stability limits. These two baffles were of 0.600- and 0.614-in. outside diameter, giving values of r_a of 0.050 and 0.057 in., respectively. The much lower values of blowout velocity for these two might indicate a quenching effect, because the inner tube is water-cooled. This hypothesis is supported by plotting the peak values for the solid baffles in terms of Peclet numbers based on flame speed, S_u, and on blowout velocity, V_{bo}, as demonstrated by Spalding and Tall.[2] The result of this is shown in Figure 17, with the correlation from the reference quoted being shown for comparison. The four points of larger r_a form a straight line of slope 1.67, while the two for the smaller values of r_a show a sharp break. This is in conformity with the theory of Spalding and Tall that no flame can exist when the stabilizer size becomes of the same order as the quenching distance. The slope of 1.67 is greater than the correlation for other types of baffles, but no great significance should be placed on this at this point in view of the limited number of points. The range of mixture strength in the stable-burning region is narrower than for the fluid baffles, and is comparable to that for other solid baffles.

Owing to the different exponents of the jet velocity for the 0.0095-in. gap width, there remain only the 0.019- and 0.0285-in. widths with which to make a general comparison of the effect of gap width. Using the correlated values of Figures 14 and 15, the peak blowout velocities are proportional to the 0.37 power of the gap width, for both air and mixture injections. Using the absolute values of peak velocity from Figure 10 for air injection at 300 fps for the 0.0095- and 0.0285-in. gap widths, *i.e.*, extremes of gap width at the highest jet velocity, V_{bo} is proportional to the 0.40 power. Thus it may be reasonably concluded that widening the injection gap has a relatively small effect and that jet velocity is the more important parameter.

Discussion of Results

The presence of the cooled inner tube at the stabilization zone produces a recirculation region bounded by one cold surface, and this must have a quenching effect. It is well established that cooling the baffle itself has a marked effect in reducing stability limits.[3] Thus the data presented here represent pessimistic conditions which might not apply in other arrangements of annular fluid baffles.

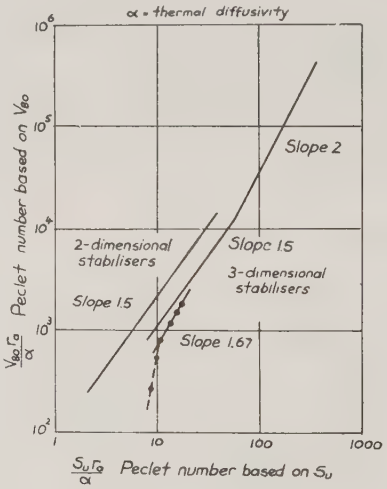

Fig. 17. Plot of Peclet numbers based on flame speed and blowout velocity.

Another variable whose effect was not investigated is that of the velocity profile of the main stream. The presence of the length of inner tube upstream of the baffle introduces a boundary layer at the baffle, and a velocity profile across the annulus at a bulk velocity of 100 fps is shown in Figure 18. The position of the flame trap close to the baffle introduces an unrepresentative factor, but this location was necessary in these tests to avoid a large-scale flashback.

These tests were carried out with what is sometimes called a "short tail-pipe"; it is well-known that an increase of duct-length following the stabilization zone decreases the stability limits and may cause combustion oscillations (see Barrere and Mestre[4] for example).

From the difference of fuel:air ratios at peak

velocity for air injection and stoichiometric-mixture injection, it is possible to estimate the mass or volume rate of flow of main-stream mixture into the recirculation zone, assuming that the peak V_{bo} occurs with a stoichiometric mixture in this zone for the case of air injection. Assuming also that this flow is obtained from a uniform annulus around the inner ½-in. pipe, it is possible to estimate the height of this annulus and thus to obtain a measure of the size of stabilizing zone. With these assumptions, the annular height varies from about 0.1 in. for the lowest values of gap width and jet velocity to just over 0.25 in. for the highest values. The outer metal duct was provided with a small window in the

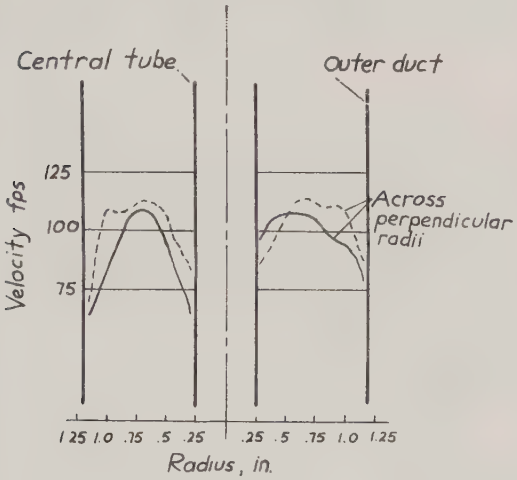

Fig. 18. Velocity profile in duct at 100 fps bulk velocity.

plane of the gap, and visual observation showed that the height of the flame zone appeared rather smaller than this, but no quantitative check was attempted.

By making the further assumption that the length of the recirculation zone is 4.5 times its dimension normal to flow, which has been shown to be approximately correct for some solid baffles,[5] then the heat-release rate for the zone can be estimated. The values obtained range from 0.8 to 1.4 $\times$ 10^8 Btu/cu ft/hr, which are to be compared with the theoretical maximum obtainable value of 8 $\times$ 10^8 put forward as a tentative value by Avery and Hart[6] and of 4 $\times$ 10^8 found by Longwell[7] in an experimental homogeneous reactor.

The exponent of ⅔ as the correlating factor for jet velocity and for the height of solid annular baffles is possibly fortuitous, but it suggests that jet penetration is proportional to jet velocity. For the solid baffles, the exponent differs from the values of about 0.5 and 1 which appear to correlate most results at low and high Reynolds numbers, respectively. More data with larger baffles at higher velocities are necessary before these results can be judged significant.

It is possible to compare the results for the solid annular baffles with previous results for baffles of other shapes by using the method of Longwell,[5] and plotting V/PD^c against equivalence ratio. Figure 19 shows the Longwell presentation together with the results for the solid annular baffles used in these tests. The units for the ordinate are V in fps, P in atmospheres and D in ft, where D is calculated as twice the mean hydraulic radius of the baffle (*i.e.*, D is equal to baffle width for a two-dimensional baffle and half of the baffle diameter for a three-dimensional baffle). Figure 19 shows that the results for annular baffles are in the same range as those for circular discs and axial cylinders.

One simple experiment was done which indicated the definite nature of the flow pattern which results in a recirculation zone. The reducing section of duct (see Fig. 1) was removed so that the injection gap was positioned a few inches above the duct carrying the main air stream; pure fuel was injected radially into an air stream of unknown, but low, velocity. The fuel was ignited and a hemispheric combustion zone resulted which is pictured in Figure 20. The unignited fuel jet was clearly seen against a white background, projecting radially about ⅜ in. from the tube. The hemispheric portion was semitransparent before the smooth envelope broke up into a bushy yellow flame. The boundary of the recirculation zone was close to the base of this turbulent region and the plane of reversal was quite sharp, as was indicated by traversing a salt-coated wire through the flame.

APPLICATION

An extrapolation of the correlated results shown in Figures 14 and 15 indicates that, with an air jet of sonic velocity, peak blowout velocities of the order of 500 fps might be obtained. Thus, for reheat or afterburning in the tail pipe of a turbo-jet, such jet velocities are possible by bleeding air from the compressor. In addition, there are the beneficial effects of a higher initial

temperature of the fuel mixture and a greater ratio of injection-air density to main-stream density. The effect of varying density of the two streams was not investigated in these tests but, using dimensional analysis and the results of this investigation to supply exponents of the right order, the blowout velocity would appear to be approximately proportional to the cube root of the ratio of injection-stream to main-stream density. The injection of stabilizing air radially from a metal disc baffle or gutter rather than from a cooled central tube would appear to be more promising both from practical constructional considerations and from a theoretical viewpoint (avoidance of the quenching effect of the cooled inner tube of these tests).

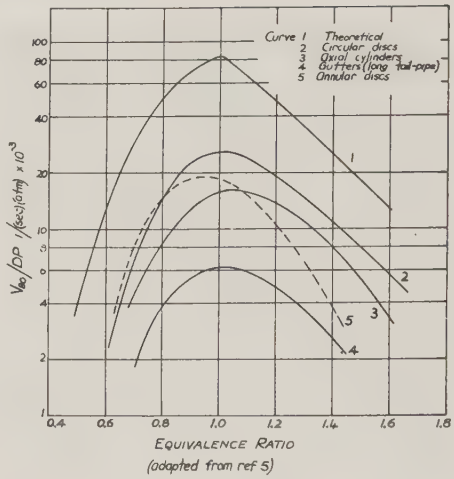

Fig. 19. Comparison of stability diagrams for solid baffles.

Conclusions

(1) Flame stabilization is possible by means of annular fluid jets with relatively narrow injection widths and low rate of injection flow.

(2) Within the range of variables used, $V_{bo}/V_j^{\frac{3}{4}}$ is a correlating parameter for injection gaps 0.019 in. wide or greater. For a gap 0.0095 in. wide, the parameter is $V_{bo}/V_j^{\frac{1}{2}}$.

(3) The effect of gap width on blowout velocity is secondary to that of jet velocity.

(4) Injection of a stoichiometric mixture gives only a slight increase of stability limits as compared with injection of pure air.

(5) Solid annular baffles with a cooled central tube can be correlated by the parameter $V_{bo}/r_a^{\frac{3}{4}}$ with a lower limit of size owing to quenching effects. The thickness in the flow direction of an annular baffle has a considerable effect for small baffle heights.

(6) Extrapolation of results indicates that flame stabilization by means of fluid jets is worth investigating for some practical applications.

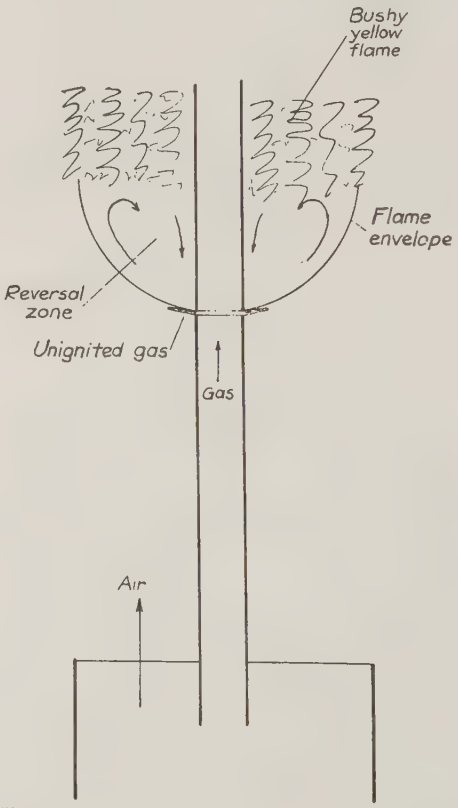

Fig. 20. Sketch of combustion zone with injection gap unenclosed.

Acknowledgments

This work was done as part of a program carried out while the author was holder of a Fellowship of the John Simon Guggenheim Foundation, and the support of the Foundation is gratefully acknowledged. The author also wishes to express his appreciation to Professor O. A. Saunders for the facilities made available at City and Guilds College, London, England, where the experimental work was done. He is also grateful to Dr. D. B. Spalding of that college for his helpful discussion of this and related combustion topics.

BIBLIOGRAPHY

1. Lee, D. H., Martin, D. G., and Moore, N. P. W.: Fuel, *34*, S107-S118 (1955).
2. Spalding, D. B., and Tall, B. S.: Aeronaut. Quart., *V*, 195–217 (1954).

3. Russi, M. J., Cornef, I., and Cornog, R.: Fourth Symposium (International) on Combustion, pp. 743–748. Baltimore, The Williams & Wilkins Co., 1953.
4. Barrere, M., and Mestre, A.: *Selected Combustion Problems, AGARD Combustion Colloquium*, pp. 426–446. London, Butterworth, 1954.
5. Longwell, J. P.: *Fifth Symposium (International) on Combustion*, pp. 48–56. New York, Reinhold Publ. Corp., 1955.
6. Avery, W. H., and Hart, R. W.: Ind. Eng. Chem., *45*, 1634–1637 (1953).
7. Longwell, J. P.: *Selected Combustion Problems, AGARD Combustion Colloquium*, pp. 508–510. London, Butterworth, 1954.

59

A CONTRIBUTION TO THE STUDY OF FLAME STABILITY IN DUCTS

By B. C. DUTTA, D. G. MARTIN and N. P. W. MOORE

Introduction

Conventional stabilizers for ducted burners consuming premixed gases normally require the establishment of a zone of recirculation in the wake of a bluff body. In the eddy region the axial velocity in the direction of flow is greatly reduced, and in this region, sustained by mass transfer across the boundary, combustion of an essentially homogeneous character occurs. From this eddy region spreads, under favorable circumstances, the turbulent flame which consumes the rest of the mixture. As an alternative to the use of a bluff body, recirculation may be achieved by suitably modifying the direction of a part or the whole of the stream at the burner inlet. A review of the literature on flame stabilization for a variety of bluff body shapes has been given by Longwell.[1] Conventional gas turbine combustion chambers frequently depend for their stability on recirculation induced by directing the air entering the primary zone. A recent discussion of high intensity combustion systems with recirculation by this means has been given by Clarke.[2]

An alternative means of producing this recirculation has been suggested by Spalding, in which a toroidal eddy region is produced by the interaction between the main stream and a normally directed jet. This system has the advantage of simplicity and ease of control, and does not require a solid baffle permanently in the stream. The stabilizing jet can either be air or a combustible mixture, thus giving a means of control of the temperature and composition in the region of flow recirculation, independently of the composition of the main streams. The addition of fuel in the stabilizing jet provides a means of increasing the stability of lean mixtures by providing a fuel enriched mixture, and therefore a hotter and more stable flame, in the eddy region. This has an obvious advantage in reducing random instabilities close to the lean stability limit. As a limiting case the combustible mixture supplied to the jet may burn as a stable flame at entry providing a pilot combustion zone. This condition may be compared with the open burners for turbulent flame studies devised by Karlovitz and his associates.[3]

Two simple realizations of jet stabilized systems are provided by either inward or outward radial flow of the stabilizing stream. The latter system, which demands an annular combustion chamber has been considered by Shepherd[4] who has been primarily concerned with the combustion stability. The present investigation of the former system, which initially proceeded parallel with that of Shepherd, has been continued in an attempt to establish a relation between some characteristic of the eddy region and the flame stability. A characteristic dimension of the eddy region has been established from experimental measurements of the axial velocity profile across a diameter downstream of the stabilizing jet in the absence of combustion. Spalding and Tall[5] have shown that bluff body data can be correlated in terms of two Peclet numbers, one based on blow-out velocity as governing the maximum tolerable rate of mass transfer into the eddy region, the other based on flame speed, being representative of the maximum reaction rate at a given mixture ratio. Both terms are expressed relative to the heat transfers by conduction from the periphery of the eddy region. By using these con-

cepts and introducing a dimension characteristic of the recirculation, and hence of the mass and heat transfer rates it has been possible to extend the Spalding and Tall type correlation to the present results.

Apparatus

A cross-section of the burner is shown in Figure 1. The main burner tube consists of two lengths of stainless steel tubing $1\frac{3}{8}$ in. internal diameter. An adjustable annular gap is arranged by separating the burner tubes, by means of the threaded sleeve. A locking ring was provided (not shown) to prevent gas leakage from this joint. The downstream length of tube, 9 in. long, was water cooled to prevent flame attachment on the hot surface as has been discussed in a previous paper.[6] Additional cooling passages were provided close to the annular gap. The gap was adjustable and could be supplied with either a metered stream of air or a combustible mixture. Air and fuel flows for both the main stream and the stabilizing jet were measured with sharp edged orifices calibrated against standard V.D.I. flow meters. The pilot stream was admitted at four points round the circumference of an annular chamber to ensure a uniform flow distribution for the annular jet.

Commercial propane and air were used in the main stream; air, propane-air, and hydrogen-air mixtures were fed to the stabilizing jet.

The burner was operated at various gap widths and stabilizing jet velocities for the evaluation of flame stability. The conventional stability limits were defined by the disappearance of flame from within the tube at various over-all mixture ratios and main stream velocities.

In order to obtain a characteristic dimension of the eddy region, in the absence of combustion a total head tube was introduced downstream of the annular gap and traversed radially across the tube. The total head distribution was measured by an inclined manometer for the range of gap widths and stabilizing jet velocities used for the flame stability experiments.

Results

Stability data expressed in terms of over-all fuel-air ratio and total mass flow are presented in Figures 2 to 5 for propane-air mixtures, stabilized by an annular air jet. Each figure shows results for a constant gap width and for four jet velocities. In each case an envelope curve has been drawn. The jet gaps are varied from 0.002 to 0.0145 in. with jet velocities from 60 to 390 ft. per sec. The jet velocities were calculated from the measured jet mass flow and gap area, and

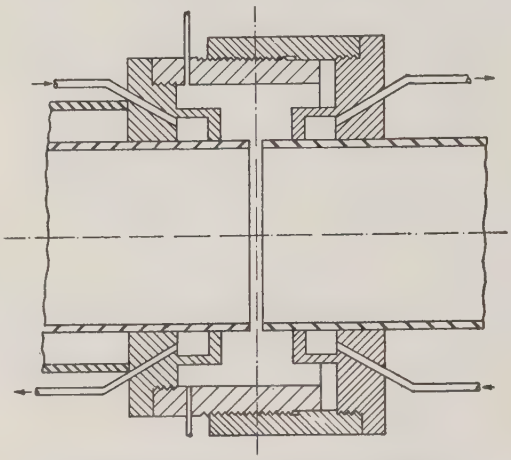

Fig. 1. Sectional view of burner.

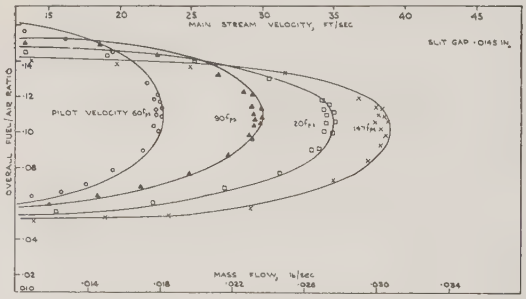

Fig. 2. Stability curves for gap width of 0.0145 in. for propane-air mixtures with air as the stabilizing stream.

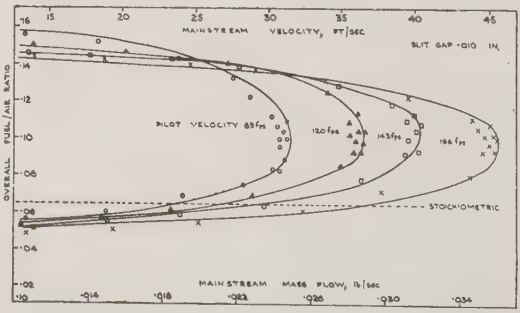

Fig. 3. Stability curves for gap width of 0.010 in. for propane-air mixtures with air as the stabilizing stream.

therefore make no allowance for any possible circumferential inequalities of flow, and assume a uniform distribution of flow over the whole jet width. The condition required to produce blow-out of a stabilized flame is that the rate of

mass transfer with the stabilizing region exceed the maximum rate of conversion of the mixture into products at the fuel-air ratio in the reaction zone. This rate reaches a maximum value when the mixture strength in the zone is stoichiometric, and therefore the blow-out velocity for a given set of conditions will presumably reach a maximum value at a stoichiometric mixture strength in the eddy region. This is well demonstrated by the bluff-body data for propane-air mixtures

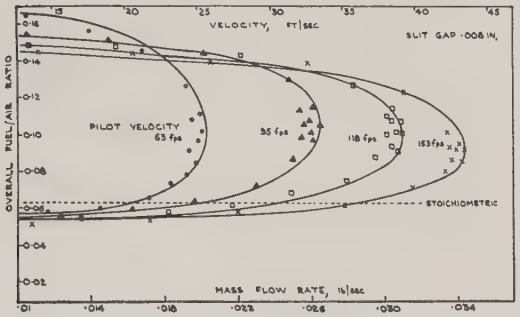

Fig. 4. Stability curves for gap width of 0.008 in. for propane-air mixtures with air as the stabilizing stream.

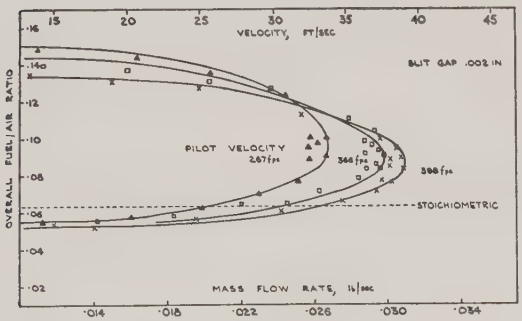

Fig. 5. Stability curves for gap width of 0.002 in. for propane-air mixtures with air as the stabilizing stream.

given by de Zubay.[7] Normally this mixture strength is close to the stream air-fuel ratio, but in the present case it will be noted that a feature of all the stability curves in which air is supplied to the jet is that they are symmetrical about a mixture strength well to the rich of stoichiometric. In the present case, however, the initial air-fuel ratio is not representative of conditions in the eddy region, and it is not surprising that the curves are displaced in view of the dilution from the pilot stream which undoubtedly occurs. It will be noted that this displacement increases as the jet velocity decreases, and this must be due to a reduced rate of mass transfer into the eddy region, requiring richer and richer mixtures in the main stream in order to obtain a stoichiometric mixture in the pilot zone. Ultimately the turbulent mass transfer processes must give way to laminar diffusion and the trend apparent in the present results would be expected to continue at progressively lower flow rates.

Similarly, at higher jet flow rates, it would be expected that mixing processes would continue to improve and that the maximum stability would ultimately be achieved at an initial fuel-air ratio nearer to stoichiometric.

For all gap widths the stability increases with jet velocity. This follows from the increased penetration of the stabilizing jet giving an extended recirculation region. The blow-out velocity, in the maximum main stream velocity defined by the stability curve, is taken throughout as the criterion of stability.

The effect of gap width at a series of constant jet velocities is shown in Figure 6, derived from the families of stability curves. It would appear that, except for small gaps, the jet velocity exerts the predominant influence on stability.

Typical stability curves with fuel-air mixtures supplied in the stabilizing jet are shown in Figures 7 and 8 for propane and hydrogen. The main stream in all cases, is a propane-air mixture, the fuel-air ratio of this mixture being given as the ordinate for the stability diagram. The curves with propane-air mixtures in the stabilizing jet are for a gap width of 0.011 in.; for hydrogen-air mixtures the gap was reduced to 0.002 in. to reduce the danger of flash-back. The corresponding stability diagram for an air jet is given in each case. The displacement of the fuel-air ratio at blow-out is marked, particularly for rich mixtures, and is to be expected from an extension of the previous argument. For hydrogen-air stabilizing jets there is a marked increase in the blow-out velocity. This follows from an increase in the reaction rate in the recirculation region. The flame was noticeably more intense under these conditions.

A satisfactory lean limit could not be expressed for the rich hydrogen-air mixture in the stabilizing jet since a stable hydrogen flame was formed at the annulus with air only in the main stream.

In an attempt to correlate the stability data determined for a range of jet velocities and gap widths the expression $V_{B.O.}/\sqrt{v}$ was evaluated for all experiments. $V_{B.O.}$ represents the main stream velocity at the maximum of the stability curves, and v, the mean jet velocity. At any gap width, l, the effect of varying jet velocity can be

satisfactorily correlated over the whole range of mixture strength. The correlation is most satisfactory in the region of the maxima. This is to be expected since this region can be accurately

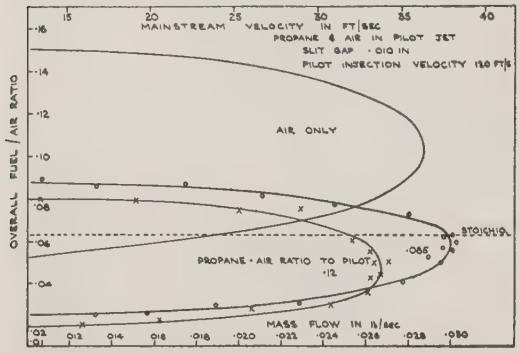
MAINSTREAM VELOCITY IN FT/SEC
PROPANE & AIR IN PILOT JET
SLIT GAP · 010 IN
PILOT INJECTION VELOCITY 130 FT/S
AIR ONLY
STOICHIO.
PROPANE-AIR RATIO TO PILOT
MASS FLOW IN lb/sec
OVERALL FUEL / AIR RATIO

Fig. 6. Stability curves for propane-air mixtures with air and propane-air mixtures as the stabilizing stream.

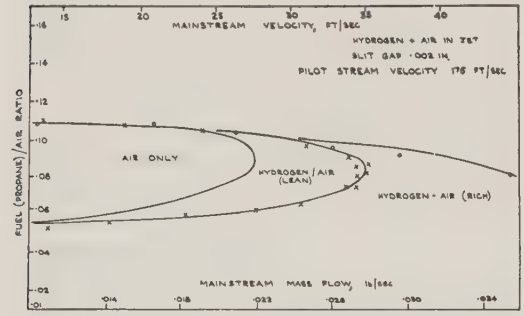
MAINSTREAM VELOCITY, FT/SEC
HYDROGEN + AIR IN JET
SLIT GAP · 002 IN.
PILOT STREAM VELOCITY 175 FT/SEC
AIR ONLY
HYDROGEN / AIR (LEAN)
HYDROGEN - AIR (RICH)
MAINSTREAM MASS FLOW, lb/sec
FUEL (PROPANE) / AIR RATIO

Fig. 7. Stability curves for propane-air mixtures with hydrogen-air mixtures as the stabilizing stream.

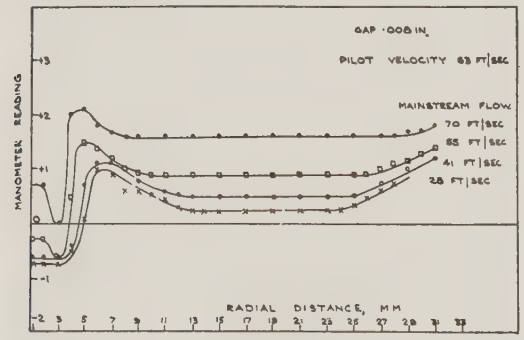

Fig. 8. Typical total head traverses in the region of recirculation.

determined experimentally. Numerical values for the functions $V_{B.O.}/\sqrt{v}$ and $V_{B.O.}\sqrt[3]{l}/\sqrt{v}$ are shown in Table 1 for the maxima of the envelope stability curves. There is some evidence that for very small gaps an inverse dependence on $\sqrt[3]{v}$ is more satisfactory, due perhaps to a reduced dependence of penetration on jet velocity for small jets. A similar trend is apparent in Shepherd's[4] results. In the range of jet widths common to the two investigations the correlation factors favor $\sqrt[1]{v}$.

Table 1. Correlation Data

Gap	Apparent F/A Ratio	Pilot Velocity	Blow Out Velocity	$\frac{V_{B.O.}}{\sqrt{v}}$	$\frac{V_{B.O.}\sqrt[3]{l}}{\sqrt{v}}$
		fps	*fps*		
0.0145	0.118	90.4	29.5	3.15	0.745
	0.108	120	34.8	3.15	0.745
	0.100	147	38.75	3.20	0.75
	0.11	60	22.75	2.85	0.71
0.01075	0.10	196	45.5	3.225	0.77
	0.10	143	40	3.45	0.73
	0.11	121	36	3.2	0.705
	0.114	83	31.3	3.15	0.7
0.0085	0.11	118	38	3.6	0.72
	0.115	95.3	33	3.4	0.68
	0.105	153	43	3.25	0.66
	0.115	63	25	3.05	0.62
				$\frac{V_{B.O.}}{\sqrt[3]{v}}$	
0.002	0.09	398	38.5	5.2	
	0.10	267	33.75	5.25	
	0.097	366	36.75	5.05	
	0.085	174	27.75	5.0	

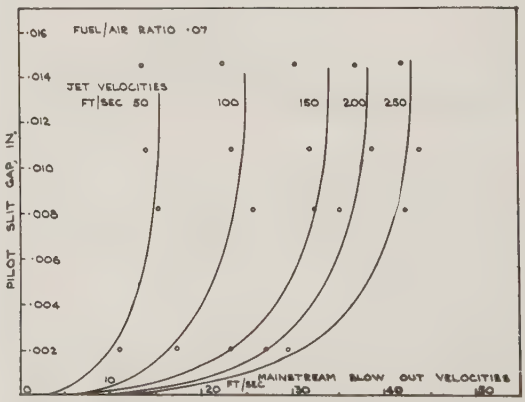

Fig. 9. Effect of gap width on stability with air as the stabilizing stream.

There is insufficient data to permit a full correlation to include the effect of variations of gap width, but within the limits of the present data, the function $V_{B.O.}\sqrt[3]{l}/\sqrt{v}$ appears satisfactory.

Velocity traverses without combustion have been obtained for the same range of jet velocities and gap widths as in the stability experiments. A typical set of traverses is reproduced in Figure 9 for a gap of 0.008 in. and for jet velocities cover-

ing the range employed in the stability experiments. From these total head traverses an estimate has been obtained of the penetration of the jet, and hence the size of the recirculation. The depth of jet penetration has been taken to be $D - d'/2$ where D = tube diameter and d' is the width of the uniform portion of the total head traverse curves. The results obtained are typical of the flow pattern to be expected in such a system showing a stable region of recirculation in the region of the walls.

Spalding and Tall[5] have shown that stability data can be correlated in terms of two dimensionless groups: one relating the blow-out velocity to the heat transferred across the boundaries of the eddy region, and the other relating the heat re-

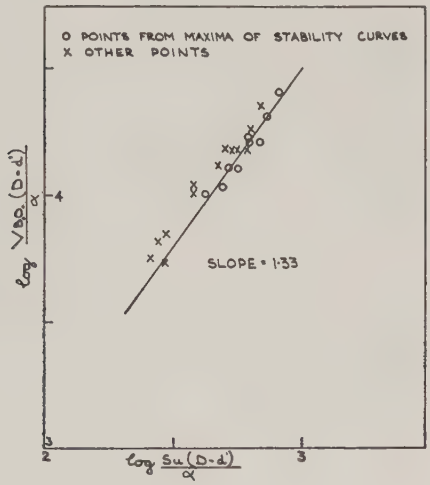

Fig. 10. Correlation of stability data.

lease by reaction to the heat conducted away, i.e., $V_{B.O.}d/\alpha = \text{constant} \left(\frac{S_u d}{\alpha}\right)^n$ (where α is the thermal diffusivity, K/cp) where n is an index depending on the Reynolds number. S_u is the laminar flame speed at the mixture ratio corresponding to the blow-out velocity, and d the baffle size. In the present work d has been replaced by $D - d'$ derived from the experimental velocity traverse.

In Figure 10 the correlation between the two dimensionless numbers is plotted logarithmically. Points have been included for all pilot velocities, gap widths, and for a range of mixture ratios. The correlation can be presented with less scatter if restricted to the velocity maxima of the stability diagrams. In view of the displacement of the stability curves into the rich region it has been necessary when calculating flame speeds for the above correlation to assume that the mixture strength in the zone of recirculation corresponding to maximum stability at each jet velocity is that for maximum flame speed. The variation of flame speed with mixture strength has been obtained from Botha and Spalding.[8]

Two marked differences between the results of the present work and the data presented for bluff-body stabilizers are apparent; the first is simply that the correlation curve is appreciably displaced to the right, the second that the slope is appreciably less than that of the main body of results.

The former is to be expected since the burner, which is of small diameter and heavily water cooled, is obviously subject to high heat losses which reduce considerably the blow-out velocities. The reaction rate term, however, has been calculated on the assumption that the combustion occurs adiabatically—in this instance, that the value of flame speed employed is the adiabatic burning velocity. This arbitrary assumption, introduced for want of accurate knowledge of the heat losses, is the reason for the displacement of the curve from that for other systems in which lower, but also unknown heat losses prevail.

The slope of the correlation curve for bluff-body data is an indication, (a) of the dependence of stability on the size of the bluff body, and (b) of the dependence of stability on the nature of the flow in the duct, i.e., on Reynolds number.

In the present case the interpretation is much more complicated. The blow-out velocity is dependent on a reduced power of the eddy size; in fact, $V_{B.O.}\alpha(D - d')^{33}$, but it is difficult to compare this effectively with the law for bluff body data for two reasons, one that the eddy size in the wake of a bluff body is not necessarily effectively represented by the bluff body size over the entire range of Reynolds numbers, the other that the estimate of eddy size for the present work was obtained in the absence of combustion, and the variation of eddy size with mass flow cold is only likely to represent approximately the variation of eddy size with mass flow in the presence of combustion.

It is supposed at this stage, however, that the reduced slope of the correlation curve is due primarily to the presence of the stabilizing jet, which augments to some extent the mixing rate due merely to the presence of an obstruction in the burner tube.

It is impossible at present to argue definite dependence of mass transfer into the eddy region

and hence of stability on Reynolds number for the main streams, since the system is complicated by the presence of the stabilizing jet, whose velocity and size provide factors which, independently of the main stream flow, can influence the mixing conditions. It is hoped to investigate this aspect in later work.

The correlation could not be extended to low Peclet numbers since this would demand more accurate determination of the mixture ratio, and hence the flame speed in the eddy region, or alternatively more sensitive velocity traverses at low jet velocities.

Conclusions

The experimental stability data has been presented for a system with a stabilizing jet directed radially inwards. The results are generally similar to those obtained in a parallel investigation by Shepherd. A similar correlation between jet velocity and the main stream velocity at blow-out applies over a range of jet velocities and jet widths. This correlation is, however, not entirely general since it is found that stability for small gaps exhibits a different dependence on pilot velocities. A similar conclusion has been reached by Shepherd for large gaps.

Certain similarities have been shown to exist between the present jet stabilized system and conventional bluff-body stabilizers by correlating the results in terms of Peclet numbers. A characteristic dimension of the recirculation zone has been obtained from experimental velocity traverses downstream of the stabilizing jet. It is found that the stability of the present system depends on a lower power of the eddy region size than that applicable for bluff-body stabilizers. It is difficult in view of the difference between the physical systems to interpret the precise meaning of this result. It is suggested, however, that this is due to the augmenting influence of the stabilizing jet on the mixing rates in the recirculation zone.

REFERENCES

1. Longwell, J. P.: *Fifth Symposium (International) on Combustion*, p. 48. New York, Reinhold Publ. Corp., 1955.
2. Clarke, J. S.: J. Roy. Aeronaut. Soc., *60*, 221 (1956).
3. Karlovitz, B., Denniston, D. W., and Wells, F. E.: J. Chem. Phys., *19*, 541 (1951).
4. Shepherd, D. G.: *Sixth Symposium (International) on Combustion*, p. 472. New York, Reinhold Publ. Corp., 1957.
5. Spalding, D. B., and Tall, B. S.: Aero Quart., *5*, 195 (1954).
6. Lee, D. H., Martin, D. G., and Moore, N. P. W.: Fuel, Vol. *34*, S107, April (1955).
7. de Zubay, E. A.: Aero Dig., 54 Vol. 61, July (1950).
8. Botha, J. P., and Spalding, D. B.: Proc. Roy. Soc., *A225*, 71 (1954).

Instability in Combustion Chambers

60

INFLUENCE OF THE INJECTOR PRESSURE DROP ON LOW FREQUENCY INSTABILITY IN LIQUID PROPELLANT ROCKETS

By M. BARRÈRE AND J. J. BERNARD

1. Introduction

The many theoretical studies made in recent years on low-frequency instability in liquid propellant rockets are based on the existence of a time lag between the injection and the combustion of active bodies in the combustion chamber.[1, 2, 3] This time lag, during which the fuel injected as liquid streamlets is atomized into droplets that are heated and then vaporized prior to combustion, evidently depends on all the physical and chemical factors which may have some effect on these phenomena. Thus, the size of the droplets, which determines the interval of time necessary for them to become hot gases—a possible assumption—is a function of the chamber pressure, and also of the injector pressure drop. Similarly, the recirculation which intensifies the energy exchanges between the droplets and the hot gases increases with the injection velocity and therefore with the injector pressure drop. Finally, the rate at which the droplets vaporize depends essentially on the difference between the temperature of the hot gases and that of the droplets. Accordingly, in the case of a monopropellant, it seems logical to consider the effect on the time lag of the gas temperature, T, and the injector pressure drop, Δp, as well as the chamber pressure, p. The presence of this additional parameter does not modify the definition of the time lag that we can always obtain by considering the amount of heat necessary for the ignition of the unit mass of monopropellant as constant:

$$\int_{t-\tau}^{t} f(\Delta p,\, p,\, T)\, dt' = c^{te} \qquad (1)$$

where $f(\Delta p, p, T)$ is the amount of heat needed to ignite a unit mass in unit time.

The assumption of a temperature-pressure relation that would reduce both parameters to a single one seems justified, but the injector pressure drop somewhat modifies the stability conditions as will be seen in the following pages.

2. General Relations

THE COMBUSTION CHAMBER EQUATION

The combustion chamber into which the liquid monopropellant is fed at an instantaneous flow-rate, $q_i(t)$ and a pressure, $p_i(t)$, operates at an average temperature, T, which is assumed to be constant and uniform, and at a pressure, $p(t)$. The mass of the combustion gases contained in the chamber at the time, t, is $M(t)$ and the fuel rate at the injection nozzle is $q_e(t)$. The equation for the reactions in the chamber, expressing the mass conservation between the injected elementary flow rate at time, $t - \tau$, that which is ejected at time, t, and the variations of mass within the chamber takes the usual form[3]

$$\frac{dM(t)}{dt} + q_e(t) - q_i(t-\tau)\left(1 - \frac{d\tau}{dt}\right) = 0 \qquad (2)$$

in which the derivative of the time lag may be obtained from Equation (1), and, following a Taylor series development which is limited to terms of the first order, reduces to

$$\frac{d\tau}{dt} = \frac{\partial \log f(\Delta p,\, p)}{\partial \log \Delta p}\left[\frac{\Delta p(t-\tau) - \Delta p(t)}{\Delta p}\right] + \frac{\partial \log f(\Delta p,\, p)}{\partial \log p}\left[\frac{p(t-\tau) - p(t)}{p}\right]$$

Discussion is possible only if linearization is assumed. With the average values designated by barred letters, $\varphi(t)$ is the perturbation

$$\varphi(t) = \frac{p - \bar{p}}{\bar{p}} = \frac{M - \bar{M}}{\bar{M}} = \frac{q_e - \bar{q}_e}{\bar{q}_e}$$

of the instantaneous values p, M, q_e, which are assumed to be in phase; similarly, ψ and μ_i represent the functions

$$\psi(t) = \Delta p - \Delta\bar{p}/\Delta\bar{p} \qquad \text{and} \qquad \mu_i(t) = q_i - \bar{q}_i/q_i$$

If the parameters, r and n, are the derivatives[a] calculated for the average values, Equation (2) becomes

$$\frac{\partial\varphi}{dt} + (1-n)\varphi(t) + n\varphi(t-\tau) + r[\psi(t-\tau) - \psi(t)] - \mu_i(t-\tau) = 0 \tag{3}$$

which is entirely dimensionless, the unit of time being the mean residence time, $ts = \bar{M}/\bar{q}$, which is usually expressed as a function of the characteristic length, L^*:

$$ts = \frac{1}{\gamma}\left(\frac{\gamma+1}{2}\right)^{(\gamma+1/\gamma-1)} \frac{\bar{q}L^*}{\bar{p}A_c}$$

($L^* = V/A_c$, ratio of the chamber volume to the injection nozzle throat area).[3]

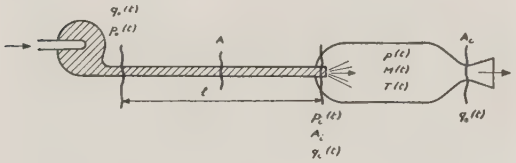

Fig. 1. Monopropellant rocket feeding diagram

EQUATION OF THE FEED LINE

It is evident that it is necessary to add to the equation expressing the behavior of the masses in the chamber the supplementary relations corresponding to the feed system. The latter comprises a pump (Fig. 1), for which the instantaneous flow-rate, q_0, and the pressure, p_0, are assumed to have the following linear relation:

$$\frac{q_o - \bar{q}_o}{\bar{q}_o} = \frac{q_i - \bar{q}_i}{q_i} = -b\frac{p_o - \bar{p}_o}{\bar{p}_o} \tag{4}$$

a pipe of length, l, and section A, terminated by an injector, the holes of which have a total cross-sectional area A_i. The effect of fluid compressibility in the pipe and the influence of a line capacitance—studied for $r = 0$[3]—are not taken into account in this paper. Under these conditions, the equation of conservation of momentum in the pipe line gives the following relation:

$$(p_o - p_i)A = \frac{d}{dt}(lq_i) \tag{5}$$

and the pressure change accompanying injection

$$\Delta p = \frac{q_i^2}{2\rho A_i^2}$$

leads to the approximation

$$\psi = \frac{q_i^2 - \bar{q}_i^2}{\bar{q}_i^2} = 2\mu_i \tag{6}$$

Equations (4), (5) and (6) reduce to the single dimensionless relation

$$P\varphi + \left(\frac{P+\frac{1}{2}}{b} + 1\right)\mu_i + IP\frac{d\mu_i}{dt} = 0 \tag{7}$$

in which the dimensionless constants, P and I, are

$$P = \tfrac{1}{2}\bar{p}/\Delta\bar{p}$$

$$I = \bar{q}l/ts\ \bar{p}\ A = \gamma\left(\frac{\gamma+1}{2}\right)^{\frac{-\gamma+1}{\gamma-1}} \frac{A_c}{A}\frac{l}{L^*}$$

STABILITY CONDITION

The characteristic equation of the system derived from equations (3) and (7) is readily obtained when a solution proportional to $e^{\lambda t}$ is sought for each function. The coefficients are calculated from a linear homogeneous algebraic system, the condition of compatibility of which gives the characteristic equation

$$(\lambda + 1 - n + ne^{-\lambda\tau})\ (\zeta + 1\ P\lambda) - P[(2r-1)e^{-\lambda\tau} - 2r] = 0 \tag{8}$$

$$\left(\zeta = \lambda + \frac{P+\frac{1}{2}}{b}\right)$$

Stability is assured if the real part of the roots in the term, λ, of Equation (8) is negative. The simplest argument uses the Nyquist criterion or, better still the variant proposed by Satche which many authors have adopted in treating problems of combustion instability.[4, 5, 6, 7] This is also the method applied below to the two special cases of a constant injection pressure and of a constant feed pressure.

3. Constant Injection Pressure

When the pipe is very short, it is possible to neglect the parameter I; the injection pressure,

[a] $r = \dfrac{\partial \log f(\Delta p, p)}{\partial \log \Delta p}$, $\qquad n = \dfrac{\partial \log f(\Delta p, p)}{\partial \log p}$

p_i, may then be considered as constant and the characteristic equation reduces to

$$\frac{1 - n + 2Pr}{n - P(2r - 1)} + \frac{\lambda}{n - P(2r - 1)} + e^{-\lambda\tau} = 0$$

When the complex variable, λ, describes the limiting contour, the point, z, such that $z = g(\lambda) = -e^{-\lambda\tau}$ describes a circle, G, of unit radius around the origin in the complex plane and the function:

$$f(\lambda) = \frac{1 - n + 2Pr}{n - P(2r - 1)} = \frac{\lambda}{n - P(2r - 1)}$$

defines a contour, F, similar to the limiting con-

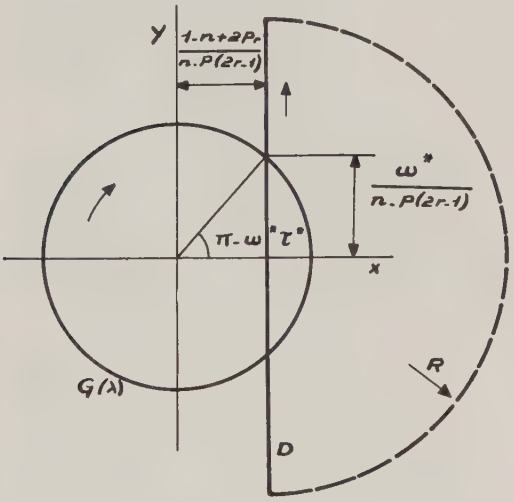

Fig. 2. Discussion of stability in the case of a constant injection pressure ($p_i = \overline{p}_i$).

tour and consisting (Fig. 2) of a semi-circle of infinite radius and a straight line, D, the abscissa of which is

$$x = \frac{1 - n + 2Pr}{n - P(2r - 1)}$$

A sufficient condition of stability, independent of τ, is obtained when the straight line, D, is outside the circle, G; this is expressed by the relation

$$P \leqslant \frac{1 - 2n}{1 - 4r}$$

which generalizes the condition given by Crocco[2] and is reduced to it for $r = 0$.

When curves, F and G, intersect, the points of intersection define a critical impulse:

$$\omega^* = \sqrt{(P + 1)\,[2n - 1 + P(1 - 4r)]}$$

and a critical time lag

$$\tau^* = \frac{\pi - \arctan\,[\omega^*/(1 - n + Pr)]}{\omega^*}$$

the variations of which are represented (Figs. 3 and 4) as function to the injection index r with

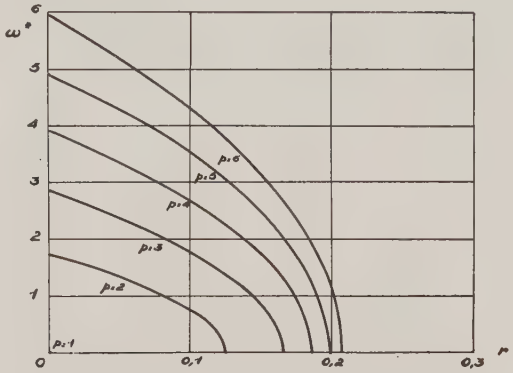

Fig. 3. Variation of the critical impulse ω^* as a function of the injection index r.

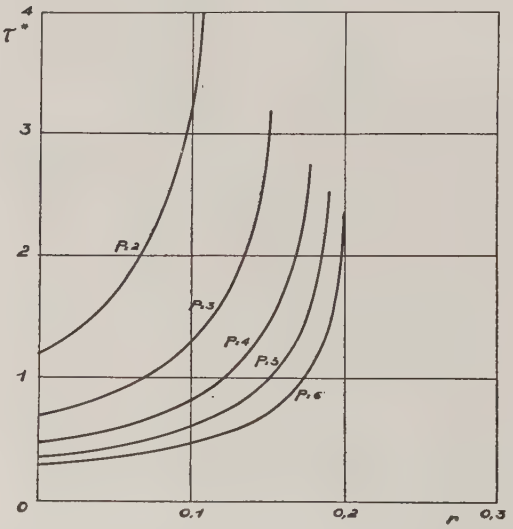

Fig. 4. Variation of the critical time lag τ^*, as a function of r, for various values of p ($p = p/2\Delta\overline{p}$); $\overline{p}$ = average chamber pressure; $\Delta\overline{p}$ injector pressure drop.

$n = 0$ and various values of P. The system being stable when the time lag is below the critical value, τ^*, the field of instability increases when P increases or when r decreases.

In a given rocket, an increase of the average feed pressure produces a simultaneous increase of $\overline{p}$ and $\Delta\overline{p}$, but decreases their ratio, P. Thus, according to Figure 5, an increase of Δp improves the stability; this is supported by experience

which gives the value of τ^* and that of the critical injector pressure drop. On the other hand, for $n = 0$ and $r = 0.1$ (a value which seems likely), the time lag connected to Δp in the vicinity of a point given by the relation:

$$\tau \Delta p^r = c^{te} \tag{9}$$

decreases when Δp increases. This confirms the existence of a critical injector pressure drop and permits an experimental check of Equation (9) between the critical values.

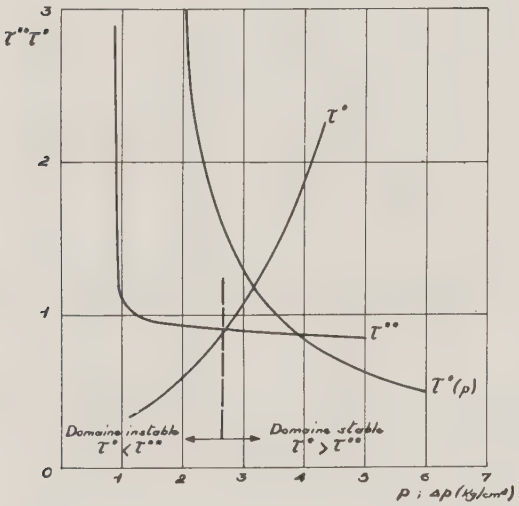

Fig. 5. Variation of the reduced time lags τ^* and τ^{**} as a function of the injection pressure drop Δp ($p = 20$ kg/cm²) ($r = 0$).

4. Constant Feed Pressure ($b \to \infty$)

In this case, the characteristic equation reduces to

$$(\lambda + 1 - n + ne^{-\lambda\tau})(1 + IP\lambda) - P[(2r - 1)e^{-\lambda\tau} - 2r] = 0$$

as before, a circle, G, defined by the function

$$g(\lambda) = -e^{-\tau\lambda}$$

can be associated with the limiting contour, but the contour, F, defined by the function

$$f(\lambda) = \frac{1 - n + 2rP - IP\lambda^2 + \lambda[1 + IP(1 - n)]}{n - P(2r - 1) + \lambda nIP}$$

is less simple and generally consists of a cubic equation and a semi-circle of infinite radius.

These cubics are symmetrical with respect to the x-axis and admit an asymptote to the abscissa

$$x_a = \frac{l - n}{n} + \frac{2r - 1}{n^2 I}$$

independent of P, a double point located on the axis, at the abscissa:

$$x_\alpha = \frac{l - n}{n} + \frac{l}{nIP}$$

independent of r, and a point with vertical tangent the abscissa of which

$$x_o = \frac{l - n + 2rP}{n - P(2r - l)}$$

is independent of I.

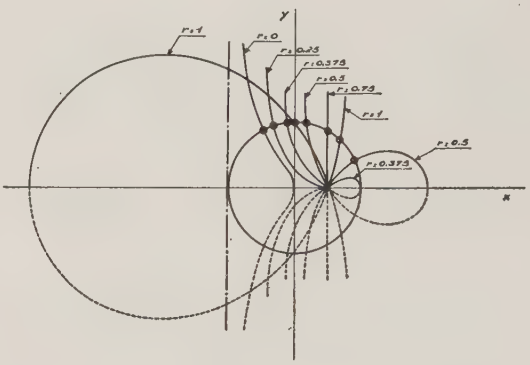

Fig. 6. Study of stability by Satche's method, for $p = 2$; $z = 2$; $L^* = 2$; $n = 1$ (for various values of r). Double points: $x_d = \frac{1}{2}$. Asymptote: $x_a = 2r - 1$. Summit: $x_0 = 4r/3 - 4r$.

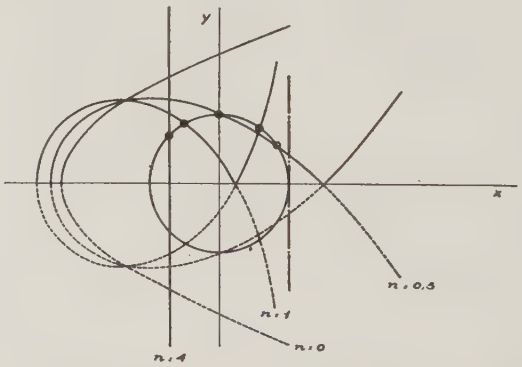

Fig. 7. Discussion of stability of system for various values of n ($r = 1$; $p = 4$; $z = 2$; $L^* = 2$).

These characteristic elements make it possible to predict conditions of stability independent of the time lag. Thus, stability is always assured when the cubic is entirely to the right of the circle, i.e., for the set of conditions:

$2n - 1 > 0$, $2r - 1 > 0$,

$$l < \frac{2r - 1}{(2n - 1)n}, \frac{2n - 1}{4r - 1} < P < \frac{n}{2r - 1}$$

Figures 6, 7, 8 and 9 show the effect of each of

the four parameters, r, n, P and I, on the shape and location of the cubic with respect to the circle of unit radius for fixed values of the three others. In most of the cases considered, the two curves intersect and the stability depends therefore on the time lag; as in the preceding cases, the points of intersection determine a critical impulse, ω^*, and a critical time lag, τ^*, both defined in

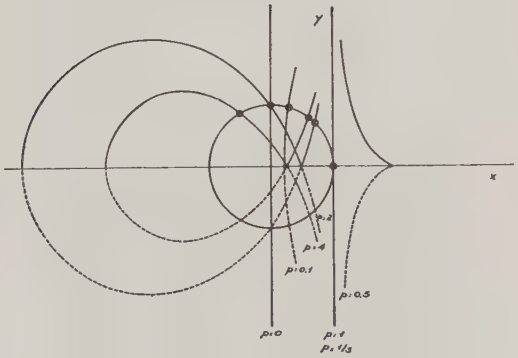

Fig. 8. Study of stability of the system as a function of p ($r = 1$; $n = 1$; $z = 2$; $L^* = 2$).

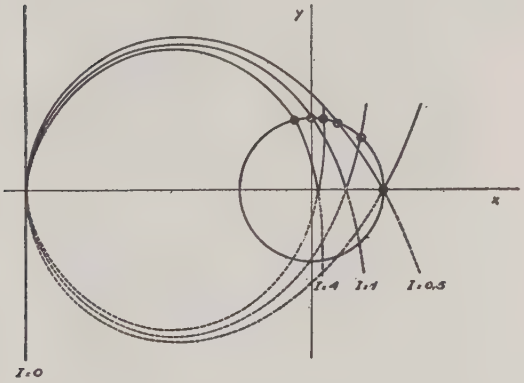

Fig. 9. The stability of the system by Satche's method for one variable ($n = 1$; $r = 1$; $p = 2$).

function of the auxiliary parameters

$$\alpha = \frac{P}{1 + I^2P^2\omega^{*2}} \quad \text{and} \quad \beta = \frac{lP^2}{1 + l^2P^2\omega^{*2}}$$

by the relations

$$n = \frac{1 - \alpha}{2} + \frac{\omega^{*2}}{2}\frac{1 - \beta^2}{1 + \alpha} + 2r\left(\alpha - \omega^*\beta\frac{1 - \beta}{1 + \alpha}\right)$$

and

$$\tau^* = \frac{1}{\omega^*}\arccos\left\{\begin{array}{c}(1 + 2rP - n - 1P\omega^{*2}) \\ \cdot[n - P(2r + 1)] \\ + nlP[1P(1 - n) + 1]\omega^{*2} \\ - \dfrac{}{[n - P(2r + 1)]^2\, n^2I^2P^2\omega^{*2}}\end{array}\right\}$$

which can be used to calculate the index, n (or r) as a function of ω^* and of the parameters of the propeller. Figure 10 shows the variations of r as a function of ω,* for several values of n.

5. Conclusion

The figures showing the variations of the characteristic parameters, ω^* and τ^*, as functions of the indexes, n and r, also show that taking into account the injector pressure drop in the determination of the time lag, modifies the stability conditions considerably without involving any

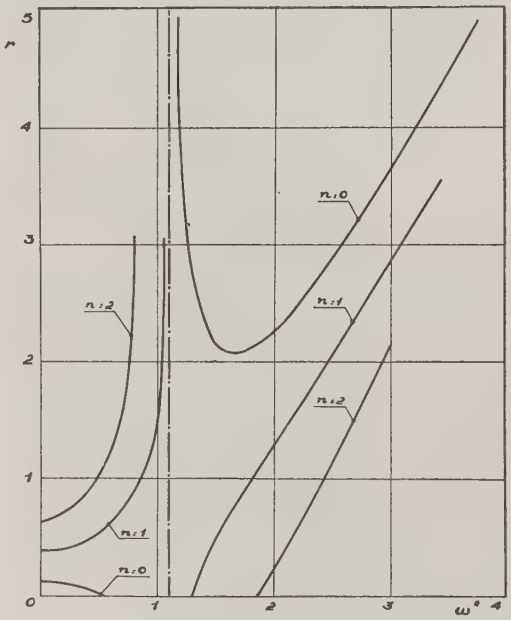

Fig. 10. Variation of the injection index r as a function of ω^*, for various values of n.

contradiction with experience. A similar generalization may be considered in the case of bipropellant rockets. Whether the oxidizer and the fuel have no affinity for each other (nitric acid and kerosene) or whether they form a hypergolic compound (nitric acid and furfurylic alcohol), the extent of mixing has a very great effect on the successive stages from the introduction of the active bodies into the chamber to the ejection. Experience has shown[8] that the time lag decreases when the momentum of the injector jets increases. This makes it possible to relate, in first approximation, the time lag, τ, to the injector pressure drops, Δp_O and Δp_H of the oxidizer and of the fuel respectively as follows:

$$\tau(C_H\Delta q_H)^{rH}\ (C_o\,\Delta q_o)^{r_o}\ q^n = c^{te}$$

which shows the concentrations

$$C_H = q_H/(q_H + q_o)$$

and

$C_o = q_o/(q_H + q_o)$ of both the propellants injected. In this case also, the discussion, which is not printed in this paper, shows important modifications of the characteristic values when the indexes, r, vary.

Thus, the injector pressure drop which is just as important in the chemical and physical phenomena of combustion as the chamber pressure has an effect on the stability conditions, not only because of the injection parameter $P = p/2\Delta p$, but also because of its effect on the time lag itself, which may not be neglected.

Nomenclature

A	cross-sectional area
b	characteristic coefficient of the feeding pump
C	concentration
$f\ (p, \Delta p, T)$	amount of heat needed to ignite the propellant unit of mass during a unit interval of time
$f\ (\lambda)$	algebraic part of the characteristic equation
$g\ (\lambda)$	exponential part of the characteristic equation
I	feed parameter
l	length of the feed line
$M\ (t)$	gas mass in the chamber at time, t
n	interaction index relating to the pressure
$p\ (t)$	instantaneous pressure
P	injection parameter
$q\ (t)$	instantaneous flow rate
r	interaction index relating to the injector pressure drop
ts	mean residence time
t, t'	time
$T\ (t)$	instantaneous temperature in the chamber
V	volume of the chamber
X, Y	coordinates in the complex plane
$\alpha\beta$	auxiliary parameters
γ	specific heat ratio
Δp	injector pressure drop
ζ	parameter connected to P and b
λ	complex variable of the characteristic equation
μ	function of perturbation of the flow rate
τ	time lag
φ	function of perturbation of the pressure in the chamber
ψ	function of perturbation of the injector pressure drop
ω	impulse of the oscillations

SUBSCRIPTS

o	pump outlet
i	injection
c	nozzle throat
e	ejection
O	oxidizer
H	fuel

A bar over a quantity indicates the average values independent of time.

REFERENCES

1. Summerfield, M.: J. Am. Rocket Soc., *21*, 5 (1951).
2. Crocco, L.: J. Am. Rocket Soc., *21*, *6*, (1951); *22*, 7 (1952).
3. Barrère, M., and Bernard, J. J.: Publication ONERA, No. 79.
4. Satche, M.: J. Appl. Mech., *16*, 4 (1949).
5. Tsien, H. S.: J. Am. Rocket Soc., *22*, 5 (1952).
6. Marble, F. E., and Cox, D. W.: J. Am. Rocket Soc., *23*, 2 (1953).
7. Marble, F. E.: Z. angew. math. phys., *6*, 1–35 (1955).
8. Barrère, M., and Moutet, A.: Rech. Aéronaut., *44*, 29–38 (1955).

61

SOME STABILITY TESTS ON AN AXIALLY SYMMETRIC COMBUSTOR

By A. A. PUTNAM AND W. R. DENNIS

The stability limits of flame-holding obstacles with small blockage in an axially symmetric combustor usually are assumed to be unaffected by the enclosing walls, provided the flame does not touch the wall and provided ocsillations are not present. Since experimental evidence supporting this assumption has been lacking, the tests reported herein were made. The tests were made in a cylindrical combustor containing a disk flame holder that was suspended in a jet of premixed propane and air issuing from an accelerating nozzle. The stability limits and noise output were measured as a function of the jet velocity, mixture ratio, and length of the combustor upstream and downstream of the flame holder. The effect of suppressing certain components of the noise spectrum was also examined.

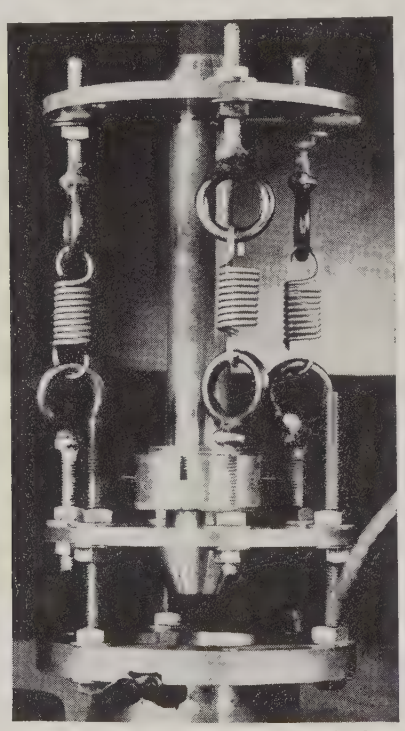

FIG. 1. ⅞-in. combustor mounted above 1-in. nozzle.

Apparatus

Figures 1 and 2 show a photograph and a schematic diagram respectively of the combustor, which was suspended directly above a one in. diam accelerating nozzle attached to a large plenum chamber. For some of the tests, a 55-gal oil drum was used as a plenum chamber, and for the remainder of the tests a section of 3-in. pipe 49 in. long was used. A combustible mixture of propane and air flowed through the plenum chamber and issued from the nozzle as a jet. Since the inside diameter of the combustor entrance was ⅞ in., an annular layer of the stream at least 1/16 in. thick spilled over into the surrounding air.

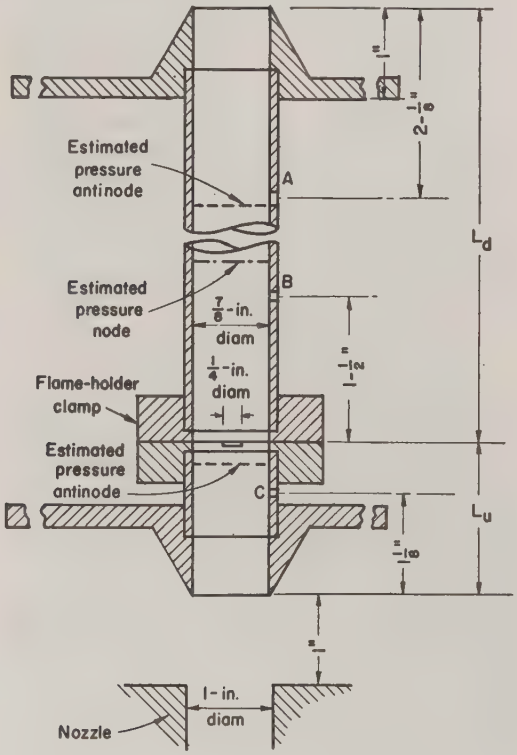

FIG. 2. Schematic diagram of ⅞-in. combustion ram jet mounted above 1-in. nozzle.

The components of the combustor were (1) a sharp-edged nose and a nose plate to which positioning bolts and expansion compensating springs were attached, (2) a stainless steel upstream tube placed in a recess in the nose plate, (3) a flame-holder section seated on the upstream tube, (4) a stainless steel downstream tube placed in a recess in the flame-holder section, and (5) a tail

plate, terminating in a sharp-edged tail, seated on the downstream tube and held in position by the springs. The lengths, L_u and L_d, of the upstream and downstream tubes, respectively, could be varied independently. A $\frac{1}{4}$-in.-diam nichrome disk flame holder was mounted on the axis, giving a blockage of about 8 per cent. Holes A, B, and C, seen in Figure 2, were used only for tests on damping of high-frequency oscillations; otherwise they were closed.

Three different Pitot-tube systems were used to measure ram velocity at different times in the course of the testing program. Each system was calibrated with known flow rates. Since the type of system used was shown to have no effect on the stability range of the combustor, a detailed description of each system will be omitted for the sake of brevity.

The noise level and noise spectrum were measured with a sound level meter and a constant percentage bandwidth sound analyzer, respectively. A laboratory-type nondirectional crystal microphone was used as the sound pick-up; it was placed 30 in. from the combustor at a level 9 in. above the top of the accelerating nozzle.

Method of Test

In blowoff tests, unless otherwise noted, a constant air flow rate was maintained through the accelerating nozzle, and the flow rate of propane was changed in small increments until the flame blew off. Successive changes were made two minutes apart to allow time for attaining equilibrium conditions. After blowoff, the combustor was re-ignited, the propane-air mixture adjusted to the composition used just prior to blowoff, and the following measurements made: (1) the reading of the Pitot-tube system, (2) the sound-pressure level in decibels, and (3) the frequency spectrum. In some tests, the frequency of oscillation at various mixture ratios and flow velocities within the stable range of combustion was also measured. This test procedure was repeated at successively higher flow velocities until combustion could no longer be stabilized.

Discussion of Test Results

Two types of oscillations were generated with the combustor just described, one a relatively high-frequency oscillation, and the other a violent low-frequency oscillation. It will be shown that (1) the high-frequency oscillations occurred when the combustor was operated above a certain ram velocity, and (2) the low-frequency oscillations occurred at velocities below this value, and were responsible for premature blowoff. The effects of each type of oscillation on blowoff limits are discussed. In addition, test results are presented which demonstrate the effects on stability limits of changes in air/fuel ratio, velocity, length of the combustor, and contraction of the combustor outlet.

STABILITY RANGE OF THE COMBUSTOR

Figure 3 shows typical observed blowoff limits for the combustor of Figure 2 with $L_u = 1\frac{3}{4}$ in. and $L_d = 6\frac{3}{4}$ in. The ordinate of Figure 3 is the average velocity at the outlet of the accelerating nozzle, and the abscissa is percentage theoretical air. For comparison, the blowoff limits for an unconfined flame burning from a $\frac{1}{4}$-in.-diam disk flame holder are also plotted. The stability range for the unconfined flame was much larger than the range for the confined flame. The discontinuity in the blowoff curve for the confined flame at 130 fps on the lean side will be discussed next.

Figure 4 shows the observed blowoff limits for all of the blowoff tests of the combustor with $L_u = 1\frac{3}{4}$ in. and $L_d = 6\frac{3}{4}$ in. The ordinate of Figure 4 is combustor velocity, or average velocity within the combustor upstream of the flame holder. Data are plotted for all three types of Pitot systems used, for each of the two types of plenum chamber used, and for several methods of damping high-frequency oscillations described in the next section. Since all of these blowoff data fell on one scatter band with no consistant deviation with any change of variable, the data points are not differentiated with respect to the various test conditions just mentioned. The fact that all of the data fell on one blowoff limit curve indicated that: (1) There was no significant variation in blowoff limits with change in the type of Pitot system used. (2) There was no appreciable change in blowoff limits when the type of plenum chamber was changed, even though other test results showed a slight, but significant, acoustic coupling between plenum chamber and combustor in each case. (3) There was no appreciable change in blowoff limits when acoustic dampers were used to suppress high-frequency oscillations. Test results using acoustic dampers are discussed in detail in the next section.

The lean blowoff limits decreased rapidly as the velocity was increased from about 30 to 45 fps. At 45 fps there was a discontinuity, with a sudden increase in the lean limit from 94 per cent

theoretical air to about 130 per cent. The lean limit then decreased again as the ram velocity continued to increase. It will be shown that the discontinuity in the lean blowoff curve, as well as the apparent discontinuity in the rich blowoff curve discussed next, results from violent low-frequency oscillations occurring when the velocity was below 45 fps.

The rich limit of combustion decreased as the combustor velocity was increased in the range above 50 fps. Below 50 fps, rich blowoff usually did not occur; instead the combustible mixture became ignited at the nose of the combustor, so that gases spilling over into the atmosphere, as well as the gases entering the combustor, started to burn. Data for the few instances when rich blowoff did occur are plotted in Figure 4. The blowoff curve shows that there was apparently a discontinuity on the rich side. The break was not as well defined as on the lean side, but premature blowoff occurred in 5 out of 6 tests at velocities below 40 fps.

Also shown in Figure 4 are the sound pressure levels, in db, 30 in. from the ramjet for several different ram velocities and mixture ratios near blowoff. For velocities above the discontinuity at 45 fps, the sound pressure level increased with velocity, as would be expected. In this velocity range, the observed frequencies were close to the computed organ-pipe frequencies of the system. This type of oscillation was observed in earlier tests, reported by Putnam and Dennis,[1] using a combustor similar to that of Figure 1; however, in those tests the combustor was directly connected to a plenum chamber.

For velocities below the discontinuity on the lean side, the sound pressure levels were much higher than would be predicted from an extrapolation of the sound pressure level data above the discontinuity. In this velocity range, violent oscillations with a frequency much lower than the computed lowest organ-pipe frequency of the system were generated. A similar low-frequency oscillation, reported by Putnam and Dennis,[2] was generated in the coupled system just mentioned.

A plot of the boundaries, in terms of velocity and mixture ratio, between low-frequency and organ-pipe oscillations for several different test conditions had the following characteristics: (1) it had roughly the shape of the burning velocity curve, (2) it moved toward higher velocities as the downstream length, L_d, was increased, and (3) it did not change in position appreciably with change in upstream length, L_u.

Before discussing in detail the effects of oscillations and configuration parameters on the blowoff limits, the following additional test result should be mentioned. Two tests were made in which the blowoff limits on the lean side were approached by gradually reducing the velocity, rather than increasing the per cent theoretical air at constant velocity, as described in the discussion of method of test. The tests started at velocities greater than 45 fps and followed the

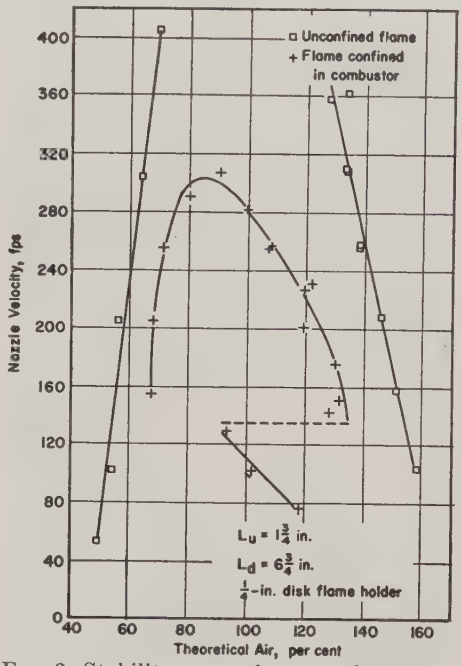

FIG. 3. Stability ranges for unconfined and confined flames.

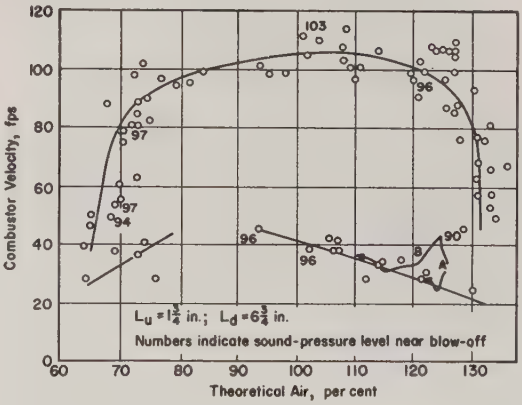
Combustor Velocity, fps
Theoretical Air, per cent
$L_u = 1\frac{3}{4}$ in.; $L_d = 6\frac{3}{4}$ in.
Numbers indicate sound-pressure level near blow-off

FIG. 4. Stability range for confined flame.

paths indicated by the curves ending in arrows on Figure 4. Blowoff occurred at the mixture ratios and velocities indicated by the tips of the arrows. In neither test did blowoff occur in the region of the discontinuity near 45 fps, as was hoped.

EFFECT OF HIGH-FREQUENCY OSCILLATIONS ON BLOWOFF LIMITS

To determine the effects of the high-frequency oscillations on blowoff limits, the oscillations were damped, using, in separate tests, a tuned quarter-wave tube, and several pressure relief ports. Each device had proved successful in earlier test programs.[3] For the present damping

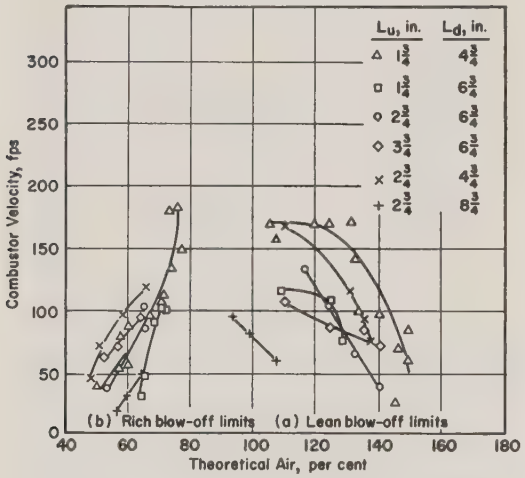

FIG. 5. Blowoff limits for uniform combustor.

tests, the combustor had the dimensions of $L_u = 1\frac{3}{4}$ in. and $L_d = 6\frac{3}{4}$ in.; the relief ports used are designated as A, B, and C in Figure 2. The position of each relief port relative to the estimated location of pressure nodes and antinodes in the combustor is also shown in Figure 2. The ports were plugged except for the tests now being discussed.

During the tests on the effect of high-frequency oscillations, the combustor generated a strong, second-mode oscillation with a frequency of about 2000 cps. Blowoff limits were obtained using each of the following damping devices: (a) a $\frac{1}{16}$-in.-diam hole at Position C, which is as close as possible to the estimated pressure antinode of the second-mode oscillation, (b) a $\frac{1}{8}$-in.-diam hole at either Station A, or B, or C, and (c) a $\frac{5}{16}$-in.-diam quarter-wave tube at Position C.

For lean mixtures, the sound-pressure level decreased with a $\frac{1}{16}$-in. orifice at Position C, and decreased even more with a $\frac{1}{8}$-in. orifice at C or A. There was no effect of an orifice at B, as might be expected since it was located at a pressure node. A significant decrease in sound-pressure level was obtained when the $\frac{5}{16}$-in.-diam quarter-wave tube at C was tuned so that it resonated at about 2000 cps. On the rich side, the mantle noise was sufficient to mask any reduction in sound-pressure level. The damping methods used had no effect on the sound-pressure level of the low-frequency oscillations.

As mentioned in discussing Figure 4, there was no change in blowoff limits when acoustic dampers were used. Since high-frequency oscillations were suppressed significantly in some cases, it was concluded that the high-frequency oscillations did not affect the blowoff limits in these tests.

EFFECT OF CONFIGURATION PARAMETERS ON BLOWOFF LIMITS

In the study of the effect of configuration on the blowoff limits, combustors of two different types were used, one with a uniform inside diameter of $\frac{7}{8}$ in., and a second type in which the exit section was contracted uniformly over the last $\frac{5}{8}$ in. to an inside diameter of $\frac{3}{4}$ in. For each type, the tube lengths upstream and downstream of the flame holder were changed.

Figure 5A shows the lean, or fuel-deficient, blowoff limits for the combustor of uniform diameter. It is seen that there was a significant decrease in lean blowoff limits with increase in downstream length, L_d. For $L_d = 6\frac{3}{4}$ in., there was no consistent effect of upstream length, L_u, on the blowoff limits. For $L_d = 4\frac{3}{4}$ in., an increase in L_u from $1\frac{3}{4}$ in. to $2\frac{3}{4}$ in. resulted in a small decrease in blowoff limits. Allowing for the scatter of the data, however, no conclusion can be drawn as to the effect of upstream length.

Figure 5B shows the rich, or air deficient, blowoff limits for the uniform combustor. Increases in the downstream length were detrimental to the flame-holding properties as was observed for the lean limits. Increases in the upstream length, however, had a beneficial effect on the flame-holding properties not observed at lean limits. This beneficial effect was probably the result of a stabilizing action of the mantle which burned above the combustor on the rich side. As the distance separating the outlet and the nozzle was increased by increasing L_u, the mantle may have been disturbed to a lesser extent by the air-

propane mixture spilling over and flowing into the air surrounding the combustor. It would be expected that if the mantle were quenched the beneficial effect of increase in upstream length would disappear.

Figure 6A shows the lean side blowoff data for the contracted combustor at velocities above 45 fps; the curve for the uniform combustor from Figure 4 is shown for comparison. Within the accuracy of the data, and from the small amount of data available, little can be said about the effects of either upstream or downstream length. Comparing Figures 5A and 6A, it appears that the uniform combustor is more stable for all combinations of L_d and L_u upon which comparison may be made, except for the combination with the longest downstream length of $8\frac{3}{4}$ in. In this instance, the contracted unit appears more stable, although the comparison rests upon one point only.

Figure 6B shows the rich side blowoff data for the contracted combustor. There is no apparent effect of upstream length within the accuracy of the data. This may be interpreted as meaning that the contraction has decreased the coupling between the mantle and the combustion region in the combustor. There may be a decreased stability with increasing downstream length, but again this conclusion can be based upon only one point.

From the discussion of Figures 5A and 5B, and 6A and 6B, it may be concluded that (1) the influences of upstream and downstream length are much more evident in the uniform combustor than in the contracted combustor, and (2) the stability range is larger for the uniform combustor than for the contracted combustor.

EFFECT OF MIXTURE RATIO ON COMBUSTOR VELOCITY AT CONSTANT NOZZLE VELOCITY

Figure 7A shows a set of velocity traverses in terms of mixture ratio of a $1\frac{3}{4}$ in. by $4\frac{3}{4}$ in. combustor, made with the air flow rate through the nozzle in each traverse held constant. In each traverse, the combustor velocity decreased to a minimum near a stoichiometric mixture. This is as expected, since the volume increase in the products of combustion accompanying a change in mixture ratio towards the stoichiometric point causes the back pressure to increase and causes more spillover at the combustor entrance. Thus the flow rate through the combustor decreases.

Figure 7B shows the traverse for a combustor with downstream length, L_d, 2 in. greater than that of the combustor of Figure 7A. For the three highest velocities, curves similar to those of Figure 7A are obtained. The increased downstream length of combustion chamber not only produces more drag, but, more importantly, increases the efficiency of combustion. Thus, the combustor velocity curves are higher on Figure 7A than in Figure 7B. The data for the 90-fps nozzle velocity show a different trend, however. These data show an increasing combustor velocity near the stoichiometric point, indicating a decreasing efficiency of combustion in this range.

One other characteristic of this particular

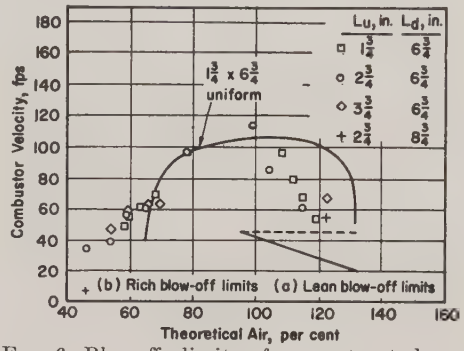

FIG. 6. Blowoff limits for contracted combustor.

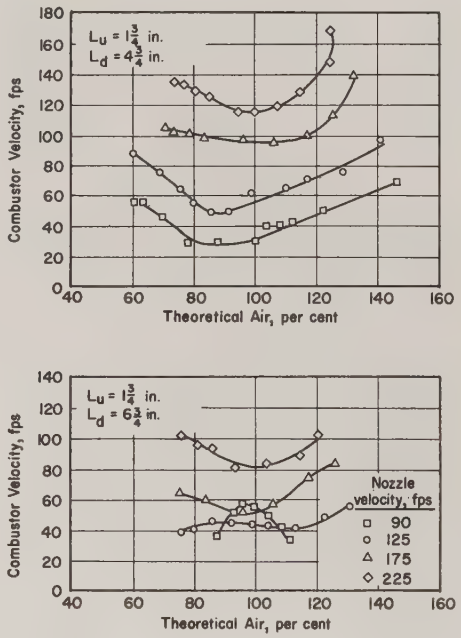

FIG. 7. Velocity traverses at constant nozzle velocity for uniform combustors.

90-fps curve is important: the end points correspond to low velocity blowoff rather than normal blowoff.

LOW-VELOCITY INSTABILITY

As pointed out in discussing Figure 3, the premature blowoff below the discontinuity at 45-fps

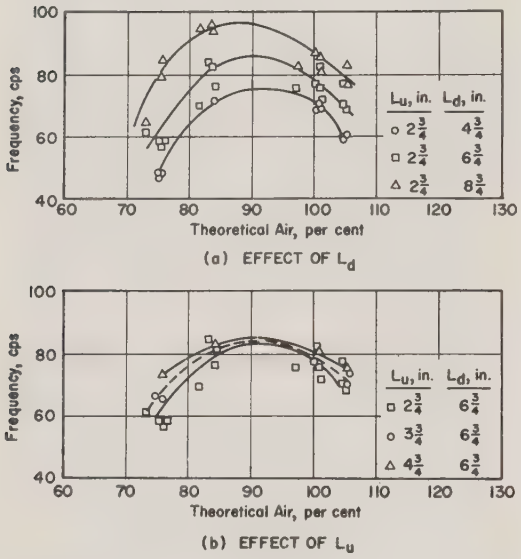

FIG. 8. Effect of L_u and L_d on frequency for various mixture compositions.

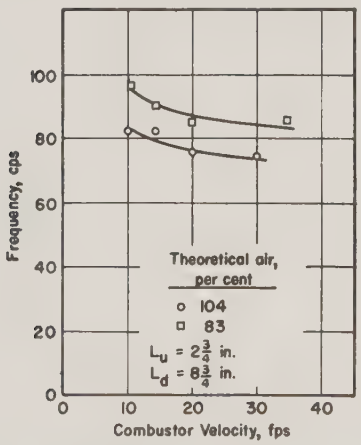

FIG. 9. Effect of combustor velocity on frequency.

combustor velocity was associated with a low-frequency oscillation. If it is assumed that the premature blowoff is a direct consequence of the low-frequency oscillation, a discussion of the premature blowoff will require an understanding of the mechanism of the low-frequency oscillation. Before proceeding with the discussion, however, some additional test results should be noted.

Only a small number of blowoff data were available for the low-frequency blowoff. However, the available data showed a consistent stabilizing effect of contracting the downstream end of the combustor. The effects of change in upstream and downstream length were small. With increase in upstream length, there was a trend toward decreasing stability. There seemed to be a similar trend with increasing downsteam length, but the experimental error was such in this instance that no conclusion could be drawn.

Figures 8A and 8B show the effects of both downstream and upstream length, at constant combustor velocity, on the frequency of the low-frequency oscillation. It is seen that the frequency curves have a shape similar to typical curves of burning velocity, with maxima at a mixture somewhat richer than stoichiometric. From Figure 8A, the frequency increased with L_d at a fairly uniform rate, for constant L_u. From Figure 8B, the frequency also increased with L_u for constant L_d, but the latter change was small.

Figure 9 shows the effect of combustor velocity on the frequency of the low-frequency oscillation. At very low velocities, an increasing velocity was accompanied by a slight decrease in frequency. The curves approach zero slope at about 35 fps, and some scattered data not shown in the figure indicated that the frequency increased with increases in velocity above 35 fps.

DESCRIPTION OF LOW-FREQUENCY BLOWOFF

It will be assumed that the low-frequency oscillation which is associated with blowoff at low velocities is the same type of oscillation as that described by Putnam and Dennis.[2] That oscillation was generated in a similar combustor attached to a plenum chamber. There are many similarities in the results for the two systems which justify this assumption. The mechanism of the oscillation consisted of periodic large-scale flame movements; during one cycle, the flame expands radially, strikes the wall, leaves the flame holder or blows out at some subsequent time, and passes downstream while a new flame starts expanding radially from a residual core of burning gases in the lee of the flame holder.

It is shown by Putnam and Dennis[2] that the low-frequency oscillation does not take place when the flame does not contact the walls of the combustor. If the flame does contact the wall,

the low-frequency oscillation does occur. This type of oscillation causes a reduction in efficiency of combustion compared to that obtained with no oscillations; this loss of efficiency with oscillation results from the escape of unburned gas periodically from the combustion system as the flame is expanding outward to the wall. As a consequence, the average pressure drop associated with the acceleration of burned gases decreases, and the average flow velocity increases when the flame is oscillating. This means that, for a given nozzle velocity, the combustion velocity is appreciably higher with than without low-frequency oscillation.

Figure 10 is a plot illustrating the relations between combustor velocity and nozzle velocity for the cases of inefficient combustion, with low-frequency oscillations, and efficient combustion, without oscillations. If the pair of curves for these two conditions are assumed to correspond to a mixture ratio near stoichiometric, pairs of curves for other mixture ratios would be closer together than the pair shown.

Assuming an increase in nozzle velocity at constant mixture ratio, the combustor velocity would increase along the "inefficient" curve, for example, from Point A through Point D to G. At Point G, blowoff occurs because the residual core flames, or pilot flame, behind the flame holder blows off; thus, the re-ignition part of the cycle of flame oscillation cannot occur. If the core flame is sufficiently tenacious that the blowoff point is not at G, but is at some higher velocity designated by G′, a point H may be reached first where the flame ceases to contact the wall even with violent oscillation. The oscillation then stops and there is a sudden decrease in combustor velocity to Point I on the "efficient" curve, from which point the velocity can then be increased further until normal blowoff occurs.

The combustor velocity, represented by Point H, at which the flame finally ceases to contact the wall probably varies directly with the product of burning velocity and downstream length, L_d. The combustor velocity at which the core flame blows off probably varies directly with the burning velocity raised to a power higher than the first. These two relations for combustor velocity lead to a prediction that above a certain burning velocity, for a given L_d, the core flame will continue to burn after the oscillation ceases. In other words, the tendency for premature blowoff would decrease as the burning velocity increases. This agrees with experimental observations. It may also be pointed out that when efficient combustion starts, the core flame is replaced by a fuller, more stable flame.

As the nozzle velocity is decreased during "efficient," or stable, burning, the combustor velocity decreases along the path through Points B, I, and C, to Point E, where the flame contacts the wall and a low frequency oscillation starts. At this point the combustor velocity immediately jumps to Point D on the "inefficient" curve. The effect of either increasing downstream length or decreasing burning velocity is to move these points away from the origin.

Paths A and B on Figure 4 illustrate a sequence of changes in mixture composition and combustor velocity in a test designed to study the factors just discussed. In Sequence B, the

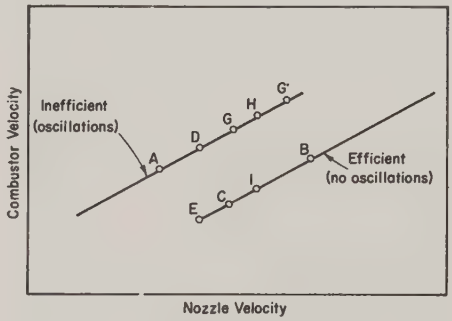

FIG. 10. Typical relations of combustor to nozzle velocity, with and without oscillations.

fuel flow rate was held constant and the air flow rate was decreased. This method resulted in a simultaneous decrease in nozzle velocity and mixture ratio, making it difficult to interpret the results, especially since the combustor velocity first decreased and then increased when low-frequency oscillation started.

In Sequence A, an attempt was made to maintain a constant mixture ratio while reducing the nozzle velocity. The attempt was not entirely successful, but was more satisfactory than that for Sequence B. A sequence of changes in velocity and mixture ratio corresponding to Path A in Figure 4 is illustrated on Figure 10 by the Sequence B, I, C, E, D, and G, allowing for change in position of G with change in composition.

Conclusions

With respect to the normal blowoff, which was unaffected by organ-pipe oscillations generated at high combustor velocities, the stability limits were much lower than for similar flames held in

a free stream of combustible mixture, even though the holder blocked less than 10 per cent of the cross section of the combustor. With a combustor of uniform diameter operating at lean mixtures in the region of normal blowoff, increases in length of the combustor downstream of the flame holder resulted in decreases in the stability range. Changes in the upstream length also appeared to have an effect, but because of the small number of tests, no positive conclusions could be drawn. Contracting the exit of the combustor caused a reduction in the magnitude of changes in stability resulting from changes in length. On the rich side, the stabilizing influence of the mantle flame at the exit of the combustor masked some of the effects of changes in length.

The low-frequency oscillation generated in the same combustor at low velocities was concluded to be the cause of observed premature blowoff. This oscillation occurred whenever it was possible for the flame front to touch the wall; thus, the oscillation tended to be generated at low velocities at long downstream lengths of combustor, and at mixture ratios near stoichiometric. It was assumed that the low-frequency oscillation was of the same type as that encountered in a similar combustor discussed by Putnam and Dennis;[2] that is, the oscillation consisted of a repeated movement of the flame downstream, each movement followed by an outward spreading of a new flame front into the oncoming combustible mixture. Energy for re-ignition was supplied by a residual core of burning gases on the axis behind the flame holder.

The results show that it may be incorrect to assume that stability tests on a flame holder are unaffected by the presence of walls. In fact, certain high amplitude oscillations may prevent even a close approach to normal free-stream flame-holding limits.

Acknowledgment

The work described in this paper was conducted under the sponsorship of the Aeronautical Research Laboratory, Wright Air Development Center, United States Air Force, Contract AF 33(038)-12656.

REFERENCES

1. Putnam, A. A., and Dennis, W. R.: *Fourth Symposium (International) on Combustion*, p. 566. Baltimore, The Williams & Wilkins Co., 1953.
2. Putnam, A. A., and Dennis, W. R.: Am. Soc. Mech. Engrs. Preprint No. 55-SA-48, Presented at the Am. Soc. Mech. Engrs. Semi-Annual Meeting, Boston, Mass., June 19–23, 1955.
3. Putnam, A. A., and Dennis, W. R.: Trans. Am. Soc. Mech. Engrs., 77, 875 (1955).

62

AN ANALYSIS OF UNSTABLE COMBUSTION OF PREMIXED GASES

By H. J. MERK

1. Introduction

Acoustic oscillations are often generated when gases are burned in combustion systems. This phenomenon goes under various names, *viz.*, unstable combustion, sonant combustion, flame-driven oscillations, etc. A qualitative explanation of this phenomenon has already been given by Rayleigh,[1] but this explanation fails to give the details of the coupling between combustion process and pulsations in gas flow. Realizing this shortcoming of Rayleigh's theory, many authors have tried to improve it, e.g., Putnam and Dennis,[2] Blackshear,[3] Kaskan,[4] and Neumark and Aronovitsch.[5] This paper contains a contribution to the theoretical explanation of unstable combustion based on the well-known principle of the dynamic stability of a gas flow through a flow system. The name "flow system" is used to designate the whole system between the feed pump and the stack. The flow system is divided into a supply system, a burner head, and a combustion system (Fig. 1). The supply system is defined as the system through which the unburned gases flow, and may be subdivided into the feed system and the mixing tube or mixing chamber. The burner head is the device on which the flames burn; its

principal parts are the burner ports or burner slits. The combustion system is defined as the system through which the combustion products flow. The principal parts of this system are the flame tube or flame chamber and the stack. The volume occupied by the flames in the combustion system is excluded and will be considered later on.

Application of the principle of dynamic stability means that small disturbances proportional to $\exp(\lambda t)$ are imposed on the steady-state flow of the gas. If the real part of λ appears to be negative, then the disturbances will die out and the flow of gas will be stable. If, however, it turns out that the real part of λ is positive, then the amplitude of the disturbances increases with time. In that case the flow is dynamically unstable and this theory is concerned only with the calculation of the instability limits determined by the vanishing of the real part of λ.

In order to calculate the instability limits we have to derive an equation for λ, the so-called characteristic equation. In deriving this equation we need the transfer functions of the flames (Section 2) and the matching conditions at the flames (Section 3) from which the characteristic equation is easily derived (Section 4). In Section 5 we have applied the theory to a very simple model of the flow system.

In the derivation of the characteristic equation, the following simplifying assumptions are introduced: (1) The fluctuating parts of all the quantities involved in the theory are small in comparison with their mean values, so that all the equations can be linearized in terms of the fluctuations. (2) The vibrations before and behind the flames are isentropic. (3) The flame length is small in comparison with the wave length. (4) If there is more than one flame on the burner head, all of them are identical and vibrate in phase with each other. (5) Either there is only primary combustion of the premixed gases, or the heat released by the secondary combustion is negligible. (6) The caloric value of the premixed gases is constant throughout the vibration. (7) The normal combustion velocity depends only on the temperature and pressure of the unburned gases and on the fuel/air ratio. (8) The fuel/air ratio is constant throughout the vibration. (9) The flow of gas through the structural parts composing the flow system is essentially one-dimensional. (10) The Mach number is small enough for the quadratic or higher terms in it to be neglected. (11) There is no heat transfer in the burner ports.

Regarding some of the assumptions, the following can be said: assumption 2 is not so obvious as it appears. It would be reasonable to expect the vibrations before the flames to be isentropic, were it not that the wall boundary conditions induce entropy fluctuations in the acoustic boundary layers along the walls of the supply system. Hence, the first part of assumption 2 means that the acoustic boundary layers are assumed to be very thin, so that the entropy fluctuations there are negligible. The flames, however, introduce entropy fluctuations which are not small, so that behind the flames there exists not only a nearly isentropic acoustic mode, but also an entropy mode of the vibrations. In an accurate analysis of the modes of vibration behind the flames allowance has to be made for the heat-conduction and friction of the gas. This analysis is rather lengthy and therefore not given in this paper. It will be

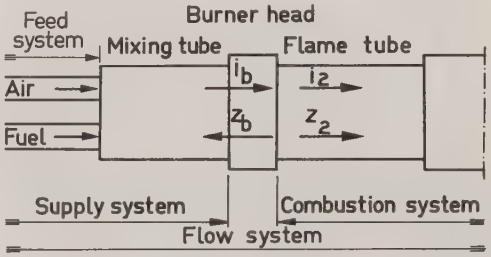

FIG. 1. Diagram of flow system in which combustion of premixed gases occurs.

published separately. We mention only that the analysis leads to the following important conclusions: in the hot gases behind the flames the entropy mode is practically damped out after travelling a distance of some centimeters. This means that generally speaking the entropy mode will not reach the output of the combustion tube, so that the boundary conditions at the exit of the combustion tube do not involve the entropy mode. Furthermore, the analysis shows that the boundary conditions for the acoustic mode at the flames have to be derived from the laws of conservation of momentum and energy, while the law of conservation of mass yields the strength of the entropy mode just behind the flames. As a result, if the boundary conditions at the flames are derived in the right manner, it is possible to consider only the acoustic mode and to ignore the existence of the entropy mode. This treatment is of course not exact and the order of approximation induced by it is of the order M^2 if $|\lambda| \nu/(aM)^2$ is considered of the order 1 or lower, so

that assumption 2 yields the same order of approximation as assumption 10.

The last-named assumption excludes the influence of the fluctuating heat transfer in the hot burner ports. This heat transfer alone may already produce sound, as is known from the Rijke-tube phenomenon (e.g., see Rayleigh[1]). If flames are present, the heat transfer in the burner ports will influence the normal combustion velocity (NCV), which is closely related to the temperature of the gas issuing from the burner ports, which again is related to the heat transfer in the burner ports. The latter effect may become important, but it is neglected in this paper and will be treated in a forthcoming paper.

Finally we remark that the theory is restricted to laminar flames. If the flow and the combustion are turbulent, then the theory is applicable only under the restricting condition that the turbulence does not affect the excitation of sound but only the magnitude of the NCV.

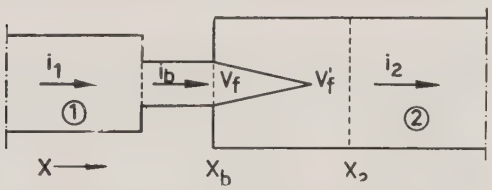

FIG. 2. Diagram of flow system near the burner ports for derivation of the matching conditions at the flame.

2. Transfer Functions of the Flames

In studying unstable combustion we have to know how the fluctuations in the heat production depend on the fluctuation conditions of the gas flow. This dependence will be characterized by the "transfer functions" of the flames. According to assumption 4, all the flames are identical, so that for the time being we may consider one flame only. The heat (Q_f) produced by the flame in a time unit can be written as:

$$Q_f = \rho_{f,1} S_{f,1} A_f H, \tag{1}$$

where the indices f, 1 refer to the conditions just upstream of the flame front. For small fluctuations we obtain from Equation (1)

$$q_f = \sigma_{f,1} + s_{f,1} + \alpha_f \tag{2}$$

The volume enclosed by the flame area (A_f) and the area of the exit of the burner port (A_b) will be denoted by V_f. The mean value of V_f is given by $\bar{V}_f$, and we define

$$\bar{l}_f = \bar{V}_f / A_b \text{ and } \tau_f = \bar{l}_f / \bar{U}_b \tag{3}$$

where $\bar{l}_f$ is a length proportional to the mean flame length, and τ_f the mean residence time of the gases in the flame volume V_f. In Appendix I it is shown that a corollary of assumptions 2, 3, and 10 is that $\tilde{P}_{f,1} \approx \tilde{P}_b$, $\tilde{T}_{f,1} \approx \tilde{T}_b$, and $\tilde{\rho}_{f,1} \approx \tilde{\rho}_b$. Furthermore, if no heat is transferred within the volume V_f, we have $\bar{P}_{f,1} = \bar{P}_b$, etc. Finally assumption 2 is used, yielding:

$$p = \gamma\sigma = \gamma\vartheta/(\gamma - 1) \tag{4}$$

for the fluctuations before (and behind) the flame. Consequently Equation (2) may be replaced by:

$$q_f = s_b + \alpha_f + p_b/\gamma_1 \tag{5}$$

The ratio α_f can be calculated from the equation of continuity applied to the volume V_f:

$$\rho_b U_b A_b = \rho_b S_b A_f + \frac{\partial}{\partial t} \int_{V_f} \rho \, dV \tag{6}$$

For the mean motion this equation yields:

$$\bar{m} = \bar{\rho}_b \bar{U}_b \bar{A}_b = \bar{\rho}_b \bar{S}_b \bar{A}_f \tag{7}$$

From Equations (3), (6) and (7) we derive for the first-order fluctuations:

$$\alpha_f + \frac{\partial}{\partial t} (\tilde{V}_f / \bar{S}_b \bar{A}_f) = u_b - s_b - \tau_f \frac{\partial}{\partial t} \sigma_b \tag{8}$$

where the volume integral in Equation (6) is approximated by $\rho_b V_f$. This approximation is of the same order as $\rho_{f,1} \approx \rho_b$. The fluctuations of V_f are closely related to the fluctuations of A_f, and we write formally:

$$\tilde{V}_f = l_f^* \tilde{A}_f \quad \text{and} \quad \tau = l_f^* / \bar{S}_b \tag{9}$$

The length l_f^* depends on λ and on the shape, size, and distortion of the vibrating flame. In Appendix II this length is calculated for a laminar cone-shaped flame without distortion during the vibration. From Equations (8) and (9) we obtain:

$$\alpha_f + \tau \frac{\partial}{\partial t} \alpha_f = u_b - s_b - \tau_f \frac{\partial}{\partial t} \sigma_b \tag{10}$$

If all the fluctuations are proportional to $\exp(\lambda t)$, the solution of Equation (10) is easily obtained. It is given by

$$(1 + \lambda\tau)\alpha_f = u_b - s_b - \lambda\tau_f\sigma_b \tag{11}$$

Substituting α_f from Equation (11) in Equation (5) and making use of Equation (4), we get

$$q_f = (1 - \Lambda_{f,u}) u_b + \frac{1}{\gamma_1} (1 - \Lambda_{f,u}\tau_f/\tau) p_b + \Lambda_{f,u} s_b \tag{12}$$

where $\Lambda_{f,u}$ is a transfer function of the flame defined by

$$\Lambda_{f,u}(\lambda) = \lambda\tau/(1 + \lambda\tau) \tag{13}$$

According to assumptions 7 and 8 the fluctuations in the NCV may be written:

$$s_b = \Lambda_{s,\vartheta}\vartheta_b + \Lambda_{s,p}p_b \tag{14}$$

At the limit $\lambda = 0$ the transfer functions $\Lambda_{s,\vartheta}$ and $\Lambda_{s,p}$ approach their quasi-steady values which can be derived from the steady NCV. By introducing

$$\chi_T = (\partial ln\bar{S}_b/\partial ln\bar{T}_b)_{\bar{P}_b}$$

and (15)

$$\chi_p = (\partial ln\bar{S}_b/\partial ln\bar{P}_b)_{\bar{T}_b}$$

and making use of Equation (4), the quasi-steady fluctuations in the NCV can be written as:

$$s_b^{(s)} = \chi p_b \quad \text{with} \quad \chi = \chi_p + (\gamma_1 - 1)\chi_T/\gamma_1 \tag{16}$$

The coefficients χ_T and χ_p can be derived experimentally (for χ_T, e.g., see Dugger and Simon,[6] for χ_p, e.g., see Lewis[7]). For a propane/air mixture with maximum NCV, at 300°K we find, e.g., $\chi_T \approx 1.5$ and $\chi_p \approx -0.05$, hence $\chi \approx 0.38$.

Equation (16) represents the fluctuations in the NCV due to slow alterations in temperature and pressure. For fast alterations, however, the combustion process is no longer in equilibrium with the fluctuations in T_b and P_b, in consequence of the inertia of the chemical and physical processes in the flame zone. Even in the steady state the processes in the flame zone are very difficult to analyze, and there does not seem to be much hope of analyzing unsteady processes in the flame zone. The unsteady behavior of the processes in the flame zone will be described by means of a hypothesis due to Grad[8] instead of by exact analysis. According to this hypothesis the rate of change of the NCV is proportional to the difference between the actual and the equilibrium NCV's, thus:

$$\partial S/\partial t = -\{S - S^{(s)}\}/\tau_c \tag{17}$$

where τ_c is the mean time lag in the various chemical and physical processes in the flame zone. If the fluctuations depend exponentially on the time, Equation (17) is again easily solved. It yields

$$s_b = s_b^{(s)}/(1 + \lambda\tau_c) = \chi p_b/(1 + \lambda\tau_c) \tag{18}$$

From Equations (12) and (18) we obtain

$$q_f = (1 - \Lambda_{f,u})u_b + (1 - \Lambda_{f,p})p_b/\gamma_1 \tag{19}$$

where

$$\Lambda_{f,p}(\lambda) = \left(\frac{\tau_f}{\tau} - \frac{\gamma_1\chi}{1 + \lambda\tau_c}\right)\Lambda_{f,u}(\lambda) \tag{20}$$

For later use it is convenient to introduce

$$\begin{aligned}\bar{\imath}_f = \bar{Q}_f/(c_{p,1}\bar{\rho}\bar{T}_b) = \{&(1 - \Lambda_{f,u})\bar{\imath}_b \\ &+ (1 - \Lambda_{f,p})G_M\bar{P}_b\}\bar{Q}_f/(c_{p,1}\bar{m}\bar{T}_b)\end{aligned} \tag{21}$$

where $\bar{\imath}_b$ is the fluctuating volume flow at the exit of the burner port ($= \bar{U}_b A_b$), and G_M a "conductance" defined by

$$G_M = \bar{U}_b A_b/(\gamma_1\bar{P}_b) = A_b M_b/(\bar{\rho}_b a_b)$$

with (22)

$$M_b = \bar{U}_b/a_b$$

In the next section we need also the fluctuating volume flow $\bar{V}_f$. From Equations (9), (11), (18) and (22) we obtain

$$\bar{\imath}_V = \partial V_f/\partial t = \Lambda_{V,u}\bar{\imath}_b - \Lambda_{V,p}G_M P_b \tag{23}$$

where $\Lambda_{V,\,u} = \Lambda_{f,\,u}$, and

$$\Lambda_{V,p}(\lambda) = \left(\lambda\tau_f + \frac{\gamma_1\chi}{1 + \lambda\tau_c}\right)\Lambda_{f,u}(\lambda) \tag{24}$$

Since the transfer functions $\Lambda_{f,p}$ and $\Lambda_{V,p}$ in Equations (21) and (23) respectively occur together with the Mach number, the transfer function $\Lambda_{f,u}$ is the most important one, since in most cases the Mach number is very small.

We conclude this section with some remarks on the experimental verification of the expression for α_f derived above. Neglecting the last two terms at the right-hand side (RHS) of Equation (11), that is, the terms proportional to the Mach number, we obtain for periodic fluctuations ($\lambda = j\omega$):

$$\alpha_f = \frac{1 - j\omega\tau}{1 + (\omega\tau)^2}\,u_b \tag{25}$$

In Appendix II, $\tau^* = \omega\tau$ is calculated and represented, in Figure 6 for constant burning rate and in Figure 7 for constant flow rate. In most cases we have $\bar{U}_b \geqslant 10\ \bar{S}_b$, so that we may write approximately (see Appendix II)

$$\omega\tau \approx \omega r_b/(3\bar{S}_b) \tag{26}$$

Equations (25) and (26) are at least qualitatively in agreement with the experiments of Blackshear.[3] The following quotations from Blackshear's paper make this clear:

"The magnitude α_f was found to depend on $\bar{U}_b$

and the average flow velocity in the cold gases $\bar{U}_b$, and in most cases varied directly as u_b."
"The phasing of α_f with $\bar{U}_b$ was found to depend primarily on the flame speed and, for the conditions studied, appeared independent of the magnitude u_b. In most cases, the phase lag of α_f behind u_b increased as the flame speed decreased."

3. Matching Conditions at the Flame

The matching conditions at the flame are derived from the three conservation laws applied to the volume $V_f + V_f'$ between the cross-sections at x_b and x_2 (Fig. 2), where, e.g., $x_2 - x_b$ may be put equal to the mean height $\bar{h}_f$ of the flame.

Neglecting dissipation by friction, heat conduction, and all the quadratic terms in the Mach numbers, the three conservation laws are given by

$$\rho_b U_b A_b = \rho_2 U_2 A_2 + \frac{\partial}{\partial t} \int_{V_f + V_f'} \rho \, dV \tag{27}$$

$$P_b A_b + P_2(A_2 - A_b) = P_2 A_2 + \frac{\partial}{\partial t} \int_{V_f + V_f'} \rho U \, dV \tag{28}$$

$$c_{p,1} \rho_b T_b U_b A_b + Q_f = c_{p,2} \rho_2 T_2 U_2 A_2 + \frac{\partial}{\partial t} \int_{V_f + V_f'} c_v \rho T \, dV \tag{29}$$

In the momentum Equation (28) it is assumed that the pressure distribution in the volume V_f' is uniform, so that the pressure on the surface $A_2 - A_b$ at x_b is equal to the pressure on the surface A_2 at x_2.

From Equations (27), (28) and (29) we derive that the steady matching conditions are given by

$$\bar{m} = \bar{\rho}_b \bar{U}_b A_b = \bar{\rho}_2 \bar{U}_2 A_2 \tag{30}$$

$$\bar{P}_b = \bar{P}_2 + O(M^2) \tag{31}$$

$$c_{p,1} \bar{m} \bar{T}_b + \bar{Q}_f = c_{p,2} \bar{m} \bar{T}_2 + O(M^2) \tag{32}$$

From Equation (32) we derive

$$B = c_{p,2} \bar{T}_2 / (c_{p,1} \bar{T}_b) = 1 + \bar{Q}_f / (c_{p,1} \bar{m} \bar{T}_b) + O(M^2) \tag{33}$$

where in most cases B is about 3 to 5. From the equation of state of ideal gases, Equation (31), and Equation (33), we derive:

$$\frac{\bar{\rho}_b}{\bar{\rho}_2} = \frac{\gamma_1}{\gamma_2} \frac{\gamma_2 - 1}{\gamma_1 - 1} B \quad \text{and} \quad \frac{a_2}{a_b} = \sqrt{\frac{\gamma_2 - 1}{\gamma_1 - 1} B} \tag{34}$$

Next the matching conditions for the first-order fluctuations have to be derived. According to assumption 3 the volume integrals in Equations (27), (28) and (29) can be calculated for uniform distributions of the temperature, pressure, and velocity throughout the volume $V_f + V_f'$. Furthermore, $V_f + V_f'$ is constant, so that

$$\tilde{v}_V = \partial \tilde{V}_f / \partial t = - \partial \tilde{V}_f' / \partial t \tag{35}$$

From the momentum Equations (28) and (31) it is derived that

$$p_b = p_2 + O(M^2) \tag{36}$$

Next we consider the energy Equations (29) and (32). The density is eliminated from Equation (29) by means of the equation of state of ideal gases, and then yields

$$\frac{\gamma_1}{\gamma_1 - 1} P_b U_b A_b + Q_f = \frac{\gamma_2}{\gamma_2 - 1} P_2 U_2 A_2 + \frac{\partial}{\partial t} \left(\frac{P_b V_f}{\gamma_1 - 1} \right) + \frac{\partial}{\partial t} \left(\frac{P_2 V_f'}{\gamma_2 - 1} \right) \tag{37}$$

From Equation (37) a second equation for the first-order fluctuations is derived. Dividing that equation by $\bar{P}_b \approx \bar{P}_2$ and making use of Equations (21), (23), (30), (34) and (36), we obtain:

$$\tilde{v}_b - \Gamma \tilde{v}_2 + \tilde{v}_f + (\Gamma - 1) \tilde{v}_V = \gamma_1 (B - 1) G_M \tilde{P}_b + \lambda C_f \Gamma \tilde{P}_b \tag{38}$$

where

$$\Gamma = \frac{\gamma_2}{\gamma_1} \frac{\gamma_1 - 1}{\gamma_2 - 1} \tag{39}$$

and

$$C_f = \left(\bar{V}_f' + \frac{\gamma_2 - 1}{\gamma_1 - 1} \bar{V}_f \right) \Big/ (\bar{\rho}_2 a_2^2) \tag{40}$$

The coefficient Γ accounts for the difference between the heat-capacity ratio of the unburned and that of the burned gases. In most cases $\gamma_1 \approx 1.4$, while for the burned gases γ_2 is about 1.2 to 1.3, so that Γ is 1.71 to 1.24. These values show that it is in general not permissible to neglect the difference between γ_1 and γ_2.

C_f represents a "capacity" or "compliance" accounting for the compressibility of the unburned gases in volume V_f and the burned gases in volume V_f'.

As already mentioned at the end of Section 1, a more accurate analysis shows that, at least to the order of approximation, Equations (36) and (38) contain only isentropic acoustic fluctuations. From the Equation of continuity (27) and the matching conditions in Equations (36)

and (38) it can easily be shown to follow that the entropy fluctuations in the volume V_f' are not zero. The entropy fluctuations calculated in this manner are the initial condition or "input" of the entropy mode behind the flames drifting downstream. Since this entropy mode decays pretty soon, it is of no further interest. As a result, Equations (36) and (38) represent the matching conditions for the acoustic vibrations to both sides of the flames, and together with Equation (4) they are sufficient for calculating whether or not sound is produced.

If the matching conditions were derived from the laws of conservation of mass and momentum they would contain acoustic as well as essentially nonisentropic fluctuations, so that they could not be used for matching the acoustic fluctuations to both sides of the flames. This is not realized, e.g., by Blackshear,[3] whose theoretical conclusions are thus not in accordance with Rayleigh's criteria.

4. Characteristic Equation

In order to obtain a general expression for the characteristic equation the concept of impedance or admittance will be introduced. The application of this concept to unsteady flow has many advantages (e.g., see Isakoff[9]), but is not common in regard to flow through industrial equipment, although it is general practice in acoustics (e.g., see Morse[10] or Beranek[11]). The alternating components of the volume flow and pressure are considered as analogous to alternating electric current and alternating voltage respectively. The admittances of the combustion and supply systems are in this paper defined by

$$Y_2(\lambda) = \tilde{v}_2/\tilde{P}_2\,, \qquad Y_b(\lambda) = -\tilde{v}_b/\tilde{P}_b \tag{41}$$

respectively. Dividing Equation (38) by $\tilde{P}_b \approx \tilde{P}_2$ and making use of Equations (21), (23) and (41), we obtain

$$\begin{aligned} &BY_b + \Gamma(Y_2 + \lambda C_f) \\ &= (B - \Gamma)\Lambda_{f,u}Y_b - (B - 1)(\gamma_1 - 1 + \Lambda_p)G_M \end{aligned} \tag{42}$$

where

$$\Lambda_p = \Lambda_{f,p} + (\Gamma - 1)\Lambda_{V,p}/(B - 1) \tag{43}$$

Equation (42) represents the characteristic equation from which the occurrence (or nonoccurrence) of the instability of the combustion can be calculated when the size and shape of the combustion and supply systems are given, that is, when relations for Y_2 and Y_b are known.

In deriving Equation (42) all terms with M^2 have been neglected. In Appendix III it is proved that:

$$Y_k = (Y_k)_{ac} + O(M^2), \qquad (k = b, 2) \tag{44}$$

where $(Y_k)_{ac}$ is the acoustic admittance calculated for $M = 0$. From Equation (44) we see that the admittances occurring in Equation (42) can be calculated according to the conventional acoustic methods. In Equation (42) the terms with G_M represent the first-order effects of the Mach number. Furthermore, terms of the order $Mk\bar{l}_f$ and $k^2\bar{l}_f^2$ have been neglected. The term with C_f represents the first-order effect of the finite flame length. In the limit $M_b = 0$ and $k\bar{l}_f = 0$, the characteristic equation reduces to:

$$BY_b + \Gamma Y_2 = (B - \Gamma)\Lambda_{f,u}Y_b \tag{45}$$

The derivation of the characteristic equation is restricted to one flame. If, however, assumption 4 is satisfied, Equation (42) can also be applied if there is more than one flame on the burner head. In that case A_b is to be defined by the total area of the exits of all the burner ports and V_f by the total volume of all the flames, but $\bar{l}_f$, l_f^*, τ_f, and τ remain the characteristic flame lengths and time lags of one individual flame.

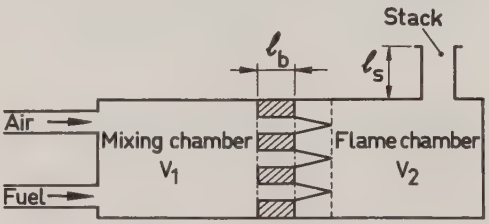

FIG. 3. Diagram of a simple low-frequency model of the flow system consisting of two coupled Helmholtz resonators.

5. Application of the Theory to a Simple Model of the Flow System

The calculation of λ from the characteristic equation is rather tedious. For that reason we will consider a very simple model of the flow system, composed of a mixing chamber with volume V_1, burner ports with length l_b, a flame chamber with volume V_2, and a stack with length l_s (Fig. 3). Even for this simple model the calculations are lengthy, so that we assume in addition that the dimensions of the flow system are small in comparison with the wave length of the gas vibrations. This assumption means that the gases in the volumes V_1 and V_2 are mainly stiffness-controlled, so that the analogous circuit

elements of these volumes are given by capacities:

$$C_i = V_i/(\bar{\rho}_i a_i^2) \qquad (i = 1, 2) \tag{46}$$

If the burner ports and the stack are short and narrow, the gas in these parts of the flow system is mainly mass-controlled and their impedances may be represented by inductances:

$$L_k = \bar{\rho}_k l_{k,e}/A_k \qquad (k = b, s) \tag{47}$$

where $l_{k,e}$ is the effective length of the ports considered. For the derivation of Equations (46) and (47) and formulae for $l_{k,e}$ we refer to the text books on acoustics, e.g., Morse[10] and Beranek.[11]

The occurrence of self-excited vibrations is the result of a balance between the dissipation and delivery of energy by the flames, so that it is not permissible to neglect all the dissipation effects. In first approximation we account only for the dissipation by radiation at the exit of the stack, as is often done in acoustics. In that case we have only to introduce a radiation resistance

$$R_s = -\bar{\rho}_s \lambda^2/(4\pi a_s) \tag{48}$$

for an unflanged open end. The admittance of the combustion system is thus given by:

$$Y_2(\lambda) = \lambda C_2 + \frac{1}{\lambda L_s + R_s} \approx \lambda C_2 + \frac{1}{\lambda L_s} + G_s \tag{49}$$

where for an unflanged open end of the stack

$$G_s = -\frac{R_s}{\lambda^2 L_s^2} = \frac{1}{4\pi} \frac{A_s}{\bar{\rho}_s a_s} \frac{A_s}{l_{s,e}^2} \tag{50}$$

Equation (48) and the RHS of Equation (49) are approximations justified for $\sqrt{A_s} < 0.07\, a_s/f$.

Assuming that the impedance of the feed system is very large, the impedance of the supply system may be approximated by:

$$Y_b(\lambda) = \left\{ \lambda L_b + \frac{1}{\lambda C_1} \right\}^{-1} \tag{51}$$

The assumptions introduced in this section mean that the flow system consists of two coupled Helmholtz resonators with flames between them. Furthermore, we will assume that the Mach number, M_b, is very small, so that the characteristic Equation (42) becomes:

$$B' Y_b + (Y_2 + \lambda C_f) = (B' - 1)\lambda\tau Y_b/(1 + \lambda\tau) \tag{52}$$

where $B' = B/\Gamma$. Upon substitution of Y_2 and Y_b from Equations (49) and (51) respectively in Equation (52), the last-named equation becomes:

$$a_5\lambda^5 + a_4\lambda^4 + a_3\lambda^3 + a_2\lambda^2 + a_1\lambda + a_0 = 0 \tag{53}$$

where

$$\left.\begin{aligned} a_5 &= \tau \\ a_4 &= 1 + \tau G_s/C_2' \\ a_3 &= \tau\{(1 + C_1/C_2')\omega_b^2 + \omega_s^2\} + G_s/C_2' \\ a_2 &= (1 + B'C_1/C_2')\omega_b^2 + \omega_s^2 + \tau\omega_b^2 G_s/C_2' \\ a_1 &= \tau\omega_b^2\omega_s^2 + \omega_b^2 G_s/C_2' \\ a_0 &= \omega_b^2\omega_s^2 , \end{aligned}\right\} \tag{54}$$

C_2' being $C_2 + C_f$, and

$$\omega_b^2 = 1/(L_b C_1) \quad \text{and} \quad \omega_s^2 = 1/(L_s C_2') \tag{55}$$

The flow system is stable with respect to infinitesimal disturbances if the real parts of the roots of Equation (53) are all negative. This is the case if all the determinantal test functions of Hurwitz are positive. According to Frazer and Duncan,[12] instability occurs first when the penultimate test function becomes negative and the coefficient a_0 is positive. In Equation (53) a_0 is positive, so that instability occurs first if:

$$\begin{vmatrix} a_4 & a_5 & 0 & 0 \\ a_2 & a_3 & a_4 & a_5 \\ a_0 & a_1 & a_2 & a_3 \\ 0 & 0 & a_0 & a_1 \end{vmatrix} \leqslant 0 \tag{56}$$

Substituting the coefficients a_i from Equation (54) in Equation (56), we obtain:

$$b_4\epsilon^2\tau^{*4} + b_3\epsilon\tau^{*3} - b_2\tau^{*2} - b_1\epsilon\tau^* + b_0\epsilon^2 \leqslant 0 \tag{57}$$

where dimensionless quantities are introduced in accordance with:

$$\tau^* = \omega_b\tau, \qquad \varphi = C_1/C_2' , \qquad \psi = (\omega_s/\omega_b)^2 ,$$
$$\epsilon = G_s(\omega_b C_2') \tag{58}$$

ϵ is the quality of the equivalent electric circuit representing the dynamic behavior of the combustion system.

The coefficients b_i are given by:

$$\left.\begin{aligned} b_4 &= \varphi\psi \\ b_3 &= (B' - 1)(\varphi + \psi - 1)\varphi\psi + 0(\epsilon^2) \\ b_2 &= (B' - 1)^2\varphi^2\psi + 0(\epsilon^2) \\ b_1 &= (B' - 1)\varphi(B'\varphi + 1 - \psi) + 0(\epsilon^2) \\ b_0 &= B'\varphi \end{aligned}\right\} \tag{59}$$

For $\tau^* = 0$ the penultimate test function is always positive. In that case the other test functions are also positive, so that for $\tau = 0$ the combustion is always stable. From this result we see

that for the occurrence of unstable combustion the time lag τ is very important. For small values of ϵ Equation (57) has a small positive root τ_1^* and a large positive root τ_2^*. Neglecting all

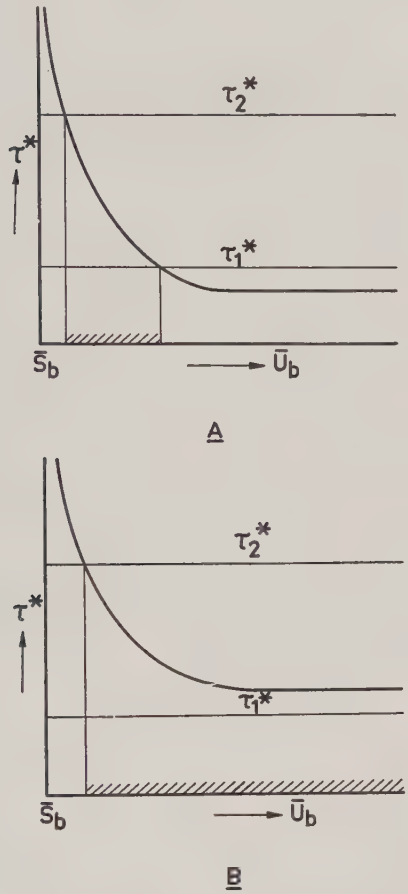

FIG. 4. Instability ranges (hatched) of $\bar{U}_b$ for constant $\bar{S}_b$.

quadratic and higher terms in ϵ, these roots are given by:

$$2(B'-1)\varphi\psi\tau_1^* = \{\psi - 1 - B'\varphi + \sqrt{(\psi-1-B'\varphi)^2 + 4B'\varphi\psi}\}\,\epsilon \tag{60}$$

$$2\tau_2^* = (B'-1)\{1-\varphi-\psi + \sqrt{(1-\varphi-\psi)^2+4\varphi}\}/\epsilon \tag{61}$$

The sign of inequality in Equation (57) indicates the instability range, which appears to be given by:

$$\tau_1^* < \tau^* < \tau_2^* \tag{62}$$

This result means that for given dimensions of the flow system unstable combustion occurs during a certain interval of the time lag τ. Since τ^* depends on the burner load and the NCV, unstable combustion occurs within ranges of the burner load and NCV. This is demonstrated in Figures 4 and 5, use being made of the results derived in the Appendix II. In Figure 4 the instability ranges of $\bar{U}_b$ are plotted for constant $\bar{S}_b$. In Figure 4A the instability range is finite, but in Figure 4B it is infinite. In the latter case it

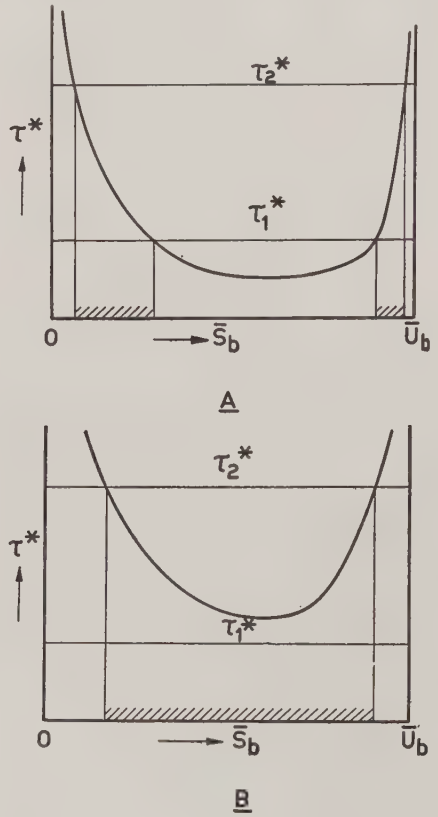

FIG. 5. Instability ranges (hatched) of $\bar{S}_b$ for constant $\bar{U}_b$.

is not possible to eliminate the instability of the combustion by putting higher loads on the burners.

Figure 5 shows the instability ranges of $\bar{S}_b$ for constant $\bar{U}_b$, where in Figure 5A two such instability ranges exist, and in Figure 5B only one. Since the NCV depends on the mixture strength of the cold gases, unstable combustion occurs within some parts of the range of the mixture strength.

6. Concluding Remarks

A more detailed investigation shows that the results of Section 5 are in accordance with Ray-

leigh's two instability criteria. These criteria may be formulated as follows: a necessary (but not sufficient) condition for the occurrence of unstable combustion is that the imaginary part of the impedance of the supply system is positive if this impedance is defined by $Z_b = -\tilde{P}_b/\tilde{\imath}_b$. This criterion is, however, rather rough and not sufficient, e.g., to determine the dependence of the instability boundaries on the burner load and NCV.

At the instability boundaries, the flow system is in resonance. In the example of Section 5 the resonance frequencies at the left-hand instability boundaries of τ^* are determined by:

$$\omega^4 - \{(1 + B'C_1/C_2')\omega_b^2 + \omega_s^2\}\omega^2 + \omega_b^2\omega_s^2 = 0 \quad (63)$$

but at the right-hand instability boundaries by:

$$\omega^4 = \{(1 + C_1/C_2')\omega_b^2 + \omega_s^2\}\omega^2 + \omega_b^2\omega_s^2 = 0 \quad (64)$$

The frequency Equation (63) has two positive roots, ω_1 and ω_2, such that $\omega_1 < \omega_b < \omega_2$. It is easily shown that only for $\omega = \omega_2$ is the imaginary part of Z_b positive, so that unstable combustion sets in at the frequency ω_2 and not at the frequency ω_1. Analogous reasonings apply to Equation (64).

For high frequencies it is no longer allowed to apply the lumped circuit approximation to the flow system. In that case we have to represent Y_2 and Y_b by transmission lines, so that the characteristic equation becomes transcendental. A simple high-frequency model of the flow system has also been investigated. The model considered is that consisting of a mixing tube with a piston for varying its length (l_1), and a flame tube with length l_2. For this configuration it appears that for a given length l_2 unstable combustion occurs during intervals in the value of l_1, and that in such an instability interval the frequency decreases with increasing l_1. These results are at least in qualitative agreement with the experiments of Putnam and Dennis.[2a]

Finally we would remark that in practice the burner ports are generally very hot, so that the unburned gases will take up heat from their walls before combustion sets in. This effect can also be calculated, and changes the formulas for the transfer functions of the flames. It may be concluded from the results of the theory that if the frequencies at which unstable combustion sets in are not too high, the heat transfer in the burner ports will promote unstable combustion.

Appendix I

Consider a tube section of length l. The equation of motion for the first-order fluctuations reads:

$$\frac{\partial P}{\partial x} = -\bar{\rho}\left(\frac{\partial}{\partial t} + \bar{U}\frac{\partial}{\partial x}\right)\tilde{U}, \quad (\text{I}, 1)$$

if $\bar{U}$ is assumed to be independent of x. If all fluctuations are proportional to $\exp(\lambda t)$, integration of the equation of motion from $x = 0$ to $x = l$ yields

$$\Delta P = \tilde{P}_0 - \tilde{P}_l = \bar{\rho}\lambda\int_0^l \tilde{U}dx + \bar{\rho}\bar{U}(\tilde{U}_l - \tilde{U}_0) \quad (\text{I}, 2)$$

Let $|\tilde{U}_m|$ be the upper limit of $|\tilde{U}|$ in $0 \leqslant x \leqslant l$; then we have

$$|\Delta\tilde{P}| \leqslant \bar{\rho}\,|\lambda|\,|\tilde{U}_m|l + 2\bar{\rho}\bar{U}|\tilde{U}_m| \quad (\text{I}, 3)$$

or, with the introduction of the velocity of sound-propagation:

$$|\Delta p| = |\Delta\tilde{P}|/\bar{P} \leqslant \gamma\left(l\frac{|\lambda|}{a} + 2M\right)|\tilde{U}_m|/a \quad (\text{I}, 4)$$

In the vicinity of the instability limits $\lambda \approx j\omega$ and $|\lambda|/a \approx k =$ wave number. According to assumption 1, at most $|\tilde{U}_m| \leqslant \tilde{U}$, so that we may write:

$$|\Delta p| \leqslant \gamma klM + 2\gamma M^2 \quad (\text{I}, 5)$$

Because γ is of the order 1, we obtain finally:

$$|\Delta p| = 0(klM) + O(M^2) \quad (\text{I}, 6)$$

Applying this result to the volume V_f, we conclude that, if, according to assumptions 3 and 10, the Mach number and $k\bar{l}_f$ are considered as small quantities of the first order, $|\Delta p|$ in this volume is of the second order. Equation (4) shows that analogous conclusions hold for the fluctuations in temperature and density.

Appendix II

For a cone-shaped flame on a burner port with circular cross-section we have

$$V_f = \pi r_b^2 h_f/3 \quad (\text{II}, 1)$$

where h_f is the height of the flame cone and r_b the radius of the burner port. From Equations (3) and (II, 1) we obtain

$$\bar{l}_f = \bar{h}_f/3 \quad (\text{II}, 2)$$

Furthermore we have

$$A_f = \pi r_b\sqrt{h_f^2 + r_b^2} \quad \text{and} \quad \bar{A}_f = \pi r_b^2\bar{U}_b/\bar{S}_b \quad (\text{II}, 3)$$

where the second equality follows from Equation (7). From Equations (II, 2) and (II, 3) we obtain

$$\bar{l}_f = \tfrac{1}{3} r_b \sqrt{(\bar{U}_b/\bar{S}_b)^2 - 1} \qquad \text{(II, 4)}$$

In order to calculate V_f the variable flame height h_f must be eliminated from (II, 1) and (II, 3):

$$V_f = \tfrac{1}{3}\pi r_b^3 \sqrt{(A_f/A_b)^2 - 1} \qquad \text{(II, 5)}$$

From the last equation and Equation (9) we derive

$$\bar{V}_f = \tfrac{1}{3} r_b \bar{A}_f \bar{A}_f / (\bar{A}_f^2 - A_b^2)^{\frac{1}{2}} = l_f^* \bar{A}_f \,. \qquad \text{(II, 6)}$$

The last equation and Equation (II, 3) yield

$$l_f^* = \tfrac{1}{3} r_b \{1 - (\bar{S}_b/\bar{U}_b)^2\}^{-\frac{1}{2}} \qquad \text{(II, 7)}$$

The time lags τ_f and τ defined by Equations (3) and (9) respectively can now be calculated from Equations (II, 4) and (II, 7):

$$\tau = \frac{r_b}{3\bar{S}_b} \{1 - (\bar{S}_b/\bar{U}_b)^2\}^{-\frac{1}{2}} \qquad \text{(II, 8)}$$

$$\tau_f = \tau\{1 - (\bar{S}_b/\bar{U}_b)^2\} \qquad \text{(II, 9)}$$

As a function of $\bar{U}_b$, Equation (II, 8) may be written as

$$\tau^* = \omega\tau = b_S\{1 - (\bar{S}_b/\bar{U}_b)^2\}^{-\frac{1}{2}} \quad \text{with} \quad b_s = \omega r_b/3\bar{S}_b \qquad \text{(II, 10)}$$

and as a function of $\bar{S}_b$ as

$$\tau^* = \omega\tau = b_U \frac{\bar{U}_b}{\bar{S}_b} \{1 - (\bar{S}_b/\bar{U}_b)^2\}^{-\frac{1}{2}} \quad \text{with } b_U = \omega r_b/3\bar{U}_b \qquad \text{(II, 11)}$$

In Figure 6, Equation (II, 10) is represented for some values of b_S, and in Figure 7, Equation (II, 11) is represented for some values of b_U. In most cases $\bar{U}_b \geqslant 10\,\bar{S}_b$, so that practically speaking $\tau^* \approx b_S$.

This should coincide with the time lag which Putnam and Dennis suggest exists for premixed flames on narrow burner ports, but the transfer function derived here differs from that of Putnam and Dennis in that according to it there is not only a time lag between q_f and u_b, but also a weakening.

For a slit burner the same formulae hold if $r_b/3$ is replaced by $d_b/2$, where d_b denotes the breadth of the burner slit.

In deriving Equations (II, 8) and (II, 9) it has been assumed that the flame retains its shape during the vibrations, that is, that no distortion of the flame cone occurs. However, many experiments have shown that the flame cone is distorted during the vibrations (e.g., see Blackshear[3] and Putnam and Dennis[13]). It may be remarked that the distortion observed may be a result of non-linear and linear effects, since the experiments

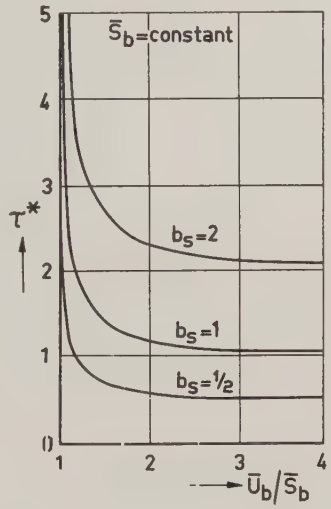

FIG. 6. Reduced time lag τ^* as function of $\bar{S}$ for constant $\bar{U}_b$.

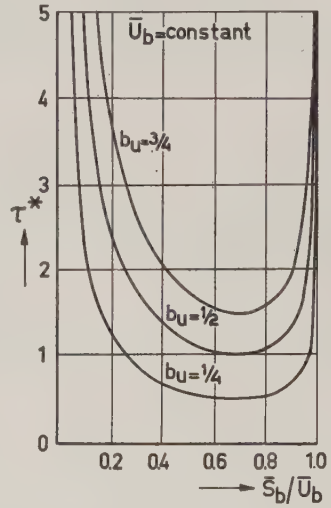

FIG. 7. Reduced time lag τ^* as function of $\bar{U}_b$ for constant $\bar{S}_b$.

deal with vibrations beyond the instability limits, outside which the amplitudes of the vibrations are no longer small. In the theoretical investigation above we are only interested in linear effects, since this theory deals only with the calculation of the instability limits, where the amplitudes of the vibrations are assumed to be small. The linear distortion may become important when it

is necessary to explain theoretically the occurrence of flame-driven oscillations, since it changes the relation for l_f^* derived above. Linear distortion has not as yet been investigated theoretically, but it may well prove to be caused by several mechanisms, e.g., nonhomogeneous distribution of pressure in the neighborhood of the flames, the flow conditions near the rim of the burner ports, and intrinsic instability of the flame front. The first mechanism is ruled out by assumptions 3 and 10, and the second mechanism would violate assumption 9. However, these assumptions are too rough to be of use in a more detailed investigation of the phenomena concerned in the nonsteady behavior of the flame front. For the time being Equation (II, 7) can be used for an elementary explanation of the occurrence of flame-driven oscillations especially as it leads to conclusions which are at least qualitatively in agreement with those derived from Blackshear's experiments.

Appendix III

Let us consider the one-dimensional propagation of an acoustic wave in a tube. If one neglects all terms of the second and higher orders and assumes that the mean motion is independent of x, the equations of motion and continuity read

$$\bar{\rho}\frac{d\tilde{U}}{dt} + \frac{\partial \tilde{P}}{\partial x} = 0 \text{ (a)}, \qquad \frac{d\tilde{\rho}}{dt} + \bar{\rho}\frac{\partial \tilde{U}}{\partial x} = 0 \text{ (b)} \tag{III, 1}$$

where $d/dt = \partial/\partial t + \bar{U}\partial/\partial x$. Since only the propagation of the isentropic acoustic wave is considered, we have also

$$\tilde{P} = a^2\tilde{\rho}. \tag{III, 2}$$

Introducing the sound velocity potential Φ, we have:

$$\tilde{U} = \frac{\partial \Phi}{\partial x} \text{ (a)}, \qquad \tilde{P} = -\bar{\rho}\frac{d\Phi}{dt} \text{ (b)} \tag{III, 3}$$

where Equation (III, 3b) follows from Equations (III, 1a) and (III, 3a). From Equations (III, 1b), (III, 2) and (III, 3) the wave equation is obtained

$$\frac{\partial^2\Phi}{\partial x^2} - \frac{1}{a^2}\frac{d^2\Phi}{dt^2} = 0 \tag{III, 4}$$

Putting Φ proportional to $\exp(\lambda t)$, we obtain from Equation (III, 4)

$$\Phi = [D_+e^{-\kappa+x} + D_-e^{-\kappa-x}]e^{\lambda t} \tag{III, 5}$$

where the + sign refers to a wave propagating to the right (R-wave) and the − sign to a wave propagating to the left (L-wave), and

$$\kappa_+ = \frac{\lambda/a}{1+M}, \qquad \kappa_- = \frac{\lambda/a}{1-M} \tag{III, 6}$$

From Equations (III, 3) and (III, 5) we get

$$\tilde{P}_+/\tilde{U}_+ = -\tilde{P}_-/\tilde{U}_- = \bar{\rho}a \tag{III, 7}$$

where $\bar{\rho}a$ represents the wave impedance of the fluid in the tube. The pressure at some point x is given by the sum of the pressures caused by the R- and the L-waves, so that

$$\begin{aligned}\bar{P}(x) &= \tilde{P}_+(x) + \tilde{P}_-(x) \\ &= D[e^{\kappa+(l)-x)} + Ne^{-\kappa-(l-x)}]e^{\lambda t}\end{aligned} \tag{III, 8}$$

where D is some constant, l the length of the tube, and N the reflection coefficient of the wave at the output impedance of the tube. From Equations (III, 7) and (III, 8) we get

$$\begin{aligned}\tilde{U}(x) = \tilde{U}_+(x) + \tilde{U}_-(x) = \frac{D}{\bar{\rho}a}[e^{\kappa\cdot(l-x)} \\ - Ne^{-\kappa-(l-x)}]e^{\lambda t}\end{aligned} \tag{III, 9}$$

At $x = l$ the ratio between the fluctuations in pressure and velocity is determined by the output impedance of the tube, so that this ratio is considered as a known quantity. From Equations (III, 8) and (III, 9) we get for $x = l$

$$z(l) = \tilde{P}(l)/\tilde{U}(l) = \bar{\rho}a\frac{1+N}{1-N} \tag{III, 10}$$

where $z(l)$ is the specific impedance of the tube at $x = l$. The specific input impedance of the tube at $x = 0$ is now easily obtained from Equations (III, 8), (III, 9) and (III, 10). The result is

$$z(0) = \tilde{P}(0)/\tilde{U}(0)$$

$$\bar{\rho}a = \frac{z(l) + \bar{\rho}a\tanh(\kappa l)}{\bar{\rho}a + z(l)\tanh(\kappa l)} \tag{III, 11}$$

where

$$\kappa = \tfrac{1}{2}(\kappa_+ + \kappa_-) = \frac{\lambda/a}{1-M^2} \tag{III, 12}$$

If it is assumed that the flows in the supply and combustion systems are essentially one-dimensional, we can derive the impedances at both sides of the flames from Equation (III, 11). This equation and Equation (III, 12) show that, if terms quadratic or higher in the Mach number are neglected, the impedances can be calculated for

$M = 0$, that is, according to the conventional acoustic methods. This is also confirmed by Carrier,[14] who shows that the influence of the Mach number on the impedance of an open end of a tube is also of the second order, and that furthermore Equations (III, 11) and (III, 12) are in accordance with the calculations of Truman and Lipstein[15] concerning the resonance frequencies of an open-ended tube for $M \neq 0$.

In the low-frequency region we may put $|\kappa l| \ll 1$, so that $\text{th}(\kappa l) \approx \kappa l$. If we put $|z(l)| = 0$ or very small, Equation (III, 11) represents a specific conductance, and for $|z(l)| = \infty$ Equation (III, 11) represents a specific capacity.

Nomenclature

a_k velocity of sound-propagation in gas of temperature T_k
A cross-sectional area
A_f flame area
B $c_{p,2}\overline{T}_2/c_{p,1}\overline{T}_1$
c_p specific heat for constant pressure
c_v specific heat for constant volume
C capacity
d_b breadth of opening of slit burner
f frequency
G conductance
G_M $A_b M_b/\bar{\rho}_b a_b$
h_f height of the flame
H caloric value of the combustible gas mixture
i volume flow $= UA$
j $\sqrt{-1}$
k wave number
l length
L inductance
m burner load
M Mach number $= \bar{U}/a$
P pressure
p dimensionless fluctuations in pressure $= \tilde{P}/\bar{P}$
Q_f heat released by the flame per unit time
q_f dimensionless fluctuations in heat release $= \tilde{Q}_f/\bar{Q}_f$
R resistance
S_k normal combustion velocity at temperature T_k and pressure P_k
s_k dimensionless fluctuations in normal combustion velocity $= \tilde{S}_k/\bar{S}_k$
t time
T temperature (°K)
U axial component of velocity in tube
u dimensionless fluctuations in axial velocity $= \tilde{U}/\bar{U}$
V volume
v dimensionless fluctuations in volume $= \tilde{V}/\bar{V}$
x co-ordinate along tube axis
Y admittance
Z impedance $= 1/Y$
z specific impedance $= ZA$
α_f dimensionless fluctuations in flame area $= \tilde{A}_f/\bar{A}_f$
γ specific heat ratio $= c_p/c_v$
ϵ quality of lumped circuit
ϑ dimensionless fluctuations in temperature $= \tilde{T}/\bar{T}$
κ complex wave number
λ characteristic value
Λ transfer function
ν kinematic viscosity of the gas
ρ density
σ dimensionless fluctuations in density $= \tilde{\rho}/\bar{\rho}$
τ time lag
τ^* reduced time lag $= \omega\tau$
φ ratio of capacities $= C_1/C_2'$
Φ sound velocity potential
ψ ratio of Helmholtz frequencies $= (\omega_s/\omega_b)^2$
χ_p pressure coefficient of NCV
χ_T temperature coefficient of NCV
ω circular frequency $= 2\pi f$

SUBSCRIPTS

1 unburned gases, mixing chamber
2 burned gases, flame chamber
b burner port or exit of burner port
f flame cone
f, 1 just before the flame front
s stack
k general index denoting one of the 6 indices above

SUPERSCRIPTS

s quasi-steady fluctuations or quasi-steady part of transfer function
$\bar{w}$ steady part of quantity w
$\tilde{w}$ fluctuating part of quantity w

ABBREVIATIONS

NCV normal combustion velocity
LHS left-hand side
RHS right-hand side

REFERENCES

1. Rayleigh, Lord: *The Theory of Sound*, Ed. 2. London, McMillan and Co., 1937.
2. Putnam, A. A., and Dennis, W. R.: (a) Trans. Am. Soc. Mech. Engrs., *75*, 15 (1953); (b) *Fourth Symposium (International) on Combustion*, p. 566. Baltimore, The Williams & Wilkins Co., 1953; (c) J. Acoust. Soc. Am., *26*, 716 (1954); (d) Trans. Am. Soc. Mech. Engrs., *77*, 875 (1955); (e) J. Acoust. Soc. Am., *28*, 246, 260 (1956).
3. Blackshear, P. L.: *Fourth Symposium (International) on Combustion*, p. 553. Baltimore, The Williams & Wilkins Co., 1953.

4. Kaskan, W. E.: *Fourth Symposium (International) on Combustion*, p. 575. Baltimore, The Williams & Wilkins Co., 1953.
5. Neumark, J. I., and Aronovitsch, G. V.: J. Exptl. & Theoret. Phys., *5*, 567 (1955) (in Russian).
6. Dugger, G. L., and Simon, D. L.: *Fourth Symposium (International) on Combustion*, p. 336. Baltimore, The Williams & Wilkins Co., 1953.
7. Lewis, B.: Selected Combustion Problems, p. 176. AGARD. London, Butterworths Sci. Publ., 1954.
8. Grad, H.: Comm. Pure & Appl. Math., *2*, 79 (1949).
9. Isakoff, S. E.: Ind. Eng. Chem., *77*, 413 (1955).
10. Morse, P. M.: *Vibrations and Sound*, Ed. 2. New York, McGraw-Hill Book Co., 1948.
11. Beranek, L. L.: *Acoustics*. New York, McGraw-Hill Publ. Co., 1954.
12. Frazer, R. A., and Duncan, W. J.: Proc. Roy. Soc., London, *A124*, 642 (1929).
13. Putnam, A. A., and Dennis, W. R.: Am. Soc. Mech. Engrs., Paper no. 55-SA-48, presented at 1955 Semi-annual Meeting.
14. Carrier, G. F.: Quart. Appl. Math., *13*, 457 (1956).
15. Truman, J. C., and Lipstein, N. J.: J. Aero. Sci., *20*, 846 (1953).

63

THE GROWTH OF DISTURBANCES IN A FLAME-GENERATED SHEAR REGION[a]

By PERRY L. BLACKSHEAR, JR.

Introduction

This paper describes a study of the growth of disturbances in a flame-generated shear region. The reasons for this work are two-fold:

(1) To shed light on the mechanism whereby the flame zone can amplify incoming turbulence.

(2) To find a way to realize the beneficial effect that burner resonance has on heat-release rates without the destructive effects that usually accompany such resonance.

Scurlock[1] has suggested that when a flame is anchored in a duct the turbulence that has the major effect on flame propagation is not that in the incoming flow but that which arises within or near the anchored flame zone. Markstein[2] has shown that the plane combustion wave is unstable under certain conditions and that such instability must be considered in formulating a theory of turbulent flame propagation.

One way of studying instabilities due to a baffle flameholder has been suggested by the work of Haddock[3] and Zukoski and Marble.[4] They showed that transition to turbulence in the flameholder boundary layer has an effect on both the flameholding process and the flame appearance. There is reason to believe that elements of the stability analyses for attached and free boundary layers may be found useful in predicting turbulent flame speeds in the near wake of the flameholder.

Further downstream of a baffle flameholder the flow is unstable, owing to the rapid acceleration of the hot gas in the core of the combustor. The velocity profile for this region was first calculated by Scurlock.[1] In the analysis part of the present paper a stability analysis is made on an idealization of the profile calculated by Scurlock.

In the experimental part of this paper an anchored "V" flame is disturbed by acoustic disturbances in such a way that transverse velocity components are present in the flame zone. The frequencies at which these transverse velocity components are amplified have been determined and compared with the results of the analysis. A comparison between analysis and experiment is also made of the phase velocity at which a disturbance moves along the flame front.

Both the analysis and experiment suggest that in many practical applications the heat release rate of a flame in a duct can be improved by supplying disturbances that a flame zone can amplify.

Analysis

In order to formulate and solve the stability problem of a flame in a duct a number of simplify-

[a] An abbreviation of a doctoral thesis at Case Institute of Technology under Professor Harold G. Elrod.

ing assumptions have been made. The most important assumption is the neglect of viscosity. Lin[5] and Pillow[6] have summarized the limitations of the inviscid analysis. In brief, we can learn something about the frequencies which a profile can amplify through an inviscid analysis only when the profile has an inflexion point. Fortunately the profile for the flame in a duct has a point of inflexion.

The profile studied is shown in Figure 1. Scurlock[1] showed that a profile similar to the one in Figure 1 arose when a flame was anchored in a duct. He found a hot-gas profile composed of slightly convex segments instead of straight-line segments. Tsien[7] found that if he assumed the profile to be as shown in Figure 1, and calculated the relationships between U^*/U_0, U_1/U_0, F, and h_2/h_1, the results obtained were in excellent agreement with Scurlock's results—which were obtained from fairly involved stepwise calculations.

In the present work the idealization employed by Tsien and shown in Figure 1 is used in calculating the steady-state profile and in the stability analysis. The details of the analysis can be found in Blackshear's work.[8] In the following paragraphs are listed the assumptions and key relationships employed in the analysis.

Assumption: The fluid is assumed incompressible, inviscid and non-heat conducting; gravity is neglected. The mean flow normal to the axis of the two-dimensional test section is assumed negligible.

The steady state results of Tsien include:

APEX VELOCITY

$$\frac{U^*}{U_0} = \sqrt{\left[1 + \frac{\rho_1}{\rho_2}\left(\frac{U_1}{U_0}\right)^2 - 1\right]} \tag{1}$$

HOT-GAS VELOCITY DISTRIBUTION

$$\frac{U}{U_0} = \sqrt{1 + \frac{\rho_1}{\rho_2}\left[\left(\frac{U_1}{U_0}\right)^2 - 1\right]} - \left\{\sqrt{1 + \frac{\rho_1}{\rho_2}\left[\left(\frac{U_1}{U_0}\right)^2 - 1\right]} - \frac{U_1}{U_0}\right\}\frac{y}{h_2} \tag{2}$$

FLAME WIDTH

$$\frac{h_2}{h_1} = \frac{\dfrac{U_1}{U_0} - 1}{\left(1 - \dfrac{1}{2}\dfrac{\rho_2}{\rho_1}\right)\dfrac{U_1}{U_0} - \dfrac{1}{2}\dfrac{\rho_2}{\rho_1}\sqrt{1 + \dfrac{\rho_1}{\rho_2}\left[\left(\dfrac{U_1}{U_0}\right)^2 - 1\right]}} \tag{3}$$

FRACTION BURNED

$$F = 1 - \frac{U_1}{U_0}\left(1 - \frac{h_2}{h_1}\right) \tag{4}$$

Assuming the flame to spread so slowly that the flow may be treated as parallel, the disturbance equation derived by Goldstein[9] may be used.

$$(U - c)\left(\frac{\partial^2 v'}{\partial y} - \alpha^2 v'\right) - v'\frac{\partial^2 U}{\partial y^2} + \frac{1}{\bar{\rho}}\frac{d\bar{\rho}}{dy}\left[(U - c)\frac{\partial y'}{\partial y} - v'\frac{\partial U_0}{\partial y}\right] = 0 \tag{5}$$

In deriving Equation (5) from the continuity and momentum equations, the first-order disturbance quantities $p'u'$, v', ρ' have been assumed to vary as $e^{i\alpha(x-ct)}$ times some function of y.

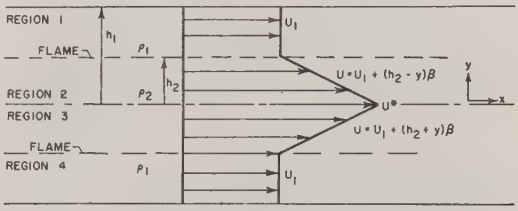

FIG. 1. Geometry of flow field.

It is easily seen that in between the corners in the profile of Figure 1, Equation (5) reduces to

$$\frac{\partial v'}{\partial y^2} - \alpha^2 v' = 0 \tag{6}$$

Solutions of Equation (6) for the four regions of Figure 1 are connected across the corners in the profile by requiring that Equation (5) hold across the corners (see Rayleigh[10]), and requiring that v' be continuous at the corners. These conditions plus the requirement that v' vanish at the walls gives eight equations in the eight unknowns A_1, $A_2 \cdots D_1$, D_2. These unknowns are the constants in the solutions of Equation (6)

$$\left.\begin{aligned} v_1' &= A_1 e^{\alpha y} + A_2 e^{-\alpha y} \\ v_2' &= B_1 e^{\alpha y} + B_2 e^{-\alpha y} \end{aligned}\right\} \tag{7}$$

etc., that apply to each of the four regions of Figure 1. The requirement that there be non-trivial solutions for these eight unknowns results in a determinantal equation that yields the relations between c, α, h_2/h_1 which we seek. If c is expressed as a function of α, h_2/h_1, there result three roots of c, one wholly real and two complex. Because the disturbance was expressed as $\sim e^{i\alpha(x-ct)}$, the real part of c corresponds to a

phase velocity c_r and the quantity αc_i corresponds to an amplification rate; *i.e.*, the $v' \sim e^{\alpha c_i t} e^{i\alpha(x-c_r t)}$.

The wholly real root corresponds to a disturbance that is symmetric to the duct axis; the complex solutions correspond to a damped and an amplified antisymmetric disturbance. Only the solution with the positive imaginary part, *i.e.*, the amplified antisymmetric disturbance, is considered. The amplification rate αc_i is most conveniently expressed by the parameter

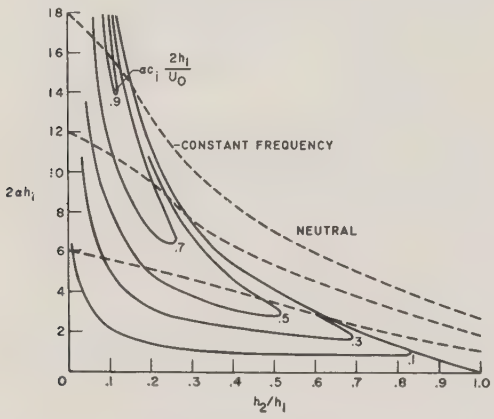

FIG. 2. Stability map for Scurlock's flow. Contours of constant amplification rate αc_i are given by lines of constant $\alpha c_i \frac{2h_1}{U_0}$. Lines of constant frequency show the path a given disturbance originating at flameholder takes as it propagates along flame zone at phase velocity c_r. $\rho_1/\rho_2 = 7$.

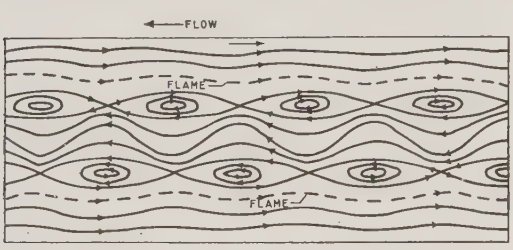

FIG. 3. Streamlines of a neutral disturbance as seen by observer moving at phase velocity c_r.

$$\alpha c_i \frac{2h_1}{U_0} = \frac{\left(\frac{U}{U_0} - \frac{U_1}{U_0}\right)\alpha h_1}{\frac{h_2}{h_1}} \qquad (8)$$

$$\sqrt{\left[\frac{\frac{h_2}{h_1} + \frac{n}{m}\frac{\rho_1}{\rho_2}\left(\mu\frac{h_2}{h_1} - \frac{1}{\alpha h_1}\right)}{\frac{n}{m}\frac{\rho_1}{\rho_2}\mu + 1}\right]^2 - 4\frac{\mu\frac{h_2}{h_1} - \frac{1}{\alpha h_1}}{\frac{n}{m}\frac{\rho_1}{\rho_2}\mu + 1}\frac{1}{\alpha h_1}}$$

for the region where the quantity under the radical is negative.

The phase velocity c_r is most conveniently expressed by

$$\frac{\frac{c_r}{U_0} - \frac{U_1}{U_0}}{\frac{U^*}{U_0}\frac{U_1}{U_0}} = \frac{1}{2\frac{h_2}{h_1}}\left\{\frac{h_2}{h_1} + \frac{n}{m}\frac{\rho_1}{\rho_2}\left(\mu\frac{h_2}{h_1} - \frac{1}{\alpha h_1}\right)\right. \qquad (9)$$

$$\left. + \sqrt{\left[\frac{\frac{h_2}{h_1} + \frac{n}{m}\frac{\rho_1}{\rho_2}\left(\mu\frac{h_2}{h_1} - \frac{1}{\alpha h}\right)}{\frac{n}{m}\frac{\rho_1}{\rho_2}\mu + 1}\right]^2 - \frac{4\left(\mu\frac{h_2}{h_1} - \frac{1}{\alpha h_1}\right)}{\frac{n}{m}\frac{\rho_1}{\rho_2}\mu + 1}}\right\}$$

where the radical is neglected unless real.

For a disturbance of given frequency that propagates along the flame front at phase velocity c_r the local wave number α is related to the wave number at the flameholder α_0 by

$$\alpha = \alpha_0 \frac{U_0}{c_r} \qquad (10)$$

Frequency f is related to α_0 by $f = (\alpha_0 U_0/2\pi)$.

Equations (1), (3), (8), (9), and (10) have been used to construct a stability map of the profile studied. The map shown in Figure 2 is for $\rho_1/\rho_2 = 7$. It consists of contours of constant amplification rate parameter $\alpha c_i(2h_1/U_0$ and constant frequency on a $2\alpha h_1$ (the dimensionless wave number) *vs* h_2/h_1 (the dimensionless flame width) grid. This map can be used to follow the amplification history of a disturbance of given frequency as it propagates from the flameholder to the station where $h_2/h_1 = 1$. These results are general in that they do not rely on a mode or rate of flame spreading. If we wish to find what frequency will possess the maximum over-all amplification, we must make an additional assumption. The following paragraphs are devoted to claryifying the reasons for making this assumption.

Figure 3 presents a qualitative picture of the nature of the disturbances propagating at phase velocity. The streamline distributions are given for a neutral disturbance in a reference plane moving at the phase velocity c_r so that the streamlines are no longer a function of time. There is motion relative to the "cat's eyes" of the disturbance centers. In the hot flame core, the gas moves faster than c_r; in the colder gas, outside the flame, the gas moves slower than c_r.

To picture what happens to an amplified disturbance, imagine the y-amplitude of the wrinkles

in Figure 3 to be growing from right to left. In addition, the flame width is increasing gradually, c_r is also increasing gradually, and, therefore, the x- and y-spacing of the "cat's eyes" is increasing in the direction of flow until a neutral situation is reached.

At each x-station the disturbance will have a local growth rate αc_i that acts over a short time, say Δt. Then (since x is related to time by $dx = c_r dt$) at any time t after the disturbance originated at the flameholder, the amplitude will be

$$v' = v_0' \exp \int_0^t \alpha c_i \, dt \tag{11}$$

where v_0' is the amplitude of the disturbance at the flameholder on the centerline of the profile.

Up to this point, the independent variables have been the dimensionless wave number $2\alpha h_1$ and flame width h_2/h_1. In order to evaluate Equation (11), it is necessary to use the relationship

$$\frac{dx}{dt} = c_r \tag{12}$$

and some assumption concerning the variation of h_2/h_1 with x. Two simple assumptions were examined:

(1) Flame front is linear with x; $(dh_2/dx) = K_1$.

(2) Combustion efficiency is linear with x; $(dF/dx) = K_2$.

The results of these two assumptions are substantially the same:

(1) The frequency that has the maximum amplification, v'/v_0', is independent of the rate or mode of flame spreading and is approximately $f = U_0/2h_1$ corresponding to a value of $2\alpha_0 h_1 = 6$.

(2) The magnitude of amplification is dependent upon the rate of flame spreading. For example: In the case of the linear flame front the amplification $v'/v_0' = (1/g^{dh_1/dx})$ where g is a function of $2\alpha_0 h_1$ and h_2/h_1 and is given in Figure 4. For the case of $2\alpha_0 h_1 = 6$, $(h_2/h_1) > 0.65$; $(v'/v_0') = 8$ for $(dh_2/dx) = (1/20)$; $(v'/v_0') = 14{,}000$ for $(dh_2/dx) = (1/100)$.

It can be seen that at values of $0 < (h_2/h_1) < 0.65$ the frequency of the disturbance that has been amplified the most will be a function of h_2/h_1. To put it another way, a given frequency less than the one corresponding to $2\alpha_0 h_1 = 6$ will at some value of h_2/h_1 have a locally higher amplification than all other frequencies. The locus of this maximum will be between the h_2/h_1 for maximum amplification rate and h_2/h_1 for neutral stability. These limiting values of h_2/h_1 are shown in Figure 5.

Owing to the fact that the disturbance v' maximizes at the center of the duct and vanishes at the wall, the neutral disturbance will undergo an apparent decay as the flame approaches the wall. Thus for any frequency the disturbance v' at the flame front will have its maximum value

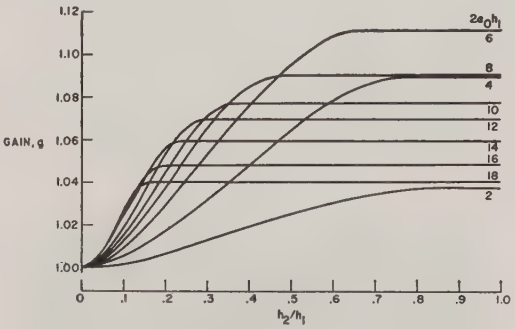

FIG. 4. Gain g as function of h_2/h_1 for a family of initial wave numbers $2\alpha_0 h_1$. $\rho_1/\rho_2 = 7$.

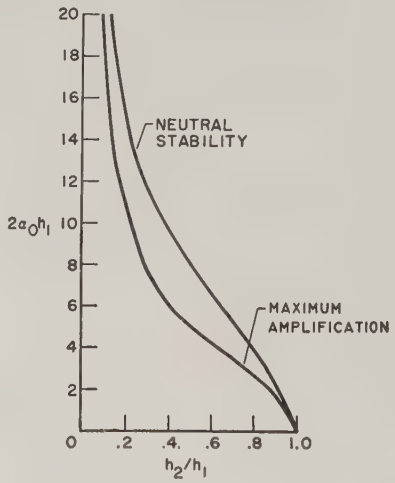

FIG. 5. Frequencies that give maximum increase in local flame speed. $\rho_1/\rho_2 = 7$.

somewhere between the two curves shown in Figure 5.

Experimental

APPARATUS

Figure 6 shows a sketch of the two-dimensional test section employed. The combustible mixture of propane and air is metered by conventional means and quieted in an 8-in. diameter plenum chamber, passing through 6 banks of 200-mesh screens, then through a nozzle plate into the

rectangular test section that is either ½ by 2 by 12 in. or 1 by 2 by 12 in.

The flame is anchored on a V-gutter flameholder which is supported by a hollow blade that

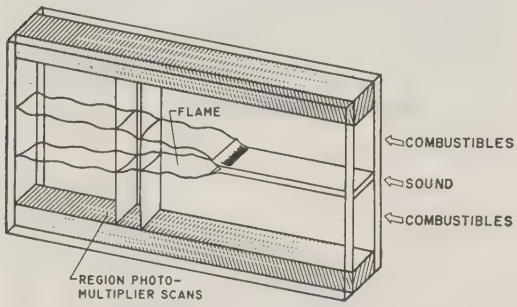

FIG. 6. Test section.

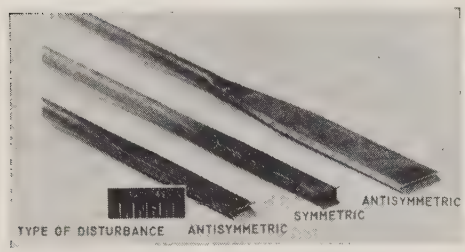

FIG. 7. Flameholders.

TABLE 1. TURBULENCE INTENSITY AND SCALE FOR SEVERAL POSITIONS AND FLOW VELOCITIES

Nominal Velocity	Distance from Nozzle Lip, x	Distance from Top Wall, y	Vertical Distance from Station, z	Turbulence Component, u'	Scale, Lx
ft/sec	*in.*	*in.*	*in.*	*ft/sec*	*in.*
50	0	½ *	¼	0.306	
100	0	½	¼	0.420	
50	6	⅛	¼	1.38	0.2
50	6	⅛	⅛	1.68	
50	6	¼	¼	0.818	0.15
50	6	¼ †	⅛	0.978	
50	6	½	¼	1.021	0.15
50	6	¾	¼	3.35	0.17
100	6	⅛	¼	2.44	

* Measured from centerline.

† Measured from flameholder lip.

extends upstream, through the plenum to a loud speaker. Standing sound waves are excited in the hollow blade and the sound is permitted to issue through slots in the flameholder. Asymmetric disturbances are furnished by cutting the slots in the blade just upstream of one edge of the gutter. Symmetric disturbances are furnished by cutting the slots in the center of the flameholder. Some of the flameholders employed are shown in Figure 7.

A probe was constructed that permitted a photomultiplier tube to scan a ¼-in. slit spanning the test section. The distance from phototube to test section was 2 ft.

The velocity profile entering the duct was flat to within 1 per cent as near to the walls as a $\frac{1}{32}$-in. diameter probe permitted measurements. Transition to turbulence occurred at a Reynolds number of 25,000, where the distance is measured in direction of flow from the plane of the nozzle. Spectra measurements were made of the turbulence at several stations and a scale L_x assigned, using the method employed by Mickelsen and Lawrence,[11] and Roshko.[12] These measurements are summarized in Table 1.

PROCEDURE

The disturbance amplitude was measured by placing a hot-wire anemometer over the sound port. The signal needed at the speaker to give the required u' at the port was determined for the various frequencies and flow velocities investigated. The effect of the disturbances on the flame was recorded as an effect on the S_T/S_L. S_T/S_L is herein defined as the ratio of the rate of change in combustion efficiency per unit length to the rate of change that would occur if the flame fronts were laminar. Two ways of sensing this quantity were employed:

(1) Momentum pressure drop measurements with the analytical results of Scurlock[1] give an average S_T/S_L for the entire flame.

(2) Radiation measurements made with a photomultiplier probe give local S_T/S_L.[13]

Two ways of calibrating the photomultiplier probe were employed:

(1) The probe scanned a laminar flame in the test section, fixing a voltage V_L proportional to S_L.

(2) The probe scanned the test section at a series of stations and an average voltage was obtained that is proportional to the fraction burned as found by measuring the momentum pressure drop.

Then in both cases $S_T/S_L = V_T/V_L$ where V_T and V_L are the voltages indicated by the photomultiplier probe for turbulent and laminar flames. The calibration consists of finding the value of V_L for a given f/a. Figure 8 shows the comparisons of fraction burned (obtained from momentum ΔP calculations) and average voltages read from the photomultiplier probe.

From this data an average value of F/V_T for each f/a is obtained. Then from

$$\frac{F}{V_T} = \frac{2S_T \times \text{length} \times \text{depth}}{U_0 \times \text{height} \times \text{depth} \times V_T}$$

(where length, height, and depth are dimensions of the combustor) a value of S_T/V_T is calculated.

If we employ an S_L value from the literature, then V_L can be calculated from $V_L = (S_L/S_T/V_T)$. In Table 2 are tabulated values of flame speed from Dugger's[14] S_L, the value of V_L calculated from the preceding relationship, and the range of V_L measured directly by viewing a pair of laminar flames in the test section.

RESULTS

The values of S_T/S_L obtained by the method just discussed are compared with Scurlock's S_T/S_L values[15] in Figure 9. The relatively high values of S_T/S_L obtained in the present work are probably due to the relatively low value of S_T/U_0 employed. The slopes, with one exception, seem to agree.

A comparison of the flame appearance and S_T/S_L distribution with and without disturbances is given in Figures 10a and 10b for two flameholder sizes. The flame is seen to be turbulent before the introduction of the disturbances, and it is distorted in a gross fashion by the disturbances. Figure 11 shows the appearance of the flame when the approach flow was substantially turbulence-free, the boundary layer transition occurring downstream of separation. The values of S_T/S_L varied but little from those shown for the smaller flameholder in Figure 10a. The flame appearance also remains substantially unchanged.

Effect of frequency of imposed disturbances

Figure 12 shows the effects on S_T/S_L of frequency f and distance x at a typical condition. If for these conditions we calculate the h_2/h_1 that corresponds to the values of x and find the range of h_2/h_1 over which a particular frequency gives the greatest S_T/S_L, we may compare the results with Figure 5 where the frequencies for maximum amplification of v' were given as functions of h_2/h_1. Such a comparison is made in Figure 13 for several conditions. The data bands appear to lie to the right of the theoretical bands, a fact which can be interpreted as indicating a lag between the time the v' reaches its maximum value and the time S_T/S_L reaches its maximum value.

Another way of demonstrating both the apparent lag and the similarity between results of theory and experiment is employed in Figure 14. Here the value of gain g from Figure 4 is plotted against frequency for three values of h_2/h_1, and compared with S_T/S_L obtained from Figure 12

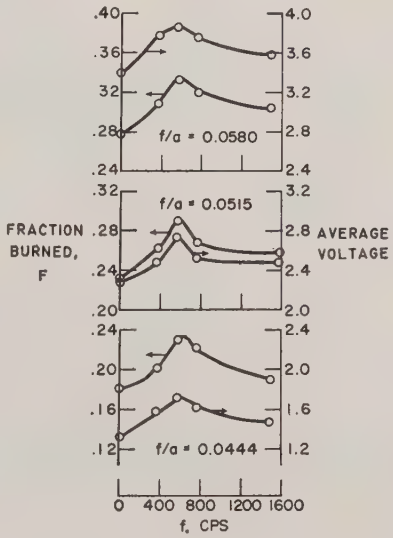

FIG. 8. Comparison of fraction burned obtained by momentum-pressure-drop measurement with average voltage obtained by photomultiplier survey. Velocity, 50 ft/sec; length, 6 in.; disturbance velocity, 2.38 ft/sec; disturbance, antisymmetric.

TABLE 2. COMPARISON OF PRESSURE-DROP CALIBRATION WITH CALIBRATION BY DIRECT VIEWING OF AN ALMOST LAMINAR FLAME

f/a	S_L[14]	$V_L = \frac{S_L}{ST/VT}$	V_L by Direct Measurement
0.0444	0.74	0.663	0.658–0.682
0.0515	1.10	1.25	1.15–1.39
0.0580	1.32	1.862	—

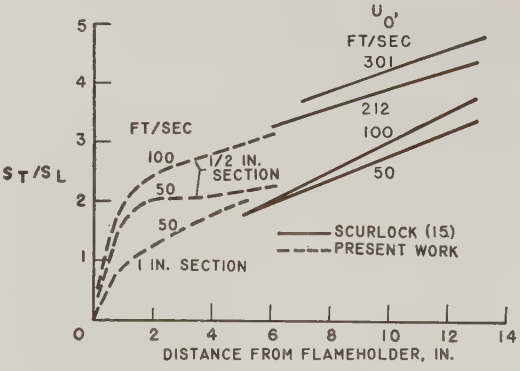

FIG. 9. Comparison of S_T/S_L taken in ½ in. and 1 in. wide ducts with Scurlock's data.

for two values of h_2/h_1. A similar plot was obtained for the 100-ft/sec condition which had a greater lag.

Disturbance-phase velocities

From a set of photographs, values of c_r/U_1 were determined, using the mean flame width to

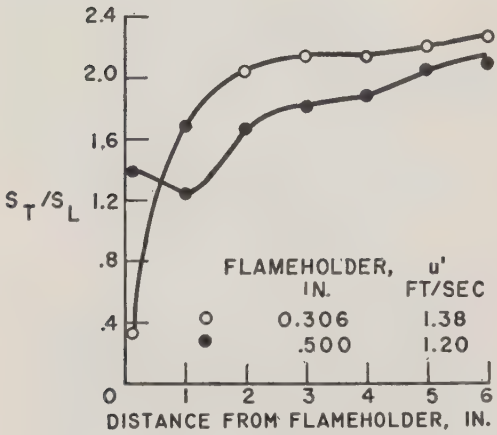

(a) Both flameholders without disturbance.

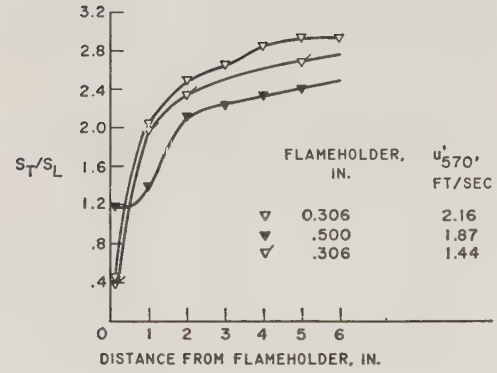

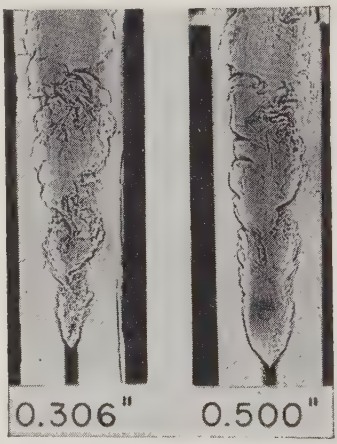

(b) Both flameholders with disturbance at 570 cps.

FIG. 10. Comparison of S_T/S_L and flame appearance for 0.500- and 0.306-in. flameholders. U, 50 ft/sec; f/a, 0.0444.

Symmetric disturbances

Tests were made with flameholders that produced symmetric disturbances. The results when compared with the antisymmetric disturbance under similar conditions indicated that:

(1) Near the flameholder the two types of disturbances affected S_T/S_L similarly.

(2) Downstream of the flameholder, $x > 3$ inches, S_T/S_L grew more rapidly for the antisymmetric disturbance.

determine h_2/h_1. The quantity U_1/U_0 was then determined from Tsien's results (Eq. (3)). Wavelengths were measured from trough to trough, and the mean position of a pair of troughs located the applicable value of h_2/h_1. The results for two frequencies are shown (Fig. 15).

The dashed lines in Figure 15 are the values of c_r/U_1 obtained from the stability analysis. The scatter of the experimental data is quite bad, but the magnitude and trends of the data remote

from the flameholder are quite good. Values of c_r/U_1 less than unity are obtained for values of $h_2/h_1 < 0.15$, implying flow reversal within this region.

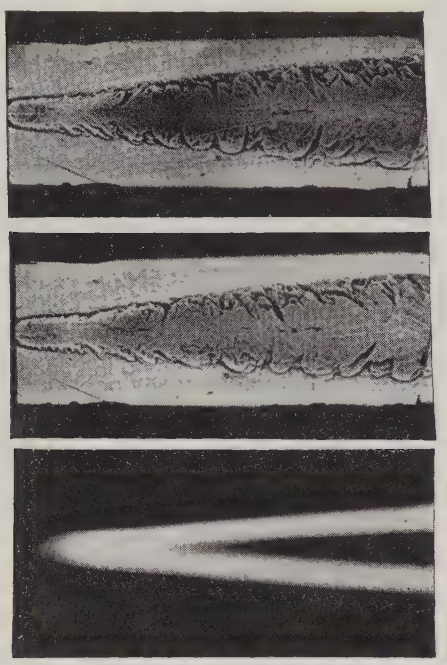

FIG. 11. Flame shadowgraphs and direct photograph of flame zone, with transition point downstream of point of separation. U, 50 ft/sec; f/a, 0.0484; $u'_{\text{turbulence}}$, 0.303 ft/sec.

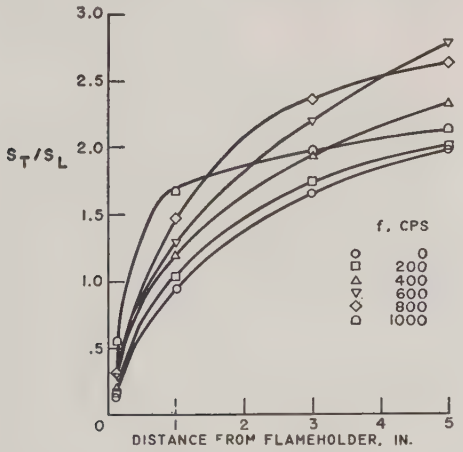

FIG. 12. Flame-speed distribution in 1 in. deep test section. U = 50 ft/sec, f/a = 0.0496.

Discussion

In the following section some questions raised by the analytical and experimental phases of the investigation are briefly discussed.

1. In what respects do the experimental results and the interpretations of the stability analysis agree? The areas of agreement are summarized in Table 3.

The details of the system that would define

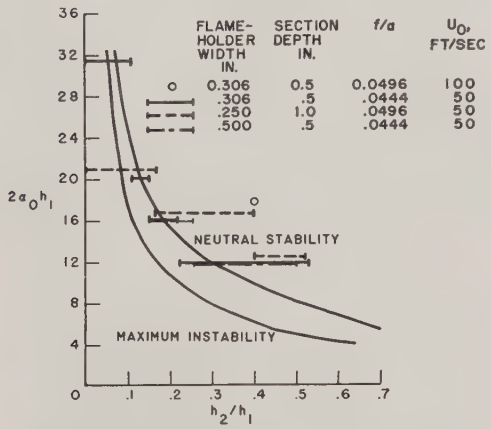

FIG. 13. Frequency giving maximum increase in flame speed as function of h_2/h_1 compared with results of stability analysis.

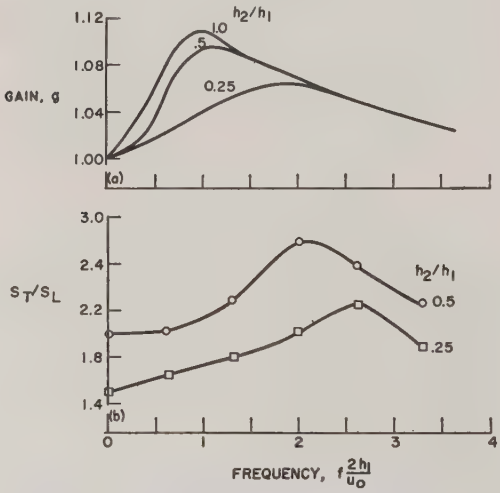

FIG. 14. Comparison of gain g, and S_T/S_L as functions of disturbance frequency. (a) Gain g for $\rho_1/\rho_2 = 7$; (b) S_T/S_L for data of Fig. 12.

more exactly the shortcomings of the stability analysis as well as the adequacies await the development of a transient-velocity measuring technique that can be used in a flame zone.

2. Would the same distribution of displacement and S_T/S_L with distance from flameholder obtain if no growth occurred in the flame zone? This seems unlikely. For example: If the input disturbance distribution simulates a source at the corner of

the flameholder, only near the flameholder would there be a marked transverse velocity component. This would mean that the highest frequencies would show the greatest increases in flame speed.

3. Do eddies shed? They certainly seem to. In Figure 16 shadowgraphs and the direct photographs of a lean flame taken through the stroboscope are compared with a smoke-trace photograph (16) of eddies shedding from a rod at Re of 73. The flame clearly has the necessary appearance for eddy shedding to be present.

4. Can the excitation at the flameholder permit increased combustion rates without destroying the burner walls? Yes. In these tests the sound level

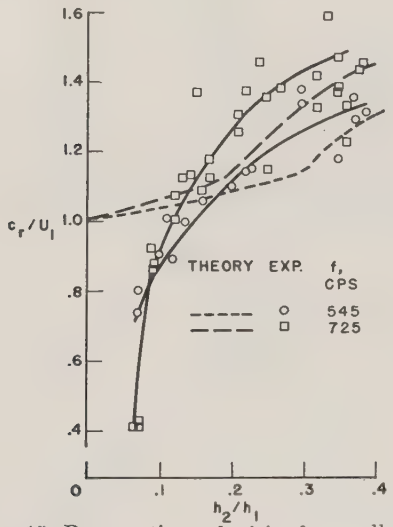

FIG. 15. Propagation velocities for small-amplitude disturbances.

at the plane of exhaust was a benign 93 db with the flame excited. When the flame is excited by the destructive duct resonance, the sound level is on the order of 200 db.

In order to apply this sort of excitation to an engine, the control exerted herein (a speaker system) would not be needed. Instead, the disturbance can be introduced by suitably placed whistles, mounted on the flameholder and driven by the flowing stream. The whistle ideally should have a number of strong overtones and a fundamental equal to the most sensitive frequency $U_0/2h$. The overtones would serve to increase the heat-release rate near the flameholder, while the fundamental would increase the heat-release rate remote from the flameholder. Another way, not investigated here, would be to use wavey walls in the combustor.

TABLE 3. COMPARISON OF STABILITY ANALYSIS AND EXPERIMENTAL RESULTS

Interpretation of Stability Analysis of Scurlock's Flow	Investigation of Sensitivity of a Flame in a Duct to Transverse Velocity Disturbance
1. The flow is stable to symmetric, unstable to antisymmetric disturbances	1. The flame seems about equally unstable to symmetric and antisymmetric disturbances near flameholder, is more unstable to antisymmetric disturbances remote from flameholder
2. In moving along the flame at phase velocity, a disturbance of given frequency grows until flame width becomes about 0.4 the wavelength, at which station an apparent decay of the disturbance begins	2. A disturbance of given frequency first grows, then decays. The critical flame width where decay starts is slightly smaller than that predicted
3. There will be a most-amplified frequency having a wave number $2\alpha_0 h_1 = 6 \rightarrow 8$	3. There is found a most-amplified frequency which, for the lengths investigated, corresponds to a $2\alpha_0 h_1 \approx 12$
4. The phase velocity ranges from a velocity = cold-gas velocity at flameholder up to 1.5 cold-gas velocity far from flameholder	4. The phase velocity behaves much as predicted save near the flameholder, where it is lower than cold-gas velocity
5. The amplification depends upon v'/S_{T_0} for given dh_2/dx	5. The amplification depends upon v'/S_{T_0} for given dh_2/dx

5. What would be the sacrifice in stability and pressure drop for such a device? Both these penalties require further investigation. The price would not seem high. For example: When the flameholder was placed $\frac{5}{8}$ in. from the nozzle entrance and a 6-in. long test section installed, lean blowout at 50 ft/sec occurred at a f/a of

0.042. At a f/a of 0.0453, the disturbance amplitudes required to cause blowout were found for several frequencies. The results are shown in Figure 17. Minimum disturbance velocity was required at 780 cps. At this condition the flameholder without flame had an eddy-shedding frequency of 420 cps. The Strouhal number is

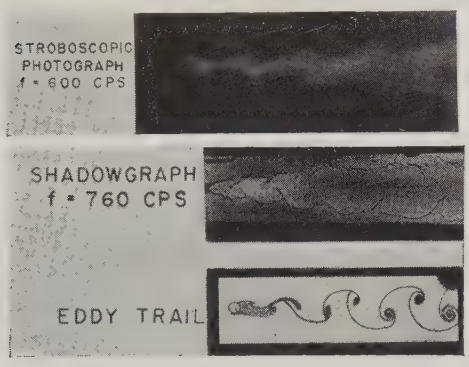

FIG. 16. Comparison of photographs of excited flame with an eddy trail.

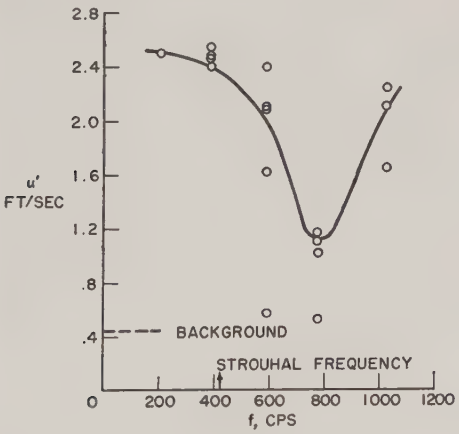

FIG. 17. Distribution with frequency of disturbance velocities required to produce blowout at a fixed velocity and fuel-air ratio. U_0, 50 ft/sec; 0.306-in. flameholder placed $\frac{5}{8}$ in. from nozzle; duct length, 5.7 in.; antisymmetric disturbances.

thus 0.206, agreeing well with the results of Roshko.[12] The duct resonance fundamental was 1000 cps cold. The reason for this result is not known. The main point here, however, is to show the effect of disturbances upon flameholder stability. It was found that, at a f/a of 0.047, it was impossible to induce blowout with speaker inputs as much as 10 times those used in the earlier tests. At this writing it seems safe to say that the imposed disturbances will narrow the stability range slightly but not prohibitively, and the amount of narrowing will depend upon the frequencies imposed.

An interesting observation was made in the study of lean blowout. As the lean blowout f/a was approached, the flame emitted a low-frequency noise at 87 cps. The average heat-release rate dropped abruptly. A survey taken with the photomultiplier probe showed the flame to be intermittently extinguished for all positions greater than $\frac{7}{8}$ in. downstream of the flameholder. Random photographs taken at this condition show intervals during which no flame is present in the downstream part of the combustor. This form of resonance accompanied by intermittent blowoff (or flame parture) downstream of the sheltered zone was the only form of excitation that reduced the heat-release rate in the combustor. On this basis it is tempting to generalize that all oscillations that do not cause flame parture must increase the heat-release rate in the combustor.

For the frequency of maximum amplification (560 cps) as much as 30 per cent increase in heat release was obtained in the 6-in. length combustor for a sound energy input of about 0.2 per cent of the kinetic energy of the flowing stream. In this case the noise level at the exhaust was 93 db.

The penalty for use of wavey walls in a combustor is unknown.

Concluding Remarks

The form of instability that has been discussed in this paper is of interest in formulating a theory of turbulent flame propagation[2] along with the plane combustion wave instability and boundary layer instability mentioned earlier. At present it is not known if the latter two forms of instability can be encouraged to influence turbulent flame propagation more than they do spontaneously. The little evidence that we have makes it appear that they can not. The type of instability that has been discussed in the present paper is of additional interest for the reason that its effect on S_T/S_L can be increased in some important applications. The ways this increase is possible lie in:

1. Increasing the v_0' in the frequency the flame zone can amplify.

2. Increasing the amplification rate by locally raising the velocity.

3. Increasing the amplification rate by locally varying the velocity profile.

A means of employing all three of these im-

proving factors would lie in building a combustor having one of its walls a wavey one.

Nomenclature

a, A, B, C, D	constants of integration
c	complex phase velocity, ft/sec
c_i	imaginary part of complex phase velocity
c_r	real part of complex phase velocity
e	Naperian base
F	fraction burned
f	frequency, cps
g	gain, $v' = v_0'(g)^{1/K}$
g'	gain, $v' = v_0'(g')^{1/K}$
h_1	duct half-width, ft
h_2	flame half-width, ft
i	$\sqrt{-1}$
K_1	constant $= \dfrac{dh_2}{dx}$ for an assumed flame-spreading mechanism
K_2	constant $= \dfrac{dF}{d\dfrac{x}{h_1}}$
L_x	Eulerian scale of turbulence, ft
$\dfrac{n}{m}$	$\dfrac{\gamma_2^2 + \gamma_1^2}{\gamma_2^2 - \gamma_1^2}$
p	pressure, lb/sq ft
p'	perturbation pressure, lb/sq ft
S_T	turbulent flame speed, ft/sec
S_L	laminar flame speed, ft/sec
t	time, sec
U	flow velocity in x-direction, ft/sec
U_0	flow velocity in x-direction at plane of flameholder
U_1	flow velocity in x-direction in cold gas, ft/sec
U^*	flow velocity in x-direction at apex of hot-gas velocity profile, ft/sec
u'	disturbance velocity in x-direction, ft/sec
v'	disturbance velocity in y-direction, ft/sec
x	coordinate in direction of duct axis (direction of mean flow), ft
f/a	fuel: air ratio
y	coordinate at right angle to direction of mean flow, ft
α	wave number of disturbance, ft^{-1}
α_0	wave number of disturbance based on initial velocity and frequency $f2\pi/U_0$
β	hot-gas velocity gradient $(U - U_1)/h_2$, sec^{-1}
γ_1	$e^{-\alpha h_1}$
γ_2	$e^{-\alpha h_2}$
μ	$\dfrac{1 + \gamma_2^2}{1 - \gamma_2^2}$
λ	wave length, ft

REFERENCES

1. Scurlock, A. C.: Meteor Rep. 19, Fuels Res. Lab., M.I.T., May 1948. (Contract NOrd 9661.)
2. Markstein, G. H.: *AGARD Selected Combustion Problems*, pp. 263–265. London, Butterworth, 1954.
3. Haddock, G. W.: Prog. Rep. 3–24, Jet Prop. Lab., Cal. Inst. Tech., May 14, 1951.
4. Zukoski, E. E., and Marble, F. E.: Combustion Res. Rev., 167–180 (1955).
5. Lin, C. C.: Quart. Appl. Math., *3*, 117–142 (1945); *3*, 218–234 (1945); *3*, 277–301 (1946).
6. Pillow, A. F.: Rep. A. 35, Dev. Aero., Council Sci. & Ind. Res. (Australia), May 1945.
7. Tsien, H. S.: Appl. Mech., *18*, 188–194 (1951).
8. Blackshear, P. L., Jr.: Ph.D. Thesis, Case Inst. of Technology, June 1956.
9. Goldstein, S.: Proc. Roy. Soc. (London), *132*, Ser. A., 524–547 (1931).
10. Rayleigh: *The Theory of Sound*, Vol. II. New York, Dover, 1945.
11. Mickelsen, W. R., and Laurence, J. C.: NACA RM E53F19, 1953.
12. Roshko, A.: NACA Rep. 1191, 1954.
13. Clark, T. P., and Bittker, D. A.: NACA RM E54F29, 1954.
14. Dugger, G. L.: NACA Rep. 1061, 1952.
15. Scurlock, A. C., and Grover, J. H.: *AGARD Selected Combustion Problems*, pp. 215–247. London, Butterworth, 1954.
16. Goldstein, S., Ed.: *Modern Developments in Fluid Dynamics*, Vols. I and II. Oxford, Clarendon, 1938.

Ignition

64

SPARK IGNITION OF FLOWING GASES USING LONG-DURATION DISCHARGES

By CLYDE C. SWETT, JR.

Introduction

To provide information for the design and operation of jet-engine combustors, research is being conducted at the NACA Lewis laboratory on the fundamental variables affecting the ignition and combustion of fuel-air mixtures. One part of this research has involved investigations of the variables that influence the energy required for a spark discharge to ignite a homogeneous fuel-air mixture. The investigations were initiated because of three starting problems in aircraft jet engines: ground starting of engines in cold climates, starting of auxiliary engines at altitude conditions, and altitude restarting of combustors in case of flame blowout. Since the program began, the ignition problem has been alleviated considerably through design and location of various components of an ignition system and through development of high-energy ignition systems. Nevertheless, research on ignition has continued to promote a better understanding of the ignition process in order that lighter-weight, more efficient, and more reliable ignition systems can be designed.

During this program many variables were investigated for both the effect that they have on the physical and electrical characteristics of discharges, and the effect that they have on the energy required for ignition.[1, 2, 3, 4, 5] Also, a theory of ignition in flowing gases has been developed[4] that relates many of these variables. The purpose of this paper is to summarize these experimental data, to present the theory, and to show to what degree the theory is substantiated by the data.

All of the experimental data presented herein were obtained at chamber pressures of 3.0 to 5.0 in. Hg abs. At these low pressures most of the discharges were glow discharges rather than arc discharges, so only glow-discharge data will be presented. Limitations of the energy-measurement equipment precluded operation at higher pressures. The data were obtained in two types of apparatus: a simple flow apparatus having no provisions for controlling turbulence and an apparatus in which turbulence could be controlled as desired. Only one combustible gas—a propane-air mixture—has been used. This gas was ignited by a single long-duration discharge obtained from a capacitance-resistance type ignition system.

Experimental Investigation

Apparatus and Procedure

Flow apparatus

The important features of the flow apparatus used are shown in Figures 1a and 1b. The complete systems are described in detail by Swett.[1, 4] Basically, the apparatus produced controlled flow conditions of premixed propane and air in a test section in which the spark electrodes were located. Provisions were made for observing the spark and the flame downstream from the electrodes; this was the criterion for ignition. In the simple flow apparatus (Fig. 1a) the pressure, temperature, and velocity of flow were controlled. No attempt was made to vary the turbulence. The controlled-turbulence flow apparatus (Fig. 1b) had a series of fine-mesh screens to reduce the turbulence in a large section, a nozzle to accelerate the flow into the test section, a means whereby different turbulence promoters could be installed upstream of the electrodes, and a means of varying the distance between the electrodes and the turbulence promoter.

Ignition system and energy measurement

The ignition and energy-measuring systems used are described by Swett[1]; they are shown

schematically in Figure 1c. The condenser is charged and then discharged through a combination of resistors to produce a spark discharge, the energy and duration of which depends upon the relative values of the condenser capacity, the voltage, and the resistances. This system was designed for laboratory use only; it would be too inefficient for engine applications.

The voltage of the discharge was reduced by means of a balanced resistance-capacitance voltage divider[2] and applied to the vertical plates of the oscillograph. A current-measuring resistance placed in series with the spark gap produced a

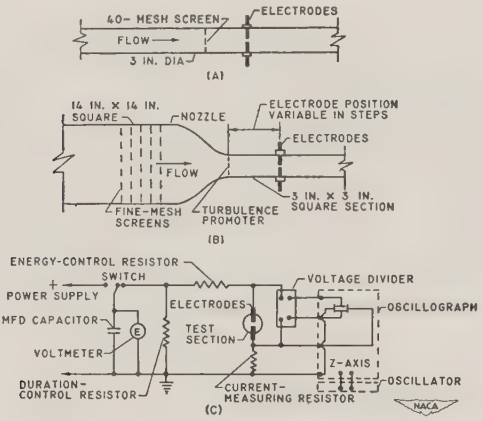

FIG. 1. Important features of flow apparatus and electrical equipment used for investigating spark ignition of flowing gases. (A) Simple flow apparatus; (B) controlled-turbulence flow apparatus; (C) ignition and energy-measuring equipment.

voltage that was applied to the horizontal plates. These two voltages in conjunction with timing marks supplied by an osciallator gave an oscillogram from which energy and duration of the discharge could be determined.

The procedure used with this apparatus was as follows: After proper flow conditions were stabilized a spark discharge was initiated. Tests were run with varying amounts of energy until the minimum amount of energy that would cause ignition was determined. Then one or more oscillograms were obtained, depending upon reproducibility at the particular condition. A more detailed description of the procedure used to obtain and analyze the ignition data is presented by Swett,[1, 2, 4, 5] and Swett and Donlon.[3]

Turbulence measurement

A description of the hot-wire anemometer apparatus and methods used to measure the turbulence is presented by Mickelsen and Laurence.[6] Single-wire probes measured the velocity fluctuations in the longitudinal direction and x-wire probes measured the velocity fluctuations in the lateral direction. A difference circuit was used in the lateral measurements to obtain the difference in velocity fluctuations from the two wires of the x-wire probes. The spectrum of the turbulence was analyzed by means of a wave analyzer. An average-square computer totaled the kinetic energy in the velocity fluctuations to give the intensity of turbulence.

Measurements of the turbulence were made as follows: With the spark electrodes removed, the probe was inserted into the test section and located so that the hot wire would be at the center of the duct. After flow conditions were established using air in place of the combustible mixture, the intensity of turbulence was determined and a spectrum analysis was made to determine the scale of the turbulence.

RESULTS OF EXPERIMENTAL INVESTIGATION

A considerable amount of data on the variables affecting ignition energy has been obtained since the first results on ignition of flowing gases were presented by Swett.[1] These new data have included the effects of fuel:air ratio, temperature, electrode spacing, electrode configuration, electrode material, gas velocity, and turbulence. One important fact shown by this research is that ignition energy also depends upon the type of discharge—arc- or glow-produced. The glow discharge requires about 70 per cent more energy for ignition than does the arc discharge. Because the glow discharge predominates at the low pressures used, only glow-discharge data will be presented and used to evaluate the theory.

Nonturbulent flow

The variation in ignition energy requirements with fuel:air ratio at one pressure, velocity, spark duration, electrode spacing, and temperature is shown in Figure 2. The smoothness of the data was quite good except in a small region around a fuel:air ratio of 0.095. The data fit somewhat better to the dashed curve which has lobes similar to those found in investigations of flammability limit. The existence of these lobes is questionable, however, and no great significance is attached to it.

The effects of some of the other variables are shown in Figures 3, 4 and 5 and Table 1. Ignition energy decreases with increasing temperature

(Fig. 3) and with increasing electrode spacing (Fig. 4). The minimum energy occurs at a spacing of 0.65 in., which is the quenching distance of quiescent mixtures for the particular pressure and fuel:air ratio. At spacings less than this the

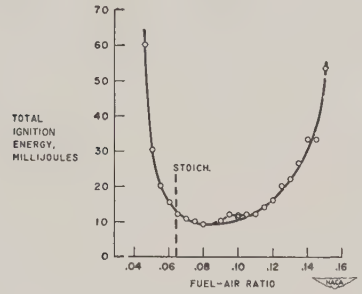

FIG. 2. Effect of fuel:air ratio on total ignition energy. Pressure, 5.0 in. Hg abs; gas velocity, 50 ft/sec; temperature, 80°F; electrode spacing, 0.723 in; spark duration, approximately 440 μsec. Data from Ref. 5.

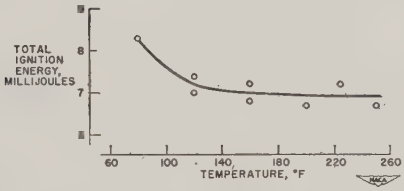

FIG. 3. Effect of initial temperature on total ignition energy. Pressures, 5.0 in. Hg abs; fuel:air ratio, 0.0835; gas velocity, 50 ft/sec; electrode spacing, 0.37 in.; spark duration, 440 μsec. Data from Ref. 5.

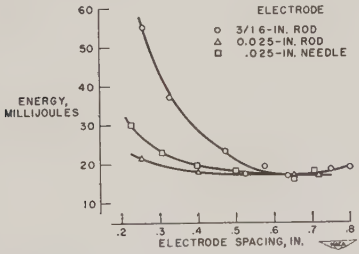

FIG. 4. Effect of electrode diameter, configuration and spacing on ignition energy of flowing propane-air mixture. Pressure, 3 in. Hg abs; temperature, 80°F; fuel:air ratio, 0.0835; velocity, 5.0 ft/sec. Data from Ref. 2.

largest electrodes require the greatest energies because of the larger surface area for flame quenching. Needle electrodes had slightly larger energy than did the small rod electrodes, possibly because of the manner in which energy is distributed along the length of the discharge.[2] Ignition energy increases with increasing velocity as shown in Figure 5a and Table 1. Although it is not readily apparent from the data presented herein, ignition energy has been found to decrease with increasing pressure and with decreasing spark duration. These effects of pressure and duration have been presented previously.[1] Ignition energy is negligibly affected by electrode material if a glow discharge is used.[2]

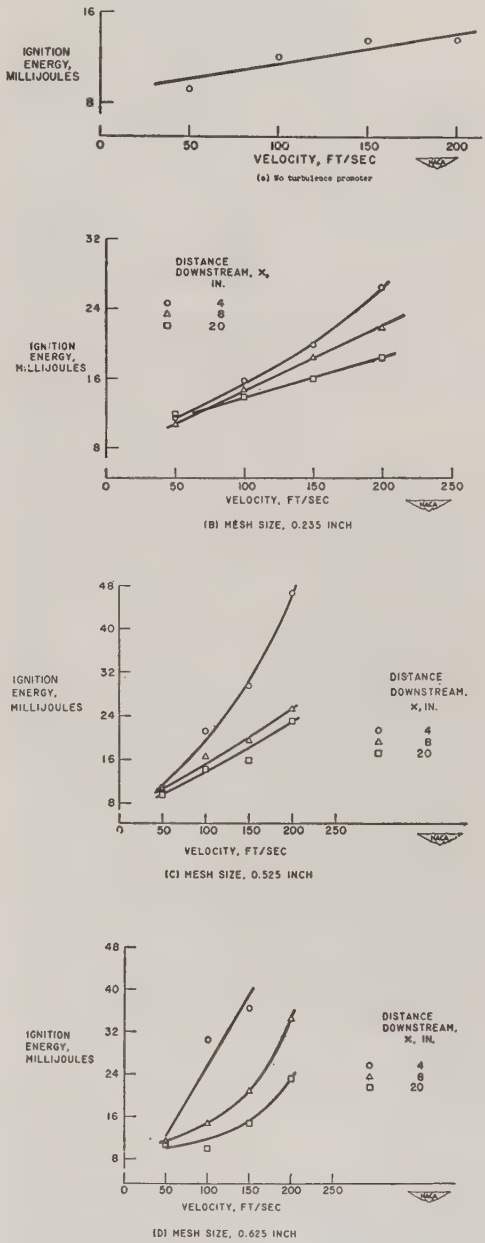

FIG. 5. Effect of velocity on ignition energy for various turbulence promoters. Fuel, propane; fuel:air ratio, 0.0835; pressure, 5.0 in. Hg abs; temperature, 80°F; spacing, 0.37 in.; electrode diameter, 0.0225 in.; spark duration, approx. 500 μsec. Data from Ref. 4.

Turbulent flow

The effects of mesh size of the turbulence promoters, of distance between turbulence promoters and the electrode, and of stream velocity on

TABLE 1. NONTURBULENT-FLOW IGNITION ENERGY DATA

Fuel:air ratio, 0.0835

Pressure	Velocity	Temperature	Spark Duration	Electrode Diameter	Ignition energy	Reference
in. Hg abs	*ft/sec*	*°F*	*μ sec*	*in.*	*mj*	
3	5	80	600	0.65	17.0	2
5	50	225	440	0.37	7.16	5
5	50	250	440	0.37	6.67	5
5	50	80	346	0.37	9.28	4
5	100	80	311	0.37	12.0	4
5	150	80	242	0.37	13.5	4
5	200	80	208	0.37	13.5	4

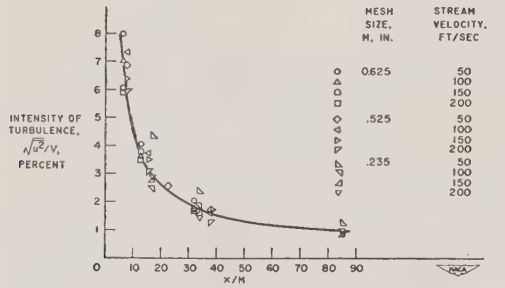

FIG. 6. Effect of x/M on $\sqrt{u^2}/V$ for various values of mesh size and velocity. Data from Ref. 4.

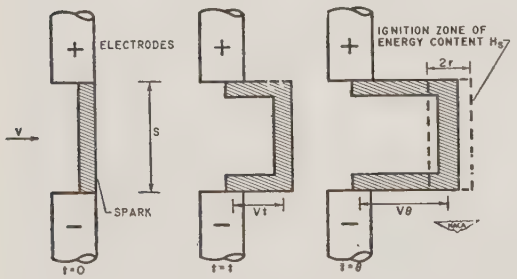

FIG. 7. Model of spark discharge in flowing gas.

ignition energy are shown in Figure 5. The energy increases with velocity and mesh size and decreases with distance between promoter and electrodes. The ignition energy increases with those factors that give increased intensity of turbulence, for, as shown in Figure 6, both increasing mesh size, M, or decreasing distance between promoter and electrodes, result in increased intensity of turbulence, $\sqrt{u^2}$, for constant stream velocity, V.

Scale of turbulence appears to have a minor effect as shown by the following data from Swett,[4] which compares values of ignition energies obtained at approximately constant values of intensities but with varying scales:

Velocity, V	Intensity, $\sqrt{u^2}$	Scale, Lx	Ignition energy, H^*
ft/sec	*ft/sec*	*in.*	*mj*
50	1.19	0.17	10.6
	1.28	0.26	10.6
100	5.76	0.15	26.4
	6.18	0.20	25.2

* Obtained at pressure, 5.0 in. Hg abs; fuel: air ratio, 0.0835; temperature, 80°F; electrode spacing, 0.37 in.

Theoretical Considerations

CONCEPT OF LINE SOURCE OF ENERGY

The model used to develop the theory for the ignition of flowing gases is shown in Figure 7. The discharge is established between two electrodes spaced S distance apart, at time $t = 0$, in a stream having a velocity V. Under influence of the gas stream the discharge moves downstream at stream velocity (as deduced from data reported by Swett[1]) so that at time t the discharge is at a distance Vt downstream. The discharge is considered to be in the shape of a square-cornered "u"; that is, rounding effects at the corners are neglected. At a time corresponding to the spark duration θ, the discharge is at its maximum distance, $V\theta$, downstream.

After the spark discharge has moved downstream, and extinguished at time θ, there exists a heated zone larger in diameter than the discharge itself but in a path coincident with that of the discharge. The vertical portion of the discharge (Fig. 7) moved at stream velocity so that the same volume of gas was continuously heated, whereas the legs of the discharge lengthened with time and fresh gas was continuously being heated at the electrode ends of the discharge. Hence, it may be considered that the zone surrounding the vertical portion of the discharge is at a much higher temperature than the legs and, therefore, constitutes a more probable zone of ignition. This vertical zone or line source of ignition is used in the development of the theory of ignition of flowing gases.

In order to establish relationships between ignition energy requirements and flow variables, the energy that goes into this line source must be determined. Swett[2] shows that the total energy of a discharge may be split into two major parts. One part is dissipated in a small region called the cathode drop region, which is extremely close to the cathode electrode. It comprises ⅓ to ½ of the total energy for the conditions used herein. The second part is dissipated in the remainder of the length or positive column. The line source of energy consists of a portion of this positive column. The energy dissipated in the cathode region is assumed to be unimportant to the ignition process. This is a reasonable assumption since, according to Cobine,[7] almost all of the cathode energy is lost to the cathode.

The energy in the line source of ignition can be calculated from total-energy data if two assumptions are made. The first assumption is that the total amount of energy in the discharge at any time varies linearly with time. Actually, for the ignition data presented herein, the energy goes into the discharge somewhat more rapidly during the first part of the discharge; however, the assumption of uniform energy release is believed sufficiently accurate for practical use. The second assumption is that the power per unit length of discharge at any time is constant. The power can be based on either the total power, if the cathode energy is assumed uniformly distributed throughout the gap, or the power in the positive column. Actually, in order to agree with the concept of the line source of energy, it should be based on the positive column only, but for practical reasons involved in measurement of cathode energies total power is used in most of the analysis. Correction of the data to include positive-column energies only will be discussed later.

The average power P_{Av} of the total energy H is H/θ where θ is the spark duration. This average power is divided into two portions: the line source and the legs of the discharge. The relative amounts dissipated in each region depend upon the respective lengths of the legs and, hence, on time and gas velocity. The amount of power available for the line source at any instant is

$$P_s = \frac{S}{2Vt + S} \cdot P_{Av}$$

The energy of the line source H_s is the integral of this instantaneous power with respect to time taken over the discharge duration or

$$\begin{aligned} H_s &= \int_0^\theta P_S dt \\ &= \int_0^\theta \frac{S}{2Vt + S} \cdot \frac{H}{\theta} \cdot dt \qquad (1) \\ &= \frac{HS}{2V\theta} \ln \frac{2V\theta + S}{S} \end{aligned}$$

Equation (1) assumes the cathode energy to be uniformly distributed over the whole length of the discharge. If the cathode energy is assumed to be lost to the electrode, H in Equation (1) may be replaced by H_p, where $H_p = H - H_c$, H_c is the cathode energy and H_p the positive column energy:

$$H_s = \frac{H_p S}{2V\theta} \ln \frac{2V\theta + S}{S} \qquad (2)$$

Equation (1) will be used herein because H_c is difficult to measure accurately.

DEVELOPMENT OF THEORETICAL EQUATIONS

The process of establishing steady burning of a homogeneous fuel-air mixture from a long-duration discharge is visualized as follows: The line source of ignition is assumed to supply the heat necessary to raise the temperature of the heated zone to flame temperature. The initial flame will then propagate if the heated zone is of proper volume to fulfill the condition of rate of heat generated in the volume equal to or greater than rate of heat loss from the volume. An additional requirement is imposed that the length of the line source must be equal to the quenching distance in order to preclude quenching effects. No heat losses from the heated zone either to the electrodes or to the gas are considered during the spark duration; also no heat is considered to be supplied from any chemical reaction during this period.

The relationship between ignition energy and the operating variables can be determined by comparing the line-source energy with the theoretical amount of energy necessary to raise the temperature of the volume under consideration to flame temperature. The radius, r, of the heated volume (Fig. 7) is the unknown dimension of the volume. Since both the rate of heat generated and the rate of heat loss are functions of the radius, equating these rates results in a value for the critical radius. The rate of heat generation in this heated zone is dependent upon the size of the

volume and upon a reaction-rate term—whereas the rate of heat loss depends upon not only the size but also the method of heat transfer, *i.e.*, thermal conduction or eddy diffusion. According to the concept of a line source of energy the zone is moving at stream velocity and therefore may be considered as a zone in a quiescent mixture if no turbulence is present. Heat will therefore be lost from the zone by thermal conduction (neglecting radiation). If turbulence is present heat can be lost by both thermal conduction and eddy diffusion. The equations have been developed for two cases: (1) heat transfer by thermal conduction when turbulence is small and (2) heat transfer by eddy diffusion when turbulence is large. In the latter case it has been assumed that thermal conduction is negligible compared to eddy diffusion.

Nonturbulent flow

The equations for the rate of heat generated and the rate of heat loss are those of Fenn[8] converted from the spherical to the cylindrical case:

Rate of heat generated

$$= \pi r^2 S_q Q N_f N_o \rho^2 A e^{-(E/RT_f)} \quad (3)$$

$$\text{Rate of heat loss} = \frac{2\pi r S_q k(T_f - T_o)}{b}$$

$$= \frac{2\pi r S_q k(T_f - T_o)}{cr} \quad (4)$$

The term cr has been substituted for the reaction zone thickness, b, as done by Fenn in his theory. This substitution is an approximation; proof for its use is as follows: Equating (3) and (4) and solving for r,

$$r = \sqrt{\frac{2k(T_f - T_o)}{cQN_f N_o \rho^2 A e^{-(E/RT_f)}}} \quad (5)$$

Equation (5) gives the critical size of the zone It also indicates that r is inversely proportional to the square root of the reaction rate. In a flame front the thickness of the reaction zone is approximately inversely proportional to the square root of the reaction rate; hence, r must be proportional to b.

The amount of heat necessary to increase the temperature of the zone from T_o to T_f is

$$H_s' = J\pi r^2 S_q \rho c_p (T_f - T_o)$$

$$= \frac{2\pi J k S_q c_p (T_f - T_o)^2}{cQN_f N_o \rho A e^{-(E/RT_f)}} \quad (6)$$

The theoretical energy should be equal to the line source energy,

$$H_s' = H_s$$

$$\frac{2\pi J k S_q c_p (T_f - T_o)^2}{cQN_f N_o \rho A e^{-(E/RT_f)}} = \frac{HS_q}{2V\theta} \ln\left(\frac{2V\theta + S_q}{S_q}\right)$$

or

$$\frac{4\pi J V\theta k c_p (T_f - T_o)^2}{cHQN_f N_o \rho A e^{-(E/RT_f)}} = \ln\left(\frac{2V\theta + S_q}{S_q}\right) \quad (7)$$

Turbulent flow

In turbulent flow the rate of heat loss depends on the rate at which mass is transferred by eddy diffusion through the cylindrical surface of area $2\pi r S_q$. The two factors that control the eddy diffusion process are the intensity and the scale of turbulence. When the scale of turbulence is large compared to the flame front thickness, as it is for this problem, the effect of scale on the diffusion process is negligible compared to the effect of intensity of turbulence; hence, the effect of scale has not been included in the analysis that follows.

The rate of heat loss is a function of the product of surface area, density, specific heat, temperature difference, and a term representing the velocity with which heat moves through the surface. The velocity term can be represented by some function of the intensity of turbulence, or $f'(\sqrt{\overline{u^2}})$. The function involves the first power of $\sqrt{\overline{u^2}}$ in order to be correct dimensionally. Thus,

$$\text{Rate of heat loss} = 2\pi r S_q \rho c_p (T_f - T_o) f' \sqrt{u^2}) \quad (8)$$

For the ignition condition, Equation (8) equals Equation (3). Solving for r gives

$$r = \frac{2c_p (T_f - T_o)}{QN_f N_o \rho A e^{-(E/RT_f)}} f'(\sqrt{\overline{u^2}})$$

The theoretical energy required to increase the temperature of the heated zone to flame temperature under turbulent flow conditions is

$$H_s' = J\pi r^2 S_q c_p \rho (T_f - T_o)$$

$$= \frac{4\pi J S_q c_p^3 (T_f - T_o)^3}{Q^2 N_f^2 N_o^2 \rho A^2 e^{-(2E/RT_f)}} f\ (\sqrt{\overline{u^2}}) \quad (9)$$

where $f(\sqrt{\overline{u^2}})$ is a new function of the intensity of turbulence.

The relationship between the theoretical and

the line-source energies is, therefore,

$$\frac{4\pi J S_q c_p^3 (T_f - T_o)^3}{Q^2 N_f^2 N_o^2 \rho A^2 e^{-(2E/RT_f)}} f(\sqrt{\overline{u^2}}) = \frac{HS_q}{2V\theta} \ln\left(\frac{2V\theta + S_q}{S_q}\right)$$

or

$$\frac{HQ^2 N_f^2 N_o^2 \rho A^2 e^{-(2E/RT_f)}}{8\pi V\theta J c_p^3 (T_f - T_o)^3} \ln\left(\frac{2V\theta + S_q}{S_q}\right) = f(\sqrt{\overline{u^2}}) \quad (10)$$

Application of Theoretical Equations to Experimental Data

Only very limited data are available to verify the theoretical equations that have been developed. Although a considerable amount of data has been obtained, much of it cannot be used in the equations because of differences in type of discharge or because electrode spacings were less than the quenching distance. The data used with the equations will be those reported herein that were obtained with glow discharges and with electrode spacing equal to the quenching distance.

NONTURBULENT FLOW

Data to be applied to the nonturbulent flow equation were obtained with one fuel and one fuel:air ratio so that Equation (7) may be reduced to

$$\frac{c_1 V\theta k c_p T_f (T_f - T_o)^2}{pHe^{-(E/RT_f)}} = \ln\left(\frac{2V\theta + S_q}{S_q}\right) \quad (11)$$

A plot of this relationship is shown in Figure 8 for the data in Table 1. The correlation is satisfactory for the limited data available.

Equation (7) indicates that there is an effect of fuel:air ratio. The data of Figure 2 were applied to this equation which, for the operating conditions of the figure, reduces to

$$\ln \frac{HN_f N_o \ln\left(\frac{2V\theta + S_q}{S_q}\right)}{T_f (T_f - T_o)^2} = c_2 + c_3\left(\frac{1}{T_f}\right) \quad (12)$$

where $\rho \propto 1/T_f$. A plot of the data using Equation (12) is shown in Figure 9. A single straight line which would be predicted by the theory was not obtained. There is a factor of about 2 between the values for the rich and the lean ends of the curve. Possible reasons for this discrepancy will be discussed later.

TURBULENT FLOW

The data used to verify the turbulent flow Equation (10) are those presented in Figure 5.

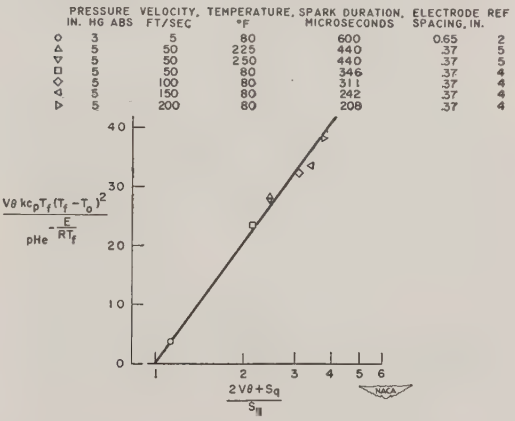
PRESSURE IN. HG ABS
VELOCITY, FT/SEC
TEMPERATURE, °F
SPARK DURATION, MICROSECONDS
ELECTRODE SPACING, IN.
REF
3 5 80 600 0.65 2
5 50 225 440 .37 5
5 50 250 440 .37 5
5 50 80 346 .37 4
5 100 80 311 .37 4
5 150 80 242 .37 4
5 200 80 208 .37 4
$\frac{V\theta k c_p T_f (T_f - T_o)^2}{pHe^{-\frac{E}{RT_f}}}$
$\frac{2V\theta + S_q}{S_q}$
NACA

FIG. 8. Correlation of nonturbulent-flow data. Fuel:air ratio, 0.0835.

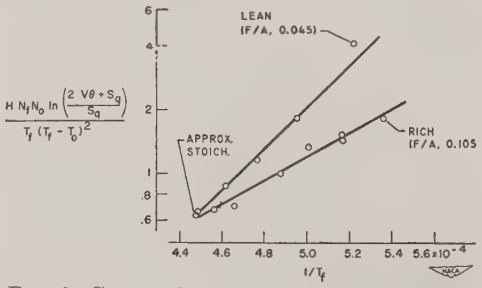

FIG. 9. Curve obtained by applying ignition energy and fuel:air ratio data to Equation (12). Data (fuel:air ratio 0.045 to 0.105) from Fig. 2.

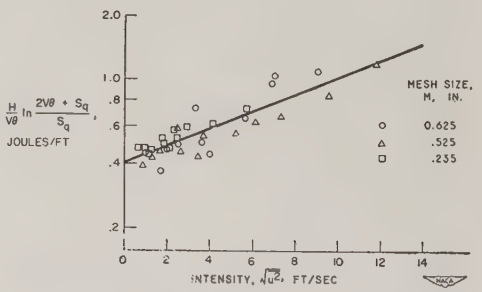

FIG. 10. Correlation of ignition data with intensity of turbulence. Fuel:air ratio, 0.0835; temperature, 80°F; pressure, 5.0 in. Hg abs. Data from Ref. 4.

For the conditions used to obtain the data Equation (10) may be reduced to

$$\frac{H}{V\theta} \ln\left(\frac{2V\theta + S_q}{S_q}\right) = c_4 f(\sqrt{\overline{u^2}}) \quad (13)$$

Data calculated according to this relation are plotted in Figure 10. The figure shows that a

reasonable relation exists among the variables of energy required for ignition, stream velocity, and the intensity of turbulence. The data correlated with an average deviation of 11 per cent and a maximum deviation of 35 per cent.

Discussion of Theory

The theory that has been described, and its experimental verification, mark the first attempt to treat ignition of flowing gases and as such is greatly simplified. The many approximations and assumptions that have been made may be summarized as follows:

(1) The analysis is based on second-order reaction for the rate of heat generation.

(2) Diffusion processes are neglected.

(3) Radiation from ignition zone is neglected.

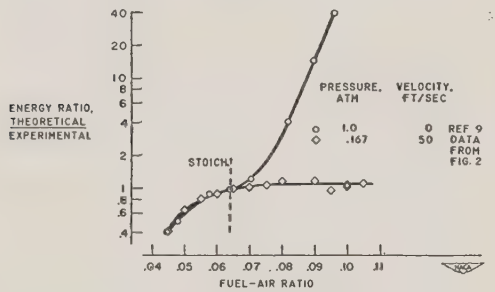

FIG. 11. Comparison of theoretical-to-experimental energy ratios with those of Ref. 9. Both sets of data adjusted to 1.0 at approximately stoichiometric fuel:air ratio.

(4) An approximation is made of the thickness of the reaction zone with a temperature difference $T_f - T_o$.

(5) The average power of the discharge is assumed to be constant.

(6) Cathode energy is assumed to be evenly distributed along length of discharge.

(7) The discharge is assumed to take the shape of a square-cornered "u"; rounding effects at the corners are neglected.

(8) There are no heat losses from the heated zone left by the spark discharge during the duration of the discharge.

(9) There is no heat resulting from chemical reaction in the heated zone during the duration of the discharge.

Many of these assumptions could have been removed from the theory, but theoretical treatment would have been unduly complicated and, in some cases, impossible.

The data used to verify the theory have been limited in scope. This has been the result of using only data from one type of discharge (glow). It has not been possible to extend the research to higher pressures, because energy measurements could not be made at higher pressures. At high pressures the small amount of energy required for ignition becomes comparable to the energy stored in the capacitance of the voltage divider. This latter energy is not measured by the oscillographic technique used.

The effects on ignition energy of all operating variables except one—fuel:air ratio—were correlated by the theoretical relationships. Other investigators have also encountered inconsistencies in variable fuel:air-ratio data. For example, in the work of Lewis and von Elbe,[9] which describes an ignition theory of quiescent gases that is separate and distinct from the one described herein, data obtained over a range of fuel:air ratios did not correlate with theoretical relations. The trends observed with the two theories may be compared by calculating the ratios of theoretical to experimental energy for the two sets of data. The term

$$\frac{4\pi JV\theta kc_p(T_f - T_o)^2}{cHQN_fN_o\rho Ae^{-(E/RT_f)} \ln\left(\dfrac{2V\theta + S_q}{S_q}\right)}$$

derived from Equation (7) represents the ratio of theoretical to experimental energy for the data contained in this report. The values of k and c_p in this equation were assumed constant, and a value of 26 kcal/mole was used for E. The energy ratios for the two sets of data were multiplied by constants in order to adjust the energy ratios to a value of 1.0 at a fuel:air ratio of approximately stoichiometric. The adjusted data are plotted against a fuel:air ratio in Figure 11. Both theories give predicted results that deviate from experimental results in the same direction. While neither theory can be used to predict trends exactly, the theory described herein more accurately predicts trends at richer-than-stoichiometric fuel:air ratios.

Swett[5] correlated the variable fuel:air-ratio data (Fig. 2) empirically by multiplying the term in the left side of Equation (12) by the factor $1 - (0.02/N_f)$, where N_f is the mole fraction of the fuel. This correlation is shown in Figure 12. A value of activation energy was calculated from the slope of the curve to be 24.8 kcal/mole, which agrees with the values in the literature. While the correction term $1 - (0.02/N_f)$ was determined empirically, it may have theoretical sig-

nificance. For example, the term may correct the total energy H to a value $H(1 - (0.02/N_f))$ or $H - (0.02H/N_f)$. This may indicate the possibility of energy loss occurring before ignition; the loss would be dependent on the total energy and on fuel concentration. Such loss may occur by heat conduction and should, therefore, be dependent on temperature and time. Considering the heated zone left by the spark, the temperature of the zone should be roughly dependent on H. The term $1/N_f$ can represent time if ignition-time lag is assumed to be inversely proportional to N_f, as is reported by Jackson and Brokaw.[10] The concept of energy loss, however, is questionable for two reasons: The theory considers the heated zone left by the spark as being at or near flame temperature, so that the time lag should be insignificant. Also, since time lag is affected by pressure,[11] a pressure term that might or might not destroy previous correlations should be included in the equations. Additional experiments would be required to prove or disprove this concept.

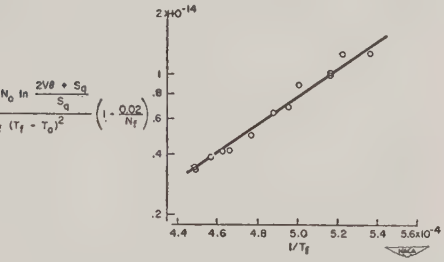

FIG. 12. Empirical correlation of ignition energy data (FIG. 2) obtained over fuel:air ratio range of 0.045 to 0.105.

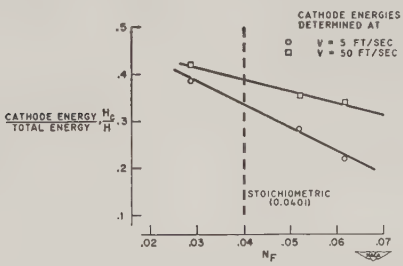

FIG. 13. Effect of fuel concentration on ratio of cathode energy to total ignition energy. Data from Ref. 5.

The term $1 - (0.02/N_f)$ might also be a correction term to the total energy for variations in in energy distribution along the spark path. As noted earlier, for practical reasons the total energy of the discharge, instead of the positive column energy, was used in the theoretical calculations—although results have indicated this latter energy to be the important factor. Therefore, if the positive column energy were used in the theory the energy would be $H - H_c$ or $H(1 - (H_c/H))$. If the ratio of cathode to total energy H_c/H were sufficiently dependent on N_f the discrepancy between theory and experiment could be explained. Figure 13 shows that H_c/H does actually decrease with increasing N_f for both low and high velocities; however, the decrease is only about 20 per cent. While this correction for cathode energy would improve the fuel:air ratio correlation somewhat, a much larger factor is needed.

There are probably other factors that may be responsible for the observed discrepancy. Preferential diffusion of the deficient reactant in the combustible mixture could be a contributing factor, as described by Lewis and von Elbe,[9] or possibly some cool flame mechanism that results in different activation energy in lean and rich mixtures may be present. Both of these items are qualitatively in the right direction to account for the difference between lean and rich data. Actually, a combination of the above factors may be responsible for the discrepancy. Further research on all the factors discussed is indicated.

Concluding Remarks

A theory of spark ignition in nonturbulent- and turbulent-flowing homogeneous gases using long-duration discharges has been developed, based on the concept that only a portion of the discharge length is important in ignition. This theory has resulted in a relation among the variables ignition energy, gas density and velocity, electrode spacing, spark duration, intensity of turbulence, and fuel constants. The limited amount of data available substantiate the relation, except for fuel:air ratio which requires empirical correction.

Nomenclature

A	constant
b	thickness of reaction zone across which the temperature change is $T_f - T_o$
c, c_1, c_2, c_3, c_4	constants
c_p	specific heat
E	energy of activation
$f(\sqrt{\overline{u^2}})$, $f'(\sqrt{\overline{u^2}})$	functions of intensity of turbulence

H	total energy of spark discharge
H_c	energy in cathode region
H_p	energy in positive column region
H_s	energy in line source of ignition
H_s'	theoretical energy required to heat ignition zone to flame temperature
J	conversion factor, heat to electrical energy
k	thermal conductivity
L_x	longitudinal scale of turbulence
M	mesh size of turbulence promoter
N_f	mole fraction of fuel
N_o	mole fraction of oxygen
P_{Av}	average power in total spark discharge
P_s	average power in line source of ignition
p	static pressure
Q	heat of combustion of fuel
R	gas constant
r	radius of heated zone caused by energy in line source of ignition
S	electrode spacing
S_q	quenching distance of quiescent mixtures
T_f	flame temperature
T_o	ambient temperature
t	time
$\sqrt{\overline{u^2}}$	intensity of turbulence
V	stream velocity
x	distance from turbulence promoter to spark electrodes
θ	spark duration
ρ	density

REFERENCES

1. Swett, C. C., Jr.: *Third Symposium on Combustion, Flame and Explosion Phenomena*, pp. 353–361. Baltimore, The Williams & Wilkins Co., 1949.
2. Swett, C. C., Jr.: NACA RM E51J12 (1951).
3. Swett, C. C., Jr., and Donlon, R. H.: NACA RM E52J28 (1953).
4. Swett, C. C., Jr.: NACA RM E54F29a (1954).
5. Swett, C. C., Jr.: NACA RM E55I16 (1955).
6. Mickelsen, W. R., and Laurence, J. C.: NACA RM E53F19 (1953).
7. Cobine, J. D.: *Gaseous Conductors*. New York, McGraw-Hill, 1941.
8. Fenn, J. B.: Ind. Eng. Chem., *43*, 2865–2868 (1951).
9. Lewis, B., and von Elbe, G.: *Combustion, Flames and Explosions of Gases*. New York, Academic Press, 1951.
10. Jackson, J. L., and Brokaw, R. S.: NACA RM E54B19 (1954).
11. Brokaw, R. S., and Jackson, J. L.: *Fifth Symposium (International) on Combustion*, pp. 563–569. New York, Reinhold Publ. Corp., 1955.

65

IGNITION AND COMBUSTION IN A LAMINAR BOUNDARY LAYER OVER A HOT SURFACE

By TAU-YI TOONG

Introduction

During the past decade, the problem of ignition in a steady stream of a combustible mixture by means of a hot surface has received increasing attention in the combustion field. Much of the research was conducted with an igniter immersed in the stream, as in the works of Mullen, Fenn and Irby[1] and Agoston.[2] Since the ignition was initiated in the wake region near the trailing edge of the igniter, the resulting complications in the flow pattern led to great difficulties in a critical examination of the theory of ignition by the use of these experimental results.

In order to further a basic understanding of the effects of reaction rate and transfer of momentum, heat, and mass on ignition, a program, both theoretical and experimental, has been started at the Massachusetts Institute of Technology. In this program, the development of combustion in the boundary layer next to a hot surface is being investigated. This hot surface is not completely immersed in the stream of a combustible mixture, but serves as a part of the combustor wall, so that the difficulties mentioned above due to the presence of wakes are entirely eliminated. Thus, both theoretical and experimental investigations can be

carried out for the same model, to permit a direct comparison of the results and a critical examination of the theory of ignition.

In the present paper, the results obtained in the first phase of the theoretical study are presented. The development of combustion in a laminar boundary layer over an isothermal flat plate is studied by the use of the well-known boundary-layer theory in fluid mechanics. The conditions for incipient ignition of a given combustible mixture predicted from the theoretical work are also compared qualitatively with the results obtained in the experimental program. However, a detailed description of the apparatus and the experimental results will be presented in a separate paper.

Problem

The model used in the theoretical analysis consists of an isothermal flat plate, over which a combustible mixture is flowing steadily. The profiles of velocity, temperature, and concentration of the combustible component in the mixture are assumed to be uniform across the entire stream at the leading edge, where a laminar boundary layer starts to grow in thickness. According to the boundary-layer theory, the viscous, thermal, and chemical effects are predominant in this region of developing boundary layer, whereas the fluid outside of this region can be assumed to be unaffected by the presence of the hot plate. Thus, the basic equations of continuity, momentum, and energy can be greatly simplified by the use of the usual boundary-layer assumptions.

In addition to these boundary-layer assumptions, it is further assumed that the fluid under consideration consists of varying proportions of only two components (*viz.*, the combustible component and the product of combustion), that it is a perfect gas with constant molecular weight, specific heats, Prandtl and Schmidt numbers, and that its viscosity varies directly with absolute temperature. The dissipation term in the energy equation is also neglected.

Analysis

Because of space limitations, only a brief outline of the analysis will be given here.

By the use of the above assumptions, the basic equations of continuity, momentum, and energy are first transformed into the following equations for the boundary-layer flow:

$$\frac{\partial}{\partial x}(\rho u) + \frac{\partial}{\partial y}(\rho v) = 0 \tag{1}$$

$$\rho\left(u\frac{\partial c}{\partial x} + v\frac{\partial c}{\partial y}\right) = \frac{\partial}{\partial y}\left(D\rho\frac{\partial c}{\partial y}\right) - a \tag{2}$$

$$\rho\left(u\frac{\partial u}{\partial x} + v\frac{\partial u}{\partial y}\right) = \frac{\partial}{\partial y}\left(\mu\frac{\partial u}{\partial y}\right) \tag{3}$$

$$\rho c_p\left(u\frac{\partial T}{\partial x} + v\frac{\partial T}{\partial y}\right) = \frac{\partial}{\partial y}\left(\lambda\frac{\partial T}{\partial y}\right) + aQ_p \tag{4}$$

For a perfect gas with a constant molecular weight and a viscosity varying directly with the absolute temperature, it has been shown, for example, by Chapman and Rubesin[3] that the equations of continuity and momentum, (1) and (3), can be solved independently of the energy equation.

Equation (1) is automatically satisfied by introducing a stream function ψ, such that

$$u = \frac{\rho_\infty}{\rho}\frac{\partial \psi}{\partial y} \tag{5}$$

and

$$v = -\frac{\rho_\infty}{\rho}\frac{\partial \psi}{\partial x} \tag{6}$$

With

$$\psi = (\nu_\infty u_\infty x)^{\frac{1}{2}} f(\eta) \tag{7}$$

and

$$\eta = \left(\frac{1}{2}\right)\left(\frac{u_\infty}{\nu_\infty x}\right)^{\frac{1}{2}} \int_0^y \frac{\rho}{\rho_\infty}\, dy \tag{8}$$

the momentum equation is reduced to the familiar Blasius equation:

$$f''' + ff'' = 0 \tag{9}$$

where primes indicate differentiation with respect to η. The boundary conditions are:

$$\left.\begin{aligned} f(0) &= f'(0) = 0 \\ f'(\infty) &= 2 \end{aligned}\right\} \tag{10}$$

It follows from Equations (5), (7), and (8) that

$$\frac{u}{u_\infty} = \frac{1}{2} f'(\eta) \tag{11}$$

Complete tables of f, f', and f'' can be found in the literature, *e.g.*, see Howarth.[4]

Without chemical reaction, the energy equation can also be transformed into an ordinary differential equation, with the relative distance ratio, η, as the independent variable. With chemical reaction, it is expected that the temperature

profiles in terms of the relative distance ratio would be modified to a different extent at different distances from the leading edge of the flat plate. Thus, it is suggested to transform the energy equation from the (x, y) plane into the (x, η) plane, as follows:

$$\frac{\partial^2}{\partial\eta^2}\left(\frac{T}{T_\infty}\right) + \sigma f \frac{\partial}{\partial\eta}\left(\frac{T}{T_\infty}\right) - 2\sigma f'\xi \frac{\partial}{\partial\xi}\left(\frac{T}{T_\infty}\right) + \left(\frac{4\sigma L}{u_\infty \rho_\infty c_\infty}\right)\left(\frac{c_\infty Q_p}{c_p T_\infty}\right)\xi a\left(\frac{T}{T_\infty}\right) = 0 \tag{12}$$

where σ is the Prandtl number, L is any characteristic length, ξ is defined as x/L, and the subscript ∞ indicates free-stream condition.

Similarly, the second continuity equation (or concentration equation) can be transformed into the (x, η) plane, as follows:

$$\frac{\partial^2}{\partial\eta^2}\left(\frac{c}{c_\infty}\right) + \sigma_s f \frac{\partial}{\partial\eta}\left(\frac{c}{c_\infty}\right) - 2\sigma_s f'\xi \frac{\partial}{\partial\xi}\left(\frac{c}{c_\infty}\right) - \left(\frac{4\sigma_s L}{u_\infty \rho_\infty c_\infty}\right)\xi a\left(\frac{T}{T_\infty}\right) = 0 \tag{13}$$

where σ_s is the Schmidt number.

As was postulated earlier that the temperature profiles (and likewise the concentration profiles), in terms of the relative distance ratio η, are modified to a different extent at different distances from the leading edge, it follows that the solutions of Equations (12) and (13) can be expressed as the following two series:

$$\frac{T}{T_\infty} = 1 + \left(\frac{T_w}{T_\infty} - 1\right)[\theta_0(\eta) + \theta_1(\eta)\xi + \theta_2(\eta)\xi^2 + \cdots] \tag{14}$$

and

$$\frac{c}{c_\infty} = 1 + \zeta_0(\eta) + \zeta_1(\eta)\xi + \zeta_2(\eta)\xi^2 + \cdots \tag{15}$$

By substituting Equations (14) and (15) into Equations (12) and (13) and assuming that the reaction is one of the second order of the Arrhenius type, such that

$$a \equiv -\frac{d\rho_r}{dt} = K\rho^2 c^2 \exp(-E/RT) \tag{16}$$

the following sets of ordinary differential equations are obtained by equating the terms of equal powers of ξ:

$$\left.\begin{aligned} \theta_0'' + \sigma f\theta_0' &= 0 \\ \zeta_0'' + \sigma_s f\zeta_0' &= 0 \end{aligned}\right\} \tag{17}$$

$$\left.\begin{aligned} &\theta_1'' + \sigma f\theta_1' - 2\sigma f'\theta_1 \\ &+ \frac{A\exp\{-E/RT_\infty[1+(T_w-T_\infty)\theta_0/T_\infty]\}}{[(T_w-T_\infty)/T_\infty][1+(T_w-T_\infty)\theta_0/T_\infty]} = 0 \\ &\zeta_1'' + \sigma_s f\zeta_1' - 2\sigma_s f'\zeta_1 \\ &- \frac{A\exp\{-E/RT_\infty[1+(T_w-T_\infty)\theta_0/T_\infty]\}}{(\sigma/\sigma_s)(c_\infty Q_p/c_p T_\infty)[1+(T_w-T_\infty)\theta_0/T_\infty]} = 0 \end{aligned}\right\} \tag{18}$$

$$\left.\begin{aligned} &\theta_2'' + \sigma f\theta_2' - 4\sigma f'\theta_2 \\ &+ \frac{A\exp\{-E/RT_\infty[1+(T_w-T_\infty)\theta_0/T_\infty]\}}{[(T_w-T_\infty)/T_\infty][1+(T_w-T_\infty)\theta_0/T_\infty]} \\ &\times\left\{\frac{(T_w-T_\infty)/T_\infty}{[1+(T_w-T_\infty)\theta_0/T_\infty]}\times\right. \\ &\left.\cdot\left[\frac{E/RT_\infty}{[1+(T_w-T_\infty)\theta_0/T_\infty]} - 1\right]\theta_1 + 2\zeta_1\right\} = 0 \\ &\zeta_2'' + \sigma_s f\zeta_2' - 4\sigma_s f'\zeta_2 \\ &- \frac{A\exp\{-E/RT_\infty[1+(T_w-T_\infty)\theta_0/T_\infty]\}}{(\sigma/\sigma_s)(c_\infty Q_p/c_p T_\infty)[1+(T_w-T_\infty)\theta_0/T_\infty]} \\ &\times\left\{\frac{(T_w-T_\infty)/T_\infty}{[1+(T_w-T_\infty)\theta_0/T_\infty]}\times\right. \\ &\left.\cdot\left[\frac{E/RT_\infty}{[1+(T_w-T_\infty)\theta_0/T_\infty]} - 1\right]\theta_1 + 2\zeta_1\right\} = 0 \end{aligned}\right\} \tag{19}$$

etc.

Here

$$A \equiv \left(\frac{4\sigma K L\rho_\infty c_\infty}{u_\infty}\right)\left(\frac{c_\infty Q_p}{c_p T_\infty}\right) \tag{20}$$

The boundary conditions are:

$$\left.\begin{aligned} \theta_0(0) &= 1, \qquad \theta_0(\infty) = 0 \\ \zeta_0'(0) &= \zeta_0(\infty) = 0 \end{aligned}\right\} \tag{21}$$

and

$$\left.\begin{aligned} \theta_m(0) &= \theta_m(\infty) = 0 \\ \zeta_m'(0) &= \zeta_m(\infty) = 0 \end{aligned}\right\} \tag{22}$$

where m is any positive integer, equal to or greater than one.

It can be shown that the solutions of Equations (17) and (21) are

$$\theta_0(\eta) = \left[\int_\eta^\infty (f'')^\sigma\, d\eta\right] \Big/ \left[\int_0^\infty (f'')^\sigma\, d\eta\right] \tag{23}$$

and

$$\zeta_0(\eta) = 0 \tag{24}$$

In other words, the terms which are independent of the variable ξ in Equations (14) and (15)

correspond to the heat-transfer solutions for a laminar flow over an isothermal plate without chemical reaction (*e.g.*, see Goldstein[5]). This further justifies the assumption that the solutions for temperature and concentration can be expressed in series form.

Discussion of Results

QUALITATIVE PREDICTIONS

The solutions of the transformed boundary-layer equations, (17), (18) and (19), together with Equations (14), (15) and (16), describe the development of combustion in the laminar boundary layer over a hot surface. Should the conditions with respect to reaction rate and transfer of heat, mass, and momentum be favorable, the combustible mixture would be ignited. However, without solving these equations, several qualitative predictions of the conditions for incipient ignition can be made by examining the dimensionless parameters which appear in these equations. These parameters are: Prandtl number σ, Schmidt number σ_s, dimensionless activation energy E/RT_∞, dimensionless enthalpy of combustion $c_\infty Q_p/c_p T_\infty$, surface temperature ratio T_w/T_∞, and a factor $(KL\rho_\infty c_\infty/u_\infty)$,† which contains the free-stream conditions ρ_∞, c_∞, u_∞, the specific reaction rate K, and the characteristic length L. It is convenient to let L be the physical length of the flat plate.

(*a*) *Effect of free-stream density and flat-plate length*

For the same values of the Prandtl and Schmidt numbers, dimensionless activation energy, and dimensionless enthalpy of combustion, and for a reaction of the second order, incipient ignition occurs at the same value of the surface temperature ratio if the value of the factor $KL\rho_\infty c_\infty/u_\infty$ remains the same. In other words, for a mixture of given composition and a flat plate of given length, incipient ignition occurs at the same value of T_w/T_∞ if the free-stream velocity varies directly with the free-stream density. Also, for a mixture of given composition and density, incipient ignition occurs at the same value of T_w/T_∞ if the free-stream velocity varies directly with the length of the flat plate. Hence, if the variation of the surface temperature ratio versus the free-stream velocity is known for given values of the mixture density and plate length, its variation for different values of the mixture density and plate length can be predicted by means of the above relationships.

(*b*) *Effect of free-stream velocity*

In order to satisfy the conditions for incipient ignition, it is expected that the profiles of temperature, concentration, and reaction rate would assume some typical forms. With Equations (14), (15) and (16), it may further be assumed that the values of θ_m and ζ_m would be nearly the same for incipient ignition, when the value of ξ is one. As the free-stream velocity increases, the factor A decreases for a given value of $\sigma KL\rho_\infty c_\infty(c_\infty Q_p/c_p T_\infty)$. To compensate for this decrease in the value of A, it is necessary to increase the value of the predominant term,

$$\exp\{-E/RT_\infty[1 + (T_w - T_\infty)\theta_0/T_\infty]\},$$

in Equations (18) and (19), so that the values of θ_m and ζ_m remain nearly the same. For a given value of the dimensionless activation energy E/RT_∞, the exponential term increases as the surface temperature ratio increases. Hence, it can be predicted qualitatively that as the free-stream velocity increases, the surface temperature ratio required for incipient ignition increases.

Because of the strong effect due to the exponential term, it is expected also that the curve representing the variation of the surface temperature ratio versus the free-stream velocity as the abscissa would be concave downward, within the usual range of values for the surface temperature.

(*c*) *Effect of free-stream temperature*

In the study of the effect of free-stream velocity in (*b*), it is observed that the value of the exponential term should increase as the free-stream velocity increases. For given values of activation energy and surface temperature ratio, the exponential term increases in value if the free-stream temperature increases. Thus, in order to ignite a given mixture at the same surface temperature ratio but at a higher free-stream velocity, the free-stream temperature should be higher.

COMPARISON WITH EXPERIMENTAL RESULTS

Tied in with the theoretical investigation presented here was an experimental program, in which the incipient ignition conditions of an ethanol-air mixture near a hot surface were studied in a steady-flow apparatus. Only a brief description of the experimental investigation is given below. The details will be presented in a separate paper.

† It can be shown that if the order of reaction is n, this factor is reduced to the form $KL(\rho_\infty c_\infty)^{n-1}/u_\infty$.

Figure 1 shows the apparatus used in the experimental program. The test section consists of a steel tube ½ in. i.d., with a Nichrome segment 2 in. long, fitted into a longitudinal slot cut in the tube, to serve as the hot surface. It can be shown that the flow in such a short test section is closely approximated by flow over a flat plate, which represents the model used in the theoretical analysis. Hence, the theoretical and experimental results can be directly compared.

The Nichrome segment is heated externally by means of an oxyacetylene torch, so that its surface temperature can be independently controlled. Three quartz windows are placed opposite to the hot surface. The surface temperature is measured by means of an optical pyrometer, and ignition is indicated by means of an ionization gap.

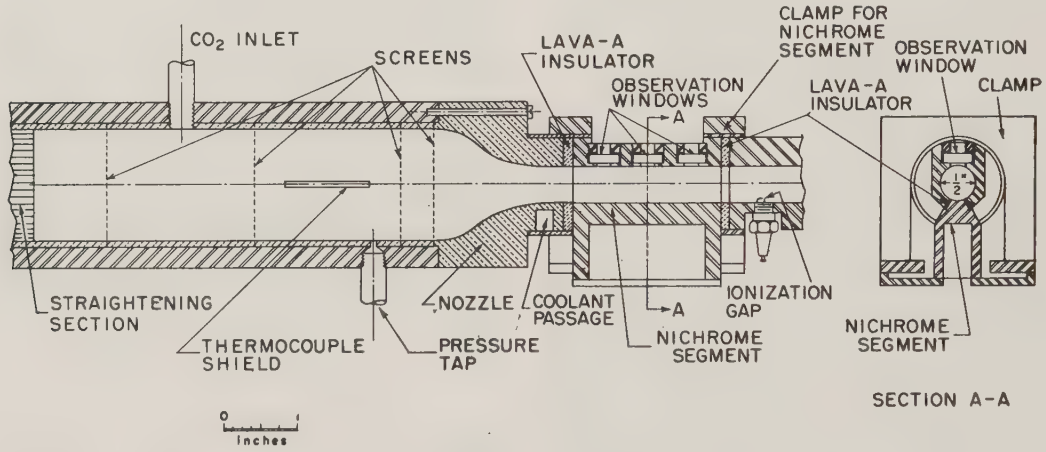

Fig. 1. Apparatus.

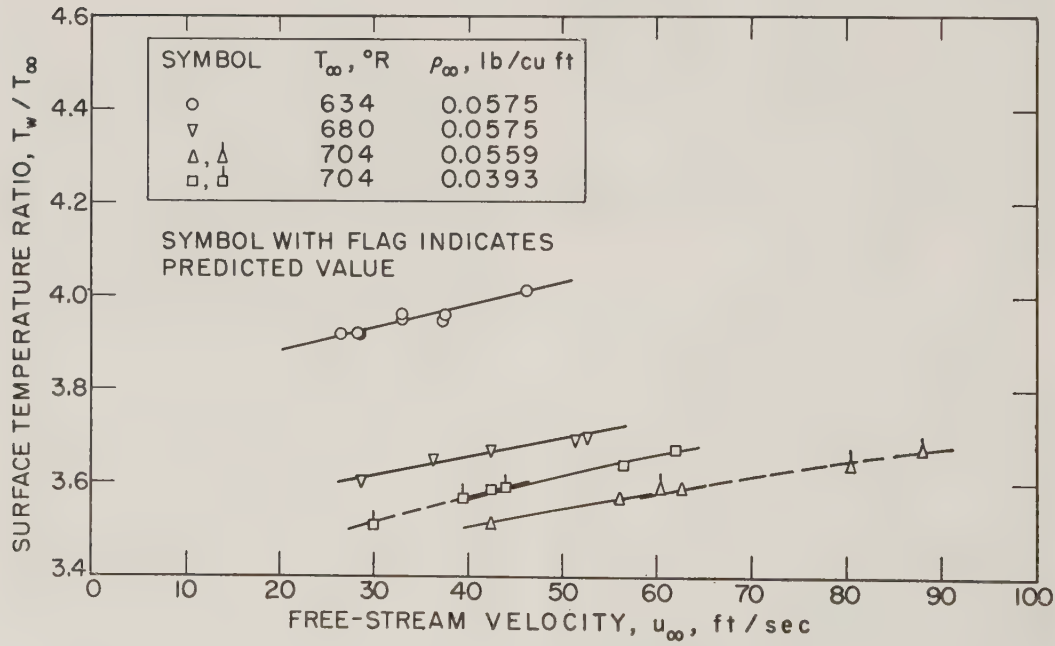

Fig. 2. Surface temperature for incipient ignition of stoichiometric ethanol-air mixture.

Preliminary tests made in this apparatus consisted of the study of the effects of velocity, density, and temperature of the free stream of a stoichiometric mixture of ethanol and air on the surface temperature required for incipient ignition. These results are summarized in Figure 2.

Within the range tested, the surface temperature ratio for incipient ignition increases with increasing velocity, decreasing density, and decreasing temperature of the free stream.

Figure 2 shows that the variation of surface temperature ratio versus free-stream velocity or temperature agrees with what is predicted qualitatively from the theory. If the over-all reaction-rate expression for an ethanol-air mixture is approximated by an Arrhenius equation of the second order, the present theory indicates that incipient ignition occurs at the same value of the surface temperature ratio, if the free-stream velocity is varied directly with the free-stream density. By the use of this relationship, two dashed curves are drawn in Figure 2. They are found to agree fairly well with the respective experimental curves. This agreement seems to indicate that the over-all reaction-rate expression for ethanol-air combustion near a hot surface is approximately second order.

PROFILES OF VELOCITY, TEMPERATURE, CONCENTRATION AND REACTION RATE

The boundary-layer equations, (17), (18) and (19), were solved with the aid of the M.I.T. Whirlwind Computer for a second-order reaction of the Arrhenius type for specific values of the dimensionless activation energy, dimensionless enthalpy of combustion, Prandtl and Schmidt numbers, and for several values of the surface temperature ratio. Figure 3 shows the profiles of velocity, temperature, concentration, and reaction rate across the laminar boundary layer at various distances from the leading edge of the hot plate for a value of T_w/T_∞ of 3.9. The specific values of the dimensionless activation energy, dimensionless enthalpy of combustion, Prandtl and Schmidt numbers are 57.5, 6.64, 0.65, and 0.65, respectively. These profiles are calculated by means of Equations (11), (14), (15) and (16), using terms up to θ_5 and ζ_5 in the temperature and concentration series. The convergence becomes poor at a distance corresponding to a value of $A\xi$ greater than 2.5×10^8, for the particular value of T_w/T_∞ of 3.9.

It is to be noted that the temperature profile at the leading edge, where the value of $A\xi$ is zero, corresponds to the one due to heat transfer only. As the distance from the leading edge increases, the temperature profiles are modified due to chemical reaction, with the temperature gradient at the wall increasing from a negative value to a positive one. In other words, when the distance is greater than a certain value, which depends on the surface temperature ratio and other factors, heat is transferred from the fluid to the wall; while heat is transferred from the wall to the fluid near the leading edge.

Note also in Figure 3 that, as the distance from the leading edge increases, the peaks in the temperature and reaction-rate profiles move in the direction toward the free stream of the combus-

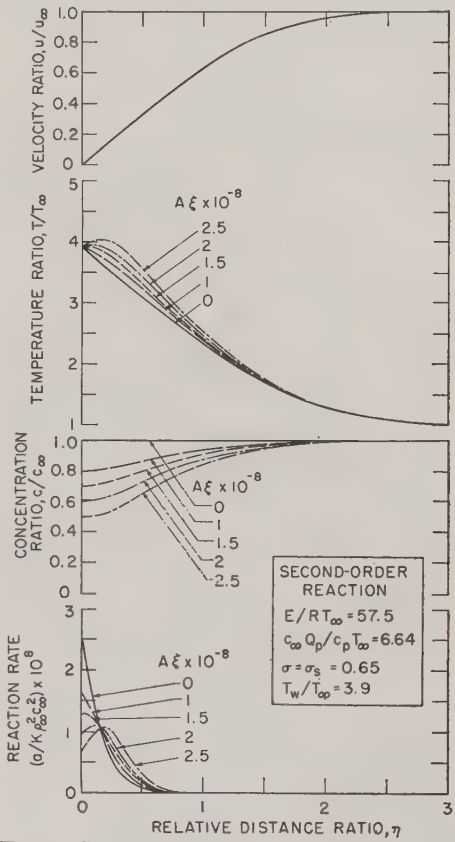

FIG. 3. Profiles of velocity, temperature, concentration, and reaction rate.

tible mixture. Meanwhile, steep gradients appear in both the temperature and the concentration profiles, thus indicating the possibility of an ignition if the distance from the leading edge is sufficiently large.

Figure 3 also shows that the reaction is significant only in a small portion of the laminar boundary layer.

Solutions of the boundary-layer equations were also obtained for other values of T_w/T_∞. The various profiles are similar to those described above. It is also found that, as the surface temperature ratio increases, the corresponding similar

features of these profiles are observed at lower values of $A\xi$. For example, the temperature gradient at the wall becomes zero at $A\xi = 1.339 \times 10^8$ for $T_w/T_\infty = 3.9$ and at $A\xi = 0.751 \times 10^8$ for $T_w/T_\infty = 4.1$.

DEVELOPMENT OF COMBUSTION IN PHYSICAL PLANE

Figure 4 shows the development of combustion in the physical (x, y) plane for the conditions of Figure 3. The ordinate and abscissa are proportional to the distances normal to the plate wall and from the leading edge, respectively. The growth of the velocity and thermal boundary layers, with and without reaction, is indicated. Here, the boundary-layer thicknesses are arbitrarily defined as those at which the velocity and the temperature are 0.999 and 1.001 times the respective free-stream values. As the effect of reaction on boundary-layer growth is rather small during the early stage of the development of combustion, it is evident from Equations (8) and (11) that the velocity profiles, with and without reaction, are nearly identical in the physical plane.

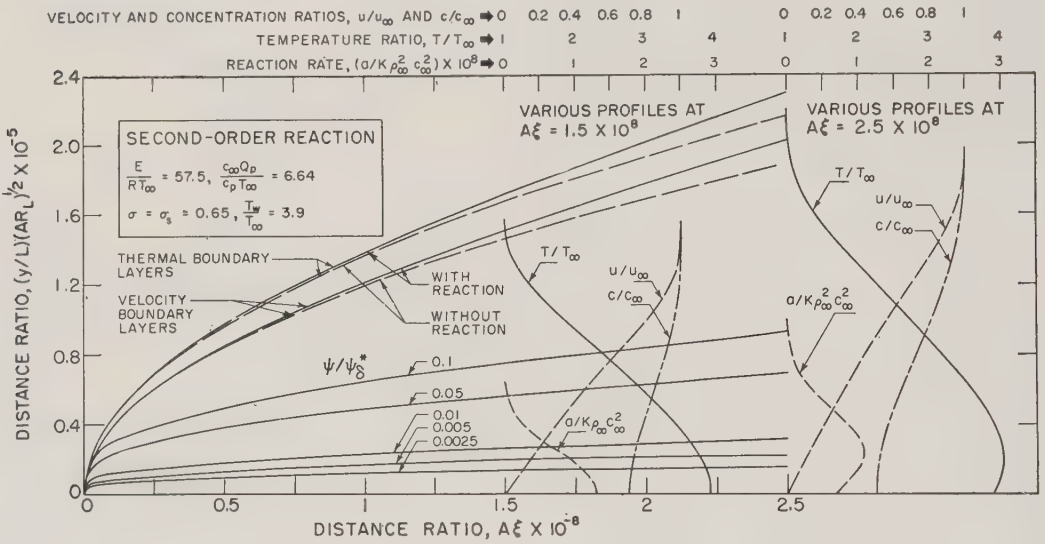

FIG. 4. Development of combustion in physical plane.

Also shown in Figure 4 are the various streamlines of different values of ψ/ψ_δ^*, which indicates the ratio of the mass rate of flow between the particular streamline and the wall to the mass rate of flow across the entire velocity boundary layer at the section where the value of $A\xi$ is 2.5×10^8. It is observed that, due to the low velocity and high temperature (and hence low density) near the wall, only about 10 per cent of the mass rate of flow is passing through that half of the boundary layer nearer to the wall.

In Figure 4 are shown also the profiles of velocity, temperature, concentration, and reaction rate at two specific sections; *viz.*, $A\xi = 1.5 \times 10^8$ and 2.5×10^8. Note again that the peaks in the temperature and reaction-rate profiles are moving toward the free stream in the physical plane.

VARIATIONS OF TEMPERATURE, CONCENTRATION, AND REACTION RATE ALONG STREAMLINES

Figure 5 shows the variations of temperature, concentration, and reaction rate along streamlines of different values of ψ/ψ_δ^* for the conditions of Figures 3 and 4. As a mass element moves downstream, its temperature rises while its concentration of combustible component decreases. Along a streamline in the immediate neighborhood of the hot plate, the reaction rate rises sharply and then decreases with the flow downstream. Along a streamline at a distance normal to the flat plate greater than a fraction of the boundary-layer thickness near the trailing edge, the reaction rate remains negligibly small. However, along a streamline somewhere between the two extreme ones described above, the reaction rate increases rapidly to a large value and remains quite high.

Figure 5 shows also a comparison of the temperature rise, with and without reaction, along two specific streamlines. The effect due to chemical reaction becomes increasingly more important as the mass element moves downstream.

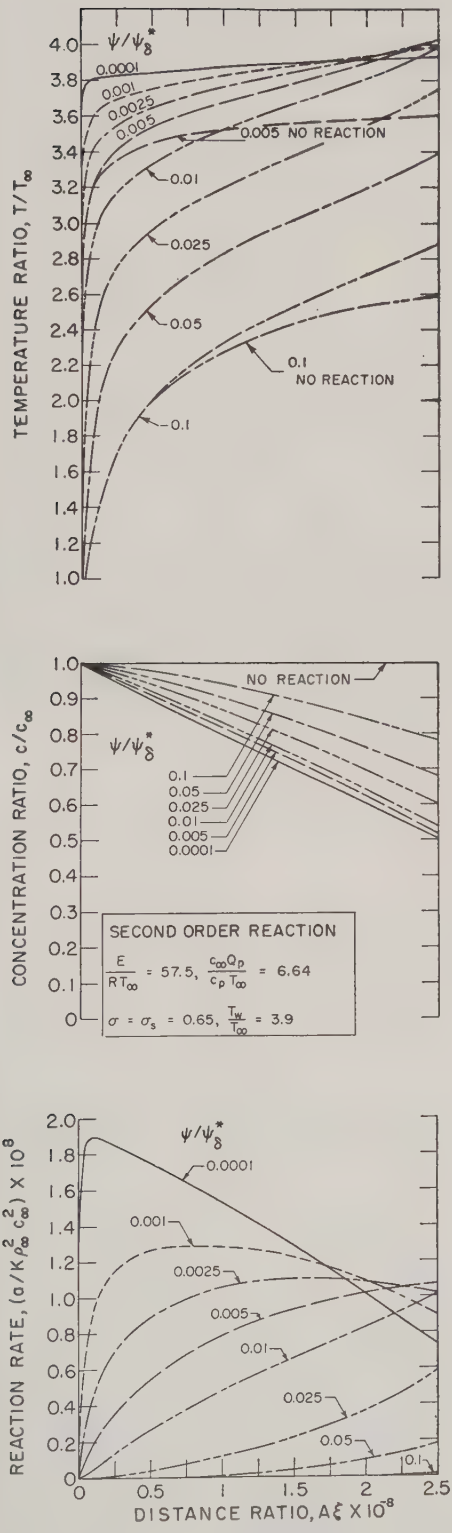

FIG. 5. Variations of temperature, concentration, and reaction rate along streamlines.

Acknowledgment

The work reported here was partially supported by the Shell-Oil-Company Research Grant. Availability of the M.I.T. Digital Computer Laboratory time for the solution of the boundary-layer equations was made possible by the Office of Naval Research. The assistance of Mr. Anthony J. Shashaty in the preparation of programs for the Whirlwind Computer is gratefully acknowledged.

Nomenclature

- A a factor, defined by Equation (20)
- a rate of consumption of combustible component per unit volume
- c mass fraction of combustible component in mixture
- c_p specific heat at constant pressure
- D binary diffusion coefficient
- E activation energy
- f function of η
- K specific reaction rate, see Equation (16)
- L length of flat plate
- m any positive integer
- n order of reaction
- Q_p enthalpy of combustion per unit mass of combustible component
- R universal gas constant
- R_L length Reynolds number, $u_\infty L/\nu_\infty$
- T absolute temperature
- t time
- u velocity component in x-direction
- v velocity component in y-direction
- x distance along flat plate
- y distance normal to flat plate
- ζ function of η, see Equation (15)
- η relative distance ratio, see Equation (8)
- θ function of η, see Equation (14)
- λ thermal conductivity
- μ absolute viscosity
- ν kinematic viscosity
- ξ distance ratio, x/L
- ρ density
- σ Prandtl number, $c_p\mu/\lambda$
- σ_s Schmidt number, ν/D
- ψ stream function, see Equations (5) and (6)

SUBSCRIPTS

- ∞ refers to free-stream condition
- r refers to combustible component
- w refers to condition at plate wall
- δ refers to outer edge of velocity boundary layer

Superscript* indicates a particular position where $A\xi = 2.5 \times 10^8$

Prime denotes differentiation with respect to η

REFERENCES

1. Mullen, J. W., II, Fenn, J. B., and Irby, M. R.: *Third Symposium on Combustion, Flame and Explosion Phenomena*, p. 317. Baltimore, The Williams & Wilkins Co., 1948.
2. Agoston, G. A.: Sc.D. Thesis, Department of Chemical Engineering, Massachusetts Institute of Technology (1949).
3. Chapman, D. R., and Rubesin, M. W.: J. Aeronaut. Sci., *16*, 547 (1949).
4. Howarth, L.: Proc. Royal Soc., *A164*, 551 (1938).
5. Goldstein, S.: *Modern Developments in Fluid Dynamics*, *2*, 623, London, Oxford University Press, (1938).

66

THE FLAMMABILITY CHARACTERISTICS OF THE SYSTEM H_2–NO–N_2O–Air[a]

By F. E. SCOTT, R. W. VAN DOLAH and M. G. ZABETAKIS

Introduction

Little information is available on the flammability characteristics of combustible-oxidant systems using oxidants other than air or oxygen. As such information often is necessary to permit the safe operation of an industrial process involving oxidants like the oxides of nitrogen, an investigation was undertaken by the Bureau of Mines to define the limits of flammability of hydrogen in mixtures of nitric oxide, nitrous oxide and air. The study also included a determination of limit-mixture flame speeds and the general appearance of the resultant flames.

Apparatus and Test Procedures

Limits of flammability of hydrogen-air-nitric oxide-nitrous oxide mixtures were determined at one atmosphere pressure and about 28°C. Tests were conducted in the standard Bureau of Mines apparatus[1] using one of two procedures. The standard procedure[1] was used for all tests involving nonreacting gas mixtures; in the other cases, no mercury mixer was used and mixing was achieved by diffusion. Adequacy of mixing was evaluated for a number of mixtures by determining the limits of flammability when the mixture components were added in various orders and by observing the motion of the flame front.[b]

The compositions of the test mixtures were calculated from the partial pressures of the n mixture components in the case of initially nonreacting mixtures and from n-1 partial pressures plus the final pressure in the case of the reacting mixtures. Thus, for nonreacting mixtures such as H_2-air-N_2O, the mixture compositions are calculated by use of the following:

$$\text{per cent i} = \frac{100p_i}{\sum_{j=1}^{n} p_j} = \frac{100p_i}{P} \qquad (1)$$

where per cent i is the concentration of the i^{th} component in the test mixture, p_i is the partial pressure of the i^{th} component and $P(\sum_{j=1}^{n} p_j)$ is the total system pressure (equal to one atmosphere in this study) for the n-component mixture.

In the case of reacting mixtures, the total pressure, P, is not equal to the sum of the partial pressures, so that Equation (1) is no longer applicable. However, the first part of Equation (1) can be used formally to determine a mixture composition based on the partial pressures of the original components before a reaction occurs. For example, consider a hydrogen-nitrous oxide-nitric oxide-air mixture in which each component is added to a constant volume system so that partial pressure measurements are made on each component except air. As the air is added, the oxygen and nitric oxide react to produce NO_2 and N_2O_4, and the quantity of air added to the system must be calculated from the final pressure. This value is then used to calculate formally the mixture composition on the assumption that Dalton's law is obeyed. The Amagat-Leduc law of

[a] This research is a part of the work being carried out at the Bureau of Mines under a program sponsored by the Atomic Energy Commission.

[b] A limit test mixture that is inadequately mixed is characterized by a non-uniform flame movement through the glass explosion chamber of the test apparatus.

partial volumes also could be applied; however, in general, it would not be as precise for a system requiring as large a volume as the standard limit-of-flammability apparatus.

To calculate the partial pressure of air added to the H_2—N_2O—NO system from the final system pressure, the quantities of gases such as NO_2 and N_2O_4 formed by addition of air to NO must be known. The equilibrium between NO_2 and N_2O_4 is temperature and pressure dependent; however, at one atmosphere pressure the equilibrium concentration can be expressed in terms of the degree of dissociation, α, which represents the fraction of the original N_2O_4 that dissociates. For example, at about 28°C and one atmos pressure, one mole N_2O_4 yields an equilibrium mixture of 2α or 0.42 mole NO_2 and $(1 - \alpha)$ or 0.79 mole N_2O_4, or 35 per cent NO_2, 65 per cent N_2O_4.[4] Then, assuming that N_2O_4 and NO_2 are formed in the ratio 65:35, and neglecting the formation of other oxides of nitrogen, a mixture of w' moles N_2O, x' moles H_2, y' moles air (taken to have a composition of 0.21 O_2 + 0.79 N_2) and z' moles NO gives:

$$w'N_2O + x'H_2 + y'(0.21\ O_2 + 0.79\ N_2) + z'NO \rightarrow w'N_2O + x'H_2 + 0.79\ y'N_2 + 0.42y'(0.21NO_2 + 0.395N_2O_4) + (z' - 0.42y');\ \text{NO } z' \geqslant 0.42y' \quad (2)$$

or

$$w'N_2O + x'H_2 + y'(0.21\ O_2 + 0.79\ N_2) + z'NO \rightarrow w'N_2O + x'H_2 + 0.79\ y'N_2 + (0.21y' - 0.5z')\ O_2 + 0.21z'\ NO_2 + 0.395z'\ N_2O_4;\ z' \leqslant 0.42y' \quad (3)$$

If Dalton's law of partial pressures is applicable, the above equations give:

$$y = 1.60\ (P\text{-}w\text{-}x\text{-}z), \qquad z \geqslant 0.42y \text{ (excess NO)} \quad (4)$$

$$y = P\text{-}w\text{-}x\text{-}0.105z, \qquad z \leqslant 0.42y \text{ (excess } O_2) \quad (5)$$

where w, x, y and z are the partial pressures of N_2O, H_2, air and NO, respectively, before the formation of N_2O_4 and NO_2 and P is the final pressure after the gases are mixed. Knowing the partial pressures, w, x, y and z (or p_1, p_2, p_3 and p_4, respectively), a mixture composition can be so defined that

$$\text{per cent i} = \frac{100\ p_i}{\sum_{j=1}^{4} p_j} \quad (6)$$

as in the case of the nonreacting gas mixtures (Eq. (1)), the only difference being that here $\sum_{j=1}^{4} p_j \neq P$, as noted above. If the total pressure, P, is substituted for the summation in Equation (6), the percentages of the nonreacting constituents are increased by the ratio $1/P$. $\sum_{j=1}^{4} p_j$, that is, the lower and upper limits are increased.

Table 1. Limits-of-flammability Data for Hydrogen-nitric Oxide-nitrous Oxide Mixtures at about 28°C and One Atmosphere Pressure

Test No.	Composition, mole % H_2	NO	N_2O	Propagated Flame?
	Lower Limit			
7	6.7	93.3	—	Yes
8	6.6	93.4	—	No
59	5.3	47.4	47.3	Yes
54	5.0	47.5	47.5	No
198	5.5	54.5	40.0	Yes
18	3.0	—	97.0	No
20	3.1	—	96.9	Yes
	Upper Limit			
17	66.0	34.0	—	Yes
16	66.9	33.1	—	No
50	67.5	25.5	7.0	No
48	67.0	25.0	8.0	Yes
39	68.4	15.8	15.8	Yes
36	68.7	15.7	15.6	No
51	72.8	10.0	17.2	No
52	71.9	10.5	17.6	Yes
40	77.9	5.5	16.6	No
42	78.1	4.5	17.4	Yes
197	68.0	16.0	16.0	Yes
25	84.6	—	15.4	No
22	83.7	—	16.3	Yes

Results

The experimental points used to plot the limit-of-flammability curves of the H_2—NO—N_2O—air system are listed in Tables 1 to 6 and presented graphically in Figures 1 to 6. The flammability curves in Figures 4, 5 and 6 differ from those in Figures 1, 2 and 3 in that they represent four-component mixtures instead of three-component mixtures and are sections within the regular tetrahedron depicted in Figure 7. Flame speeds of various limit mixtures were determined by measuring the time required for the passage of the flame front between two reference points 110

cm apart with a manually operated stopclock. These varied from 24 to 100 cm/sec, the fastest flames being those of hydrogen-rich mixtures. The colors of the flames were white or pale blue for all mixture compositions tested except those near the maximum and minimum points on the H_2—NO—air limit-of-flammability curves. Near these points the flames appeared to have a reddish-orange hue. Lower limit flames of the hydrogen-nitrous oxide-air system appeared to be diffusion flames; that is, the flames had the appearance of clouds of luminous balls of fire

Table 2. Limits-of-flammability Data for Hydrogen-nitrous Oxide-air Mixtures at about 28°C and One Atmosphere Pressure

Test No.	Composition, mole % H_2	N_2O	Air	Propagated Flame?
	Lower Limit			
18	3.0	97.0	—	No
20	3.1	96.9	—	Yes
—[1]	4.0	—	96.0	Limit mixture
47	3.9	48.1	48.0	Yes
44	3.5	48.2	48.3	No
195	4.5	25.0	70.5	Yes
	Upper Limit			
25	84.6	15.4	—	No
22	83.7	16.3	—	Yes
—[1]	75.0	—	25.0	Limit mixture
191	81.0	9.5	9.5	Yes
—[3]	83.4	13.3	3.3	Limit mixture
—[3]	82.1	10.7	7.2	Limit mixture
—[3]	80.0	8.0	12.0	Limit mixture
—[3]	77.4	4.5	18.1	Limit mixture

similar to those described by Coward and Jones[1] for lower limit hydrogen-air mixtures.

The broken lines in Figures 1 to 6 represent the limit-of-flammability curves that would result if Le Chatelier's law applies.[1] The lower limit mixtures of the H_2—NO—N_2O system and both the upper and lower limit mixtures of the H_2—N_2O—air system follow this law. The greatest deviations are observed with the H_2—NO—Air system. The upper limit deviation is quite pronounced due to the method of calculating the mixture compositions. It is interesting to note that similar limit curves were obtained for a nonreacting system of hydrogen-bromine and air by Simmons and Wolfhard.[2]

Smith and Linnett[3] determined upper limits of flammability for hydrogen in mixtures of nitrous oxide and air. Part of this work was repeated in the present investigation; the agreement was quite good (Fig. 2).

Table 3. Limits-of-flammability Data for Hydrogen-nitric Oxide-air Mixtures at about 28°C and One Atmosphere Pressure

Test No.	Composition, mole % H_2	NO	Air	Propagated Flame?
	Lower Limit			
103	5.3	13.2	81.5	No
104	6.8	9.3	83.9	Yes
101	7.1	24.8	68.1	No
102	7.5	24.6	67.9	Yes
108	14.2	41.7	44.1	No
188	14.4	53.6	32.0	No
89	14.8	35.3	49.9	No
109	15.6	36.8	47.6	No
114	16.0	42.2	41.8	Yes
190	16.0	53.7	30.3	Yes
88	16.2	38.1	45.7	Yes
110	17.3	35.4	47.3	Yes
111	10.8	63.3	25.9	Yes
113	8.3	71.2	20.5	No
	Upper Limit			
150	69.8	2.0	28.2	No
149	64.9	2.0	33.1	Yes
138	57.5	4.8	37.7	No
187	57.1	3.7	39.2	Yes
139	46.7	7.4	45.9	Yes
154	46.0	9.1	44.9	No
153	43.1	9.2	47.7	Yes
152	39.1	12.5	48.4	No
140	33.9	17.0	49.1	Yes
146	31.1	20.4	48.5	Yes
145	32.2	21.4	46.4	No
144	32.0	26.1	41.9	Yes
147	36.1	25.7	38.2	No
186	34.4	27.9	37.7	Yes
151	44.9	27.8	27.3	No
143	51.2	30.8	18.0	Yes
147	57.2	30.5	12.3	Yes
155	62.2	30.1	7.7	No
193	63.0	32.4	4.6	Yes

The minimum point, *a*, on the upper limit of the H_2—NO—air curve (Fig. 3) occurs at the mixture composition corresponding to a stoichiometric nitric oxide-oxygen mixture whereas the maximum point, *b*, on the corresponding lower

TABLE 4. LIMITS-OF-FLAMMABILITY DATA FOR HYDROGEN-NITRIC OXIDE-NITROUS OXIDE-AIR MIXTURES AT ABOUT 28°C AND ONE ATMOSPHERE PRESSURE (PER CENT NO/PER CENT N_2O = 2.57)

Test No.	Composition, mole % H_2	NO	N_2O	Air	Propagated Flame?
		Lower Limit			
185	6.2	66.4	25.9	1.5	Yes
184	6.4	64.1	24.9	4.6	Yes
183	5.9	63.3	24.6	6.2	No
122	6.4	51.7	20.2	21.7	Yes
118	6.1	42.8	16.6	34.5	No
120	7.2	28.9	11.3	52.6	Yes
121	5.5	24.3	9.4	60.8	No
119	6.6	19.1	7.5	66.8	Yes
123	4.3	15.6	6.0	74.1	No

TABLE 5. LIMITS-OF-FLAMMABILITY DATA FOR HYDROGEN-NITRIC OXIDE-NITROUS OXIDE MIXTURES AT ABOUT 28°C AND ONE ATMOSPHERE PRESSURE (PER CENT NO/PER CENT N_2O = 1.0)

Test No.	Composition, mole % H_2	NO	N_2O	Air	Propagated Flame?
		Lower Limit			
130	4.2	7.3	7.3	81.2	No
131	6.3	12.4	12.4	68.9	Yes
126	6.9	15.9	15.9	61.3	Yes
124	5.9	18.0	18.0	58.1	No
127	7.0	19.4	19.4	54.2	Yes
128	5.1	27.2	27.1	40.6	No
129	6.3	32.5	32.5	28.7	Yes
		Upper Limit			
160	69.3	1.0	1.2	28.5	Yes
159	70.1	1.5	1.5	26.9	No
196	59.8	4.8	4.8	30.6	Yes
200	61.3	4.8	4.8	29.1	No
176	52.9	9.2	9.2	28.7	Yes
174	53.3	9.2	9.2	28.3	No
178	52.9	10.0	10.0	27.1	No
177	52.1	10.8	10.8	26.3	Yes
180	59.0	13.8	13.8	13.4	No
181	59.3	14.4	14.3	12.0	Yes
168	66.2	15.3	15.3	3.2	No
182	66.1	15.9	15.9	2.1	Yes

limit curve is a mixture composition that is rich in nitric oxide. However, both these points correspond to maximum concentrations of NO_2 and N_2O_4 along their respective curves, so that the addition of NO_2 and N_2O_4 to a hydrogen-air or a

TABLE 6. LIMITS-OF-FLAMMABILITY DATA FOR HYDROGEN-NITRIC OXIDE-NITROUS OXIDE-AIR MIXTURES AT ABOUT 28°C AND ONE ATMOSPHERE PRESSURE (PER CENT NO/PER CENT N_2O = 0.33)

Test No.	Composition, mole % H_2	NO	N_2O	Air	Propagated Flame?
		Lower Limit			
136	5.3	15.3	45.9	33.5	Yes
135	4.5	12.5	37.3	45.7	No
132	6.3	10.9	32.5	50.3	Yes
133	4.5	10.9	32.6	52.0	No
134	5.6	8.7	26.3	59.4	Yes
137	4.1	8.4	25.0	62.5	No

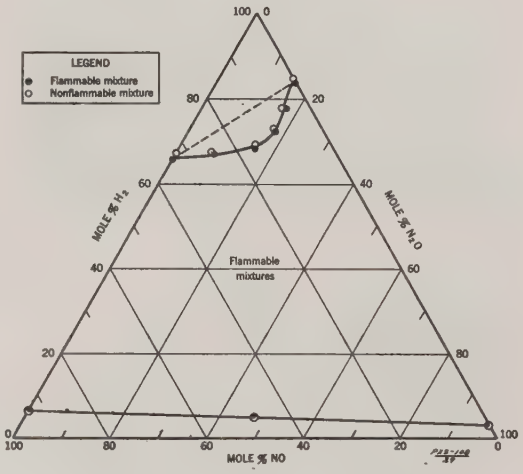

FIG. 1. Limits of flammability of the system H_2—NO—N_2O at ca. 28°C and 1 atmos pressure.

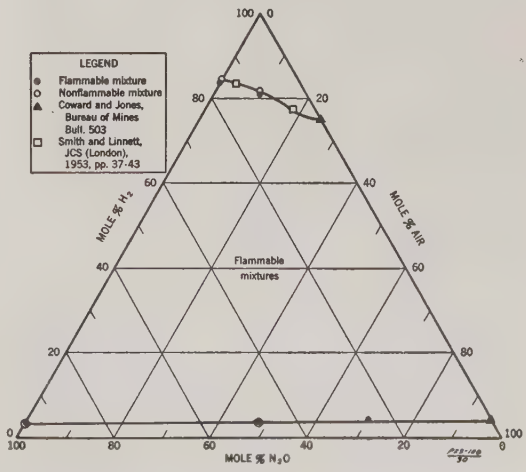

FIG. 2. Limits of flammability of the system H_2—N_2O-Air at ca. 28°C and 1 atmos pressure.

hydrogen-nitric oxide mixture inhibits the combustion of hydrogen in air and in nitric oxide.

Before limit-of-flammability tests were initiated on the above reacting mixtures, tests were conducted to determine whether a reaction occurs between hydrogen and oxygen when nitric oxide is added to a hydrogen-air mixture due to the heat of the oxygen-nitric oxide reaction. Test mixtures made with a gas burette, on the assumption that the Amagat-Leduc law was applicable, showed that only the nitric oxide-oxygen reaction occurs.

In addition to the above limits of flammability, the lower limit of hydrogen was determined in a stoichiometric nitric oxide-oxygen mixture. The test mixtures were prepared by introducing measured volumes of the gas components in the limit-of-flammability apparatus; the gas compositions were determined by assuming the Amagat-Leduc law applied. The lower limit of hydrogen in a stoichiometric nitric oxide-oxygen mixture was found to be 7.5 per cent hydrogen, which is the same as the lower limit of hydrogen in a stoichiometric nitric oxide-air mixture. This is rather surprising, as the specific heats of nitrogen dioxide and nitrogen tetroxide that were in excess

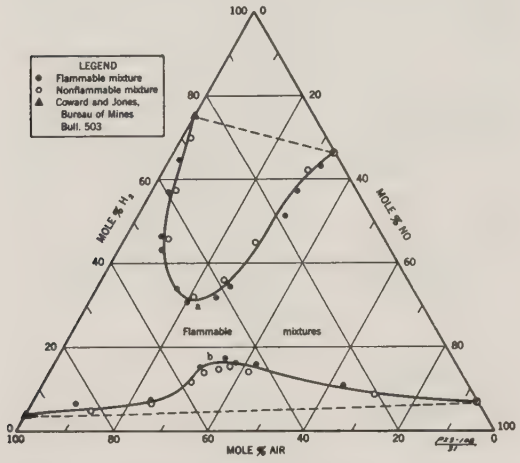

FIG. 3. Limits of flammability of the system H_2—NO-Air at ca. 28°C and 1 atmos pressure.

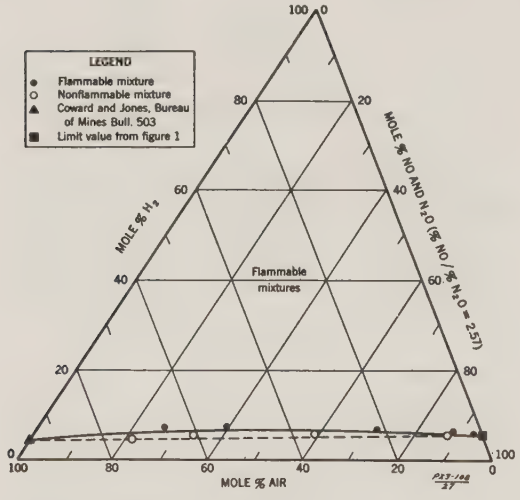

FIG. 4. Limits of flammability of the system H_2—NO—N_2O-Air at ca. 28°C and 1 atmos pressure (% NO/% N_2O = 2.57).

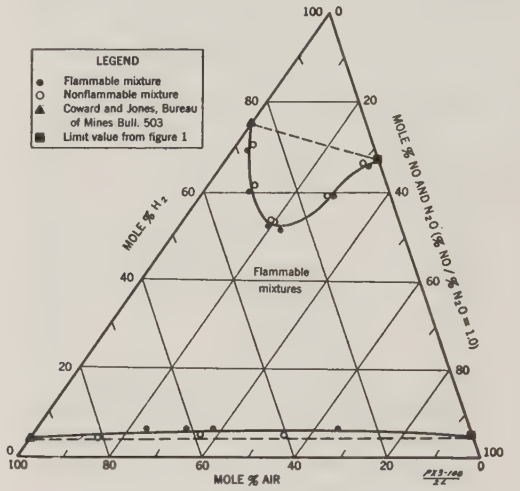

FIG. 5. Limits of flammability of the system H_2—NO—N_2O-Air at ca. 28°C and 1 atmos pressure (% NO/% N_2O = 1.0).

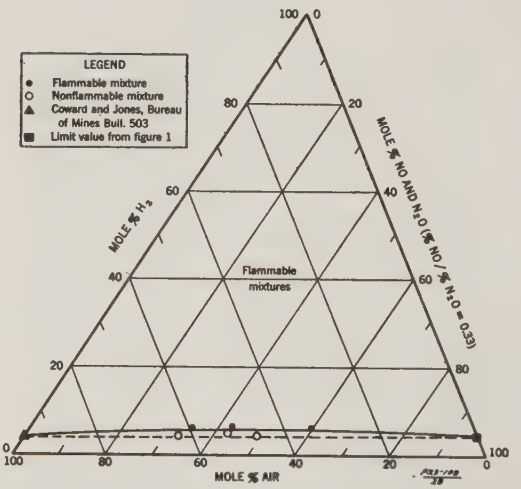

FIG. 6. Limits of flammability of the system H_2—NO—N_2O-Air at ca. 28°C and 1 atmos pressure (% NO/% N_2O = 0.33).

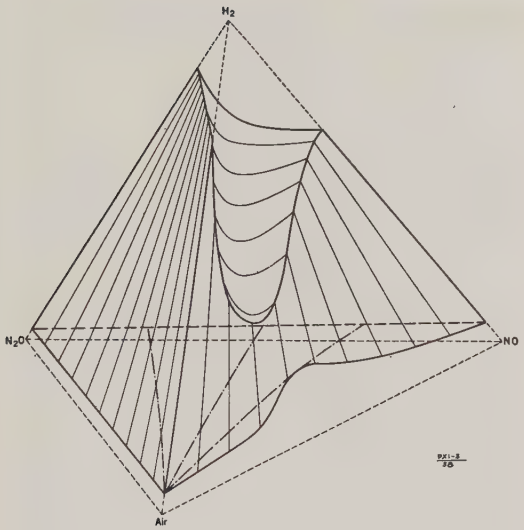

FIG. 7. Limits of flammability of the system H_2—NO—N_2O-Air at 1 atmos pressure and ca. 28°C.

in the second mixture are higher than that of nitrogen which was in excess in the first mixture.

Conclusions

Limits of flammability of the H_2—NO—N_2O—air system were determined at about 28°C and one atmosphere pressure. Some of the limit curves obey Le Chatelier's law for limit mixtures, while others show a marked deviation. The points of maximum deviation on the upper and lower limit-of-flammability curves were found in H_2—NO—air mixtures in which maximum quantities of NO_2 and N_2O_4 were formed in the precombustion reaction. As these points were approached along the limit-of-flammability curves, the flame colors changed from white to orange. In a study of flame-speed measurements of limit mixtures, the range of flame speeds was 24 to 100 cm/sec.

REFERENCES

1. COWARD, H. F., AND JONES, G. W.: U. S. Bureau of Mines Bulletin 503, 1952.
2. SIMMONS, R. F., AND WOLFHARD, H. G.: Trans. Faraday Soc., *51*, part 9, (1955).
3. SMITH, S., AND LINNETT, J. W.: J. Chem. Soc. (London), Part 1, 37–43, (1953).
4. DANIELS, F.: *Outlines of Physical Chemistry*, p. 259. New York, John Wiley & Sons, 1948.

67

THERMAL THEORY OF IGNITION OF GAS MIXTURES: LIMITING CONDITIONS

By L. N. KHITRIN AND S. A. GOLDENBERG

Ignition is the most typical and important phenomenon of combustion. The most common type of ignition is so-called artificial ignition by an electric spark. Recently this type of ignition was treated successfully from the standpoint of excess enthalpy.[1] In this connection, the ignition of gas mixtures is treated here from the standpoint of general thermal concepts, based on the theory of Zeldovich,[2] adequate development of which has proved quite fruitful.

Introduction

Unlike the ignition of quiescent mixtures, ignition of a gas flow has not been studied extensively, although investigations to date have dealt with the most important problem, namely, the relation between the critical ignition parameters (temperature and size of the ignition source, composition of the mixture) and the flow velocity.[3, 4, 5] Silver[3] has attempted a theoretical analysis of experimental data on ignition by a heated body, based on a greatly simplified application of Semyonov's theory of spontaneous thermal ignition.[6]

Zeldovich[2] formulated this problem more accurately although he limited himself to a simplified analysis of the simplest cases of ignition (quiescent medium, spherical or flat igniting wall). Subsequently, Semyonov[7] extended Zeldovich's results to the case of natural convection.

Later, related problems of the theory of ignition and quenching were developed by Blinov[8] and Frank-Kamenetzki[9] for a first order reaction and then for a reaction of any order.[10] A similar problem was considered recently by Spalding,[11] and the general questions of thermal conditions of combustion have been dealt with in detail in a monograph by Vulis.[12]

According to ideas expressed at an early date by Van't Hoff, ignition by a hot body takes place when the temperature gradient in the gaseous medium near the wall $(dT/dx)_s$ becomes greater than zero. The limiting condition of the stationary state is $(dT/dx)_s = 0$, unless the wall possesses catalytic properties. This condition implies that there is no flow of heat from the wall to the gas and that the heat, q_2 released by the reaction at the wall is sufficient to compensate for the quantity of heat q_1 lost to the surrounding unheated gaseous medium, i.e., $q_1 = q_2$. In this case, the heated wall merely brings the adjacent gas layer to a temperature such that an additional increment of temperature causes local spontaneous ignition with formation of a primary flame, which then spreads in all directions from the heated body, independent of the properties of the source.

The procedure for computing the critical conditions of ignition proposed by Zeldovich for the case of a flat heated wall and a spherical body, takes into account the fact that the reaction develops mainly in a relatively thin layer, ξ, in the immediate proximity of the "hot" wall, in the temperature interval $T_s - T_\xi \approx RT_s^2/E$, where Ts is the temperature of the wall, T_ξ the temperature of the outer boundary of the layer, ξ, and E is the activation energy of the chemical reaction. Within this layer the process is described by the equation[a]

$$\lambda \frac{d^2 T}{dx^2} + qW(C, T) = 0 \qquad (1)$$

where λ is the thermal conductivity coefficient of the mixture and q is the thermal effect; $W(C,T)$ is the expression for the rate of the reaction employed by Zeldovich in simplified form: $W(C,T) = K_0 c_0^\nu e^{-(E/RT)}$. (Here c_0 is the molar concentration of one of the reagents in the initial state, and ν is the total order of the reaction). It is assumed that the concentration near the wall is the same as at some distance from it, and that the mixture is stoichiometric. From Equation (1) we get

$$q_2 = -\lambda \left(\frac{dT}{dx}\right)_\xi = \sqrt{2\lambda q \int_{T_\xi}^{T_s} W(C, T)\, dT} \qquad (2)$$

Outside the layer, ξ, where the heat released by the reaction can be neglected, the value, q_1, is determined by the usual laws of thermal conductivity or heat transfer.

[a] In the case of a spherical body this equation remains practically true when $\xi \ll d$, where d is the diameter of the sphere.

The Problem of Ignition in the General Case

A precise solution of this problem for a moving medium is, of course, rather difficult, owing to the complexity of the flow of the gas around the body. Hence the necessity of employing a simplified model. In first appoximation, let us assume that the boundary layer surrounding the body is quiescent. The temperature in this layer drops from T_s to T_0, and the chemical reaction takes place there. Such schematizations are not unknown in computational practice for many processes, particularly in computations involving the combustion of solid bodies.[13, 14, 15] Experience shows that in the long run this model has been very satisfactory and has made it possible to attain a number of fundamental results in the field of the diffusion theory of solid combustion.

As for q_2, in this general case, the values of q_1 should be written as $q_1 = \alpha(T_\xi - T_0) \approx \alpha(T_s - T_0)$ where α is the coefficient of heat transfer. For the conditions at the boundary we obtain

$$\frac{Nu}{d}(T_s - T_0) = \sqrt{\frac{2q}{\lambda} \int_{T_\xi}^{T_s} W(C, T)\, dT} \qquad (3)$$

The chief computational task becomes the most accurate possible determination of the value $\mathfrak{I} = \int_{T_\xi}^{T_s} W(C, T)\, dT$.

In its general form

$$W(C, T) = Ka, b, c$$

where K is the velocity constant, and a, b, c are the effective molar concentrations of the reacting substances. There is always a definite relation between the initial concentrations of these substances, a_0, b_0, c_0. If we express the reaction in terms of c, then $a_0 = \beta_1 c_0$, $b_0 = \beta_2 c_0$, etc. If the concentration, c_0, is deficient, then

$$\left.\begin{aligned} a &= c_0\left(\beta_1 - 1 + \frac{cT}{c_0 T_0}\right)\frac{T_0}{T} \\ b &= c_0\left(\beta_2 - 1 + \frac{cT}{c_0 T_0}\right)\frac{T_0}{T} \end{aligned}\right\} \qquad (4)$$

and

$$W(C, T) = Kc_0^\nu\left(\beta_1 - 1 + \frac{cT}{c_0 T_0}\right) \cdot\left(\beta_2 - 1 + \frac{cT}{c_0 T_0}\right)\cdots\frac{c}{c_0}\left(\frac{T_0}{T}\right)^{\nu=1} \qquad (5)$$

If we express c as the relative concentration, then since $(c/c_0) = (N/N_0)(T_0/T)$, we can write,

$$W(C, T) = K_0 c_0^{\nu} \left(\frac{T_0}{T}\right)^{\nu} \Pi\left(\beta - 1 + \frac{N}{N_0}\right) \quad (5')$$

where $\Pi(\beta - 1 + (N/N_0))$ is the product of all the terms of the form $(\beta - 1 + (N/N_0))$, in which $\beta = \beta_1, \beta_2 \cdots 1$ and are determined by the initial composition of the mixture. Ultimately, therefore, expression Π is a polynomial of the νth power of N/N_0. If $N/N_0 = Z$, we have

$$\Pi(Z) = Z^{\nu} + \alpha_1 Z^{\nu-1} + \alpha_2 Z^{\nu-2} \cdots \alpha,$$

and

$$W(C, T) = K c_0^{\nu} \left(\frac{T}{T_0}\right)^{\nu} \Pi(Z) \quad (6)$$

In the particular case of a stoichiometric mixture,

$$W(C, T) = K c^{\nu} = K c_0^{\nu} \left(\frac{T_0}{T}\right)^{\nu} \left(\frac{N}{N_0}\right)^{\nu} \quad (7)$$

These expressions are widely used in various computations involving combustion phenomena, such as ignition, flame propagation, and especially, in the flame propagation theory of Zeldovich and Frank-Kamenetski.[16, 17, 18]

Making use of Equation (6), we have

$$\mathfrak{I} = \int_{T_\xi}^{T_s} W(C, T)\, dT = \int_{T_\xi}^{T_s} K_0 c_0^{\nu} \left(\frac{T_0}{T_0}\right)^{\nu} \Pi(Z) e^{-(E/RT)}\, dT$$

Keeping in mind that the relation $(N/N_0) = (T_k - T)/(T_k - T_0)$ is true,[12] taking into account that $T_0/T \approx T_0/T_s$, and making use of the resolution of $e^{-(E/RT)}$ into a series in the vicinity of $T = T_s$[19] we get

$$\mathfrak{I} = K_0 c_0^{\nu} \left(\frac{T_0}{T_s}\right)^{\nu} e^{-(E/RT_s)} \int_{T_\xi}^{T_s} \Pi(Z) \cdot e^{-(E/RT_s^2)(T_s - T_0)}\, dT = W_s^0 \int_{T_\xi}^{T_s} \Pi(Z) \cdot e^{-(E/RT_s^2)(T_s - T_0)} \cdot dT$$

Integrating under the condition of integral values of ν, we get the following general expression:

$$\mathfrak{I} = W_s^0 \frac{RT_s^2}{E} \left[\sum_0^{n=\nu} \left(\frac{RT_s^2/E}{T_k - T_0}\right)^n \Pi^{(n)} \cdot \left(\frac{T_k - T_s}{T_k - T_0}\right) - e^{-(E/RT_s^2)(T_s - T_\xi)} \cdot \sum_0^{n=\nu} \left(\frac{RT_s^2/E}{T_k - T_0}\right)^n \Pi^{(n)} \left(\frac{T_k - T_\xi}{T_k - T_0}\right) \right] \quad (8)$$

This expression contains the indefinite value, T_ξ. However, taking into account the fact that the second term in brackets diminishes rapidly as T decreases, it may be considered approximately, with a somewhat augmented result, that:

$$\mathfrak{I} \approx W_s^0 \frac{RT_s^2}{E} \sum \left(\frac{RT_s^2/E}{T_k - T_0}\right)^n \Pi^{(n)} \left(\frac{T_k - T_s}{T_k - T_0}\right) \quad (9)$$

Returning to Equation (3) therefore, we can write the general expression for the boundary condition of ignition in the form

$$\left(\frac{Nu}{d}\right)^2 (T_s - T_0)^2 = \frac{2q}{\lambda} W_s^0 \frac{RT_s^2}{E} \cdot \sum \left(\frac{RT_s^2/E}{T_k - T_0}\right)^n \Pi^{(n)} \left(\frac{T_k - T_s}{T_k - T_0}\right) \quad (10)$$

This general relation leads to a number of corollaries of theoretical and practical importance.

Conditions of Ignition by a Heated Body

If we consider a mixture with a composition very different from that of a limit mixture and close to stoichiometric, the difference $T_k - T_s$ is always large, and $\Pi^{(n+1)}/\Pi^{(n)} \ll 1$. By somewhat curtailing the right side of Equation (10) we may write approximately

$$\left(\frac{Nu}{d}\right)^2 (T_s - T_0)^2 = \frac{2q}{\lambda} W_s^0 \frac{RT_s^2}{E} \Pi \left(\frac{T_k - T_s}{T_k - T_0}\right)$$

or

$$\left(\frac{Nu}{d}\right)^2 (T_s - T_0)^2 = \frac{2q}{\lambda} W_s \frac{RT_s^2}{E} \quad (11)$$

where W_s is the reaction rate at T_s, i.e., in the gas layer immediately adjacent to the wall. Incidentally, the latter equation shows that the value of the integral of the reaction rate in the layer, ξ, in the temperature interval, $T_s - T_\xi$, is approximately equal to the reaction velocity at the temperature of the wall multiplied by the value RT_s^2/E. In the particular case of a first order reaction

$$\left(\frac{Nu}{d}\right)^2 \left[\frac{(T_s - T_0)^2}{T_0 \cdot T_s} \cdot \frac{T_k - T_0}{T_k - T_s}\right] = \frac{2qR}{\lambda E} K_0 c_0 e^{-(E/RT_s)} = K \cdot e^{-(E/RT_s)} \quad (12)$$

In the case of a second order reaction

$$\left(\frac{Nu}{d}\right)^2 \left(\frac{T_s - T_0}{T_0} \cdot \frac{T_k - T_0}{T_k - T_s}\right)^2 = c_0 K \left(1 + \frac{\beta - 1}{\frac{T_k - T_s}{T_k - T_0}}\right) \cdot e^{-(E/RT_s)} \quad (13)$$

and with $\beta \approx 1$ (near stoichiometric)

$$\left(\frac{Nu}{d}\right)^2\left(\frac{T_s - T_0}{T_0}\cdot\frac{T_k - T_0}{T_k - T_s}\right)^2 = c_0 K \cdot e^{-(E/RT_s)} \qquad (13')$$

With the help of equations (12) and (13), reliable values of the chief kinetic characteristics of combustible gases, K_0 and E, can be found from experimental data.

Thus, in the case of ignition by heated rods and spherical igniters, if $Nu = A \cdot Re^{0.5} = A'W^{0.5}$ it follows from Equations (12) and (13) that

$$\frac{W}{W_0}\left(\frac{T_s - T_0}{T_s^0 - T_0}\sqrt{\frac{T_s^0}{T_0}\frac{T_k - T_s^0}{T_k - T_s}}\right) = e^{(E/R)((1/T_s^0)-(1/T_s))} \qquad (14)$$

and

$$\frac{W}{W_0}\left(\frac{T_s - T_0}{T_s^0 - T_0}\cdot\frac{T_k - T_s^0}{T_k - T_s}\right)^2 = e^{(E/R)((1/T_s^0)-(1/T_s))} \qquad (15)$$

where T_s^0 is the temperature of the body at a certain flow velocity W_0 selected as the initial value. Treatment of experimental results obtained with city gas[4] for values of W ranging from 29 to 60 m/sec (d = 2 mm) according to both equations, shows (Fig. 1) that the experimental points corresponding to two gas concentrations (16 and 20 per cent) ignited by a glass sphere, and to one concentration (20 per cent) ignited by a platinum sphere, coincide well with a straight line in the corresponding coordinate system if a second order reaction is assumed. The corresponding value of E is 38,000.

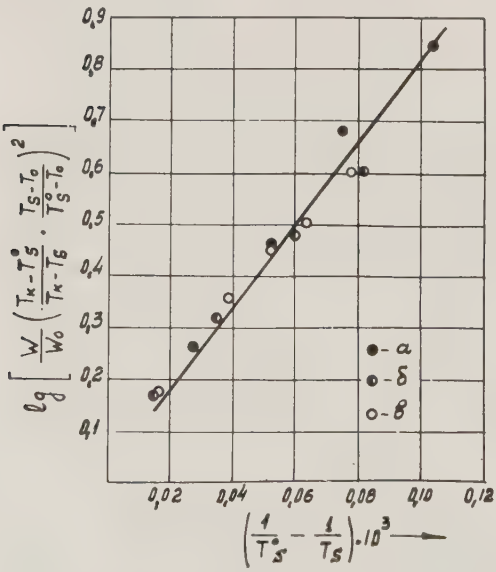

FIG. 1. Correlation of data on the velocity of heated spherical pellets and the ignition temperature (size of pellets is constant).

α—city gas 20%; glass sphere
δ—city gas 20%; platinum sphere
β—city gas 16%; glass sphere.

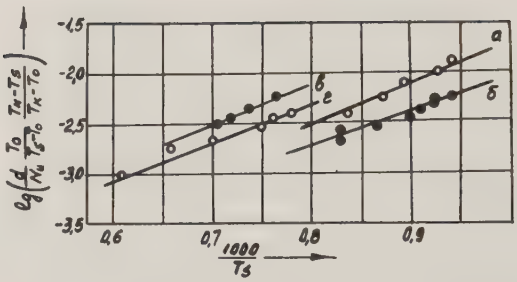

FIG. 2. Correlation of data on size of heated spherical pellets and ignition temperature (velocity of pellets is constant).

α—city gas 20%
δ—hydrogen 20%
β—pentane 3% (W = 1.2 m/sec)
γ—pentane 3% (W = 4.0 m/sec)

Analogous treatment of experimental data for ignition by hot spherical bodies of various size but with W = const according to the relations

$$\frac{d}{Nu}\frac{\sqrt{T_0 T_s}}{T_s - T_0}\sqrt{\frac{T_k - T_s}{T_k - T_0}} = \frac{1}{\sqrt{K}}e^{(E/2RT_s)}$$

(first order)

and

$$\frac{d}{Nu}\frac{T_0}{T_s - T_0}\frac{T_k - T_s}{T_k - T_0} = \frac{1}{\sqrt{c_0 K}}e^{(E/2RT_s}$$

(second order)

shows linear dependence in both cases and close values of E. Figure 2 shows a treatment of the results of experiments carried out by different authors with various fuels, according to the relation for a second-order reaction. It should be noted that the numerical value of E when determined by this method (from data for various values of d) depends essentially on the accuracy of Nu. If we use certain data for Nu and the experimental data obtained for city gas (20 per cent) with d varying from 1 to 5 mm and with W = 1.2 m/sec[3] we get 37,000 cal/mole for a first order reaction and 38,000 to 40,000 cal/mole for a second order reaction. Thus, there is good agreement between both methods of determining E, even when applied to widely differing experimental conditions. The other data in Figure 2 are for a 20 per cent mixture of hydrogen and air[3] with W = 4 m/sec; a 3 per cent mixture of

pentane and air[3] with $W = 4$ m/sec. and[4] $W = 1.2$ m/sec. The slight parallel displacement of the lines for pentane (with different K_0) is evidently due to differences in the measuring procedures used by different authors in these two series of experiments.

Concentration Limits of Ignition

A second important corollary to the general condition of Equation (10) is the relation for the concentration limits of ignition. The concentration limits of flammability of gas mixtures have been treated as a consequence of critical changes in the velocities of the chemical transformations[6, 20, 21] or of disturbance of the stability of the reacting system.[22] In induced ignition, we are dealing with the conditions governing the formation and propagation of the initial flame front, conditions which do not imply any necessary assumption as to a critical change in the state of the reacting system.

As we have already indicated, the role of the heated body is simply to produce in the surrounding gas a temperature $T = T_s$, such that the temperature in the layer, ξ, rises spontaneously to that of the flame, which begins to spread away from the body as from a source. Obviously, the necessary T_s level cannot be higher than the flame temperature, T_f, in the given mixture. If we introduce this temperature into Equation (10), the latter becomes the general condition for the critical (limit) temperatures of a flame, the size of which is predetermined by its source. Accurate temperature values in the flame front can be obtained only by special experiments. Taking into account that the temperature T_f is close to the computable final burning temperature T_k, in other words that $T_f \approx T_k$, we obtain from Equation (10)

$$\left(\frac{Nu}{d}\right)^2 (T_k - T_0)^2 = \frac{2q}{\lambda} W_s^0 \frac{RT_k^2}{E} \left[\nu! \left(\frac{\frac{RT_k^2}{E}}{T_k - T_0}\right)^{\nu} + \sum_{\nu}^{\nu-1} n! a_{\nu-n} \left(\frac{\frac{RT_k^2}{E}}{T_k - T_0}\right)^{n}\right] \quad (16)$$

since with $T_k - T_s = 0$ only one term remains in each of the derivatives $\Pi^{(n)}$. Here $a_{\nu-n}$ are constant factors expressed through β_1, β_2, etc.

Accordingly, for a first order reaction

$$\frac{Nu}{d} = K_1 \sqrt{p_0} \sqrt{\left(\frac{T_k}{T_k - T_0}\right)^3} \cdot \sqrt{N_0}\, e^{-(E/RT_k)} \quad (17)$$

where P_0 is the pressure, and $K_1 = \sqrt{2qR/\lambda E^2}$. Taking into account the fact that $T_k/(T_k - T_0) \approx 1$, Equation (17) can be simplified to

$$\frac{Nu}{d} = K_1 \sqrt{P_0} \sqrt{N_0}\, e^{-(E/2RT_k)} \quad (17')$$

For a second order reaction

$$\frac{Nu}{d} = K_2 P_0 \sqrt{N_0 \left[2N_0 + (1 - 2N_0) \frac{T_k - T_0}{\frac{RT_k^2}{E}}\right]} \cdot e^{-(E/2RT_k)} \quad (18)$$

because

$$\beta - 1 = \frac{1 - N_0}{N_0}$$

In the latter relation the radical changes very little with changes in N_0 in comparison with the term $e^{-(E/2RT_k)}$ which also depends on N_0 through T_k. Whereas the radical changes only by a factor of about four, $e^{-(E/2RT_k)}$ changes by a factor of several hundred. Accordingly, even more simply, but with sufficient accuracy, for a second order reaction, we can write

$$\frac{Nu}{d} = BP_0 e^{-(E/2RT_k)} \quad (19)$$

where $B \approx$ const.

The condition in Equation (19) gives the simplest relation for determining the limits of ignition under various conditions.

Two cases are of interest—the ignition of a quiescent medium and that of a moving medium. In the quiescent medium, $Nu = 2$ and from Equation (19) we have

$$T_k^{\lim} = \frac{\frac{E}{2R} lge}{lg\left[BP_0 \frac{d}{2}\right]} \quad (20)$$

Typical curves showing the dependence of the limits on d and P_0 are given in Figure 3, based on computations made for city gas and hydrogen, the constants of which were determined from Figure 2. The curves show that as the diameter and/or P_0 increase the boundary curves tend towards assymptotic (limit) values, just as observed experimentally. In particular, the picture of the influence of pressure is in good

qualitative and even quantitative agreement with experiment, (see, for example, Abesgaus[23]).

Another characteristic example is concerned with the form of the boundary curves for the case of combustible mixtures diluted with inert additives. In this case, assuming again that B

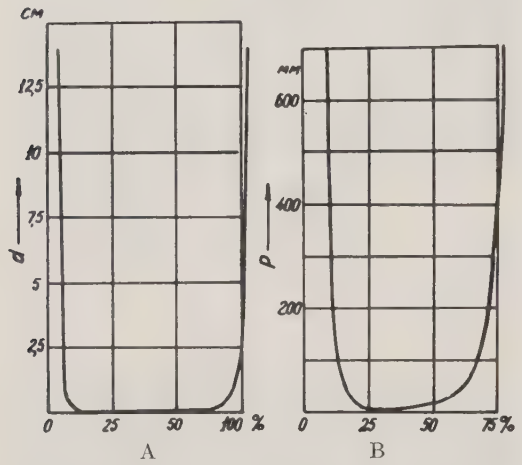

FIG. 3. Ignition size and pressure composition limits. A, City gas; B, hydrogen.

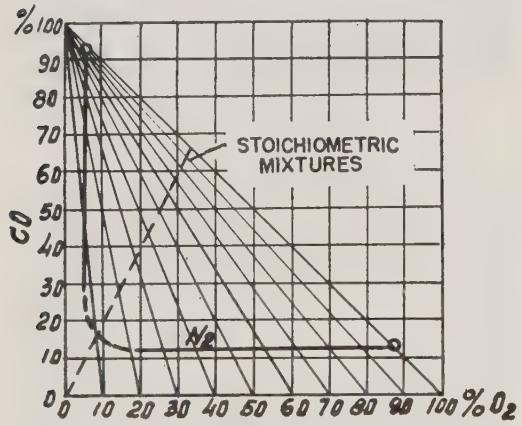

FIG. 4. Limits of flammability of carbon monoxide-oxygen-nitrogen mixtures.

changes little, we come to the simplest and most important condition:

$$T_k^{\lim} \approx \text{const} \qquad (21)$$

At the lower limit, especially in the case of dilution with nitrogen, this condition is equivalent to

$$N_0 \approx \text{const} \qquad (21')$$

as the heat capacity of nitrogen is close to that of oxygen.

In the case of an excess of fuel, the analogous expression for N_0 is less accurate as the heat capacity of the fuel is not always close to that of nitrogen. However, Equation (21′) is applicable to both the lower and upper limits in the ignition of carbon monoxide. In this case the ignition region in a triangular co-ordinate system has the shape of an isosceles triangle, as can be seen in Figure 4. This is confirmed by familiar experimental relationships, (see, for instance, Bunte and Jahn[24]).

Another important characteristic of the initial state of a gas mixture is its initial temperature. Equation (20) does not include the initial temperature in its right half. This means that the temperature of the mixture at the boundary also remains approximately constant. This has been

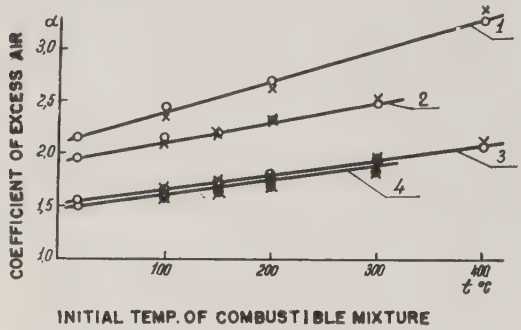

FIG. 5. Effect of initial temperature of combustible mixtures on lean-limit mixtures. Coefficient of excess air $= \frac{\text{air}}{\text{air/(stoich)}}$. 1, Carbon monoxide; 2, ethylene; 3, methane; 4, pentane.

proved experimentally for a number of fuels with the mixture temperatures changing from 20° to 400°C,[25] independent of the initial temperature. Hence, introduction of the preheating heat into the expression determining the value, T_k, gives us a relation for computing the dependence of the concentration limits on the temperature of preheating of the mixture to be ignited. Computations of this kind[26] are shown in Figure 5. The indefinite value of the constant in Equation (20) was computed for each gas from experimental data on ignition without preheating. The agreement between the curves and the experimental data is quite satisfactory. In connection with our discussion of Equation (20), it should be stated that an attempt was made by Fenn[27] and Fenn and Calcote[28] to determine the activation energy of various combustible mixtures on the basis of experimental data on the ignition of stagnant mixtures at the lower limit. It can easily be shown

that the relation $E = \text{const}\ T_k^{\lim}$ follows from Equation (20) as a particular case.

In a moving medium, for which the law of heat transfer is different $Nu = ARe^{0.5}$

$$T_k^{\lim} = \frac{\frac{E}{2R}\, lge}{lg\left[\left(\frac{B}{A}\right)^2 \frac{d}{w}\nu\right]} \qquad (22)$$

where ν is the kinematic viscosity.

The nature of the dependence of the ignition limits on the flow velocity for various d is shown in Figure 6 for the combustion of pentane. In this computation, use was made of the data of treatment of the experiments by Peterson[4] shown in Figure 2. The curves are the typical ones observed when the flame is stabilized by bluff bodies. It is significant that the computation gives critical velocity values that are quite close to the experimental values.

To obtain quantitative agreement, the values, B and E, must be known for any given combustible gas. They can be obtained from Equations (18) and (19) for any system of critical data obtained experimentally, such as experimental data on flame stabilization by baffles. Results of a computation based on experiments carried out in our laboratory by L. Volodina (see Fig. 7) lead to a linear relation between $lg\ (W/d)$ and $1/T_k$ for methane, in agreement with Equation (19). The value of E was found to be 25,000.

Thus, the general method developed for computing the concentration ignition limits of quiescent and moving gas mixtures leads to correct qualitative conclusions concerning the main relations for the limits and make it possible, in principle, to determine the values of the effective kinetic characteristics of flame processes in gas mixtures necessary for detailed quantitative computations. Using only these chief characteristics and the corresponding law of heat transfer, the values of the critical ignition parameters can be computed under various conditions (various P_0, T_0, W, d and the presence of additives). Development of the computation will make it possible also to examine the question of limits in the case of a mixture of several combustible gases, and thus to analyze the conditions and properties of Le-Chatelier's law for combustible mixtures.

Flame Stabilization

Flame stabilization in a flowing combustible mixture is effected by setting up a zone of recirculation of hot combustion products. Bluff bodies are known to be the simplest types of stabilizers.[29, 30, 31] In this case, ignition is caused by

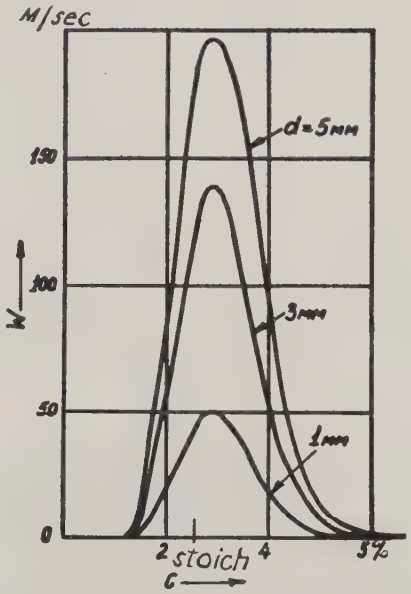

FIG. 6. Blowoff velocities vs flameholder size (calc. data).

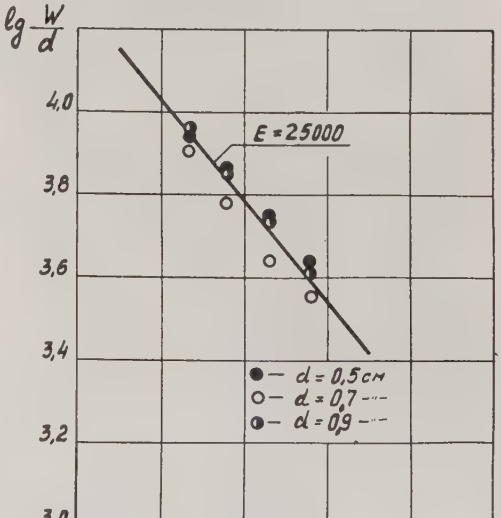

FIG. 7. Correlation of data on blowoff velocities vs combustion temperature.

circulating hot combustion products at a combustion temperature of T_k, offering an analogy with the case considered above, concerning ignition of a flow by a gas film heated by a body. In the present instance, the body is the aggregate

of the hot products which come into contact with the cold gas right at the edge of the stabilizer (along the blowoff line of the boundary layer), where the thin initial flame front usually makes its appearance. As before, the conditions of thermal equilibrium in this thin layer of gas determine the possibility of the flame propagating through the flow.

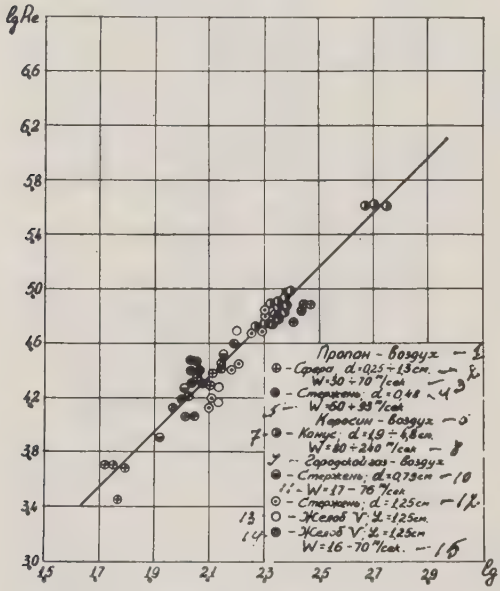

FIG. 8. Correlation of data on the stability parameter.

Propane-Air

⊕ Sphere; d = 0.25/1.3 cm W = 30/70 m/sec
● Rod; d = 0.48 W = 60/93 m/sec

Naphtha-Air

◑ Cones annular; d = 1.9/4.8 cm W = 80/240 m/sec

City gas-Air

◒ Rod; d = 0.79 cm W = 17–76 m/sec
⊙ Rod; d = 1.25 cm
○ Gutter: L = 1.25 cm
◎ Gutter; L = 1.25 cm W = 16 − 70 m/sec

Returning to Equation (3), but bearing in mind that $T_s \approx T_k$, we get

$$Nu = \frac{\sqrt{\frac{2q}{\lambda}\int_{T_\xi}^{T_k} W(C, T)\, dT}}{T_k - T_0}$$

From the theory of flame propagation,[16, 17, 18] identifying T_ξ with the temperature of perceptible development of the reaction in the flame, we have

$$\frac{\sqrt{2\lambda q \int_{T_\xi}^{T_k} W(C, T)\, dT}}{C_p(T_k - T_0)} = \psi m$$

where ψ is a factor of the order of unity, and m is the mass burning velocity (g/cc/sec). Hence

$$Nu = \psi \frac{C_p}{\lambda} dm = \psi \frac{C_{p\rho 0}}{\lambda} ud$$

where u is the linear normal velocity of the flame, ρ_0 the density of the mixture, or

$$Nu = \psi \frac{ud}{a} \tag{23}$$

Thus, the critical value of Nu is related through a very simple condition with a fundamental physicochemical characteristic of the combustible mixture—its fundamental burning velocity. As we know, various other attempts to analyze the phenomenon of stabilization[32, 33, 34] have already led to the existence of such a relation.

Denoting the non-dimensional value[b] ud/a by S and taking into account that $Nu = ARe^n$, we may write finally

$$Re^{cr} = AS^{1/n} \tag{24}$$

as the general condition for the stabilization of the flame front. A relation of this type, as already noted has been derived by a number of authors from other considerations, but in the present case it is a direct corollary of the theory of thermal ignition developed above. Experiment shows that this condition is satisfied for mixtures that are not too lean or too rich.

Figure 8 illustrates the application of Equation (24) to various available experimental data on stabilities by various stabilizers. The points lie along a relatively straight line, showing good agreement with Equation (24), which in this case takes the following concrete form:

$$Re^{cr} = 1.45S^2 \tag{25}$$

This means that here the law of heat transfer has the form $Nu = 0.83\ Re^{0.5}$. The factor 0.83 differs somewhat from that usually given for heat transfer in the case of a sphere, *viz.*: 0.54[35] or 0.62.[36] However, this discrepancy is not essential, since in ignition by bluff bodies heat transfer occurs practically only in the blowoff zone of the boundary layer, and in this case the temperature difference is considerably greater than the difference for the above values of the constant A'.

[b] This value may be called the stabilization criterion; in analyzing the phenomenon of flashback of a laminar flame in a gas burner and its blowoff from wires[32], an analogous value has been termed the Peckle of the flame.

Limit Burning Velocities

Equation (23) gives another interesting and important characteristic—the mass burning velocity at the ignition limit. In the case of a quiescent medium $Nu = 2 = \text{const}$. Hence

$$M_{\text{lim}} \approx \frac{2}{\psi} \frac{\lambda}{C_p} \frac{1}{d} \tag{26}$$

This relation shows that for an igniter of a given size M_{lim} depends only on the physical characteristics of the mixture. The λ/C_p values for various gases differ relatively little and are of the order of 0.1×10^{-3} or 0.2×10^{-3} (for air, $\lambda/C_p = 0.232 \times 10^{-3}$; for benzene, 0.075×10^{-3}). In accord with this, the limit velocities for all gases should also differ little from each other, and the order of their values should be close to those computed from Equation (26).

This conclusion explains earlier observations to the effect that not only the mass but also the linear border velocities of all gas mixtures are approximately equal. In particular,[37] at pressures from 100 to 700 mmHg (experiments in a tube)[37] the burning velocity ranges only from 8.1 to 9.2 mg/cc/sec. If we assume that the ignition spark was 0.1 cm in diam, the computed values will all be within 4.3 to 4.6 mg/cc/sec.

According to the data of A. V. Bondarenko (Moscow State University), in the case of hydrogen mixtures diluted with various non-combustible gases, M_{lim} in the tube remained at approximately the same level of 6 to 7 mg/cc/sec. From the latest data on limit velocity measurements, obtained with the aid of a flat flame,[38] it also follows that the limit velocities u and M are quite constant.

Equation (23) leads to a physically clear treatment of the value M_{lim}, which, in essence, is a measure of the heat transfer coefficient under conditions of a real flame front of a given size, for from Equation (23) we have

$$\alpha = \psi \cdot C_p \cdot M_{\text{lim}} \tag{27}$$

Thus the value M_{lim} as such, although it is a result of the chemical process in the flame front, does not by any means characterize that process. However, the chemical process has an essential influence over the values of the reagent concentrations in the mixture at which a given value of M_{lim} is attained.

Summary

The thermal theory of ignition of quiescent and moving combustible gas mixtures developed in this paper makes it possible to obtain the entire system of critical (limit) characteristics of flammability, including:

(1) Concentration limits and their dependence on the pressure, initial temperature and additive content.

(2) Limit burning velocities.

(3) Flame front stabilization criteria.

The results of computations are in agreement with the known experimental relationships for flammability (ignition) limits. The relations obtained also make it possible to find the most likely values for the effective kinetic constants of gas combustion from systems of limit characteristics, and on this basis to carry out quantitative computations of the ignition limits.

REFERENCES

1. Lewis, B., and von Elbe, G.: *Combustion, Flames and Explosions of Gases*. New York, Academic Press, 1951.
2. Zeldovich, J. B.: J. Exp. Tech. Phys. (USSR), *9*, 1530 (1939).
3. Silver, R. S.: Phil. Mag., *23*, 633 (1937).
4. Peterson, S.: Phil. Mag., *28*, 1 (1939); *30*, 437 (1940).
5. Mullen, J., Fenn, J., and Irby, M.: *Third Symposium on Combustion, Flame and Explosion Phenomena*. Baltimore, The Williams & Wilkins Co., 1949.
6. Semyonov, N. N.: *Chain Reactions*. USSR, 1934.
7. Semyonov, N. N.: Uspekhi fizicheskikh nauk (USSR), *23*, 3 (1940).
8. Blinov, W. I.: Proceedings of the Voronezh Univers. (USSR), vol. 11, 1, (1939).
9. Frank-Kamenetzki, D. A.: *Diffusion and Heat Transfer in Chemical Kinetics*. New York, Academic Press, 1947.
10. Buben, N. Y.: J. Phys. Chem., *19*, 250 (1950).
11. Spalding, D.: J. Inst. Fuel, *26*, 289 (1953).
12. Vulis, L. A.: *Thermal Conditions of Combustion*. 1954.
13. Tu, C. M., Davis, H., and Hottel, H. C.: Ind. Eng. Chem., *26*, 629 (1934).
14. *Carbon Combustion*, part III. New York, Academic Press, 1953.
15. Khitrin, L. N.: Reports of the USSR Academy of Sciences, No. 4, 1953.
16. Zeldovich, J. B., and Frank-Kamenetzki, D. A.: J. Phys. Chem., *12*, 100 (1938).
17. Semyonov, N. N.: Uspekhi fizicheskikh nauk (USSR), *24*, 4 (1940).
18. Zeldovich, J. B.: J. Phys. Chem., *22*, 27 (1948).
19. Frank-Kamenetski, D. A.: J. Phys. Chem., *13*, 738 (1939).
20. Nalbandjan, A. P., and Voevodsky, V. V.:

The Mechanism of Hydrogen Oxidation and Combustion. Inst. Khim. Fiz. Izdatl. Akad. Nauk. SSSR. 1949.
21. Akulov, N. S.: *The Theory of Chain Processes.* Moscow, Gosndarst. Izd. Tekhn. Teor. Literatury. (1951).
22. Predvoditelev, A. S.: Proceedings of the Moscow University, No. 10, 1951.
23. Abesgaus, E. M.: Report of the Moscow University, No. 10, 1946.
24. Bunte, K., and Jahn, G. Gas u. Wasserfach *76*, 89 (1933).
25. White, A. G.: J. Chem. Soc., *127*, 672 (1925).
26. Pechkin, M. A.: J. Phys. Chem., *28*, 433 (1954).
27. Fenn, J. B.: Ind. Eng. Chem., 43, 2865 (1951).
28. Fenn, J. B., and Calcote, H. F.: *Fourth Symposium (International) on Combustion.* Baltimore, The Williams & Wilkins Co., 1953.
29. Longwell, J. P.: J. Aero. Sci., *16*, 707 (1948).
30. Williams, G. W.: J. Aero. Sci., *16*, 714 (1949).
31. Longwell, J. P.: *Fourth Symposium (International) on Combustion.* Baltimore, The Williams & Wilkins Co., 1953.
32. Putnam, A., and Jensen, R.: *Third Symposium on Combustion, Flame and Explosion, Phenomena*, p. 89. Baltimore, The Williams & Wilkins Co., 1949.
33. Spalding, D.: Aircraft Eng., *25*, 264 (1953); Spalding, D., and Tall, B.: Aeronaut. Quart., *5*, 195–217 (1954).
34. Lies, L.: Jet Prop., *24*, 234 (1954).
35. Vuirubov, D. N.: J. Tech. Phys., *10*, 12 (1940).
36. Lyahovsky, D. N.: J. Tech. Phys., *10*, 12 (1940).
37. Khitrin, L. N.: J. Phys. Chem., *22*, 7 (1948).
38. Badami, G. N., and Egerton, A.: Proc. Roy. Soc., *A228*, 297 (1955).

68

IGNITION OF FLOWING GASES BY HEATED WIRES

By SEIICHIRO KUMAGAI and ITSURO KIMURA

I. Introduction

Considerable attention has been given the ignition of combustible mixtures by heated surfaces.[1, 2, 3] In the present paper, we have studied the ignition of flowing gases by heated wires in connection with ignition and combustion in engines.

It is generally recognized that ignition by the surface of a heated wire is the more readily accomplished the lower the flow velocity or, for a fixed flow velocity, the larger the diameter of the wire. The ignition of high velocity streams of combustible gases has been investigated intensively by Mullen, Fenn and Irby[3] at velocities ranging from 80 to 200 ft/sec, using heated rods with diameters ranging from $\frac{1}{4}$ to $\frac{1}{16}$ in. In these experiments, the approach flow was always turbulent, but the degree of turbulence was undetermined.

To obtain a better understanding of the ignition mechanism, we conducted experiments on laminar flows or turbulent flows of known intensity and scale. Velocities ranged from 0.2 to 30 m/sec and wire diameters from 0.3 to 5 mm.

II. Apparatus and Procedure

The flow system is shown in Figure 1. Orifices 1 and 2 for air and city gas, respectively, are used to determine the mixture strength, and orifice 3 is used to determine the mass flow in the ignition unit.

Two types of ignition unit were used. The larger one is shown in Figure 2. It is composed of a duct (3 cm i.d.), across which a nichrome wire is inserted. The smaller ignition unit has a duct which measures 1.245 cm i.d. and is similar in construction to the larger one. The nichrome wire is thinner at the center of its span (Fig. 3). This slender section is heated electrically and acts as an igniter, its temperature being measured by an optical pyrometer through a glass window of the ignition unit.

The degree of turbulence in the ignition unit can be varied by placing a perforated plate (Fig. 4) at different distances upstream. Nonturbulent flow in the velocity range above the critical Reynolds number is achieved by placing a twofold 200 mesh screen 1.5 cm upstream from the heated wire.

In the case of laminar flow, gas velocity along the axis of the ignition unit duct was determined from the mass flow. In the other cases (ordinary turbulent flow, turbulent flow by use of the perforated plate and nonturbulent flow by use of the screen) it was measured with a Pitot tube. The

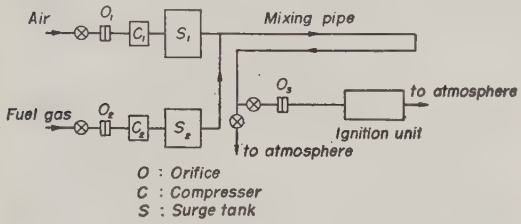

FIG. 1. Mixture control system.

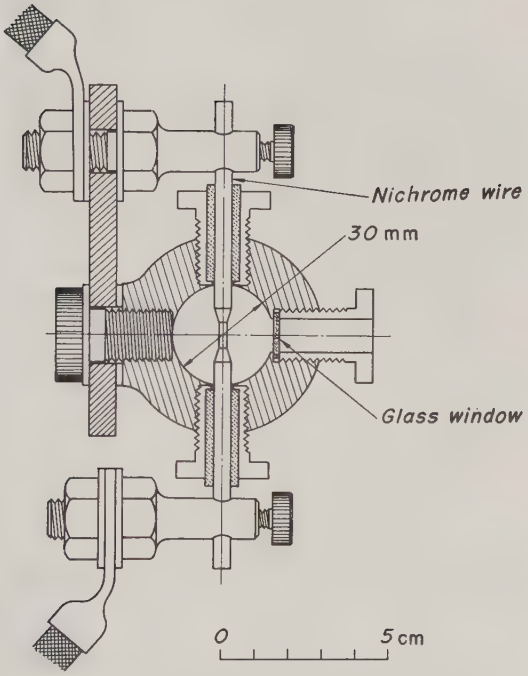

FIG. 2. Large ignition unit.

gas velocity can be regulated by control valves from 0 to 30 m/sec in the ignition unit, where the pressure and temperature of flowing gas are virtually atmospheric.

The intensity and scale of turbulence in the gas flow at the heated wire was measured by a hot-wire turbulence meter,[4] in which the probe element was a platinum wire, 5 μ in diam and about 0.5 mm long. The thermal lag of the probe was compensated by an R-C circuit inserted in the amplifier.

III. Results

Figure 5 is a typical plot of wire temperature for ignition versus gas velocity. The small ignition

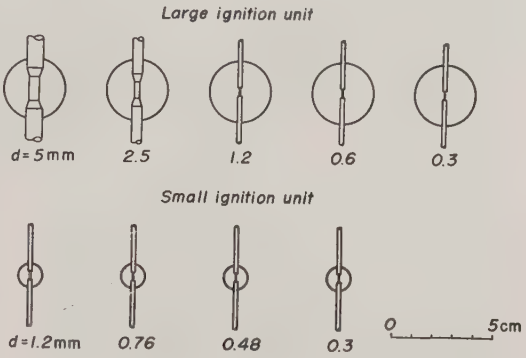

FIG. 3. Nichrome wires used.

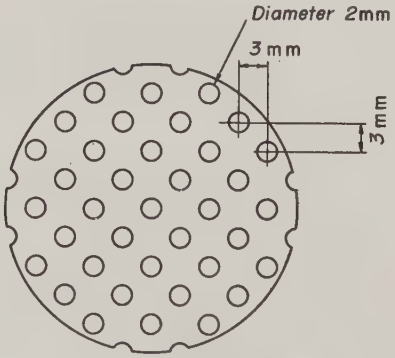

FIG. 4. Perforated plate.

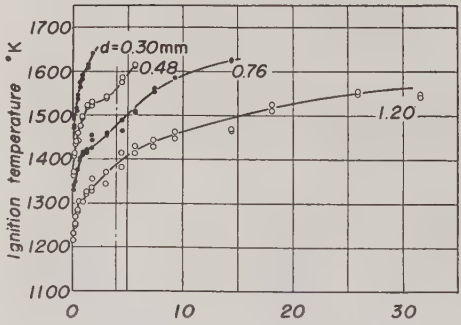

FIG. 5. Ignition temperature vs flow velocity, small ignition unit, 22 per cent by volume.

unit was used in this experiment so the wire diameter was less than 1.2 mm. The mixture strength was kept 22 per cent by volume. The velocity profiles for laminar and turbulent flows were established perfectly in the ignition unit, as the length of piping upstream was sufficient. The transition velocity from laminar to turbulent flow

was about 4 m/sec in this case. The ignition curves generally show downward concavity.

Figure 6 is a logarithmic replot of Figure 5 against the Reynolds number. In the Reynolds number, Ud/ν, U is the velocity along the axis of the duct, d is the diameter of the thin section of the nichrome wire and ν is the kinematic viscosity, evaluated at the mean temperature of hot wire and flowing gas. The ignition curves in Figure 6 are made up of three characteristic parts. For small Reynolds numbers, the ignition temperature rises almost linearly, but from the point corresponding to $Re = 9$ the rising rate of ignition temperature becomes remarkably small. If the Reynolds number continues to increase, the temperature rise recovers its rate gradually. This remarkable change corresponds to growth of a wake behind the wire as follows. As long as the flow velocity (or Reynolds number) is small, the wake is not noticeable, but in the vicinity of the flow velocity corresponding to $Re = 10$ the wake appears distinctly and two stable eddies form behind the wire. For further increases in velocity, they become unstable eddies which are dropped from the wake one by one. We were able to confirm by the schlieren method that the wake appears at much the same Reynolds number in the case of high wire temperature. Thus, the wake behind the wire plays an important part in ignition, as this problem can be divided into the following three separate regions: the first where no wake appears; the second where two stable eddies exist; the third where unstable eddies appear.

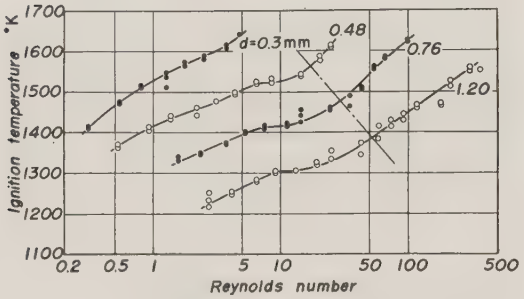

FIG. 6. Replotting of Fig. 5, ignition temperature vs Reynolds number.

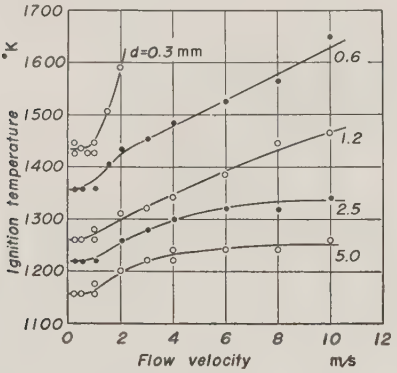

FIG. 7. Ignition temperature vs flow velocity, large ignition unit, 18 per cent by volume.

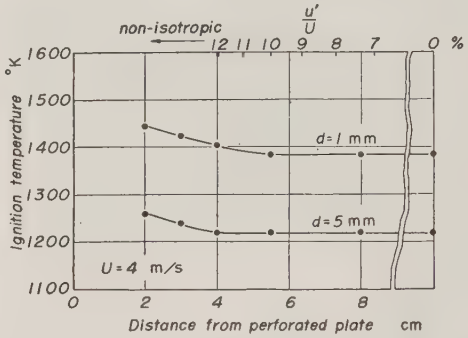

FIG. 8. Effect of turbulence on ignition temperature, large ignition unit, 18 per cent by volume, 4 m/sec.

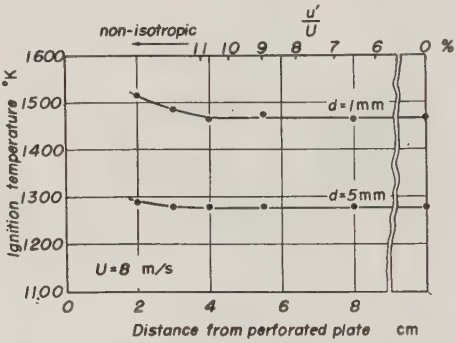

FIG. 9. Effect of turbulence on ignition temperature, large ignition unit, 18 per cent by volume, 8 m/sec.

The experimental results obtained with the large ignition unit are shown in Figure 7. The wire diameter ranges from 0.3 to 5 mm; the mixture strength is kept at 18 per cent by volume. In this experiment, turbulence in the ignition unit in the velocity range beyond the critical Reynolds number is rendered negligible by use of the screen. For velocities smaller than 1 m/sec, the ignition temperature is virtually constant, in contrast with the results in Figure 5 or 6, suggesting the influence of increased natural convection due to the large inner diameter of duct. The effect of the wake on ignition is not

clear in this experiment, being masked by natural convection.

Figures 8 and 9 show the effect of turbulence in the approach flow on ignition. In this experiment, two wire diameters (1 and 5 mm) and two flow velocities (4 and 8 m/sec) were used. The mixture strength is kept 18 per cent by volume. The relative turbulence, u'/U, shown in these figures, is measured at the heated wire. Measurements have established that the scale of turbulence, L, defined as $\int_0^\infty Rydy$,[5] is kept in the range from 1.5 to 2 mm in the case of turbulence caused by the perforated plate. When the perforated plate is placed nearer than about 4 cm, the turbulence at the heated wire is no longer isotropic, making measurement by the hot wire turbulence meter impossible.

IV. Discussion

We consider first the temperature rise of the fluid in the boundary layer along a plane surface of high temperature, which is placed parallel to the flow (Fig. 10). The velocity and temperature of approach flow are U and T_0, respectively, and the temperature of plane surface of length X is denoted by T_w. In the case of $Pr = 1$, the velocity, U', and temperature, T', at any position in the laminar boundary layer are given approximately as follows:

$$U' = U\left[\frac{3}{2}\left(\frac{y}{\delta}\right) - \frac{1}{2}\left(\frac{y}{\delta}\right)^3\right] \tag{1}$$

and

$$T_w - T' = (T_w - T_0)\left[\frac{3}{2}\left(\frac{y}{\delta}\right) - \frac{1}{2}\left(\frac{y}{\delta}\right)^3\right] \tag{2}$$

where y is the distance from the surface, and δ is the width of the laminar boundary layer, defined as

$$\delta = 4.64\sqrt{\frac{\nu x}{U}} \tag{3}$$

If a fluid particle moving along the surface at $y = y^*$ is designated by y^*, Equations (1) and (2) concerning y^* are simplified in the case of $y^*/\delta < 1$ as follows:

$$U' = \frac{3}{2}\frac{U}{\delta}y^* \tag{1'}$$

and

$$T_w - T' = \frac{3}{2}\frac{(T_w - T_0)}{\delta}y^* \tag{2'}$$

The time interval, t_c, in which the fluid particle y^* moves from $x = 0$ to $x = X$, is obtained from Equations (1') and (3) as follows:

$$t_c = \int_0^x \frac{dx}{U'} = \frac{4}{9}\frac{\delta_{x=X}}{y^*}\frac{X}{U} \tag{4}$$

or

$$t_c \propto \left(\frac{X}{U}\right)^{3/2} \tag{4'}$$

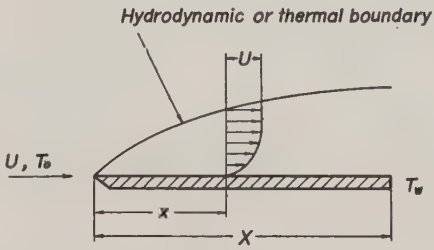

FIG. 10. Hydrodynamic and thermal boundary layer along plane surface.

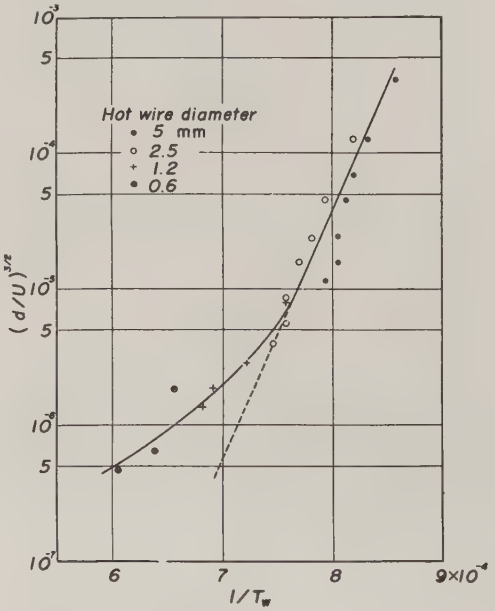

FIG. 11. Relationship between contact time and ignition temperature.

From Equation (2'), the temperature of the fluid particle y^* at $x = X$, T_X, is expressed as

$$T_X = T_w - \frac{3}{2}\frac{(T_w - T_0)}{\delta_{x=X}}y^* \tag{5}$$

We can apply Equations (4) or (4') and (5) to the boundary layer around a cylindrical surface, if the width of the boundary layer is small compared to the radius of cylinder.

The relation between ignition temperature and ignition lag may be expressed as

$$r = \text{const} \cdot e^{(E/RT_{ig})} \tag{6}$$

Substituting t_c for r and T_X for T_{ig}, Equation (6) becomes the equation which determines the condition of ignition. In this equation, the characteristic length y^* is unknown, but it can be determined experimentally from the condition required to keep the plot log t_c versus $1/T_X$ a straight line.

The experimental points of ignition temperature in the region where no appreciable wake is observed are obtained from the left part of Figure 6. These data, however, are affected to some extent by natural convection, making it impossible to estimate the value of y^* by Equation (6).

Next, let us consider ignition in the region where unstable eddies appear. As a first approximation, we assume that the relation of the peripheral velocity of the eddies to the velocity of approach flow and the relation of the contact length of the eddies along the hot wire surface to the diameter of the wire are constant. This assumption would be more accurate for a fixed Reynolds number. Thus, in this case, the time interval during which a fluid particle in the eddy is in contact with the hot wire is proportional to $(d/U)^{3/2}$ also. Figure 11 is the replotting of some data on Figure 7, where T_w is the wire temperature. The Reynolds number of the points on this graph ranges from 40 to 600. The decrease of the gradient at small values of $(d/U)^{3/2}$ can be explained by the decrement of $\delta_{x=X}$ in Equation (5). Taking T_0 as the temperature of the eddies, the decrease in the contact time of the eddies and hence the low value of T_0 may be another cause of this deviation. For large values of $(d/U)^{3/2}$, the second term in the right hand of Equation (5) becomes negligible and the activation energy is obtained directly from the straight line in Figure 11. The activation energy obtained is 37 kcal/mole, which is considered a reasonable value.

V. Conclusions

Wire temperatures for ignition were obtained for laminar flows and for turbulent flows of known intensity and scale. For the velocities and wire diameters used, the plot of ignition temperature versus gas velocity generally shows downward concavity. The growth of the wake behind the wire has a marked effect upon ignition. The influence of turbulence in the approach flow on ignition is not remarkable in the velocity range used.

Acknowledgment

The authors acknowledge their indebtedness to Messrs. F. Deguchi, T. Fujimura, and H. Ukawa for their co-operation in the experimental work and their part in the discussions.

REFERENCES

1. Silver, R. S.: Phil. Mag. (7), *23*, 633 (1937).
2. Paterson, S.: Phil. Mag. (7), *28*, 1 (1939); Phil. Mag., *30*, 437 (1940).
3. Mullen, J. W., Fenn, J. B., and Irby, M. R.: *Third Symposium on Combustion, Flame and Explosion Phenomena*, p. 317. Baltimore, The Williams & Wilkins Co., 1949.
4. Kovásznay, L. S. G.: NACA Tech. Note No. 2839, 1953.
5. Dryden, H. L.: Quart. Appl. Math., *I*, 37 (1943).

Combustion of Solid Fuels

69

REPORT ON PROGRESS IN COMBUSTION OF SOLID FUELS

By A. A. ORNING

The eight papers, which follow this report, give a cross-section of current activity in fundamental research on combustion of solid fuels. Three papers by Russian authors, Khitrin, Chukhanov[a] and Tsukhanova, together with one by a Japanese author, Koizumi, deal primarily with the kinetics and mechanisms of carbon reactions. A second Japanese paper, by Yagi and Kunii, applies thermodynamic balances to data obtained from a model cyclone generator. A third paper by a Japanese author, Hattori, a paper from India, by Ghosh, Basu and Roy, and one from the United States, by Cassel, Liebman and Mock, present experimental data on conditions needed for production of stable flames of pulverized fuels and on the importance of radiation in energy transfer within such flames.

Reference will be made to these papers by names of the first authors. A topical summary will be attempted with a hope, but no promise, that each paper will be adequately covered.

The bibliography given by Khitrin includes many reports of intensive work on carbon combustion that have been carried on in the Soviet Union. This work has been concerned largely with analyses of mass and heat transfer, both outside and inside carbon bodies, and with the specific chemical processes occurring at the carbon surface and within the gas stream. Assuming a first order reaction, the apparent rate constant relating the reactant concentration at the superficial surface to the overall reaction rate is made up of two terms

$$K^* = K + \frac{D_i}{c_s}\left(\frac{\partial c}{\partial n}\right)_s$$

the first being the rate constant of the chemical process at the gas solid interface and the second an estimate of the contribution of diffusion into the porous solid. If the quantity

$$r\sqrt{\frac{S_i K}{D_i}}$$

is sufficiently small, where S_i is the specific surface in area per unit volume of porous solid, the apparent rate constant for a spherical body becomes

$$K^* = K\left(1 + \frac{S_i r}{3}\right)$$

Under these conditions reaction occurs uniformly throughout the porous solid. As K increases with temperature, or for very small r, a transition occurs until

$$K^* = K$$

and reaction appears to occur only at the superficial surface. The temperature range of this transition region becomes narrower the smaller the particle size and the temperature level of the transition depends upon the type of carbon, higher for instance for an anthracite carbon than for an electrode carbon.

Khitrin writes the specific combustion rate, expressed in grams of carbon reacted per cm^2 per sec, in the form

$$K_s^c = \beta\alpha_{\text{dif}} C \frac{1}{1 + \frac{\alpha_{\text{dif}}}{K^*}}$$

where

$$\alpha_{\text{dif}} = \frac{D}{d} Nu_{\text{dif}}$$

The quantity, β, is a complex expression that accounts for the effect of specific surface reactions,

[a] Based on abstract only.

$C + \frac{1}{2} O_2 = CO$ or $C + O_2 = CO_2$ plus the gas phase reaction $CO + \frac{1}{2} O_2 = CO_2$. This quantity varies between the limits $1\frac{2}{3}2$ and $2\frac{4}{3}2$. It is of lesser importance, in controlling the magnitude of the reaction rate, than the Nusselt's diffusion criterion and the ratio of this last to the apparent surface reaction rate, K^*, which appears in the last factor. When this ratio is high, as at low temperatures and favorable mass transport conditions, the rate expression becomes

$$K_s^c = 6K^*C$$

and the system is in the reaction rate controlled region. When this ratio is low, and may be neglected in comparison to unity, the rate expression becomes

$$K_s^c = \beta\alpha_{dif}c$$

and the system is in the mass transport controlled region.

A last subject considered by Khitrin is that of combustion of a system of many particles as in the burning of pulverized fuel in suspension or of solid fuel in a bed. In such systems it has been found that the disappearance of oxygen can be expressed in the form

$$\frac{dc}{dx} = -ac$$

where

$$a = S\frac{\alpha_{dif}}{W}\frac{1}{1+\frac{\alpha_{dif}}{K^*}}$$

the coefficient, a, shows the same transition, indicated above, from reaction rate to mass transport control. It is further, and even more significantly in the high rate mass transport controlled region, a function of the specific surface, S, expressed in area per unit volume of the combustion system. The surface per unit weight is higher for pulverized fuels, but this is offset by the large expansion when the pulverized fuel is suspended in the entire amount of air needed for combustion. Turbulence and cyclonic forces may be used to increase the efficiency of mass transport but the intensity of combustion in suspension remains in a lesser order of magnitude than that in fuel beds because of the dominant effect of the surface concentration.

Chukhanov has considered the role of carbon dioxide reduction in the burning of coke. Unfortunately, his complete paper has not yet been received. The reaction $CO_2 + C$ occurs with a velocity of lesser magnitude than that of the $C + O_2$ reaction at temperatures up to 1500 to 1600°C. The speed of supplying CO_2 to the coke surface has no influence upon the reaction rate within this region. The oxygen reaction passes from the kinetic into the diffusion controlled region at much lower temperatures. At temperatures up to 1300 to 1400°C the CO_2 reaction is not intensified by pulverization of the coke below 1 mm, while the oxygen reaction rate rises abruptly with pulverization under the same conditions.

Chukhanov proposes the quantity

$$S_m = \frac{\alpha_{dif}}{K_r}$$

as a criterion of the regions in which reaction kinetics or diffusion may be controlling. α_{dif} is the mass transfer constant and K_r is the reduced heterogenous reaction rate constant. In the diffusion region $S_m < 0.1$. For values of $S_m > 10$ the process is reaction rate controlled.

The equation

$$\frac{T_c - T_0}{T_r - T_0} = \frac{1}{1 + S_m}$$

is given for the relation of the reacting surface temperature, T_c, the initial gas temperature, T_0, and the theoretical temperature, T_r, provided there is no radiant heat transfer and heat loss is only into the reacting gas. With transition into the diffusion region the reacting surface approaches the theoretical temperature.

The process becomes somewhat different when the oxidizing agent is supplied by mass transport through a channel. Tsukhanova treated this problem for a straight circular channel. Within the gas stream, diffusion terms in the direction of flow may be neglected in favor of mass transfer by convection. This condition fails in the layer immediately adjacent to the solid surface but if the influence of this layer might be neglected Tsukhanova's Equation (1) results. If volume changes due to reaction may be neglected, the gas velocity may be considered a function of the radius only and this equation becomes integrable with respect to the radius. Tsukhanova considered the effect of dependence of W upon the radius but continued the analysis with a simplifying assumption that the velocity profile was flat and W could be taken outside the integral and the differential. With the boundary condition that the concentration sur-

face was proportional to the rate of diffusion to the surface:

$$\frac{\partial \bar{c}}{\partial z} = -\frac{2\alpha}{WR} C_R$$

Further progress requires some assumption as to the form of the concentration function. Tsukhanova assumed that

$$C = A(z)\{1 + \gamma(z)\psi(r)\}$$

without explicitly noting that the boundary condition then demanded that γ should be a constant without dependence upon z. This function is also complicated by the need for ψ to become negative if the concentration is ever to vanish at the boundary. For this reason, I will depart from the paper and assume that

$$C = S(z)T(r)$$

and define a further quantity

$$U = \frac{2}{R^2}\int_0^R Tr\, dr$$

which is the mean value of $T(r)$. Then

$$C_R = ST_R$$

$$\bar{C} = SU$$

and from the boundary condition

$$-DT'_R = \alpha T_R$$

The assumption as to the form of the concentration function thus reduces the equation to an ordinary differential equation

$$\frac{\partial \bar{C}}{\partial z} = -\frac{2\alpha}{WR}\frac{T_R}{U}\bar{C}$$

$$\frac{dT'_R}{U} = \frac{1}{4} Pe_{\text{dif}} \frac{d}{z} \ln \frac{\bar{C}}{C_0}$$

where

$$Pe_{\text{dif}} = \frac{Wd}{D}$$

Tsukhanova recognized the right hand member of this solution, from an exact analysis, as Nusselt's diffusion criterion. This permits an estimate of dT'_R/U through analogy between heat transfer and diffusion processes. This quantity might also be estimated by assuming a form of the radial concentration function.

The author gives data for the problem of simultaneous reactions of combustion and carbon dioxide reduction for which an exact analysis had been obtained. The data agree quite well with the carbon dioxide concentration passing through a maximum as the oxygen concentration fell rapidly to a minimum. Details of the system considered, whether for instance oxygen was assumed to react with carbon monoxide, or of the calculations were not given.

Koizumi considered a problem somewhat similar to that treated by Tsukhavnoa, but under boundary conditions and with mixing in the gas stream such that the analysis becomes entirely different. As applied to zones of active combustion in a bed of solid fuel, it was assumed that turbulent flow through irregular channels produced perfect mixing across the channel but not in the direction of flow. It was further assumed that temperatures were so high that carbon dioxide was immediately reduced at the carbon surface and that oxygen was reduced by carbon monoxide as these gases diffused in counter direction through the stagnant layer adjacent to the carbon surface.

The fraction of oxygen remaining in the gas stream was found as

$$r_a = (1 + A)e^{-Ky} - A$$

where the mass transfer rate in the oxidation zone of the fixed bed is

$$K = \frac{DS}{Ub}$$

and D is the diffusion coefficient, S is surface per unit volume of bed, U is the superficial velocity through the bed, b the thickness of the stagnant layer, y is the distance through the bed; and $B = ln(1 + P_{a0})/P_{a0}$ where P_{a0} is the volume concentration of oxygen in the air. From the point of complete disappearance of oxygen the fraction of carbon dioxide reduced to the monoxide was found as

$$r_g = \frac{2(1 - e^{-K'y})}{2 - e^{-K'y}}$$

where K' is the mass transfer rate in the reduction zone. These formulas were checked with 10 to 14 mesh fuel in a shallow bed in a fused silica tube which was, in turn, placed in a furnace at 900°C. The change in gas composition with distance through the bed was inferred from the change in exit gas composition with time as fuel was burned. Air deficient in oxygen, about 7 per cent oxygen, was used to minimize temperature

gradients and to avoid ash fusion. Data observed for a low ash active carbon were in agreement with the equations with $K = 1.305$ cm^{-1} and $K' = 1.82$ cm^{-1}. Data for a high temperature coke gave similar results but with greater scatter about the theoretical curves.

Koizumi also considered blow out due to interference of ash residues with combustion. It was assumed that the temperature of the carbon under the ash layer was so low that the reaction of CO_2 with carbon could not occur. Balancing heat and mass flows through the various layers with the reaction rate and heat release at the carbon surface led to Koizumi's Equation (17) relating the temperature of the carbon under the ash layer to the temperature of the gas stream and other parameters describing oxygen diffusion through the ash layer.

The temperature under the ash layer, other factors remaining constant, is a multiple valued function of either the outer air temperature or of the thickness of the ash layer. Once active burning is started the insulating effect of the ash layer permits a considerable drop in the outer air temperature with little loss in reaction temperature until a critical point is reached. At this point, the temperature drops to a lower branch of the curve where the rate of burning is that essentially at the temperature of the air stream. If the temperature is again raised another critical point is reached, the ignition point, where the temperature of the reacting surface rises substantially above that in the gas stream. The first critical point may be reached as a combustion wave moves through the bed while considerable combustible remains under the ash layer. Active combustion is blown out and little additional burning occurs within any reasonable time. Experiments with a high ash coke and with high ash coals showed that the fraction of residual carbon was reduced with increasing oxygen partial pressure and increased with ash percentage as predicted by the equation given.

Yagi used a model cyclone combustion chamber for study of factors controlling the amount of unburned carbon remaining in ash residues under conditions of combustion and gasification. The cyclone was made of moldable refractory. It was set in an electrically heated chamber so that radiation losses could be minimized. Fuel in suspension was introduced tangentially into the cyclone through a water cooled tube. Gases were removed through a second water cooled tube from the top center of the cyclone. Bypassing was reduced by forming the top of the cyclone as a cylindrical annulus surrounding the refractory shielded outlet tube. Effective volume was about 6.8 liters. The inside wall temperature and that in the center of the cyclone were measured by thermocouples. Using a high volatile coal with an ash fusion temperature, in air, about 1250°C, there was no difficulty in operation of the unit as a slagging gas generator with the slag collecting in the bottom of the generator.

The author used equations based upon thermal balances for correlating the experimental data. Heat contents and losses were expressed for this purpose as fractions of the calorific value of the fuel. Low values of gas yield and high oxygen requirements were due to high heat loss. The equations permitted estimates of these quantities in larger equipment with more favorable heat loss ratios.

Experiments were run both under conditions of combustion in air and of gasification either with steam and air or steam and oxygen. Steam to coal ratios were on the order of unity. The product gas was largely CO_2, CO, H_2, H_2O, N_2, and up to 3 per cent of methane. The methane content was primarily a function of the generator temperature, falling to zero at 1300 to 1400°C. The carbon efficiency varied between 80 and 95 per cent. It appeared to vary with oxygen supply primarily as a result of rising generator temperature passing through 90 per cent at about the ash fusion temperature. The carbon efficiency appeared almost independent of the steam to coal ratio in the range from zero to two with generator temperature otherwise held nearly constant. The efficiency also appeared to fall off with gasification rate in the range from 100 to 350 kg/m^3/hr. The percentage of ash entrained in the product gas fell off with rising generator temperature, passing through 50 per cent at about the ash fusion temperature and reaching about 15 per cent under slagging conditions. The mean temperature of the reduction zone appeared to be the most important factor in determining the performance of the generator and its efficiency.

The three papers on the combustion of pulverized fuels may be considered together. These papers present interesting experimental arrangements for production of stable flames and provide limited bases for judging the important modes of energy transfer within such flames. Cassel presented data on flat flames of aluminum powder. Mache-Hebra nozzles were used for production of a flat velocity profile. This had a minor dis-

advantage that low velocities in the chamber below the nozzle allowed elutriation of coarser particles out of the gas stream. The particle-streak photograph shows the flame produced. The change of momentum in the flame front produced a back pressure that expanded the stream below the flame. The stream continued to expand through the flame front and then contracted. This suggests that whatever device may have been placed over the flame it had little effect upon stabilizing the flame. This flame was produced with 210 mg/l of -5 μ aluminum dust. Flames were produced with concentrations from 200 to 310 mg/l and also with -5 μ graphite in concentrations from 200 to 230 mg/l. The burning velocity increased with concentration from 15 to 21.5 cm/sec for aluminum and from 12 to 15.5 for carbon. There was a further small increase in velocity with flame area, the areas ranging from 0.8 to 1.2 for aluminum and from 1.2 to 2.9 for the carbon.

Hattori produced stable flames of coal dust by means of an acetylene flame in the center of a concentric stream of coal dust suspension. Photographs showed the flame propagating as an inverted cone from the central ignition flame into the coal stream. A sharp change in flow direction was due to momentum change in the flame front. The author indicated a further change due to an outward bending of flow lines below the flame. The formula

$$V_f = V_0 \operatorname{Sin}\theta$$

was used for estimation of flame velocities. The author presented a more complicated analysis depending upon conservation of mass and of parallel components of momentum across the flame front together with an application of the Bernoulli principle. The analysis led to results significantly different than given by the above formula only at low discharge velocities. With an adequate ignition flame, acetylene velocity about 0.3 or more of the coal air velocity, the estimated flame velocities were nearly independent of the velocity ratio or of the total discharge velocity. Using a -100-mesh size of high volatile B coal, 47 per cent volatile matter on a dry, ash-free basis, the flame velocity in air reached a maximum of about 0.2 m/sec at a stoichiometric ratio, air over coal, of 0.3, or air over volatile matter of about 0.5. With oxygen enrichment the maximum was pushed into the fuel rich region of flash back and the decrease at high enrichment could not be observed. The velocity in 35 per cent oxygen reached 0.5 m/sec at a ratio of 0.15.

Ghosh has continued experimental work along the lines that were the subject of his thesis at the Coal Research Laboratory. His apparatus consisted in part of a tight circulatory system. Coal suspension was circulated through a loop of streamline tubing by an enclosed blower. Vibration was needed to keep coal from adhering to the tube walls. Introducing a metered flow of air, the coal air mixture was ejected through a water cooled tube into an externally heated furnace. In the earlier work a burner tube with an i.d. of 0.12 in. was used. In the present work the tube was 0.25 in. in diam.

When a suspension of coal in air was blown into a hot furnace, the appearance of ignition depended upon the coal to air ratio. At low concentrations the coal particles ignited at random at different points in the furnace. With increasing concentration a flame front appeared. The furnace temperature required depended upon the coal; with -200-mesh samples, two coals of about 45 per cent volatile matter content required 850°C, a coal of 34 per cent and one of 25 per cent required 950°C. Stable flame fronts could be produced with air supply in the range from 30 to 80 per cent of the stoichiometric. The burner mouth velocity could be varied over a considerable range; with a coal of 43 per cent volatile matter content, a 950°C furnace and 50 per cent stoichiometric air supply, the velocity could be varied from 40 to 150 cm/sec. As the velocity increased the flame front moved further from the burner mouth. Furnace temperature had a similar effect on the flame position, closer to the burner mouth with higher temperature, but this effect could not be studied in detail because of the significant effect of the flame upon the furnace temperature.

Oxygen enrichment of the air supply produced a brighter flame and increased the flame velocity, (Ghosh's Fig. 3). With an established flame the furnace temperature could be lowered but if the flame was lost the furnace had to be reheated to establish a new flame.

It was found that stable flames could be maintained in the open air with oxygen enrichment and a somewhat larger flame. Flames were maintained over a 1.1-cm tube but not over the next smaller size. Sixty per cent oxygen was needed for high volatile matter content coals, 70 per cent oxygen for 34 per cent V M coal and 100 per cent oxygen for a 27 per cent V M coal. Burner mouth

velocities could be varied from about 25 to 50 cm/sec excepting flash back below 35 cm/sec at 70 per cent and below 40 cm/sec at 100 per cent oxygen.

Using a −200-mesh to 40 μ coal as compared to a 100- to 160-mesh high volatile coal, it was found that stable flames for the fine coal could be produced in a somewhat narrower and lower range of coal concentration excepting instability at the highest burner mouth velocity, 55 cm/sec.

Ghosh (Fig. 6) shows an open air flame under blow off conditions. There is little expansion of the jet of coal in air suspension below the flame. The flame expands immediately to a size considerably larger than the jet.

Estimates of flame velocities in each of the three papers, under widely different conditions, are of the same magnitude, 10 to 100 cm/sec. Estimates found in the literature for commercial furnaces, on the order of 10 m/sec, either do not correspond to stable flames of the type considered here or are the result of larger flame size.

Cassel and Ghosh both attempted analyses of the effect of radiation in flame propagation. According to Cassel

$$SC(T_i - T_u) = k\left(\frac{dT}{dx}\right)_i + ASP$$

where S is the burning velocity, C the heat capacity of the unburned mixture, k, a coefficient of thermal conductivity, the subscript i refers to the ignition point, u refers to the initial state, A is the area of the flame and P depends only on the radiating quality of the flame. The equation is a modification, to include radiation, of an analysis of heat transfer in flame fronts as given by Mallard and Le Chatelier in 1885. Ghosh cites the same equation but does not elaborate upon the form of the "geometrical view factor." Cassel, in an earlier paper, did not specify the form of this factor but in the present paper sets it equal to the area of the flame. On the basis of this assumption, which is correct in direction but incomplete in that it does not include angle factors, Cassel has continued a detailed analysis which leads to estimates that the fraction of the heat transfer, needed for ignition, that is provided by radiation ranges from 30 to 60 per cent of the total. Ghosh points out that the basic equation is not free from objection in that it does not recognize the heterogeneous nature of the fuel suspension.

Although theoretical analyses are poor, the experimental data show the importance of radiation in production of pulverized fuel flames. Flames were stabilized by placing them in an environment at high radiant temperature while the fuel entered in a jet of cold air. In the distance from the burner mouth to the flame the jet showed little expansion. As the burner mouth velocity was increased, within the hot furnace, the flame moved away from the burner mouth. The necessary flame velocity was slightly smaller at the greater distance but the more important factor was the greater time available for radiant heat transfer from the environment. Unless the jet of fuel and air was too dense to permit penetration of radiant energy, conical cones of the Bunsen type were not formed. Angle factors within the cone are so effective for radiant energy transfer that the flame velocity becomes higher and a nearly flat flame is produced in spite of the higher velocities in the center of the stream. Stable flames in the open air required more intensely radiant flames and larger flames giving more favorable angle factors for radiation than those found for stable flames in hot furnaces.

70

FUNDAMENTAL PRINCIPLES OF CARBON COMBUSTION AND FACTORS INTENSIFYING THE BURNING OF SOLID FUELS

By L. N. KHITRIN

Introduction

In the combustion of any solid fuel, the combustion of the carbon residue is now generally recognized to play a major role. Thus the investigations of carbon combustion that have been actively pursued in recent years, particularly in the Soviet Union,[1-26] have been of great practical importance and have at the same time permitted the successful development of the theory of one of the most significant and complex heterogeneous chemical processes—the combustion of solid carbon.[27]

The problem of carbon combustion involves the combined analysis of mass and heat transfer both outside and inside the carbon mass, and of the complex of specific chemical processes (reactions of carbon with oxygen and its combustion products, reactions of the products of incomplete combustion of carbon with oxygen, etc.). The comprehensive solution of this problem is very complicated, but reasonable simplifications make it possible to clarify the principal properties of the process, thus establishing substantiated methods of simplifying the problem, and to obtain reliable characteristics of the process, above all the chemical (reaction) characteristics of carbon.

The purpose of the present paper is to analyze, on the basis of the foregoing studies, the principal regularities of the phenomenon of carbon combustion, which are represented as simple, approximate relationships that take into account the chief factors of the process and are acceptable for practical use.

The following three features of the carbon combustion process are worth noting:

(1) Possible diversity of composition of the carbon oxides so produced, which probably results not only from the primary chemical process (the reaction $C + O_2$), but also from the fact that under suitable conditions the presence of CO and CO_2 leads to concomitant secondary reactions, $C + CO_2$ and $CO + O_2$.

(2) Possible penetration of oxygen and other gaseous products into the porous carbon mass, resulting in the development of reactions not only on the surface, but within the mass. This phenomenon and the process of inner diffusion are of great significance in appraising the reactivity of carbon.[4, 27-33] It is evident that the presence of this factor alone, i.e., the reaction inside the carbon piece, indicates that the composition of the carbon oxides released outside by the burning surface ("surface" oxides) cannot, generally speaking, correspond to the composition of the primary products of carbon combustion.

(3) Specificity, from the mathematical viewpoint, of the problem of the combustion of a carbon mass. Without additional conditions, this problem is not reduced in the broad sense to the similar problem of heat transfer even if a definite law of interaction between the ambient gas and the surface of the body can be accepted as a boundary condition at the surface of the body. As we know, in a thermal problem, either the temperature or the heat flow at the surface of the body must be assumed whereas, in a combustion problem, the flow of reacting matter and its concentration at the surface of the body are determined by the law of reaction, and the values of surface concentrations are determined simultaneously by diffusion and chemical processes, in other words, they are unknown quantities.

Reactivity Characteristics

In calculating the combustion and appraising the reactivity of a given carbon (coke), it is very important to be able to characterize the over-all process by an equation similar to the law of heterogeneous chemical processes of the type $W = Kf(c)$, where W is the velocity of consumption of the gas reagent, K is a rate constant, and $f(c)$ is some function of concentration of the gas reagent.

Analysis of this problem, for the special case of the combustion of a spherical body, shows[27, 34] that strictly speaking such an approach to the problem, i.e., treating it as a purely surface process, is permissible only in the simplest case, namely when the chemical reactions involving carbon are first order. In this case the over-all process of interaction of oxygen at the surface of the phase boundary has the form $W_{O_2} = K^* C$

(or $W_{CO_2} = K_{21}^* C_2$ for carbon dioxide), where K^* and K_{21}^* are independent of C or C_2 and play a role similar to that of ordinary rate constants in heterogeneous chemical reactions. It follows from the analysis of the conditions at the surface, S, of the boundary between the gas phase and the porous body that

$$K^* = K + \frac{D_i}{c_s}\left(\frac{\partial c}{\partial n}\right)_s. \qquad (1)$$

where K is the rate constant of the chemical process, C_s is the concentration of O_2 at the surface of the body, and D_i is the coefficient of inner diffusion.

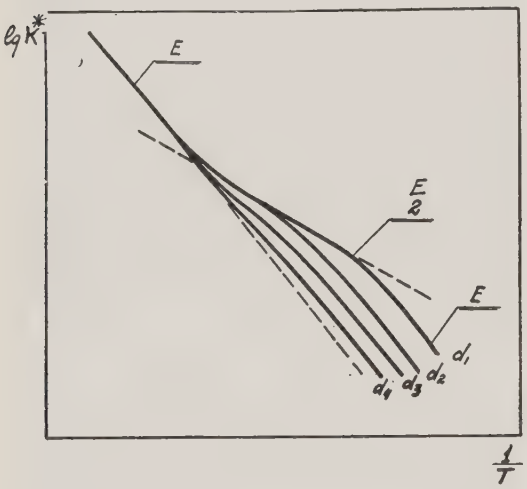

FIG. 1. Dependence of K^* upon temperature and particle size.

K^* as well as K_{21}^* is the effective or reduced constant of interaction between the gas and the porous solid; it has also been called the reaction coefficient of gas exchange.[27] It is this constant or coefficient that must be considered as the practical characteristic of the reactivity of a given carbon in relation to a given gaseous reagent.

Experience has shown[21, 27, 35] that ordinarily the heterogeneous process of the reaction of oxygen with carbon is governed by the law

$$W_{O_2} = \frac{K'}{c + A} \qquad (2)$$

which for $c \ll A$ becomes the equation of a first order reaction. The latter condition is realized in a natural way when the temperature of the process is raised due to retardation of the reaction by diffusion, that is, precisely when it becomes necessary to analyze the general problem of the combustion of a carbon body. The course of the reaction $C + CO_2$ is similar, although in this case retardation due to diffusion sets in at higher temperatures. For this reason, it is somewhat arbitrary to treat this process as part of the general problem of combustion by introducing the linear law of reaction; further analysis and experimental control are needed. When assuming magnitudes K^* and K_{21}^* as characteristics of reactivity, it should be noted that, generally speaking, they are functions of a point on a surface of variable concentration of O_2 and CO_2. As a result, one has to deal with the mean values of K^* and K_{21}^*.

For a spherical body the mean value of K^* is

$$K^* = K + \lambda D_i\left(\coth \lambda r - \frac{1}{\lambda r}\right)\frac{\text{cm}}{\text{sec}} \qquad (3)$$

where

$$\lambda = \sqrt{\frac{K_i}{D_i}}, \qquad K_i = Ks_i$$

(s_i is the specific reaction surface of a porous body in cm^2/cm^3.).

K^* depends on the dimensions of the body and the temperature. This type of dependence is shown in Figure 1.

There are three typical regions:

(1) The case of small values of λr (low temperatures or small dimensions of the body) when

$$K^* = K\left(1 + \frac{s_i r}{3}\right)$$

or

$$K^* \approx \frac{s_i r}{3}, \qquad \text{if} \qquad \frac{s_i r}{3} \gg 1$$

In this case the reaction takes place throughout the volume of the body, and K^* is proportional to its dimensions and the magnitude of the kinetic constant $K = K_0 e^{-E/RT}$. The magnitude $K^*/K' = 1 + s_i r/3$ defines the ratio of the whole reaction surface to the outer surface of the body; the smaller its dimensions, the closer this relationship approaches unity.

(2) The case of larger values of K (high temperatures), when $K^* \approx K$. The reaction virtually proceeds only on the outer surface of the body, and K^* coincides with the kinetic constant of the reaction of carbon with oxygen.

Between these two regions there exists a

transient region where K^* depends both on the kinetic and diffusion characteristics of the carbon. It is precisely this region that most frequently fits the conditions of actual processes. The smaller the dimensions of the particles, the narrower are the temperature boundaries of this region. Figure 2 shows, for instance, the dimensions of the transient region for the two types of carbon, depending on the dimensions of the particle. The equation $K^* = K(1 + s_i r/3)$ may be valid for temperatures for small-sized particles, becoming $K^* = K$ for small r.

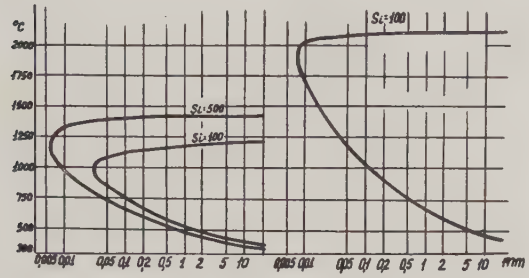

(a) (b)

FIG. 2. Boundaries of the influence of the internal process on the reactivity characteristics. (a) electrode carbon, (b) anthracite. Dimensions of the particles in mm are plotted along the axis of the abscissa.

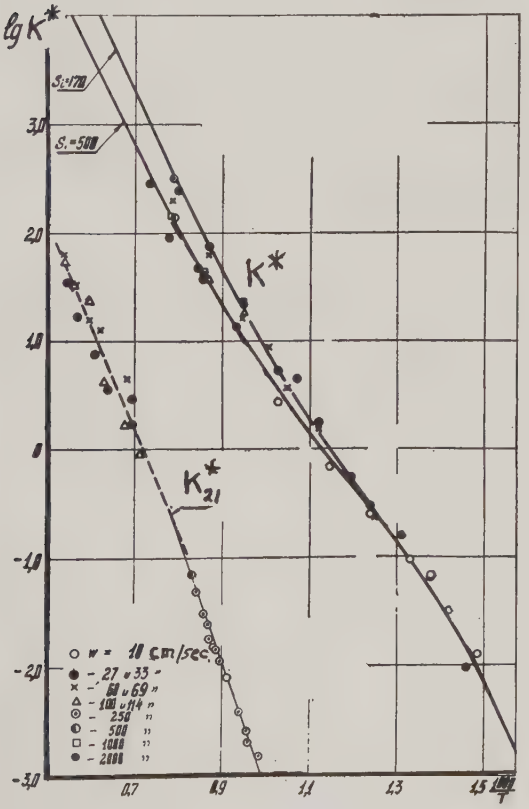

FIG. 3. Values of K^* and K^*_{21} for electrode carbon; d = 15 mm.

A similar pattern has been established for the coefficient K^*_{21}. However, in this case, the transition region (Fig. 2) is shifted to higher temperatures. At ordinary temperatures of combustion, particles on the order of 1 to 2 mm react throughout their volume.

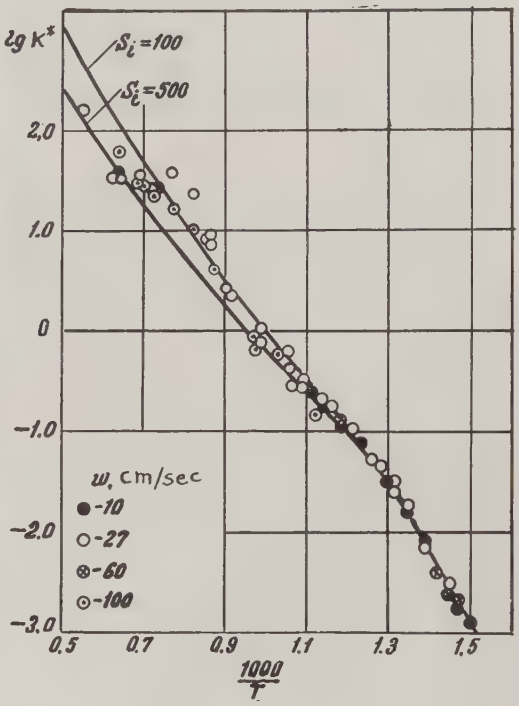

FIG. 4. Values of K^* for anthracite (coke); d = 15 mm.

The changes of K^* and K^*_{21} (for a given carbon) with the temperature observed experimentally and analyzed,[3, 10, 27, 39] are shown in Figures 3, 4 and 5 for large particles. A comparison of the course of K^* for large and small particles is shown in Figure 6.

SPECIFIC RATE OF COMBUSTION AND THE ROLE OF SECONDARY REACTIONS

The specific rate of combustion of carbon K_s^c (g carbon/cm² sec) is a characteristic of the process of combustion as a whole. Unlike the analogous quantity frequently used $K_s^{O_2}$ (g oxygen/cm² sec) $= -D(\partial c/\partial n)_s$, the quantity

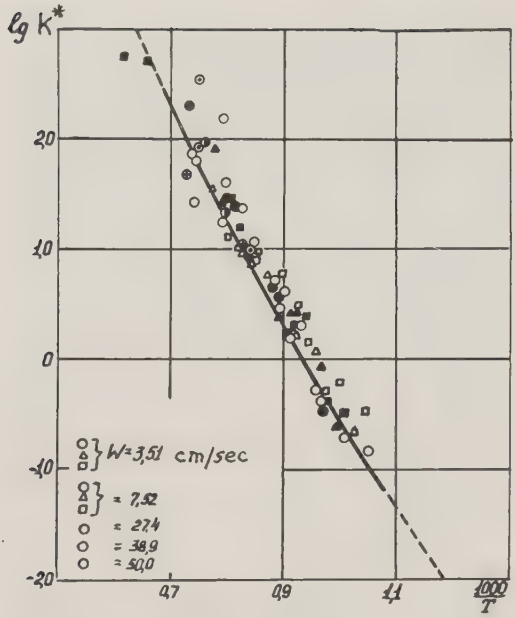

FIG. 5. Values of K^* for brush carbon (experimental data of Parker and Hottel); $d = 25.4$ mm.

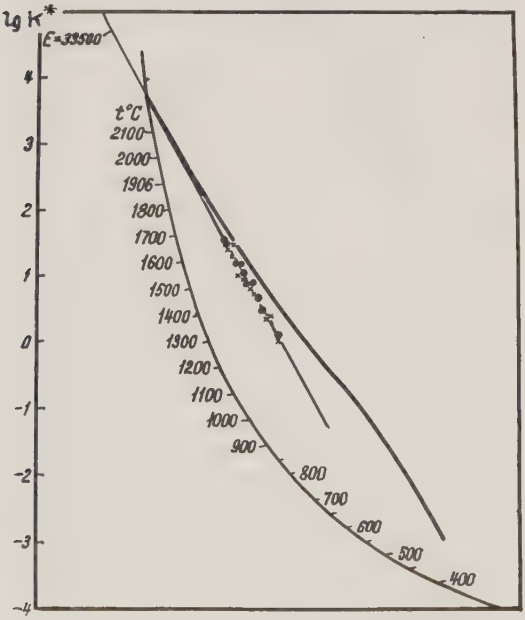

FIG. 6. Values of K^* for large and small particles (anthracite). Solid line, $d = 15$ mm; dotted line, $d = 100\ \mu$.

$K_s^c = -12/32[2(\partial c_1/\partial n)_s + (\partial c_2/\partial n)_s]D^a$ where C, C_1 and C_2 are weight concentrations of O_2, CO and CO_2 (the latter two expressed as the weight of oxygen contained in these oxides); D is the diffusion coefficient.[34]

[a] In this relationship an increase in the number of molecules during the combustion of carbon to CO is not taken into account.

It is generally accepted that $K_s^c = K_s^{O_2} \cdot \beta$. This cannot be valid under all conditions since a limiting case is possible, when oxygen does not reach the carbon surface at all,[36] and combustion becomes a kind of "relay race" between the reactions of $C + O_2$ and $CO + O_2$. The introduction of β is expedient for characterising the effectiveness of oxygen consumption in gasification of carbon (the conversion of solid carbon into gaseous products).

By using the effective value β_{eff},[27] we obtain an approximate expression for K_s^c of the ordinary type:[1, 3, 9, 27, 37, 38, 39]

$$K_s^0 = \beta_{eff}\alpha_{dif}C\,\frac{1}{1+\dfrac{\alpha_{dif}}{K^*}} = \beta_{eff}\alpha_{dif}CR \qquad (4)$$

where

$$\beta_{eff} = \frac{12}{32}\cdot\frac{2K_{21}^* + (1+\xi)(\nu z\coth\nu\delta + 1)\dfrac{D}{r}}{\left\{K_{21}^* + \alpha_{dif} + (\nu z\coth\nu\delta + 1 - 0{,}5Nu_{dif})(1+\xi R)\right\}} \qquad (5)$$

$\alpha_{dif} = (D/d)Nu_{dif}$ (diffusion analogue of the coefficient of heat exchange), ν is the parameter connected with constant κ of the velocity of CO combustion: $\nu = \sqrt{\kappa/2D}$; $\delta = d/(Nu_{dif} - 2)$ is the thickness of the reduced stagnant film; ξ is the fraction of K^* corresponding to the consumption of oxygen for CO. The limits of the change of β_{eff} are from 12/32 to 24/32 and of R from 0 to 1.

Magnitude R may serve as a convenient criterion for appraising the regime of the combustion process. With $R < 0.1$, $\alpha_{dif}R \approx K^*$ and $K_s^c = \beta_{eff}K^*C$, the process is determined by the coefficient, K^* (quasi-kinetic conditions). With $R > 0.9$, $\alpha_{dif}R \approx \alpha_{dif}$ and $K_s^c = \beta_{eff}\alpha_{dif}C$, the process does not depend on the characteristic of the fuel, K^*. Accordingly, in the first regime, for a given temperature, K_s^c remains constant or increases with an increase in d; in the second regime, K_s^c always decreases with an increase in d. Under the latter conditions, a decrease in d by crushing is effective; under quasi-kinetic conditions crushing is advisable to a definite size only. This last observation is of particular importance for the reduction of carbon dioxide where K_{21}^* is

always $\ll K^*$ (under ordinary conditions of combustion, K_{21}^* is at least two orders smaller than K^*).

The expression, β_{eff}, indicates that the combustion of carbon monoxide in a gas volume is accounted for by the expression $\nu z \coth \nu\delta$. The smaller the relative velocity between air stream and particle is, and the larger the particle, the greater the influence of CO combustion will be. Figure 7 shows the nature of the change in β_{eff} for a small and for a large particle burning in a slow flow with various ratios of "surface" oxides $M = -CO/CO_2$ (different ξ). It will be seen that the behavior of K_s^c differs in these two cases (Fig. 8). When large particles burn, there is a more (II) or less (I) pronounced slowing up of combustion in the region of ~750° (ignition temperature of CO).

It is worth noting that the limiting diffusion conditions of combustion do not conform to the limiting diffusion conditions governing the oxygen flow (lower dotted line), but are shifted far to the right toward the region of very high temperatures. The dotted line in Figure 8 with index, K^*, designates the limit value of K_s^c determined by magnitude K^* (the law of quasi-kinetic conditions of combustion). It will be seen from the graphs that after ignition of CO the velocity of combustion of a large particle (10 to 15 mm) in a slow flow is virtually independent or the composition of "surface" oxides and conforms solely to the apparent formation of CO_2. On the other hand, m exerts a marked influence on the combustion rate of small particles ($d < 500\ \mu$).

After a certain delay in the growth of K_s^c with an increase in temperature, the new rise of the curves, particularly noticeable on Figure 8, is accounted for by the onset of a considerable development of the reaction $C + CO_2$. The rise of the curve, K_s^c, begins approximately in the region of 1300 to 1500°C. It is only around 2500°C that the limiting condition of combustion is virtually attained and β_{eff} corresponds to the formation of CO alone. These conditions correspond to those of two-stage combustion analyzed elsewhere.[36] The existence of the reaction $CO + O_2$ near the carbon surface is a prerequisite. This becomes possible at small particle velocities. At higher flow velocities, the carbon monoxide flame blows off from the particle front, leading to a decrease, instead of an increase, in K_s^c. This is due to the fact that the delaying action of the flame is concentrated at the rear of the particle. The combustion of CO then proceeds

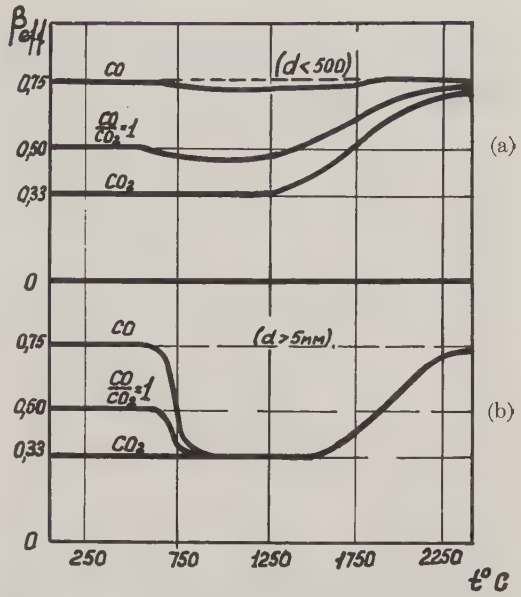

FIG. 7. Changes in β_{eff} depending on the temperature. (a) Small particle, $d < 500\ \mu$; (b) large particle, $d > 5$ mm.

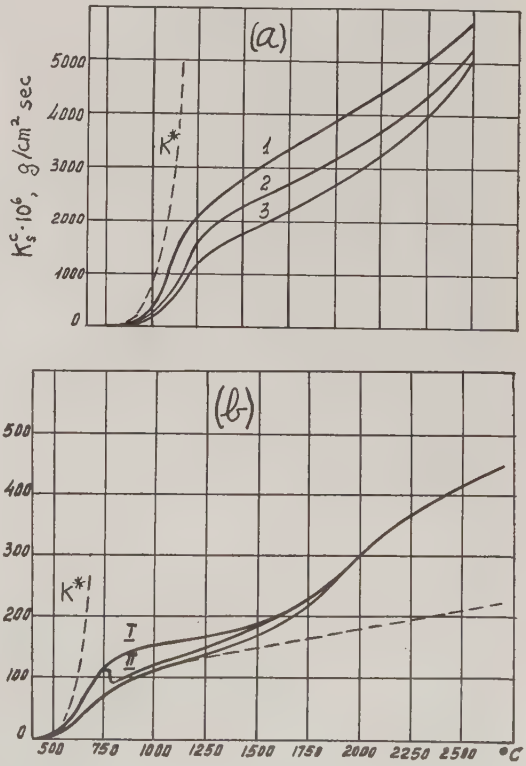

FIG. 8. K_s^c as a function of the temperature (calc.). (a) Particle $d = 2$ mm; (b) Particle $d = 15$ mm.

as gas mixtures in the wake of a spherical stabilizer. The experimental results illustrating the behavior of K_s^c in this case are shown on Figure 9. It is difficult to judge the probable value of m for "surface" oxides on the basis of β_{eff}. An appraisal of m can be made in two ways: (1) By

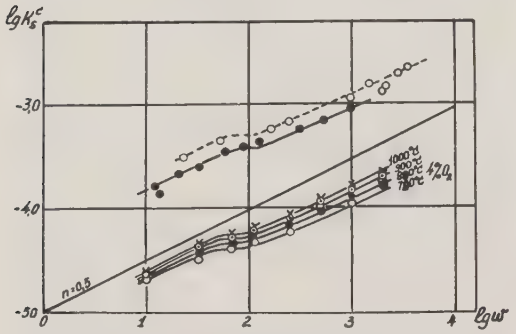

FIG. 9. K_s^c as a function of the flow velocity for large particles. (1) (- ∘ - - ∘ shows experiments by Tsukhanova and Kolodkina; (2) —•—• shows experiments by Khitrin and Oleschuk; (3) Bottom lines show experiments by Khitrin and Oleschuk, O_2 = 4 per cent.

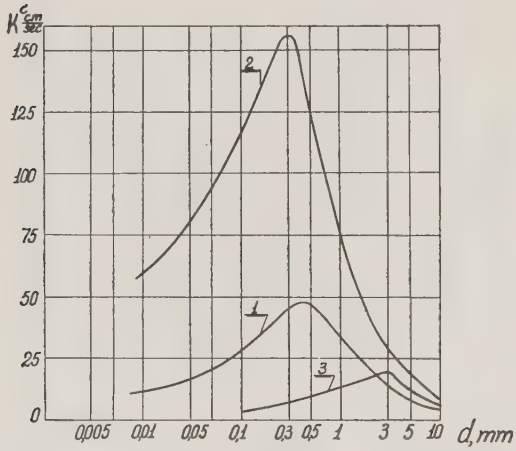

FIG. 10. K^c as a function of the particle size (S_i = 500). (1) Combustion at 1000°C; (2) combustion at 1600°C; (3) reduction of CO_2 with carbon at 1300°C.

comparing β_{eff} (or K_s^c) before or after ignition of CO, when $m \approx 0$; (2) By changing K_s^c before or after the CO flame blows off due to the increased flow velocity. For electrode carbon, these calculations give m = 1.0 (at 800° to 1000°C).

From the practical viewpoint, the relationship between changes in the combustion rate of particles and changes in their dimensions is of considerable interest.

For small particles, $Nu_{dif} \approx 2$, and $\nu r = 0$. Hence, if $K_{21}^* \ll D/z$, then

$$\beta_{eff} = (1 + \xi)\frac{12}{32} \qquad \text{and for}$$

$$\xi = 0.33 \quad (m = 1.0)$$

$$K^c = \frac{K_s^c}{c} = \frac{\dfrac{D}{r}}{1 + \dfrac{2D}{K^* d}} \tag{6}$$

As has been shown above, K^* is related to s_i and K and also depends on d. If this dependence and the probable value of s_i are considered, the dependence of K^c on d has the form indicated on Figure 10 where curves 1 and 2 correspond to the case of combustion, and curve 3 to the process of carbon dioxide reduction. These curves indicate that there is always a rational lower limit of the carbon particle size below which the velocity of the process again decreases. These dimensions depend on the type of carbon (porosity) and the constant, K. As seen from the graph, in the case of combustion, this limit is much lower than in the case of reduction (gasification process). This type of dependence (Fig. 11) is confirmed by experimental data for the combustion of particles of different sizes.[40]

COMBUSTION OF A MULTIPLICITY OF PARTICLES

In practice the combustion of fuel always proceeds in a fuel bed, a suspension of pulverized fuel, or in a fluidized bed. It has been shown[27, 41, 42] that in the simplest but very common case of a one-dimensional flow, the combustion process can be described by the following averaged equations:

$$\frac{dc}{dx} = -ac \tag{7}$$

$$\frac{dc_2}{dx} = \zeta ac - a_{21}c_2 \tag{8}$$

where

$$\zeta = 1 - \xi$$

The parameter, a, is related to K_s^c for the individual particle and the outer surface (area) of the particles in a unit volume S_i: $a = S_i \varphi R$, (where $\varphi = \alpha_{dif}/w$ is often termed the Margulis criterion). Similarly $a_{21} = S_i \varphi R$, where $R_{21} = 1/1 + (\alpha_{dif}/K_{21}^*)$.

Equation (7) for oxygen is the basic equation. The intensity of the process is determined by the parameter, a, whose numerical value and properties depend upon conditions of combustion.

The combustion of a fixed bed of particles and that of suspended fine dust illustrate two extremes. For a bed where the particles are not too small, φ proves to be approximately constant;[16] it approximates 0.3 and, theoretically,[43] has the form $\varphi = 0.28\, Re^{-0.18}$. We obtain $\varphi R \approx$ const $\approx$ 0.3, irrespective of w and d. In an air suspension of dust $\varphi \approx 2D/w\,d$, and φR approximates K^*/w, as $R \approx K^*\, d/2D$. Figure 11 illustrates the change in φR for a dust suspension, as a function of w and d. The corresponding dotted line represents φR for a bed. It follows from the graph that there is no substantial difference in φR for a dust suspension or a bed for values of K^* on the order of 500 to 1000 cm sec (system of curves 3) and where the particle diameters range from 25 to 250 μ. This conclusion is of interest as it proves that a very great reduction in the particle size, is not effective because the combustion of fine dust approximates the conditions of quasi-kinetic combustion.

The value S_i is determined by the size of the fuel particle and the weight concentration of the fuel C_f(g/cm³). In a bed, S_i is of the order of $3/d$. Experience has shown[18] that S_i is approximately constant throughout the entire depth of the combustion zone. In a dust suspension

$$S_i = \frac{6}{d_0}\frac{c_f}{\gamma_f}\left(\frac{d}{d_0}\right)^2 \tag{9}$$

where γ_f is the specific weight of the coal particle (g/cm³). As combustion proceeds, S_i tends toward zero. The numerical values of S_i in a bed and in a dust suspension differ by about two orders. Thus, in a bed where $d = 5$ mm S_i is 600(m²/m³), and in a dust suspension where $d = 100\ \mu$ it is 6 (m²/m³). This is due to the great difference between the concentration of carbon in a bed, where it is approximately 0.5 γ_f, i.e., generally 500 to 800 kg/m³, and in a dust suspension where, with a stoichiometric ratio of unity, $C_f \approx 0.112$ kg/m³. It is evident that crushing the fuel leads to decreased intensity of combustion, for the amount of reaction surface in a unit volume is inevitably decreased because burning in a suspended state sets in.

Thus, analysis of the influence of S_i and φR on the value of a indicates that S_i, or, in other words, the fuel concentration, is the most effective factor determining the difference between combustion in a bed and combustion in a dust suspension. It attains its maximum in a bed, and is at its minimum in a dust suspension. All other types of suspended burning must be considered as intermediate.

As the behavior of a changes, so does the major technical characteristic of combustion, namely, the rate of the heat release, Q/V (kcal/m³ hr), where Q is the heat evolved during combustion, and V is the volume of combustion.

From Equation (7)

$$\frac{c}{c_0} = e^{-ax} \tag{10}$$

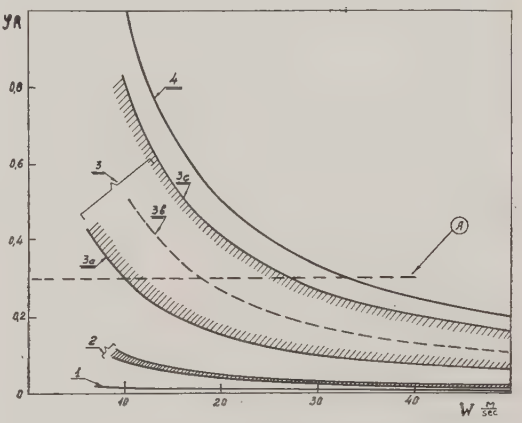

FIG. 11. φR as a function of the flow velocity for dust suspensions. (1) Change at K^* 10 cm/sec. (2) Change at K^* 100 cm/sec. (3) Change at K^* 1000 cm/sec: 3a—250 μ; 3b—100 μ; 3c—25 μ. (4) Change for the limiting case, $K^* \to \infty$. (A) Approximate value of φR for the combustion of a fuel bed.

By assuming the end of the combustion zone to be magnitude $x = L$, where $C/C_0 = 0.05$, we obtain in the case of a bed

$$L = \frac{3}{S_i\varphi} \simeq 3d \tag{11}$$

and

$$\frac{Q}{v} = 3600 w\gamma \frac{(Q_{CO_2} - Q_{CO})\dfrac{CO}{CO_2 + 0.5CO} + Q_{CO}}{3d} \tag{12}$$

where Q_{CO} and Q_{CO_2} are the heats of burning 1 kg of air to CO and CO_2, γ is the specific weight of air, and w is the velocity of filtration. It follows from Equation (12) that Q/V increases in direct proportion to w and γ, i.e., to the pressure, and inversely to d. The simplest way of increasing

Q/V is to raise w. The order of Q/V in a bed where $w = 1$ m/sec is 100 to 200 million kcal/m³ hr. These conclusions are confirmed experimentally[15, 16, 17, 18].

In a dust suspension:

$$L = \phi(\alpha) \frac{wd_0}{K^* c_f} \tag{13}$$

where $\phi(\alpha)$ is a coefficient dependent on the excess air coefficient α. Hence

$$\frac{Q}{V} = 3600 \frac{\gamma}{\gamma_f} \frac{K^* c_f}{\alpha \phi(\alpha) d_0} \cdot Q_{CO_2} \tag{14}$$

since usually it is only CO_2 that is found in the burning dust suspension. In this case, Q/V does not depend on w, but increases greatly with the pressure ($Q/V \sim p^2$). The decrease in particle sizes also may lead to an increase in Q/V, unless K^* is proportional to d_0. This latter possibility is illustrated in Figure 10. For ordinary conditions of combustion (Fig. 11), Q/V proves to be of the order of 1 million kcal/m³ hr, or less, for dust suspensions.

As has been pointed out, S_i is the principal means of intensifying combustion. The more the flow velocity of the air differs from that of the fuel particles, the greater this value. In a dust suspension, it is at its minimum. The increase of the relative velocities (increasing the residence time of the solid phase as compared with the residence time of the gas) increases the concentration of fuel and also the transfer function φ. The burning of pulverized and fine-grained fuels, using vortex and cyclone furnaces, is to a great extent, based on this general conclusion.

REFERENCES

1. Blinov, V. I.: J. (Izvestiya) USSR Heat Engr. Inst., No. 7, 1934; Proc. Voronezh University, *12*, Installment 1 (1941).
2. Blinov, V. I., and Khaikina, S. I.: J. (Isvestiya) USSR Heat Engr. Inst., No. 6 (1935).
3. Blinov, V. I., and Golovina, E. S.: Proc. Voronezh University, *11*, Installment 1, 7 (1939).
4. Blinov, V. I., and Smirnov, P. G.: Proc. Voronezh University, *11*, Installment 1, 33, 55 (1939).
5. Blinov, V. I., and Rozet, T. A.: Reports USSR Acad. Sci., *47*, No. 3 (1949); *48*, No. 2 (1950).
6. Predvoditelev, A. S.: J. Tech. Phys. (USSR), *10*, Installment 16 (1940); *11*, Installment 10 (1941).
7. Predvoditelev, A. S., and Tsukhanova, O. A.: J. Tech. Phys. (USSR), *10*, Installment 13 (1940).
8. Tsukhanova, O. A., J. Tech. Phys. (USSR), *9*, Installment 4 (1939); Izvestiya Akademii Nauk SSSR, Tech. Sci. Sec., No. 4 (1947); J. Phys. Chem. (USSR), *21*, Installment 6 (1947).
9. Khitrin, L. N.: Izvestiya Akademii Nauk SSSR, Tech. Sci. Sec., No. 4 (1948); No. 7 (1948); No. 4 (1953).
10. Golovina, E. S.: Ozvestiya Akademii Nauk SSSR, Tech. Sci. Sec., No. 9 (1949).
11. Goldenberg, S. A.: Izvestiya Akademii Nauk SSSR, Tech. Sci. Sec., No. 4, 5, 8 (1950).
12. Chukhanov, Z. F., and Grodzovsky, M. K.: Reports USSR Acad. Sci., *3*, No. 5, (1934); J. Appl. Chem. (USSR), *7*, Installment 8m (1934); Installment 1 (1936); Chem. Solid Fuel (USSR), No. 9–10 (1936); Fuel, No. 11 (1936).
13. Chukhanov, Z. F.: J. Tech. Phys. (USSR), *8*, Installments 2 and 7 (1938); *9*, Installment 21 (1939); 10, Installment 15 (1940); Reports USSR Acad. Sci., *26*, No. 4 (1940); *27*, No. 3 (1940); *28*, No. 1 (1940); Fuel, *18*, No. 10 (1939); *19*, Nos. 1, 2, 3 (1940); Reports USSR Acad. Sci., *44*, No. 7 (1944); *42*, No. 3 (1948); *59*, No. 5 (1948); *72*, No. 3 (1950); *77*, No. 4 (1951); *81*, No. 5 (1951); Izvestiya Akademii Nauk SSSR, Tech. Sci. Sec., No. 1 (1948); No. 4 (1953).
14. Chukhanov, Z. F., and Karzhavina, N. A.: J. Tech. Phys. (USSR), *9*, No. 21 (1939); *10*, No. 15 (1940); Fuel, *20*, No. 3, 4, 8 (1941).
15. Chukhanov, Z. F., and Chirkin, A. P.: Reports USSR Acad. Sci., *95*, No. 6 (1954).
16. Kolodtsev, K. I.: J. Tech. Phys. (USSR), *9*, Installment 4 (1939); J. (Izvestiya) USSR Heat Engr. Inst., No. 1 (1940); J. Phys. Chem., *19*, Installments 9 and 12 (1945); J. (Izvestiya) USSR Heat Engr. Inst., No. 4 (1948); No. 8 (1949); Nos. 1 and 10 (1951); Heat Power, No. 1 (1954).
17. Kolodtsev, K. I., and Orelchenko, I. F.: J. (Izvestiya) USSR Heat Engr. Inst., No. 8 (1952); No. 5 (1953).
18. Babiy, V. I., and Kolodtsev, K. I.: Heat Power, No. 1 (1954); No. 7 (1955).
19. Frank-Kamenetzki, D.: J. Phys. Chem. (USSR), *13*, Installment 6 (1939); J. Tech. Phys. (USSR), *10*, Installment 14 (1940); J. Phys. Chem. (USSR), *14*, Installment 3 (1940); Uspekhi Khimii (USSR), *7*, No. 9 (1938).
20. Syromyatnikov, M. I.: Reports USSR Acad. Sci, *97*, No. 2 (1954).
21. Khaikina, S. E.: J. Tech. Phys. (USSR), *8*, Installment 1 (1938).

22. Vulif, L. A.: J. Tech. Phys. (USSR), *11*, Installment 6 (1941); *16*, Installment 1, 83, 85 (1946).
23. Kantorovich, B. V.: J. Tech. Phys. (USSR), *12*, Installment 7 (1942); Isvestiya Akademii Nauk SSSR, Tech. Sci. Sec., No. 3 (1945); No. 4 (1947); No. 4 (1953).
24. Savvinov, M. I.: Proc. Voronezh University, *12*, Installment 1 (1941).
25. Predvoditelev, A. S.: *The Process of Coal Combustion*. State Publishing House of Technical Literature, 1938.
26. Knorre, G. F.: *Investigating the Processes of Combustion of Natural Fuel*. Power Industry State Publishers, 1948.
27. Predvoditelev, L. N., Tsukhanova, O. A., Kolodtsev, K. I., and Grodzovsky, M. K.: Carbon combustion. USSR Academy of Sciences Publishing House, 1949.
28. Zeldovich, Y. B.: J. Phys. Chem. (USSR), *13*, Installment 2 (1939); Acta Phys.-chim. (USSR), *10*, 583 (1939).
29. Thiele, E. W.: Ind. Eng. Chem., *31*, 916 (1939).
30. Mayers, M. A.: J. Am. Chem. Soc., *61*, 2053 (1939).
31. Wagner, C.: Z. Phys. Chem., *A198* (1944).
32. Wicke, E.: *Fifth Symposium (International) on Combustion*, p. 245. New York, Reinhold Publishing Corp., 1954.
33. Wicke, E., and Brotz, W.: Chem. Ind. Tech., *21*, 219 (1949).
34. Khitrin, L. N.: Izvestiya Akademii Nauk SSSR, Tech. Sci. Sec., No. 3 (1948).
35. Lambert J. D.: Trans. Faraday Soc., *32*, 452 (1936).
36. Burke, S., and Schumann, T.: Proc. Third Intern. Conference on Bituminous Coal, *2*, 485 (1931).
37. Tu, C. M., Davis, H., and Hottel, H. C., Ind. Eng. Chem., *26*, 749 (1934).
38. Davis, H., and Hottel, H. C.: Ind. Eng. Chem., *26*, No. 8 (1934).
39. Parker, A., and Hottel, H. C.: Ind. Eng. Chem., *28*, 1334 (1936).
40. Katsnelson, B. D.: Private communication.
41. Tsukhanova, O. A., Izvestiya Akademii Nauk SSSR, Tech. Sci. Sec., No. 6 (1947).
42. Predvoditelev, A. S.: Izvestiya Akademii Nauk SSSR, Tech. Sci. Sec., No. 10 (1947).
43. Chukhanov, Z. F.: Reports USSR Acad. Sci., *65*, No. 5 (1949).

71

SOLVING PROBLEMS OF HETEROGENEOUS COMBUSTION BY THE METHOD OF AVERAGING EQUATIONS[a]

By O. A. TSUKHANOVA

The combustion process of carbon is described in a general way by two systems of diffusion equations. One system describes the diffusion process in the gas phase at the outer surface of the coal; the other pertains to the processes taking place inside the porous mass. With rare exceptions, when solving the problem of carbon combustion, one system of diffusion equation is sufficient for the gas phase, with boundary conditions which take into account the chemical process at the surface and the conditions of delivering the reaction gases to the surface. The complex process of gas exchange at the outer surface of coal, including the processes inside the porous coal mass and at the surface of coal, can be determined with the aid of reaction gas exchange coefficients. These numerical values are determined by special experimental methods.[b] Their value depends only on the chemical nature of the reaction gas, the kind of fuel, and the temperature; it does not depend on the physical parameters determining the process of transfer of the gas reagent to the coal surface. These parameters include the velocity of the gas, the geometric configuration and the diffusion coefficient.

Generally speaking, if the values of the reaction gas exchange coefficients are known, the

[a] This work was carried out in the laboratory of physics of combustion, Krzhizhanovsky Institute of Energetics, USSR Academy of Sciences, and supervised by A. S. Predvoditelev, Corresponding Member of the USSR Academy of Sciences.

[b] The derivation of the combustion equation and the properties of the reaction gas exchange coefficients are discussed in detail by Predvoditelev *et al.*[1]

equation system can be solved numerically and the field of concentrations of the reaction gas and reaction products can be determined. Consequently, the other characteristics of the combustion process can also be determined.

Because of mathematical difficulties, this equation is not capable of a general solution. However, a small number of problems raised in connection with the study of particular aspects of the process of carbon combustion have been solved individually.

An attempt to solve the system analytically for practical applications, such as the process of gas formation in a fuel bed, could hardly prove successful.

This is confirmed, for instance, by the development of the heat exchange theory. The heat exchange equations are similar to diffusion equations. The problem of heat transmission is far simpler than that of combustion, since in heat exchange only one equation has to be solved, and not a system of equations. However, analytical methods have proved useful only for problems of heat conductivity in solids. The solution of the problem of heat transmission in fluids gave no positive results. The theoretical values and experimental results were not in good agreement. The discrepancy of the results is explained by the fact that, to avoid mathematical difficulties, assumptions were made which distorted the process itself.

In the theory of heat exchange, a solution was found in the theory of analogy and the use of models. Application of these methods to the calculation of the processes of combustion appears promising. Attempts have been made, for instance, to make use of the analogy between heat transmission and diffusion. However, in the general sense, this is inadmissible, because the boundary conditions in heat transmission and combustion are different.

Let us analyze, for instance, the actual process of combustion at the wall of a coal tube and the heat transmission in the tube. The two processes are defined by the following similar differential equations:

$$w \frac{\partial C}{\partial z} = D \left(\frac{\partial^2 C}{\partial r^2} + \frac{1}{r} \frac{\partial C}{\partial r} \right) \tag{1}$$

(diffusion equation)

$$w \frac{\partial t}{\partial z} = a \left(\frac{\partial^2 t}{\partial r^2} + \frac{1}{r} \frac{\partial t}{\partial r} \right) \tag{2}$$

(heat transmission equation)

where w = velocity of gas, C = concentration of oxygen, D = diffusion coefficient, t = temperature, a = thermal diffusivity, z, r = coordinates, and R = radius of the tube.

Let us consider the boundary conditions. The problem of combustion can be solved with the boundary condition as follows

$$-D \left(\frac{\partial C}{\partial r} \right)_R = \alpha C_R$$

showing that the diffusion flow of reaction gas to the surface of coal is proportional to the concentration of reaction gas at the surface C_R. The reaction gas exchange coefficient, α, is constant, whereas the concentration of reacting gas at the surface, C_R is proportional to the gradient of concentrations at the surface and depends on the transfer number. The concentration at the wall of the tube C_R is similar to the t_R in the problem of heat transfer. This problem can be solved on the assumption that the temperature at the surface is constant. It can be assumed, for instance, to equal zero. The surface coefficient is variable and depends on the transfer number. Consequently, the boundary conditions of these problems differ and, except in special applications, there is no analogy between the processes of combustion and heat transmission. Thus, when the rate of reaction of carbon with the gas is very high, it may be assumed that $\alpha \to \infty$. Then since the diffusion flow to the coal surface remains a finite value, it follows that $C_R = 0$. We can speak of an analogy between the processes of heat exchange and combustion only in this special case.

The impossibility of applying the method of analogy to combustion processes with a finite chemical reaction rate has led to a research for other methods of solving the problem. As far back as 1939, A. S. Predvoditelev, of the USSR Academy of Sciences, outlined a general approach to the problem of combustion, using the calculation of gas formation during the gasification of a fuel bed.[2] For practical purposes, the calculation can be limited to determining the average cross-sectional concentrations of gas through the fuel bed. Then a system of ordinary differential equations with constant coefficients can be formulated for mean gas concentrations. These constant coefficients, which Predvoditelev called "summary" coefficients of gas exchange, depend upon the chemical parameters, the structure of the bed, and the velocity of gas filtration.

In many cases it is advisable to apply an approximate method of solving the problem of combustion, based on averaging the differential equations over one of the independent variables. This method has been suggested to us by M. V. Keldysh. It has been applied to the problem of combustion at the walls of a carbon channel, taking into account the secondary reaction of carbon monoxide combustion,[3] and later to other problems. By averaging, the system of differential equations in partial derivatives of the second order is reduced to a system of ordinary differential equations of the first order with constant coefficients.

Let us consider the application of the method to the combustion of carbon in a channel with the assumption that oxygen reacts at the wall to give carbon dioxide. Suppose we have a carbon channel with a radius, R, through which the gas flows with a constant velocity of W m/sec. If $Z = 0$ at the channel inlet, the initial concentration of oxygen is constant and equals C_0. The distribution of mean concentrations along the length of the channel must be determined.

The process is described by the equation of forced diffusion of oxygen:

$$w\frac{\partial C}{\partial Z} = D\left(\frac{\partial^2 C}{\partial r^2} + \frac{1}{r}\frac{\partial C}{\partial r}\right)$$

with the following initial conditions:

$$Z = 0$$

$$c = C_0$$

The boundary condition is taken so that the diffusion of oxygen to the carbon surface is proportional to the concentration of oxygen at the surface

$$-D\left(\frac{\partial C}{\partial r}\right)_R = \alpha C_R \qquad (2)$$

where α is the reaction gas exchange coefficient. Let us assume that the solution can be approximated by the following function:

$$C = A(1 + \gamma\Psi) \qquad (3)$$

where

$$A = A(z),\ \gamma = \gamma(z)$$

$$\Psi = \Psi(r)$$

Let us determine the mean cross section concentration

$$\bar{C} = \frac{2}{R^2}\int_0^R A(1 + \gamma\Psi)r\,dr = A + A_\gamma\psi \qquad (4)$$

where

$$\psi = \frac{2}{R^2}\int_0^R \Psi r\,dr$$

To average Equation (1) over r, multiply each term by $2r\,dr/R_2$ and integrate from 0 to R. Assume, by virtue of symmetry, that $\Psi_0' 0$.

We then obtain

$$w\frac{d\bar{C}}{dz} = \frac{2D}{R}A\gamma\Psi_R' \qquad (5)$$

where Ψ_R' is the value of derivative $d\Psi/dr$ at $r = R$.

In order to eliminate the unknown function $A\gamma$ from Equation 5, let us use the boundary condition 2 and substitute expression 3

$$-DA_\gamma\Psi_R' = \alpha R(1 + \gamma\Psi_R] \qquad (6)$$

Here Ψ_R is the value of function Ψ at the wall.

We obtain the following equation for the mean concentrations of oxygen:

$$\frac{dC}{dz} = -\frac{2D}{wR^2}\frac{\bar{C}}{\frac{D}{\alpha R} + \frac{\Psi_R - \psi}{R\Psi_R'}} \qquad (7)$$

Let us write

$$\eta = \frac{\Psi_R - \psi}{R\Psi_R'} \qquad (8)$$

The solution of Equation (7) may be expressed as follows:

$$\ln\frac{\bar{C}}{C_0} = -\frac{4z}{Pe_d d}\frac{1}{\frac{D}{\alpha d} + 2\eta} \qquad (9)$$

where

$$Pe_d = \frac{wd}{D}$$

In order to use Equation 9 in calculations, the value of coefficient, η, must be known. η is a constant dependent on the law of distribution of velocity and concentration along the cross section.

In the case of high reaction velocities, coefficient, η, can be determined as follows.

If $\alpha d/D \to \infty$, then it follows from Equation 9 that:

$$\frac{1}{2\eta} = -\frac{1}{4}Pe_d\frac{d}{z}\ln\frac{\bar{C}}{C_0} \qquad (11)$$

As we know from the analytical solution of the problem, the right part of Equation 11 is

$$\bar{N}u_d = -\frac{d}{z}\int_0^z \frac{1}{\bar{C}}\left(\frac{\partial C}{\partial R}\right)_R dz$$

The number Nu has been determined experimentally for many cases. Thus for larger values of $\alpha d/D$, the numerical values of η can be found by the analogy with friction, heat exchange and diffusion processes.

It sometimes suffices to find the approximate value η by assuming a function of concentration disrtibution and of cross-section velocity. It may be assumed, for example, that $\psi = (r/R)^n$; then $\eta = 1/(n + 2)$.

For instance, given a parabolic type of concentration distribution and a flat velocity distribution profile, we have $n = 2$ and $\eta = 0.25$.

In this case, the approximate equation yields good results not only when $D/\alpha d > 2\eta$, but also when $D/\alpha d \approx 2\eta$.

The method of averaging was used in solving the well-known problems of cooling a plate, a cylinder and a sphere at an initial temperature of t_0 in a medium of zero temperature. If the parabolic law of temperature distribution along the cross section is assumed, the mean temperature, $\bar{t}$, of a cylinder is determined by the following formula:

$$\bar{t} = t_0 \exp -\frac{a\tau}{R^2}\frac{2}{\frac{1}{hR} + 0.25} \qquad (12)$$

where a = thermal diffusivity, τ = time, and $h = \alpha/\lambda$ = reduced surface coefficient.

Comparison of the mean temperature values

Table 1

	Z/R	0.1	0.2	0.4	0.6	0.8	1.0	1.5	2.0	5.0
Relative concentration of carbon dioxide	Exact equation	0.1583	0.2187	0.2709	0.2838	0.2819	0.2747	0.2511	0.2279	0.1269
	Approximate equation	0.139	0.216	0.278	0.287	0.284	0.276	0.251	0.228	0.127
Relative concentration of oxygen	Exact equation	0.5104	0.3120	0.1204	0.04657	0.018				
	Approximate equation	0.569	0.319	0.121	—	—				

The range in which an approximate solution of the problem can be used depends on the purpose of the calculation. Let us consider two important cases.

(1) The distribution of mean concentrations along the length of the reaction zone has been determined by experiment. The values $Pe_d(d/z)$ can be calculated from the conditions of the experiment. The values of the reaction gas exchange coefficients must be determined. From equation (9) $\alpha d/D$ is calculated as the difference between the value $(4/Pe_d)\,(z/d)/\ln\,(C_0/C)$ and the coefficient 2η. Therefore the approximate equation can be used only when $D/\alpha d \gg 2\eta$.

(2) The values of the reaction gas exchange coefficients are known. The values of $Pe_d(d/z)$ are given. The distribution of the mean reaction gases concentrations along the length of the reaction zone is sought.

derived from Equation (12) with those calculated on the basis of an accurate solution of the heat conductivity equation has shown that the results coincide to $1/hR \geqslant 0.5$ down to the third place, and in the region of $0.1 \leqslant 1/hR \ll 0.5$ the divergence does not exceed several per cent.

In the region where $D/\alpha d \ll 2\eta$, values of Nu_d should be substituted for the coefficient $1/2\eta$. They can be found by the analogy between the friction, diffusion and heat transmission processes.

The method of averaging equations has made it possible to solve problems in cases of several reactions that take place together. In addition to the above-mentioned problem of carbon combustion accompanied by the combustion of carbon monoxide, the problem of combustion reactions accompanied by carbon dioxide reduction has been solved.[1] In the latter case, calculations ac-

cording to the exact and to the approximate equations were compared (Table 1). An accurate solution has been obtained by B. V. Kantorovich.[4]

Summary

Use of the approximate method of averaging equations to solve the problem of gas formation is discussed. With this method, the system of partial differential equations of diffusion of the second order is reduced to a system of ordinary differential equations containing mean cross-section concentrations of the reaction gases. The solution of the problem gives a distribution of mean concentrations along the length of the reaction zone, depending on the hydrodynamic and physical and chemical parameters and constants. The values of the constants can be found approximately by the method of analogy. The method of averaging equations makes it possible to solve problems of gas formation in several given joint volume and surface reactions.

REFERENCES

1. Predvoditelev, A. S., Khitrin, L. N., Tsukhanova, Kolodtsev, K. I., and Grodsovsky, M. K.: *Carbon Combustion.* USSR Academy of Sciences Publishing House, 1949.
2. Predvoditelev, A. S.: J. Tech. Sci., No. 10 (1947).
3. Tsukhanova, O. A.: J. Tech. Sci., No 6 (1947).
4. Kantorovich, B. V.: J. Tech. Sci., No. 3 (1945).

72

THE COMBUSTION OF SOLID FUELS IN FIXED BEDS

By MUTSUO KOIZUMI

Introduction

The combustion of solid fuels in fixed beds is complicated, for it includes many factors such as the packing of particles, the flow pattern in bed, the mass and heat transfer, chemical and physical properties of solid particles, etc. Consequently, the analytical explanation of this process is very difficult.

Recently, however, some aspects of this process have been clarified by several investigators.[1, 2] Using the rate of mass transfer in the fixed bed, they calculated the burning rate related to the distance through the bed.

In the first part of this report the author develops an analytical treatment of this aspect, and derives a theoretical formula, which gives the rate of carbon consumption against the thickness of the burning zone in the bed, by assuming the boundary layer in which carbon monoxide burns. On the other hand, the relation between the thickness of the fuel bed and the composition of the combustion gas is obtained experimentally by using a small combustion tube of silica glass. This relation may be explained by the theoretical formula.

When solid fuels containing some quantity of ash are burned, the ash layer covers the surface of particles as combustion proceeds. This ash layer restricts the rate of mass transfer to the surface. In over-feed firing of high ash fuels with oxygen lean air some combustible remains in cinders after the burning zone in the bed has passed. This phenomenon may be explained by the effect of the ash layer. In the second part of this report the analytical attack of this aspect is made considering the limit point of steady burning. Some experiments concerning the relation between oxygen concentration in the air and the quantity of combustible in the cinder are carried out and compared with the theory.

The Relation Between the Thickness of Fuel Bed and the Combustion Gas Composition

THEORETICAL ANALYSIS

Although the combustion process in a fixed bed is complicated, many authors have pointed out that the temperature of the burning surface is so high that the chemical reaction rate may be instantaneous as compared to the rate of molecular transfer to the surface. Therefore the rate of burning is controlled by the rate of transfer of reactant molecules to the solid surface.

Most solid fuels contain volatile matter, but

in this paper solid carbon or fuels after loss of their volatile matter are dealt with.

The initial combustion product of carbon is not certain, but it is probable that the chemical equilibrium is almost attained at the surface of solid carbon where the temperature is high. It is well known that the equilibrium of the reaction, $CO_2 + C = 2CO$, predominantly gives carbon monoxide at high temperatures. It is assumed, therefore, that at the surface of carbon, carbon dioxide is instantaneously and completely reduced to carbon monoxide.

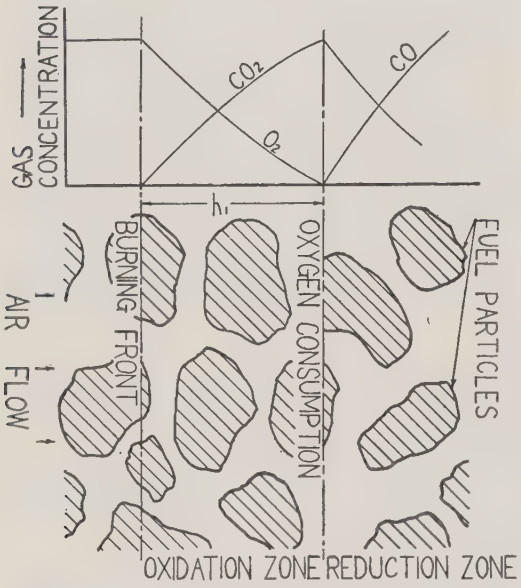

FIG. 1. Constitution of a burning fuel bed.

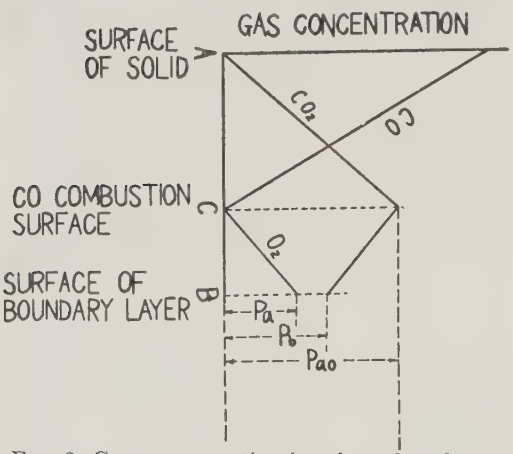

FIG. 2. Gas concentration in a boundary layer.

In fixed bed burning, the air passes through the void between particles, and at the burning front (Fig. 1) oxygen is consumed and successively converted to carbon dioxide and carbon monoxide along the gas flow in the bed. In an early state of burning the combustion gas in the void contains some oxygen, and this oxygen encounters carbon monoxide before it reaches the surface of the solid by diffusion. Again, as the chemical reaction rate is very high, the reaction, $2CO + O_2 = 2CO_2$, is assumed to occur instantaneously.

The flow pattern in fixed beds is complicated, but it is recognized that a stagnant gas layer exists in contact with the surface of the solid. The rate of mass or heat transfer in the bed is often explained by diffusion rates in such a stagnant boundary layer. Accordingly, it is assumed that the burning rate in beds is controlled by the rate of gas diffusion in the boundary layer. Although the boundary layer around the particles may not be regular, a boundary layer of uniform thickness, $\overline{AB}$ in Figure 2, is assumed. Combustion of carbon monoxide may occur in this boundary layer.

Figure 2 shows the gradient of gas composition in the boundary layer. As the gas mixing rate in the void is very high, it is assumed that a gas composition in the void is constant throughout a certain cross section of the bed. As shown in Figure 2, the gradient of gas concentration exists only in the boundary layer, and carbon monoxide reacts with oxygen on a surface, C in Figure 2, in this layer.

By these assumptions gas diffusion equations for oxygen, carbon dioxide and carbon monoxide are obtained. For simplification, however, the effect due to the difference between diffusion coefficients is neglected. Thus, for the b_1 zone in Figure 2, considering the increase of volume of the reaction, $CO_2 + C = 2CO$,

$$D_b \frac{dp_b}{dx} = v(p_b + 1) \tag{1}$$

for b_2 zone

$$D_a \frac{dp_b}{dx} = -v \tag{2}$$

where D_b, D_a = the diffusion coefficients in b_1 and b_2 zone, ($\overline{AC}$ and $\overline{CB}$ in Fig. 2), respectively; p_b = the volume concentration of CO_2; v = the volume of CO_2 which is reduced to CO at the surface of unit area per unit time; x = the scale of distance. For Equation (1), $p_b = 0$ at A, $p_b = P_{ao}$ at C, $p_b = P_b$ at B. Symbols, P_a, P_b, P_c and P_{ao}, mean volume concentrations of

O_2, CO_2 and CO in the void gas and that of O_2 in the air respectively. In the oxidation zone the relation, $P_{ao} = P_a + P_b$, exists.

From Equations (1) and (2), as $b_1 + b_2 = b$

$$v = \frac{D_b \ln\left(1 + \frac{D_a}{D_b} P_a + P_b\right) + D_a P_a}{b} \tag{3}$$

substituting $D_a = D_b$

$$v = \frac{D_b}{b} \{\ln (1 + P_{ao}) + P_a\} \tag{4}$$

After the oxygen in the void gas is completely consumed, the b_2 zone is eliminated and $p_b = P_b$ at B. Thus,

$$v = \frac{D_b}{b} \ln (1 + P_b) \tag{5}$$

The decreasing rate of oxygen in the void gas flow is derived from Equation (4) considering the flow rate, e.g.,

$$\frac{dP_a}{dy} = -\frac{v}{U} S = -\frac{D_b S}{U_b} \{\ln (1 + P_{ao}) + P_a\} \tag{6}$$

where U = superficial gas velocity in the bed; S = summed up surface area of particles per unit volume of the bed; y = the scale of height of the fuel bed (see Fig. 1); $D_b S/Ub$ shows the ordinary mass transfer rate in the fixed bed and is substituted as K. Then,

$$\frac{dP_a}{dy} = -K\{\ln (1 + P_{ao}) + P_a\} \tag{7}$$

From this equation it is clear that oxygen is completely consumed in a definite thickness of bed, h_1.

$$h_1 = \frac{\ln\left(\frac{\ln (1 + P_{ao}}{\ln (1 + P_{ao}) + P_{ao}}\right)}{K} \tag{8}$$

The solution of Equation (7) shows the change of oxygen concentration in the void gas against the thickness of the bed. Substituting $P_a/P_{ao} = r_a$

$$r_a = \left\{\frac{\ln (1 + P_{ao})}{P_{ao}} + 1\right\} e^{-ky} - \frac{\ln (1 + P_{ao})}{P_{ao}} \tag{9}$$

The decreasing concentration of carbon dioxide after the complete consumption of oxygen is derived from Equation (5). For simplicity of calculation, substituting $\ln(1 + P_b) \approx P_b$

$$\frac{dP_b}{dy} = -K' P_b (1 + P_b) \tag{10}$$

where K' = the mass transfer rate in the reduction zone of the fixed bed. Solution of this equation is simplified by use of "gasification ratio," $r_g = Pc/(Pb + Pc)$

$$r_g = \frac{2(1 - e^{-k'y})}{2 - e^{-k'y}} \tag{11}$$

EXPERIMENTAL RESULTS AND DISCUSSION

The relation between the thickness of the bed and the composition of combustion gas can be calculated by Equations (9) and (11). But, it is very difficult to determine the relation by experimental methods owing to the following facts: (1) As the rate of burning in a fixed bed is high and the thickness of the oxidation zone is only one or two particle diameters, gas sampling is very difficult. (2) As fixed beds may be somewhat irregular, reproductivity of results is apt to be poor. (3) The high temperature of combustion gas may cause ash fusion and exaggerate the irregularity of the bed.

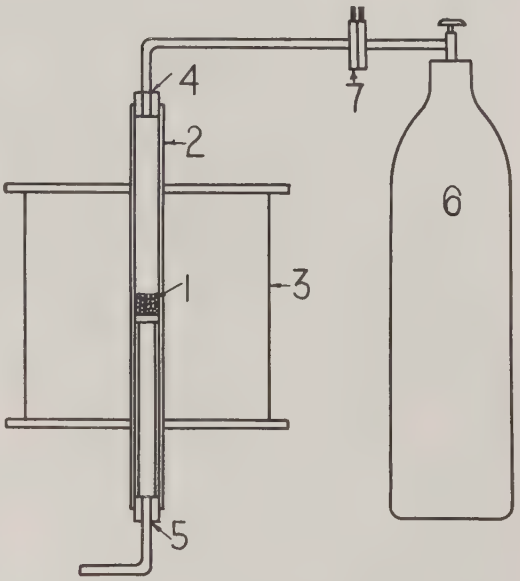

FIG. 3. The experimental apparatus. 1, fuel bed; 2, silica glass combustion tube; 3, electric furnace; 4, air inlet; 5, combustion gas outlet; 6, air container; 7, flow meter.

To avoid these difficulties the following experimental method was adopted. Figure 3 is a di-

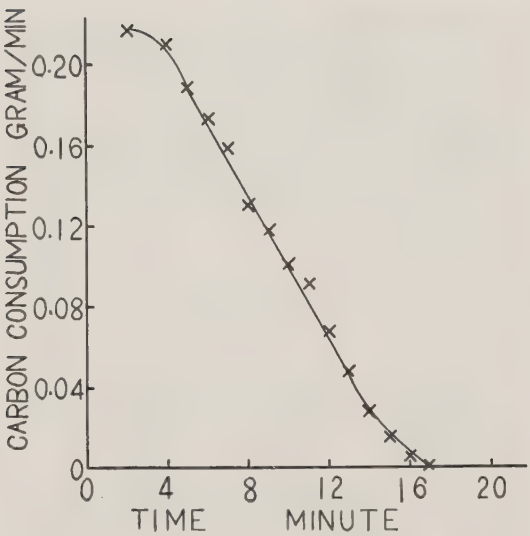

FIG. 4. The carbon consumption rate against time.

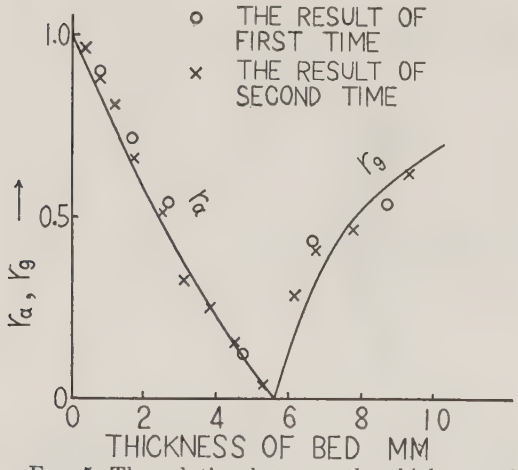

FIG. 5. The relation between the thickness of the bed and the combustion gas composition; activated carbon.

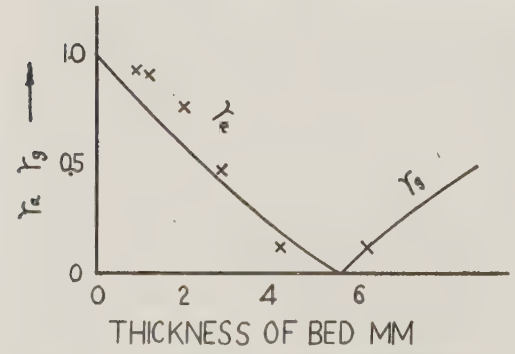

FIG. 6. The relation between the thickness of the bed and the combustion gas composition; high temperature coke.

agrammatical drawing of the apparatus. The solid fuel bed, 1, is set in the silica glass combustion tube, 2, with a thickness slightly over the oxidation zone. The combustion tube is heated by an electric furnace, 3, whose temperature is maintained at about 900°C. Oxygen lean air (about 7 per cent oxygen, 93 per cent nitrogen) flows into the tube from the upper end, 4. The fuel is burned with this air and combustion gas is taken out from the lower end, 5, of the tube. Combustion gas is sampled at constant intervals and analyzed by a Hempel apparatus.

By this experimental method the scale of thickness of the bed is replaced by a scale of time, so error due to the location of a probe is eliminated. As the oxygen concentration is small, the temperature gradient in the bed is small. The furnace temperature is controlled so that ash fusion does not occur and the combustion can be maintained well.

From the composition of gas samples, carbon consumption in the bed per unit time can be calculated (Fig. 4). The total carbon consumption calculated from Figure 4 is almost equal to the quantity of carbon initially contained in the bed. Therefore, the carbon consumption integrated after a certain time may correspond to the quantity of carbon contained in the bed at that time.

To determine the relation between the quantity of carbon and the thickness of bed, the following assumption is made: the carbon consumption occurs only in the direction perpendicular to the axis of the tube. Accordingly the carbon quantity may not be proportional to the thickness of bed, and the ratio of the thickness to the carbon quantity increases as the carbon consumption increases.

Figure 5 shows the relation between the combustion gas composition and the thickness of the bed thus calculated. The fuel used was almost ash free activated carbon, graded from 10 to 14 mesh size. The superficial velocity is kept at 10 cm/sec (N.T.P.). In this figure the results of two experiments with similar condition are plotted. The reproducibility is fairly good.

The results show good agreement with theoretical Equations (9) and (11) using $K = 1.305$ l/cm and $K' = 1.82$ l/cm. This value of the rate of mass transfer is somewhat smaller than is found in the literature.[3]

Experimental results with high temperature coke are shown in Figure 6, where theoretical curves are drawn. Considerable deviation of the experimental results from the curves could be

ascribed to the effect of the ash which remains around coke particles. The ash layer around a particle restricts the rate of mass transfer to the particle and decreases the rate of burning.

"Blowout" Condition in Fixed Bed Burning

THEORTEICAL ANALYSIS

In over-feed firing of high ash fuels with oxygen lean air, even if the bed can be ignited, combustible matter often remains behind the burning zone. This condition, where combustion ceases in spite of the existence of some quantity of carbon, will be called a "blowout" condition. "Blowout" may be caused by an effect of the ash layer which restricts the transfer of oxygen to the combustible

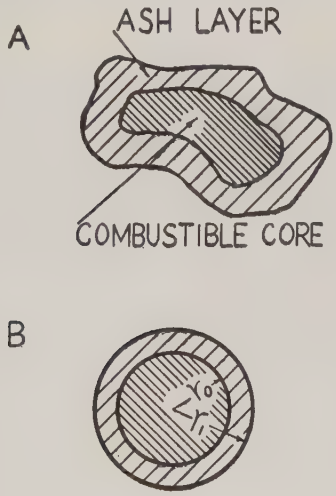

FIG. 7. A burning particle with ash layer.

core (Fig. 7A). To determine this "blowout" condition, the condition of steady state burning is formulated.

The following assumptions are made. (1) For simplification a particle is replaced by a sphere which has equal specific surface (Fig. 7B). (2) Oxygen diffusion and heat transfer to or from the particle are assumed only in the radial direction. (3) At the vicinity of the "blowout" condition, the temperature of the particle is rather low, so that the reaction, $CO_2 + C = 2CO$, does not occur. Consequently, oxygen diffusing to the surface of the combustible core is converted to carbon dioxide at the surface. (4) The chemical reaction rate at the surface is expressed by an Arrhenius' equation, first order with respect to oxygen.[4] (5) Radiant heat loss from the surface of the ash layer is neglected, because only the conditions in a fuel bed burning are dealt with.

The following symbols are used in equations:

r_0, r_1 = radii of the combustible core and the particle containing ash layer, respectively; P_0, P_1, P_2 = volume concentration of oxygen at the surface of the combustible core, at the surface of the ash layer, and in the external air, respectively; T_0, T_1, T_2 = temperature at the surface of the combustible core, at the surface of the ash layer, and in the external air, respectively. ρ_1, ρ_2, ρ_3 = the density of oxygen at the surface of the combustible core, in the ash layer, and in the external air, respectively; β = the oxygen transfer coefficient from the external air to the surface of the ash layer; D_a = the oxygen diffusion coefficient in the ash layer; α = the heat transfer coefficient from the surface of the ash layer to the external air; λ = the heat conductivity in the ash layer; C = the frequency factor of the reaction $C + O_2 = CO_2$; A = the activation energy of the reaction $C + O_2 = CO_2$; R = the universal gas constant; m = the mass of carbon consumed at the combustible core surface per unit time; H = the calorific value of carbon; s = the mass ratio of oxygen to carbon in carbon dioxide; b_a = the equivalent thickness of the ash layer $= r_1(r_1 - r_0)/r_0$.

Consequently the following equations are derived: (1) The mass of oxygen transferred to the ash layer from the external air per unit time

$$4\pi r_1^2 \beta \rho_2 (P_2 - P_1) = sm \tag{12}$$

(2) The mass of oxygen passing through the ash layer per unit time

$$4\pi r_1^2 \frac{D_a}{b_a} \rho_1 (P_1 - P_0) = sm \tag{13}$$

(3) The mass of oxygen reacting at the surface of the combustible core per unit time

$$4\pi r_0^2 \rho_0 C e^{-A/RT_0} = sm \tag{14}$$

(4) The heat passing through the ash layer per unit time

$$4\pi r_1^2 \frac{\lambda_a}{b_a} (T_0 - T_1) = Hm \tag{15}$$

(5) The heat transferred from the surface of the ash layer to the external air

$$4\pi r_1^2 \alpha (T_1 - T_2) = Hm \tag{16}$$

Eliminating m, P_1, P_0, and T_1 from these equations,

$$T_0 - T_2 = HsP_2 \frac{\rho_0 r_0^2 \left(\frac{1}{\alpha} + \frac{b_a}{\lambda_a}\right)}{\frac{r_1^2}{Ce^{-A/RT_0}} + r_0^2 \left(\frac{1}{\beta} + \frac{b_a}{D_a}\right)} \tag{17}$$

Equation (17) represents the temperature of the surface of the combustible core in steady-state

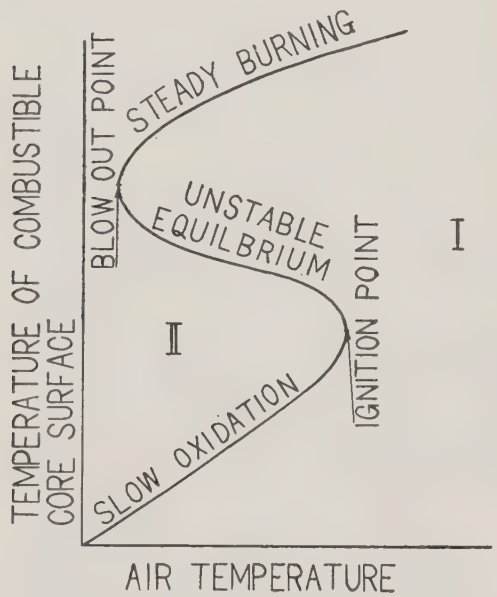

FIG. 8. The temperature of the combustible core surface against the air temperature. I: temperature increasing region; II: temperature decreasing region.

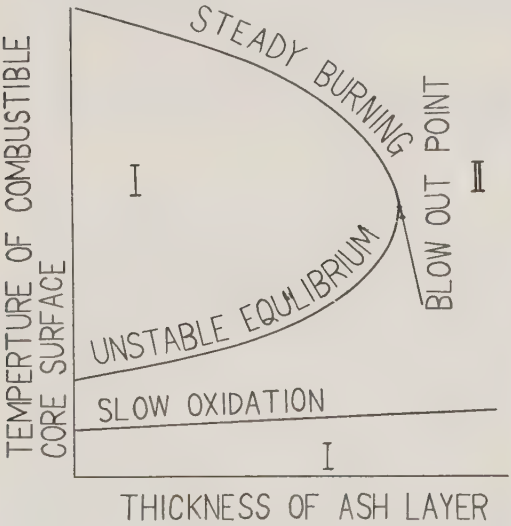

FIG. 9. The temperature of the combustible core surface against the thickness of ash layer. I: temperature increasing region; II: temperature decreasing region.

burning as a function of external conditions—the oxygen concentration in air, the temperature of air, the thickness of the ash layer, the reactivity of carbon, the rate of heat and mass transfer in the ash layer, the heat and mass transfer rates in the bed, etc.

The temperature of the combustible core surface is shown against the air temperature and the thickness of the ash layer, with other variables held constant (Figs. 8 and 9). Curves in these figures represent equilibrium temperatures and divide the graph plane into two regions—the temperature increasing region and the temperature decreasing region. When the temperature of the combustible core surface is set in the former region, the temperature increases, whereas in the latter the temperature decreases. From this viewpoint equilibrium curves are generally divided into three parts—the steady-state burning, the unstable equilibrium, and the slow oxidation. The critical points correspond to "blowout" and ignition.

These points can be determined by an analytical procedure, e.g., T_0 is partially differentiated by a certain variable and the term equated to zero.

By carrying out this procedure, it is found that the thickness of the ash layer at "blowout" decreases, (1) as the air temperature decreases, (2) as the oxygen concentration in the air decreases, (3) as the diffusion coefficient in the ash layer decreases, (4) as the rate of mass and heat transfer in the bed increases, (5) as the particle size decreases, (7) as the reactivity of carbon decreases. Moreover, in case of low air velocity, as the particle size decreases, the fraction of residual combustible in particles increases in spite of the increase of the specific surface.

EXPERIMENTAL RESULTS AND DISCUSSION

Experiments determining the quantity of combustibles (carbon) after "blow out" were carried out in a silica glass combustion tube (Fig. 3) without external heating. The solid fuel, graded between 8 and 12 mesh, was packed in about 100 mm height, and the air was introduced from the upper end. The fuel bed was ignited at its top. The burning zone formed in the bed gradually went down, and passed through the bed. After the combustion was over, the cinder was taken out and the quantity of combustibles in it was analyzed.

Results with two combustion tubes, whose inner diameters were 18 mm and 30 mm, respectively, were almost equal. This fact shows that "blowout" is little affected by heat losses from the bed. Air velocity only slightly affected the fraction of combustible in cinder, probably because

in the range of this experiment the flow pattern was almost laminar.

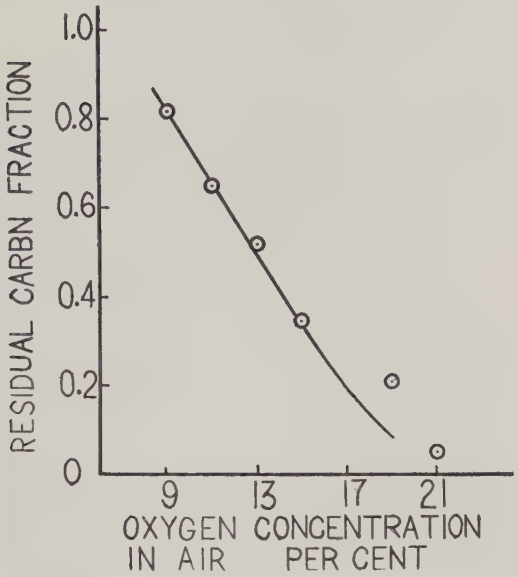

FIG. 10. The relation between the oxygen concentration in air and the residual carbon fraction; high temperature coke.

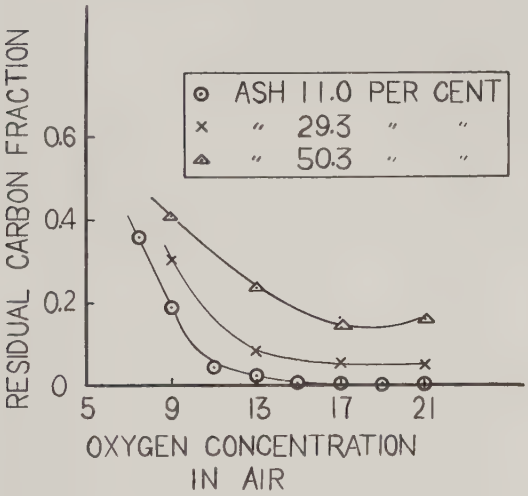

FIG. 11. The relation between the oxygen concentration in air and the residual carbon fraction; Nagakura coal.

Figures 10 and 11 show the relation between the oxygen concentration in air and the residual carbon fraction, the ratio of the total quantity of carbon in the cinder to the total quantity of fixed carbon in the original solid fuel. Figure 10 shows the results for high temperature coke and the curve is the value calculated by the above procedure substituting $C = 7.21 \times 10^9$ cm/sec $A/R = 1.5 \times 10^4\,1/°K, \beta = 80 = \alpha/C_p\rho_2$ cm/sec, $D_a = 0.705 = 0.294\,\lambda_a/C_p\rho_2$ cm^2/sec (C_p = specific heat of oxygen), $T_2 = 300°K$.

The oxygen concentration, where the curve of residual carbon fraction reaches 1, almost corresponds to the concentration at which the combustion becomes impossible initially.

Figure 11 shows the residual carbon fraction for different ash contents in the original coal. The ash layer of high ash coal may be denser and may restrict the oxygen diffusion more than that of low ash coal.

Conclusion

To clarify the combustion process in the fixed bed some attempts on theoretical analysis concerning the rate of burning through the bed and the "blowout" condition in the fixed bed have been made. Some experiments concerning these aspects have been carried out, and from a qualitative point of view the results agree with the theoretical formulae fairly well. But quantitatively the agreement cannot be verified owing to the lack of quantitative knowledge of some variables in the formula. The following properties in fixed bed burning are clarified.

(1) In burning ash free fuels, oxygen in air is completely consumed in a very small thickness of bed, within two particle diameters or so. This thickness can be calculated theoretically.

(2) The ash layer formed around fuel particles retards the rate of combustion and lengthens the thickness of oxygen consumption.

(3) "Blowout" is apt to occur in fixed bed burning of a high ash coal with oxygen lean air.

(4) The cause of "blowout" may be explained by the effect of an ash layer whose thickness attains the critical condition of steady-state burning.

(5) Combustibles in the cinder after "blowout" increase, as the oxygen concentration in air decreases, and as the ash in coal increases.

REFERENCES

1. THRING, M. W.: Fuel, *31*, 355 (1952).
2. SILVER, R. S.: Fuel, *32*, 121 (1953).
3. RANZ, W. E.: Chem. Eng. Progress, *48*, 247 (1952).
4. WEISZ, H. L., AND ORNING, A. A.: Fuel, *32*, 435 (1953).

73

STUDIES ON COMBUSTION AND GASIFICATION OF PULVERIZED COAL IN A MODEL CYCLONE GENERATOR

By SAKAE YAGI AND DAIZO KUNII

Introduction

In slagging gas generators and pulverized coal-fired boiler furnaces, the amount both of fly ash and of unburned carbon must be reduced to obtain high efficiency. Furthermore, unburned carbon entrained with the produced gas is sometimes a chief cause for low gasification efficiency in generators using entrainment systems. Therefore, to design a more efficient burner or gas generator, it is important to know factors affecting the value of carbon efficiency, i.e., per cent of carbon gasified. The authors designed and constructed a model gas generator, resembling the ordinary cyclone collector, in which pulverized coal was burned and gasified to study the effect of the general control variables upon the values of carbon efficiency.

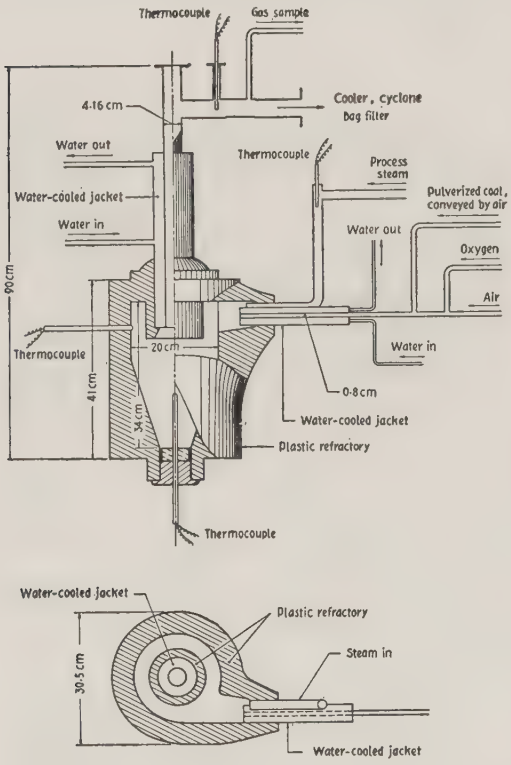

FIG. 1. Experimental gas generator.

Theoretical Considerations

According to the authors' thermodynamic studies on gas generators,[1] both the volume of carbon monoxide and hydrogen produced, and the total oxygen requirement per unit weight of raw coal, can be formulated theoretically as follows:

$$CO + H_2 = 0.3279 \left(\frac{Q_g}{1{,}000}\right) \cdot \{\alpha + \beta - (\gamma + \delta)\} \text{ nm}^3/\text{kg} \quad (1)$$

$$O_2 = 0.5303 c\eta_c + 0.1640 \cdot \left(\frac{Q_g}{1{,}000}\right)(\gamma + \delta - \beta) \text{ nm}^3/\text{kg} \quad (2)$$

where c = weight fraction of carbon in raw coal; η_c = carbon efficiency, i.e., fraction of carbon gasified; Q_g = gross calorific value (kcal/kg); $\alpha = 1 - \dfrac{8{,}150c(1-\eta_c)}{Q_g}$; β = total heat of steam, nitrogen and oxygen blown in (containing the latent heat of steam)/Q_g ; γ = total heat of gas produced (containing the latent heat of steam)/Q_g ; δ = total heat loss/Q_g . Equations (1) and (2) can explain gasification data in industrial generators, not only for entrainment systems but also for moving bed or fluidized bed systems, as reported previously.[1] In generators of industrial or pilot plant scale, in which $\beta = 0.05 \sim 0.07$, $\delta = 0.05 \sim 0.08$ and $\gamma = 0.10 \sim 0.18$, the carbon efficiency η_c is the most effective factor for determining the total efficiency of gasification.

According to results obtained in a pilot plant gasification with oxygen and highly superheated steam, performed by the U. S. Bureau of Mines at its Morgantown station, carbon efficiency increases with the increase of the per cent ash remaining in the generator. The authors, therefore, designed a new type of gas generator, resembling an ordinary cyclone collector, in order to make the ash move toward the wall of the generator and to flow down as molten slag, anticipating a higher value of carbon efficiency than had been obtained in any previous type of gas generator. As the coal inlet tubes are situated at the top position on the inside wall, the possibility of slag attacking the inlet tube is reduced considerably.

In small gas generators, as reported in this paper, the ratios of heat loss to the gross calorific value of the fuel used are calculated as high as

$\delta = 0.4 \sim 0.7$ when ordinary thermal insulation is used.

Model Generator and Purpose of Experiments

The model gas generator of the cyclone collector type was made of plastic refractory manufactured by the Nihon Kokan Company. The pulverized coal conveyed pneumatically by the air and oxygen, was blown tangentially into the generator (Fig. 1.). The steam generated in a small boiler was slightly superheated, about 140° $\sim$ 200°C, and was blown into the generator from an adjacent inlet parallel to the coal inlet. To prevent the breaking down of the inner cylinder, as well as the accumulation of the molten slag, the outlet tube was water cooled. Temperatures, both of the inside wall and of the reduction zone, were measured by thermocouples, which indicated mean values of these zones respectively. In Figure 2, both the external heating systems and the dust removal train are outlined; the latter can catch the entrained dust completely, bricks keeping a clearance of 3 $\sim$ 4 cm, where the fuel-gas burners and carborundum electric heaters compensate heat loss by conduction.

As described in the preceding section, the value of carbon efficiency is an important factor in gas generators. The authors conducted several

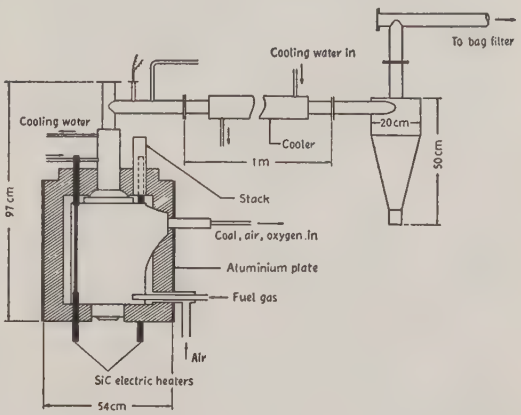

FIG. 2. Heating chamber, cooler and cyclone collector.

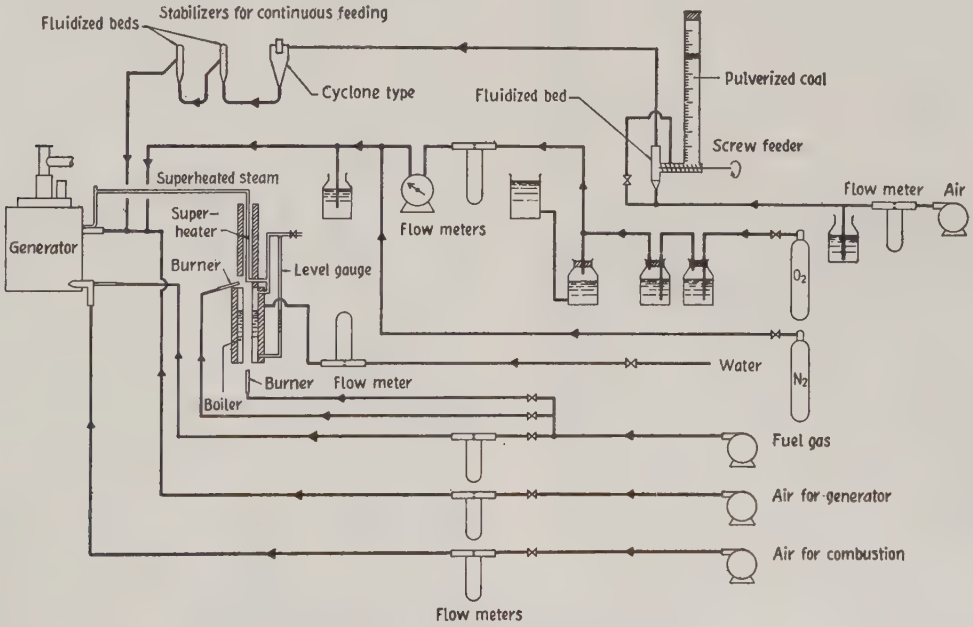

FIG. 3. Flow sheet for experimental gasification.

in dry state. Pulverized coal, fed by a screw feeder into a stabilizer of fluidized bed type, was conveyed by the air through three stabilizers, and was fed into the generator after being mixed with oxygen (Fig. 3). The model generator was covered with the special insulator as shown in Figure 2, which was made of insulating fire

series of combustion and gasification experiments, looking for the effects upon carbon efficiency over a wide range of operating conditions. Heat loss by conduction was compensated by the external heating. Nevertheless, the ratio of total heat loss to the gross calorific value of coal was considerably larger than that of gas generators of industrial

or pilot plant scale because of the thin insulators on the water-cooled jackets. This ratio would be negligible on the industrial or pilot plant scale. Therefore, in this experiment, values of $CO + H_2$ nm³/kg, larger than that of industrial generators were not expected.

Another object was to determine whether slag would flow down as liquid of low viscosity along the generator wall without any trouble.

Table 1. Characteristics of Coal Used: Miyanoura Coal

Size distribution

Mesh	*Per cent*
+100	3.7
+100, −160	5.1
+160, −200	10.7
+200, −250	9.1
−250	71.4

Analysis (per cent)

Moisture	1.63
V.M.	40.49
F.C.	47.92
Total sulfur	2.1
Ash	9.90

Ultimate (sample without moisture) (per cent)

Carbon	73.67
Hydrogen	5.59
Oxygen	7.97
Nitrogen	1.18
Sulfur	1.49
Ash	10.10

Moisture in coal as used: 2.1 per cent

Gross calorific value

Without moisture	7350 kcal/kg
With moisture	7380 kcal/kg

Composition of ash (per cent)

SiO_2	35.44
Al_2O_3	17.42
Fe_2O_3	10.72
CaO	14.75
MgO	1.87
SO_3	14.32

Melting point of ash, measured in the air: 1200 ~ 1280°C

Experimental Procedures

The characteristics of the coal used in these experiments are described in Table 1; the ash melting point was comparatively low, 1200° ~ 1280°C. A typical procedure for gasification with oxygen was as follows:

(a) The model generator was heated by external heaters to the scheduled temperature in about 4 to 7 hours.

(b) Air was blown in.

(c) Pulverized coal was blown in immediately, and the ignition was confirmed.

(d) Oxygen was blown in at once.

(e) Process steam was blown in, and operation was continued about one or two hours in steady state. Gas samples were bottled.

(f) Feeding of both the coal and oxygen were stopped simultaneously.

(g) At the same moment, gas remaining in the generator was purged with nitrogen.

(h) The process steam was stopped.

(i) The cooler, cyclone, and bag filter were disconnected and the total entrained dust was collected.

(j) The generator was cooled by air blown into the external combustion chamber.

(k) After cooling, the slag was removed from the bottom of the generator.

(l) The weight of dust was measured after drying.

(m) The gas samples were analysed for CO_2, O_2, CO, H_2, and CH_4, using an Orsat apparatus.

(n) Dust samples were analyzed for carbon and ash, and the slag samples for carbon.

Experimental Results

Five combustion runs, five gasification runs with air, and 26 gasification runs with oxygen were made; some examples of experimental data are shown in Table 2.

In spite of the severe conditions, the generator operated without any trouble; the coal inlet tube never clogged with coal or slag under ordinary operations. According to the observation made after cooling the generator, the molten slag seems to have flowed down as liquid of low viscosity along the inside wall of the generator, staying on the bottom slightly cooled, because of the considerable heat loss in this position.

As proof of complete melting of slag for runs in which the temperature of the reduction zone was higher than 1200°C, one could see numerous small crystals of minerals, both on the inside wall surface of the generator and on the sample pieces of slag, containing negligible carbon. Also there were swellings of slag ready to fall down as droplets on the bottom surface of the inner cylinder of the generator. The ranges of experimental data for gasification runs with oxygen are described in Table 3.

Discussion on Experimental Data

It was not a chief object to get a large volume of carbon monoxide and hydrogen per unit weight

TABLE 2. EXAMPLES OF EXPERIMENTAL DATA*

	Combustion		Gasification with Air		Gasification with Oxygen		
Exp. No.	1–1	1–3	2–1	2–4	3–2–2	3–3–6	3–5–3
Duration (min)	180	50	185	95	63	57	60
Feed rate (g/min)	15.9	24.5	18.0	23.4	24.6	26.9	38.0
Rate of combustion or gasification† (kg/m^3h)	131	217	159	207	217	237	336
Air rate (l/min)	136	238	78.0	88.2	22.8	20.5	25.7
Oxygen rate (l/min)	0	0	0	0	12.2	23.8	23.0
Steam (g/min)	0	0	22.0	24.0	18.3	16.0	14.3
Oxygen/coal (nm^3/kg)	0	0	0.910	0.791	0.690	1.04	0.748
Steam/coal (kg/kg)	0	0	1.22	1.03	0.744	0.595	0.376
Temperature °C							
Process steam	—	—	163	160	200	210	232
Inside wall	1330	1340	1000	1260	1220	1280	1330
Generator	1250	1340	1040	1210	1170	1230	1200
Heating chamber (outside)	1260	1260	1070	1240	1430	1270	1410
Gas, Produced (per cent)							
CO_2	15.3	15.0	12.6	12.2	11.6	18.8	13.3
O_2	4.9	1.2	0.3	0.5	0.3	0.2	0.1
CO	1.3	2.8	8.3	6.5	30.9	33.0	36.1
H_2	0	0	4.4	4.5	28.8	18.8	24.4
CH_4 + H. C.	0.9	0.8	0.8	0.6	1.5	0.7	1.2
N_2	75.6	81.2	74.6	75.7	26.9	28.5	24.9
Carbon efficiency (per cent)	97.7	93.4	87.0	89.6	84.8	91.3	86.3
Per cent ash in dust	11.6	27.2	37.0	25.0	81.0	34.0	38.0
CO + H_2 (nm^3/kg)	—	—	0.630	0.560	1.60	1.26	1.35

* Total data will be reported in Chemical Engineering (Japan) in 1957.

† Rate of combustion or gasification per unit volume of a gas generator. (The effective volume of the model generator for combustion or gasification is 6.80 l.)

of raw coal in the small generator. Analyzing the results of the combustion runs, the ratio of heat loss to the gross calorific value of coal can be estimated as $0.2 \sim 0.4$, even with external heating. For example, the data of both Exp. Nos. 3-3-6 and 3-5-3 in Table 2 are analyzed with Equations (1) and (2), as shown in Table 4. Both relatively low values of CO + H_2 nm^3/kg, and high requirements of O_2, nm^3/kg, depend upon the higher values of heat loss than those in gas generators of industrial or pilot plant size. Assuming the values of carbon efficiency to remain the same as those in Table 4, values of CO + H_2, nm^3/kg, can be estimated as shown in Table 5, as well as values of oxygen requirements, if gas generators of this type of industrial or pilot plant size were operated.

Percentages of methane in the dry gas are shown in Figure 4 where it is apparent that reduction zone temperatures higher than 1300°C gave methane percentages below 1 per cent.

The entrained dust was caught principally by the cyclone collector and the bag filter, although some fractions precipitated in the outlet of the

TABLE 3. RANGES OF DATA OBTAINED IN GASIFICATION RUNS WITH OXYGEN*

Rate of gasification per unit volume of generator (kg/m^3h)	$164 \sim 360$
Total oxygen requirement per unit weight of raw coal (nm^3/kg)	$0.615 \sim 1.280$
Process steam/raw coal (kg/kg)	$0.191 \sim 1.85$
Temperature (°C)	
Process steam	$120 \sim 280$
Upper inside wall	$1160 \sim 1380$
Mean value of reduction zone	$1030 \sim 1370$
Gas produced (per cent)	
CO_2	$11.6 \sim 31.0$
CO	$21.1 \sim 36.1$
H_2	$9.6 \sim 29.2$
CH_4	$0.5 \sim 3.2$
N_2	$2.16 \sim 35.6$
CO + H_2 produced per unit weight of raw coal (nm^3/kg)	$0.71 \sim 1.60$
Carbon efficiency (per cent)	$71.5 \sim 97.8$
Ash in dust entrained (per cent)	$19 \sim 92$

* All data will be reported in Chemical Engineering (Japan) in 1957.

generator, the cooler and the duct. The percentages of ash in entrained dust as caught in different positions in gasification runs with oxygen are plotted in Figure 5.

Table 4. Analysis of Experimental Data

Gross calorific value of coal with moisture, 7,380 kcal/kg

Carbon percentage in coal with moisture,

$$C = 0.7367 \times (1 - 0.021) = 0.722$$

(1) *Exp. No. 3-3-6:* $\eta_c = 0.913$

$$\alpha = 1 - \frac{8{,}150 \times 0.722 \times (1 - 0.913)}{7{,}380} = 0.931$$

Results of calculation:

$$\beta = 0.056, \quad \gamma = 0.250, \quad \delta = 0.240$$

$$CO + H_2 = 0.3279 \times (7{,}380/1{,}000)\ (0.931 + 0.056 - 0.250 - 0.240) = 1.20\ nm^3/kg \text{ (exp. data 1.26)}$$

$$O_2 = 0.5303 \times 0.722 \times 0.913 + 0.1640 \times (7{,}380/1{,}000) \times (0.250 + 0.240 - 0.056) = 0.88\ nm^3/kg \text{ (exp. data 1.04)}$$

(2) *Exp. No. 3-5-3:* $\eta_c = 0.863$

$$\alpha = 1 - \frac{8{,}150 \times 0.722 \times (1 - 0.863)}{7{,}380} = 0.891$$

Results of calculation:

$$\beta = 0.036, \quad \gamma = 0.200, \quad \delta = 0.150$$

$$CO + H_2 = 0.3279 \times (7{,}380/1{,}000)\ (0.891 + 0.036 - 0.200 - 0.150) = 1.40\ nm^3/kg \text{ (exp. data 1.35)}$$

$$O_2 = 0.5303 \times 0.722 \times 0.863 + 0.194 \times (7{,}380/1{,}000) \times (0.200 + 0.150 - 0.036) = 0.71\ nm^3/kg \text{ (exp. data 0.748)}$$

Table 5. Estimations for Gas Generators of Industrial Scale

$$\beta = 0.08, \quad \delta = 0.08, \quad \gamma = 0.180$$

(1) $\eta_c = 0.913, \quad \alpha = 0.931$

$$CO + H_2 = 0.3279(7{,}380/1{,}000) \times (0.931 + 0.08 - 0.18 - 0.08) = 1.82\ nm^3/kg$$

$$O_2 = 0.5303 \times 0.722 \times 0.913 + 0.164 \times (7{,}380/1{,}000) \times (0.08 + 0.18 - 0.08) = 0.568\ nm^3/kg$$

(2) $\eta_c = 0.863, \quad \alpha = 0.891$

$$CO + H_2 = 0.3279(7{,}380/1{,}000) \times (0.891 + 0.08 - 0.18 - 0.08) = 1.73\ nm^3/kg$$

$$O_2 = 0.5303 \times 0.722 \times 0.863 + 0.164 \times (7{,}380/1{,}000) \times (0.08 + 0.18 - 0.08) = 0.548\ nm^3/kg$$

The effects of total oxygen requirement on the carbon efficiency and the mean temperature of the reduction zone for gasification runs with oxygen are shown in Figure 6, but the comparatively low values of carbon efficiency seem to depend upon the temperature, rather than upon the total oxygen required. Therefore, values of carbon efficiency for runs within some ranges are plotted with respect to the mean temperature

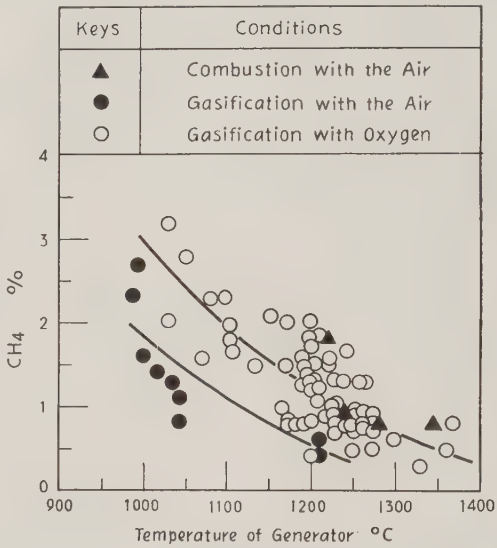

Fig. 4. Effect of temperature on percentage of methane in dry gas produced.

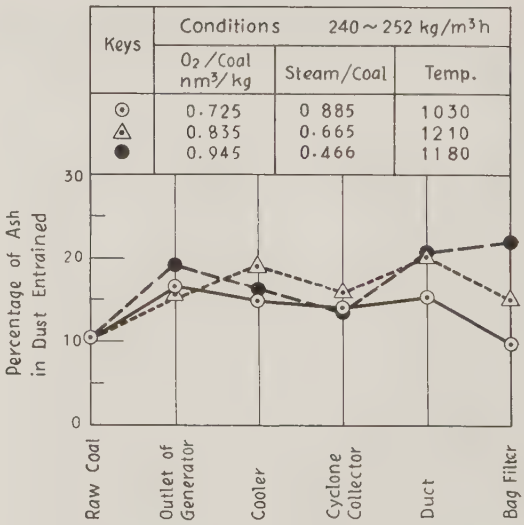

Fig. 5. Percentage of ash content in dust entrained.

of reduction zone in the model generator as in Figure 7, where the difference of carbon efficiency seems small considering the three series of runs; the first being combustion, the second, gasification with air, and the third, gasification with oxygen.

Figure 8 indicates the influence of the process steam to raw coal ratio on the carbon efficiency in two cases of gasification with air or oxygen, respectively.

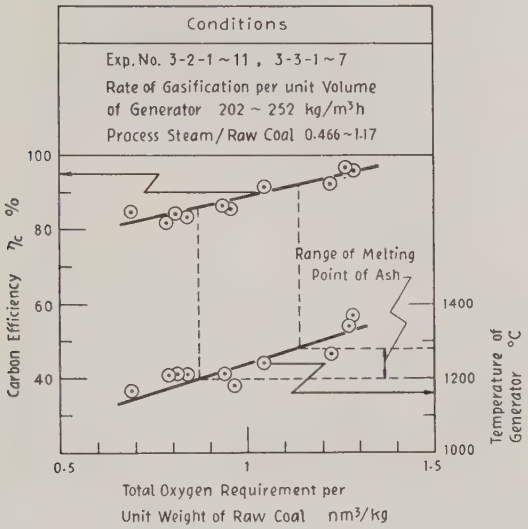
Conditions
Exp. No. 3-2-1 ~ 11 , 3-3-1 ~ 7
Rate of Gasification per unit Volume of Generator 202 ~ 252 kg/m³h
Process Steam / Raw Coal 0.466 ~ 1.17
Carbon Efficiency ηc %
Range of Melting Point of Ash
Temperature of Generator °C
Total Oxygen Requirement per Unit Weight of Raw Coal nm³/kg

FIG. 6. Effects of oxygen requirement on both temperature of gasification zone and carbon efficiency.

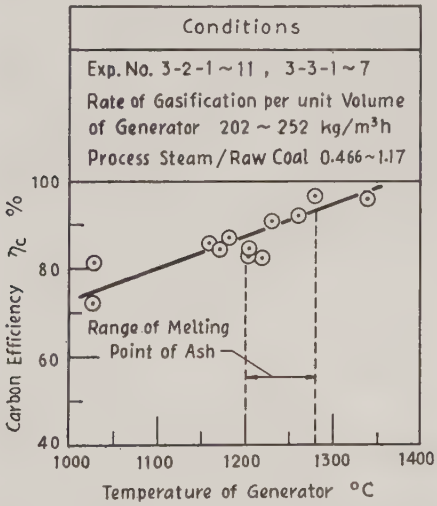
Conditions
Exp. No. 3-2-1 ~ 11 , 3-3-1 ~ 7
Rate of Gasification per unit Volume of Generator 202 ~ 252 kg/m³h
Process Steam / Raw Coal 0.466 ~ 1.17
Carbon Efficiency ηc %
Range of Melting Point of Ash
Temperature of Generator °C

FIG. 7. Efficiency of temperature in gasification zone on carbon efficiency.

The rate of gasification per unit volume of generator seems to affect considerably the values of carbon efficiency, as shown in Figure 9, where the experimental data correspond to comparatively high gasification rates, as compared with 150 ~ 200 kg/m³h in a Koppers-Totzek gas generator.

All data of per cent ash in the entrained dust are plotted in Figure 10, against the mean temperature of the reduction zone. It is interesting to note the sharp decrease of the per cent ash

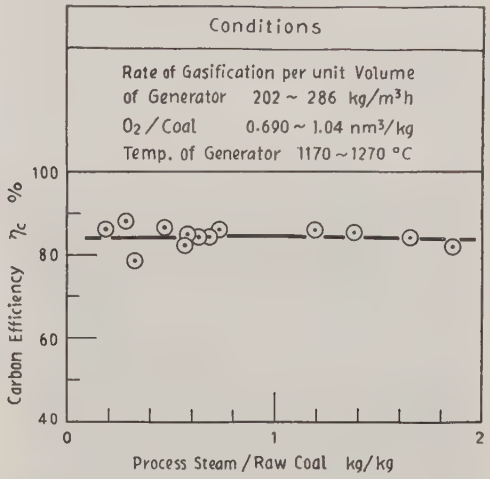
Conditions
Rate of Gasification per unit Volume of Generator 202 ~ 286 kg/m³h
O₂ / Coal 0.690 ~ 1.04 nm³/kg
Temp. of Generator 1170 ~ 1270 °C
Carbon Efficiency ηc %
Process Steam / Raw Coal kg/kg

FIG. 8. Effect of steam-coal ratio on carbon efficiency.

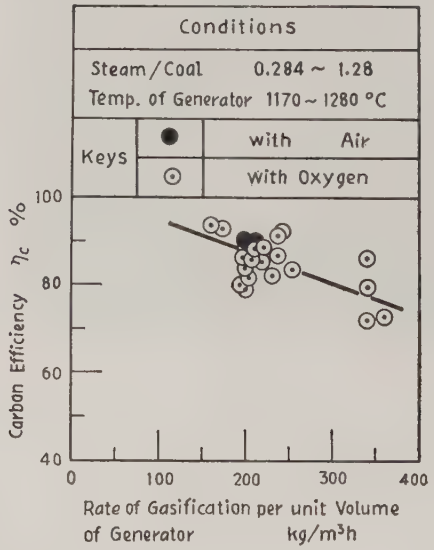
Conditions
Steam / Coal 0.284 ~ 1.28
Temp. of Generator 1170 ~ 1280 °C
Keys
with Air
with Oxygen
Carbon Efficiency ηc %
Rate of Gasification per unit Volume of Generator kg/m³h

FIG. 9. Effect of gasification rate on carbon efficiency.

corresponding to the ranges of the melting point of ash measured in air. Almost 70 ~ 80 per cent of the ash remains as slag in the generator when the temperature is higher than 1300°C.

Figure 11 shows the relation between carbon efficiency and the per cent of the ash remaining in the generator as slag for all the data obtained in these experiments. It seems there are no

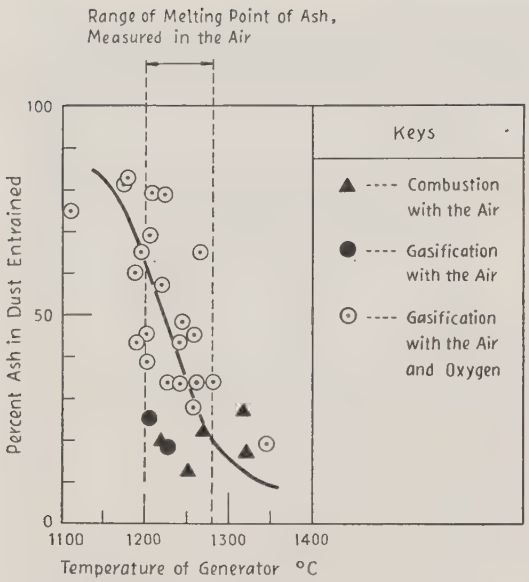

FIG. 10. Effect of temperature on percentage of total ash in entrained dust.

great differences between the data for combustion runs and those for gasification runs.

Conclusions

(1) A model cyclone gas generator of the slagging type was constructed and operated without any trouble, obtaining fairly good gas yields per unit weight of raw coal. Values for generators of this type of industrial size were estimated with the authors' theoretical equations.

(2) Many factors affecting the values of carbon efficiency were analyzed over wide ranges of operation in three series of runs; the first for combustion, the second for gasification with air, and the third for gasification with oxygen. It became apparent that the mean temperature of the reduction zone was the essential factor affecting carbon efficiency.

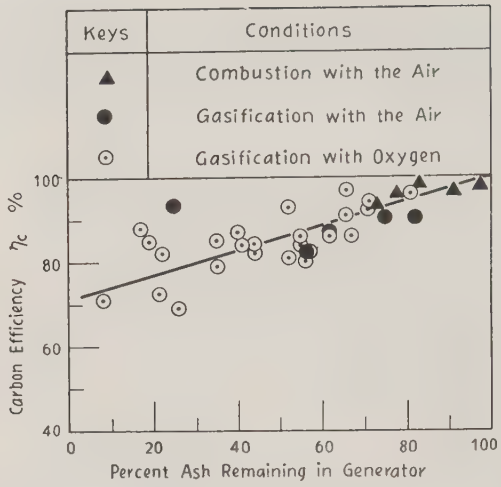

FIG. 11. Relation between percent ash remaining in generator and carbon efficiency.

REFERENCES

1. YAGI, S., KUNII, D., AND IKEDA, Y.: J. Japan Soc. Fuel, *34*, 426 (1955).
2. STRIMBECK, G. R., *et al.*: U. S. Bureau of Mines, Rep. Inv., 4733 (1950).
3. SEBASTION, J. J. S., *et al.*: U. S. Bureau of Mines, Rep. Inv., 4742 (1951).
4. TOTZEK, F.: Chem. Eng. Prog., *50*, 182 (1954).
5. GROSSMAN, P. R., AND CURTIS, R. W.: Trans. Am. Soc. Mech. Engr., *76*, 689 (1954).

74

FLAME PROPAGATION IN PULVERIZED COAL-AIR MIXTURES

By HISAO HATTORI

Introduction

It is still controversial, in pulverized coal combustion, whether ignition is caused by flame propagation as in a gaseous mixture or by radiation in the furnace.

The characteristics of flame propagation of aerosols or clouds of pulverized coal have not been fully investigated compared with those of gaseous mixtures. Also there are no reliable values for the velocity of flame propagation.

A new experimental method was devised; pulverized coal-air mixtures were discharged from a burner into free air, and ignited by an ignition source placed in the centre of the burner. Flame

propagated into the mixture and an inverted cone flame front was formed in the mixture, similar to a Bunsen cone.

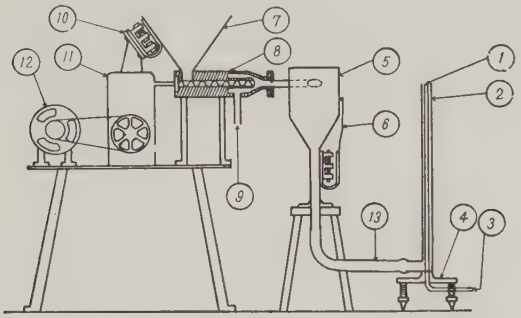

FIG. 1. Experimental apparatus. 1, acetylene gas burner for ignition; 2, burner tube of pulverized coal-air mixture; 3, acetylene gas inlet; 4, adjustable legs of burner tube; 5, cyclone type mixer; 6, vibrator for mixer; 7, hopper of pulverized coal; 8, screw feeder; 9, air inlet; 10, vibrator for hopper; 11, gear box; 12, D. C. motor; 13, rubber tube connecting the mixer and the burner tube.

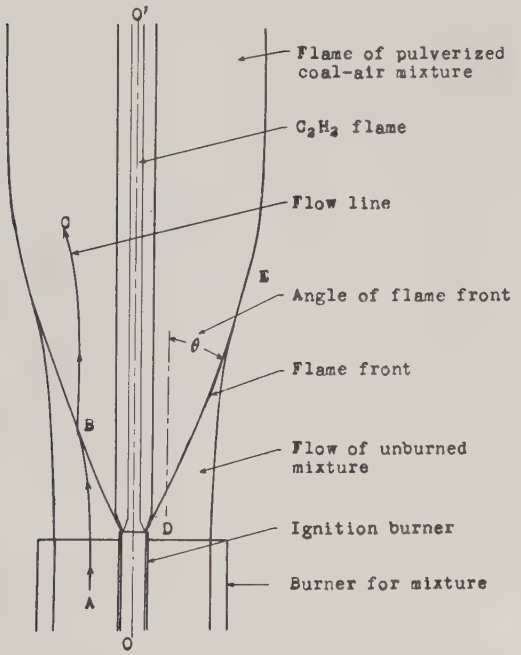

FIG. 2. Shape of the flame.

From these experiments the mechanism of propagation of flame in coal-air mixtures was studied.

Experimental

The apparatus is shown in Figure 1. Pulverized coal stored in hopper, 7, was fed continuously by screw feeder, 8, driven by variable speed D.C. motor, 12. A strobometer was attached to the shaft of the screw feeder, 8, to measure revolution speed.

Compressed air was measured by an orifice meter and introduced to the screw feeder, 8, at the inlet, 9. Coal and air from the screw feeder were uniformly mixed in a cyclone mixer, 5, and led into the burner tube, 2. The mixture passed through an annular space formed by the burner tube, 2, and ignition gas tube, 1, and was discharged upward to open atmosphere. The inner diameter of the burner tube, 2, was 27.2 mm, and the outer and inner diameters of the ignition gas tube, 1, were 5 mm and 4 mm, respectively. Velocity of the coal air mixture at the burner head was about 0.7 to 2.0 m/sec.

FIG. 3. Photograph of a flame.

Acetylene (as ignition gas), measured by a capillary flow meter was also discharged upward to open air through the ignition gas tube, 1.

Electromagnetic vibrators, 10 and 6, were attached to the hopper, 7, and the mixer, 5, lest the pulverized coal should adhere to the walls.

When the acetylene was ignited a steady inverted cone flame was formed as shown in Figures 2 and 3. In each experiment, the flame was photographed, and the angle of the flame front

(Fig. 2) was measured on the photograph. Exposures were 1/100 to 2 sec. The amounts of air, C_2H_2 and coal were also recorded. The analytical data for the coal used (Mayachi coal) is shown in Table 1.

TABLE 1. ANALYSIS OF MAYACHI COAL UNDER 100-MESH SIEVE

Proximate Analysis (as used)	
Moisture	4.00 per cent
Ash	6.24 per cent
Volatile matter	42.41 per cent
Fixed carbon	47.35 per cent
Total	100.00 per cent
Gross calorific value	7160 kcal/kg

Ultimate Analysis (moisture free)	
Hydrogen	5.58 per cent
Carbon	74.78 per cent
Oxygen	11.35 per cent
Sulfur	0.14 per cent
Nitrogen	1.65 per cent
Ash	6.50 per cent
Total	100.00 per cent

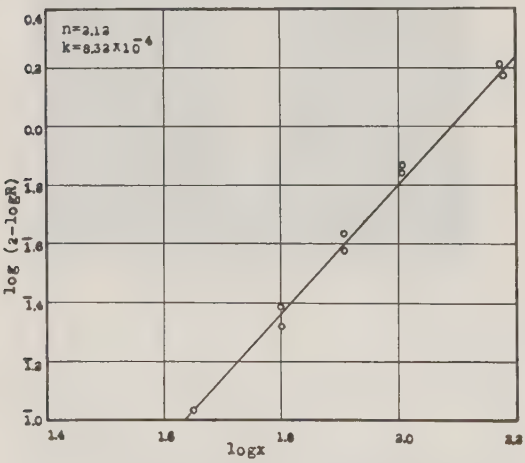

FIG. 4. Size distribution of Mayachi coal. x, opening of sieves (micron); R, residue (weight per cent). (By Rodin's law).

In the Bunsen cone used for the measurement of burning velocity of gas-air mixtures, the following relation exists:

$$\sin\theta = v_f/v_0 \tag{1}$$

where v_0 (m/sec) = velocity of mixture at the burner head; v_f (m/sec) = burning velocity, θ = angle of flame front.

In the inverted cone, the relations become more complex, as the gas flow lines (ABC — line, Fig. 2) are bent by thermal expansion at the flame front, and the tangents of AB and BC at B are not parallel to OO′. With several reasonable assumptions, the following equation might be derived from theoretical calculations

$$\sin\theta = \frac{v_f}{\sqrt{v_0^2 + v_f^2 - v_c v_f}} = \frac{v_f}{\sqrt{v_0^2 + v_f^2\left(1 - \frac{\rho_2}{\rho_1}\right)}} \tag{2}$$

where ρ_1 = density of the cold mixture kg/m³; ρ_2 = density of burnt gas kg/m³; v_f = flame propagation velocity (relative velocity of flame front to combustion gas) m/sec; v_c = ignition velocity (relative velocity of flame front to unburned gas) m/sec.

As seen from theoretical calculations, Equation (2) holds strictly only in the vicinity of the top of the inverted cone, because the flame front deflects slightly outward.

The flame front observed, however, is not clear at the top and the bottom, because, at the top of inverted cone, combustible matter and heat from the flame of the ignition burner affect the flame front and at the bottom, air diffuses into the mixture, and the flow lines are disturbed. Therefore, the angle of flame, θ, was measured on the assumption that the portion of flame front clearly visible on the photograph was approximately straight. The value of ρ_2/ρ_1 was calculated on the assumption that only the volatile matter of coal burns instantaneously. In the following calculations v_{f_2} means v_f in Equation (1) and v_{f_1}, v_f in Equation (2).

Experimental Results

THE RELATION BETWEEN IGNITION GAS VELOCITY AND FLAME VELOCITY

Effects of the flow velocity of acetylene from the ignition burner on v_f were observed, by keeping the concentration of the main gaseous mixture and its flow velocity constant (Fig. 5). The ratio of flow velocities shown on the abscissa was that of acetylene to the main gas mixture; v_f remains almost constant as the velocity of acetylene increases, which shows that the angle of the flame front was controlled mainly by the flame velocity.

When oxygen was added to the primary air to promote combustion (upper curve, Fig. 5), the flame velocity of the main gas mixture was little affected until the ratio of flow velocity reached 0.01 (height of ignition flame was only 3 mm). At a ratio of flow velocities of 0.01, the flame of the main gas mixture suddenly became unstable, fire-ball like flames appeared one after another at irregular intervals, rose upward and disappeared.

As the ratio decreased further, the main gas mixture ceased to ignite, and the ignition flame was left alone. In combustion by air (lower curve, Fig. 5), below the ratio, 0.3, the flame attenuated gradually and left the ignition flame alone at 0.05 or thereabout. The limit, as in the upper curve, was not observed in this case. In the following experiments the ratio of flow velocities was kept at 0.3.

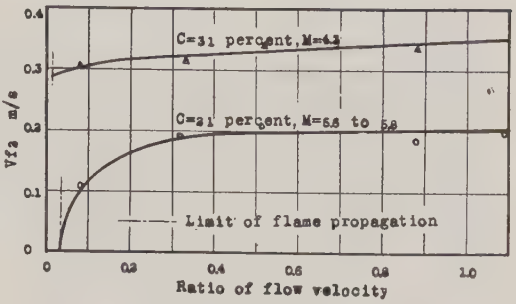

FIG. 5. Relation between ratio of flow velocity and flame propagation velocity. Temperature, 10.8 to 15.3°C; barometric pressure, 757 to 763 mm Hg; used coal, Mayachi coal under 100 mesh; discharge velocity of mixture, 1.60 to 1.62 m/sec.

THE RELATION BETWEEN DISCHARGE VELOCITY AND FLAME VELOCITY

In this experiment the effect of discharge velocity on the shape of the flame was examined by changing the velocity. As seen clearly from the photographs the flame front angle increased as the discharge velocity diminished. The flame velocities v_{f_2}, v_{f_1}, calculated from Equations (1) and (2), are shown in Figure 6. Although the observed points were dispersed widely because exact measurement of the flame front angle was difficult, it may be fairly concluded that the flame velocity was little affected by the flow velocity and was determined by properties of the gas mixture.

Therefore v_{f_1} is more reasonable than v_{f_2}, as flame propagation velocity; in other words, Equation (2) is preferable to Equation (1).

In these experiments, the mean velocity v_0 was changed only from 0.7 to 2.0 m/sec. For, below 0.7 m/sec, the flame became unstable owing to fluctuation of the coal air ratio, and over 2.0 m/sec, angle of the flame became so small that v_f could not be calculated correctly.

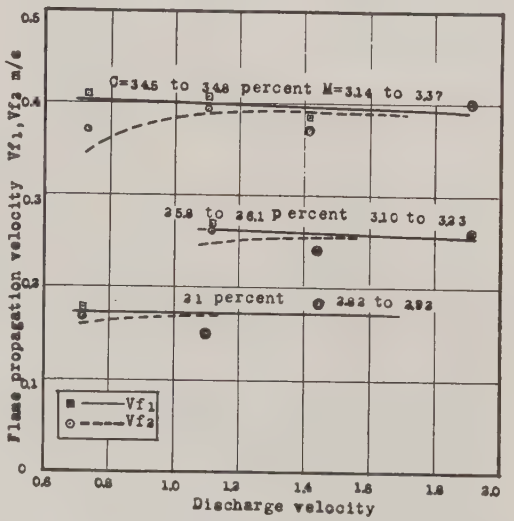
C=34.5 to 34.8 percent M=3.14 to 3.37
25.8 to 26.1 percent 3.10 to 3.23
21 percent 2.82 to 2.92
Vf1
Vf2
Flame propagation velocity Vf1, Vf2 m/s
Discharge velocity

FIG. 6. Relation between discharge velocity and flame propagation velocity. Temperature, 10.2 to 12.4°C.; barometric pressure, 760 to 761.2 mm Hg.; used coal, Mayachi coal under 100 mesh; ratio of flow velocity, 0.76 to 0.82.

RELATION BETWEEN CONCENTRATION OF MIXTURE AND FLAME VELOCITY

Coal-air mixtures, similar to gas-air mixtures, have maximum values of v_f. This maximum with air occurs at $M \approx 3$ (M is air-coal ratio).

Upon increasing the concentration, the flame is blown off. Decreasing the concentration, the flame front becomes indistinct at about $M = 7$,

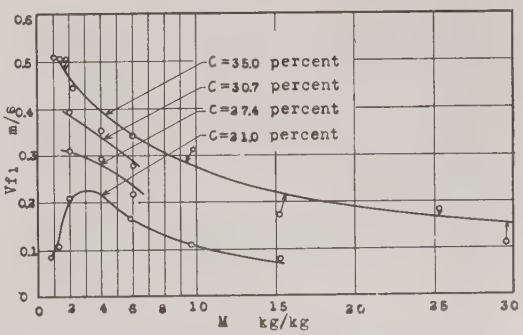

FIG. 7. Relation between air-coal ratio and flame propagation velocity. Temperature, 6.8 to 23.2°C; barometric pressure, 732.4 to 767.8 mm Hg; used coal, Mayachi coal under 100 mesh.

and finally combustion ceases. These regions are shown by broken lines in Figure 7.

It is a remarkable fact that with air-coal mixtures (total stoichiometric ratio is $M = 10$, and stoichiometric ratio of air-volatile matter is $M = 5$) the maximum flame propagation velocity was obtained at $M = 3$, while with air-gas mixtures this value is obtained at the stoichiometric ratio.

The flame velocity increased with air enriched to 35 per cent oxygen (upper curve, Fig. 7). With oxygen enrichment, the flame velocity does

Table 2. The Moisture and Ash Contents of Mayachi Coal

Grain size	Moisture	Ash
	per cent	*per cent*
Under 100 mesh	4.0	6.2
100 to 160 mesh	3.7	4.8
160 to 200 mesh	4.0	5.3
200 to 250 mesh	4.0	6.2
Under 250 mesh	4.2	7.3

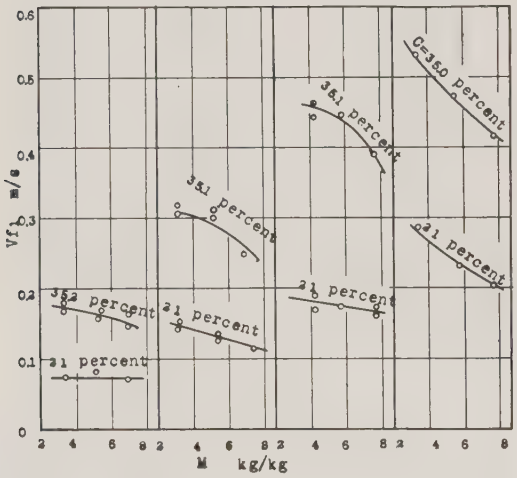

Fig. 8. Relation between size of coal, air coal ratio and flame propagation velocity.

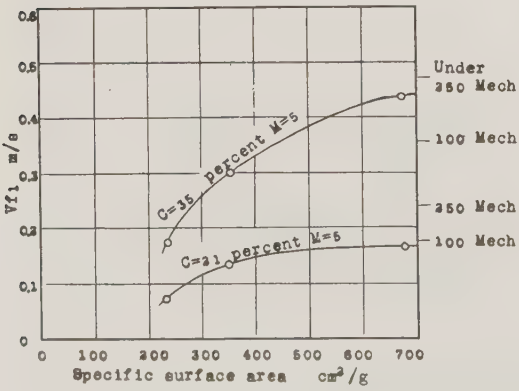

Fig. 9. Relation of specific surface area of pulverized coal and flame propagation velocity.

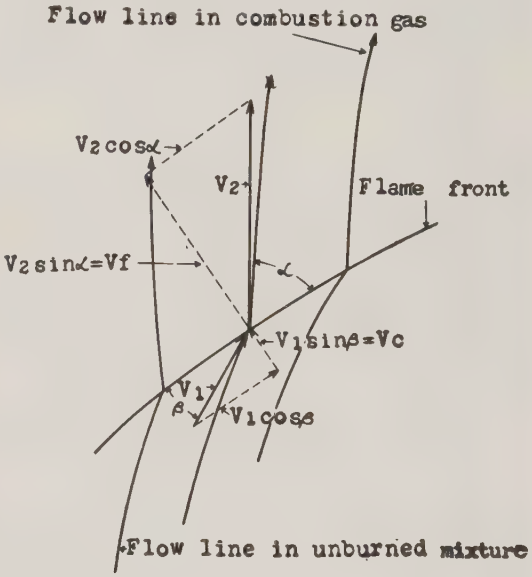

Fig. 10. Flow lines before and after flame front.

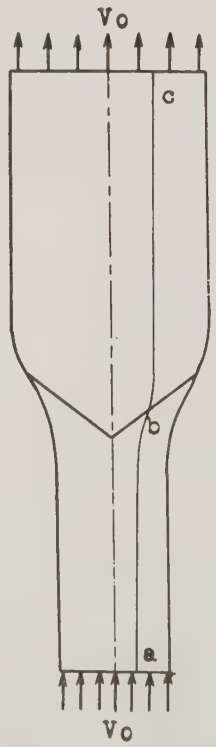

Fig. 11. Flow lines in flame.

not decrease even at $M = 1$. At this point, due to high propagation velocity, backfiring occurs.

THE RELATION BETWEEN GRAIN SIZE OF PULVERIZED COAL AND FLAME VELOCITY

The moisture and ash contents of samples used in this experiment, classified according to the grain size, are shown in Table 2.

The flame velocities measured are shown in Figure 8. The flame velocity increased remarkably as the grain size of coal decreased. Mean Gudman diameters, d_g, were measured from microscopic photographs of each sample and the specific surface area cm^2/g was calculated from the equation,

$$\frac{6}{\text{density of grains}} \times \frac{1}{d_g} = \text{specific surface area}$$

The relation between specific surface area and flow velocity is shown in Figure 9, and three points on the curves correspond to the sample, 100 to 160, 160 to 200, 200 to 250 mesh. The flame velocity increases as the grain becomes finer.

Ash content increases as grain diameter becomes finer as shown in Table 2. The effect of grain size on flame velocity might be greater, if the ash content did not change. Flame velocity decreases suddenly at about 100 mesh, and over this range flame propagation may be difficult.

Conclusion

The values of the velocity of pulverized coal flame propagation as given in the literature, about 10 m/sec, may be considered to be too high. Perhaps these values might be obtained due to turbulence of the flame or radiation from furnace walls. The flame velocity, 0.2 to 0.5 m/sec, obtained in this experiment may correspond to that of gas mixtures.

75

STUDIES OF PULVERIZED COAL FLAMES

By B. GHOSH, D. BASU AND N. K. ROY

Introduction

Propagation of flame through a suspension of coal dust is encountered in the commercial utilization of pulverized coal as fuel, as well as in mine hazards caused by coal dust explosion. In the former case, the rates of ignition and combustion are within control; in the latter, the reactions are out of control. Stable flames are formed by collective ignition of coal particles at a flame front, and, therefore, fundamental work in this field began with a study of the mechanism of ignition and combustion of individual coal particles. Newall and Sinnatt[1] investigated the behavior of coal particles in a heated atmosphere and observed that at temperatures somewhat below the ignition point, coal particles usually swelled up and formed thin hollow spherical bubbles which they termed cenospheres. Furnace temperature necessary for steady ignition of coal particles in suspension was on the order of 800°C which was considerably higher than the ignition temperature of coal in a fuel bed. From photographic studies Orning[2] found that when coal particles were introduced within a properly heated furnace, the volatile matter escaping from the particles burned with candle like flames around the coke residues. The coke particles burned later. Ghosh and Orning[3] studied the formation of small flames within a furnace and observed that the transition from scattered ignition of individual particles to collective ignition at a flame front was a gradual process. Fuhrmann and Koettgen[4] tired to produce stationary flames of coal dust but were unsuccessful, except when methane was introduced continuously in the suspension. The present work was undertaken with a view to studying the conditions necessary for producing stationary flames, and the influence of various physico-chemical factors like coal and oxygen concentrations in the coal dust suspension, particle size, furnace temperature, etc., on the velocity of the coal dust suspension at the burner mouth which would maintain a stable flame position within a furnace or in the open air.

Experimental

The apparatus used for studying pulverized coal flames inside a furnace, schematically shown

in Figure 1, consisted of a circulatory system for producing a coal dust suspension, and an electrically heated furnace within which combustion took place with the formation of a flame. The circulatory system consisted of a blower, the inlet and outlet of which were connected by a loop formed by 1¼-in. tubing. Coal dust and air were circulated through this loop and the suspension produced was fed into the burner through an outlet tube (¼ in. diam) attached vertically, axially to the elbow of the descending limb of the

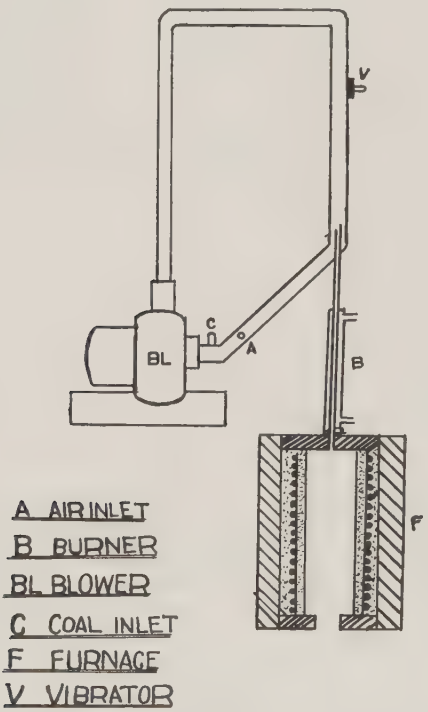

FIG. 1. Schematic diagram of apparatus for studying pulverized coal flame within a furnace.

loop. The speed of the blower, and hence the rate of circulation of coal dust and air, could be regulated. Dry air and coal dust were separately introduced into the system at the inlet side of the blower. The rate of air flow was measured by a capillary flow-meter. A vibrator was placed against the descending limb of the apparatus in order to minimize settling of coal dust on the tube walls.

The burner tube was a vertical water cooled copper tube, 5 mm i.d., connected to the outlet tube of the circulatory system by means of a short piece of rubber tubing. The tip of the burner tube projected one inch from the cooling jacket. When placed in the operating position the tip was flush with the ceiling of the furnace cavity. The furnace was made from a 3-in. diam., 12-in. long refractory tube wound with a heating coil and properly insulated. The top and the bottom of the refractory tube were closed with asbestos disks. The top disk was provided with an axial hole for inserting the tip of the burner tube, and also an inclined peep hole for viewing the flame. The bottom disk was provided with a 2-in. diam hole for allowing the ash to fall through. A mirror placed below this hole allowed observation of the flame from the bottom.

The circulatory system was air-tight. Therefore, the rate of flow of suspension was obtained

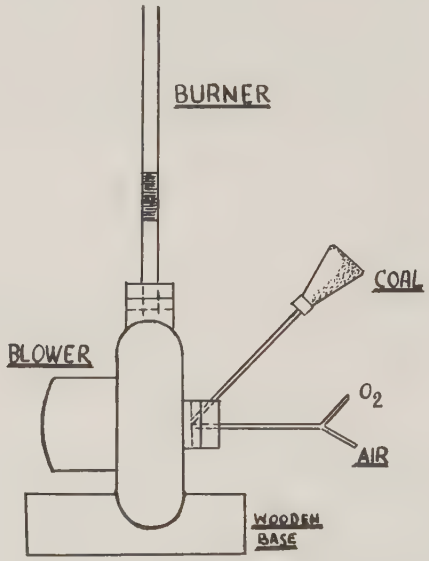

FIG. 2. Schematic diagram of apparatus for studying pulverized coal flames in the open air.

from the rate at which air was introduced into the system. The rate of coal flow was determined by removing the burner tube, collecting the coal flowing through the coal outlet of the loop for one minute, and weighing. At the beginning of an experiment the furnace was heated up to the desired temperature and the heating current was so adjusted as to maintain the temperature within ±10°C. The temperature was checked periodically. The flame could be seen through the peep hole and the position of the flame front could be estimated by introducing a thin refractory rod along the wall of the refractory tube till the centre of the peep hole, the flame front and the tip of the refractory rod were on a straight line. The distance of the flame front from the tip of the burner tube was then calculated from the geom-

etry of the system. This estimate was within a tenth of an inch from the actual value.

The apparatus used for studying flames in open air, shown in Figure 2, consisted of a blower for producing coal dust suspensions. The inlet and the outlet of the blower were closed with tightly fitting ruber stoppers. Measured quantities of dry air and/or oxygen were introduced through an axial hole, while coal dust was fed through an oblique hole bored through the stopper closing the inlet of the blower. Pulverized coal was kept in an inclined conical flask and was introduced into the blower by gently vibrating the flask. The coal concentration in the suspen-

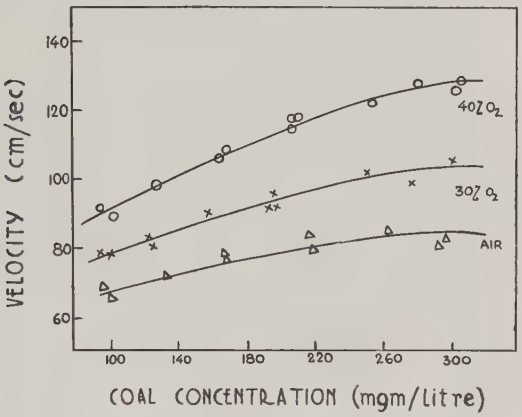

Fig. 3. Effect of oxygen enrichment on burner mouth velocity. Assam coal, minus 200 mesh, furnace temperature 950°C.

Coal Suspended in:

△ air
× 30 per cent oxygen
○ 40 per cent oxygen

sion could be varied by varying the speed of the blower and the rate of vibrating the flask. The stopper at the outlet side of the blower was bored axially, vertically, for introducing the burner tube which consisted of two sections of Pyrex tube joined by rubber tubing so that in case the flame started to flash back into the burner tube the top portion could be easily disconnected, because, otherwise, the flame might flash back into the blower and cause an explosion. In case of an explosion the rubber stoppers acted as safety valves and blew off.

Dry air and oxygen were separately metered through capillary flow meters and introduced into the blower through a Y-connection. The coal concentration in the suspension was measured by aspirating a known volume of the suspension through a dust filter and weighing the coal collected. The suspension was ignited with a Bunsen flame. The velocity of the suspension at the burner mouth was determined by dividing the volume rate of flow by the cross-section of the burner tube.

Table 1. Proximate Analyses of Coals Used for Studying Flames within a Furnace (as Received Basis)

Coal field	Moisture	Ash	Volatiles
	per cent	*per cent*	*per cent*
Assam	3.5	9.5	37.7
Raniganj (I)	1.9	15.5	37.3
Raniganj (II)	0.9	15.1	28.5
Jharia	0.8	21.5	19.7

Table 2

In addition to Assam, Raniganj (I) and Raniganj (II) coals mentioned in Table 1, the following coals were used for studying flames in the open air.

Coal field	Moisture	Ash	Volatiles
	per cent	*per cent*	*per cent*
East Sitalpur	5.0	18.1	34.9
Ekrakhas	1.0	21.1	21.4

Table 3. Regions of Stable Flame Formation in the Open Air

Minimum oxygen concentration in suspension (volume per cent), ranges of coal concentration (g/l) and burner mouth velocity (cm/sec) within which flames could be maintained are indicated. The extreme values of the ranges are approximate.

Type of Coal	Minimum Oxygen	Coal Concentration	Burner Mouth Velocity
	per cent	*g/l*	*cm/sec*
E. Sitalpur	60	0.2 –1.0	27–45
Assam	60	0.2 –0.5	28–57
Raniganj (I)	60	0.2 –0.5	28–43
Raniganj (II)	70	0.2 –0.3	35–45
Ekrakhas	100	0.25–0.35	40–45

Proximate analyses of coals used in these studies are given in Tables 1 and 2. The effect of oxygen concentration in the suspension on the Burner mouth velocity necessary for maintaining a stable and fixed position of the flame front is shown graphically in Figure 3. Data on stable flames in open air are summarized in Tables 3 to 5.

Discussion

Maintenance of stable flames within a furnace depended upon furnace temperature and coal concentration in the coal dust-air suspension. The minimum furnace temperature necessary for igniting minus 200-mesh coals in stable flames was found to be about 850°C for Assam and Raniganj (I) coals, about 900°C for Raniganj (II), and 950°C for Jharia coals. It was observed that when combustion started, the temperature of the furnace increased by approximately 50°C within a short time making it difficult to study the effect of variation of furnace temperature. It was apparent, however, that coals of lower volatile matter and higher ash content needed higher furnace temperatures for ignition in stable flames. The ignition characteristics of these coals were not widely different from those of some American coals studied by Ghosh and Orning.[3] When the quantity of air in the suspension was less than 20 per cent of the air theoretically necessary for complete combustion, no ignition took place. Ignition at stable flame fronts was observed when coal dust was associated with about 30 to 80 per cent of the theoretical air. With larger quantities of air in the suspension, there was a gradual transition from collective ignition at a flame front to scattered ignition of individual coal particles at different distances from the mouth of the burner tube.

Table 4. Burner Mouth Velocity *vs.* Coal Concentration Necessary for Maintaining Stable Flames with Minus 200-Mesh East Sitalpur Coal with 60 Per Cent (by Volume) Oxygen in the Suspension

Velocity at Burner Mouth	Coal Concentration in Suspension
cm/sec	*g/l*
26.3	0.23–1.0
35.0	0.20–1.0
43.8	0.20–0.50

Note. At the extreme limits of coal concentration reported above, the flame was occasionally stable and not always.

Table 5. Effect of Particle Size on the Range of Stable Flame Formation

Fine fraction is below 200 mesh and the coarse fraction is 100- to 160-mesh particles of East Sitalpur coal. Particles below 40μ size were removed by elutriation with air.

Burner Mouth Velocity	Range of Coal Concentration	
	Coarse coal	Fine coal
cm/sec	*g/l*	*g/l*
31.8	0.95–1.19	0.70–0.78
42.4	0.74–1.49	0.50–0.73
55.0	0.72–0.87	Unstable flame

Note. The extreme limits are approximate though they represent the extreme values of at least ten observations for each velocity.

Under conditions of stable flame formation, the burner mouth velocity could be varied over a considerable range without affecting the stability of the flame while furnace temperature and coal concentration in the suspension were kept constant. Thus, with Assam coal the velocity could be varied (at 950°C. temperature and 50 per cent theoretical air in the suspension) between 40 to 150 cm/sec. The distance of the flame front from the burner mouth varied with the burner mouth velocity, and increased with increase in velocity. Velocities lower than 40 cm/sec could not be used because of difficulties in maintaining proper flow of the suspension. At velocities higher than 150 cm/sec the flame front was not steady. Diameter of the flame as observed through the bottom was much larger than that of the burner tube.

The effect of furnace temperature on the flame was studied by varying the temperature and observing the position of the flame front. At higher initial temperature of the furnace the flame front was formed closer to the burner mouth. However, since the formation of a flame increased the temperature of the furnace, the effect of this factor could not be studied independent of that of the flame. After the establishment of a flame the temperature of the furnace could be lowered by cutting off the power supply, and the flame front moved away from the burner mouth until the temperature was so low that ignition could not be maintained. The furnace temperature required to start ignition at a stable flame front was approximately 100°C higher than the temperature at which an already established flame became extinguished. Although these observations were of a qualitative nature, they indicated that an already established flame helped considerably the ignition of the on-coming coal stream.

The temperature of a pulverized coal flame is determined by the degree and the rate of combustion of coal particles. The flame temperature could be increased by increasing the oxygen con-

centration in the suspension. The effect of oxygen enrichment on the burner mouth velocity necessary for maintaining a fixed flame position is shown in Figure 3. The data were obtained with minus 200-mesh Assam coal at a furnace temperature of 950°C. With 40 per cent oxygen in the primary air, the furnace temperature could be lowered to about 600°C after the establishment of a flame without affecting its stability. But if the flame were extinguished, the furnace temperature had to be raised to 800°C before re-ignition took place. With oxygen enrichment the flame became brighter.

Since the flame temperature had a considerable effect on the ignition of on-coming coal particles, attempts were made to obtain high temperature flames by increasing the oxygen concentration of the primary air and to find out whether such flames would be self-maintaining in the open air. The apparatus shown in Figure 2 was used and various burner tube diameters were tried. It was observed that with proper concentrations of coal and oxygen in the dust suspension, stable flames could be produced with a burner tube of 1.1 cm i.d. Using the next smaller size of tube available, no stable flame could be maintained with any of the coals mentioned in Table 2. A vertical position of the burner tube was also essential, since the flame could not be maintained when the burner tube was kept in a horizontal or inclined position. In order to determine the regions of stable flame formation with the 1.1-cm burner tube, the feed rates of air, oxygen and coal were changed until a stable flame was obtained. The flame was then blown off and coal concentration determined. The oxygen concentration was determined from the flow rates of air and oxygen, and the burner mouth velocity was computed by dividing the volume flow rate by the cross-section of the burner tube. The results are summarized in Table 3. Stable flames could be obtained only when the burner mouth velocity was kept within a definite range. At lower velocities the flame flashed back into the burner tube, while at higher velocities it blew off. However, within this range of stable flame formation, the coal concentration and the burner mouth velocity did not show any definite interdependence. The diameter of the flame was larger than that of the burner tube, and the color and the shape of the flame also varied from time to time without any apparent reason. Coal concentrations for maintaining stable flames with minus 200-mesh East Sitalpur coal at 60 per cent oxygen concentration in the fuel stream are given in Table 4.

The effect of particle size on flame propagation was also studied. Minus 200-mesh East Sitalpur coal was elutriated with air to obtain a fine fraction containing particles below 40μ. This fraction had poor dispersing characteristics and could not be used for making coal suspensions. The coarse fraction of the minus 200-mesh coal was compared with a 100 to 160-mesh fraction (of the same coal) with regard to their flame forming characteristics. A much higher concentration of

FIG. 4. A long flame of pulverized coal. East Sitalpur coal, minus 200 mesh, with 60 per cent by volume of oxygen in suspension.

the coarser coal was necessary for producing stable flames. The results are presented in Table 5.

Flames of pulverized coal in the open air showed blowoff and flashback characteristics similar to flames of other finely divided solids but did not show any inner cones. Some photographs of pulverized coal flames are shown in Figures 4 to 7, together with explanatory notes.

From theoretical considerations, Nusselt[5] and Traustel[6] presented equations for estimating the rate of rise of temperature of coal particles prior to ignition. In the pre-ignition zone where heat evolution due to chemical reaction may be neglected, the net gain of heat by the coal particles

is given by the difference between heat transfer to coal particles by radiation and heat loss from the particles by conduction to the immediately surrounding atmosphere. If a coal dust suspension

FIG. 5. A short flame of pulverized coal. Conditions similar to those shown in Fig. 4.

FIG. 6. Blowoff of a pulverized coal flame due to increase in velocity of the fuel stream.

at temperature t_0, at zero time, be exposed to radiation from all directions at a temperature, T_r, the temperature, t, of the coal particles will rise initially according to the relation:

$$t = t_0 + \frac{3\sigma\phi T_y^4}{c\rho r}\theta \qquad (1)$$

where c is the heat capacity, ρ is density and r is the radius of the coal particles, θ is the time, σ is the radiation constant, and ϕ is a geometric view factor. After some time the two heat transfer processes reach a quasi-equilibrium, and the rise

FIG. 7. Pulverized coal flame photographed through a yellow filter. The zone of intense combustion is seen close to the flame front.

of particle temperature after this is given by the approximate relation:[7]

$$t = t_0 + \sigma\phi T_r^4 \left\{ \frac{N_r^2}{(N+1)^2 k} + \frac{3\theta}{(N+1)c\rho r} \right\} \qquad (2)$$

where k is the thermal conductivity of the atmosphere and N is the ratio of heat capacities of associated quantities of atmosphere and coal.

If a suspension of coal particles of 60μ diam in 30 per cent of the air theoretically necessary for complete combustion be introduced into a furnace heated to a temperature of 1000°C, then according to these theoretical estimates the particle surface would be heated to a temperature of of approximately 250°C in 50 msec. In an actual

case, however, chemical reactions (oxidation of coal) bring about ignition under these circumstances and the temperature of the coal particles rises to that of the flame. After ignition the rate of combustion is determined by the rate of diffusion of oxygen to the coal surface.

Three distinct zones exist in the process of ignition and combustion of pulverized coal, *viz.*, (1) the pre-ignition zone where the temperature rise is slow because of insignificant evolution of heat by chemical reactions, (2) the ignition zone where chemical reactions rapidly raise the coal particles to the flame temperature, and (3) the combustion zone where the combustion rate is controlled by the rate of diffusion of oxygen to the coal surface while the temperature of the flame remains more or less constant. Nusselt's and Traustel's equations are valid only for the pre-ignition zone. Mallard and Le Chatelier's[8] treatment of the combustion wave can be modified to obtain a suitable expression for the burning velocity of dust suspensions. The following relation may be derived:

$$S_0 = \frac{\lambda(T_f - T_i)/\delta + \beta w\sigma\alpha\phi T_f^4/\rho r}{(c_a\rho_a + cw)(T_i - T_0)} \qquad (3)$$

where S_0 is the burning velocity or the approach velocity (burner mouth velocity) of the suspension, λ is the coefficient of heat conduction of the suspension, T_0, T_i, and T_f are respectively the initial, the ignition, and the flame temperature, σ is the radiation constant, α is a correction factor, ϕ is a geometric-view factor, c_a is the specific heat and ρ_a is the density of the atmosphere, w is the weight of the coal per unit volume of the suspension, r is the average radius of the coal particles, δ is the thickness of the ignition zone, and β is the equivalent thickness of the zone in which the particles receive radiation from the flame. Equation 3 is slightly different from the equation presented by Cassel, Das Gupta and Guruswamy[9] in which they assume that δ and β are equal to the thickness of the combustion zone.

Equation 3 is not free from objections on theoretical grounds. The temperatures of coal and associated atmosphere have been assumed to be equal at the end of the pre-ignition zone. Cenosphere formation, combustion of the escaping volatile matter, etc., have not been taken into consideration in deriving the equation. However, it gives a dimensionally correct correlation of the factors affecting the propagation of a pulverized coal flame.

Combustion reactions are not directly considered in Equation 3. Higher combustion rates, as obtained by oxygen enrichment, influence the rate of flame propagation by decreasing the thickness of ignition and reaction zones and increasing the flame temperature. When a flame is established, Equation 3 may be used for predicting the flame propagation (or the burner mouth) velocity provided that it is possible to evaluate all the terms which appear in the equation, but the equation can not be used for predicting whether a stable flame would result under a given set of conditions. For attaining ignition the coal particles must be heated to a minimum temperature which is determined by the nature of the coal and the experimental conditions. If a suspension of coal dust is assumed to consist of parallel layers of coal particles separated by a constant distance, propagation of flame may be viewed as progressive ignition of successive layers of coal particles. Thus, when one layer of particles is ignited, heat is transferred to the next layer by both conduction and radiation, and the particles in the next layer are heated up to the ignition point. It is not necessary to assume complete combustion of particles for flame propagation. With this picture it is easy to visualize that increasing coal concentration in suspension or using finer coal would have the effect of reducing the distance between successive layers of particles, and therefore, the rate of flame propagation would increase. Radiation plays a very important role in the propagation of flame through a suspension of coal dust. Since radiant heat transfer does not depend on distance but on angle factors, the propagation of flame through a coal dust suspension is determined by the size and geometry of the flame, the fuel distribution, and aerodynamic pattern. In this respect a pulverized coal flame differs from a gaseous flame.

Acknowledgments

Thanks are due to the Council of Scientific and Industrial Research for sponsoring the investigation, and to Dr. A. Lahiri, Director, Fuel Research Institute, for his kind interest.

REFERENCES

1. Newall, H. E., and Sinnatt, F. S.: Fuel, *3*, 424 (1924); Fuel, *5*, 335 (1926); Fuel, *6*, 118 (1927).
2. Orning, A. A.: Trans. Am. Soc. Mech. Engrs., *64*, 497 (1942).

3. Ghosh, B., and Orning, A. A.: Ind. Eng. Chem., *47*, 117 (1955).
4. Fuhrmann, E. A., and Koettgen, H.: Z. physik. Chem., *A169*, 388 (1934).
5. Nusselt, W.: Z. Verhandl. deut. Ing., *68*, 124 (1924).
6. Traustel, S.: Feuerungstech., *29*, 1, 25, 49 (1941).
7. Omori, T. T., and Orning, A. A.: Trans. Am. Soc. Mech. Engrs., *72*, 591 (1950).
8. Mallard, E., and Le Chatelier, H. L.: Ann. des mines, *4*, 274 (1883).
9. Cassel, H. M., Das Gupta, A. K., and Guruswamy, S.: *Third Symposium on Combustion, Flame and Explosion Phenomena*, p. 185. Baltimore, The Williams & Wilkins Co., 1949.

76

RADIATIVE TRANSFER IN DUST FLAMES[a]

By H. M. CASSEL, I. LIEBMAN and W. K. MOCK

Introduction

Ordinarily radiation plays a minor part in the heat transfer across the combustion zone of explosive gas mixtures. However, its effect might be appreciable in dust flames.

Fig. 1. Bunsen-type aluminum dust flame burning in air (160 mg./liter).

In the course of research on laminar aluminum dust flames, evidence of such an effect was first sought by comparing burning velocities of stationary Bunsen-type flames of equal concentrations, burning in air on burner tubes of different diameters, i.e., 1.4 and 1.9 cm. Burning velocities were evaluated from flame photographs (Fig. 1) by the truncated cone method.[1] The dust concentrations covered the range from 85 to 300 mg/l—

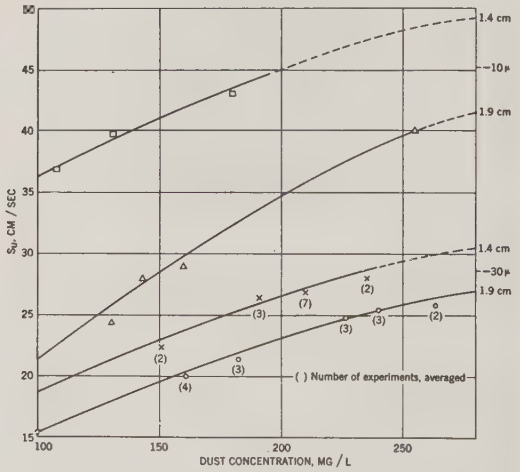

Fig. 2. Burning velocities of Bunsen-type aluminum dust flames in air (cm/sec) vs. dust concentration (mg/liter).

stoichiometric concentration 315 mg/l—with dispersions of minus 10 and minus 30μ particle size. Results are shown in the burning velocity versus concentration diagram of Figure 2.

Contrary to expectation, the burning velocities on the small burner exceed those on the large burner by as much as 15 per cent for the coarse dust and about 23 per cent for the fine dust. The increase in burning velocity with decreasing

[a] Work partly sponsored by Office of Ordnance Research, Durham, N. C.

burner size may be interpreted as a curvature effect that overshadows radiation and is due to the comparatively great thickness of the reaction zone in dust flames.[2] For it can be expected that the burning velocity, S_r, of a flame front of radius, r, concave toward the unburned fuel, increases with curvature according to a function of the form, $S_r = S_\infty (1 + 2\Delta/r)$, where Δ is the thickness of the flame. Consequently, the investigation was extended to the behavior of *flat* laminar dust flames.

Flat Flame Experiments

As the method of channeled matrices[3] is not suitable for producing uniform velocity profiles in dust currents, circular Mache-Hebra[4] nozzles were used. Once ignited, flat laminar dust flames floating within one inch above the burner port are self-sustaining when stabilized by an enveloping divergent gas stream, thus requiring no pilot flame.

The use of Mache nozzles in dust burners entails gravity elutriation in the supporting tube where the flow rate is 3 to 5 times smaller than at the throat. As a result, the poly-disperse dust becomes deficient in coarse particles, and flames of the same over-all concentration may appear to burn faster on smaller nozzles. This source of error can be minimized by reducing the particle size. In the present work, minus 5-μ pulverized aluminum and graphite were prepared (maximum sedimentation velocity 0.2 cm/sec). Fuel concentrations in the dispersions were determined from the volume, by flow rate and time (15 sec) measurement, and from the weight of filtered dust aspirated at the burner port. Burning velocities were determined by two procedures: (1) By measuring the ratio of volume flow into a central stream tube and its cross section at a level of the burning zone where stream lines are parallel, as derived from particle streak photographs on the basis of total flow measurement. Flame diameters were determined from the same photographs (Fig. 3). (2) From the velocity minimum in the unburned zone of central stream tube particles as micrographed on rotating film (magnification 6.3 ×) (Fig. 4). Flame diameters were determined from enlarged natural size photographs (Fig. 5). Experimental data are listed in Table 1. The results clearly show an increase in burning velocity with flat flame area.

Theoretical Considerations

The dependence of burning velocity on flame area can be interpreted by the contribution of radiation in heat transfer to the unburned fuel on the basis of the elementary theory of flame propagation through dust clouds[2] as follows.

The heat flux across the flame is given by the energy balance equation

$$S\rho(H_i - H_u) = k\left(\frac{dT}{dx}\right)_i + R \qquad (1)$$

where S = burning velocity; H = enthalpy per unit mass of unburned mixture; ρ = its density; k = coefficient of thermal conductivity; T = absolute temperature. Subscript i refers to the igni-

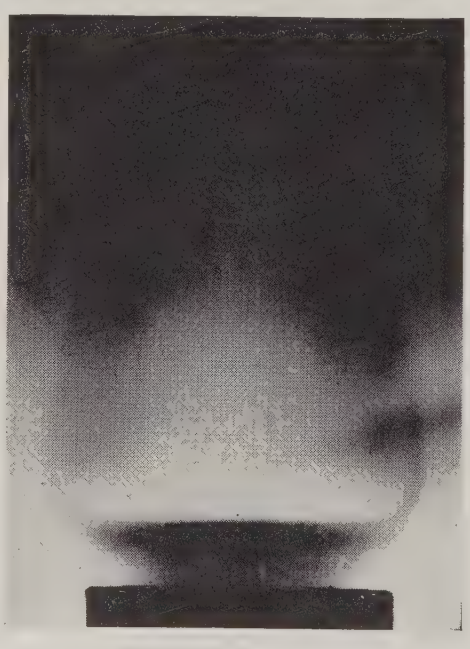

FIG. 3. Flat graphite dust flame burning in oxygen (200 mg/liter).

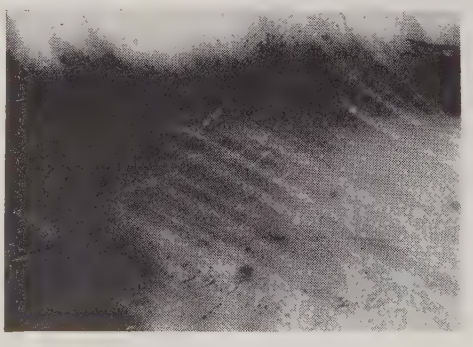

FIG. 4. Rotating-film micrograph of aluminum particle tracks approaching flame front, showing minimum slope.

tion point, and u to the initial state. The radiation

$$R = ASP \tag{2}$$

where A = flame area; and P = product of

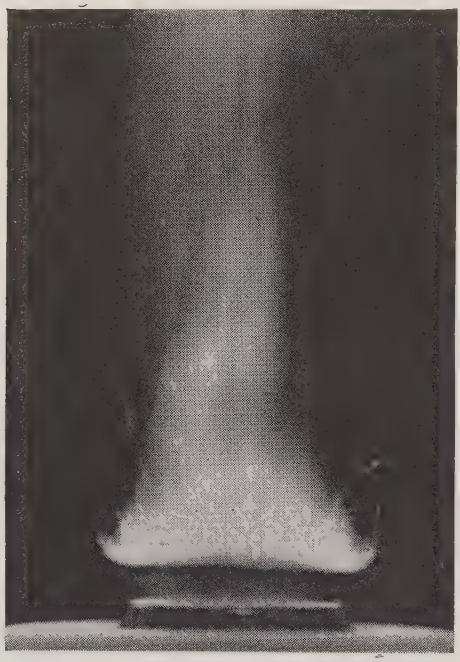

FIG. 5. Flat aluminum dust flame in air (225 mg/liter).

with thickness

$$\delta = S/U \tag{4}$$

U being the average rate of reaction. Therefore Equation (1) can be written

$$S^2\rho(H_i - H_u) = kU(T_f - T_i) + S^2AP \tag{5}$$

From differentiation with respect to A

$$2\frac{dS}{dA}\rho S(H_i - H_r) = kU\left\{1 + \frac{T_f - T_i}{U}\frac{dU}{dT}\right\} \cdot \frac{dT_f}{dA} + ASP\left\{2\frac{dS}{dA} + \frac{S}{A} + \frac{S}{P}\frac{dP}{dA}\right\} \tag{6}$$

Since P varies proportionately to T_f^4 we have

$$\frac{d\log P}{dA} = 4\frac{d\log T_f}{dA} \tag{7}$$

Therefore, the ratio of radiative transfer to total heat flux $ASP/\rho S(H_i - H_u) = f$ can be expressed as

$$f = \frac{\dfrac{dS}{dA} - \dfrac{kU}{2}\left\{1 + \dfrac{T_f - T_i}{U}\dfrac{du}{dt}\right\}\dfrac{dT}{dA}\Big/\rho S(H_i - H_u)}{\dfrac{dS}{dA} + \dfrac{S}{2A} + 2S\dfrac{d\log T_f}{dA}} \tag{8}$$

If, in a first approximation, it is assumed that

TABLE 1. BURNING VELOCITIES OF ALUMINUM- AND GRAPHITE-DUST FLAMES

	Flat (minus-5-micron) Aluminum Flames in Air								Flat (minus-5-micron) Graphite Flames in Oxygen			
	Method 1				Method 2				Method 1			
Dust concentration, mg/l.	200	200	240	240	260	260	310	310	200	200	230	230
Nozzle ϕ, cm	0.80	0.95	0.95	1.10	0.80	0.95	0.80	0.95	0.99	1.10	1.26	1.47
Flame area, cm^2	.81	.88	1.16	1.55	1.05	1.40	1.00	1.20	1.30	1.65	2.45	2.90
Burning velocity, cm/sec	15.0	16.0	16.5	18.0	19.5	21.0	21.5	22.5	12.0	14.8	15.5	17.5
Brightness temperature, °C.	1440	1445	—	—	1700	1710	1740	1760	—	—	1600	1610
f_A	0.60(?)		0.36		0.35		0.32		0.63		0.58	

emissivity and concentration of reaction products, absorptivity and concentration of fuel particles, and, approximately, of the fourth power of flame temperature, T_f.

In Equation (1) the temperature gradient can be taken as that of the reaction zone

$$\left(\frac{dT}{dx}\right)_i = \frac{T_f - T_i}{\delta} \tag{3}$$

temperatures are virtually independent of flame area

$$f_A = \frac{dS}{dA}\Big/\left(\frac{dS}{dA} + \frac{S}{2A}\right) \tag{9}$$

It should be noticed that according to Equation (8) f varies only little with change in ignition temperature while f_A, according to Equation

(9), is independent of the ignition temperature. However, f and f_A are functions which approach zero with decreasing, and unity with increasing flame area.

Values of f_A computed from experimental results (Table 1) are overestimated, but the error is small as shown by measurement of flame brightness temperatures which increase insignificantly with stepwise increasing flame area.

Conclusions

Within the range of flame areas studied the average radiative contribution in heat transfer amounts to about 60 per cent for graphite dust flames burning in oxygen and to about 35 per cent for aluminum flames burning in air. The greater effect in graphite flames is in line with the greater absorptivity of this fuel.

REFERENCES

1. Lewis, B., and von Elbe, G.: *Combustion, Flames and Explosions*, p. 464. New York, Academic Press, 1951.
2. Cassel, H. M., Das Gupta, A. K., and Guruswamy, S.: *Third Symposium on Combustion, Flame and Explosion Phenomena*, p. 185. Baltimore, The Williams & Wilkins Co., 1949.
3. Powling, J.: Fuel, *28*, 25 (1949).
4. Mache, H., and Hebra, A.: Sitzber. Akad. Wiss. Wien, *150*, 157 (1941).

77

IGNITION OF EXPLOSIVES[a]

By C. H. JOHANSSON, A. PERSSON and H. L. SELBERG

Introduction

Liquid explosives are known for their impact sensitivity, but under certain conditions they can be subjected to very intense impacts without igniting or detonating. Striking examples of this apparent anomaly are observed for nitroglycerin. Bowden and Yoffe[1] have found that a drop of nitroglycerin can be initiated by the impact of a 40-g striker, with a cavity in the impact surface, falling from a height of only 5 mm. On the other hand, Zippermayr[2] was able to fire spherical bullets at velocities of 300 to 1050 m/sec against a nitroglycerin target without ignition or detonation. This was the case even for bullets with small surface cavities similar to the cavity in Bowden's striker. The present investigation was performed to gain a better insight into the hazards of igniting explosives by blow or rapid compression.

Wall Temperature of Compressed Air Inclusions

A basic point in the investigation was the idea that the increase in temperature of the explosive during compression is only a fraction of the increase of the air temperature.[3] As a first step, we calculated the temperature increase of the wall, ϑ_w, due to a sudden increase of the air temperature, ϑ_a, produced by rapid compression to p atmos, neglecting convection. The following values were obtained:

p atmos	5	10	50	100	500
ϑ_a°C	170	265	560	720	1180
ϑ_w°C	3	6	25	47	160

Experiments with rapid compression of air were carried out in a cylinder 27 mm in diam and 200 mm long. The compression times ranged from 50 to 300 ms, with compression ratios up to 27. The volume and pressure of the air versus time were recorded, and the mean temperature of the compression chamber was calculated according to the perfect gas law as a function of the time. Use of a piston with a Bridgman[4] packing and a suitable lubricant prevented leakage during compression.

The increase in the surface temperature was measured on a glass plate with 0.4 μ thick silver foil, the temperature of which was determined by measuring the electric resistance. Figure 1 gives an example of experimental curves for volume, pressure, air temperature, and the temperature in the silver foil at the compression ratio of $V_1:V_2 = 25$. The recorded maximum increase of the surface temperature is only 30°C, making the maximum increase of the air temperature (mean value of the chamber) about 410°C.

The measured increase in the wall temperature is in good agreement with values calculated from the experimental temperature-time curve of the air according to the equation

$$\vartheta_w = \frac{2}{\sqrt{\pi}} h \sqrt{a} \int_{\tau=0}^{t} \sqrt{t-\tau}\, d\theta \qquad (1)$$

in which $h = \alpha/\lambda$, α being a coefficient of heat transfer; $a = \lambda/\rho c$; λ, ρ and c being the thermal conductivity, density and specific heat of the explosive respectively; t = time. Equation (1) is derived from

$$\vartheta_w/\vartheta_a = 1 - e^{h^2 at}\, erfc\, h\sqrt{at} \qquad (2)$$

for the special case where $h\sqrt{at} \ll 1$. The heat transferred to the walls was determined from the

[a] This investigation was performed at Nitroglycerin AB, Physical Research Laboratory, Stockholm, Sweden, with support of the Swedish Research Foundation of Detonics.

rate of cooling. During compression and immediately afterwards, the measured heat transfer was several times greater than the transfer according to Schmidt's experimental formula.[6]

$$Nu = 0.65\ (Gr\ Pr)^{0.25} \qquad (3)$$

When the compression was completed, the transfer of heat decreased slowly, approximating the value calculated from Equation (3).

To estimate the temperature in the interior of the chamber, the temperature of a 0.1-mm platinum wire was measured by recording the variation of the resistance with time (Fig. 2). The wire reached its maximum temperature after about 315 ms. At this point the mean temperature of the air was about 30°C lower than in the interior of the chamber. If the temperature of the air is assumed to decrease linearly to the temperature of the wall in a thin boundary layer, it will be found that the mean thickness of the layer is 0.03 cm. The variations in the temperature of the platinum wire also show that flow and turbulence in the air, during and immediately after compression, play an important part in the transmission of heat.

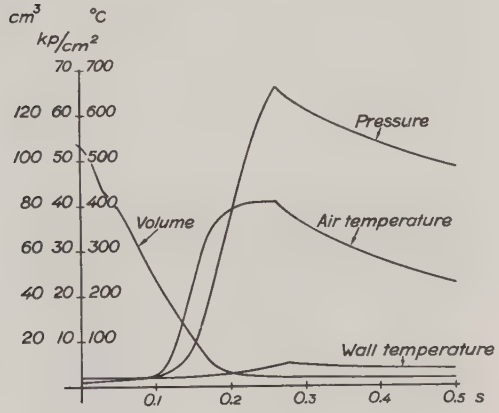

Fig. 1.

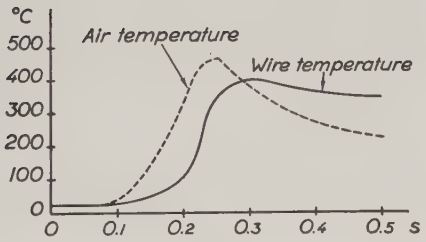

Fig. 2.

Ignition of Vapors and Small Particles or Droplets

Air inclusions with smooth walls must be compressed to several hundreds of atmospheres to heat the explosive to its ignition temperature. The case is quite different if the air inclusions contain explosives or combustible substances in the form of vapor with sufficient pressure, small particles or drops, thin membranes between neighboring bubbles or convex parts, or fibers that project into the air from the wall.[3] In this case, compression to 10 and 20 atmos may be quite sufficient to initiate the reaction and the rise in temperature due to the heat liberated by the exothermal reaction can in its turn ignite the smooth walls of the explosive.

To investigate the conditions for ignition, tests were made with ether-air mixtures and different flammable materials. At compression ratios of 20 to 25 and air temperatures of 400 to 450°C, newsprint paper, cotton and wood filings were completely consumed. A sheet of cardboard 1 mm thick remained perfectly intact when the surface was smooth and the edges rounded off, but when the surface was burred, the projecting sections caught fire and were burned, leaving smooth, charred surfaces. This can be explained by the fact that the thickness of the boundary layer between the surface and the hot air was only about 0.03 cm.

When blasting gelatin was spread out in a thin layer and its surface flattened by careful heating, it remained unaffected on a brass plate, but ignited and burned on a 0.01-mm sheet of mica with an area of 7 by 25 mm. When the layer was spread on 0.015-mm tinfoil of the same area, it remained unaffected, but when placed on a strip only 1 mm wide it burned up.

Figure 3 shows temperature curves obtained by compressing air containing a small quantity of powdered PETN. The temperature is determined from the recorded volume and pressure curves. With a compression degree of 9.7 and a maximum mean temperature of 390°C, the PETN powder ignited 24 ms after compression was terminated at a mean temperature of 330°C (Point A). With a compression degree of 8.4 and a maximum mean temperature of 340°C, a slight inflection at a mean temperature of about 290°C (Point B) indicates some reaction about 55 ms after compression was terminated. Photographs of the compression chamber observed through a transparent glass cylinder bottom show that

only the smallest PETN grains were ignited. The grains that did not ignite, melted and acquired a

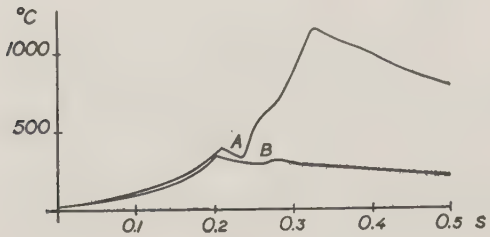

FIG. 3.

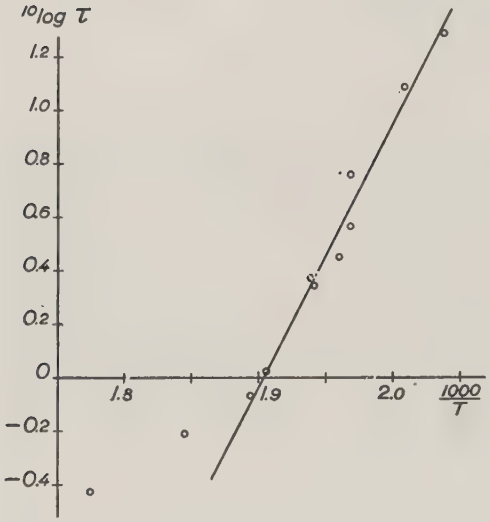

FIG. 4.

spherical form or, in certain cases, the form of droplets. The induction time for thermal ignition of PETN was measured by heating PETN in an oven. The values obtained up to 255°C lie along a straight line (Fig. 4)

$$^{10}\log t = 10100/T - 19.27 \qquad (4)$$

where t is the induction time in seconds and T the absolute temperature. These induction times are in reasonable agreement with the delays observed in the experiments mentioned above. Equation (4) corresponds to an "activating energy" $E = 46.6$ kcal/mole in closest agreement with the activating energy of 47 kcal/mole derived by Robertson[7] from the rate of decomposition.

Conclusions

The investigation showed that a high explosive is very sensitive to ignition by a blow or rapid compression if its air inclusions contain small particles or drops, thin membranes, convex parts, fibers projecting into the air from an uneven wall, or a combustible substance in the form of vapor with sufficient pressure. The high sensivity of liquid explosives, such as nitroglycerin, may be explained simply by the fact that small drops are easily released by a blow and ignited by compressed air.

REFERENCES

1. BOWDEN, F. P., AND YOFFE, A. D.: *Initiation and Growth of Explosion in Liquids and Solids*. London, Cambridge University Press, 1952.
2. ZIPPERMAYR, M.: Explosivstoffe, *3*, 25 (1955).
3. JOHANSSON, C. H., AND SELBERG, H. L.: Appl. Sci. Res., *A5*, 439 (1955).
4. BRIDGMAN, P. W.: *The Physics of High Pressure*. London, G. Ball & Sons, Ltd., 1949.
5. CARSLAW, H. S., AND JAEGER, J. C.: *Conduction of Heat in Solids*. Oxford University Press, 1948.
6. SCHMIDT, E. Z.: Zeit. des Ver. dent Ing., *81*, 1041 (1937).
7. ROBERTSON, A. J. B.: J. Soc. Chem. Ind., *67* 221 (1948).

78

THE COMBUSTION AND EXPLOSION OF CRYSTALS

By F. P. BOWDEN, B. L. EVANS AND A. D. YOFFE

Introduction

When a crystal of a material such as cadmium azide or lead azide is heated at a temperature below the ignition temperature, there is a tendency for the decomposing crystal to crack and break up in a regular manner along crystallographic planes. Some experiments made by Bowden and Singh[1] gave the results shown in Figure 1. Figure 1a is a crystal of cadmium azide which on heating to 317°C breaks up into small blocks as shown in Figure 1b. Lead azide behaves in the same way and Figures 1b and c show a crystal before and after heating at 325°C. Electron diffraction studies by Sawkill[7] provide further evidence that decomposition can occur at cracks or defects inside the crystal.

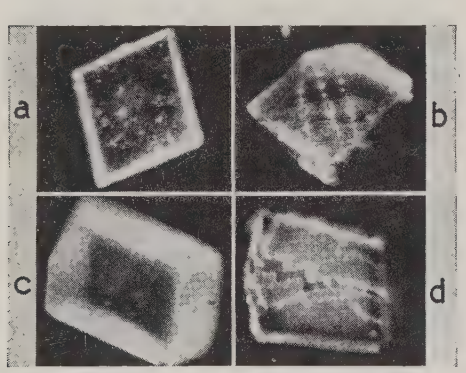

FIG. 1. (a) Slow decomposition of crystals. Crystal of cadmium azide before heating (×100). (b) Same crystal as shown in Fig. 1(a) after heating at 317°C showing the regular cracking and breaking up of the crystal (×100). (c) Crystal of α-lead azide before heating (×140). (d) Same crystal as shown in Fig. 1(c) after heating at 325°C showing cracking and breaking up into blocks (×140).

A study is now being made[2] of the combustion and explosion of single crystals of a number of explosive materials, partly to obtain data on the burning speed of single crystals and the influence of crystal size, and also to determine whether the spreading of cracks in the crystal plays any part in the propagation process.

Apparatus

A high speed cine-microscope recently developed by Courtney-Pratt has been used. A full description of the instrument used in these experiments has already been published.[3] This microscope enables events lasting several msec to be recorded at magnifications up to 500. The framing rate of the camera can be of the order of 30,000/sec or higher. It has been possible with the instrument to record the combustion of crystals as small as 0.1 mm in length. Ignition is usually brought about by a hot platinum wire, but in some instances a high intensity light flash has been used to initiate the combustion or explosion (McAuslin[4]). Apparatus is also being developed to determine velocities in single crystals by means of a spiral-type cathode ray oscilloscope, and by an image converter-type camera designed by Courtney-Pratt.[5]

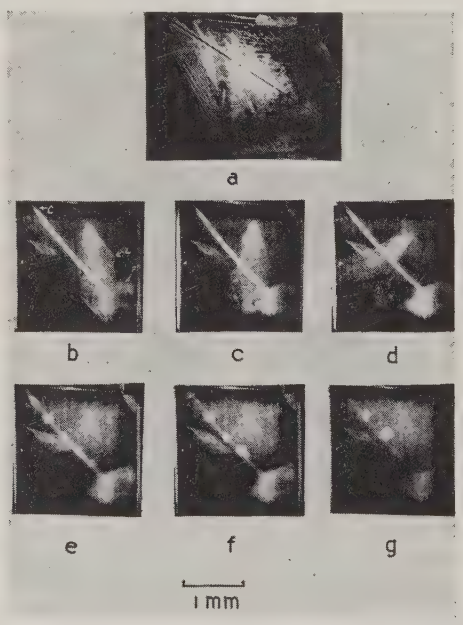

FIG. 2. Fast decomposition of crystals. (a) Crystal of mercury fulminate containing numerous faults (× 28). (b) to (g) sequence in the combustion of a mercury fulminate crystal *a* ignited by a hot platinum wire *c*. The flame and region of ignition is at *F*. In Fig. 2(d) *d* shows a fragment of mercury fulminate breaking away from the crystal.

The compounds which have been studied are mercury fulminate, lead styphnate, cyanuric triazide, trinitrotriazido benzene, silver azide and thallous azide.

Results

Some typical results are shown in Figures 2, 3, 4 and 5. Figure 2a shows a crystal of mercury fulminate which contains numerous faults. When such a crystal is ignited by a hot platinum wire there is a marked tendency for it to break up into a number of fragments which fly off at high speed. In Figure 2b the crystal, *a*, is ignited by the hot platinum wire, *c*, at *F*. The sequence

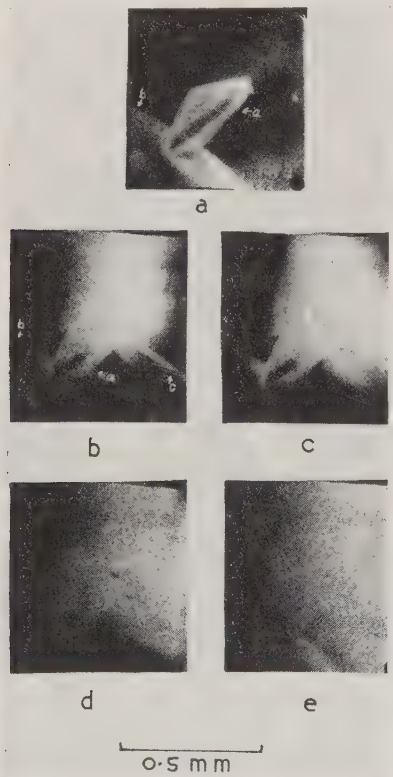

FIG. 3. Sequence in the combustion of a mercury fulminate crystal *a* ignited by a hot platinum wire *c*. The crystal is held at one end by means of "lustrex" *b*. The burning speed in this experiment was 20 cm/sec.

shows the crystal moving off in Figure 2c, and a fragment, *d*, is seen to come away in Figure 2d. The fusing of the platinum wire to give a number of oscillating molten blocks of metal is shown in Figures 2e, 2f and 2g. The total sequence time for Figures 2b to 2g is about 6 msec. Numerous experiments with mercury fulminate and other materials have shown that this break up of the crystal when faults are present is general.

When the crystals are relatively free from faults then burning speeds may be measured as shown in Figures 3 and 4. In Figure 3a which shows the burning of a mercury fulminate crystal the crystal, *a*, is held at one end by a thin film of "lustrex" cement, and ignited by the wire, *c* (Fig. 3b). The burning speed in this experiment was 20 cm/sec. The combustion of a crystal of lead styphnate is shown in Figure 4. Figure 4a illustrates the kind of crystal used in these experiments. In Figure 4b the crystal, *a*, which is held at one end by means of the "lustrex" film, *b*, is ignited by the platinum wire, *c*. In Figure 4c the flame front, *F*, may be seen and the sequence of events is shown in Figures 4b to 4g. The burning

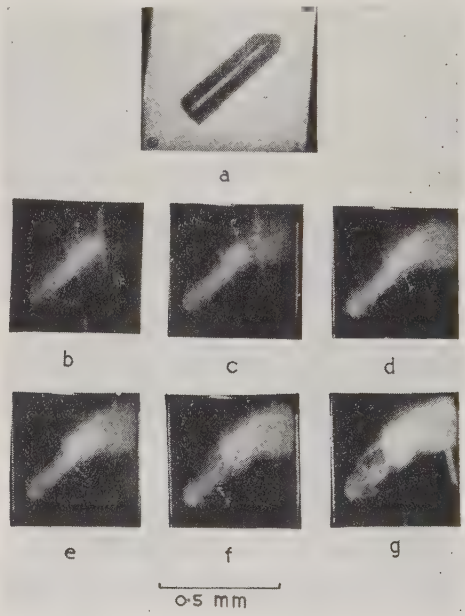

FIG. 4. Sequence in the combustion of a crystal of lead styphnate similar to that shown in Fig. 4(a). The crystal *a* is held at one end by means of the "lustrex" film *b* and ignited by the hot platinum wire *c*. The flame front is at *F*. The burning speed in this experiment is 4 m/sec.

speed calculated from this experiment is 4 m/sec. The values for the burning speeds obtained from this investigation are very similar to those for thin films (*ca.* 0.5 mm thick) of the same materials.

If the diameter of the crystal is increased there is an increase in the burning speed and eventually detonation will occur. For example a crystal of cyanuric triazide 0.35 mm in diam burns with a speed of 30 cm/sec. When the diameter is 0.6 to 0.7 mm the burning speed is *ca.* 1 to 2 m/sec. Crystals larger than this may burn for a short time and then explode. These observations can be explained in terms of heat losses to the surroundings.

The behavior of the compounds which have melting points is somewhat different from those which explode without melting. For example a single crystal of silver azide in the form of a needle explodes when its diameter is of the order of 0.025 mm. When the diameter is *ca.* 0.01 mm the silver azide in some cases appears to burn with a velocity of the order of 7 m/sec. When very fine needles less than 0.01 mm in diam are used, part of the needle near the hot platinum wire melts to form a molten blob of decomposing

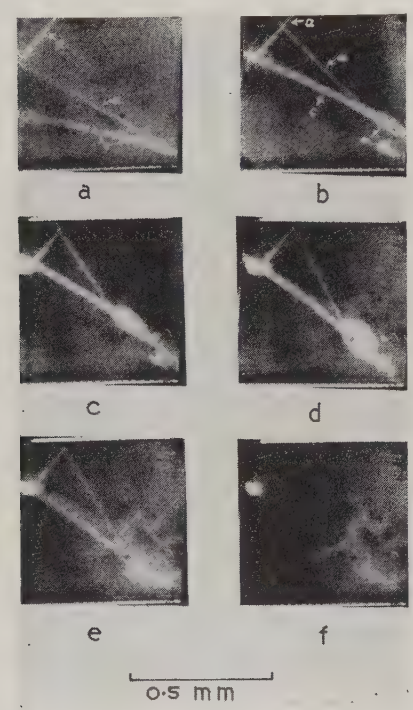

FIG. 5. Sequence in the explosion of a thin silver azide needle *a*. Ignition by means of a hot platinum wire *c*. Melting occurs prior to explosion at *m*.

azide which explodes after a fraction of a msec and the explosion spreads to the solid crystal. A typical sequence is shown in Figures 5a to f. In Figure 5a two small needles of silver azide, *a*, may be seen near the platinum wire, *c*. In Figure 5b local melting of the silver azide occurs at *m*. The mass of molten decomposing azide continues to increase until there is an explosion of the liquid as shown in Figure 5e. The explosion then spreads to the solid needle as illustrated in Figure 5f. One possible explanation of these results is that a critical size of decomposing azide is necessary for explosion (*cf.* Bowden and Yoffe[6] and Bowden and Singh[1]). If this critical size is not exceeded then rapid decomposition takes place and the heat losses are sufficiently great to prevent explosion.

Crystal Structure of Azides and Sensitivity to Explosion

For the decomposition of silver azide, the exothermic nature of the reaction

$$2AgN_3 \rightarrow 2Ag + 3N_2$$

is generally attributed to the heat liberated when two azide radicals react

$$2N_3^\circ \rightarrow 3N_2$$

If a "hot spot" of sufficient size is formed during the decomposition, the reaction becomes self supporting and the material explodes.

Potassium azide does not possess the explosive properties of silver azide and it is clear that the metal (*K*) must influence the explosive sensitivity. For this reason a study is being made of the Group I metal azides and isoelectronic cyanates, fulminates and thiocyanates.[8] Values for the lattice energies of the azides and the electron affinity of the azide radical have been obtained by Gray and Waddington.[9] An indication of the way in which the metal ion influences the azide ion will be found from the crystal structure. The tetragonal structure of potassium, rubidium and caesium azide may be compared with the orthorhombic structure of silver azide. The electron affinity of the N_3 radical is 3.52 ev and the crystal structure of KN_3, RbN_3, and CsN_3 is compatible with that of an ionic structure. It has been possible to explain the orthorhombic symmetry of AgN_3 only by assuming a partial covalent character. This assumption has been shown to be valid by studying the optical properties of crystals of AgN_3. The first ionization potential of thallium is 6.07 ev and the valence electron is 6 p. If, however, we include TlN_3 (tetragonal structure) in the series of Group I metallic azides we see that an increase in explosive sensitivity results from increasing the ionization potential of the metal. In this connection a knowledge of the crystal structure and explosive sensitivity of monovalent gold azide (AuN_3) would be of interest. The greater the ionization potential of the metal forming the metallic azide the more completely the binding electron is under the influence of the metal. The corresponding electrical neutrality of the azide group facilitates the reaction $2N_3^\circ \rightarrow 3N_2$. By an extension of these calculations and experiments it is hoped to ex-

plain the relation between crystal structure and explosive sensitivity.

Conclusions

(1) The slow decomposition of explosive crystals does not proceed in a uniform manner. The crystals tend to crack and break up into small blocks along crystallographic planes.

(2) The rapid combustion of single crystals which contain faults is also accompanied by the formation of cracks which run ahead of the flame and by the break up of the crystal into fragments which fly off at high speed.

(3) Crystals which are relatively free from faults burn in a uniform manner and combustion speeds may be determined.

(4) The burning speed depends on the crystal diameter and on the initial temperature.

(5) The behavior of compounds which melt prior to explosion (silver azide) is different from those which explode or burn while they are still solid.

(6) The relation between crystal structure and explosion sensitivity is discussed. The nature of the metal ion is considered to be the significant variable due to the changing ionization potential.

Acknowledgment

We are grateful to Dr. J. S. Courtney-Pratt for making the cine-microscope available to us and to Mr. G. J. Dean for assistance with the photographic work.

REFERENCES

1. Bowden, F. P., and Singh, K.: Proc. Roy. Soc. *A227*, 22 (1954).
2. Evans, B. L., and Yoffe, A. D.: To be published.
3. Courtney-Pratt, J. S.: *International Symposium on Photography*. Paris, 1954; Second O.N.R. Symposium on Detonation, Washington, 1955.
4. McAuslan, J.: Unpublished work.
5. Courtney-Pratt, J. S.: Research, *2*, 287 (1949).
6. Bowden, F. P., and Yoffe, A. D.: *Initiation and Growth of Explosions in Liquids and Solids*. Cambridge, Cambridge University Press, 1952.
7. Sawkill, J.: Proc. Roy. Soc., *A229*, 135 (1955).
8. Evans, B. L.: Unpublished work.
9. Gray, P., and Waddington, T.: Proc. Roy. Soc., in press (1956).

79

DEFLAGRATION OF AMMONIUM PERCHLORATE[a]

By RAYMOND FRIEDMAN, R. G. NUGENT, K. E. RUMBEL and A. C. SCURLOCK

Introduction

Ammonium perchlorate is an important ingredient of composite propellants, yet little is known about its mechanism of decomposition under combustion conditions. Bircumshaw and Newman[1] studied the thermal decomposition at subatmospheric pressure and temperatures up to 450°C. They found that (1) the decomposition initiated at discrete points on the crystal surface and spread through the crystal as a decomposition interface; (2) only a portion (about 30 per cent) of the ammonium perchlorate was decomposed by the passage of the interface; (3) the reaction was accelerated by the addition of manganese dioxide or ferric oxide; (4) a phase transformation from orthorhombic to cubic crystal form occurred at 240°C, with a corresponding change in decomposition rate; (5) the product gas composition differed greatly from equilibrium products.

The results of this investigation were analyzed further by Schultz and Dekker[2] who applied the transition-state theory of reaction rates to the velocity of the decomposition interface. They compared their result with values deduced from Bircumshaw and Newman's sigmoid-shaped rate curves.

Adams, Newman and Robins[3] and Adams[4] have shown that a deflagration wave will propagate through ammonium perchlorate at pressures above 68 atmos. This is a rapid process involving steep temperature gradients, as contrasted with

[a] This work was supported by the Office for Advanced Studies, United States Air Force, Office of Scientific Research, Air Research and Development Command.

the isothermal, slow-moving decomposition interface observed by Bircumshaw and Newman.[1] Adams, Newman and Robins[4] found that the deflagration wave progressed through pressed pellets at roughly one cm/sec. The rate increased with the 0.57 power of pressure and was somewhat dependent on the particle size of the powder from which the pellets were pressed.

In the current investigation, further studies have been made of the deflagration of pressed pellets of ammonium perchlorate. The effects of ambient pressure and temperature, initial particle-size distribution, and catalyst addition have been explored. Thermocouples have been used to measure the temperatures of the gases evolved from the decomposing perchlorate.

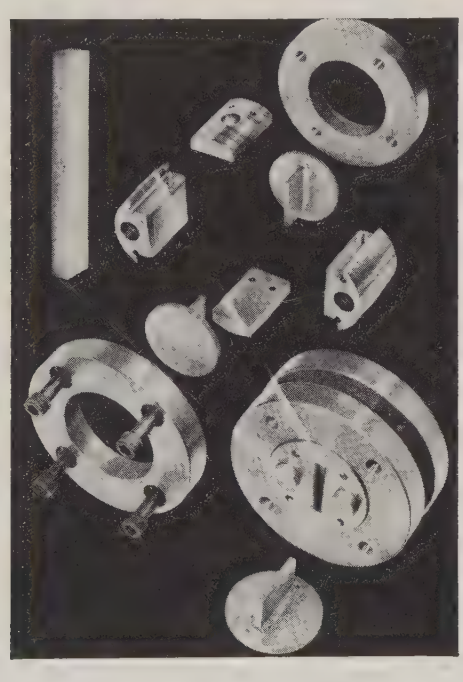

FIG. 1. Mold used for pressing ammonium perchlorate powder into pellets.

Experimental Procedures

Reagent-grade ammonium perchlorate was used. The powder was pressed into pellets 4 mm square and 38 mm long in a mold with hardened steel faces, shown in Figure 1. A pressure of 100,000 psi was applied to the crystals by means of a hydraulic press. In certain selected experiments, sieved particle-size fractions were pressed; in all other cases the powder was pressed "as received." The as-received material contained particles ranging from a few microns to several hundred μ in diam.

Density of the pressed pellets, as determined by micrometer measurements and weighings, was found to be as follows: 1.908 gm/cc for the as-received material (average of seven specimens); 1.894 gm/cc for the 74-to-105μ fraction (average of three specimens); and 1.896 gm/cc for the minus-53 μ fraction (average of three specimens). The single-crystal value is 1.95 gm/cc. These results indicate that the material was not perfectly compacted although the molding pressure of the pellets was 100,000 psi. Dye-penetration experiments confirmed the presence of voids. The degree to which these imperfections influence the burning characteristics reported below could perhaps be determined by burning large single crystals. Such experiments are planned.

Most of the deflagration rates were measured in a conventional Crawford strand burner[5] with nitrogen pressurization and hot-wire ignition. The deflagration wave proceeded downward. The timing fuse wires were placed through holes of 0.34 mm diam drilled horizontally through the pellets 1.9 cm apart. It was not necessary to inhibit the sides of the pellets.

Some of the deflagration rates were determined by motion-picture photography with a window bomb. The burning surface was seen to be somewhat tilted and irregular at times. This is very probably associated with imperfections in the pressed pellets and is likely to be the main cause of scatter of the data. Also, the presence of tilted surfaces implies that the "true" burning rates must be somewhat lower than the measured values. Inspection of the motion pictures, however, suggests that this difference is not very large.

No luminosity of the products of deflagration was observed, except for occasional flashes believed to be due to impurities. Condensation of the combustion products was evident as the high-pressure, moisture-laden gases mixed with the cold ambient nitrogen to form an acid fog.

To assess the effects of catalysts on the deflagration, a weighed quantity of finely powdered catalyst was thoroughly mixed with the as-received ammonium perchlorate powder, and pellets were pressed from the mixture. The particle-size distribution of each catalyst was measured with a Sharples Micromerograph, with results shown in Figure 2.

Temperature measurements of the product gases were made by mounting thermocouples of

platinum versus platinum plus 10 per cent rhodium in holes of 0.34 mm diam drilled transversely through the pressed pellets. The wires were fastened to supports which were aligned with the drilled hole on either side of the strand. Electrical connections were brought out of the pressurized test chamber by insulated bushings in the bomb wall, and records of emf *vs.* time were obtained with a Consolidated Engineering Corporation recording oscillograph, Type 5-101B. The majority of the work was done with thermocouples of 25 μ wire, the gas-welded beads averaging 46 μ in diam. A few experiments were made with 13 μ and with 51 μ wire, the beads again being somewhat less than twice the wire diameter in each case.

Results

The deflagration-rate measurements which were made for pure ammonium perchlorate are shown in Figure 3. At an ambient temperature of 21°C, lower and upper deflagration limits of about 45 atmos and about 300 atmos, respectively, were found for the perchlorate pressed from as-received powder, with a wide distribution of particle sizes. Tests with perchlorate pressed from a 74-to-105 μ sieve fraction gave lower deflagration rates that agreed rather well with the results of Adams, Newman and Robins[4] from 110 to 160 atmos, but possessed a surprisingly high lower limit, namely about 90 atmos. The upper limit appears to be slightly below that for the as-received material.

Data are also shown for pellets made of a minus-53 μ sieve fraction. Deflagration rates compare closely with the as-received material above 110 atmos, but the material would not burn at all at 100 atmos or below.

Since the as-received material yielded higher pellet densities and wider pressure limits of burning than sized fractions, and at least as high burning rates, this material was chosen for further studies of ambient-temperature and catalyst effects.

When such pellets were preheated to 70°C instead of to 21°C before ignition, deflagration rates were increased at all pressures, as Figure 3 shows. Further, deflagration could be maintained down to nearly 20 atmos, and the pressure above which the deflagration rate began to decrease was raised from 150 atmos to 200 atmos.

When the pellets were precooled to minus 18°C, ignition could not be obtained at any pressure from 70 to 270 atmos.

To recapitulate, the main features of the above findings are: deflagration rate of ammonium perchlorate below 150 atmos increases with increasing pressure, increasing ambient temperature, and decreasing particle size from which the pellets are pressed. These results are not unexpected and agree in general with those of Adams, Newman and Robins.[3] At higher pressures, however, a novel phenomenon is encountered, the existence of an upper pressure limit, which is only slightly dependent on particle size but may be raised by preheating.

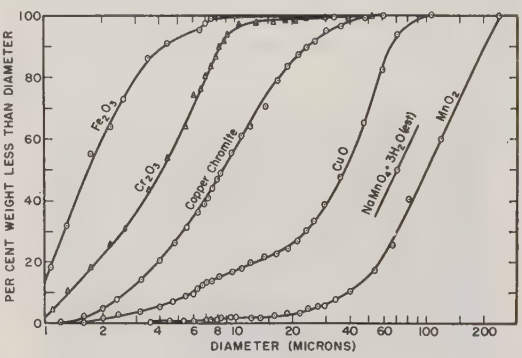

FIG. 2. Particle size distribution curves for powders used as catalysts.

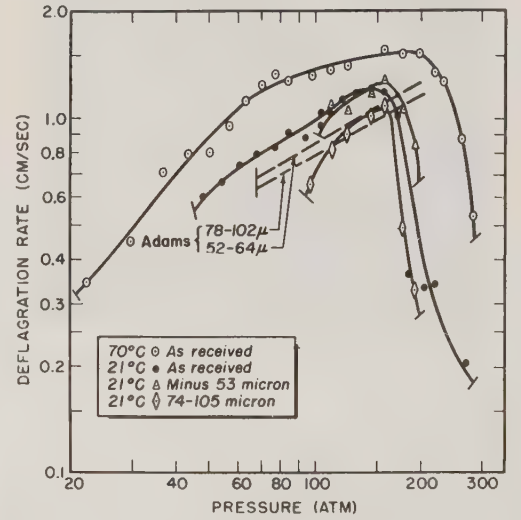

FIG. 3. Rate of deflagration of ammonium perchlorate pellets pressed from powders of various size distributions.

The presence of catalysts markedly changes the behavior of this system. Figure 4 shows deflagration rates as a function of pressure when 3 per cent by weight of each of six powders was mixed with as-received perchlorate before press-

ing. In all cases, the upper pressure limit was eliminated, or at least shifted above 340 atmos (the highest pressure at which operation of the apparatus was feasible). However, it should not be concluded that addition of *any* foreign substance will produce this effect. Perchlorate containing 1.3 per cent of either CaO or $CaCO_3$ was not ignitable in tests at pressures from 140 to 340 atmos.

The greatest increase in deflagration rate was produced by copper chromite, which is a well-known hydrogenation catalyst. A commercial

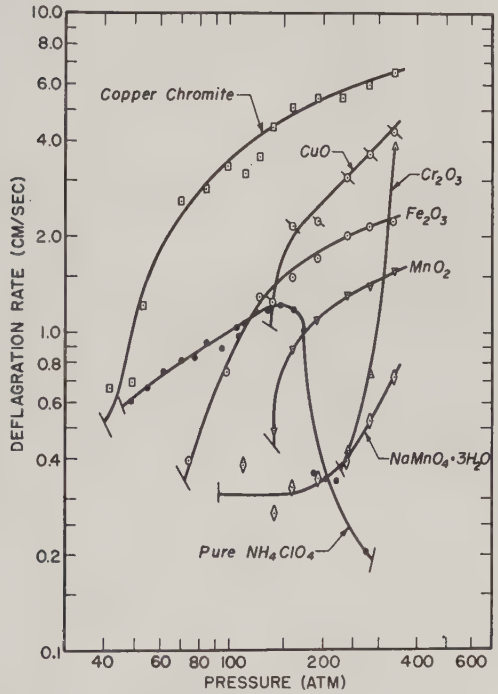

FIG. 4. Rate of deflagration of "as received" ammonium perchlorate with three per cent additions of various catalysts.

grade of copper chromite prepared by Harshaw Chemical Company, designated as Cu-0202, and analyzing 85 per cent by weight CuO and 15 per cent by weight Cr_2O_3, was employed. Pure CuO, when substituted for copper chromite as a 3-percent additive to perchlorate, augmented the deflagration rate above 135 atmos but prevented deflagration from occurring below this pressure. Reference to Figure 2 shows that the mean particle size of the CuO was not nearly as fine as that of the copper chromite, so no rigorous conclusions about the relative effectiveness of these catalysts may be drawn.

The catalyst Cr_2O_3 was effective only above 230 atmos, preventing deflagration below this pressure. The other three catalysts, Fe_2O_3, MnO_2 and $NaMnO_4 \cdot 3H_2O$, decreased the burning rate below that of pure perchlorate at low pressures and promoted it at high pressures, the crossover pressures being 116, 175, and 205 atmos, respectively. These pressures may well be functions of catalyst particle size and concentration, but such effects have not yet been investigated.

Inasmuch as copper chromite was the most effective catalyst, its characteristics were studied in more detail. Figure 5 shows the behavior observed when various concentrations of copper chromite ranging from 0.1 per cent to 5 per cent were added to as-received perchlorate. The most striking feature of the results is the characteristic that the catalyst would either augment the deflagration rate or completely prevent burning, depending on the concentration and pressure; but it never produced finite burning rates below that of the pure perchlorate. This contrasts with the behavior of other catalysts shown in Figure 4.

It may be noted from Figure 5 that at 200 atmos deflagration rate appears to increase monotonically with copper chromite concentration from zero per cent up to a saturation point between 3 and 5 per cent. However, at a lower pressure, say 100 atmos, any copper chromite addition in excess of perhaps 2 per cent will augment the rate, while smaller additions prevent burning. Presumably an *extremely* small addition would permit burning, but no tests were made at concentrations below one part in a thousand.

At 100 atmos, where the slopes of the curves for pure ammonium perchlorate and for ammonium perchlorate with 5 per cent additive are similar, the catalyst augmented the rate by the very substantial factor of 3.7.

At this point the measurements of product-gas temperature will be described. A typical oscillograph trace is shown in Figure 6. The product-gas temperature was assumed to correspond to the plateau immediately following the region of rapid rise. The irregular nature of this rapid rise is believed to be associated with the relatively large drilled hole in which the thermocouple bead was located, and could perhaps be eliminated by pressing the thermocouple into the pellet when the latter is formed. However, these considerations probably have no bearing on the magnitude of the plateau temperature. The hot gases seem to maintain their temperature for a substantial period, which varied, however, from test to test.

Values of indicated plateau temperature, as obtained with 25 μ thermocouples, are shown in Figure 7 as a function of pressure. At 100 atmos the mean value is 930°C. There is possibly a tendency for this temperature to increase slightly with increasing pressure, but the precision of the measurements is insufficient to be sure about this. Some tests with pellets containing 3 per cent copper chromite gave much more precise results, with a more definite indication of pressure dependence. The presence of copper chromite appears to increase the temperature by about 25°C.

The true gas temperature will tend to be higher than the thermocouple temperature by an amount ΔT, because of radiative heat loss from the couple. If the thermocouple bead be represented by a sphere of diameter d, emissivity ϵ, and absolute temperature T_c, surrounded by gas of thermal conductivity k, and Nusselt number Nu, and radiating to absolute zero, where σ is the Stefan-Boltzmann constant, it follows that

$$\Delta T = \epsilon\sigma d T_c^4 / kNu.$$

If ϵ is taken as 0.15, d as 0.0046 cm, T_c as 1200°K, k as 1.8×10^{-4} cal/cm-sec-°K, and Nu as 3, ΔT is only 3.6°C, which is negligibly small for the present purposes. Accordingly, the temperatures reported are uncorrected for thermocouple radiation.

For an experimental evaluation of the effect of thermocouple size on the results, two tests were made with thermocouples of 13 μ wire, at 100 atmos. Temperatures of 930° and 906°C were obtained. These values may be compared with the average value of 930°C obtained with couples twice this size. If the radiation error were appreciable, one would expect smaller couples to yield substantially higher temperatures; such results were not found.

The possibility remains that the results may be influenced by catalytic heating on the platinum surface. To test this, two thermocouples of 25 μ wire were coated with the National Bureau of Standards' ceramic glaze A-418. The emissivity of this coating is given by De Corso and Coit[6] as 0.87. The coated couples were about 0.0051 cm in diam. These values lead to a computed radiation error of 23°C. Deflagration experiments were made at 136 atmos, and peak temperatures of 907° and 943°C were measured in the two tests. This result suggests that platinum-induced catalysis is not influencing the data reported in Figure 7.

The dash-line curve of Figure 7, giving theoretical product-gas temperature as a function of pressure, was calculated by the conventional

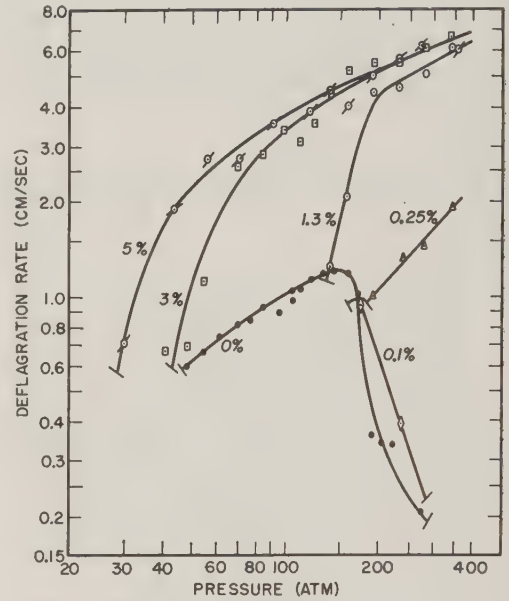

FIG. 5. Rate of deflagration of "as received" ammonium perchlorate pellets with various concentrations of copper chromite catalyst.

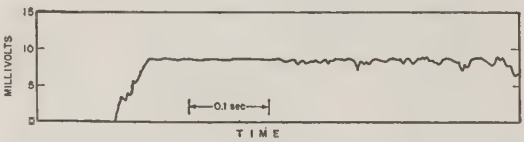

FIG. 6. A typical oscillograph trace for a 25-micron thermocouple mounted in a deflagrating ammonium perchlorate pellet.

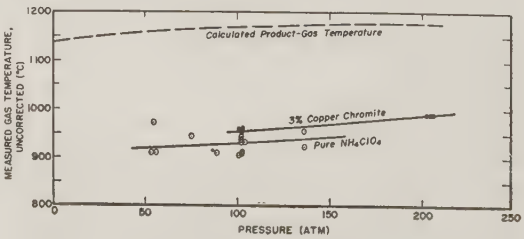

FIG. 7. Calculated and measured product-gas temperatures for deflagrating ammonium perchlorate.

thermodynamic procedure. An adiabatic constant-pressure process was assumed, with initial state consisting of pure crystalline NH_4ClO_4 at 25°C ($\Delta H_f^0 = -69.42$ kcal/mole), and a final state satisfying the conservation and equilibrium relationships was found by trial and error for

each pressure of interest. At 100 atmos, for example, the equilibrium products, at 1167°C, were found to consist of mole fractions as follows: H_2O, 0.378; O_2, 0.286; HCl, 0.195; N_2, 0.119; Cl_2, 0.021; Cl, 0.00050; NO, 0.00043; NO_2, 0.00006.

Figure 7 shows the measured temperatures to be more than 200°C below the calculated values. Since it has been established that the radiation error with uncoated couples is negligibly small, this difference must be due to a failure of the deflagration reactions to reach equilibrium. The actual gases may possibly contain a large proportion of undecomposed nitric oxide. Gas-analysis experiments would shed further light on this question.

Discussion

Of the characteristics of ammonium perchlorate deflagration which have been revealed by this investigation, three findings are particularly intriguing, and call for explanation. First is the existence of an upper-pressure limit of deflagration. Second is the surprisingly large augmentation of burning rate by catalysts. Third is the fact that an additive which catalyzes the reaction at higher pressures may inhibit it strongly at lower pressures. Any proposed explanation for the mechanism of the deflagration process should be tested by attempting to rationalize these facts within the framework of the hypothesis.

With this viewpoint in mind, some of the physicochemical processes which might conceivably be involved will now be discussed.

One possible explanation of the upper-pressure limit involves the assumption that one of the gaseous reaction intermediates does not have a very high vapor pressure at the prevailing surface temperature. The postulated mechanism is then that the constituent cannot vaporize and deflagration ceases when the total pressure is raised above a critical value. Catalysts might raise the upper-pressure limit by raising the surface temperature.

The data of this study have shown that preheating the perchlorate from 21° to 70°C, which corresponds to a temperature rise of similar magnitude in the product gases, produces only a modest increase in the upper-pressure limit, particularly in comparison with the effect of 3 per cent copper chromite. Therefore, if the proposed explanation is correct, copper chromite addition must be far more efficient than preheating in raising the surface temperature. It is recalled that product-gas temperature was found to be only slightly increased by 3 per cent copper chromite addition. Although the above facts do not permit any rigorous conclusion to be reached, they tend to cast doubt on the hypothesis in question. A reliable technique for measuring the surface temperature would be very helpful in testing this hypothesis.

Other explanations may be offered for the upper-pressure limit. The reaction may be supposed to occur in two distinct stages. In the first stage, the solid decomposes to give intermediates. In the second stage, these intermediates diffuse to various active sites on the surface where they react further to give the final products. The first stage is rate-controlling unless the pressure is so high that diffusion is too slow; hence, above a critical pressure, an abrupt change of rate would occur. Catalysts elevate the upper-pressure limit by providing additional sites which catalyze the second stage.

This model seems to be inconsistent with the finding that 3 per cent or more of copper chromite augments the deflagration rate at low as well as high pressures.

Another model may be put forth which is consistent with Bircumshaw and Newman's[1] observation that at much lower temperatures decomposition initiates at discrete surface points and spreads through the crystal as a reaction interface. Let this be taken as the mode of propagation of a deflagration through a pressed aggregate of perchlorate crystals, with the additional feature that each decomposition interface can only propagate a very short distance before it encounters intercrystalline matter and dies out. Hence, for steady deflagration, new initiation sites are continuously needed. In pure perchlorate, these sites are some sort of crystal imperfection. At sufficiently high pressure, the initiation sites can become poisoned in some manner by adsorption of a reaction intermediate or product. Catalysts eliminate the upper-pressure limit by providing a new type of nonpoisonable initiation site. Catalysts also promote deflagration well below the upper-limit pressure (e.g., 3 to 5 per cent copper chromite) simply because they provide more initiation sites.

This model also provides an explanation of why the as-received perchlorate continued to deflagrate at much lower pressures than the minus-53μ fraction. Conceivably the decomposition interfaces could progress a relatively long distance uninterruptedly through the large

crystals in the as-received material, and this effect would favor propagation.

The above model, however, completely fails to give a clue to the observation that under certain conditions catalysts strongly inhibit deflagration. All of the other models, it is true, suffer the same limitation.

A final model may be mentioned, which involves a rate-controlling gas-phase reaction from which heat is transferred to the surface. The exothermic gas reaction might well be of the chain-branching type, with competition between second-order branching and third-order breaking processes. At a sufficiently high pressure, the chain-breaking processes overtake the chain-branching processes. Catalyst additions are assumed to promote gas-phase chain-branching and, accordingly, to postpone or eliminate the upper limit.

The following argument casts some doubt on whether a gas-phase reaction can indeed be controlling. Huggett[7] reports that a mixture of ammonium perchlorate and an organic binder at 136 atmos has a burning rate of 0.76 cm/sec and a flame temperature of 1930°C. As shown in Figure 3, pure ammonium perchlorate at the same pressure deflagrates at 1.2 cm/sec with a measured product-gas temperature of about 940°C. It is seen that the much higher gas-phase temperature in the first case does not lead to a higher deflagration rate. An obvious way to account for this is to suppose that the rate-controlling process does not occur in the gas phase at all, but at the solid surface, where the temperature might be similar in the two cases.

The foregoing speculative discussion is presented in the hope that it will stimulate further efforts to determine the mechanism of this interesting rate process. Obviously, more experimental studies are needed before this phenomenon can be entirely understood.

REFERENCES

1. Bircumshaw, L. L., and Newman, B. H.: Proc. Royal Soc. (London) *A227*, 115 (1954); *A227*, 228 (1955).
2. Schultz, R. D., and Dekker, A. O.: Office of Scientific Research TN-55-142, July 1955, Aerojet-General Corp., Azusa, Calif.
3. Adams, G. K., Newman, B. H., and Robins, A. B. *Selected Combustion Problems: Fundamentals and Aeronautical Applications*, p. 387. Butterworths Scientific Publications, London, 1954.
4. Adams, G. K.: Private communication, Feb. 8, 1956.
5. Crawford, B. L., Jr., Huggett, C., Daniels, F., and Wilfong, R. E., Anal. Chem., *19*, 630 (1947).
6. De Corso, S. M., and Coit, R. L.: Am. Soc. Mech. Engrs. Trans., *77*, 1189 (1955).
7. Huggett, C.: *Combustion Processes*, p. 515. Princeton University Press, Princeton, N. J., 1956.

80

TRANSITION-STATE THEORY OF THE LINEAR RATE OF DECOMPOSITION OF AMMONIUM PERCHLORATE[a]

By ROBERT D. SCHULTZ and ALBERT O. DEKKER

Introduction

Bircumshaw and Newman[1] have recently summarized the results of an exceptionally detailed investigation of the kinetics of decomposition of ammonium perchlorate. The present writers sometime ago obtained a report[2] of well over a hundred pages containing the excellent original data which facilitated the following theoretical analysis. The present paper is based upon a discussion[3] originally presented in 1952 and recently modified in the light of recent studies on the linear vaporization rate of ammonium chloride[4, 5] and on the sublimation rates of molecular[6] and ionic crystals.[7]

By a series of excellent photomicrographs on individual crystals of ammonium perchlorate, Bircumshaw and Newman[1] demonstrated that

[a] This work was supported under Contract AF18(600)-1026 by the United States Air Force, through the Office of Scientific Research of the Air Research and Development Command OSR-TN-55-142.

the slow decomposition at 230°C proceeds by the formation of opaque spots (i.e., nuclei) on the crystal surface. These spots then grow in size and eventually coalesce to form a continuous opaque region whose boundary with the transparent region was observed to move uniformly inward toward the center of the crystal. When the boundary reaches the center of the crystal, decomposition ceases, leaving a porous pseudomorph which is still pure ammonium perchlorate but which has a density only 70 per cent of that of the original crystal.

In the following discussion, it is shown that a single consistent treatment of the kinetic data can be made in terms of the linear rate of progression of the interface between partially decomposed and undecomposed crystal. A modification of a treatment by Mott[8] is used to analyze the acceleratory (or nucleation) period, and a modification of a treatment by Topley and Hume[9] is used to analyze the deceleratory (or postcoalescence) period. An explanation for the observed cessation of the reaction at 30 per cent completion is proposed on the basis of the concept of mosaic structure in crystals. The experimental linear rates derived by this analysis provide a basis for a transition-state absolute rate treatment in the manner of Glasstone, Laidler, and Eyring. These latter calculations suggest that the intermosaic material of the orthorhombic crystal decomposes below 250°C via a primary rate-controlling step requiring the attainment of nearly free rotation of the perchlorate ion. On the other hand, the intermosaic material of the cubic crystal appears to decompose above 250°C via a rate-controlling step which involves desorption of a loosely bound NH_3:$HClO_4$ complex from its physically adsorbed state at the decomposition interface.

Theory of the Nucleation Process in the Acceleratory Period

Bircumshaw and Newman[1, 2] have suggested that the formation of centers of decomposition on the crystal surface may be associated with the formation of free adsorbed perchloric acid. To support this hypothesis, they have demonstrated that the induction period for decomposition is considerably shortened by crystallizing some of the salt with perchloric acid as a 2 per cent impurity. Moreover, they find that the induction period is considerably lengthened by a small pressure of ammonia over the salt, presumably caused by the neutralization of adsorbed perchloric acid. Accordingly, the following mechanism is assumed for the nucleation process:

$$NH_4ClO_4 \underset{b}{\overset{a}{\rightleftharpoons}} NH_3{:}HClO_4 \underset{d}{\overset{c}{\rightleftharpoons}} NH_3 + HClO_4 \quad (1)$$

(crystal surface) (physically adsorbed surface complex) (gas) (adsorbed on surface)

state symbol:

(ss) (ad) (g) (ad)

Let dz/dt be the rate of escape of NH_3 (g) from the surface of the crystal in molecules sec^{-1} cm^{-2}. As a first approximation, the back reactions (1b) and (1d) are neglected and reaction (1c) is assumed to be rate controlling, so that

$$\frac{dz}{dt} = k_c(NH_3{:}HClO_4)_{ad} = K_z \quad (2)$$

where k_c is the specific rate constant for reaction (1c) and where K_z is a combination constant. (The alternate assumption that reaction (1a) is rate-controlling will not affect the mathematical form of the decomposition pressure-time relationship (13) below.) Assume in this first approximation that the rate of escape of perchloric acid from the surface is negligible. Assume also that the time required to attain temperature equilibrium is negligible compared to the duration of the nucleation period. At time, t, after start of heating, the concentration of perchloric acid in the surface is

$$(HClO_4)_{ad} = z = K_z t \quad (3)$$

provided that no adsorbed $HClO_4$ or NH_3 is present prior to $t = 0$. A nucleus will be considered to be in existence when a certain number, j, of $HClO_4$ (ad) molecules have migrated to a potential nucleus site (i.e., surface discontinuity) and have decomposed to leave a surface hole. The mobility of the adsorbed perchloric acid could be the result of a surface lattice migration process of a type discussed by MacDonald.[10] For NH_4ClO_4 the migration process might be visualized as

$$\begin{array}{ccccccccc} ClO_4^- & & H^+ & & ClO_4^- & & H^+ & ClO_4^- & NH_4^+ \\ & & \rightarrow & & & \nearrow & & \rightarrow & \\ NH_4^+ & ClO_4^- & {}^+H & \boxed{NH_3} & & ClO_4^- & {}^+H & ClO_4^- & \end{array} \quad (4)$$

The formation of an empty space in the surface lattice caused by a decomposition reaction of j molecules of $HClO_4$ at a potential nucleus site

should loosen the lattice restraints on the immediately adjacent ions, thereby permitting them to enter decomposition reactions. (This situation is comparable to the calcium carbonate decomposition discussed by Langmuir.[11] The latter used the phase rule to show that the lattice vacancy left by the removal of a CO_2 group weakens the bonds by which adjacent groups are held.) The rate of nuclei formation per unit area of crystal is then

$$\frac{dn}{dt} = k_n\gamma z^j = k_n\gamma K_z^j t^j \tag{5}$$

where γ is the number of potential nucleus sites per unit area and k_n is the specific rate constant of the nucleation process.

It has been observed in many crystal decompositions that the radial growth rate (dr/dt) of a nucleus is constant under isothermal conditions and varies with temperature, T, according to the equation

$$B = dr/dt = B_0 \exp(-E/RT) \tag{6}$$

At the time, τ, the radius of a nucleus born at time, t, is

$$r = B(\tau - t) \tag{7}$$

Both τ and t are measured from the commencement of heating. The volume of a hemispherical nucleus is

$$V = (2/3)\pi B^3 (\tau - t)^3 \tag{8}$$

and the total volume V_n of all n nuclei existing at anytime τ before coalescence (i.e., before appreciable interference of decomposition zones occurs) is

$$V_n = \int_0^n (2/3)\pi B^3(\tau - t)^3 \, dn \tag{9}$$

where dn is given by Equation (5). Hence

$$V_n = \int_0^\tau (2/3)\pi B^3 k_n\gamma K_z^j t^j (\tau - t)^3 \, dt \tag{10}$$

Integration gives

$$V_n = \frac{4\pi B^3 k_n\gamma K_z^j}{(j+1)(j+2)(j+3)(j+4)} \tau^{j+4} \tag{11}$$

If it is assumed that perchloric acid decomposes by a bimolecular reaction at a potential nucleus site, $j = 2$, so that

$$V_n = (\pi B^3 k_n\gamma K_z^2/90)\tau^6 \tag{12}$$

In the absence of secondary reactions at time, t, the pressure, p, of decomposition products above the salt is proportional to V_n, so that

$$p = (C\pi B^3 k_n\gamma K_z^2/90)\tau^6 \tag{13}$$

where C is a constant of proportionality. Equation (13) is identical in form to the power expression, $p = kt^x$ (where $x = 6.2 \pm 0.5$) which Bircumshaw and Newman[2] found to hold for the acceleratory period at 220–275°C. Secondary reactions in the gaseous decomposition products which involve volume changes will not affect the experimental value of the exponent, x, provided that the final decomposition is attained in a time which is either very small or very large compared to the duration of the acceleratory period.

The above calculations suggest that some kind of bimolecular reaction is responsible for the formation of a nucleus but it is by no means certain that the reaction involves perchloric acid. An alternative assumption that a nucleus is formed by two holes (or even two charged particles) which migrate through the crystal lattice and coalesce at a discontinuity in the crystal would lead to a mathematical expression of the same form as Equation (13) (see Mott[8]).

The Maximum Rate Period

Once coalescence of the growing nuclei has occurred so that the surface is completely covered by a layer of residue, Equation (13) is no longer valid. At this time, the reaction interfaces no longer increase in area. Instead, the resulting single interface decreases in area as it progresses toward the center of the crystal. Let the shape of a given crystal at coalescence time, t_y, be approximated as a sphere of radius, r_y. The volume, V_y, of undecomposed crystal inside this sphere at time, t_y, is

$$V_y = (4/3)\pi r_y^3 \tag{14}$$

At the later time, t, the volume, V_t, of undecomposed crystal is

$$V_t = (4/3)\pi[r_y - B(t - t_y)]^3 \tag{15}$$

Differentiation gives

$$dV_t/dt = -4\pi B[r_y - B(t - t_y)]^2 \tag{16}$$

The rate of increase of decomposition product pressure dp/dt is proportional to the rate of volume decrease $-dV_t/dt$ and to Q the number of crystals assumed uniform in size and shape, so that

$$dp/dt = 4\pi QBG[r_y - B(t - t_y)]^2 \tag{17}$$

where G is a proportionality constant. The maximum rate occurs at the time, $t = t_y$, so that

$$(dp/dt)_y = 4\pi QBG\, r_y^2 \tag{18}$$

The number of crystals, Q, in a fixed initial weight, W, of uniform NH_4ClO_4 crystals (assumed spherical in shape) is

$$Q = \frac{3W}{4\pi r_0^3 \rho} \tag{19}$$

where r_0 is the initial crystal radius and ρ its density. Insertion of Equation (19) into (18) gives

$$(dp/dt)_y = 3\,\frac{WBG}{\rho}\,\frac{r_y^2}{r_0^3} \tag{20}$$

Let the difference between the initial radius of

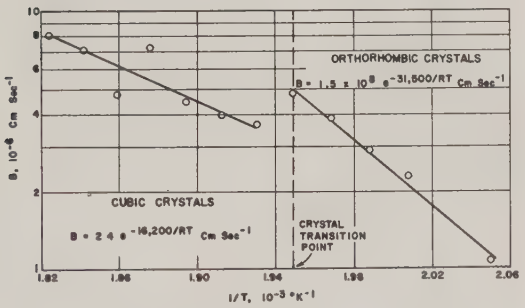
ORTHORHOMBIC CRYSTALS
B = 1.5 x 10^8 e^-31,500/RT Cm Sec^-1
CUBIC CRYSTALS
B = 2.4 e^-16,200/RT Cm Sec^-1
CRYSTAL TRANSITION POINT
B, 10^-4 Cm Sec^-1
1/T, 10^-3 °K^-1

FIG. 1. Arrhenius plot of the linear rate of decomposition of ammonium perchlorate as a function of temperature.

the crystal and the radius of the spherical reaction interface at coalescence be δ so that

$$r_y = r_0 - \delta \tag{21}$$

and

$$(dp/dt)_y \propto (r_0 - \delta)^2/r_0^3 \propto (r_0^2 - 2r_0\delta + \delta)^2/r_0^3 \tag{22}$$

For large crystals, δ is small compared to r_0 so that

$$(dp/dt)_y \propto 1/r_0 \tag{23}$$

Thus, the maximum rate for a given mass of large NH_4ClO_4 crystals should vary inversely as the initial crystal radius. Indeed, this is nearly the relationship observed by Bircumshaw and Newman[2] for crystals greater than 0.004 in. in diam. Below this size, the maximum rate was found to decrease with decrease in diameter. This results from the fact that coalescence occurs at greater percentages of decomposition for the smaller particles (i.e., δ is no longer small compared to r_0). Mampel[12] reached a similar conclusion about the effect of decreased particle size on the rate of solid decomposition.

For a given batch of uniform crystals, the point of inflection of the commonly observed sigmoid decomposition pressure-time curves correspond approximately to t_y, the time of coalescence of the nuclei on the surface of the crystal. At time, $t = t_y$ the decomposition rate, in terms of fraction of original crystal volume, V_0, is from Equation (16)

$$\left(\frac{dV_t/V_0}{dt}\right)_y = -3B\,\frac{r_y^2}{r_0^3} \tag{24}$$

But V_0 is proportional to p_f, the final decomposition pressure, so that Equation (24) becomes

$$\left(\frac{dp/p_f}{dt}\right)_y = 3B\,\frac{r_y^2}{r_0^3} \tag{25}$$

The ratio of the volume, V_y, of undecomposed crystal to the original volume, V_0, is at time, t_y,

$$\frac{V_y}{V_o} = \frac{r_y^3}{r_0^3} = \frac{p_f - p_y}{p_f} \tag{26}$$

The radius of the decomposition interface at time, t_y, is, therefore,

$$r_y = r_0\,(p_f - p_y)^{\frac{1}{3}}\, p_f^{-\frac{1}{3}} \tag{27}$$

The maximum rate of linear progression of the decomposition interface, $B = dr_y/dt$, at time, t_y, is

$$B = \frac{r_0(dp/dt)_y}{3p_f^{1/3}(p_f - p_y)^{2/3}} \text{ cm sec}^{-1} \tag{28}$$

where r_0 = initial crystal radius, cm; $(dp/dt)_y$ = slope at the point of inflection of sigmoid decomposition product pressure-time curve, mm Hg sec^{-1}; p_y = decomposition product pressure at point of inflection; mm Hg; p_f = final product pressure (assuming no change in volume of system during run), mm Hg. By means of Equation (28), experimental values of B (plotted in Figure 1 as $\log_{10} B$ versus $1/T$) were derived directly from the sigmoid p-t curves of the original Bircumshaw and Newman data[2] using their estimated mean value of $r_0 = 1.98 \times 10^{-2}$ cm. Below 513°K the linear decomposition rate of the intermosaic material of the orthorhombic NH_4ClO_4 crystal is given by

$$B_{NH_4ClO_4\ (\text{orthorhombic})} = 1.5 \times 10^8 \exp(-31{,}500/RT) \text{ cm sec}^{-1} \tag{29}$$

At 513°K, the crystal of NH_4ClO_4 assumes the cubic NaCl type lattice. Above this temperature, the linear decomposition rate of the intermosaic material of the cubic NH_4ClO_4 crystal is

$$B_{NH_4ClO_4\ (cubic)} = 2.4 \times 10^{1} \exp(-16{,}200/RT) \text{ cm sec}^{-1} \quad (30)$$

It is of interest to compare Equation (29) with an equation[7] recently estimated for the maximum linear rate of advance in vacuo of the decomposition interface between $CaCO_3$ and CaO

$$B_{CaCO_3:CaO} = 7.7 \times 10^{7} \exp(-37{,}600/RT) \text{ cm sec}^{-1} \quad (31)$$

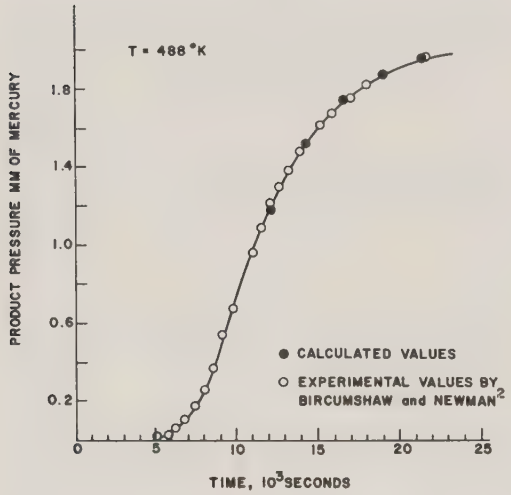

FIG. 2. Decomposition pressure vs. time for NH_4ClO_4 at 488°K.

It is also of interest to compare Equation (30) with the equation for the linear rate of vaporization of ammonium chloride obtained by an analysis[4] of the experimental data of Spingler.[13]

$$B_{NH_4Cl} = 1.2 \times 10^{2} \exp(-13{,}500/RT \text{ cm sec}^{-1} \quad (32)$$

The Deceleratory Period

It follows from the previous mathematical analysis that the equation of the deceleratory portion of the sigmoid $p - t$ curve is

$$\frac{p_f - p}{p_y} = \frac{[r_y - B(t - t_y)]^3}{r_0^3} \quad (33)$$

where r_y is given by Equation (27). Figures 2, 3, and 4 compare the deceleratory curves derived by Equation (33) with the experimental curves. At 215°C, the agreement is excellent but becomes progressively poor with increasing temperature. The discrepancy at higher temperatures may be the result of an increase in the vaporization rate of the salt without oxidation-reduction reactions in the gas phase or perhaps may be the result of an impedance or hindering effect of the layer of residue on the escape of gaseous products from the decomposition interface.

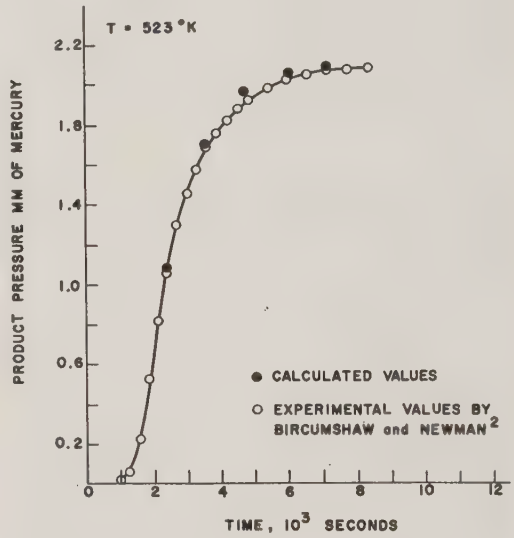

FIG. 3. Decomposition pressure vs. time for NH_4ClO_4 at 523°K.

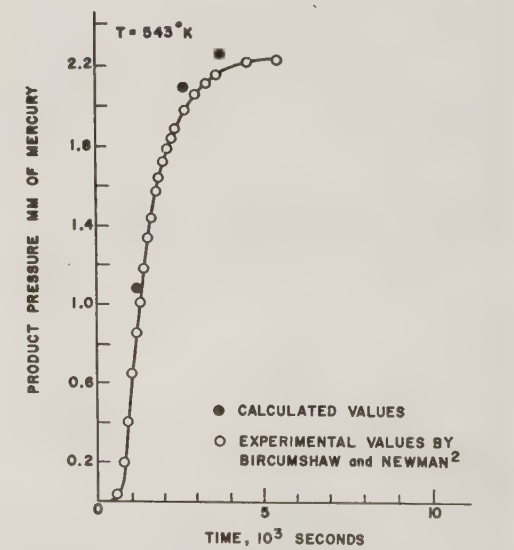

FIG. 4. Decomposition pressure vs. time for NH_4ClO_4 at 543°K.

The Thermodynamics of the Simple Dissociation Process

An enthalpy balance for the dissociation of orthorhombic ammonium perchlorate to gaseous ammonia and perchloric acid may be written as

$$NH_4ClO_4 \rightleftharpoons NH_3 + HClO_4 + \text{heat of reaction} \quad (34)$$

	NH_4ClO_4	NH_3	$HClO_4$	heat of reaction
State:	(ortho-rhombic crystal)	(gas)	(gas)	
$\Delta H_f^0(298^\circ K)$ kcal g-mole^{-1}	−69.4	−11.0	−2.3	$\Delta H = -56.0$
Reference	14	14	(Calculated)	(By Difference)

A value of 8.8 kcal g-mole^{-1} for the enthalpy of vaporization of anhydrous perchloric acid was estimated from vapor pressure data[15] by use of the Clausius-Clapeyron equation. This enthalpy of vaporization was added to the −11.1 kcal g-mole^{-1} heat of formation of $HClO_4$ (liq)[14] to obtain the estimated value ΔH_f^0 (298°K) [$HClO_4$ (gas)] $\simeq$ −2.3 kcal g-mole^{-1}. Reaction (34), as written, is endothermic to the extent of about 56 kcal g-mole^{-1}. This value is somewhat uncertain because the heat of aqueous solution of $HClO_4$ (liq) is not known accurately.[16] Since the endothermicity of the simple dissociation process (34) is much higher than the observed activation energies for the vaporization process, it follows that the latter must occur in stages rather than as a single step.

The Nature of the Residue

Garner and Hailes[17] have suggested that, in certain cases, solid decomposition might proceed preferentially along the boundaries of the mosaic blocks comprising a crystal. If the decomposition paths at 215 to 280°C travel exclusively through the strained intermosaic lattice in NH_4ClO_4 crystals and do not penetrate the interior of the mosaic blocks, the formation of a residue stable at these temperatures is understandable. The minimum size of the mosaic blocks in ammonium perchlorate may be estimated on the assumption that the thickness of the strained transition lattice is about equal to the side of a unit cell of the cubic lattice. If the residue consists mainly of the original mosaic blocks with the intermosaic material removed, it follows that

$$\frac{\text{Mass residue}}{\text{Mass original crystal}} = \left[\frac{D}{D+d}\right]^3 = 0.7 \quad (35)$$

where D is the side dimension of the mosaic block; d is the thickness of the intermosaic layer; 0.7 is the fraction of the original mass remaining after cessation of decomposition. Setting d equal to 7.64 Å, the side dimension of the unit cell in cubic NH_4ClO_4,[18] gives a minimum average value of about 62 Å for the side dimension of a mosaic block or about 69 Å for the spacing of successive intermosaic layers.

Transition-State Decomposition Rate Theory for Intermosaic Cubic NH_4ClO_4

Assume that the final stages of the mechanism of decomposition of the intermosaic material in the cubic form of ammonium perchlorate is

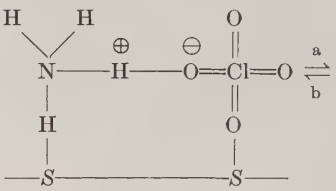

(36)

Reaction Intermediate

$$\underbrace{NH_3(\text{gas}) + HClO_4(\text{gas})}_{\downarrow} + S_2 \quad (37)$$

Irreversible Oxidation-Reduction

where S_2 is a dual adsorption site and where the reaction intermediate is a loose NH_3:$HClO_4$ complex which is physically adsorbed at the decomposition interface. Reactions (36a) and (36b) are similar to those assumed in a recently revised absolute rate treatment[5] of the ammonium chloride decomposition $NH_4Cl(s) \rightleftharpoons NH_{3(g)} + HCl_{(g)}$. A possibility exists, therefore, of analyzing the reverse reaction (36b) by a straightforward application of the absolute rate treatment formulated by Laidler, Glasstone, and Eyring[19] for a bimolecular surface reaction proceeding by a Langmuir-Hinshelwood mechanism. By analogy

with the treatment for NH_4Cl, the maximum exchange rate, reaction (36b), should be equal to the maximum forward rate of reaction (36a). Assuming the latter to be rate-controlling, the maximum decomposition rate of the intermosaic material of the cubic form of ammonium perchlorate should correspond to the equation

$$\frac{-d(NH_4ClO_4)}{dt} = [NH_3]_g[HCl]_g C_{S_2} \frac{kT}{h} \cdot \frac{F^*}{F_{NH_3(g)} F_{HClO_4(g)} f_{S_2}} e^{-E_0/RT} \text{ ion-pairs cm}^{-2} \text{ sec}^{-1} \quad (38)$$

where $-d(NH_4ClO_4)/dt$ = the decomposition rate per unit area of exposed surface of intermosaic material, ion-pairs cm^{-2} sec^{-1}; $[NH_3]_g$ = steady-state gas phase concentration of ammonia in contact with the reaction interface, molecules cm^{-3}; $[HClO_4]_g$ = steady-state gas phase concentration of perchloric acid in contact with the reaction interface, molecules cm^{-3}; C_{S_2} = concentration of bare dual adsorption sites, cm^{-2}; F^* = partition function of activated complex over all degrees of freedom except the vibrational mode included in kT/h; $F_{NH_3(g)}$ = partition function of ammonia per unit volume of gas phase; $F_{HClO_4(g)}$ = partition function of perchloric acid per unit volume of gas phase; f_{S_2} = partition function of a bare dual adsorption site; E_0 = activation energy of surface reaction, calories g-mole^{-1}; kT/h = Eyring frequency for passage over potential energy barrier, $sec.^{-1}$. By a procedure nearly identical to that used for ammonium chloride[5] Equation (38) may be simplified to

$$B_{NH_4ClO_4(cubic)} = \frac{1}{2}\left(\frac{M}{\rho N}\right)^{\frac{1}{3}} \frac{kT}{h} \frac{f^*(\text{trans})}{f(\nu_{NH_3}) f(\nu_{HClO_4})} \cdot \exp -(E_0 + E_{NH_3} + E_{HClO_4})/RT \quad (39)$$

where kT/h = Eyring transition-state frequency for passage over a potential energy barrier, sec^{-1}; M = formula weight of NH_4ClO_4, g g-mole^{-1}; ρ = density of NH_4ClO_4 (cubic) $\simeq$ 1.95, g cm^{-3}; N = Avogadro's number, molecules g-mole^{-1}; f^* (trans) = partition function for a one-dimensional translation motion of the center of gravity of the complex in the plane of the crystal surface. As an approximation f^* (trans) $\simeq$ 1; $f(\nu)$ = single mode vibrational partition function of the form $[1 - \exp(-h\nu/kT)]^{-1}$. As an approximation $f(\nu) \simeq kT/h$; ν_{NH_3}, ν_{HClO_4} = frequencies for translational oscillation of physically adsorbed ammonia and perchloric acid in the plane of the adsorbed layer at the decomposition interface, sec^{-1}; E_0 = activation energy for surface reaction, calories g-mole^{-1}; E_{NH_3} = energy of adsorption of ammonia, calories g-mole^{-1}; E_{HClO_4} = energy of adsorption of perchloric acid, calories g-mole^{-1}. Implicit in Equation (39) is the assumption that the rotational oscillation of physically adsorbed $HClO_4$ is nearly free gas-type rotation. The frequencies ν_{NH_3} and ν_{HClO_4} may be estimated in the manner of Hill[20] and Drenan and Hill[21] by use of the equation

$$\nu = (v_0/4ms^2)^{\frac{1}{2}} = 1.025 \times 10^{13} (V_0/MS^2)^{\frac{1}{2}} \text{ sec}^{-1} \quad (39)$$

where $\nu = \nu_x = \nu_y$ = translational oscillation frequency in the x or y directions in the plane of the physically adsorbed layer, sec^{-1}; v_0 = maximum potential energy barrier to translation in x or y direction, ergs; m = mass of adsorbed molecule, g; s = distance between potential minima along x or y axis of surface lattice (assumed simple cubic), cm; V_0 = same as v_0 except for unit, kcal g-mole^{-1}; M = molecular weight of adsorbed molecule, g g-mole^{-1}; S = same as s except for unit, Å. Hill[20] has estimated the potential barrier V_0 to be about 0.3 — 1.0 kcal g-mole. If $HClO_4$ is adsorbed preferentially on a NH_4^+ ion and NH_3 is adsorbed preferentially on a ClO_4^- ion, the distance, S, should be about equal to the 7.64 Å side dimension of the unit cell in cubic NH_4ClO_4. Thus, the estimated frequencies are

$$\nu_{NH_3} \simeq 1.8 \text{ to } 3.3 \times 10^{11} \text{ sec}^{-1} \quad (40)$$

$$\nu_{HClO_4} \simeq 0.7 \text{ to } 1.3 \times 10^{11} \text{ sec}^{-1} \quad (41)$$

As in the treatment for ammonium chloride

$$E_0 \simeq 2V_0 \simeq 600 \text{ to } 2000 \text{ calories g-mole}^{-1} \quad (42)$$

$$E_{NH_3} \simeq \Delta H_{cg\ NH_3} - RT_{cg} \simeq 6460 \text{ calories g-mole}^{-1} \quad (43)$$

$$E_{HClO_4} \simeq \Delta H_{cg\ HClO_4} - RT_{cg} \simeq 10{,}700 \text{ calories g-mole}^{-1} \quad (44)$$

where ΔH_{cg} signifies an enthalpy of sublimation measured at the temperature, T_{cg}. Therefore, the theoretical value of $B_{NH_4ClO_4(cubic)}$ at $T_{average}$ = 532°K is between

$$B_{NH_4ClO_4(cubic)} = 2.8 \times 10^1 \text{ Theory} \cdot \exp(-17{,}800/RT) \text{ cm sec}^{-1} \quad (45)$$

(V_0 assumed to be 0.3 kcal g-mole^{-1})

and

$$B_{NH_4ClO_4(cubic)} = 9.0 \times 10^1 \text{ Theory} \cdot \exp(-19{,}200/RT) \text{ cm sec}^{-1} \quad (46)$$

(V_0 assumed to be 1.0 kcal g-mole^{-1})

in fair agreement with the experimentally derived value

$$B_{NH_4ClO_4(cubic)} = 2.4 \times 10^1 \text{ Experiment} \cdot \exp(-16{,}200/RT) \text{ cm sec}^{-1} \quad (47)$$

Use of energies of liquefaction instead of energies of sublimation to approximate E_{NH_3} and E_{HClO_4} would have given an activation energy of 13,900 to 15,500 calories g-mole^{-1} also in fair agreement with the experimental value. In these calculations the enthalpies of sublimation and liquefaction of ammonia were taken from a compilation by the U. S. Bureau of Standards.[22] The enthalpy of fusion of perchloric acid was estimated to be about 2.5 kcal g-mole^{-1} by comparison with nitric, sulfuric, and phosphoric acid. The enthalpy of vaporization of perchloric acid was estimated above to be 8.8 kcal g-mole^{-1} from vapor pressure data at 16 and 39°C.

Transition-State Decomposition Rate Theory for Intermosaic Orthorhombic NH_4ClO_4

For the linear decomposition of the intermosaic material in orthorhombic NH_4ClO_4, the experimentally derived pre-exponential factor of 1.5×10^8 cm sec^{-1} is about the same as for sublimation of simple ionic crystals and for the decomposition of calcium carbonate.[7] In these cases, the chief statistical difference between the initial and activated states appears to be that rotation or nearly free rotation is possible only in the activated state. Accordingly, it will be assumed that the formation of the activated complex for the decomposition of intermosaic orthorhombic NH_4ClO_4 requires the attainment of an almost free rotational motion of the ClO_4^- ion at the decomposition interface. A reasonable estimate of the initial state torsional oscillation frequency of the ClO_4^- ion is about 7.5×10^{12} sec^{-1} corresponding to a characteristic temperature $\theta = h\nu/k = 360$°K. It will be assumed, in accordance with a suggestion by Bircumshaw and Newman,[1] that the ammonium ion is rotating almost freely in the initial state in both orthorhombic and cubic NH_4ClO_4. Apropos of this assumption, the neutron diffraction experiments of Levy and Peterson,[23] the infrared spectra studies of Plumb and Hornig,[24] and the Raman spectra studies of Couture-Mathieu and Mathieu[25] provide evidence that one-dimensional rotation of the NH_4^+ ion is possible in the ammonium halides (i.e., ND_4Br, ND_4I, NH_4I) possessing the NaCl-type structure. Moreover, the neutron diffraction experiments[23] provide evidence for appreciable rotatory oscillation of the NH_4^+ ion in ND_4Br. The fact that ClO_4^- is larger than either the Br^- or I^- ion makes nearly free rotation of NH_4^+ ion in crystalline NH_4ClO_4 a distinct possibility.

The attainment of the activated complex for decomposition probably also involves a translational motion of the ClO_4^- ion. In a manner analogous to that used for the escape velocity during sublimation,[6, 7] the activated state translational motion of the ClO_4^- ion is divided into three components. The partition function for one of these components is included in the kT/h factor of the Eyring formulation of transition state theory. The other two components are assumed to be normal-state translational lattice vibrations. It is further assumed that the translational lattice vibrations of the NH_4^+ ion remain unaltered during the formation of the activated state.

It is now possible to write an absolute rate expression for the pre-exponential linear decomposition rate factor of intermosaic orthorhombic NH_4ClO_4, identical in form to that used for sublimation of a non-linear molecule, namely

$$B_{0\ NH_4ClO_4\ (ortho)} = \left(\frac{M}{\rho N}\right)^{\frac{1}{3}} \frac{kT}{h} \frac{\frac{\pi^{\frac{1}{2}}}{\sigma}\left(\frac{8\pi^2 IkT}{h^2}\right)^{\frac{3}{2}}}{[1 - \exp(-\theta/T)]^{-4}} \quad (48)$$

cm sec^{-1}

where $\rho \simeq$ density of NH_4ClO_4 (orthorhombic) $\simeq 1.95$, g cm^{-3}; θ = characteristic temperature for lattice vibration frequency, assuming equal frequencies for translational and torsional oscillation $\simeq 350$, °K; $\sigma = 12$ = symmetry number of ClO_4^- ion; I = moment of inertia of ClO_4^- ion $= 1.57 \times 10^{-38}$, g cm^{-2}; T = average temperature = 501, °K. Insertion of the above numerical constants into Equation (48) yields

$$B_{0\ NH_4ClO_4\ (orthorhombic)} = 4 \times 10^7 \text{ cm sec}^{-1} \quad (49)$$

Theory

in reasonable agreement with the experimentally derived value of 1.5×10^8 cm sec^{-1}.

A theoretical calculation of the activation energy for the linear decomposition of intermosaic orthorhombic NH_4ClO_4 is not possible on the basis of present knowledge.

Acknowledgment

The authors are indebted to Mr. Richard D. Geckler and Dr. S. C. Burket of Aerojet-General Corporation and to Professor S. S. Penner of the California Institute of Technology for valuable criticism in connection with an early version of this paper. Sylvia Davison assisted in the calculations. The authors are also indebted to the British Ministry of Supply for an interim report containing the excellent original data of Bircumshaw and Newman. The help of Dr. Hoyt Anderson in correcting the final proofs is also acknowledged.

REFERENCES

1. Bircumshaw, L. L., and Newman, B. H.: Proc. Roy. Soc. (London), *A227*, 115–132, 228–241 (1954).
2. Bircumshaw, L. L., and Newman, B. H.: Interim Report, March, 1951.
3. Schultz, R. D., and Dekker, A. O.: Paper presented at the 122nd National Meeting, American Chemical Society, Atlantic City, New York, September, 1952.
4. Schultz, R. D., and Dekker, A. O.: *Fifth Symposium (International) on Combustion.* New York, Reinhold Publ. Corp., 1955.
5. Schultz, R. D., and Dekker, A. O.: J. Phys. Chem., *60*, 1095–1100 (1957).
6. Schultz, R. D., and Dekker, A. O.: J. Chem. Phys., *23*, 2133–8 (1955).
7. Schultz, R. D., and Dekker, A. O.: To be published.
8. Mott, N. F.: Proc. Roy. Soc. (London), *A172*, 325 (1939).
9. Topley, B., and Hume, J.: Proc. Roy. Soc. (London), *A120*, 211 (1929).
10. MacDonald, J. Y., Trans. Faraday Soc., *47*, 860–863 (1951).
11. Langmuir, I. J. Am. Chem. Soc., *38*, 2263–2267 (1916).
12. Mampel, K. L.: Z. Physik. Chem., *A187*, 43–57, 235–249 (1940)
13. Spingler, H.: Z. Physik. Chem., *B52*, 90–106 (1942).
14. National Bureau of Standards, Circular 500, 1952.
15. Mellor, J. W.: *Comprehensive Treatise on Inorganic and Theoretical Chemistry*, Vol. 2, p. 377. London, Longmans, Green and Co., (1946).
16. Goodeve, C. F., and Marsh, A. E. L.: J. Chem. Soc., *1816* (1937).
17. Garner, W. E., and Hailes, H. R.: Proc. Roy. Soc. (London), *A139*, 576–595 (1933).
18. Hermann, K., and Illge, W.: Z. Krist, *75*, 41–66 (1931).
19. Laidler, K. J.: *Catalysis*, Vol. I, Part 1, 195–243, particularly pp. 214–217. New York, Reinhold Publ. Corp., 1954.
20. Hill, T. L.: J. Chem. Phys., *16*, 181–189 (1948).
21. Drenan, J. W., and Hill, T. L.: J. Chem. Phys., *17*, 775–781 (1949).
22. U. S. Bureau of Standards, Circular 500, 1952.
23. Levy, H. A., and Peterson, S. W.: J. Chem. Phys., *21*, 366 (1953); J. Am. Chem. Soc., *75*, 1536–1542 (1953).
24. Plumb, R. C., and Hornig, D. F.: J. Chem. Phys., *21*, 366–367 and 1113 (1953).
25. Couture-Mathieu, L., and Mathieu, J. P.: J. Chem. Phys., *49*, 226 (1952).

81

SOME DEVELOPMENTS IN THE THEORY OF THERMAL EXPLOSIONS

By G. B. COOK

1. Introduction

The decomposition of an explosive substance is accompanied by the liberation of energy as heat and it may be that the rate of liberation of heat by chemical reaction exceeds the rate of loss of heat by radiation, convection or conduction into cooler surroundings. If this is the case, the chemical reaction may accelerate to a great rate and a thermal explosion will develop. Such explosions depend on the thermal properties of the system and the physical constants determining the chemical reaction rate as well as the initial state and geometry of the system and its boundary conditions. The field of problems under examination, therefore, is one in which energy is supplied by some mechanism, such as a constant temperature bath or an external source of radiation, to an explosive which is assumed to undergo decomposition with the liberation of heat according to some definite rule. In fact, a classical Arrhenius heat generation term has been taken. The heat conduction equation is set up, including

this heat generation term, in the appropriate coordinate system and with the appropriate initial and boundary conditions; it is desired to find the conditions under which explosion will be initiated. Analytical methods of solution are possible, in principle, if the heat generation term is large compared with the heat conduction term and *vice versa*, but, in most cases of practical interest, heat conduction and heat generation become at some stage of a comparable order of magnitude, the latter becoming progressively more important until it is the dominant factor. In these cases, analytical methods of solution appear impossible and numerical integration procedures have to be employed. Such numerical procedures are quite feasible when the services of a high-speed digital computer are available. The object of solving such problems is to correlate ignition time with the various physical parameters of the system and, in particular, to determine the critical conditions under which explosion just, and only just, manages to occur. In addition, a comparison of the behavior of different explosives under similar physical conditions is possible and a comparison of the effect of various possible types of energy input can be made. In short, an attempt at a general theory of explosive sensitivity is possible.

In this paper, three problems are considered, one of which is discussed in detail. In this problem, a sample of explosive is placed in contact with a constant temperature bath and the time to explosion is calculated. No critical parameters are involved in this problem, but, for a given explosive, the ignition time can be correlated with the two physical parameters of the system, namely, the temperature of the bath and the initial temperature of the sample. The remaining two problems are rather more briefly mentioned. In the first of these, a time-dependent flux of thermal radiation is assumed to fall on a steel plate covering a mass of explosive. The radiation is partly absorbed at the steel surface and heat is conducted through the steel and hence into the explosive. Critical parameters are involved in this problem; for example, for a given total absorbed radiation, there exists a critical thickness of steel plate such that, if it is exceeded, explosion will not be initiated. In the remaining problem, the initiation of explosion by spherical hot spots of grit is considered. The model taken is a small hot sphere of chemically inert material embedded in a mass of cold explosive. Critical parameters are again involved; for a given hot spot size, there exists a critical hot spot temperature such that, if it is exceeded, explosion will be initiated. Conversely, for a given hot spot temperature, there exists a critical size.

2. The Initiation of Explosion by a Thermal Bath

In this problem, one face of a slab of solid explosive is assumed to be placed in contact with a constant temperature bath, the dimensions of the slab being such that a one-dimensional semi-infinite approximation is sufficient. In actual practice, this is a reasonable approximation for quite small samples since explosion commences very close to the surface of the sample. If it is assumed that the thermal constants of the explosive are independent of temperature and that the chemical decomposition is unimolecular, the governing equation may be written

$$\rho c \frac{\partial T}{\partial t} = k \frac{\partial^2 T}{\partial x^2} + \rho Q Z \exp(-E/RT) \qquad (1)$$

under the initial condition

$$T = T_1 ; \qquad x \geq 0, t = 0 \qquad (2)$$

and the boundary conditions

$$T = T_0 ; \qquad x = 0, t > 0 \qquad (3)$$

$$T \to T_1 ; \qquad x \to \infty, t > 0 \qquad (4)$$

where T_0 denotes the bath temperature and T_1 the initial (uniform) temperature of the sample, T being the temperature in degrees absolute. In Equation (1), ρ, c and k denote the density, specific heat and thermal conductivity of the explosive respectively and E, Z and Q denote the activation energy, the frequency factor and the heat liberated per gram of explosive respectively. As far as the author is aware, only one solution of this equation has been obtained previously. It is reported in the Proceedings of a Symposium[2] in a paper by Seeger.

Certain physical assumptions have to be made in order to make the problem reasonably tractable. It was mentioned above that k, ρ and c are assumed to be independent of temperature; this approximation is mathematically very convenient but it should be noted that data on these physical constants are very scarce. The use of a simple Arrhenius term to describe the heat generation is undoubtedly an over-simplification but probably at temperatures where heat evolution is important, it is a reasonable approximation. The way in which this heat generation term is written

also neglects the material consumed by chemical reaction but this is not a serious approximation since most of the reaction occurs in a comparatively short period of time close to the time at which explosion occurs. The effects arising from the liquefaction of the explosive are ignored.

It is convenient at this stage to introduce the dimensionless variables ξ, τ and θ defined by

$$\xi = 10^{-7}\left\{\frac{\rho RQZ}{kE}\right\}^{\frac{1}{2}} x = \alpha x$$

$$\tau = 10^{-14}\frac{RQZ}{cE}\, t = \beta t \qquad (5)$$

$$\theta = \frac{RT}{E} = \delta T$$

so that Equations (1), (2), (3) and (4) may be written

$$\frac{\partial\theta}{\partial\tau} = \frac{\partial^2\theta}{\partial\xi^2} + 10^{14}\exp(-1/\theta) \qquad (1')$$

under the initial condition

$$\theta = \theta_1\,; \qquad \xi \geq 0,\ \tau = 0 \qquad (2')$$

and the boundary conditions

$$\theta = \theta_0\,; \qquad \xi = 0,\ \tau > 0 \qquad (3')$$

$$\theta \to \theta_1\,; \qquad \xi \to \infty,\ \tau > 0. \qquad (4')$$

In order to illustrate the transformations in Equation (5), the constants β and δ are given in Table 1 for several explosives. The data for Q, Z and E are taken from Rideal and Robertson[1] and, for all explosives, it has been assumed that

$$c = 0.35 \text{ cal/g(°C)}$$

$$k = 6 \times 10^{-4} \text{ cal/cm sec(°C)}$$

On account of the uncertainty in the physical data, these transformation constants may not be very accurate and, while the solutions of (1′) may be satisfactory, the corresponding physical solutions may indicate an order of magnitude only.

Equation (1′) was replaced by finite differences and a step-by-step integration in τ was carried out using the high-speed Ferranti Mark I* computer, AMOS, in operation at the Armament Research and Development Establishment. This aspect of the calculation will be referred to more fully in the Appendix. The integration was continued until a sharp maximum appeared near $\xi = 0$ in the temperature distribution in the explosive. When this stage was reached, it was assumed that explosion had been initiated and τ has the value τ_e, say. In all, some 30 solutions of Equation (1′) were obtained for various values of θ_0 and θ_1.

The results obtained may be expressed empirically as follows. For a fixed θ_1, (i.e., for a fixed initial temperature)

$$\log \tau_e = A/\theta_0 + B \qquad (6)$$

where A and B are constants and for a fixed θ_0 (i.e., for a fixed bath temperature)

$$\tau_e = -\,|\,C\,|\log\theta_1 + D \qquad (7)$$

where C and D are constants. More generally, Equation (7) may be regarded as holding for an arbitrary θ_0, C and D now being functions of θ_0. The dependence of C and D on θ_0 was found to be

$$\log|\,C\,| = A_1/\theta_0 + B_1 \qquad (8)$$

$$\log D = A_2/\theta_0 + B_2 \qquad (9)$$

where A_1, A_2, B_1 and B_2 are constants which

Table 1

	Tetryl	PETN	RDX
β	0.713	17800	3250
$10^4\delta$	0.517	0.423	0.418

were determined numerically. These three empirical relationships in Equations (7), (8) and (9) together with the data of Table 1 are sufficient to determine t_e given T_0 and T_1. An example will make the procedure clear: consider a slab of Tetryl initially at 15°C placed in contact with a bath at 225°C. We have

$$T_0 = 498°\text{K} \quad \text{and} \quad T_1 = 288°\text{K}$$

Using Table 1, it will be found that

$$\theta_0 = 0.0257 \quad \text{and} \quad \theta_1 = 0.0149$$

Using this value of θ_0 in Equations (8) and (9), the values of $|\,C\,|$ and D may be determined. These are used in Equation (7) with the value of θ_1 to give

$$\tau_e = 38$$

and hence from Table 1,

$$t_e = 53.3 \text{ sec}$$

The working just given may be repeated for other explosives for which the transformation constants are listed in Table 1 and a comparison of the behavior of the explosives under similar

physical conditions made. In Table 2, the three explosives are shown in order of increasing ignition time at $T_0 = 225°C$, 250°C and 300°C, T_1 having been fixed at 15°C. The change of order between 250°C and 300°C should be noted. Because of the inaccuracy of the transformation constants given in Table 1, the orders given in Table 2 may be incorrect. However, if explosives existed for which these constants were accurate and if values of t_e (for fixed T_0 and T_1) are used to compare "thermal sensitivities," then it follows that, according to the present model, the order of sensitivity is not the same for all temperatures. It should finally be pointed out that the nondimensional solutions have a permanent significance and may be translated into more accurate physical solutions as more reliable data become available.

TABLE 2

225°C	250°C	300°C
PETN	PETN	PETN
Tetryl	Tetryl	RDX
RDX	RDX	Tetryl

3. The Initiation of Explosion by High Intensity Thermal Radiation

In this problem, a one-dimensional semi-infinite model is again taken. A time-dependent flux of thermal radiation of the form

$$\Phi(t) = At \exp(-\alpha t) \tag{10}$$

is assumed to fall on a steel plate of thickness d covering a mass of explosive. The radiation is partly absorbed at the steel surface; heat is conducted through the steel and hence into the explosive which again is assumed to undergo unimolecular chemical reaction with the liberation of heat according to the classic Arrhenius formula. The theoretical procedure consists of setting up heat conduction equations to describe heat flow in the steel and in the explosive together with the appropriate boundary conditions at the surface of the steel plate and at the steel/explosive interface. If x denotes the distance measured inwards from the surface of the steel plate, the required equations are

$$\rho_1 c_1 \frac{\partial T_1}{\partial t} = k_1 \frac{\partial^2 T_1}{\partial x^2} \qquad 0 < x < d$$

$$\rho_2 c_2 \frac{\partial T_2}{\partial t} = k_2 \frac{\partial^2 T_2}{\partial x^2} + \rho_2 Q Z \exp(-E/RT_2) \qquad x > d$$

under the initial conditions

$$t = 0; \qquad T_1 = T_2 = T_0$$

and the boundary conditions

$$x = d; \qquad T_1 = T_2$$

$$x = d; \qquad k_1 \frac{\partial T_1}{\partial x} = k_2 \frac{\partial T_2}{\partial x}$$

$$x \to \infty; \qquad T_2 \to T_0$$

$$x = 0; \qquad -k_1 \frac{\partial T_1}{\partial x} = F$$

where suffixes "1" and "2" refer to steel and explosive respectively. The notation employed is the same as that given in Section 2 except that here T_0 refers to the initial (uniform) temperature of the system. F denotes the resultant flux at $x = 0$ and will have the form

$$F = Bte^{-\alpha t} - H \tag{11}$$

The first term in Equation (11) represents the incident flux in Equation (10) modified by some absorption coefficient and the second term represents an emitted flux due to radiation and convection. In practice, H has been set equal to zero since detailed examination shows that the total emitted flux is small in comparison with the total absorbed flux.

The above system of equations presents many more difficulties than the system involved in the thermal bath theory. In the first place, the system cannot be completely nondimensionalized and, second, the numerical integration and organization for the computer is rather more complicated since two media with different thermal properties are involved. In addition, the ignition time, t_e, is a function of four physical parameters, namely, T_0, B, α and d. It is also important to consider the parameter, S, the total absorbed radiation given by

$$S = \int_0^\infty Bte^{-\alpha t}\, dt = B/\alpha^2 \tag{12}$$

Detailed results will not be given here but the following is a summary of the physical conclusions which may be drawn from the results which have been obtained. (a) If T_0, B and α are fixed (i.e., for a given initial temperature and for a given radiation pulse), there exists a critical value of d, equal to d^*, say, such that if $d > d^*$, explosion will not occur. Conversely for a given T_0 and d, there exists a critical value of S, equal to S^*, say, such that if $S < S^*$, explosion will

not occur. (b) Consider two radiation flashes

$$\Phi_1(t) = At \exp(-\alpha_1 t) \quad \text{and} \quad \Phi_2(t) = At \exp(-\alpha_2 t)$$

such that

$$S_1 = S_2$$

i.e., the two flashes have different flux-time relationships but the total absorbed radiation is the same in both cases. Then, for a fixed T_0, to within one or two per cent, the critical value of d in each case is the same. For values of d rather less than this common critical value, the two ignition times are quite different but the curves showing the variation of ignition time with steel thickness tend to a common asymptote $d = d^*$. Hence, in approaching the critical thickness, where the ignition time is large compared with the effective duration of the flash, the detailed shape of the flash is unimportant; the important quantity is the total energy absorbed. If d is rather less than d^*, the ignition time is of the same order of magnitude as the effective duration of the flash and the detailed shape of the flash is important. (c) The critical steel thicknesses may be determined for a range of total absorbed energies and an empirical relationship derived. In principle, this could be done for several explosives and an order of sensitivity for thermal radiation constructed by comparing the critical thicknesses of steel required to prevent initiation of explosion by a given total absorbed radiation.

4. The Initiation of Explosion by Hot Spots of Grit

In this problem, a small hot sphere of chemically inert material of radius, a, and uniform temperature T_0 is supposed to be embedded at time $t = 0$ in a mass of cold explosive at uniform temperature T_1. The governing equations may be set up in much the same way as those for the problem discussed in Section 3 except that spherical polar coordinates are involved and the initial and boundary conditions are somewhat different. A scheme for the numerical integration of the equations has been worked out and has been organized for the computer, but, at the time of writing, no results of interest have been obtained. It is to be expected, however, that critical sizes and temperatures of hot spot will appear. An approximate treatment of *explosive* hot spots has been given by Rideal and Robertson,[1] and critical radii and temperatures estimated. The full nonsteady heat conduction equation for explosive hot spots has been solved on the Aiken computer and three solutions are reported in the Proceedings of a Symposium.[2]

Appendix

Three different finite difference procedures were employed in the numerical integration of Equation (1′) appearing in Section 2. The first of these is essentially the well-known Schmidt method and has been found to be the most satisfactory. The disadvantage of the Schmidt method is that for a given spatial interval, $\Delta\xi$, the size of interval in τ is limited by the relation

$$(\Delta\xi)^2 = 2(\Delta\tau)$$

On the other hand, the essential simplicity of the finite difference equation tends to compensate for this limitation in interval size. The second method used is an adaptation of one recently suggested by Du Fort and Frankel.[3] In this method, there is no such definite limitation on interval size but the finite difference equation is rather more involved and the organization of the method for an electronic computer is considerably more complicated (although quite feasible). The third method depends upon the knowledge of an analytical solution of the same problem for a chemically inert medium (where there is no heat generation). The method appeared to be very accurate but rather slow to use. All the results for the thermal bath problem of Section 2 were obtained by using the Schmidt approximation and two or three of the solutions were extensively checked, on the one hand, by varying the interval size in the Schmidt method and, on the other, by employing the other two approximations and also varying the interval sizes. It was estimated that the nondimensional solutions of Equation (1′) were accurate to within one or two per cent.

The Ferranti Mark I* computer at Armament Research and Development Establishment is characterized by a high-speed electronic store of moderate capacity (832 words of 20 binary digits each) and an auxiliary magnetic store of very large capacity (32,768 words of 20 digits each). The principal difficulty in programming a calculation of the present type is in obtaining an efficient method of organization, in particular, in making the best use of the high-speed store. The problem discussed in Section 2 may be regarded as one of a class of problems for a one-dimensional, semi-infinite medium for which the boundary condition at infinity is $\partial T/\partial x \longrightarrow 0$ together with a specified boundary condition at $x = 0$. A

general approach to such a class of problems is possible: much of the programming can be done once and for all, different problems requiring only special routines (corresponding effectively to the particular boundary condition involved). Similarly, the problem in Section 3 may be regarded as one of a class of problems for a semi-infinite composite solid.

REFERENCES

1. Rideal, E. K., and Robertson, A. J. B.: Proc. Roy. Soc., *A195*, 135 (1948).
2. Proceedings of a Symposium on Large-Scale Digital Calculating Machinery, pp. 157–168. Harvard University Press, Cambridge, Mass., 1948.
3. Du Fort, E. C., and Frankel, S. P.: MTAC VII, 135 (1953).

82

EFFECT OF THE CHARGE DIAMETER ON THE VELOCITY OF DETONATION WAVES IN GAS MIXTURES

By N. MANSON and H. GUÉNOCHE

Introduction

(1) Zeldovitch[1] has analyzed the possible structure of a plane detonation wave, taking into account energy losses that may occur (heat lost to the walls, friction). He concludes that the velocity, D, of the wave must be a decreasing function of the charge radius, R.

On the basis of completely different hypotheses, Jones,[2] on the one hand, and Eyring, Powel, Duffey and Parlin[3] on the other, reached a similar conclusion for solid explosives. Jones attributes the loss of energy to the lateral expansion of the gases in the wave, the walls which confine the charge being ruptured by the shock wave. Eyring and his associates consider the curvature of the wave, which is a function of the charge diameter, to be responsible for changes in the propagation velocity. This theory has been adopted by Wood and Kirkwood.[4]

(2) As regards the Zeldovitch theory, it should be noted that its author makes the assumption that the fundamental equations of hydrodynamics are applicable within the detonation wave, considered as a shock wave followed by a reaction zone. The use of these equations, which take into account heat lost to the walls and friction against the walls by the gas within the reaction zone, is justified *a posteriori* by numerical calculations. These calculations show, for instance, that the wave thickness, e, measured as the distance between the shock wave front and the Chapman-Jouguet plane, would be of the order of $3R$ when D_{th}-D/D_{th} is of the order of 5 per cent (see Zeldovitch and Kompaneez[5]).

However, under these conditions, for $R = 1$ cm and $D = 3.10^5$ cm/sec, the time during which the gas is in the reaction zone is $\tau \cong 10^{-5}$ sec. Moreover, these gases are in a state of reaction. Accordingly, there is some question as to whether we have any right to make such calculations, attributing the usual numerical values to the quantities involved (frictional coefficient, ratio, γ, of the specific heats), or whether we can call upon hypotheses such as Reynolds' analogy.

Eyring, Powel, Duffey and Parlin followed by Wood and Kirkwood, describe a nonplane wave for which certain characteristic terms become negligible as the calculations proceed. In this way they obtain "corrected" equations for plane waves which take into account wave curvature and thickness. We feel that these approximations are too difficult to evaluate and too numerous to judge the validity of their theory.

As for the Jones' theory, it does not apply to gas mixtures as the relation between D and R is independent of the resistance of the tube walls.

(3) In interpreting the effect of R on D, the above theories introduce another characteristic: the time, τ, or the wave thickness, e, which are equivalent. However, this parameter does not appear to be absolutely necessary for the relation between D and R, at least in the case of gas mixtures.

If we assume that the chemical reaction is in-

hibited, or at least profoundly modified, in a layer of gas of thickness, ϵ, adjacent to the walls,[a] the reaction is complete only in a cross section of radius $R - \epsilon$. When ϵ tends toward R, the reaction becomes such that the detonation wave can no longer be maintained and it ceases to propagate. Thus, at the limit, the parameter 2ϵ can be considered as the limiting diameter $2R_l$. However, this latter value has been measured only for solid explosives (see, for instance, Taylor[6]). What of experimental results for gas mixtures?

The experiments in the literature rarely are useful for defining the influence of R on D, because in most cases the accuracy of the measured values of D do not exceed 4 to 5 per cent. The first systematic investigation of the problem is that of Kistiakowsky, Knight and Malin,[7] working with C_2N_2-O_2 and C_2H_2-O_2 mixtures in tubes which measured $2R > 12$ mm. Their chief objective was to obtain values of D_{th} for a charge of infinite diameter, to calculate certain energies of dissociation. We also studied[8] the effect of R on the detonation wave velocity, but we used C_2H_2-O_2 and C_3H_8-O_2 mixtures with tube diameters ranging from 0.9 to 24 mm.

The extent and shape of the curve representing changes in the function $D = f(R)$ depend on the nature and composition of the mixture. Usually, the change is very small for stoichiometric mixtures of oxygen and combustible (at atmospheric pressure, room temperature). The change becomes increasingly significant as we approach the detonation limits. For instance Table 1 gives values obtained for $C_2H_2 + aO_2$ mixtures.

The relation D^*/D varies less for $C_3H_8 + aO_2$, but it is different from 1 for the stoichiometric mixture ($a = 5$). For mixtures close to stoichiometric, there is a proportionality relation between D and $1/R$.[b]

However, as Kistiakowsky, Knight and Malin have noted, this is not a general law, and in a region where R^*/R varies more extensively, the curve $D^*/D = f(R^*/R)$ would have the shape shown in Figure 1 as for a $C_2H_2 + \frac{1}{2}O_2$ mixture very different from stoichiometric.

We were not able to establish experimentally what happens to the curve for high values of R^*/R. If we assume that there is a limiting diameter $2R_l$ (diameter for which the detonation wave no longer propagates), the curve should terminate at a point, L, of the abscissa R^*/R_l, or tend asymptotically to the straightline which equation is $R^*/R = R^*/R_l$. The fact that this has not been observed so far can be explained as follows:

(a) Mixtures with oxygen as the oxidant which do not differ appreciably from the stoichiometric may have a very small limiting diameter ($< \frac{1}{10}$ mm).

TABLE 1.

a	0.5	2.5	4	12.3
$2R^*$	11.5	11.5	11.5	100
$2R$	1.1	0.9	1.3	12
D	0.92	1	0.99	0.97
D^*				
References	8			7

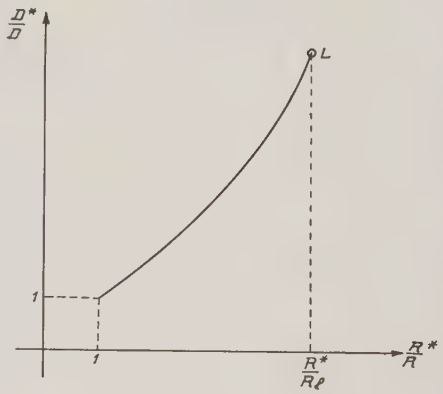

FIG. 1. Variation of $\frac{D^*}{D}$ vs $\frac{R^*}{R}$ as observed with $C_2H_2 + \frac{1}{2}O_2$ mixture.

(b) Mixtures with air as oxidant are not actinic enough to be recorded.

However, it does appear possible to learn something about the existence of $2R_l$ from detonation limit measurements. To determine the lower and upper limits of detonation, C_I and C_S, means that we are really determining the limiting diameter for mixtures of concentration C_I and C_S. The results of Kogarko and Zeldovitch[9] show that for H_2-air mixtures, C_I drops from 19.6 per cent to 15 per cent, and that C_S increases from 58.8 per cent to 63.5 per cent when the tube diameter goes from 10-20 mm to 305 mm. Thus, for mixtures with 19.6 and 58.8 per cent H_2, the limiting diameter would be about 10-20 mm, whereas it would be about 300 mm for mixtures

[a] Function of the nature, composition, initial pressure and temperature of the mixture; even of the surface of the charge wrapper and of its radius, R.

[b] As a matter of convenience, we have written the relation as: $D^*/D = 1 + \alpha(R^*/R - 1)$.

with 15 per cent and 63.5 per cent. Similarly, experiments by Rivin and Sokolik[10] on the effect of the initial pressure of the mixture on the limits indicate that R_l will increase as the pressure decreases.[c]

Assuming the existence of a limiting diameter $2R_l$, an attempt was made to modify the hydrodynamic theory of shock and combustion waves by introducing correction factors that would take into account the effect of the charge radius, R, on the detonation wave velocity, D.

The following calculations are limited to waves in gas mixtures, as calculations for solid explosives require additional assumptions as to the thermodynamic parameters of the detonation gases.

Modified Hydrodynamic Theory of Detonation Waves

(1) If we assume that incomplete release of the heat of reaction within the detonation wave is

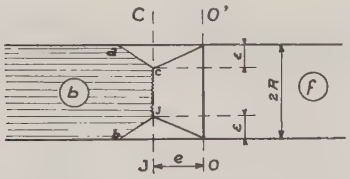

FIG. 2. Model of detonation wave (wall effect included).

due to the fact that complete reaction is possible only in gases located at a certain distance, ϵ, from the walls, without explicitly describing the details of the reaction zone and thus retaining the main results and the hypotheses of the classic hydrodynamic theory, we can change this theory so as to introduce correction factors that are functions of the charge radius R.[13]

The above hypothesis leads us to divide the gases behind the shock wave OO′ (Fig. 2) into two fractions: one in the central part of the reaction zone which has an area of $\pi\ (R - \epsilon)^2$ and where the chemical reaction is normal; the other ("primed") in the section of thickness, ϵ, adjacent to the charge walls where the reaction is quite different and may even be completely inhibited.

The fraction, λ, of the burned gas mass which has traversed the central part of the reaction zone is defined by the ratio of its area to the area of the charge.

$$\lambda = \frac{\pi(R - \epsilon)^2}{\pi R^2} = \left(1 - \frac{\epsilon}{R}\right)^2 \tag{1}$$

If we consider only the average stage of the gases in each section of the charge, we still can write the fundamental equations of the hydrodynamic theory of shock and combustion waves in their classic form:

$$\rho_f u_f = \rho_b u_b \tag{2a}$$

$$p_f + \rho_f u_f^2 = p_b + \rho_b u_b^2 \tag{2b}$$

$$\tfrac{1}{2}u_f^2 + H_f = \tfrac{1}{2}u_b^2 + H_b \tag{2c}$$

between the OO′ surface (wave front) and the CJ surface (Chapman-Jouguet plane which retains its usual meaning and properties throughout the entire section, except in the region of thickness, ϵ).[d]

The fact that the reaction is incomplete, or totally inhibited in one part of the wave, is introduced by stating the enthalpy difference $(H_b - H_f)$. If L_p is the heat of reaction and $(\Delta H_b)_{T_f}^{T_b}$ is the change between T_f and T_b of the enthalpy of the burned gas emitted by the central part of the wave, and L'_p and $(\Delta H'_b)_{T_f}^{T_b}$ are the corresponding parameters for the burned gas from the periphery of the wave:

$$H_b - H_f = \lambda[(\Delta H_b)_{T_f}^{T_b} - L_p] + (1 - \lambda)[(\Delta H'_b)_{T_f}^{T_b} - L'_p] \tag{3}$$

Taking into account the perfect gas law

$$p = NRT\rho \tag{4}$$

we arrive at the expression of the Rankine-Hugoniot curve

$$\frac{1}{2}(p_b - p_f)\left(\frac{1}{\rho_b} - \frac{1}{\rho_f}\right) + \lambda L_p + (1 - \lambda)L'_p = \lambda(\Delta H_b)_{T_f}^{T_b} + (1 - \lambda)(\Delta H'_b)_{T_f}^{T_b} \tag{5}$$

which is similar to that obtained when λ rep-

[c] As far as we know, the effect of the nature of the walls on these limits has not been studied. Tests by us[8] to determine the effect of this factor on the wave velocity D have confirmed the conclusions of Berthelot and Vieille[11] and of Laffitte[12] that the nature of the walls does not affect D. However, as our mixtures were close to stoichiometric, it would be interesting to repeat these tests with other mixtures before drawing any definite conclusion.

[d] Strictly speaking, the average Chapman-Jouguet plane, CJ, shifts farther and farther behind cj as ϵ increases with respect to R, because the surface where $u_b = a_b$ must follow the outline ac, cj, jb.

resents the degree of progress of the reaction (For bibliography, see Lewis and von Elbe[14]).

To plot this R-H curve and establish the average state of the gases at the CJ surface by the condition $u_b = a_b$, we must know: (a) the heat, L'_p, liberated by the incomplete reaction; (b) the corresponding composition of the burned gas; (c) the thickness, ϵ.

(2) With respect to L'_p and the composition of the gas which we need in order to calculate $(\Delta H'_b)_{Tf}^{Tb}$, very simple hypotheses are possible only for mixtures such as H_2/air, H_2/O_2, CO/air, CO/O_2.

We can, for instance, assume that $L'_p = 0$ and consider $(\Delta H'_b)_{Tf}^{Tb}$ as identical with $(\Delta H_b)_{Tf}^{Tb}$, since the components of the unburned gas (O_2, N_2, H_2, or CO) are the same as those of the burned gas.[e] As against that, for mixtures of hydrocarbons with oxygen or air, such calculations appear impossible unless we make certain assumptions which might ultimately obscure the consequences of the main hypothesis.

It seemed preferable to base our calculations on the Chapman-Jouguet method which leads to an approximate relation between the wave velocity, D, and the heat of reaction L_p (see, for instance, Jouguet[15]).

Equation (5) becomes:

$$\frac{1}{2} NRT_f \left[\frac{p_b}{p_f} - 1\right]\left[1 + \frac{\rho_f}{\rho_b}\right] + \lambda L_p + (1 - \lambda) L'_p = \frac{\gamma NRT_f}{\gamma - 1}\left[\frac{p_b \rho_f}{p_f \rho_b} - 1\right] \tag{6}$$

and

$$D_{th} = \sqrt{2(\gamma^2 - 1)L_p} \tag{7}$$

with

$$D_l = \sqrt{2(\gamma^2 - 1)L'_p} \tag{8}$$

leads to

$$D = D_{th} \cdot \sqrt{\left(1 - \frac{\epsilon}{R}\right)^2 + \left[1 + \left(1 - \frac{\epsilon}{R}\right)^2\right]\left(\frac{D_l}{D_{th}}\right)^2} \tag{9}$$

(3) According to this equation, D_l is the wave velocity when ϵ tends toward R, i.e., when the charge diameter becomes equal to the limiting diameter $2R_l$. Although, in view of the above approximations, the limiting velocity cannot be defined by Equation (8), it may be noted that the limiting value ϵ_l of ϵ is close to R_l. More especially, we may assume that ϵ can be expressed as $\epsilon = R_l\, f(R_l/R)$ where R_l would be a function of the nature, composition, pressure and temperature of the mixture, and of the state of the walls. The function $f(R_l/R)$ would be such that for $R \to R_l$, we would have $f(R_l/R) \to 1$, for instance, $f(R_l/R) = R_l/R$.

However, here again, so as not to mask the consequences of the main hypothesis, we will restrict our discussion to the case where $R \gg R_l$, for which it would appear that the error involved in setting ϵ equal to R_l cannot be very great.

Given the two conditions that $R \gg R_l$ and $\epsilon \cong R_l$, Equation (9) can be written as:

$$D \cong D_{th}\left(1 - \frac{R_l}{R}\right) \tag{10}$$

or, as it results from the calculations in the appendix (H_2-air mixture for which it is assumed that $L'_p = 0$)

$$D \cong (D_{th} - a_f)\left(1 - \frac{R_l}{R}\right) + a_f \tag{10'}$$

Comparison with Experimental Data

Having summarized our experiments by referring for each mixture to the wave velocity, D^*, in a reference tube of radius, R^*, it can be seen that for this type of representation Equation (10) leads to:

$$\frac{D^*}{D} = \frac{1 - \frac{R_l}{R^*}}{1 - \frac{R_l}{R}}$$

or, if $k = R_l/R^*$,

$$\frac{D^*}{D} - 1 = \frac{k}{1 - k\frac{R^*}{R}}\left(\frac{R^*}{R} - 1\right) \tag{11}$$

Figure 3 shows changes in D^*/D as a function of R^*/R for various values of k (from 0 to 0.0075). These curves were compared with the $D^*/D = f(R^*/R)$ curves plotted by us to derive values of R_l. If we adopt Equation (10'), we again reach Equation (11) and the same conclusions provided that

$$k = \left(1 - \frac{a_f}{D_{th}}\right)\frac{R_l}{R^*} \tag{12}$$

[e] See appendix; calculations of this type have been summarized for H_2-air mixtures.

Table 2 gives R_l values for different mixtures which we tested, using the latter definition for k and the values listed in the table for a_f and D_{th}.

Figure 4 shows $2R_l$ as a function of the nature and composition of the mixtures studied. It is clear that the result, $R_l = 0$, for the stoichiometric C_2H_2-O_2 mixture is due to the precision of our

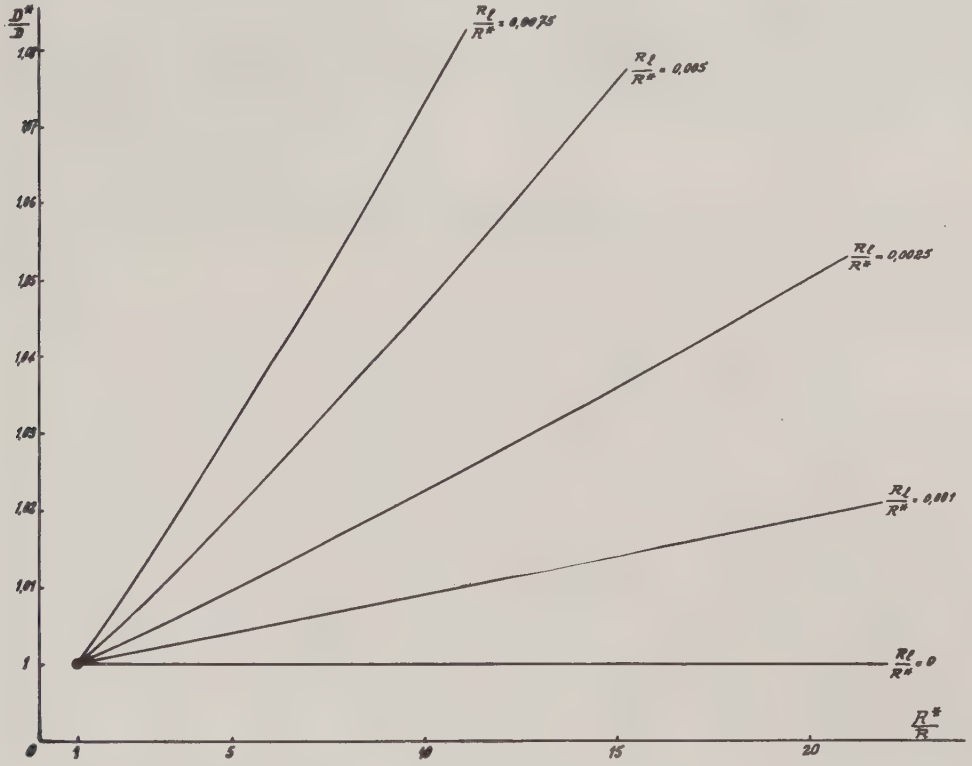

FIG. 3.

TABLE 2

Mixture	$C_2H_2 + aO_2$				$C_3H_8 + aO_2$				Observations
a	0.5	1	2.5	4	3	4	5	6.1	
D_{th} m/sec	2420	2960	2700	2150	2620	2500	2300	2250	(a)
a_f m/sec	380	347	326	324	295	297	304	307	(b)
$10^3\alpha$	6.1	2.0	0	1.0	3.2	1.8	1.6	3.2	(c)
$10^3 \times 2R_l$ mm	84	26	0	14	41	23	21	42	

(a) Values adopted using the information from Figures 7 and 8 of Reference 16.
(b) Calculated values.
(c) According to Reference 8.

It will be seen that R_l was calculated in this way from

$$R_l = \alpha \frac{R^*}{1 - \frac{a_f}{D_{th}}}$$

where α is the slope of the linear portions of the experimental $D^*/D = f(R^*/R)$ curves.[8]

measurements; no change in D with R could be observed for experimental values of R.

Substituting the experimental values of Kistiakowsky and Zimmann[17] in Equation (10) or (10′), we again find that there is qualitative agreement. However, calculation of $2R_l$ for mixtures of C_2H_2 + a O_2 where $0.5 < a < 1$ leads to values that are appreciably different from those

of our experimental curves. Thus, for a = 0.89, we should obtain $2R_l = 0.84$ mm.[f] whereas we actually find $2R_l = 0.04$ mm. In spite of the very accurate measurements of Kistiakowsky and Zimmann, we believe that the resulting $2R_l$ value is too high. Moreover, one of us [18] was able to observe detonation waves in mixtures where $a \cong 1$ with 0.30 mm diam tubes, without noting anything anomalous.

Conclusions

(1) According to the proposed interpretation the definition of the upper (C_S) and the lower (C_I) detonation limits as the "concentration C of combustible in the mixture, at a given p_f and T_f such that if $C \ll C_I$ and $C \gg C_S$, the detonation cannot propagate," must be completed at least by specifying the charge diameter, $2R$.

This means that the existing detonation

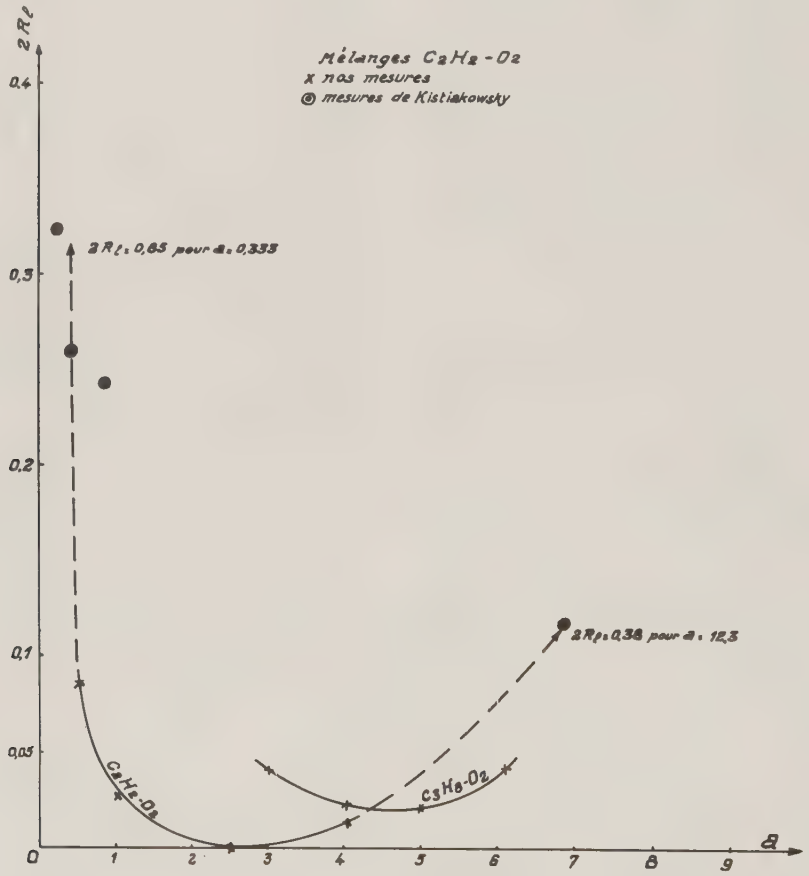

FIG. 4. Variation of limit diameter vs $a = \dfrac{\text{O}_2 \text{ moles}}{\text{fuel moles}}$.

However, we do not feel that this divergence is particularly significant at this time, first, because of the difficulty of making accurate measurements and second, because of the approximate nature of the equations derived from the theory which, as already stated, assumes that R_l is of the same order as the thickness ϵ of the zone where the reaction is influenced by the walls.

limits C_I and C_S are no longer characteristic of the combustible mixture, if the tube diameter changes. As against that, they do define the limiting diameters $2R_l$, corresponding to mixtures of concentration, C_I and C_S, these diameters being precisely those of the tubes in which these concentrations are determined.

As the latter are functions of p_f[g] and of T_f,[h]

[f] Average of three calculations with $D_{th} = D_{R_\infty} = 2827$ m/sec and $2R = 25; 50; 100$ mm.

[g] Breton[19] has shown that C_I decreases when p_f increases.

[h] Rivin[20] has shown that C_I decreases when T_f increases.

the study of the conditions for which the detonation wave no longer propagates in a given mixture appears to offer difficulties comparable to those associated with the study of flammability limits, taking into account the probable effect of the nature of the walls when $R \to R_l$.

(2) Another problem presents itself, along the same lines. Experiments by one of us in collaboration with Ferrié,[21] and experiments by Freiwald and Uhde[22] have shown that in the case of spherical detonation waves, the lower concentration limit, C_I, is greater than for "plane" waves, whereas the upper concentration limit, C_S, is smaller.

(3) If we compare our interpretation with other theories, we find that it is not in contradiction with the accepted hypotheses, but that it interprets them differently.

From what has been said above, the assumption of a width, ϵ, where the reaction is inhibited leads to an expression for the detonation wave velocity which has the following form:

$$D = D_{th} f(\epsilon/R)$$

where D_{th} is a function solely of the mixture (nature composition, p_f and T_f), whereas ϵ may also be a function of R and of the surface of the tube.

TABLE 3. Characteristics of the Explosive Wave in the Mixtures $H_2 + a(O_2 + 3.76N_2)$ where (1) a = 0.5; (2) a = 1 for Different Values of the Parameter $\lambda = \left(1 - \frac{R_l}{R}\right)^2$

λ	1		0.75		0.5		0.25		0	
$\frac{R_l}{R}$	0		0.134		0.292		0.5		1	
Mixture a =	0.5	1	0.5	1	0.5	1	0.5	1	0.5	1
P_b atmos	17.2	11.9	14.1	9.7	10.5	7.5	6.5	4.6	1	1
T_b°K	3370	2245	2710	1830	2020	1410	1250	780	298	298
D	2085	1620	1910	1475	1670	1295	1310	992	407	379
$\frac{D}{a_f}$ (a)	5.12	4.275	4.68	3.89	4.10	3.41	3.2	2.62	1	1
$\frac{D}{a_f}$ (b)	5.12	4.275	4.44	3.70	3.62	3.02	2.56	2.14	0	0
$\frac{D}{a_f}$ (c)	5.12	4.275	4.57	3.84	3.92	3.32	3.06	2.63	1	1

(a) Calculated with the values of D indicated in the preceding line.
(b) Calculated according to Equation 10. Mixture 1; D_{th} = 2085 m/sec; mixture 2: D_{th} = 1620 m/sec.
(c) Calculated according to Equation 10′. Mixture 1; D_{th} = 2085 m/sec; mixture 2: D_{th} = 1620 m/sec.

However, it is probably more accurate to consider the limits determined in this way as the limits of formation C_{IF} and C_{SF} of the detonation wave, and to compare them with the corresponding values measured in tubes, especially by Rivin and Sokolik.[10†]

More especially for mixtures of C_2H_2 and air, where Freiwald and Uhde report C_{IF} = 9 per cent, C_{SF} = 19 per cent and Rivin and Sokolik report C_{IF} = 6 per cent, C_{SF} = 14 per cent, we find better agreement than if we consider the results of Breton (C_I = 4 per cent, C_S = 50 per cent) obtained in a 14-mm wide tube.

† The difference between the detonation limits and the limits of formation has already been noted, in particular by Laffitte[23] who noted that the latter depend not only on the parameters of the combustible mixture, but on the ignition process.

The other theories lead to a similar relation

$$D = D_{th} f(e/R)$$

where the thickness, ϵ, is replaced by the thickness, e, of the reaction zone which is proportional to the reaction time, τ, that is, to the same variables as ϵ.

In the last analysis, the two parameters, ϵ and e, characterize the same process, i.e., the chemical reaction, and thus the role of ϵ is equivalent to that attributed to e by Zeldovitch or Döring.[24] Similarly, there is no contradiction with the hypothesis of a curved Chapman-Jouguet surface postulated by Eyring, Powel, Duffey and Parlin, and by Wood and Kirkwood; it simply means that we are considering a different reaction time along the axis and near the tube walls. In particular, the fact that, according to our interpretation, R_l (R_l = lim ϵ) is smallest for a

stoichiometric mixture, i.e., that for these mixtures the effect of the walls does not extend as far into the central part of the charge, is directly related to the fact that the reaction is exceptionally rapid in these mixtures, i.e., that the reaction zone is narrowest, approximating most nearly a section between two planes. Although there is no fundamental incompatibility between these various theories, the one presented here offers the advantage of relating D and R without involving any rough numerical data. Moreover, it emphasizes the importance of the limiting diameters, which studied in conjunction with the ratio $D = f(R)$, should lead to a better understanding of the processes that take place in the detonation wave.

Appendix

CALCULATIONS OF DETONATION WAVE PARAMETERS FOR TWO HYDROGEN-AIR MIXTURES, ASSUMING NO LIBERATION WHATSOEVER OF THE HEAT OF REACTION

The $H_2 + a(O_2 + 3.76\ N_2)$ mixtures for which detonation wave parameters were calculated are mixtures containing 29.6 and 17.4 per cent hydrogen, in other words, mixtures for which (A) $a = 0.5$, and (B) $a = 1$. We have assumed that: (a) $p_f = 1$ atmos; $T_f = 298°K$; and (b) the average composition of the burned gas corresponds to $H_2 + a(O_2 + 3.76\ N_2) \rightarrow \lambda\ (H_2O + 3.76\ a\ N_2) + (1 - \lambda)\ (H_2 + a[O_2 + 3.76\ N_2]) + 57.6\ \lambda$ kcal/mole.

For each of these mixtures, the R-H curves for $\lambda = 0; 0.25; 0.50; 0.75$ and 1 have been plotted in the p, $1/\rho$ plane, according to the method described in reference,[25] but neglecting dissociations and adopting the values of $\Delta Hj)_{Tf}^{Tb}$ ($j = H_2O, H_2, O_2, N_2$) given in reference.[26]

The results of these calculations are summarized in Table 3, together with values of D/a_f calculated (a) from these data; (b) from Equation (10); (c) from equation (10′).

This latter leads to results that are closer to those obtained under (a). We conclude that, for conditions where our calculations hold,[j] the relation between D and R obtained by the approximate Chapman-Jouguet method (Equation (10)) may be used in first approximation provided that $R_l/R < 0.15$. However, Equation (10′) is preferable, at least for cases where we can assume that $L'_p = 0$.

[j] For mixture (B), the error introduced by neglecting the dissociations is not significant owing to the values of T_b and p_b, but this undoubtedly is not the case for mixture (A). The results of calculations for this mixture have been given here only for purposes of comparison.

Nomenclature

D_{th} theoretical velocity of a plane detonation wave, considered as the velocity of a wave in a tube of infinite radius
D velocity of a detonation wave in a charge of radius, R
D^* velocity of a detonation wave in a charge of radius, R^*, taken as the reference radius
e thickness of the reaction zone, usually defined as $e = \tau D_{th}$, extending from the shock wave which is assumed to be infinitely thin to the Chapman-Jouguet plane
τ time during which the gases are in the reaction zone
CJ Chapman-Jouguet plane defined by the condition $u_b = a_b$
u_b velocity of the burned gas with respect to the detonation wave
a_b velocity of sound in the burned gas
ϵ thickness of the layer where the reaction in the wave is more or less inhibited
$2R_l$ limiting diameter

INDICES

f unburned gas
b burned gas
$'$ gas traversing the detonation wave in the layer of thickness, ϵ

REFERENCES

1. Zeldovitch, J. B.: Phys. Exp. et Théor. URSS, *10*, 542 (1940).
2. Jones, H.: Proc. Roy Soc., *A189*, 415 (1947).
3. Eyring, H., Powel, R. E., Duffey, G. H., and Parlin, R. B.: Chem. Rev., *45*, 69 (1949).
4. Wood, W. W., and Kirkwood, J. G.: J. Chem. Phys., *22*, 1920 (1954).
5. Zeldovitch, J. B., and Kompaneez, A. S.: *Théorie de la Détonation*. Moscow, 1955.
6. Taylor, J.: *Detonation in Condensed Explosives*. Oxford, Clarendon Press, 1952.
7. Kistiakowsky, G. B., Knight, H. T., and Malin, M. E.: J. Chem. Phys., *20*, 884 (1952); *20*, 876 (1954).
8. Guénoche, H., and Manson, N.: Rev. I. F. P., *9*, 214 (1954).
9. Kogarko, S. M., and Zeldovitch, J. B.: C. R. Acad. Sci. URSS, *63*, 553 (1948).
10. Rivin, M. A., and Sokolik, A. C.: Acta Phys. Chim. URSS, *4*, 301 (1936); *7*, 825 (1937).
11. Berthelot and Vieille: C. R. Acad. Sci., Paris, *94*, 101 (1882).
12. Laffitte, P.: Thèse, Paris, 1925.

13. Guénoche, H., and Manson, N.: C. R. Acad. Sci., Paris, *240*, 1318 (1955).
14. Lewis, B., and von Elbe, G.: *Combustion Flames and Explosions of Gases*. New York, Academic Press, 1951.
15. Jouguet, E.: *La Mécanique des Explosifs*, p. 284. Paris, Ed. Doin, 1917.
16. Manson, N.: Rev. I. F. P., *9*, 133 (1954).
17. Kistiakowsky, G. B., and Zimmann, W. G.: J. Chem. Phys., *23*, 1889 (1955).
18. Guénoche, H.: Rev. I. F. P., *4*, 15 (1949).
19. Breton, J.: Thèse, Nancy, 1936.
20. Rivin, M. A.: Les Progrès de la Chimie, U. R. S. S., *20*, 473 (1951).
21. Manson, N., and Ferrie, F.: *Fourth Symposium on Combustion*, p. 486. Baltimore, The Williams & Wilkins Co., 1953.
22. Freiwald, H., and Uhde, H.: C. R. Acad. Aci., Paris, *236*, 1741 (1953); *241*, 736 (1955).
23. Laffitte, P.: Rocznikow Chemii, *18*, 195 (1938).
24. Doring, W.: Ann. Phys., *5*, 421 (1943).
25. Manson, N.: *Propagation des Détonations et des Déflagrations dans les mélanges Gazeux, I. F. P.*, ONERA, Paris, 1947.
26. Ribaud, G.: Publ. Sc. et Tech. Min. Air, No. 266, Paris, 1952.

83

DETONATION IN MEDIA OF VARIABLE DENSITY

By L. I. SEDOV

When analyzing theoretically the phenomena of detonation, it has been assumed heretofore that the density of the explosive material is uniform throughout.[1] The aim of this paper is to show that the laws of density variation in detonating material may accelerate the propagation of the detonation wave, raise the temperature and the pressure behind the wave front, and greatly influence the motion of the detonation gases. Similar effects are bound to occur in tubes of variable cross section with a constant density of detonating material.

To substantiate these qualitative conclusions, let us examine the problem of detonation with spherical waves in an ideal gas where the initial density is distributed according to the law

$$\rho_0 = \frac{A}{r^\omega} \tag{1}$$

where A and $1 < \omega < 3$ are constants, and r is the distance to the center of symmetry. The study of such a problem can be directly instrumental in explaining the coruscation of novae and supernovae.

To describe the gas motion behind the front of the detonation wave, we will apply the equations of one-dimensional adiabatic gas motion of spherical symmetry.

In considering a detonation wave, it is quite permissible to neglect the initial pressure as compared with the very high pressure behind the wave front. Moreover, having in mind the astro physical application, it is permissible to neglect Newtonian gravitation in the equations of motion for short intervals of time after the onset of detonation. The perturbation of the gas is determined by a system of independent values

$$\gamma, \omega, A, Q, r, t \tag{2}$$

where $\gamma = C_p/C_v$; $Q > 0$ is the reaction heat, and t is the time; detonation begins in the center of symmetry at $t = 0$.

We may regard all the dimensionless values as functions of three dimensionless values:

$$\gamma, \omega, \lambda = \frac{r}{\sqrt{Q}\, t} \tag{3}$$

with only λ variable. Thus the gas motion is automodeling, and the problem of determining it is reduced to integration of ordinary differential equations.

The following equations give the detonation front velocity D, the temperature, T_2, and the pressure, p_2 (behind the wave front)

$$D = k_1 \sqrt{Q}; \qquad T_2 = k_2 Q; \qquad \frac{p^2}{\rho_0 Q} = \frac{p_2 r_2^\omega}{AQ} = k_3 \tag{4}$$

where r_2 is the wave radius, and k_1, k_2, k_3 are constants that depend on γ and, in general, on ω.

Taking into consideration the shock wave conditions and the Chapman-Jouguet conditions, we can easily define the constants k_1, k_2, k_3 as functions only of γ.

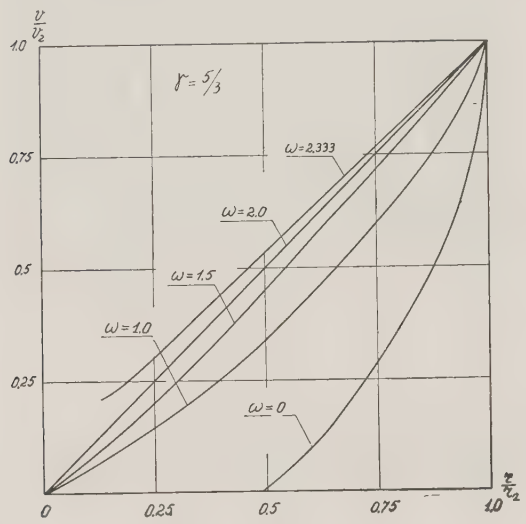

FIG. 1.

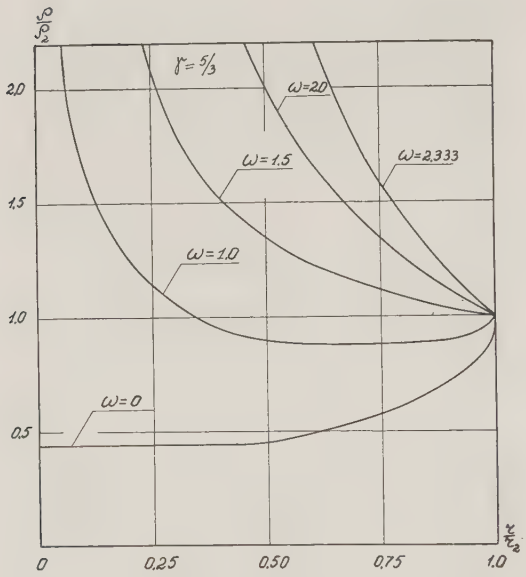

FIG. 2.

The influence of ω is due to nonfulfilment of the Chapman-Jouguet conditions.

A qualitative mathematical analysis of the corresponding system of ordinary differential equations and complementary conditions has led to the following conclusions.

If

$$0 \leq \omega < \frac{2\gamma}{\gamma + 1}$$

then at the center of symmetry the pressure, p^*, is finite, the density, $\rho^* = \infty$, and the temperature, $T^* = 0$. In front of the detonation wave the Chapman-Jouguet conditions are fulfilled.

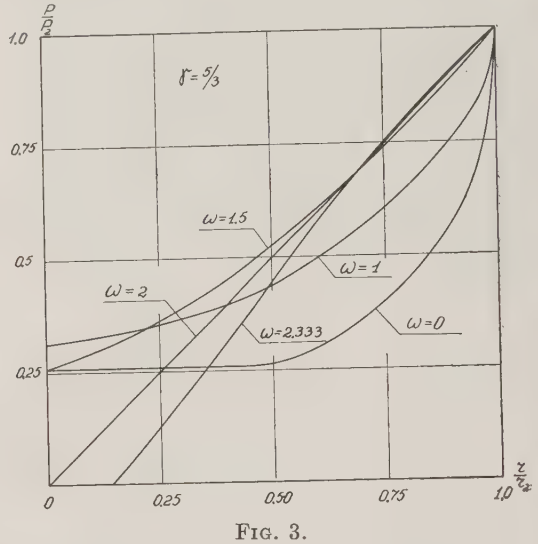

FIG. 3.

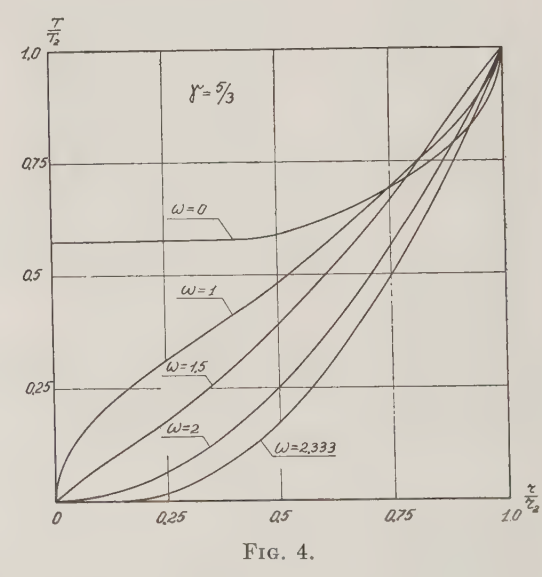

FIG. 4.

If

$$\frac{2\gamma}{\gamma + 1} < \omega < \frac{3(\gamma + 1)}{3\gamma - 1}$$

then at the center of symmetry $p^* > 0$, $\rho^* = \infty$ and $T^* = 0$, but the Chapman-Jouguet conditions are not fulfilled in the detonation wave; the values, k_1, k_2 and k_3, in Equation (4) increase with the increase of ω.

If $\omega = 3(\gamma + 1)/3\gamma - 1$, the solution of the

problem is very simple:

$$\frac{v}{v_2} = \frac{r}{r_2}; \qquad \frac{\rho}{\rho_2} = \frac{r_2}{r}; \qquad \frac{p}{p_2} = \frac{r}{r_2} \tag{5}$$

If

$$\omega > \frac{3(\gamma + 1)}{3\gamma - 1}$$

a spherical cavity forms at the center of symmetry and its radius r^* increases proportionately

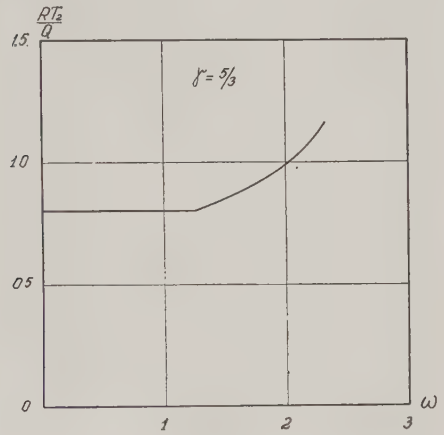

FIG. 5.

with the time. The ratio r^*/r_2 is constant with time and increases with ω. On the inner surface the pressure, p^*, and temperature, T^*, are equal to zero.

Distributions of velocity, density, pressure and temperature behind the detonation wave front as functions of $\gamma = 5/3$ and various values of ω are given in Figures 1, 2, 3 and 4. Curves in Figures 5 and 6 give the pressure and temperature in the detonation wave as functions of ω; as soon as

$$\omega = \left.\frac{2\gamma}{\gamma + 1}\right|_{\gamma=(5/3)} = 1.25$$

the Chapman-Jouguet conditions do not hold.

It must be noted that the above conclusions do not depend on the magnitude of heat release, Q; they depend only on the law of density decrease, determined by the value of ω.

The outlined results indicate possible ways of obtaining high temperatures and pressures through the use of detonation at velocities corresponding to the points of the Hugoniot curve which are above the Chapman-Jouguet points.

It is obvious that there may be various experi-

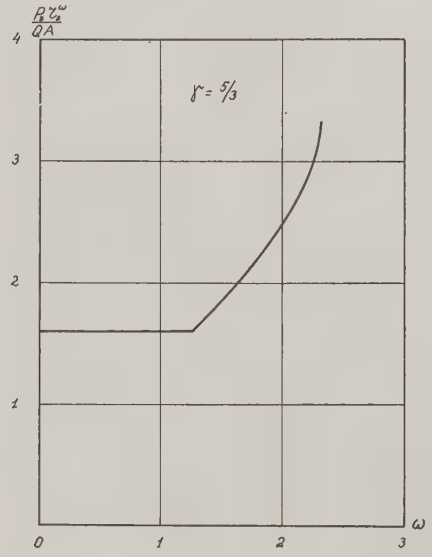

FIG. 6.

mental procedures for achieving such effects. In a similar way, it is possible to work out the problem of detonation in a medium of varying density for the case of cylindrical and plane waves.

Acknowledgment

The author concludes by thanking I. M. Yavorskaya who took part in analyzing and solving the above problem.

REFERENCE

1. ZELDOVICH, Ya. B.: Zhur. Exp. Theor. Fiz, *12*, No. 9 (1942).

84

THE EFFECT OF SLIGHT CONFINEMENT ON THE DETONATION WAVES IN SOLID EXPLOSIVES

By L. DEFFET AND J. BOUCART

A. Introduction. Statement of the Problem

Confinement of solid explosives in rigid tubes has long been known to influence their velocity of detonation.[1] In all cases, such confinement leads to an increase in the detonation velocity, a fact which has been explained by various authors, on the basis of the hydrodynamic theory of detonation. Two methods of calculation have been proposed, one based on the Jones expanding jet theory[2] and the other on the Eyring theory of a curved wave front.[3] However, Eyring, Powell, Duffey and Parlin[3] were concerned mainly with the effect of the charge diameter on the detonation velocity; accordingly, in our study we will draw chiefly on the principles set forth by Jones.

We need not go back to the development of this theory, with its quantitative explanation of earlier observations by other authors, who established an initial distinction between thin and thick confinements. Thus, a 1-mm thick lead tube increases the velocity of detonation more than a steel one of the same thickness, whereas the opposite is true if the thickness of the tubes exceeds a few millimeters. Briefly, it can be said that the resistance of the confining material is not important, the important factors being density and inertia for thin confinement, and compressibility for a thick confinement, which explains the above observations. If the thickness of confinement attains and exceeds the thickness of the reaction zone of the explosive confined, that is to say, if the time required for the shock wave to traverse the tube is longer than the reaction time, we go from the first to the second state of confinement.

Thus, the Jones equations governing the variations in the detonation velocity are necessarily different depending upon whether they apply to thin or to thick confinement.

(1) For the former, the velocity of lateral expansion of the detonation products, of which the detonation velocity is a function, is determined by the velocity at which the tube is projected outwards. This velocity thus depends on the inertia of the tube which must have a fairly high density for it to act. The following formula, proposed by Jones, can be used to calculate the effect of such a confinement:

$$\frac{V_m - V}{V} = \frac{E^2\Delta}{2mR} \tag{1}$$

where V_m = maximum detonation velocity, corresponding to zero radial expansion at the reaction zone; V = detonation velocity under the experimental conditions; E = thickness of the reaction zone; Δ = loading density of the explosive; m = mass of the confining tube, per unit of surface, before expansion; and R = charge radius.

(2) Equations governing the case of thick tubes also have been derived from Jones' theory, in particular by Copp and Ubbelohde.[4] The latter authors have shown that when the thickness of confinement is such that the shock wave does not reach the outer wall of the tube within the reaction time, compressibility is the major factor in the action of this confinement. The formula corresponding to this effect is

$$\left(\frac{V_m}{V}\right)^2 = 1 + 9E\,\frac{tgB}{R} \tag{2}$$

where, in addition to the factors already known, B is the angle which the inner wall forms during expansion, with respect to its initial direction. In order to check this equation experimentally, Copp and Ubbelohde, who had no way of defining angle B, derived it from the values of the compressibility at high static pressures, which naturally involves considerable approximation. However, this check showed the validity of these hypotheses, which were further supported by Cybulski, Payman and Woodhead[5] in the course of other experiments.

Belgian permissible explosives generally consist of an explosive core surrounded by an inert sheath. At the Fourth Symposium on Combustion we presented a study[6] on explosives of this type provided with active sheaths; i.e., which contained 10 to 15 per cent nitroglycerin. The present investigation is limited to inert sheaths, more particularly to rigid sheaths. In point of fact, for about two years, Belgium has been developing a new type of sheath—a rigid sheath of compressed sodium chloride. In the

course of a careful study of such sheaths, we were led to determine the various characteristics of explosives sheathed in this way, and in particular their velocities of detonation, the shape and thickness of the detonation waves (by the x-ray flash method), and the external shock waves (by the shadow method). This study showed first that explosives with rigid sheaths have considerably higher detonation velocities than explosives with unsheathed charges. This, in turn, led us to examine more closely the working of these sheaths, which we were able to compare with that of thick

TABLE 1. VELOCITIES OF DETONATION IN M/SEC

Unsheathed Cartridges	Sheathed Cartridges	Difference
2.230	2.400	170
2.780	3.015	235
2.200	2.520	320
2.250	2.560	310
1.990	2.330	340
2.320	2.650	330
2.205	2.650	445
2.330	2.800	470
2.165	2.700	535
2.085	2.705	620
3.480	4.100	620
2.520	3.150	630
2.545	3.225	680
2.430	3.160	730
2.570	3.330	760
3.000	3.930	930
2.620	3.600	980

confinement. Observations on the detonation wave curve confirm this hypothesis which could be used to assess changes in the detonation reaction caused by rigid sheaths.

B. Experimental Study

1. VELOCITIES OF DETONATION

The variations in the detonation velocities of unsheathed and sheathed explosives are always positive and sufficiently well-defined to show that, independent of other findings, rigid sheaths are responsible for these variations. The tests covered different types of industrial explosive, the compositions of which varied little and always included nitroglycerin, nitroglycol, trinitrotoluene, ammonium nitrate, sodium chloride, wood meal, and sometimes small amounts of nitrocotton. These constituents separate them from the explosives used ordinarily in theoretical studies and make comparisons of a physico-chemical nature on the effect of confinement more difficult. Accordingly, we have limited ourselves to physical data, which are quite sufficient.

Detonation velocities of unconfined explosives were determined in thin cardboard tubes, which offer virtually no obstacle to radial expansion of the products. The inner diameter of the tubes was 26 mm. The confined explosives were studied in their industrial form; i.e., a diameter of 26 mm and a 5 mm-thick compressed sodium chloride sheath, making the external diameter 36 mm. Table 1 gives detonation velocities of various explosives cartridged in the two manners. It will be noted that the velocities of detonation undergo increases that range from 170 m/sec to 980 m/sec. Such an increase in detonation velocity at first may seem inconsistent with the effect that a slight confinement can produce. However, the following observations indicate that these increases in detonation velocity must be attributed solely to this confinement.

2. SHOCK WAVES

We have already shown that shock waves emitted laterally by the detonation wave of sheathed cartridges are very different in form from those emitted by unsheathed cartridges.[7] We shall not linger over this point, but will simply recall that, for a few microseconds, the shock waves of sheathed cartridges form a rather slight angle and that they form a connection cone between their starting point and their intersection with the shock waves preceding the expanding detonation gases (Fig. 1). Shadow photographs of this type also show that the rigid sheaths do not burst upon passage of the detonation wave, which in itself is qualitative evidence of their confining action. We shall see, moreover, that the angles formed by these expanding sheaths can be used in the equation which links this parameter with the detonation velocities of unconfined charges (Equation (2).

3. DETONATION WAVES

The structure of detonation waves can be studied by the x-ray flash method which gives direct indications as to their curvature and thickness. In addition to the usual difficulties of this type of recording, x-ray photography of sheathed cartridges offers considerable complications due to the fact that sodium chloride sheaths absorb x-rays strongly which makes it difficult to obtain clear records of the detonation waves and the reaction zone. However, Figures 2 and 3 show

that these difficulties can be overcome, and that the great difference in convexity between the detonation waves of unsheathed and sheathed cartridges can be observed.

The detonation waves of sheathed cartridges are more nearly plane, showing that radial expansion is slight and inhibited by the sheath. The difference in curvature of the waves can be used to calculate the changes in the detonation velocity. This would also be proof of the confining

FIG. 1.

action of the sheaths, but it seemed more interesting to apply the equations of Jones, and of Copp and Ubbelohde directly to sodium chloride sheaths in order to confirm their action.

C. Preliminary Calculations

We have seen that, in first approximation, compressed sodium chloride sheaths can be likened to thick confinements, the classical examples of which are lead or steel tubes. Copp and Ubbelohde have shown that calculations based on compressibilities determined by Bridgman[8] up to 12,000 kg/cm² roughly confirm theoretical predictions. To avoid any basic error, we began by comparing the compressibilities of different materials in accordance with new experimental data by Bridgman given in Table 2.

It is noted that the compressibilities of steel lead, and sodium chloride at 30,000 kg/cm² are 1:3.5 and 1:5.5, respectively. The order of magnitude of the compressibilities is thus the same,

FIG. 2.

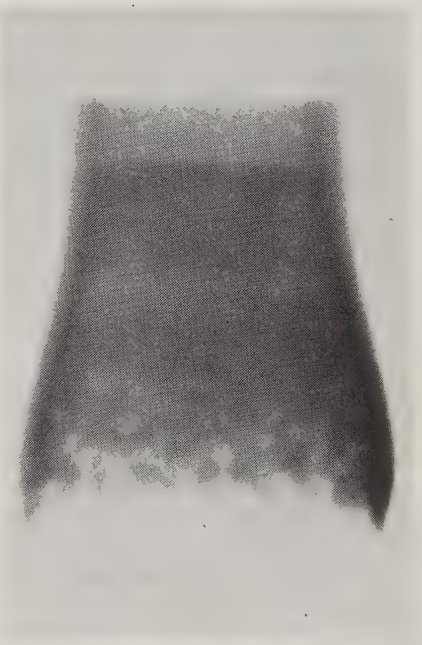

FIG. 3.

and the remarks made previously on the difference in the behavior of steel and lead tubes apply to the case of sodium chloride tubes. Just as a lead tube has a less satisfactory confining action than a steel tube of the same thickness, so the action of a sodium chloride tube is somewhat less favorable with respect to lead than that of lead with respect to steel. This comparison would be really exact if the sodium chloride tubes were formed of a single crystal without any interposition of air. It is evident that the air located between the sodium chloride crystals decreases the action of the sheath by diminishing its compressibility. Correspondingly, sheaths of similar, less compressed substances or pulverulent sheaths have an even slighter effect on the confinement of the explosive. However, the x-ray photographs show that even the pulverulent sheaths remain intact for a certain length of time and are compressed by the passage of the shock wave. Thus, it appears that confinement due to sodium chloride sheaths can be considered a thick confinement.

TABLE 2

Substance (x)	Pressures kg/cm²	V/V_0	$\frac{V/V_{0x}}{V/V_0 \text{ steel}}$ (taking the steel values as 30,000 kg/cm² = 0.1)
Stainless steel H 26	30,000	0.0167	0.01
	20,000	0.0113	
Stainless steel H 29	30,000	0.0175	0.01
	20,000	0.0119	
Iron	30,000	0.01676	0.01
	20,000	0.01133	
Lead	100,000	0.145	
	50,000	0.0892	
	30,000	0.0587	0.0351
	20,000	0.041	
NaCl	100,000	0.210	
	50,000	0.135	
	30,000	0.093	0.0556
	20,000	0.068	

D. Applications of the Experimental Results

Having established that the equations for thick confinement can be applied accurately to inert sheaths of permissible explosives regardless of their rigidity, i.e., their resistance, we used the experimental results obtained by our three methods of study to check these equations, in particular the following:

$$\left(\frac{V_m}{V}\right)^2 = 1 + 9E\,\frac{tgB}{R}$$

In making this check, rather than determine the maximum velocity, V_m, experimentally, we calculated it from the other quantities which are all accessible to experiment. In fact, V, E, B and R can be determined experimentally with sufficient precision to calculate the maximum speed with good approximation, as shown by the estimated error.

The two quantities that can be defined by photographic and x-ray methods can be determined with the following maximum errors: E (thickness of the reaction zone): 0.5 mm; B (angle of expansion): 1°.

The following calculation shows the effect of these errors on the final result: Let V = 3,000m/sec, E = 2.5 mm, B = 10°; then V_m = 3,427.5 m/sec. For E = 3.0 mm, V_m = 3,507 m/sec, i.e., a difference of 80 m/sec. For B = 11°, V_m = 3,478.5 m/sec, i.e., a difference of 51 m/sec.

It will be seen that we remain within the acceptable limits of precision, assuming experimental errors that are certainly larger than in reality. Moreover, these errors are of the same order as the initial errors in the detonation velocity, V, and of those due to the lack of precision in the measurement of the charge radius. Starting from the maximum velocity thus obtained, which is the same for a given explosive no matter how it is cartridged, we can calculate, in accordance with other experimental data, the detonation velocities of explosives sheathed in various manners. Thus we have a method of determining whether the calculated detonation velocities agree with the observed velocities.

An initial series of approximate calculations was performed taking 2.5 mm as the reaction zone thickness, and measuring the angles, B, on photographic recordings by the shadow method. Table 3 gives the results of these measurements.

Taking the average values of the angle formed by the sheath (21° for pulverulent sheaths and 13° for rigid sheaths), the difference in the average detonation velocities of explosives with different sheaths can be determined. This difference is of the order of 300 m/sec, which agrees with the experimental results. However it is rather hazardous to base calculations of the maximum velocity on observations for sheathed industrial explosives because it is often difficult to measure the thickness of the reaction zone. The results would have

to be confirmed by calculations on explosives of different diameters.

The difficulty in measuring the thickness of the reaction zone arises from the fact that the sodium chloride sheath is not very transparent to x-rays. Moreover, the increase in the density of the sheath, due to compression by the shock wave precisely at the point of the detonation wave, diminishes this transparency still further. We have tried to circumvent this difficulty by using polyethylene (polythene) sheaths of two different diameters. These plastic sheaths are less opaque to x-rays and make it possible to measure more exactly the thickness of the reaction zone, and also give a better value for the angle formed by the sheath upon passage of the detonation wave (Fig. 4). The results of these tests are given in Table 4.

Table 3. Angles Formed by the Sheath (Shadow Photographs)

Type of Explosive	Type of Sodium Chloride Sheath	Mean Angle
A	Pulverulent	23°
B	Pulverulent	22°
B	Semi-rigid	19°
B	Semi-rigid	21°
C	Pulverulent	20°
	Average:	21°
B	Rigid	13°
B	Compressed	14°30′
B	Compressed	12°
C	Compressed	12°30′
C	Compressed	13°
	Average:	13°

The Jones formula (Equation (2)) can be applied to sheathed explosives to calculate the maximum velocity, V_m, by using the experimental values in Table 5 measured on x-ray photographs.

These results as a whole indicate that the compressed sodium chloride sheath exerts a confining action comparable to a thick confinement as defined by Jones, since the increases in the detonation velocity for the 26-mm explosive diameter are greater than those observed for confinement by a polythene tube which is certainly not as compressible as the sodium chloride tube. Moreover, the maximum detonation velocities obtained for these few experimental values by the Jones formula are in good enough agreement to be considered reliable and to supply new evidence of the action of rigid compressed sheaths.

This discussion has been limited to the application of the Jones equation, and the Copp and Ubbelohde equation to confinement by inert sheaths. In the course of this study, we recorded a large number of detonation speeds, shock waves and reaction zones of unsheathed explosives, with a view to studying the influence of the cartridge

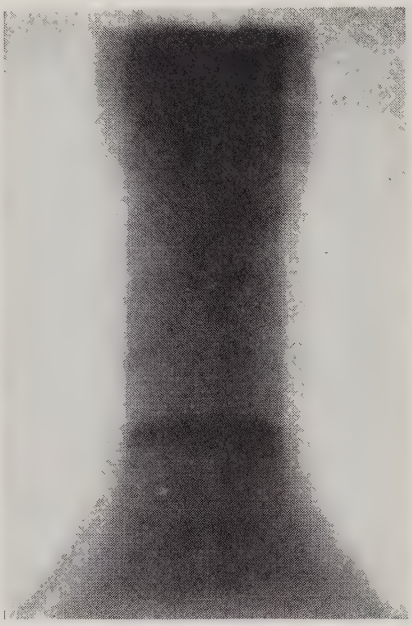

Fig. 4.

Table 4
Detonation Velocities in m/sec

Diameter	Unsheathed	NaCl Sheath	Polythene Sheath
mm			
20	1,805	—	1,885
26	1,965	2,305	2,170
30	2,200	—	—
36	2,250	—	—

Table 5

	E	B	V_m
	mm		
Explosive with NaCl sheath	4.6	13°	3,070
Explosive with polythene sheath, 20 mm.	3.7	28°4′	3,110
26 mm.	4	23°	3,185

diameter for cases that are easier to observe experimentally. Moreover, it seemed interesting to us to test against actual experience the accuracy of another theoretical equation proposed by Eyring, Powell, Duffey and Parlin[3], for calculating the maximum speed as a function of the reaction zone thickness

$$\frac{V}{V_m} = 1 - 0.5\frac{E}{R}$$

This equation offers the advantage that Dr. R. Schall—the only other investigator besides us to have studied detonation waves by instantaneous x-rays—employed it to check the influence of the particle size on the thickness of the reaction zone. In addition, it is interesting to see to what extent the Eyring and Jones equations lead to similar results for the maximum detonation velocity.

Table 6 has been drawn up for the same

TABLE 6

Cartridge Diameter	Detonation Velocity	E	Maximum Velocity
mm		*mm*	
20	1,805	4	2,260
26	1,965	3.7	2,315
30	2,200	—	—
36	2,250	2.5	2,410

standard industrial explosive as was used for the confinement tests. The reaction zone thicknesses determined for this explosive were confirmed by a large number of experiments bearing on other explosives.

A check was made on a square cartridge (20 mm²). By treating such a cartridge as a cylindrical cartridge, we obtain 2,305 m/sec as the maximum velocity, the real speed being 1,800 m/sec and the thickness of the reaction zone, 4.4 mm. We must take into account the lack of precision of the measurements, and the fact that the difference in the particle size of the explosive has a certain effect on the thickness of the reaction zone. In spite of this lack of precision, we get an average maximum velocity of 2,315 m/sec, with divergences of 55 and 100 m. The agreement between these values and those obtained by applying Jones' formula to sheathed explosives is far from good. The average maximum speed determined from experiments on sheathed explosives is 3,120 m/sec, with divergences of about 50 and 65 m/sec. The difference of the average values is 800 m/sec, which is obviously higher than the experimental error. Thus, the Eyring and Jones equations appear to lead to aberrant results, although it is not possible for us to decide which of the equations is the more exact. Taylor[10] had already pointed out this discordance between the values of the reaction zone thickness calculated by these two equations, without however indicating which he believes to be the more accurate.

There is a direct method of determining the maximum velocity based on graphic extrapolation for infinite diameters of the curves established as functions of the detonation velocities and the cartridge diameters. This method is applicable separately to unsheathed and to sheathed explosives, as the maximum velocities must be identical in both cases. It is not possible for us to effect these extrapolations for sheathed explosives as we have studied only two diameters (20 and 26 mm). In the case of unsheathed explosives, we have studied the explosive for four diameters, which allows a certain evaluation. However, as the maximum diameters are certainly over 100 mm, extrapolation from diameters which do not exceed 36 mm also runs the risk of being somewhat inaccurate. The chart shows that extrapolation leads to values of the order of 2,400 m/sec, which agrees much better with values obtained by Eyring's equation than by Jones'.

E. Conclusions

The results show that sodium chloride sheaths act as thick confinements. Direct comparison of the x-ray photographs of explosives with polythene and sodium chloride sheaths confirms the hypothesis proposed by us on the basis of observed detonation velocities. Consequently, sodium chloride sheaths, and more particularly rigid sheaths of that substance, give the detonation wave and the reaction zone special qualities and make the explosive safer with respect to fire-damp and dust, quite apart from that safety which it acquires as a result of materially better sheathing. Detailed discussion of this problem would exceed the scope of this symposium. However, it seems well to mention it as a reminder that the research which we have undertaken and are continuing in this field bears on the improvement of permissible explosives.

Acknowledgment

This research work was carried out with the support of the Association of Belgian Explosive

Manufacturers and the Institute for the Promotion of Scientific Research in Industry and Agriculture (I. R. S. I. A.), to whom we tender our sincere thanks.

REFERENCES

1. Berthelot, M.: Ann. Chim. Phys., *6*, 556 (1885); Berthelot, M., and Vieille, P.: Memorial des Poudres, *4*, 7 (1891).
2. Jones, H.: Proc. Royal Soc., *A189*, 415, (1947).
3. Eyring, H., Powell, R. E., Duffey, G. H., and Parlin, R. B.: Chem. Rev., *45*, 69 (1949).
4. Copp, J. L., and Ubelohde, A. R.: Trans. Faraday Soc., *44*, 658 (1948).
5. Cybulski, W. B., Payman, W., and Woodhead, D. W.: Proc. Royal Soc., *A197*, 51 (1949).
6. Deffet, L., De Coster, M., and Vande Wouwer, P. J.: *Fourth Symposium on Combustion*, p. 481. Baltimore, The Williams & Wilkins Co., 1953.
7. Deffet, L., and Boucart, J.: Explosifs, *8*, 83 (1955).
8. Bridgman, P. W.: The Physics of High Pressure. London, Bell & Sons, 1931; Proc. Am. Acad. Sci., *76*, 1 (1945); Proc. Am. Acad. Sci., *77*, 187 (1949).
9. Schall, R.: Nobel Hefte, *20*, 75 (1954).
10. Taylor, J.: *Detonation in Condensed Explosives*. Oxford, Clarendon Press, 1952.

85

POST-DETONATION PRESSURE AND THERMAL STUDIES OF SOLID HIGH EXPLOSIVES IN A CLOSED CHAMBER

By WILLIAM S. FILLER

Introduction

Current methods and principles involved in determining the heat energy released by high explosives have been very well presented by Lothrop and Handrick.[1] Measurements of heat of detonation usually involve small quantities of explosive initiated in a small space within a strong container filled with inert gas.[2, 3, 4] The quantity of explosive used has been limited by practical considerations of calorimetric technique. Since many explosives will not detonate in small quantities, this limits the type of explosives that may be used. Also, many explosives, although they apparently detonate, do not undergo the same chemical transformation as they do in larger quantities. If an explosive booster is used even in small amounts, its interaction chemically with the test explosive must introduce uncertainties in the measured heat of detonation values.

Values for heat of detonation of organic explosives can also be computed if products of detonation are known. The chief drawback of this method is the lack of exact knowledge regarding the products formed on detonation of many explosives.

Due to these difficulties of measurement and computation, heat of detonation for many explosives is not well established, and few published measurements exist. Yet, the energy which can be released by detonation is one of the most fundamental properties of explosives.

This paper describes studies of pressures that develop shortly after the detonation of high explosives in a closed chamber and how these pressures may be used to measure heat of detonation of high explosives. It was found that a hydrostatic pressure developed within the enclosure a few msec after the initial shock wave traversed the chamber space and that the maximum value of this pressure (before decay due to heat conduction) was in good agreement with simple theory for adiabatic heating of a perfect gas in a fixed volume.

If a quantity of heat, H, is added to a gas with a ratio of specific heats, $C_p/C_v = \gamma$, contained in a volume, V, the pressure rise, P, is given by the relation

$$P = \frac{H(\gamma - 1)}{V} \qquad (1)$$

This relationship applies to the ambient gas initially present in the chamber. The correction

for the addition of explosion product gases is small (on the order of 2 per cent) since the chamber initially contained a volume of gas that was large (72.4 cu ft) compared with the quantity of gaseous products released by two ounces of explosive. Deviations from the perfect gas law are not significant since the hydrostatic pressure did not exceed two atmos and temperatures did not exceed 500°C.

Measured values of maximum static pressure were used in Equation (1) to compute H for a number of explosives detonated in a variety of ambient gases. The values so computed were close to values for heat energy measured or computed by other means for comparable explosion conditions.

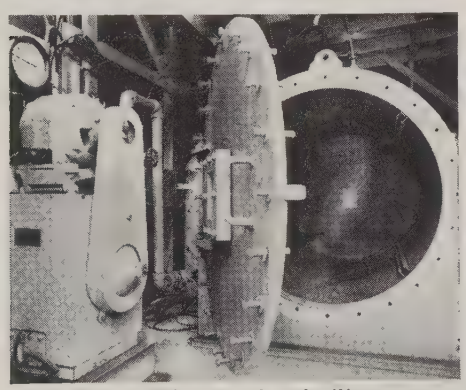

FIG. 1. The chamber facility.

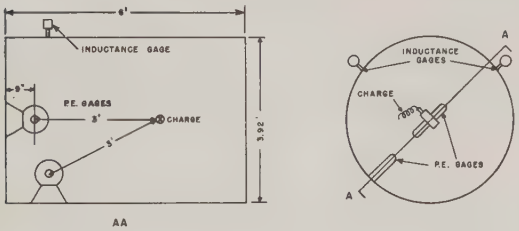

FIG. 2. Gauge-charge arrangement.

Apparatus

THE CHAMBER FACILITY

The chamber (Figs. 1 and 2) is a ½-in.-thick steel cylinder 6 ft long and 4 ft in diameter. The doors are 1½ in. thick and are secured over the chamber opening with 24 bolts. A large rubber "O" ring is used as a seal. Access holes with rubber sealing glands are arranged about the cylinder walls and doors to accommodate cables, gauges, piping, etc. Brackets are welded to the inside of the chamber for conveniently bolting gauges and other objects into place.

PIEZOELECTRIC GAUGE SYSTEM

To provide a detailed picture of the pressure of the explosion shock wave and its reflections from the chamber wall, a tourmaline piezoelectric gauge[5] was used with an appropriate amplifier, cathode ray tube, and photographic recording system.[6] The gauge system had a time resolution of about 50 μsec. This was adequate to produce records which provided a good qualitative picture of the shock phenomena.

INDUCTANCE GAUGE SYSTEM

The most useful data were collected by means of a variable inductance gauge of the Bendix type[7,8] and its associated system. This gauge, although slow responding (1000 cycles/sec) can be used to indicate static or slowly changing pressure levels—a task which formed the major part of these investigations and for which the piezoelectric gauge is not suitable. The inductance gauge proper is located outside of the chamber. Gas pressure from the chamber is led to it through a tube mounted in a gland hole. Calibration of this gauge is performed statically by means of a dead weight tester. Two such gauges were used in all work. Absolute differences in measurement between gauges were found to be statistically insignificant.

RECORDING METHODS

Two methods of recording have been used. The first method employed a cathode ray tube and a rotating drum camera. The record consisted of a 10-in. long, 35-mm strip of film. In practice two signal scopes and a timing scope, used to calibrate the time base, are photographed simultaneously. Amplitude calibration lines are also put on the film before firing. The drum speed could be set to study pressure fluctuations over a wide range of durations, from incident shock waves of 0.5 msec duration to static pressure decay out to 0.2 sec (later extended to 3.0 sec) in time. Measurements are made from enlargements of the film.

The second recording method employs a Brush Instrument Company pen and ink recorder. This recorder is more suitable for static pressure measurements since pressure decay information can be recorded conveniently for as long a time as desired. Its frequency response (100 cycles/sec) is completely adequate for the purpose, and the data reduction is simple and direct.

Experimental Design

This work was performed in two phases. The object of the first phase was to establish the characteristic features of shock wave and later pressure phenomena from explosions in a confined space and to correlate the later pressure phenomena (static pressure) with theory. The ambient gas was atmospheric air except for exploratory shots in nitrogen. The second phase was a more carefully controlled attempt to measure heat of detonation using the static pressure theory. Argon and nitrogen were used as the ambient gas. Shots were also fired in air and in air diluted with nitrogen. Table 1 is a summary of the experiments performed.

EXPLOSIVE MATERIALS

All explosives were pressed with the exception of pentolite (PETN/TNT) which was cast. The charges were cylinders one in. in diameter with length varying according to the pressing properties of the explosive. In the center on one end of each charge a ¼-in. diameter hole, ½ in. deep was drilled for an electrical blasting cap. Materials of sufficient sensitivity or in a sufficiently sensitive form (pressed TNT for example) were used so that reliable detonation might be expected without the use of boosters. Thus contaminating effects of initiating materials was minimized. Comparison of measurements on the initial shock wave with established values was made as a check for proper detonation. These shock wave comparisons were satisfactory and indicated normal detonation was achieved.

The detonator was a Hercules special blasting cap, commercially available. In the first phase a weaker detonator, No. 6 Hercules, was used for one shot of each explosive to check for possible variation in measured pressures with the variation in the strength of detonator. None was observed.

GASEOUS MATERIALS

Atmospheric air and commercial grade nitrogen—0.2 per cent impurity—were employed in phase one. Gas changing was accomplished by evacuation. The estimated total oxygen content in the chamber at the time of firing was 25 g or about 5 per cent of sea level air.

An ambient gas purity requirement for phase two was established in terms of a 5 per cent maximum allowable error in heat of detonation values assuming the detonation products utilized all of the residual ambient oxygen. To meet this requirement for the size chamber being used, the oxygen content of the bottled gas used did not exceed 0.01 per cent. This total oxygen impurity requirement proved extremely conservative in practice, since post-detonation combustion appeared to cut off completely for TNT, an explosive potentially most sensitive to this source of error, even though the chamber contained a total of as much as 100 grams of oxygen or about 20 per cent of the concentration of oxygen in sea level air (see Discussion). In the light of this, phase one data for shots in nitrogen may be considered valid in spite of the substantial amount of residual oxygen present in the chamber during those shots.

Table 1. Summary of Experiments

	Explosive Composition	Ambient Gas	No. of Shots (½ No. of Data)	Density
				g/cc
Phase One	PETN/TNT (cast)	Air	3	1.66
	50/50	N_2	3	
	RDX/wax	Air	3	1.71
	98/2	N_2	1	
	RDX/Aluminum/wax			
	76/22/2	Air	3	1.83
		N_2	1	
	63/35/2	Air	3	1.93
		N_2	1	
Phase Two	TNT	Air	1	1.55
	100	Air & N_2	3	
		N_2	3	
		A	3	
	RDX/wax	N_2	3	1.67
	98/2	A	3	
	PETN/wax	Air	2	1.64
	98/2	N_2	1	
		A	4	

TNT = $C_7H_5N_3O_6$ = Trinitrotoluene.

RDX = $C_3H_6N_6O_6$ = Cyclotrimethylenetrinitramine.

PETN = $C_5H_8N_4O_{12}$ = Pentaerythrite tetranitrate.

PROCEDURE

All gauges were located near one end of the chamber (Fig. 2); the charge was positioned on the chamber axis 2 ft from the other end. The string and tape used for suspension weighed a

fraction of a g, most of which was left intact after a shot. The charge was then armed by connecting the detonator leads to the firing cable, and inserting the detonator into the hole provided in the charge. The door was then closed and bolted.

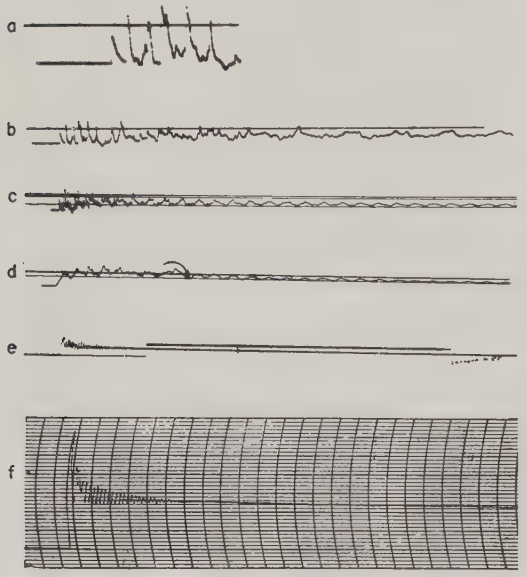

FIG. 3. Representative pressure-time histories: *T.L.* = Time Length of signal trace from start of trace.

(a) Initial shock and reflections; 1.5 fold magnification of initial portion of 4b. *T.L.*, 3 msec.
(b) Piezoelectric gauge. *T.L.*, 58 msec.
(c) Piezoelectric gauge. *T.L.*, 185 msec.
(d) Inductance gauge. *T.L.*, 185 msec.
(e) Inductance gauge. *T.L.*, 1.780 sec.
(f) Inductance gauge, pen and ink record. *T.L.*, 0.970 sec.

If air was to be the ambient gas, the chamber was ready for firing. If argon or nitrogen was to be the ambient gas, the chamber was evacuated to less than 1 mm, then filled to atmospheric pressure.

Experimental Results

QUALITATIVE ANALYSIS OF RECORDS

The six records in Figure 3 reveal the nature of the pressure phenomena in the chamber in a progressive manner, timewise, from highly resolved piezoelectric gauge records to highly condensed and smoothed inductance gauge records. Each record is representative of a type obtained at some stage in the work. The characteristics discussed in this section are independent of type of charge or ambient gas.

Figures 3a, b, c, d, and e are all film records. Figures 3a, b, c, and d are of the same shot. Figures 3a and b show the initial shock wave and later reflections. The initial shock is the first rise and fall. It is well formed and free from extraneous oscillations until the first reflected shock front arrives. Figure 3c is a simultaneous recording of the same gauge signal at a slower drum speed. The shock fluctuations are compressed and several important new features are apparent. The shock fluctuations are well above the base line rather early in the record. This is the static pressure. Notice also the periodic fluctuation which persists for the length of the record. These features are suggested in Figure 3b, but are clearly brought out in Figure 3c.

In Figure 3d we have an inductance gauge record made at the same drum speed as Figure 3c. The limited frequency response of this gauge results in the smooth appearance of the initial portion of the record, but the character of the remainder of the record is essentially the same as Figure 3c. Figure 3e is an inductance gauge recording highly condensed in time compared with Figure 3d. The relatively broad periodic fluctuations of Figure 3d now appear sharp and narrow, and the static pressure appears in a new light with features of its over-all development and decay directly apparent. Figure 3f is an inductance gauge record obtained with a pen and ink recorder. It differs from Figure 3e in the increased amplitude of deflection and in its smoother appearance due to the low frequency response of the recorder itself compared with that of the inductance gauge system. The oscillation is the same periodic fluctuation observed in Figures 3c and 3d.

The sequence of happenings in the chamber which have been illustrated by Figure 3 appears to be as follows:

(1) The usual initial shock wave from explosions is propagated to the walls of the chamber. Reflection occurs followed by shock interactions and further reflections. The resultant complex, aperiodic wave-form obtained with the piezoelectric gauges lasts for about 50 msec and, far from being random, is reproduceable from shot to shot in surprising detail.

(2) A few msec after the initial shock wave has traversed the chamber, a periodic pressure phenomenon with an amplitude of large magni-

tude (several lb per sq in.) develops and persists for several hundred msec.

(3) About the same time that the periodic fluctuation develops, a hydrostatic pressure also develops and rises to a maximum, and then decays to nearly atmospheric pressure in 20 to 30 sec. The shock and periodic waves, while they last, both overlay the static pressure.

QUANTITATIVE ANALYSIS OF RECORDS—PHASE ONE

Shock wave measurements were not of direct quantitative interest for the purpose of this paper and will not be discussed further.

shock waves as the cause of the overshoot. It is possible that the inductance gauge overshoots in response to the successive reflected shocks impinging on it. The overshoot could also result from the fact that the gauges will give an integrated response to the many shock reflections reaching it, while at the same time responding to the static pressure. Thus, while shocks persist, the records would show pressure values higher than would occur otherwise. In either case, the initial overshoot must be ignored in determining a value for maximum static pressure.

The sloping portion of the static pressure curve

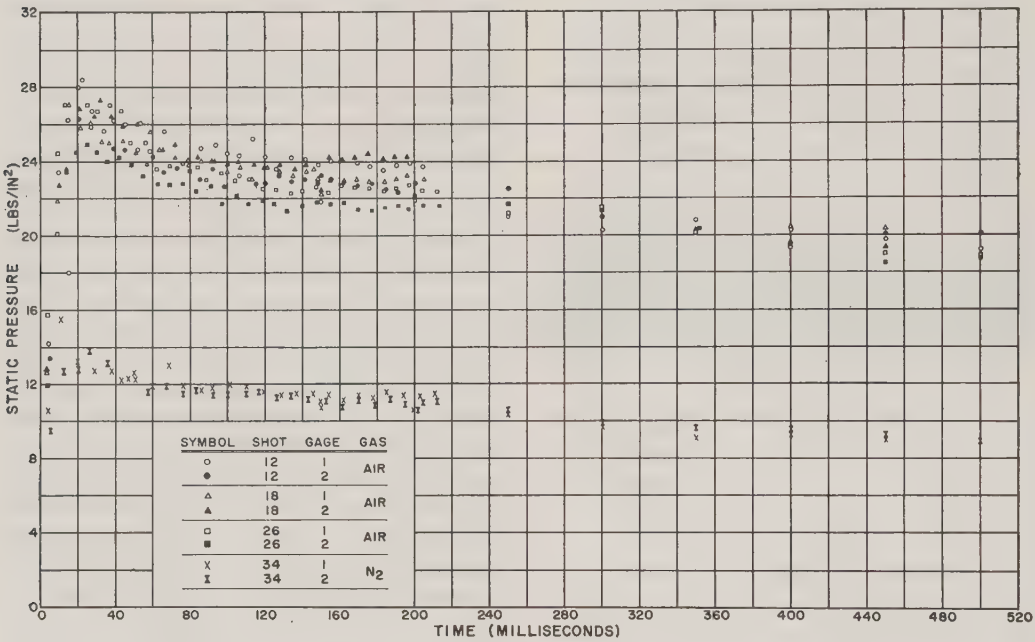

FIG. 4. Pressure—time scatter plot for one explosive RDX/AI/wax 63/35/2, three shots in air, one shot in nitrogen, two gauges on each shot.

Pressure-time histories

All static pressure measurements for phase one were made from records of the Figure 3c type. The characteristic shape of these pressure-time histories may be observed when the traces have been transformed to suitable axes as in Figures 4 and 5. It consists of an initial overshoot followed by a relatively flat sloping curve for the first ½ sec. This is identical to the curve obtained directly in phase two and shown in Figure 3f. An analysis of the overshoot amplitude shows no correlation with static pressure amplitude. However, its duration is nearly the same as the time it takes the shock waves on the piezoelectric gauge records to die out. This points to the is due to heat loss from the gas to its surroundings. A model which successfully describes this decay consists of a hot gas in turbulent motion and thus always at a uniform temperature. The chamber wall, being of steel and of such high conductivity and specific heat compared with the gas, remains uniformly at atmospheric temperature through the conduction period. Then, if the temperature difference between gas and wall is T and the surface area of the chamber is A, the heat transfer from gas to wall will be at a rate

$$Q = KAT \tag{2}$$

where K is a proportionality constant depending

on the material of the boundary (rust, paint, stagnant air, etc.).

With this understanding of the pressure-time curves, the method used to get maximum static pressure was to draw a straight line through the portion of the curve from 100 to 500 msec, extrapolate back, and read pressure at zero time. Values so obtained are listed in Table 2.

Chamber resonance measurements

Measurements on the periodic oscillations found on all records proved of considerable interest. Their amplitude was of the order of several psi. It was assumed, however, that they followed ordinary acoustic relationships and were treated as resonance of the chamber space, considered as a pipe closed at both ends. The temperature rise of the gas due to the explosion should increase the velocity of sound in the ambient gas and result in an increase of the resonance frequency of the chamber cavity. Since pressure is proportional to the temperature with no change in density, the static pressure could be determined from measurement of this frequency. The equation for velocity of sound, c, in a gas is

$$c = \sqrt{\frac{\gamma P_a}{\rho}} \tag{3}$$

where P_a is the absolute pressure, γ is the ratio of specific heats, and ρ the density of the gas. For a closed tube of length, L, the fundamental resonance frequency has a period

$$\tau = \frac{2L}{c} \tag{4}$$

If we combine Equations (3) and (4) and solve for the pressure, we have

$$P_a = \frac{4\rho L^2}{\gamma \tau^2} \tag{5}$$

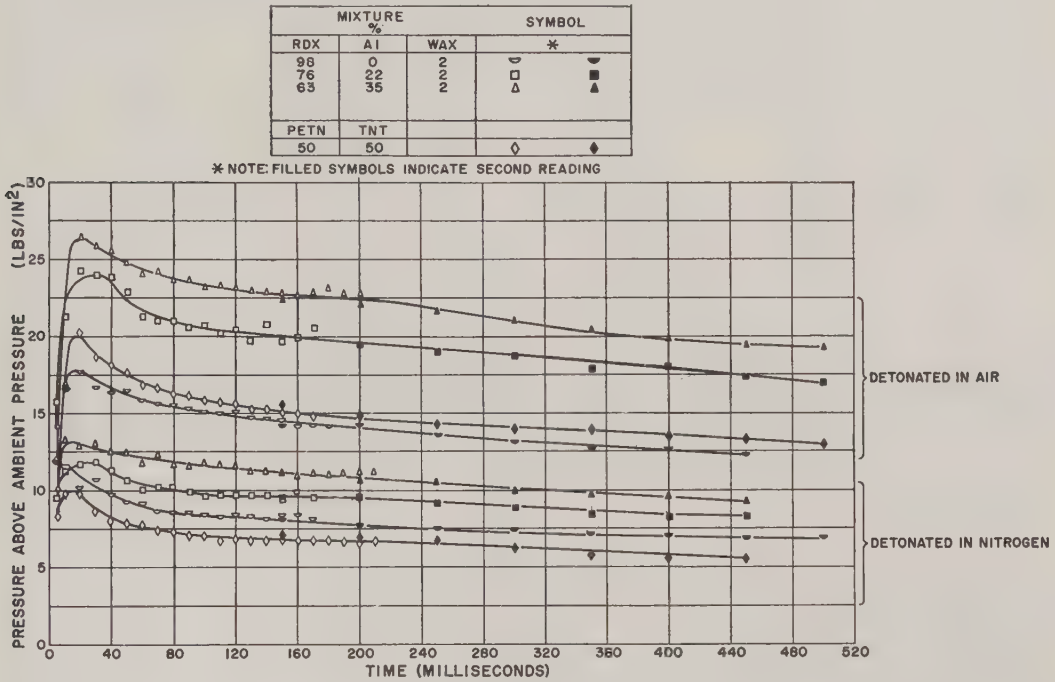

FIG. 5. Composite pressure—time histories of static pressure for explosives detonated in air and nitrogen.

TABLE 2. AVERAGE STATIC PRESSURES IN PSI UNITS FROM PHASE ONE

Explosive	Air		N_2	
	Pressure-time	Resonance	Pressure-time	Resonance
PETN/TNT 50/50	16.0	14.9	7.5	6.0
RDX (2% wax)	15.6	13.5	8.7	6.8
RDX/Al/wax 76/22/2	21.3	20.8	10.3	8.0
63/35/2	24.3	22.1	12.2	—

Note. These values are uncorrected for volume of gas products.

Since ρ, L, and γ are known, P_a may be calculated by measuring τ.

Average values (corrected for conduction decay) for each explosive listed in Table 2 are close to values obtained directly from pressure-time histories. A surprising fact is that they are about 10 per cent low as a whole, although one would expect waves of such large amplitude to move faster than sound waves, thus resulting in a shorter period and higher pressure values from Equation (5).

Table 3. Typical Set of Static Pressure Values in Psi Units From Phase Two

TNT in Nitrogen			TNT in Argon		
Shot	Gauge 1	Gauge 2	Shot	Gauge 1	Gauge 2
1	6.30	6.51	6	10.13	9.84
2	6.39	6.25	7	9.80	9.84
3	6.18	6.78	8	9.79	9.70

Note. These values are uncorrected for volume of gas products.

from 5 sec out to 20 or 30 sec is much slower but the loss rate still is linear as a function of temperature. This would be consistent with a model comprised of relatively still rather than turbulent hot gases (as in the first ½ sec) in a constant temperature enclosure. The conductivity of the gas now dominates the heat loss rate, and since gas conductivity is much lower than the boundary materials which were important during the first ½ sec, the heat loss rate would be expected to be lower than that of the earlier model.

Discussion

HEAT ENERGY VALUES

Heat energies released by the various explosives when fired in the various ambient gases were computed from Equation (1). H in Equation (1) is the total heat released for the weight of charge, W. Since the heat released per gram of explosive, h, is desired, we may write

$$h = \frac{H}{W} \tag{6}$$

Table 4. Heat Computation Data

Explosive	Air				Nitrogen				Argon			
	P	T	γ	W	P	T	γ	W	P	T	γ	W
	psi	°C		*g*	*psi*	°C		*g*	*psi*	°C		*g*
TNT	19.9	389	1.368	56.7	6.3	123	1.398	56.8	9.7	190	1.669	56.9
PETN/TNT 50/50	15.7	308	1.378	56.2	7.3	144	1.397	56.3	—	—	—	—
RDX (2% wax)	15.3	300	1.378	56.6	7.8	153	1.396	56.7	12.2	240	1.668	56.5
PETN (2% wax)	12.5	245	1.384	56.6	7.7	152	1.396	56.7	12.3	242	1.668	56.8
RDX/Al/wax 76/22/2	21.3	410	1.366	56.4	10.3	198	1.393	56.9	—	—	—	—
63/35/2	24.3	468	1.359	56.2	12.2	235	1.390	56.2	—	—	—	—

QUANTITATIVE ANALYSIS OF RECORDS—PHASE TWO

The maximum static pressure data of phase two were developed from records of the Figure 3f type. A straight edge was placed directly on each record, an average line drawn through the record for the interval from 100 to 500 msec and extended back to zero time where the maximum amplitude was read, just as was done with the phase one composite curves. A typical set of data for one explosive is given in Table 3. Average values for all explosives are listed in Table 4.

Analysis of the entire pressure decay curve obtained with the pen and ink recorder revealed that the method of heat transfer changes drastically after the first half second. Heat conduction

Combining Equation (6) with Equation (1) and using the units cu ft for volume, g for weight, and psi for pressure, the heat release per unit weight of explosive is given in calories per gram by the expression

$$h = 46.64 \frac{PV}{W(\gamma - 1)} \tag{7}$$

For these experiments the value for V, computed from measurements of the chamber, was 72.4 cu ft. From the U. S. Bureau of Standards[9] γ was obtained in accordance with the measured static pressure and computed temperature, all of which are listed in Table 4. The charge weights are also listed in Table 4. They are average values; individual values varied ±0.3 g. From

this data, heat values were computed (Table 5). Final values, except for the aluminum mixtures, have been corrected for the change in the volume of gas before and after explosion due to addition of product gases. The correction varied from 1.5 to 2.5 per cent. Adjacent to the heat values are heat of combustion and heat of detonation values obtained from other sources.

General agreement is found between chamber measurements in air and heat of combustion. Similarly, agreement is found between nitrogen and argon chamber values and heat of detonation. Some exceptions are apparent. PETN is especially low. The explanation is not immediately clear. The low value for heat of combustion of TNT suggests the inadequacy of the oxygen concentration of air at one atmosphere to complete the oxidation of explosion products before cooling of the products causes the reaction to cut off.

Some light is thrown on this matter by data collected for TNT fired in various concentrations of oxygen obtained by mixing nitrogen with air at one atmosphere. Figure 6 is a plot of that data. It shows the nature of the shift in energy release from 940 to 3,220 cal/g as the ambient gas changes from effectively pure nitrogen to air with a 23 per cent oxygen content (by weight). Notice that the heat energy released is not substantially affected by the increase in total oxygen content until past the 100 g point, although 100 g are more than sufficient to oxidize completely the amount of TNT used. Also note the rather narrow region on the oxygen concentration scale within which the transition occurs. This indicates that oxygen concentration is a critical variable.

TABLE 5. HEAT ENERGY VALUES IN CAL/G

Explosive	NOL Measurements			Other Values			
	Air	Nitrogen	Argon	Heat of combustion[10]	Heat of detonation [10]	[11]	[12*]
TNT	3220	940	860	3589.5	925	1080	768
PETN/TNT 50/50	2500	1100	—	2782†	1220	1265†	1056†
RDX (2% wax)	2250	1190‡	1110	2307.2	1300	1260	1239
PETN (2% wax)	1770	1180	1110	1974	1385	1450	1343
RDX/Al/wax							
76/22/2	3480	1560	—	3509†			
63/35/2	4070	1880	—	4124†			

Note 1. All values are for water in gaseous form.

Note 2. Heat of detonation values in the Encyclopedia of Chemical Technology[10] were computed; the Armament Research Establishment[11] used a recently developed calorimeter for approximately 100 g charges; Tonegutti[12] employed 2 g charges in the conventional calorimetric method.

* Original values for water liquid corrected by author to water gas.

† Obtained by combining values for components. Heat of combustion of aluminum to Al_2O_3 was taken as 7039 cal/g.

‡ The single value from phase one was not included.

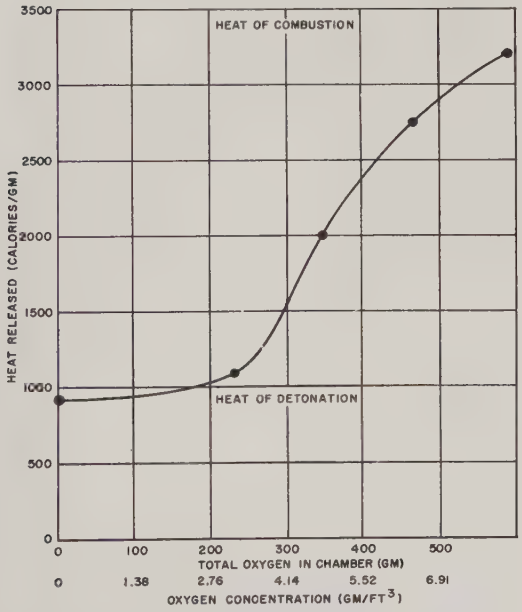

FIG. 6. Chamber heat released by TNT fired in an oxygen-nitrogen mixture of varying proportions at one atmosphere.

SIGNIFICANCE AND POSSIBLE EXTENSIONS OF THIS TYPE OF MEASUREMENT

The results of these experiments show that efforts to measure the heat of detonation need

no longer be restricted to surmounting the difficulties of designing calorimeter bombs to withstand extreme pressures. Also, convenient experimental determinations of heat of detonation values may serve as a guide to the actual detonation products formed and improve the accuracy of computation methods of determining heat of detonation. Although 2 oz charges were used in these experiments, use of larger charges is desirable and chambers may easily be designed for several pounds of explosives. Construction of such a facility is being considered by this Laboratory.

Conclusions

(1) The static pressure rise resulting from detonation of high explosives in a closed chamber has been measured and found to be in agreement with simple theory.

(2) The theory makes possible the measurement of the energy released by an explosive under various ambient gas conditions.

(3) Heat of detonation values for several explosives have been determined and, in the main, are in agreement with values from other sources.

(4) In this method for measuring heat of detonation, temperatures and pressures are relatively low and are easily dealt with in the design of apparatus. Also, this method permits the use of relatively large quantities of explosives in energy measurements.

Acknowledgment

This work is an extention of some experiments performed in World War II by W. E. Gordon for the Office of Scientific Research and Development.

REFERENCES

1. Lothrop, W. C., and Handrick, G. R.: Chem. Revs., *44*, 419 (1949).
2. Robertson, R.: J. Chem. Soc., *119*, 1 (1921).
3. Robertson, R., and Garner, W. E.: Proc. Roy. Soc. (London), *A103*, 539 (1923).
4. Taylor, J., and Hall, C. R. L.: J. Phys. Colloid Chem., *51*, 593 (1947).
5. Arons, A. B., and Cole, R. H.: Rev. Sci. Inst., *21*, 31 (1950).
6. Cole, R. H.: *Underwater Explosions*. Princeton. Princeton University Press, 1948.
7. *Bumblebee Telemetering Handbook*, Applied Physics Laboratory, Johns Hopkins University, 1949 (see Bendix Model No. TTP-3).
8. *Physical Measurements in Gas Dynamics and Combustion*, p. 129. Princeton, Princeton University Press, 1954.
9. U. S. Bureau of Standards Circular 544, Tables of Thermodynamic Properties of Gases, U. S. Gov. Printing Office, 1955.
10. *Encyclopedia of Chemical Technology*, Vol. 6, New York, Interscience Publishers, Inc., 1951.
11. Armament Research Establishment Memo 1/51: Ministry of Supply, United Kingdom (1951).
12. Tonegutti, M.: Z. ges. Schiess-u Sprengstoffw., *32*, 93–97 (1937).

Discussion by Cyrus G. Dunkle*

Heat of detonation is given by deducting the heat of formation of the explosive, from that of the mixture of products as formed at the Chapman-Jouguet (C-J) point, where they are still hot and at high pressure. Both heats of formation refer to the same standard temperature, e.g., 298°K. Heat of detonation, like heat of explosion, can be corrected to give the standard enthalpy change on formation of the respective products from the explosive.

In any explosion calorimeter, the heat measured is that evolved by the time the products have cooled to calorimeter temperature. Interaction beyond the C-J point when possible, as in an oxygen deficient system, is difficult to prevent. We try to, in determining heat of detonation, by strong confinement which keeps pressures higher and thus allows faster cooling; also the products work against resistance by shattering a steel capsule within the bomb while still at high pressure. This too speeds cooling, in hopes of "freezing" the chemical equilibria at what Springall and Roberts term their "high pressure" values. Here there are more C, CO_2 and H_2O but less CO and H_2 than at low pressures. Heats of detonation usually exceed heats of explosion because energy is evolved in forming C, CO_2 and H_2O from CO and H_2 at calorimeter temperature.

In determining heat of explosion, on the other hand, no such attempt is made. Pressure drops quickly from detonation values, but temperature stays high longer because the products make only a free expansion and do no work. They thus have time to react, and approach their "low pressure" composition before the equilibria freeze.

Filler's heats in ambient nitrogen or argon resemble in magnitude our heats of explosion. Those in air resemble heats of combustion in excess of oxygen.

Author's Reply

The values presented in this paper are low compared with values obtained with cased charges in

* Picatinny Arsenal.

a calorimeter (see reference[11]). Although this might be explained by the Springall-Roberts mechanism described by Mr. Dunkle, it is also possible that factors such as heat losses not yet established, corrections yet to be applied, and other experimental factors yet to be investigated may also be the cause. Further experiments with larger charges may also throw some light on the confinement effect.

Although the interpretation of the chamber energies as heats of detonation in the defined sense is not at all established, we believe that further work will demonstrate the probability of this interpretation.

86

THE DETONABILITY OF CERTAIN ROCKET PROPELLANTS[a]

By JOHN R. SCHOLL, H. W. BYINGTON, AND R. L. POTTER

Introduction

The development of rocket engines in this country has been hampered by the lack of a clear understanding of the combustion process. The problem has been particularly severe in the case of rocket engines utilizing fuming nitric acid and jet fuels as propellants. The manifestations of these problems are large chamber pressure oscillations of various frequencies. These are often of sufficient amplitude to destroy the thrust chamber and associated hardware. In the rocket industry this phenomenon is labeled "combustion instability." In many cases this "combustion instability" has been overcome by design changes. Unfortunately, at this time, there seem to be no definite rules to guide the rocket designer so that this problem can be overcome.

The fact that the same propellants can perform so differently in essentially the same rocket engine calls for a theoretical explanation. Several attempts have been made to explain "combustion instability" on a theoretical basis.[1] The physical basis for these theories can certainly be improved, and in fact must be, in order that the rocket designer may benefit from them. If the normal combustion process in a rocket engine can suddenly change to detonation, in some as yet unexplained manner, then qualitatively all the effects of "combustion instability" can be accounted for. Thus "high frequency combustion instability" can be explained away as spinning detonation. The other low frequency instabilities can be considered as detonations of succeeding portions of propellants injected into the thrust chamber. Each detonation results in a rise in chamber pressure, thus causing the propellant flows to oscillate severely. The destructive effects follow immediately, since the pressure rise in the gas across such a front is about 45 times the initial pressure.

In order to find out if this is indeed possible, it is necessary to find out whether fuming nitric acid and jet fuel can detonate under any conditions, and in particular, whether they can detonate under conditions similar to those encountered in a rocket engine. The experimental portion of this paper is concerned with the first question which has been answered in the affirmative by work at Bell Aircraft Corporation; at this time the second question has not been answered unequivocally, although qualitative arguments may be put forth in support of this idea. A brief discussion of the implications of these experimental results concerning the foundations of present "combustion stability" theories is presented after the experimental section of this paper.

Experimental Equipment and Technique

A schematic diagram of the equipment used to determine the conditions under which nitric acid and jet fuels detonate is shown in Figures 1a and 1b. Figures 2a and 2b are photographs of the test unit. The essential parts of this unit are a stainless steel reaction tube 3.75 cm in diam and 3 m long, separate evaporators for hydrocarbon fuel and acid and the instrumentation required to determine detonation velocities. The apparatus grew slowly as components were added to permit finer control of the acid-fuel

[a] Work supported by Contract W33(038)-ac-14169, U. S. A. F.

mixtures at a safe distance from the reaction tube. Hot nitrogen was used as the heat source for both the evaporators and the reaction tube, since all operations with the vaporized propellants had to be carried out above their condensation temperatures, but below their ignition temperatures.

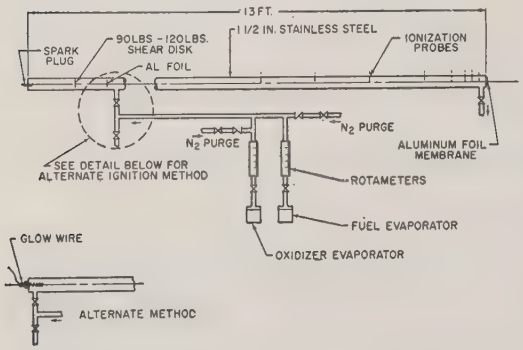

FIG. 1a. Schematic diagram of reaction tube.

in accordance with MIL-N-7254B(USAF), Type I.

Since such work with propellants that are normally liquid at room temperature has rarely been reported, the experimental procedure is given in more detail than usual. Acid and *n*-heptane were boiled under pressure in separate stainless steel evaporators. The vapors were passed through separate motorized needle valves, which permitted flows to be throttled remotely, and then through glass Fischer-Porter flow-meters to separate pairs of remotely operated, nitrogen-actuated valves. Beyond these valves, the propellants were brought together in a mixing tube, at the end of which there was another remotely controlled valve that allowed the mixed propellants either to be dumped into a flowing stream of water (bypass condition) or to be passed into the reaction tube.

When the flows of oxidizer and fuel had been stabilized to the desired mixture ratio in the

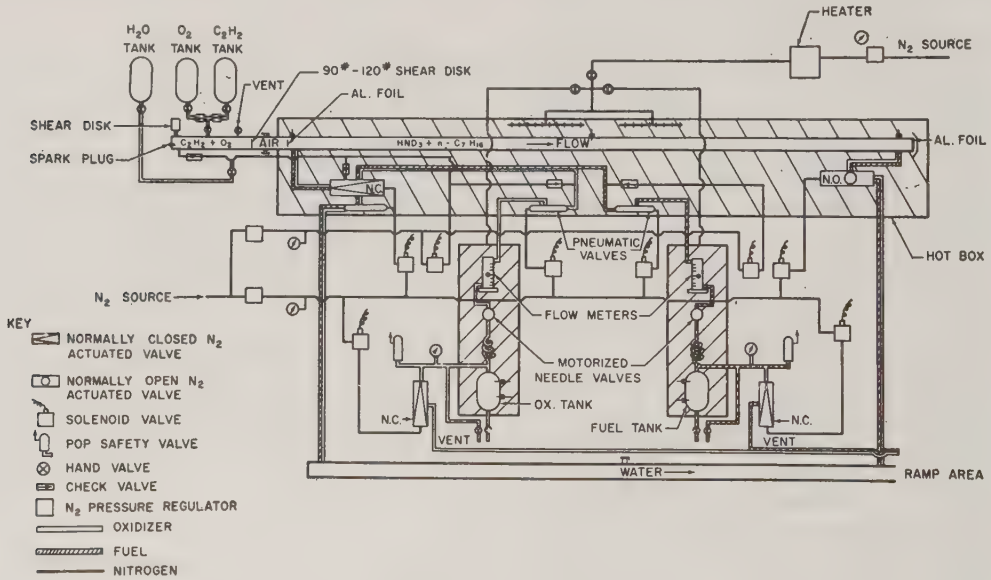

FIG. 1b. Reaction tube.

It would have been desirable to work directly with the jet fuel used in rocket engines but the difficulties involved in vaporizing such a mixture were out of proportion to the technical gain. Therefore, *n*-heptane, a typical hydrocarbon component of jet fuel, was purchased from Phillips Petroleum Company at a stated purity of 99 mole per cent and used for all the tests. Nitric acid was purchased from General Chemical Division, Allied Chemical and Dye Corporation

bypass condition, they were passed into the reaction tube itself. The mixed propellants were allowed to flow through the reaction tube for a sufficient time to displace the air and provide a homogeneous mixed propellant vapor in the reaction tube. Then the flows were stopped and the mixed propellants trapped in the reaction tube. This mixture was immediately ignited with a glow plug. Hot nitrogen was employed to maintain the vaporizing, metering and mixing

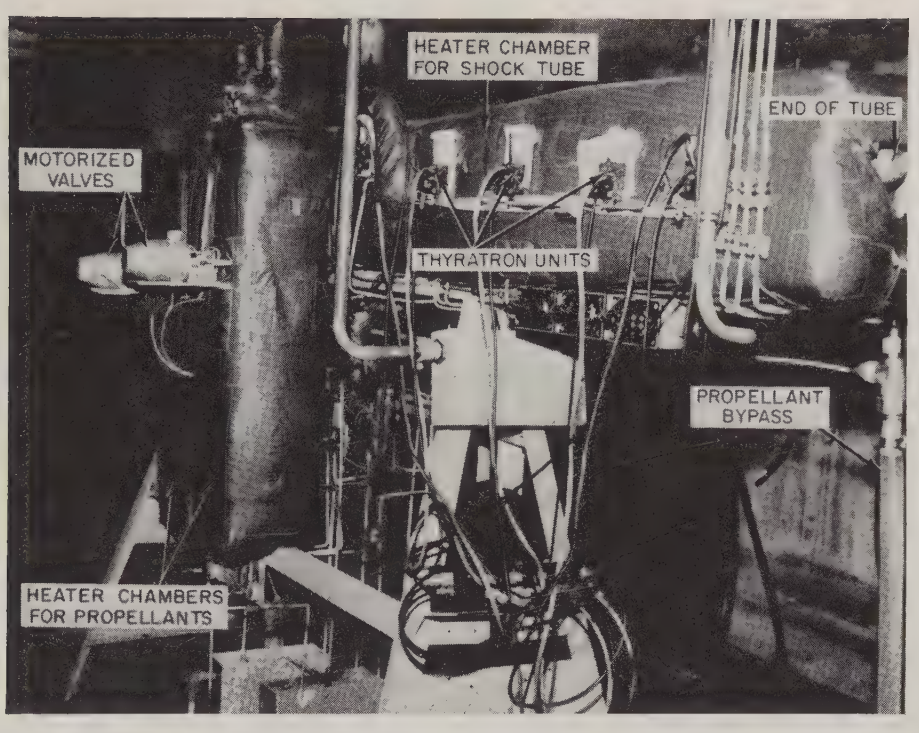

FIG. 2a. View of tube and support equipment.

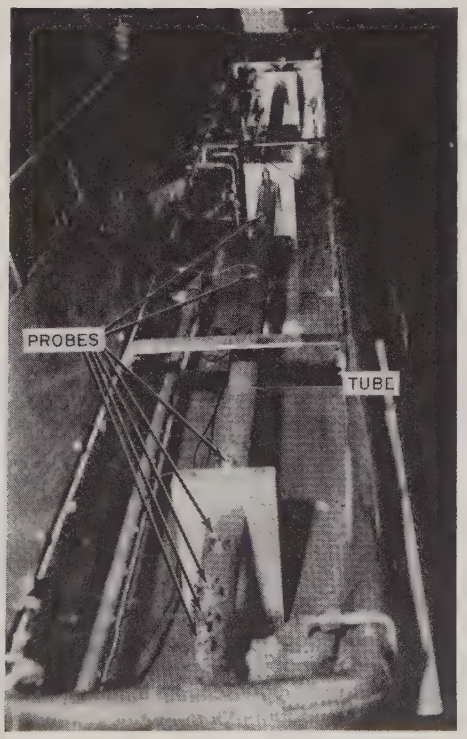

FIG. 2b. View of shock tube.

apparatus above the condensation temperatures of the propellants.

Wave velocities were measured by recording the signal from small ionization gauges set into the walls of the reaction tube at various intervals. The signals from these gauges were displayed as blanking pulses on a spiral sweep oscilloscope, and recorded photographically as shown in Figure 4. The velocity over each interval was calculated by dividing the distance between probes by the time interval between pulses. The spiral sweep was started by a pulse which was generated by the first ionization probe. A second sweep was prevented from starting by a special stop circuit. The spiral was divided into eight radial segments of 5 μsec each, thus one complete spiral corresponds to an elapsed time of 40 μsec. A crystal-controlled oscillator fixed the time basis. The accuracy of the measurements depended upon the crystal, the time of discharge of the thyratron tubes, and upon the measurements on the photograph. The crystal had an accuracy of 5 parts/100,000. Interchange of the thyratrons on the ionization probes indicated some small, just detectable, variation in their firing time. The accuracy of the results obtainable from the

photographs was no better than ±1.5 per cent. The error introduced by the measurement of the distance between the successive ionization gaps was less than 0.2 per cent in the final velocity measurement.

The flow-meters were calibrated by flowing *n*-heptane and nitric acid through them, and the effluent gases were condensed and weighed. The error in the measured flow rates was estimated to be ±3 per cent, or the mixture ratio (mass of acid per unit mass of fuel) might be in error by approximately 6 per cent. Such an error in mixture ratio, according to the theoretical curve produces about 1 per cent uncertainty in the expected detonation velocity. The uniformity of the mixture throughout the length of the pipe before initiation was not checked; however, as pointed out above, the velocity does not depend too strongly upon mixture ratio. In some cases appreciable decomposition of the acid occurred. In one case, the nitric acid gas mixture was condensed and chemical analysis showed the weight per cent of HNO_3, NO_2, H_2O and O_2 to be respectively 67.6, 26.6, 1.0, and 4.8. The calculated effect on the expected detonation velocity with this composition is to raise it about 1 per cent above that expected with 100 per cent HNO_3.

It was very difficult to keep the temperature of the gases in the pipe constant from run to run; however, calculations showed that the detonation velocity is insensitive to temperature variations of ±15°C such as were encountered in this work. The overall accuracy in the measurements of velocity is estimated to be ±2 per cent.

On one occasion ignition was attempted by electrical spark, but no flame resulted. Later a few tests were made with a driver section containing an equimolar mixture of acetylene and oxygen.[2] The driver section consisted of a 3.75 cm tube 61 cm in length separated from the main chamber by a section 15 cm in length that was filled with an inert gas, or air. This driver section was located outside the box used to thermostat the reaction tube. Aluminum diaphragms were used to separate the various sections of the assembly. A spark plug served to ignite the driver mixture.

Results and Interpretation

The results of the tests are plotted in Figure 3 which shows the experimental velocities from the runs initiated by the glow plug superimposed on the theoretical detonation velocity curve. The results are the average of velocities measured between at least three, and, in many cases, four ionization probes located in the reaction tube. As can be seen the majority of values lie above the curve. However, in most of these cases the velocity was not steady, and in fact it generally decreased down the length of the tube. Since the velocity was not steady there is no conflict between these results and the hydrodynamical theory of one-dimensional steady-state detonations. Such results have been found by other investigators.[3] Thus when a detonation is started by a deflagration in a tube, a shock develops in front of the combustion wave, and in this region a detonation wave may form. The region where this develops has been previously heated and pressurized by the compression waves sent out

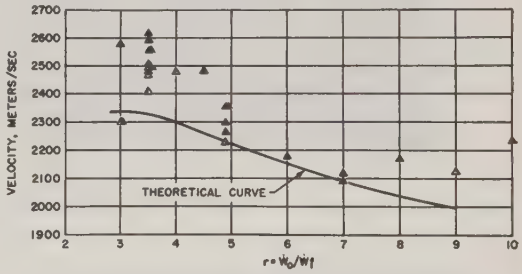

FIG. 3. Experimental velocity of HNO_3 and *n*-heptane (ignition by glow wire).

in front of the deflagration waves and the detonation develops in a non-stationary zone; the speed of the wave is often much larger than the steady-state velocity. A clear example of this phenomenon is fully discussed by Lewis and von Elbe.[4]

In run H-4 (18), the oscilloscope record of which is shown in Figure 4, the velocity was constant within the accuracy of the measurements over a distance of 1.3 m divided into four intervals. Thus the standard deviation amounted to 20 m/sec. In this rather good case, the velocity was roughly 3 per cent higher than the theoretical curve for 100 per cent HNO_3. However, this velocity is, within the limits of error, close to that expected if allowance is made for the dissociation of the acid prior to the start of the test. In this run, ignition was achieved by the glow coil system. The runs which were started by a shock show better agreement with theory (Fig. 5); in addition they exhibited constant velocity within the accuracy of measurements. There was no detectable evidence that these waves were overdriven.

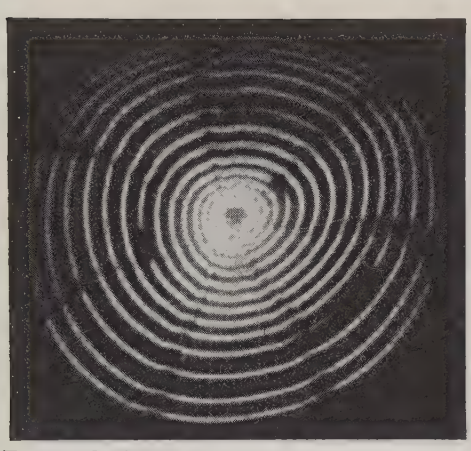

FIG. 4. Oscillograph trace of test H4-18. Mixture ratio 4.9.

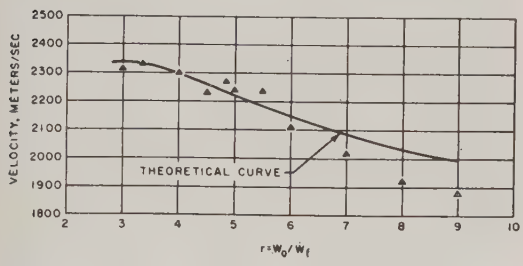

FIG. 5. Experimental velocity of HNO_3 and *n*-heptane (ignition by shock).

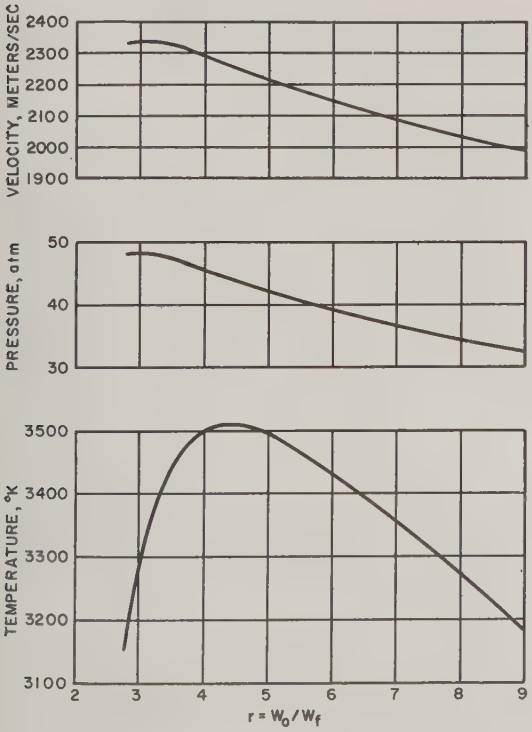

FIG. 6. Detonation parameters for HNO_3 and *n*-heptane (P_o = 1 atm.).

High flame velocities were obtained with gaseous *n*-heptane and nitric acid down to a mixture ratio of 2.8 and as high as 10. Mixtures outside these limits could be ignited by the glow coil, but the flame was so slow that the spiral sweep was all over before the flame could traverse the distance to the next ionization probe.

The theoretical curves were calculated on an IBM 650 machine. The IBM 650 program included 16 burned gas species. Only CH, C_2, and HO_2 out of all the more common radicals were ignored. The Bureau of Standards[5] tabulation of thermodynamic properties of gases provided most of the thermochemical data. Other information was taken from Kistiakowsky and associates[6] and Johnston and associates.[7] The calculations were made assuming frozen sound speed at the Chapman-Jouguet point.[8] Other detonation parameters of interest are shown in Figure 6.

The agreement between the calculated and the experimental velocities (under demonstrated steady conditions in the case of the shock initiated detonations) constitutes irrefutable evidence that gaseous nitric acid and *n*-heptane can support detonation waves.

Discussion of Results and Application to Rocket Engines

The evidence from the experiments presented here points out that some common liquid rocket propellants, besides being combustible, are also detonable. Experience at Bell Aircraft Corporation and other investigations of combustion stability in rocket engines strongly indicate that "combustion instability" is the manifestation of combustion changing to detonation. Thus when instability is encountered, it is usually sudden and very destructive. In Figure 7, the pressure arising from a one-dimensional detonation is plotted *vs.* initial pressure for a mixture of nitric acid and *n*-heptane. These calculations are for ideal conditions and the results must be lower in a thrust chamber where the gases would not be so concentrated. Thus droplets above a few μ would not contribute to the combustion wave behind the front, and the combustible gases are very likely diluted by hot, burned gases. In any event, pressure transducers do not exist that can follow the pressure rise in such circumstances. Calculations indicate that the time required for the peak pressure in such a wave to decay to $1/e$ of its original amount is of the order of magnitude of $\frac{1}{2}$ msec.[9] Therefore, the fact that large pressures have not been measured in

rocket engines during "instability" does not rule out their presence. Weak mixtures, diluted with combustion products, etc., would have a much smaller pressure rise across their fronts, and very likely would tend to spin just as observed in cases of premixed gases in tubes that are near the limits of detonability. Published work at NACA,[10] General Electric,[11] and Jet Propulsion Laboratories[12] gives photographic evidence of strong pressure waves or shocks in the combustion chamber during "instability." Those presented by workers at NACA[10] are especially interesting, as clear photographic evidence is obtained which can be simply explained as spinning detonation. The energy to support these waves can come from no other source than the chemical energy in the unburned propellants.

Our own experience indicates that design changes can overcome "combustion instability" problems. The injector seems to hold the key to these problems, and, in fact, its influence apparently dominates the whole situation. Thus experiments here have shown that pressure oscillations of considerable magnitude in the feed system of a rocket engine are not sufficient to cause instabilities. Further, flash pictures indicate that substantial amounts of unburned propellants are present in a combustion chamber during normal operation. This is also confirmed by the large L^* required for reasonable performance of liquid bipropellant rocket engines. If these unburned propellants were mixed, they would almost certainly detonate.S ince engines do operate normally, the propellants must either not be completely mixed, or they must be diluted by hot combustion products to a point where they cannot support a detonation, or some combination of these two possibilities. The preparation of the propellant and hence subsequent combustion is fixed by the injector and chamber geometry, and the role played by the successful injector is evidently to provide a combustible mixture which burns just as fast as it forms. The details of this process are at present shrouded in ignorance. However, an obvious way to reduce the influence of the injector and chamber geometry is well known. If propellants are used that burn on contact at a rate faster than they are mixed by normal injection processes, e.g., are extremely hypergolic, then no substantial amount of propellant mixture can accumulate. This idea has been demonstrated in practice; thus such propellant combinations are usually characterized by smooth combustion in a rocket engine.

A word concerning current theories of "combustion instability" should be added. That rocket propellants can detonate has been established, and that the results of "combustion instability" can be understood qualitatively, if the plausible assumption is made that the propellants are detonating, has been shown above. If detonations of rocket propellants are indeed responsible for the results of "combustion instability," then the problem of predicting when "combustion instability" will occur reduces to the problem of predicting when the normal combustion process (this includes injection, liquid mixing, evaporation, further mixing in the gas phase, chemical reactions, etc.) will turn into a detonation. But this problem has not yet been solved in the much simpler case of premixed combustible gases. Therefore, it seems premature to attempt a mathematical-theoretical treatment of combustion instability in rocket engines at this time. It is to be hoped that experiments designed to elucidate the various steps in heterogeneous combustion will reveal significant information as to the importance of these processes. A satisfactory combustion theory must instruct a rocket engineer how to design an injector first off; there is not much solace in having to design an engine, build and fire it in order to find out if the engine will perform satisfactorily.

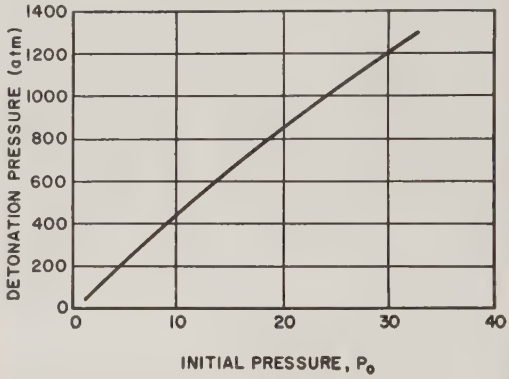

FIG. 7. Detonation pressure of nitric acid and *n*-heptane vs initial pressure at a mixture ratio of 5.

Acknowledgment

The authors thank D. Wayman, who is continuing this work, for furnishing the experimental data used in Figure 5.

REFERENCES

1. Crocco, L.: J. Am. Rocket Soc., *21*, No. 6, 163–178 (1951); *22*, 7–16 (1952). Summerfield, M.: J. Am. Rocket Soc., *21*, 108 (1951).
2. Berets, D. J., Greene, E. F., and Kistiakowsky, G. B.: J. Am. Chem. Soc., *72*, 1086 (1950).
3. Bone, W. A., Fraser, R. P., and Wheeler, W. H.: Trans. Roy. Soc. (London), *A235*, 29 (1936).
4. Lewis, B., and von Elbe, G.: *Combustion, Flames, and Explosions of Gases*, p. 616. New York, Academic Press, Inc., 1951.
5. Rossini, F. E., et al.: NBS Circular 500, and Series III; Rossini, F. E., et al.: NBS Circular C461.
6. Kistiakowsky, G. B., Knight, H. T., and Malin, M.: J. Chem. Phys., *20*, 876 (1952).
7. Johnston, H. L., Belzer, J., and Savedoff, L.: Ohio State University Research Foundation, Columbus 10, Ohio, TR316-7, 1 May 1950.
8. Brinkley, S. R., Jr., and Richardson, J. M.: *Fourth Symposium (International) on Combustion*, p. 450. Baltimore, The Williams & Wilkins Co., 1953; Kirkwood, J. G., and Wood, W. W.: J. Chem. Phys., *22*, 1915 (1954).
9. Taylor, G. I.: Proc. Roy. Soc., *A200*, 235 (1950).
10. Tischler, A. O., and Male, T.: Proceedings, Gas Dynamics Symposium on Aerothermochemistry, p. 71, Evanston, Illinois, Northwestern University Press, 1956.
11. Berman, K., and Cheney, S. H., Jr.: Jet Propulsion, *25*, 513 (1955).
12. Ellis, H., Odgers, I., Stosick, A. J., Van de Verg, N., and Wick, R. S.: *Fourth Symposium (International) on Combustion*, p. 880. Baltimore, The Williams & Wilkins Co., 1953.
13. Hirschfelder, J. O., Curtiss, C. F., and Campbell, D. E.: *Fourth Symposium (International) on Combustion*, p. 190. Baltimore, The Williams & Wilkins Co., 1953; Courant, R., and Friedricks, K. O.: *Supersonic Flow and Shock Waves*. New York, Interscience Publishers, Inc., 1948.

87

A MATHEMATICAL METHOD TO PREDICT THE EFFECTS OF EROSIVE BURNING IN SOLID-PROPELLANT ROCKETS[a]

By J. M. LENOIR and G. ROBILLARD

A burning-rate law for solid propellants is proposed based on the postulate that the erosive component of the burning rate is proportional to the heat-transfer rate from the core of the combustion gas stream to the propellant walls. A transpiration model for the core gas is used to compute the heat-transfer rate. The burning-rate law developed from theoretical considerations is:

$$r = aP^n + \frac{\alpha G^{0.8}}{L^{0.2} e^{(\beta r \rho_c / G)}}$$

By digital-machine computations on a limited range of propellants and burning conditions, this new burning-rate law was found to predict the results of interrupted burning of solid-propellant rocket motors within the limits of experimental error.

As a solid propellant burns, its surface recedes at a rate known to be a function of the gas pressure and the velocity of the combustion gases flowing parallel to the burning surface. Customarily, the effect of pressure and velocity on the burning rate is correlated by a dimensional expression of the form

$$r = aP^n + acVP^n \qquad (1)$$

The term, aP^n, represents the component of the burning rate, r_p, controlled by pressure alone. The term, $acVP^n$, represents the additional effect of gas velocity on the burning rate and is called the erosive-burning increment; the propellant constant, c, is obtained from the analysis of many tests in which the burning of solid-propellant rockets is interrupted and is specific for a par-

[a] This paper presents one phase of research carried out at the Jet Propulsion Laboratory, California Institute of Technology, under Contract No. DA-04-495-Ord 18, sponsored by the Department of the Army, Ordnance Corps.

ticular propellant. Equation (1) is not satisfactory because it gives only a fair estimation of the erosive-burning rates. Further, a great many interrupted-burning tests must be made, requiring considerable time, money, and effort in order to get results of moderate accuracy. It is the object of this report to develop a method for predicting erosive burning that gives a more adequate representation of erosive burning and that can be applied with accuracy after only limited experimental work has been done.

To develop a new erosive-burning law, the following model is postulated. To maintain combustion, the propellant wall receives heat to bring each succeeding layer of propellant to the burning temperature. The main source of heat is from the primary-burning zone in the first few milli-inches adjacent to the propellant wall. The mechanism of heat transfer from this primary-burning zone to the wall is by a complex combination of conduction, heterogeneous turbulent convection, and radiation. The mechanism is such that the heat-flow rate is independent of the core-gas velocity. The narrower the primary-burning zone, the less resistance exists to heat transfer by this complex mechanism. Increased pressure is considered to narrow the primary-burning zone through an increase in the gas-phase reaction rate. The burning rate is thus pressure-dependent. The second source of heat is from the core of the hot combustion gases. This second source of heat flow acts through convective mechanism and is therefore dependent upon gas-flow rates. The total burning rate is thus the sum of two effects, a rate dependent upon pressure and an erosive rate dependent upon combustion-gas-flow rate, as

$$r = r_p + r_e \tag{2}$$

As a picture, a burning rocket is considered to consist of a central core of combustion gases, surrounded by a cylindrical primary-burning zone only m-in. thick, which is in turn surrounded by the propellant walls. Focusing attention only on the central core of combustion gases, this is an on-rushing gas stream with gas transpiring into the core from all sides. This transpiring gas enters the core at right angles to the direction of gas flow, with a mass velocity equal to the product of the burning rate and the propellant density. The heat-transfer model is therefore not that of a gas flowing down a simple tube, but rather heat transfer in a tube under conditions of vigorous transpiration.

It is this specific consideration of transpiration as a pertinent part of the burning mechanism that differs from previous propellant burning theories. For example, a theory of burning was advanced by Corner[1] relating the burning rate to the thermal conductivity of the laminar gas layer and an eddy conductivity dependent on flow rate for flow in a simple tube without transpiration. Corner's relation under conditions where it can be practically evaluated reduces to the form of Equation (1).

It is of interest to consider the effects of physical drag on the propellant walls as a factor contributing to the erosive-burning increment. The physical nature of the propellant walls makes this picture of flow erosion unlikely as a significant contributing factor. But, more important, drag and convective heat transfer are dependent upon the same gas-flow parameters. For this reason, it is considered not necessary to distinguish between heat-flow and drag effects in the ensuing discussion.

It has been established[2, 4, 5, 6, 9] that the result of transpiration into flowing gas stream is to reduce both heat-transfer rate and drag. The degree of reduction is very considerable, so much so that for the conditions of strong transpiration, the core gas approaches the conditions of being insulated from the propellant walls and also lubricated from contact with the propellant walls. Complete insulation and lubrication is substantially attained near the head end of the rocket motor. As the nozzle end of the grain is approached, the degree of insulation and lubrication becomes continuously poorer. The self-lubricating properties of the combustion core gas mean small drag losses. The energy losses suffered by the flowing gas are thus only in a minor way due to friction but are primarily caused by momentum losses suffered in accelerating the transpiring gas.

The relationship between the heat-transfer coefficient, h, under conditions of transpiration, and the heat-transfer coefficient, h_0, with zero transpiration, can be expressed in exponential form,[5, 6, 7] as

$$h = h_0 e^{-\beta Q/G} \tag{3}$$

The erosive burning rate is postulated to be proportional to the heat-transfer coefficient. Substituting Equation (3) in Equation (2),

$$r = aP^n + k\, h_0\, e^{-\beta Q/G} \tag{4}$$

The heat-transfer coefficient under conditions of zero transpiration is correlated by the Chilton-

Colburn equation for flow over a flat plate,[3]

$$h_0 = 0.0288\ G\ C_p\ R_x^{-0.2}\ Pr^{-0.667} \quad (5)$$

Combining Equations (4) and (5),

$$r = aP^n + [0.0288\ C_p\mu^{0.2}\ Pr^{-0.667}]k\left(\frac{G^{0.8}}{L^{0.2}e^z}\right) \quad (6)$$

where

$$z = \beta r\rho_c/G \quad (7)$$

The combustion gases of many solid propellants have similar heat capacity, viscosity, and Prandtl number. Because of this fact, the expression in

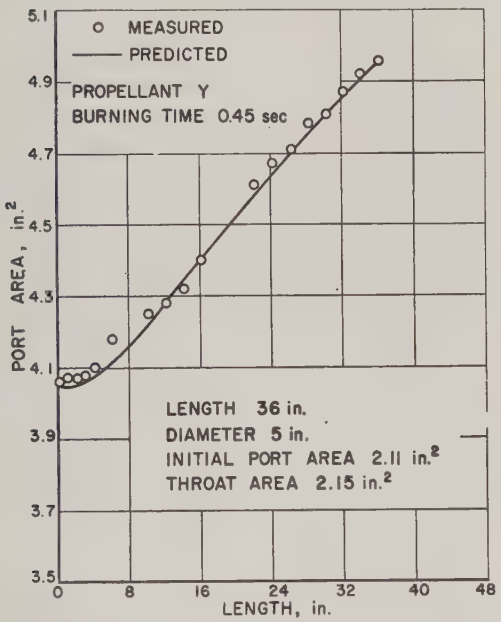

FIG. 1. Interrupted burning of port area vs grain length.

the brackets of Equation (6) is reasonably insensitive to changes in propellant identity. For simplicity,

$$\alpha = [0.0288\ C_p\ \mu^{+0.2}\ Pr^{-0.667}]k \quad (8)$$

The resulting form of the erosive burning law is

$$r = aP^n + \alpha G^{0.8}/L^{0.2}e^z \quad (9)$$

Because of the self-lubricating effects of transpiration, the drag of the combustion gas on the propellant walls is negligible with large values of r/G. Under these conditions the gas flow is frictionless with mass addition. On this consideration, the pressure along the grain is given by

$$P = P_F/(1 + \gamma M^2) \quad (10)$$

The mass velocity along the grain is similarly:[8]

$$G = G^*M\sqrt{\frac{2(\gamma+1)\left(1+\left(\frac{\gamma-1}{2}\right)M^2\right)}{1+\gamma M^2}} \quad (11)$$

Instantaneous values of mass rate were obtained by use of a nozzle throat tap, and the relation:

$$\dot{w} = \frac{gA_tP_t}{c^*}\left(\frac{\gamma+1}{2}\right)^{\frac{\gamma}{\gamma-1}} \quad (12)$$

The simultaneous combination of Equations (9), (10), (11) and (12) with necessary geometric relations, makes a procedure for computing the burning rate and port area at any time or position in the rocket grain. This calculation is adaptable to digital-machine computers, using iteration over incremental lengths of propellant grain, and incremental time intervals.

To effect machine computations, a value of α of Equation (9) and a value of β of Equation (7) must be established. One procedure employs laborious trial and error. It was assumed that α and β were constants for a particular propellant. By guessing values of α and β and matching the computed total mass rate of flow out of the rocket nozzle to the measured mass rate, the constants can be established. By repeated machine computations of this sort, values were obtained that gave the best fit to the results of interrupted-burning tests. For example, for a particular propellant, Y, a value of $\alpha = 2.12 \times 10^{-4}$ and a value of $\beta = 53$ were obtained. The numerical value of α is dependent on units, and the number given is for burning rates of ft/sec. The closeness of the fit with measured values is illustrated in Figure 1 where the experimental and computed port area after 0.45 sec burning time is as a function of position down the grain. It is of special interest that this new burning rate law predicts the "threshold velocity" effect,[3] where the erosive effect is not observed over a portion of the head end of the propellant grain. Predictions based on Equation (1) do not show this "threshold" phenomenon, nor does the theory of Corner[1] under circumstances where the numerical values can be ascertained. The results of studies on similar type of propellants have shown that β is apparently independent of propellant identity, and α shows some small variation with different propellants. For a given propellant, the values of α and β remain constant, independent of grain length, initial port to throat ratio, and pressure level, within the accuracy of the erosive interrupted-burning tests

and applied to the limited number of similar type propellants tested. That $\beta = 53$ has been further substantiated by recent as yet unreported measurements[4] made under transpiration conditions in geometries similar to that of a rocket engine. As it stands, this mathematical system is valid for predicting erosive-burning rates. A single interrupted-burning test, satisfactorily performed, seems adequate to determine α and β.

For such a test, the pressure-time curves for both the head-end of the rocket and at the nozzle throat are needed, together with geometric measurements.

In addition to obtaining α by trial and error computation, an estimate can be made based on a semi-theoretical analysis. Referring to Equation (6), the constant, k, is the proportionality factor between the erosive-burning increment and the heat transfer from hot core gas to the propellant wall. This transferred heat causes the temperature of the propellant wall to rise from the ambient temperature, T_i, to the burning surface temperature, T_s. If T_F is the flame temperature, a heat balance per unit area gives:

$$h(T_F - T_s) = r_e \rho[C_{ps}(T_s - T_i)] \qquad (13)$$

This equation assumes that no significant exothermic or endothermic processes occur in the solid phase during heating to the burning-surface temperature. Solving for r_e,

$$r_e = \frac{h}{\rho_c C_{ps}} \left(\frac{T_F - T_s}{T_s - T_i} \right) \qquad (14)$$

Realizing from Equation (4) that $r_e = hk$,

$$k = \frac{1}{\rho c C_{ps}} \left(\frac{T_F - T_s}{T_s - T_i} \right) \qquad (15)$$

and

$$\alpha = \frac{0.0288 C_p \mu^{+0.2} Pr^{-0.667}}{\rho_c C_{ps}} \left(\frac{T_F - T_s}{T_s - T_i} \right) \qquad (16)$$

In order to determine T_s, let us now consider the burning rate under nonerosive conditions. For the propellants under consideration, and for very short grain rockets the burning law that applies is the simple one,

$$r = aP^n \qquad (17)$$

The exponent, n, has been experimentally found to be essentially independent of ambient temperature, T_i, but the value of a varies somewhat with changing ambient temperature. It has been established that

$$a = b/(T_s - T_i) \qquad (18)$$

From firing a series of short grain rockets with significantly different ambient temperatures, say at 160°F and −40°F, a high and low temperature value of a can be obtained. Then, as a first approximation

$$a_{160}/a_{-40} = (T_s - T_{-40})/(T_s - T_{160}) \qquad (19)$$

and a solution for T_s results. Using the value of flame temperature determined from thermochemical calculations, the quantity $(T_F - T_s)/(T_s - T_i)$ was computed.

The terms of Equation (15) can now be evaluated without recourse to trial and error fitting. By substituting the appropriate properties of propellant, Y, in Equation (15), and with knowledge of a_{160} and a_{-40}, a value of $\alpha = 2.25 \times 10^{-4}$ ft$^{2.8}$/lb$_m^{0.8}$ sec$^{0.2}$ was computed. When it is realized that it is difficult to ascertain with accuracy the heat capacities, viscosities, etc., of gas or propellant that are needed to insert in Equation (15), it is seen that excellent agreement is obtained between the computed value and the value of $\alpha = 2.12 \times 10^{-4}$ obtained by trial and error fitting. The excellence of the agreement is probably fortuitous but the magnitude of this result gives confidence to the heat-transfer theory of erosive burning and to the use of Equation (9).

It is of interest qualitatively that Equation (9) predicts a large degree of erosive burning for slow-burning propellants, and conversely, small amounts of erosive burning with fast-burning propellants. This conclusion is in accord with the known behavior of solid propellant burning.

The transpiration model and heat-transfer theory of erosive burning gives promise of being an effective method to predict erosive burning in solid-propellant rockets. From theoretical considerations it has been possible to develop the form of an equation relating the effect of gas velocity on the burning rate of solid propellants. Values of the appropriate constants as determined from the physical and chemical properties of the propellants thus far considered show excellent agreement with those determined by interrupted-burning techniques. Future efforts will be devoted to extending the theoretical treatment to other solid-propellant systems in order to determine whether it is universally applicable.

Nomenclature

a constant in burning-rate law, dependent upon ambient propellant temperature and specific to propellant identity
A_t area of nozzle throat
b constant
c old erosive-burning constant
c^* characteristic velocity
C_p heat capacity of combustion gas, Btu/lb F
C_{ps} heat capacity of solid propellant, Btu/lb F
G mass velocity of combustion gas, lb_m/ft^2 sec
G^* mass velocity of gas where $M = 1$
h heat-transfer coefficient with transpiration, Btu/sec ft^2 F
h_0 heat-transfer coefficient with zero transpiration
k proportionality constant
L length from head of grain, ft.
M Mach number
n exponential constant
P pressure, lb_f/ft^2
P_F pressure at head end of propellant grain
Pr Prandtl number of combustion gas
P_T pressure at nozzle throat
Q Mass velocity of transpiring gas, lb_m/ft^2 sec.
Re Reynolds number, based on distance from flow origin, LG
r burning rate, ft/sec
r_e erosive-burning rate
r_p burning rate dependent upon pressure
T_F flame temperature, R
T_i ambient propellant temperature, R
T_s propellant surface temperature, R
V core-gas velocity, ft/sec
z exponent, $\beta_{Q/G}$
α erosive constant, $ft^{2.8}/lb_m^{0.8}sec^{0.2}$
β dimensionless exponential constant
γ heat-capacity ratios
μ viscosity of combustion gases, lb_m/ft-sec
ρ density of gas, lb_m/ft^3
ρ_c density of propellant, lb_m/ft^3

REFERENCES

1. Corner, J.: Trans. Faraday Society, *43*, 635 (1947).
2. Duwez, P., and Wheeler, H. L.: J. Aeronaut. Sci., *15*, 509 (1948).
3. Green, L. J.: Am. Rocket Soc., *24:* 9 (1954).
4. Lenoir, J. M.: Unpublished studies on heat transfer rates under conditions of transpiration, 1956.
5. Mickley, H. S., Ross, R. C., Squyers, A. C., and Stewart, W. E.: NACA TN 3208, July 1954.
6. Rannie, W. D.: Progress Report 4–50, Jet Propulsion Laboratory, Pasadena, California.
7. Rubesin, M. W., Pappas, C. C., and Okuno, A. F.: NACA RM A55 119, Dec. 21, 1955.
8. Shapiro, A. H.: *The Dynamics and Thermodynamics of Compressible Fluid Flow*, Vol. I, p. 239. New York, The Ronald Press, 1953.
9. Wheeler, H. L., and Duwez, P.: J. Am. Rocket Soc., *25*, 519 (1955).

Evaporation and Combustion of Droplets and Sprays

88

COMBUSTION OF FUEL SPRAYS

By SEIICHIRO KUMAGAI

Introduction

The combustion of fuel sprays is of practical importance in diesel engines, gas turbines, various types of jet engines, liquid propellant rocket motors, and industrial furnaces. It is a very complex phenomenon, involving atomization and evaporation, mixing processes, and chemical kinetics. As a first step in attacking this complicated problem we have considered the combustion of fuel droplets and the diffusion flame of fuel gases, which represent extreme cases of the combustion of fuel sprays. The combustion of fuel droplets has been investigated actively in recent years, and the diffusion flame of fuel gases long has been a subject of combustion research. On the other hand, the study of the combustion of fuel sprays is in the initial stage, and a considerable effort will be needed for advances in this field.

In the present paper, we have limited our discussion to the combustion of fuel droplets and to certain special topics.

Theoretical Analyses and Experimental Work

The phenomenon of droplet combustion has been treated as a case of heat transfer, accompanied by mass transfer. However, droplet combustion cannot be attacked successfully by such a treatment alone. Theoretical analyses on this subject have been made by Godsave,[1] Spalding,[2] Goldsmith and Penner,[3] Okazaki and Gomi,[4] and others. Some of the analyses are general, others are particular. Although they differ in minor points, these theories all are similar in essence. They assume a steady state of burning for a combustion model of spherical symmetry. The assumption of spherical combustion is valid, as we are concerned with the combustion of very fine droplets where neither forced nor natural convection plays an important role. The steady state is to be expected for the combustion of most hydrocarbon droplets, but not for certain liquid propellant droplets.

Based on these theories, we have

$$D_0^2 - D^2 = kt$$

where D is the droplet diameter, D_0 is the initial droplet diameter, t is the time, and k is the evaporation constant and is independent of both time and initial diameter. This relation is known as the first power of the diameter law. The ratio of flame diameter to droplet diameter remains constant. Deviation from these laws occurs when the composition and physico-chemical properties of the droplet change during combustion.

If the physico-chemical parameters of the fuel and the ambient condition are given, the evaporation constant and other quantities, such as the flame diameter and the flame temperature, can be calculated from these theories. In this way, the effect of ambient temperature, ambient pressure and ambient oxygen concentration on droplet combustion of various kinds of fuel has been predicted theoretically. However, the calculated values are not in satisfactory agreement with the observed values, except in the case of the evaporation constant. These discrepancies cannot be attributed solely to neglect of thermal dissociation, radiation effect and the unavailability of physico-chemical properties.

Experimental investigations have been made, using various techniques. Two methods are available for handling droplets. One is to suspend the droplet from a filament; the other is to leave the droplet free. The latter is divided into falling droplets and droplets ejected upward. The falling

droplet is inevitably subjected to the relative velocity or forced convection of the surrounding gases. Investigation of an upward moving droplet at the crest of its trajectory is restricted within narrow limits of experimental conditions. The suspended droplet method, using silica filaments, is applied most frequently and conveniently, although it is not free from undesirable effects due to the filament. As there is no perfect method, we must select the one best suited to the objective of the experiment.

The best suited of the methods of observation are silhouette photography for the burning rate of droplets, direct photography for flame boundaries, and schlieren photography for hot gas zones. A pressurized, heated combustion chamber is used to vary the ambient conditions over a wide range. A droplet of about 0.1 mm initial diameter is the easiest to treat. It is difficult to reduce the initial droplet diameter below 1 mm by conventional techniques. A burning droplet is not spherical, but has a tear-drop shape. Unless the lateral diameter of a burning droplet, or some mean value of diameters, as applied to Godsave, is considered, the droplet is treated as an equivalent sphere of equal volume or surface area.

The evaporation constant for various kinds of fuel has been determined and compared with the theoretically predicted values. The agreement between the two sets of data is relatively good but depends on the numerical values of the physicochemical properties used.

Observations as to the effect of the ambient conditions on a burning droplet may be summarized as follows.

AMBIENT PRESSURE

It has been shown empirically that the burning rate, or the evaporation constant, is roughly proportional to the n^{th} power of the absolute pressure.[5, 11] The values of n range from 0.2 to 0.4, i.e., the influence of the ambient pressure on a burning droplet is rather small. This is not surprising considering that the evaporation constant contains various factors, some of which increase it whereas others decrease it, with increasing ambient pressure. However, at higher pressures near the critical state, the pressure effect would be considerable.

AMBIENT TEMPERATURE

Goldsmith has correlated data obtained by him at lower temperatures with Kobayashi's data obtained at higher temperatures for n-heptane and benzene, both sets of values being very scattered.[6, 11] Experimental data for cetane, n-heptane and ethyl alcohol at temperatures ranging from room temperature to 700°C were given in our previous paper.[8] Roughly speaking, the experimental data show an increase of burning rate of the order predicted theoretically as the ambient temperature increases.

AMBIENT OXYGEN CONCENTRATION

Experiments with n-heptane and ethyl alcohol droplets burning in various oxygen-nitrogen mixtures show that the increase of burning rate with increasing oxygen concentration is in satisfactory agreement with the theoretically calculated value.[11] Introduction of chemical kinetics into the theory of droplet combustion has been suggested in view of the carbon and residue formation noticed in the combustion of aromatic fuel droplets at higher weight fractions of oxygen.[11]

The combustion of fuel droplets in a vibrating air field and the effect of forced convection on a burning droplet also have been investigated.[1] The latter will be mentioned later in this paper. The increase of the evaporation constant caused by air vibration cannot exceed some limit as shown by the following empirical formula:

$$\dot{k} = k_0 + Afa^2(B - fa^2)$$

where k_0 is the evaporation constant in still air, a and f are the amplitude and the frequency of air vibration, respectively, and A and B are constants. Taking fa^2 as a kind of diffusivity, the above relation can be applied to the case of a turbulent air field.

Ignition Problems[9]

In considering ignition problems, we feel that the spontaneous ignition of a fuel can be treated as a statistical phenomenon, like electric sparking and the fracture of solid materials. The probability, μ, that ignition will occur in unit time is a function of the time, t. Denoting the probability in which the ignition lag falls between t and $t + dt$ by $q(t)dt$, and the probability in which the ignition lag exceeds t by $p(t)$, we have

$$p(t) = \int_t^\infty q(t)\, dt$$

and

$$p(0) = 1$$

As the probability that ignition will occur in the

time dt (there having been no ignition up to t) is expressed by $p\mu dt$ and is equal to $-dp$, we have

$$\mu\, dt = -dp/p = -d(\log p)$$

If the frequency distribution of ignition lags, $Nq(t)\, dt$, is measured experimentally, $\mu(t)$ can be obtained by the above equation. N denotes the total number of measurements.

Application of this treatment to actual ignition problems shows that, in general, μ is equal to zero for a certain period, t_0, and then rises rapidly to a finite value. In the special case where $\mu = 0$ for $0 < t < t_0$ and $\mu =$ constant, m, for $t_0 < t$,

$$p(t) = \exp(-mt) \qquad (t_0 < t)$$
$$= 1 \qquad (0 < t < t_0)$$

and

$$q(t) = m \exp(-mt) \qquad (t_0 < t)$$
$$= 0 \qquad (0 < t < t_0)$$

Denoting the mean value of ignition lags by $\bar{t}$, we have

$$\bar{t} = \int_0^\infty qt(t)\, dt = \int_0^\infty tm \exp(-mt)\, dt = t_0 + \frac{1}{m}$$

This equation shows that the ignition lag consists of two parts, the mean values of which are t_0 and $1/m$, respectively.

The ignition lag is considered as a succession of so-called physical lag and chemical lag. Compression ignition of a premixed gas plays no physical part in its ignition lag. In the combustion of a liquid propellant rocket, the chemical lag may be very small compared to the physical lag, but in most fuel vapor-droplet systems, the physical and chemical lags must be considered separately, because they are different in nature. In actual combustion problems, the two components of the ignition lag introduced in the above equations could be interpreted as the physical and the chemical lag, although we have no reason *a priori* for this.

An experiment on the ignition of fuel droplets in a heated cup may be mentioned, the results of which are given in Figure 1 and Tables 1, 2 and 3. The physical lag is not affected by addition of small quantities of so-called ignition inhibitors and ignition promoters, such as tetraethyl lead and amyl nitrite (see Tables 1 and 3). The interpretation of the experimental results in Table 2 is that in this case amyl nitrite evaporates and ignites earlier than gas oil. It is known that there are two classes of ignition promoters. In one, the ignition promoter acts as a catalyst in the preflame combustion; in the other, the promoter itself acts as the ignition source.

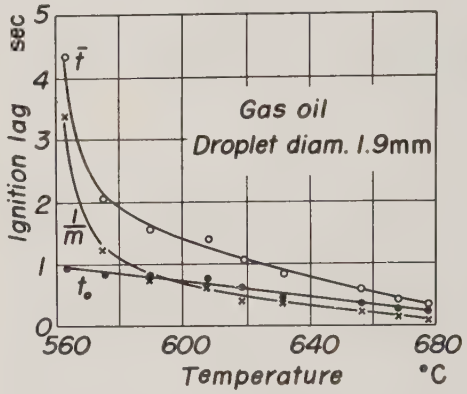

FIG. 1. Temperature dependence of physical lag and chemical lag.

TABLE 1. EFFECT OF TETRAETHYL LEAD ON IGNITION LAG OF GAS OIL

(Cup Temperature = 660°C, Initial Droplet Diameter = 1.9 mm)

	t_0	$1/m$
	sec	sec
Gas oil	0.275	0.130
Plus ethyl fluid 0.2 per cent	0.275	0.365

TABLE 2. EFFECT OF AMYL NITRITE ON IGNITION LAG OF GAS OIL

(Cup Temperature = 630°C, Initial Droplet Diameter = 1.9 mm)

	t_0	$1/m$
	sec	sec
Gas Oil	0.50	0.33
Plus amyl nitrite ? per cent	0.16	0.08

TABLE 3. EFFECT OF AMYL NITRITE ON IGNITION LAG OF *N*-HEPTANE

(Cup Temperature = 630°C, Initial Droplet Diameter = 1.9 mm)

	t_0	$1/m$
	sec	sec
n-Heptane	0.39	0.23
Plus amyl nitrite 2 per cent	0.38	0.16

In combustion in diesel engines, the chemical lag, although small, cannot be neglected by comparison with the physical lag under the normal operating condition. The physical lag is of the same order as the chemical lag in the initial cold stage. Ignition promoting additives, especially of a catalytic type, can be effective only under operating conditions where the chemical lag plays a considerable part in the ignition lag and for fuels having a relatively low cetane number, because the cetane number of diesel fuels is considered a practical measure of the chemical lag. The relative importance of the atomization and mixing characteristics increases with increasing compression ratio of the engine.

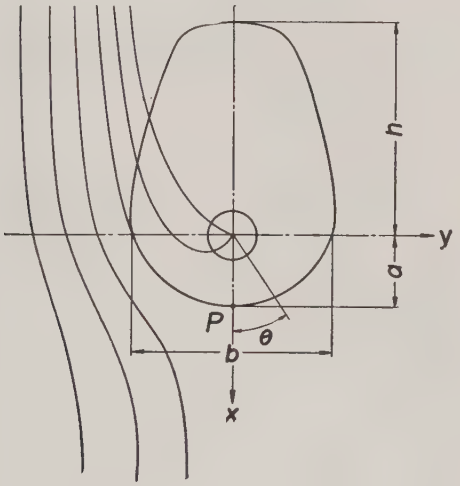

FIG. 2. Schematic diagram of fuel droplet burning under natural convection.

In the study of ignition problems of fuel vapor-droplet systems, it is important to measure separately the physical lag and the chemical lag by means of the above or any other good method, although the boundary between the two lags is more or less ambiguous.

Convection Effects

The combustion of a suspended droplet in still air is affected by the upward current due to natural convection. In this type of combustion of fuel droplets, the first power of the diameter law applies precisely. In fact, most experimenters first confirmed this law for the above type of combustion of fuel droplets, and there appeared to be good agreement between the experimental data and the theory based on a combustion model of spherical symmetry. On the contrary, however, the combustion of fuel droplets under natural convection is very different in nature from that assumed in the theory. The most striking fact is that the lower height and the diameter of the flame on the horizontal section through the center of the droplet remain constant, whereas the upper height of the flame is directly proportional to the droplet diameter. This is a contrast to the theoretical prediction that the ratio of flame diameter to droplet diameter remains constant.

Our previous experimental results and a theoretical analysis of the combustion of fuel droplets with natural convection[10] have been referred to by United States scientists in a recent paper.[15] In this investigation, a three dimensional flow was assumed which is a combination of the uniform air flow and the source of fuel vapor as shown in Figure 2. Using symbols given in the figure, the stream function is

$$\psi = -\pi U y^2 + \frac{m}{2}(1 - \cos\theta)$$

where m is the energy source. The contact surface is described by the following equations:

$$y = R \sin \tfrac{1}{2}\theta$$

$$x = \frac{R \cos\theta}{2 \cos \tfrac{1}{2}\theta}$$

$$R = \sqrt{\frac{m}{\pi U}}$$

It is assumed that the air flow comes in contact with the vapor flow at the point, P, and that interdiffusion between these two gases originates at this point. The observed shape of the lower half of the flame is very close to such a contact surface. The theoretical value of b/a is $2\sqrt{2}$, and is in agreement with the experimental value.

The source energy is directly proportional to the burning rate and consequently to the droplet diameter by the first power of the diameter law. Therefore, U must be directly proportional to D, for the lower half of the flame to remain unchanged during combustion, i.e., R is independent of D. This means that the quantity of air brought into the flame zone per unit time is directly proportional to the droplet diameter and accordingly to the burning rate of the droplet, suggesting that the upward current produced by natural convection supplies the air required for this type of combustion of fuel droplets.

For simplicity, the upper half of the flame is approximated to a cylindrical diffusion flame of the type treated by Burke and Schumann. If the

fuel droplet is considered to burn mainly in the upper flame zone, the mean velocity of the fuel vapor at $x = 0$ is

$$u = m/A$$

where A is the cross-sectional area of the flame at $x = 0$. As m is directly proportional to D, and A is independent of D, u is directly proportional to D. Therefore, the fact that the height of the upper half of the flame is directly proportional to the droplet diameter can be explained by the nature of cylindrical diffusion flames.

As regards the influence of forced convection on a burning droplet, Goldsmith[11] has reported his experiment in his paper on Spalding's work.[2] Nevertheless, it may help in understanding this phenomenon to present our experiment on cetane, the result of which is illustrated by Figure 3.

Even in this type of combustion of fuel droplets, the first power of the diameter law applies fairly well, and the evaporation constant can be evaluated. At room temperature (20°C), the evaporation constant increases with increasing upward air velocity, and the flame is blown off at the critical air velocity (45 cm/sec in this case). The flame retains an oval shape as in still air. The order of magnitude of the change in burning rate caused by forced convection depends on the ambient temperature as well as on the air velocity. The air velocity for blow-off, and consequently the maximum value of the evaporation constant, increases with increasing ambient temperature. A peculiar phenomenon is observed at still higher ambient temperatures. At 310°C, the evaporation constant increases up to an air velocity of 90 cm/sec, and the flame surrounding the droplet blows off, but combustion continues beyond the air velocity of 90 cm/sec with a kind of lifted flame which establishes itself above the droplet. It is only at an air velocity of 123 cm/sec that the burning droplet is extinguished completely. The evaporation constant for the lifted flame is notably smaller than for a normal flame. As the air velocity increases and the distance between the droplet and the lifted flame increases correspondingly, the evaporation constant tends toward the value observed in the absence of combustion.

Empirical expressions and a hydrodynamic interpretation of the effect of both natural and forced convection on the burning rate have been presented by Spalding[2] for the steady-state combustion of a liquid fuel at the surface of a sphere.

Effects of Filaments

The heat transfer to a burning droplet from its flame through the silica filament cannot be disregarded. The experimental result given in Figure 4 shows the dependence of the evaporation constant on filament materials.[8] In this experiment (on liquid paraffin), filaments of 0.1 mm diam attached to a glass rod were used and the

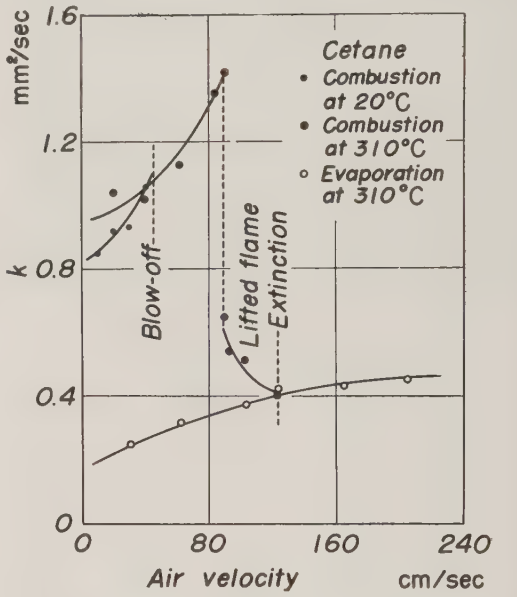

FIG. 3. Increase of evaporation constant due to forced convection.

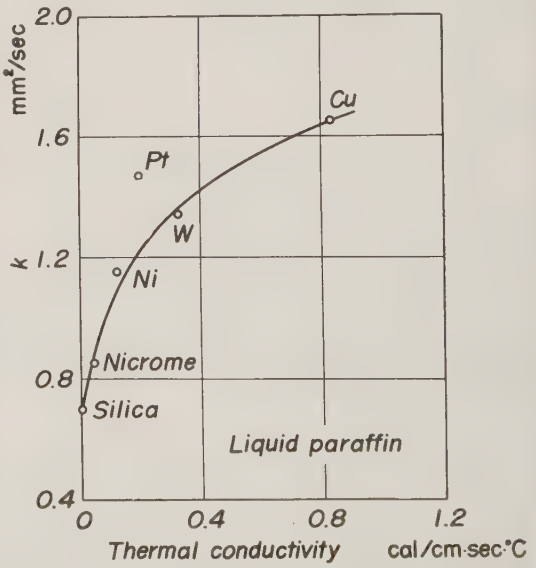

FIG. 4. Effects of filament materials on evaporation constant.

values of thermal conductivity at 800°C were recorded, as it was difficult to measure the temperature of each filament in the flame. As the thermal conductivity of silica lies between that of metals and that of gases, the true value of the evaporation constant should be considerably smaller than that determined by the conventional method.

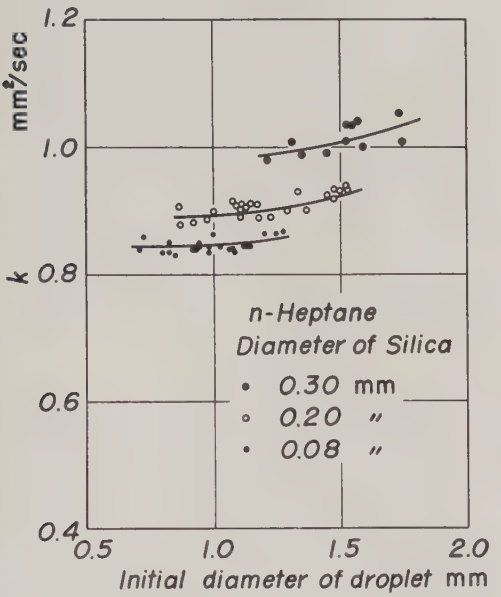

FIG. 5. Effects of initial droplet diameter and filament size on evaporation constant.

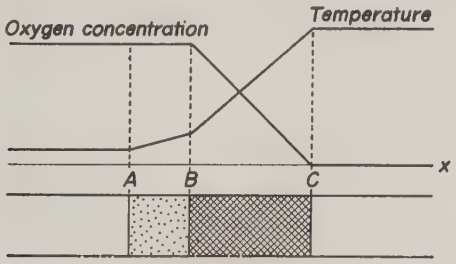

FIG. 6. Model of combustion of fuel sprays.

Most experimenters undoubtedly were aware of the dependence of the evaporation constant on the filament diameter and even the initial droplet diameter, although they have made no specific mention of this relation in their papers. It is rather difficult to distinguish between the effect of the filament diameter and that of the initial droplet diameter on the evaporation constant, because to some extent they are related. Our recent experiment has revealed, however, that the initial droplet diameter has little effect on the evaporation constant (Fig. 5), suggesting the validity of the theoretical prediction that the evaporation constant is independent of the initial droplet diameter. In this experiment (on *n*-heptane), silica filaments with a hump at the end were used. With regard to the effect of the filaments alone, the heat capacity of the filaments is presumably responsible for reversing the tendency of change in the evaporation constant with the initial droplet diameter observed for very fine filaments. Materials and sizes of filaments can be considered similar in their effects on the evaporation constant. The true value of the evaporation constant is extrapolated to zero filament diameter.

Approaches to Spray Combustion

An approach to spray combustion has been attempted as follows. The law of combustion of single droplets was applied to individuals in a group of droplets, and the percentage of burned or unburned fuel was computed by Probert[12] and by Tanasawa[13] as a function of over-all time for a known drop-size distribution. The treatment is mathematical rather than physical. The theoretically predicted change of evaporation characteristics is not significant for a range of drop-size distributions with a fixed value of the mean droplet diameter. Needless to say, the percentage of burned fuel, i.e., the combustion efficiency, increases with the over-all time on a saturation curve.

We should not overestimate the virtue of considering the drop-size distribution in actual problems of spray combustion. The drop-size distribution itself is of secondary importance, and in most cases it may suffice to take the mean size of the droplets into consideration.

Graves and Gerstein[14] compared the combustion efficiency observed in a certain type of combustor with the combustion efficiency calculated according to Probert, using the evaporation constant of a single droplet, but this comparison showed the limited applicability of the above treatment. Its inadequacy was attributed to the fact that the evaporation constant suitable to spray combustion is different from the constant for a single droplet. In this connection, some authors have sought a solution in studies on interference between two or more closely spaced droplets.

The case of two droplets burning in close proximity has been investigated in detail by Rex, Fuhs and Penner.[15] It is interesting to note that the linear relation between the square of the droplet diameter and time applies also to this

type of combustion of fuel droplets. In general, the average evaporation constant for two droplets takes on a maximum value for a certain value of the initial minimum distance between adjacent droplet surfaces. This is attributed to a balance between two opposing factors, *viz.*, the decreased heat loss from the flame of one droplet because of the presence of the other droplet which acts as a heat source, and the decreased oxygen supply to the region between two droplets. Experiments also have been conducted on five droplets arranged with a droplet at each corner of a square and one in the center of the square (Rex, Fuhs and Penner), and on nine droplets arranged in a body-centered cubic lattice (Kanevsky). With these arrangements, the evaporation constant of the center droplet is reported to be larger than the average evaporation constant for two droplets burning in close proximity.

Another approach to spray combustion is suggested here. As a model of spray combustion we can introduce a structure similar to the combustion wave in a premixed gas as illustrated schematically by Figure 6. In the air flow along the x-axis, a group of fuel droplets is dispersed at A. The fuel droplets, which for simplicity are assumed to be uniform in size, are suspended in the flow. They ignite at B, and burn out at C. Distribution of temperature and oxygen concentration, respectively, through the pre-heating zone and the burning zone, is established as shown in Figure 6. The fuel droplets in the flow burn with the evaporation constant of a single droplet, which is a known function of the temperature and of the oxygen concentration. On the other hand, gas molecules in a combustion wave react at a rate that depends on the temperature and on the concentration of the reactants. The two systems could be treated similarly in theoretical analyses.

In our opinion, effective treatment must be necessarily particular, from case to case, because the combustion of fuel sprays assumes different forms in individual problems. To solve problems of spray combustion perfectly, it would probably be necessary to consider not only droplet combustion, but also diffusion flames and even combustion phenomena in premixed gases.

Conclusions

Although there have been many theoretical and experimental investigations on the combustion of fuel droplets, application to problems of spray combustion has not yet been successful. In conclusion, I should like to point out one more problem, namely, the fact that most experiments have been conducted on fuel droplets burning under the influence of natural convection, whereas theories have been derived for a combustion model of spherical symmetry. We have reached a crossroad: one road leads to the theoretical analysis of actual droplet combustion under natural convection; the other leads to experimental work on spherical droplet combustion, such as has been treated theoretically. Two methods are available for eliminating the effect of natural convection on the combustion of fuel droplets to attain spherical combustion. One is to observe the combustion of extremely fine fuel particles. The other is to burn fuel droplets of ordinary size in a freely falling chamber. This latter method will be discussed in detail at this symposium in our paper on experiments in a combustion chamber designed to fall with a constant acceleration.

REFERENCES

1. Godsave, G. A. E.: *Fourth Symposium (International) on Combustion*, p. 818. Baltimore, The Williams & Wilkins Co., 1953.
2. Spalding, D. B.: *Fourth Symposium (International) on Combustion*, p. 847. Baltimore, The Williams & Wilkins Co., 1953.
3. Goldsmith, M., and Penner, S. S.: Jet Propulsion, *24*, 245 (1954).
4. Okazaki, T., and Gomi, M.: Trans. Japan Soc. Mech. Engr., *19*, 1 (1953).
5. Hall, A. R., and Diederichsen, J.: *Fourth Symposium (International) on Combustion*, p. 837. Baltimore, The Williams & Wilkins Co., 1953.
6. Kobayashi, K.: *Fifth Symposium (International) on Combustion*, p. 141. New York, Reinhold Publ. Corp., 1955.
7. Kumagai, S., and Isoda, H.: *Fifth Symposium (International) on Combustion*, p. 129. New York, Reinhold Publ. Corp., 1955.
8. Kamagai, S., and Isoda, H.: Science of Machine (Japan), *4*, 337 (1952).
9. Kumagai, S., and Kimura, I.: Trans. Japan Soc. Mech. Engr., *18*, 16 (1952).
10. Kumagai, S., and Kimura, I.: Science of Machine (Japan), *3*, 431 (1951).
11. Goldsmith, M.: Jet Propulsion, *26*, 172 (1956).
12. Probert, R. P.: Phil. Mag., *37*, 94 (1953).
13. Tanasawa, Y.: Technology Reports of Tohoku University (Sendai, Japan), *18*, 195, 1954.
14. Graves, C. C., and Gerstein, M.: *Combustion Researches and Reviews*, p. 23. London, Butterworths Scientific Publications, 1955.
15. Rex, J. F., Fuhs, A. E., and Penner, S. S.: Jet Propulsion, *26*, 179 (1956).

89

APPLICATION OF THE ONSAGER THEORY TO THE TRANSFER PHENOMENON IN EVAPORATION AND COMBUSTION PROCESSES

By A. V. LUIKOV

Evaporation, drying, and other thermal treatments of solid fuel, involve heat and mass transfer. Mass transfer is a necessary consequence of phase transitions (evaporation) or chemical transitions (burning). Solid fuels (coal, slates, peat, etc.) are capillary porous solids, in which heat transfer cannot be separated from mass transfer of bounded matter.

The internal heat and mass transfer, as well as external heat exchange, must be considered as a single complex process to which we apply

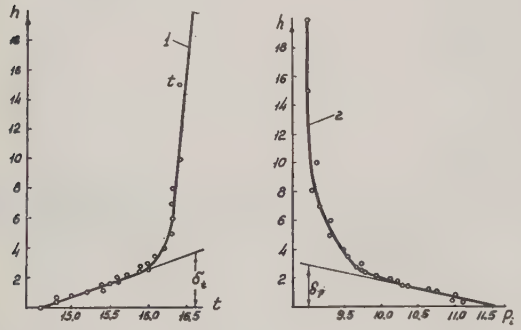

FIG. 1. Distribution curves of temperature and partial steam pressure.

TABLE 1. VALUE OF CONSTANTS IN EQUATIONS (3) AND (4)

Limits of Changing *Re* Criterion	*A*	*n*	*m*	*A'*	*n'*	*m'*
1 to 200	1.07	0.48	0.175	0.83	0.53	0.135
3.15×10^3 to 2.2×10^4	0.51	0.61	0.175	0.49	0.61	0.135
2.2×10^4 to 3.15×10^5	0.027	0.90	0.175	0.0248	0.90	0.135

methods for studying molecular processes that are physically and thermodynamically irreversible (Onsager theory).

External Heat and Mass Transfer

The intensity of heat and mass transfer during the evaporation of liquids is determined by the following relations:

$$q = \alpha(t_a - t_b) = Nu \frac{\lambda_a}{l} \Delta t, \qquad (1)$$

$$q' = \alpha'(p_a - p_b) = Nu' \frac{\lambda_a'}{l} \Delta p \qquad (2)$$

Usually, Nu and Nu' are derived experimentally from the flux densities of heat and matter (q and q'), the temperature drops, Δt, and partial pressure change, Δp. Coefficients λ_a and λ_a' are computed or taken from tables.

The best results are obtained by determining Nu and Nu' from the experimental curves for temperature distribution and partial pressure in the boundary layer, based on special temperature measurements and the pressure of condensing gas.

Figure 1 shows distribution curves for temperature and partial vapor pressure: $t = f(h)$ and $p = f(h)$ during evaporation of the liquid. It will be seen that the conventional boundary layer thickness of the temperature field δ_t is 3.7 mm, and the partial pressure field δ_p is 3.0 mm. Consequently, the Nusselt criteria will be respectively:

$$Nu = \frac{l}{\delta_t} = \frac{0.165}{0.0037} = 45; \qquad Nu' = \frac{l}{\delta_p} = \frac{0.165}{0.0030} = 55$$

where l is the characteristic dimension (0.165 m for this test).

Nu and Nu' for various conditions of evaporation of the liquid were determined by this method. It was established that in conditions of forced convection, Nu and Nu' depend not only on flux hydrodynamics, defined by the Reynolds criterion and the physical properties of gas-vapor medium (criteria Pr and Pr'), but also on the thermodynamic properties of the medium, K_T.

The thermodynamic criterion of evaporation K_T is derived from the primary thermodynamic correlation; it defines the cumulative capacity of the gas-vapor mixture for the absorption of liquid vapor.

By treating numerous experimental data Nesterenko[3] obtained the following empirical formulas

$$Nu = A\, Pr^{0.33}\, Re^n\, K_T^m \qquad (3)$$

$$Nu' = A' Pr'^{0.33}\, Re^{n'}\, K_T^{m'} \qquad (4)$$

The constants in these formulas are shown in Table 1. For $Re < 200$, we must deduct 2 from the value of Nu obtained according to Equation (3), writing $Nu - 2$ instead of Nu. The same applies to the diffusion criterion Nu'.

Calculation of Equation (3) shows that heat exchange coefficients in the presence of mass transfer are 10 to 15 per cent higher than the corresponding heat transfer coefficients without mass transfer.

This difference increases sharply during evaporation of the liquid from the solids, reaching the order of 150 to 200 per cent. Simultaneously it was established that, under constant drying conditions, the heat exchange coefficient in the first stage of the drying process is constant, whereas in the second stage of the drying process it decreases continuously, gradually approaching the value of the coefficient of heat transfer in the absence of mass exchange (coefficient of heat transfer "proper").

On the basis of experimental drying data for different materials, Lebedev[4] obtained the following empirical relation

$$Nu = ARe^{0.5}\left(\frac{T_a}{T_b}\right)^2\left(\frac{T_h}{T_a}\right)^{0.4}\left(\frac{U}{U_c}\right)^n \qquad (5)$$

Constants A and n are given in Table 2.

Table 2. Value of Constants in Equation (5)

Materials	A	n
Peat	—	0.8
Quartz sand	0.65	1.8
Wood	0.50	0.3
Clay	0.45	0.9

In this equation, the parameter T_a/T_b is a thermodynamic criterion of evaporation, which is a modification of K_T.

The presence of a radiational heat transfer influences the convective heat transfer, and is taken into account by the parameter T_h/T_a.

Equation (5) holds for the second stage of the drying process, when the moisture content of the solid changes from the critical moisture content, U_c, to the equilibrium moisture contents ($U_e < U < U_c$).

In the first stage of the drying process ($U \geq U_c$), the parameter (U/U_c) must be equal to unity.

To determine the cause of the sharp increase in heat transfer coefficients during the evaporation of the liquid from the solid, special tests were carried out to study the boundary layer of the vapor-gas mixture at the surface of the solid during the drying process.

The field temperature of the boundary layer in one of the tests is shown in Figure 2, together

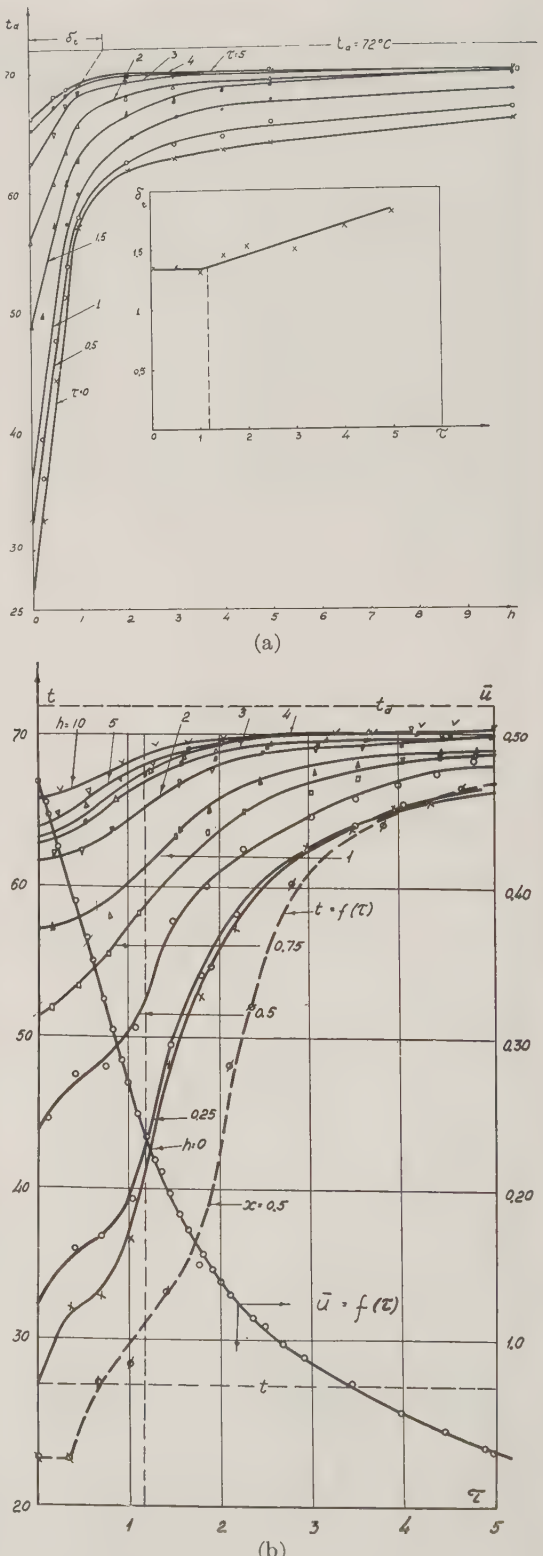

Fig. 2. Temperature fields in the boundary layer during drying.

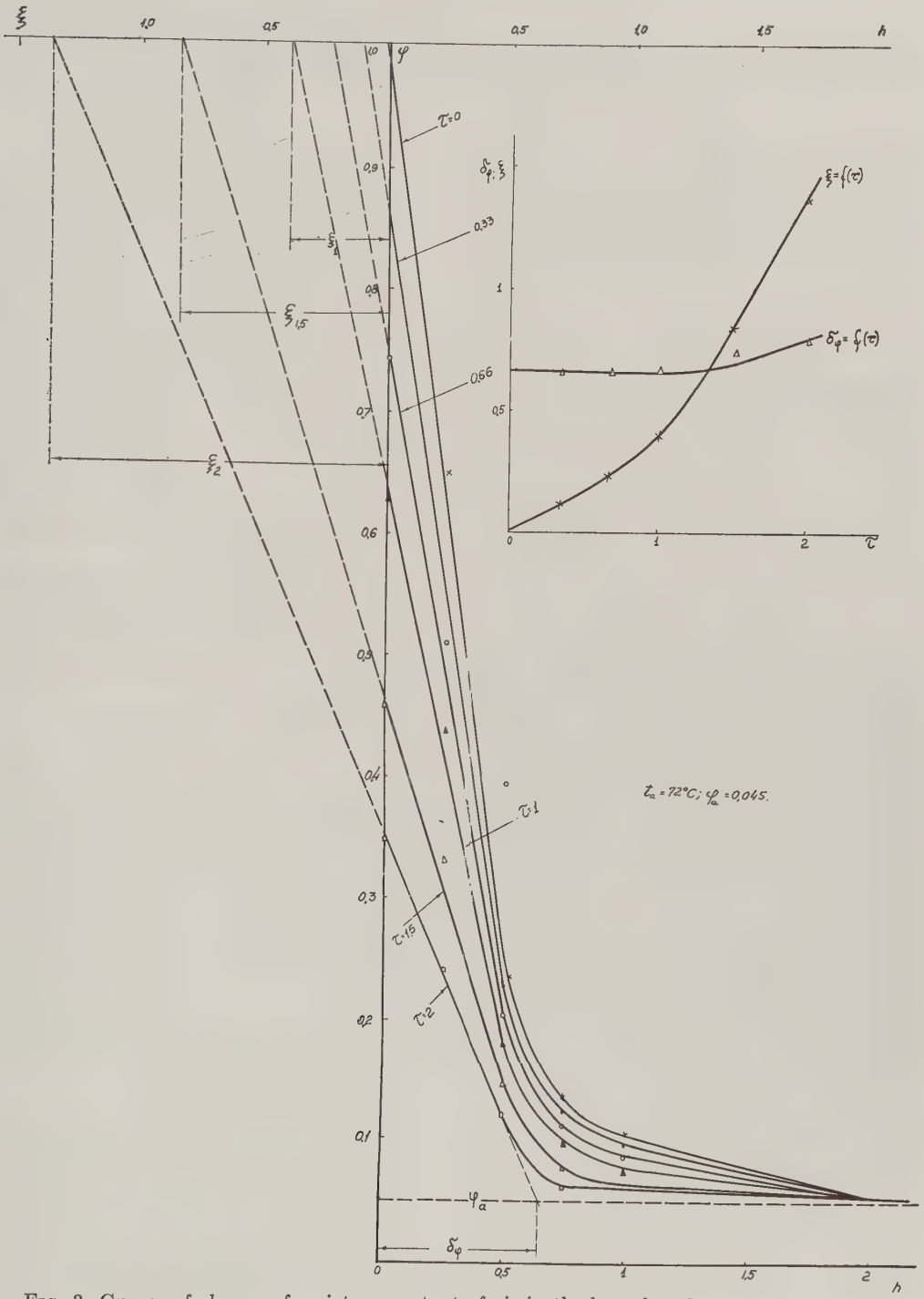

FIG. 3. Curves of change of moisture content of air in the boundary layer during drying.

with the kinetic drying curve, $u = f(\tau)$. From Figure 2 it is evident that, in the first stage, the conventional boundary layer thickness of the temperature field is always constant (δ_t = 1.35 mm) but beginning from a critical point that corresponds to the drying time τ_c = 1.2 hr δ_t increases continuously.

The curves in Figure 3 show the air moisture changes in the boundary layer at various drying times. From Figure 3 it is evident that the

conventional boundary layer thickness of the moisture field δ_φ is equal to 0.65 mm in the first stage (plot of changes with time also is shown in Figure 3). Figure 3 shows that air moisture at the surface of the material ($h = 0$) is continuously decreasing from the very beginning of the process, in spite of the constant velocity of evaporation during the first drying stage. If we were to extend the straight portion of the curve $\varphi = f(h)$ for air moisture distribution into the solid up to the intersection with the horizontal line $\varphi = 1$ (complete saturation of moist air), we would obtain the conventional thickness ξ of the evaporation area (distance of evaporation surface from the surface of the solid).

It is evident from Figure 3 that during the drying process the evaporation surface is continuously moving deeper into the solid, and that during the first stage, the rate of withdrawal of the evaporation surface is constant ($d\xi/d\tau$ = const), whereas in the second stage it increases continuously (see curve $\xi = \mathcal{F}(\tau)$, Fig. 3).

The vapor transfer through the evaporation area, which accompanies evaporation of the liquid within the solid, is considerably more intensive than the vapor transfer in the boundary layer of the vapor-gas mixture at the surface of the solid. In the boundary layer, at the surface of the solid, the transfer of vapor takes place by molecular diffusion. In the evaporation area (within the solid) the transfer of vapor takes place not only by diffusion (in macroscopic capillaries), but by effusion (in microscopic capillaries). Vapor diffusion in macroscopic capillaries is increased by the molecular motion of the vapor-gas mixture (phenomenon of heat slide). As a result, the intensity of vapor transfer in the evaporation area of the solid is many times higher than that of diffusion transfer. The vapor from the evaporation area affects the state of the laminar sublayer at the surface of the body, i.e., turbulizes the boundary layer, sharply increasing the intensity of the heat transfer. The main correlation of the Onsager theory can be used to show, in the presence of a heat-barrier (porous wall, membrane, etc.) in the vapor-gas mixture in the direction of the transfer, a gradient of the total pressure. The magnitude of the pressure drop is determined by the relation

$$\frac{dp}{dT} = -\frac{Q^* p}{RT^2} \tag{6}$$

In the event of a pure effusion transfer, the heat transfer is equal to $Q^* = \frac{1}{2}RT$. Then from Equation (6) we obtain

$$\frac{p}{\sqrt{T}} = \text{const}$$

i.e., the potential of mass transfer is not the partial vapor pressure, but the relation $p/\sqrt{T}$.

The temperature of the surface of the solid is higher than that of the evaporation surface. Thus at the surface of evaporation, the total pressure of moist air will be greater than the barometric pressure, i.e., along the thickness of the surface layer of the body (evaporation area) there exists a difference in the total pressure, which considerably speeds up the vapor transfer.

With a mixed transfer mechanism (diffusion and effusion) the heat transfer, Q^*, will be less than $\frac{1}{2}RT$, but will be different from zero. Therefore, the total pressure gradient in the evaporation area will be lower.

In the second stage of the drying process, the evaporation intensity decreases steadily, causing a decrease of the heat transfer coefficient which gradually approaches the value of the pure heat transfer coefficient.

Vapor transfer in the evaporation area influences not only heat transfer, but also the hydrodynamics of heat transfer. This conclusion is confirmed by the drying tests of solids of different shapes, made of plaster of Paris. Samples for tests were prepared in the form of a plate, a cylinder, a sphere and cones of different sizes. They were arranged in various ways with respect to the direction of the air flux. It was found that the intensity of evaporation does not depend upon the shape and position of the sample; but for a given set of conditions, it is a function of the surface of evaporation (Fig. 4). This conclusion holds for a range of Reynolds numbers from 9,000 to 35,000.

If we take the square root of the area A of evaporation surface $l = \sqrt{A}$ as the determining size, l, we obtain a simple relation between Nu and Re, provided that the thermodynamic value, K_T, remains constant (Fig. 4).

On the basis of the plot of Figure 4 we can write the following empirical relation:

$$Nu = 4.66\ Re^{0.4}$$

Consequently, in this case, the hydrodynamic factor of heat transfer is somewhat lower because of changes in the transfer mechanism at the boundary layer.

Internal Heat and Mass Transfer

Let us consider heat and mass transfer of a bounded substance during its evaporation from the solid (heating of the solid in the presence of evaporation).

Most hard fuels are capillary-porous solids containing a bound substance in various states.

The total specific mass content, U, is equal to the sum of specific mass contents of the bounded substance in the solid, liquid, and vaporous states (three-phase system)

$$U = \sum_{i=1}^{3} U_i \tag{8}$$

Local changes of the bounded substance in any phase i may take place at the expense of phase reduction dU_{ij} and as a result of transfer dU_{if}

$$dU_i = \sum_j dU_{ij} + dU_{if} \tag{9}$$

Let us introduce a criterion of phase reduction of a bounded substance from phase i into phase j and conversely, by relations:

$$E_{ij} = \frac{dU_{ij}}{dU_i}. \tag{10}$$

Here we have an equation

$$E_{ij}\, dU_i = E_{ij}\, dU_j \tag{11}$$

which reflects the law of conservation of mass during its transition from phase i into phase j.

It will be seen that E_{ij} goes from 1 without transfer of substance in phase i to zero (change of the mass content in phase i occurs only as a result of transfer).

Thus Equation (9) may be written in the following form

$$dU_i = \sum E_{ij}\, dU_i + dU_{if}$$

hence

$$E_{ii} = E_{jj} = 0$$

Let us isolate a certain volume of the solid confined in a closed surface (reference surface). Then the change of mass content in the body in this volume will take place only at the expense of mass transfer, because phase reduction within the isolated volume does not change the mass content of the bounded substance in this volume, i.e.,

$$dU = \sum_i dU_{if}\,; \qquad \sum_i \sum_j E_{ij}\, dU_i = 0. \tag{12}$$

Consequently, the local rate of change in the mass content of the bounded matter is equal to the divergence from the sum of specific fluxes of the mass of various phases

$$\gamma_0 \frac{\partial u}{\partial \tau} = -\mathrm{div} \sum_i q_i' \tag{13}$$

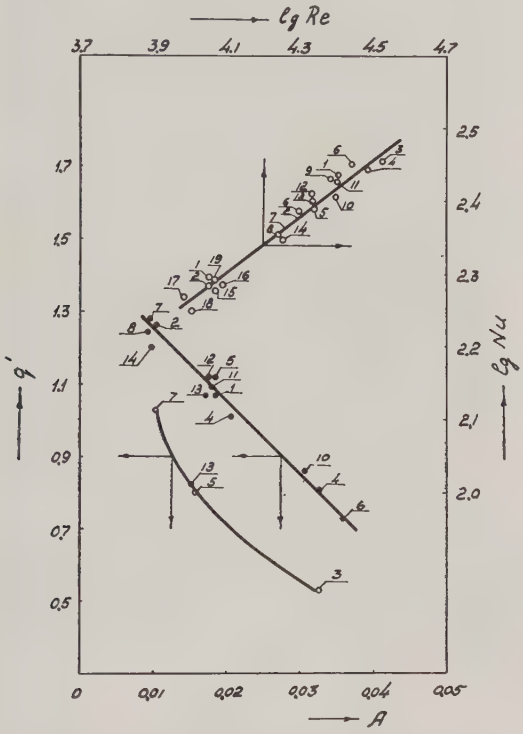

FIG. 4. Dependence of the intensity of heat and mass-transfer upon the shape and the position of samples.

(1) v = 3.0 m/sec.

1. A bounded plate located along the flow.
2. A bounded plate with the lateral surface isolated.
3. An unbounded plate.
4. An unbounded plate with the lateral surface isolated.
5. A bounded cylinder.
6. An unbounded cylinder.
7. A cone; the bottom facing the flow.
8. A cone; the vertex facing the flow.
9. A bounded plate perpendicular to the flow.
10. A sphere.
11. A bounded plate, located vertically.
12. A bounded cylinder perpendicular to the flow.
13. A bounded cylinder located vertically.

(2) v = 1.5 m/sec.

14. A cone located vertically.
15. A bounded plate located along the flow.
16. A bounded plate perpendicular to the flow.
17. A cone; bottom facing the flow.
18. A cone; vertex facing the flow.
19. A bounded cylinder located vertically.
20. A bounded cylinder, located along the flow.

The differential equation for transfer from phase i of the bounded substance then takes the form:

$$\gamma_0 \frac{\partial u_i}{\partial \tau} = -\text{div}\, q_i' + \sum_j E_{ij} \frac{\partial u_i}{\partial \tau} \qquad (14)$$

The second member of the right-hand side of Equation (14) must be considered as a sink or drain of phase i of the bounded substance, as a result of its reduction from phase i into phase j.

The differential equation for heat transfer is derived from the equation for the energy transfer: the local rate of energy change in an infinitely small volume is equal to the divergence from the specific flow of energy

$$\gamma_0 \frac{\partial}{\partial \tau}\left(H_0 + \sum_i H_i U_i\right) = -\text{div}\left(q + \sum_i H_i q_i'\right) \qquad (15)$$

According to the linear law, under isothermal conditions, the specific flow of mass is directly proportional to the thermodynamic motive force or to the gradient of the potential of transfer of the substance.

A total transfer potential of the liquid phase of the substance is equal to the sum of potentials of the corresponding fields (gravitational, capillary, electric and molecular). It is possible to show that the potential of transfer of liquid is a function of the substance of bounded mass content (moisture content) and temperature.

The moisture content of the solid is not a potential of the transfer of liquid, since the moisture content is not analogous to the enthalpy of the solid. That is why at the limit of solids in contact, such as peat and quartz sand, there is a jump of moisture content. As a potential of liquid transfer in capillary-porous solids we assume a specific moisture content of the model (cellulose) in contact with the substance studied under conditions of thermodynamic equilibrium.

By analogy with heat capacity, we may introduce a conception of isothermal mass capacity, numerically equal to the derivative quotient of the specific moisture content along the potential of liquid transfer at a constant temperature. This scheme was used by the author who studied various cases of transfer of the liquid in capillary-porous substances.

If heat and mass transfer take place through a molecular course, the specific flows of mass and heat are determined by a system of Onsager's linear equations

$$\begin{aligned} q_e &= q_1 = L_{11} X_1 + L_{12} X_2 \\ q' &= q_2 = L_{21} X_1 + L_{22} X_2 \end{aligned} \qquad (16)$$

where thermodynamic motive forces of heat transfer X_1 and of the mass X_2 are determined by the relations

$$X_1 = -\frac{1}{T} \operatorname{grad} T; \qquad X_2 = -T \operatorname{grad} \frac{\mu}{T} \qquad (17)$$

On the basis of Onsager's reciprocity principle, cross kinetic coefficients are equal ($L_{12} = L_{21}$).

The chemical potential μ_i of the bounded substance in any phase is a function of temperature and concentration or specific mass content of the substance U_i. Then, the linear law of mass transfer may be written as:

$$q_i' = -a_i' \nabla U_i - a_i' \delta_i \nabla t \qquad (18)$$

Here the thermogradient coefficient δ_i is numerically equal to the gradients relating the specific mass content and the temperature of the bounded substance in a fixed state, without mass transfer ($q_i' = 0$)

$$\delta_i = -\left[\frac{\nabla u_i}{\nabla t}\right]_{q_{i=0}'} \qquad (19)$$

Equation (18) also describes molar liquid transfers under the influence of a capillary potential gradient, since the latter is a function of U and t.

Specific flow of heat is determined by the relation:

$$q = -\lambda \nabla t \qquad (20)$$

where the heat conduction coefficient λ is an equivalent coefficient that takes into account heat transfer by heat conduction and transfer of substance.

Let us consider in detail the heat and mass transfers in the drying process of solids. The capillary-porous solid contains a bounded substance (moisture) in the form of liquid and vapor ($U_3 = 0$). Vapor in the pores and capillaries of the solid is in molecular and thermal equilibrium with the liquid, its temperature being equal to that of the liquid, and, consequently, the temperature of the solid skeleton.

At atmospheric pressure, the mass of the moist gas (vapor and air) in the pores and capillaries of the solid is negligibly small ($M_1 = 0$). Therefore, the specific mass content of the

solid is equal to the mass content of the liquid ($U = U_2$). Consequently, the heat consumed in heating the moist gas in the pores is insignificant, and the volumetric heat capacity of the moist substance is equal to the volumetric heat capacity of an absolutely dry substance ($C_0\gamma_0$) and to the volumetric heat capacity of the

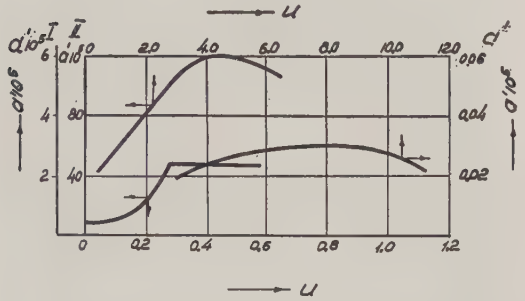

FIG. 5. The coefficient of potential conductivity as a function of the moisture content.

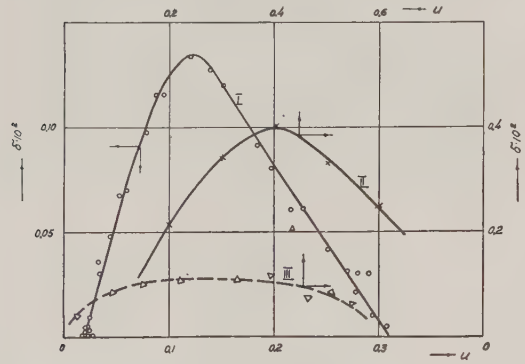

FIG. 6. The thermogradient coefficient as a function of the moisture content. I. clay; II. peat; III. kaolin.

liquid present in the substance ($C_2U_2\gamma_0$)

$$C\gamma_0 = (C_0 + C_2 U)\gamma_0 \tag{21}$$

Under these conditions the differential equation for the transfer of the bounded substance (vapor and liquid) within the body according to Equations (13) and (14) may be written

$$\frac{\partial U}{\partial \tau} = \nabla\cdot\left\{\sum_{i=1}^{2}\left(a_i'\nabla U + a_i'\delta_i\nabla t\right)\right\} = \nabla\cdot\left\{a_2'\nabla U + a_2'\delta_2\nabla t\right\} + E\frac{\partial U}{\partial \tau} \tag{22}$$

where $E = E_{21}$ is the phase criterion of the reduction of the liquid to vapor.

The differential equation of heat transfer, Equation (15), is converted into the following equation

$$C\gamma_0\frac{\partial t}{\partial \tau} = \nabla\cdot(\lambda\nabla t) + E\rho\gamma_0\frac{\partial U}{\partial \tau} - \sum_{i=1}^{2} C_i\gamma_i v_i\nabla t \tag{23}$$

where $\rho = \rho_{21} = \rho_{12}$ is the specific heat of liquid evaporation or the condensation of vapor.

In addition, it was assumed that the vapor enthalpy is equal to:

$$H_1 = H_2 + \rho \approx 595 - 0.47t \tag{24}$$

Differential Equation (23) is similar to the Fourier-Kirchhoff equation of heat transfer, which is derived for the heat transfer in a moving liquid. In Equation (23) the first member on the right-hand side takes into account the conductive component of heat transfer; the second member is the heat sink or drain, stipulated by a phase reduction; and the third member determines the magnitude of heat transfer as a result of transfer of the substance. The magnitude of heat transfer in the drying process is negligible, if the Reynolds criterion for the moving liquid or vapor within the substance is less than unity ($Re_i < 1$).

The transfer coefficients λ, a_i', δ_i are variables. However, over a short interval of temperature and moisture content (Δt and ΔU) they may be considered as constant. Then, for such a system of computation for separate areas (Δt_k, ΔU_k), the differential transfer equations may be written

$$\frac{\partial U}{\partial \tau} = a_2'\nabla^2 U + a_2'\delta_2\nabla^2 t + E\frac{\partial U}{\partial \tau} = a'\nabla^2 U + a'\delta\nabla^2 t \tag{25}$$

$$\frac{\partial t}{\partial \tau} = a\nabla^2 t + E\frac{\rho}{C}\frac{\partial U}{\partial \tau} \tag{26}$$

where: $a' = a_2'/(1 - E)$ is the equivalent coefficient of the potential conductivity of the substance ($\delta_1 = \delta_2 = \delta$).

From the systems of Equations (25) and (26), together with conditions of single value, the criteria of heat and mass exchange similarities are determined.

Transfer Coefficients

The basic transfer coefficients of the substance are the coefficient of potential conductivity, a', of the substance and the thermogradient coefficient, δ. For most capillary-porous substances the coefficient, a', increases with increasing U. At higher moisture contents, a' becomes constant (Fig. 5). The increase of coefficient, a', is characteristic of the vapor transfer.

The invariability of coefficient, a', is conditioned by the transfer of the liquid under the influence of capillary forces. For capillary-porous colloidal substances (peat) in the region of high moisture contents, the coefficient is decreased with the increase of moisture content. This is characteristic of the transfer of liquid under the influence of osmotic forces. At a constant moisture content, coefficient a' is directly proportional to the absolute temperature in powers of $n(a' = CT^n)$. The index of powers varies for various substances, ranging from 10 to 14.

The thermogradient coefficient, δ, increases with increase of the moisture content, reaches a certain maximum value, and then decreases (Fig. 6). The character of the changes of coefficient, δ, depends on the capillary-porous structure and on the type of transfer of the bounded substance.

The changes in the coefficient of heat transfer (coefficient of heat conductivity, λ, and coefficient of temperature conductivity a) as a result of the moisture content of the substance are shown in Figure 7. It should be kept in mind that the coefficient of heat conductivity is equivalent; it also takes into account heat transfer by transfer of the substance,

$$\lambda = \lambda_C + \rho a' \gamma_0 \delta \qquad (27)$$

where λ_C is the true coefficient of heat conduction.

Therefore, the character of the coefficient change is determined also by the regularity of change of the thermogradient coefficient, δ, as a result of the moisture content of the substance.

The relation of the potential conductivity coefficient of substance transfer, a', to the coefficient of temperature conductivity, a, is the criterion of inertia for the development of the moisture content field in relation to the temperature field and is expressed by LU

$$LU = \frac{a'}{a}$$

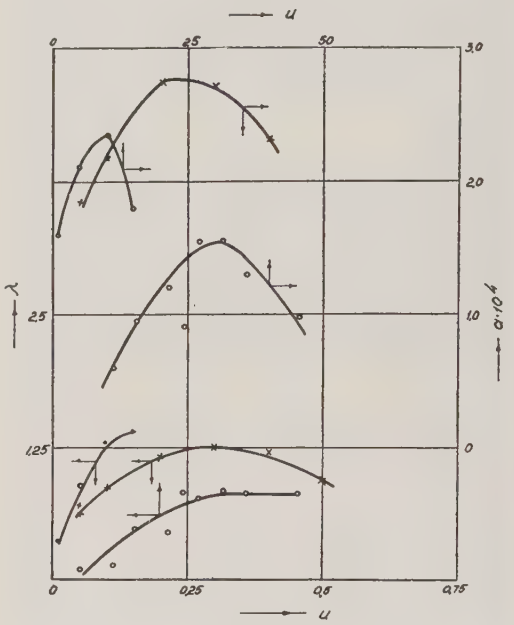

FIG. 7. The coefficients of heat conductivity and thermal conductivity as functions of the moisture content.

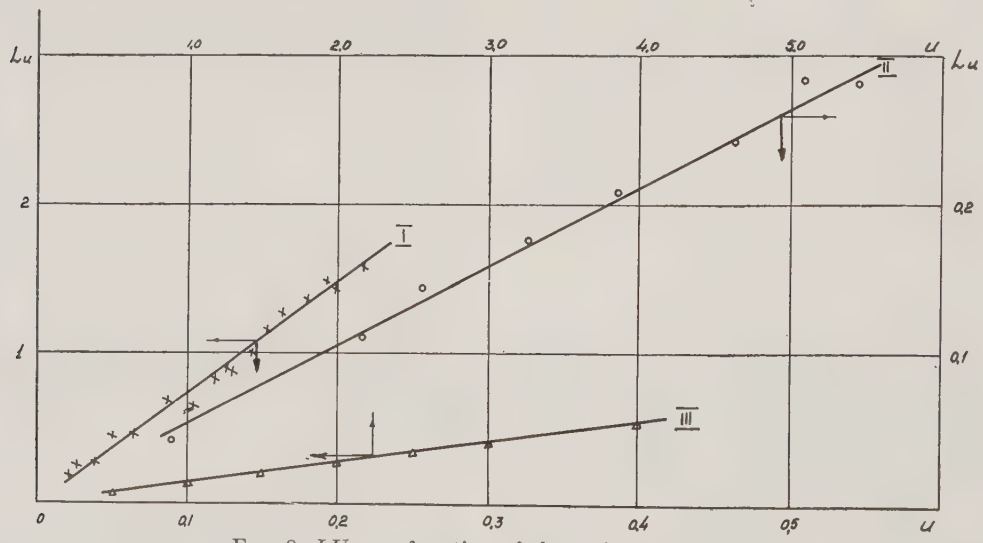

FIG. 8. LU as a function of the moisture content.

Figure 8 shows plots of the change of criterion, L, with the moisture content, U, for certain substances. Figure 8 shows that criterion, LU, increases linearly with the increase of the moisture content.

When the moisture content of quartz sand is higher than 15 per cent ($U \geqslant 0.15$), the criterion, LU, is higher than unity. In this case, the mass propagation precedes heat propagation, i.e., the temperature field lags behind the development of the field potential of the substance transfer.

The system of differential equations for heat and mass transfers, Equations (14) and (15), holds in the case of chemical reductions. The criterion E_{ij} becomes the criterion of chemical reduction of the substance i to the substance j. In this case, it is more convenient to introduce the volume concentration ω_i of the substance ($\omega_i = \gamma_0 U_i$) instead of the specific mass content U_i of bounded substance.

The above regularities of heat and mass exchange during phase and chemical reductions may be used to determine the optimum conditions for energetic and technologic processes (drying, gasification, burning).

Nomenclature

q and q' — specific flows (fluxes) of heat and mass in kcal/m² hr and kg/m² hr respectively

$\Delta t = (t_a - t_b)$ — temperature difference between gas and liquid surface or substance in °C

$\Delta p = (p_a - p_b)$ — difference of partial vapor pressure in surrounding gas-vapor medium and at surface of liquid or substance in mm Hg

α and α' — coefficients of heat and mass transfer in kcal/m² hr °C and kg/m² hr respectively

λ and λ' — coefficients of heat and mass conductivity of gas-vapor mixtures at liquid surface in kcal/m hr °C and kg/m hr mm Hg

l — specific dimension in m

Nu and Nu' — Nusselt's thermal and diffusion criterion (number)

Re — Reynolds number ($Re = vl/\nu$)

v — velocity of movement of the gas-vapor medium in m/sec

ν — coefficient of kinematic viscosity in m²/sec

Pr — Prandtl's diffusion number ($Pr = \nu/a_a$)

a_a — temperature conductivity coefficient of gas-vapor mixture in m²/sec

Pr' — Prandtl's diffusion number ($Pr' = \nu/a_a'$)

a_a' — coefficient of vapor diffusion in m²/sec

K_T — thermodynamic evaporation number $\left(K_T = \dfrac{T_a - T_b}{T_a}\right)$

T — temperature in °K ($T = 273 + t$)

T_b — temperature of adiabatic air saturation in °K

T_h — temperature of the screen of the radiating solid in °K

U — specific mass content (moisture content) of substance (moisture mass in substance referred to absolutely dry substance mass in kg/kg)

U_c — substance moisture content at the beginning of the second drying stage (substance moisture content at critical point of drying process) in kg/kg

τ — time in hr

h — distance from surface of liquid or solid substance in normal direction to surface, in m

φ — air moisture, equal to partial vapor pressure p_a in the relation to the saturated vapor pressure p_0 at a given temperature ($\varphi = p_a/p_0$).

ξ — conventional distance of evaporation surface from substance surface, in m

p — total pressure of gas-vapor mixture in mm Hg

R — universal gas constant

Q^* — heat transport (heat transported by the substance at p = const and T = const)

A — surface area of substance evaporation, in m²

E_{ij} — criterion of bounded substance phase transformation from phase i to phase j (dimensionless quantity)

ρ_{ij} — specific heat of phase transformation, ij.

C — specific capacity of substance (calculated per unit of mass of constant substance in kcal/kg °C)

γ_0 — density of substance (mass of constant substance of the solid per unit volume) in kg/m³

C_i specific heat capacity of bounded substance phase, in kcal/kg °C

γ_i density of bounded substance phase, in kg/m³

v_i linear transfer velocity of bounded substance phase in m/hr ($v_i = q_i'/\gamma_i$)

μ_i chemical potential of substance in phase i

a_i' transfer diffusion coefficient of bounded substance phase in m²/hr

δ_i thermal gradient coefficient of bounded substance phase in 1/grad

H_0 and C_0 respectively, the specific enthalpy (kcal/kg) and specific heat capacity (kcal/kg °C) of the substance of the solia ($H_0 = C_0 t$).

H_i specific enthalpy of bounded substance phase, in kcal/kg

ω_i volume concentration of bounded substance in kg/m³

REFERENCES

1. De Groot, S.: *Thermodynamics of Irreversible Processes*. Interscience Publishers, New York, 1952.
2. Denbigh, K.: Thermodynamics of the Steady State. John Wiley & Sons, Inc., New York, 1951.
3. Nesterenko, A. B.: J. Tech. Phys., USSR, *24*, (1954).
4. Lebedev, P. D.: *Drying by Infrared Rays*. Moscow, 1955.
5. Luikov, A. V.: *Transfer Phenomena in Capillary-porous Substances*. Moscow, 1954.
6. Luikov, A. V.: Ind. Eng. Chem., *27*, 406 (1935).
7. Luikov, A. V.: Phil. Mag., *22*, 239 (1936).

90

ATOMIZATION, ACCELERATION, AND VAPORIZATION OF LIQUID FUELS

By ROBERT D. INGEBO

Introduction

Fuel-spray vaporization rates are important in determining jet-engine burning characteristics, such as ignition delay, flame stability, and completeness of burning.[1] The droplets formed by atomization simultaneously accelerate and evaporate in the air stream to give combustible fuel-air mixtures. Thus, vaporization rates may be calculated when the size distribution, drag coefficients, and heat-transfer coefficients for the droplets in the spray are known. Such fuel-spray data are difficult to obtain in high-velocity air streams, since the droplets are microscopic in size and attain relatively high velocities in a very short time.

Recent research with a high-speed camera at the NACA Lewis Laboratory has provided data on droplet sizes and acceleration rates in high-velocity streams. The object of this paper is to present these recent results with the high-speed camera and to compare and correlate these data with other data obtained in previous studies using different techniques to study the evaporation rates of fuel sprays and of single droplets.

Apparatus and Procedure

A diagram of the test section, camera, and lens system is shown in Figure 1; auxiliary components are described by Ingebo.[2] The camera utilized a rotating mirror which tracked the droplets and stopped motion of their images on the film during an exposure time of approximately 4 μsec. A typical photomicrograph (Fig. 2) shows droplets produced by contrastream injection of isooctane from a simple orifice. The diameter of the stopped-droplet image was measured from the film with an accuracy of ± 3 μ and the corresponding drop velocity was calculated from the mirror speed with an accuracy of ± 5 ft/sec.

A picture was taken at a low mirror speed, the film advanced in the magazine, and another picture was taken at a higher mirror speed until a range of mirror speeds had been tested. At too low or too high a mirror speed, droplet images were smeared, but intermediate speeds gave stopped images on the film.

Fuel Spray Drop-size Distributions

Several investigators (e.g., Lee[3] and Houghton[4] have obtained drop-size-distribution data for the

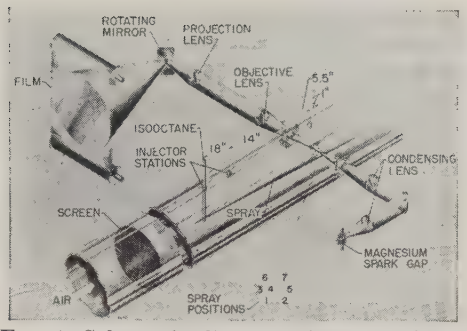

FIG. 1. Schematic diagram of test section and camera unit.

FIG. 2. Photomicrograph of isooctane spray in 180 ft/sec air stream.

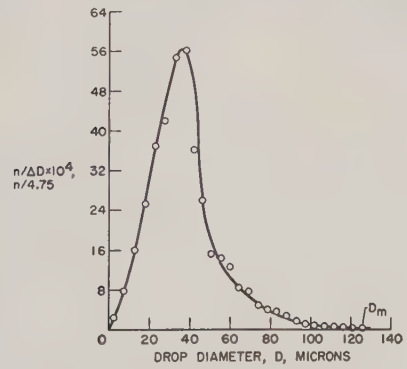

FIG. 3. Droplet-size distribution. Air-stream velocity, 140 ft/sec; distance from injector, 5.5 in.

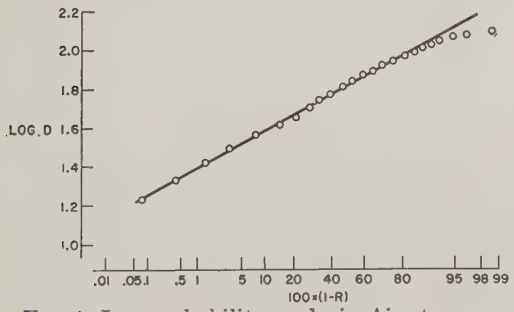

FIG. 4. Log-probability analysis. Air-stream velocity, 140 ft/sec; distance from injector, 5.5 in.

atomization of liquid jets in air streams. However, the problem of correlating drop-size distribution parameters with physical characteristics of the atomization process is still unsolved. This is primarily due to the lack of instrumentation capable of giving drop-size data accurately and rapidly.

The method of photographing the spray was fast, but measuring droplet images on the film was quite slow. As a result, only eight drop-size distributions were obtained. A typical plot of the data is shown in Figure 3. The applicability of the Rosin-Rammler, Nukiyama-Tanasawa, and log-probability distribution equations to the data was tested.[2] Good agreement was found for most mean-drop sizes calculated from the three equations. However, the Rosin-Rammler expression was found to have limited application in calculating median-drop sizes. A plot is shown for the log-probability analysis of the data in Figure 4. Some disagreement is shown for large drops since the existence of a maximum drop size is not accounted for in the distribution equation.

Drag Coefficients for Droplets in Accelerating Sprays

Considerable data are available for steady-state momentum transfer from air streams to fixed solid spheres,[5] but very little data for accelerating spheres. Thus, it is often assumed that steady-state drag coefficients may be used directly for accelerating drops. This would mean friction drag due to viscous shear and form drag due to surface pressure variations would be the same in both cases. However, data for "free-falling" spheres[6, 7] gave disagreement with steady-state drag coefficients even though terminal velocities were reached and nearly steady-state conditions existed. Thus, it is questionable whether steady-state rates are applicable to unsteady momentum transfer.

The high-speed camera used in the present investigations[8] gave drop-size and drop-velocity data quite accurately and rapidly. Although many pictures were taken, a large count of droplets was not required as in the atomization studies. Isooctane (2,3,4 trimethylpentane), water, and trichloroethylene in turn were injected from a nozzle which spread a flat sheet of liquid on a 50 by 40-mesh screen, thus fixing the initial point of droplet acceleration. Figure 5 shows a typical plot of drop velocity-squared against distance downstream of the screen.

Linear accelerations were determined from the

slopes of these curves, and droplet drag coefficients were calculated by equating the force accelerating the sphere to the aerodynamic pressure force of the air stream. A plot of droplet Reynolds number against drag coefficient is shown in Figure 6, and the following empirical expression was derived:

$$C_D = 27\ Re^{-0.84} \tag{1}$$

In Figure 6, Stokes' law and drag-coefficient data for fixed solid spheres[5] and falling water drops[6] are included for comparison. This figure shows that drag coefficients for droplets accelerating in clouds fall in between Stokes' law and steady-state values. A fundamental explanation of this disagreement with steady-state data could not be obtained directly from the camera data. However, some possible explanations are discussed by Ingebo.[8]

Heat-Transfer Coefficients for Single Drops

Heat-transfer-coefficient data for droplets in accelerating sprays could not be obtained directly with the high-speed camera used in these investigations. However, heat-transfer-coefficient data were obtained for several pure liquids evaporating from the surface of porous spheres,[9, 10] and applied to drop-size-distribution data to test the applicability of single droplet data to sprays.

Ingebo[9, 10] derives the following expression for the vaporization rate $dm/d\theta$ of single drops

$$\frac{dm}{d\theta} = \frac{\pi D k_g \Delta t}{H_v} \cdot \left[2 + 2.58 \cdot 10^6 \left(ReSc \frac{g\ell}{\bar{c}^2} \right)^{0.6} (k_g/k_v)^{0.5} \right] \tag{2}$$

where

D drop diameter
k_g gas thermal conductivity
k_v vapor thermal conductivity
Δt temperature of gas relative to that of drop surface
H_v latent heat of vaporization.
The term in brackets is the heat-transfer Nusselt number
Re Reynolds number
Sc Schmidt number
g acceleration due to gravity
ℓ mean free-path of gas molecules
$\bar{c}$ root-mean-square velocity of gas molecules.

Nine pure liquids and a range of air-stream pressure, temperature, and velocity conditions were tested in this study. Also, drop-surface temperatures were found to be approximately equal to wet-bulb temperatures, and a method of relating boiling point to wet-bulb temperature was derived.

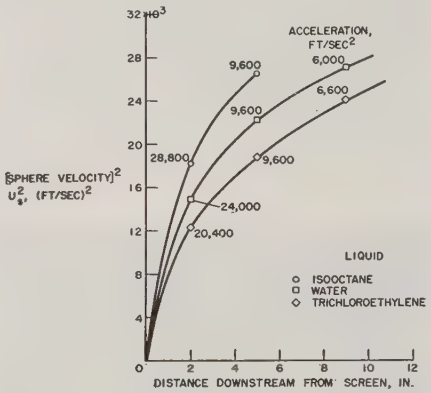

FIG. 5. Data plot for determining acceleration of 40 micron diameter droplets. Air-stream velocity, 180 ft/sec; static-pressure, 29.3 in. Hg abs; air temperature 82°F.

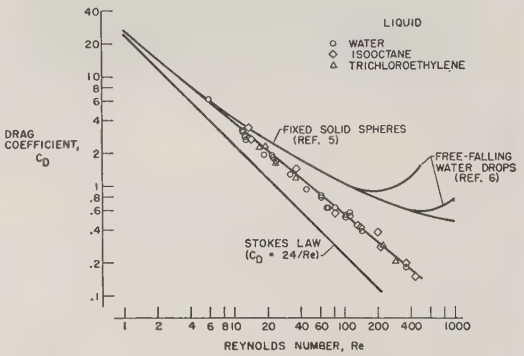

FIG. 6. Correlation of drag coefficients of droplets in accelerating clouds with Reynolds numbers.

TABLE 1

Air Velocity	Percentages Evaporated		
	Calculated	Camera data	Probe data
ft/sec			
140	14.1	14.4	17
180	16.9	15.1	19

Spray Vaporization-Rate Calculations

Spray vaporization rates were calculated by starting with isooctane drop-size-distribution data obtained with the camera stationed a few inches downstream of the injector.[2] Vaporization rate based on an average drop size for each size increment (0 to 5, 5 to 10 μ, etc.) was calculated by means of a graphical integration method

utilizing Equations (1) and (2). From this, a new drop-size distribution was calculated for the next downstream camera station, and compared with the experimental size distribution obtained with the camera. Good agreement was found as shown by the percentages evaporated given in Table 1. This table also includes data which were obtained by means of a continuous sampling probe technique.[11]

Conclusions

A graphical integration method for calculating spray vaporization rates gives good results when atomization, drag coefficient, and heat-transfer coefficient data are available. The need for drop-size-distribution data is probably the most critical requirement at present. Also, a more fundamental picture of simultaneous heat, momentum, and mass transfer is needed for a general treatment of spray vaporization.

REFERENCES

1. Clarke, J. S.: Inst. Mech. Engrs. (London), and Am. Soc. Mech. Engrs., Joint Conf. on Comb., Sect. 5 Gas Turbines, June 1955, pp. 24–31.
2. Ingebo, R. D.: NACA TN 3265, 1954.
3. Lee, D. W.: NACA Rep. 425, 1932.
4. Houghton, H. G.: Chem. Engrs. Handbook, Ed. 3, pp. 1170–1175. New York, McGraw-Hill Book Co., Inc., 1950.
5. Perry, J. H., ed.: Chem. Engrs'. Handbook. Ed. 3, p. 1018. New York, McGraw-Hill Book Co., Inc., 1950.
6. Laws, J. O.: Trans. Am. Geophys. Union, *22*, part 3, 709 (1941).
7. Lunnon, R. G.: Proc. Roy. Soc. London, *A110*, 302 (1926).
8. Ingebo, R. D.: NACA TN 3762, 1956.
9. Ingebo, R. D.: NACA TN 2368, 1951.
10. Ingebo, R. D.: NACA TN 2850, 1953.
11. Bahr, D. W.: NACA RM E53I14, 1953.

91

LIQUID FUEL ATOMIZATION

R. P. FRASER

Introduction

The combustion of liquid fuels through the process of atomization occurs in furnaces, in boilers for steam raising, in air heaters, and in internal combustion piston engines, jet engine combustion chambers and rocket motors. The rate of burning in a liquid fuel diffusion flame, as expressed by the heat release per unit time per unit volume of combustion chamber, is primarily dependent on the rate of mixing with the gaseous oxident. The first phase of mixing with a low volatility liquid is the disintegration of the fuel by atomization. Mixing involves the rate of production of liquid surface by the reduction of drop size and the spatial distribution of the spray within the combustion chamber. Ignitability of the spray is influenced by the drop size distribution of the spray near the atomizer by the presence of sufficient small drops to obtain flame homogeneity. Ignition point stability, and thus flame stability, is aided by a stable aerodynamic pattern in the air-spray mixture close to the atomizer. This may be created by the fluid flow from the atomizer itself or by a pattern induced in the secondary air-stream leaving the atomizer housing or burner register.

In liquid fuel combustion, therefore, the object of the atomizer is to disintegrate the fuel into the smallest drops possible to increase the specific surface of the liquid and thus the rate of mixing and vaporization. The functions of the atomizer are to accelerate and disintegrate the liquid by the production of a liquid sheet from which threads and finally drops will be produced, and also to disperse the resulting drops in a controlled pattern and direction.

Principles of Disintegration

The disruption of the liquid as it is discharged from the orifice of the atomizer is affected by: (1) the disturbances in the fuel flow within the atomizer, which cause turbulence in the liquid; (2) the properties of the gaseous medium into which the stream is discharged, and (3) the physical properties of the liquid itself.

The fundamental principle of the disintegra-

tion of a liquid consists in increasing the surface area of a rod or sheet until it becomes unstable and disintegrates. In liquid jets, when the major velocity component is in the axial direction and the jet is in laminar flow, a vibration in the jet, or an external disturbance, causes disintegration as predicted by the Rayleigh[1] break-up mechanism. When the jet is fully turbulent it can break up without the application of any external force. Radial components of velocity within it, when no longer confined by the orifice walls are only restrained by surface tension and the jet disintegrates when the surface tension is overcome. High viscosity in the liquid favors a longer break-up distance, whereas with increase of pressure and velocity break-up distance decreases. Regardless of all other effects the disintegration is always favored by air reaction which increases with air density.

The method usually employed to produce small drops at lower working pressures, for the purpose of producing diffusion flames, is to spread the liquid into a thin sheet (usually under 5 μ). Such sheets of liquid may be produced by using orifices with specially shaped approach passages (see Fig. 3a), by making it issue from a narrow annulus, by feeding the liquid to the center of a rotating disc or cup (Fig. 3e), or by spinning the liquid in an air vortex (Fig. 3h and i).

It is convenient to classify the numerous designs of atomizer according to the source of energy used but it is agreed that no fundamental difference exists in the mechanism of break-up of the liquid (Table 1).

The development of the sheet is greatly influenced by the spraying pressure, liquid properties, and ambient atmosphere. To open the sheet against the contracting force of surface tension, a minimum sheet velocity is required which is produced by the pressure or centrifugal force. Increasing the pressure expands and lengthens the sheet to an optimum distance when, with further increase, the sheet contracts towards the orifice by disintegrating earlier.

The formation of ligaments or fine threads is a necessary stage before the production of drops, and these can be formed directly from a free edge or in any boundary. A leading edge is formed when equilibrium exists between surface tension and inertia forces.

Three modes of disintegration in the sheet have been defined by Fraser and Eisenklam,[2] although there is only one mechanism of disintegration, namely the break-up of the liquid threads. Because of surface tension any liquid boundary is continually contracting and this phenomena produces "rim" disintegration (Fig. 1a). Threads are pulled out from the rim during contraction and these produce larger drops than those formed from the leading edge of the sheet. This mode is most prominent under conditions of low velocity, high surface tension and high viscosity.

In "perforated" sheet disintegration (Fig. 1b) the leading edge disintegrates to a network of threads. Disturbances on the sheet puncture it when they have reached a thin enough region and the resulting holes expand regularly by sur-

Table 1. Classification of Atomizers[29]

Pressure Energy Used for Pressure Atomizers	Centrifugal Energy Used for Rotary Atomizers	Gaseous Energy Used for Twin-Fluid or Blast Atomizers
Single hole nozzles Fan sprays 25 to 125 lb/sq in.	Spinning disks 100 to 600 ft/sec	Low pressure air (0.25 to 2 lb/sq in.) Air velocity 100 to 400 ft/sec Air/liquid ratio, 15 to 25 lb/lb 210 to 350 cu ft at 100°F/lb
Swirl spray nozzles Hollow sprays Drowned sprays 40 to 1000 lb/sq in.	Spinning cups 20 to 100 ft/sec	Medium pressure air or steam (2 to 20 lb/sq in.) Air velocity, 400 to 1000 ft/sec Air/liquid ratio 0.02 to 1 lb/lb 0.3 to 14 cu ft at 100°F/lb
Impact nozzles Solid surface, impact up to 400 lb/sq in. Impinging jets 20 to 140 lb/sq in.		High pressure steam or air (above 20 lb/sq in.) Air velocity sonic or above Air or steam/liquid ratio 0.2 to 1.0 lb/lb

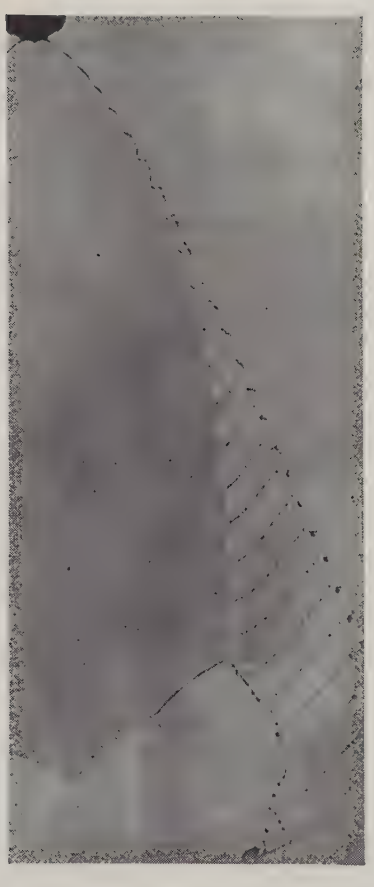

(a) "Rim" disintegration, glycerine and water, 15 centipoises viscosity. Velocity of sheet 58 ft/sec. (in vacuo)

(b) "Perforated sheet" disintegration, water. Velocity 85 ft/sec. (in vacuo)

(c) "Wavy sheet" disintegration, water. Velocity 120 ft/sec. (in atmosphere)

(d) "Air reaction" disintegration, water. Velocity 350 ft/sec. (in atmosphere)

FIG. 1. Modes of disintegration.

face tension so that they remain nearly circular until they coalesce, forming long threads which disintegrate when they become unstable. Threads which escape strong air reaction and which are formed in an orderly manner disintegrate uniformly according to theory. But the irregular areas of liquid which occur when a number of holes expand towards each other and coalesce produce a wide variety of drop sizes. The sheet also disintegrates in the absence of perforations in another mode—"wavy sheet" disintegration (Fig. 1c)—where the stability is such that major wave disturbances caused by the atmosphere disintegrate the sheet by tearing whole surfaces away before the leading edge is reached. A fourth mode may be defined where the velocity of the liquid leaving the nozzle is so high that air reaction plays the major role and the disintegration of a small but thicker sheet takes place close to the nozzle (Fig. 1d). This case is the inverse of the airblast atomizer.

Clearly the orderliness of the manner of disintegration of the sheet and the uniformity of production and diameter of threads has a great influence on the drop size distribution. "Rim" disintegration gives large drops together with numerous small satellite drops, as is obtained from a spinning disc at a medium flow rate (see Fig. 12a). Perforations occurring in the sheet at the same distance from the orifice have a similar life and thus the threads can be uniform, producing uniform drops. Wavy sheet disintegration is highly irregular and thus the drop sizes are very varied.

The atomization process, therefore, depends on a combination of different forces: viscosity, surface tension, air reaction and inertia. The combined effect of viscosity and surface tension with an approximately constant density (about 1.0) is illustrated in Figure 2. The photographs are of flat sheets of different liquids from the same nozzle at the same liquid velocity. They show the marked effect of increasing the viscosity approximately ten times at two levels of surface tension, and also the effect of increasing the surface tension approximately three times at two levels of viscosity. Increase in viscosity lengthens the sheet, and increase of surface tension contracts it and makes it more placid.

THE EFFECT OF SPRAYING ATMOSPHERE ON DROP SIZE

The spraying atmosphere has a marked effect on the resulting drop size. Thus high pressure in a combustion chamber causes a shortening of the liquid sheet and a "wavy" disintegration, whereas low pressure, as might occur in a high altitude vehicle, causes the sheet to become flat, and elongated, and perforations appear on it.

There are two separate effects of the atmosphere. First, the effect on the sheet and the mode of its disintegration, and second, the effect on the drops as they fly through the atmosphere.

Experiments have been carried out at room temperature by spraying water from a single hole nozzle (Fig. 3a) at a constant differential

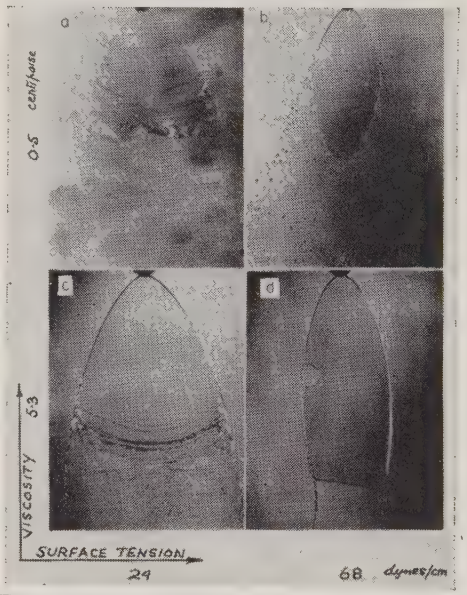

FIG. 2. Influence of liquid properties on the development of the sheet.

pressure into saturated air in a confined space, the density of which could be controlled at subatmospheric levels.[3] It was observed that as the density is reduced to about 18 in. mercury absolute, the sheet continues to break up through waves, but as the density is further reduced the sheet becomes flat, elongated and perforations appear on it.

The changes in mean drop sizes are plotted in Figure 4. It is seen that the results fall into two separate groups depending upon the mode of disintegration prevailing. The larger mean drop sizes obtained under subatmospheric conditions are caused by the effect of air density and a sudden change in the mode of disintegration. At atmospheric density the sheet is relatively short and thick. Waviness caused by air friction helps

in the formation of fine ligaments and the resulting drops are small and fairly uniform in size. As the density is reduced, the sheet flattens out and the intensity of the waves is reduced so that the resulting mean drop size increases. At the air

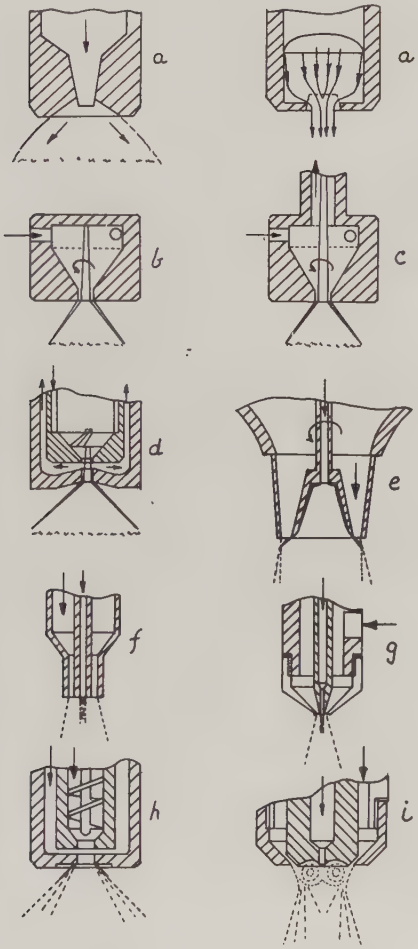

FIG. 3. Characteristic types of atomizer. (a) Rectangular orifice fan spray nozzle; (b) simple swirl chamber; (c) spill type swirl chamber, axial return; (d) spill type swirl chamber, nozzle boundary return; (e) rotary cup with air blast; (f) twin-fluid simple injection; (g) twin-fluid simple injection, convergent orifice; (h) twin-fluid internal mixer with swirl; (i) twin-fluid simple vortex cup.

density corresponding to the change in mode of disintegration from waves to flat perforated sheet, the sheet is thinner since it is longer. But the drops now originate from thicker ligaments because the drops are almost entirely formed from the rims of holes occurring in the sheet. Because the sheet is long the holes have a longer life and more liquid is contained in them. With still lower density the mean drop size decreases again nearly linearly, but never reaches the small size associated with a wavy sheet disintegration at atmospheric density.

Figure 5 shows the effect on drop size of spraying at varying differential pressure into atmospheric and low subatmospheric density. The tests were carried out with distilled water and the same nozzle. It is seen that over the liquid

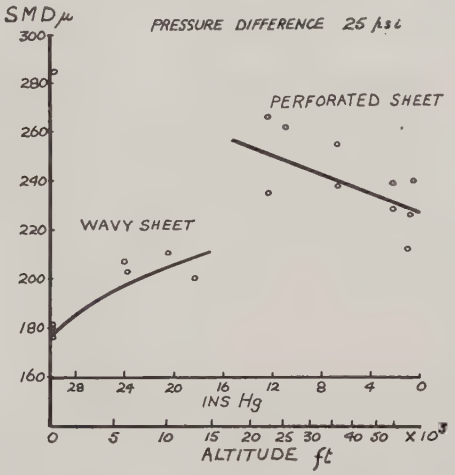

FIG. 4. Drop size variation in partial vacuum with water.

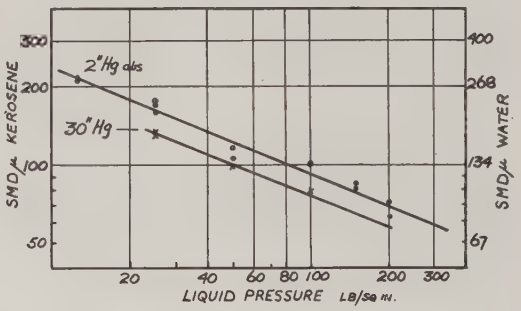

FIG. 5. Effect of differential pressure on drop size under atmospheric and subatmospheric conditions.

pressure range investigated the mean drop sizes are always greater at the low atmospheric density. The SMD difference at any pressure diminishes as the pressure rises, but the difference in the specific surface of the drops remains the same. The abrupt change in drop size at about two-thirds of an atmospheric pressure, particularly at low atomizing liquid pressure, indicates the possibility of a sudden change in particle size and dispersion from a pressure atomizer working in a combustion chamber under high altitude conditions.

The Atomizer and Attendant Drop Sizes With Fuel Oils

The energy for atomization can be applied in several different ways and because viscosity is one of the forces to be overcome, the first and simplest form of energy which can be applied is heat to the liquid to reduce the viscosity before the atomizer deals with it. Table 2 gives a comparison of the liquid properties of a number of common liquids with fuel oils at working preheat temperatures, in order of kinematic viscosity. It will be noticed that the fuel oils under working conditions have much the same density, surface tension and kinematic viscosity. In combustion practice the effect of the two former properties on the atomization of oils is therefore small; thus absolute viscosity and air reaction become of major importance.

Table 2. Comparison of Liquid Properties of Fuel Oils with Common Liquids, in Order of Viscosity

	Temp	Kinematic Viscosity	Redwood	Saybolt Universal	Absolute Viscosity	Density	Surface Tension
	°C	cs	sec		cp	g/cm	d/cm
Mercury	20	0.114			1.55	13.6	476
Methyl iodide	20	0.219			0.5	2.28	27
Acetone	20	0.405			0.32	0.79	24
Water	55	0.505			0.50	0.99	67
Sodium	148	0.60			0.55	0.92	187
Benzene	20	0.74			0.65	0.88	29
Water	20	1.00			1.00	1.00	73
Kerosene	20*	2.04	31.5	35	1.60	0.80	26
Gas oil (100°F)	40*	4.0	36.0	39.1	3.3	0.836	23
Analine	15	5.3	39.5	43.0	5.3	1.0	40
Gas oil (60°F)	15	7.0	43	48.6	5.95	0.85	24
Light fuel oil (180°F)	83*	9.4	51	57	8.3	0.88	21
Medium fuel oil (220°F)	105*	15.0	68	70	13.4	0.897	20
Heavy fuel oil (260°F)	127*	17.0	75	86	15.3	0.90	20
Glycerine and water (71 per cent)	20	21.0	90	104	25.0	1.19	68
Heavy fuel oil (200°F)	93*	40	160	190	37.0	0.92	21
Light fuel oil (100°F)	40	51	220	227	47.0	0.916	23
Glycerine and water (84 per cent)	20	82	313	375	100	1.22	66
Light fuel oil (60°F)	15	185	750	854	172	0.93	25
Medium fuel oil (100°F)	40	230	950	1060	215	0.936	23
Heavy fuel oil (100°F)	40	585	2700	3300	567	0.97	23

* Fuels at working preheat temperature.

ATOMIZATION BY PRESSURE

In combustion practice the swirl spray nozzle has attracted the greatest attention. Many forms of it are employed in land installations and aerogas turbines (Shell,[4] Joyce[5, 6]). All simple pressure atomizers (Fig. 3a, b) suffer from low flexibility or turn-down ratio because the discharge varies approximately as the $\sqrt{P}$ and, in commercial practice, the pressure is usually limited to less than 350 lb/sq in., although in special applications pressures up to 8,000 lb/sq in. have been employed. Greater turn-down ratio can be obtained with the "spill" type swirl spray nozzle where the rotational velocity of the liquid in the swirl chamber is maintained at low discharge rates by a large proportion of the liquid which enters the swirl chamber being returned to the supply side. The return path can either be from the axis of the swirl chamber (Fig. 3c) or by removing part of the boundary flow at the nozzle (Fig. 3d), or by designs which vary the swirl slot area as the flow pressure changes.

Many theories for the design of swirl spray atomizers of given flow characteristics have been proposed and it has taken the work of many investigators to derive the necessary design data to obtain an efficient solution for a nozzle for a particular liquid, pressure, spray angle and drop size (Harvey and Hermandorfer;[7] Watson;[8] Doble;[9] Doble and Halton;[10] Taylor;[11] Ellis;[12] Sohngen and Grigull;[13] Radcliffe[14]). According

to ideal flow analysis the discharge coefficient and the spray angle should depend only on the geometry of the nozzle expressed by the dimensionless number.

$$\Delta = A_s/D_2D_3$$

where A_s = total area of inlet swirl grooves, D_2 = orifice diameter, D_3 = swirl chamber diameter. The higher Δ, the lower the spray angle and the higher the discharge coefficient. These deductions hold in practice, but it is found that the flow characteristics depend also on additional dimensions of the nozzle, in particular the ratios of the orifice length/diameter (L/D_2) and of the swirl chamber/orifice diameter (D_3/D_2), as well as on the liquid properties, in particular pressure and viscosity.

Recent work has shown that for a nozzle of given Δ, the discharge coefficient increases with increasing D_3/D_2 and with diminishing L/D_2. The spray angle increases with both diminishing D_3/D_2 and L/D_2, for there is a unique relationship between discharge coefficient and spray angle which is determined only by the ratio L/D_2. These phenomena have been satisfactorily explained by examining the frictional decay of the vortex in the swirl chamber.

DROP SIZE FROM PRESSURE ATOMIZERS

The drop size resulting from the liquid sheet depends upon its velocity, thickness and the physical properties of the liquid. The factors which determine the film thickness and thus the drop size with a swirl atomizer are the flow number, the spray angle, the liquid pressure, viscosity and surface tension. The flow number is a product of the orifice area and of the discharge coefficient

$$FN = \frac{\text{Flow rate (Imp. Gal/hr.)}}{\sqrt{\text{Pressure (lb/sq in)}}}$$

$$\propto K_Q \times \text{orifice area} \times \sqrt{\frac{2g}{\rho_L}}$$

A = area in sq cm
K_Q = discharge coefficient
ρ_L = density

Since drop size depends on discharge coefficient and, to some extent, spray angle, both of which are determined by nozzle geometry, as mentioned above, the nozzle dimensions in this atomizer have considerable influence on the drop size. Empirical relationships have been derived by many workers which are of the form

$$\text{SMD} \quad \text{or} \quad d_s \frac{\gamma^a \nu^b FN^c}{P^d}$$

where γ = surface tension, ν = kinematic viscosity (centistokes), P = pressure (lb/sq (in.). There is considerable variation in the values of the indices obtained by different authors and because the spray angle is excluded in most of these relationships, the results are only strictly applicable to those angles at which the drop sizes were measured.

Recently Knight[15] has correlated a large number of drop size results (obtained by the wax method) of Lubbock and Bowen,[16] Joyce,[5] Needham,[17] Watson,[8] and others, with nozzles of 85°-angle and surface tensions of 24 d/cm, in the range of FN up to 4 and pressures up to about 200 lb/sq in. into the form

$$\text{SMD} = 220\, P^{-0.458}\, Q^{0.209}\, \nu_L^{0.215} \qquad (1)$$

where Q is in lb/hr.

The influence of nozzle dimension on drop size for various heat outputs or flow rates from a single swirl spray atomizer passing two typical industrial fuels at working preheat temperatures is shown in Figure 4. The figures for these curves have been calculated for

	ρ g/cc	γ d/cm	ν_L c/stokes
Gas oil at 100°F	0.836	23	4
Medium fuel oil at 220°F preheat	0.894	20	15

with the assumption that SMD varies according to SMD $\propto \gamma^{0.33}$ and density $\rho^{0.2}$. Substituting in Equation (1) these liquid properties give

$$\text{SMD} = 454 \frac{FN^{0.209}}{P^{0.353}} \qquad (2)$$

Gas oil

$$\text{SMD} = 585 \frac{FN^{0.209}}{P^{0.353}} \qquad (3)$$

Medium fuel oil

To obtain the least combustion loss the combustion chamber must be designed to consume the largest drops. Thus large drops must be few in number and the SMD to be aimed for should be less than 100μ, and the drop size dispersion such that the largest drops are few in number and not greater than 200μ. Figure 6 shows that at small flow rates of 6 Imp. gal/hr or 1 million Btu/hr output, fuel pressures of 100 to 200 lb/sq

in. can achieve a satisfactory drop size with either fuel. With flow rates about 240 Imp. gal/hr or 1 ton/hr an SMD of 100μ is only obtainable with a pressure of 400 lb/sq in. for gas oil and 700 lb/sq in. with medium fuel oil. (See Table 2 for properties.) Thus to achieve the least combustion loss with large swirl spray nozzles up to 500 Imp. gal/hr a pressure of about 1,000 lb/sq in. must be employed. For still higher heat outputs of over 100 million Btu/hr the necessity of employing a large number of atomizers is evident. To achieve the desired drop size at a commercial pressure of 350 lb/sq in. about 75 gal/hr or 12½ million Btu/hr is the maximum size. Above this figure the curves in Figure 6 are extrapolations.

To summarize the characteristics of swirl spray nozzles

At constant liquid pressure

Flow $\propto$ to nozzle diameter^2

SMD $\propto$ to (nozzle diameter)$^{\frac{3}{4}}$

With constant nozzle size:

Flow increases $\propto$ to $\sqrt{\text{Pressure}}$

SMD reduces $\propto$ to $\sqrt{\text{Pressure}}$

IMPINGING JET AND SINGLE HOLE FAN SPRAY NOZZLES

With the exception of the rocket motor, impinging jet nozzles have had little application for use in combustion but are commonly used in other fields. Where two jets of liquid are produced from two separate orifices and made to impinge they produce a fan-shaped sheet in a plane perpendicular to that containing them. In the single-hole fan spray nozzle there is only one shaped orifice which forces the liquid into two opposing streams within itself so that the resulting fan-shaped sheet issues directly from the single hole (Fig. 3a). The drop sizes from such fan spray nozzles are generally larger than those from swirl spray nozzles of equal flow rate (Fraser and Eisenklam[3]). With this form of nozzle the discharge coefficient remains constant for a very wide range of liquid properties. Experimental evidence has so far been obtained for property ranges of 0.4 to 81 cs viscosity, 0.8 to 21 g/cm^3 density and surface tension 23 to 73 d/cm (Dombrowski and Fraser[18]).

An attempt to relate the design characteristics of this kind of atomizer to the properties of the sheet and finally to the drop size obtained on disintegration led to the following formula applicable to fuel oils

$$\text{SMD} = \frac{340}{K_Q} (P)^{-0.25} \left(\frac{FN}{\alpha}\right)^{0.37} \qquad (4)$$

where α is the exit angle of the atomizer orifice in radians.

ATOMIZATION BY MEANS OF A SECOND FLUID (TWIN-FLUID ATOMIZERS)

In twin-fluid or blast atomizers a high velocity gas stream is made to impinge on the liquid, either externally or within the body of the atomizer. The amount of energy available for atomization being independent of the fuel quantity, no strict limitation of drop size to liquid discharge rate, turn-down ratio or spray angle exists. Spray angles up to 180° and SMD below 20μ can be achieved with large flow rates, and satisfactory atomization for ignition can be accomplished with the fuel at a higher jet viscosity, namely about 100 cs (400 Redwood sec).

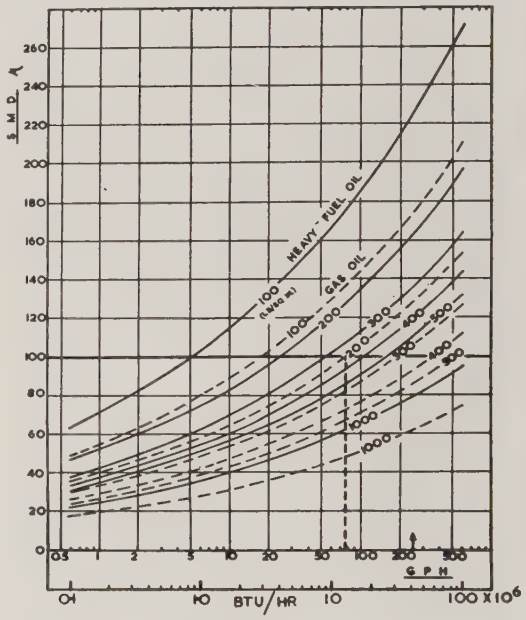

FIG. 6. Drop size heat output relation for swirl spray nozzles.

Much less study has been made with twin-fluid atomizers because of their very varied design, the difficulties of measurement of the relative fluid velocities, variability of spray pattern and the photographing and sampling of very small drops.

Nukiyama and Tanasawa[19] derived an empirical expression for the assessment of SMD. It is

based on experiments with small twin-fluid nozzles of the internal mixing type operating with a high volumetric ratio of air to liquid. Their work leads to the following formula:

$$\text{SMD} = \frac{585}{V}\sqrt{\frac{\gamma}{\rho_L}} + 597\left(\frac{\eta}{\sqrt{\gamma\rho_L}}\right)^{0.45}\left(\frac{1000}{j}\right)^{1.5} \quad (5)$$

where V = velocity of air relative to liquid m/sec (subsonic at nozzle exit); γ = surface tension d/cm, range 30 to 73; ρ_L = liquid density g/cm³, range 0.8 to 1.2; η = absolute viscosity

FIG. 7. Disintegration of a cylindrical liquid jet in an air stream 115 ft/sec.

poise, range 0.01 to 0.3; j = actual air/liquid volume ratio at air and liquid orifice respectively; i.e., at pressure of surrounding atmosphere.

This relation shows that the SMD is determined by the amount of air used per unit of liquid, and the relative fluid speeds. Thus the SMD is reduced as the air pressure and air/liquid ratio are raised. The relation also shows that to obtain SMD 20μ air velocities greater than 700 ft/sec and air/liquid weight ratios above 10 lb/lb may be required. At such high ratios the effect of the viscosity term is small and the first term of the equation is the most influential. In Figure 11, Curve A, the mean drop sizes predicted by this equation for a fuel of the following properties: viscosity 10 cs, density 0.94 g/cm³ and surface tension 28 d/cm at 10 lb/sq in. air pressure and different mass ratios; is compared with the drop sizes from a number of industrial and experimental atomizers.

Golitzine, Sharp and Badham[20] explored two types of small venturi injection atomizer, one with a convergent and the other with a convergent-divergent orifice, using water, and correlated drop size against the air/liquid ratio and air and liquid orifice jet diameters. Air/liquid ratios were high, between 3 and 5 lb/lb and the air orifice diameters were from 0.125 in. to 0.247 in. The smallest drop size for the lowest air/liquid ratio was found with the smallest orifice diameters with the convergent nozzle.

Wetzel and Marshall,[21] experimenting with venturi injection type atomizers and using molten wax, density 0.38 g/cc, viscosity 9 cp, surface tension 29.5 d/cm, expressed their results as

$$\text{MMD} = 4.2 \times 10^6 (V_a - V_L)^{-1.68} x\, d_0^{0.35} \quad (6)$$

where MMD = Mass Median diameter (50 per cent volume oversize); V_a = velocity of air stream in ft/sec, V_L = velocity of liquid jet in ft/sec, d_0 = diameter of liquid jet in inches. Their results show good agreement with the Nukiyama-Tanasawa results when wax was used and the air velocity was above 400 ft/sec (about 2 lb/sq in.). But no agreement was obtained when spraying a high density, high surface tension molten alloy, indicating that the Nukiyama-Tanasawa equation should be employed only within the range of liquid properties for which it was established (see Equation (5)). Bitron,[22] however, has confirmed the formulae for supersonic velocities.

A great number of twin-fluid atomizers have been designed for combustion purposes. In these simple injection types already referred to (Fig. 3f, g), the air is made to impinge externally on a solid jet of fuel, the angle of the spray produced is small (*ca* 12°), and the spatial uniformity in the cone of spray is uneven. High-speed pictures of the simple injection atomizer show the disruption of the jet to result in an intermittent process; the liquid jet being pinched off into sections before being blown into drops, with the result that the axial distribution of the drops is in successive groups. Figure 7 shows water disintegrating within a jet of air at a velocity of 115 ft/sec.

The importance of filming the liquid in twin-fluid atomizers has not been sufficiently realized. Methods of prefilming are to cause the liquid to issue from a swirl-spray nozzle or a spinning cup,

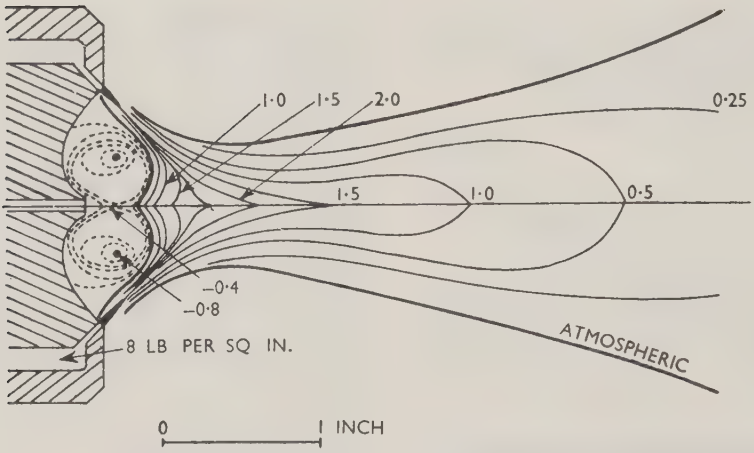

(a) Simple annulus without swirl producing a vortex ring.

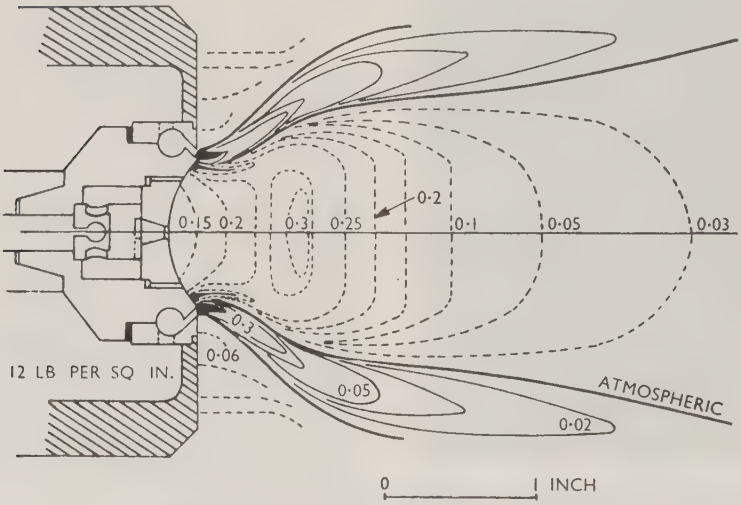

(b) With swirl, producing a cylindrical vortex.

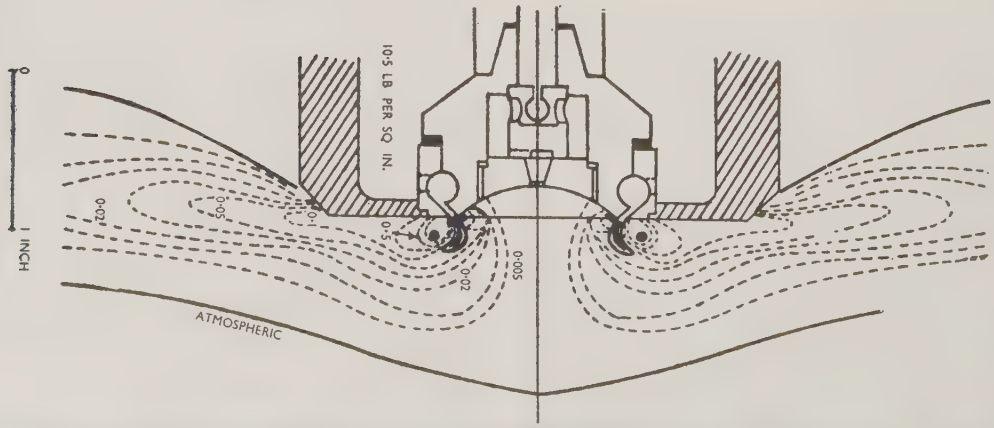

(c) Maximum spray angle adjustment of (b). Figures against full lines indicate positive pressures, and dotted lines negative pressures.

FIG. 8. Isobar diagrams of a twin-fluid vortex cup atomizer.

or issue through a narrow annulus, or, by means of the air itself, to rotate the liquid in a stationary cup (vortex cup).[23] This last method is achieved by greatly broadening the tip of the liquid orifice and allowing the air at high velocity to issue from a very narrow annulus at its periphery some distance from the liquid orifice.

Isobars from a design of this type are shown in Figure 8. These diagrams represent lines of equal pressure or isobars without liquid flow. Dotted lines indicate pressures below atmospheric. (These contours are plotted from measurements with a very fine search tube, not a Pitot tube; thus the direction of flow cannot be immediately assessed. Nevertheless, they give valuable information for design purposes and define changes of the flow pattern and the appearance of asymmetry.)

The pattern of flow in the three examples is different, dependent on the relation of rotational to translational velocity in the air stream leaving the annulus. Figure 8a represents the case of no rotational air velocity, and thus the converging cone of air leaving the annulus causes a vortex ring to form within the cup and a positive pressure to be created in front of the liquid orifice. These conditions constrain the liquid to flow radially from the orifice over the surface of the cup and meet the sheet of air issuing from the annulus at right angles. The time of contact of the air with the liquid is increased and atomization is improved.

In Fig. 8b a very high rotational component of velocity obtains, and the sheet of air leaving the annulus proceeds to diverge from it almost immediately. What may be defined as a cylindrical vortex exists at the lip of the vortex cup and the liquid within it is constrained to rotate rapidly as if the cup itself were rotating. The liquid finally meets the very rapidly rotating air at the periphery of the cup and is rapidly disintegrated.

Figure 8c shows the interesting case of the atomizer as in (b) adjusted to give practically no forward velocity but only high rotational velocity, so that the air leaving the annulus rotates and spreads outwards at 90° to the axis, giving an effective cone angle of spray of 180°.

Figure 9 shows a series of msec photographs of this atomizer operating as adjusted in Figure 8b. Figure 9a shows the airstream only photographed by shadow photography. Figure 9b shows the delivery of liquid from the central swirl-spray nozzle only; Figure 9c shows the addition of a small quantity of air from the annulus at 2 lb/sq in. The sheet is seen to have expanded towards and leaves from the edge of the cup. Figure 9d is with increased air pressure and shows the considerable reduction in particle size. Figure 9e shows a further photograph of the case of the atomizer adjusted as in Figure 8c and indicates the manner in which the liquid rotates in the cup. The air core in the liquid jet can be seen with spirals of liquid expanding outwards to the air annulus where it is blown out into sheets and atomized and where, photographically speaking, it disappears.

The drop size distribution of twin-fluid atomizers will change with nozzle design and size and, also, by adjustment of component parts in any one design. Some examples of the distribution obtained with a 1 in. diam vortex cup atomizer with water are shown in Figure 10 and Table 3. Differences are observed with change of air/liquid ratio, air pressure, annulus width and sampling distance. A smaller SMD is obtained when the sample is taken near the atomizer due to loss of small particles by drift and coalescence of particles with distance.

It is interesting to note that although there is much variation in design, fluid pressure, physical properties, and method of drop-size measurement, the SMD given by several practical types of this kind of atomizer can be correlated reasonably well when plotted against air/liquid ratio, as shown in Figure 11 and Table 4. The correlation illustrates the large expenditure of air required to reduce the SMD below 40μ with any design or viscosity compared with that required to obtain SMD = 100μ. The large expenditure of air for a given drop size at 10 lb/sq in. by the Tanasawa and Nukiyama equation is shown in Curve A. This is confirmed by Curve B calculated from determinations of Courshee, Byass and Waring,[24] using a simple injection atomizer of the type shown in Figure 3f. These figures are in contrast to the results with more modern designs where rotating streams of air are employed.

In the internal-mixing type the liquid and air interact at high density and the pressures counterbalance, whereas with external mixing they intersect at ambient density and the pressures are independent; and this may be the explanation of a distinction between these types. In the internal mixer, reduction of the liquid pressure and flow at the same air pressure reduces the drop size. In the external-mixing type, reduction of the liquid flow at the same air pressure and annulus adjustment does not materially alter the drop

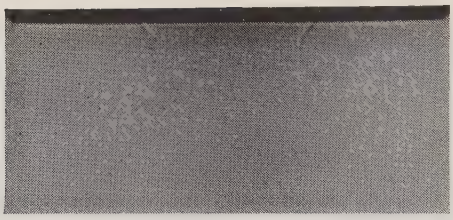

(a) Liquid nil; air 14 psi.

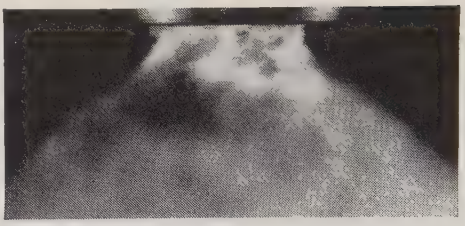

(d) As (b) with air at 14 psi.

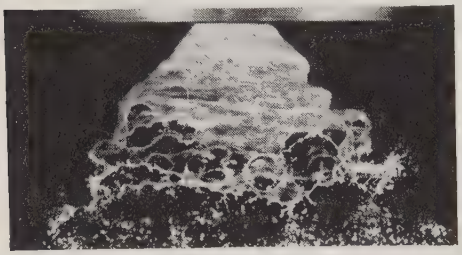

(b) Liquid flow 100 lb/hr from central swirl spray nozzle; air nil.

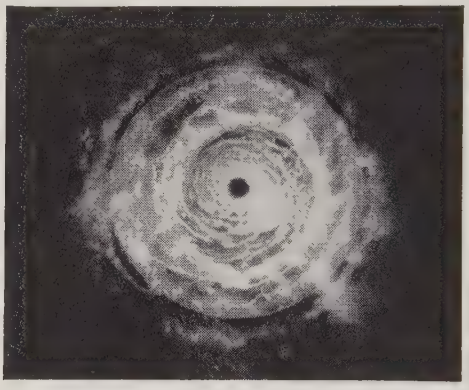

(e) View of vortex cup from axis with maximum spray angle setting as in Fig. 8(c).

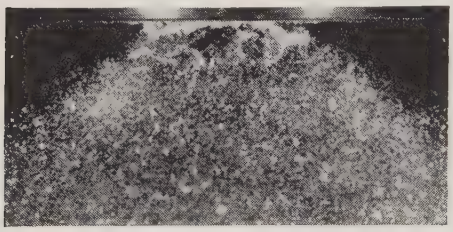

(c) As (b) with air at 2 psi.

FIG. 9. Microsecond photographs of the vortex atomizer, as in Fig. 8(b).

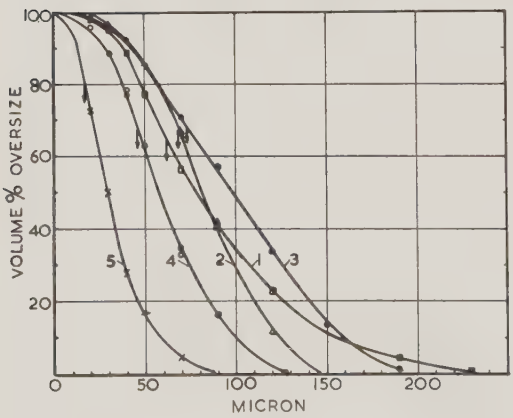

FIG. 10. Drop size distributions of water from twin-fluid vortex cup atomizer, as in Fig. 8(b).

size (Curves C and D). The effect of increasing air pressure is shown by the figures against each point. Higher pressure is beneficial in reducing drop size at lower mass ratio.

TABLE 3

Curve No.	Air Annulus	Pressure		Water Flow-rate	Air/ Water Ratio	SMD	Sampling Distance
		Air	H_2O				
	10^{-3} in.	*lb/sq in.*	*lb/sq in.*	*gal/hr*	*lb/lb*	μ	*in.*
1	50	9	50	26.5	0.465	63	9
2	50	9	22	17.7	0.69	69	9
3	50	8.5	40	11.4	1.05	74.5	12
4	50	16	10	5.9	3.0	47	36
5	50	35	10	5.9	5.1	18	36

ROTARY ATOMIZERS

Photographs have shown (Hinze and Millborn[25] and Dombrowski and Fraser[18]) that the mechanism of drop formation from a spinning disc by centrifugal force is similar to that observed by gravity at the end of a stationary circular tube, the diameter of which is equal to the thickness of the rim of the disc Figure 12a shows

that each drop is connected to the rim by a thread which on detachment forms itself into satellite drops. It is important to realize that the conditions of uniform main drop size only exist when the drops are formed at the rim of the disc between the upper and lower edge, and there is a critical flow rate range which produces such conditions. Below it, starved conditions and incomplete wetting exists so that the drops are shot off from the upper edge only and a wider drop size dispersion results. Above this range flooding occurs and drops are formed from long ligaments away from the rim and, again, a wide drop size distribution results (Fig. 12a). At still greater flow rates flooding produces a sheet of liquid in the atmosphere away from the disc perimeter which disintegrates irregularly at its leading edge in the manner of a normal sheet from a pressure atomizer (Figure 2). Under this condition of working the spinning disc atomizer may be regarded as the limiting case of swirl spray nozzles, where the axial velocity is zero and the spray cone angle is 180°.

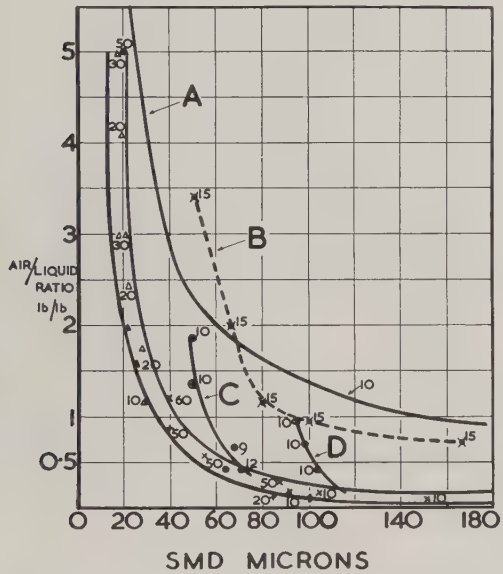

FIG. 11. Drop size correlation of twin-fluid atomizers. Figure against each point represents the air pressure in psi.

In most combustion applications the spinning cup is small in diameter and driven by mechanical means. Where it is directly coupled with a fan impeller the peripheral velocity of the cup is often limited to below 50 ft/sec. In such cases, under full load conditions, the cup is in a flooded condition. In this case also the low pressure air jet from the fan around the cup plays the largest part in the disintegration, for the centrifugal energy in the liquid is small in comparison with the energy content in the airstream.

TABLE 4

Symbol	Type of Atomizer	Liquid Delivery Range	Liquid Used	Liquid Properties			Author
				Viscosity	Density	Surface Tension	
		lb/hr				*d/cm*	
△	Internal mixing	Up to 0.115	Petroleum ether	0.69	0.734	20*	Garner and Henny[27]
×	Internal mixing (Fig. 3h)	54 to 269	Wax	40	0.93	23*	Clare and Radcliffe[28]
+	Internal mixing	86 to 218	Wax	20	0.9	23*	
⊕	External mixing	50 to 280	Wax	40	0.93	23*	
●	Vortex Cup (Fig. 7b)		Water	1.0	1.0	73	Fraser[29]
○	External mixing Vortex Cup (Fig. 3i)	166 to 400	Wax	40	0.93	23*	
✱	External mixing Simple Injection (Fig. 3f)	9 to 59	Water	1.0	1.0	73	Coursheé et *al.*[24]

* Approximate.

The main drop sizes obtained from small diameter discs or cups for an oil of $\gamma = 28$ d/cm, $\rho_L = 0.94$ g/cm^3 is given in Figure 13. The curves show that a 10 cm diam disc requires to rotate at 6,500 rpm to achieve a main drop diameter of

100μ. They also show that small diameter cups without air assistance must rotate at speeds in the region of 20,000 rpm to achieve main drop

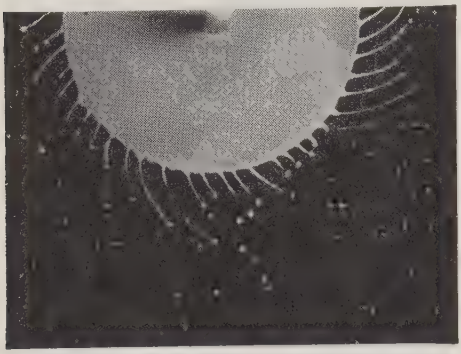

(a) Thread formation

(b) Sheet disintegration, by flooding disc.

FIG. 12. Disintegration from a spinning disc.

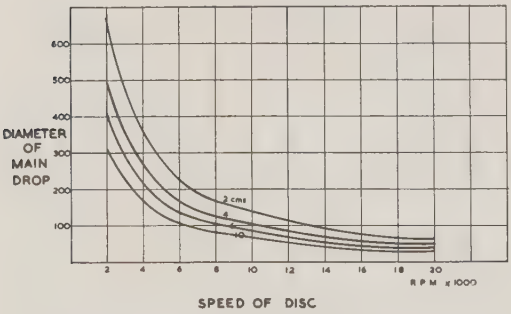

FIG. 13. Main drop size from a non-flooded spinning disc with fuel oil.

sizes equivalent to the SMD of twin-fluid atomizers using 0.4 to 0.7 lb of air/lb of fuel.

Lane[26] has shown that in a steady stream of gas a critical relative velocity is reached at which large drops are further disintegrated. Under atmospheric conditions the relative velocity, V, corresponding to a critical diameter, d, below which shatter will not occur is given by

$$V \propto \sqrt{\frac{\gamma}{d}}$$

which, for a fuel oil, becomes

$$V^2 d = 2.1 \times 10^6 \qquad (7)$$

where V is in ft/sec; d is in μ within the range 500 to 5000μ.

If it is assumed that this relationship holds for sizes below 500μ, Fraser and Eisenklam[3] have made a comparison of the critical diameter with the SMD from several types of atomizer. This shows that the larger drops from fuel atomizers will begin to shatter at velocities given by pressures of about 150 lb/sq in. for a fan spray nozzle of $FN = 2$, and about 250 lb/sq in. for a swirl spray nozzle of $FN = 2$, while the corresponding peripheral speed of a spinning disc is over 300 ft/sec (i.e., 18,000 rpm for a 4 in. diam disc).

REFERENCES

1. RAYLEIGH, LORD: Proc. London Math. Soc., *10*, (1878).
2. FRASER, R. P., AND EISENKLAM, P.: J. Imp. Coll. Sci. Chem. Eng. Soc., *7* (1953).
3. FRASER, R. P., AND EISENKLAM, P.: Trans. Inst. Chem. Engrs., 1956.
4. Shell Report: TR ICT/*12* (1947); *17* (1948).
5. JOYCE, J. R.: J. Inst. Petroleum, *39*, 350 (1953).
6. JOYCE, J. R.: J. Inst. Fuel, 150–156 (1949).
7. HARVEY, J. F., AND HERMANDORFER, A. S.: Trans. Soc. Naval Architects & Marine Engrs, *51*, 61–82 (1943).
8. WATSON, E. A.: Jos. Lucas Report L.1258 (1944); L.1675 (1945); L.2671 (1947).
9. DOBLE, S. M.: Engineer *21*, 61, 103 (1945).
10. DOBLE, S. M., AND HALTON, E. M.: Trans. Inst. Eng. Mech. (1947).
11. TAYLOR, G. I.: Quart. J. Mech. Appl. Math., *111*, 129 (1950).
12. ELLIS, J.: London University Thesis, 1950.
13. SOHNGEN, E., AND GRIGULL, U.: Forschung, *17*, 77 (1951).
14. RADCLIFFE, A.: Proc. Inst. Mech. Engrs., *169*, 3, 93 (1955).
15. KNIGHT, B. E.: Proc. Inst. Mech. Engrs., *169*, 93 (1955), written discussion.
16. LUBBOCK, I., AND BOWEN, I. G.: Proc. Inst. Petroleum and Inst. Fuel Joint Conf. on Liquid Fuels, p. 231 (1948).
17. NEEDHAM, H. C.: Power Jet Report, R1209, 1946.
18. DOMBROWSKI, N., AND FRASER, R. P.: Phil. Trans. Roy. Soc., *A924*, 247 (1954).

19. Nukiyama, S. T., and Tanasawa, Y.: Trans. Soc. Mech. Engrs., Japan, *4*, 86–138 (1938); Trans. Soc. Mech. Engrs., Japan, *5*, 63, 68 (1939); Trans. Soc. Mech. Engrs., Japan, *6*, II, 7, II, 18 (1940). (In Japanese; refer to Lewis and others, 1948.)
Lewis, H. C., Edwards, D. G., Goglia, M. J., Rice, R. I., and Smith, L. N.: Ind. Eng. Chem., *40*, 67 (1948).
20. Golitzine, N., Sharp, C. R., and Badham, L. G.: Nat. Aero. Estab. Canada, R14ME-186, 1951.
21. Wetzel, R. H., and Marshall, W. R.: Washington, D. C., Nat. Meeting Am. Soc. Mech. Engrs., 1954.
22. Bitron, M. D.: Ind. Eng. Chem., *47*, 23 (1955).
23. Fraser, R. P.: Brit. Pat. No. 405,308, 1934; 664,076, 1947.
24. Courshee, R. J., Byass, J. B., and Waring, N. D.: N.I.A.E. Tech. Memo No. 125, 1955.
25. Hinze, J. O., and Milborn, H.: J. Appl. Mech., *17*, 145 (1950).
26. Lane, W. R.: Ind. Eng. Chem., *43*, 1312 (1951).
27. Garner, F. H., and Henny, V. E.: Fuel, *32*, 151 (1953).
28. Clare, H., and Radcliffe, A.: J. Inst. Fuel, *27*, 510 (1954).
29. Fraser, R. P.: Inst. Mech. Engrs. and Am. Soc. Mech. Engrs. Joint Conf. on Combustion, 1955.

92

FLAME PROPAGATION THROUGH AIR-FUEL FOAMS

By A. THOMAS

In connection with the evaluation of a practical hazard, the question arose whether explosive flames could propagate through foams of air in fuels well below their flash points. It was known that flames could propagate through mists and sprays of nonvolatile liquids, but no information on the explosive behavior of foams was available. The air and fuel would be in intimate contact in these foams, so that a considerable degree of premixing would have been achieved; explosive flame propagation would not be unlikely. An experimental investigation into the matter was therefore carried out at the Thornton Research Centre. Although the work was planned to give information about a specific hazard, it is here presented with the emphasis upon features of general interest in the study of flame propagation through air-fuel dispersions.

Apparatus

A technique analogous to that of measuring limits of inflammability of gaseous mixtures was developed. Foams were produced in a trough 2 ft 6 in. long and 6 in. wide and ignited at one end. A flame was adjudged to propagate only if it travelled to the other end of the trough.

A diagram of the apparatus is shown in Figure 1. The liquid under investigation filled the trough to a depth of ¾ in. leaving an ullage 2½ in. deep. The bottom of the trough was covered with a perforated plate, below which was a compartment into which gas could be passed. Bubbles arose from the perforations and collected on top of the liquid to form a layer of foam.

A considerable problem was to achieve uniformity in foam over the whole length of the trough, since foams of the fuels investigated were not very stable, and did not persist long enough to level out by flowing in a horizontal direction. The compartment underlying the trough was therefore subdivided into 28 sections, as indicated in Figure 1. Oxygen-nitrogen mixtures were fed into a manifold which discharged through precision-drilled orifices of 0.015 in. diam to each section. Both oxygen and nitrogen were metered separately through critical flow orifices and conditions were such that critical flow also occurred through the entry holes to the sections, thereby insuring equal delivery to each. The metal plate covering the sections was perforated all over with holes 0.002 in. diam spaced 0.02 in. apart. Bubbles arose from only a few of the holes above each air compartment, but enough horizontal flowing of the foam on the surface of the liquid took place to give a fairly even covering. Most of the foam bubbles had a diameter of about 1 mm but larger bubbles were also present.

Fuel temperature was measured by means of

a thermocouple and controlled by circulation of fuel through external heating or cooling coils.

The trough was contained in a small altitude chamber which was a steel vessel of 10 in. i.d. fitted with a window and a relief valve, and connected to a large capacity vacuum pump. The pressure in the vessel was adjusted by throttling the pump, and measured by a mercury-in-glass manometer.

The development of a source of ignition presented some difficulty in view of the low pressures within the chamber. An extremely powerful source was required which would nevertheless

Procedure

It was found that flame propagation was critically affected by the oxygen concentration in the bubbles. This is in itself significant, and will be referred to in the discussion. The most convenient experimental procedure was to find the critical concentration of oxygen at which propagation first occurred.

Fuel temperature, gas flow rates and ambient pressure were set to required values and the foam was ignited at one end. If propagation to the other end did not take place, oxygen flow rate was increased, and the experiment repeated until

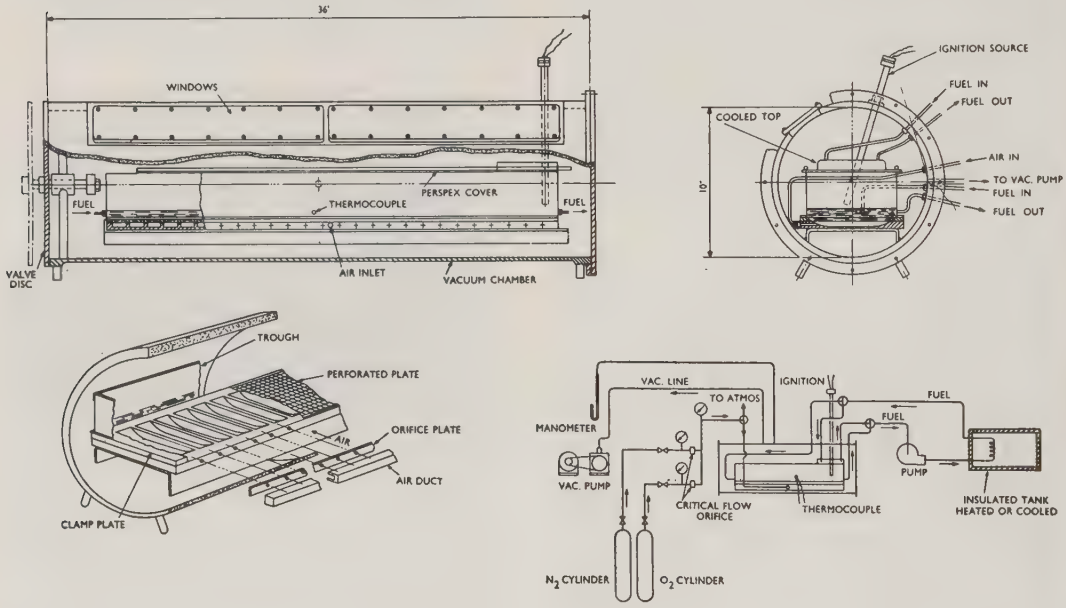

FIG. 1. Diagram of apparatus.

vaporize very little fuel other than in the immediate vicinity. Both a hot wire and an electric arc were successfully used, and gave results very close to one another, but the arc was preferable insofar that ignition took place with more certainty, and in a shorter time than with the hot wire.

It was found that a lid placed on the trough, leaving a gap for the exhaust at one end, significantly enhanced flame propagation, and thereby provided more hazardous conditions. The effect was greatest when the vent was at the end remote from the source of ignition. For the bulk of the work, the trough was covered with a lid except for a length of $1\frac{1}{2}$ inches at the remote end.

the critical oxygen concentration for propagation was found. For reproducibility it was necessary always to approach the limit from the nonpropagating side; otherwise the thermal state of the system was considerably disturbed for a long period by the very considerable flames that were produced, even though the fuel itself could be quickly cooled by circulation. Sometimes at conditions below the critical oxygen concentration for full propagation small fires would stabilize around the igniter. These also induced irregular behavior until a liquid-cooled lid was placed over the trough around the igniter.

It was frequently found that the critical oxygen concentration went through a minimum and then increased again as bubbling rates were increased.

Since the work was related to the defining of a hazard, this minimum value was the quantity immediately required, and curves were not taken very far beyond the minimum point. Only where a minimum was not found were the bubbling rates increased to the maximum of which the apparatus was capable. The limit was then set at higher pressures by the maximum gas flow rates that could be conveniently obtained, and at lower pressures by the overflowing of foam from the trough.

One variable which was not investigated systematically was bubble size. Preliminary work indicated that the smaller the bubble size the more easily did flames propagate. Consequently most of the work was carried out with the smallest bubble sizes that could be obtained with the equipment.

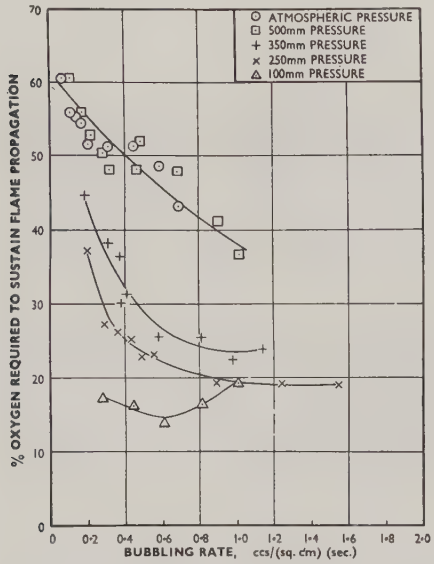

FIG. 2. Limiting conditions for flame propagation through gas oil foams at 30°C (P_F = 75 mm).

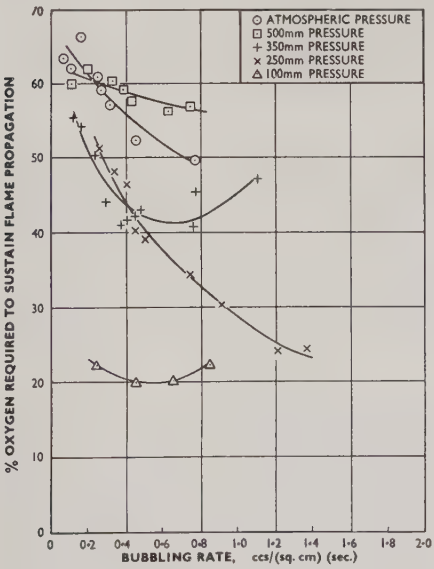

FIG. 3. Limiting conditions for flame propagation through gas oil foams at 20°C (P_F = 40 mm).

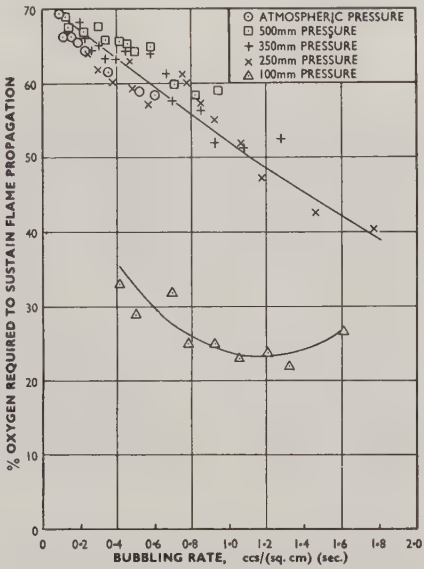

FIG. 4. Limiting conditions for flame propagation through gas oil foams at 10°C (P_F = 18 mm).

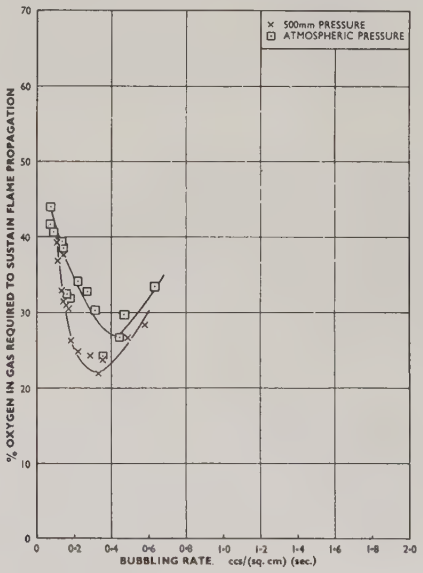

FIG. 5. Limiting conditions for flame propagation through kerosene (JP1) foams at 26°C (P_F approx. 220 mm).

Results and Discussion

The critical oxygen concentration was determined at increasing bubbling rates for various fuel temperatures and at various pressures. The results obtained are illustrated in Figures 2 to 9. Figures 2, 3 and 4 show the relationship between bubbling rate and oxygen requirement for gas oil foams at various temperatures and pressures, and Figures 5, 6, 7, 8 and 9 show similar results for kerosene foams. The bubbling rate is expressed as the volume of gas, measured at conditions prevailing in the chamber, emerging from each sq. cm. of surface/sec. This is equal to the mean gas velocity upwards through the foam, and determines the height of foam.

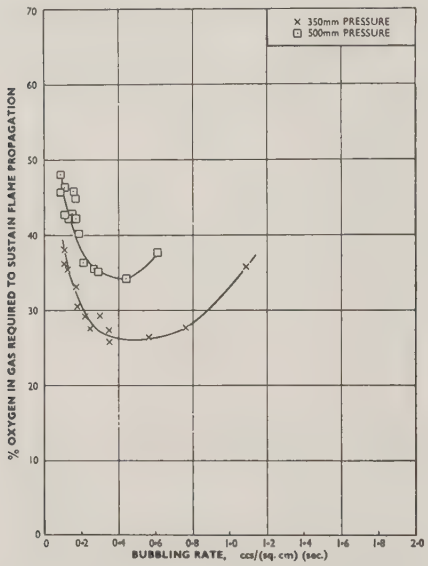

FIG. 6. Limiting conditions for flame propagation through kerosene (JP1) foams at 18°C (P_F = approx. 150 mm).

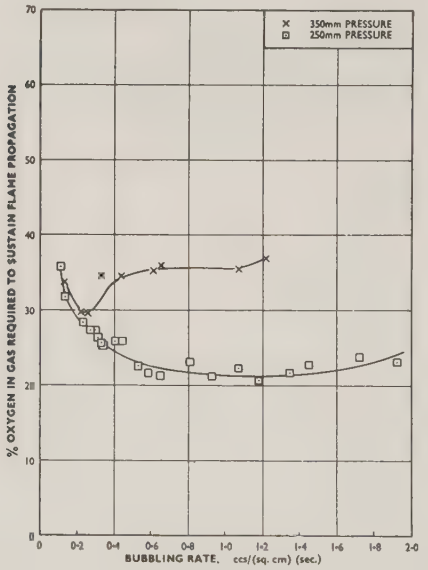

FIG. 7. Limiting conditions for flame propagation through kerosene (JP1) foams at +10°C (P_F = approx. 90 mm).

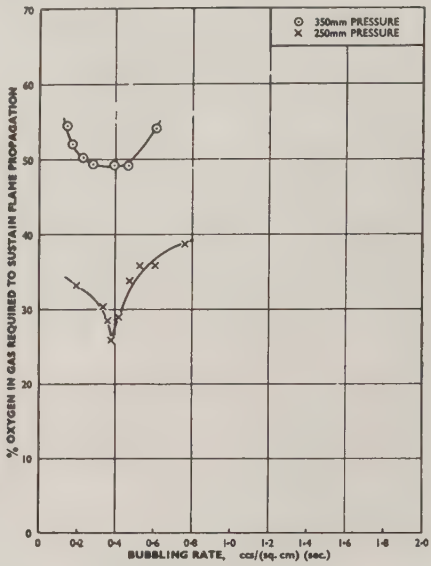

FIG. 8. Limiting conditions for flame propagation through kerosene (JP1) foams at 0°C (P_F approx. 45 mm).

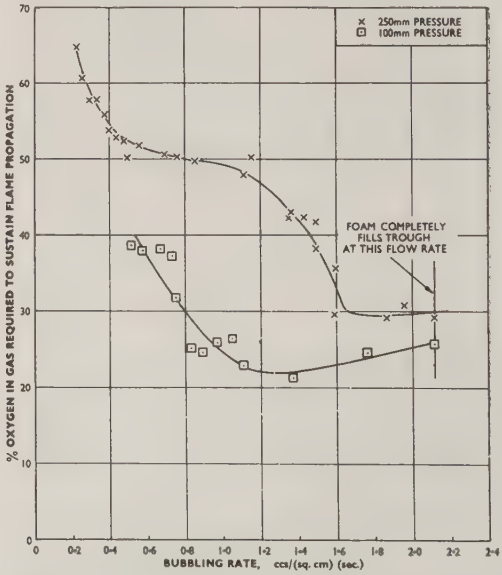
× 250mm PRESSURE
□ 100mm PRESSURE
FOAM COMPLETELY FILLS TROUGH AT THIS FLOW RATE
% OXYGEN IN GAS REQUIRED TO SUSTAIN FLAME PROPAGATION
BUBBLING RATE, ccs/(sq. cm) (sec.)

FIG. 9. Limiting conditions for flame propagation through kerosene (JP1) foams at −10°C (P_F approx. 20 mm).

MODE OF FLAME PROPAGATION

The interpretation of the results is considerably assisted by a picture of the mode of flame propagation through the mixture.

Figure 10 shows successive stills from a ciné film (24 frames/sec) of a "flame" propagating through a thin kerosene foam composed of large bubbles. The film was taken during preliminary work, the bubbles being larger and the foam less uniform than in the subsequent quantitative

FIG. 10. Successive stills from a ciné film (24 frames per sec) showing flame propagating through a thin foam

work, but the mode of propagation was the same. Close examination of these pictures shows that flame propagation occurs essentially by the physical movement of burning droplets which are projected presumably by the bursting of bubbles. When a burning droplet alights on a new bubble it can give rise to a number of new burning droplets which carry on the process. The analogy that this mode of propagation bears to a chain reaction is striking, and it seems reasonable that the critical conditions for continued flame propagation are achieved when, on the average, one burning droplet produces one new burning droplet during its lifetime.

Thick foams present a somewhat different picture. Here the heat flow from the flame breaks down the foam just in front of it, so that a dense spray of droplets is produced through which the flame propagates with a front which is better defined. It is not clear whether propagation involves the successive ignition of droplets by already burning droplets, or whether the premixing of vaporized fuel with air in advance of the flame front contributes significantly.

EFFECT OF BUBBLING RATE

The flame makes use of the whole of the space above the liquid in the trough, so that the average concentration of fuel in the burning mixture will be to a large extent related to the fraction of the free space above the liquid which is occupied by foam. Since the foam height varies linearly with bubbling rate, the overall fuel concentration will increase as bubbling rate increases, and the abscissae in Figures 2 to 9 can be regarded as an index of fuel concentration. As mentioned previously, many of the curves in these figures show minima, and the possibility suggests itself that the left-hand branches might be likened to lower limits of inflammability, and the right-hand branches to upper limits.

EFFECT OF OXYGEN CONCENTRATION

The lower limit of a gaseous mixture is set by a deficiency of fuel; oxygen concentration has very little effect upon this limit once sufficient is present for flame to be at all possible. With foams, however, the "lower limit" appears to be related to the propagation of a chain of burning droplets, and here it is very likely that the oxygen concentration will affect the temperature and size of the flame surrounding an already burning droplet, and also the ease with which a flame may be initiated around a new droplet. It is not very surprising therefore that the lower limiting rate of bubbling for a foam is affected by oxygen concentration. (Of more general interest it might be pointed out that the influence or otherwise of oxygen concentration upon a lower limit could form a test to establish whether, in a given dispersion of fuel in air, flame propagation takes place by a heterogeneous process, one burning droplet igniting another, or by a more homogeneous process as in gaseous mixtures or in very fine mists.)

Oxygen concentration naturally has a very large effect upon the upper limit of inflammability of a gas, because the limit is here set by oxygen deficiency. The right-hand branches of the curves in Figures 2 to 9 are therefore not unexpected. What is surprising is the absence of such a branch in some curves even when the flow rate is such that the whole of the ullage above the liquid is filled with foam. It is remarkable that flame is at all possible here, for the foam contains approximately 97 per cent by weight of fuel before it breaks down. (Even in pure oxygen, the upper limit of propane occurs at only 59 per cent by weight[1]). It is therefore likely that during collapse of the foam much of the liquid present simply falls out in large aggregates, the droplets which are dispersed forming but a fraction of the total.

EFFECT OF PRESSURE

At pressures below about 350 mm the flames surrounding individual droplets became blue in color and very greatly enlarged. At 100 mm total pressure their diameters were about double those at 250 mm pressure. Their cross-sectional areas were correspondingly increased so that the sphere of influence of a burning droplet became very much greater. Flame propagation would thus be enhanced, and this is reflected in the results in Figures 2 to 9 where reduced pressure frequently lowers the oxygen concentration necessary to sustain flame propagation. When fuel temperatures are low, however, pressure has little effect above 250 mm Hg.

The vapor pressure of the fuels used is small, but not negligible. The pressures at which explosive vapor-air mixtures would be formed have been estimated for both fuels at various temperatures and are given beneath the captions as P_F on each of Figures 2 to 9. The estimations are approximate and are based upon the flash points of the fuels and their vapor-pressure-temperature curves.

Air bubbling through gas oil at 30°C and 100

mm pressure would pick up enough vapor to form about three-quarters of the lower limit concentration. It is not surprising therefore that the corresponding curve on Figure 2 shows that the critical concentration of oxygen does not vary greatly with flow rate, and that it approaches the minimum required for flame propagation through a completely gaseous mixture.

EFFECT OF FUEL TEMPERATURE

Figures 2 to 9 show that increased fuel temperatures result in enhanced flame propagation. Both the viscosity and the vapor pressure of the fuel will vary with temperature. Decreased viscosity will result in greater foam drainage rates, and probably in a more finely dispersed spray upon breakdown of the foam. Increased vapor pressure will result in an enrichment with fuel of the atmosphere around the droplets. The effects of both these properties with increasing temperature would be expected to favor flame propagation, which is the effect observed.

Practical Hazards

It has been established that flames can propagate through foams of air in fuels below their flash points over a range of conditions. However, in the assessment of a hazard these conditions must be compared with those occurring in practice. For example, neither kerosene (JP1 type) nor gas oil gave explosive foams with air containing 21 per cent oxygen at atmospheric pressure at the temperatures and flow rates investigated. It therefore appears very unlikely that foam formation during normal handling of these fuels at these temperatures or below would constitute an explosive hazard. However, where reduced pressures, elevated temperatures, or increased oxygen concentrations are found, hazards may exist.

Velocities of flame propagation were not measured but appeared to be considerably less than those of vapor-air mixtures. It was frequently observed that secondary explosions of much higher flame speed occurred in the burned gases in the wake of the primary flame. These probably resulted from the mixing of fresh air, which was still bubbling through the fuel, with fuel which had been vaporized by the primary flame. Far greater pressures were generated by the secondary explosions than by the primary ones. The sequence of events giving rise to the highest explosion pressures is therefore: (1) breakdown of foam to form a spray, (2) slow primary flame propagation through this spray, and (3) fast secondary flame propagation through vapor-air mixtures in the wake of the primary flames.

Conclusions

The general conclusions drawn from the work are here summarized.

(1) Flames can in certain conditions propagate through foams of oxygen-nitrogen mixtures in fuels below their flash points.

(2) Foams break down during the approach of flame which propagates through the spray of droplets so formed. When foams are thin, the flame is seen to consist of a number of burning droplets which are projected some distance by the bursting of bubbles. These droplets alight on fresh bubbles which burst, and send out a spray of newly ignited droplets to carry on the process.

(3) Flame propagation is favored by reduced pressures, increased oxygen concentration and increased fuel temperatures. Up to an optimum value increase in bubbling rate also favors flame propagation, but beyond this point it has an adverse effect.

(4) Primary flames are relatively slow moving, but fast secondary flames producing much higher explosion pressures may occur in their wake. These present the more serious explosion hazard.

Acknowledgments

The author wishes to thank a number of the members of the staff of the Thornton Research Centre, particularly Mr. C. P. Rimmer, for assistance during the course of the work. He is indebted to the Directors of "Shell" Research, Ltd., for permission to publish this paper.

REFERENCE

1. Laffitte, P., and Delbourgo, R.: *Fourth Symposium (International) on Combustion*, p. 114. Baltimore, The Williams & Wilkins Co., 1953.

93

DYNAMIC FACTORS AFFECTING THE COMBUSTION OF LIQUID SPHERES[a]

By GEORGE A. AGOSTON, HENRY WISE AND WILLIS A. ROSSER

I. Introduction

In recent years, considerable progress has been made in the study of the mechanism of combustion of individual drops of liquid fuel or oxidizer. Much of this work has been performed with stationary fuel drops burning under natural convection conditions. However, aside from the experiments of Spalding[1] and Goldsmith,[2] relatively little experimental data have been reported on the influence of hydrodynamic factors on droplet combustion. The present work was undertaken to provide further experimental information on the effects of forced convection and turbulence on droplet combustion.

In this investigation a porous sphere, wetted with fuel and surrounded by a flame envelope in a gas stream, was employed to simulate a burning droplet. Such models were used successfully under natural convection conditions in a previous experimental study of steady-state combustion.[3] The mass burning rates obtained by this technique are comparable with those found for small suspended liquid fuel drops whose radii decreased with time.[4] Similarly, it is believed that with forced convection, information on the burning of a fuel wetting a porous sphere will be useful in elucidating the combustion characteristics of a freely moving fuel droplet. The contributions of internal circulation and of droplet deformation from spherical shape which may occur under conditions of forced convection and turbulence have not been taken into account in this study.

II. Experimental Apparatus

The apparatus employed in this study is shown schematically in Figure 1. A small wind tunnel consisting of a long diffuser-cone entry, a settling chamber with four equally spaced fine mesh screens, and an ASME long radius nozzle[5] was employed to deliver at a measured flow-rate a uniform, relatively nonturbulent, stream of air at environmental temperature downward through a transparent cylindrical Lucite test section. Provision was made for the addition of oxygen to the air stream before its entry into the wind tunnel.

Each porous alundum sphere[b] (0.315, 0.635, 0.952, and 1.32 cm in diam) was supported in the Lucite section by a short, stainless-steel, hypodermic-tubing feed line to which it was cemented (Sauereisen cement). Liquid fuel was fed to the center of the sphere by means of a mechanically driven syringe. Use of a servo-controlled fuel-supply apparatus permitted precise regulation of the rate of fuel delivered to the surface liquid film which coated the entire sphere including the cemented joint. The mass burning rate was determined by a critical value of the fuel flow below which a full steady flame could not be maintained and above which excess fuel dripped from the sphere. In Figure 2, a 0.635-cm sphere is shown supporting a steady flame of *n*-butyl alcohol burning in an air stream moving at 108 cm/sec.

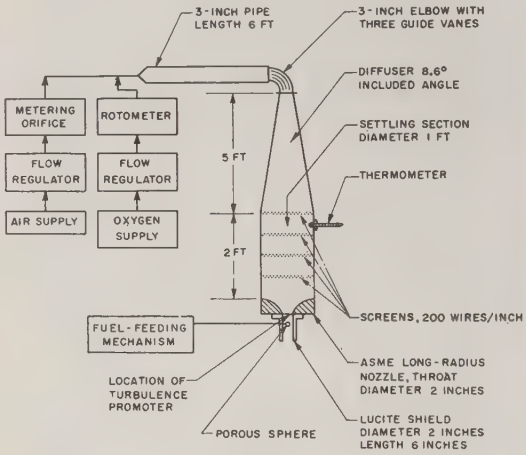

FIG. 1. Schematic diagram of apparatus.

In a number of tests, various uniform screens and drilled plates (Figure 3 and Tables 1 and 2) were employed to introduce different levels of turbulence into the air stream. These turbulence promoters were mounted across the wind-tunnel nozzle-exit (Figure 1). Additional variation in local turbulence was achieved by changing the distance between promoter and sphere.

[a] This paper represents the results of one phase of research carried out at the Jet Propulsion Laboratory, California Institute of Technology, under Contract No. DA-04-495-Ord-18, sponsored by the Department of the Army, Ordnance Corps.

[b] Manufactured by the Norton Company, Worcester 6, Mass.

In this study no measurements of turbulence levels were performed. Isotropic turbulence data reported in the literature were considered adequate for estimating the values of the intensity and scale parameters characterizing the turbulence conditions encountered. A comprehensive study of turbulence intensity downstream from

FIG. 2. Burning of fuel from wetted porous sphere (forced air flow in downward direction). $D_s = 0.635$ cm; $m = 9.6 \times 10^{-3}$ g/sec; $V = 108$ cm/sec.

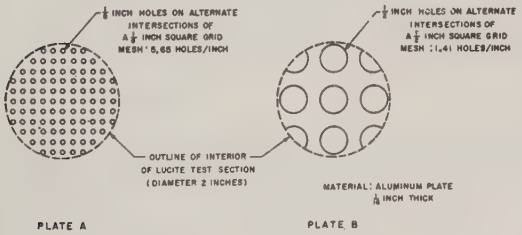
1/4 INCH HOLES ON ALTERNATE INTERSECTIONS OF A 1/4 INCH SQUARE GRID MESH : 5.65 HOLES/INCH
1/4 INCH HOLES ON ALTERNATE INTERSECTIONS OF A 1/4 INCH SQUARE GRID MESH : 1.41 HOLES/INCH
OUTLINE OF INTERIOR OF LUCITE TEST SECTION (DIAMETER 2 INCHES)
MATERIAL: ALUMINUM PLATE 1/4 INCH THICK
PLATE A
PLATE B

FIG. 3. Drilled plate turbulence promoters.

screens has been made by Davis.[6] His isotropic data can be represented by the empirical relation:

$$\xi = \frac{49}{\left(\frac{X}{M}\right)^{0.7}\left(\frac{M}{d}\right)^{0.53}} \qquad (1)$$

Equation 1 is based on data obtained in the ranges $M/d = 3$ to 6 and $X/M = 10$ to 100. When X/M is below 10, nonisotropic conditions are considered to prevail.[7, 8] The measurements of other investigators[8, 9, 10, 11] are in fair agreement with the data of Davis.

Information on the Eulerian scale in an isotropic turbulent field generated by a screen is rather fragmentary. The data reported by Williams, Hottel, and Scurlock[10] were arbitrarily selected because their values are intermediate between those reported from the other sources considered.[8, 9] Their data can be approximated by the following:

$$\frac{X}{d} = 36\left(\frac{L}{d}\right)^2 \qquad (2)$$

Equation (2) is based on values of $L/d = 0.8$ to 4.0 and $X/d = 23$ to 550.

For high levels of turbulence scale and intensity, the drilled plates were employed. An estimate of the resulting turbulent conditions was gained from the data of Maisel and Sherwood,[12] who used similar plates in an air stream passing through a four-inch diameter pipe.

III. Experimental Results

A. MASS BURNING RATES OF LIQUID SPHERES UNDER CONDITIONS OF FORCED CONVECTION

Burning-rate measurements were performed with four porous spheres in gas streams whose velocity, oxygen concentration, and turbulence were varied. Figure 2 illustrates a typical flame obtained during the tests. At the leading point of the sphere (i.e., the forward stagnation point) the distance between the visible flame and the sphere surface is a minimum. The progressive increase of this flame distance downstream from the forward stagnation point reflects the simultaneous increase in boundary layer thickness. Finally the boundary layer separates, resulting in formation of a wake region downstream of the sphere where the formation of smoke and increase in luminosity of the flame are noted. Also, at high gas velocities, an odor typical of aldehydes was detected.

The experimental data in Figure 4 show the influence of relative air velocity on the mass burning rate of *n*-butyl alcohol for spheres of different sizes. In each case the air flow was increased up to a limiting velocity where a flame envelope could no longer be maintained. Below velocities of about 20 cm/sec the influence of natural convection opposing the downward flow of the air stream was apparent. At a gas velocity sufficiently low so that the natural and forced convective effects seemingly balanced, it was

possible to produce a stable cylindrical flame open at each end, with the sphere at its midpoint. The curves in Figure 4 are based on an empirical relation (discussed in the following section) which serves to correlate the data in a region where the effect of natural convection relative to forced convection is negligible. Extending the empirical relation into the low velocity region (dashed lines) yields the burning rate behavior expected and 5 at zero forced air stream velocity fall above the corresponding theoretical values indicating directly the influence of natural convection.

The influence of air-stream turbulence on heterogeneous combustion represents another variable investigated in this study. Earlier tests[12] on the evaporation of water from the surfaces of porous spheres showed that turbulence in the ambient air stream significantly affected the

Table 1. Influence of Air Stream Turbulence on Extinction Velocity

Turbulence Generators: Screens.* Fuel: *n*-Butyl alcohol

Screen	Mesh†	Wire Diameter†	Screen Critical Velocity‡	Screen Distance§	Turbulence Intensity ¶	Turbulenc Scale‖	Extinction Velocity			
							D_s = 0.315 cm	D_s = 0.635 cm	D_s = 0.952 cm	D_s = 1.32 cm
	wires /in.	*in.*	*cm/sec*	*cm*	*per cent*	*cm*	*cm/sec*	*cm/sec*	*cm/sec*	*cm/sec*
a	3	0.063	29	5.1	(5.8)**	(0.15)**	66	63	91	94
a	3	0.063	29	10.2	3.6	0.20	—	—	—	130
a	3	0.063	29	15.2	2.7	0.25	—	—	—	143
b	8	0.025	72	5.1	3.0	0.10	—	107	—	134
b	8	0.025	72	10.2	1.9	0.13	—	—	—	166
b	8	0.025	72	15.2	1.4	0.15	—	—	—	—
c	4	0.092	20	10.2	4.2	0.25	51	101	—	134
d	6	0.063	29	10.2	3.2	0.20	77	—	—	—
d	6	0.063	29	15.2	2.4	0.25	73	101	—	137
e	8	0.047	38	5.2	4.2	0.13	82	101	—	122
e	8	0.047	38	10.2	2.6	0.18	88	—	—	—
e	8	0.047	38	20.3	1.6	0.25	75	119	—	149
f	16	0.023	78	10.2	1.6	0.13	88	99	—	165

* Screens were manufactured by W. S. Tyler Co., Cleveland, Ohio.

† Information supplied by manufacturer.

‡ Estimated on basis of data presented by Schubauer, Spangenburg and Klehanoff.[20] Air velocities must exceed the critical velocity of a given screen in order to produce a turbulence field.

§ Distance between screen and center of sphere.

¶ Evaluated by means of Equation (1).

‖ Evaluated by means of Equation (2).

** Parentheses indicate nonisotropic turbulence, although the values given apply to isotropic conditions. Nonisotropic conditions persist downstream from screens in the region where $X/M < 10$ (*cf.* Davis[7] and Swett[8]).

if natural convection did not occur. The ordinate intersections correspond to calculated burning rates in the absence of natural and forced convection (*cf.* Equation (3)). Similar measurements were made of the mass burning rates of ethyl alcohol (95.5 per cent by weight, 4.5 per cent water), the results of which are shown in Figure 5. Under free convection, the experimental mass burning rates of a sphere (0.635 cm diam) in air are 5.6×10^{-3} g/sec for *n*-butyl alcohol, and 5.1×10^{-3} g/sec for ethyl alcohol (95.5 weight per cent). These two values plotted in Figures 4

evaporation rate. In recent tests[13] with suspended burning drops, modest increases in mass burning rates were attained under free convection conditions when high frequency vibrations were introduced into the ambient air. In the present program, rather extreme turbulence conditions were introduced into the air stream. However, as shown in Figure 6, wide variations in turbulence intensity and scale had negligible effect on the mass burning rate. This is evidenced by the close agreement of the data for turbulent and nonturbulent conditions.

B. CORRELATION OF MASS BURNING RATE DATA

In the present investigation, the *n*-butyl alcohol and ethyl alcohol data were individually

TABLE 2. INFLUENCE OF AIR STREAM TURBULENCE ON EXTINCTION VELOCITY

Turbulence Generators: Drilled Plates.
Fuel: *n*-Butyl alcohol

Drilled Plate (Fig. 3)	Plate Distance*	Turbulence Intensity†	Turbulence Scale†	Extinction Velocity D_s = 0.315 cm	D_s = 0.952 cm	D_s = 1.32 cm
	cm	*per cent*	*cm*	*cm/sec*	*cm/sec*	*cm/sec*
A	5.1	32‡	0.5‡	63	73	91
A	10.2	20	0.5	51	—	122
A	15.2	15	0.5	74	—	132
A	20.3	11	0.5	74	—	—
B	5.1	(60)‡	(1.3)‡	—	—	49
B	10.2	(37)‡	(1.3)‡	61	—	93
B	15.2	(28)‡	(1.3)‡	68	98	128
B	20.3	23	1.3	69	—	—

* Distance between drilled plate and center of sphere.

† Turbulence intensity and scale are based on measurements of Maisel and Sherwood.[12] Parentheses indicate nonisotropic turbulence, although the values given apply to isotropic conditions. Nonisotropic conditions persist downstream from plates where $X/M < 10$ (Davis[7]).

‡ Values obtained by extrapolation of published data of Maisel and Sherwood.[12]

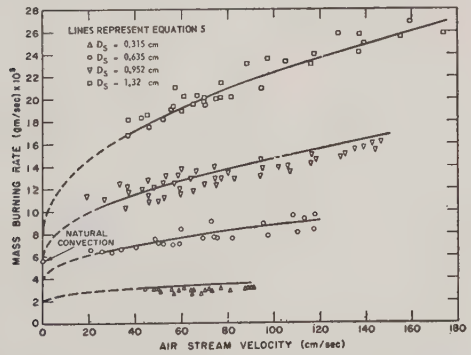
LINES REPRESENT EQUATION 5
Δ D_s = 0.315 cm
○ D_s = 0.635 cm
▽ D_s = 0.952 cm
□ D_s = 1.32 cm
NATURAL CONVECTION
MASS BURNING RATE (gm/sec) x 10^3
AIR STREAM VELOCITY (cm/sec)

FIG. 4. Mass burning rate as a function of sphere diameter and air stream velocity. Fuel: *n*-butyl alcohol; air stream temperature: 26–40°C.

correlated by plotting the fractional increase in burning rate with forced convection over that in the absence of convection effects, i.e., $(m - m_0)/m_0$, versus the square root of the Reynolds number based on sphere diameter. The theoretical mass burning rate without convection, m_0, based on a spherico-symmetrical model,[3] is given by

$$m_0 = 2\pi D_s \frac{\lambda_a}{C_a} \ln \cdot \left[1 + \frac{q}{H}\frac{Y_{xg}}{i} - \frac{C_a(T_s - T_g)}{H}\right] \tag{3}$$

This type of correlation of the data is suggested by the semi-empirical equation of Frössling[14]

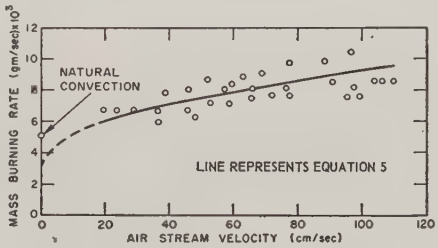

FIG. 5. Mass burning rate as a function of air stream velocity. Fuel: ethyl alcohol (95.5 per cent by weight); sphere diameter: 0.635 cm; air stream temperature: 18–31°C.

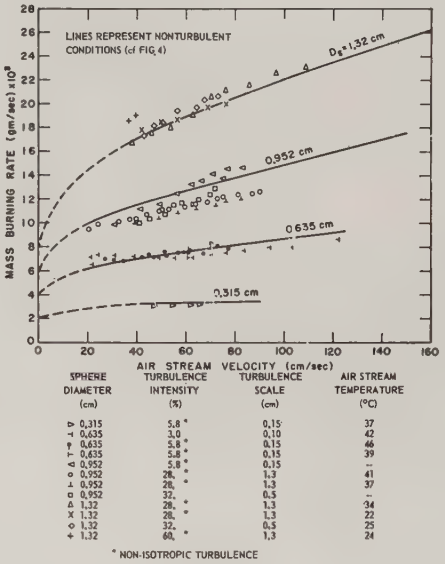
LINES REPRESENT NONTURBULENT CONDITIONS (cf FIG. 4)
D_s = 1.32 cm
0.952 cm
0.635 cm
0.315 cm
MASS BURNING RATE (gm/sec) x 10^3
AIR STREAM VELOCITY (cm/sec)
SPHERE DIAMETER (cm)
TURBULENCE INTENSITY (%)
TURBULENCE SCALE (cm)
AIR STREAM TEMPERATURE (°C)
▷ 0.315 5.8 * 0.15 37
→ 0.635 3.0 0.10 42
↑ 0.635 5.8 * 0.15 46
← 0.635 5.8 * 0.15 39
◁ 0.952 5.8 * 0.15 --
○ 0.952 28. * 1.3 41
⊥ 0.952 28. * 1.3 37
□ 0.952 32. 0.5 --
△ 1.32 28. * 1.3 34
X 1.32 28. * 1.3 22
◇ 1.32 32. 0.5 25
+ 1.32 60. * 1.3 24
* NON-ISOTROPIC TURBULENCE

FIG. 6. Mass burning rates with and without air stream turbulence. Fuel: *n*-butyl alcohol.

based on a diffusion-controlled mechanism

$$\frac{m - m_0}{m} = 0.276 Re^{\frac{1}{2}} Sc^{\frac{1}{3}} \tag{4}$$

which was derived for droplet evaporation with relative gas motion in the absence of combussion or large temperature differences. A similar correlation was presented by Spalding.[15]

For droplet combustion, where heat transfer

rather than diffusion is the rate-controlling transport mechanism, the combustion rate probably should be expressed as a function of the Prandtl number rather than the Schmidt number (*cf.* Spalding[1]). On the basis of the work of Ranz and Marshall[16] it appears that it is necessary merely to substitute $Pr^{\frac{1}{3}}$ for $Sc^{\frac{1}{3}}$ in Equation (4) to make it apply to droplet combustion. However, since the Prandtl number may be assumed constant in the present investigation, the relationship tested is

$$\frac{m - m_0}{m_0} = KRe_a^{\frac{1}{2}} \tag{5}$$

In the evaluation of the Reynolds number, the kinematic viscosity employed was that for air at a temperature corresponding to the arithmetic average of the adiabatic flame temperature and the ambient gas temperature.

In Figure 7 the *n*-butyl alcohol data are presented for the four sphere sizes (see Table 3 for values of physical properties). Also given are the data for ethyl alcohol burning in air (*cf.* Figure 5) and in different oxygen concentrations in the gas stream. Separate correlations are obtained for each of the fuels used, in accordance with Equation (5), and the constant K is found to have the value of 0.28 for ethyl alcohol and 0.20 for *n*-butyl alcohol. The difference in K for the two fuels may be due partly to the chosen values for the fluid properties. The use of air properties at a mean temperature was found to be more satisfactory than that of fuel vapor properties at the temperature of the liquid surface.[15]

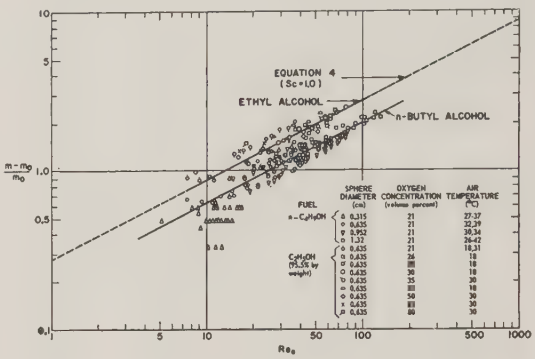

FIG. 7. Correlations of burning rate data.

TABLE 3. NUMERICAL VALUES OF PARAMETERS AND PHYSICAL PROPERTIES

Fuel	Oxygen	T_c	ν_a^*	C_f	μ_f‡	λ_f§	m_0/D_s¶	C_a‖	λ_a/C_a**
	vol. per cent	°K	cm^2/sec	*cal/g °K*	*(poise)* $\times 10^6$	*(cal/cm sec °K)* $\times 10^6$	*(g/cm sec)* $\times 10$	*cal/g °K)*	*g/cm sec)* $\times 10^4$
C_2H_5OH	21	2200	1.67	0.86	295	282	5.43	0.283	6.40
(95.5 weight per cent)	26	2395	1.89	0.87	311	301	6.33	0.285	6.66
	28	2445	1.94	0.87	314	304	6.62	0.286	6.73
	30	2490	1.99	0.87	318	308	6.99	0.287	6.86
	35	2580	2.10	0.87	324	313	7.15	0.288	7.00
	40	2640	2.16	0.87	329	317	8.21	0.289	7.05
	50	2740	2.28	0.87	336	325	9.10	0.290	7.14
	65	2845	2.40	0.87	344	333	10.28	0.291	7.28
	80	2920	2.49	0.87	349	338	11.25	0.292	7.38
n-C_4H_9OH	21	2265	1.75			293††	6.19	0.283	6.50

* Hilsenrath and Touloukian;[21] $T_g = 300°K$.

† Glasstone;[22] $T_s = 351°K$.

‡ Perry;[23] Sutherland equation used.

§ Lange;[24] based on $Pr = 0.9$.

¶ Equation (3). In calculating m_0/D_s, use was made of the tabulated values of C_a and λ_a/C_a and of the following information:

	q *cal/g*	H *cal/g*	i *g/g*
C_2H_5OH (95.5 wt per cent)	6325	254	1.99
n-C_4H_9OH	8051	196	2.59

‖ Keenan and Kaye.[25]

** Ref. 21; based on $Pr = C_a\mu_a/\lambda_a = 0.735$.

†† Thermal conductivity of butanol assumed equal to that of ethanol; $T_s = 390°K$.

The burning rate of a liquid sphere may be expressed in terms of the Nusselt number,

$$Nu_f = \frac{mL}{\pi D_s(T_c - T_s)\lambda_f} \tag{6}$$

In Table 4, Nusselt numbers based on two burning rate observations may be compared with the Nusselt numbers (Nu') computed using the Ranz and Marshall relationship[16] for heat transfer with relative gas motion, which applies when mass transfer is absent (or negligible) and the heat source (or sink) is located at a large distance from the sphere. Also presented in Table 4 are Nusselt numbers (Nu'') evaluated using the Ranz and Marshall equation modified to account for a concentric heat source (the combustion surface) located at a relatively small distance from the sphere. The magnitude of the effect of mass transfer on heat transfer is apparent from a comparison of the observed Nusselt number (Nu_f) and Nu''.

TABLE 4. COMPARISON OF NUSSELT NUMBER FOR *n*-BUTYL ALCOHOL BURNING IN AIR

D_s	V	y^*	D_c†	Re_a	Nu_f‡ (observed)	Nu'§	Nu''¶
cm	*cm/sec*	*cm*	*cm*				
0.635	100	0.1	0.84	36.6	1.5	5.6	23.6
1.32	100	0.1	1.32	75.5	1.9	7.2	55.0

* *Cf.* Figure 12.

† In this calculation the relation $D_c = D_s + 2y^*$ is assumed.

‡ *Cf.* Equation (6). $Nu_f = Nu_{f0}(1 + K\ Re_a^{\frac{1}{2}})$.

§ Ranz and Marshall equation (16), $Nu' = Nu_0'\ (1 + 0.3\ Re^{\frac{1}{2}}\ Pr^{\frac{1}{3}})$, where $Nu_0' = 2$. Pr is taken equal to 1.0.

¶ Modified Ranz and Marshall equation, $Nu'' = Nu_0''\ (1 + 0.3\ Re^{\frac{1}{2}}\ Pr^{\frac{1}{3}})$, where $Nu_0'' = 2D_c/(D_c - D_s)$. Pr is taken equal to 1.0.

C. EXTINCTION VELOCITY

Of special interest in the analysis of the effect of dynamic parameters on the combustion of a liquid fuel is the critical gas velocity (extinction velocity, V_e) above which a flame envelope can not be maintained around a fuel-wetted sphere. When this extinction velocity is exceeded, the flame is extinguished at the leading half of the sphere and a tiny flame is stabilized within the wake, as observed previously by Spalding.[17] Under these conditions, the wetted sphere acts merely as a flameholder. Since the flame no longer envelops the sphere, the rate of heat flow to the sphere is greatly diminished and the consumption of liquid fuel is reduced to about 25 per cent of the value measured with a full flame envelope just below the extinction velocity.

In this investigation the extinction velocity was measured as a function of sphere diameter and oxygen concentration in the gas stream, with *n*-butyl alcohol as fuel (Figure 8). It is apparent that with increasing sphere diameter the extinction velocity grows. A cross-plot of the data presented in Figure 9 relates the extinction velocity to the sphere diameter at various partial pressures of oxygen. These data suggest that V_e is proportional to the square root of the diameter for the spheres studied. On the other hand, Spalding[18] reports a proportionality between extinction velocity and diameter to the first power. Of interest is the marked change in the value of V_e with oxygen content of the gas stream. For any given sphere size the extinction velocity increases exponentially with the oxygen concentration.

Although turbulence in the gas stream was found to have little or no effect on the mass burning rate, it became evident that near the extinction velocity the flame envelope could sometimes be extinguished by minor disturbances in the gas flow. A series of tests was then conducted with *n*-butyl alcohol to reveal effects of variations of turbulence scale and turbulence intensity on the extinction velocity. In Figure 10 the extinction velocity (represented nondimensionally as the ratio of the turbulent to nonturbulent extinction velocity) is plotted against the turbulence intensity.

It was possible to sketch isoscale lines for all but one of the scale levels investigated (L = 0.20 cm). Owing to considerable scatter, tag lines were drawn between individual data points and the corresponding isoscale curves. Points enclosed by parentheses were obtained under nonisotropic turbulence conditions not fully represented, for example, by Equations (1) and (2). In Figure 10 a limiting curve based on the following equation is presented for the condition of infinitely large turbulence scale:

$$(V_e)_{t_\infty} = \frac{V_e}{1 + \frac{\xi}{100}} \qquad (7)$$

It is observed that curve II (Figure 10), corresponding to a turbulence scale of 0.25 cm, deviates from the pattern set by other curves. Insufficient data were obtained to resolve whether curves I and II cross, bringing the positions of the isoscale lines into conformity at high turbulence intensities. However, at least within a certain range of the data, it is apparent that at a fixed turbulence intensity the turbulence extinc-

tion velocity is a minimum for a critical scale and frequency (defined as V_{et}/L).

A second significant observation is that the positions of the isoscale lines appear to be independent of sphere diameter, suggesting that the dimensionless ratio V_{et}/V_e is a function not of L/D_s but rather of the ratio of scale to a linear dimension which did not vary in these tests. Such a dimension which has been found constant at flame extinction under nonturbulent conditions is the distance of the luminous flame at the forward stagnation point (discussed below). Thus, the ratio of turbulence scale to flame distance may be one of the parameters which govern the conditions leading to flame extinction. It is believed that the decrease in extinction velocity as a result of stream turbulence is brought about by the intermittent penetration of the flame zone to a point closer to the liquid surface than the minimum distance adequate for stable combustion (*cf.* Fig. 12). Additional experimental data are needed in order to permit a more detailed analysis of this phenomenon.

D. FLAME DISTANCE

In the absence of convective flow, fuel vapor evaporating from the surface of a burning spherical drop diffuses radially to a concentric spherical reaction shell where interaction with oxidizer molecules leads to the formation of combustion products. The location and thickness of the spherical flame shell with respect to the liquid surface are controlled by physico-chemical properties and chemical kinetics. When flow of the ambient gas (e.g., by either free convection or forced convection) is superimposed on the system of a burning spherical drop, the fuel vapor issuing from the upstream hemisphere is deflected, forming a vapor layer which moves along the surface to a location where it finally separates. The visible flame envelope is probably an accurate delineation of the hottest portion of the reaction zone, wherein combustibles and oxidizer combine in stoichiometric proportion.

In Figure 11 data are presented which show the increase in distance of the visible flame from the surface at succeeding positions downstream from the forward stagnation point. Since the luminous zone appearing in the photographs has appreciable thickness, distances were measured radially from the surface to the outer visible edge of the flame. The measurements are reported as the ratio of flame distance to the distance at the forward stagnation point. In this series of tests

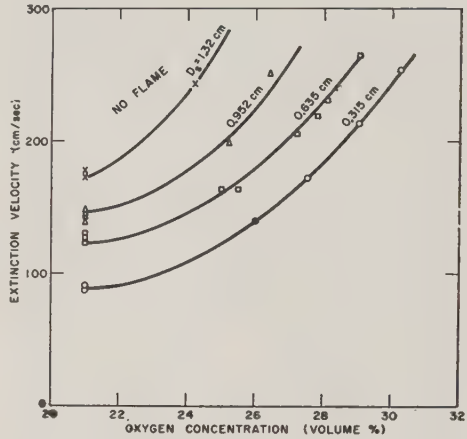

FIG. 8. Extinction velocity as a function of sphere diameter and oxygen concentration. Fuel: *n*-butyl alcohol; gas stream temperature: 29–38°C.

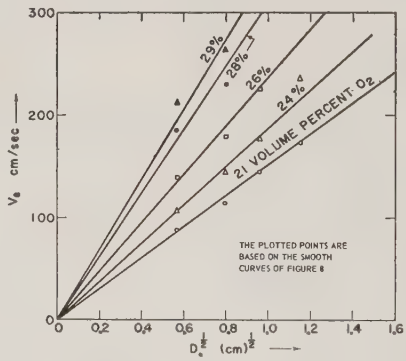

FIG. 9. Extinction velocity as a function of sphere diameter.

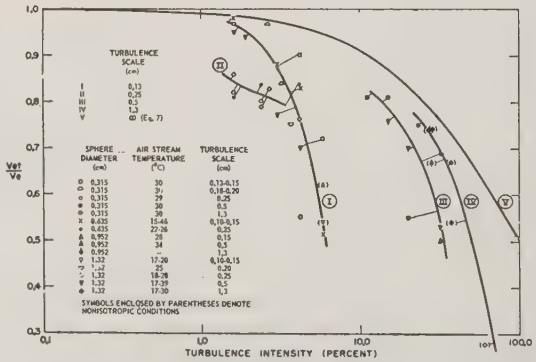

FIG. 10. Extinction velocity as a function of turbulence scale and intensity of the air stream. Fuel: *n*-butyl alcohol.

with a 0.635-cm sphere, one curve serves as a satisfactory representation of the flame distance.

The flame distances at the forward stagnation point employed in preparing Figure 11, as well as those pertaining to a 1.32-cm sphere, are given

in Figure 12. Under natural convection conditions, the flame distances for spheres wetted by ethyl alcohol have been found to be independent of diameter over the range of 0.36 to 1.25 cm (3). With forced convection conditions, however, the data suggest a dependency of flame distance on sphere diameter at the lower gas stream velocities

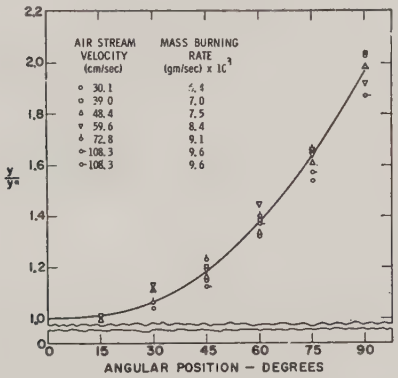

FIG. 11. Distance of flame zone from sphere surface as a function of angular distance from forward stagnation point. Fuel: *n*-butyl alcohol; sphere diameter: 0.635 cm; temperature of air stream: 32°C.

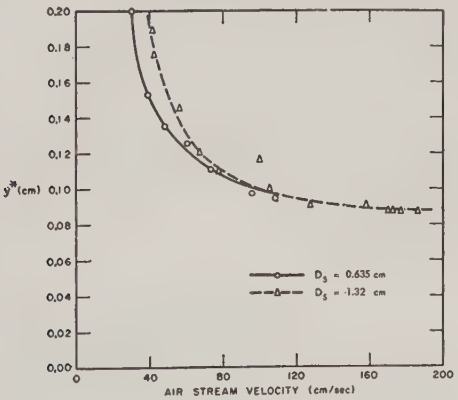

FIG. 12. Distance of flame from forward stagnation point of sphere as a function of air stream velocity. Fuel: *n*-butyl alcohol; air stream temperature: 23–32°C.

(Fig. 12). It is possible that this dependency is due to buoyancy effects which oppose the downward forced-flow of air.

At air velocities exceeding 120 cm/sec the flame distance at the forward stagnation point for both spheres appeared to level off at a constant value of about 0.9 mm. This fact is of particular interest because it implies that the flame distance at the maximum velocity at which a flame envelope surrounding a liquid sphere may be maintained is a constant for spheres in this size range. This is in agreement with the work of Spalding[1] who noted flame distances at extinction of 0.9 mm for kerosene-coated spheres ranging from 0.7 to 2.6 cm in diam. It remains to be demonstrated whether this distance at flame extinction is independent of diameter for smaller spheres.

IV. Discussion

The experimental results demonstrate the pronounced influence which relative gas motion may have on the mass burning rate of a fuel droplet. The maximum gain in the rate of combustion of a droplet of given diameter as a result of forced convection is limited, however, by the phenomenon of flame extinction. It is apparent from the data in Figure 9 that extrapolation of the experimental data down to droplet sizes encountered in industrial fuel sprays yields, for combustion in air, extinction velocities of the order of 50 cm/sec. It must be remembered, however, that during combustion of a fuel spray the proximity of other burning droplets and the increased gas temperature may have a significant influence on the limits of flame extinction. Also, it has been observed that the heterogeneous characteristics of burning fuel sprays disappear as the diameters of the fuel droplets approach approximately 10 μ. The combustion of a fuel cloud composed of such small liquid particles more closely resembles that of a prevaporized, premixed fuel-oxidizer mixture.[19]

Acknowledgment

The experimental investigation was performed at the Jet Propulsion Laboratory, California Institute of Technology. The final preparation of the manuscript was carried out at Stanford Research Institute.

Nomenclature

C	specific heat (constant pressure), cal/°C g
d	wire diameter (screen), cm
D	diameter, cm
$\mathfrak{D}$	diffusion coefficient, cm²/sec
h	heat transfer coefficient, cal/°C sec cm²
H	heat of vaporization (sensible plus latent heats), cal/g
i	stoichiometric oxygen-fuel ratio, g/g
K	constant (*cf.* Equation (5))
L	Eulerian turbulence scale, cm
m	burning (or evaporation) rate with relative gas motion, g/sec
m_0	theoretic burning (or evaporation) rate in

absence of natural and forced convection, g/sec

M (screen mesh size)$^{-1}$ = (wires/cm)$^{-1}$

Nu Nusselt number, $\frac{hD_s}{\lambda}$

Nu_0 Nusselt number in absence of natural and forced convection

q heat of combustion (fuel vapor to vapor products), cal/g

Sc Schmidt number, $\mu/\rho\mathfrak{D}$

Re Reynolds number, $\frac{D_s V}{\nu}$

Pr Prandtl number, $\frac{C\mu}{\lambda}$

T temperature, °K

V velocity of ambient gas, cm/sec

X distance downstream from turbulence generator, cm

y radial distance of flame from sphere surface, cm

y^* radial distance of flame at forward stagnation point, cm

Y_x weight fraction of oxygen, g/g

λ thermal conductivity, cal/°C cm sec

μ viscosity, poises

ν kinematic viscosity, cm^2/sec

ξ turbulence intensity, per cent

ρ density, g/cm^3

SUBSCRIPTS

a gas film properties corresponding to $(T_g + T_c)/2$

c flame zone

e extinction conditions

f fuel vapor properties corresponding to $(T_s + T_c)/2$

g ambient gas

s liquid surface

t turbulent conditions

t_∞ infinite turbulent scale

REFERENCES

1. Spalding, D. B.: *Fourth Symposium (International) on Combustion*, p. 847. Baltimore, The Williams & Wilkins Co., 1953.
2. Goldsmith, M.: Jet Propulsion, *26*, 172 (1956).
3. Wise, H., Lorell, J., and Wood, B. J.: *Fifth Symposium (International) on Combustion*, p. 132. New York, Reinhold Publ. Corp., 1955.
4. Wise, H., and Agoston, G. A.: Presented at the 129th Meeting, American Chemical Society, Dallas, Texas, April 1956.
5. Marks, L. S.: Mechanical Engineers' Handbook, Ed. 5, p. 2080. New York, McGraw-Hill Book Co., 1951.
6. Davis, L.: Jet Propulsion Laboratory Progress Report 3-22, California Institute of Technology, Pasadena, California, November 17, 1950.
7. Davis, L.: Jet Propulsion Laboratory Report No. 3-17, California Institute of Technology, Pasadena, California, June 5, 1952.
8. Swett, C. C.: NACA Res. Memo. E54F29a, August 1954.
9. Dryden, H. L.: Quart. Appl. Mat., *1*, 7 (1943).
10. Williams, G. C., Hottel, H. C., and Scurlock, A. C.: *Third Symposium on Combustion, Flame, and Explosion Phenomena*, p. 21. Baltimore, The Williams & Wilkins Co., 1949.
11. Hottel, H. C., Williams, G. C., and Levine, R. S.: *Fourth Symposium (International) on Combustion*, p. 636. Baltimore, The Williams & Wilkins Co., 1953.
12. Maisel, D. S., and Sherwood, T. K.: Chem. Eng. Progress, *46*, 172 (1950).
13. Kumagai, S., and Isoda, H.: *Fifth Symposium (International) on Combustion*, p. 129. New York, Reinhold Publ. Corp., 1955.
14. Frössling, N.: Gerlands Beitr. Geophys., *52*, 170 (1938).
15. Spalding, D. B.: *Some Fundamentals of Combustion*, p. 135. New York, Academic Press Inc., 1955.
16. Ranz, W. E., and Marshall, W. R.: Chem. Eng. Progress, *48*, 173 (1952).
17. Spalding, D. B.: Fuel, *32*, 169 (1953).
18. Spalding, D. B.: Fuel, *33*, 255 (1954).
19. Burgoyne, J. H., and Cohen, R.: Proc. Roy. Soc., *A225*, 375 (1954).
20. Schubauer, G. B., Spangenburg, W. G., and Klebanoff, P. S.: NACA Tech. Note 2001, January 1950.
21. Hilsenrath, J., and Touloukian, Y. S.: Trans. Am. Soc. Mech. Engrs., *76*, 967 (1954).
22. Glasstone, S.: *Thermodynamics for Chemists*. New York, Van Nostrand, 1947.
23. Perry, J. H.: *Chemical Engineers' Handbook*, Ed. 3. New York, McGraw-Hill Book Co., 1950.
24. Lange, N. A.: *Handbook of Chemistry*, Ed. 8. Sandusky, Ohio, Handbook Publishers Inc., 1952.
25. Keenan, J. H., and Kaye, J.: *Thermodynamic Properties of Air*. New York, John Wiley & Sons, Inc., 1945.

Discussion by C. C. Miesse

The present paper constitutes a notable advance in the technology of droplet combustion. It is with particular interest that we note the author's ability to correlate burning-rate data with a Frössling-type equation. For this fact confirms the similarity between evaporation and combustion of a liquid droplet, and indicates the

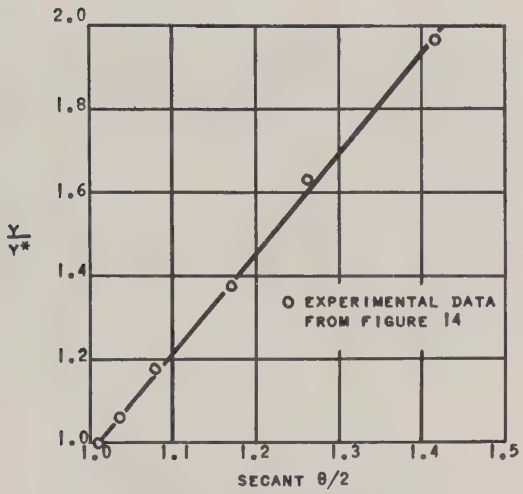

FIG. 1. Angular variation of relative radial distance from droplet surface to flame.

applicability of evaporating droplet theories to the combustion process.

Consideration of Kumagai and Isoda's* Equation (2) indicates that the relative radial distance (y/y^*) from droplet surface to flame should vary linearly with the secant of the half-angle:

$$y/y^* = (r - D/2)/y^*$$

$$= \left[R\sqrt{(\sin\theta/2)^2 + \left(\frac{\cos\theta}{2\cos\theta/2}\right)^2} - \frac{D}{2}\right]\cdot\frac{2}{R}$$

$$= \sec\theta/2 - D/R.$$

where r is the flame radius and R is defined by Equation (3) Kumagai and Isoda.[1] From the following variation of (y/y^*) with $\sec\theta/2$, it is apparent that the present authors' data, as shown in Figure 14 of subject paper, vary linearly with the secant of the half-angle, although with a coefficient of approximately 1.2 rather than 1.0. Perhaps this deviation in coefficient can be reconciled by a more detailed analysis of the phenomenon.

* S. Kumagai and H. Isoda: *Sixth Symposium (International) on Combustion*, p. 726. New York, Reinhold Publ. Corp., 1957.

94

COMBUSTION RATES OF FREELY FALLING FUEL DROPS IN A HOT ATMOSPHERE

By J. A. BOLT AND M. A. SAAD

Introduction

The combustion of fuel sprays has received much recent attention because of its importance in power-generating equipment, especially in high output military aircraft propulsion systems. However, because of the complexity and difficulties involved, most research workers have approached the problem by analyzing and conducting experiments involving single drops. This is an indication of how much remains to be accomplished before the factors involved in the process of burning a fuel spray can be fully understood and evaluated. The bibliography indicates some of the most important work that has been accomplished.

The main purpose of the present investigation was to obtain fundamental data concerning the combustion of individual drops in a hot atmosphere under controlled temperatures. The experimental method permitted small fuel drops to fall freely through a vertical furnace. Each drop was photographed at several positions as it fell through a heated furnace, and a record of drop diameter and elapsed time was obtained. This method is applicable only to volatile fuels, since the evaporation of residual fuels and heavy fuel oils is generally accompanied by swelling.

Description of Equipment and Experimental Procedure

The two measurements necessary to determine the evaporation and burning rates of light fuels were the changes in the drop diameters and the time intervals between these changes. The ex-

perimental equipment consisted of four units: the furnace and fuel dropper, the photographing equipment, the detection equipment, and the timing equipment.

The furnace, as shown in Figure 1, consisted of two main heating elements placed opposite to each other and one inch apart. The heating wire was cast in two vertical alundum pieces which constituted the sides of the furnace. The volume between the alundum walls (1 by 4 by 45 in.) constituted the furnace atmosphere through which the drops fell. The total power of the furnace was 7.64 kw and the maximum furnace atmosphere temperature reached was 1700°F. The furnace was insulated on two sides with firebrick and vermiculite contained within a sheet-metal steel shell.

Two opposite walls of the furnace consisted of nearly continuous tempered glass windows which allowed the drop to be photographed at any position in the furnace.

Three iron-constantan thermocouples were used to determine the temperature within the furnace, their junctions being shielded by platinum foil.

The furnace test section was completely closed, except for a $\frac{1}{4}$-in. hole at the top of the furnace for the entrance of the fuel drops. Air was admitted into the furnace, normally after the fall of every five droplets, by removing a plug at the bottom of the test section and allowing the furnace to purge itself.

The formation of fuel drops was accomplished by a small-bore tube from which the drops were thrown by a concentric jet of air. Experience showed that the drop size can be controlled by capillary bore size, pressure of the concentric air jet, head of the fuel, and the distance the capillary protrudes beyond the air nozzle.

The fuel dropper consisted of a hypodermic needle of 0.0185 in. o.d. The tip of the needle was cut square and carefully finished. The needle was centered in a brass tube through which the air blast was supplied. Drops leaving the tip of the dropper fell through a Pyrex glass tube $\frac{1}{2}$-in. in diam before entering the furnace, to eliminate any air currents that might cause deviation of the falling drops from their vertical path.

Three of the four photographing positions were used to record the drop diameter as it fell through the furnace. The fourth position was not used, because the bottom section of the furnace was slightly cooler than the rest of the furnace. The photolights provided a flash of light of approximately one μsec which permitted the use of the open-shutter technique so that the shutters of the cameras were kept open during the entire time of fall of the drop. The exposure was thus determined by the intensity and duration of the illumination. Due to the high intensity of illumination supplied by the photolights, the silhouette of the drop without the flame appeared on the film. The magnification ratio was about 1:1, which was established by photographing an accurately measured wire.

A photo multiplier tube was used at each

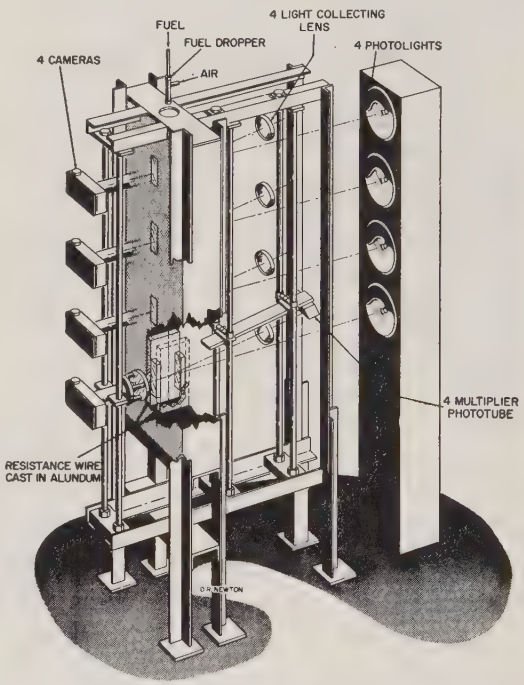

FIG. 1. Furnace, lights and camera equipment.

photographing position for the detection of the falling drop. The multiplier phototube was totally enclosed, except for a small horizontal slit of dimensions $\frac{1}{16}$ by $1\frac{1}{4}$ in. The function of the photo multiplier tubes and the triggering circuit was to flash the GE photolights at the instant when the drop was in the field of view of the camera. A 5-in.-focal-length lens was used to collect the light from the burning drop and focus it on the multiplier phototube. A $\frac{1}{32}$-in. horizontal slit, placed in front of the phototube box, served as a knife edge so that the light from the burning drop had to pass through the two slits in order to reach the photo multiplier tube.

The timing pulses produced when the photolights flashed were recorded on the screen of a

Teckronix oscilloscope. At the same time, pulses from a 60-cycle square-wave generator were fed to the scope. To reduce the square wave into a pulse, a differentiating circuit, consisting of a capacitor and a resistance, was introduced in the main circuit. Also a crystal diode was connected to the output of the generator before it was fed to the scope. The crystal diode acted as a rectifier, eliminating alternate pulses produced by the generator. The pulses were photographed for each falling drop by means of a Polaroid camera mounted on the oscilloscope. Knowing the exact timing between the pulses produced by the photograph the timing pips. The flame attending the droplet energized the multiplier phototubes, which in turn triggered the high-intensity photolights. The shutters were closed as soon as the photolights flashed.

By means of a comparator, the drop images were magnified about 20 times to permit accurate measurements of the diameters. The diameters were measured in two perpendicular directions and the average was taken, the result of any drop with its greatest and least diameters differing by more than 5 per cent being discarded. The timing intervals between the photolights flashes were

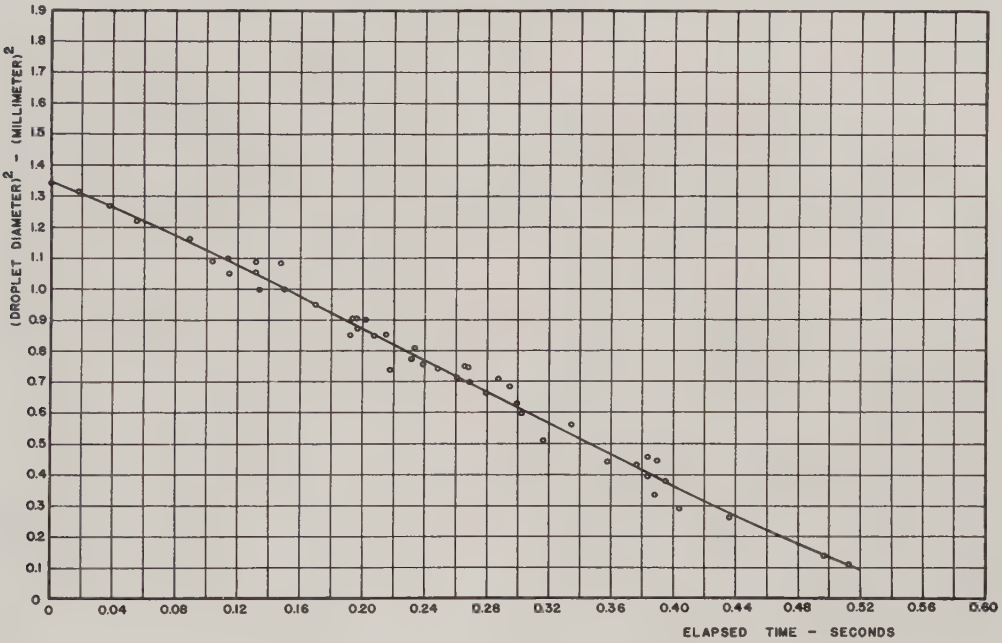

FIG. 2. Combustion of *n*-heptane in air at 1500°F—(diameter)² vs time.

square-wave generator, it was possible to know the time intervals between the flashes of the photolights.

PROCEDURE FOR OBTAINING DATA

After the furnace temperature was brought to the desired value (1500°F), fuel was introduced into the dropper and the air pressure was adjusted to give the required size of drops. The drops fell through the small hole at the top of the furnace and were ignited by the heat of the furnace.

At the instant before a drop left the dropper, the camera shutters were opened by a master cable release. At the same time, the shutter of the Polaroid camera was opened in order to accurately measured by comparing the distance between these pulses and the equal distances between the pulses of the square-wave generator. The error in measuring the drop images on the comparator and the timing intervals was estimated to be within ±1 per cent.

Curves of diameter *vs.* time were plotted for the fuels investigated. By knowing three diameters and two timing intervals, it was possible to draw a curve of diameter *vs.* time for each drop. The curves shown in Figures 2, 3 and 4 were obtained by superimposing the individual curves of the different sizes of drops.

Results and Discussion

The combustion of two pure hydrocarbons, *n*-heptane and isooctane, and kerosene were

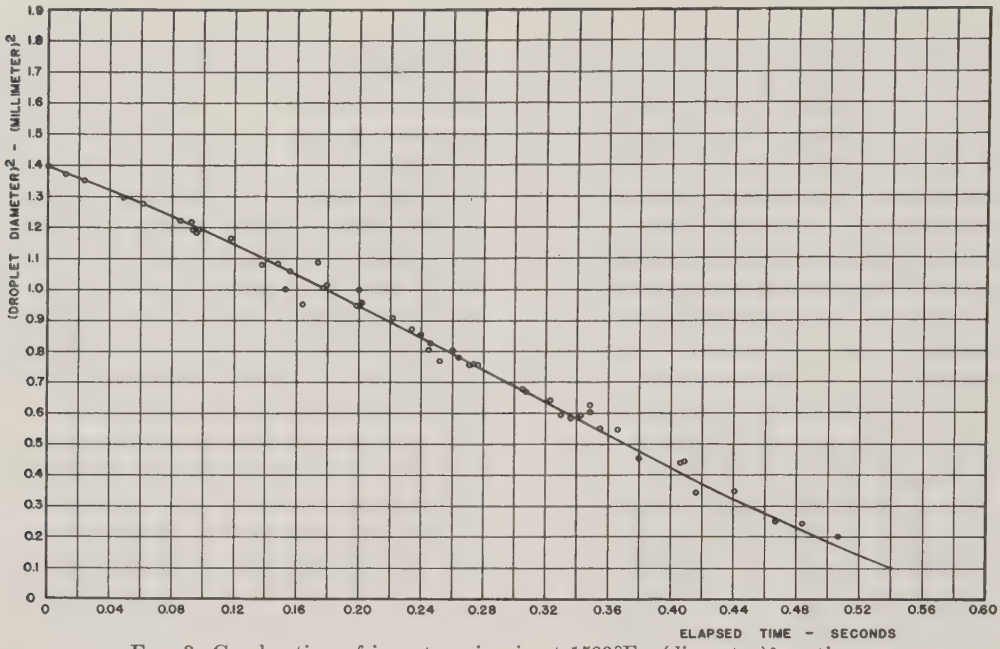

FIG. 3. Combustion of isooctane in air at 1500°F—(diameter)² vs time.

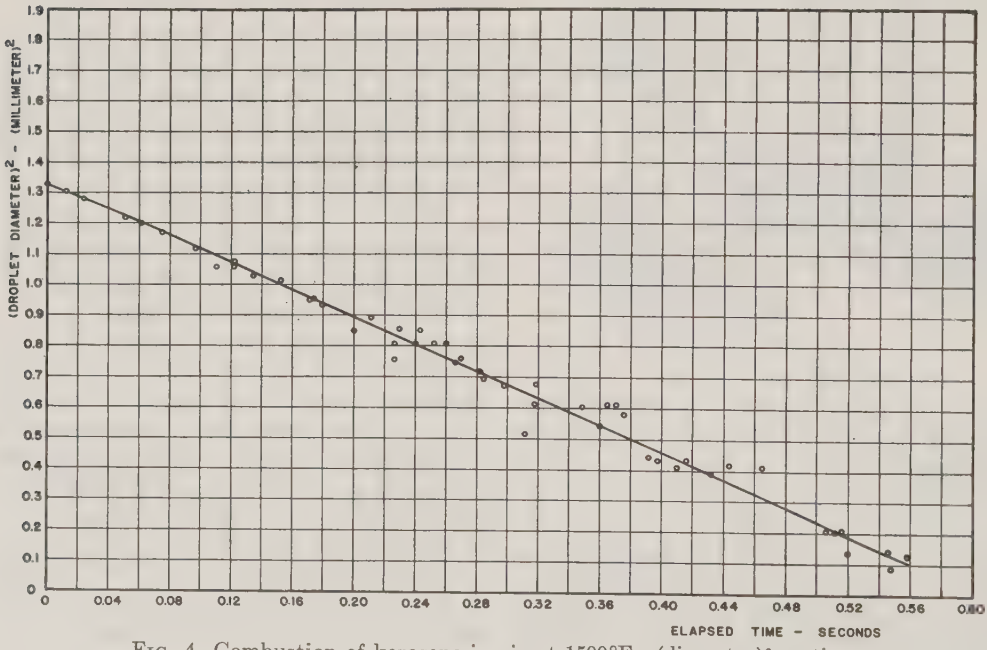

FIG. 4. Combustion of kerosene in air at 1500°F—(diameter)² vs time.

investigated at an ambient temperature of 1500°F. The range of the drop diameters was approximately from 1150 to 300 μ.

The results of the combustion studies are presented in Figures 2, 3 and 4, which show the square of the diameters of the drop as a function of elapsed time following the first photographing event.

EFFECT OF FLAME ON DRAG

The existence of the flame around and in the wake of the drop tends to decrease the drag force.

This is in agreement with Spalding.[1] It was found that the mean velocity of the falling drops, between the second and third photographing stages, was much higher than the terminal velocities for solid spheres of the same size and under the same conditions of surrounding atmosphere. Although it is believed that the drag on liquid spheres is less than for solid ones, the big increase in velocity was more than could be accounted for by this fact alone. As an example, a 487-μ *n*-heptane drop was falling between the second and third photographing stages at a mean velocity of 7.22 ft/sec. The corresponding value for a nonevaporating solid sphere falling at its terminal velocity is only 4.2 ft/sec. This increase in velocity was more noticeable in the case of small drops.

The reduction of drag is explained by the fact that the flame increases the rate of mass transfer from the drop and, consequently, the velocity of vapor leaving the drop surface. The circulation of the liquid near the surface of the drop and the vaporization of the fuel are believed to cause a reduction in the relative velocity of the gas close to the liquid surface.

The velocity of vapor leaving the drop surface is evaluated as follows. The rate of the mass transfer of the vapor is given by

$$\frac{dm}{dt} = -\rho_v A V \tag{1}$$

where

$\frac{dm}{dt}$ = the rate of mass transfer

ρ_v = the density of the vapor

A = the area of the drop

V = the velocity of the vapor

If ρ_l is the mean density of the liquid of the droplet, then

$$\frac{dm}{dt} = \frac{1}{2}\pi\rho_l D^2 \frac{dD}{dt} \tag{2}$$

Equating Equations (1) and (2), the velocity of the vapor is given by

$$V = -\frac{1}{2}\frac{\rho_l}{\rho_v}\frac{dD}{dt} = -\frac{1}{4}\frac{\rho_l}{\rho_v}\frac{1}{D}\frac{dD^2}{dt} \tag{3}$$

The density of the vapor can be calculated from the characteristic gas equation:

$$\rho_v = \frac{P}{\mu RT} \tag{4}$$

where

P = atmospheric pressure

R = gas constant

T = absolute temperature

The symbol μ is a dimensionless constant depending on the ratios of T/T_c and P/P_c, where T, P, T_c and P_c are the temperature, pressure, critical temperature and critical pressure of the vapor, respectively. μ is called the compressibility factor; values of μ are found in Maxwell's *Data Book on Hydrocarbons*.[2]

The value of dD^2/dt is the slope of the combustion curves of D^2 *vs.* t at the corresponding diameter. Thus Equation (3) can be written

$$V = \frac{1}{4}\frac{\rho_l}{\rho_v}\frac{1}{D}C \tag{5}$$

where C is the slope of the D^2-*vs.*-t curve.

As an example, for a 1000-μ *n*-heptane drop, $C = -0.0251$ cm^2/sec. At boiling point and at atmospheric pressure $T/T_c = 0.4075$, $P/P_c = 0.0373$, giving $\rho_v = 0.219$ lb/ft^3 and $V = 0.362$ ft/sec. For a 300-μ drop, $C = -0.0195$ cm^2/sec, which gives $v = 0.938$ ft/sec.

It must be noted that the mole fraction of the fuel at the drop surface is in general less than one, causing the surface temperature to be less than the boiling point.

It has been pointed out that the velocity of the vapor leaving the surface of the drop increases as the diameter decreases. For a small drop, the falling velocity is small and at the same time its vapor velocity is high, resulting in an appreciable reduction of the relative velocity between the drop and the surrounding atmosphere. Consequently, the drag force on the drop is reduced.

The mean velocity of the falling drop was determined by measuring the distance of fall and the time interval between the photographing positions.

Further work is necessary on this point, and the determination of the exact velocity history of the drop rather than average velocities is needed. This could be done by taking two pictures of the drop in quick succession while passing in front of the camera, or by replacing the still cameras by motion picture cameras.

OBSERVATIONS ABOUT THE FLAME ENVELOPING THE DROP

Visual observation indicated that the luminous region was at the wake of the droplet. The lu-

minosity of the flame was due to the presence of incandescent carbon particles which burned slowly, radiating the bright yellow color. At lower temperatures and in the absence of carbon particles, the pure hydrocarbon fuels burned with a blue flame which was characteristic of the reaction zone.

The combustion of kerosene caused more soot and carbon particles to be formed, which increased the luminosity of the flame, in comparison with the pure hydrocarbon fuels. Figure 5 shows a drop in the middle of a white zone appearing on the film. This white zone was caused by the luminous flame when the burning drops passed in front of the open-shutter cameras. The width of the zone is the lateral dimension of the flame.

Due to the open-shutter technique, the vertical dimension of the flame could not be determined. The surrounding flame was from 1.9 to 2.1 times the diameter of the drop in the lateral direction for large and small droplets respectively, for the fuels investigated under the conditions of the present experiments.

HEAT TRANSFER TO THE DROP

As the drop entered the furnace, it was first preheated, receiving heat by radiation from the furnace walls and by conduction and convection from the ambient air.

The heat transfer by radiation is given by

$$q_r = h_r \pi D^2 (T_W - T_S) = \pi D^2 \sigma \epsilon T_W^4$$

and

$$h_r = \frac{\sigma \epsilon T_W^4}{T_W - T_S} \tag{6}$$

where

h_r = the radiation heat transfer coefficient

σ = the Stefan-Boltzmann constant

ϵ = emissivity of the furnace wall

T_W = the absolute temperature of the furnace wall

T_S = the absolute temperature of the surface of the drop

The Nusselt number is used to determine the forced-convection heat transfer coefficient

$$Nu = \frac{h_c D}{k_g} \tag{7}$$

where

h_c = the convection heat transfer coefficient

D = the diameter of the droplet

k_g = the average thermal conductivity of the surrounding atmosphere

The term k_g is estimated at an average temperature $(T_W + T_S)/2$. The ratio of the two heat transfer coefficients is given by

$$\frac{h_r}{h_c} = \frac{\sigma \epsilon D T_W^4}{k_g Nu (T_W - T_S)} \tag{8}$$

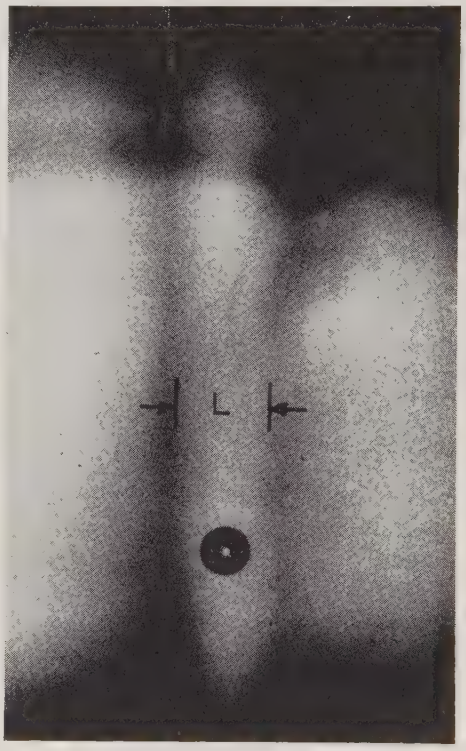

FIG. 5. Lateral dimension of the flame surrounding a falling droplet. L = lateral dimension of flame.

The temperature of the furnace wall was measured by a Leeds and Northrup optical pyrometer and was found to be 1630°F when the ambient-air-temperature was 1500°F. Taking T_s as 200°F, k_g was estimated at 915°F, and was found to be 0.031 Btu/(hr)(ft²)(°F/ft). The emissivity of alundum was taken as 0.3 at 1630°F and σ = 0.173×10^{-8} Btu/(ft²)(hr)(°R)⁴. For a 1000-μ drop falling in the furnace at a Reynolds number of 20, Nu is about 4.4. Inserting these values in Equation (8) gives $h_r/h_c = 0.167$.

Due to the transparency of the volatile hydrocarbon fuels, the ratio h_r/h_c must be multiplied by the absorptivity of the drop, which is in the order of 0.1. This reduces the value of h_r/h_c appreciably. Thus it can be stated that in the present experiments most of the heat received by the drop in the preheating region is by convection and conduction.

The evaluation of the luminous and nonluminous radiation for an 800 μ n-heptane droplet is as follows: The emission of the nonluminous gas to the droplet is given by the generally accepted equation

$$q_{r,n} = \sigma \epsilon_g T_g^4 \tag{9}$$

where

$q_{r,n}$ = the radiant heat due to nonluminous gases, Btu/(hr)(ft^2)

σ = the Stefan-Boltzmann constant = 0.173×10^{-8} Btu/(ft^2)(hr)(°R)^4

ϵ = the gas emissivity defined as the ratio of radiation from gas to drop to the radiation from a black body at the same temperature, and

T_g = the temperature of the gas, °R.

For the emitting gases, ϵ_g depends on T_g, the total pressure and the partial pressure-path length product P_gL, L being the mean beam length in evaluating gas emissivity. The net radiant-heat interchange per unit area is given by

$$q_{r,n} = \sigma \epsilon_g T_g^4 - \sigma \alpha_g T_S^4 \tag{10}$$

where α_g is the absorptivity of the gas for blackbody radiation from the droplet surface and T_S is small compared to T_g, the second term in the right hand side of Equation (10) can be neglected.

Assuming a relatively high flame temperature for n-heptane (2300°K), the partial pressures of carbon dioxide and water vapor were found to be 0.1104 and 0.136 atmos, respectively. This gives $\epsilon_{CO_2} = 3.48 \times 10^{-4}$ and $\epsilon_{H_2O} = 0.501 \times 10^{-4}$ and the total emissivity is 3.981×10^{-4}. Hence, $q_{r,n} = 203$ Btu/hr ft^2.

For the estimation of the radiated heat from the luminous flame, a reasonable value for the absorption strength of the flame KL is assumed 0.8. The flame emissivity was found to be $\epsilon_F = 0.28$ and the luminous radiation $q_{r,l} = 142{,}500$ Btu/hr ft^2. The total radiation to the 800-μ diameter drop is, $Q_r = 3.095$ Btu/hr $= 0.216$ cal/sec.

If the absorption factor is taken to be 0.07 of the total radiation received,[3] then

$$Q_r = 15.12 \times 10^{-3} \text{ cal/sec}$$

For an 800-μ n-heptane dm/dt is found from the relation

$$\frac{dm}{dt} = \frac{1}{4} \pi \rho_l D \frac{dD^2}{dt} \tag{3}$$

From Figure 2, $dD^2/dt = -0.0253$ cm^2/sec, then $dm/dt = 9.82 \times 10^{-4}$ g/sec. It follows that the radiation absorbed per gram of fuel evaporated is 15.4 cal/g and the contribution of radiation is less than 15 per cent of the total heat requirement to evaporate an 800-μ n-heptane drop. The rest of the heat required by the drop is evidently supplied by conduction and convection.

EXPLANATION OF THE COMBUSTION CURVES

The curves for the three fuels investigated have the same shape as shown in Figure 2, 3 and 4.

The equation of these curves can be written as

$$D^2 = D_0^2 - Ct \tag{11}$$

where

D = the diameter of the droplet at time t

D_0 = the initial diameter of the droplet

C = the slope of the curve.

The change in the rate of combustion is thus a function of C, which is usually termed the coefficient of combustion. C depends on Nu, and in the case of small stationary drops or drops moving at a constant Re, the values of Nu and C are constants. C, in this case, is called the combustion constant. In this investigation, the Reynolds number of the falling drop was continuously changing as both the velocity and the diameter changed. For the range of Re_{mean} (7 to 25) of this investigation, the mean Nu ranged from 3.4 to 4.6. This is believed to be the reason why the variation of D^2 *vs.* t is not a straight-line relation.

Taking as an example Figure 3 for isooctane, it is seen that the first part of the curve is slightly convex, the middle part is fairly straight and the last part is concave.

As the drop entered the furnace it was relatively cool, especially near the center. The heat transferred to the drop is partly used in heating up the liquid and partly in evaporating it. The amount of heat per unit mass necessary to heat the drop is larger in big drops than in small ones.

The convexity of the first part of the curve is very small because the drop was heated to near its final stable temperature when the first photographing position was reached.

The middle part of the curve is nearly a straight line, indicating that the value of C is nearly constant. This is explained by the fact that the Re of the drop did not change appreciably in this region. As a large drop reached the first photographing stage at about 85 per cent of its terminal velocity, two factors were counteracting each other in changing its Re. The drop was attaining a higher percentage of its terminal velocity, but at the same time it was reducing in size and consequently, in velocity. The first factor was helped by the presence of the flame, which reduced the drag on the droplet. It seemed that these two factors had approximately equal effects on Re and the drop moved at a fairly constant Re. The small variation of Re for different-sized drop in this region had no appreciable effect on Nu to change the linearity of this part of the curve. This means that Nu and C were fairly constant in that region.

The third part of the curve of Figure 3 is concave. The Re is reduced as time proceeded, because of the reduction in size and velocity of the drop. The gain in velocity due to the flame or toward the terminal velocity is negligible as this latter is believed to be reached at this stage.

As indicated by Figure 4, the combustion curve of kerosene is similar to n-heptane and isooctane. The main physical properties of the fuel that affect the combustion process are the thermal conductivity, specific heat, latent heat, and heat of combustion. The values of these properties do not differ greatly in the fuels investigated and, consequently, the combustion curves are of the same general shape. The values of the curve slope, C, for kerosene were lower than the corresponding values for the pure hydrocarbons during most of the range of the drops investigated. C varied from 0.02 to .0255 cm²/sec during this investigation.

Conclusions

The following conclusions are believed justified by the experimental work:

(1) The appreciable decrease in the drag coefficient of the burning drops is due to the presence of the flame.

(2) At the early stage of combustion the heat required to heat the interior of the drop retarded the rate of combustion. The heat per unit mass absorbed by the drop increased with the increase of initial drop size.

(3) Radiation from the flame was only a small portion of the heat necessary to evaporate the drop. Most of the heat received is believed to be from conduction and convection.

(4) The change of drop size of n-heptane, isooctane, and kerosene due to evaporation during combustion, can be represented by the equation

$$D^2 = D_0^2 - Ct \tag{11}$$

The combustion coefficient, C, depended on the type of fuel, the diameter of the drop, and the relative velocity between the falling drop and the surrounding atmosphere.

Data

Tables of data and details of the experimental equipment and procedure of this paper are given by Saad.[4]

Acknowledgment

The financial assistance of the Power Plant Laboratory, Wright Air Development Center, in support of the Engineering Research Institute Projects 1988 and 2253-3 is gratefully acknowledged. The second author also wishes to express his gratitude for a grant from the Horace H. Rackham School of Graduate Studies at the University of Michigan.

REFERENCES

1. Spalding, D. B.: *Some Fundamentals on Combustion*, Gas Turbine Series, Vol. 2. New York, Academic Press, 1955.
2. Maxwell, J. B.: *Data Book on Hydrocarbons*. New York, Van Nostrand Co., 1950.
3. Wolfhard, H. G., and Parker, W. G.: J. Inst. Petrol., *35*, 118 (1949).
4. Saad, M. A.: Ph.D. Dissertation, Mechanical Engineering Dept., University of Michigan, 1955.
5. Chang, T. Y.: Sc.D. Dissertation, Chemical Engineering Dept., M.I.T., 1941.
6. Godsave, G. A. E.: NTGE (England), Memorandum M95, 1950.
7. Godsave, G. A. E.: NGTE (England) Part I, Report R66, 1950; Part II, Report R87, 1951; Part III, Report R88, 1952.
8. Godsave, G. A. E.: *Fourth Symposium (International) on Combustion*, p. 818. Baltimore, The Williams & Wilkins Co., 1953.
9. McAdams, W. H.: *Heat Transmission*, Ed. 2. New York, McGraw-Hill Book Co., 1942.

10. Simpson, H. C.: Sc.D. Dissertation, Chemical Engineering Dept., M.I.T., 1954.
11. Spalding, D. B.: Fuel, *29*, 2, 25 (1950).
12. Spalding, D. B.: Fuel, *32*, 169 (1953).
13. Spalding, D. B.: Aeronautical Res. Council (Combustion of Fuels Subcommittee), *13*, 711, C. F. 159 (1951).
14. Spalding, D. B.: *Fourth Symposium (International) on Combustion*, p. 847. Baltimore, The Williams & Wilkins Co., 1953.

Discussion by C. C. Miesse

The authors are to be complimented on this vital contribution in a basic field which is so plagued by large areas of ignorance. It is interesting to note that the shape of the correlation curves presented in Figures 2, 3, and 4 of subject paper can be predicted theoretically by consideration of Frössling's equation, which was shown to be valid for burning droplets by Agoston, Wise, and Rosser.* This equation for the variation in surface area (D^2) with time can be written

$$\frac{dD^2}{dt} = -C(1 + k\sqrt{D}v) \qquad \text{(A)}$$

where v is the velocity of the droplet, and k is a constant which is determined by the physical properties of the droplet and its vapor.

The shape of the D^2 *vs.* t curve is best characterized by its second derivative:

$$\frac{d^2(D^2)}{dt^2} = -Ck\left(\sqrt{D}\,\frac{d\sqrt{v}}{dt} + \sqrt{v}\,\frac{d\sqrt{D}}{dt}\right) \qquad \text{(B)}$$

For $t = 0$, $v = 0$ (in free fall), and its derivative is positive. Hence the second derivative defined by Equation (B) is negative, thus predicting the initial convexity of the curves shown in Figures 2, 3, and 4. As the droplet vanishes ($D = 0$), the first term in the parentheses of Equation (B) disappears, and the second term is negative by virtue of the decreasing size of the droplet. Hence, the second derivative defined by Equation (B) is positive, and the ultimate concavity of the D^2 *vs.* t curves is predicted by theory.

Author's Comments

Dr. Stewart Way and others have raised questions concerning the correlation of the results of the single drop studies with the processes that occur in the burners of gas turbine engines. Questions have also been asked whether the flame surrounds the individual drops in the case of fuel spray combustion.

Concerning the last question, studies which we have reported,† lead us to believe that the term "burning rate" may be misleading, since it implies that the drop is intimately associated with its flame. Actual combustion of fuel spray involves evaporation, followed by the burning of the vapor. The vapor may burn at some distance from the drop that was its source, and the resulting flame and the drop will almost certainly not be concentric.

The values of the burning rates of the drops in a fuel spray of original size of 100 microns are approximately one-half those reported by Godsave‡ for much larger drops burned individually in still air. The discrepancy in values suggests that the phenomena associated with a burning fuel spray of very small drop size may be more nearly similar to drop evaporation in a hot atmosphere without combustion than to burning in a relatively cool atmosphere of a single large fuel drop surrounded by flame from its own vapor.

As to the first question concerning the correlation of the single drop studies with the combustion in a turbine burner, this is impossible to judge, because little is known concerning the circumstances of burning of the individual drops in the engine burner. Published data concerning the actual fuel burning conditions within the burner are quite lacking. For example, little or no quantitative data is available concerning the air temperatures in the several burning zones within the gas turbine burner, the relative air and fuel drop velocities, the concentrations of fuel, air, and the products of combustion, or the rates of burning of the fuel drops. This all points to the need for further laboratory activity involving probing of the inside of burners to fill these gaps in our knowledge. Only after more information is available will we be able to evaluate the correlation of the single drop combustion data with the actual burning conditions.

* G. A. Agoston, H. Wise and W. A. Rosser: *Sixth Symposium (International) on Combustion*, p. 708. New York, Reinhold Publ. Corp., 1957.

† J. A. Bolt and T. A. Boyle: Trans. Am. Soc. Mech. Engr., *78*, 3 609–617 (1956).

‡ Godsave, G. A.: Fourth Symposium (International) on Combustion. Baltimore, The Williams & Wilkins Co., 1953.

· 95

COMBUSTION OF FUEL DROPLETS IN A FALLING CHAMBER

By SEIICHIRO KUMAGAI AND HIROSHI ISODA

I. Introduction

As one aspect of the combustion of sprayed fuels, the combustion of individual droplets has been studied for various fuels and ambient conditions. It is known empirically that the mass burning rate of droplets is directly proportional to the droplet diameter. This relation is applicable to a wide range of experimental conditions. Theoretical analyses of droplet combustion also have been reported.[1, 2, 3, 4] Most of these analyses are based on a spherically symmetrical combustion model. Starting from these theories, it can be shown that the mass burning rate of droplets is directly proportional to the droplet diameter, and the quantities, such as temperature and diameter of flame boundary, can be calculated. These calculated quantities have been compared with experimental results. But the influence of natural convection on the burning process of droplets is too severe to be neglected under these experimental conditions. This problem has been treated both experimentally and theoretically by Spalding[2] and by Kumagai and Kimura.[10] It is undoubtedly meaningless to compare the results of these experiments with calculated spherically symmetrical theoretical analysis and based on a model of combustion.

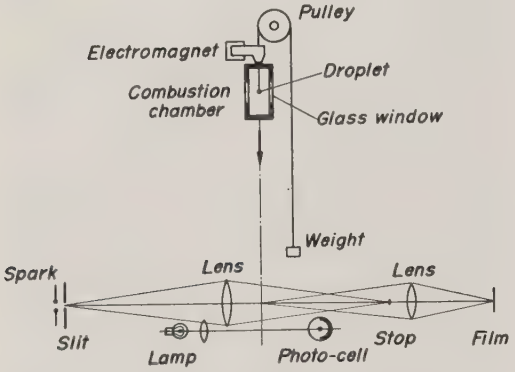

FIG. 1. Schematic diagram of apparatus.

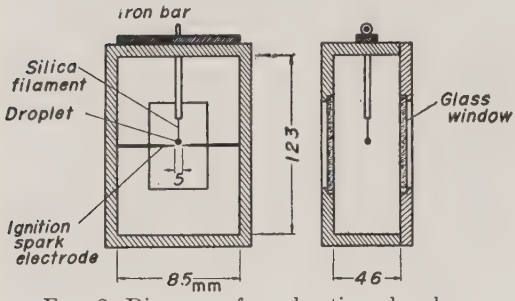

FIG. 2. Diagram of combustion chamber.

In real combustion processes, fuel droplets are so fine that the influence of both natural and forced convection is negligible, and consequently the flames may be treated as spheres. The effect of natural convection can be avoided in two ways. One is to observe the combustion of very fine droplets, and the other is to observe the combustion of droplets used in ordinary experiments in a field with little or no gravitational acceleration. The latter method was adopted in the present investigation, and the effect of natural convection on droplet combustion was studied in a combustion chamber that falls with a constant acceleration. The experiment on the combustion of droplets in a freely falling chamber can be reasonably compared with the theory of spherical combustion.

II. Experimental Apparatus and Procedure

The apparatus used is shown schematically in Figure 1. The combustion chamber is a closed wooden box (Fig. 2) with one wall that opens to permit introduction of a droplet. This box contains a silica filament from which the fuel droplet is suspended and a pair of spark electrodes for ignition. A counter-weight connected to the chamber by a silk string through a pulley system is pulled up as the chamber drops. The acceleration of the fall can be varied by changing the mass of this counter-weight. Denoting mass of the chamber by M and mass of the counter-weight by m, the acceleration of fall is expressed as $g(M - m)/(M + m)$ in the case of negligible drag and friction, where g is the gravitational acceleration. Therefore, acceleration, α, in the moving system fixed to the falling chamber is equal to $2gm/(M + m)$. Using this device we can vary the value of α from zero to g.

The chamber is held at a given height by an electromagnet supported by a stand, and a fuel droplet is suspended at the end of the silica filament. Just before the chamber drops, the droplet is photographed to measure its initial diameter.

Ignition of the droplet by an electric spark is made simultaneously with the start of the fall. A schlieren photography system is provided along the path of the falling chamber. When the chamber reaches its optical axis, the light beam of a photo-relay is cut off to initiate the light source spark. Dimensions of the droplet and the hot air zone around it can be measured on a schilieren photograph. Direct photographs also are taken, because the flame boundary cannot be observed clearly on the schlieren photograph. The apparatus used in direct photography is the same in principle as that used previously except that a camera is connected to the combustion chamber. A photo-relay clicks the shutter of the camera electromagnetically when desired.

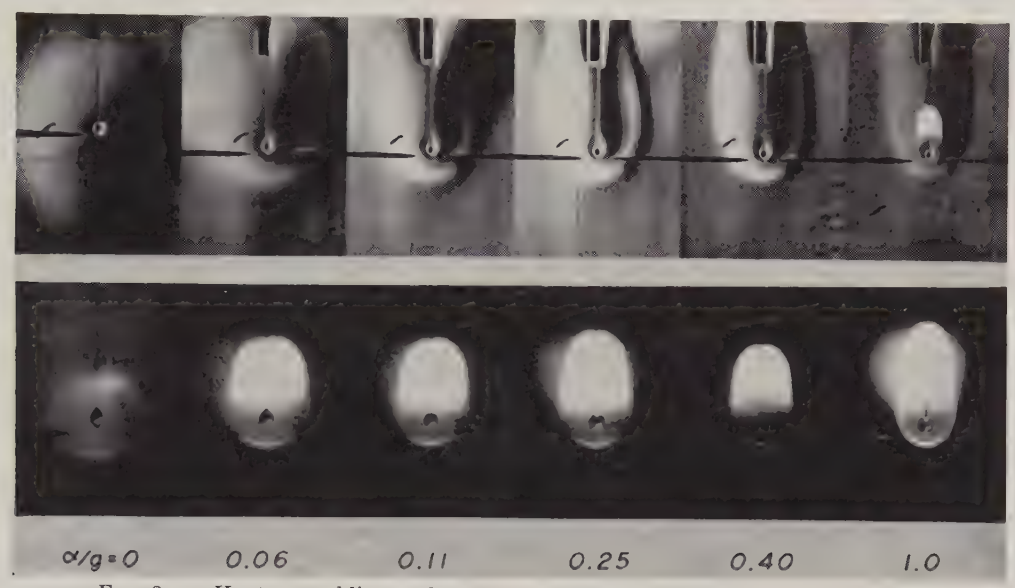

FIG. 3a. *n*-Heptane, schlieren photographs (top), direct photographs (bottom).

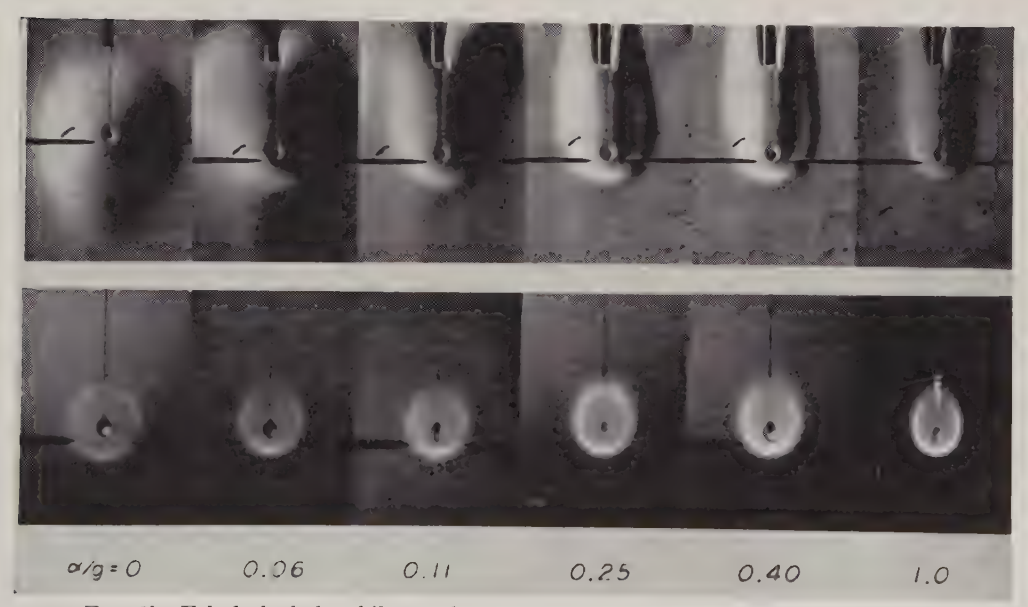

FIG. 3b. Ethyl alcohol, schileren photographs (top), direct photographs (bottom).

III. Results

Fuels used in this experiment were *n*-heptane and ethyl alcohol. Schlieren photographs of burning droplets and direct photographs of their

flames at various values of the acceleration, α, are shown in Figure 3. In the case of combustion of fuel droplets at $\alpha = 0$, *viz.*, combustion in a freely-falling chamber, the flame boundary and the surrounding hot-air zone are almost spherical and concentric with the droplet. But, if there is any acceleration, the hot-air zone is transformed into an upward flow and the flame takes an oval shape. In the case of *n*-heptane, the upper part of the flame is very luminous and seems to be a little inside the lower flame which is less brilliant. In the case of ethyl alcohol, however, a brighter region of the type observed in the flame of *n*-heptane does not appear even at $\alpha = g$. As the value of α increases, the flame boundary becomes higher and brighter, the hot-air zone becomes narrower and the temperature gradient appears to increase (Fig. 3). Figures 4, 5

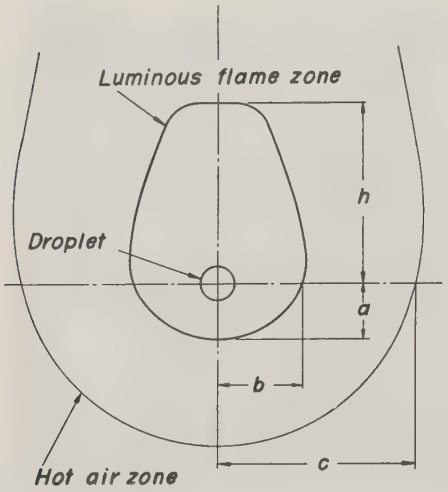

FIG. 4. Schematic presentation of burning droplet.

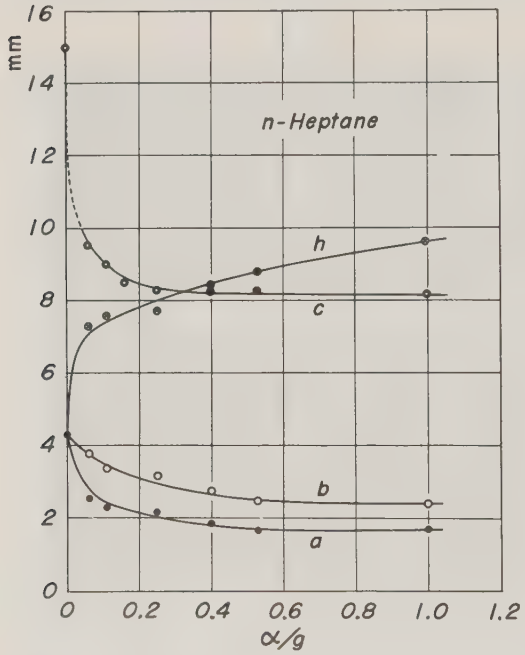

FIG. 5. Dimensions of flame boundary and hot-air zone of *n*-heptane, 1.3 mm in diameter.

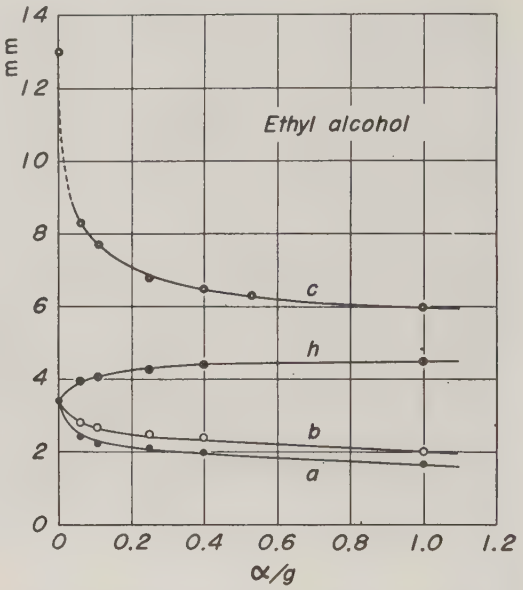

FIG. 6. Dimensions of flame boundary and hot-air zone of ethyl alcohol, 1.3 mm in diameter.

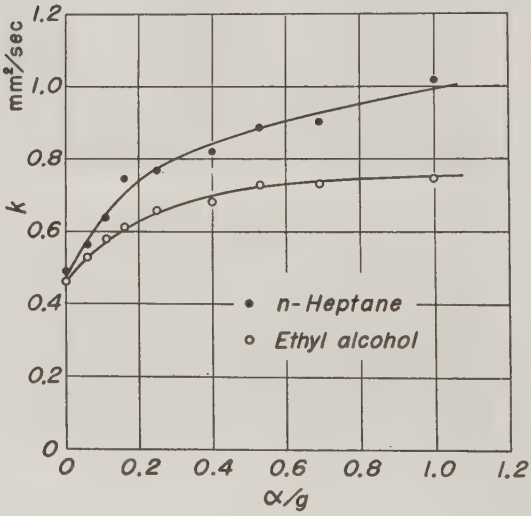

FIG. 7. Evaporation constant κ as a function of α.

and 6 show the relation between the value of α and the dimensions of the burning droplets. The change of these dimensions is remarkable in the region of smaller values of α.

The evaporation constant, k, can be determined from the relation, $D_0 - D^2 = kt$, where D_0 and D are the initial and the instantaneous diameter, respectively, and t is the time. These data are shown in Figure 7. As the value of α decreases, the evaporation constant also decreases, especially in the region of smaller values of α, as a result of the decrease of natural convection. In the case of n-heptane the value of k at $\alpha = 0$ is almost half of the value at $\alpha = g$. Excluding the influence of natural convection, these experimental results can reasonably be compared with the results of the theoretical analysis based on a spherical combustion model.

IV. Discussion

Theoretical analyses of burning droplets are generally treated under the assumption of a steady state of combustion and a combustion model having spherical symmetry. The important result derived from these theories is that the evaporation constant and the ratio of flame diameter to droplet diameter should be independent of droplet diameter for fixed values of physicochemical parameters. In Table 1, the experimental values obtained in a freely-falling chamber are contrasted with the theoretical values calculated by Goldsmith and Penner.[3] The observed values of the evaporation constant are about half of the calculated values.

The observed flame diameter values in Figure 8 are not likely to be directly proportional to the droplet diameters. This is contrary to theoretical predictions and suggests that the burning process is not in a steady state, at least in the period observed. In our experiment, where the initial droplet diameter ranges from 1.0 mm to 1.5 mm and the observed time from ignition is 0.1 − 0.4 sec, the burning process seems to be unsteady as shown in Table 2. The flame diameter is still increasing in this period although the droplet diameter is decreasing. The data in Figure 8 correspond to various cases of initial droplet diameter (0.7 − 1.6 mm), but the observed time from ignition is kept nearly constant for all droplets (0.3 sec). Accordingly, the burning process has progressed considerably for the smaller droplets, whereas it is still in an early stage for the larger droplets. This means that we are considering values of flame diameters at different stages of combustion for droplets of different sizes. For larger droplets observed in a later stage, the flame diameter might possibly be proportional to the droplet diameter. To confirm the validity of assuming a steady state, the successive stages of the burning process of droplets must be observed.

Table 1. Calculated Values of the Ratio of Flame Diameter to Droplet Diameter, D_f/D, and of the Evaporation Constant, k, and Observed Values of the Evaporation Constant, k

	$\frac{Df}{D}$	Calculated Value of k mm²/sec	Observed Value of k mm²/sec
n-Heptane	8.6	0.86	0.49
Ethyl alcohol	5.3	0.79	0.46

Table 2. Observed Values of the Flame Diameter as a Function of Time, n-Heptane

Time from ignition, sec	0.12	0.22	0.32
Droplet diameter, mm	1.28	1.26	1.24
Flame diameter, mm	7.4	8.1	8.6
Ratio of flame diameter to droplet diameter	5.8	6.4	6.9

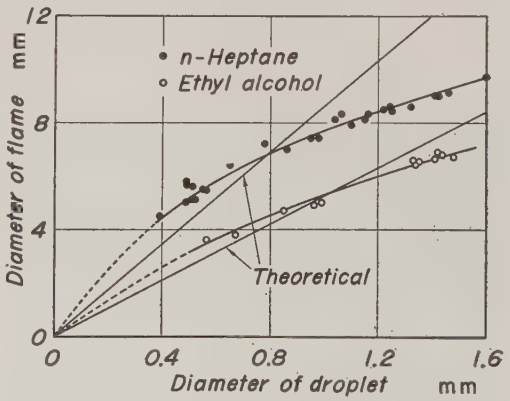

Fig. 8. Flame diameter as a function of droplet diameter.

This problem will be treated in a future program, using a falling chamber equipped with a motion picture camera.

Ordinarily the flame of a burning droplet takes on an oval shape under the influence of natural convection. It is observed experimentally that the lower part of the flame remains unchanged, whereas the upper portion of the flame is directly proportional to the droplet diameter.[7, 9, 10]

Kumagai and Kimura[10] investigated a burning droplet under the influence of natural convection both experimentally and theoretically. Their analysis involved the following assumptions: (a) Steady-state combustion for a fixed droplet diameter; (b) Uniform upward flow of air caused by natural convection; (c) Burning droplet considered as a source of fuel vapor at uniform strength; (d) Interdiffusion across the contact plane between air and fuel vapor; (e) Flame boundary at which delivery of oxygen and fuel vapor is in stoichiometric ratio. The burning droplet and the flow lines of fuel vapor and air are shown schematically in Figure 9. If $\dot{m}$ is the

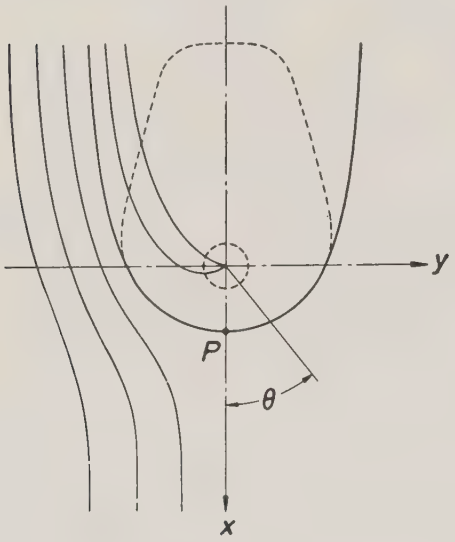

FIG. 9. Schematic diagram of flow and coordinate of burning droplet.

volume flow of fuel vapor per unit time and U is the uniform velocity of air, the stream function, χ, can be expressed as follows:

$$\chi = -\pi U y^2 + \dot{m}(1 - \cos\theta)/2 \qquad (1)$$

The contact plane between air and fuel vapor is determined by $\chi = 0$, namely

$$\left.\begin{aligned} y &= R \sin\frac{\theta}{2} \\ x &= \frac{R\cos\theta}{2\cos\frac{\theta}{2}} \end{aligned}\right\} \qquad (2)$$

$$R = \sqrt{\dot{m}/\pi U} \qquad (3)$$

Air and fuel vapor come in contact with each other first at the point, P, and therefore the flame boundary begins at this point. The lower part of flame observed coincides well with the calculated contact plane, and the lower height, a, and the radius of flame on the horizontal section through the center of the droplet, b, remain nearly constant during combustion. In the upper part of flame, however, the flame boundary lies inside the calculated contact plane and is approximately of the nature of a cylindrical diffusion flame,[11] e.g., direct proportionality between the upper height of flame and the droplet diameter. According to Equation (2), the ratio b/a should be equal to $\sqrt{2}$. The experimental results seem to support this prediction.

As the value of $a(= R/2)$ remains constant and, experimentally, $\dot{m}$ is directly proportional to the droplet diameter D, U should be directly proportional to D. As

$$\dot{m} = \frac{22.4\pi k\rho_l}{4M}\frac{Tv}{273} D \times 10^3 \text{ cm}^3/\text{sec} \qquad (4)$$

where T_v and ρ_l denote the temperature of the fuel vapor and density of liquid fuel, respectively, and M is the molecular weight. U is calculated from Equations (3) and (4). For example, when $k = 0.0075$ cm^2/sec, $\rho_l = 0.79$ g/cm^3, $T_v = 773$°K, $D = 0.1$ cm and $R = 0.25$ cm for ethyl alcohol, $U = 3.3$ cm/sec is derived as the order of upward air velocity caused by natural convection.

The actual combustion process of fuel droplets may lie between two theories, one in which natural convection is neglected[3, 4] and the other in which the diffusion process is neglected in the lower part of the flame.[10]

V. Conclusion

(1) Combustion of fuel droplets at various accelerations is observed by using a combustion chamber that drops with a constant acceleration.

(2) Combustion of fuel droplets in a freely falling chamber is not affected by natural convection, and therefore the combustion process corresponds to that of a spherically symmetric combustion model.

(3) Dimensions of the flame boundary and the hot-air zone become higher and narrower as acceleration increases, because natural convection becomes stronger. Burning rates of fuel droplets at various accelerations are also obtained. They decrease as acceleration decreases, and both burning rates and dimensions of flame boundary change rapidly at the region of smaller values of acceleration.

(4) The experimental results obtained in the case of no or little acceleration are compared with the results of the theory, assuming a steady state on a combustion model of spherical symmetry. The experimental values of burning rate give about half of the values calculated by Goldsmith and Penner, and the theoretical prediction that the ratio of flame diameter to droplet diameter remains constant seems not to be supported, at least in the early stage of combustion. However, we must not conclude prematurely that there is no steady state in the combustion process of fuel droplets. Further investigation is needed on this point.

(5) The influence of natural convection on the shape of the flame is treated theoretically, assuming that interdiffusion of fuel vapor and oxygen occurs across the contact plane between uniform upward flow of air and a source of fuel vapor of uniform strength. The lower part of the flame observed coincides well with the calculated contact plane, and the upper part of the flame is approximately of the nature of a cylindrical diffusion flame.

REFERENCES

1. Godsave, G. A. E.: *Fourth Symposium (International) on Combustion*, p. 818. Baltimore, The Williams & Wilkins Co., 1953.
2. Spalding, D. B.: *Fourth Symposium (International) on Combustion*, p. 847. Baltimore, The Williams & Wilkins Co., 1953.
3. Goldsmith, M., and Penner, S. S.: J. Am. Rocket Soc., *24*, 245 (1954).
4. Okazaki, T., and Gomi, M.: Trans. Japan Soc. Mech. Engr., *19*, 1 (1953).
5. Kobayashi, K.: Trans. Japan Soc. Mech. Engr., *20*, 826 (1954).
6. Kumagai, S., and Isoda, H.: Nature, *166*, 1111 (1950). Kumagai, S., and Isoda, H.: *Fifth Symposium (International) on Combustion*, p. 129. New York, Reinhold Publ. Corp., 1955.
7. Hall, A. R., and Diederichsen, J.: *Fourth Symposium (Internationl) on Combustion*, p. 830. Baltimore, The Williams & Wilkins Co., 1953.
8. Hottel, H. C., Williams, G. C., and Simpson, H. C.: *Fifth Symposium (International) on Combustion*, p. 101. New York, Reinhold Publ. Corp., 1955.
9. Wise, H., Lorell, J., and Wood, B. J.: *Fifth Symposium (International) on Combustion*, p. 132. New York, Reinhold Publ. Corp., 1955.
10. Kumagai, S., and Kimura, I.: Sc. Machine (Japan), *3:* 431 (1951).
11. Burke, and Schumann: Ind. Eng. Chem., *20*, 998 (1928).

Discussion by C. C. Miesse

The authors are to be congratulated on this outstanding contribution to the technical literature. Moreover, the experimental variation of flame/droplet diameter ratio with droplet diameter, as shown in Figure 8 of subject paper, can be readily predicted on the basis of the equations presented.

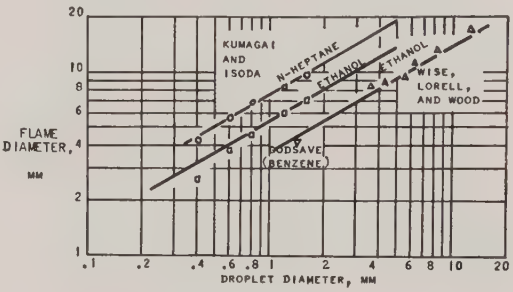

Fig. 1. Variation of luminous flame diameter with droplet diameter.

Mass burning rate: $\dot{m} = \alpha D$

Vapor source: $\rho_f v_f = \dfrac{\dot{m}}{4\pi y^2}$

Stoichiometric: $k\rho_f v_f = \rho_0 v_0$

Flame diameter: $D_c = \dfrac{k\alpha D}{\pi \rho_0 v_0}$

Under the stated assumption of a uniform air velocity, U, simultaneous consideration of Equations (2), (3) and (4) of subject paper reveals that the flame "diameter" should vary as the square root of the droplet diameter. The apparent validity of this derivation is indicated by the remarkable degree to which correlations of various sets of data,*† including those of the present authors, are effected in the following figure.

* G. A. E. Godsave: *Fourth Symposium (International) on Combustion*, p. 826. Baltimore, The Williams & Wilkins Co., 1953.

† H. Wise, J. Lorell, and B. J. Wood, *Fifth Symposium (International) on Combustion*, p. 134. New York, Reinhold Publ. Corp., 1955.

96

ON THE COMBUSTION OF A LIQUID FUEL SPRAY[a]

By C. C. MIESSE

Introduction

The increasing demands for greater efficiency in jet propulsion engines have stimulated widespread research in the fields of atomization, evaporation, and combustion in recent years. Outstanding among the numerous surveys on atomization are those by Browning,[3] De Juhasz and Meyer,[7] and Giffen and Muraszew,[9] and the present status of knowledge on spray evaporation is best represented by Ingebo,[12] Foster and Ingebo,[8] and Ranz and Marshall.[17] The combustion of single droplets has been extensively investigated by Godsave,[10] Spalding,[19] Goldsmith and Penner,[11] and Wise, Lorell, and Wood;[21] the combustion of fuel sprays has been studied experimentally by Bolt and Boyle,[2] Burgoyne and Cohen,[5] and Browning and Krall.[4] The effect of atomization characteristics on performance has been outlined by Anson,[1] Ross,[18] and Trent,[20] and was summarized by the present author.[15]

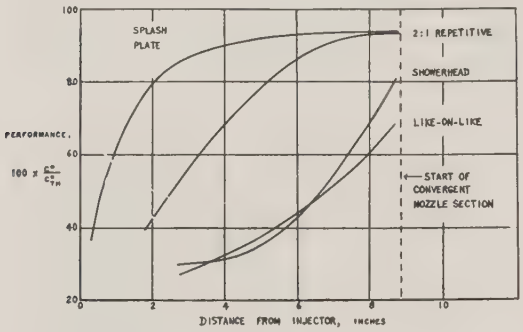

FIG. 1. Axial variation of performance for various injectors (Ross).

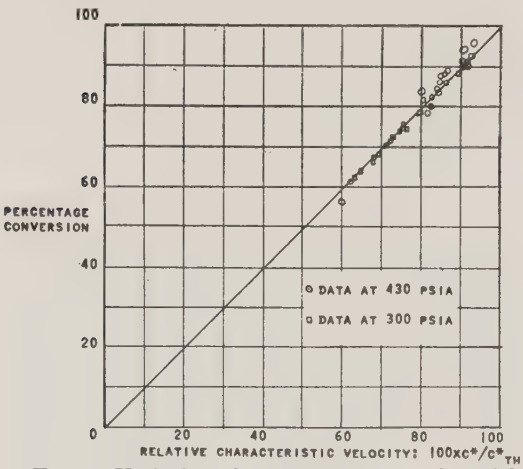

FIG. 2. Variation of percentage conversion with local characteristic velocity (Trent).

The purpose of the present paper is to present several theoretical concepts which may be of aid in explaining some of the phenomena which have been observed. Of primary interest is the variation of performance characteristics due to changes in the method of injection, as reported by Ross[18] and shown in Figure 1. From this figure, it is apparent that the finer atomization of the splash-plate and 2:1 impinging injectors leads to a rapid increase in performance close to the injector, while the coarser atomization of the like-on-like and shower-head injectors results in a more gradual increase in performance. This apparent correspondence of increased performance with finer atomization suggests the hypothesis that performance characteristics are related directly to evaporation processes. Trent[20] has shown the direct variation of local values of performance with the ratio of weight burned to weight unburned, as presented in Figure 2, and plotting of Ingebo's[12] drop size data on the graph of gas composition (obtained by sampling) versus distance, as reported by Foster and Ingebo[8] and shown in Figure 3, indicates that the variation of available propellant vapors with distance can be calculated from drop-size data. From Figures 2 and 3, it is apparent that performance characteristics, as indicated by percentage conversion, should be determinable in terms of the spatial variation of average drop size. By making various simplifying assumptions, the effect of atomization and evaporation on burning characteristics will be analyzed theoretically in a subsequent section.

A second, and more fundamental, aspect of the combustion of sprays, which is worthy of theoretical consideration, is the apparent difference in the burning rates of large (1000 μ) single droplets, as reported by Godsave,[10] and of smaller (53 μ) spray droplets, as reported by Bolt and Boyle.[2] One clue as to the possible explanation lies in the

[a] The work reported in this paper was performed at the Aerojet-General Corporation under the sponsorship of the United States Air Force, Wright Air Development Center.

fact that the flame/drop radius ratio for the larger drop was 3:1, whereas the same ratio for the smaller drops was approximately 19:1. This latter observation concurs quite well with Wise, Lorell, and Wood's[21] report that, in their experiments, the surface-to-flame distance appeared to be invariant and independent of droplet radius. The diffusion concept, presented by the author in an analysis of the flame front between two unlike droplets in a bipropellant system,[14] will be applied to the combustion of a single droplet, and several proposed mechanisms will be investigated in order to derive an analytical explanation for the phenomena observed.

Performance Characteristics

For the purpose of determining the variation of performance with distance from the injector in a liquid propellant combustion chamber, the configuration shown schematically in Figure 4 is considered. From this figure, it is apparent that the elementary volume under consideration is a cross-sectional slice which proceeds downstream from the injector at a velocity, U, equal to the average velocity of the propellants (both liquid and gas) at the corresponding axial position. According to this model, the observer is thus seen to travel with the propellants, implying a Lagrangian coordinate system. The quantities of propellant unreacted or reacted can then be specified by percentages of the total weight in the slice, and the relation between time and distance can be expressed by the familiar equation

$$dz = dx/L = U(x)\, dt/L \tag{1}$$

where x is the axial coordinate, L is the length of the chamber, t is time, and the velocity, U, may vary in the axial direction but is considered to be independent of the transverse coordinates.

The present simplified theory is based upon the following idealized assumptions regarding the chemical kinetics of the system: (1) the propellants react only in the vapor phase; (2) the propellant vapors react as a single chemical substance, hence implying that perfect mixing occurs immediately upon vaporization of the spray; and (3) the system is isothermal. Under these assumptions, the law of mass action can be expressed by the equation[20]

$$-\frac{dC}{dt} = AC^n \tag{2}$$

where C is the concentration of the unburned propellant, A is the specific reaction rate constant, and n is the order of the reaction. The assumption of a two-component system permits Equation (2) to be written in a form which facilitates the consideration of various assumptions regarding the rate of supply of the combustible vapors in a two-phase (liquid and vapor) system:

$$dw = rW^n dt \tag{3}$$

where dw is the incremental percentage of propellant converted in time dt, r is the relative reaction rate (or "reaction frequency," as referred to by Penner[16]) in fraction of propellant converted per second, and W is the percentage of unreacted propellant available. The performance characteristics for the various types of injectors, as depicted in Figure 1, will depend upon the assumptions regarding the distribution of available propellant W.

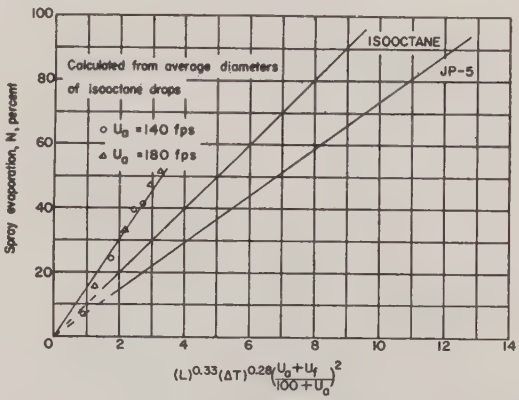

FIG. 3. Comparison of variations in percentage of fuel evaporated as determined by gas-sampling and average droplet diameters (Foster and Ingebo).

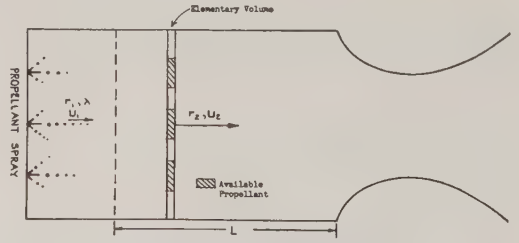

FIG. 4. Idealized thrust chamber configuration.

VAPORIZED PROPELLANTS

For those injectors which produce a very finely-atomized spray which vaporizes completely within a short distance from the injector, the gas in the combustion chamber can be considered

as a homogeneous mixture of combustibles. Hence, the weight of unreacted propellant at any point in the chamber is equal to the total weight of combustibles minus the weight previously reacted:

$$W = 1 - w \tag{4}$$

Substitution of Equations (1) and (4) into Equation (3) results in the following first-order differential equation for w

$$\frac{dw}{dz} = \frac{rL}{U}(1 - w)^n \tag{5}$$

where the parameter rL/U can be identified as Damköhler's first similarity ratio.[16]

For a first-order reaction ($n = 1$), Equation (5) can be solved for the case in which rL/U

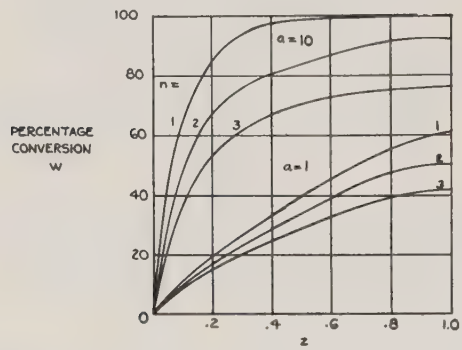

FIG. 5. Variation of performance with axial distance for various values of a and n.

is allowed to vary with z:

$$w = \exp\left\{-\int\frac{rL}{U}\,dz\right\}\cdot\left[\int\frac{rL}{U}\exp\left\{\int\frac{rL}{U}\,dz\right\}dz - 1\right] = 1 - \exp\left\{-\int\frac{rL}{U}\,dz\right\} \tag{6}$$

For constant (average) values of $rL/U = rT_g$, where T_g is the gas residence time in the combustor, Equation (6) reduces to

$$w = 1 - \exp(-rLz/U). \tag{7}$$

Equation (7) indicates immediately that the per cent reacted will increase sharply near the injector end of the chamber, and then proceed more gradually as noted in Figure 1 for the splash-plate and 2:1 impinging injectors, for which cases finer atomization leads to complete vaporization close to the injector. For higher orders of reaction and constant values of rL/U, the solution of Equation (5) can be written

$$w = 1 - \frac{U}{(n-1)rLz - U}^{1/(n-1)} \tag{8}$$

Typical variations for various values of rL/U and n are shown in Figure 5, which indicates that more rapid increases in performance result from either high values of rL/U or low values of n. It is seen that the parameter rL/U is essentially a measure of the predominance of the reaction rate over the gas velocity (convection).

ATOMIZED PROPELLANTS

For those combustors in which the propellants persist in droplet form for a large percentage of the length of the chamber, it is apparent that the available propellant must be represented as a heterogeneous mass of liquid and vapor, in which the vapor concentration will vary with distance from the injector. Since Figure 3 shows that the vapor concentration can be determined from droplet evaporation considerations, the equation for available propellant vapor, W, can be written in terms of the square of the relative droplet diameter

$$y = (D/D_0)^2 \tag{9}$$

where D and D_0 are the instantaneous and original values, respectively, of the drop diameter:

$$W = 1 - y^{3/2} - w \tag{10}$$

By assuming a constant evaporation or burning rate, λ, the relation between droplet diameter and time can be expressed by the equation

$$dy = -\lambda dt \tag{11}$$

Substitution of Equations (10) and (11) into Equation (3) (with $n = 1$) yields the following equation for the assumed first-order reaction:

$$\frac{dw}{dy} = \frac{rD_0^2}{\lambda}(w - 1 + y^{3/2}) = b(w - 1 + y^{3/2}) \tag{12}$$

For constant values of rD_0^2/λ, which is analogous to Damköhler's second (diffusion) similarity group,[16] the solution of Equation (12) can be written:

$$w = 1 - y^{3/2} + \frac{3}{2b}(e^{-b(1-y)} - y^{\frac{1}{2}}) - \frac{3\sqrt{\pi}}{4b^{3/2}}e^{by}(erf\sqrt{b} - erf\sqrt{by}) \tag{13}$$

where

$$erf(x) = \frac{2}{\sqrt{\pi}} \int_0^x e^{-u^2}\, du \qquad (14)$$

is designated as the error function. The performance of a heterogeneous system is thus characterized by the parameter $rD_0^2/\lambda = rT_d$, where T_d is the lifetime of the drop, which represents the ratio of the reaction rate to the rate at which combustible vapors are being supplied.

Figure 6 shows several representative curves as determined from Equations (7) and (13) for a first-order reaction with constant values of the parameters. It is noted that a low value of the heterogeneous parameter b results in gradual progressive combustion, as noted in Figure 1 for the shower-head and like-on-like injectors. The criterion for gradual progressive combustion can be expressed by the inequality which is satisfied by values of y close to unity:

$$\frac{2}{\sqrt{\pi}} e^{-b} > (erf\sqrt{b} - erf\sqrt{by})/\sqrt{b} \qquad (15)$$

It is noted that, as the droplet approaches complete vaporization ($y \rightarrow 0$), Inequality (15) is no longer satisfied, and the character of the performance curve resembles that predicted by Equation (7) for the vaporized case.

From these preliminary remarks, it is indicated that the concept of distribution of available propellant may be of aid in determining the performance characteristics of any combustor under consideration and may thereby prove valuable in the design of future combustors. It is suggested that most combustors will fit neither of the above cases exactly, but will be represented by a combination of these extreme models. The precise method by which the two models are combined will be determined by the penetration characteristics of the liquid jets in that the vaporized propellants analysis will become valid upon the complete disappearance of the droplets due to evaporation.

Variation of Flame Drop Radius Ratio

The variation of flame/drop radius ratio with droplet radius, as reported by Wise, Lorell, and Wood[21] for ethanol drops burning in air, is shown graphically in Figure 7. For comparison purposes, the single data points reported by Godsave[10] and Burgoyne and Cohen[5] for benzene drops burning in air are plotted on the same graph. From this figure, it is apparent that, as the drop size increases, the flame/drop radius ratio decreases in all cases. A theoretical explanation for this variation will be sought by investigating the conditions necessary for the establishment of a flame front in a liquid-vapor system.

The basic equations for determining the position of the flame envelope surrounding a single fuel droplet burning in an oxidizing atmosphere were presented in a previous paper,[14] and are

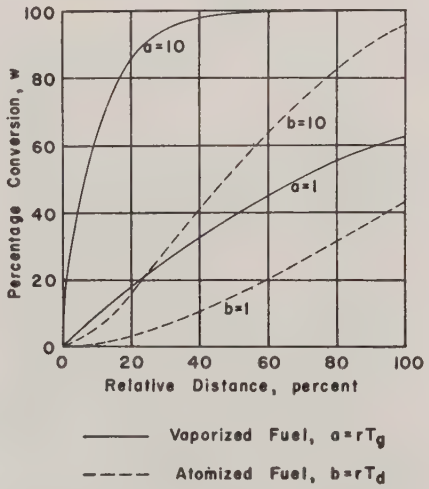

FIG. 6. Theoretical variation of performance with axial distance in combustor.

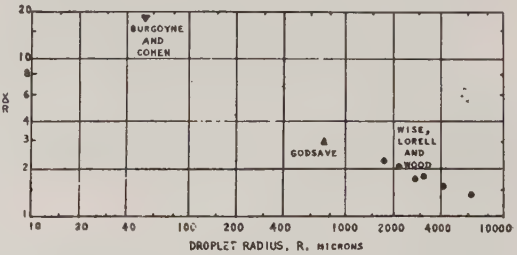

FIG. 7. Experimental variation of flame drop radius ratio.

listed here for convenience. If it is assumed that the combustion takes place at the locus where the ratio of mass flows of fuel vapor and oxidizing atmosphere is stoichiometric, then the following condition can be prescribed:

$$k\rho_f v_f = \rho_o v_o \qquad (16)$$

where ρ_f and ρ_o are the densities and v_f and v_o are the linear velocities of the fuel and oxidizing vapors, respectively, at the flame front, and k is the stoichiometric mixture ratio. An expression for v_f can be obtained by considering the fuel

droplet to be a vapor source:

$$v_f = \frac{M}{4\pi\rho_f X^2} \tag{17}$$

where M is the mass rate of evaporation (considered as the strength of the vapor source) and X is the radius of the flame front. An expression for M was given by Godsave[10]:

$$M = \frac{F}{1/R - 1/X} \tag{18}$$

where R is the radius of the droplet and F is a

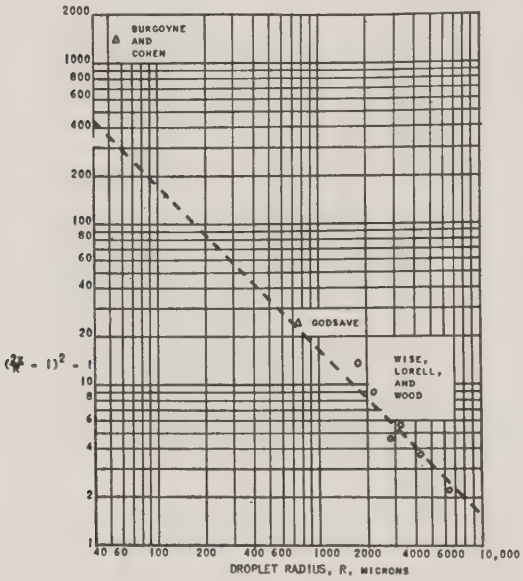

FIG. 8. Variation of flame/drop radius ratio with droplet radius for benzene and ethanol drops burning in air. - - - Theoretical curve: $K^* = 1.6$ cm.

function of the thermodynamic properties of the fuel vapor. The equation for flame front position is obtained by substituting Equations (17) and (18) into Equation (16), the final expression depending upon the assumptions made regarding the dependence of the oxidizer flow rate $\rho_o v_o$ on the radius of the fuel droplet.

THE DIFFUSION HYPOTHESIS

If it is assumed that the fuel droplet acts as a vapor sink for the oxidizer vapors, using a negative concentration concept similar to that employed by Burke and Schumann[6] and applying Fick's First Law of Diffusion,[13] then a derivation similar to that of Goldsmith and Penner[11] and Wise, Lorell, and Wood[21] leads to the following equation for the flame-front radius:

$$X/R = \tfrac{1}{2}(1 + \sqrt{1 + k''}) \tag{19}$$

where

$$k'' = kF/\pi\rho_o v_o R \tag{20}$$

From Equation (19), it is apparent that the assumption of diffusion flow of oxidizer vapors in toward the fuel droplet leads to a constant flame/drop radius ratio, independent of droplet radius, which is contrary to the experimental evidence cited above.

CONSTANT OXIDIZER FLOW-RATE

If the mass flow-rate of the oxidizing vapors is assumed to be determined solely by the flame temperature and pressures, hence to remain constant with respect to the size of the fuel droplet, then substitution of a constant value for $\rho_o v_o$ into Equation (16) results in the following equation for the flame radius:

$$X/R = \tfrac{1}{2}(1 + \sqrt{1 + k^*/R}) \tag{21}$$

where

$$k^* = kF/\pi\rho_o v_o \tag{22}$$

It is thus seen that Equation (21) predicts a decrease in the flame/drop radius ratio with drop diameter, as noted experimentally. Figure 8 shows a comparison of the experimental data with the theoretical curve, for $k^* = 1.6$ cm, and suggests that the theoretical concepts proposed above may indeed provide the proper mechanism for the combustion of a fuel droplet. The variation of flame/drop radius ratio, as given by Equation (21), when combined with Godsave's[10] burning rate Equation (18), provides further theoretical justification for the decreased burning rates for smaller droplets, as reported by Bolt and Boyle.[2]

Consideration of the time lag (T) between formation of the vapors and their consumption at the flame front leads to the following perturbation equation for the time-lag component (*cf.* Equation (8) of Miesse[14]):

$$g[t - T] + 2\,(X/R - 1)\,g[t] = 0 \tag{23}$$

By letting

$$g[t] = e^{ct}\,(\cos\omega t + i\,\sin\omega t) \tag{24}$$

substitution of Equation (24) into Equation (23) reveals that

$$\omega = (2N + 1)\pi \qquad N = 0, 1, 2 \tag{25}$$

and

$$e^{-cT} = 2(X/R - 1) \tag{26}$$

Since stability of the oscillating flame front is assured for negative values of c, the stability criterion becomes

$$2(X/R - 1) > 1 \tag{27}$$

or

$$X/R > \tfrac{3}{2} \tag{27}$$

Substitution of Equation (27) into Equation (21) results in the following condition for stability of the flame front.

$$k^* > 3R \tag{28}$$

Equation (28) indicates that stability is increased by an increase in the vaporization rate, F, or by a decrease in the droplet diameter. Since a decrease in droplet diameter results in an increase in flame/drop radius ratio, it appears that stability is assured if the flame is far enough from the droplet surface. This criterion might help to explain the conditions for extinction of the flame surrounding a drop in an air stream, in that a flame which is blown close to the droplet surface will be highly unstable, according to the above conditions, and will be subject to rapid extinction.

Conclusions

As a result of these theoretical analyses, the following conclusions can be drawn:

(1) The performance of a liquid propellant combustor is dependent upon two dimensionless groups which are equal to the product of the reaction frequency and the gas residence time or droplet lifetime.

(2) An increase in the value of either of the above dimensionless parameters leads to higher performance.

(3) The flame/drop radius ratio decreases with droplet diameter, with a corresponding increase in burning rate.

(4) The stability of the flame front surrounding a single fuel droplet is increased by an increase in the burning rate, or by a decrease in the size of the droplet.

Nomenclature

A specific reaction rate constant
a $rL/U = rT_g$, Damköhler's first similarity group
b $rD_0^2/\lambda = rT_d$, Damköhler's second similarity group
C concentration of unburned propellant
c exponential rate of growth of flame-front oscillation
c^* characteristic velocity
D droplet diameter
D_0 initial droplet diameter
F function of thermodynamic properties of fuel vapor
g perturbation component of flame-front radius
k stoichiometric mixture ratio
k'' $kF/\pi\rho_o v_o R$
k^* $kF/\pi\rho_o v_o$
L length of vapor portion of combustion chamber
M mass burning rate
N integer
n order of reaction
R radius of droplet
r reaction frequency
T time lag between formation of vapors and their consumption at flame-front
T_d droplet lifetime
T_g gas residence time
t time
U axial gas velocity
v vapor velocity normal to flame-front
W fraction of available gaseous propellant
w fraction of propellant converted
X steady-state radius of flame-front
x axial coordinate
y $(D/D_o)^2$, relative droplet surface area
z x/L, relative axial distance
λ evaporation or burning rate of droplet surface
ρ density
ω angular frequency of flame-front oscillation

SUBSCRIPTS

f fuel
o oxidizer
th theoretical

REFERENCES

1. Anson, D.: *Fuel*, *32*, 39 (1953).
2. Bolt, J. A., and Boyle, T. A.: Trans. Am. Soc. Mech. Engrs., *78*, 609 (1956).
3. Browning, J. A.: Presented at the Symposium on the Literature of the Combustion of Petroleum, 129th Meeting of the American Chemical Society, Dallas, Texas, 1956.
4. Browning, J. A., and Krall, W. G.: *Fifth Symposium (International) on Combustion*, p. 159. New York, Reinhold Publ. Corp., 1955.
5. Burgoyne, J. H., and Cohen, L.: Proc. Roy. Soc., *A225*, 375 (1954).
6. Burke, S. P., and Schumann, T. E. W.: Ind. Eng. Chem., *20*, 998 (1928).
7. De Juhasz, K. J., and Meyer, W. E., *Bibliography on Sprays*. New York, The Texas Company, 1949; see also *The Penn State*

Bibliography on Sprays. New York, The Texas Company, 1953.

8. Foster, H. H., and Ingebo, R. D.: NACA RM E55KO2 (1956).
9. Giffen, E., and Muraszew, A.: *The Atomization of Liquid Fuels*. New York, John Wiley and Sons, 1953.
10. Godsave, G. A. E.: *Fourth Symposium (International on Combustion*, p. 818. Baltimore, The Williams and Wilkins Co., 1953.
11. Goldsmith, M., and Penner, S. S.: Jet Propulsion, *24*, 245 (1954).
12. Ingebo, R. D.: NACA TN 3265 (1954).
13. Jost, W.: *Diffusion*, p. 2. New York, Academic Press, 1952.
14. Miesse, C. C.: *Fifth Symposium (International) on Combustion*, p. 190. New York, Reinhold Publ. Corp., 1955.
15. Miesse, C. C.: Presented at the Symposium on the Literature of the Combustion of Petroleum, 129th Meeting of the American Chemical Society, Dallas, Texas, 1956.
16. Penner, S. S.: *Combustion Researches and Reviews (AGARD)*, p. 140. London, Butterworths Scientific Publications, 1955.
17. Ranz, W. E., and Marshall, W. R., Jr.: Chem. Eng. Prog., *48*, 141, 173 (1952).
18. Ross, C. C.: Presented at AGARD Symposium on Combustion, Liege, Belgium, 1955.
19. Spalding, D. B.: *Selected Combustion Problems (AGARD)*, p. 340. London, Butterworths Scientific Publications, 1954.
20. Trent, C. H.: Ind. Eng. Chem., *48*, 749 (1956).
21. Wise, H., Lorell, J., and Wood, B. J.: *Fifth Symposium (International) on Combustion*, p. 132. New York, Reinhold Publ. Corp., 1955.

Experimental and Analytical Techniques in Combustion

97

PYROMETRY OF HIGH VELOCITY GASES

By I. WARSHAWSKY

Introduction

This report presents results of some studies by members of the Lewis laboratory staff of methods that may be suited to measuring temperatures in the exhausts of turbo-jet, ram-jet, and rocket engines. The studies have been limited to techniques that are usable routinely by test engineers, and that will serve to yield a value of "temperature" that can be inserted in conventional engineering calculations on propulsion systems. In the temperature range of present interest, this ordinarily implies a temperature representative of the translational energy of the gas molecules.

Several different techniques have been studied not only because each has properties that make it better suited to any one application, but also because a comparison of methods based on distinctly different physical principles may reveal the existence and the probable absolute magnitude of unknown systematic errors in these methods. The importance of this second reason is confirmed by the fact that such comparisons have yielded disagreements, among different types of instruments, that are considerably larger than the sensibility or reproducibility of any one of the instruments.

The ranges of extrinsic gas properties that have been covered in the experiments are 2500° to 5500°R in temperature (T), 0.1 to 1 in Mach number (M) and 0.2 to 2 atmospheres in pressure (p); however, many of the results are applicable to wider property ranges.

Most of the measurement techniques depend on the high gas velocities for their accurate operation; several also depend on the fact that appreciable amounts of energy may be abstracted from the gas without materially affecting the extrinsic gas properties. Particular attention has been given to methods that yield local ("point") measurements rather than averages over an extended path.

Extensive bibliographies have been published by Freeze,[1] Hase,[2] and Mullikin.[3] An inclusive discussion of measuring methods appears in the Journal of the Institute of Fuel.[4]

Descriptions of Pyrometers

THERMOCOUPLES

Considerations entering into the selection of thermocouple probes for jet engines have been discussed by Probert and Singham[5] and Scadron and his associates.[6] In any probe suited for routine engineering use at $M > 0.1$, $T > 2000$°R, the effects of conduction, radiation, and incomplete stagnation ("recovery") must be considered; generally, at least one of these is sufficiently large that a correction must be applied before acceptable accuracy is obtained in steady-state measurement. At $T > 2500$°R, the uncertainties in knowledge of these corrections are so large that they overshadow errors in wire calibration or in the metering instruments. For dynamic measurements, the time-constant of response is the most important performance parameter.

As gas velocity past the thermocouple junction increases, the conduction error, the radiation error, and the time constant all decrease (the latter two approximately as the square root of the mass flow rate), and the recovery error increases (approximately linearly with the Mach number of the stream passing the junction itself). These facts, together with additional considerations of ruggedness, reproducibility, ease and cost of construction, have led to a variety of designs that represent different compromises among these factors. Scadron and his associates[6] have sum-

marized the recovery errors reported by a number of probe designers and have estimated the magnitudes of the radiation errors and time constants for these designs. Stickney[7] and Glawe and his associates[8] provide more detailed data on these and other designs, giving exact dimensions of the probes tested; Stickney reports on recovery- and time-constant determinations at

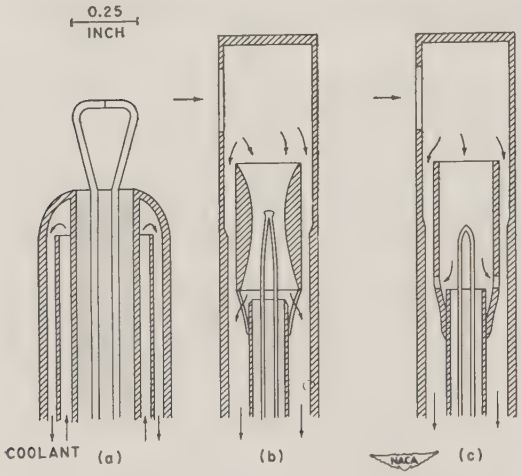

FIG. 1. Thermocouple probes. (a) Crossflow, with water-cooled shell; (b) sonic-velocity, aspirated, radiation-shielded; (c) high-stagnation, aspirated, radiation-shielded.

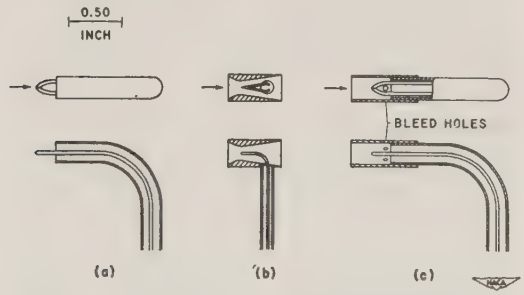

FIG. 2. Wedge-type thermocouple probes. (a) Open type; (b) high-velocity, radiation-shielded; (c) high-stagnation, radiation-shielded.

room temperature; Glawe and his associates report on radiation-error-, recovery-, and time-constant determinations at temperatures to 2500°R.

The probe designs may be grouped into the following classifications:

(1) Open ("bare-wire") designs, in which gas velocity is approximately the same as free-stream velocity. *Examples:* Crossflow-type (Fig. 1a)[6, 9] and wedge-type (Fig. 2a).

(2) High-velocity radiation-shielded designs, in which the gas velocity near the junction is increased by ram pressure or by aspiration. *Examples:* "Sonic-velocity aspirated" type (Fig. 1b)[3, 8, 10] and venturi-shielded wedge type (Fig. 2b).

(3) High-stagnation types, in which stagnation around the junction is relieved by small bleed holes only enough to reduce conduction errors and time lag. *Examples:* Double-shielded aspirated type (Fig. 1c),[8] and wedge with stagnation shield (Fig. 2c).

In the aspirated designs, the radiation error is reduced by passing high-velocity gas through the annulus between the shields.

Radiation corrections and time constants

The radiation correction may be represented as

$$\left(\begin{matrix}\text{Radiation}\\ \text{correction}\end{matrix}\right) = \frac{\left(\begin{matrix}\text{Radiative heat transfer}\\ \text{rate from junction}\end{matrix}\right)}{\left(\begin{matrix}\text{Convective heat transfer rate to junction per unit temperature difference between junction and gas}\end{matrix}\right)} \qquad (1)$$

From a determination of the Nusselt No.-Reynolds No. relation for round wires transverse to the airstream, Scadron and Warshawsky[9] established that, for the crossflow design, the radiation correction and the time constant could conveniently be represented by the approximations:

$$\text{Radiation correction} \propto \sigma \varepsilon_w \frac{1}{\sqrt{Mp}} \left(\frac{T_w}{T_0}\right)^{-0.2} (T_w^4 - T_d^4) \qquad (2)$$

$$\text{Time constant} \propto \frac{1}{\sqrt{Mp}} \left(\frac{T_w}{T_0}\right)^{-0.2} \qquad (3)$$

where the constants of proportionality are functions of wire diameter and of wire and gas properties at reference temperature T_0, (Mp) is representative of free stream static and total pressures, ε_w is junction emittance, σ is the Stefan-Boltzmann constant, T_w is junction temperature, T_d is the equivalent black-body temperature of the surroundings to which the junction radiates, and $(T_w/T_0)^{-0.2}$ represents the variation of heat transfer coefficient with temperature because of the variation of intrinsic gas properties with temperature.

It was then postulated[6] that expressions similar to Equations (2) and (3) would apply for other probe designs, if the constant of proportion-

ality were considered a function of junction- and probe-geometry. This postulate was confirmed by Glawe and his associates[8] for all but the aspirated designs.

Conduction correction

This correction, for the crossflow design, is given by

$$\text{Conduction correction} = (T_w - T_b)\ \text{sech}\ (\eta L/2) \quad (4a)$$

where T_b is wire temperature near the base of the loop and, approximately,

$$(\eta L)^2 \propto \sqrt{Mp}\ (T_w/T_0)^{0.2} \quad (4b)$$

In precise instrument-research work, this correction is determined by attaching auxiliary thermocouple wires at the base of the loop in order to measure T_b. This refinement is omitted in routine testing because proper design can always make the conduction correction smaller than the uncertainty in the radiation correction.

Comparisons among thermocouple probes

Table 1 lists a typical set of corrections for the probes shown in Figure 1, assuming that the junction temperature itself is the same for each probe. The crossflow probe (a) is characterized by rapid response, moderate but reproducible recovery correction, and a large radiation correction. The sonic-velocity aspirated probe (b) has a rapid response but a high recovery correction which, although independent of free-stream Mach number, varies from one probe to another, so that each probe must be individually calibrated. The high-stagnation aspirated type (c) has a very long time constant but a low recovery correction, invariant with Mach number, and reproducible from one probe to another.

The accuracy of measurement with the crossflow probe is determined largely by the accuracy of the radiation correction; the uncertainty in this correction arises primarily from uncertainty in wire emittance. Using a wire of known emittance, G. E. Glawe, in hitherto unreported work, has compared a crossflow probe (Fig. 1a) with a sonic-velocity aspirated probe with inner and outer shields of platinum, up to 3500°R. He obtains agreement to ±20°F limit of error when corrections are applied in accordance with Scadron and Warshawsky.[9] Further evidence of the validity of these formulas is provided by tests[11] wherein a gradual decrease, totalling 125°F, in the output emf from a Pt Rh-Pt thermocouple was produced by continued exposure to a dirt-laden, rich exhaust gas. No change in thermoelectric power as great as 0.2 per cent was found, but the independently measured increase in wire emittance due to the dirt deposition was precisely the increase required to produce the observed 125°F drop in wire temperature.

Extension of range

The above tests, and the sample values listed in Table I for the crossflow design, confirm that this design can be used to measure gas temperatures beyond the melting point (3676°R) of the wire itself by deliberately cooling the wire by radiation. Such cooling can be increased by enlarging wire diameter, D (the radiation correction $\propto \sqrt{D}$) or by increasing wire emittance ε_w. Experience to date[11] indicates that a stable value of $\varepsilon_w = 0.4$ might be obtained by deliberate dirtying of the wire. Gas temperatures to 3700°R have been measured by such techniques. It is believed that ε_w can be estimated to 20 per cent;[11] this sets an upper limit on attainable accuracy.

Table 1. Typical Corrections for Three Thermocouple Designs

Assumed conditions: $M = 0.4$, $p = 1$ atmos., Pt Rh-Pt Thermocouple

Design	Fig. 1a	Fig. 1b	Fig. 1c
Wire temperature	3350°R	3350°R	3350°R
+ Radiation correction	290	0	10
+ Conduction correction	20	0	0
+ Recovery correction	45	100	20
= Gas Temperature	3705	3450	3380
Time Constant =	0.4	0.2	>1 sec

Still higher temperatures appear attainable in routine engineering work by recourse to noble thermocouple materials of higher melting points. Droms and Dahl[12] report progress in the development of a 40 per cent Ir 60 per cent Pt-Ir thermocouple (melting point $\approx$ 4020°R). The exact degree of reproducibility and stability of thermoelectric power have yet to be established. The emittance is reported to be probably no greater

than that of platinum. A wedge-type thermocouple has been used at $M = 0.5$, $p = 1$ atmos., $T_g = 3950°R$. An upper limit of 4300°R in measurement of gas temperature with this thermocouple appears a reasonable speculation.

COOLED TUBE

An alternate approach to extending measurements beyond the usual range of the thermocouple is represented by the design shown in Figure 3. A tube of dimensions similar to that of the crossflow thermocouple is cooled by liquid flowing through it. The temperature rise $T_2 - T_1$ and mass flow rate w of this coolant are measured. If c is the specific heat capacity of the coolant,

$$wc(T_2 - T_1) = h(T - T_w)(\pi DL) \qquad (5)$$

where h is the convective heat transfer coefficient

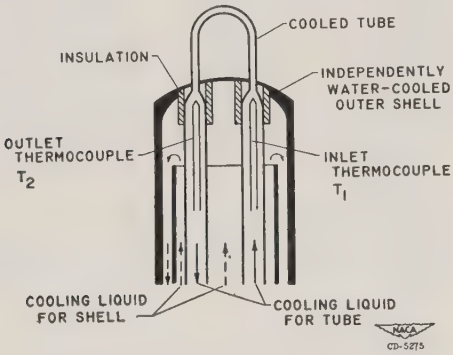

FIG. 3. Cooled-tube pyrometer probe.

from gas to outside of the tube (h = power per unit surface area per unit temperature difference), T_w is the average tube temperature, and (πDL) is the effective surface area. Since previous experience[8, 9, 11] with the crossflow thermocouple lends validity to the assumption that, approximately,

$$h \propto \sqrt{Mp}\ (T_e/T_0)^{0.2} \qquad (6)$$

where T_e is an effective gas temperature, it follows that, if coolant flow rate and inlet temperature were held constant, one might write

$$(T - T_w)(T_e/T_0)^{0.2} = \text{constant} \times [(T_2 - T_1)/\sqrt{Mp}] \qquad (7)$$

Thus, if the constant in Equation (7) were determined at some lower temperature where the thermocouple is an acceptable standard, extrapolation to higher temperatures would be possible by measuring $(T_2 - T_1)$ and (Mp). This latter quantity is obtained from static- and total-pressure measurements and rarely involves serious experimental difficulties.

Advantages of the cooled-tube method are the negligible effects of emittance, independence of the heat-transfer mechanism between tube and coolant, and an upper operating limit set only by cooling ability.

Disadvantages of the method are the complexity of construction, the need to control several secondary variables such as the temperature of the outer shell, and the increased dependence on Equation (6). Although this relation has proved adequate for computing thermocouple radiation corrections on the order of 10 per cent of the gas temperature, it is now being relied upon to yield the whole of the gas temperature.

Other assumptions implicit in Equation (7) are that the average tube temperature T_w is substantially equal to the average coolant temperature, that T_e can be defined in terms of measured quantities, and that gas composition at high temperatures will always be known sufficiently to permit insertion of reasonably correct values of gas constants.

C. D. Lanzo, at this laboratory, has designed the cooled-tube and is now engaged in comparing it with other thermometers.

PNEUMATIC PROBE

Another method providing local temperature measurement beyond the range of the thermocouple is the pneumatic-probe technique used by Schmick,[13] Cassan,[14] and, more recently, by Moore.[15] The basic principle is that the mass flow rate, w, of a gas through a restriction of area, A, is a function of the total temperature, T, total pressure, P, and static pressure, p, of the gas. Thus, by measuring w, P, and p, the total temperature, T, may be computed. Furthermore, if sonic flow velocity is established at the restriction, by ram pressure or by aspiration, measurement of p is unnecessary and gas temperature is obtainable from

$$w = CAP\sqrt{m_w/(R_0T)} \cdot f(\gamma) \qquad (8)$$

$$f(\gamma) = [(\gamma + 1)/2]^{-(\gamma+1)/(2\gamma-2)} \cdot \sqrt{\gamma} \qquad (9)$$

where R_0 is the universal gas constant, m_w the molecular weight, γ the specific heat capacity ratio, and C the discharge coefficient of the restriction.

The gas aspirated through the restriction may be cooled immediately and w then measured by

any convenient instrument: positive-displacement meter, rotameter, orifice, hot-wire- or vane-anemometer. Most workers find it convenient to use a second sonic-velocity nozzle ("critical flow nozzle") or orifice, which requires measurement of total temperature and total pressure at this restriction. The probe thereby acquires the appearance shown in Figure 4; relations such as Equation (8) exist at each restriction, so that with the measuring-station location (Fig. 4) used as a subscript

$$T_1 = T_3 \left(\frac{P_1}{P_3}\right)^2 \cdot \left\{\left[\frac{C_2 A_2 \cdot f(\gamma_1)}{C_4 A_4 \cdot f(\gamma_3)}\right]^2 \frac{m_{w1}}{m_{w3}}\right\} \quad (10)$$

$$= T_3 (P_1/P_3)^2 \times \{F_P\} \quad (11)$$

The quantity F_P is a "calibration constant" only under idealized conditions. To attain accurate measurements, it is necessary to examine possible variations in this "constant" and to find how they may be minimized by appropriate design. Factors that may produce deviations from the ideal situation may be itemized:

(1) *Non-conservation of mass.* Maximum accuracy in measurement of T_3 is obtained when T_3 is near to room temperature. However, cooling of any portion of section 2–3, Figure 4, must not be so great as to produce condensation of exhaust gas products; such condensation was encountered in some early applications of the pneumatic probe.

(2) *Non-constant geometry.* For circular restrictions, F_P varies with the fourth power of the restriction diameter. Erosion by dirt particles, or accretion of dirt will modify the effective diameter; they will also modify the discharge coefficient, C. Thermal expansion due to heating by the gas will produce an increase of about 3 per cent in F_P per 1000°R increase in temperature of the restriction.

Various compromises are possible. Blackshear[16] chooses an orifice on the basis of simplicity of construction, lesser over-all heat transfer, and lesser variation of C with Reynolds number. Baker[17] and Simmons and Glawe[18] choose nozzles, based on the experimental finding that the short straight section of the nozzle tended to remain clean even in a moderately dirty stream, while deposition of dirt on the upstream face produced a much smaller change in C than it did in the case of an orifice plate.

(3) *Non-isentropic flow processes.* Several factors, particularly influential at the upstream nozzle, contribute to deviations from the isentropic conditions postulated in deriving Equation (10).

(a) *Friction,* leading to boundary-layer formation, leads to a value of C different from unity and dependent on the Reynolds number of the flow; hence (C_2/C_4) will not remain constant as T_1 changes.

(b) *Aspiration-rate* also affects C. In supercritical flow, the value of C changes continuously with downstream pressure in the case of a sharp-edged orifice,[19] becomes constant for a thick-plate orifice at pressure ratios P/p exceeding 3,[16, 19] and changes very little for $(P/p) > 2$ in the case of nozzles.[19]

(c) *Heat transfer* between the gas and the restriction also affects the value of C. For the nozzle, Simmons and Glawe[18] and Simmons[20] have made a rough analytical estimate of magnitude of this effect. It is of the same order of magnitude, but of opposite sign, as the effect of friction. These effects may each be on the order of 2 to 5 per cent of the gas temperature.

(d) *Dissociation* of the hot gas and reassociation on cooling may alter the ratio (m_{w1}/m_{w3})

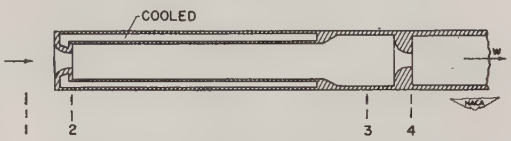

FIG. 4. Pneumatic probe.

in Equation (10). Dissociation of hydrocarbon-air combustion products starts at about 3300°R and can involve a molecular-weight change of about 4.5 per cent at 4000°R.[21]

(e) *Specific-heat-capacity variation* with temperature causes the value of γ_1 to differ from γ_3 by an amount dependent on T_1 and on gas composition. In a representative case of gasoline-air combustion, the value of γ is 1.24 at 4000°R and 1.36 at room temperature; this change represents a 6 per cent change in the value of F_P. Such an effect, like dissociation, introduces a non-linearity with respect to temperature into Equation (10).

(f) *Thermal-relaxation* complicates the choice of the appropriate value of γ_1 because the vibrational mode of internal energy of the gas does not always remain in equilibrium with the translational and rotational modes while the gas is decelerated in front of the probe and then accelerated through the nozzle. This temporary deviation from the equilibrium partition of energy manifests itself in two ways in Equation (10); (1) The total pressure P_1 measured by

stopping the aspiration through the probe, or else with a separate total-head tube, is slightly lower than the true stagnation pressure (the difference is termed the "total-head defect" by Kantrowitz.[22] (2) The specific heat capacity ratio γ no longer has the value associated with equilibrium conditions but a value somewhat closer to the room-temperature value.

It is expedient to combine effects (e) and (f) by inserting into Equation (10) an "effective" value of γ and inserting for P_1 the actually measured total pressure. Using this technique, Blackshear[16] concludes that, for his design and application, γ_{eff} is the room-temperature value. Simmons and Glawe[18] empirically determine that, for their design and application, γ_{eff} varies from

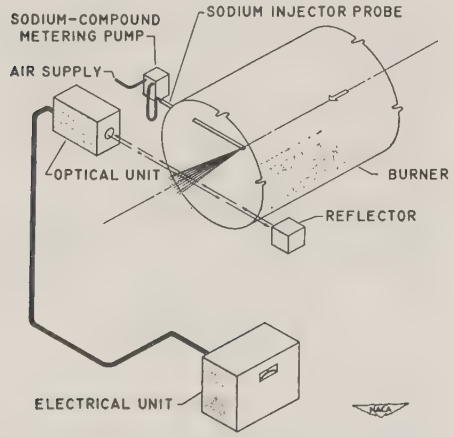

FIG. 5. Self-balancing line-reversal pyrometer.

the room-temperature value at $M = 0$ to the high-temperature equilibrium value at $M = 1$.

The value of γ_{eff} depends on the ratios of the thermal relaxation time constant τ to the time taken for gas deceleration in front of the probe and the time taken for gas acceleration through the nozzle. In typical instances, these values may be 10 to 100 μsec for deceleration and 0.5 to 2 μsec for acceleration. These times are comparable to the relaxation times of some of the gaseous products of combustion,[23] so that the vibrational mode of the gas may neither be considered as fully "relaxed" (in equilibrium with other internal energy modes) or as fully "unrelaxed" (unchanged during the flow process). The concept of "partial relaxation" must be introduced.[18, 23]

Kuhns[24] summarizes numerous results reported in the literature on the value of τ and treats in detail the combined effects of thermal relaxation and of specific-heat-capacity changes on pneumatic-probe indications. The technique of estimating γ_{eff} is also outlined briefly by Blackshear.[16] The corrections that must be applied for thermal relaxation are of the same order as the corrections for specific heat capacity changes.

Although the various sources of deviation from the idealization of Equation (11) may individually introduce corrections up to 5 or 10 per cent, the signs and magnitudes of these corrections are such that considerable cancellation results, and the remaining random error is acceptably small. In any practical application this error will overshadow any errors due to the instruments that measure P_1, P_3, and T_3.

LINE-REVERSAL PYROMETER

Inclusive reviews[4, 25, 26, 27] of optical methods of temperature measurement have been published. In particular, the resonance-line-reversal method[28] has been shown by various observers to be capable of yielding reliable results. A self-balancing instrument of this type[29] has been constructed for providing local-temperature measurements of the relatively nonluminous exhaust gases of jet engines.

For this purpose, Buchele[29] employs the following features (Fig. 5): (1) By adopting a double-path design, the reference source (a tungsten strip lamp), spectroscope, photoelectric reversal detector, and most of the intervening optical elements are housed in a single permanently aligned assembly within a fully enclosed protective box. (2) The beam through the gas is essentially parallel, the reflector is of the corner-cube type, and the spectroscope requires only a narrow central core of the reflected beam; hence appreciable angular and translational motion of the reflector, such as that due to vibration, can be tolerated. For the same reason, it has been possible to mount all elements of the internal assembly on a flexible vibration absorber. (3) Localized injection of sodium-containing powder, from a probe nozzle upstream of the point of measurement, permits local-temperature measurement over a cross-section 0.2 by 0.7 in.; in view of the parallelism of the projected beam, this means that a temperature survey across the stream requires only motion of the powder-injecting probe, the optical system remaining fixed.

Flux from the D-line and flux from the continuum 12Å on each side of the line are alter-

nately (120 times per sec) directed at a photomultiplier tube. The current resulting when reversal does not exist is used to operate a servomechanism that readjusts the lamp current to restore the state of reversal. This lamp current, read remotely, provides a measure of temperature. Thus, the apparatus does not require the presence of an operator in the often-hazardous location of the exhaust gas stream.

The sensibility of temperature measurement is determined by photocell sensitivity, photocell noise, radiant flux available at the photocell, and spectral band-width of the D-lines. Optimum values of the latter two quantities are obtained by specifying the sodium injection rate, for any given gas pressure and path length, so as to yield an absorptivity of 0.5 at wavelengths 0.5 A from each side of the center wavelength of the 5896 Å line. Fourfold reductions or increases in this value of injection rate can be tolerated without appreciable loss of sensibility.

Although the idealized line-reversal equation merely requires equality of the monochromatic areal intensities[30] $N_{\lambda,g}$ and $N_{\lambda,\ell}$ of black bodies at gas and lamp temperature, respectively, the actual equation is of the form

$$N_{\lambda,g} = (\tau_1 \varepsilon_\ell N_{\lambda,\ell})\tau_3 + \Delta N \qquad (12)$$

The first term on the right-hand side applies to any line-reversal instrument; the second term is primarily due to the automatic features of the instrument described above. The quantity in parentheses is established by calibration with an optical pyrometer, and includes effects of lamp emissivity ε_ℓ and transmission factor τ_1 of the optical elements between lamp and gas. The transmission factor τ_3 includes effects of ε_ℓ, τ_1, gas absorptivity, window- and reflector-transmission factors (which, like τ_1, may be affected by dirt on the windows), emission from solid particles, and self-absorption by sodium-containing cooler boundaries of the colored stream. Although corrections for window dirt, solid-particle emission, and self-absorption can be made (through auxiliary measurements of radiant intensities) during laboratory testing, such corrections cannot conveniently be made in routine engineering usage. Uncertainties in gas absorptivity, if controlled through control of injection rate as described in the preceding paragraph, do not lead to errors greater than 0.4 per cent in gas temperature.

The term ΔN represents effects of the variation with wavelength of photocell sensitivity, prism dispersion, lamp emissivity, and Planck's distribution function for black-body radiation. The error is partially corrected by circuitry within the electrical unit shown in Figure 5; the remaining error varies from 0.6 per cent of the temperature at the low end of the scale to 0.1 per cent at the high end.

Other performance features of the self-balancing instrument are:

Upper limit of range: 4500°R for 100-hr lamp life; 4800°R for 10-hr lamp life. (The line-reversal principle itself is, of course, usable at higher temperatures if other types of adequately stable radiators are available.)

Lower limit of range: 2900°R.

Lamp stability: Equivalent black-body-temperature change at constant current is generally less than 2 per cent during first 75 per cent of the lamp's life.

Sensibility: 10°R

Path length: Up to 5 ft

Path cross-section: 0.2 by 0.7 in.

Misalignment tolerances: ±0.5 inch transverse displacement of reflector relative to impinging beam; ±10-degree rotation of reflector.

Speed of response: ¼-sec lag when $(dT/dt) = 500$°R/sec

Atomic concentration required: ~1 in 10^4. Over the gas density and velocity ranges usually encountered, this requires $NaHCO_3$-powder injection rates from 0.01 to 6 g/min. These are provided by a motor-driven variable-speed mechanical powder feeder (Fig. 5).

Average deviation in comparison with manually operated instrument used under laboratory conditions: 20°R.

MICROWAVE-ATTENUATION PYROMETER

Rudlin[31] demonstrated the feasibility of measuring gas temperature by determining the attenuation of a microwave beam passing through the gas. The attenuation is produced by free electrons; an adequate supply is conveniently obtained by injection of an alkali halide (the halide element is immaterial). The required amount of injected alkali is only about $\frac{1}{100}$ of that required for the line-reversal pyrometer.

A typical arrangement of apparatus is shown in Figure 6. The attenuation equations have been developed by Belcher and Sugden[32] and, with particular reference to temperature measurement, by Kuhns.[33] If P' and P'' are the microwave

power (flux) before and after passage through a gas of depth L and temperature T,

$$\log (P'/P'') = F_M L \nu (\nu^2 + \omega^2)^{-1} \sqrt{N}\, T^{3/4} \exp(-q/2kT) \quad (13)$$

where ω is the microwave frequency, ν is the electron-molecule collision frequency, N is the volume-concentration of atoms producing free electrons, q is their ionization potential, and k is Boltzmann's constant.

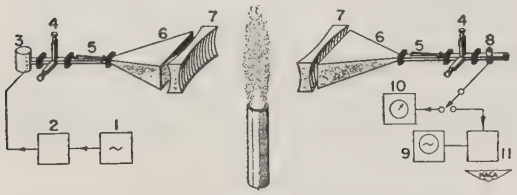

FIG. 6. Microwave-attenuation pyrometer. 1. Modulation oscillator, 2. klystron power supply, 3. klystron, 4. tuner, 5. attenuator, 6. horn, 7. lens, 8. crystal, 9. oscilloscope, 10. averaging vacuum-tube volt-meter, 11. amplifier and filter.

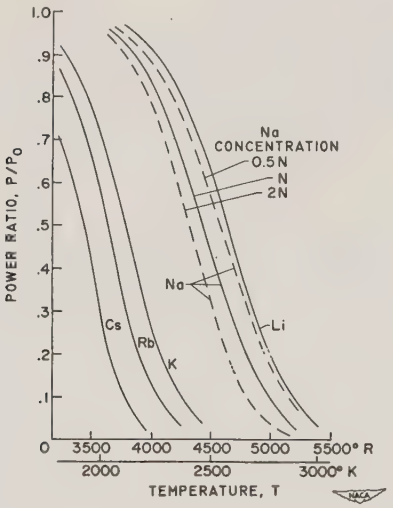

FIG. 7. Microwave attenuation for various alkalis and concentrations. $N = 10^{13}$ atoms cm^{-3}, path length = 8 cm.

The quantity F_M is a constant only under idealized conditions. In practice, it includes corrections for the spatial distributions of beam intensity and of electron concentration in the gas. The path length, L, must be measured independently; various methods have been employed[32, 33]—electric-conductivity probe, total-head probe, length of melted area on a salt-coated tube—and all give moderately consistent results (about ±10 per cent average deviation from the mean of all three methods).[33] The collision frequency ν is variously reported by Belcher and Sugden[32] and Kuhns[33]; it may be assumed to be 1×10^{11} sec^{-1} at 4000°R and 1 atmos, and to be proportional to $p/\sqrt{T}$, where p is pressure.

Over a limited temperature span of about 1000°R, the attenuation (P''/P') varies almost linearly with temperature (Fig. 7), and the temperature indication is relatively insensitive to variations in F_M, L, ν, or N (see dotted curves of Fig. 7), so that large uncertainties can be tolerated in these quantities. The relative sensitivities are treated in detail in Kuhns.[33] However, the indication is directly proportional to the ionization potential, q; for sodium, this presently appears known to ½ per cent.

Comparison of a microwave instrument with a D-line reversal measurement in the range 3400° to 4500°R yielded an average deviation of 100°R in absolute temperature.

In the usable linear region, the slope of the (P''/P') *vs* T curve is quite high, not strongly dependent on the alkali element used or on its concentration (Fig. 7), and dependent almost solely on q and the average value of T. Thus, the instrument has high sensitivity to temperature fluctuations that lie within the linear region; these can be measured to probable errors of 10°R in fluctuation amplitude. The upper limit of frequency response is set by the requirement that the period t_1 of the fluctuation shall be long compared to the time of transit t_2 of the gas through the microwave beam. If $t_1 > 3t_2$, the error in fluctuation amplitude is less than 10 per cent.[33]

The instrument has been used to record 3000-cps screaming of a liquid oxygen-heptane burner at $T_{Av} = 4500$°R and has yielded results comparable with those of a two-color pyrometer.[34] The characteristics of a typical instrument are:

Range: 3600° to 5400°R

Operating frequency: 24,000 Mcps (1.25 cm wavelength)

Separation between lenses: 1 to 3 ft

Beam cross section: 1.5 in. square

Frequency response at $M = 1$, $T = 4500$°R: to 10,000 cps.

Concentration of alkali atoms required: ~1 in 10^6

In common with the line-reversal pyrometer, the microwave-attenuation pyrometer has the advantage (derived from the fact that T appears in the exponent of e in Equation (13) and in the Planck distribution law) that the radiant intensities are more sensitive to temperature than to

most of the other parameters. Other advantages of the microwave method are that the apparatus in the hazardous area is relatively rugged and inexpensive (involving only waveguides, horns, and lenses), that high sensitivity and high frequency response are possible in studying fluctuations, and that the upper limit of the range is well above that of a line-reversal pyrometer using a tungsten reference lamp.

Disadvantages are the limited temperature span over which the attenuation ratio is linear with temperature, the limited accuracy in absolute temperature measurement, the limitation to gas streams of dimensions much larger than the microwave beam wavelength, and the need to know the ionization potentials of all copious sources of free electrons.

X-RAY AND α-PARTICLE ABSORPTION

E. M. Winkler has effectively summarized[35] the use of these techniques for air-density measurement. Their application to temperature measurement is based on the inverse proportionality between density and temperature, as contained in the perfect-gas law. Because of this inverse relation, the attenuation of a beam of x-rays passing through a hot-gas stream is affected more strongly by the cooler gases bounding the jet than by the hot gases of the jet itself. The governing relation is

$$(I''/I') = \exp\left[-\int (F_X/T)\, dx\right] \qquad (14)$$

where I' and I'' are incident and emerging beam intensities, x is distance along the beam, F_X is a function of gas composition and of the spectrum of x-radiation, and the integration is performed over the path from the x-ray target to the radiation detector. Weltmann and Kuhns[36] show that reasonably accurate temperature measurement is possible only if the gas-density distribution outside the hot-gas stream is accurately estimated or established by an auxiliary survey.

In additional unpublished work, Weltmann concluded that similar problems arise when α-particles are used. In this case, the experimental technique would use the range of the α-particles as a measure of gas density, rather than the intensity of radiation after traversing a fixed path length.

Thus, as the flowing-gas temperature to be measured increases, methods using nuclear- and x-radiation appear to involve increasingly great experimental inaccuracies.

Comparison of Point-Temperature Indicators

The accuracy of absolute measurement of any inferential instrument can be determined only by comparison with an accepted reference "standard." The "standard" must itself include the specification of the experimental means by which the comparison is made. Such standards exist for thermometers designed to measure the temperature of solid objects. They do not exist, at present, for thermometers designed to measure the temperature of hot, flowing gases, especially when the instruments draw appreciable energy from the flowing gas.

The alternative expedient is to compare different thermometers in the same gas stream. If three or more thermometers, each operating on distinctly different principles, should yield the same temperature indication, the probability that that indication is wrong would be very small. Such probability would exist only to the extent (a) that the various thermometers shared some common experimental measurements or physical assumptions of uncertain validity and (b) that these common doubtful measurements or assumptions entered with equal importance into the results yielded by each of the thermometers. More realistically, if the several thermometers yielded almost the same indication, the weighted mean of these indications would constitute the most probable value of gas temperature, and the deviations from the mean would provide an estimate of the probable error of temperature indication.

This philosophy has been carried out by comparing three local-temperature thermometers—a crossflow thermocouple[9] (Fig. 1a), a pneumatic probe,[18] and a line-reversal pyrometer[29]—in the exhaust from a 4-in. diameter nozzle of the test apparatus shown in Figure 8a.

In this apparatus, air, oxygen, and gasoline are injected at the inlet, and a long mixing chamber is used to assure completeness of combustion. Separate control of fuel-, air-, oxygen-, and dilution-air-flow rates and of inlet-, exhaust-, and bleed-off-pressures provide independent control of pressure, Mach number, and temperature at the test section. The baffle and the liner are used to flatten the temperature profile; a typical profile is shown in Figure 8b. Four observation ports, 90-degrees apart, allow cyclic observations with the three instruments, the thermocouple and pneumatic probe being moved alternately on to

the center line of the jet, while the other instrument is retracted.

The possible range of test conditions obtainable is $0.1 < M < 1$, $0.15 < p < 2$ atmos, $1500 < T < 4000$°R (but not in all combinations); however, the comparison was made only at $p \approx 1$ atmos., $M \approx 0.5$, and thus suffers somewhat in completeness.

Results of the comparison are shown in Figure 9. The common basis of comparison is the computed "stagnation temperature," defined as the temperature that would be obtained if the free

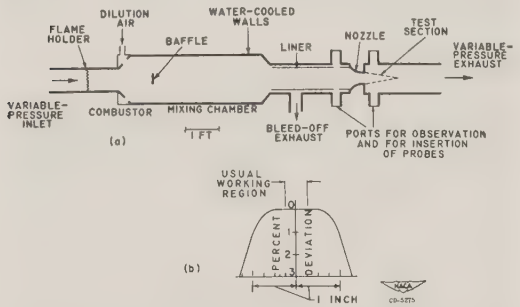

FIG. 8. High-temperature test facility. (a) Arrangement of equipment; (b) test-section temperature profile at 2800°R, $M = 0.5$, $p = 1$ atmos.

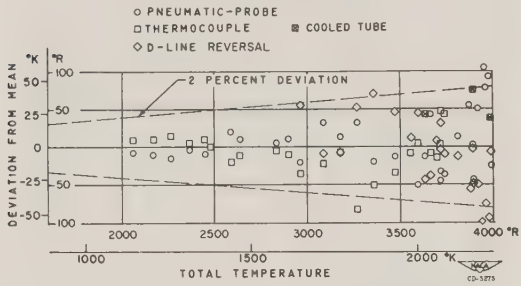

FIG. 9. Comparison of pyrometers used for local-temperature measurement.

stream at the test section were brought to rest isentropically. Equal weight was assigned to each instrument. The comparison among the three instruments was possible only in the range $2900 < T < 3750$°R. However, Figure 9 includes also (a) three comparisons, in the range $3600 < T < 4000$°R, in which the cooled tube was treated as an alternate to the thermocouple, (b) six comparisons, in the range $3800 < T < 4000$°R, between line reversal and pneumatic probe, and (c) 8 comparisons, in the range $2000 < T < 2900$°R, between pneumatic probe and thermocouple. The average deviation from the mean is about 1 per cent at 3600°R.

This agreement was achieved only under circumstances more favorable than can be expected in most routine engineering tests. Thus, each instrument's reading was carefully corrected for progressive systematic changes of instrument parameters from the beginning to the end of the tests (e.g., changes in thermocouple emittance, pneumatic-probe-nozzle area, and line-reversal pyrometer window dirtying). Under ordinary engineering test conditions, errors considerably greater may reasonably be expected.

Comparison of Average-Temperature Indicators

The indication of the microwave-attenuation thermometer represents the average temperature defined by

$$\int_0^L N^{1/2} T^{3/4} \exp[-q/(2kT)]\, dx = LN_{\mathrm{Av}}^{1/2}\, T_{\mathrm{Av}}^{3/4}\, \exp[-q/(2kT_{\mathrm{Av}})] \tag{15}$$

The indication of the X-ray attenuation thermometer, in accordance with Equation (14), represents the harmonic mean temperature,

$$\left[L^{-1} \int_0^L T^{-1}\, dx \right]^{-1} \tag{16}$$

if F_X is assumed independent of x.

An example of the averages yielded by these instruments is shown in Figure 10a. It is assumed that the line of sight is along a diameter of an axially-symmetric profile shown by the solid curve, that both N and F_X are constant at all points of the traversing beam, and that the beam cross section is small compared to the radius, R. The linear average is $R^{-1}\int_0^R T dr$. It is assumed further that the temperature drops linearly to room temperature in a distance $0.1\,R$ on each side outside of the circle $-R \leq r \leq R$. The average temperature yielded by the x-ray method is shown both for the case where this fact is included and for the artificial case where absorption outside the circle is neglected. The effect of the cooler boundaries is thus clearly evident.

In Figure 10b are shown the averages that would be yielded by a line-reversal instrument sighting through a gas stream having the profile of Figure 10a, if only a central core, of radius ρ, were uniformly colored with sodium. The indication depends both on the diameter of this core and on the optical depth $2k_{\lambda,0}\rho$, which is proportional to sodium-atom concentration ($k_{\lambda,0}$ is the monochromatic absorption coefficient at center wave length of the D-line). In the self-balancing

instrument described above, the optical depth is always greater than 30 and is >200 at pressures below 1.5 atmos.

If c_2 is Planck's constant, k_λ is the monochromatic absorption coefficient and is assumed independent of x, and optics transmissivities are neglected, the averaging law followed is, to an adequate approximation,

$$\iint_0^L k_\lambda \exp\left[-(c_2/\lambda T) - \int_x^L k_\lambda \, dx\right] dx \, d\lambda = [\exp(-c_2/\lambda T_{Av})] \int [1 - \exp(-k_\lambda L)] \, d\lambda \quad (17)$$

where the integration with respect to wavelength λ is performed over the interval accepted by the spectroscope slit (in a low-resolution instrument, this may be taken as $0 < \lambda < \infty$ without serious error).

Strong and Bundy[37] describe a convenient technique of performing the averaging and give numerical results for a two-zone path.

Figure 10 shows that both the microwave and the line-reversal instrument read higher than the linear average, when the entire gas stream is uniformly colored.

Dynamic Measurements

High frequency temperature fluctuations are measurable with the thermocouple if static- and total-pressures, p and P, of the gas stream are known and remain reasonably constant. Then, the thermocouple time constant, τ can be predicted[6, 9] and electrical methods of lag compensation applied.[38, 39] The low-lag thermocouple is of modified crossflow design.[6] A butt-welded pair of 3-mil wires has a time constant of 0.02 sec at $M = 0.4$, $p = 1$ atmos; a 300-fold reduction of this time constant is possible by electrical compensation,[38] resulting in an upper cut-off frequency of 2400 cps. This performance can not be attained if the temperature fluctuations are accompanied by large velocity or pressure fluctuations; thus, the indicated fluctuation amplitude will be 30 per cent in error, at the upper end of the frequency range, if the value of (Mp) should change by a factor of 2.

The approximate proportionalities

$$\tau \propto D^{3/2}(Mp)^{-1/2} \propto D^{3/2}[(P - p)^2 p^3/P]^{-1/8} \quad (18)$$

are useful in estimating time constants of the low-lag crossflow design.

The pneumatic probe is adaptable to dynamic measurements if pressure P_1 and flow rate w (Eq. (8)) can be measured. If w is measured with a second critical-flow nozzle, pressure P_3 and temperature T_3 (Fig. 4) must be measured, the latter with a lag-compensated thermocouple. The lag in T_3 may be reduced by measuring T_4 instead of T_3 and P_4 in addition to P_3. The method is awkward if simultaneous fluctuations in P_1 are large. In addition to previously indicated problems associated with thermocouple measurements, the method is also subject to serious distortions of the wave form of high-amplitude fluctuations because of the long distance required for transmission of pulsations along the length of the cooled section of the probe.

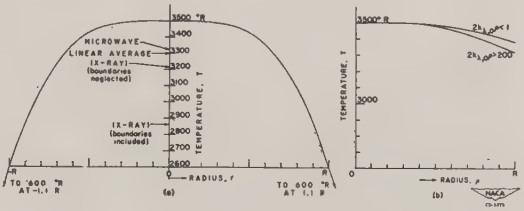

FIG. 10. Averages yielded by various radiation-type instruments. (a) Assumed temperature distribution, and resultant averages; (b) readings yielded by line-reversal pyrometer, as functions of optical density and radius of central sodium-containing core.

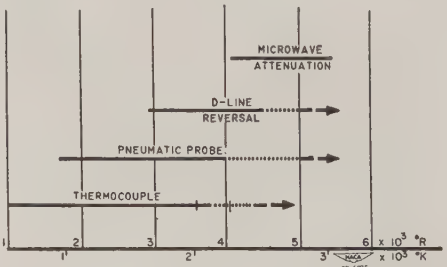

FIG. 11. Ranges of various gas pyrometers described in this report.

The line-reversal method in its present self-balancing form is not suited to dynamic measurements, although other optical methods[34, 40] are. The microwave method is well adapted to convenient dynamic measurements, if space-averaged rather than local measurements are acceptable. Nuclear- and x-radiation absorption techniques require long counting periods to achieve adequate statistical accuracy and hence are not suited to high frequency measurements.

Concluding Remarks

Figure 11 shows the ranges that appear attainable with the thermometers described herein. Solid lines represent ranges in which measurements have actually been made at this laboratory;

where these ranges overlap, comparisons have been made. Dotted lines show extensions of range that appear attainable with reasonable certainty. Arrows indicate possible further extensions whose upper limit is not yet known.

Although the sensibilities of the various thermometers are on the order of 10°R, the probable error in absolute temperature measurement is about one per cent for the local-temperature devices and about three per cent for the microwave-attenuation method. Even such accuracy is attainable only if all systematic corrections are carefully itemized, evaluated, and applied.

REFERENCES

1. Freeze, P. D.: National Bureau of Standards Circular 513 (1951).
2. Hase, R.: Z. Ver. deut. Ing., *81*, 571 (1937).
3. Mullikin, H. F.: In *Temperature—Its Measurement and Control in Science and Industry*, p. 775. New York, Reinhold Publ. Corp., 1941.
4. Symposium on Gas Temperature Measurement. J. Inst. Fuel (London) *12*, No. 64 (1939).
5. Probert, R., and Singham, J. R.: J. Sci. Instr., *23*, 72 (1946).
6. Scadron, M. D., Warshawsky, I., and Gettelman, C. C.: ISA Proc., *7*, 142 (1952).
7. Stickney, T. M.: NACA Technical Note 3455 (1955).
8. Glawe, G. E., Simmons, F. S., and Stickney, T. M.: NACA Technical Note 3766 (1956).
9. Scadron, M. D., and Warshawsky, I.: NACA Technical Note 2599 (1952).
10. Assman, R.: Abhandlg. Kgl. Pr. meteorologischen Institute, *1*, 117 (1892).
11. Glawe, G. E., and Shepard, C. E.: NACA Technical Note 3253 (1954).
12. Droms, C. R., and Dahl, A. I.: Gas Turbines. A.S.M.E. and Inst. Mech. Eng. (London) Joint Conference on Combustion, Section 5, June 17, 1955, pp. 6–9.
13. Schmick, H.: Z. tech. Physik, *10*, 146 (1929).
14. Cassan, M. H.: J. Usines à Gaz., *53*, 527 (1929).
15. Moore, D. W., Jr.: Aero. Eng. Rev., *7*, 30 (1948).
16. Blackshear, P. L.: NACA Technical Note 2167 (1950).
17. Baker, D. I.: Jet Propulsion, *25*, 217 (1955).
18. Simmons, F. S., and Glawe, G. E.: NACA Technical Note 3893 (1957).
19. Grace, H. P., and Lapple, C. E.: Trans. A.S.M.E., *73*, 639 (1951).
20. Simmons, F. S.: NACA Technical Note 3447 (1955).
21. Fehling, H. R., and Leser, T.: *Third Symposium on Combustion, Flame and Explosion Phenomena*, p. 634. Baltimore, The Williams & Wilkins Co., 1949.
22. Kantrowitz, A.: NACA ARR 4A22 (1944). Also J. Chem. Phys., *14*, 150 (1946).
    Kantrowitz, A., and Huber, P. W.: NACA Wartime report L-21 (RB-L4E29-1944). Also J. Chem. Phys., *15*, 275 (1947).
23. Spooner, R. B.: NACA Technical Note 2193 (1950).
24. Kuhns, P. W.: NACA Technical Note 4026 (1957).
25. Penner, S. S.: Am. J. Phys., *17*, 422, 491 (1949).
26. Lewis, B., and von Elbe, G.: In *Temperature—Its Measurement and Control in Science and Industry*, p. 707. New York, Reinhold Publ. Corp., 1941.
27. Broida, H. P.: In *Temperature—Its Measurement and Control in Science and Industry*, Vol. 2, p. 265. New York, Reinhold Publ. Corp., 1955.
28. Féry, Ch.: Compt. Rend., *137*, 909 (1903).
29. Buchele, D. R.: NACA Technical Note 3656 (1956).
30. *American Standard Letter Symbols for Heat and Thermodynamics Including Heat Flow.* ASA Z10.4-1943. New York, Am. Soc. of Mech. Engrs.
31. Rudlin, L.: NACA Research Memorandum E51G20 (1951).
32. Belcher, H., and Sugden, T. M.: Proc. Roy. Soc. (London), *A201*, 480, *202*, 17 (1950).
33. Kuhns, P. W.: NACA Technical Note 3254 (1954).
34. Heidmann, M. F., and Priem, R. J.: NACA Technical Note 3033 (1953).
35. Winkler, E. M.: In *Physical Measurements in Gas Dynamics and Combustion*, p. 97. Princeton, Princeton University Press, 1954.
36. Weltmann, R. N., and Kuhns, P. W.: NACA Technical Note 2580 (1951).
37. Strong, H. M., and Bundy, F. P.: J. Appl. Phys., *25*, 1521, 1527 (1954).
38. Shepard, C. E., and Warshawsky, I.: NACA Technical Note 2703 (1952).
39. Shepard, C. E., and Warshawsky, I.: ISA Proceedings, *7*, 149 (1952).
40. Myers, P. S., and Uyehara, O. A.: SAE Quarterly Trans. *1*, 592 (1947).

98

PHOTOPYROMETRIC DETERMINATION OF THE TEMPERATURE OF A BURNING, MOVING PARTICLE

By V. A. POPOV

It is well known that when luminescent bodies are photographed in their own radiation, there is a definite relation between the quantity of silver reduced in the light-sensitive emulsion and the quantity of energy that strikes it, i.e., between the optical density of the image and the brightness temperature of the surface of the body being photographed. Knowing the character of this relation, it is possible to determine the brightness temperature of the body's surface from the optical density of the image. This method of temperature determination is known as photopyrometry.

The present paper considers the photopyrometric method of determining the temperature of a burning moving particle. The method was developed by the author during an investigation of problems connected with the burning processes of different fuels. It can, of course, be used to determine the temperature of nonburning moving bodies, provided the temperature is sufficiently high.

The temperature distribution, within the range of infrared radiation, at the surface of an electrically heated (up to 380°C) iron tube was first determined by the photopyrometric method in 1930 by Hencky and Neubert. Subsequently, these authors, and especially Neubert published several more papers[1, 2, 3] in which the photopyrometric method was developed and applied to various technical problems: the temperature distribution in a high pressure water trap, in a steam line with superheated steam (up to 400°C), in the pipe of a steam boiler (365°C). Hencky and Neubert were the first to point out the dependence between the temperature of a body and the density of its image on a photographic emulsion. In the thirties, the method of infrared pyrometry attracted the attention of several other investigators,[4, 5, 6] who determined the heat losses of furnaces due to imperfect heat insulation, the temperature of incandescent metal ingots, and of cylinder blocks and hot parts in internal combustion engines. This method was used to determine temperature gradients at the anodes and cathodes of powerful radio valves, at the surface of rheostats, etc. Hase[7] was the first (1932) to use photopyrometry in the visible region of the spectrum. Later, using motion pictures, the method was employed to measure the rapidly changing temperature of molten steel.[8]

In recent years,[9, 10] the photopyrometric method has been applied in the investigation of problems which cannot be solved by existing pyrometric methods. This is precisely the advantage that it has over such methods.

The photopyrometric method of determining the temperature of a moving burning body, or of a body heated to a sufficiently high temperature, differs but slightly from the photopyrometric method described in the historical sketch given above. It will become clear from what is to follow that the modification introduced complicates slightly the measurements. However, the possibility of determining the temperature of a moving body is extremely attractive and compensates for the difficulties encountered. The basic theoretical principles of the photopyrometric method are as follows.

The Dependence of Brightness on the Temperature

The relation between brightness and the temperature of a true black body is given by the well-known Planck ratio

$$r_{\lambda,T} = 2\pi hc^2\lambda^{-5}\frac{1}{\exp\,(hc/\lambda kT) - 1}$$

where h is the Planck constant, c the velocity of light, k the Boltzmann constant, λ the wave length; T is the absolute temperature, and $r_{\lambda T}$ the spectral brightness.

Since the spectral brightness is a function not only of the temperature, but also of the wave length, strict monochromatization of the light flux is necessary for a general case in the practical application of this ratio. Here a filter with a sufficiently narrow pass band is used, or a filter with a broad pass band which only partially covers the spectral sensitivity curve of the film. In this case, if the body is not absolutely black, Planck's formula determines not its true temperature, but the brightness temperature, T_{br}. The latter is always lower than the true tempera-

ture, and the difference increases as the monochromatic emissivity, e_λ of the nonblack body decreases. Knowing the value of the emissivity, it is possible to determine the true temperature from the brightness temperature

$$\frac{1}{T} - \frac{1}{T_{br}} = \frac{\lambda}{c_2} \ln e_\lambda$$

where $c_2 = 1.436$ cm. degree.

The value of e_λ depends on many factors, including the material of the body photographed and its surface finish. For this reason, the value of e_λ is hardly ever known exactly. Approximate data for various materials are given in reference works.

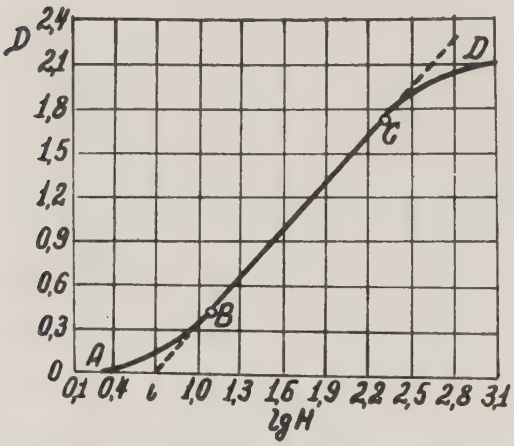

FIG. 1. Characteristic curve $D = f(\lg H)$.

Density of the Image as a Function of the Brightness

The relation of the exposure, H, of the light-sensitive layer, and therefore the brightness of the body for a constant exposure time, to the optical density of the image, D, is given by a curve which is characteristic of the photographic emulsion shown in Figure 1. The initial section of the curve (section AB) corresponds to the region of underexposure, the straight part of the curve (section BC) to the region of proportional exposure, and the upper section of the curve (section CD) to the region of overexposure.

As the exposure increases indefinitely, the curve acquires a saturated character that corresponds to the maximum density of blackening. It is difficult to give the analytical form of the characteristic curve which depends not only on the type of emulsion, but on the particular batch of emulsion, on the storage time of the material, and on the method of treatment (the composition of the developing solution, its weakness and temperature, the developing time, etc.). Consequently, photopyrometry employs the comparative method, which consists in calibrating on a reference standard of known temperature each part of the photographic material. This method makes it possible to exclude completely the influence of the large variety of uncontrollable factors mentioned above. The density-temperature calibration curve D-T is similar in character to the curve shown in Figure 1. Naturally, in order to attain greater accuracy in the measurements it is best to work in the linear region of this curve.

The Spectral Characteristic

As already mentioned, the photopyrometer measures the brightness temperatures, i.e., the "apparent" temperatures of the surface. To pass to the true temperatures, one must know the emissivity of this surface. This is extremely inconvenient if true temperatures are required, and a photograph is made of an evenly heated surface where different points have different emissivities and these emissivities are unknown. Such a photograph shows different degrees of blackness at different points. This difference may be attributed erroneously to different brightness temperatures, and consequently to different true temperatures of the surface, given one and the same emissivity. It should be remembered that different degrees of darkness on the negative may be caused not only by a change in the temperature, but also by a change in the emissivity. The value of the latter may vary not only when passing from one region of the surface to another, but also during heating of a given portion of the surface due to alterations in the surface structure. The law of such alteration in emissivity is not generally known, thus complicating the process still further. Finally, both the temperature and the emissivity may be different at different points. In this case, photopyrometry cannot give a correct answer as to the distribution of the true temperatures.

Therefore, precisely as in the case of optical pyrometry, photopyrometry can be used only for measuring the temperatures of surfaces that are homogeneous in material and in the character of the surface finish.

The Temperature Interval

The interval of temperatures that may be reproduced by a layer during a given exposure is

determined by the differences of the strongest and weakest (overexposure and underexposure) densities, which may be obtained on a given emulsion. It is usually not great because, according to the Stephan-Boltzmann law, the brightness of an incandescent body is proportional to the fourth power of the temperature. In the majority of cases, only the linear part of the "density-temperature" curve, where the accuracy is greatest, is worth using. This, in its turn, leads to an additional reduction of the temperature interval.

The lower temperature limit that may be measured by the photopyrometer is determined only by the sensitivity of the film and the value of exposure. It may be decreased by prolonging the exposure, by increasing the sensitivity of the film, and by increasing the aperture ratio of the lens, etc. The upper temperature limit depends exclusively on the possibility of precise calibration and a reduction in the quantity of light acting on the layer. This latter is achieved through shorter exposures, less sensitive photo emulsions, smaller diaphragms, and also by using devices employed in optical pyrometry—revolving sectors and absorbing filters. The temperature limits within which photopyrometry can be applied extend from 200°C using inframaterials with a very great exposure, to 6000°K when applying dense light filters to attenuate the light.

Film Calibration

Each piece of the film employed in photopyrometry must undergo a series of calibration exposures that establish the *D-T* relation. Any heated surface, the temperature of which has been measured accurately by any independent method, may be used as a reference body. The surface must be homogeneous as to temperature and emissivity. The calibration is carried out either by consecutive photography of one reference body, the temperature of which is varied in a definite manner, or by simultaneously photographing several standards at different temperatures. The temperature of the calibration body may be measured by an instrument, such as a thermocouple or a pyrometer. Lamps with a tungsten filament heated by an electric current are most commonly used. They are the equivalent of a black body for the given wave length as they are calibrated for this wave length by an absolutely black body.

A fast method for establishing a calibration curve with the aid of a reference lamp kept at a constant temperature and of absorbing filters has been described.[10] The essence of this method is that the filament of the lamp is at a temperature which gives the density corresponding to the upper part of the calibration curve. One or several absorbing filters that give a series of lesser degrees of darkness are placed in the beam of light from the lamp. These darknesses are compared with the true *D-T* curve of the film, obtained by varying the current passing through the lamp. In this way we find the temperature that corresponds to the introduction of a given filter or of a combination of filters. These filters can then be used to establish other calibration curves simply by introducing them into the beam of light from the lamp, and not by varying its current. This, of course, is true only of a given current passing through the lamp, i.e., for a given value of the temperature.

Measuring the Temperature of Moving Bodies

All that has been said of the photopyrometric method for use in measuring the temperature of stationary bodies can be applied to measuring the temperature of a moving body with a sufficiently high temperature, or of a burning body. This case presents the following complications: (1) The moving object is photographed not on a stationary film, but on a film moving at a definite speed. (2) Calibration of the reference standard is also done on a film, moving at exactly the same speed.

Naturally, the fact that the film moves reduces considerably the temperature interval that may be measured, because in this method the exposure is determined by the speed of the film as well as by the speed of the object. The low-temperature region which requires prolonged exposure does not come within the limits of this method. The lower the temperature, the less must be the speed of the object if this method is to be used. However, the temperature of an object that corresponds to the visible portion of the radiation spectrum may be measured if the speed of the object is sufficiently high.

The image of the reference calibration standard, which always remains stationary, will acquire the character of a straight line that runs parallel to the direction of the film. Thus, calibration yields a family of straight lines, each of which corresponds to a very definite temperature of the reference standard. It should be noted that varying the speed of the film may give the same

results as varying the time of the shutter or diaphragm of the lens in photopyrometry of stationary objects.

In general, the trace of a moving body on the film (a simple case is when the body is moving vertically, and the film horizontally) will have the form of a certain curve, the inclination angle of which at each point determines the speed of the object. If the various experimental parameters (film speed, size of diaphragm of lens, etc.) have been correctly selected, so that the optical density of the image of the moving object is in the linear part of the characteristic curve of the film, the value of the density of the image of the object, measured and corrected to the value $v \cdot tg\varphi \cdot (\sec \alpha - 1)$, (where v is the speed of the film, α is the angle between the trace of the object at a given point and the direction of motion of the film, and φ is the angle of the D-v curve with the axis, v) may serve as a criterion for determining

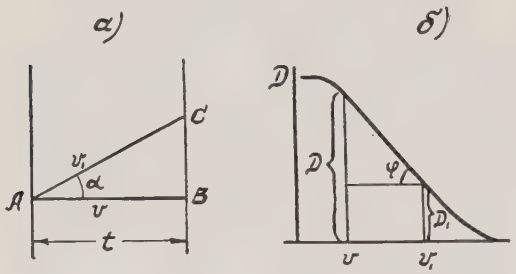

Fig. 2.

the temperature from the D-T curve in the usual way. The correction value of the density of the image (caused by the shape of the particle track) is determined from the following considerations. Figure 2a gives a diagram of the traces of the reference standard and of the particle track on a moving photographic film. The image of the reference standard was exposed for the time, t, on section AB, and the image of the particle was exposed during this same period of time on section AC. The speeds of the particle, v_1, and of the reference standard, v, with respect to the film are not equal to each other, and therefore the optical densities of their images cannot be compared. The density of the image of the particle must be recalculated and must be reduced to a value that corresponds to the speed of the particle with respect to the film, this speed being equal to the speed of the reference standard with respect to the film. It is easily seen that $v_1 = v/\cos \alpha$. However, the optical density of the image depends in a definite manner on the relative speed of the object and film; Figure 2b shows this dependence. It is obvious that the true density of the particle track, D, is equal to the sum of the measured density, D_1, and the correction connected with the difference of the relative speeds, i.e., $D + D_1 + v \cdot tg\varphi \cdot (\sec \alpha - 1)$.

The value, $tg\varphi$, is a standard characteristic of the film, and is limited in a definite manner with the contrast coefficient given in reference works on photography. Attention should be directed to one more extremely important circumstance, the neglect of which leads to completely distorted results. The dimensions of the graduated standard and the particle should be strictly equal. In the present instance, this was achieved by placing a telescopic slit in front of the temperature lamp, the width of the slit being equal to the diameter of the particles to be photographed.

If this essential condition is not observed, it is easy to see that the reference standard and the object will be photographed under different exposures, which is absolutely not acceptable. Complying with this condition reduces the possibilities of applying the method; however, if the dimensions of the object exceed the dimensions of the calculated standard, a photograph may be made not of the whole object, but only of a part of it, the characteristic dimensions of which are equal to the dimensions of the standard.

If the dimensions of the object vary during a change in its temperature, corrections must be introduced. In the case of insignificant variations in the dimensions of the object, which was the case in our experiments, the corrections lie within the limits of the accuracy of the method.

Evaluation of the Method

The method described for measuring temperatures has the basic advantage of any optical method: it does not introduce distortions into the process being investigated. This fact is especially important when working with bodies heated to a level below the temperature of visible luminescence (the infrared region of 200° to 450°), where other optical methods cannot be applied, and nonoptical methods which require that the measuring instrument be placed at the surface under investigation cannot be used because of a heat loss that disturbs perceptibly the actual temperature field.

At temperatures above 800°C, use should be made of simpler and faster methods if they can be applied and if they give satisfactory accuracy. However, here too, photopyrometry is of value

in the solution of problems whose conditions are outside the technical possibilities of other methods.

Such problems include: (1) Measuring temperature simultaneously at several points, i.e., an investigation of the temperature field of the surface at a given instant. Obviously, here the use of other methods is either difficult, inaccurate, or impossible, as for example when the sections of the surface under investigation are less than the dimensions of the filament of the pyrometer or other measuring instruments. In this case, the problem is easily solved by macrophotography on calibrated light-sensitive material. This variant is simple since all that is needed is an ordinary camera. (2) Recording of the process of temperature change of the object, if the rate of change is such that other optical methods are not applicable due to their inertia, or due to other factors. In this case, a common camera is not sufficient, and motion picture photography or photography on a revolving film is required. The temperature variation may be estimated from changes in the density of the continuous image track. (3) A combination of the first and second cases: investigation of temperature fields varying in time. (4) Measuring the temperature of a moving body within the limits mentioned above.

The biggest defect of the photopyrometric method is the necessity of treating the photomaterial in order to determine the temperature. In other words, a calculation cannot be made immediately.

In addition, the use of a reference standard is obligatory, and this standard must be photographed on every developed piece of photomaterial. This is a drawback as far as "mobility" is concerned; however, this latter difficulty may be overcome if the interval of temperature to be measured is known approximately. Calibration of the film within this interval may be done as desired, and measurement may be separated from calibration both in time and in space if necessary. Another shortcoming of the photopyrometric method for moving bodies is the preliminary selection of film speeds and lens diaphragms that can give a value for the optical density of the object image which lies in the linear part of the characteristic curve. Finally the temperature interval given by the linear part of the characteristic curve is relatively narrow.

Experimental Determination of the Temperature of a Moving Burning Particle

The above method was used to measure the temperature of a freely falling spherical particle of burning coal.

The burning particles were coal particles with diameters of 4.5, 4.0, 3.2, and 2.4 mm. Their temperature was raised to 800°C in a special furnace in an atmosphere of nitrogen. They were then delivered, particle by particle, into a vertical transparent tube 1500 mm long. The composition of the oxidizing atmosphere in the tube could be varied, thus changing the combustion temperature of the coal particles. This paper does not attempt to discuss the laws that govern the changes in the combustion temperature of a moving particle, however, it may be noted that as the speed of the falling particle increases, its temperature changes. The technique applied here made it possible to determine not only the absolute temperature of the particles, but also the changes in the temperature of the particles during their displacement. The optical system used was a broad-angle Jupiter lens 12.1:2.8. The lamp was calibrated at a distance equal to the distance between the lens and the axis of the tube. A slit equal to the diameter of the particle was placed in front of the lamp. A motor shaft that supported a drum camera was used to move the film. The film used was type $\Delta\kappa$ 350° (State

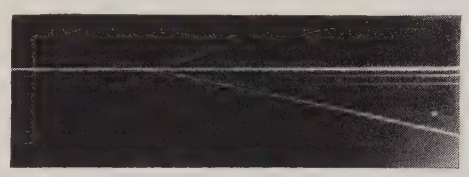

FIG. 3. Photograph of the tracks of a moving particle and the temperature lamp.

TABLE 1

No.	y	T	D
	a	°C	
1	8.2	876	0.03
2	8.38	908	0.10
3	8.52	928	0.17
4	8.8	977	0.28
5	9.0	1006	0.38
6	9.2	1035	0.45
7	9.4	1064	0.52

Standard, 8000°X and D). It was developed in a NIKFI-I developer.

TABLE 2

	l	$tg\alpha$	D_1	D
1	0.61	0.305	0.051	0.060
2	0.65	0.325	0.055	0.065
3	0.67	0.335	0.060	0.072
4	0.68	0.340	0.068	0.080
5	0.73	0.365	0.082	0.096
6	0.74	0.370	0.093	0.107
7	0.83	0.415	0.105	0.122
8	0.88	0.440	0.113	0.133
9	0.89	0.445	0.119	0.139
10	0.94	0.470	0.131	0.156

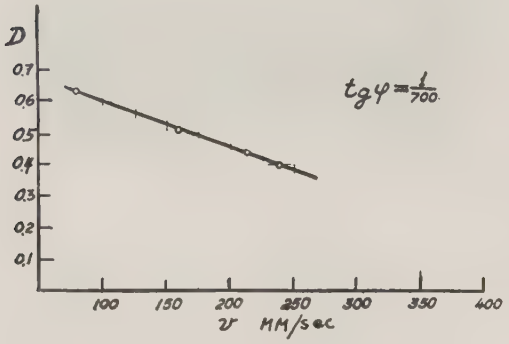

FIG. 4. Dependence, D-v.

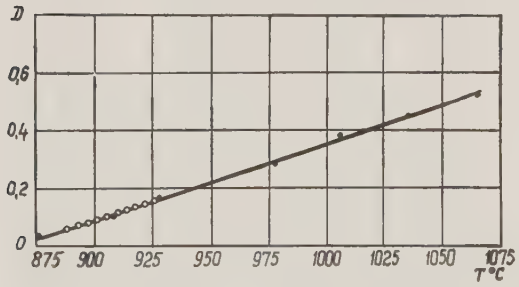

FIG. 5. Dependence, D-T. ● Calibration points. ○ Temperature of particle at different instants of its displacement.

Figure 3 shows a typical photograph. The horizontal calibration lines, corresponding to the extended images of the temperature lamp, agree with the various values of current intensity that heat the filament. Table 1 shows the values of the current intensity, and the corresponding values of the temperatures and image densities.

Table 2 contains the results of an analysis of the track of a moving, burning particle. The angle of inclination, α, of the track and its optical density were measured every two mm along the film ($tg\alpha = l/2$). Figure 4 shows the experimentally obtained dependence, D-v.

An analysis of the results obtained (Fig. 5) leads to the conclusion that under the given experimental conditions, the temperature of the particle varied from 885° to 930°C which is in good agreement with the physical chemical calculations. The error of the data does not exceed 2 per cent.

Acknowledgment

The author wishes to express his deep gratitude to Professor L. N. Khitrin, Corresponding Member of the Academy of Sciences, USSR, for his aid and interest in the work, and also to A. V. Sheklein, a student of the Moscow State University, for his active participation in the first stages of the work.

REFERENCES

1. NEUBERT, P.: Arch. tech. Messen, *5*, 1114–1115 (1936).
2. NEUBERT, P.: Glastech. Ber. *18*, 245–246, (1940); Ceram. Abstr., *20*, 66, (1941).
3. NEUBERT, P.: Arch. Wärmewirtsch., and Dampfkesseln, *19*, 29–32, (1938).
4. Photography with Invisible Light. Science in Industry, the MBS Bull., January–June, No. 3–4, 1936.
5. WALLES, M. B.: Thesis, Massachusetts Institute of Technology, Boston, Mass., 1936.
6. SCHWABE, E.: Bestimmungen von Oberflächentemperaturen durch Infrarotphotographie, Elektro-wärme, *11*, 65–68 (1941).
7. HASE, R.: Z. tech. Physik, *13*, 410–415 (1932); Ceram. Abstr., *2*, 625 (1932).
8. HALLE, I. A.: Phot. J., *86B*, 117–32, (1946).
9. MALE, D. W.: Rev. Sci. Instr., *22*, 769 (1951).
10. LONDEREE, J. W.: J. Am. Ceram. Soc., *37*, 354 (1954).

99

THERMOELECTRIC PROBES FOR MEASURING HIGH TEMPERATURES IN GAS STREAMS: THEIR APPLICATION TO THF STUDY OF FLAMES STABILIZED BY OBSTACLES

By G. MATTON AND C. FOURÉ

A New Type of Thermoelectric Probe[1]

1. APPLICATION

Ordinarily thermoelectric probes are used only for temperatures up to 1200°C. At higher temperatures, difficulties are encountered due to the behavior of the materials and to uncertainties regarding the corrections to be applied to the data provided by the probe, depending upon the working conditions. In addition there may be certain catalytic effects. Optical methods are not always practical and local measurements are questionable.

2. APPARATUS

All the elements of a probe can be cooled so as to keep them at a temperature lower than that limiting its use. As the thermoelectric junction also undergoes cooling, the temperature recorded by the thermocouple must be related to the true temperature of the gases in a known, simple and reproducible manner. At moderate temperatures, where cooling is not necessary, a sonic flow induced near the thermocouple makes it possible to obtain a reliable relation between the temperature at the junction and the true temperature of the gas.[2] Basically, this is possible because exchanges by convection vary with the product of the density and the speed of the gases. This product reaches a maximum when the flow is sonic and varies little over a wide range (for $0.8 < M < 1.2$, the relative variation of ρV is less than 3 per cent). This allows for the unavoidable local divergencies with respect to the sonic velocity.

As the quantity of heat supplied by convection to the junction is well defined, if the heat transferred by convection and radiation from the probe to its surroundings is appreciable due to the necessary cooling, this heat must virtually be a function only of the temperature to be measured. It will be least dependent on the other parameters that affect the temperature of the surrounding system if the temperature level of the system is kept as low as possible (to minimize the relative variations of the temperature difference between the thermocouple and its surroundings). This is why a cooling fluid is circulated through the probe. We restricted ourselves to water which is convenient for bench tests, but any low temperature cooling fluid would be suitable.

Figures 1 and 2 show diagrams of probes based on this principle. They are designed to be placed across the flow, the temperature of which is to be measured. It will be seen that they are of two kinds: in type A the gas flow forms an angle downstream of the neck; in type B the angle is upstream from the neck. The dimensions of probe B allowed for a static pressure intake at the wall of the neck and a thermocouple that measured the temperature at that wall.

3. EXPERIMENTAL PROCEDURE

The temperature recorded by the probes was studied systematically as a function of the design parameters, the flow rate of the cooling water, and the suction pressure.

It was established that the readings were not affected by the gas velocity at the point of sampling nor by the conditions of radiation external to the probe.

Up to 900°C, the gas temperature taken as reference was supplied by a thermocouple that was carefully protected from the effects of radiation and conductivity; from 900°C to 2000°C the reference temperature was given by an optical measurement according to Fery's method in the hot gases of a Meker burner. The effect of absolute pressure in the flow where sampling takes place has not been studied yet because no suitable setup was available.

4. RESULTS

It was found that: (a) The readings were sensitive enough to design parameters to require calibration of each probe, particularly as regards the position of the junction with respect to the axis of the neck for probes of type A (Fig. 3). (b) The flow rate of the cooling water has no effect, within wide limits, although the temperature of the water increases appreciably as it passes through the probe (Fig. 4) and the temperature at the wall of the neck is perceptibly higher than the water temperature at the intake

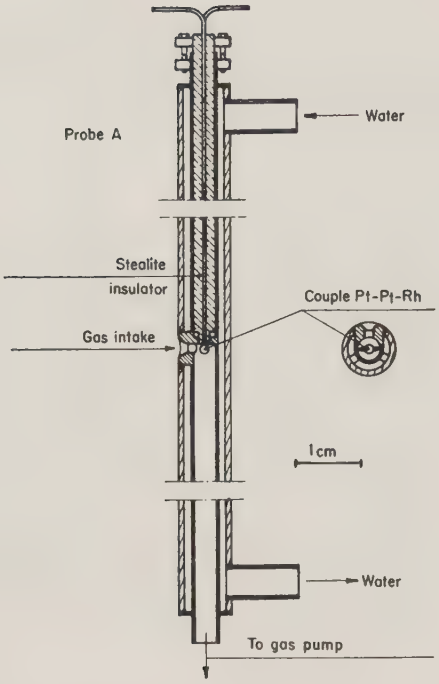

(1)

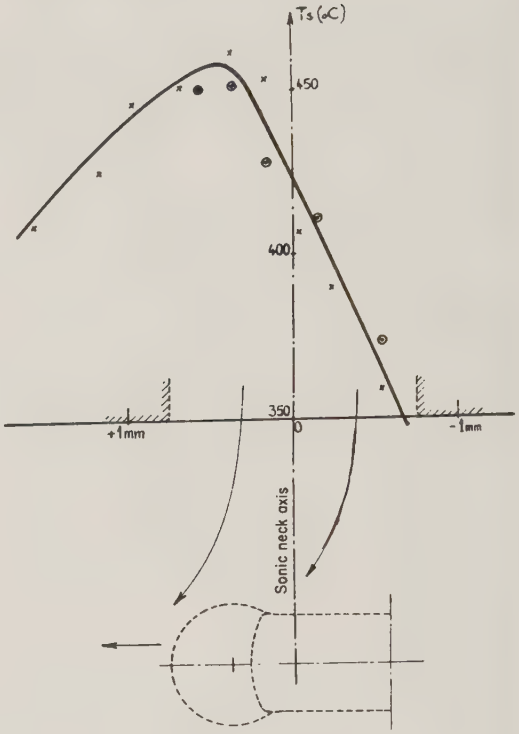

FIG. 3. Type A Probe. Influence of junction location in relation to the sonic neck axis.

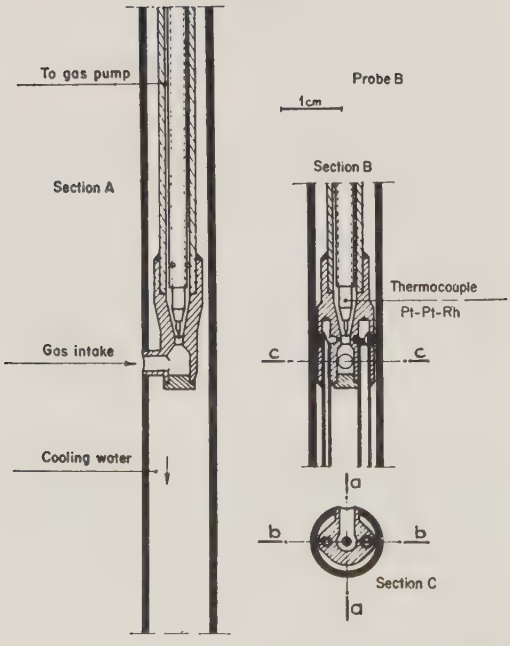

(2)

FIGS. 1 AND 2. Diagram of a water-cooled sonic-flow probe.

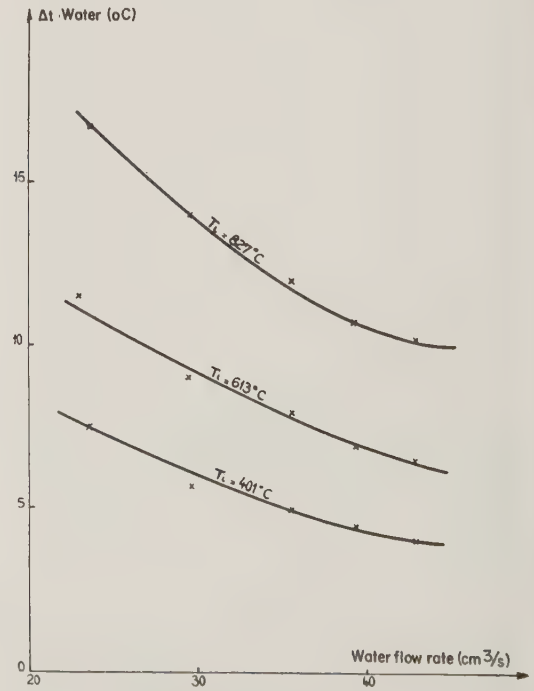

FIG. 4. Water temperature increase through the probe vs cooling water flow.

(Fig. 5). (c) The suction pressure has no influence once sonic flow is established at the neck (Fig. 6).

Analysis of the heat exchange in these probes (summarized in Appendix I) shows that it is possible to represent the readings on a diagram $T_i - T_e = f(T_s - T_e)$, where T_i is the gas temperature to be determined, T_s is the temperature indicated by the thermocouple, and T_e is the temperature of the cooling water at the intake.

Calibration curves were established (Fig. 7);

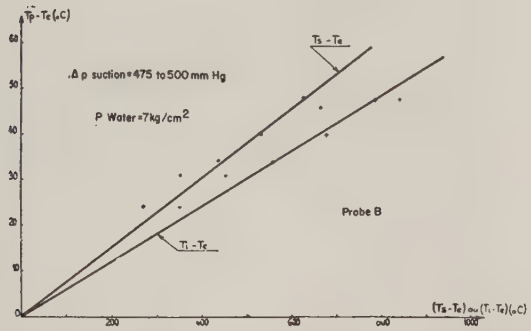

FIG. 5. Wall temperature vs gas or junction temperature (all temperatures expressed as differences to water intake temperature).

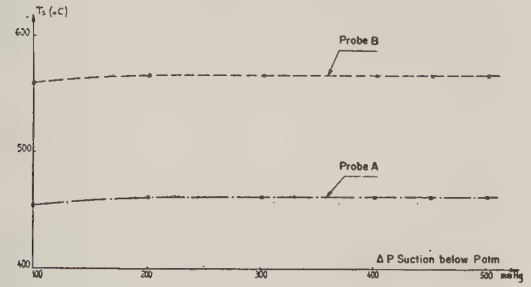

FIG. 6. Influence of suction pressure.

they are valid only for measurements near atmospheric pressure.

At high temperatures, the temperature T_0 measured by the sodium line reversal method was taken as the temperature T_i of the gases; the calibration curves show an inflexion towards the $(T_s - T_e)$ axis, whereas the radiation term would lead us to expect the opposite.

Application to Temperature Measurements in the Wake of a Flame Stabilizer

1. THE STABILIZER PROBE ASSEMBLY

The stabilizer is derived from the ONERA-AGARD standard and is fitted at the upstream end of a probe: the streamlined arms placed at right angles to the flow in the working section provide access for the cooling fluid and the thermocouple wires (platinum 10 per cent rhodium platinum) (Fig. 8).

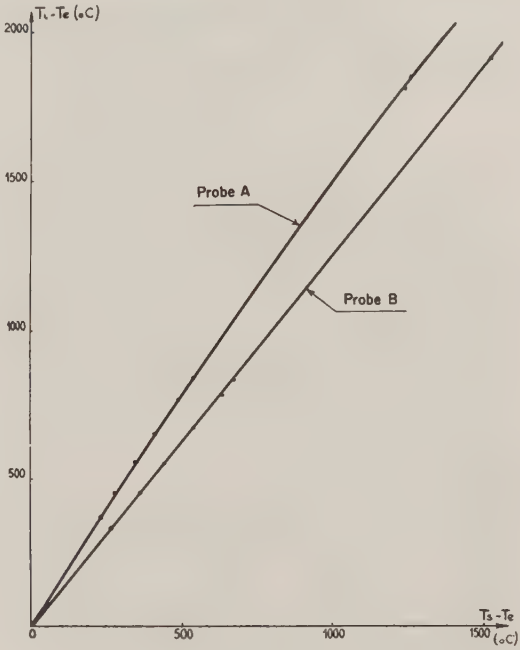

FIG. 7. Calibration curves.

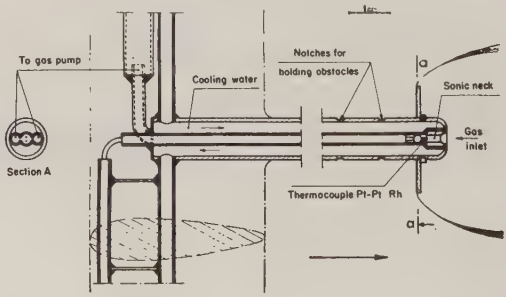

FIG. 8. Diagram of a temperature probe—disc flameholder assembly.

2. EXPERIMENTAL SETUP

The obstacle is situated at the outlet of a nozzle through which a homogeneous vaporized air-kerosene mixture of known composition flows at velocities ranging from 50 m/s to 200 m/s, and temperatures ranging from 250°C to 650°C, attained in a preheating chamber (Fig. 9).

A bench for optical temperature measurements, by Fery's method, is mounted in such a way that the image of the tungsten filament forms a few mm from the probe opening. In this way the optical beam traverses only a very small thick-

ness of the reaction zone located at the edges of the wake of the disc. Moreover, it was found that the ionic density in the neighborhood of the probe opening was constant and low enough to indicate the absence of strong reaction in this region. The radiation intensity of the sodium colored flame is too great to allow optical measurement in rich mixtures.

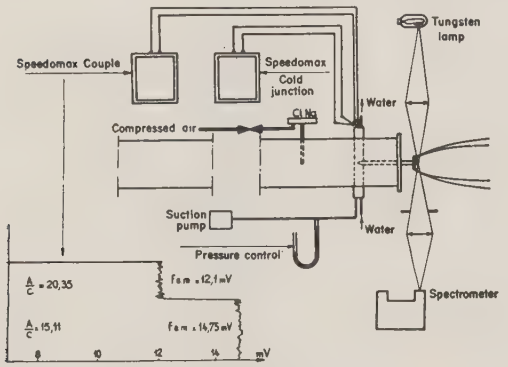

FIG. 9. Experimental setup.

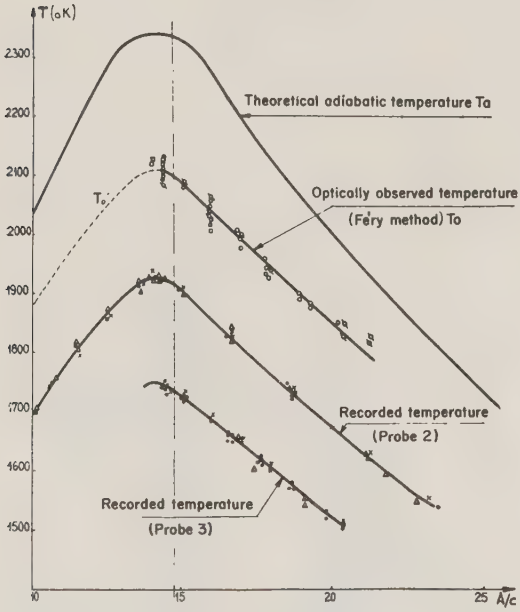

FIG. 10. Gas temperatures recorded in the core.

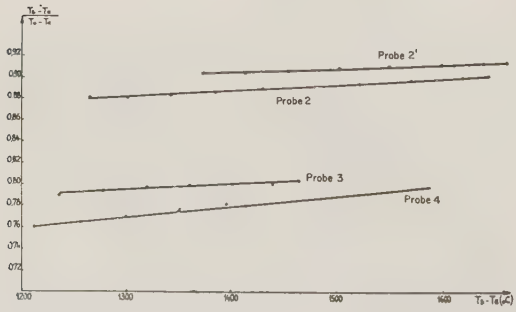

FIG. 11. Calibration curves.

3. RESULTS

The reproducibility is satisfactory, both for the optical measurements and for the probe.

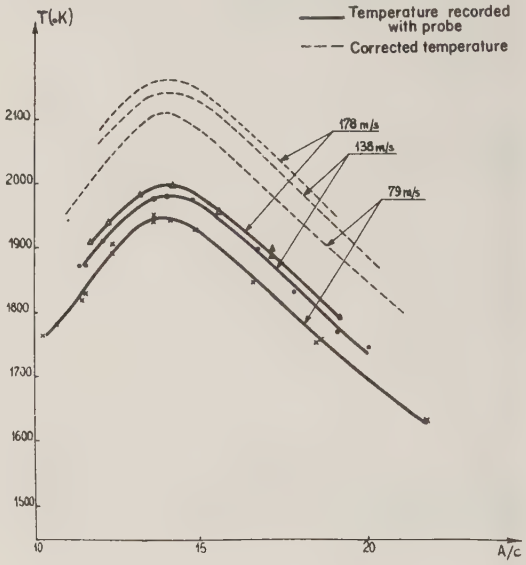

FIG. 12. Effect of flow velocity.

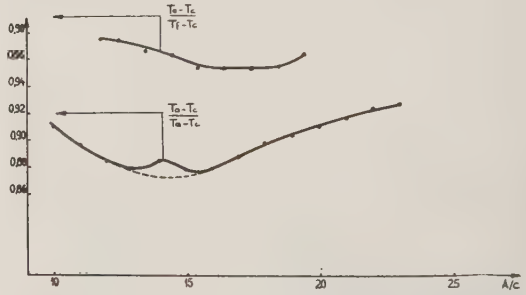

FIG. 13. Relative temperature increase in the core.

In Figure 10, the air-fuel ratio (A/F) of the mixture is plotted against the flow velocity to give curves for the calculated adiabatic temperature, T_a,[3] taking into account dissociations and the initial air temperature; the optically measured temperature, T_0 ; and the temperature indicated by the probe, using two different probes. All these curves reach a peak near $A/F = 14$ and have the same general shape. It was established that the temperatures in Figure 10 are independent of the preheating temperature in

the present case where the A/F dilution is derived from the over-all consumption of the fuel.

If we assume that the optically measured temperature, T_0, is really equal to the temperature, T_i, of the gas, these measurements represent a calibration of each probe against the phenomenon itself that can be expressed by a curve (Fig. 11). It then becomes possible to use the probe alone—which is much simpler—to study the influence of different parameters, such as the flow velocity (Fig. 12).

The optical temperature, T_0 is considerably lower than the calculated adiabatic temperature, T_a. Figure 13 shows the ratio of the optically observed temperature increments to the calculated increase (with respect to the initial air temperature, T_0). Its average value of 0.9 is in good agreement with that reported by Zukoski.[4]

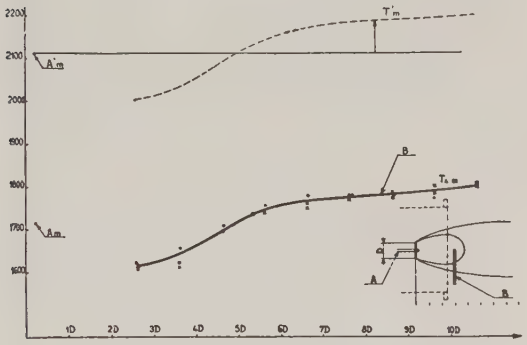

FIG. 14. Temperatures along the axis of the disc wake.

A series of measurements were made in which the end of a probe, similar to that used as a stabilizer support, was moved along the wake axis for the flow that gave the highest temperature. As the distance from the disc increases, the temperature indicated by the probe (position B, Fig. 14) rises. After about 10 diam no further change is observed. The temperature readings were virtually the same whether the obstacle was supported by another cooled probe (dots) or by an uncooled support (crosses). Figure 14 also shows the temperature indicated by the probe when it supports the obstacle (point A_m). As before, the presence or absence of a probe at position B in the recirculation core has no appreciable effect upon the temperature, A_m. Although there is no doubt that a probe at B disturbs the regime of temperatures in the core, at least locally, these measurements show that the temperature is higher downstream from the core than inside it.

The data of the calibration curves can be used to find the values of the corrected temperatures A'_m and T'_m. The temperature downstream from the core was recorded as a function of the air-fuel ratio; if the corrected temperature, T'_m, is considered as the actual flame temperature, T'_f, we can take T_f as reference for calculating the relative temperature rise within the core (upper curve, Fig. 13).

Conclusions

It is possible to make thermoelectric probes for use in flames of air-kerosene mixtures. They must be calibrated by an optical method; the calibration curve is virtually linear. The gas temperature measured immediately downstream of a flameholder, plotted against the air-fuel ratio gives a curve that is very similar to the adiabatic temperature curve. The temperature in the recirculation core is lower than the temperature of the flame downstream; the relative temperature increase in the core is of the order of 0.9 or 0.96, depending upon whether it is referred to the calculated adiabatic temperature or to the measured flame temperature.

Appendix

ANALYSIS OF THE HEAT EXCHANGES INSIDE A PROBE

In the steady state, the rate of heat transfer by convection to the junction is equal to the rate of the heat lost by radiation to the surrounding walls and by conductivity along the wire. Assuming that the wall temperature, T_p, is uniform, we can write

$$hS(T_g - T_s) - \epsilon\sigma S(T_s^4 - T_p^4) + \Lambda \frac{\pi d^2}{2} \left(\frac{\partial T_x}{\partial x}\right)_{x=0} = 0 \qquad (1)$$

The heat loss across the wire boundaries can be expressed as:

$$dq = k\pi d\ (T_x - T_p)\ d_x$$

The temperature, T_x along the wires decreases from the junction following a curve, the tangent of which has an angular coefficient at the origin that can be evaluated:

$$\left(\frac{\partial T_x}{\partial x}\right)_{x=0} = -\alpha(T_s - T_p) \qquad (2)$$

where

$$\alpha^2 = \frac{4k}{\Lambda d}$$

Rearranging and using Equation (2), Equation (1) becomes

$$T_g - T_p = \left(1 + \frac{\sqrt{k\Lambda\Pi^2 d^3}}{hS}\right)(T_s - T_p) + \frac{\epsilon\sigma}{h}(T_s^4 - T_p^4) \quad (3)$$

The platinum emission factor ϵ can hardly be greater than 0.2 whereas the sonic convection coefficient, h, is of the order of 5000 kcal/hm^2°C for a junction of 0.1 cm diam; the radiation term reaches only 32°C for $T_s = 2000$°K. Thus we can write

$$T_g - T_p = (1 + A)(T_s - T_p) + BT_s^4 \quad (3')$$

BT_s^4 is a small correction term.

Before reaching the thermocouple, the gases are in contact with cold walls and their stagnation temperature, T_i, can be reduced to an average value T_i'.

Let us write

$$T_i - T_i' = (T_i - T_p)l \quad (4)$$

(by evaluating l, we reach the maximum in the order of 0.1).

The temperature, T_g, that the thermocouple would indicate if there were no losses is different from the stagnation temperature, T_i'.

If β is the recovery coefficient defined as $\beta = T_g - T/T_i' - T$ and if the flow is sonic, we have

$$\frac{T_g}{T_i'} = 1 - (1 - \beta)\frac{\gamma - 1}{\gamma + 1} = 1 - \delta \quad (5)$$

δ is generally of the order of 0.03.

In practice, the walls and the water are not at the same temperature (Fig. 5); we can write

$$T_p - T_e = m(T_i - T_e)$$

with $m < 0.06$.

Finally, we have

$$T_i - T_e = \frac{1}{1 - m - \delta}\left[(1 + A)\frac{1 - m(1 + A)}{1 - l}(T_s - T_e) \cdots + \frac{B}{1 - l}T_s^4 + \delta T_e\right]$$

If A, l, m and δ did not vary with temperature, the calibration curve would be a straight line starting from a point very close to the origin since $\frac{\delta T_e}{1 - m - \delta}$ is of the order of 10°C.

With regard to the effect of temperature and pressure on the parameters used in the probe equation, we have

$$A = \frac{\sqrt{k\Lambda\Pi^2 d^3}}{hS}$$

where

$$h = 0.33\frac{\lambda}{D}\left(\frac{\rho^a D}{\mu}\right)^{0.6}$$

Inspection of the variations of ρ, a, λ and μ shows that h varies very little with temperature, but varies with $p^{0.6}$. Similarly $\frac{(1 + A)(1 - mA)}{1 - l - \delta}$ varies little with temperature, which explains why the calibration curves are virtually linear.

However, it seems unrealistic to calculate the calibration curve of a probe for a given pressure from the curve plotted at the atmospheric pressure.

Nomenclature

- T_i adiabatic stagnation temperature of the gas
- T_g temperature indicated by the thermocouple if there were no losses by radiation or conduction
- T_s temperature indicated by the thermocouple
- T_0 optically measured temperature
- T_s water temperature at intake
- T_p temperature of the internal metal wall (all temperatures are in °K)
- h convective exchange coefficient (between gas and junction)
- l relative cooling coefficient of the gas before reaching the junction
- m relative heating coefficient of the internal wall
- ϵ emission factor of the junction
- σ Stefan-Boltzmann constant
- S surface of junction exposed to convection and radiation
- Λ thermal conductivity of the couple wires
- d wire diameter
- k heat exchange coefficient of the wires with the surrounding medium
- λ thermal conductivity of the gas
- μ absolute viscosity of the gas
- a gas velocity following sonic expansion
- γ specific heat ratio

REFERENCES

1. Fouré, C.: Brève information, La Recherche Aéronautique, No. 50, 1956.

2. Lalos, G. T.: J. Research Nat. Bureau of Standards, *47*, 3, (1951).
3. Rappeneau, J.: Thèse. Publications Scientifiques at Techniques du Secrétariat á l'Air, 1956.
4. Zukoski: AGARD. Liège, 1955 (film).

100

A SELF-CALIBRATING HIGH SPEED PHOTOGRAPHIC PYROMETER

By J. TYROLER

Introduction

This instrument was designed to study the brightness temperature distribution of explosive phenomena as a function of time. Because of the nature of the phenomena being observed, most testing had to be done under field conditions and consequently a portable, easily operated apparatus was particularly desirable. There is no theoretical maximum brightness temperature to which this instrument is limited. It is operated in a manner similar to an ordinary high speed fastax camera, and can be used to obtain brightness temperature distribution up to a maximum rate of 2000 times per second, which is the limit of the particular camera used.

Description of Instrument

The instrument consists of a 35 mm high speed fastax camera, a method for recording only "monochromatic" light, and a calibrator. The function of the calibrator is to put stripes of various density along the edge of the film, each stripe simulating a specific brightness temperature.

In order to utilize only monochromatic light, a Number 2412 Corning Glass cut-off filter is placed in front of the camera lens. The combined effects of the filter and the wavelengths sensitivity distribution of the Super XX film used in the instrument permits only "monochromatic" light to be recorded (Fig. 1).

The calibrator (Fig. 2c) consists of a tungsten filament lamp, a Number 2412 Corning Glass filter of the same melt and stock thickness as the one placed in front of the camera lens, and a small collimating lens. The top of the calibrating device consists of a disc with three slits of different widths (Fig. 2b). Essentially, the fastax camera consists of a prism which rotates in synchronism with the sprocket wheel which drives the film smoothly but at a continually increasing speed (Fig. 3).

The film runs across the calibrating disc in the direction of the slit widths (Fig. 2b). The lamp in the calibrating device is operated on a six-volt storage battery in series with a variable resistor and an ammeter. With the proper combination of lamp voltage and slit width, it is possible to obtain three stripes of different densities on the film. The filament is placed at the focus of the lens, so that small displacements in the film will have little effect on the densities of the stripes.

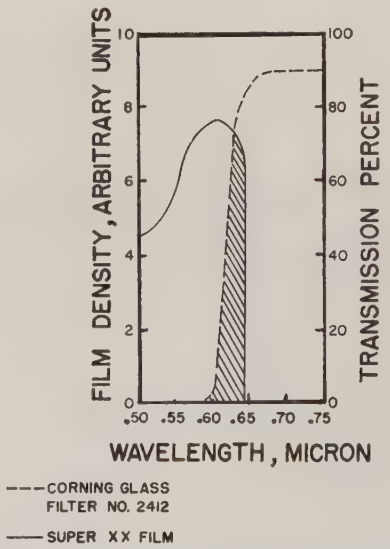

Fig. 1. Curve illustrating combined effect of both the filter and film sensitivity to give "monochromatic" light.

The image exposures on the film for the stripes and for the phenomenon measured is inversely proportional to the speed of the film. These stripes correspond to densities of images for three

different brightness temperature sources. The stripes are recorded at one edge of the film and the phenomena on the opposite side.

Calibration

The method used for calibrating the stripes is very similar to that used by D. W. Male in his photographic pyrometer.[1] The stripes are calibrated by taking pictures of several tungsten ribbon filament lamps at various known brightness temperatures in place of the phenomena, and interpolating the densities on the film to find the simulated temperatures.

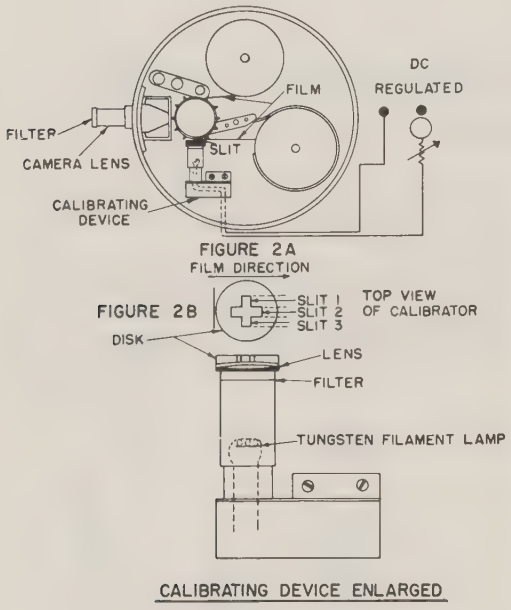

Fig. 2. Complete photographic pyrometer.

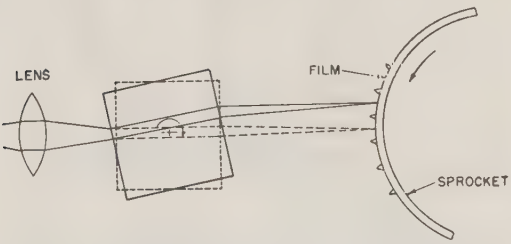

Fig. 3. Illustration of synchronous arrangement of sprocket wheel and prism in fastax camera.

The small calibrating lamp is aged by operating it at its rated voltage for 10 per cent of its rated life. The filament of the lamp in the "calibrating device" is placed at the focus of the lens so that small displacements in the distance of the film from the top of the disc will have little effect on the "image" (the stripes) of the filament on the film. With a proper selection of voltage on the lamp and slit widths in the disc on the "calibrating device" it is possible to obtain three stripes simulating different brightness temperatures on the film.

Since during actual testing of explosive items, the event occurs at a distance of greater than 100 feet. The 105 mm lens on the camera was fixed permanently so as to focus on infinity. The ribbon filament lamps during calibration were placed approximately 12 feet away from the camera and kept in sharp focus on the film with the aid of large field lenses placed directly in front of the ribbon filament lamps. The f number and brightness temperatures of the calibrating ribbon filament lamp are then adjusted so that the densities of the images of the ribbon filament lamps are in the range of the densities of the stripes from the "calibrating device." The f number on the camera lens is then fixed permanently (in this particular case f 16). The brightness temperature of the ribbon filament lamps are measured by a Leeds and Northrup optical pyrometer placed in the same position as the camera. This procedure also automatically adjusts for any small radiation losses through the field lenses. The simulated brightness temperatures of the stripes are then calibrated by comparing these densities to the densities due to the images of the tungsten ribbon filament lamps. Once the stripes are calibrated for a particular voltage across the lamp of the "calibrating device" there is no further need for the ribbon filament lamps. It is possible to utilize a range of densities on the film in which the brightness temperatures are proportional to the densities at any particular film speed.

Method for Measuring Brightness Temperatures Beyond Range of Calibration

Frequently phenomena are observed whose peak brightness temperatures are above the simulated brightness temperature range of the stripes (2700°K in the instrument as presently used). In such cases brightness temperature measurements can still be made by placing a "neutral filter" of known transmission, at the wavelength utilized (630 mμ), in front of the camera lens so that the densities of the image of the phenomena being observed are attenuated

to that of simulated stripes. If the temperature is within the range where Wien's law may be applied, the following equation may be used:

$$C_1\lambda^{-5}e^{-C_2/\lambda T} = T_r C_1\lambda^{-5}e^{-C_2/\lambda T_H}$$

where λ is the best effective wavelength (630 mμ), T is the brightness temperature of the phenomena interpolated from the calibrated stripes as if the neutral filter was not there, T_H is the true brightness temperature of the phenomena, C_1 and C_2 are constants, T_r is the transmission of the "neutral filter" at 630 mμ. Therefore

$$T_H = \frac{C_2 T}{T\lambda \ln T_r + C_2}$$

If the temperature is beyond the accurate range of Wien's law, Planck's expression must be utilized.

Accuracy of Method

Temperature measurements made of a ribbon filament lamp calibrated by the National Bureau of Standards to have a brightness temperature of 2800°K ± 8°K when determined by this instrument have been found to be 2802°K with an average deviation of 10.0°K.

Temperatures of greater magnitude would be expected to have larger errors.

REFERENCE

1. Male, D. W.: Rev. Sci. Instr., *22*, 769–772, (1951).

101

APPLICATION OF OPTICAL METHODS TO COMBUSTION RESEARCH

By F. J. WEINBERG

1. Introduction

The experimental study of combustion processes is rendered difficult by the extreme conditions of high temperatures, short times of residence and large magnitudes of concentration and temperature gradients under which reaction occurs in flame zones. These conditions imply the need for "*in situ*" studies on actual flames and at the same time are responsible for the sensitivity of combustion zones to external interference which renders such studies difficult. In this sphere of activity optical methods offer some obvious advantages, the most notable perhaps being their noninterference with combustion processes, their absence of inertia and their ability of producing instantaneous records by photographic means of transient phenomena.

The purpose of this communication is to summarize recent advances in research carried out at the Department of Chemical Engineering of the Imperial College of Science and Technology, London, into the analytical applications of optical methods to combustion research. The summary is confined to optical methods based on ray deflections applied to premixed flames of simple geometry.

2. Schlieren and Shadowgraphs

Preliminary analytical work and calculations have shown that the maximum rate of change of refractive index in premixed flames occurs at temperatures well below those at which reaction becomes appreciable. The greatest magnitudes of deflection of incident light rays occur, in fact, within a zone where refractive index variations due to any composition changes are rendered negligible by those due to temperature changes. Since the temperature distribution in this region is calculable from heat transfer considerations alone, the distribution of ray deflections there can be deduced theoretically.

From the point of view of both schlieren and shadow photography, this zone is the most important region within the flame. Thus in the case of schlieren methods the local image intensity is determined by θ, the angle of ray deflection. The calculation of the complete intensity distribution, however, is rendered somewhat uncertain by the superimposed diffraction pattern due to the knife edge which is determined by the exact position and orientation of the latter. For this reason, our calculations have, in the main, been confined to the location of the posi-

tions and temperatures, T_s, within flames of simple geometry giving rise to the "schlieren image," *i.e.*, the maximum deflection.

Thus in the case of a flat flame, parallel to the initial ray direction (Fig. 1a), the deflection is given, to a close approximation,[1] by

$$\theta = -\frac{dn}{dy} \cdot D = -\frac{d\delta}{dy} \cdot D \qquad (1)$$

where y is the distance coordinate perpendicular to the flame, n = refractive index, $\delta = n - 1$ and D is the length of the light beam within the flame. The variation of refractive index with temperature, T, is given by

$$\delta = \delta_0 T_0 / T \qquad (2)$$

so that the condition for maximum deflection is

$$\frac{d^2\delta}{dy^2} = 0, \textit{ i.e.,} \; T\frac{d^2T}{dy^2} = 2\left(\frac{dT}{dy}\right)^2 \qquad (3)$$

In the zone before the onset of appreciable heat

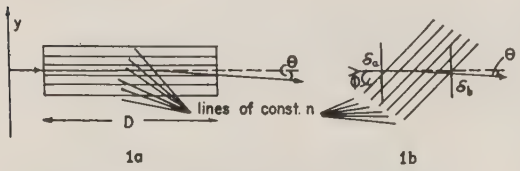

FIG. 1. Ray deflections by flame facets.

release due to reaction, the variation of temperature with distance is governed by

$$k\frac{dT}{dy} = Mc(T - T_0) \qquad (4)$$

neglecting the effects of radiation for transparent gases, where k = thermal conductivity, c = mean specific heat at constant pressure, M = mass burning rate, and the subscript denotes the initial state.

The solution of Equation (3) with Equation (4) yields T_s, the temperature of maximum deflection. The results depend on the manner of variation of k and c with T. If $k/c \propto T^a$ over the relevant range, it can be shown[2] that

$$T_S = T_0\frac{a+2}{a+1} \qquad (5)$$

(All temperatures in °K.)

For air in the range of immediate interest, a is close to unity and T_s becomes $3/2\ T_0$. This theoretical prediction has been found to be in excellent agreement with experimental results.[2]

In the case of flames inclined to the direction of the beam at an angle ϕ (Figure 1b), Equation (1) can be shown[3] to become

$$\theta = -(\delta_a - \delta_b)\cot\phi \qquad (6)$$

the subscripts a and b referring to the points of entry and exit of the ray into the region of disturbance. The combination of Equations (1) and (6) permits an approach to the problem of curved flames, since (i) the deviation of the beam during its flame traverse is very small, and (ii) the thickness of the flame (in terms of the region of refractive index variation) is, in general, negligible in comparison with the radius of curvature of the flame, so that the flame curve may be regarded as constituted of infinitesimal flat facets. Equation (6) then applies to each facet unless ϕ is so small that Equation (1) must be used.

Application of these concepts to axial sections of curved flames in cylindrically symmetric systems[3] has led to the following conclusions for flames whose curvature is concave towards the approaching stream of reactants: The temperature of maximum deflection within the flame is even lower than its corresponding value in flat flames parallel to the direction of the incident beam. For the purely mechanical model of a perfectly conical flame surface, maximum deflection would, in fact, occur at the lowest axial temperature available. However, no real flame can conform to this artificial model, because the large curvature at the tip would result in augmented transfer processes there. The consequent local increase in burning velocity and flow line distortion causes all the flame tips to be rounded in practice. Now even a small horizontal portion of the flame surface exercises a profound effect on ray deflection leading to results closely similar to that of the flat flame. Thus for the model of a conical flame-front whose inclination to the horizontal is ϕ having a flattened apex of diameter p,

$$T_S = T_0\frac{a+2}{a+1+\dfrac{2\nu\cot\phi}{ps}} \qquad (7)$$

where ν = thermal diffusivity of reactants, s = normal burning velocity and other symbols correspond to those of Equation (5). Equation (7) implies that for the model chosen $(a+2)/(a+1) \geq T_s/T_0 \geq 1$ always. Insertion of numerical values, however, shows that for an inclination of 45° and a burning velocity of 50

cm/sec, for instance, a flattened apex of only 0.05 cm radius suffices to raise this temperature of maximum deflection to within less than 4 per cent of the flat flame solution.[3]

Shadowgraph interpretation was approached in a similar manner. The mode of interpretation depends greatly on the distance separating the flame from the shadowgraph screen or photographic plate. The general statement that local shadowgraph intensities depend only on the rate of change of deflection with distance neglects the fact that points on the shadowgraph are often illuminated by superimposed light rays deriving from more than one position in the flame and applies therefore only to shadowgraphs close to the flame. The general problem is obviously very complex, but a complete solution has been obtained[4] in the case of a flat flame parallel to the beam of light. The full results are too cumbersome for presentation here but a few numerical consequences may be quoted to illustrate the conclusions.

In the case of the shadowgraph close to the flame, for reactants containing largely air at an initial temperature of 18°C, the first intensity maximum (from the upstream side) corresponds to a temperature of only 59°C, while the subsequent minimum originates at a flame temperature of 364°C. For shadowgraphs distant from the flame, a new point of reference on the image has been suggested in the first discontinuous rise in intensity and this has been correlated with the temperature of maximum deflection. The distance ranges within which each type of interpretation is applicable were defined and expressed in terms of the properties of the flame. An interesting conclusion which emerged is that the more generally accepted type of correlation between shadowgraph intensity distribution and the refractive index field, namely, that referred to here as the "shadowgraph close to the flame" is applicable only to separations between flame and screen which may frequently be too small for practical purposes. Comparison with the conclusions on schlieren interpretation suggest that in the case of shadowgraphs also, results for curved flames may not differ greatly from those derived for the flat flame case.

3. Analytical Studies

A method has been developed[1, 5] in which the refractive index distribution across a flat flame-front is measured by recording the instantaneous distribution of deflections and is used to calculate the corresponding temperature profile. This temperature distribution together with the measured burning velocity, used in conjunction with the steady-state conservation equations of flame propagation makes possible the calculation of the distributions of the "over-all" variables across the flame-front. It has yielded the distributions of temperature, fraction of total reaction, rates of heat release and reaction, flow velocities, etc., together with values of "ignition temperature," periods of residence, forces on the flame and other parameters.

The principle of the method is illustrated schematically in Figure 2. An accurately parallel beam of light is produced by concentrating light from a high intensity source on a pin-hole placed at the focus of a collimating lens of long focal length. If the beam is confined by a slit inclined

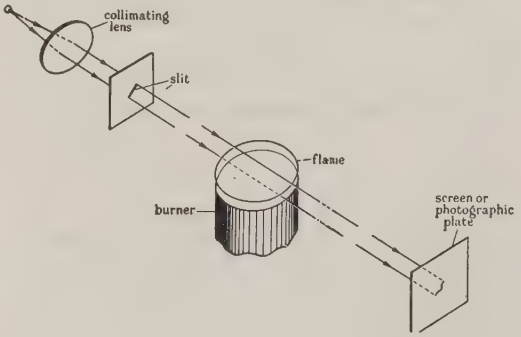

FIG. 2. The "inclined slit" method.

with respect to a flat flame stabilized on a modified form of the Egerton-Powling burner,[6] the distribution of ray deflections can be recorded as a distortion of the slit image on a screen or photographic plate at some distance beyond the flame. In practice, a number of parallel slits are used extending across the entire field of disturbance in order that corrections may be made for any heating up of the surrounding atmosphere or deviations from flatness of the flame. The full theory of the interpretation is given by Burgoyne and Weinberg.[1] A few of the results are shown below to illustrate the scope of the method; these refer to a lean ethylene-air flame. Figures 3 and 4 show the distribution of temperature (T°K) and fraction of total reaction (ϵ) in space (distance y cm perpendicular to the flame) and time (t sec) respectively. The magnitude of energy flow rates is shown in Figure 5, while Figure 6 illustrates the distribution of the over-all

reaction rate from which the distribution of volumetric heat release rates can be deduced.

Many other conclusions can be drawn from the results concerning the physics, chemistry and aerodynamics of the flame, but for the purpose of the present communication these illustrations must suffice to indicate the potentialities of the method as a tool in the study of flames. This method as used for the fullest interpretation possible will henceforth be referred to as "the complete interpretation."

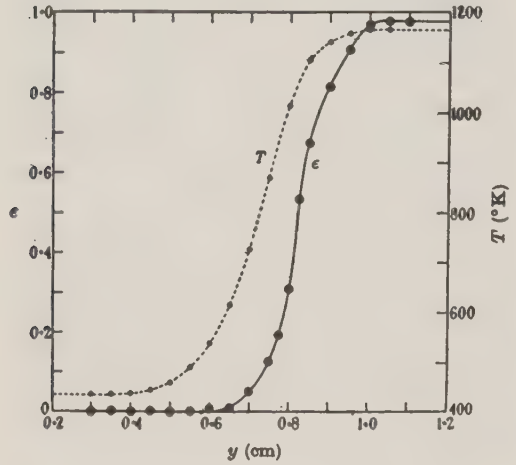

FIG. 3. Curve of ϵ distribution.

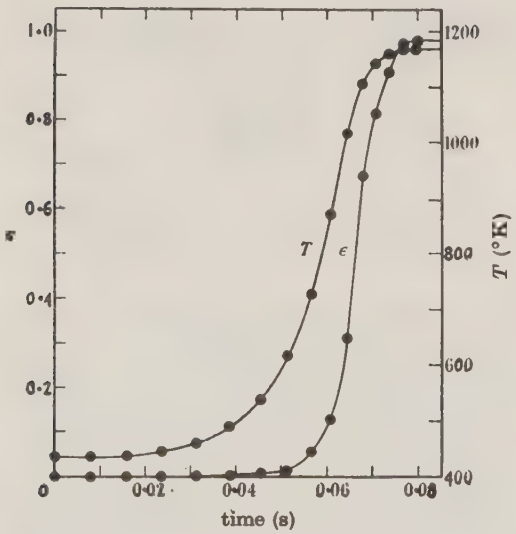

FIG. 4. Distribution of temperature and ϵ in time.

In some of the research projects in progress, the nature of the investigation does not warrant the mathematical labor of such complete analysis or the experimental refinements associated with the production of an accurately flat flame. In such cases, the measurement of only some of the important parameters by a method identical in experimental principle to that of the "complete interpretation" outlined above is sufficient. A very simple procedure has been evolved for the partial interpretation of the deflected slit image based on some of the more obvious aspects of its shape and this will henceforth be referred to as "partial interpretation." The extent of the information desired and the method by which it is deduced from experimental results depends somewhat on the nature of the particular investigation, but a few of the parameters obtainable are discussed below.

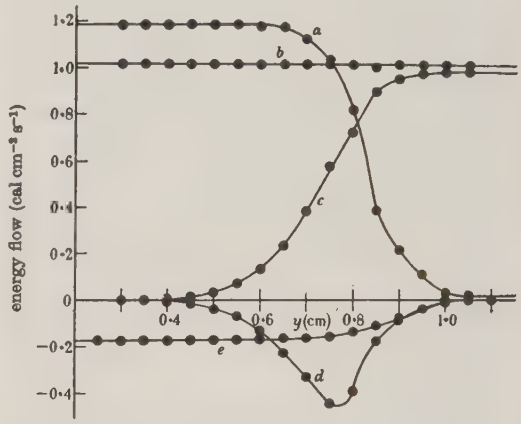

FIG. 5. Distribution of energy transfer. *a*, chemical energy flow; *b*, total flow; *c*, mass flow of thermal energy; *d*, conduction flow; *e*, radiation flow.

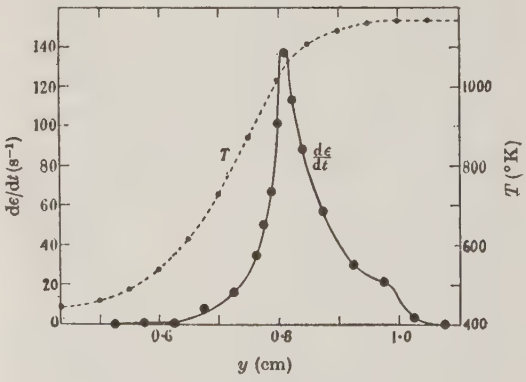

FIG. 6. Distribution of $d\epsilon/dt$.

If the flame under investigation is flat, the distance perpendicular to it over which deflections of the image occur is obviously a measure of the total "flame thickness." The purpose of

the quotation marks is to emphasize that, since all the variables across the flame-front tend to their initial and terminal values asymptotically, the term "flame thickness" has quantitative significance only within the framework of its definition. The vertical distance over which ray deflections occur furnishes a definition in terms of the sensitivity of the optical method. This sensitivity, however, is less at the higher than at the lower flame temperatures. For this reason, an alternative definition based on a given fraction of the total temperature rise has been correlated with the deflected image shape. This "flame thickness" is deducible from a simple geometric construction upon an enlargement of the image. Its magnitude is of importance in studying the mechanism of flame propagation and the measurement has been carried out successfully for hydrocarbon flames containing a gaseous inhibitor. The conclusions of this work will be published in the near future.

Another aspect of the "partial interpretation" is the location of particular values of temperature in the "pre-ignition zone" of the flame, particularly the temperature of maximum deflection, T_s, which is easily calculable (see Section 2). It can be shown that maximum deflection occurs where the tangent to the curved image becomes parallel to its undeflected extremities and the height within the flame at which this deflection occurs is given by the point of intersection of the vertical through the point of tangency with the undeflected line of the slit. Here again simple geometric construction upon the image suffices.

Perhaps the most important aspect of the "partial interpretation" consists of the measurement of final flame temperature, T_f. Its importance lies not only in its applicability to nonflat flames but also in that other flame properties, extremely difficult to measure in other ways, can be deduced by this method if T_f is known.

It has been shown[7, 8] that the final temperature is related to the area, A, enclosed between the deflected and undeflected slit images in the following manner

$$T_f = \frac{T_0}{1 - \dfrac{Am}{Dd\delta_0}} \left(\frac{\delta_p}{\delta_r}\right) \qquad (8)$$

where m is the slope of the inclined slit with respect to the part of the flame traversed, D is the path of the ray within the flame region, d is the separation between burner axis and photographic plate, $\delta = n - 1$, and the subscripts 0, p, r, denote initial state, products and reactants respectively. Equation (8) applies to flat, curved and corrugated flames and the method is applicable, in principle, to any two dimensional flame geometry. The reason is that although the *shape* of the deflected image depends on flame geometry, the *area* A does not, other quantities remaining constant. In practice, however, excessive curvature introduces experimental difficulties and the method, up to the time of writing, has been applied only to flames of very gradual curvature.[8]

In special cases, Equation (8) may be used for the determination of one of its variables other than T_f. Thus, if the flame surface is interrupted, calculation of D will yield the total size of the discontinuities. An illustration of this use of the method is cited in the next section. It does, of course, necessitate knowledge of T_f, which can be obtained conveniently by burning the same mixture under different conditions of geometry and using the method described.

4. Applications

Of the research projects currently in progress, the "complete interpretation" forms the basis of one attack on the mechanism of flame propagation. In this investigation, which was initiated in October, 1954, the initial temperature of the reactants is varied by uniform preheating and the effect on burning velocities, limits of inflammability as well as on the complete flame structure is studied. The highest degree of accuracy is aimed at by refinements of the optical technique. This constitutes a direct experimental approach to the theory of flame propagation since the initial variable is simple and directly controllable and its final consequences together with the mechanism of their attainment can be measured accurately.

The method of "partial interpretation" is in use on two projects investigating the mode of action and the effects of flame inhibitors.[8] In one of these, the inhibitor is gaseous ("Freon 12," CCl_2F_2) and is uniformly premixed with the reactants. The dependence of burning velocity and limits of inflammability on inhibitor concentration is measured. The optical method furnishes flame thicknesses and final flame temperatures. The latter gives a measure not only of the over-all heat release due to the "inhibited reaction" but also of the increase in flame temperature required

to maintain a particular flame for various inhibitor concentrations and therefore of the effectiveness of the inhibitor. To eliminate the purely physical components of the inhibition process, control experiments with an inert diluent are carried out.

In the second project the effects of solid inhibitors in the form of monodisperse alkali halide (in particular NaCl) crystal clouds are investigated. The mechanism of these effects is likely to be rather different from those governing homogeneous gaseous inhibition if the particles do not have time to evaporate and their vapor to diffuse uniformly through the gas before the major part of the flame thickness has been traversed. Unevaporated particles and undiffused vapor spheres might then be expected to disrupt the flame surface locally, introducing "holes" in the flame. From a knowledge of the final flame temperature, Equation (8) can be used to deduce D and comparison with its apparent value yields the mean fraction of flame area occupied by these disruptions. Preliminary measurements based on this principle have yielded reasonable results.

Another investigation of the early stages of ignition of premixed reactants by optical means is in hand.

Details and results of all these investigations have been or will be published elsewhere. In the present summary they are intended merely to illustrate the scope of the current applications of the optical tool. In the immediate future it is intended to extend its field of application to turbulent and to diffusion flames. The former in particular promises to become a fruitful field of study whose importance is emphasized by the present state of theory in the field of turbulent flame propagation.

Acknowledgments

The author is indebted to Dr. J. H. Burgoyne for many helpful discussions and to his colleagues in this work Messrs. A. Levy, J. Reck, J. Sage and K. Sumi.

REFERENCES

1. Burgoyne, J. H., and Weinberg, F. J.: Proc. Roy. Soc., *A224*, 286 (1954).
2. Weinberg, F. J.: Fuel, *34*, S84 (1955).
3. Weinberg, F. J.: Fuel, *35*, 161 (1956).
4. Weinberg, F. J.: Proc. Roy. Soc., *A235*, 510 (1956).
5. Burgoyne, J. H., and Weinberg, F. J.: *Fourth Symposium in (International) Combustion*, p. 294. Baltimore, The Williams & Wilkins Co., 1953.
6. Powling, J. A.: Fuel, *28*, 25 (1949).
7. Weinberg, F. J.: Fuel, *35*, 359 (1956).
8. Reck, J., Sumi, K., and Weinberg, F. J.: Fuel, *35*, 364 (1956).

102

IONIZATION STUDIES OF FLAMES STABILIZED IN RAPID FLOW

Measurement of Ionic Density in The Flame

By G. MATTON

1. Ionic Density and Reaction Zone

There have been a number of qualitative and quantitative studies of ionic density distribution in burner flames.[1, 2] As the value of this density is much higher in the neighborhood of the flame front than in the hot gases, it offers a means of studying the reaction zone distribution. The present paper reports an investigation of this type, applied to flames stabilized by obstacles in a rapidly flowing air-kerosene mixture.

2. Experimental Device

In these measurements, the positive ions are collected by raising the probe electrode to a constant potential that is very negative with respect to the flame gases. All insulating materials tested for insulation of the electrode were found to be conductors at high temperature. After considerable testing, a probe was adopted, consisting of a 0.6-mm diam chromel electrode in a 4-mm diam water-cooled support (Fig.

1). Good insulation is provided by a silica tube between the electrode and its support. This tube is kept at a low temperature. The electrode protrudes from the support by a constant length of 2 mm.

In the course of this first investigation, the virtually instantaneous qualities of the procedure were not exploited and the ionic currents were simply recorded with a Speedomax-type electronic potentiometer and an amplifier. The DC amplifier is a differential setup with a 6 SN 7 G double tube, one element of which is held at the tension investigated. The power is stabilized and amplification is linear. This amplifier is used to lower the impedance so as to obtain good results with the recording electronic potentiometer.

The flame is held by a disc of the ONERA-AGARD type (diameter, 25 mm), located at the end of the nozzle to facilitate probing. However, this is not essential and the procedure can be applied to flames in confined flow.

3. Ionic Structure of the Obstacle Wake

Figure 2b shows traces of the ionic current obtained during flame traverses made downstream, at distances expressed in function of the disc diameter. It will be seen that there is a region of moderate density (hot gases) between two zones of high density (reaction zone). It was also found that the ionic density and the recorded fluctuations increase gradually in the wake as the distance from the obstacle increases, whereas they both decrease in the lateral reaction zones.

The difference is very marked at a distance of about 5 diameters which would correspond to the end of the recirculation zone (checked by introduction of sodium.)[3]

Figure 2a gives a typical series of traces obtained across poor mixture limits, with the tip of the probe located in the wake axis at the indicated distances. There is a characteristic increase of the ionic density before quenching. The phenomenon is not as clear across a rich mixture limit.

Varying the dilution of the mixture has little effect on the ionic current which reflects the ionic density of the gases of the core, except, as we have already seen, near the quenching point. On the other hand, in the reaction zone, the ionic current is a function of the dilution. Its intensity is maximum for a stoichiometric mixture ratio of 1:14.7 and it is about 15 times as high as that of the core under the experimental conditions used.

4. Interpretations

Although the relative ionic concentration of hot gases is considerably lower than that of the reaction zone, it is rather high. In the course of transversal probing, above a laminar blue cone, the residual ionic concentration is also remarkable.

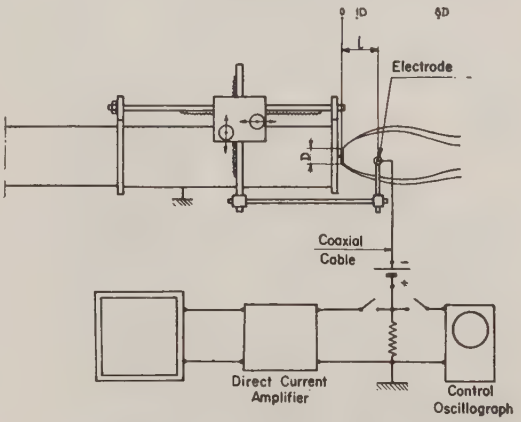

FIG. 1. Setup for recording ionic currents in flames.

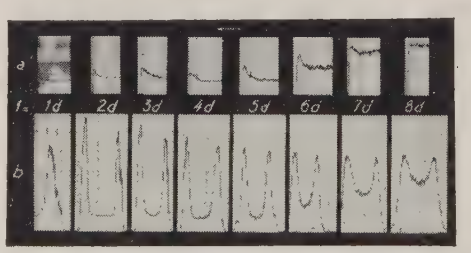

FIG. 2. Records of relative ionic density in the flame. (a) Ionic current; picked up by the probe in the core before and during lean blow out. (b) Ionic current picked up by the probe crossing the flame at different distances from the disc. Disc d = 25 mm; v = 110 m/s; A/F = 18.65.

This residual ionization is attributed to the relatively slow rate at which the ions formed in the reaction zone recombine.

In a flame stabilized by an obstacle, the interval between the time when the positive ions and the negative ions (electrons) produced in the reaction zone start to recombine, and the time when they are detected in the recirculation zone of the core is very short. The average recirculation time, τ, is of the order of 10 msec, under the experimental conditions considered.[4, 5] In the following we will assume that the time needed for

the ions to recombine is of the same order ($t \sim 10^{-2}$ sec).

Assuming that, in a flame, the positive ion concentration is about the same as that of the negative ions, we can write

$$n_+ = n_- = n$$

where n is the ion concentration per cu cm of gas.

The rate of recombination, dn/dt, varies with the square of the concentration

$$dn = -\alpha n^2 \, dt$$

If we assume that the recombination coefficient,

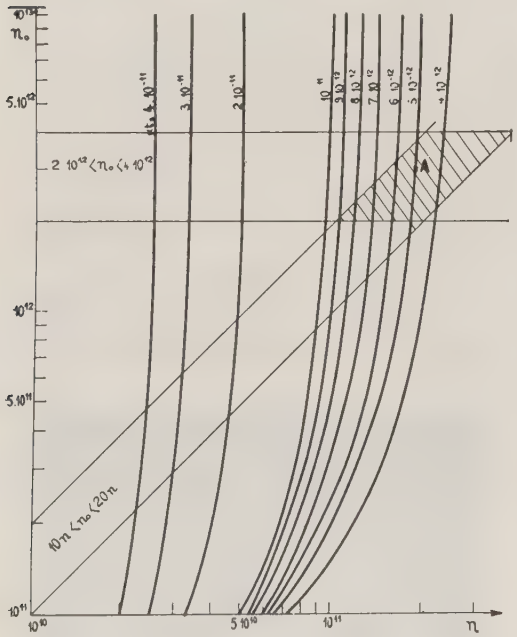

FIG. 3. Residual ionic density vs initial ionic density and recombination time. α = recombination factor.

α, remains constant, a simple integration gives the residual concentration, n, as a function of the initial concentration, n_0, and of the time interval, t:

$$n = \frac{n_0}{1 + n_0 \alpha t} \qquad (1)$$

Figure 3 shows a network of parts of hyperbolas for initial concentrations varying between 10^{11} and 10^{13} ions per cu cm and different values of αt. These curves make it possible to obtain the residual concentration as a function of these various parameters.

At this stage, it is necessary to discriminate so as to eliminate the regions of the graph which do not correspond to the assumed or measured experimental data. Thus: (a) For the stoichiometric mixture ratio, n_0 is maximum and its value n_{0s} is of the order of 2.10^{12} to 4.10^{12} ions/cm^3 for hydrocarbon flames at atmospheric pressure.[2, 6] We have the conditions

$$2.10^{12} < n_{0s} < 4.10^{12} \qquad (2)$$

(b) As seen in Section 3, the ionic current in the reaction zone with stoichiometric regime was about 15 times that of the core; this gives approximately the order of the value of the ratio n_{0s}/n_0. We will assume that

$$10_n < n_{0s} < 20_n \qquad (3)$$

Both of these two conditions are satisfied simultaneously inside the parallelogram formed by the intersection of the couples of parallels defining the conditions (a) and (b) on the diagram (Fig. 3).

Let us consider point A on the curve $\alpha t = 5.10^{-12}$ for which the initial concentration is $n_{0s} = 3.10^{12}$ and the residual concentration is $n \sim 2.10^{11}$, making the ratio n_{0s}/n close to 15.

If the dilution, n_0, varies from 3 to 1, it will be seen that the variation of n is only 10 per cent, which corresponds to the variations of the ionic current observed in the core (Section 3).

It remains to examine the compatibility of the value of α with the assumed experimental values for the flames: for $t = 10^{-2}$, $\alpha_A = 5.10^{-10}$. The few rather rough studies carried out in this field give values ranging from 2.10^{-10} to 5.10^{-10}.[5, 6, 7] Thus the elementary calculation leads to a series of cross-checks which suggest that these relative ionization measurements may be of some value.

The successive tests, first with a disc-stabilized flame and then with a cone-stabilized flame,[a] show the same type of phenomenon, except that the ionization level is higher in the core of the cone. As the volume of the cone core is smaller, both the recirculation time and the recombination time are shorter, raising the level of residual ionization.

As the mixture deviates from the stoichiometric ratio, n_0 decreases and it will be seen from Figure 3 that n should not increase if there were no longer any reactions. However, we do observe an increase of the ionic density in the hot gases of the core before extinction. The closer we are to the disk, the nearer the dilution for which

[a] Both the disc and cone had a diameter of 25 mm.

this increase of the ionic density appears will be to the quenching dilution of the mixture.

It seems that as we get closer to a quenching limit, the core is penetrated increasingly at its downstream end by small volumes of gases in process of reaction. This hypothesis had already been advanced by Williams and Shipman[9] to explain the striograms obtained by them.

In rich mixtures, the increase of the ionic current is less marked and occurs much closer to the quenching limit. It does not even occur at lower speeds where a slight and progressive decrease of the ionization level is observed, indicating that chemical conversion is virtually eliminated in the core.

5. Conclusions

Use of an ionization probe to explore the wake of a flame stabilizer in a constant mixture showed that there is a core where the ionic density is low. Its edges are thin at the beginning, gradually growing wider downstream until they meet to give a high density. The ionic density in the core varies very little with the dilution of the incident mixture, contrary to what is found in the lateral zones where this density has a relative value, with respect to that in the core, that reaches a maximum of 15 near the stoichiometric. When the probe is maintained at a given point in the core and the mixture concentration is changed, an increase in ionic density is observed near the quenching limit. The time lag decreases as the probe is brought closer to the stabilizer. Thus, it appears that for a wide range of mixture dilutions, there is no chemical reaction in the core. However, near the limits, gases in process of reaction seem to penetrate increasingly from the downstream gas into the core.

As far as optical temperature measurements are concerned, that require complete chemical equilibrium for the application of Kirchhoff's law, we must concentrate on the region near the obstacle. As the reaction zone explored by the optical beam is thin, the possible error will be small, whereas near the quenching limits, or at a point too far downstream, the beam passes through appreciable thicknesses of reacting gas and the resulting error may be large.

Nomenclature

τ recirculation time
t time required for the ion recombination
α ion recombination coefficient
n ion concentration (per cc)
n_0 initial ion concentration (per cc)
n_{0s} initial ion concentration at the stoichiometric ratio
A air mas flow (g)
C in English: F, fuel mass flow

REFERENCES

1. Karlovitz, B., Denniston, D. W., Knapschaefer, D. H., and Wells, F. E.: *Fourth Symposium (International) on Combustion*, p. 617. Baltimore, The Williams & Wilkins Co., 1953.
2. Calcote, H. F., and King, I. R.: *Fifth Symposium (International) on Combustion*, p. 423. New York, Reinhold Publ. Corp., 1955.
3. Mestre, A.: AGARD, *Combustion Researches and Reviews*, p. 72. London, Butterworths Scientific Publications, 1955.
4. Nicholson, H. M., and Field, J. P.: *Third Symposium on Combustion, Flame and Explosion Phenomena*, p. 44. Baltimore, The Williams & Wilkins Co., 1949.
5. Longwell, J. P., Frost, E. E., and Weiss, M. A.: Ind. Eng. Chem., *45*, 1629 (1953).
6. Gaydon, A. G., and Wolfhard, H. G.: *Flames: Their Structure, Radiation, and Temperature*. London, Chapman and Hall, Ltd., 1953.
7. Loeb, L. B.: *Basic Process of Gaseous Electronics*. Berkeley, University of California Press, 1955.
8. Loeb, L. B.: *Fundamental Process of Electrical Discharge in Gases*. New York, John Wiley and Sons, Inc., 1939.
9. Williams, G. C., and Shipman, C. W.: *Fourth Symposium (International) on Combustion*, p. 733. Baltimore, The Williams & Wilkins Co., 1953.

103

A DETECTOR FOR COMBUSTIBLE HYDROCARBONS IN AIR

By HAROLD M. BREWSTER[a]

An automatic and portable explosive gas-air detector has been developed for atmospheric conditions. The detector is applicable for sampling in open combustion facilities and fuel rooms.

Detectors which have been previously developed are suitable and can be calibrated for a given hydrocarbon in air, or for a mixture of hydrocarbons in air where the proportion of each hydrocarbon to the total hydrocarbon content remains constant. However, the wide limits set by the present gas turbine (jet engine) fuel specifications has led to a unique problem in determining the explosive hazard created when the fuel is exposed and some of the fuel constituents evaporate. Not only will the proportions of these constituents vary with different batches of fuel, but they will also change depending upon the pressure and temperature to which the fuel is exposed and the length of exposure time at a given condition.

Development of this detector was based upon published information which showed that the total heat content per unit volume of the possible constituents evaporating from reciprocating and gas turbine fuels at their lean explosive limit in air is practically the same.[1]

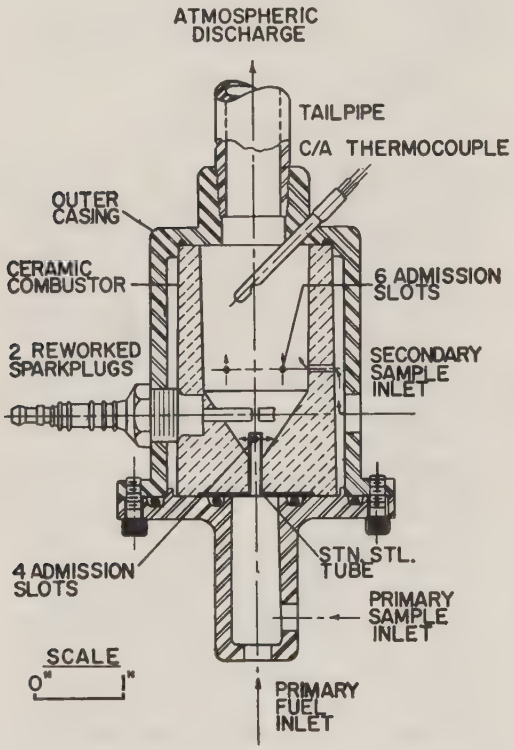

FIG. 1. Cross-sectional view of the detector combustor.

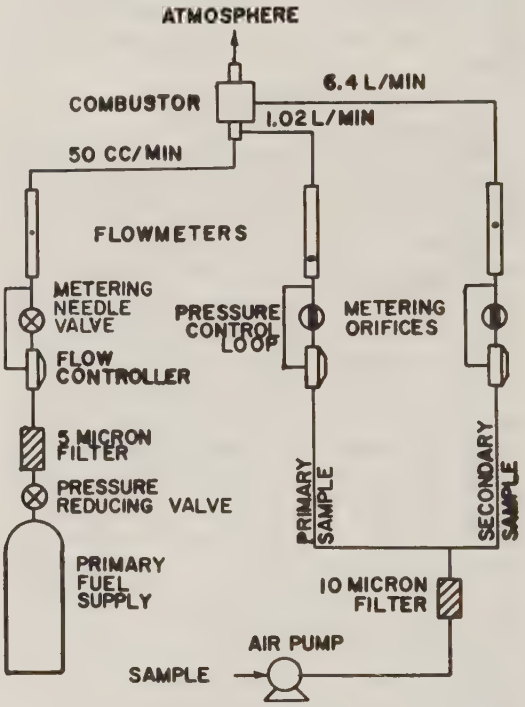

FIG. 2. Schematic of the detector flow system.

Description of Detector

As shown in Figure 1, the detector consists of a small combustor to which primary gaseous fuel and a sample of air or air and fuel from the area under investigation are delivered at known rates of flow. The mixture is ignited and combustion is then self-sustaining. Credit for the basic idea goes to W. Slivka and J. Daley of the Naval Air Development and Material Center.

[a] The opinions stated in this article are the private ones of the writer and are not to be construed as official or reflecting the views of the Navy Department or the Naval Service at large.

The burner consists essentially of a ceramic liner enclosed in a stainless steel casing, to which primary fuel and a portion of the sample (primary sample) are metered. The remainder of the sample (secondary sample) is admitted downstream for the purpose of lowering the temperature of the combustion products. The exhaust gases are discharged to atmosphere. The entire combustor and tailpipe are insulated with a ¼-in. layer of asbestos.

The rates of flow (in l/min) used in the present test were: primary fuel (propane), 0.05; primary sample, 1.02; and secondary sample, 6.40. As shown in Figure 2, these flows were maintained by conventional flow controllers, which provide constant downstream pressure and constant flow through the metering orifices regardless of upstream pressure or flow variations. The flows were indicated visually by float type flowmeters.

The sample is forced by a vane-type pump through a 10-μ filter, to prevent clogging of the metering orifices, and is then divided into the aforementioned primary and secondary sample flows. The primary fuel from a small tank (150 psig) passes through a pressure reducing valve and a 5-μ filter.

Thermocouples, connected differentially, indicate the temperature rise across the combustor. An increase in this temperature rise to a predetermined limit, due to a given fuel vapor concentration in the sample, activates an electrical relay to produce an audible and visual alarm signal.

A thermal relay, located in the combustor discharge tailpipe, deactivates the ignition system after combustion has been initiated.

Calibration Procedure

The detector was calibrated using samples containing known amounts of propane and of acetylene in air. Sample strengths were calculated by use of Dalton's law of partial pressures, with corrections made to the dry basis from psychrometric and barometer readings.

The detector was activated and allowed to come to equilibrium while the sample consisted of pure air. A propane- or acetylene-air sample of known composition was then admitted to the detector. The combustor temperature rise was noted after equilibrium conditions had been observed for a period of at least ten minutes. It was found that, regardless of sample strength, the time required for attainment of equilibrium was practically a constant. The detector was again operated on an air sample until another gas-air sample strength could be prepared and admitted. This test procedure was repeated on subsequent days to determine the reproducibility of results.

Discussion

The observed values of temperature rise, shown as a function of the gas-air sample strengths, are given in Figure 3, in which the open symbols denote propane-air and the closed symbols denote acetylene-air samples. From the known combustion characteristics of propane and acetylene,

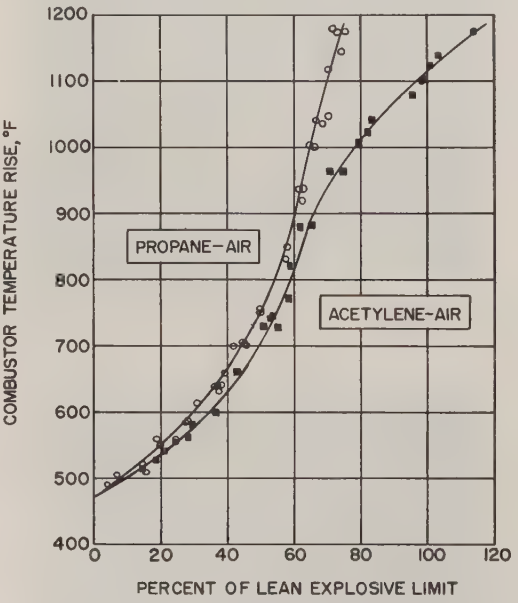

Fig. 3. Effect of gas-air sample strength on the detector temperature rise. Primary fuel: propane.

a possible explanation of the differences between the two curves can be presented. However, the explanation is highly speculative and does not affect the operation of the detector.

The propane-air curve, shown in Figure 3, adequately represents the combustor temperature rise expected when sampling areas in which the vapors of gas turbine fuels may be present.[1]

During initial tests of the detector, it was noted that nearly an hour elapsed between the introduction of a gas-air sample and the attainment of combustor equilibrium. If the sample strength was that for which the alarm system had been set to activate, this time lag could not be tolerated. Derivative action was added to the alarm system to minimize the time lag.

Conclusions

The detector as evaluated is useful only in test facilities operating at atmospheric conditions. However, it is believed that a second air pump placed in series with the existing air pump, and capable of delivering the required flow at atmospheric pressure, would suffice to adapt the detector for low pressure use, provided that the temperature rise due to compression prevents condensation of the hydrocarbon constituents.

In conclusion, the detector is relatively simple to operate, and its usefulness is not affected by a wide variation in the proportions of hydrocarbons being detected.

Acknowledgments

The author would like to thank W. Slivka for his help and close association during the initial development work, W. Wastallo and I. Stoltze for their contribution to the detector development and evaluation, and to F. Koehler and R. Weiss, test mechanics for their invaluable assistance in the overall development of the detector.

REFERENCE

1. Spakowski, A. E.: NACA RM52H15, Sept. 1951.

104

A MICROPHOTOGRAPHIC DEVICE FOR THE STUDY OF RAPIDLY MOVING MISTS AND ITS APPLICATION TO RESEARCH ON CARBURIZATION IN INTERNAL COMBUSTION ENGINES

By WILLY DIAMANT

An experimental study has been made of a device designed for direct observation and instantaneous photography of pulverized liquid jets. With this device it becomes possible to determine the speed and dimensions of the liquid particles—essential factors for the study of the microstructure of mists—and to establish the instantaneous distribution of the droplets throughout the jet.

Objectives

Let us consider briefly the principal methods used in previous investigations of the macro- and microstructure of jets. Lee, Zahn, and Schweitzer employed a method of impressions in a plastic substance produced by the observed structure. This method gives the mean diameter of the particles, but unfortunately it cannot be used to carry out experiments within the combustion chamber. Woeltjen made use of a jet which he directed into an absorbing liquid. Other workers in the field have collected droplets on smoked glass, microphotographed the emulsion and studied the mist statistically. The modern trend is to study the jet *in nascendo* in the combustion chamber with the aid of instantaneous photography and high-speed motion pictures. Continuous observation leads to a better appreciation of modifications designed to improve the pulverization of the combustible. Accordingly, our purpose is not only to photograph the process of pulverization at any moment and any point in the jet, but to carry out observations in a continuous manner. Except for stroboscopic techniques, none of the previous methods of observation achieves this.

The problem was to find a new and simple method of observation that could easily be applied to the investigation of carburization. For this we needed an optical system that would not be affected by the observation chamber placed between the carburetor and the inlet duct. To simplify the apparatus, an electric spark illumination was replaced by a tungsten-filament source. Even a very rapid flash of light tends to blur the photographic plate unless the light moves with the illuminated particle. It is possible, however, to arrest the image for the duration of pulverization and we shall see how this can be accomplished.

Experimental Procedure

Let us consider a rotating mirror whose vertical plane of reflection is perpendicular to the optical

axis of an objective lens associated with it and let us assume that this objective lens is situated between the jet and the mirror. With the lighting correctly adjusted, let us assume the speed of rotation of the mirror to be such that it sweeps the field of vision in a time equal to the time that it takes a liquid particle to traverse the same field. We can then consider the two velocities as equal, and the image formed by the objective will be stationary and permanently observable. Moreover, by moving the reflected image of the jet into the object plane of a microscope we obtain all the space we need between the light source and the objective lens, which can have any suitable focal distance. Another important advantage lies in the use of an ordinary light source.

Theoretical Considerations

Let V be the velocity of liquid particles in the plane of the jet and V' be the speed of the corresponding image formed by the objective lens. Let p' be the distance of the principal objective lens from the virtual image plane of the jet and let A be the distance from the center of rotation of the mirror to the principal objective lens. If p is the distance from the objective to the principal objective lens, and ω_0 is the angular velocity of the real image, the velocity of the real image becomes

$$V' = \omega_0(p' - A)$$

where ω_0 is the angular velocity of the image, and ω_m the angular velocity of the mirror. If N is the number of revolutions per minute of the mirror, we have

$$2\omega_m = \omega_0 = \frac{4\pi N}{60}$$

$$V' = \frac{4\pi N}{60} \cdot (p' - A)$$

If γ is the magnification by the objective lens, we have

$$\gamma = p'/p \text{ and } V' = \gamma V$$

$$\gamma V = \frac{4\pi N}{60} \cdot (p' - A)$$

$$V = \frac{4\pi N(p' - A)}{60\gamma}$$

$$N = \frac{60\gamma V}{4\pi(p' - A)}$$

Thus the rpm of the mirror necessary to obtain a stationary image is directly proportional to the speed of the particles V and inversely proportional to $(p' - A)$. Both the distance p' and γ are constants.

The only variable in the formula for N being A, it is sufficient to control that distance in order to keep the image of the droplets stationary at various points along the jet. A continuous control is thus available, which can be as accurate as desired.

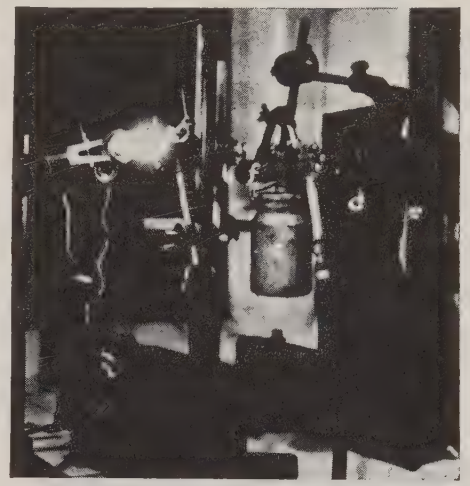

FIG. 1. Laboratory Apparatus. (a) Light; (b) slit; (c) spray; (d) photographic objective; (e) mirror; (f) microscope.

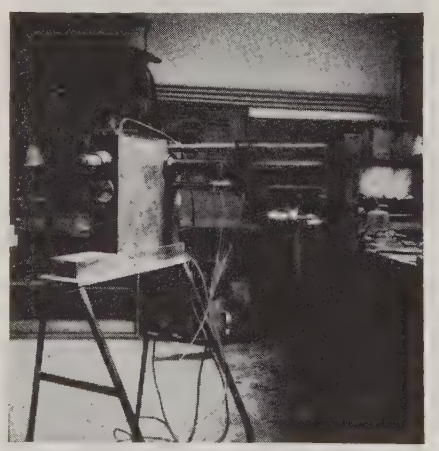

FIG. 2. Laboratory Apparatus.

Experimental Set-up

The light source is a flat tungsten filament supplied from a 6-v electrical source. A variable resistor is used to adjust the intensity of the light

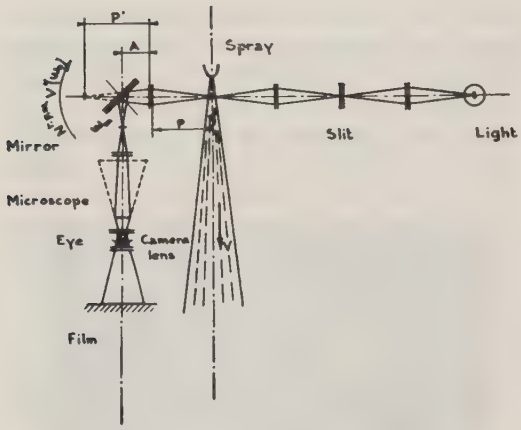

FIG. 3. Diagram of optic method.

the first, we obtain illumination "in the flame." The illuminated slit becomes the slit source and its image is formed in the plane of the jet. Each droplet which passes through the viewing field (its image being equal to that of the source since the magnification chosen is $\gamma = 1$) becomes an illuminated particle. To satisfy the same condition, the objective lens must have the same aperture as the condensing lens, that is f/1.9. The focal distance of the objective being 9.6 cm, its distance to the jet is equal to 19 cm, for $\gamma = 1$.

The rotating mirror placed behind the objective lens reflects the image of the jet perpendicularly to the optical axis. It is formed in the frontal plane of a microscope with a magnification of 10. The particles which constitute the jet can thus be

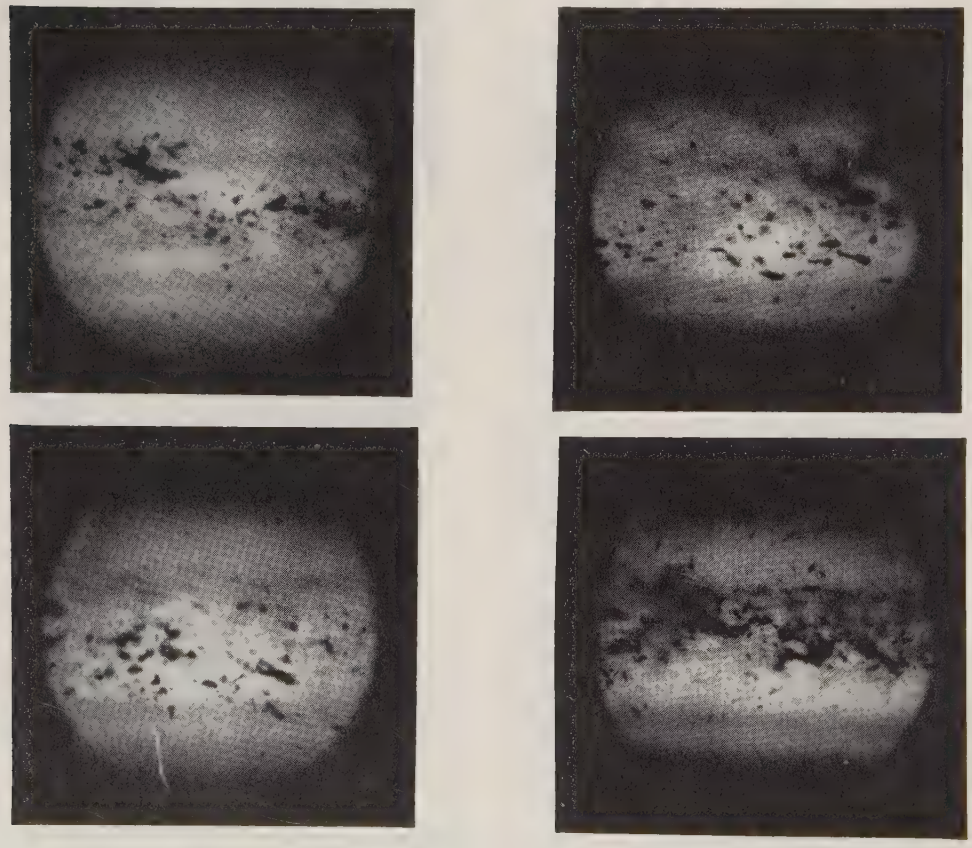

FIG. 4. Photographs of spray (water). $V = 30$ m/sec. (Magnification, 15×)

source, reduced intensity being sufficient for observation and adjustment.

A first condensing lens with an f/1.9 aperture forms the image of the filament in the plane of a vertical slit (4 mm × 0.10 mm). With the aid of another condenser having the same aperture as

observed at any time. A photographic camera may be placed against the eyepiece in order to obtain a record of the droplets. It is sufficient to choose an exposure time that is slightly inferior to the time required for complete revolution of the mirror.

Efficiency of the Method

The optical image supplied by the microscope is of excellent quality owing to high contrast, and is readily observable. The changes in the jet can be observed easily with a slit of 10/100 mm. In fact, the narrower the slit, the smaller are the amplitudes of observable movements of the particles and the better the images.

We were able to observe jets under excellent conditions of visibility using a 10-mm wide slit. The disintegration of liquid filaments could readily be observed. Thus in the case of water at pulverization velocities of about 40 m/sec, disintegration of the liquid filaments begins near the orifice (within 0.1 to 0.2 cm). Consequently the time of resolution of the jet is of the order of 1/30,000 sec. During the observation, a micrometric image screen placed in the object plane of the microscope makes it possible to determine the dimensions of the droplets and their distribution in the optical field. This makes it possible to determine the statistics of the jet distribution. With A held constant, N is controlled by a variable resistor. Owing to variations in the velocities of the droplets at different points along the jet, it is necessary to control the speed of the mirror with precision. The variable resistor should be graduated in m/sec of speed instead of rpm. The method described enables us to obtain at any instant the chief parameters defining pulverization, the velocity of particles, their dimensions and their distribution in a given space.

Conclusions

A simple method has been developed to be used in research on carburization in combustion engines. A chamber possessing transparent windows can be placed between the carburetor and the inlet duct. In practice, there is a distance of 40 cm between the condensing lens and the objective lens. Thus, when an interesting new detail appears, it can be recorded conveniently.

105

AN APPARATUS FOR STUDYING THE BURNING OF DUST CLOUDS[a]

By LLOYD E. LINE, JR., WENDALL J. CLARK AND JAMES C. RAHMAN

Introduction

Although a considerable amount of work has been carried out over the past 20 years or longer in the field of dust explosions,[1-10] relatively little effort has been expended to learn the physicochemical processes underlying the combustion of finely divided solids suspended in an oxidizer gas. Most of the methods for producing and igniting dust clouds have been developed to simulate conditions in a coal mine or in other technological processes and to define the conditions under which a dust cloud in air becomes hazardous.

The apparatus described in this paper has been built to gain an understanding of the processes underlying the burning of dust suspensions by studying the phenomenon under a wide variety of controlled conditions. While it is similar in some respects to systems previously described, it has certain novel features which include: (a) generation of a nonturbulent dust cloud, (b) production of the cloud in a wall-free as well as a wall-confined condition, (c) provision for varying the percentage of oxygen in an oxygen-diluent gas mixture continuously from 0 to 100 per cent, as well as for varying the dust concentration and spark ignition energy over wide limits, (d) instantaneous measurement of the concentration of the dust cloud, and (e) provision for studies at initial pressures up to 100 psi.

[a] This research was supported by the United States Air Force, through the Office of Scientific Research of the Air Research and Development Command, and the United States Navy, Bureau of Aeronautics.

Description of the Apparatus

PRINCIPLE OF OPERATION

The dust cloud is produced in the form of a continuously moving column. A turbulent dust cloud is created in a dust generator (Fig. 1) by means of jets of premixed oxidizer gas passing through

a bed of the finely divided solid. This cloud is then directed downward through a vertical cylindrical tube from which it emerges continuously into the combustion chamber as a nonturbulent, wall-free column of dust particles moving at a velocity of about 30 cm/sec. To provide a wall-

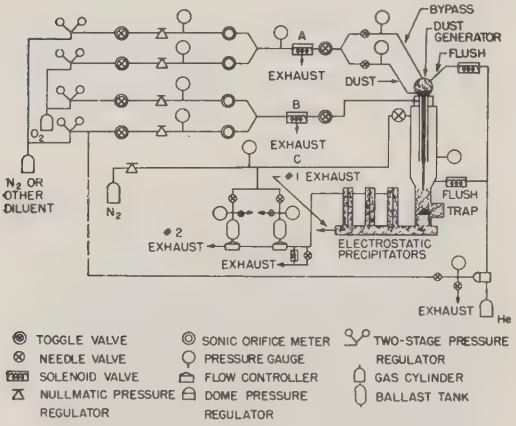

FIG. 1. Schematic diagram of dust explosion apparatus and flow system.

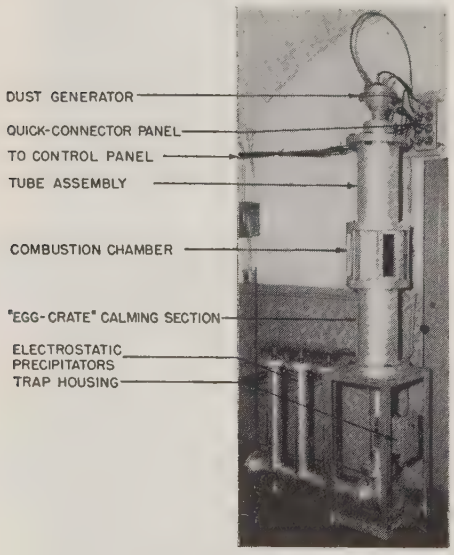

FIG. 2. Dust explosion apparatus.

confined system the wall-free column is surrounded by an open-end glass tube of the same diameter. When the desired dust and oxidizer concentrations are established, the column is ignited in the explosion chamber by means of a capacitance spark, and the resulting flame propagates along the moving dust column. The dust-laden gas and combustion products are vented directly to the atmosphere (No. 1 Exhaust) in experiments at ambient pressure or through pressure regulators (No. 2 Exhaust) in experiments at elevated pressures.

FLOW SYSTEM

Gas flows continuously into the apparatus through three lines A, B, and C (Fig. 1). Premixed gas from line A passes into the dust generator. For controlling the dust concentration the flow may be split so that only a part of it flows into the dust bed, while the remainder goes through the "by-pass." Premixed gas from line B, of the same composition as that in A, passes into an annular space between the dust tube and a surrounding tube of slightly larger diameter in order to stabilize the wall-free dust column. Nitrogen from line C passes into a second annular space to confine the turbulent dust mixture to the lower part of the apparatus. The gas flows in lines A and B are accurately measured and controlled with sonic orifices and pressure regulators.[11]

Figure 1 shows two positions (flush lines) at which inert gas (helium, nitrogen) may be introduced through solenoid valves for extinguishing the flame. In the experiments described below the burning rates at ambient pressure were slow enough that manual discharging of the inert gas through the top line was adequate. In some cases the flame self-extinguished in the dust tube. Seldom has the flame propagated below the combustion chamber. Experiments at higher pressures or with faster-burning materials will require improved methods for confining the burning to the region of the combustion chamber.

DUST EXPLOSION APPARATUS

The dust explosion apparatus proper (Fig. 2), of steel construction, stands about 8 ft high and rests on a support made of 0.5-in. steel plate and 1.5-in. angle iron. It is constructed of a number of flanged sections to facilitate alteration and replacement of parts where necessary. The essential parts of the apparatus are dust generator, concentric tube assembly, combustion chamber, "egg-crate" calming section, and dust-collection equipment.

The dust generator shown in Figure 3 was designed originally for use with boron up to initial pressures of 100 psi. It consists of a spherical steel chamber approximately 11 in. in diameter divided into halves for access and given a high inside polish to reduce the caking of dust on the wall. Through the bottom half, a smooth-walled

tube (dust tube), 1 in. in diameter and 28 in. long, extends 3.5 in. The dust is blown into a cloud by passing the premixed gas through an annular ring with several evenly spaced holes 0.3 mm in diameter. Agitation of the dust bed, necessary for materials like boron which tend to channel, is accomplished by means of a nest of screens attached to a Bourdon tube. The latter is pulsed with gas from a cylinder at pressures up to 125 psi through a 3-way solenoid valve. This valve is opened and closed by means of an electronic circuit which allows pulsing frequencies from approximately 1 to 10 cycles/sec.

The generator shown in Figure 3 does not appear to be as suitable for freely flowing powders (such as atomized magnesium and lycopodium) as the one shown in Figure 4. With this generator charged with freely flowing powders, no agitation mechanism is required. It is particularly suitable when one must work with small charges.

The concentric-tube assembly, an exploded view of which is shown in Figure 3, consists of (a) the smooth-walled dust tube 1 in. i.d. and 28 in. long, (b) a smooth-walled 2.5-in. i.d. tube, 18 in. long, and (c) the 8-in. pipe. Between the walls of the 1-in. and 2.5-in. tubes is a calming assembly of seven horizontal screens (25-mesh) distributed at equal intervals along the length of the assembly. The gas for this enveloping stream is introduced at the top through an annular ring with equally spaced holes. Calming sections also exist between the 2.5-in. tube and the 8-in. pipe at the top and at the bottom of the assembly.

The combustion chamber, constructed from a 12-in. length of 8-in. steel pipe, is fitted with four equally spaced Pyrex windows 3.5 x 9 x 1 in. for observation, photography, and measurement of dust concentration. It is also fitted with removable plates through which electrical leads are introduced.

An "egg-crate" calming section 18 in. in length and constructed of thin strips of stainless steel is placed below the combustion chamber to assist in keeping dust from "boiling up" between the dust column and chamber walls.

The trap shown in Figures 5 is used to collect unburned dust and the products of combustion for examination. In addition it relieves the electrostatic precipitators of a considerable load and should aid in the quenching of the downward moving flame. Two metal plates 90° apart are fastened to a hinge. During establishment of the dust column plate 1 is horizontal and plate 2 is vertical. Most of the dust piles up on plate 1, while the remainder passes with the flowing gas through the annular space (about ¼ in.) between the plate and the 3-in. pipe. When the solenoid is energized (a second or two prior to igniting), the horizontal plate strikes the frame, whereupon the adhering powder is thrown into the housing. At the same time plate 2 moves into a horizontal position for collection of the burned

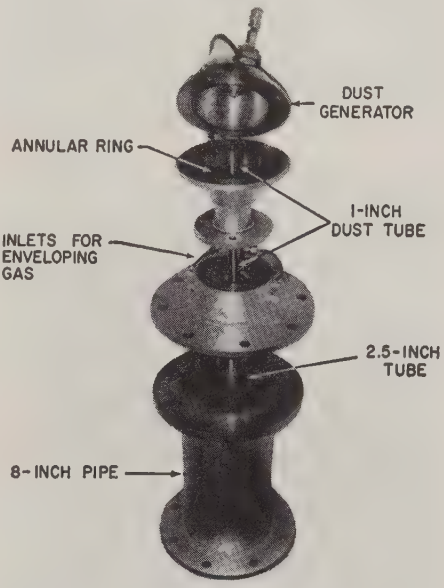

FIG. 3. Dust generator and exploded view of concentric tube assembly.

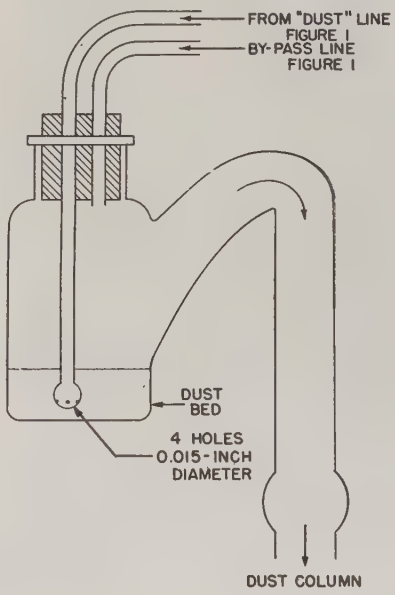

FIG. 4. Alternate type of dust generator.

powder. When the trap is thrown, there is a slight disturbance, but the column re-establishes itself quickly. When the pressure regulators are employed to control the system pressure, the exhaust must be dust-free, and the removal of the dust is accomplished by three electrostatic precipitators in parallel. These are constructed (Fig. 2) from 3-in. steel pipe and concentri-

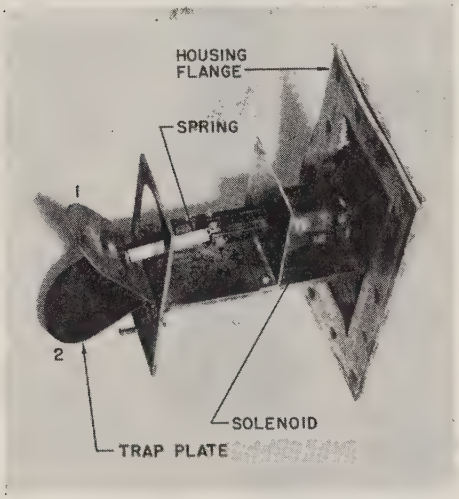

FIG. 5. Dust trap.

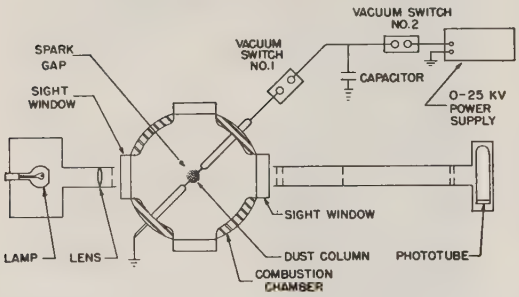

FIG. 6. Schematic diagram of densitometer and spark-ignition circuit. Combustion chamber is shown in horizontal cross section.

cally spaced rods $\frac{1}{8}$ in. in diameter. The latter are brought to a dc potential less than the breakdown potential for the dust-gas system, and the dust particles collect on the rods and on the walls. This system, in conjunction with a glass wool filter, completely removes boron dust from the exhaust gas.

SPARK-IGNITION SYSTEM

The dust column is ignited by passing a capacitance spark across the column between two tungsten probes 0.014 in. in diameter. The probes are given a small amplitude vibration during a run to keep dust from collecting on them. The joules of energy stored in the capacitance is given by $CV^2/2$, where C is the capacitance in farads and V is the voltage.

The circuit is shown in Figure 6. Solenoid-operated vacuum switches and low-resistance leads are employed to minimize energy losses. In operation Switch No. 2 is closed for a time sufficient to charge the condenser. The condenser is then discharged by simultaneously closing Switch No. 1 and opening Switch No. 2.

With dust clouds, the spark lag (*i.e.*, the time required for breakdown after the voltage has been applied) must be minimized; otherwise the column is distorted before the spark passes, and the dust concentration in the gap is different from that measured. This has been done by using condenser voltages in excess of the breakdown potential. Measurements of spark lags with excess voltage with various O_2-N_2 and O_2-He mixtures and different gap distances indicate that a very large majority of the spark lags are well under 5 msec. Experiments with nitrogen carrier gas also indicate that the spark lag is not greatly affected by the presence of dust. A calculation shows that the predischarge displacement in 5 msec of a spherical particle 15 μ in radius carrying 10 electrostatic charges and having a density of 1 g/cc should be only about 3×10^{-4} cm when placed with zero lateral velocity in an electric field set up by 25 kv across a 1-cm gap. The disturbance due to the drift of charged particles in an electric field is therefore probably very small unless each particle carried 1000 or more charges.

MEASUREMENT OF DUST CONCENTRATION

The concentration of dust immediately before the spark discharge is measured with a light-absorption apparatus, hereafter referred to as a "densitometer" (Fig. 6). A defined beam of parallel light originating from a source of fixed intensity I_0 is passed through the dust column and emerges with reduced intensity I. The ratio I/I_0 corresponds to a definite concentration of dust. This is given by a calibration curve of the type shown in Figure 7.

Each point is obtained from (a) the loss in weight from the dust generator divided by the volume flow rate times the time, and (b) the time-average value of I/I_0 held to a nearly constant value by manual adjustment of the dust concentration.

The optical system of the densitometer employs a 50-cp automobile headlamp placed at the

focal point of an achromatic lens of 17-mm diameter and 80.8 mm focal length. The emergent rays, approximately parallel, are collimated with perforations 0.25 in. in diameter. The beam strikes a 929 phototube, and the output of the latter is measured with a conventional bridge circuit and microammeter. After ignition there is normally a thin dust deposit on the windows. This is compensated for by adjustment of the bridge circuit prior to each firing to give full scale deflection of the microammeter. The microammeter reading (full scale, 100 μa) can be read or controlled to ± 0.5 μa. The dust concentration of lycopodium is therefore controlled to about ± 10 per cent in the dust-concentration range 40 to 180 mg/l.

When wall-free dust columns are ignited, the densitometer light beam is nearly in the same plane as that of the spark electrodes and is located about 2 in. from the end of the dust tube. When the glass confining tube is employed, the densitometer light beam is located just below the glass tube, about 5 in. from the probes. The glass tube is 8.5 in. long, with spark electrodes introduced through side arms of capillary tubing at the midpoint of the tube.

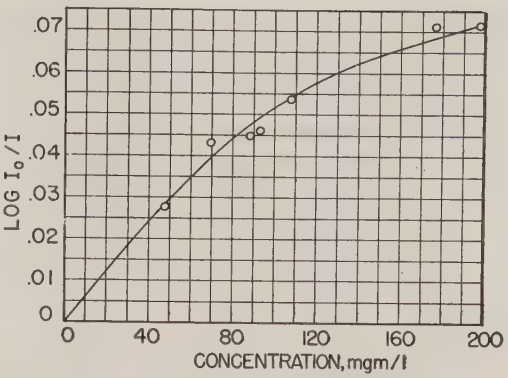

FIG. 7. Densitometer calibration curve for lycopodium.

FIG. 8. Wall-free moving column of boron dust. Atmospheric pressure; side illumination.

WALL-FREE DUST COLUMNS

The conditions for producing stable, wall-free dust columns must be carefully controlled. The velocity of the enveloping annular stream is determined by experiment and appears not to be critical. However, its flow must be perfectly concentric and axial. The column stability is sensitive to thermal gradients and to small volume disturbances in the dust generator. The appropriate conditions for producing stable columns must be determined in advance for each dust used.

Figure 8 shows a wall-free, moving column of boron dust (particles up to 10 μ in diameter) at atmospheric pressure as viewed through the chamber windows. It was created with the spherical type of dust generator (Fig. 3) and with the Bourdon tube shaker mechanism. The linear velocity of the dust column was 15 cm/sec, while that of the enveloping stream was 7 cm/sec. Satisfactory wall-free dust columns of charcoal, atomized magnesium, and lycopodium have also been produced.

Results on the Ignition of Dust Clouds

This section presents some examples of results which serve to indicate the usefulness of the apparatus. While eventually it will be desirable to measure flame propagation rates along the moving dust cloud, initial experiments have been carried out to find the critical oxygen concentration (with a fixed spark energy) or critical

spark energy (with a fixed oxygen concentration) for ignition of a dust cloud of given characteristics. The purpose of these experiments has been to explore possibilities for future study and to define the precision of the data and the importance of certain apparatus parameters. Explanation of the results in terms of fundamental processes will form the subject of a future paper.

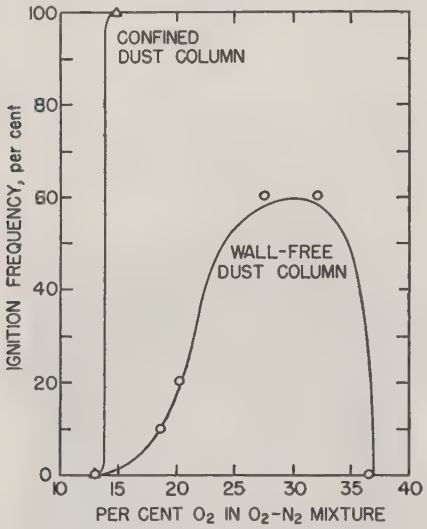

FIG. 9. Ignition frequency vs O_2 concentration for lycopodium in O_2-N_2 mixtures. Dust concentration, 180 mg/l; condenser energy, 5.3 joules; spark gap, 12.5 mm.

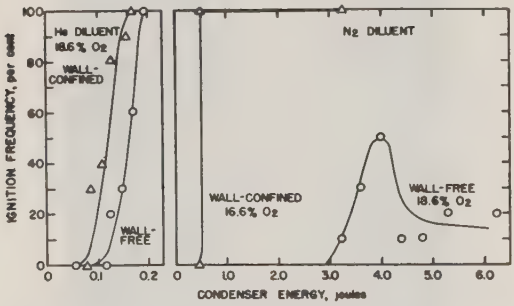

FIG. 10. Ignition frequency vs condenser energy for lycopodium in O_2-diluent mixtures. Dust concentration, 180 mg/l; spark gap, 12.5 mm.

In carrying out these experiments lycopodium has been a convenient material for study because of its flow properties and uniform particle size (*ca.* 30 μ in diameter).

The results have been obtained at a pressure of one atmosphere with the use of the dust generator shown in Figure 4. The pressure regulators, trap, and electrostatic precipitators were not employed. In all experiments the flow rate in the dust tube was 150 cc/sec, corresponding to an average linear velocity of 30 cm/sec. For wall-free experiments the flow rate of the enveloping stream was 150 cc/sec corresponding to an average velocity of about 6 cm/sec. We arbitrarily include in the definition of "ignition" a minimum flame propagation of 4 in. along the dust column. In almost all trials the propagation was 4 in. or more or not at all.

The critical oxygen concentration or condenser energy for the spark ignition of dust clouds in this apparatus is not sharply defined. Instead there is a certain range over which the ignition appears to be statistical. In this range a plot is made of the ignition frequency (the percentage of trials igniting, normally based on 10 trials) as the ordinate against the condenser energy or oxygen concentration as the abscissa. Example of these plots are given by Figures 9, 10, and 11.

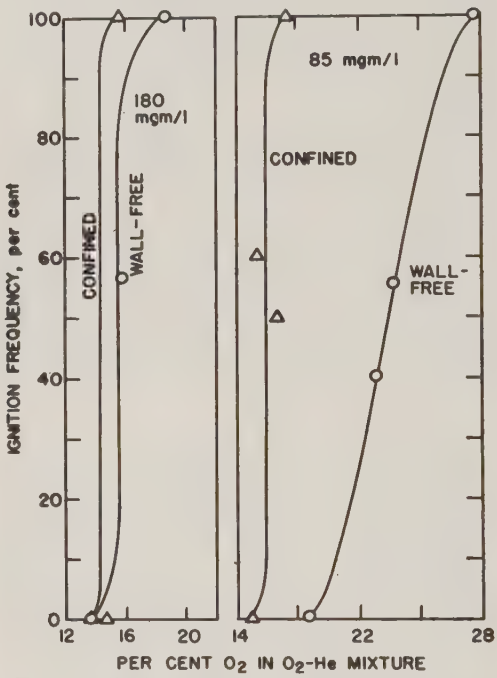

FIG. 11. Ignition frequency vs O_2 concentration for lycopodium in O_2-He mixtures. Condenser energy, 5.3 joules; spark gap, 12.5 mm.

One would expect the ignition frequency to rise continuously with increasing oxygen concentration to 100 per cent ignition frequency and remain there as the oxygen concentration is increased to 100 per cent. However, many experiments with wall-confined and wall-free dust clouds yield curves that go through a maximum. An example of this behavior is given by the curve

for the wall-free dust column in Figure 9. Experiments are now being carried out to determine whether this behavior reflects a real property of dust clouds or some behavior of the spark or of the apparatus as yet not clearly understood.

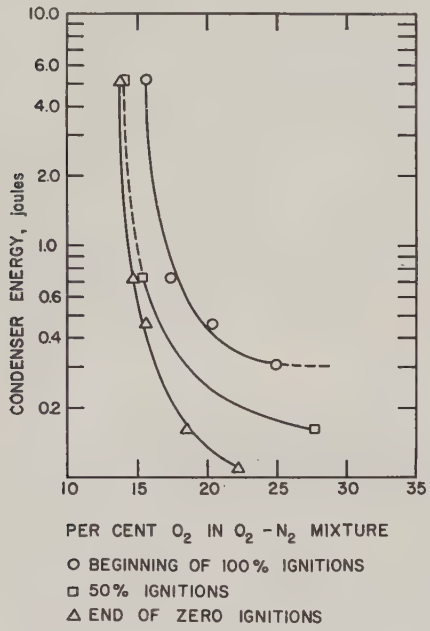

FIG. 12. Effect of O_2 concentration on minimum condenser energy for ignition of lycopodium. Dust concentration, 180 mg/l; confining wall; N_2 diluent; spark gap, 12.5 mm.

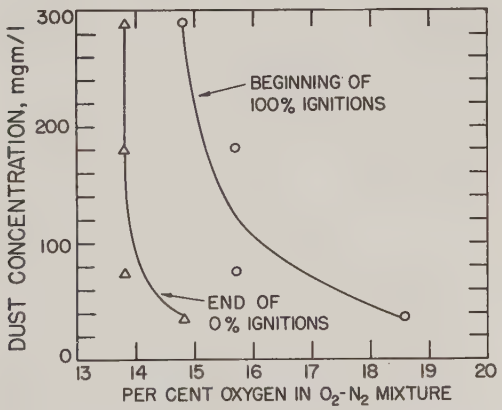

FIG. 13. Effect of O_2 concentration on minimum dust concentration for ignition of lycopodium. Confining wall; N_2 diluent; spark gap, 12.5 mm; condenser energy, 5.2 joules.

A similar phenomenon has been observed for both confined and unconfined dust columns when the ignition frequency is measured for different condenser energies at a fixed concentration of oxygen. The meaning of this behavior, exemplified in Figure 10, is also being studied.

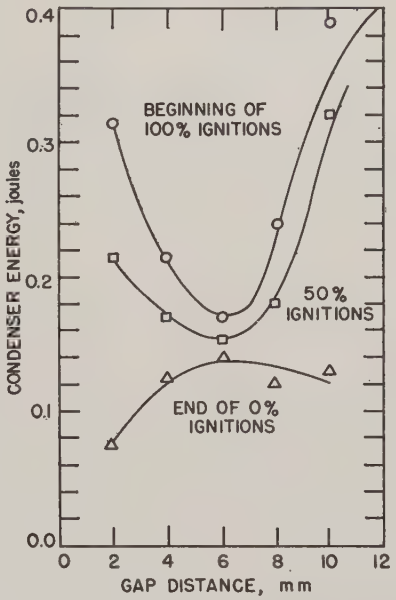

FIG. 14. Effect of spark gap length on minimum condenser energy for ignition of lycopodium. Confining wall; dust concentration, 180 mg/l; 23% O_2 in O_2-N_2 mixture.

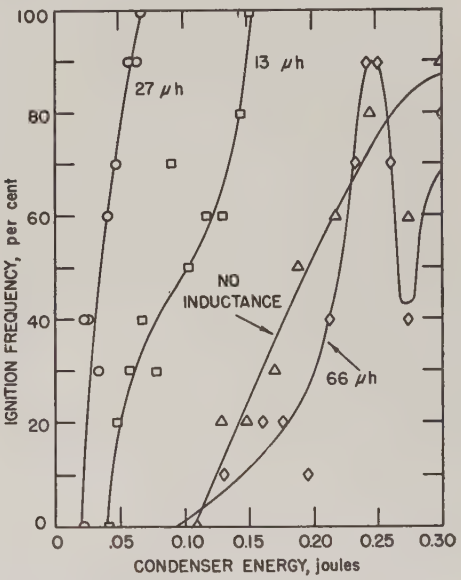

FIG. 15. Effect of inductance on minimum condenser energy for ignition of lycopodium. Confining wall; dust concentration 80 mg/l; 23% O_2 in O_2-N_2 mixture; spark gap, 6 mm.

Figures 9, 10, and 11 present contrasts with respect to wall-confinement and the employment of diluents of different transport characteristics. With a nitrogen diluent and a wall-confined dust

column the ignition frequency rises sharply with per cent oxygen or ignition energy, whereas with the wall-free column the rise is initially more gradual. Considering the minimum oxygen concentration or minimum energy to be that corresponding to 50 per cent ignitions, one sees that nearly twice as much oxygen and about eight times as much energy are required for the wall-free column as were required for the wall-confined one. With a helium diluent these differences between wall-free and wall-confined conditions are less pronounced.

The results presented in Figures 12, 13, 14 and 15 refer only to the region in which the ignition frequency is increasing with oxygen concentration or condenser energy. Figure 12 shows how the minimum energy decreases with the per cent oxygen. It was obtained from plots of the ignition frequency as the ordinate against oxygen concentration as the abscissa for five different condenser energies. The results show how the spread between the end of zero ignitions and beginning of 100 per cent ignitions increases as the condenser energy is reduced.

Figure 13 shows how the minimum dust concentration for ignition varies with the oxygen concentration. It was obtained from plots of ignition frequency as the ordinate against oxygen concentration as the abscissa for three different dust concentrations. Here the region of partial ignition broadens somewhat as the dust concentration is reduced.

Both Figures 12 and 13 show that the dust concentration and condenser energy are very sensitive to the oxygen concentration for low oxygen concentrations, becoming less sensitive at higher oxygen concentrations. They resemble the results obtained by Hartmann with powdered aluminum.[3]

Figure 14 was obtained from plots of the ignition frequency as the ordinate against the condenser energy as the abscissa for five different gap distances between the probes. An optimum gap distance of 6 mm is indicated for the 50 per cent and 100 per cent levels.

Inductances of 13 and 27 μh were placed in the circuit shown in Figure 6 to test the effect of reducing the rate and manner of introduction of spark energy into the gap. These consisted of coils of $\frac{1}{4}$ and $\frac{1}{8}$ in. copper tubing, respectively, to minimize resistance losses. The inductances were computed from the physical dimensions of the coil. The effect of a third inductance of 66 μh made from No. 20 B. and S. gauge insulated wire and having resistance of 9 ohms was also tested. The results (Fig. 15) show a significant decrease in the energy required for ignitions for inductances of 13 and 27 μh. Also the slopes of these curves become steeper and the scatter of the data was diminished. The 66 μh inductance brings the required energy back to about that required for no inductance, indicating either that the inductance has passed through an optimum value or some energy has been lost in the resistance, or both.

Acknowledgments

The authors wish to thank H. F. Calcote for valuable discussions, James L. Gibson, Jr. for assistance with the experiments, Carlton M. Slough for assistance with the electronic equipment, and F. R. Scott for help in preparing the manuscript.

REFERENCES

1. Edwards, P. W., and Leinbach, L. R.: U. S. Dept. Agr. Tech. Bull. No. 490, 1935.
2. Mason, R. B., and Taylor, C. S.: Ind. Eng. Chem., *29*, 626 (1937).
3. Hartmann, I., Ind. Eng. Chem: *40*, 752 (1948).
4. Boyle, A. R., and Llewellyn, F. J.: J. Soc. Chem. Ind. (London), *69*, 173 (1950).
5. Hartmann, I.: Sci. Monthly, *79*, 97 (1954).
6. Meek, R. L., and Dallavalle, J. M.: Ind. Eng. Chem., *46*, 763 (1954).
7. Costa, D., and Costantinides, G.: Pubbl. fac. sci. ing. univ. Trieste, *B8*, 3–8 (1947).
8. Fuhrmann, E. A., and Koettgen, H.: Z. physik. Chem., *A169*, 388 (1934).
9. Cassel, H. M., Das Gupta, A. K., and Guruswamy, S.: *Third Symposium on Combustion, Flame and Explosion Phenomena*, p. 185. Baltimore, The Williams & Wilkins Co., 1949.
10. Schlaepfer, P.: Schweiz. Ver. Gas. u. Wasserfach. Monats.-Bull., *31*, 69 (1951).
11. Andersen, J. W., and Friedman, R.: Rev. Sci. Instr., *20*, 61 (1949).

Applications of Combustion

106

THE SUPPRESSION OF METHANE/AIR IGNITIONS BY FINE POWDERS

By J. E. DOLAN

Introduction

Modern coal mining explosives are the result of fifty years experience in explosives technology, during which time many problems, particularly those associated with the risk of firedamp explosions have been investigated. Indeed the development of the permitted explosive is concomitant with research into the mechanism of firedamp ignitions. The present day coal mining explosive, as exemplified by the British Equivalent to Sheathed Explosive,[1, 2, 3] has attained a very high degree of safety. In these explosives a flame suppressant material is incorporated in the explosive composition. The function of such materials is twofold. There is, firstly, a reduction in the temperature of the detonation reaction, and in the flame associated with it. Secondly, subsequent to the process of detonation, the suppressant material penetrates into the atmosphere in the form of a dust cloud, which affects the ignition characteristics of the firedamp ahead of the igniting source. It is, therefore, of importance to the explosive technologist to have as complete a knowledge as possible of the function of those materials which might be included in explosives for the purpose of improving their safety. In particular, it is important to know how suppressant-loaded detonation products are likely to affect the safety of the explosive containing the suppressant when a cartridge train is fired in a shothole which is either inadequately stemmed or is broken along its length and communicates with gas-filled partings in the coal strata.

The most widely used suppressant material is common salt, although any material which has proven effective with the earlier sheathed explosives should be suitable, provided there is no reaction between the suppressant and the explosive material. A great deal of practical work has been done on various sheathing materials[4, 5, 6] the effectiveness being measured by the effect on the charge limit of an arbitrarily chosen explosive when fired into the inflammable gas under various test conditions.[7]

The fundamental study of these substances was first undertaken by Jorissen who extended his studies on the effect of vapors on the explosion of gases[8] to include the quenching effect of powders on methane/air explosions in open[9] and closed vessels.[10] Jorissen and his co-workers expressed the efficiency of a material as a flame suppressant in terms of the concentration (by weight) required to extinguish a methane/air flame propagated in a glass tube or sphere. This work was continued by Dijksman[11] who showed that the size of the material used was of importance and that the extinction effect was roughly proportional to the surface area. Jorissen found the halides, and in particular the alkali halides, to be the most efficient suppressants. The ability of the alkali halides to suppress gas explosions has also been demonstrated by Hinshelwood and others (in Lewis and von Elbe[12]) in their study of chain breaking efficiency at the walls of ignition tubes used in hydrogen/oxygen reactions, and iodine itself has been shown to be capable of suppressing both slow and explosive reactions of hydrogen and oxygen.[13] Similar effects have been observed with bromine, chlorine and organic halides.[14] The effect of alkali salts on firedamp ignitions has received the attention of Dufraisse.[15, 16] The marked efficiency of the alkali halides has been attributed to the combination of low melting and boiling points and comparatively high latent heats of fusion and vaporization. Sperckaert[17] who has studied the effect of inhibitor salts on the luminosity of explosive

detonation reactions photographically, has correlated flame reduction efficiency and thermal characteristics.

The introduction of a dust suspension into a methane/air flame will alter the velocity of the combustion. As the burning velocity of a methane/air flame in a tube is fairly high,[18] the heating effect of the flame will be momentary only, and thus it might well be expected that there is a limiting size of dust particle above which the thermal conductivity of the material will be too low to allow the whole mass of the solid to reach the temperature of the burning gases. For particles greater than this limiting size, the major factor controlling the extent of heat transfer from gases to solid will be the surface area of the solid in contact with the flame. For particles smaller than this limiting size, the maximum amount of heat transfer will take place and the cooling effect of the dust will be a maximum. If the substance is an inert, infusible material whose effect is purely thermal, then the mass and specific heat of the material will then control the speed of the methane/air reaction, which will be independent of further size reduction. If, on the other hand, the material behaves as an explosion suppressant due to some surface activity, then it might be expected that the suppressing effect will continue to be a function of surface area, and therefore of particle size, even though thermal equilibrium with the gases be attained.

Experimental

In order to obtain material in a sufficiently finely divided form to produce dust suspensions, the substances under examination were subjected to various reductionizing treatments. The preliminary reduction of the coarse material was effected in either a mechanical mortar or a high speed rotating hammer mill, both of which were followed by an air-milling treatment in a Kiddiwell type of unit.[19] The specific surface and average particle diameters of the resultant dusts were determined by the Rigden air permeability method.[20] The size ranges of the materials obtained by these processes were, in certain cases further narrowed by means of air elutriation so that the dusts to be used in the experiments were as closely ranged as possible. A photograph of the apparatus in its final form is shown in Figure 1 and the arrangement of the explosion tube is shown diagrammatically in Figure 2.

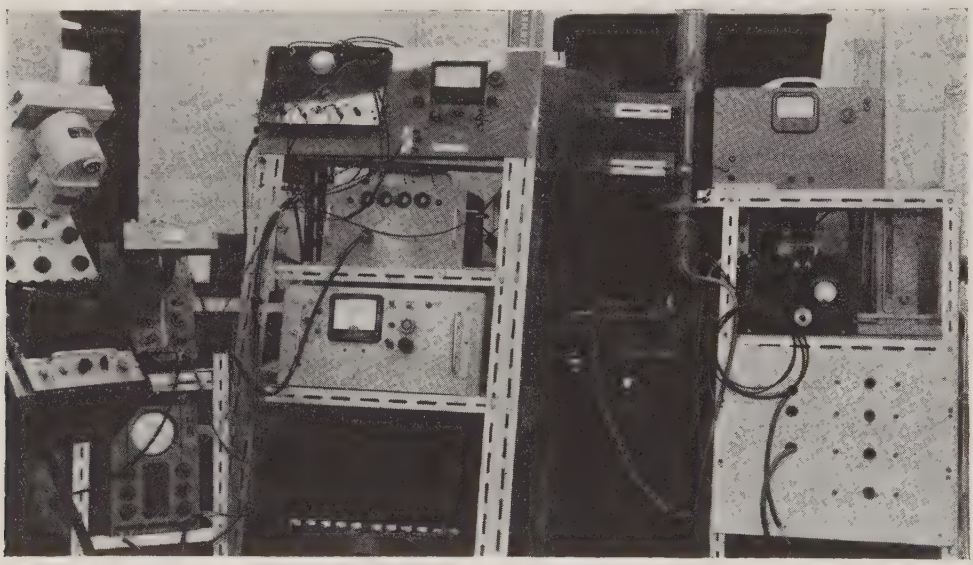

Fig. 1. General layout of apparatus.

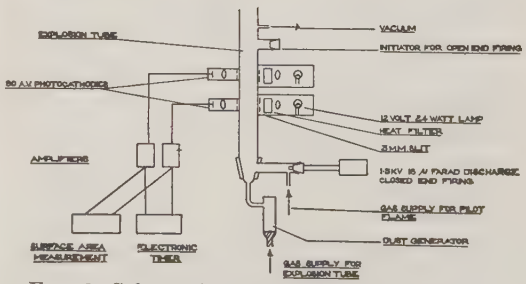

Fig. 2. Schematic diagram of explosion tube.

The principle employed was to create a dust suspension in a known mixture of methane and air, and observe the effect of various methods of initiation of the gases in a 7-cm diameter open-ended tube. To do this the requisite volumes of methane and air were metered by water aspiration, and after drying by passage through calcium chloride tubes, were stored under pressure. The methane used throughout these experiments was natural mine gas of approximately 90 per cent methane content, and free from carbon monoxide, hydrogen and unsaturated hydrocarbons. The dust under examination was placed in the dust generator and the premixed gases from the reservoir allowed to flow through it into the evacuated explosion tube, so fluidizing the bed of powder and entraining the dust in the gas stream.

In the early stages of the investigation[21] the concentration of dust in suspension was obtained by weight difference of the dust generator before and after the experiment, and this was then expressed as cm^2/ml (of gas), using the value of specific surface obtained by the air permeability method. This system suffers from the disadvantages that some of the dusts tend to aggregate, also the fluidization of the dust bed itself constitutes a size separation process, which detracts from the evaluation of the dust in suspension. In later experiments, the surface area of the dust within the tube was measured *in situ* by a modification of the photoextinction method[22] employing the experimental techniques suggested by Rose.[23] The dust concentration was measured at two points within the tube, at 20 and 35 cm from the point of initiation. Four methods of initiation were employed.

(a) A fusehead, such as is used in low tension electric detonators, where the active igniting component is the charcoal/potassium chlorate mixture of the match-head composition.[24]

(b) A gasless fusehead of the type employed in delay detonator designs, where the active igniting source is essentially a 50/50 mixture of a cerium/magnesium alloy and red lead.

(c) A capacitance spark discharge of 16 f charged to 1.5 kv.

(d) The capacitance discharge of (c) fired in a 2.5-cm diameter 16-cm pilot tube filled with a dust-free methane/air mixture, where the igniting source is the flame advancing from the pilot tube into the dust laden gases in the explosion tube. In order to obviate gas and dust locks at the mouth of the pilot tube, the explosion tube constitutes the plug of a 6-cm diameter stopcock with the pilot tube mounted on the barrel (Fig. 2).

The effect of a dust suspension on a methane/air flame is progressive. At high concentrations the gas fails to ignite and the inhibiting dust is regarded as having suppressed the flame. Lower concentrations allow a region of slow, quenched flames. The spatial velocities of the flames in this region and in the region of faster propagating flames were measured either by a rotating drum camera or by using the photo-cathodes of the dust measuring apparatus to trigger an electronic timing device. In either case the flame speeds

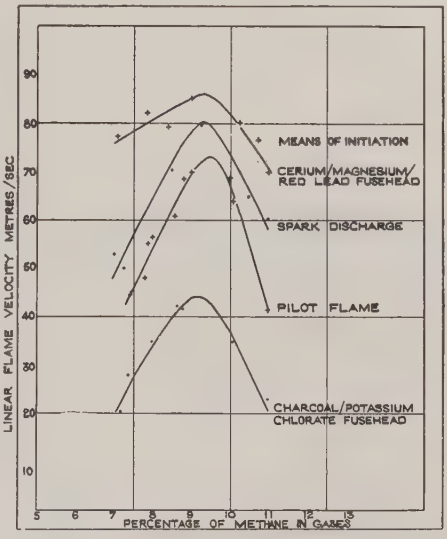

FIG. 3. The effect of the initiator on the flame velocities observed with upward propagating flames.

were measured only between the two points at which the dust concentration readings were taken.

Initiation of the Gas at the Closed End of the Explosion Tube

The quasi-detonations of firedamp caused by a gunned shot[25] is best simulated by this type of initiation. The behavior of these accelerating flames under the influence of an inhibiting dust is therefore of great practical importance in assessing the value of a suppressant for inclusion in an explosive. Under the experimental conditions observed in this investigation, the spatial velocity of the flame in the explosion tube is dependent on the nature of the initiating source as is shown in Figure 3. The fastest flames were

obtained with cerium fuseheads but the reproducibility was poor, owing to probable irregularities in the weight of fusehead composition. Much better regularity was obtained with the spark discharge and pilot flames, which were adopted as the standard methods of ignition.

When a noninhibiting dust is introduced into the gas the effect on the flame speed is very

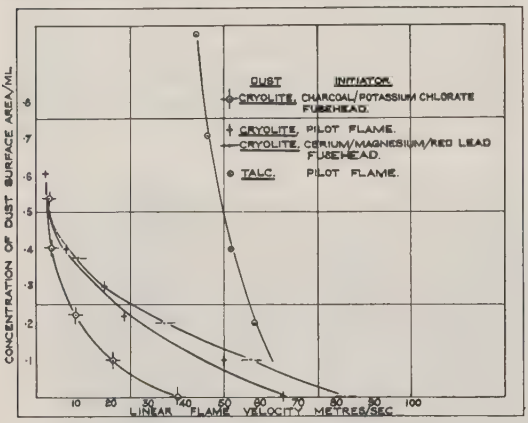

FIG. 4. The effect of dusts on the flame velocities of upward propagating flames.

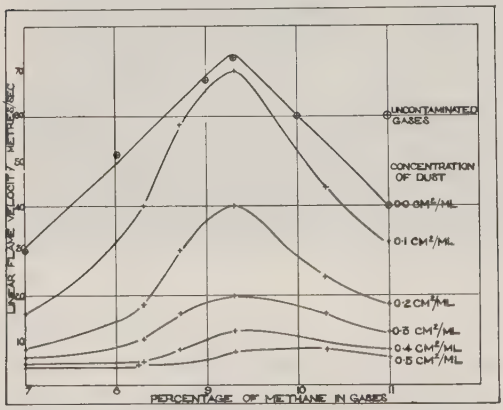

FIG. 5. The effect of sodium aluminium fluoride (cryolite) of specific surface 4,000 cm²/g on upward propagating flames.

limited. Some depression does occur, but even with heavy concentrations of dust the drop is seldom more than about 20 per cent. The effect is illustrated by the sample of talc of specific surface 11,000 cm²/g in suspension with a methane/air mixture containing 10.0 per cent methane, shown in Figure 4. When the gases are laden with an inhibiting dust, however, the effect on the flame speed is most marked. The results obtained with naturally occurring sodium aluminium fluoride dust (cryolite) of specific surface 4,000 cm²/g are interpreted graphically in Figure 4, and are typical of suppressant materials. This graph also serves to illustrate that, with upward propagation, the effect of low concentrations of dust on the linear flame velocity is dependent on the nature of the igniting source. The variation in flame speeds associated with the use of different initiators becomes less as the dust concentration is increased, until, at the concentrations at which quenching of the flame occurs, the velocity is the same for all initiators.

The linear velocity/percentage of methane in air relationships for various concentrations of cryolite dust, when the gases are ignited by means of a pilot flame, are shown in Figure 5. These curves are typical of most suppressant dusts. For light concentrations the linear flame velocity shows the maximum associated with the uncontaminated flame, but as the concentrations approach those at which propagation fails, the speed of the flame becomes more or less independent of the percentage of methane in the mix. Further increases in the concentration of dust result in slow, decelerating flames, which are quenched within the length of the tube, and whose linear velocity is indeterminate. A point is finally reached at which the flame is effectively suppressed. The suppression point, the quenching point and the change in linear velocity of the flame effected by a 0.1 cm²/ml increase in concentration at low dust concentrations, were taken as adequately evaluating the effect of a dust for the purposes of the investigation. The figures obtained in the suppression of spark initiated 9.8 to 10 per cent methane in air flames by the alkali halides, together with those for sodium bicarbonate, are listed in order of effectiveness in Table 1. The lithium chloride and bromides could not be investigated, because of the difficulties involved in air-milling these deliquescent compounds and the impracticability of obtaining dust suspensions with the powders available. When working with the alkali halides it was observed that quenching was accompanied by the characteristic metal ion flame color. It is to be remarked that potassium salts are more effective inhibitors than the sodium salts, which is the reverse of what one might be led to expect from the specific heat relationship.[17]

That the efficiency of the powders is a function of the surface area and not the weight of the suspension is shown by the results for the various sodium chloride and sodium bicarbonate samples listed in Table 2. These results justify the expres-

sion of the concentrations as a surface area, because the concentrations by weight are obviously meaningless unless accompanied by a statement of particle size.

Initiation of the Gas at the Open End of the Explosion Tube

Flame propagation under these conditions simulates that which occurs in practice with the ignition of firedamp in gas-filled partings, where the flame is advancing into a more or less quiescent mixture of gases. The linear flame velocities measured under such experimental conditions are, of course, much lower than those observed for an accelerating flame. The flame fronts resulting from ignition by the fuseheads were not very uniform in velocity and in the case of the charcoal/potassium chlorate fusehead tended to be rather broken. The observed velocities for 10 per cent methane/air mixtures using capacitance spark discharges, charcoal/potassium chlorate fuseheads and cerium/magnesium/red lead fuseheads were 70, 75 and 220 cm/sec respectively. The linear flame velocity of the inhibitor laden gases was found to be independent of the initiator.

The flame velocity/dust concentration curve for sodium chloride suspended in 10 per cent of methane in air shown in Figure 6 illustrates this point. While the velocity of the propagating and quenched flames is more or less independent of the initiating source, the concentration of dust at which complete suppression of the flame occurs is affected as is shown by the results quoted in Table 3. It will be noted that the concentrations required to effect these suppressions are considerably less than those required to suppress flames initiated from the closed end of the explosion vessel. With the exception of the superiority of sodium silicofluoride over the naturally occurring cryolite dust, the order of effectiveness remains the same. The rearrangement of these two materials might be accounted for by the fact that two different batches of mined cryolite were employed.

Other Salts

Apart from sodium bicarbonate and the alkali halides, 13 substances capable of quenching methane/air ignitions have been placed in order of effectiveness using surface area/ml of gas as the measure of efficiency in suppressing closed end initiated 10 per cent methane/air flames. These are listed in Table 4 together with the equivalent suspension weights. Some 30 other

Table 1. Suppression Effect of the Alkali Salts

Substance	Specific Surface	Suppression Point	Quenching Point	Velocity Change
	cm /g	*cm²/ml*	*cm²/ml*	*ms/sec/0.1 cm²/ml*
Potassium fluoride	800	0.25	0.08	—
Potassium iodide	900	0.50	0.04	52
Sodium aluminium fluoride	2,200	0.61	0.40	45
Potassium chloride	5,700	0.64	0.40	32
Sodium silicofluoride	8,000	0.68	0.47	35
Sodium bicarbonate	4,600	0.75	0.52	36
Sodium chloride	6,500	1.84	0.57	32
Calcium fluoride	4,000	2.16	0.92	22

Table 2. Suppression Points of Sodium Chloride and Sodium Bicarbonate Powders of Varying Grist

Substance	Specific Surface	Average Particle Diameter	Suppression Point	
			By Weight	By Surface Area
	cm²/g	*μ*	*g/l*	*cm²/ml*
Sodium chloride	6,500	4.3	0.284	1.84
	3,100	9.0	0.590	1.83
	2,300	12.0	0.810	1.86
Sodium bicarbonate	11,500	2.4	0.066	0.76
	4,600	5.9	0.160	0.74
	3,200	8.5	0.231	0.74

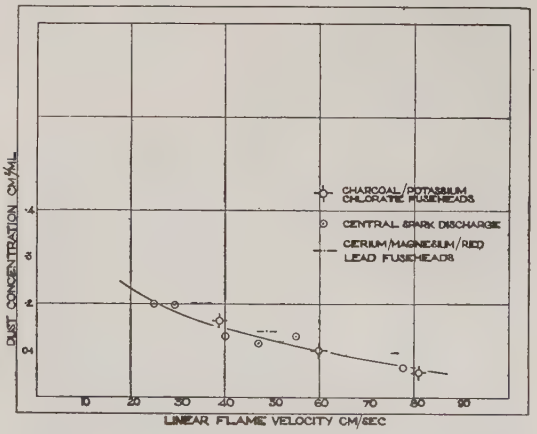

Fig. 6. The effect of cryolite dust of specific surface 4,000 cm²/g on the velocity of downward propagating flames using different initiators.

materials, which for various reasons suggested themselves as possible inhibitors, have been shown to be ineffective both in suppressing and quenching methane/air flames under the conditions of experiment. These inert materials include: chalk, magnesium carbonate, copper carbonate, lead acetate, barium sulfate, cupric oxide, alum, magnesium sulfate tetrahydrate, ammonium nitrate, litharge, sodium thiosulfate, zinc sulfate, hydrated zinc sulfite and talc.

Table 3. Suppression Points of Representative Suppression Dusts, the Gas Being Initiated at the Open End of the Explosion Tube

Substance	Suppression Point	
	Charcoal/ Chlorate Fusehead	Spark Discharge
	cm^2/ml	cm^2/ml
Sodium silicofluoride	0.13	0.37
Sodium aluminium fluoride (cryolite)	0.20	0.32
Sodium bicarbonate	0.27	0.45
Sodium chloride	0.37	0.50

Table 4. Suppression Points of Miscellaneous Inorganic Salts

Substance	Specific Surface	Suppression Point	
	cm^2/g	g/l	cm^2/ml
Aluminium chloride	1,400	0.072	0.10
Ammonium bicarbonate	1,200	0.221	0.27
Sodium sulfite	1,200	0.420	0.50
(exsiccated)	6,200	0.870	0.54
Sodium acetate trihydrate	7,600	0.116	0.87
Potassium carbonate	8,000	0.114	0.91
Cuprous oxide	4,000	0.230	0.92
Cobaltous chloride hexahydrate	2,200	0.450	0.99
Barium hydroxide octahydrate	6,400	0.388	2.48
Copper acetate monohydrate	13,200	0.202	2.66
Ammonium chloride	4,200	Quenches at 0.8	
Sodium carbonate	5,500	Quenches at 0.98	
Sodium sulfate decahydrate	3,500	Quenches at 1.00	
Barium chloride	6,300	Quenches at 2.19	

A study of Tables 1 and 4 does not allow many general conclusions to be drawn. It can be said, however, that on a broad basis salts with melting points below 200°C are more effective than those with melting points above this temperature, the exceptions to this being the alkali salts and cuprous oxide. With isolated exceptions the alkali salts, particularly the alkali halides, are the most effective compounds. The potassium salt is, in general, more effective than the sodium salt, the fluoride more effective than the iodide, which in turn is more effective than the chloride and the halides are more effective than the carbonates.

Salts which decompose are generally effective if their decomposition temperatures are below 200°C, *e.g.*, aluminium chloride, ammonium bicarbonate, ammonium chloride and copper acetate monohydrate. If the decomposition temperature is above 200°C the salts are usually ineffective, *e.g.*, basic copper carbonate, magnesium carbonate and magnesium sulfate. Ammonium chloride has a low quenching point (0.8 cm^2/ml) and a wide quenching range with no real suppression point. Heavily hydrated salts proved to be unexpectedly ineffective with two exceptions, cobalt chloride hexahydrate and barium hydroxide octahydrate.

Discussion of Results

A generalization which can now be made is that, apart from chemical specificity, the major physical factor determining the ability of an inorganic dust suspension to inhibit the explosion of methane/air mixtures is the surface area of the powder exposed to the advancing flame.

The fact that quenching of upward propagating flames by any particular suppressant dust occurs at, or about, the same linear velocity, and therefore temperature, in spite of large differences in the initial velocity, would lead one to suggest a thermal mechanism for the quenching of these flames, the flame temperature dictating whether or not propagation occurs. The effects observed with flames initiated at the open-end of the explosion tube are not inconsistent with this view. The dependence of the concentration of dust at which suppression of these flames occurs on the nature of the igniting source is to be expected as the ease with which a given gas mixture ignites, and conversely the difficulty with which the ignition is prevented is dependent on the temperature and duration of the event causing the ignition. Once the flame is established, however, the effect of a dust on its velocity is a function

only of the gas mixture and the concentration of dust in suspension, the speed of the flame being dictated by the temperature of the combination.

On the other hand, if reduction of gas temperature by the suppressant were the sole determinant, then one would expect the suppression concentration with very small particles to be weight rather than size dependent. That the suppression point continues to be size dependent, even with those particle sizes where thermal equilibrium is feasible,[26] argues that some form of surface activity is playing a part.

A. G. White[27] in a discussion of the explosive properties of gaseous media points out that despite differences in ignition temperatures of various fuel/air mixtures, the effective temperature so far as the propagation of flame is concerned seems to be much the same for all the gases and vapors reviewed. It would appear that sustained propagation of flame only occurs if the flame temperature reaches the critical value of about 1,400°C. Deductions from Kaveler and Lewis's[28] sodium line reversal determination of flame temperatures would put the limiting temperature slightly lower than this, at about 1,330 to 1,350°C.

If, therefore, the presence of an inorganic dust in a methane/air mixture lowers the temperature of the burning gases to below 1,330°C, the flame will be quenched. The ability of any dust to do this will depend on whether the particle size of the dust is sufficiently small to allow appreciable heat transfer to take place. If it is assumed that in the extreme case, with very fine dusts, thermal equilibrium between the solid and the burning gases is established, the equilibrium temperature can then be obtained by means of a simple graphical method. Figure 7 for potassium chloride is typical and shows the heat absorbed by the solid particle and the heat losses of the gas envelope plotted against temperature. The point where the two curves intersect is the equilibrium temperature attained by the system. The equilibrium temperature associated with some of the alkali halides, the most effective class of inhibitor materials examined, has been estimated in this way and the results, together with that for ferric oxide (an inefficient material) tabulated in Table 5. Taking a limiting flame temperature of 1,330°C as the criterion of a nonpropagating flame, then in no case does this thermal treatment explain the suppressions obtained with the alkali halides.

Objections can be raised against the postulate of thermal equilibrium for these calculations. However, at thermal equilibrium the heat absorbed by the solid will be a maximum, and since it has been shown that even at thermal equilibrium the heat absorbed by the solid is insufficient to reduce the flame temperature to below that required for propagation, then, if thermal equilibrium is not reached, the amount of heat absorbed by the solid will be even smaller

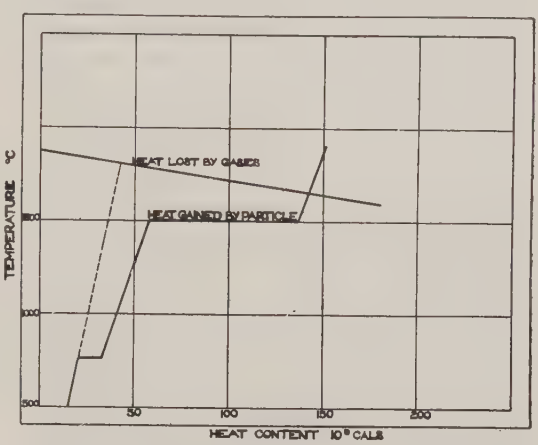

FIG. 7. Graphical determination of the equilibrium temperature for potassium chloride dust.

TABLE 5. EQUILIBRIUM TEMPERATURES ASSOCIATED WITH SUPPRESSIVE CONCENTRATIONS OF THE ALKALI HALIDES

Substance	Suppression Point	Equilibrium Temperature
	cm^2/ml	°C
Ferric oxide	15.0	1,230
Potassium fluoride	0.25	1,500
Potassium iodide	0.50	1,500
Potassium chloride	0.64	1,650
Sodium aluminium fluoride	0.61	1,600
Sodium chloride	1.84	1,400

and a thermal explanation of the flame suppression even less likely.

Using a mathematical treatment based on Paterson's,[26] analysis of the effect of solid spheres of small dimensions on the temperature of the fluid surrounding them shows that, for the ferric oxide used in these experiments, thermal equilibrium is feasible and the total possible amount of heat is transferred from the burning gases to the solid particle. As the equilibrium temperature of 1,230°C is below the melting point of ferric oxide (1,560°C), fusion does not occur and the suppression can be accounted for by the absorp-

tion of heat from the flame by the ferric oxide dust.

It appears then, that the dependence of the suppressive effect on surface area is due, in the first instance, to the more complete heating of the smaller particles and consequent effect on the temperature of the burning gases. In the case of materials where fusion does not occur, the suppression of the methane/air flame can be accounted for by the lowering of the temperature of the gases to the point where the flame ceases to propagate. In the case of the alkali halides, however, this purely thermal explanation does not appear complete because, even at thermal equilibrium, the gas temperature has still not been reduced sufficiently to prevent propagation. The efficiency of these salts must therefore lie in some other property.

The practical significance of the data obtained during this work is that particle diameter and flame retarding efficiency will be most important factors when considering the effect of diluents on the safety of explosives. If one considers that an inhibiting dust is dispersed into the firedamp as a suppressant cloud, then smaller weights of very fine material will be as effective as much larger quantities of coarse materials. As an illustration consider the hypothetical case where the dust cloud from a detonating explosive inhibits the ignition of 25 l of a 10 per cent methane/air. Then for sodium chloride where the suppression value is 1.84 cm^2/ml, a surface area of some 2×10^6 cm^2 would be required. Using milled material of 5 μ average particle diameter would require some 300 g to effect this suppression, whereas with run of plant material the prohibitive quantity of some 8 kg would be necessary. Optimum particle sizes for the maximum suppressive efficiency have been calculated from the suppression values and have been used in explosive design with some degree of success.

REFERENCES

1. Taylor, J.: Trans. Inst. Mining Engrs., London, *109*, 358 (1949–50).
2. Taylor, J., and Sillito, G. P., Trans. Inst. Mining Engrs., London, *110*, 355 (1950–51).
3. Haslam, R., and Hancock, J.: Trans. Inst. Mining Engrs., London, *110*, 40 (1950–51).
4. Lemaire, E.: Ann. Mining Belg., *19*, 587 (1914).
5. Lemaire, E., Ann. Mining Belg., *22*, 749 (1921).
6. Grimshaw, H. C.: Colliery Guard., *163*, 520 (1941).
7. Jones, E.: Colliery Engr., London, *31*, 145 (1954).
8. Jorissen, W. P., and Hermans, J. J.: Rec. Trav. Chim. Pays-Bas, *52*, 271 (1933).
9. Jorissen, W. P., Van Der Dussen, A. A., Maltla, W. P. M., and de Liefde, J. H.: Rec. Trav. Chim. Pays-Bas, *52*, 403 (1933).
10. Jorissen, W. P., Snijders, H. G., and Vink, H. J.: Rec. Trav. Chim. Pays-Bas, *59*, 957 (1940).
11. Dijksman, A. J.: Chem. Weekbl., *12.1*, 718 (1934).
12. Lewis, B., and von Elbe, G.: *Combustion, Flames and Explosions of Gases*. New York, Academic Press, 1951.
13. Cook, G. A., and Bates, J. R.: J. Am. Chem. Soc., *57*, 1775 (1935).
14. Hinshelwood, C. N., and Williamson, A. T.: *Reactions between Hydrogen and Oxygen*. London, Oxford Press, 1934.
15. Dufraisse, C., and German, M.: C. R. Acad. Sci., Paris, *207*, 1221 (1938).
16. Dufraisse, C.: C. R. Acad. Sci., Paris, *236*, 164 (1953).
17. Sperckaert, P.: Explosifs, *2*, 65 (1952).
18. Gerstein, M., Levine, O., and Wong, E. L.: J. Am. Chem. Soc., *73*, 418 (1951).
19. Murphy, E., Ross, F. F., and Sharpe, G. C. H.: Non-mechanical methods of size-reduction, in *Report of the Conference on Pulverized Fuel*. London, Odhams Press, 1947.
20. Rigden, P. J.: J. Soc. Chem. Ind., *62*, 1 (1943).
21. Dolan, J. E., and Dempster, P. B.: J. Appl. Chem., *5*, 510 (1955).
22. Richardson, E. G.: Trans. Inst. Mining Engrs., London, *88*, 265 (1934–35).
23. Rose, H. E.: J. Appl. Chem., *2*, 80, 217 (1952).
24. Taylor, W., and Hall, C. R. L.: Trans. Inst. Mining Engrs., London, *107*, 409 (1948–49).
25. Payman, W., and Shepherd, W. C. F.: Proc. Roy Soc., *158*, 348 (1937).
26. Paterson, S.: Proc. Phys. Soc., *59*, 50 (1947).
27. White, A. G.: J. Chem. Soc., *125*, 2, 387 (1924).
28. Kaveler, H. H., and Lewis, B.: Chem. Rev., *21*, 421 (1937).

107

FIRE EXTINGUISHMENT BY MEANS OF DRY POWDER

By C. S. McCAMY, H. SHOUB AND T. G. LEE

1. Introduction

A common type of commercial fire extinguisher is charged with dry powder which is expelled by the discharge of compressed gas. The powder, known in the trade as "dry chemical," is finely-ground sodium bicarbonate with small amounts of additives to improve its flow properties. Numerous experiments have demonstrated the effectiveness of such extinguishers in fighting flammable-liquid fires. In a series of tests to determine the relative effectiveness of various types of small portable devices, commercially available 4- and 5-pound dry-chemical extinguishers proved equal to 10-pound carbon dioxide extinguishers on flammable liquid fires of ten different conformations. The Factory Mutual Laboratories consider dry-chemical extinguishers about twice as effective as carbon dioxide extinguishers of equal weight capacity on the basis of the relative areas of gasoline spill fires for which these devices are considered adequate protection.[1]

Although dry sodium bicarbonate has been used in one manner or another since the beginning of this century, or before, the prototype of our modern dry chemical did not appear until 1928, when D. J. Block applied for a patent on a dry chemical composed of sodium bicarbonate with enough magnesium stearate added to keep the powder free flowing.[2] About 1943 it was found that the effectiveness of the extinguishers was somewhat improved by the use of more finely powdered material. Fire-fighters generally believed that the sodium bicarbonate decomposed when heated and liberated enough carbon dioxide to extinguish the fire. This belief seems to have been the basis upon which the dry-powder method of extinguishment was developed.

As plausible as the carbon dioxide theory seemed, it was not very satisfactory when considered quantitatively. On this basis, how could 5 pounds of sodium bicarbonate be as effective as 10 pounds of pure carbon dioxide? If it were *completely* decomposed, the sodium bicarbonate would liberate about 26 per cent of its weight as carbon dioxide. Samples of dry chemical were collected after an actual extinguishment and were quantitatively analyzed. According to this analysis less than 15 per cent of the bicarbonate had decomposed, therefore less than 4 per cent by weight of the powder was liberated as carbon dioxide. It appears that the carbon dioxide theory which motivated the development of the dry chemical extinguisher does not account for a large part of the extinguishing action.

The ultimate objective of the investigation of which this work was a part was to determine the mechanism of dry chemical extinguishment.

2. Mechanisms of Extinguishment

A brief consideration of the general nature of flammable-liquid fires suggests some possible mechanisms. Once the vapors are ignited, the flame provides heat to vaporize more fuel. The rising vapors are heated by the energy liberated in the reaction zone until they are hot enough to react and produce more heat. The reactions occurring in hydrocarbon flames are not well known but spectral studies and other experiments indicate that they are complex branched-chain type reactions involving short-lived free radicals which carry the impetus of the reaction to succeeding links in the chain.[3] In a continuous cycle, the flame heats the fuel and the heated fuel and oxygen feed the flame. Any mechanism which interrupts this cycle extinguishes the flame.

There are a number of conceivable physical mechanisms of extinguishment of flammable-liquid fires, including the following:

(1) *Throttling.* The influx of fuel is stopped.

(2) *Cooling.* So much heat is removed that combustion ceases.

(3) *Blowing-out.* The velocity of the gaseous fuel or air exceeds the velocity of the combustion wave and the combustion wave recedes, finally disappearing as a result of other mechanisms.

(4) *Smothering.* The influx of air or oxygen is stopped.

(5) *Diluting.* Inert gas is mixed with the atmosphere.

(6) *Shielding.* Material is interposed between the flame and the fuel to prevent the transfer of energy by radiation.

Chemical mechanisms of extinguishment include the following:

(1) *Chain-breaking.* Material is introduced

into the flame so that potentially reactive particles encountering this material will not propagate the reaction chain.

(2) *Preferential oxidation.* A material with a strong tendency to unite with oxygen is introduced into the flame so that the available oxygen combines with the extinguishing agent rather than the fuel.

It is quite likely that this list of mechanisms is incomplete, but it will serve as a basis for the present discussion.

3. Preliminary Experiments with Various Powders

In view of the many conceivable mechanisms, it was felt that the more likely ones should be determined by a comparison of the effectiveness of a variety of powders in extinguishing gasoline fires. Powders were selected on the basis of their physical properties. The fineness ranged from 85 per cent through 200 mesh to over 85 per cent through 400 mesh. Three tests were performed on each powder, under actual fire-fighting conditions. The fuel, ⅝ gal of leaded gasoline, was placed on a slightly indented 4 x 4-ft concrete surface, ignited and allowed to burn 5 sec before the extinguisher was discharged into the fire. An effort was made to keep the discharge operation uniform for various powders, the extinguisher being aimed at the base of the flames and advanced slowly while sweeping from side to side. The extinguisher was a commercial "stored-pressure" device of 2.5 lb capacity, pressurized with dry nitrogen at 350 psi gauge. The powder charge weighed 2 to 2.5 lb, depending on the bulk density of the powder. The average discharge rate ranged from 0.4 to 0.5 lb/sec for the various powders.

Extinguishment efficiency was based on the average time rate of extinguishment or extent to which flames were suppressed, as evaluated by two observers. The most effective powders were rated +3, the least effective −3 and the others were rated between these values in algebraic order. Positive numbers were used if the fire was extinguished, negative numbers if not. The most easily dispersed powders were rated A, the least C, on the basis of visual observation during use. Table 1 lists the various powders, some of their properties, and their extinguishment efficiencies. In Table 1, the powders are listed in order of apparent effectiveness based on efficiency and dispersibility.

To determine whether or not the discharge was merely blowing the fire out, an extinguisher charged with dry nitrogen at a pressure of 450 psi gauge was tried. The gas discharge fanned the flames and increased the intensity of the fire. This result shows that the flame is not merely blown out by the discharge of a dry chemical extinguisher, and also indicates that the mechanism by which such devices operate is neither smothering nor diluting, for these mechanisms should be provided as well or even better by the inert gas.

It was noted that immediately after extinguishment the fire could be re-ignited, indicating that the powder was not forming a film on the gasoline and throttling the fire.

The effectiveness of borax and silica proves that the release of carbon dioxide is not the principal mechanism of extinguishment by means of dry powder. The results shown in Table 1 seem to indicate that the combination of fine particle size and good dispersibility is an important requirement for extinguishment by means of dry powder. The salts of the alkali metals were more effective than other types of materials tested.

Among the materials tested, there was no observable correlation between the effectiveness of powders and their heat capacities. The number of calories required to heat one gram of each material from 18°C to 300°C was calculated and is shown in Table 1. Heat of reaction was included where decomposition or dehydration would occur. With the materials listed in order of effectiveness, there is no apparent order among the heat capacities. It must be noted that mechanisms involving the heating of particles are not necessarily ruled out by this observation alone, since heat transfer phenomena are not governed only by heat capacity. Nonetheless, heat transfer theory shows that heat transfer from gases to fine particles is very efficient, due to the high surface to mass ratio involved.

The results of these preliminary experiments indicated that the mechanisms of throttling, cooling, blowing-out, smothering, and diluting are of minor importance if operative at all. Since the preferential oxidation theory was inapplicable to the best dry powders tested, the original list of mechanisms under consideration was reduced to two principal mechanisms, shielding and chain-breaking. These mechanisms would depend upon the projected or other area of material in a cloud and therefore would require fine particle size and

TABLE 1. THE PROPERTIES AND EFFECTIVENESS OF VARIOUS POWDERS FOR FIRE EXTINGUISHMENT

Powder*	Special Characteristics	Sieve Mesh† (passing 85 per cent)	Estimated‡ Heat Capacity (18°C–300°C)	Dispersibility	Efficiency
Potassium bicarbonate with 2 per cent zinc stearate	Decomposes on heating, fine particles	270 est.	238	A	3+
Dry chemical (contains 95 + per cent sodium bicarbonate)	Decomposes on heating, free flowing	325	259	A	3
Borax with 2 per cent zinc stearate	High heat capacity, loses water on heating	270 est.	463	A	3
Sodium carbonate§	High interior surface area	325	79	A	2
70 per cent sodium carbonate 30 per cent magnesium carbonate	Better flow than magnesium carbonate	325	72	A	2
50 per cent sodium carbonate 50 per cent Portland cement; dried at 120°C		325	68	B	2
60 per cent silicon dioxide 40 per cent sodium carbonate; heated at 280°C, 3 hr	Better flow than silicon dioxide	400 est.	67	B	2
30 per cent silicon dioxide 70 per cent sodium carbonate	Better flow than silicon dioxide	325	74	B	2
Sodium carbonate (derived from untreated sodium bicarbonate)		170 est.	79	A	2
Sodium bicarbonate dried at 120°C	Poor dispersibility	200	259	B	1
Silica with 2 per cent zinc stearate¶	Inert, hard and irregular surface	400 est.	60	B	1
Borax with 2 per cent zinc stearate	Coarse particles	170 est.	463	A	−2
Gypsum plaster ($CaSO_4 \cdot \frac{1}{2}H_2O$)	Loses water on heating	400 est.	61	B	−2
Portland cement dried at 120°C	Dark gray color	325	58	C	−2
Talc	Soft surface	Impalpable	66	C	−2
Fire clay	Light gray color, low heat conductivity	200	63	A	−3
Sodium bicarbonate, not dried	Poor dispersibility	200	259	C	−3

* Powders were either technical or commercial grade.

† ASTM Standard Specification for Sieves for Testing Purposes, E11-39.

‡ Includes sensible heat and heat of reaction where applicable (cal/gm).

§ All sodium carbonate except as noted was derived from commercial dry chemical, decomposed by heating.

¶ Improved performance was obtained in a later test when discharge pressure was increased about 25 per cent.

good dispersibility, in accord with the results of these experiments. There is a considerable amount of corroborating evidence for these conclusions, based upon combustion experiments not simulating fire-fighting conditions.[4, 5, 6, 7, 8]

4. Optical Properties of Dry Chemical

In order to determine the possibilities of the shielding hypothesis, measurements were made of some optical properties of commercial dry chemical dispersed in the air. Measurements were made to determine how much of the incident radiant energy would be transmitted undeviated through a cloud of powder and how much would be deflected through various angles. It was felt that, with the aid of the theory of scattering, the deflection measurements might reveal information concerning the relative magnitudes of the

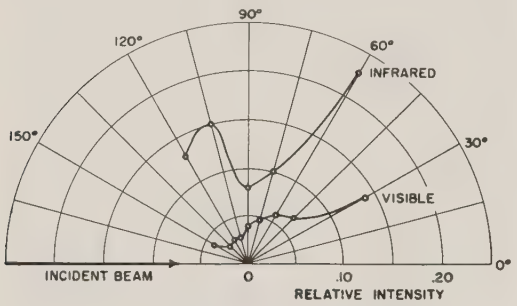

FIG. 1. The observed relative intensity of energy deflected through various angles by a dispersion of commercial dry chemical in air.

effective particle diameters and the wavelengths of the bulk of the radiant energy.

Since commercial dry-chemical extinguishers discharge powder at a rate which is initially very high, and which decreases very rapidly, they were not considered suitable for use in controlled optical experiments. It was found that commercial dry chemical would remain on a fixed 100-mesh sieve but would flow if the sieve were vibrated. This fact made it possible to dispense a stream of powder which could be irradiated and observed under controlled conditions. The powder was placed in a light metal cylinder 12 cm in height and 5 cm in diameter, open at the top and bottom, resting on the center of a round 100-mesh sieve 20 cm in diameter. An electric vibrator was used and the rate of powder discharge was controlled by adjusting the voltage on the vibrator. To avoid interference from particles floating around in the air, a vacuum cleaner was used to remove the powder as it fell. The vacuum cleaner was equipped with a conical attachment 20 cm in diameter placed 20 cm below the dispensing sieve. At this distance, the exhaust system had no apparent effect on the free fall of the powder in the first 8 cm of fall. The diameter of the falling powder stream contracted from 5.0 cm at the sieve to 4.0 cm at 2.5 cm below the sieve and remained fairly constant for an additional 5 cm. On the basis of previous estimates of the discharge rate employed in fire-fighting, the powder was discharged so that its flow rate was 0.012 gm/sec-cm^2 in the region under observation.

Measurements were made using radiant energy in the visible region of the spectrum and in the infrared. For the visible region, the optical system consisted of a 100-watt incandescent lamp, projection lenses, a photovoltaic cell, and a recording potentiometer. The photocell was mounted so that it could view the powder stream from various angles. The lamp and photocell combination gave an effective spectral distribution similar to the relative visibility curve for the normal human eye but shifted about 0.05μ toward the long wavelengths.

Previous investigations had shown that the spectral distribution of the energy emitted by hydrocarbon diffusion flames is similar to that of a blackbody at 1470°K, having a maximum in the infrared at a wavelength of about 2 μ.[9] To approximate this distribution, an electrically powered hot-wire source was operated at 1200°K and gave a spectral distribution with a maximum around 2.4 μ. A radiation pyrometer was used as a detector.

Measurements were made of the fraction of the incident energy which was transmitted directly and the fraction deflected through angles from 30° to 150° at 15° intervals. The observed relative intensities of the deflected energy are shown in Figure 1. It was found that 85 per cent of the visible light and 81 per cent of the infrared energy were transmitted directly through the 4.0–cm stream. There was much more energy deflected at forward angles than at backward angles and the observed relative intensity of deflected energy (within the angular range covered) was 2 to 5 times as great in the infrared as it was in the visible. This would be expected if the particle diameters were greater than the effective wavelength of the infrared source. An independent analysis of the particle diameter distribution with a Roller Analyzer (an elutriation type separator) indicated 3 per cent by weight less than 10 μ, 14

per cent from 10 to 20 μ, 38 per cent from 20 to 40 μ, and 45 per cent above 40 μ.

In a gasoline spill-fire on an area four feet square, flames often rise six to eight feet in the air. The powder cloud used in extinguishing such fires would have a depth of the order of 45 cm. If the concentration were the same as that of the powder stream in these experiments and Bouguer's exponential law of transmission may be assumed, it appears that less than 10 per cent of the energy radiated in the direction of the gasoline would be transmitted through the powder cloud. It would seem that this effect should make a substantial contribution toward the extinguishment of the fire.

If the shielding effect is a substantial part of the mechanism, and the size distribution of particles in the dispersion is that indicated above, one would predict on the basis of optical principles that powders having a larger part by weight in smaller particles would be more effective if the small particles were discrete in the dispersed state. The preliminary experiments seem to show such a trend for the range of particle sizes used.

5. Transmittance Measurements During Extinguishment

The uncertainties involved in interpreting laboratory data in terms of fire-fighting conditions made it desirable to simulate actual conditions. For this reason, a group of measurements was made of the effect of dry chemical on the radiant energy from a flame during actual extinguishment. The objective was to determine how much of the energy radiated toward the fuel was transmitted by the dry chemical cloud. The adverse conditions at the surface of the fuel made it impractical to place a detector there, so a burner was constructed with a window in the bottom. The burner was a thin steel cylinder 10 cm in diameter and 6 cm deep, open at the top. The window in the bottom was made of clear fused quartz.

The powder was placed in a cylinder 8 cm in diameter and 45 cm in height with a compressed air inlet at the bottom and a nozzle at the top (Fig. 2). The 1 x 10 mm nozzle opening discharged a stream having a cross section of greater width than height. To avoid the transient flow conditions produced when the compressed air was turned on or off, the extinguisher was allowed to discharge continuously. Except when it was desired to apply powder to the flame, the powder stream was caught by a funnel connected to a vacuum dust collector. The funnel could be pulled aside for a given time interval, by means of a solenoid and an electronic timer. This arrangement provided short bursts of powder with a nearly constant flow rate during the discharge.

A lead sulfide infrared photoconductive cell was placed below the window to detect the energy radiated toward the fuel and another such cell was placed above and to one side of the burner to detect the energy radiated in that direction. This arrangement is shown in Figure 2. In order to limit the effect of radiation from other sources, infrared filters were used to limit the spectral sensitivity of the detectors to the wavelength region from 0.7 to 2.6 μ.

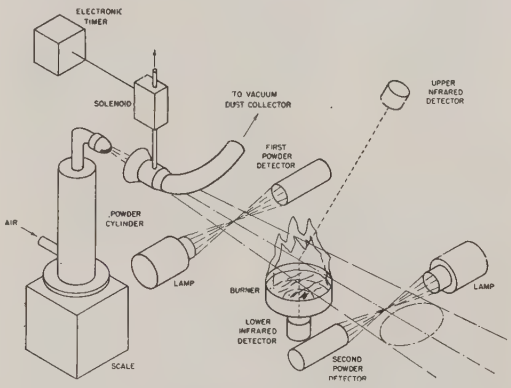

FIG. 2. Equipment used to measure the transmittance and concentration of powder clouds.

The fuel was a commercial mixture of heptanes with a boiling point range of about 88°C to 100°C. This fuel was chosen because it represents a major component of gasoline, the most common hazardous flammable liquid, but has a much more uniform burning rate in a spill-type fire. The fuel was floated on a thin layer of water to prevent overheating of the window and its mounting gaskets. The thickness of the water layer was 1.1 cm and the thickness of the fuel layer was 0.4 cm at the start of the experiment. The metal rim of the container extended about 3 cm above the fuel level. When the burner had warmed up, the flame measured about 10 cm in diameter, at its widest part, and about 40 cm in height.

In the part of the spectrum used, thin layers of water and quartz transmit nearly 100 per cent at all wavelengths. A 4 mm layer of heptane transmits nearly all energy in the wavelengths from the visible spectrum to 1.6 μ with the exception of

sharp absorption bands at 1.25 and 1.45 μ, and about 77 per cent from 1.6 to 2.3 μ, with the exception of a narrow absorption band at 1.7 μ. Thus the spectral sensitivity of the lower detector was little different from that of the upper one. There was practically no change in these absorbing layers during the small fraction of a second involved in making a measurement. Aside from these considerations it was not necessary to take into account the transmittance and reflectance of these various layers because only relative values of the irradiance at the receiver were required for transmittance measurements.

In the usual measurement of transmittance, a radiant source of constant intensity is employed and a determination is made of the ratio of the relative amounts of energy received with and without a sample interposed between the source and receiver. In the present case, the source was a flame which decreased in intensity when the powder cloud was injected. The upper detector measured the decrease in intensity in the upward direction and it was assumed that the intensity in the downward direction changed in the same ratio. The transmittance, measured by the lower detector, was then corrected for the decrease in flame intensity.

Because the extinguishment occurred so quickly, it was necessary to record the data with a high speed automatic recorder. The recorder used was essentially a row of 2-in. cathode ray oscilloscopes that were photographed simultaneously by a 35 mm camera in which the film was exposed continuously as it moved at right angles to the deflections of the spots on the tubes. The output of a 40 cps fixed frequency oscillator was applied to one channel to provide a time scale.

The radiant intensity of the flames dropped very rapidly after the appearance of the powder. The time required to extinguish the flame averaged about 200 msec as observed by means of the upper detector but only about 170 msec as observed by means of the lower detector. During the time that the radiant intensity was diminishing, slight fluctuations in the intensity produced relative maxima and minima in the two radiometric records. The measurements of transmittance were made at the maxima because such corresponding points on the two curves presumably represented events which occurred simultaneously.

Thirty measurements of this kind were made with the powder concentration near the minimum value required for extinguishment. The average transmittance was found to be 53 per cent. This result seems to support the belief that even in a small fire, the shielding effect of the powder may contribute materially to the extinguishing process. The cloud of powder used in these experiments had a depth of about 6 cm. In larger fires, where thicker and more concentrated clouds are used, a somewhat greater effect would be likely.

6. Concentration Measurements During Extinguishment

Quantitative considerations of the mechanism of extinguishment hinge ultimately upon knowledge of the concentration of material required for extinguishment. The relative effectiveness of different powders can be expressed quantitatively if the minimum effective concentration of each is known. The quantitative control of concentration during a series of experiments depends upon measurement of concentration. A satisfactory method of measurement should give the concentration during extinguishment. Direct sampling techniques were not employed because such methods disturb the distribution of the powder and disrupt the normal course of events during extinguishment. To avoid these difficulties, optical methods were employed to measure several related physical quantities from which the concentration was calculated.

The average weight rate of discharge for a time period of a few seconds could be obtained by direct weighing and timing, but during a small fraction of a second the weight change was too small to be differentiated from variations in the recoil of the discharging cylinder. It was found that the average rate of discharge was proportional to the average optical density of the powder stream. (This is a manifestation of Beer's Law, usually applied to the relationship of optical density and concentration in solutions.) This fact was utilized in calculating the instantaneous rate of discharge from the optical density of the powder stream measured by projecting a light beam through the stream onto a photoelectric cell and recording the response automatically.

Another such photoelectric system was placed a fixed distance downstream and when a short burst of powder was injected, the elapsed time between the appearance of powder at these two points was recorded. The burner was placed below a point midway between the light beams as shown in Figure 2. The data obtained were used

to calculate the velocity of the stream at the burner. The average observed velocity was 43 cm/sec.

A photoelectric system such as those described was used to scan the stream horizontally and vertically at the burner position to determine the distribution of the powder in the stream. The distribution determined in this way appeared to be nearly uniform over an area approximating an ellipse and to drop rapidly to zero outside this region. From the plotted density, an estimate was obtained of the lengths of the axes of an ellipse which would encompass all of the powder if it were uniformly distributed. This ellipse had axes of 6 and 10 cm, giving an area of 47 cm^2.

The measured values of weight rate, R, velocity, v, and cross sectional area, A, were used to calculate the concentration of powder, c, by means of the equation $c = R/vA$. All of these measurements, except the area scanning, were recorded simultaneously with the transmittance measurements during extinguishment by the use of six channels on the oscillograph. It was found that when the concentration exceeded 2.8×10^{-4} gm/cm^3 the flame was always extinguished but when the concentration fell below 0.7×10^{-4} gm/cm^3 the flame was not extinguished. At concentrations between these values, both successes and failures were recorded. These values may be applicable to this flame only but the order of magnitude is established for theoretic considerations. The technique described here was the only practical method of concentration measurement found which met the conditions imposed by the nature of the experiments.

7. Conclusions

The theory of extinguishment involving the evolution of carbon dioxide is not satisfactory because powders that do not release carbon dioxide are effective agents. The combination of fineness and dispersibility of powders appears to have some correlation with their effectiveness. Salts of alkali metals appear to be particularly effective. The evidence indicates that the mechanism of dry-powder extinguishment is not principally that of excluding oxygen, diluting the atmosphere, cutting off the fuel supply, or blowing out the fire. A minimum concentration of the order of 10^{-4} gm/cm^3 of commercial dry chemical is required to extinguish small fires involving heptane under the conditions of the experiments. In the light of prevailing theories of combustion and flame propagation, it appears that dry-powder extinguishment may be largely attributable to the interruption of chain-reactions in the combustion process. The rapidity of the action, the apparent dependence of effectiveness on fineness, and the small concentration required, as determined in these experiments, seem to support this view. However, it appears that a full account of the mechanism of dry-powder extinguishment of flammable-liquid fires must also include the factor of radiation shielding.

REFERENCES

1. Approved Equipment for Industrial Fire Protection. Factory Mutual Laboratories, 184 High Street, Boston 10, Massachusetts.
2. Block, D. J.: Fire Extinguishing Material, U. S. Patent 1,793,420, filed September 22, 1928.
3. Lewis, B., and von Elbe, G.: *Combustion, Flames and Explosions of Gases*. New York, Academic Press, Inc., 1951.
4. Dufraisse, C., and German, M.: Compt. Rend., *207*, 1221 (1938).
5. Jorissen, W. P., et al.: Rec. Trav. Chim. (Amsterdam), *52*, 403 (1933).
6. Dijksman, A. J.: Chem. Weekblad, *31*, 718 (1934).
7. Jorissen, W. P., et al.: Rec. Trav. Chim. (Amsterdam), *59*, 957 (1940).
8. Muraour, H., and Michel-Levy, A.: Compt. Rend., *218*, 551 (1944).
9. Roeser, W. F., and McCamy, C. S.: Principles of Fire Detection in Aircraft Engine Spaces. WADC Technical Report 54-307, Wright Air Development Center (1954).

108

THE EFFECT OF CERTAIN HALOGENATED METHANES ON PRE-MIXED AND DIFFUSION FLAMES

By F. H. GARNER, R. LONG, A. J. GRAHAM AND A. BADAKHSHAN

1. Pre-mixed Flames

INTRODUCTION

It is well known that some of the halogenated methanes are valuable as vaporizing liquid-fire extinguishing agents. The influence of these substances on the limits of inflammability of hydrocarbon/air mixtures has been investigated[1, 2] but there appears to be little information concerning their influence on burning velocities. Zentler-Gordon,[3] from approximate calculations of burning velocities from flame heights, found that organic halides caused a reduction, with bromides more effective than iodides or chlorides. Recently Simmons and Wolfhard[4] have shown that methyl bromide reduces the burning velocity of ethylene/air mixtures.

The present work was undertaken to provide further information concerning the influence of additives and in the hope that the results might throw some light on the mechanism of inhibition.

EXPERIMENTAL

The method adopted for the determination of burning velocities involved the use of a nozzle burner (brass, 1 cm in diameter) and a schlieren optical system as described elsewhere.[5] This method was used because the experimental technique is relatively simple.

There is a disadvantage in this method as the results obtained by the use of the angle method on the schlieren cone are dependent upon the gas flow rate;[5, 6] however, in the present work relative results only were required and the mixture flow rate to the burner was at all times maintained constant. Since burning velocities determined at 50°C are only quoted as relative values, all results for mixtures containing the additives have been expressed in the following form:

The maximum burning velocity of the fuel/air mixture with a given amount of additive is expressed as a percentage of that of the maximum burning velocity of fuel/air mixture alone.

This method of expressing the results provided the simplest way of making allowance for the small amount of extra fuel introduced in the form of additive. The mole percentage of additive was, in general, below 1 per cent.

Gaseous additives were metered and controlled in the same way as the fuel supply while liquid additives were introduced from a "micro doser" and vaporized into the air stream.

The flames as burned were surrounded by air; the outer diffusion flame has been shown to have a stabilizing influence on the flame.[4, 7]

RESULTS

The effects of water vapor, hydrogen chloride, methyl chloride, methylene chloride, chloroform, carbon tetrachloride, methyl iodide, methyl bromide and chlorobromomethane upon the maximum burning velocity of propane/air mixtures are shown in Figure 1.

Only small proportions of additive were used in the case of the halogenated methanes and it can be seen that the reduction in burning velocity is almost linear with the increase in concentration of additive (although there is evidence of a slight falling off in effectiveness as the concentration increases).

The order of effectiveness of the additives in reducing the burning velocity is $H_2O < HCl < CH_3Cl < CH_2Cl_2 < CHCl_3 < CCl_4 < CH_3Cl < CH_3Br < CH_2ClBr$. The last three additives show a markedly higher inhibiting effect than that of the series of chlorinated methanes.

DISCUSSION

The presence of halogenated methane as additive in the fuel/air mixture leads to two effects; the first is that of additional fuel (when part of the additive molecule is combustible) which causes an apparent shift in the position of the burning velocity *vs.* mixture strength curves, while the second is the marked inhibiting effect on flame propagation.

It has been suggested that flame propagation is controlled either by thermal conduction or radical diffusion from the flame front into the unburned mixture or by a combination of these mechanisms. Egerton and Powling[8] suggested that the main criterion for inflammation is the maintenance of a sufficient rate of heat release

in the flame which will provide active radicals, and the flame temperature must be sufficient for this.

Additives might influence flame propagation in three ways: (1) by altering the properties of the unburned mixture so as to influence heat conduction or radical diffusion; (2) by altering the flame temperature; (3) by specific chemical inhibition of the combustion reactions.

It seems most unlikely that the very small concentrations of additive employed in the present work could have any appreciable influence upon the physical properties of the unburned mixture. No measurements appear to have been made of the experimental flame temperatures of fuel/air mixtures containing small amounts of additives. Recent calculations by Simmons and Wolfhard,[4] however, indicate that the flame temperatures of stoichiometric hydrocarbon/air flames are not greatly affected by the introduction of small amounts of bromine.

It can be seen from Figure 1 that the addition of 1 per cent of water vapor reduces the maximum burning velocity by roughly 5 per cent and this is most likely due to the increased heat capacity of the moist mixture. Hydrogen chloride as additive has a greater effect, the addition of 1 per cent reducing the maximum burning velocity by 10 per cent. The halogenated methanes are considerably more effective in reducing the burning velocity.

It appears that hydrogen chloride and to an even greater extent, the halogenated methanes, exert a specific chemical inhibition of the flame reactions.

This supports the conclusions of Burden, Burgoyne and Weinberg[9] and of Simmons and Wolfhard[4] who have recently shown that methyl bromide, while not greatly reducing the calculated flame temperature of stoichiometric hydrocarbon + air mixtures, causes a marked increase in the limit flame temperature. This presumably implies that the additive removes chain-carriers.

Simmons and Wolfhard have also shown that the action of methyl bromide can be interpreted in terms of the addition of an equivalent amount of bromine and fuel.

It therefore seems reasonable to suppose that the main effect of the halogenated methane additive is to cause a reduction in the concentration of active free radicals in the flame boundary. The halogenated methane might be expected to be largely dissociated in the flame and the halogen itself to act as the inhibitor. Whether atomic or molecular halogen is the inhibitor cannot be decided from available evidence but at the flame temperature at least partial dissociation of halogen molecules to atoms will occur.

The fact that methyl chloride is more effective as an inhibitor than hydrogen chloride suggests that the halogenated methane molecule itself might be involved also.

$$H + CH_3X \rightarrow HX + CH_3$$

If the molecule acts in this way, the effective concentration of inhibitor may be greater, for HX itself may remove H atoms.

The order of effectiveness of the chlorinated

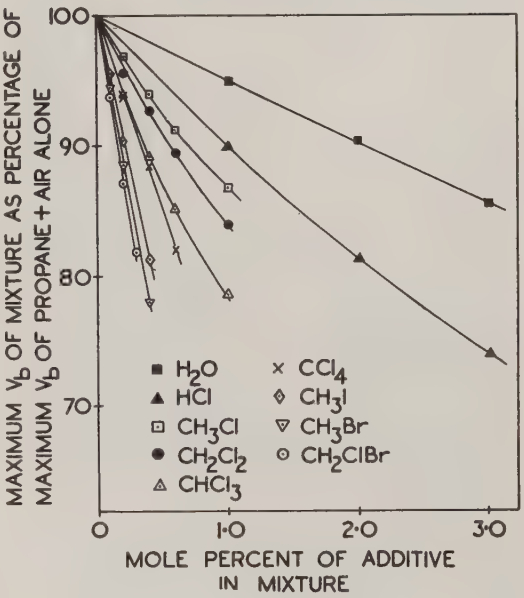

Fig. 1.

methanes in reducing the maximum burning velocity is

$$CH_3Cl < CH_2Cl_2 < CHCl_3 < CCl_4$$

which is the same as the order of their total inhibitory effect as assessed by the values for the limiting safe mixtures.[10]

It is interesting to note, however, that the effect on the upper limit of *n*-hexane[10] is in the reverse order to that given above.

2. Diffusion Flames

Halogens are known to exert a profound effect upon some combustion processes; it was considered that a study of the influence of halogenated methanes upon the carbon deposition from diffusion flames would be of interest and might

lead to increased knowledge concerning the processes leading to carbon formation in flames.

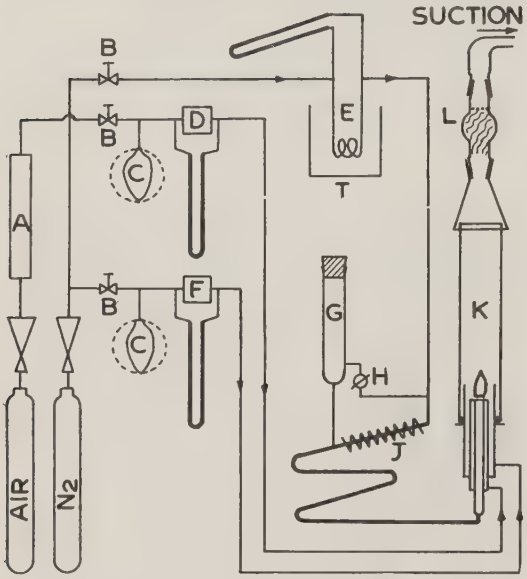

FIG. 2. Diagrammatic sketch of the diffusion flame apparatus.

A—$CaCl_2$ drier
B—Needle valves
C—Surge balloons
D—Air flowmeter
E—N_2 flowmeter (carrier gas)
F—N_2 flowmeter (outer jacket)
G—Burette
H—By-pass valve
J—Heated vaporizer tube
K—Circular diffusion burner
L—Soot filter
T—Thermostat

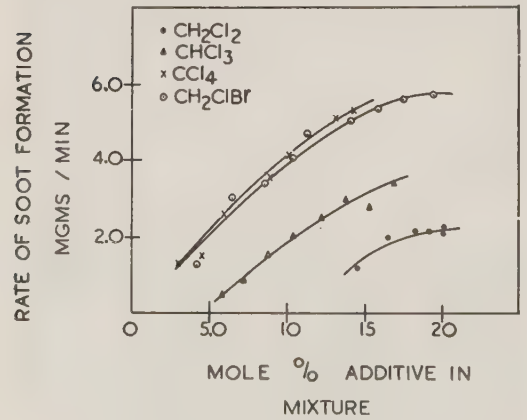

FIG. 3. Effect of additives on the rate of soot formation from a *n*-heptane/air diffusion flame.

There has been increased interest in the mechanism of carbon formation in recent years and the various theories have been discussed by Gaydon and Wolfhard[11] and by Schalla and McDonald.[12]

Since this work was started it has come to our notice that Sachs and Ziebell[13] have reported that atoms and radicals such as those found in the pyrolysis of halogen compounds increase smoke formation presumably by dehydrogenation of the fuel molecules. Street and Thomas[14] have also reported that halogenated compounds increased the amount of air required to inhibit carbon formation in their experiments.

In the present work the effects of methylene chloride, chloroform, carbon tetrachloride and chlorobromomethane upon hydrocarbons of the paraffin and naphthene series *viz.* *n*-heptane and methylcyclohexane, were studied.

EXPERIMENTAL

A known fuel/additive mixture was burned with air as a diffusion flame under steady conditions and the quantity of soot produced in a certain length of time measured.

Fuel/additive mixture was allowed to drip from a constant head reservoir through a capillary tube into a heated inclined Pyrex tube in which it vaporized and mixed with a pre-heated stream of nitrogen which acted as a carrier-gas. The vaporized fuel/additive mixture was burned with air in a diffusion flame burner circular in cross-section. The rate of flow of nitrogen as carrier gas was kept constant and the liquid flow-rate could be determined from the burette readings.

The apparatus with the burner is shown in Figure 2. The burner consisted of three concentric Pyrex tubes with the fuel and carrier-gas passing up the inner, air through the middle, and nitrogen through the outer tube. The purpose of the stream of nitrogen through the outer tube was to improve the steadiness of the diffusion flame.

The air-rate was adjusted so that no soot formation could be detected when no additive was present in the fuel. The air-rate was kept constant with each hydrocarbon throughout the experimental work.

Soot from the flame was collected in a filter shown in Figure 2. The cotton wool in this filter retained the soot particles when the products of combustion were drawn through it and after drying, the weight of soot deposited in a given period could be determined. Soot deposited in the chimney tube was extracted by a known volume of carbon tetrachloride and the amount (not more than 5 per cent of the total) was estimated approximately by measuring the light absorption of the suspension using a photoelectric colorimeter. The instrument was calibrated

with suspensions made up to contain known concentrations of soot.

A study was made of the effect of increasing the proportion of additive in the fuel (with the volume rate of flow of the mixture maintained constant) upon the rate of soot formation.

RESULTS AND DISCUSSION

The effect of the additives, methylene chloride, chloroform, carbon tetrachloride and chlorobromomethane, upon the smoke formation in diffusion flames of *n*-heptane and methylcyclohexane is illustrated in Figures 3 and 4 respectively.

It can be seen that the order of effectiveness of the additives in promoting soot formation is

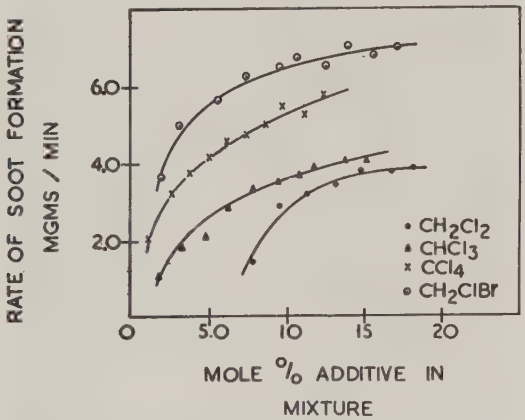

FIG. 4. Effect of additives on the rate of soot formation from a methylcyclohexane/air diffusion flame.

$CH_2ClBr \simeq CCl_4 > CHCl_3 > CH_2Cl_2$ for *n*-heptane, and $CH_2ClBr > CCl_4 > CHCl_3 > CH_2Cl_2$ for methylcyclohexane.

It seems clear from these results that as the proportion of halogen in the molecule increases, the additive becomes more effective (when the additive is expressed as mole percentage in the liquid mixture). Bromine appears to be more effective than chlorine. The evidence is insufficient to allow a decision to be made as to whether the halogen acts in the molecular or atomic form although dissociation to atoms to a considerable extent might be expected.

The authors favor the explanation already advanced by Schalla and McDonald,[12] namely, that the halogen leads to more extensive dehydrogenation of the fuel molecule which is probably a most important stage in the complex process of carbon formation in diffusion flames. C—C bond scission and dehydrogenation might be expected to lead to simpler molecules but the evidence obtained so far is insufficient to allow a decision to be made as to whether acetylene, as suggested by Porter[15] or a diene as suggested by Garner, Long and Thorp[16] is the important fragment leading to carbon formation. In fact, these two suggestions do not seem to be mutually exclusive.

It seems significant that colored substances have been found both in the "self-combustion" of acetylene (Westbrook, Hellwig and Anderson[17]) and associated with the carbonaceous deposits from hydrocarbon diffusion flames (Garner, Long and Thorp[16]). The latter workers have suggested that colored substances with a fulvenic structure may be precursors of the carbonaceous deposits.

REFERENCES

1. BURGOYNE, J. H., AND WILLIAMS-LEIR, G.: Proc. Roy. Soc., *A193*, 525 (1948).
2. COLEMAN, E. H.: Fuel, *30*, 114 (1951).
3. ZENTLER-GORDON, H. E.: Ph.D. Thesis, London (1940).
4. SIMMONS, R. F., AND WOLFHARD, H. G.: Trans. Faraday Soc., *51*, 1211 (1955).
5. GARNER, F. H., LONG, R., AND THORLEY, B.: *Fourth Symposium (International) on Combustion*, p. 386. Baltimore, The Williams & Wilkins Co., 1953; Fuel, *33*, 394 (1954).
6. CALDWELL, F. R., BROIDA, H. P., AND DOVER, J. J.: Ind. Eng. Chem., *43*, 2731 (1951).
7. GARSIDE, J. E., FORSYTH, J. S., AND TOWNEND, D. T. A.: J. Inst. Fuel, *18*, 175 (1945).
8. EGERTON, A. C., AND POWLING, J.: Proc. Roy. Soc., *A193*, 172 (1948).
9. BURDEN, M. C., BURGOYNE, J. H., AND WEINBERG, F. J.: *Fifth Symposium (International) on Combustion*, p. 647. New York, Reinhold Publ. Corp., 1955.
10. Report of the Fire Research Board for the Year 1951. H.M.S.O. London (1952).
11. GAYDON, A. G., AND WOLFHARD, H. G.: *Flames, Their Structure, Radiation and Temperature*. London, Chapman and Hall, 1953.
12. SCHALLA, R. L., AND MCDONALD, G. E.: *Fifth Symposium (International) on Combustion*, p. 316. New York, Reinhold Publ. Corp., 1955.
13. SACHS, W. AND ZIEBELL, M. T. I.: National Aeronautical Establishment Lab. Report LR-30 (1952).
14. STREET, J. C., AND THOMAS, A.: Fuel, *34*, 4 (1955).
15. PORTER, G.: *Fourth Symposium (International) on Combustion*, p. 248. Baltimore, The Williams & Wilkins Co., 1953.

16. Garner, F. H., Long, R., and Thorp, N.: Fuel, *32*, 116 (1953); Fuel, *34*, S.I. (1955).
17. Westbrook, E. A., Hellwig, K., and Anderson, R. C.: *Fifth Symposium (International) on Combustion*, p. 631. New York, Reinhold Publ. Corp., 1955.

109

EFFECTS OF HALOGENATED EXTINGUISHING AGENTS ON FLAME QUENCHING AND A CHEMICAL INTERPRETATION OF THEIR ACTION

By FRANK E. BELLES and CLEVELAND O'NEAL, Jr.

Introduction

Various halogenated hydrocarbons have much greater power to extinguish flames than have inert diluents, and it has been pointed out that these compounds evidently operate by means of some chemical effect.[1, 2] The present work was undertaken to study the effects of several halogenated agents on flame quenching, in order to obtain estimates of the chemical activity. It was hoped that the results would lead to a better understanding of the chemical processes of flame extinction, and that they would be of value in rating the agents.

The usual way to assay the effectiveness of an agent is to examine its effect on the flammability of a fuel.[1, 3, 4] Various mixtures of fuel, agent, and air are tested, until enough data are gathered to define the region of flammable mixtures in a plot of per cent fuel against per cent agent required for extinction. From such a plot, one may read off the amount of agent required to prevent flame propagation in all possible mixtures, and this is called the flammability peak agent concentration. The smaller the peak concentration, the better is the agent.

In recent years, the flammability test has turned up some highly effective agents. For example, 4.2 volume per cent dibromodifluoromethane will prevent flame propagation in all *n*-heptane-air mixtures, whereas 29.5 per cent of the relatively inert carbon dioxide is required.[4] Furthermore, there is some correlation between the order of effectiveness of various agents as indicated by flammability peaks and by practical tests on standard fires.[4]

However, it is desirable to understand something of the chemistry of fire extinction, in order to guide the selection of agents for test and to help decide whether still more effective agents remain to be found. There are some well-developed concepts of flame quenching by means of which the chemical effect of an agent may be evaluated. It has been found possible to interpret the wall-quenching of laminar flames by equations developed from the idea that quenching is due to destruction of the active particles H, O, and OH at the walls.[5, 6, 7] The concepts have been extended to the case in which there is also chain-breaking by destruction of these active particles in the gas phase.[7] Inasmuch as it has been suggested[1, 2, 8] that halogenated agents extinguish flames by this gas-phase chain-breaking mechanism, it was anticipated that data showing the effects of agents on quenching distance might be used to calculate rate constants for the crucial agent-active particle reaction.

The method has already been applied to the case of propanemethyl bromide-air mixtures, with encouraging results.[2] The present work was therefore undertaken. Pressure limits of flame propagation were measured for propane-air mixtures in the presence of small amounts (0.5 volume per cent or less) of extinguishing agents. The tube method of Simon, Belles, and Spakowski[5] was used. It has been shown that this method gives the pressure at which the quenching distance of a given mixture is just equal to the tube diameter.[5, 9] Downward flame propagation was used to avoid convection effects. The following agents were tested: CH_3Br, CCl_4, CH_2BrCl, CH_3I, CBr_2F_2, and $CBrF_2CBrF_2$.

Apparatus and Procedure

Figure 1 shows the apparatus used. Mixtures were made up by the method of partial pressures in the two large tanks, A and B, after they had first been pumped out to 0.1 mm Hg or less. In tank A, agent vapor and air were introduced to

give a mixture of reasonably high concentration, for example, 2 per cent. A predetermined partial pressure of propane was admitted to tank B, the appropriate pressure of agent-air mixture was added, and finally air was admitted to give the required concentrations of fuel and agent. The agent concentration was always 0.5 volume per cent or less of the total mixture, and for any given agent, all mixtures prepared had the same agent concentration. Water and carbon dioxide were removed from the air in a train of absorption towers.

The flame tube, and the plenum used to give essentially constant-pressure combustion, were very similar to apparatus previously described.[5] However, two changes were incorporated:

(1) The flame tube was made in two pieces, a wide ignition section and a narrower propagation section; a brass adapter plate connected the two and provided an abrupt transition between them. This arrangement has been found[10] to give results superior to those obtained with a one-piece tube, having a smooth transition from the ignition section to the propagation section.

(2) The direction of flame propagation was downward, to avoid effects of convection.

One tube was used for all the work. It had a diameter of 3.73 cm and was 50 cm long.

In order to determine a pressure limit for flame propagation, the flame tube was first evacuated. The desired pressure of propane-agent-air mixture was admitted from tank B to the flame tube. The air pressure in the plenum was equalized to that in the flame tube, and the stopcock between the two was opened. The mixture was ignited by a condensed spark, and the flame observed. If the test pressure was greater than the limit, the flame propagated through the mouth of the 3.73-cm tube and all the way to its lower end. If the test pressure was less than the limit, the flame was quenched at the mouth of the 3.73-cm tube. Repeated trials at various pressures established the limit, in most cases to within ±2 mm of mercury.

Experimental Results

PROPANE-AIR MIXTURES

Inasmuch as downward flame travel was used in the present work to avoid convection effects, the pressure limits for downward flame propagation in propane-air mixtures were determined and compared with those previously obtained[10] for upward propagation. Figure 2 shows the curves of pressure limit against propane concentration for the two cases. The curves are surprisingly close together, actually coinciding on the lean side. As expected, where deviations do occur, they show that upward-propagating flames do get some small assistance from convection and are therefore not quite so easily quenched.

Although the effects are small, they are sufficient to resolve a question about which there has been some discussion. It has been predicted[5, 11] that the quenching distances for cylindrical tubes

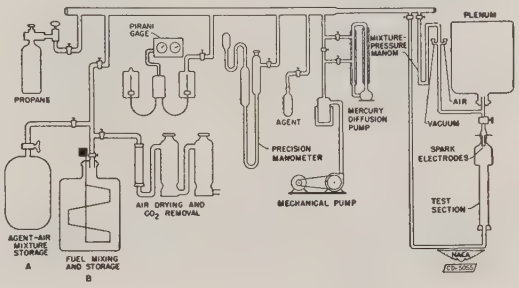

FIG. 1. Pressure limit apparatus.

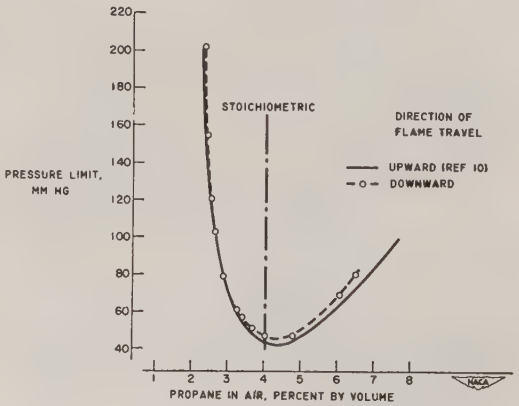

FIG. 2. Effect of direction of flame travel on pressure limits of flame propagation. Propane-air mixtures, 3.73 cm diameter tube.

(d_2) and plane parallel plates (d_1) should be related as follows:

$$d_1/d_2 = 0.61 \qquad (1)$$

However, previous data for quenching by cylinders that were used to test Equation (1) were taken with upward propagating flames, and the observed value of the ratio d_1/d_2 was about 0.7 for lean mixtures.[5] The present data (which consist of the pressures and propane concentrations at which the cylindrical-tube quenching distance is 3.73 cm) agree much more closely with the predicted ratio; with quenching distances for

rectangular slots,[12] corrected for end effects to reduce them to equivalent plane-parallel plate data,[11] values of d_1/d_2 from 0.57 to 0.60 were obtained. Both lean and rich mixtures are represented in this range of values.

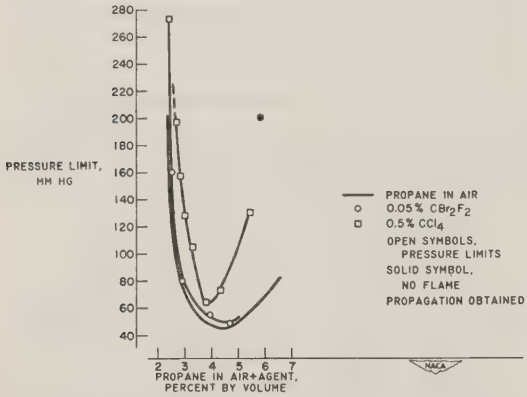

FIG. 3. Effect of CBr_2F_2 and CCl_4 on pressure limits of flame propagation. Propane fuel, 3.73 cm diameter tube.

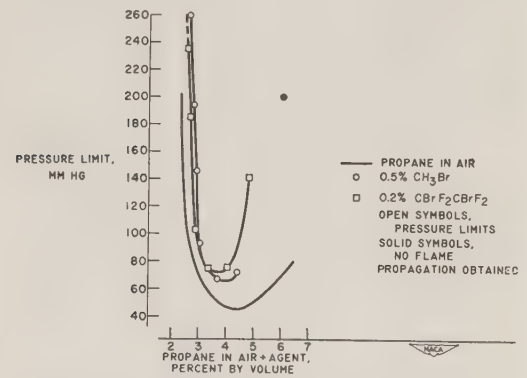

FIG. 4. Effect of CH_3Br and $CBrF_2CBrF_2$ on pressure limits of flame propagation. Propane fuel, 3.73 cm diameter tube.

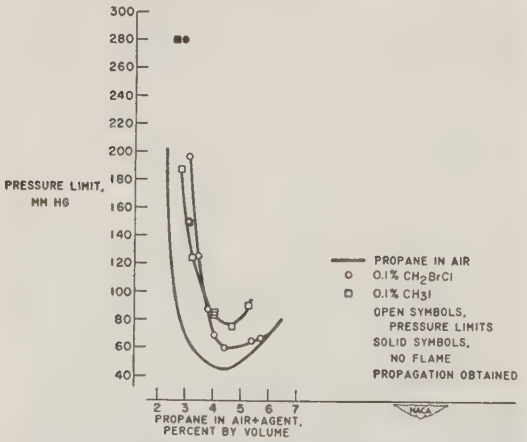

FIG. 5. Effect of CH_3I and CH_2BrCl on pressure limits of flame propagation. Propane fuel, 3.73 cm diameter tube.

PROPANE-AGENT-AIR MIXTURES

Figures 3, 4 and 5 show curves of pressure limit of flame propagation against fuel concentration for the propane-agent-air mixtures studied. Both propane and agent concentrations are given as volume per cent of the total mixture. The concentration of each agent was held constant for all tests. Only small additions of agent were used, 0.05 to 0.5 per cent; this was done to avoid changing the thermodynamic properties of the mixtures appreciably, so that calculations of flame temperature and burned-gas composition made previously for propane-air mixtures[5] would still apply.

The pressure limit curve for downward flame propagation in propane-air mixtures is included in each figure for comparison. It is seen that despite the small additions of agent used, there were very pronounced effects on the pressure limits. For example, with 0.1 per cent methyl iodide, the minimum pressure limit is 77 mm of mercury compared to 45 for propane-air. In addition, the range of fuel concentrations for propagating flames, at constant pressure, is less when agent is present. The concentration at which the minimum pressure limit occurs is also affected; for propane-air the minimum falls at an equivalence ratio φ of 1.08, while for the propane-agent-air mixtures it occurs at $\varphi = 0.95$ to $\varphi = 1.16$.

It does not appear feasible to attempt any correlation of the effects shown in Figures 3, 4 and 5 with the usual criteria of agent effectiveness, that is, with the flammability peak concentration.[4] The main difficulty is that various agent concentrations were used; the amount chosen in each case was just enough to produce a reasonable change in the pressure limits. Furthermore, a limited number of tests (not reported here) showed that the changes for a given agent are not directly proportional to its concentration. Thus, it is not possible to reduce all the data to a common agent concentration.

However, two qualitative comparisons may be made. One might expect that the lower the flammability peak and hence the more effective the agent, the higher the minimum pressure limit should be. Table 1 compares the minimum pressure limits and flammability peaks for two pairs of agents that were used at the same concentrations; it is seen that the expectation is borne out in one case, while in the other the comparison is not conclusive.

Calculation of Rate Constants for Agent-Active Particle Reactions

The quenching-distance equations based on the concept that flame quenching is due to destruction of H, O, and OH at the walls have been used quite successfully to interpret the effect of pressure, temperature, mixture composition (lean to stoichiometric mixtures only), and geometry of the quenching surface.[5, 6, 7, 11] The original equations[5] have been generalized to include the case of a small amount of chain-breaking in the gas phase, such as may occur when a halogenated agent is present.[7] The following result was obtained:

$$d_1^2 = \frac{12\left[A - \dfrac{(1-\epsilon)0.7}{1 - \dfrac{g-b}{k_f N_f}} \sum_i \frac{p_i}{P}\right]\left(\frac{T_R}{To}\right)^n}{k_f N_f \left[1 + \dfrac{(1-\epsilon)0.7}{1 - \dfrac{k_f N_f}{g-b}}\right] \sum_i \frac{p_i}{D_i^0}\left[1 - \frac{Pd_1^2(g-b)}{10D_i^0}\left(\frac{To}{T_R}\right)^n\right]} \tag{2}$$

It should be noted that it is not really necessary to invoke the diffusion mechanism. An expression analogous to Equation (2) might be derived on the assumption that loss of heat, rather than loss of active particles, governs flame propagation in ducts, while retaining the notion that the fuel-active particle reaction is the rate-controlling step. Flame quenching has indeed been treated in this manner;[13] however, an equation for the case of gas-phase chain breaking is not derived.

Analysis of a large amount of quenching data indicated that chain-branching may be neglected ($b = 0$), and that the efficiency of the wall for destruction ϵ may be set equal to unity for the purposes of the theory.[7] With these simplifications, Equation (2) becomes:

$$d_1^2 = \frac{12A\left(\frac{T_R}{To}\right)^n}{k_f N_f \left[\sum_i \frac{p_i}{D_i^0} - \frac{Pd_1^2 g}{10}\left(\frac{To}{T_R}\right)^n \sum_i \frac{p_i}{(D_i^0)^2}\right]} \tag{3}$$

Now, the frequency of chain-breaking reactions per unit concentration of active particles is given by

$$g = k_a N_a \tag{4}$$

where k_a is an average or over-all rate constant for the chain-breaking reaction between active particles and agent. Solving for k_a from Equations (3) and (4) gives:

$$k_a = \frac{-120A\left(\frac{T_R}{To}\right)^n + 10d_1^2 k_f N_f \sum_i \frac{p_i}{D_i^0}}{Pd_1^4 k_f N_f N_a \left(\frac{To}{T_R}\right)^n \sum_i \frac{p_i}{(D_i^0)^2}} \tag{5}$$

Of the quantities in Equation (5), the quenching distance and pressure are measured directly. In the present work, the pressure was the pressure limit of flame propagation. The quenching distance required is that for plane parallel plates; however, in view of the good agreement between predicted and observed values of d_1/d_2, d_1 may be set equal to (0.61) (3.73) = 2.28 cm. Except for To, which was 300°K, the remaining quantities were either assigned or calculated. The considerations used were the same as those adopted in previous work:[2, 5, 7] (1) The fraction A was set equal to the mole fraction of propane at the lean flammability limit, 0.0201.[14] (2) The mean reaction temperature T_R was set equal to 0.7 T_F. (3) The partial pressure of active particles of one kind in the reaction zone p_i was taken as 0.7 of $p_{i,\,eq}$. (4) The equilibrium adiabatic quantities T_F and $p_{i,\,eq}$ were computed by the method of reference 15, and were taken from Simon, Belles and Spakowski.[5] (5) The amounts of fuel and agent in the reaction zone, N_f and N_a, were taken as half the amounts computed by the perfect gas law from fuel and agent concentrations and reaction-zone temperature T_R.

Table 1. Comparison of Minimum Pressure Limits and Flammability Peaks for Various Agents

Agent	Agent Concentration	Minimum Pressure Limit	Flammability Peak
	per cent by vol	*mm Hg*	*per cent by vol*
CH_2BrCl	0.1	61	7.6
CH_3I	0.1	77	6.1
CH_3Br	0.5	65	9.7
CCl_4	0.5	63	11.5

* See Table 3.[4]

This allows for the fact that the average concentrations in the reaction zone must be less than would be present in fresh gas at the same temperature, owing to reaction. (6) The following numerical values were used[7]: $n = 2$; $D_H^0 = 1.80$ cm²/sec; $D_O^0 = 0.40$ cm²/sec; $D_{OH}^0 = 0.28$ cm²/sec; and $k_f = 2.25 \times 10^{-13}$ cm³ molecule^{-1} sec^{-1}.

All of the data needed for Equation (5) are therefore at hand. Values of k_a were calculated constants were calculated, the corresponding pressure limits of flame propagation (read from Figures 3, 4 and 5), and the calculated values of k_a.

Discussion

AVERAGE RATE CONSTANTS

The calculated values of k_a shown in Table 2 vary with propane concentration, increasing

TABLE 2. CALCULATED RATE CONSTANTS FOR AGENT-ACTIVE PARTICLE REACTIONS

Agent	Agent Concentration	Propane Concentration	Pressure Limit	Reaction Temperature, T_R[5]	Rate Constant cm³ mol^{-1} sec^{-1}
	per cent by vol	*per cent by vol*	*mm Hg*	°K	
CBr_2F_2	0.05	3.50	61	1465	2.94×10^{-13}
		4.03	52	1528	3.84×10^{-13}
					Av. = 3.39×10^{-13}
CH_2BrCl	0.10	3.25	173	1462	0.79×10^{-13}
		3.50	122	1474	1.60×10^{-13}
		4.03	70	1538	3.49×10^{-13}
					Av. = 1.96×10^{-13}
CH_3I	0.10	3.00	157	1354	0.66×10^{-13}
		3.50	109	1472	1.83×10^{-13}
		4.03	85	1540	3.17×10^{-13}
					Av. = 1.89×10^{-13}
$CBrF_2CBrF_2$	0.20	2.50	270	1203	0.78×10^{-14}
		3.00	92	1352	3.19×10^{-14}
		3.50	73	1467	10.89×10^{-14}
		4.03	75	1536	17.28×10^{-14}
					Av. = 8.04×10^{-14}
CH_3Br	0.50	2.75	210	1281	0.66×10^{-14}
		3.00	115	1352	1.74×10^{-14}
		3.50	71	1467	4.30×10^{-14}
		4.03	65	1533	6.77×10^{-14}
					Av. = 3.37×10^{-14}
CCl_4	0.50	2.50	230	1203	0.31×10^{-14}
		3.00	132	1353	1.66×10^{-14}
		3.50	82	1469	4.57×10^{-14}
		4.03	66	1533	6.78×10^{-14}
					Av. = 3.33×10^{-14}

for each agent at several lean-to-stoichiometric mixture compositions, 4.03 per cent propane being taken as stoichiometric. Actually, a fuel-agent-air mixture containing 4.03 per cent propane is not exactly stoichiometric, because part of the air is replaced by agent; however, even with 0.5 per cent agent present, the equivalence ratio is only changed from $\varphi = 1.000$ to $\varphi = 1.004$. Rich mixtures were not treated, because previous work[5, 6, 7] has shown that the assumed active-particle reactions do not interpret flame quenching satisfactorily on the rich side. Table 2 lists the propane concentrations for which rate from lean to stoichiometric. The reaction temperatures also increase, suggesting that the effect might be due to the temperature dependence of the reaction rates. However, Arrhenius plots of log k_a against $1/T_R$ lead to activation energies from 30 to 40 kcal/mole, much larger than the values of about 5 to 10 kcal/mole that might be expected for the agent-active particle reactions.[16] It seems quite possible that there may be another factor contributing to the variations in k_a. This is bound up with the assumption, inherent in Equation (5), that H, O, and OH all react similarly with the agent, and that the contribu-

tion of each species to the reaction is proportional to its concentration in the reaction zone. The relative concentrations of H, O, and OH change from lean to stoichiometric mixtures, so if the assumption were incorrect, a variation in the calculated k_a's over and above that expected from temperature change would be introduced. In view of the lack of knowledge of the reactions of H, O, and particularly OH, with halogenated hydrocarbons, it is not possible to resolve this question at present.

In order to obtain a single number for each agent for purposes of discussion, simple averages of the k_a's were taken, and are listed in Table 2. This procedure is probably justified. Figure 6 shows that the curves of k_a against propane concentration are similar for the various agents; therefore, the averages may be expected to express the over-all reactivities of the agents relative to one another in a satisfactory manner.

RELATIONS OF AVERAGE RATE CONSTANTS TO OTHER DATA

Previous work

In the preliminary work in which rate constants were calculated from pressure limits for upward flame propagation in propane-methyl bromide-air mixtures,[2] the average k_a obtained was 3.45×10^{-14} cm^3 molecule^{-1} sec^{-1}. The present value of 3.37×10^{-14} cm^3 molecule^{-1} sec^{-1}, from data for upward propagation, is very nearly the same, and again shows that the direction of flame travel has little influence on quenching in lean to stoichiometric mixtures.

Extinguishing ability of halogenated agents

In the model of flame propagation used, the flame can exist only if the average chain length is equal to or greater than 1. The chain length is reduced both by destruction of active particles at the walls and by reaction with agent molecules in the gas phase. At pressures near 1 atmosphere and for large tubes, the wall effects are small. If one uses reasonable values for the quantities appearing in the equation for chain length (Belles and Berlad,[7] Equation (A 17)), it reduces very closely to the following form under conditions of small wall effects:

$$k_a N_a = k_f N_f \tag{6}$$

Equation (6) states that the flame cannot continue to propagate if the frequency of gas-phase chain-breaking reactions $k_a N_a$ becomes equal to the frequency of chain-propagating reactions $k_f N_f$. It should therefore apply at the flammability peak. Writing Equation (6) in terms of the volume percentages of fuel and agent at the flammability peak, c_f and c_a, respectively, and

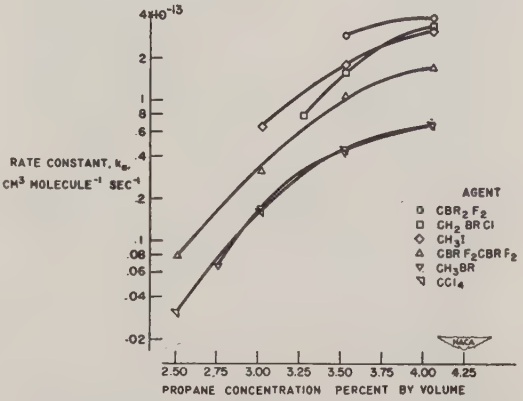

FIG. 6. Variation of agent-active particle rate constants with propane concentration.

TABLE 3. ESTIMATED AND OBSERVED AGENT CONCENTRATIONS AT FLAMMABILITY PEAK

Agent	*n*-Heptane Concentration at Flammability Peak[4]	Observed Agent Concentration at Flammability Peak[4]	Estimated Agent Concentration at Flammability Peak
	per cent by vol	*per cent by vol*	*per cent by vol*
CBr_2F_2	4.4	4.2	2.9
CH_2BrCl	2.2	7.6	2.5
CH_3I	2.1	6.1	2.5
$CBrF_2CBrF_2$	3.3	4.9	9.2
CH_3Br	1.4	9.7	9.4
CCl_4	3.2	11.5	21.6

solving for c_a, gives

$$c_a = \frac{k_f}{k_a} c_f \tag{7}$$

No flammability peak data for propane-agent-air mixtures were found in the literature. However, k_f is the same for a large number of saturated hydrocarbons,[17] and k_a should not depend on the fuel used in its determination. Therefore, Equation (7) should apply to the flammability-peak data for *n*-heptane.[4] Table 3 lists these data for the six agents tested in this work, and the estimated values of c_a obtained from Equation (7); k_f was taken as 2.25×10^{-13} cm^3 molecule^{-1} sec^{-1}, and k_a was the average value from table 2.

It is seen that the estimated agent concentrations required to produce a flammability peak are

of the proper size. They range from 2.5 to 21.6 volume per cent, while the observed amounts are 4.2 to 11.5 volume per cent. In the case of methyl bromide, the agreement is very good, 9.7 per cent observed and 9.4 per cent calculated. The deviations are somewhat greater in the other cases. Furthermore, the observed order of c_a is not the same as the estimated order. But it is probably expecting too much to hope for agreement in detail, since the k_a's were averages for lean-to-stoichiometric mixtures whereas the flammability peaks occur in 5 out of 6 cases in rich mixtures. Significantly, the sixth case, methyl bromide, gives a flammability peak on the lean side and does show agreement.

Despite this lack of detailed agreement, however, inspection of the data in Tables 2 and 3 shows that the average rate constants and peak agent concentrations fall into 2 corresponding groups: (1) Poorer agents: CH_3Br and CCl_4. Average k_a is of the order of 10^{-14} cm^3 molecule^{-1} sec^{-1}. Average peak agent concentration is 10.6 per cent. (2) Better agents: CH_2BrCl, CH_3I, CBr_2F_2, and $CBrF_2CBrF_2$. Average k_a is of the order of 10^{-13} cm^3 molecule^{-1} sec^{-1}. Average peak agent concentration is 5.7 per cent.

Thus, in general, the average k_a is larger for the better agents, and a factor of 10 in the rate constant corresponds to a factor of about 2 in the peak agent concentration.

Finally, the question arises as to whether better agents may be found in the future. In other words, can one reasonably expect average k_a's an order of magnitude or so greater than 10^{-13} cm^3 molecule^{-1} sec^{-1}? A tentative approach to an answer may be made as follows: Reaction cannot occur more frequently than reactants can collide. The gas-kinetic estimate of the frequency factor, Z, in the expression

$$k_a = pZe^{-E/RT_R} \qquad (8)$$

is 10^{-10} cm^3 molecule $^{-1}$ sec^{-1} for $T_R = 1500$°K, in reactions of H, O, or OH with a typical agent having a molecular weight of 150 and a molecular diameter of 4Å. The steric factor, p, should be 10^{-2} for reactions involving H and O, and 10^{-4} for reactions involving OH.[18] If the activation energy is 5 to 10 kcal/mole, the exponential term introduces an additional factor of approximately 10^{-2} to 10^{-1}. Therefore, the total estimated range of rate constants for active particle-agent reactions is 10^{-13} to 10^{-16} cm^3 molecule^{-1} sec^{-1}. It is thus unlikely that halogenated hydrocarbons dramatically superior to those already tested will be found.

Nomenclature

A	fraction of total molecules present in gas phase that must react if flame is to propagate
b	average chain-branching coefficient, sec^{-1}
c_a	agent concentration at flammability peak, per cent by volume
c_f	fuel concentration at flammability peak, per cent by volume
D_i^0	diffusion coefficient for active particles of one kind into unburned gas at atmospheric pressure and initial mixture temperature, cm^2/sec
D_H^0, D_O^0, D_{OH}^0	diffusion coefficients for H, O, and OH, respectively, into unburned gas at atmospheric pressure and initial mixture temperature, cm^2/sec
d_1	distance between parallel plates, cm
d_2	diameter of cylindrical tube, cm
E	activation energy, cal/mole
g	average chain-breaking coefficient, sec^{-1}
k_a	average specific rate constant for reaction of H, O, and OH with agent molecules, cm^3 molecule^{-1} sec^{-1}
k_f	average specific rate constant for reaction of H, O, and OH with fuel molecules, cm^3 molecule^{-1} sec^{-1}
N_a	number of agent molecules per unit volume, molecules/cm^3
N_f	number of fuel molecules per unit volume, molecules/cm^3
n	power expressing temperature dependence of diffusion coefficient, $D \propto T^n$
P	total pressure of mixture, atmos
p	steric factor in Arrhenius expression for rate constant
p_i	partial pressure of active particles of one kind, atmos
$p_{i,eq}$	equilibrium adiabatic partial pressure of active particles of one kind, atmos
R	universal gas constant, cal/(mole)(°C)
T_F	equilibrium adiabatic flame temperature, °K
T_R	mean reaction temperature, 0.7 T_F, °K

T_o initial mixture temperature, °K

Z frequency factor in Arrhenius expression for rate constant, cm^3 $molecule^{-1}$ sec^{-1}

ϵ fraction of total number of active particles striking walls that is destroyed

φ equivalence ratio, mass fuel-air ratio divided by mass fuel-air ratio in stoichiometric mixture

REFERENCES

1. Fryburg, G.: NACA TN 2102 (1950).
2. Belles, F. E.: NACA TN 3565 (1955).
3. Coward, H. F., and Jones, G. W.: Bulletin 503, Bureau of Mines, 1952.
4. Malcolm, J. E.: Report 1177, Dept. Army, Engineering Research and Development Laboratories, Fort Belvoir (Va.), Aug. 18, 1950 (Proj. 8-76-04-003.)
5. Simon, D. M., Belles, F. E., and Spakowski, A. E.: *Fourth Symposium (International) on Combustion*, p. 126. Baltimore, The Williams & Wilkins Co., 1953.
6. Berlad, A. L.: J. Phys. Chem., *58*, 1023 (1954).
7. Belles, F. E., and Berlad, A. L.: NACA TN 3409 (1955).
8. Burdon, M. C., Burgoyne, J. H., and Weinberg, F. J.: *Fifth Symposium (International) on Combustion*, p. 647. New York, Reinhold Publ. Corp., 1955.
9. Belles, F. E., Simon, D. M., and Weast, R. C.: Ind. & Eng. Chem., *46*, 1010 (1954).
10. Belles, F. E., and Simon, D. M.: NACA RM E53I29 (1953).
11. Berlad, A. L., and Potter, A. E., Jr.: *Fifth Symposium (International) on Combustion*, p. 728. New York, Reinhold Publ. Corp., 1955.
12. Friedman, R., and Johnston, W. C.: J. Appl. Phys., *21*, 791 (1950).
13. Potter, A. E., Jr., and Berlad, A. L.: NACA TN 3398 (1955).
14. Egerton, A. C., and Thabet, S. K.: Proc. Roy. Soc., *A211*, 445 (1952).
15. Huff, V. N., Gordon, S., and Morrell, V. E.: NACA Report 1037 (1951).
16. Steacie, E. W. R.: *Atomic and Free Radical Reactions*, Ed. 2. New York, Reinhold Publ. Corp., 1954.
17. Simon, D. M.: Ind. & Eng. Chem., *43*, 2718 (1951).
18. Frost, A. A., and Pearson, R. G.: *Kinetics and Mechanism*, p. 92. New York, John Wiley and Sons, Inc., 1953.

110

THE ROCKET MOTOR AS A CHEMICAL REACTOR (ILLUSTRATED BY NITROGEN FIXATION)

By I. J. WEISENBERG and P. F. WINTERNITZ

Introduction

The purpose of this investigation was to determine the feasibility of applying rocket motor design principles to the design of a reactor for the production of nitric oxide by the direct fixation of nitrogen and oxygen using oxygen enriched air and ethane.

Within the last few years, considerable experimentation has been carried out by many groups on the direct fixation of nitrogen and oxygen by thermal processes.[1, 2, 3] Recent work has dealt mainly with the kinetics of nitrogen fixation; equilibrium concentrations and the rate of decomposition of nitric oxide.[4, 5, 6, 7, 8, 9, 10, 11] It has been shown that the equilibrium concentration of nitric oxide can be doubled by increasing the temperature from 2400°K to 2800°K, but the rate of cooling of the reaction must be increased from 10^4°K per sec to about 10^6°K per sec in order to freeze the reaction and minimize the loss of nitric oxide due to decomposition.

The inherent capabilities of the rocket motor to contain high reaction temperatures at residence times in the order of 1×10^{-3} sec as well as the very rapid adiabatic expansion cooling obtained through the nozzle at a rate in the order of 10^6°K per sec, particularly suits this device for application as a reactor in the nitrogen fixation process. According to a preliminary analysis by Altman and Penner[5] the gas temperature changes so rapidly during adiabatic expansion through a typical rocket nozzle that reaction

$2NO \rightleftarrows O_2 + N_2$ produces insignificantly small composition changes when the rocket chamber temperature is 3000°K.

mum NO formation. The necessary weight ratio of the oxygen enriched air to ethane (called in this paper "over-all mixture ratio") was calcu-

Table 1. Theoretical Performance Calculations

Fuel	C_2H_6 ΔH_f^0 − 13,660 at 298°K from elements at 0°K
Oxidizer	O_2 ΔH_f^0 + 2070 at 298°K from elements at 0°K
	N_2 ΔH_f^0 + 2072 at 298°K from elements at 0°K
P_{ch} (psia)	300 (reaction pressure)
P_{exh} (psia)	14.7 and 6.1 (exhaust pressure)
Stoichiometric mixture ratio for heating reaction	O_2/C_2H_6 = 3.7 (b.w.)

Frozen Equilibrium

O/F (b.w.)	4.0	6.0	7.0	9.0	10.0	11.0
% of Oxidizer O_2 (b.w.)	97%	82%	78%	73%	71%	69%
% of Oxidizer N_2 (b.w.)	3%	18%	22%	27%	29%	31%
T_{ch} (°K)	3478	3296	3204	3013	2918	2781
T_{exh} (°K) at P_{ch} = 300, P_{exh} = 14.7	2009	1898	1838	1713	1650	1558
$C_{p_{exh+ch}}$	10.9171	10.8593	10.7859	10.6154	10.5069	10.3330
T_{exh} (°K) at P_{ch} = 300, P_{exh} = 6.1	1695	1600	1548	1438	1382	1301
$C_{p_{exh+ch}}$	10.7671	10.7105	10.6348	10.4605	10.3539	10.1862
$C_{p_{ch}}$	11.2914	11.2479	11.1655	11.0077	10.9129	10.7476
$\bar{M}$	23.7392	26.2809	27.1022	28.2300	28.5926	29.0106
γ at T_{ch}	1.2135	1.214	1.216	1.220	1.223	1.227

Mole Fractions of Combustion Products

O/F (b.w.)	4.0	6.0	7.0	9.0	10.0	11.0
H	0.02802	0.01156	0.00726	0.00279	0.00169	0.00077
OH	0.08946	0.06795	0.05802	0.03907	0.03098	0.02189
O	0.03352	0.02572	0.02167	0.01361	0.01024	0.00655
O_2	0.09383	0.15348	0.18180	0.23674	0.25803	0.29738
NO	0.00788	0.02399	0.02709	0.02877	0.02818	0.02597
H_2	0.05033	0.02099	0.01367	0.00579	0.00379	0.00191
H_2O	0.36472	0.31386	0.29207	0.25498	0.23923	0.21939
CO_2	0.15223	0.16628	0.16755	0.16150	0.15588	0.14646
CO	0.16363	0.08346	0.05802	0.02628	0.01702	0.00863
N_2	0.01638	0.13720	0.17284	0.23047	0.25496	0.27104

Thermodynamic data is from NBS unless otherwise noted.
Heats of formation, ΔH_f, are at 298°K unless otherwise noted.
O/F = Over-all mixture ratio ($O_2 + N_2/C_2H_6$).
T_{ch} = Reaction temperature.
T_{exh} = Static temperature of effluent at nozzle exhaust station.
C_p = Specific heat.
$\bar{M}$ = Mean molecular weight.
A large number of significant numbers have been retained in the tables to avoid inconsistencies and rounding-off errors. This is not meant to imply that the data are necessarily accurate to such high order of precision.

Combustion of ethane with an excess of oxygen enriched air in a rocket motor simultaneously provided the required reaction temperature of 2800–3000°K and approximately equimolecular oxygen-nitrogen mixtures, as required for optilated from available thermodynamic data for a fixed chamber pressure of 300 psia and two exhaust pressures of 14.7 and 6.1 psia. Results are summarized in Table 1.

The reactor itself had to be designed for a suffi-

ciently long residence time to attain near equilibrium concentration of nitric oxide. The chosen residence time of 8.3×10^{-3} sec was based on kinetic data available in the literature and on earlier nitrogen-fixation tests at Reaction Motors, where a chamber residence time of 2.9×10^{-3} seconds had been estimated to give only 60 to 70 per cent of equilibrium nitric oxide formation.

Reactor Design

The actual reactor shown in Figure 1 is typical of a conventional rocket motor with the exception of the extra long combustion chamber, provided to give the long residence time. The design chamber pressure was 315 psia and the nozzle was designed for overexpansion to 6.1 psia giving a theoretical exhaust temperature below the 1800°K limit where the reaction is frozen and with some reserve for reheat at the exhaust gas sampling probe.

The total flow rate of 0.3 lb per sec of reactants chosen for convenience consisted of flows of approximately 0.17 lb per sec of gaseous oxygen premixed with 0.11 lb per sec of gaseous air and 0.03 lb per sec of gaseous ethane. An over-all mixture ratio O/F (b.w.) range from 7 to 11 was selected for investigation as this range indicated the maximum concentration of nitric oxide (Table 1).

The effects of reactant mixing upon the NO yield was determined by the use of two widely different injection patterns in a showerhead injector and an intersecting sheet injector shown in Figure 1. The showerhead injector consisted of seventeen fuel tubes silver-soldered to the inner body of the injector with each tube located so that it was concentric with an oxidizer hole in the face of the injector. Thus each fuel stream was surrounded by a concentric sheet of oxidizer with the total flow in an axial direction. All of the oxidizer holes were fed from an annular passage surrounding the fuel body of the injector.

The intersecting sheet injector consisted of one central fuel hole surrounded by an annulus for the oxidizer. A commercial oil burner nozzle spinner was incorporated into the fuel body of this injector to form a hollow cone fuel "spray" which intersected with the axial sheet of oxidizer. The oxidizer annular opening was fed in the same way as with the showerhead injector.

To further promote mixing of the reactants, and to insure complete combustion, a turbulence ring was welded to the combustion chamber liner just downstream of the injector.

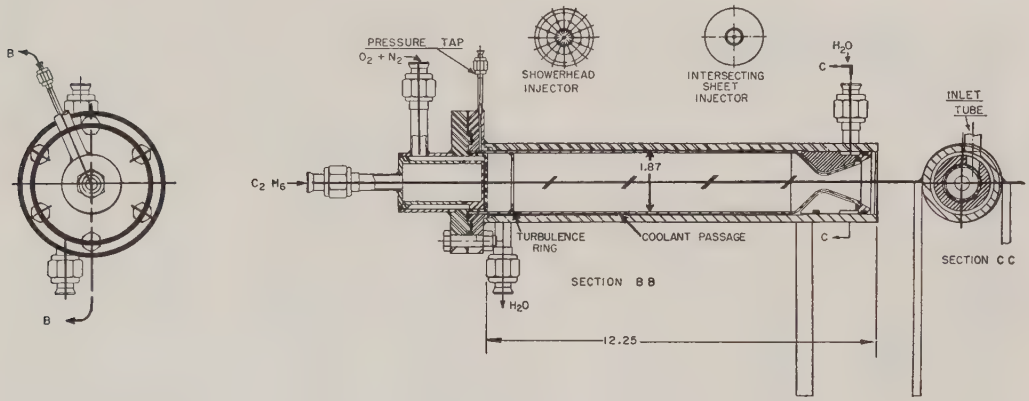

Fig. 1. Reactor.

Most of the reactor was fabricated from Type 304 stainless steel with the chamber exit nozzle, the turbulence ring, and the injector face plates fabricated of nickel for better heat transfer. Combustion chamber and cooling jacket were welded into an integral assembly at the injector bolting flange thus allowing axial expansion of the inner liner and nozzle at the exit end.

The exit nozzle and combustion chamber were water cooled. The cooling passages were designed for a water flow of 2 lb per sec. The injectors were cooled by the oxidizer flow.

Apparatus

The standard re-enforced concrete rocket test cell with a control room and test bay included the complete reactor installation with controls, feed stock supply, sampling apparatus, and instrumentation.

Gaseous oxygen with a guaranteed purity of

99.5 per cent was supplied from standard 16-lb bottles. Filtered air was supplied from 15-cu ft steel flasks. The air and oxygen were mixed in a special mixing chamber provided with turbulence type baffles. The mixture of air and oxygen was then fed to the control valves and into the injector. Temperature at the point of injection into the reactor was approximately 0°C.

Ethane of 96.7 per cent purity was supplied from standard 32-lb bottles which were placed in a steam heated water-filled storage tank and held at approximately 55°C to obtain sufficient feed pressure. Condensation of the vaporized ethane in the exposed manifold was prevented by applying heat up to the point of pressure regulation.

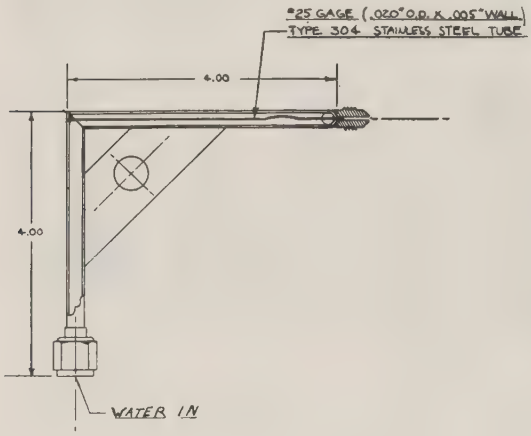

FIG. 2. Water cooled sampling probe.

After regulation the temperature dropped to approximately 0°C.

Safety circuits in conjunction with pneumatically operated valves were installed to stop injection of feedstock if the reactor coolant supply fell below 1.7 lb per sec. Flow control orifices in the oxygen and air lines allowed pressure regulation of the regulators while still maintaining the common pressure at the inlet to the mixing chamber.

All data collected during stable operation were permanently recorded. Pressures were measured by Bourdon type pressure gages, gaseous feedstock flows by flat plate orifice type flowmeters, and temperatures by thermocouples. In addition the sample pressure and temperature were accurately measured after each run by a mercury manometer and by a thermometer immersed in the sample bath.

A sample of the exhaust gases was collected in a water cooled probe. The sampling probe consisted of one hypodermic needle tube 0.010 in. inside diameter through which the sample gases passed. This tube was placed in one leg of a right angle formed by the coolant water inlet and outlet lines. Figure 2 is a drawing showing the probe. The large surface to volume ratio of the gas inlet tube surrounded by high velocity water provided sufficiently rapid cooling[12] to compensate for the reheat of the gases entering the sampling system. The sample gases flowed from the probe, through a solenoid valve, into a 200-ml sample balloon and 2000-ml reservoir bottle. A 10:1 flush of the sample balloon was thereby obtained before the sample was collected.

To minimize water condensation during sampling the connecting tubes from the probe to the sample balloon and to the reservoir bottle were wrapped with a nichrome ribbon wire insulated with asbestos tape and the sample balloon was immersed in a hot water bath. Auxiliary equipment served to flush the system before each test with nitrogen and to remove water vapor. In addition the system was evacuated to reduce the sampling time and to remove most of the gas from the system before collecting the sample.

Two series of tests were made. In the first series, only wet samples were collected. During the second test series, dry samples were also collected by connecting a second sampling system in parallel, downstream of the probe. The gases passed through a calcium chloride drying agent into a 250-ml sample bottle and then into two 2000-ml reservoir bottles to provide flushing volume similar to the wet sample system. Thus, the sample gases, collected at the same point, were divided after passing the probe, into a wet and a dry sample.

Testing Procedure

Before each run the sampling system was purged with dry nitrogen for a period of approximately five minutes. The hot water bath was maintained at or near boiling water temperature by means of a Calrod heater. The ribbon heaters around the tubes were energized and the sampling system was then evacuated to about 2 psia.

In all tests the reaction mixture was ignited by first starting the reactor and probe coolant flows, next turning on the electric spark igniter, and then admitting the gaseous oxygen-nitrogen oxidizer and gaseous ethane as nearly simultaneously as possible.

The initially closed solenoid valve of the sampling system was opened only after equilibrium operating conditions had been reached. During the test run, the sample gas flowed through the balloon and then into the reservoir bottle, thus flushing the sample balloon during the run, and ensuring a more representative sample.

TABLE 2. FIRST TEST SERIES—WET SAMPLE DATA

Run No.*	Fixed Nitrogen as NO	Over-all Mixture Ratio	Oxygen to Nitrogen Ratio O_2/N_2	Ratio of Theoretical to Actual O_2/N_2 Ratio	Total Through-Put	Chamber Pressure	Probe Angle	Injector
	Vol per cent	*b.w.*			*lb/sec*	*psia*	*degrees*	
31	1.8	5.90	2.59	1.81	0.308	310	28	B
5	0.9	6.72	2.59	1.45	0.320	326	28	B
8	1.1	6.85	2.85	1.28	0.299	306	28	B
27	2.3	6.88	2.65	1.37	0.312	342	28	A
28	2.2	6.94	2.71	1.32	0.311	339	28	A
11	1.8	6.98	2.83	1.25	0.301	307	45	B
12	1.1	7.07	2.87	1.22	0.298	306	28	B
24	1.5	7.17	1.78	1.93	0.286	291	28	B
15	1.2	7.25	2.77	1.23	0.296	304	28	B
41	2.0	7.45	1.67	1.97	0.303	310	45	C
7	1.5	7.47	1.91	1.72	0.293	297	45	B
25	1.7	7.48	1.79	1.83	0.285	292	28	B
42	0.7	7.49	1.53	2.14	0.290	302	28	C
18	1.1	7.52	1.82	1.79	0.292	300	28	B
13	1.6	7.55	2.42	1.34	0.306	302	45	B
22	2.4	7.64	2.75	1.17	0.294	299	45	B
2	1.8	7.64	2.30	1.39	0.321	329	28	A
23	1.4	7.67	2.75	1.17	0.298	301	28	B
29	1.3	7.79	2.03	1.55	0.296	296	28	B
14	1.5	7.82	2.48	1.26	0.315	306	0	B
20	1.7	7.87	1.90	1.64	0.299	300	45	B
30	0.7	7.89	2.36	1.31	0.298	301	28	B
19	1.1	7.91	1.79	1.73	0.291	297	28	B
36	1.8	7.95	2.25	1.37	0.311	311	28	C
40	1.8	7.96	1.875	1.64	0.303	308	45	C
32	2.4	7.98	2.48	1.23	0.330	332	45	C
34	2.2	8.02	2.25	1.35	0.321	320	28	C
43	1.0	8.09	1.76	1.72	0.302	306	28	C
33	1.9	8.18	2.74	1.10	0.322	324	28	C
17	1.3	8.25	2.15	1.38	0.298	297	28	B
21	2.7	8.35	2.18	1.34	0.304	302	45	B
35	1.6	8.45	2.30	1.26	0.316	316	28	C
39	1.9	8.65	2.05	1.38	0.311	306	45	C
37	1.8	8.66	2.45	1.15	0.324	306	45	C
26	1.5	8.76	2.68	1.04	0.318	317	28	A
38	2.1	8.81	2.32	1.20	0.320	308	45	C
4	0.8	8.90	2.52	1.08	0.314	319	28	B
6	1.3	9.28	2.19	1.20	0.318	308	45	B
9	1.7	8.93	2.43	1.13	0.315	310	45	B
1	2.0	10.25	2.19	1.08	0.324	314	28	A
33	0.6	10.30	2.25	1.05	0.319	317	28	B
10	1.1	10.85	2.11	1.07	0.321	297	45	B
16	1.6	16.8	2.21	0.91	0.310	257	28	B

* Runs arranged in order of over-all mixture ratio.

The solenoid valve was closed when the rate of increase in the sampling system pressure began to approach zero, usually at from 12 to 30 in. of mercury with the probe at an angle of 28° with

respect to the axis of the effluent jet, and between 20 and 30 in. with the probe angle at 45° with respect to the axis of the effluent jet. The sample balloon was sent to the laboratory for analysis, after recording temperature and pressure.

Tests

Successful ignition and stable combustion were obtained on the first checkout, but most of the uncooled turbulence ring shown in Figure 1 was burned and melted away. All subsequent runs

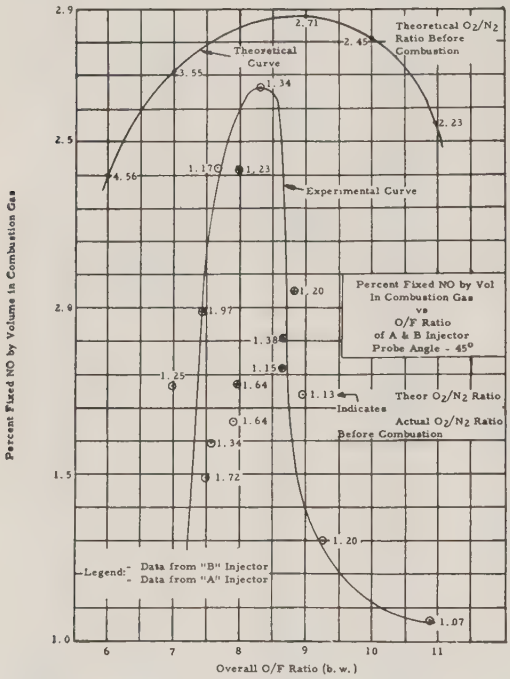
Theoretical O2/N2 Ratio Before Combustion
Theoretical Curve
Experimental Curve
Percent Fixed NO by Vol In Combustion Gas vs O/F Ratio of A & B Injector Probe Angle - 45°
Theor O2/N2 Ratio Indicates
Actual O2/N2 Ratio Before Combustion
Legend:- Data from "B" Injector
- Data from "A" Injector
Percent Fixed NO by Volume in Combustion Gas
Overall O/F Ratio (b. w.)

FIG. 3. Fixed NO in combustion gas (per cent by volume) plotted against over-all mixture ratio (O/F by weight).

were conducted without any additional burning by completely eliminating this element. The temperature rise of the coolant across the reactor was approximately 60°F. Most of the runs lasted approximately 4 minutes. The maximum run duration was over 7 minutes.

Samples were taken over a range of over-all mixture ratio from 5.9 to 16.8. The oxygen to nitrogen ratio in the feedstock was also varied. In addition, samples were taken at several probe positions. Satisfactory samples were obtained at angles of 28° and 45°, but during two attempts at a 60° angle the probe melted.

The characteristic brown color of NO_2 (formed upon combination of NO with the excess oxygen present in the sample) appeared to a varying extent in all samples.

In some of the wet samples the color would disappear as the NO_2 was absorbed in the water. In the dry samples the brown color remained the same indefinitely. During the first test series of 49 runs, 45 samples were taken and analyzed. During the second series of 21 runs, 20 wet and 20 dry samples were collected.

Operation of both injectors, described before was satisfactory over a mixture ratio range of 7 to 11. Some burning of the first showerhead unit (injector A) was encountered when operation was inadvertently carried out at a mixture ratio of 5.6 resulting in extremely high temperatures. The intersecting sheet type injector (injector B) was used while the showerhead injector was being repaired.

Sample Analytical Procedure

For the present investigation the analytical method described by Koerner,[9] with some modifications because of the small amounts of nitrogen to be determined, was used.

The dry samples obtained during the second test series were analyzed with conventional Orsat equipment. The CO_2 measurement which included the NO_2 was corrected from the wet sample analysis and all residuals assumed to be N_2.

Results and Discussion

Table 2 gives the results of the analyses of the samples obtained in the first test series which are considered reliable together with reactor operating data. Over 2 per cent NO by volume was reached in 8 of the 45 samples with a maximum value of 2.7 per cent corresponding to a maximum yield of over 90 per cent of theoretical.

Figure 3 shows some of the data obtained with both injectors at a probe angle of 45°, plotted as per cent NO *vs* over-all mixture ratio. The uppermost curve shows the maximum theoretical yield of NO *vs* over-all mixture ratio calculated under the assumption that at equilibrium in the reactor equimolecular amounts of oxygen and nitrogen are present. The required theoretical weight ratio of oxygen to nitrogen is indicated by numbers at the calculated points. The numbers noted against the experimental points represent the ratio of this theoretical weight ratio to the actual experimental weight ratio.

The shape of the calculated curve indicates that the increase in NO formation at higher

theoretical temperatures is more than compensated for by the increased dilution of the effluent with the combustion products of the ethane. Preheating of the feedstock and increasing of the pressure ratio to obtain the faster quench required would minimize this effect.

The experimental curve deviates from the theoretical curve based on thermodynamic equilibrium in that it reaches a peak and drops off much more rapidly than does the theoretical. This sharp maximum would necessarily result from a proper combination of (a) incompleteness of the reaction at large oxidizer to fuel ratio where the chamber temperature is insufficient for completion within the effective residence time; and (b) reversal of the reaction during expansion at small oxidizer to fuel ratios where the chamber temperature is excessively high. However, the optimum mixture ratio is nearly the same both theoretically and experimentally because the equipment was designed to operate at this mixture ratio. Considerable scatter in the data are

Table 3. Second Test Series—Complete Effluent Analysis

Run No.	NO_2	CO_2	C_2H_2	C_3H_8 etc.	C_2H_4	O_2	H_2	CO	CH_4	C_2H_6	N_2	H_2O
	vol per cent	*vol per cent*	*vol per cent*	*vol per cent*	*vol per cent*	*vol per cent*	*vol per cent*	*vol per cent*	*vol per cent*	*vol per cent*	*vol per cent*	*vol per cent*
44	2.1	13.8	0.3	0	0	24.2	1.0	0.2	0	1.7	36.3	20.5
45	2.6	17.0	0.3	0	0	17.5	0.6	0.6	4.9	0.9	31.7	23.9
46	2.7	16.7	0	0	0	18.7	0.5	0.4	0.6	0.7	34.9	24.8
47	2.3	16.4	0.3	.1	0	19.4	0.1	0.1	1.1	0.4	35.0	24.8
48	2.3	16.1	0.4	0	0	20.4	0	0.2	3.4	0	33.7	23.5
49	1.8	15.5	0.2	0	0	22.4	0	0.3	2.3	0	34.5	23.0
50	1.7	15.4	0.1	0	0	23.7	0.2	0.2	1.0	0.5	34.4	22.8
51	2.0	14.1	0.2	0	0	25.4	0	0.2	1.9	0	25.1	21.1
52	2.2	13.7	0.2	*	*	25.4	0	0.1	2.0	0	36.2	20.1
59	2.5	16.9	0.6	*	*	17.9	0.1	0.2	0	0.6	34.4	26.8
60	2.5	17.4	0.1	*	*	17.5	0	0.1	2.5	0	34.6	25.3
61	2.4	17.9	0.1	*	*	16.3	0	0.1	2.7	0	34.1	26.4
63	2.2	18.0	0.1	*	*	19.7	0	0	3.5	0	31.0	25.5
64	2.5	16.7	0.1	*	*	19.5	0	0.1	2.8	0	34.2	24.1

* Not determined.

Table 4. Second Test Series—Reactor Operating Conditions

Run No.	Total Through-Put W_T	Oxygen Flowrate W_o	Air Flowrate W_a	Ethane Flowrate W_e	Chamber Pressure P_{ch}	Measured Over-all Mixture Ratio O/F	Calculated Over-all Mixture Ratio O/F*	Ratio of Theoretical to Actual O_2/N_2 Ratio
	lb/sec	*lb/sec*	*lb/sec*	*lb/sec*	*psia*			
44	0.490	0.156	0.109	0.025	282	10.43	8.71	1.08
45	0.281	0.149	0.101	0.031	296	8.11	6.69	1.35
46	0.296	0.159	0.106	0.031	304	8.49	9.21	1.27
47	0.297	0.157	0.109	0.031	304	8.53	9.07	1.32
48	0.296	0.159	0.107	0.030	305	8.75	9.05	1.25
49	0.313	0.175	0.108	0.030	315	9.36	9.47	1.08
50	0.316	0.174	0.109	0.033	308	8.52	10.1	1.21
51	0.318	0.179	0.109	0.030	313	9.76	10.7	1.02
52	0.317	0.183	0.107	0.027	311	10.73	11.0	1.02
59	0.313	0.168	0.114	0.031	309	9.04	8.96	1.22
60	0.301	0.157	0.118	0.033	315	8.25	8.57	1.46
61	0.305	0.158	0.114	0.033	318	8.21	8.15	1.41
63	0.320	0.182	0.103	0.035	330	8.16	7.91	1.15
64	0.321	0.172	0.116	0.033	332	8.65	8.75	1.25

* Calculated from effluent analysis.

indicated when plotted as per cent NO *vs* over-all mixture ratio.

Although changing the probe angle did not appear to alter significantly the results, the data scatter increased for the 28° sampling probe angle. No significant difference was noticeable in the results between operation with the showerhead or intersecting sheet injector.

Table 3 summarized the results obtained by combining the wet sample and dry sample analyses for the second test series to determine the complete effluent constituents. Reactor operating data are included in Table 4. The fixed nitrogen is here reported as NO_2 because the large amount of oxygen present tended to oxidize the NO. The NO_2 mole fraction of over 2 per cent in nearly all of the runs confirms the results obtained during the first series of tests. The highest yield again was 2.7 per cent by volume of the total gas sample, at an over-all mixture ratio of 8.49 as compared to 8.35 for the first test series and at an oxygen to nitrogen ratio of 2.26 as compared to 2.18 for the first test series. These data further substantiate that over 90 per cent of the theoretical NO can be recovered with this reactor.

Table 5. Mole Fractions of Combustion Products

O/F (b.w.)	9.0
O_2	0.24637
NO_2	0.02975
H_2	0.00599
H_2O	0.28534
CO_2	0.16702
CO	0.02718
N_2	0.23835

Assumptions:

1. Products at room temperature.
2. Products frozen at conditions in chamber as shown in Table 2 with equimolar concentrations of O_2 and N_2 at these conditions.
3. NO is oxidized by excess O_2 to NO_2.

The amounts found for the additional primary constituents of the effluent namely CO_2, O_2, N_2, and H_2O are in good agreement with the theoretical results shown in Table 5 which were obtained from Table 1 assuming that NO was oxidized to NO_2 and all species unstable at room temperature had disappeared. For instance, run 59 performed at a measured mixture ratio of 9.04, shows good agreement for most of the constituents. The experimental values should in most cases be corrected slightly upward because the excess of nitrogen over oxygen used reduced the theoretical yield. The relatively small amounts of the intermediates C_2H_2 and CH_4 and also C_2H_6, indicates that combustion was carried essentially to completion. The observed completion of reaction for various over-all mixture ratios agreed roughly with accepted rate equations for a bimolecular reaction if somewhat arbitrary assumptions were made for the reduction in effective residence time due to mixing, feedstock heating and temperature differences within the chamber. The same is, however, not true for changes during expansion in the nozzle for tests at high temperatures. Here the decomposition of NO exceeded by far the values predicted by theory. The catalyzing effect of oxygen at high temperatures[10] might explain this discrepancy.

In Table 4 the mixture ratio as calculated from the analysis of the effluent gases is compared with the measured mixture ratio. Agreement is considered acceptable particularly in view of the experimental error present in measurements during reactor tests as compared to the analytical accuracy.

These results prove that the reactor used will give high yields of NO by direct fixation of nitrogen and operates with high efficiency. With some improvements the method should give sufficient rapid quenching to permit the use of reaction temperatures of 3200°K to 3400°K.

The development of a decelerating device, such as a turbine, to reduce high velocity of the effluent with a minimum of reheat, might present serious cooling problems, but these problems should not be unsurmountable. However, the separation of the products still appears to require considerable development for this particular process before the method can be put to practical use.

Acknowledgment

This work was carried out under the auspices of the Mathieson Chemical Corporation. The authors wish to thank Mr. D. Chatfield and Mr. P. Barbaccia for their engineering work, Dr. J. Irgon and co-workers for the equilibrium thermochemical calculations, and Mr. G. Evans for the sample analyses. All of the above personnel are with Reaction Motors, Inc.

1. Riegel, E.: *Industrial Chemistry*, p. 114. New York, Reinhold Publ. Corp., 1949.
2. Gilbert, N., and Daniels, F.: Ind. & Eng. Chem., *40*, 1719–1723 (1948).
3. Cottrell, F. G.: U. S. Patent No. 2,422,081, June 10, 1947.

4. Wise, H., and Baker, D.: J. Chem. Phys., *21*, 1904 (1953).
5. Altman, D., and Penner, S.: J. Chem. Phys., *17*, 56 (1949).
6. Jet Propulsion Laboratory, California Institute of Technology Progress Report No. 9-5, May, 1947.
7. Jet Propulsion Laboratory, California Institute of Technology, Progress Report No. 9-46, March, 1950.
8. Jet Propulsion Laboratory, California Institute of Technology, Progress Report No. 20-150, October, 1951.
9. Koerner, W. E.: Thesis, University of Wisconsin, 1949 (unpublished).
10. Kaufman, Kelso: J. Chem. Phys., *23*, 1702 (1955).
11. Yuan, Slaughter, Daniels: Nitrogen Symposium. Food Machinery and Chemical Corporation and Wisconsin Alumni Research Foundation, November 21–22, 1955.
12. Cornell Aeronautical Laboratory, Project Squid Technical Memorandum No. CAL-8, September 1, 1948.

Discussion by A. L. Thompson*

Professor Mordell, George Yano and I have been studying nitrogen fixation for several years at this laboratory. Preheated air and propane are burned in a zirconia brick furnace and the products are quenched by passing through a water-cooled tube. The yield of fixed nitrogen is approximately the percentage predicted by theory and has reached about 3.5 per cent in air enriched with oxygen. A preliminary economic study of several possible systems has been made. Studies are continuing with S. K. Fang in place of G. Yano on details of quenching rate and rechecks on the influence of oxygen concentration and temperature on yield.

* Gas Dynamics Laboratory, McGill University.

Author's Reply

The authors appreciate the comment by Dr. Thompson and are pleased to see that work on direct nitrogen fixation is being continued. The use of zirconia should permit higher temperatures than have been used to date in ceramic furnaces. It should be noted, however, that the rocket type reactor as described by us permits the use of relatively common metals at the same high temperatures. The life of a reactor using these metals as compared to a ceramic reactor is still not known but it would appear to be longer. In addition, a supersonic nozzle should provide a more rapid quench rate than a water cooled tube and should therefore ultimately allow the use of higher reaction temperatures.

111

CHEMICAL REACTIONS IN ADIABATIC COMPRESSION

By V. N. KONDRATIEV, A. M. MARKEVITCH, Yu. N. RYABININ, and I. I. TAMM

In view of the part played by chemical kinetics in detonation, the study of chemical processes under conditions approaching those of a compression wave can give valuable information on chemical transformations in the detonation wave, for instance on their rates. The adiabatic machine, designed at the Institute of Chemical Physics some years ago,[1] makes such investigations possible. The operation of this machine and earlier data have been discussed elsewhere. The present paper gives certain new data[2, 3, 4] obtained by Ryabinin and co-workers at our Institute.

The dependence of nitrogen oxide yields on maximum pressure is shown for two nitrogen-oxygen mixtures in Figure 1 (in the presence of 5.5 per cent methane which raises the combustion temperature).[5] The nitrogen oxide concentration obtained under these conditions appears to be close to the equilibrium concentration, corresponding to the maximum compression temperature, which follows from yield values and from their agreement with the mass action law.

Different combustion rates of hydrogen and of carbon monoxide are shown in Figure 2. The amounts of gases added to the nitrogen-oxygen mixture were chosen to give equal heat production.[5] Nevertheless, equal nitrogen oxide yields were obtained in both cases at widely different maximum pressures, showing a great difference in the combustion rates of hydrogen and carbon monoxide. It is possible that the combustion of CO, whose concentration lies outside the combustion region, is not completed at the moment of maximum compression.

The influence of the maximum compression

temperature and of the nature of the gases on the reaction rate, manifested by different hydrocyanic

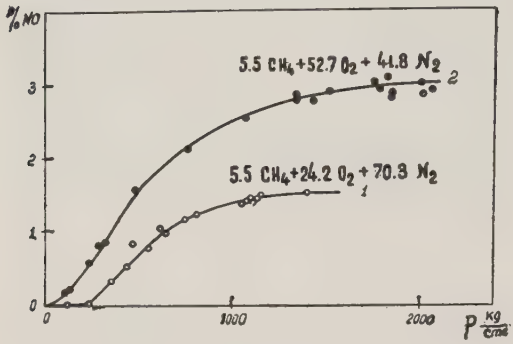

FIG. 1. Formation of nitrogen oxide in nitrogen-oxygen mixtures containing methane.

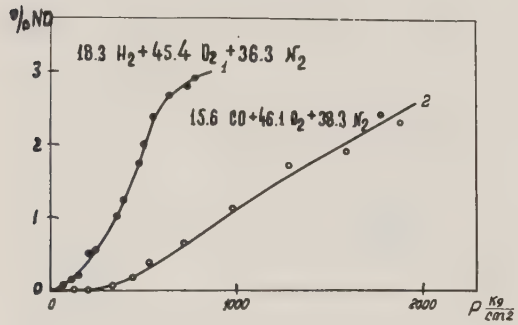

FIG. 2. Formation of nitrogen oxide in nitrogen-oxygen mixtures containing hydrogen and carbon monoxide.

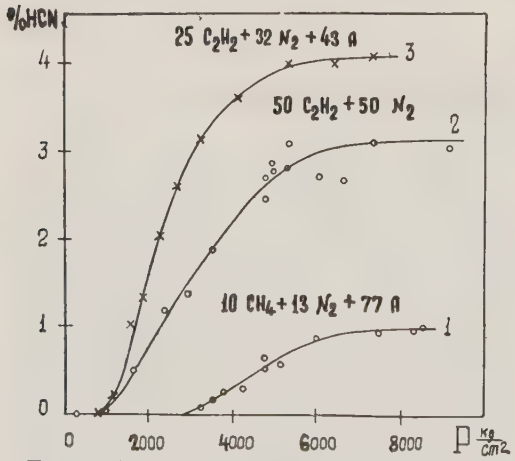

FIG. 3. Formation of hydrocyanic acid in mixtures of acetylene and methane with nitrogen.

acid yields in the combustion of methane-nitrogen and acetylene-nitrogen mixtures, can be seen in Figure 3.[6] In the case of a methane-nitrogen mixture, hydrocyanic acid is not observed, even at the maximum pressure of 10,000 kg/cm²; it appears only after addition of a considerable amount of argon, which raises the combustion temperature. The more active acetylene-nitrogen mixture gives a much higher yield of hydrocyanic acid which increases with the addition of argon.

Finally, Figure 4 shows formaldehyde yields obtained with adiabatic compression of rich methane-oxygen mixtures.[7] The HCHO yield increases with the oxygen content if its concentration is less than 12 per cent, but begins to decrease at 12 per cent, after the pressure reaches about 1500 kg/cm². This effect is accounted for by the beginning of further HCHO

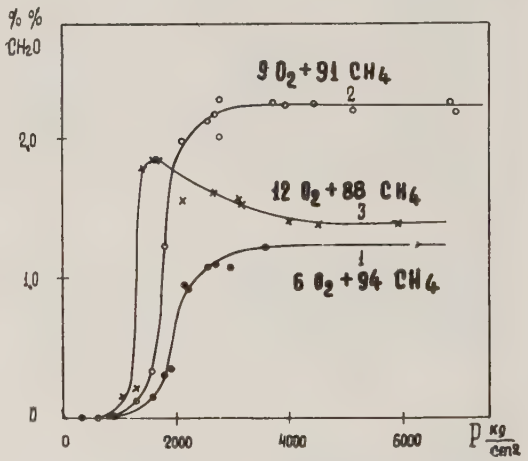

FIG. 4. Formation of formaldehyde in methane-oxygen mixtures. Curve 3 was obtained under conditions close to ignition.

oxidation. With a still larger amount of oxygen (more than 15%) the beginning of compression is accompanied by a flash and practically no HCHO is observed in this case. Obviously these results can be interpreted as evidence of a two- or multi-stage mechanism of an adiabatic compression reaction. These data reveal possible applications of the adiabatic machine in the study of the mechanism of chemical reactions at very high temperatures and pressures.

REFERENCES

1. RYABININ, Yu. N.: J. Exp. Theor. Phys., USSR, *23*, 461 (1952).
2. RYABININ, Yu. N., MARKEVITCH, A. M., AND TAMM, I. I.: J. Exp. Theor. Phys., USSR, *24*, 107 (1953); Doklady Akademii Nauk, SSSR, *94*, 1121 (1954); *95*, 111 (1954).
3. KARPENKO, A. S., MARKEVITCH, A. M., AND

Ryabinin, Yu. N.: J. Exp. Theor. Phys., USSR, *23*, 468 (1952).
4. Ryabinin, Yu. N., Sobolev, N. N., Markevitch, A. M., and Tamm, I. I.: J. Exp. Theor. Phys., USSR, *23*, 564 (1952).
5. Ryabinin, Yu. N., Markevitch, A. M., and Tamm, I. I.: Doklady Akademii Nauk USSR, in press.
6. Ryabinin, Yu. N., Markevitch, A. M., and Tamm, I. I.: In press.
7. Ryabinin, Yu. N., Markevitch, A. M., and Tamm, I. I.: In press.

112

THE EFFECT OF PIPE DIAMETER ON THE THERMAL DECOMPOSITION OF ACETYLENES

By HERBERT H. NELSON

Introduction

A large amount of information is available concerning the thermal decomposition characteristics of acetylene as a result of extensive investigations conducted by various groups in Germany and by the Bureau of Mines and others in this country. However, very few experimental data are available on the higher acetylenes, such as methyl acetylene, monovinyl acetylene and bi-acetylene. This paper describes an experimental technique developed for investigating the explosive characteristics of acetylenes and presents some new data on acetylene and monovinyl acetylene.

It was considered important that the experimental technique correspond closely to that employed by the Germans, or at least produce comparable results, so that a basis would exist for correlation of data on the higher acetylenes with the large amount of existing data on acetylene accumulated by the Germans.

The portion of the German work concerned with the effect of pipe diameter on the minimum initial gas pressure at which acetylene will undergo self-sustaining thermal decomposition was repeated and extended. The experimental technique developed was then applied to a similar investigation of monovinyl acetylene.

Experimental

A. Purification of acetylenes

Commercial cylinder acetylene was purified by passing it through a series of five cold traps maintained at −50°C to remove acetone and moisture. The purity of the acetylene exceeded 99 mole per cent as determined by mass spectrometer analysis.

Monovinyl acetylene was obtained as a 50 per cent solution in xylene. It was purified by fractionation through a low-temperature column followed by scrubbing through 10 per cent NaOH. The pure gas was dried with anhydrous $CaCl_2$ and stored under refrigeration. Purity exceeded 99 mole per cent.

B. Apparatus

Commercially available Pyrex pipes were employed as explosion vessels. The pipes were three feet in length and were closed on each end with steel blinds, one of which contained an inlet valve and the igniter, the other a pressure transducer and outlet valve. During experiments the vessels were placed in a horizontal position behind a sturdy barricade. Visual observation of the decompositions was afforded by a mirror suspended above the barricade.

The igniter was a sparkplug fitted with elongated electrodes which extended 8 cm into the vessel. Ignition was effected by fusing a 10 mm length of 0.127 mm diameter Copel resistance wire, soldered across the ends of the electrodes, with the discharge from a condenser charged to 800 v.

In series with the Copel wire was placed a Manganin resistance wire which served to decrease the current through the Copel wire and to round off the pulse of current from the condenser. This prevented the Copel wire from exploding or sputtering as it fused. By changing the length of the Manganin wire and by adjusting the voltage applied to the condenser, both the energy

and the characteristics of the igniter could be altered.

The ignition energy was adjusted in this manner so that the minimum decomposition pressure for acetylene in the 4-in pipe matched the corresponding German data. The energy of ignition was then assumed to be equivalent to that employed in the German investigations. The energy of ignition is estimated to be 8 j.

This system permitted exactly reproducible ignition energies which is extremely important, for the minimum decomposition pressures were found to be highly sensitive to ignition energy. With increased ignition energy, decomposition occurs at much lower pressures, other conditions being equal.

The pressure transducer used in the experimental work with acetylene comprised a thin-walled, cup-shaped stainless steel cylinder, 2 in. long and 2 in. in diameter. The open end was threaded into the center of the steel blind which formed the end closure of the explosion vessel. A strain gauge (SR-4, type A-11) bonded to the outer curved wall of the cylinder formed the variable resistance arm of a Wheatstone bridge circuit. This was tied to a strain gauge amplifier recorder (Sanborn amplifier Model 140S, recorder Model 127) which was calibrated to read directly in pounds per square inch.

A commercially available transducer (Statham Laboratories, Model P 11-300G-180) was used in the experiments with monovinyl acetylene.

The surfaces of both transducers which were exposed to the flame were coated with an insulating plastic to eliminate the effect of temperature changes. This did not noticeably affect pressure response.

Both the velocity of the flame and magnitude of the pressure increase were measured on the strip chart of the strain gauge recorder.

C. PROCEDURE

The scrupulously cleaned vessel was first flushed with nitrogen gas, then evacuated, before filling with acetylene. The measurement of the initial system pressure was accurate to within 1 or 2 mm Hg.

An explosion was defined as a decomposition in which the flame propagated the entire length of the pipe and also resulted in a pressure increase.

In determining the minimum decomposition pressures for acetylene, 10 runs or experiments were made at each initial pressure under identical conditions. The initial pressure was then changed by 10 mm (increased or decreased) and another 10 experiments were made at the new pressure and so on. This procedure was repeated until an upper pressure was reached at which at least 9 of the 10 runs resulted in explosions and a lower pressure was reached at which not more than one of the ten runs was an explosion. The range between these two pressures was defined as the "minimum decomposition pressure range" for the particular pipe diameter being used.

The experiments with monovinyl acetylene were conducted in the same manner except that the pressure increments between each series of 10 runs was increased from 10 to 25 mm Hg.

D. ESTIMATION OF PROBABILITY LEVELS

If the numbers of explosions occurring in each of the 10 runs made at each initial pressure in a pipe of given diameter are expressed as percentages and plotted as a function of initial pressure, an S-shaped curve is obtained. If the percentages (or frequencies) above 50 per cent are plotted on the same graph as (100–frequency) the resultant curve approximates a normal distribution curve.

When the amount of data is restricted, as is the case here, the normal distribution curve is best approximated by plotting the data on probability graph paper. This yields a straight line which may be extrapolated. This method was employed in determining the minimum decomposition pressure at the 1 per cent, 50 per cent, and 99 per cent probability levels for both acetylene and monovinyl acetylene.

Experimental Data and Discussion

The acetylene data are summarized in Table 1. In every case except the 1-in. pipe the number of flame propagations equalled the number of explosions. This is explained by the polymerization reactions occurring in the 1-in. pipe along with the decomposition into carbon and hydrogen. This polymerization was evidenced by the oily nature, brown color and odor of the soot residue.

It is also noticed that the explosibility of acetylene in a pipe of given diameter seems to pass through a minimum within the pressure range defined by the experiments. No reasonable explanation is seen for this behavior, and it is not believed to be due to experimental error. Since this anomaly occurred in almost every case, it seems possible that it may be characteristic of such acetylene decompositions.

The acetylene data are presented in graphical form in Figure 1, with probability levels as

TABLE 1. ACETYLENE DATA

1-in. ID Pipe			2-in. ID Pipe		3-in. ID Pipe		4-in. ID Pipe		6-in. ID Pipe	
P_i	Expl.	Prop	P_i	Expl.	P_i	Expl.	P_i	Expl.	P_i	Expl.
1650	0	0	1120	1	1030	0	1020	0	1030	0
1660	0	1	1140	0	1040	0	1030	3	1040	2
1670	0	1	1150	5	1050	1	1040	2	1050	6
1680	0	6	1160	7	1060	0	1050	2	1060	4
1690	6	10	1170	5	1070	0	1060	5	1070	7
1700	3	10	1180	6	1080	0	1070	9	1080	9
1710	0	7	1190	9	1090	1				
1720	1	7			1100	4				
1730	5	10			1110	5				
1740	5	10			1120	6				
1750	6	10			1130	8				
1760	4	8			1140	10				
1770	4	10								
0780	5	10								
1790	10	10								
1800	10	10								

Legend: P_i Initial (charging) pressure (mm Hg, abs)
Expl. Number of explosions in 10 runs
Prop. Number of flame propagations in 10 runs

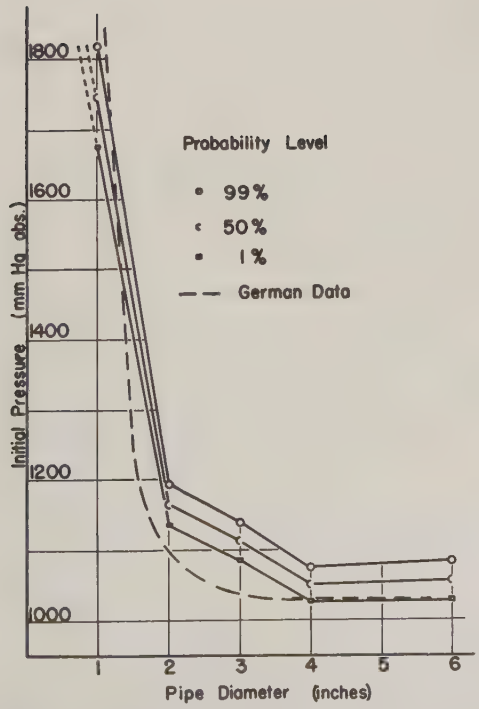

FIG. 1. Minimum decomposition pressure of acetylene as a function of pipe diameter with probability levels as parameters.

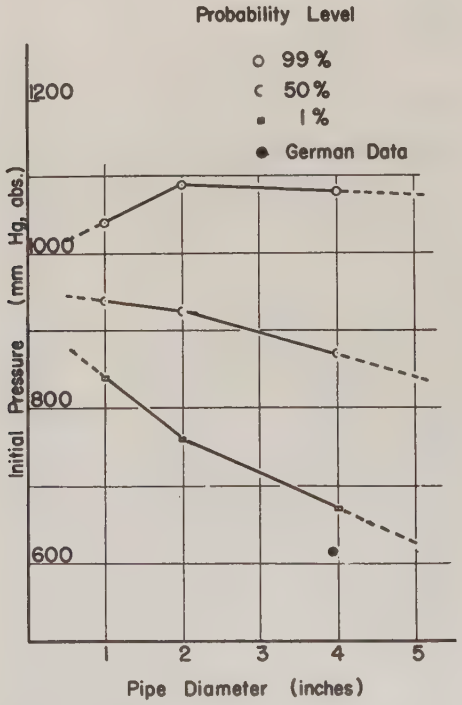

FIG. 2. Minimum decomposition pressure of monovinyl acetylene as a function of pipe diameter with probability levels as parameters.

parameters. The German data are shown for comparison. It is seen that the data do not fall in a smooth curve. The most reasonable explanation for this would appear to be the competing reactions of polymerization and decomposition.

It is seen that the minimum decomposition pressures change little with increasing pipe diameter beyond 4 in. This has been explained on the basis that the cooling effect exerted on the flame by the wall of the vessel does not change appreciably above this diameter.

The velocities of the decomposition waves were found to be on the order of feet per second, about as expected on the basis of the German data.

Table 2. Monovinyl Acetylene Data

1-in. ID Pipe		2-in. ID Pipe		4-in. ID Pipe	
P_i	Expl.	P_i	Expl.	P_i	Expl.
850	1	800	0	775	0
875	3	825	1	800	2
900	4	850	2	825	3
925	0	900	2	975	7
950	2	1000	7	1000	10
975	3	1025	9		
1000	4				
1025	3				
1050	10				

Legend: P_1 Initial charging pressure (mm Hg, abs)
Expl. Number of explosions occurring in 10 runs

Note: The number of explosions equalled the number of flame propagations in every case.

However, the velocities were by no means constant, even for identical experiments in the same vessel. In pipes of less than 3-in. diameter, velocities were commonly less than 1 ft/sec.

The final pressures resulting from the explosions were on the order of 10 times the initial pressure, again supporting the previous German data. The ratio of final pressure to initial pressure was found to increase with pipe diameter, initial pressure, and with energy of ignition.

The monovinyl acetylene data are shown in Table 2. The single value reported in the German literature is 614 mm Hg, absolute, for a pipe diameter of 100 mm, whereas the corresponding minimum decomposition pressure range defined by this work is approximately 775 to 1000 mm Hg, absolute. No readily apparent explanation for this considerable difference is seen unless a much stronger source of ignition was used in the determination of the German value. It is considered possible that the higher acetylenes may not be as unstable to thermal decomposition as has been believed. It is noted (see Fig. 2) that the minimum decomposition pressure ranges are considerably broader than in the case of acetylene. It is further observed that the minimum decomposition pressures do not increase sharply at small diameters as with acetylene.

Summary

The experimental technique developed in this work differs considerably from methods used in previous investigations of this type. It was possible to essentially duplicate the German data concerning the effect of pipe diameter on the thermal decomposition of acetylene; however, the more detailed investigation disclosed additional information of interest. It was shown that acetylene passes from explosibility to non-explosibility through a pressure range rather than abruptly through a so-called boundary pressure as described in the German data. It was further observed that the explosibility of acetylene, in a given size pipe, apparently passes through a minimum within the minimum decomposition pressure range as defined by the experiments. Since no reasonable explanation is seen for this phenomenon, it is concluded that it may be characteristic of such thermal decompositions of acetylenes.

The minimum decomposition pressures obtained with monovinyl acetylene are much higher than the single value reported in the German data. This may indicate a greater degree of stability to thermal decomposition than has heretofore been attributed to the higher acetylenes.

Although this work has shown that the probability of thermal decomposition of acetylene and monovinyl acetylene has a statistical dependence on the initial system pressure, in view of the dominant effect of ignition energy on the minimum decomposition pressures, it is concluded that such precise definition is of little practical value in predicting acetylene explosibility unless the energy of ignition can be precisely specified.

Acknowledgments

The author wishes to express his appreciation to the Plastics Division of Monsanto Chemical Company for releasing the information contained in this report for publication. We are particularly indebted to Mr. J. L. Masten and Dr. W. B. Howard under whose direct supervision the work

was carried out. The interest and support of Drs. W. H. Lane and H. E. Morris is acknowledged with pleasure.

We should also like to express our gratitude to Drs. R. F. Wall and J. F. Draffen for their assistance in designing, constructing, and maintaining the instruments involved in the work, to Mr. J. G. McQuarrie for assistance in the statistical design of the experiments, and to Mr. J. C. Burleson for the graphs and drawings contained in the report.

REFERENCES

1. Copeland, N. A. and Youker, M. A. FIAT Final Report No. 720, PB No. 20078 (1946).
2. Cousins, E. W. and Cotton, P. E.: Chem. Eng., *58*, No. 8, 133, (1951).
3. T. O. M. Reel 32, Bag 2078, Section G. Translated from the German by Charles A. Meyer and Co., Inc.
4. P. B. 70248, Frames 2351–2388, Office of Technical Services (in German).
5. Farben, I. G.: P. B. 25610, Frames 4658–5661, (Patent Application, dated July 16, 1941).
6. Jones, E.: J. Appl. Chem., *1*, 411 (1951).
7. Jones, G. W. and Kennedy, R. E.: Bureau of Mines Report of Investigations No. 3809 (1945).
8. Jones, G. W., Kennedy, R. E., and Spolan, I.: Bureau of Mines Report of Investigations No. 4196 (1948).
9. Jones, G. W., Kennedy, R. E., Spolan, I., and Huff, W. J.: Bureau of Mines Report of Investigations No. 3826 (1945).
10. Jones, G. W., Kennedy, R. E., Scott, G. S., and Huff, W. J.: Bureau of Mines Report of Investigations No. 3755 (1944).
11. Jost, W.: *Explosion and Combustion Processes in Gases*. New York, McGraw-Hill Book Co., Inc., 1946.
12. Kammermeyer, K.: P. B. 60886, FIAT 1017, Office of Technical Services.
13. Lavine, P.: Mech. Eng., *24*, 483–485, 489 (1952).
14. Prout, W. E. and Anderson, R. C.: Texas J. Sci., *4*, 521–530 (1952).
15. Reppe, W.: Chem.-Ing.-Tech., *22*, 273–283, (1950).
16. Rotzler, R. W., Confidential report, Plastics Division, Monsanto Chemical Company.
17. Timry: P. B. 35675-T, Office of Technical Services.

113

THE PRODUCTION OF HYDROGEN PEROXIDE VIA COMBUSTION: CONDITIONS FOR THE SYNTHESIS AND ISOLATION IN HIGH YIELD FROM THE COMBUSTION OF ALIPHATIC ALCOHOLS

By C. F. CULLIS and E. J. NEWITT

It has long been known that peroxides are formed during the slow oxidation of the paraffin hydrocarbons and their simple derivatives. The exact nature of these peroxides and the role which they play are matters on which opinion is still divided. There is evidence for the formation of alkyl hydroperoxides and acyl peroxides under certain conditions, but it is also clear that hydrogen peroxide is sometimes an important intermediate product.

Much earlier work was concerned with methods of distinguishing between hydrogen peroxide and organic peroxides (e.g., see Egerton, Smith and Ubbelohde[1]), and more refined techniques have recently become available which facilitate this distinction.[2] With the application of these improved analytical methods, it has become apparent that in many gaseous mixtures undergoing slow oxidation, hydrogen peroxide is the main, if not the only, peroxide present. Minkoff and Salooja[3] found that the peroxide formed in the slow oxidation of methane was almost exclusively hydrogen peroxide and that, if other peroxides were present, their concentration was less than 2 per cent of that of hydrogen peroxide. Knox and Norrish[4] were unable to find any evidence for the presence of alkyl hydroperoxides during the oxidation of propane, although considerable amounts of hydrogen peroxide were formed. According to Batten, Gardner and Ridge,[5] the peroxides present during the oxidation of isobutane consist of hydrogen peroxide and of alkyl and acyl peroxides, hydrogen peroxide and its derivatives accounting for about 50 per cent of the total peroxide.

Several recent investigations have been es-

pecially concerned with the conditions for obtaining high yields of peroxides, particularly hydrogen peroxide, from hydrocarbon combustion.[6, 7, 8] In general, however, the yields are small[3, 9] and studies of the oxidation of certain hydrocarbon derivatives have revealed the formation of much larger amounts of peroxides. Ethers, for example, are known to be remarkably prone to peroxidation,[10] and during their gaseous oxidation the quantities of peroxides are considerably greater than those found in hydrocarbon oxidation.[11, 12] The nature of the peroxides formed during ether oxidation has not been established with certainty, but such compounds are of exceptional stability and are able to survive the passage of a cool flame. Alcohols have received less attention than ethers, but it has recently been shown that the slow combustion of isopropyl alcohol gives rise to high yields of peroxides under appropriate conditions.[13] During studies of the oxidation of ethanol and *n*-propanol in this laboratory, it has become apparent that exceptionally large amounts of peroxides (principally hydrogen peroxide) are sometimes formed. In this paper, the conditions for the synthesis and isolation of peroxides in high yield are outlined and discussed.

Experimental

Gaseous reactants were admitted to a Pyrex reactor maintained at constant temperature in an electric furnace, and the products were analyzed at various stages of reaction. In most of the work described, permanent gases (oxygen, carbon monoxide, nitrogen, methane and ethane) were separated from residual alcohol and other products by condensation of the latter at −196°C. The condensate was dissolved in water and the resulting solution was rapidly analyzed. Experiments involving other methods of sampling are described later (Table 7).

The apparatus, the method of purifying the reactants and the analytical procedure used in studies of the oxidation of ethanol have been described in detail elsewhere.[14, 15] A brief outline is given below of the analytical methods used for the estimation of unchanged reactant and condensable products.

Total alcohols. Oxidation with potassium dichromate, after destruction of aldehydes and peroxides with silver oxide.

Methanol. Colorimetrically, by the method of Boos.[16]

Ethanol. By difference.

Total aldehydes. Oxidation with silver oxide by the method of Bailey and Knox.[17]

Formaldehyde. Colorimetrically, by a modification of the chromotropic acid method of Bricker and Johnson.[18]

Acetaldehyde. By difference.

Peroxides. Iodometrically by a method which distinguishes between (1) acyl peroxides, (2) hydrogen peroxide, (3) alkyl hydroperoxides, dialkyl peroxides and hydroxy-alkyl peroxides.

(1) Acyl peroxides were estimated by iodine liberation from a slightly acidified aqueous solution of potassium iodide under carbon dioxide at 0°C. Hydrogen peroxide reacts very slowly under these conditions and the alkyl peroxides do not react at all.

(2) Hydrogen peroxide was determined from the iodine liberated within three minutes at 5°C, following the addition of 5 ml 2*N* hydrochloric acid and one drop of 20 per cent ammonium molybdate solution. The alkyl peroxides react only very slowly under these conditions.

(3) Alkyl hydroperoxides, dialkyl peroxides and hydroxy-alkyl peroxides were estimated by iodine liberation after thirty minutes' heating at 40°C.

The values of total peroxides determined by this procedure were in very good agreement with those obtained by the hydrogen iodide-glacial acetic acid method.[19]

Results

The gaseous oxidation of ethanol and *n*-propanol proceeds at a conveniently measurable rate above 250°C. Rapid (autocatalytic) reaction is preceded by an induction period which varies exponentially with temperature. The detailed kinetics of the slow combustion of these alcohols will be described elsewhere. Oxidation below 300°C leads to the formation of carbon oxides and a mixture of condensable, water-soluble products.

Ethanol

The consumption of ethanol and the formation of condensable products during reaction are shown in Figure 1 (ethanol-rich mixture) and Figure 2 (oxygen-rich mixture). Product yields with respect to ethanol consumed are shown for partial oxidation (excess ethanol) in Figure 3; under these conditions, two important results may be noted. (1) In the early stages of reaction, ethanol is converted quantitatively into acetaldehyde and hydrogen peroxide according to the

overall equation:

$$CH_3CH_2OH + O_2 = CH_3CHO + H_2O_2$$

(2) During rapid oxidation, acetaldehyde and hydrogen peroxide continue to be produced in closely parallel amounts. Although the yields of both products decrease with increasing extent of reaction, acetaldehyde and hydrogen peroxide still account for about 40 per cent of the alcohol consumed at the end of reaction.

Under all conditions studied, hydrogen peroxide is by far the most abundant peroxide present. The organic hydroperoxides "RO_2H" are tentatively assumed to be methyl hydroperoxide and/or α-hydroxy-ethyl hydroperoxide. Peracetic acid is usually found only in small amounts in the oxidation products at 295°C.

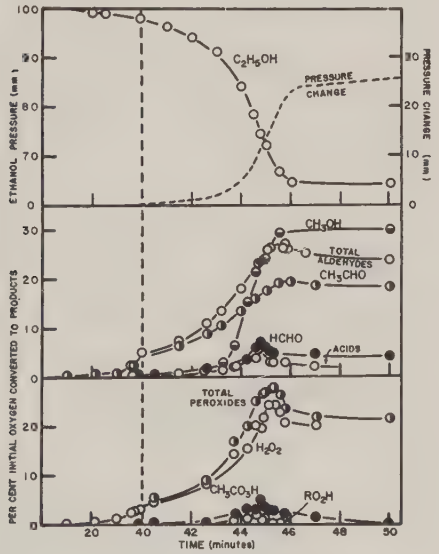

FIG. 1. The consumption of ethanol and the formation of condensable products. Temp. 295°C. Ethanol pressure, 100 mm; oxygen pressure, 50 mm.

INFLUENCE OF REACTANT PRESSURES

Increase in pressure of either reactant favours the formation of both hydrogen peroxide and organic peroxides, particularly during partial oxidation (Table 1). Analysis of the data shows that at low pressures the maximum amount of hydrogen peroxide produced is proportional to the product of the reactant pressures, i.e.,

$$[H_2O_2]_{max} \propto [C_2H_5OH]\,[O_2]$$

At higher pressures the relationship becomes complex, the order with respect to oxygen tending towards zero.

In the presence of excess oxygen, production of hydrogen peroxide remains an important process (Fig. 2), but the yields are somewhat reduced;

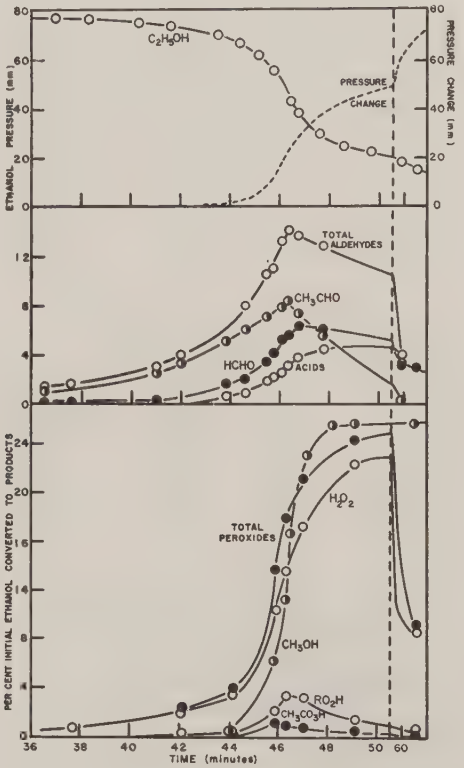

FIG. 2. The consumption of ethanol and the formation of condensable products. Temp. 295°C. Ethanol pressure, 80 mm; oxygen pressure, 300 mm.

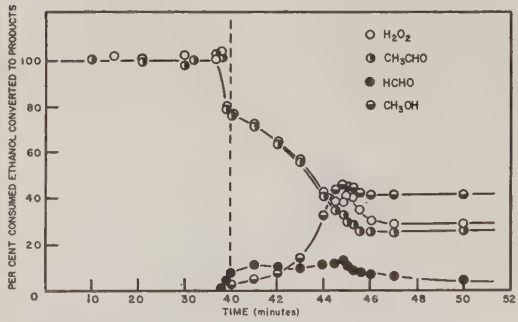

FIG. 3. Yields of condensable products. Temp. 295°C. Ethanol pressure, 100 mm; oxygen pressure, 50 mm.

values at various stages of reaction are given in Table 2.

INFLUENCE OF NITROGEN

The presence of added nitrogen has little effect on the formation of hydrogen peroxide during the

Table 1. The Influence of Reactant Pressures on the Maximum Peroxide Pressures Attained
Temp. 295°C

Ethanol Pressure	Oxygen Pressure	Total Peroxides	H_2O_2
mm	*mm*	*mm*	*mm*
(a) Influence of oxygen pressure			
80	80	16.2	13.8
80	300	20.1	18.6
100	30	7.56	6.93
100	50	12.1	11.1
100	80	17.2	14.4
(b) Influence of ethanol pressure			
100	30	7.60	7.00
120	30	8.45	7.90
80	80	16.2	13.8
100	80	17.2	14.4
160	80	20.7	17.1
230	80	23.9	20.6

Table 2. The Formation of Hydrogen Peroxide in the Presence of Excess Oxygen
Temp. 295°C; ethanol pressure, 80 mm; oxygen pressure, 300 mm

Pressure Change	Yields of Hydrogen Peroxide
mm	*per cent of ethanol consumed*
0.5	46.3
1.2	42.6
3.0	33.6
15.5	31.3
24.3	30.9
30.4	30.2
39.0	31.4
48.0	31.1

Table 3. The Effect of Nitrogen Pressure on Hydrogen Peroxide Formation
Temp. 295°C; ethanol pressure, 120 mm; oxygen pressure, 30 mm

Nitrogen Pressure	$(H_2O_2)_{max.\ rate}$
mm	*mm*
0	8.32
80	7.78
110	9.01
150	8.80
228	8.36

rapid oxidation of an ethanol-rich mixture. The values in Table 3 were obtained from analysis of the products present at the maximum reaction rate.

INFLUENCE OF TEMPERATURE

Analysis shows that between 270°C and 400°C the nature of the products of the combustion of ethanol and the extent of their formation remain sensibly unchanged. Figure 4 shows the consumption of ethanol and the formation of aldehydes and peroxides at 370°C (compare Figure 1). Almost all the peroxide present at the higher

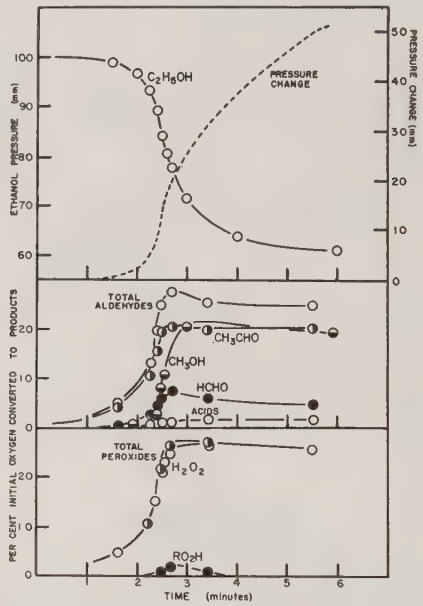

Fig. 4. The consumption of ethanol and the formation of condensable products. Temp. 370°C. Ethanol pressure, 100 mm; oxygen pressure, 50 mm.

temperature consists of hydrogen peroxide. During the region of autocatalytic reaction, the yields of hydrogen peroxide are considerably higher at 370° than at 295°; comparative data are given in Table 4.

INFLUENCE OF SURFACE

Surface : Volume ratio

Increase in surface area leads to a marked reduction in peroxide yields, particularly those of hydrogen peroxide. Table 5 shows the effect of surface on the amounts of hydrogen peroxide present at the maximum rate of reaction. An increase in the extent of even a relatively "inert"

surface (Pyrex, "aged" by numerous reactions carried out under similar conditions) sharply decreases the yields of hydrogen peroxide.

KCl-coating

A coating of potassium chloride on the walls of the reactor promotes the decomposition of peroxides[20] and is also believed to facilitate destruction of HO_2 radicals.[21] No peroxide was detected in the products of ethanol combustion at 295°C or at 370°C in a KCl-coated reactor. Apart from an increased yield of water, there was no other change in the nature of the products, although the overall reaction was strongly retarded.

INFLUENCE OF SAMPLING CONDITIONS

Observations on the effect of condensation temperature on the products formed in the dissociation of water vapor[22] and in the interaction between H and O_2[23] suggest that hydrogen peroxide may arise from reactions of OH or HO_2 radicals below about −120°C. In one series of experiments, the products of reacting ethanol-oxygen mixtures were rapidly withdrawn (1) by "sharing" into a heated gas pipette (ca. 60°C), (2) by condensation in separate traps cooled to −78°C and −196°C respectively. The products were quickly extracted with water and, except where specified, the resulting solution was rapidly analysed for peroxides. The results in Table 6 show that the different sampling methods have no effect on the amount of total peroxides present, but only influence the ratio of hydrogen peroxide to organic peroxides. This ratio is governed largely by the extent to which aldehyde—hydrogen peroxide interaction can occur; the latter is clearly a function of both product condensation temperature and time of standing of the aqueous extract before analysis or separation. There is no evidence from these results that hydrogen peroxide is produced from a reaction, in the cold trap, of radicals such as HO_2.

n-Propanol

Oxidation of *n*-propanol at 295°C resembles that of ethanol in that parallel formation of aldehydes and peroxides occurs. Hydrogen peroxide is the only peroxide detected during the early stages of oxidation and remains the predominant peroxidic product throughout the reaction. The quantities of peroxides present at various stages of the partial oxidation of *n*-propanol are given in Table 7; they are comparable to those obtained

TABLE 4. THE INFLUENCE OF TEMPERATURE ON THE YIELDS OF HYDROGEN PEROXIDE

Ethanol pressure, 100 mm; oxygen pressure, 50 mm

Pressure Change	Yields of Hydrogen Peroxide 295C°	370°C
mm	*per cent of ethanol consumed*	
0.5	77.0	100
1.5	62.6	93.0
3.0	52.0	90.0
6.0	43.0	82.8
12.0	38.6	78.2
20.0	34.0	60.1
28.0	—	45.2

TABLE 5. THE INFLUENCE OF SURFACE ON HYDROGEN PEROXIDE FORMATION

Temp. 295°C

Surface:Volume Ratio of Reactor	Ethanol Pressure	Oxygen Pressure	$(H_2O_2)_{max}$ rate
cm^{-1}	*mm*	*mm*	*per cent of inital* O_2
0.88	100	50	24.0
3.94	100	50	8.0
8.27	150	80	1.6
21.4	150	80	<1

TABLE 6. THE EFFECT OF SAMPLING CONDITIONS ON PEROXIDE FORMATION

Temp. 295°C; ethanol pressure, 100 mm; oxygen pressure, 50 mm

Method of Sampling	Total Peroxides	H_2O_2
	mm	*mm*
Heated pipette	10.3	7.08
Trap at −78°C	10.8	8.79
Trap at −196°C	10.6	9.70
*Trap at −196°C	10.6	7.00

* Aqueous solution analyzed after 18 hr.

TABLE 7. THE FORMATION OF PEROXIDES DURING PARTIAL OXIDATION OF *n*-PROPANOL

Temp. 295°C; *n*-propanol pressure, 100 mm; oxygen pressure, 50 mm

Pressure Change	Total Peroxides	H_2O_2
mm	*mm*	*mm*
1.0	1.43	1.27
3.0	3.28	2.97
9.0	6.57	5.62
15.0	9.48	7.44
19.0	11.10	8.75
24.0	11.20	9.18
31.0	8.22	6.45

in the oxidation of a similar ethanol-oxygen mixture.

Potential Application of Alcohol Combustion to the Large-Scale Production of Hydrogen Peroxide

The formation of high yields of hydrogen peroxide during the partial combustion of ethanol and *n*-propanol raises the possibility that the oxidation of alcohols might form the basis of an economic method for the manufacture of hydrogen peroxide. Under favorable conditions, the sole reaction occurring in the early stages of the partial combustion of ethanol is:

$$CH_3CH_2OH + O_2 = CH_3CHO + H_2O_2$$

Ethanol is a relatively inexpensive commercial product and since the presence of nitrogen does not affect the yields of peroxides, oxidation could be carried out with air instead of oxygen. The working temperature for maximum peroxide yields from ethanol combustion (300 to 400°C) is considerably lower than from hydrocarbon oxidation (400 to 500°C).[6, 7] Following separation of hydrogen peroxide, reduction of acetaldehyde and recycling of the alcohol distillate should result in little loss in organic starting material. The presence of water vapor in the recycled alcohol distillate has no appreciable effect on the combustion of the alcohol.[15]

Separation of hydrogen peroxide from aldehyde and residual alcohol and prevention of aldehyde/hydrogen peroxide condensation are the principal difficulties in economic production. The presence of excess alcohol appears to stabilize the products and might be expected to reduce the extent of peroxide/aldehyde condensation.[24] The separation of hydrogen peroxide from aldehydes and other combustion products has been discussed by Satterfield and Wilson,[8] who conclude that precipitation with slaked lime at 0°C leads to recovery of over 90 per cent of the hydrogen peroxide from solutions containing acetaldehyde and hydrogen peroxide.

Summary

The combustion of ethyl and *n*-propyl alcohols in the temperature range 250 to 400°C leads, under suitable conditions, to high yields of hydrogen peroxide. Peroxide formation is, however, highly sensitive to the nature and extent of surface, and hydrogen peroxide readily undergoes chemical reaction with aldehydic products in aqueous solution. Yields are improved by (1) oxidation in the presence of excess alcohol, (2) reaction at relatively high temperatures (350 to 400°C), (3) inert reactor surfaces (e.g., "aged" Pyrex), (4) low surface:volume ratio, and (5) removal of products by condensation at low temperatures and rapid separation after extraction with water. During the early stages of the oxidation of ethanol, acetaldehyde and hydrogen peroxide are the sole products, presenting a relatively simple water-soluble mixture for separation. Inert gases and water vapor are without effect on the formation of hydrogen peroxide, and hence combustion in air and the recycling of "wet" alcohol distillates is permissible.

Acknowledgments

The authors would like to express their gratitude to the Shell Petroleum Company and to the University of London Central Research Fund for generous financial assistance.

REFERENCES

1. Egerton, A. C., Smith, F. L., and Ubbelohde, A. R.: Phil. Trans. Roy. Soc., *234*, 433 (1935).
2. Shtern, V., and Pollyak, S.: Acta. physchim. U.R.S.S., *11*, 797 (1939); Brüschweiler, H., Minkoff, G. J., and Salooja, K. C.: Nature, *172*, 909 (1953); Brüschweiler, H., and Minkoff, G. J.: Anal. Chim. Acta, *12*, 186 (1955).
3. Minkoff, G. J., and Salooja, K. C.: Fuel, *32*, 516 (1953).
4. Knox, J. H., and Norrish, R. G. W.: Proc. Roy. Soc., *A221*, 151 (1954).
5. Batten, J. J., Gardner, H. J., and Ridge, M. J.: J. Chem. Soc., 3029 (1955).
6. U. S. Patent, 2,376,257.
7. Kooijman, P. L.: Rec. Trav. Chim., *66*, 5 (1947).
8. Satterfield, C. N., and Wilson, R. E.: Ind. Eng. Chem., *46*, 1001 (1954).
9. Kahler, E. J., Bearse, A. E., and Stoner, G. G.: Ind. Eng. Chem., *43*, 2777 (1951).
10. Clover, A. M.: J. Am. Chem. Soc., *44*, 107 (1922); *46*, 421 (1924).
11. Eastwood, T. A., and Hinshelwood, C. N.: J. Chem. Soc., 733 (1952).
12. Lemay, A., and Ouellet, C.: Can. J. Chem., *33*, 1316 (1955).
13. Baccareda, M., and Pedrazzini, C.: Riv. combustibili., *8*, 417 (1954).
14. Newitt, E. J.: *Fifth Symposium (International) on Combustion*, p. 558. New York, Reinhold Publ. Corp., 1955.
15. Cullis, C. F., and Newitt, E. J.: Proc. Roy. Soc., A237, 530 (1956).

16. Boos, R. N.: Anal. Chem., *20*, 964 (1948).
17. Bailey, H. C., and Knox, J. H.: J. Chem. Soc., 2741 (1951).
18. Bricker, C. E., and Johnson, H. R.: Anal. Chem., *17*, 400 (1945).
19. Dickey, F. H., Raley, J. H., Rust, F. F., Treseda, R. S., and Vaughan, W. E.: Ind. Eng. Chem., *41*, 1673 (1949).
20. Pease, R. N., and Munro, W. P.: J. Am. Chem. Soc., *56*, 2034 (1934); Harris, E. J., and Egerton, A. C.: Chem. Rev., *21*, 287 (1937); Harris, E. J.: Trans. Faraday Soc., *44*, 764 (1948).
21. Hoare, D. E., and Walsh, A. D.: *Fifth Symposium (International) on Combustion*, p. 467. New York, Reinhold Publ. Corp., 1955; Egerton, A. C., Minkoff, G. J., and Salooja, K. C.: Proc. Roy. Soc., *A235*, 158 (1956).
22. Jones, R. A., and Winkler, C. A.: Can. J. Chem., *29*, 1010 (1951); Sanders, T. M., Schawlow, A. L., Dousmanis, G. C., and Townes, C. H.: J. Chem. Phys., *22*, 245 (1954); Giguère, P.: J. Chem. Phys., *22*, 2085 (1954).
23. Geib, K. H., and Harteck, P.: Ber. deut. chem. Ges., *65*, 1551 (1932); Badin, E. J.: J. Am. Chem. Soc., *70*, 3651 (1948).
24. Dutch Patent, 61,465.

114

TECHNIQUES FOR THE STUDY OF AIR FLOW AND FUEL DROPLET DISTRIBUTION IN COMBUSTION SYSTEMS

By B. V. POULSTON and E. F. WINTER

Introduction

Until recently active research into the fundamental processes of chemical reaction, evaporation, burning of single droplets, etc. has proceeded in parallel with largely *ad hoc* development of engineering equipment which employs combustion for specific purposes. The fundamental research has rightly concerned itself with homogeneous systems or idealized droplet systems; the practical equipment uses far more complex systems.

The techniques which are described in this paper were developed so that detailed studies of fuel and air mixtures under practical conditions could be carried out in order to link fundamental combustion data with the performance of practical systems.

The Approach to the Problem

The efficient combustion of liquid fuel in a practical combustion chamber requires that atomization, evaporation from the droplets, mixing the vapor and air, ignition, and completion of chemical reaction should proceed unhindered in many different parts of the combustion zone simultaneously. Complete understanding of the system thus demands a knowledge of the physical and chemical state of the mixture in every element of volume of the combustion zone. It is obviously nearly impossible to satisfy such an exacting demand but progress can be made if the velocity of air flow and the mixture strength are known for a number of elements at the more important regions, thus reducing the problem mainly to that of investigating the air flow pattern and the distribution of fuel droplets within the combustion zone, although knowledge of the size spectrum of fuel droplets produced by the atomizer and the temperature distribution within the zone is also required.

It would be desirable to study the air flow pattern and the behavior of the fuel droplets while combustion is occurring in the combustion zone but the experimental difficulties are so great that a simplified approach is necessary to allow the use of convenient, rapid and relatively simple techniques. One simplification consists in carrying out the investigations in the absence of flame. It will be shown that this procedure does not invalidate the results as much as might be expected, and that separate investigations—one dealing with the air flow pattern only, and the other dealing with the fuel distribution only—can be coordinated so that our understanding of the combustion zone performance is improved.

The Study of the Air Flow

THE EFFECT OF THE FLAME

As the first part of the investigation, a comparison was made between the flow patterns in the flame zone of a gas turbine combustion chamber with and without the flame present. The water-cooled combined yawmeter and Pitot-static probe

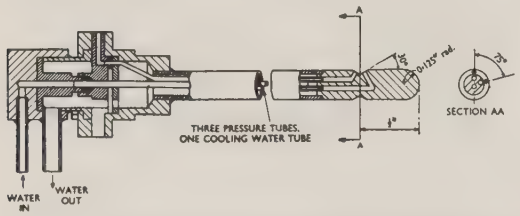

FIG. 1. Water-cooled three-dimensional probe.

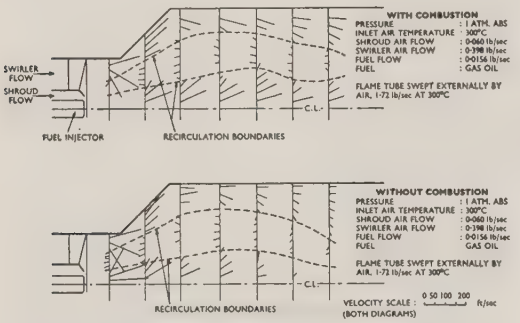
WITH COMBUSTION
PRESSURE : 1 ATM. ABS
INLET AIR TEMPERATURE : 300°C
SHROUD AIR FLOW : 0·060 lb/sec
SWIRLER AIR FLOW : 0·398 lb/sec
FUEL FLOW : 0·0156 lb/sec
FUEL : GAS OIL
FLAME TUBE SWEPT EXTERNALLY BY AIR, 1·72 lb/sec AT 300°C
SWIRLER FLOW
SHROUD FLOW
C.L.
FUEL INJECTOR
RECIRCULATION BOUNDARIES
WITHOUT COMBUSTION
PRESSURE : 1 ATM. ABS
INLET AIR TEMPERATURE : 300°C
SHROUD AIR FLOW : 0·060 lb/sec
SWIRLER AIR FLOW : 0·398 lb/sec
FUEL FLOW : 0·0156 lb/sec
FUEL : GAS OIL
FLAME TUBE SWEPT EXTERNALLY BY AIR, 1·72 lb/sec AT 300°C
C.L.
RECIRCULATION BOUNDARIES
VELOCITY SCALE : 0 50 100 200 ft/sec
(BOTH DIAGRAMS)

FIG. 2. Results of radial probe traverses in the combustion zone of a gas-turbine system, with and without combustion. The vectors refer to components in the central plane; swirl components are not shown.

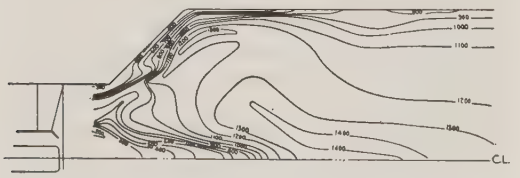

FIG. 3. Temperature contours, in °C, for the case illustrated in the upper diagram of Fig. 2.

illustrated in Figure 1 was traversed across the flame zone at a number of points successively along its length. The design of the instrument was based on Fechheimer's work[1] and it required calibration over the operating range. When the flame was present a further traverse with a pyrometer was necessary in order that gas velocities could be computed.

The results of this laborious technique are shown in Figure 2, where comparisons are drawn between the "hot," or variable density, and the "cold," or constant density, flow patterns in a particular combustion zone. The general design of this type of combustion zone is shown diagrammatically in this figure and has been fully described elsewhere.[2] In Figure 2, vector diagrams of the flow components in a plane through the longitudinal axis are shown, and in Figure 3, approximate temperature contours for the hot conditions are shown.

It can be seen that, at least in this combustion system, the effect of density change on the flow pattern was small, and was confined largely to changes in vector quantities which would be approximately predicted from observation of the temperature contours and flame position.

Hence on this type of system a study of the airflow pattern at constant density would yield information applicable to the behavior of the system in the presence of flame.

CONSTANT-DENSITY FLOW VISUALIZATION

The probe method already described has several disadvantages compared with methods of direct flow visualization, which permit a more complete and detailed examination of a flow field, avoid the errors and flow disturbances due to probing instruments and can both reduce the test time and eliminate the delay between the test run and the assessment of the results.

Although the flow may easily be rendered visible in air flowing through transparent models, the use of air is unsatisfactory for the observation of details in highly turbulent systems, principally because of the difficulty of obtaining a tracing material of suitable properties. Solid tracers must be used in such systems, but the large difference in density between the available materials and air necessitates the use of solids of very small particle size if gravitational errors are to be reduced to a reasonable level. Clouds of very fine particles, however, are difficult to observe and record in practice.

It has been found that the substitution of water for air offers advantages in this respect, since it is possible to provide tracers which are of similar density to the fluid and which also have excellent optical properties. The water method also offers the advantage of dynamic similarity, for a given linear scale, at much lower velocities than when air is used, so that observation and recording are facilitated. Furthermore, the optical clarity through a transparent model is generally greater in water than in air.

Details of the water circuit and associated

apparatus used have been given elsewhere.[3] The transparent plastic models are normally mounted horizontally within a water-filled rectangular glass tank, which has the principal purpose of eliminating optical distortion through models with curved walls.

THE VISUAL STUDY OF FLOW PATTERNS IN A WATER MODEL

Scale models of the combustion zone under investigation are made in moulded Perspex (acrylic plastic) and are operated on water at conditions which give Reynolds number similarity with the real operating conditions. It has been verified that the value of Reynolds number has little effect when fully developed turbulence prevails but is sometimes important where low local Reynolds numbers occur in certain parts of the system. Since the constant-density technique precludes over-all similarity, it is usual to relate the Reynolds number to the inlet air conditions.

Because of the turbulent nature of the majority of the flow systems studied, solid tracers are desirable for indicating the "mean" or basic flow pattern and spherical pellets of polystyrene, up to 500 μ in diam, have generally been used. This material, when slightly impure, has been obtained with a specific gravity within 0.02 of that of water. It is also satisfactorily reflective to light.

Visual observations have usually been made with tracers circulating continuously through the water system, with a tracer concentration of about 0.1 per cent. In two-dimensional systems, and in three-dimensional systems where motion in one of the dimensions is relatively insignificant, the flow may be observed on a single plane through the system. This has been achieved by the use of a narrow, flat beam of light from a 2 kw tungsten lamp projected through the model so that the dimension in which the motion is substantially zero is normal to the plane of the beam. Only the tracers which pass into the beam are illuminated, so that in a three-dimensional flow field a two-dimensional section of the pattern can be observed without obstruction by the surrounding flow.

Directions of flow and areas of extreme turbulence can be readily seen by this method, although in complex flow it is sometimes difficult to determine which way the motion occurs along some of the flow lines. Figure 4 gives an impression of the appearance of the flow round a two-dimensional baffle viewed in this way.

SEMI-QUANTITATIVE PHOTOGRAPHIC RECORDING OF FLOW PATTERNS

Photographic records of instantaneous flow characteristics have been obtained with the aid of a 700-j electronic flash unit. Linear quartz flash tubes (Mullard LSD17) are used and are

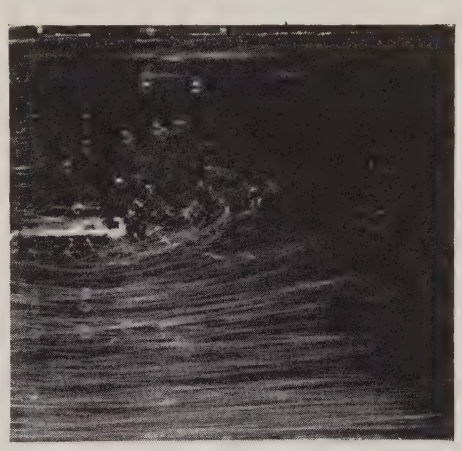

FIG. 4. Two-dimensional flow observed by continuous light.

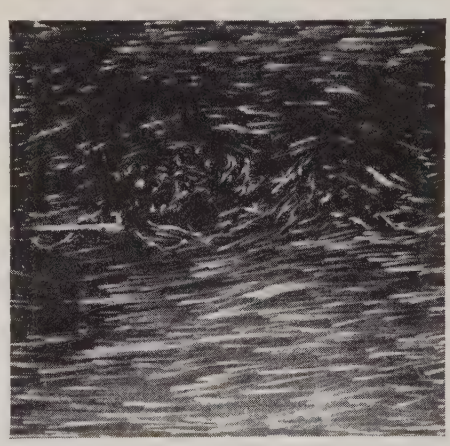

FIG. 5. Two-dimensional flow photographed by electronic flash.

arranged to project a narrow, flat beam across the flow field. Because of the flash characteristics of this system, namely a rapid rise to maximum intensity followed by exponential decay, the recorded trace of each illuminated particle varies in brilliance in such a way that the direction of motion is clearly defined. Typical traces are shown in Figure 5; the direction of motion is in each case from the broad to the narrow end of the trace. This directional feature of flash photographs has been previously exploited in similar

work by Howes and Philip.[4] Comparison with Figure 4 shows the greater amount of information obtained with the flash technique.

The flash duration is variable over the range 500 μsec to 6 msec by switching inductance and resistance into the flash-tube circuit. A rough time base is thus imposed, since the duration of the flash affects the length of the trace. The actual trace length recorded depends not only on flash duration but also on the properties of the photographic material. Moreover, the length of trace is not a linear function of the tracer velocity, since the effective exposure is inversely proportional to velocity. Nevertheless, a fair idea of relative flow velocities can be obtained from measurements of trace length, and an approximate absolute datum may be obtained on each record if necessary by the inclusion of an upstream steady-flow section.

The situation is more complicated when fully

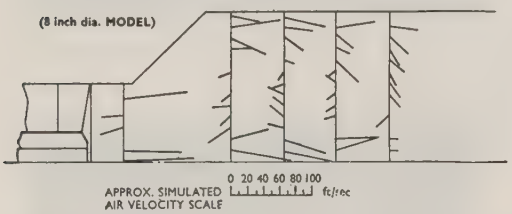

FIG. 6. Result obtained by photography of water in a model of a combustion chamber. Comparable with Fig. 2.

three-dimensional turbulent flow fields are observed. By means of a suitable beam width, it is usually possible to ensure that a high proportion of the recorded traces are contained wholly within the beam. From a viewpoint substantially perpendicular to the plane of the beam, records may be obtained of the instantaneous components of motion in this plane. A number of successive photographs will show that the flow at each point varies with time but that in most cases the flow vectors at each point form a group which generally indicates a preferred direction of flow. The basic two-dimensional flow pattern can then be determined by measuring these preferred vectors.

The vector diagram of Figure 6 shows the basic flow components in the central plane of a particular system determined in this way. This diagram is directly comparable with the lower diagram of Figure 2, which was produced by the probe technique. The resemblance between the two records is very close and probably no greater error is involved in the measurements by visualization than by probing.

TECHNIQUE FOR STUDYING RESIDENCE TIME

Variants of the methods described above can be applied to the study of particular flow problems, such as the penetration of dilution air jets, but of special interest is the adaptation to study residence time in any zone of the combustion chamber.

For this purpose a single tracer particle is injected and rendered visible throughout the whole of the time it remains in the zone under study. Inasmuch as it is itself nondiffusible and large compared with fluid molecules, the tracer is not subject to small-scale turbulence and molecular mass transport, but nevertheless its random motion will be related to the random molecular flow of the fluid. It is probably justifiable to consider that statistical observations of the tracers apply also to the fluid. In particular, the extremes of behavior, such as the minimum and maximum residence times, should be closely related. Comparisons of different combustion systems can be made on this basis.

The photography of an individual tracer by means of tungsten light is restricted by the fact that the whole model must usually be illuminated and exposures of more than about two seconds result in the obscuration of the observed trace by the light reflected from the surroundings.

A technique of selective illumination has therefore been devised, in which a polystyrene tracer with a fluorescent coating is illuminated by ultra-violet light from mercury discharge lamps. A suitable filter at the camera transmits the greater part of the reradiated light from the tracer while transmitting only a minor portion of the initial ultra-violet radiation. Adequate records can thus be obtained up to ten seconds or more total exposure, and a time base is automatically imposed by the variation in discharge intensity in synchronism with the main supply frequency.

As an illustration of the records produced by this technique, Figure 7 shows flow paths of three single tracers passing at different instants through a model of a particular combustion zone.

The tracers were introduced successively upstream of the air director into the fluid before entering the combustion zone. The particles thus occupied random initial positions in this zone and followed random paths which varied in length

from the direct route of the top photograph to the intricate route of the bottom photograph.

In this experiment, the residence times of two hundred tracers were observed, half being introduced into the swirling main air stream and half in the subsidiary stream in the annular jet surrounding the fuel injector. The results are shown in Figure 8, and it is interesting to observe the high proportion of particles which had residence times less than that of fluid flowing at the same volumetric rate but with uniform velocity across the stream.

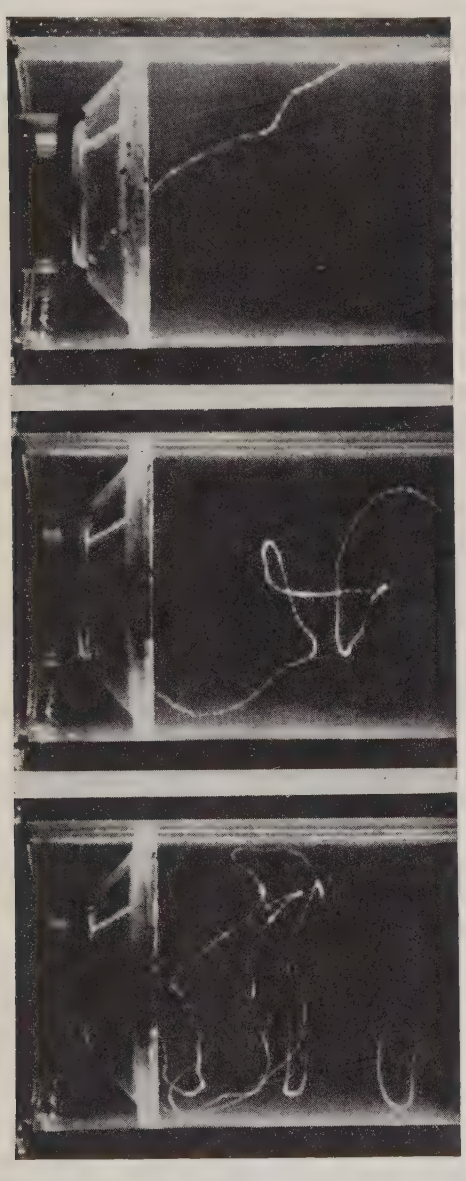

FIG. 7. Paths of three individual tracers through the same system.

With this technique the effects of disposable variables on residence time can be studied, with reference to its adequacy for combustion at high altitude and for combustion of slow burning fuels at ground level. The method might also be of value in the study of "refreshment efficiency" as defined by Clarke.[5]

The Fuel Droplet Distribution

GENERAL

The open-spray-type pressure jet atomizer achieves a fine degree of atomization by causing the fuel to rotate at high velocity in its swirl chamber. During this process an air core is set up and in consequence the fuel, traveling through the fluid orifice as a thin spinning cylindrical film, is distributed on emergence so that the paths of the droplets trace out a hollow cone with its apex at or near the orifice. The droplet path is very quickly modified by aerodynamic drag depending upon the usual variables,[6] including the velocity of the droplet relative to the medium through which it travels, which may itself be moving.

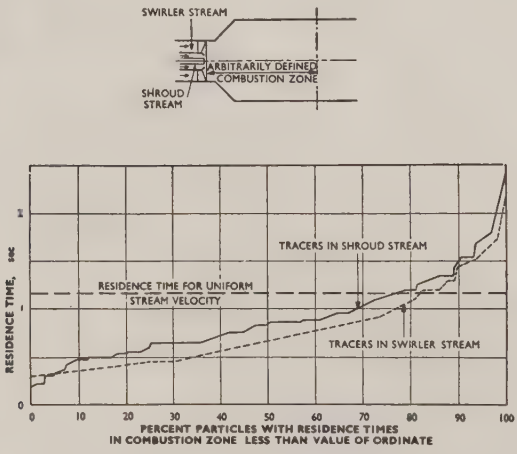

FIG. 8. Residence times of tracers in model of a combustion zone.

Even without directed air streams around the atomizer, induced air currents are sufficient to produce the familiar diffuse "tulip" spray, the fuel distribution on a cross-section of which is sketched in Figure 9.

Heterogeneity in the flow of fuel droplets per unit area of cross-section of combustion zone is thus inherent in the pressure jet atomizer, and if this is to be matched with a heterogeneity in

air flow per unit area so that nowhere in the combustion zone will unacceptable mixture strengths be developed, it is necessary to know how the method of introduction of the air into the combustion zone reacts upon, and modifies, the spatial distribution of the fuel droplets.

APPARATUS

Apparatus has been built to measure the fuel flow across a small area of cross-section placed

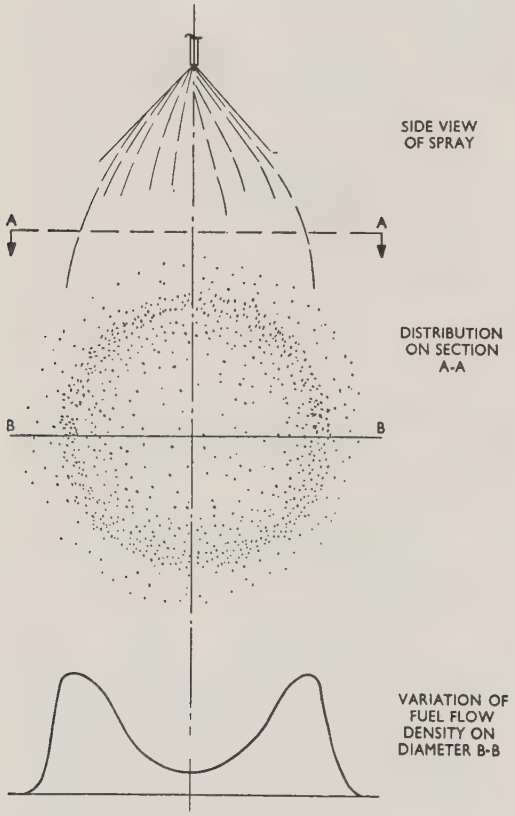

FIG. 9. Characteristics of fuel spray from pressure atomizer.

at different radii in a transverse plane at a given distance downstream from the atomizer, with the air flow pattern around the atomizer simulating as closely as possible that which would exist in the actual combustion zone under investigation. Although an absolute measure of the local fuel flow would be desirable it is considered more important to concentrate on obtaining quickly the effect of any change in conditions rather than to strive for absolute accuracy. The effect of the change can be directly checked on the combustion rigs.

Models of combustion zones under investigation are mounted vertically with their atomizers spraying downwards. Air is supplied exactly as it would be if combustion were occurring and the fuel spray is sampled at a plane some inches downstream of the atomizer.

The original sampling apparatus consisted of a rack of closed tubes of equal bores placed with their mouths along a diameter.[7] A remotely operated shutter allowed the tubes to be exposed for a given time, during which each tube filled up to a level dependent upon the fuel flow density where its mouth was situated.

In certain combustion zones which have been investigated, some of the air was given a rotating motion about the axis of the zone. The fuel droplets at the sampling plane therefore possessed a tangential velocity component, and to allow for this readings were taken with the tube rack tilted at different angles to the axis. Plotting the fuel levels for each tube against angle of tilt then showed a maximum where the tube mouth was truly normal to the direction in which the fuel droplets were traveling.

Although this technique allows a large number of changes in air- and fuel-flow conditions to be investigated very quickly, the tube rack and shutter mechanism disturbs the air-flow pattern sufficiently to affect the fuel spray upstream of the tubes, and radial velocity components cannot be measured. Another scheme has therefore been developed which employs only one sampling probe and eliminates the shutter. The probe is arranged to traverse across a diameter, separate readings being taken at set intervals. The arrangement is sketched in Figure 10.

The air and fuel mixture entering the mouth of the probe passes continuously along a flexible pipe to a small cyclone situated outside the model combustion zone. Here the fuel is disengaged and the flow measured. Tangential droplet velocity components are allowed for by repeating traverses with the straight sampling probe replaced by probes having their mouths inclined to the axis. This sampling method goes some way towards overcoming the lack of *iso*kinetic sampling inherent in the original method.

In a combustion zone in which an upstream current of air is induced for the purpose of stabilizing the flame the tube rack technique will not detect fuel droplets carried upstream by this current. The single probe might be adapted for the purpose but this has not yet been attempted.

Investigations have been carried out for the

combustion zone design referred to in a previous section (see Figure 2) in which the combustion air was supplied in two streams, one rotating or "swirling" about the axis. In order that test conditions could be altered rapidly, these two air supplies were separately ducted, controlled and metered. The fuels used were kerosene and gas oil and the model combustion zone was mounted over a large closed disengaging tank, from which the air was ducted away while the fuel was recirculated back to the atomizer.

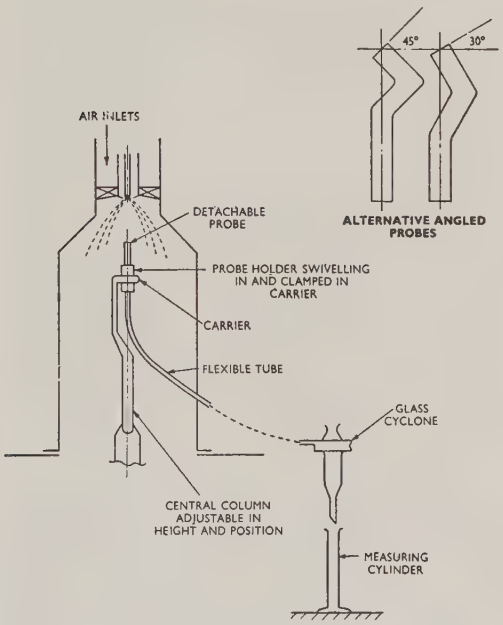

FIG. 10. Sketch of single probe sampling apparatus.

RESULTS

Results obtained from the rig cannot be adequately discussed without extensive reference to parallel investigations of air flow pattern and combustion performance, but examples can be quoted to show that the more obvious predictions of the effects of certain changes are confirmed, and some unexpected ones are revealed.

The inherent fuel distribution as fixed by the cone angle of the atomizer is shown in Figure 11 to persist in spite of the air streams. Here the distributions at a particular section of the combustion zone given by two atomizers with the same flow number but with cone angles 75° and 85° are compared for identical air- and fuel-flow conditions. The outer peaks of concentration occurred at a smaller radius with the narrower cone angle, and a change in the combustion performance would be predicted.

Figure 12 compares tests in which the only

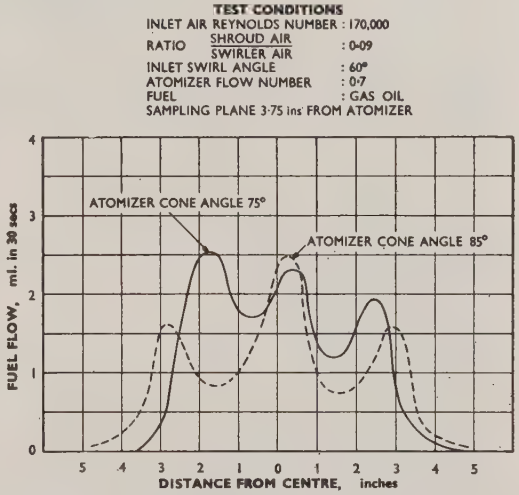
TEST CONDITIONS
INLET AIR REYNOLDS NUMBER : 170,000
RATIO SHROUD AIR / SWIRLER AIR : 0·09
INLET SWIRL ANGLE : 60°
ATOMIZER FLOW NUMBER : 0·7
FUEL : GAS OIL
SAMPLING PLANE 3·75 ins FROM ATOMIZER
ATOMIZER CONE ANGLE 75°
ATOMIZER CONE ANGLE 85°
FUEL FLOW, ml. in 30 secs
DISTANCE FROM CENTRE, inches

FIG. 11. Effect of atomizer cone angle on fuel distribution.

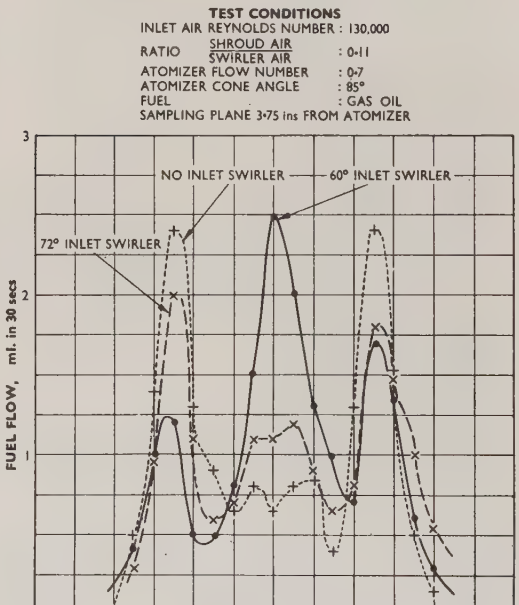
TEST CONDITIONS
INLET AIR REYNOLDS NUMBER : 130,000
RATIO SHROUD AIR / SWIRLER AIR : 0·11
ATOMIZER FLOW NUMBER : 0·7
ATOMIZER CONE ANGLE : 85°
FUEL : GAS OIL
SAMPLING PLANE 3·75 ins FROM ATOMIZER
NO INLET SWIRLER
60° INLET SWIRLER
72° INLET SWIRLER
FUEL FLOW, ml. in 30 secs
DISTANCE FROM CENTRE, inches

FIG. 12. Effect of inlet air rotation on fuel distribution.

variable altered was the tangential velocity component of the swirler air supply. Fuel supply conditions and the small axial air supply were identical. A curve is also included for a test without the swirling air stream. Although some centrifuging action upon the droplets might have

been expected with the swirling air supply this was small, and the main effect was that the lower swirl angle induced much more fuel to travel towards the axis of the combustion zone than with either no swirling air or the higher swirl angle. An explanation of this result might be found in the effects of the different amounts of recirculating air induced by the two swirlers.

When using a simplified air flow pattern without any tangential velocity component, good agreement was obtained between experimental results and those predicted by calculating the trajectories of solid spheres of sizes equal to those of the fuel droplets,[8] provided that the accepted drag coefficients[6] were multiplied by a factor 1.5. Considering the disturbing effects of evaporation[9] and fluid distortion,[10] the modification of the rigid sphere drag coefficients is not surprising.

Table 1. Summary of Combustion, Air-Flow Pattern and Fuel Distribution Tests

A. Combustion zone operation		
Atomizer flow number $\left\{\frac{\text{Fuel Flow—g.p.h.}}{\sqrt{\text{Fuel Pressure—p.s.i.}}}\right\}$	1.42	
Atomizer cone angle	85°	
Fuel	Gas Oil	
Axial air inlet annulus width	0.31 in.	
Inlet angle of swirled air	60°	72°
B. Flow pattern tests on water model		
Inlet Reynolds number	100,000	100,000
Ratio $\frac{\text{Axial flow}}{\text{Total flow}}$	0.13 (See Figure 13)	0.13 (See Figure 13)
Note:—Small departures from this ratio have no measurable effect.		
Diameter of core at plane 3.75 in. from atomizer	2 in.	2 in.
Proportion of air flow in core	11 per cent	11 per cent
Outer Diameter of recirculation zone at plane 3.75 in. from atomizer	7.6 in.	7.6 in.
Proportion of air flow in recirculation zone at this plane	25 per cent (See Figure 14)	60 per cent (See Figure 14)
C. Fuel distribution tests		
Inlet Reynolds number	170,000	170,000
Ratio $\frac{\text{Axial flow}}{\text{Total flow}}$	0.133	0.133
Fuel flow	227 lb/hr (See Figure 15)	227 lb/hr (See Figure 15)
Note:—Moderate departures from this fuel flow have no measurable effects on distribution.		
Proportion of fuel flow within central 2-in. diam. core at plane 3.75 in. from atomizer	19 per cent	15.4 per cent
D. Combustion rig tests		
Pressure	2 atmos	2 atmos
Inlet temperature	100°C	100°C
Smoke limited fuel flow for		
(a) Equivalent Reynolds number to Section C	98 lb/hr	130 lb/hr
(b) Equivalent inlet momentum to Section C	140 lb/hr	170 lb/hr

The Relationship between Air-Fuel Distribution Data and Combustion Performance

The premise that it is possible to investigate component processes in a practical combustion system and marry the results so that the actual performance of the system is explained has been confirmed in a number of cases. The marked change in fuel distribution due to a change in air swirl has already been mentioned and this example will be discussed further.

The effect of changing the angle of swirl from

60° to 72° without altering other variables has been investigated also on the water-flow rig and on the combustion rig. The swirl angle is defined as the angle between the swirler blades and the axis of the primary zone. On the combustion rig, compact suspended flames were obtained for each swirler and the fuel flow was increased until smoke appeared in the exhaust sufficient to give a reading on a photo-electric smoke meter equivalent to a just visible smoke level.

It was found that more fuel could be burned satisfactorily with the 72°-swirler than with the 60°-swirler. The ratio between the two, compared at inlet air velocities equal to those of the fuel distribution tests, was 1.41, while it was noted that the latter tests and the flow pattern tests showed that the 60°-swirler gave for the same fuel flow a fuel concentration on the axis larger than that given by the 72°-swirler by quite a similar factor (1.56) although air pattern changes were small. For a more complete study of this point, the results of the tests on the combustion rig, the water-flow rig and the fuel distribution rig are set out in Table 1 and Figures 13, 14 and 15.

The flow patterns show that the axial air supply travels relatively smoothly along the axis of the combustion zone: the diameter of this core and the relative amount of air flowing along it at a plane 3.75 in. downstream of the atomizer are given in Table 1 for each swirler. Similarly the relative amounts of fuel reaching the core at this plane have been derived from the fuel distribution tests.

If the local air/fuel ratio for the core at this plane is now calculated the following figures appear: (a) Core air/fuel ratio for combustion tests compared on the basis of Reynolds number equal to that used in fuel distribution tests:

For 60°-inlet angle: 17.2

For 72°-inlet angle: 16

(b) Core air/fuel ratio for combustion tests compared on the basis of inlet momentum equal to that used in fuel distribution tests:

For 60° inlet angle: 16.7

For 72° inlet angle: 16.3

The significant conclusion now emerges that, although the over-all air/fuel ratios in the combustion zone were widely different for the two swirlers, the core air/fuel ratios coincided at the smoke-limited fuel flow, i.e., a critical air/fuel ratio leading to excessive smoke formation was reached first in this core for the particular zone configuration under discussion.

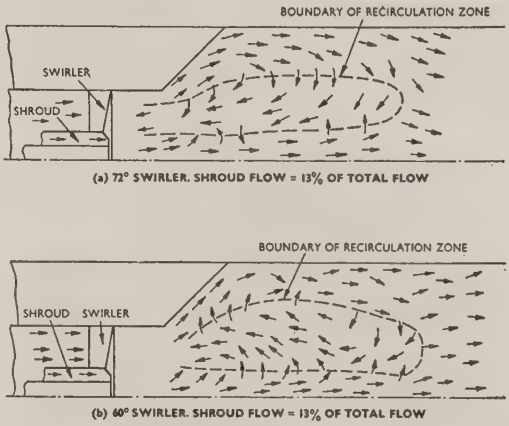
BOUNDARY OF RECIRCULATION ZONE
SWIRLER
SHROUD
(a) 72° SWIRLER. SHROUD FLOW = 13% OF TOTAL FLOW
BOUNDARY OF RECIRCULATION ZONE
SHROUD SWIRLER
(b) 60° SWIRLER. SHROUD FLOW = 13% OF TOTAL FLOW

FIG. 13. Directional flow diagrams for combustion system with two degrees of swirl.

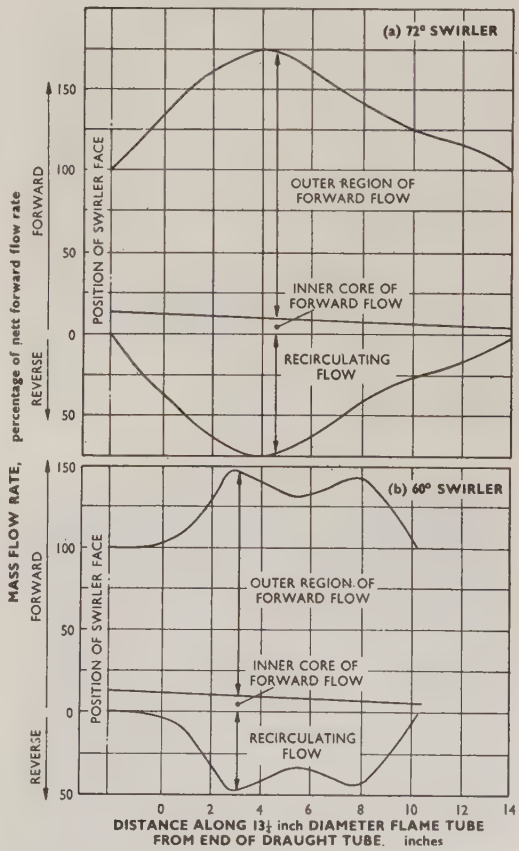

FIG. 14. Approximate mass distribution (corresponding to Fig. 13) produced from flash photographs on water model.

It is probable that this example could have been dealt with on the combustion rig by developing a technique for measuring local air/fuel ratios. The difficulties of probing in the presence of partially evaporated fuel droplets and partially burned vapor are extreme, and it is submitted that the inferential procedure outlined above is capable of obtaining valid results far more quickly. Also it gives a far broader picture of the details of flow and fuel distribution and thereby

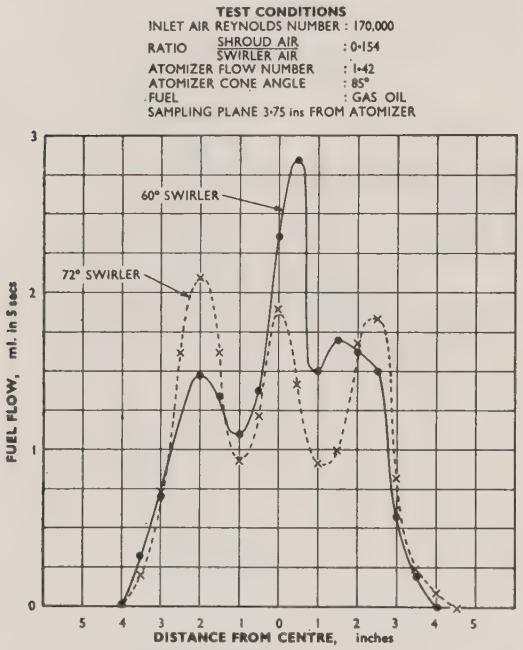
TEST CONDITIONS
INLET AIR REYNOLDS NUMBER : 170,000
RATIO SHROUD AIR / SWIRLER AIR : 0·154
ATOMIZER FLOW NUMBER : 1·42
ATOMIZER CONE ANGLE : 85°
FUEL : GAS OIL
SAMPLING PLANE 3·75 ins FROM ATOMIZER
60° SWIRLER
72° SWIRLER
FUEL FLOW, ml. in 5 secs
DISTANCE FROM CENTRE, inches

FIG. 15. Fuel distribution tests for correlation with combustion tests.

means for improving a given system may be more readily devised.

Conclusions

Reducing the investigation of a combustion system to separate investigations of its component processes involves certain simplifications which must be carefully verified before the separate investigations become valuable. It is believed that the techniques described in this paper for investigating flow pattern and fuel distribution, together with the technique described elsewhere[8] for measuring the sizes of droplets produced by an atomizer, are sufficient to provide information about the most important processes occurring in a practical combustion zone. Experience in using the techniques, in particular that involving ultra-violet selective illumination, and relating the results to combustion system performance is continually being gained, and it appears that the simplifications referred to are valid, within certain limits, so that some quantitative predictions of performance can be attempted.

It must be recognized that there are limitations to the techniques, although further development is possible, but where the techniques are applicable to a problem there will be considerable saving in time, when covering a wide range of variables, by carrying out these simplified component investigations without combustion rather than concentrating on combustion rig work.

Acknowledgments

It is desired to acknowledge, with thanks, the permission for, and assistance in, publishing this paper given by the Directors of "Shell" Research, Ltd., and the cooperation of colleagues at Thornton Research Centre, Chester, and Shell Petroleum Co., London.

The development of the three-dimensional probe and the aerodynamic traverses referred to on page 834 were carried out by R. M. Palmer and G. E. Powell at the laboratories of Ricardo & Co., Ltd., Sussex, England.

REFERENCES

1. FECHHEIMER, C. J.: Trans. Am. Soc. Mech. Engrs., *48*, 392 (1926).
2. LUBBOCK, I.: Trans. North-East Coast Inst. Eng. & Shipbuilders, *67*, 131 (1951).
3. WINTER, E. F., AND DETERDING, J. H.: To be published in British Journal of Applied Physics.
4. HOWES, R. S., AND PHILIP, A. R.: J. Iron & Steel Inst., *162*, 392 (1949).
5. CLARKE, J. S.: Am. Soc. Mech. Engrs./I. Mech. E. Joint Conference on Combustion, Section 5, 1955.
6. GOLDSTEIN, S.: *Modern Developments in Fluid Mechanics*, vol. 2, p. 491. Oxford University Press, 1950.
7. RUPE, J. H.: *Third Symposium on Combustion, Flame and Explosion Phenomena*, p. 688. Baltimore, The Williams & Wilkins Co., 1949.
8. JOYCE, J. R.: J. Inst. Fuel, *22*, 150 (1949).
9. INGEBO, R. D.: NACA Technical Note 3265, 1954.
10. HINZE, J. O.: Appl. Sci. Res., Sec. A., *1*, 263–272 (1949).

115

EXPERIMENTAL INVESTIGATION OF RAPID COMBUSTION OF LOW GRADE GASEOUS FUEL

By TEIKICHI ŌTSUKA AND HISAO HATTORI

Introduction

Low grade gaseous fuels, such as blast-furnace gas, producer gas from refuse coal, underground gasification gas, etc., appear promising for stationary gas turbines. However, they tend to burn unstably or incompletely at high combustion rates. Therefore, the practical application of such fuels involves both the construction of a suitable combustor and the study of their combustion.

In the present experiments, a small metallic combustor with suitable burners was used to investigate a number of characteristics, including the stable combustion region, combustion efficiency, pressure loss, etc.

Apparatus

The combustor used in these experiments is shown in Figure 1. In principle, it is similar to the ordinary gas turbine combustors for liquid fuel, but it offers the following differences:

(1) It has a cylindrical flame tube, and primary and secondary air are fed separately through the ducts. The flame tube has secondary air holes only at the end of the tube, thus preventing secondary air from entering the combustion zone. It is assumed that the flame tube is cooled sufficiently by convection of the surrounding flow of secondary air, as radiation from the flames of such fuels is weak and the temperature of the flame is not high. Moreover, the supply of air to the combustion zone is inefficient as it may lower the temperature of the burning zone.

(2) The burner can be moved along the axis of the combustor, thus changing the volume of the flame tube and of the burner itself.

(3) The auxiliary outer tubes are designed to control the cooling action of the secondary air on the flame tube.

Figure 2 and Table 1 show seven different burners used in these experiments. Their design is based on the following considerations:

(1) Premixing of fuel and air prior to combustion is replaced by diffusion combustion, which improves both the safety and simplicity of the operation, and the stability of the combustion.[1]

(2) Stabilization of the flame utilizing recirculation caused by the swirl.

(3) Stabilization of the flame utilizing recirculation originating in the wake of a bluff body.

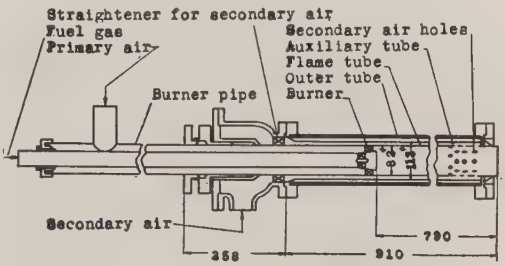

FIG. 1. Details of combustor.

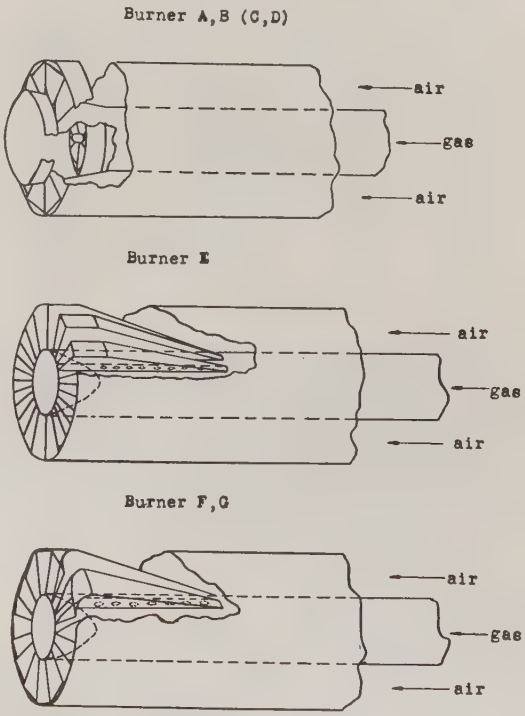

FIG. 2. Burners.

(4) Separation as far as possible of air and fuel gas into thin layers in order to facilitate mixing.

Burners A and B have swirl vanes with the same rotational direction at the air and fuel outlets. Burners C and D are similar to A and B, but the vanes have opposite directions. Burner E

has a plug at the front end of the fuel gas pipe around which forty slots are arranged radially, and air and gas flow out parallel to each other. The construction of burners F and G, is similar to that of E. However, they are equipped with swirl vanes, the number of which is determined so that the minimum width of slots may be equal to that of E.

Experimental Method, Results and Discussion

The fuel gas used in the experiments is coke producer gas with the following composition (volume per cent): carbon dioxide, 4.8; oxygen, 0.1; carbon monoxide, 24.5; hydrogen, 7.0; and nitrogen, 63.6. Its net heating value is 920 kcal/m^3

Table 1. Details of Experimental Burners

Burner	Mean Vane Angle Relative to Axis at Outlet (Degree)		Rotational Directions of Air and Gas	Number of Vanes	
	Air side	Gas side		Air side	Gas side
A	55	69	Same	16	8
B	70	75	Same	16	8
C	45	69	Counter	16	8
D	74	75	Counter	16	8
E	0		—	40	
F	58		Same	30	
G	76		Same	16	

at 760 mm Hg and 0°C, which is nearly the same as for blast furnace gas, although the former contains less carbon monoxide and more hydrogen than the latter. Air and fuel gas were not preheated and their temperatures ranged from 15°C to 40°C at the combustor inlet.

STABLE COMBUSTION REGION

In order to determine the stable combustion region, the burner was removed from the combustor and inserted into a transparent quartz tube (i.d., 82 mm; length, 30 cm). A metallic tube was attached to the quartz tube to make the combustion chamber the same length as the combustor in Figure 1. Once combustion was established, the stable region was determined by observation in which the flame was generated in contact with the burner port. The flame was photographed from the side and downstream of the burner. Only the quartz tube region was photographed.

The primary excess air factor, n_1 and the specific heat release, W, are defined as follows:

$$n_1 = \frac{\text{(mass flow of primary air, kg/hr)}}{\text{(mass flow of fuel gas, kg/hr)} \times \text{(stoichiometric air-fuel ratio, kg/kg)}}$$

$$W = \frac{\text{(mass flow of fuel gas, kg/hr)} \times \text{(heating value of fuel gas, kcal/kg)}}{\text{(volume of flame tube, m}^3\text{)}}$$

Figure 3 shows the stable combustion regions of seven burners taking W and n_1 for abscissa and ordinate, respectively. Figure 4 shows photographs taken from the side and downstream.

The stable combustion regions of the burners are summarized as follows:

(1) In general, burners with swirl vanes have a wide stable combustion region, particularly when W is small. However, in the case of burners F and G, the strong swirl produces a rapid jet of air and gas, leading to insufficient recirculation, which in turn results in flame instability and narrow stable combustion limits.

(2) With burner D, the flame is divided near the upper limit of the stable region. As this division generally occurs when there is an excess of primary air, the swirl of air predominates and limits recirculation along the axis downstream of the burner. At the point where the swirl of gas is inhibited the flame disappears, but again it is regenerated in the new recirculation zone formed by the swirl of air.

(3) For burner E, the width of the stable region along the ordinate is virtually constant, independent of W within the limits of our experiments. It is somewhat narrower than that of the other burners.

COMBUSTION EFFICIENCY

Combustion efficiency was determined varying the burner, fuel flow and primary excess air, provided that temperature increases up to about 500°C through the combustor produced complete combustion. The distance between the burner port and the flame tube outlet was kept constant at 790 mm, and the auxiliary outer tube with an i.d. of 113 mm was used, as shown in Figure 1.

To compute combustion efficiency, gas analyses were made of burned gas collected in a water-cooled sampling tube located in the center of the outlet of a steel pipe (i.d., 82 mm; length, 600 mm) attached to the outlet of the combustor. Preliminary investigation showed that the composition of the burned gas was almost uniform

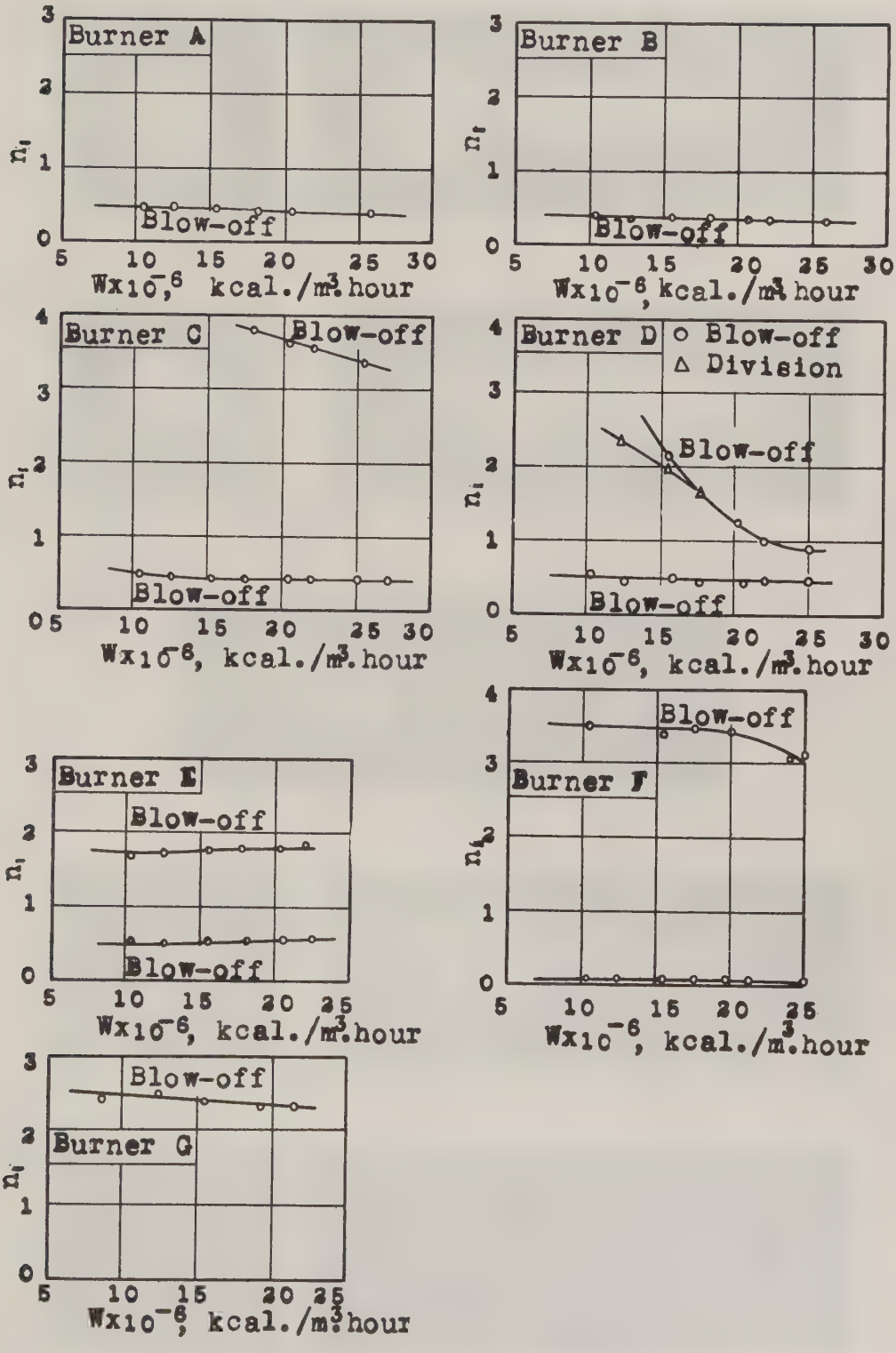

FIG. 3. Stable combustion regions for each burner.

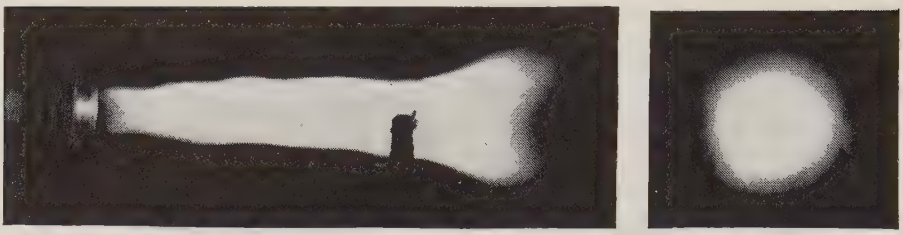

(a) Burner B; $n = 1.23$; $W = 20.3 \times 10^6$ kcal/m^3 hour

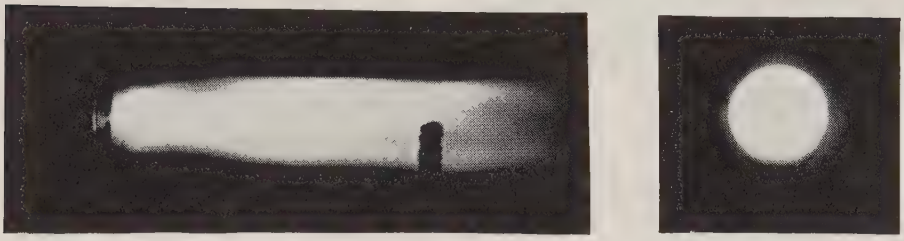

(b) Burner D; $n = 1.16$; $W = 19.9 \times 10^6$ kcal/m^3 hour

(c) Burner D; $n = 2.68$; $W = 12.5 \times 10^6$ kcal/m^3 hour

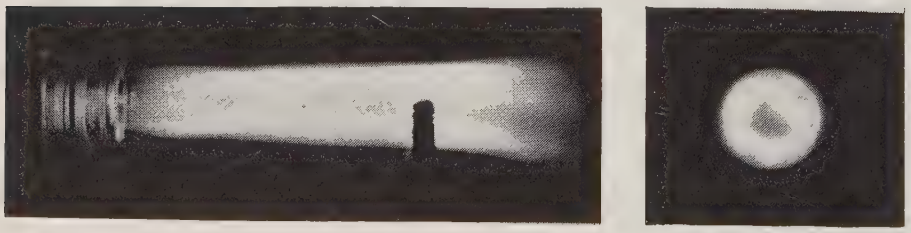

(d) Burner E; $n = 1.12$; $W = 19.5 \times 10^6$ kcal/m^3 hour

(e) Burner G; $n = 1.08$; $W = 20.1 \times 10^6$ kcal/m^{3}hour

FIG. 4. Flame photographs.

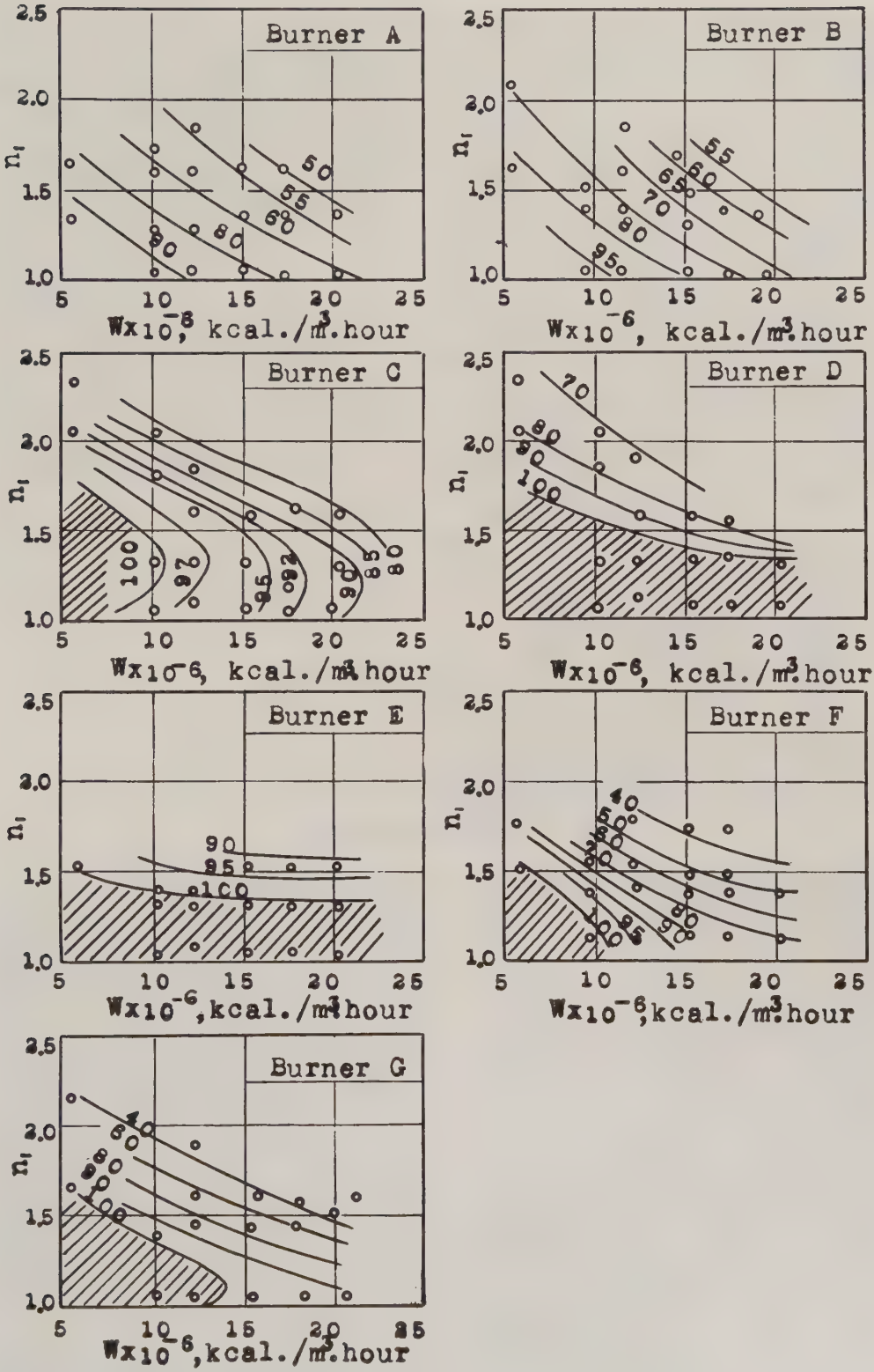

FIG. 5. Combustion efficiency for each burner.

over the section of the steel pipe. An electric gas analyzer was used. The maximum errors of unburned carbon monoxide and hydrogen measured by this method were 0.1 per cent by volume per

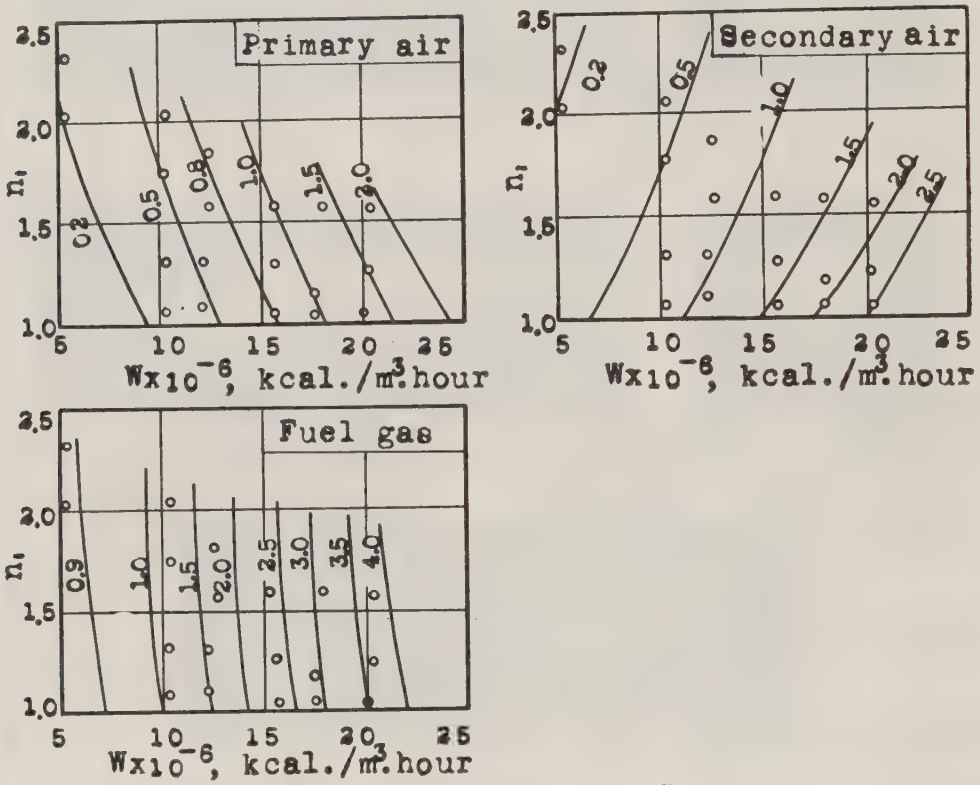

Fig. 6. Pressure losses for burner C.

Table 2. Factors for Pressure Losses

Burner	Primary Air	Fuel Gas
A	0.85	0.95
B	3.2	1.1
C	1.0	1.0
D	5.0	1.2
E	1.2	0.55
F	1.7	1.2
G	5.5	3.0

cent in the burned gas which was equivalent to an error of combustion efficiency of 1.8 per cent.

In Figure 5, the resulting combustion efficiency is plotted, taking W and n_1 for abscissa and ordinate respectively. The circles show the conditions under which the experiments were carried out. The curves show the combustion efficiency contours, and the shaded regions correspond to 100 per cent combustion efficiency.

Observations on combustion efficiency can be summarized as follows:

(1) For burners with swirl vanes, the stronger the swirl is, the greater combustion efficiency is for a high specific heat release. It is probable that this is due to the increase of turbulent mixing. However, when n_1 is large, increased turbulent mixing often cools the flame too fast to obtain very good combustion when the specific heat release is low.

(2) Of the burners with swirl vanes, burners A, B, F and G in which air and gas revolve in the same direction are less efficient than C and D in which air and gas revolve in the opposite direction. The photographs show that the volume of the combustion chamber is effectively utilized in the latter burners, whereas in the former the flame formed by the swirl lingers along the inner surface of the tube where it is liable to be cooled, and thus the central portion of the chamber is scarcely utilized.

(3) For burner E, the curves of combustion efficiency contour are distinguished by the fact that they are almost parallel to the abscissa.

PRESSURE LOSS

All pressure loss data were obtained together with the combustion efficiency data in the experiment described under *Combustion Efficiency.* As the combustor was supplied with primary air, secondary air, and fuel gas separately through the ducts, three values of the pressure loss were obtained for any given condition.

Losses are expressed as

$$\left(\frac{\Delta P}{P}\right)_{pa}, \left(\frac{\Delta P}{P}\right)_{sa}, \left(\frac{\Delta P}{P}\right)_{g} = \frac{\text{total pressure loss of the combustor}}{\text{total pressure at the combustor entry}}$$

where

$\left(\frac{\Delta P}{P}\right)_{pa}$ = pressure loss of primary air (per cent)

$\left(\frac{\Delta P}{P}\right)_{sa}$ = pressure loss of secondary air (per cent)

$\left(\frac{\Delta P}{P}\right)_{g}$ = pressure loss of fuel gas (per cent)

Figure 6 shows each pressure loss for burner C as expressed in combustion efficiency. The values for losses of primary air and fuel gas with the other burners correlate to Figure 6, and are obtained by multiplying the values in Figure 6 by the values in Table 2. Pressure losses of secondary air were virtually the same for all burners. The temperature of the flame tube was measured mainly by irreversible thermocolor and was below 500°C under all experimental conditions, except for burner G where the flame tube became dark red for a high specific heat release.

Taking into consideration the three points of stable combustion region, combustion efficiency, and pressure loss, we can conclude that burners C, D and E give the best performance as regards the rapid combustion of low grade gaseous fuels. These burners could find application in gas turbine design.

REFERENCE

1. HERSHEY, A. E.: Joint Conference on Combustion, Section 5, Gas Turbine, 1955.

116

SIMILITUDE STUDY OF IDEALIZED COMBUSTORS

By E. C. WOODWARD

1. Introduction

The intense interest one finds directed toward studies of similitude is well justified. A theory of similitude verified by experiment would be most useful in designing new combustors on the basis of experience with old ones, in comparing the performance of different combustors, and in the model testing of large combustors. Some progress in this field of scaling and similitude in systems involving chemical reactions has been made in recent years.[1, 2, 3, 4, 5] More recent treatments, in the form of general review studies, clearly define the currently accepted laws of similitude as well as emphasize the great need for more immediate experimental investigation in the scaling of both liquid and gaseous fired systems.[6, 7, 8, 9, 10, 11 a]

Gas turbine combustor development has in the past usually been by "trial and error" methods and has been greatly hindered by the lack of any effective knowledge of a scaling technique. The problem of scale effect in combustion chambers has become more acute recently with the introduction of large annular chambers which demand tremendous test facilities for full-scale testing. The economic factors concerned with full-scale testing quickly reach staggering proportions.

In short, most workers in the combustion field, in both jet and rocket propulsion, are quick to concur on the very great need for scaling techniques based on theoretical and experimental approaches.

Basically, this study is experimental in nature. Data were taken for two classes of idealized

[a] Since preparation of this paper, there has come to the author's attention the recent work of Longwell and Weiss on experimental "can" type combustors, in which some attention was directed to similitude considerations. Reference: Jet Propulsion, September, 1956.

combustors, each class containing three geometrically similar combustors of different diameters. The primary object of the study described herein was to check theoretically predicted scaling correlation parameters.

2. Theoretical Concepts

It has been shown by Way[12] and others that for geometrically similar combustors, operating on the same fuel at the same inlet temperature and having gaseous fuel injection, the factors that would be expected to play a role in determining the behavior of the combustor are:[b] W_f/W_a = fuel-air ratio; uL/ν = flow Reynolds number; $\Delta t_2/\Delta t_1$ = reaction time to residence time ratio.

It is pointed out by Way that the combustion efficiency, η, for a combustor operating as described above, may be considered a dependent variable and expressed as a function of the three above dimensionless parameters.

$$\eta = \varphi(W_f/W_a\ ,\ Re,\ \tau) \tag{1}$$

Here, $Re = uL/\nu$ and $\tau = \Delta t_2/\Delta t_1$.

If an average reaction rate, $\overline{U}$, in the reaction zone of the flame front is assumed proportional to the density raised to some power, we may say

$$\overline{U} = c\rho^n \tag{2}$$

where ρ is the mixture density and c depends on inlet temperature and mixture conditions; then n, in this instance, could be considered as an "effective over-all reaction order." In a combustor, a reaction time factor can be defined as $\rho/\overline{U}$ which, by Equation (2), is

$$\Delta t_2 = \frac{\rho}{\overline{U}} = \frac{1}{c\rho^{n-1}} \tag{3}$$

A residence time factor may be set proportional to L/u such that the reaction time to residence time ratio, τ, may be written

$$\tau = \frac{c'u}{L\rho^{n-1}} \tag{4}$$

where c' is a new proportionality constant.

[b] Certain other factors such as Schmidt number, Prandtl number, and Mach number would also enter, but these are either essentially constant or, in the case of Mach number, of negligible effect at moderate velocities. Other ratios such as ratio of scale factor to quenching distance or flow velocity to burning velocity are shown to be redundant.

Clearly, τ may be expressed in terms of variables which could be measured directly. Assuming the longitudinal combustor length to be proportional to the radial combustor dimension (the diameter, D), τ may be expressed as proportional to the mass flow, combustor volume, and combustor pressure, P, as

$$\tau = \frac{c''W_a}{P^nD^3} \tag{5}$$

where c'' is a new proportionality constant and W_a is the mass flow of primary air.

Therefore, for a geometrically similar family of combustors operating at a constant inlet temperature, at constant fuel-air ratio, on the same fuel and having gaseous fuel injection, the combustion efficiency becomes

$$\eta = \psi(Re,\ W_a/P^nD^3) = \psi(Re,\ \beta) \tag{6}$$

To insure the same level of performance of a large combustor as for a small combustor, the two should be compared at conditions of thermodynamic similitude. This implies, in addition to the stipulations previously covered, constancy of the Reynolds number and time ratio, τ, or, since τ is proportional to β,

$$Re_1 = Re_2 \text{ and } \beta_1 = \beta_2 \tag{7}$$

where subscripts 1 and 2 refer to the two combustors in question. Suppose now $L_2 = L_1\alpha$, then

$$\frac{u_1\rho_1}{u_2\rho_2} = \alpha \qquad \text{and} \qquad \frac{u_1}{u_2} = \frac{1}{\alpha}\left(\frac{\rho_1}{\rho_2}\right)^{n-1} \tag{8}$$

It follows that

$$\frac{\rho_2}{\rho_1} = \alpha^{-2/n} \qquad \text{and} \qquad \frac{u_2}{u_1} = \alpha^{(2-n)/n} \tag{9}$$

Equation (9) has been suggested by other investigators and sometimes appears as

$$\frac{P_m}{P_p} = \left(\frac{D_m}{D_p}\right)^{-2/n} \qquad \text{and} \qquad \frac{u_m}{u_p} = \left(\frac{D_m}{D_p}\right)^{(2/n)-1}$$

where m refers to "model" and p to "prototype."

The objects of this similitude study are to check the validity of Equation (6) and to explore the character of the functional relation which is represented by Equation (6) under the stipulations: geometric similitude; constant fuel-air ratio; burning a given fuel; gaseous injection; moderate Mach number; and a constant inlet temperature.

3. Experimental Test Equipment. Phase I

Construction details of the similitude test passage and the idealized "can" type combustors used in the first phase of this investigation are shown in Figures 1 and 2.

Reference to Figure 1 shows the fluid flow paths, method of fuel injection, combustor location, etc. By varying the per cent of open area of the register, any desired fraction of the total air supply could be selected to serve as the primary air. The ignition of the homogeneous fuel-air mixture was accomplished with a standard model airplane type spark plug. A mixing baffle was incorporated, as shown, to help assure rapid quenching of the combustion products at the combustor exit by the cooling air (remainder of the total air supply not used as primary air).

The quenched combustion products pass directly to the thermocouple measuring section containing six couples at "equal area" positions.

The fuel used was commercial propane having a guaranteed composition of a minimum of 95 per cent propane with the remaining gases being ethane and butane.

4. Experimental Test Program. Phase I

Basically, the test program consisted of two parts designed to investigate the detailed character of Equation (6). One part was the investigation of the effect of the time ratio, τ (or the proportional variable, $\beta = W_a/P^nD^3$), on the combustion efficiency, η, at various values of the flow Reynolds number. The other part was the investigation of the effect of the Reynolds number on the combustion efficiency for various values of the time ratio, W_a/P^nD^3. The pressure, P, used in the time ratio is that measured just upstream of the combustor and designated P_c on Figure 1. Throughout this paper the Reynolds numbers are based on cold flow primary quantities and the diameter of the combustor.

At the outset, it was decided to operate at a primary fuel-air ratio of 0.0545 and a constant inlet temperature of approximately 550°R.

The methods used in obtaining the significant data were rather straight forward. For the effect of the time ratio on combustion efficiency, a given diameter combustor was operated at a given primary mass flow rate over a range of absolute combustor pressures (constant Reynolds number, as the product $Du\rho$ = constant). Families of curves of η versus P were obtained with W_a serving as the parameter. Sufficient quantities of secondary air were supplied, when possible, to assure reasonable outlet temperatures. The operating range of a particular combustor was generally limited by one of two things: the combustor stability limit; or the limitation imposed by the flow area range of the control register. In respect to this latter point, conditions arose where one could not arrive at a desired primary air rate

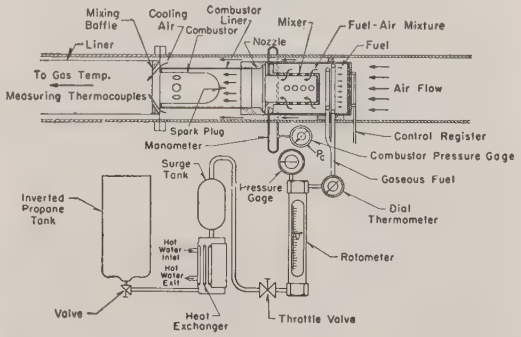

FIG. 1. Similitude test facility and instrumentation—Phase I.

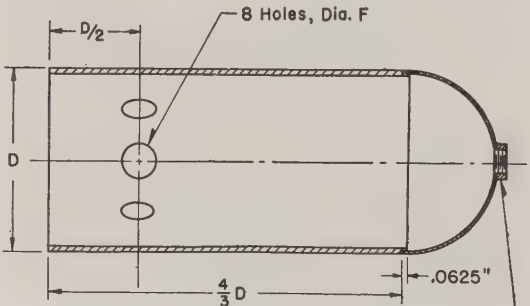

Combustor	D	4/3 D	F
1	1 1/2"	2"	3/8"
2	3"	4"	3/4"
3	4"	5 1/3"	1"

FIG. 2. Similitude combustor details—Phase I.

and combustor pressure and still be able to supply sufficient secondary air. This condition was often evident in testing the 4-in. diam combustor.

Combustion efficiency was computed by means of a heat balance. The data described above were correlated, by means to be described later, to predict the effect of the time ratio, β, on the combustion efficiency, η, for two values of the Reynolds number. In changing from one combustor diameter to another at constant Reynolds number, some decision had to be made about the

choice of the new operating conditions. For simplicity, the points at which to operate were chosen on the basis of an assumed n value of two. Thus, if the combustor size were halved, velocity

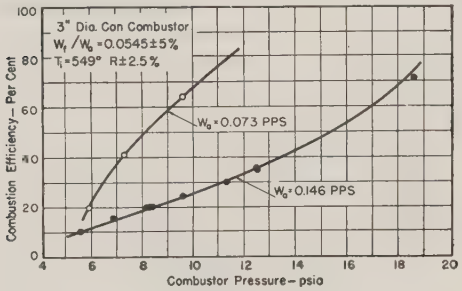

FIG. 3. Data from 3-in. diameter combustor—Phase I.

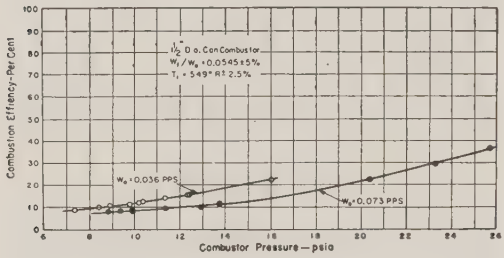

FIG. 4. Data from 1½-in. diameter combustor—Phase I.

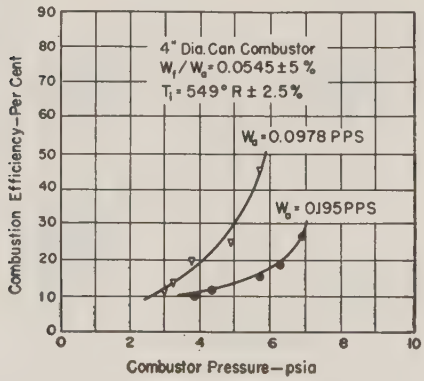
4" Dia. Can Combustor
W_f / W_a = 0.0545±5%
T_i = 549° R ± 2.5%
W_a = 0.0978 PPS
W_a = 0.195 PPS
Combustion Efficiency—Per Cent
Combustor Pressure—psia

FIG. 5. Data from 4-in. diameter combustor—Phase I.

was held constant and the pressures used were double those used in the previous (larger) combustor. This led to a satisfactory test range for operation. The actual β values for the new combustor could be calculated corresponding to the most realistic n value.

The data for the effect of Reynolds number on combustion efficiency were obtained in a similar manner. Families of curves of η versus Re were obtained with the time ratio, β, serving as parameter. When changing from one combustor to another, the approximate scaling procedure already described was followed to arrive at the proper ranges for the operating variables.

5. Discussion of Results. Phase I

The basic data, combustion efficiency versus combustor pressure, for the three combustors used in the first phase of this investigation are shown in Figures 3 to 5.

Perhaps the major observation to be made from Figures 3 to 5 is that, as one may suspect, the rate of change of combustion efficiency with combustor pressure increases rapidly as the Reynolds number is decreased.

It is worthwhile mentioning at this point that the data for the 3-in. diam combustor were taken before importance was attached to the possibility of a long flame "tail" extending from the combustor exit, or the possibility of flashback or burning in the region upstream of the combustor. If a flame tail were present, combustion efficiency would depend somewhat on the ratio of cooling air to primary air, as well as on β and Re, and this ratio was not always closely controlled in the Phase I tests. If flashback burning occurred, it would be reflected as a higher η value. Such occurrences could, therefore, give misleading results in correlations of η with β and Re. To check on these points, a small observation port was installed just downstream of the combustor exit, and a thermocouple was installed upstream of the combustor. In the testing of the 1.5-in. and 4-in. diam combustors, flame "tails" of various lengths were observed. It was not always possible to reduce these due to flow limitations. Rather than attempt a complete redesign of the quenching section in the middle of the project, it was decided to simply regard the flame "tail" as part of the combustion process under observation. Lack of close control of the ratio of cooling air to primary air could conceivably have some effects, but they are felt to be of a secondary magnitude. With the added thermocouple present upstream of the combustor and a revised "light-up" procedure, it was possible to operate without flashback.

The low efficiencies exhibited on Figures 3 to 5 strongly suggest that a large portion of the fuel-air mixture supplied to the combustor passes directly downstream and is quenched with little, if any, opportunity to burn.

To correlate the effect of the time ratio, β, on

the combustion efficiency, η, the most probable curve was calculated for the data points (for a given Reynolds number) by the method of "least squares." Curves were computed for various n values between 1.5 and 2.0 for Reynolds numbers of 30,000 and 60,000. The n value yielding the curve of minimum deviation (rms) was found to be 1.64 for both Reynolds numbers. The calculated curve was of the form

$$\eta = a\sqrt{|C|}\beta \exp(-C\beta^2) \qquad (10)$$

where a and C are constants determined in the solution of "least squares." For the n value of 1.64, the rms deviation was less than 6 per cent for both Reynolds numbers.

It is significant to mention here that the "best n value" reported to date for hydrocarbon combustion is 1.8. This value was determined by Longwell and Weiss[13] with their "homogeneous spherical reactor." Despite the shortcomings of the test passage already discussed, it is encouraging that the experimental data contained herein would predict a value of n so close to 1.8. It is felt that human judgment in curve fitting has been reduced to a minimum in the present treatment, whereas this factor was present to some degree in the work of Longwell and Weiss.[13]

Figures 6 and 7 contain the data for Reynolds numbers of 30,000 and 60,000, respectively. The combustion efficiency is shown plotted versus the time ratio for $n = 1.64$. The curves shown are "faired in."

Concurrent with the calculation of the best n value, data were taken for the effect of Reynolds number on combustion efficiency. Since, originally the exact value of n was unknown, these tests were made for two values of W_a/P^nD^3 for two arbitrarily chosen n values of 1.8 and 2.0. It is perhaps more instructive to consider these data on the basis of $n = 1.64$. The data obtained for constant β with $n = 1.8$ have been calculated and plotted for $n = 1.64$ on Figure 8. Although the data of Figure 8 are not for two constant values of W_a/P^nD^3, the trend exhibited in each case is sufficient evidence to imply that over the Reynolds number range investigated changes in Reynolds number do not appreciably affect flow or combustion patterns in the burner.

The data of Figures 6, 7, and 8 may be combined to show the combustion efficiency correlation expected from Equation (6). This three dimensional plot is shown on Figure 9.

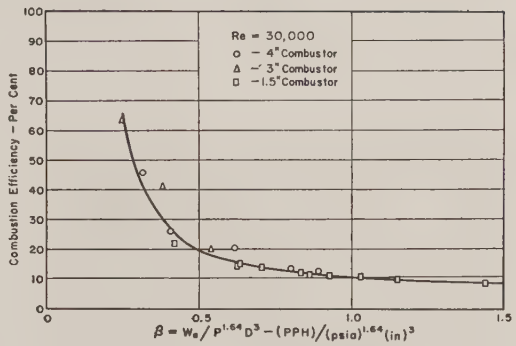

FIG. 6. Variation of combustion efficiency with $W_a/P^{1.64}D^3$ for Re = 30,000—Phase I.

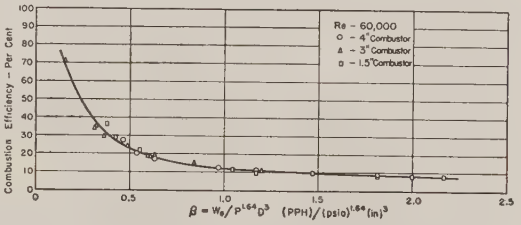

FIG. 7. Variation of combustion efficiency with $W_a/P^{1.64}D^3$ for Re = 60,000—Phase I.

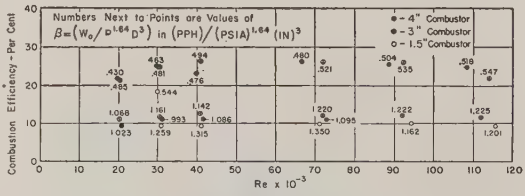
Numbers Next to Points are Values of
β=(Wa/P^1.64 D^3) in (PPH)/(PSIA)^1.64 (IN)^3
• - 4" Combustor
• - 3" Combustor
o - 1.5" Combustor
Combustion Efficiency - Per Cent
Re x 10^-3

FIG. 8. Variation of combustion efficiency with Reynolds number for various time ratio (β) values—Phase I.

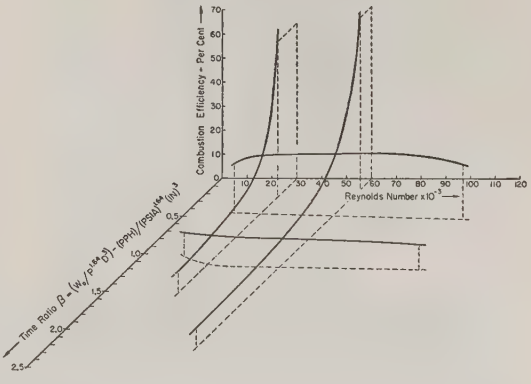

FIG. 9. Combustion efficiency correlation: gas fired combustors, fixed fuel-air ratio, fixed inlet temperature, geometric similarity—Phase I.

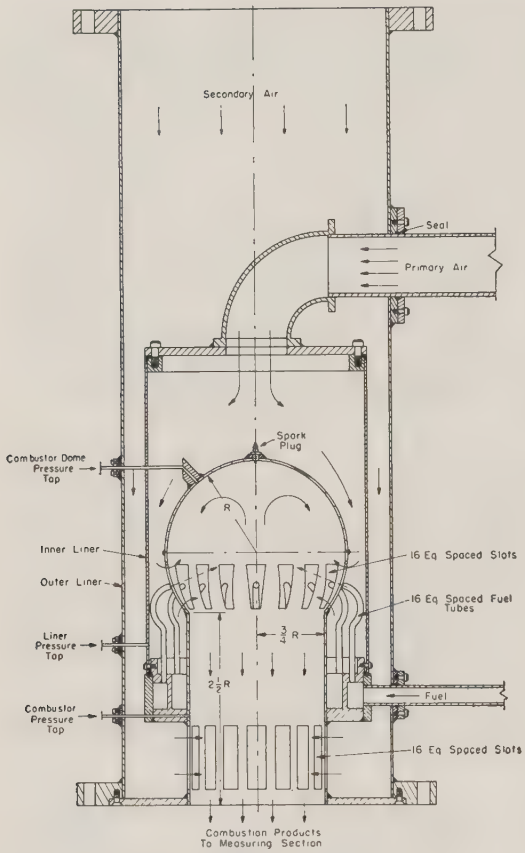

FIG. 10. Similitude test passage—Phase II.

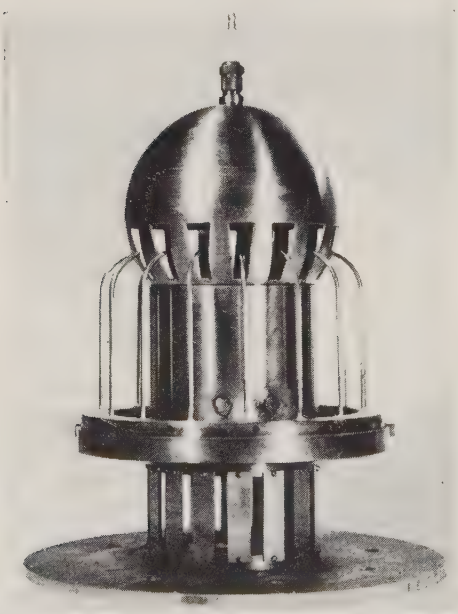

FIG. 11. Photograph of the 5.89-in. diameter spherical dome combustor and fuel injection tubes—Phase II.

6. Conclusions. Phase I

The experimental data from this phase of the combustor similitude studies permit the following to be concluded about a geometrically similar family of gaseous-fired combustors operating at a constant inlet temperature and at a constant fuel-air ratio of thoroughly premixed reactants:

(1) Combustion efficiency correlates very well with a modified time ratio (reaction time to residence time ratio) of W_a/P^nD^3.

(2) For the combustors investigated, the most probable effective reaction order, n, for propane-air combustion is between 1.6 and 1.7 with 1.64 appearing to yield the best data correlation.

(3) The effect of Reynolds number on combustion efficiency appears to be very slight over the range 30,000 to 100,000 for the particular combustors investigated, showing a preponderant influence of residence time:reaction time ratio.

7. Experimental Test Equipment. Phase II

Details of the similitude test passage and the idealized spherical dome type combustors used in the second phase of this investigation are shown in Figures 10 and 11. The configuration shown in Figure 10 has several advantages over that employed in the first phase. Some of these advantages are: (a) completely independent control of primary and secondary air permits a wider choice of flow conditions; (b) fuel injection takes place at a point such that any flashback is impossible; (c) a certain degree of diffusion flame burning will be present, owing to fuel jets injecting fuel directly into the burner. The results will, therefore, provide a check of theoretical concepts relating to similitude in diffusion burning systems; (d) better over-all mixing between products and fresh mixture is expected as well as better recirculation patterns because of the radial type flow of the fuel jets and primary air jets; (e) more combustor volume has been made available before the addition of quenching (secondary) air. This should raise the combustion efficiencies to more realistic values; (f) the secondary air is added in such a manner that much better quenching is expected, giving a sharp cut-off to combustion. This should reduce or eliminate the undesirable "flame tail"; and (g) more area is available for the recirculating products in the upstream dome (spherical section) to turn and pass downstream. It is believed that this will encourage more recirculation in the upstream end and will

cause much less of the fresh mixture to flow directly downstream.

Three different diameter (spherical dome diameter) combustors were investigated, the diameters being 5.89, 3.90, and 1.95 in. Geometric similarity was everywhere preserved through careful construction of the combustors.

The fuel used in this phase, as in Phase I, was commercial propane.

8. Experimental Test Program. Phase II

The test program for the second phase of the investigation was similar in most respects to that employed in the first phase. However, rather than attempt a series of tests for the effect of Reynolds number on combustion efficiency for various values of the time ratio, W_a/P^nD^3, it was decided to perform several sets of tests on the effect of the time ratio on the combustion efficiency for several values of the Reynolds number. These results would permit one to "cross-plot" the effect of Reynolds number on combustion efficiency for several constant values of the time ratio. These two sets of results would be sufficient to permit the determination of another three dimensional plot similar to that shown as Figure 9.

The pressure, P, used in the time ratio is that measured on the combustor dome (Fig. 10). The second phase was conducted with a primary fuel-air ratio, f/a, of 0.040 and an inlet temperature, T_i, of 595°R. Throughout this phase the ratio of secondary (quenching) air, W_n, to primary air was maintained at a value of 2.0.

The actual method of conducting the tests and of changing conditions from one combustor to another is the same as previously described under Phase I.

A few tests were made to see what effect changes in fuel-air ratio would have on the combustion efficiency.

9. Discussion of Results. Phase II

The basic data from the 5.89-in. and 3.90-in. diam combustors are shown in Figures 12 and 13. Insufficient data were obtained from the 1.95-in. diam combustor to present in this form. The difficulties involved in maintaining the low mass flows and high system pressures necessary to test the 1.95-in. diam combustor over the desired range of Reynolds numbers forced a curtailment of the test program. The several points which were obtained from the 1.95-in. diam combustor are used in the eventual determination of the three dimensional representation of Equation (6), however.

From Figure 12, one may see that the combustor is relatively insensitive to changes in the primary fuel-air ratio. However, the results indicate that the combustor operates as though it receives a fuel-rich mixture compared to the measured fuel-air ratio supplied. This would be expected since the type of fuel injection em-

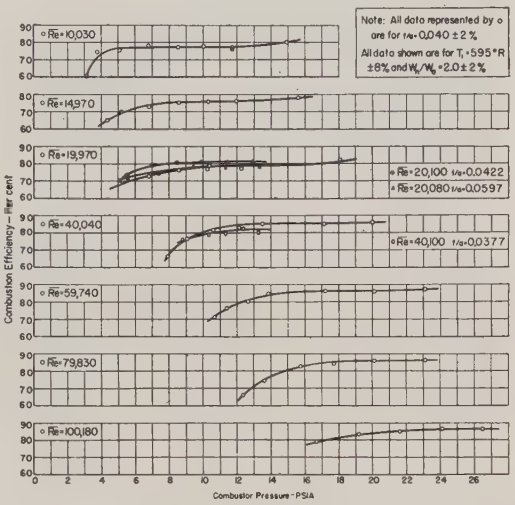
Note: All data represented by ○ are for f/a=0.040 ± 2 %
All data shown are for T_i = 595°R ±8% and W_n/W_p = 2.0 ± 2 %
○ Re=10,030
○ Re=14,970
○ Re=19,970
○ Re=20,100 f/a=0.0422
△ Re=20,080 f/a=0.0597
○ Re=40,040
○ Re=40,100 f/a=0.0377
○ Re=59,740
○ Re=79,830
○ Re=100,180
Combustion Efficiency – Per cent
Combustor Pressure - PSIA

FIG. 12. Data from 5.89-in. spherical dome combustor—Phase II.

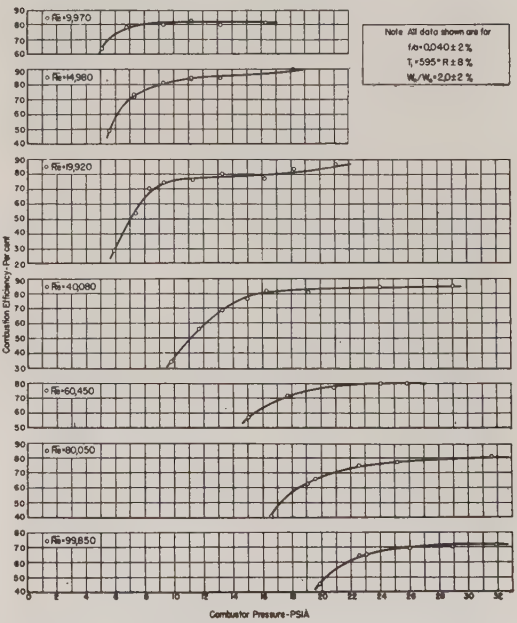

FIG. 13. Data from 3.90-in. spherical dome combustor—Phase II.

ployed may well cause local fuel-rich conditions, which would not exist were the combustor supplied with a completely homogeneous fuel-air mixture. These data on changes in fuel-air ratio are too few to permit any generalizations concerning the effects of these changes on the three dimensional representation of Equation (6).

The method of "least squares" was again used to correlate the effect of the time ratio, β, on the

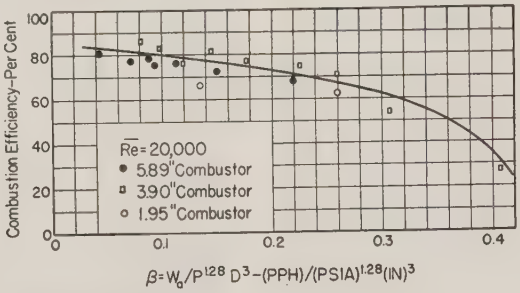

FIG. 14. Variation of combustion efficiency with $W_a/P^{1.28}D^3$ for Re = 20,000—Phase II.

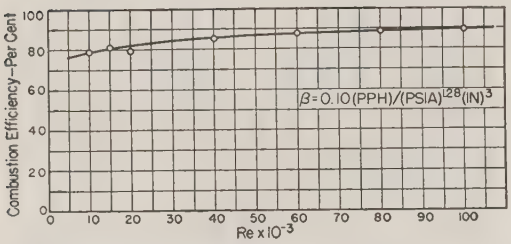

FIG. 15. Variation of combustion efficiency with Reynolds number for a constant value of the time ratio β—Phase II.

combustion efficiency, η. The most probable curve for the data of a given Reynolds number was computed for n values of 1.2, 1.3, and 1.4 for each Reynolds number investigated between 10^4 and 10^5. The n value yielding the minimum "rms" deviation was found for each Reynolds number. These seven n values yielded an average n value of 1.28. The calculated curve was of the form

$$\eta = a_0 + a_1\beta + a_2\beta^2 + a_3\beta^3$$

where the a's are constants determined in the solution of "least squares." A typical plot of the data from all three combustors tested, at a Reynolds number of 20,000, is shown in Figure 14 for an n value of 1.28. The curve shown is "faired in."

It was previously mentioned in this paper that the "best n value" reported for hydrocarbon combustion is 1.8. However, some recent work by Hottel, Williams and Baker[14] using similar equipment to that of Longwell and Weiss predicts an n value of 1.0 to 1.2. Recent work by White and Lewis[15, 16] predicts an n value of 1.5 to 4.0. A most significant point to be remembered is that here we are speaking of an effective overall reaction order, n. Clearly, then, anything which alters the various chemical reactions (each with its own reaction order) would reflect itself

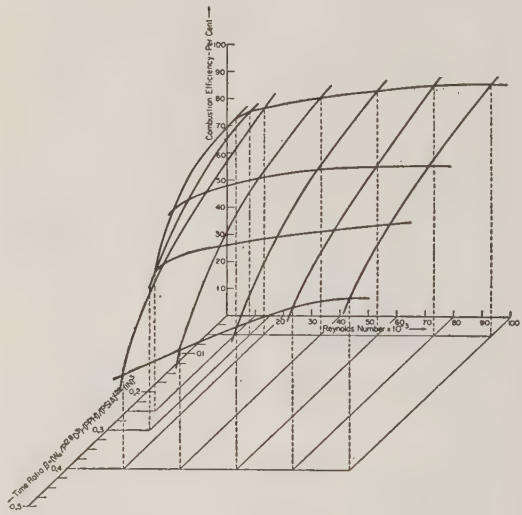

FIG. 16. Combustion efficiency correlation: gas fired combustors, fixed fuel-air ratio, fixed inlet temperature, geometric similarity—Phase II.

in the ultimate value of n determined. Is it not within the realm of possibility that such factors as geometry and fuel injection methods could easily effect changes in the pattern of reaction kinetics? The present tests of Phase II, when compared to those of Phase I, strongly suggest that it would be unrealistic to expect a unique value of n to be determined from widely different experimental approaches.

A typical "cross-plot" of the effect of Reynolds number on combustion efficiency is shown

in Figure 15 for a constant value of β of 0.10. The three dimensional representation of Equation (6) for the spherical dome type combustors is seen in Figure 16. The dependent and interdependent effects of changes in Reynolds number and/or the time ratio on the combustion efficiency may be clearly seen from Figure 16.

At the close of this phase of the investigation some question was raised as to the accuracy of the temperature measurements obtained with bare thermocouples. Checks were made using aspirating type thermocouples. The results of these checks indicate that the measured temperatures could be off by as much as five per cent This difference in readings, however, was due mostly to circumferential temperature gradients and not to basic differences in the readings of the bare and the aspirating thermocouples.

10. Conclusions. Phase II

The experimental data from this phase of the combustor similitude studies permit the following to be concluded about a geometrically similar family of diffusion type gaseous-fired combustors operating at a constant inlet temperature and at a constant fuel-air ratio:

(1) Combustion efficiency correlates very well with a modified time ratio (reaction time to residence time ratio) of W_a/P^nD^3.

(2) For the diffusion type combustors investigated, the most probable effective reaction order, n, for propane-air combustion is between 1.0 and 1.4 with an average value of 1.28 appearing to yield the best data correlation.

(3) The effect of Reynolds number on combustion efficiency appears rather pronounced over the Reynolds number range 10,000 to 100,000 for the particular combustors investigated. The indications are that an extrapolation of these results to Reynolds numbers above 100,000 would show a diminishing effect of Reynolds number and a preponderant influence of residence time:reaction time ratio as would be expected.

(4) The results described herein indicate that the effective over-all reaction order may depend strongly on geometric configuration and other factors.

Experiments as here described appear to yield results which should prove useful in future scaling predictions. They support the procedure of changing pressure and velocity, while testing a scaled model, in such a way as to simulate the performance of a prototype combustor and indicate the correct manner in which this should be done.

Acknowledgment

The writer gratefully acknowledges the many helpful comments of Dr. S. Way, Manager, Thermodynamics Section, throughout the project. The basic design of the similitude test passage used in Phase I was by Dr. E. A. DeZubay, formerly of these laboratories. Special thanks are due Mr. W. M. Rohrer, University of Pittsburgh, for his able assistance during Phase II. At various times during the course of this investigation, the writer was fortunate to have the aid of some student engineers in the performance of tests and the calculation of data, their names being: Mr. C. Miller, Mr. J. B. Hammer, Mr. R. R. Leyendecker, Mr. C. R. Price, and Mr. T. E. Lund.

REFERENCES

1. Damköhler, G.: Z. Elektrochem. *42*, 846 (1936).
2. Edgeworth-Johnstone, R.: *Trans.* Inst. Chem. Engr., *17*, 129 (1939).
3. Bosworth, R. C. L.: *Trans.* Faraday Soc., *43*, 399 (1947).
4. Wolfhard, H. G.: Z. tech. Phys., *24*, 206 (1943).
5. Putnam, A. A., and Jensen, R. A.: *Third Symposium on Combustion, Flame and Explosion Phenomena*, p. 89. Baltimore, The Williams & Wilkins Co., 1949.
6. Stewart, D. G.: Paper presented at the Second AGARD Combustion Colloquium, Liêge, Belgium, December, 1955.
7. Bragg, S. L., and Holliday, J. B.: Paper presented at the Second AGARD Combustion Colloquium, Liêge, Belgium, December, 1955.
8. Way, S.: Paper presented at the Second AGARD Combustion Colloquium, Liêge, Belgium, December, 1955.
9. Penner, S. S.: Tech. Rep. No. 8, California Institute of Technology, Guggenheim Jet Propulsion Center, November, 1954.
10. Crocco, L.: Discussion of paper by C. C. Ross at the Second AGARD Combustion Colloquium, Liêge, Belgium, December, 1955.
11. Probert, R. P.: Paper presented at the Joint Conference on Combustion, Am. Soc. Mech. Engrs. and the Inst. of Mech. Engrs., Boston, Mass., June, 1955.
12. Way, S.: Westinghouse Research Laboratory Report 60-8-05-24-R5, June, 1954.

13. Longwell, J. P., and Weiss, M. A.: Ind. Eng. Chem., *47*, 1634 (1955).
14. Hottel, H. C., Williams, G. C., and Baker, M. L.: *Sixth Symposium (International) on Combustion.* New York, Reinhold Publ. Corp., 1952.
15. White, S. W., and Lewis, W. G. E.: National Gas Turbine Establishment Report No. R.165, May, 1955.
16. White, S. W.: National Gas Turbine Establishment, Hants, England, 1956, private communication.

117

SOME APPLICATIONS OF COMBUSTION THEORY TO GAS TURBINE DEVELOPMENT

By V. W. GREENHOUGH and A. H. LEFEBVRE

Introduction

The development of combustion systems for the gas turbine is governed to a large extent by the rate at which new designs can be tested. Most of the initial testing can be carried out on laboratory rigs, although with the gradual trend towards higher operational altitudes the demand for larger air flows at lower pressures is becoming increasingly difficult to meet. To assist in this problem, combustion theory is being used to provide (a) techniques which allow high altitude conditions to be simulated on rigs operating at relatively high pressures, usually atmospheric; (b) correlating parameters whereby test data obtained over a restricted range may be used to predict combustion performance at any other operating condition.

Two theoretical approaches have been made, the first based on a burning velocity concept and the second on homogeneous reaction rate theory.

Introduction to Burning Velocity Theory

The process of combustion in a gas turbine is usually one in which liquid fuel is injected into a region of flow reversal and combustion is initiated after a time interval during which partial or complete evaporation is achieved. Analysis of the factors governing the rate at which chemical enthalpy of fuel is liberated as heat can only proceed from a knowledge of the form and structure of the burning zone and an understanding of the mechanism whereby a progressive explosion is maintained. However, although the associated processes of atomization and fuel evaporation are largely understood, most theoretical and experimental studies of flame propagation have so far been confined to plane combustion waves and premixed gases. Much of the data obtained could be applied directly to gas turbine combustion systems if the fuel were assumed to be completely vaporized at entry to the burning zone, an assumption partly justified by the experiments of Burgoyne and Cohen[1] in which flame propagation through fuel/air mists containing droplets 10 μ in diam was observed to proceed at the same rate as for homogeneous mixtures.

A more serious objection to the use of data obtained by burner methods has been that measured burning velocities have always been much too low to account for the high rates of heat release attained. This difference, however, can be fully explained by the important influence of turbulence on the rate of flame propagation. From studies of Bunsen burner flames Damkoehler[2] concluded that the effect of turbulence on burning velocity depends primarily on whether the scale of turbulence is small or large compared to the thickness of the flame front. He showed that the effect of small scale turbulence is to increase the transport processes within the burning zone, and derived the following expressions for turbulent burning velocity

$$\frac{S_t}{S_L} = \sqrt{\frac{\epsilon}{\nu}}$$

where S_t is the turbulent flame speed, S_L the laminar flame speed, ϵ the turbulent exchange

coefficient and ν the kinematic viscosity. Alternatively,

$$S_t = S_L\, k\, \sqrt{\mathrm{Re}} \tag{1}$$

where Re = Reynolds No. and k is a constant.

Of more practical importance, however, is the effect of large scale turbulence on flame propagation, since this could account for flame survival in the relatively high gas velocities in the reversal. It is generally agreed that large scale turbulence distorts or destroys the flame front and thereby increases its effective surface area and hence the burning velocity. The actual mechanism of this process is not yet fully established; the picture of flame propagation in a turbulent explosive mixture presented by Karlovitz[3] is used here but amended in the following manner. Instead of flame fronts propagating from small "volumina" at normal burning velocity it is assumed that individual flame fronts progress at a speed governed by the small scale turbulence in the approach stream. In the following analysis, therefore, the combustion zone is visualized as a region in which strong turbulence produces small volumina of gas which propagate with a burning velocity governed by the small scale turbulence present. Karlovitz's equation becomes

$$S_T = \sqrt{2S_t \cdot \bar{u}} \tag{2}$$

where u = rms value of fluctuating velocity.

ANALYSIS

We have

Heat supplied to combustion zone

$$= q.\ M.H.\ \text{[Chu/sec]} \tag{3}$$

Heat released in combustion

$$= \rho.A_f.S_T.C_p.\Delta T\ \text{[Chu/sec]} \tag{4}$$

Then

$$B = \frac{\rho A_f.S_T.C_p.\Delta T}{q.M.H}$$

and since

$$\frac{C_p.\Delta T}{q.H} = 1$$

$$B = \frac{\rho.A_f.S_T}{M} \tag{5}$$

Substitution for S_T in Equation (5) using Equations (1) and (2) and squaring gives

$$B^2 = \frac{2.k\rho^2.A_f^2.S_L.\bar{u}\ \mathrm{Re}^{0.5}}{M^2} \tag{6}$$

In the reversal

$$\mathrm{Re} = \frac{\mathrm{V}D\rho}{\mu} = \frac{M.D.}{A.\mu}$$

Viscosity varies little with pressure; its variation with temperature may be expressed as

$$\mu = k_1^2.T^{0.75}$$

Hence

$$\mathrm{Re} = \frac{M.D.}{k_1^2.A.T^{0.75}} \tag{7}$$

Large scale turbulence can be related to pressure loss in the form

$$\Delta P = \frac{\rho\bar{u}^2}{2.g.k_2.}$$

where k_2 = fraction of pressure loss promoting useful turbulence or

$$\bar{u} = \left[\frac{k_2.2g.\Delta P}{\rho}\right]^{.5} \tag{8}$$

The dynamic head

$$d = \frac{\rho\mathrm{V}^2}{2g.} = \frac{M^2}{2.\rho A^2} \tag{9}$$

Substituting in Equation (6) for Re and $\bar{u}$ from Equations (7) and (8) respectively and introducing d from Equation (9) gives

$$B^2 = \left(\frac{2k}{k_1}\right)\left(\frac{A_f^2.D^{0.5}}{A^{1.5}}\right)\left[\frac{\rho^2.S_L^2}{MT^{0.75}} \times \frac{k_2\Delta P}{d}\right]^{0.5} \tag{10}$$

For any given fuel, S_L depends only on equivalence ratio, inlet temperature and pressure. The effect of temperature is expressed in Semenov's equation but in a complex and unwieldy form.[4] Pressure dependence is related to reaction order by the equation

$$S_L \propto P^{(n-2)/2}$$

Equation (10) thus becomes

$$B^2 \propto [f(\phi)]\left(\frac{2k}{k_1}\right)\left(\frac{A_f^2D^{0.5}}{A^{1.5}}\right)\left[\frac{P^n[f(T_0)]}{M}\ \frac{k_2\,\triangle P}{d}\right]^{0.5} \tag{11}$$

and since $A_f \propto A$.

$$B^2/f(\phi) \propto \left[\frac{P^n[f(T_0)]A.D.}{M} \cdot \frac{k_2\Delta P}{d}\right]^{0.5} \quad (12)$$

Equation (12) relates combustion efficiency to the dimensions and pressure loss factor of the combustion system and to the operating conditions of pressure, temperature and air mass flow. For any individual system operating a fixed equivalence ratio Equation (12) reduces to

$$B \propto \left[\frac{P^n f(T_0)}{M}\right]^{0.25} \quad (13)$$

Equation (12) has been used to correlate experimental data on combustion efficiency obtained over a wide range of pressures, temperatures and air mass flows using various designs of combustion chamber. The best correlation was achieved using a value for n of 1.75.[5] The temperature dependence was found to vary according to the degree of vitiation incurred in preheating the entry air. In the absence of suitable experimental data an explanation for this effect was sought from reaction rate theory.

Reaction Rate Theory

Longwell and Weiss[6] consider a steady-state reactor into which unburned mixture is fed at a constant rate and is instantaneously mixed with all the other material within the zone. Burned material leaves the zone at a constant rate with a temperature and composition identical to that within the zone. On these and other assumptions Longwell has derived reaction rate equations for octane burning in air. The conventional gas turbine fuel is, however, kerosene; also in many practical combustion systems the air at entry is vitiated by products of combustion. Reaction rate equations for kerosene burning in air and/or combustion products are stated below. They relate to a reaction order of 1.75 as suggested from the burning velocity analysis.

LEAN MIXTURES

$$\frac{M}{VP^{1.75}} = \frac{C.\,(1-B)^{0.75}[1-\phi_1) - B(\phi_2-\phi_1)\,]}{T^{1.25}\exp E/RT\; B(\phi_2-\phi_1)^{0.25}\,[(85.7+6\phi_2) - 5(1-B)\;(\phi_2-\phi_1)]^1} \quad (14)$$

RICH MIXTURES

$$\frac{M}{VP^{1.75}} = \frac{C.(1-B)^{1.75}(\phi_2-\phi_1)^{.75}}{T^{1.25}\exp E/RT\; B[(67.7+24\phi_2) + (1-B)(18-23\phi_2+5\phi_1)]^{1.75}} \quad (15)$$

These equations describe the performance of a homogeneous reactor supplied with air and/or combustion products plus kerosene fuel of which a fraction (1-B) leaves the reactor unburned. ϕ_1 is the equivalence ratio of combustion processes occurring upstream of the reactor. It is assumed that any such process takes place with 100 per cent combustion efficiency. ϕ_2 is the over-all equivalence ratio.

A weakness of Equations (14) and (15) is that combustion performance is related to reaction temperature, T. In practical combustion systems this is a somewhat nebulous entity dependent upon, but not easily related to B, ϕ_1 and ϕ_2. It is clearly advantageous to obtain reaction rates in terms of the gas temperature at entry to the system since this is usually accurately known.

THE EFFECT OF AIR INLET TEMPERATURE ON REACTION RATES

In normal combustion chamber operation any increase in inlet air temperature above ambient which is achieved by compression and combustion performance is described by Equations (14) and (15) in which ϕ_1 is zero. The application of these equations is illustrated by reference to Figure 1 in which $\frac{M}{VP^{1.75}}$ is shown plotted against B for a stoichiometric mixture at various levels of inlet temperature. These calculated results are based on values for E/R and C of 21,000 and $8 \cdot 10^{14}$ respectively. It is observed that the peaks of the curves, corresponding to blowout, shift slightly towards lower values of B as the inlet temperature is increased. Their absolute values obey the relation

$$\left(\frac{M}{VP^{1.75}}\right)_{max} \propto \exp \frac{T_0}{340}$$

In Figure 2 calculated values of $\left(\frac{M}{VP^{1.75}}\right)_{max}$ are plotted against equivalence ratio for various inlet air temperatures ranging from 200 to 600°K. It has been shown[7] that all results can be ex-

pressed in the form

$$\left(\frac{M}{VP^{1.75}}\right)_{max} \propto \exp \frac{T_0}{b}$$

where b is a constant dependent only on ϕ. The variation of b with ϕ is described by the full line in Figure 3. From Figures 2 and 3 it is apparent that although absolute values of reaction rate decrease as the mixture strength is reduced their dependence on inlet air temperature is raised. Rich mixtures show a similar increase in temperature dependence as ϕ is increased above unity. This is illustrated in Figure 4 where $\left(\frac{M}{VP^{1.75}}\right)_{max}$, expressed as a ratio of its value at T_0 to that at 288°K, is shown plotted against T_0 for three values of ϕ, namely 0.5, 1.0 and 1.5.

The dotted line in Figure 3 is the result of more recent calculations by Herbert.[8] He relates b to ϕ by the empirical relation

$$b = 220\left(\sqrt{2} \pm \log_e \frac{\phi}{1.03}\right)$$

(where + refers to $\phi < 1.03$, and − to $\phi > 1.03$), the peak reaction rate having been found to occur at $\phi = 1.03$.

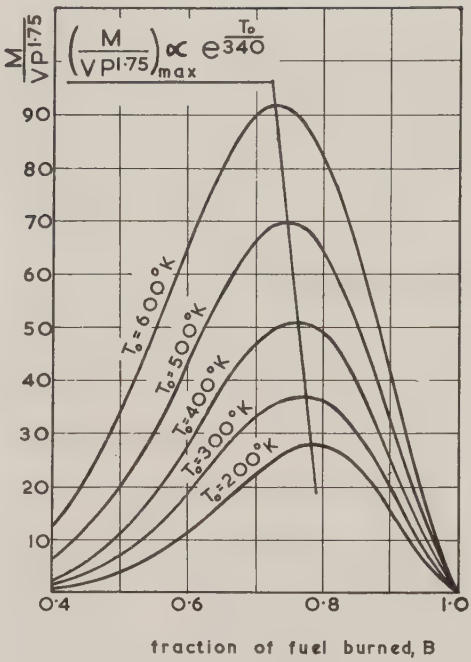

FIG. 1. Performance curves for a stoichiometric mixture.

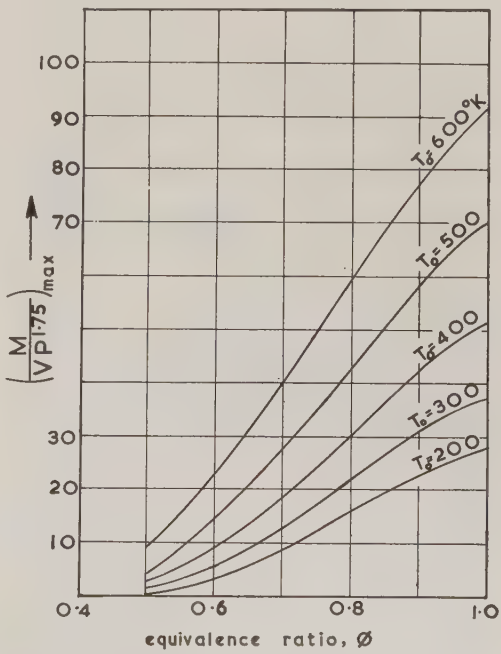

FIG. 2. Variation of air loading parameter with equivalence ratio.

THE EFFECT OF VITIATION ON REACTION RATES

Systems affected by vitiation include combustion chambers on rig test using a slave combustor to heat up the incoming air, and reheat systems where the entry air is contaminated by combustion products from the main engine.

Performance curves for a reheat system operating at $\phi_2 = 1$ are shown in Figure 5. They were obtained using Equation (14) and are based on an air temperature at entry to the engine of 15°C. The results are described by the above equation in which $b = 1660$. This high value of b emphasizes the relative insensitivity to jet pipe gas temperature of reheat gutter stability. This is further illustrated in Figure 6 where $\left(\frac{M}{VP^{1.75}}\right)_{max}$ is plotted against T_0 for three combustion systems: (a) A combustion chamber operating under normal engine conditions. In the primary zone $(\phi_2 - \phi_1) = 1.\phi_1 = 0$. (b) A combustion chamber on rig test with primary zone $(\phi_2 - \phi_1) = 1.\phi_1 = f(T_0 - 288)$. (c) A reheat system in which $\phi_2 = 1, \phi_1 = f(T_0 - 288)$. This corresponds to Figure 5.

The difference between Curves (a) and (b) represents the extent to which rig results are likely to prove pessimistic with regard to actual engine performance when testing is carried out

in vitiated atmospheres. It also explains why correlating parameters for combustion efficiency require a reduced temperature dependence when the inlet air is vitiated. Curves (a) and (b) both refer to a stoichiometric mixture. The difference between them is less for leaner mixtures; when $\phi = 0.5$ the two curves practically coincide.

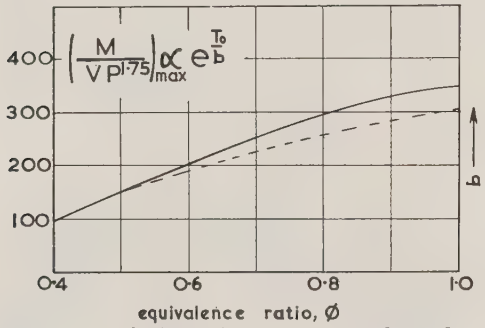

FIG. 3. Variation of temperature dependence with equivalence ratio.

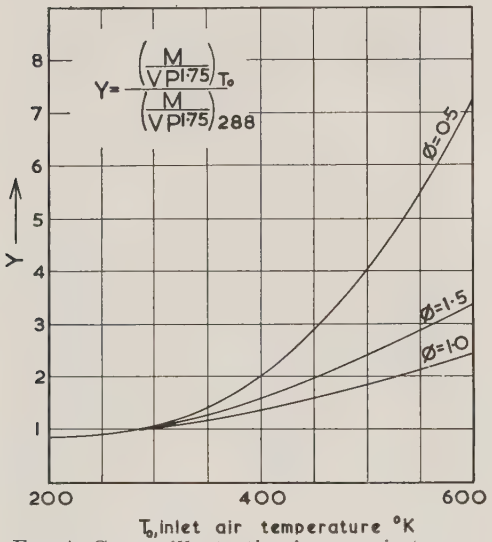

FIG. 4. Curves illustrating increase in temperature dependence as equivalence ratio departs from unity.

Experimental data on the effect of gas temperature on gutter stability in vitiated mixtures are provided by Barrère and Mestre.[9] Their results for a kerosene/air mixture (17.5 AFR) are plotted in Figure 7 and show reasonable agreement with the corresponding theoretical curve.

Comparison of Burning Velocity and Reaction Rate Theories

If the temperature dependence $f(T_0)$ in the burning velocity parameter is expressed in the

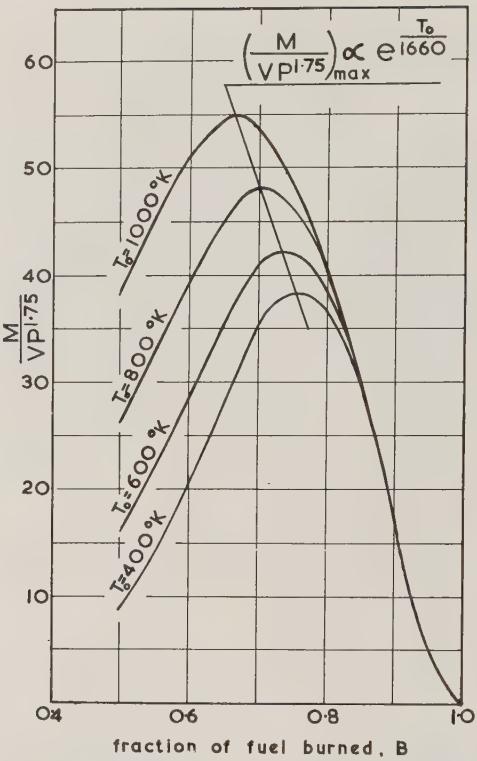

FIG. 5. Effect of inlet gas temperature on reheat performance.

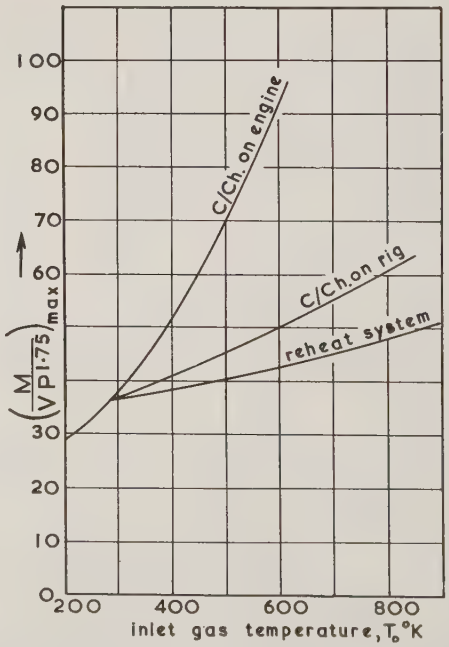

FIG. 6. Effect of inlet temperature on performance of three typical combustion systems.

exponential form exp T_0/b the performance equations become, for burning velocity

$$\frac{M}{P^{1.75} \exp T_0/bA.D.\frac{\Delta P}{d}} = f(\phi, B) \qquad (16)$$

for reaction rate

$$\frac{M}{P^{1.75} \exp T_0/b.V.} = f(\phi, B) \qquad (17)$$

Alternative forms of the above expressions are

$$\frac{U}{P^{0.75} D.T_0 \exp T_0/b.\frac{\Delta P}{d}} = f(\phi, B) \qquad (18)$$

and

$$\frac{U}{P^{0.75} D.T_0 \exp T_0/b} = f(\phi, B) \qquad (19)$$

respectively.

Thus the two theories yield parameters of almost identical form. This is hardly surprising since the same pressure and temperature dependence has been attributed to both. For many practical purposes, e.g., the correlation of experimental results of combustion efficiency obtained from a fixed combustion system or from geometrically similar systems, the two parameters are effectively the same. It is in the comparison of combustion systems of basically different design that the important differences between the two parameters emerge. In the burning velocity parameter the dimensions of the burning zone appear as AD as against V or AL (L = length of burning zone) in the reaction rate parameter. A more significant difference is the pressure loss factor in the burning velocity expression since this could explain the important effect of pressure loss on combustion performance which has been known qualitatively for some time. Confirmation of the pressure loss term is provided by Mestre.[10] He correlates experimental results on gutter stability with the equation,

$$\frac{2U}{P^{\alpha} D\, Cx.} = f(\phi)$$

which, since drag coefficient $C_x \propto \Delta P/d$, is a special case for constant T_0 of the more general Equation (18).

It may be considered that the pressure loss term in the burning velocity parameter makes it the more realistic, although final judgement on the relative merits of the two theories must await more detailed knowledge of the physical and chemical processes involved in the burning zone. In the meantime some insight into these processes is being gained from analyses of the performance of basically dissimilar combustion systems.

Application of Theory

A. TO CORRELATION OF COMBUSTION EFFICIENCIES

According to Equation (13) when experimental values of combustion efficiency are plotted against the parameter $\left[\frac{P^{1.75} \exp T_0/b}{M}\right]^{0.25}$ the points

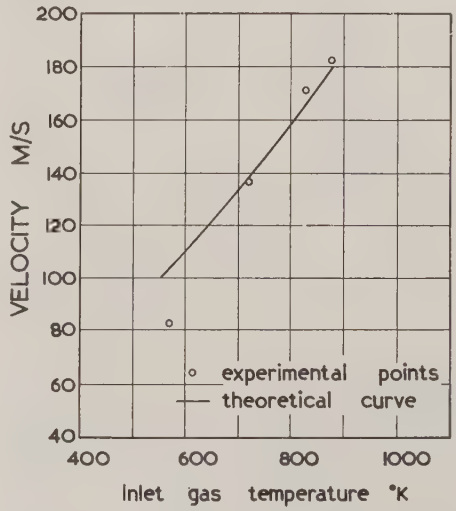

FIG. 7. Effect of inlet temperature on gutter blowout points. Comparison of theoretical curve and experimental results (9) for $\phi_2 - \phi_1 = 0.85$.

should fall on a straight line passing through origin of the graph. This is never achieved in practice for reasons which are best explained by reference to Figure 8. In this figure the two broken lines emanating from the origin represent primary zone performance as predicted by Equation (13) for two equivalence ratios. The line having the steeper slope represents a stoichiometric mixture. The other line is drawn for a leaner mixture, its reduced slope being due to a lower burning velocity. The upper limit to both lines is reached when all the fuel has been converted. At this stage the effective combustion efficiency is less than 100 per cent owing to losses by chemical dissociation of the combustion products. (The stoichiometric mixture has the higher loss because of its higher flame temperature.) The function of the secondary zone

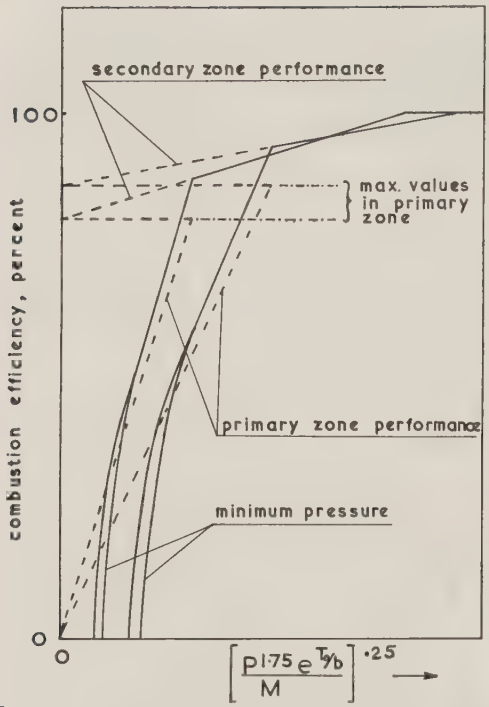

FIG. 8. Theoretical combustion efficiency curves.

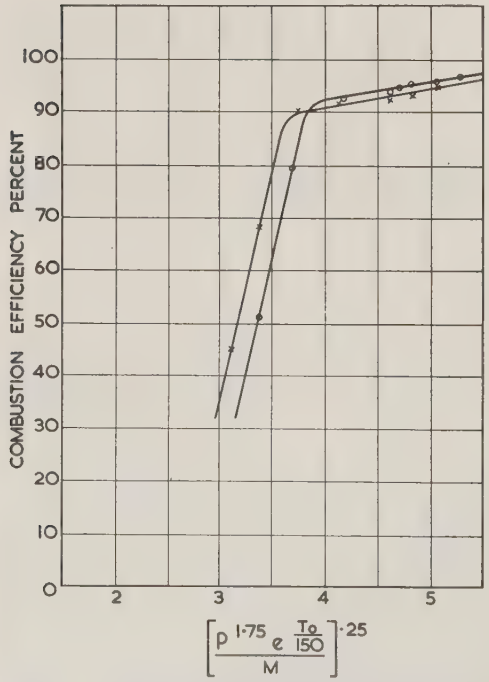

FIG. 9. Combustion efficiency correlation for a tubular combustion chamber at two equivalence ratios.

is to recover this dissociation loss by discreet addition of secondary air. Its performance is represented by the broken lines drawn from origins corresponding to the maximum combustion efficiency attained in the primary zone. The full lines in Figure 8 describe the combined performance of primary and secondary zones and should, therefore, represent the performance as actually measured in practice.

As the pressure is reduced it should be possible in theory to maintain a high combustion efficiency by reduction in mass flow. However, with falling gas pressure heat losses become increasingly significant and for any given combustion chamber there is a minimum pressure below which no combustion is possible. The effect of heat losses is indicated on the diagram by lines drawn for various pressures falling away from the overall performance curve to intercept the base line at finite values of

$$\left[\frac{P^{1.75} \exp T_0/b}{M}\right]^{0.25}$$

The characteristic features of Figure 8 are evident in Figure 9 in which experimental results of combustion efficiency are shown plotted against

$$\left[\frac{P^{1.75} \exp T_0/b}{M}\right]^{0.25}$$

for a tubular combustion chamber operating at two equivalence ratios. Figure 10 shows similar plots for tubo-annular and fully annular combustion chambers respectively. Quite often the best correlation is obtained using a value of b lower than the theoretical one. This is not necessarily a condemnation of the theory, it could also be due to maldistribution of fuel. Since both lean and rich mixtures are more sensitive to temperature than a stoichiometric mixture, when $\phi \simeq 1$ any unmixedness of fuel and air must inevitably decrease b. More experimental work is needed on the effect of inlet temperature for completely uniform fuel/air mixtures. If the theoretical relationship between b and ϕ could be definitely established then the value of b determined experimentally for a given combustor would indicate the degree of fuel/air mixing achieved.

The performance of various combustor designs is compared using Equation (16). The best design

is regarded as having the lowest value of

$$P^{1.75} \exp T_0/b \ A.D. \frac{\Delta P}{d}/M$$

at a stipulated combustion efficiency and equivalence ratio.

B. TO CORRELATION OF STABILITY DATA

There is ample evidence both in the literature and from our own results to show that stability data can be correlated by parameters of the form of Equation (18). Figure 11 shows reliable stability data from a tubo-annular combustor plotted as U against $P^{0.75}\ D$ for various air/fuel ratios and constant inlet temperature. According to Equation (18) these experimental results should plot as a straight line through the origin: they quite obviously do not. This figure cannot be entirely explained by heat losses or the use of an incorrect value of n. It is included here to demonstrate that although correlating parameters of the type derived herein are an invaluable tool they are by no means infallible. Their reliability will undoubtably improve as more data obtained under controlled experimental conditions are collated.

C. TO SCALING OF COMBUSTION SYSTEMS

The operating conditions at which a small scale combustion system should be tested to simulate the performance of the full size unit were first defined by Stewart in 1951.[11] He suggested that similarity might be achieved if both systems were to operate at the same gas velocity and temperature and obey the relation $P^{n-1}\ D$ = constant, a conclusion also reached in Equations (18) and (19). A further stipulation for constant Mach number and Reynolds number was that $n = 2$. It followed that if reaction kinetics required a different value of n then perfect aerodynamic similarity could not be attained. Furthermore, such factors as fuel particle size and penetration, heat losses and metal temperatures could not be expected to conform to the simple scaling law. However, at Stewart's suggestion some available experimental data relating to a one-third scale model reheat system were re-analyzed and found to correlate on the basis PD = constant, corresponding to a reaction order of 2.[12]

This reaction order, since definitely established for reheat scaling, is apparently inconsistent with

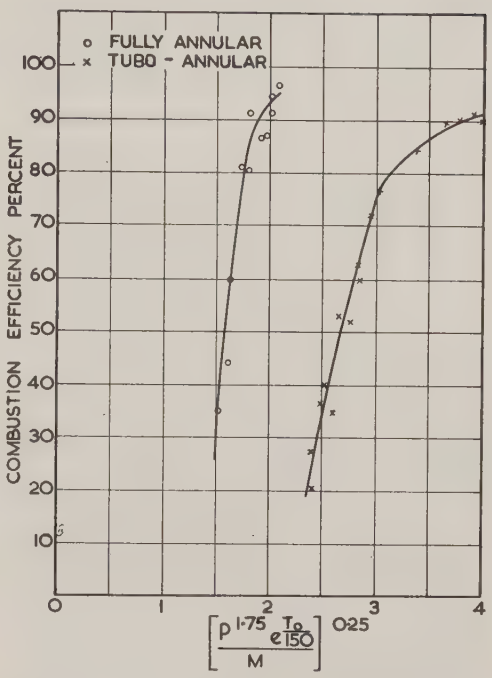

FIG. 10. Combustion efficiency correlations for fully annular and tubo-annular combustion chambers.

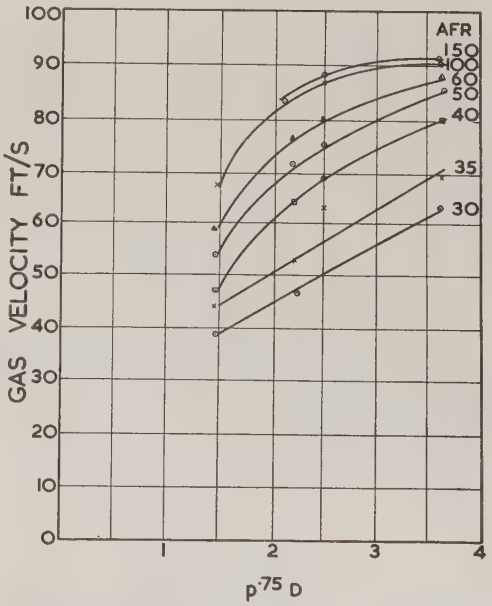

FIG. 11. Blowout data from a tubo-annular combustion chamber.

the value of 1.75 derived from burning velocity analysis and also Longwell and Weiss' more recent experimental value of 1.8.[6] These would

suggest the parameters $P^{0.75}\,D$ and $P^{0.8}\,D$ respectively. The reasons for this anomaly are not yet clear. Experimental data for propane on the effect of pressure on burning velocity[13] and on the critical tube diameter for flame propagation[14] suggest that n decreases numerically with decreasing equivalence ratio below unity. At an equivalence ratio of 1, n is almost 2. A possible explanation, therefore, is that unburned mixture may reach the gutter in pockets of varying mixture strength. Since the volumetric reaction rate is considerably higher in mixtures at or near unit equivalence ratio, these burn first and thus control the process. An antithetical explanation is that in current designs of reheat system mixing processes so predominate that constant Reynolds number and Mach number are the primary criteria for simularity. Further investigation into this problem is being made using stabilizers of simple design and uniform fuel/air mixtures. Meanwhile the scaling parameter, PD = constant, is being currently applied to reheat design.

Correct air-flow conditions upstream of the gutter are obtained by accurate scaling of all the engine components downstream of the turbine plane; upstream a parallel annular duct serves for instrumentation and allows a boundary layer build up similar to that obtaining in the engine. A precise reproduction of the residual swirl or even the velocity profile at the turbine plane is unnecessary although this may be required with shorter systems. Accurate scaling of the main engine nozzle is essential to ensure that the rig operates with the correct relationship of mass flow to gas pressure at all equivalence ratios. It is also essential that the final nozzle runs "choked" under all conditions.

In scaling the fuel system it was at first assumed that the relative fuel penetration should be made the same on the scale model and prototype. From fuel penetration tests

$$d_{\text{model}} = d_{\text{engine}} \times r^x \qquad (20)$$

where

d = diam of fuel jet

r = scaling factor

and $x = 0.74$, 0.81 and 0.5 according to references Rice,[15] Chelko[16] and Longwell and Weiss[17] respectively. Equation (20) was originally used to determine the jet size with $x = 0.74$. It was later found that, within limits, combustion efficiency is largely independent of jet size. It is concluded, therefore, that fuel penetration is not a controlling factor in these systems and that the dispersion of fuel by diffusion is of greater importance. This process has been analyzed by Longwell and Weiss.[17] From the equations derived it can be shown that the process of fuel dispersion can be scaled if the eddy diffusivity is proportional to the rig or duct size. Some experimental results suggest that eddy diffusivity is not necessarily directly proportional to scale of turbulence and therefore not directly proportional to the duct dimensions, but as Longwell points out, "the scale of turbulence in these tests probably depended primarily on the upstream perforated plate and not on the duct size (as there was insufficient length for normal pipe turbulence to develop)."

A typical reheat burner is shown in Figure 12 together with its ¼-scale counterpart. Results of tests carried out over a range of flight conditions are shown in Figure 13 for five burners; the full and broken lines refer to ¼-scale rig and full scale flight results respectively. Although plots of fuel flow against altitude have been adopted for simplicity it should be realized that correlation on this basis automatically implies correlation of all other factors such as combustion efficiency and burner pressure loss. The results satisfy practical requirements of accuracy, the maximum error as measured on an altitude basis being less than 2,000 ft. Moreover, the onset of rough combustion which occurs in flight at high altitudes can be identified with the toe of the fuel flow/altitude curves.

It is concluded, therefore, at least for this type of burner, that provided care is taken in the construction and testing of the models, the scale rig tests are as accurate as routine flight testing.

D. LOW PRESSURE COMBUSTION SIMULATED BY FUEL DILUTION

From a rig test aspect the most arduous conditions to be met are undoubtably those corresponding to limiting stability at low pressure.

Following a suggestion by A. C. Lovesey[a] a method has been devised whereby stability tests are carried out at atmospheric pressure, lower gas pressures being simulated by diluting the fuel with water. The method has general application to all types of combustion systems where the

[a] Chief Development Engineer, Rolls-Royce, Ltd.

aerodynamics of the burning zone are not unduly influenced by the fuel injection process. It is thus particularly suited to systems in which the fuel and air are uniformly premixed. This type of fuel distribution is used to obtain basic data on reheat cone and gutter stability.

The test procedure is quite simple. The temperature and velocity of the gas approaching the stabilizer are first adjusted to appropriate engine values. A flame is then established and water gradually admixed with the fuel until blowout occurs. This procedure is carried out at sufficient equivalence ratios to enable a complete stability loop to be drawn.

Figure 14 shows a typical stability loop obtained, in this instance, using a 1-in. Vee gutter of 30° included angle. This figure also illustrates how easily and clearly defined is the point of peak stability, a most useful characteristic of stability loops obtained using this technique.

Curves of this type provide useful data whereby the basic stability of various designs of gutter may be compared. The only assumption involved is a reasonable one, namely that the gutter requiring the largest amount of water per pound of fuel has the highest stability. The value of the technique would obviously be considerably enhanced by a relationship between the fraction of water in the mixture and the equivalent fall in pressure. Such a relationship can be derived from reaction rate theory. For lean mixtures ($\phi_2 \gg 1$)

The theoretical relationship between K and equivalent pressure ratio is illustrated in Figure 15 for the following conditions:

(a) $\phi_2 = 1$	$\phi_1 = 0$
(b) $\phi_2 = 1$	$\phi_1 = 0$
(c) $\phi_2 = 0.75$	$\phi_1 = 0$
(d) $(\phi_2 - \phi_1) = 1$	$\phi_1 = 0.1124$
(e) $\phi_2 = 1$	$\phi_1 = 0.214$,
(a) $T_0 = 300°K$	
(b) $T_0 = 600°K$	
(c) $T_0 = 300°K$	
(d) $T_0 = 600°K$ (from 300°K by vitiation)	
(e) $T_0 = 873°K$ (from 300°K by vitiation)	

Curves (a), (b) and (c) represent typical combustor chamber operating conditions. Curve (d) is the test rig equivalent of (b); increase in inlet air temperature above 300°K incurring vitiation. Curve (e) is a typical reheat condition. In general, the effect of adding a pound of water to each pound of fuel is roughly the same as halving the gas pressure. This result may be verified experimentally by operating a combustion system at constant air mass flow and temperature and recording the degree of fuel dilution required to produce blowout at different pressure levels. An easier, but less direct method, is to make similar measurements at various mass flows for a constant pressure.

Experimental results obtained by this latter method using various cone and gutter designs

$$\frac{M}{VP^2} \propto \frac{(1 - B)[1 - \phi_1 - B(\phi_2 - \phi_1)]}{T^{1.5}\, e^{\frac{21000}{T}B[85.7 + 6\phi_2) - 5(1 - 1.87K - B)(\phi_2 - \phi_1)]^2}} \tag{21}$$

where K = water/kerosene ratio by weight. For rich mixtures ($\phi_2 \ll 1$)

$$\frac{M}{VP^2} \propto \frac{(1 - B)^2(\phi_2 - \phi_1)}{T^{1.5}\, e^{\frac{21000}{T}B[67.7 + 24\phi_2 + (1 - B)(18 - 23\phi_2 + 5\phi_1) + 9.34K(\phi_2 - \phi_1)]^2}} \tag{22}$$

The above equations are similar to Equations (14) and (15) respectively but take into account the reduction in fuel and oxygen concentration due to the presence of additional water vapor. Another effect of the water is to reduce the calculated reaction temperature by an amount corresponding to the heat absorbed in converting water at 15°C to steam at temperature, T. In deriving Equations (21) and (22) a second order reaction has been assumed because peak stability always occurs at or near unit equivalence ratio.

are presented in Figure 16 together with the corresponding theoretical curve.

Conclusions

The combustion theories discussed in this paper are at best approximations based on simple concepts of what is actually a very complex process. Nevertheless, they enable combustion performance to be related to the geometry of the system and the operating variables of pressure, temperature, velocity and equivalence ratio. This

is a valuable aid in design and also provides a basis for the various techniques whereby rig testing is made easier and cheaper and the development of new systems speeded.

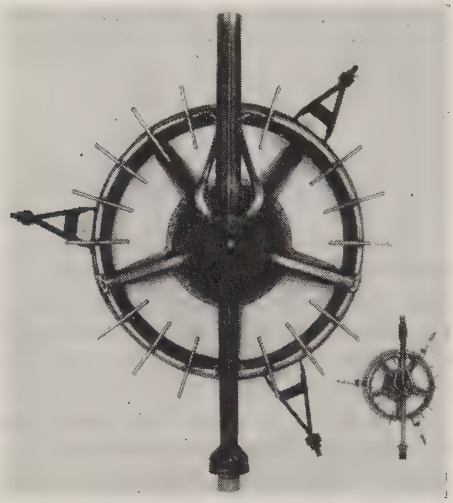

FIG. 12. Comparison of engine and scale model reheat burners.

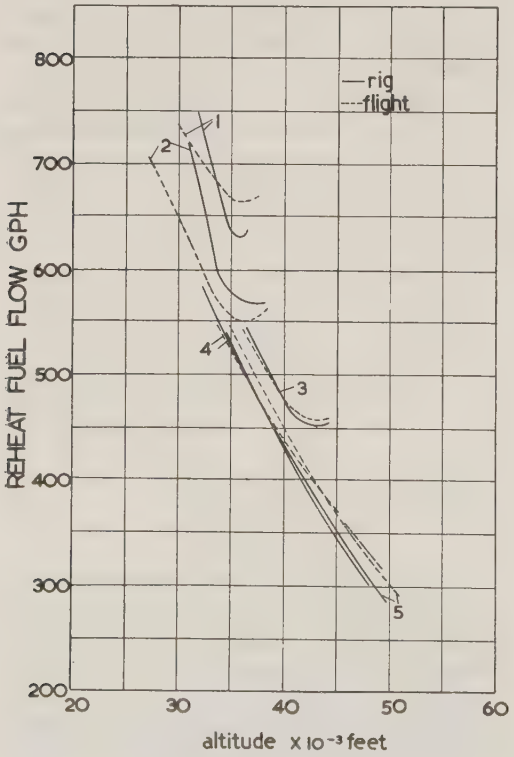

FIG. 13. Comparison of engine and scale rig performance for five different reheat systems.

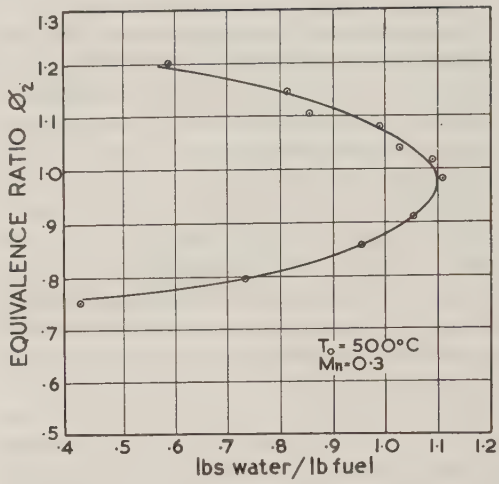

FIG. 14. Typical stability loop obtained by water injection technique. Experimental data related to a 1-in. Vee gutter of 30° included angle.

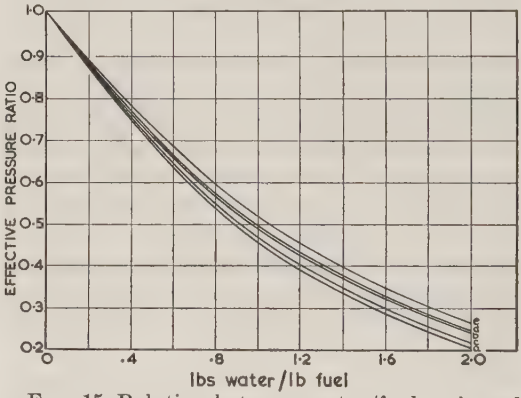

FIG. 15. Relation between water/fuel ratio and equivalent pressure ratio for five typical combustion systems ($n = 2$).

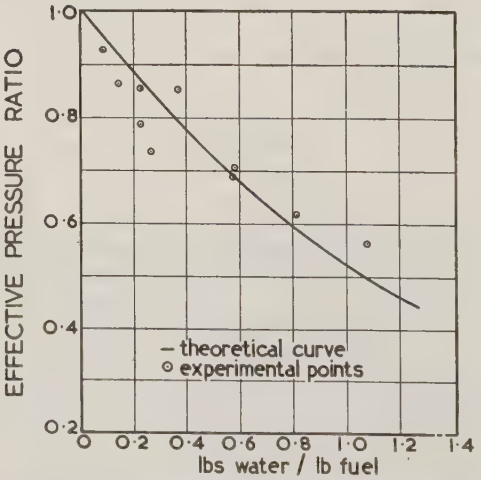

FIG. 16. Experimental results showing the equivalent fall in gas pressure produced by the addition of water to kerosene fuel. The full line is the corresponding theoretical curve.

Acknowledgments

The authors' thanks are due to Messrs. Rolls-Royce, Ltd. and the British Ministry of Supply for permission to write and publish this paper.

Nomenclature

M air rate, lb/sec
T_0 inlet air temperature, °K
P gas pressure, atmos
q fuel/air ratio
ϕ equivalence ratio
H LCV of fuel, Chu/lb
C_p specific heat of mixture, Chu/lb/°C
ρ gas density, lb/ft^3
μ gas viscosity, lb/ft sec
D characteristic dimension, ft (e.g., for a circular combustion chamber D = flame tube diam)
A cross sectional area of combustion system. (=0.785 D^2 for a circular flame tube)
U gas velocity, ft/sec
d dynamic head = $\frac{1}{2}\rho U^2$
A_f flame area, ft^2
ΔT theoretical temperature rise due to combustion.
ΔP pressure loss across system, lbs/ft^2
S_T turbulent burning velocity, ft/sec (including effect of small and large scale turbulence.)
B fraction of fuel burned.

REFERENCES

1. Burgoyne, J. H., and Cohen, L.: Proc. Roy. Soc., *A227*, 375 (1954).
2. Damkoehler, G.: Z. Elektrochem., *46*, 601 (1940).
3. Karlovitz, B.: *Fourth Symposium (International) on Combustion*, p. 60. Baltimore, The Williams & Wilkins Co., 1953.
4. Semenov, N.: NACA Tech. Memo. No. 1026, 1942.
5. Greenhough, V. W., and Lefebvre, A. H.: Unpublished Rolls-Royce Report, April, 1954.
6. Longwell, J. P., and Weiss, M. A.: Ind. Eng. Chem., *47*, 1634 (1955).
7. Lefebvre, A. H.: Unpublished Rolls-Royce Report, October, 1955.
8. Herbert, M. V.: Unpublished M.O.S. Report, 1956.
9. Barrère, M., and Mestre, A.: *Selected Combustion Problems*. London, Butterworth Scientific Publications, 1954.
10. Mestre, A.: *Combustion Researches and Reviews*, p. 72. London, Butterworth Scientific Publications, 1955.
11. Stewart, D. G.: Unpublished M.O.S. Report, 1951.
12. Johnson, F. M., and Greenhough, V. W.: Unpublished A.R.C. Report, June, 1952.
13. Egerton, A. C., and Lefebvre, A. H.: Proc. Roy. Soc., *A222*, 206 (1954).
14. Simon, D. M., Belles, F. E., and Spakowski, A. E.: *Fourth Symposium (International) on Combustion*, p. 126. Baltimore, The Williams & Wilkins Co., 1953.
15. Rice, R. A.: Unpublished Rolls-Royce Report, October, 1952.
16. Chelko, L. J.: NACA/RM/E50, F21, 1950.
17. Longwell, J. P., and Weiss, M. A.: Ind. Eng. Chem., *45*, 667 (1953).

118

CORRELATION OF TURBINE-ENGINE COMBUSTION EFFICIENCY WITH THEORETICAL EQUATIONS

By J. HOWARD CHILDS and CHARLES C. GRAVES

Introduction

Early in 1944 a turbo-jet powered aircraft encountered the problem of flameout at altitude. Subsequent tests in the NACA Altitude Wind Tunnel at Cleveland, Ohio, established that this phenomenon was the direct result of the combustor behavior rather than a secondary effect resulting from malfunctioning of some other engine component. Consequently, research was begun to learn more about the causes of these flameouts and to investigate remedial measures to cope with them. This research was started by testing production-model turbo-jet combustors in ducts that permitted control of operating conditions to values simulating high flight altitudes.

It was demonstrated[1] that combustion efficiency and maximum obtainable temperature rise decreased as the combustor pressure and inlet temperature were decreased and as the combustor velocity was increased. At the low combustor pressures and inlet temperatures encountered at high altitudes, the obtainable temperature rise in some cases was less than that required to maintain engine rpm. When such a condition was reached, the pilot would advance the throttle until a flameout occurred due to a too-rich fuel-air mixture in the combustor.

The observed behavior of turbo-jet combustors (Childs, McCafferty and Surine,[1] and other unpublished NACA data) in response to changes in such operating variables as pressure, inlet temperature, and flow velocity was very similar to that to be expected if the chemical reaction rate controlled the over-all turbo-jet combustion process. An effort was therefore made to correlate the experimental combustion efficiency data with theoretical equations derived from chemical reaction kinetics. The object of this paper is to review the NACA work on correlation of turbo-jet combustion efficiency and theoretical analyses of the combustion process. For several years this work was subject to security classification. However, the various reports on this work[2, 3, 4, 5] have recently been declassified. This paper will summarize the material contained in these reports.

A correlation of turbo-jet combustion efficiency is of obvious value for several reasons. It provides for interpolation and extrapolation to predict combustion efficiency at operating conditions that have not been investigated in combustor tests. Also, where the correlating equations are derived from theory, it provides insight into the mechanism of combustion. This, in turn, indicates the combustor design changes that should be made.

A theoretical treatment of turbo-jet combustion is difficult because of the many different conversion steps which must occur. The fuel must be vaporized, mixed with air, ignited, and oxidized to the final products of combustion. These combustion products must then be mixed with dilution air to reduce the temperatures to values that can be tolerated by the turbine blades. The combustion can be visualized as a competition between these conversion steps (vaporization, mixing, ignition, and oxidation) and the quenching that occurs when the reacting mixture is cooled by the dilution air and when the reacting mixture comes in contact with the relatively cool walls of the combustor liner. If the quenching occurs before the conversion steps have proceeded to completion, then the combustion efficiency will be low. Because of the complicated nature of the over-all process, no exact theoretical treatment is currently possible.

By making simplifying assumptions regarding the turbo-jet combustion process, it is possible, however, to apply theoretical considerations in the analysis of the process. If the rate of any one of the conversion steps is substantially less than the rates of the others, this one step will then govern the over-all rate and hence will determine the combustion efficiency. The existence of a single, slow conversion step in the over-all chain of processes was assumed. The chemical reaction was selected as the most probable rate-determining step, and the first theoretical analysis was based on this assumption. However, theoretical treatment of turbo-jet combustion was also made, assuming each of the various other conversion steps to be the slow rate-determining step. This paper describes the details of the analysis and demonstrates the application of the results of the analysis to experimental data obtained with various turbo-jet combustors.

Analysis

CHEMICAL REACTION KINETICS

One theoretical analysis of the turbo-jet combustion process is based on the assumption that the chemical reaction (oxidation of the fuel) constitutes the over-all rate-determining step in the combustor. This oxidation occurs by some chain mechanism. It is sometimes true, however, that the kinetics of chain reactions are dependent entirely upon the kinetics of a single, slowly occurring reaction within the chain. The analysis described herein was therefore based on the kinetics of a bimolecular chemical reaction.[2]

For the bimolecular reaction

$$A + B \rightarrow C + D$$

in which A is the reactant present in smaller quantity, the reaction rate is given by the equation

$$\frac{dw}{d\theta} = \frac{Z\varphi\beta}{N_A} \tag{1}$$

Substituting appropriate relations from the

kinetic theory of gases[6] leads to

$$\frac{dX}{d\theta} = \frac{1}{\rho}\frac{dw}{d\theta}$$

$$= \frac{K_1(\sigma_A + \sigma_B)^2 \cdot N_M(1 - X)\left(1 - \frac{N_A}{N_B}X\right)Pe^{-E/RT}}{R^{\frac{1}{2}}T^{\frac{1}{2}}} \quad (2)$$

Equation (2) applies to any sample of the reacting mixture as it passes through the combustor.

At this point in the analysis, two somewhat different approaches are taken. These are treated as the nonhomogeneous reactor and the homogeneous reactor, respectively.

Nonhomogeneous reactor

Figures 1 and 2 show values of fuel-air mixture composition within the burning zone of a typical turbo-jet combustor; these data were obtained by a water-cooled sampling probe. The vapor fuel-air ratio decreases progressively along the length of the combustor, and marked variations in composition occur over the combustor cross section. The data of Figures 1 and 2 indicate that homogeneity is not approached. The rate of mixing of fuel and air may nevertheless be quite rapid. The assumption of rapid fuel-air mixing is made in this portion of the paper; possible effects of slow mixing rates will be subsequently treated in the section, Other Processes.

The major assumptions contained in this analysis may be summarized as follows:

(1) Reaction occurs in local stoichiometric fuel-air ratio zones which exist at the interface between the fuel-rich and air-rich regions.

(2) The mixing process whereby fuel and air are introduced to the reaction zone is sufficiently rapid so that the chemical reaction rate controls the over-all process.

(3) The temperature in the reaction zone is constant along the combustor at a value close to the stoichiometric flame temperature.

(4) The mean concentration of each reactant in the reaction zone varies along the combustor and is equal to the initial concentration minus the fraction, X, that has already reacted at any position in the combustor.

The foregoing assumptions do not necessarily constitute those characterizing the simplest or most plausible physical model of the combustion process. Rather, they constitute the assumptions necessary to arrive at a final equation which fits the experimental data.

At the outlet of the reaction zone, X is equal to η_b, because the particular reaction under consideration is the one governing the over-all process. Thus,

$$X = \eta_b \text{ when } l = L \text{ and } \theta = L/V_a \quad (3)$$

Integrating Equation (2) with the assumption

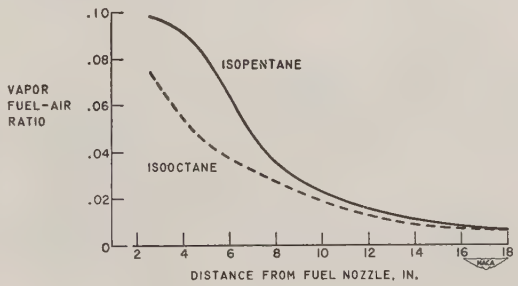

FIG. 1. Variation of vapor fuel-air ratio with distance from fuel nozzle in typical tubular turbojet combustor. Simulated high altitude; over-all fuel-air ratio, 0.007.

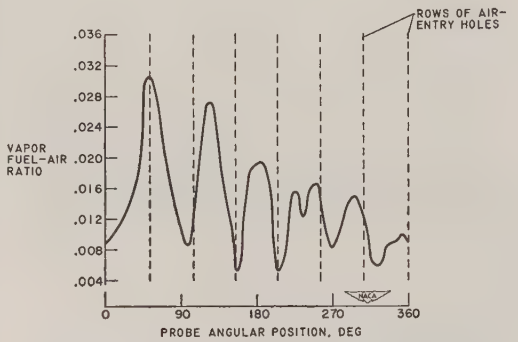

FIG. 2. Variation of fuel-air ratio with angular position of sampling probe 12½ in. downstream of fuel nozzle in a typical tubular turbojet combustor. Fuel, isooctane; over-all fuel-air ratio, 0.014.

that the temperature in the zone where the reaction

$$A + B \rightarrow C + D$$

occurs is substantially constant, and substituting from Equation (3),

$$\ln \frac{1 - \frac{N_A}{N_B}\eta_b}{1 - \eta_b} + K_2 = \frac{K_1(\sigma_A - \sigma_B)^2(N_B - N_A)LPe^{-E/RT}}{V_a R^{\frac{1}{2}}T^{\frac{1}{2}}} \quad (4)$$

The foregoing equation is expressed in terms of the values of P, T, and V_a in the reaction zone. In experimental investigations, these variables

are not measured; the values of the combustor-inlet variables, P_i, T_i, and V_r, are usually determined, however. The values of P, T, and V_a must therefore be expressed in terms of combustor-inlet conditions; when appropriate ap-

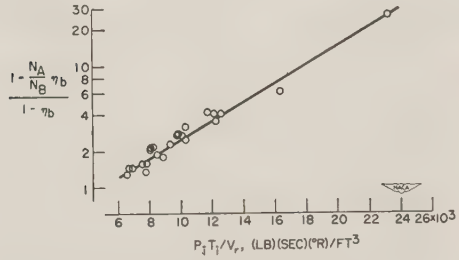

FIG. 3. Experimental data obtained with combustor A plotted in accordance with Equation (6). Fuel, gasoline; variable fuel-air ratio.

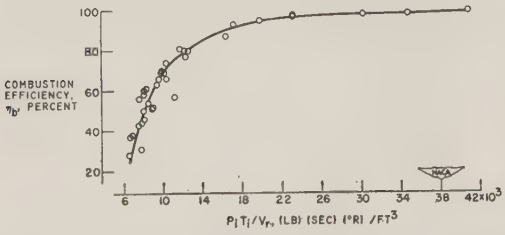

FIG. 4. Experimental data obtained with combustor A plotted in accordance with Equation (7). Fuel, gasoline; variable fuel-air ratio.

proximations and substitutions are made,

$$\ln \frac{1-\frac{N_A}{N_B}\eta_b}{1-\eta_b} + K_2 = \left[K_1 \frac{(\sigma_A+\sigma_B)(N_B-N_A)e^{-E/RT}}{R^{\frac{1}{2}}T^{\frac{3}{2}}}\right] \left[\frac{L\left(1-\frac{\Delta P}{P_i}\right)^2}{\frac{A_{H.P}}{A_{H.T}}\frac{A_r}{A_a}}\right]\left(\frac{P_iT_i}{V_r}\right) \quad (5)$$

On the right side of Equation (5) the terms are grouped into (1) those dependent upon fuel type and fuel-air ratio, (2) those dependent upon combustor design, and (3) those dependent only upon the operation conditions.

For a given combustor operating with a given fuel at a fixed fuel-air ratio and assuming negligible pressure drop across the combustor, Equation (5) becomes

$$\ln \frac{1-\frac{N_A}{N_B}\eta_b}{1-\eta_b} + K_2 = K_3 \frac{P_iT_i}{V_r} \quad (6)$$

The same relation can be expressed as

$$\eta_b = f\left(\frac{P_iT_i}{V_r}\right) \quad (7)$$

Figures 3 and 4 show experimental data obtained with turbo-jet combustor A plotted in accordance with Equations (6) and (7), respectively. A straight-line data correlation is obtained in Figure 3, as predicted by Equation (6). Data for a range of fuel-air ratios are included in both Figures 3 and 4. The theoretical equations apply only for a fixed fuel-air ratio; however, it was noted that for this particular combustor, the efficiency did not vary appreciably with change in fuel-air ratio in the range investigated.

Childs[2] presents a detailed derivation of Equations (6) and (7) and discusses the application of Equation (7) to data obtained with 14 turbo-jet combustors. For some combustors, the correlation is good, but for others, the data scatter is great and the parameter, P_iT_i/V_r cannot be used to predict combustion efficiency. Equation (7) has nevertheless been widely used to correlate combustion-efficiency data obtained at the NACA Lewis laboratory in single combustor tests (for example, Childs[2]) and in full-scale engine tests. For combustors in which combustion efficiency varies appreciably with fuel-air ratio, a satisfactory correlation may be obtained by using a different correlation curve for each narrow range of fuel-air ratio.

Homogeneous reactor

With the assumption that the mixing in the combustor is sufficiently rapid to produce a homogeneous mixture throughout the combustor volume, for given operating conditions the value of X is constant over the combustor reaction zone, and it is no longer necessary to integrate the equation as was done in the preceding analytical approach. The assumption of a homogeneous reactor was also made by Avery and Hart[7] in analyzing the combustion process in a can-type combustor having a premixed fuel-air feed and in reference 8 by Longwell, Frost and Weiss[8] in analyzing flames in the wake of bluff bodies.

For this condition $T \cong T_i + K_4 \Delta T_s \eta_b$,

$$\eta_b \equiv \left(\frac{dw}{d\theta}\right)\left(\frac{1}{\rho}\right)\theta$$

$$= \frac{K_1(\sigma_A + \sigma_B)^2 N_B(1 - \eta_\eta)\left(1 - \frac{N_A}{N_B}\eta_b\right) PLe^{-E/R(T_i + K_4\Delta T_s\eta_b)}}{R^{1/2}(T_i + K_4\Delta T_s\eta_b)^{\frac{1}{2}}V_a} \quad (8)$$

Rearranging terms yields

$$\frac{\eta_b(T_i + K_4\Delta T_s\eta_b)^{\frac{3}{2}}e^{E/R(T_i+K_4\Delta T_s\eta_b)}}{(1 - \eta_b)\left(1 - \frac{N_A}{N_B}\eta_b\right)} = \left[\frac{K_1(\sigma_A + \sigma_B)^2 N_B}{R^{\frac{1}{2}}}\right]\left[\frac{L\left(1 - \frac{\Delta P}{P_i}\right)^2}{\left(\frac{A_{H.P}}{A_{H.t}}\right)\left(\frac{A_r}{A_a}\right)}\right]\left(\frac{P_iT_i}{V_r}\right) \quad (9)$$

Here again the terms on the right side of the equation are grouped into (1) those dependent upon fuel type and fuel-air ratio, (2) those dependent upon combustor design, and (3) those dependent only upon operating conditions. For a given combustor, a given fuel, and a single fuel-air ratio, Equation (9) becomes

$$\frac{\eta_b(T_i + K_4\Delta T_s\eta_b)^{\frac{3}{2}}e^{E/R(T_i+K_4\Delta T_s\eta_b)}}{(1 - \eta_b)\left(1 - \frac{N_A}{N_B}\eta_b\right)} = K_3\frac{P_iT_i}{V_r} \quad (10)$$

The data for combustor A were plotted in accordance with Equation (10). The predicted straight-line relation was not obtained, thereby indicating that the assumption of nonhomogeneity (Eq. (6)) better fits the experimental data than does the assumption of homogeneity (Eq. (10)) for this particular combustor. This is in accord with expectations, since Figures 1 and 2 indicate that a condition of homogeneity is not approached within a typical turbo-jet combustor. For combustors having higher rates of mixing in the combustion space, Equation (10) may afford a better correlation of the data. Equation (10) can also be expressed as

$$\eta_b = f\left(\frac{P_iT_i}{V_r}, T_i\right) \quad (11)$$

and since T_i is small compared with $K_4\Delta T_s$, for a reasonable correlation of engineering data for which T_i does not vary widely, it might be assumed

$$\eta_b = f\left(\frac{P_iT_i}{V_r}\right) \quad (7)$$

This is the same equation as that obtained for the nonhomogeneous reactor.

FLAME SPREADING

An analysis was also made, assuming combustion efficiency to be controlled by the rate of flame spreading. The combustion process was visualized as the burning of fuel-air mixture zones of random size and shape, which are surrounded by a flame surface and which are consumed as they pass through the combustor. The flame surface advances into the adjacent unburned mixture at a rate determined by the physical conditions of the unburned mixture. The effect of turbulence on the rate of flame spreading is considered solely in terms of its effect on the flame surface area. This picture of the combustion process was suggested by the analysis of Wohlenberg,[9] in which the concept of reaction interface extension was introduced in a study of the combined effects of diffusion and chemical reaction in gaseous fuel combustion.

The combustion efficiency can be expressed approximately by the relation

$$\eta_b = \left(\frac{1}{f}\right)\left(\frac{u_f}{V_r}\right)\left(\frac{A_f}{A_r}\right) \quad (12)$$

The numerator of this expression is proportional to the rate of consumption of fuel-air mixture in the flame, and the denominator is proportional to the rate of flow of combustible mixture through the combustor. A detailed derivation of Equations (12) through (17) appears in the report by Graves.[3] Equation (12) is based on the assumptions of low pressure drop across the combustor and a temperature in the unburned mixture equal to the combustor-inlet temperature. The total flame surface, A_f, corresponds to the reaction interface extension that is treated in detail by Wohlenberg.[9] The value, A_f, represents an integration of the flame surface area per unit volume, a_f, over the total combustor volume.

The principal changes in a_f would appear to be associated with (1) the changes in turbulence accompanying the energy release per unit mass of air along the combustor, (2) the reduction in flame area resulting from consumption of the combustible mixture, and (3) the effect of com-

bustor-inlet variables on flame area. For a given fuel and over-all fuel-air ratio, the energy release per unit mass of air is proportional to the combustion efficiency, while the fractional volume occupied by the unburned mixture is a function of both the combustion efficiency and the inlet temperature. The effect of combustor-inlet variables on the flame surface area is treated similarly to the reaction zone interface extension by Wohlenberg.[9] The value, a_f, is a measure of the average hydraulic radius of the unburned mixture zones, or the average distance through which the flame must travel to complete the combustion process. The product of a_f, with its dimensions of reciprocal length, and a characteristic length of the combustor has a physical significance similar to that of the Nusselt number for heat transfer. As suggested by Wohlenberg,[9] a_f would probably be related to inlet conditions in terms of the Reynolds number. Increase in density of the unburned mixture alone will increase the flame surface area "packed" in a unit volume of the combustor, since the surface-volume ratio of any individual zone within the unit volume increases with density. As was also shown by Wohlenberg,[9] a_f would be proportional to the cube root of the density. If the effects of inlet-flow variables and the actual burning process on a_f can be treated as separate functions, the total flame area, A_f, could be expected to be related to combustor-inlet conditions and combustion efficiency by

$$A_f = K_5 \left[(Re)^p \left(\frac{P_i}{T_i} \right)^{\frac{1}{3}} \right] [f(\eta_b , T_i)] \quad (13)$$

Here the terms in the first set of brackets account for the effect of combustor-inlet variables in flame area, while the term in the second brackets accounts for the effect of energy release and reduction in volume of unburned mixture on flame area. Substituting Equation (13) in Equations (12) and neglecting the probable small effect of inlet temperature on the fractional volume occupied by unburned mixture yields

$$\eta_b = f K_6 \left[\left(\frac{P_i}{T_i} \right)^{\frac{1}{3}} \left(\frac{u_f}{V_r} \right) Re^p \right] \quad (14)$$

Here K_6 is a constant for a given combustor, fuel, and over-all fuel-air ratio.

The use of Equation (14) for normal combustor operating data requires knowledge of the effect of ambient temperature and pressure on laminar flame speed and the effect of Reynolds number on turbulent flame speed. In the report by Dugger and Graab,[10] the laminar flame speeds of vapor isooctane-oxygen-nitrogen mixtures at atmospheric pressure and various equivalence ratios were found to be proportional to the 1.4 power of the initial mixture temperature. This temperature dependency was assumed to be representative for the fuel used in combustor A.

The effect of variations in ambient pressure on the laminar flame speeds of hydrocarbon fuel-air mixtures has not been definitely established. The effect, if any, is small and appears to vary with fuel type. In general, the relation between the flame speed and pressure can be expressed in the form

$$u_f = K_7 P_i^q \quad (15)$$

for hydrocarbon fuel-air mixtures. Here q generally has a value ranging from $-\frac{1}{3}$ to approximately 0. Gaydon and Wolfhard[11] concluded that the flame speeds of hydrocarbon fuel-air mixtures should be independent of pressure provided that the tube diameter is large enough to prevent surface effects from becoming important. The report by Garner, Ashforth and Long,[12] the flame speed of vaporized isooctane-air mixtures was found to be inversely proportional to the cube root of the ambient pressure. Hawthorne and Fabri[13] show the exponent q in Equation (15) to be dependent on the flame speed of the fuel. For fuels having flame speeds of the order of that isooctane, the value of q is zero. In view of the conflicting data available in the literature, indicating that the reported trends may be influenced by the experimental methods used, the effect of ambient pressure on laminar flame was assumed negligible.

In an investigation of turbulent Bunsen-type flames,[14] the turbulent flame speed $u_{f,t}$ was correlated by means of the following relation

$$u_{f,t} = 0.18\, u_f Re^{0.24}\, d^{0.26} \quad (16)$$

where d is the tube diameter. If the turbulent flame speed is controlled by the increase in flame surface area resulting from "wrinkling" of the flame, and Equation (16) is used to estimate the effects of combustor-inlet Reynolds number on the total flame area, A_f, the exponent, p, in Equation (14) would be equal to 0.24. However, there are no data available for the case of the intense mixing conditions existing in turbo-jet combustors as the result of the impinging air jets and very high Reynolds numbers.

For the normal combustor operating conditions, it was assumed that the effects of both pressure and combustor-inlet Reynolds number on flame speed were minor. Equation (14) then reduces to

$$\eta_b = f\left(\frac{P_i^{1/3}T_i^{1.1}}{V_r}\right) \tag{17}$$

if the effect of temperature on the normal flame speed of isooctane[10] is included. It is noted, however, that if both pressure[12] and Reynolds number[14] effects on flame speed are included, the relative exponents of inlet pressure and velocity would be approximately the same as presented in Equation (17).

The parameter derived from the assumption that flame spreading governs the over-all combustion rate did not correlate the data for combustor A, as evidenced by the scatter of data points in Figure 5. A majority of the data points do, however, lie close to a common curve.

It is therefore indicated that the flame-speed parameter might possibly serve to correlate data over a part of the combustor operating range, and a more critical evaluation of this parameter appears to be warranted.

OTHER CONVERSION PROCESSES

In addition to those already discussed, analyses of the turbo-jet combustion process were also made with the assumption that (1) fuel vaporization, (2) fuel-air turbulent mixing, and (3) fuel-droplet burning (governed by heat transfer into the droplet) were the rate-determining steps in the over-all combustion process. With each of these three analyses, the predicted effects on combustion efficiency of operating variables such as combustor-inlet pressure, combustor velocity, and combustor-inlet temperature, differed markedly from the effects observed experimentally; that is, the equations relating P_i, T_i, and V_r derived in these analyses differed markedly from Equation (7) and gave no correlation of experimental data. Graves[15] presents the change in burning rate of single fuel droplets resulting from a change in oxygen concentration of the ambient atmosphere. This change in droplet-burning rate is shown to be much less than that required for this phenomenon to account for the observed change in combustion efficiency with change in inlet oxygen concentration in a typical turbo-jet combustor.

Since none of these three analyses provided agreement between theoretical and experimental data, the tentative conclusion may be drawn that neither fuel vaporization, fuel-air mixing, nor fuel-droplet burning alone constitutes the rate-determining, slowest step in the combustion process. The analyses were, however, based on certain simplifying assumptions similar to the assumptions included in the analyses of the chemical reaction kinetics and flame spreading, which were previously discussed. Therefore, the possibility can not be overlooked that difference assumptions in these analyses might result in closer agreement between theoretical and experimental data.

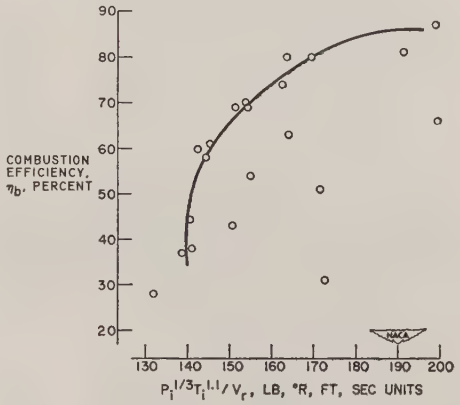

FIG. 5. Experimental data obtained with combustor A plotted in accordance with Equation (17). Fuel, gasoline; variable fuel-air ratio.

Experiments to Verify Theory

VARIATION OF OXYGEN CONCENTRATION

In order to test the applicability of the equations previously derived, a number of special experiments were conducted. Investigations of vapor-fuel-oxygen-nitrogen mixtures have shown marked effects of oxygen concentration on such fundamental combustion properties as minimum spark-ignition energy, quenching distance, and flame speed.[10, 16] Oxygen concentration appreciably affects equilibrium flame temperature at stoichiometric or richer fuel-air ratios and also affects the concentration of the chemical species involved in the combustion; oxygen concentration is therefore a means of varying the kinetics of the chemical reactions. In combustor tests, variations in oxygen concentrations should affect the rate of combustion without appreciably changing such factors as inlet velocity, turbulent mixing as associated with inlet conditions, and the fuel-spray characteristics. This experimental device

should simplify interpretation and application of the test data. Accordingly, an investigation was conducted to determine the effect of inlet-oxygen concentration on the combustion efficiency of turbo-jet combustor B.

The reaction kinetics equation (Eq. (5)) and the flame spreading equation (Eq. (14)) were modified to include the effects of changes in oxygen concentration. It was found that both of the resulting equations gave good correlation of the experimental data.[3, 4, 5]

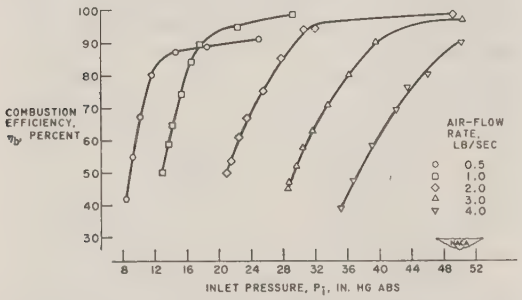

FIG. 6. Sample of data obtained with combustor B for wide variation in inlet pressure and air-flow rate. Fuel, propane; fuel-air ratio, 0.012; inlet temperature, 80°F.

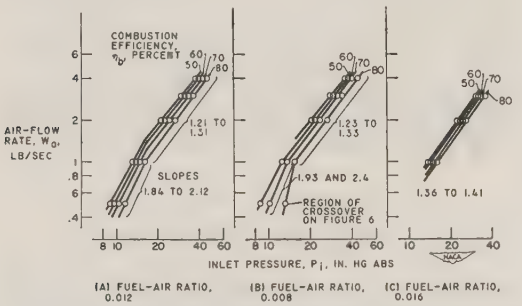

FIG. 7. Cross plot from faired curves of Fig. 6 to determine relative effects of inlet pressure and air-flow rate on combustion efficiency.

INDEPENDENT VARIATION OF COMBUSTOR-INLET PRESSURE AND AIR-FLOW RATE OVER WIDE RANGES

The assumption that chemical reaction kinetics govern the over-all combustion rates led to the prediction that combustion efficiency could be correlated as a function of the parameter, $P_i T_i / V_r$, and this parameter is equal to a dimensional constant times the parameter P_i^2 / W_a. The assumption that the rate of flame spreading governs the over-all combustion rate led to the prediction that combustion efficiency should correlate as a function of the parameter $P_i^{1/3} T_i^{1.1} / V_r$. This parameter is equivalent to a dimensional constant times $P_i^{1.3} T_i^{0.1} / W_a$. The reaction kinetics analysis therefore yields a ratio of exponents on the pressure and air-flow rate terms of 2, while the flame-speed analysis yields a ratio of these same exponents of 1.3. Obviously both of these parameters cannot adequately correlate the combustion-efficiency data where the combustor pressure and combustor air-flow rate are varied through wide ranges.

In order to determine conclusively whether the ratio of exponents on the pressure and air-flow rate terms should be 2 or 1.3, it was therefore necessary to conduct a series of combustor tests in which the pressure and air-flow rate were independently varied over wide ranges of operating conditions. Such an investigation was conducted in turbo-jet combustor B, using gaseous propane fuel and a single-orifice fuel injector. A sample of the experimental data is shown in Figure 6, where combustion efficiency is plotted against combustor-inlet pressure with parametric lines of air-flow rate. The data of Figure 6 are for a fuel-air ratio of 0.012; similar data were obtained for fuel-air ratios of 0.008 and 0.016.

Figure 7a shows a cross plot of the data of Figure 6; combustor air-flow rate is plotted against combustor pressure with parametric lines of combustion efficiency. The slope of the lines in Figure 7a indicates the ratio of exponents on the pressure and air-flow rate terms of the correlating parameter which best fits the experimental data. A transition is evident in the vicinity of a combustor pressure of 15 inches of mercury. At the very low values of combustor pressure and air-flow rate, the slope of the curves is approximately 2, which agrees with the slope predicted by the parameter $P_i T_i / V_r$. At high values of combustor air-flow rate and pressure, however, the slope of the curves is of the order of 1.3, which agrees with the value predicted by the parameter $P_i^{1/3} T_i^{1.1} / V_r$.

Similar plots of the data obtained at fuel-air ratios of 0.008 and 0.016 are shown in Figures 7b and c, respectively. The data of Figure 7b again indicate a transition in the curves, with the slope being approximately 2 at low values of pressure and air-flow rate and approximately 1.3 at the higher values of pressure and air-flow rate. The data for a fuel-air ratio of 0.016 do not extend to pressures below about 14 in. of mercury; hence the transition in slope of the curves was not obtained in Figure 7c.

The data of Figure 7 indicate that for this particular combustor, the parameter, $P_i T_i / V_r$,

will correlate data obtained at the low values of pressure and air-flow rate, while the parameter, $P_i^{1/3}T_i^{1.1}/V_r$, will correlate the data obtained at higher values of pressure and air-flow rate. Neither parameter, however, adequately correlates data obtained over the entire range of pressures and air-flow rates.

Although the data of Figure 7 are meager and therefore insufficient to warrant conclusions regarding the combustion mechanism, there is some indication that a shift from one rate-controlling process to some other rate-controlling process occurs as combustor operating conditions are varied through wide ranges. The data of Figure 7, together with the analyses presented earlier in this paper, indicate that at very low values of pressure in the combustor, the chemical reaction kinetics is the rate-controlling process. At higher pressures, however, the rate of flame spreading would appear to be the rate-determining process. This trend of events is at least in qualitative accord with expectations, for the chemical reaction kinetics are a function of the square of combustor pressure and would therefore be expected to be very slow at low-pressure conditions and increase rapidly with increase in pressure until some pressure is reached above which kinetics no longer constitute the slowest step in the over-all chain of processes. More extensive investigations with other combustors are required, however, before any definite conclusions could be made in this regard.

Conclusion

The experimental data indicate that a shift from one rate-controlling step to another probably occurs as combustor pressure is increased, and the reaction kinetics parameter P_iT_i/V_r therefore best correlates the data at low pressure while the flame-spreading parameter $P_i^{1/3}T_i^{1.1}/V_r$ is better at higher pressures. No single correlating parameter can therefore be expected to be adequate for all combustors and for the entire range of operating conditions. For some combustors[2] the P_iT_i/V_r parameter has provided a good correlation of combustion efficiency; this is probably due to the fact that at the higher pressures, where flame spreading controls the combustion rate, the efficiency is close to 100 per cent.

Because of the complexity of the over-all process of turbine-engine combustion, it would appear unlikely that this simplified theoretical treatment (which assumes one step in the chain of conversion processes to be rate-controlling) would be adequate for all combustors. Childs[2] shows that the parameter, P_iT_i/V_r, is not adequate for correlating the data for certain turbojet combustors, even for the limited range of conditions required to simulate flight operation. In addition, experimental data are available that indicate fuel vaporization and fuel air mixing play an important role in some combustors. Consequently, the equations derived in this paper must be applied judiciously and with due regard for their limitations.

Nomenclature

$A_{H,P}$	liner open-hole area in combustor reaction zone, sq ft
$A_{H,T}$	total liner open-hole area, sq ft
A_a	average cross-sectional area of combustor reaction zone, sq ft
A_f	total flame-surface area in combustor, sq ft
A_r	maximum cross-sectional area of combustor flow passage, sq ft
a_f	flame surface-area per unit volume, ft^{-1}
d	tube diameter
E	energy of activation for reaction, ft-lb/lb
f	over-all fuel-oxygen-nitrogen-mixture ratio
K_1, K_2, K_3, etc.	constants
L	length of reaction zone, ft
l	distance from upstream end of reaction zone to plane of any point within reaction zone, ft
N_A, N_B	number of molecules of reactant A and B per lb original mixture, lb^{-1}
P	static pressure in combustor reaction zone, lb/sq ft abs
ΔP	static pressure drop across combustor, lb/sq ft abs
P_i	combustor-inlet static pressure, lb/sq ft abs
R	gas constant, ft-lb/lb °R
Re	Reynolds number
T	absolute static temperature in combustor reaction zone, °R
T_{eq}	equilibrium flame temperature, °R
T_i	combustor-inlet absolute static temperature, °R
ΔT_s	temperature rise for complete combustion on stoichiometric mixture, °F

u_f	laminar flame speed, ft/sec
$u_{f,t}$	turbulent flame speed, ft/sec
V_a	velocity based on density, mass flow, and average cross-sectional area of reaction zone, ft/sec
V_r	reference velocity based on combustor-inlet density, total air flow, and maximum cross-sectional area of combustor flow passage, ft/sec
W_a	combustor air-flow rate, lb/sec
$dw/d\theta$	reaction rate, lb mixture reacting/(sec)(cu ft)
X	fraction of N reacted at any time θ or at any location within reaction zone
Z	number of molecular collisions of type involved in reaction, per unit volume per unit time, ft^{-3} sec^{-1}
α	volume percent oxygen concentration at combustor inlet
β	probability factor, fraction of collisions involving sufficient energy for reaction to occur which actually result in reaction
η_b	combustion efficiency
θ	time, sec
ρ	density, lb/cu ft
σ_A , σ_B	effective molecular diameter of reactants A and B, ft
φ	fraction of collisions involving sufficient energy for reaction to occur

REFERENCES

1. Childs, J. H., McCafferty, R. J., and Surine, O. W.: NACA TR 881.
2. Childs, J. H.: NACA RM E50F15, 1950.
3. Graves, C. C.: NACA RM E52F13, 1952.
4. Graves, C. C.: NACA RM E53A27, 1953.
5. Childs, J. H., and Graves, C. C.: NACA RM E54G23, 1954.
6. Kassel, L. S.: *The Kinetics of Homogeneous Gas Reactions*. New York, Chemical Catalog Co. 1932.
7. Avery, W. H., and Hart, R. W.: Ind. Eng. Chem., *45*, 1634–1637 (1953).
8. Longwell, J. P., Frost, E. E., and Weiss, M. A.: Ind. Eng. Chem., *45*, 1629–1633 (1953).
9. Wohlenberg, W. J.: Trans. Am. Soc. Mech. Engr., *70*, 143–156 (1948); discussion, pp. 156–160.
10. Dugger, G. L., and Graab, D. D.: NACA TN 2680, 1952.
11. Gaydon, A. G., and Wolfhard, H. G.: Proc. Roy. Soc., *196*, 105–113 (1949).
12. Garner, F. H., Ashforth, G. K., and Long, R.: Fuel, *30*, 17–19 (1951).
13. Hawthorne, W. R., and Fabri, J.: *Selected Combustion Problems: Fundamentals and Aeronautical Applications*, p. 177. London, Butterworths Scientific Publications, 1954.
14. Bollinger, L. M., and Williams, David T.: NACA Rep. 932, 1949 (supersedes NACA TN 1707).
15. Graves, C. C.: Proc. Third Midwestern Conference on Fluid Mechanics, University of Minnesota, pp. 759–778, 1953.
16. Lewis, B., and von Elbe, G.: *Combustion, Flames and Explosions of Gases*. New York, Academic Press, 1951.

119

A DETONATION WAVE THEORY OF GASOLINE ENGINE KNOCK

By J. C. FIREY

Introduction

Past studies of knock in gasoline engines have produced two different theories of the knock process—the detonation wave theory and the autoignition theory. The detonation wave theory describes knock as a completion of the combustion of the unburned fuel-air mixture ahead of the normal flame front (the end gas) by the action of a shock wave or true detonation wave. The autoignition theory proposes that knock is caused by a rapid acceleration of the slow oxidation reactions known to occur in end gas.

Photographs of knocking combustion show the transformation from slow oxidation to knock to be abrupt, and this is the evidence usually used to support the detonation wave theory. As early

as 1936 two Russian investigators, Sokolik and Voinov,[1] interpreted their photographs of engine combustion to indicate that knock was a detonation wave process. More recently, C. D. Miller[2] and others drew an essentially similar conclusion from very high speed photographs of knocking combustion.

The similarity between the knock properties and the slow oxidation properties of various hydrocarbons and antiknock additives is the principle evidence supporting the autoignition theory. Hydrocarbon structure and antiknock additives greatly affect knock but are found not to influence detonation wave speeds. Slow hydrocarbon oxidations are influenced by hydrocarbon structure and antiknock additives in a directionally similar manner as knock.[3]

The autoignition theory either fails to describe clearly how the slow oxidation reaction becomes abruptly transformed into the extremely rapid process of knock or describes the transformation essentially as a branched chain, homogeneous explosion. Although this latter explanation is entirely reasonable, few if any explosions are known to occur as homogeneous branched chain reactions. Detonation wave explosions, on the other hand, are commonplace.

The theory described in this paper reconciles the autoignition and detonation wave theories by proposing that the slow oxidation reactions (preflame reactions) in the end gas generate the shock wave needed to cause a detonation of the remaining unburned fuel-air mixture. This detonation, together with the gas vibrations to which it gives rise, is knock.

Engine Experiments

To test the proposed knock theory, engine experiments were run to determine if knock exhibited some of the known properties of detonation waves, and further tests were run to determine if preflame reactions are capable of forming shock waves. The engine used in these experiments is an adjustable compression ratio engine constructed by the Christie Machine Works of San Francisco, California. This engine is of 3-in. bore and 4.5-in. stroke and has a flat, disk-shaped combustion chamber of diameter equal to the bore.

I. IMPACT PRESSURE WAVES FROM COMPRESSION IGNITION

If knock and compression ignition are a detonation wave process, then they will exhibit the properties of a detonation wave. Among other properties, a detonation wave possesses a high component of impact pressure in the direction of wave motion as a result of the high forward velocity of the compressed material immediately behind the wave front. Hence, engine tests were run to determine whether directional impact pressures existed in the combustion chamber when compression ignition occurred.

As described by Pastell,[4] compression ignition of homogeneous fuel-air mixtures appears to take place by the same process as knock. Hence, compression ignitions were investigated in these experiments in order to avoid complications from the normal, spark-ignited flame.

FIG. 1. Holder for statically balanced beams.

To detect the presence of impact pressures, thin beams were inserted in the engine combustion chamber in such manner that they could only be loaded by impact pressure. The fixture shown in Figure 1 was constructed to suspend two small cantilever beams in the combustion chamber. The fixture was mounted in the engine cylinder head so that the wide face of one beam (beam A) was parallel to the axis of the engine cylinder, whereas the wide face of the other beam (beam B) was normal to the axis of the cylinder.

The beams were positioned about one fourth of a diameter inward from the cylinder wall. The location of the beams in the engine combustion chamber is shown diagrammatically in Figure 2. Steel beams were used of 0.125-in. width, 0.500-in. free length and of thickness varying from 0.0015 in. to 0.020 in. Static pressures on both faces of these beams are equal, and thus any bending of the beams must be a result of impact pressure.

The test procedure consisted merely of inserting the beam holder and beams into the engine, allowing the engine to undergo one or more cycles of compression ignition, and then removing the beam holder and examining the beams for permanent deformation. During these tests the engine was motored at 1000 rpm and at a compression ratio of 11.3 to 1. These conditions insured immediate and audibly sharp compression ignitions whenever the test fuel, normal heptane, was turned on.

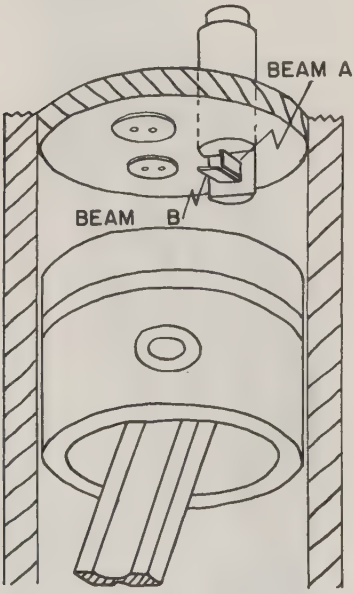

FIG. 2. Cylinder cutaway view showing beam locations.

A. Multiple compression ignition tests

When the beams were exposed to several cycles of compression ignition (from 5 to 10 cycles) beams of up to 0.010-in. thickness were severely bent as shown in Figure 3.

Beam A was almost always bent either straight backward or forward or a combination of both. Beam B, on the other hand, was almost always twisted. The extent of deformation of beam A appeared somewhat greater when it faced directly across a diameter of the cylinder.

These results indicate that directional impact pressures are present when compression ignition occurs. The impact pressure waves appear to be largely directed at right angles to the cylinder axis. These results were open to some question, however, since the beams were subjected to several different waves of impact pressure and had clearly become quite hot and correspondingly weak during the test.

B. Single compression ignition tests

To avoid the questionable features of the multiple tests, the procedure was modified so that the test beams were subjected to but a single cycle of compression ignition. This was accomplished with the aid of a selector valve in the engine intake manifold, which permitted the operator to admit either air or air-fuel mixture to the engine. By turning the selector valve quickly past the air-fuel mixture position, a single cycle of compression ignition could be obtained.

Single cycles of compression ignition bent beams of up to 0.010-in. thickness as shown in Figure 4, but the extent of damage was distinctly less than with multiple cycles. In particular, beam B was not always damaged, but when damaged was twisted as previously. Beam A was always damaged, and by bending as previously. In these single cycle tests the steel beams became straw-colored, demonstrating that they were cooler than in the multiple cycle tests where a black and partially flaked oxide film was formed.

These results again demonstrate the presence of impact pressures and more clearly show their directional nature. The impact pressure waves appear to travel parallel to a diameter of the disc-shaped combustion chamber. The impact pressure is thus applied directly to a wide face of beam A, and it is bent directly backward or forward. On beam B the impact pressure acts on the thin edge of the beam and either no failure results or beam B buckles and becomes twisted.

C. Normal spark ignition tests

Several cycles (5 to 10) of normal, spark ignited, engine combustion or ordinary air compression failed to damage the thinnest (0.0015 in.) beams as shown in Figure 5, runs 1, 2, 6, and 7. However, when knock was obtained, as in runs 8 and 9 of Figure 5, beam A was bent slightly, indicating the presence of impact pressures.

These tests show that normal combustion and

air compression do not create appreciable impact pressures, even though they greatly increase cylinder pressures. Knock, on the other hand, creates impact pressure waves but has relatively little effect on average cylinder pressures.

The mechanical strength properties of the beam steel, needed for the above calculations, were estimated from measurements of indentation hardness and ultimate tensile strength. These properties are presented in Table 1.

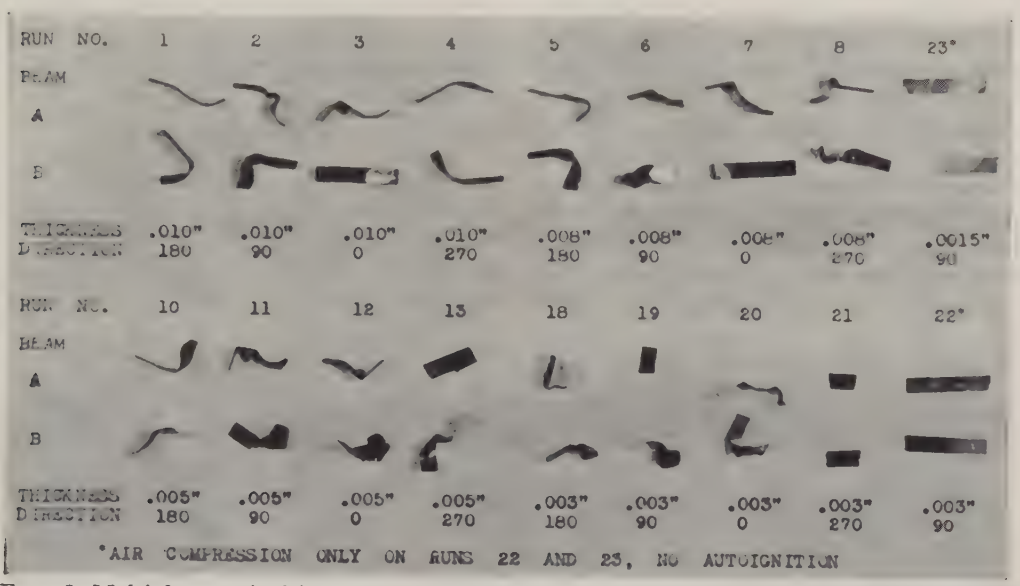

FIG. 3. Multiple autoignition tests in the Christie engine. Normal heptane fuel at 11.3 to 1 compression ratio.

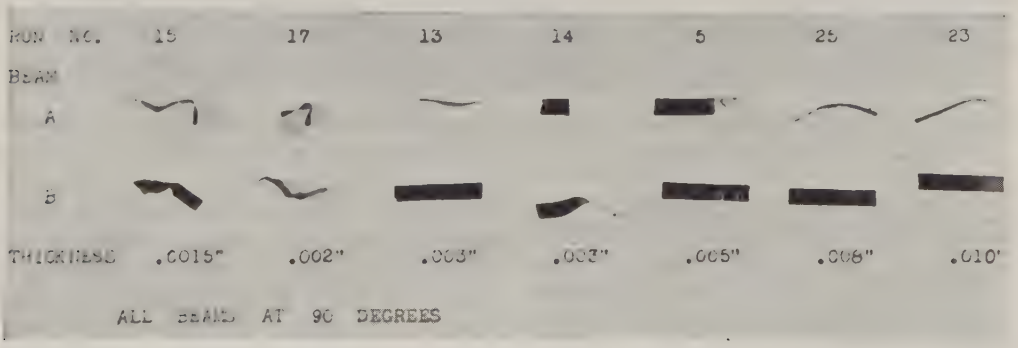

FIG. 4. Single autoignition tests in the Christie engine. Normal heptane fuel at 11.3 to 1 compression ratio.

D. Analysis of beam failures

The magnitude of the impact pressure can be estimated by assuming that the 0.010-in. beam was bent by a simple impact pressure load and that the 0.003-in. beam was sheared off by a similar load. Two very different values of impact pressure result from this calculation: 10 psi for bending and about 700 psi for shear. This wide discrepancy of results is attributed to the fact that the impact pressure applies only briefly to the beam and the inertia of the beam itself resists bending.

If beam inertia is the major resistance to deformation from abrupt loads, then shorter beams, being of reduced inertia, should be about as easily deformed as the longer beams. This was indeed found to be the case, as shown in Figure 6. In these single compression ignition tests 0.005 in. and 0.008 in. beams were about equally deflected whether 0.250 in. long or 0.500 in. long.

A theoretical analysis of the beam loading and resultant stresses was undertaken with allowances for the effect of the beam inertia. The following simplifying assumptions were made: (1) Impact

pressure is applied as a square wave of short time duration. (2) The beam behaves elastically throughout the duration of the impact pressure wave. (3) The angular velocity of the beam, at a particular time, is constant over the beam length. (4) Strain energy is distributed in the beam as it would be if the beam were statically deflected with a uniformly distributed load. It is difficult to estimate the magnitude or direction of error introduced by these assumptions.

One result of this analysis was the demonstration that the 700-psi impact pressure, calculated by assuming simple shear, is probably the correct value. Throughout the application of the impact pressure, the total shear load at the clamped root of the beam was found to be equal to at least 90 per cent of the product of the impact pressure times the beam area. Hence the 700-psi impact pressure calculated from the observed shear failure of the 0.003-in. beam is approximately correct. This conclusion is largely independent of the simplifying assumptions.

By applying conservation of energy and momentum, a mathematical relation was obtained between the magnitude, p, and the duration, t, of the impact pressure pulse capable of permanently bending the 0.010-in. beam as observed experimentally.

$$pt = 3.55 \times 10^{-4} \text{ psi sec}$$

The reasonableness of this relation was checked very approximately by assuming the thickness of the impact pressure wave to be about the same as the thickness of the supporting chemical reaction zone behind the detonation wave. Detonation wave velocities of 5500 ft/sec are known for hydrocarbon-air mixtures.[5] Using this velocity and the above relation, a wave thickness of 0.034-in. (0.85 mm) is calculated for an impact pressure of 700 psi. Reaction zone thicknesses of about 1 cm have been estimated for gaseous reactants[6] initially at room temperature and atmospheric pressure. If we assume reaction zone thickness to decrease directly with reactant density, reaction zone thickness would be about 0.9 mm at the engine operating conditions used for these tests. This agreement suggests that the experimental results on beam bending are in reasonable harmony with the results on beam shearing and that beam inertia is indeed the principle resistance to bending from brief impact pressure loads.

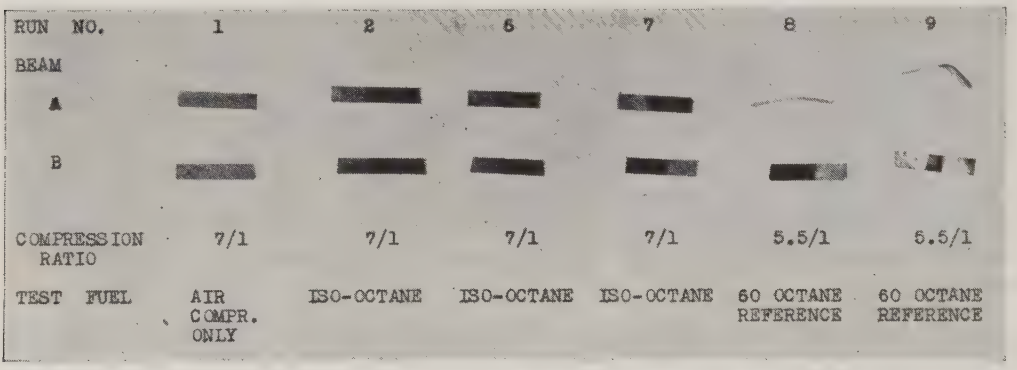

FIG. 5. Spark ignition tests in the Christie engine at 1000 rpm. All beams 0.0015-in. thickness.

TABLE 1. MECHANICAL PROPERTIES OF STEELS USED IN THE TEST BEAMS

Beam Thickness	Rockwell Superficial Hardness 15T	Ultimate Tensile Strength*	Tensile Yield Strength†	Ultimate Shear Strength‡
in.		*psi*	*psi*	*psi*
.0015	94.9	147,000	95,500	98,500
.002	93.5	145,000	94,200	97,100
.003	94.9	146,500	95,200	98,200
.004	92.5	133,000	86,500	89,000
.005	91.4	131,000	85,000	87,800
.008	87.0	115,000	74,700	77,000
.010	79.5	94,300	61,300	63,200

* Measured in a Laucks tension test machine.

† Calculated as 0.65 times ultimate tensile strength.

‡ Calculated as 0.67 times ultimate tensile strength.

E. Summary of beam tests

The foregoing experiments and analysis show that compression ignition generates directional impact pressure waves and that these waves possess an impact pressure component of the

order of 700 psi. Although these results do not prove that compression ignition is a detonation wave process, they strongly support this theory. It is difficult to postulate a process, other than a detonation wave, capable of generating these very strong waves of impact pressure. These results, combined with the photographic evidence cited previously, constitute a compelling argument in support of the detonation wave theory of knock.

II. SHOCK WAVES FROM PREFLAME REACTIONS

A chemical reaction which proceeds in such a manner as to cause an accelerating pressure increase can set up a shock wave and thus a detonation wave. The individual pulses of pressure increase will merge to form a shock wave when the pressure increase is accelerating.[5] After such a shock wave has been formed, the material immediately behind the shock front may be sufficiently compressed to react rapidly and in turn send pressure pulses forward to maintain the shock front. This latter condition is a detonation wave which is very stable, provided the supporting chemical reaction immediately behind the shock front can keep up with the shock front. There are thus two independent chemical reactions, the shock-wave-initiating reaction which need only accelerate and the detonation-wave-supporting reaction which must be sufficiently rapid to keep up with the wave front.

To obtain shock waves experimentally from preflame reactions without also obtaining a detonation wave in an engine requires that the supporting chemical reaction behind the shock front be drastically inhibited without a concurrent inhibition of the initiating preflame reaction. Tetraethyl lead antiknock material is ideally suited to this purpose, since it is known to suppress both knock and compression ignition without significantly inhibiting preflame reactions.[4]

Motoring tests were accordingly run in the engine, using normal heptane fuel to which was added 6 cc of tetraethyl lead per gal. To discern pressure waves a conventional magnetostrictive, rate-of-change-of-pressure indicator, manufactured by the Phillips Petroleum Company, was installed in the engine. The electrical output of this indicator was connected to the vertical deflection plates of a cathode ray oscilloscope, so that a diagram of rate-of-change-of-pressure (dp/dt) against time could be examined on the oscilloscope or photographed.

At low compression ratio, a simple compression diagram is obtained, as shown on upper Figure 7, without evidence of any reaction occurring. At higher compression ratio preflame reaction (i.e., cool flame reaction) occurs and produces a diagram such as that shown on lower Figure 7. This preflame reaction releases little energy, is incapable of running the engine and causes only about 150°F rise of exhaust temperature. The pressure increase caused by the preflame reaction is seen to accelerate (d^2p/dt^2 is positive) initially, indicating that the preflame reaction is capable of generating a shock wave, provided sufficient reactant volume is available.

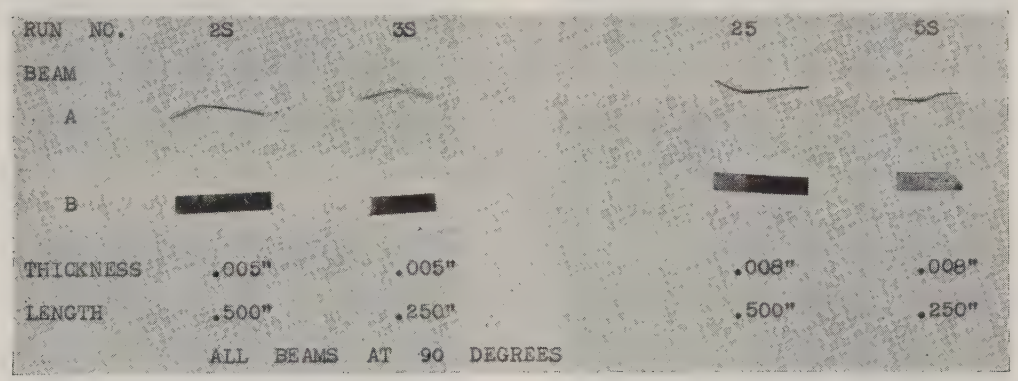

FIG. 6. Single autoignition tests in the Christie engine. Normal heptane fuel at 11.3 to 1 compression ratio.

When compression ratio is further increased or mixture ratio made somewhat richer than the above condition, distinct pressure waves are created by the preflame reaction of the leaded normal heptane as shown on Figure 8.

When the pressure fluctuations became about twice as large as those shown on Figure 8, com-

pression ignition occurred during the expansion stroke sometime after the preflame reaction. Unfortunately a photograph of this latter phenomenon could not be obtained as the engine speeded up when compression ignition occurred and the diagram drifted rapidly off the oscilloscope screen. It was consistently observed that compression ignition was obtained only when severe pressure fluctuations were created by the preflame reaction.

When the preflame reaction was occurring with pressure waves, but without compression ignition,

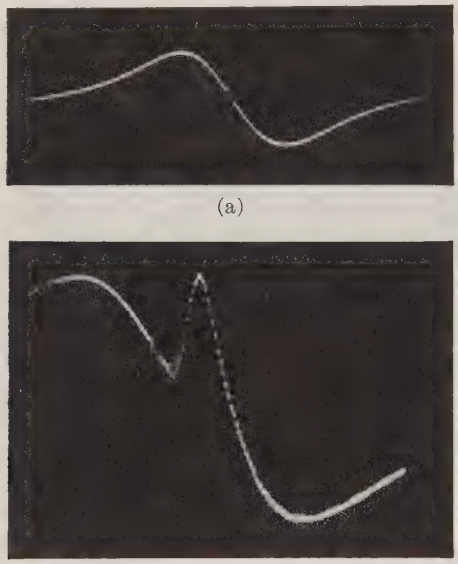

(a)

(b)

Fig. 7. Motoring tests in Christie engine at 8.5 to 1 compression ratio and 1000 rpm. (a) Rate of change of pressure diagram for air compression only. (b) Rate of change of pressure diagram for compression of normal heptane and 6 ml TEL at 0.07 fuel-air ratio showing cool flame reaction.

a sound came from the engine closely resembling a light knock. This sound could only be eliminated by turning off the fuel or eliminating the pressure waves by reduced compression ratio. This latter observation, together with the observation of pressure fluctuations, indicates that shock waves were formed by the preflame reaction.

The presence of these pressure fluctuations and sounds does not prove that the preflame reaction generated a shock wave. However, if a shock wave is generated by the preflame reaction then the pressure fluctuations and sounds must be present as they are. Although the data are not conclusive, the concept that preflame reactions can form shock waves is supported by the results, particularly the observation that compression ignition occurred whenever strong pressure fluctuations were obtained.

Discussion

The foregoing experimental results strongly support the theory that knock and compression

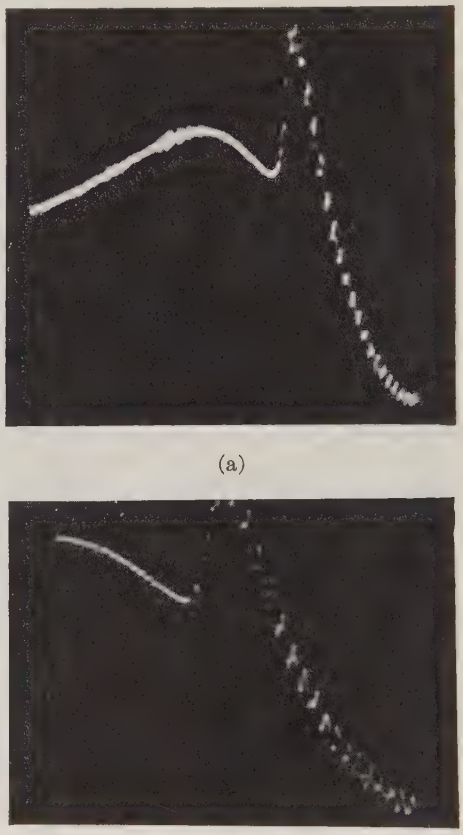

(a)

(b)

Fig. 8. Motoring tests in Christie engine at 8.5 to 1 compression ratio and 100 rpm. Rate of change of pressure diagrams for compression of normal heptane and 6 ml TEL at 0.08 fuel-air ratio showing cool flame reaction with pressure wave formation.

ignition are a detonation wave process initiated by a shock wave formed by the preflame reaction. Both knock and compression ignition generate impact pressure, as do detonation waves. The preflame reaction creates pressure fluctuations which appear to be the direct cause of compression ignition. These observations and many other known properties of the knock and compression ignition processes are most easily explained by the detonation wave theory of knock.

APPLICATION OF THEORY TO KNOCK PHENOMENA

In the measurement of gasoline octane ratings the engine operating conditions needed to obtain a detonation wave in the end gas are measured and the preflame or slow oxidation properties of the gasoline determine what these conditions must be. Hence gasoline octane ratings correlate well with slow oxidation properties.[3]

The gross geometric arrangement of a mass of detonable reactant about the shock-wave-initiating source can make the attainment of a detonation easier. Generally large linear dimensions are needed since the shock wave must achieve the required strength within the volume of the reactant. Thus in a nonspherical reaction mass the most probable direction of a detonation wave is along the greatest linear dimension. In the disk-shaped combustion chamber of the test engine the most probable direction of a detonation wave and its impact pressure is along a diameter of the cylinder. We can thus account for the consistently greater damage to beam A than to beam B in these compression ignition tests. The well known cycle-to-cycle irregularity of knock in engines can also be explained as due to changes of the geometry of the reactant mass resulting from cycle-to-cycle changes of position of the preflame reaction within the end gas. Occasionally the preflame reaction will be ideally located to produce detonation of a large volume of end gas and a severe knock thus results.

No theory of knock is complete without an explanation of the very large effect of tetraethyl lead as a knock inhibitor. Tetraethyl lead appears to make the fuel-air mixture more difficult to detonate without greatly affecting its ability to undergo preflame reaction and form shock waves. Evidence supporting this theory of tetraethyl lead antiknock action is obtained when we seek to discern shock waves produced by the preflame reactions of unleaded fuels. Preflame reaction diagrams of two unleaded fuels are shown on Figure 9. The engine conditions were such that occasional cycles of compression ignition occurred.

The preflame reactions are clearly evident but the pressure fluctuations are not. Visual examination of the oscilloscope revealed that pressure fluctuations did occur occasionally and that compression ignition always followed these fluctuations. The pressure fluctuations needed to detonate these unleaded fuels were much smaller than those needed to detonate the leaded normal heptane even though all three fuels are of about the same octane rating. Tetraethyl lead did not inhibit the ability of normal heptane to undergo preflame reaction and form shock waves, but so severely inhibited the supporting reaction behind the shock front that it could not keep up with the shock wave. Hence no detonation was obtained. To detonate the leaded fuel required that compression ratio be increased so that stronger shock waves were obtained from the preflame reaction. Although a stronger shock wave travels faster, the supporting chemical reaction is even more accelerated by the shock compression and can eventually keep up with the shock wave and produce detonation.

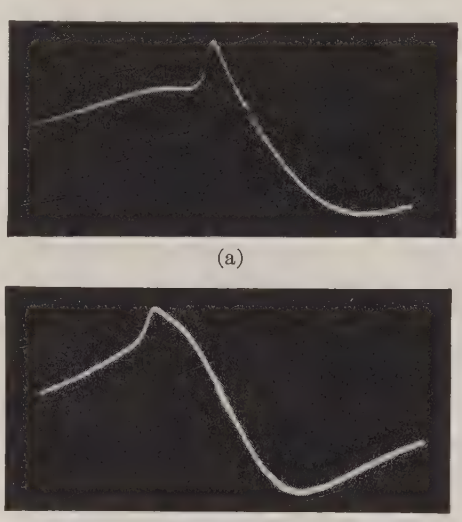

(a)

(b)

FIG. 9. Motoring tests in Christie engine at 9.0 to 1 compression ratio and 1000 rpm. Rate of change of pressure diagrams for two fuels at 0.08 fuel-air ratio showing cool flame reaction. (a) Heptane plus 50 per cent benzene. (b) Heptane plus 50 per cent isooctane.

REFERENCES

1. SOKOLIK, A., AND VOINOV, C.: Bull. Acad. Sci. (USSR), 123 (1927).
2. MILLER, C. D.: Soc. Aut. Engr. Quarterly Trans., *1*, 98 (1947).
3. BARUSCH, M. R., AND PAYNE, J. Q.: Ind. Eng. Chem., *43*, 2329 (1951).
4. PASTELL, D. L.: Soc. Aut. Engr. Quarterly Trans., *4*, 571 (1950).
5. JOST, W.: *Explosion and Combustion Procesess in Gases*, p. 179 and p. 196. New York, McGraw-Hill Book Co., 1946.
6. GORDON, W. E.: *Third Symposium on Combustion, Flame and Explosion Phenomena*, p.

579. Baltimore, The Williams & Wilkins Co., 1949.

Discussion by Cyrus G. Dunkle*

I concur in the suggested criterion of detonation, a highly unidirectional component of impact pressure; this component is applied by the particle velocity, or material velocity, which is of course one-dimensional.

The concept that the cool flame reaction can generate shock waves has support from the findings of both Germans and Russians during World War II.†

Both agreed that knock is always a two-stage process, there being always a cool flame followed by a normal flame. Such ignition ahead of the moving flame front characterizes the oxidation at moderate temperatures of all hydrocarbons, possibly including even methane and benzene, and is due to a peroxide-catalyzed autoxidation. The view that knock occurs only in a mixture previously traversed by a cool flame is supported also by papers presented in previous combustion symposia, e.g., the paper in the Third Symposium Proceedings (1949) by Spence and Townend, pp. 404–424, those in the Fourth Symposium Proceedings (1953) by Egerton *et al.*, pp. 396–402, Grove and Walsh, pp. 429–439, and Schmidt *et al.*, pp. 658–666, and those in the Fifth Symposium Proceedings (1955) by Ball, pp. 366–372, Levendahl, pp. 372–376, and others. The Report of the Fourth Symposium in "Chemical and Engineering News," Sept. 15, 1952, pp. 3832–3837 is of interest also.

Author's Reply

I certainly concur with the several comments made by Mr. Dunkle.

The generality of detonations as a reaction mechanism is probably widely recognized, but this important point appears to have escaped the emphasis it deserves. Apparently any exothermic, pressure generating reaction can occur detonatively. Professor A. R. Ubbelohde in his paper, "The Possibility of Weak Detonation Waves," Fourth Symposium (International) on Combustion, speculates that low energy crystalline transformation reactions could occur detonatively in very large reaction masses such as might exist in underground magma chambers.

In analyzing very fast reactions we need only ascertain whether they occur as detonations and, if so, whence came the needed shock wave, to have a basic understanding of the process.

The exact source of the shock wave needed to produce gasoline engine knock remains to be clearly demonstrated. In the paper the preflame reaction was proposed as the source. In further research we hope to ascertain more clearly the shock wave source in the engine.

* Picatinny Arsenal.

† A. Sokolik and S. Yantovskii: Acta physicochim. (URSS), *19*, 329–359 (1944); and F. A. F. Schmidt: Motortech. Z., *5*, 41–46 (1943).

120

FLAME QUENCHING AT THE WALLS OF AN INTERNAL COMBUSTION ENGINE

By W. A. DANIEL

Introduction

Hydrocarbons which are found in the exhaust gas of automobiles are considered partially responsible for the Los Angeles smog. About $\frac{1}{3}$ of the total amount of unburned hydrocarbons exhausted by automobiles in the Los Angeles area is emitted during deceleration operation.[1] During deceleration the concentration of unburned hydrocarbons in the exhaust gas may be as high as 60 per cent when expressed as the weight per cent of the fuel supplied to the engine. The reasons for the high concentrations have been established.[2] The other $\frac{2}{3}$ of the total amount of unburned hydrocarbons is exhausted during full-throttle, road-load, and idle operation. Under these conditions the concentrations are usually less than 5 per cent. Three possible explanations for these low concentrations are: (1) the hydrocarbons are an equilibrium product of the combustion reaction, (2) the highly turbulent gases in the combustion chamber enable small pockets of unburned mixture to pass through the reaction zone without igniting, and (3) flame quenching at the relatively cool walls of the combustion chamber may prevent a portion of the fuel-air mixture from reacting.

This paper presents experimental evidence which indicates that the low concentrations of unburned hydrocarbons found in the exhaust gas of automobiles may be due to the quenching of the combustion reaction at the walls of the combustion chamber.

Equipment

A laboratory single-cylinder engine was used for the investigation. The top of the combustion chamber was a quartz window with which it was possible to observe the region next to the vertical walls of the combustion chamber in a direction parallel to the wall surface. Figure 1 is a view looking down through the quartz window into the combustion chamber. The combustion chamber was of the L-head type, and the engine was operated at a compression ratio of 6.7.

Engine speed was maintained at 500 ± 10 rpm by means of a dynamometer, and a spark timing of top dead center was used. Engine cooling water temperature and the engine oil temperature were 150° ± 5°F. Propane was used as the fuel, and both fuel flow and air flow were measured by means of critical flow nozzles. Engine inlet pressure was adjusted by regulating the rate at which air was admitted to the engine.

To obtain photographs of the flame radiation in the vicinity of the wall of the combustion chamber, a portrait-type camera was equipped with an extension to increase the lens to film distance so that a magnification of ten could be obtained. The focal length of the lens was 3 in. and an aperture of f/40 was used to obtain a depth of field comparable to the depth of the combustion chamber (0.375 in.). The field of view of the camera is indicated in Figure 1 and measured approximately 0.4 by 0.5 in.

A stroboscopic disc was used between the lens and the film to limit to about 10 crank-angle degrees the time during which an observation was made of the flame front passing a given wall location. Film exposure times ranged from about 1 hr to 23 hr; therefore, each photograph represented an average of from about 15,000 to about 300,000 cycles.

An Eastman high speed motion picture camera was used to photograph the entire combustion chamber so that the time required for the flame to propagate across the chamber could be determined. One frame of a sequence is reproduced as Figure 2 to show an average flame front position at the time the quench photographs were obtained. The film speed for this picture was about 1500 frames/sec.

The exhaust gas of the engine operated at full throttle was analyzed for hydrocarbons by infrared absorption spectroscopy. An absorption path length of two meters was obtained using a multiple pass absorption cell. The gases were analyzed at room temperature at a pressure of 750 mm of mercury. A Perkin-Elmer Model 99 monochromator was used to determine the absorption at a wavelength of 3.35 μ, and the total

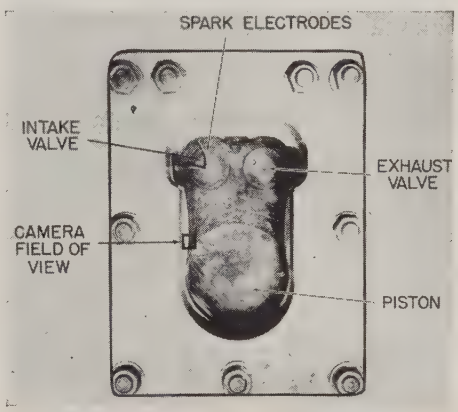

FIG. 1. Top view of combustion chamber.

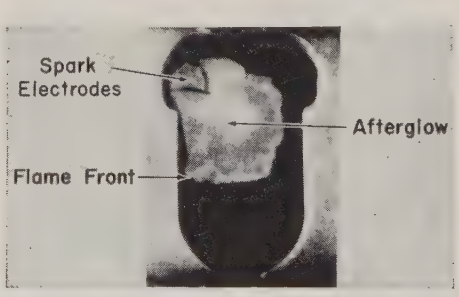

FIG. 2. Photograph showing approximate position of flame front at time quench photographs were obtained.

hydrocarbon concentration was assumed proportional to the absorption at 3.35 μ.

Photographs of the Quench Zone in an Engine

For most engine conditions visible radiation is emitted from both the flame front and the hot gases behind the flame front (see, for example, Figure 2). The latter radiation is usually referred to as the afterglow and may have no relation to any chemical reaction. As a result of turbulence the afterglow might conceivably approach closer to the wall surface, or through heat loss might

end further from the wall surface than the flame front; therefore, to determine photographically if a quench zone exists at the wall of the combustion chamber at the time the flame front passes the wall surface, it was necessary to record preferentially the radiation from the flame front.

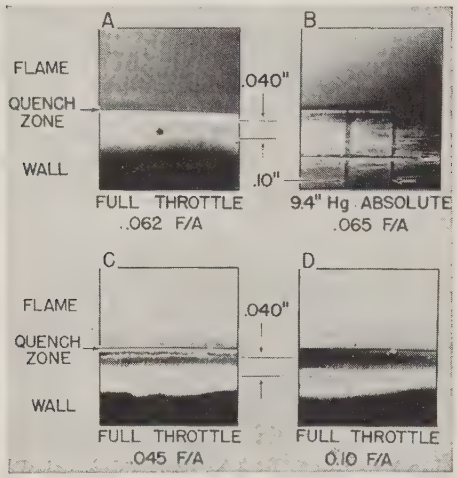

FIG. 3. Photographs showing the apparent quench zone at the combustion chamber wall.

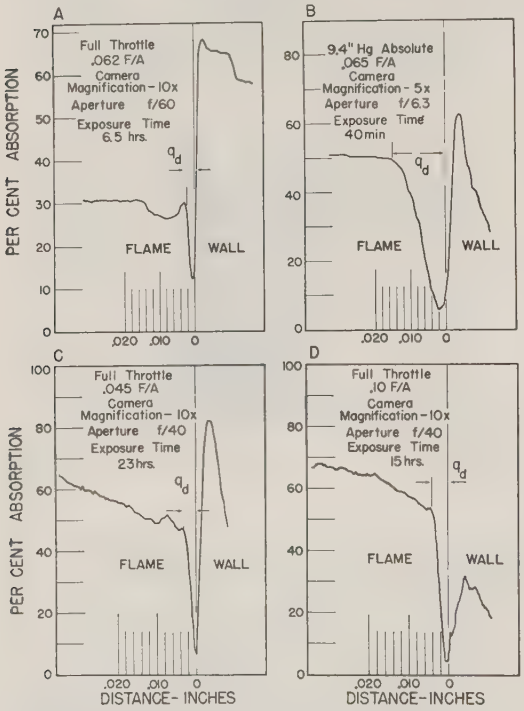

FIG. 4. Densitometer traces of the negatives of the photographs shown in Fig. 3.

It was experimentally difficult, however, to obtain a separation of the radiation of the flame front from that of the afterglow due to cyclic variation. Variation occurred in both the time at which radiation could pass through the opening in the stroboscopic disk due to gear backlash, and in the position of the flame front with respect to the field of view for a given timing of the stroboscopic disc. In addition, the relative flame front speed was great enough so that during the time radiation could pass through the opening in the stroboscopic disk and be recorded on the film, the flame front could move across the field of view. (Shorter stroboscopic disc opening times were prohibited by the exposure time required to obtain a film image which in turn was limited by how long the window remained clean.) As a result of these complications only a partial separation of the flame front radiation from that of the afterglow was obtained. This partial separation was achieved by adjusting the stroboscopic disk timing so that a flash of radiation from the combustion chamber was visible through the lens in about $\frac{1}{2}$ of the cycles.

In Figure 3 are shown four quench photographs which serve to indicate the effects of both fuel-air ratio and engine inlet pressure. The wall surface is perpendicular to the plane of the photograph and the top of the wall is located in the lower half of each photograph. The radiation from the combustion chamber is recorded in the top half of each photograph. A dark zone or quench zone may be seen between the wall and the chamber. The width of the quench zone may be estimated from the indicated distances between the reference lines which were scribed on the top surface of the wall. The top of the wall was illuminated by a projected spot of light which spilled over into the combustion chamber.

The apparent quench zone extends along the entire length of the wall surface in the pictures, and no definite flame front position is apparent. If the radiation from the combustion chamber were divided into thirds by two lines drawn perpendicular to the wall, then the image in the right hand third is probably due essentially to radiation from the flame front but also due to some afterglow radiation. The image in the middle third is probably due to partly flame front radiation and partly to afterglow, and the image in the left hand third is probably due to mostly afterglow radiation. Within the accuracy of the measurements no difference in quench zone thickness across a given picture was detected.

In Figure 4 are shown densitometer traces of the negatives of each of the quench photographs

of Figure 3 and are located in the corresponding positions. The different exposure times noted were required since the flame intensity decreased as the fuel-air ratio was changed from stoichiometric and also as the engine inlet pressure was decreased. With a change in exposure time the illumination of the wall was changed in an attempt to obtain about the same image density for both flame and wall for a given picture. In Figures 3B and 4B the camera magnification was five but in the printing process an enlargement was made so that an effective magnification of ten was obtained and these figures are thus directly comparable with the others.

Each quench photograph negative was traversed by the densitometer at right angles to the wall surface and in about the middle of each negative. The per cent absorption of the densitometer beam by the negative is indicated along the ordinate and the distance in inches in a plane parallel to the combustion chamber floor is indicated along the abscissa. The apparent quench zone thickness (q_d) is indicated on each trace. It may be seen that at full throttle the quench distance increased from about two thousandths of an inch (Fig. 4A) at a propane-air weight ratio near stoichiometric (0.062) to about 0.004 in. at a fuel-air ratio of 0.10 (Fig. 4D) and to about 0.003 in. at a fuel-air ratio of 0.045 (Fig. 4C). With approximately stoichiometric mixtures, the quench distance increased from about 0.002 in. (Fig. 4A) to about 0.0015 in. (Fig. 4B) when the engine intake manifold pressure was decreased from about 29.4 in. of mercury to about 9.4 in. of mercury absolute.

Another factor to be considered in interpreting the quench photographs arises from a consideration of Figure 5. To observe the quench zone the optical axis of the camera was aligned with the wall surface. Upon examination of the relative position of the camera lens and the cross sectional view of the combustion chamber, it becomes apparent that if point sources of uniform intensity of radiation were assumed along the floor of the combustion chamber all the way over to the wall surface (no quench zone), the lens would discriminate against those point sources located closer to the wall than the point m since a portion of the lens area would be lost to those point sources due to the top edge of the wall at t. Thus an apparent decrease in radiation in the vicinity of the wall would be recorded on the film. This discrimination by the lens or "wall-shadow effect" would reach a maximum for the point source located at the intersection of the wall surface and the floor of the combustion chamber and the intensity decrease would amount to a factor of one-half, since one-half the lens area would be in the shadow of the top edge of the wall for this point. The distance from the wall to m is easily calculated knowing the distance from the lens to the top edge of the wall, the lens diameter, and the depth of the combustion chamber. For the camera settings used for Figure 4A the distance from the wall to m is 0.0025 in.; for Figure 4B, 0.0250 in.; and for Figures 4C and 4D, 0.0045 in.

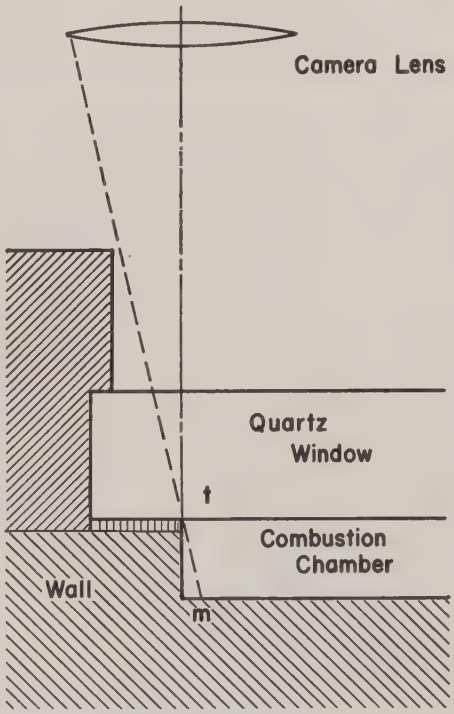

FIG. 5. Schematic showing relative positions of camera lens and combustion chamber.

A comparison of these values with the corresponding apparent quench distances indicates that the wall-shadow effect must be considered.

A photograph of a standard gray scale taken with similar film and developed in a similar manner was used to convert the density of the negative of Figure 4D to the relative intensity of the source. It was found that the minimum intensity of radiation recorded in the apparent quench zone was less than one-third the intensity of radiation found further from the wall than m. Since the wall-shadow effect could only decrease the intensity of radiation to one-half it may be concluded that the decrease in radiation in the

vicinity of the wall is due to some factor in addition to the wall-shadow effect.

Although the possibility exists that still other unknown optical effects may cause the decrease in radiation in the vicinity of the wall, the variation of the width of the decrease in radiation zone determined two relations for predicting the quench distance (q_d). For stoichiometric and rich mixtures q_d is proportional to

$$\frac{1}{P^{0.91}T^{0.50}} \tag{1}$$

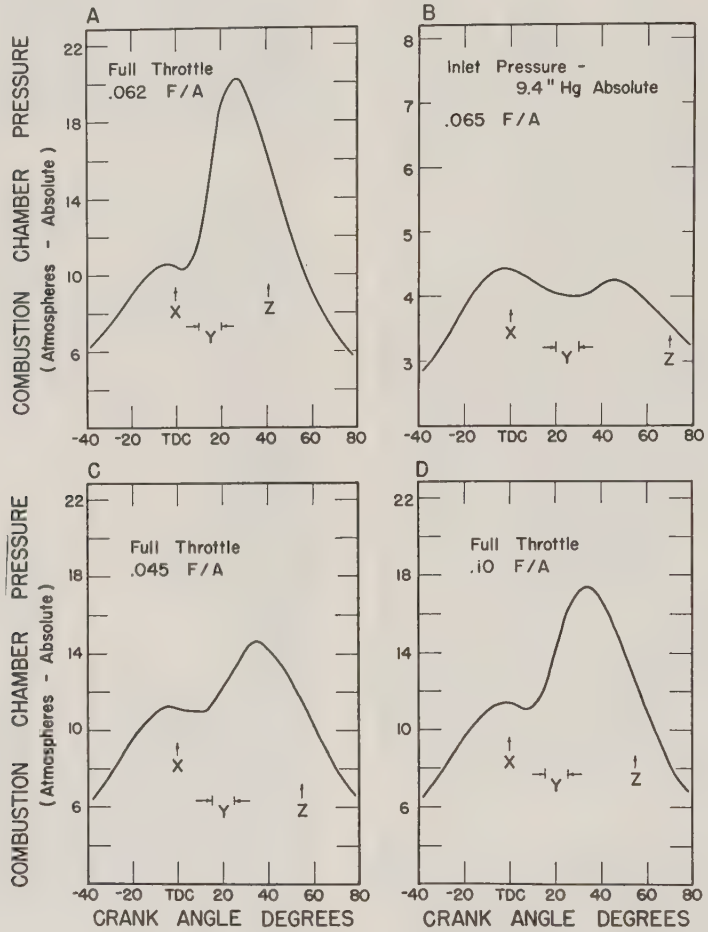

FIG. 6. Combustion chamber pressure as a function of crank angle degrees.

with engine conditions supports the assumption that the decrease in radiation is primarily due to wall-quenching phenomena.

A Comparison of the Experimental Quench Distance with Calculated Quench Distances

Friedman and Johnston[3] determined quench distances for propane-air flames by a rectangular-slot-burner flash back method at pressures between 0.0832 and 2.77 atmos, at temperatures between 75°F and 715°F, and at fuel-air ratios between 0.10 and 0.042. From their data they and for lean mixtures q_d is proportional to

$$\frac{1}{P^{0.76}T^{0.85}} \tag{2}$$

where P is the absolute pressure and T is the absolute temperature of the gas in the quench zone.

A quench distance in the engine may be calculated using relations (1) and (2) by determining the pressure and temperatures existing in the engine. Pressure records were obtained at the engine conditions used for obtaining the data shown in Figures 3 and 4 and are shown in Figure

6. Three points are indicated on each pressure record: the time of occurrence of the ignition, X, the time during which the quench photographs of figure 3 were obtained, Y, and the time at which combustion was complete, Z. The temperatures of the gases in the quench zone are estimated to differ only slightly from the engine coolant temperature (Table 1). By choosing a value for the quench distance determined by Friedman and Johnston at a known pressure and temperature a quench distance may be calculated for other pressures and temperatures. Using the Friedman and Johnston value of 0.0355 in. for q_d at $P = 1$ atmos and $T = 535°R$ and determining P' (the average pressure) from Figure 6 for the time during which the quench photographs were obtained, the quench distances given in Table 1 were obtained.

The calculated and experimentally determined values of the quench distance as shown in Table 1 agree remarkably well considering the assumptions involved in the calculations and all the possible differences between the engine and a burner. This agreement provides additional evidence for the existence of wall-quenching in an internal combustion engine.

In Figure 7 are shown results obtained by analyzing the exhaust gas of the single cylinder engine operated at full throttle for unburned hydrocarbons. The ordinate is the relative hydrocarbon concentration with the concentration at stoichiometric arbitrarily chosen as one and the abscissa is the fuel-air weight ratio. A minimum hydrocarbon concentration occurred at a somewhat leaner mixture than stoichiometric.

To evaluate the possibility that these unburned hydrocarbons are due to a wall-quenching of the flame-reaction, the following assumptions were made: (1) the dark region between the wall and the flame radiation (Fig. 4) actually defines the limits of a quench zone; (2) a homogeneous mixture of fuel and air exists in the combustion chamber prior to inflammation; (3) none of the hydrocarbons existing in the quench zone are completely oxidized, either during or after the flame front passage; and (4) the quench zone is of uniform thickness over all the combustion chamber surface exposed to the flame front. The fourth assumption ignores the effects of changing pressures and temperatures during the cycle as well as the hotter surface of the quartz window which was used as the top of the combustion chamber.

Using these four assumptions and the measured quench distances indicated in Figure 4 and the surface area and volume of the combustion chamber at the time the combustion was completed, a quench volume, V_q, was calculated. The ratio of the quench volume to the total volume, V_t, at the time of the completion of combustion is given in Table 2.

In Table 2 a comparison may be made between the relative values of V_q/V_t and the relative unburned hydrocarbon concentrations obtained from Figure 7. The corresponding relative values of V_q/V_t and of hydrocarbon concentration are

TABLE 1

F/A	Engine Pressure P'	Engine Temperature T'	Calculated q_d	Experimental q_d(Fig. 4)
	atmos	°F		
0.100	13.4	650	0.0030	0.004
0.062	15.0	675	0.0027	0.002
0.045	13.4	650	0.0042	0.003
0.065	4.0	625	0.0093	0.015

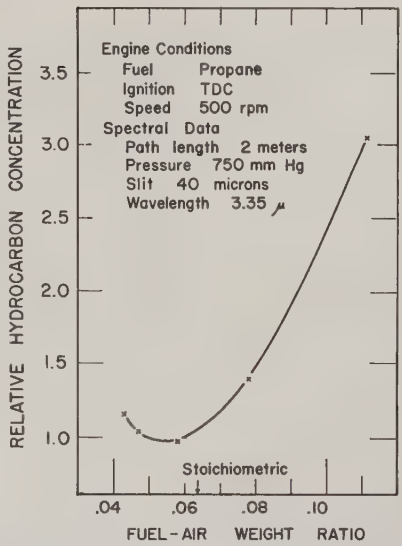

FIG. 7. Relative hydrocarbon concentration in engine exhaust gas as a function of fuel-air ratio.

TABLE 2

F/A	V_q/V_t	Relative V_q/V_t	Relative Hydrocarbon Concentration (Fig. 7)
0.100	0.0147	1.65	2.4
0.062	0.0089	1.00	1.0
0.045	0.0110	1.24	1.1

in fair agreement and would indicate that a large part of the unburned hydrocarbons found in the exhaust gas could occur because of a wall-quenching of the combustion reaction.

Converting the ratio V_q/V_t to percent unburned hydrocarbons at the end of combustion and calculating a similar value for the light load engine condition (9.4 in. of mercury inlet pressure) values of 0.89 and 3.1 per cent unburned hydrocarbons respectively are obtained for a stoichiometric fuel-air ratio. These values are comparable to the values obtained by other workers[4, 5] from an analysis of automobile exhaust gases for comparable engine inlet pressures.

Summary

Experimental evidence is given which indicates that wall-quenching of the combustion reaction occurs in an internal combustion engine. The apparent quench distances observed are in agreement with the quench distances calculated from burner data at approximately the same pressures and temperatures. In addition, the observed quench distances are of the right order of magnitude to account for the unburned hydrocarbons found in the exhaust gas of automobiles operated in the range of full throttle and road load.

REFERENCES

1. Magill, et al.: Proc. Second National Air Pollution Symposium, p. 71, 1952.
2. Wentworth, J. T., and Daniel, W. A.: Soc. Am. Engr. Trans., *63*, 602 (1955).
3. Friedman, R., and Johnston, W. C.: J. Appl. Phys., *21*, 791 (1950).
4. Air Pollution Foundation, Report No. 8, 1955.
5. Twiss, et al., J. Air Pollution Control Assoc., *5*, 75 (1955).

Discussion by Walter Cornelius*

Mr. Daniel has shown by means of photographs of flame radiation in a single-cylinder internal combustion engine that a dark zone exists at the walls of the combustion chamber at the time the flame front passes the wall surface. In addition, he has presented data that indicate a reasonable agreement between the widths of the observed dark zone and flame quench distances calculated by the procedure of Friedman and Johnston for comparable operating conditions. As a result, Mr. Daniel has assumed that no combustion reactions were taking place in the dark zone observed by him and hence that wall-quenching of the combustion reaction occurs in an internal combustion engine.

The thermal efficiency of an internal combustion engine may be decreased significantly if appreciable wall-quenching of the combustion reaction takes place. In 1940, Withrow and Cornelius† reported that only about 81 per cent of the heat energy supposedly liberated during an explosion in a spark-ignited single cylinder internal combustion engine could be accounted for by pressure development during the combustion process. In other words, 19 per cent of the liberated heat energy is apparently lost from the working fluid. But the most important observation and the one that was not fully understood at the time was the fact that the greatest energy loss ocurred when the flame front first contacted the walls of the combustion chamber. Now in view of Mr. Daniel's experimental findings, this apparent loss in liberated heat energy of the working fluid may have been the result of a wall-quenching phenomenon.

Withrow and Cornelius employed two different procedures to determine the amount of heat energy that was released during nonknocking engine explosions. In the first procedure, the rate at which the fuel-air charge was apparently burned was calculated from high-speed flame picture and pressure data recorded simultaneously during engine explosions in a single cylinder quartz-window engine.‡ In the second method, thermodynamic charts which were developed by H. C. Hottel and co-workers,§ were used to determine the percentage of the liberated heat energy that could be accounted for by pressure developed during the recorded engine explosions.

Figure 1 presents a series of flame pictures illustrating the inflammation of an iso-octane-air mixture containing 89 per cent theoretical air. Presented below the flame pictures are the following: (1) Increments of mass burned from one flame

* Research Staff, General Motors Corporation.

† See SAE Transactions, December, 1940, pp. 526–548: "Effectiveness of the Burning Process in Non-Knocking Engine Explosions" by Lloyd Withrow and Walter Cornelius.

‡ See SAE Transactions, May 1938, pp. 185–204: "Motion Pictures of Engine Flames Correlated with Pressure Cards" by Gerald M. Rassweiler and Lloyd Withrow.

§ See "The Internal Combustion Engine" by Taylor and Taylor, book published by the International Textbook Company.

¶ Chart showing the thermodynamic properties of the combustion products of a benzene-air mixture containing 85 per cent theoretical air was supplied by Prof. H. C. Hottel of Massachusetts Institute of Technology.

picture to another calculated from observed pressures and inflamed volumes (Mass Increments Burned); (2) Increments of mass required to be burned under adiabatic conditions to produce the observed pressure increase from one flame picture to another as determined from the Hottel thermodynamic charts (Mass Increments Required); (3) Increments of mass unaccounted for (Diff. Unaccounted For—Item 2 minus Item 1).

containing 85 per cent theoretical air. Mass burned data similar to that tabulated in Figure 1 are also presented below the flame pictures.

In this explosion, only 81 per cent of the liberated heat energy could be accounted for by pressure development. As in the previously illustrated explosion, 15 per cent of the total 19 per cent of apparent energy loss occurred between Frames 8 and 10 when the flame front reached a maximum

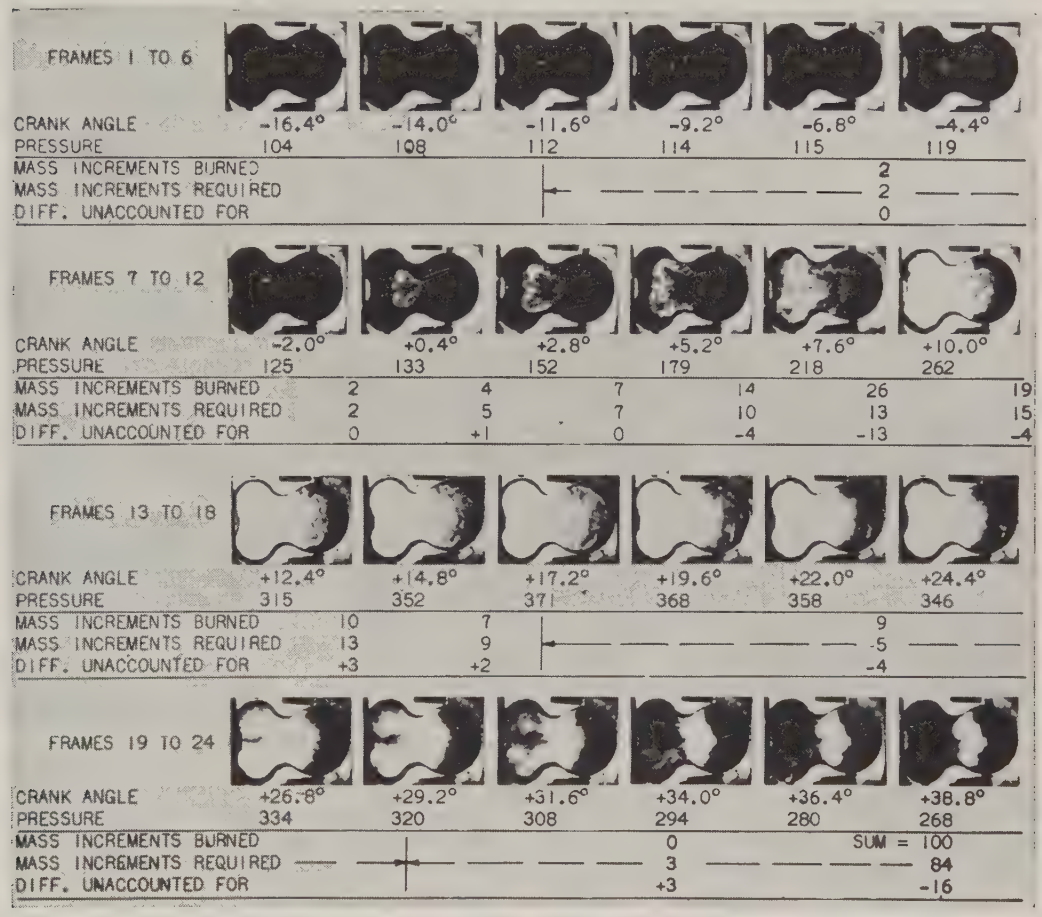
FRAMES 1 TO 6
CRANK ANGLE -16.4° -14.0° -11.6° -9.2° -6.8° -4.4°
PRESSURE 104 108 112 114 115 119
MASS INCREMENTS BURNED 2
MASS INCREMENTS REQUIRED 2
DIFF. UNACCOUNTED FOR 0
FRAMES 7 TO 12
CRANK ANGLE -2.0° +0.4° +2.8° +5.2° +7.6° +10.0°
PRESSURE 125 133 152 179 218 262
MASS INCREMENTS BURNED 2 4 7 14 26 19
MASS INCREMENTS REQUIRED 2 5 7 10 13 15
DIFF. UNACCOUNTED FOR 0 +1 0 -4 -13 -4
FRAMES 13 TO 18
CRANK ANGLE +12.4° +14.8° +17.2° +19.6° +22.0° +24.4°
PRESSURE 315 352 371 368 358 346
MASS INCREMENTS BURNED 10 7 9
MASS INCREMENTS REQUIRED 13 9 -5
DIFF. UNACCOUNTED FOR +3 +2 -4
FRAMES 19 TO 24
CRANK ANGLE +26.8° +29.2° +31.6° +34.0° +36.4° +38.8°
PRESSURE 334 320 308 294 280 268
MASS INCREMENTS BURNED 0 SUM = 100
MASS INCREMENTS REQUIRED 3 84
DIFF. UNACCOUNTED FOR +3 -16

FIG. 1. Inflammation of an isooctane-air-mixture containing 89 per cent theoretical air.

It will be noted that in this particular explosion only 84 per cent of the supposedly liberated heat energy could be accounted for by pressure development. Of the total 16 per cent apparent energy loss occurring during the explosion, 13 per cent was lost between Frames 11 and 12. At this time, the flame front reached its maximum extent and came in contact with the walls of the combustion chamber.

Figure 2 presents a series of flame pictures illustrating the inflammation of a benzene-air mixture and came in contact with the walls of the combustion chamber.

Results similar to those shown in Figures 1 and 2 were obtained from analyses of other engine explosions involving different fuels, fuel-air ratios and ignition locations. An extension of this thermodynamic analysis through the expansion stroke of the engine after combustion had ended showed that no detectable energy liberation occurred after combustion was completed.

At the time that these studies were performed, the effect of flame quenching at the walls of the

combustion chamber on the amount of energy liberated during an engine explosion was not considered. However, in view of Mr. Daniel's observations this flame quenching phenomenon may prove to be significant. As a result, it would appear to be worthwhile to repeat some of this earlier work including Mr. Daniel's technique for measuring the magnitudes of the flame quench zone and the amount of unburned hydrocarbons exhausted in order to arrive at a more exact explanation for the energy loss that occurs during a nonknocking engine explosion.

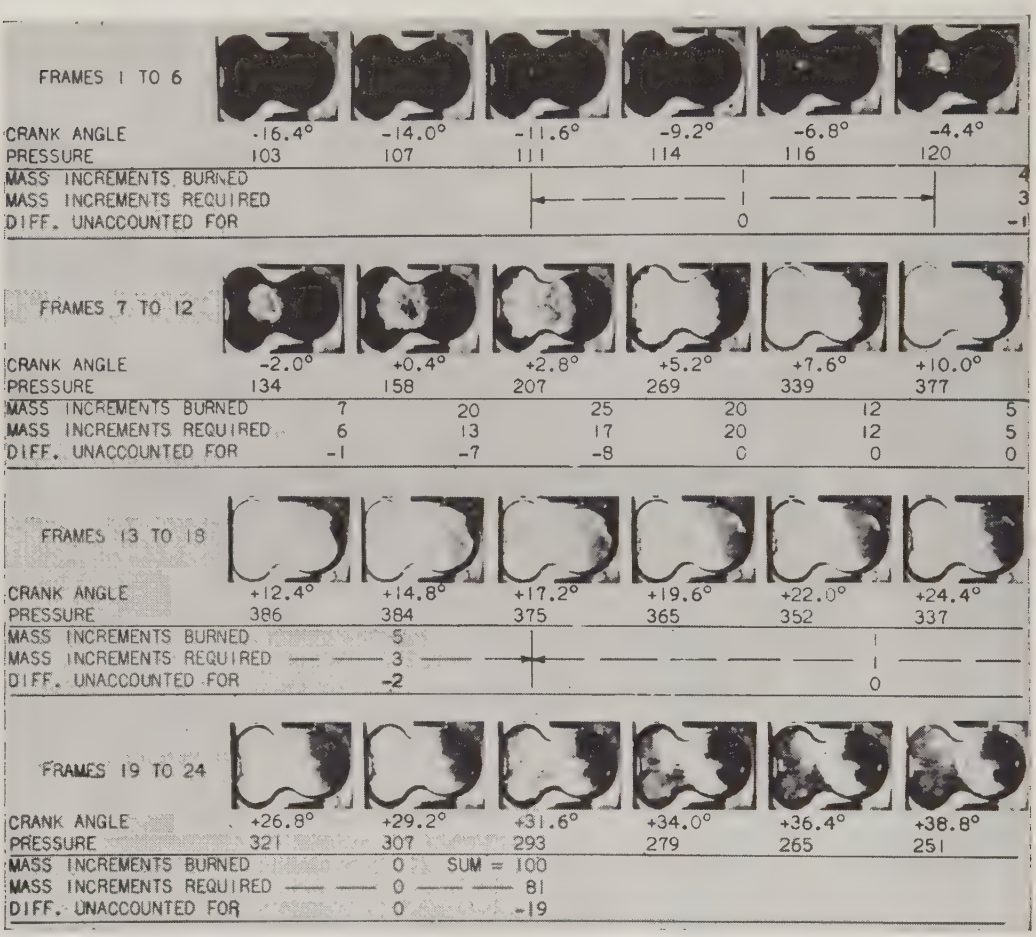
FRAMES 1 TO 6
CRANK ANGLE -16.4° -14.0° -11.6° -9.2° -6.8° -4.4°
PRESSURE 103 107 111 114 116 120
MASS INCREMENTS BURNED 1 4
MASS INCREMENTS REQUIRED 1 3
DIFF. UNACCOUNTED FOR 0 -1
FRAMES 7 TO 12
CRANK ANGLE -2.0° +0.4° +2.8° +5.2° +7.6° +10.0°
PRESSURE 134 158 207 269 339 377
MASS INCREMENTS BURNED 7 20 25 20 12 5
MASS INCREMENTS REQUIRED 6 13 17 20 12 5
DIFF. UNACCOUNTED FOR -1 -7 -8 0 0 0
FRAMES 13 TO 18
CRANK ANGLE +12.4° +14.8° +17.2° +19.6° +22.0° +24.4°
PRESSURE 386 384 375 365 352 337
MASS INCREMENTS BURNED 5 1
MASS INCREMENTS REQUIRED 3 1
DIFF. UNACCOUNTED FOR -2 0
FRAMES 19 TO 24
CRANK ANGLE +26.8° +29.2° +31.6° +34.0° +36.4° +38.8°
PRESSURE 321 307 293 279 265 251
MASS INCREMENTS BURNED 0 SUM = 100
MASS INCREMENTS REQUIRED 0 81
DIFF. UNACCOUNTED FOR 0 -19

FIG. 2. Inflammation of a benzene-air mixture containing 85 per cent theoretical air.

121

COMPARISON OF EMISSION SPECTRA OF LOW TEMPERATURE COMBUSTION REACTIONS PRODUCED IN AN ENGINE AND IN A FLAT-FLAME BURNER

By J. T. AGNEW, W. G. AGNEW AND K. WARK, JR.

Introduction

It has been known for many years that mixtures of many hydrocarbon fuels with air give rise to low temperature combustion reactions which are in some cases termed "cool flames." These low temperature combustion processes affect the operation of all types of internal combustion engines. In spark-ignition engines they are associated with self-ignition of the "end-gas" mixture ahead of the flame front, the phenomenon commonly referred to as knock. In diesel engines

they constitute an important feature of the ignition system and may contribute also to the exhaust gas odor problem. Thus, large benefits might result from a better understanding of low temperature combustion reaction kinetics and, more specifically, the transition from low temperature, partially complete reactions to the normal high temperature, complete reactions.

For practical application it is, of course, most desirable to study these reactions in operating engines. Unfortunately, such studies are beset with difficulties arising both from instrument requirements and from uncontrolled or interrelated variables. Thus it is also useful to study the same, or similar, reactions under idealized conditions outside engines.

The authors described in the Fifth Combustion Symposium[1] preliminary work performed in a spectroscopic survey of low temperature combustion reactions produced in a flat-flame burner and in a motored single-cylinder engine. The present paper describes the continuation of that work and may be considered a second progress report. In the present study attempts have been made to obtain comparable emission spectra of the two-stage cool flames stabilized in the flat-flame burner and corresponding motored-engine preflame reactions. These spectra cover the range from 2900 Å in the ultraviolet through the visible to 11 μ in the infrared. This comparison has been made to determine if the reactions, as evidenced by emission spectra of the transient molecular species present, are similar and at the same time to obtain basic information concerning the use of emission spectroscopy for the identification of transient intermediates present during low temperature combustion reactions.

Equipment and Procedure

The spectroscopic equipment, the flat-flame burner, and the single-cylinder engine have all been previously described,[1, 2, 3] and only minor changes were made for the present work.

The Perkin-Elmer Model 99 monochromator was used with a lithium fluoride prism in the ultraviolet, visible, and near infrared portions of the spectrum. Beyond 4 μ a sodium chloride prism was used. Detectors employed were 1P21 and 1P28 photomultiplier tubes for the ultraviolet and visible, a lead sulfide photoconductive cell for the near infrared, and a radiation thermocouple at wavelengths greater than 3 μ.

Complete spectra were recorded for each of the various stages in the multistage burner flames by focusing just one portion of the stabilized flame on the monochromator slit and slowly traversing the entire ultraviolet, visible, and infrared regions. However, this was not possible in the case of the engine spectra. With the fast-response photomultiplier and lead sulfide detectors the radiation signal at a given wavelength was presented as a function of time in the engine cycle on an oscilloscope screen, and spectra were obtained by reading the average peak signal height point-by-point at successive wavelength settings. Thus, the data represent average spectra recorded over a number of engine cycles at one specific crankangle during the cycle (the peak occurred at the same crankangle for all wavelengths).

The thermocouple detector, which was the only detector available with sensitivity beyond 3 μ, has insufficient speed of response to indicate the variation in radiation intensity as a function of crankangle in a given engine cycle. It was thus necessary with this detector to integrate all of the radiation emitted in each motored-engine cycle in order to obtain a spectrum. Since the normal Perkin-Elmer detection system employs a 13 cps chopper and amplifier, it was decided to operate the engine at this frequency (13 engine cycles per second equal 1560 rpm). Selsyn motors driven from the engine camshaft and connected to the monochromator chopper shaft permitted synchronization and phasing of the chopper and engine.

Since there could be no discrimination between single and double-pass radiation in the monochromator with the engine operating at 13 cps, it was necessary to mask half of the monochromator entrance and exit slits in order to record clear double-pass spectra. This, in turn, roughly halved the instrument sensitivity for the engine thermocouple spectra.

The fuels used and spectra available for comparison in this study are indicated in Table 1. It may be noted that in only a few cases was it possible to closely duplicate conditions in the engine and burner for direct comparison of spectra. This was because the different environments of the two systems only permitted the formation of low temperature combustion reactions under certain critical conditions. Cool flames were only obtained with three fuels in the flat-flame burner, and for these only at rich mixtures. In the engine, detectable preflame reactions (without autoignition) were only obtained at very lean fuel-air mixtures, and the rich mixture infrared spectra were obtained only for the

purpose of identifying the hot fuel spectra. Diethyl ether had to be diluted with the relatively unreactive isooctane in order to obtain engine operation without severe autoignition.

Table 1. Spectra Available for Comparison

Fuel	Diethyl Ether	50% Diethyl Ether 50% Isooctane (by volume)	Acetaldehyde	*n*-Heptane	70% Isooctane 30% *n*-Heptane (by volume)	Isooctane
Flat-flame burner	Visible and ultraviolet: Various rich fuel-air mixtures Near infrared: Various rich fuel-air mixtures Infrared: One rich fuel-air mixture		Infrared: One rich fuel-air mixture	Infrared: One rich fuel-air mixture		
Motored engine		Visible and ultraviolet: One lean fuel-air mixture Near infrared: One lean fuel-air mixture Infrared: One lean fuel-air mixture One rich fuel-air mixture		Infrared: One lean fuel-air mixture One rich fuel-air mixture	Infrared: One lean fuel-air mixture One rich fuel-air mixture	Infrared: One lean fuel-air mixture One rich fuel-air mixture

Results

VISIBLE AND ULTRAVIOLET SPECTRA (2900 Å to 7000 Å).

Figure 1 shows a comparison of spectra recorded for the motored-engine preflame reaction with a diethyl ether-isooctane blend and for the burner second-stage cool flame with pure diethyl ether as the fuel. The slit widths were 350 and 400 μ respectively for the engine and burner spectra, and the fuel-air ratios were 0.058 and 0.818 respectively. (Stoichiometric fuel-air ratio is 0.0737 by weight for the ether-isooctane blend and 0.0895 for ether.) In both cases all of the emission bands are readily identified as the well-known chemiluminescence bands from excited formaldehyde molecules formed in the reaction. The underlying continuum may arise simply from band overlapping or may result from some other process.

The comparison has been made in Figure 1 using a rich burner second-stage flame because the burner first-stage cool flame (often called simply the "cool flame") shows certain differences. Figure 2 shows a burner first-stage cool flame spectrum. The same formaldehyde bands appeared in the first-stage flame between 3400 Å and 5200 Å, but in this case some additional

radiation appeared at longer wavelengths. The long wavelength emission is unidentified as yet, but it was not detected either in the burner second-stage flame or in the engine preflame reaction.

Fuel-air ratio had very little effect on the burner first-stage cool flame spectra. Spectra recorded at ether-air ratios of 0.428 and 1.00 both appeared much like that at 0.538 in Figure 2. However, some remarkable changes occurred in the second-stage flame as the mixture was leaned from 0.818 fuel-air ratio. Figure 3 shows a second-stage flame spectrum at 0.333 fuel-air ratio in which the formaldehyde bands have been almost entirely replaced by HCO bands. The CH band at 4313 Å also appears, and a strong continuum seems to underlie the whole region. This spectrum represents just one point in a gradual transition from the second-stage cool flame spectrum of Figure 1 to a rich normal flame spectrum consisting of CH, C_2, and OH which appears at a fuel-air ratio of about 0.176.[2] In the burner this transition occurs slowly as the mixture approaches stoichiometric from very rich values.

In the engine, on the other hand, the preflame reaction spectrum was only obtained at fuel-air ratios considerably leaner than stoichiometric, and transition occurred very suddenly and violently to normal autoignition as the mixture was enriched. No HCO has been detected in the engine preflame reaction spectra.

NEAR INFRARED SPECTRA (1.0 μ to 3.0 μ)

Figure 4 compares the motored-engine preflame reaction spectrum with a diethyl ether-isooctane blend to the burner second-stage flame spectrum of diethyl ether in the near infrared region of the spectrum. The slit widths were 300 μ for the engine spectrum and 500 μ for the burner. Fuel-air ratios were 0.047 and 0.333 by weight respectively.

Again the spectra appear nearly identical. The peaks at about 1.4, 1.85, and 2.5 μ are attributed to H_2O, and those near 1.9 to 2.0 and 2.7 μ have contributions from both H_2O and CO_2. The peak at about 2.3 μ is as yet unidentified, but probably arises from some compounds containing C—H bonds either in the fuel itself or produced in the reaction. In the flat-flame burner the 2.3-μ peak tended to decrease in intensity relative to the H_2O and CO_2 emission as (a) the two-stage flame was traversed from the first-stage cool flame up through and beyond the second-stage flame, and (b) in all regions of the flame as the fuel-air mixture was made leaner. These trends are indicated by Figures 5 and 6. Figure 5 shows the spectrum

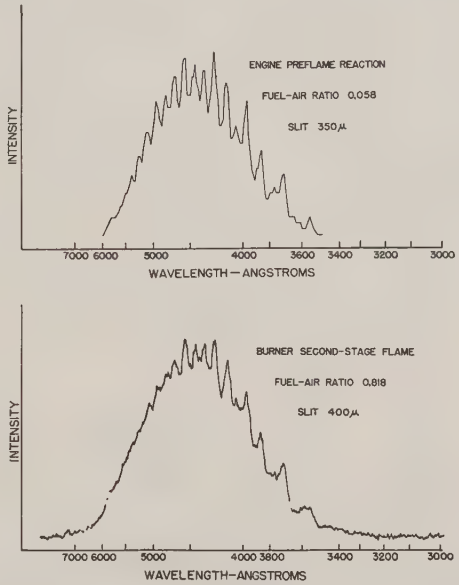

FIG. 1. Comparison of engine and burner spectra in the visible and ultraviolet range.

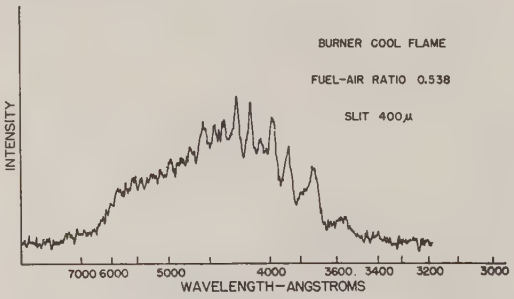

FIG. 2. Burner first-stage cool flame spectrum in the visible and ultraviolet range.

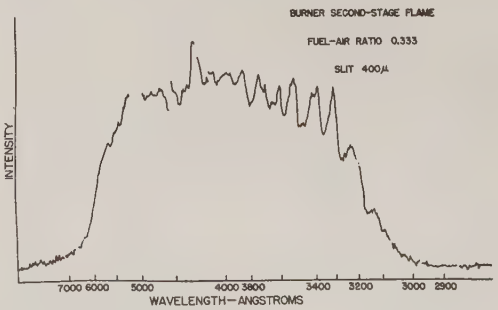

FIG. 3. Burner second-stage flame spectrum at a reduced fuel-air ratio.

of the burner first-stage cool flame at the same fuel-air ratio as in Figure 4 (a higher gain was required because of the much lower over-all in-

tensity), and Figure 6 shows a second-stage flame spectrum at a leaner mixture ratio (about 0.30).

The near infrared engine spectra were not obtained at fuel-air ratios other than that shown in Figure 4, since preflame reactions were not detected at appreciably different ratios.

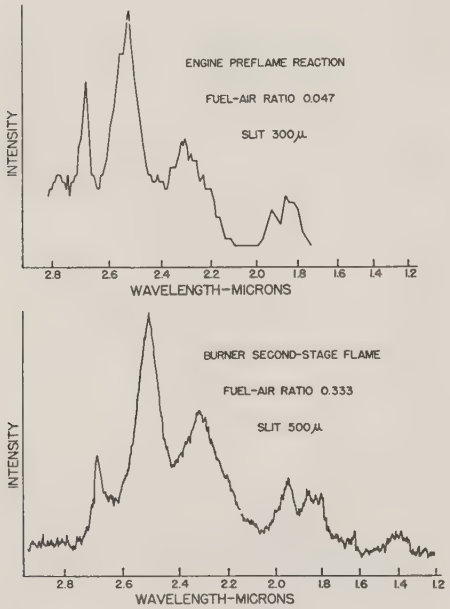

FIG. 4. Comparison of engine and burner spectra in the near infrared region.

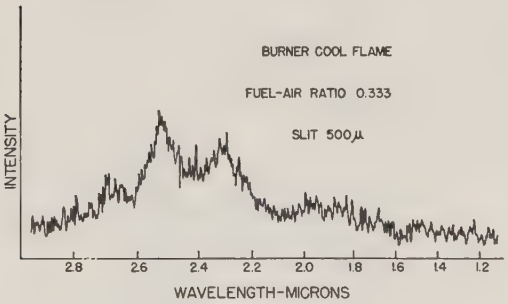

FIG. 5. Burner first-stage cool flame spectrum in the near infrared range.

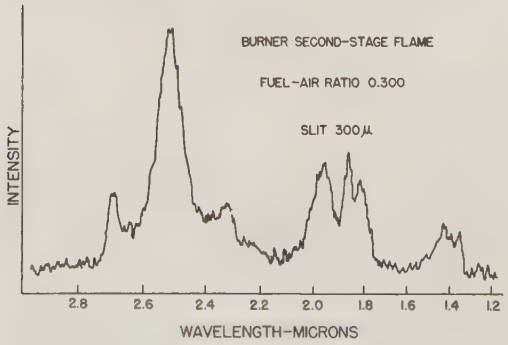

FIG. 6. Burner second-stage flame spectrum at a reduced fuel-air ratio.

INFRARED SPECTRA (3 μ to 11 μ)

Infrared spectra from 3 to 11 μ for the engine preflame reactions and the burner two-stage flames are shown in Figures 7 and 8 respectively.

The engine spectra obtained at two fuel-air ratios are shown for the ether-isoctane blend and for *n*-heptane. The rich mixture (0.15 fuel-air ratio) was included to illustrate a hot fuel emission spectrum for reference purposes. Preflame reactions, as evidenced by a decrease in required motoring friction torque (due to power development from chemical reaction), did not occur with the rich fuel-air mixture in the engine.

The burner spectra for ether and heptane include both the cool flame and second-stage flame spectra. The nominal fuel-air ratio in all the burner spectra was 0.43.

It is difficult to compare the absolute intensities of the burner and engine emission, since the engine emission was intermittent and of only a very short duration. However, an analysis of the slit width settings required to give adequate signal strengths indicates that the engine emission in the 3- to 4-μ region of the spectrum is relatively weaker than the corresponding burner emission.

The 3- to 4-μ region of the spectra is complicated since the original fuel molecules, as well as most of the intermediate and final products of the low temperature combustion reactions, possess CH bonds capable of emitting radiation in this portion of the spectrum. The fact that the spectra recorded with a rich fuel-air mixture (presumably due entirely to hot fuel emission) are very similar to the lean mixture spectra (for which preflame reaction was extensive) indicates that much of the preflame reaction emission in this region may be due simply to the fuel itself.

The burner spectra in all four cases have maximum CH emission near 3.4 μ, and the engine spectra all have deep minima at this wavelength. This immediately suggests that the engine spectra all suffer from considerable self absorption which was not present in the burner flames. This self-absorption perhaps resulted from a layer of cold gas near the inside surface of the observation window in the engine combustion chamber. Self-absorption helps explain the relatively weaker CH emission from engine preflame reactions as compared to burner flames and also why the lean mixture spectra in this region required considerably smaller slit widths than the rich

mixture spectra in spite of the reduction of fuel concentration by a factor of ten.

The 3.48-μ peak appearing in the engine preflame reaction spectra may simply represent a decrease in absorption, but it also appears in the heptane first-stage cool flame and ether second-stage flame, and there it appears to result from formaldehyde formed in the low temperature reaction. Emission in the 3.6-μ region, appearing most clearly in the ether first-stage cool flame, may result from acetaldehyde. The 3.21- and 3.32-μ peaks in the burner second-stage flame spectra are most likely due to compounds containing carbon double or triple bonds.

Large quantities of CO_2 and CO were formed both in the engine and burner reactions. This was evidenced by the CO_2 emission band at 4.4 μ and the CO bands at 4.6 and 4.8 μ (atmospheric CO_2 self-absorption appeared at 4.25 μ). The ratio of CO to CO_2 emission in both systems was considerably greater for heptane than for either the ether flames in the burner or the ether-isooctane blend in the engine. The 4.85-μ band, which appeared only in the ether two-stage flame spectra, may have resulted from dimethyl ether.

The 5- to 6-μ region shows strong emission from C=O linkages for all the low temperature reaction spectra. As with the 3.5-μ CH-stretching region, the engine spectra again appear to suffer from large self-absorption effects at 5.75 μ. This wavelength, which shows a minimum in the engine preflame reaction spectra, produces the maximum C=O emission in the burner spectra, and apparently results from aldehydes. Other possibilities for emitters in the 5- to 6-μ region are open chain ketones, saturated aliphatic acids, dialkyl peroxides, and open chain anhydrides.[4]

The complete disappearance of the diethyl ether emission band at 5.15 μ as the mixture in the engine was leaned from 0.15 to 0.015 indicates considerable reaction of the ether in the fuel.

Most of the emission peaks at wavelengths greater than 6 μ are due to fuel molecules. The rich mixture engine spectra are complicated somewhat by self-absorption at some wavelengths (7.3 and 8.9 μ particularly with the ether-isooctane blend). The sharp peak at 7.81 μ in the ether second-stage burner flame spectrum is attributed to formaldehyde, and that at 10.57 μ is due to ethylene. The ethylene band also appeared in the heptane burner spectrum, but is not shown in Figure 8. Neither the ethylene nor the formaldehyde bands were detected in the engine spectra.

No comparison spectra are available for the engine and burner low temperature reactions using other fuels. The engine spectra using isooctane as a fuel showed no signs of emission from reaction products except that the CO_2 intensity was slightly greater with the lean mixture than with the rich. This increase may have resulted either from a slight reaction or from the somewhat higher temperature with the lean mixture. Isooctane exhibited no detectable change in motoring friction torque between the rich and

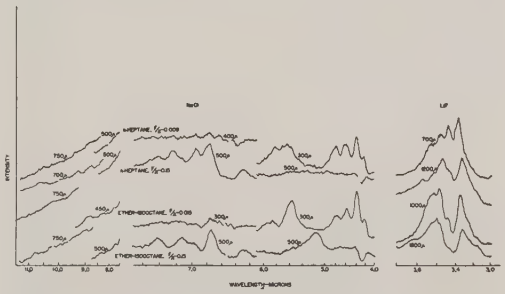

FIG. 7. Infrared spectra of engine preflame reactions.

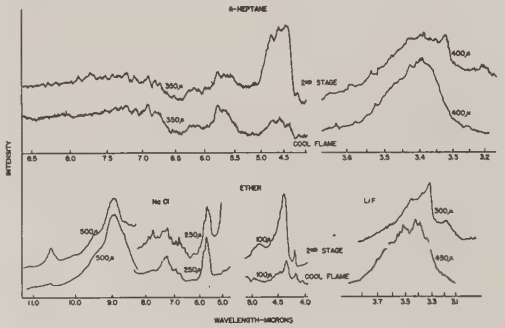

FIG. 8. Infrared spectra of burner two-stage flames.

lean mixtures. The 70 per cent isooctane-30 per cent heptane blend gave spectra intermediate between those of pure isooctane and heptane. The acetaldehyde two-stage burner flame was more nearly like that of diethyl ether than *n*-heptane. The most notable differences were the complete absence of the 10.57-μ ethylene, the 7.81-μ formaldehyde, and the 4.86-μ dimethyl ether bands, and the accentuation of aldehyde bands at 3.6- and 5.64-μ and the bands of unsaturates at 3.2 and 3.3 μ.

Discussion

It was expected in this work that, in the first place, it would prove difficult to simulate closely

the engine preflame reactions in a steady flow system, and in the second place, that the simpler steady flow reaction would provide a considerably broader range of information on low temperature reaction mechanisms than would the engine system. Both of these expectations were realized.

Engine preflame reactions were most easily obtained with extremely lean fuel-air ratios. Only a narrow range of fuel-air ratios was feasible, since the ratio had to be set just short of the autoignition limit in order to obtain the maximum emission intensity. Even so, the signal-to-noise ratio for radiation at wavelengths greater than 3 μ was generally insufficient to permit adequate resolution of the engine spectra. The fuel-air ratios producing maximum preflame emission intensity were generally near or leaner than the normal lean inflammability limits for the fuels in question.

It is true that the autoignition region could also be entered by leaning the mixture from an extremely rich fuel-air ratio, but in the few tests made of this limit, autoignition was found to occur very suddenly with little indication of preflame reaction. The nonpredictability of this "rich limit" operation did not lend itself to spectroscopic studies, and no further investigations were made.

In contrast to the engine preflame reactions, no burner cool flames were obtained at fuel-air ratios leaner than stoichiometric for any of the fuels tested. In fact, cool and two-stage flames are generally found in the flat-flame burner only at fuel-air ratios richer than the usual rich "inflammability limit" for the fuel in question. Thus it was impossible to study the burner cool flames under fuel-air ratio conditions simulating those of the engine. On the other hand, a wider range of fuel-air ratios could be observed with the burner than with the engine, and for the visible and ultraviolet portion of the spectrum brief studies of this variable were made.

In the investigations made so far there has been no provision for pressurizing the flat-flame burner, so that it has been impossible to simulate engine cylinder pressures. It may be that the differences in fuel-air ratio at which low temperature reactions occur in the two systems are explained by the difference in pressure.

In view of this generally poor simulation of experimental conditions in the engine by the flat-flame burner, it is somewhat surprising that the low temperature reaction spectra resemble each other at all. Of course, the resemblance is closest in the visible, ultraviolet, and near infrared regions of the spectrum which probably have less significance than the longer wavelength infrared region from a reaction mechanism standpoint. The longer wavelength region includes emission from most of the intermediate chemical species expected in the reactions, and it is just this region which presents the most difficulties in engine instrumentation. The only certain identifications of reaction products obtained in the present work from the engine spectra were those of H_2O, CO_2, compounds containing C=O, and chemiluminescent formaldehyde (visible spectrum). All of these emissions appeared similar in the engine and burner spectra. Perhaps rather more emphasis should be placed on the fact that numerous reaction product emissions observed in the burner spectra were not detected in the engine spectra. There was evidence for the existence of HCO radicals, formaldehyde, acetaldehyde, unsaturates, dimethyl ether, and ethylene in the burner flames but not in the engine reactions.

In addition to the differences in the environments for the burner and engine reactions, the detection system itself may be responsible for some apparent dissimilarities of the reactions. This is particularly noticed in a consideration of the multistage character of the burner reactions as opposed to the single-stage observed for the engine spectra. For wavelengths greater than 3 μ it was necessary to integrate all of the preflame emission occurring in a given engine cycle in order to obtain engine spectra. This technique would be expected to de-emphasize any intermediate emissions which might occur only during a short interval of the engine cycle. That is, if the engine reaction were multistaged, as is the burner flame, some reaction intermediates might be masked in the integration process.

In the case of the visible, ultraviolet, and near infrared portions of the spectrum, the engine preflame emissions were actually recorded as functions of time in the engine cycle, and it might be expected that any multistaged character of the reaction would be evident. The photomultiplier and lead sulfide cell detector traces on the oscilloscope, however, gave no indications of a multistage engine reaction under the conditions of these spectra.

Cornelius and Caplan,[5] Downs, Street, and Wheeler,[6] Olson, Wentworth, and Daniel,[7] and Sturgis[8] have all described work in which multistage preflame reactions have been observed in engines. The stages were made evident by double

peaks in the visible radiation *vs.* crankangle oscilloscope traces and in the pressure development *vs.* crankangle curves. Sturgis has called this second-stage engine reaction the "blue flame" and indicated that it involves considerably more heat release and light emission than the first stage. He states that it was obtained by the use of "leaner mixtures." Downs, Street, and Wheeler also obtained double-peak radiation traces primarily with mixtures leaner than stoichiometric.

This work of previous investigators with photomultiplier detectors (but no spectrometer), by demonstrating that two-stage reactions can occur in engines, that the second stage is considerably brighter than the first, and that they occur most readily with lean mixtures, suggests that the engine preflame reaction observed in the present investigation was actually a "second-stage" reaction. In the present work the engine reactions were only detected with very lean mixtures, and the similarity of the engine preflame reaction and burner second-stage flame spectra strengthens the conclusion. The interposition of a spectrometer between the engine cylinder gases and the detector apparently accounts for the failure to detect the much weaker engine first-stage reaction.

The question then remains as to why HCO radicals were not detected in the engine preflame reactions, although they did appear strongly when the very rich burner second-stage flame was slightly leaned. The answer to this may be complicated by the widely different fuel-air ratios of the burner and engine reactions. However, two bits of evidence suggest a different conclusion. Moore[9] and Gaydon, Moore and Simonson[10] have observed HCO spectroscopically while enriching methane-air mixtures in a motored engine toward the lean autoignition limit, indicating that the phenomenon does occur in engines with a lean mixture of at least one fuel. In addition, Gaydon and Moore[11] have recently described work with propane-air mixtures flowing through a heated tube in which similar spectral transitions involving HCO occurred as temperature was increased with both lean and rich fuel-air mixtures. In all cases HCO appears momentarily in the transition region between cool flames and normal self-ignition of the fuel-air mixture. It seems quite likely that in the present work the failure to detect HCO was simply due to fact that the autoignition limit was not approached closely enough. The engine was not designed to operate under autoigniting conditions, and a rather large factor of safety was used to prevent cyclic variations from inadvertently starting autoignition.

Summary

The visible, ultraviolet, and near infrared spectra of low temperature combustion reactions produced in a motored engine and in a flat-flame burner indicate a similarity between the engine preflame reaction and the burner second-stage flame. This conclusion is in agreement with a consideration of other general characteristics of the engine preflame reactions, which also suggests that they are "second-stage" in nature. The longer wavelength infrared spectra show more discrepancies which may indicate real differences in reaction mechanisms or may simply result from difficulties in instrumenting the engine for long wavelength spectroscopic studies. In addition to hot fuel emission the engine spectra exhibited emission from H_2O, CO_2, CO, compounds containing C=O, and chemiluminescent formaldehyde, while the burner spectra included bands from other intermediate and final products of the reaction.

The effects of environmental conditions on the reactions in the two systems, particularly fuel-air ratio and pressure, have received only the briefest attention so far and appear to represent fruitful areas for future study. It is believed that the transition region between low temperature reactions and the normal hot flame ignition reaction in which HCO is importantly involved deserves special effort. In the long wavelength infrared region of the spectrum, improved resolution appears necessary before appreciable gains can be made in the engine studies.

REFERENCES

1. Agnew, W. G., Agnew, J. T., and Wark, K., Jr.: *Fifth Symposium (International) on Combustion*, pp. 766–778. New York, Reinhold Publ. Corp., 1955.
2. Agnew, W. G., and Agnew, J. T.: Ind. Eng. Chem., *48*, 2224 (1956).
3. Donovan, R. E., and Agnew, W. G.: J. Chem. Phys., *23*, 1592 (1955).
4. Bellamy, L. J.: *The Infra-Red Spectra of Complex Molecules*. New York, John Wiley & Sons, 1954.
5. Cornelius, W., and Caplan, J. D.: Soc. Auto. Engr. Quart. Trans., *6*, 488 (1952).
6. Downs, D., Street, J. C., and Wheeler, R. W.: Fuel, *32*, 279 (1953).
7. Olson, D. R., Wentworth, J. T., and Daniel W. A.: Soc. Auto. Engr. Trans., *62*, 606 (1954).

8. Sturgis, B. M.: Soc. Auto. Engr. Trans., *63*, 253 (1955).
9. Moore, N. P. W., and Simonson, J. R.: Nature, *173*, 543 (1954).
10. Gaydon, A. G., Moore, N. P. W., and Simonson, J. R.: Proc. Roy. Soc., *A230*, 1 (1955).
11. Gaydon, A. G., and Moore, N. P. W.: Proc. Roy. Soc., *A233*, 184 (1955).

122

STUDIES OF THE SPONTANEOUS IGNITION TENDENCIES OF SULFUR-CONTAINING ORGANIC COMPOUNDS WITH WHITE FUMING NITRIC ACID BY THE DROP-TEST METHOD

By MURRAY P. STRIER and LOUIS R. RAPP

Introduction

The influence of the chemical structure of fuels on their spontaneous ignition tendencies with white fuming nitric acid indicates that such tendencies are at least partially controlled by the chemical reactivity of fuel and oxidizer. At the Fifth Combustion Symposium, Kilpatrick and Baker[1] reported that efficient mixing of several hypergolic fuel and oxidizer combinations reduced the ignition delay values to less than 3 msec. One of these propellants had manifested an ignition delay value of 400 msec by less efficient mixing techniques. However, it was concluded that the reduced ignition delay values were based on ignition by impact rather than on the rate of homogenous chemical reaction.

By resorting to the simple "drop-test" technique wherein less than 1 ml of fuel is dropped by its own weight into a few ml of oxidizer it is possible to arrive at ignition delay values that are based partially on rate of mixing and partially on rate of chemical reaction. Studies conducted at 25°C involving isomeric fuels having relatively similar physical properties such as boiling points, densities, surface tensions and viscosities reveal that considerably greater differences exist in ignition delay values. This indicates that, if the physical parameters are held constant essentially, the ignition delay obtained by the "drop-test" technique is dependent to a significant extent on chemical reactivity.

As a result of the evaluation of the qualitative and quantitative ignition delay tendencies with white fuming nitric acid of various sulfur-containing fuel systems it is possible to arrive at basic concepts relating hypergolic tendencies with fuel chemical structure. In an effort to evaluate the effect of various physical parameters on the ignition delay, a comparative study was made of six entirely different fuels by various organizations throughout the United States employing several different types of apparatus. These studies indicated that spontaneous ignition characteristics evaluated at ambient temperature by the "drop-test" method agreed with the results obtained by the impinging jet method which simulates the injection pattern employed in the rocket engine. Hence, the results of a correlative program involving determination of spontaneous ignition tendencies by the "drop-test" technique should greatly aid in the selection of optimum hypergolic propellant combinations for rocketry.

In this presentation the results obtained with organic sulfur compounds as fuels will be given and discussed.

Experimental

During this investigation ignition delay measurements were performed by means of the apparatus shown in Figure 1. A calibrated 1-ml pipette having an internal bore diameter of 3 mm (partially narrowed down at the tip) is mounted so that the tip is 9.9 cm above a 30 by 70 mm Pyrex weighing bottle serving as the reaction vessel. The weighing bottle is enlarged at the top so that a ground glass joint could be sealed to it. Both the pipette and the reaction vessel are jacketed in order that the temperature at which fuel and oxidizer are mixed can be controlled.

Fixed volumes of fuel are dropped by gravity feed into a fixed volume of acid. The light from a 50-watt projection lamp is focused through a diaphragm and then through the walls of the reaction vessel. The light is transmitted through

the transparent oxidizer and is picked up by photocell A which is an RCA No. 921 photocell. The photocell is connected to an electronic timer. Upon striking the surface of the oxidizer, the fuel causes an indentation in the surface. The light beam striking this surface is refracted so that it can no longer be picked up by photocell A at the original intensity. This change in light intensity activates the electronic timer indicating

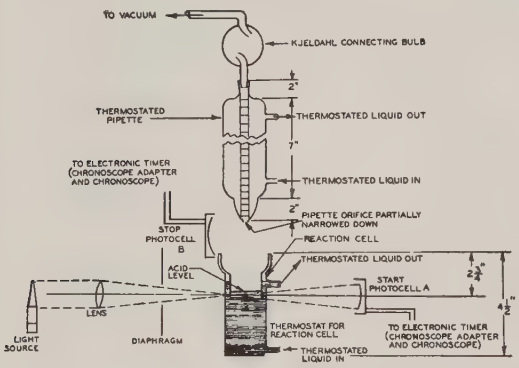

FIG. 1. Schematic diagram of apparatus for measuring ignition delay values by the "drop-test" method.

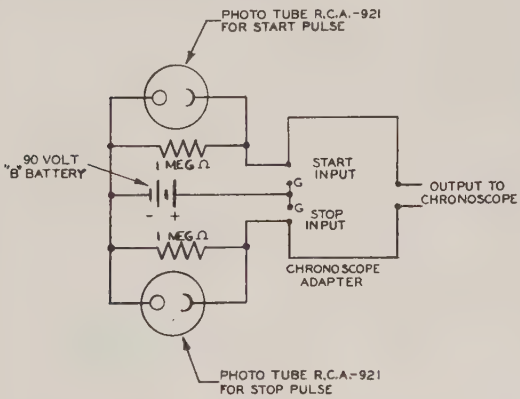

FIG. 2. External wiring circuit for timing mechanism.

the starting time. The flame resulting from the reaction of fuel with oxidizer sensitizes RCA No. 921 photocell B, activating the stop mechanism of the timer.

The timing mechanism is an American Chronoscope Corporation Input Adapter, Model 211, which furnishes start and stop signals to the American High Speed Chronoscope. The Chronoscope operates on the principle that a charged capacitor loses a definite percentage of its charge when connected across a resistor for a fixed period of time. The adapter serves as an electronic relay by utilizing the start and stop signals to turn on or off a rectangular timing voltage to the Chronoscope. Thus, the Chronoscope receives a constant pulse during the timing period which in turn controls the time of discharge of the charged capacitor. The percentage of charge lost is determined by a self-balancing potentiometer in the Chronoscope circuit. The external wiring circuit for the timing mechanism is shown in Figure 2.

During operation, volumes of fuel of 0.15, 0.3, 0.6 and 0.9 ml were dropped into 2.5 ml of acid. From two to five determinations were conducted at each oxidizer-to-fuel level. Generally ignition delay values were reproducible to ± 10 per cent.

TEST MATERIALS

Most of the fuels used in this investigation were purchased and were of the highest purity commercially available. No efforts were made at further purification unless the appearance and physical constants obviously warranted it. The white fuming nitric acid employed in this investigation was procured from the General Chemical Co. and came from batches having the following ranges of composition by weight: HNO_3, 96.8 to 98.0 per cent; NO_2, 0.3 to 1.3 per cent; H_2O, 1.8 to 2.3 per cent. The acid was analyzed in the following way. The total HNO_3 content is determined by standardization with a standard base. The NO_2 content is then ascertained by titration with $Ce(SO_4)_2$ and back titration with Fe_2SO_4-$(NH_4)_2SO_4$. The H_2O content is subsequently obtained by difference.

Measurements were performed under thermostatic conditions at 25° ± 0.5°C.

Results and Discussions

Ignition delay values reported herein are generally averages of values obtained when volumes of fuel of 0.15 ml, 0.3 ml, 0.6 ml and 0.9 ml are added to 2.5 ml of acid. Whenever exceptions prevailed, they were noted.

A. ALIPHATIC MERCAPTANS

(1) *Linear aliphatic-unsubstituted*

The results obtained for this class of compounds are summarized in Table 1. Hypergolicity is evident as the length of the hydrocarbon chain varies from two to five carbon atoms and vanishes beyond this point. Allyl mercaptan having the shortest ignition delay value of this group of compounds, indicates that unsaturation in the hydrocarbon moiety of the molecule is conducive

to hypergolic tendencies. No explanation can be advanced for propyl mercaptan having the shortest ignition delay of the linear saturated mercaptans.

(2) Effect of substitution at the alpha carbon

The results obtained for these compounds are given in Table 2. Although isopropyl mercaptan is hypergolic, its ignition delay value is higher than that for propyl mercaptan (i.d. = 53 ms, Table 1). Tert-butyl mercaptan is not hypergolic whereas butyl mercaptan (i.d. = 61 ms, Table 1) has a fairly short ignition delay period. The nonhypergolicity of tert-hexyl mercaptan is consistent with the nonhypergolic characteristics of hexyl mercaptan (Table 1).

It is apparent that substitution of methyl groups for secondary hydrogen atoms at the alpha carbon is deleterious to spontaneous ignition tendencies.

Hypergolicity of the aliphatic mercaptans may be dependent on dissociation of the S—H bond and attack on the sulfur atom. The presence of methyl groups at the alpha carbon makes this carbon more negative through inductive influences. This could retard the dissociation of the S—H bond. Also the presence of methyl substituents at the alpha carbon could sterically hinder any direct attack on the sulfur atom. These trends point to a possible mechanism for hypergolic activity of the subject compounds with white fuming nitric acid to be discussed later in this paper.

Table 1. Ignition Delay Values of Linear Aliphatic Mercaptans, Unsubstituted

Compound	Structure	Average Ignition Delay
		ms at 25°C
Ethyl mercaptan	$CH_3—CH_2—SH$	95
Allyl mercaptan	$CH_2=CH—CH_2—SH$	12
Propyl mercaptan	$CH_3—CH_2—CH_2—SH$	53
Butyl mercaptan	$CH_3—CH_2—CH_2—CH_2—SH$	61
Amyl mercaptan	$CH_3—CH_2—CH_2—CH_2—CH_2—SH$	149
Hexyl mercaptan	$CH_3—CH_2—CH_2—CH_2—CH_2—CH—SH$	No ignition
Heptyl mercaptan	$CH_3—CH_2—CH_2—CH_2—CH_2—CH_2—CH_2—SH$	No ignition

Table 2. Ignition Delay Values of Aliphatic Mercaptans: Substituents at the Alpha Carbon

Compound	Structure	Average Ignition Delay
		ms at 25°C
Isopropyl mercaptan	$CH_3—CH(CH_3)—SH$	183
Tert-butyl mercaptan	$CH_3—C(CH_3)_2—SH$	No ignition
Tert-hexyl mercaptan	$CH_3—CH_2—CH_2—C(CH_3)_2—SH$	No ignition

(3) Effect of substitution at the beta carbon

The results of spontaneous ignition studies on these compounds are given in Table 3. Isobutyl mercaptan, has a slightly higher ignition delay period than does butyl mercaptan (Table 1); nevertheless, its positive hypergolic activity is to be contrasted to the nonhypergolic nature observed for tert-butyl mercaptan (Table 2). The relative order of results noted for the butyl mercaptans indicates that their hypergolic tend-

encies may be based on dissociation of hydrogen from sulfur and attack on the —S— atom.

Both 2-hydroxyethyl mercaptan and ethylene dimercaptan have shorter ignition delay periods than does ethyl mercaptan (i.d. = 95 ms, Table 1). However, 2-phenylethyl mercaptan is not hypergolic at all.

ignition delay period than does propyl mercaptan (Table 1) which is rather surprising, but does indicate that there may be an optimum ratio of mercapto to methylene groups for shortest ignition delay periods. The inactivity of 3-phenylpropyl mercaptan demonstrates further the deactivating influence of phenyl groups on spontaneous ignition tendencies of aliphatic mercaptans.

Table 3. Ignition Delay Studies of Aliphatic Mercaptans: Substituents at the Beta Carbon

Compound	Structure	Average Ignition Delay
		ms at 25°C
Isobutyl mercaptan	$CH_3—CH(CH_3)—CH_2—SH$	77
2-Ethylhexyl mercaptan	$CH_3—CH_2—CH_2—CH_2—CH(CH_2—CH_3)—CH_2—SH$	No ignition
2-Hydroxyethyl mercaptan	$HO—CH_2—CH_2—SH$	67
Ethylene dimercaptan	$HS—CH_2—CH_2—SH$	35
2-Phenylethyl mercaptan	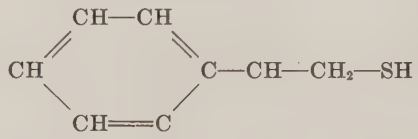	No ignition

Table 4. Ignition Delay Studies of Aliphatic Mercaptans: Substituents at the Gamma Carbon

Compound	Structure	Average Ignition Delay
		ms at 25°C
Isoamyl mercaptan	$CH_3—C(H)(CH_3)—CH_2—CH_2—SH$	975
Trimethylene dimercaptan	$HS—CH_2—CH_2—CH_2—SH$	74
3-Phenylpropyl mercaptan	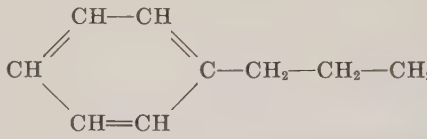	No ignition

(4) *Effect of substitution at the gamma carbon*

The results obtained for three mercaptans belonging to this category are summarized in Table 4. The longer ignition delay period for isoamyl mercaptan compared to that of amyl mercaptan (i.d. = 149 ms, Table 1) is further evidence that branching in the alkyl chain is deleterious to spontaneous ignition tendencies for alkyl mercaptans. Trimethylene dimercaptan has a longer

(5) *Aliphatic dimercaptans*

The ignition delay values obtained for this class of compounds are given in Table 5. In Figure 3 the average ignition delay values for these compounds are plotted against the number of carbon atoms in the molecule. It is seen that

the compound having the minimum ignition delay value is ethylene dimercaptan, which has the lowest molecular weight. Conversely the compound having the highest molecular weight has the longest ignition delay period.

Referring to Table 5, the inactivity of 1,2-dimercaptopropanol can be attributed to the substitution of alkyl groups for secondary hydrogen atoms at the alpha position which has been shown earlier to be deleterious to spontaneous ignition tendencies. Although earlier, substitution of a hydroxy group for a primary hydrogen atom was found to be conducive to spontaneous ignition tendencies (2-hydroxyethyl mercaptan, Table 3), it may have deleterious effects when substituted for a secondary hydrogen atom at the alpha carbon.

B. SULFIDES

From the results of Table 6 it is evident that the only sulfides that are hypergolic are those containing the ethylene sulfide ring, and those aliphatic compounds containing ethylenic groups. Apparently for aliphatic systems, the —C=C—C—S—C— and —C=C—S—C groupings are similar to the —C—C—C—S—H grouping as far as spontaneous ignition characteristics are concerned.

C. DISULFIDES

The ignition delay values obtained for these compounds are summarized in Table 7. The nonhypergolic nature of tert-butyl disulfide follows the trend established earlier for the butyl mercaptans (Table 1). The average ignition delay value for methyl disulfide is believed to be too high. It is believed that the nonluminous nature of the flame obtained with this fuel prevented obtaining a realistic ignition delay period.

Table 5. Ignition Delay Studies of Aliphatic Dimercaptans

Compound	Structure	Average Ignition Delay
		ms at 25°C
Ethylene dimercaptan	$HS—CH_2—CH_2—SH$	35
Trimethylene dimercaptan	$HS—CH_2—CH_2—CH_2—SH$	74
1,2-Dimercaptopropanol	$CH_3—\underset{\displaystyle SH}{\underset{\vert}{CH}}—\underset{\displaystyle SH}{\underset{\vert}{CH}}—OH$	No ignition
Tetramethylene dimercaptan	$HS—CH_2—CH_2—CH_2—CH_2—SH$	118
Pentamethylene dimercaptan	$HS—CH_2—CH_2—CH_2—CH_2—CH_2—SH$	62
Nonamethylene dimercaptan	$HS—C_9—H_{18}—SH$	96
Decamethylene dimercaptan	$HS—C_{10}H_{20}—SH$	237

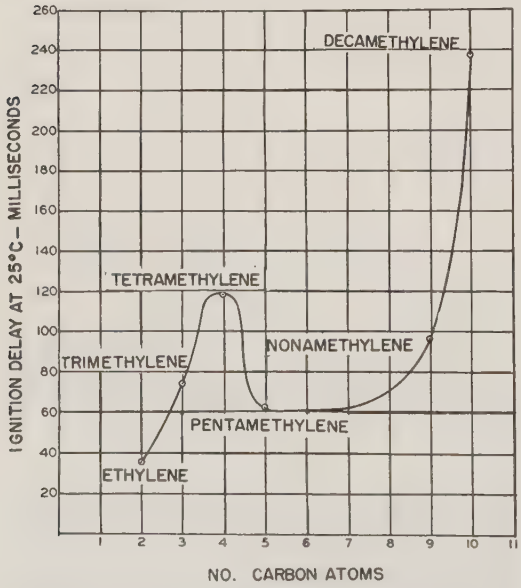

Fig. 3. Variation of ignition delays with increasing number of carbon atoms for the methylene dimercaptans.

D. THE RELATIONSHIP BETWEEN IGNITION DELAY VALUES AND CARBON ATOM TO SULFUR ATOM RATIO FOR THE THREE SULFUR-CONTAINING HYPERGOLIC SYSTEMS—MERCAPTANS, DIMERCAPTANS AND DISULFIDES

In Figure 4 the ignition delay values are plotted versus carbon atom to sulfur atom ratio for these three classes of compounds. The mercaptan and dimercaptan curves are fairly close together which is significant since increasing molecular weight is apparently deleterious to spontaneous ignition tendencies especially when the length of the uninterrupted hydrocarbon chain is greater than four carbon atoms. Also of interest is the fact that the dimercaptans are more hypergolic than their disulfide isomers, with one exception,

i.e., ethyl disulfide has a shorter ignition delay period than tetramethylene dimercaptan. It can be concluded from the trends in Figure 4 that for hypergolic sulfur-containing compounds, the shortest ignition delay periods occur in the region wherein the carbon atom to sulfur atom ratio varies from 1 to 3 but not higher.

Table 6. Ignition Delay Studies of Sulfides

Compound		Average Ignition Delay
		ms at 25°C
Ethylene sulfide	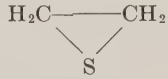	435
Methyl sulfide	$CH_3—S—CH_3$	No ignition
Methyl vinyl sulfide	$CH_3—S—CH=CH_2$	100
Propylene sulfide,	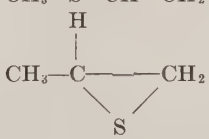	198
Ethyl methyl sulfide	$CH_3—CH_2—S—CH_3$	No ignition
Ethyl sulfide	$CH_3—CH_2—S—CH_2—CH_3$	No ignition
Thioxane	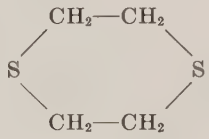	No ignition
Allyl sulfide	$H_2C=CH—CH_2—S—CH_2—CH=CH_2$	75
Allyl propyl sulfide	$H_2C=CH—CH_2—S—CH_2—CH_2—CH_3$	300
p-Cresyl ethyl sulfide	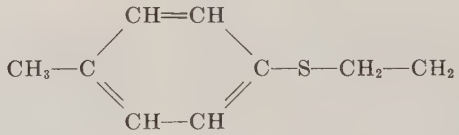	No ignition
Phenyl sulfide	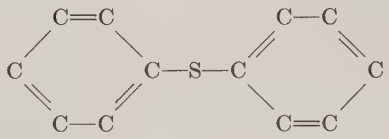	

E. The Relationship Between Ignition Delay Values and Physical Constants for Sulfur-Containing Fuels

In Table 8 are given average ignition delay values together with corresponding boiling points and densities for a number of mercaptans and disulfides. Comparing compounds having similar numbers of carbon atoms, it is evident that ignition delay values increase with decreasing boiling points and densities. Branching of the hydrocarbon moieties in these compounds, as has already been shown, is deleterious to spontaneous ignition tendencies and apparently reduces intermolecular forces of attraction, as manifested by the trends in boiling points and densities.

Discussions

On the basis of spontaneous ignition studies conducted at 25°C with different classes of sulfur compounds, i.e., mercaptans, sulfides and disulfides with white fuming nitric acid as oxidizer, certain generalizations regarding the relationship between chemical structure and spontaneous ignition tendencies are possible.

TABLE 7. IGNITION DELAY STUDIES OF DISULFIDES

Compound	Structure	Average Ignition Delay
		ms at 25°C
Methyl disulfide	$CH_3—S—S—CH_3$	330* · †
Ethyl disulfide	$CH_3—CH_2—S—S—CH_2—CH_3$	41*
Propyl disulfide	$CH_3—CH_2—CH_2—S—S—CH_2—CH_2—CH_3$	540
Butyl disulfide	$Ch_3—CH_2—CH_2—CH_2—S—S—CH_2—CH_2—CH_3$	1000
Isobutyl disulfide	$CH_3—CH(CH_3)—CH_2—S—S—CH_2—CH(CH_3)—CH_3$	960
Tert-butyl disulfide	$CH_3—C(CH_3)_2—S—S—C(CH_3)_2—CH_3$	No ignition
Amyl disulfide	$CH_3—CH_2—CH_2—CH_2—CH_2—S—S—CH_2—CH_2—CH_2—CH_2—CH_3$	Occasional‡ ignition
Isoamyl disulfide	$CH_3—CH(CH_3)—CH_2—CH_2—S—S—CH_2—CH_2—CH(CH_3)—CH_3$	Occasional‡ ignition
Tert-hexyl disulfide	$CH_3—CH_2—CH_2—C(CH_3)_2—S—S—C(CH_3)_2—CH_2—CH_2—CH_3$	No ignition

* Values obtained for 0.15 ml of fuel not included in average because they were highly erratic.

† Flames were barely luminous; ignition delay values obtained varied considerably and appeared to be too high.

‡ Ignition delay values were greater than 1 sec.

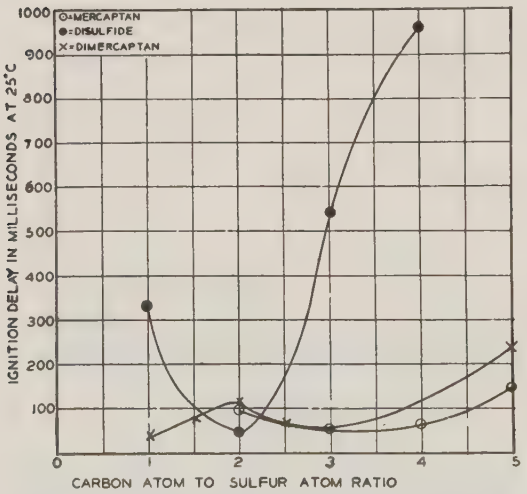

FIG. 4. Ignition delays vs carbon to sulfur ratio for three sulfur-containing hypergolic systems.

Mercaptans, sulfides and disulfides can ignite spontaneously, providing certain requirements of chemical structure are met. Also, the magnitude of ignition delay values of spontaneously igniting compounds is regulated by certain aspects of chemical structure. The presence of an ethylenic (—C=C—) function, that is not aromatic, lowers the ignition delay value considerably. In the case of sulfides either the presence of an ethylenic function or the presence of sulfur as one constituent of a three-membered ring, is required for hypergolicity. Methyl branching increases ignition delay values in nearly all cases. When there is complete substitution by methyl groups at the alpha carbons, then spontaneous ignition tendencies vanish entirely. As a result of such trends, spontaneous ignition tendencies vary directly with densities and boiling points. It is not claimed that high densities and high boiling points in sulfur compounds are conducive to hypergolicity but, rather, the same characteristics of chemical structure of these compounds that aid hypergolicity also lead to higher densities and boiling points. It appears that the carbon atom to sulfur atom ratio should not be greater than three to

TABLE 8. COMPARISON OF IGNITION DELAY VALUES WITH PHYSICAL CONSTANTS FOR MERCAPTANS AND DISULFIDES

Compound	Structure	Boiling* Point °C	Density† g/ml at 24°C	Average Ignition Delay at 25°C
Mercaptans Containing 3 Carbon Atoms				
Allyl mercaptan	$CH_2{=}CH{-}CH_2{-}SH$	67-68‡	0.923	12
Propyl mercaptan	$CH_3{-}CH_2{-}CH_2{-}SH$	67.61	0.843	53
Isopropyl mercaptan	$CH_3{-}\underset{\displaystyle CH_3}{\overset{\displaystyle H}{\overset{\displaystyle \vert}{\underset{\displaystyle \vert}{C}}}}{-}SH$	52.56	0.808	183
Mercaptans Containing 4 Carbon Atoms				
Butyl mercaptan	$CH_3{-}CH_2{-}CH_2{-}CH_2{-}SH$	98.46	0.840	61
Isobutyl mercaptan	$CH_3{-}\underset{\displaystyle CH_3}{\overset{\displaystyle H}{\overset{\displaystyle \vert}{\underset{\displaystyle \vert}{C}}}}{-}CH_2{-}SH$	88.72	0.834	77
Tert-butyl mercaptan	$CH_3{-}\underset{\displaystyle CH_3}{\overset{\displaystyle CH_3}{\overset{\displaystyle \vert}{\underset{\displaystyle \vert}{C}}}}{-}SH$	64.22	0.795	No ignition
Mercaptans Containing 5 Carbon Atoms				
Amyl mercaptan	$CH_3{-}CH_2{-}CH_2{-}CH_2{-}CH_2{-}SH$	126.64	0.847	149
Isoamyl mercaptan	$CH_3{-}\underset{\displaystyle CH_3}{\overset{\displaystyle \vert}{CH}}{-}CH_2{-}CH_2{-}SH$	117.78	0.835§	975
Disulfides Containing 8 Carbon Atoms				
Butyl disulfide	$CH_3{-}CH_2{-}CH_2{-}CH_2{-}S{-}S{-}CH_2{-}CH_2{-}CH_2{-}CH_3$	—	0.938	100
Isobutyl disulfide	$CH_3{-}\underset{\displaystyle CH_3}{\overset{\displaystyle \vert}{CH}}{-}CH_2{-}S{-}S{-}CH_2{-}\underset{\displaystyle CH_3}{\overset{\displaystyle \vert}{CH}}{-}CH_3$	—	0.931	960
Tert-butyl disulfide	$CH_3{-}\underset{\displaystyle CH_3}{\overset{\displaystyle CH_3}{\overset{\displaystyle \vert}{\underset{\displaystyle \vert}{C}}}}{-}S{-}S{-}\underset{\displaystyle CH_3}{\overset{\displaystyle CH_3}{\overset{\displaystyle \vert}{\underset{\displaystyle \vert}{C}}}}{-}CH_3$	—	0.926	No ignition

* Data taken from Rossini[2] unless stated otherwise.

† Determined at Reaction Motors, Inc., except where noted.

‡ Reported in Handbook of Chemistry and Physics,[3] p. 1116.

§ Reported in Handbook of Chemistry and Physics,[3] p. 813.

one in order to achieve minimum ignition delay values for any of the saturated compounds in the spontaneously igniting series. The actual size of the fuel molecule is apparently not the controlling factor.

Studies performed by Trent and Zucrow[4] on the rate of temperature rise of saturated and unsaturated hydrocarbons with anhydrous nitric acid indicate that the reaction of unsaturates is decidedly more exothermic than for saturated hydrocarbons. Also the rate of heat release is greater for hydrocarbons containing a conjugated unsaturated linkage than for hydrocarbons containing isolated unsaturated linkages. This could explain the enhancing influence of ethylenic functions on spontaneous ignition tendencies. The mechanism proposed for the exothermicity noted was based on the relative ease of nitration of the double bond. The spontaneous ignition tendencies of mercaptans may be based on the formation of a sulfanion in solution according to the equation

$$R - SH \rightarrow RS^- + H^+$$

The sulfanion formed is presumed to be highly reactive towards nitration reactions.

In exploratory studies conducted at Reaction Motors, Inc., thioxane, 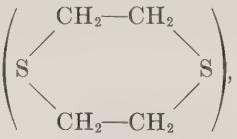 , was not found capable of igniting spontaneously with white fuming acid at ambient temperature. However, as described above, ethyl disulfide (CH_3—CH_2—S—S—CH_2—CH_3) ignites with a relatively short ignition delay period. This means that the disulfide linkage imparts greater reactivity towards white fuming nitric acid than two sulfide functions (—S—) separated by methylene groups.

An analogous case exists for diolefin compounds wherein the conjugated olefins are more reactive than the non-conjugated isomers. The enhanced electronic polarizability of the —S—S— linkage over that of the —S— linkage has been demonstrated in ultra-violet absorption spectra studies reported by Braude.[5] Similar enhanced electronic polarizability exists for conjugated diolefins over non-conjugated isomers. It is of interest to note that the —S— function has been considered to be isosteric with the —C=C— function.[6] Reactivity with nitric acid offers another method for depicting the analogy between the two systems.

Conclusions

(1) By employing the simple "drop test" technique wherein a fixed volume of fuel is dropped by its own weight into a fixed volume of white fuming nitric acid (O/F = 2.8 to 16.6 by volume), it is possible to establish correlations between chemical structure of the fuel molecules and spontaneous ignition tendencies at 25°C.

(2) Employing several different classes of sulfur compounds as fuels, i.e., mercaptans, sulfides and disulfides the following correlations between the chemical structure of fuels and spontaneous ignition tendencies are deduced. (a) Among the saturated mercaptans and disulfides, the carbon atom to sulfur atom ratio should not be greater than three to one in order to achieve optimum spontaneous ignition tendencies (shortest ignition delay). (b) Nonlinearity in the hydrocarbon chain is deleterious to spontaneous ignition tendencies. Because of this the more reactive fuels have higher boiling points and densities. (c) In the case of mercaptans it appears that spontaneous ignition tendencies are based on the ease of dissociation of the S—H bond and the reactivity of the resulting sulfanion. (d) The presence of a non-aromatic ethylenic function (—C=C—) enhances hypergolicity and in the case of sulfides is actually required if an ethylene sulfide function is not present. (e) Generally, factors concerning the chemical structures of fuels which favor increased exothermicity upon reaction with oxidizer tend to enhance spontaneous ignition tendencies. This is based on comparison of sulfur compounds with unsaturated hydrocarbons.

REFERENCES

1. Kilpatrick, M., and Baker, L. L., Jr.: *Fifth Symposium (International) on Combustion*, pp. 196–205. New York, Reinhold Publ. Corp., 1955.
2. Rossini, F. D.: *Selected Values of Physical and Thermodynamic Properties of Hydrocarbons and Related Compounds*. Pittsburgh, Carnegie Press, Carnegie Institute of Technology, 1953.
3. *Handbook of Chemistry and Physics*, Ed. 36. Cleveland, Chemical Rubber Publishing Co., 1954.
4. Trent, C. H., and Zurcow, M. J.: Ind. Eng. Chem., *44*, 2668 (1952).
5. Braude, E. A.: Annual Reports, London Chem. Soc., *105* (1945).
6. Gilman, H.: *Organic Chemistry*, Vol. *1*, pp. 838, 879. New York, John Wiley and Sons, 1943.

123

THE BEHAVIOR OF THE SYSTEM TRIETHYLAMINE—WHITE FUMING NITRIC ACID UNDER CONDITIONS OF RAPID MIXING

By ROSE L. SCHALLA AND EDWARD A. FLETCHER

Introduction

The rocket engine has created a great deal of interest in the processes which lead to ignition when self-igniting propellants are brought together. Ignition delays have been studied by many techniques which have been adequately described in the literature.[1, 2, 3, 4] They have proved useful in rating various propellant combinations with respect to relative ease of ignition. It has been suggested that they may be related to combustion instabilities in a rocket engine.[5, 6] There is, however, a great need for experimental study of the individual events which contribute to the over-all phenomenon of ignition. A knowledge of these events would be useful in predicting the behavior of various propellant combinations and would contribute to the art of designing propellant injection systems for rockets.

The effects on ignition delay of initial temperature, fuel-oxidant ratio, and ambient atmosphere have been studied. However, the work of Kilpatrick and Baker[7] suggests that the rate of mixing is an extremely important factor which has often been neglected in the interpretation of the results of ignition delay experiments. Ignition delays measured in an apparatus which does not mix the reactants efficiently are unnecessarily complicated to the extent that temperature and concentration gradients exist; an attempt to deduce facts about individual ignition phenomena from such data is difficult.

Kilpatrick and Baker found that, with the propellant combinations they studied (e.g., hydrazine-nitric acid, and aniline-nitric acid), ignition was essentially as fast as mixing. This suggests that all the steps subsequent to mixing, i.e., the reactions leading to ignition, were extremely fast. In order to use their technique for a study of the steps which follow mixing and lead to ignition, it was felt that a slower-reacting propellant combination should be used. By minimizing the importance of mixing in this way, the effects of other important variables were expected to show up.

Accordingly, a study of this kind was made at the NACA Lewis Laboratory using triethylamine-white fuming nitric acid. The rate of pressure rise in a constant volume bomb was studied as a function of: (1) the fuel-oxidant ratio; (2) the bomb volume; (3) the size of the propellant charge; (4) the oxygen content of the bomb prior to injection of the propellants; and (5) the water content of the acid.

High speed motion pictures taken simultaneously in some of the runs were used to help interpret the pressure traces.

Apparatus and Procedure

The apparatus used was similar to that of Kilpatrick and Baker except for several modifications made to adapt it to the present study. The component parts are shown in Figure 1a. The plastic bomb used when the reaction was photographed is also shown in this figure. Figure 1b is a cutaway illustration of the assembled apparatus ready for firing. A quick opening valve, not shown in the figures, was located above the reactor; it discharged nitrogen at 1500 psig into the space above the driving piston and simultaneously closed a switch to start a sweep on an oscilloscope. As the driving piston descended, four smaller pistons having diameters of 0.523, 0.725, 0.888, and 1.016 cm were simultaneously driven downward. The reactants were initially contained below these four pistons. They were prevented from mixing before firing by a teflon diaphragm located between the block and mixing plate. Since all the cylinder diameters were different, 13 different fuel-oxidant ratios could be obtained. When the apparatus was fired the diaphragm ruptured; the propellants were mixed in the mixing plate and ejected into the closed 430 ml bomb. The pressure rise was sensed with a strain gauge transducer of the catenary diaphragm type whose natural frequency was 35,000 cps. It was mounted in the side of the bomb. The electrical output was displayed on a dual beam cathode ray oscilloscope and photographed. A sine wave of known frequency on the second channel of the oscilloscope served as a time base. The sweep normally began several milliseconds before the beginning of injection.

The time required for total injection was obtained by placing several wire leads between the

driving piston and the top of the block (a distance of 1.6 cm). As the driving piston descended it made contact with these wires and registered a displacement on the oscilloscope. The second beam was simultaneously used to record either time or pressure. When the second beam recorded time it was shown that the total time of descent of the driving piston, and consequently the time for injection of propellants into the bomb, was

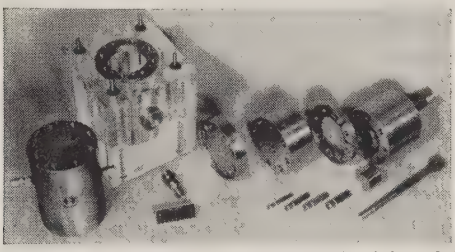

FIG. 1a. Component parts of the ignition delay apparatus. The plastic and stainless steel reaction chambers are interchangeable.

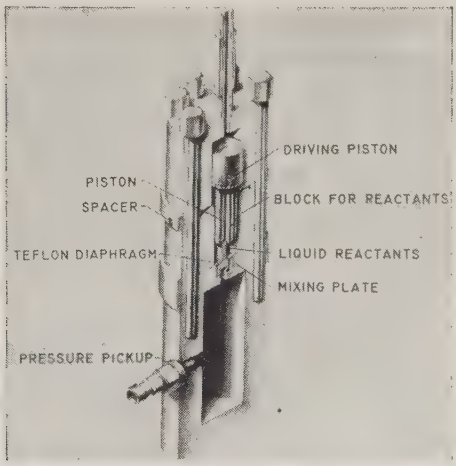

FIG. 1b. Ignition delay apparatus assembled and ready for firing.

less than one msec. When the second beam recorded pressure, it was observed that the pressure had started to rise before the driving piston had finished its descent. When water alone was injected into the bomb, there was no pressure rise.

With the lucite bomb shown in Figure 1a in place of the stainless steel bomb the reaction could be photographed. The timing light in the high speed motion picture camera was synchronized with the sine wave on the oscilloscope permitting the various steps in the pressure trace to be correlated with the phenomena recorded on the motion picture film.

The triethylamine was redistilled before use. It had an n_D^{20} of 1.4003. The white fuming nitric acid contained 98.05 per cent HNO_3, 0.33 per cent NO_2, and 1.62 per cent H_2O. The red fuming nitric acid contained 78 per cent HNO_3, 18.88 per cent NO_2, and 3.12 per cent H_2O.

Results and Discussion

TIME-PRESSURE CURVES

There was considerable experimental variation of the time-pressure curves even when the runs were nominally identical. However, the ignition phenomenon usually consisted of three well defined steps. This can be seen in Figure 2, where typical time pressure curves obtained in this study are shown for amine mole fractions (m) of 0.23, 0.305, and 0.545 (fuel-oxidant weight ratios of 0.478, 0.705, and 1.94). For the very rich

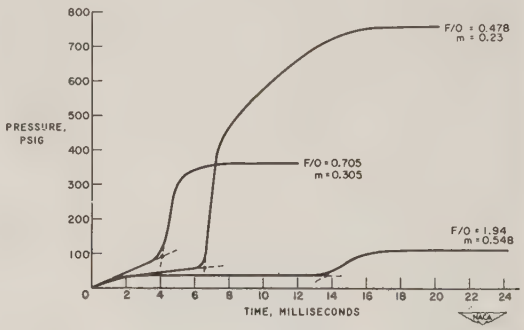

FIG. 2. Experimental pressure vs time curves for three fuel-oxidant ratios. Ignition delays are indicated by ●.

fuel-oxidant ratio of 1.94 (m = 0.545), the first step was accompanied by an initial pressure rise of about 35 psi in about 2 ms. This was followed by a second step during which the pressure remained almost constant. Finally, after about 13 ms, the mixture ignited, and the pressure rose rapidly to its maximum value of about 110 psig. These three steps are also indicated for the ignition of the mixture with the fuel-oxidant ratio of 0.478 (m = 0.23) where the ignition delay was somewhat shorter. The initial slope was the same as that for the very rich mixture. The transition to the second step took place after the same time interval, but the pressure rose appreciably faster during the second step of this run, and the ignition delay was shorter. With the fuel-oxidant ratio of 0.705 (m = 0.305), the second slope approached the first in magnitude and it is difficult to distinguish between them. Ignition followed very quickly. It is noteworthy, however, that even in this run, the initial slope was not

greatly different from that for the other two, and that all three curves indicated a similar rate of pressure rise during the mixing and injection period.

The small scale of the original traces and the experimental discrepancies among the various runs precluded a precise determination of the slopes associated with each step. In spite of these discrepancies, however, trends can be observed in the way these slopes changed with fuel-oxidant ratio. This is shown in Figure 3, where individual data points and average values of the slopes are plotted for a number of different mixtures. The initial slopes showed a relatively small variation over the fuel mole fraction range of 0.15 to 0.55 with a maximum at about 0.4. At the lower fuel mole fraction of 0.12, the slope was probably less, but the errors in measurement were too great to justify their inclusion on the plot. The slope corresponding to the second step showed a very marked variation over the range of fuel-oxidant ratios studied. The highest slopes occurred at the fuel-oxidant ratios having the shortest ignition delays. The variation of slopes for the third step (the actual ignition) with fuel-oxidant ratio is shown in Figure 3c. A rather large variation is observed with the maximum values occurring between fuel mole fractions of 0.15 and 0.35. The stoichiometric mole fraction of amine, based on complete combustion to carbon dioxide, water, and nitrogen, is 0.114.

In Figure 4 is shown the maximum pressure rise obtained at each fuel-oxidant ratio studied. The pressure was highest at the fuel-oxidant ratio of 0.478 ($m = 0.23$) and fell off very rapidly with leaner mixtures, the decrease on the rich side was not quite as pronounced.

IGNITION DELAYS

The ignition delay was arbitrarily selected from each curve by extending the flat portion near the beginning of each curve to the point where it intersects the tangent to the point of inflection on the steep portion.

Effect of fuel-oxidant ratio

A plot of ignition delays for seven mixtures having mole fractions of amine ranging from 0.116 to 0.548 is presented in Figure 5 for the propellant combination of triethylamine-white fuming nitric acid (WFNA), and for one mixture consisting of triethylamine and red fuming nitric acid (RFNA). Mixtures having amine mole fractions of 0.07 or less did not ignite. The ignition delay decreased from about 12 ms at a fuel-oxidant ratio of 0.21 ($m = 0.116$) to a minimum of about 3.5 ms at the fuel-oxidant ratio of about one ($m = 0.38$ to 0.4) and then increased as the mixtures became richer. Under the conditions of

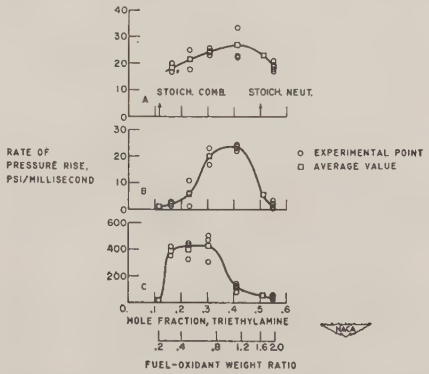

FIG. 3. Average rate of pressure rise vs mixture composition. (A) initial reaction; (B) during induction period; (C) during ignition.

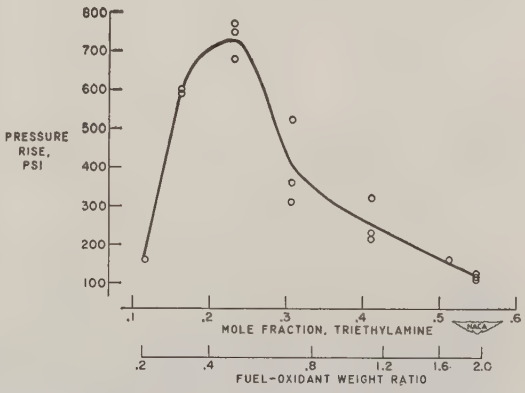

FIG. 4. Variation of maximum pressure rise with mixture composition.

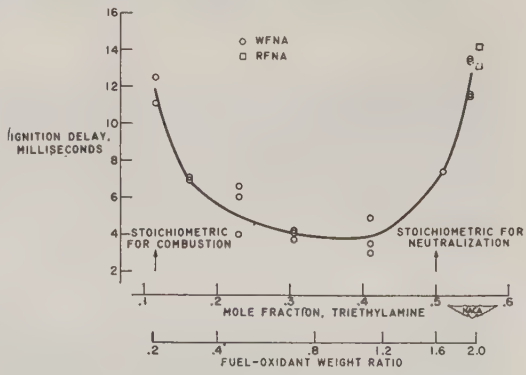

FIG. 5. Variation of ignition delay with mixture composition.

this investigation a four fold variation in ignition delay was observed with this range of fuel-oxidant ratios. The delay with RFNA for the one mixture studied was substantially the same as that for WFNA.

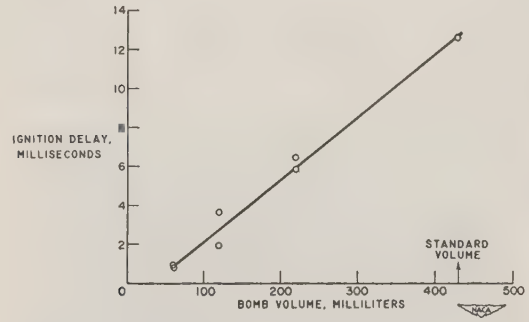

FIG. 6. Variation of ignition delay with bomb volume. Fuel-oxidant ratio 1.94, $m = 0.55$. The charge volume is 2.88 ml.

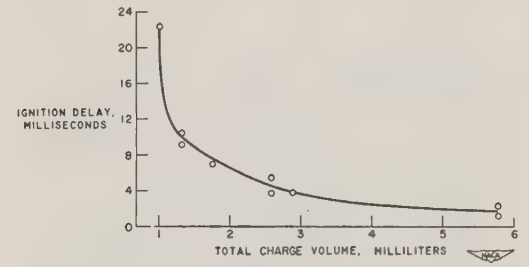

FIG. 7. Variation of ignition delay with volume of propellant charge at a fuel-oxidant ratio of approximately 0.98 ($m = 0.38$). The bomb volume is 430 ml.

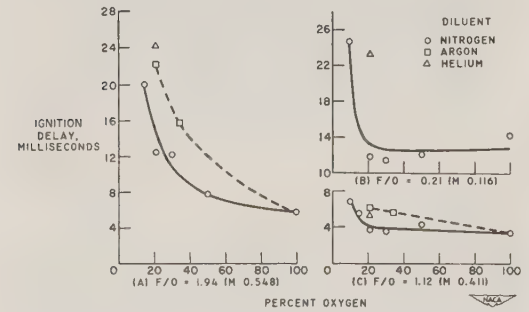

FIG. 8. Variation of ignition delay with oxygen concentration.

Effect of bomb volume

The volume of the bomb was varied from its standard value of 430 ml to 61 ml by the insertion of aluminum blocks. The variation in ignition delay over this range for a constant fuel-oxidant ratio of 1.94 ($m = 0.545$) is shown in Figure 6. There is a linear decrease in delay with decreasing bomb volume. Although the duration of the first step of the reaction was not affected, the pressure rise during this step increased as the bomb volume decreased.

Effect of size of the propellant charge

For most of the experiments the total volume of the propellants was 2.88 ml. The total volume was varied from 1 to 5.75 ml with the results shown in Figure 7. The fuel-oxidant ratio was approximately 0.97 ($m = 0.38$). The delay increased as the total charge was reduced. Here, too, the duration of the first step was not affected, but the pressure rise increased as the propellant volume was increased.

A correlation between these results and the results described in the preceding paragraph suggests that the ignition delays observed at a given fuel-oxidant ratio were approximately proportional to the ratio of the bomb volume to the charge volume.

Effect of the initial atmosphere in the bomb

Most of the data were obtained with the bomb initially filled with air at atmospheric pressure. Surprisingly when inert gases were substituted for air, no ignition occurred. The effect of varying the oxygen content of the atmosphere from 10 per cent to 100 per cent with nitrogen as the diluent was studied at three different fuel-oxidant ratios. The results are shown in Figure 8, for three fuel-oxidant ratios of 1.94, 0.21, and 1.12. With the very rich mixture, ignition delays consistently decreased with increasing oxygen concentration. With the less rich mixtures, decreasing the initial oxygen content below that of air increased the delays or quenched the reaction, but increasing the oxygen content had practically no effect. Apparently with these mixtures (0.21 and 1.12), the acid was furnishing sufficient amounts of oxidizing agents to propagate the reaction once it had started. One run was made with a very rich mixture ($F/O = 1.94$) with N_2O_4 substituted for the air. This run produced a delay of 2.7 ms, the shortest ignition delay observed in the present study with the standard bomb volume to propellant volume ratio. In view of this system's behavior with oxygen, the fact that the N_2O_4 was originally in the gas phase, and the fact that N_2O_4 reacts quite readily with triethylamine itself,[8] the short ignition delay obtained in this experiment was not at all surprising.

It thus appears that with triethylamine, mere mixing with nitric acid is not a sufficient requirement for ignition. There must be present oxidizing agents in the gas phase. If gaseous oxidizing agents are not initially present, ignition probably will not take place unless the acid decomposes enough to furnish the necessary gas phase oxidizers. Since no ignition was obtained in inert atmospheres, it appears that under the conditions of this research, decomposition of the nitric acid alone did not provide sufficient gaseous oxidizers.

In addition, several data points obtained with oxygen-argon and oxygen-helium atmospheres are shown in Figure 8. The effect of substituting argon or helium for nitrogen was to increase the ignition delay. It is noteworthy that variation of the initial oxygen content had no effect on the initial reaction step, even when the oxygen content was so low that there was no subsequent ignition.

Effect of dilution of WFNA with water

The water content of the WFNA was varied from the standard value of 1.6 weight per cent to 10.4 per cent for the fuel-oxidant ratio of 0.705. The delay increased with increasing water content as shown in Figure 9. With 15 per cent water no ignition was obtained. These results are somewhat similar to those of Gunn.[9] It is noteworthy that this parameter is the only one studied

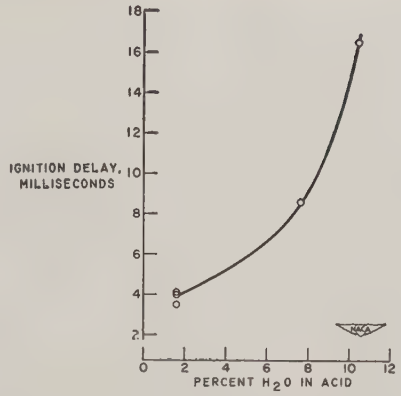

FIG. 9. Variation of ignition delay with water content of the acid. Fuel-oxidant volume ratio is 1.47.

which appreciably affected the behavior of the reaction in the first step. As the initial water content of the acid was increased the vigor of the first step decreased as evidenced by a decrease in the rate of pressure rise.

Observation from films

High speed motion pictures were taken of a number of runs with the plastic bomb substituted for the stainless steel bomb. A run made with water is shown in Figure 10a. A run made with propellants is shown in Figure 10b. Two photofloods were used for illumination of these runs.

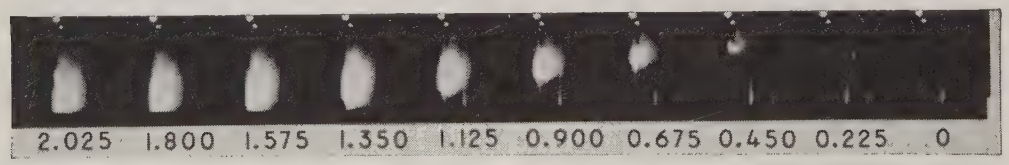

(A) Injection of water into plastic bomb

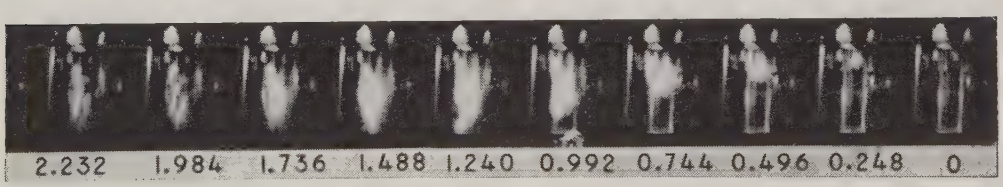

(B) Injection of propellents into the plastic bomb

(C) Ignition

FIG. 10. High-speed motion pictures (time, milliseconds).

The time after the start of injection is indicated by each frame. It appears that liquid injection was completed in both runs within approximately 1 ms, in agreement with the results obtained by measuring the time of descent of the pistons. A comparison of films from the water injection runs and live runs showed a marked distinction after approximately 2 ms. The pictures from the propellant runs were less opaque at this time probably indicating that much of the liquid had evaporated. It was found that the illumination from the photofloods made it almost impossible to recognize the appearance and growth of flame. Consequently, instead of constant illumination from the photofloods, an electronic flash unit was set up to fire at the same time the scope was triggered. The intensity and duration of the flash were sufficient to illuminate the injection and vaporization portion of the run, but no external illumination was present when flame appeared in the bomb. Therefore, the initiation and growth of the flame could be followed. Pictures of an ignition are shown in Figure 10c. Here, too, injection was complete in about 1 ms and a correlation with the oscilloscope pressure trace indicated that the pressure started to rise 2 frames (0.5 ms) after the first appearance of liquid. This is in agreement with the piston descent measurements which indicated that the pressure started to rise during the descent time. As can be seen in Figure 10c, the flame started at several places and grew rapidly. The appearance of flame accompanied the steep pressure rise on the pressure-time curve.

General Discussion

It had been hoped that these results would lend themselves to quantitative kinetic interpretation. However, initial composition and temperature must be known before such an interpretation can be made. The uncertainties introduced into the composition and temperature by the first step as described below complicated the problem to such an extent that the results of such an interpretation could have only doubtful value. Still, a gross interpretation of the pressure traces and the way they change with different parameters yields a plausible qualitative picture of the steps leading to an ignition with this system.

The present study suggests that the first step in the ignition process, after mixing, is common to all of the runs. It takes place, regardless of whether or not ignition is ultimately achieved and is always essentially complete in 1 to 2 ms. The pressure rise observed during this step and the observations made with the high speed motion picture camera are consistent with the hypothesis that the first step results in the production of gases. The liquid spray disappears very quickly. As the size of the charge is increased or the volume of the bomb decreased, the first step pressure rise increases. The variation of the pressure rise observed in the first step with fuel-oxidant ratio suggests that the initial reaction is most vigorous at a fuel-oxidant mole ratio of about 0.7. This suggests a rapid, liquid phase, ionic reaction using roughly equimolar quantities of fuel and oxidant (perhaps a neutralization reaction) which liberates sufficient heat to bring about thermal decomposition or evaporation of some of the reactants. In connection with this, the heat of neutralization of triethylamine with nitric acid is estimated to be about 13.5 kcal/mole from the heats of formation of the species involved.[10, 11]

The initial reaction is then followed by an induction period (the second step) during which it is determined whether or not an ignition will subsequently take place and how fast. The reaction rate in the induction period is the principal factor determining the ignition lag. The greater the rate, the shorter the lag. Increasing the pressure at the beginning of the induction period (by increasing the over-all concentration of propellants in the bomb) greatly lowered the ignition lag. This indicates that the rate in the induction period is quite pressure sensitive. In addition, it is quite likely that at least three other factors determine the behavior of the system during the induction period:

(1) The temperature to which the mixture is raised in the initial reaction. This will be determined by the reactivity of the fuel with nitric acid in the liquid phase. Although neutralization is indicated for this combination, other fuels could undergo nitration or neutralization and nitration reactions. For a stoichiometric neutralization, if there are no subsequent endothermic processes such as re-dissociation, vaporization, or decomposition, the temperature might easily be expected to rise as much as 160°C. This, of course, is impossible. The figure is quoted only to illustrate the magnitude of the thermal effect which neutralization may produce.

(2) The composition of the gaseous mixture after completion of the initial reaction. If the initial reaction uses up the nitric acid without

supplying a sufficient amount of oxidizing agents to the gas phase for consumption in the second step, the ignition will be delayed or quenched.

(3) The ease with which the fuel or its decomposition products can be attacked by oxygen or oxides of nitrogen.

If neutralization is the first chemical reaction in ignitions involving triethylamine-nitric acid, the contribution of this step to a successful ignition would be greatest when the mixture consists of equimolar quantities of amine and acid. Unfortunately, however, when this situation exists, the second requirement, namely the availability of oxidizing agents in the gas phase is satisfied to a much lesser extent than it is with leaner mixtures, so ignitions with this system have their shortest delays at a fuel-oxidant ratio somewhat leaner than that for complete neutralization. The effect of substituting oxygen or N_2O_4 for the air in the bomb was to make oxidizers available for the second step without incurring a loss of the heat of neutralization of the first step. As a result these ignition delays were among the shortest measured in the present study. The importance of oxidizing agents in the second step is further indicated by the observation that inert gas completely quenched the reaction.

One might speculate that, in the absence of chemical factors like those whose importance was demonstrated by Rapp and Strier[3] the best amine-acid propellant combinations would be those whose stoichiometries for both neutralization-nitration and fast efficient combustion are about the same. For a given rocket application the stoichiometry is chosen with complete combustion in mind. The optimum stoichiometry for ignition or preparation for combustion may be only a secondary consideration. It is quite conceivable that neglect of propellant preparation may lead to deleterious effects on performance. This effect was mentioned in connection with engine starting by Barrere and Moutet.[6] With propellant combinations like hydrazine-WFNA, and aniline-WFNA, the stoichiometries for a neutralization-nitration reaction and complete combustion are quite close together; with amines having larger and larger aliphatic groups the practical fuel-oxidant ratio is farther and farther removed from that which gives the greatest boost to the reaction in the initial step. This could conceivably result in an unnecessarily long combustion time lag and increase the tendency toward combustion instabilities.[5]

Since completion of the first step depends only on mixing of the reactants, it appears that minimization of the ignition delay or the combustion time lag—in a system where ignition and combustion are not achieved solely by propagation from an existing combustion zone—might be achieved by minimizing the second step induction period, making use of a combination of the principles suggested here and in other studies.[3, 6]

REFERENCES

1. Broatch, J. D.: *Fuel*, 24–5, pp. 106–109 (1950).
2. Pino, M. A.: Jet Propulsion, No. 9, Part 1, 1955, 463–466 (1955).
3. Rapp, L. R., and Strier, M.: Second AGARD Combustion Colloquium, University of Liege, Liege, Belgium, December 5–9, 1955.
4. Ladanyi, D. J., and Miller, R. O.: Jet Propulsion, *26*, 157 (1956).
5. Crocco, L., Grey, J., and Matthews, G. B.: *Fifth Symposium (International) on Combustion*, pp. 164–170. New York, Reinhold Publ. Corp., 1955.
6. Barrere, M., and Moutet, A.: *Fifth Symposium (International) on Combustion*, 170–181. New York, Reinhold Publ. Corp., 1955.
7. Kilpatrick, M., and Baker, L. L., Jr.: *Fifth Symposium (International) on Combustion*, 196–205. New York, Reinhold Publ. Corp., 1955.
8. Davenport, D. A., Burkhardt, H. J., and Sisler, H. H.: J. Am. Chem. Soc., *75*, 4175–4178 (1953).
9. Gunn, S. V.: J. Am. Rocket Soc., *22*, No. 1, 1952.
10. Cottrell, T. L., and Gill, J. E.: J. Chem. Soc., 1798 (1951).
11. *Handbook of Chemistry and Physics*, Ed. 35 Cleveland, Chemical Rubber Publishing Co., 1954.

124

SOME FLUID DYNAMIC ASPECTS OF LAMINAR DIFFUSION FLAMES

By H. N. POWELL AND W. G. BROWNE

It may be argued that fluid dynamic factors do not alter the basic physicochemical processes which occur in laminar diffusion flame burning zones. Unfortunately, however, it is not easy to make a clear separation of these factors in treating experimental data—a circumstance which appears to have undermined the confidence with which the combustion public regards much of the previous analytical work on diffusion flame structure. Consequently, we feel that the following development of certain fluid dynamic aspects will help to place our own and some previous work in a more clearly defined context.

Hydrodynamic Aspects

Our preliminary investigations pointed out a fluid dynamic aspect of laminar diffusion flame structure which, it appears, has not been adequately appreciated, namely, the influence of a density difference in the fuel and oxidant streams. If the horizontal dimensions of these streams are large in comparison to the flame zone thickness, *we may then regard the system as hydrodynamically equivalent to one composed of two immiscible liquid streams of different densities.* In this picture the flame zone is a comparatively minor variation in stream properties near the interface of the two streams. It is apparent then, that under the influence of gravity, the heavier fluid will tend to constrict the flow of the lighter, thereby increasing its velocity. Obviously these considerations are most applicable to the lower parts of diffusion flames; for the present we will leave open the question of their influence on the over-all structure.

We may investigate this picture by considering the streams a and b to have the mean velocities u_a and u_b at some point y above the lip of their initially separating wall. Then let the kinetic energy balance form for the Bernoulli equation be applied to each stream separately, neglecting the friction term. These two equations are then combined by equating the static pressures $p_a = p_b$ at the same y in accord with the fact that the interface of the two fluids is a free surface. Finally, noting that at the same T and p the density of a gas is proportional to its molecular weight, m, and for the condition that both streams have the same initial velocity, u_0, we obtain:

$$\left(\frac{u_a}{u_0}\right)^2 - \left(\frac{m_b}{m_a}\right)\left(\frac{u_b}{u_0}\right)^2 = \left[\frac{y}{(u_0^2/2g)} - 1\right]\left[\frac{m_b}{m_a} - 1\right] \tag{1}$$

The geometric constraints of a particular system are introduced by the volume flow rate balances in terms of the flow areas A_a, A_b and the total area A_t

$$A_a u_a = (A_{a,0})(u_0), \qquad A_b u_b = (A_{b,0})(u_0), \qquad \text{and} \quad A_a + A_b = A_t \tag{2}$$

Upon the assumption of a constant total A_t, Equations (2) can be combined to give:

$$(u_a/u_0) = \frac{(u_b/u_0)}{(1 + r)(u_b/u_0) - r} \tag{3}$$

in which $r = A_{b,0}/A_{a,0}$. Unfortunately the form of Equations (1) and (3) do not lend themselves to an analytic simultaneous solution, but they can be solved readily by numerical or graphic means.

The one-dimensionality of the Bernoulli equation limits this analysis to situations in which the average horizontal component of a flow stream is small relative to its vertical component. Also no detail on the effects of mixing or viscous interaction between the streams or with the walls is revealed. We can, however, make some qualitative deductions about the effects of momentum exchange between the streams.

First we note that for a fixed u_0 there are no pressure dependent variables in Equations (1), (2) or (3). The shear force per unit area of interface is therefore independent of pressure. The distribution of this shear stress in the region about the "interface" depends on the kinematic viscosity, ν, which may be regarded as a "coefficient of momentum diffusion." However, ν, like the molecular diffusion coefficient, D, varies as p^{-1} so that we would expect increased pressures to concentrate the shear stress in a thin region of steep velocity gradients about the interface—conditions which tend to favor low frequency hydro-

dynamic instability. An analogy to rather irregular wave formation by wind blowing over water suggests itself. If a diffusion flame sheet is present, it must, of necessity, locate in this same interface-mixing region. A low frequency flickering and roughness would therefore appear to be a phenomenon which is associated with the flame itself, whereas actually it is independent of the flame.

Strong evidence for this purely hydrodynamic point of view is shown in Figure 1, a and b, schlieren photographs of a butane-air system, with and without a flame, respectively. The initial stream velocities are equal (9.3 cm/sec) and the pressure is 1.0 atmos. Butane is approximately twice as dense as air and is seen to constrict the air flow into a narrow channel. It is also seen that, other than to intensify the contrast of the schlieren pattern, the presence of the flame does little to alter the position of the interface region or character of the instability. The presence of a series of fine mesh screens in both flow streams just below the lower edges of the photographs eliminates upstream turbulence as an explanation for the instability. The duct Reynolds numbers were too low for turbulence generation in both up and downstream sections.

However, if the pressure is decreased, ν increases, the diffusion rate of momentum increases, the velocity gradients become less steep and the shear stress is distributed over a wider zone, *i.e.*, the interface region should become more stable. When we decreased the pressure on the butane-air flame of Figure la, (holding u_0 constant), the flickering did diminish until at 0.15 atmos the flame zone was completely stable and indeed, for a flame of double this velocity, we were able to obtain a quantity of data as reported in a subsequent paper.[1]

All the foregoing hydrodynamic effects follow originally from a density difference of the fuel and oxidant streams. Consequently, the simplest and most stable hydrodynamic system should be one with a negligible density difference between the two streams. The stability of ethane-air diffusion flames ($m_{C_2H_6} = 30.04$ and $m_{air} = 28.97$) over the whole range of pressures which we investigated, 0.15 to 1.0 atmos, was one of the principal reasons for choosing this system for the majority of our work. Figure lc shows a schlieren photograph of an ethane-air flame at identically the same flow conditions as Figures la and lb.

Since the foregoing hydrodynamic considerations seem to be pertinent, it would be interesting to make a few speculations. Equation (1) suggests that a characteristic height is $y = y_1 = u_0^2/2g$, *i.e.*, the height which is equal to the initial velocity head of the streams. This height corresponds to a Froude number of unity (Fr = inertia forces/gravitational forces). A reference to the original Bernoulli equation shows that the total kinetic pressures of the two streams are equal at this height. Therefore, it would seem plausible to associate an average velocity with this point for flame height calculations. When

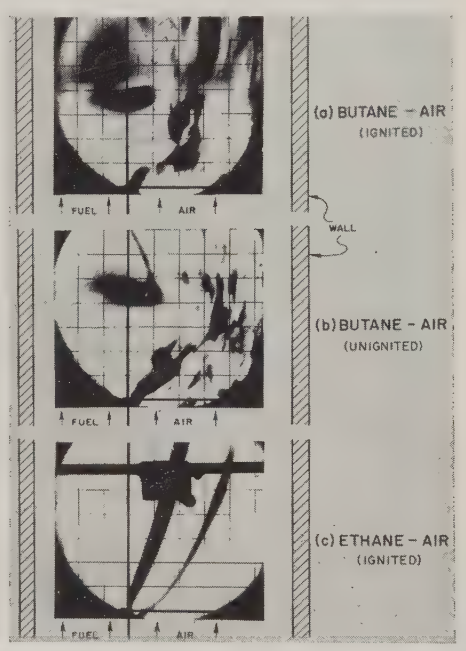

FIG. 1. Schlieren photographs of three fuel-air systems with all initial stream velocities = 9.3 cm/sec and at 1 atmos pressure.

$y/(u_0^2/2g) = 1$, Equation (1) yields:

$$(u_a/u_b)_1 = \sqrt{m_b/m_a} \tag{4}$$

Then, since the flame locates in the interface region between the streams, let the interface velocity, u_{in}, be defined as the average of the two stream velocities,

$$\frac{u_{in}}{u_0} = \frac{1}{2}\left[\left(\frac{u_a}{u_0}\right)_1 + \left(\frac{u_b}{u_0}\right)_1\right] \tag{5}$$

using the Equations (2) or (3) to evaluate (u_a/u_0) and (u_b/u_0) from Equation (4).

An important result of the Burke and Schumann[2] analytical development is that for a fixed geometry with equal fuel and oxidant stream

u_0's, the flame height $h_f \sim u_0/D$. Therefore, noting that for H_2 and CO diffusion in air the diffusion coefficient ratio is $D_{H_2}/D_{CO} \simeq 4$, they predicted the flame height ratio $h_{fCO}/h_{fH_2} \simeq 4$ for CO-air and H_2-air flames when all the u_0's are equal. However their experimental result was $h_{f(CO)}/h_{f(H_2)} \simeq 2.5$. Of the several tests which they ran to check various analytical predictions, this is the only result which is in marked disagreement with their theory, and has been a focal point for criticism of their analytical development ever since.

From a hydrodynamic viewpoint, the density ratio, $m_{air}/m_{CO} = 28.97/28.01$, is so close to unity that we may say $u_{in} = u_0$. However, the ratio $m_{air}/m_{H_2} \simeq 14$ is very large and should cause a marked velocity increase of H_2, thereby causing a higher flame height than if the velocities were equal as they assumed. Most of their work was methane-air systems which involve less pronounced differences in density. Table 1 was prepared from Equations (1), (4) and (5) and the pertinent geometric and flow data in the Burke and Schumann Tables I and II.[2]

In support of the reasonableness of these results, it is seen that the small values of the ratio y_1/h_f is fair justification for neglecting (up to y_1) the fluid dynamic influences of both the flame zone and momentum exchange between the streams. The last column in Table 1 shows that the hydrodynamic effects in their particular methane-air flames are relatively constant and are not sufficiently drastic to invalidate a theoretical interpretation which neglects these factors.

In the H_2-air flame however, the ratio of the interface velocity to the initial velocity, u_{in}/u_0, is markedly different from unity. Therefore, by taking ratios of the general formula

$$h_f \sim u_0 \left(\frac{u_{in}}{u_0}\right) \Big/ D \qquad (6)$$

and noting that $(u_{in}/u_0)_{CO} \simeq 1$, we obtain a "modified" theoretical ratio,

$$\frac{h_{fCO}}{h_{fH_2}} = \frac{1}{(u_{in}/u_0)} \left(\frac{D_{H_2}}{D_{CO}}\right) = \frac{4}{1.61} = 2.48$$

as compared to their experimental ratio 2.5. In view of the partly intuitive definition of y_1, the close agreement of our calculated result with experiment may be fortuitous, but it does provide a physically reasonable explanation of their results.

Hydrodynamic factors will certainly have some influence in the lower structure of unconfined laminar fuel jets as well as in enclosed systems.

At first thought it might appear that mixing and combustion would override purely hydrodynamic considerations in the upper parts of any initially laminar flame, but since the flame height and the hydrodynamic forces tend to vary with u_0 and u_0^2, respectively, it would not seem advisable, *a priori*, to neglect possible contributions of the latter mechanism. For example, in a laminar fuel jet discharging into air, if the volume flow rates are sufficiently large, strong hydrodynamic effects may assert themselves before all of the fuel is consumed. If the fuel is heavier than air, then at some height the fuel will expend its initial velocity head and fall back on itself like a water fountain, tending to promote turbulence. On the other hand if the fuel is markedly lighter than air, it will continuously tend to accelerate and may exceed the critical Reynolds number, tending to promote turbulence. The point is that, in principle, here are two turbulence promoting mechanisms which have no connection with combustion and which depend entirely on the choice of the system and flow variables.

Table 1. Hydrodynamic Effects in Some Burke and Schumann Flames

a = fuel and b = air

Flame	$\frac{u_0}{\frac{\text{in.}}{\text{sec}}}$	$\frac{h_f}{\text{in.}}$	$\frac{y_1}{\text{in.}}$	$\frac{y_1}{h_f}$	r	$\frac{m_b}{m_a}$	$\frac{u_a}{u_b}$	$\frac{u_a}{u_0}$	$\frac{u_b}{u_0}$	$\frac{u_{in}}{u_0}$
6 (a) CH_4-Air	4.89	0.87	0.031	0.036	5.25	1.806	1.34	1.29	0.96	1.12
6 (e) CH_4-Air	8.73	8.1	0.099	0.012	6.10	1.806	1.34	1.30	0.96	1.13
H_2-Air	21.7	2.75	0.608	0.220	1.25	14.36	3.79	2.55	0.67	1.61

Some Results of Streamline Tracing

In our flat flame burner, which used fine mesh screens to achieve flat velocity profiles prior to burning, the choice of an ethane-air system did

not eliminate all the gross fluid dynamic effects. The flow patterns in the first 5 in. of the flame region were investigated at 1 atmos pressure by using the well known titanium smoke technique for tracing streamlines. Titanium tetrachloride was introduced through a very small probe just above the last screen into the previously humidified gases passing up the burner. The resulting titanium dioxide smoke traces were photographed with a Speed Graphic camera set on bulb exposure using Kodak Super XX film. Illumination was provided in the plane of the trace through a slit in the side of the burner with an Amglo flash bulb (model 78R9D at 2000 volts and with 20 mfd) which provided a flash duration of 0.1 msec. The brief high intensity flash was necessary to make the trace illumination strong in comparison to the steady flame radiation. The slit was covered with glass to prevent flow communication between the interior of the burner and the room.

Two of these photographs are shown in Figure 2, a and b. It is immediately apparent that the whole flow pattern is being shifted to the air side of the burner by a recirculation flow which originates in the chimney above the top of the photograph. The lower edge of this recirculation zone is made visible by the cross flowing trace at the top of Figure 2b. The position of the flame front is indicated by the luminous diagonal zone which seats on the indicated partition. Many such photographs established the fact that it was a stable and reproducible phenomenon.

From these photographs we conclude that no purely physicochemical significance can be

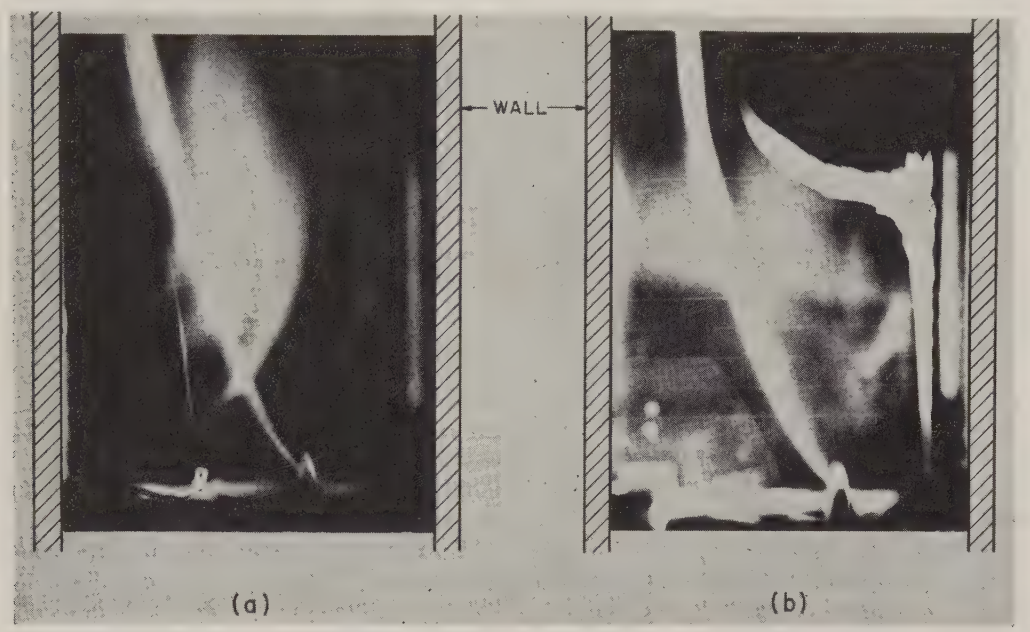

FIG. 2. Streamline traces in a flat flame burner (ethane-air with initial velocity = 9.3 cm/sec and at 1 atmos).

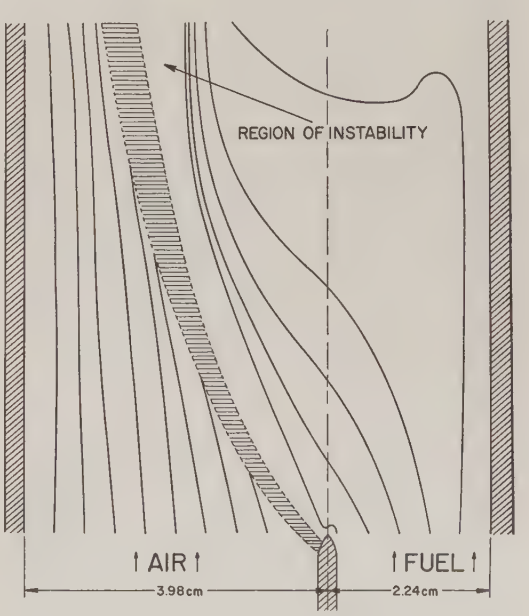

FIG. 3. Flow map of flat flame burner as formulated from streamline traces (ethane-air with initial velocity = 9.3 cm/sec and at 1 atmos).

attached to the position of the flame zone as is the case for the idealized flow situation which Burke and Schumann treated. It should be noted, however, that the axial flow symmetry of cylindrical diffusion flames, should markedly lessen effects of this kind.

From a quantitative scaling of many such photographs a composite flow map of the burner was made and is shown in Figure 3. For the sake of clarity, Figure 3 shows the appearance of the flow field with streamlines having an equal initial spacing, rather than showing the actual experimental traces. The mass flow rate, (ρu), can be determined relative to the initial $(\rho u)_0$ by the relative distance between two streamlines as they pass up the burner. The wide spacing of the streamlines to the right of the flame zone indicates the lower mass flow rate-region in the wake of the initially separating partition. This map shows that the streamlines which enter the region of the visible flame zone have a definite tendency to crowd. It is seen that the streamlines in the flame front region tend to crowd by a factor of at least 2, but no more than 4, times closer than the same streamlines in the initial stream, depending on whether or not the wake region is included. The corresponding mass flow rate ratio is $(\rho\ u)/(\rho\ u)_0 = 2$ to 4 in this region. Then let us empirically relate this ratio to a corresponding average temperature ratio, (T_{Av}/T_0), for this region by $(\rho\ u)/(\rho\ u)_0 \simeq (T_{Av}/T_0)^a = (3 \pm 1)$ in which a is a constant. By assuming $(T_{Av}/T_0) \simeq (1500°K/300°K) = 5$ it is found that for a crowding ratio of 3, $a = 0.7$. By allowing for considerable variations in the assumed (T_{Av}/T_0) and in the crowing ratio, reasonable limits for a can be established; $0.3 < a < 1$. Despite the clear-cut appearance of Figure 3, in reality the experimental accuracy of the method is such that a more quantitative treatment is not justified. Therefore, since $\rho \sim T^{-1}$ and $D \sim T^{1.75}$ we obtain $(D/u) \sim T^{1.75-1-a)} = T^b$ in which $-0.25 < b < +0.45$ with a likely value $b \simeq 0.1$. It is this group, (D/u), which Burke and Schumann and other investigators have had to regard as independent of T for mathematical reasons. From the above crude analysis it appears that in reality this may be a very reasonable approximation.

Some Conclusions on Fluid Dynamic Factors

(Based on the foregoing analytical and experimental investigations)

(a) Gross departures in flame shape and height from the Burke and Schumann analytical predictions are primarily due to hydrodynamic effects which stem from density differences in the fuel and oxidant streams. These same factors may also cause a low frequency instability which is enhanced by increasing pressures.

(b) In the absence of strong hydrodynamic effects, the flame zone will generally conform in shape and appearance to that predicted by the Burke and Schumann analysis, but its position depends on an over-all flow field which may contain marked directional departures from the one-dimensional vertical flow of their analysis. In this respect a cylindrically symmetric geometry is most favorable.

(c) The local buoyancy and velocity effects within a single flame zone are such as to justify regarding the group (D/u) as approximately independent of temperature.

(d) In view of the considerable experimental support which the Burke and Schumann formulation has received since 1928 from a number of applications, we conclude that there is no clear evidence for questioning the *physicochemical* validity of their analysis for describing the gross structure of flames in which it is reasonable to regard the flame zone as a surface; its experimentally revealed weaknesses are due to inadequately accounted for fluid dynamic effects. A more general physicochemical approach, applicable to both the gross and detail structure of inhomogeneous combustion systems, is presented in this volume by the present authors.

Acknowledgment

The authors wish to gratefully acknowledge the skill and ingenuity which Mr. Maynard Cook has brought to bear in developing the special photographic technique for streamline tracing employed in this paper.

REFERENCES

1. Browne, W. G., and Powell, H. N.: *Sixth Symposium (International) on Combustion*, p. 37. New York, Reinhold Publishing Corp., 1957.
2. Burke, S. P., and Schumann, T. E. W.: Ind. Eng. Chem., *20*, 998–1004 (1928).

125

PHYSICAL METHODS FOR IMPROVING COMBUSTION

By YUKICHI ASAKAWA

Introduction

Physical phenomena of so-called flame ionization have been treated by several authors.[1, 2] A flame is generally considered to have positive ions in its outer region and negative ions in its inner region, the two types of ions being in a state of over-all equilibrium. Application of a powerful magnetic field to a flame ordinarily splits it into two parts,[1] corresponding to the direction of force exercised on the two types of ions by the magnet.

The present author has long been concerned with a new method of increasing the flow velocity of combustible media (solid particles, oils, gases) by physical means.[3] This method has led to the theory that the shape and character of a burning flame can easily be modified simply by applying an electric or magnetic field.[4] Moreover, with this method the rate of combustion of fuel oils could easily be increased up to 3-4 times, which is not to be expected with other procedures.

Experimental Results

1. DISPERSION AND ROTATION OF A COMBUSTIBLE MEDIUM, ASSOCIATED WITH A LARGE INCREASE OF VOLUME OF THE FLOW

A high voltage was applied to the nozzle emitting a stream of solid particles, as shown in Figure 1. Thus, the particles passing through the nozzle become charged equally with ions of the same sign. As a result, a downward stream of solid particles charged with ions of the same sign becomes a divergent flow due to the mutual repulsion between the charged particles. The phenomena thus observed are shown in Figure 2. The angle of divergence observed in Figure 2 naturally increases with the applied voltage (Fig. 3). In this case, the downward volume per unit time is observed to increase up to 30 per cent as shown in Figure 4. Similar results are obtained when a flow of heavy diesel oil is subjected to a high voltage. In this case, diesel oil was directed downward through a metal nozzle, 1.0 mm in diam (Fig. 5). Owing to the narrow passage and to its own high viscosity the oil does not form a continuous stream, but passes drop by drop. However, if a high voltage (several kv) is applied to the nozzle orifice, the oil flows in a continuous stream, as shown in Figure 6. As in the case of solid particles, this downward stream of oil is electrically charged as may easily be ascertained by using an electrometer or by approaching a foreign body connected to earth (Fig. 6). A charged oil stream will tend to deflect toward a grounded body owing to the mutual attraction between a certain type of ion and ions of a different type produced by induction. The resulting increase in the downward flow velocity of a diesel oil has been measured (Fig. 7).

The next step was to substitute an ac for the dc source, with similar results for a flow of solid particles (see D, E, F, Fig. 2) or an oil stream (Fig. 8).

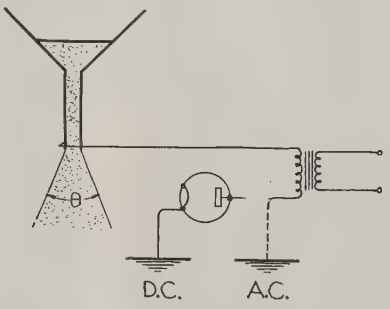

FIG. 1.

In the case of ac source, we must first consider the fact that ionization produced by the application of ac high voltage would certainly change its intensity at every instant cyclically, as the same cycle of an applied ac source. Consequently, a flowing stream of oil will generally be affected by this ionization. Ordinarily, the phenomena associated with ionization cannot be observed directly because of the frequency (25 or 50 cycle) of fluctuation of an observable image.

To observe a true image of these phenomena, the author inserted a neon lamp in the same circuit of the applied source. With this neon illumination, a true image at a certain instant of a flowing stream of oil could be observed as a stationary column of the stream (Fig. 8).

These photographs were obtained by a long exposure of 10 sec. From the nature of a neon lamp, we may consider that if the phase of flash of a neon lamp is shifted by a certain angle, the new image also will be shifted by that angle.

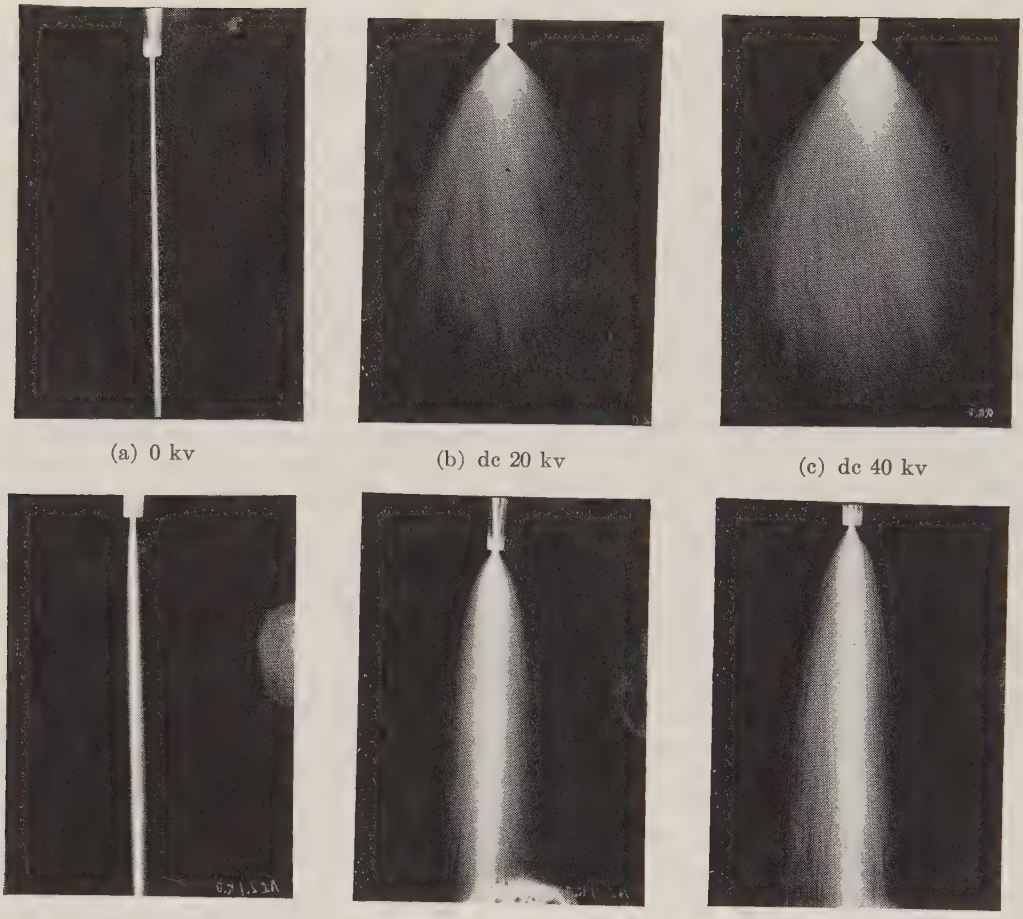

(a) 0 kv (b) dc 20 kv (c) dc 40 kv

(d) ac 2.1 kv (e) ac 7 kv (f) ac 9 kv

FIG. 2.

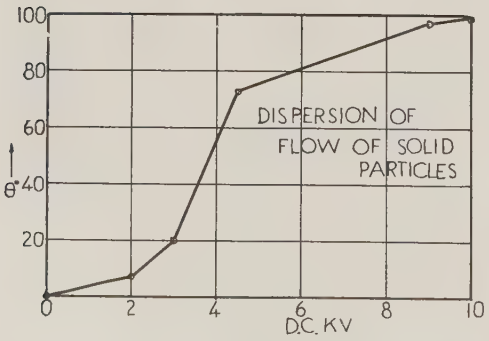

FIG. 3.

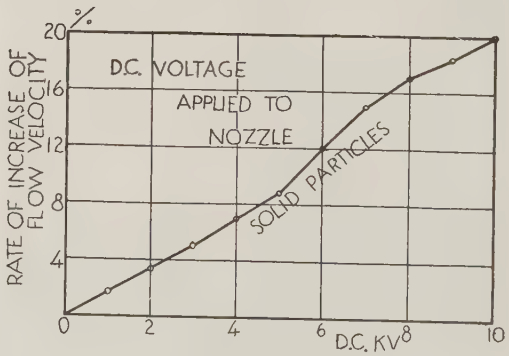

FIG. 4.

Accordingly, if we shift the phase of flash continuously by a complete cycle (360°), then the image thus observed will change its features continuously, corresponding to the angle of shifting.

From these photographs, we can see that a node of the stream corresponds to a zero point of a voltage curve of the applied ac source, and a loop corresponds to a peak of the voltage curve. On this basis, the fact that an oil flow increases its volume per unit time can be explained by the loop phenomena shown in the photographs.

2. APPLICATION OF SECONDARY EXCITATION TO A FLOWING MEDIUM THAT HAS ALREADY BEEN EXCITED

Starting from the above phenomena, the author applied a new excitation to a flow of oil which

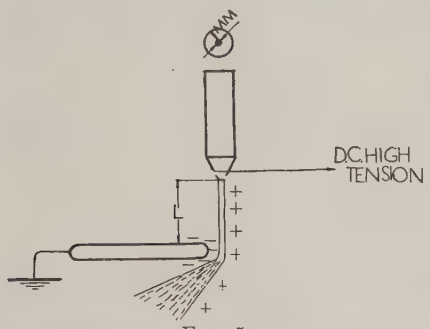

FIG. 5.

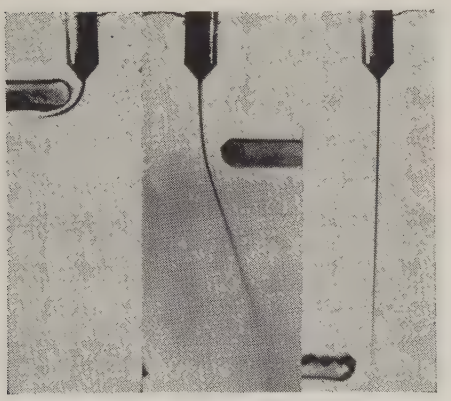

FIG. 6.

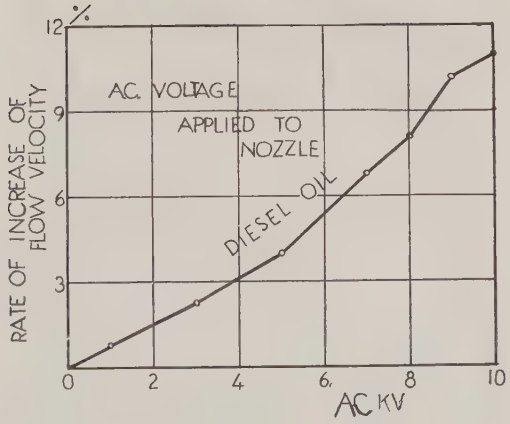

FIG. 7.

had already been excited, on the assumption that this would increase the flow of oil thus treated. The results obtained were just as expected by the author.[3] They suggest that the behavior of a

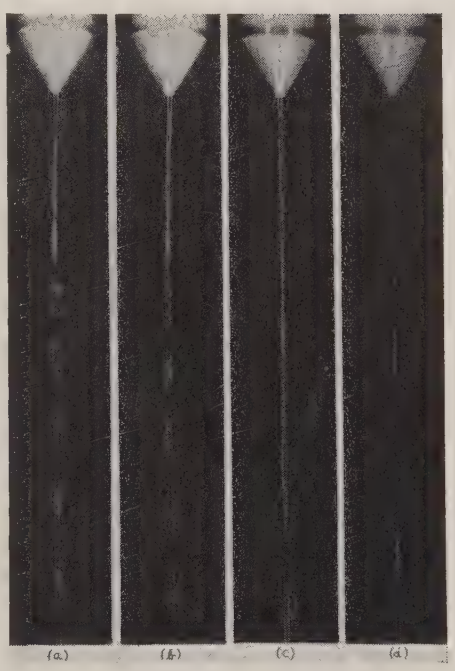

FIG. 8. (a) 50 cycle excited; (b) 50 cycle excited; (c) 25 cycle excited; (d) 25 cycle excited.

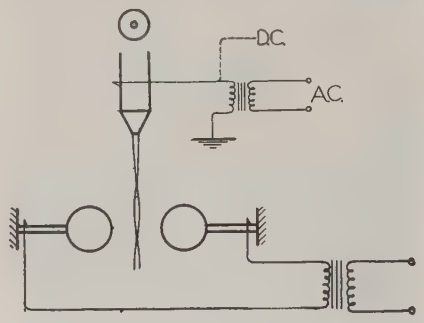

(a)

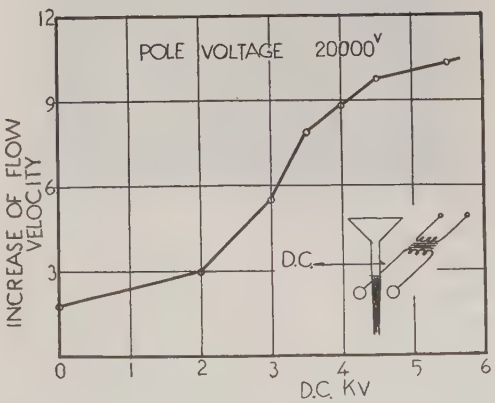

(b)

FIG. 9.

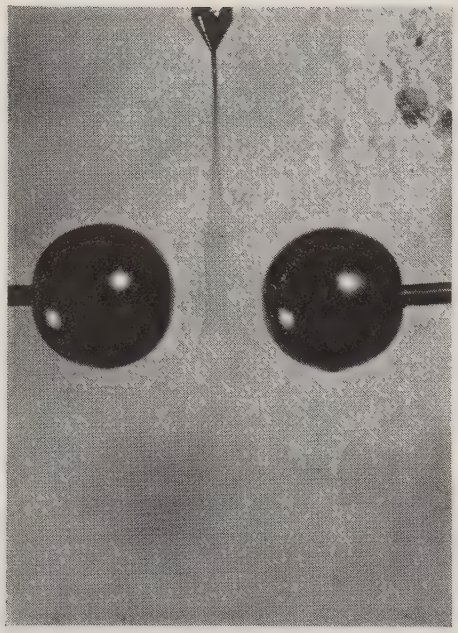

FIG. 10a. Nozzle: dc 10 kv; Pole: ac 20 kv.

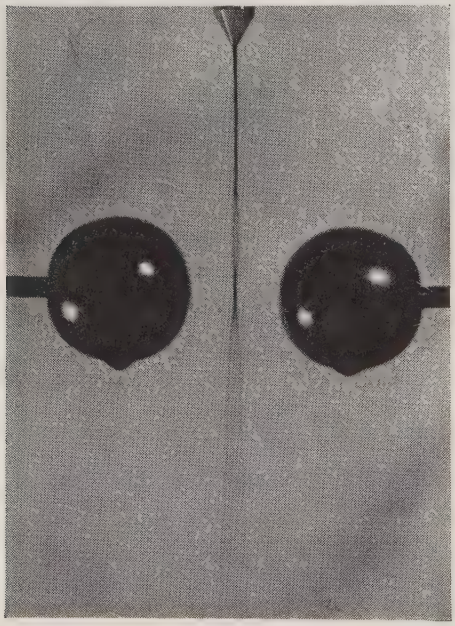

FIG. 10b. Nozzle: dc 6 kv; Pole: ac 20 kv.

flowing oil may easily be modified in the same way as a stream of electrons in a vacuum tube. In particular, the velocity of a flowing oil may be accelerated by a new application of an electric (Fig. 9) or magnetic field. Moreover, if a rotating field is applied to an ionized flow of oil, the flow of oil will be accompanied by a rotational motion having the same cycle as the rotating field applied.

In practice, a flow of oil with a rotational motion can be obtained simply by surrounding the ionized oil stream with a pair of poles connected to an ac source, or a rotating magnetic field. Figure 10 shows a downward stream of oil that

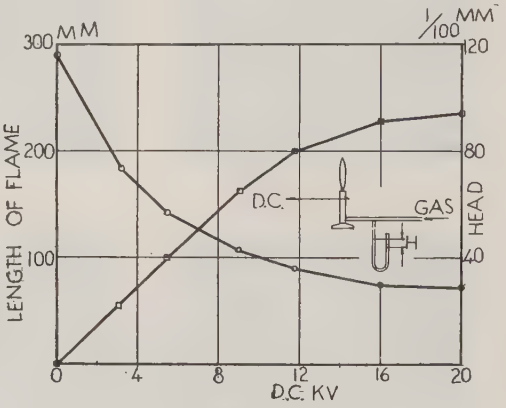

FIG. 11.

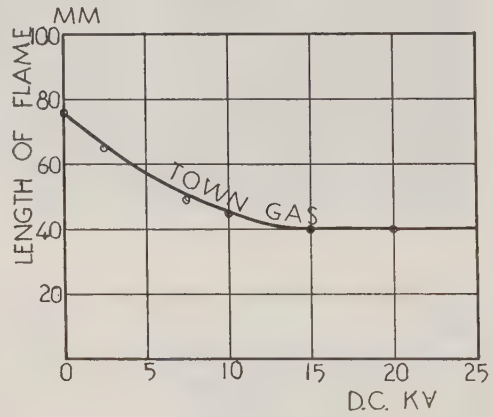

FIG. 12.

describes a spherical envelope. In this case, the cycle forming the spherical envelope is the same as the cycle of the source applied to the pole, as ascertained from a neon illumination of the type mentioned above.

It is suggested that a flowing combustible will generally change its shape and form by mere physical means, independent of the surrounding sphere. This flow generally rises spontaneously to a certain high rotational speed having the cycle of the ac source. Thus a stream of fuel oil may newly be forced into a high speed turbulence, independent of the surrounding sphere.

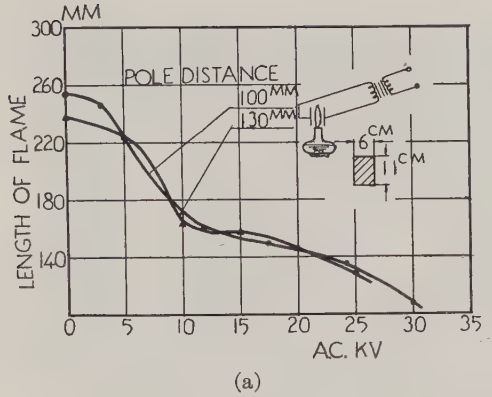

(a)

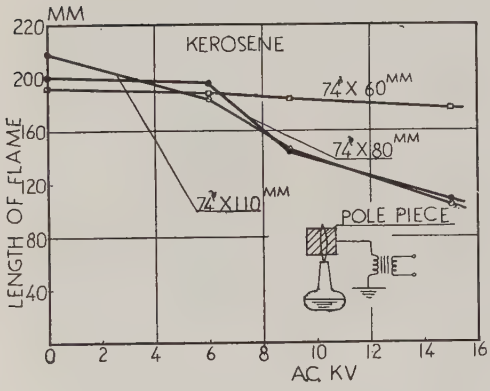

(b)

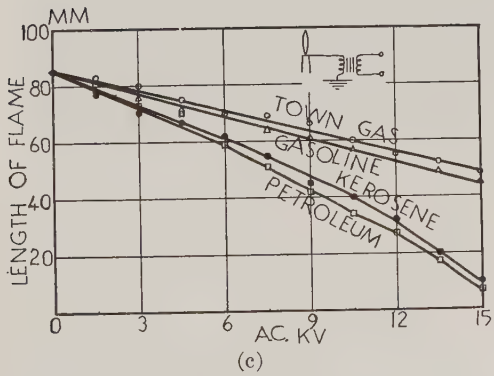

(c)

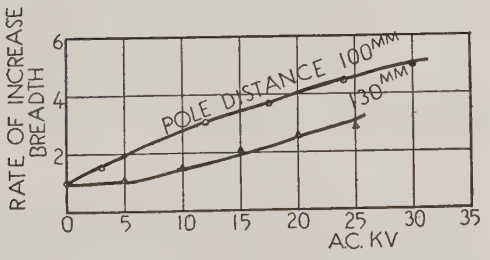

(d)

FIG. 13.

3. BEHAVIOR OF A BURNING FLAME AFFECTED BY AN ELECTRIC OR MAGNETIC FIELD

(a) A flame excited by dc or ac voltage

The author tried to excite the orifice of a Bunsen burner by a dc source. In this case, the

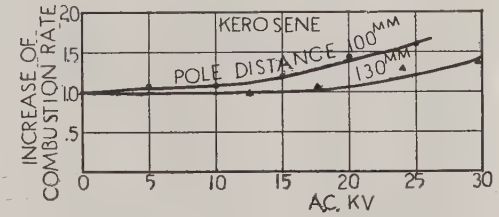

FIG. 14.

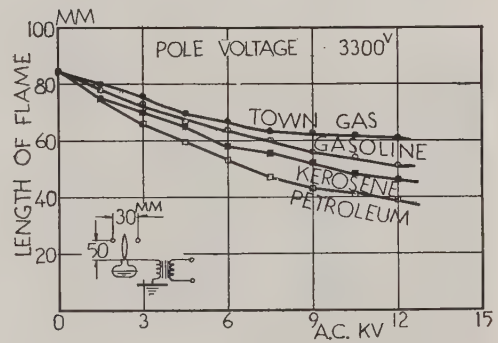

(a)

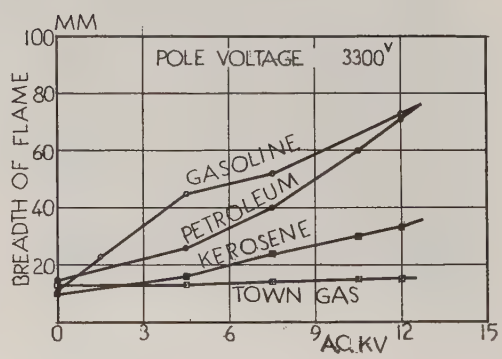

(b)

FIG. 15.

increase in the velocity of the town gas flow was ascertained by an increment of negative head (0.50 to 0.60 mm water head) which could be measured by Chattock micromanometer (Fig. 11).

On the other hand, a flame treated in this way changes its features, the length of a flame, especially the length of a reducing flame decreases considerably and the flame itself will fluctuate

slightly (Fig. 12). If we excite a burning flame with an ac source, the flame fluctuates with the same cycle as the cycle of the applied ac source; the cycle of this fluctuation may be traced by a series of continuous motion picture films.

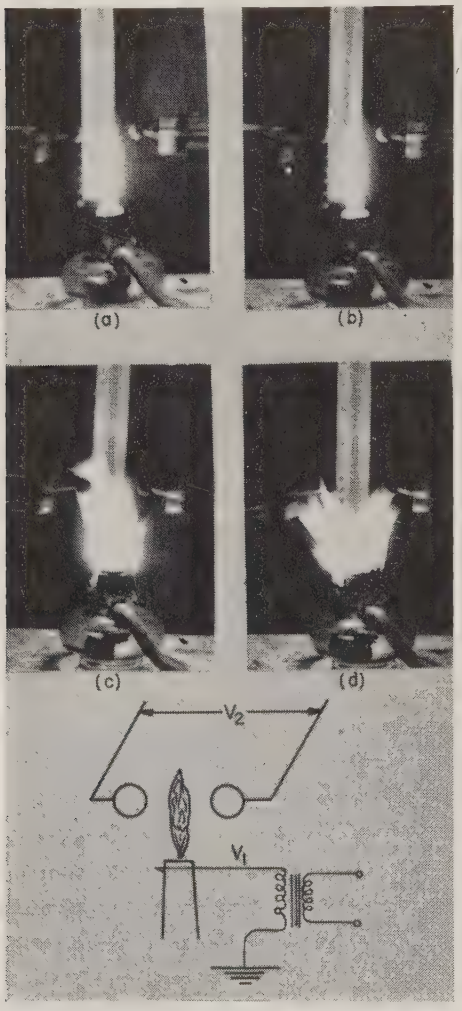

FIG. 16.

(a) V_1 =	0^V	V_2 = 0^V
(b) V_1 =	0	V_2 = 3300
(c) V_1 =	7800	V_2 = 3300
(d) V_1 =	12000	V_2 = 3300

If a high tension is applied to a pole near a burning flame, the burning flame grows shorter and wider as shown in Figure 13. Figure 14 shows an increase in the rate of combustion of kerosene.

(*b*) *Flame excited by a high ac voltage and exposed to a pair of pole pieces of ac high voltage or to a pair of magnet poles*

A flame normally contains positive and negative ions, but when it is excited by a high voltage, one type of ion is neutralized. A flame excited in this way may generally be considered as a singly ionized flow, similar to an oil column charged by an excitation. The singly ionized flame column thus obtained fluctuates more readily toward the surrounding pole pieces than in the case of a single application of excitation.

This concept gives us a new idea of how to produce high-speed combustion and to improve it. A diagram of the experiment is shown in Figure 15A. A pair of pole pieces surrounding a burning flame are connected to 3300 v. and a series of high

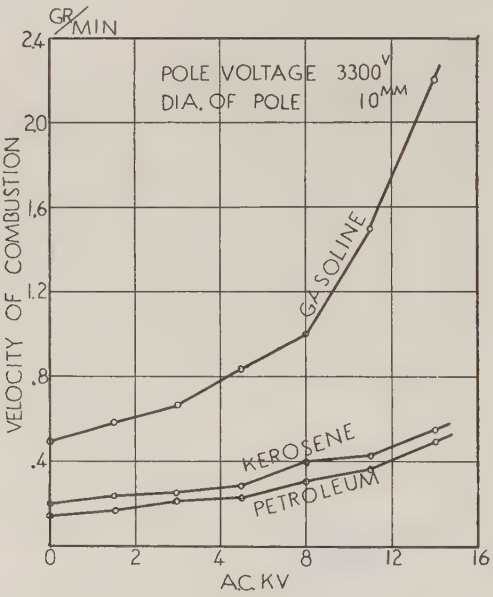

FIG. 17.

voltages (several kv) are applied successively to the base of the burning flame which fluctuates between the pole pieces, forming a violently fluctuating column. Figure 16 shows a fluctuating kerosene flame.

The rate of combustion of the fuel oils is given in Figure 17, showing that the burning velocity increases up to 3-4 times in gasoline, and up to 2-3 times in kerosene or petroleum when an ordinary high voltage is applied. Similar results are obtained if a pair of permanent magnets is substituted for the pole pieces (Fig. 18).

Conclusion

The author has ascertained that the shape and character of a burning flame can be modified, independent of the surrounding sphere, simply by

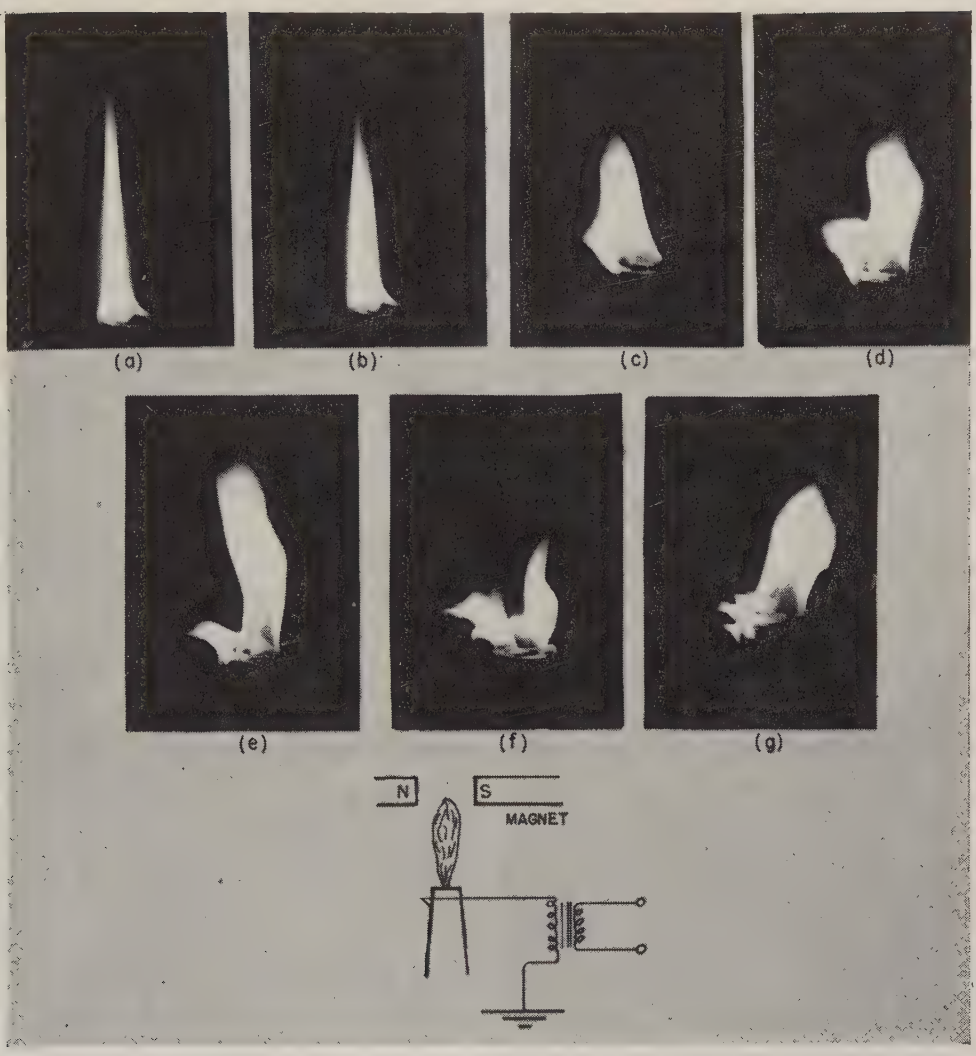

FIG. 18.

(a) Magnet^{ac} 500^{v}
(b) Magnet 1000
(c) Magnet 1500
(d) Magnet 2000
(e) Magnet^{ac} 2500^{v}
(f) Magnet 3000
(g) Magnet 3500

application of an electric or magnetic field. The rate of combustion increases up to 3-4 times in gasoline and up to 2-3 times in kerosene or petroleum.

REFERENCES

1. THOMSON, J. J.: *Ionization through Gases.* Cambridge, Cambridge Press, 1914.
2. VON ENGLE, A.: *Ionized Gases.* London, Oxford Press, 1955.
3. ASAKAWA, Y.: Kogyozashi No. 886 (1934); J. Soc. Mech. Engr., (1935); Proc. First National Congress for Applied Mechanics, 1951.
4. ASAKAWA, Y.: Advance copy of research meeting, Soc. Mech. Engr., June, November, 1954.

Panel Discussions

1

FUTURE PROBLEMS IN COMBUSTION RESEARCH

Panel Members

Walter T. Olson, *Chairman*
Louis Deffet
Carl Hugo Johansson
Tsutomu Hikita
V. N. Kondratiev
H. Gg. Wagner
Guenther von Elbe
J. S. Clarke

The chairman introduced the subject and called on each panel member to speak for ten minutes, after which the meeting was opened for discussion. A resumé of the remarks of each panel member follows.

Dr. Deffet:

When one examines the surveys submitted at previous combustion symposia, one notes that the phenomena that have been dealt with are those of "combustion" in its generally accepted meaning. The particular nature of the comments I should like to make is, however, that they differ somewhat from that line, and I should like to include in this term "combustion" the phenomena of deflagration and detonation which the promotors of the combustion symposia and The Combustion Institute have moreover inserted in their programs of investigation and of work.

There is no doubt that the investigations into the combustion of gases, liquids and solids are the most important. In Belgium, independent of the investigations carried out by Professor A. Van Tiggelen, plans are being drawn up for practical work in the field of liquid and solid propellants.

But there are two other problems which I consider urgent and which are related to industries of great importance in Europe and in the United States, *viz.*, the coal industry and the explosives industry.

The problems, which are set by the conditions of the use of explosives in underground coal mines, are those of the transition from detonation to deflagration and of the ignition of fire-damp by explosives.

There are several aspects of these problems to which satisfactory answers have not been given at the present time. However, as the solutions to these problems are certainly of interest, especially in Europe, it would seem that their investigation should be urged forward more actively.

The only laboratories now dealing with these investigations are those of the official institutions for safety in mines, such as the U. S. Bureau of Mines, and the research laboratories connected with the coal or explosives industries, for example the "Centre d'Etudes et Recherches des Charbonnages de France" and the "Centre Belge de Recherches pour l'Industrie des Explosifs."

In the course of the International Conferences of Directors of Safety in Mines Research, meetings between specialists take place, but it is noted that the lack of cooperation with other investigators working in related fields is rather unfavorable to the futherance of these investigations.

It would be desirable that consideration be given within the framework of The Combustion Institute and of future combustion symposia to the promotion of studies bearing on the following questions:

(*1*) Transition from detonation to deflagration and combustion for explosives of diverse compositions and in different conditions.

(*2*) Ignition of air-methane mixtures (fire-damp) by explosives in the regime of detonation. Determination of the causes of such ignition (shock waves, gas compression, free radicals, undetonated particles, etc.).

The objection that may be raised to such a program is that it is not a new one. As a matter of

fact, this is only an appearance, because, although it has already been investigated in numerous laboratories, particularly in the U. S. Bureau of Mines in the course of researches promoted by Dr. B. Lewis, one realizes that the solutions to the afore-mentioned questions are far from being established.

These solutions are of greater importance for the European coal-producing countries than for the United States, where the danger of fire-damp is less. But independently of this directly useful aspect, the theoretical problems set by such a program seem almost sufficient to expedite its realization.

Dr. Johansson:

I should like to draw your attention to some problems concerning ignition and combustion in high explosives.

The ignition by blows of liquid or plastic explosives containing air bubbles is to a great extent a question of heat transmission. It is very easy to heat air to high temperatures by rapid compression, but the temperature of the explosive around an air bubble will only be a small fraction of that of the air. For heating the explosive to the ignition temperature, a rapid compression to many hundred atmospheres is necessary. The conditions are, however, quite different if the explosive is in the form of small particles or drops in the hot air or has thin layers between air bubbles. In this case the maximum temperature of the explosive will be nearly as high as in the air, and light blows with compressing pressures of 10 to 20 atmos are quite sufficient for ignition.

With regard to safety in handling high explosives, I think it is important to investigate more thoroughly how the impact sensitivity of plastic and liquid explosives depends on their interior structure. It should be noted, however, that the original structure is not always decisive, because in some cases it will be completely changed by the impact. A clear example of this is given in tests with vertically suspended closed tubes of steel containing liquid and a small volume of air at the top. Zippermayr has shown that tubes with a liquid high explosive explode when dropped a few meters against an anvil. By photographing tubes with water at the impact and measuring the pressure at the top we have found that a scum is formed and compressed to high pressures. The liquid evidently bounces better than the tube and moves upward in relation to the tube. Photos taken with a camera with rotating mirror of impacting tubes with an explosive liquid shows that the detonation starts at the top and propagates with high velocity to the bottom. I think it is easily understood that a combustor is ignited at the top, as the foamed structure that forms there is very favourable for that.

Little is known as to how a detonation can be initiated by burning. This is another very important question for safety. It demands and deserves much experimental work.

Professor Hikita:

I wish to make some remarks on future problems in the field of detonation.

First of all, exact knowledge concerning the state of gases at high temperatures and pressures is highly desirable. An equation of state for detonation gases should be expressed entirely in molecular terms. For that purpose it seems to be most important for us to accumulate experimental data on the compressibility of gases at high temperature in order to minimize idealizations involved in any theoretical treatment. Furthermore, the compressibility data for a solid phase are also necessary for a treatment of heterogeneous reaction in a condensed phase.

Next, regarding the structure of the detonation wave, the heterogeneity of the reaction zone should be properly evaluated. A group of Hugoniot curves along the reaction path in the detonation zone should be drawn for the heterogeneous phase. Consequently, the pressure and temperature profiles of the reaction zone in a condensed explosive may not be so simple as predicted by the Von Neuman-Döring theory.

How do we understand the detonation reaction processes? To seek answers for this difficult question, we have many things, experimental and theoretical, to do; especially, further development of new tools for the measurement of such transient phenomena is badly needed. For instance, high speed spectrography, microwave techniques, and X-ray radiography may be useful.

Among the detonation characteristics other than the velocity of propagation, the temperatures in the detonation zone are most accessible and should be quite useful. For example, if a transparent liquid like nitroglycerine or its mixture with a solvent is used, a spectrograph in the visible or infrared region may be made of the curved front of the detonation wave.

Also, physicochemical studies of detonation should be carried out from various standpoints, because the mechanisms of initiation and propagation of detonation, gap transmission of detonation, and transition of combustion to detonation, and so on are still quite obscure.

Let me cite an example. Heretofore it has been said that pure ammonium nitrate is difficult to detonate unless very large quantities are used. But recently Mr. Fukuyama has found that even a small quantity of pure ammonium nitrate can

very easily detonate if the low density crystal prepared by some means is charged at a loading density of 0.5 $\sim$ 0.7 g/cc in a steel or tin tube of more than 13 mm diam. and initiated by an ordinary blasting cap; the bulky, porous state of the salt is realized (1) at its transition point of 125° or 84°C on the way of drying, or (2) at room temperatures by keeping the state realized at the transition points through a method of rapid cooling to the room temperature, or (3) by growth of the crystal of an abnormal habit. The sensitivity and power of this pure ammonium nitrate are comparable to that of a commercial ammonium nitrate explosive.

On the other hand, Mr. Yamasue has found that nitroglycerine mixed with a mixture of mono- and di-nitro-naphthalene becomes very insensitive, just like a gelatinized propellant.

Thus we know that the sensitiveness of explosives depends not only on chemical composition, but also on the state of aggregation, number of active points, and their distribution.

In order to elucidate the mechanisms of initiation and propagation of detonation, the modes of energy transfer in various phases, such as gaseous, liquid, solid, gelatinous or other heterogeneous phases, must be clearly understood. Thus shock behaviors in various phases and chemical kinetics of rapid reactions under extreme conditions of turbulence and heterogeneity should be studied.

In conclusion, I think it is most desirable to measure detonation temperature and its change with the initial loading densities by spectroscopic analysis or some other means. It would also be of great interest to determine the critical conditions of detonation activation: What is the critical energy for an initiation? What is the critical composition? What is the limit of lower and higher densities of explosives? Or what is the influence of porosity or surface nature of the explosive grain on its explosibility? Or how will the transition of combustion to detonation occur and what is the difference between the mode of detonative activation and that of combustion? These are questions to be solved.

Dr. Kondratiev:

Processes taking place in nature and industry rarely correspond to our classification of sciences, being usually an intricate complex of phenomena, each belonging to a different branch of science. The combustion process appears to be a striking instance of such a complicated process, where chemical, physical, and mechanical factors often play an equally important role. Since the chemical reaction is the origin of the combustion process, the chemical factor should naturally be recognized as basic. The chemical reaction promotes thermal and mechanical effects. These effects influence in turn the reaction and this accounts for the complicated nature of the combustion process.

This conception of the combustion process was arrived at some thirty years ago, mainly as a result of kinetic studies of combustion reactions. It was then that the modern chain theory was founded, as a result of the work of various research laboratories and scientific schools, including the kinetic school that I belong to. The mechanism of self-ignition, the nature of ignition limits and the chain explosion were discovered at that time. They confirmed the belief that chemical kinetics actually is an essential part of the theory of flame propagation.

Kinetic data were first used in 1934 by Lewis and von Elbe in their work on the ozone decomposition flame. Diffusion was also first taken into account in this pioneer work, where the similarity of the temperature and concentration fields was postulated.

The theory of the laminar flame propagation suggested by Lewis and von Elbe was further developed and has taken an analytical form defining its application limits in the works of Zeldovitch and Frank-Kemenetzki (1938), of Semenov (1940) and of Zeldovitch in 1948.

Many features of normal combustion were explained by means of this theory on grounds of known data on kinetics and the mechanism of combustion reactions.

The theory assuming the similarity of temperature and concentration fields, sometimes misnamed as thermal theory, is often set off against the so-called diffusion theory, claiming that flame propagation is caused by diffusion of active centers from the combustion zone into the unburned mixture.

Indeed, the possibility of the diffusion mechanism of flame propagation is confirmed by experimental facts. The isothermic cold flame of very poor carbon disulfide-air mixtures, investigated by Semenov and Voronkov in 1939, is a striking example of such a mechanism. After Semenov, the possibility of isothermic flame propagation in this case is due to the positive chain interaction. The role of this phenomenon in common hot flames is not yet defined.

It has been often suggested that the diffusion mechanism of flame propagation is peculiar to reactions with hydrogen atoms as active centers. However, the decisive role in this process is played not by the rapid diffusion itself, but by the effects produced by hydrogen atoms in the unburned gas. The importance of this effect should be proved by means of careful analysis, based on kinetics of combustion reactions. Thus, since the total heat in the hydrogen-chlorine reaction proceeding by

the mechanism of simple Nernst chains, in accordance with equation

$$H + Cl_2 + H_2 = 2\,HCl + H + 44.0\ kcal$$

is liberated in the course of the reaction, we may suggest that in this case the importance of the diffusion effect is not to be expected. On the other hand, only ten per cent of the total energy is liberated in the course of the branching chain hydrogen-oxygen reaction, as can be seen from the equation

$$H + O_2 + 3\,H_2 = 2\,H_2O + 3\,H + 11.0\ kcal$$

This leads to the conclusion that the effect of hydrogen atom diffusion is apparently more pronounced in this case and incidentally can play a certain role in flame propagation. Naturally, these considerations are based on the assumption that the reaction mechanisms both in hot and low-temperature flames are similar.

It follows that the role of the diffusion factor, and consequently the applicability of various approximate analytical forms of the laminar flame propagation theory, should in every case be defined by the mechanism and kinetics of the combustion reaction.

The leading role of the chemical factor can also be seen from the works of Hirschfelder and Curtiss, von Kármán, Spalding, and other authors, whose methods consist in the solution of complete (or not fully complete) systems of diffusion and energy equations, not limited by the condition of temperature and concentration fields similarity. Thus, von Kármán, assuming a simple one-stage reaction of hydrazine molecule decomposition, obtained a hydrazine flame velocity that was much too small, as compared with the experimental value. Solving essentially the same system of equations, but using the more complicated chain mechanism, Spalding gets a quite good agreement between calculated and measured values of hydrazine decomposition flame velocity. Another example is given by the calculations of ozone decomposition flame velocity. Lewis and von Elbe give a flame speed value much in excess of the measured one, on supposition that ozone and atomic oxygen are in equilibrium. On the other hand, assuming a somewhat different reaction mechanism, von Kármán obtains a close agreement of calculated and experimental values of ozone flame speed.

The important role of the chemical factor in flame propagation makes the development of the combustion theory on the basis of chemical kinetic studies very real. Yet the present state of kinetic investigations on combustion reactions should be considered to be rather unsatisfactory. Chemical kinetics has still much to do for the combustion theory. The establishment of the chemical mechanism of hydrogen combustion, thought to be in many respects a model reaction, and the rate evaluation of most important elementary processes, participating in this mechanism, can be considered to be a great achievement of chemical kinetics. But the knowledge of kinetics and of the mechanism even of the nearest important reaction —of the carbon monoxide combustion—is inadequate, to say nothing of more complicated reactions, in particular, such as hydrocarbon combustion reactions.

The study of kinetics and of the mechanism of preflame reactions—slow oxidation and cold flame combustion—is also of great importance, particularly in connection with combustion processes in engines. Considerable attention is now paid to these processes, and we are very near to quantitative kinetic investigations of slow oxidation and combustion of hydrocarbons.

From the combustion theory point of view, the kinetic investigation of a reaction can be considered to be completed if: (1) the rates of the most important elementary processes are known; (2) a brutto-reaction kinetic equation can be derived from them, giving the correct dependence of the reaction rate—and consequently the heat liberation rate—on the temperature, concentrations and other factors; and (3) we are convinced that the kinetic equations are also valid in complex conditions of the flame. No combustion reaction has been investigated to that extent, with the possible exception of several simple decomposition reactions and perhaps of hydrogen-halogen and of the hydrogen combustion reaction.

Quantitative investigations of the role played by kinetics and gas dynamic factors in the turbulent combustion phenomena can be considered exceedingly important in view of the great abundance and significance of turbulent flames. The interaction of these factors is not excluded.

The degree of departure of atoms and radicals, as well as of charged particle concentrations, from equilibrium values, together with the problem of radiation equilibrium in flames is an essential aspect of kinetic investigations on combustion reactions. There is no unity of opinion concerning these problems, although considerable deviation from equilibrium usually occurs in rarified flames.

Essential questions arise in connection with the problem of equilibrium in flames, the limits of possible applications of common ideas on the chemical reaction mechanism and of the usual conception of gas temperature in the course of a rapid reaction. Studies of equilibrium in flames might help to resolve these questions as well as the old problem of energy chains raised again by Shuler and Ubbelohde at the Fifth Symposium on

Combustion in connection with high temperature reactions.

The significance of the problem of equilibrium in flames is certainly not confined to combustion reaction kinetics. It is also of great importance for the energy balance in flames. The investigations of departures from equilibrium in various parts of the turbulent flame front might prove to be an effective method in turbulent flame studies. All this shows the necessity of a more detailed research on flame equilibrium.

I have tried to emphasize the general significance of the kinetic or chemical trend in the combustion theory, which is one of the most promising lines in the development of this theory. The scope of work in this field demands great efforts on the part of many scientific schools, wider cooperation and better coordination of work. I think it to be the principal aim of this symposium. Soviet scientists are glad to take part in the joint efforts of the many distinguished scientists, who are assembled here, in the promotion of one of the most important branches of science.

Dr. Wagner:

Two essentially different groups of phenomena may be observed in all combustion processes: (1) The chemical reaction. Generally speaking one has to consider two domains; the low temperature region up to temperatures of about 700°C and the high temperature region above this temperature. (2) Flow phenomena comprising laminar and turbulent flow, as well as shock waves and transport phenomena as heat conduction, diffusion and viscosity are to be considered. In analyzing combustion processes essential difficulties are encountered due to the fact that the above-mentioned phenomena are coupled in a very complicated way. It would be of great importance to separate experimentally the different particular processes. These have to be investigated in the same pressure and temperature regions as those prevailing in flames. A thorough study of transport phenomena under the extreme conditions existing in flames should bring marked progress.

Up to now, only a few conclusive experiments dealing with the mechanism of the chemical reaction at very high temperatures have been published. From a solution of this problem we may expect even more interesting results. In the high temperature region the concentration of atoms is high and radicals may be in highly excited states; the energy distribution may deviate considerably from equipartition. One has to test experimentally to what extent the usual formulas for the rate of reaction are applicable under such conditions or to what extent they ought to be modified.

May I sketch some methods of investigation.

A labile mixture of, for example, water-gas is used, its composition corresponding to equilibrium at a temperature of, say, 1000°C. This mixture is suddenly heated to a temperature in the neighborhood of the temperature of equilibrium, for example, 1300°C. The transition of the mixture from its initial equilibrium composition to the equilibrium at 1300°C is followed experimentally. The heating might be produced, e.g., by a shock wave or by adiabatic compression.

Another method may use the sudden cooling of a hot equilibrium mixture, the mixture being, for example, the combustion products of a flame generated by a pressure burner or by a burning chamber. Cooling may be obtained by flow of the gas through a Laval nozzle. The emanating gases may be analyzed by physical methods after a certain time of reaction, corresponding to a definite distance from the nozzle. Another possibility consists in freezing gas composition by injection of a liquid.

Still another method of investigation is obtained by producing deviations from equilibrium in a streaming equilibrium mixture. This may be achieved by injecting in a gas mixture flowing isothermally one of its original components or an additional component. The establishment of equilibrium is observed under constant pressure and essentially at constant temperature.

All the methods of investigation so far discussed contain an inherent difficulty; this is the analysis of the mixture approaching equilibrium composition. In addition to physical methods the direct taking of samples of the mixture for analysis has to be considered. This method has proved successful up to 1500°C in investigations of the water-gas reaction.

Finally, I should mention the application of flames of simple systems for investigation of reaction rates. It is known that it is very difficult to reach conclusions as to the reaction mechanism, but in some cases this does not seem hopeless.

A very rewarding task in the investigation of high temperature reactions might be the testing of the influence of additives on the rate of reaction. In the combustion of CO small additions of hydrogen or water strongly raise the rate of reaction. On the other hand, addition of halides reduce the rate of reaction considerably.

As in the case of CO, one should try to find compounds which, when added in small amounts, catalyze the rate of reaction either homogeneously or heterogeneously. Thus it might be possible, in different fields of application, to increase or to reduce the time necessary for reaction, or to direct, or to suppress the reaction altogether.

Considering the question of inhibition of reaction, which is of importance for fire extinguishing, application of halogens and of halogenated components has shown encouraging results although

the mechanism has not been completely understood.

In addition to an acceleration or an inhibition of the rate of reaction, an attempt at steering the reaction into a definite direction in order to obtain valuable end products might prove of increasing importance. On the other hand, one has the possibility of freezing the reaction in a definite phase, on the other hand, one may try to increase or to reduce the concentration of certain products by properly chosen additives. Up to now flame and combustion processes have found practical application in the synthesis of products only in a few cases, e.g., the Bartholome-Sachsse process for acetylene.

The problem of influencing high-temperature reactions is not only of scientific interest. In technical combustion processes, too, chiefly in cases where the temperature of the emanating gases is relatively low, e.g., when starting, a noticeable part of the heat of reaction is liberated outside of the engine under consideration or the products of incomplete reaction are strongly cooled at the walls, with increased soot formation. In technical combustion processes, it may have a considerable influence on the efficiency factor, and serious air pollution results, too. Here a reduction of the time of reaction would give an improvement in many cases.

In Germany, examples proving this statement are given at every railway station and on every highway. Photographs of running engines often indicate that great quantities of precious fuel only serve for heating and illuminating the atmosphere.

An old problem which nevertheless is still interesting and important arises from the question of ignition. It is known that pre-ignition reactions below the ignition temperature, e.g., for paraffin hydrocarbons, take place with a marked temperature rise. This increase in temperature is strongest for mixtures near the upper limit of ignition. In stoichiometric mixtures this increase in temperature due to reactions preceding ignition is very small in the region of the temperature of ignition, as determined by the method of the American Society for Testing Materials.

The problem dealing with the exact mechanism of the reaction in a homogeneous mixture which determines the transition from low-temperature reaction to normal combustion is of particular interest. Here, too, the mechanism in the high temperature region should be of great importance.

Dr. von Elbe:

We seem to agree that combustion research is not just a matter of academic intellectual curiosity but is urged on us by important and difficult problems associated with the diagnosis and prevention of disasters, with the development of internal combustion engines of all kinds, with the use of burners for a multitude of purposes, and with the development and use of explosives and propellants. By means of research we hope to make combustion problems amenable to a scientific approach based on an understanding of combustion fundamentals. Such fundamentals, as I see it, comprise the thermodynamics of combustion products, the mechanism and kinetics of chemical reactions of fuels and explosives, and the physics and chemistry of the propagation of combustion by shock or by diffusion processes.

Now there are some subjects that are rather well explored, as for example, the thermodynamic computation of combustion equilibria and the hydrodynamic theory of detonation waves, and there are other subjects on which we possess considerable insight, such as the chemical kinetics of some combustion reactions. However, there remain vast unexplored or insufficiently explored fields of study. In particular, the reactions of organic fuels with oxygen continue to present problems taxing the resourcefulness of the ablest investigators; but to my mind the main challenge is offered by problems of diffusive propagation of combustion, such as combustion wave propagation in homogeneous gaseous and nongaseous mono-explosives or explosive mixtures, propagation of flame in fuel suspensions and unmixed fuel-oxidant systems of all kinds, under laminar and turbulent conditions; the development of combustion waves from ignition source; the stabilization of combustion waves in flowing gases; the stability limits due to the proximity of sinks or dilution with inerts; and the transition from combustion to detonation. We must devise models which present the essential physical features of such problems in simple form so that theoretical analysis and comparison with experimental data becomes possible. Some progress has already been achieved in this manner with respect to minimum ignition energy of electric sparks, turbulent flame propagation, and scaling of diffusion flame parameters, and it seems reasonable to expect that much more can be achieved. There is also a noteworthy parallel effort of developing the theoretical mathematical basis of the combustion wave theory. It is by such work that progress will be carried forward. As the field develops we must not shrink from hypothesis and argument which historically have been the driving forces in the development of great sciences. We must stimulate interest by a continuous flow of ideas and discussions. Otherwise, as we become beset by frustrations due to the complexities and difficulties of the subject matters that we deal with, our efforts may well become stale and infertile and we shall fail to discharge the obligation to progress that is upon us.

Dr. Clarke:

The following several problem areas relate to the application of combustion, and particularly to application in gas turbine engines.

Attention should be directed to the problems of preparing reactants properly for combustion. Proper comminution and distribution of both solid and liquid fuels is in need of closer study and definition in the future. New techniques might be helpful. For example, one might try means to lower the surface tension of liquid fuels for better atomization.

One problem will certainly be the correlation of the extensive data to be reported at this Sixth Combustion Symposium. It has taken a number of years to digest and to start to use data from each of the earlier Symposia; similarly, future effort will be the assimilation of this Symposium.

Then, too, future problems in combustion research will continue to embrace the classical problems of internal combustion engines, for example, high combustion efficiencies, short reaction times, low carbon deposition.

Chemical kinetics has started to play a stronger part in the engineer's experience. In some cases the controlling rate of a practical combustion system has been found to be set by an overall reaction rate. Also, kinetics may influence the course, and thus the products, of gross combustion processes. In the future, the engineer will have to study the role of chemical kinetics in his work with applied combustion.

A final problem is that of oscillations in combustion systems. Unexpected and unexplained shrieks, howls, or buzzings may be encountered in a high-heat release system. The accompanying high heat transfer and high-amplitude, high-frequency pressure waves often destroy the combustion chamber or parts of it. Research is needed to find the causes and cures for this phenomenon.

Dr. Olson

As a sample of future problems, I have chosen to select six items that represent current or clearly foreseen needs in the general combustion field. This section undoubtedly is biased by my background in aircraft propulsion research. Further, I stress application of combustion in order to complement and round out the panel discussion. Here are my six items:

(1) A deficiency, or shortcoming in current work is our lack of an adequate description of turbulent combustion. For the case of homogeneous mixtures, a big need is for the relations between aerodynamics and flame to be described so that an engineer can use pressure drop to give optimum turbulence. Optimum turbulence means the size and strength of flow disturbances, and the statistical distribution of these, which maximize efficient heat release rates for the pressure expended.

(2) In the case of nonhomogeneous mixtures, we have the complicated picture found with most technical applications. The highly stirred reactors fed with homogeneous mixtures give heat release rates that are several to many orders of magnitude greater than those of technical devices: Furnaces, gas turbine combustors, and the like. Now if heat release rate, or conversely, combustion space, is important (and we know it is, in aircraft at least!), clearly there is need to examine the physical, and aerodynamic processes other than chemical reaction alone. The flame itself is not necessarily the large space consumer; droplet evaporation and spreading, gas mixing, heat transfer, and their interactions with flame present, need to be put together to give an adequate, conceptual model of the gross combustion process.

(3) Literature has appeared that describes the dynamics of combustion oscillations in high heat release devices: pressure waves, usually of tangential form, cross the chamber at high frequency and high amplitude. Heat release from combustion is phased to sustain them. Important future work would be to find the effect of this oscillation of pressure and velocity on atomization and mixing, and on reaction rate with the intent of better describing how oscillations are sustained, or driven. The results could lead either to utilization or elimination of the oscillations.

(4) This next item has to do with rockets. Combustion of hydrocarbons in air has been studied exhaustively—especially flame speed and related phenomena, such as quenching and ignition, and the pressure and temperature dependence of these. A future problem is to acquire similar information about rocket propellants. A need is indicated for reaction studies of liquid rocket propellants at high pressures and temperatures.

(5) Chemical synthesis via combustion represents a fascinating area for future work. There are a few papers in this Symposium on chemical syntheses. There is other work that the sponsors are not ready to discuss publicly.

(6) This problem area introduced the last item. There is need for knowledge on high speed, high temperature reactions. Technology in several areas is encountering high speed phenomena at high temperatures, and, in cases, with unusual materials. Basic research is needed on states and rates in chemistry at high temperatures and with short times. Applied research in this area is manifold: chemical synthesis, heat transfer, high temperature materials, hypersonic flight, energetics, and so on.

Doubtless important future problems will stem from ideas yet unborn.

Dr. Bahn

In the sense of a problem concerning application of combustion, the need for gas properties data over ever wider ranges of independent variables, such as inlet air temperature and fuel type, is a continuing one. More than this, however, the emergence of practical interest in the region of substantial dissociation has raised the question of whether equilibrium gas properties are suitable for combustor performance evaluation and engine performance prediction. Where there is, of necessity for the engine and exhaust nozzle size of interest, an assurance that some reassociation reactions will go essentially to completion during exhaust nozzle expansion, and that others will proceed essentially insignificantly, it may be hoped that investigation of the chemical kinetics of the various reactions will allow eventual preparation of gas properties consistent with all of the laws governing nozzle processes, instead of with just a portion of them concentrating upon equilibrium considerations. Furthermore, it would be very helpful, for attempting to interpret combustor performance, if such provision for the limitations of chemical kinetics could be carried to conditions of appreciably overrich fuel concentrations, where materials may be formed which subsequently will have a negligible rate of combustion. Attempts to interpret combustor performance in terms of overall ideal values are expediencies and present problems. If the interpretation can be made in terms of what is the very best possible *under the circumstances*, chances for success, in distinguishing between chemical and physical sources of inefficiency, should improve considerably.

2

HIGH SPEED REACTIONS

Panel Members

Arthur Kantrowitz, *Chairman*
James A. Fay
David Garvin
J. O. Hirschfelder
Paul Kydd
A. A. Westenberg

Dr. Kantrowitz:

High speed reactions which we shall discuss are those which occur in high temperature gases. Our attention will be concentrated briefly on techniques for the study of these reactions. To start the discussion, I would like to mention the advantages of shock tubes as an experimental tool for the study of high temperature gases. These advantages are: (1) In the shock tube you can produce a gas of accurately known enthalpy and density; (2) The enthalpies can be made high enough (currently up to 0.3 × molecular weight electron volts per particle) to cover and go beyond the range of temperatures important to gas chemistry; (3) The shock waves produced in well designed shock tubes are accurately plane and almost the entire enthalpy jump occurs in the shock thickness of only a few mean free paths. These facts have been used by Hornig, Davidson, Kistiakowsky, and others, to achieve beautifully clean gas kinetics experiments.

Dr. Westenberg:

A common approach to the experimental study of fast gas reactions is to set up a flow system which is time-invariant and can be studied at leisure. Problem in all such methods is to initiate reaction rapidly enough so as not to be rate-determining.

A stabilized laminar flame is such a time-invariant flow system in which these initiation difficulties are avoided.

The lack of kinetic data has been the main stumbling-block to complete solutions of the laminar flame problem. There are now available techniques for detailed, microscopic flame structure studies which should permit the opposite approach, i.e., get kinetic information from the flame structure data. It is now possible, by flame sampling and by particle-track techniques, to get temperature and aerodynamic profiles, and composition profiles for all stable species in a laminar flame front. With diffusion data, these provide all

the information necessary for determining the reaction rates of each stable species at many different temperatures in the flame. With the exception of information on free radical distributions (which may be handled by the steady-state approximation in appropriate cases), this is all one needs for deriving kinetic data.

This method has the advantage of giving rates under actual combustion conditions, thus avoiding the necessity of extrapolating low temperature data to flame conditions. At the very least it should provide a good testing ground for reaction mechanisms.

Two outstanding needs at present are free radical distributions and good high temperature diffusion data. It is highly desirable that such an experimental analysis be carried out on a "simple" flame for which a theoretical study is available, e.g., the H_2-Br_2 flame.

A comment from the U.S.S.R. delegation was that methods of analysis with the mass spectrograph need to be worked out for many of the products.

Dr. Kydd:

He mentioned experiments now in progress utilizing the opposite approach to that stated above. In this method a static system is utilized in which it is hoped that a homogeneous flame reaction can be established in a combustible mixture by the method of flash photosensitisation developed by Norrish, Porter, and Thrush. This should result in a situation in which concentrations, particularly those of reaction intermediates, such as free radicals, are independent of their position in the burning gas, thus avoiding many of the difficulties encountered in conventional flame sampling. It is hoped that the variations in concentration with time can then be comprehensively investigated with the aid of a time-of-flight mass spectrometer, which is capable of producing a complete mass spectrum at a frequency of twenty kilocycles. The mass spectrometer leak is incorporated directly in the quartz reaction cell, and precautions have been taken to prevent collisions of sample molecules within the spectrometer, so that the spectra obtained will be truly representative of the instantaneous chemical state of the gas.

Dr. Thrush:

He pointed out the difficulties of obtaining truly homogeneous reactions in this manner especially in vessels of large size. He also stressed the effect of the surface in a small vessel in rendering the induction period between the flash illumination and the explosion of the gas irreproducible. This unavoidable effect of the walls of the vessel appears at present to be the most serious disadvantage of this approach, and indeed of all flame sampling methods.

Dr. Fay:

As an alternative to the stabilized laminar flame or the homogeneous reaction initiated by flash photolysis, the shock tube permits the study of homogeneous reactions over a wide temperature range, reactions in which wall effects and transport processes are inoperative during the experiment. It is, of course, restricted to reactions of several milliseconds duration or less.

Vibrational and dissociational relaxation processes, and some simple chemical processes, have already been studied by such techniques. It appears feasible to study some of the chemistry of combustion in this manner.

Dr. Hirschfelder:

He considered that those using physical or chemical analysis of product species "are like blind men feeling the elephant." The need is to measure free radicals, activated species, ionized gas molecules and the like, and to determine their energy states, in order to get at the kinetics. He pointed out that even two oxygen atoms have 81 potential energy curves, with *a priori* odds for the distribution of energy among each of them.

Dr. Garvin:

One approach to the complex phenomenon of combustion is to study the chemical transformations and, in particular, to place emphasis upon the elementary chemical reactions. The reason for attempting to pinpoint individual steps is a practical one, based upon the present experience with combustion chemistry.

Most chemical processes related to combustion are complex sequences of chain and competitive reactions. Studies of explosion limits, slow oxidations, and thermal decompositions give valuable information about those particular gross processes, but it is extraordinarily difficult to apply the results to high speed burning. On one hand, the relative importance of gas phase as opposed to surface reactions is a strong function of temperature. On the other, certain unstable intermediates present at high temperature are unimportant at lower temperatures, while the intermediates that predominate in the lower region disappear as the temperature increases.

When attention is paid to the high speed elementary (one or two step) reactions some of these difficulties disappear. A reaction with a low intrinsic activation energy is temperature insensitive, and may be studied under the convenient

laboratory conditions. Many of the intermediate steps in combustion fall in this category.

In this discussion I wish to remind the panel of some of the sources of chemical kinetic knowledge about these high speed elementary reactions. It is a personal opinion that the present knowledge and techniques have not been exploited adequately for the benefit of the combustioneer. Some of these are summarized below.

(*1*) *Photochemistry and free radical reactions.* The activity in this field has been high. Bimolecular radical recombination and disproportionation rates are currently being determined. The former are more efficient than the latter, though usually they are of the same order of magnitude. A large number of hydrogen abstraction reactions:

$$R + RH \rightarrow RH + R'$$

important as chain propagators, have been studied. Each year much new information is presented on the activation energies (usually low) of these steps. The current interest in the field is mainly in abstractions from oxygenated organic molecules. Some of this information has been summarized recently.[1]

Another approach to hydrogen abstraction reactions has been made by Rice and Varnerin[2] who have pyrolyzed a large number of organic compounds in the presence of isotopically substituted reactive substances. The extent of isotopic mixing leads to an evaluation of the abstraction process.

Hydrogen peroxide photolysis studies recently have added to our knowledge of the mechanism of hydrogen-oxygen explosions. For example, Volman's work on peroxide photolysis[3] in the presence of hydrogen and oxygen points up the importance of the chain propagation step.

$$OH + H_2 \rightarrow H_2O + H$$

(*2*) *Direct studies of atom reactions.* The technique of preparing atoms by means of photolysis or an electric discharge is well known. Systems in which these atoms are mixed with reactive molecules continue to be of interest and provide information. Examples of recent work include the spectroscopic studies of "atomic flames" by Ferguson and Broida,[4] Cvetanovic's work on oxygen atom reactions with ethylene,[5] the use of a calorimetric method by Callear and Robb[6] to study the hydrogen-oxygen reaction and the mass spectroscopic studies of the HO_2 radical by Foner and Hudson.[7]

An allied field is that of low pressure diffusion controlled reactions. The modern work is an outgrowth of the Polyanyi diffusion flame technique. It has been applied recently to recombination rates[8] and to atom reactions.[9] While some of this information will apply directly to combustion phenomena, it is of more importance in providing a general background for the development of a theoretical approach to high speed, low activation energy reactions.

(*3*) *Molecular beam experiments.* A very fundamental problem of chemical kinetics is the determination of the precise influence of the energy contained in the reagents upon the rate of reaction. For very simple reaction, crossed molecular beam experiments offer one method of attack. The recent work of Taylor and Datz[10] on $K + HBr \rightarrow KBr + H$ should promote renewed interest in the field. The results of such experiments will undoubtedly influence our interpretation of processes occurring in the combustion zone.

(*4*) *Oxidations triggered by active species.* Low temperature auto-oxidations in which the initiating step is bypassed by means of a "catalyst" offer a chance to study the rapid propagation steps without them being limited by a slow initiation step. A recent example of such work is that of Schubert and Pease on the oxidation of light hydrocarbons by ozonized oxygen.[11]

(*5*) *Shock tubes.* Simple reactions may be studied under conditions approaching those found in combustion using the shock tube. Hornig[12] has recently used the method to determine recombination rate of bromine atoms. Britton and Davidson[13] have studied the hydrogen-bromine reaction at temperatures above 1000°K.

(*6*) *Spectrographic information.* Spectroscopy long has been a valuable tool for the study of combustion. It is mentioned here only because recent advances in instrumentation permit the study of very weak emission. Spectrographs have been designed for use in examination of the aurorea and night sky, both of which have very low surface brightness. These have speeds of f/0.8 while maintaining adequate dispersion to permit analysis of bands.[14] They have been employed profitably for the study of chemically produced nonequilibrium energy distributions and should be used for detailed study of combustion processes.

REFERENCES

1. Garvin, D., and Naumann, R. A.: Ind. Eng. Chem., *48*, 570 (1956).
2. Rice, F. O., and Varnerin, R. E.: J. Am. Chem. Soc., *77*, 221 (1955).
3. Volman, D. H.: J. Chem. Phys. *23*, 2458 (1935).
4. Ferguson, R. E., and Broida, H. P., *Fifth Symposium (International) on Combustion.* New York, Reinhold Publ. Corp., 1955.
4. Cvetanovic, R. J.: J. Chem. Phys., *23*, 1375 (1955).
6. Callear, A. B., and Robb, J. C.: Trans. Faraday Soc., *51*, 630, 638, 649 (1955).

7. Foner, S. N., and Hudson, R. L.: J. Chem. Phys., *23*, 1364, 1974 (1955).
8. Kistiakowsky, G. B., and Williams, R.: J. Chem. Phys., *23*, 334 (1955).
9. Garvin, D., and McKinley, J. D., Jr.: J. Chem. Phys., *24*, 1266 (1956).
10. Taylor, E. H., and Datz, S.: J. Chem. Phys., *23*, 1711 (1955).
11. Schubert, C. C., and Pease, R. N.: J. Am. Chem. Soc., *78*, 2044 (1956).
12. Hornig, D. F.: Conference on Unstable Species. New York Academy of Sciences, March 1956 (unpublished).
13. Britton, D., and Davidson, N.: J. Chem. Phys., *23*, 2461 (1955).
14. Petrie, W., and Small, R.: Astrophys. J., *116*, 433 (1952).

A comment by Dr. Melvin Gerstein, NACA, was that all available methods should be trained on some one, single decomposition, or other simple reaction. Thus the several methods—mass spectra, sampling, shock tubes, detonations—would complement each other and help overcome deficiencies.

Dr. Kantrowitz:

He observed that when activation energy controls the course of reaction, the reaction paths are quite complicated. He suggested that at high temperatures, the paths available for reaction might be much simpler.

Discussion with Dr. Hirschfelder established that statistical methods are required to select reaction paths at high temperature.

Dr. Garvin

With regard to the importance of energetically excited species in combustion processes, there are two cases that should be considered. Where the temperature is high enough to support an appreciable population of molecules or radicals in vibrational energy states above the lowest level of the ground state then the enhanced reactivity of these species should be quite important. One recent theoretical treatment of an exchange reaction in which the reagents have high input energy shows that a moderate decrease in the transmission coefficient should be expected.[1]

The second case is that where radicals are produced chemically with excess energy and in numbers far above the thermal equilibrium values. While these must be very reactive, I suspect that they are not important in the combustion process. This is because either the lifetime of the excited species is very short (electronic excitation) or, when the lifetime is long, collisional deactivation can remove the excess energy in a few collisions (a number small compared to the average number required for reaction). These remarks apply, of course, only to reactions with low pre-exponential factors in the rate expression and moderately low activation energies.

REFERENCE

1. de Vogelaere, R., and Boudart, M. J.: J. Chem. Phys., *23*, 1236 (1955).

Dr. Kydd:

After the chairman had introduced another item for discussion, the chemistry of detonation waves, Dr. Kydd mentioned work in press in which the variation of gas density with time throughout the reaction zone has been measured by X-ray absorption. Detonations in mixtures of hydrogen, carbon monoxide, methane, and acetylene with oxygen have been studied, the first two relatively intensively. For these, an apparent second order dependence of over-all reaction rate on total pressure has been established. In the case of mixtures of both hydrogen and carbon monoxide with oxygen, the reaction rate appears to increase proportionally to the square root of the partial pressure of hydrogen at low partial pressures. Other results of a chemical nature have also been obtained.

The Von Neuman theory of the detonation wave has been verified qualitatively by these measurements; however, a difficulty has arisen with respect to occurrences at the wave front. The theory predicts that the detonation wave consists of a normal shock wave in the unburned gas, which initiates chemical reaction, presumably after an induction period in which chain carriers build up. For a hydrogen-oxygen mixture this would predict a discontinuous shock transition to a density five times the initial value, followed by a region of constant density terminating in a self-accelerating drop. Instead, what is observed is a rise to a value of roughly 3.5 characteristic of a shock in a monatomic gas with no internal degrees of freedom, followed immediately by a rapid decrease which approaches the predicted chemical equilibrium (Chapman-Jouquet) state asymptotically. This behavior appears to be characteristic of all the mixtures studied and is very difficult to explain. The possibilities of lack of internal equilibration, or an immeasurably fast initial reaction which slows to an operable rate at roughly the same point for all reactions seem equally unattractive.

It was suggested from the floor that diffusion of active particles forward in the reaction zone might produce the required effect, but it was pointed out that diffusion, in the ordinary sense at least, is much too slow a process to be effective at these high flow velocities.

Dr. Kantrowitz remarked that for diffusion and heat conduction to play as important a role as the

pressure wave in a detonation requires large gradients; but they are not observed.

Dr. George Kistiakowsky, Harvard, joined with the opinion that diffusion is unimportant in detonation in view of the speed of the wave

Dr. J. O. Hirschfelder maintained, on the other hand, that diffusion and heat conduction play a role, and that reactions after passage of the shock wave are important. Dr. Kantrowitz agreed with this point of view.

3

FLAME STABILIZATION IN FAST STREAMS

Panel Members

E. D. Brown, *Chairman*
M. Barrère
Béla Karlovitz
J. P. Longwell
G. C. Williams
E. E. Zukoski

The chairman welcomed the group and introduced the subject for discussion. Each panel member was invited to speak for ten minutes on his concept of the physical picture of the mechanism of flame stabilization, with particular reference to his own experiences which led to these conclusions. In the discussion period that followed, contributions also were made by Professor Kurt Wohl, Dr. Arch Scurlock, Mr. William Bennet, Dr. Walter Olson, Dr. Robert Gross, Dr. Walter Berl, and others.

Dr. Barrèrre:

He opened the discussion by describing some of the research work being done at O.N.E.R.A. In this work three important zones in the flame stabilization process were pictured as follows: (1) The boundary layer zone near the bluff body; (2) The recirculation and mixing zone; (3) The turbulent flame zone. *Dr. Barrère's* group briefly investigated the importance of the boundary layer zone with an apparatus consisting of a rotating cylindrical flameholder, which modified the boundary layer approaching the stabilizer by varying the rotational speed. With his particular device, however, he was not able to study the characteristics of the stabilization at high velocity. Consequently, his efforts were directed toward the second important zone, the recirculation and mixing zone.

The recirculation and mixing zone was investigated by a spectroscopic method (similar to *Summerfield*) which indicated local mixture ratio in the wakes of baffles by comparing the radiation intensity of the CH and C_2 bands. Both a simple disk and a cone flameholder were investigated. The measurements, which were similar for both baffles, clearly defined the wake thickness and the length of the recirculation zone. The distribution of intensity ratio indicating fuel-air ratio varied as follows: large variations close to the flameholder between the recirculation zone and the flame, decreasing with distance from the flameholder. These variations decreased as the mixture ratio increased.

Similar results were noted in a combustor made up of two parallel streams, a fresh combustible gas in half the duct, and a hot, burned gas in the other stream. With this device, it also was possible to determine ignition distance for various inlet conditions, study temperature distributions and the diffusion process.

Dr. Longwell:

He continued the discussion, also speaking of the recirculation and mixing zone as most important in the stabilization problem. He spoke briefly of experiments concerning heat release and composition in the wakes of baffles and concluded that homogeneity throughout the recirculation zone could not be expected. However, the most important area was certainly the mixing zone, as indicated by Zukoski and others. He pointed out that the paper by Weiss, reporting on the results of tests of fuels with varying reactivity, indicated to him that the important "chemical factor" in the stabilization problem was reaction rate rather than ignition delay or laminar flame velocity. He concluded that a better understanding of the mixing zone and over-all reaction rates from

spherical reactor studies would eventually give a complete analytical model for the stabilization problem.

Dr. Williams:

He spoke of the many problems that require more research work. In particular, he spoke of the complexity introduced in the stabilization problem with partially vaporized liquid fuel mists, situations where there has been evidence that the heat transfer from the flameholder and flame is even more important and more complex than with premixed mixtures. More fundamental work also is required with pilot flames which may be used in practical combustion devices to improve stability limits and extend the altitude operating range. Finally, scaling studies are required so that these fundamental problems above can be studied successfully in small research facilities. In these studies, the Reynolds number, Schmidt number, and the Prandtl number should be kept constant so that the turbulent mixing and molecular mixing would be similar.

Mr. Karlovitz:

Describing his concept of the mechanism of flame stabilization, he spoke of the region where the combustion wave must propagate across a steep velocity gradient as the most critical zone. He pointed out that a study of the combustion wave in this region indicates that the heat flowing by conduction from the wave into the unburned gas is returned to an increased flame surface reducing the burning velocity and flame temperature until the wave is interrupted. The critical condition at which the combustion wave breaks is reached when the velocity increases several fold within the thickness of the combustion wave, that is when the following quantity exceeds a critical value, which is approximately 2.

$$\frac{\eta_0 \, du}{\mu \, dy}$$

where μ = approach velocity; du/dy = velocity gradient; η_0 = thickness of wave. Since the interruption of the wave does not depend on velocity gradient alone, the wave must be maintained up to a minimum flow velocity to enable it to traverse a given velocity gradient. In high speed flow, this must be accomplished by an outside heat source such as a pilot or flameholder. Consequently, stabilization is more difficult at low pressures because this heat source must supply the excess enthalpy, which is independent of pressure, while the heat release rate of the combustion wave is proportional to pressure.

Mr. Karlovitz pointed out that solution of the practical flame stabilization problem is difficult since a flameholder produces both the velocity gradient and the return eddy, and these depend in a complex way on the conditions of the approach flow and the flameholder geometry. However, his criterion enables us to calculate the amount of heat required for flame stabilization, and thereby it opens up the possibility of dividing the problem into simpler ones which can be handled separately.

Dr. Zukoski:

He pictures the critical zone in flame stabilization as the shear layers outside the recirculation zone where the cool combustibles are heated by mixing with combustion products. In this concept the critical time characteristic of the stabilization process is the residence time of the material in the shear layers, which is given roughly by (L/u). Here, L is the measured length of the recirculation zone and (u) is the gas speed past the wake. If this time is greater than the chemical time, τ, required for ignition of a propagating flame then flame stabilization will be possible; however, if (L/u) is less than the chemical time, the flame will blow off. Therefore, the correct similarity parameter for the description for the stabilization phenomena is $(u\tau/L)$; when this dimensionless group is less than 1, stabilization will be possible. This parameter is particularly useful because L and u have been found experimentally to depend only on the fluid dynamic variables of the system and τ only on the chemical variables.

Dr. Zukoski also reported that recent experiments at JPL have indicated that the blockage ratio alone is an important parameter for flameholders of certain geometries and may be responsible for some of the observed differences in scaling laws. A correlation was shown for cylindrical flameholders which indicated that the L/D of the recirculation zone varied with the square root of the blockage ratio. This results because the spreading of the wake from a cylindrical flameholder decreases with increasing blockage. The effect causes the blowoff limit to vary with the square root of the diameter for cylindrical flameholders. However, for other flameholder shapes, such as the cone cylinder, wedge plates, etc., blockage has no effect on the wake geometry or the length of the recirculation zone and, therefore, the blowoff limit will vary directly with flameholder diameter.

In the discussion period that followed the presentations by panel members, several questions concerning stability problems were raised. Dr. Arch Scurlock pointed out that his blowout data still correlated with the 0.5 power of the flameholder width, even at very low blockage. Dr. Zukoski replied that the Jet Propulsion Laboratory data indicated that the maximum blowoff velocity was independent of scale for flameholders

operating at low blockage ratios and with laminar shear layers, but pointed out that for this result the extinction of the residual flame rather than the propagating flame had been used as the blowoff criteria. He added that it was quite possible that a .5 power law was appropriate to describe blowoff of propagating flame in this laminar flow regime.

The fact that tailpipe length, choked exit nozzles and disturbances in the flow upstream of flameholders all affect stability was generally agreed. However, much of the research work done on stability avoids these problems by the choice of apparatus. Dr. Scurlock stated that tailpipe lengths of 2.5 to 5 flameholder diameters (widths) seemed to have a minimum of effect on limits. Mr. Bennet mentioned that he had noted peculiar happenings and discontinuities at low pressures. Stability was not the problem, but performance seemed to deteriorate.

On the problem of screech, it was generally agreed that systems were needed to predict when screech would occur and what amplitude would result. A question was raised as to whether designers should not take advantage of screech rather than to avoid it. Of course, one of the difficulties is that a designer cannot be sure screech will result over the range of conditions he may require. In addition, severe pressure fluctuation made it difficult to design parts for extended life.

It appears to the Chairman that the various theoretical and experimental approaches to the flameholding problem which were presented are not contradictory but rather supplement each other. It is believed that the fusion of the fundamental concepts that were introduced here, such as heat release rate in the wake, time required for transfer of excess enthalpy to the fresh mixture, and the flame propagation across the boundary layer, will ultimately lead to a complete understanding of the flameholding process. This can result in substantial advances in flameholder design.

LIBRARY USE ONLY

10 002069814
UNIVERSITY OF HAWAII

QD516
S92
1956